

Review

# Speciation of arsenic and selenium compounds by HPLC hyphenated to specific detectors: a review of the main separation techniques

T. Guerin<sup>a</sup>, A. Astruc<sup>b</sup>, M. Astruc<sup>b,\*</sup>

<sup>a</sup> Agence Française de Sécurité Sanitaire des Aliments (A.F.S.S.A.), ex-CNEVA-Paris, 10 rue Pierre Curie, 94704 Maisons-Alfort Cedex, France

<sup>b</sup> Université de PAU et des Pays de l'Adour, Laboratoire de Chimie Analytique Bio-Inorganique et Environnement, EP CNRS 132, Avenue de l'Université 64000 Pau, France

Received 29 July 1998; received in revised form 22 April 1999; accepted 3 May 1999

## Abstract

This review deals with liquid phase separation of major arsenic and selenium species followed by element specific detection. It concerns papers published since 1980 and describing only currently used methods that were or could be applied to As and Se speciation in environmental matrices. Methods performances are compared on the basis of efficiency, rapidity, absolute and concentration detection limits and applicability to real world environmental samples. © 1999 Elsevier Science B.V. All rights reserved.

*Keywords:* Arsenic; Selenium; Speciation; HPLC

## 1. Introduction

For many elements, especially those belonging to the VA and VIA groups, HPLC separation of species is a most satisfying procedure in speciation studies because, contrary to GC separation, it does not imply complicated derivatisation steps of the analytes to form volatile derivatives. Detec-

tion limits and sensitivity to interference depends on the detector hyphenated to the HPLC separation. Element specific detectors involving atomic emission, absorption or fluorescence or else mass spectrometry are the most interesting ones in these respects.

There are many review papers dealing with analytical methods used for the determination of total concentration and of the speciation of arsenic and selenium.

The most recent ones are due to Irgolic [1], Morita and Edmonds [2], Greschonig and Irgolic

\* Corresponding author. Tel.: +33-05-59-92-31-52; fax: +33-05-59-02-93-77.

*E-mail address:* michel.astruc@univ-pau.fr (M. Astruc)

[3], Iffland [4], Crompton [5] and Van Loon and Barefoot [6] for arsenic; Roberecht and Van Grieken [7], Ihnat [8], Potin-Gautier et al. [9], Kölbl et al. [10], Dauchy et al. [11], Munoz Olivas et al. [12], Crompton [5], Van Loon and Barefoot [6], Cámara et al. [13], Sanz Alaejos and Diaz Romero [14], D’Ulivo [15] and Pyrzyńska [16–18] for selenium.

However, few reviews deal with liquid phase separation of species followed by element specific detection. Some papers [19–24] remain quite general and do not deal in depth with arsenic and selenium speciation. There are only two reviews devoted to this subject for arsenic [25,26] and one for selenium [27].

The following review deals with papers published since 1980. It describes the most commonly used speciation methods that were or could be applied to As and Se speciation in matrices such as water, soils and sediments thus limiting the study to the main compounds occurring in the different environmental compartments.

Synthesis Tables have been drawn so as to ease comparisons and help the reader in selecting the most suitable method adapted to his aim. Parameters in these tables are either taken directly from the original papers or recalculated by ourselves to unify the presentation, or presented as ‘ns’ (non specified).

Absolute detection limits or DL (in element mass unit) are the minimal mass of the element—whatever the species—that must be injected in the HPLC to obtain a significant signal. Most DL data concern standard solutions, they should certainly be reconsidered for the analysis of complex matrices. DL data marked with a star have been evaluated by the authors in the actual sample matrix.

Retention times given are only indicative because as they were often not reported by the authors most of them were evaluated from published figures; moreover it was usually impossible to know if reported values were corrected retention times or not.

We have used many symbols to simplify the Tables, we tried to choose them as obviously as possible. However a list of symbols is in Appendix A.

## 2. Selenium speciation methods

Two modes of liquid chromatography are of current use: direct ion exchange or ion-pairing reversed-phase separation. Vesicular chromatography, a particular reversed phase chromatography was recently introduced in an Se, As and Hg speciation study [28]. Several papers dealing with this mode of separation are considered below.

### 2.1. Reversed-phase or vesicle-mediated separation of Se species (Table 1)

This mode of separation concerns a third of published papers, using most often  $C_{18}$  columns. Typical mobile phase contains a tetrabutylammonium salt in isocratic water–methanol solution. This allows most authors to separate inorganic Se species, and using a  $1 \text{ ml min}^{-1}$  flow rate, retention times are lower than 10 min, Se(VI) being always the most retained species.

A recent paper by Kölbl et al. [29], at the cost of a solvent composition gradient, presents a method separating seven selenium species, five of which are organoselenium compounds. However the detector used (FAAS) is of very low sensitivity and the large methanol content (50%) of the solvent does not seem easily compatible with the plasma torch of ICP detectors. In a preceding paper Kölbl et al. [27], as well as Jabukowski et al. [30], indicate also the sensitivity of this separation to extreme pH values and salinity.

Few of these publications deal with the analysis of actual unspiked samples (urine [31–34], vegetables [35] and animal food additives [27]).

In urine, the use of vesicle-mediated chromatography and a gradient mode leads to separation of seven selenium species instead of four with reversed phase chromatography but DL obtained with the same system of detection used are not so good for inorganic selenium [33,34].

The lowest detection limits are obtained by non-classical methods such as post column on-line hydruration before ICP-MS detection [33] or ultrasonic nebulizer ICP-MS [30,31]; they are in the low  $\mu\text{g l}^{-1}$  range for solutions. Direct use of commercial ICP-MS as the detector [36] leads to DLs similar to those obtained with on-line

Table 1  
Separation of selenium species by ion-pairing reversed-phase or vesicle-mediated chromatography

Column	Mobile phase	Flow (ml min <sup>-1</sup> )	Matrix	Species (Rt (min))	Detection	DL (ng Se)	Ref.
<sup>PB</sup> Hamilton PRP-1 10 μm (250 × 4 mm)	2 mM TBAP+50% MeOH (v/v)	1	Animal Supplementa- tion	Se(IV) (3.3); Se(VI) (5.0)	FAAS	31; 51	[27]
<sup>PB</sup> Hamilton PRP-1 10 μm (250 × 4 mm)	Gradient: 2 mM TBAP then 2 mM TBAP+ 50% MeOH (v/v)	1	Standards	TMSe (1.9); SeCys (2.4); Se h-Cys (3.5); SeMet (4.6); SeEth (10.2); Se(IV) (11.8); Se(VI) (13.6)	FAAS	ns (Between 10 ng)	[29]
Cyanopropyl LC-SN 5 μm (150 × 4.6 mm)	0.015% (v/v) acetic acid+0.1 % (w/v) AAC	0.6	Spiked tap water, spiked ground wheat	Se(VI) (2.7); Se(IV) (3.1); SeCys (4.0); SeMet (4.4); SeEth (4.8)	THG-AAS (on- line)	1.3; 1.3; 1.1; 1.0; 1.4	[37]
C <sub>18</sub> Altex Lichro- sorb RP-1 10 μm (250×4.6 mm)	Gradient: 1 mM HTAB then MeOH, pH 7	0.5	Spiked synthetic river water	Se(IV) (3.0); Se(VI) (16)	GFAAS (on- line)	25; 25	[40]
<sup>PB</sup> Hamilton PRP-1 5 μm (400 × 4.1 mm)	0.625 mM TEAB, pH 4, +1% CH <sub>3</sub> CN (v/v)	0.4	White clover (CRM 402)	SeCys (9.0); Se(IV) (12); Se(VI) (14); SeMet (17)	GFAAS (on- line)	1.0; 1.0; 1.2; 0.8	[35]
C <sub>18</sub> Waters μBondapak 10 μm (150 × 3.9 mm)	2.5 mM TBAHS+10 mM K <sub>2</sub> HPO <sub>4</sub> +10 mM KH <sub>2</sub> PO <sub>4</sub> , pH 6.55	0.5	Spiked waters, spiked animal feed premixes	Se(IV) (4.0); Se(VI) (6.0)	DCP-AES	50; 50	[41]
C <sub>18</sub> Alltech Kro- masil 10 μm (250 × 4.6 mm)	5 mM TBAP, pH 3.4+50% MeOH (v/v)	1	Spiked tap water	Se(IV) (3.3); Se(VI) (4.9)	ICP-AES	ns; ns	[42]
Vydac 201 TP 10 μm (250 × 4.6 mm)	5 mM TBAP, pH 7.4	1.5	Standards	Se(IV) (3.1); Se(VI) (5.1)	USN-ICP-AES	2–3; 2–3	[43]
C <sub>18</sub> Spherisorb ODS 1 5 μm (250 × 4.6 mm)	5 mM TBAP+5% MeOH (v/v)	1	Spiked waters	Se(IV) (<10); Se(VI) (<10)	ICP-MS	1.25; 2.00	[36]
<sup>PB</sup> Hamilton PRP-1 5 μm (150 × 4.6 mm)	5 mM TBAP,pH 7.6+ 3% MeOH (v/v)	1.7	Urine (NIST SRM 2670)	TMSe (1.0); Se(IV) (2.3); Se(VI) (7.8)	USN-ICP-MS	0.022; 0.040; 0.074	[31]
C <sub>18</sub> Eurospher RP 100 5 μm (60 × 4 mm)	10 mM TBAA+40% MeOH (v/v)	1	Spiked tap water	Se(IV) (1.5); Se(VI) (2.7)	HHPN-ICP-MS	0.028; 0.028	[30]
C <sub>18</sub> <sup>SB</sup> Spherisorb 5 μm (250 × 4.6 mm)	0.1 M ammonium ethanoate, pH 4.5	1	Urine	Se(IV) (3.0); Se(VI) (3.0); SeMet (4.8); SeEth (9.2)	MD-HG-ICP- MS	0.019; 0.016; 0.059; 0.066	[33]

Table 1 (Continued)

Column	Mobile phase	Flow (ml min <sup>-1</sup> )	Matrix	Species (Rt (min))	Detection	DL (ng Se)	Ref.
<i>Vesicle-mediated chromatography</i>							
C <sub>18</sub> <sup>SB</sup> Spherisorb 10 μm (250 × 4.6 mm)	Gradient: 5 mM AAC, pH 5.0 + 0.5% MeOH (v/v) + 0.1 mM DDAB then 0.2 M AAC, pH 7.5, + 0.5% MeOH (v/v) + 200 mM DDAB	1	Standards	SeCys (3); SeMet (3.8); SeEth (5.6); Se(IV) (6.6); Se(VI) (8.2)	ETAAS (off-line)	2.5; 2.5; 2.5; 2.5; 2.5	[28]
C <sub>18</sub> <sup>SB</sup> Spherisorb 10 μm (250 × 4.6 mm)	Gradient: 10 mM CH <sub>3</sub> COONa, pH 5.0 + 0.5% MeOH (v/v) + 0.01 mM DDAB then 0.2 M CH <sub>3</sub> COONa, pH 7.5, 0.5% MeOH (v/v) + 0.01 mM DDAB	1	Urine	SeCys (4.5); SeMet (5.5); SeEth (7.3); Se(IV) (9.7); Se(VI) (10.4)	MD-HG-AAS	0.50; 0.50; 0.50; 0.50; 0.50	[32]
C <sub>18</sub> <sup>SB</sup> Spherisorb 5 μm (210 × 4.6 mm)	Gradient: 10 mM AAC, pH 4.0 + 0.5% MeOH (v/v) + 0.01 mM DDAB then 100 mM AAC, pH 6.5 + 0.5% MeOH (v/v) + 0.01 mM DDAB	1	Urine	TMSe (3.9); SeCys (4.1); SeC(NH <sub>2</sub> ) <sub>2</sub> (4.9); SeMet (5.7); SeEth (8.9); Se(IV) (11.6); Se(VI) (12.5)	MD-HG-ICP-MS	2.585 <sup>a</sup> ; 0.265; 0.080; 0.051; 0.105; 0.225; 0.115	[34]

<sup>a</sup> DL data have been evaluated in the actual sample matrix.

GFAAS [35] or THG-AAS [37]. However the slow sequential detection by on-line GFAAS induces the necessity of low solvent flow rates to maintain a satisfying selectivity [38]; this seriously increases analysis time [39].

## 2.2. Ion exchange separation of Se species (Table 2)

Various anion exchange columns have been used, Hamilton PRP-X100 being often preferred for this purpose together with ESA Anion III. Most authors elaborated isocratic eluents based on either phosphate, carbonate, citrate or phthalate anions. Eight out of the 23 papers reviewed deal with inorganic selenium species. Their order of elution does not vary, Se(VI) being the most strongly retained.

Organoselenium compounds studied are essentially Se–cystine and Se–methionine; trimethylselenonium (TMSe) is not retained and elutes in the dead volume. Kölbl et al. [39] show that analysis in these conditions is possible at extreme pH values and high salinity, Cai et al. [36] indicate however that high chloride concentrations may affect the separation, working at analyte concentrations lower by two orders of magnitude.

Sequential detection by on-line GFAAS induces long analysis time [39,44], shorter anyway than detection by off-line GFAAS analysis of collected fractions [45], and allows the analysis of complicated matrices (yeasts).

On-line ICP-MS detection is the most frequently used method nowadays and leads to the lowest detection limits (approximately  $2 \mu\text{g l}^{-1}$ ) or even less with an unusual DIN nebulizer [46].

Most papers deal with the analysis of standard solutions. Actual samples analysed are animal food additives, yeasts, urine, fish (cod), vegetables and certified reference materials.

## 3. Arsenic speciation methods

Ion pairing in reverse mode and ion exchange are also the favourite chromatographic processes used by most authors. However vesicular chromatography has also been the object of some attempts.

### 3.1. Reversed-phase or vesicle-mediated separation of As species

For sake of convenience, methods using ICP-MS as the detector have been separated from the others.

#### 3.1.1. Detectors other than ICP-MS (Table 3)

Most authors use  $C_{18}$  columns and isocratic conditions and consider methylated as well as inorganic As species. The elution order of the various species is different and may even vary drastically for the same authors with slight differences in eluent composition [62–65].

The majority of these publications present analysis of actual samples such as water [43,66–70], urine [63,71] or certified reference materials [48,64,65,68,70,72].

The lowest DL are obtained through post column hydride generation (approximately  $1 \mu\text{g l}^{-1}$ ). Hyphenating optical ICP to HPLC, on the contrary, leads to DL in the range of 50–100  $\mu\text{g l}^{-1}$ , i.e. far too high to allow direct application to tap water analysis (the usual As recommended maximum total concentration is  $50 \mu\text{g l}^{-1}$ ).

The recent vesicular chromatography has been essentially used for analysis of synthetic samples or standards. It has often been coupled to atomic fluorescence detector but the detection limits obtained are not better than those obtained for reversed-phase chromatography. However, interfacing hydride generation improves, once more, the DL by a factor of 6–14 [73,74].

#### 3.1.2. ICP-MS detection (Table 4)

$C_{18}$  and PRP-1 columns are prevalent as well as isocratic elution. The species studied are most often those that may be found in water or soil samples: As(III), As(V), MMA and DMA, a few authors dealing also with AsB and AsC that occur only in living organisms.

Overall analysis time are close to 10 min except for Shum et al. [78] who use a very low flow rate of chromatographic eluent. Most of these methods have been applied to actual samples.

DLs with ordinary commercial equipment are close to  $1 \mu\text{g l}^{-1}$  per species in solution, i.e. similar to those obtained via hydride generation-

Table 2  
Separation of selenium species by anion exchange chromatography

Column	Mobile phase	Flow (ml min <sup>-1</sup> )	Matrix	Species (Rt (min))	Detection	DL (ng Se)	Ref.
ESA Anion III 10 µm (250 × 4 mm)	10 mM KHP, pH 7.0	2.5	Animal supplementa- tion	Se(IV) (1.3); Se(VI) (2.1)	FAAS	8; 11	[39]
ESA Anion III 10 µm (250 × 4 mm)	Gradient: 2 mM KHP, pH 9 then 12 mM KHP, pH 9, +20% MeOH (v/v)	2	Standards	TMSe (1.1); SeCys (1.6); Se(IV) (2.5); Se h-Cys (3.1); SeMet (3.9); Se(VI) (7.2); SeEth (8.3)	FAAS	ns (Between 10 ng)	[29]
<sup>PB</sup> Merck Polyspher IC AN-2 10 µm (120 × 4.6 mm)	6 mM salicylate ion, pH 8.5+3% MeOH	1	Standards	SeMet (2.3); Se(Cys) <sub>2</sub> (3.6); Se(IV) (5.2); Se(VI) (7.9)	FAAS	90; 100; 100; 120	[47]
<sup>PB</sup> Polymer PL-SAX 8 µm (150 × 4.6 mm)	0.1% (w/v) (NH <sub>4</sub> ) <sub>2</sub> CO <sub>3</sub> + 10 mM NH <sub>4</sub> OH	0.6	Standards	Se(IV) (4.7); Se(VI) (7.0)	THG-AAS	2.0; 2.0	[48]
<sup>PB</sup> Hamilton PRP-X100 10 µm (250 × 4.1 mm)	0.1 M phosphate buffer, pH 6.8	1.5	Spiked tap waters	TMSe (1.8); Se(IV) (2.5); Se(VI) (4.3)	MR-HG-QFAAS	1.1; 1.4; 2.2	[49]
Dionex AS12A (ns)	8.3 mM Na <sub>2</sub> HPO <sub>4</sub> , pH 9.2	1.5	Standards	SeMet (3.1); Se(IV) (4.8); Se(VI) (7.7)	MR-HG-QFAAS	10.3; 1.5; 1.2	[50]
Benson BAX-10 ns µm (50 × 4.6 mm)	0.1 M K <sub>2</sub> SO <sub>4</sub> , pH 5	2	NIST SRM 1643c; trace elements in H <sub>2</sub> O	Se(IV) (2.8); Se(VI) (9.2)	MR-HG-AFS	0.22; 0.31	[51]
ESA Anion III 10 µm (250 × 4 mm)	3 mM KHP saturated with Ni(OH) <sub>2</sub> , pH 7.0	0.4	Standards	Se(IV) (10); Se(VI) (31)	GFAAS (on-line)	1.00; 0.60	[39]
<sup>SB</sup> Nucleosil 100-SB 10 µm (50 × 2 mm)	Gradient: 10 mM am- monium citrate, pH 3 then 7	0.6	Spiked water; urine	TMSe (1.2); Se(IV) (5.2); Se(VI) (8.8)	GFAAS (off- line)	1.67; 1.27; 0.76	[45]
<sup>PB</sup> Hamilton PRP-X100 10 µm (250 × 4.1 mm)	Gradient: 2 g l <sup>-1</sup> nickel ethanoate then nickel sulphite, pH 6.5	0.4	Yeast	SeCys (6); SeMet (15); Se(IV) (20); Se(VI) (30)	GFAAS (on-line)	0.80; 1.50; 1.70; 1.20	[44]
Dionex PAX 100 Guard column ns µm (50 × 2 mm)	15 mM (NH <sub>4</sub> ) <sub>2</sub> CO <sub>3</sub> , pH 10, +2% MeOH	0.08	BCR CRM 402 (white clover)	SeMet (1.3); Se(IV) (2.5); Se(VI) (4.5); Se- Cys (5.5)	GFAAS (off- line)	0.062; 0.047; 0.042; 0.048	[52]
HPIC-AS4 ns µm (150 × 3 mm)	25 mM Na <sub>2</sub> CO <sub>3</sub>	2	Standards	Se(IV) (1.8); Se(VI) (2.9)	DCP-AES	ns; ns	[53]
Waters IC-PAK 10 µm (150 × 4.0 mm)	80 mM ammonium ci- trate	1	Standards	TMSe (1.4); Se(IV) (3.0); Se(VI) (7.6)	Thermospray- ICP-AES	14; 14 < x < 54; 54	[54]
<sup>PB</sup> Hamilton PRP-X100 10 µm (250 × 4.1 mm)	Gradient: 25 mM phosphate buffer then 50 mM, pH 6.7	1	Standards	SeCys (2.5); Se(IV) (4.7); SeMet (7.1); Se(VI) (15.3)	ICP-AES	380; 700; 760; 440	[55]
Dionex PAX 100 Guard column ns µm (50 × 2 mm)	10–20 mM (NH <sub>4</sub> ) <sub>2</sub> CO <sub>3</sub> , pH 10, + 2% MeOH	0.08	BCR CRM 402 (white clover)	SeMet (1.2); Se(IV) (1.9); Se(VI) (3.1); Se- Cys (4.2)	DIN-ICP-AES	0.57; 0.35; 0.53; 0.30	[56]

Table 2 (Continued)

Column	Mobile phase	Flow (ml min <sup>-1</sup> )	Matrix	Species (Rt (min))	Detection	DL (ng Se)	Ref.
CETAC MCANX1710 5 µm (100 × 1.6 mm)	5 mM (NH <sub>4</sub> ) <sub>2</sub> CO <sub>3</sub> /5 mM NH <sub>4</sub> HCO <sub>3</sub>	0.1	Standards	Se(IV) (3.4); Se(VI) (9.0)	DIN-ICP-MS	0.014; 0.015	[46]
<sup>PB</sup> Hamilton PRP-X100 10 µm (250 × 4.6 mm)	80 mM (NH <sub>4</sub> ) <sub>2</sub> CO <sub>3</sub> /80 mM NH <sub>4</sub> HCO <sub>3</sub>	0.8	Spiked waters	Se(IV) (3.3); Se(VI) (5.9)	ICP-MS	0.40; 0.42	[36]
ESA Anion III 10 µm (250 × 4 mm)	5 mM KHP, pH 7.0	0.92	Standards	Se(IV) (4.1); Se(VI) (9.6)	ICP-MS	0.10; 0.10	[57]
<sup>PB</sup> Merck Polyspher IC AN-2 ns µm (120 × 4.6 mm)	5 mM salicylate, pH 8.5	0.75	Cooked cod	SeMet (2.8); SeCys (4.1); Se(IV) (6.7); Se(VI) (10.9)	ICP-MS	0.20	[58]
<sup>PB</sup> Hamilton PRP-X100 PEEK (150 × 4.6 mm)	5 mM ammonium cit- rate, pH 4.8	1	Selenium enriched veg- etables	SeCys (2); MetSeCys (2.5); Se(IV) (3.2); SeMet (4.4); SeallylSeC (9); Se(VI) (11)	ICP-MS	ns	[59]
<sup>SB</sup> Spherisorb 5 ODS- AMINO 5 µm (250 × 4.6 mm)	Gradient: 3.5 mM then 7 mM phosphate buffer, pH 6	1	Certified water for Se(IV) and Se(VI); (BCR CRM 603)	SeCys (3); SeMet (4.2); Se(IV) (6.3); Se(VI) (12.2)	ICP-MS	0.20; 0.10; 0.16; 0.12	[60]
<sup>PB</sup> Hamilton PRP-X100 ns µm (150 × 4.6 mm)	5 mM ammonium cit- rate, pH 4.8, +2% MeOH	1	Garlic	SeCys (1.9); MetSeCys (2.6); Se(IV) (3.3); SeMet (4.3); AllylSeCys (9); Se(VI) (11.1)	ICP-MS	ns	[61]
<sup>PB</sup> Merck Polyspher IC AN-2 10 µm (120 × 4.6 mm)	6 mM salicylate ion, pH 1 8.5, +3% MeOH	1	BCR CRM 402 (white clover)	SeMet (2.0); Se(Cys) <sub>2</sub> (2.7); Se(IV) (4.2); Se(VI) (7.3)	ICP-MS	0.07; 0.11; 0.08; 0.11	[47]

Table 3

As species separation by ion-pairing reversed-phase or vesicle-mediated chromatography coupled to detectors other than ICP-MS

Column	Mobile phase	Flow (ml min <sup>-1</sup> )	Matrix	Species (Rt (min))	Detection	DL ((ng As))	Ref.
C <sub>18</sub> ChromSpher 5 μm 2 × (100 × 3 mm)	10 mM TBA + 20 mM NaH <sub>2</sub> PO <sub>4</sub> , pH 6	1	Urine	As(III) (1.0); DMA (1.5); MMA (2.0); As(V) (2.7)	HG-AAS	0.05; 0.08; 0.06; 0.24	[71]
<sup>PB</sup> Dionex NS-1 (ns)	5 mM TBAP + 5% MeOH, pH 7.3	1	Groundwaters	As(III) (2.1); DMA (3.2); MMA (4.0); As(V) (6.3)	HG-AAS	0.07; 0.15; 0.10; 0.10	[67]
<sup>PB</sup> Dionex NS-1 5 μm (250 × 4.6 mm)	0.15 mM TBAP pH 5.8	1	Groundwaters NIST SRM 1643b	As(III) (2.7); DMA (5.3); MMA (8.4); As(V) (18.5)	HG-AAS	0.07; 0.11; 0.12; 0.30	[68]
<sup>PB</sup> Hamilton PRP-1 10 μm (150 × 4.1 mm)	10 mM TBAOH/TBAP, pH 6.15	1	Tuna powder; EEC mussel material (BCR CRM 278); Cod sam- ple	As(III) (2.4); DMA (4.2); MMA (6.0); As(V) (13.1)	HG-AAS	0.15; 0.43; 0.33; 0.84	[72]
C <sub>18</sub> Phenomenex Bond- clone 10 μm (300 × 3.9 mm)	10 mM hexanesul- fonate, pH 3.5	1	Standards	As(V) (4.0); As(III) (4.9); DMA (6.0); MMA (8.7); AsB (12.6)	MD-HG-AAS	ns	[62]
C <sub>18</sub> Phenomenex ODS(3) 5 μm (250 × 4.6 mm), 70°C	Gradient: 10 mM hep- tanesulfonate, pH 3.5, then 10 mM methane- sulfonic acid + 4 mM malonic acid + 2% MeOH, pH 3.0	1	Standards	As(V) (4.0); As(III) (5.1); MMA (6.8); DMA (9.0); AsB (11.8); AsC (24); TMAs (30)	MD-HG-AAS	ns	[64]
C <sub>18</sub> Phenomenex ODS(3) 5 μm (30 × 4.6 mm), 30°C	10 mM TBAH + 1 mM malonic acid + 5% MeOH, pH 6.0	1	Standards	As(III) (0.3); DMA (0.7); MMA (1.0); As(V) (1.5)	MD-HG-AAS	ns	[65]
Supelcosil LC CN 5 μm (150 × 4.6 mm)	0.01% Acetic acid (v/v)	0.6	Dogfish muscle (DORM-1)	As(V) (2.0); MMA (3.0); DMA (4.0); As(III) (6.9)	THG-AAS	0.70; 1.00; 1.00; 0.80	[48]
Phenomenex Spherisorb ODS 1 5 μm (150 × 4.6 mm)	12 mM phosphate buffer, pH 10.7	2	Ground water; waste water; synthetic sedi- ment extract	As(III) (2.8); AsB/ AsC (3.7); DMA (6.5); MMA (7.2); As(V) (8.0)	MO-HG-AAS	9.70; 10.0; 12.2; 12.8; 14.3	[69]
C <sub>18</sub> Altex Lichrosorb RP-1 10 μm (250 × 4.6 mm)	Gradient: 1 mM HTAB, pH 9.5, then H <sub>2</sub> O/MeOH/ACN (6:4:1)	0.4 Then 0.5	Spiked synthetic river water	As(III) (3.0); DMA (11); MMA (28); As(V) (45)	GFAAS (on- line)	15; 15; 15; 15	[40]
C <sub>18</sub> Phenomenex 10 μm (300 × 3.9 mm), 70°C	10 mM hexanesul- fonate + 1 mM TEAH + 0.5% MeOH, pH 4	1	Urine	As(V) (3.8); As(III) (4.3); AsB (5.0); MMA (6.0); DMA (7.0); AsC (10); TMAs (12)	HG-AFS	ns	[63]
C <sub>18</sub> Phenomenex ODS(3) 5 μm (250 × 4.6 mm), 70°C	10 mM hexanesul- fonate + 1 mM TEAH + 0.5% MeOH, pH 4	0.8	Urine (NIST SRM 2670)	As(V) (3.4); As(III) (4.3); AsB (5.1); MMA (6.6); DMA (7.8); AsC (10.2); TMAs (11.6)	HG-AFS	ns	[64]



Table 3 (Continued)

Column	Mobile phase	Flow (ml min <sup>-1</sup> )	Matrix	Species (Rt (min))	Detection	DL ((ng As))	Ref.
C <sub>18</sub> Phenomenex ODS(3) 5 μm 2 × (30 × 4.6 mm), 30°C	5 mM TBAH+2 mM malonic acid+0.5% MeOH, pH 5.9	0.9	Urine (NIST SRM 2670)	As(III) (1.0); DMA (1.4); MMA (2.1); As(V) (3.1)	HG-AFS	<sup>a</sup> 0.010; 0.014; 0.008; 0.016	[65]
C <sub>18</sub> Phenomenex ODS(3) 5 μm (250 × 4.6 mm), 70°C	5 mM TBAH+4 mM malonic acid+5% MeOH, pH 6.0	1	Standards	As(III) (2.8); DMA (4.2); MMA (5.7); As(V) (8.0)	HG-AFS	ns	[65]
C2 Lichrosorb 10 μm (120 × 4.6 mm)	H <sub>2</sub> O/MeOH 95:5 (v/v) saturated with TBAP, pH 7.3	1	Standards	As(III) (2.5); As(V) (4.2)	ICP-OES	155; 75	[76]
<sup>PB</sup> HAMILTON PRP-1 10 μm (150 × 4.1 mm)	Gradient: 0.5 then 20 mM TBAP, pH 9.5	1	Tuna powder; EEC mussel material (BCR CRM 278); cod sample	AsC (1.9); AsB (2.5); As(III) (3.9); DMA (6.7); MMA (10.1); As(V) (12.3)	ICP-OES	120; 110; 120; 130; 100; 130	[72]
C <sub>18</sub> Whatman Partisil 5 ODS-3 10 μm (250 × 4.6 mm)	5 mM TBAP, pH 7.5+ 10% MeOH (v/v)	1	Undergroundwaters	As(III) (4.0); MMA (5.0); DMA (5.6); As(V) (7.7)	USN-ICP-AES	6–9	[43]
C <sub>18</sub> Excalibar Spherisorb ODS 5 μm (150 × 4.6 mm)	5 mM TBAP, pH 7.15	1	Groundwaters	As(III) (2.4); DMA (3.0); As(V) (8.0)	HG-ICP-AES	10; 21; 10	[66]
<i>Vesicle-mediated chromatography</i>							
C <sub>18</sub> <sup>SB</sup> LKB Lichrosorb RP 18 10 μm (240 × 4 mm), 30°C	10 mM NaH <sub>2</sub> PO <sub>4</sub> , pH 5.75, +0.01 mM DDAB+0.5% MeOH	1	Spiked tap water; spiked human urine	As(III) (2.9); DMA (4.5); MMA (5.8); As(V) (9.4)	HG-ICP-AES	0.5; 1.0; 0.6; 1.2	[77]
C <sub>18</sub> <sup>SB</sup> Spherisorb ODS 2 10 μm (250 × 4.6 mm)	5 mM NaH <sub>2</sub> PO <sub>4</sub> , pH 5.75, +0.01 mM DDAB+1% MeOH	1.3	Spiked sea water; spiked tap water; spiked urine	As(III) (2.8); DMA (4.6); MMA (5.9); As(V) (9.8)	HG-ICP-AES	0.5–1.2	[28]
C <sub>18</sub> <sup>SB</sup> Spherisorb ODS 2 10 μm (250 × 4.6 mm)	10 mM NaH <sub>2</sub> PO <sub>4</sub> , pH 5.75, +0.01 mM DDAB+0.5% MeOH	1	Spiked tap water; spiked urine	As(III) (2.3); DMA (4.1); MMA (9.5); As(V) (12.0)	HG-MIP-AES	0.10; 0.60; 0.12; 0.50	[75]
C <sub>18</sub> BST Rutin 10 μm (25 × 4.6 mm), 24°C	20 mM phosphate buffer, pH 6, +0.1% (v/v) of 10 mM DDAB+0.5% (v/v) MeOH	1	Standards	As(III) (3); DMA (3.7); MMA (4.8); As(V) (9.3)	USN-AFS	35; 20; 20; 50	[73]
C <sub>18</sub> BST Rutin 10 μm (25 × 4.6 mm), 24°C	Gradient: 10 mM to 50 mM phosphate buffer, then 50 mM phosphate buffer+0.01 mM DDAB+0.5% MeOH (v/v), pH 6	2	Six drilled well waters; fresh water (NIST 1643c)	As(III) (1.4); DMA (2.2); MMA (5.1); As(V) (6.3)	HG-AFS	3.2; 2.9; 4.3; 4.5	[70]
C <sub>18</sub> BST Rutin 10 μm (25 × 4.6 mm), 24°C	20 mM phosphate buffer, pH 6, +0.1% (v/v) of 10 mM DDAB+0.5% (v/v) MeOH	0.8 To 2	Standards	As(III) (3.9); DMA (4.9); MMA (6.6); As(V) (10.9)	HG-USN-AFS	2.5; 3.2; 2.0; 6.0	[74]

<sup>a</sup> DL data have been evaluated in the actual sample matrix.

Table 4  
Separation of arsenic species by ion-pairing reversed-phase chromatography coupled to ICP-MS detector

Column	Mobile phase	Flow (ml min <sup>-1</sup> )	Matrix	Species (Rt (min))	Detection	DL (ng As)	Ref.
<sup>PB</sup> Hamilton PRP-1 10 μm (150 × 4.1 mm)	5 mM TBAH + 4% MeOH, pH 6	1	Dogfish muscle (DORM-1)	AsB (1.9); As(III); (2.0); DMA (3.5); MMA (5.5); As(V) (12.3)	ICP-MS	0.15; 0.15; 0.15; 0.15; 0.15	[82]
Inertsil ODS-2 (250 × 4.6 mm)	10 mM TEAH + 0.05% MeOH (v/v), pH 6.8	0.75	Urine	As(III) (3.8); MMA (4.4); DMA (4.8); As(V) (5.0) + 11 As <sup>orga</sup>	ICP-MS	0.02–0.05	[83]
C <sub>18</sub> Phenomenex Bondclone 10 μm (300 × 3.9 mm)	10 mM hexanesulfonate, pH 3.5	1	Standards	As(V) (3.2); As(III) (4.0); DMA (5.1); MMA (7.6); AsB (11.8)	ICP-MS	ns	[62]
<sup>PB</sup> Hamilton PRP-1 10 μm (250 × 4.6 mm)	0.5 mM TBAP + 4mM Na <sub>2</sub> HPO <sub>4</sub> , pH 9, + 2% MeOH	0.9	Three mineral bottle waters; 12 spring waters	AsC (2.0); AsB (2.3); As(III) (2.5); DMA (3.5); MMA (5.6); As(V) (10.0)	ICP-MS	0.07; 0.07; 0.05; 0.08; 0.15; 0.13	[84]
<sup>PB</sup> Hamilton PRP-1 10 μm (250 × 4.6 mm)	0.5 mM TBAP + 4mM Na <sub>2</sub> HPO <sub>4</sub> , pH 9	0.85	Fish muscle; mussel tissue (BCR CRM 278)	AsC (2.0); AsB (2.4); As(III) (2.8); DMA (3.5); MMA (7.0); As(V) (10.1)	ICP-MS	0.18; 0.12; 0.12; 0.20; 0.44; 0.50	[85]
C <sub>18</sub> Alltech Nucleosphere 5 μm (250 × ns mm)	5 mM TBAP	0.9	Urine (NIST SRM 2670)	As(III) (4.8); DMA (6.7); MMA (11.2); As(V) (11.2)	HG-ICP-MS	0.046; ns ;ns; ns	[86]
C <sub>18</sub> Vydac 201TP 5 μm (250 × 4.6 mm)	1 mM TBAP + 2 mM AAC + 2% MeOH, pH 6	1	Tap water; spring water; underground water; river water SLRS-2	As(III) (3.2); DMA (5.1); MMA (6.8); As(V) (9.8)	HG-ICP-MS	0.0022; 0.0036; 0.0056; 0.0102	[81]
SGE Inertsil ODS-2 5 μm (100 × 1.0 mm)	5 mM HTEAP, pH 6, + 5% MeOH	0.03	Standards	As(III) (2.0); DMA (5.0); MMA (7.6); As(V) (29.7)	DIN-ICP-MS	0.0006; 0.0006; 0.0005; 0.0006	[78]
SGE Inertsil ODS-2 5 μm (100 × 1.0 mm)	Gradient: 5 mM HTEAP, pH 7, + 5% MeOH then 5 mM HTEAP + 25% MeOH, pH 7	0.03	Standards	As(III) (2.4); DMA (4.3); MMA (9.5); As(V) (14.1)	DIN-ICP-MS	0.0002; 0.0002; 0.0002; 0.0002	[78]
C <sub>18</sub> <sup>SB</sup> Spherisorb 3 μm (150 × 1 mm)	1 mM TEAH, pH 5.28 + 0.5% MeOH (v/v)	0.04	Standards	As(III) (2.1); DMA (3.8); MMA (5.9); As(V) (6.7); p-As (7.4)	HEN-ICP-MS	0.0006; 0.0012; 0.0011; 0.0004; 0.0009	[79]
C <sub>18</sub> <sup>SB</sup> Spherisorb 3 μm (150 × 1 mm)	5 mM TEAH, pH 5.8, + 0.5% MeOH (v/v)	0.04	Water (NIST SRM 1643a); soil extract (NIST SRM 2709); urine (NIST SRM 267(n))	As(III)/AsB (1.9); DMA (3.0); MMA (3.4); p-As (4.5); As(V) (5.0); 4-OH (8.3)	HEN-ICP-MS	0.0006; ns; ns; 0.0009; 0.0004; 0.0008	[80]

AAS. Shum et al. [78] using a DIN nebuliser or Pergantis et al. [79,80] using a HEN nebuliser claim to reach absolute DL lower than 1 pg, i.e. for a 100  $\mu\text{l}$  injection a concentration DL lower than 10  $\text{ng l}^{-1}$  per species. Hwang and Jiang [81] interfacing hydride generation between HPLC and ICP-MS proposed a very sensitive method also (DL in the 20–100  $\text{ng l}^{-1}$  range).

However, Beauchemin et al. [82] or Szpuńar-Lobinska et al. [23] point out that reversed-phase chromatography is hardly applicable to real world samples, as this mode of separation is prone to severe matrix interferences and pH effects and suggest that the ion exchange mode, although producing a poorer selectivity, is much less sensitive to these phenomena because of the higher buffering capacity of the mobile phase.

### 3.2. Ion exchange separation of As species

#### 3.2.1. Detectors other than ICP-MS (Table 5)

Many publications appeared especially during the last 10 years dealing with ion exchange separation of As species coupled to various specific detectors. Many different columns have been tested, Hamilton PRP-X100 being the most commonly used with phosphate eluents in isocratic or gradient modes, gradients being often associated with post column hydride generation. Common analytes are As(III), As(V), MMA and DMA but other organoarsenical derivatives are sometimes considered, i.e. AsB, AsC, TMAs or some exotic compounds.

At pH lower than 10, the order of elution is usually As(III), DMA, MMA, As(V) and at higher pH, DMA appears first [62,87] or after MMA [88–91]. These apparently surprising differences of behaviour may probably be explained by rather strong hydrophobic interactions of organoarsenical species with some stationary phases. Some authors indicate however that the separation performances of silica-based (SB) columns may degrade quite rapidly. After a few tens of analysis the efficiency and reproducibility may be seriously affected [92]. What is more, the pH range that may be used with SB columns is more reduced than with polymer-based stationary phases and cannot exceed pH 8.5 [93]. Using

another type of column Chana and Smith [89] and Rauret et al. [90] noted similar—although slower—degradation phenomena.

On the other hand, Heitkemper et al. [94] indicated a fast degradation of performances of their polymer-based column after only 50 urine analysis and Zhang et al. [91] preferred an SB phase giving a higher resolution and found it stable. Too fast a degradation may be overcome by lowering the mobile phase concentration, with the following side effects: longer analysis and some loss of resolution for the most retained species.

Half of the publications deal with actual environmental samples such as water, urine, soil leachates, estuarine sediments, fish or mollusc tissues, i.e. a wide diversity of matrices. The most recent studies contain applications to reference materials certified for their total arsenic content such as DORM-1 (dogfish) This is a very important point as these certified reference materials are available to all experimentators and should be analysed by every new method proposed to allow rational performance comparisons.

DLs vary widely; it is only when hydride generation is used in conjunction with ICP-AES or QFAAS that DL low enough to analyse directly tap water are obtained.

#### 3.2.2. ICP-MS detection (Table 6)

This set of methods (ion exchange HPLC-ICP-MS) appears to be spreading quite rapidly. There are several reasons. On the separation side it appears possible to separate by ion exchange HPLC most of the significant As species: As(III), As(V), MMA, DMA, AsB and AsC. TMAsO is not considered except by Inoue et al. [124] and Kawabata et al. [125]. Interfacing ICP-MS to HPLC is extremely simple and, provided that the compatibility of the mobile phase with plasma torch behaviour and mass detection interference has been carefully established, low DLs may be obtained. Absolute DL which were in the 0.05–2  $\text{ng}$  range 10 years ago have now been divided by 10, i.e. concentration DL close to 0.1  $\mu\text{g l}^{-1}$  became common thus allowing direct As speciation in drinking water or easy handling of other more complicated matrices such as fish [126] or mollusc samples [127], soft drinks or wine [128],

Table 5  
Separation of arsenic species by anion exchange chromatography coupled to detectors other than ICP-MS

Column	Mobile phase	Flow (ml min <sup>-1</sup> )	Matrix	Species (Rt (min))	Detection	DL (ng As)	Ref.
<sup>PB</sup> Merck Polyspher IC AN 2 10 µm (120 × 4.6 mm), 50°C	0.1 M NaHCO <sub>3</sub> , pH 10.25	1	Aqueous extract of soil samples	AsB (1.5); DMA (1.8); As(III) (2.1); MMA (2.5); As(V) (3.0)	FAAS	30; 70; 110; 140; 140	[87]
<sup>PB</sup> Hamilton PRP-X100 10 µm (250 × 4.1 mm)	30 mM ethanoate buffer, pH 5	1.5	Standards	As(III) (1.3); DMA (1.8); MMA (4.7); As(V) (7.2)	FAAS	1000	[95]
<sup>PB</sup> Hamilton PRP-X100 10 µm (250 × 4.1 mm)	6 mM sodium sulphate, pH 5.9	1.5	Standards	As(III) (2); DMA (2.7); MMA (4.1); As(V) (8.9)	FAAS	1000	[95]
<sup>PB</sup> Hamilton PRP-X100 10 µm (250 × 4.1 mm)	15 mM tartaric acid, pH 2.91	1	Standards	AsC (2.0); AsB (2.6); As(III) (2.9); DMA (3.7); MMA (4.7); As(V) (9.8)	FAAS	ns	[96]
<sup>SB</sup> Synchropak Q300 6.5 µm (100 × 4.6 mm)	10 mM malonic acid, pH 6.6	1	Standards	AsC (1.2); AsB (1.3); As(III) (1.6); DMA (2.0); MMA (2.3); As(V) (6.3)	FAAS	ns	[96]
<sup>PB</sup> Benson BAX-10 5 µm (200 × 5.0 mm)	Gradient: 0.1 M NH <sub>4</sub> CO <sub>3</sub> then 10–4% (v/v) H <sub>2</sub> SO <sub>4</sub>	4	10 Mineral bottle waters; waterlogged soil	As(III) (0.8); DMA (1.6); MMA (1.85); As(V) (2.75)	HG-AAS	2; 1; 2; 2	[97]
<sup>SB</sup> Nucleosil 10SB ns µm (250 × 4.6 mm)	50 mM phosphate buffer, pH 6.75	0.5	Hijiki extract	As(III) (3.6); DMA (7.4); MMA (9.1); As(V) (18.9)	HG-AAS	1; 2; 2; 7	[98]
<sup>PB</sup> Hamilton PRP-X100 10 µm (250 × 4.1 mm)	Gradient: 2.5 mM phosphate buffer, pH 6.0, then 100 mM, pH 6.5	2	Drinking water; Adit + 6 creek waters of a old mining area	As(III) (3.9); DMA (4.9); MMA (6.6); As(V) (10.9)	HG-AAS	0.5	[99]
<sup>PB</sup> Dionex OmniPak PAX-500 or IonPak AS11 ns µm (250 × 4.6 mm)	30 mM NaOH + 1% MeOH	1	Estuarine sediments (MESS-1, PACS-1, NBS-1646); coal fly ash (NBS-1633b)	As(III) (2.2); As(V) (4.2)	HG-AAS	0.2; 0.2	[100]
<sup>PB</sup> Hamilton PRP-X100 10 µm (250 × 4.1 mm)	17 mM phosphate buffer, pH 6.0	3	Spiked river; spiked mineral waters	DMA (1.4); MMA (2.3); As(V) (5.5)	HG-AAS	0.2; 0.3; 0.6	[101]
IC-Pak AHR 6 µm (75 × 4.6 mm)	Gradient: 12.5 mM NaHCO <sub>3</sub> , pH 8.0, then H <sub>2</sub> O	1 Then 0.5	Geothermal water	As(III) (7); DMA (20); As(V) (32)	HG-AAS (off-line)	ns	[102]
<sup>PB</sup> BDH Polyspher SAW ns µm (120 × 4.6 mm)	50 mM phosphate buffer, pH 10.3	1	Standards	DMA (2); As(III) (3.4); MMA (6.3); As(V) (8.7)	MD-HG-AAS	0.2; 0.2; 0.3; 0.4	[62]

Table 5 (Continued)

Column	Mobile phase	Flow (ml min <sup>-1</sup> )	Matrix	Species (Rt (min))	Detection	DL (ng As)	Ref.
<sup>B</sup> Benson BAX-10 ns µm (150 × 4.6 mm) 60°C	Gradient: 0,1 mM at 75 mM K <sub>2</sub> SO <sub>4</sub> , pH 10.4	1	Lobster hepatopan- creas (TORT-1); dogfish muscle (DORM-1)	AsB (5.5); DMA (7.1); MMA (13.4); As <sub>inorg</sub> (15.1)	MD-HG-AAS	2.5; 5.3; 3.3; 5.9	[103]
<sup>PB</sup> Hamilton PRP- X100 10 µm (250 × 4.1 mm)	12 mM phosphate buffer, pH 10.7	2	Ground water; waste water; synthetic sedi- ment extract	AsB/AsC (1.6); As(III) (2.0); DMA (2.7); MMA (4.0); As(V) (7.5)	MO-HG-AAS	1.54; 1.43; 1.46; 1.60; 2.10	[71]
<sup>PB</sup> Hamilton PRP- X100 10 µm (250 × 4.1 mm)	12 mM phosphate buffer, pH 6	2	Ground water; waste water; synthetic sedi- ment extract	AsC (1.2); As(III)/AsB (1.6); DMA (2.4); MMA (3.5); As(V) (8.8)	MO-HG-AAS	1.17; 1.21; 1.59; 1.56; 1.18	[71]
Spherisorb ODS/NH <sub>2</sub> mixed column 5 µm (250 × 4.6 mm) 25°C	5 mM NaH <sub>2</sub> HPO <sub>4</sub> / Na <sub>2</sub> HPO <sub>4</sub> , pH 5.0	1.5	Mineral waters	AsC (1.6); As(III) (2.5); AsB (3.0); DMA (5.0); MMA (7.1); As(V) (8.6)	MO-HG-AAS	2.4; 1.4; 1.7; 1.9; 2.2; 2.1	[104]
Partisil SAX 10 µm (250 × 4.6 mm)	30 mM KH <sub>2</sub> PO <sub>4</sub> , pH 4.6	2	Standards	As(III) (2.9); AsC (3.2); DMA (3.3); AsB (3.7); TMAsH (4.3); MMA (4.9); p-As (6.0); PhAs (7.4); o-As (7.4); As(V) (9.3)	Photo-oxidation-HG-0.078; QFAAS (lamp off and lamp on)	0.050; 0.052; 0.023; ns; 0.048; 0.065; 0.056; 0.027; 0.061	[105]
<sup>PB</sup> Hamilton PRP- X100 10 µm (250 × 4.1 mm)	17 mM phosphate buffer, pH 6.0	2	Mineral water; waste water; synthetic fish extract	AsC (1.5); AsB (1.85); As(III) (1.85); DMA (2.45); MMA (3.7); As(V) (7.2)	Thermo-oxidation- HG-QFAAS (lamp off and lamp on)	0.4; 0.4; 0.5; 0.6; 0.6; 0.8	[106]
<sup>PB</sup> Hamilton PRP- X100 10 µm (250 × 4.1 mm)	Gradient: 12 mM then 1 24 mM phosphate buffer, pH 6.22	1	Spot urine samples; urine (NIST SRM 2670); Bio-Rad Lyphochek urine Urine	AsB (4.4); As(III) (4.4); DMA (5.5); MMA (6.7); As(V) (11.7)	UV photo-oxidation- HG-QFAAS (lamp off and lamp on)	0.20 <sup>a</sup> ; 0.10; 0.20; 0.15; 0.30	[107]
<sup>SB</sup> Supelcosil SAX1 5 µm (250 × 4.6 mm)	20 mM phosphate buffer, pH 4.64	1	Urine	AsC/TMAs (5.0); As(III) (6.0); AsB (6.6); DMA (7.8); TMAsO (7.8); MMA (14.5); As(V) (15.6)	UV photo-oxidation- HG-QFAAS (lamp off and lamp on)	ns	[107]
<sup>SB</sup> Chrompak Iono- spher 10 µm (250 × 4.5 mm)	30 mM phosphate buffer, pH 6.2	1.7	Urine	As(III) (2.8); MMA (4.8); DMA (6.9); As(V) (8.6)	HG-QFAAS	0.2; 0.2; 0.2; 0.2	[89]
Elite AS3 ns µm (250 × 4.6 mm) and Dionex HPIC- CAS1 ns µm (250 × 4.6 mm)	5 mM NH <sub>4</sub> H <sub>2</sub> PO <sub>4</sub> - and NH <sub>4</sub> OH, pH 5.8	1	Spiked river water; spiked lake water	As(III)+AsB (4); DMA (4.6); MMA (6.8); AsC (7.8); As(V) (9.5); p- APAs (12)	HG-ETAAS (off- line)	0.16/0.19; 0.19; 0.16; 0.19; 0.16; 0.16	[108]

Table 5 (Continued)

Column	Mobile phase	Flow (ml min <sup>-1</sup> )	Matrix	Species (Rt (min))	Detection	DL (ng As)	Ref.
<sup>PB</sup> Hamilton PRP-X100 10 µm (250 × 4.1 mm)	Gradient: 20 mM then 100 mM phosphate buffer, pH 6		Spiked mineral water at 5 and 10 times the DL	As(III) (2.3); DMA (3.4); MMA (5.7); As(V) (9.3)	HG-QFAAS	0.13; 0.48; 0.38; 0.46	[109]
<sup>SB</sup> Supelcosil LC-SAX 5 µm (250 × 4.6 mm)	30 mM NaH <sub>2</sub> PO <sub>4</sub> , pH 4.5		Urine	As(III) (6.2); DMA (7.0); As(V) (7.9); MMA (8.9)	HG-QFAAS	0.075; 0.060; 0.066; 0.138	[91]
<sup>PB</sup> Hamilton PRP-X100 10 µm (250 × 4.1 mm), 28°C	Gradient: 20 mM then 100 mM phosphate buffer, pH 5.75		Dogfish muscle (DORM-1); seafood products	As(III) (2.7); DMA (3.6); MMA (5.8); As(V) (8.5)	HG-QFAAS	ns; 0.03 <sup>a</sup> ; 0.02; ns	[110]
Dionex ns 3 µm (250 × 3 mm)	Gradient: H <sub>2</sub> O/MeOH 80:20 then 20 mM (NH <sub>4</sub> ) <sub>2</sub> CO <sub>3</sub> /MeOH 85:15 (v/v)	1.2	Soils	As(III) (4); DMA (13); MMA (22); As(V) (31)	GFAAS	5–25	[111]
<sup>PB</sup> Aminex Biorad A-27 ns µm (100 × 8 mm)	Gradient: H <sub>2</sub> O then 0.2 M (NH <sub>4</sub> ) <sub>2</sub> CO <sub>3</sub>	1.4	Herbicide (MMA)	As(III) (10); DMA (19); MMA (27); As(V) (36)	GFAAS	ns; ns; 0.25; ns	[112]
<sup>PB</sup> Hamilton PRP-X100 10 µm (250 × 4.1 mm)	5 mM nickel sulphate, pH 6.3		Standards	As(III) (15.6); DMA (21.2); MMA (26.3); As(V) (37.5)	GFAAS	10	[95]
IC-Pak AHR 6 µm (75 × 4.6 mm)	Gradient: 12.5 mM NaHCO <sub>3</sub> , pH 8.0, then H <sub>2</sub> O	1 Then 0.5	Geothermal water	As(III) (6); DMA (18); p-APAs (26); As(V) (37)	GFAAS (off-line)	ns	[102]
<sup>PB</sup> Hamilton PRP-X100 10 µm (250 × 4.1 mm)	Gradient: 10 then 60 mM then 10 mM phosphate buffer, pH 5.75	1	Seronorm <sup>TM</sup> ; urine	As(III) (2.3); DMA (3.6); MMA (6.4); As(V) (8.4)	HG-AFS	0.034; 0.009; 0.006; 0.008	[113]
<sup>PB</sup> Hamilton PRP-X100 10 µm (250 × 4.1 mm)	15 mM KH <sub>2</sub> PO <sub>4</sub> , pH 6.1	1	Stability of As compounds (in aqueous media) related to food treatment procedures	As(III) (2.8); DMA (4.0); MMA (5.3); As(V) (11.3)	UV-HG-AFS	ns	[114]
<sup>PB</sup> Hamilton PRP-X100 10 µm (250 × 4.1 mm)	15 mM KH <sub>2</sub> PO <sub>4</sub> , pH 6.0	1	Mushroom extract	As(III) (3.9); DMA (5.1); MMA (6.7); As(V) (15.1)	UV-HG-AFS	0.05; 0.05; 0.05; 0.05	[115]
HPIC-AS4 ns µm (150 × 3 mm)	3 mM NaHCO <sub>3</sub> + 2.4 mM Na <sub>2</sub> CO <sub>3</sub>	2	Standards	As(III) (2.0); As(V) (6.4)	DCP-AES	250	[53]
<sup>SB</sup> Supelcosil LC-SAX 5 µm (250 × 4.6 mm)	20 mM phosphate buffer, pH 3.75	1	Standards	AsC (2.5); As(III) (3.8); DMA (4.3); AsB (5.7); MMA (6.9); As(V) (10)	ICP-OES	34; 22; 41; 41; 152; 87	[116]
<sup>PB</sup> Hamilton PRP-X100 10 µm (250 × 4.1 mm)	Gradient: 10 mM Na <sub>2</sub> HPO <sub>4</sub> /NaH <sub>2</sub> PO <sub>4</sub> , pH 6.5, then 100 mM Na <sub>2</sub> HPO <sub>4</sub> , pH 7.2	1	Marine organisms	AsC (2.5); AsB (3.0); DMA (4.0); MMA (6.9); As(V) (9.9)	ICP-OES	ns	[117]

Table 5 (Continued)

Column	Mobile phase	Flow (ml min <sup>-1</sup> )	Matrix	Species (Rt (min))	Detection	DL (ng As)	Ref.
<sup>PB</sup> Hamilton PRP-X100 10 μm (250 × 4.1 mm)	Gradient: 5 mM then 35 mM phosphate buffer, pH 6.0	1	Dogfish muscle (DORM-1); mussel tissue (BCR CRM 278); cod muscle (BCR CRM 422)	AsC (3.0); AsB (3.3); DMA (5.2); MMA (9.5); As(V) (13.5)	UV-HG-ICP-OES	0.46; 0.56; 0.60; 0.62; 0.60	[118]
Nucleosil-N(CH <sub>3</sub> ) <sub>3</sub> -10 10 μm (305 × 3.2 mm)	50 mM phosphate buffer	1	Hiziki extract	AsB (3.8); As(III) (4.9); As(V) (11.8)	ICP-AES	ns; 30; 19; 41; 30	[88]
<sup>PB</sup> Aminex A-27 Radial-PAK 15 μm (100 × 8 mm)	Gradient: H <sub>2</sub> O then 0.5 M (NH <sub>4</sub> ) <sub>2</sub> CO <sub>3</sub>	1	Spiked cultured cell medium	As(III) (6.3); DMA (9.4); MMA (13.4); As(V) (16.7)	ICP-AES	390; 60; 57; 126	[119]
<sup>SB</sup> Nucleosil 10SB ns 10 μm (250 × 4.6 mm)	20 mM phosphate buffer, pH 7.0	1	Shellfishes	As(III) (4.7); DMA (5.9); MMA (7.1); As(V) (11.9)	ICP-AES	ns	[120]
<sup>PB</sup> Dionex HPIC AS4A ns 10 μm (250 × 4.6 mm)	Gradient: H <sub>2</sub> O then 50 mM (NH <sub>4</sub> ) <sub>2</sub> CO <sub>3</sub> + 0.2% MeOH	501	Standards	As(III) (ns); DMA (4.6); As(V) (11.3); PhAs (12.0)	Thermospray-ICP-AES	234; 31; 3.4; 2.4	[121]
<sup>SB</sup> Nucleosil SB 5 μm (200 × 4 mm)	50 mM phosphate buffer, pH 6.75	1	Spiked mineral water at 5 and 10 times the DL	As(III) (2.7); MMA (3.4); DMA (4.6); As(V) (6.3)	HG-ICP-AES	0.35; 0.38; 2.13; 0.92	[90]
<sup>PB</sup> Hamilton PRP-X100 10 μm (250 × 4.1 mm)	Gradient: 20 then 100 mM phosphate buffer, pH 5.75	1	Synthetic fish extract	As(III) (2.4); DMA (3.1); MMA (5.9); As(V) (8.5)	HG-ICP-AES	0.27; 0.94; 0.92; 1.14	[122]
<sup>SB</sup> Supelcosil LC-SAX 5 μm (250 × 4.6 mm) + (V)iosfer NH <sub>2</sub> -based 5 μm (100 × 4.0 mm)	5 mM NH <sub>4</sub> H <sub>2</sub> PO <sub>4</sub> , pH 4.5	1	Standards	As(III) (5.25); DMA (9.24); MMA (29.8); As(V) (37.8); AsC (45.1); AsB (48.6)	UV-HG-ICP-AES	1; 10; 5; 5; 10; 5	[123]

<sup>a</sup> DL data have been evaluated in the actual sample matrix.

Table 6

Separation of arsenic species by anion exchange chromatography coupled to ICP-MS detector

Column	Mobile phase	Flow (ml min <sup>-1</sup> )	Matrix	Species (Rt (min))	Detection	DL (ng As)	Ref.
Waters Radial-Pak SAX (ns)	25 mM phosphate buffer + 5% MeOH, pH 8	1	Dogfish muscle (DORM-1)	DMA (4.7); MMA (5.1); AsB (5.5); As(III) (6.9); As(V) (8.5)	ICP-MS	0.3	[82]
<sup>RB</sup> Benson 7–10 μm (100 × 4.0 mm)	50 mM K <sub>2</sub> SO <sub>4</sub> , pH 10.5	1.5	Standards; fish	AsB (0.5); DMA (0.8); As(III) (2.25); MMA (3.3); As(V) (5.4)	ICP-MS	0.875–1.75	[92,126]
<sup>PB</sup> Alltech Adsorbosphere-NH <sub>2</sub> 5 μm (250 × 4.6 mm)	15 mM NH <sub>4</sub> H <sub>2</sub> PO <sub>4</sub> + 2 mM CH <sub>3</sub> COONH <sub>4</sub> + 30% MeOH, pH 5.75	1 then 2 (after 6 min)	Urine	As(III) (3.7); DMA (4.7); MMA (6.9); As(V) (8.7)	ICP-MS	0.038; 0.020; 0.044; 0.091	[94]
Wescan Anion/R ICns μm (250 × 4.1 mm)	Gradient: 2% propan-1-ol then 50 mM carbonate buffer, pH 7.5	1 Then 2 (after 6.5 min)	Urine (NIST SRM 2670); wine; club soda	As(III) (3.1); DMA (4.0); MMA (5.5); As(V) (10.7)	ICP-MS	0.063 <sup>a</sup> ; 0.032; 0.080; 0.037	[128]
<sup>PB</sup> Merck Polyspher ICAN 2 10 μm (120 × 4.6 mm), 50°C	0.1 M NaHCO <sub>3</sub> , pH 10.25	1	Aqueous extract of soil samples	AsB (1.5); DMA (1.8); As(III) (2.2); MMA (2.8); As(V) (3.3)	ICP-MS	0.2; 0.3; 0.7; 0.3; 0.3	[87]
ION 120 ns μm (125 × 4.6 mm)	0.1 M NH <sub>4</sub> HCO <sub>3</sub> , pH 10.3	1	Urine	DMA (2.0); As(III) (2.9); MMA (5.1); As(V) (8.0)	ICP-MS	0.16 <sup>a</sup> ; 0.23; 0.20; 0.26	[129]
<sup>PB</sup> Dionex IonPac AS7 (ns)	Gradient: H <sub>2</sub> O then 30 mM NaHCO <sub>3</sub> , pH 9	0.7 Then 1.5	Fish and mussel extracts	AsB (2.1); As(III) (3.4); DMA (8.8); AsC (10.9); MMA (16.8); PhAs (23.1); As(V) (29.5)	ICP-MS	2.7 <sup>a</sup> ; 1.5; 2.5; 2.4; 2.7; IS; 1.3	[127]
<sup>PB</sup> Hamilton PRP-X100 10 μm (250 × 4.1 mm)	Gradient: 10 mM Na <sub>2</sub> HPO <sub>4</sub> /NaH <sub>2</sub> PO <sub>4</sub> + 2% CH <sub>3</sub> CN, pH 6.5, then 100 mM, pH 8, + 2% CH <sub>3</sub> CN	1	Synthetic sediment and synthetic fish	AsC (1.8); AsB (2.1); As(III) (2.4); DMA (3.7); MMA (4.7); As(V) (6.8)	ICP-MS	0.01; 0.01; 0.01; 0.02; 0.02; 0.03	[132]
<sup>PB</sup> Excelpak ICS-A35 2 × 10 μm (150 × 4.6 mm), 50°C	10 mM tartaric acid, pH 3–3.5	1	Urine	TMA <sub>5</sub> O (2.7); AsB (3.3); DMA (3.8); MMA (5.1); As(III) (5.8); As(V) (14)	ICP-MS	0.0050; 0.0044; 0.0056; 0.0088; 0.0078; ns	[124,125]
<sup>PB</sup> Alltech Adsorbosphere-NH <sub>2</sub> 5 μm (250 × 4.6 mm)	15 mM NH <sub>4</sub> H <sub>2</sub> PO <sub>4</sub> + 15 mM CH <sub>3</sub> COONH <sub>4</sub> + 10% MeOH, pH 5.75	1	Urine	As(III) (5); AsB (5.9); MMA (8.8); DMA (12.4); As(V) (19.1)	ICP-MS	ns; (<0.1)	[133]



Table 6 (Continued)

Column	Mobile phase	Flow (ml min <sup>-1</sup> )	Matrix	Species (Rt (min))	Detection	DL (ng As)	Ref.
<sup>PB</sup> Waters IC-Pak A HC 10 μm (150 × 4.6 mm) + <sup>PB</sup> Waters Guard-Pak cation-exchange CM/D 5 μm (5 × 3.9 mm)	Gradient: 0.3–2.5 mM 2 NaHCO <sub>3</sub> /Na <sub>2</sub> CO <sub>3</sub> , pH 9.3, + HNO <sub>3</sub> 4–6 mM at 40 mM		Spiked river water	AsB (1.2); DMA (2.1); As(III) (3.2); MMA (4.9); As(V) (6.1); AsC (10)	ICP-MS	0.010; 0.010; 0.015; 0.028; 0.040; 0.028	[134]
<sup>PB</sup> Waters IC-Pak A HC 10 μm (150 × 4.6 mm)	20 mM KNO <sub>3</sub> , pH 9.8	2	Drinking water; waste waters	AsB (1.0); DMA (1.3); As(III) (1.9); MMA (3.1); As(V) (3.6)	ICP-MS	ns; ns; 0.125; ns; 0.125	[135]
<sup>PB</sup> Hamilton PRP-X100 10 μm (250 × 4.6 mm)	Gradient: 10 mM (NH <sub>4</sub> ) <sub>2</sub> HPO <sub>4</sub> /NH <sub>4</sub> H <sub>2</sub> PO <sub>4</sub> , pH 7.0, +3% MeOH, then 100 mM, pH 8.5, +3% MeOH	1	In-house soil; in-house sediment; river sediment (BCR CRM 320)	As(III) (2.8); DMA (3.9); MMA (5.7); As(V) (13.1)	ICP-MS	0.039; 0.039; 0.039; 0.051	[131]
<sup>PB</sup> Hamilton PRP-X100 10 μm (150 × 4.1 mm)	Gradient: 5 mM phosphate buffer, pH 6, then 10 mM citrate buffer, pH 6	Then 2	Certified river sediment (NIST SRM 2704)	As(III) (2.0); DMA (2.7); MMA (3.5); As(V) (5.3)	ICP-MS	ns; ns; 0.16; ns	[136]
<sup>SB</sup> Supelcosil LC SAX1 (ns)	15 mM NH <sub>4</sub> H <sub>2</sub> HPO <sub>4</sub> , pH 5.1		Estuarine water	As(III) (2.8); AsB (3.5); DMA (4.4); As(V) (5.1); MMA (5.8)	ICP-MS	ns	[137]
Capillary ION 120 IAC (ns)	Gradient: 0.01 then 0.1 M NH <sub>4</sub> HCO <sub>3</sub> , pH 10.3	ns	Estuarine water	AsB (1.4); DMA (2.5); As(III) (3.0); MMA (6.5); As(V) (8.3)	ICP-MS	ns	[137]
ICPAK A HR 6 μm (75 × 4.6 mm)	10 mM NaH <sub>2</sub> HPO <sub>4</sub> /Na <sub>2</sub> HPO <sub>4</sub> , pH 6.0	0.5	Mung bean seeds	AsB (2.0); As(III) (2.4); DMA (3.1); MMA (3.6); As(V) (11.4)	ICP-MS	0.110; 0.097; 0.180; 0.170; 0.140	[138]
Dionex AS 4A-SC ns μm (ns × 4 mm)	5 mM Na <sub>2</sub> CO <sub>3</sub> + 40 mM NaOH + 4% MeOH (v/v)	1	DORM-2; seepage water samples	As(III) (1.5); As(V) (4.5)	ICP-MS	0.0065; 0.0073	[139]
Ion 120 ns μm (125 × 3 mm)	Gradient: 5 mM NH <sub>4</sub> HCO <sub>3</sub> , pH 10.3 then 0.2 M NH <sub>4</sub> HCO <sub>3</sub> , pH 10.3	1	Urine (NIST SRM 2670)	AsB (1.5); DMA (2.4); As(III) (3.1); MMA (6.4); As(V) (7.1)	ICP-MS	0.03 <sup>a</sup> ; 0.04; 0.04; 0.03; 0.04	[130]
Spherisorb ODS/NH <sub>2</sub> mixed column 5 μm (250 × 4.6 mm), 25°C	5 mM NaH <sub>2</sub> HPO <sub>4</sub> /Na <sub>2</sub> HPO <sub>4</sub> , pH 5.0	1.5	Urine; mineral waters	AsC (1.3); As(III) (2.1); AsB (2.4); DMA (3.6); MMA (5.7); As(V) (8.0)	ICP-MS	0.15; 0.20; 0.28; 0.04; 0.06; 0.08	[104]

Table 6 (Continued)

Column	Mobile phase	Flow (ml min <sup>-1</sup> )	Matrix	Species (Rt (min))	Detection	DL (ng As)	Ref.
<sup>SB</sup> Supelcosil LC SAX 1 5 µm (250 × 4.6 mm), 30°C	20 mM NaH <sub>2</sub> HPO <sub>4</sub> / Na <sub>2</sub> HPO <sub>4</sub> , pH 4.16	1.5	Soils; earthworms	As(III) (2.4); DMA (2.8); AsB (3.4); As(V) (8.7); MMA (11.2)	ICP-MS	ns	[140]
<sup>SB</sup> Supelcosil LC SAX 5 µm (250 × 4.6 mm), 25°C	20 mM NaH <sub>2</sub> HPO <sub>4</sub> , pH 3.9, +1% MeOH	1	Urine; mineral waters	AsC (2.6); As(III) (3.5); DMA (4.2); AsB (5.2); As(V) (6.2); MMA (7.3)	TN-ICP-MS	0.012; 0.012; 0.006; 0.006; 0.004; 0.008	[141]

<sup>a</sup> DL data have been evaluated in the actual sample matrix.

Table 7  
Simultaneous separation of arsenic and selenium

Column	Mobile phase	Flow (ml min <sup>-1</sup> )	Matrix	Species (Rt (min))	Detection	DL ((ng As/Se))	Ref.
<i>Ion-pairing Reversed-phase chromatography</i>							
<sup>PB</sup> Hamilton PRP-1 (ns)	Gradient: 2 mM HTAB, pH 9.6, then 1% (v/v) acetic acid then 10% (v/v) DMF	1.5	Standards	As(III) (2.6); DMA (6.4); MMA (11.3); Se(IV) (13.4); As(V) (14.1); PhAs (22.2)	ICP-AES	13; 13; 13; 13; 13; ns	[145]
C <sub>18</sub> Whatman Partisil 5 ODS-3 (250 × 4.2 mm)	5 mM TBAP + 5% MeOH (v/v)	0.7	Coal process stream; shale oil; solvent refined oil; crude oil	As(III) (5); MMA (7.5); DMA (8.5); Se(IV) (9); As(V) (18); Se(VI) (27)	DIN-ICP-AES	19.6; 11.2; 11.2 < x < 19.6; 4.6; 11.2 < x < 19.6; 8.4	[146]
C <sub>18</sub> Alltech Spherisorb ODS 5 μm (150 × 4.6 mm)	5 mM TBAP + 3 or 10% MeOH (v/v)	1	Spiked river water; spiked tap water	As(III) (2); DMA (3); Se(IV) (8.6); As(V) (11)	HG-ACP-AES	2.8; 3.0; 4.0; 4.0	[147]
C <sub>18</sub> Alltech Econosphere 5 μm (250 × 4.6 mm)	5 mM TBAP, pH 7.1 + 5% MeOH (v/v)	1	Standards	As(III) (3.5); MMA (3.7); Se(IV) (3.9); DMA (4); As(V) (5.7); Se(VI) (7.3)	USN-ICP-MS	0.20; 0.08; 0.20; 0.10; 0.10; 0.10	[148]
<sup>PB</sup> Hamilton PRP-1 10 μm (250 × 4.6 mm)	0.5 mM TBAP/4mM Na <sub>2</sub> HPO <sub>4</sub> , pH 8.5, + 2% (v/v) MeOH	0.9	Mineral water (As); two certified waters (Se(IV) + Se(VI))	As(III) (2.7); DMA (3.7); MMA (5.6); Se(IV) (8.6); As(V) (10.6); Se(VI) (14)	ICP-MS	0.030; 0.045; 0.055; 0.050; 0.200; 0.275	[149]
<i>Anion exchange chromatography</i>							
<sup>B</sup> Nucleosil-NH(CH <sub>3</sub> ) <sub>2</sub> ns μm (250 × ns mm)	Gradient: 2 mM ADP + 5 mM AAC, pH 4.6, then 80 mM ADP, pH 6.9	1.4	Standards	As(III) (3.5); Se(IV) (6.8); As(V) (9.0); Se(VI) (14.5)	ICP-AES	52; 140; 57; 91	[150]
Sarasep ANX 1710 (100 × 1.7 mm)	5 mM carbonate buffer, pH 8.6	0.08	Standards	As(III) (0.8); MMA (1.7); Se(IV) (3.6); As(V) (4.3); Se(VI) (7.2)	DIN-ICP-AES	0.10; 0.10; 0.10; 0.04; 0.04	[151]
<sup>PB</sup> Hamilton PRP-X100 10 μm (125 μm × 4.0 mm), 25°C	1 mM <i>p</i> -hydroxybenzoate + 0.4 mM benzoate + 2.5% MeOH, pH 8.5	2	Standards	As(III) (3.2); DMA (4.2); Se(IV) (5.2); As(V) (13.8)	HG-ICP-AES	1.70; 1.00; 0.64; 2.30	[152]
<sup>PB</sup> Hamilton PRP-X100 10 μm (250 × 4.6 mm)	12.5 mM phosphate buffer, pH 8.5	1.5	Standards	As(III) (1.9); DMA (2.3); MMA (3.7); Se(IV) (6.3); As(V) (7.4); Se(VI) (15.2)	ICP-MS	0.016; 0.011; 0.014; 0.200; 0.021; 0.417	[142,143]
Cetac ANX1606As ns μm (100 × 2 mm)	5 mM malonate acid, pH 8.5	0.1	Water (Se); spiked groundwater; soil extracts (As)	As(III) (1.0); As(V) (1.9); Se(IV) (2.3); Se(VI) (3.0)	MCN-ICP-MS	0.01; 0.01; 0.04; 0.04	[144]

urine [129,130], soil lixiviates [87] and sediments [131].

It is quite interesting to consider further Hansen et al.'s [87] results obtained under the same chromatographic conditions with both FAAS and ICP-MS detectors: the factor of improvement of DLs vary between 150 and 450 depending on species.

#### 4. Simultaneous arsenic and selenium speciation methods

Quite a few papers appeared dealing with the simultaneous speciation of As and Se; this is possible when detectors such as ICP-AES or ICP-MS are used provided that powerful enough data treatment hardware and software are available.

Arsenic and selenium have some common chemical properties: predominant inorganic forms appear as oxygenated acids and/or anions, they give birth to organic species. In pH conditions where As(III), As(V), MMA and DMA appear as anions, Se(IV) and Se(VI) are ionised also. It is therefore possible to find chromatographic conditions such that these six species may be simultaneously analysed [142,143].

Reverse phase and ion exchange modes have been evaluated for this purpose (Table 7). Selenite usually elutes before arsenate (except in Woller et al. [144]); it appears sometimes between MMA and DMA, and selenate is always the most retained species.

DLs are similar to those presented in papers devoted to the speciation of a single element.

Other As and Se species which are quite significant in biological samples (AsB, AsC SeCys and SeMet) do not form anions in these conditions and have not been considered in these papers.

#### Appendix A. Abbreviations used

##### Techniques

AAS atomic absorption spectrometry

ACP	alternating current plasma
AES	atomic emission spectrometry
AFS	atomic fluorescence spectrometry
DCP	direct current plasma
DIN	direct injection nebulization
ETAAS	electroThermal atomic absorption spectrometry
F/GF/QF-AAS	flame/graphite furnace/quartz furnace-atomic absorption Spectrometry
HG	hydride generation
HEN	high efficiency nebulizer
HHPN	hydraulic high pressure nebulization
HPLC	high performance liquid chromatography
ICP	inductively coupled plasma
MCN	micro-concentric nebulizer
MD/MO	microwave digestion/microwave Oxidation
MIP	microwave induced plasma
MR	microwave reduction
MS	mass spectrometry
OES	optical emission spectrometry
THG	thermochemical hydride generating
TN	thermospray nebulizer
USN	ultraSonic nebulizer
UV	ultraviolet
<i>Units</i>	
°C	Celsius degree
µg l <sup>-1</sup>	micrograms per litre
ml	millilitre
mM	millimole per litre
min	minutes
ng	nanograms
<i>Terms</i>	
DL	detection limits
IS	internal standard
ns	not specified
PB	polymer-based
Rt	retention time
SB	silica-based

##### Mobile phases

AAC ammonium acetate

ADP	ammonium dihydrogen phosphate
CTAB	cetyltrimethylammonium bromide
DDAB	didodecyldimethylammonium bromide
DMF	<i>N,N</i> -dimethylformamide
HTAB	hexadecyltrimethylammonium bromide
HTEAP	heptyltriethylammonium phosphate
KHP	potassium hydrogen phthalate
TBA	tetrabutylammonium ion
TBAA	tetrabutylammonium acetate
TBAH	tetrabutylammonium hydroxide
TBAHS	tetrabutylammonium hydrogen sulphate
TBAP	tetrabutylammonium phosphate
TEAB	tetraethylammonium bromide
TEAH	tetraethylammonium hydroxide
<i>Standards</i>	
As(III)	arsenite
As(V)	arsenate
AsB	arsenobetaine
AsC	arsenocholine
DMA	dimethylarsinic acid
MMA	monomethylarsonic acid
<i>o</i> -As	<i>o</i> -arsinilic acid
<i>p</i> -APAs	<i>p</i> -aminophenylarsenate
<i>p</i> -As	<i>p</i> -arsinilic acid
PhAs	phenylarsonic acid
4-OH	4-hydroxy-phenylarsonic acid
Se(IV)	selenite
Se(VI)	selenate
SeC(NH <sub>2</sub> ) <sub>2</sub>	selenourea
Se h-Cys	selenohomocystine
SeCys	selenocystine
Se(Cys) <sub>2</sub>	selenoamino acid dimer selenocystine
AllylSeCys	allyl-DL-selenocysteine
MetSeCys	methyl-DL-selenocysteine
SeEth	selenoethionine
SeMet	selenomethionine
TMA <sub>s</sub>	tetramethylarsonium ion
TMA <sub>s</sub> H	tetramethylarsonium hydroxide
TMA <sub>s</sub> O	trimethylarsine oxide
TMSe	trimethylselenonium iodide

## References

- [1] K.J. Irgolic, Arsenic, in: M. Stoeppler (Ed.), *Hazardous Metals in the Environment*, Elsevier, Amsterdam, 1992, pp. 288–350.
- [2] M. Morita, J.S. Edmonds, *Pure Appl. Chem.* 64 (4) (1992) 575.
- [3] H. Greschonig, K.J. Irgolic, *Appl. Organomet. Chem.* 6 (1992) 565.
- [4] R. Iffland, Arsenic, in: H.G. Seiler, A. Sigel, H. Sigel (Eds.), *Handbook of Metals in Clinical and Analytical Chemistry*, Marcel Dekker, New York, 1994, pp. 237–253.
- [5] T.R. Crompton, Detection, identification and determination, in: S. Patai (Ed.), *The Chemistry of Organic Arsenic, Antimony and Bismuth Compounds*, Wiley, New York, 1994, pp. 169–235.
- [6] J.C. Van Loon, R.R. Barefoot, Trends and developments, in: A.M. Ure, C.M. Davidson (Eds.), *Chemical Speciation in the Environment*, Chapman and Hall, London, 1995, pp. 335–388.
- [7] H. Robberecht, R. Van Grieken, *Talanta* 29 (1982) 823.
- [8] M. Ihnat, Selenium, in: M. Stoeppler (Ed.), *Hazardous Metals in the Environment*, Elsevier, Amsterdam, 1992, pp. 475–515.
- [9] M. Potin-Gautier, M. Astruc, P. Vermeulin, *Analisis* 20 (1992) 73.
- [10] G. Kölbl, K. Kalcher, K.J. Irgolic, R.J. Magee, *Appl. Organomet. Chem.* 7 (1993) 443.
- [11] X. Dauchy, M. Potin-Gautier, A. Astruc, M. Astruc, *Fresenius J. Anal. Chem.* 348 (1994) 792.
- [12] R. Munoz Olivas, O.F.X. Donard, C. Cámara, P. Quevauviller, *Anal. Chim. Acta* 286 (1994) 357.
- [13] C. Cámara, M.G. Cobo, M.A. Palacios, R. Munoz, O.F.X. Donard, Selenium speciation analyses in water and sediment matrices, in: Quevauviller, Maier, Griepink (Eds.), *Quality Assurance for Environmental Analysis*, Elsevier, Amsterdam, 1995, pp. 235–262.
- [14] M. Sanz Alaejos, C. Diaz Romero, *Chem. Rev.* 95 (1995) 227.
- [15] A. D'Ulivo, *Analyst* 122 (1997) 117R.
- [16] K. Pyrzyńska, *Chem. Anal. (Warsaw)* 40 (1995) 677.
- [17] K. Pyrzyńska, *Analyst* 121 (1996) 77R.
- [18] K. Pyrzyńska, *Anal. Sci.* 14 (1998) 479.
- [19] D. Heitkemper, J. Caruso, Chromatographic sample introduction for plasma mass spectrometry, in: I.S. Krull (Ed.), *Trace Metal Analysis and Speciation*, Amsterdam: Elsevier, 1991, pp. 288–350.
- [20] G. Lespes, M. Potin-Gautier, A. Astruc, *Environ. Technol.* 13 (1992) 207.
- [21] S.J. Hill, M.J. Bloxham, J. Worsfoldp, *J. Anal. Atom. Spectrom.* 8 (1993) 499.
- [22] N.P. Vela, J.A. Caruso, *J. Anal. Atom. Spectrom.* 8 (1993) 787.
- [23] J. Szpunar-Lobinska, C. Witte, R. Lobinski, F.C. Adams, *Fresenius J. Anal. Chem.* 351 (1995) 351.

- [24] H. Garraud, A. Woller, P. Fodor, O.F.X. Donard, *Analisis* 25 (1997) 25.
- [25] K.J. Irgolic, R.A. Stockton, *Mar. Chem.* 22 (1987) 265.
- [26] B. Amran, F. Lagarde, M.J.F. Leroy, et al., Arsenic speciation in environmental matrices, in: P. Quevauviller, E. Maier, B. Griepink (Eds.), *Quality Assurance for Environmental Analysis*, Elsevier, Amsterdam, 1995, pp. 285–304.
- [27] G. Kölbl, J. Lintschinger, K. Kalcher, K.J. Irgolic, *Mikrochim. Acta* 119 (1995) 113.
- [28] A. Sanz-Medel, B. Aizpun, J.M. Marchante, E. Segovia, M.L. Fernandez, E. Blanco, *J. Chromatogr.* 683 (1994) 233.
- [29] G. Kölbl, K. Kalcher, K.J. Irgolic, Identification and determination of selenium compounds in samples of environmental importance, in: V.G. Kumar Das (Ed.), *Main Group Elements and Their Compounds*, Narosa Publishing House, New Delhi, 1996, pp. 161–172.
- [30] N. Jakubowski, C. Thomas, D. Stuewer, I. Dettlaff, J. Schram, *J. Anal. Atom. Spectrom.* 11 (1996) 1023.
- [31] K.L. Yang, S.J. Jiang, *Anal. Chim. Acta* 307 (1995) 109.
- [32] J.M. Marchante-Gayón, J.M. González, M.L. Fernández, E. Blanco, A. Sanz-Medel, *Fresenius J. Anal. Chem.* 355 (1996) 615.
- [33] J.M. González LaFuente, M.L. Fernández Sánchez, A. Sanz-Medel, *J. Anal. Atom. Spectrom.* 11 (1996) 1163.
- [34] J.M. González LaFuente, M. Dlaska, M.L. Fernández Sánchez, A. Sanz-Medel, *J. Anal. Atom. Spectrom.* 13 (1998) 423.
- [35] M. Potin-Gautier, C. Boucharat, A. Astruc, M. Astruc, *Appl. Organomet. Chem.* 7 (1993) 593.
- [36] Y. Cai, M. Cabañas, J.L. Fernández-Turiel, M. Abalos, J.M. Bayona, *Anal. Chim. Acta* 314 (1995) 183.
- [37] T. Lei, W.D. Marshall, *Appl. Organomet. Chem.* 9 (1995) 149.
- [38] A. Astruc, R. Pinel, M. Astruc, *Anal. Chim. Acta* 228 (1990) 129.
- [39] G. Kölbl, K. Kalcher, K.J. Irgolic, *Anal. Chim. Acta* 284 (1993) 301.
- [40] D. Chakraborti, K.J. Irgolic, Separation and determination of arsenic and selenium compounds by high pressure liquid chromatography with a graphite furnace atomic absorption spectrometer as the element-specific detector, in: T.D. Lekkas (Ed.), *5th Heavy Metal Environment, International Conference*, vol. 2, CEP Consultants, Edinburgh, UK, 1985, p. 484.
- [41] W.L. Childress, D. Erickson, I.S. Kruss, in: *Element-Specific Chromatographic Detection by AES*. ACS Symp. Ser., 1992, 479, 257.
- [42] J. Yang, T.S. Conner, J.A. Koropchak, *Anal. Chem.* 68 (1996) 4064.
- [43] S.R. Wang, S.J. Jiang, *J. Chin. Chem. Soc.* 38 (1991) 327.
- [44] N. Gilon, M. Potin-Gautier, M. Astruc, *J. Chromatogr.* 750 (1996) 327.
- [45] F. Laborda, D. Chakraborti, J.M. Mir, J.R. Castillo, *J. Anal. Atom. Spectrom.* 8 (1993) 643.
- [46] S.C.K. Shum, R.S. Houk, *Anal. Chem.* 65 (1993) 2972.
- [47] G.A. Pedersen, E.H. Larsen, *Fresenius J. Anal. Chem.* 358 (1997) 591.
- [48] G.M. Momplaisir, T. Lei, W.D. Marshall, *Anal. Chem.* 66 (1994) 3533.
- [49] M.G. Cobo-Fernández, M.A. Palacios, D. Chakraborti, P. Quevauviller, C. Cámara, *Fresenius J. Anal. Chem.* 351 (1995) 438.
- [50] N. Ellend, C. Rohrer, M. Grasserbauer, J.A.C. Broekaert, *Fresenius J. Anal. Chem.* 356 (1996) 99.
- [51] L. Pitts, A. Fisher, P. Worsfold, S.J. Hill, *J. Anal. Atom. Spectrom.* 10 (1995) 519.
- [52] H. Emteborg, G. Bordin, A.R. Rodriguez, *Analyst* 123 (1998) 893.
- [53] I.T. Urasa, F. Ferede, *Anal. Chem.* 59 (1987) 1563.
- [54] F. Laborda, M.T.C. De Loos-Vollebregt, L. De Galan, *Spectrochim. Acta* 46B (6/7) (1991) 1089.
- [55] A. Hagège, S. Niemczyk, M.J.F. Leroy, *Analisis* 23 (1995) 476.
- [56] H. Emteborg, G. Bordin, A.R. Rodriguez, *Analyst* 123 (1998) 245.
- [57] G. Kölbl, *Mar. Chem.* 48 (1995) 185.
- [58] H.M. Crews, P.A. Clarke, D.J. Lewis, L.M. Owen, R. Strutt, A. Izquierdo, *J. Anal. Atom. Spectrom.* 11 (1996) 1177.
- [59] H. Ge, X.J. Cai, J.F. Tyson, P.C. Uden, E.R. Denoyer, E. Block, *Anal. Commun.* 33 (1996) 279.
- [60] M.A. Quijano, A.M. Gutiérrez, M.C. Pérez-Conde, C. Cámara, *J. Anal. Atom. Spectrom.* 11 (1996) 407.
- [61] S.M. Bird, H. Ge, P.C. Uden, J.F. Tyson, E. Block, E. Denoyer, *J. Chromatogr.* 789 (1997) 349.
- [62] X.C. Le, W.R. Cullen, K.J. Reimer, *Talanta* 41 (4) (1994) 495.
- [63] X.C. Le, M. Ma, A. Wong, *Anal. Chem.* 68/24 (1996) 4501.
- [64] X.C. Le, M. Ma, *J. Chromatogr.* 764 (1997) 55.
- [65] X.C. Le, M. Ma, *Anal. Chem.* 70/9 (1998) 1926.
- [66] D.S. Bushee, I.S. Krull, P.R. Demko, S.B. Smith, *J. Liq. Chromatogr.* 7 (5) (1984) 861.
- [67] S.L. Chen, S.R. Dzung, M.H. Yang, K.H. Chlu, G.M. Shieh, C.M. Wai, *Environ. Sci. Technol.* 28/5 (1994) 877.
- [68] F.-H. Ko, S.-L. Chen, M.-H. Yang, *J. Anal. Atom. Spectrom.* 12 (1997) 589.
- [69] I. Martín, M.A. López-González, M. Gómez, C. Cámara, M.A. Palacios, *J. Chromatogr.* 666 (1995) 101.
- [70] Z. Mester, P. Fodor, *J. Chromatogr.* 756 (1996) 292.
- [71] E. Hakala, L. Pyy, *J. Anal. Atom. Spectrom.* 7 (1992) 191.
- [72] M.B. Amran, F. Lagarde, M.J.F. Leroy, *Mikrochim. Acta* 127 (1997) 195.
- [73] A. Woller, Z. Mester, P. Fodor, *J. Anal. Atom. Spectrom.* 10 (1995) 609.
- [74] Z. Mester, A. Woller, P. Fodor, *Microchem. J.* 54 (1996) 184.
- [75] J.M. Costa-Fernández, F. Lunzer, R. Pereiro-Garcia, A. Sanz-Medel, N. Bordel-Garcia, *J. Anal. Atom. Spectrom.* 10 (1995) 1019.

- [76] W. Nisamanepong, M. Ibrahim, T.W. Gilbert, J.A. Caruso, *J. Chrom. Sci.* 22 (1984) 473.
- [77] Y.M. Liu, M.L. Fernández Sánchez, E.B. Gonzalez, A. Sanz-Medel, *J. Anal. Atom. Spectrom.* 8 (1993) 815.
- [78] S.C.K. Shum, R. Neddersen, R.S. Houk, *Analyst* 117 (1992) 577.
- [79] S.A. Pergantis, E.M. Heithmar, T.A. Hinners, *Anal. Chem.* 67 (1995) 4530.
- [80] S.A. Pergantis, E.M. Heithmar, T.A. Hinners, *J. Anal. Atom. Spectrom.* 122 (1997) 1063.
- [81] C.J. Hwang, S.J. Jiang, *Anal. Chim. Acta* 289 (1994) 205.
- [82] D. Beauchemin, K.W.M. Siu, J.W. McLaren, S.S. Berman, *J. Anal. Atom. Spectrom.* 4 (1989) 285.
- [83] Y. Shibata, M. Morita, *Anal. Sci.* 5 (1989) 107.
- [84] P. Thomas, K. Sniatecki, *J. Anal. Atom. Spectrom.* 10 (1995) 615.
- [85] P. Thomas, K. Sniatecki, *Fresenius J. Anal. Chem.* 351 (1995) 410.
- [86] W.C. Story, J. Caruso, D.T. Heitkemper, L. Perkins, *J. Chrom. Sci.* 30 (1992) 427.
- [87] S.H. Hansen, E.H. Larsen, G. Pritzl, C. Cornett, *J. Anal. Atom. Spectrom.* 7 (1992) 629.
- [88] M. Morita, T. Uehiro, K. Fuwa, *Anal. Chem.* 53 (1981) 1806.
- [89] B.S. Chana, N.J. Smith, *Anal. Chim. Acta* 197 (1987) 177.
- [90] G. Rauret, R. Rubio, A. Padró, *Fresenius J. Anal. Chem.* 340 (1991) 157.
- [91] X. Zhang, R. Cornelis, J. De Kimpe, L. Mees, *J. Anal. Atom. Spectrom.* 11 (1996) 1075.
- [92] S. Branch, K.C.C. Bancroft, L. Ebdon, P. O'Neill, *Anal. Proc.* 26 (1989) 73.
- [93] C. Demesmay, Spéciation de l'arsenic par couplages chromatographie en phase liquide et méthodes spectrales d'analyse élémentaires spécifiques, Thèse de Doctorat, Université de Lyon I, 1992.
- [94] D. Heitkemper, J. Creed, J. Caruso, F.L. Fricke, *J. Anal. Atom. Spectrom.* 4 (1989) 279.
- [95] J. Gailer, K.J. Irgolic, *Appl. Organomet. Chem.* 8 (1994) 129.
- [96] J. Zheng, W. Goessler, W. Kosmus, *Chromatographia* 47 (5/6) (1998) 257.
- [97] C.T. Tye, S.J. Haswell, P. O'Neill, K.C.C. Bancroft, *Anal. Chim. Acta* 169 (1985) 195.
- [98] T. Maitani, S. Uchiyama, Y. Saito, *J. Chromatogr.* 391 (1987) 161.
- [99] J. Stummeyer, B. Harazim, T. Wippermann, *Fresenius J. Anal. Chem.* 354 (1996) 344.
- [100] B.A. Manning, D.A. Martens, *Environ. Sci. Technol.* 31/1 (1997) 171.
- [101] M. Gómez, C. Cámara, M.A. Palacios, A. López-González, *Fresenius J. Anal. Chem.* 357 (1997) 844.
- [102] E. Büyüktuncel, S. Bektaş, B. Salih, M.M. Evirgen, Ö. Genç, *Fresenius Environ. Bull.* 6 (1997) 494.
- [103] K.J. Lambie, S.J. Hill, *Anal. Chim. Acta* 334 (1996) 261.
- [104] M. Moldovan, M.M. Gómez, M.A. Palacios, C. Cámara, *Microchem. J.* 59 (1998) 89.
- [105] A.G. Howard, L.E. Hunt, *Anal. Chem.* 65/21 (1993) 2995.
- [106] M.A. López, M.M. Gómez, M.A. Palacios, C. Cámara, *Fresenius J. Anal. Chem.* 346 (1993) 643.
- [107] D.L. Tsalev, M. Sperling, B. Welz, *Analyst* 123 (1998) 1703.
- [108] H. Han, Y. Liu, S. Mou, Z. Ni, *J. Anal. Atom. Spectrom.* 8 (1993) 1085.
- [109] R. Rubio, A. Padró, G. Rauret, *Fresenius J. Anal. Chem.* 351 (1995) 331.
- [110] D. Vélez, N. Ybáñez, R. Montoro, *J. Anal. Atom. Spectrom.* 11 (1996) 271.
- [111] R. Iadevaia, N. Aharonson, E.A. Woolson, *J. Assoc. Off. Anal. Chem.* 63/4 (1980) 742.
- [112] F.E. Pick, P.R. De Beer, S.M. Prinsloo, L.P. Van Dyk, *Pestic. Sci.* 21 (1987) 45.
- [113] J.L. Gomez-Ariza, D. Sánchez-Rodas, R. Beltran, W. Corns, P. Stockwel, *Appl. Organomet. Chem.* 12 (1998) 439.
- [114] J.T. van Elteren, Z. Slejkovec, *J. Chromatogr.* 789 (1997) 339.
- [115] Z. Slejkovec, J.T. van Elteren, A.R. Byrne, *Anal. Chim. Acta* 358 (1998) 51.
- [116] R. Rubio, I. Peralta, J. Albertí, G. Rauret, *J. Liq. Chromatogr.* 16/16 (1993) 3531.
- [117] A. El Moll, R. Heimbürger, F. Lagarde, M.J.F. Leroy, *Fresenius J. Anal. Chem.* 354 (1996) 550.
- [118] J. Albertí, R. Rubio, G. Rauret, *Fresenius J. Anal. Chem.* 351 (1995) 415.
- [119] W.D. Spall, J.G. Lynn, J.L. Andersen, J.G. Valdez, L.R. Gurley, *Anal. Chem.* 58 (1986) 1340.
- [120] K. Shiomi, M. Orii, H. Yamanaka, T. Kikuchi, *Nippon Suisan Gakkaishi* 53 (1) (1987) 103.
- [121] S.B. Roychowdhury, J.A. Koropchak, *Anal. Chem.* 62/5 (1990) 484.
- [122] R. Rubio, A. Padró, J. Albertí, G. Rauret, *Mikrochim. Acta* 109 (1992) 39.
- [123] N. Violante, F. Petrucci, F. La Torre, S. Caroli, *Spectroscopy* 7 (7) (1992) 36.
- [124] Y. Inoue, K. Kawabata, H. Takahashi, G. Endo, *J. Chromatogr.* 675 (1994) 149.
- [125] K. Kawabata, Y. Inoue, H. Takahashi, G. Endo, *Appl. Organomet. Chem.* 8 (1994) 245.
- [126] S. Branch, L. Ebdon, P. O'Neill, *J. Anal. Atom. Spectrom.* 9 (1994) 33.
- [127] S. Caroli, F. La torre, F. Petrucci, N. Violante, *Environ. Sci. Pollut. Res.* 1 (4) (1994) 205.
- [128] B.S. Sheppard, J.A. Caruso, D.T. Heitkemper, K.A. Wolnik, *Analyst* 117 (1992) 971.
- [129] E.H. Larsen, G. Pritzl, S.H. Hansen, *J. Anal. Atom. Spectrom.* 8 (1993) 557.
- [130] R. Ritsema, L. Dukan, T. Roig i Navarro, et al., *Appl. Organomet. Chem.* 12 (1998) 591.
- [131] P. Thomas, J.K. Finnie, J.G. Williams, *J. Anal. Atom. Spectrom.* 12 (1997) 1367.

- [132] C. Demesmay, M. Olle, M. Porthault, Fresenius J. Anal. Chem. 348 (1994) 205.
- [133] P. Bavazzano, A. Perico, K. Rosendahl, P. Apostoli, J. Anal. Atom. Spectrom. 11 (1996) 521.
- [134] P. Teräsahde, M. Pantsar-Kallio, P.K.G. Manninen, J. Chromatogr. 750 (1996) 83.
- [135] M. Pantsar-Kallio, P.K.G. Manninen, J. Chromatogr. 779 (1997) 139.
- [136] P. Yehl, J.F. Tyson, Anal. Commun. 34 (1997) 49.
- [137] M.H. Florêncio, M.F. Duarte, S. Facchetti, et al., Analusis 25 (1997) 226.
- [138] K. Van den Broeck, C. Vandecasteele, J.M.C. Geuns, Anal. Chim. Acta 361 (1998) 101.
- [139] J. Mattusch, R. Wennrich, Anal. Chem. 70 (1998) 3649.
- [140] A. Geiszinger, W. Goessler, D. Kuehnelt, K. Francesconi, W. Kosmus, Environ. Sci. Technol. 32 (1998) 2238.
- [141] S. Saverwyns, X. Zhang, F. Vanhaecke, R. Cornelis, L. Moens, R. Dams, J. Anal. Atom. Spectrom 12 (1997) 1047.
- [142] T. Guérin, M. Astruc, A. Batel, M. Borsier, Talanta 44 (1997) 2201.
- [143] T. Guérin, A. Astruc, M. Astruc, A. Batel, M. Borsier, J. Chromatogr. Sci. 35 (1997) 213.
- [144] A. Woller, H. Garraud, J. Boisson, A.M. Dorthé, P. Fodor, O.F.X. Donard, J. Anal. Atom. Spectrom. 2 (1998) 141.
- [145] K.J. Irgolic, R.A. Stockton, D. Chakraborti, W. Beyer, Spectrochim. Acta 38B (1/2) (1983) 437.
- [146] K.E. Lafreniere, V.A. Fassel, D.E. Eckels, Anal. Chem. 59 (1987) 879.
- [147] L.A. Colon, E.F. Barry, J. High Res. Chromatogr. 14 (1991) 608.
- [148] J.J. Thompson, R.S. Houk, Anal. Chem. 58 (1986) 2541.
- [149] P. Thomas, K. Pereira, D. Koller, Analusis 25 (1997) 19.
- [150] J.P. McCarthy, J.A. Caruso, F.L. Fricke, J. Chrom. Sci. 21 (1983) 389.
- [151] D.T. Gjerde, D.R. Wiederin, F.G. Smith, B.M. Mattson, J. Chromatogr. 640 (1993) 73.
- [152] D. Schlegel, J. Mattusch, K. Dittrich, J. Chromatogr. 683 (1994) 261.



# Industrial sludge reference material for the analysis of acid-extractable metals

Stuart J. Nagourney \*, Nicholas J. Tummillo Jr., John Birri, Kenneth Peist, Bruce MacDonald, Jean S. Kane

*Division of Science Research and Technology, New Jersey Department of Environmental Protection, PO Box 409, Trenton, NJ 08625-0409, USA*

Received 24 August 1998; received in revised form 22 January 1999; accepted 1 February 1999

## Abstract

An interlaboratory study describing the assignment of reference values to the extractable concentrations of metals in industrial sludge using NJDEP and USEPA methods is presented. Industrial waste containing high concentrations of alkali, alkaline earth, ferrous and transition metals was dried, size-reduced and homogenized. Multiple aliquots of this material were analyzed in two different government laboratories by several different combinations of extraction and analysis methodologies. Reference values for the acid-extractable concentrations of more than 15 metals were determined and will be included in the NIST Certificate of Analysis for SRM 2782, Industrial Sludge. © 1999 Elsevier Science B.V. All rights reserved.

*Keywords:* Sludge; Standard Reference Materials®; Reference materials; Metals determination; Quality assurance; Acid-extractable; Microwave digestion; Flame atomic absorption spectrometry; Graphite furnace atomic absorption spectrometry; Inductively coupled plasma atomic emission spectrometry

## 1. Introduction

New Jersey Department of Environmental Protection (NJDEP) regulations limit the levels of discharged toxic substances in sludge effluents by sewage treatment plants. Once maximum contaminant levels are established, they become part of the facility's operating permit. When chemical analyses indicate that these permit levels are exceeded, the NJDEP has statutory authority to

assess significant monetary penalties.

Sludge samples vary widely in their physical and chemical composition, ranging from liquids with low dissolved solid content and small quantities of organics and metals, to multi-phase samples and cakes with solid contents often greater than 50% and concentrations of metals and other constituents at percent levels. Since permit limits for metals are based on the amount leached during mineral acid digestion, these acid-extractable concentrations, rather than total concentrations, are the values of interest. With several options for methods of sample preparation and measurement

\* Corresponding author. Fax: +1-292-7340.

E-mail address: snagourney@dep.stse.nj.us (S. Nagourney)

being proposed by State and Federal agencies, comparability of data and robustness among methods is a critical issue. Reference materials of similar matrix and composition to the various sludge matrices, and having known metal levels with defined uncertainties, are essential to ensuring comparability of data.

The National Institute of Standards and Technology (NIST) certifies the chemical composition of a wide variety of Standard Reference Materials® (SRMs) to ensure the quality of physical and chemical measurements. SRM certified concentrations are generally provided only for total constituent values. A NIST reference value is the best estimate of the true value provided by NIST when all known or suspected sources of bias have not been fully investigated. The uncertainty associated with a reference value may not include all sources of uncertainty and may only represent a measure of the precision of the measurement method(s). Environmental professionals, including soil scientists and geochemists, often require information about labile or extractable concentrations of metals to address issues such as ionic mobility and vegetative uptake. To expand the utility of existing environmental SRMs, NIST has initiated efforts to provide data on the acid-extractable levels of metals in selected new solid sample environmental SRMs [1].

A recent paper by these authors described a collaborative project among the NJDEP, USEPA, Region II Technical Support Branch and NIST to develop sludge reference materials from domestic and industrial sources having reference values for their acid-extractable metals content [2]. The study was successful for the domestic material, resulting in the derivation of reference values for EPA acid-extractable methods as part of SRM 2781, Domestic Sludge. The addendum to SRM 2781 contains leachable mass fractions for 14 metals and compares the leach recoveries to total metal concentrations obtained separately [3]. However, difficulties cited in the evaluation of the more complex industrial sludge prohibited the derivation of leachable mass fraction values for that material at that time. This paper discusses subsequent studies on the industrial sludge material, resulting in improved quality of the data for

SRM 2782. Information is also provided on the comparability of various methods for sample preparation and measurement

## 2. Experimental

### 2.1. Reference Samples

The candidate industrial sludge standard reference material SRM 2782, was prepared from more than 100 kg of electroplating waste supplied by AT&T Bell Laboratories (Murray Hill, NJ). This material was shipped to NIST, wherein it was freeze-dried, processed, radiation-sterilized and homogenized by contractors according to procedures used to prepare United States Geological Survey and NIST geological reference materials [4]. Samples were placed in 125 ml glass bottles and supplied to the NJDEP Bureau of Radiation and Inorganic Analytical Services (BRIAS) and USEPA, Region II, Technical Support Branch laboratories for chemical analysis.

### 2.2. Experimental reagents

The NJDEP and USEPA laboratories used Class A glassware and calibrated microliter pipettes to perform all volumetric dilutions. ACS reagent grade chemicals, double-distilled water and re-distilled acids were employed for sample preparation and digestion. Individual NIST aqueous SRMs (SRM 3100 series) were used for spike recovery studies.

### 2.3. Sample preparation

The NJDEP used open vessel hot plate digestion (NJDEP Method 100) for all of their acid digestions. The USEPA used open vessel hot plate digestion (USEPA Method 3050) for the industrial sludge, and Method 3050 and closed vessel microwave digestion techniques (USEPA Method 3051) to prepare the domestic sludge for measurement. EPA prepared two sets of samples using microwave digestion, one without and one with HCl.

Previous work established the homogeneity of the various aliquots of the domestic and industrial sludge reference materials. The USEPA and NJDEP independently analyzed six aliquots from separate bottles of the industrial material (SRM 2782); the mean value for each metal is reported as the grand mean of six determinations. In this study, two replicates from separate bottles of the domestic material (SRM 2781) were also analyzed by these procedures, by each laboratory, for purposes of comparison and quality assurance.

#### 2.4. Instrumentation<sup>1</sup>

The NJDEP used a Perkin-Elmer (PE) Model 5000 atomic absorption spectrometer (AAS) for its flame atomic absorption (FAAS) metal measurements. A similar unit, equipped with a PE Model 500 furnace and a PE AS-50 autosampler, was used for the graphite furnace atomic absorption (GFAAS) measurements. The NJDEP also employed a Thermo-Jarrell Ash Model 25 sequential inductively coupled plasma emission spectrometer (ICPOES) for some of its metal determinations. The USEPA used a CEM Model MDS-2000 microwave digestion system for some sample preparations, and a Thermo Jarrell-Ash Model 61 Simultaneous ICPOES and a PE 5100 GFAAS, equipped with a model AS-600 furnace and AS-60 autosampler for its metal determinations. The USEPA performed the metal measurements by either simultaneous ICPOES and GFAAS, using one technique per metal. The NJDEP used FAAS, sequential ICPOES and GFAAS and, where possible, employed more than one technique to measure most of the metals.

Calibration standards were prepared by serial dilution from commercial concentrates; the working level concentrations are prepared daily. A minimum correlation coefficient value of 0.999 for the linear calibration curve was required. Contin-

uing calibration check samples were analyzed at a frequency of one per every 10 determinations. Aqueous quality assurance samples, with known values and from sources other than those used for the calibration solutions, were analyzed at a frequency of one per every 10 determinations. Blank solutions, consisting of the reagents used in the sample digestion procedure(s), were prepared and analyzed at a frequency of one per every 10 samples. All values are corrected for any blank concentration. Instrumental conditions were identical to the manufacturer's nominal values.

#### 2.5. Sample processing

Each laboratory analyzed its own digests by one or more instrumental methods. Once completed, the two laboratories exchanged extracts and conducted another series of measurements using the same techniques.

### 3. Results and discussion

Assessment of measurement uncertainty is an integral part of reference value assignment. Components of uncertainty include measurement and procedure variability as well as sample-to-sample variability ascribable to heterogeneity of materials. Complex materials can offer analytical challenges at all concentration levels. While relative uncertainties of  $-20\%$  to  $+20\%$  are expected when EPA methods such as FAAS, GFAAS and ICPOES are applied to non-aqueous media, reference values based upon these methods are still useful for confirmation of results of environmental monitoring, such as the analysis of sludge effluents from treatment plants.

Procedural options in sample preparation and analysis are now available to those who analyze environmental samples and report the results to regulatory agencies. With the emergence of the concept of performance-based analytical methodology as an alternative to the traditional, prescriptive procedurally-based approach, more responsibility is being placed on the reporting entity and, ultimately, the analyst, to understand how the various stages of the analytical process

<sup>1</sup> Certain commercial materials and equipment are identified to specify adequately the experimental procedure. Such identification does not imply recommendation or endorsement by the National Institute of Standards and Technology, nor does it imply that the materials or equipment denoted are the best available for the purpose.

affect their results. In addition to NIST's historical emphasis on certifying the total metals content in non-aqueous environmental samples, the interest of regulatory agencies such as the USEPA and the NJDEP in the environmentally available fraction has led NIST to expand its scope to include evaluations of the efficacy of analytical methods that report only the amount of metal leachable by acid digestion test protocols. The amount of metal liberated from a non-aqueous environmental sample can vary widely depending upon the matrix, metal and extraction procedure. It is important that reference materials exist to benchmark these analyses and procedures as needed to assure results submitted for regulatory purposes, such as those required by NJDEP and USEPA, and help to develop environmental policy standards that protect public health.

### *3.1. Comparison of results for domestic sludge and industrial sludge*

The data for the analysis of the domestic sludge material (SRM 2781) were discussed in detail in an earlier publication by these authors. Issues such as the intralaboratory differences between methods of sample preparation and analysis and comparisons of the overall means between the two laboratories were evaluated for 17 metals. For most elements, small methodological biases were seen; NJDEP means obtained separately by FAAS and ICPOES agreed to within 10% for 13 of 17 elements and within 5% for nine of 17 elements. The between method means of data obtained by the NJDEP and the USEPA laboratories differed by more than 10% only for Ba, Be, Ca, K and Pb. Differences of less than 10% were seen for the means of leach results obtained by Methods 3050 and 3051 for all but one element. Mean values of spike recoveries obtained by the two laboratories were 97.3% for the NJDEP; for the USEPA hot plate digestion, results showed a mean recovery of 102.8%; using microwave digestion, the mean value was 105.3%. This demonstrated minimal bias or matrix interferences in the measurements of the acid-extractable metals in the domestic sludge. The relative uncertainty level compared very favorably with the uncertainties

for total concentrations of inorganic environmental SRMs whose certifications are based primarily on NIST laboratory analyses. Overall uncertainty levels of the interlaboratory means of the leach data for most elements were in the 6% range at the 95% confidence interval, which is four to five times less than typical between-laboratory comparisons. Consequently, acceptable levels of relative uncertainties were determined. This enabled the derivation of reference values for leach concentrations for 14 metals for the NIST SRM 2781.

Our initial attempts at measuring leachable metal concentrations in the industrial sludge SRM 2782 were not nearly as successful. The complex composition of this material and >25% iron mass fraction greatly complicated the reproducibility of extraction of less abundant elements and made it difficult to select interference-free analytical lines for plasma spectrometry for most analyses. For the initial attempt at the analysis of NIST SRM 2782, 12 of the 18 elements analyzed showed between-laboratory differences of greater than 10%, with eight elements exceeding 20%.

### *3.2. Current results for industrial sludge*

Along with the experience gained through our first attempt, recent efforts to analyze the leachable content of this material included several procedural enhancements:

- use of multiple dilutions for flame AAS measurements;
- use of yttrium as an internal standard for ICP measurements;
- use of multiple analytical lines for sequential ICP measurements;
- close matching of acid content of samples and standards;
- customized, updated interelement correction factors for Fe.

This second series of analyses were not without a unique circumstance that unfortunately limited the extent of comparative analyses which could be performed: the DEP closed the BRIAS laboratory in June 1996. The work shown reflects all efforts made up to that date, but resulted in the absence of some information that otherwise would have been obtained.

The improvements in the most recent series of measurements as compared to those conducted earlier, as well as the impacts of methods of sample preparation and measurement, can be demonstrated through several comparisons of individual data sets presented in this paper. All standard deviations are  $\pm 2\sigma$  in the tables:

- mean NJDEP and USEPA results for individual metals (Table 1);
- data from concurrent analysis of NIST SRM 2781 (Table 3);
- USEPA analyses by Method 3050 and Method 3051 (Table 5).

Precision of the six aliquots of NIST SRM 2782 ranged from 0.2 to 2.0% for all elements measured by both participating laboratories. There is no discernible change in the level of precision of the replicate measurements obtained in the earlier and later studies. Table 1 compares the results obtained by both laboratories in the initial (1994) and most recent (1996) studies. There is no discernible pattern in the NJDEP data from 1994 to 1996; the more recent series of USEPA results are generally higher than those obtained previously. The grand means of all elemental results, obtained for each element by the two laboratories for the more recent set of measurements, agreed within

6% for six elements and 10% for 12 of the 17 metals studied; two others were within 12%. Cd, Cr and K were the only elements outside this range. This represents a considerable improvement from the earlier study, the agreement now being comparable to that seen for the analysis of NIST SRM 2781. Three elements exhibited ratios of NJDEP/USEPA data that differ significantly from unity. For Cd, the unavailability of a graphite furnace caused the NJDEP to use only FAAS in the more recent work; given the complex matrix and low concentration, the difference in results is not unexpected. The USEPA results for K are quite variable, both between aliquots exposed to the same sample preparation method and among different sample preparation methods; this was also seen for the data for the domestic sludge material. DEP data for K using hot plate digestion and FAAS as the measurement method showed a relative standard deviation from the mean of only 1.7%. Results for Cr continue to differ between the two laboratories; no assignable cause is evident for either the K or Cr data.

Analysis of variance (ANOVA) [5] can be utilized to evaluate whether the individual element means obtained by the two laboratories for each element, generated by different methods of sample

Table 1  
Comparison of NJDEP and USEPA data SRM 2782<sup>a</sup>

Element	Mean DEP 1994	Mean DEP 1996	Mean EPA 1994	Mean EPA 1996	Ratio DEP/EPA 1996
Al	150 ± 43	1587 ± 107	1380 ± 50	1528 ± 46	1.038
Ba	150 ± 1	161 ± 11	132 ± 4	144 ± 4	1.118
Ca	4687 ± 470	4950 ± 144	4320 ± 141	4685 ± 151	1.056
Cd	4.0 ± 0.1	11.4 ± 3.0	15.4 ± 0.8	2.3 ± 0.1	–
Co	70.0 ± 6	51.6 ± 7	54.4 ± 2	56.0 ± 3	0.921
Cr	79.8 ± 1	76.7 ± 4	55.3 ± 2	58.3 ± 1	–
Cu	2485 ± 146	2459 ± 37	2270 ± 53	2420 ± 42	1.016
Fe	255 020 ± 170 00	256 600 ± 2300	232 000 ± 5600	253 000 ± 14 000	1.014
K	116 ± 1	121 ± 2	58.9 ± 6	78.6 ± 21	–
Mg	508 ± 37	498 ± 69	441 ± 17	470 ± 15	1.059
Mn	274 ± 13	274 ± 7	224 ± 7	247 ± 7	1.109
Na	2430 ± 18	2431 ± 20	2000 ± 123	2573 ± 307	0.945
Ni	125 ± 2	95.5 ± 6	90.8 ± 2	96.1 ± 4	0.994
Pb	581 ± 18	558 ± 9	519 ± 30	553 ± 22	1.010
V	23.2 ± 1	17.5 ± 2	20.6 ± 1	15.9 ± 1	1.100
Zn	1266 ± 31	1181 ± 59	1170 ± 21	1158 ± 71	1.019

<sup>a</sup> Units in mg/kg; uncertainties are  $2\sigma$ .

Table 2  
ANOVA: NIST SRM 2782

Element	<i>F</i> value	<i>P</i> value
Al	0.82	0.38
Ba	33.9	0.00
Ca	1.73	0.22
Co	0.25	0.62
Cr	3.67	0.00
Cu	0.51	0.49
Fe	4.09	0.06
Mg	2.25	0.14
Mn	69.6	0.00
Na	0.06	0.81
Ni	4.20	0.09
Pb	3.52	0.09
V	2.32	0.14
Zn	0.07	0.79

preparation and analysis, are statistically significant. This is shown in Table 2 for the 14 metals where agreement between the grand means was within 12%. ANOVA analyses, as shown by the *F* value (ratio of variance between data sets to the variance within a data set) and *P* value (measure of the probability the actual sample set fell within hypothetical frequencies for infinitely large data populations) showed that the means obtained by the two laboratories agreed within specified tolerances for 11 of the 14 metals; the exceptions being Ba, Cr and Mn. This serves as further corrobora-

Table 3  
Recoveries for Leach Methods: NIST SRM 2781<sup>a</sup>

Element	NIST Leach values from SRM 2781	DEP mean	DEP/NIST	EPA mean	EPA/NIST
Al	8040 ± 980	8844	1.100	7920	0.985
Ba	570 ± 65	475	0.833	534	0.936
Ca	36 440 ± 1830	38 950	1.069	35 050	0.962
Cd	11 ± 2	-	-	12.7	1.155
Cr	143 ± 14	129	0.900	132	0.923
Cu	601 ± 16	588	0.979	590	0.982
Fe	24 300 ± 2100	2540	01.045	26867	1.106
Mg	4850 ± 290	4558	0.940	4588	0.946
Mn	743 ± 33	722	0.984	727	0.978
Ni	72.3 ± 6	63.9	0.884	64.3	0.889
Pb	183 ± 15	180	0.985	194	1.060
V	81.9 ± 4	79.5	0.970	77.6	0.947
Zn	1120 ± 34	1092	0.975	1100	0.982

<sup>a</sup> Units in mg/kg; uncertainties are 2σ.

Table 4  
Linear Regression, NIST SRM 2782: NJDEP and USEPA results

Method of comparison	<i>R</i>	Slope
AAS vs. ICP DEP digestions, hot plate digestion, DEP analyses	0.996	1.039
3050 vs. 3051 EPA analyses, microwave digestions	0.999	0.966
3051 with vs. without HCl EPA analyses, microwave digestions	0.996	1.085

tion to the extent of the agreement between the results.

Comparisons of recoveries of aliquots of NIST SRM 2781, Domestic Sludge analyzed concurrently with the SRM 2782, Industrial Sludge are shown in Table 3. The grand mean for the ratio of each individual NJDEP metal result ( $N = 12$ ) to its NIST reference value is 0.972; the ratio for USEPA data ( $N = 13$ ) is 0.989. There are several interesting sub-sets of the data that address specific issues related to sample preparation and measurement. One method of comparison is a linear regression of the NJDEP data (abscissa) against the USEPA data (ordinate); the regression (*R*) and slopes (*m*) of the line are shown in Table 4; values of 1.000 represent ideal agreement.

- *Comparison of AAS and ICP-OES.* Extensive comparisons of both absorption and emission

spectroscopic methods of analyses were made for the domestic material. A limited sub-set (only seven owing to the closure of the DEP laboratory) of metals for the industrial material were analyzed by both procedures. The grand mean of the ratio of AAS to ICP-OES results was 1.043; the slope of the regression line is 1.039. This is evidence that good agreement between detection methods exists for this SRM.

- *Method 3050 versus Method 3051.* The USEPA obtained good results for 14 metals where extractions were obtained by both methods and analyses performed by ICP-OES. Agreement is within  $\pm 6\%$  for all metals studied except for Na and K; with a range in bias from  $-4.8\%$  for Al to  $+5.2\%$  for Zn. These results are shown in Table 5. The values for the alkali metals Na and K are approximately 30–40% higher for the microwave technique. When the *t*-test for means assuming unequal variance is applied [6], the differences between the calculated means obtained by each method were statistically significant for six metals (Ba, Ca, Cu, Mn, Pb and Zn). However, these detected differences are relatively small, especially when compared to the control limits assigned to

acid-extractable analyses measured in non-aqueous media.

- *Method 3051 with and without HCl.* The agreement of data from the two sets of USEPA digestions is good for all metals but K. The range in bias is  $-1.7$  to  $+12.1\%$ . The generally high bias (11 out of 13 metals had higher values when the extraction was performed with the addition of HCl) and positive slope for the regression suggests the addition of acid increases the extraction efficiency for the metals studied in this matrix. This data suggests that the USEPA should consider allowing the use of HCl in the digestion of non-aqueous samples for the acid-extractable content of metals. The data are shown in Table 6.
- *USEPA analysis of EPA and DEP digests.* The closure of the DEP laboratory limited the comparisons of analyses of extracts where analyses were performed in both laboratories. There are analyses of extracts done in the DEP facility (Method 100) and the EPA laboratory (Method 3050), where both sets were analyzed by the same laboratory (EPA by ICP-OES); these data are shown in Table 7. The long time (approximately 10 months) between extraction and analysis, combined with low analysing

Table 5  
2782, comparison of extraction methods: EPA3050 and 3051<sup>a</sup>

Element	Method 3050		Method3051		Ratio 3050/3051
	Mean	SD	Mean	SD	
Al	1520	18	1580	59	0.962
Ba	148	2	142	5	1.042
Ca	4870	58	4640	169	1.050
Cd <sup>b</sup>	2.19	0.40	2.21	0.57	0.991
Co	58.5	0.9	56.2	2.2	1.041
Cr	57.9	0.6	60.3	2.4	0.960
Cu	2500	37	2400	87	1.042
Fe	260 000	4500	269 000	1400	0.967
Mg	470	5	455	17	1.033
Mn	256	3	246	9	1.041
Ni	99.6	0.8	99.3	3.7	1.003
Pb	545	6	513	22	1.062
V	16.0	0.1	16.7	0.6	0.958
Zn	1210	15	1150	45	1.052

<sup>a</sup> Units in mg/kg; uncertainties are  $2\sigma$ .

<sup>b</sup> Analyses by GFAAS.

Table 6  
NIST SRM 2782, comparison of Method 3051 with and without HCl<sup>a</sup>

Element	Method 3051 with HCl		Method 3051 without Cl		Ratio extracted w & w/o HCl
	Mean	SD	Mean	SD	
Al	1580	59	1470	21	1.075
Ba	142	5	142	3	1.000
Ca	4640	169	4510	70	1.029
Co	56.2	2.2	51.9	1.0	1.083
Cr	60.3	2.4	56.8	2.4	1.062
Cu	2400	87	2360	39	1.017
Fe	269 000	1400	248 000	5850	1.085
Mg	455	17	463	7	0.983
Mn	246	9	238	4	1.034
Ni	99.3	3.7	90.2	2.0	1.101
Pb	513	22	492	8	1.043
V	16.7	0.6	14.9	0.2	1.121
Zn	1150	45	1060	22	1.085

<sup>a</sup> Units in mg/kg; uncertainties are  $2\sigma$ .

level, contributed to the poorer agreement for Cd and V. For 14 metals, the grand mean of comparisons of DEP to EPA sample preparation methods was 1.009, showing that again for the industrial sludge material there is little difference between values derived from different sample preparation methods.

### 3.3. Comparison of leachable concentrations for domestic sludge and industrial sludge

Addenda to the Certificates of Analysis for NIST SRM 2781, Domestic Sludge and NIST SRM 2782, Industrial Sludge [7] compare the percentage leach recoveries of selected metals with the values obtained for their total mass fractions. For elements where leachable metal results were obtained from both the USEPA and NJDEP laboratories, a ratio of leachable metal concentration to total metal concentration (obtained by NIST) was calculated. For the domestic sludge, these ratios were between 0.82 and 0.96 for nine out of 11 elements; only Al (0.50) and Cr (0.71) were below this range. Preliminary values supplied by NIST for the industrial sludge material shows a different pattern; for the 14 elements for which such data is available, only six have ratios of leachable to total that are greater than 0.80. Na,

K, Mg, Al have ratios below 0.20; the ratio for V is 0.21, Ba and Ni are 0.60 and 0.62, respectively, while Ca is 0.72. Only certain transition elements (Cu, Pb, Zn, Mn, Fe and Co) have leachable/total ratios for the industrial sludge that are greater than 0.80. The results are summarized in Table 8. Note that for the industrial sludge, all of the ratios for the alkali and alkaline earth metals as well as Al are 0.72 or below. While the reasons for the specific analyte–matrix interactions are uncertain, it is apparent that the more complex nature of the industrial sludge plays a key role in how much metal is leached by the regulatorily-approved digestion methods, and the amount that leaches varies significantly by element and group. This issue must be considered when evaluations of leachable metal concentrations are made for environmental assessment and policy considerations.

## 4. Conclusions and recommendations

Reference values have been determined for the leachable concentration of 14 metals in an industrial sludge standard reference material (NIST SRM 2782). Both open vessel hot-plate acid digestion (NJDEP Method 100 or USEPA Method 3050) or microwave digestion (USEPA Method



Table 7  
2782, comparison of NJDEP and USEPA extracts: analyses by USEPA<sup>a</sup>

Element	Method 3050		Method 100		Ratio 3050/100
	Mean	SD	Mean	SD	
Al	1520	18	1540	8	0.987
Ba	148	2	144	1	1.027
Ca	4870	58	4720	34	1.032
Co	58.5	0.9	57.0	0.9	1.026
Cr	57.9	0.6	58.2	2.4	0.994
Cu	2500	37	2420	45	1.033
Fe	260 000	4500	236 000	1100	1.102
K	72.4	11.8	80.1	1250	0.904
Mg	470	5	490	7	0.959
Mn	256	3	246	3	1.041
Na	2300	39	2470	60	0.931
Ni	545	6	524	13	1.040
Pb	545	6524	13	1.040	
Zn	1210	15	1210	11	1.000

<sup>a</sup> Units in mg/kg; uncertainties are  $2\sigma$ .

3051) are appropriate methods for sample preparation of these materials and the leachable concentrations may be measured by either FAAS, sequential or simultaneous ICPOES. This information supports the application of performance-based methodology since there are several combinations of sample preparation and measurement systems that can achieve similar results. Reference materials from both sludge sources are commercially available. Reference values for their acid-extractable metal content and associated uncertainties are provided and are available to support the quality assurance of sludge metal measurements. Analyses of these SRMs should be recommended as part of a POTW's compliance data submitted to regulatory agencies such as the USEPA and NJDEP. It is also recommended that these materials become part of any future laboratory certification program for sludge effluents.

### Acknowledgements

The authors wish to thank the NJDEP's Bureau of Pretreatment and Residuals for providing the funding for this study and Mary Jo Aiello and Tony Pilawski of that Bureau for many helpful discus-

sions. Thomas LaFisca and Gail Suozzo are New Jersey state chemists who conducted some of the chemical analyses. Robert Markow of AT&T Bell Laboratories supplied the industrial sludge. Dr Gregory Turk of NIST assisted with the data assessment.

Table 8  
Comparison of leachable concentrations: NIST SRM 2781 and 2782<sup>a</sup>

Element	Domestic sludge ratio (leachable/total)	Industrial sludge ratio (leachable/total)
Ag	0.88	–
Al	0.50	0.11
Ba	–	0.60
Cd	0.86	–
Ca	0.93	0.72
Co	–	0.82
Cr	0.71	–
Cu	0.96	0.94
Fe	0.87	0.95
K	–	0.02
Pb	0.91	0.97
Mg	0.82	0.18
Mn	0.82	0.86
Na	–	0.19
Ni	0.90	0.62
V	–	0.21
Zn	0.88	0.93

<sup>a</sup> Units in mg/kg; uncertainties are  $2\sigma$ .

Stuart J. Nagourney is a Research Scientist with the NJDEPs Division of Science and Research; he was Chief of the Bureau of Radiation and Inorganic Analytical Services for the NJDEP while this study was conducted. Nicholas Tummillo is a Principal Chemist with the New Jersey Department of Health and Senior Services. John Birri is Special Projects Coordinator and Kenneth Peist a staff scientist with the USEPA's Region II Technical Support Branch laboratory. Bruce MacDonald is the current, and Jean S. Kane the former Project Manager with the United States Department of Commerce, NIST Standard Reference Materials Program who provided oversight for this project.

## References

- [1] J.S. Kane, *Fres. J. Anal. Chem.* 352 (1995) 309.
- [2] S.J. Nagourney, N.J. Tummillo, J. Birri, K. Peistand, J.S. Kane, *Talanta* 44 (1997) 189.
- [3] National Institute of Standards and Technology, Office of Standard Reference Materials, Addendum to Certificate 2781, October 1996.
- [4] J.F. Flanagan, *United States Geological Survey Bulletin* 1582, 1986.
- [5] L.L. Havlicek, R.D. Crain, *Practical Statistics for the Physical Sciences*, American Chemical Society, Washington, DC, 1988.
- [6] J.K. Taylor, *Quality Assurance of Chemical Measurements*, Lewis Publishers, Chelsea, Michigan, 1989.
- [7] National Institute of Standards and Technology Office of Standard Reference Materials Addendum to Certificate 2782, December 1998.

# Determination of the cyclodextrin inclusion constant with the constant current coulometric titration method

Jun Gu, Jinghao Pan \*

*Department of Chemistry, Shanxi University, Taiyuan 030006, People's Republic of China*

Received 5 March 1998; received in revised form 12 August 1998; accepted 8 March 1999

## Abstract

With fluorometry this paper has proved that  $\alpha$ -cyclodextrin (CD) and  $\gamma$ -CD do not form inclusion complexes with procaine, while  $\beta$ -CD and HP- $\beta$ -CD do. Their molar ratios are demonstrated both 1:1 with the equimolar variation method. The constant current coulometric titration method (CCCT) is first proposed and applied in the determination of the CD inclusion constant. To compare with this method, the fluorescence experiment has been done with the satisfactory results. © 1999 Elsevier Science B.V. All rights reserved.

*Keywords:* Cyclodextrin; Inclusion constant; The constant current coulometric titration method; Procaine

## 1. Introduction:

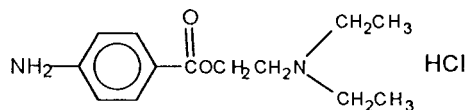
Cyclodextrins (CDs) are cyclic oligosaccharides produced by the action of the CD-*trans*-glycosidase enzyme on a medium containing starch. Due to their special molecular cavity structure, CDs can include other 'guest' molecules as 'hosts' to form inclusion complexes. The formation of CD complexes improves physical, chemical and biological properties of the guest molecular. This leads to the wider application of CD in the fields of medicine, food, organic synthesis, environmental protection and analytical chemistry etc. [1]. As the quantitative descrip-

tion of the inclusion equilibrium between CD and guest molecule, the inclusion constant reflects the strength of the binding force between them. So, the inclusion constant is an important and basic parameter to the applications of CD. In pharmaceuticals, the inclusion constants of pharmaceuticals-CD complexes are of especial importance to guide the CD's application directions. Until now, the reported determination methods for the CD inclusion constant are: spectroscopic method [2]; surface tension method [2]; nuclear magnetic resonance method [3–5]; phase-solubility technique [7]; high pressure liquid chromatography [6]; fluorometry [8]; electrochemistry [9,10] (potentiometry; polarography and voltammetry). There have been no reports on the coulometric determination of the CD inclusion constant.

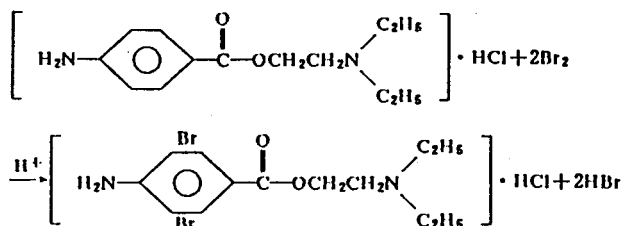
\* Corresponding author.

## 2. The basic principles

The structural formula of procaine hydrochloride:

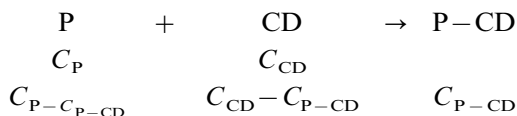


The quantities of procaine hydrochloride can be accurately measured with the constant current coulometric titration method (CCCT) [11]. This method is based on the bromo reaction. According to the following reaction, under the acidic condition, H in the benzene ring was exchanged by the titrant bromine produced by electrolysis.



It will be proven that the benzene ring in procaine hydrochloride would be included into the cavities of  $\beta$ -CD and HP- $\beta$ -CD. As a result, the included benzene ring could not react with bromine and the quantity of the procaine measured with CCCT is the one that was not included by CDs.

For 1:1 complex inclusion: (procaine hydrochloride is denoted as 'P' and procaine-CD complex as 'P-CD').



where  $C_{\text{P}}$ ,  $C_{\text{CD}}$  are procaine's and CD's known starting concentration respectively,  $C_{\text{P}-\text{P-CD}}$ ,  $C_{\text{CD}-\text{P-CD}}$  and  $C_{\text{P-CD}}$  are procaine's, CD's and procaine-CD complex's equilibrium concentrations respectively.

The inclusion constant is calculated from Eq. (1):

$$K = \frac{[\text{P-CD}]}{[\text{P}][\text{CD}]}$$

$$= \frac{C_{\text{P-CD}}}{(C_{\text{P}} - C_{\text{P-CD}})(C_{\text{CD}} - C_{\text{P-CD}})} (\text{l mol}^{-1}) \quad (1)$$

$$C_{\text{P}} = \frac{iT}{96487nV} (\text{mol l}^{-1})$$

$$C_{\text{P}} - C_{\text{P-CD}} = \frac{it}{96487nV} (\text{mol l}^{-1})$$

$$C_{\text{P-CD}} = \frac{i(T-t)}{96487nV} (\text{mol l}^{-1})$$

so

$$K = \frac{\frac{(T-t)}{i}}{t \left\{ C_{\text{CD}} - \frac{i}{96487nV}(T-t) \right\}} (\text{l mol}^{-1}) \quad (2)$$

where  $T$  and  $t$  are the titration end point time in the absence and presence of CD (second).  $i$  is the constant current (0.96 mA).  $n$  is the transferred electron number of the substances in the electrode reaction (here,  $n = 4$ ).  $V$  is the total volume of the electrolyte (100 ml).

Thus, after we determine  $T$  and  $t$ , we can calculate  $K$  from Eq. (2).

## 3. Experimental

### 3.1. Reagents

$\alpha$ -CD and  $\gamma$ -CD were from Casei, Tokyo (Japan); HP- $\beta$ -CD (MS 0.6) was from Aldrich (USA);  $\beta$ -CD from Yunan (China) was recrystallized three times in the laboratory. Procaine hydrochloride that was kindly provided by Shanxi Pharmaceutical Testing Institute was of pharmaceutical purity grade. Other reagents used were of analytical purity grade, and redistilled deionized water was used throughout.

### 3.2. Apparatus

The coulometric titration was carried out on the self-assembling coulometer, which consist of the SKD-A coulometer (Wuhan, China), the double platinum electrode, the magnetic stirrer and the current detector (Shanghai, China). The fluorescence spectrum and the fluorescence intensity were measured on a RF-540 spectrofluorometer (Shimadzu, Japan). The molar ratios were measured on a UV-265 recording spectrophotometer (Shimadzu).

### 3.3. Procedures

(1) 10 ml  $1\text{ mol l}^{-1}$  KBr, 0.5 ml 10%  $\text{H}_2\text{SO}_4$ , 0.5 ml  $1 \times 10^{-3}$  mol  $\text{l}^{-1}$  procaine solution and certain amounts of  $\alpha$ ,  $\beta$ ,  $\gamma$ , HP- $\beta$ -CD ( $1 \times 10^{-2}$  mol  $\text{l}^{-1}$ ) were added and diluted to 100 ml. After stirring for 5 min, the titration end point time was measured.

(2) 1 ml  $1\text{ mol l}^{-1}$  KBr, 0.05 ml 10%  $\text{H}_2\text{SO}_4$ , 0.5 ml  $1 \times 10^{-3}$  mol  $\text{l}^{-1}$  procaine solution and 0.5, 1, 2, 3, 4, 5 ml  $\alpha$ ,  $\beta$ ,  $\gamma$ , HP- $\beta$ -CD ( $1 \times 10^{-2}$  mol  $\text{l}^{-1}$ ) were added into a 10 ml volumetric flask, respectively. The fluorescence spectrum and the fluorescence intensity were obtained after diluting to final volume.

(3) The equimolar variation experiment (the continuous method): The total concentration of CD and procaine will be kept constant ( $[\text{CD}] + [\text{procaine}] = 5\text{ mM}$ ), and the ratio  $r = [\text{CD}]/[\text{P}] + [\text{CD}]$  varied from 0 to 1. This is accomplished by preparing equimolar solutions of CD and procaine and mixing them to constant volume to the desired ratio  $r$ . The absorbances at 290 nm were measured.

## 4. Results and discussions

### 4.1. The proof of formation of inclusion complex with the fluorescence spectrum of procaine hydrochloride in the different CD ( $\alpha$ , $\beta$ , $\gamma$ , HP- $\beta$ -CD) media

In the presence of  $\alpha$ -,  $\beta$ -,  $\gamma$ -, HP- $\beta$ -CD, the fluorescence spectra of procaine hydrochloride were measured. The results show that in the pres-

ence of  $\alpha$ -CD or  $\gamma$ -CD, the fluorescence intensities of procaine increase little or do not increase; while in the presence of  $\beta$ -CD or HP- $\beta$ -CD, the fluorescence intensities of procaine increase greatly (Fig. 1). This shows that  $\alpha$ -CD and  $\gamma$ -CD do not form an inclusion complex with procaine, while  $\beta$ -CD and HP- $\beta$ -CD do. It is because that CD's cavity offers a protective microenvironment that can shield the excited singlet species from quenching and nonradiative decay process occurred in bulk aqueous solution [12].

### 4.2. The constant current coulometric titration of procaine hydrochloride in the presence of $\alpha$ , $\beta$ , $\gamma$ , HP- $\beta$ -CD

In the absence and presence of  $\alpha$ ,  $\beta$ ,  $\gamma$ , HP- $\beta$ -CD, the titration end point time of procaine hydrochloride was measured on the self-assembling coulometer. The results show that in the presence of  $\alpha$ -CD or  $\gamma$ -CD the titration end point time of procaine has no change, while in the presence of  $\beta$ -CD or HP- $\beta$ -CD the titration end point time shifts earlier. The earlier shift of the titration end point time shows that the quantity of benzene ring in procaine reacted with bromine was less. Thus the conclusion can be drawn that the benzene ring was included into the cavity of  $\beta$ -CD and HP- $\beta$ -CD.

### 4.3. The determination of the molar ratios of the inclusion complexes (the equimolar variation experiment)

The determination of the stoichiometry of the complex was performed using the equimolar variation experiment as described in the Section 3. Plots of the  $\Delta A$  as a function of  $r$  leads to the Job Plots presented in Fig. 2. They show a maximum at  $r = 0.5$ , indicating that both complexes have 1:1 stoichiometry and that no other complex is present.

### 4.4. The determination of cyclodextrin inclusion constants by constant current coulometric titration method

According to the method in basic principle, the titration end time ( $t$ ) was measured and  $K$  was

calculated according to Eq. (2). In order to confirm and compare the experimental and theoretical methodology described above, the fluorometric determination of CD inclusion constants has been done [8](Benesi–Hildebrand method)

$$\frac{C_G}{\Delta F} = \frac{1}{\alpha K} \times \frac{1}{C_{CD}} + \frac{1}{\alpha} \quad (3)$$

where  $C_G$  and  $C_{CD}$  are the concentrations of guest and CD, respectively.  $\Delta F$  is the fluorescence inten-

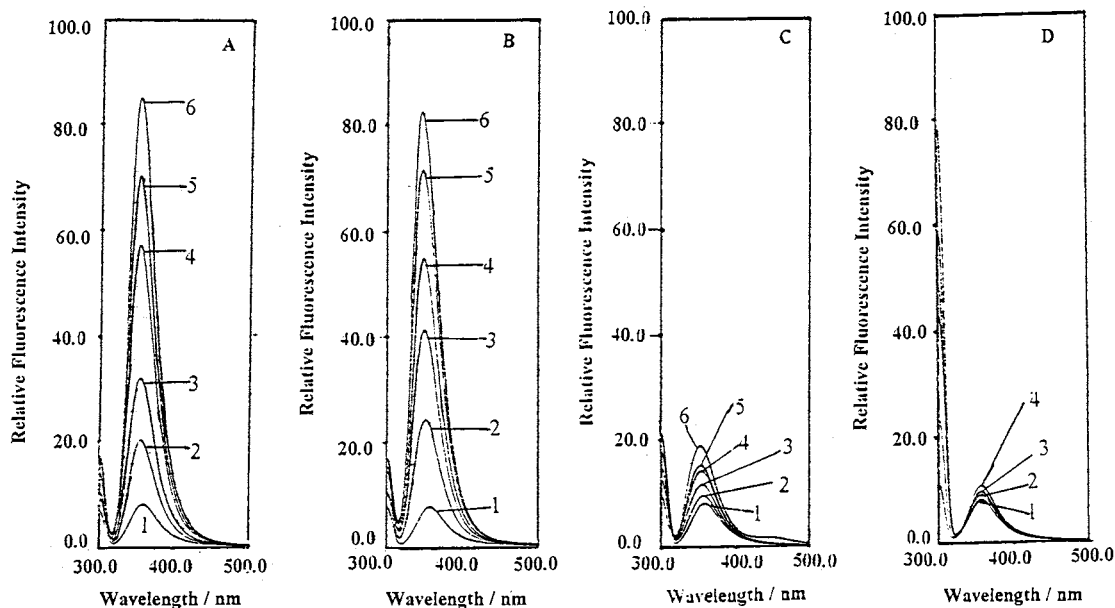


Fig. 1. The fluorescence spectrum of 0.05 mmol procaine hydrochloride in the presence of  $\beta$ -cyclodextrin (CD) and HP- $\beta$ -CD. (A) [ $\beta$ -CD] = 0 M (1), 0.0005 M (2), 0.001 M (3), 0.002 M (4), 0.003 M (5), 0.004 M (6); (B) [HP- $\beta$ -CD] = 0 M (1), 0.001 M (2), 0.002 M (3), 0.003 M (4), 0.004 M (5), 0.005 M (6); (C) [ $\alpha$ -CD] = 0 M (1), 0.001 M (2), 0.002 M (3), 0.003 M (4), 0.004 M (5), 0.005 M (6); (D) [ $\gamma$ -CD] = 0 M (1), 0.001 M (1), 0.002 M (3), 0.003 M (2), 0.004 M (4), 0.005 M (3).

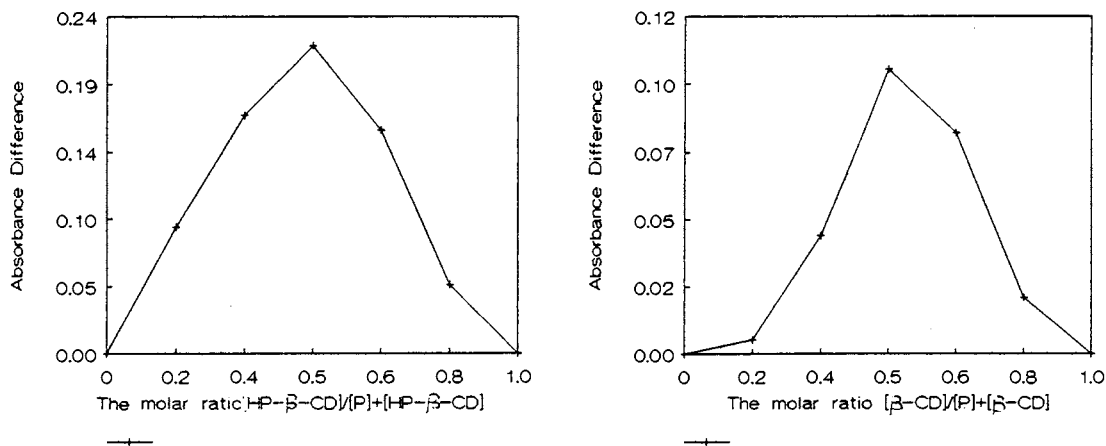


Fig. 2. Continuous variation plot (Job Plot).

Table 1

The inclusion constants of procaine- $\beta$ -cyclodextrin (CD) complex and procaine-HP- $\beta$ -CD complex

$K$ (l mol <sup>-1</sup> )	$\beta$ -CD				HP- $\beta$ -CD		
	1	2	3	4	1	2	3
Exp. no.							
CCCT ( $\times 10^2$ )	1.47	1.06	1.43	1.51	2.85	2.86	2.26
Average ( $\times 10^2$ )		1.37				2.66	
Fluorescence ( $\times 10^2$ )		1.00				2.32	

sity difference,  $\alpha$  is the coefficient; and  $K$  is the inclusion constant. Following procedure 2, the relative fluorescence intensities were measured. The curve of  $1/\Delta F \sim 1/C_{CD}$  was drawn, and  $K$  was the ratio of the intercept to the slope.

Table 1 shows that the results of coulometric titration method and the fluorometry are basically the same.

## 5. Conclusions

Till now, there has been no report on determining the CD inclusion constant with the constant current coulometric titration method. This method expands the electrochemical ways with which the CD inclusion constants can be measured.

Moreover, more accurate, more sensitive, simpler, quicker and easier to operate automatically are advantages of coulometry. It has wide applications in the fields of medicine, food and environment monitoring, etc.

The coulometric titration method has some restrictions. The guest molecular must have the group that can be included into the cavity of CD and that can react with the titrant produced by electrolysis.

## Acknowledgements

This work was supported by Returnee Research Item Fund from Shanxi Province (China).

## References

- [1] J. Gu, Y. Chang, J. Pan, *Chin. J. Appl. Chem.* 13 (4) (1996) 5–9.
- [2] O. Bekers, E.V. Uijtendaal, J.H. Beijnen, A. Bult, W.J.M. Underberg, *Drug Dev. Ind. Pharm.* 17 (11) (1991) 1503–1549.
- [3] R.J. Bergeron, M.A. Channing, G.J. Gibeily, D.M. Pillor, *J. Am. Chem. Soc.* 99 (1977) 5146.
- [4] D.J. Wood, F.E. Hruska, W. Saenger, *J. Am. Chem. Soc.* 99 (1977) 1735.
- [5] Y. Inoue, Y. Miyata, *Bull. Chem. Soc. Jpn.* 54 (1981) 809.
- [6] K. Uekama, F. Hirayama, T. Irie, *Chem. Lett.* 7 (1978) 661.
- [7] T. Higuchi, K.A. Connors, Phase-solubility techniques, *Adv. Anal. Chem. Instrum.* 4 (1965) 117.
- [8] Y. Wang, X. Huang, G. Chen, *Chin. J. Chem.* 9 (1990) 46.
- [9] T. Osa, T. Matsue, M. Fujihira, *Heterocycles* 6 (1977) 1833.
- [10] P.M. Bersier, T. Bersier, B. Klingert, *Electroanalysis* 3 (1991) 443.
- [11] Y.C. Sheng, J. Pan, M. Dong, Yaoi Fenxi Zazhi (China) 8 (20) (1988) 91.
- [12] W. Qi, Z. Qi, Xin. Fenxi Zhengxiao Shiji (China), the publish house of Hangzhou University, 1994.

# Flow-injection determination of copper(II) based on its catalysis on the redox reaction of cysteine with iron(III) in the presence of 1,10-phenanthroline

Norio Teshima <sup>a,\*</sup>, Hideyuki Katsumata <sup>a</sup>, Makoto Kurihara <sup>a</sup>, Tadao Sakai <sup>b</sup>,  
Takuji Kawashima <sup>a</sup>

<sup>a</sup> *Laboratory of Analytical Chemistry, Department of Chemistry, University of Tsukuba, Tsukuba 305-8571, Japan*

<sup>b</sup> *Department of Applied Chemistry, Aichi Institute of Technology, Toyota 470-0392, Japan*

Received 21 January 1999; received in revised form 11 March 1999; accepted 16 March 1999

## Abstract

A redox reaction of cysteine with iron(III) proceeds slowly in the presence of 1,10-phenanthroline (phen). However, this reaction is accelerated in the presence of copper(II) as a catalyst, producing an iron(II)–phen complex ( $\lambda_{\max} = 510$  nm). A sensitive spectrophotometric flow-injection method is proposed for the determination of copper(II) based on its catalytic action on this redox reaction. The dynamic range was 0.1–10 ng ml<sup>-1</sup> of copper(II) with a relative standard deviation of 1.0% ( $n = 10$ ) for 1.0 ng ml<sup>-1</sup> of copper(II) at a sampling rate of 30 h<sup>-1</sup>. The detection limit ( $S/N = 3$ ) is 0.04 ng ml<sup>-1</sup>. The proposed method was successfully applied to the determination of copper in river water as a certified reference material. © 1999 Elsevier Science B.V. All rights reserved.

*Keywords:* Catalytic reaction; Copper determination; Cysteine; Flow-injection spectrophotometric method; Iron(III); 1,10-Phenanthroline

## 1. Introduction

Much attention has been focused on kinetic–catalytic methods of analysis based on catalytic reactions because these methods have been applied to trace and/or ultratrace analyses for vari-

ous elements [1–3]. Recent developments in kinetic–catalytic methods have been reviewed by Mottola and Perez-Bendito [4] and Crouch et al. [5]. Numerous catalytic methods have still been proposed for the determination of copper(II) with various monitoring systems such as fluorimetric [6], amperometric [7] and photometric [8–14] detections. For example, an oxidative coupling of 3-methyl-2-benzothiazolinone hydrazone with *N*-ethyl-*N*-(2-hydroxy-3-sulfopropyl)-3,5-dimethoxyaniline has been used as an indicator reaction for the catalytic determination

\* Corresponding author. Present address: Department of Applied Chemistry, Aichi Institute of Technology, Toyota 470-0392, Japan. Fax: + 81-565-48-0076.

*E-mail address:* teshima@ac.aitech.ac.jp (N. Teshima)



of copper(II) at the 0.002–0.1 ng ml<sup>-1</sup> levels [14]. The method is very sensitive, but its analytical conditions in the batchwise procedure should be strictly controlled.

It is well known that copper ion catalyzes the oxidation of cysteine to cystine with oxygen in aqueous medium [15,16]. Watanabe and co-workers [17,18] first adapted the redox reaction to a catalytic method for the determination of copper(II) in a mixed solution of water and *N,N*-dimethylformamide. In the method the decrease in the concentration of cysteine was measured spectrophotometrically by adding 2,2'-dithiobis(5-nitropyridine) for the determination of copper(II). However, the batchwise method is laborious and the sensitivity of the method is not enough to determine copper in natural water: the detection limit is 2.5 ng ml<sup>-1</sup> for copper(II).

On the other hand, flow-injection analysis has been recognized as a suitable device for improving the kinetic-catalytic methods of analysis [2,19]. On-line monitoring of trace amounts of copper(II) in steam condensate and boiler feed-water was carried out by flow-injection catalytic method at a rate of 30 h<sup>-1</sup> [11]. By using flow-injection catalytic method, applications to the determination of copper(II) in blood plasma [7] and natural water [13] were also reported.

The redox potential of a system involving metal ions is modified by complexation of metal ions with a suitable ligand [20]. By using this phenomenon, we have recently proposed novel redox systems, which are applicable to potentiometric titrimetries for the determination of metal ions [21–25]. We also developed a new flow-injection spectrophotometric method for the simultaneous determination of vanadium(IV) and vanadium(V), based on the effect of 1,10-phenanthroline (phen) and diphosphate on the redox potential of the Fe(III)/Fe(II) system [26]. Thus, it is worthwhile to propose novel redox systems based on the ligand effect from the viewpoint of analytical chemistry.

In this paper, the effect of phen on the redox reaction of cysteine with iron(III) is potentiometrically studied. The presence of phen causes an increase in the oxidizing power of iron(III) as a result of the formation of the iron(II)–phen com-

plex ( $\lambda_{\max} = 510$  nm). Furthermore, we propose the redox reaction as a new indicator reaction in the catalytic spectrophotometric flow-injection method for the determination of trace amounts of copper(II). The present method can determine copper(II) in the range 0.1–10 ng ml<sup>-1</sup> at a sampling rate of 30 h<sup>-1</sup> and was successfully applied to the determination of copper in river water as a certified reference material.

## 2. Experimental

### 2.1. Reagents

A commercially available copper standard solution for atomic absorption spectrometry (1.0 mg ml<sup>-1</sup>) (Wako Junyaku, Japan) was used and working standard solutions were prepared daily by diluting the standard solution with 0.01 mol l<sup>-1</sup> nitric acid. A stock solution of iron(III) (0.1 mol l<sup>-1</sup>) was prepared by dissolving 4.82 g of iron(III) ammonium sulfate dodecahydrate in 100 ml of 0.5 mol l<sup>-1</sup> sulfuric acid and was standardized with EDTA. Working solutions of iron(III) were prepared by suitable dilution with  $5 \times 10^{-3}$  mol l<sup>-1</sup> sulfuric acid. A solution of cysteine ( $1 \times 10^{-2}$  mol l<sup>-1</sup>) was prepared by dissolving 0.43 g of L-cysteine hydrochloride monohydrate in 250 ml of water. A phen solution (0.2 mol l<sup>-1</sup>) was prepared by dissolving an appropriate amount of the reagent in 0.1 mol l<sup>-1</sup> sulfuric acid. Working solutions of cysteine and phen were prepared by suitable dilution with water.

All reagents were of analytical-reagent grade and were used without further purification. All solutions were prepared with deionized water purified with a Millipore Milli-Q PLUS system.

### 2.2. Apparatus

Fig. 1 shows a schematic FIA diagram for the determination of copper(II). Two double-plunger micropumps (Sanuki Kogyo, DMX-2000, Tokyo) and a six-way injection valve (Sanuki Kogyo, SVM-6M2) were used to assemble the system. The flow lines were made from Teflon tubing (0.5 mm i.d.). The absorbance was monitored at 510 nm

with a spectrophotometer (Soma Optics, S-3250, Tokyo) equipped with a 10-mm micro flow cell (8  $\mu$ l) and recorded on a recorder (Chino, EB 22005, Tokyo). The pH of the waste solution was continuously monitored with a pH/mV meter (Horiba, Model F-8 AT, Kyoto).

Potentiometric titrations of cysteine with iron(III) were performed using a Mitsubishi Chemical Model GT-05 automatic titrator installed with a Mitsubishi Chemical Model GTPR10 combination platinum electrode (the reference electrode, a silver–silver chloride electrode) and a Model GT5TSN thermometer. A Taiyo Kagaku Kogyo (Tokyo) C-630 thermostat was used to maintain the temperature (50°C).

### 2.3. Procedure

In the flow system as shown in Fig. 1,  $1 \times 10^{-2}$  mol  $l^{-1}$  nitric acid as a carrier solution in reservoir C, a mixed solution of cysteine ( $1 \times 10^{-3}$  mol  $l^{-1}$ ) and acetate buffer (0.1 mol  $l^{-1}$ , pH 4.8) in  $R_1$ , a solution of iron(III) ( $2 \times 10^{-3}$  mol  $l^{-1}$ ) in  $R_2$  and a solution of phen ( $4 \times 10^{-3}$  mol  $l^{-1}$ ) in  $R_3$  were pumped at a flow rate of 1.0 ml  $min^{-1}$ , respectively. An aliquot (200  $\mu$ l) of copper(II) solution was injected into the carrier stream (C). The copper(II)-catalyzed reaction of cysteine with iron(III) in the presence of phen took place in the reaction coils at room temperature. The absorbance of the iron(II)–phen complex produced was continuously monitored at 510 nm.

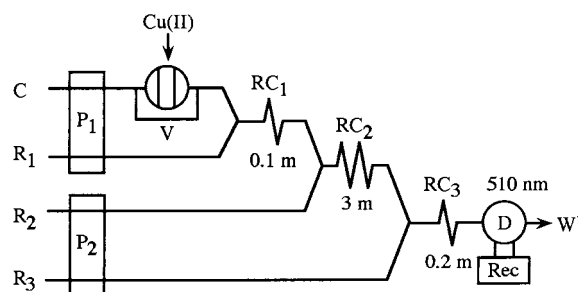


Fig. 1. Flow system for the catalytic determination of copper(II). C, carrier solution ( $HNO_3$ ,  $1.0 \times 10^{-2}$  mol  $l^{-1}$ );  $R_1$ , cysteine ( $1 \times 10^{-3}$  mol  $l^{-1}$ ) + acetate buffer (0.1 mol  $l^{-1}$ , pH 4.8);  $R_2$ , iron(III) ( $2 \times 10^{-3}$  mol  $l^{-1}$ );  $R_3$ , phen ( $4 \times 10^{-3}$  mol  $l^{-1}$ );  $P_1$  and  $P_2$ , pump; V, six-way valve (200  $\mu$ l);  $RC_1$ ,  $RC_2$  and  $RC_3$ , reaction coil; D, detector; Rec, recorder; W, waste.

## 3. Results and discussion

### 3.1. Redox reaction of cysteine with iron(III) in the presence of phen

The conditional redox potential of the Fe(III)/Fe(II) system in the presence of phen,  $E'_{Fe}$ , can be written as

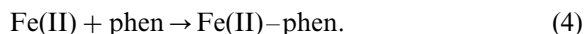
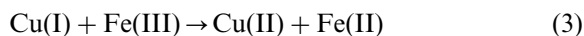
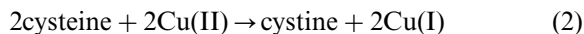
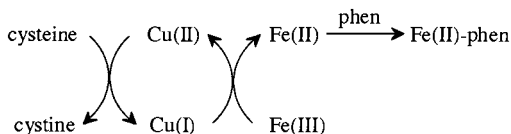
$$E'_{Fe} = E^{\circ}_{Fe} + 0.059 \log \frac{\alpha_{Fe(II)(phen)}}{\alpha_{Fe(III)(phen)}} + 0.059 \log \frac{C_{Fe(III)}}{C_{Fe(II)}} \quad (1)$$

where  $C_{Fe(III)}$  and  $C_{Fe(II)}$  refer to the total concentrations of iron(III) and iron(II), respectively, and  $\alpha$  refers to the side reaction coefficient taking into account the complex formation of the relevant metals with phen:  $\alpha_{Fe(II)(phen)} = 1 + \sum \beta_n(Fe(II)(phen)) [phen]^n$  with  $\beta_n(Fe(II)(phen)) = [Fe(II)(phen)]_n [Fe]^{-1} [phen]^{-n}$  ( $n = 1, 2, 3$ ) and  $\alpha_{Fe(III)(phen)}$  are defined similarly. It is obvious from Eq. (1) that  $E'_{Fe}$  is higher than the standard redox potential of the Fe(III)/Fe(II) system,  $E^{\circ}_{Fe}$ , in the presence of phen, that is, the oxidizing power of iron(III) increases because the formation constant,  $\log \beta_3$ , of the Fe(II)–phen complex ( $\log \beta_3$ , 21.3) is higher than that of the Fe(III)–phen ( $\log \beta_3$ , 14.1) [27]. Thus, the oxidation reaction of cysteine with iron(III) should be favored in the presence of phen. The oxidation reaction of cysteine with iron(III) in the presence of phen was studied potentiometrically prior to utilization of the reaction as an indicator reaction for the development of catalytic method of copper(II) determination. To a 50-ml volumetric flask, 25 ml of acetate buffer (1 mol  $l^{-1}$ , pH 5), 5 ml of phen (0.1 or 0.2 mol  $l^{-1}$ ) and 5 ml of cysteine ( $1 \times 10^{-2}$  mol  $l^{-1}$ ) solutions were added and the solution was then diluted to the mark with water. A 20 ml aliquot of the solution was taken into the titration vessel. The solution was then titrated with a standard iron(III) solution ( $1 \times 10^{-2}$  mol  $l^{-1}$ ) by an automatic titrator under a nitrogen atmosphere. All titrations were performed at 50°C to promote the reaction. The potential data were recorded in  $\pm 1$  mV  $min^{-1}$  at each addition of iron(III) solution. A clear poten-

tial break was not obtained in the absence of phen, while remarkable potential break was obtained in the presence of phen; the potential change in the vicinity of the equivalence point was ca 63 mV per 0.01 ml of iron(III) solution in the presence of  $2 \times 10^{-2}$  mol l<sup>-1</sup> phen. This result indicates that the oxidation reaction of cysteine with iron(III) quantitatively takes place due to the presence of phen because the redox potential of the Fe(III)/Fe(II) system increases by forming an iron(II)–phen complex which is a very stable complex. This redox reaction has been utilized as the indicator reaction for the catalytic determination of copper(II).

### 3.2. Effect of variables on the flow-injection determination of copper(II)

As described above, the redox reaction of cysteine with iron(III) proceeds completely in the presence of phen, but the reaction at room temperature is slow. We predicted that copper(II) would catalyze the redox reaction of cysteine with iron(III) in the presence of phen. Although there are several possible mechanisms, the following pathway which mainly permits the experimental observations is thought to proceed in the copper(II)-catalyzed reaction:



Copper(I) produced by reaction (2) should reduce iron(III) to iron(II) because the equilibrium constant of the redox reaction of copper(I) with iron(III) calculate to be  $10^{10.5}$  from both standard redox potentials of the Cu(II)/Cu(I) (0.15 V vs. NHE) and Fe(III)/Fe(II) (0.77 V vs. NHE) systems [20]. In other words, copper(I) is oxidized again by iron(III) to copper(II) which participates in reaction (2). Iron(II) produced by reac-

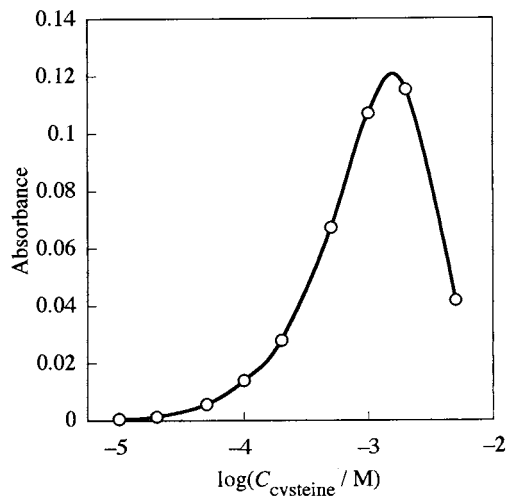


Fig. 2. Effect of cysteine concentration on the peak height for copper(II).  $C_{\text{copper(II)}}$ , 2 ng ml<sup>-1</sup>. Other conditions as in Fig. 1.

tion (3) reacts with phen to form an iron(II)–phen complex ( $\lambda_{\text{max}} = 510$  nm) in proportion to the concentration of copper(II) injected into the carrier stream. Thus, trace amounts of copper(II) can be determined by measuring the absorbance of the iron(II)–phen complex produced.

The optimum conditions were studied by injecting an aliquot of 2 ng ml<sup>-1</sup> copper(II) solution into the FIA system shown in Fig. 1.

The effect of pH on the peak height was examined over the range 2.6–5.1. The peak height rapidly increased with increasing pH up to 4.8, decreasing at pH above 4.8. Therefore, the copper(II)-catalyzed reaction was carried out at pH around 4.8. The effect of cysteine concentration was examined over the range  $1 \times 10^{-5}$ – $5 \times 10^{-3}$  mol l<sup>-1</sup>. As shown in Fig. 2, the peak height for copper(II) increased with increasing cysteine concentration up to the range  $1 \times 10^{-3}$ – $2 \times 10^{-3}$  mol l<sup>-1</sup>, and then rapidly decreased at a concentration higher than this range. The decrease in the peak height at higher cysteine concentration might be attributable to the formation of a stable iron(III)–cysteine complex ( $\log \beta_3$ , 32.1) [28] which can not participate in the regeneration of copper(II). A  $1 \times 10^{-3}$  mol l<sup>-1</sup> cysteine concentration was used for the procedure.

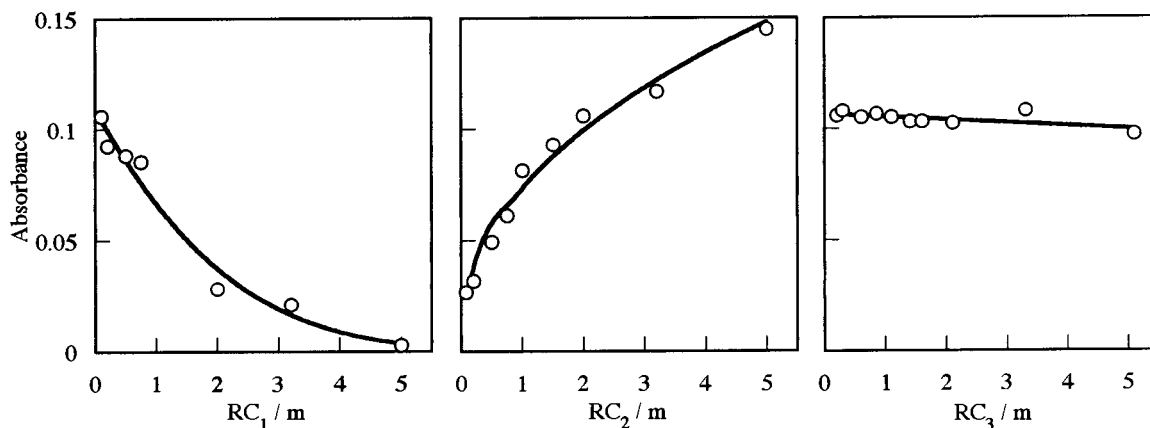


Fig. 3. Effects of lengths of reaction coils on the peak height for copper(II).  $C_{\text{copper(II)}}$ , 2 ng ml<sup>-1</sup>. Other conditions as in Fig. 1.

The effects of reaction coil lengths of  $RC_1$ ,  $RC_2$  and  $RC_3$  were examined. The results are shown in Fig. 3. The peak height rapidly decreased with increasing the length of  $RC_1$  up to 5 m, although the reason is not fully understood. When the length of  $RC_2$  was varied, the peak height increases with increasing the length up to 5 m; iron(II) was produced as a result of the regeneration of copper(II) based on reactions (2) and (3) in the  $RC_2$ . While, the peak height was maximum and almost constant over the length of  $RC_3$  examined. Reaction coil lengths of  $RC_1$ ,  $RC_2$  and  $RC_3$  were selected as 0.1, 3 and 0.2 m, respectively, for the sake of sensitivity and sampling rate.

The effect of iron(III) concentration was examined in the range  $2 \times 10^{-5}$ – $2 \times 10^{-3}$  mol l<sup>-1</sup>. The peak height for copper(II) increased with increasing iron(III) concentration up to  $1 \times 10^{-3}$  mol l<sup>-1</sup>, above which it changed little (Fig. 4). As described later in Section 3.4, when a sample solution containing iron(III) was injected into the system, iron(III) causes a positive interference for the determination of copper(II). The interference from iron(III) was minimized when pumping the  $2 \times 10^{-3}$  mol l<sup>-1</sup> iron(III) from  $R_2$ . Fig. 5 shows the effect of phen concentration on the peak height for copper(II). Maximum and almost constant peak height was obtained over the phen concentration range  $1 \times 10^{-3}$ – $1 \times 10^{-2}$  mol l<sup>-1</sup>. A  $4 \times 10^{-3}$  mol l<sup>-1</sup> phen concentration was chosen.

### 3.3. Analytical characteristics

Calibration graphs were prepared by using the flow system shown in Fig. 1. The dynamic range for the copper(II) determination was from 0.1 to 10 ng ml<sup>-1</sup> at a sampling rate of 30 h<sup>-1</sup>. Though the calibration graph in the concentration range 2–10 ng ml<sup>-1</sup> displayed downward curvature, the linear graph was obtained over the range 0.1–2 ng ml<sup>-1</sup> copper(II):  $A = 0.0501C$  with a correlation coefficient of 0.999 where  $A$  is the absorbance and  $C$  is the concentration of copper(II) in ng

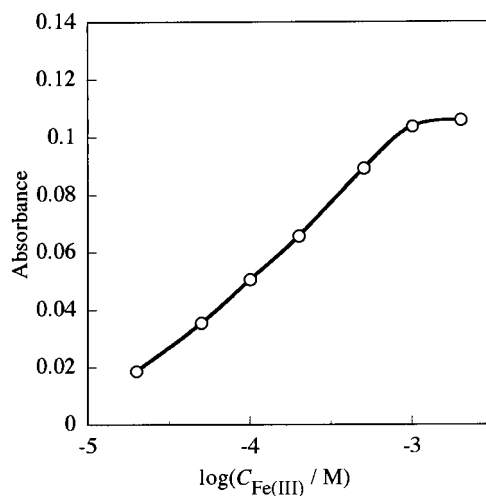


Fig. 4. Effect of iron(III) concentration on the peak height for copper(II).  $C_{\text{copper(II)}}$ , 2 ng ml<sup>-1</sup>. Other conditions as in Fig. 1.

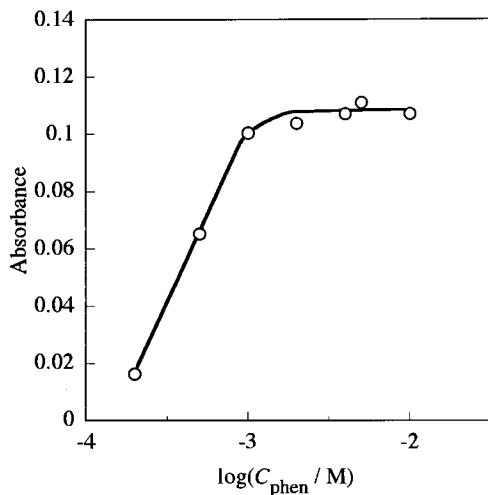


Fig. 5. Effect of phen concentration on the peak height for copper(II).  $C_{\text{copper(II)}}$ , 2 ng ml<sup>-1</sup>. Other conditions as in Fig. 1.

ml<sup>-1</sup>. The relative standard deviation was 1.0% for ten determinations (1 ng ml<sup>-1</sup> copper(II)). The detection limit ( $S/N = 3$ ) was 0.04 ng ml<sup>-1</sup>.

### 3.4. Interferences

Table 1 summarizes the tolerance limits for foreign ions on the determination of 2 ng ml<sup>-1</sup> copper(II); an error of  $\pm 5\%$  is considered to be tolerable. Most ions examined did not interfere in concentrations up to at least 500-fold excess (1000 ng ml<sup>-1</sup>). Iron(III) at the amounts of 1000 ng ml<sup>-1</sup> showed a positive interference because of the oxidation of cysteine with iron(III) in the presence of

Table 1  
Effect of foreign ions on the determination of 2 ng ml<sup>-1</sup> copper(II)

Tolerance limit (ng ml <sup>-1</sup> )	Ion or compound added
10 000	Na(I), K(I), Mg(II), Ca(II), Al(III), Co(II), Ni(II), Pb(II), NH <sub>4</sub> <sup>+</sup> , Cl <sup>-</sup> , Br <sup>-</sup> , NO <sub>3</sub> <sup>-</sup> , SO <sub>4</sub> <sup>2-</sup>
5000	Zn(II), ClO <sub>3</sub> <sup>-</sup> , BrO <sub>3</sub> <sup>-</sup>
2000	Mn(II)
1000	V(V), IO <sub>3</sub> <sup>-</sup>
500	Fe(III), PO <sub>4</sub> <sup>3-</sup> , citrate
200	V(IV), Cr(III), Cr(VI)

Table 2

Determination of copper in river water<sup>a</sup>

Copper found <sup>b</sup> (ng ml <sup>-1</sup> )	Certified value (ng ml <sup>-1</sup> )
10.6 $\pm$ 0.1 <sup>c</sup>	10.4 $\pm$ 0.3 <sup>d</sup> 10.5 $\pm$ 0.2

<sup>a</sup> Issued by the Japan Society of Analytical Chemistry.

<sup>b</sup> Average value for three determinations.

<sup>c</sup> Calibration method.

<sup>d</sup> Standard addition method.

phen. Without any treatments such as the use of a suitable masking agent for iron(III), most catalytic methods for copper determination are subject to interference from a few hundred-fold excess of iron(III) [6,8,11,13,15]. In the proposed method, however, iron(III) did not interfere even when present in 250-fold excess (500 ng ml<sup>-1</sup>). This advantage can be attributable to the use of iron(III) at high concentration as a reagent for copper determination. Vanadium(IV) and chromium(III,VI) at the amounts of 500 ng ml<sup>-1</sup> caused positive and negative interferences, respectively; they did not interfere at amounts below 200 ng ml<sup>-1</sup>. In general, the concentration levels of these ions are tolerable in the case of application to natural waters.

### 3.5. Application

The method was applied to the determination of copper in river water as certified reference material (spiked) issued by the Japan Society for Analytical Chemistry. The water sample was diluted 40 times with 0.01 mol l<sup>-1</sup> nitric acid as a carrier solution. Analytical results were obtained by both calibration and standard addition methods (Table 2). The results were in good agreement with the certified value.

## 4. Conclusions

A sensitive, selective and rapid flow-injection spectrophotometric method is proposed for the determination of copper(II) in the range 0.1–10 ng ml<sup>-1</sup> by using copper(II)-catalyzed reaction of cysteine with iron(III) in the presence of phen.

The proposed method was subject to few interferences from coexisting foreign ions. The accurate result of application to river water confirms that the method is suitable for the determination of sub-nanogram levels of copper in natural waters.

### Acknowledgements

We gratefully acknowledge the financial support of this study by Grants-in-Aid for Scientific Research No. 09640715 from the Ministry of Education, Science, Sports and Culture.

### References

- [1] D. Perez-Bendito, M. Silva, *Kinetic Methods in Analytical Chemistry*, Horwood, Chichester, 1988.
- [2] T. Kawashima, S. Nakano, *Anal. Chim. Acta* 261 (1992) 167.
- [3] T. Kawashima, S. Nakano, M. Tabata, M. Tanaka, *Trends Anal. Chem.* 16 (1997) 132.
- [4] H.A. Mottola, D. Perez-Bendito, *Anal. Chem.* 68 (1996) 257R.
- [5] S.R. Crouch, T.F. Cullen, A. Scheeline, E.S. Kirkor, *Anal. Chem.* 70 (1998) 53R.
- [6] S. Kawakubo, H. Kato, M. Iwatsuki, *Analyst* 119 (1994) 2119.
- [7] J. Michalovoski, M. Trojanowicz, *Anal. Chim. Acta* 281 (1993) 299.
- [8] B.F. Shraydeh, M.A.A. Eid, N.A. Zatar, A.A. Obeid, M. Khamis, K. Kanan, *Instrum. Sci. Technol.* 22 (1994) 355.
- [9] M.I. Prodromidis, C.D. Stalikas, P.T. Veltsistas, M.I. Karayannis, *Talanta* 41 (1994) 1645.
- [10] K. Satoh, N. Iwamura, N. Teshima, S. Nakano, T. Kawashima, *J. Flow Injection Anal.* 10 (1993) 245.
- [11] S. Cao, J. Zhong, K. Hasebe, W. Hu, *Anal. Chim. Acta* 331 (1996) 257.
- [12] H. Mao, *Microchem. J.* 53 (1996) 303.
- [13] S. Nakano, K. Nakaso, K. Noguchi, T. Kawashima, *Talanta* 44 (1997) 765.
- [14] S. Ohno, N. Teshima, T. Watanabe, H. Itabashi, S. Nakano, T. Kawashima, *Analyst* 121 (1996) 1515.
- [15] J. Zwart, J.H.M.C. Van Wolput, D.C. Koningsberger, *J. Mol. Catal.* 12 (1981) 85.
- [16] A. Hanaki, H. Kamide, *Bull. Chem. Soc. Jpn.* 56 (1983) 2065.
- [17] T. Kamidate, K. Itoh, H. Watanabe, *Anal. Sci.* 6 (1990) 769.
- [18] A. Katayama, K. Itoh, M. Furukawa, T. Kamidate, H. Watanabe, *Nippon Kagaku Kaishi* 1992 (1992) 318.
- [19] N. Teshima, S. Nakano, T. Kawashima, *J. Flow Injection Anal.* 11 (1994) 7.
- [20] E.P. Serjeant, *Potentiometry and Potentiometric Titrations*, Wiley, New York, 1984.
- [21] H. Itabashi, K. Umetsu, K. Satoh, T. Kawashima, *Anal. Sci.* 6 (1990) 721.
- [22] K. Umetsu, H. Itabashi, K. Satoh, T. Kawashima, *Anal. Sci.* 7 (1991) 115.
- [23] N. Teshima, T. Kawashima, *Bull. Chem. Soc. Jpn.* 69 (1996) 1975.
- [24] H. Katsumata, N. Teshima, T. Kawashima, *Bull. Chem. Soc. Jpn.* 70 (1997) 2151.
- [25] H. Katsumata, N. Teshima, T. Kawashima, *Anal. Sci.* 13 (1997) 825.
- [26] N. Teshima, H. Itabashi, T. Kawashima, *Anal. Sci.* 10 (1994) 207.
- [27] W.A.E. McBryde, *A Critical Review of Equilibrium Data for Proton- and Metal Complexes of 1,10-Phenanthroline, 2,2'-Bipyridyl and Related Compounds*, Pergamon Press, Oxford, 1978.
- [28] N. Tanaka, I.M. Kolthoff, W. Stricks, *J. Am. Chem. Soc.* 77 (1955) 1996.

# Flow-injection fluorimetric determination of vitamin K<sub>1</sub> based on a photochemical reaction

Tomás Pérez-Ruiz \*, Carmen Martínez-Lozano, Virginia Tomás, Jesús Martín

*Department of Analytical Chemistry, Faculty of Chemistry, University of Murcia, 30071 Murcia, Spain*

Received 11 March 1999; accepted 16 March 1999

## Abstract

The sensitizing effect of vitamin K<sub>1</sub> on the photo-oxidation of glucose has been used for the determination of the vitamin. The hydrogen peroxide formed in the photochemical reaction reacts with Fe(II) to yield hydroxylradical and this radical is scavenged by benzoic acid to form the fluorescent hydroxybenzoic acids, which are analysed by fluorescence detection. This analytical scheme was adapted to a flow-injection system, which permits the determination of vitamin K<sub>1</sub> between  $1 \times 10^{-6}$  and  $1 \times 10^{-4}$  M with a throughput of 20 samples h<sup>-1</sup> and relative standard deviation between 0.2 and 1%. The applicability of the method was demonstrated by determining vitamin K<sub>1</sub> in pharmaceutical preparations and vegetables. © 1999 Elsevier Science B.V. All rights reserved.

*Keywords:* Flow-injection; Photochemical reaction; Vitamin K<sub>1</sub>

## 1. Introduction

Vitamin K<sub>1</sub> (phylloquinone; 2-methyl-3-phytyl-1,4-naphthoquinone) is known to be involved in the production of certain blood clotting factors [1] and a protein called osteocalcin, which is found in bone [2]. It is ubiquitous within the chloroplast of green plants, which constitute the major dietary source of this vitamin.

Several methods have been proposed for the determination of phylloquinone: spectrophotometry [3], polarography [4], adsorptive stripping

voltammetry [5], fluorometry [6] and gas-liquid chromatography [7]; however, high-performance liquid chromatography (HPLC) appears to be a more appropriate approach. The detection systems used with this technique in order of their increasing sensitivity are: UV spectrophotometry, amperometry and fluorometry. Since vitamin K<sub>1</sub> does not possess native fluorescence, it has to be reduced to the highly fluorescent hydroquinone form. Methods based on post-column chemical [8,9], electrochemical [10] and photochemical [11] reduction have been described.

There is growing interest in a combination of photochemical reactions and automated systems that permit continuous determinations of the analytes, e.g. in flow-injection or continuous-flow analysis [12–15], because photochemical reactions

\* Corresponding author. Tel.: +34-968-367407; fax +34-968-364148.

have characteristics that are well suited to reactor technology. First, such reactions only require the addition of photons and so there is no need for reagent-addition pumps and mixing cells, which cause additional band broadening. Second, many photochemical reactions are rapid because they proceed via free radical intermediates, and so lengthy reaction times can be avoided.

The objective of the present work was to develop a simple, sensitive and rapid assay for vitamin K<sub>1</sub> using a flow-injection (FI) system coupled to photochemically induced fluorescence. The method uses the photo-oxidation of glucose sensitized by vitamin K<sub>1</sub>. The hydrogen peroxide generated in the photochemical reaction is determined through the Fe(II)-catalyzed oxidation of benzoic acid to form hydroxybenzoic acid isomers, which fluoresce strongly [16,17]. This method is shown to be a good alternative to routine vitamin K<sub>1</sub> analysis in pharmaceutical preparations and vegetables.

## 2. Experimental

### 2.1. Reagents

All chemicals were of analytical reagent grade and demineralized water from a Milli-Q system was used in all experiments.

Aqueous standard solutions of vitamin K<sub>1</sub> were prepared in 5% (w/v) triton X-100 and diluted with 5% (w/v) triton X-100 as required. All glassware containing vitamin K<sub>1</sub> solutions was protected from light. Vitamin K<sub>1</sub> solutions were also prepared in ethanol.

### 2.2. Apparatus

A Hitachi F-3010 spectrofluorimeter was used to record spectra and carry out fluorescence measurements. Adsorption spectra and absorbance measurements were made with a Unicam UV2 UV/visible spectrophotometer. A Gilson Mini-plus-3 peristaltic pump was used to introduce the reagents into the system. An Omnifit rotary valve and a Hellma (176.052 QS, inner volume 25  $\mu$ l) flow cell were also used. A rod-shaped low-pres-

sure mercury discharge lamp from Spectronic was employed to irradiate the reactor. A timer synchronized to the injection system allowed the flow to be stopped at any delay time and for any length of time.

### 2.3. Manifold and procedure

The schematic diagram of the instrumental setup is shown in Fig. 1 with optimum conditions as stated. The sample was injected into the carrier (0.03 M phosphate buffer of pH 7.5) stream with the aid of a rotary valve with a loop of 115  $\mu$ l. This stream joined the glucose stream at a mixing point prior to the photo-reactor. The photo-reactor (L<sub>1</sub>) consisted of a PTFE tubing (i.d. 0.5 mm, length 100 cm) helically coiled around the lamp and wrapped with aluminium foil to enhance the photon flux. The irradiated solution (containing the H<sub>2</sub>O<sub>2</sub> generated in the photochemical reaction) merged with a stream carrying Fe<sup>2+</sup> ( $4.5 \times 10^{-4}$  M), benzoic acid ( $9 \times 10^{-4}$  M), sulphuric acid (0.2 M) and Triton X-100 (5%, w/v). After passing through the coil, L<sub>2</sub>, in which the hydroxybenzoic acids are formed, the solution was

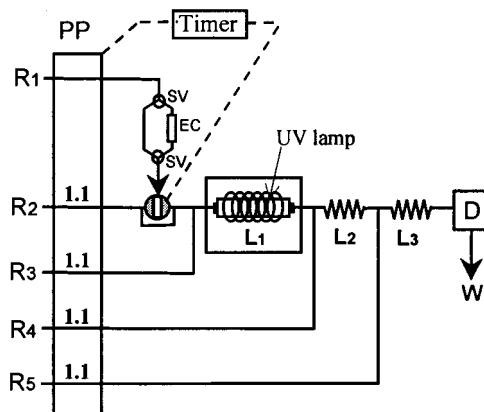


Fig. 1. Flow-injection manifold for the determination of vitamin K<sub>1</sub>. PP, peristaltic pump (with flow rates given in ml min<sup>-1</sup>); R<sub>1</sub>, sample; R<sub>2</sub>, 0.03 M phosphate buffer; R<sub>3</sub>, 1.25 M glucose; R<sub>4</sub>,  $4.5 \times 10^{-4}$  M Fe(II),  $9 \times 10^{-4}$  M benzoic acid, 0.2 M sulphuric acid and 5% (w/v) Triton X-100; R<sub>5</sub>, 0.5 M sodium hydroxide; SV, selection valve; EC, exchange column; L<sub>1</sub>, photo-reactor, length, 100 cm, i.d., 0.5 mm; L<sub>2</sub> = L<sub>3</sub> = 50 cm; D, spectrofluorimeter ( $\lambda_{\text{ex}} = 305$  nm,  $\lambda_{\text{em}} = 412$  nm); W, waste.



merged with a 0.5 M sodium hydroxide stream. Thus, the sample plug becomes strongly fluorescent prior to passing through the flow cell.

To enhance the sensitivity of the method by increasing the residence time, an intermittent pumping was used. The stop–go periods were set by means of a timer synchronized to the injection valve. At a delay time of 25 s after the injection, coinciding with the time when the sample plug reached the photo-reactor ( $L_1$ ), the flow was stopped for 60 s in order to increase the development of the photochemical reaction. After this time, the pump was switched on again for 15 s to enable the photolyzed sample plug and the reagents to flow through the system and be mixed in the reactor  $L_2$ . Then the flow was stopped in order to increase the yield in the monitored species. After 60 s, the pump was started and a transient FI peak was obtained due to the passage of the fluorescent hydroxybenzoic acids through the detector (measured at 412 nm with excitation at 305 nm).

### 3. Results and discussion

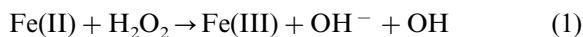
#### 3.1. Photochemical reaction sensitized by vitamin $K_1$

Hydrogen atom donor (HAD) substrates, which typically have an electron-withdrawing element (O or N) bound to a carbon with  $\alpha$ -hydrogens, can be easily photo-oxidized using vitamin  $K_1$  as a sensitizer. The first step is the absorption of a photon by phyloquinone. After excitation, phyloquinone rapidly decays to the excited singlet state ( $S_1$ ) by internal conversion. The vast majority of  $S_1$  vitamin  $K_1$  molecules undergo intersystem crossing to the triplet state and subsequent internal conversion to the lowest excited triplet state ( $T_1$ ). Once formed, the  $T_1$  state of phyloquinone rapidly extracts a hydrogen atom from the HAD substrate to produce a semiquinone radical and an  $\alpha$ -hydroxyl alkyl radical. Under aerobic conditions, both intermediates will react with molecular oxygen to produce hydrogen peroxide, vitamin  $K_1$  and the oxidized substrate. Vitamin  $K_1$  can therefore be determined

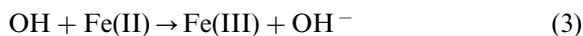
by analysing the hydrogen peroxide produced in the photochemical reaction.

#### 3.2. Detection of hydrogen peroxide

The most sensitive and widely used methods for monitoring hydrogen peroxide were coupled to the photochemical reaction in order to check their suitability for determining vitamin  $K_1$ . The chemiluminescence (CL) oxidation of luminol by  $H_2O_2$  catalyzed by Co(II), Cu(II), hexacyanoferrate(II) or hemin [18,19] led to absorption of the CL by phyloquinone and interference from transition metals. The peroxyoxalate CL technique [20] could not be used because CL is also emitted when peroxyoxalate is irradiated in the presence of an HAD species [21]. The method based on the reaction between hydrogen peroxide and (*p*-hydroxyphenyl) acetic acid, catalyzed by horseradish peroxidase, to generate a fluorescent dimer [22], was highly sensitive and relatively free from interference; however, it suffers the disadvantage of reagent instability and high cost. The detection system based on the reaction of hydrogen peroxide with Fe(II) and benzoic acid to form the fluorescent hydroxybenzoic acids [23] was selected based on criteria of sensitivity, selectivity and low cost. This analytical scheme is summarized in the following steps:



(*o*-, *m*- and *p*-isomers)



Where BA and OHBA represent benzoic acid and hydroxybenzoic acid, respectively. The BA concentration was always kept higher than the Fe(II) concentration in order to minimize scavenging of OH radical by reaction (3).

#### 3.3. Selection of the HAD substrate

Organic compounds such as alcohols, ethers, aldehydes, and saccharides with weak carbon–hydrogen bonds were used to produce hydrogen peroxide through their vitamin  $K_1$ -sensitized

photo-oxidation. Ethanol and glucose were the two substrates that gave the highest photochemical yield of hydrogen peroxide.

The effect of the presence of ethanol and glucose on the  $\text{H}_2\text{O}_2$ –Fe(II)–BA fluorescent system was studied. Glucose did not affect the sensitivity of this system, but ethanol strongly decreased the fluorescence. Glucose was selected as the HAD substrate in subsequent experiments.

As phyloquinone is poorly water soluble, the presence of surfactants was tested in order to work in aqueous medium. In addition to overcoming the solubility problem, surfactants also alter the pathway of the photochemical and fluorescent processes and can be effective means of enhancing the sensitivity [24]. Thus, the effect of aqueous micellar systems of each charge type (i.e. cationic, anionic, zwitterionic or nonionic) were studied. The surfactants employed were hexadecyltrimethylammonium chloride and bromide, sodium dodecylsulphate, Triton X-100, 3-(*N*-dodecyl-*N,N*-dimethylammonium)-propane-1-sulphonate, poly(vinyl alcohol) and Span-20. Triton X-100 gave the best results as regards sensitivity and reproducibility, and was chosen for further studies.

#### 3.4. Optimization of the flow-injection manifold

The FI manifold (Fig. 1) was optimized by using the univariate method. Chemical variables affecting both photochemical and indicator reactions were optimized before the FI variables.

#### 3.5. Chemical variables

The effect of pH on the photo-oxidation of glucose sensitized by vitamin  $\text{K}_1$  is shown in Fig. 2. The rate of the photochemical reaction increased with increasing pH values, although alkaline media must be avoided since vitamin  $\text{K}_1$  undergoes a photo-degradation reaction. A pH value of 7.5 was chosen for further experiments. The concentration of the phosphate buffer used as carrier must be such that the solution in the photo-reactor is buffered at pH 7.5; however, its concentration should be as low as possible so that

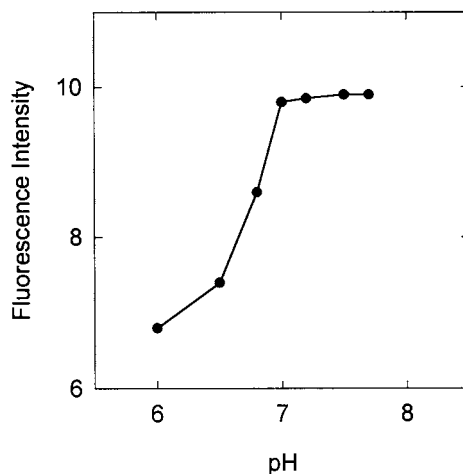


Fig. 2. Effect of pH on the photochemical reaction.

the pH in the reactor  $L_2$  remains close to the optimum value. A 0.03 M phosphate buffer of pH 7.5 was used as carrier.

The rate of the photochemical reaction increased with increasing glucose concentration up to about 1 M, above which it remained virtually constant (Fig. 3). A 1.25 M glucose solution was pumped in subsequent studies.

Special attention was paid to the influence of the irradiation on the peak height. Different irradiation times were achieved by halting the flow

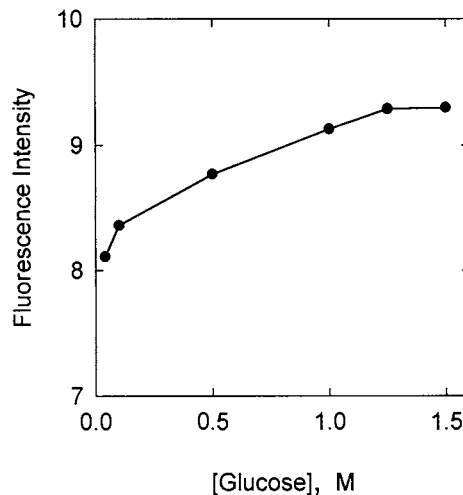


Fig. 3. Influence of glucose concentration on the photochemical reaction.

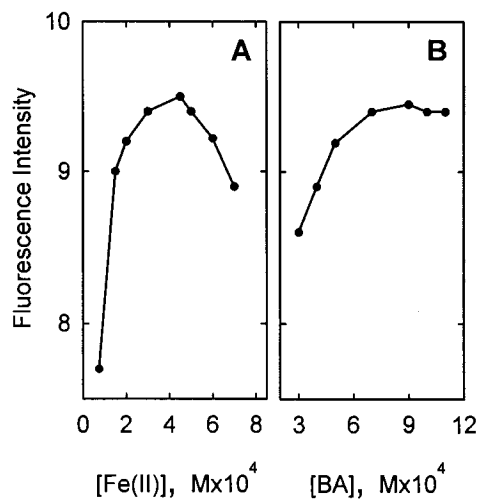


Fig. 4. Influence of Fe(II) (A) and benzoic acid (B) concentrations on the fluorescence intensity.

when the samples were located in the photo-reactor and then irradiating them for different times. As expected, the longer the time the higher the development of the photochemical reaction; however, the analysis time was also longer. An irradiation time of 60 s was taken as a compromise between sensitivity and analysis time.

The optimum conditions for production of the fluorescent products were determined by varying Fe(II) and BA concentrations and pH.

The concentrations of Fe(II) and BA were studied using separate channels for each reagent. The Fe(II) and BA concentrations, which give the maximal signal, can be deduced from Fig. 4. A solution containing  $4.5 \times 10^{-4}$  M Fe(II) and  $9 \times 10^{-4}$  M BA was selected for further experiments. This solution is stable to air oxidation for several days, as long as the pH is kept below 2.5.

The fluorescence signal was virtually insensitive to changes in pH when the reaction between Fe(II) and  $\text{H}_2\text{O}_2$  (reaction 1) was carried out below pH 2.5. In these experiments, the HOBA isomers were produced in the reaction coil  $L_2$  at pH 2. As HOBA exhibits very much stronger fluorescence in a basic medium [16], two sequential reactions were thus required. The solution emerging from the reactor  $L_2$  was mixed with a 0.5 M sodium hydroxide stream, ensuring that the

sample plug becomes strongly fluorescent prior to passing through the flow cell. In basic medium, the ferrous ion is rapidly oxidized to ferric ion. This is unstable and precipitates slowly, presumably in the form of hydroxide or oxide, thus causing instability of the signal and blocking of the tubes. The precipitate is colloidal and can be stabilized by addition of surfactants. The presence of 5% (w/v) Triton X-100 was sufficient to avoid these deleterious effects.

A solution containing Fe(II) ( $4.5 \times 10^{-4}$  M), BA ( $9 \times 10^{-4}$  M), sulphuric acid (0.2 M) and Triton X-100 (5%, w/v) was pumped to merge with the stream emerging from the photo-reactor.

### 3.6. FI variables

The effects of FI variables were investigated by performing four injections of  $1 \times 10^{-5}$  M vitamin  $\text{K}_1$  solution per value of the variable studied. The values adopted as optimum were those resulting in the best possible compromise between peak height, reproducibility and throughput.

The volume of sample injected was varied between 35 and 150  $\mu\text{l}$ . The peak fluorescence obtained increased with increasing volume up to 115  $\mu\text{l}$ , above which it remained virtually constant. A sample volume of 115  $\mu\text{l}$  was selected.

The flow rates of the different reagent streams were varied over the range 0.5–1.5  $\text{ml min}^{-1}$ . The maximum peak height was observed at a flow rate of 1.1  $\text{ml min}^{-1}$  for each channel.

A study of the influence of photo-reactor length showed the need for a long reactor because the sample was not totally irradiated in small volume reactors and hence the sensitivity was low. A photo-reactor of 100 cm length and 0.5 mm i.d. was used.

### 3.7. Analytical features

Under optimum conditions, the effect of the concentration of vitamin  $\text{K}_1$  on fluorescence intensity was studied by measuring the peak height when 125  $\mu\text{l}$  of vitamin  $\text{K}_1$  solution of different concentrations were injected. The calibration graph gave a straight line from  $1 \times 10^{-6}$  to  $1 \times 10^{-4}$  M with a correlation coefficient of 0.999.

The relative standard deviations of ten injections of each solution containing  $1 \times 10^{-5}$  and  $8 \times 10^{-5}$  M of vitamin K<sub>1</sub> were 0.4 and 0.2%, respectively. The detection limit calculated according to IUPAC recommendations [25] was  $4 \times 10^{-7}$  M. The sample throughput was 20 samples h<sup>-1</sup>.

The reproducibility of the method was studied by analysing, on five consecutive days, ten identical solutions of phylloquinone ( $1 \times 10^{-5}$  M). Every day three injections of each solution were made; the relative standard deviation was 1%.

### 3.8. Interferences

The influence of foreign species was studied by preparing solutions containing  $5 \times 10^{-6}$  M vitamin K<sub>1</sub> and increasing concentrations of the potential interferent up to  $2.5 \times 10^{-3}$  M. The tolerance of each foreign specie was taken as the largest amount yielding an error of less than 3% in the analytical signal of vitamin K<sub>1</sub>. Sodium, potassium, calcium, magnesium, chloride, sulphate, phosphate and nitrate were tolerated in large amount (500-fold excess was the maximum tested); a 200-fold excess of lactose, fructose, sorbitol and benzyl alcohol, 100-fold excess of rutin, hesperidin, starch and cyanocobalamin, and 20-fold excess of ascorbic acid, thiamine and saccharin were also tolerated. Citrate, oxalate and menadione interfere seriously (0.8-fold excess was the maximum ratio tolerated) because the two anions for complexing Fe(III) altered the reactions concerning the fluorescent signal and because menadione acted as a sensitizer on the photo-oxidation of glucose. The interference of

citrate and oxalate was avoided by incorporating an anion exchanger minicolumn before the injection valve. Oxalate was also removed by precipitation with calcium chloride before injecting the sample.

### 3.9. Analysis of real samples

To investigate the applicability of the proposed method to real samples, vitamin K<sub>1</sub> was determined in pharmaceutical preparations and plants.

#### 3.9.1. Pharmaceutical preparations

For the determination of vitamin K<sub>1</sub> in Konakion (from Roche, Madrid, Spain), 23 µl of the ampoules or 28 µl in drop form were diluted with 5% (w/v) Triton X-100 to 25 ml in a calibrated flask. The data in Table 1 show that the vitamin K<sub>1</sub> contents measured by the proposed method were in good agreement with the values supplied by the manufacture and with those obtained by a manual spectrophotometric method. The recoveries obtained by adding phylloquinone to each pharmaceutical formulation are shown in Table 2.

#### 3.9.2. Vegetable samples

The extraction of vitamin K<sub>1</sub> from alfalfa or spinach was performed using the following procedure. An amount of alfalfa or spinach equivalent to 1 mg of vitamin K<sub>1</sub> was shaken with a mixture of 100 ml dichloromethane and 50 ml of iso-octane. The extract was evaporated to dryness in a rotary evaporator. The residue was dried by adding acetone, rinsing the flask and drying in an evaporator. The residue was dissolved in 5% (w/v) Triton X-100 and diluted to 25 ml in a calibrated

Table 1  
Determination of vitamin K<sub>1</sub> in pharmaceutical preparations

Product <sup>a</sup>	Content (mg ml <sup>-1</sup> )	Found <sup>b</sup> (mg ml <sup>-1</sup> )	
		Proposed method	Reference method
Konakion (ampoules)	10.0	9.9 ± 0.1	9.8 ± 0.1
Konakion (drops)	20.0	20.2 ± 0.2	20.1 ± 0.3

<sup>a</sup> Composition of samples: *Konakion ampoules* (amount per ml), vitamin K<sub>1</sub>, 10 mg; excipients, glycocholic acid, lecithin, sodium hydroxide, hydrochloric acid, water. *Konakion drops* (amount per ml), vitamin K<sub>1</sub> 20 mg; excipient, polyethoxylated castor oil.

<sup>b</sup> Means ± SD of three determinations.

Table 2  
Recoveries of vitamin K<sub>1</sub> added to real pharmaceutical formulations

Product	Concentration added (mg ml <sup>-1</sup> )	Concentration found (mg ml <sup>-1</sup> )	Recovery <sup>a</sup> (%)
Konaktion (ampoules)	0.30	0.31	103 ± 0.8
	0.50	0.49	98 ± 0.6
	0.70	0.69	99 ± 1.5
Konaktion (drops)	0.10	1.10	100 ± 0.9
	0.30	0.30	100 ± 0.8
	0.60	0.62	103 ± 1.7

<sup>a</sup> Average values of three determinations ± SD.

flask. The solution was passed through an Ione-naustauscher III (Merck) anion exchanger column (length, 10 cm, i.d. 0.5 cm) before filling the sample-loop in order to ensure the absence of oxalate and/or citrate.

The determinations of vitamin K<sub>1</sub> in alfalfa and spinach are summarized in Table 3. The results show that the phyloquinone content, as measured by the proposed FI method, was in excellent agreement with that obtained by a manual spectrophotometric method.

#### 4. Conclusions

The method proposed for determining vitamin K<sub>1</sub> combines the advantages of photochemical reactions (e.g. selectivity, sensitivity, cleanliness and easy manipulation) with those associated with the use of flow-injection systems (e.g. simplicity, rapidity and low cost).

Compared to the other fluorescent methods, which are based on the reduction of phyloquinone to its fluorescent dihydroquinone form by means of chemical, electrochemical or photochemical reactions, the approach presented here is much simpler because deoxygenation of the samples and reagents is unnecessary. In addition, the photo-oxidation pathway is easier to adapt to FI methodology than the photo-reduction pathway because the tube materials used in FI systems have permeability for oxygen. The applicability of the method to real samples has been demonstrated by analysing pharmaceutical preparations and alfalfa and spinach samples.

Table 3  
Determination of vitamin K<sub>1</sub> in vegetal samples

Sample	Found <sup>a</sup> (µg g <sup>-1</sup> )		
	Proposed method	Reference method	
Alfalfa	Sample 1	17.7 ± 0.6	20.3 ± 0.3
	Sample 2	20.4 ± 0.3	19.9 ± 0.3
	Sample 3	19.6 ± 0.3	20.0 ± 0.2
Spinach	Sample 1	24.3 ± 0.3	23.8 ± 0.3
	Sample 2	24.4 ± 0.8	24.6 ± 0.2
	Sample 3	23.3 ± 0.5	23.4 ± 0.2

<sup>a</sup> Means ± SD of three determinations.

#### Acknowledgements

The authors gratefully acknowledge financial support from Fundación Séneca de la Comunidad Autónoma de Murcia and the Dirección General de Investigación Científica y Técnica.

#### References

- [1] J.W. Suttie, in: L. Machlin (Ed.), *Handbook of Vitamins*, 2, Marcel Dekker, New York, 1991, pp. 145–194.
- [2] P.V. Hauschka, J.B. Lian, P.M. Gallop, *Trends Biochem. Sci.* 3 (1978) 75.
- [3] G. Milch, E. Szabo, *Analysis* 16 (1988) 59.
- [4] J.P. Hart, A.M. Nahir, J. Chayen, A. Catteral, *Anal. Chim. Acta* 144 (1982) 267.
- [5] J.P. Hart, S.A. Wring, I.C. Morgan, *Analyst* 114 (1989) 933.
- [6] M. Holasova, J. Blatna, *Cesk. Farm.* 31 (1982) 119.
- [7] M. Shino, T. Yamashiro, K. Yamada, Y. Mori, T. Sato, K. Kawabe, K. Okada, *J. Pharm. Soc. Jpn.* 102 (1982) 651.

- [8] Y. Haaron, D.S. Bacon, J.A. Sadowski, *J. Chromatogr.* 384 (1987) 386.
- [9] M. Shino, *Analyst* 113 (1988) 393.
- [10] J.P. Langenberg, U.R. Tjaden, *J. Chromatogr.* 305 (1984) 61.
- [11] M.F. Levefere, R.W. Frei, A.H. Scholten, U.A. Brinkman, *J. Chromatogr.* 181 (1980) 227.
- [12] C. Martínez-Lozano, T. Pérez-Ruiz, V. Tomás, E. Yagüe, *Analyst* 113 (1988) 1057.
- [13] L.E. Leon, A. Rios, M.D. Luque de Castro, M. Valcárcel, *Anal. Chim. Acta* 308 (1995) 299.
- [14] M.C. Mahedero, J.J. Aaron, *Anal. Chim. Acta* 269 (1992) 193.
- [15] T. Pérez-Ruiz, C. Martínez-Lozano, A. Sanz, *Anal. Chim. Acta* 308 (1995) 299.
- [16] A. Lazrus, G. Kok, S. Gitlin, J.A. Lind, S. McLaren, *Anal. Chem.* 57 (1985) 917.
- [17] J.H. Lee, I.N. Tang, J.B. Weinstein-Lloyd, *Anal. Chem.* 62 (1990) 2381.
- [18] K. Robards, P.J. Worsfold, *Anal. Chim. Acta* 266 (1992) 147.
- [19] F. Shaw, *Analyst* 105 (1980) 11.
- [20] G. Scott, W.R. Seitz, W.R. Ambrose, *Anal. Chim. Acta* 115 (1980) 221.
- [21] R.E. Milofsky, J.W. Birks, *Anal. Chem.* 62 (1990) 1050.
- [22] A. Lazrus, G. Kok, S. Gitlin, J.A. Lind, S. McLaren, *Anal. Chem.* 57 (1985) 912.
- [23] J.H. Lee, I.N. Tang, J.B. Weinstein-Lloyd, *Anal. Chem.* 62 (1990) 2381.
- [24] T.E. Riehl, C.L. Malchorn, W.L. Hinze, *Analyst* 111 (1986) 931.
- [25] G.L. Long, J.A. Winefordner, *Anal. Chem.* 55 (1983) 712A.

# Determination of vitamin D<sub>3</sub> hydroxymetabolites in plasma at the sub-part per trillion levels using on-line cleanup/preconcentration and HPLC-fluorimetric post-column derivatisation

F. Ortiz Boyer<sup>a</sup>, J.M. Fernández Romero<sup>a</sup>, M.D. Luque de Castro<sup>a,\*</sup>,  
J.M. Quesada<sup>b</sup>

<sup>a</sup> Analytical Chemistry Division, Faculty of Sciences, University of Córdoba, Córdoba E-4004, Spain

<sup>b</sup> Mineral Metabolism Unit, Hospital Reina Sofía, University of Córdoba, Córdoba E-14004, Spain

Received 12 March 1999; accepted 16 March 1999

## Abstract

A new method for the determination of the hydroxymetabolites of vitamin D<sub>3</sub> (24,25-(OH)<sub>2</sub>-D<sub>3</sub>, 1,25-(OH)<sub>2</sub>-D<sub>3</sub> and 25-OH-D<sub>3</sub>) in plasma is reported. The method is based on the integration of three subsystems: continuous cleanup/preconcentration, HPL separation and post-column fluorimetric derivatisation. The derivatising subsystem is based on the dehydration reaction undergone by the secosteriod molecules in a strong-acid medium. The calibration graphs were run between 0.1 pg ml<sup>-1</sup> and 100 ng ml<sup>-1</sup> for each analyte with excellent regression coefficients ( $\geq 0.9933$ ) in all cases. The precision at two concentration levels was established with acceptable RSDs (%) in all instances (values between 2.1 and 5.2%). The method was also checked by applying it to human plasma samples spiked with the target analytes and the recoveries ranged between 86 and 106%. © 1999 Elsevier Science B.V. All rights reserved.

**Keywords:** Continuous cleanup/preconcentration; HPLC/post-column fluorimetric derivatisation; Plasma samples; Vitamin D<sub>3</sub> hydroxymetabolites

## 1. Introduction

Vitamin D<sub>3</sub> has scarce biological activity, but it is converted into biologically active metabolites

(25-hydroxyvitamin D<sub>3</sub>, 1,25-dihydroxyvitamin D<sub>3</sub> and 24,25-dihydroxyvitamin D<sub>3</sub>) by oxidation. Measurements of circulating levels of 25-OH-D<sub>3</sub> are presently useful both in the diagnosis of vitamin D<sub>3</sub> deficiency (a determinant factor of hip fracture in elderly people) and intoxication. The most biologically active metabolite, 1,25-dihydroxyvitamin D<sub>3</sub>, is the major hormonal regulator of calcium metabolism and its quantification is

\* Corresponding author. Tel.: +34-957-218614; fax: +34-957-218614.

E-mail address: qallucam@uco.es (M.D. Luque de Castro)

widely used as a means of assessing the vitamin D<sub>3</sub> level in humans. Circulating 1,25-(OH)<sub>2</sub>-D<sub>3</sub> is altered in several pathophysiological states (e.g. parathyroid gland disorders, renal failures, vitamin D-dependent rickets, types I and II, and sarcoidosis [1,2]).

Simultaneous determination of these metabolites in different samples have been reported and reviewed in the literature [3,4]. This determination in clinical samples has been considered to be a difficult goal owing to: low concentration of circulating hydroxymetabolites in human fluids; presence of several metabolites which exhibit similar chemical behaviour; large amounts of other related compounds; instability of their chemical structures in presence of UV light and heat; and low reactivity of these secosteroids. Vitamin D<sub>3</sub> and its metabolites are currently determined by radioimmunoassay (RIA) [5,6] and competitive protein binding assay (CPBA) [7,8] after tedious and time-consuming pretreatment which involves liquid–liquid [9–11], solid–liquid extractions [12–15] for both and different separation procedures (LC [16–21] or GC [13,14,22–27]) coupled with photometric [17,18,28,29], and fluorimetric detection [30–33] and, more recently, with mass spectrometry [13,14,24,34,35] in the case of GC. These methodologies are commonly used in clinical analysis in order to evaluate the vitamin D<sub>3</sub> hydroxymetabolites status in human fluids with severe limitations in quality assurance of the results obtained by RIA owing to cross-reactions.

The poor chemical reactivity of these compounds was one of the most important restrictive aspects in the development of new analytical methods for their determination. However, several methods based on derivatisation (dehydration [3,35,36,40], cycloaddition [12,30,34,37,38], silanization [13,14,22,23,32] and charge-transfer complex formation[39]) have been implemented.

Derivatisation based on dehydration reactions occurs by exposure of the secosteroids to high temperatures. Non-specific dehydration takes place under these conditions, producing B-ring cyclation to yield pyro and isopyro isomers [3]. Some other methods for the derivatisation of vitamin D<sub>3</sub> hydroxymetabolites have been aimed at obtaining more thermostable products by for-

mation of the corresponding isotachysterol [25,41,42]. Dehydration based on the use of a strong acid has been reported by Li et al. [42]. Fig. 1 depicts the reaction undergone by vitamin D<sub>3</sub> or its hydroxymetabolites in strong acid solution. The isotachysterol formed exhibits both an absorption displacement to longer wavelengths and fluorescence emission. An enhanced sensitivity is foreseeable by implementing this derivatisation in a continuous system.

The aim of this paper has been the development of a new post-column derivatisation procedure based on dehydration of the vitamin D<sub>3</sub> hydroxymetabolites in strong acid solution and fluorescence monitoring of the common isotachysterols formed at their maximum wavelengths ( $\lambda_{\text{ex}} = 366\text{--}389$  nm and  $\lambda_{\text{em}} = 472\text{--}482$  nm). This derivatisation reaction has been used as a final step of the development of a method for the determination of 24,25-(OH)<sub>2</sub>-D<sub>3</sub>, 1,25-(OH)<sub>2</sub>-D<sub>3</sub> and 25-OH-D<sub>3</sub> in human plasma using the continuous cleanup/preconcentration procedure and HPLC separation approach previously proposed by the authors [43].

## 2. Experimental

### 2.1. Reagents

All solutions were prepared using bidistilled water (Millipore Milli-Q System). Bond-Elut cartridges of (NH<sub>2</sub>) 500 mg, 2.8 ml (no. 01210-2037) from Varian SPP was used. All organic solvents used were of HPLC grade. A 20:80 acetonitrile:phosphate buffer (50 mmol l<sup>-1</sup>, pH 6.5) (v/v) mixture was used as initial mobile phase. A linear gradient was programmed in order to obtain a 10:90 isopropanol–methanol (v/v) mobile phase in 1.7 min then stabilised for 20 min. Standard solutions of 24,25-(OH)<sub>2</sub>-D<sub>3</sub>, 1,25-(OH)<sub>2</sub>-D<sub>3</sub> and 25-(OH)-D<sub>3</sub> were prepared by dissolving separately the content of a vial of each (Solvay Duphar, The Netherlands) in methanol. Less concentrated solutions were prepared daily by dilution in 50 mmol l<sup>-1</sup> phosphate buffer adjusted to pH 6.5. No appreciable analyte degradation was detected during the overall analytical process.



Plasma samples from hospitalized patients and from healthy volunteers were stored at  $-45^{\circ}\text{C}$  for a maximum of 10 days, then centrifuged at  $65\,000 \times g$  for 5 min before analysis.

## 2.2. Apparatus and instruments

A Vac elut sps24 vacuum station incorporated to an Eyle4 A-3S evaporator was used. A modular Hitachi liquid chromatograph consisting of an L-6200A high-pressure ternary gradient pump, a Rheodyne 7125 high-pressure manual injection valve (whose loop was exchanged by a 100-cm stainless-steel tubing of 0.25 mm I.D.), an F-1050 spectrofluorimeter and a D2500 integrator was used. An Altech high-pressure pump, a Gilson Minipuls-2 low-pressure peristaltic pump, a Rheodyne 5041 low-pressure injection valve, a Rheodyne 5010 low-pressure selecting valve, an Omnifit 50-mm length glass minicolumn, and Teflon tubing of 0.5 mm inner diameter and different lengths, were also used for construction of the flow manifold. A Selecta thermostat containing vaseline oil was used as calefactor and an ice bath

was also used as a cooler. An Ultrabase  $\text{C}_{18}$  column ( $25 \times 4.6$ ;  $5.0 \mu\text{m}$ , Scharlau Science) was used as analytical column.

## 2.3. Sample pre-treatment

The effect of related neutral lipids and other macromolecules present in the samples was reduced using a previous liquid–liquid extraction procedure, which, in summary, is as follows: 2 ml of plasma were first extracted by vortexing four times with 1 ml isopropanol, centrifuged for 5 min, collected and evaporated under  $\text{N}_2$  flow at room temperature in order to reduce the volume to 1 ml. This solution was mixed four times with 2 ml hexane, vortexed and centrifuged for 2 min. The four hexane aliquots were mixed and evaporated to dryness under  $\text{N}_2$  flow at room temperature. After this treatment, the residue was kept refrigerated at  $4^{\circ}\text{C}$  for 2 weeks without appreciable degradation. The residue was dissolved in 7 ml of  $10 \text{ mmol l}^{-1}$  phosphate buffer, pH 6.5, then being ready for aspiration into the continuous cleanup/preconcentration and separation system.

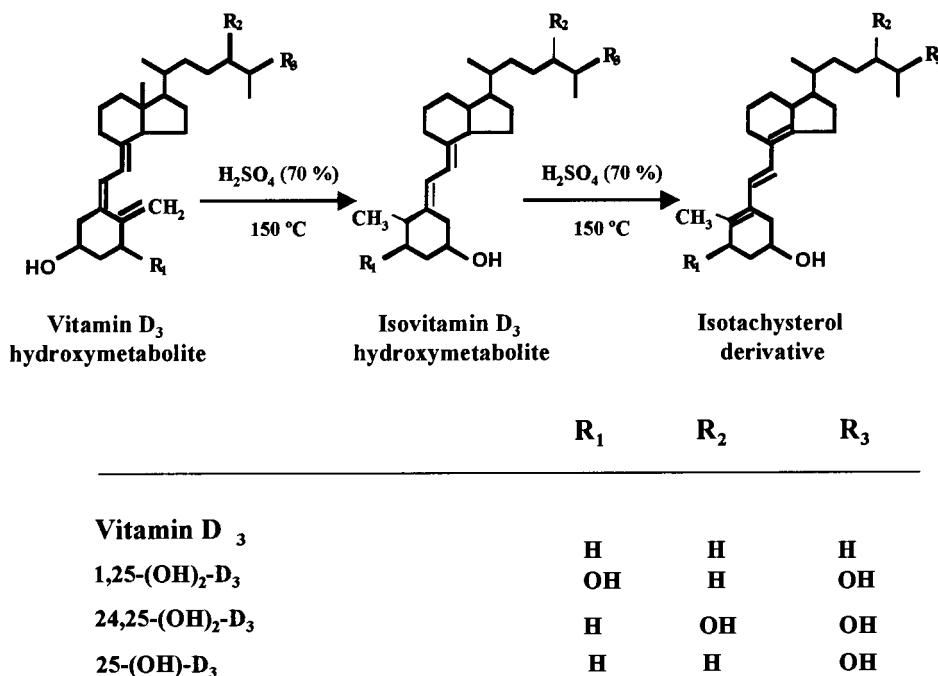


Fig. 1. Dehydration reaction of vitamin  $\text{D}_3$  and its hydroxymetabolites based on the use of a strong acid solution.

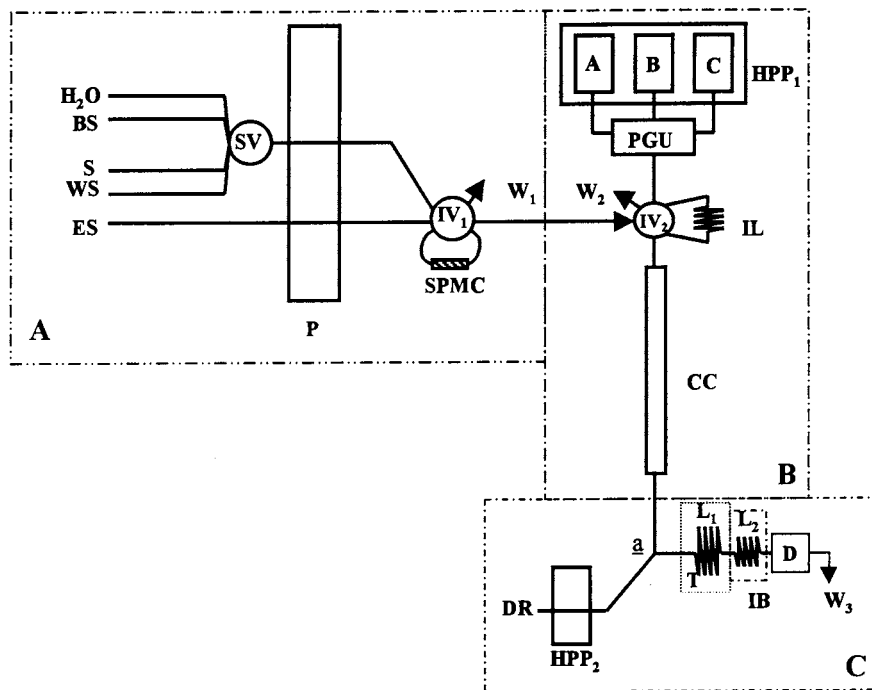


Fig. 2. Integrated continuous assembly for monitoring hydroxyvitamin D<sub>3</sub> metabolites in human plasma. (A) Continuous cleanup/preconcentration subsystem; (B) modular chromatograph subsystem; and (C) post-column derivatisation and fluorimetric detection subsystem. P, peristaltic pump; SV, selecting valve; BS, buffer solution; S, sample; WS, washing solution; ES, eluting solution; IV<sub>1</sub>, low-pressure injection valve; SPMC, solid-phase minicolumn; HPP<sub>1</sub> and HPP<sub>2</sub>, high-pressure pumps; A, B, C, solvent reservoirs; PGU, programmable gradient unit; IV<sub>2</sub>, high-pressure injection valve; IL, injection loop; CC, chromatographic column; a, mixing point; DR, derivatising reagent; L<sub>1</sub> and L<sub>2</sub>, open reactors, T, thermostat; IB, ice-bath; D, fluorimetric detector; and W, waste.

Under these conditions the time required for the development of the manual sample pre-treatment was less than half of that necessary for previous liquid–liquid extraction procedures [12,14,15].

#### 2.4. Manifold and procedure

Fig. 2 shows the integrated continuous cleanup-preconcentration/HPLC/post-column derivatisation/fluorescence detection assembly in which parts A and B have been previously used by the authors [43]. The overall setup works as follows: the pre-treated sample is passed through the pre-concentration aminopropyl minicolumn (inserted in the sample loop of a low-pressure injection valve in the position for sample aspiration), and both the target analytes and interferents with similar features are retained. After a 20-min pre-

concentration time, the minicolumn is washed in 2-min cycles with 50 mmol l<sup>-1</sup> phosphate buffer, pH 6.5, and 70:30 methanol:water (v/v) solution in order to remove the interferents and, finally, the analytes are eluted by methanol solution (by manually switching the low-pressure injection valve) and driven to the injection valve of the chromatograph. The volume of methanol containing the eluted analytes is trapped by switching the HPLC injection valve 95 s after switching the low-pressure injection valve, and the analytes are thus introduced into the column. The gradient starts simultaneously with injection. The analytes are removed from the column as a function of their relative polarity. The eluate containing the separate analytes merges at point a with a strong acid stream, and the mixed solution passes through to reactor L<sub>1</sub> placed in the high tempera-

ture bath where the dehydration reaction takes place, then through reactor L<sub>2</sub> cooled at 4°C before reaching the detector. The fluorescence intensity is monitored on passage of the fluid through the flow-cell as a compromise wavelength of 482 and a ( $\lambda_{\text{ex}} = 389$  nm).

### 3. Results and discussion

#### 3.1. Preliminary studies of the dehydration reaction

A preliminary study consisted of selecting the best dehydration reagent in order to obtain the reaction product that exhibited the highest fluorescence emission. With this aim HCl, H<sub>2</sub>SO<sub>4</sub>, Lewis' acids (such as SnCl<sub>2</sub>, AlCl<sub>3</sub>, SbCl<sub>3</sub> and BF<sub>3</sub>) and trifluoroacetic anhydride were used. Individual solutions of 24,25-(OH)<sub>2</sub>-D<sub>3</sub>, 1,25-(OH)<sub>2</sub>-D<sub>3</sub> and 25-OH-D<sub>3</sub> at the same concentration were mixed with the reagents at several concentrations and, after heating, the excitation and emission spectra of each mixture were recorded. Only two of the reagents (namely, H<sub>2</sub>SO<sub>4</sub> and AlCl<sub>3</sub>) formed the fluorescent product. Table 1 shows the excitation and emission wavelength and the highest relative fluorescence intensity achieved with these two reagents and the concentration at which the maximum fluorescence was obtained. As can be seen, the derivatised products achieved using 60% sulphuric acid (v/v) exhibit the highest relative fluorescence intensity ( $\lambda_{\text{ex}} = 389$  nm and  $\lambda_{\text{em}} = 482$  nm).

Table 1  
Fluorimetric features of the isotachysterol derivative

Reagent	Analyte	$\lambda_{\text{ex}}$ (nm)	$\lambda_{\text{em}}$ (nm)	Relative fluorescence intensity (A.U.)
H <sub>2</sub> SO <sub>4</sub> <sup>a</sup>	24,25-(OH) <sub>2</sub> -D <sub>3</sub>	389	482	1700.2
	1,25-(OH) <sub>2</sub> -D <sub>3</sub>	387	482	1004.4
	25-(OH)-D <sub>3</sub>	387	476	1350.0
AlCl <sub>3</sub> <sup>b</sup>	24,25-(OH) <sub>2</sub> -D <sub>3</sub>	370	485	114.1
	1,25-(OH) <sub>2</sub> -D <sub>3</sub>	369	482	187.7
	25-(OH)-D <sub>3</sub>	366	472	108.8

<sup>a</sup> Concentration 60%.

<sup>b</sup> Concentration 70%.

#### 3.2. Continuous cleanup/preconcentration and analyte separation

The continuous cleanup/preconcentration and separation subsystems of the experimental setup were similar to those previously reported by the authors [43]. Table 2 shows the optimum values of the variables affecting these steps, which were used as such.

#### 3.3. Continuous post-column derivatisation

The hydrodynamic and chemical variables that affected the post-column subsystems were studied using the univariate method. Table 3 shows the variables, the range studied and the optimum value found in each case. The derivatising subsystem consisted of a continuous manifold in which the chromatographic eluate was mixed at point a with a stream containing a concentrated acid solution for development of the derivatisation reaction.

##### 3.3.1. Effect of temperature

The derivatising reaction occurred at temperatures over 70°C. Temperatures higher than 110°C caused the formation of bubbles in the system as a consequence of the evaporation of the organic solvent present in the mobile phase. The location of an ice-bath between the thermostat and the detector, circumvented this drawback. A temperature of 150°C provided the optimal conditions for the dehydration reactions.

Table 2  
Optimum values of the variables of the cleanup/preconcentration and HPLC separation steps

Type	Variable	Optimum value
Physical	Temperature (°C)	25
Cleanup/pre-concentration	Mode	Single
	Sorbent	NH <sub>2</sub>
	Particle size (µm)	63
	pH	6.5
	Washing solution	
	Methanol:water	70:30
	(% , v/v)	
	Elution solution	
	Methanol (%)	100
	Flow-rate (ml min <sup>-1</sup> )	100
	Minicolumn length (cm)	0.32
Stainless-steel tubing	100	
(cm, 0.25 mm ID)		
Chromatographic	Type of chromatography	Reverse-phase gradient
	Column	C <sub>18</sub> (5 µm, 250 × 4.6 mm)
	Flow-rate (ml min <sup>-1</sup> )	1.2
	Injection volume (µl)	100
	Initial mobile phase	
	Acetonitrile:phosphate buffer (v/v)	20:80
	Final mobile phase	
	Isopropanol:methanol	10:90
	Gradient time (min)	1.7
Stabilised time (min)	20	

### 3.3.2. Flow-rate of the derivatisation reagent

The flow-rate of the acid solution was changed by keeping constant the flow-rate of the chromatographic effluent at the optimum value (see Table 2).

Table 3  
Study of variables of the derivatisation subsystem

Type of Variable	Variable	Range studied	Optimum value
Physical	Temperature (°C)	30 – 200	150
Chemical	[H <sub>2</sub> SO <sub>4</sub> ] (%)	25–80%	70
Hydrodynamic	Flow rate (ml min <sup>-1</sup> )	0.5–1.5	0.8
	Length of reactor L <sub>1</sub> (cm)	50 – 500	150
	Length of reactor L <sub>2</sub> (cm)	50 – 500	200
Chemical	H <sub>2</sub> SO <sub>4</sub> concentration (% , v/v)	25 – 80	80

Flow-rates higher than 1.2 ml min<sup>-1</sup> caused high pressure at the mixing point and produced back-flowing through the separation system. A flow-rate of 0.8 ml min<sup>-1</sup> of the acid stream provided the optimum acid solution–column effluent ratio.

### 3.3.3. Length of the reactors

After fixing the flow-rate, the length of reactors L<sub>1</sub> and L<sub>2</sub> was optimised in order to obtain an appropriate residence time for both development of the derivatisation reaction and cooling of the solution prior to passage through to detector. A length of 150 cm for L<sub>1</sub> provided enough residence time for formation of the isotachysterol products. A length of 200 cm for L<sub>2</sub> provided enough residence time for cooling the fluid. Higher lengths increased considerably the analytes dispersion thus decreasing the separation efficiency.

**3.3.3.1. Concentration of sulfuric acid.** Under the above optimised conditions, an aqueous solution containing a 70% sulfuric acid (v/v) provided the most appropriate medium for development of the derivatisation reaction. Solutions with concentrations higher than 70% caused damage to the high-pressure pump and connections in stainless-steel.

A chromatogram of a mixture of the target analytes obtained under the optimal working conditions is shown in Fig. 3A.

### 3.4. Features of the method

Calibrations graphs were run using the optimum values of the variables listed in Tables 2 and

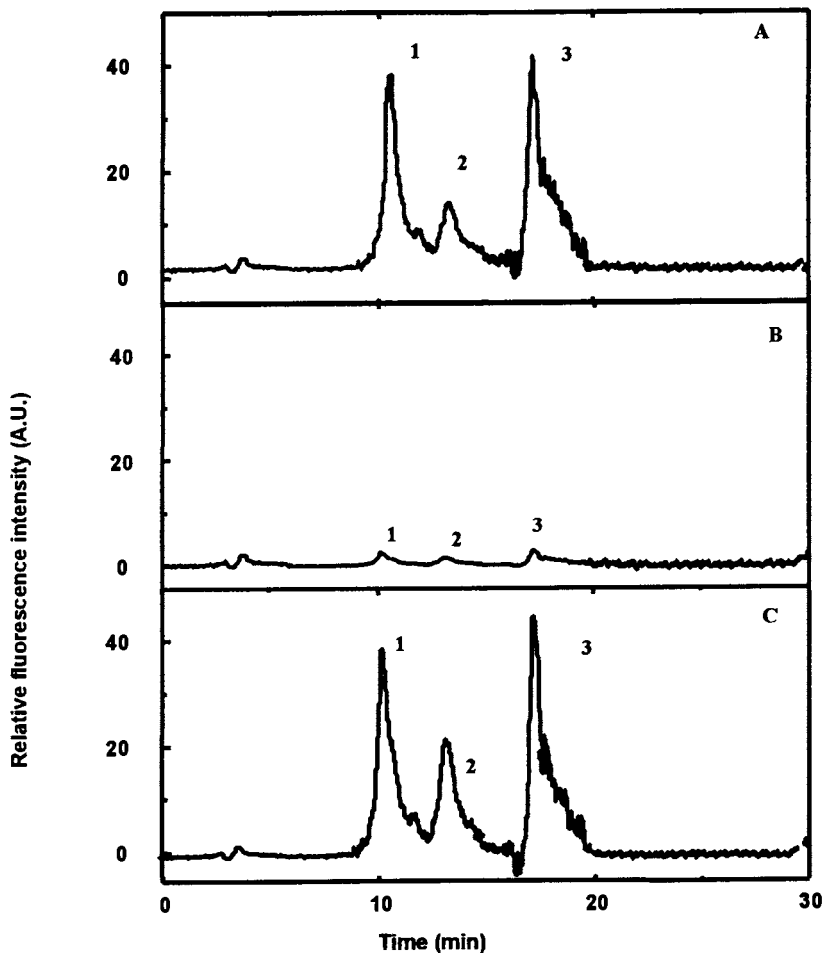


Fig. 3. Chromatograms of three solutions processed under the optimal working conditions listed in Tables 2 and 3. (A) Chromatogram of the derivatised analytes from a standard solution  $10 \text{ ng ml}^{-1}$  for 24,25-(OH) $_2$ -D $_3$  (1 in the figure), and 25-OH-D $_3$  (3), and  $10 \text{ pg ml}^{-1}$  for 1,25-(OH) $_2$ -D $_3$  (2); (B) chromatogram of other standard solution containing  $0.5 \text{ ng ml}^{-1}$  of 24,25-(OH) $_2$ -D $_3$  and 25-OH-D $_3$ , and  $0.5 \text{ pg ml}^{-1}$  of 1,25-(OH) $_2$ -D $_3$ ; and (C) chromatogram of the derivatised target analytes from a human plasma (for concentration values see No. 6 in Table 5) (A.U., arbitrary units).

3. Standard solutions of 24,25-(OH) $_2$ -D $_3$ , 1,25-(OH) $_2$ -D $_3$  and 25-OH-D $_3$  were mixed at concentrations between  $0.01 \text{ pg ml}^{-1}$  and  $500 \text{ ng ml}^{-1}$  of each analyte. Both standards and plasmas were subjected to the same procedure and injected in triplicate into the system. Table 4 summarises the features of the method (equations, regression coefficients, linear ranges and RSD% values). As can be seen, two linear ranges for each analyte were obtained at the sub-part per trillion and sub-part per billion

levels. The former ranged between  $0.1$  and  $1000 \text{ pg ml}^{-1}$ , with a LOD and LOQ of  $0.06$  and  $0.1 \text{ pg ml}^{-1}$ , respectively (estimated as  $3\sigma$  and  $10\sigma$ , respectively), which provides enough sensitivity for quantification of 1,25-(OH) $_2$ -D $_3$  at the normal level in human plasma. The latter linear range (between  $0.1$  and  $100 \text{ ng ml}^{-1}$ ) was the most appropriate for determining the other two analytes. In comparison with the UV-detection used in the previous method [43], the sensitivity was increased 50 times using

post-column derivatisation and fluorescence detection method [43], the sensitivity was increased 50 times using post-column derivatisation and fluorescence detection.

In order to establish the precision of the method, two series of seven solutions containing  $5 \text{ pg ml}^{-1}$  and  $10 \text{ ng ml}^{-1}$  of each analyte were assayed in triplicate. The repeatability of the method yielded acceptable RSD% values in all instances, with values between 2.1 and 5.2. Similar RSD% values were achieved using plasma samples (see Table 5).

### 3.5. Application of the method to clinical samples

Due to the lack of certified reference materials for the target analytes, the proposed method was validated by applying it to the determination of 24,25-(OH)<sub>2</sub>-D<sub>3</sub>, 1,25-(OH)<sub>2</sub>-D<sub>3</sub> and 25-OH-D<sub>3</sub> in plasma in two ways, namely: (a) determination of the analytes in six plasma samples from individuals from hospitals who had received or not vitamin D<sub>3</sub> treatment; and (b) study of the recovery afforded after addition of two standard solutions containing  $5 \text{ pg ml}^{-1}$  and  $10 \text{ ng ml}^{-1}$  of each analyte to the five previous plasma samples. Fig. 3 depicts three chromatograms, which correspond to two derivatised standard solution of the analytes (at a normal

concentration level Fig. 3A), and at concentration close to the LOQ of the method, Fig. 3B); and a chromatogram of the derivatised target analytes from human plasma (for concentration values see Table 5, sample No. 6). Table 5 also summarises the concentration found and the recoveries achieved by the standard addition method. As can be seen, acceptable recoveries were obtained in all instances (between 86 and 106%).

## 4. Conclusions

In comparison with the methods published so far, that proposed here presents the following advantages:

1. The method incorporates a shorter manual sample treatment and conditioning than previous methods [12,14,15].
2. The continuous cleanup step provides an effective removal of interferences.
3. The preconcentration of the target analytes makes possible the determination of vitamin D<sub>3</sub> hydroxymetabolites at the concentrations occurring in human fluids.
4. The miniaturisation of the continuous cleanup step based on the use of continuous solid-phase extraction reduces sorbent consumption

Table 4  
Features of the method

Analyte	Equation <sup>a</sup>	$r^2$	Linear range <sup>a</sup>	RSD% <sup>b</sup>	
				Low level	High level
First linear range ( $n = 7$ )					
24,25-(OH) <sub>2</sub> -vitamin D <sub>3</sub>	$y = 3.96 + 0.25x$	0.9994	0.1 <sup>c</sup> –1000	2.4	–
1,25-(OH) <sub>2</sub> -vitamin D <sub>3</sub>	$y = 2.36 + 0.27x$	0.9986	0.1 <sup>c</sup> –1000	4.9	–
25-(OH)-vitamin D <sub>3</sub>	$y = 4.82 + 0.33x$	0.9984	0.1 <sup>c</sup> –1000	5.2	–
Second linear range ( $n = 5$ )					
24,25-(OH) <sub>2</sub> -vitamin D <sub>3</sub>	$y = 7615.8 + 2.57x$	0.9966	0.1–100	–	2.1
1,25-(OH) <sub>2</sub> -vitamin D <sub>3</sub>	$y = 8072 + 2.73x$	0.9933	0.1–100	–	3.6
25-(OH)-vitamin D <sub>3</sub>	$y = 10087 + 3.4x$	0.9966	0.1–100	–	2.6

<sup>a</sup>  $y$  denotes area in arbitrary units,  $x$  concentration in  $\text{pg ml}^{-1}$  and  $\text{ng ml}^{-1}$  for the first and second linear ranges, respectively ( $n$  = number of standards).

<sup>b</sup> For  $5 \text{ pg ml}^{-1}$  and  $10 \text{ ng ml}^{-1}$  low and high level, respectively.

<sup>c</sup> Quantification limit (calculated as  $10\sigma$  of the blank signal).

Table 5  
Application of the method

Sample no.	Concentration and recoveries% <sup>a</sup>	Analyte		
		24,25-(OH) <sub>2</sub> -D <sub>3</sub> <sup>b</sup>	1,25-(OH) <sub>2</sub> -D <sub>3</sub> <sup>c</sup>	25-(OH)-D <sub>3</sub> <sup>b</sup>
1	Concentration	16.2 ± 2.6	6.5 ± 3.8	38.4 ± 3.4
	First addition	86	96	98
	Second addition	96	91	92
2	Concentration	8.8 ± 3.1	4.9 ± 2.2	15.6 ± 4.9
	First addition	103	101	89
	Second addition	101	102	91
3	Concentration	9.8 ± 2.0	12.5 ± 2.8	22.4 ± 2.3
	First addition	101	96	95
	Second addition	106	89	99
4	Concentration	10.1 ± 1.8	60.3 ± 4.2	14.2 ± 3.1
	First addition	98	99	91
	Second addition	87	92	99
5	Concentration	12.2 ± 0.39	48.5 ± 1.2	22.1 ± 1.76
	First addition	99	101	101
	Second addition	98	103	102
6	Concentration	13.4 ± 0.28	26.2 ± 0.98	15.2 ± 4.8
	First addition	98	99	100
	Second addition	102	97	98

<sup>a</sup> Recoveries after addition of 5 pg ml<sup>-1</sup> and 10 ng ml<sup>-1</sup>, first and second additions, respectively.

<sup>b</sup> Concentration (± S.D.) in ng ml<sup>-1</sup>.

<sup>c</sup> Concentration (± S.D.) in pg ml<sup>-1</sup>.

due to the minicolumn reusability (for at least 200 times without loss of capacity or deterioration).

- The sensitivity is increased due to the use of on-line derivatisation and fluorescence detection (estimated as 50 times in comparison with the previous method [43] based on UV-detection). It is remarkable that, for the first time, a method makes possible the quantification of 1,25-(OH)<sub>2</sub>-D<sub>3</sub> at concentrations lower than part-per trillion (that is, lower than its usual concentration in human plasma).
- Easy adaptation to commercial devices and reduction of the derivatisation cost as compared with methods either based on GC-MS or RIA.

For these reasons, the proposed method constitutes the basis for both implementation of low-cost routine analyses of vitamin D<sub>3</sub> hydroxymetabolites in hospital and easy, cheap automation of the overall process.

## Acknowledgements

Comisión Interministerial de Ciencia y Tecnología (CICYT) is thanked for financial support (project No. PB97/0505). The Fondo de Investigaciones Sanitarias (FIS) is also thanked (Grant No. 98/1040).

## References

- A. Brown, A. Dusso, E. Slatopolsky, Vitamin D, in: D.W. Seldin, G. Giebisch (Eds.), *The Kidney: Physiology and Pathophysiology*, 2, Raven Press, New York, 1992, p. 1505.
- N.H. Bell, P.H. Stern, E. Panther, T.K. Sinha, H.F. DeLuca, *J. Clin. Invest.* 64 (1979) 218.
- G. Jones, D.H.J. Trafford, H.L.J. Makin, B.W. Hollis, Vitamin D: cholecalciferol, ergocalciferol and hydroxylated metabolites, in: A.P. Delleheer, W.E. Lambert, H.J. Nelis (Eds.), *Modern Chromatographic Analysis of Vitamins*; Chromatographic Science Series, vol. 60, Marcel Dekker, New York, 1992, pp. 73–151.

- [4] K. Shimada, N. Kobayashi, Trends Anal. Chem. 10 (3) (1991) 103.
- [5] H. Koyama, J.M. Prahl, A. Uhland, M. Nanjo, M. Inaba, Y. Nishizawa, Y. Morii, Y. Nishii, H.F. DeLuca, Anal. Biochem. 205 (2) (1992) 213.
- [6] M.L. Traba, M. Babe, C. de la Piedra, A. Marín, Clin. Chim. Acta 29 (10) (1983) 1806.
- [7] F.H. Johannsen, Landwirtsch. Forsch. 40 (1) (1987) 32.
- [8] M.A. Haughton, R.S. Mason, Clin. Chem. 38 (9) (1992) 1796.
- [9] E. Stary, A.M.C. Cruz, C.A. Donomai, J.L. Mondardini, J. High Resolut. Chromatogr. 12 (6) (1989) 421.
- [10] E.C. Bligh, W.J.A. Dyer, Can. J. Biochem. Physiol. 37 (1959) 911.
- [11] G. Jones, Clin. Chem. 24 (2) (1978) 287.
- [12] M. Shimizu, Y. Gao, T. Aso, K. Nakatsu, S. Yamada, Anal. Biochem. 204 (2) (1992) 258.
- [13] R.D. Coldwell, D.J.H. Trafford, H.L. Makin, J. Clin. Chem. 31 (11) (1985) 1919.
- [14] R.D. Coldwell, D.J.H. Trafford, M.J. Varley, D.N. Kirk, H.L. Makin, J. Clin. Chim. Acta 180 (2) (1989) 157.
- [15] F. Ortiz-Boyer, J.M. Fernández-Romero, M.D. Luque de Castro, J.M. Quesada, J. Chromatogr. B 693 (1997) 43.
- [16] R.D. Coldwell, D.J.H. Trafford, H.L. Makin, M.J. Varley, D.N. Kirk, J. Chromatogr. Biomed. Appl. 39 (1985) 289.
- [17] E.B. Mawer, J.T. Hann, J. Chromatogr. Biomed. Appl. 59 (1987) 305.
- [18] R.L.G. Norris, M.J. Thomas, P.W. Craswell, J. Chromatogr. Biomed. Appl. 54 (1) (1986) 53.
- [19] S. Shimada, K. Mitamura, N. Kitama, Biomed. Chromatogr. 9 (5) (1995) 229.
- [20] A. Benmoussa, J.L. Lacout, P.R. Loiseau, M. Mikou, Chromatographia 42 (3-4) (1996) 177.
- [21] A. Benmoussa, G. Dlaurent, J.L. Lacout, P.R. Loiseau, M. Mikou, J. Chromatogr. 731 (1-2) (1996) 153.
- [22] J.M. Halket, I. Ganschow, B.P. Lisboa, J. Chromatogr. 192 (2) (1980) 434.
- [23] S. Komuro, I. Nakatsuka, A. Yoshizake, K. Iba, Biol. Mass. Spectrom. 23 (1) (1994) 33.
- [24] R.D. Coldwell, D.J.L. Trafford, H.L. Makin, J. Mass. Spectrom. 30 (1995) 348.
- [25] P.P. Nair, C. Bucana, D. DeLeón, D.A. Turner, Anal. Chem. 37 (1965) 631.
- [26] I. Bjorkhem, I. Holmberg, T. Kristiansen, J.I. Pedersen, Clin. Chem. 25 (4) (1979) 584.
- [27] P.M.K. Poon, I.T. Mak, C.P. Pang, Clin. Biochem. 26 (6) (1993) 461.
- [28] K. Shimada, K. Mitamura, M. Mukouyama, T. Okura, K. Sagaya, J. Chromatogr. Sci. 32 (2) (1995) 82.
- [29] D.A. Seamark, D.J.H. Trafford, P.G. Hiscocks, H.L. Makin, J. Chromatogr. 197 (2) (1980) 271.
- [30] T. Iwata, M. Yamaguchi, H. Hanazono, Y. Imazato, M. Nakamura, Y. Ohkura, Anal. Sci. 6 (3) (1990) 361.
- [31] M. Shimizu, Y. Gao, T. Aso, K. Nakatsu, S. Yamada, Anal. Biochem. 204 (2) (1992) 258.
- [32] K. Shimada, I. Nakatani, K. Saito, K. Mitamura, Biol. Pharm. Bull. 19 (4) (1996) 491.
- [33] P.H. Jordan, G. Read, T. Hargreaves, Analyst 116 (12) (1991) 1347.
- [34] B. Yeung, P. Vouros, G.S. Reddy, J. Chromatogr. 645 (1) (1993) 115.
- [35] R.J. Vreeken, M. Honing, B.L.M. Van-Baar, R.T. Ghijssen, G.J. De-Jong, U.A.T. Brinkman, Biol. Mass-Spectrom. 22 (11) (1993) 621.
- [36] D.J.H. Trafford, D.A. Seamark, H. Turnbull, H.L.J. Makin, J. Chromatogr. Biomed. Appl. 15 (1981) 351.
- [37] M. Shimizu, Y. Iwasaki, H. Ishida, S. Yamada, J. Chromatogr. 672 (1995) 63.
- [38] M. Shimizu, S. Kamachi, Y. Nishii, S. Yamada, Anal. Biochem. 194 (1991) 77.
- [39] A. Sánchez-Pérez, M.J. Gallego-Matilla, J.S. Hernández-Méndez, Anal. Lett. 26 (4) (1993) 721.
- [40] D.J.T. Trafford, R.D. Colwell, H.L. Makin, J. Pharm. Biomed. Anal. 9 (1991) 1095.
- [41] V.K. Agarwal, Anal. Chem. 72 (6) (1989) 1007.
- [42] H. Li, H. Shang, C. Liu, Shenyang-Yaoxueyuan-Xuebao 8 (4) (1991) 248.
- [43] F. Ortiz-Boyer, J.M. Fernández-Romero, M.D. Luque de Castro, J.M. Quesada, Analyst 124 (1999) 401.



# Determination of chloride in drinking and ground water by AlCl molecular absorption spectrometry using graphite furnace atomic absorption spectrometer

Pekka Parvinen <sup>a,b,\*</sup>, Lauri H.J. Lajunen <sup>b</sup>

<sup>a</sup> VTT Chemical Technology, Mineral Processing, FIN-83500 Outokumpu, Finland

<sup>b</sup> Department of Chemistry, University of Oulu, FIN-90570 Oulu, Finland

Received 15 March 1999; accepted 16 March 1999

## Abstract

The use of high temperature molecular absorption spectrometry for the determination of chloride in drinking and ground water samples is described. The chloride is measured by monitoring the absorbance of vaporised aluminium chloride molecule. The effect of various components commonly present in natural waters were studied and any serious interference was found. The accuracy was assessed by comparing the results obtained using the proposed method with those got by conventional titrimetric method. © 1999 Elsevier Science B.V. All rights reserved.

*Keywords:* Chloride determination; Electrothermal atomisation; Electrothermal evaporation; Ground water; Molecular absorption

## 1. Introduction

In lake and ground waters, chloride is a common anion because the chlorides in soil are relatively easily dissolved in water. Waste waters contain often great amounts of chloride, and that may increase the amount of chloride in some natural waters.

Chloride is usually determined by titrimetric methods, like iodometric titration, Hg(NO<sub>3</sub>)<sub>2</sub> titration, ion chromatography or various spectrophotometric methods. However, these methods

are seriously interfered with by many cations and anions and, hence, sample pre-treatment may be difficult. Atomic spectroscopy has commonly used simple methods for the determination of a wide range of elements. However non-metallic elements are difficult to determine because their resonance lines lie in the vacuum ultraviolet region [1]. That is the reason why molecular spectroscopic methods have been developed for the determination of those elements. When we compare molecules to atoms, we find that the energy terms are complicated by additional possibilities that the molecule may possess energy of both rotation and vibration. Each atomic spectrum line is then replaced by a system of bands [2]. The electronic transition determines the region of the spectrum in which a

\* Corresponding author. Tel.: +358-13-557-960; fax: +358-13-557-870.

E-mail address: pekka.parvinen@vtt.fi (P. Parvinen)

band system occurs, while the distribution of individual bands depends on the changes in the rotational energy. The intensity of any line of a band system depends on the probability of the electronic transition, on the vibrational intensity distribution, on the population of the molecules in the initial energy level, and on the branch type of the rotational fine structure of a band and  $J$  value [2].

The strong and single band-heads in the molecular spectra may behave like atomic lines when measuring the absorption caused by this band using a hollow cathode lamp emitting suitable radiation. When measuring this kind of narrow band, deuterium lamp background correction can also be used in the determinations. The determination of fluorine in different types of samples has been for some time performed by AIF molecular absorption using a deuterium lamp background correction system [3,4].

Molecular absorption spectrometry was developed for the ultra-trace determination of chloride by Dittrich and Vorberg [5] and Fuwa et al. [6]. These methods are based on the formation of aluminium monochloride in a graphite furnace at high temperatures. We introduced the use of a lead hollow cathode lamp as a light source [7]. By this method it is possible to perform background correction at the same wavelength with a deuterium lamp background correction system. Aluminium monochloride has a strong absorption spectrum at 259–264 nm, and measurements have been done near the sharp molecular band at 261.4 nm.

In this study we have examined the matrix effects which may have an influence on the accuracy and precision of AlCl molecular absorption measurements, with ions commonly present in drinking and ground waters that have an influence on the formation of the diatomic AlCl molecule, and the sample pre-treatment needed in order to avoid these interferences.

## 2. Experimental

### 2.1. Apparatus

The molecular absorption of AlCl was measured using Pye Unicam SP 9 and PU 9200

atomic absorption spectrometers equipped with a deuterium lamp background correction system for simultaneous background correction. The measurements have been done in ordinary, uncoated graphite furnaces. Nitrogen gas (4 l/min) was used to purge air from the furnace. A lead hollow-cathode lamp was used as an irradiation source for AlCl molecular absorption measurements (Cathodeon). The measurements were performed using the Pb line at 261.4 nm [5,6] with the spectral band pass of 0.2 nm, and deuterium lamp background correction.

### 2.2. Chemicals

All the reagents were pro analysis grade from Merck. A chlorine standard solution was prepared from NaCl. All the metal ions used were in the form of nitrates. Other halogens tested were added as NaX. The concentration of the aluminium solution (as [Al (NO<sub>3</sub>)<sub>3</sub>]) was 0.01 M.

### 2.3. Procedure

The experimental procedure for the determination of chloride is summarised in Table 1. Drinking water and other chloride-containing solutions were added to the furnace after ashing of the aluminium solution. In the most cases, a dilution with distilled water was necessary in order to be able to do the measurements.

Table 1  
Experimental procedure for the determination of chloride as AlCl with a graphite furnace<sup>a</sup>

(1) Injection of Al solution	10 µl	
Drying	120°C	20 s
Ashing	700°C	20 s
Cooling		5 s
(2) Injection of Cl solution	5 µl	
Drying	120°C	20 s
Ashing	700°C	20 s
(3) Evaporation and measurement	1900°C	5 s

<sup>a</sup> The aluminium solution contain 0.01 M of Al, Sr and Co as nitrates.

Table 2  
Determination of chloride (1 mg/l) in solutions containing increasing amounts of nitric acid using different aluminium solutions

Al solution	A			
	0.0 M	0.1 M	0.5 M	1.0 M HNO <sub>3</sub>
Al–Ag–Sr solution	0.74	0.77	0.85	0.85
Al–Co–Sr solution	0.81	0.81	0.40	
Al–Sr solution	0.82	0.33	0.16	
Al solution	0.33	0.27	0.23	

### 3. Results and discussion

#### 3.1. Matrix modifier

A matrix modification is necessary for the formation of the AlCl molecule, to increase the sensitivity and to improve the precision of the analysis, as reported earlier [5–7]. Usually Sr, Co, Ni and Ba are used to reduce the volatilisation of chlorine during the drying and ashing steps by binding it in the graphite furnace until the AlCl formation temperature is reached. Ag was also tested for the binding of chlorine. The results obtained by these matrix modifiers are compared in the form of calibration curves. These show that an aluminium solution with strontium and cobalt gives the best results, providing an absorption of 0.82 from solution containing 1 mg/l of chloride. The corresponding absorption by solution where cobalt was replaced by silver gave an absorption of 0.76, aluminium solution containing strontium in addition to aluminium gave an absorption of 0.63, and an aluminium solution gave an absorption of 0.33. However, if the sample solution is very acidic (pH 2), the results are slightly better when using aluminium solution containing strontium and silver (Table 2). Silver seems to form a AgCl molecule with chloride during the drying step and so the easy escape of chloride as HCl in acidic conditions is prevented. Almost as good results were obtained using an aluminium solution containing barium, when the measurements were performed from slightly acidic chloride solutions.

The increase of aluminium concentration in the matrix modifier will cause an increase in background absorption. An increase in the injection volume of the aluminium solution also increases the background absorption. For different aluminium solutions, the strongest background absorption was caused by solutions containing silver.

#### 3.2. Interferences

The most common cations and anions present in drinking and raw water were tested in order to determine their effect on the evaporation and formation of AlCl molecule. The interference of cations is mainly caused by the formation of other metal chloride molecules that are volatile at lower temperatures or significantly stable at the AlCl formation and evaporation temperature. In the drying and ashing step the main problem is the thermal hydrolysis which causes the evaporation of HCl. This can be avoided by the addition of metals that have high  $pK_a$  values like Sr<sup>2+</sup>. The effects of these cations, when using an aluminium solution containing strontium and cobalt as matrix modifiers, are presented in Table 3. The metals studied have little effect up to concentrations of 100 mg/l, except for Ba. The concentrations of these cations are generally so small in water samples, especially after dilution, that they do not have to be taken into account when determining chlorine. However, if the amount of some

Table 3  
The interference caused by some metals in the determination of Cl by molecular absorption when measured solutions containing 1 mg/l of chlorine<sup>a</sup>

Element	Chloride found (%)	
	0.1 g/l	1.0 g/l
Cu	97	96
Sr	98	80
Na	98	71
Ba	82	74
Mg	100	74
Ca	98	73
K	100	61

<sup>a</sup> The interfering elements were added, 0.1 and 1.0 g/l, in chlorine solutions.

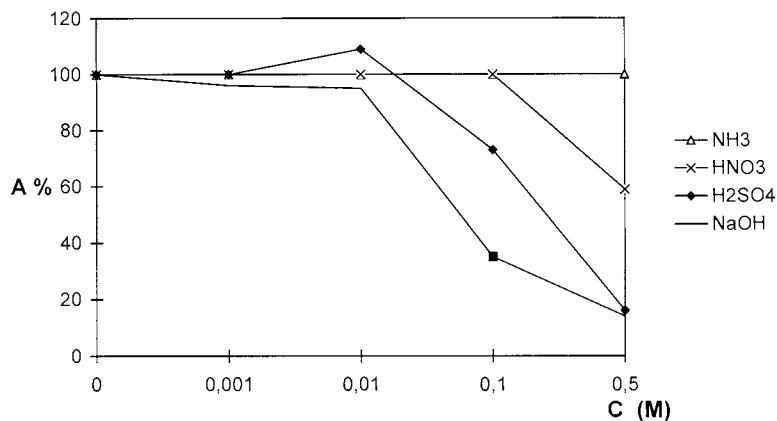


Fig. 1. Chloride found in solutions containing different concentrations of some acids and bases.

metals is too high in the sample, the interference can be avoided by ion exchange, after which the sample should only be neutralised by  $\text{NH}_3$ . The effects of some acids and bases on the evaporation and formation of  $\text{AlCl}$  molecules was studied by measuring chloride in these solutions (Fig. 1). In Fig. 1 it can be seen that the effects of acids and bases studied are not serious in the concentration range in which they may generally exist in natural waters.

Other halogenides interfere because they form stable AIX molecules in the same conditions as chloride. The most severe interference is caused by fluoride, because it forms the most stable molecule with aluminium. The effect of bromide is not serious because the dissociation energy of  $\text{AlBr}$  is lower than that of  $\text{AlCl}$ , and iodide has no effect at all [7]. As the aim of this work was to determine the chloride in different types of water samples, the effects of the other halogenides do not have to be taken into account, because their concentrations lie much below the interfering levels.

### 3.3. Determination of chloride in real and artificial water samples

The present method was applied to natural and artificial drinking and raw water samples taken from different sources and with different metal concentrations. The experimental conditions are described in Section 2.3. The working range was

estimated to be from 0.03 mg/l (1% A) to 3 mg/l. The precision (RSD) of the analysis at 1.0 mg/l level was about 3%. In order to test the accuracy of the method, artificial water samples containing (1) 0.1 mg/l of Cl as NaCl, 100 mg/l  $\text{Na}_2\text{SO}_4$ , 10 mg/l  $\text{Fe}(\text{NO}_3)_2$  and 10 mg/l  $\text{NH}_4\text{NO}_3$  and (2) 10 mg/l of Cl as NaCl, 10 mg/l NaBr, 100 mg/l  $\text{Na}_2\text{SO}_4$  and 0.01 mg/l of NaF were prepared. The results obtained by measuring those artificial water samples were in good agreement with the known amounts of chloride added. Generally, the chloride content in the drinking and ground water was so high that 2–20-fold dilution with distilled water was required in order to get the chloride concentrations low enough for the measurements. After the dilution, the other substances present in the samples did not show any interference. In ordinary drinking water samples, no matrix effect was found and it was possible to perform the analysis using a conventional calibration graph. The method was used for the determination of chloride in ground water wells for the water supply in the region of Raahe on the west coast of Finland. Table 4 lists the results obtained by present MAS method and conventional titrimetric method. The titration procedure was chosen because it is a standard method SFS-3006 (others: DS/R 239, NS 4756 and SS 028136), which is the basic one used in water and environmental laboratories in Finland. The precision of the method on the basis of the comparison as  $P_{0.95}$  was 3.9%.

Table 4

Determination of chloride in water samples by coulometric titration and molecular absorption (MAS) in ground water wells for the water supply in the region of town of Raahe in the middle of Finland

Sample	Titration (Cl mg/l)	MAS (Cl mg/l)	MAS (RSD)
Ra I 1	6.0	6.0	
Ra I 2	9.9	9.2	
Ra II 1 <sup>a</sup>	11.2	10.9	
Ra II 2 <sup>a</sup>	6.3	6.1	
Ra II 3	4.3	4.2	1.8%
Ra II 4	2.4	2.5	2.6%
Ra II 5	1.8	1.8	2.4%
Ra II 6	5.9	5.6	1.5%
Ra III 1 <sup>a</sup>	32.7	34	
Ra III 2	6.3	6.0	
Ra III 3 <sup>a</sup>	6.6	6.2	
Ra III 4	6.8	6.7	
Ra III 5	5.7	5.4	

<sup>a</sup> Special pre-treatment was needed in measurement of chloride by titration because of high iron content of these samples.

#### 4. Conclusions

The method using molecular absorption of AlCl affords a high potential with respect to the analysis for chloride in water samples. The sample preparation is rapid and simple, only dilution is often needed, which makes the method easy to

automate. The measurement is easy to realise from the same samples in the autosampler, either after or before the analysis of metals has been performed. For example, in our case it was easy to perform the chlorine determinations from the same dilutions that had been done for determination of iron by the graphite furnace. The sensitivity and precision of the present system are good, and the method can be applied to a great variety of water samples. Also, in determinations using the described method no interference caused by the matrix was found. These experimental results suggest that the method proposed is useful for the practical analysis of chloride in different kinds of water samples.

#### References

- [1] L.H.J. Lajunen, *Spectrochemical Analysis by Atomic Absorption and Emission*, Royal Society of Chemistry, Cambridge, 1992.
- [2] A.G. Gaydon, *Dissociation Energies and Spectra of Diatomic Molecules*, Chapman and Hall, London, 1968.
- [3] K. Tsunoda, et al., *Anal. Chem.* 51 (1979) 2059.
- [4] M. Gomez, et al., *Microchem. J.* 47 (1993) 399.
- [5] K. Dittrich, B. Vorberg, *Chem. Anal.* 28 (1983) 539.
- [6] K. Fuwa, et al., *Anal. Chem.* 41 (1969) 188.
- [7] P. Parvinen, L.H.J. Lajunen, *Spectroscopy Lett.* 22 (1989) 533.

# Complexation and fluorescence behavior of 9,10-bis[bis( $\beta$ -hydroxyethyl)aminomethyl]anthracene

Kanji Kubo <sup>a,\*</sup>, Tadamitsu Sakurai <sup>b</sup>, Akira Mori <sup>a</sup>

<sup>a</sup> Institute of Advanced Material Study, 86, Kyushu University, Kasuga-koen, Kasuga, Fukuoka 816-8580, Japan

<sup>b</sup> Department of Applied Chemistry, Faculty of Engineering, Kanagawa University, Kanagawa-ku, Yokohama 221-8686, Japan

Received 19 October 1998; received in revised form 11 March 1999; accepted 18 March 1999

## Abstract

9,10-Bis[bis( $\beta$ -hydroxyethyl)aminomethyl]anthracene (**1**) showed weak emission, suggesting that photoinduced electron transfer (PET) from amine group to excited anthracene occur. The PET fluoroionophore (**1**) was found to display unique photophysical properties in the presence of the guest metal cations in H<sub>2</sub>O–CH<sub>3</sub>OH (1:1, v/v). Complexation of **1** with guest metal cations increased the fluorescence intensity. © 1999 Elsevier Science B.V. All rights reserved.

*Keywords:* Fluoroionophore; Fluorescence behavior; Photoinduced electron transfer

## 1. Introduction

Photoresponsive supramolecular systems are of great significance particularly for their potential application to nanoscale devices for cation sensor and switch [1]. There are extensive investigations toward the characterization of fluoroionophores including crown ether, calixarene, and cyclodextrin derivatives with naphthalene, umbelliferone, anthracene, or pyrene fluorophore [2–13].

Recently, a number of fluoroionophores has been designed for metal ions [3–13]. Most of them operate by a photoinduced electron transfer

(PET) mechanism. In a classic example from the de Silva group [5–8], the binding component of the sensor is *N*-(9-anthrylmethyl)-18-azacrown-6. The uncomplexed fluoroionophore is weak fluorescent, as the photoexcited fluorophore is quenched by the electron transfer from amine group. Following metal incorporation (Na<sup>+</sup> and K<sup>+</sup>), the metal–ligand interaction decreases the amine oxidation potential drastically and prevents the electron transfer. As a consequence, the intense and characteristic anthracene emission is largely restored. We were interested in developing PET fluoroionophore for metal ion using the same supramolecular approach [9–13]. However, the complexation behaviors were investigated in the organic solvents, which were of no practical use. As an approach to the manipulation of PET fluoroionophores, we now report the complexa-

\* Corresponding author. Tel.: +81-92-583-7807; fax: +81-92-583-7810.

E-mail address: kubo-k@cm.kyushu-u.ac.jp (K. Kubo)

tion and fluorescence behavior of 9,10-bis[bis( $\beta$ -hydroxyethyl)aminomethyl]anthracene (**1**) [6,14] with metal salts in H<sub>2</sub>O–CH<sub>3</sub>OH (1:1, v/v).

## 2. Experimental

Elemental analyses were performed by Perkin-Elmer PE2400 series II CHNS/O analyzer. Melting points were obtained with a Yanagimoto Micro Melting Point Apparatus and are uncorrected. NMR spectra were measured on a JEOL JNM-500 Model spectrometer in CDCl<sub>3</sub>; the chemical shifts are expressed by a  $\delta$  unit using tetramethylsilane as an internal standard. IR spectra were recorded on a Hitachi Model 270-30 infrared spectrophotometer. Fluorescence spectra were measured with a Hitachi Model F-4500 spectrofluorimeter.

### 2.1. Preparation of 9,10-bis[bis( $\beta$ -hydroxyethyl)aminomethyl]anthracene (**1**)

Recrystallization from ethanol gave analytically pure samples with the following physical and spectroscopic properties. pale yellow crystals, mp 172–173°C, <sup>1</sup>H NMR (500 MHz, CDCl<sub>3</sub>):  $\delta$  = 2.67 (8H, t,  $J$  = 6.7 Hz), 3.45 (8H, q,  $J$  = 6.7 Hz), 4.29 (4H, t,  $J$  = 6.7 Hz), 4.62 (4H, s), 7.53 (4H, dd,  $J$  = 6.7, 3.1 Hz), and 8.63 (4H, dd,  $J$  = 6.7, 3.1 Hz); <sup>13</sup>C NMR (125.7 MHz, CDCl<sub>3</sub>) = 51.4 (2C), 56.0 (4C), 59.3 (4C), 125.1 (4C), 125.6 (4C), 130.6 (4C), and 130.9 (2C). IR (KBr): 732, 1035, 1236, 1440, 1611, 2806, 2878, and 3274 cm<sup>-1</sup>. FABMS found:  $m/z$  413.2. Calcd for C<sub>24</sub>H<sub>33</sub>N<sub>2</sub>O<sub>4</sub>: 413.2. Anal. calcd for C<sub>24</sub>H<sub>32</sub>N<sub>2</sub>O<sub>4</sub>: C, 69.88; H, 7.82; N, 6.79. Found: C, 69.58; H, 8.10; N, 6.79.

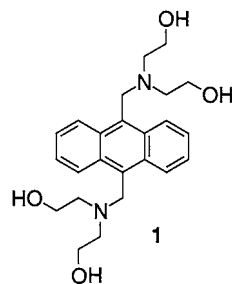
### 2.2. Fluorescence measurement of **1** and its complexes

Fluorescence intensities of **1** ( $4.00 \times 10^{-6}$  M,  $1 \text{ M} = 1 \text{ mol l}^{-1}$ ) and 9,10-dimethylantracene ( $4.00 \times 10^{-6}$  M) excited at 378 nm, measured in H<sub>2</sub>O–CH<sub>3</sub>OH (1:1, v/v) under nitrogen at room temperature, as shown in Fig. 1.

The titrations were conducted by adding a solution (2.0 cm<sup>3</sup>) containing metal salts ( $0\text{--}4.00 \times 10^{-2}$  M NaCl, KCl, CaCl<sub>2</sub>, BaCl<sub>2</sub>, PbCl<sub>2</sub>, NiCl<sub>2</sub>, CuCl<sub>2</sub>, ZnCl<sub>2</sub>, CdCl<sub>2</sub>, and HgCl<sub>2</sub> in H<sub>2</sub>O), to a cuvette containing 2.0 cm<sup>3</sup> of the fluoroionophore solution ( $8.00 \times 10^{-6}$  M for **1** in methanol). The solutions were homogenized by ultrasonic waves for 10 min. The spectrum was recorded after each addition. The added equivalents of the cation were then plotted against the emission-intensity change at 429 nm (excited at 378 nm). The association constants ( $K$ ) were determined by curve-fitting method in the previous study [12,15].

## 3. Result and discussion

The anthracene-functionalized ionophore (**1**) was prepared by the *N*-alkylation of 9,10-bis(chloromethyl)anthracene with diethanolamine [6,14]. The purity of **1** was ascertained by <sup>1</sup>H, <sup>13</sup>C NMR spectroscopic data, and elemental analysis.



Fluorescence spectral behavior of **1** ( $4.00 \times 10^{-6}$  M), (when excited at 378 nm), gave weak emission bands at 406, 428 and 452 nm. The emission-band intensities of **1** was reduced to approximately one-98th that of standard substance (9,10-dimethylantracene,  $4.00 \times 10^{-6}$  M, 9,10-DMA). This indicates that the quenching of the excited-state anthracene chromophore by the diethanolamine unit proceeds in a mechanism similar to that for the classical fluorescent-aliphatic amine system [16–18]. The emission intensity ( $I_1/I_{9,10\text{-DMA}}$ ,  $1.0 \times 10^{-2}$ ) of **1** for 9,10-DMA is lower than that ( $I/I_{9\text{-MA}}$ ,  $2.5 \times 10^{-2}$ ) of *N*-(9-anthrylmethyl)-18-azacrown-6 for 9-methylantracene (9-MA) [5,19]. This means the

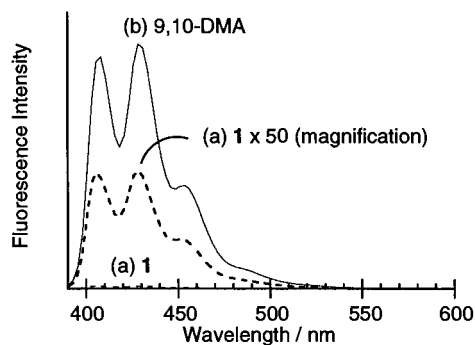


Fig. 1. Fluorescence spectra of **1** ( $4.00 \times 10^{-6}$  M) and 9,10-dimethylanthracene ( $4.00 \times 10^{-6}$  M) in  $\text{H}_2\text{O}-\text{CH}_3\text{OH}$  (1:1, v/v), as excited at 378 nm.

PET from the nitrogen atoms in the diethanolamine to excited fluorescent moieties occur efficiently.

Fig. 2 illustrates the fluorescence spectral behavior of **1** ( $4.00 \times 10^{-6}$  M) in  $\text{H}_2\text{O}-\text{CH}_3\text{OH}$  (1:1, v/v) at room temperature. A dramatic change in the emission intensity of **1** ( $I_1$ ) was observed upon the addition of various amounts of metal cations ( $\text{Na}^+$ ,  $\text{K}^+$ ,  $\text{Ca}^{2+}$ ,  $\text{Ba}^{2+}$ ,  $\text{Pb}^{2+}$ ,  $\text{Ni}^{2+}$ ,  $\text{Cu}^{2+}$ ,  $\text{Zn}^{2+}$ ,  $\text{Cd}^{2+}$ , and  $\text{Hg}^{2+}$ ). When the metal salts were added ( $5 \times 10^3$  molar equivalent), the relative emission intensity ( $I_{\text{complex}}/I_1$ ), being used as a measure of the molecular recognition sensing, changed from 0.9 to 46 depending on the nature of metal cations as shown in Fig. 2. Interestingly, the complexation of **1** with quenching metal cation [4,20] such as  $\text{Ni}^{2+}$ ,  $\text{Cu}^{2+}$ , and  $\text{Hg}^{2+}$  enhanced the emission intensity (Fig. 3). This means that the complexation inhibit the PET from nitrogen atom to anthracene.

Fig. 4 illustrates the relative emission intensity of **1** against the metal salt concentration. Clearly,

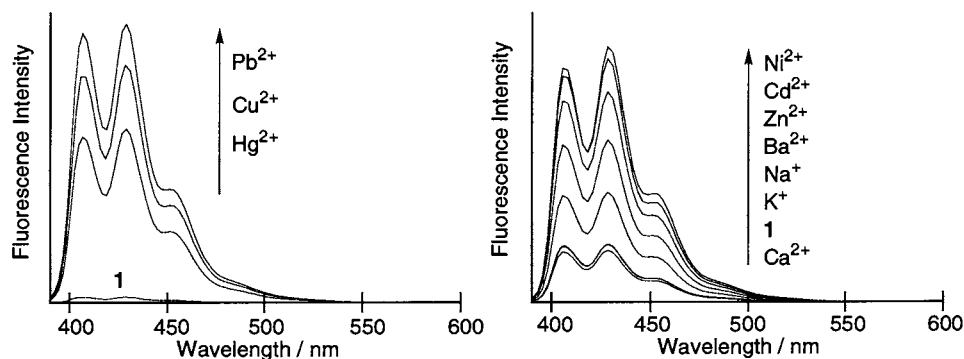


Fig. 2. Fluorescence spectra of **1** ( $4.00 \times 10^{-6}$  M) with and without various metal salts ( $2.00 \times 10^{-2}$  M) in  $\text{H}_2\text{O}-\text{CH}_3\text{OH}$  (1:1, v/v), as excited at 378 nm.

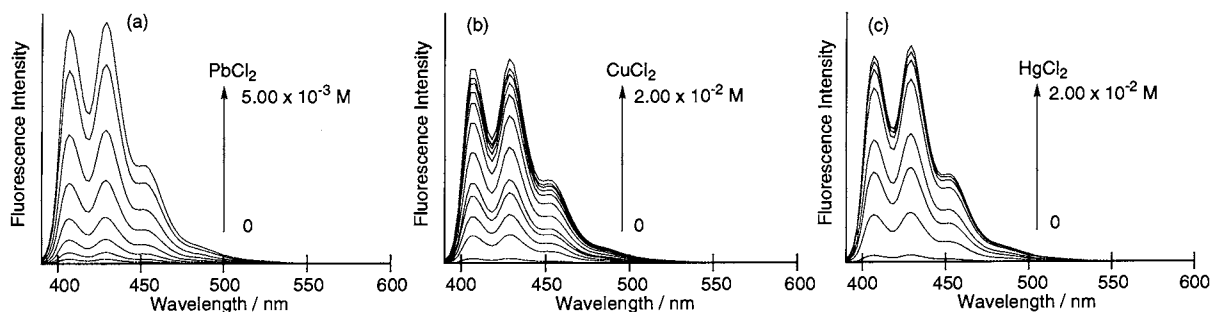


Fig. 3. Fluorescence spectra of **1** ( $4.00 \times 10^{-6}$  M) with (a)  $\text{PbCl}_2$  ( $0-5.00 \times 10^{-3}$  M), (b)  $\text{CuCl}_2$  ( $0-2.00 \times 10^{-2}$  M), and (c)  $\text{HgCl}_2$  ( $0-2.00 \times 10^{-2}$  M) in  $\text{H}_2\text{O}-\text{CH}_3\text{OH}$  (1:1, v/v), as excited at 378 nm.



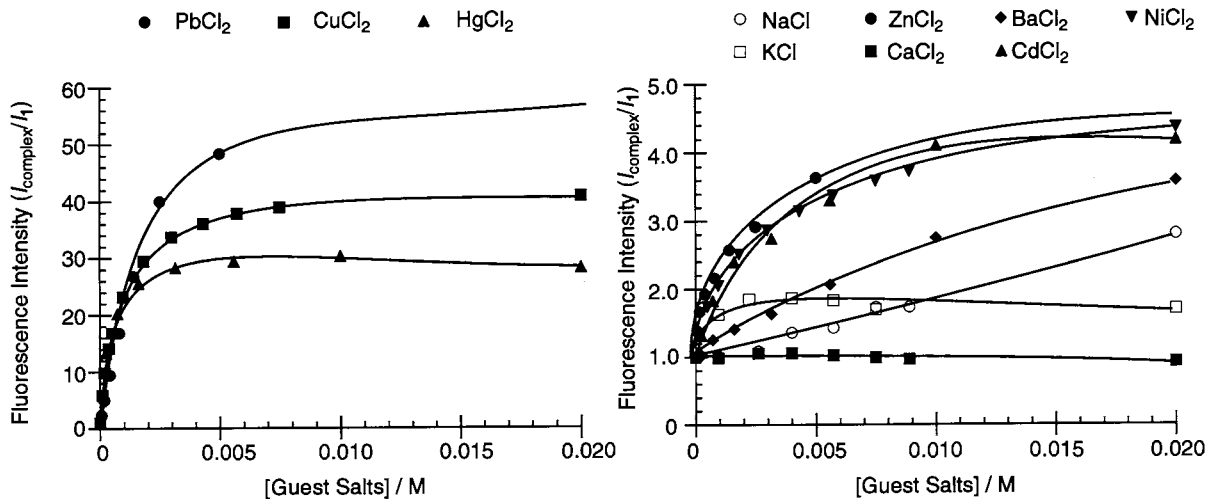


Fig. 4. Dependence of fluorescence intensities of **1** ( $4.00 \times 10^{-6}$  M) at 429 nm on the concentration of various metal salts in  $\text{H}_2\text{O}-\text{CH}_3\text{OH}$  (1:1, v/v), as excited at 378 nm.

the emission intensity increases with an increase in the metal salt concentration. The intensity ratio ( $I_{\text{complex}}/I_1$ ) was different among bound metal ions and decreased in the following order:  $\text{Pb}^{2+}$  (48, with 0.005 M  $\text{Pb}^{2+}$ ) >  $\text{Cu}^{2+}$  (41) >  $\text{Hg}^{2+}$  (30) >  $\text{Ni}^{2+}$  (4.4) >  $\text{Cd}^{2+}$  (4.2) >  $\text{Zn}^{2+}$  (3.63, with 0.005 M  $\text{Zn}^{2+}$ ) >  $\text{Ba}^{2+}$  (3.59) >  $\text{Na}^+$  (2.8) >  $\text{K}^+$  (1.9) >  $\text{Ca}^{2+}$  (0.9).

Instead of emission quantum yield, a measure of the guest cation-induced fluorescence recovery would express as a emission intensity ratio ( $I_{\text{complex}}/I_{\text{standard substance}}$ ) of guest cation complexes for the corresponding standard substance (9,10-DMA). The guest cation-induced fluorescence recovery ( $I_{1-\text{guest cation complexes}}/I_{9,10\text{-DMA}}$ ) of **1** were 0.03 for  $\text{Na}^+$ , 0.02 for  $\text{K}^+$ , 0.01 for  $\text{Ca}^{2+}$ , 0.04 for  $\text{Ba}^{2+}$ , 0.49 for  $\text{Pb}^{2+}$ , 0.04 for  $\text{Ni}^{2+}$ , 0.42 for  $\text{Cu}^{2+}$ , 0.04 for  $\text{Zn}^{2+}$ , 0.04 for  $\text{Cd}^{2+}$  and 0.31 for  $\text{Hg}^{2+}$ . The fluorescence intensity of **1**- $\text{PbCl}_2$  and **1**- $\text{CuCl}_2$  complexes were approximately one-half that of 9,10-DMA. This means that **1** has a high fluorescence switch-on ability as PET fluoroionophore.

Metal-ion concentration dependence of the emission intensity (Fig. 4) allowed us to determine the association constants ( $K$ ,  $\text{M}^{-1}$ ) by the non-linear curve-fitting method [12,15]. The sensor (**1**) showed the following cation selectivity:  $\text{Na}^+$

( $<1$ ) <  $\text{Ba}^{2+}$  ( $47 \pm 4$ ) <  $\text{Cd}^{2+}$  ( $167 \pm 34$ ) <  $\text{Ni}^{2+}$  ( $290 \pm 10$ ) <  $\text{Zn}^{2+}$  ( $523 \pm 90$ ) <  $\text{Pb}^{2+}$  ( $543 \pm 79$ ) <  $\text{Cu}^{2+}$  ( $1430 \pm 50$ ) <  $\text{Hg}^{2+}$  ( $2680 \pm 80$ ). In spite of the small association constant for **1** in  $\text{H}_2\text{O}-\text{CH}_3\text{OH}$  (1:1, v/v), the emission intensity of this host was greatly enhanced in the presence of  $\text{Pb}^{2+}$ ,  $\text{Cu}^{2+}$ , and  $\text{Hg}^{2+}$ , establishing that **1** has a high fluorescence switch-on ability for complexation within wide concentration range.

In conclusion, the PET fluoroionophore (**1**) could be utilized as a fluorescent sensing ionophore for  $\text{Pb}^{2+}$ ,  $\text{Cu}^{2+}$ , and  $\text{Hg}^{2+}$ .

## References

- [1] J.-M. Lehn (Ed.), *Supramolecular Chemistry*, VCH, Weinheim, 1995.
- [2] H.G. Löhr, F. Vögtle, *Acc. Chem. Res.* 18 (1985) 65.
- [3] L. Fabrizzi, A. Poggi, *Chem. Soc. Rev.* 95 (1995) 197.
- [4] A.W. Czarnik, *Acc. Chem. Res.* 27 (1994) 302.
- [5] A.P. de Silva, S.A. de Silva, *J. Chem. Soc. Chem. Commun.* 23 (1986) 1709.
- [6] A.B. Richard, E. Calle, A.P. de Silva, S.A. de Silva, H.Q.N. Gunaratne, J.L. Habib-Jiwan, S.L.A. Peiris, R.A.D.D. Rupasinghe, T.K.S.D. Samarasinghe, *J. Chem. Soc. Perkin Trans. 2* (9) (1992) 1559.
- [7] A.P. de Silva, H.Q.N. Gunaratne, T. Gunnlaugsson, C.P. McCoy, R.S. Maxwell, J.T. Rademacher, T.E. Rice, *Pure Appl. Chem.* 48 (1996) 1443.

- [8] A.P. de Silva, H.Q.N. Gunaratne, T. Gunnlaugsson, A.J.M. Huxley, C.P. McCoy, J.T. Rademacher, T.E. Rice, *Chem. Rev.* 97 (1997) 1515.
- [9] K. Kubo, R. Ishige, N. Kato, E. Yamamoto, T. Sakurai, *Heterocycles* 45 (1997) 2365.
- [10] K. Kubo, N. Kato, T. Sakurai, *Bull. Chem. Soc. Jpn.* 70 (1997) 3041.
- [11] K. Kubo, R. Ishige, T. Sakurai, *Heterocycles* 48 (1998) 347.
- [12] K. Kubo, R. Ishige, J. Kubo, T. Sakurai, *Talanta* 48 (1999) 181.
- [13] K. Kubo, R. Ishige, T. Sakurai, *Talanta* 49 (1999) 339.
- [14] K.D. Petrov, L.M. Runova, *Zh. Org. Khim.* 4 (1968) 1234.
- [15] K.A. Connors (Ed.), *Binding Constants*, Wiley, New York, 1987.
- [16] H. Leonhardt, A. Weller, *Ber. Bunsen-Ges. Phys. Chem.* 67 (1963) 791.
- [17] R.S. Davidson, K.R. Trethewey, *J. Chem. Soc. Chem. Commun.* 20 (1976) 827.
- [18] R. Foster (Ed.), *Photophysical Aspects of Exciplexes Molecular Association*, Academic Press, London, 1979.
- [19] K. Kubo, T. Sakurai, *Heterocycles* (submitted).
- [20] G.G. Giulbault (Ed.), *Practical Fluorescence: Theory, Methods, Techniques*, Marcel Dekker, New York, 1973.

# Synergistic extraction of rare earths with bis(2,4,4-trimethylpentyl) dithiophosphinic acid and trialkyl phosphine oxide

M.L.P. Reddy <sup>a,\*</sup>, J.R. Bosco Bharathi <sup>b</sup>, Smitha Peter <sup>a</sup>, T.R. Ramamohan <sup>a</sup>

<sup>a</sup> Regional Research Laboratory (CSIR), Trivandrum 695 019, India

<sup>b</sup> Department of Chemistry, The American College, Madurai 625 002, India

Received 17 November 1998; received in revised form 10 March 1999; accepted 18 March 1999

## Abstract

Synergistic extraction of trivalent rare earths from nitrate solutions using mixtures of bis(2,4,4-trimethylpentyl)dithiophosphinic acid (Cyanex 301 = HX) and trialkyl phosphine oxide (Cyanex 923 = TRPO) in xylene has been investigated. The results demonstrate that these trivalent metal ions are extracted into xylene as  $MX_3 \cdot 3HX$  with Cyanex 301 alone. In the presence of Cyanex 923, La(III) and Nd(III) are found to be extracted as  $MX_2 \cdot NO_3 \cdot TRPO$ . On the other hand, Eu(III), Y(III) and heavier rare earths are found to be extracted as  $MX_3 \cdot HX \cdot 2TRPO$ . The addition of a trialkylphosphine oxide to the metal extraction system not only enhances the extraction efficiency of these metal ions but also improves the selectivities significantly, especially between yttrium and heavier lanthanides. The separation factors between these metal ions were calculated and compared with that of commercially important extraction systems like di-2-ethylhexyl phosphoric acid. © 1999 Elsevier Science B.V. All rights reserved.

**Keywords:** Synergistic extraction; Rare earths; Cyanex 301; Cyanex 923; Separation factors

## 1. Introduction

With increasing demand for rare earth elements and their compounds individually and collectively, the separation and purification of these elements has gained considerable importance in recent years. Various kinds of acidic organophosphorus extractants such as di-2-ethylhexyl phosphoric acid (DEHPA), 2-ethylhexyl phosphoric acid mono-2-ethylhexyl ester (EHEHPA) and

bis(2,4,4-trimethylpentyl) phosphinic acid (Cyanex 272) have been widely used in the Rare Earth Industry for the separation and purification of these metal ions [1,2]. However, even with the above extractants, a large number of separation steps are necessary to obtain highly purified rare earth elements. Thus, there is a growing interest in the development of new extraction systems for the separation of rare earths as a group or from one another.

Synergistic extraction systems have been applied to rare earths, numerous times, with a large increase in the extraction efficiency being ob-

\* Corresponding author. Fax: +91-471-91712/490186.

E-mail address: reddy@csrrlrd.ren.nic.in (M.L.P. Reddy)

served [3,4]. Moreover, a few synergistic systems have also shown improved separation among trivalent rare earths [5,6]. Recently, from our laboratory we have reported enhanced extraction and separation for trivalent lanthanides and yttrium using mixtures of bis(2,4,4-trimethylpentyl) phosphinic acid and trialkyl phosphine oxide [7]. The separation factors observed between yttrium and heavier lanthanides ( $\text{Lu/Y} = 37$ ;  $\text{Tm/Y} = 9$ ;  $\text{Ho/Y} = 1.6$ ) were found to be significantly higher than the separation factors reported with DEHPA, which is a commonly used extractant in rare earth separations. This prompted us to investigate new synergistic extraction systems involving Cyanex 923 as a synergist in the extraction of rare earths using bis(2,4,4-trimethylpentyl)dithiophosphinic acid in xylene as an extractant, with a view to elucidate the nature of the complexes extracted into the organic phase and also to investigate the selectivity among these trivalent metal ions.

## 2. Experimental

### 2.1. Reagents

Bis(2,4,4-trimethylpentyl)dithiophosphinic acid (Cyanex 301) and Cyanex 923 (a mixture of four trialkylphosphine oxides), supplied by Cytec Canada Inc., were used as such without further purification. Their composition and properties have been described elsewhere [8,9]. Xylene of analytical reagent quality obtained from Fischer, India, was used as a diluent in the present work.

Stock solutions of rare earths were prepared from their oxides (Rare Earth Products, Chesire, UK, 99.99%) by dissolving in concentrated hydrochloric acid and diluting to 100 cm<sup>3</sup> with distilled water. These solutions were then standardised by titration with a standard solution of EDTA at pH 5.0 using an acetate buffer with xylenol orange as the indicator. Initial metal ion concentration was maintained at  $1 \times 10^{-4}$  mol dm<sup>-3</sup> for all the studies. All extraction experiments were performed at constant ionic strength (1 mol dm<sup>-3</sup>).

Arsenazo 1 (Fluke, Switzerland) solution was prepared by dissolving 25 mg of this reagent in

250 cm<sup>3</sup> of distilled water. Ammonium acetate buffer (pH 7.5) was prepared by dissolving 19.25 g in 250 cm<sup>3</sup> of distilled water and adjusting the pH with HCl/NaOH. All the other chemicals used were of analytical grade.

### 2.2. Apparatus

A Hitachi 220 double beam microprocessor based spectrophotometer was used for measuring absorbances. An ECIL, India digital pH meter was used for pH value measurements. All the computer programs were written in FORTRAN 77 and executed on a Pentium PC.

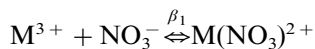
### 2.3. Solvent extraction procedure

Distribution ratios were determined by shaking equal volumes of aqueous and organic phases for 60 min in a glass stoppered vial with the help of a mechanical shaker at  $303 \pm 1$  K. Preliminary experiments showed that the extraction equilibrium was attained within 10 min. After allowing the phases to settle, 5 cm<sup>3</sup> aliquots of aqueous phase were pipetted in to a 25 cm<sup>3</sup> beaker and 1 cm<sup>3</sup> of ammonium acetate buffer and 5 cm<sup>3</sup> of Arsenazo I solution were added. After adjusting the pH to 7.5, the solution was transferred into a 25 cm<sup>3</sup> volumetric flask and made up to the mark. The absorbances of the solutions were measured at 575 nm and the metal ion concentrations were computed from the respective calibration graphs. The concentration of the metal ion in the organic phase was obtained by material balance. These concentrations were used to obtain the distribution ratio,  $D$ .

## 3. Results and discussion

### 3.1. Extraction of rare earths with Cyanex 301

The trivalent rare earth ion in the aqueous phase forms a variety of complexes in the presence of nitrate ions. However, under the experimental conditions, it is sufficient to consider only the first complex as defined by



Then the total metal in the aqueous phase ( $M_t$ ) is given by

$$M_t = M^{3+} + M(NO_3)^{2+} = M^{3+} \{1 + \beta_1 [NO_3^-]\} \quad (1)$$

The values of the stability constant ( $\beta_1$ ) for different rare earths were taken from the literature [10].

The extraction equilibria of trivalent rare earths from nitrate solutions with an acidic organophosphorus extractant, Cyanex 301 (HX) may be expressed as,



where  $K_{ex}$  is the equilibrium constant. It is assumed that the extractant exists predominantly as dimeric species,  $(HX)_2$  in the range of concentrations used [8,11].

$$K_{ex} = \frac{[MX_3 \cdot 3HX]_{org} [H^+]_{aq}^3}{[M^{3+}]_{aq} [(HX)_2]_{org}^3} \quad (2)$$

Then the distribution ratio,  $D$ , of the metal can be written from Eq. (1) and Eq. (2) as

$$D = \frac{[MX_3 \cdot 3HX]_{org}}{[M^{3+}]_t} = \frac{K_{ex} [(HX)_2]_{org}^3}{[H^+]^3 (1 + \beta_1 [NO_3^-])}$$

For confirming the above mechanism, the extraction of trivalent La, Nd, Eu, Tb, Ho, Tm, Lu and Y from 1.0 mol dm<sup>-3</sup> sodium nitrate solutions with Cyanex 301 alone in xylene as a function of extractant concentration (0.008–0.6 mol dm<sup>-3</sup>) and pH (at constant Cyanex 301 = 0.03 mol dm<sup>-3</sup> for Y and heavier rare earths; 0.5 mol dm<sup>-3</sup> for La(III), Nd(III) and Eu(III) respectively has been studied. The relevant log–log plots (Figs. 1 and 2) were linear with a slope of 3.0, indicating the extraction of complexes,  $MX_3 \cdot 3HX$ .

The equilibrium constants ( $K_{ex}$ ) for the above species were determined by non-linear regression analysis as described in our earlier publications [6,12] and the values are shown in Table 1. It is clear from Table 1 that the equilibrium constant values of these trivalent lanthanides increase with atomic number, presumably as a result of the increase in strength of the electrostatic inter-

action between the extractant anion and the lanthanide cation as the size of the latter decreases. The extraction of yttrium lies between that of Ho and Tm, as would be expected on the basis of its cationic radii. A similar trend has been observed by Reddy et al. [7] in the equilibrium constants of rare earths from nitrate media with bis(2,4,4-trimethylpentyl)phosphinic acid in xylene as an extractant. Further, the equilibrium constants of Cyanex 301 ( $K_{ex}$  of Ho =  $2.97 \times 10^{-3}$ ; Y =  $5.43 \times 10^{-3}$ ) are found to be much smaller than that of the DEHPA [13] ( $K_{ex}$  of Y = 35;  $K_{ex}$  of Ho = 24) system. The present results clearly suggest that the lower the  $pK_a$  of the extractant, the higher its extractability ( $pK_a$  of DEHPA = 0.98; Cyanex 301 = 2.61).

### 3.2. Extraction of trivalent rare earths with Cyanex 301 in the presence of Cyanex 923

The extraction of rare earths from 1.0 mol dm<sup>-3</sup> sodium nitrate solution of pH = 3.0 with mixtures of Cyanex 301 (0.005–0.5 mol dm<sup>-3</sup>) and Cyanex 923 (0.006–0.04 mol m<sup>-3</sup>) in xylene has been studied. About a twofold synergistic enhancement in the extraction of heavier rare earths (synergistic enhancement factor =  $D_{Mixture} / (D_{cyanax\ 301} + D_{cyanax\ 923})$  for Lu = 2; Tm = 2; Ho = 1; Y = 2; has been observed with mixtures of 0.01 mol dm<sup>-3</sup> Cyanex 301 and

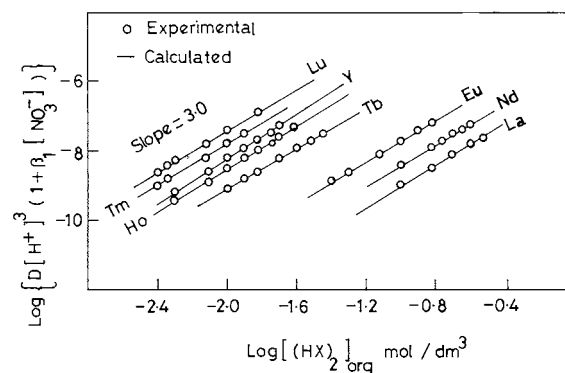


Fig. 1. Effect of Cyanex 301 concentration on the extraction of rare earths. Aqueous phase, 1.0 mol dm<sup>-3</sup> sodium nitrate at pH 3.0 + M(III) =  $1 \times 10^{-4}$  mol dm<sup>-3</sup>.

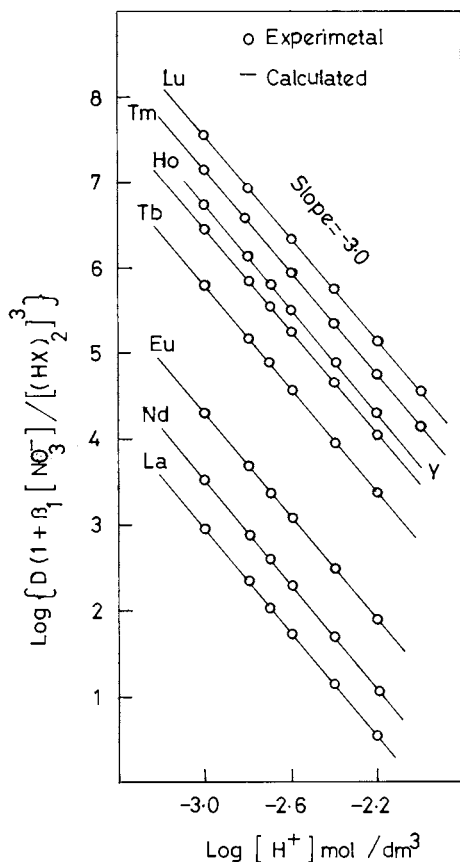


Fig. 2. Effect of pH on the extraction of rare earths. Aqueous phase,  $1.0 \text{ mol dm}^{-3}$  sodium nitrate +  $M(\text{III}) = 1 \times 10^{-4} \text{ mol dm}^{-3}$ .

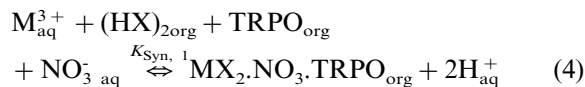
$0.01 \text{ mol dm}^{-3}$  Cyanex 923. In the case of Eu(III) about threefold enhancement and one to twofold enhancement in the extraction of lighter lanthanides has been observed with mixtures of  $0.2 \text{ mol dm}^{-3}$  Cyanex 301 and  $0.01 \text{ mol dm}^{-3}$  Cyanex 923. Further, the results clearly demonstrate that at constant concentration of Cyanex 923, the synergistic enhancement factor for these metal ions marginally increases with the increase of Cyanex 301 concentration. On the other hand, at a given concentration of Cyanex 301, the synergistic enhancement factor decreases with the increase of Cyanex 923 concentration.

It is clear from the plots (Fig. 3) of  $\log \{D[\text{H}^+]^3\{1 + \beta_1[\text{NO}_3^-]\}\}$  versus  $\log [(\text{HX})_2]_{\text{org}}$

$\text{mol dm}^{-3}$  that at constant Cyanex 923 concentration ( $0.01 \text{ mol dm}^{-3}$  for Lu, Tm, Ho and Y;  $0.02 \text{ mol dm}^{-3}$  for Eu) two molecules of the cyanex 301 are involved in the extracted complexes of Eu(III), Ho(III) Tm(III), Lu(III) and Y(III). On the other hand, in the case of La(III) and Nd(III), it is clear from the plot ( $\log \{D[\text{H}^+]^2(1 + 0\beta_1[\text{NO}_3^-])\}$  versus  $\log [(\text{HX})_2]_{\text{org}} \text{ mol dm}^{-3}$ ) that only one molecule of Cyanex 301 is involved in the extractable complexes.

The plots (Fig. 4) of  $\log \{D[\text{H}^+]^3(1 + \beta_1[\text{NO}_3^-])\}$  versus  $\log [\text{TRPO}]_{\text{org}} \text{ mol dm}^{-3}$  at constant Cyanex 301 concentration ( $0.01 \text{ mol dm}^{-3}$  for Ho, Tm, Lu and Y;  $0.02 \text{ mol dm}^{-3}$  for Eu), give slopes of 2 for Eu(III), Ho(III), Tm(III), Lu(III) and Y(III), indicating the participation of two TRPO molecules in these synergistic extraction systems.

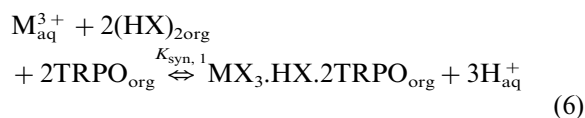
On the other hand, in the case of La(III) and Nd(III), it is clear from the plot ( $\log \{D[\text{H}^+]^2(1 + \beta_1[\text{NO}_3^-])\}$  versus  $\log [\text{TRPO}]_{\text{org}} \text{ mol dm}^{-3}$ ) that only one molecule of TRPO is involved in the extracted complexes. These in conjunction with the slope value of 2 and 3 observed in the extraction of lighter and heavier rare earths, respectively, with the pH variation experiments (pH 2.0–3.0) at constant Cyanex 301 + Cyanex 923 (for the sake of conciseness, the data not included) indicates the synergistic extraction equilibria as follows:



where  $M^{3+} = \text{La(III)}$  and  $\text{Nd(III)}$ .

Then from Eq. (1) and Eq. (4), the distribution ratio,  $D$ , can be written as

$$D = \frac{K_{\text{syn}, 1} [(\text{HX})_2] [\text{NO}_3^-] [\text{TRPO}]}{[\text{H}^+]^2 (1 + \beta_1 [\text{NO}_3^-])} \quad (5)$$



where  $M^{3+} = \text{Eu(III)}, \text{Ho(III)}, \text{Tm(III)}, \text{Lu(III)}$  and  $\text{Y(III)}$ .

$$D = \frac{K_{\text{syn. 1}}[(\text{HX})_2]^2[\text{TRPO}]^2}{[\text{H}^+]^3(1 + \beta_1[\text{NO}_3^-])} \quad (7)$$

The above synergistic extraction mechanisms were further confirmed by analysing the equilibrium data using Eq. (5) for  $\text{La(III)}$  and  $\text{Nd(III)}$ , and Eq. (7) for  $\text{Eu(III)}, \text{Ho(III)}, \text{Tm(III)}, \text{Lu(III)}$  and  $\text{Y(III)}$ , as described in our earlier publications [6,12]. The equilibrium constants of the extracted complexes for these trivalent rare earths were determined by non-linear regression analysis and the values are given in Table 1.

The present study clearly shows that the complex  $\text{MX}_2\cdot\text{NO}_3\cdot\text{TRPO}$  seems to be involved in the extraction of  $\text{La(III)}$  and  $\text{Nd(III)}$  from nitrate solutions with Cyanex 301 in the presence of Cyanex 923 as a synergist. On the other hand,  $\text{Eu(III)}$ , and heavier rare earths are extracted as  $\text{MX}_3\cdot\text{HX}\cdot 2\text{TRPO}$ . This difference possibly arises due to the presence of nitrate ions in the aqueous phase which compete with Cyanex 301 during the metal chelate formation in the case of lighter rare earths. This competition may be less pronounced in the extraction of heavier rare earths and yttrium, resulting in the extraction of the above complexes. The authors have also observed the formation of mixed-ligand complexes  $\text{M}(\text{NO}_3)_3(\text{BTMPP})_2(\text{TRPO})_2$  in the extraction of lighter lanthanides with mixtures of Cyanex 272 (HBTMPP) and Cyanex 923 from nitrate solutions [7]. The ability of a neu-

tral donor, TBP to replace a chelated molecule of thenoyltrifluoroacetone (HTTA) has been reported by Davies et al. [14,15] in the extraction of rare earths from nitrate solutions. The above authors have postulated that this replacement was due to steric factors.

Table 2 gives the separation factors (SF) between these trivalent rare earths defined as the ratio of the respective equilibrium constants with Cyanex 301 and Cyanex 301 + Cyanex 923 systems. It is interesting to note that the selectivities observed between yttrium and heavier lanthanides with mixtures of Cyanex 301 and Cyanex 923 are higher than that of the Cyanex 301 system alone. Further, the SF values between  $\text{Tm/Y}$  are found to be much higher than that of the DEHPA system, which is widely used in the Rare Earth Industry. The SF values of the  $\text{Lu/Y}$  and  $\text{Ho/Y}$  pairs are also found to be comparable with that of the DEHPA system. On the other hand, the addition of trialkylphosphine oxide to the Cyanex 301 system, decreases the SF values between lighter rare earths. The improvement in separation factors observed in this study clearly indicates that yttrium can be separated from heavier lanthanides in a fewer number of stages as compared to Cyanex 301 and DEHPA alone.

#### 4. Conclusion

The extraction equilibria of trivalent rare earths with Cyanex 301 and also with mixtures

Table 1

Two phase equilibrium constants of trivalent rare earths with Cyanex 301 and Cyanex 301 + Cyanex 923 systems

Extractant	Log equilibrium constant							
	La(III)	Nd(III)	Eu(III)	Tb(III)	Ho(III)	Tm (III)	Lu(III)	Y(III)
Cyanex 301	$-6.05 \pm 0.04$	$-5.46 \pm 0.02$	$-4.70 \pm 0.02$	$-3.17 \pm 0.04$	$-2.53 \pm 0.03$	$-1.84 \pm 0.04$	$-1.44 \pm 0.02$	$-2.27 \pm 0.04$
Cyanex 301 + Cyanex 923	$-2.57 \pm 0.03$	$-2.16 \pm 0.02$	$-1.75 \pm 0.03$	–	$-0.38 \pm 0.02$	$0.58 \pm 0.02$	$0.87 \pm 0.02$	$-0.28 \pm 0.02$

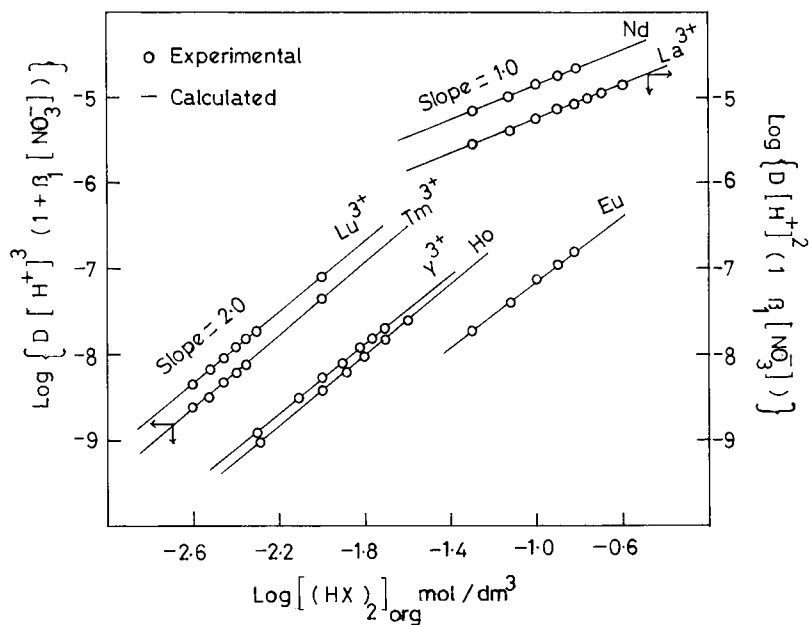


Fig. 3. Effect of Cyanex 301 concentration on the extraction of rare earths at constant Cyanex 923 concentration. Aqueous phase,  $1.0 \text{ mol dm}^{-3}$  sodium nitrate at pH, 3.0 +  $M(\text{III}) = 1 \times 10^{-4} \text{ mol dm}^{-3}$ .

of Cyanex 301 and Cyanex 923 have been investigated. It was found that La(III) and Nd(III) are extracted into xylene as  $\text{MX}_2 \cdot \text{NO}_3 \cdot \text{TRPO}$ . On the other hand, Eu(III), Y(III) and heavier rare earths are found to be extracted as  $\text{MX}_3 \cdot \text{HX} \cdot 2\text{TRPO}$ . The addition of a tri-alkylphosphine oxide to the metal-Cyanex 301 system not only improves the extraction efficiency of these metal ions but also improves the selectivities significantly among yttrium and heavier lanthanides, as compared to the Cyanex 301 system alone. Hence such a mixed-ligand system would be of practical value in the extraction and separation of these trivalent lanthanides and yttrium.

### Acknowledgements

The authors wish to thank Dr W.A. Rickelton, Research Manager of Cytec, Canada for providing Cyanex reagents and Dr G. Vijay Nair, Director, Regional Research Laboratory (CSIR), Trivandrum for giving permission to

publish this work. Financial support for JRBB from the Tamil Nadu State Council for Science and Technology is also acknowledged.

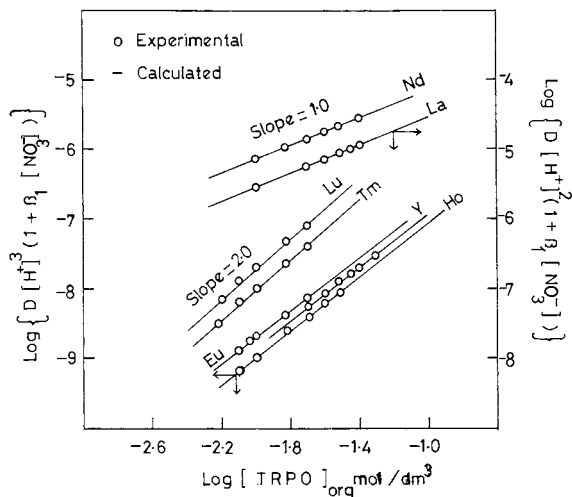


Fig. 4. Effect of Cyanex 923 concentration on the extraction of rare earths at constant Cyanex 301 concentration. Aqueous phase,  $1.0 \text{ mol dm}^{-3}$  sodium nitrate at pH, 3.0 +  $M(\text{III}) = 1 \times 10^{-4} \text{ mol dm}^{-3}$ .



Table 2

Separation factors for trivalent rare earths with Cyanex 301 and Cyanex 301 + Cyanex 923 systems

Extraction system	Separation factors				
	Nd/La	Eu/Nd	Ho/Y	Tm/Y	Lu/Y
Cyanex 301	3.87	5.86	0.55	2.68	6.68
Cyanex301 +Cyanex 923	2.60	2.56	0.79	7.16	14.06
DEHPA [16]	8.40	12.50	0.60	3.40	19.60

## References

- [1] M.L.P. Reddy, T. Prasada Rao, A.D. Damodaran, *Miner. Process. Extr. Metall. Rev.* 12 (1995) 91.
- [2] J.S. Preston, A.C. duPreez, *Process Metall.* 7 (1992) 883.
- [3] J.N. Mathur, *Solvent Extr. Ion Exch.* 1 (1983) 349.
- [4] G. Duyckaerts, J.F. Desreux, *Int. Solvent Extr. Conf.*, Toronto, Canada, 1977, pp.73.
- [5] Y. Kitatuji, Y. Meguro, Z. Yoshida, T. Yamamoto, K. Nishizawa, *Solvent Extr. Ion Exch.* 13 (1995) 289.
- [6] M.L.P. Reddy, S. Sujatha, R. Luxmi Varma, et al., *Talanta* 44 (1997) 97.
- [7] M.L.P. Reddy, T.R. Ramamohan, C.S.P. Iyer, *Solvent Extr. Research and Dev. (Japan)* 5 (1998) 1.
- [8] Y. Zhu, J. Chen, R. Jiao, *Solvent Extr. Ion Exch.* 14 (1996) 61.
- [9] F.J. Alguacil, C. Carvaca, S. Martirez, A. Cobo, *Hydrometallurgy* 30 (1992) 345.
- [10] R.M. Smith, A.E. Martell, *Critical Stability Constants*, vol. 4, Plenum Press, New York, 1976.
- [11] G.M. Ritcey, A.W. Ashbrook, *Solvent Extraction principles and Applications to Process Metallurgy*, Part 1, Elsevier, Amsterdam, 1984, p. 98.
- [12] P.B. Santhi, M.L.P. Reddy, T.R. Ramamohan, et al., *Solvent Extr. Ion Exch.* 12 (1994) 633.
- [13] K. Ohto, K. Inoue, M. Goto, et al., *Bull. Chem. Soc. (Japan)* 66 (1993) 2528.
- [14] R.A. Tournier, M.W. Davis, *Sep.Sci.* 7 (1972) 159.
- [15] E.C. Cox, M.W. Davis, *Sep.Sci.* 8 (1973) 205.
- [16] T.B. Pierce, P.F. Peck, *Analyst* 88 (1963) 217.

# A new enzyme electrode based on ascorbate oxidase immobilized in gelatin for specific determination of L-ascorbic acid

Erol Akyilmaz \*, Erhan Dinçkaya

*Department of Biochemistry, Faculty of Science, Ege University, 35100 Bornova-Izmir, Turkey*

Received 16 December 1998; received in revised form 15 March 1999; accepted 18 March 1999

## Abstract

A biosensor for the specific determination of L-ascorbic acid in fruit juices and vitamin C tablets was developed using ascorbate oxidase (EC 1.10.3.3) from cucumber (*Cucumis sativus* L.) in combination with a dissolved oxygen probe. Ascorbate oxidase immobilized with gelatin using glutaraldehyde and fixed on pretreated teflon membrane served as an enzyme electrode. The phosphate buffer (50 mM, pH 7.5) and 35°C were established as providing the optimum conditions. The biosensor response depends linearly on L-ascorbic acid concentration between  $5.0 \times 10^{-5}$  and  $1.2 \times 10^{-3}$  M with a response time 45 s. The biosensor is stable for more than 2 months, while more than 200 assays were performed. The results obtained for fruit juices and tablets were compared with DCIP (2,6 dichlorophenolindophenol) method. © 1999 Elsevier Science B.V. All rights reserved.

*Keywords:* Ascorbic acid; Ascorbate oxidase; Biosensor; Enzyme immobilization; Enzyme electrode; Fruit juices; Vitamin C tablets

## 1. Introduction

The importance of vitamin C arises from its being essential for humans. Beyond its function in collagen formation, ascorbic acid is known to increase absorption of inorganic iron, to have essential roles in the metabolism of folic acid, some amino acid and hormones, and to act as an antioxidant [1,2]. Consequently, the determination of L-ascorbic acid in various natural and prepared foods, drugs and physiological fluids is very im-

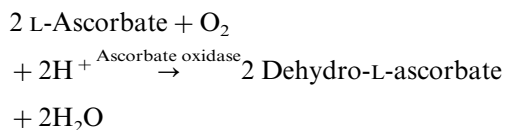
portant [3–5]. Many methods have been developed for the determination of L-ascorbic acid, however, most of them have been based on its reducing properties. These methods lack specificity and are prone to interferences by other reducing agents in the sample [6,7]. The alternative method for measurement in complex materials such as physiological fluids or foodstuffs is to use high-performance liquid chromatography; however, this is a time-consuming technique [8–10]. Recently, enzymatic methods that are more practical, accurate and faster than chemical methods have been developed. Since soluble enzymes are uneconomically for routine measurements, some

\* Corresponding author. Fax: +90-232-3888264.

E-mail address: akyilmaz@fenfak.ege.edu.tr (E. Akyilmaz)

immobilization methods have also been developed [11–13]. For the preparation of ascorbate oxidase electrodes, the enzyme has been combined with an appropriate sensor [14–16]. The aim of the present study is to develop a inexpensive, specific and simple procedure for L-ascorbic acid determination with ascorbate oxidase enzyme electrode.

Ascorbate oxidase catalyzes the oxidation of L-ascorbic acid as follows:



In this study, the consumption of O<sub>2</sub> was detected by YSI 5739 model dissolved oxygen probe. The enzyme was immobilized directly on probe by copolymerization with gelatin, using the bifunctional agent glutaraldehyde.

## 2. Experimental

### 2.1. Chemicals

Ascorbate oxidase (EC 1.10.3.3) was isolated from cucumber (*Cucumis sativus* L.) and partially purified [17]. The enzyme activity was measured according to modified DCIP (2,6 dichlorophenolindophenol) method [17]. The 225 bloom calf skin gelatin and glutaraldehyde were obtained from Sigma (St. Louis, USA). All other chemicals were purchased from Merck (Darmstadt, Germany).

### 2.2. Apparatus

YSI 5739 model dissolved oxygen (DO) probes based on amperometric mode consists of Au (cathode), Ag–AgCl (anode), half-saturated KCl (electrolyte) and a teflon membrane (0.0005" thick FEP teflon membrane) which is selective for oxygen. DO probes were connected to a YSI 54A model oxygenmeter (YSI, Yellow Springs, OH, USA). For this system, polarizing voltage is 0.8 V. Ultra-thermostat (Colora, Germany) were also used.

### 2.3. Preparation of bioactive layer

In this study, the teflon membrane of dissolved oxygen probe was pretreated with a 0.5% sodium dodesylsulphate (SDS) solution in 50 mM phosphate buffer (pH 7.5). Ascorbate oxidase (140 IU ml<sup>-1</sup>) and 225 bloom gelatin (33.5 mg ml<sup>-1</sup>) were mixed at 38°C in phosphate buffer (pH 7.5, 50 mM). The mixed solution (200 µl) was spread over the DO probe membrane and allowed to dry at 4°C overnight. Finally, it was immersed in 2.5% glutaraldehyde in 50 mM phosphate buffer (pH 7.5) for 3 min. The enzyme electrode contained 24.8 IU cm<sup>-2</sup> enzymatic activity.

### 2.4. Measurements of the oxygen consumption by the enzyme electrode

The concentrations of L-ascorbic acid were obtained by measuring the reduction current of oxygen. The steady-state current depends on the amount of oxygen that is consumed by the enzymatic reaction at the immobilized enzyme membrane which is placed on top of the dissolved oxygen probe. Measurements were carried out by standard curves which were obtained by the determination of consumed oxygen level, related to L-ascorbic acid concentration in the enzymatic reaction. In the steady-state method, addition of L-ascorbic acid caused a rapid current decrease, due to oxygen consumption in the enzyme layer, which reached a steady-state within 45 s and dissolved oxygen concentrations were recorded using an oxygenmeter. All measurements were carried out using a specifically developed thermostatic cell at 35°C. An oxygen-saturated working buffer (50 mM, phosphate buffer, pH 7.5) was also used.

### 2.5. Sample preparation

For the determination of L-ascorbic acid in vitamin C tablets Ca-Sandoz (1000 mg L-ascorbic acid/tablet) and Redoxan (500 mg L-ascorbic acid/tablet) tablets were used. The solution of each tablet was prepared in the phosphate buffer (pH 7.5, 50 mM) containing 0.6 mM L-ascorbic acid after they were powdered. The L-ascorbic

acid content of vitamin C tablet solution was determined both by using the ascorbate oxidase and modified DCIP methods.

For the determination of L-ascorbic acid in some fruit juices, oranges and lemons were used. After the fruits (100 g) were peeled, they were homogenized with Braun blender. The homogenate was filtered through cheese-cloth to remove the cellulose residue and then the filtrate was centrifuged at 10 000 rpm for 5 min at 4°C. The supernatant obtained was kept at 4°C in dark and measurements were carried out on the same day.

The amounts of L-ascorbic acid in each vitamin C tablet solution and fruit juices prepared were determined using the ascorbate oxidase and DCIP methods. The two methods were compared.

### 3. Results and discussion

#### 3.1. Enzyme electrode optimization

##### 3.1.1. Effect of pH

According to optimization of the biosensor the optimum pH was found to be 7.5. Fig. 1 shows the results obtained for the determination of the optimum pH value for the enzyme electrode.

##### 3.1.2. Effect of buffer concentration

Phosphate buffer at varying concentrations (25, 50 and 100 mM) was tested for maximum electrode response. When the buffer concentration was increased the electrode response was decreased. This can be explained in terms of the increasing effects of the ionic strength on enzymatic activity as negative. As the buffer capacity of the 50 mM buffer concentration was higher than the 25 mM one, it was preferred for the determination of L-ascorbic acid in natural samples. Moreover, it was observed that the increase in buffer concentration from 25 to 50 mM decreased the electrode response only by 5.0%, and this decrease was thought not to be important for getting sensitive results. Therefore, 50 mM phosphate buffer was used in all measurements throughout this work.

##### 3.1.3. Effect of temperature

The effect of assay temperature (15–45°C) was examined. The highest electrode response was observed at 35°C. Below and above 35°C, decrease in electrode response was recorded. Deviation from linearity at high concentrations occurred at temperatures such as 35 and 40°C. Since higher enzyme activity observed at these temperatures, the deviation from linearity was due to the insufficient amount of dissolved oxygen which was a co-substrate of the enzyme. On the other hand at lower temperatures, the standard curve at high concentration of L-ascorbic acid showed no deviation from linearity as the concentration of the dissolved oxygen was higher.

##### 3.1.4. Effect of the amount of the enzyme

The effect of enzyme amount on the electrode response is shown in Fig. 2. The enzymatic activity of the bioactive membrane layer depended upon the amount of enzyme. When the amount of the enzyme on the bioactive layer increased, by 2.95, 5.9 and 8.85 mg enzyme cm<sup>-2</sup> (12.4, 24.8 and 37.2 IU cm<sup>-2</sup>, respectively) an increase was

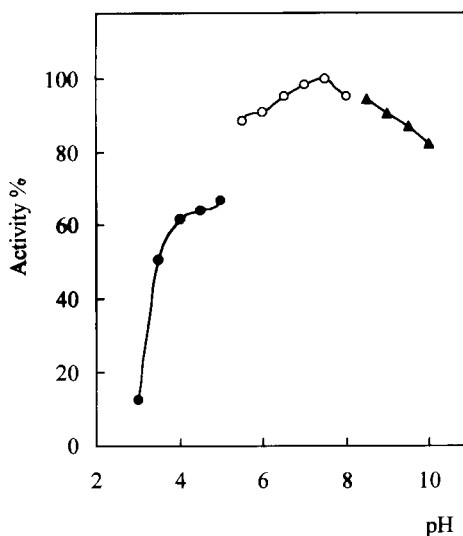


Fig. 1. Optimum pH for selected response. (●) Citrate buffer, 50 mM; (○) phosphate buffer, 50 mM; (▲) glycine buffer, 50 mM. The amount of ascorbate oxidase, gelatin and the percentage of glutaraldehyde were kept constant as 5.9 mg enzyme cm<sup>-2</sup> (24.8 IU cm<sup>-2</sup>), 5.9 mg gelatin cm<sup>-2</sup> and 2.5%, respectively.

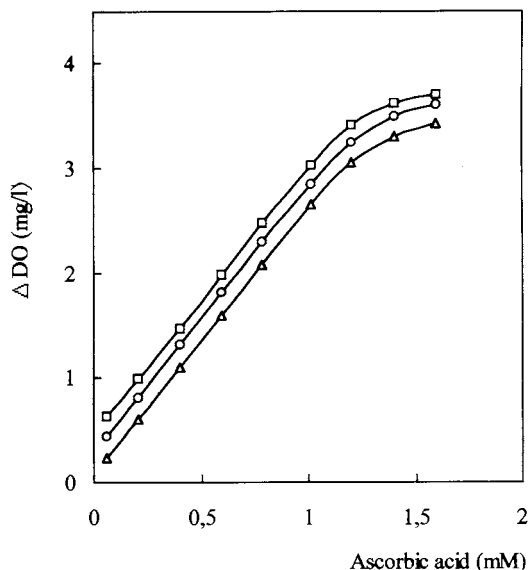


Fig. 2. Effect of enzyme amount on the electrode response. Bioactive membrane layers containing fixed concentration of gelatin ( $5.9 \text{ mg cm}^{-2}$ ) and varying levels of activity of ascorbate oxidase were assayed at  $35^\circ\text{C}$  in phosphate buffer. The amount of ascorbate oxidase; ( $\Delta$ )  $2.95 \text{ mg enzyme cm}^{-2}$  ( $12.4 \text{ IU cm}^{-2}$ ); ( $\circ$ )  $5.9 \text{ mg enzyme cm}^{-2}$  ( $24.8 \text{ IU cm}^{-2}$ ); ( $\square$ )  $8.85 \text{ mg enzyme cm}^{-2}$  ( $37.2 \text{ IU cm}^{-2}$ ).

observed for the electrode response. Although the best electrode response is obtained by  $8.85 \text{ mg enzyme cm}^{-2}$  ( $37.2 \text{ IU cm}^{-2}$ ), this amount causes some disadvantages in membrane preparation and membrane stability. Under these conditions, a homogeneous membrane could not be prepared due to its high viscosity, and it decomposed after ten measurements. As a result,  $5.9 \text{ mg enzyme cm}^{-2}$  ( $24.8 \text{ IU cm}^{-2}$ ) was found to be the most suitable amount of the enzyme. In this case, the bioactive layer could easily be formed and was stable.

### 3.2. Analytical characteristics

#### 3.2.1. Linear range

Ascorbate oxidase enzyme electrode response depends linearly on L-ascorbic acid concentration between  $5.0 \times 10^{-5}$  and  $1.2 \times 10^{-3} \text{ M}$  at a response time of 45 s. At higher concentrations than  $1.2 \times 10^{-3} \text{ M}$ , the standard curve showed a deviation from linearity. The deviation from linearity

was due to insufficient amounts of dissolved oxygen which is a co-substrate of the enzyme.

#### 3.2.2. Specificity

L-Ascorbic acid, oxalic acid, L-aspartic acid, L-glutamic acid, succinic acid, citric acid, glycolic acid, D(+)-glucose, D(-)-fructose, hydroquinone, 8-hydroxyquinoline and catechol were examined for the substrate specificity of the enzyme electrode. For the determination of substrate specificity of ascorbate oxidase enzyme electrode, 0.4 and 1.0 mM of standard of various compounds and L-ascorbic acid solutions were used. The electrode response obtained for L-ascorbic acid was accepted as 100% and compared with the electrode responses of other substances. The substrate specificity of the enzyme electrode is given in Table 1. Ascorbate oxidase oxidizes ascorbic acid by introducing two hydroxyl groups at the double bond. Hydroquinone (0.4 and 1.0 mM) and catechol (1.0 mM), which contain similar hydroxyl groups, were also oxidized by the ascorbate oxidase. However, electrode response

Table 1

The substrate specificity of ascorbate oxidase enzyme electrode<sup>a</sup>

Substrate	Relative activity (%)	
	Substrate concentrations (0.4 mM)	Substrate concentrations (1.0 mM)
L-Ascorbic acid	100.0	100.0
Oxalic acid	0.0	0.0
L-Aspartic acid	0.0	0.0
L-Glutamic acid	0.0	0.0
Succinic acid	0.0	0.0
Citric acid	0.0	0.0
Glycolic acid	0.0	0.0
Glucose	0.0	0.0
Fructose	0.0	0.0
Hydroquinone	2.2	7.5
8-Hydroxy-quinoline	0.0	0.0
Catechol	0.0	1.9

<sup>a</sup> Working conditions: phosphate buffer, pH 7.5, 50 mM,  $T = 35^\circ\text{C}$ . The amount of ascorbate oxidase, gelatine and the percentage of glutaraldehyde were kept constant as  $5.9 \text{ mg enzyme cm}^{-2}$  ( $24.8 \text{ IU cm}^{-2}$ ),  $5.9 \text{ mg gelatin cm}^{-2}$  and 2.5%, respectively.

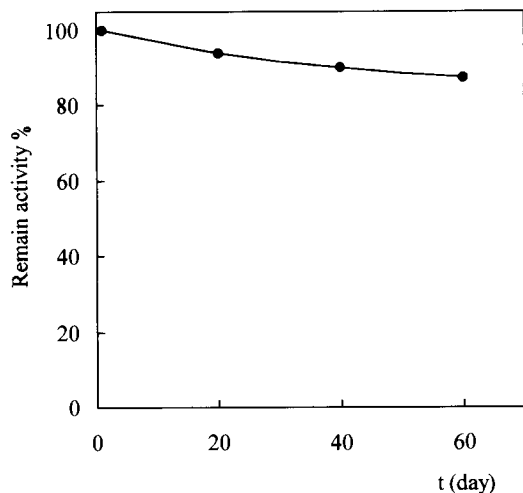


Fig. 3. Stability of ascorbate oxidase enzyme electrode. The amount of ascorbate oxidase, gelatin and the percentage of glutaraldehyde were kept constant as  $5.9 \text{ mg enzyme cm}^{-2}$  ( $24.8 \text{ IU cm}^{-2}$ ),  $5.9 \text{ mg gelatin cm}^{-2}$  and  $2.5\%$ , respectively.

levels for hydroquinone and catechol were not important for the substrate specificity of the enzyme electrode.

### 3.2.3. Reproducibility

The reproducibility of responses of the enzyme electrode was tested by 11 average standard solutions containing equal amounts of L-ascorbic acid ( $0.4 \text{ mM}$ ). The average value ( $\bar{x}$ ), standard deviation (SD) and variation coefficient (CV) were calculated as  $0.399 \text{ mM}$ ,  $\pm 0.001$ ,  $0.251\%$ , respectively. In this study a phosphate buffer ( $\text{pH } 7.5$ ,  $50 \text{ mM}$ ) was used and the experiments were carried out at  $35^\circ\text{C}$ .

### 3.2.4. Storage and operational stability

The stability of the enzyme electrode was assessed by its storage and operational efficiency. In order to determine the biosensor storage stability, measurements were carried out periodically every 20 days for 2 months. The biosensor was used for only this purpose and it was stored at  $4^\circ\text{C}$ . In the experiments,  $0.05 \text{ mM}$  L-ascorbic acid concentration was used. After the storage period (2 months), it was determined that the retained activity of enzyme electrode is more than  $85\%$  of its initial activity (Fig. 3).

On the other hand, another ascorbate oxidase electrode which has same properties was used for the determination of operational stability of the electrode. Two or three measurements were done in every day during a 2-month period. In this study,  $0.05 \text{ mM}$  L-ascorbic acid concentration was used. During that period more than 200 assays were carried out with the same electrode.

### 3.3. Applications

#### 3.3.1. L-Ascorbic acid determination in vitamin C tablets

The analytical results for vitamin C tablets are given in Table 2 and suggest that the results obtained with ascorbate oxidase enzyme electrode are in fairly good agreement with those obtained by DCIP method.

As can be seen in Table 2, the L-ascorbic acid amounts determined using the enzyme electrode were  $0.3\text{--}0.7\%$  smaller than the tablet's original content. Whereas, in the case of the DCIP

Table 2

Comparison between the ascorbate oxidase enzyme electrode and the DCIP methods for determination of L-ascorbic acid in vitamin C tablets

Method	Sample	L-Ascorbic acid contents of tablets (mg/tablet)	Found L- ascorbic acid content <sup>a</sup> (mg/tablet)	Recovery (%)
Ascorbate Oxidase Enzyme Electrode	Ca-Sandoz	1000	992.5	99.3
	Redoxan	500	497.8	99.6
DCIP	Ca-Sandoz	1000	1015.0	101.5
Method	Redoxan	500	510.0	102.0

<sup>a</sup> The average of five analyses.

Table 3

Determination of L-ascorbic acid in fruit juices using the two different methods

Sample	Ascorbate oxidase electrode method			DCIP method		
	Average (mg/100 g)	<i>n</i> = 5		Average (mg/100 g)	<i>n</i> = 5	
		SD	CV (%)		SD	CV (%)
Orange	39.19	0.00204	2.35	31.15	0.0153	2.42
Lemon	26.42	0.00167	2.76	25.50	0.0158	3.04

method, the amount of L-ascorbic acid was found to be 1.5–2.0% larger. As a result, it can be suggested that the obtained data, using both methods, are very sensitive. It was understood that better results were obtained by the ascorbate oxidase electrode in comparison to the DCIP method. In addition, that method is more practical, specific, and useful than the DCIP method and not time-consuming.

### 3.3.2. L-Ascorbic acid determination in fruit juices

The contents of L-ascorbic acid in fruit juices were determined by ascorbate oxidase electrode and compared with the DCIP method. The results are given in Table 3.

As a result of this work, the method developed by the ascorbate oxidase enzyme electrode was found to be more advantageous in comparison to other methods reported in the literature so far; it was determined that the method is sensitive, economic, practical and less time-consuming. L-Ascorbic acid determination at low concentrations is possible by HPLC methods, although very expensive equipment and chemicals are necessary [10,18,19]. Ion chromatographic and gas chromatographic methods are time-consuming and also very expensive for the determination of L-ascorbic acid [20,21]. The enzymatic methods are known to be very sensitive, specific, simple and useful methods, in which the immobilized forms of the enzymes are generally used [12]. Since biosensor technology provides economical, practical, specific and sensitive results for the determination of L-ascorbic acid, it was improved very efficiently [15,22].

The ascorbate oxidase electrode developed in this study has major advantages, such as long-

term stability, sensitivity and linear range. The major advantage as compared with the original electrode described by Uchiyama and Umetsu [15], lies in lowering of the linear range from  $2.5 \times 10^{-4}$  to  $1.6 \times 10^{-3}$  M L-ascorbic acid to  $5.0 \times 10^{-5}$ – $1.2 \times 10^{-3}$  M. For the L-ascorbic acid sensor described by Uchiyama and Umetsu [15], response time and life time have been reported to be 3–6 min and 11 days, respectively. On the other hand, the response time and life time of our biosensor are 45 s and at least 2 months, respectively. In addition, after carrying out 200 measurements for 2 months, the biosensor is still found to be active. The reproducibility of the analysis results is very high and there are no important interference effects from diverse substances. Consequently, it can be suggested that the method developed would be an original and useful procedure for L-ascorbic acid determination.

## References

- [1] S.N. Gershoff, *Nutr. Rev.* 51 (11) (1993) 313.
- [2] S.R. Tannenbaum, J.S. Wishnok, *Ann. NY Acad. Sci.* 498 (1987) 354.
- [3] T. Moeslinger, M. Brunner, I. Volf, P.G. Spieckermann, *Clin. Chem. (Washington, DC)* 41 (1995) 1177.
- [4] H. Hemila, *Br. J. Nutr.* 67 (1992) 3.
- [5] H. Sies, W. Stahl, A.R. Sundquist, *Ann. NY Acad. Sci.* 669 (1992) 7.
- [6] R. Strohecker, H.M. Henning, Verlag Chemie, Weinheim, 1965.
- [7] S.P. Arya, M. Mahajen, *Anal. Sci.* 11 (5) (1995) 853.
- [8] P.W. Washko, R.W. Welch, K.R. Dhariwal, Y. Wang, M. Levine, *Anal. Biochem.* 204 (1) (1992) 1.
- [9] M. Irache, I. Ezpeleta, F.A. Vega, *Chromatographia* 35 (3-4) (1993) 232.
- [10] C. Xi, S. Masanori, *Anal. Sci.* 11 (5) (1995) 749.

- [11] R. Stevanato, L. Avigliano, A. Finazzi-Agro, A. Rigo, *Analytical Biochem.* 149 (1985) 537.
- [12] G.M. Greenway, P. Ongomo, *Analyst* 115 (10) (1990) 1297.
- [13] D. List, W. Knechtel, *Flüessiges. Obst.* 47 (2) (1980) 57.
- [14] B.J. Vincke, M.J. Deuleeschouwer, G.J. Patriarche, *Anal. Lett.* 18 (B13) (1985) 1593.
- [15] S. Uchiyama, Y. Umetsu, *Anal. Chim. Acta* 255 (1991) 53.
- [16] S. Uchiyama, S. Suzuki, *Sensors Actuators B* 13-14 (1993) 76.
- [17] E. Akyılmaz, H.B. Dinçkaya, *Natural Sci. Eng.* 25 (1996) 135.
- [18] S. Zapata, J.P. Bufour, *J. Food. Sci.* 57 (2) (1992) 506.
- [19] J.T. Vanderslice, D.J. Higgs, *J. Nutr. Biochem.* 4 (3) (1993) 184.
- [20] M. Yasuyuki, M. Takashi, K. Tomozo, *Anal. Sci.* 11 (4) (1995) 617.
- [21] J.C. Deutsch, J.F. Kolhouse, *Anal. Chem.* 65 (4) (1993) 321.
- [22] L. Macholan, B. Chmelikova, *Anal. Chim. Acta* 185 (1986) 187.



# Detection of ferritin in human serum with a MAP–H<sub>2</sub>O<sub>2</sub>–HRP voltammetric enzyme-linked immunoassay system

Shusheng Zhang<sup>a</sup>, Kui Jiao<sup>b,\*</sup>, Hongyuan Chen<sup>a</sup>, Manxia Wang<sup>b</sup>

<sup>a</sup> Department of Chemistry, Nanjing University, 22 Hankou Road, Nanjing, 210093 Jiangsu, People's Republic of China

<sup>b</sup> Department of Applied Chemistry, Qingdao Institute of Chemical Technology, 53 Zhengzhou Road, Qingdao, 266042 Shandong, People's Republic of China

Received 16 October 1998; received in revised form 18 March 1999; accepted 24 March 1999

## Abstract

A voltammetric enzyme-linked immunoassay based on new system of *m*-aminophenol (MAP)–H<sub>2</sub>O<sub>2</sub>–horseradish peroxidase (HRP) has firstly been developed and used for the detection of HRP, labelled HRP and ferritin in human serum. HRP or labelled HRP catalyzes the oxidation reaction of MAP with H<sub>2</sub>O<sub>2</sub>, the product of which produces a sensitive voltammetric peak at potential of  $-0.46$  V (vs. SCE) in Britton–Robinson (BR) buffer solution. By using this voltammetric peak, HRP can be measured with a detection limit of  $9.5 \times 10^{-1}$  mU/l and a linear range of  $2.5-2.5 \times 10^2$  mU/l. The detection limit to ferritin is 0.25 ng/ml and the linear range 0.25–320 ng/ml. The processes of the electro-reduction of the product of the enzyme-catalyzed reaction have been investigated in detail. © 1999 Elsevier Science B.V. All rights reserved.

**Keywords:** Electrochemical immunoassay; Ferritin; Horseradish peroxidase (HRP); *m*-Aminophenol; Voltammetry

## 1. Introduction

Immunoassay with electrochemical detection is an attractive method in bioanalytical chemistry due to its high sensitivity and low detection limit. Technique with enzyme labels is by far mostly used in electrochemical immunoassay. Heineman and co-workers, and others, have applied alkaline

phosphatase to the detection of some antigens and drugs [1–8], most of which are involved in amperometric enzyme-linked immunoassay. There are only a few documents on voltammetric enzyme-linked immunoassay [9,10].

The sensitive detection of ferritin in human serum is very important. Agar double diffusion, immunoelectrophoresis, immuno-osmophoresis, reverse indirect hemagglutination and the enzyme-linked immunosorbent spectrophotometric assay (ELISA) are now employed for the detection of ferritin, but the sensitivity of these techniques is somewhat low [11,12].

\* Corresponding author. Tel.: +86-532-4022750; fax: +86-532-4879146.

E-mail address: jiaokui@public.qd.sd.cn (K. Jiao)

In this paper, a new system of MAP–H<sub>2</sub>O<sub>2</sub>–HRP voltammetric enzyme-linked immunoassay was advanced for the first time, which also had not been investigated in spectrophotometric ELISA method. The oxidation of MAP by H<sub>2</sub>O<sub>2</sub> catalyzed by HRP yields a stable product 2-amino-5-[(3-hydroxyphenyl)amino]-2,5-cyclohexadiene-1,4-dione. The product has two unsaturated bonds, which are subject to electro-reduction, and can be detected by voltammetry. So, MAP was chosen as the substrate. The method has been successfully applied to the detection of ferritin in human serum.

## 2. Experimental

### 2.1. Apparatus

MP-1 voltammetric analyser, produced by Shandong No. 7 Electric Communication Factory, with a three-electrode system, composed of a dropping mercury electrode or a hanging mercury drop electrode as working electrode, a platinum wire electrode as auxiliary electrode and a saturated calomel electrode (SCE) as reference electrode; JM-01 hanging mercury drop electrode was made by Jiangsu Electric Analysis Apparatus Factory. Incubation for the immune reaction is carried out in a Model HH.W21.Cr420 incubator, produced by Guangdong Shantou Instrument Factory.

### 2.2. Reagents

*m*-Aminophenol (MAP): Fluka,  $2.5 \times 10^{-2}$  mol/l MAP solution was prepared by dissolving 0.2730 g MAP in water and diluted to 100 ml. HRP solution: Dongfeng Biochemical Technique, Shanghai Institute of Biochemistry, 250 units per mg enzyme (RZ > 3.0),  $2.5 \times 10^8$  mU/l stock solution of HRP was prepared by dissolving 0.0500 g HRP in 50 ml water, which was stored in a refrigerator at 4°C. H<sub>2</sub>O<sub>2</sub> solution:  $4.0 \times 10^{-4}$  mol/l, prepared before using. Britton–Robinson buffer solution: 0.2 mol/l, pH 7.25 and 0.2 mol/l, pH 10.5. Carbonate buffer (0.1 mol/l, pH 9.6):

1.60 g Na<sub>2</sub>CO<sub>3</sub> + 2.90 g NaHCO<sub>3</sub>, diluted to 1 l. PBS–Tween 20 buffer solution: 8.00 g NaCl + 2.90 g Na<sub>2</sub>HPO<sub>4</sub>·12H<sub>2</sub>O + 0.20 g KH<sub>2</sub>PO<sub>4</sub> + 0.20 g KCl + 0.5 ml 1% Tween 20, diluted to 1 l, pH 7.4. Substrate solution: to a colorimetric tube of 10 ml the following solutions were added in sequence: 1.0 ml of  $2.5 \times 10^{-2}$  mol/l MAP solution, 2.0 ml of  $4.0 \times 10^{-4}$  mol/l H<sub>2</sub>O<sub>2</sub> solution and 4.0 ml of pH 7.25 BR buffer solution, then diluted to the desired scale and shaken to uniform. The Ferritin EIA Kit was purchased from Beijing Biotinge Biomedicine. The kit included: a 96-well immunoplate precoated by anti-ferritin serum, horseradish peroxidase (HRP)-conjugated anti-ferritin (FtAb-HRP), 0 ng/ml of ferritin negative control serum, 320 ng/ml of ferritin quality control serum. The other reagents were all analytical reagents prepared with doubly deionized water.

### 2.3. Procedures

#### 2.3.1. Measurement of HRP activity

A total of 1.0 ml ( $2.5 \times 10^{-2}$  mol/l) MAP + 2.0 ml ( $4.0 \times 10^{-4}$  mol/l) H<sub>2</sub>O<sub>2</sub> + 4.0 ml, pH 7.25 (0.2 mol/l), BR buffer + 1.0 ml ( $2.5 \times 10^2$  mU/l) HRP, diluted to 10 ml with deionized water. Then it sat for 30 min at room temperature. A total of 5.0 ml of the above solution was transferred into a colorimetric tube of 10 ml, and 2.5 ml of pH 10.5 BR buffer solution were subsequently added, then diluted to the scale and shaken to uniform solution. The solution was transferred into a 10-ml electrolyte cell. The second-order derivative linear-sweep voltammogram was recorded with an MP-1 voltammetric analyser. The instrumental conditions were as follows: initial potential, –0.20 V; potential scanning rate, 535 mV/s; mercury drop standing time, 12.8 s.

#### 2.3.2. Determination of ferritin

The wells of the polystyrene immunoplate precoated by anti-ferritin serum were rinsed with PBS–Tween 20 buffer (300 µl) three times for 3 min each. After removing the rinsing solution, 100 µl of the ferritin quality control serum diluted with PBS buffer or the serum sample were added to each well and incubated at 37°C for 30 min. The wells were then rinsed as above, and 100 µl of

FtAb-HRP were added to each well and incubated at 37°C for 30 min. The wells were then rinsed as above and once more with dideionized water. Following this step, 400  $\mu\text{l}$  of the substrate solutions were added to each well and incubated at room temperature for 30 min. The reaction solution was transferred into a cell of 2 ml. A total of 200  $\mu\text{l}$  of 0.2 mol/l BR buffer (pH 10.5) and 200  $\mu\text{l}$  dideionized water were added into the cell. The second-order derivative linear-sweep voltammogram was recorded. The ELISA detection of the immuno-reaction solutions prepared as above was conducted with a Minireader II (Dynatech).

### 3. Results and discussion

#### 3.1. The second-order derivative linear-sweep voltammograms

Differential pulse voltammetry, modern square wave voltammetry and linear sweep second-order derivative polarography all have excellent voltammetric peaks or polarographic waves in the detection of the product formed by  $\text{H}_2\text{O}_2$  oxidizing MAP, which is catalyzed by HRP in pH 10.5 BR buffer solution. Among these methods, linear sweep second-order derivative polarography has advantages, such as the highest sensitivity, the lowest detection limit, the short experimental time or fastest electrochemical procedure, and simple manipulation. The product of the enzyme-catalyzed reaction has a well-defined voltammetric peak. Fig. 1 shows the results of the second-order derivative linear-sweep voltammograms. Curve 1 is the voltammogram of BR buffer solution, which has no voltammetric peak. Curve 2 is that of BR + MAP +  $\text{H}_2\text{O}_2$ , which has a small voltammetric peak at  $-0.46$  V. The small peak is due to the product of slow oxidation of MAP by  $\text{H}_2\text{O}_2$ . Curve 3 is that of the enzyme-catalyzed reaction solution. Owing to the addition of HRP, which quickens greatly the oxidation of MAP with  $\text{H}_2\text{O}_2$ , the reaction product produces a large and well-defined voltammetric peak at  $-0.46$  V. Al-

though the HRP content is as low as 2.5 mU/l, a distinctive increase of this voltammetric peak can still be observed. In this concentration of HRP, the response current is 0.8  $\mu\text{A}$ . On the basis of analytical data [13], the oxidation of MAP by  $\text{H}_2\text{O}_2$  yields a stable product, 2-amino-5-[(3-hydroxyphenyl)amino]-2,5-cyclohexadiene-1,4-dione, if the enzyme-catalyzed reaction happens in BR buffer solution of pH 7.25. In BR buffer solution of pH 10.5, the product of the enzyme-catalyzed reaction can be reduced through two-electron transfer. With the electro-reduction peak, free HRP and different labelled HRPs can be determined. By means of immunoassay, different antibodies and antigens can also be identified.

#### 3.2. Conditions for enzyme-catalyzed reaction

HRP intensely catalyzes the oxidation reaction of MAP by  $\text{H}_2\text{O}_2$  in BR buffer solution. From the structure of the product [13] and the catalytical cycle of HRP in reaction [14], the process of the enzyme-catalyzed reaction can be expressed as follows:

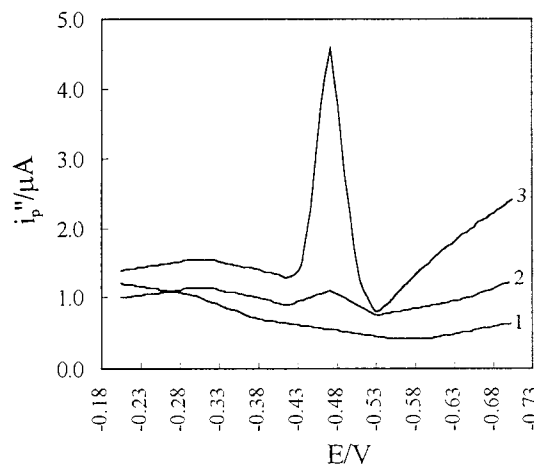
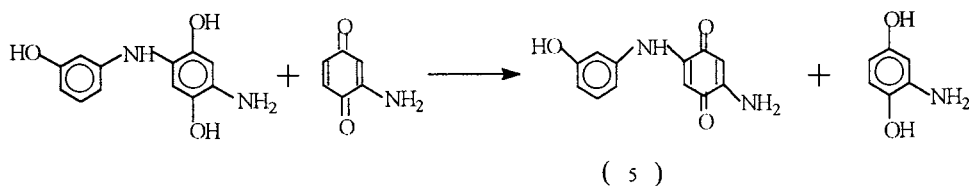
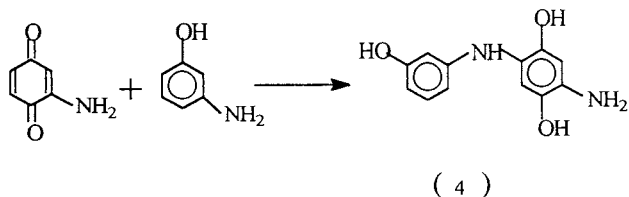
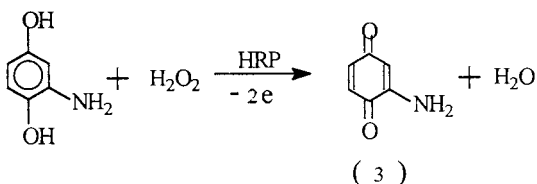
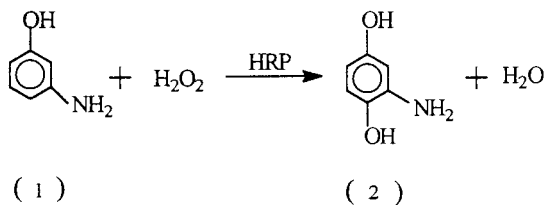


Fig. 1. Second-order derivative linear-sweep voltammograms: (1) 0.08 mol/l pH 7.25 BR buffer; (2) reaction without HRP (0.08 mol/l pH 7.25 BR buffer +  $2.5 \times 10^{-3}$  mol/l MAP +  $8.0 \times 10^{-5}$  mol/l  $\text{H}_2\text{O}_2$ ); (3) reaction with HRP: 2 + 25 mU/l HRP.



In a pH range from 2.0 to 10.0, the effect of the pH value of BR buffer solution on the reaction was tested. At pH 7.0–7.5, a sensitive and stable voltammetric peak can be obtained. So, BR buffer at pH 7.25 was chosen as optimal enzymatic reaction solution. The concentrations of BR buffer solution, MAP and  $\text{H}_2\text{O}_2$  were also investigated. When 10 ml of the overall reaction solution included 4.0 ml of 0.2 mol/l pH 7.25 BR buffer solution, 1.0 ml of  $2.5 \times 10^{-2}$  mol/l MAP solution and 2.0 ml of  $4.0 \times 10^{-4}$  mol/l  $\text{H}_2\text{O}_2$  solution, the peak was the highest and also stable.

Under the selected enzyme-catalyzed reaction conditions, the equilibrium will be achieved in 25 min at room temperature. And the peak height keeps stable within 2 h and the small blank peak also has no change. A total of 30 min was selected as the time for the enzyme-catalyzed reaction at room temperature.

### 3.3. Detection conditions

A fine second-order derivative linear-sweep voltammetric peak of the product of the enzyme-catalyzed reaction can be obtained in some buffer solutions, such as BR, HOAc–NaOAc,  $\text{NH}_3$ – $\text{NH}_4\text{Cl}$ ,  $\text{H}_3\text{BO}_3$ –KCl–NaOH and  $\text{KH}_2\text{PO}_4$ – $\text{Na}_2\text{HPO}_4$ . In this work, BR buffer solution was selected as the supporting electrolyte for the polarographic measurement. The effect of pH value of BR buffer on the voltammetric peak was investigated. The peak potential shifts negatively and the peak height advances with the increase of pH, and with a relative stability before the peak height

decreases with the further increase of pH. At pH 10.5, the peak is the highest and also stable. When 10 ml of the overall solution includes 2.0–3.0 ml of 0.2 mol/l BR buffer solution (pH 10.5), the highest peak appears.

For pH 7.25 BR buffer solution, the linear-sweep voltammetric peak increases with the increase of the scanning rate. But the plot of the peak current against the square root of the scanning rate is not linear but an upward curve in the range of 120–735 mV/s. The peak potential values shift to more negative values with the increase of the scanning rate. The peak potential value shifts about 10 mV negatively, while the scanning rate increases 100 mV/s. That is to say, the product of the enzyme-catalyzed reaction is adsorbed on the mercury electrode. Because the second-order derivative linear-sweep voltam-

mogram is recorded on a dropping mercury, the phenomenon that the product of the enzyme-catalyzed reaction is adsorbed on the dropping mercury electrode does not interfere the detection.

Under the selected conditions, the multiple-sweep voltammograms of the product of the enzyme-catalyzed reaction were recorded. On the first scanning curve, there are good cathodic and anodic peaks and these two peaks are similar in height. Based on the theory advanced by Nicholson [15], this is a two-electron reversible electrode process. In the multiple-sweep cyclic voltammograms, the peak lowers gradually to nothing with the increase of the scanning time. This is the adsorptive behaviour of the product of the enzyme-catalyzed reaction.

The cyclic voltammetric experiment was run for the solution of the enzyme-catalyzed reaction. After reaction in pH 7.25 BR buffer solution, the cyclic voltammograms were recorded at different pH values from 3.0 to 13.0. There is no cyclic voltammetric peak when  $\text{pH} < 5.0$ . Between pH 5.0 and 12.0, one pair of reversible redox peaks appears. In the pH range of 5.0–12.0, the two peak heights are almost equal, which indicates the reversible electrode process. When  $\text{pH} > 12.0$ , there is only a small cathodic peak, and the anodic peak disappears.

The influence of pH on the peak potential was investigated for BR buffer solution of different pH values. The peak potential value has a good linear relation with the pH value in the range of 3.0–12.0, with an equation of linear regression  $E_p = -0.170 - 0.067 \text{ pH}$  ( $n=9$ ,  $\gamma = -0.9962$ ). According to the formula [16]:  $-0.059 x/n = -0.067$ , where  $n$  is the number of the electron transfer,  $x$  is the hydrogen ion number participating the reaction,  $x \approx n = 2$ .

From the above experimental results, there is a two-electron reversible redox process of 2-amino-5-[(3-hydroxyphenyl) amino]-2,5-cyclohexadiene-1,4-dione in pH 5.0–12.0 BR buffer solution, which can be expressed as follows:

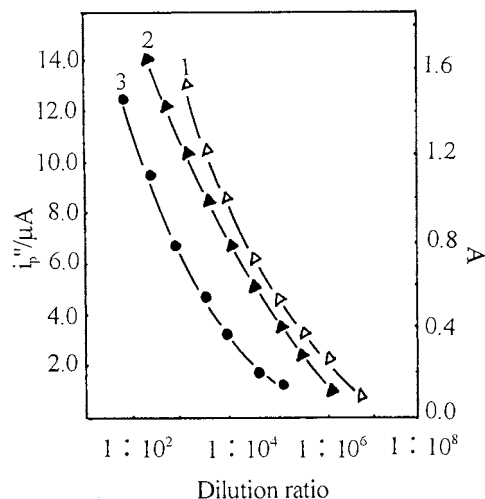
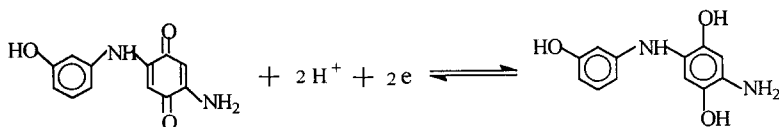


Fig. 2. Dilution curves of detecting FtAb-HRP with this method (1); the *o*-dianisidine spectrophotometric ELISA method (2); and the *o*-phenylenediamine spectrophotometric ELISA method (3).

If  $\text{pH} > 12.0$ , there is a two-electron irreversible reduction process of 2-amino-5-[(3-hydroxyphenyl) amino]-2,5-cyclohexadiene-1,4-dione.

#### 3.4. Determination of HRP and labelled HRP

According to the experimental method, different quantities of HRP were used to catalyze the oxidation reaction of MAP with  $\text{H}_2\text{O}_2$  and the second-order derivative linear-sweep voltammograms were recorded. The HRP concentration from 2.5 to  $2.5 \times 10^2$  mU/l has a good linear relation with the peak height in BR buffer solution. The relative standard deviation is 4.8% for 11 parallel determinations with 5.0 mU/l HRP, and the detection limit of HRP is  $9.5 \times 10^{-1}$  mU/l ( $3\sigma$ ).

In order to use the new system in the immunoassay of ferritin, the HRP-conjugated anti-ferritin (FtAb-HRP) was detected under the

optimum experimental conditions. The result is shown in curve 1 of Fig. 2; that of the *o*-dianisidine spectrophotometric ELISA method in curve 2 of Fig. 2; that of *o*-phenylenediamine spectrophotometric ELISA method in curve 3 of Fig. 2. The highest dilution ratio detected by this method is  $1: 1.0 \times 10^7$ . The highest dilution ratio detected by the *o*-dianisidine spectrophotometric ELISA method is  $1:1.3 \times 10^5$  and that by the *o*-phenylenediamine spectrophotometric ELISA method  $1:2.1 \times 10^6$ . The detection limit of this method is lowered by 64 times compared with that of the *o*-dianisidine spectrophotometric ELISA method; and four times compared with those of the *o*-phenylenediamine spectrophotometric ELISA method. The presented method is a highly sensitive detection method.

### 3.5. Determination of ferritin

The determination of ferritin was carried out with double-antibody-sandwich immunoassay method, the advantage of which is that the manipulation is simpler and faster; the detection cost is lower and the application is easier. It needs no more than 2 h to detect a batch of samples. The more ferritin detected in serum, the more the FtAb-HRP combined on the solid-phase carrier, the more the product of oxidizing MAP by  $H_2O_2$  catalyzed by FtAb-HRP, the higher the voltammetric peak. Nonspecific adsorption of ferritin and labelled antibody can be suppressed using not only Tween 20 but also this method. In this assay, the commercial ferritin kit was used directly. The conditions of the immune reaction were controlled according to the procedure recommended by conventional ELISA.

#### 3.5.1. The linear range, the detection limit and the precision of ferritin determination

Under optimum conditions, the linear range of the ferritin quality control serum is 0.25–320 ng/ml and the detection limit is 0.25 ng/ml. The equation of linear regression is  $i_p'' = 3.912 + 1.461 \log_2 C$  ( $i_p''$  is the peak current,  $\mu A$ ;  $C$  is the concentration of ferritin, 0.25–320 ng/ml,  $n = 12$ ),  $r = 0.9976$ . The repeatability of the assay was studied by running 11 replicate assays on 7.8 ng/ml of ferritin in serum,

Table 1

The comparison of results of this method with the *o*-phenylenediamine spectrophotometric ELISA method for the detection of ferritin in human serum

Sample	This method (ng/ml)	<i>o</i> -Phenylenediamine spectrophotometric ELISA method (ng/ml)
1	4.0	5.0
2	3.6	2.6
3	154.0	140.0
4	48.0	42.0
5	279.0	250.0
6	255.0	260.0
7	8.0	8.0
8	10.0	5.0
9	46.6	30.0
10	37.0	48.0

and the relative standard deviation is 3.4%. Under the same conditions, the linear range of the ferritin quality control serum is 1.0–320 ng/ml and the detection limit is 1.0 ng/ml with the *o*-phenylenediamine spectrophotometric ELISA method. The equation of linear regression is  $A = -0.492 + 0.9191 \log C$  ( $A$  is the absorbance,  $C$  is the concentration of ferritin, 1.0–320 ng/ml,  $n = 6$ ),  $r = 0.9960$ . Under the same conditions, the detection limit is 160 ng/ml with *o*-dianisidine spectrophotometric ELISA method.

#### 3.5.2. The determination of human serum samples

Under the optimum conditions, the human serum samples were detected. The compared results with *o*-phenylenediamine spectrophotometric ELISA method were listed in Table 1. The results are corresponding to each other. The result of this method is linear proportional to that of spectrophotometric ELISA method, and the equation of linear regression is  $y = 2.17 + 1.04x$  ( $x$  is the results of this method;  $y$  is the results of *o*-phenylenediamine spectrophotometric ELISA method;  $n = 10$ ),  $r = 0.9947$ .

### Acknowledgements

We greatly appreciate the support of the National Natural Science Foundation of China (No. 29775012, No. 29835110).

**References**

- [1] W.R. Heineman, H.B. Halsall, K.R. Wehmeyer, M.J. Doyle, D.S. Wright, *Anal. Proc.* 24 (1987) 324.
- [2] K.R. Wehmeyer, H.B. Halsall, W.R. Heineman, C.P. Volle, I.W. Chen, *Anal. Chem.* 58 (1986) 135.
- [3] K. Kronkvist, U. Lovgren, L.E. Edholm, G. Johansson, *J. Pharm. Biomed. Anal.* 11 (1993) 459.
- [4] N. Kaneki, Y. Xu, I.A. Kumar, H.B. Halsall, W.R. Heineman, P.T. Kissinger, *Anal. Chim. Acta* 278 (1994) 253.
- [5] C. Duan, M.E. Meyerhoff, *Anal. Chem.* 66 (1994) 1369.
- [6] O. Niwa, Y. Xu, H.B. Halsall, W.R. Heineman, *Anal. Chem.* 65 (1993) 1559.
- [7] H. Yao, S.H. Jenkins, A. Pesce, H.B. Halsall, W.R. Heineman, *Clin. Chem.* 39 (1993) 1423.
- [8] D. Athey, M. Ball, C.J. Mcneil, *Ann. Clin. Biochem.* 30 (1993) 570.
- [9] K. Jiao, S.S. Zhang, L. Wei, C.F. Liu, C.L. Zhang, Z.F. Zhang, J.Y. Liu, P. Wei, *Talanta* 47 (1998) 1129.
- [10] K. Jiao, S.S. Zhang, L. Wei, *Sci. China (Series B)* 39 (1996) 135.
- [11] L.J. Kricka, *J. Pharm. Biomed. Anal.* 8 (1987) 829.
- [12] M. Mesako, et al., *Anal. Chim. Acta* 167 (1985) 241.
- [13] S.S. Zhang, K. Jiao, H.Y. Chen, H.J. Li, *Acta Chim. Sinica* 57 (1999) 1.
- [14] J. Everse, K.E. Everse, M.B. Crisham, *Peroxidase in Chemistry and Biology*, vol. 2, CRC Press, Boston, MA, 1991, p. 5.
- [15] R.S. Nicholson, *Anal. Chem.* 37 (1965) 1351.
- [16] I.M. Kolthoff, J.J. Lingane, *Polarography*, Interscience, New York, 1952, p. 247.

## Evaluation of phenolic assays for the detection of nitrite

James Davis <sup>a</sup>, Kenneth J. McKeegan <sup>a,b</sup>, Marco F. Cardosi <sup>b</sup>,  
D. Huw Vaughan <sup>a,\*</sup>

<sup>a</sup> *Department of Chemistry and Chemical Engineering, University of Paisley, Paisley, PA1 2BE, UK*

<sup>b</sup> *Department of Biological Sciences, University of Paisley, Paisley, PA1 2BE, UK*

Received 8 December 1997; received in revised form 8 March 1999; accepted 29 March 1999

### Abstract

A series of generic nitrite assay systems based on the single step nitrosation of phenol derivatives are presented. The chemical reactivity offered by the C-nitroso compounds provides an opportunity to pursue a number of analytical strategies of which three spectroscopic (UV/Vis) and two electrochemical options (linear sweep voltammetry/differential pulse voltammetry) were evaluated. The capacity for multiple detection options from a single analyte species without significant sample manipulation is a major advantage with each assay system providing sub ppm detection limits with linear ranges up to milli-molar concentrations of nitrite. The influence of common interferents such as nitrate, ascorbate and paracetamol was investigated. The applicability of the assay procedures to the analysis of authentic biological samples (saliva and urine samples) was assessed with the analytical accuracy independently corroborated with a standard Griess protocol. In addition, a brief comparison with alternative nitrite detection strategies is also presented. © 1999 Elsevier Science B.V. All rights reserved.

*Keywords:* Phenol; Phloroglucinol; Nitrite; Electrochemical; Spectroscopy

### 1. Introduction

The nitrite ion is an important intermediate in the biological nitrogen cycle and is present in soils and surface waters [1,2]. Nitrite is also a versatile chemical agent which has found numerous applications ranging from dye manufacture to food preservation [3,4]. While the commercial utilisation

of this agent has found numerous beneficial applications, health concerns over its implication in certain cancers has led to the establishment of a significant knowledge base for its determination in a wide variety of matrices [4–7]. A large number of detection techniques are available with the majority based upon either chromatographic or spectroscopic methodologies. Selection of the appropriate analytical procedure will generally depend upon the equipment available, sample nature and the expected nitrite level. Spectroscopic procedures require relatively simple instrumentation but the need for several preparative stages and the potential interference from other

\* Corresponding author. Tel.: +44-141-848-3217; fax: +44-141-848-3204.

E-mail address: vaug-ch0@wpmail.paisley.ac.uk (D.H. Vaughan)



coloured species within the matrix often limits their applicability. This problem is highlighted by the large number of spectroscopic detection strategies available in the literature such that one particular procedure will fit the requirements of an application under a given set of circumstances. There is clearly a need for a versatile yet simple assay which can be analysed using a number of techniques but which retains a single, common preparative stage.

This report details one such procedure which is based upon the single step nitrosation of commercially available phenolic compounds with the resulting products providing a diverse range of analytical possibilities. The production of nitroso compounds from the reaction of nitrous acid with phenolic species is well established and is known to result in the incorporation of nitroso functional groups onto the aromatic ring system (C-nitrosation) [8–10]. The typical reaction scheme which forms the foundation of the assay systems described herein is detailed in Fig. 1.

The resulting phenolic species are often coloured and could be applied to the detection of nitrite. The reaction of various phenolic compounds with acidified nitrite was investigated and their suitability for nitrite determination assessed. Phenol, hydroquinone, catechol, resorcinol, pyrogallol, phloroglucinol and gallic acid were all assessed but only three successfully fulfil the criteria of providing a quick and stable response. This article will therefore examine the results obtained from the investigations into phenol, resorcinol and, particularly, phloroglucinol which has been found to possess several beneficial qualities for nitrite detection.

The chemical versatility of the C-nitroso species is such that many analytically distinct procedures can be developed from a single species. In this report we present three spectroscopic strategies and detail a number of electrochemical alternatives. Each assay is evaluated and factors such as colour stability, response and the influence of interferents assessed. In addition, the ability to detect nitrite in a range of complex matrices (saliva, urine and river water) using the assay systems presented herein was investigated.

## 2. Experimental

All reagents were of the highest grade available and were used without further purification. Each reagent solution, with the exception of HCl, was prepared in deionised water immediately before a given analytical session. Spectroscopic measurements were obtained using a Hewlett Packard HP8452 diode array spectrophotometer. Cyclic voltammetry was conducted using a Cypress Systems CYSY-I potentiostat. Differential pulse voltammetry was conducted using an Autolab (Windsor Scientific) potentiostat. A three-electrode configuration was adopted throughout with a bare glassy carbon (0.1 cm<sup>2</sup>) electrode serving as the working electrode with a platinum wire auxiliary and an Ag/AgCl (3 M KCl) reference electrode.

### 2.1. Spectroscopic assay procedures

The development of each assay is presented in turn and the relevant  $\lambda_{\max}$  and molar absorptivity data summarised in Table 1. Each system is based on the reaction pathway detailed in Fig. 1 with excess phenolic reagents added to minimise the possibility of multiple substitution. Condensation of the resulting nitroso species with the excess phenol to form the corresponding indophenol derivative (Liebermann Reaction) [11] was not observed irrespective of the assay conditions specified and phenol indicator.

### 2.2. The acidic assay

A solution containing the phenolic species (2 ml, 20 mM) was placed in a quartz cell (1 cm path

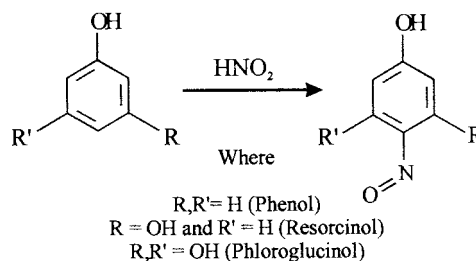
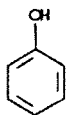
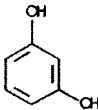
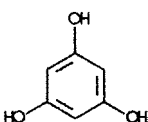


Fig. 1. Nitrosation reaction scheme.

Table 1  
Comparison of the spectroscopic assay parameters

Assay procedure							
Reagent	Development time <sup>a</sup>	Acidic		Alkaline		Cu(II)	
		$\lambda_{\max}$	$\epsilon^b$	$\lambda_{\max}$	$\epsilon^b$	$\lambda_{\max}$	$\epsilon^b$
	5 h	300	1.2	398	1.75	N/A	N/A
	1 h	300 <sup>c</sup>	1.48	352	1.84	362	1.47
	10 min	312	1.08	N/A	N/A	348	1.58

<sup>a</sup> The nitrosation of the phenolic ring is the rate determining step and as such only one development time is shown for each indicator reagent.

<sup>b</sup> Molar absorptivity,  $\epsilon/10^4 \text{ l mol}^{-1} \text{ cm}^{-1}$ . Each calculation based on 10–20 points covering a linear nitrite range extending from 6  $\mu\text{M}$  to 0.2 mM with  $R^2 = 0.999$ .

<sup>c</sup> Absorption Shoulder—no defined peak.

length) and HCl (100  $\mu\text{l}$ , 0.1 M) added. A given quantity of nitrite (10–300  $\mu\text{l}$ , 1 mM  $\text{NaNO}_2$ ) was then added and the solution gently mixed. The absorption spectrum was recorded after the nitrite addition with a band at 300–320 nm, corresponding to the production of the appropriate nitroso phenol derivative developing. The nitrite response of the phloroglucinol assay is shown in Fig. 2. The kinetics of the nitrosation reaction are known to be complex and depend on the nature of the nitrosating species, the pH and the aromatic species present. While the reader is directed to more comprehensive treatments [4,12,13] of the kinetics for this type of reaction a comparison of the time required for nitrosation to reach completion for the three phenolic reagents under the assay conditions is provided. In general, the reaction with phloroglucinol was complete within 2 min, rising

to several hours for the phenol indicator. This sequence effectively mirrors the reactivity of the target molecule in that phloroglucinol, being the most activated with three hydroxy groups, reacts most quickly under identical conditions. The highly reactive nature of both the nitrosating species and the phenolic compound requires a large excess of the latter to prevent multiple substitution of the aromatic rings from occurring. The mono substituted derivatives provide an analytical band that is just within the visible region (as shown by the  $\lambda_{\max}$  values in Table 1). Multiple substitution pushes the analytical band into the UV region (not shown) and thus requires a greater degree of instrumental expense. The position of both the phenol and resorcinol nitroso band is at the limits of the visible range and their analytical utility may be questioned where large

concentrations of organics are present as any absorption tail may significantly affect the analytical signal.

### 2.3. The alkaline assay

This procedure builds upon the previous stage and provides a substantial improvement in both signal intensity and clarity as detailed by the molar absorptivity data in Table 1. The acidic procedure is completed as previously described and once the nitroso signal is stable, NaOH (100  $\mu$ l, 1 M) is added. The resulting nitroso phenolate derivative produces an absorption band at 352 and 400 nm for resorcinol and phenol, respectively. The transformation between the neutral nitroso compound and corresponding nitroso phenolate anion is shown in the inset diagram in Fig. 2 for the phenol assay. This approach is similar to the use of *p*-nitrophenol esters in colourimetric enzyme assays wherein release of the anion provides a strong absorption at 400 nm [13]. The presence of the nitroso species rather than the nitro compound was confirmed by the electrochemical reduction (discussed later) and the

spectrum signature. Oxidation of the nitroso group to nitro functionality does not occur under the induced alkaline conditions as re-acidification of the sample returns the initial spectrum. Phloroglucinol was unsuitable for this procedure as its own phenolate ion produces a band at 350 nm which masks the analytical absorption signal. While resorcinol was found to provide a positive response to nitrite, the stability of the colour was compromised with oxidation of the reagent effectively masking the analytical response after 5 min. The nitroso phenolate ion however exhibited excellent stability over 24 h with no change in signal magnitude.

### 2.4. Ion complex assay

The presence of nitroso functionality in the ortho position relative to a phenol group (*o*-quinone monoximes) is known to have extensive applications in the complexation of metals [9,14–16]. A previous assay procedure based upon the action of nitrous acid on resorcinol employed zirconium ion complexation with the nitroso derivative to provide the analytical absorbance band [16]. Given the structural similarity between resorcinol (1,3-dihydroxy) and phloroglucinol (1,3,5-trihydroxy) the effect of transition metal complexation, or interaction, on the position, shape and intensity of the phenolic-nitroso absorption band was also assessed. The zirconium ion approach was not repeated in this instance as the complexity of the procedure and reagent expense ran counter to the principal aims of this investigation. A range of common, environmentally significant ions were however investigated and their effects on the assay response assessed in terms of beneficial or detrimental influence. The acidic assay procedure detailed previously was modified slightly with various concentrations of Cd(II), Co(II), Cr(III), Cu(II), Fe(II), Fe(III), Ni(II) and Zn(II) (typically 0.1–1.5 mM) added before the nitrite sample (the order of addition was found to have no effect on the final signal response).

There was no modification of the signal response in the phenol assay which is consistent with literature reports where the para nitroso

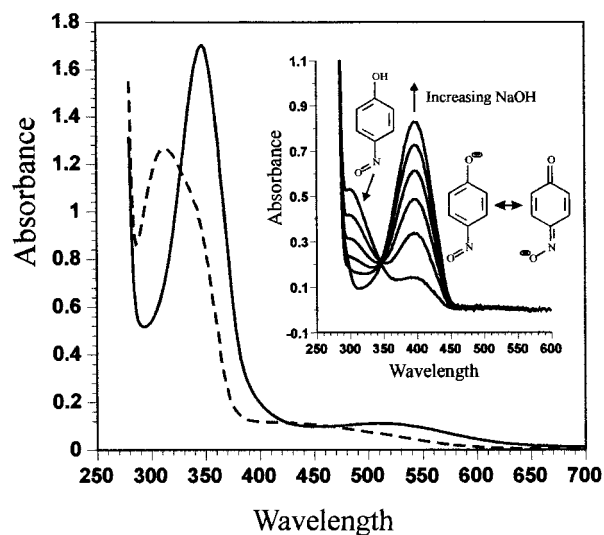


Fig. 2. Spectra profile comparison for the spectroscopic assays. Simple acidic phloroglucinol (dashed line), copper modified phloroglucinol assay (solid line). Inset: The transition from nitrosophenol to nitroso phenolate forms the basis of the alkaline assay system.

derivative is known to be the major product. The position of substitution in the nitrosation reaction is crucial in terms of complexing ability as only nitroso groups ortho to the phenol groups (*o*-quinone monoximes structures) are generally capable of metal co-ordination. Thus, both resorcinol and phloroglucinol are likely to form ortho nitroso groupings as in both cases the vacant 2 and 4 positions, where the electrophilic substitution would occur, are adjacent to a hydroxy group.

The presence of Cu(II), Fe(III), or Ni(II) ions were found to influence the analytical response. Excess cupric ion (1 mM) had a beneficial affect upon the nitroso analytical absorbance band, increasing the sharpness, shifting the peak position and increasing the signal intensity as detailed in Table 1. A comparison between the simple phloroglucinol assay response and that observed with the copper modified procedure to similar nitrite concentrations is detailed in Fig. 2. Both the nickel(II) and iron(III) ions, however, were found to interfere with the acidic and the copper modified assay. While the nickel ions broadened the shape of the peak leading to a depression in the phloroglucinol analytical signal at 312 nm, the overall error was found to be typically  $-2\%$  (0.31 mM Ni(II)) and  $-6\%$  (1.56 mM Ni(II)). It is likely that the nickel ion is weakly co-ordinating to the nitroso group in a similar way to that observed with the cupric ion. The presence of ferric ion had by far the greatest effect on the simple acidic assays as exemplified by the errors of  $+57\%$  (0.16 mM Fe(III)) and  $+130\%$  (0.31 mM Fe(III)) for the phloroglucinol procedure. Interaction between the ferric ion and the aromatic hydroxy groups are responsible for the interference. This is to be expected as the reaction of ferric chloride with phenolic species is a standard laboratory test for their identification[11]. Each of the three phenols give a similar response with a shoulder at around 300 nm and a broad, weaker band at 540 nm.

Thus, the simple acidic procedure would be severely limited in situations where significant levels of oxidising agents may be present. The procedure utilising cupric ion to enhance the assay response to nitrite does fare better in the presence

of ferric ion. Its affect on the phloroglucinol copper modified procedure is reduced through the shift in the analytical absorption band to a longer wavelength resulting in errors of  $-5\%$  (0.13 mM Fe(III)) and  $+8\%$  (0.31 mM Fe(III)), compared with  $+57\%$  and  $+130\%$  for the simple assay. It is important to note that the relatively high concentrations of iron(III) investigated here are unlikely to be found at such levels within either routine food or soil samples and therefore simply highlight the worst case scenario.

### 2.5. Electrochemical detection

The presence of coloured species within a sample matrix will affect most spectroscopic analytical methods to at least some degree. The phenolic assay procedures detailed in this communication provide a limited option for effectively ‘tuning’ the analytical absorption band such that if the simple acidic procedure is masked then secondary positions can be obtained through the addition of either base or cupric ion. Unfortunately, the magnitude of the wavelength shift is not large and in highly coloured matrices may still be insufficient for clear resolution. Electrochemical reduction of the nitroso functionality, however, provides a third option which is independent of the coloured nature of the matrix and whose reduction potential ( $-150$  mV vs. Ag/AgCl) is in a region where there are few competing interferents in the case of either food (with the notable exception of ascorbate) or soil analysis. The main restriction would however be the need to ensure the complete removal of oxygen from the sample before reduction took place.

The reagents used for the spectroscopic assay were also utilised for the electrochemical procedure. The analysis solution consisted of the phenol solution (5 ml, 20 mM) in 0.1 M KCl, HCl (300  $\mu$ l of 0.1 M) and the nitrite sample (10–1000  $\mu$ l, 1 mM). The electrochemical reduction can be carried out at either glassy carbon or platinum electrodes. These investigations were carried out under nitrogen to preclude oxygen interference with the irreversible reduction of the nitroso group in each case observed at approximately  $-150$  mV versus Ag/AgCl. Linear sweep voltam-

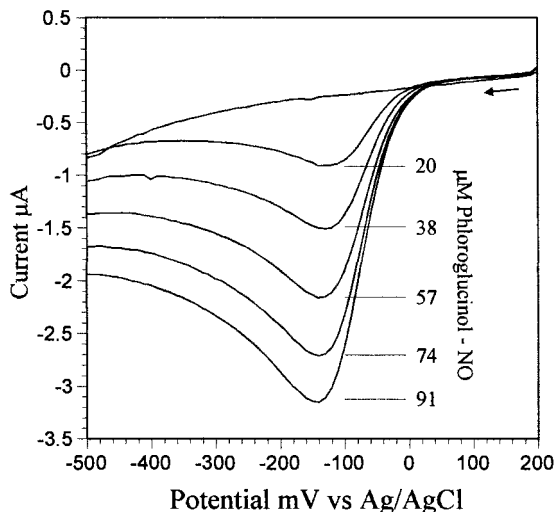


Fig. 3. Linear sweep voltammograms recorded on a glassy carbon electrode detailing the reduction of phloroglucinol-nitroso derivative.

mograms recorded at a glassy carbon electrode covering the potential range +200 to –500 mV are detailed for the phloroglucinol nitroso derivative in Fig. 3. A linear response was observed for concentrations of nitrite from 4 up to 80 mM. The regression data relating peak current ( $I_{pc}$ ) to nitrite concentration under the phloroglucinol assay conditions are detailed below.

LSV:

$$I_{pc} (\mu A) = 3.2 \times 10^4 [\text{NO}_2^-] + 0.0828, R^2 = 0.999$$

## 2.6. Analytical performance

The applicability of the simple acidic assay protocol to the analysis of nitrite in authentic samples was evaluated for a number of differing matrices. These were principally biological in nature (saliva and urine) but nitrite recovery tests were also performed in river water. In the case of the saliva and urine samples, the nitrite concentration was independently verified through standard Griess protocols determined by the local hospital from which the sample originated. The phloroglucinol assay has been shown to be the most

promising of the systems evaluated thus far and its applicability for the detection of nitrite in these matrices has been assessed. Both spectroscopic and electrochemical (DPV) procedures were examined.

The analysis was carried out using standard addition procedures. In the interest of brevity the procedures followed for the analysis of each type of sample are specified for the electrochemical assay only. Near identical conditions were applied for the spectroscopic analysis. The results obtained from the various investigations are compared in Table 2.

### 2.6.1. Analysis of nitrite in saliva and urine

The saliva sample was centrifuged using a Centaur bench top micro-centrifuge. An aliquot of the supernatant (0.3 ml) was then injected into an electrochemical cell containing phloroglucinol (5 ml, 20 mM) with KCl (0.1 M) as supporting electrolyte. The sample was then acidified with HCl (300  $\mu$ l, 0.1 M) and incubated at room temperature for 10 min. The solution was degassed with helium and electrochemical measurement initiated. Three aliquots of nitrite (5  $\mu$ l, 20.3 mM) of stock sodium nitrite solution were then added to the cell and the increase in peak current noted for each case. The differential pulse voltammograms recorded are shown in Fig. 4. The standard addition plot is detailed in the inset diagram

Table 2

Detection of nitrite in authentic biological and environmental matrices

Biological sample	UV/Vis	DPV ( $\mu$ M nitrite)	Griess
Saliva	360	367	347.5
Urine	156	146.5	144

### Recovery in river water by DPV

Sample	Actual ( $\mu$ M)	Expected ( $\mu$ M)	Recovery (%)
1	25.35	25	101
2	51.92	50	104
3	59.0	60	98

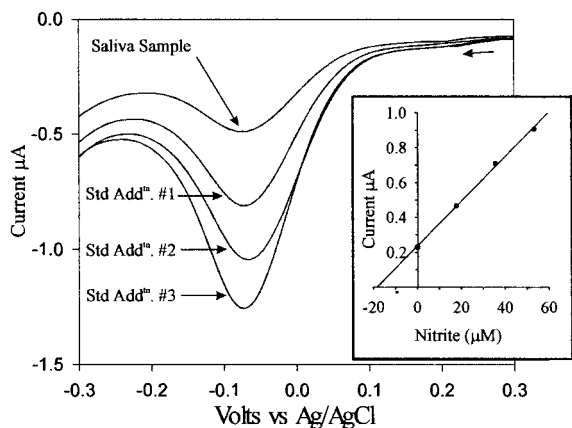


Fig. 4. Differential pulse voltammograms recorded during the standard addition determination of nitrite in saliva.

with the initial nitrite level (after taking into account preparatory dilutions) determined as 367  $\mu\text{M}$ . An analogous routine was conducted for the analysis of nitrite in urine.

#### 2.6.2. Analysis of river water

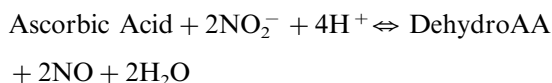
A sample of water (250 ml) was collected from the banks of the River Calder, Scotland, and stored in an opaque plastic bottle. The sample was kept overnight at 4°C in the dark. Prior to analysis the water sample was filtered through a 0.2-mm bacteriological filter into a sterile glass bottle. No further pre-treatment was carried out. The assay procedure specified for the biological samples was again used with the exception that the river water itself was used to make up the reagent solution, i.e. the phloroglucinol and KCl were dissolved in the river water to give the final respective concentrations of 20 and 100 mM. A portion (5 ml) was transferred to the electrochemical cell and acidified by the addition of HCl (300  $\mu\text{l}$ , 0.1M). The cell was assembled, and the sample degassed. The electrochemical measurement was then initiated. After the first electrochemical scan (blank) an aliquot of stock sodium nitrite (10  $\mu\text{l}$ , 10 mM) was added. The solution was stirred and the electrochemical measurement performed. Two further aliquots of nitrite were added representing a low, medium and high level of nitrite. The measured level of nitrite in the river water matrix was calculated by reference to a calibration curve

performed under standard conditions. The percentage recovery was calculated from the ratio of the determined concentration of nitrite to the expected concentration of nitrite.

In summary, it can be seen that the results obtained from the analysis of nitrite in the two biological samples, Table 2, are in close agreement with the values obtained from the standard Griess analysis. Neither the spectroscopic nor the electrochemical system exhibited any distinct analytical disadvantage in respect to one another or in comparison with the Griess method. However, the spectroscopic system proved fallible in the analysis of the river water samples. This can be attributed to the coloured nature of the sample (possessing an absorption tail leading significantly into the visible region) and could possibly be addressed by the way in which the sample was processed. It does serve to highlight the versatility of the assay detection system with the electrochemical detection option providing nitrite recovery results that are within  $\pm 5\%$  of the expected values, detailed in Table 2, despite the sample colouration.

#### 2.7. Influence of interferences

All three spectroscopic assays and the electrochemical options were unaffected by the presence of nitrate, perchlorate, phosphate, chloride or alkali metals. These were assessed at a 100-fold excess over an initial nitrite concentration of 40  $\mu\text{M}$ . The influence of transition metals has been previously mentioned. The most potent interferent likely to be encountered (especially in food and physiological matrices) is ascorbic acid. This analyte is a common antioxidant which is extremely effective at removing nitrous acid and thus a major problem in assays that utilise acidified nitrite as the reaction step. Ascorbic acid reduces the nitrous acid resulting in the production of nitric oxide which under normal circumstances will be lost from the solution [17]



As each assay system described in this report is based upon the reaction of nitrous acid with the appropriate phenol reagent each is therefore susceptible to the influence of ascorbate. However the extent of the induced error is reduced in magnitude such that at 100-fold excess of ascorbate (based on an 18 mM nitrite sample) a depression of 11% was observed in the case of the simple acidic phloroglucinol assay procedure. The copper modified procedure again performed significantly better resulting in the signal being depressed by only 3%. These results compared extremely favourably with previous studies where a 15-fold excess led to a 19.3% recovery of nitrite using standard Griess protocol [4]. Repeating the ascorbate experiment with phenol as the phenolic indicator reagent produced no nitrite response. The superior ability of the copper/phloroglucinol assay to scavenge  $\text{NO}^+$  (the principal nitrosating species) can be attributed to three factors—the large excess of phloroglucinol, its high reactivity towards nitrous acid and the fact that copper(II) salts are known to promote nitrosation through the co-ordination of nitric oxide thus minimising the loss [17]. In this case the order of reagent addition is important with the presence of cupric ion required before the introduction of the nitrite sample. It should also be noted that the resulting nitroso derivatives are stable in the presence of ascorbic acid.

The presence of activated aromatics such as phenol and amines will also pose a threat as indeed they would with the traditional spectroscopic procedures based upon the Griess method. Aromatics containing deactivating groups such as carboxyl (i.e. phthalate) are less susceptible to nitrosation and, with the exception of coloured species such as nitrophenolate, do not exert any influence on the assay response. Paracetamol contains an activated aromatic ring system and its influence on the performance of the nitrite system will be of particular importance when considering physiological samples such as the saliva and urine matrices. The effect of this potential constituent was assessed at a concentration of 0.312 mM and represents dangerous circulating levels 4 h after overdose administration of the drug. This level therefore serves to highlight the worst case sce-

nario for paracetamol interference within a physiological matrix. The influence exerted by the paracetamol additive on the nitrite assay was determined by examining the percentage recovery of various nitrite concentrations. The simple phloroglucinol assay system was used in combination with DPV detection and the results obtained are shown in Table 3. It can be seen that the paracetamol exerts little effect on the recovery of nitrite. This can be attributed to the large excess of the phloroglucinol indicator and its highly activated ring system whose combination leads to the efficient scavenging of the available nitrite.

## 2.8. Technique comparison

A number of reviews relating to the determination of nitrite and nitrate analysis have been published [3,4,18] in which comparisons of the various methods for nitrite determination have been made. In many of these methods, although it is nitrate that is the primary concern, the nitrate is first reduced to nitrite which is then determined by a variety of methods (e.g. colourimetric and fluorimetric methods). Consequently the detection limits of these methods are equally applicable to nitrite analysis. The most widely used method for the detection and determination of nitrite is a colourimetric method based on the formation of a diazo dye, i.e. the Griess method. It is generally accepted that this method has a detection limit for nitrite of 1  $\mu\text{M}$  (50 ppb). Other methods are compared in Table 4. Further details on the various methods are given in references [4,18].

Table 3  
Influence of paracetamol on the recovery of nitrite using the simple phloroglucinol assay

Results in the presence of 0.312 mM paracetamol		
Nitrite concentration ( $\mu\text{M}$ )	Ratio paracetamol: $\text{NO}_2^-$	% Recovery
11.83	26:1	103
23.66	13:1	96
35.49	9:1	99
47.32	7:1	93
71.04	4:1	100

Table 4  
Detection limit comparison for alternative nitrite detection strategies

Detection limits for various methods of nitrite detection	
Method	$\mu\text{M}$
Phloroglucinol	6
Enzyme ( $\text{NH}_3$ electrode)	100
Complex formation	40
Catalytic voltammetry	10
Optical absorption of NOX gases	4
Pneumatoamperometry	4
Diffusion conductivity method	1.4
Electrode	1
Colourimetric (Griess)	1
Titration	1
Fluorescence quenching	1
Direct optical absorption	0.4
Catalysis	0.4
Conductimetric	0.2
Indirect photometric chromatography	0.2
Electron capture	0.1
Chemiluminescence	0.1–0.02
Resonance Raman	0.1
Solvent extraction	0.1
Fluorescence	0.04–0.01
GLC (derivatisation)	0.02
Polarography	0.006
Dye absorption	$2 \times 10^{-5}$

It should be noted that a low detection limit is not necessarily a good indication of the superiority of a particular method. The more steps involved in the procedure the greater the chance of loss of nitrite or generation of reaction intermediates due to side reactions, with less of the desired product being formed. It is thus somewhat surprising that the Griess method which involves the formation of a diazo dye in a four-step reaction, is such a widely used method. A technique such as fluorescence, with its low detection limit, requires several steps in the preparation of the fluorescing products and consequently the method is not convenient for routine analysis. Similarly, chemiluminescence has not proved to be a method suitable for general applicability. A recent report [19] on nitrate and nitrite in food described the analysis for nitrite by HPLC with UV detection at 214 nm. The limit of detection using this technique was reported as  $10 \mu\text{M}$  (0.5 ppm).

### 3. Conclusion

In the majority of cases, assay development tends to be application driven and while this can lead to ever decreasing detection limits, the cost is usually paid through increasing specificity which ultimately leads to reduced transferability. The main aim of this report has been to detail a series of generic procedures which retain both simplicity and sensitivity. The assay procedures possess common preparative stages which could be easily employed in food, soil or health care screening applications. The value of the systems presented are principally that where one may be inappropriate to a given circumstance an alternative may be readily applied using standard laboratory equipment and reagents without recourse to a completely new method. This is demonstrated in the case of the interference caused by ferric ion on the simple assay systems which was easily remedied through the use of cupric ion.

There have been many reported assay procedures for nitrite determination however the speed, simplicity and flexibility offered by the phenol protocols, and in particular that of phloroglucinol, should make the assay system described here a worthy contribution to existing nitrite detection strategies. More importantly, the assay is accurate and covers an analytically valuable detection range which is suitable for environmental, food and physiological analytical applications. In addition, the complementary electroanalytical detection options are shown to be attractive alternatives to the spectroscopic procedures especially where highly coloured matrices are problematic. They also demonstrate their potential to rival spectroscopy as the primary detection system for traditional assay procedures with comparable sensitivity and selectivity.

### Acknowledgements

Urine samples were obtained from the Department of Medicine, Royal Infirmary, Glasgow and many thanks are due to Dr John Lockhart for providing Griess test comparison data.



## References

- [1] J.R. Dojlido, G.A. Best, *Chemistry of Water and Water Pollution*, Ellis Horwood, Chichester, UK, 1993.
- [2] R.E. Hester, R.M. Harrison (Eds.), *Agricultural Chemicals and the Environment*, Royal Society of Chemistry, Cambridge, 1996.
- [3] J.B. Fox, *CRC Crit. Rev. Anal. Chem.* 15 (1985) 283.
- [4] C.D. Usher, G.M. Telling, *J. Sci. Fd. Agric.* 26 (1975) 1793.
- [5] J.K. Foreman, K.J. Goodhead, *J. Sci. Fd. Agric.* 26 (1975) 1771.
- [6] S.S. Mirvish, *Cancer Lett.* 93 (1995) 17.
- [7] C.S. Bruning-Fann, J.B. Kaneene, *Vet. Human Toxicol.* 35 (1993) 521.
- [8] J. Gibert, M.E. Knowles, D.J. McWeeny, *J. Sci. Fd. Agric.* 26 (1975) 1785.
- [9] M. Cameron, B.G. Gowenlock, *Chem Soc. Rev.* 19 (1990) 355.
- [10] H. Feuer (Ed.), *The Chemistry of the Nitro and Nitroso Groups*, Wiley, New York, 1969, pp. 215–300.
- [11] F.G. Mann, B.C. Saunders, *Practical Organic Chemistry*, Longman, Harlow, 1990.
- [12] S. Patai, *The Chemistry of Hydrazo, Azo and Azoxy Groups*, Wiley, London, 1975.
- [13] R.M.C. Dawson, D.C. Elliot, W.H. Elliot, K.M. Jones, *Data For Biochemical Research*, Oxford Science, 1986.
- [14] O. Carugo, K. Djinovic, M. Rizzi, C.B. Castellani, *J. Chem Soc. Dalton Trans.* (1991) 1225.
- [15] E. Colacio, J.M. Dominguez-Vera, A. Escuer, R. Kivekas, A. Romerosa, *Inorg. Chem.* 33 (1994) 3914.
- [16] J. Gabbay, Y. Almog, M. Davidson, A.E. Donagi, *Analyst* 102 (1977) 371.
- [17] A.R. Butler, D.L.H. Williams, *Chem. Soc. Rev.* 23 (1993) 233.
- [18] R.N. Sah, *Commun. Soil Sci. Plant Anal.* 25 (1994) 2841.
- [19] MAFF Food Surveillance Information Sheet, FS1S 137, Dec 1997.

# Extraction-chromatographic preconcentration with chromatomembrane separation of extract from aqueous phase for luminescence determination of oil products and phenols in natural water by flow injection analysis

A.L. Moskvina<sup>a,\*</sup>, L.N. Moskvina<sup>b</sup>, A.V. Moszhuchin<sup>a</sup>, V.V. Fomin<sup>a</sup>

<sup>a</sup> Joint Stock Company 'Granit-NEMP', Gospitalnaja st. 3, 191014, St. Petersburg, Russia

<sup>b</sup> Department of Chemistry, Saint-Petersburg State University, Universitetskij pr. 2, Stary Petergof, 198904 St. Petersburg, Russia

Received 5 July 1998; received in revised form 26 March 1999; accepted 29 March 1999

## Abstract

The new method of preconcentration by extraction for flow injection analysis (FIA) with luminescence and photometric detection is proposed. Preconcentration is carried out on extraction-chromatographic column, extract is eluted by extragent with the following separation of extract from aqueous phase in chromatomembrane cell. Possibilities of the proposed method are illustrated in the examples of FIA with luminescence determination of oil products and phenols in natural water. © 1999 Elsevier Science B.V. All rights reserved.

**Keywords:** Extraction-chromatographic preconcentration; Chromatomembrane extraction; Oil products and phenols; Natural water; Flow injection analysis

## 1. Introduction

Preconcentration by chromatomembrane extraction in flow injection analysis (FIA) [1,2] has several advantages over the traditional system of extraction in segmented flows [3]. These advantages are displayed in greater values of coefficients

of concentration and experimental conveniences of introduction the chromatomembrane cells in flow systems of analyzers. In the simplest case, which has been realized, for example, in the case of FIA photometric determination of anionic surfactants in water [4], in such cells the separation of analyzed substances is carried out to the extragent's phase, the flow of which is passing later through the corresponding flow detector.

The main disadvantage of the method is the clogging of biporous hydrophobic matrix by suspended particles represented in analyzed samples, which requires frequent replacement of chromatomembrane cells. This disadvantage occurs

\* Corresponding author. Present address: Department of Chemistry, Saint-Petersburg State University, Universitetskij pr. 2, Stary Petergof, 198904 St. Petersburg, Russia. Tel.: +7-812-2740126; fax: +7-812-4586939.

E-mail address: moskvina@pobox.spbu.ru (A.L. Moskvina)

especially during the analysis of natural and waste waters, when the initial filtration of a sample is not allowed, due to a danger of the loss of analyzed impurities.

In this article the combined scheme of preconcentration by extraction is proposed, and is more valuable in the case of analysis of natural and waste waters by FIA. According to the proposed method, the preconcentration is carried out on an extraction-chromatographic column. Stationary phase with separated on it impurities is eluted from the column by the extractant. Separation of the combined flow of aqueous and organic phases is carried out on chromatomembrane cells.

Elution from the preconcentration column can be carried out in the case of stop of the aqueous phase flow, as well as in continuous flow through it of aqueous and organic phases. In the first case, we deal with a mode of FIA with the injection of a sample to an analyzer system, and the second we deal with a mode of continuous flow analysis (CFA). In the conditions of the complete extraction of the analyzed substances into the extractant and periodic elution, which are realized in CFA, and with the great values of coefficients of distributions in a system 'sample-extractant', the coefficient of concentration will be proportional to a volume of a sample, passing through the column. In a mode of CFA, as in a case of a direct chromatomembrane separation, the coefficient of concentration will be equal to the ratio of the velocities of aqueous and organic phases.

Independently of the used mode, all suspensions from the analyzed water, will clog the easily exchangeable extraction-chromatographic column, which protects from the suspended material the chromatomembrane cell. The main advantage of the proposed mode of preconcentration is that separated commutation of aqueous and organic phases is not necessary, which simplifies the flow system of the analyzers.

Among the problems of analytical control of natural water, usually when the preconcentration by extraction is used, the most important is the

determination of total contents of oil products and phenols. In any method of their determinations, the main problems show up during the stage of extraction's preconcentration and the extraction to an organic phase. In this work, when trying to find the uniform solution for determination of both classes of substances and to allow the lowest limits of detection, the luminescence method has been chosen as a method of final determination. In order to minimize the influence of phenols on the determination of oil products, hexane has been chosen as an extractant for oil products. Both modes of extraction-chromatographic preconcentration, mentioned above, were taken into consideration: one with periodical introduction of a sample and the other with continuous separation. In both cases the separated oil products have been detected in an extractant's phase.

It is well known, that during extraction of phenols, the maximum values of coefficient of distributions are reached when tributyl phosphate (TBPh) is used [5]. The possibility of its application in FIA are limited due to its relatively high viscosity. In such a case it is more preferable that its mixtures are with less viscous organic solvents, for example with hexane. In such a case it is impossible to use the identical systems of preconcentration of oil products and phenols, because of interference of aromatic hydrocarbons as a consequent part of the oil products on luminescence determination of phenols. Interference of oil products on luminescence determination of phenols during their common preconcentration by extraction can be avoided by introduction of the stage of reextraction in an alkaline aqueous solutions with the following detection of phenols in reextract after its acidification. But it is necessary to take into consideration the possible influence of gummy acids, usually present in natural water. The introduction, in flow system of FIA analyzers, of the stage of separation of gummy acids will lead to its complication. That is why the possibility of separation of gummy acids was counted as a byway process during preconcentration of phenols by extraction.

## 2. Experimental

The initial stock solution of oil products with concentration 1 mg/l was prepared by dissolving in water the ethanol solution of the transformer oil. One milliliter of transformer oil solution with concentration 1 g/l was dissolved by water up to the volume of 1 l. The rest working solutions have been prepared by the dilution of the main stock solution. Water, used for preparation of working solutions, has been cleaned from non-polar organic impurities by way of filtration through extraction-chromatographic column with hexane as a stationary phase.

Working solutions of phenol in water were prepared by the proportional dilution of initial phenol solution with concentration 1 g/l. The initial phenol solution has been prepared from freshly sublimated phenol, kept at a low temperature. The solutions with concentration less than 10 mg/l have been used freshly prepared. For the phenol reextraction the 0.2 M solution of potassium hydroxide was used. The acidification of reextract before, the detection, was done by the 0.6 M solution of hydrochloric acid. Water used for the preparation of solutions has been purified from phenol compounds by way of filtration through the extraction-chromatographic column with TBPh as a stationary phase.

To separate aqueous and organic phases the chromatomembrane cells with the volume of mass exchangeable layer 1.27 cm<sup>3</sup> were used. The cross section of mass exchangeable layer, limited by membrane, was 1.59 cm<sup>2</sup>. Membranes and mass exchangeable layer were prepared from PTFE. The medium radius of porous in membrane was 0.2 μm. The medium radius of micro- and macroporous in mass exchangeable layer were 0.5 and 150 μm. Extraction-chromatographic column used for preconcentration were from 15 to 100 mm high with the diameter of 6 mm. The porous PTFE was used that as an organic phase carrier, the same as used in chromatomembrane cells for mass exchangeable layer.

Hexane and TBPh (qualification 'clean') were used for extraction. After analysis hexane was recovered by distillation. The TBPh-hexane mixture was separated by fractional distillation and

further TBPh was purified by fractional distillation with depression.

Flow systems for flow-injection determination of oil products and phenols with extraction-chromatographic preconcentration and chromatomembrane separations of aqueous and organic flows are shown on Fig. 1(a, b), for determination of oil products in the mode of continuous flow analysis on the Fig. 1(c). We had to reject the CFA mode with the stage of reextraction for determination of phenols due to its complexity and that its application was unjustified when compared to the limits of detection with the mode of FIA. On Fig. 1(a, b) the position of the switches of flows, shown by continuous lines corresponds to the conditions of preconcentration on extraction-chromatographic column. The position shown by the dashed lines-by elution of concentrate by extragent.

The common feature for both modes is the position of the level of waste on the lines of aqueous phase 12, which should always be higher than the level of the position of chromatomembrane cells in order to create the conditions for separation of aqueous and organic phases. Experimentally this position is taken in such a way, that in a flow of aqueous phase, coming from chromatomembrane cells, should absent the bubbles of extragent. Under chosen parameters of chromatomembrane cells and extragent flow rate of 0.5–0.7 ml/min, the minimal difference in the position of chromatomembrane cell and the level of waste, was 30 cm in the case of hexane application and 40 cm in the case of the mixture TBPh-hexane. This difference creates, inside the chromatomembrane cell, the excess of aqueous phase's pressure over organic app. by 0.3 and 0.4 atmospheres. Practically, there is no upper limit of the difference in the position of layers, because the value of capillary pressure, initiated in porous of applied membranes, is more than 1 atm.

Detection of oil products and phenols has been done with the help of fluorimeter with the flow cell. The conditions of detection were: excitation wavelength, 270 ± 10 nm; and fluorescence recording wavelength, 310 ± 10 nm. A PC was used for the governing of the analyzer and for the processing the measurement results.

### 3. Results and discussion

In a usually applied mode of chromatomembrane extraction the processes of extraction-chromatographic preconcentration and separation of the flows of a sample and extractant are carried out inside of the chromatomembrane cell. In a proposed mode the preconcentration and separation of the analyzed substances to extractant is carried out in extraction-chromatographic column. The elution of the concentrate from extraction-chromatographic column is done by extractant via intermedium chromatomembrane cell, the main function of which is to separate the flows of extractant and aqueous phase before the detection.

In the cycle of analysis of operation for extraction-chromatographic preconcentration, the limiting stage of the whole cycle of the analysis would be the elution of concentrate from chromato-

graphic column. The chosen schemes for realization of FIA (Fig. 1(a, b)) are allowed to reduce the durability of the elution stage in a cycle of analysis during the time necessary for the elution of concentrate from the column. After that, the transition to a stage of preconcentration of the next sample is possible. During this stage the flow of eluate will continue to move along tubes to a detector and after that to the waste. In such modes the total time of analysis' cycle should not be less than the time from the beginning of elution until the return of the recording system on the base line, after the elution's peak. As in any chromatographic process, the time of the return of the recording system on the base line depends on, under all other equal conditions, the quantity of analyzed substance.

In the case of oil products determinations, under chosen geometrical dimensions of extraction-chromatographic column (length, 15 mm;

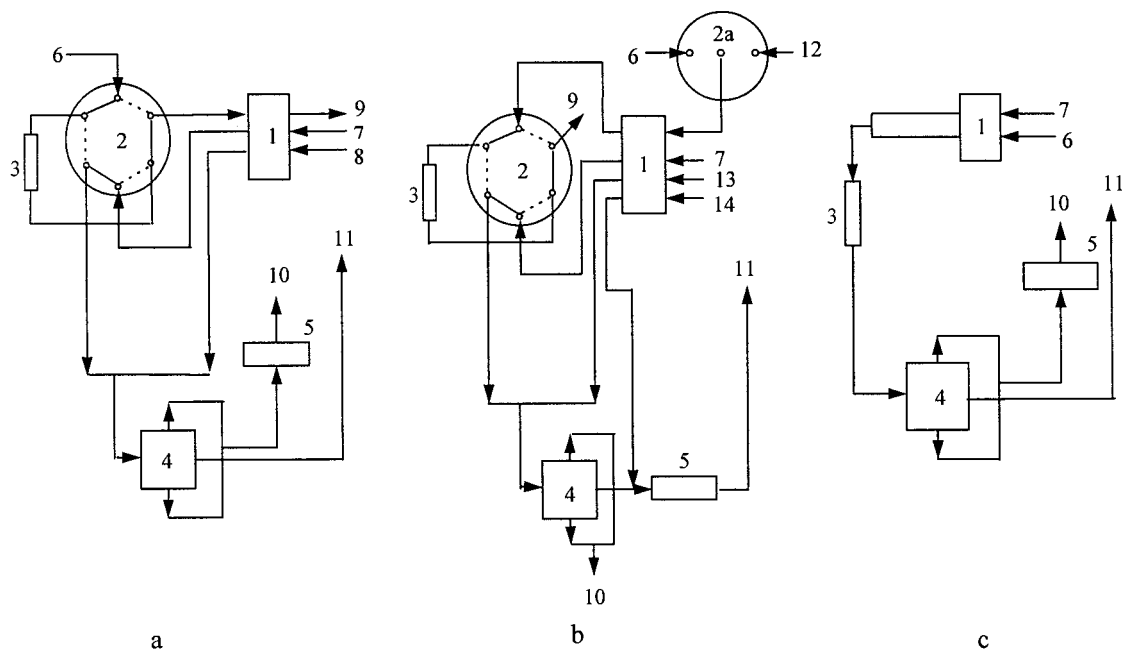


Fig. 1. Flow systems for the flow-injection (a, b) and continuous flow (c) determination with extraction-chromatographic preconcentration and chromatomembrane separations of aqueous and organic flows of oil products (a, c) and phenols (b). 1—pump; 2, 2a—valves; 3—extraction-chromatographic column; 4—chromatomembrane cell; 5—flow detector; 6–8—sample, extractant and distilled water for stabilization the extractant flow in chromatomembrane cell accordingly; 9–11—waste of sample, extract and aqueous phase from chromatomembrane cell accordingly; 12—distilled water for washing the column; 13 and 14—alkaline and acid solutions.

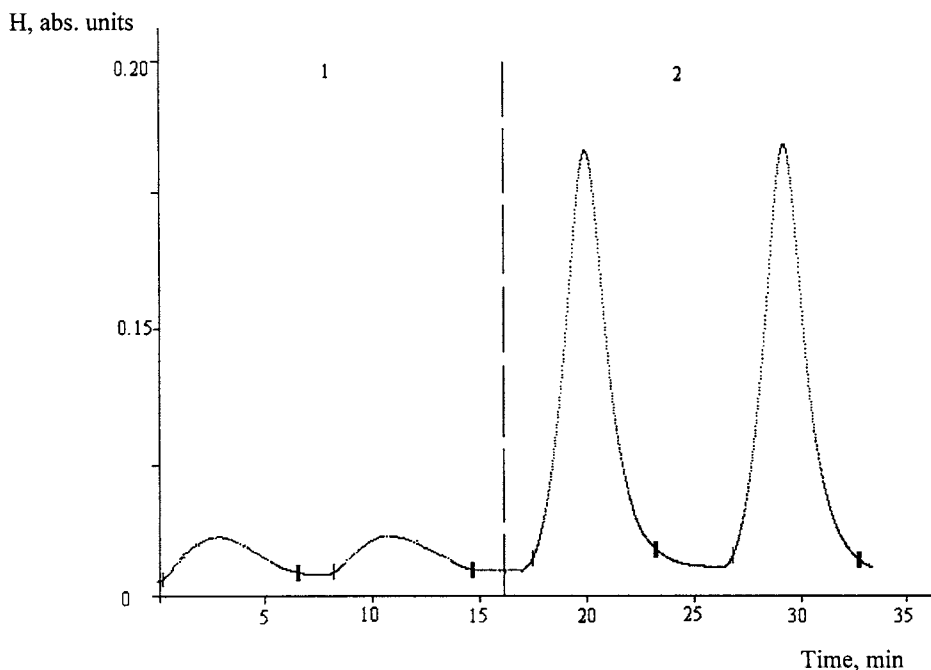


Fig. 2. General features of the analytical signal in the FIA mode with the variable of oil products concentration (1—5 µg/l; 2—50 µg/l). Flow rate of hexane = 0.5 ml/min, flow rate of sample = 2.5 ml/min.

diameter, 6 mm) and the size of particles of the carrier of the organic phase (250–500 µm), the required time of the elution's stage was 1 min; the minimal total time of the cycle was 5 min. The general features of the analytical signal in the mode of FIA with the variable of oil products concentration is illustrated by the Fig. 2. It was found that the degree of the total extraction of oil products practically does not change when the aqueous solution (sample) flow rate is in the range 0.9–9 ml/min. Under these conditions the amplitude of the elution's peak is increased proportionally to the volume of the sample in the investigated range of 10–200 ml of sample. Accordingly, there is a possibility to vary the value of the coefficient of concentration depending on the requirements to the lower level of oil products' concentrations. For determination of oil products on a level of 1 µg/l by luminescence detection only 20 ml of a sample is required.

It was elicited that phenols, until the level in the sample equals to 100 µg/l, anionic surfac-

tants equals 1 mg/l and gummy acids equals 70 mg/l, did not influence on the signal height.

In a proposed method the following parameters have been fixed: the sample flow rate was in a range shown above, the hexane flow rate was 0.5 ml/min, and the total time of a cycle was 5 min. At chosen parameters the calibrating curve was linear in a range from 1 to 1000 µg/l. In Table 1 the results of oil products determination in model aqueous solutions are shown ( $n = 7$ ,  $P = 0.95$ ).

For two stage mode of preconcentration, including the separation of analyzed substances to an extractant's phase and reextraction to aqueous

Table 1  
Results of determination of oil products in model solutions

Introduced (µg/l)	Determined (µg/l)	S (%)
5.0	6.6	22.2
100.0	98.1	11.4
250.0	248.8	5.1
500.0	461.4	3.0
1000.0	1009.7	5.0

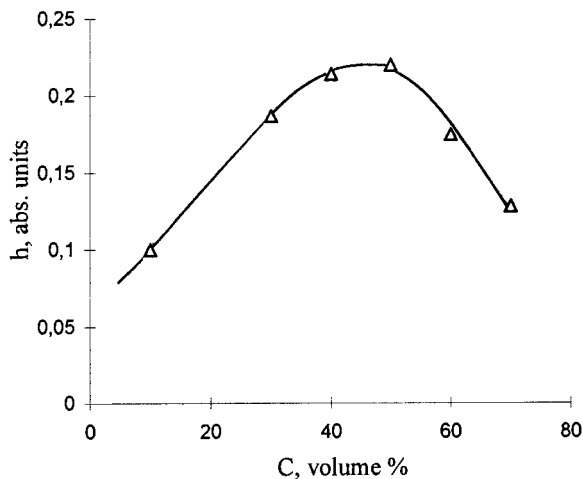


Fig. 3. Dependence of the amplitude of analytical signal ( $h$ ) from the concentration of TBPh in hexane ( $C$ ). Concentration of phenol in sample = 10  $\mu\text{g/l}$ , sample volume = 15 ml.

solutions, there is no evident criteria for the choice of extragent's compositions. In order to chose the optimal composition of extragent for phenol's determination, the dependence of the amplitude of analytical signal from the concentration of TBPh in hexane and constant quantity of phenol in samples of the initial solutions has been investigated (Fig. 3). On the base of the obtained dependence, the solutions of 50% (by volume) TBPh in hexane were chosen for the extraction of phenols. Investigations of the influence of a samples' pH on the results of determinations of phenols shows, that the variation of pH in the interval from 2 to 9 practically does not affect the value of the analytical signal. Under the fixed composition of extragent, the factor which influences the concentration of substances under determination in the phase of extragent, are the dimensions of extraction-chromatographic column. The column length, under the same diameter, governs the allowed volume of a sample before the phenols leak through the column and has an influence on the position of the eluated concentrate's peak. The optimal length of the column for a given mode of preconcentration can be chosen on the basis of dependence on analytical signal's amplitude from volumes of samples for columns of different length under the fixed

concentration of phenol in samples (Fig. 4). The obtained results show that the enlargement of the column sizes is expedient if it is necessary to reduce the limit of the detected phenols concentration. In most cases, the use of small extraction-chromatographic columns for preconcentration would be more profitable, because for determination of phenols on the level of 0.5  $\mu\text{g/l}$ , only the volume of 20 ml of a sample is needed. Under this condition the time of the eluation stage is reduced and the total time of measurement cycle can be minimized.

As was mentioned above, the main impurities affecting the determination of phenols in natural water are the gumatic acids. But the results of the experiments show, that gumatic acids are not extracted by the mixture of TBPh-hexane and only mechanically filtrate into the extraction-chromatographic column and are not eluated from it. In order to avoid the penetration of gumatic substances to reextract from the volume of a sample, which is left in free space of column, it is necessary to introduce the stage of 'washing out' of the column by the distilled water after preconcentration in order to remove the residue of a sample. The clogging force changes the column relatively often during the analysis of water with relatively high concentration of gumatic acids, but completely

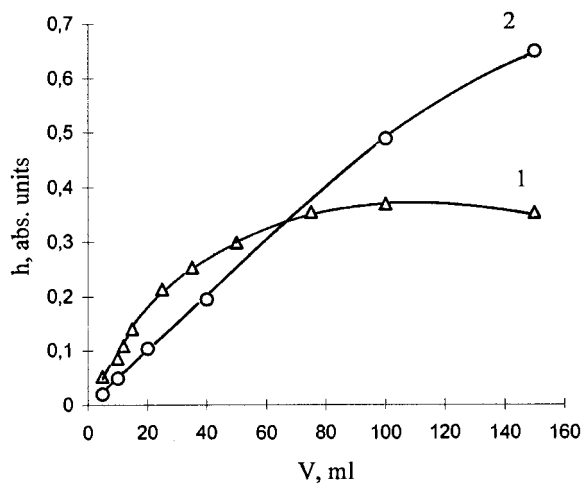


Fig. 4. Dependence of the amplitude of analytical signal ( $h$ ) from volumes of sample for the columns of different length ( $L$ ). Curve 1— $L = 30$  mm; curve 2— $L = 100$  mm. Concentration of phenol in sample = 10  $\mu\text{g/l}$ .

Table 2  
Results of determination of phenols in model solutions

Introduced ( $\mu\text{g/l}$ )	Determined ( $\mu\text{g/l}$ )	S (%)
1.0	1.1	27.6
5.0	5.3	12.3
10.0	10.1	3.1
30.0	30.5	3.3
100.0	101.9	3.2

removes their influence on the results of phenols determinations up to 70 mg/l of gamic acids in a sample. Oil products, when the level in the sample equals 1 mg/l and anionic surfactants when 1 mg/l did not influence on the phenols determination.

Following the technical possibilities of a used model of phenols analyzer, the proposed method of phenols determinations, the following parameters were chosen: the sample flow rate—5 ml/min; the extragent flow rate—0.7 ml/min; the alkaline solution 0.2 M flow rate—0.5 ml/min; the hy-

drochloric acid 0.6 M flow rate—0.2 ml/min; time of the stage of washing the column by distilled water—1 min; and total time of a cycle of analysis 8 min. Under chosen conditions the calibrating curve is linear in the range of 0.5–100  $\mu\text{g/l}$ . Table 2 gives the results of phenol determination in model solutions ( $n = 7$ ,  $P = 0.95$ ).

All given above results of determination of oil products and phenols in water has been obtained using FIA mode. For 'on line' monitoring more profitable could be CFA mode, which does not allow the loss of information about the object under monitoring during the stage of elution of extract from extraction-chromatographic column. The general features of the analytical signal in the CFA mode with the variable of oil products concentration are illustrated by Fig. 5. Contrary to a FIA mode, the possibility of variations of the coefficient of concentration, and, therefore, the limit of determined concentrations, the CFA mode is limited by the ratio of the velocities of

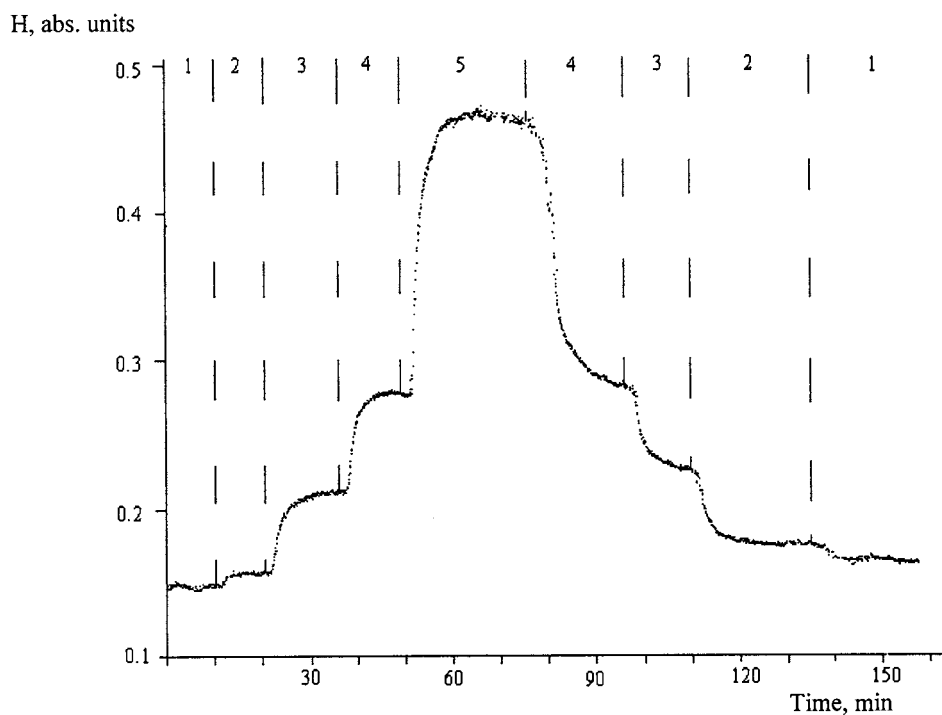


Fig. 5. General features of the analytical signal in the CFA mode with the variable of oil products concentration (1—distilled water; 2—5  $\mu\text{g/l}$ ; 3—50  $\mu\text{g/l}$ ; 4—100  $\mu\text{g/l}$ ; 5—250  $\mu\text{g/l}$ ). Flow rate of hexane = 0.74 ml/min; flow rate of sample = 6.7 ml/min.



aqueous and organic phases. The given limitation is not essential for ecoanalytical control of polluted natural and waste waters by oil products. For the determination of oil products by the CFA mode, with the ratio of the velocities of aqueous and organic phases equal to 9, the range of analyzed concentrations of oil products in water has been found to be 5–1000 µg/l. This range covers the most problems, connected with ecoanalytical investigations. As it was mentioned above, such mode can not be applied for luminescence determination of phenols due to the necessity of introduction of the stage of their reextraction into a aqueous solutions and by the influence of the gumic acids.

In comparisons with established methods of water analysis such as ISO 9377 (gravimetric and IR determination of oil products) and ISO 6439 (spectrophotometric determination of phenolic compounds with 4-aminoantipyrine) or the same EPA standards the proposed methods require far less time (5–10 min instead of 40–60 min) and sample volume (15–50 ml instead of 1–2 l). Luminescence method of phenols determination by FIA had shown better sensitivity than the photometric one (ISO 14402) with good recovery (60–90%). In the case of the oil products determination, a luminescence detector employment permit to detect aromatic structures, sub-

stantially a PAH with very high sensitivity. Thus all saturated hydrocarbons are ignored. This fact lead to essential reduction results of determination of the oil products by this method when the sample content benzene, kerosene and the other same fractions. However, proposed method could be used successfully for samples screening purposes, for example for the on-line environmental monitoring.

The investigations carried out show the wide analytical possibilities of the proposed methodological way to the realization of the processes of extraction's preconcentration using FIA. The mode including extraction-chromatographic preconcentration and chromatomembrane separation of extract can be adapted to any extraction system, used in extraction photometric and extraction luminescence methods of analysis.

## References

- [1] L.N. Moskvina, J. Chromatog. A 669 (1994) 81–87.
- [2] L.N. Moskvina, J. Simon, Talanta 41 (1994) 1765–1769.
- [3] H. Lui, P.K. Dasgupta, Anal. Chim. Acta 288 (1994) 237–245.
- [4] L.N. Moskvina, J. Simon, P. Löffler, N.V. Michailova, D.N. Nicolaeva, Talanta 43 (1996) 819–824.
- [5] Ya.I. Korenman, N.N. Selmanshchik, V.A. Minasyants et al., Fresenius J. Anal. Chem. 335 (1989) N 2, 131–136.

# Flow injection spectrophotometric determination of lactic acid in skimmed milk based on a photochemical reaction

E. Gómez-Álvarez, E. Luque-Pérez, A. Ríos, M. Valcárcel \*

*Department of Analytical Chemistry, Faculty of Sciences. University of Córdoba, E-14004 Córdoba, Spain*

Received 30 September 1998; received in revised form 3 March 1999; accepted 30 March 1999

## Abstract

A spectrophotometric method for the determination of lactic acid in milk samples based on the use of a photochemical reaction carried out in a Flow Injection System is proposed. Determination is based on the reaction between lactic acid and Fe(III), which is reduced to Fe(II) in the presence of UV light, being the latter made to react with *o*-phenanthroline. The complex formed between Fe(II) and *o*-phenanthroline, Fe(*o*-phen)<sub>3</sub><sup>2+</sup> (ferroin) is a coloured compound and it can be spectrophotometrically monitored at 512 nm. The method shows a linear range between 0.5 and 50 µg ml<sup>-1</sup> with a limit of detection of 0.16 µg ml<sup>-1</sup>. The precision was ± 2.15 expressed as relative standard deviation (*n* = 11) and the sample throughput of 30 samples h<sup>-1</sup>. Also non-linear adjustments have been made and validated by ANOVA. The proposed method has been applied to the determination of lactic acid in both synthetic and milk samples. © 1999 Elsevier Science B.V. All rights reserved.

*Keywords:* Flow injection; Photochemical reaction; Lactic acid; Milk samples

## 1. Introduction

Milk is a heterogeneous natural product composed of inorganic species, vitamins, proteins, lipids and carbohydrates (lactose). Aerobical degradation of lactose produces lactic acid. Therefore pH, lactose and lactate concentration measurements should be checked for determining potability of milks. The normal lactate concentration in fresh milk samples is about 1–2 mmol l<sup>-1</sup> (i.e. 90–180 µg ml<sup>-1</sup>) but it can increase to 10–20

mmol l<sup>-1</sup> (i.e. 900–1800 µg ml<sup>-1</sup>) because of microbial fermentation [1]. The content of lactic acid in food is regulated by the legislation in the different countries. It is therefore very important to determine lactic acid in a simple, reliable and inexpensive way. According to the Spanish legislation, acidity is expressed as weight of lactic acid and the maximum allowed is 0.19 g per 100 ml what corresponds to a concentration of 1900 µg ml<sup>-1</sup> [2]. However, no regulation on lactic acid concentration is found in this same source for other dairies such as butter, yoghurt, sour cream, etc. When it comes to contrast the concentration of lactic acid in numerical terms there seems to be some contradictions. In addition, this type of

\* Corresponding author. Tel.: +34-957-218614; fax: +34-957-218606.

*E-mail address:* qa1meobj@uco.es (M. Valcárcel)

information is often missing in the literature. Sechaud et al. [3] found a concentration of lactic acid of 0.92 mM in half-skimmed milk and values of concentration significantly higher were found in some other dairies (ranging from 83.2 mM for cream cheese to 116.1 mM for bulgarian yoghurt), whereas a concentration of 2.8 mM in milk has been found by using an enzyme electrochemical sensor [4], in a determination, using an electrochemical sensor based on the use of lactate oxidase immobilised in a poly-(vinyl alcohol) matrix platinized graphite electrode by chemical cross-linking with isocyanate. Also, the enantiomeric discrimination between L- and D-forms has been reported by using HPLC with polarized photometric detector [5]. Morales et al. [6] described the enzymatic determination of lactic acid and glucose, using for this an automatic sequential flow-injection analysis (FIA) method for the determination of both analytes based on enzymatic reactions with Hexokinase (HK) and glucose-6-phosphate dehydrogenase (GDH) immobilized on controlled-pore glass. Other enzymatic methods have been also proposed [7–10].

The use of photochemical reactions in flow injection (FI) systems has demonstrated its usefulness from an analytical point of view. Thus, oxalate was determined by using its reaction with Fe(III) using a specially designed flow-cell, which allowed the irradiation of the sample–reagent mixture and the simultaneous monitoring of the progress of the photochemical reaction [11]. In a later work [12], a similar system was applied to the determination of oxalate in urine samples. The photochemical determination of citrate in beverages and fruit juices has been also proposed by using a flow system [13]. Moreover, several continuous-flow manifolds were developed to implement the photochemical reaction between ascorbic acid and methylene blue [14]. Pérez Ruiz et al. [15] based their determination of citrate on the photochemical decomposition of the iron (III)-citrate. Detection was based on the catalytic effect of this complex on the chemiluminiscent luminol in the absence of added oxidant. The same principle was also extended to the determination of oxalate [16].

Determination of lactic acid using a photochemical reaction in a FI system has not been reported so far. It is well known that a number of carboxylic acids, such as citric acid and lactic acid, are oxidised when their solutions containing  $\text{Fe}^{3+}$  are irradiated with visible or UV light [17]. The photochemical process consists of the reduction of  $\text{Fe}^{3+}$  to  $\text{Fe}^{2+}$ , evolution of carbon dioxide and formation of oxidation products ( $\text{CH}_3\text{COCH}_3$  in the case of lactic acid). In this work, it is reported how this photochemical reaction can be used to determine lactic acid, using for detection the complex formation reaction between the  $\text{Fe}^{2+}$  originated and 1,10-phenanthroline. The red–orange coloured complex formed is spectrophotometrically measured at 512 nm, where the complex shows a maximum absorption. In principle, the method hereby proposed should be valid for the determination of all isomeric forms of lactic acid, thus serving as a good procedure for determination of total lactic acid in milk as means of establishing a quality rank based on this parameter. In addition, it could be an appropriate method for determining acidity of milk that is often expressed in terms of lactic acid concentration. The use of luminous light to develop derivatising reactions in FI systems simplifies the set-up by eliminating the need for additional channels and confluence points for the reagents. The main advantages of the method here proposed are those derived from using light as a reagent and the fact that dilution is the only sample treatment applied.

## 2. Experimental

### 2.1. Apparatus

A UNICAM 8625 UV/Vis Spectrophotometer equipped with a Hellma QS 1000 flow cell of 18  $\mu\text{l}$  inner volume and 10 mm light path was used, and it was connected to a REC-80 SERVOGRAPH recorder. A Gilson Minipuls-3 peristaltic pump allowed the introduction of the reagents into the system. A Rheodyne 5041 injection valve and two laboratory made poly(methyl methacrylate) mixing points were also used. Poly(vinyl chloride)

pump tubing of different diameters, suited to the required flow rate, and PTFE tubing of 0.8 mm inner diameter completed the flow system. A 500-W visible light lamp from Larelco (Italy) and a power regulator were also used.

In addition, a Diode Array Hewlett Packard 8453 interfaced to a Hewlett Packard Vectra 500 computer connected to a Hewlett Packard DeskJet 400 printer was also used to study the effect of dispersion caused by the sample plug injected.

## 2.2. Chemicals

A standard stock solution containing  $1000 \mu\text{g ml}^{-1}$  of lactic acid was prepared from DL-lactic acid syrup provided by Sigma. Standard working solutions were made by appropriate dilution of the stock solution. A stock solution of  $\text{Fe}^{3+}$  was prepared by dissolving 0.1 g of  $\text{Fe}(\text{NO}_3)_3 \cdot 9 \text{H}_2\text{O}$  (Merck) in 100 ml of 0.01 M HCl, and kept in a PVC bottle. A working solution containing  $100 \mu\text{g ml}^{-1} \text{Fe}^{3+}$  was then prepared by dilution from the stock. The solution of reagent was prepared by dissolving 1 g of 1,10-phenantrolinium-chloride monohydrate (Merck) in 100 ml of water. A 0.1-M nitric acid was used as washing solution. All solutions were prepared in MilliQ water, to avoid possible contamination from  $\text{Fe}^{3+}$ , which due to its abundance could be present in water, air, etc.

The stability of the standard solutions of lactic acid was also investigated. A  $30\text{-}\mu\text{g ml}^{-1}$  solution of lactic acid was analysed over a few days for

stability studies. The results of these experiments showed that the solutions were reasonably stable for more than a week. However, some increase in the absorbance yielded by the solutions started to occur for longer times, possibly indicating that some decomposition was taking place.

## 2.3. Manifold

The manifold used is depicted in Fig. 1, and consisted of four channels. The sample channel filled the loop of an injection valve (IV), being carried into the system by a second stream of buffer, which provided the appropriate pH for the photochemical and chemical reactions to take place. The third stream, carrying  $\text{Fe}^{3+}$  joined the sample/buffer stream in a mixing point prior the reactor (R). This reactor was placed in a water bath, which helped to prevent excessive heating of tubing and reactor. Light from a 500-W halogen lamp was made to fall on the reactor and a box was used to prevent it from dispersing in all directions. Once the reduction of  $\text{Fe}^{3+}$  to  $\text{Fe}^{2+}$  by lactic acid and light had taken place, the stream that contained  $\text{Fe}^{3+}$ ,  $\text{Fe}^{2+}$  and buffer joined another stream of 1,10-phenanthroline, giving rise to the formation of an orange-red  $\text{Fe}(\text{phen})_3^{2+}$  complex (ferroin). As the coloured complex was passing through the flow-cell placed at the detector, a transient peak arose which was measured at 512 nm.

The operational sequence was as follows. First, the pump was switched on and the reagents let flow through the system for some minutes. Then

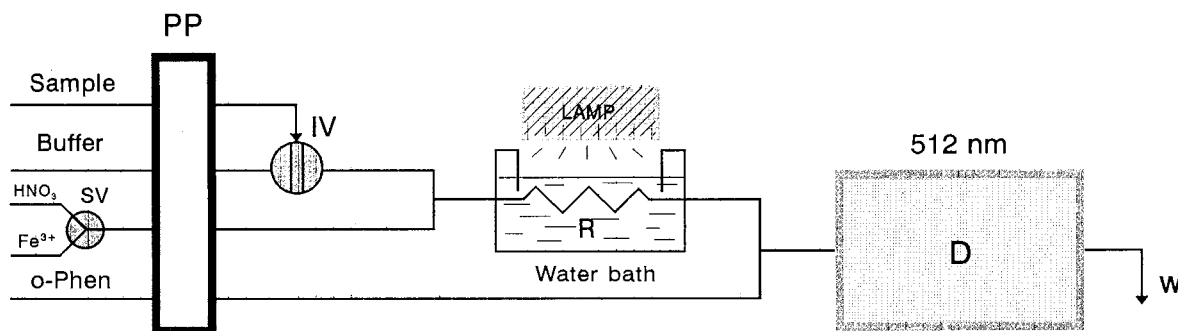


Fig. 1. FIA manifold for the determination of lactic acid based on the proposed photochemical reaction.

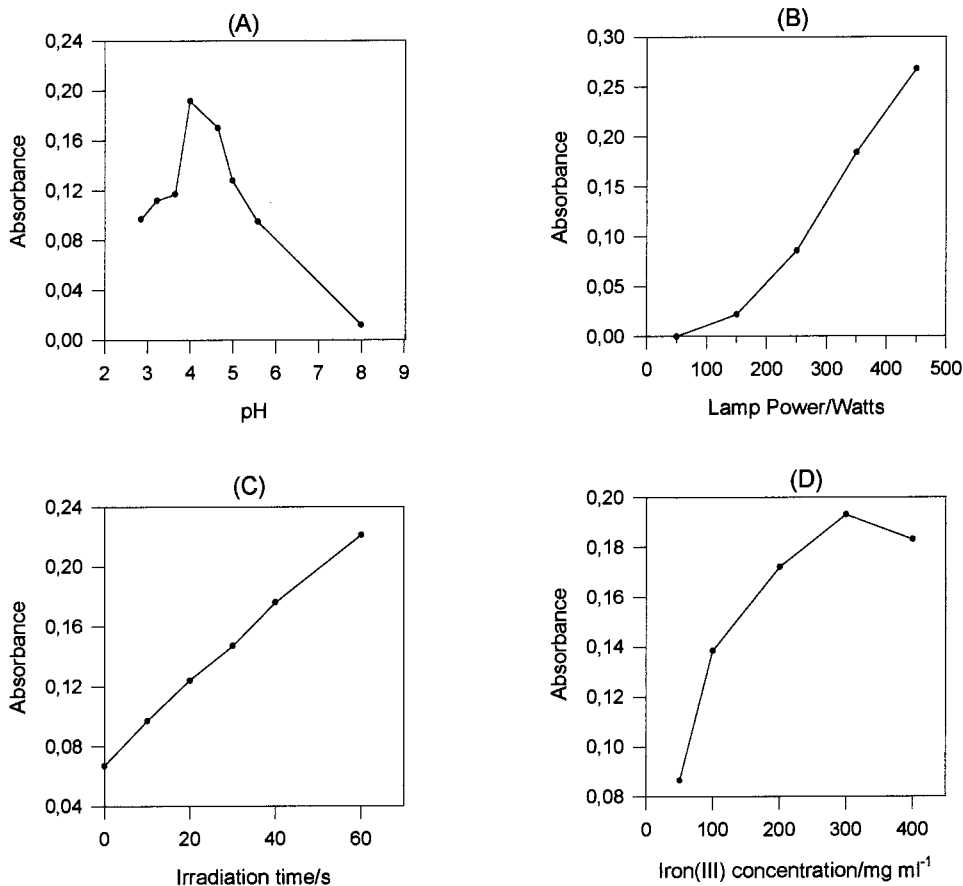


Fig. 2. Influence of pH (A), lamp intensity (B), irradiation time (C), iron(III) concentration (D) on the response obtained in the FI system.

the lamp was switched on and the instrument zeroed, with all the reagents passing through the flow-cell except the sample that was filling the loop of the injection valve. This injection valve was then actuated, and the sample was led by the buffer into the system and joined the stream of  $\text{Fe}^{3+}$ . When the sample reached the reactor (R), the flow was stopped for a fixed time (Section 3.1), in order to irradiate the sample and activate the development of the photochemical reaction between  $\text{Fe}^{3+}$ , lactic acid and light. After this time, the pump was switched on again and a transient FIA peak was obtained due to absorption of the coloured  $\text{Fe}(\text{phen})_3^{2+}$  complex while passing through the detection point. Once the maximum of the peak appeared, the injection

valve was actuated back to the filling position and the system was ready for a new experiment.

### 3. Results and discussion

#### 3.1. Optimisation

As it is usual in FIA systems, attention should be focused on physical, chemical and hydrodynamic variables for optimisation purposes. Among the physico-chemical variables, the effect of pH, light intensity, irradiation time, Fe(III) and *o*-phenanthroline concentration were studied. As FIA variables, time before stopping the flow, flow rates in each line and reactor volume. Fig. 2 comprises some of the results obtained.

The buffer was prepared at a pH = 4 since this proved to be the optimum value (Fig. 2(A)). Initially, it was feared that this value of pH could lead to precipitation of casein and proteins present in milk giving rise to a cloudy solution. However, no problem occurred when working with real samples, probably due to the high dilution factor employed. From Fig. 2(B and C), it can be easily appreciated that light is a reagent of a paramount importance for the reaction to take place. When a low light intensity was applied, the reaction did not occur or occurred only in a small extent. The higher the lamp power applied the better the sensitivity attained. However, 460 W was finally chosen as optimum since good sensitivity was obtained while moderating in some extent heating of the system with respect to the maximum value of 500 W. On behalf of the irradiation time, although the higher the irradiation time the better the sensitivity, a time of 30 s was chosen as a compromise between sensitivity and analysis time. Fig. 2(D) shows that a concentration of Fe(III) of 300  $\mu\text{g ml}^{-1}$  resulted in better sensitivities, but it could also give rise to problems of carryover and contamination of the lines, and it makes it more difficult to clean the system afterwards by the use of a dilute solution of nitric acid. Therefore, a Fe(III) concentration of 200  $\mu\text{g ml}^{-1}$  was chosen.

The time allowed before the flow was stopped was also optimised. Initially, the time that it took for the sample plug to arrive to the reactor was measured using a coloured solution. Then, a range of times was chosen about this value in order to find the optimum time that contributed to the increase in the sensitivity. A neat increase was observed up to 40 s. After this time, an irregular dependence of the response versus time was observed. A time of 30 s was chosen as optimum. The response versus phenanthroline concentration reached a maximum for 0.25% (w/v) and started to decrease after this value, which was consequently chosen as optimum. The flow rates in the different lines were also optimised. In the buffer line, it was observed that the response decreased with the buffer flow rate. A flow rate of 0.8  $\text{ml min}^{-1}$  was chosen as a com-

promise between sensitivity and sample throughput. This was also the case for the  $\text{Fe}^{3+}$  line, and an optimum value of 0.8  $\text{ml min}^{-1}$  was chosen for the same reason. The phenanthroline flow rate was assessed in a narrower range (0.15–1.1  $\text{ml min}^{-1}$ ). The behaviour obtained was similar as for the other lines, i.e. a decrease in the response with the flow rate. Chosen as optimum was 0.25  $\text{ml min}^{-1}$ . The plot of response versus sample loop volume reached a plateau when the latter was 200  $\mu\text{l}$ . However, a slight increase was still observed up to 350  $\mu\text{l}$  that was therefore chosen as the optimum value. The reactor volume influence on the response was assayed in the range 108–550  $\mu\text{l}$ . The response kept increasing up to the highest volume assayed although an irregular pattern was observed in some intervals. A reactor volume of 550  $\mu\text{l}$  was chosen as optimum for subsequent experiments. The assayed range for all the variables subject to study, as well as the optimum conditions picked finally are displayed in Table 1.

Table 1  
Optimum conditions found for the determination of lactic acid by the proposed method

	Optimum value	Assayed range
<i>Chemical variables</i>		
pH	4.0	2.8–8.0
1,10 phenanthroline concentration	0.5%(m/v)	0.25–1.95
$\text{Fe}^{3+}$ concentration	200 $\mu\text{g ml}^{-1}$	50–400 $\mu\text{g ml}^{-1}$
<i>FIA variables</i>		
Buffer flow rate	0.8 $\text{ml min}^{-1}$	0.6–1.4 $\text{ml min}^{-1}$
$\text{Fe}^{3+}$ flow rate	0.8 $\text{ml min}^{-1}$	0.4–2 $\text{ml min}^{-1}$
1,10-phen line flow rate	0.25 $\text{ml min}^{-1}$	0.15–1.1 $\text{ml min}^{-1}$
Sample volume	350 $\mu\text{l}$	150–500 $\mu\text{l}$
Reactor volume	550 $\mu\text{l}$	108–550 $\mu\text{l}$
Time before stop flow	30 s	20–50 s
<i>Photochemical variables</i>		
Irradiation time	30 s	0–60 s
Lamp power	460 W	50–500 W

Table 2

Figures of merit for the first, second and third order adjustments for the calibration equation

Equation <sup>a</sup>	Conditions	Regression coefficient	Determination range ( $\mu\text{g ml}^{-1}$ )	Throughput (samples $\text{h}^{-1}$ )	Precision ( $n = 11$ ) (%RSD)	LOD ( $\mu\text{g ml}^{-1}$ )
$A = 6.59 \times 10^{-3}C + 1.37 \times 10^{-2}$	460 W–30 s stop	0.9984	0.5–50	30	2.15	$7.13 \times 10^{-2}$
$A = -3.34 \times 10^{-5}C^2 + 7.73 \times 10^{-3} C + 1.24 \times 10^{-2}$	460 W–30 s stop	0.9092	0.5–150	30	2.15	$1.07 \times 10^{-2}$
$A = 1.48 \times 10^{-7}C^3 - 6.56 \times 10^{-5} C^2 + 9.38 \times 10^{-3}C + 3.35 \times 10^{-3}$	460 W–30 s stop	0.9979	1–150	30	2.15	1.04

<sup>a</sup> A, absorbance; C, concentration of lactic acid in  $\mu\text{g ml}^{-1}$

Table 3  
Validation by ANOVA for the first, second and third order-degree curves<sup>a</sup>

Degree	SV	SS	DF	MS	$R^2$ (%)	$R'^2$ (%)
First order	Regression	$9.71 \times 10^{-2}$	1	$9.71 \times 10^{-2}$	99.7	99.6
	Residuals	$3.00 \times 10^{-4}$	6	$5.00 \times 10^{-5}$		
	Total	$9.74 \times 10^{-2}$	7	$1.39 \times 10^{-2}$		
Second order	Regression	0.413	2	0.206	91.0	88.9
	Residuals	0.042	11	$3.86 \times 10^{-3}$		
	Total	0.454	13	$3.49 \times 10^{-2}$		
Third order	Regression	0.411	3	0.137	99.8	99.7
	Residuals	$8.24 \times 10^{-4}$	10	$8.24 \times 10^{-5}$		
	Total	0.411	13	$3.16 \times 10^{-2}$		

<sup>a</sup> SV, source of variation; SS, sum of squares; D.F., degrees of freedom; MS, mean of squares;  $R$ , determination coefficient;  $R'$ , adjusted coefficient of determination.

### 3.2. Calibration curve

Different-order curves were adjusted to the absorbance readings obtained for a series of experimental points obtained on injection of lactic acid standards and the quality of the adjustment was estimated according to a mathematical model of ANOVA [18]. In Table 2, the figures of merit for each curve are presented. The limit of detection (LOD) was calculated as the value obtained for the blank (water) plus three times its standard deviation. As can be seen in the table a good linear adjustment was obtained in the range 0.5–50  $\mu\text{g ml}^{-1}$ . The aim when adjusting to higher order curves was to widen the range of concentrations (0.5–50  $\mu\text{g ml}^{-1}$ ) to which the calibration curve could be applied since the very high concentration of lactic acid in milk is what adds difficulty to its determination. The model [19] assumes that random errors only occur in the direction of the  $y$ -axis.  $R^2$  is defined as:

$$R^2 = \frac{\text{SS due to regression}}{\text{Total SS}} = 1 - \frac{\text{SS residuals}}{\text{Total SS}}$$

where SS represents the sum of squares. In order to consider the different number of degrees of freedom in the polynomial regression, the adjusted  $R'^2$  value was used:

$$R'^2 = 1 - \frac{\text{AS of residuals}}{\text{Total AS}}$$

being AS the average of squares. The results obtained for the application of the model can be found in Table 3. An adjustment to a second order polynomial curve is not appropriate in the range 0.5–150  $\mu\text{g ml}^{-1}$  in the view of the values for  $R^2$  yielded (91%), and regression coefficient of 0.909 (Table 2). Conversely, very good values were obtained for the third order curve ( $R^2 = 99.8\%$ ). In addition, higher orders than the third are not used normally. This is the reason why the third order equation was considered to fit best the experimental points in the range of concentrations that went up to 150  $\mu\text{g ml}^{-1}$ .

### Interferent species

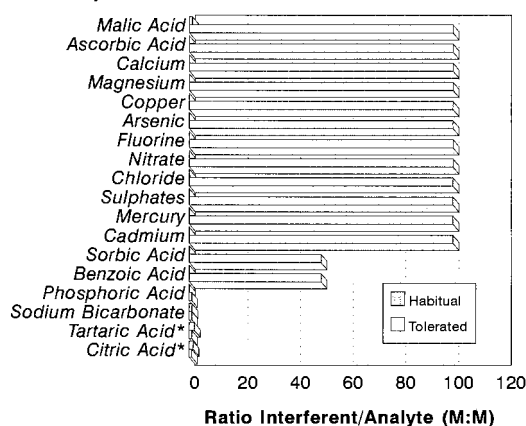


Fig. 3. Graphical study of the interferences.



Table 4

Experimental results obtained for the analysis of synthetic samples by the proposed method by using different adjustment orders for the calibration

Degree of adjustment and equation	Conc. added ( $\mu\text{g ml}^{-1}$ )	Conc. found ( $\mu\text{g ml}^{-1}$ )	Recovery (%)
First degree $y = 1.78 \times 10^{-2} + 5.96 \times 10^{-3} x$	0.78	0.60	77.0
	4.20	4.22	105.5
	8.25	7.58	91.9
	22.02	25.53	115.9
	34.02	37.45	110.1
	48.00	46.34	96.5
	50.00	48.69	97.4
	56.00	55.23	98.6
Second degree $y = 0.01 + 7.33 \times 10^{-3}x - 2.97 \times 10^{-5} x^2$	0.78	0.54	69.2
	4.20	4.09	97.4
	8.25	6.95	84.2
	22.02	23.61	107.2
	34.02	36.41	107.0
	48.00	47.36	98.7
	50.00	50.53	101.1
	56.00	60.19	107.5
Third degree $y = 6.26 \times 10^{-3} + 8.57 \times 10^{-3}x - 5.56 \times 10^{-5}x^2 + 1.23 \times 10^{-7}x^3$	0.78	1.14	146.1
	4.20	4.41	105.0
	8.25	6.93	84.0
	22.02	22.13	100.5
	34.02	34.54	101.5
	48.00	45.82	95.5
	50.00	49.22	98.4
	56.00	60.05	107.2

### 3.3. Interferences

Fig. 3 presents in a graphical mode the results obtained in the study of interferences carried out. The figure illustrates a comparison between the habitual ratio in which the studied species are present in food [2], together with the limits tolerated by the proposed method, taken as the largest amount of interferent yielding a relative error lower than  $\pm 3\%$  of the signal obtained for  $30 \mu\text{g ml}^{-1}$  lactic acid. The tolerated ratios (likely/potential interferent:lactic acid) were in most of the cases far higher than those in which they are normally encountered in real samples. The only serious problems encountered were for citric and tartaric acids. For those two, interferences appeared at low ratios interferent:lactic acid. However, these carboxylic acids are not expected to be

present in milk. Therefore, these potential interferences do not pose any major risk in the determination pursuit. The use of an enzymatic reaction to decompose these interferences into other derivatives that would not interfere with the reaction could also be considered if needed.

Pilloton et al. [1] found interferences from ascorbic acid that they tried to eliminate by the use of an acetate dialysis membrane. Also in a previous work [13], we found interferences from ascorbic acid when determining citric acid in beverages and fruit juices by a similar method based on a photochemical reaction. The interference was minimised by using an immobilised enzymic reactor (IER). In the work hereby presented, that type of interference was not a problem as shown in Fig. 3. The presence of ascorbic acid was not expected in milk. Spanish legislation gives only a

maximum allowed value of ascorbic acid added as antioxidant for powder milk but not for other types of milk, such as fresh, pasteurised or UHT milk. Therefore, a molar ratio of 1:20 000 ascorbic:lactic acid was assayed. This was the habitual ratio at which these two acids were normally allowed in the legislation for other types of food in which both could be present such as beverages

and fizzy drinks. The ratio was increased up to a numerical value of 1:200 ascorbic:lactic acid, and it still exercised no influence on the determination.

### 3.4. Validation of the method

The applicability of the proposed method was checked by analysing standards of lactic acid of known concentration. Table 4 displays the concentrations found and percentage recoveries for a series of these samples in the range of concentrations 2–56  $\mu\text{g ml}^{-1}$  when applying the first, second and third order calibration curves. As can be seen in the table, recoveries were very good in all cases. Percentage recoveries ranged from 77 to 115% when they were calculated from the first order calibration curve, 69–107% for the second order and 84–107% for the third order.

## 4. Analytical applications

### 4.1. Application to the analysis of real samples

The official method [19] for the analysis of lactic acid in milk samples as suggested by the AOAC involves several extraction steps with different organic solvents and is therefore prone to introducing errors throughout the different steps. Trying to separate lactic acid from the matrix would unavoidably give rise, to a lengthy process, difficult to automate (to integrate in a FIA system). The reason is that lactic acid seems to remain in the solid organic phase together with casein and fats after treatment with trichloroacetic/acetic acid, as can be figured out from the successive extraction steps with ether involved in the official method. Initial experiments gave favourable results by simple dilution of the sample. Therefore, an appropriate dilution factor was investigated for the analysis of real samples.

Fig. 4 presents DAD (Diode Array Detection) spectra obtained for aqueous solutions of lactic acid (A–C) and ten-times diluted milk (D–F). It is obvious from the second group of spectra that a dilution factor of 10 is not enough since the light is obviously being dispersed by the sample.

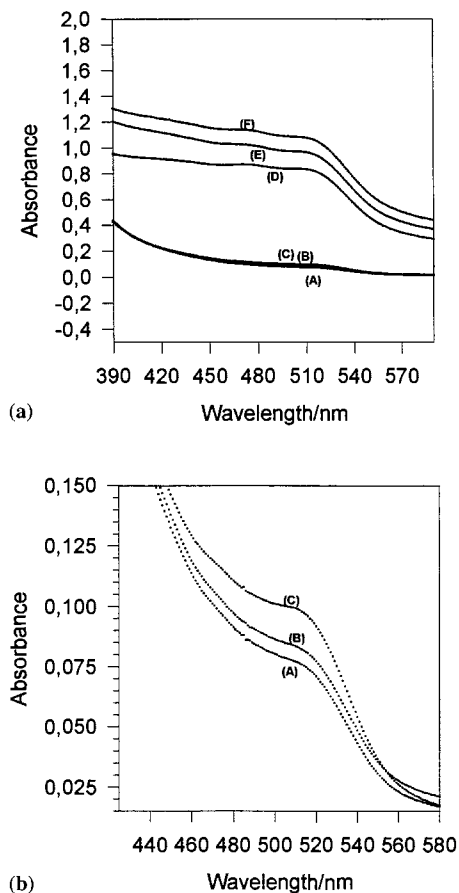


Fig. 4. (a) Spectra showing the effect of the direct introduction of milk samples (in all cases: 5 ml buffer  $\text{AcO}^-/\text{AcOH}$ ,  $\text{pH} = 4.0$ , 3 ml  $100 \mu\text{g ml}^{-1}$   $\text{Fe(III)}$  solution and 1 ml *o*-phen solution were added). Curves (A), (B) and (C) correspond to water and lactic acid solutions and (D), (E) and (F) to samples containing milk. The composition of each sample is as follows: (A) blank (water); (B) =  $1.5 \mu\text{g ml}^{-1}$  of lactic acid (without irradiation); (C) = (B) with irradiation; (D) = milk sample diluted ten times (without irradiation); (E) = (D) with irradiation, and (F) = (E) +  $1.36 \mu\text{g ml}^{-1}$  of lactic acid. (b) Zoom of curves (A), (B), (C) in last figure (the scale has been expanded).

Table 5  
Analysis of milk samples by the proposed method

Sample	Concentration added ( $\mu\text{g ml}^{-1}$ )	Concentration found ( $\mu\text{g ml}^{-1}$ )	Recovery (%)	Total conc. found <sup>a</sup> ( $\mu\text{g ml}^{-1}$ )
A	2.00	1.92	95.8	2020.0
	4.00	4.21	105.2	
	6.00	6.50	108.3	
	8.00	8.58	107.2	
	10.00	10.04	100.1	
	12.00	12.12	101.0	
B	2.00	1.87	93.5	878.4
	4.00	4.00	100.0	
	6.00	5.48	91.3	
	8.00	8.24	103.0	
	10.00	10.11	101.1	
	12.00	12.05	100.4	
C	2.00	1.64	82.0	1336.4
	4.00	3.69	92.3	
	6.00	5.74	95.6	
	8.00	7.79	97.4	
	10.00	9.59	95.9	
	12.00	10.98	91.5	
D	2.00	1.54	77.0	1672.4
	4.00	4.35	108.7	
	6.00	6.63	110.0	
	8.00	8.74	109.2	
	10.00	10.58	105.8	
	12.00	12.59	104.9	

<sup>a</sup> Calculations made by applying the dilution factor.

As it is widely known, Lambert Beer's law should be applied to values of absorbance not higher than 1. When that is the case, absorbance values cannot be used for quantitation. Obviously, the higher the dilution factor the more the effect of dispersion can be overcome. However, the dilution cannot be as high as to bring the concentration of lactic acid lower than the LOD. Since lactic acid can be present in milk in a concentration ranging on average between 1000 and 3000  $\mu\text{g ml}^{-1}$ , an intermediate value, i.e. 1500  $\mu\text{g ml}^{-1}$  will be taken. A dilution factor of 1000 would bring the concentration of lactic acid down to 1.5  $\mu\text{g ml}^{-1}$ . By doing this, the effects originated by dispersion of light will be reduced greatly while maintaining the concentration of lactic acid over the LOD. Fig. 4(a) displays the spectra obtained on direct introduction of milk samples. Two sets of curves are represented in the graph, i.e. those

corresponding to standard solutions (A–C) and those corresponding to milk samples (D–F). A closer look at curves A–C (Fig. 4(b)) allows to see clearly that a 1.25- $\mu\text{g ml}^{-1}$  lactic acid solution (B) can be clearly distinguished from pure water (A) and shows also the enhancing effect of the light on the signal (C). Spectra of aqueous solutions of 1.5  $\mu\text{g ml}^{-1}$  of lactic acid (B) show that the system responds sensitively to this concentration. Although as has already been said, spectra D, E and F in Fig. 4 cannot be used for quantitation, the enhancing effect produced by light (E) and by small differences in lactic acid concentration can still be noticed (in F, the concentration of lactic acid has been increased in 1.36  $\mu\text{g ml}^{-1}$  over the concentration in E).

The method of standard additions was applied to eliminate any likely matrix effect produced by the sample of 1000-time diluted milk. When the

method of standards additions was applied to the sample diluted 1000 times, good sensitivities were obtained and a good linearity was observed (higher than 0.999 in all instances). The method of standard additions was applied to four different brand names of skimmed milk. The absorbance values readings were recorded for the solutions of diluted milk together with their additions of 2, 4, 6, 8, 10 and 12  $\mu\text{g ml}^{-1}$ . The results obtained are presented in Table 5.

## 5. Conclusion

The application presented in this work constitutes a rapid and inexpensive method for the monitoring of the amount of lactic acid present in milk. Several methods to achieve determination of lactic acid have been described so far in the literature. The determination procedure should work at an acidic pH in order to detect all the lactic acid present. This is another asset of the method hereby proposed. Although the optimum pH was 4.0, no precipitation or change in the physical properties of the solution were observed at the working pH used perhaps due to high working dilution factors. This photochemical method provides the appropriate selectivity to be applied to real milk samples.

The high concentrations of lactic acid found in milk pose a difficulty to its determination. However, determination of the concentration of lactic acid in milk should be done accurately since this is an important parameter, which determines quality of milk and other dairy products. Therefore, an attempt to widen the concentration range used for the calibration curve has been made. For larger concentration ranges, non-linear adjustments have been made which have been validated using an ANOVA mathematical model.

## Acknowledgements

Financial support provided by DGICyT (PB95-0977) is gratefully acknowledged.

## References

- [1] R. Pilloton, T.N. Nwosu, M. Mascini, *Anal. Lett.* 21 (5) (1988) 727–740.
- [2] A. Madrid, *Manual de Utilización de los Aditivos en Alimentos y Bebidas*, Madrid, Ediciones, 1987, p. 170.
- [3] F. Sechaud, S. Peguin, P.R. Coulet, G. Bardeletti, *Process Biochem.* 24 (1) (1989) 33–38.
- [4] K. Hajizadeh, B. Halsall, W.R. Heineman, *Talanta* 38 (1991) 37–47.
- [5] A. Yamamoto, A. Matsunaga, K. Hayakawa, M. Miyazaki, M. Nishimura, *J. Chromatogr.* 727 (1996) 55–59.
- [6] M.T. Morales, P. Linares, M.D. Luque de Castro, M. Valcárcel, *Anal. Chim. Acta* 238 (1990) 411–415.
- [7] F.K. Mizutani, S. Yabuki, Y. Hirata, *Talanta* 43 (1996) 1815–1820.
- [8] S. Benthin, J. Nielsen, J. Villadsen, *Anal. Chim. Acta* 247 (1991) 45–50.
- [9] J. Nielsen, K. Nikolajsen, S. Benthin, J. Villadsen, *Anal. Chim. Acta* 237 (1990) 165–175.
- [10] K. Nikolajsen, J. Nielsen, J. Villadsen, *Anal. Chim. Acta* 214 (1988) 137–145.
- [11] L.E. León, A. Ríos, M.D. Luque de Castro, M. Valcárcel, *Anal. Chim. Acta* 234 (1990) 227–232.
- [12] L.E. León, A. Ríos, M.D. Luque de Castro, M. Valcárcel, *Analyst* 115 (1990) 1549–1552.
- [13] E. Luque Pérez, A. Ríos, M. Valcárcel, *Anal. Chim. Acta* 366 (1998) 231–240.
- [14] A. Sanz-Martínez, A. Ríos, M. Valcárcel, *Analyst* 117 (1992) 1761–1765.
- [15] T. Pérez Ruiz, C. Martínez-Lozano, V. Tomás, O. Val, *Analyst* 120 (1995) 471–475.
- [16] T. Pérez Ruiz, C. Martínez-Lozano, A. Sanz, O. Val, *Anal. Chim. Acta* 284 (1993) 173–179.
- [17] V. Balzani, V. Carassiti, *Photochemistry of Coordination Compounds*, Academic Press, London, 1970, pp. 172–174.
- [18] J.C. Miller, J.N. Miller, *Statistics for Analytical Chemistry*, 3rd ed., Ellis Horwood, 1993, pp. 133–137.
- [19] AOAC Official Methods of Analysis 15th ed., Association of Official Analytical Chemists, Arlington, USA, 1990, pp. 806–807.

# Adsorptive stripping voltammetric assay of phenazopyridine hydrochloride in biological fluids and pharmaceutical preparations

Suzy M. Sabry \*

*Pharmaceutical Analytical Chemistry Department, Faculty of Pharmacy, University of Alexandria, Alexandria, Egypt*

Received 27 October 1998; received in revised form 5 March 1999; accepted 30 March 1999

## Abstract

A sensitive method for the measurement of phenazopyridine hydrochloride (PAP) by differential pulse polarography (DPP) based on adsorptive stripping technique, using a hanging mercury drop electrode (HMDE) is described. The voltammetric peak is obtained at  $-0.760$  V, which corresponds to the reduction of the azo group in Britton–Robinson buffer. The redox behaviour is reversible. Optimum conditions were found to be: accumulation potential  $-50$  mV (vs. Ag/AgCl), accumulation time 60 s, scan rate  $5$  mV s $^{-1}$ , pulse amplitude  $-100$  mV and supporting electrolyte Britton–Robinson buffer (0.04 M, pH = 11). The relative standard deviation (at 20 ng ml $^{-1}$  level) was  $\pm 0.6\%$  for six measurements. The calculated detection limit was 0.0299 ng ml $^{-1}$  with a 60-s accumulation time. The applicability of such a method was evaluated through the assay of PAP in human plasma and urine samples after a simple extraction procedure and in pharmaceutical preparation. The mean recovery was  $97 \pm 2$  (100 ng ml $^{-1}$  plasma). © 1999 Elsevier Science B.V. All rights reserved.

*Keywords:* Adsorptive stripping voltammetry; Differential pulse mode; Phenazopyridine hydrochloride; Plasma and urine samples

## 1. Introduction

Phenazopyridine hydrochloride exerts an analgesic effect on the mucosa of the urinary tract and is used to provide symptomatic relief of pain in conditions such as cystitis and urethritis [1]. It is given in conjunction with an antibacterial agent for the treatment of urinary-tract infections.

The USP 20 (1980) recommends a direct spectrophotometric procedure for the assay of phenazopyridine hydrochloride (PAP) bulk drug and tablets [2]. The USP 23 (1995) gives a HPLC method for PAP tablets assay [3].

A variety of analytical techniques have been used to assay PAP including amperometry in a flowing stream at the glassy carbon electrode [4], UV spectrophotometry [5], and colorimetry [6,7]. Quantitation of PAP combination with nitrofurantoin has been achieved by spectrophotometric [8–10], HPLC [11], polarographic [12], and

\* Tel.: +20-3-4833810/4222692; fax: +20-3-4833273.

E-mail address: pharmacy.alex.univ.mac@cns-egypt.com (S.M. Sabry)

gravimetric [13] methods. Simultaneous determination of PAP and sulfonamides has also been reported [14–16].

The polarographic reduction of PAP has been investigated by Surmann and Aswakun [12]. The studies have been performed with differential pulse polarography using Pt electrode (vs. Ag/AgCl) in Britton–Robinson buffer of pH 5.5. The method was adopted for simultaneous determination of PAP and nitrofurantoin in tablets.

The adsorption behaviour of PAP at the mercury electrode has not yet been studied. So it would be of interest to investigate the properties of adsorption process of PAP at hanging mercury drop electrode (HMDE). The work presents a study of the factors that may influence both the accumulation process and the voltammetric response. A sensitive adsorptive stripping procedure for voltammetric measurement of PAP was developed.

Reviewing the literature, it was revealed that up to the present time, nothing has been published concerning the determination of PAP in human biological fluids using electrochemical method. This article deals with the application of the proposed voltammetric method to the assay of PAP in biological fluids and its dosage form.

## 2. Experimental

### 2.1. Apparatus

The voltammograms were obtained with a Metrohm 693 VA Processor. A Metrohm 694 VA Stand was used in the HMDE mode. The three-electrode system was completed by means of a Ag/AgCl (3 M KCl) reference electrode and a Pt auxiliary electrode.

### 2.2. Chemicals and reagents

Phenazopyridine hydrochloride was purchased from Kahira Pharm., Egypt and used as received. All experiments were performed with analytical-reagent grade chemicals and pure solvents.

Urisept tablets (Kahira Pharm., Egypt) labelled to contain 100 mg phenazopyridine hydrochloride per tablet

Stock standard solution (1.00 mg ml<sup>-1</sup>) of PAP was freshly prepared in distilled water. From this solution, intermediate dilution steps were made with distilled water in accordance with the concentration range used in the analytical technique.

The studies were carried out in Britton–Robinson buffer (0.04 M in each of acetic, *o*-phosphoric and boric acids) adjusted to the required pH with 0.2 M sodium hydroxide solution.

### 2.3. Procedure for voltammetric analysis

Supporting electrolyte (10 ml) was placed in the voltammetric cell and the required volume of standard PAP solution was added by micropipette (1–20 ng ml<sup>-1</sup>). The stirrer was switched on and the solution was purged with nitrogen gas for 5 min. The accumulation potential was then applied to a new mercury drop, whilst still stirring the solution. Following the accumulation period, the stirring was stopped and allowed to equilibrate for 10 s. The voltammogram was obtained by applying a negative going potential scan. Unless otherwise stated the following parameters were used; accumulation time 60 s, accumulation potential –50 mV, –100 mV pulse amplitude for differential pulse stripping, scan rate 5 mV s<sup>-1</sup> and a potential interval 10 mV. The maximum drop size, 9 (Ca. 0.60 mm<sup>2</sup> drop area) and constant stirrer speed, 2000 rpm were used.

### 2.4. Pharmaceutical formulation

A quantity of the mixed contents of 20 tablets equivalent to 100 mg of PAP was dissolved in 50 ml of distilled water with stirring. The solution was filtered into a 100-ml calibrated flask, the residue washed several times with distilled water and the solution diluted to the mark. Suitable dilution steps were made with distilled water. For the analysis, the experimental work described in the previous section was followed using the pharmaceutical sample solution instead of the standard one.

## 2.5. Preparation of biological samples

Frozen plasma (or urine) was thawed at room temperature, saturated with sodium chloride (ca. 0.5 g of NaCl for each ml) and alkalised to a pH ~ 13 with 2 N sodium hydroxide solution. Into a set of separators, separate aliquots of the prepared sample, 1 ml each, were spiked with varying amounts (ranged from 500 to 100 ng) of the standard PAP solution and extracted with four 5-ml portions of chloroform. Each extraction was shaken for 2 min. The extracts were filtered through anhydrous sodium sulfate. The combined chloroform extracts (relevant for each sample) were carefully evaporated to dryness. The remaining residue was reconstituted in Britton–Robinson buffer (pH 11) and the volume was completed to 25 ml. The resulting solution was taken for voltammetric analysis following the op-

timised instrumental adjustments. The recovery was calculated with reference to the data obtained from standard PAP solution.

## 3. Results and discussion

### 3.1. Adsorptive behaviour of phenazopyridine hydrochloride

Adsorption of the analyte was confirmed by the results obtained with cyclic voltammetry. Fig. 1 shows two sets of sequential cyclic voltammograms for 200 ng ml<sup>-1</sup> PAP. For 10 s accumulation, only a small peak is observed at -0.760 V (A). When the experiment is repeated with 40 s accumulation period (-50 mV), a significantly (~ three-fold) larger adsorptive stripping peak is observed (B), indicating an interfacial accumula-

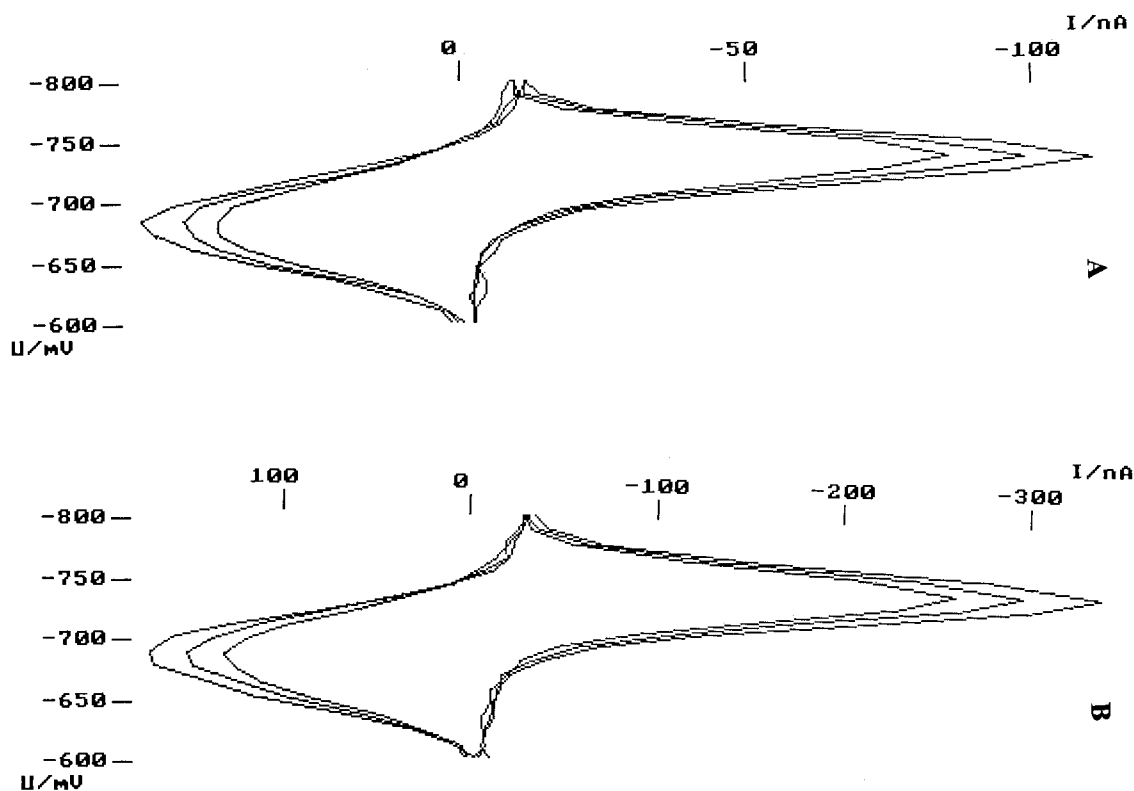


Fig. 1. Cathodic-anodic sequential cyclic voltammogram for PAP (200 ng ml<sup>-1</sup>) in pH 11 Britton–Robinson buffer using a scan rate of 500 mV s<sup>-1</sup>.  $t_{\text{acc}}$  = (A) 10 s and (B) 40 s. Accumulation potential = -50 mV.

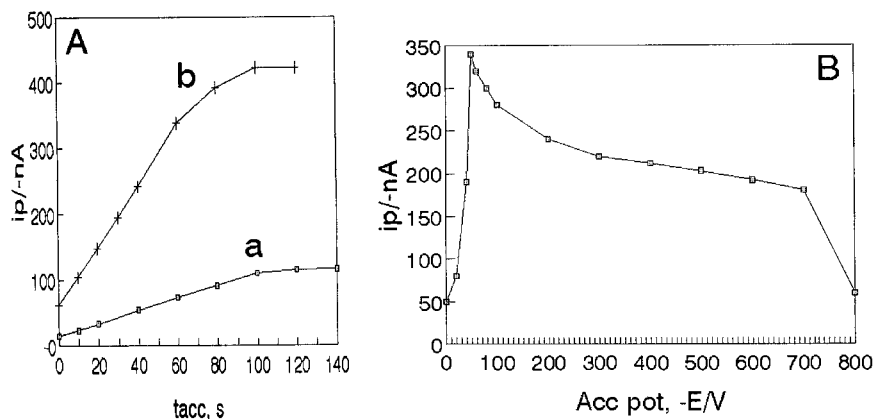


Fig. 2. A: Effect of accumulation time on the peak current, PAP concentration = a, 4; and b, 20 ng ml<sup>-1</sup> in pH 11 Britton–Robinson buffer (scan rate = 5 mV s<sup>-1</sup>, accumulation potential = -50 mV, pulse amplitude = -100 mV). B: Effect of accumulation potential on the response to 20 ng ml<sup>-1</sup> PAP.  $t_{acc}$  = 60 s, other conditions as in A.

tion of PAP. Clearly the reduction of PAP is totally reversible, with the product of reduction also being adsorbed. The peak decreased rapidly upon repetitive scan, indicating rapid desorption of the compound from the surface.

### 3.2. Factors influencing the accumulation step

The spontaneous accumulation of PAP can be exploited for effective preconcentration prior to the voltammetric scan. Fig. 2A displays the resulting peak current versus preconcentration time plot for 4 (a) and 20 (b) ng ml<sup>-1</sup> PAP. The rapid increase of the current observed at short preconcentration time, is followed by a levelling-off for longer periods. The plots do not pass through the origin possibly because of the strong adsorption of the analyte at the electrode surface at the equilibrium time which was fixed at 10 s. Hence to maximise sensitivity, a 60-s accumulation time was generally used for subsequent quantitative determinations. However, the ultimate choice of accumulation time should depend on the concentration range studied.

The effect of the accumulation potential on the adsorptive stripping peak current was evaluated over the range -0.800–0 V (Fig. 2B). Larger peaks were obtained over the range from -0.050 to -0.060 V, the peak decreased rapidly at lower and higher potentials. Therefore an adsorption

potential of -0.050 V was adopted for analytical determination of PAP.

### 3.3. Influence of the pH of the supporting electrolyte

The effect of pH on the peak current and the reduction potential was studied over the range 4.0–11.0 (20 ng ml<sup>-1</sup> PAP). Plots of peak potential versus pH and peak current versus pH are given in Fig. 3 (curves a and b, respectively). The potential of the adsorptive stripping peaks moves to more negative values with increasing pH, with

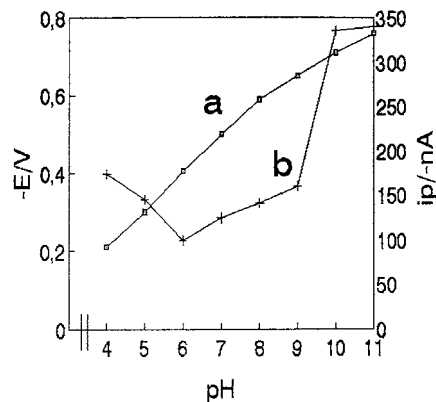


Fig. 3. Influence of pH on the DP adsorptive stripping peak potential, a, and peak current, b, of PAP (20 ng ml<sup>-1</sup>) in Britton–Robinson buffer. Other conditions as in Fig. 2.



Table 1

Parameters of calibration graphs and limit of detection (DL) of phenazopyridine hydrochloride by DP cathodic stripping voltammetry

Concentration range (ng ml <sup>-1</sup> )	<i>t</i> <sub>acc</sub> (s)	Slope, <i>b</i> (nA ml ng <sup>-1</sup> )	Intercept, <i>a</i> (nA)	Correlation coefficient ( <i>r</i> )	DL (ng ml <sup>-1</sup> )
1–20	30	10.0119	0.4762	0.9999	0.0725
1–20	60	17.2636	-1.7415	1	0.0299

a change of slope at pH > 8. The slope of the linear portion from pH 4 to 8 being 95 mV pH<sup>-1</sup>. The peak current has its maximum value at pH 10–11.

### 3.4. Calibration graph and detection limit

Under the optimised conditions of a preconcentration potential of -50 mV, a scan rate of 5 mV s<sup>-1</sup> and a pulse amplitude of -100 mV, the peak current monitored was found to be proportional to the PAP concentration. Data recorded in Table 1 summarises the characteristics of the calibration plots following 30 and 60 s of preconcentrations. Both plots are highly linear over the entire range examined (1–20 ng ml<sup>-1</sup>) with slopes, 10.01 and 17.26 nA ng<sup>-1</sup> ml, respectively.

According to IUPAC [17], the detection limit DL = 3 *s*/*k*, where *s* is the standard deviation of replicate determination values under the same conditions as for the sample analysis in the absence of the analyte; *k* is the sensitivity, namely the slope of the calibration graph. Now, *n* = 6, *s* = 0.1722 nA, *k* = 17.26 nA ng<sup>-1</sup> ml, hence DL = 3 *s*/*k* = 0.0299 ng ml<sup>-1</sup>.

### 3.5. Precision

The adsorptive accumulation of PAP results in reproducible adsorptive stripping peak currents. For six successive measurements of 20 ng ml<sup>-1</sup> of the analyte, the mean peak current was 346.3 nA, with a range of 344–350 nA and a relative standard deviation of 0.6%.

### 3.6. Pharmaceutical applications

The proposed method was applied to the determination of PAP in its dosage form. The re-

coveries were calculated with reference to the calibration graph (Table 1). As can be seen from the results shown in Table 2, the method gave satisfactory recovery data. The statistical calculations for the assay results show good precision of the method. According to the *t*- and *F*-test, there were no significant differences between the calculated and theoretical values at *P* = 0.05, demonstrating that the proposed method is as accurate and precise as the official spectrophotometric method [2].

### 3.7. Interferences from co-formulated drugs

Interference studies were carried out in order to investigate the effect of sulphamethoxazole, sulphadiazine, nalidixic acid, oxytetracycline and nitrofurantoin that are co-formulated with PAP in some of its dosage forms.

The determination of PAP (10 ng ml<sup>-1</sup>) by the proposed procedure in the presence of each of the

Table 2

Application of the voltammetric and spectrophotometric methods for the assay of Urisept tablets<sup>a</sup>

Voltammetric declared (ng ml <sup>-1</sup> )	Recovery ± <i>s</i> <sup>b</sup> (%) <sup>c</sup>	Spectrophotometric <sup>d</sup> recovery ± <i>s</i> <sup>b</sup> (%) <sup>c</sup>
8	98.7 ± 0.7	99.6 ± 0.4
20	98.6 ± 0.4	
	<i>t</i> = 3.71; <i>F</i> = 1.25 <sup>e</sup>	

<sup>a</sup> Urisept tablets (Kahira Pharm., Egypt) labelled to contain 100 mg phenazopyridine hydrochloride per tablet.

<sup>b</sup> *s* refers to standard deviation.

<sup>c</sup> Mean of five determinations.

<sup>d</sup> Ref. [2].

<sup>e</sup> Tabulated value for *t*-test = 3.83 and for *F*-test = 6.39 at *P* = 0.05.

aforementioned ingredients, at 40 ng ml<sup>-1</sup> level, was evaluated. The recovery of PAP ranged from 98 to 101%.

The voltammograms were recorded in the range from -0.2 to -1.4 V. Under the instrumental parameters adjusted for PAP determination, only nitrofurantoin exhibits a signal at -0.470 V.

Another factor has to be considered is the solubility of the tested drugs in water. Nalidixic acid, sulphamethoxazole, sulphadiazine, oxytetracycline and nitrofurantoin are known to be very slightly soluble in water. So, whenever water is used as a solvent, negligible amounts, or even nil, of the latter drugs will co-extracted with PAP.

It could be concluded that using the proposed procedure with the specified instrumental parameters, the signal monitored at -0.760 V can be used for selective measurement of PAP.

### 3.8. Application to biological samples

Preliminary experiments were carried out to recover the analyte from spiked plasma (or urine) samples (200 ng ml<sup>-1</sup>) after a prior purification step of protein deposition with ethanol, methanol or acetonitrile. A flow of nitrogen was used to flush out the organic solvent (supernatant) and the residue was reconstituted with Britton–Robinson buffer. Under the optimised instrumental conditions, the voltammetric signal was monitored. About 90% of the peak current decreased.

The previous results indicated that the natural components of human plasma (or urine) interfere with the analyte signal, possibly the surface active compounds that can competitively adsorb on the electrode surface. This necessitates the development of extraction procedure to efficiently recover the drug from plasma or urine to exclude the matrix interferences.

The extraction of PAP from aqueous solutions alkalised with 2 N sodium hydroxide solution (pH ~ 13) was carried out using chloroform. The percent recovery obtained for the extraction of 500 ng ml<sup>-1</sup> of PAP from an aqueous solution with four 5-ml portions of

Table 3

Analytical results of phenazopyridine hydrochloride in biological samples

Spiked plasma per 1 ml (ng)	Recovery ± s <sup>a</sup> (%) <sup>b</sup>	Standard addition procedure Recovery ± s <sup>a</sup> (%) <sup>b</sup>
500	80 ± 3	99 ± 2 <sup>c</sup>
100	71 ± 3	97 ± 1
Spiked urine per 1 ml, ng		
500	84 ± 4	100 ± 1 <sup>d</sup>
100	81 ± 7	99 ± 2

<sup>a</sup> s refers to standard deviation.

<sup>b</sup> Mean of four determinations.

<sup>c</sup> Day-to-day precision (98 ± 1).

<sup>d</sup> Day-to-day precision (98 ± 2).

chloroform was ~98%. The extraction with chloroform has been described in the USP [3] for PAP in its combined dosage form with oxytetracycline and sulfamethizole.

The applicability of the proposed voltammetric method following the extraction procedure was evaluated through the analysis of biological samples, fortified with varying amounts of PAP (500–100 ng ml<sup>-1</sup>). The recoveries of PAP were calculated comparing the signals provided by the examined samples after following the procedure in the experimental section with the direct measure of a PAP standard of the same theoretical concentration in Britton–Robinson buffer.

At a concentration level of 500–100 ng ml<sup>-1</sup> PAP in biological sample, the peak current obtained was ~75%. Obviously this does not mean that the yield of PAP extraction is worst, but some amount of interferences can be co-extracted with it, resulting in a decrease of the adsorption capacity for PAP.

To assess the reproducibility, four determinations for each concentration examined were conducted and the standard deviation was calculated. The results obtained are listed in Table 3. As can be seen, recovery varies between 70 and 80%. So, if a direct calibration with standards is employed, a 20–30% of error in defect will be obtained.

Fig. 4 shows the voltammograms of a plasma blank and a 10-ng ml<sup>-1</sup> PAP in plasma (prepared by spiking 1 ml plasma with 250 ng PAP) obtained following the proposed procedure. No electrochemical signal appears in the blank at the potential where reduction of PAP occurs.

### 3.9. Standard addition procedure and precision study

The relatively low recovery makes it advisable to employ a standard addition procedure for the determination of PAP in biological samples rather than the employment of a calibration with standards. Samples can be determined using the following standard addition procedure: a sample is first treated following the general procedure described in the experimental section and after that the sample is spiked with a known amount of PAP and the voltammetric measurement is taken again. The increase on peak current can be used to determine the amount of PAP present in the sample. Determination of a 100-ng per 1 ml plasma (spiking) or urine sample based on this procedure, showed errors between 2 and 4%.

Day-to-day precision was studied by analysing plasma and urine samples spiked with PAP at a concentration level of 500 ng per 1 ml (ca. combined before and after extraction). The analysis was followed up to 4 days using standard addition technique. The results presented were acceptable (Table 3).

### 3.10. Metabolites

Studies [18] of urinary metabolites of PAP in man showed that the drug is subjected to in vivo reductive metabolism with the cleavage of the azo linkage. The metabolites identified in man's urine included; aniline, *N*-acety-*p*-aminophenol, *p*-aminophenol and traces of *o*-aminophenol. About 45% of the drug is excreted unchanged.

Voltammetric measurement of solutions of aniline, *N*-acety-*p*-aminophenol and *o*-aminophenol in Britton–Robinson buffer, pH = 11, under the specified instrumental parameters indicated only a signal for *o*-aminophenol at -0.530 V.

However, theoretically the phenolic metabolites can not be extracted from urine samples alkalinised with 2 N sodium hydroxide into the chlo-

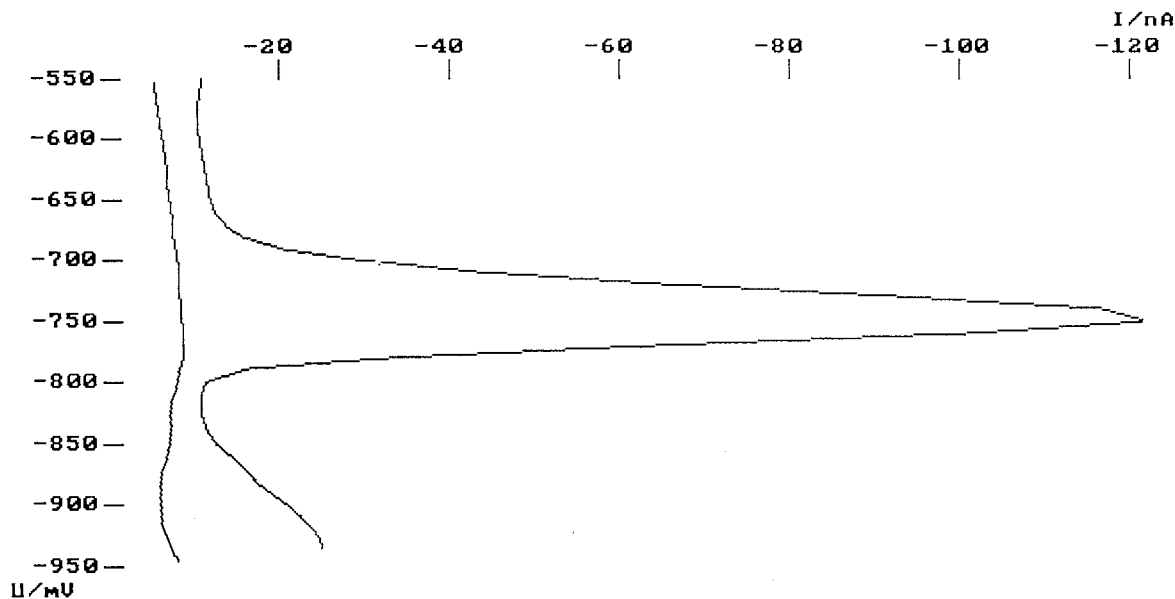


Fig. 4. Voltammograms obtained from A, a plasma blank and B, 10 ng ml<sup>-1</sup> PAP in prepared plasma sample, after following the general procedure described in the experimental section. Other conditions as in Fig. 2.

roform layer. Accordingly the procedure described for PAP extraction (Section 2.5) from biological samples excludes interference, if any, of these metabolites.

In conclusion, the method described provides a sensitive approach to the determination of PAP in biological samples. Moreover, the proposed method is simple, sensitive and accurate, and can be applied to the quality control analysis of PAP pharmaceutical formulations.

## References

- [1] Martindale, in: E.F. Reynolds (Ed.), *The Extra Pharmacopoeia*, 30th ed., Pharmaceutical Press, London, 1993, p. 29.
- [2] *United States Pharmacopeia XX*, US Pharmacopoeial convention, Rockville, MD, 1980.
- [3] *United States Pharmacopeia XXIII*, US Pharmacopoeial convention, Rockville, MD, 1995.
- [4] F. Belal, *J. Assoc. Off. Anal. Chem.* 68 (1985) 1207.
- [5] L. Szabolcs, *Acta Pharm. Hung.* 48 (1978) 155.
- [6] F. Belal, M.E.-S. Metwally, *Anal. Lett.* 17 (1984) 1637.
- [7] S.C. Mathur, Y. Kumar, N. Murugesan, Y.K.S. Rathore, P.D. Sethi, *Indian Drugs* 29 (1992) 375.
- [8] M.I. Walash, A.M. El-Brashy, M.S. El-Din, M.A. Abuirjeie, M.A. El-Rahman Sultan, *Pharmazie* 49 (1994) 698.
- [9] J.J. Berzas Nevado, J. Rodriguez Flores, M.L. De la Morena Pardo, *Analisis*, 21 (1993) 33; *Anal. Abstr.* 55 (1993) 7G39.
- [10] S.M. Hassan, F. Belal, M.K. Sharaf El-Din, M. Sultan, *Anal. Lett.* 21 (1988) 1199.
- [11] F. Belal, *Chromatographia* 25 (1988) 61.
- [12] P. Surmann, P. Aswakun, *Arch. Pharm.* 318 (1985) 14.
- [13] M.N. Vora, K. Maheswaran, *Indian J. Pharm.* 38 (1976) 98.
- [14] B. Nickerson, S. Scypinski, H. Sokoloff, S. Sahota, *J. Liq. Chromatogr.* 18 (1995) 3847.
- [15] M.H. Abdel-Hay, A.M. El-Walily, *Spectrosc. Lett.* 26 (1993) 1745.
- [16] J.L. Du Preez, S.A. Botha, A.P. Lotter, *J. Chromatogr.* 333 (1985) 249.
- [17] J.N. Miller, *Analyst* 113 (1991) 3.
- [18] W.J. Johnson, J. Burba, *Fed. Proc.* 25 (1966) 734.

# Diamine oxidase and putrescine oxidase immobilized reactors in flow injection analysis: a comparison in substrate specificity

M.-A. Carsol, M. Mascini \*

*Dipartimento di Sanità Pubblica, Epidemiologia e Chimica Analitica Ambientale, Sezione di Chimica Analitica, Via Gino Capponi 9, 50121 Firenze, Italy*

Received 25 January 1999; received in revised form 22 March 1999; accepted 30 March 1999

## Abstract

Enzyme reactors for the determination of biogenic amines have been developed using diamine oxidase (DAO) from porcine kidney and from lentil and putrescine oxidase (PUO) from microorganism (*Micrococcus roseus*). Determination is based on the electrochemical oxidation of enzymatically produced  $H_2O_2$  at platinum electrode poised at 600 mV versus Ag/AgCl. The enzymes are immobilized on controlled pore glass beads activated by glutaraldehyde in a small reactor (diameter 5 mm, length 50 mm) and included in a flow injection analysis assembly. The reactor using DAO from porcine kidney as the biochemical component responds mainly to histamine (with a detection limit of 0.5  $\mu M$ ), and it can be used for the evaluation of fish spoilage. The PUO reactor shows a significant response only to putrescine. It is linear in the range 0.07–500  $\mu M$ . The reactor using DAO from lentil is sensitive to several amines and it could be useful to evaluate a total value. The buffer used for both types of oxidase based sensors is phosphate 0.10 M pH 7.0 containing 0.10 M NaCl. © 1999 Elsevier Science B.V. All rights reserved.

*Keywords:* Biogenic amines; Diamine oxidase; Putrescine oxidase; Fish spoilage

## 1. Introduction

Biogenic amines, low molecular weight organic bases, possess biological activity [1]. In foods, amine levels are a good index of food decomposi-

tion: they are formed upon degradation of proteins and amino acids by decarboxylase-positive microorganisms [2]. Putrescine, cadaverine and histamine, have been confirmed useful chemical indicators [3] of bacterial spoilage of food. The most frequent intoxication involves histamine, and histamine poisoning is referred to as ‘scombroid fish poisoning’ because is often associated with the consumption of scombroid fish: tuna, mackerel and sardines [1].

\* Corresponding author. Tel.: +39-55-2757267; fax: +39-55-2476972.

E-mail address: mascini@cesit1.unifi.it (M. Mascini)

The analytical methods used for their separation and quantification are mainly based on chromatographic methods: gas chromatography [4], thin-layer high-performance liquid chromatography (HPLC) [5,6], reversed phase HPLC [7–9] and HPLC with precolumn [7,10], post-column [11,12] or oncolumn derivatization techniques [13].

Official AOAC methods for analysis of histamine in seafood involve biological, colorimetric or fluorometric procedures [14].

The maximum level allowed in fish samples by Italian law is 100 mg/kg, and similar limits are adopted by EC regulations.

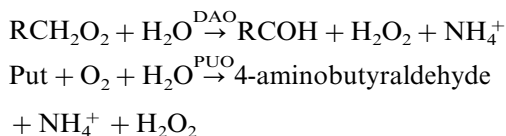
Recently due to the commercially availability of enzymes like monoamine oxidase (MAO) and putrescine oxidase (PUO) several groups tried to couple the enzymatic reactions with electrochemical sensors in order to obtain simple and reproducible biogenic amine biosensors. In some cases the amines have been coupled with oxygen sensors [15,16] or hydrogen peroxide sensors [17–19]. In such attempts several immobilization procedure were proposed.

Also in this laboratory, previous attempts [20] to obtain biogenic amine biosensor with a flow injection analysis (FIA) arrangement and several procedures using one or two enzymes with or without a mediator dissolved in the carrier stream have been worked out.

In this paper, three other approaches were developed using different enzymes (diamine oxidase (DAO) from porcine kidney commercially available, from lentil not commercially available and PUO again commercially available from *Micrococcus roseus*) immobilized in a small reactor (diameter 5 mm, length 50 mm) in FIA and a Pt electrode for amperometric detection of hydrogen peroxide at an applied potential of 600 mV (vs. Ag/AgCl). The system was chosen as it allows great flexibility: the amperometric sensor for hydrogen peroxide can be coupled with the different enzyme reactors.

The different enzymes have been evaluated for sensitivity, lifetime and selectivity.

The enzyme systems chosen operated according to the following reaction sequence:



H<sub>2</sub>O<sub>2</sub> production due to the oxidative activity of the enzyme immobilized in the reactor increased the output current of the Pt electrode.

## 2. Experimental

### 2.1. Chemicals

DAO (EC 1.4.3.6; from porcine kidney; 0.14 U/mg solid), amines and amine hydrochlorides were purchased from Sigma, St. Louis, MO (USA). PUO (EC 1.4.3.10, from *Micrococcus roseus*, Toyobo Enzymes, PUO-301; 38 U/mg solid) was used as received.

The enzyme DAO from lentil (26 U/mg solid, 5.4 mg/ml) has been obtained and purified by Dr Volpe G. (Istituto Superiore Sanità, Rome, Italy).

Amine standard solutions were prepared by dissolving the amines or their hydrochlorides in phosphate buffer. The amines selected in this work were the most commonly found in fish samples. Glutaraldehyde (25% aqueous solution) was obtained from Merck.

### 2.2. Immobilization

DAO and PUO were immobilized on controlled pore glass beads (aminopropyl glass, average pore size 700 Å, particle size 80–120 mesh from Sigma) activated by glutaraldehyde. One hundred milligrams of controlled pore glass were gently stirred in a 2.5% glutaraldehyde solution (1 ml of buffer pH 7.0) for 1 h at room temperature. After the reaction, this mixture was washed with water. Sixty milligrams of DAO from porcine kidney, 600 µl of DAO from lentil or 0.8 mg of PUO were added and stirred at 4°C for 24 h. The enzyme-immobilized beads were put into a reactor column (Tygon™ tube of 5 mm internal diameter and 50 mm long) and flowed continuously until the beads were uniformly packed.

The working buffer for the procedure was 0.10 M phosphate buffer at pH 7.0 containing 0.10 M

NaCl. The reactor is stored at about 4°C in the working buffer when not in use.

### 2.3. Apparatus and assay procedure

The FIA system included a peristaltic pump (Minipuls 3 Peristaltic Pump Gilson), a sampling device (Rheodyne 5020) and an amperometric biosensor detector (Universal Sensors) used as potentiostat and connected with an Amel model 868 recorder.

The electrodes were placed in a suitable flow cell. The carrier buffer solution was continuously pumped to the flow cell at a constant rate by the peristaltic pump. When the current reached a stable value (drift less than 1% in 10 min), a known volume of sample solution was injected through the sampling valve. A flow rate of 0.8 ml min<sup>-1</sup> with an optimum sample volume fixed at 1 ml was used throughout. This system had a delay time of 3 min (time elapsed between sample injection to current peak maximum observed with sampling rate of 20 h<sup>-1</sup>).

The working electrode is a platinum wire (diameter of 0.7 mm), and the reference (Ag/AgCl) surrounding it has the form of a tube. The silver tube was placed in a stirred solution of sodium hypochlorite for about 5 min, then it was rinsed with water and placed on UV light for 5 min). A thin (20 µm) membrane of cellulose acetate was stretched over the platinum electrode surface and secured to it by an O ring.

The cellulose acetate membrane was prepared as follows: cellulose acetate (1.98 g) and polyvinylacetate (20 mg) were dissolved in 20 ml of cyclohexanone and 30 ml of acetone. The solution was cast on a glass plate with a thickness of 200 µm with the aid of a casting tool. After complete evaporation (10 h) the membrane was immersed in water and peeled off the glass surface. The dried membrane has a thickness of about 20 µm.

All standard solutions were prepared by dissolving reagent in phosphate buffer 0.10 M pH 7.0 containing 0.10 M NaCl and were diluted with the buffer solution.

### 2.4. Preparation of samples for fish spoilage determination

Several authors proposed a treatment of fish sample according to Ehira's methods [21] for deproteinization.

For storage experiments mackerels and sardines were used. These fish samples were purchased from a local fish market in Florence, Italy. They were stored at room temperature (20–25°C) for 2 days. The fish extracts were obtained by pressing fish muscle (without skin) placed in a membrane of nylon with a suitable squeezer. The extracts were analyzed immediately and in some cases stored at -40°C until use.

The fish extracts were generally diluted ten or 100 times with phosphate buffer 0.10 M pH 7.0 containing 0.10 M NaCl, filtered through 0.45 µm pore filters, and immediately injected into the sampling valve. The results of such procedures are reported as mg of amine/l of sample extract.

Some samples (sardine, mackerel, tuna, salami, sausage and cheeses) were homogenized with 20 ml of phosphate buffer 0.1 M NaCl 0.1 M pH 7.0 and centrifuged at 4000 rpm for 30 min. The aqueous phase was separated and filtered through a 0.45 µm filter and injected directly after dilution into the buffer solution. The results in this case are expressed as mg of amine/kg of sample.

## 3. Results

### 3.1. Selectivity of the sensor

Uric and ascorbic acid are commonly associated with physiological liquids, and are electrochemical interferents at the platinum electrode.

Permeable membranes such as Nafion (Nafion 117, perfluorinated membrane, 0.007 in. thick, Aldrich) and cellulose acetate covering the platinum electrode were used to reduce the interference effect [22,23].

Table 1 shows that with Nafion in the concentration range 10–100 µM, 15–16% of these

two compounds was still interferent, whereas the cellulose acetate membrane eliminated almost completely such interfering effects.

### 3.2. Selectivity of enzyme

Diamine oxidase has been obtained in two preparations: from lentil (20 U/mg) and porcine kidney. Only this latter form is commercially available.

In the pea seedling, DAO is predominantly found in the cotyledons, and activity reaches a peak at 8–16 days after germination in the dark [24]. Pea seedlings are the most active source of DAO, exceeding the classical hog kidney 105-fold in terms of crude material and 58 times in terms of purified enzyme [25]. When isolated from pea seedlings, the enzyme shows broad specificity, but there can be differences in oxidation rates between substrates as reported [26].

With the enzyme DAO (from porcine kidney) for 60  $\mu\text{M}$  substrate concentrations, the calibration with histamine was set as 100%, agmatine represents 37%, the putrescine 28%, the cadaverine 14%, the tyramine 1% and spermine, tryptamine and spermidine below 1%.

With the enzyme DAO (from lentil), several amines gave a current signal. For 50  $\mu\text{M}$  substrate concentrations, we obtained 100% response to cadaverine, 98% to agmatine, 93% to histamine, 76% to spermidine, 74% to putrescine, 60% to tyramine, 37% to tryptamine and 9% to spermine. Though this system did not allow the determination of the concentrations of the individual amines in the mixture, it could be used as a useful indicator of total amines.

The sensor PUO with 10  $\mu\text{M}$  substrate concentrations showed 100% response to putrescine, 12% to cadaverine, 10% to agmatine and tyramine, 9% to spermidine, and 8% to tryptamine. For this system, both spermine and histamine levels are undetectable (1%, and <1%, respectively).

The enzyme preparation from lentil was obtained with the higher activity (20 U/mg, cadaverine as main substrate). The preparation from the porcine kidney has histamine as major substrate and cadaverine gave ca. 1/7 of the response (14%). The preparation from the lentil has cadaverine as main substrate and histamine gave 93% of relative response.

The sensitivity of the different systems did not change using a pool of amines instead of single amine standard solutions.

Hypoxanthine and histidine were examples of a possibly interfering substance in histamine analysis because the concentrations of these two compounds are important in the fish extracts. However any response was obtained at the electrode if the reactor was or not excluded from this system.

### 3.3. Calibration curves

Calibration plots were always obtained in buffer phosphate 0.1 M-NaCl 0.1 M pH 7.0. The dynamic response of a typical histamine (using DAO from porcine kidney) and putrescine (using PUO) sensor is illustrated in Fig. 1.

The sensor for histamine (with DAO from porcine kidney) has a useful detection range of up to 60  $\mu\text{M}$  (Fig. 2) with a detection limit of 0.5

Table 1  
Electrochemical interferents (uric acid, ascorbate)<sup>a</sup>

	Uric acid		Ascorbate		Hydrogen peroxide	
	<i>i</i> (nA)	%	<i>i</i> (nA)	%	<i>i</i> (nA)	%
Without membrane	150 ± 7	100	75 ± 7	100	500 ± 5	100
Cellulose acetate	0.30 ± 0.01	0	0.50 ± 0	1	150 ± 2	30
Nafion	22 ± 4	15	12 ± 2	16	50 ± 2	10

<sup>a</sup> Current increase (nA) for 50  $\mu\text{M}$  concentration equivalent. Carrier solution (0.1 M phosphate buffer containing 0.1 M NaCl pH 7.0) was pumped at a flow rate of 0.8 ml min<sup>-1</sup>.



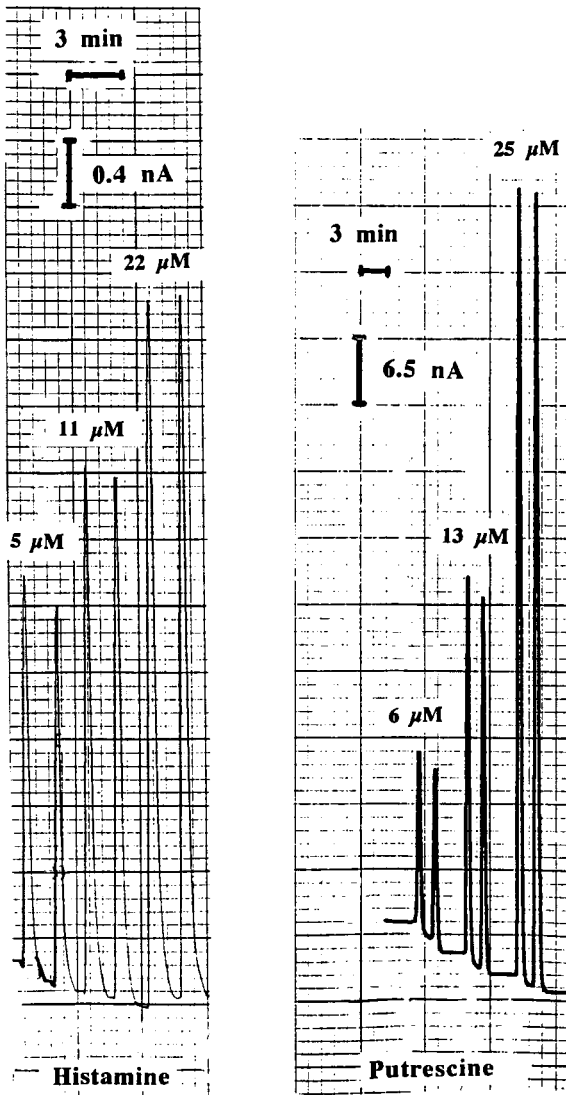


Fig. 1. Typical FIA peaks of the histamine (using the system assembled with the immobilized enzyme DAO from porcine kidney) and putrescine (using the system assembled with the immobilized enzyme PUO) standards detected at Pt electrode. Flow rate, temperature, pH and sample volume were  $0.8 \text{ ml min}^{-1}$ ,  $20^\circ\text{C}$ , 7.0 and 1 ml, respectively.

$\mu\text{M}$ ; we obtained a standard deviation of 1% when  $20 \mu\text{M}$  standard solution was injected.

The sensor for putrescine (Fig. 3; using PUO) has a linear response range of up to  $400 \mu\text{M}$  with a detection limit of  $0.07 \mu\text{M}$  and with a standard deviation of 1% for  $8 \mu\text{M}$  putrescine standard

solution. Previous work reported a smaller range ( $0\text{--}20 \mu\text{M}$ ) in putrescine determination [2].

### 3.4. Reactor stability

The present system based on FIA and one reactor (DAO or PUO) has the advantage of simplicity of manual operation. The enzyme reactor was stored at  $4^\circ\text{C}$  when not in use and the intermittent tests were done at room temperature. In these conditions, 20–30 measurements were realized with each reactor.

Both DAO reactors (obtained from porcine kidney and from lentil) kept nearly 70% initial

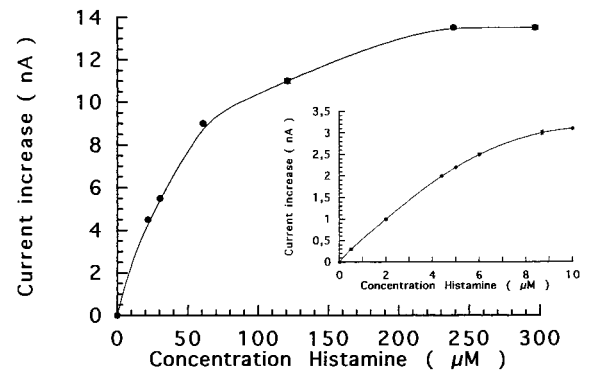


Fig. 2. Typical calibration curves of the DAO (from porcine kidney) sensor for histamine. Flow rate, temperature, pH and sample volume were  $0.8 \text{ ml min}^{-1}$ ,  $20^\circ\text{C}$ , 7.0 and 1 ml, respectively.

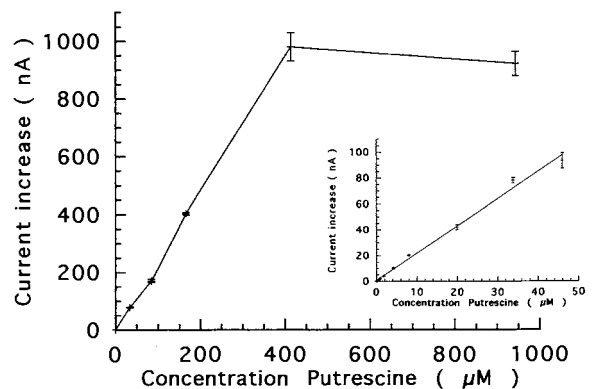


Fig. 3. Typical calibration curves of the PUO sensor for putrescine. Flow rate, temperature, pH and sample volume were  $0.8 \text{ ml min}^{-1}$ ,  $20^\circ\text{C}$ , 7.0 and 1 ml, respectively.

Table 2

Recovery study performed by adding standard solutions of cadaverine, histamine or putrescine to fish samples

Amines found in the sample before spiking ( $\mu\text{M}$ )	Cad added ( $\mu\text{M}$ )	Expected value ( $\mu\text{M}$ )	Found value ( $\mu\text{M}$ )	Recovery (%)
$6.0 \pm 0.5$	6.0	12.0	$13 \pm 1$	108
$6.0 \pm 0.5$	12.0	18.0	$19 \pm 1$	106
His found in the sample before spiking ( $\mu\text{M}$ )	His added ( $\mu\text{M}$ )			
$5.0 \pm 0.1$	5.0	10.0	$11.0 \pm 0.1$	110
$5.0 \pm 0.1$	10.0	15.0	$15.5 \pm 0.1$	103
Put found in the sample before spiking ( $\mu\text{M}$ )	Put added ( $\mu\text{M}$ )			
$7.0 \pm 0.5$	7.0	14.0	$13 \pm 1$	93
$7.0 \pm 0.5$	14.0	21.0	$20 \pm 1$	95

Table 3

Changes in biogenic amines (histamine and putrescine) measured as fish extracts content in two different species of fish during storage at 20–25°C<sup>a</sup>

Days of storage	Histamine content (Eq. mg/l)		Putrescine content (Eq. mg/l)	
	Sardine	Mackerel	Sardine	Mackerel
0	$26 \pm 8$	0	$36 \pm 6$	$60 \pm 5$
1	$132 \pm 11$	$19 \pm 7$	$161 \pm 8$	$291 \pm 5$
2	$141 \pm 7$	$40 \pm 6$	$509 \pm 5$	$482 \pm 4$

<sup>a</sup> Measurements were obtained with DAO from porcine kidney and PUO-reactors.

sensitivities in the first month while the PUO reactor can be used for about 1 month with nearly 90% of initial sensitivity.

### 3.5. Application to real samples

Preliminary experiments have been realized with fish samples prepared as described in Section 2.4.

For all measurements with real samples (DAO or PUO reactors), the fish extracts were diluted with buffer in order to fall in to the linear range of the sensors.

When the sensor was not coupled with reactors, no electrochemical signals were obtained, therefore it was concluded that any significant amount of electrochemically interfering substances was present in fish extracts.

PUO reactor was calibrated with standard solution of putrescine, DAO (from porcine kidney) reactor with histamine and DAO (from lentil) with cadaverine. The current values obtained with the three different systems when assaying real samples were therefore expressed, respectively, as histamine content (DAO obtained from porcine kidney), as cadaverine content (DAO from lentil) and as putrescine content (from PUO).

We can again be reminded that histamine and putrescine values are very near to the real amount of such amines, because the respective enzymes are very selective, while the cadaverine values obtained are more near to the total amount of amines because of the low selectivity of the DAO from lentil.

The procedure of extraction with 0.1 M phosphate buffer, 0.10 M NaCl pH 7.0 was tested for

Table 4

Concentration of biogenic amines in can seafood and other food samples performed with DAO (from porcine kidney, from lentil) and PUO reactors measured after homogenization, centrifugation and filtration<sup>a</sup>

Samples	Histamine (Eq. mg/kg)	Putrescine (Eq. mg/kg)	Cadaverine (Eq. mg/kg)
Salmon	7 ± 1	8 ± 2	27 ± 3
Mackerel	3 ± 1	8 ± 2	20 ± 2
Tuna	8 ± 1	11 ± 2	33 ± 6
Salami	77 ± 9	110 ± 10	510 ± 25
Sausage	23 ± 2	37 ± 5	160 ± 12
Parmesan	23 ± 7	20 ± 4	470 ± 20
'Pecorino' cheese	148 ± 20	9 ± 1	1280 ± 40

<sup>a</sup> The dilution of the original sample was in the range of 10–50 according to the result obtained.

recovery (Table 2). Standard solutions of cadaverine (using the system assembled with the immobilized enzyme DAO from lentil), histamine (using the system assembled with the immobilized enzyme DAO from porcine kidney) or putrescine (using the system assembled with the immobilized enzyme PUO) were added to the extracts of fish samples.

In all cases a recovery from 93 to 110% was observed.

Table 3 shows in two fish samples, the changes in biogenic amines expressed as histamine and putrescine content during storage at room temperature (20–25°C) using the DAO (from porcine kidney) and PUO reactors. During storage, histamine and putrescine were formed and, hence, a marked increase of the signal of the DAO and PUO reactors was observed. It can be observed that during such a period of storage at 20–25°C, the putrescine values were higher in comparison with histamine levels.

Table 4 shows preliminary results on the determination of biogenic amines (histamine, putrescine and cadaverine) in several foods obtained, respectively, with the reactor assembled with the immobilized enzyme DAO from porcine kidney, with PUO and with DAO from lentil. Cheese was found to be the food with the highest amine content.

#### 4. Conclusions

A simple and rapid method for the evaluation of biogenic amines was developed. This method is based on an hydrogen peroxide probe coupled with

a reactor with immobilized enzyme DAO (from lentil and porcine kidney) and PUO.

The three enzyme reactors have a different pattern of selectivity, which can be exploited in some specific study of fish spoilage. The DAO (from porcine kidney) reactor and the PUO reactor are quite selective and therefore give sharp information on individual amine content (histamine and putrescine, respectively) while the DAO (from lentil) reactor is quite unselective and allows the measurement of the total amines.

In all cases, the biosensor procedure has advantages, such as low cost, short analysis time, simplicity of use and it can be used outside an organized laboratory like directly in the market place or in a custom office. Moreover, the biosensors show a low detection limit with a lifetime estimated at 1 month with a 10–30% loss of sensitivity.

In view of these facts, the whole procedure can be considered a valuable approach for the quality control of fish processing and storage.

#### Acknowledgements

M.-A. Carsol acknowledges ECC Programm (Contact FAIR GT-97-3791).

#### References

- [1] A. Halasz, A. Barath, L. Simon-Sarkadi, W. Holzapfel, *Trends Food Sci. Technol.* 51 (1994) 42–49.
- [2] X. Yang, G.A. Rechnitz, *Electroanalysis* 7 (2) (1995) 105–108.

- [3] Y. Yano, K. Yokoyama, E. Tamiya, I. Karube, *Anal. Chim. Acta* 320 (1996) 269.
- [4] W.F. Staruszkiewicz Jr., J.F. Bond, *J. Assoc. Off. Anal. Chem.* 64 (1981) 584.
- [5] P. Nadeau, S. Delaney, L. Chouinard, *Plant Physiol.* 84 (1987) 73.
- [6] A.R.G. Dibble, P.J. Davies, M.A. Mutschler, *Plant Physiol.* 86 (1988) 338.
- [7] R. Reggiani, P. Giussani, A. Bertani, *Plant Cell Physiol.* 31 (1990) 489.
- [8] P.J. Oefner, S. Wongyai, G. Bonn, *Clin. Chim. Acta* 205 (1992) 11.
- [9] M.Z. Hauschild, *J. Chromatogr.* 630 (1993) 397.
- [10] P.G. Zambonin, A. Guerrieri, T. Rotunno, F. Palmisano, *Anal. Chim. Acta* 251 (1991) 101.
- [11] T. Hyvönen, T.A. Keinänen, A.R. Khomutov, T.O. Eloranta, *J. Chromatogr.* 574 (1992) 17.
- [12] H. Ohta, Y. Takeda, K.-I. Yoza, Y. Nogata, *J. Chromatogr.* 628 (1993) 199.
- [13] K. Saito, M. Horie, N. Nose, K. Nakagomi, H. Nakazawa, *Anal. Sci.* 8 (1992) 675.
- [14] *Official Methods of Analysis*, 15 ed., Arlington, VA, secs 957.07, 977.13, 954.04, 1990.
- [15] I. Karube, I. Satoh, Y. Araki, S. Suzuki, H. Yamada, *Enzyme Microb. Technol* 2 (1980) 117.
- [16] U. Bilitewski, G.C. Chemnitz, P. Rüger, R.D. Schmid, *Sensors Actuators B* 7 (1992) 351.
- [17] G.C. Chemnitz, M. Suzuki, K. Isobe, J. Kimura, I. Karube, R.D. Schmid, *Anal. Chim. Acta* 263 (1992) 93.
- [18] G.C. Chemnitz, U. Bilitewski, *Sensors Actuators B32* (1996) 107–113.
- [19] S.A.M. Marzouk, C.X. Xu, B.R. Cosofret, R.P. Buck, S.S.M. Hassan, M.R. Neuman, R.H. Sprinkle, *Anal. Chim. Acta* 363 (1998) 57–65.
- [20] S. Tombelli, M. Mascini, *Anal. Chim. Acta* 358 (1998) 277.
- [21] S. Ehira, H. Uchiyama, *Bull. Jpn. Soc. Sci. Fish.* 35 (1969) 1080.
- [22] S. Dong, Q. Qiu, *J. Electroanal. Chem.* 314 (1991) 223.
- [23] J.P. Lowry, R.D. O'Neill, *J. Electroanal. Chem.* 334 (1992) 183.
- [24] T.A. Smith, *Anal. Biochem.* 92 (1979) 331.
- [25] D. Wijesuriya, G.A. Rechnitz, *Anal. Chim. Acta* 243 (1991) 1.
- [26] Z. Toul, L. Macholan, *Coll. Czech. Chem. Commun.* 40 (1975) 2208.

# Experimental design methodologies to optimize monobutyltin chloride determination by hydride generation gas phase molecular absorption spectrometry

Jesús Sanz \*, Margarita Pérez, María T. Martínez, María Plaza

*Department of Chemistry (Analytical Chemistry), University of La Rioja, Obispo Bustamante 3, Logroño 26001, Spain*

Received 15 December 1998; received in revised form 19 March 1999; accepted 1 April 1999

## Abstract

A hydride generation gas phase molecular absorption spectrometry (HG-GPMAS) method for the determination of butyltin compound is optimized by experimental design. This method is based on the conversion of the butyltin chloride into gaseous monobutyltin hydride by adding a sodium tetrahydroborate (III) solution. The hydride generated is collected in a liquid nitrogen cryogenic trap. This is revolatilized, driven to the quartz flow cell and measured with GPMAS with diode array detection. A Plackett–Burmann design is used for the study of the factors that influence the absorption signal. The optimization of the parameters affecting the production and collection of the monobutyltin hydride is achieved using a central composite design. Partial least square (PLS), multiple linear regression (MLR) and univariate calibration are applied to the spectra obtained. The quality parameters (detection limits and precision) for the butyltin chloride are reported. An interference study is made. © 1999 Elsevier Science B.V. All rights reserved.

*Keywords:* Hydride generation; Gas phase molecular absorption spectrometry; Butyltin chloride; Factorial design

## 1. Introduction

One of the most important steps in the development of a new analytical method is its optimization: the study of those factors which have an influence on the analytical signal, and selection of the values that produce the best results for the analytical method. In the traditional strategy of

one variable at a time, only one variable is changed while all the others remain constant. This approach requires a large number of experiments and does not allow the study of any response changes which may occur when two or more factors are modified simultaneously.

Experimental design is an alternative to this strategy. It allows a large number of factors to be screened simultaneously to determine which of them has a significant effect on the analytical signal; in addition, the factors can be optimized to give the best possible results with a relatively low

\* Corresponding author. Tel.: +34-941-244-811; fax: +34-941-259-431.

*E-mail address:* [jesus.sanz@dq.unirioja.es](mailto:jesus.sanz@dq.unirioja.es) (J. Sanz)

number of experiments. This methodology also allows for sequential experimentation, in such a way that each group of experiments is based on the previous group.

A variety of analytical techniques have been described for the determination of organotin compounds. Many of these are based on separation via high performance liquid–liquid chromatography (HPLC) [1,2] or more often using gas chromatography (GC) [3–5]. The derivatization by hydride generation with sodium tetrahydroborate (III) [1,6], sodium tetraethyl borate [5,7] and alkylation by Grignard reagents [8] are the most commonly used methods for the analysis of these compounds by conversion to volatile species. Several detection techniques have been coupled to GC and HPLC for the determination of derivatized organotin compounds. These include atomic absorption spectrometry (AAS) [9], atomic emission spectrometry (AES) [4], mass spectrometry (MS) [10], flame photometric detection (FPD) [11] and microwave-induced plasma atomic emission spectrometry (MIP-AES) [5,12].

Gas phase molecular absorption spectrometry (GPMAS) is a consolidated technique; analytical applications of GPMAS have been independently developed by Syty [13] and by Cresser [14] since 1973. The technique is based on the measurement of the absorption of molecular species in the gas phase, generated at room temperature. Its application has focused on sulphur compounds [15], nitrogenated compounds [16], halides [17], covalent hydride volatiles [18] and more recently, arsenic and tin organo-metals [19]. The introduction of a diode-array system as the detector has widened the technique's application range. Obtaining the volatile spectrum generated over a wide wavelength range allows the study of the changes produced in the structure of the molecule generated [20] or the simultaneous determination of the various analytes involved [21].

The aim of this study was to establish the best possible experimental conditions for the determination of monobutyltin chloride using the generation of monobutyltin hydride, carried out by continuous addition of the reducing agent and subsequent determination by GPMAS. The optimization study was performed in a sequential

way. Owing to the numerous experimental factors that influence the response of the analyte, a statistical model of the Plackett–Burmann [22] design was used to evaluate the significance of each factor. A statistical model of central composite design [23] was then used to study the influence of the interaction between variables and the optimum conditions.

## 2. Experimental

### 2.1. Apparatus

All measurements were made with a Hewlett-Packard (model HP 8451) diode-array Spectrophotometer equipped with an HP 98155A keyboard, an HP 9121 disk drive for bulk data storage, an HP Thinkjet printer and an HP 7475A graphics plotter. A Hellma 174QS 1 cm quartz flow cell was used, together with a Masterflex peristaltic pump Ref. E07523-37 (Cole-Parmer, USA), a Heidolph MR 3003 agitomatic (Heidolph, Kelheim, Germany) with platinum probe, a Mettler PJ 3600 Delta Range, a Dilvac Dewar (2 l) and a Schott ISO 250/1000 ml generator flask.

For mathematical treatment, a Hewlett-Packard Vectra VL was used; the statistical designs were created and analyzed with the Statistica 5.0 software package [24]. For multicomponent analysis, Parvus 3.0 [25] was used.

### 2.2. Reagents

All reagents used were of analytical grade quality. Double distilled water was used.

A stock solution of tin compound was prepared, of  $1000 \mu\text{g ml}^{-1}$  of Sn as follows: butyltin trichloride,  $\text{C}_4\text{H}_9\text{SnCl}_3$  from Aldrich (Sigma–Aldrich, USA) dissolved in double-distilled water. Working standards were prepared by serial dilution of the stock solutions with double-distilled water, immediately before use.

Aqueous solutions of sodium tetrahydroborate (III),  $\text{NaBH}_4$  from Carlo Erba (Milan, Italy) were prepared immediately prior to use.

Hydrochloric acid (37% m/m,  $1.186 \text{ g ml}^{-1}$ ) and acetic acid (80% m/m,  $1.070 \text{ g ml}^{-1}$ ) from

Carlo Erba-RPE (Milan, Italy). Working solutions were prepared daily by diluting concentrated solutions with double-distilled water.

Dried granular calcium chloride from Carlo Erba-RE (Milan, Italy).

The carrier gases were nitrogen and hydrogen (C-50 Carbuos Metálicos).

### 2.3. System description. Basic procedure

The system used for the generation and measurement of the butyltin hydride is shown in Fig. 1; the scheme consists of: (i) the hydride generator; (ii) the trapping section; (iii) the revolatilizing section; and (iv) UV detection.

A volume of the acidified standard solution was added to the generation vessel, the peristaltic pump introduced the reducing agent and a gas flow was applied through the solution. Once the reducing agent was consumed, the gas flow was maintained for some minutes more. The volatiles generated were condensed in the U-tube immersed in liquid nitrogen.

The U-tube was then removed from the liquid nitrogen and left for a short period at room temperature. Volatilization of the hydrides was achieved by a controlled heating of the trap. The trap was connected to the flow cell with a Teflon tube. The butyltin hydrides were detected using the BASIC program as given in the experimental procedure; a time overlap was obtained of the

volatile absorbance spectra from 190 to 220 nm every 0.2 s for 7 s (enough time for the absorbance to fall to zero).

Using the determination system selected, the total absorbance spectrum of monobutyltin hydride, shown in Fig. 2, was obtained.

## 3. Results and discussion

### 3.1. Study of significant factors

In order to achieve the significant factors, a Plackett–Burman design was used. This experimental design allows a large number of factors to be screened simultaneously to determine which of them has a significant effect on the response. This design supposes that only the principal effects influence the absorbance signal; the interactions among the variables are not considered.

Several variables could potentially affect the absorbance signal: reducing agent flow, reductor concentration, acid type, gas flow rate during hydride generation, revolatilizing temperature, carried time, carrier gas type, time at room temperature, revolatilizing time, sample volume and pH. Each variable was studied at two levels; these levels were selected on the basis of previous results [19], in function of the bibliography found [1,6], and taking into account the limitations of the experimental system. The levels of control are

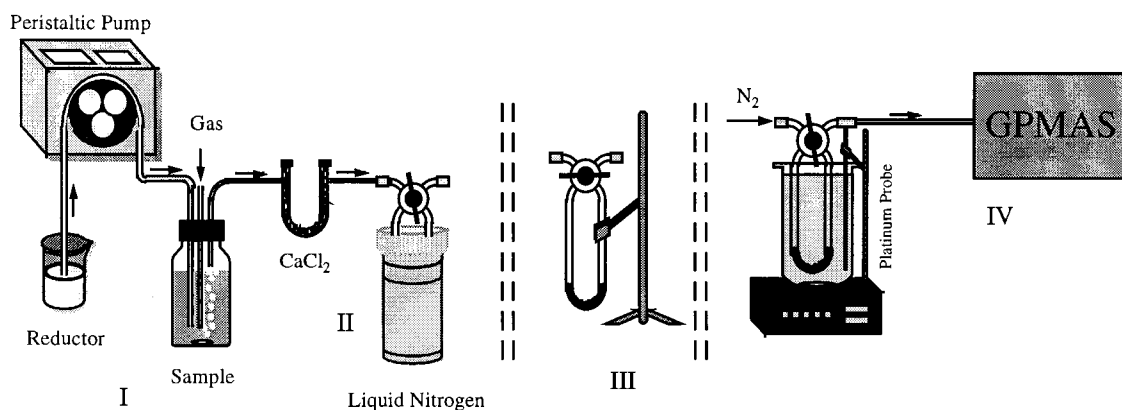


Fig. 1. Schematic diagram of the determination system. (i) The hydride generator; (ii) the trapping section; (iii) the revolatilizing section; (iv) UV detection.

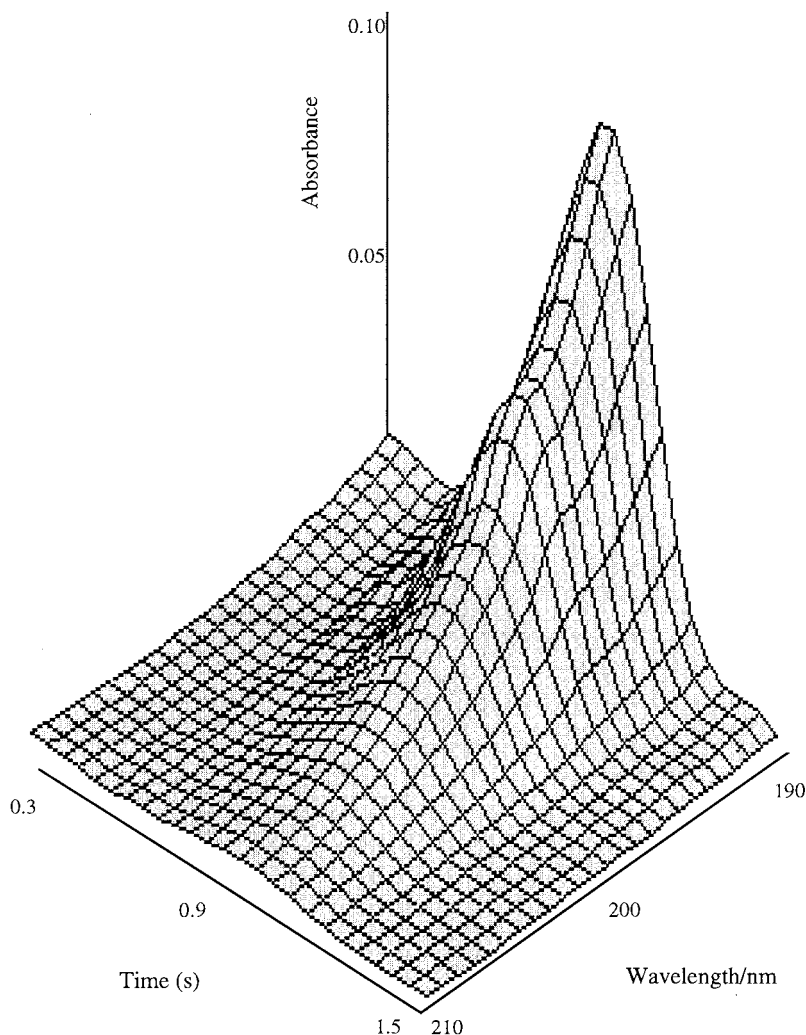


Fig. 2. Three-dimensional absorption molecular spectrum of monobutyltin hydride.

listed in Table 1. The experiments were carried out with three replicates per run, to obtain a value for the experimental error. Randomization was used in order to obtain a random distribution of unknown systematic errors. The sample amount was 208.5  $\mu\text{g}$  for butyltin chloride. Table 2 gives the design matrix for the Plackett–Burman design, the mean response obtained (absorbance of the monobutyltin hydride measured at 192 nm) and the main effects of the factors.

The analysis of the results given in Table 2 produced the bar chart shown in Fig. 3. In this chart, the bar lengths are proportional to the

absolute value of the estimated main effects; those which exceed the reference line, corresponding to the 95% confidence interval (CI), are significant as regards to the response.

The factors which gave significant effects on the signal were reductor concentration, gas flow rate during hydride generation, carried time, carrier gas type, time at room temperature, revolatilizing time and sample volume. The sign of the main effects showed whether the response would be improved or decreased on passing a given factor from the lower level to the higher level, and determined the new experimental domain to be



Table 1  
Factors and levels used in Plackett–Burman design

Factors	Level	
	Low (–)	High (+)
(A) Reductor flow (ml min <sup>-1</sup> )	2	10
(B) Reductor concentration (%)	0.5	4
(C) Acid	Acetic acid	Hydrochloric acid
(D) Generation flow (ml min <sup>-1</sup> )	170	500
(E) Revolatilizing temperature (°C)	60	90
(F) Carried time (min)	2	5
(G) Carrier gas	H <sub>2</sub>	N <sub>2</sub>
(H) Time at room temperature (min)	1.5	3
(I) Revolatilizing time (min)	0.5	1.5
(J) Sample volume (ml)	150	750
(K) pH	1	4

explored to obtain response optimization. The sample volume and carrier gas type were not continuous variables and showed negative signs, and these were therefore fixed as 150 ml and

hydrogen gas. The reductor agent concentration, gas flow rate during hydride generation, carried time, time at room temperature and revolatilizing time were significant and positive effects, so that the region of their higher level was studied further. The reducing agent flow, acid type, revolatilizing temperature and pH were not significant effects and these were fixed at the values of 2 ml min<sup>-1</sup>, hydrochloric acid, 90°C and pH 1. The results of this first study led to the elimination of four variables of the sequential optimization (reducing agent flow, acid type, revolatilizing temperature and pH) and also allowed the fixing of those variables which were non-continuous (carrier gas type, acid type and sample volume).

### 3.2. Optimization of the experimental conditions

A second-order polynomial function was postulated with the aim of obtaining a response map. A five level central composite design with three central points was carried out. This design gave the surface response; the experimental data were fitted to the polynomial mathematical model:

$$y_{\text{pred.}} = \beta_0 + \sum \beta_i x_i + \sum \beta_{ij} x_i x_j + \sum \beta_{ii} x_i^2 + \varepsilon$$

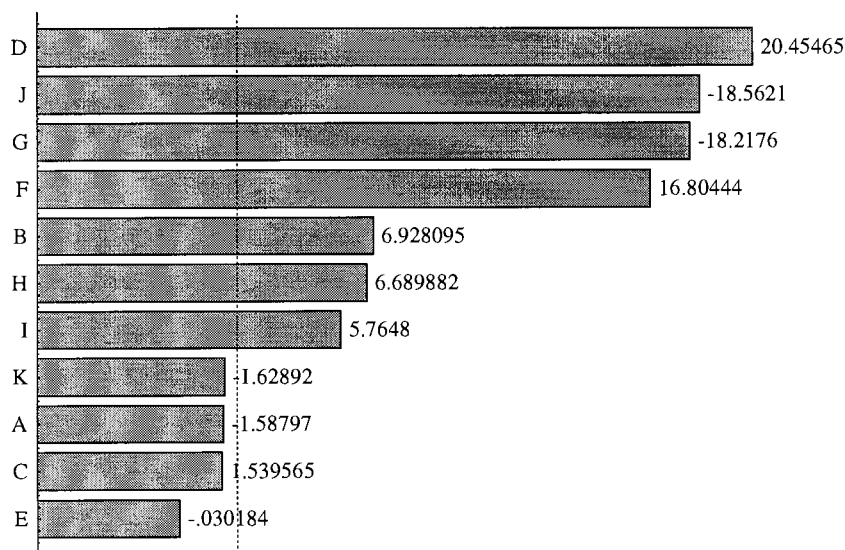


Fig. 3. Graphic analysis of the main effects obtained from the Plackett–Burman design. The vertical line defines the 95% confidence interval (CI).

Table 2  
Experimental matrix and results for Plackett–Burman design

Runs	Factors											BT response
	A	B	C	D	E	F	G	H	I	J	K	
7	+	–	+	–	–	–	+	+	+	–	+	0.0398
3	+	+	–	+	–	–	–	+	+	+	–	0.1666
5	–	+	+	–	+	–	–	–	+	+	+	0.0466
1	+	–	+	+	–	+	–	–	–	+	+	0.1541
4	+	+	–	+	+	–	+	–	–	–	+	0.1023
10	+	+	+	–	+	+	–	+	–	–	–	0.2164
9	–	+	+	+	–	+	+	–	+	–	–	0.2301
2	–	–	+	+	+	–	+	+	–	+	–	0.0366
11	–	–	–	+	+	+	–	+	+	–	+	0.2992
6	+	–	–	–	+	+	+	–	+	+	–	–0.0010
12	–	+	–	–	–	+	+	+	–	+	+	0.0373
8	–	–	–	–	–	–	–	–	–	–	–	0.0746
Effect	–0.008	0.033	0.007	0.096	–0.000	0.078	0.085	0.032	0.027	–0.087	–0.007	

(with  $i$  and  $j$  ranging from  $A$  to  $E$ ) where  $\beta_{ii}$  and  $x_i^2$  are the quadratic regression coefficients and the quadratic settings respectively.

Time limitations on the great number of experiments potentially involved led to the selection of a minimum set of experiments to estimate the model coefficients. In this case, the number of experiments was reduced by running a fractional factorial design,  $2^{5-1}$ . In this design, the main effects were confused with four-way interactions, normally not significant, whereas the interactions of order two were confused with the interactions of order three. The central composite design consisted of the points of fractional factorial design augmented with ten star points. These star points were located at  $+\alpha$  and  $-\alpha$  from the centre of the experimental domain. An axial distance ( $\alpha$ ) was selected with a value of 2 in order to establish the rotatability condition.

On the basis of the previous results, the experimental domain for the remaining variables was adjusted as follows: reductor agent concentration (A): 1–5 (%), gas flow rate during hydride generation (B): 250–750 ( $\text{ml min}^{-1}$ ), carried time (C): 2–6 (min), time at room temperature (D): 2–4 (min) and revolatilizing time (E): 0.5–2.5 (min). The sample amount was 88  $\mu\text{g}$  for butyltin chloride. Due to anticipated problems of overpressure in the system as a result of an excessive quantity of gas, it was not possible to investigate reductor agent concentration of over 5% or carried time of over 6 min. The results obtained are shown in Table 3, together with the corresponding matrix design. The experimental runs were randomized and were carried out with three replicates per run.

Variance analysis (ANOVA) was used to estimate the significance of the main effects and interactions (Table 4). In this table, the sum of squares (SS) is the information that was used to estimate the F-ratios ( $F$ ), which are the ratios of the respective mean square effect and the mean square error. The  $P$ -values indicate when the effect of each factor is statistically significant ( $P < 0.05$ ) or statistically not significant ( $P > 0.05$ ).

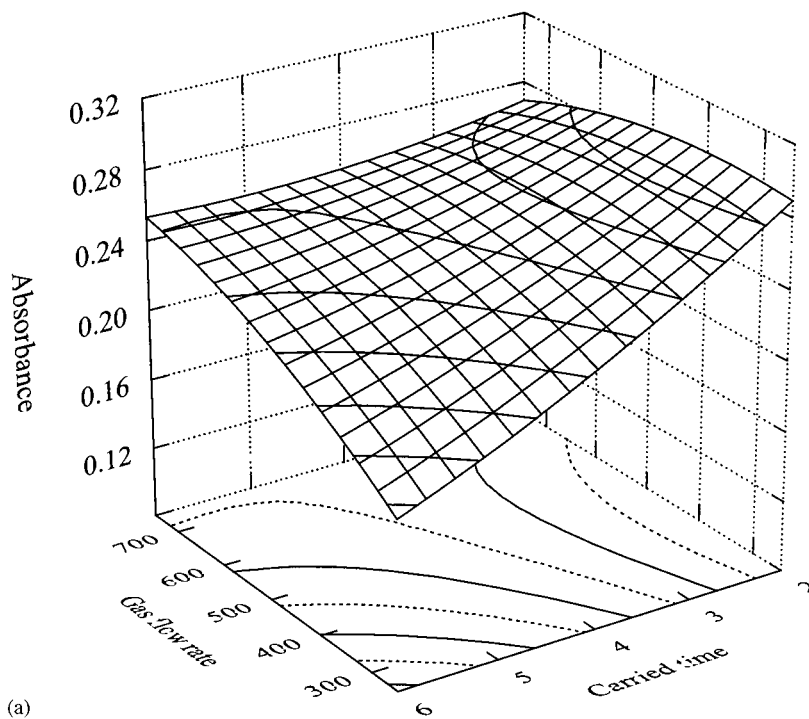
The analysis of the results showed that, out of all the factors studied in this experimental design, the reductor concentration and the revolatilizing time had the highest influence on the response.

Several interactions and quadratic terms were also significant.

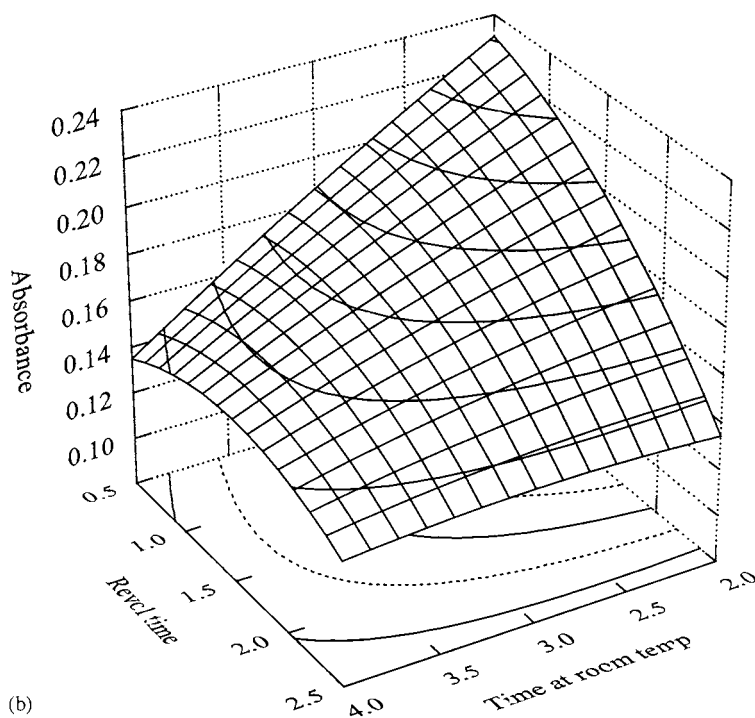
The design allows the obtaining of the response surface. This is an effective way of locating the optimum and for the interpretation of the most influential interactions if a mathematical relationship between the variables is known. Fig. 4 shows the response surfaces including the significant interactions. Fig. 4(a) shows the response surface function developed by the model for gas flow rate during hydride generation and carried time. The response obtained showed a maximum between 200 and 600  $\text{ml min}^{-1}$  when the carried time was at its lowest level. Fig. 4(b) shows the response surface function developed by the model for revolatilizing time and time at room temperature; the response obtained was greatest when the two factors were at their lowest levels; when one of the two factors was at its highest level and the other at its lowest level, the response was minimum. The response was inversely proportional to the two factors. Fig. 4(c) shows the function for carried time and time at room temperature. In this case, the function showed a maximum when the two factors were at the lowest or the highest level.

Fig. 4(d) shows the function for reductor concentration and time at room temperature; the response obtained was a maximum when the first factor was at its high level and the other at its low level. The response is directly proportional to the reductor concentration. Fig. 4(e) shows the response surface function developed by the model for revolatilizing time and carried time. The function was at a maximum when the two factors were at their lowest levels. Fig. 4(f) shows the function for revolatilization time and gas flow rate during hydride generation. As can be seen, the response surface presents a maximum for high flows and low times.

It can be seen that these results confirm those obtained in the above study. Of all the factors investigated, the reductor concentration and the revolatilization time are those which most affect the response. This design completes the previous study, since it permits the obtaining of the interactions between the factors and the optimum working conditions. The most important interactions were seen between the parameters affecting the



(a)



(b)

Fig. 4. Response surfaces estimated from the central composite design for (a) carried time vs gas flow rate, (b) time at room temperature vs revolatilizing time, (c) time at room temperature vs carried time, (d) reductor agent concentration vs time at room temperature, (e) revolatilizing time vs carried time, and (f) revolatilizing time vs gas flow rate.

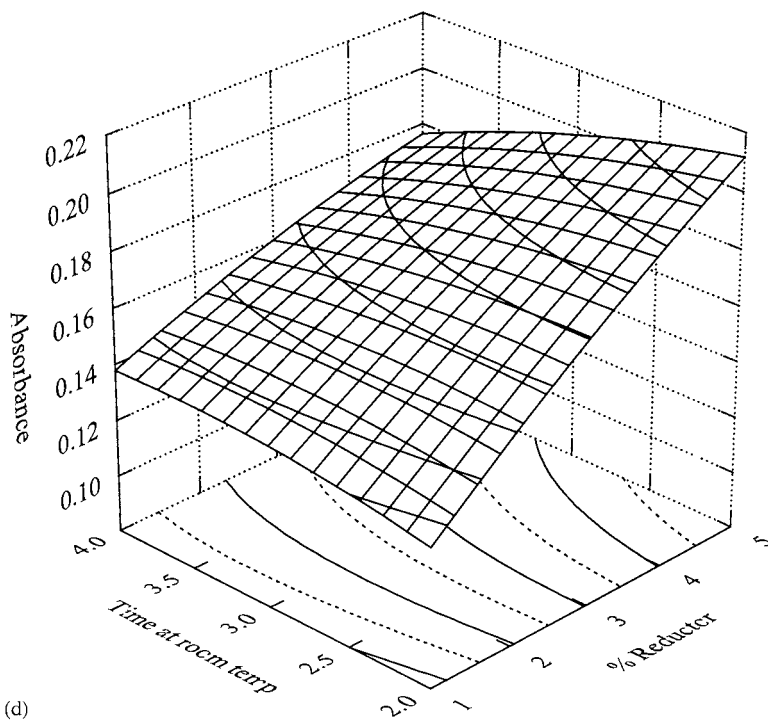
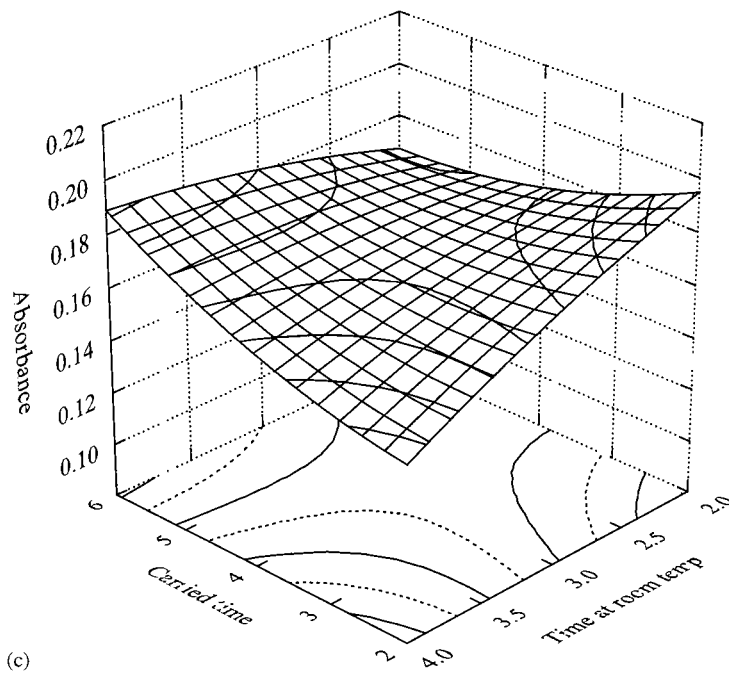


Fig. 4. (Continued)

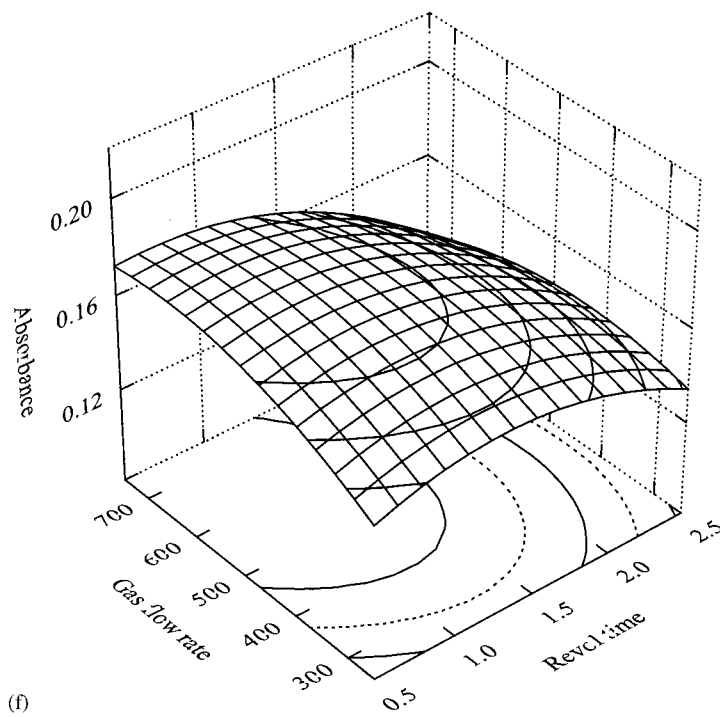
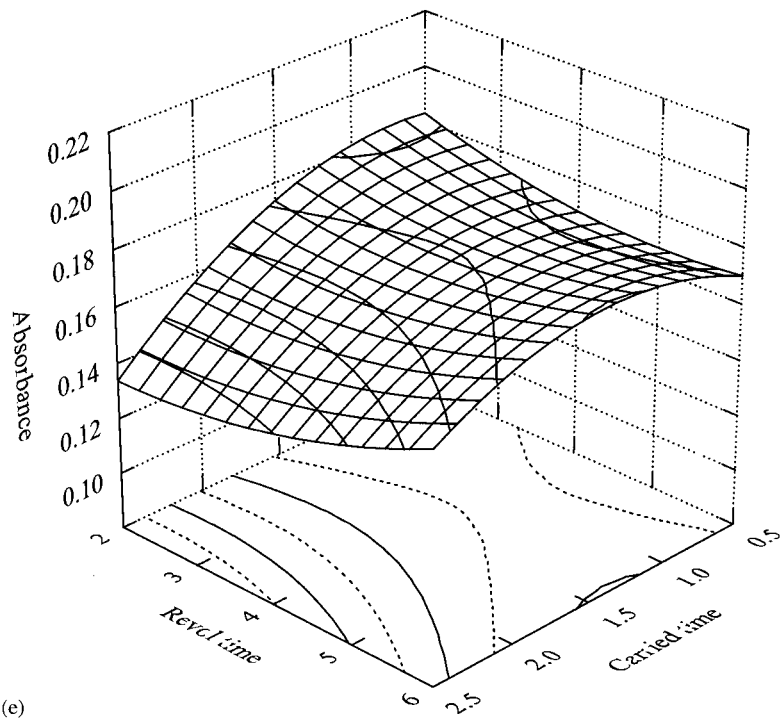


Fig. 4. (Continued)

Table 3  
Design matrix and response of fractional factorial central composite design

Runs	Factors					BT response (192 nm)
	Reductor (%)	Gas flow rate (ml min <sup>-1</sup> )	Carried time (min)	Time room $T^a$ (min)	Revol. time (min)	
1	+	+	+	+	+	0.1774
2	+	+	+	-	-	0.1575
3	+	+	-	+	-	0.1537
4	+	+	-	-	+	0.1700
5	+	-	+	+	-	0.1381
6	+	-	+	-	+	0.1188
7	+	-	-	+	+	0.1474
8	+	-	-	-	-	0.1244
9	-	+	+	+	-	0.1967
10	-	+	+	-	+	0.1578
11	-	+	-	+	+	0.1617
12	-	+	-	-	-	0.2025
13	-	-	+	+	+	0.1612
14	-	-	+	-	-	0.1590
15	-	-	-	+	-	0.1339
16	-	-	-	-	+	0.1372
17	$-\alpha$	0	0	0	0	0.1568
18	$+\alpha$	0	0	0	0	0.1141
19	0	$-\alpha$	0	0	0	0.1053
20	0	$+\alpha$	0	0	0	0.1948
21	0	0	$-\alpha$	0	0	0.1338
22	0	0	$+\alpha$	0	0	0.1483
23	0	0	0	$-\alpha$	0	0.1598
24	0	0	0	$+\alpha$	0	0.1650
25	0	0	0	0	$-\alpha$	0.1654
26	0	0	0	0	$+\alpha$	0.1344
27	0	0	0	0	0	0.1659
28	0	0	0	0	0	0.1643
29	0	0	0	0	0	0.1659

volatile's generation (carried time and gas flow rate during hydride generation) and those affecting the revolatilization (time at room temperature and revolatilizing time).

During the volatile generation, a displacement of water vapor from the generator was seen. To ensure that this vapor was not carried to the four-way valve, a CaCl<sub>2</sub> U-tube was used; however, it was seen that the elimination of the vapor was not complete in some experimental conditions (high reducer concentration or high gas flow during hydride generation). This circumstance could be due to the increase in water vapor in the gas or to the higher velocity of the gas passing through the water trap. To avoid overpressure problems in

the system, the gas flow rate during hydride generation had to be sufficiently high to guarantee the correct carrying of the volatiles to the liquid nitrogen trap; a low carried time allows for control of the movement of water vapor without causing volatile loss.

The effect of the water vapor carried to the four-way valve explains the interaction between the factors which affect the revolatilization. In the optimum conditions found for the generation, a displacement of water vapor to the four-way valve is seen, in such a way that short times at room temperature and of revolatilization act against the dissolving of the analyte in the aqueous phase, thus favoring its revolatilization.

Resulting from this study, the optimum working conditions to obtain the highest absorbance responses were selected. There are: revolutizing time 0.5 min; reductor agent concentration 5%; carried time 2 min; gas flow rate during hydride generation 550 ml min<sup>-1</sup>, and time at room temperature 2 min.

### 3.3. Analytical characteristics

Under the instrumental and chemical conditions obtained in Section 2, calibration studies were made for the butyltin chloride. The regression equation was obtained by simple linear regression, multiple linear regression (MLR) and partial least square regression (PLSR). The absorbance was obtained on a wavelength interval from 190 to 220 nm. For the univariate regression, the wavelength selected was 192 nm; the MLR results were obtained after reducing by stepwise selection the total set of 20 predictors to an optimum subset (192 and 214 nm). For PLS, in

order to select the number of factors, a cross-validation method, leaving out one sample at a time, was used.

The detection limit of 5.6 ng ml<sup>-1</sup> was calculated according to the IUPAC; the value reported is the mean of five replicates, using the absorbance signal measured at the peak height at 192 nm. The relative standard deviation (RSD) value for precision, calculated from 20 determinations from a solution containing ten times the corresponding detection limit and taken on different days, was 5.1%.

Table 5 shows the root mean square difference (RMSD) and  $R^2$  of the calibration model. The RMSD is an indication of the average error in the analysis

$$\text{RMSD} = \left[ \frac{1}{N} \sum_{i=1}^N (\hat{y}_i - y_i)^2 \right]^{0.5}$$

and the square of the correlation coefficient ( $R^2$ ) is an indication of the quality of fit of all the data to a model:

Table 4  
Analysis of variance (ANOVA) for the fractional factorial central composite design

Source of variation	Sum of squares	Degrees of freedom	Mean square	F-ratio	P-value
(A) Reductor (L)	0.02379	1	0.02379	320.48	0.0000
(AA) Reductor (Q)	0.00008	1	0.00008	1.06	0.3078
(B) GAS FLOW RATE (L)	0.00052	1	0.00052	7.02	0.0100
(BB) GAS FLOW RATE (Q)	0.00084	1	0.00084	11.37	0.0012
(C) CARRIED TIME (L)	0.00036	1	0.00036	4.82	0.0315
(CC) CARRIED TIME (Q)	0.00035	1	0.00035	4.72	0.0332
(D) TIME ROOM $T^A$ (L)	0.00115	1	0.00115	15.53	0.0002
(DD): TIME ROOM $T^A$ (Q)	0.00009	1	0.00009	1.15	0.2881
(E) REVOL. TIME (L)	0.00541	1	0.00541	72.82	0.0000
(EE): REVOL. TIME (Q)	0.00173	1	0.00173	23.28	0.0000
(AB)	0.00020	1	0.00020	2.71	0.1041
(AC)	0.00029	1	0.00029	3.96	0.0507
(AD)	0.00052	1	0.00052	7.02	0.0100
(AE)	0.00000	1	0.00000	0.02	0.8981
(BC)	0.00259	1	0.00259	34.94	0.0000
(BD)	0.00027	1	0.00027	3.63	0.0609
(BE)	0.00035	1	0.00035	4.74	0.0329
(CD)	0.00135	1	0.00135	18.20	0.0001
(CE)	0.00045	1	0.00045	6.02	0.0167
(DE)	0.00243	1	0.00243	32.80	0.0000
Error	0.00512	69	0.00007		
Total SS <sup>a</sup>	0.04794	89			

<sup>a</sup> Sum of squares.



$$R^2 = 1 - \frac{\sum_{i=1}^N (y_i - \hat{y}_i)^2}{\sum_{i=1}^N (y_i - \bar{y})^2}$$

where  $y_i$  is the standard concentration of analyte in the sample  $i$ ,  $\hat{y}_i$  is the estimated concentration of the analyte in the sample  $i$ ,  $\bar{y}$  represents the mean of standard concentrations and  $N$  is the total number of samples. It can be seen that the best results were obtained using MLR, which gave the best correlation coefficient and the lowest RMSD.

The proposed simple linear regression, MLR and PLS methods applied to the absorption spectra allowed the resolution of drinking waters fortified with butyltin compound. In Table 6, the results obtained for the determination of the butyltin in the synthetic samples of butyltin chloride are shown. It can be seen that the RSD values were significantly lower when multivariate methods were used. The accuracy values obtained for the MLR and PLS methods were greater than for the univariate regression; within this group, the best results were obtained using PLS.

### 3.4. Interference study

The effect of several ions on a monobutyltin chloride standard of  $0.30 \text{ mg ml}^{-1}$  Sn are shown in Table 7. Solutions containing butyltin chloride (BT) and various concentrations of the potential interferents, one at a time, were subjected to the generation and determination procedure and the signals obtained by this method were compared with the signals obtained without the interference. All experiments were performed in triplicate.

No effects were observed for up to  $200 \text{ } \mu\text{g ml}^{-1}$  of Na (I), K (I), Ca (II), Ba (II), Sr (II), Mg (II), Mn (II), Hg (II), Cd (II), Zn (II), V (V), Mo (VI), Al (III), Cr (III),  $\text{NH}_4^+$ , Te (VI), Sn (IV), Bi (III), Pb (II), Ge (IV),  $\text{MnO}_4^-$ ,  $\text{Br}^-$ ,  $\text{F}^-$  and  $\text{I}^-$ ; up to

$1000 \text{ } \mu\text{g ml}^{-1}$  of chloride, sulphate and nitrate did not interfere. Those elements which gave rise to a signal depression of less than 1 S.D. of the expected response were deemed not to interfere.

Depression of the signal was observed in the presence of Co (II), Ni (II), Cu (II), Ag (I), Fe (II), Fe (III) and Cr (VI).

Significant interference effects were seen from the sulphite ion and the elements which form volatile hydrides under the generation conditions. Sb (III), Sb (V), Sn (II), As (III), As (V) and the  $\text{S}^-$  anion caused a quantitative increase in the absorbance signal which can be used for the simultaneous determination of mixtures of several elements. The Se (IV) showed a different behavior: for low interferent/analyte ratios, the error was almost the same, but when the [ $\mu\text{g ml}_{\text{int}}^{-1} / \mu\text{g ml}_{\text{BT}}^{-1}$ ] ratio increased, the interference increased also. This behavior may be due to the equilibria which becomes established between the butyltin chloride and the selenium species in the liquid or gas phase.

## 4. Conclusions

With the Plackett–Burman design used in this work, the variables which affect the determination of butyltin chloride by HG-GPMAS were identified: reductor agent concentration, gas flow rate during hydride generation, carried time, time at room temperature and revolatilizing time. This design allows a reduction in the number of factors to be studied, from 11 to 5, and establishes a new region to study.

The proposed experimental design methodology allows the finding of the optimal conditions for the determination of butyltin chloride by HG-GPMAS, together with an identification of the interactions between the factors studied, parameters which cannot be obtained when optimization of one factor at a time is used. It can be concluded that the most influential parameters on the response are reductor agent concentration, revolatilizing time and the interactions between carried time and gas flow rate during hydride generation and between time at room temperature and revolatilizing time.

Table 5  
Statistical parameters of the calibration

	Univariate	MLR	PLS
$R^2$	0.9991	0.9991	0.9989
RMSD	0.2178	1.7166	0.8651

Table 6  
Results obtained from the resolution of the artificial samples of butyltin chloride

Added (ng ml <sup>-1</sup> )	Univariate			MLR			PLS		
	Found <sup>a</sup> (ng ml <sup>-1</sup> )	Recov. (%)	RSD <sup>a</sup> (%)	Found <sup>a</sup> (ng ml <sup>-1</sup> )	Recov. (%)	RSD <sup>a</sup> (%)	Found <sup>a</sup> (ng ml <sup>-1</sup> )	Recov. (%)	RSD <sup>a</sup> (%)
42.9	45.8	107	8.3	42.6	99	1.9	43.2	101	1.1
53.6	54.8	102	5.9	53.1	99	1.4	54.1	101	1.8
74.3	68.9	92	7.8	74.5	100	1.4	74.4	100	0.89
148.6	140.2	94	12.9	145.8	98	1.6	147.9	99	0.95

<sup>a</sup> Mean of three independent determinations.

Table 7  
Results from the interference study

Interferent	Ratio [Int.]/[BT] <sup>a</sup>	% Error	Interferent	Ratio [Int.]/[BT] <sup>a</sup>	% Error
Co (II)	10	–	Sb (III)	0.1	17.56
	25	–20.61		0.2	50.85
	75	–45.25		0.3	88.02
	125	–73.27		0.5	151.7
	200	–96.3		1	257.1
Ni (II)	10	–44.05	Sb (V)	0.25	24.15
	25	–57.18		0.5	42.56
	100	–90.9		1	106.21
	150	–98.02		1.5	178.25
Cu (II)	10	–34.01	As (III)	0.25	67.66
	50	–71.25		0.5	101.49
	100	–80.74		0.75	135.32
	250	–88.06		1	202.98
Ag (I)	5	–21.96	As (V)	0.25	67.79
	25	–40.3		0.5	134.2
	50	–70.67		0.75	179.55
	100	–98.5		1	265.32
Fe (II)	10	–	Se (IV)	0.25	74.2
	25	–38.28		0.5	71.38
	75	–51.07		1.5	69.28
	150	–78.16		3.5	87.59
	300	–91.58		5	102.8
Fe (III)	25	–	Sn (II)	5	28.3
	75	–13.8		10	100.14
	150	–25.11		25	240.65
	300	–75.74		50	322.7
	400	–95.97			
Cr (VI)	5	–	NO <sub>2</sub> <sup>–</sup>	10	–38.23
	25	–46.37		25	–49.44
	75	–67.2		75	–58.69
	125	–77.42		100	–98.23
	325	–86.84	S <sup>=</sup>	0.25	99.25
		0.5		120.59	
		1		161.9	
			2	254.14	

<sup>a</sup> [ $\mu\text{g ml}_{\text{int}}^{-1}$ ]/ $\mu\text{g ml}_{\text{BT}}^{-1}$ (as Sn)].

The use of a diode-array molecular absorption spectrophotometer as the detector allows the spectra of generated volatiles to be obtained over a wide wavelength range, making possible the application of a multivariate calibration system. Fur-

thermore, the different effects that the various interferences present on the analytical signal can be observed. The spectra obtained for the interfering compounds allows, in some cases, the simultaneous determination of several compounds.

## Acknowledgements

The authors would like to thank the University of La Rioja and the Instituto de Estudios Riojanos for the financial support given to carry out this research. The authors also want to thank the CAICYT (Project No. 541-A783). Margarita Pérez Clavijo would like to thank the MEC for the FPI grant.

## References

- [1] P. Rivaro, L. Zaratín, R. Frache, A. Mazzucotelli, *Analyst* 120 (1995) 1937.
- [2] S. White, T. Catterick, B. Fairman, K. Webb, *J. Chromatogr. A* 794 (1998) 211.
- [3] D. Rosales, F. Pablos, I.L. Marr, *Appl. Organomet. Chem.* 6 (1992) 27.
- [4] Y.K. Chau, F. Yang, M. Brown, *Anal. Chim. Acta* 304 (1995) 85.
- [5] Y. Rodríguez-Pereiro, V.O. Schmitt, R. Lobinski, *Anal. Chem.* 69 (1997) 4799.
- [6] G. Schulze, C. Lehmann, *Anal. Chim. Acta* 288 (1994) 215.
- [7] A. Prange, E. Jantzen, *JAAS* 10 (1995) 105.
- [8] V. Lopez-Avila, Y. Liu, W.F. Beckert, *J. Chromatogr. A* 785 (1997) 279.
- [9] Y.K. Chau, S. Zhang, R.J. Maguire, *Analyst* 117 (1992) 1161.
- [10] S. Reader, E. Pelletier, *Anal. Chim. Acta* 262 (1992) 307.
- [11] H. Harino, M. Fukushima, M. Tanaka, *Anal. Chim. Acta* 264 (1992) 91.
- [12] V. Minganti, R. Capelli, De Pellegrini, *Fresenius J. Anal. Chem.* 351 (1995) 471.
- [13] A. Syty, *Anal. Chem.* 45 (1973) 1744.
- [14] M.S. Cresser, P.J. Isaacson, *Talanta* 23 (1976) 885.
- [15] A. Safavi, B. Haghghi, *Talanta* 44 (1997) 1009.
- [16] Y. Nakamoto, T. Tomiyama, T. Kumamaru, *Anal. Sci.* 13 (1997) 379.
- [17] Y. Duan, H. Zhang, X. Jiang, Q. Jin, *Spectrosc. Lett.* 29 (1996) 69.
- [18] J. Sanz, F. Gallarta, J. Galban, *Anal. Chim. Acta* 255 (1991) 113.
- [19] J. Sanz-Asensio, M.T. Martínez-Soria, M. Plaza-Medina, M. Pérez Clavijo, *Anal. Chim. Acta* 381 (1999) 331.
- [20] J. Sanz-Asensio, M. Pérez-Clavijo, M.T. Martínez Soria, *Anal. Chim. Acta* 343 (1997) 39.
- [21] S. Cabredo, I. Sanz, J. Sanz, J. Galban, *Talanta* 42 (1995) 937.
- [22] G.E.P. Box, W.G. Hunter, J.S. Hunter, *Statistic for Experiments*, Ed. Reverté, Barcelona, 1993.
- [23] N. Saim, J.R. Dean, Md.P. Abdullah, *Anal. Chem.* 70 (1998) 420.
- [24] STATISTICA/W + QC, Loll + Nielsen/StatSoft of Europe (ref. No 953746-1995).
- [25] PARVUS, M. Forina, S. Lanteri, C. Armanino, R. Leardi, G. Drava, Università degli Studi di Genova (invoice No 18/5002).

# Determination of selenium species in human urine by high performance liquid chromatography and inductively coupled plasma mass spectrometry

M. Angeles Quijano <sup>a</sup>, Ana Maria Gutiérrez <sup>b,\*</sup>, M. Concepción Pérez-Conde <sup>b</sup>,  
Carmen Cámara <sup>b</sup>

<sup>a</sup> *Departamento de Ciencias Básicas, E.U.I.T. de Obras Públicas, Universidad Politécnica de Madrid, 28014 Madrid, Spain*

<sup>b</sup> *Departamento de Química Analítica, Facultad de Química, Universidad Complutense de Madrid, 28040 Madrid, Spain*

Received 18 December 1998; received in revised form 31 March 1999; accepted 1 April 1999

## Abstract

A method developed to determine organic and inorganic selenium species in human urine samples is presented in detail. After a simple sample treatment based on elimination of non-charged organic compounds, selenium species were separated by high performance liquid chromatography (HPLC) on a Spherisorb 5 ODS/AMINO column using two different chromatographic conditions: phosphate buffers at pH 2.8 and 6.0. Detection was carried out using an on-line inductively coupled plasma mass spectrometer (ICP-MS). Trimethylselenonium ion and two unknown selenium species in urine samples were found. Selenium species were shown to have stability problems, with the maximum allowed storage time of 1 week. © 1999 Elsevier Science B.V. All rights reserved.

*Keywords:* Inductively coupled plasma mass spectrometry; High performance liquid chromatography; Selenium speciation; Human urine

## 1. Introduction

Selenium has been recognised as an essential trace element, based on its presence as a structural component of the enzyme glutathione peroxidase [1]. This element has a complex impact on man and animals depending on the concentration and

the chemical form in which it is present [2]. However, the difference between the necessary daily intake and the toxic dose is narrow.

Selenium exists in many different chemical forms in the environment and in biota. The inorganic species selenite and selenate are very important in the biochemical cycle of selenium. Seleno-amino acids take part in the biological selenium cycle and are incorporated into proteins [1,2]; selenomethionine (SeMet) is used as selenium supplements for man and animals and has been found in plants, selenocysteine is part of the

\* Corresponding author. Tel.: +34-91-3944222; fax: +34-91-3944329.

*E-mail address:* carreras@eucmax.sim.ucm.es (A.M. Gutiérrez)

active site of the enzyme glutathione peroxidase. The trimethylselenonium ion ( $\text{TMSe}^+$ ) is known to be a detoxified form of other more toxic selenium compounds [3,5]. The relationship between  $\text{TMSe}^+$  and other selenium compounds, such as selenocysteine, is not yet clear, though excess amounts of selenomethionine and several other amino acid derivatives administered to rats were shown to be metabolised to trimethylselenonium [4].

Detailed information concerning analytical methods for speciation of selenium will be found in some reviews [5–8]. Unfortunately, applications of selenium speciation techniques to real samples is scarce.

Urinary selenium concentration is used as an indicator of selenium status. Some articles have been published reporting clinical studies of the total selenium concentrations in biological fluids [5,9]. In human urine, amounts between 20 and 200  $\mu\text{g day}^{-1}$  are considered as normal excretion, but knowledge of the total concentration gives only poor information.

A few studies of analytical methods for determining selenium species in urine samples have been reported, most of them were performed on spiked urine samples [10–12]. A knowledge of the chemical form and concentration of selenium in urine is of interest; however, reports on the identification of Se species in urine are contradictory.  $\text{TMSe}^+$  has been identified as an important selenium metabolite in urine, ranging from 10 to 70% of total selenium [2,16], while other studies detected a major inorganic contribution [13–15].

Blotcky et al. [16] found that  $\text{TMSe}^+$  made up about 30% of total selenium in urine for a normal diet, and that the excretion level increased when the diet was supplemented by selenium-containing vitamins.  $\text{TMSe}^+$  was determined using a polystyrene column packed with cation exchange resin and neutron activation detection.

Yang and Jiang [14] determined  $\text{TMSe}^+$ , selenite and selenate in urine samples by ion-pairing chromatography coupled to ICP-MS with ultrasonic nebulisation. They found a major selenite contribution (between 100 and 400  $\mu\text{g l}^{-1}$ ), while  $\text{TMSe}^+$  was detected in a few samples at a level of 10  $\mu\text{g l}^{-1}$ .

Fodor and Barnes [15] differentiated selenate and selenite in urine samples using different pH-values for complexation with a poly(dithiocarbamate) resin. Analysis of the urine of 11 healthy persons showed that the average selenite content (8.6  $\mu\text{g l}^{-1}$ ) was about three times higher than the selenate concentration (3.1  $\mu\text{g l}^{-1}$ ).

Other peaks present in chromatograms of urine samples were considered to be possible seleno-amino acids. Muñoz Olivas et al. [17] differentiated selenocysteine (SeCys), selenomethionine and trimethylselenonium ion by ion-pairing chromatography and ICP-MS detection. They found a principal peak attributed to SeCys, without any presence of  $\text{TMSe}^+$ . No quantification was possible due to the overlapping of peaks.

Sample complexity makes it necessary to deal with sample storage and stability problems. Some studies have been carried out on the stability of selenium species in aqueous solution [18,19]. The best storage conditions for organic selenium species in aqueous solution, were found to be Pyrex containers at 4 and 20°C in the dark [19]. The authors observed excellent stability of  $\text{TMSe}^+$ , SeCys and SeMet for 3 months under all conditions studied. Inorganic species in aqueous solution are stable for 12 months in polyethylene and PTFE containers at  $-20^\circ\text{C}$ , and in these conditions it is not necessary to acidify the samples [18]. In biological fluids, the sampling and storage conditions may differ due to the presence of the matrix. In contrast to most elements, selenium sampling and storage are essentially free from contamination problems, but selenium species stability is a problem to be considered. At ambient temperature, bacterial growth transforms urea into ammonia, causing an alkaline urine. pH changes can affect urine composition [20]. Sanz Alaejos and Díaz Romero [5] reported no losses of Se when urine samples are stored at 4°C in polyethylene bottles for 12 h, but the study determined total selenium without monitoring transformation of species.

The aim of this work is to present a sensitive method for determination of selenium species in human urine samples and to describe a sample treatment that obviates immediate analysis. The analytical developments presented complete the

method proposed by us for the simultaneous separation of SeCys, SeMet, selenite and selenate by HPLC with ICP-MS detection [21]. For the application of this method to human urine samples, we included two more selenium species: TMS<sup>+</sup> and selenoethionine (SeEt).

## 2. Experimental

### 2.1. Apparatus

The chromatographic system used consisted of a Milton Roy CM4000 HPLC pump with a Milton Roy six-port sample injection valve fitted with a 100- $\mu$ l loop (Milton Roy LDC Division, Riviera Beach, FL, USA). Separations were performed on a Spherisorb ODS (octadecyl silica)/AMINO 5-mm, 250  $\times$  4.6 mm i.d. column (Phenomenex, Torrance, CA, USA).

Detection was performed using an ICP-MS instrument, VG Instrument PQ3 (Thermo Instruments, Uxbridge, Middlesex, UK). The PQ3 was first optimised separately from the chromatographic system, for nebuliser gas flow rate, ion lens voltages, quadrupole resolution and pole bias, using a standard solution containing elements spanning the mass range from beryllium to uranium at concentrations of 10  $\mu$ g l<sup>-1</sup>. The optimisation was also performed using a 20- $\mu$ g l<sup>-1</sup> standard selenium solution.

The chromatographic system was then coupled to the ICP-MS instrument by 20 cm of poly(tetrafluoroethylene) capillary tubing (0.5 mm i.d.) from the column outlet to the inlet of the standard Meinhard nebuliser.

During the HPLC-ICP-MS runs only m/z = 82 was monitored. The conditions used are summarised in Table 1. Total selenium concentration was performed by flow injection, using the same system without an analytical column and employing 2% HNO<sub>3</sub> as a carrier solution.

Bond Elut C<sub>18</sub> cartridges (3.0 ml and 500 mg) from Varian (CA, USA) were used to remove the organic matrix from urine samples and Millipore 0.45- $\mu$ m nylon filters (Bedford, MA, USA) to filter all HPLC solutions.

### 2.2. Reagents and standards

Selenium stock standard solutions (10 mg l<sup>-1</sup> of Se) were prepared by dissolving the appropriate amount in ultra-pure Milli-Q water (Millipore). Inorganic selenium solutions were obtained by dissolving sodium selenate and sodium selenite (Merck, Darmstadt, Germany), selenocystine (SeCys), selenomethionine (SeMet) and selenoethionine (SeEt) purchased from Sigma (St. Louis, MO, USA). Trimethylselenonium chloride was synthesised in our laboratory following the procedure of Palmer et al. [22]. Stock solutions were stored in the dark at 4°C. Working standards were obtained daily.

The eluents used for separations were 3.5 and 7.0 mmol dm<sup>-3</sup> phosphate buffer at pH = 6.0 (both concentrations) and 5.0 mmol dm<sup>-3</sup> phosphate buffer at pH = 2.8. Solutions were prepared by mixing separately prepared solutions of Na<sub>2</sub>HPO<sub>4</sub> and H<sub>3</sub>PO<sub>4</sub> (Panreac, Barcelona, Spain) until the desired pH was reached.

Table 1  
Operating conditions of the chromatographic and ICP-MS system

<i>Chromatographic system</i>	
HPLC column	Spherisorb ODS/AMINO (250 $\times$ 4.6 mm i.d.), 5 $\mu$ m
Mobile phases	Phosphate buffers: 5 mmol dm <sup>-3</sup> at pH = 2.8 3.5 and 7.0 mmol dm <sup>-3</sup> at pH = 6.0
Flow rate	1.0 ml min <sup>-1</sup>
Sample injection volume	100 $\mu$ l
Dead volume <sup>a</sup>	2.02 $\pm$ 0.01 ml
<i>ICP-MS</i>	
Forward power	1350 W
Reflected power	0.5 W
Coolant gas flow rate	14 l min <sup>-1</sup>
Auxiliary gas flow rate	0.8 l min <sup>-1</sup>
Nebuliser gas flow rate	0.9 l min <sup>-1</sup>
Data collection mode	Single ion monitoring
Integration time	2.0 s

<sup>a</sup> Measured with 10  $\mu$ g l<sup>-1</sup> of Lithium (LiNO<sub>3</sub>) at m/z = 7.

Methanol, HPLC grade, was purchased from Scharlau (Barcelona, Spain).

All solutions used were filtered through a 0.45- $\mu\text{m}$  nylon filter and de-gassed before use.

### 2.3. Procedure

#### 2.3.1. Separation and determination of selenium species in urine samples

Selenium species were separated by HPLC using two different sets of chromatographic conditions:

Chromatographic separation of organic selenium standard solutions (TMSe<sup>+</sup>, SeCys, SeMet and SeEt) was performed by injecting solutions containing the four compounds onto the column and eluting with 5.0 mmol dm<sup>-3</sup> phosphate buffer at pH = 2.8, at a flow rate of 1.0 ml min<sup>-1</sup>.

Chromatographic separation of organic and inorganic selenium standards solutions (TMSe<sup>+</sup>, SeCys, SeMet, SeEt, selenite and selenate) was carried out by elution with 3.5 mmol dm<sup>-3</sup> phosphate buffer at pH = 6.0. After 7 min, the eluent concentration was changed to 7.0 mmol dm<sup>-3</sup> at pH = 6.0, by applying a linear concentration gradient over a 1-min period. The flow rate was 1.0 ml min<sup>-1</sup>.

Human urine samples (4 ml) were processed in a vacuum manifold system by passage through Bond-Elut C<sub>18</sub> cartridges previously conditioned with 5 ml of methanol followed by 5 ml of Milli-Q water. The cartridge was washed with 5 ml of 3.5 mmol dm<sup>-3</sup> phosphate buffer at pH 6.0. The eluate was diluted to 10 ml with Milli-Q water, resulting in a 2/5 dilution of the sample.

Detection of the eluted selenium species was carried out by the ICP-MS using the operating conditions given in Table 1. The analytical peaks obtained were evaluated by peak area measurements.

#### 2.3.2. Design of the stability study

The storage containers used for the stability test were 10 ml vials of polyethylene and Pyrex. Vials were previously washed and immersed in a 10% HNO<sub>3</sub> bath for 24 h and rinsed with Milli-Q water several times before use.

Different aliquots of an urine sample were processed as it is above indicated. All of them were mixed and split into vials and maintained in the dark at -18 and 4°C. Storage flasks were sealed with paraffin paper.

A total of ten vials was prepared for storage under each experimental condition. In order to determine the reference signal values ( $S_{\text{Ref}}$ ), two different vials taken randomly from each series were analysed immediately after sample preparation. Measurements for the stability study were made after 1, 7, 14 and 28 days.

## 3. Results and discussion

### 3.1. Analytical performance

In previous work, we evaluated chromatographic parameters such as mobile phase pH and concentration for SeCys, SeMet, selenite and selenate separation, and found that the best working conditions were achieved using a phosphate concentration gradient from 3.5 to 7.0 mmol dm<sup>-3</sup> at pH 6.0 [21]. High resolution was obtained in organic selenium species separation at pH = 2.8, but inorganic selenium species did not elute below pH 6. Selenium species separation over a pH gradient from 2.8 to 6.0 was not feasible, due to the long time required for the column equilibrium.

As there is considerable controversy over the selenium species present in urine samples, this study included two more selenium species in addition to the four above mentioned: SeEt and TMSe<sup>+</sup>. The latter necessarily had to be included because most authors agree that it is present in this kind of samples [2,14,16].

Table 2 lists the chromatographic parameters for the six selenium species mentioned above. The mobile phase pH exerts little influence on SeEt retention, as occurs with other amino acids (SeCys and SeMet). TMSe<sup>+</sup> elutes in the dead volume at low pH, but its retention time increases when pH is increased, possibly due to interaction with deprotonated silanol groups (Si-O<sup>-</sup>) in the stationary phase. The capacity factor ( $k'$ ) for the two selenium species studied was independent of buffer concentration, and only inorganic selenium species were affected by this parameter [21].



Table 2  
Chromatographic parameters for aqueous selenium species<sup>a</sup>

	TMSe <sup>+</sup>	SeCys	SeMet	SeEt	Se(IV)	Se(VI)
<i>k'</i> at pH = 2.8	0.14	0.58	1.16	2.35	–	–
Resolution		1.02	1.19	2.30		
<i>k'</i> at pH = 6.0	0.27	0.89	1.47	3.17	5.64	14.8
Resolution		0.70	0.76	1.65	1.68	5.66

<sup>a</sup> *k'* is the capacity factor.

The chromatogram of standard solutions at pH 2.8 is shown in Fig. 1(a). There is a good separation between organic selenium species. The chromatogram at pH 6.0 (Fig. 1(b)) shows that SeEt elutes between SeMet and selenite with a good resolution, but that TMSe<sup>+</sup> elutes close to SeCys. In conclusion, at pH = 6.0 it is possible to obtain separation of selenium species, but in the presence of TMSe<sup>+</sup> it is necessary to carry out the separation of organic selenium species at pH = 2.8. These results suggest that both chromatographic conditions (pH 6.0 and 2.8) will have to be used in the speciation of urine samples.

### 3.2. Urine sample analysis

#### 3.2.1. Qualitative analysis

Urine samples can be analysed by simple dilution, generally 1/5, in distilled water and direct injection into the chromatographic column [14]. The proposed method was applied to urine samples collected from three healthy subjects, all having a normal diet. In all cases the chromatographic profiles were the same.

Urine chromatograms showed two peaks at pH = 2.8 (Fig. 2(a)) and three peaks at pH = 6.0 (Fig. 2(b)).

At pH = 6.0, the first peak elutes at 2.9 min; at this pH TMSe<sup>+</sup> cannot be differentiated from SeCys. This peak was identified as TMSe<sup>+</sup> at pH = 2.8 because of the increase in its area when standard TMSe<sup>+</sup> solutions were added, though it could be other cationic selenium species that also eluted in the dead volume. The absence of SeCys under this chromatographic condition was confirmed.

The second peak found in urine analysis eluted around 5.2 min at pH = 2.8 and around 5.7 min at pH 6.0, between SeMet and SeEt under both chromatographic pH conditions. This peak cannot be attributed to any selenium species studied,

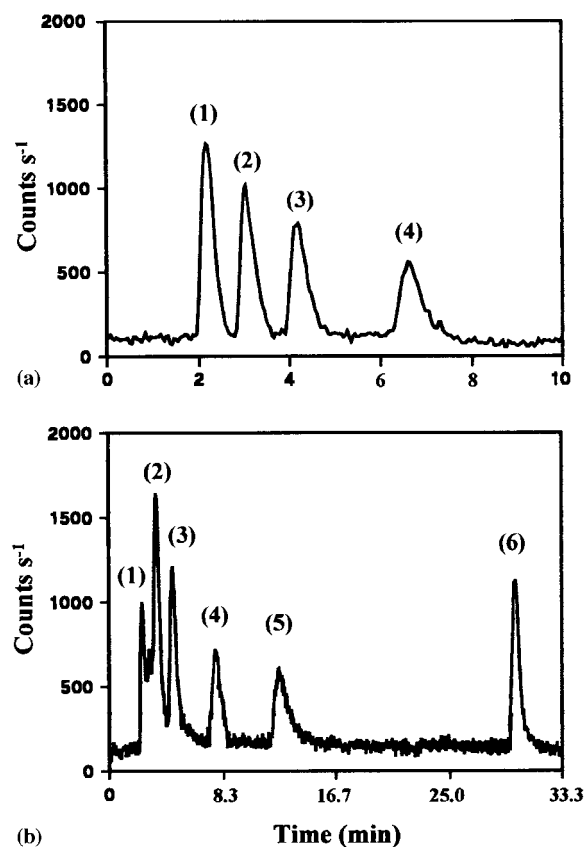


Fig. 1. HPLC-ICP-MS chromatogram of a standard mixture of (1) TMSe<sup>+</sup>; (2) SeCys; (3) SeMet; (4) SeEt; (5) Se(IV) and (6) Se(VI) ( $5 \mu\text{g l}^{-1}$  of selenium each). Mobile phase: (a) phosphate buffer  $5.0 \text{ mmol dm}^{-3}$  at pH = 2.8; (b) phosphate buffers  $3.5$  and  $7.0 \text{ mmol dm}^{-3}$  at pH = 6.0.

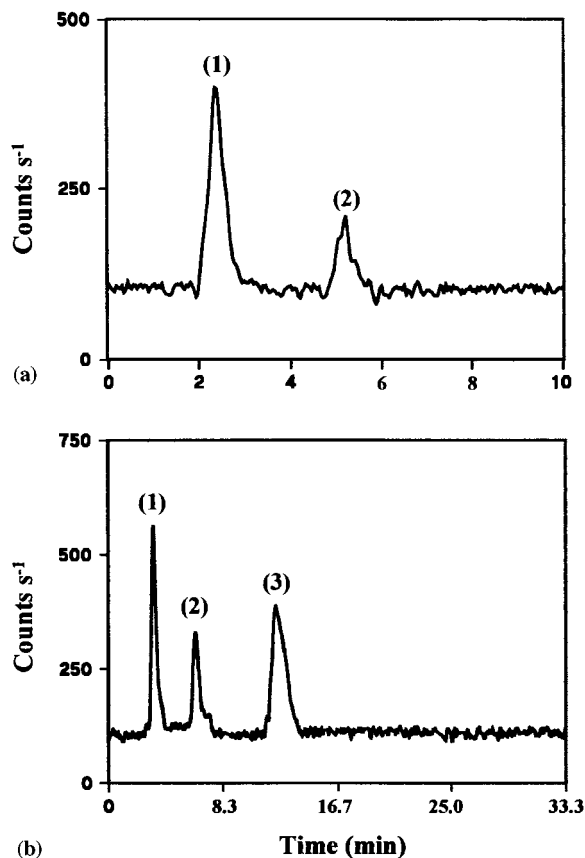


Fig. 2. HPLC-ICP-MS chromatogram of urine<sub>A</sub> (1) TMS<sup>+</sup>; (2) U<sub>1</sub>; (3) U<sub>2</sub>. Mobile phase: (a) phosphate buffer 5.0 mmol dm<sup>-3</sup> at pH = 2.8; (b) phosphate buffers 3.5 and 7.0 mmol dm<sup>-3</sup> at pH = 6.0.

because as was proved by adding the other known selenium species. The retention time suggests that this selenium species could be a different seleno amino acid or a methylated form of selenomethionine. We will refer to this selenium species as U<sub>1</sub>.

The third peak found in all urine samples only eluted at pH = 6.0 as an inorganic selenium species, and the retention time of 10.5 min was similar to that of selenite elution; however, when selenite was added, it yielded a different retention time. We will refer to this selenium species as U<sub>2</sub>. A better resolution between these two selenium species was achieved using a 3.5-mmol dm<sup>-3</sup> mobile phase, without a concentration gradient, because selenite is retarded at this lower buffer

concentration. U<sub>2</sub> eluted close to selenite, which could create confusion in its identification. The fact that this unknown selenium species only elutes at pH = 6.0 suggests a strong negative charge on the molecule.

As there was no evidence of the presence of SeCys, which overlapped with TMS<sup>+</sup> at pH = 6.0, and the unknown peaks (U<sub>1</sub> and U<sub>2</sub>) did not overlap, the selenium species in these urine samples can be analysed in a single chromatographic run.

### 3.2.2. Sample treatment

Because of instability, the urine samples had to be stabilised to avoid the need for immediate analysis. Some authors have added compounds such as toluene, formaldehyde, hydrochloric acid, nitric acid and others to prevent bacterial growth and minimise selenium adsorption losses [5]. However, these additives can induce species transformation and create interferences in the instrumental detector used. Other authors describe complex methods of sample treatment based on protein precipitation and selenium species preconcentration by evaporation to dryness and redissolution of the residue in a reduced volume [12].

To improve stability of urine samples, we attempted to remove the organic matrix using a simple treatment consisting of phase solid extraction with C<sub>18</sub> cartridges.

In the working pH range (2.8–6.0), all the selenium species studied are charged. Inorganic selenium species are present as HSeO<sub>3</sub><sup>-</sup> and SeO<sub>4</sub><sup>2-</sup>, trimethylselenonium is a cation and seleno amino acids (selenocystine, selenomethionine and selenoethionine) are present as zwitterions. As non-charged species are retained in C<sub>18</sub> cartridges, selenium species will be eluted and separated from the retained organic matrix. However, it is possible that in the presence of urine matrix, some selenium species could form ion-pairs with a resulting change in their behaviour.

Recovery from the C<sub>18</sub> cartridges was studied by addition of known amounts of selenium standards to the urine sample. Aliquots of human urine (8 ml) were spiked with 0.1 μg of each selenium standard, and half of each aliquot was diluted directly to 10 ml with Milli-Q water and

the other half was processed through C<sub>18</sub> cartridges. The study was extended to the unknown selenium species present in the sample (U<sub>1</sub> and U<sub>2</sub>), by comparing the results obtained after clean-up step with those obtained after simple dilution.

Recoveries were evaluated as the ratio of the selenium signal for processed samples to that for unprocessed samples. C<sub>18</sub> cartridges were washed with Milli-Q water (method 1) and with 3.5 mmol dm<sup>-3</sup> mobile phase at pH = 6 (method 2). Table 3 shows losses of about 30% for SeCys and SeEt using method 1, while method 2 provides good recoveries for all selenium species. Losses of seleno amino acids and unknown selenium species could be attributed to a partial retention on C<sub>18</sub> stationary phase. An increase of the eluent ionic strength produces an improvement of recoveries. Thus, we chose the method 2 for further experiments.

### 3.2.3. Stability study

Selenium species stability in urine was evaluated by measuring the analytical peaks of TMSe<sup>+</sup>, U<sub>1</sub> and U<sub>2</sub>. The addition of other selenium species, absent in the original sample, was avoided because it could cause chemical interaction with the selenium species present in urine.

Stability was calculated as the ratio between the mean signal obtained under the different storage conditions (*S<sub>x</sub>*) and the mean value taken as reference (*S<sub>Ref</sub>*), expressed as a percentage (%*R*). Results are shown in Fig. 3.

Table 3  
Recovery percentage (± standard deviation) on spiked urine samples processed by passage through C<sub>18</sub> cartridges<sup>a</sup>

Species	Method 1	Method 2
TMSe <sup>+</sup>	97 ± 4%	101 ± 3%
SeCys	73 ± 8%	94 ± 4%
SeMet	89 ± 7%	98 ± 3%
SeEt	71 ± 5%	95 ± 5%
Selenite	102 ± 4%	99 ± 4%
Selenate	96 ± 5%	98 ± 3%
U <sub>1</sub>	85 ± 5%	97 ± 6%
U <sub>2</sub>	90 ± 4%	102 ± 5%

<sup>a</sup> Cartridges were washed with Milli-Q water (method 1) and 3.5 mmol dm<sup>-3</sup> mobile phase at pH = 6.0 (method 2). Results are the mean of three separate experiments.

Severe losses of U<sub>1</sub> species appears after only a week of storage in all cases, except in polyethylene vials maintained at 4°C in which losses were detected after 2 weeks of storage. This species tends to be lost with time in all the storage conditions tested. TMSe<sup>+</sup> and U<sub>2</sub> seem to be more stable, but samples kept frozen at -18°C in two storage materials underwent a gradual loss.

Losses observed upon samples storage cannot be attributed to species conversion, because there are no new peaks in the sample chromatograms. We did not observe the appearance of any precipitate in samples that could adsorb these compounds. Slightly better results were obtained in polyethylene than in Pyrex containers, possibly due to their better resistance to light and oxidising agents. The effect of temperature was similar for the two materials tested. Losses of TMSe<sup>+</sup> and U<sub>2</sub> species were more notable at -18°C and, contrary to expectations, better results were obtained at 4°C. The possible loss of selenium through volatilisation into DMS<sub>2</sub>Se is not ruled out, however, it would be minimal at the storage temperatures used.

The results show that the best storage condition was in polyethylene vials at 4°C. If held in these storage conditions and subjected to the sample treatment indicated, the selenium species present in urine samples remain stable for a week, avoiding the need for immediate analysis.

### 3.2.4. Quantitative analysis

Total selenium content in urine samples was determined by flow injection ICP-MS, using standard selenite solution. Previously we verified that there were no differences in the selenium signal produced by the six selenium species studied. No appreciable matrix effect was found at a sample dilution of 1/10, as evidenced by the similar slopes of the aqueous and standard addition flow injection calibrations (Table 4). The total selenium concentrations found in the three human urines analysed are shown in Table 5.

Table 4 shows the slopes obtained for the six selenium species in aqueous and standard addition HPLC calibrations. No significant differences were found at the 95% confidence level and, therefore, it was concluded that there is no matrix

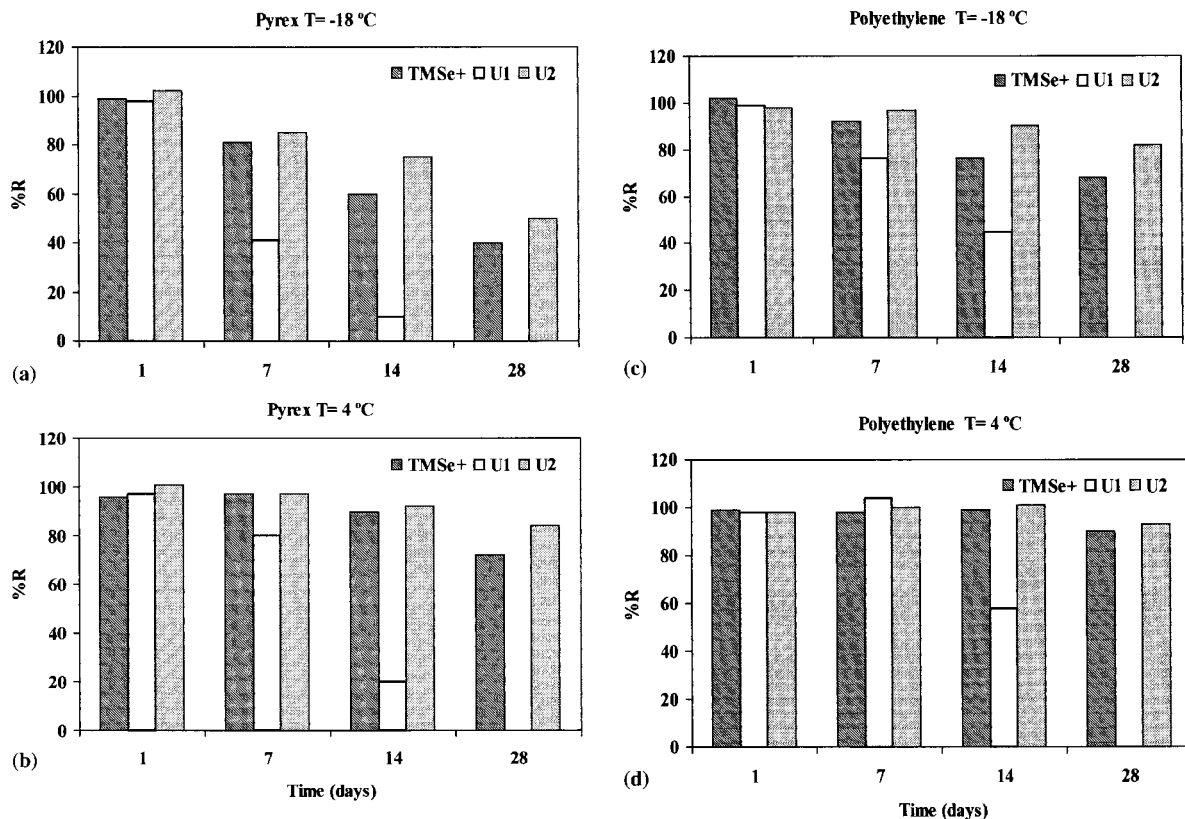


Fig. 3. Stability of seleno compounds present in urines stored in two kinds of container at two different temperatures: (a) Pyrex at  $-18^{\circ}\text{C}$ ; (b) Pyrex at  $4^{\circ}\text{C}$ ; (c) polyethylene at  $-18^{\circ}\text{C}$ ; and (d) polyethylene at  $4^{\circ}\text{C}$ .

effect in species quantification at the 1/5 sample dilution used.

The concentrations of the two unknown selenium species ( $U_1$  and  $U_2$ ) were estimated as selenium analyte, by calibration against the nearest neighbouring peak of a known substance, which was SeEt for  $U_1$  and selenite for  $U_2$ . The concentrations of different species in three human urines are shown in Table 5.

There was an excellent recovery calculated by comparison of the sum of selenium species concentration and the total selenium found in urine. The recoveries were 95.0, 87.6 and 90.5% for urine A, B and C, respectively.

The analytical characteristics in urine matrix were evaluated for the six selenium compounds. The precision of the method was found to be better than 5%, and detection limits in urine matrix was

0.05 ng using a 100- $\mu\text{l}$  injection volume, slightly worse than for the aqueous standard (0.04 ng).

#### 4. Conclusion

Three different human urines were analysed. Qualitative urine analysis showed the presence of  $\text{TMSe}^+$  and two unknown selenium peaks denoted  $U_1$  and  $U_2$ , which were present in all urines. Based on its retention times and acidic nature,  $U_1$  could be a seleno amino acid or a methylated form of selenium.  $U_2$  does not elute at  $\text{pH} = 2.8$ , possibly due to a strong negative charge. Research is now in progress to elucidate the structure of these two unknown species. No appreciable presence of selenite and selenate was found in any of the all urines analysed.

Table 4

Calibration slopes ( $\pm$  standard deviation,  $s_b$ ) for total selenium (1/10 dilution) and selenium species (1/5 dilution) in aqueous and standard additions calibration

	Aqueous calibration	Standard additions calibration
Total Se	6898 $\pm$ 28 ( $r = 0.9998$ ) <sup>a</sup>	6743 $\pm$ 72 ( $r = 0.9992$ )
TMSe <sup>+</sup>	6734 $\pm$ 40 ( $r = 0.9997$ )	6509 $\pm$ 58 ( $r = 0.9993$ )
SeCys	6505 $\pm$ 27 ( $r = 0.9998$ )	6366 $\pm$ 38 ( $r = 0.9997$ )
SeMet	6179 $\pm$ 26 ( $r = 0.9998$ )	6102 $\pm$ 48 ( $r = 0.9995$ )
SeEt	5987 $\pm$ 34 ( $r = 0.9997$ )	6058 $\pm$ 73 ( $r = 0.9987$ )
Se(IV)	6035 $\pm$ 47 ( $r = 0.9996$ )	5940 $\pm$ 70 ( $r = 0.9988$ )
Se(VI)	6615 $\pm$ 28 ( $r = 0.9998$ )	6302 $\pm$ 56 ( $r = 0.9993$ )

<sup>a</sup>  $r$  is the correlation coefficient of regression.

Table 5

Quantitative results for selenium species in human urine expressed as  $\mu\text{g l}^{-1}$  of selenium (mean  $\pm$  s,  $n = 3$ )

	TMSe <sup>+</sup>	U <sub>1</sub>	U <sub>2</sub>	Total Se
Urine <sub>A</sub>	17.8 $\pm$ 0.6	7.7 $\pm$ 0.3	17.5 $\pm$ 0.6	45 $\pm$ 1
Urine <sub>B</sub>	14.3 $\pm$ 0.5	14.9 $\pm$ 0.6	16.9 $\pm$ 0.6	53 $\pm$ 2
Urine <sub>C</sub>	19.8 $\pm$ 0.7	8.5 $\pm$ 0.3	6.1 $\pm$ 0.2	38 $\pm$ 1

Simple sample treatment with Bond-Elut C<sub>18</sub> cartridges removes organic matrix without loss of selenium species, there by improving storage characteristics.

The stability study focused on finding a storage method in order to avoid the immediate need for analysis. The possible seleno amino acid U<sub>1</sub> was more unstable than the others species present, and limited the storage time. The selenium species present in the urines studied were stable for 1 week in polyethylene vials maintained at 4°C.

## Acknowledgements

The authors are grateful for financial support from DGCYT under project PB 95-0366-C01-C02 and the Measurements and Testing Programme (EC) and to Max Gormann for revising the manuscript.

## References

- [1] L. Fishbein, in: E. Merian (Ed.), *Metals and their Compounds in the Environment*, UHC Verlagsgesellschaft, Germany, 1991, pp. 1153–1190.
- [2] Y. Shibata, M. Morita, K. Fuwa, *Adv. Biophys.* 28 (1992) 31.
- [3] M. Sanz Alaejos, C. Díaz Romero, *Clin. Chem.* 39/10 (1993) 2040.
- [4] R.J. Kraus, S.J. Foster, H.E. Ganther, *Anal. Biochem.* 147 (1985) 432.
- [5] M. Sanz Alaejos, C. Díaz Romero, *Chem. Rev.* 95 (1995) 227.
- [6] R. Muñoz Olivas, O.F.X. Donard, C. Cámara, P. Quevauviller, *Anal. Chim. Acta* 286 (1994) 357.
- [7] G. Kölbl, K. Kalcher, K.J. Irgolic, R. Magee, *J. Appl. Organomet. Chem.* 7 (1993) 443.
- [8] X. Dauchy, M. Potin-Gautier, A. Astruc, M. Astruc, *Fresenius J. Anal. Chem.* 348 (1994) 792.
- [9] S. Caroli, A. Alimonti, E. Coni, F. Petrucci, O. Senofonte, N. Violante, *Crit. Rev. Anal. Chem.* 24 (5 & 6) (1994) 363.
- [10] J.M. González LaFuente, M.L. Fernández Sánchez, A. Sanz-Medel, *J. Anal. At. Spectrom.* 11 (1996) 1163.
- [11] J.M. Marchante-Gayón, J.M. González, M.L. Fernández, E. Blanco, A. Sanz-Medel, *Fresenius J. Anal. Chem.* 355 (1996) 615.
- [12] J-S. Blais, A. Huyghues-Despointes, G.M. Mompalaisir, W.D. Marshall, *J. Anal. At. Spectrom.* 6 (1991) 225.
- [13] A.K. Das, R. Chakraborty, M.L. Cervera, M. de la Guardia, *Mikrochim. Acta* 122 (1996) 209.
- [14] K.-L. Yang, S.-J. Jiang, *Anal. Chim. Acta* 307 (1995) 109.
- [15] P. Fodor, R.M. Barnes, *Spectrochim. Acta* 38B (1983) 229.
- [16] A.J. Blotcky, G.T. Hansen, L.R. Opeliano-Buencamino, E.P. Rack, *Anal. Chem.* 57 (1985) 1937.
- [17] R. Muñoz Olivas, O.F.X. Donard, N. Gilon, M. Potin-Gautier, *J. Anal. At. Spectrom.* 11 (1996) 1171.
- [18] M.G. Cobo, M.A. Palacios, C. Cámara, F. Reis, Ph. Quevauviller, *Anal. Chim. Acta* 286 (1994) 371.
- [19] R. Muñoz Olivas, Ph. Quevauviller, O.F.X. Donard, *Fresenius J. Anal. Chem.* 360 (1998) 512.
- [20] Ames, D., in: Miles (Ed.), *Urianálisis Moderno*. Martin Lab., S.A.E. Barcelona, Spain, 1987, pp. 12–15.
- [21] A. Quijano, A.M. Gutiérrez, C. Pérez-Conde, C. Cámara, *J. Anal. At. Spectrom.* 11 (1996) 407.
- [22] I.S. Palmer, D.D. Fisher, A.W. Halverson, O.E. Olson, *Biochem. Biophys. Acta* 117 (1969) 336.

# The use of ozone as the primary digestion reagent for the cold vapor mercury procedure

K. Sasaki <sup>a</sup>, G.E. Pacey <sup>b,\*</sup>

<sup>a</sup> College of Science, Rikkyo University, Tokyo, Japan

<sup>b</sup> Department of Chemistry, Miami University, Oxford, OH 45056, USA

Received 13 April 1998; received in revised form 20 March 1999; accepted 2 April 1999

## Abstract

Ozone was tested as an alternative digestion/oxidation system to the permanganate/peroxodisulfate currently used in the cold vapor mercury method. The results indicate that the digestion of comparable size samples to the 'Standard Method' was complete in less than 2 min. A 0.5 ml (10 ppb) sample size was completely oxidized in less than 30 s. The batch system used produced a limit of detection (LOD) for mercury(II) chloride, methylmercury chloride, and phenylmercury acetate of about 0.5 ppb. © 1999 Elsevier Science B.V. All rights reserved.

*Keywords:* Ozone; Cold vapor mercury method

## 1. Introduction

The determination of mercury in environmental samples has been complicated by the fact that the discharged inorganic mercury can be converted to organomercury species. In the cold vapor atomic absorption method, these organomercury species must be digested and the mercury ion stabilized in its  $\text{Hg}^{2+}$  valence state before subsequent reduction to the volatile  $\text{Hg}^0$  species. To accomplish the reduction, the standard method subjects the sam-

ple to a digestion process that includes potassium permanganate, potassium persulfate and heating for 2 h [1]. The excess oxidant is reduced by a hydroxylamine salt and then the digested sample has stannous chloride added, followed immediately by a gas purging of the  $\text{Hg}^0$  into the atomic absorption spectrometer cell.

This method has suffered from poor precision and accuracy because of the 2-h digestion step. Until now, automation of this method has only been possible for the steps after the digestion. Obviously, if the mercury procedure is to be fully automated, the time required for the digestion step must be reduced. Some attempts using flow injection analysis (FIA) have been made [2–6]. Birnie used a strong oxidizing acid concurrently

\* Corresponding author. Fax: +1-513-529-5715.

E-mail address: chmcwis@miaavx1.muohio.edu (G.E. Pacey)

with a strong oxidizing agent and external heating [2]. The poor detection limit of 20 ng/ml Hg was attributed to the large internal volumes of the system. Attempts at utilizing on-line microwave digestion still require off-line oxidation [6]. Hanna et al. eliminated the external heating source by taking advantage of the heat of mixing between the concentrated sulfuric acid and the carry stream [7]. Potassium persulfate was still used. A detection limit of 0.23 ng/ml was reported. The recovery from this system was good. The down side to this approach was a significant problem with water vapor. The increased temperatures produced problematic fogging of the cell windows.

The problem for the oxidation has been in the oxidants used. The use of a stronger and kinetically more vigorous oxidant like ozone is necessary. Ozone readily decomposes to produce radicals that are believed to be responsible for the majority of the observed reactivity [8]. Therefore, unlike the permanganate/peroxodisulfate system where excess oxidant and by-products must be destroyed, the excess ozone can be removed by degassing. This means that the hydroxylamine reduction step currently in 'Standard Methods' can be eliminated. The only potential downside is that ozone cannot be generated and saved for later use. Ozone must be generated on site. This paper reports the preliminary data on the oxidation of organomercury compounds.

## 2. Experimental

### 2.1. Apparatus

Fig. 1 shows the manifold diagram for the batch ozone digestion system used for the organomercury determination. The typical cold vapor system was modified to allow for the ozonizer.

A small ozonizer was constructed consisting of a glass discharger (Fig. 2) with aluminum and copper electrodes coupled with a Tesla coil. Ozone was generated by passing oxygen at 140 kPa. The feedstock oxygen contacts only the glass sheath and the aluminum electrode. The copper counter electrode is located in a closed compartment isolated from the feedstock oxygen and the ozone. This is necessary to minimize the potential for corrosion. The design of the discharger may be simplified more if all aluminum wire is used instead of copper.

A 100 ml of standard or sample was placed into the standard mercury digestion glass bottle. The sparger/stopper was placed in the digestion bottle. The sparger and bottles were used only after a cleansing procedure where they were soaked with mercury-free concentrated nitric acid for at least 5 min.

For the smaller scale 0.5 ml experiments, a fish-tank ozonizer (SANDEL Model 50) was used as the ozone source. For these experiments, a homemade digestion bottle and a bubbling capil-

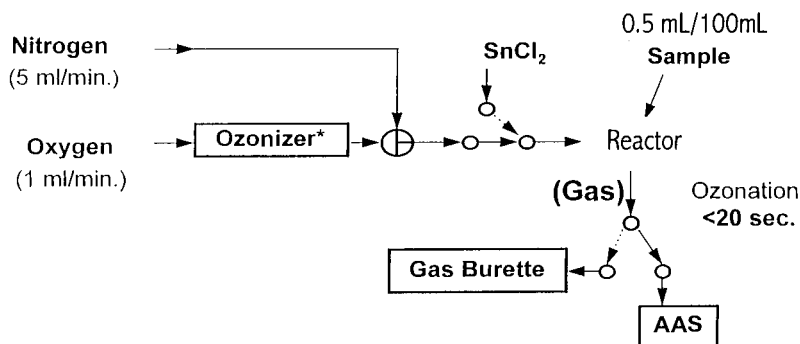


Fig. 1. Manifold design for the batch ozone digestion system.

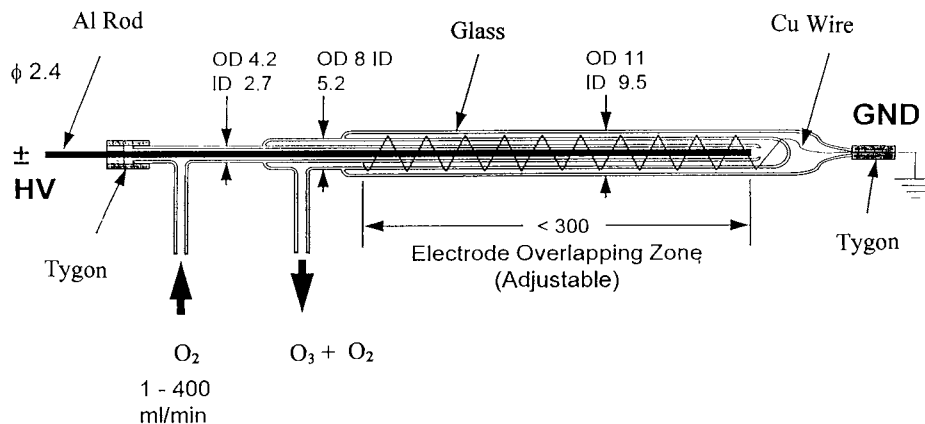


Fig. 2. Small ozonizer used in this work.

lary (0.5 mm i.d.) that had a glass plate at the gas outlet was used. This design provided better control of the bubble size (Fig. 3). The bottle was connected with glass capillaries and tygon joints to the atomic absorption spectrometer (AAS) flow cell. A switching valve was used to direct the ozone to waste in order to eliminate the possibility of ozone adsorption on the tubing or AAS cell. Use of this design minimized the area that produced the major delay in removal of ozone from the system. The bottles and capillary were used only after a cleansing procedure where they were soaked with mercury-free concentrated nitric acid for at least 5 min.

A model 3110 Perkin Elmer AAS, equipped with a mercury electrodeless discharge lamp operated at 210 mA, was used for the measurement of mercury. Wavelength, slit width, and slit height of the spectrophotometer were adjusted to 253.7 nm, 0.7 nm, and low position, respectively. A plastic spectrophotometric flow cell (Perkin Elmer) of 14.5 mm i.d. and 145 mm in length with quartz windows of 11 mm in diameter on the end of the cell was used for the 100 ml scale samples. All connections in this system were made with tygon tubing. For 0.5 ml scale samples, a T-shaped flow cell of 3.2 mm i.d. and 200 mm length with quartz windows placed 1 mm apart from the vapor outlets was used. All connections for this system were made using 0.5 mm teflon tubing.

The gas flow rates were determined manually using a flowmeter or a gas burette at the outlet of

digestion bottle in real time or after AAS signal reading.

## 2.2. Reagents

The standard solution of mercury(II) ion was prepared by dissolving mercury(II) chloride (Fisher) into 0.14 M nitric acid and diluted by triple-distilled water immediately before use. The standard solution of methylmercury(II) chloride and phenylmercury(II) acetate (Aesar) were prepared by dissolving each compound in triple distilled water. Commercially available standard solution of methylmercury(II) chloride ( $1000 \pm 10$  mg/l mercury) (Alfa) was also used, but the concentration was lower than our laboratory-prepared standard solution and its use discontinued. A tin(II) solution was prepared by dissolving tin(II) chloride dehydrate (5 g; Fisher) in concen-

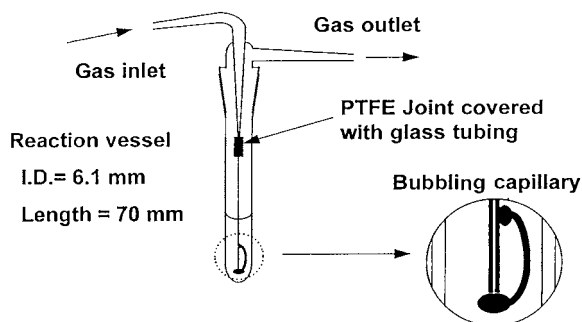


Fig. 3. Reactor design.



trated hydrochloric acid (20 ml), and the solution was diluted (to 100 ml) with triple-distilled water and was flushed with nitrogen. All the other chemicals used in the present work were of analytical reagent grade or higher, and used without purification.

### 2.3. Procedure

For the initial experiments, the 100 ml sample size was chosen since the current standard method for organomercury determinations used 100 ml [1,2]. A 100 ml sample solution was placed in a 295 ml glass digestion bottle with a sparger/stopper. Sodium hydroxide solution and water were added to adjust the hydroxide ion concentration ( $7 \times 10^{-4}$  M) and the volume to 140 ml, the same reaction volume as the standard method. Ozone was produced using the large-scale ozonizer (Fig. 2) at an oxygen flow rate of 0.35 l/min. This flow rate produced about 0.015 moles of ozone/min. The ozone was bubbled into the digestion bottle for 1 min. After the excess ozone was removed using a 1-min air bubbling step, the outlet of the digestion bottle was connected to the AAS flow cell. Two milliliters of a 5% tin(II) chloride solution (in 2.5 M hydrochloric acid) was added, quickly pipetted into the solution, and the mercury(II) was reduced to mercury(0). The volatile mercury(0) was purged using bubbled nitrogen with a flow rate between 11 and 15 ml/min. Peak absorbance was read on an AAS display.

The flow rates of oxygen and nitrogen for ozone purging were measured using a direct reading flow meter at the gas outlet of digestion bottle when the flow cell was disconnected from the outlet in real time. The nitrogen flow rate for the mercury purging was measured after atomic absorption measurement in the same way.

Once it was clear that the ozone digestion was viable on the large scale, the smaller version that could be used on-line in a flow injection system was tested. A 0.5 ml sample solution was placed in the small digestion bottle (Fig. 3). The concentration of hydroxide ion was adjusted to  $5 \times 10^{-4}$  M with sodium hydroxide. The ozone was generated using the Sandel ozonizer model 50 at oxygen flow rates between 0.8 and 1.0 ml/min, and

bubbled through the microcapillary sparger with a glass blocking plate for 20 s. The ozone concentration was about  $1.2 \times 10^{-5}$  moles of ozone/min. The nitrogen used for ozone-purging at a flow rate of 5 ml/min. was bubbled for 2 min. The outlet of the digestion bottle was connected to the AAS flow cell. After the absorbance from residual ozone was confirmed to be negligibly small, 0.05 ml of 5% tin(II) chloride solution was added to the bottle using a peristaltic pump connected through the microcapillary sparger. Mercury(0) was vaporized, purged and transferred to the small T-shaped flow cell with nitrogen at a flow rate of 5 ml/min. The peak absorbance was read on the display panel of the AAS.

The flow of ozone and nitrogen into the aerator was switched using a PTFE multi-way rotary valve. The flow rates were measured using gas burettes placed at the end of an outlet of the aerator. The flow rates of ozone/oxygen and nitrogen for ozone purging were monitored in real time, but nitrogen flow rate for mercury purging was monitored after atomic absorption measurement.

### 3. Results and discussion

The first question to be answered was whether ozone would digest organomercury species completely and rapidly. Fig. 4 shows the observed peak absorbances for mercury as a function of the volume of oxygen feed into the ozonizer at various sodium hydroxide concentrations. All excess ozone was removed before the mercury determination was made. The optimized concentration of hydroxide ion was between 0.0005 and 0.001 M. At these concentrations of hydroxide ion, the digestion of a 0.5 ml (10 ppb) sample of methylmercury was complete in less than 0.5 ml ozone/oxygen or, in other words, a 30 s ozonation at a flow rate of 1 ml/min. Assuming a uniform ozone production rate, the mole ratio of mercury to ozone was about  $1:3 \times 10^6$ . Using the home-made ozonizer, similar quick saturation curves were obtained. The 100 ml sample scale exhibited a complete digestion within 1 min or 350 ml ozone/oxygen at a flow rate of 0.35 l/min. From

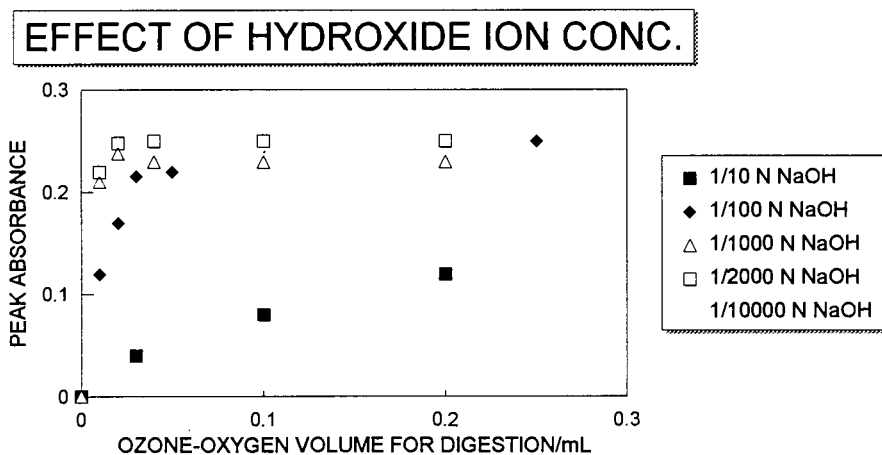


Fig. 4. The observed peak for mercury as a function of oxygen volume at various concentrations of sodium hydroxide at 1 ml/min.

these types of test, it is clear that the rapid digestion of organomercury species can be accomplished using ozone. In addition, it was clear that the smaller sample volumes envisioned for a completely automated system would require less than 30 s of ozone contact time.

The next problem to address was the removal of excess ozone. Any ozone that remains will be sparged into the spectrometer cell and will absorb photons at the 253 nm mercury line produced by the electrodeless discharge lamp. Residual ozone in the system was removed by flushing air or nitrogen for 1 or 2 min. This residual ozone was monitored using the AAS. Once the AAS signal returned to baseline, the stannous chloride could be added and the absorbance from the mercury observed. It was clear from the length of time that it took to remove the ozone from the system that the ozone was being held up in the system. Most likely, this was adsorption to the walls of the flow system. The automated system would have to be designed with a valve system to direct the excess purged ozone out of the system prior to the AAS connection. With this approach, the ozone would be more efficient and less time consuming.

The reducing activity of the stannous chloride was good for more than 2 weeks in a glass stoppered bottle. However, the glass walls of the digestion bottle adsorb significant amounts of tin(II). Ozone and concentrated nitric acid could not completely oxidize or remove it from the glass

surfaces. It was clear that the residue was tin(II) since mercury(II) chloride was readily reduced by the species adsorbed on the wall of the previously-used bottle even after soaking with concentrated nitric acid, even though no additional tin(II) chloride was added. This often caused poor reproducibility in determining mercury and potentially limits the types of materials that can be used in the fully automated system.

The dissolved mercury metal was readily sparged using an air/nitrogen mixture. However, it was desired to increase the sparging rate, thereby making a more concentrated mercury vapor. This was accomplished by redesigning the sparger in order to produce smaller bubbles. The specific design uses a capillary tube having a plate at the outlet shown in Fig. 3. Fig. 5 shows a comparison study of the response difference between capillaries with and without the plate. Although the difference was relatively small, poor reproducibility ( $\pm 8\%$ ) was observed for the capillary without the plate. By placing the plate in front of the capillary, the reproducibility for the mercury system improved to  $\pm 3\%$ .

Once this batch system was optimized, the response for three mercury species, mercury(II) chloride, methyl mercury chloride and phenylmercury acetate was observed (Fig. 6). All three species gave comparable results. A linearity range for methyl mercury from 0.5 to 10 ppb with a linear regression of  $y = 0.0225x + 3 \times 10^{-5}$  and a corre-

lation coefficient of 0.9998 was observed. A LOD of 0.3 ppb was calculated. For phenyl mercury(II) acetate, a linear range from 0.5 to 10 ppb with a linear regression of  $y = 0.0229x + 0.0007$  and a

correlation coefficient of 0.9996 was observed. A LOD of 0.3 ppb was calculated. For mercury(II) chloride, a linear range from 0.5 to 10 ppb with a linear regression of  $y = 0.0223x + 0.0039$  and a

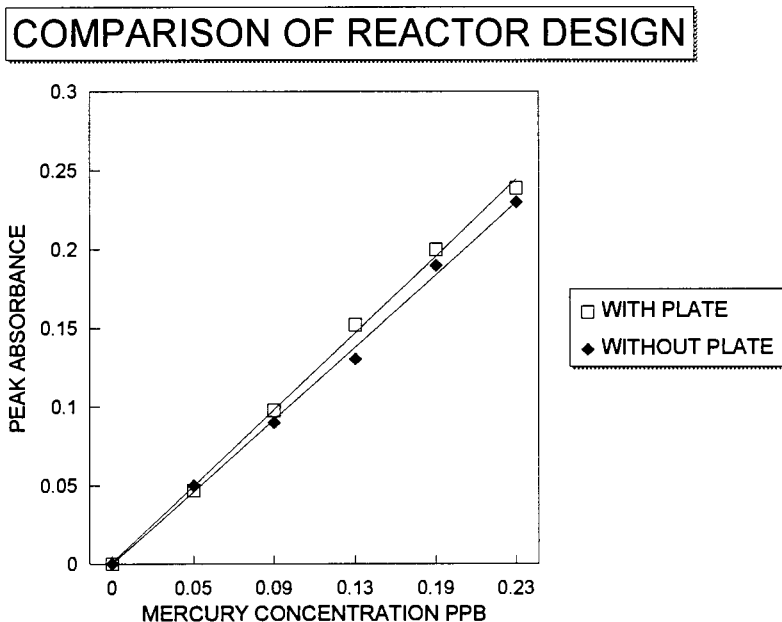


Fig. 5. Comparison of reactor designs.

### OZONATION TIME VS PEAK ABSORBANCE

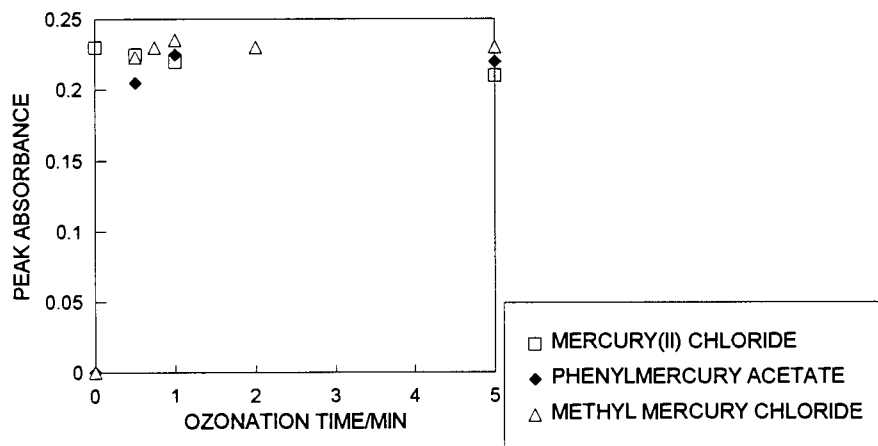


Fig. 6. A plot of ozonation time versus peak absorbance for mercury(II) chloride, methyl mercury chloride, and phenyl mercury acetate.

correlation coefficient of 0.9990 was observed. A LOD of 0.5 ppb was calculated. A combined methyl mercury(II) chloride and mercury(II) chloride sample produced a linear range from 1 to 10 ppb with a linear regression of  $y = 0.0215x + 0.0033$  and a correlation coefficient of 0.9990. A LOD of 0.6 ppb was calculated. The linearity began to be lost after the upper limits.

#### 4. Conclusion

From this preliminary work, it is clear that the ozone digestion system meets the requirements for a fully automated system. The ozone digestions are quick, being less than 30 s. The equipment requirements are simple, meaning that they can be added to a flow injection system. The entire operation is at room temperature. As compared with 'Standard Methods', there is a significant reduction in the amount and number of reagents needed. The reagents were not overly reactive with traditional tubing materials like PTFE and Tygon, since they lasted 2 months or longer.

#### Acknowledgements

The Perkin-Elmer Corporation is gratefully acknowledged for the donation of atomic absorption equipment.

#### References

- [1] A.D. Eaton, L.S. Clesceri, A.R. Greenberg (Eds), *Standard Method for the Examination of Water and Wastewater*, 19th ed., American Public Health Association (APHA), American Water Works Association (AWWA) and the Water Environmental Federation (WEF) 1990.
- [2] S.E. Birnie, *J. Autom. Chem.* 10 (1988) 140–143.
- [3] J.C. de Andrade, C. Pasquini, N. Baccan, J.C. Van Loon, *Spectrochim. Acta* 38B (1983) 1329–1338.
- [4] Z. Fang, S. Xu, X. Wang, S. Zhang, *Anal. Chim. Acta* 179 (1986) 325–340.
- [5] C. Pasquini, W.F. Jardim, L.C. de Faria, *J. Autom. Chem.* 10 (1988) 188–191.
- [6] B. Welz, D. Tsalev, M. Sperling, *Anal. Chim. Acta* 261 (1992) 91–103.
- [7] C.P. Hanna, J.F. Tyson, S. McIntosh, *Anal. Chem.* 65 (1993) 653–656.
- [8] G. Gordon, G. Pacey, An introduction to chemical reactions of ozone pertinent to its analysis, in: R.G. Rice, L.J. Bollyky, W.J. Lacy (Eds.), *Handbook of Ozone Technology and Applications*, vol. Vol. 1, Lewis Publishers, Chelsea, MI, 1986, pp. 41–52.

# Simultaneous determination of iron and ruthenium as ternary complexes by extractive second derivative spectrophotometry

M. Inés Toral <sup>a,\*</sup>, Pablo Richter <sup>a</sup>, A. Eugenia Tapia <sup>b</sup>, Jimmy Hernández <sup>b</sup>

<sup>a</sup> *Department of Chemistry, Faculty of Sciences, University of Chile, P.O. Box 653, Santiago, Chile*

<sup>b</sup> *Department of Chemistry, Faculty of Natural Sciences, Mathematics and Environment, Technological Metropolitan University, P.O. Box 9845, Santiago, Chile*

Received 9 November 1998; received in revised form 24 March 1999; accepted 2 April 1999

## Abstract

A highly sensitive and selective second derivative spectrophotometric method has been developed for the determination of ruthenium and iron in mixtures. The method is based on the formation of the binary complexes of iron and ruthenium with 4,7-diphenyl-1,10-phenanthroline (bathophenanthroline) in the presence of ethyleneglycol. These complexes are formed at pH 4.0–6.0 upon heating at 90°C for 60 min. The ternary perchlorate complexes are then separated by liquid–liquid extraction. The extracts were evaluated directly by derivative spectrophotometric measurement, using the zero-crossing approach for determination of both analytes. Ruthenium and iron were thus determined in the ranges 9.6–450 and 16.3–280 ng/ml, respectively, in the presence of one another. The detection limits achieved ( $3\sigma$ ) were found to be 2.9 ng/ml of ruthenium and 4.9 ng/ml of iron. The relative standard deviations were in all instances less than 1.5%. The proposed method was applied to the determination of both analytes in synthetic mixtures. © 1999 Elsevier Science B.V. All rights reserved.

*Keywords:* Extractive second derivative spectrophotometry; Iron determination; Ruthenium determination

## 1. Introduction

The increasing importance of the use of ruthenium in widely different fields, particularly in metallurgy and in high technology components, has made it necessary to develop simple, inex-

pensive and sensitive methods for the determination of traces of ruthenium in different samples. Various spectrophotometric methods have been proposed for ruthenium determination, but they present low sensitivity which makes them unsuitable for the determination of trace ruthenium [1–3]. Compared with other organic reagents when the heterocyclic azo derivatives [4–7] and sulfur containing compound [8,9] are used as chromophore reagents the sensitivity is consider-

\* Corresponding author. Fax: +56-2-2713888.

E-mail address: analitic@abello.dic.uchile.cl (M.I. Toral)

ably increased. On the other hand, it is well known that the sensitivity and the selectivity can be increased also by ion-pair solvent extraction [10–12] and by using derivative spectrophotometry [13–18].

From an analytical point of view, the development of analytical methods for the determination of ruthenium together with other metals is more attractive. There are a number of methods reported using classical spectrophotometry and derivative spectrophotometry, for example the simultaneous determinations of ruthenium with other analytes such as osmium [19,20], palladium [21–23] and platinum [24]. Other analytical techniques which have been used for these pairs include polarography [25], thin-layer chromatography [26], differential pulse voltammetry [27], high performance liquid-chromatography [28], graphite-furnace atomic absorption spectrometry (AAS) [29–32], inductively coupled plasma atomic Auger electron spectroscopy (ICP-AES) [33] and inductively coupled plasma mass spectrometry (ICP-MS) [34–36]. These last two spectroscopic methods are specifically designed for multielement determination, but required the use of expensive and sophisticated instrumentation.

The simultaneous determination of iron and ruthenium is also important because interest in development of methods for catalytic systems containing both metals is increasing, for example in  $\text{NH}_3$  synthesis. The simultaneous determination of ruthenium and iron has been achieved using techniques such as radiochemical neutron activation analysis [37] and XRF, using an empirical inter-element correction method [38]. The latter case proposed the simultaneous determination of ruthenium with iron and other metallic analytes in corrosion resistant steels. In this method, it is also necessary to use expensive and sophisticated instrumentation.

This work reports a simple, sensitive and selective method by second derivative extractive spectrophotometry for the simultaneous determination of iron and ruthenium. The method is based on the formation of the complexes of iron and ruthenium with 4,7-diphenyl-1,10-phenan-

throline (bathophenanthroline) in the presence of ethyleneglycol.

## 2. Experimental

### 2.1. Apparatus

A Shimadzu UV-160 spectrophotometer with 10-mm cells was used for measurements of the absorbance and derivative absorption spectra. For all solutions, the second derivative spectra were recorded over the range 700–400 nm against solvent, at a scan speed of 480 nm/min with  $\Delta\lambda = 17.5$  nm. An Orion Research Digital Ion-Analyzer 701 with glass and saturated calomel electrodes was used for pH determinations.

### 2.2. Reagents

All reagents were of analytical grade and the solutions were prepared with high-purity water from a NANOpure Barnstead ultrapure water system device: ruthenium(III) standard solution (Sigma ruthenium atomic absorption standard solution, 1005  $\mu\text{g/ml}$  Ru in 5% HCl); standard iron(II) solution (Titrisol Merck, 1000  $\mu\text{g/ml}$ ). Solutions of 10  $\mu\text{g/ml}$  of the analytes were prepared by diluting these standard solutions, and other ranges of concentrations were prepared by appropriate dilution. A solution of bathophenanthroline  $1 \times 10^{-3}$  mol/l was prepared by dissolving 0.03324 g in 100 ml of methanol. A 1 mol/l solution of sodium perchlorate was prepared by dissolving 140.46 g of sodium perchlorate monohydrate in 1000 ml of water. Hydroxylamine hydrochloride ( $\text{NH}_2\text{OH}\cdot\text{HCl}$ ) solution was prepared by dissolving 100 g of the salt in 1000 ml of water. Sodium acetate–acetic acid buffer pH 5.0 was prepared by dissolving 164.0 g of sodium acetate (Merck) in 100 ml of water and then adding 64.4 ml of acetic acid (Merck) and diluting to 1000 ml with water. Solutions of various foreign ions for the interference studies were prepared by dissolving the calculated amount of each compound to give 10–1000  $\mu\text{g/ml}$  solutions of each species. All these solutions were stored in polyethylene con-

tainers. 1,2-Dichloroethane (DCE) Extrapure (specific gravity 1.25) was used.

### 2.3. Procedure

To an aliquot of sample solution containing less than 28  $\mu\text{g}$  of iron and 45  $\mu\text{g}$  of ruthenium in a glass beaker were added 1 ml of acetic acid–acetate buffer (pH 5.0), 1 ml of 10%  $\text{NH}_2\text{OH}\cdot\text{HCl}$  solution, 0.5 ml of ethyleneglycol, 10 ml of  $1 \times 10^{-3}$  M bathophenanthroline solution and 30 ml of high-purity water, and heated at  $90 \pm 5^\circ\text{C}$  for 60 min. After cooling, the solution was transferred into a 250-ml separating funnel, 5 ml of 1 M sodium perchlorate solution were added, the total volume adjusted to 100 ml, mixed and set aside. The mixture was shaken for 3–4 min with 5 ml of DCE. The phases were allowed to separate and the organic layer was run into a dry flask. The zero-order spectrum of the DCE extract was recorded over the range 700–400 nm against a reagent blank prepared under the same experimental conditions, using 10-mm cells. The second derivative spectrum was recorded over the same wavelength range, using  $\Delta\lambda = 7.5$  nm.

## 3. Results and discussion

The reaction between Ru(III) and bathophenanthroline to give the binary complex Ru(III)–bathophenanthroline is very slow at room temperature. Consequently the rate of reaction depends on the heating time, temperature and the presence of the water-soluble organic compound, in order to promote the complex formation and prevent the hydrolysis of the Ru(III). In contrast, Fe(II) reacts quickly under the same conditions. The simultaneous determination proposed in study is therefore only possible by heating the reaction mixture.

### 3.1. Spectral characteristics

The analyte Fe(II), in the presence of hydroxylamine hydrochloride, bathophenanthroline, ethyleneglycol and sodium perchlorate (pH 5.0), forms a ternary complex that is extractable into

1,2-dichloroethane. The zero-order spectrum of the extract of the Fe(II)–bathophenanthroline–perchlorate complex over the range 700–400 nm exhibits one band centred at 532 nm, corresponding to the absorption of Fe(II)–bathophenanthroline chromophore (Fig. 1A). Under the experimental conditions described above, Ru(III) can be extracted also as the ternary complex. The zero-order spectrum of the extract of this complex shows one band centred at 466 nm, over the same range of wavelengths (Fig. 1B).

Under these conditions, when iron and ruthenium are simultaneously present in a sample, both analytes are quantitatively extracted, after heating, into the organic phase, in which the formation of the mixed complexes Fe(bathophen)<sub>3</sub>–(ClO<sub>4</sub>)<sub>2</sub> and Ru(bathophen)<sub>2</sub>(ClO<sub>4</sub>)<sub>3</sub> takes place. This extraction process permits both analytes to be separated and preconcentrated by a factor of 20.

As derivative spectrophotometry provides additional possibilities because it enhances the detectability of minor spectral features, this technique was adopted. In this context the first and second derivative spectra of the extracts of Ru(III)–bathophen–perchlorate, Fe(II)–bathophen–perchlorate and the mixture of the complexes were recorded, respectively (Figs. 2 and 3). It can be seen by comparing Fig. 2 and Fig. 3 that

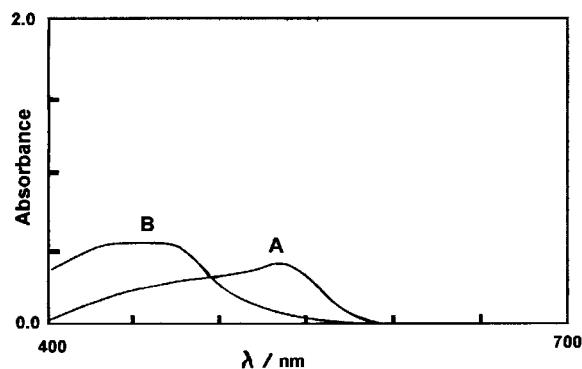


Fig. 1. Absorption spectra of the DCE extract of the Fe(II)–bathophen–perchlorate and Ru(III)–bathophen–perchlorate complexes measured against a reagent blank. (A) Fe(II)–bathophen–perchlorate, 0.04  $\mu\text{g}/\text{ml}$ ; (B) Ru(III)–bathophen–perchlorate, 0.10  $\mu\text{g}/\text{ml}$ .

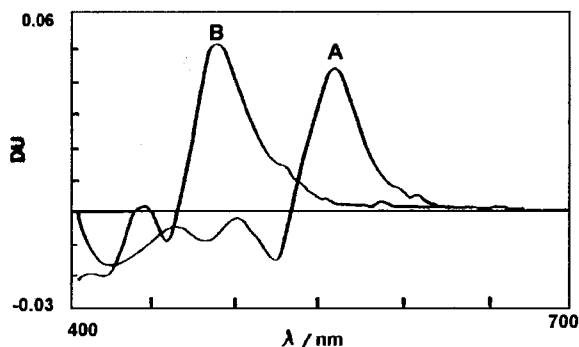


Fig. 2. First derivative spectra of the DCE extract of the Fe(II)-bathophen-perchlorate and Ru(III)-bathophen-perchlorate complexes measured against a reagent blank. (A) Fe(II)-bathophen-perchlorate, 0.04  $\mu\text{g/ml}$ ; (B) Ru(III)-bathophen-perchlorate, 0.10  $\mu\text{g/ml}$ .  $\Delta\lambda = 17.5$  nm. DU, derivative units.

the second derivative spectra are more resolved than those obtained for the first derivative. However, even higher derivative orders yield sensitive but irreproducible signals, so this possibility was discarded.

In order to make the proposed simultaneous determination more sensitive, selective, reproducible and simple, the second derivative spectrophotometry was adopted and the zero-crossing approach can be used for determination of both analytes. The measurement of the second deriva-

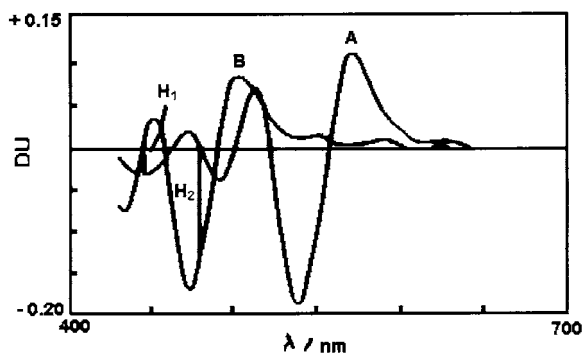


Fig. 3. Second derivative spectra of the DCE extract of the Fe(II)-bathophen-perchlorate and Ru(III)-bathophen-perchlorate complexes measured against a reagent blank. (A) Fe(II)-bathophen-perchlorate, 0.04  $\mu\text{g/ml}$ ; (B) Ru(III)-bathophen-perchlorate, 0.10  $\mu\text{g/ml}$ .  $\Delta\lambda = 17.5$  nm.  $H_1$  at 445.0 nm is used for Fe determination and  $H_2$  at 445.0 nm for Ru determination. DU, derivative units.

tive spectrum at an abscissa value at 445.0 nm, corresponding to the zero-crossing point in the spectrum of Ru(III)-bathophen-perchlorate ( $H_1$ ) can be satisfactorily used for the determination of iron. In contrast, the ruthenium determination can be carry out at 481.5 nm, corresponding to the zero-crossing point in the spectrum of Fe(II)-bathophen-perchlorate ( $H_2$ ). In summary, the following parameters were selected: second derivative, using the zero-crossing approach with  $\lambda = 445.0$  nm for iron determination and  $\lambda = 481.5$  nm for ruthenium determination.

### 3.2. Study of the physicochemical variables

The chemical and spectral variables were optimized by the univariate method, for each element separately. Table 1 shows the range studied, the optimum ranges found for chemical and spectral variables and the working values selected.

The ruthenium reaction depends on the heating time and temperature. In order to obtain the optimum condition for the complex formation, the effect of temperature in the range 25–95°C (for 60 min) was examined. It was found that at  $90 \pm 3^\circ\text{C}$  the signal was at a maximum and constant and remained stable for over 48 h at room temperature. Heating time at  $90 \pm 3^\circ\text{C}$  was then studied. The results show that after 50 min the formation and extraction of Ru(III)-bathophen-perchlorate complex is quantitative. In contrast, Fe(II) reacts quickly under the same conditions. A value of 60 min was selected for further experiments.

As the reaction of each analyte depends on pH, the optimum pH value for simultaneous determination of ruthenium and iron was selected to ensure that the formation and extraction of both ternary complexes was quantitative. In this context, the pH value selected was pH 5.0, which was achieved with an acetic acid-acetate buffer.

The bathophenanthroline and sodium perchlorate concentrations were selected by taking into account not only the presence of both species but also that foreign cations can be present in the sample, with the consequential additional consumption of both reagents.



Table 1  
Study of variables and selection of working values

Variable	Range studied	Optimum range		Working value
		Iron	Ruthenium	
<i>Physics and chemistry</i>				
Temperature (°C) (60 min)	25–95	25–95	87–93	90
Heating time (min) (90 ± 3°C)	20–100	NN <sup>a</sup>	50–100	60
pH	1.0–13.0	3.0–6.0	4.0–7.0	5.0
bathophenanthroline (10 <sup>-3</sup> mol/ml/ml)	1.0–12.0	1.0–12.0	7.0–12.0	12.0
Sodium perchlorate (1.0 mol/ml/ml)	0.0–5.0	2.0–5.0	2.0–5.0	5.0
Aqueous/organic phase ratio	4.0–40	12–23	12–23	20
<i>Spectral</i>				
Derivative order	1–4	1–2	1–2	2
Δλ (nm)	–	–	14.0–21.0	17.5
Wavelength Δλ (nm)	400–700			Ru, 481.5; Fe, 445.0

<sup>a</sup> Not necessary.

In the solvent-extraction process the maximum enrichment factor was obtained with an aqueous/organic phase volume ratio of 20. Above this value, miscibility of the phases occurred.

The derivative order and Δλ values for differentiation were the spectral variables studied, because these variables affect the shape and the resolution of the spectra. The second-order derivatives were selected for this simultaneous determination of Ru and Fe because the best spectral resolution was then obtained. In order to select the Δλ value for differentiation, a series of second derivative spectra of mixtures of 0.1 μg/ml ruthenium with increasing concentrations of iron ranging from 0.02 to 0.1 μg/ml were evaluated under the selected conditions, at different Δλ values. The results are shown in Fig. 4.

Similarly, the second derivative spectra of mixtures of 0.04 μg/ml iron with increasing concentrations of ruthenium from 0.05 to 0.25 μg/ml were obtained (Fig. 5). After evaluating these results, a Δλ of 17.5 nm value was used for differentiation, because using this value in these conditions a good sensitivity and also no interference between the analytes were observed.

Under the selected conditions, the simultaneous determination of iron and ruthenium by the zero-crossing method at 445.0 nm and 481.5 nm, respectively, is possible.

### 3.3. Features of the method

Calibration graphs were obtained by plotting the second-derivative value  $H_1$  for iron and  $H_2$  for ruthenium with Δλ = 17.5 nm, versus the respective analyte concentrations. The linear regression equations and the correlation coefficients calculated for mixtures of both analytes were:

Iron:

$$H_1 = (7.80 \times 10^{-1} \times C) + (2.0 \times 10^{-4})$$

$$r = 0.996$$

Ruthenium:

$$H_2 = (1.63 \times C) + (3.0 \times 10^{-4}) \quad r = 0.999$$

where  $H$  is in derivative units and the concentration ( $C$ ) is in μg/ml.

The ranges in which determinations could be made were found to be 0.0163–0.28 μg/ml for iron and 0.0096–0.45 μg/ml for ruthenium. The detection limits (calculated by using the 3σ recommendation) were found to be 0.0049 μg/ml for iron and 0.0029 μg/ml for ruthenium. The relative standard deviations for ten standard samples containing 0.02 μg/ml of each element were 1.1% and 1.4% for iron and ruthenium, respectively.

### 3.4. Interference studies.

The effect of various foreign ions on the simultaneous determination of iron and ruthenium was studied by adding known quantities of a selected foreign ion to solutions of 40 ng/ml of iron and 100 ng/ml of ruthenium. The tolerance limit was taken as being the amount causing an error  $\pm 4\%$  in the signals. Table 2 indicates the levels at which different ions can be tolerated. Because the tolerance for some ions was rather small, in all cases a  $5 \times 10^{-3}$  mol/l batho-phenanthroline solution and appropriated masking agents were used. The tolerance limits of Au(III) and Cu(I) were improved by using KBr and NaNO<sub>2</sub>, respectively, as masking agents. The masking agents were added before heating the solution.

It was found that the most common anions are tolerated even when present in large amounts.

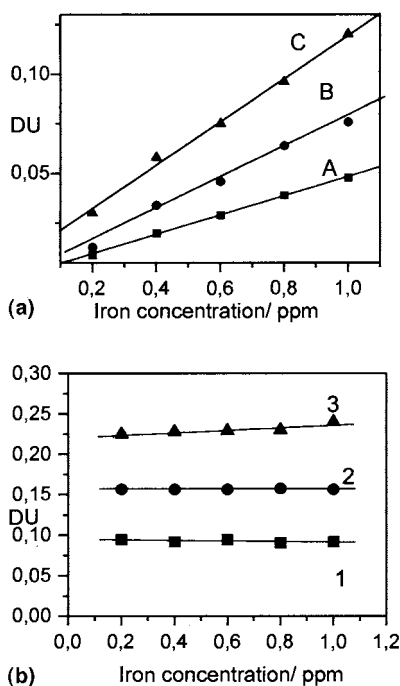


Fig. 4. (a) Calibration graph of iron in the presence of 0.10  $\mu\text{g/ml}$  ruthenium for second derivative spectra at 445 nm, using different  $\Delta\lambda$  values: (A) 14.0 nm; (B) 17.5 nm; (C) 21.0 nm. (b) Effect of the iron concentration on the signal from 0.10  $\mu\text{g/ml}$  ruthenium for second derivative spectra at 481.5 nm, using different  $\Delta\lambda$ : (1) 14.0 nm; (2) 17.5 nm; (3) 21.0 nm.

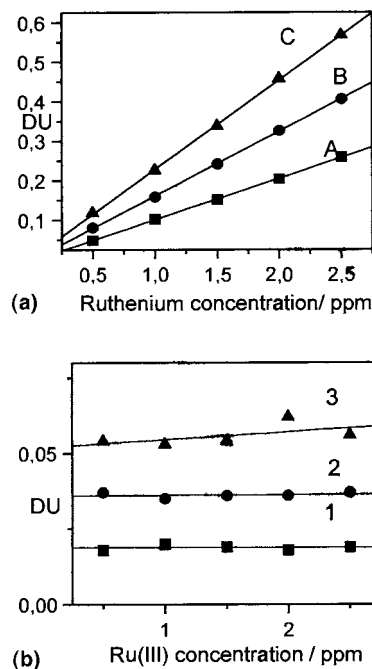


Fig. 5. (a) Calibration graph of ruthenium in the presence of 0.04  $\mu\text{g/ml}$  iron for second derivative spectra at 481.5 nm, using different  $\Delta\lambda$  values: (A) 14.0 nm; (B) 17.5 nm; (C) 21.0 nm. (b) Effect of the ruthenium concentration on the signal from 0.04  $\mu\text{g/ml}$  iron for second derivative spectra at 445 nm, using different  $\Delta\lambda$  values: (1) 14.0 nm; (2) 17.5 nm; (3) 21.0 nm.

### 3.5. Application of the proposed method

The proposed method was applied to the determination of both analytes in synthetic mixtures. In this context, the recoveries of samples containing standard solutions of ruthenium and iron in different ratios were carried out. It can be seen from Table 3 that the content of each cation can be reliably determined using this second derivative spectrophotometric method. It was found that the recovery was between 98.3% and 102.5% and that, in all cases, the relative standard deviation was less than 1.5%.

Samples containing trace amounts of iron and ruthenium were not available. Therefore, synthetic samples containing iron 30 ng/ml, ruthenium 70 ng/ml and metals of the VIII group and other possible interfering ions were prepared. Iron and ruthenium contents were determined

using the proposed method. As can be seen from Table 4, in all cases good recoveries were obtained.

#### 4. Conclusions

In this work a simple, sensitive, selective and inexpensive method has been developed for the simultaneous determination of ruthenium and

Table 2  
Effect of foreign ions on solutions containing iron (40 ng/ml) and ruthenium (100 ng/ml)

Foreign species	Tolerance limit <sup>a</sup> (ng/ml)	
	Iron	Ruthenium
<i>Cations</i>		
K(I), Na(I), Al(III), Mg(II), Ca(II), Sr(II), Zn(II), Cd(II), Cr(III)	1.0 × 10 <sup>4</sup>	1.0 × 10 <sup>4</sup>
Ni(II)	5.0 × 10 <sup>2</sup>	1.5 × 10 <sup>3</sup>
Co(II)	7.0 × 10 <sup>2</sup>	2.0 × 10 <sup>3</sup>
Mn(II)	1.7 × 10 <sup>3</sup>	1.7 × 10 <sup>3</sup>
Bi(III)	1.0 × 10 <sup>4</sup>	1.0 × 10 <sup>3</sup>
Hg(II)	1.0 × 10 <sup>4</sup>	1.5 × 10 <sup>3</sup>
Zn(II)	1.0 × 10 <sup>4</sup>	4.0 × 10 <sup>3</sup>
Cd(II)	1.0 × 10 <sup>4</sup>	3.0 × 10 <sup>3</sup>
Ir(II)	1.0 × 10 <sup>4</sup>	1.5 × 10 <sup>3</sup>
Pt(IV)	1.0 × 10 <sup>4</sup>	5.0 × 10 <sup>2</sup>
Pd(IV)	5.0 × 10 <sup>2</sup>	5.0 × 10 <sup>2</sup>
Au(III)	1.0 × 10 <sup>3</sup>	1.0 × 10 <sup>2b</sup>
Cu(II)	5.0 × 10 <sup>2</sup>	5.0 × 10 <sup>2c</sup>
<i>Anions</i>		
NO <sub>3</sub> <sup>-</sup> , SO <sub>4</sub> <sup>2-</sup> , Br <sup>-</sup> , Cl <sup>-</sup>	5.0 × 10 <sup>6</sup>	5.0 × 10 <sup>6</sup>
F <sup>-</sup>	1.5 × 10 <sup>6</sup>	4.0 × 10 <sup>6</sup>
PO <sub>4</sub> <sup>3-</sup>	1.0 × 10 <sup>6</sup>	1.0 × 10 <sup>6</sup>
I <sup>-</sup>	5.0 × 10 <sup>6</sup>	2.0 × 10 <sup>6</sup>
SCN <sup>-</sup>	4.0 × 10 <sup>6</sup>	1.0 × 10 <sup>3</sup>
S <sub>2</sub> O <sub>3</sub> <sup>2-</sup>	1.4 × 10 <sup>6</sup>	1.0 × 10 <sup>5</sup>
Citrate	2.0 × 10 <sup>5</sup>	1.0 × 10 <sup>3</sup>
Tartrate	1.8 × 10 <sup>6</sup>	5.0 × 10 <sup>3</sup>
Oxalate	5.0 × 10 <sup>4</sup>	1.0 × 10 <sup>3</sup>
EDTA	1.0 × 10 <sup>5</sup>	1.0 × 10 <sup>3</sup>
P <sub>2</sub> O <sub>7</sub> <sup>4-</sup>	6.0 × 10 <sup>5</sup>	6.0 × 10 <sup>5</sup>

<sup>a</sup> The tolerance limit was taken as the amount causing an error of ±4% in the signals.

<sup>b</sup> 0.3–0.4 g of KBr.

<sup>c</sup> 0.3–0.4 g of NaNO<sub>2</sub>.

Table 3  
Simultaneous determination of ruthenium and iron in synthetic mixtures

Concentration added (µg/ml)		Concentration found <sup>a</sup> , µg/ml (recovery, %)	
Ruthenium	Iron	Ruthenium	Iron
0.180	0.020	0.1797 (99.8)	0.0205 (102.5)
0.150	0.040	0.1503 (100.2)	0.0397 (99.3)
0.130	0.060	0.1294 (99.6)	0.0602 (100.4)
0.110	0.080	0.1110 (100.9)	0.0795 (99.4)
0.090	0.100	0.0914 (101.5)	0.0980 (98.0)
0.070	0.120	0.0720 (102.8)	0.1190 (99.4)
0.050	0.140	0.0509 (101.8)	0.1410 (100.7)
0.050	0.020	0.0496 (99.4)	0.0205 (102.5)
0.070	0.040	0.0699 (99.8)	0.0397 (99.3)
0.090	0.060	0.0908 (100.8)	0.0602 (100.4)
0.110	0.080	0.1092 (99.3)	0.0792 (99.4)
0.130	0.100	0.1319 (101.4)	0.0987 (98.7)
0.150	0.120	0.1509 (100.6)	0.1179 (98.3)

<sup>a</sup> Average of eight determinations.

iron by second-order extractive derivative spectrophotometry. In this method the binary complexes are formed at pH 4.0–6.0, upon heating at 90°C for 60 min, in order to obtain the quantitative formation of these complexes. The formation of the ternary complexes using NaClO<sub>4</sub> as counter-ion permits the separation of the analytes, by liquid–liquid extraction in 1,2-dichloroethane, increasing the sensitivity and selectivity of the method. In this conditions the determination of microamounts of ruthenium and iron is favoured. The use of the masking agent allows the selectivity to be increased considerably. According to the high sensitivity and selectivity reached, the proposed method can be applicable to a variety of different samples.

#### Acknowledgements

The authors are grateful to the National Fund for Development of Sciences and Technology (FONDECYT), project 1961024, for financial support.

**Table 4**  
Simultaneous determination of ruthenium and iron in synthetic mixtures by second derivative spectrophotometry

Sample	Synthetic mixtures (ng/ml)													Recovery <sup>a</sup> Ru (%)	RSD (%)	Recovery <sup>a</sup> Fe (%)	RSD (%)
	Fe(II)	Ru(III)	Pt(IV)	Pd(IV)	Cu(II)	Ir(II)	Co(II)	Zn(II)	Cd(II)	Mn(II)	Hg(II)	Bi(III)	Ni(II)				
1	30	70	50	50	50	50	50	50	50	50	50	50	50	101.6	1.2	102.5	1.3
2	30	70	50	50	50	100	50	100	100	100	100	100	100	99.9	1.4	104.1	1.3
3	30	70	100	50	–	–	150	600	300	–	100	–	100	98.2	1.4	99.4	1.2
4	30	70	200	100	–	300	100	–	300	–	–	50	–	98.7	1.2	99.4	1.4
5	30	70	–	150	300	–	–	50	–	50	–	50	50	100.1	1.3	98.9	1.3
6	30	70	200	200	50	–	–	100	–	100	100	–	–	99.0	1.3	101.6	1.2
7	30	70	400	–	200	–	–	150	–	100	100	50	–	100.7	1.2	102.1	1.4
9	30	70	200	200	200	50	50	50	50	100	50	50	50	98.7	1.4	99.0	1.4
10	30	70	–	–	–	50	200	300	200	200	100	100	100	100.7	1.3	99.4	1.3

<sup>a</sup> Values are the average of five determinations. Determinations were carried out in the presence of the 0.3–0.4 g of KBr and 0.3–0.4 g of NaNO<sub>2</sub> as masking agents.

**References**

- [1] H.S. Gowda, A.T. Gowda, *J. Indian Chem. Soc.* 59 (1982) 1201.
- [2] P. Jain, R.P. Singh, M. Katyal, *Chem. Era* 19 (1983) 159.
- [3] A.T. Gowda, H.S. Gowda, N.M.M. Gowda, *Anal. Chim. Acta* 154 (1983) 347.
- [4] L.C. Kamra, G.H. Ayres, *Anal. Chim. Acta* 78 (1975) 423.
- [5] Y. Sasaki, *Anal. Chim. Acta* 98 (1978) 335.
- [6] W.A. Embry, G.H. Ayres, *Anal. Chem.* 40 (1968) 1499.
- [7] M.A. Islam, W.I. Stephen, *Talanta* 39 (1992) 1429.
- [8] S.C. Shome, P.K. Gangopadhyay, S. Gangopadhyay, *Talanta* 23 (1976) 603.
- [9] B. Morelli, *Analyst* 108 (1983) 386.
- [10] Z. Marczenko, R. Lobinski, *Talanta* 357 (1988) 1001.
- [11] S.A. Abbasi, A.S. Hameed, P.C. Nipanay, R. Soni, *Analyst* 113 (1988) 1561.
- [12] I. Kasahara, T. Isomi, E. Tsuda, N. Hata, S. Taguchi, K. Goto, *Analyst* 114 (1989) 1479.
- [13] G. Talsky, S. Gotzmaier, H. Betz, *Microchim. Acta* II (1981) 1.
- [14] H. Ishii, K. Satoh, *Fresenius Z. Anal. Chem.* 312 (1982) 114.
- [15] B. Morelli, *Fresenius Z. Anal. Chem.* 325 (1986) 415.
- [16] J. Medimilla, F. Ales, F.G. Sánchez, *Talanta* 33 (1986) 329.
- [17] S. Kus, Z. Marczenko, *Analyst* 112 (1987) 1503.
- [18] A. Morales, M.I. Toral, P. Richter, M. Silva, *Anal. Lett.* 25 (1992) 1765.
- [19] Z. Marczenko, M. Balcerzak, *Anal. Chim. Acta* 109 (1979) 123.
- [20] S. Jaya, T.V. Ramakrishna, *Bull. Chem. Soc. Jpn.* 57 (1984) 267.
- [21] B.J. Desai, V.M. Shinde, *Fresenius Z. Anal. Chem.* 298 (1979) 158.
- [22] V.V. Yeole, A.D. Langade, V.M. Shinde, *Mikrochim. Acta* II (1980) 117.
- [23] B. Morelli, *Analyst* 108 (1983) 1506.
- [24] S.K. Singh, R.K. Sharma, S.K. Sindhvani, *Bull. Chem. Soc. Jpn.* 59 (1986) 1223.
- [25] R.S. Sindhu, S. Sharey, R.P. Singh, *Orient. J. Chem.* 2 (1986) 154.
- [26] N. Singh, M. Mehrotra, K. Rastogi, T.N. Srivastava, *Analyst* 110 (1985) 71.
- [27] R. Palaniappan, T.A. Kumar, *Analyst* 118 (1993) 293.
- [28] H. Wang, Y.X. Miao, W.Y. Mou, H.S. Zhang, J.K. Chen, *Mikrochim. Acta* 117 (1994) 65.
- [29] H.A. Hamid, *Atom. Spectrosc.* 10 (1989) 16.
- [30] M. Hoashi, R.R. Brooks, R.D. Reeves, *Anal. Chim. Acta* 232 (1990) 317.
- [31] Z. Aneva, S. Arpadyan, I. Kalaidzhieva, *Anal. Chim. Acta* 236 (1990) 385.
- [32] J.G. Sen Gupta, *Talanta* 40 (1993) 791.
- [33] T. Adachi, H. Takeishi, Y. Sasaki, K. Motojima, *Anal. Chim. Acta* 218 (1989) 77.
- [34] J. Enzweiler, P.J. Potts, K.E. Jarvis, *Analyst* 120 (1995) 1391.
- [35] S.M. Graham, R.V.D. Robert, *Talanta* 41 (1994) 1369.
- [36] D.C. Gregoire, *J. Anal. Atom. Spectrom.* 3, 1988, p 309.
- [37] C. Chai, Y. Liu, X. Mao, *J. Radioanal. Nucl. Chem.* 204 (1996) 159.
- [38] B.T. Eddy, *Mintek M269* (1986) 26.

# The active and passive sampling of benzene, toluene, ethyl benzene and xylenes compounds using the inside needle capillary adsorption trap device

S. Shojania, R.D. Oleschuk, M.E. McComb, H.D. Gesser, A. Chow \*

*Department of Chemistry, University of Manitoba, Winnipeg, Manitoba R3T 2N2, Canada*

Received 30 November 1998; received in revised form 30 March 1999; accepted 5 April 1999

## Abstract

A new and simple method of solventless extraction of volatile organic compounds (VOCs) from air is presented. The sampling device has an adsorbing carbon coating on the interior surface of a hollow needle, and is called the inside needle capillary adsorption trap (INCAT). This paper describes a study of the reproducibility in the preparation and sampling of the INCAT device. In addition, this paper examines the effects of sample volume in active sampling and exposure time in passive sampling on the analyte adsorption. Analysis was achieved by sampling the air from an environmental chamber doped with benzene, toluene, ethyl benzene and xylenes (BTEX) compounds. Initial rates of adsorption were found to vary among the different compounds, but ranged from 0.0099 to 0.016 nmol h<sup>-1</sup> for passive sampling and from 2.2 to 10 nmol h<sup>-1</sup> for active sampling. Analysis was done by thermal desorption of the adsorbed compounds directly into a gas chromatograph injection port. Quantification of the analysis was done by comparison to actively sampled activated carbon solid phase extraction (SPE) measurements. © 1999 Elsevier Science B.V. All rights reserved.

*Keywords:* INCAT; Microextraction; VOC; BTEX

## 1. Introduction

Developing analytical methods for investigating hazardous substance release into indoor air and the environment for public health assessments is important. The impact on human health from exposure to hazardous substances has created the

need for determining the sources of exposure (i.e. drinking water, air, soil, food sources, etc.). The sheer number of analyses required for environmental/public health assessments implies a need for the development of simple and economical techniques for such investigations.

Humans are exposed to volatile organic compounds (VOCs) via the environment, workplace, or consumer products. As a result, detecting and monitoring these compounds to determine human exposure is required. Several VOCs have severe

\* Corresponding author. Tel.: +1-204-474-9504; fax: +1-204-474-7608.

*E-mail address:* achow@cc.umanitoba.ca (A. Chow)

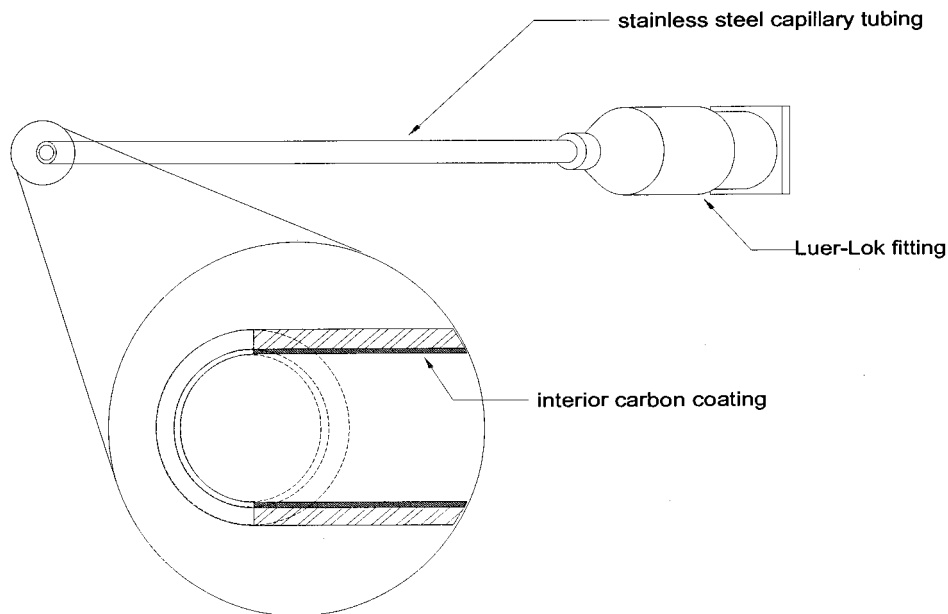


Fig. 1. Schematic representation of an inside needle capillary adsorption trap (INCAT) device.

health effects depending on the duration and levels of exposure. An abundance of human evidence, and supporting animal studies, have shown some of these VOCs to have carcinogenic or mutagenic effects. Some VOCs will harm the im-

mune system while others have adverse effects on tissue development [1–3]. VOCs will enter the body easily through the air and therefore pose health risks from long term exposure to even low concentration levels (as low as 0.05 ppm) [1]. As

Table 1

Molecular weights, order of elution, response factors, and concentrations of the benzene, toluene, ethyl benzene and xylenes (BTEX) compounds in a 70 l environmental test chamber

Compound	Molecular weight (g mol <sup>-1</sup> )	Order of elution	Response factor	Chamber concentration <sup>a</sup>		
				in mg m <sup>-3</sup>	in μmol m <sup>-3</sup>	in ppm <sup>b</sup>
Benzene	78.11	1	1.48	6.89 ± 0.07	88.2 ± 0.9	2.19
Toluene	92.13	2	1.24	4.95 ± 0.05	53.7 ± 0.5	1.33
Ethyl benzene	106.16	3	1.3	2.28 ± 0.02	21.5 ± 0.2	0.533
<i>p</i> -Xylene	106.16	4	1.13	6.01 ± 0.06	56.6 ± 0.6	1.40
<i>m</i> -Xylene	106.16	5	1.12	2.50 ± 0.03	23.7 ± 0.2	0.588
<i>o</i> -Xylene	106.16	6	1.18	4.27 ± 0.04	40.2 ± 0.4	0.997
sec-Butyl benzene <sup>c</sup> (internal standard)	134.22	7	1	Absent		

<sup>a</sup> Chamber concentration values based on four activated carbon solid phase extraction (SPE) tube measurements during the course of these analyses.

<sup>b</sup> The concentration in ppm refers to parts per million by molar volume for an ideal gas at standard ambient temperature and pressure (SATP) conditions of 298.15 K and 1 bar. The molar volume of a gas under these conditions is 24.79 l.

<sup>c</sup> The internal standard sec-Butyl benzene was used with the extraction solvent (107 μg g<sup>-1</sup>) for the activated carbon SPE tube.

Table 2

Mean amounts of benzene, toluene, ethyl benzene and xylenes (BTEX) compounds adsorbed, relative standard deviations (RSD) from the mean, and the proportion adsorbed relative to the amount present, determined by repeated measurements ( $n = 10$ ) of an actively sampled 5 ml volume using a 26 gauge inside needle capillary adsorption trap (INCAT) device

Compound	Mean amount (nmol)	%RSD	Percent adsorbed <sup>d</sup>
Benzene	0.072	6.3	16.3
Toluene	0.14	9.3	52.1
Ethyl benzene	0.043	8.7	40.0
<i>p</i> -Xylene	0.2	9.4	70.7
<i>m</i> -Xylene	0.059	8	49.8
<i>o</i> -Xylene	0.12	8.1	59.7

<sup>d</sup> The proportionate amount of the analyte adsorbed relative to the amount actually sampled from the test chamber, defined by the relation:

$$\text{Percent adsorbed} = \frac{\text{moles of compound adsorbed}}{(\text{volume sampled})(\text{concentration})} \times 100$$

such, a simple method of determining VOCs in ambient air is needed.

A new method of solventless extraction of VOCs has been achieved using the inside needle

capillary adsorption trap (INCAT) [4]. The INCAT device (Fig. 1) has an adsorbing carbon coating on the interior surface of a hollow stainless steel needle. Sampling of a gaseous or aqueous mixture can then be done by actively drawing a fixed volume of the gaseous mixture or headspace of an aqueous sample through the device via a syringe. For aqueous samples, an analyte will partition between the aqueous and vapour phases to reach an equilibrium concentration in the static headspace above the aqueous sample. Direct sampling of the VOCs in the absence of the nonvolatile matrix can then be achieved by sampling the static headspace rather than the aqueous mixture [5,6]. The volatile analytes adsorbed and concentrated inside the device can then be thermally desorbed in the heated injection port of a gas chromatograph (GC) for separation.

The passive sampling of VOCs in air can also be achieved by letting the vapour slowly diffuse into the INCAT device. Passive sampling of VOCs then allows for the determination of air contaminants at very low concentrations by simply extending the exposure time of the device to

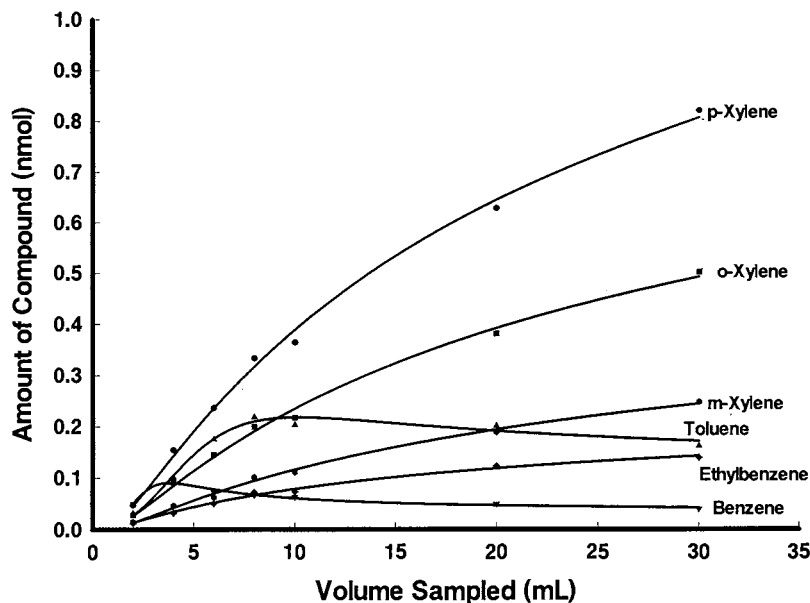


Fig. 2. The amounts of benzene, toluene, ethyl benzene and xylenes (BTEX) compounds determined by active sampling with a 26 gauge inside needle capillary adsorption trap (INCAT) device.



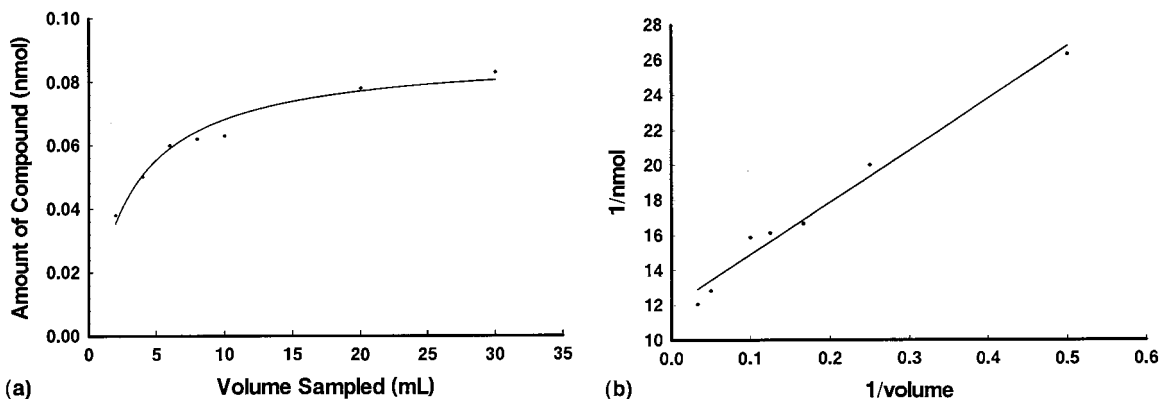


Fig. 3. (a) The amount of benzene determined by active sampling with a 26 gauge inside needle capillary adsorption trap (INCAT) device in the absence of all other benzene, toluene, ethyl benzene and xylenes (BTEX) compounds. (b) The Langmuir fit for benzene active sampled with a 26 gauge INCAT device in the absence of all other BTEX compounds.

obtain an average concentration over the time exposed. A concentration profile of a 'sick' building may be achieved by the passive sampling method by simultaneously exposing the passive INCAT samplers at various locations within the building.

This paper reports the use of the INCAT device to sample benzene, toluene, ethyl benzene, and xylenes (BTEX) compounds. Sampling was performed actively for a fixed volume to determine the sampling reproducibility with the device, actively at varying volumes, and passively over varying exposure times to investigate the saturation effects with this type of carbon adsorbent. In addition, the rates of adsorption in both the active and passive modes of sampling were investigated. Quantitation of the INCAT results was based on comparison to measurements with actively sampled activated carbon solid phase extraction (SPE) tubes.

## 2. Experimental

The INCAT devices used in this study were prepared from stainless steel capillary tubing (Small Parts, Logansport, IN) to which a Luer-Lok was fitted. For these devices, the stainless steel capillaries were either 26 gauge (0.25 mm i.d., 0.46 mm o.d.), or 22 gauge (0.41 mm i.d.,

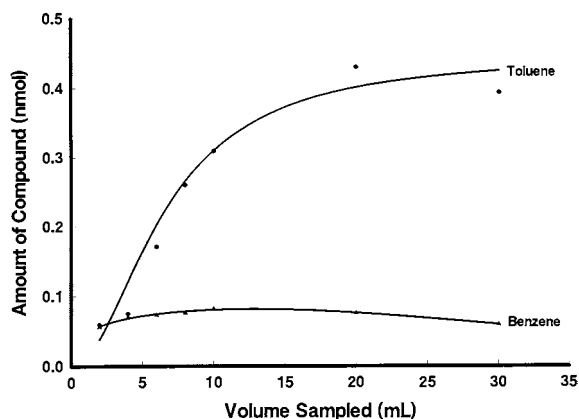


Fig. 4. The amount of benzene and toluene determined by active sampling with a 26 gauge inside needle capillary adsorption trap (INCAT) device in the absence of heavier benzene, toluene, ethyl benzene and xylenes (BTEX) compounds.

Table 3

Mean absolute passive rates of adsorption and relative standard deviations (RSD) from the mean, for 22 gauge inside needle capillary adsorption trap (INCAT) devices ( $n = 3$ )

Compound	Mean rate (pmol h <sup>-1</sup> )	%RSD
Benzene	3.4	13
Toluene	12.4	8.6
Ethyl benzene	7.7	11
<i>p</i> -Xylene	46.3	10
<i>m</i> -Xylene	13.9	9.5
<i>o</i> -Xylene	28.7	11

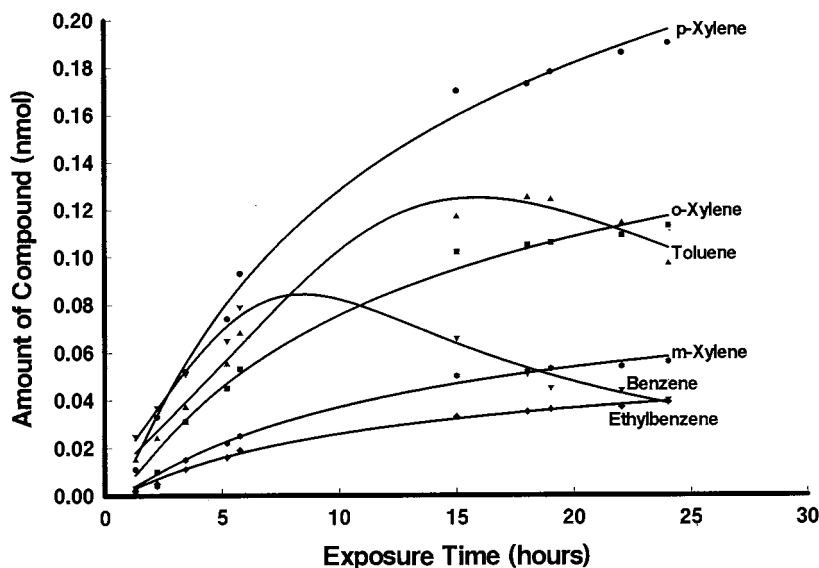


Fig. 5. The amounts of benzene, toluene, ethyl benzene and xylenes (BTEX) compounds determined by passive sampling with a 26 gauge inside needle capillary adsorption trap (INCAT) device over a range of exposure times.

0.71 mm o.d.). The entire length of the interior surface of the capillary was coated with a layer of colloidal graphite paint (SPI Supplies, West Chester, PA). The coated device was heated at 300°C for 20 min while passing helium gas through its length to dry the coating, and to ensure that the capillary was not clogged. Following the drying of the carbon coating, the device was inserted into the injection port of a GC to determine if any off-gassing occurred.

Gas chromatographic analysis was performed using a Hewlett Packard 5710A GC with a flame ionization detector (FID). BTEX compounds were separated using a 2 m × 3 mm packed column of 5% bentone, 5% isodecylphthalate on Chromosorb W. This packed column was chosen since it can resolve all of the BTEX compounds [7]. Most GC columns do not resolve *para* and *meta*-xylene. The injection port temperature for the GC was at 300°C, the column temperature was 90°C, and the detector temperature was 200°C. For each analysis, the thermal desorption of a sample from an INCAT device was followed with a second desorption in the injection port of the GC to verify that the sample had been completely desorbed in the first injection.

BTEX compounds were placed into individual sample vials sealed with a small opening in the cap. A layer of polyethylene membrane was placed inside the vial cap to act as a semipermeable barrier. The sample vials were placed into a 70 l environmental test chamber that had dry air (9–11% relative humidity) flowing in at a rate of 32 l h<sup>-1</sup>. Three fans were used to circulate the air inside the chamber.

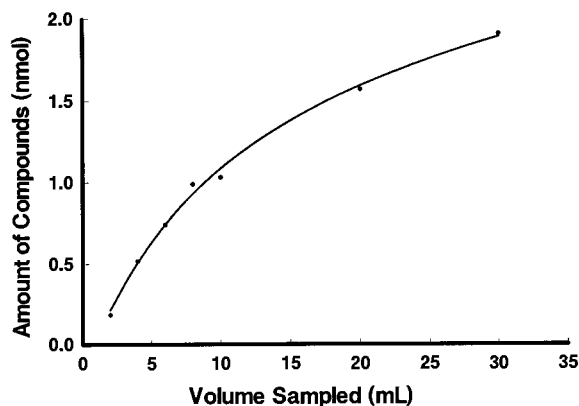


Fig. 6. The total amount of benzene, toluene, ethyl benzene and xylenes (BTEX) compounds determined by active sampling with a 26 gauge inside needle capillary adsorption trap (INCAT) device.

Table 4

Initial slopes and absolute rates of adsorption for the 26 gauge inside needle capillary adsorption trap (INCAT) device in active sampling of the benzene, toluene, ethyl benzene and xylenes (BTEX) compounds (based of the initial five data points in the 0–8 ml range)

Compound	Initial slope (nmol ml <sup>-1</sup> )	Coefficient of determination ( <i>r</i> <sup>2</sup> )	Initial rate of adsorption (nmol h <sup>-1</sup> ) <sup>f</sup>
Benzene <sup>e</sup>	0.023		5.5
Toluene	0.029	0.985	7.0
Ethyl benzene	0.0091	0.991	2.2
<i>p</i> -Xylene	0.043	0.988	10
<i>m</i> -Xylene	0.013	0.976	3.1
<i>o</i> -Xylene	0.026	0.989	6.2

<sup>e</sup> The values determined for benzene are based on only the first three data points since the profile becomes clearly curved after sampling 4 ml of chamber air. Thus, the values are only included for the purpose of an approximate comparison and cannot be considered as relevant as the values for the other compounds. It is for this reason that the *r*<sup>2</sup> value for benzene has been omitted since it was based on only three points it is deceptively high.

<sup>f</sup> The active rates of adsorption were determined by the relation: Initial rate of adsorption = (initial slope in nmol ml<sup>-1</sup>)(flow rate through the INCAT of 4 ml min<sup>-1</sup>).

The BTEX concentrations in the test chamber were measured using activated carbon SPE tubes (SKC, Eighty Four, PA) attached to a Dräger bellows pump (BGI, Waltham, MA) that reproducibly sampled a 0.5 l volume (sampled five times at 100 ml per sample) of the chamber air. The BTEX compounds were extracted from the carbon tube using 1.0 ml of CS<sub>2</sub> doped with an internal standard (sec-butyl benzene at 107 μg g<sup>-1</sup>). The molar amount of each BTEX compound relative to the internal standard was obtained using the relation:

$$D_c = \frac{A_c D_{\text{std}}}{A_{\text{std}} f} \quad (1)$$

where *D<sub>c</sub>* is number of moles of an individual BTEX compound obtained by the carbon tube, *D<sub>std</sub>* is the number of moles of the internal standard in the extract, *A<sub>std</sub>* is the area of the standard peak in the chromatogram, *A<sub>c</sub>* is the area of an individual BTEX peak in the chromatogram, and *f* is the response factor for the BTEX peak of interest.

The peaks in the INCAT chromatograms can then be determined by comparison to the peaks from the carbon tube using the relation:

$$D = \frac{A}{A_c} D_c F \quad (2)$$

where *D* is the number of moles of an individual BTEX compound obtained by the INCAT, *A* is the area of the BTEX peak of interest, and *F* is the fraction of the SPE tube extract injected into the GC (*V<sub>inj</sub>**V<sub>extract</sub>*<sup>-1</sup>).

The results of the activated carbon SPE tube measurements of the BTEX concentrations in the test chamber are listed in Table 1. To test the INCAT device, higher BTEX concentration levels (relative to environmentally significant levels)

Table 5

Initial absolute rates of adsorption for the 26 gauge inside needle capillary adsorption trap (INCAT) device in passive sampling of the benzene, toluene, ethyl benzene and xylenes (BTEX) compounds (based on the initial six data points in the 0–5.75 h range)

Compound	Initial rate of adsorption <sup>g</sup> (nmol h <sup>-1</sup> )	Coefficient of determination ( <i>r</i> <sup>2</sup> )
Benzene	0.013	0.977
Toluene	0.011	0.991
Ethyl benzene	0.0034	0.981
<i>p</i> -Xylene	0.016	0.984
<i>m</i> -Xylene	0.0048	0.950
<i>o</i> -Xylene	0.0099	0.960

<sup>g</sup> The initial rates of adsorption are the initial slopes of the adsorption profiles in Fig. 5.

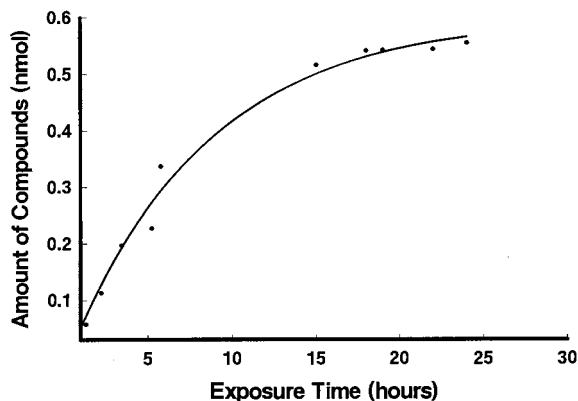


Fig. 7. The total amount of benzene, toluene, ethyl benzene and xylenes (BTEX) compounds determined by passive sampling with a 26 gauge inside needle capillary adsorption trap (INCAT) device.

were used to determine if the device could work in both the active and passive sampling modes, to determine the effect of varying volume and exposure time when dealing with concentration levels that might saturate the adsorbent, and to determine the usefulness of the colloidal graphite adsorbent.

### 2.1. Active sampling with the INCAT device

Using the INCAT device, the reproducibility of sampling was investigated by repeated measurements ( $n = 10$ ) of the BTEX compounds within the chamber. Actively sampled 5 ml volumes of the chamber air were drawn through the device using a 10 ml glass gas-tight syringe (Hamilton, Reno, NV). Samples were taken at 30 min intervals to allow the chamber to return to a steady state. The temperature inside the chamber ranged from 22.0 to 24.6°C and the relative humidity was 9–11%. All of the measurements were obtained from a 26 gauge INCAT device. Active sampling was performed by drawing the air sample through the INCAT device via the syringe, and then pushing the same volume of air back through the device into the chamber. The rate at which the sample volume was withdrawn and expelled by the syringe was approximately 4 ml min<sup>-1</sup>.

In addition to the constant volume measurements of the BTEX compounds in the chamber, the effect of different sample volumes on the molar amounts of BTEX compounds adsorbed by the device was also investigated. The interval

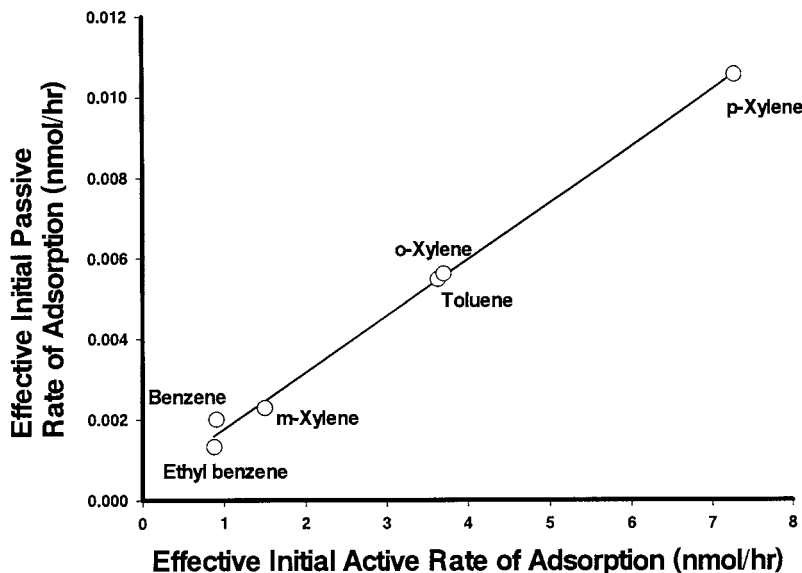


Fig. 8. Plot of the effective initial adsorption rates for passive sampling against active sampling, of the benzene, toluene, ethyl benzene and xylenes (BTEX) compounds with a 26 gauge inside needle capillary adsorption trap (INCAT) device.

between samples here was 60 min, and the flow rate through the device was again  $4 \text{ ml min}^{-1}$ . All of the measurements were performed using the same 26 gauge INCAT device in the same manner as the constant volume measurements. The variable volume measurements involved the chamber containing (i) all of the BTEX compounds; (ii) only benzene; and (iii) benzene and toluene.

### 2.2. Passive sampling with the INCAT device

Application of the INCAT device to passive sampling was investigated by preparing three needles (22 gauge) made from a single continuous piece of stainless steel capillary tubing, which was subsequently cut into sections. The three devices were left in the chamber for approximately 24 h. Reproducibility of the coating process was measured relative to the passive rates of adsorption ( $\text{nmol h}^{-1}$ ).

The effect of exposure time on the INCAT device in passive sampling was investigated over a period of several days. To account for any instrumental drift over time, a toluene standard was run each day and the results of the BTEX analysis scaled relative to the toluene standard. Sampling was performed using the same 26 gauge INCAT device used in the active sampling experiments. The device was placed in a 3.5 ml cryogenic vial (Evergreen Scientific, Los Angeles, CA). The open end of the vial was then inserted into a small, snug-fitting opening on top of the chamber, thus exposing the INCAT device to the chamber air.

Once the VOC sample was adsorbed inside the INCAT device (via active or passive method), the Luer-Lok end was plugged with a piece of septum. Subsequently, the device was immediately inserted into the injection port of the GC instrument for thermal desorption of the sample. A 60 s injection time was suitable for the desorption of the BTEX compounds. A second thermal desorption injection of the device was performed to ensure that the entire sample had been desorbed in the first 60 s injection, and showed that no carry-over occurred.

## 3. Results

### 3.1. Active sampling with the INCAT device

The mean molar amount of each compound obtained from actively sampling 5 ml of the chamber air are presented in Table 2. The peak areas of the BTEX compounds were quantified by comparison to the SPE tube measurements using the relationships presented in Eqs. (1) and (2). The mean molar amounts of BTEX compounds were calculated based on ten sequential samples of the test chamber air. The relative standard deviations from the mean amount of compound sampled (RSD) ranged from 6.3 to 9.4%. The proportional amount of each compound adsorbed relative to the amount present in the volume sampled from the chamber ranged from 16.3 to 70.7%. These results show that despite the manual sampling procedure, the sampling reproducibility is comparable to the sampling error for direct liquid injections onto packed GC columns, as evidenced by the RSD values (Table 2) that were calculated at less than 10%. The variation in the efficiency of sampling (percent adsorbed relative to the amount sampled) is independent of the sampling reproducibility, and is likely due to the individual affinities of the compounds for the adsorbent.

The results of the adsorption profiles of all of the BTEX compounds actively sampled at varying volumes are presented in Fig. 2. The adsorption profiles suggested that the amount of each compound determined with the INCAT device were dependent on the presence of other compounds. Active sampling of all of the BTEX simultaneously showed a distinctive trend among the heavier compounds (ethyl benzene and the xylenes) for a Langmuir-like adsorption curve [8,9]. However, the adsorption profiles for benzene and toluene reached a maximum and then 'tailed off' as the sample volume increased. This decrease in the amounts of the compounds adsorbed implies some sort of competition for space on the surface of the carbon coating. The competition for space seemed to favour the heavier compounds.

The adsorption profile of benzene, when sampled in the absence of other BTEX compounds

(shown in Fig. 3a), shows an initial rapid increase in the amount adsorbed with increasing sample volume. This rate of change begins to decrease as the interior carbon surface becomes saturated. Analysis of this single component system showed that the adsorption of benzene followed a Langmuir-like isotherm, i.e. the reciprocal of the amount adsorbed was directly proportional to the reciprocal of the volume sampled as shown in Fig. 3b. However, the presence of an additional compound again showed that competition for space on the coating favouring the heavier species, thus disturbing the Langmuir-like behaviour. This trend was seen in the analysis of benzene and toluene sampled in the absence of the heavier compounds, shown in Fig. 4. The constant volume active sampling results listed in Table 2, showed an efficiency value (percent adsorbed) of 52.1% for toluene relative to 16.3% for benzene. As such, it is not surprising that benzene is the compound affected as the capacity of the device becomes a significant factor—even in a two component system. Thus, when sampling several compounds at once, a competitive adsorption profile is likely to occur. It should also be noted that benzene adsorbed in the absence of all other compounds from ten replicate 5 ml measurements, had a mean of  $0.062 \pm 0.004$  and RSD of 7.2%. These constant volume results for the single component system are consistent with the multi-component system where all of the BTEX compounds were sampled. The proportional amount of benzene adsorbed, relative to the amount sampled, was 15.3% (the test chamber concentration of benzene was again  $88.2 \pm 0.9 \mu\text{mol m}^{-3}$ ). This low efficiency, even in the absence of other compounds, implies that benzene has a low affinity for the adsorbent despite the numbers of compounds in the system being sampled.

### 3.2. Passive sampling with the INCAT device

Mean passive rates of adsorption for the 22 gauge INCAT devices were determined from passive sampling with three devices for a 24 h period. The mean passive rates of adsorption (absolute) for the three 22 gauge INCAT devices are listed in Table 3. Since competition for space on the car-

bon coating between the various species being sampled was apparent, the mean adsorption rates serve only to show consistency in sampling for a specific amount of time. It is likely that a different set of mean adsorption rates would result if the devices were used to sample the BTEX compounds passively for different lengths of time. Thus, only information on the reproducibility of the carbon coating and reproducibility in passive sampling for a fixed time of exposure may be obtained from these results.

The adsorption profiles for the BTEX compounds, passively sampled over a range of exposure times, are shown in Fig. 5. The competitive effects observed in the active sampling of all of the BTEX compounds are again present, but are not as severe. Profiles for the passive adsorption closely resemble the active sampling adsorption profiles (in shape only but not magnitude) up to a 10 ml sample volume (Fig. 2). This similarity suggests that similar adsorption phenomena occur, but on a slower (smaller) scale due to the slower rate of uptake in the passive mode of sampling.

## 4. Discussion

Active sampling of the BTEX compounds over a wide volume range revealed an inconsistency in the various adsorption profiles that was not directly related to their actual concentration. The differences in the adsorption curves suggest a preferential or competitive adsorption affect on the carbon surface. The total molar amount of compounds obtained from the INCAT shows a typical adsorption profile (Fig. 6) similar to that of benzene sampled in the absence of the other compounds. This suggests that differences in the profiles of the individual compounds when sampled simultaneously, are the result of competition for space on the carbon surface where the individual affinities of the compounds for the adsorbent become more significant.

The competition for space on the adsorbing surface of the INCAT device becomes significant only as the coating is nearing saturation. Therefore, looking more closely at the initial regions of

the active and passive sampling results may be prudent. The initial rates of adsorption for the active samples are found in Table 4. Considering the molar amount of each compound obtained with the device in the actively sampled range of 0–8 ml, it appears that the adsorption of each compound, with the exception of benzene, was approximately linear. The coefficient of determination for the linear relationship was at least 97% for all compounds other than benzene. Benzene was not included as it reached its maximum and then began to decrease within the initial range of volume sampled. The best fit line for benzene could not be determined to same degree of certainty as the other compounds since too few data points were collected prior to the 5 ml sample. An estimate of the slope and adsorption rate based on the initial three data points is included in Table 4 for comparison. The coefficient of determination for the linear fit for benzene has been omitted since it is the result of only three data points and is therefore misleadingly high.

In addition to the molar amounts of each compound adsorbed (except benzene), having an initial linear relationship with the sample volume, the initial slopes were in order of increasing chamber concentration (see Table 1). The rates of adsorption of the BTEX compounds, listed in Table 4, are obtained from the initial slopes and the flow rate at which they were actively sampled. The sampling efficiencies of each compound with this type of carbon surface (or affinities for the adsorbent) are reflected by the initial slopes and rates of adsorption. Differences in the amount of each compound adsorbed, relative to the amount sampled from the chamber (listed in Table 2), also reflect the individual affinities of the BTEX compounds for the adsorbent.

In comparison, analysis of the BTEX compounds by passive sampling resulted in the same linear trends being observed in the initial region of sampling (0–5.75 h of exposure). The initial slopes, or passive rates of adsorption, are listed in Table 5. For each compound, the coefficient of determination for the linear relationship ( $r^2$ ) was greater than 95%. Although the curvilinear shape to the benzene profile is present in the initial passive sampling data, it is not as extreme as

observed in the active data. As such, benzene can be included in the analysis to the same degree of certainty as the other compounds.

The initial rates of adsorption listed in Table 5 are not meant to be compared with the mean passive rates of adsorption found in Table 3. The mean adsorption rates listed in Table 3 resulted from sampling with three INCAT devices (22 gauge) over a 24 h period, whereas Table 5 lists the initial adsorption rates for a single INCAT device (26 gauge) exposed for up to 5.75 h. Even if the devices used in the two analyses were the same size (gauge), and had the same surface area of adsorbent, the periods of sampling would not be the same and are unlikely to result in equivalent passive adsorption rates.

Passive sampling the BTEX compounds over the entire range of exposure times, showed that the amounts of benzene and toluene both reached a maximum, but were still obtained in high amounts relative to the heavier compounds being sampled. Ethyl benzene is consistently adsorbed to a lesser degree than all of the other compounds, which is similar to the initial portion of the active sampling curve of all of the BTEX compounds (Fig. 2). Similarity between the passive sampling profiles and the initial portion of the active sampling profiles (up to 10 ml) suggests consistency of the adsorbing material. Again, the shape of the total amount of compounds adsorbed in Fig. 7 shows a typical adsorption profile, as observed in the active sampling. The correlation coefficient ( $r$ ) between the active and passive initial rates of adsorption (Tables 4 and 5) was calculated to be 0.930, indicating reasonable agreement between the independent sets of results. The correlation coefficient between the active and passive sampling rates is even greater,  $r = 0.999$ , when the benzene point is excluded due to the higher error associated with its initial active rate of adsorption. Moreover, if the efficiency of adsorption of the individual analytes is taken into account, the initial rates of adsorption in the passive and active sampling modes show very good agreement. The proportional amount of each compound adsorbed (listed as the percent adsorbed in Table 2) may be considered as the efficiency for sampling the individual species in

the initial linear region of the adsorption profiles. Then, the passive and active rates of adsorption may be scaled to account for the variation in the individual affinities of the analytes for the adsorbent. Fig. 8 shows the 'effective' initial active and passive rates of adsorption plotted against each other, with the best fit line through the data. The coefficient of determination for the linear fit through the data in Fig. 8 was calculated to be  $r^2 = 0.996$  with the benzene point included, and  $r^2 = 0.999$  with the benzene point excluded. The result of this correlation is that the INCAT device can serve as both a passive or active sampler for these VOCs. Direct correlation between the rate of adsorption (active and passive) and the analyte partition coefficient was poor. The lack of correlation between the adsorption rates and partition coefficients is likely due to the influence of the individual efficiency or affinity factors for the compounds.

Active sampling a 10 ml volume takes only 5 min, with the flow rate through the device of 4 ml  $\text{min}^{-1}$  (to draw through and expel the sample volume). Therefore, one can obtain relatively the same amounts of the compounds in 5 min of active sampling as one does in 24 h of passive sampling with this device. If the rate of actively drawing the air through the INCAT is reduced, then the same sample volume would be sampled over a longer period. As such, the analytes in the sample volume would have more time to interact with the adsorbing coating and increase the amount adsorbed, thus raising the sensitivity of analysis. In addition, longer periods of exposure for passive sampling may be better for situations where VOC levels vary with time, allowing an integrating effect averaged over time.

## 5. Conclusions

BTEX compounds were chosen as an indicator of the effectiveness of the INCAT device to act as a representative set of VOCs that occur frequently in urban environments and pose particular occupational hazards [1]. BTEX compounds are found in gasoline and automobile exhaust, in tobacco smoke, and in commercial or industrial solvents.

Thus, the potential for human exposure to these compounds is quite high, especially for individuals in occupations involving the use of these compounds. Furthermore, the severe impact of the BTEX compounds on human and animal health has been observed and documented. Benzene is listed as the fifth compound in the top 20 hazardous substances by the Agency for Toxic Substances and Disease Registry (ATSDR) of the US Department of Health and Human Services [1]. Benzene has been found to cause leukemia and to have adverse effects on blood production and the immune system. It is because of this level of impact on humans that the need for passive monitors for VOCs in certain occupational areas is particularly necessary.

The reproducibility of the INCAT device in measuring the BTEX compounds sampled actively at a fixed volume showed a variation in sampling error ranging from 6.3 to 9.3% for the different compounds when sampled simultaneously. The implication of the sampling error for the individual analytes, all being less than 10%, is that although the active samples were performed manually, the consistency in sampling is very good for packed column GC. Variation between the sampling errors is likely due to the influences of the individual analytes on each other resulting from the high levels that the BTEX compounds are present in the test chamber. The reproducibility of the coating surface, determined from passive sampling of three INCAT devices for a fixed amount of time, showed relative standard deviations from the mean adsorption rate ranging from 8.6 to 12.9% for the different compounds. Again, the variation in the sampling error was perhaps due to the effect of the compounds on each other leading to different adsorption profiles when sampling a mixture as opposed to a single component. Variation in the adsorption profile for benzene and toluene appeared dependent on other compounds present. This variation implies that a specific calibration would be required for quantitative analysis or that measurements would have to be restricted to the range in which the adsorption is essentially linear. Although these analyses were performed using a packed column, the INCAT has been used with capillary columns



with split injection system. The use of a packed column was to resolve all of the BTEX compounds.

The adsorption profiles for both active and passive sampling suggested competitive effects between the lighter and heavier compounds. These effects become more pronounced as the carbon coating inside the device nears saturation at which point the individual affinities for the surface become more evident. Since the competitive effects were observed in the passive sampling mode as well, it was concluded that an adsorbing coating with a higher surface area, to raise the capacity of the device, was needed. Colloidal graphite tended to capacity too quickly with the BTEX concentrations at such levels. It should be noted that some concentration levels in the test chamber are much higher than what the minimum risk levels (MRL) are for indoor air (e.g. the test chamber concentration for benzene is approximately 2.2 ppm and the MRL is 0.05 ppm) [10].

In general, it can be concluded that most of the shortcomings of the INCAT sampling methods are directly related to the use of colloidal graphite for the adsorbing coating. The colloidal graphite was chosen only because it was commercially available and of reasonable consistency to easily coat the interior surface of the capillary. The concept of principal importance is that 'a carbon coating material' on the interior of the device can be used to adsorb VOCs, either actively or passively, and that the device may then be inserted into a GC or GC/MS instrument for thermal desorption of the analytes. The simplicity of this sampling method is related to: the INCAT device being relatively robust and may therefore be used many times before the adsorbing coating begins to degrade; sampling is achieved in the solventless extraction process; the active sampling of analytes can be achieved for indoor air; the passive sampling can be done for any amount of time and in various locations of a site (a 'sick' building) to obtain a profile of VOCs; and the device is technically simple for sampling and injecting. The aim is to see if an INCAT sampler can sent by mail to a site for passive sampling and then mailed back for analysis.

The INCAT device is analogous to the activated carbon SPE air sampler used to measure the test chamber concentrations in these analyses. Rather than containing loosely packed adsorbent particles that allow air flow, as with the activated carbon SPE tubes, the INCAT has an adsorbing coating on the interior surface of capillary. However, the fact that the adsorbent is present in the device much like a GC capillary column, analyte partitioning between air and the adsorbent should not be confused with analyte partitioning in open tubular gas chromatography (OTGC). OTGC involves a 'sample plug' being transported through the column via an inert carrier gas. The INCAT device in the active sampling mode, involves the continuous flow of analytes that are uniformly distributed throughout the air volume sampled. Although both systems are flow/velocity dependent, the partitioning of the analytes between the air and the INCAT adsorbent are not likely to occur in the same manner as in OTGC. The dependence on analyte velocity, in active sampling with the INCAT device, is related whether the analyte has sufficient time to interact with the carbon adsorbent, and sufficient numbers of sites available for adsorption. Physical adsorption interactions are relatively weak, but occur readily when the adsorbate comes into contact with the adsorbent. As such, the proximity to an adsorbing site and the speed at which the analyte moves through the device, are two variables that will affect analyte adsorption. The effect of these variables would then be more significant as the adsorbing surface nears its capacity.

The passive adsorption rates do partially involve the diffusion coefficient of the analytes through air. As with SPME, the sampling rate will depend on the rate of analyte mass transport through a matrix (air in this study) to the adsorbent. However, in the environmental chamber used here, the air is being constantly circulated via fans and clean air is being blown in ( $32 \text{ l h}^{-1}$ ). Thus, the environmental chamber is not a static headspace where the diffusion of the analyte would be such an important variable.

This paper presents a new method of sampling VOCs using a particular adsorbing coating in the device. The use of carbon coatings with greater

surface areas should reduce the problem of the competitive effects for space by raising the level at which the interior carbon coating becomes saturated. The INCAT sampling method is still very much in its infancy, and at this point the investigations of its usefulness have been directed at obtaining reproducible samples. Competitive effects and variation in sampling efficiencies for the different compounds are the result of the low capacity of the graphite adsorbent, not with the sampling method. In summary, these results show that the INCAT device may be used to sample BTEX compounds from air in both the active and passive modes. Future work is directed to improving the adsorbent in the device, to reduce the variation in sampling efficiencies. New INCAT devices will be made with activated carbon coatings for similar studies. These new devices should prove to have a much higher capacity and less variation in sampling efficiencies for aromatic VOCs.

### Acknowledgements

The authors would like to thank P. Marvroudis, C. Morrison and E. Giller for their preliminary work on the sampling of BTEX

compounds with the INCAT device and activated carbon cloth. We also thank H. Perreault, K.J. Keen and K. Lalbiharie for helpful advice, and the Sustainable Development Innovations Fund of the Government of Manitoba, the University of Manitoba and NSERC Canada for financial assistance.

### References

- [1] Agency for Toxic Substances and Disease Registry Public Health Statement, ATSDR Science Corner, <http://atsdr1.atsdr.cdc.gov:8080/cx.html>, 1989.
- [2] H.N. MacFarland, *Am. Ind. Assoc.* 47 (1986) 704.
- [3] M. Tancrede, R. Nilson, L. Zeise, E.A. Crouch, *Atmos. Environ.* 21 (1987) 2187.
- [4] M.E. McComb, R.D. Oleschuk, E. Giller, H.D. Gesser, *Talanta* 44 (1997) 2137.
- [5] C.J. Koester, R.E. Clement, *Crit. Rev. Anal. Chem.* 24 (4) (1993) 263–316.
- [6] B. Kolb, L.S. Ettre, *Static Head-Space Gas Chromatography*, Wiley-VCH, New York, 1997, pp. 13–20.
- [7] S.F. Spencer, *Anal. Chem.* 35 (1963) 592.
- [8] D.M. Ruthven, *Principles of Adsorption and Adsorption Processes*, Wiley, New York, 1984, pp. 80–96.
- [9] V. Ponec, Z. Knor, S. Cerny, *Adsorption on Solids*, Butterworths, London, 1974, pp. 326–332.
- [10] Minimal Risk Levels (MRLs) for Hazardous Substances, Agency for Toxic Substances and Disease Registry Division of Toxicology, <http://www.atsdr.cdc.gov/mrls.html>, 1998.

# Urinary selenium speciation by high-performance liquid chromatography–inductively coupled plasma mass spectrometry: advantages of detection with a double-focusing mass analyser with a hydride generation interface

J.M. González LaFuente, J.M. Marchante-Gayón, M.L. Fernández Sánchez, A. Sanz-Medel \*

*Department of Physical and Analytical Chemistry, University of Oviedo, c/ Julián Clavería 8, 33006 Oviedo, Spain*

Received 29 September 1998; received in revised form 29 March 1999; accepted 7 April 1999

---

## Abstract

A detailed comparison of the performance of inductively coupled plasma mass spectrometry (ICP-MS), with quadrupole and double-focusing instruments for the speciation of selenium in urine has been carried out. Selenium sensitivity about 23–59 times higher with double-focusing ICP-MS detection was observed, but limits of detection were only 1–8.7 times better because of background noise. Selenium species separation has been carried out by both reversed-phase and vesicle-mediated high-performance liquid chromatography (HPLC), coupled on-line with the detector via conventional nebulization and via on-line focused microwave digestion–hydride generation. A remarkable improvement in sensitivity (28–110 times better for  $^{77}\text{Se}$  depending on the chromatographic system) and elimination of interference problems from the urinary matrix or the components of the mobile phases were achieved when an on-line microwave digestion–hydride generation interface was used, but the background noise was much higher than with conventional nebulization. Therefore, the limits of detection were not as low as expected from such improvement in the sensitivity. More selenocompounds can be separated, and a slight improvement in the sensitivity and limits of detection was obtained when the vesicle-mediated HPLC system was used as compared with reverse-phase chromatography. However, the use of several complementary chromatographic systems, such as reverse-phase HPLC, is recommended to bring some light on the selenocompounds present in basal human urine. Comparative data of rat urine speciation are also given. © 1999 Elsevier Science B.V. All rights reserved.

*Keywords:* Quadrupole inductively coupled plasma mass spectrometry; Double-focusing sector field inductively coupled plasma mass spectrometry; Urinary selenium speciation; High-performance liquid chromatography

---

\* Corresponding author. Tel.: +34-98-510-3480; fax: +34-98-510-3125.

E-mail address: asm@sauron.quimica.uniovi.es (A. Sanz-Medel)

## 1. Introduction

The present situation in the speciation of trace elements in biological materials is characterised by its great complexity. In the clearly better developed field of environmental chemical speciation, we are usually dealing only with a few toxic elements and their species, e.g. different oxidation states or chemical forms of a particular trace element [1,2]. However, in clinical and biological chemical speciation, we found also many essential and therapeutical trace elements, which can be bound or interact with a huge number of possible biocompounds of extremely complex chemical structure [1,2] (proteins, enzymes, DNA, LMM and MMM biocompounds, etc.). Only very sensitive analytical detectors can evidence the possible beneficial or detrimental role of the extremely low amounts of such elements and species as they are in the body at physiological levels.

In this sense, inductively coupled plasma mass spectrometry (ICP-MS) has opened new avenues for biological research when coupled to a powerful separation technique such as high-performance liquid chromatography (HPLC): an increasing number of unknown trace element species are being reported in the latest analytical literature [3] at such low levels. Therefore, the greater sensitivity of ICP-MS is now allowing biological toxic or essential trace elements studies at basal levels [4–6] (unspiked samples), useful to evidence the presence of both unknown and known species in the organisms at extremely low concentration levels (only dreamed of a few years ago).

In this vein, the use of the ICP-Sector Field-MS at low resolution can provide increased sensitivity for HPLC–ICP-MS experiments [7]. Some Sector Field instruments allow three resolution settings (low, medium and high). Of course, the higher the resolution, the lower the sensitivity. In the low resolution mode, the sensitivity is about two orders of magnitude better than that of quadrupole ICP-MS, but a major problem is keeping blank levels low enough to exploit the extreme sensitivity obtainable in such low resolution mode.

So far, the advantages and disadvantages of different ICP-mass spectrometers coupled to HPLC for the speciation of trace elements in

biological samples are not clearly evaluated in the literature. Therefore, from our previous experience [8,9], the first objective of this research is to perform a detailed comparison of quadrupole ICP-MS and double-focusing sector field ICP-MS for the speciation of selenium in urine, comparing also different HPLC–ICP-MS interfaces (e.g. direct nebulization and on-line microwave digestion–hydride generation).

On the other hand, selenium speciation in biological fluids such as urine is of growing interest [10,11] because controversial selenium speciation results have been reported: at least, five species of selenium have been found in urine [12], but only trimethylselenonium, selenite and monomethylselenol have been identified so far [12–14]. Trimethylselenonium seems to be a minor Se species (1–7% of the total selenium in urine) in normal conditions, but if nutritional selenium intake increases, this species becomes predominant in urine (probably due to the detoxification process taking place in liver and kidney). The ingestion of trimethylselenonium produces a rapid urinary excretion of the non-metabolised species [12]. Monomethylselenol has been found as the predominant species in the urine of rats fed with normal levels of selenium [13]. However, the urinary concentrations of trimethylselenonium in rats increased by  $\text{Na}_2^{82}\text{SeO}_3$  intravenous injections. Three species of selenium in human urine from subjects with high urinary levels of the element (137–427  $\mu\text{g l}^{-1}$  of total selenium) were recently reported [14]: in two cases, trimethylselenonium was not detected, while in another two cases, a concentration of 10  $\mu\text{g l}^{-1}$  was found. In all cases, selenite was reported as the predominant species (98–423  $\mu\text{g l}^{-1}$ ), while the third species was not identified.

At present, there is an urgent need for pure Se biocompounds and reference urine samples with certified selenium species. In order to tackle the present problems of identification/confirmation of metal bio-molecules, the use of different complementary analytical methodologies/techniques able to confirm speciation results is recommended [7]. So, the speciation information obtained by different principle-based separation approaches is one of the practical ways to proceed further in specia-

tion work. In this paper, speciation information of reversed-phase and vesicle-mediated HPLC is compared, with the aim of shedding some light on catabolism of selenium in mammals. This methodology has been applied to human and rat urine.

## 2. Experimental

### 2.1. Instrumentation

For the chromatographic separations, an LKB (Browman, Sweden) Model 2150 HPLC pump with a Rheodyne sample injection high pressure valve (Berkeley, CA, USA) equipped with a 50  $\mu\text{l}$  loop was used for eluent delivery and sample introduction. The two analytical columns (210 mm  $\times$  4.6 mm id) were packed with 5  $\mu\text{m}$  Spherisorb  $\text{C}_{18}$  bonded silica stationary phase (Phase Separations, Deeside, UK). One of them was modified for vesicle-mediated speciation with didodecyldimethylammonium bromide (DDAB) from Merck (Darmstadt, Germany)  $10^{-3}$  mM in methanol 50% (v/v) at a flow rate of 0.5 ml  $\text{min}^{-1}$  during 3 h. This modified column was cleaned daily with filtered DDAB  $10^{-5}$  M in Milli-Q water. A pre-column (30 mm  $\times$  4.6 mm id) was packed with 10  $\mu\text{m}$  Spherisorb  $\text{C}_{18}$  bonded silica stationary phase. This pre-column was cleaned

after 40 injections, first with methanol and, second, with filtered DDAB  $10^{-5}$  M in Milli-Q water. A glass home-made three-way valve was used for mobile phase change in vesicle-mediated experiments. An ultrasonic device from Sonics&Materials (CT, USA), Mod. VC (250 W), was used for the preparation of vesicles from surfactant (DDAB) solution.

The quadrupole inductively coupled plasma mass spectrometer used in this work was a Hewlett-Packard model HP4500 (Yokogawa Analytical Systems, Tokyo, Japan). The double-focusing sector field inductively coupled plasma mass spectrometer used was an Element from Finnigan Mat (Bremen, Germany).

For on-line microwave digestion–hydride generation interface (Fig. 1), a focused microwave digester Microdigest M301 from ProLabo (Paris, France), two multi-channel peristaltic pumps from Gilson Minipuls (Middleton, WI, USA), a laboratory-made glass cylinder for reaction coil wrapping [15] and a glass gas–liquid separator [8] were used.

### 2.2. Reagents and urine samples

Seleno-L-methionine, seleno-D,L-ethionine and seleno-L-cystine (Sigma Chemicals, St. Louis,

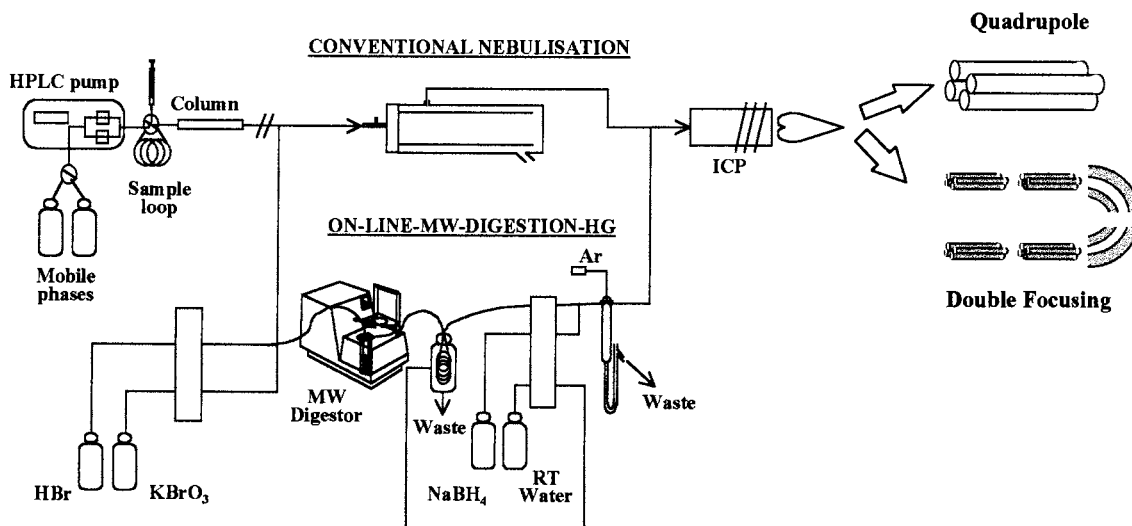


Fig. 1. Schematic diagram of the coupling HPLC interface ICP-MS used in this work.

MO, USA) stock solutions containing  $10 \text{ mg l}^{-1}$  Se were obtained by dissolving the appropriate amount of the corresponding compounds with filtered (0.22 mm) 18 M $\Omega$  deionized water (ultrapure water). This water was obtained from a Milli-Q 185 system (Millipore, Molsheim, France). Inorganic Se(IV) stock solution ( $1000 \text{ mg l}^{-1}$ ) was obtained from Merck (Darmstadt, Germany). The Se(VI) stock solution ( $1000 \text{ mg l}^{-1}$ ) was prepared by dissolving  $\text{Na}_2\text{SeO}_4$  from Merck in ultrapure Milli-Q water.

Sodium tetrahydroborate (III) (0.5% w/v) was prepared by dissolving 2.0 g of  $\text{NaBH}_4$  (Probus, Barcelona, Spain) in 400 ml of 0.1% (w/v) NaOH solution from Merck and filtering this solution. Potassium bromate from Merck solution ( $1.5 \times 10^{-2} \text{ M}$ ) was prepared by dissolving the appropriate amount of the salt in ultrapure Milli-Q water. Hydrobromic acid (47% w/v) and hydrochloric acid (37% w/v) were from Merck. A DDAB solution ( $10^{-2} \text{ M}$ ) was prepared by adding 0.4626 g of the surfactant (Fluka, Buchs, Switzerland) to 100 ml of Milli-Q water. The DDAB  $10^{-2} \text{ M}$  solution was sonicated for 10 min with a power output of 60 W, and this solution was used for preparing, by simple appropriate dilution, all other vesicular mobile phases. Ammonium acetate was obtained from Merck. Methanol (Suprapure) was from Teknokroma (Barcelona, Spain). All other chemicals were of analytical-reagent grade.

Human urine samples were obtained from healthy volunteers. Urine from normal fed rats were provided by the 'Hospital Central de Asturias' in Oviedo, Spain. All urine samples were kept at 4°C in the dark before analysis.

### 2.3. Procedure

Urine samples are diluted 1:1 with ultrapure Milli-Q water, filtered through a Millipore 20  $\mu\text{m}$  membrane and 50  $\mu\text{l}$  of sample injected in the chromatographic system (Fig. 1). Aqueous standard calibration by direct nebulization is carried out by injecting 50  $\mu\text{l}$  of standards containing 0, 25, 50, and 75  $\mu\text{g l}^{-1}$  of each Se species (as selenium) under study. For on-line focused microwave digestion–hydride generation

coupling, these concentrations were lowered to 0, 5, 10, 15 and 20  $\mu\text{g l}^{-1}$ .

For reversed-phase separations, the mobile phase consisted of 0.1 M ammonium acetate buffer solution (pH 4). For vesicle-mediated experiments, the mobile phase A consisted of 0.01 M ammonium acetate buffer solution (pH 4) with 0.5% v/v methanol and DDAB  $10^{-5} \text{ M}$ . The mobile phase B consisted of 0.2 M ammonium acetate solution (pH 6.5) with 0.5% v/v methanol and DDAB  $10^{-5} \text{ M}$ . Phase A is replaced by B by turning the three-way valve 5.5 min after the sample injection. Once the chromatogram is finished, phase B must be switched again to phase A with the three-way valve. In order to re-equilibrate the column, 15 min are allowed before a second injection is carried out. In both chromatographic systems, the carrier flow is  $1 \text{ ml min}^{-1}$ .

For on-line focused microwave digestion–hydride generation coupling, the eluate from the chromatographic system is first continuously mixed with HBr 47% w/v at a flow rate of  $1.2 \text{ ml min}^{-1}$  and  $\text{KBrO}_3$   $1.5 \times 10^{-2} \text{ M}$  solution at a flow rate of  $0.6 \text{ ml min}^{-1}$  going through the focused microwave digester setting at a power of 15% (see Fig. 1). During the digestion time (around 1 min), the liquid sample rotates inside the PTFE reaction coil immersed in the microwave field. The emerging flow, cooled by passing through the additional PTFE coil immersed in a room-temperature water bath, then merges with  $\text{NaBH}_4$  0.5% w/v solution at a flow rate of  $2 \text{ ml min}^{-1}$  pumped by the second peristaltic pump [15] to form volatile  $\text{SeH}_2$ , which is carried by a flow of argon to the atomiser via the gas–liquid separator [8] (see Fig. 1).

Optimum operating conditions for Se detection by ICP-MS at the exit of the chromatographic columns using the quadrupole HP-4500 and the sector field Element are shown in Table 1.

### 3. Results and discussion

Under the instrumental conditions given in Table 1 and the procedure already described, the

Table 1

Optimum operating conditions for Se detection by ICP-MS at the exit of the chromatographic column for quadrupole HP-4500 and double-focusing Element instruments

	Quadrupole	Double focusing
Isotopes monitored	$^{77}\text{Se}$ , $^{78}\text{Se}$ , $^{82}\text{Se}$	$^{77}\text{Se}$ , $^{78}\text{Se}$ , $^{82}\text{Se}$
Radiofrequency power	1200 W	1300 W
Sample depth	5.7 mm	Manually optimised
Carrier gas flowrate	1.29 l min $^{-1}$	1.05 l min $^{-1}$
Intermediate gas flowrate	1.0 l min $^{-1}$	0.91 l min $^{-1}$
Outer gas flowrate	15 l min $^{-1}$	14.2 l min $^{-1}$
Nebulizer	Meinhard	Meinhard
Spray chamber temperature	2°C	Room temperature
Samples and skimmer cones	Nickel	Nickel
Resolution	300	300
Points per mass	3	25
Integration time	0.5 s	0.025 s

selenium response to selenocystine, selenomethionine, selenoethionine, selenite and selenate was evaluated using the double-focusing ICP-MS by aqueous calibration and standard additions in human urine. The obtained limits of detection, calculated as  $3\sigma C/I_C$  ( $n = 3$ ),  $C$  being equal to 25 and 5  $\mu\text{g l}^{-1}$  of each selenospecies (as selenium) for conventional nebulization and microwave digestion–hydride generation, respectively, and  $I_C$  being the respective peak height in counts per second, and the sensitivities (calculated from calibration graphs for 0, 25, 50 and 75  $\mu\text{g l}^{-1}$  and 0, 5, 10, 15 and 20  $\mu\text{g l}^{-1}$  of each selenospecies as selenium for conventional nebulization and microwave digestion–hydride generation, respectively) are summarised in Tables 2 and 3.

### 3.1. Mass detectors: quadrupole versus double focusing

In previous papers [8,9], it was demonstrated that the limits of detection obtained by an ICP quadrupole mass analyser allows the direct reliable speciation of selenium in urine while the limits of detection obtained by more classical photon detectors, e.g. electrothermal atomic ab-

sorption spectroscopy, ICP-OES (optical emission spectroscopy) etc. are too high to follow directly the selenium species concentrations normally found in this kind of sample. Of course, if the sensitivity of the analytical technique is low enough, unknown or new species present at low levels in biological fluids could be detected.

An ICP-MS with double-focusing mass analyser, working in the ‘low resolution’ mode ( $R = 300$ ), can be used to provide enhanced sensitivity at the exit of the chromatographic column, compared with the quadrupole. In order to compare the performance of both mass detectors for selenium speciation in urine, different species of selenium (selenocystine, selenomethionine, selenoethionine, selenite and selenate) in human urine were investigated in terms of sensitivity and limits of detection with the two instruments, and the results were compared always using the HPLC–microwave–hydride generation system of Fig. 1.

Comparing the data obtained in the Element (see Tables 2 and 3) with previously published quadrupole data [9], the use of a double-focusing mass detector, working in the ‘low resolution’ mode, enhanced the sensitivity 23–59 times compared with the quadrupole. However, the observed limits of detection were just 1–8.7 times better than those found with the quadrupole mass analyser. These results can be rationalised considering that background noise (from polyatomic ions of Ar) and effects of selenium contamination of the reagents also increased substantially in the Element. Although further studies are guaranteed to lower such negative factors, the double-focusing instrument is still more sensitive to Se and was selected for subsequent experiments.

### 3.2. HPLC–mass detector interface: conventional nebulization versus on-line focused microwave–hydride generation

Conventional nebulization and on-line focused microwave–hydride generation interfaces (Fig. 1) were compared in terms of limits of detection, sensitivities and interferences.

Fig. 2A shows a typical chromatogram obtained for a pure aqueous mixture of  $25 \mu\text{g l}^{-1}$  of each selenocompound (monitoring  $^{77}\text{Se}$ ,  $^{78}\text{Se}$  and  $^{82}\text{Se}$ ), and Fig. 2B shows the corresponding chromatograms attained for spiked human urine ( $25 \mu\text{g l}^{-1}$ ), using reversed-phase separation and conventional nebulization. As can be seen, selenite was eluted in the dead volume and its ICP-MS signal in urine samples did not change when the

amount of selenite increased; in other words, urine matrix interferences occur, rendering this determination impossible. However, selenomethionine and selenoethionine were not interfered with, sensitivities being virtually the same in both matrices.

Similarly, Fig. 3A shows a typical chromatogram obtained for an aqueous mixture of  $5 \mu\text{g l}^{-1}$  of each selenocompound (monitoring  $^{77}\text{Se}$  and  $^{78}\text{Se}$ ), and Fig. 3B shows basal and spiked

Table 2

Absolute detection limits (pg selenium) obtained by double-focusing ICP-MS (Element)<sup>a</sup>

	Se-Cys	Se-Met	Se-Eth	Se(IV)	Se(VI)
<b>Water</b>					
<i>VESICLE-MEDIATED HPLC</i>					
<i>Conventional nebulization</i>					
$^{77}\text{Se}$	90	111	107	128	81
$^{78}\text{Se}$	173	176	216	253	98
$^{82}\text{Se}$	868	806	872	1104	562
<i>Microwave digestion-hydride generation</i>					
$^{77}\text{Se}$	38 (35)	45 (60)	52 (105)	49 (220)	42 (100)
$^{78}\text{Se}$	60	88	71	95	72
<i>REVERSED-PHASE HPLC</i>					
<i>Conventional nebulization</i>					
$^{77}\text{Se}$	Overlapped	123	155	98	Overlapped
$^{78}\text{Se}$	Overlapped	153	177	136	Overlapped
$^{82}\text{Se}$	Overlapped	164	209	134	Overlapped
<i>Microwave digestion-hydride generation</i>					
$^{77}\text{Se}$	Overlapped	41	93	67	Overlapped
$^{78}\text{Se}$	Overlapped	57	88	63	Overlapped
<b>Human urine</b>					
<i>VESICLE-MEDIATED HPLC</i>					
<i>Conventional nebulization</i>					
$^{77}\text{Se}$	703	142	187	248	203
$^{78}\text{Se}$	311	218	290	422	275
$^{82}\text{Se}$	Interfered	797	1332	Interfered	556
<i>Microwave digestion-hydride generation</i>					
$^{77}\text{Se}$	88 (265)	41 (51)	45 (105)	26 (225)	26 (115)
$^{78}\text{Se}$	130	57	67	32	37
<i>REVERSED-PHASE HPLC</i>					
<i>Conventional nebulization</i>					
$^{77}\text{Se}$	Overlapped	129	195	Interfered	Overlapped
$^{78}\text{Se}$	Overlapped	188	238	Interfered	Overlapped
$^{82}\text{Se}$	Overlapped	157	234	Interfered	Overlapped
<i>Microwave digestion-hydride generation</i>					
$^{77}\text{Se}$	Overlapped	63	84	132	Overlapped
$^{78}\text{Se}$	Overlapped	50	68	100	Overlapped

<sup>a</sup> Values in parentheses are LDs obtained by quadrupole ICP-MS (HP4500) [9].



Table 3  
Sensitivity (cps  $\mu\text{g}^{-1}$  l) obtained by double-focusing ICP-MS (Element)<sup>a</sup>

	Se-Cys	Se-Met	Se-Eth	Se(IV)	Se(VI)
<b>Water</b>					
<i>VESICLE-MEDIATED HPLC</i>					
<i>Conventional nebulization</i>					
<sup>77</sup> Se	935	922	868	847	2233
<sup>78</sup> Se	3361	2939	3229	2830	7884
<sup>82</sup> Se	1460	1450	1173		3604
<i>Microwave digestion–hydride generation</i>					
<sup>77</sup> Se	38 580	40 367	39 804	37 884	49 067
<sup>78</sup> Se	134 119	137 208	128 099	117 781	158 272
<i>REVERSED-PHASE HPLC</i>					
<i>Conventional nebulization</i>					
<sup>77</sup> Se	Overlapped	1035	733	1236	Overlapped
<sup>78</sup> Se	Overlapped	3326	2310	3913	Overlapped
<sup>82</sup> Se	Overlapped	1387	907	1634	Overlapped
<i>Microwave digestion–hydride generation</i>					
<sup>77</sup> Se	Overlapped	100 518	62 056	116 432	Overlapped
<sup>78</sup> Se	Overlapped	327 726	234 973	457 793	Overlapped
<b>Human urine</b>					
<i>VESICLE-MEDIATED HPLC</i>					
<i>Conventional nebulization</i>					
<sup>77</sup> Se	235	1188	1082	1508	1717
<sup>78</sup> Se	1010	3959	3705	4754	5380
<sup>82</sup> Se	Interfered	1392	1424	Interfered	2259
<i>Microwave digestion–hydride generation</i>					
<sup>77</sup> Se	15 757 (674)	33 360 (1028)	31 171 (532)	44 311 (993)	46 987 (1737)
<sup>78</sup> Se	57 351	119 418	96 338	138 881	168 761
<i>REVERSED-PHASE HPLC</i>					
<i>Conventional nebulization</i>					
<sup>77</sup> Se	Overlapped	1021	787	Interfered	Overlapped
<sup>78</sup> Se	Overlapped	3694	2462	Interfered	Overlapped
<sup>82</sup> Se	Overlapped	1421	953	Interfered	Overlapped
<i>Microwave digestion–hydride generation</i>					
<sup>77</sup> Se	Overlapped	111 937	68 401	117 597	Overlapped
<sup>78</sup> Se	Overlapped	343 779	237 380	406 651	Overlapped

<sup>a</sup> Values in parentheses are LDs obtained by quadrupole ICP-MS (HP4500) [9].

human urine ( $5 \mu\text{g l}^{-1}$ ) when a reversed-phase separation and on-line microwave digestion–hydride generation (MW–HG) system were used. As can be seen, the ionisation suppression due to the urinary matrix now disappears. As an example, the observed sensitivity for <sup>77</sup>Se was about 87–110 times higher by MW–HG than by conventional nebulization. Unfortunately, again, the limits of detection observed were only around two times

better by hydride generation because the observed background noise increased using our on-line digestion system.

Fig. 4A shows a typical chromatogram obtained for an aqueous mixture of  $25 \mu\text{g l}^{-1}$  of each selenocompound (monitoring <sup>77</sup>Se, <sup>78</sup>Se and <sup>82</sup>Se), and Fig. 4B shows the corresponding chromatogram attained for basal and spiked human urine ( $75 \mu\text{g l}^{-1}$ ) with vesicle-mediated separation

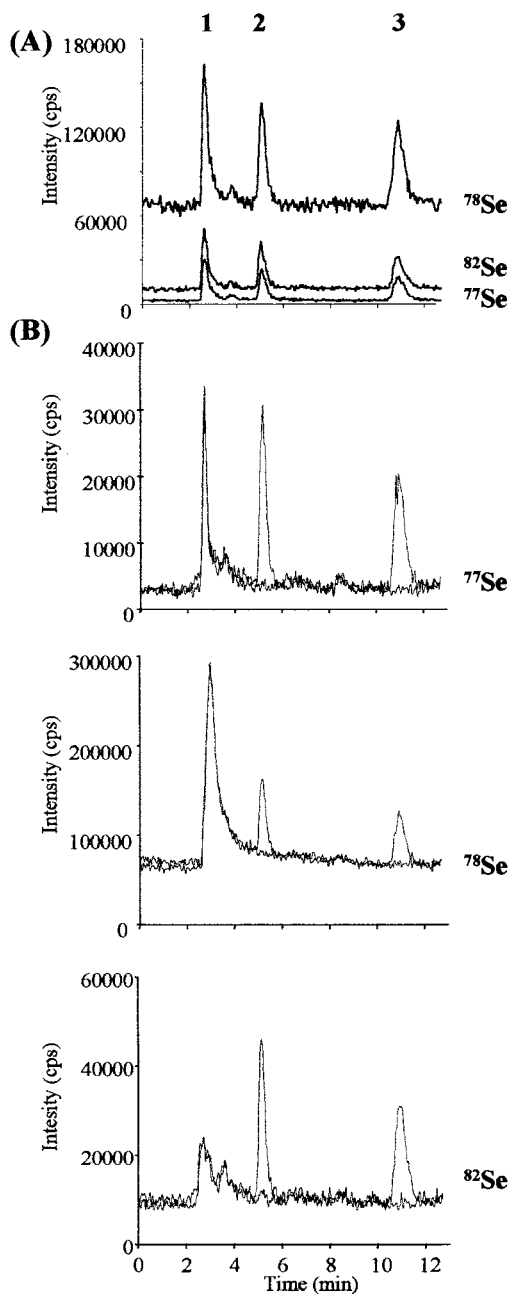


Fig. 2. Typical chromatograms obtained by reversed-phase chromatography conventional nebulization double-focusing ICP-MS: (A) aqueous mixture of  $25 \mu\text{g l}^{-1}$  of each selenocompound; (B) basal and spiked human urine ( $25 \mu\text{g l}^{-1}$ ) of each selenocompound. (1) selenite, (2) selenomethionine, and (3) selenoethionine.

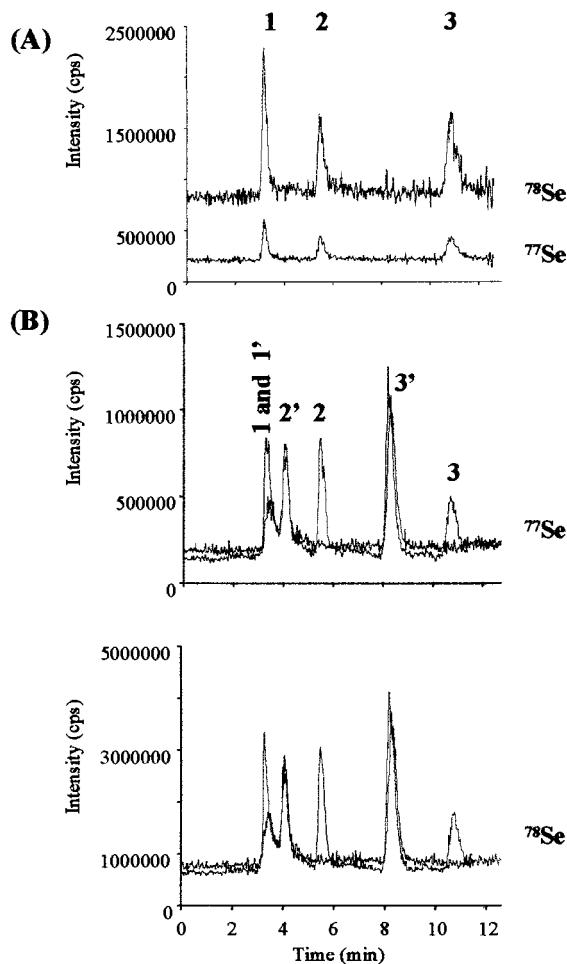


Fig. 3. Typical chromatogram obtained by reversed-phase chromatography microwave digestion-hydride generation double-focusing ICP-MS: (A) aqueous mixture of  $5 \mu\text{g l}^{-1}$  of each selenocompound; (1), (2) and (3) as in Fig. 2; (B) basal and spiked human urine ( $5 \mu\text{g l}^{-1}$ ) of each selenocompound; (1'), (2') and (3') unspiked basal urine Se species.

and conventional nebulization. It is worth noting the background  $^{82}\text{Se}$  signal strongly affected by changing the mobile phase because of  $^{81}\text{Br}^1\text{H}$  (from DDAB) interference: bromide ion from the DDAB of the mobile phase is continuously eluted from the column so the background signal is high at mass 82. When the mobile phase change and the concentration of acetate anion increases rapidly, the bromide anions are eluted until a new equilibrium is reached [9]. This explains the odd behaviour of the chromatogram ( $^{82}\text{Se}$ ) in Fig. 4B

at 10–12 min. Again, the selenocompound eluting at the dead volume (selenocystine in this case) is strongly interfered with in urine samples, probably

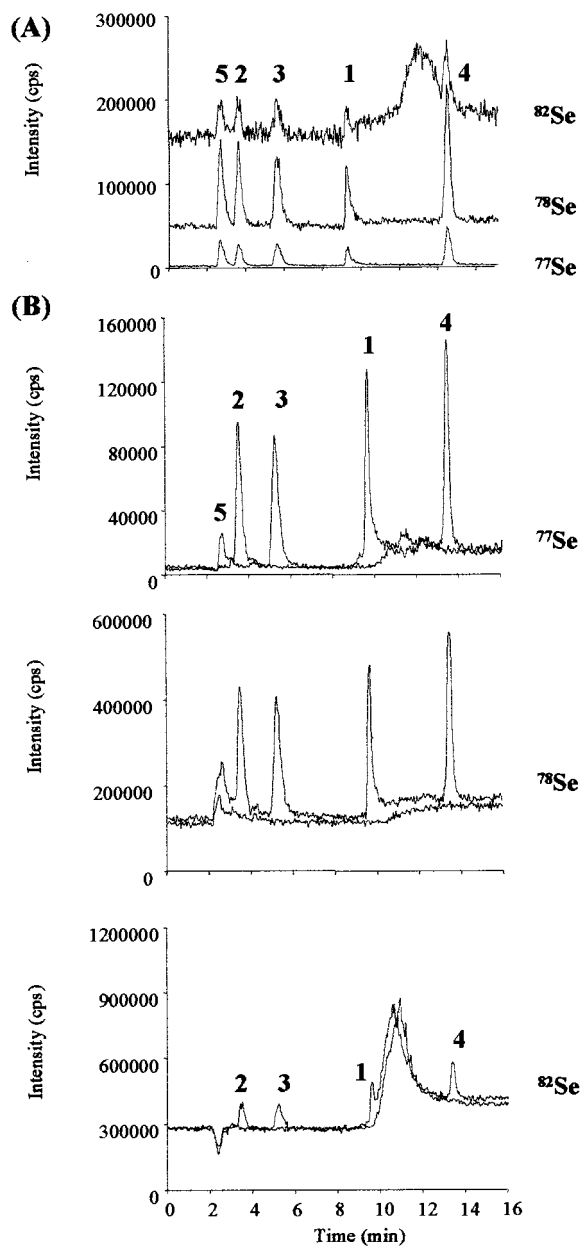


Fig. 4. Typical chromatograms obtained by vesicle-mediated chromatography conventional nebulization double-focusing ICP-MS: (A) aqueous mixture of 25  $\mu\text{g l}^{-1}$  of each selenocompound; (B) basal and spiked human urine (75  $\mu\text{g l}^{-1}$ ) of each selenocompound. (1) selenite, (2) selenomethionine, (3) selenoethionine, (4) selenate, and (5) selenocystine.

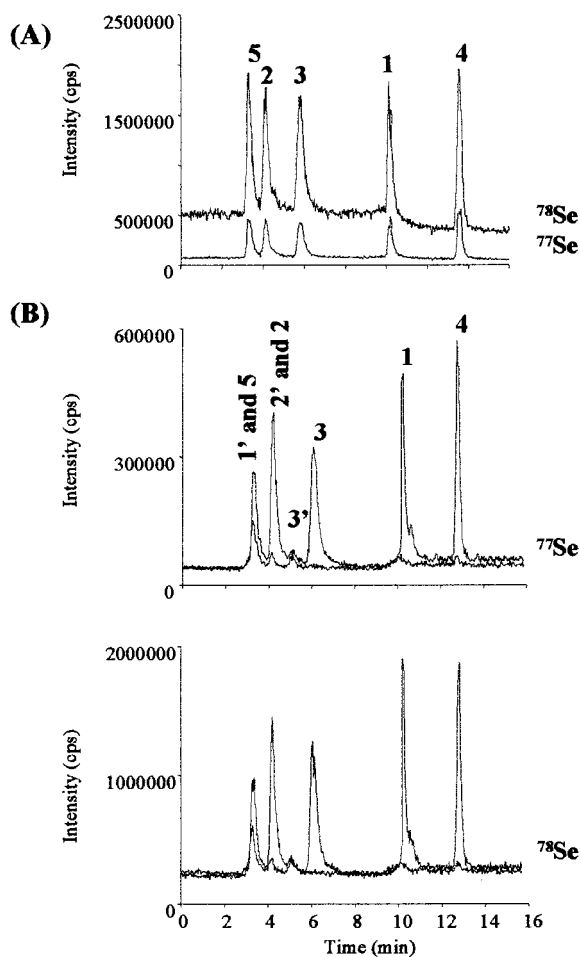


Fig. 5. Typical chromatogram obtained by vesicle-mediated chromatography microwave digestion-hydrate generation double-focusing ICP-MS: (A) aqueous mixture of 10  $\mu\text{g l}^{-1}$  of each selenocompound; (B) basal and spiked human urine (10  $\mu\text{g l}^{-1}$ ) of each selenocompound. (1), (2), (3), (4), (5) as in Fig. 4. (1'), (2') and (3') as in Fig. 3.

due to changes in the plasma conditions when the bulk of the urinary matrix reaches the plasma by conventional nebulization.

Similarly, Fig. 5A shows a typical chromatogram obtained for an aqueous mixture of 10  $\mu\text{g l}^{-1}$  of each selenocompound (monitoring <sup>77</sup>Se and <sup>78</sup>Se), and Fig. 5B shows that for basal and spiked human urine (10  $\mu\text{g l}^{-1}$ ) when a vesicle-mediated separation and on-line microwave digestion-hydrate generation system (Fig. 1) was used. As can be seen in Fig. 4B and Fig. 5B, the

selenocystine signal is now less depressed in the urine matrix than that by conventional nebulization. Once again, sensitivity for each Se species (as  $^{77}\text{Se}$ ) is between 28–67 times higher by MW–HG than by conventional nebulization, although limits of detection are only 3.5–9.5 times better by hydride generation because the background noise increased. The effect on signals of phases change was not so accused by hydride generation as by conventional nebulization.

It can be concluded that the on-line microwave digestion–hydride generation interface has two main advantages over conventional nebulization: (a) a remarkable improvement in the sensitivity, and (b) elimination of interference problems coming from the urinary matrix or from the components of the mobile phases. However, it was clear that with hydride generation, the background noise was much higher than with conventional nebulization in the Element. This explains why the limits of detection for Se were not improved as much as it should be expected from such improvement in sensitivity.

### 3.3. HPLC separation: reverse phase versus vesicle mediated

When the analytical performance of the two chromatographic systems was compared, vesicle-mediated HPLC showed two main advantages over reverse phase: first, a slight improvement in the sensitivity and limits of detection (Tables 2 and 3); and, second, more selenocompounds can be separated [9]. However, using vesicle-mediated HPLC, a change of mobile phases is necessary in order to elute inorganic species of selenium.

In order to compare speciation results obtained by reversed-phase and vesicle-mediated HPLC, a pool of human urine and a pool of rat urine fed with normal selenium content (feed A04, Panlab<sup>®</sup>) was speciated in the same day. Fig. 6 shows the  $^{77}\text{Se}$  chromatograms obtained for basal rat and human urine by both chromatographic methods. One main peak was obtained for basal rat urine (3'), while three peaks were obtained for basal human urine (1', 2' and 3'). Monomethylselenol has been found to be the predominant species in the urine of rats fed with normal levels of sele-

nium [13], so the peak found for this kind of sample could be attributed to such a compound and, consequently, peak 3' found in the human urine could also be attributed to such species. By vesicle-mediated HPLC (Fig. 6B), peak 2' could be ascribed to selenomethionine, because its retention time coincides with this species. However,

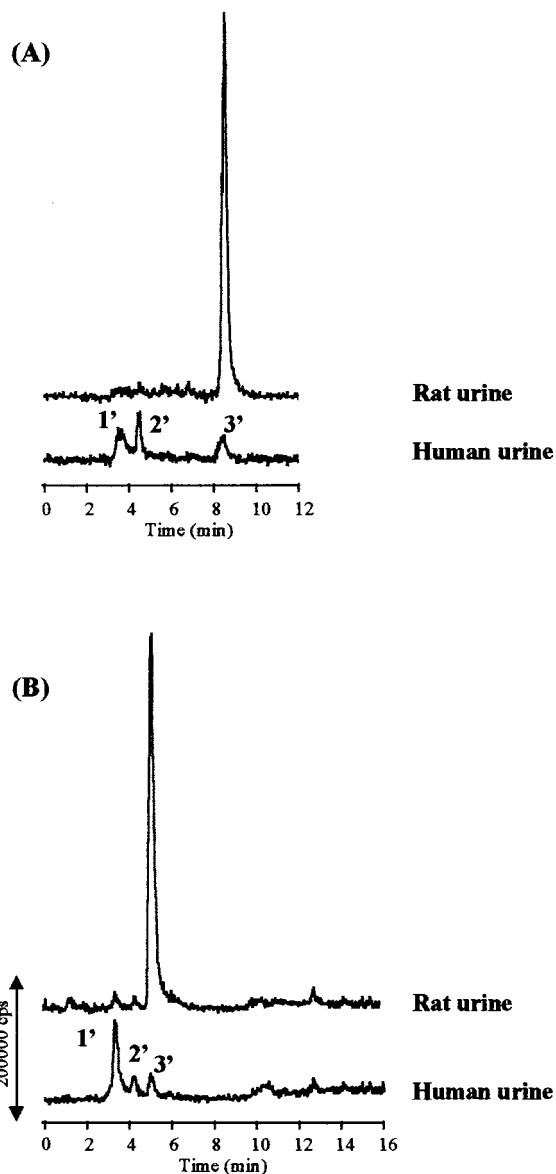


Fig. 6. Chromatograms obtained for basal rat urine and basal human urine, by both chromatographic methods: (A) reversed-phase HPLC, and (B) vesicle-mediated HPLC ( $^{77}\text{Se}$ ).

no peak was obtained at the retention time of selenomethionine by reversed-phase HPLC. Thus, it could be concluded that peak 2' is not selenomethionine. Finally, peak 1' corresponds to a species eluting at the dead volume in both chromatographic systems, so it could be selenocystine, but this is just a hint which should be pursued further for possible confirmation.

#### 4. Conclusions

The use of a double-focusing mass detector, working in the 'low resolution' mode, to detect selenium enhanced the sensitivity 23–59 times, as compared with a quadrupole mass detector. However, the limits of detection are only 1–8.7 times better than those found with the quadrupole due to a serious background noise increase (from polyatomic ions of Ar and also selenium contamination of the reagents).

On the other hand, the proposed on-line microwave digestion–hydride generation interface (Fig. 1) has important advantages over conventional nebulization: (a) sensitivities 28–110 times better depending on the chromatographic system, and (b) elimination of interference problems coming from the urinary matrix or from the components of the mobile phases. Unfortunately, the hydride generation system increases substantially the background noise, observed using conventional nebulization, so the limits of detection were only 2–9.5 times better (depending again on the chromatographic system). Thus, work to decrease background and contamination is guaranteed. On the other hand, selectivity and slight improvement in the sensitivity and limits of detection was obtained when vesicle-mediated HPLC was used instead of reverse-phase separations. However, the use of only one chromatographic system to tackle a problem like this (many species unknown in human urine) could lead to erroneous results. For example, from the chromatograms obtained by vesicle-mediated HPLC, one of the peaks found (Se species 2' in Fig. 6B) could be ascribed to selenomethionine on the basis of just retention time observed (Fig. 5B). However, by resorting to complementary chromatographic systems, re-

versed-phase HPLC in this case, the erroneous assignment becomes clear (Fig. 3B). In other words, most of the data available so far about Se species present in human urine [12–14] have been derived from HPLC retention time values experimentally observed with only one technique (that of the concerned authors). As already shown, that approach is rather limited for reliable identification of species. Thus, complementary techniques for confirmation [7] should be applied more and more to tackle this modern problem of unknown trace element speciation.

#### Acknowledgements

The authors are grateful to Hewlett Packard and Prolabo for the loan of the HP 4500 and Microdigest M301 instruments, respectively. Financial support from DGICYT Project PB94-1331 is acknowledged. Provision of samples from the 'Hospital Central de Asturias' (Oviedo, Spain) is also highly appreciated.

#### References

- [1] R. Lobinski, *Appl. Spectrosc.* 51 (1997) 260A.
- [2] J. Szpunar-Lobinska, C. Witte, R. Lobinski, F.C. Adams, *Fres. J. Anal. Chem.* 351 (1995) 351.
- [3] G.K. Zoorob, J.W. McKiernan, J.A. Caruso, *Mikrochim. Acta* 128 (1998) 145.
- [4] M. Patriarca, *Microchem. J.* 54 (1996) 262.
- [5] R.M. Barnes, *Anal. Chim. Acta* 283 (1993) 115.
- [6] R.M. Barnes, *Fres. J. Anal. Chem.* 355 (1996) 433.
- [7] A. Sanz-Medel, *Spectrochim. Acta B* 53 (1998) 197.
- [8] J.M. González LaFuente, M.L. Fernández Sánchez, A. Sanz-Medel, *J. Anal. Atom. Spectrom.* 11 (1996) 1163.
- [9] J.M. González LaFuente, M. Dlaska, M.L. Fernández Sánchez, A. Sanz-Medel, *J. Anal. Atom. Spectrom.* 13 (1998) 423.
- [10] M.S. Alaejos, C.D. Romero, *Clin. Chem.* 39 (1993) 2040.
- [11] C.D. Thomson, *Analyst* 123 (1998) 827.
- [12] R. Hasunuma, M. Tsuda, T. Ogawa, Y. Kawanishi, *Bull. Environ. Contam. Toxicol.* 51 (1993) 756.
- [13] K.T. Suzuki, M. Itoh, M. Ohmichi, *Toxicology* 103 (1995) 157.
- [14] K.L. Yang, S.J. Jiang, *Anal. Chim. Acta* 307 (1995) 109.
- [15] J.M. González LaFuente, M.L. Fernández Sánchez, J.M. Marchante-Gayón, J.E. Sánchez Uría, A. Sanz-Medel, *Spectrochim. Acta Part B* 51 (1996) 1849.

# A miniaturized urea sensor based on the integration of both ammonium based urea enzyme field effect transistor and a reference field effect transistor in a single chip

Anne Senillou <sup>a,\*</sup>, Nicole Jaffrezic-Renault <sup>a</sup>, Claude Martelet <sup>a</sup>, Serge Cosnier <sup>b</sup>

<sup>a</sup> *Laboratoire d'Ingénierie et Fonctionnalisation des Surfaces, UMR CNRS 5621, Ecole Centrale de Lyon, BP 163, F-69131 Ecully Cedex, France*

<sup>b</sup> *Laboratoire d'Electrochimie Organique et de Photochimie Rédox, UMR CNRS 5630, Université Joseph Fourier, BP 53, F-38041 Grenoble Cedex 9, France*

Received 18 December 1998; received in revised form 16 March 1999; accepted 7 April 1999

---

## Abstract

A urea biosensor prepared by covalent binding of urease directly to the surface of an ammonium-sensitive field effect transistor (FET) is described. Nonactin incorporated in carboxylated polyvinyl chloride was used to obtain the sensitive membrane of the ammonium-sensitive FET. The grafting of urease on the polyvinylchloride–COOH membrane surface was performed through carbodiimide coupling. The activity of the immobilized enzyme was spectrometrically controlled through the time-dependent disappearance of the absorbance of NADH at 340 nm. An apparent activity of 50% was found, compared with free enzyme. The sensitivity of the urea enzyme FET is 50 mV/pUrea working in a differential mode of 2 μM to 1 mM, this sensitivity being constant during 15 days. Finally, in order to test the potentialities of the urea biosensor for the environmental applications, the detection of heavy metal ions such as Cu(II) and Hg(II) in solution was performed by measuring the remaining activity of the inhibited enzyme. © 1999 Elsevier Science B.V. All rights reserved.

*Keywords:* Biosensor; Enzyme field effect transistor; Urease; Urea

---

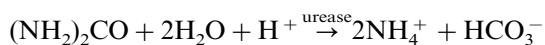
## 1. Introduction

The urea determination is of great interest in biomedical and clinical analysis applications. The determination of urea in biological serum has been realized with biosensors. Most of these biosensors are based on the immobilization of

\* Corresponding author. Tel.: + 33-4-7218-6243; fax: + 33-4-7833-1577.

*E-mail address:* njaffre@ec-lyon.fr (A. Senillou)

urease, an enzyme which catalyses the hydrolysis of urea according to the reaction:



Among these biosensors, the enzyme field effect transistor (ENFET) is based on the ion-sensitive field effect transistor (ISFET), the urease enzyme being immobilized onto the surface of the gate insulator. Effectively, the advance in semiconductor technology in the past few years has allowed the development of this type of sensor. For the determination of urea, two methods of detection have been exploited with ENFET. Detection of pH changes due to the enzymatic reaction was measured around the gate surface of a pH-FET [1–7] or detection of  $\text{NH}_4^+$  ions enzymatically formed was obtained with an ammonium ISFET [7,8].

With the pH-FET biosensor, the membrane containing urease is directly deposited onto the sensitive area of the sensor. The most commonly used matrix was based on the cross-linking of a mixture of bovine serum albumin and urease by glutaraldehyde as the bifunctional agent. Results obtained with this type of sensor were not satisfactory. In particular, the sensitivity of the biosensor for urea was low and detection limit was 50 to 100  $\mu\text{M}$ , these characteristics being decreased by an increase of the ionic strength and of the buffer capacity [4]. These drawbacks have been minimized by adding additional permselective membranes [4] or using feedback with an integrated pH actuator [9].

On the other hand, ENFET sensors for urea have been developed through the elaboration of a  $\text{NH}_4^+$ -sensitive membrane such as plasticized polyvinyl chloride [7,8] containing nonactin and their deposition on the FET. Then, urease molecules were immobilized on the  $\text{NH}_4^+$ -sensitive membrane surface by cross-linking with an inert protein. Ammonium ions produced by the enzymatic reaction were detected by the ammonium-sensitive FET. The analytical characteristics of the resulting biosensor were better than those reported for the pH-FET biosensor. However, our preliminary experiments focused on the elaboration of this type of biosensor have highlighted a major drawback of the biosensor configuration.

The low affinity between the two different membranes induces a poor adhesion between them.

For the pH-FET and the  $\text{NH}_4^+$ -ISFET, the immobilization of the enzyme molecules was carried out by a cross-linking process. Unfortunately, this method induces a loss of the protein flexibility and hence a deactivation of the immobilized enzyme. Moreover, this biologically sensitive coating exhibits a cross-linked structure which hinders markedly the diffusion of substrates and products of the enzymatic reaction. High stability, good sensitivity and short response time are mainly dependent on the method of enzyme immobilization and on the thickness of the resulting biological layer. In order to obtain these characteristics and to improve the mechanical stability of the immobilized enzyme, we have investigated the potentialities of a chemical grafting of the enzyme molecules directly on the ammonium-sensitive membrane [10]. It is expected that this approach may improve the accessibility to enzyme molecules and hence the sensitivity of the biosensor.

The analytical performances of the ammonium ISFET elaborated as previously described [11] and working in the differential mode are studied and discussed. After the functionalization of this  $\text{NH}_4^+$ -ISFET by urease molecules, the enzymatic activity and the analytical characteristics of the resulting ENFET for the detection of urea have been investigated.

In addition, the determination of heavy metal cations via an inhibition process of the biosensor activity has been examined.

## 2. Experimental

### 2.1. Materials

#### 2.1.1. ISFET sensors

n-Channel depletion-mode ISFETs were fabricated at the Research Institute of Microdevices (Kiev, Ukraine) on a p-Si wafer with a (100) crystal orientation and 7.5  $\Omega\text{ cm}$  was made by ion implantation of phosphorus, the implanted amount depended on the threshold voltage required. In the experiments, ISFETs with a chan-

nel length of 20  $\mu\text{m}$  and with a threshold voltage of about  $-3\text{ V}$  were used.

Sensor chips including two ISFETs were glued on a ceramic support made of fused alumina measuring 28 mm  $\times$  6 mm (thickness 1.0 mm). The sensor contact pads were electrically bonded by ultrasonic wiring to aluminum conducting paths which were photolithographically patterned on the ceramic support. After wiring, the contact pads and wires were encapsulated with epoxy resin. Details about the construction and operation of the ISFETs can be found in Ref. [12].

### 2.1.2. Solutions and reagents

Nonactin from streptomyces tsusimaensis, diisobutyl phtalate (DNP; approximately 80%) and tetrahydrofuran (THF; 99 + %) were purchased from Sigma. Solutions of ammonium, sodium, copper and mercury chloride were obtained by salts (from Sigma and Prolabo, ACS reagents) diluted in bidistilled water. Polyvinylchloride (PVC) was purchased from Solvay and carboxylated polyvinylchloride (PVC-COOH) from Aldrich.

Urease (EC 3.5.1.5 type VI from Jack Beans, 118 U/mg), glutamic dehydrogenase (EC 1.4.1.3 type III from bovine liver 40 U/mg), 1-ethyl-3-(3-dimethylaminopropyl)-carbodiimide (EDAC),  $\alpha$ -ketoglutaric acid, nicotinamide adenine dinucleotide reduced form (NADH), dithiothreitol, sodium azoture ( $\text{NaN}_3$ ) glycerol and EDTA were purchased from Sigma.

### 2.1.3. Ammonium-sensitive FET fabrication

#### 2.1.3.1. Composition of the membranes.

- $\text{NH}_4^+$ -ISFET. For the preparation of the membrane of the  $\text{NH}_4^+$ -ISFET, a typical procedure was applied using PVC-COOH, DNP and nonactin as ionophore in a mass ratio of 28.5:68.5:3, respectively. This mixture was diluted in THF, and  $\text{NH}_4\text{Cl}$  was added to the resulting solution in order to obtain identical concentrations of  $\text{NH}_4^+$  and nonactin.
- REFET. The REFET is an ISFET, non-sensitive to ammonium ions and without any enzymatic membrane, which allows one to work in a differential mode. The non-sensitive FET

membrane was elaborated with a PVC without nonactin. In order to avoid any coupling of the urease on the REFET surface, the polymeric matrix is polyvinylchloride. The composition of the REFET membrane was PVC and DNP in a ratio of 3:7 (w/w) diluted in THF.

2.1.3.2. *Deposition of the membrane.* Before deposition of the polymeric membranes, a surface treatment was performed: the ISFET insulator surface was treated with hexamethyldisilazane (HMDZ) in order to functionalize surface sites (hydroxyl groups). This treatment allows one to neutralize the acid–base properties of these sites and thus to obtain a blocking insulator–PVC interface. Moreover, the hydrophobic methyl groups at the grafted surface insure a good adhesion of the polymer membrane. This type of treatment can avoid the use of an intermediate hydrogel layer as was recommended by Bergveld et al. in order to eliminate the effect of  $\text{CO}_2$  diffusion on the surface charge of the insulator [13].

Next, the plasticized polymeric membranes were formed by depositing 0.5  $\mu\text{l}$  of each of the previous solutions on the surface of one ISFET (for differential measurement) and the solvent was evaporated under nitrogen flow.

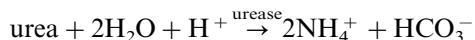
### 2.1.4. Urea-sensitive FET fabrication

2.1.4.1. *Covalent grafting of urease.* Once the ammonium-sensitive FET was realized, it was soaked in a solution containing 10 mg/ml urease and 4 mg/ml carbodiimide and left for 12 h. Then the sensor was soaked, during 1 h, in a 5 mM phosphate buffer, pH 7.4, solution vigorously stirred in order to eliminate adsorbed enzyme molecules.

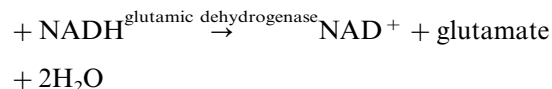
2.1.4.2. *Storage conditions of urease electrodes.* All electrodes were conditioned in a special mixture to prevent the loss of enzyme activity during storage [14]. The mixture composition used was 50 wt.% glycerol (protects urease crystalline suspension for several months), 1 mM EDTA (prevents the enzyme inhibition by heavy metals ions), 0.01%  $\text{NaN}_3$  (stops the development of harmful microorganisms) and 1 mM dithiothreitol in 5 mM phosphate buffer, pH 7.4.



**2.1.4.3. Spectrophotometric method for the measurement of the activity of the immobilized enzyme.** The urease activity was determined by following the time-dependent disappearance of the absorbance of NADH at 340 nm. This decrease results from the oxidation of NADH by glutamic dehydrogenase in the presence of enzymatically generated  $\text{NH}_4^+$  ions.



$\text{NH}_4^+ + \alpha$  – ketoglutaric acid



One unit of activity corresponds to the disappearance of 1  $\mu\text{mol}/\text{min}$  of urea and hence the oxidation of 2  $\mu\text{mol}/\text{min}$  of NADH at 20°C and pH 7.4.

The apparent activity of urease covalently bound to the ammonium-sensitive membrane was determined as follows. Assays were carried out at 20°C in a cuvette containing a total volume of 3 ml of 0.01 M phosphate buffer, pH 7.4, 1 mM urea, 1 mM  $\alpha$ -ketoglutaric acid, 1.5 mM NADH and 0.1 mg/ml glutamic dehydrogenase. The EN-FET was immersed in the mixture and the decrease of the absorbance at 340 nm versus time was recorded.

## 2.2. Measurements

The output voltage of the modified ISFETs immersed in double-distilled water were measured with the source and drain follower type ISFET amplifier. This system allowed the source voltage ( $V_s$ ) to be measured, while the drain current ( $I_d$ ) and the drain voltage ( $V_d$ ) remained constant ( $V_d = 1$  V,  $I_d = 100$   $\mu\text{A}$ ).  $V_s$  was directly plotted on a recorder.

- *Individual.* The voltage was measured against a platinum electrode.
- *Differential.* Two ISFETs were connected to two identical amplifiers: output signals  $V_s$  and  $V'_s$  were measured against the common silicon substrate. A differential amplifier enabled the difference of these two signals to be obtained as well.

The composition of the solutions of test was 0.1 M  $\text{NH}_4\text{Cl}$  in bidistilled water. All the measurements were carried out at room temperature.

## 3. Results and discussion

### 3.1. Analytical characteristics of the ammonium ISFET

#### 3.1.1. Sensitivity, repeatability and detection limit

Fig. 1 shows the response of the REFET (with a PVC membrane) and the  $\text{NH}_4^+$ -ISFET (with a PVC-COOH membrane) for the two modes of measurement to  $\text{NH}_4^+$  concentration in the range  $10^{-7}$  to  $10^{-3}$  M.

The REFET sensor, with a PVC membrane, is insensitive to  $\text{NH}_4^+$  until 0.1 mM, while a response (20 mV/p $\text{NH}_4^+$ ) is observed for higher concentrations. This behavior shows that the potential difference at the water-plasticized PVC interface is influenced by the concentration of the ammonium ion, the partition coefficient of this ion in plasticized PVC not being nil [15]. This phenomenon is due to the cationic permselectivity through anionic defects of the PVC. The responses to ammonium ions are quite similar to those obtained with REFET and  $\text{NH}_4^+$ -ISFET covered with a PVC membrane. This shows that PVC and PVC-COOH behave similarly towards the ionic sensitivity. Consequently, both poly-

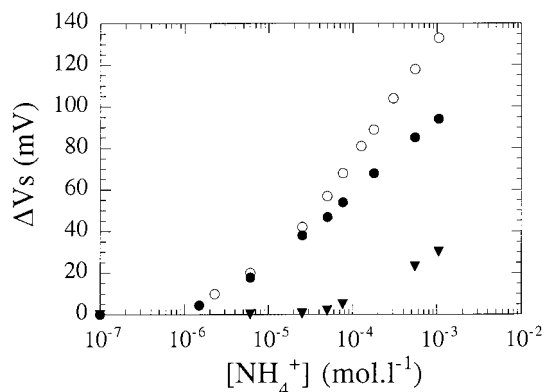


Fig. 1. Sensitivity of the ammonium ISFET in the two modes of measurements and that of the REFET in double-distilled water: ○, normal mode; ●, differential mode; ▼, REFET.

meric membranes can be chosen indifferently. PVC was thus kept for REFET in order to avoid any chemical grafting of the enzyme on its surface. It should be noted that the REFET sensitivity to  $\text{NH}_4^+$  should be markedly reduced if the  $\text{NH}_4^+$  source is spatially restricted to the urease membrane deposited on the ISFET.

In the normal mode, the calibration curve is linear in the range of concentration  $10^{-5}$  to  $10^{-3}$  M, the  $\text{NH}_4^+$ -FET response being quasi-Nernstian with a slope of about 56 mV/p $\text{NH}_4^+$ . A less sensitive response (23 mV/p $\text{NH}_4^+$ ) is recorded for lower concentrations.

As expected, in the differential mode, the value of the  $\text{NH}_4^+$ -FET response (36 mV/p $\text{NH}_4^+$ ) is diminished because the signal of REFET is substrated from the signal of the sensitive FET. This sensitivity decrease is counterbalanced by a slight increase in the linear range of the calibration curve ( $6 \times 10^{-6}$  to  $1 \times 10^{-3}$  M) the detection limit being 2  $\mu\text{M}$ . The response time (determined as the time required to reach a steady-state potential value after a  $\text{NH}_4^+$  injection) was within 30 s. Consequently, the differential mode was used for the subsequent investigations. Effectively, this type of measurement allows one to increase the selectivity of the sensor for  $\text{NH}_4^+$  ions and to suppress the utilization of the reference electrode as previously reported in Ref. [11]. In order to investigate the repeatability of the  $\text{NH}_4^+$ -FET response, 10 successive calibration curves in the  $\text{NH}_4^+$  range  $10^{-5}$  to  $10^{-3}$  M were recorded in the differential mode with the same sensor. A relative standard deviation of 15% was calculated for the sensitivity values determined from the slope of the successive calibration curves.

### 3.1.2. Influence of the ionic strength

The influence of the ionic strength has been studied to simulate a utilization in a natural serum (hemodialysis solution). One  $\text{NH}_4^+$ -FET was tested in different solutions of NaCl in range of concentration  $10^{-3}$  to  $10^{-1}$  M and in 0.01 M phosphate buffered saline, pH 7.4 (137 mM NaCl, 2.7 mM KCl). The sensitivity values of the  $\text{NH}_4^+$ -FET sensor, determined as the slope of the resulting calibration curves for  $\text{NH}_4^+$ , are summarized in Table 1. It appears that the sensor sensitivity

Table 1

Influence of the ionic strength on the  $\text{NH}_4^+$ -FET sensitivity for  $\text{NH}_4^+$

	NaCl (mM)			PBS
	1	10	100	
Sensitivity (mV/p $\text{NH}_4^+$ )				
$[\text{NH}_4^+] < 10^{-4}$ M	30	30	17	7
$[\text{NH}_4^+] > 10^{-4}$ M	30	30	30	15

for  $\text{NH}_4^+$  decreases only for high concentrations of NaCl (above 10 mM). It should be noted that the loss of sensitivity due to the ionic strength is more important for concentrations of  $\text{NH}_4^+$  lower than  $10^{-4}$  M. In addition, the sensitivity decreases markedly in phosphate buffered saline (PBS) solutions. This effect may be attributed to the high concentration of cations (0.15 M) and to the presence of  $\text{K}^+$ , which can hinder the recognition of  $\text{NH}_4^+$  by nonactin. Nevertheless, a linear response of the sensor for  $\text{NH}_4^+$  is observed above  $10^{-4}$  M in pseudo-physiological conditions, the sensitivity (15.4 mV/p $\text{NH}_4^+$ ) being 50% of the value recorded in 1 mM NaCl.

### 3.2. Determination of the enzymatic activity of ENFET

An  $\text{NH}_4^+$ -FET made of carboxylated PVC membranes was immersed in a urease and coupling agent solution for 15 h, and washed vigorously during 2 h. In order to detect the presence of grafted urease, the enzymatic activity of the ENFET has been examined. For this purpose, the increase in concentration of the enzymatically generated  $\text{NH}_4^+$  was followed by a coupled enzymatic reaction involving a decrease in NADH concentration (see Section 2). The evolution of the NADH absorbance at 340 nm ( $\epsilon_{340} = 6.22 \text{ mM}^{-1}/\text{cm}$ ) with the immersion time of the ENFET in the NADH solution has been recorded (Fig. 2). It appears that the absorbance decreases linearly with time. The slope ( $0.01 \text{ DO min}^{-1}$ ,  $r = 0.997$ ) corresponds to 27 mU/cm. In addition, the specific activity of the free enzyme under the same conditions has been determined. Taking into account that the theoretical maximum coverage of a

urease monolayer on the PVC–COOH membrane can be estimated as  $10^{-12}$  mol/cm<sup>2</sup>, the urease monolayer exhibits an enzymatic activity of 53 mU/cm<sup>2</sup>. Consequently, the apparent specific activity of the grafted urease is 50% of the expected value for the free enzyme. Nevertheless, it should be noted that this value is markedly higher than those (1, 3 and 9%) previously reported for enzyme entrapped in organic polymers [16,17] or inorganic gels [18]. Furthermore, the estimation of the apparent specific activity of urease is based on the most unfavorable hypothesis, namely the obtention of a complete urease monolayer by chemical grafting.

The same chemical grafting of urease was attempted with the REFET covered by a plasticized PVC membrane. After the immersion of the REFET for 2 h in the NADH solution, no decrease of the NADH absorbance was recorded. This clearly indicates the absence of grafted urease on the plasticized PVC membrane. Consequently, the immobilized urease molecules are only located on the carboxylated PVC membrane.

### 3.3. Analytical characteristics of the urea sensor

Since the pH change in the range 6–8 induces no response of the ammonium sensor [11], the influence of the pH on the urea sensor must be solely due to its conventional effect on the enzyme activity. Consequently, the measurements were

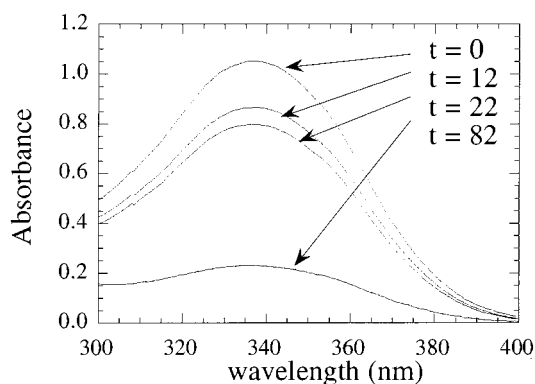


Fig. 2. Absorbance of NADH, in the range of wavelength 300–400 nm, after different times of soak of a PVC–COOH sensor.

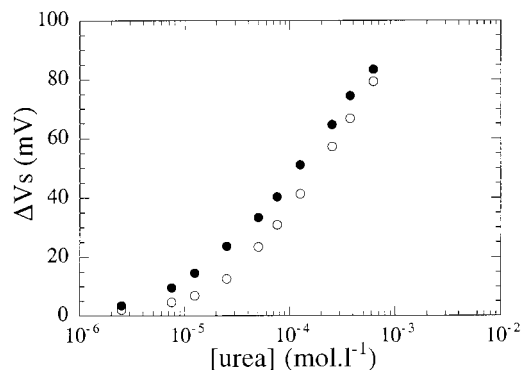


Fig. 3. Sensitivity of the urea ISFET in the two modes of measurements in double-distilled water, at pH 7.4: ●, differential mode; ○, normal mode.

carried out at pH 7.4, the optimum pH value recorded for the free urease.

Ammonium ions enzymatically produced at the interface-sensitive membrane/solution do not affect the response of the REFET. So, as expected, the biosensor sensitivity for urea is identical (50 mV/pUrea) with the two modes of measurement, the detection limit being 2 μM (Fig. 3). This detection limit is markedly lower than those (50–100 μM) previously reported for pH-FET biosensors [1,2] and similar to the value (1 μM) recently obtained with potentiometric biosensors [19]. It appears clear that the better detection limit is obtained when the detected species is NH<sub>4</sub><sup>+</sup>. This may be attributed to the procedure used for urease immobilization. The chemical grafting of enzyme on the carboxylic groups of the PVC coating does not deteriorate the ammonium sensitivity of this membrane, whereas the cross-linking method decreases the H<sub>3</sub>O<sup>+</sup> sensitivity [20].

It should be noted that the influence of the ionic strength on the response of the urea sensor is the same that previously obtained with the ammonium sensor. A loss of sensitivity of 55% is observed between a calibration curve recorded in a 1 mM NaCl solution and one in PBS solution.

The ENFET sensors were also examined for the storage and operational stabilities. The ENFET was stored in a special storage solution at 4°C (see Section 2) and its calibration curve for urea was recorded periodically. The biosensor sensitivity ( $48 \pm 5$  mV/pUrea) was approximately constant

during 15 days. However, a detachment of the enzymatic membrane is observed after 15 days, inducing a complete loss of the ENFET sensitivity for urea.

The operational stability of the sensor was checked at room temperature through the stability of biosensor response to 100 mM urea. No appreciable change in the steady-state voltage response of the biosensor was observed after 3 h, illustrating the good stability of the ENFET.

The ENFET construction was also quite reproducible: eight ENFETs were prepared by following identical chemical steps and their responses towards urea were investigated. The comparison of the sensitivity determined from the resulting calibration curves indicates that the relative standard deviation is only 10%.

#### 3.4. Detection of heavy metal ions by inhibition of the enzymatic sensor

Heavy metals (such as Cu, Pb, Hg or Zn) can inhibit enzymes, usually by reacting with cysteine side chains. As a consequence, the enzymatic activity of the biosensor is decreased or totally suppressed. Since it has been reported that Cu(II) and Hg(II) inhibited urease molecules [21], the urea ENFET was applied to the determination of copper and mercuric ions in solution. For this purpose, a urea biosensor was placed in a 1 mM urea solution and left until stabilization of the output signal. Then, the effect of increasing concentrations of Cu(II) or Hg(II) on the biosensor response was investigated. It appears that the addition of metal ions induces a rapid inhibition ( $t_{90\%} = 5$  min) of the immobilized urease. A decrease of source voltage depending on the metal ions concentration was recorded. Fig. 4A,B shows the inhibition percentage of the biosensor response as a function of Cu(II) and Hg(II) concentration, respectively. The calibration curves indicate detection limits of 0.2 and 0.1  $\mu\text{M}$  for Cu(II) and Hg(II), respectively. It should be noted that these values of detection limit are markedly lower than those previously reported by Volotovsky et al., namely 4  $\mu\text{M}$  for Hg(II) and 3  $\mu\text{M}$  for Cu(II) [22]. In addition, these authors

use a multistep procedure involving the measurement of the biosensor sensitivity in a separate solution before and after the immersion of the urea sensor for 5–15 min in the inhibitor solution [22,23].

The possibility to regenerate the enzymatic activity of the biosensor has been investigated after a 80% inhibition. The remaining activity was measured after soaking the biosensors in a 100 mM EDTA solution for 15 min. It appears that 75 and 60% of the initial sensitivity is restored for Cu and Hg inhibition, respectively, illustrating the efficiency of the reactivation process.

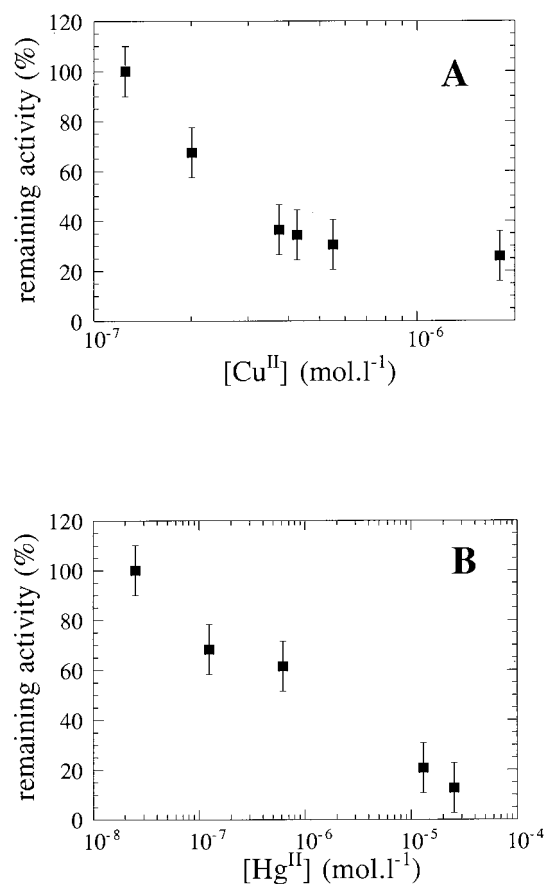


Fig. 4. Dependence of remaining activity of the sensor on the concentration of the inhibitor metal ions: (A) Cu (II) ions, (B) Hg (II) ions. The data points are the average of three measurements carried out with three different sensors.

#### 4. Conclusion

In this report, we have described the successful functionalization of an ammonium FET by urease molecules and its application to the selective determination of urea. It is expected that the attractive potentialities offered by the functioning principle of the ENFET based on a differential mode will be exploited for the *in vitro* and *in vivo* measurements of biologically important metabolites.

#### Acknowledgements

This work was in part supported by the GDR 517 'Reconnaissance et détection des espèces chimiques' of CNRS (France). The authors thank Dr A. Deronzier for laboratory facilities.

#### References

- [1] C. Colapicchioni, A. Barbaro, F. Porcelli, *Sensors Actuators B* 6 (1992) 202–207.
- [2] A.P. Soldatkin, A.V. El'skaya, A.A. Shulga, L.I. Netchiporouk, A.M. Nyamsi-Hendji, N. Jaffrezic-Renault, C. Martelet, *Anal. Chim. Acta* 283 (1993) 695–701.
- [3] O.A. Boubriak, A.P. Soldatkin, N.F. Starodub, A.K. Sandrovsky, A.K. El'skaya, *Sensors Actuators B* 26-27 (1995) 429–431.
- [4] D.V. Gorchkov, A.P. Soldatkin, S. Poyard, N. Jaffrezic-Renault, C. Martelet, *Mater. Sci. Eng. C5* (1997) 23–28.
- [5] D.V. Gorchkov, S. Poyard, A.P. Soldatkin, N. Jaffrezic-Renault, C. Martelet, *Mater. Sci. Eng. C5* (1997) 29–34.
- [6] D.G. Pijanowska, W. Torbicz, *Sensors Actuators B* 44 (1997) 370–376.
- [7] S. Alegret, J. Bartroli, C. Jiménez, E. Martínez-Fàbregas, D. Martorell, F. Valdès-Perezgasga, *Sensors Actuators B* 15–16 (1993) 453–457.
- [8] Y. Miyahara, K. Tsukada, H. Miyagi, *Sensors Actuators B* 3 (1991) 287–293.
- [9] B.H. Van der Schoot, P. Bergveld, *Biosensors Bioelectron.* 3 (1987) 161.
- [10] R. Koncki, E. Leszczynska, A. Cybulska, S. Glab, *Anal. Chim. Acta* 321 (1996) 27–34.
- [11] A. Senillou, N. Jaffrezic-Renault, C. Martelet, F. Griffe, *Mater. Sci. Eng. C6* (1998) 59–63.
- [12] A.A. Shulga, L.I. Netchiporouk, A.K. Sandrovsky, A.A. Abalov, O.S. Frolov, Y.a.G. Kononenko, H. Maupas, C. Martelet, *Sensors Actuators B* 30 (1996) 101.
- [13] P. Bergveld, A. Van Den Berg, P.D. Van Der Wal, M. Skowronska-Ptasinska, E.J.R. Sudhölter, D.N. Reinhoudt, *Sensors Actuators* 18 (1989) 309.
- [14] S. Poyard, D.V. Gorchkov, A. Jdanova, N. Jaffrezic-Renault, C. Martelet, A.P. Soldatkin, A.V. El'skaya, *C. R. Acad. Sci. Paris* 319 (1996) 257–262.
- [15] A. Van den Berg, P.D. Van der Wal, M. Skowronska-Ptasinska, E.J.R. Sudhölter, D.N. Reinhoudt, P. Bergveld, *Anal. Chem.* 59 (1987) 2827.
- [16] S. Cosnier, C. Innocent, *Bioelectrochem. Bioenerg.* 31 (1993) 147–160.
- [17] L. Coche-Guerente, S. Cosnier, C. Innocent, P. Mailley, *Anal. Chim. Acta* 311 (1995) 23–30.
- [18] S. Poyard, N. Jaffrezic-Renault, C. Martelet, S. Cosnier, P. Labbé, *Anal. Chim. Acta* 364 (1998) 165.
- [19] J.H. Shin, S.Y. Yoon, I.J. Yoon, S.H. Choi, S.D. Lee, H. Nam, G.S. Cha, *Sensors Actuators B* 50 (1998) 19–26.
- [20] S. Poyard, Ph.D. Thesis, University Claude Bernard, Lyon, France, 1996.
- [21] J.L. Webb, *Enzyme and Metabolic Inhibitor*, vol. II, Academic Press, New York, 1966, pp. 635–653.
- [22] V. Volotovskiy, Y.J. Nam, N. Kim, *Sensors Actuators B* 42 (1997) 233–237.
- [23] G.A. Zhylyak, S.V. Dzyadevich, Y.I. Korpan, A.P. Soldatkin, A.V. El'skaya, *Sensors Actuators B* 24–25 (1995) 145–148.

## Determination of dihaloacetonitriles and halophenols in chlorinated sea water

Anne-Sophie Allonier <sup>a</sup>, Michel Khalanski <sup>a</sup>, Valérie Camel <sup>b,\*</sup>,  
Alain Bermond <sup>b</sup>

<sup>a</sup> EDF, Direction des Etudes et Recherches, Département Environnement, 6 Quai Watier, 78401 Chatou Cedex, France

<sup>b</sup> Institut National Agronomique Paris-Grignon, GER Chimie Analytique, 16 Rue Claude Bernard, 75231 Paris Cedex 05, France

Received 15 February 1999; received in revised form 7 April 1999; accepted 7 April 1999

### Abstract

The cooling effluents in power stations are chlorinated to avoid excessive biofouling. However, this disinfecting treatment leads to the formation of halogenated by-products, mainly trihalomethanes, haloacetonitriles and halophenols. There is therefore a need for precise and accurate methods that allow trace level determinations of these compounds. Experimental procedures combining liquid–liquid extraction and gas chromatography coupled to mass spectrometry were developed in this study to determine dihaloacetonitriles and halophenols. The extraction step was improved and the performance of both methods evaluated. Precise and accurate determinations were obtained, allowing the measurement of the investigated compounds in chlorinated sea water samples from three French nuclear power stations. © 1999 Elsevier Science B.V. All rights reserved.

**Keywords:** Chlorination; Dihaloacetonitriles; Halophenols; Sea water

### 1. Introduction

As coastal nuclear power stations use sea water in their cooling systems, a wide range of fouling organisms are entrained in the system, thereby leading to possible organism growth on the solid surfaces (also called biofouling). Two types of biofouling can be distinguished: macrofouling (due to organisms such as mussels, barnacles and

hydroids) which leads to blockages of pipework and culverts, and microfouling (involving bacteria and fungi) which reduces heat transfer efficiency, thus decreasing power output. In practice, both biofoulings are related, as the successful settlement of large organisms often requires the formation of a biofilm. To reduce biofouling, chlorination of sea water is usually performed, with typical applied doses of 0.5–1.5 mg l<sup>-1</sup> (expressed as Cl<sub>2</sub>) and a resultant residual oxidant level of 0.1–0.2 mg l<sup>-1</sup> in the cooling water (the reduction being due to the sea water oxidant demand). However, chlorine is very reactive towards natural organic matter, leading to the for-

\* Corresponding author. Tel.: + 33-1-44-081725; fax: + 33-1-44-081653.

E-mail address: camel@inapg.inra.fr (V. Camel)

mation of several by-products [1]. While trihalomethanes are the major compounds formed, other by-products are of concern due to their possible toxicity towards aquatic organisms: dihaloacetonitriles (DHANs) and halophenols (HPhs).

Evidence has been given that DHANs are formed upon chlorination of water [2–7]. In addition, the presence of bromide ion in water samples favours the formation of brominated compounds [2,3]. Amino acids, as well as humic and fulvic acids, are known to be good precursors of DHANs [2,3,5]. Also, 2,4,6-trichlorophenol is formed upon chlorination of humic substances in fresh waters [8].

The presence of dihaloacetonitriles and halophenols in chlorinated sea water is of great concern, due to possible toxicity of such compounds towards aquatic organisms. Due to the presence of high contents of bromide in sea water, this study focused on the determination of brominated compounds. It was conducted to develop a reliable method for the determination of these pollutants in sea water samples that had been chlorinated in power stations. The methods employed were liquid–liquid extraction (LLE) followed by gas chromatography coupled to mass spectrometry (GC–MS).

## 2. Experimental

### 2.1. Standards

All solvents used were of analytical grade (Merck, HPLC grade). In addition, blank chromatograms were obtained by injecting all solvents in GC–MS.

The EPA 551 mix, containing dichloroacetonitrile, bromochloroacetonitrile and dibromoacetonitrile (each at  $100 \mu\text{g ml}^{-1}$  in acetone), was obtained from Merck (Darmstadt, Germany). A standard solution containing 3-bromophenol, 2,4-dibromophenol, 2,6-dibromophenol and 2,4,6-tribromophenol (at  $500 \mu\text{g ml}^{-1}$  in methanol) was obtained from Merck. These standard solutions were further diluted with methanol to obtain stock solutions at the desired concentrations.

For dihaloacetonitriles, 2-bromo-1-chloropropane was used as an internal standard. A standard solution ( $2 \text{ g l}^{-1}$  in methanol) of this compound was supplied by Supelco (Saint-Quentin Fallavier, France). For bromophenols, 2,3,5-trichlorophenol was used, and supplied by Supelco (solution at  $2 \text{ g l}^{-1}$  in methanol).

Sodium sulphate, sodium carbonate and acetic anhydride (analytical grade) were obtained from Merck.

### 2.2. Sea water samples

The cooling sea water effluent samples were collected during spring and summer periods at the nuclear power station sites of Gravelines, Paluel and Penly. These stations are located on the English Channel and the North Sea coast of France. The samples were collected in the outlet of the power stations.

Sampling recipients (50 or 100 ml) were equipped with a Teflon septum. According to the USEPA recommendations, the recipients were heated for 1 h at  $105^\circ\text{C}$  and kept in a pure atmosphere before sampling [9]. Care was taken to ensure a similar volume ratio between the liquid and the gaseous phases inside the recipients for all the samples. Besides, the samples were kept at  $4^\circ\text{C}$  before their analysis (which was performed within 14 days) to avoid losses of the compounds, particularly DHANs [2].

### 2.3. Extraction procedures

All compounds were extracted from sea water samples using liquid–liquid extraction, as this method affords acceptable efficiencies for DHANs and HPhs in water [2,3,5,8–12]. Extraction solvent volumes and extraction times were chosen based upon preliminary experiments conducted in our laboratory. In case of halophenols, acetylation was performed simultaneously with the extraction [8].

For the extraction of dihaloacetonitriles, 50 ml of sea water (with pH adjusted to 3 by adding 0.5 ml of nitric acid at 65%) were put into a 60-ml flask. Ethyl acetate (4 ml) spiked with the internal standard (2-bromo-1-chloropropane at the 2 mg

$l^{-1}$  level) was added. The flask was sealed, and mixed (using a magnetic mixer) for 2 min at 800 rnds  $min^{-1}$ . Then, the two phases were allowed to separate for 2 min. In the case of incomplete separation, the sample was submitted to ultrasounds. Finally, 0.5 ml of the ethyl acetate phase was sampled and placed into a sealed vial. An aliquot (1  $\mu l$ ) of this extract was further injected in gas chromatography.

For extracting halophenols, 500 ml of sea water were placed into a flask (1 l). After addition of the internal standard (20  $\mu l$  of a standard solution of 2,3,5-trichlorophenol at 10  $\mu g l^{-1}$  in methanol), sodium carbonate (10 g) was added to the sample. Then, acetic anhydride was added (5 ml) in order to derivatise the phenolic compounds. The flask was sealed and the sample mixed during 15 min at 800 rnds  $min^{-1}$ . Then, the sample was extracted with  $3 \times 30$  ml of dichloromethane. The organic phases were mixed and dried over anhydrous sodium sulphate. The extract was further concentrated to 1 ml using a rotary evaporator. The final extract was placed in a sealed flask, and 1  $\mu l$  was injected into the gas chromatograph.

#### 2.4. Chromatographic conditions

Separations were carried out on a Hewlett-Packard 6890 gas chromatograph coupled to a mass spectrometer (Hewlett-Packard 5973). The column used was a narrow-bore HP-5MS (30 m  $\times$  0.25 mm i.d., film thickness 0.25  $\mu m$ ). Helium (high purity) was used as the carrier gas (flow-rate at the end of the column: 2.5 ml  $min^{-1}$ ). Injections (1  $\mu l$ ) were made in the pulsed splitless mode (1.2 bar for 1 min). The initial analytical conditions were chosen according to the USEPA Method 551 [9]: detector at 280°C, injector at 200°C, MS source at 230°C, MS manifold at 150°C. The  $m/z$  range was 50–350. For dihaloacetonitrile separation, the column temperature programme was as follows: 35°C (5 min) to 110°C at 5°C  $min^{-1}$ , then to 240°C at 20°C  $min^{-1}$ , the final temperature being held for 15 min. For halophenol determination, the column temperature was held 5 min at 35°C, before being increased to 220°C at 8°C  $min^{-1}$ , and further to 240°C at 30°C  $min^{-1}$ , the final temperature being held for 2 min.

The following target and qualifier  $m/z$  values were recorded respectively: 82, 74 for dichloroacetonitrile; 118, 199 for dibromoacetonitrile; 155, 74 for bromochloroacetonitrile; 77, 107 for 2-bromo-1-chloropropane; 172, 93 for 3-bromophenol; 252, 250 for 2,4-dibromophenol and 2,6-dibromophenol; 332, 141 for 2,4,6-tribromophenol; 196, 132 for 2,3,5-trichlorophenol. Examples of separations are given in Fig. 1.

### 3. Results and discussion

#### 3.1. Choice of the extraction solvent

For the extraction of dihaloacetonitriles, three solvents were tested: hexane, methyl-*tert*-butyl ether (MTBE) and ethyl acetate. The extraction recoveries for standard solutions (at 4  $\mu g l^{-1}$  in sea water) are presented in Fig. 2. As the best extraction efficiencies seemed to be obtained with ethyl acetate, this solvent was chosen for extracting dihaloacetonitriles. The results obtained for halophenols (at 2  $\mu g l^{-1}$  in sea water) are also shown in Fig. 2, using the following solvents: hexane, ethyl acetate and dichloromethane. Dichloromethane was selected for further experiments due to its better efficiency in the extraction of these compounds.

#### 3.2. Figures of merit

For dihaloacetonitriles, calibration was performed by means of seven standard solutions (1, 2, 4, 8, 10, 16 and 20  $\mu g l^{-1}$ ) prepared by diluting standard solutions in sea water (in the inlet of Gravelines station). 2-Bromo-1-chloropropane (solution at 2  $mg l^{-1}$  in ethyl acetate) was added as an internal standard. In case of halophenols, calibration was performed by means of five standard solutions (0.2, 1, 2, 4 and 10  $\mu g l^{-1}$ ) prepared by diluting standard solutions in sea water. 2,3,5-Trichlorophenol (solution at 10  $\mu g l^{-1}$  in methanol) was added as an internal standard. For each concentration, three extractions were performed. Analyses were conducted in a random order.



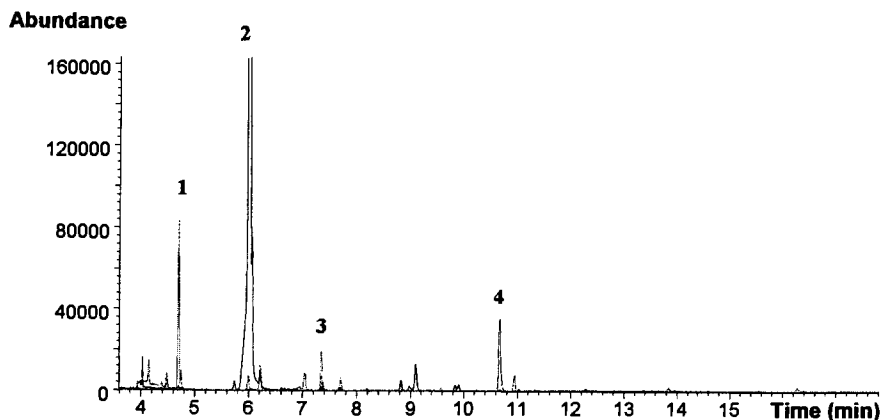
Calibration curve equations were obtained using a linear regression; the following equations were found:

$$\text{Dichloroacetonitrile: } A = 1.002 \times C \quad r = 0.987$$

$$\text{Dibromoacetonitrile: } A = 0.999 \times C \quad r = 0.997$$

$$\text{Bromochloroacetonitrile: } A = 1.003 \times C \quad r = 0.988$$

(a)



(b)

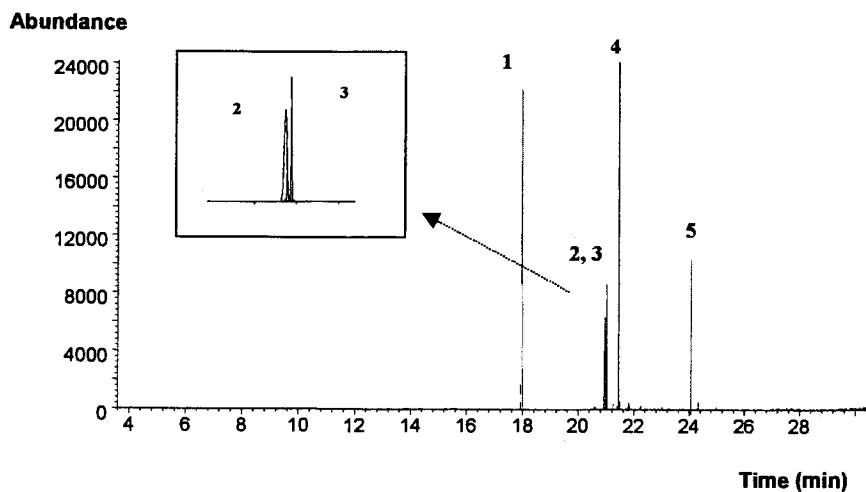


Fig. 1. Chromatogram of a solution containing either dihaloacetonitriles or halophenols at  $2 \mu\text{g l}^{-1}$  in sea water (detection in the SIM mode). (a) Analysis of a dihaloacetonitrile solution (after solvent extraction): (1) dichloroacetonitrile ( $m/z$  82); (2) 2-bromo-1-chloropropane (internal standard) ( $m/z$  77); (3) bromochloroacetonitrile ( $m/z$  155); (4) dibromoacetonitrile ( $m/z$  118). (b) Analysis of a halophenol solution (after solvent extraction and simultaneous derivatisation): (1) 3-bromophenol ( $m/z$  172); (2) 2,4-dibromophenol ( $m/z$  252); (3) 2,3,5-trichlorophenol (internal standard) ( $m/z$  196); (4) 2,6-dibromophenol ( $m/z$  252); (5) 2,4,6-tribromophenol ( $m/z$  332).

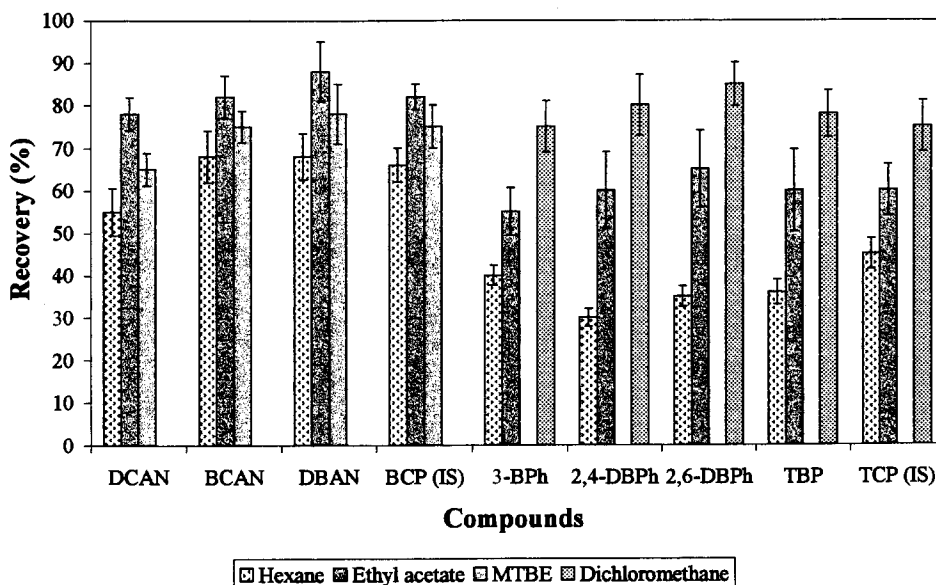


Fig. 2. Influence of the extraction solvent on the recoveries of halogenated compounds from standard solutions in sea water. Methyl-*tert*-butyl ether (MTBE) and dichloromethane were tested only for haloacetonitriles and halophenols, respectively. The S.D.s are indicated as lines above the bar graphs (experiments were done in triplicate). DCAN, dichloroacetonitrile; BCAN, bromochloroacetonitrile; DBAN, dibromoacetonitrile; BCP, 2-bromo-1-chloropropane (internal standard); 3-BPh, 3-bromophenol; 2,4-DBPh, 2,4-dibromophenol; 2,6-DBPh, 2,6-dibromophenol; TBP, 2,4,6-tribromophenol; TCP, 2,3,5-trichlorophenol (internal standard).

3-Bromophenol:  $A = 1.004 \times C$   $r = 0.988$

2,4-Dibromophenol:  $A = 0.996 \times C$   $r = 0.978$

2,6-Dibromophenol:  $A = 0.995 \times C$   $r = 0.976$

2,4,6-Tribromophenol:  $A = 1.001 \times C$   $r = 0.999$

A statistical evaluation of the calibration curves was performed according to the French norm NF X20-300 [13]. The homogeneity of variances was established using a Cochran test, the linearity confirmed by a Student test, and the linear regression was validated by means of a Fischer test.

The relative standard deviation (R.S.D.) on the peak area and the estimated concentration ( $C_{est.}$ ), along with its confidence interval (CI) for a 5% risk, were determined for each concentration ( $C_{real}$ ) and compound. Results are presented in Tables 1 and 2. Acceptable precision was achieved for the calibration (R.S.D. lower than 10%), except for low concentrations of dichloroacetonitrile and bromochloroacetonitrile. In addition, in most cases, the true concentration falls within the estimated concentration confidence interval.

The calibration precision and accuracy were tested for low concentrations. They were estimated upon ten extractions and analysis of sea water samples containing each component at the  $4 \mu\text{g l}^{-1}$  level. Results are presented in Table 3. Acceptable precision was obtained (R.S.D.s between 4 and 8%). Mean recoveries were between 96 and 104%, and a good correlation was observed between the measured concentration and the real concentration (slopes ranged from 0.999 to 1.042, with correlation coefficients from 0.996 to 0.999). All the above results show that our experimental procedure allows a satisfactory determination of haloacetonitriles and bromophenols at low level concentrations in sea water.

Finally, the limits of detection (LOD) and quantification (LOQ) were determined according to the NF X20-300 norm [13]. This was performed by injecting the lowest concentrated standard solution three times. Results are presented in Table 4. For dihaloacetonitriles, detection limits

were slightly lower than previous reported results (i.e. 0.1–0.5  $\mu\text{g l}^{-1}$  [2]). However, they remained higher than the LODs reported in the USEPA Method 551 (i.e. 0.011–0.092  $\mu\text{g l}^{-1}$  [9]); we believe this might be attributed to the higher sensitivity of the electron capture detector (used in the USEPA Method 551) compared to the mass spectrometer for such compounds. In case of bromophenols, detection limits were very low (0.02–0.05  $\mu\text{g l}^{-1}$ ), enabling the determination of these compounds in sea water samples at trace levels.

Accuracy was determined for the LOQ by injecting ten times a dihaloacetonitrile solution at a concentration near the LOQ (i.e. 0.5  $\mu\text{g l}^{-1}$ ). Acceptable R.S.D.s were obtained (near 10%).

### 3.3. Application to the determination of dihaloacetonitriles and halophenols in chlorinated sea water samples

The type and relative amounts of the by-products formed upon chlorination varies with the organic content and the nature of the inorganic species present in the water. Hence, when bromide is present at high concentrations, such as in sea water, brominated compounds are mainly formed

[1]. This is due to the bromide oxidation by chlorine, leading to the formation of bromine, so that bromination reactions can take place. So our experimental procedures were applied to the determination of dihaloacetonitriles and halophenols in cooling effluents that had been chlorinated in several French power stations (Gravelines, Penly and Paluel). Among the dihaloacetonitriles, only dibromoacetonitrile could be detected in the chlorinated samples (around the 4.4  $\mu\text{g l}^{-1}$  level). This is in agreement with a previous study reporting the preferential formation of this compound in waters containing high levels of bromide [3]. Similarly, 2,4,6-tribromophenol was the only halophenol detected in the samples (at a concentration ten times lower than dibromoacetonitrile, i.e. around 0.4  $\mu\text{g l}^{-1}$ ).

Chlorinated sea water samples from the outlet of the three power stations were analysed during the chlorination period in 1997 and 1998. Only dibromoacetonitrile and 2,4,6-tribromophenol were detected, with variable concentrations as shown in Table 5 (as the chlorine dose varied during the chlorination period). The concentrations of brominated compounds formed in the sea

Table 1  
Precision and estimated concentrations from dihaloacetonitrile calibration<sup>a</sup>

$C_{\text{real}}$ ( $\mu\text{g l}^{-1}$ )	Dichloroacetonitrile			Bromochloroacetonitrile			Dibromoacetonitrile		
	RSD (%)	$C_{\text{est.}}$ ( $\mu\text{g l}^{-1}$ )	CI for $C_{\text{est.}}$	RSD (%)	$C_{\text{est.}}$ ( $\mu\text{g l}^{-1}$ )	CI for $C_{\text{est.}}$	RSD (%)	$C_{\text{est.}}$ ( $\mu\text{g l}^{-1}$ )	CI for $C_{\text{est.}}$
0.50	53.80	0.40	0.25–0.56	16.52	0.78	0.69–0.87	7.86	0.35	0.33–0.37
1.00	30.86	1.15	1.13–1.27	21.74	1.29	1.13–1.45	5.27	1.10	1.07–1.13
2.00	14.44	2.32	2.15–2.50	7.88	2.21	2.11–2.31	2.62	2.09	2.06–2.12
4.00	2.23	3.77	3.73–3.82	4.09	3.73	3.64–3.82	8.33	3.91	3.73–4.09
8.00	9.73	8.15	7.60–8.70	0.97	8.05	8.00–8.11	10.70	8.78	8.13–9.43
10.00	3.12	10.06	9.89–10.25	1.92	9.99	9.88–10.09	10.96	10.56	9.75–11.36
16.00	0.04	16.33	16.33–16.34	0.90	16.66	16.55–16.76	2.61	16.18	15.88–16.47
20.00	2.31	19.97	19.72–20.24	1.23	19.90	19.76–20.04	3.78	19.28	18.77–19.78

<sup>a</sup> The confidence interval (CI) for each concentration is calculated for a 5% risk. For  $A_{\text{mean}}$ :

$$\text{CI} = A_{\text{mean}} \pm S_{(A,C)} \frac{t}{\sqrt{n}}$$

where  $S_{(A,C)}$  is the standard deviation of  $n$  measurements of the solution at concentration  $C$  from which  $A_{\text{mean}}$  has been determined,  $t$  is the Student–Fisher coefficient for a probability of 0.975 with  $(n-1)$  degrees of freedom (e.g. for  $n=3$ ,  $t/\sqrt{n}=3.46$ ).

Table 2  
Precision and estimated concentrations from bromophenol calibration<sup>a</sup>

$C_{\text{real}}$ ( $\mu\text{g l}^{-1}$ )	3-Bromophenol			2,4-Dibromophenol			2,6-Dibromophenol			2,4,6-Tribromophenol		
	RSD (%)	$C_{\text{est.}}$ ( $\mu\text{g l}^{-1}$ )	CI for $C_{\text{est.}}$	RSD (%)	$C_{\text{est.}}$ ( $\mu\text{g l}^{-1}$ )	CI for $C_{\text{est.}}$	RSD (%)	$C_{\text{est.}}$ ( $\mu\text{g l}^{-1}$ )	CI for $C_{\text{est.}}$	RSD (%)	$C_{\text{est.}}$ ( $\mu\text{g l}^{-1}$ )	CI for $C_{\text{est.}}$
0.20	3.18	0.20	0.18–0.22	1.06	0.19	0.18–0.21	1.64	0.17	0.16–0.18	5.29	0.18	0.17–0.19
1.00	0.47	1.00	0.98–1.01	0.40	0.96	0.95–0.97	0.31	0.92	0.91–0.93	0.49	0.98	0.96–1.00
2.00	0.45	2.02	1.99–2.05	0.11	1.95	1.94–1.97	0.08	1.94	1.93–1.95	0.34	2.08	2.05–2.10
4.00	0.70	4.22	4.11–4.32	0.09	4.01	3.99–4.02	0.79	4.02	3.91–4.13	0.23	4.05	4.00–4.10
10.00	0.40	9.91	9.77–10.05	0.04	10.01	9.99–10.02	0.16	10.01	9.96–10.06	0.27	9.97	9.88–10.05

<sup>a</sup> See footnote to Table 1.

Table 3  
Precision and accuracy of dihaloacetonitrile and bromophenol analysis

Compounds	R.S.D. (%)	Mean recovery (%)	CI for recovery (%)	Slope for the correlation between $C_{est}$ and $C_{real}$	Correlation coefficient ( $r^2$ ) for the correlation between $C_{est}$ and $C_{real}$
<i>Dihaloacetonitriles</i>					
Dichloroacetonitrile	8	104	[99–108]	1.042	0.999
Bromochloroacetonitrile	4	104	[98–110]	0.999	0.998
Dibromoacetonitrile	8	103	[98–108]	1.032	0.996
<i>Bromophenols</i>					
3-Bromophenol	8	100	[99–101]	1.000	0.999
2,4-Dibromophenol	7	98	[97–99]	0.999	0.999
2,6-Dibromophenol	8	96	[94–98]	1.000	0.999
2,4,6-Tribromophenol	8	99	[97–101]	1.000	0.999

water are globally the highest at the Gravelines station, and the lowest at the Penly station. Hence, the mean concentrations were 4.05 and 0.37  $\mu\text{g l}^{-1}$  for dibromoacetonitrile and 2,4,6-tribromophenol at the Gravelines station, compared to 2.1 and 0.14  $\mu\text{g l}^{-1}$  at the Paluel station, and 0.36 and 0.10  $\mu\text{g l}^{-1}$  at the Penly station. These results seem to be correlated to the chlorine dose, as slightly lower chlorination levels were used in the latter station (mean applied chlorine dose of 0.87  $\text{mg l}^{-1}$  at the Gravelines station, instead of 0.56  $\text{mg l}^{-1}$  and 0.20  $\text{mg l}^{-1}$  at the Paluel and Penly stations respectively).

### 3.4. Conclusions

Two methods for determining either dihaloacetonitriles or halophenols in sea water are presented that combine liquid–liquid extraction and gas chromatography coupled to mass spectrometry. Their performances were evaluated in order to prove that they are applicable to the determination of such halogenated components in chlorinated sea water samples. The precision was satisfactory and the concentrations estimated based upon the calibration curves were closed to the real sample concentrations for spiked sea water samples. In addition, the limits of detection and quantification (LODs ranged from 0.10 and 0.20  $\mu\text{g l}^{-1}$  for dihaloacetonitriles

and from 0.02 to 0.05  $\mu\text{g l}^{-1}$  for halophenols) enabled the determination of such compounds at trace levels in sea water. Both methods were also successfully applied to chlorinated cooling effluents from three French power stations. Due to the presence of high bromide concentrations in sea water, only brominated compounds could be detected, namely dibromoacetonitrile and 2,4,6-tribromophenol, the former being the major compound formed. In addition, evidence was given that increased concentrations of brominated compounds were formed at elevated chlorine doses.

Table 4  
Limits of detection and quantification for dihaloacetonitriles and bromophenols in sea water

Compounds	LOD ( $\mu\text{g l}^{-1}$ )	LOQ ( $\mu\text{g l}^{-1}$ )
<i>Dihaloacetonitriles</i>		
Dichloroacetonitrile	0.20	0.70
Bromochloroacetonitrile	0.10	0.50
Dibromoacetonitrile	0.10	0.50
<i>Bromophenols</i>		
3-Bromophenol	0.02	0.10
2,4-Dibromophenol	0.05	0.10
2,6-Dibromophenol	0.05	0.10
2,4,6-Tribromophenol	0.03	0.10

Table 5  
Concentrations of dibromoacetonitrile (DBAN) and 2,4,6-tribromophenol (TBP) found in cooling effluents from nuclear units of three French power stations

Sampling date	Nuclear unit	Chlorine dose (mg l <sup>-1</sup> )	DBAN (µg l <sup>-1</sup> )	TBP (µg l <sup>-1</sup> )
<i>Gravelines station</i>				
24/07/1997	1	1.18	9.7	nd
	1	1.18	5.0	nd
	2	1.14	7.0	nd
	2	1.14	6.4	nd
26/08/1997	2	0.94	4.3	0.4
	2	0.94	3.8	0.2
	5	0.42	2.9	0.4
	5	0.42	2.3	0.3
11/05/1998	5	0.76	0.5	0.4
	6	0.86	0.7	0.2
29/06/1998	5	0.65	0.85	0.43
	6	0.87	2.1	0.4
16/07/1998	5	0.92	3.6	0.43
	6	1.0	3.8	0.38
12/08/1998	1	0.83	7.4	0.4
	2	0.63	4.4	0.5
<i>Paluel station</i>				
11/05/1998	1	0.65	0.3	0.01
	2	0.59	0.5	0.01
8/06/1998	1	0.25	0.86	0.26
	4	0.21	1.04	0.09
30/06/1998	1	0.68	3.8	0.2
	2	0.68	4.6	0.2
15/07/1998	2	0.66	2.25	0.23
	3	0.48	2.8	0.21
10/08/1998	1	0.71	4.07	0.11
	2	0.69	0.79	0.07
<i>Penly station</i>				
25/08/1997	1	0.22	0.36	0.1
	2	0.13	0.47	0.1
11/05/1998	1	0.16	0.2	0.05
	2	0.21	0.1	0.05
8/06/1998	1	0.21	0.13	0.27
30/06/1998	1	0.24	0.5	0.1
15/07/1998	1	0.21	0.2	0.07
11/08/1998	1	0.21	0.7	0.09
	2	0.23	0.6	0.11

#### 4. Nomenclature

*A* Peak area of the compound relative to the internal standard peak area  
*C* Concentration of the compound relative to the internal standard concentration

$C_{est.}$  Estimated concentration (from the calibration curve)  
 $C_{real}$  Real concentration  
 CI Confidence interval  
 DBAN Dibromoacetonitrile  
 DHAN Dihaloacetonitrile  
 EPA Environmental protection agency

GC	Gas chromatography
HPhs	Halophenols
i.d.	Internal diameter
LLE	Liquid–liquid extraction
LOD	Limit of detection
LOQ	Limit of quantification
MS	Mass spectrometry
<i>r</i>	Linear correlation coefficient
R.S.D.	Relative standard deviation
TBP	Tribromophenol

### Acknowledgements

The authors wish to thank the French company Electricité de France for its financial and technical support.

### References

- [1] A.S. Allonier, M. Khalanski, *J. Rech. Oceanogr.* 23 (1998) 21.
- [2] B.G. Oliver, *Environ. Sci. Technol.* 17 (1983) 80.
- [3] T.I. Bieber, M.L. Trehy, Dihaloacetonitriles in chlorinated natural waters, in: *Water Chlorination: Environmental Impact and Health Effects*, vol. 4, Ann Arbor Science, Ann Arbor, MI, 1983, pp. 85–96.
- [4] R.J.B. Peters, E.W.B. de Leer, L. de Galan, *Water Res.* 24 (1990) 797.
- [5] M.L. Trehy, R.A. Yost, C.J. Miles, *Environ. Sci. Technol.* 20 (1986) 1117.
- [6] J.D. McKinney, R.R. Maurer, J.R. Haas, R.O. Thomas, Possible factors in the drinking water of laboratory animals causing reproductive failure, in: L.H. Keith (Ed.), *Identification and Analysis of Organic Pollutants in Water*, vol. 5, Ann Arbor Science, Ann Arbor, MI, 1976, pp. 417–432.
- [7] W.E. Coleman, J.W. Munch, W.H. Kaylor, H.P. Ringhand, J.R. Meier, *Environ. Sci. Technol.* 18 (1984) 674.
- [8] S. Karlsson, S. Kaugare, A. Grimvall, H. Boren, R. Sävenhed, *Water Sci. Technol.* 31 (1995) 99.
- [9] J.W. Hodgeson, A.L. Cohen, 1990. Method 551. Determination of chlorinated disinfection byproducts and chlorinated solvents in drinking water by liquid–liquid extraction and gas chromatography with electron-capture detection. US Environmental Protection Agency, Cincinnati, OH.
- [10] L.H. Keith, R.C. Hall, R.C. Hanisch, J.E. Henderson, R.G. Landolt, New methods for gas chromatographic analysis of water pollutants, in: *Water Chlorination: Environmental Impact and Health Effects*, vol. 4, Ann Arbor Science, Ann Arbor, MI, 1983, pp. 563–582.
- [11] R.C. Barth, P.S. Fair, *J. AWWA* 84 (1992) 94.
- [12] L.H. Keith, R.C. Hall, R.C. Hanish, R.G. Landolt, J.E. Henderson, *Water Sci. Technol.* 14 (1982) 59.
- [13] Norme Française NF X20-300. Recueil de normes françaises pour la qualité de l'air. AFNOR, Paris, 1994.

# 'Hidden parameters' of infrared drying for determining low water contents in instant powders

H.-D. Isengard \*, J.-M. Färber

*University of Hohenheim, Institute of Food Technology, Garbenstr. 25, D-70593 Stuttgart, Germany*

Received 10 July 1998; received in revised form 9 September 1998; accepted 16 September 1998

---

## Abstract

Drying techniques are very frequently used and in many cases official methods for moisture determination. These methods, however, do not yield the water content as a result but a mass loss which is caused not only by the evaporation of water but by all substances volatile under the drying conditions, be they original components of the product or be they produced by decomposition reactions during the drying process. This mass loss varies therefore with the parameters applied like time, temperature, form of energy transfer, atmospheric pressure or surrounding humidity. To shorten determination times of many hours in common air ovens with convective heating, techniques with more efficient heating principles have been developed. One of these is infrared drying. With such methods, however, the danger of product decomposition and, consequently, of wrong results rises, particularly when the water content is low. It could be shown, however, that analyses are possible, even for beverage instant powders with very low water contents. Moreover, parameter sets could be found to match the infrared results exactly with the true water content determined by Karl Fischer titration. Another essential finding was that not only the parameters for the drying programme itself like time, temperature and end-point criterion are important, but also, and this to a surprisingly great extent, the number of consecutive measurements and the duration of the intervals between analyses. This effect again depends extremely on the type of apparatus. © 1999 Elsevier Science B.V. All rights reserved.

*Keywords:* Water content; Infrared drying; Parameters; Karl Fischer titration

---

## 1. Introduction

Water content is for a number of reasons one of the most important general properties of food-stuffs. Very rapid methods like NMR and even

on-line methods like NIR spectroscopy and microwave techniques exist for its determination. These methods do not measure the water content specifically but a property of the product that depends on the water content. As the correlation between the measured entity and the water content is extremely complex in most of the real situations, these methods need an extremely product-specific calibration, which must be based on a direct and selective method [1].

---

\* Corresponding author. Tel.: +49-711-397-4670; fax: +49-711-397-4674.

*E-mail address:* isengard@uni-hohenheim.de (H.-D. Isengard)



Drying methods are still the most common way to determine the moisture of a product. The term 'water content' was deliberately avoided in this context. Drying techniques do in fact not determine the water content but only a mass loss under certain conditions. This mass loss is not only caused by water, but by all substances volatile under the drying conditions, by those originally contained in the sample but also those produced during and by the drying process itself. Moreover, as the drying conditions may be principally freely chosen, the results for a given product are variable. The results of a drying method should therefore not be called water content, even though in some cases (but rarely for foodstuffs) the mass loss may come very close or even correspond to the water content.

The danger of decomposition reactions with consecutive production of volatile matter is particularly high with drying techniques with an intensive energy input. The widely used infrared dryers are an example. Nevertheless, the drying parameters can be chosen in a way that the result of the infrared drying corresponds to the true water content found by a reference method such as the Karl Fischer titration. In such cases the two main (and conflicting) sources of error (undetected water remaining in the sample, and the determination of other volatile substances) compensate for each other [1,2]. If the results are reproducible using this parameter set, the infrared drying method can be used to determine the water content of this particular sort of product [2,3], and only from time to time is it necessary to check if the results still match those found by Karl Fischer titration. A discrepancy may occur when the matrix of the product analysed differs from the one of the 'original' sample or when the technical conditions such as the effectiveness of the heating source and with it the emission spectrum of the dryer change. The parameter set may also not be appropriate for samples with a water content outside the range which was the base of the calibration.

Instant powders have a very low water content. This makes the infrared drying process difficult. Right from the beginning the matrix takes up much energy, because there is only a low evapora-

tion enthalpy due to the low amount of water in the sample. Products that contain much water are protected from this high energy transfer at the beginning of the drying process by the evaporation of water (and possibly other substances).

## 2. Experimental

### 2.1. Samples

Four beverage instant powders from Nestlé were analysed: Caro coffee substitute, Frappé iced coffee, Nesquik (cocoa-containing beverage powder), Nestea lemon low calorie. Several batches of each product with different water content were examined.

### 2.2. Determination of the water content by Karl Fischer titration

The water content was determined by Karl Fischer titration using the KF-Titrino 701 from Metrohm, Herisau, Switzerland. The main titration parameters and end-point criteria were the following: polarising current 50  $\mu\text{A}$ , stop voltage 250 mV, maximal titration rate 1 ml  $\text{min}^{-1}$ , minimal volume increment 2  $\mu\text{l}$ , stop delay time 17 s. The drift was measured before each analysis and registered by the titrator. The consumption due to the drift, taking the titration time into account, was then automatically deducted from the titration volume. The two-component volumetric technique was used with Hydranal-Titrant 5 or Hydranal-Titrant 2 as titrating solution and a mixture of 13 ml Hydranal-Solvent and 7 ml formamide as working medium. All chemicals were from Riedel-de Haën, Seelze, Germany.

### 2.3. Determination of the mass loss by infrared drying

Two different infrared dryers were used, the Moisture Analyzer MA30 and the Moisture Analyzer MA50, both from Sartorius, Göttingen, Germany. Both apparatuses offer the feature of a time controlled measurement (time mode): the temperature is set (in steps of 5°C with the MA30

and in steps of 1°C with the MA50) and the drying process is stopped after a set time. With the MA50 three consecutive time periods, each with an individual temperature and duration can be used (time programme). Both the MA30 and the MA50 have also an automatic mode. The analysis is terminated when, at a set temperature, the mass loss within the last time interval of measurements is inferior to a minimum. The amount of the difference and the length of the time interval can be chosen with the MA50, this is the so-called semi-automatic mode. The heating source of the MA30 are two infrared dark metal emitters of 180 W each. At full power the surface temperature is 750°C, this corresponds—according to Wien's law—to a maximum of the emission spectrum at 2.8  $\mu\text{m}$ . The MA50 has a 250-W infrared lamp. The surface temperature at full power is 1950°C with a spectral maximum at 1.3  $\mu\text{m}$ . The built-in balance of the MA30 has a resolution of 1 mg, the one of the MA50 of 0.1 mg.

The aim of the infrared experiments was to find parameter sets with which results could be obtained equal to the water content found by Karl Fischer titration with good repeatability and small standard deviations. Only those parameter sets were finally accepted which yielded good results for samples with different water contents of a specific product.

The general procedure with the MA30 was the following. Batches of a product with different water contents (within the range of practically occurring products) were measured in the automatic mode at different temperatures in steps of 5°C (two replicates each) to find temperatures that yield results close to the Karl Fischer value. The experiment was then repeated with 10–15 replicates for one of the batches at the most suitable temperatures. In some situations the time

mode was also applied for optimisation. The applicability on samples with other water contents was also tested. The proceeding with the MA50 was principally the same, but for the possibility to adjust the temperature in steps of 1°C and to use the 3-step time programme.

Finally, experiments were carried out to investigate the dependence of the measurements on other conditions than the parameters to be set with the apparatus, particularly the number of consecutive measurements and the duration of the intervals between analyses.

### 3. Results and discussion

#### 3.1. Water content of the products

The water content of the original products determined by Karl Fischer titration varied according to the different batches:

Caro coffee substitute (15 replicates each)	from $2.46 \pm 0.05$ to $3.13 \pm 0.06\%$ ,
Frappé iced coffee (10–15 replicates each)	from $0.53 \pm 0.02$ to $0.73 \pm 0.02\%$ ,
Nesquik (10–12 replicates each)	from $0.99 \pm 0.02$ to $1.10 \pm 0.02\%$ ,
Nestea lemon low calorie (ten replicates each)	from $0.58 \pm 0.01$ to $0.63 \pm 0.01\%$ .

#### 3.2. Infrared drying of Caro coffee substitute

##### 3.2.1. Moisture Analyzer MA30

Using the automatic mode the results obtained at 80 or 85°C were close to the water content. The experiment was repeated with more replicates for the batch with a water content of 2.99%. The results are given in Table 1.

Table 1

Mass loss of Caro coffee substitute by infrared drying with the MA30 at different temperatures in the automatic mode (n replicates); water content found by Karl Fischer titration  $2.99 \pm 0.07\%$  (15 replicates)

Temperature (°C)	70 (n = 5)	75 (n = 10)	80 (n = 10)	85 (n = 15)	90 (n = 11)	95 (n = 12)
Mass loss (%)	$2.76 \pm 0.06$	$2.91 \pm 0.08$	$2.93 \pm 0.09$	$3.04 \pm 0.09$	$3.16 \pm 0.07$	$3.34 \pm 0.12$
Drying time (min)	5.0–6.3	4.2–5.5	3.7–5.0	2.3–4.5	3.1–4.7	2.9–5.3

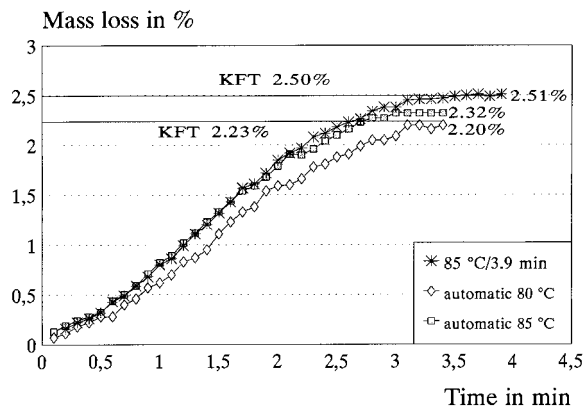


Fig. 1. Drying curves for two batches of Caro with the MA30.

The standard deviation intervals of the results obtained in the automatic mode at 80 and 85°C include the Karl Fischer result and can be recommended for determining the water content. An intermediate temperature cannot be set with the MA30. A better approximation of the Karl Fischer value can be achieved by setting the higher temperature (85°C) and shortening the determination time by using the time mode. For a batch with  $2.61 \pm 0.06\%$  water (15 replicates) a mass loss of  $2.59 \pm 0.05\%$  (ten replicates) was found at 85°C after a set drying time of 3.9 min. Instead of 2.46% water a mass loss of 2.48% was found and a 2.78% batch gave 2.77% under the same conditions. Fig. 1 depicts the drying curves in the automatic mode and the time mode for batches with 2.23 and 2.50% water respectively and shows that the methods are applicable for these water contents, too. The time to be fixed in the time mode, however, depends to a certain extent on the water content and this variety is therefore not generally possible for all ranges of water content, particularly when it lies clearly outside the normal range of the product.

### 3.2.2. Moisture Analyzer MA50

By a similar proceeding with the same batches as above, 110°C was found to be the best temperature in the automatic mode to reproduce the water content with the MA50. The batch with a water content of  $2.61 \pm 0.06\%$  was then

inspected more closely. Ten replicates yielded a mass loss of  $2.59 \pm 0.02\%$  in 4.8–6.4 min. Determinations are also possible using the time programme. A batch with  $2.58 \pm 0.05\%$  water (15 replicates) had a mass loss of  $2.56 \pm 0.05\%$  (ten replicates) after 4.5 min at 132°C + 0.9 min at 129°C + 1.5 min at 128°C (total time 6.9 min) and a mass loss of  $2.62 \pm 0.06\%$  (ten replicates) after 2.0 min at 160°C + 0.5 min at 150°C + 0.4 min at 145°C (total time 2.9 min). The corresponding values for a 3.13% batch were 3.13 and 3.15%, respectively.

This shows that the temperature settings are not transferable from one dryer type to another. The different wavelength spectra of the heating sources (Section 2.3) affect the heating effect to a great extent. The temperatures to be set with the MA50 are higher than those with the MA30. It should be mentioned that the temperatures set do not necessarily correspond exactly to the real temperatures in the sample.

### 3.3. Infrared drying of Frappé iced coffee

#### 3.3.1. Moisture Analyzer MA30

This product proved to be very sensitive to infrared heating. In most of the experiments no end point was found in the automatic mode at temperatures from 45 to 110°C within 1 h. Obviously a continuous decomposition of the sample takes place and not even an approximate mass constancy can be achieved. At higher temperatures the measurements were, in some cases, automatically stopped by the dryer when the decomposition had obviously progressed to an extent—the sample had visibly changed extremely—that the sample lost mass slowly enough to fulfil the end-point criterion in the automatic mode. The indicated ‘moisture’ was however about twice the Karl Fischer value. In such situations the time mode can be applied and the drying process has to be stopped at the ‘right’ moment. Table 2 shows the results.

A fixed drying time of 2.2 min at 85°C can be recommended. This was checked with other batches. The result for a batch with 0.67% water was  $0.67 \pm 0.02\%$  (ten replicates). A batch

with 0.62% water showed  $0.64 \pm 0.02\%$  (eight replicates) mass loss, and instead of 0.57% water a mass loss of  $0.56 \pm 0.02\%$  was found.

The usual water content of Frappé lies in this range. To investigate the applicability of the method beyond this range, samples were moistened in an atmosphere over salt solutions. It was found that the drying time is too short. Mass losses of 1.30, 1.28 and 1.15% were found for samples with 1.68, 1.51 and 1.38% water, respectively. If, therefore, a water content higher than the usual range is found, this is only a hint that the water content is too high but does not necessarily indicate the correct value.

### 3.3.2. Moisture Analyzer MA50

The MA50 heats the samples less vigorously. It was in fact possible to use the automatic mode. For a sample with  $0.60 \pm 0.02\%$  water (15 replicates) a mass loss of  $0.61 \pm 0.01\%$  was found for ten replicates at 70°C with determination times of 6.5–9.8 min. Using the time mode, the determination time could be shortened by raising the temperature to 85°C and limiting the duration to 2.4 min. The result for ten replicates was also  $0.61 \pm 0.01\%$ . A time reduction was also possible using the 3-step time programme. For ten replicates a mass loss of  $0.62 \pm 0.02\%$  was found after 0.9 min at 89°C + 0.9 min at 85°C + 2.2 min at 77°C (in total 4.0 min). Using 0.9 min at 160°C + 0.3 min at 100°C + 0.1 min at 80°C (in total only 1.3 min) the result obtained for ten replicates was  $0.59 \pm 0.03\%$ .

As with the MA30, these procedures are only applicable for samples with a water content in the usual range. Instead of the water content of 1.44% of a moistened sample a mass loss of only 1.27% was found after 2.4 min at 85°C.

## 3.4. Infrared drying of Nesquik

### 3.4.1. Moisture Analyzer MA30

For all batches—they had very similar water contents—the Karl Fischer value was well approached at 80°C in the automatic mode. Table 3 gives the results for the example that was more closely examined.

At higher temperatures the correct results can be obtained by enforcing a shorter drying time in the time mode. For 3.2 min/85°C and for 2.9 min/90°C ten replicates each gave a mass loss of  $1.01 \pm 0.02\%$  with both settings. The water content of 1.02% of a batch was also correctly found with the automatic mode at 80°C.

### 3.4.2. Moisture Analyzer MA50

A temperature of 94°C proved to be the most appropriate temperature setting with the MA50 in the automatic mode. For the batch with the lowest water content ( $0.99 \pm 0.02\%$ , 12 replicates) a mass loss of  $0.98 \pm 0.01\%$  was found for 11 replicates with drying times from 5.6 to 11.2 min. The drying times can be shortened by applying a time programme. A batch with  $1.03 \pm 0.02\%$  water (ten replicates) gave a mass loss of  $1.04 \pm 0.01\%$  after 6.1 min (4.6 min at 100°C + 0.8 min at 97°C + 0.7 min at 95°C) and a mass loss of  $1.03 \pm 0.01\%$  after only 2.3 min (1.6 min at 160°C + 0.5 min at 120°C + 0.2 min at 105°C). The first programme with the more moderate temperatures is safer. Whereas the correct value was found for the batch with the highest water content (1.10%), the second time programme yielded 1.12%.

## 3.5. Infrared drying of Nestea lemon low calorie

The water content of the batches investigated lay in a very narrow range. In two cases 0.58

Table 2

Mass loss of Frappé iced coffee by infrared drying with the MA30 at different temperatures after different times (time mode) (12 replicates each); water content found by Karl Fischer titration  $0.73 \pm 0.02\%$  (15 replicates)

Temperature (°C)	70	80	85	95
Drying time (min) (set)	3.4	2.3	2.2	2.0
Mass loss (%)	$0.72 \pm 0.02$	$0.72 \pm 0.03$	$0.74 \pm 0.02$	$0.76 \pm 0.03$

Table 3

Mass loss of Nesquik by infrared drying with the MA30 at different temperatures in the automatic mode (n replicates); water content found by Karl Fischer titration  $1.00 \pm 0.02\%$  (12 replicates)

Temperature (°C)	70 (n = 11)	75 (n = 11)	80 (n = 14)	85 (n = 10)
Mass loss (%)	$0.89 \pm 0.03$	$0.94 \pm 0.04$	$0.99 \pm 0.02$	$1.08 \pm 0.03$
Drying time (min)	3.7–4.5	3.7–4.4	3.7–4.7	3.7–4.8

0.01% and in four cases  $0.63 \pm 0.01\%$  was measured by Karl Fischer titration for ten replicates each.

### 3.5.1. Moisture Analyzer MA30

The product is very heat sensitive. No appropriate automatic method could be found. For a 0.58% batch several time-mode methods gave good results:  $0.56 \pm 0.01\%$  after 8.0 min at 80°C,  $0.58 \pm 0.01\%$  after 4.3 min at 85°C,  $0.60 \pm 0.01\%$  after 3.7 min at 90°C and  $0.58 \pm 0.01\%$  after 3.2 min at 95°C. These methods are nevertheless problematic, especially those at the higher temperatures which resulted in a very visible change of the product. Therefore the risk is great to find inadequate values for other water contents. The decomposition seems to occur in an uncontrollable way and the results may be arbitrary to a certain extent. Thus, for a 0.63% batch the automatic mode at 95°C yielded a mass loss of  $0.60 \pm 0.04\%$  for four replicates with drying times between 2.9 and 39 min (!), but in four other assays the mass loss had already reached values of up to 1.63% after 25 min and the apparatus did still not stop the determination. The drying curve is ascending very slightly but the gradient is obviously not small enough to fulfil the end-point criterion.

### 3.5.2. Moisture Analyzer MA50

In contrast to the MA30, the MA50 can be used in the automatic mode for this product. Nine replicates of a 0.63% batch had a mass loss of  $0.62 \pm 0.04\%$  at 99°C with drying times of 5.2–13.2 min. Times can be shortened by using a time programme. The result for a batch with 0.63% water was  $0.62 \pm 0.01\%$  (ten replicates) after 4.7 min (3.1 min at 115°C + 0.6 min at 108°C + 1.0 min at 107°C). Ten replicates of a 0.58% batch gave a mass loss of  $0.58 \pm 0.01\%$ .

### 3.6. Repeatability of results in consecutive measurements

All the experiments described above were made starting a new analysis exactly 2 min after the end of the preceding one. Before starting the first measurement of a series of analyses the dryers were kept in the stand-by position for half an hour. The first measurements had nevertheless to be discarded in some cases, depending on the apparatus, the operation mode and the used temperatures. This is shown for the example of Frappé iced coffee. Similar effects were also observed for the other products investigated.

#### 3.6.1. Moisture Analyzer MA30

With several temperature/time-settings the water-content values could be reproduced (Table 2). Fig. 2 shows the results of consecutive measurements using the time mode at 85°C. The interval between the measurements was in all cases 2 min. The first measurements are extremely different from the found water content values. The infrared dryer must obviously be heated up first to reach a certain working temperature. The effect depends, of course, on the temperature chosen. Thus, the

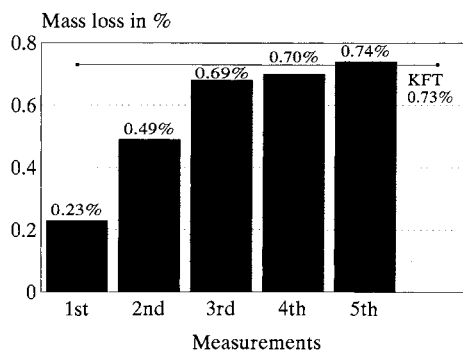


Fig. 2. Mass loss of Frappé with the MA30 at 85°C for 2.2 min (time mode).

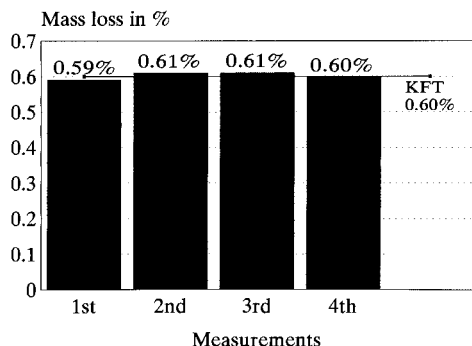


Fig. 3. Mass loss of Frappé with the MA50 using a 3-step time programme: 0.9 min at 89°C + 0.9 min at 85°C + 2.2 min at 77°C.

corresponding values for a sample with a found water content of 0.53% using the time mode at 95°C were 0.10, 0.35, 0.43, 0.48 and 0.51%, respectively.

When the obtained values are once in the range of the water content found, the results scatter from then on around this value. The effect is repeatable. Using, for instance, the time mode in Fig. 2, the first result with a ‘cold’ apparatus is always in the range of 30% of the value obtained with a ‘warmed-up’ dryer. The results in Table 2 were obtained taking this effect into account. ‘12 replicates’ means that 16 analyses were made and the results of the first four were discarded.

This effect was also considered for the other products.

### 3.6.2. Moisture Analyzer MA50

The heating source of the MA50 is much swifter than the one of the MA30. When the set temperature is not too high, even the first analysis of a series is therefore correct, as is shown in Fig. 3. The analyses were carried out with intervals of 2 min each as in the case of the MA30 measurements discussed above.

The higher the temperature, however, (in a 3-step programme the first temperature counts), the bigger is the risk to obtain wrong results in the first measurement(s). Thus, the values for a sample with a water content of 0.62% using the 3-step programme 0.9 min at 160°C + 0.3 min at 100°C + 0.1 min at 80°C were 0.53, 0.59, 0.64 and 0.62%, respectively.

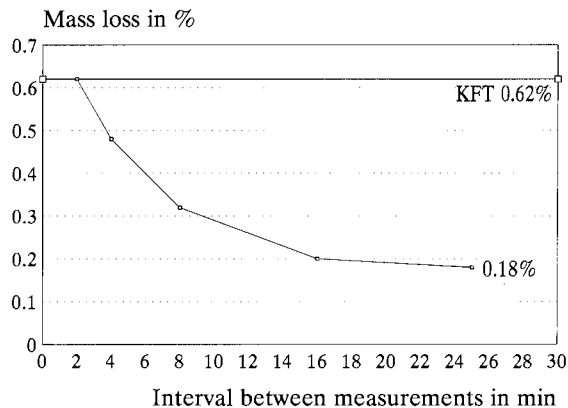


Fig. 4. Mass loss of Frappé with the MA30 at 85°C for 2.2 min with different time intervals between the measurements.

### 3.7. Intervals between measurements

Measurements were always started exactly 2 min after the end of the preceding one. The dependence of the results on the duration of the time intervals between measurements was also investigated, because the status of the dryers at the beginning of an analysis affects the results, as was shown for consecutive measurements.

The results are again reported for Frappé iced coffee as example. For the other products similar observations were made.

The values in Figs. 4 and 5 are those obtained after the results were approximately constant. The first results were discarded. Such rejections were,

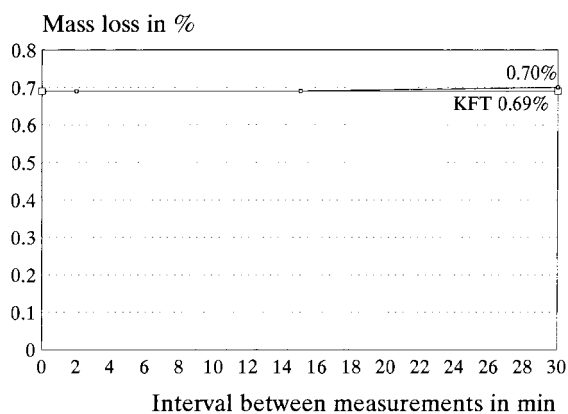


Fig. 5. Mass loss of Frappé with the MA50 at 85°C for 2.4 min with different time intervals between the measurements.

logically, particularly necessary for shorter measurement intervals.

### 3.7.1. Moisture Analyzer MA30

The Karl Fischer value is reached after 2.2 min drying at 85°C (Section 3.2.1). Fig. 4 gives the values for various time intervals between the measurements. The values for 2, 4 and 8 min were obtained with five replicates, those for 16 and 25 min with four replicates. In accordance with the findings concerning the consecutive measurements, results were only accepted, after they had become nearly constant. Rejections were, logically, particularly necessary for short intervals, for the 25-min measurement no value had to be discarded. For such long intervals each analysis is practically a 'new' one.

### 3.7.2. Moisture Analyzer MA50

The findings concerning the consecutive measurements show that the MA50 with its swifter heating source is distinctly less sensitive to variations of the intervals between analyses. Using the time mode mentioned in Section 3.2.2, the duration of the pause between analyses has no influence on the results (Fig. 5). The same holds for the 3-step time programme of Fig. 3. Only for high initial temperatures are deviations of the results observed, though less important than with the MA30. For a sample with 0.62% water the 3-step time programme 0.9 min at 160°C + 0.3 min at 100°C + 0.1 min at 80°C yielded 0.61, 0.55 and 0.53% mass loss with intervals of 2, 15 and 30 min, respectively. The values are based on four replicates (2 min) or three replicates (15 and 30 min).

## 4. Conclusions

The water content of several beverage instant powders was determined by Karl Fischer titration.

It could be shown that the water content of these products can also be determined by infrared drying. The parameters can principally be ad-

justed in such a way that the results of the mass loss by infrared drying (caused not only by the evaporation of water!) correspond to the water-content values found by Karl Fischer titration. A certain parameter set may, however, lead to inexact results when the water content of the sample falls out of the range for which the method has been developed. A certain reserve must be made concerning the MA30 with its more efficient heating source which more likely induces decomposition reactions. No end point may then be found in the automatic mode.

With various parameter settings and operation modes repeatable but very different results can be obtained. This repeatability is treacherous, as it may give the impression of correct results. Infrared-drying methods must therefore be developed by product-specific calibration against a chosen reference method, particularly in the case of products with very low water content and of those that tend to decomposition reactions. If the water content is to be measured, the Karl Fischer titration is usually the best reference.

A most important observation is the fact that it is not sufficient to fix only the parameters that can directly be set with the instrument like the working mode (stop criteria), time and temperature or the details of a time programme. It is also necessary to define and then to respect the interval between measurements and to find out how many values have to be discarded before the results become approximately constant. This necessity is not at all immediately obvious, because the results obtained without taking these requirements into account may be even very well repeatable. This good repeatability can conceal the (in some cases extreme) falseness of such results.

## References

- [1] H.-D. Isengard, *Trends Food Sci. Technol.* 6 (1995) 155–162.
- [2] H. Brack, H.-D. Isengard, *Dtsch. Milchwirtsch.* 46 (1995) 73–77.
- [3] H. Präger, H.-D. Isengard, *GIT-Labor-Fachzeitschrift* 41 (1997) 1094–1101.

# A flow system with an electrochemical reduction cell for spectrophotometric determinations of major constituents in Fe/V alloys

Antonio O. Jacintho <sup>a</sup>, Luiz F.R. Machado <sup>b</sup>, Amauri A. Menegário <sup>a</sup>,  
Iolanda A. Rufini <sup>a</sup>, Maria Fernanda Giné <sup>a,\*</sup>

<sup>a</sup> Centro de Energia Nuclear na Agricultura, Universidade de São Paulo, Av. Centenário 303, C. Postal 96,  
13400-970 Piracicaba, Brazil

<sup>b</sup> Instituto de Química de São Carlos, Universidade de São Paulo, São Paulo, Brazil

Received 22 July 1998; received in revised form 29 September 1998; accepted 2 October 1998

## Abstract

Insertion of an electrochemical cell in a flow injection system to evaluate the on-line reduction of ionic species is presented. The cell comprised Pt electrodes installed in two sections separated by a Nafion membrane. The sample was injected into an acidic carrier stream and passed through the cathode compartment of the electrolytic chamber where the species were reduced as consequence of an applied DC voltage. The sample solution leaving the cell received a confluent reagent stream (1,10-phenanthroline buffered at pH 4.7) and the reacted products were dropped off in an open tube for gas/liquid separation. Efficiency of the Fe<sup>3+</sup> to Fe<sup>2+</sup> reduction in acidic medium was evaluated in the presence of strongly reducing species of V and Mo by monitoring the Fe(II) colored complex. Interferences from Pb<sup>2+</sup>, Co<sup>2+</sup>, Ni<sup>2+</sup>, Zn<sup>2+</sup>, Cu<sup>2+</sup>, V<sup>5+</sup> and Mo<sup>6+</sup> were evaluated. Production of strongly reducing species of V at the electrolytic cell presented higher efficiency for Fe reduction than the electrolytic chamber itself. Total reduction of Fe<sup>3+</sup> in solutions containing up to 10 mg l<sup>-1</sup> Fe plus 100 mg l<sup>-1</sup> V or 100 mg l<sup>-1</sup> of Mo was achieved by the electrolytic process at 2 A. The quantitative determination of Fe and V in low silicon Fe/V alloys was achieved. Accuracy was assessed with the certified Euro-standard 577-1 ferrovandium alloy produced by the Bureau of Analysed Samples Limited and no difference at the 95% confident level was found. © 1999 Elsevier Science B.V. All rights reserved.

**Keywords:** Electrochemical cell; Iron reduction; Flow analysis; Iron alloys

## 1. Introduction

In flow injection analysis reducing columns have been used for different applications. A column with copperized cadmium filings was em-

\* Corresponding author. Tel.: +55-194-292-4636; fax: +55-194-294-610.

E-mail address: mfgine@cena.usp.br (M.F. Giné)



ployed for reduction of nitrate to nitrite [1]. Several applications used the Jones reductor of amalgamated Zn packed in an on-line column to reduce  $\text{Cr}^{3+}$  to  $\text{Cr}^{2+}$  [2,3],  $\text{V}^{4+}$  and  $\text{V}^{5+}$  to  $\text{V}^{2+}$  [2] and  $\text{U}^{6+}$  to  $\text{U}^{3+}$  [4]. In these papers, the generation of strongly reducing agents in flow systems which are unstable under atmospheric conditions was demonstrated. The determination of total Fe and  $\text{Fe}^{2+}$  was also attained after reduction in a column with the Jones reductor in a flow system [5].

Electrochemical reduction of ionic species was reported for the hydride forming elements [6]. The approach was accomplished by using a flow-through electrolytic cell [7,8]. Papers published on the last years described the electrochemical hydride generation (EchG) of selenides, arsines, stibines and others coupled to different spectrometers, atomic absorption with a T-tube atomizers (ETAAS) [7,8] or with graphite furnaces (GFAAS) [9] or atomic emission microwave induced plasmas (MIP-AES) [10]. Electrodes of different materials: vitreous carbon [7], platinum [7,8,10], lead and pyrolytic graphite [9] were described.

In the present work the electrochemical approach using a flow-through cell is proposed to reduce  $\text{Fe}^{3+}$  to  $\text{Fe}^{2+}$ . The spectrophotometric detection of the ferrous complex was used to estimate the reduction process. The on line production of reduced species of V and Mo and the effect on reducing  $\text{Fe}^{3+}$  was evaluated. The determination of Fe in ferrovanadium alloys and the possibility of the indirect determination of V is presented.

## 2. Experimental

### 2.1. Apparatus

The flow system comprised a peristaltic pump (mp-13R Ismatec, Zurich, Switzerland) provided with Tygon pumping tubing, an automatic injector (Model 352, Micronal, São Paulo, Brazil) a flow-through electrolytic cell described below, a spectrophotometer (Model 432, Femto, São Paulo, Brazil) furnished with a flow cell (10 mm

optical path, 80  $\mu\text{l}$  inner volume) and a strip-chart recorder (REC 61, Radiometer, Copenhagen, Denmark). Accessories such as Y-shaped connectors, and mixing coils of polyethylene tubing (0.8 mm i.d.) were used.

The electrochemical cell was constructed by assembling layers of Perspex of different thickness, with two compartments, (anode 1.6  $\text{cm}^3$  and cathode 0.4  $\text{cm}^3$ ) separated by a Nafion membrane and electrodes of platinum sheets (3.2  $\text{cm}^2$ ) connected to a home made electrical source, which could be varied from 0.2 to 3.0 A. The Nafion membrane was conditioned by immersing it in hot water 20 min before installing at the cell protected between two rubber layers.

The gas phase separator (PS) was constructed from a 10 cm  $\times$  5 mm i.d. glass tube, with two lateral exits at opposite sides as described earlier [11].

### 2.2. Reagents and solutions

All reagents were of analytical grade and distilled, de-ionized water was always used. The electrolyte solution was 2.0 M  $\text{H}_2\text{SO}_4$ . The 1,10-phenanthroline solution (0.25% w/v) was prepared weekly by dissolving 0.6250 g of 1,10-phenanthroline hydrochloride in 250 ml of 0.1 M HCl. Acetate buffer solution (pH 4.7) was prepared with 1.0 M ammonium acetate plus 1.0 M acetic acid.

Stock solution containing 1000  $\text{mg l}^{-1}$   $\text{Fe}^{3+}$  was prepared from  $\text{Fe}(\text{NO}_3)_3 \cdot 9\text{H}_2\text{O}$  (Merck, Darmstadt, Germany). Solutions of the individual concomitants containing 1000  $\text{mg l}^{-1}$   $\text{Zn}^{2+}$ ,  $\text{Co}^{2+}$  and  $\text{Cr}^{3+}$  from the metals and  $\text{Ni}^{2+}$  from  $\text{NiSO}_4 \cdot 6\text{H}_2\text{O}$  (Johnson and Matthey Chemicals JMC),  $\text{Pb}^{2+}$  from  $\text{Pb}(\text{NO}_3)_2$ ,  $\text{V}^{5+}$  from  $\text{NH}_4\text{VO}_3$  and  $\text{Mo}^{6+}$  from  $(\text{NH}_4)_6\text{MO}_7\text{O}_{24} \cdot 4\text{H}_2\text{O}$  (Merck, Darmstadt, Germany) were prepared. Solutions used to test interference containing 10.0  $\text{mg l}^{-1}$   $\text{Fe}^{3+}$  plus 10.0 and 100  $\text{mg l}^{-1}$  of each element were used. A freshly prepared solution containing 10.0  $\text{mg l}^{-1}$   $\text{Fe}^{2+}$  was employed to estimate the reduction efficiency.

Working standard solutions, 0.00, 2.50, 5.00 and 10.0  $\text{mg l}^{-1}$   $\text{Fe}^{3+}$  plus 100  $\text{mg l}^{-1}$  of  $\text{V}^{5+}$ , were used to determine Fe in the diluted sample.

Standard solutions, 0.00, 2.00, 5.00 and 10.0 mg l<sup>-1</sup> V or Mo plus 10.0, 20.0 and 30.0 mg l<sup>-1</sup> of Fe were prepared. Three synthetic solutions containing Fe and V concentrations in different proportions (50/50; 60/40 and 40/60 w/w) in 0.25 M HCl, simulating alloy samples with low silicon contents were analyzed together with the standard reference material Euro-standard 577-1 produced by the Bureau of Analysed Samples Limited (Middlesborough, UK). About 100 mg of the reference alloy were accurately weighted, received 10 ml of aqua-regia and were heated in a hot plate until complete dissolution. After cooling to room temperature 5 ml of perchloric acid (70% v/v) were added and heated until evolution of white fumes. The residual solution was diluted to 100 ml [12]. Aliquots of 5.0 ml of this solution received 50 ml of 2.5 M HCl and 50 ml of 1000 mg l<sup>-1</sup> of V before diluting to 500 ml.

### 2.3. The flow system

The electrochemical reduction of Fe<sup>3+</sup> was performed by using the flow set up depicted in Fig. 1. The electrolyte solution was continuously recycled

through the anode compartment of the electrochemical cell (EC). In the situation specified in Fig. 1, the sample solution at loop L was carried by C through the EC cathode compartment and the mixing coil B<sub>1</sub>. At the confluent point X, the sample solution received a buffered reagent stream (B + R). After passing reaction coil B<sub>2</sub> the solutions was dropped off in an open tube PS to separate gaseous components. Part of this solution was aspirated from the bottom of the tube towards the detector D with wavelength adjusted to 512 nm. Moving down the central part of the injector, L was filled with another sample solution while part of solution at the PS was drained. After 30 s, the injector returned to the position shown in Fig. 1 and simultaneously the electrical power at the EC was switched on during 30 s. The injector rested in this position during 60 s and the spectrophotometric detection occurred.

Speciation of Fe<sup>2+</sup> and Fe<sup>3+</sup> in acidified water samples (0.25 M HCl) could be accomplished with the flow system in Fig. 1. The injection of the sample allowed the direct Fe<sup>2+</sup> determination and in a second injected sample volume simultaneously the EC is switched on and the reduction

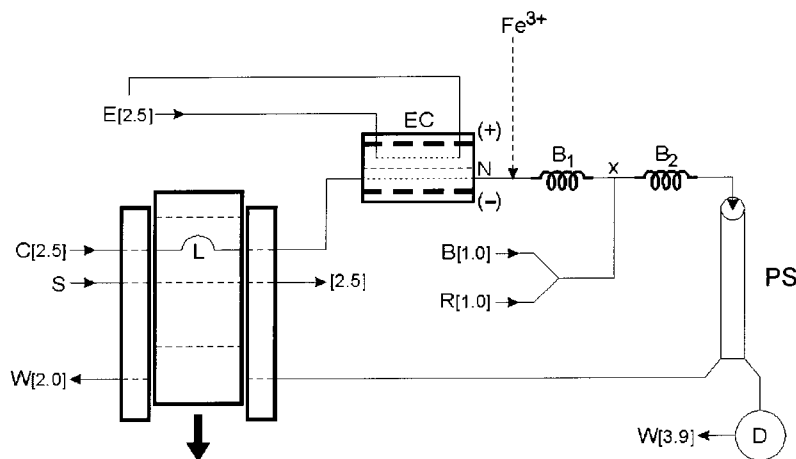


Fig. 1. A. Flow diagram for electrochemical reduction of Fe<sup>3+</sup> to Fe<sup>2+</sup>. The three rectangles at the left represent the injector in the injection position with sample in loop L. The arrow below represent the displacement of the central part to the alternative position. Lines indicate the tubing used for flowing solutions of electrolyte E, carrier C, sample S, reagent R, buffer B, and the residual W. Numbers in brackets indicate the flow rates in ml min<sup>-1</sup>, and arrows indicate the pumping direction. The electrochemical cell (EC) is schematized with the Nafion membrane N and the electrodes connections. Other devices are the mixing and reaction coils B<sub>1</sub> and B<sub>2</sub> of 25 cm tubing each, the connector X, the phase separator (PS) and the detector D. Dashed line after the EC, indicates the optional inlet to introduce the Fe<sup>3+</sup> solutions.

Table 1

Regression data obtained with solutions from 0.00 to 10.0 mg l<sup>-1</sup> Fe<sup>3+</sup> at electrolytic currents of 1.0, 2.0 and 3.0 A

Current (A)	$y = ax + b$	$r^2$	R.S.D. <sub>10Fe<sup>3+</sup></sub> <sup>a</sup>
1.0	0.012x + 0.002	0.9990	0.98
2.0	0.018x + 0.001	0.9999	2.04
3.0	0.026x + 0.004	0.9990	2.93

<sup>a</sup> Relative standard deviations (R.S.D.) for the 10 mg l<sup>-1</sup> Fe standard based on three replications.

of Fe<sup>3+</sup> occurred permitting the determination of total iron.

The flow system in Fig. 1 presents an alternative configuration to introduce the Fe<sup>3+</sup> solutions (dashed line after the cell), to study the effect of the reduced species of V and Mo produced at EC.

### 3. Results and discussion

The efficiency of the proposed electrolytic reduction of Fe<sup>3+</sup> to Fe<sup>2+</sup> is dependent on several parameters such as flow-rates, cell compartment dimensions, type and electrode surface, sample acidity and electrolytic voltage. One liter of the electrolyte solution (2 M H<sub>2</sub>SO<sub>4</sub>) was continuously pumped at 2.5 ml min<sup>-1</sup>, through the anode compartment. This solution was replaced periodically to maintain its characteristics. Under DC current the electrolyte solution yielded H<sub>3</sub>O<sup>+</sup> which crossed the Nafion membrane towards the cathode compartment. The temperature at the EC increased when the current was raised just to 3 A, sample flow rate was lower than 1.0 ml min<sup>-1</sup> and the sample acidity was < 0.05 M HCl. Under these conditions a damage of the Nafion membrane was observed. On the other hand, after increasing the sample acidity beyond 0.25 M HCl the large quantity of gases evolved impaired the Fe<sup>3+</sup> reduction. Therefore, sample solutions at 0.25 M HCl flowing at 2.5 ml min<sup>-1</sup> were employed throughout.

Effect of raising the electrolytic current at the EC to reduce solutions of Fe<sup>3+</sup> produced data in Table 1. Despite higher absorbances being attained with 3 A data presented poor precision probably due to higher gas evolution at the cham-

ber. Thus, further experiments were carried out at 2 A yielding results characterized by good linearity and precision.

Solutions containing 10.0 mg l<sup>-1</sup> of Fe<sup>3+</sup> plus 10.0 and 100 mg l<sup>-1</sup> of Pb<sup>2+</sup>, Co<sup>2+</sup>, Ni<sup>2+</sup>, Zn<sup>2+</sup>, Cu<sup>2+</sup>, V<sup>5+</sup> and Mo<sup>6+</sup> were injected using the electrolytic current switched on and off to verify the possibility of being interfering either on reduction or on the complexation reaction. The effects of concomitant additions are presented in Table 2. Cobalt solutions were colored and raised the background at 512 nm. Using a EC with clean Pt electrodes a signal increase of 10% due to Pb addition was observed. After passing repeatedly the Pb solution (total mass of 0.1 mg Pb) the signal stabilized. When the EC was opened, Pb deposition on the Pt cathode could be observed by naked eyes.

Addition of V<sup>5+</sup> and Mo<sup>6+</sup> increased the signal proportionally to the applied current emphasizing the formation of strongly reducing species [2].

The efficiency of reduction was evaluated at different electrolytic currents by comparing absorbances of a 10 mg l<sup>-1</sup> Fe<sup>3+</sup> after reduction with that corresponding to a 10 mg l<sup>-1</sup> Fe<sup>2+</sup>

Table 2

Results after addition of different ionic species to 10 mg l<sup>-1</sup> Fe<sup>3+</sup><sup>a</sup>

Ions	Added amount (mg l <sup>-1</sup> )	Absorbance
Cu <sup>2+</sup>	10	0.188 ± 0.003
	100	0.199 ± 0.010
Ni <sup>2+</sup>	10	0.189 ± 0.001
	100	0.191 ± 0.001
Zn <sup>2+</sup>	10	0.189 ± 0.003
	100	0.183 ± 0.003
Mn <sup>2+</sup>	10	0.177 ± 0.001
	100	0.179 ± 0.001
Co <sup>2+</sup>	10	0.320 ± 0.003
	100	0.407 ± 0.008
Cr <sup>3+</sup>	10	0.189 ± 0.006
	100	0.196 ± 0.009
Mo <sup>6+</sup>	10	0.315 ± 0.005
	100	0.472 ± 0.004
V <sup>5+</sup>	10	0.353 ± 0.005
	100	0.471 ± 0.009

<sup>a</sup> The analytical signal related to 10 mg l<sup>-1</sup> Fe<sup>2+</sup> was 0.180 ± 0.004 A ( $n = 3$ ).

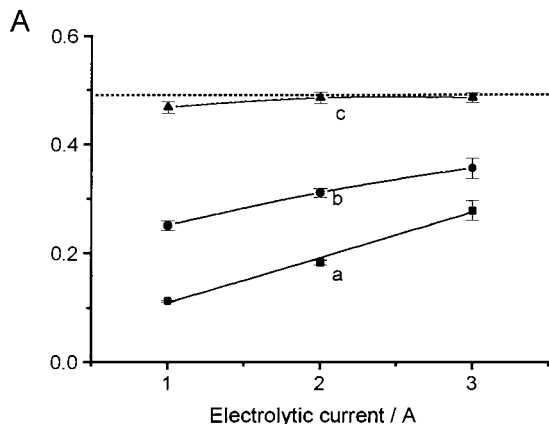


Fig. 2. Effect of the electrolytic current and the presence of  $V^{5+}$  on  $Fe^{3+}$  reduction (a)  $10\text{ mg l}^{-1} Fe^{3+}$ ; (b)  $10\text{ mg l}^{-1} Fe^{3+} + 10\text{ mg l}^{-1} V^{5+}$ ; and (c)  $10\text{ mg l}^{-1} Fe^{3+} + 100\text{ mg l}^{-1} V^{5+}$ . A is absorbance. Dashed line indicates the signal obtained by injecting a solution of  $10\text{ mg l}^{-1}$  of  $Fe^{2+}$ .

solution injected in the same way. Results are presented in Fig. 2. No signal was observed for  $Fe^{3+}$  without current at the EC. Increasing the current up to 3 A the reduction of  $Fe^{3+}$  alone increased linearly ( $r = 0.9968$ ) attaining 55% of reduction. The effect of reducing  $10\text{ mg l}^{-1} Fe^{3+}$  alone or together with 0.00, 10.0 or  $100\text{ mg l}^{-1}$  of  $V^{5+}$  could be appreciated by comparing curves at Fig. 2. The addition of  $100\text{ mg l}^{-1} V^{5+}$  to  $Fe^{3+}$  provided the best reduction efficiency, attaining total reduction after a current of 2 A (curve c, Fig. 2).

To elucidate the influence of V and Mo reduced species on the reduction of iron, an experiment involving addition of a  $Fe^{3+}$  solution after the EC was performed. Solutions of  $V^{5+}$  and  $Mo^{6+}$  were injected instead of the sample and while flowing through the EC (2 A) produced reduced species which merged with the  $Fe^{3+}$  solution. The reduction of  $10\text{ mg l}^{-1} Fe^{3+}$  occurred in an extent of 80% with  $100\text{ mg l}^{-1} V^{5+}$  and 45% with  $100\text{ mg l}^{-1} Mo^{6+}$ . Therefore, the reduced V species which formed from  $100\text{ mg l}^{-1} V^{5+}$  at the EC cell at 2 A allowed the attainment of 80% efficiency on  $Fe^{3+}$  reduction, while the efficiency of the EC alone was 38% (curve a, Fig. 2). No signal corresponding to the reduced species of V and Mo was observed probably due to their oxidation until reaching the detector unity.

The expected probable competition of  $Fe^{2+}$  and  $V^{2+}$  for 1,10-phenanthroline [5] was not observed even though a diluted solution of the reagent (0.1% w/v) and a concentrated solution of  $V^{5+}$  ( $100\text{ mg l}^{-1}$ ) reduced at 2 A was used.

The quantification of iron in dissolved ferrovanadium alloys (dilution factor of  $10^5$ ) was achieved by adding  $100\text{ mg l}^{-1} V$  to the samples and standards, assuming complete reduction of  $Fe^{3+}$  (Fig. 2).

The analytical curves in Fig. 3 were used for V quantification. The effect of increasing the V concentrations up to  $10\text{ mg l}^{-1}$  in solutions with 10, 20 and  $30\text{ mg l}^{-1}$  of Fe was characterized by linear coefficients and slopes depending on the  $Fe^{3+}$  concentrations following the relationship  $A = 0.018 C_{Fe} + 0.0008 C_{Fe} \cdot C_V$ . For the dissolved samples, the Fe concentration previously determined was used to calculate the V concentration, but this is only valid for V concentrations lower than  $10\text{ mg l}^{-1}$ . When  $C_V = 10 C_{Fe}$  maximum absorbance was attained (Fig. 2). Thus, the proposal is to add Fe to the diluted samples to ensure the determination of V in the linear analytical range (Fig. 3) for samples with a  $C_{Fe} < C_V$ . The effect of adding up to  $10\text{ mg l}^{-1} Mo$  to solutions in three different iron concentrations presented good correlation (Fig. 3 dashed lines). In this situation, the slope of the curves were not depen-

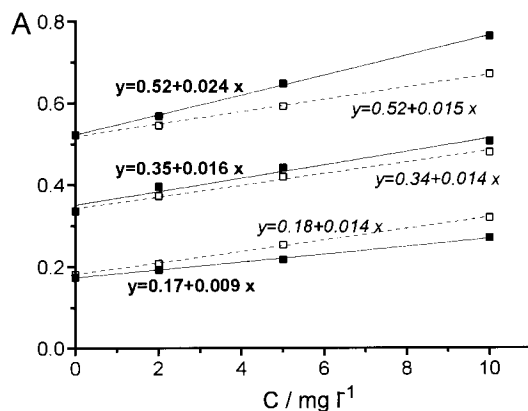


Fig. 3. Effect of adding different V (solid lines) and Mo (dashed lines) concentrations to solutions containing  $10.0$ ,  $20.0$  and  $30.0\text{ mg l}^{-1} Fe^{3+}$ . A is absorbance and C is the concentration of V or Mo added. Regression curves in bold correspond to V and those in italic to Mo.

Table 3

Results of a reference standard ferrovanadium alloy and V results in three synthetic Fe–V solutions containing 50, 40 and 60% w/w V

Sample		Fe (% w/w)	V (% w/w)
EURO-ST5771	Certified value	47.21	50.16 ± 0.13
EURO-ST5771	Found value <sup>a</sup>	47.2 ± 0.5	50.1 ± 1.8
1			52.1 ± 1.7
2			38.9 ± 0.9
3			60.5 ± 0.8

<sup>a</sup> Mean ± S.D., *n* = 3.

dent on the Fe concentration as found for V. Results for three ferrovanadium synthetic solutions and one certified reference material Euro-standard 577-1 are shown in Table 3. The certified and found results were not statistically different from each other at the 95% confidence level.

#### 4. Conclusions

The proposed electrochemical reduction approach is efficient for on-line reduction of Fe<sup>3+</sup> to Fe<sup>2+</sup> in acid solutions. Addition of V and Mo increased significantly the Fe<sup>3+</sup> reduction to Fe<sup>2+</sup>.

The proposal suits well for the quantitative determination of Fe<sup>2+</sup> and total Fe, the determination of Fe and V or Fe and Mo in the respective solubilized iron alloys by using the electrolytic chamber reduction and 1,10-phenanthroline. Application of this approach could not be used to determine V or Mo in samples contain-

ing both elements, once these elements are determined indirectly by its effect on iron reduction.

#### Acknowledgements

Financial support from FAPESP (Fundação de Amparo à Pesquisa do Estado de São Paulo) and CNPq (Conselho Nacional de Desenvolvimento Científico e Tecnológico) was greatly appreciated.

#### References

- [1] M.F. Gine, H.F. Bergamin, E.A.G. Zagatto, B.F. Reis, *Anal. Chim. Acta* 114 (1980) 191.
- [2] R.C. Schothorst, J.M. Reijn, H. Poppe, G. den Boef, *Anal. Chim. Acta* 145 (1983) 197.
- [3] R.C. Schothorst, G. den Boef, *Anal. Chim. Acta* 153 (1983) 133.
- [4] R.C. Schothorst, M. van Son, G. den Boef, *Anal. Chim. Acta* 162 (1984) 1.
- [5] A.T. Faizullah, A. Townshend, *Anal. Chim. Acta* 167 (1985) 225.
- [6] L. Tomlinson, *J. Electrochem. Soc.* 111 (1964) 593.
- [7] Y. Lin, X. Wang, D. Yuan, P. Yang, B. Huang, Z. Zhuang, *J. Anal. At. Spectrom.* 7 (1992) 287.
- [8] A. Brockmann, C. Nonn, A. Golloch, *J. Anal. At. Spectrom.* 8 (1993) 397.
- [9] W.W. Ding, R.E. Sturgeon, *J. Anal. At. Spectrom.* 11 (1996) 225.
- [10] C. Schickling, J. Yang, J. Broekaert, *J. Anal. At. Spectrom.* 11 (1996) 739.
- [11] T. Blanco, N. Maniasso, M.F. Gine, A.O. Jacintho, *Analyst* 123 (1998) 191.
- [12] Annual Book of ASTM Standards, Section 3. Metals Test Methods and Analytical Procedures E31, Philadelphia, USA, 1991, p. 29.

# Determination of transition metals in human hair by high-performance liquid chromatography using sodium hexadecane-sulfonate coated columns

Agostinho A. Almeida, Xiao Jun, José L.F.C. Lima \*

*CEQUP/Departamento de Química-Física, Faculdade de Farmácia, Universidade do Porto, Rua Anibal Cunha, 164, 4050 Porto, Portugal*

Received 7 September 1998; accepted 13 October 1998

## Abstract

A chromatographic method for the determination of transition metals in human hair samples is described. The method involves the separation of Cu, Pb, Zn, Ni, Co, Cd and Mn in a C18 column coated with sodium hexadecane-sulfonate (SHS) and spectrophotometric detection (520 nm) after post-column reaction of the eluted metals with 4-(2-pyridylazo)-resorcinol (PAR). The eluent was a 100 mM tartrate solution adjusted to pH 3.1 with a 2 M sodium hydroxide solution (flow-rate = 1.0 ml min<sup>-1</sup>). A good separation of the eluted metals (specially for Cu/Pb and Zn/Ni) has been achieved. The detection limits, expressed as µg l<sup>-1</sup>, were 2.2 (Cu), 8.0 (Pb), 2.8 (Zn), 1.5 (Ni), 1.5 (Co), 12.0 (Cd), and 1.4 (Mn). A microwave-assisted closed vessel acid digestion procedure with HNO<sub>3</sub> + HClO<sub>4</sub> (4 + 1 ml) was used for the hair samples solubilisation. Nineteen hair samples were analysed with the proposed method. The results were in good agreement with those obtained by atomic absorption spectrometry (AAS). © 1999 Elsevier Science B.V. All rights reserved.

*Keywords:* Hair; Transition metals; HPLC; Coating column

## 1. Introduction

Human hair is an excretory system for trace metals, can act as an accumulating tissue and its metal content can reflect the body status for a long period [1–5]. Therefore, and considering the simplicity of sampling, storing and handling, hu-

man hair is an attractive biological material for determining the body's trace element status either for nutritional, toxicological or clinical diagnostic purposes [1,2,5].

The most used techniques for the determination of elements in hair are neutron activation analysis, X-ray fluorescence analysis, particle induced X-ray emission, anodic stripping voltammetry, atomic fluorescence spectrometry, mass spectrometry and atomic emission spectrometry with inductively coupled plasma and atomic absorp-

\* Corresponding author. Tel.: +351-2-207-8900; fax: +351-2-200-3977.

*E-mail address:* limajlfc@ff.up.pt (J.F.C. Lima)

tion spectrometry (AAS) with electrothermal (ET) atomisation or with flame (F) atomisation [5,6].

In this context, the techniques allowing multi-element determinations are of particular interest, since the number of potentially relevant elements is high and antagonist or synergistic effects can be taken into account [2]. However, even considering that chromatographic techniques enable multi-metal determination, there are only few reports dealing with its application in the determination of metals in hair. Yang et al. [7] used a complex sample treatment before the chromatographic analysis with UV detection (254 nm). Sturaro et al. [8] used dynamic ion-exchange chromatography for the separation of transition metals in human hair and colorimetric detection after post-column derivatisation with 4-(2-pyridylazo)-resorcinol (PAR), but the resolutions of ion pairs Zn/Ni and Cu/Pb were not enough for an accurate determination of Ni and Pb at a single wavelength owing to the intense chromatographic peaks of Cu and Zn. Another chromatographic determination of some alkaline-earth and transition metals using conductivity detection was proposed by Xu et al. [9], though the detection limits were high, considering the normal expected values of transition metals in hair.

One of the main reasons why analytical atomic techniques are clearly preferred when metals determination in hair is intended and that further clarifies the scarce use of chromatographic techniques is the fact that the latter procedure is much more dependent on the sample digestion. In this work a high performance liquid chromatography (HPLC) method for the simultaneous determination of transition metals in human hair samples is described. Special attention was given to chromatographic resolution and sample digestion. Different wet ashing procedures have been tested, either in opened or closed vessels. Finally, a microwave-assisted acid digestion procedure using  $\text{HNO}_3$  and  $\text{HClO}_4$  was chosen for this analytical purpose. The method has been applied to 19 human hair samples and the results are in good agreement with those provided by AAS.

## 2. Experimental

### 2.1. Apparatus

The chromatographic system used was a Waters ACTION Analyser (Millipore, Bedford, MA). The analytical column was a sodium hexadecane-sulfonate (SHS)-coated Waters Nova-Pak C18 reversed-phase column ( $3.9 \times 150$  mm, with  $4 \mu\text{m}$  diameter particles). A Pye Unicam Model SP9 spectrophotometer (Philips Scientific, Cambridge, UK), equipped with a Hellma (Baden, Germany)  $8 \mu\text{l}$  flow-cell, was used for the colorimetric detection at 520 nm and a Gilson Minipuls 3 peristaltic pump for the post-column PAR delivery. A single-bead string reactor (5 cm length) and a T-piece were used for mixing the column effluent with the PAR solution. All tubes were made of PTFE and obtained from Omnifit (Cambridge, UK). A personal computer equipped with Gilson 712 HPLC software and connected to the chromatographic system by a Gilson 506C interface was used to acquire, store and process the analytical data. The pH measurements were made with a Metrohm electrode (Herisau, Switzerland) coupled to a Model pH 300 pH meter (Anatron Instruments, Matosinhos, Portugal). For ETAAS determinations, a Perkin-Elmer (Uberlingen, Germany) Model 4100 ZL atomic absorption spectrophotometer equipped with a transverse heated graphite atomiser (THGA) and an AS 70 auto-sampler was used. Graphite tubes were of end-capped type (Perkin-Elmer Part. No. B300-0644). The determinations have been made according to the instrumental and analytical conditions (e.g. graphite furnace programs and matrix modifiers) recommended by the manufacturer. FAAS determinations have been carried out using a Perkin-Elmer Model 3100 instrument, also operated according to the manufacturer recommended conditions. Hollow cathode lamps were used for both ETAAS and FAAS. Microwave-assisted acid digestions have been made using a Milestone (Soriso, Italy) MLS 1200 mega high performance microwave digestion unit, equipped with a HPR-1000/10 S rotor.

## 2.2. Reagents and solutions

SHS and PAR were obtained from Fluka (Buchs, Switzerland) and concentrated nitric acid of Suprapur grade was obtained from Merck (Darmstadt, Germany). All the other chemicals were obtained from Riedel-deHaen (Seelze, Germany) and were of analytical-reagent grade, except the methanol and the acetonitrile which were of HPLC grade. Spectrosol atomic absorption standards obtained from BDH (Poole, UK) were used as stock solutions for preparing the calibration standards. Chemical modifier solutions for Pb ETAAS determinations were prepared from commercial solutions of magnesium nitrate and palladium nitrate supplied by Merck. Purified water (18 M $\Omega$ ) was obtained with a Milli-Q system (Millipore).

## 2.3. Preparation of the column

To prepare the analytical column, a 2 mM SHS solution in an acetonitrile:water (0.25:0.75 v/v) mixture was pumped through the C18 column at a flow-rate of 0.5 ml min<sup>-1</sup> for 6 h [10]. Before use, the coated column was equilibrated with the eluent for 1 h (1.0 ml min<sup>-1</sup> flow-rate).

## 2.4. Samples analysis

Prior to acid digestion, 1–2 g of hair samples was finely grind and washed according to the procedure proposed by the International Atomic Energy Agency [11]. Afterwards, samples were dried overnight at 110°C. For the samples decomposition 0.5 g was weighted into the PTFE digestion vessels and 4 ml of concentrated HNO<sub>3</sub> plus 1 ml of concentrated HClO<sub>4</sub> acid were added. Then the following microwave oven program was run: 250 W, 1 min; 0 W, 2 min; 250 W, 5 min; 400 W, 5 min; 600 W, 5 min. After cooling, the samples digests were transferred into conic flasks and slowly evaporated to near dryness. Using volumetric flasks, the residues were then brought to a final volume of 20 ml with the eluent. The solutions obtained were analysed by both the HPLC method and AAS. The conditions for the HPLC determinations are summarised in Table 1.

## 3. Results and discussion

### 3.1. Chromatographic separation conditions

The separation of transition metals in human hair digests using ion-pair chromatography with sodium octane-sulphonate as the ion-pair agent has been investigated [8]. However, the resolution between Pb and Cu as well as between Zn and Ni was not good enough for the analytical purpose, especially considering that the hair has a much higher Zn level than Ni (about 250-fold) [2].

The ion-pair agents having a sufficiently long carbon chain can be adsorbed onto the stationary phase, which enables permanently coated columns to be obtained. In a previous work [10] the utilisation of SHS as a coating agent of C18 columns for the separation of transition metals was studied. SHS provided a good stability of the column coating due to being strongly adsorbed to the stationary phase as a consequence of its long carbon chain. The SHS-coated column could be continuously used for 5 months with no significant changes in retention times. In this work, a SHS-coated Nova-Pak C18 column was prepared for the separation of the transition metals in hair digests. The eluent was a 100 mM tartaric acid solution adjusted to a pH value of 3.1 with a 2 M sodium hydroxide solution. Figs. 1 and 2 show representative chromatograms of a standard and a digested sample solution, respectively. As can be observed, a fair separation between all the elements, including Zn and Ni, is achieved.

Table 1  
Operating conditions for the chromatographic determinations

Separating column	Nova-Pak C18 (3.9 × 150 mm), permanently coated with sodium hexadecane-sulphonate (SHS)
Mobile phase	100 mM tartaric acid solution; pH adjusted to 3.1 with 2 M sodium hydroxide solution
Flow-rate	1.0 ml min <sup>-1</sup>
Colour reagent	0.2 mM PAR solution, containing 1 M of acetic acid and 3 M ammonium hydroxide
Detection	Post-column derivatisation; $\lambda = 520$ nm



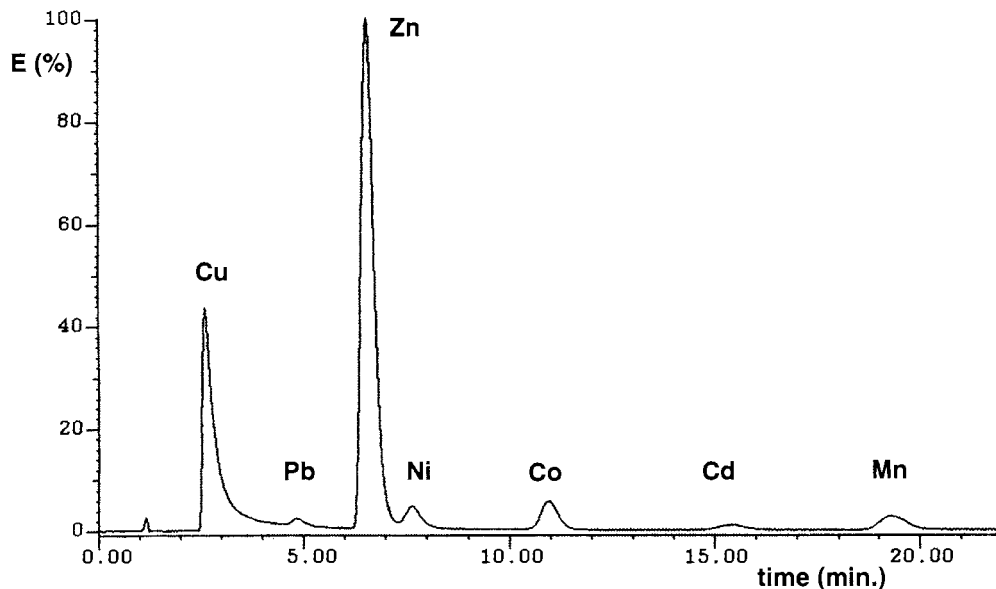


Fig. 1. Typical chromatogram of a 2.5 (Cu), 0.4 (Pb), Zn (5.0), 0.2 (Ni), 0.2 (Co), 0.4 (Cd) and 0.2 (Mn)  $\text{mg l}^{-1}$  standard solution (full scale = 609.3 mV).

### 3.2. Digestion conditions

In this work, the digestion of hair samples by both open vessels on a hot plate and closed vessels in a microwave oven unit was studied. The latter is currently considered the most universal and powerful technique for solid sample solubilisation [12]. In fact, microwave energy dramatically speeds up the sample dissolution process and microwave-assisted wet digestions in closed vessels minimise the reagents consume [12–16] and the problems related to the losses of analytes or sample contamination [13–16]. Nevertheless, it is described that an incomplete oxidation of organic compounds may occur [13]. For some techniques (e.g. ICP-AES, ICP-MS, FAAS and ETAAS) the presence of organic carbon residues is not critical, but for others, that can be crucial for obtaining accurate results [13,16]. That is particularly true with the chromatographic methods combined with UV/VIS spectrophotometric detection, which imposes a special attention to the samples digestion, since the majority of the described procedures are related with atomic spectrophotometric techniques. To develop the microwave-assisted wet digestion procedure, a mixture of different

hair samples has been prepared and divided into ten aliquots of the same size (0.5 g). Aliquots 1–3 have been treated with the digestion mixture  $\text{HNO}_3 + \text{H}_2\text{O}_2$  (4 + 1 ml) and aliquots 4–6 with  $\text{HNO}_3 + \text{HClO}_4$  (also 4 + 1 ml). In all the cases the microwave oven program used was as referred in Section 2, except for aliquot 1 (a microwave programme with a final step at 650 W was used). Aliquots 7–10 were treated exactly as aliquots 1–3, but after the first microwave digestion 1 ml of  $\text{HClO}_4$  acid was added and the microwave digestion program was repeated. Aliquot 6 was also submitted to this second treatment with 1 ml  $\text{HClO}_4$  acid and a second microwave digestion step. After cooling, all the digested solutions were slowly evaporated to near dryness (in conic flasks, enabling acid refluxing), the residue was diluted with the eluent (final volume = 20 ml) and 100  $\mu\text{l}$  sample solution was injected into the chromatographic system.

The criteria used for considering that the digestion was adequate was the attainment of a sample digest chromatogram with a peak resolution similar to the chromatogram of the standard solutions. Clear chromatograms were obtained for aliquots 4–10 (see Fig. 2 for example), what led to

the conclusion that  $\text{HClO}_4$  was necessary whereas the  $\text{HNO}_3 + \text{H}_2\text{O}_2$  (4 + 1 ml) mixture was not strong enough for the complete digestion of the hair (see Fig. 3).

Moreover, the open vessels procedure required the use of 16 ml of concentrated  $\text{HNO}_3$  and 4 ml of concentrated  $\text{HClO}_4$  for the complete digestion of 0.5 g of sample. The amount of  $\text{HClO}_4$  plays an important role on the digestion. In both cases (open vessels or closed vessels) it seems that the reflux with  $\text{HClO}_4$  is essential to decompose the residual organic matter. Therefore, the boiling-off of the acid mixture after acid digestion procedure has to be done slowly in a conic flask rather than in a beaker and under conditions that assure the perchloric acid refluxing.

### 3.3. Application to the analysis of hair samples

The developed chromatographic method has been applied to the analysis of 19 hair samples. The same solutions prepared for the chromatographic determination were also analysed by AAS (FAAS for Cu and Zn and ETAAS for Pb and Ni). The accuracy of the ETAAS determinations

of Pb and Ni was assessed by performing recovery measurements in two different samples, being obtained 93.7 and 98.5% for Pb and 101.5 and 104.0% for Ni.

From a statistical point of view, there were no significant differences between the results obtained by HPLC and atomic absorption techniques (Table 2).

Using the present method, the intense chromatographic peaks for Zn and Cu did not influence the results of Pb and Ni due to the good resolution. Under the selected digestion conditions, the chromatograms for hair samples are as clear as those for standard solutions. Nevertheless, no chromatographic peaks for Cd and Mn were found with all the hair samples tested, indicating that their concentration levels in the samples are lower than the quantification limits of the proposed HPLC method.

## 4. Conclusions

The developed method proved to be an alternative procedure for measuring transition metals in

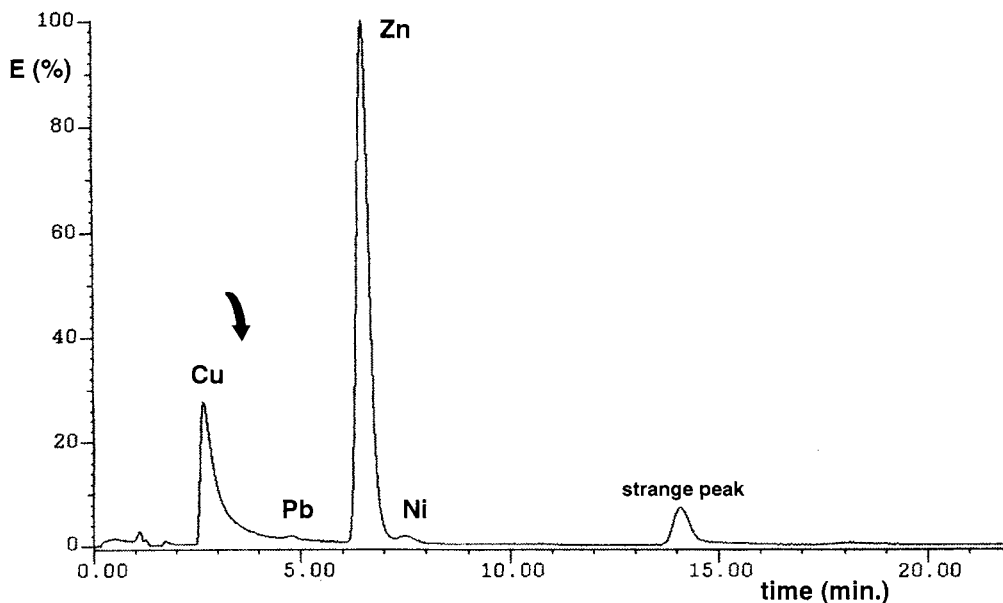


Fig. 2. Typical chromatogram of a completely digested hair sample (4 ml  $\text{HNO}_3 + 1$  ml  $\text{HClO}_4$  mixture) (full scale = 463.7 mV).

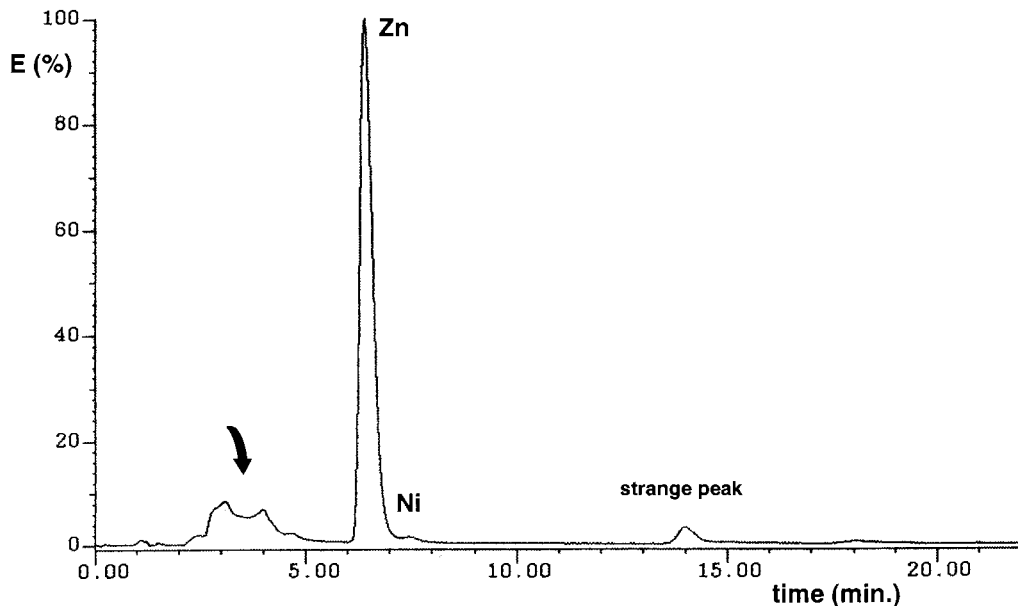


Fig. 3. Chromatogram of an incompletely digested hair sample (4 ml  $\text{HNO}_3$  + 1 ml  $\text{H}_2\text{O}_2$  mixture (full scale = 617.1 mV).

hair samples. Its main advantage lays on the simultaneous determination of four elements of great importance in human hair analysis being carried out with the widely available and inexpensive HPLC instruments. For example, using atomic absorption techniques, and considering the final concentrations of the solutions obtained, both F (for Zn and Cu) and ET atomisation (for Ni and Pb) are required.

For sample preparation, both open vessels or microwave-assisted closed vessels acid digestion can be used if enough quantity and refluxing of  $\text{HClO}_4$  are assured.

The permanently coated reversed-phase column used presents the advantage of its low cost and large flexibility over the commercial ion columns. Additionally, it provides a better chromatographic efficiency than that achieved with dynamically coated reversed-phase columns [8], demonstrated by the good separation between Zn and Ni.

Compared to other chromatographic procedures described, the proposed method is simpler [7], presents better chromatographic efficiency [8] or better detection limits [9]. Its accuracy, evalu-

ated by comparison with AAS determinations, proved to be good.

### Acknowledgements

The authors thank the financial support obtained from Projecto Praxis XXI (Project 2/2.1/SAU/1190/95). One of us (A.A.A.) thanks PRODEP for a PhD grant.

Table 2  
Results of the statistical evaluation of the method accuracy<sup>a</sup>

Regression analysis	$R^2$	$t_{\text{calc.}}^b$	Range ( $\mu\text{g g}^{-1}$ )
$\text{Cu}_{\text{HPLC}} = 0.938$ $\text{Cu}_{\text{FAAS}} + 0.856$	0.9867	0.0611	16.0–375
$\text{Pb}_{\text{HPLC}} = 1.051$ $\text{Pb}_{\text{ETAAS}} - 0.416$	0.9837	0.9528	0.81–34.8
$\text{Zn}_{\text{HPLC}} = 1.002$ $\text{Zn}_{\text{FAAS}} - 0.934$	0.9975	0.5890	126–498
$\text{Ni}_{\text{HPLC}} = 0.943$ $\text{Cu}_{\text{ETAAS}} + 0.296$	0.9855	0.0065	1.14–11.6

<sup>a</sup>  $n = 19$  for all the elements, except for Ni ( $n = 8$ ).

<sup>b</sup>  $t_{\text{tab}} = 2.101$  (2.365 for Ni).  $t_{\text{calc.}}$  and  $t_{\text{tab}}$  are the calculated and tabulated values for a Student's  $t$ -test at a 95% confidence level, respectively.

## References

- [1] S.A. Katz, *Int. Lab.* 3 (1979) 181.
- [2] O. Senofonte, N. Violante, L. Fornarelli, E. Beccaloni, A. Powar, S. Caroli, *Ann. Ist Super. Sanità* 3 (1989) 385.
- [3] K. Bencze, *Fresenius J. Anal. Chem.* 337 (1990) 867.
- [4] J.A. Cargnello, J.J. Powell, R.P.H. Thompson, P.R. Crocker, F. Watt, *Analyst* 120 (1995) 783.
- [5] J. Kubová, V. Hanáková, J. Medved, V. Stresko, *Anal. Chim. Acta* 337 (1997) 329.
- [6] A. Taylor, S. Branch, H.M. Crews, D.J. Halls, *J. Anal. At. Spectrom.* 7 (1992) 89R.
- [7] S. Yang, J. Xu, Q. Shen, X. Zhang, L. Yang, Y. Ma, Y. Lin, *Zhonghua Yixue Jianyan Zazhi* 13 (1990) 71.
- [8] A. Sturaro, G. Parvoli, L. Doretto, S. Zanchett, G. Allegri, G.A. Battiston, *Anal. Chim. Acta* 274 (1993) 163.
- [9] H.S. Xu, Z.Y. Xian, W. Qian, J. Yao, *Fenxi Kexue Xuebac* 11 (1995) 33.
- [10] A.A. Almeida, X. Jun, J.L.F.C. Lima, *Analyst* 123 (1998) 1283.
- [11] Y.R. Ryabukhin, Report of The Advisory Group on the Applications of Nuclear Methods in Environmental Research, IAEA, 1976.
- [12] M. Zischka, G. Knapp, *Anal. Eur.* 11 (1997) 18.
- [13] W. Jiang, S.J. Chalk, H.M. 'Skip' Kingstom, *Analyst* 122 (1997) 211.
- [14] M.A.Z. Arruda, R.E. Santeli, *Quím. Nova* 20 (1997) 638.
- [15] M. Burguera, J.L. Burguera, *Quím. Anal.* 15 (1996) 112.
- [16] I. Novozamsky, H.J. van der Lee, V.J.G. Houba, *Mikrochim. Acta* 19 (1995) 183.

# Micellar electrokinetic capillary chromatography as an alternative method for the determination of ethinylestradiol and levo-norgestrel

J.J. Berzas <sup>a,\*</sup>, B. Del Castillo <sup>b</sup>, G. Castañeda <sup>a</sup>, M.J. Pinilla <sup>a</sup>

<sup>a</sup> Departamento de Química Analítica y Tecnología de Alimentos, Facultad de Químicas, Universidad de Castilla-La Mancha, E-13071 Ciudad Real, Spain

<sup>b</sup> Sección departamental de Química Analítica, Facultad de Farmacia, Universidad Complutense de Madrid, Madrid, Spain

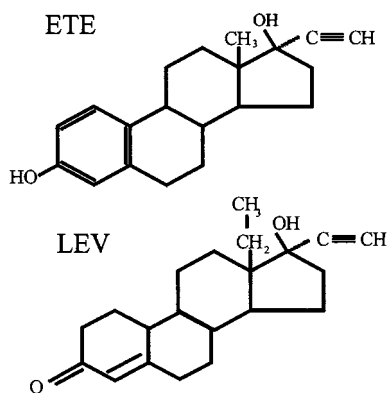
Received 7 September 1998; received in revised form 9 October 1998; accepted 13 October 1998

## Abstract

A method for quantifying of ethinylestradiol (ETE) and levo-norgestrel (LEV) in pharmaceutical products by micellar electrokinetic chromatography (MEKC) is described. The separation was carried out at 25°C and 25 kV, using a 20 mM borate buffer (pH 9.2), 15 mM sodium dodecylsulfate (SDS) in 30% acetonitrile/water (v/v). Under these conditions the analysis takes about 7 min. The method has been applied for quantifying both compounds in six different commercial contraceptives and the proposed method gave good results when compared with a reference liquid chromatographic (LC) method. © 1999 Elsevier Science B.V. All rights reserved.

**Keywords:** Ethinylestradiol; Levo-norgestrel; Micellar electrokinetic chromatography (MEKC); Oral contraceptives

## 1. Introduction



Ethinylestradiol (ETE) is a semisynthetic estrogen female sex hormone, which is present at a very low dosage level (30–100 µg tablet<sup>-1</sup>) in combination with levo-norgestrel (LEV), an orally active synthetic progestin which is present at a level of 1–4 times that of the estrogen. The structure of LEV has a characteristic D<sup>4</sup>-3-Keto group in A-ring with a different chromophoric power to ETE. Oral contraceptives have had an enormous positive impact on public health for the past three decades and, overall, there has been a remarkably low incidence of troublesome side-effects.

At present three types of oral contraceptives are available. In the sequential type, estrogen is administered alone for the first week, followed

\* Corresponding author. Tel.: +34-926-29-53-39; fax: +34-926-29-53-18.

E-mail address: jjberzas@qata-cr.uclm.es (J.J. Berzas)

by a lower dosage of the estrogen in conjunction with progestogen for the remainder of the course. In the second type, commonly used, both estrogen and progestogen are present in the tablets (as either a single dose or in three different doses). In the progestogen type, progestogen alone is administered.

Several studies [1–12] on the determination of contraceptive agents including the use of radioimmunoassay [1], radioactively labeled derivatives [2,3], dansyl or other fluorescent derivatives [4–6], spectrophotometry [7–9] and liquid chromatographic (LC) [10–12]. No references were found for ETE and LEV in capillary electrophoresis (CE). Since capillary electrophoresis offers important advantages, such as rapid set-up of instrumentation, versatility and low cost, and has proved to be a valuable method in the quality control of drugs substances [13,14], its performance in the determination of ETE and LEV was evaluated in this paper. Similar studies were made with gestodene (GTD) and ETE in previous works.

## 2. Experimental

### 2.1. Apparatus

A Beckman P/ACE 5510 (Fullerton, CA) capillary electrophoresis system equipped with a diode-array detector was used. The system was controlled by a Dell DIMENSION™ P133V with P/ACE Station Software. Separation was carried out on a 57 cm (50 cm to the detector)  $\times$  75  $\mu$ m i.d. fused silica capillary housed in a cartridge with a detector window 800  $\times$  100 mm.

A Shimadzu (Kyoto, Japan) liquid chromatography equipped with a Nova-Pak C<sub>18</sub> column (15  $\times$  0.39 cm i.d., 4 mm), a diode-array detector, a Rheodyne injection valve and connected to a computer fitted with CLASS LC-10 software was used.

A Crison (Barcelona, Spain) MicropH 2002 pH meter was used for the pH measurements.

A Beckman (Fullerton, CA) DU-70 spectrophotometer equipped with 1.0 cm quartz cells

and connected to an IBM-PS 2 Model 30 computer, fitted with Beckman Data Leader software, was used.

### 2.2. Reagents and solutions

Ovoplex, Ovoplex 30/150 and Triciclor formulations were obtained from WYETH-ORFI S.A. (Spain), and Microgynon, Neogynona and Triagynon formulations from SCHERING AG (Spain).

ETE and LEV were obtained from Sigma (St. Louis, MO). Standard solutions were prepared in 50% acetonitrile/water (v/v) (200 mg l<sup>-1</sup>) and their stabilities were evaluated over a period of 7 days by spectrophotometric measurements of diluted solutions, in 50% acetonitrile/water (v/v), of LEV and ETE at a concentration of 15 mg l<sup>-1</sup>. The spectra were recorded between 190 and 315 nm at a scan speed of 300 nm min<sup>-1</sup>. ETE and LEV were assumed to be stable under the operating conditions.

All chemicals and solvents used were of analytical-reagent grade.

### 2.3. Sample pretreatment

#### 2.3.1. LC

The described method is a slight modification of the one proposed by the Pharmacopoeia [15].

The mobile phase was a deaerated mixture of acetonitrile/methanol/water in a relation 3.5:1.5:4.5 (v/v/v), the flow rate was about 1 ml min<sup>-1</sup> and spectrophotometric detection was performed at 214 nm. Twenty tablets were finely powdered and an appropriate aliquot (equivalent to the medium mass of three tablets) was dissolved in 10 ml of mobile phase by sonication for 10 min, followed by shaking by mechanical means for 20 min and finally centrifuged for 5 min.

#### 2.3.2. MECC

Twenty tablets were washed with 40 ml of water by shaking for 45 s. The washing water was eliminated. Then, the same treatment was carried out with 10 ml of water for 3 s. These two washed steps were necessary for removing the cover which

showed interferences in the determination of ETE and LEV. Later, the tablets were dissolved in 40 ml of electrolyte (20 mM borate buffer, 15 mM sodium dodecylsulfate (SDS) and 30% acetonitrile (v/v)) by shaking by mechanical means for 30 min and lastly, they were centrifuged for 5 min.

#### 2.4. Operating conditions

Separations were conducted using 4 ml glass vials. The rinse step was carried out using different vials from the separation vials in order to keep the level of buffer constant in the anodic separation vial.

The capillary was conditioned prior to its first use by flushing first with 0.1 M NaOH for 20 min and then with water for 10 min.

In the optimized method, the capillary was filled under high pressure for 2 min with NaOH 0.1 N, later was filled for 3 min with the separation buffer, followed by a 5 s hydrodynamic sample injection. The separation was performed at 25 kV for 10 min (with a 125 kV min<sup>-1</sup> ramp voltage) at 25°C; under the selected conditions the current was 68  $\mu$ A.

The data generated from the first two injections in a sequence were not used because of the requirement for system equilibration.

### 3. Results and discussion

#### 3.1. Preliminary studies

The study was carried out using a borate buffer (20 mM, pH 9.2) with SDS (20 mM) and the aqueous phase was modified by using an organic solvent (acetonitrile) in order to get a better selectivity. These initial conditions were selected according to another study made with similar drugs.

##### 3.1.1. Influence of acetonitrile

This organic solvent was used as an additive to micellar solution to manipulate the capacity factors or the selectivity. The organic modifier

alters the retention mechanism by changing the polarity of the aqueous phase, the electrolyte viscosity and the zeta potential.

Concentrations of acetonitrile up to 40% (v/v) were tested and an improvement of resolution was found up to 30% acetonitrile/water (v/v) that can be explained by peak broadening decrease with decreasing retention times. However, for higher concentration the resolution is slightly reduced because of the breakdown of micellar structure. Acetonitrile 30% concentration (v/v) was selected due to high resolution and low analysis time as can be seen in Fig. 1.

##### 3.1.2. Influence of SDS concentration on migration time and separation

Now, the effect of surfactant concentration on the retention times of the drugs is studied. The separation potential was 20 kV and the operating temperature 25°C. Fig. 2 shows the effect of different concentrations of SDS added to the buffer (20 mM borate, pH 9.2; 30% acetonitrile). For SDS concentration of zero, ETE and LEV eluted with the electroosmotic flow (EOF). Results demonstrate that the SDS concentration has low effect on the velocity of EOF but dramatic influ-

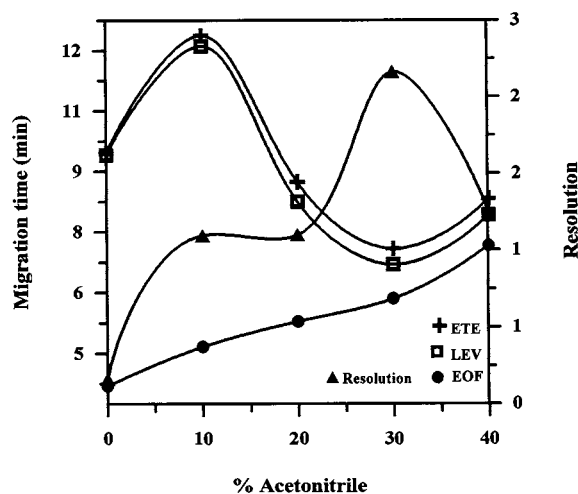


Fig. 1. Influence of acetonitrile on migration times (MT) and resolution. Operating conditions: variable % acetonitrile containing 20 mM borate buffer (pH 9.2), 15 mM sodium dodecylsulfate (SDS); 20 kV and 25°C.

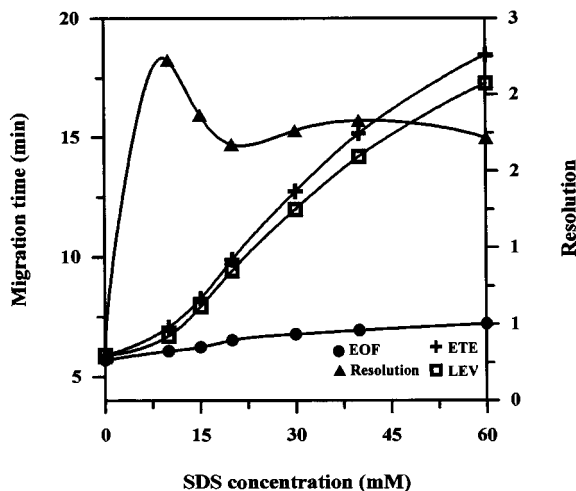


Fig. 2. Influence of sodium dodecylsulfate (SDS) concentration on migration times (MT) and resolution. Operating conditions: 20 mM borate buffer (pH 9.2), 30% acetonitrile with SDS concentrations between 10 and 60 mM; 20 kV and 25°C.

ences in the mobility of the two compounds. A concentration of 15 mM SDS was selected for the experiment because it gave narrow high peaks and good resolution with an acceptable current intensity (60  $\mu$ A) and analysis time (10 min).

### 3.1.3. Influence of borate buffer concentration

The ionic strength of buffer has significant effects on solutes mobilities and separation efficiency [16]. When the capillary temperature is controlled, increasing the buffer concentration will lower the EOF (because it lowers the zeta potential) which prolongs the analysis times [17]. While very lower buffer concentrations will give shorter analysis times and it may cause broadened and asymmetric peaks [18]. Using 20 kV and 25°C, the effect of varying the buffer concentration from 10 to 35 mM was investigated (Fig. 3). While short separation times and high efficiencies are desirable, the most important aspect is resolution. It takes into account how narrow and how far apart adjacent peaks are.

Borate buffer (20 mM) was selected as a compromise between resolution and analysis time. As can be seen in Fig. 3, the resolution increases very fast with the buffer concentration up to 30 mM and finally decreases for high concentrations.

### 3.1.4. Effect of temperature

A temperature lower than 20°C was not considered for the following reasons. Firstly, the surfactant has sufficient solubility to form micelles only at temperatures above the Kraft point (16°C for SDS). Secondly, temperature regulation with the instrument is efficient only until 4°C below room temperature. The effect of temperature on the separation between 20 and 40°C was investigated.

The resolution remains unaffected by temperatures between 20 and 30°C. For temperatures higher than 30°C, contributions of Joule heating and temperature gradient become more pronounced giving band broadening. A temperature of 25°C was selected as a compromise between run time (Fig. 4(a)), resolution and current intensity (Fig. 4(b)) and acceptable level of baseline noise.

### 3.1.5. Influence of running voltage

The maximum voltage was determined from graph of observed current versus applied voltage (Ohm's law plot). Running voltages in the range 5–30 kV were tested by using the experimental conditions selected above. This graph was linear up to 25 kV. Later increments given a deviation

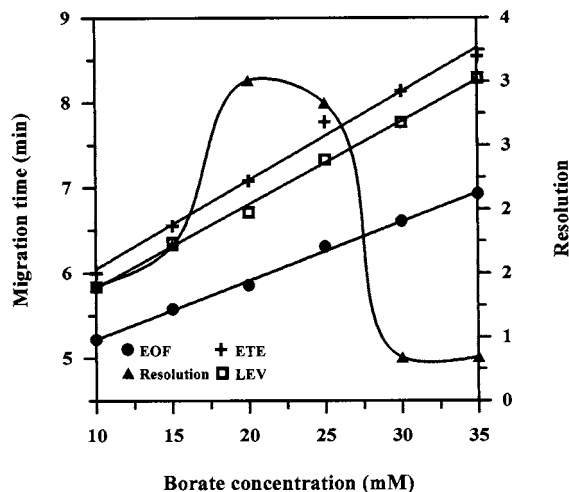


Fig. 3. Influence of buffer molarity. Operating conditions: variable buffer molarity pH 9.2 containing 30% acetonitrile and 15 mM sodium dodecylsulfate (SDS); 20 kV and 25°C.



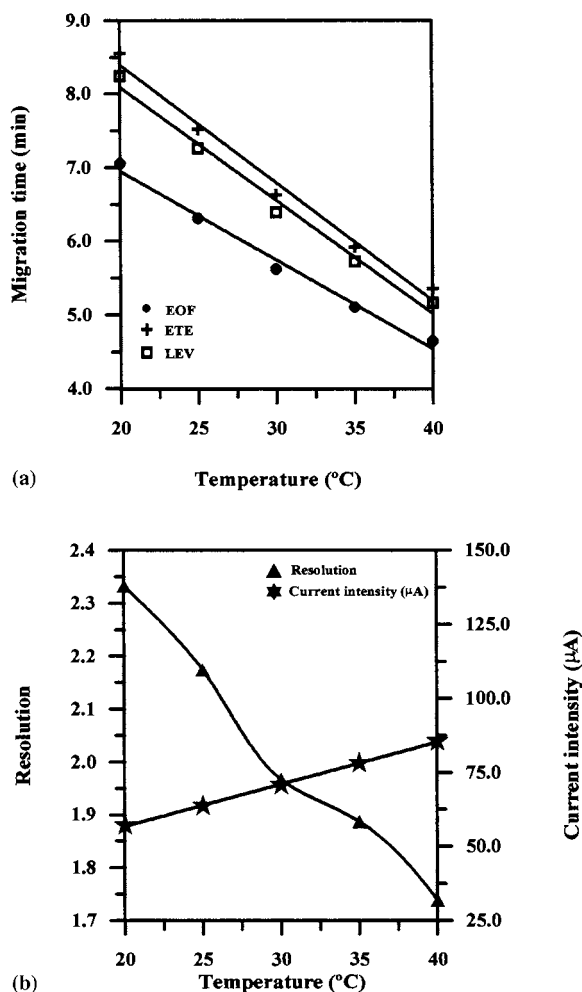


Fig. 4. Influence of temperature on migration times (MT) (a), resolution and current intensity (b). Operating conditions: 20 mM borate buffer (pH 9.2), 30% acetonitrile with 15 mM sodium dodecylsulfate (SDS); 20 kV and variable temperature.

from linearity and an increase in the slope of the plot. Because of this, a potential of 25 kV was selected as optimum. As expected, decreasing migration time was obtained with increasing applied voltages. Since higher voltages give shorter analysis times, higher efficiencies and in the other way higher currents and increased Joule heating.

Ramp voltage was varied from 0.2 to 1 min (0.42–2.1 kV s<sup>-1</sup>) and 0.2 min was selected as it gave the best migration times for ETE and LEV. (Separations were performed at 25 kV.)

### 3.1.6. Optimization of rinse and wash steps

A wash step of 2 min with 0.1 M sodium hydroxide, followed by a 3-min buffer wash, was adequate to restore the capillary wall surface and re-equilibrate the capillary between sample injections.

## 3.2. Performance evaluation

### 3.2.1. Linearity of the response

In all cases the results were obtained using corrected peak areas (CPA) for calculations (for obtaining CPA, the peak area of each peak was divided by its corresponding migration time) [19]. Linearity was assessed both by injecting solutions of ETE and LEV in the concentration range 2–60 mg l<sup>-1</sup> ( $n = 7$ ) at a constant injection time (5 s), and by injecting a solution (25 mg l<sup>-1</sup> ETE and 25 mg l<sup>-1</sup> LEV) with variable injection times (from 2 to 10 s,  $n = 5$ ).

The regression equations were:

Constant injection time:

$$\text{LEV: CPA} = -23.8 \pm (84.47) + 132.96 \pm (2.81) \times \text{conc. (mg l}^{-1}\text{); } r^2 = 0.9994$$

$$\text{ETE: CPA} = 0.51 \pm (161.45) + 308.22 \pm (5.04) \times \text{conc. (mg l}^{-1}\text{); } r^2 = 0.9996$$

Constant concentration:

$$\text{LEV: CPA} = 101.75 \pm (187.63) + 758.35 \pm (28.29) \times \text{time (s); } r^2 = 0.9992$$

$$\text{ETE: CPA} = 90.52 \pm (296.37) + 1826.2 \pm (44.68) \times \text{time (s); } r^2 = 0.9996$$

The satisfactory correlation coefficient values showed that ETE and LEV responses are linear in the studied concentration and time injection ranges.

Graphs obtained with different concentration passed through the origin, but, as expected, graphs obtained with different injection times ( $P = 0.05$ ) showed a slight bias; this can be explained easily in terms of 'spontaneous injection' [20].

### 3.2.2. Limits of detection (LOD) and quantitation (LOQ)

LODs were about 1.7 and 0.75 mg l<sup>-1</sup> for ETE and LEV and the LOQs were estimated to be about 5.5 and 2.5 mg l<sup>-1</sup>, respectively. These limits were estimated on basis to the base-line-noise. The base-line-noise was evaluated by

recording the detector response over a period about 10-fold the peaks width. The LOD was obtained as the sample concentration that caused a peak with a height three times the level of the base-line-noise [21]. The LOQ was calculated as 3-fold the LOD.

### 3.2.3. Precision

Repeatability was assessed under the conditions which have been shown to optimize the precision in quantitative assays [22], using the experimental conditions previously selected and a constant injection time of 5 s. The most characteristic statistical data obtained from the ten replicate injections of a standards containing 16.048 mg l<sup>-1</sup> ETE and 32.48 mg l<sup>-1</sup> LEV are given in Table 1.

Acceptable precision in terms of migration times and CPA was obtained on the order of 0.2–2% for main peaks assays.

### 3.2.4. Reproducibility

The reproducibility was evaluated over 2 days by performing 11 successive injections each day. The results (Table 1) show that the repeatability for both hormones on each day is satisfactory. The comparison of averages with the Snedecor test did not show any significant difference at a confidence level of 95%.

### 3.3. Application to pharmaceutical formulations

The Spanish pharmacological industry has at present six different low-dose commercial oral contraceptives (Microgynon, Neogynona, Ovo-

plex, Ovoplex 30/150, Tricilor and Triagynon) containing ETE and LEV. Two of these contraceptives (Triagynon and Triciclor) have three different doses in the formulation (different ratios of ETE and LEV); in these contraceptives the amount of LEV starts at 0.05 mg tablet<sup>-1</sup> at the beginning of the treatment, later it is 0.07 mg tablet<sup>-1</sup> and at the end is 0.100 mg tablet<sup>-1</sup>. Each oral contraceptive packet contains 21 tablets, six of them corresponding to the lowest dosage of LEV, five to the intermediate dosage and ten to the highest dosage. The amount of ETE starts at 0.03 mg tablet<sup>-1</sup>, becomes 0.04 mg tablet<sup>-1</sup> and at the end is once more 0.03 mg tablet<sup>-1</sup>.

Fig. 5 shows an electropherogram obtained for a commercial preparation by using the selected conditions. The results obtained for the determination of ETE and LEV mixtures in pharmaceuticals are given in Table 2. The study was made in terms of CPA and the measurements were performed at 197 nm for ETE and 244 nm for LEV. The injection time was 5 s. Quantification assay was performed using standardization. A typical sequence contain a number of injections of the calibration solutions and sample solution was used (calibration 1, sample 1, calibration 2, sample 2, calibration 1) and the response factor was calculated as the average of two consecutive calibration injections. The relative differences between LC and micellar electrokinetic chromatography (MEKC) results were between  $\pm 3\%$  for LEV and ETE determinations in all oral contraceptives.

Table 1

Precision for migration times (MT), areas and corrected areas on different days ( $n = 10$  determinations on each day)

	MT			Area			Corrected area		
	Av.	S.D.	R.S.D.%	Av.	S.D.	R.S.D.%	Av.	S.D.	R.S.D.%
<i>LEV</i>									
Day A	6.37	0.01	0.18	37379.5	473.7	1.27	5868.1	63.7	1.3
Day B	6.43	0.02	0.33	37877.2	402.9	1.06	5890.7	40.7	0.83
<i>ETE</i>									
Day A	6.61	0.01	0.21	46972.8	386.1	0.82	7106.3	54.7	0.92
Day B	6.67	0.02	0.23	47287.3	574.2	1.21	7089.6	37.1	0.63

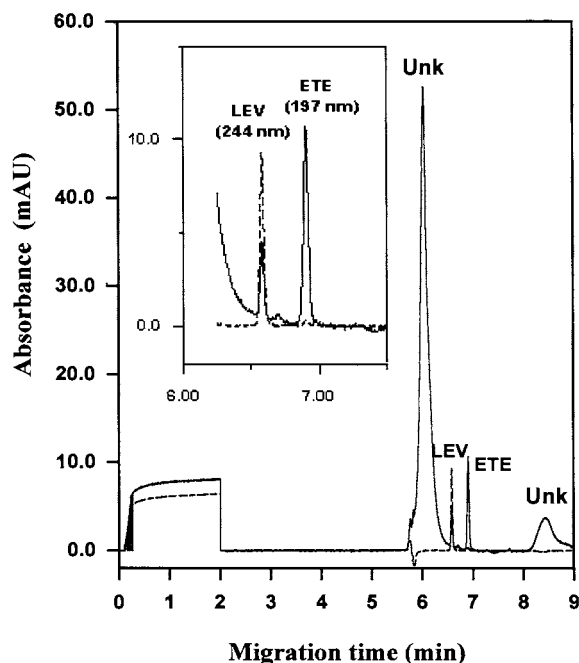


Fig. 5. An electropherogram obtained from a commercial preparation by using the selected conditions.

### 3.3.1. Peak purity

Peak purity was obtained for both LEV and ETE by overlay of the spectra captured at the

apex, upslope and downslope and no interference was noted for ETE and LEV.

## 4. Conclusions

The described MEKC method is very suitable for the simultaneous determination of ETE and LEV and can be used to analyze commercial formulations of low-dose oral contraceptives. This method gave good results when compared with the LC method.

MEKC, as an alternative method to LC, is suitable for routine use and offers advantages of simplicity of operation, flexibility and low cost (requiring only a few milliliters of buffer and inexpensive capillaries).

## Acknowledgements

The authors want to thank Dr Vicente Trigo (Wyeth-Orfi Laboratory) and Dr Carmen Barona (Schering Laboratory) for their help and information. Financial Support from DGICYT of the Ministerio de Educación y Ciencia of Spain (Project PB-94-0743) is acknowledged.

Table 2

Comparison between liquid chromatographic (LC) and micellar electrokinetic chromatography (MEKC) methods in the assays of commercial formulations (average of two determinations)

Commercial formulation <sup>a</sup>	Label claim/tablet (mg)		%Label claim (MEKC)		%Label claim (LC)	
	LEV	ETE	LEV	ETE	LEV	ETE
Microgynon	0.15	0.03	98	99	100	98
Triclor A*	0.125	0.03	100.5	97	99	97
Triclor B*	0.075	0.04	98.5	100	99	101
Triclor C*	0.05	0.03	104	102	103	101
Ovoplex	0.25	0.05	96	96	95	94
Triagynon A*	0.125	0.03	99.5	99	98	99
Triagynon B*	0.075	0.04	95	95.5	94	97
Triagynon C*	0.05	0.03	100	104	100	102
Neogynona	0.25	0.05	100.5	99	100	100
Ovoplex 30/150	0.15	0.03	100.5	99.5	98	99

<sup>a</sup> A\*, yellow; B\*, white; C\*, brown.

## References

- [1] B. Nieuweboer, J. Tack, U. Taeuber, M. Hempel, H. Wendt, *Contraception* 40 (3) (1989) 313.
- [2] K. Pollow, R. Sinnecker, B. Pollow, *J. Chromatogr.* 90 (1974) 402.
- [3] P. Verma, C. Curry, C. Crocker, P.T. Dillon, B. Ahluwalia, *Clin. Chim. Acta* 63 (1975) 363.
- [4] J.A. Skrivanek, M. Ruhlig, R. Schraer, *Abstr. Pap. Am. Chem. Soc. Meet Biol.* 58 (1973) 166.
- [5] L.P. Penzes, G.W. Oertel, *J. Chromatogr.* 74 (1972) 359.
- [6] M.P. Short, C.T. Rhodes, *Can. J. Pharm. Sci.* 8 (1973) 26.
- [7] J.J. Berzas, J. Rodríguez, G. Castañeda, *Anal. Lett.* 30 (12) (1997) 2221.
- [8] M.A. Eldawy, A.S. Tawfik, S.R. Elshabouri, *J. Pharm. Sci.* 64 (1975) 1221.
- [9] J.J. Berzas, J. Rodríguez, G. Castañeda, *Anal. Sci.* 13 (1997) 1029.
- [10] J.K. Paliwal, R.C. Gupta, *Drug Metab. Disposition* 24 (2) (1996) 148.
- [11] P. Barditchcrovo, F. Witter, F. Hamzeh, J. Mcpherson, P. Stratton, J.N. Alexander, C.B. Trapnell, *Contraception* 55 (4) (1997) 261.
- [12] P. Horvath, G. Balogh, J. Brlik, A. Csehi, F. Dravec, Z. Halmos, A. Lauko, M. Renyei, K. Varga, S. Gorog, *J. Pharm. Biomed. Anal.* 15 (9–10) (1997) 1343.
- [13] G. Castañeda, E. Julien, H. Fabre, *Chromatographia* 42 (1996) 159.
- [14] K.D. Altria, *J. Chromatogr.* 646 (1993) 245.
- [15] United States Pharmacopeia, XXIII Revision, US Pharmacopeial Convention, Rockville, MD, 1995, pp. 881–883.
- [16] S.F.Y. Li, *Capillary Electrophoresis Principles, Practice and Applications* (J. Chromatogr. Library, Vol. 52), Elsevier, Amsterdam, 1992.
- [17] M.B. Harrold, M.J. Wajtusik, J. Riviello, P. Henson, *J. Chromatogr.* 640 (1993) 463.
- [18] D.R. Baker, *Capillary Electrophoresis*, Wiley-Interscience, New York, 1995.
- [19] K.D. Altria, *Chromatographia* 35 (1993) 177.
- [20] E.V. Dosc, G. Guiochon, *Anal. Chem.* 64 (1992) 123.
- [21] K.D. Altria, Y.L. Chanter, *J. Chromatogr.* 652 (1993) 459.
- [22] K.D. Altria, H. Fabre, *Chromatographia* 40 (1995) 313.

# Analytical evaluation of polyunsaturated fatty acids degradation during thermal oxidation of edible oils by Fourier transform infrared spectroscopy

M.C.M. Moya Moreno <sup>a,\*</sup>, D. Mendoza Olivares <sup>b</sup>, F.J. Amézquita López <sup>b</sup>,  
J.V. Gimeno Adelantado <sup>a</sup>, F. Bosch Reig <sup>a</sup>

<sup>a</sup> Department of Analytical Chemistry, Faculty of Chemistry, University of Valencia, C/Dr. Moliner 50, 46100-Burjassot, Valencia, Spain

<sup>b</sup> Department of Chemistry, Instrumental Laboratory, Faculty of Chemistry, University of Guanajuato, Noria Alta, 36050 Guanajuato, Mexico

Received 7 September 1998; received in revised form 19 October 1998; accepted 20 October 1998

## Abstract

The oxidative deterioration of polyunsaturated fatty acids (PUFAs) in culinary oils and fats during episodes of heating associated with normal usage (80–300°C, 20–40 min) has been monitored by Fourier transform infrared spectroscopy (FTIR). The thermal oxidation of PUFAs is a free radical chain reaction, in which hydroperoxides are generally recognized as the primary major products. Hydroperoxides of PUFAs are easily decomposed into a very complex mixture of secondary products with the decrease in unsaturation. The oxidative advance of PUFAs during heating was studied by the determination of unsaturation percentage at different temperatures and heating times. Oils frequently used in food frying such as olive oil, sunflower oil, corn oil and seeds oil (sunflower, safflower and canola seed) were studied. The results show there is a decrease in unsaturation starting at 150°C and becoming more pronounced at temperatures around 250°C. The following variations were found in the unsaturation percentage, expressed as methyl linoleate, between the original sample and the sample heated at 300°C for 40 min: olive oil (19–6%), sunflower oil (29–12%), corn oil (28–18%) and seeds oil (23–11%). This variation in unsaturation grade provides evidence of the transformation of essential PUFAs and subsequent decrease in the oils' nutritional value. The internal standard method is suitably precise when the *n*-valeronitrile is used as standard as shown by the 1–2% relative standard deviation (R.S.D.) found for seven replicates. © 1999 Elsevier Science B.V. All rights reserved.

**Keywords:** Oils; Polyunsaturated fatty acids; Unsaturation grade; FTIR spectroscopy

## 1. Introduction

Oils and fats are an important part of the human diet and more than 90% of global production is used as food or as ingredients in food

\* Corresponding author. Tel.: +34-96-386-4533; fax: +34-96-386-4436.

*E-mail address:* montse.moya@uv.es (M.C.M. Moya Moreno)

products. Oils and fats in the diet are a rich source of energy, they contain certain fatty acids, which are nutritionally indispensable and their functional and textural characteristics add to the flavour and acceptability of many natural and processed foods. The polyunsaturated fatty acids (PUFAs) which can not be synthesised by the human body must be present in the diet to avoid symptoms caused by a shortage. They can be considered as vitamin factors and linoleic and linolenic acids must be considered specifically as they are PUFAs which are necessary for the normal development and functioning of human tissues and are known as essential fatty acids [1].

Oils and fats begin to decompose from the moment they are isolated from their natural environment when changes occur causing a disagreeable taste and smell. Atmospheric oxidation is the most important cause of deterioration in fats. This oxidative rancidity is accelerated by exposure to heat, light, humidity and the presence of trace transition metals [2]. The intense frying of oils causes an oxidizing thermal degradation with the formation of decomposition products [3–6], and a change in physical properties [7]. When oxygen travels through a fat, it is adsorbed by the fat and reacts mainly in the double links, thus the polyunsaturated components of fats oxidise much faster than saturated ones [8].

Spectroscopic methods can be employed to evaluate deterioration in oils subjected to intense heat [9]. Fourier transform infrared spectroscopy (FTIR) provides a quick and accurate way of evaluating thermal degradation in these lipids.

This paper reports a methodology to evaluate the degradation of the PUFAs initially present in the oil when it is subjected to intense heat (80–300°C, 20–40 min), and which are consequently related with the oxidative deterioration of the lipid. The unsaturation percentage was determined by FTIR for different temperatures and heating times, using *n*-valeronitrile as internal standard, so sample preparation was quick and optic pathlength does not have to be determined.

Four types of oils commonly used to fry food and high in unsaturated fats were studied, sunflower oil, corn oil, olive oil and seeds oil (canola, safflower and sunflower).

## 2. Experimental

### 2.1. Instrumentation

Perkin Elmer 1600 Fourier transform infrared spectrometer with deuterated triglycine sulphate (DTGS) detector. Number of co-added scans, 16; resolution: 4 cm<sup>-1</sup>. Data acquisition and processing software Spectrum for Windows, Perkin Elmer.

### 2.2. Reagents

*n*-Valeronitrile Aldrich analysis grade; nujol Aldrich IR grade; methyl linoleate Aldrich analysis grade; and chloroform Baker analysis grade.

### 2.3. Samples

Oils from the Mexican and Spanish market were analyzed: Virgin olive oil (Domeq), corn oil (Mazola), sunflower oil (Cristal), seeds oil (sunflower, safflower and canola, As).

### 2.4. Procedure

#### 2.4.1. Thermal treatment

Approximately 80 ml of oil were placed in 9.7 cm diameter porcelain capsule and were subjected to heating on an electric device, stirring manually with a glass rod. A thermometer was introduced in the capsule and held by a support to control

Table 1  
Thermal treatment of the oils

Sample	Temperature (°C)	Time (min)
1	$T_{amb}$	–
2	80	20
3	80	40
4	150	20
5	150	40
6	200	20
7	200	40
8	250	20
9	250	40
10	300	20
11	300	40

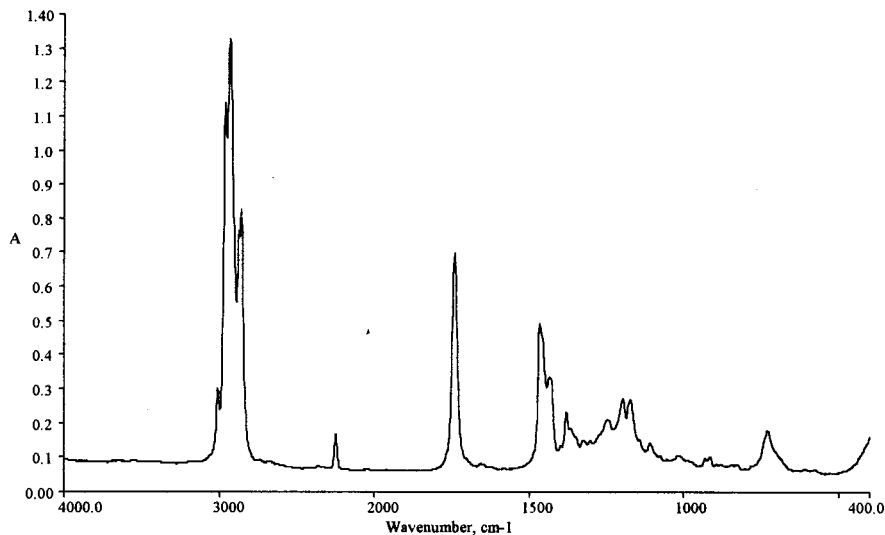


Fig. 1. Infrared spectrum of a methyl linoleate/n-valeronitrile/nujol mixture.

sample temperature. To follow the oxidation process in the oil during the period of frying, the samples were subjected to increasing heat up to a temperature of 300°C, during this process heating was maintained for 20 and 40 min at the following temperatures: 80, 150, 200, 250 and  $300 \pm 5^\circ\text{C}$ . Table 1 shows the samples analysed.

#### 2.4.2. FTIR quantitative analysis

The oil samples and internal standard n-valeronitrile were mixed in a test tube, weighed on an analytical scale and the sample was shaken manually to ensure total homogenization. The proportion in weight of n-valeronitrile in the prepared samples was between 35 and 65%. To obtain the infrared spectra using a Pasteur pipette, one or two drops of the prepared samples were placed between two circular pieces of well polished potassium bromide crystal without using a spacer so sample thickness was not controlled but was variable in each prepared sample.

In the IR spectra of the prepared samples absorbance was measured as peak height at 3008  $\text{cm}^{-1}$  with respect to the base line tangent at 3116–2718  $\text{cm}^{-1}$  and the peak 2246  $\text{cm}^{-1}$ , corresponding to n-valeronitrile, with respect to the base line tangent at 2408–2144  $\text{cm}^{-1}$ .

Eight mixtures of known composition of n-valeronitrile, methyl linoleate and nujol were prepared to obtain the calibration straight line. In these mixtures, the absorbance quotient  $A(3008)/A(2246)$  was measured with respect to the above-mentioned base lines.

### 3. Results and discussion

The percentage of unsaturation expressed as a percentage in weight of methyl linoleate (l) was obtained for the eleven prepared samples, for each type of oil. The internal standard method was used with n-valeronitrile (v) as internal standard.

The infrared spectrum of n-valeronitrile shows an absorbance band at 2246  $\text{cm}^{-1}$ , due to the stretching vibration of the triple  $\text{C}\equiv\text{N}$  link which can be used as reference band as it does not interfere with any of the sample bands. The analytical signal used to determine unsaturation was the peak at 3008  $\text{cm}^{-1}$ , due to the stretching vibration of the  $\text{C}-\text{H}$  link adjoining the double  $\text{C}=\text{C}$  link.

From eight mixtures of n-valeronitrile/methyl linoleate/nujol whose infrared spectrum is shown in Fig. 1, the calibration straight line was obtained representing the quotient  $A(3008)/A(2246)$

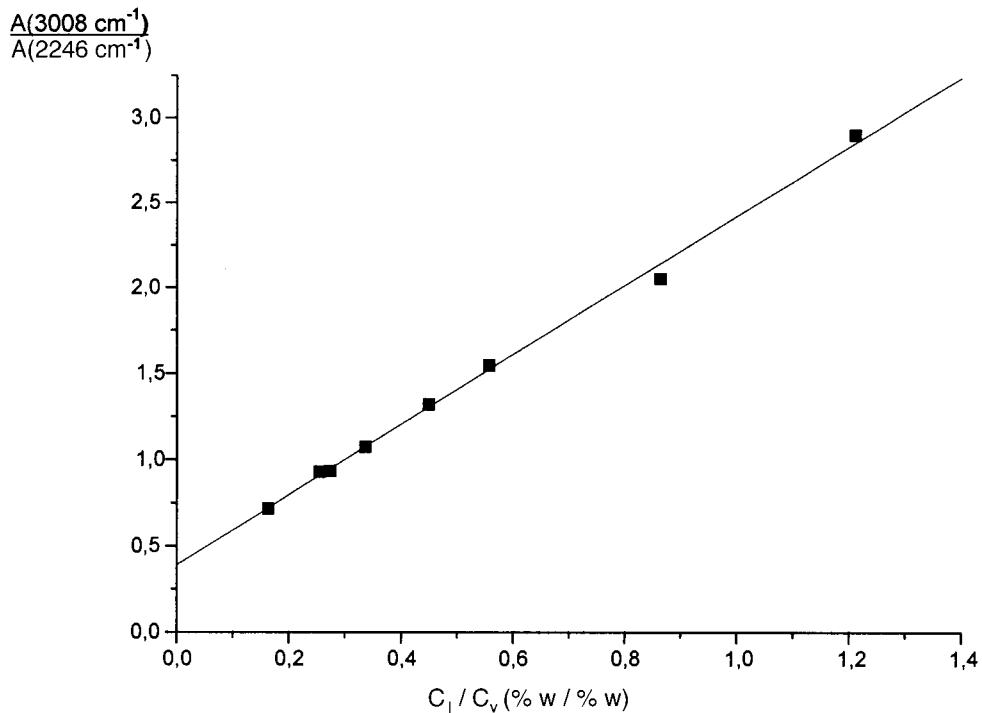


Fig. 2. Calibration straight line to obtain the unsaturation percentage of methyl linoleate.

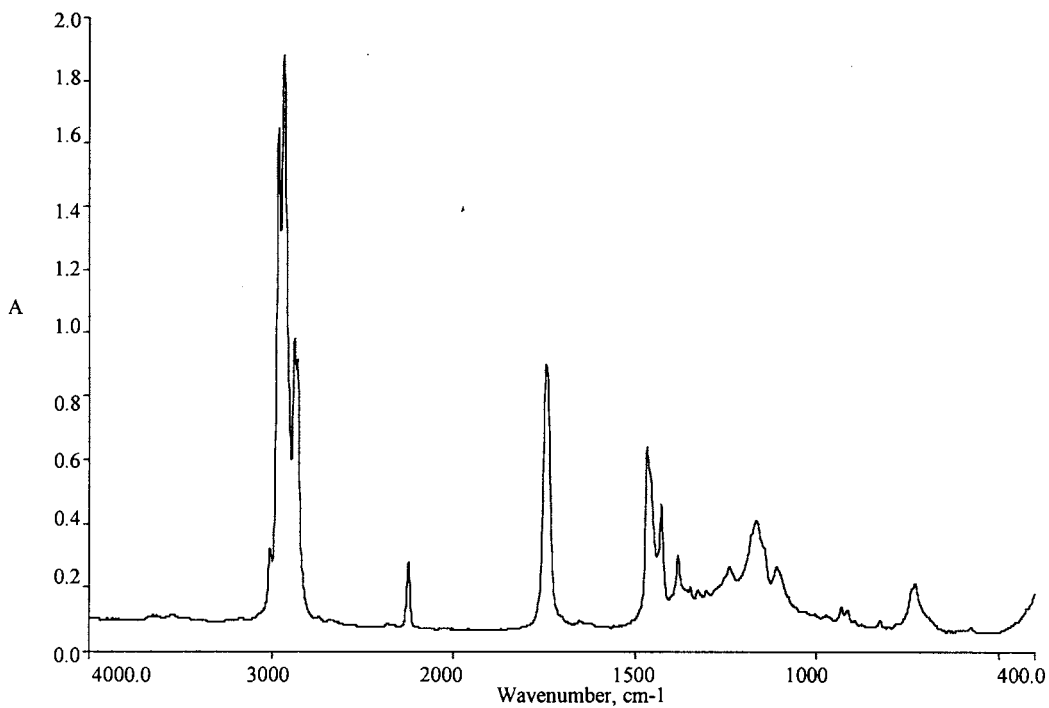


Fig. 3. Infrared spectrum of a prepared sample of corn oil unheated.



Table 2

Unsaturation expressed as percentage in weight of methyl linoleate, in the oils at different temperatures and heating times<sup>a</sup>

Sample	Heating (°C min <sup>-1</sup> )	Olive oil	Sunflower oil	Corn oil	Seeds oil
1	$T_{amb}$	18.9	29.6	27.4	23.2
2	80–20	18.8	29.3	27.8	23.3
3	80–40	18.2	29.7	27.0	22.5
4	150–20	18.3	29.2	27.1	22.0
5	150–40	18.5	29.2	26.4	21.2
6	200–20	16.7	28.3	24.6	20.7
7	200–40	12.4	26.9	24.1	19.6
8	250–20	11.8	26.3	24.0	18.8
9	250–40	11.5	24.9	23.2	18.1
10	300–20	9.8	19.0	18.7	16.4
11	300–40	5.6	11.9	18.3	10.9

<sup>a</sup> Results obtained by the internal standard method with Fourier transform infrared spectroscopy (FTIR).

against the  $C_1/C_v$  concentration quotient, where  $C_1$  is methyl linoleate concentration and  $C_v$  the n-valeronitrile concentration both expressed as % (weight/weight). This is shown in graph form in Fig. 2.

Linear regression provided the following behaviour with a correlation index 0.998 for the eight standard mixtures:

$$A(3008)/A(2246) = 0.3888 + 2.0326C_1/C_v$$

The unsaturation percentage was calculated from the spectra of the samples prepared with n-valeronitrile (Fig. 3) using the calibration equation. The values obtained are shown in Table 2. The precision for the different samples analyzed was studied, the relative standard deviation

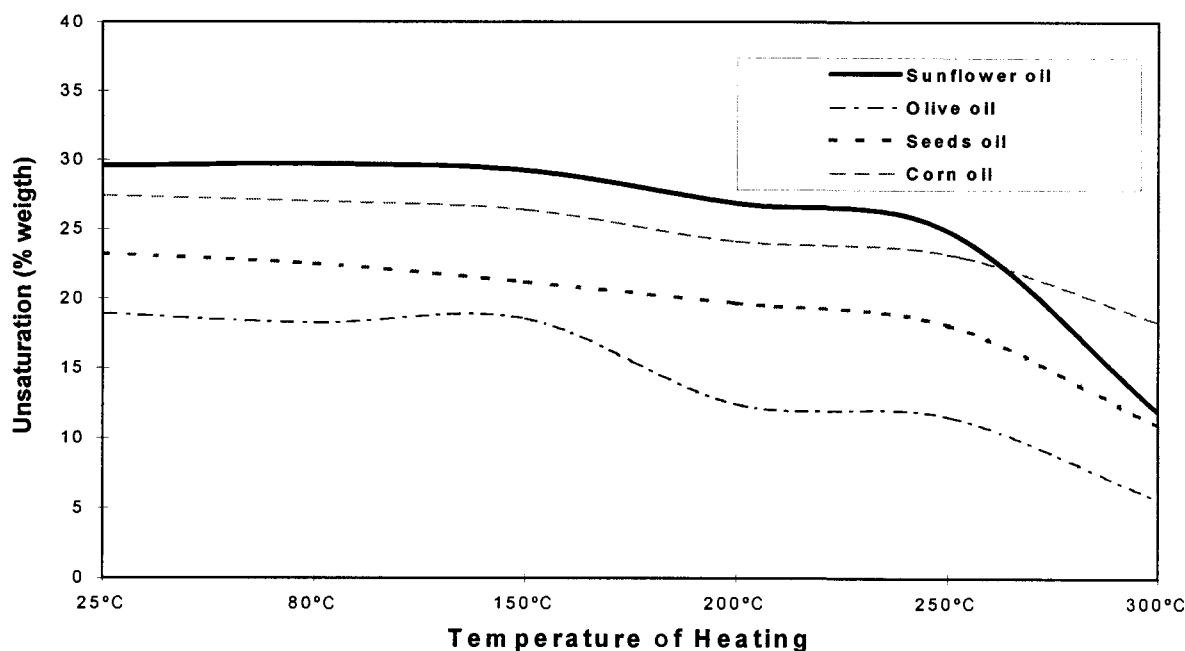


Fig. 4. Unsaturation expressed as percentage in weight of methyl linoleate, in the studied oils at different temperatures and 40 min heating time.

(R.S.D.) obtained for seven replicates was statistically satisfactory, with values between 1 and 2%.

The difference in unsaturation can be seen for each type of oil, at ambient temperature sunflower oil and corn oil have the highest content of unsaturates and the lowest is olive oil. The results obtained show how the intense heating of oils causes a decrease in unsaturation. It has been possible to establish that in all the oils studied this degradation starts becoming considerable after 150°C (Fig. 4) and at higher temperatures, a more significant decrease in unsaturation of between 40 and 70% is apparent.

The peroxide index obtained for each sample by the iodimetric method [10], reveals that the decrease in unsaturation coincide with the decomposition of hydroperoxides. Fig. 5 shows the variation of unsaturation grade and peroxide value in sunflower oil when subjected to different temperatures. The same behaviour is observed in the rest of the studied oils.

#### 4. Conclusions

FTIR provides very useful information on the composition and extent of thermal self-oxidation

in oils subjected to intense heat, equivalent to that used in the ordinary preparation of food.

The methodology developed in this study permitted determination of the percentage of unsaturated components in the samples at different heating temperatures, with no prior treatment. The use of absorbance quotient measurements permitted quantitative analysis without requiring a constant and known cell thickness thus facilitating sample handling and reducing analysis time. Furthermore, it permits quantification in cases where it is impossible to know the optic path-length accurately.

The determination of unsaturation in oils makes it possible to classify them and evaluate their oxidative deterioration which is directly related with the degradation of polyunsaturated fatty acids in the lipids and which are indispensable nutrients in human tissue development.

It can be said then, that when an edible oil is subjected to a heating process or frying, the initial nature of the triglyceride changes significantly and the decrease in unsaturation is evidence of the transformation occurring in the essential PUFAs which the oil initially contains, thus indicating a decrease in the oils' nutritional value.

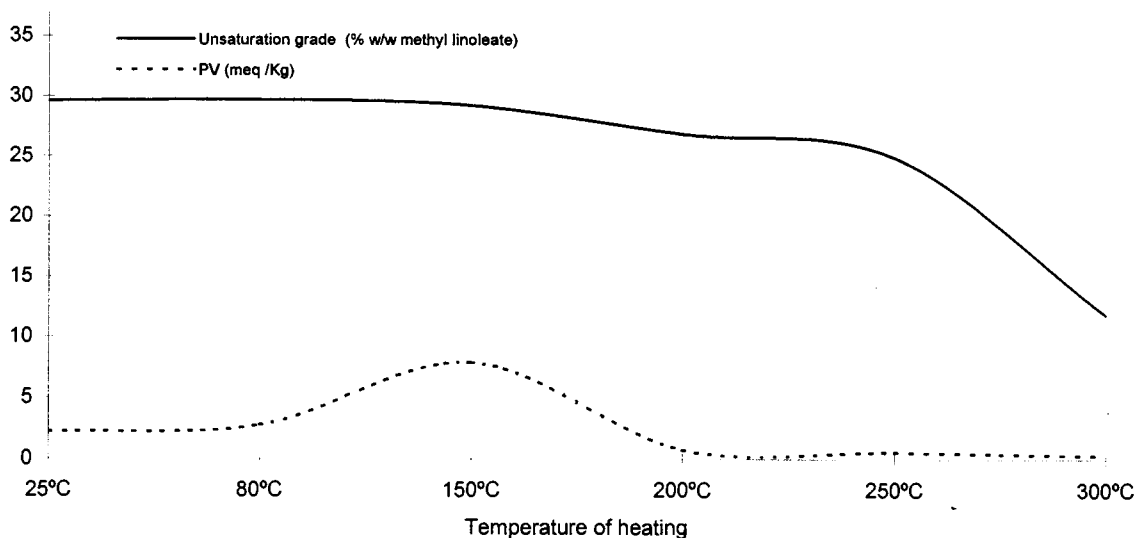


Fig. 5. Variation in unsaturation grade and peroxide value in sunflower oil when subjected to different heating and 40 min heating time.

## Acknowledgements

Authors are very grateful to the Department of Foreign Affairs of Mexico for a research grant for one of the authors.

## References

- [1] Dietary Fats and Oils in Human Nutrition. Food and Nutrition Paper, Rome, FAO, 1978.
- [2] E. Primo Yúfera, Química Agrícola III, Alimentos, E. Alhambra, Madrid, 1978.
- [3] A. Kamal-Eldin, L.A. Appelqvist, *Grasas y Aceites* 47 (5) (1996) 342–348.
- [4] G. Takeoka, C. Perrino, R. Buttery, *J. Agri. Food Chem.* 44 (3) (1996) 654–660.
- [5] G.R. Takeoka, G.H. Full, L.T. Dao, *J. Agri. Food Chem.* 45 (8) (1997) 3244–3249.
- [6] G. Dobson, W.W. Christie, J.L. Sebedio, *Chem. Phys. Lipids* 82 (2) (1995) 101–110.
- [7] V.K. Tyagi, A.K. Vasishtha, *J. Am. Oil Chem. Soc.* 73 (4) (1996) 499–506.
- [8] G. Dobson, W.W. Christie, M.C. Dobarganes, *Grasas y Aceites* 47 (1–2) (1996) 34–37.
- [9] S.B. Engelsens, *J. Am. Oil Chem. Soc.* 74 (4) (1997) 1495–1508.
- [10] Official press of European Community, No 1248, 8–9, 5 September 1991.

# Integrated flow injection-solid phase spectrophotometric determination of minoxidil

A. Ruiz-Medina, M.L. Fernández-de Córdoba, A. Molina-Díaz \*

*Department of Physical and Analytical Chemistry, Faculty of Experimental Sciences, University of Jaén, 23071 Jaén, Spain*

Received 7 September 1998; received in revised form 4 November 1998; accepted 10 November 1998

## Abstract

A flow-through solid phase spectrophotometric (SPS) sensing device is proposed for the determination of minoxidil. The analyte is concentrated on Sephadex SP-C25 ion-exchanger packed in a flow cell and it is monitored by UV-Vis spectrophotometry at 282 nm, without derivatization reaction. When a HCl ( $10^{-2}$  mol l $^{-1}$ )/NaCl ( $5 \times 10^{-2}$  mol l $^{-1}$ ) solution is used as carrier/desorbing solution, the sensor responds linearly in the measuring range of 0.2–7, 0.1–4 and 0.05–2  $\mu$ g ml $^{-1}$  with detection limits of 60, 33 and 6 ng ml $^{-1}$  for 600, 1000 and 2000  $\mu$ l of sample, respectively. The relative standard deviations (%) for these volumes are 0.38, 1.06 and 2.63, respectively. The method was satisfactorily applied to the determination of minoxidil in pharmaceutical preparations and the results were compared with those obtained by high performance liquid chromatography (HPLC). © 1999 Elsevier Science B.V. All rights reserved.

*Keywords:* Minoxidil determination; Solid-phase spectrophotometry; FIA; Pharmaceuticals

## 1. Introduction

Molecular absorption spectroscopy is the most frequently used detection technique in analytical laboratories because of its high flexibility for adaptation to a wide variety of analytical problems [1]. This characteristic is clearly apparent from the large number and variety of flow injection analysis (FIA) assemblies that include an UV-Vis detector. The literature abounds with references to determinations of pharmaceuticals by

using this type of detection; however, few of these applications [2,3] rely on UV absorbance measurements of the pharmaceuticals themselves. It is due to the poor selectivity of spectrophotometric measurements in this region.

Solid phase spectrophotometry (SPS) is today widely used. It is a spectrophotometric method based on the direct measurement of the absorbance of an active solid support (usually an ion-exchanger) that has sorbed a sample component by previous equilibration with sample solution (batch methodology) [4]. It combines the steps of preconcentration, separation and determination, and provides sensitivities several orders of magnitude higher than those obtained with solu-

\* Corresponding author. Tel.: +34-53-212-147; fax: +34-53-212-141.

*E-mail address:* amolina@ujaen.es (A. Molina-Díaz)

tion phase spectrophotometry [5,6]. SPS has also been integrated with FIA systems [7,8]. In the present work, this SPS-FIA integration has been applied to the determination of minoxidil in the UV region.

Minoxidil, 2,6-diamino-4-piperidinopyrimidine-1-oxide is an orally active peripheral vasodilator useful in the treatment of severe hypertension. It can cause marked fluid retention and hirsutism. Now it is used in male pattern baldness (alopecia androgenetica) and alopecia areata. Methods proposed for the determination of minoxidil include GC [9], high performance liquid chromatography (HPLC) [10], radioimmunoassay [11], differential pulse polarography [12], ion-pair extraction [13] and electro-analysis [14]. The US Pharmacopeia gives a method that involves liquid chromatography for its estimation [15].

Most of spectrophotometric methods for the determination of minoxidil are by derivatization [16–20] and all of them are less sensitive than that proposed here. This paper describes the development of a spectrophotometric procedure for the determination of minoxidil in pharmaceuticals by an integrated SPS-FIA method, based on the monitorization of its intrinsic absorbance at 282 nm.

## 2. Experimental

### 2.1. Apparatus and instrumentation

A schematic diagram of the manifold used is shown in Fig. 1. An UV-Vis Lambda 2 Perkin Elmer spectrophotometer was used to make spectra and direct measurements of absorbance. This instrument was connected to a 386 personal computer (PC) connected by means of a serial port and fitted with the PECSS V.5.0. software package (from Perkin Elmer) and a HP Deskjet 690C printer was used for obtaining graphs. A Hellma 138 QS flow-through cell (1 mm optical path length, 50  $\mu$ l inner volume), packed with the ion exchanger, was used as the active microzone. A peristaltic pump (Gilson Minipuls-3) and a six-port rotary Rheodyne type 50 injection valve were used. The single-line manifold for the FI measure-

ments was employed with 0.8 mm i.d. PTFE tubing. All reported measurements were made at room temperature.

A digital CRISON model 2002 pH-meter fitted with a glass/saturated calomel electrode assembly and a temperature probe was used for all pH measurements.

### 2.2. Reagents

All solutions were prepared with doubly distilled water and analytical-reagent grade chemicals.

Minoxidil standard solutions. A stock standard solution of 1000  $\mu$ g ml<sup>-1</sup> of pure analytical generic form of minoxidil supplied by SIGMA was prepared by directly dissolving the drug in water containing 50 ml of ethanol 96% (v/v) l<sup>-1</sup>.

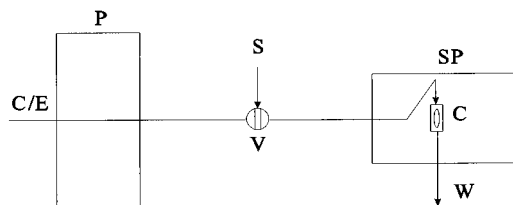


Fig. 1. Schematic diagram of the flow injection analysis (FIA) system: C/E, carrier/eluent; P, peristaltic pump; V, injection valve; S, sample; SP, spectrophotometric detector; C, flow cell; W, waste.

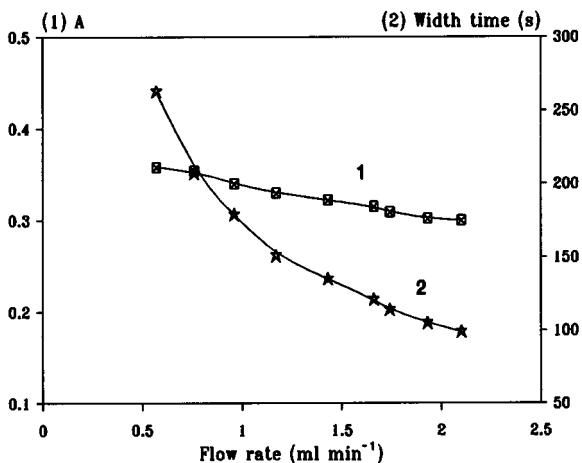


Fig. 2. Effect of flow rate: (1) on absorbance and (2) on width time. Minoxidil 2  $\mu$ g ml<sup>-1</sup> (sample volume 600  $\mu$ l and flow rate 1.60 ml min<sup>-1</sup>).

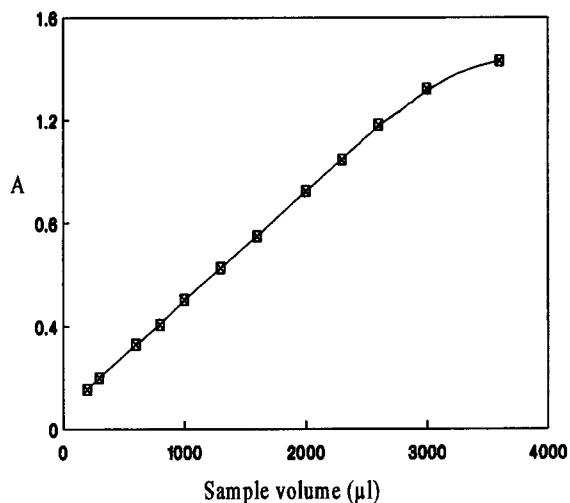


Fig. 3. Sample volume effect in increasing order (Minoxidil  $2 \mu\text{g ml}^{-1}$  and flow rate  $1.60 \text{ ml min}^{-1}$ ): 200, 300, 600, 800, 1000, 1300, 1600, 2000, 2300, 2600, 3000 and 3600  $\mu\text{l}$ .

Table 1  
Figures of merit

Parameter	Volume of sample loop ( $\mu\text{l}$ )		
	600	1000	2000
Linear dynamic range ( $\mu\text{g ml}^{-1}$ )	0.2–7.0	0.1–4.0	0.05–2.0
<i>Calibration graph</i>			
Intercept	0.028	0.026	0.024
Slope ( $\text{ml } \mu\text{g}^{-1}$ )	0.143	0.229	0.430
Correlation coefficient	0.9998	0.9995	0.9997
Detection limit ( $\mu\text{g ml}^{-1}$ )	0.060	0.033	0.006
R.S.D. (%) ( $n = 10$ )	0.38	1.06	2.63
Sampling frequency ( $\text{h}^{-1}$ )	26	22	16

Working standard solutions were prepared daily by appropriate dilutions of the stock standard solution (with doubly distilled water).

The carrier used in FIA experiments was HCl ( $10^{-2} \text{ mol l}^{-1}$ )/NaCl ( $5 \times 10^{-2} \text{ mol l}^{-1}$ ) solution. The eluting solution consisted of the same carrier solution. Nitrate, citrate, tartrate, sulphate and phosphate as sodium salts (from Panreac)

were also used as  $5 \times 10^{-2} \text{ mol l}^{-1}$  together with HCl  $10^{-2} \text{ mol l}^{-1}$  solutions. Sephadex SP-C25 (Aldrich) was used in the  $\text{H}^+$  form as the solid support without any pretreatment to avoid contamination, and packed into a Hellma 138 QS flow cell (1 mm light path) with the aid of a syringe by impelling it in a water suspension and using glass-wool in the outlet to retain the resin.

### 2.3. Treatment of the sample

Pharmaceuticals containing minoxidil were treated in a different form.

(a) Minoxidil tablets. A solution was prepared by crushing four tablets (Loniten, Upjohn) and dissolving an amount of the powder equivalent to 10 mg of minoxidil in about 5 ml of ethanol 96% (v/v) with shaking for 5 min in an ultrasonic instrument. The solution was filtered through a  $0.45 \mu\text{m}$  pore size Millipore membrane filter, and the filtrate plus washings were diluted to the mark in a 100 ml calibrated flask. Appropriate dilutions were made from this solution with doubly distilled water.

(b) Minoxidil solutions. All of them were in a concentration of 2% (w/v) (Lacovin, Galderma; Pilovital, Lesvi; Regaine, Farmoquímica; Riteban, Centrum). These solutions were dissolved in doubly distilled water without previous pretreatment and suitable dilutions were made from this solution.

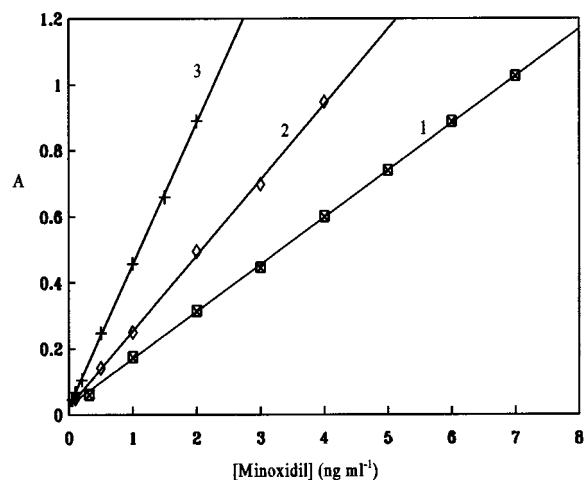


Fig. 4. Calibration graphs obtained from different sample volumes injected: (1) 600, (2) 1000 and (3) 2000  $\mu\text{l}$ .

Table 2  
Determination of minoxidil in pharmaceutical preparations

Sample	Minoxidil labeled	% Recovery $\pm$ R.S.D. by <sup>a</sup>	
		Proposed method	USP method
Loniten (Upjohn)	10 <sup>b</sup>	98 $\pm$ 1	98.2 $\pm$ 0.9
Lacovin (Galderma)	20 <sup>c</sup>	103 $\pm$ 1	102 $\pm$ 2
Pilovital (Lesvi)	20 <sup>c</sup>	103 $\pm$ 1	101 $\pm$ 2
Regaine (Farmoquímica)	20 <sup>c</sup>	101.7 $\pm$ 0.8	99.8 $\pm$ 0.8
Riteban (Centrum)	20 <sup>c</sup>	99.0 $\pm$ 0.9	99.2 $\pm$ 0.9

<sup>a</sup> Mean of three determinations.

<sup>b</sup> mg tablet<sup>-1</sup>.

<sup>c</sup> mg ml<sup>-1</sup>.

### 3. Results and discussion

#### 3.1. Absorption spectra

In solution, minoxidil shows a maximum absorption at 289 nm. This analyte is easily sorbed on a cation-exchanger, Sephadex SP-C25, showing a maximum absorption at 282 nm. Other cation-exchange resins were tested (Sephadex CM-C25, SP-C50 and CM-C50) and several resins for gel filtration (G-15 and G-75). Of all them, Sephadex SP-C25 gave the best results and fixation became quicker. Dowex resins were discarded due to their high background in the UV region.

The wavelength was fixed at 282 nm for the flow analysis. The slight change of the absorbance spectrum with respect to the solution can be attributed to the modification of the surrounding environment of minoxidil in the solid phase. The sorption on the resin (from a sample volume of 600  $\mu$ l) resulted in a signal about 20-fold higher than that obtained in aqueous solution in the same flow cell and in the same working conditions. This strong increase in sensitivity is due to the concentration of the analyte by ion exchange on the active solid support in the detection area of the spectrophotometer.

#### 3.2. Procedure

A single-channel FIA configuration was used in which the carrier HCl ( $10^{-2}$  mol l<sup>-1</sup>)/NaCl

( $5 \times 10^{-2}$  mol l<sup>-1</sup>) was pumped at 1.60 ml min<sup>-1</sup> and in which the sample was injected. The analyte was retained on the cationic Sephadex SP-C25 resin when passing through the flow cell (preconcentration step). The retention signal was monitored at 282 nm. When the tail end of the sample plug reached the active zone the analyte was desorbed by the carrier itself. Three different calibration lines were constructed for 600, 1000 and 2000  $\mu$ l of sample volume. The absorbance was continuously monitored on the screen of the PC (with the software package), saved on the floppy disk and printed on the PC printer.

Table 3  
Recovery study of minoxidil in pharmaceutical preparations

Sample	Amount of minoxidil added	% Recovery $\pm$ R.S.D. <sup>a</sup>
Loniten	1 <sup>b</sup>	98.2 $\pm$ 0.9
(Upjohn)	2 <sup>b</sup>	99.5 $\pm$ 0.9
Lacovin	1 <sup>c</sup>	101 $\pm$ 1
(Galderma)	2 <sup>c</sup>	99.8 $\pm$ 0.8
Pilovital	1 <sup>c</sup>	102 $\pm$ 1
(Lesvi)	2 <sup>c</sup>	100 $\pm$ 1
Regaine	1 <sup>c</sup>	101.2 $\pm$ 0.9
(Farmoquímica)	2 <sup>c</sup>	99 $\pm$ 1
Riteban	1 <sup>c</sup>	99.4 $\pm$ 0.9
(Centrum)	2 <sup>c</sup>	99.5 $\pm$ 0.9

<sup>a</sup> Mean of three determinations.

<sup>b</sup> mg tablet<sup>-1</sup>.

<sup>c</sup> mg ml<sup>-1</sup>.

### 3.3. Influence of the pH of the carrier and of the sample

The influence of the pH of the carrier solution was investigated by varying it in the range 1–10 by adjusting it with HCl or NaOH and suitable conditions for the fixation of the analyte were obtained between pH 2 and 3. The analyte was not fixed on the resin for pH values between 8 and 10. It was decided to work at pH 2 (HCl  $10^{-2}$  mol  $l^{-1}$ ). Several electrolyte solutions at pH 2 were tested as carriers (sodium chloride, sodium nitrate, sodium citrate, sodium tartrate, sodium sulphate and sodium phosphate). The best results were obtained by using sodium chloride; the influence of its concentration on both the analytical response and the eluting action was tested by varying it from 0.02 to 0.1 mol  $l^{-1}$ . A decrease was observed in the response of the sensor when electrolyte solution concentration increased but on the other hand the peak width time decreased. A 0.05 mol  $l^{-1}$  concentration was chosen as a compromise solution. So, a solution HCl ( $10^{-2}$  mol  $l^{-1}$ )/NaCl ( $5 \times 10^{-2}$  mol  $l^{-1}$ ) was used as a carrier solution.

The sample pH value did not influence the analytical signal when its value was maintained in the 1–8 range and, hence, there is no need to adjust the sample pH.

### 3.4. Influence of flow rate

The effect of the flow-rate was investigated by injecting sample solutions at the same concentration of the analyte into the flow system at various flow-rates. The resulting peak heights and peak width times are shown in Fig. 2.

When the flow-rate is reduced from 2.10 to 0.57 ml  $min^{-1}$ , an increase in peak height of 30% (absorbance) is observed but the maximum number of samples analyzed per hour is also reduced from 34 to 13. This is an usual observation in this type of system. The sorption of the analyte on the resin is influenced (sometimes strongly) by the flow rate when the kinetic of the diffusion-retention process of the analyte in the solid support is slow: if the sorption is not instantaneous, an increase in the flow rate obviously decreases the

amount of the analyte retained on the resin from the sample plug. Consequently, a decrease in the peak height is observed, but the sampling frequency is increased. In all subsequent experiments, the total flow-rate was maintained at 1.60 ml  $min^{-1}$  as a compromise solution.

### 3.5. Effect of sample volume

Sample volumes from 0.2 to 3.6 ml at the same concentration of minoxidil (2  $\mu g$   $ml^{-1}$ ) were studied. Fig. 3 shows that absorbance ( $A$ ) increases linearly with an increase in the sample volume from 0.2 to 3.0 ml (but this increase is not linear for a sample volume between 3.0 and 3.6 ml);  $A$  is expressed as a function of the sample volume for the former mentioned range ( $V$  in ml):  $A = 0.420 \times V + 0.075$  (correlation coefficient = 0.9998).

Consequently, the use of a large volume of sample solution yields a much higher sensitivity but more time is required for each determination. So, the selection of the sample volume should reflect a consideration of sensitivity and analysis speed. In this paper, three working sample volumes were selected: 600, 1000 and 2000  $\mu l$ .

## 4. Analytical figures of merit

Table 1 contains the figures of merit of the method proposed for the three calibration volumes and Fig. 4 shows the three calibration graphs. The data were fitted by standard least-squares treatment. The calibration graphs are linear for the concentration range 0.05–2, 0.1–4 and 0.2–7  $\mu g$   $ml^{-1}$  for 2000, 1000 and 600  $\mu l$ , respectively.

The reproducibility was established for ten analyses of solutions containing 0.2, 2 and 5  $\mu g$   $ml^{-1}$  of minoxidil, respectively; the detection limit, by using  $3\sigma$  recommendation [21], was calculated from the relative standard deviation (R.S.D.) of the background absorbance and values of 6, 33 and 60 ng  $ml^{-1}$  were obtained for 2000, 1000 and 600  $\mu l$  of sample volume, respectively. The effect of foreign ions was not examined because minoxidil appears without another ac-



companion species in tablets or solutions pharmaceuticals.

## 5. Application of the method

The proposed sensor was applied to the determination of minoxidil in pharmaceutical preparations using a 1000  $\mu$ l sample volume injection. The results obtained are summarized in Table 2. As can be seen, in all the cases the data were in good agreement with the labeled amounts and were comparable with USP method [15]. In addition, the accuracy of the proposed method was further checked by adding known amounts of minoxidil to previously analyzed pharmaceuticals (Table 3).

## 6. Conclusions

The most salient advantages of the proposed method respect to the batch method, are as follows: reduced human participation (automation capability), higher throughput than the batch alternatives (SPS batch methodology and homogeneous solution phase spectrophotometry), reusability of the resin, i.e. the sensor can be regenerated by elution of the retained analyte (in the batch method the resin is wasted) and simplicity, as reflected in the fact that all the steps involved are performed in the flow system (the batch method requires manual mixing of the reactants, addition of a previous weighed amount of resin for each sample to the medium, shaking, filtration and collection of the resin with the retained product in a conventional cell, followed by measurement).

This SPS-FIA integrated method is a significant contribution owing to the urgent need for simple, rapid, automated and more sensitive methods for this analyte with a very good sampling frequency. This method will be quite suitable for routine analysis of a wide variety of pharmaceuticals.

## Acknowledgements

The authors are grateful to the Dirección General de Enseñanza Superior (DGES) of the Ministerio de Educación y Cultura (Project No. PB97-0849), for financial support.

## References

- [1] J. Martínez Calatayud, *Flow Injection Analysis of Pharmaceuticals*, Taylor and Francis, UK, 1996.
- [2] J. Martínez Calatayud, A. Sánchez Sampedro, P. Villar Civera, *Pharmazie* 44 (1989) 795.
- [3] R.M. Alonso, P.M. Jiménez, A. Carvajal, *Talanta* 36 (1989) 761.
- [4] M.L. Fernández de Córdova, A. Ruiz Medina, A. Molina Díaz, *Fresenius J. Anal. Chem.* 357 (1997) 44.
- [5] P. Ortega Barrales, M.I. Pascual Reguera, L.F. Capitán Vallvey, A. Molina Díaz, *Anal. Chim. Acta* 353 (1997) 115.
- [6] P. Ortega-Barrales, M.L. Fernández-de Córdova, A. Molina-Díaz, *Anal. Chem.* 70 (1998) 271.
- [7] A. Molina Díaz, A. Ruiz Medina, M.L. Fernández de Córdova, *Fresenius J. Anal. Chem.* 363 (1999) 92.
- [8] L.F. Capitán Vallvey, M.C. Valencia, G. Mirón, *Anal. Chim. Acta* 289 (1994) 365.
- [9] T. Koniewska, E. Kublin, E. Wedawowicz, *Acta Pol. Pharm.* 43 (1986) 588.
- [10] G. Carrum, D.R. Abernethy, M. Sadhaukhan, C. Wright, *J. Chromatogr.* 381 (1986) 127.
- [11] M.E. Rajer, H. Ko, T.J. Wilberston, J.M. McCall, K.T. Jonston, *J. Pharm. Sci.* 66 (1977) 1266.
- [12] L. Amankwa, L.G. Chatter, S. Pons, *Analyst* 108 (1983) 1221.
- [13] C.S.P. Sastry, D.M. Krishna, A. Sailaja, *Ind. Drugs* 29 (1992) 275.
- [14] J. Arcos, B. García, A. Munguia, J. López Palacios, *Anal. Lett.* 24 (1991) 357.
- [15] The United States Pharmacopoeia, IIIth revision, US Pharmacopoeial Convention, Rockville, MD, 1985, p. 1867.
- [16] Ahmet Araman, *Acta Pharm. Turc.* 28 (1986) 9.
- [17] C.S.P. Sastry, A. Sailaja, T. Thirupathi Rao, M.V. Suryanarayana, *Microchem. J.* 44 (1991) 268.
- [18] M. El-Sayed Mahrous, *Anal. Lett.* 24 (1991) 2017.
- [19] C.S.P. Sastry, A. Sailaja, T.T. Rao, D.M. Krishna, *Ind. Drugs* 29 (1992) 473.
- [20] M.B. Devani, S.S. Pandya, S.A. Shah, *Ind. Drugs* 28 (1991) 197.
- [21] IUPAC, Nomenclature, symbols, units and their usage in spectrochemical analysis, *Pure Appl. Chem.* 105 (1976) 45.

# Near infrared (NIR) spectroscopy for in-line monitoring of polymer extrusion processes

Thomas Rohe \*, Wolfgang Becker, Sabine Kölle, Norbert Eisenreich, Peter Eyerer

*Fraunhofer-Institut für Chemische Technologie (ICT), Joseph-von-Fraunhofer-Strasse 7, D-76327 Pfinztal-Berghausen, Germany*

Received 7 September 1998; received in revised form 9 November 1998; accepted 10 November 1998

---

## Abstract

In recent years, near infrared (NIR) spectroscopy has become an analytical tool frequently used in many chemical production processes. In particular, on-line measurements are of interest to increase process stability and to document constant product quality. Application to polymer processing e.g. polymer extrusion, could even increase product quality. Interesting parameters are composition of the processed polymer, moisture, or reaction status in reactive extrusion. For this issue a transmission sensor was developed for application of NIR spectroscopy to extrusion processes. This sensor includes fibre optic probes and a measuring cell to be adapted to various extruders for in-line measurements. In contrast to infrared sensors, it only uses optical quartz components. Extrusion processes at temperatures up to 300°C and pressures up to 37 MPa have been investigated. Application of multivariate data analysis (e.g. partial least squares, PLS) demonstrated the performance of the system with respect to process monitoring: in the case of polymer blending, deviations between predicted and actual polymer composition were quite low (in the range of  $\pm 0.25\%$ ). So the complete system is suitable for harsh industrial environments and could lead to improved polymer extrusion processes. © 1999 Elsevier Science B.V. All rights reserved.

*Keywords:* Near infrared spectroscopy; Polymer extrusion; In-line monitoring

---

## 1. Introduction

Growing demands on the quality of plastic products as well as reduction of costs in production and processing require fast and reliable control methods. These methods have to record quality parameters relevant to the process as early

as possible. In the case of polymer extrusion, mainly spot check off-line measurements of e.g. composition, mechanical properties, moisture, MFI, etc. are implemented. In-/on-line measurements have been introduced for only a few process parameters like melt temperature or pressure. Other parameters are neglected. This low level of information about the processed product can lead to huge losses due to the time lag between detection of insufficient product quality in the laboratory and the reaction to restore the process itself.

---

\* Corresponding author. Tel.: +49-721-4640-154; fax: +49-721-4640-566.

*E-mail address:* ro@ict.fhg.de (T. Rohe)

This time lag can exceed several hours and would result in up to several tons of polymeric waste, because products not fulfilling the quality demands of customers cannot be reprocessed in many cases. Fast near infrared (NIR) spectroscopy [1,2] is a very promising measurement method to improve the knowledge on the melt by in-line measurements. Results of in-line NIR spectroscopy can be, for example, composition [3–5]. With these and other parameters it could be possible to steer the complete extrusion process automatically.

Problems in realising this measurement technology are many: the probes are exposed to hot and pressurised polymer melts, which can be corrosive; the applied spectrometer has to withstand harsh industrial environments; data handling has to be fast and reliable; the complete system has to be economic and very robust. These demands are hard to fulfil.

In this paper a measurement system for in-line transmission NIR spectroscopy of polymer extrusion processes is presented. Application to the determination of polymer melt composition is demonstrated for a PE/PP blend, where different data preparation techniques have been tested.

### 1.1. Near infrared (NIR) spectroscopy

In the near-infrared (NIR) spectral range (700–2500 nm), molecules absorb incoming light by overtone or combination vibrations. Absorbance is reduced by an order of magnitude compared to fundamental vibrational transitions in the infrared (IR). The reduced absorbance in the NIR allows registration of spectra of thick samples which are of practical interest in process analysis. C–H, O–H, N–H and C–O bands observed in NIR spectra are characteristic for polymers and can be used for determination of composition of polymers.

Further advantages of NIR compared to IR are the NIR-photodetectors (germanium Ge, indium arsenide InAs, or indium gallium arsenide InGaAs), having shorter response times and higher detectability. Also, quartz fibre optics with low attenuation and low costs can still be used.

## 2. Experimental

### 2.1. Extruder system

A 20-mm single-screw extruder (Haake Rheomex 252) with length to diameter ratio of 25 is used to melt particulate solid polymers. Maximum torque is 100 N m, maximum melt pressure is 7 GPa. The temperature profile can be adjusted with four independent temperature zones (including nozzle). Maximum wall temperature at the cylinder is 400°C. A control unit regulates the extrusion conditions and automatically records torque and speed of screw.

Between end of screw and nozzle there is an adapter, which was transformed to a flow cell combining adapter and insertion for probes (Fig. 1). Hence, molten polymer passes the measuring zone inside the extruder, where the two probes are installed facing each other. Fibre optic probes are used to transmit light through the polymer stream. The distance between these probes can be varied by insertion of spacers, and consequently pathlength ranges from 0 to 10 mm. Fibre optic probes installed in the flow cell are connected to an AOTF-NIR spectrometer via optical fibres (core diameter 1 mm, length of each fibre is 1 m, numerical aperture 0.22). This spectrometer was developed at the Fraunhofer-Institut für Chemische Technologie (ICT) and uses a tungsten halogen lamp, a germanium detector, and an

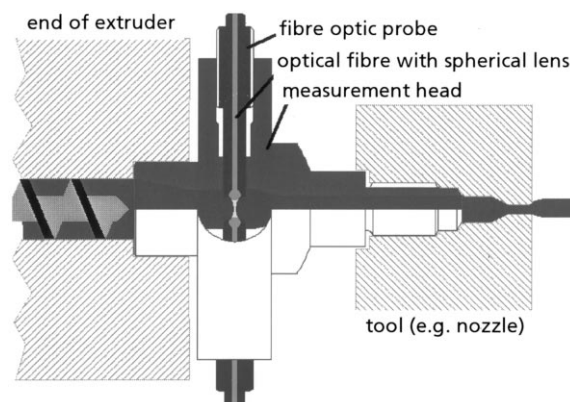


Fig. 1. Scheme of measurement head with integrated fibre optic probes for in-line measurement.

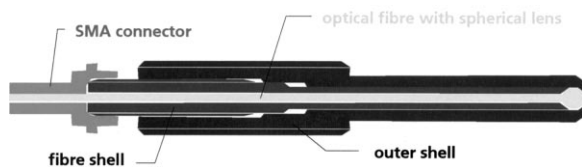


Fig. 2. Scheme of fibre optic probes.

acousto-optic tunable filter (AOTF) as dispersive element. Details on the spectrometer are described elsewhere [6,7].

## 2.2. Fibre optic probes

The fibre optic probes have to withstand extreme conditions: high temperature, high pressure, high viscosity and corrosiveness of the polymer melt. Thermal cycling due to process start-up and shutdown is another difficulty. The probes have to transport radiation effectively, so damping of optical components has to be low. From a chemical point of view it must be guaranteed that the probes do not affect polymeric properties in a negative way.

To fulfil these demands the probe design shown in Fig. 2 has been developed, which can be divided into two main parts. The first part consists of a spherical lens, which is welded onto an optical fibre (diameter 1 mm, length 70 mm, numerical aperture 0.22). Both components are made of quartz. This central optics is embedded in a sleeve made of stainless steel. The space between sleeve and optics is filled with a high temperature resistant glue. A protective housing in the form of another sleeve is the second part of the probe. It contains the first part and has an opening for the spherical lens, so that only part of the lens has contact with the polymer melt. On the other side of the housing there is a standard SMA connector for an optical fibre. The connection between the two parts is again made by a glue.

The advantages of this design are obvious. Use of spherical lenses reduces intensity losses due to the numerical aperture of the optical fibres. This results in an overall transmission ratio of 12%. By choosing quartz as lens material the optics withstand temperatures up to 800°C, which is

much higher than normal extrusion temperatures lying in the range of 200–350°C. Internal tensions due to the difference between the thermal coefficient of expansion of quartz and the housing material are eliminated by use of glue as connector. On the other hand coefficients of expansion of housing and flow cell material are the same, so that there is a clearance fit between these two parts. The result of this arrangement is an effective gasket.

## 2.3. Materials

Materials used are polyethylene (PE-LD) and polypropylene (PP) (Table 1). These materials are widely used in extrusion applications. Materials were used as pure material and as mixtures for blending. Mixtures were produced by weighing with an accuracy of  $\pm 0.01$  g, so all mixing ratios are given in weight percent.

## 2.4. Measurement procedure

The extruder is heated to a predefined temperature profile corresponding to the processed material. Before processing the polymer a reference spectrum is taken which is used for all other measurements. Then the extruder is filled with polymeric material. After processing inside the extruder near infrared spectra of the polymer melt are taken while passing the measurement head. The recorded spectra are stored and evaluated on a separate personal computer. During the measurement, melt temperature, melt pressure and torque of screw as well as the spectrometer adjustments are documented. Measurement time for one single spectrum is only about 10 ms; for calibration development and analytical determination 500 single spectra were averaged.

The mixtures were varied step by step, i.e. 1 kg of material was filled into the funnel of the extruder and extruded until the funnel was empty. Then the funnel was re-filled with the next material mixture. This procedure is sufficient due to the self-cleaning effect of the extruder, i.e. the screw not only homogenises and transports the polymer melt to the nozzle, but also cleans the walls of residual material.

Table 1  
Materials used

	Name	Manufacturer	MFI	Viscosity
Polyethylene (PE-LD)	ESCORENE	Exxon Chemical	MFI (190°C; 2.16 kg): 0.3 g/10 min	High
Polypropylene (PP)	Hostalen PP	Hoechst AG	MFI (230°C/2.16 kg): 47 g/10 min	Low

## 2.5. Data analysis

For processing, evaluation and analysis of the obtained spectra the software package ‘The Unscrambler’<sup>®</sup> (CAMO) was used. Common statistical analysis (e.g. principal component analysis (PCA), principal component regression (PCR), partial least squares analysis (PLS)) can be carried out with it. For the investigations on polymer blends only PLS analysis [8] was used. The PLS model was generated with one set of spectra and the prediction ability of this model was tested with another set of spectra. These sets were recorded subsequently, so that spectra of the same mixture were obtained. For generation of the PLS model 20 spectra of each mixture were used, but these spectra were prepared in different ways before generating a new PLS model:

1. no preparation (raw): raw data were used for calibration,
2. averaging (av- $x$ ):  $x$  spectra (replicates) of the same mixture were averaged to one new spectrum,
3. smoothing (sm): moving average smoothing with segment size 5,
4. data reduction (red- $x$ ):  $x$  points of a spectrum were averaged to one new data point,
5. differentiation ( $x$ -diff): the spectrum is differentiated  $x$  times,
6. multi-scattering correction (MSC): off-set and/or slope correction.

The spectra preparation tools were combined in different ways to evaluate an optimised PLS model. This model was tested by a leverage correction, which is a ‘quick and dirty’ validation method using all samples for calibration. Leverage is a measure of the effect of an object on the model, which is related to its distance from the model center. To make a leverage corrected error estimate for the individual error, the residuals for

each object are weighted [9]. After the validation the deviation between measured and predicted composition is investigated. The resulting parameter RMSEP (root mean square error of prediction) can be used for comparison of the different spectrum preparation techniques.

## 3. Results

### 3.1. Technical results on developed probes

In an initial investigation it was tested whether the developed probes would withstand the normal extrusion conditions. For this, different materials were extruded. Melt temperature of 300°C and pressure of up to 37 MPa were unproblematic. The complete measuring head was sealed, so that no melt could leave the melt channel. Although the probes are within the melt channel the melt flow is essentially not disturbed with respect to throughput and obvious flow inhomogeneities.

The optical properties of the probes are sufficient for the described application. Light leaving the probe forms a cone with a focal point at about 2.5 mm, i.e. illuminating light is not parallel at all. Therefore these probes are not applicable for sophisticated spectroscopic measurements aimed at correct extinction values. But for spectroscopic measurements aimed at the relative simple statement if an observed process is running stable or unstable the presented probes are absolutely sufficient. For such applications the overall maximum light transmission of 12% at a distance of about 2 mm between the probes is more important than high quality spectra, because high transmission allows longer absorption pathlengths, e.g. to go to higher extruder diameters or to decrease surface effects on the probes. Therefore for all measurements a distance of approximately 2.3 mm between the probes was used.

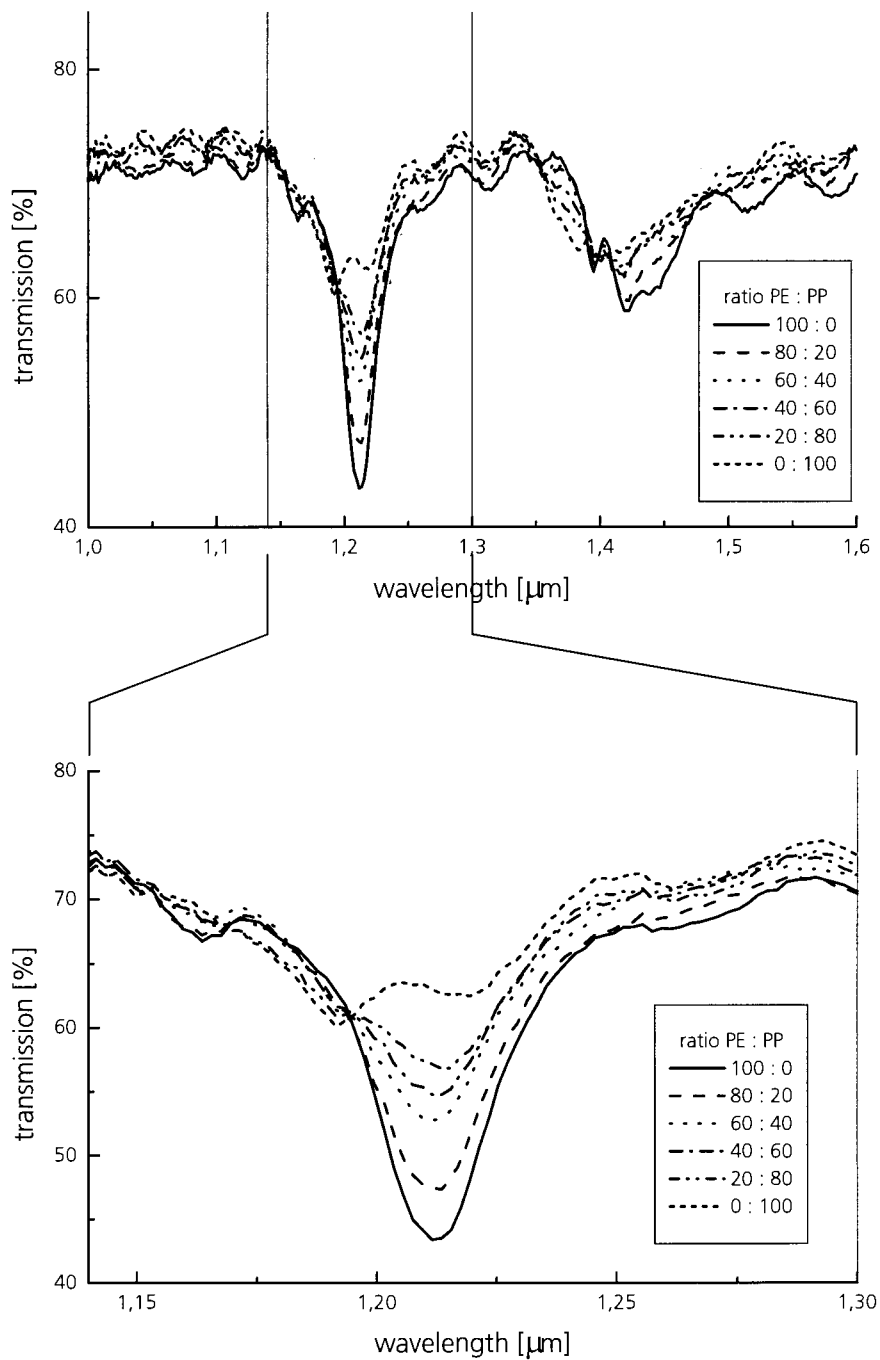


Fig. 3. Spectra of PE/PP blends with different mixture ratios varying from pure PE to pure PP in steps of 20%. PE/PP blend was extruded at 240°C and 50 rpm. Number of averaged spectra: 500, scan frequency: 100 spectra  $\text{s}^{-1}$ , spectral resolution: 2 nm at 1.523  $\mu\text{m}$ .

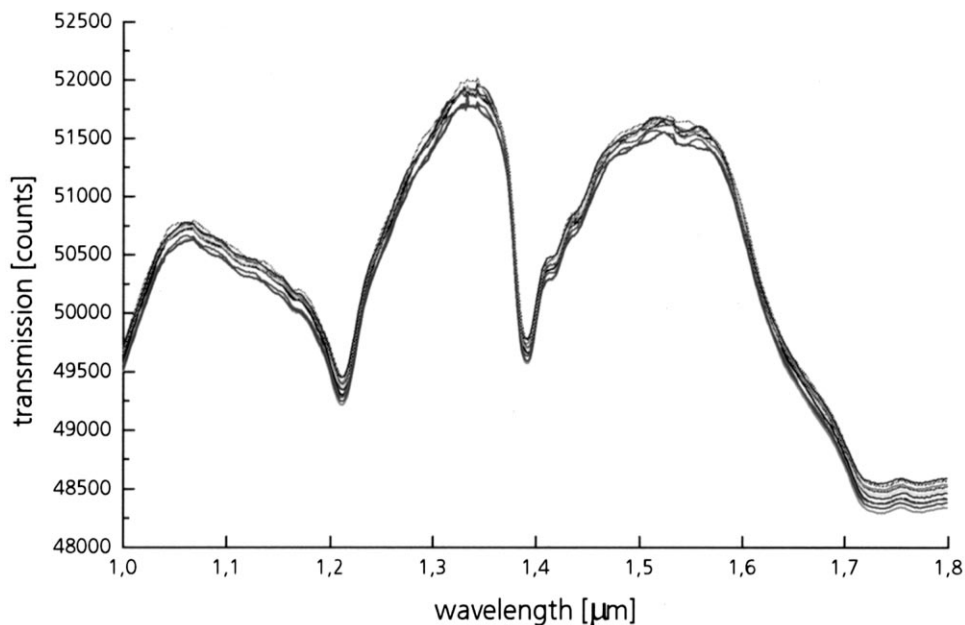


Fig. 4. Averaged transmission spectra of calibration set of PE/PP blends. The mixture ratios vary from pure PE to 90% PE with 10% PP. PE/PP blend was extruded at 240°C and 50 rpm. Number of averaged spectra: 500, scan frequency: 100 spectra  $s^{-1}$ , spectral resolution: 2 nm at 1.523  $\mu\text{m}$ .

Hence, it can be concluded that the developed probes are appropriate sensors for in-line observation of polymeric melts in an extruder leading to quality statements concerning actual process status and actual processed material.

### 3.2. PE/PP-blends

Different PE/PP-blends were investigated, varying the content of PE (PP respectively) from 0 to 100% in different percentage steps. In Fig. 3 spectra are shown for 20% steps. It is obvious that the main spectral information concerning the composition of the blend is in the second overtone of the C–H stretching band around 1.21  $\mu\text{m}$ . Transmission in the area of 1.21  $\mu\text{m}$  decreases if the PE content is increased. A contrary effect can be observed in the wavelength area of 1.19  $\mu\text{m}$  where a shoulder develops to a side maximum with increasing PP content. This side maximum of PP can be explained by the

fact that besides C–H vibrations of  $\text{CH}_2$  groups, vibrations of CH and  $\text{CH}_3$  groups also appear, which are slightly shifted compared to  $\text{CH}_2$  group vibrations. This leads to band splitting and displacement of the band's centre.

In the next step, the percentage difference of the PE/PP blend was reduced. Mixtures varied between pure PE and 90% PE + 10% PP in steps of 1%. These mixtures were chosen to simulate (1) different amounts of an additive in a polymer matrix and (2) blending of two different polymers. A PLS model was applied for prediction of the polymer mixture, i.e. ratio of PE to PP, and covers 11 different PE/PP blends, with 20 spectra of each mixture used for calibration and validation. Averaged spectra of the calibration set are shown in Fig. 4.

For each PLS model, five principal components were used, which explain over 95% of the spectral variance and also over 95% of the compositional variance of the PP/PE system. The

combination of different spectrum preparation techniques was tested to generate an optimised PLS model. The results for the RMSEP are shown in Table 2. From this table it can be seen that best results were received by simple spectral averaging and smoothing (RMSEP, 0.38%).

It is important to note that model 1 through 11 were generated based on two measurement series (measurements were conducted at different times), whereas model 12 and 13 are based only on the first of these measurement series. This explains the enormous decrease of the RMSEP comparing model 11 and model 12, although the same data preparation was applied. Here it becomes obvious that the transfer of the PLS model from one measurement to another is very difficult and produces additional errors (RMSEP increases by a factor of about two). This is a problem to be dealt with in the future.

Table 2  
RMSEP for different spectral preparation techniques<sup>a</sup>

PLS model no.	Combination of preparation techniques	RMSEP (%)
1	raw	0.5
2	1-diff	0.6
3	2-diff	0.85
4	red-3	0.4
5	red-3, MSC	0.45
6	red-4	0.38
7	red-4, MSC (only off-set correction)	0.42
8	red-5	0.4
9	red-5, MSC (only off-set correction)	0.4
10	red-4, av-5, MSC (only off-set correction)	0.38
11	av-2, sm	0.38
12	av-2, sm	0.21
13	av-2, red-4, sm (instead of leverage correction ⇒ test set validation)	0.25

<sup>a</sup> Models 1 through 11 are based on two measurements, models 12 and 13 are based only on the first measurement series; raw, no preparation; *x*-diff, differentiation; red-*x*, data reduction; MSC, multi scattering correction; av-*x*, averaging.

Reduction of the spectra by a factor of four (four points were averaged to one new point) were used for a test set validation in model 13. This reduction has the main effect that the PLS model becomes more stable. The test set validation uses six samples for calibration and four samples for validation. The resulting RMSEP of 0.21% indicates an averaged error of  $\pm 0.21\%$  in prediction, which is a very good result. Fig. 5 shows the predicted mixture ratios of the calibration samples (leverage correction) and of the validation samples. As expected the leverage correction delivers better results than the test set validation, because the samples for the leverage correction were already used for generation of the PLS model. Nevertheless all samples build very dense clusters around the real mixture ratio.

#### 4. Discussion

A measurement system for in-line NIR spectroscopy for polymer extrusion processes had been developed at Fraunhofer ICT. It consists of a measurement head adapted to a single screw extruder with integrated fibre optic probes and an AOTF-NIR spectrometer. Transmission measurements at typical extrusion conditions (temperature 300°C, pressure 35 MPa) yielded good results with respect to mechanical and optical properties of the probes. The developed system is capable of measuring different polymer compositions as demonstrated for PE/PP blends. Various data preparation techniques were tested. Best results were received with spectral averaging, smoothing, and data reduction. In this case the prediction ability of a partial least squares (PLS) model was in the range of  $\pm 0.25\%$ .

These results demonstrate the capabilities of in-line NIR spectroscopy with respect to process control in the area of polymer extrusion. Future investigations have to focus on improvement of optical probes and data treatment. Also further polymeric materials have to be investigated to demonstrate fully the enormous advantages of this new technology.



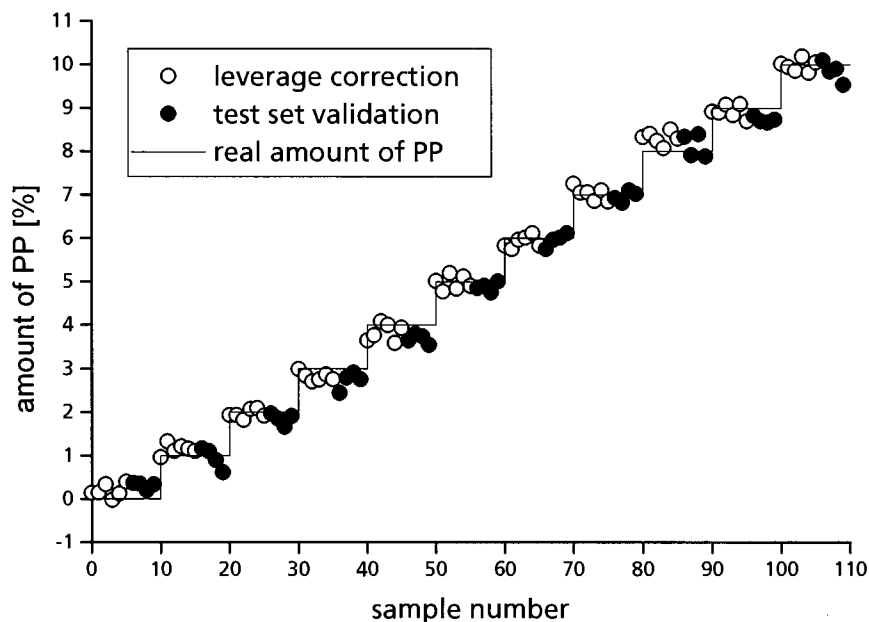


Fig. 5. Validation of the best PLS model. Six samples were used for generation of the PLS model, four samples were used as test set. As expected leverage correction is almost better than test set validation.

## References

- [1] I. Murray, I.A. Cowe (Eds.), *Making Light Work: Advances in Near Infrared Spectroscopy*, Proceedings of the 4th International Conference on NIR Spectroscopy, Aberdeen, UK, August 19–23, 1991, VCH, Weinheim, 1992.
- [2] J. Workman Jr, *J. Near Infrared Spectrosc.* 1 (1993) 221.
- [3] D. Fischer, T. Bayer, K.-J. Eichhorn, M. Otto, *Fresenius J. Anal. Chem.* 359 (1997) 74.
- [4] M.G. Hansen, A. Khettry, *Polym. Eng. Sci.* 34 (1994) 1758.
- [5] A. Khettry, M.G. Hansen, *Polym. Eng. Sci.* 36 (1996) 1232.
- [6] A. Blanc, N. Eisenreich, H. Kull, W. Liehmann, in: 19th International Annual Conference of ICT, 1988, 74-1.
- [7] N. Eisenreich, J. Herz, H. Kull, W. Mayer, T. Rohe, *ANTEC '96*, (1996) 3131.
- [8] H. Martens, S.A. Jensen, in: J. Holasand, J. Kratochvil (Eds.), *Progress in Cereal Chemistry and Technology, Part A*, Proceedings of 7th World Cereal and Bread Congress, Elsevier, Amsterdam, 1983, p. 607.
- [9] K. Esbensen, S. Schönkopf, T. Midtgaard, *Multivariate Analysis in Practice*, CAMO, Trondheim, Norway, ISBN 82-993330-1-6, 1996.

# Application of FT-Raman spectroscopy to quality control in brick clays firing process

J.M. Alia <sup>a,\*</sup>, H.G.M. Edwards <sup>b</sup>, F.J. Garcia-Navarro <sup>a</sup>,  
J. Parras-Armenteros <sup>c</sup>, C.J. Sanchez-Jimenez <sup>a</sup>

<sup>a</sup> *Departamento de Química Física y Laboratorio de Mineralogía Aplicada, Universidad de Castilla-La Mancha, E-13071 Ciudad Real, Spain*

<sup>b</sup> *Chemistry and Forensic Science Department, University of Bradford, Bradford BD7 1DP, UK*

<sup>c</sup> *Departamento de Ingeniería Geológica y Minera, Universidad de Castilla-La Mancha, Almadén, Ciudad Real, Spain*

Received 7 September 1998; received in revised form 13 November 1998; accepted 16 November 1998

---

## Abstract

This paper reports the study of the mineralogical evolution during the firing process (800–1150°C) of the main types of raw materials used for the brick industry in Santa Cruz de Mudela (Ciudad Real, Spain). The mineralogical diversity observed in these materials leads to different behaviour during the shaping, drying and firing stages. Traditional use of similar working conditions in local industries, despite the mineralogical differences in the starting material, promotes the presence of defects in the drying and/or firing stages. This study attempt to implement some analytical guideline for the raw materials in order to improve the final product. Three types of raw materials obtained in different quarries have been characterised by means of chemical analysis with electron microprobe, powder X-ray diffraction and FT-Raman spectroscopy. The main difference between the clays studied is the carbonate content: one of the analysed samples is deficient in this component, while it is present as calcite (8%) or as calcite (14%) plus dolomite (10%) in the rest. The observed compositional differences seem to be relevant in the firing process. FT-Raman spectra reveal the onset of early vitrification (at about 900°C) in the sample without carbonate. The importance of calcium and magnesium oxides, obtained from the corresponding carbonates, for the synthesis of new mineral phases that could slow down the vitrification process is discussed. © 1999 Elsevier Science B.V. All rights reserved.

*Keywords:* Industrial clays; Quality control; Vitrification; FT-Raman spectroscopy

---

## 1. Introduction

The application of Raman spectroscopy to the identification and characterisation of mineral species is well-established [1,2]. Recent papers and reviews [3,4] have stressed the use of Fourier-

\* Corresponding author. Fax: +34-926-295-351.  
E-mail address: jmalia@qifi-cr.uclm.es (J.M. Alia)

transform Raman spectroscopy (FT-Raman) in the study of both natural as well as synthetic mineral analogues. However, Raman investigations on silicates and, specifically, layer silicates (clays) have been relatively scarce despite their importance and extensive utilisation. The main explanation for this shortage of data are the strong fluorescence that is excited in the natural clays due to the presence of iron(III) hydroxide, which is observed even using the near-infrared laser, and their intrinsic low scattering power due to the relatively small polarizability of the corresponding Si–O and Si–O bonds. The presence of organic matter, frequent in these types of materials, could obviously contribute to the fluorescence, particularly with the use of visible laser excitation. This fact, and the easy destruction of the red coloured samples under effect of the visible lasers, justify the use of the FT-Raman in the present study.

On the other hand, the usefulness of vibrational spectroscopy techniques (infrared and Raman) to study short-range order/disorder phenomena is well-documented [5,6]. Since in the firing of ceramic materials the vitrification of some components starts at moderate temperature (900–950°C), it seems interesting to assess the ability of FT-Raman spectroscopy to monitor such a process in the early stages which needs to be quite extended to become observable by means of X-ray diffraction techniques. The main objective of the present investigation is a practical one, because the presence of vitrified phases modifies the physical and technical properties of the final product and therefore it is important to improve the analytical techniques available to detect and study the appearance of such phases.

## 2. Experimental

### 2.1. Chemical and mineralogical characterisation of the samples

Chemical composition of the samples was analysed by X-ray fluorescence using a Philips PW 1404/10 apparatus. Mineralogical characterisation was carried out using a Philips PW 1710

automatic X-ray diffractometer with Cu K $\alpha$  radiation. Scanning rate for general identification diffractograms (from  $2\theta = 5\text{--}70^\circ$ ) was  $0.5^\circ \text{ min}^{-1}$ . The diffractometer was calibrated using Si as an external standard. X-ray source conditions were 40 kV and 50 mA with 2200 W of power.

### 2.2. FT-Raman spectra

FT-Raman spectra were excited at 1064 nm using a Nd:YAG laser and a Bruker IFS66 optical bench with a FRA 106 Raman accessory. Laser power was set at ca. 80 mW and 2000 scans were accumulated with a resolution of  $2 \text{ cm}^{-1}$ . Powdered samples were lightly pressed in the Bruker powder holder and mounted with  $180^\circ$  scattering geometry.

The mathematical treatment of the spectra and diffractograms was carried out using the commercial software GRAMS/32<sup>®</sup> (Galactic Industries). Smoothing procedures or baseline correction routines were not applied in this work.

### 2.3. Firing process

As the main interest of this work is to assess the changes that occur in the clays during the industrial firing process, powdered raw materials (particle size  $< 50 \mu\text{m}$ ) were fired in air atmosphere during 2 h at the desired temperature (heating speed:  $10^\circ\text{C min}^{-1}$ ). Once finished the firing process, the oven was switch off and allowed to cool down to room temperature. The full process usually takes 24 h.

## 3. Results

Table 1 gives the chemical and mineralogical compositions of the raw materials. In all the samples studied, layer silicates (kaolinite, illite and smectite) are the main components accounting for 78 (SC1), 83 (SC2) and 70% (SC3), respectively, of the total mineral content. From the mineralogical point of view, the principal difference between the samples studied stems from the carbonate (calcite and dolomite) contents. Such minerals are not observed in the SC2 sample, although they

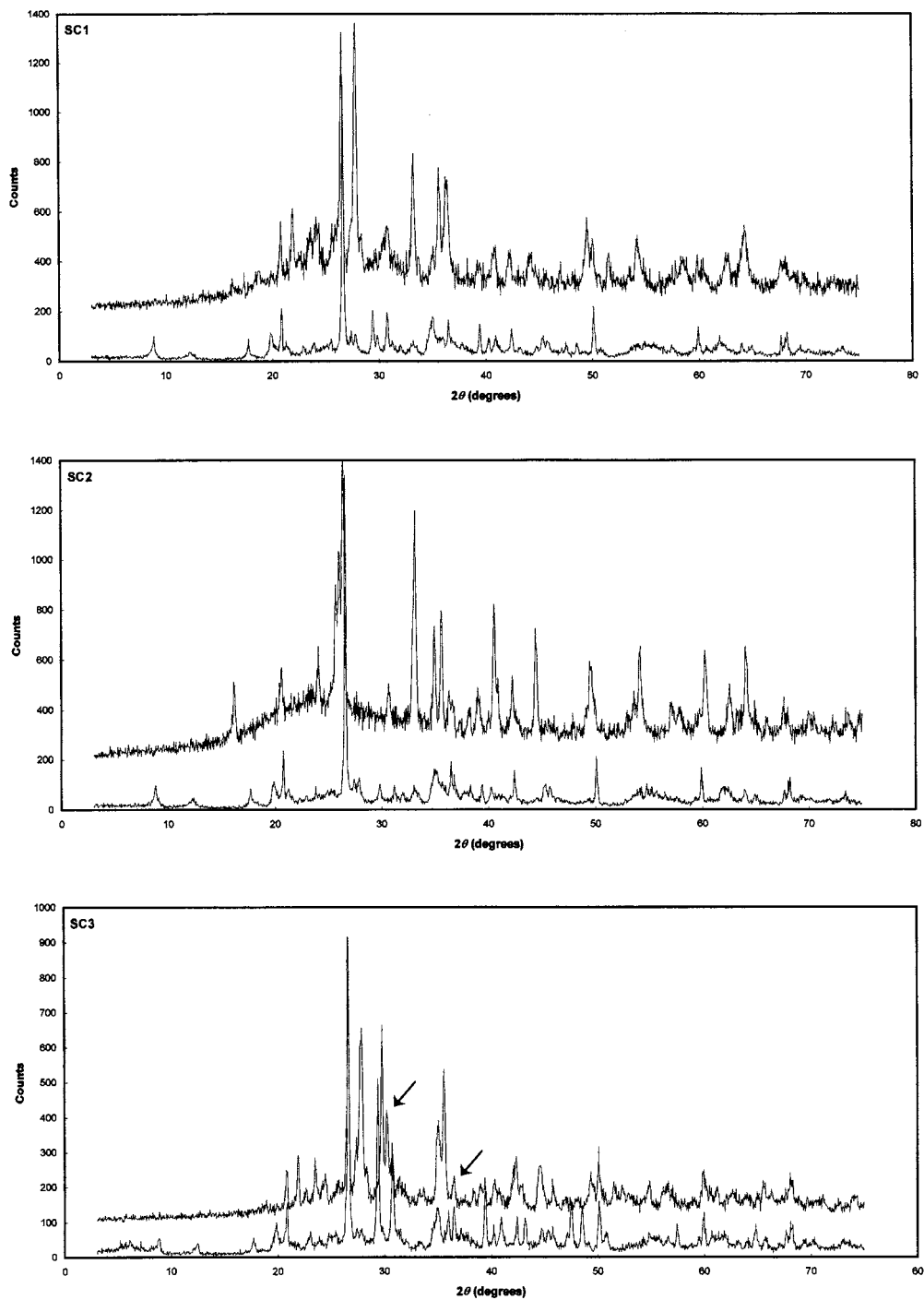


Fig. 1. X-ray diffraction patterns of the samples studied. Bottom: raw material. Top: heated for 2 h at 1150°C. Marked features in the SC3 (top) pattern are diffraction peaks from gehlenite at  $2\theta = 31.28$  and  $36.56^\circ$  (2.85 and 2.45 Å).

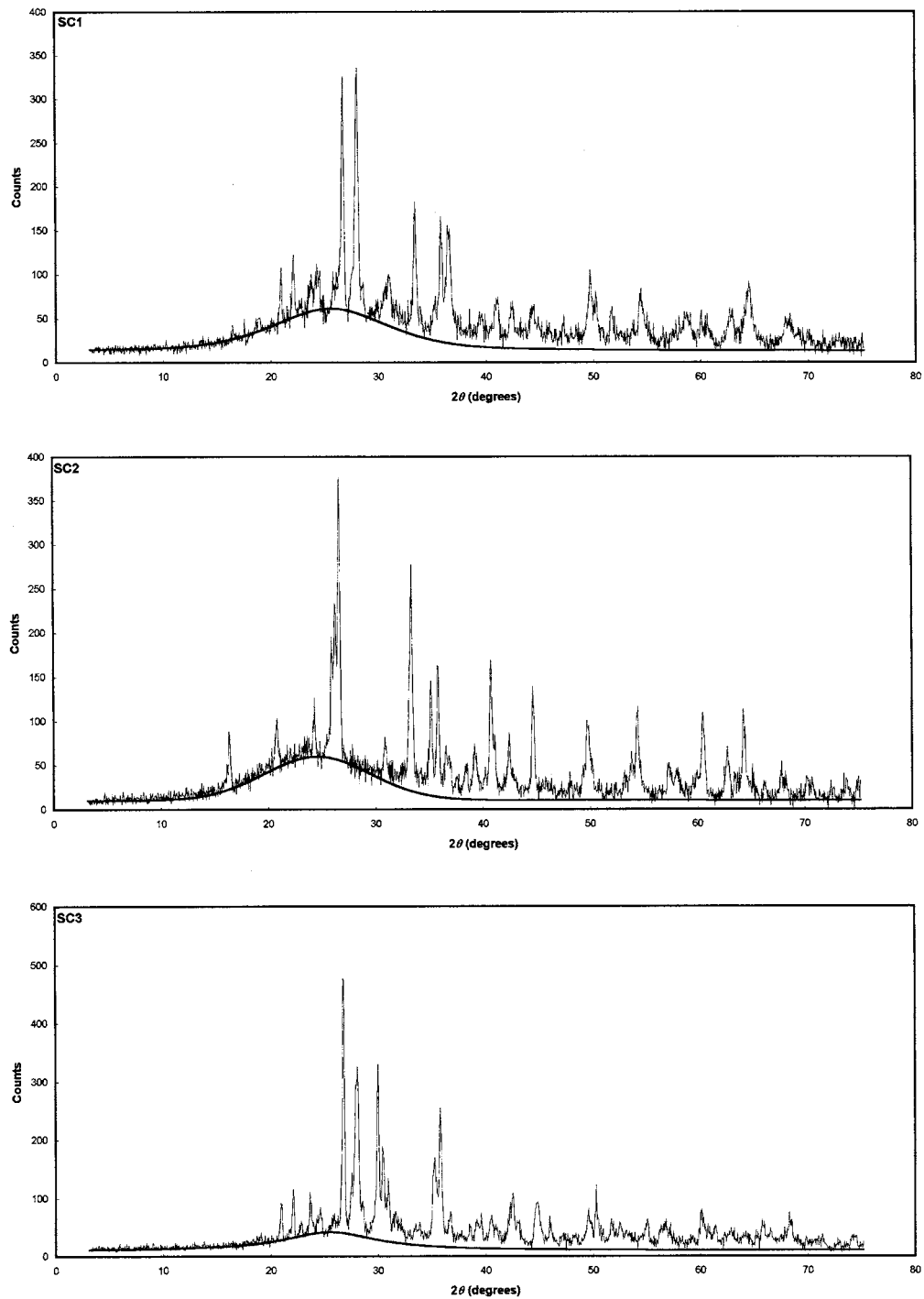


Fig. 2. Resolution and fitting of the amorphous phase diffraction feature. Samples heated for 2 h at 1150°C.

Table 1  
Chemical and mineralogical composition of the raw materials studied in the present work

	SC1	SC2	SC3
<i>Component (%)</i>			
SiO <sub>2</sub>	43.9	45.3	36.9
Al <sub>2</sub> O <sub>3</sub>	22.6	23.6	17.5
Fe <sub>2</sub> O <sub>3</sub>	8.9	9.0	5.1
Na <sub>2</sub> O+K <sub>2</sub> O	6.9	6.6	5.3
CaO	4.0	0.9	9.6
MgO	1.0	0.5	3.2
TiO <sub>2</sub>	1.9	2.0	1.3
Ignition losses	10.9	12.1	21.1
<i>Mineral (%)</i>			
Quartz	6	6	5
Feldspar	8	11	7
Calcite	8	0	14
Dolomite	0	0	10
Kaolinite	16	22	6
Illite	62	61	55
Smectite	0	0	9

constitute 8% (calcite) in the sample SC1 and up to 24% (calcite + dolomite) in the sample SC3.

X-ray diffraction patterns corresponding to the raw materials and the samples fired at 1150°C are shown in Fig. 1. In all the samples studied the appearance of a broad diffraction feature centred at ca.  $2\theta = 26^\circ$  is evident. This is particularly clear in the sample SC1 and more so in sample SC2. Such a broad and ill-defined component can be ascribed to the presence of amorphous phases (glasses) originating from the abundant layer silicates originally present in the raw material [7,8]. This component can be separated from the rest of the diffraction pattern after the appropriate fitting using a Gaussian and Lorentzian linear combination function. The curve-fitting results are given in Fig. 2. Table 2 shows the corresponding numeri-

Table 2  
Band-fitting numerical results and statistics of the amorphous phase component in the powder diffraction patterns given in Fig. 2<sup>a</sup>

Sample	Center/ $2\theta$	S.E.	FWHH/ $2\theta$	S.E.	Reduced $\chi^2$	$r^2$	S.E.E.
SC1	24.874	0.139	15.768	0.745	2.2176	0.9678	7.6739
SC2	24.542	0.116	13.448	0.611	2.0369	0.9736	6.4015
SC3	25.502	0.249	14.408	0.937	2.7964	0.9542	9.3679

<sup>a</sup> S.E., standard error; S.E.E., standard error of the estimate; FWHH, full width at half height.

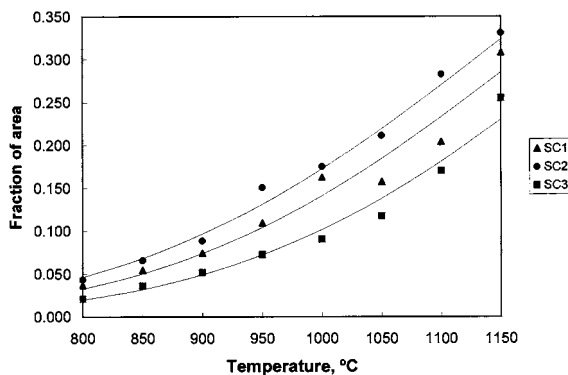


Fig. 3. Fraction of area corresponding to the X-ray diffraction pattern amorphous phase feature vs the heating temperature.

cal information. The fraction of area corresponding to the fitted component increases non-linearly when the temperature is increased as can be observed in Fig. 3. As can be seen in this figure, the sample richer in amorphous fraction over the full range of studied temperatures is SC2, in which the band arising from the amorphous material in the sample fired at 1150°C reaches 35% of the total area of the corresponding diffraction pattern.

Since the presence of vitrified phases has great influence over the physical and mechanical properties of the ceramic materials [8–10] and FT-Raman spectroscopy is an efficient analytical technique to detect short range disorder phenomena, the possibility of early detection of the vitrification processes was investigated. To this end, the FT-Raman spectra of samples fired at different temperatures were obtained (Fig. 4). The Raman spectra of the unheated samples show high fluorescence background. In spite of this fact, the carbonate anion symmetric stretching band at  $1085\text{ cm}^{-1}$  is clearly observable in the samples SC1 and SC3. This feature remains, although with

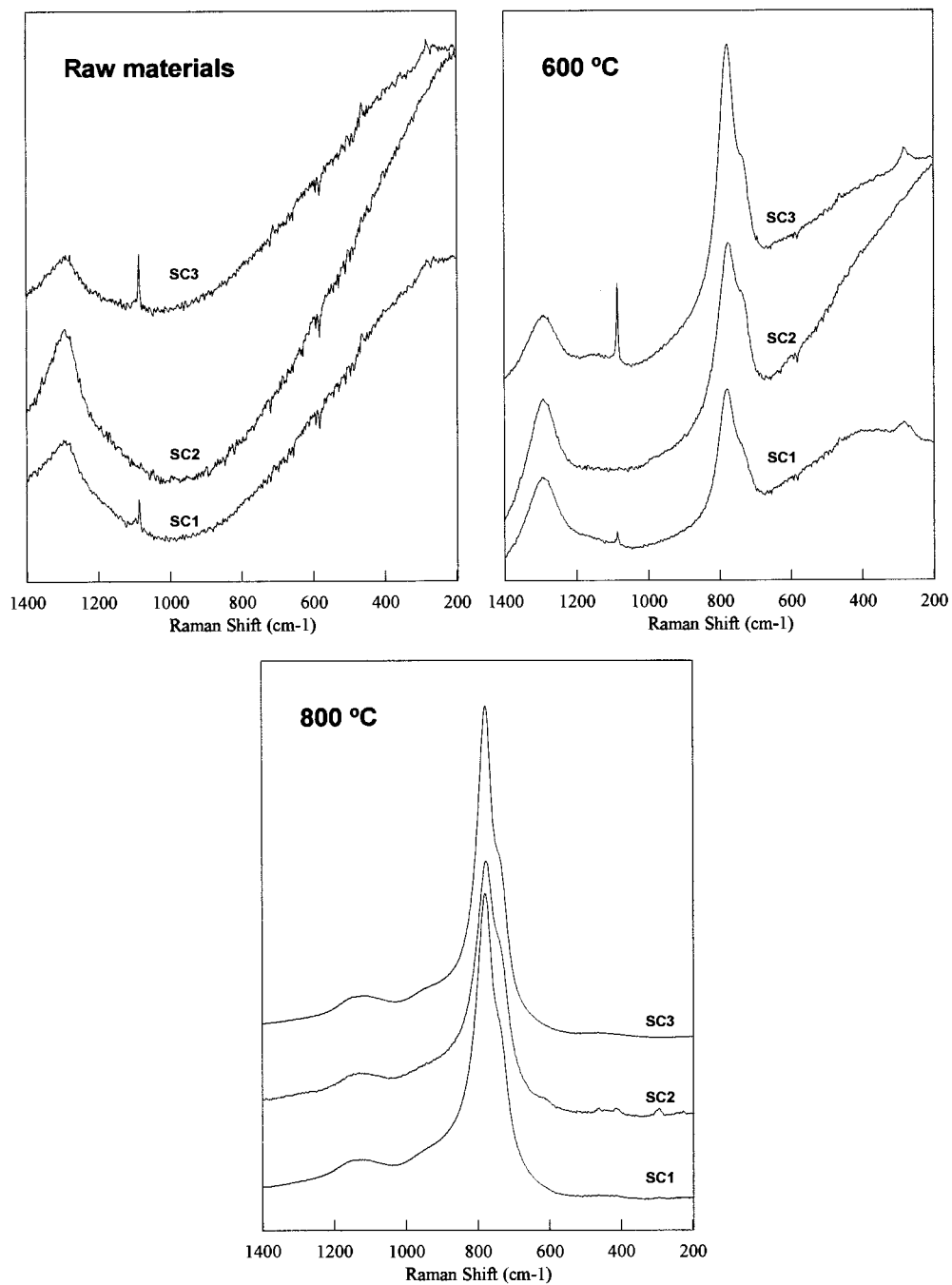


Fig. 4. FT-Raman spectra of the samples studied at different temperatures. In the spectra corresponding to the raw materials SC1 and SC3 the peak from  $\text{CO}_3^{2-}$  symmetric stretching is clearly visible at  $1086 \text{ cm}^{-1}$ . These peaks are much less intense in the spectra at  $600^\circ\text{C}$  (intensity  $\times 2$ ). The fluorescence background and noise are also less important.

less intensity, in the samples heated at 600°C. It is evident that the decrease of the fluorescence background suggests the organic origin of this process.

At 800°C, all the samples studied present a quite simple FT-Raman spectrum whose most intense feature is a poorly resolved doublet with compo-

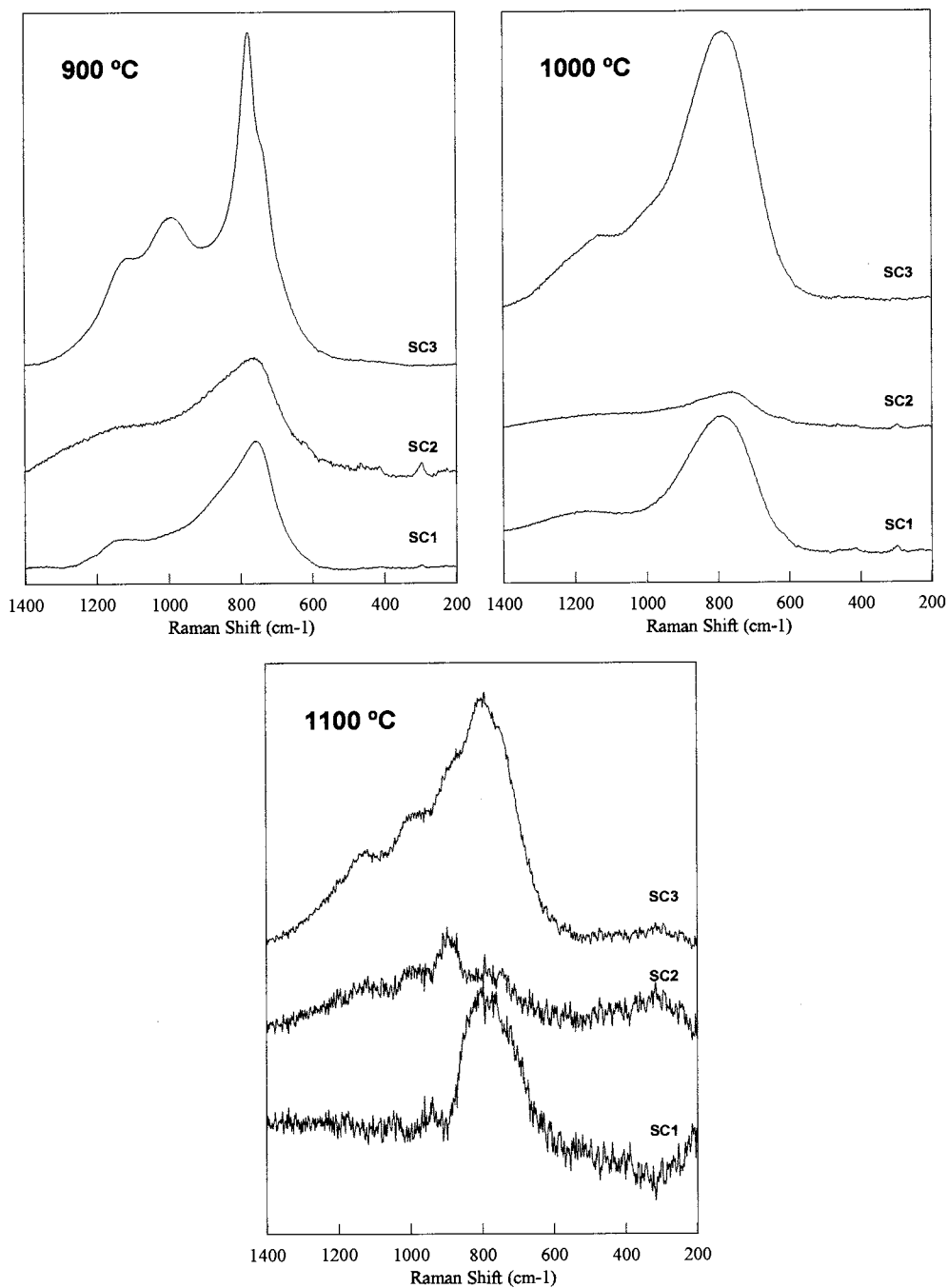


Fig. 4. (Continued)



nents at 745 (shoulder) and 776  $\text{cm}^{-1}$ . This band can be assigned to the symmetric stretching of the Si–O–Si group in the tetrahedral layer of the phyllosilicates [11]. An Al-for-Si substitution could be responsible for the lower wavenumber component [12]. At 900°C, a strong decrease of the integrated band intensity accompanied by a relevant enlargement of that feature are detected in the FT-Raman spectrum of the sample SC2. Similar, although less pronounced, effects are evident in the spectrum of the sample SC1. The sample SC3, however, maintains the structure of the doublet relatively intact, furthermore showing two well-resolved new features at 991 and 1108  $\text{cm}^{-1}$ , which could be attributed to the high temperature phase of the feldspar albite [5] (ideal stoichiometry:  $\text{NaAlSi}_3\text{O}_8$ ). In contrast, the minimal differences observed in the X-ray diffraction patterns corresponding to the same samples fired at 800 and 900°C must be pointed out. Intensity decrease and enlargement of the same doublet are evident in the FT-Raman spectra of the samples fired at 1000°C. In fact, the Raman signal corresponding to the sample SC2 has almost vanished at this temperature. Finally, in the FT-Raman spectra of the samples fired at 1100°C the vibrational bands are hardly discernible from the noisy background in the samples SC1 and SC2, and are very weak in the sample SC3.

The weakening of the Raman signal that accompanies the loss of short-range order in this type of material is well-documented [11]. In the samples studied, the modifications in the tetrahedral layer of the phyllosilicates provoked by the firing process seem to promote the weakening in intensity and later disappearance of the observed vibrational bands. This can be explained by the loss of short-range order that precedes the vitrification process. Thus, Raman spectroscopy is able to detect the local order loss earlier than X-ray diffraction, as has already been demonstrated in other solid systems [6]. The persistence of the

Raman signal observed in the sample SC3 can be explained by considering its higher content in  $\text{Ca}^{2+}$  ion arising from the corresponding carbonates (calcite and calcic dolomite) which decomposed at 600–700°C, giving rise to highly reactive calcium oxide. Formation of non-amorphous phases such as gehlenite ( $\text{Ca}_2\text{Al}_2\text{SiO}_7$ ), whose characteristic diffraction peaks are observable in the corresponding diffraction pattern, could explain the persistence of the Si–O–Si symmetric stretching Raman signal in the spectrum of the sample SC3.

## References

- [1] W.P. Griffith, in: V.C. Farmer (Ed.), *The Infrared Spectra of Minerals*, 1st edition, The Mineralogical Society, London, 1974, p. 119.
- [2] P.F. McMillan, A.M. Hofmeister, in: F.C. Hawthorne (Ed.), *Spectroscopy Methods in Mineralogy and Geology*, vol. 18, Ch. Review in Mineralogy, 1st edition, Mineralogical Society of America, Chelsea, Michigan, 1988, p. 99.
- [3] E.E. Coleyshaw, W.P. Griffith, R.J. Bowell, *Spectrochim. Acta Part A* 50 (1994) 1909.
- [4] M. Mehicic, J.G. Graselli, in: J.G. Graselli, B.J. Bulkin (Eds.), *Analytical Raman Spectroscopy*, 1st edition, Wiley, New York, 1991.
- [5] W.B. White, in: V.C. Farmer (Ed.), *The Infrared Spectra of Minerals*, 1st edition, The Mineralogical Society, London, 1974, p. 87.
- [6] F. Rull, J. Rodríguez, J.M. Alía, F. Arroyo, H.G.M. Edwards, *Makromol. Chem. Macromol. Symp.* 94 (1995) 189.
- [7] F. González-García, V. Romero-Acosta, G. García-Ramos, M. González-Rodríguez, *Appl. Clay Sci.* 5 (1990) 361.
- [8] B. Sonuparlak, M. Sarikaya, I.A. Aksay, *J. Am. Ceram. Soc.* 70 (1987) 837.
- [9] T. Peters, R. Iberg, *Am. Ceram. Soc. Bull.* 57 (1978) 503.
- [10] K. Srikrishna, G. Thomas, R. Martínez, M.P. Corral, S. De Aza, J.S. Moya, *J. Mater. Sci.* 25 (1990) 607.
- [11] E. Dowty, *Phys. Chem. Miner.* 14 (1987) 122.
- [12] V.C. Farmer, in: V.C. Farmer (Ed.), *The Infrared Spectra of Minerals*, 1st edition, The Mineralogical Society, London, 1974, p. 331.

# Separation of poly(ethylene glycols) into fractions by sequential liquid–liquid extraction

Krzysztof Tomaszewski, Andrzej Szymanski, Zenon Lukaszewski \*

Poznan University of Technology, Institute of Chemistry, ul. Piotrowo 3, PL-60-965 Poznan, Poland

Received 27 July 1998; received in revised form 7 December 1998; accepted 8 December 1998

Dedicated to: Professor Kazimierz Sykut of Maria Curie, Sklodowska University on the occasion of his 75th birthday.

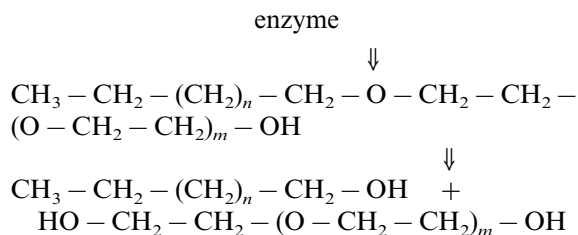
## Abstract

Poly(ethylene glycols) (PEG) are the major metabolites of non-ionic surfactants (NS). Chains of PEG may be shortened due to further biodegradation. The separate determination of short- and long-chained PEG (SC- and LC-PEG) may be useful to control the biodegradation of NS and PEG. A scheme for the separation of a whole mixture of PEG into SC- and LC-fractions and their subsequent determination is developed. A sequential extraction of a water sample with *n*-hexane and ethyl acetate is used to separate NS and other interferences as well as dichloromethane and chloroform for the separation of PEG into LC- and SC-fractions. The indirect tensammetric technique (ITT) is used for the final quantification of PEG into separated fractions as well as for the control of every separation step. The boundary between fractions is not sharp due to the similarity of the properties of neighbouring homologues which may be approximately 15 oxyethylene subunits. The developed scheme is successfully used for the separation into fractions of PEG from river water and raw and treated sewage. An initial separation of PEG from these samples by extraction with chloroform is carried out. © 1999 Elsevier Science B.V. All rights reserved.

**Keywords:** Non-ionic surfactants; Poly(ethylene glycols); Tensammetry; Extraction

## 1. Introduction

Poly(ethylene glycols) (PEG) are a major by-product of the biodegradation of ethoxylates—the dominating group of non-ionic surfactants (NS). The most probable pathway for ethoxylates is central fission [1], as may be seen in the reaction given in the example of oxyethylated alcohols:



in which PEG are formed together with free fatty alcohol. Industrial applications of PEG, mainly in the textile industry and in cosmetic formulations,

\* Corresponding author. Tel.: +4861-8782-786; fax: +4861-8782-571.

E-mail address: lukasz@et.put.poznan.pl (Z. Lukaszewski)

is an additional source of PEG in the aquatic environment. Chains of PEG may be shortened due to further biodegradation in sewage treatment or in surface water. This shortening may occur both by a split in terminal ethylene glycols as well as by random fragmentation of longer PEG molecules into shorter PEG. The more intensive the PEG biodegradation, the higher the concentration of short-chained PEG (SC-PEG). Therefore a separate determination of SC- and long-chained PEG

(LC-PEG) may be useful in the control of the biodegradation of ethoxylates and PEG. However, this analytical task is as yet unresolved.

The aim of this work was to develop a scheme for the separation of a whole mixture of PEG into SC- and LC-fractions and their subsequent determination. PEG of molecular weight (MW) within the range of 150–1000 were investigated. PEG longer than 23 oxyethylene subunits (MW approximately 1000) are unlikely to be the metabo-

Table 1

Liquid–liquid extraction of triethyleneglycol (E<sub>3</sub>), PEG 400, PEG 600 and PEG 1000 into dichloromethane and chloroform<sup>a</sup>

	E <sub>3</sub>	PEG 400	PEG 600	PEG 1000
No. oxyethylene subunits	3	8.7	13.2	22.3
<i>Dichloromethane</i>				
Ratio of phases (ml/ml)	10/100	5/100	2/100	2/100
Found in (µg):				
Water phase	930	930	850	280
Organic phase	40	120	180	820
Total	970	1050	1040	1100
Extraction coefficient	0.39	2.8	10.5	145
<i>Chloroform</i>				
Ratio of phases (ml/ml)	5/100	5/100	1.6/100.4	5/100
Found in (µg):				
Water phase	910	830	794 ± 30 <sup>b</sup>	90
Organic phase	120	180	278 ± 15 <sup>b</sup>	880
Total	1030	1010	1072 ± 35 <sup>b</sup>	970
Extraction coefficient	1.3	4.3	22 ± 1.3 <sup>b</sup>	490

<sup>a</sup> Water phase: 100 g l<sup>-1</sup> of sodium chloride. Spike of E<sub>3</sub> or PEG: 1000 µg.

<sup>b</sup> n = 7.

Table 2

The influence of sodium chloride concentration on the extraction of triethyleneglycol (E<sub>3</sub>) into chloroform<sup>a</sup>

Sodium chloride concentration (g l <sup>-1</sup> )	Found (µg)			Extraction coefficient
	Water phase	Organic phase	Total	
0	970	80	1050	0.80
50	940	85	1025	0.90
100	910	120	1030	1.3
150	840	200	1040	2.3
200	690	300	990	4.4
250	540	450	990	8.4
300	420	610	1030	15

<sup>a</sup> Spike of E<sub>3</sub>: 1000 µg.

Table 3

A recovery of 50 µg spike of Marlipal 1618/25, PEG 600, PEG 1000 and triethyleneglycol in sequential extraction with *n*-hexane, ethyl acetate, dichloromethane and chloroform ( $n = 5$ )

Surfactant or PEG	Fraction-solvent	Found [µg]	Confidence interval [µg]
Marlipal 1618/25	Ethyl acetate	48.9	4.2
	Dichloromethane	1.5	
	Chloroform	0.3	
	Total	50.7	
PEG 1000	Ethyl acetate	0.3	6.5 2.7
	Dichloromethane	43.4	
	Chloroform	8.5	
	Total	52.2	
PEG 600	Ethyl acetate	0.6	3.5 4.0
	Dichloromethane	24.6	
	Chloroform	26.2	
	Total	51.4	
Triethyleneglycol	Ethyl acetate	0.3	2.9
	Dichloromethane	2.0	
	Chloroform	48.3	
	Total	50.6	

lites of ethoxylates. The presence of non-biodegraded NS as possible interferents in the analysed samples should be taken into account. Oxyethylated alcohol Marlipal 1618/25 was used as a representative of this group in the study.

Sequential liquid–liquid extraction was selected as a possible means of resolving the problem. The separation of NS and PEG may be achieved by sequential extraction of the water sample with ethyl acetate to separate NS and then with chloroform for the extraction of PEG [2,3]. The possible use of dichloromethane and chloroform for the separation of PEG from water samples was preliminarily reported [3]. However, a further separation of PEG into fractions is as yet unreported in the literature.

The indirect tensammetric technique (ITT) was used for the final quantification of PEG into separated fractions as well as for the control of every separation step. This electroanalytical technique was developed for the determination of electroinactive NS [4,5]. The lowering of the tensammetric peak of the monitoring substance-ethyl acetate is the analytical signal in the ITT. PEG can also be determined by ITT [3], though signals

of SC-PEG are relatively weak compared to LC-PEG or NS.

## 2. Experimental

### 2.1. Apparatus and reagents

A Radelkis OH-105 polarograph and an ECO Chemie General Purpose Electroanalytical System µAUTOLAB were alternatively used for tensammetric measurements. A standard mode of mea-

Table 4

Recovery and precision of separation of a synthetic mixture of non-ionic surfactants (50 µg Triton X-45 and 50 µg Marlipal 1618/25) and PEGs (50 µg PEG 1000 and 50 µg triethyleneglycol) into fractions by sequential extraction with *n*-hexane, ethyl acetate, dichloromethane and chloroform ( $n = 5$ )

Fraction	Found (µg)	S.D. (µg)	R.S.D. (%)
Ethyl acetate	51.1 ± 2.6	2.1	4.1
Dichloromethane	46.0 ± 2.7	2.2	4.8
Chloroform	57.5 ± 4.0	3.2	5.6

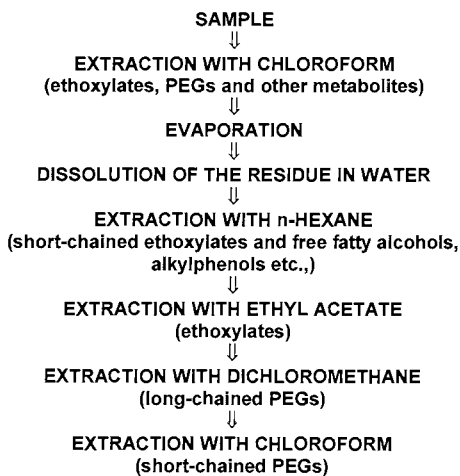


Fig. 1. Outline for sequential extraction of the mixture of non-ionic surfactants (NS) and poly(ethylene glycols) (PEGs).

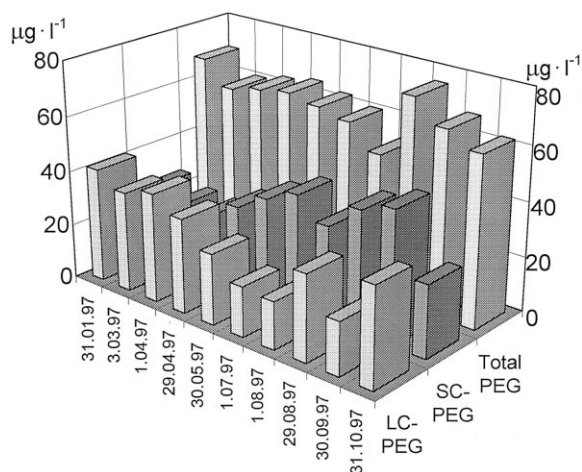


Fig. 2. The results of screening long-chained poly(ethylene glycols) (LC-PEG), short-chained PEG (SC-PEG) and total concentration of PEG (Total PEG) in the River Warta (Poznan, Poland).

surement (without phase sensitivity), a frequency of 60 Hz, a superimposed alternating voltage amplitude of 2 mV and a scan voltage rate of 400 mV min<sup>-1</sup>, were applied. Controlled-temperature HMDE equipment (Radiometer) was used having an additional platinum wire auxiliary electrode. A quartz beaker instead of a glass beaker was used. A ceramic frit on the end of a salt bridge was protected by a short polyethylene tube; both these

changes were adopted to prevent adsorptive loss of surfactant [6]. All potentials cited are against the saturated calomel electrode.

Triton X-45 and Triton X-100 (both Rohm and Haas), Marlipal 1618/25 (Hüls), PEG 400, PEG 600, PEG 1000 (all Karl Roth), and triethyleneglycol (Fluka) were used without additional purification. Methanol and sodium chloride of Analar grade were also used.

Purified sodium sulphate was used for the preparation of the aqueous base electrolytes. All solutions were prepared in water triply distilled from a quartz apparatus using only freshly distilled water.

Freshly distilled dichloromethane, ethyl acetate, *n*-hexane and chloroform were used.

## 2.2. Procedures

### 2.2.1. Single liquid–liquid extraction

Water and organic phases (dichloromethane, chloroform, ethyl acetate, *n*-hexane) were preliminarily mutually saturated. Spikes of PEG or Marlipal 1618/25 were introduced into water phase. Usually 5 min shaking with 15 min quiescent periods were applied. PEG or Marlipal 1618/25 were determined both in water and organic phases, as in Sections 2.2.2 and 2.2.3, respectively.

### 2.2.2. Determination of PEG or Marlipal 1618/25 in water phase

An aliquot of water phase was transferred into a quartz beaker. A stream of nitrogen was passed through the sample for 15 min to remove the dissolved organic solvent. The sample was transferred into a 25 ml volumetric flask. 12.5 ml of 1 M aqueous sodium sulphate and a precisely measured 1.50 ml of ethyl acetate were added and the flask filled to the mark with water. The mixture was vigorously shaken and transferred into the voltammetric cell. The mixture was stirred (approximately for 10 min in an open cell) to evaporate excessive ethyl acetate until droplets and turbidity disappeared. A saturated solution of ethyl acetate was prepared in this manner. The droplets of excess ethyl acetate can extract surfactants and cause their loss. Therefore this excess should be removed, as evidenced by the disappearance of turbidity or droplets. After a quies-

cent period (30 s) the tensammetric curve of ethyl acetate was recorded in the cathodic direction using a new mercury drop and starting from  $-1.20$  V (vs SCE). The difference between the peak height of ethyl acetate (recorded in a separate measurement) and the peak height of ethyl acetate in the presence of NS was the analytical signal. The results were quantified using a calibration curve of the investigated PEG or surfactant.

### 2.2.3. Determination of PEG or Marlipal 1618/25 in organic phase

An aliquot of organic phase was transferred into a quartz beaker and evaporated with gentle heating. The residue was dissolved in a precisely measured 1.50 ml of ethyl acetate and transferred into a 25 ml volumetric flask. A total of 12.5 ml of 1 M aqueous sodium sulphate was added and the flask filled to the mark with water.

The rest of the procedure was performed as in Section 2.2.2.

### 2.2.4. Initial separation of PEG from surface water samples

River water (800 ml) was sampled and preserved with 1% formaline. The sample was transferred into a 1000 ml separation funnel and 280 g of sodium chloride was dissolved into the sample. This stage required 90–120 min for the salt to be completely dissolved. Chloroform (40 ml) was added and extraction performed. After separation of phases the extraction was repeated twice with two 30 ml portions of chloroform. The joint extracts were collected in a 100 ml volumetric flask and the flask filled to the mark with chloroform.

### 2.2.5. Initial separation of PEG from raw and treated sewage samples

A 100 ml raw or treated sewage sample was taken and preserved with 5% formaline. The sample was transferred into a 250 ml separation funnel and 35 g of sodium chloride was dissolved into the sample. Chloroform (20 ml) was added and extraction performed. After separation of phases the extraction was repeated four times with 20 ml portions of chloroform. The joint extracts were collected in a 100 ml volumetric flask and the flask filled to the mark with chloroform.

### 2.2.6. Removal of NS and separation of PEG into fractions by a sequential liquid–liquid extraction

A chloroform extract of surface water (made as in Section 2.2.4) or sewage (made as in Section 2.2.5) was evaporated with gentle heating. The residue was leached with five 20 ml portions of water which were then transferred into a 250 ml separation funnel. Sodium chloride (1 g) was added and dissolved. The solution was twice extracted with 10 ml portions of *n*-hexane. The *n*-hexane solution was discarded and the water phase used in the further procedure.

Sodium chloride (10 g) was added to the water phase and dissolved. The solution was twice extracted with 15 and 10 ml portions of ethyl acetate, respectively. The organic phase, which contained NS, was used for their determination, while the water phase, which contained PEG, was used in the further procedure.

The water phase was twice extracted with 5 ml portions of dichloromethane. The joint extracts were collected in a 25 ml volumetric flask and the flask filled to the mark with dichloromethane (LC-PEG fraction). Sodium chloride (25 g) was

Table 5  
Screening of long- and short-chained PEG (LC- and SC-PEG) in three sewage treatment plants (STP) ( $\mu\text{g l}^{-1}$ )

STP	Raw sewage			Treated sewage		
	Long-chained PEG	Short-chained PEG	Total PEG	Long-chained PEG	Short-chained PEG	Total PEG
Goluchow	635	186	821	204	333	537
Hohland	542	524	1066	365	1430	1795
Biedrusko	1250	1310	2560	240	945	1185

added to the water phase and dissolved. The solution was thrice extracted with 20, 15 and 15 ml portions of chloroform, respectively. The joint extracts were collected in a 50 ml volumetric flask and the flask filled to the mark with chloroform (SC-PEG fraction).

An aliquot of dichloromethane fraction or chloroform fraction was transferred into a quartz beaker and evaporated with gentle heating. The residue was dissolved in a precisely measured 1.50 ml of ethyl acetate and transferred into a 25 ml volumetric flask. The rest of the procedure was performed as in Section 2.2.3.

The results were quantified using a calibration curve of PEG 1000 in the case of the dichloromethane fraction or triethyleneglycol in the case of the chloroform fraction.

### 3. Results and discussion

#### 3.1. Extraction of single PEG

A series of extractive experiments were performed in order to measure the partition of PEG of different MW, between water on the one hand and dichloromethane or chloroform on the other. Polydispersal PEG 400, PEG 600, PEG 1000 and homogeneous triethyleneglycol ( $E_3$ ) were investigated. The water phase was sodium chloride solution with a concentration of  $100 \text{ g l}^{-1}$ . PEG (1000  $\mu\text{g}$ ) was introduced into the water phase. The ratio of phases varied from 1.6:100.4 to 10:100. The extraction was performed as in Section 2.2.1 and the determination of PEG in the water and organic phases—as in Sections 2.2.2 and 2.2.3, respectively. The extraction coefficient was calculated by dividing concentrations in the organic and water phases. The results are shown in Table 1. The majority of results represent an average of two to three measurements, apart from the case of the extraction of PEG 600 with chloroform, where seven separate measurements were performed. Two conclusions may be drawn: the higher the MW, the better the extraction; the extraction coefficients for chloroform are higher than those for dichloromethane. In a single extraction almost 75% of PEG 1000 is

extracted with dichloromethane, while only several percent of  $E_3$  is extracted.

In order to find better extraction conditions for  $E_3$ , a series of experiments was carried out with varied concentrations of sodium chloride in the water phase. The extraction was carried out as in Section 2.2.1 and the determination of  $E_3$  in the water and dichloromethane as in Sections 2.2.2 and 2.2.3, respectively. The average results of two to three measurements are shown in Table 2. The conclusion is that the best conditions for  $E_3$  separation may be achieved at a maximum concentration of sodium chloride. The conclusions drawn on the basis of Tables 1 and 2 were applied in the further experiments.

#### 3.2. Sequential extraction of a mixture of NS and PEG

The idea of the sequential extraction of a mixture of NS and PEG by *n*-hexane, ethyl acetate, dichloromethane and chloroform was based on the previous series as well as on the literature. The extraction with *n*-hexane was expected to remove the most hydrophobic substances (free fatty alcohols, ethoxylates with very short oxyethylene chains, etc.). The next step—the extraction with ethyl acetate was expected to ensure the removal of NS. Only PEG was expected to remain in the water phase after the first two steps. The sequential extraction with dichloromethane and chloroform was expected to divide PEG into two fractions: LC and SC, respectively. In order to check this conception the behaviour of Marlipal 1618/25 and PEG 1000, PEG 600 and  $E_3$  was investigated under conditions of sequential extraction. Marlipal 1618/25 here represents the NS group. Fifty  $\mu\text{g}$  spikes of the NS or PEG were treated as in Section 2.2.6. *n*-Hexane extraction was applied as a preliminary treatment and the extracts discarded. Ethyl acetate, dichloromethane and chloroform extracts were treated as separate fractions. The results are given in Table 3. Marlipal 1618/25 passes almost completely into the ethyl acetate fraction. Above 85% of PEG 1000 passes into the dichloromethane fraction, though only approximately 50% of PEG 600. However, triethyleneglycol almost completely passes into the chloroform fraction. The results for

PEG 600 and PEG 1000 reflect the polydispersal nature of these PEG: longer components pass into the dichloromethane fraction while shorter ones remain in the water phase and are then extracted by chloroform. It would be important to fix the boundary length of PEG passing into dichloromethane during the sequential extraction. Unfortunately this is not realistic at present because of a lack of homogeneous PEG, though it may eventually be resolved, when homogeneous PEG will be available. However, this boundary cannot be sharp due to the similarity of the properties of neighbouring homologues and may be approximately 15 oxyethylene subunits.

In order to check the recovery and precision of separation by the proposed sequential extraction, a synthetic mixture of two NS and two PEG was treated according to the procedure. Fifty  $\mu\text{g}$  Triton X-45, Marlipal 1618/25, PEG 1000 and  $\text{E}_3$  were spiked into water and separated by sequential extraction with *n*-hexane, ethyl acetate, dichloromethane and chloroform, as in Section 2.2.6. The Triton X-45 spike represented the group of highly hydrophobic surfactants, while Marlipal 1618/25 represented typical NS. The *n*-hexane fraction was discarded without determination. The results are shown in Table 4. The removal of Marlipal 1618/25 was satisfactory. The recovery of PEG 1000 was not complete (92%) and therefore the chloroform fraction contained more than a 50  $\mu\text{g}$  spike of  $\text{E}_3$ . The precision of the determination was satisfactory.

### 3.3. Separation into fractions and the determination of PEG from environmental samples

#### 3.3.1. River water

The developed procedure was used for the determination of LC- and SC-PEG in river water. Water was sampled from the River Warta in Poznan, Poland over the period January–October 1997. An outline of the full procedure is shown in Fig. 1. The first step of the procedure was the initial separation of PEG from the river water sample, as in Section 2.2.4, and then sequential extraction was performed, as in Section 2.2.6. The results of the screening of LC- and SC-PEG in the

River Warta are given in Fig. 2. A relatively high total concentration of PEG was observed over the whole period of screening. The ratio of LC- and SC-PEG varied greatly and seems to have a seasonal nature: lower concentrations of SC-PEG over the winter season and a higher level during the summer period.

Precision of determination was estimated for one of the water samples as well as the results for NS (ethyl acetate fraction). The precision of measurements was 7.1% for NS (ethyl acetate fraction), 6.8% for LC-PEG (dichloromethane fraction) and 10.5% for SC-PEG (chloroform fraction) at a concentration of  $55.8 \pm 5.0$ ,  $36.0 \pm 3.0$  and  $26.3 \pm 3.5 \mu\text{g l}^{-1}$ , respectively. This precision is satisfactory and typical for a trace level of concentration.

#### 3.3.2. Raw and biologically treated sewage

Raw and biologically treated sewage from three sewage treatment plants (STPs) in the Poznan region (Poland) were processed as in Fig. 1. The first step was performed as in Section 2.2.5, and then as in Section 2.2.6. The results of these screenings are given in Table 5. A high level of PEG in treated sewage was observed. The ratio of LC- and SC-PEG changed dramatically during sewage treatment to the advantage of SC-PEG. However, these observations cannot be generalised. The aim of this part of the study was not to consider river water or STPs but the feasibility of the developed procedure in relation to the environmental samples, as well as to demonstrate the utility of the procedure in environmental studies.

### Acknowledgements

This work was supported by Poznan University of Technology (Grant No. BW 31-541/98).

### References

- [1] R.D. Swisher, *Surfactant Biodegradation*, 2nd edition, Revised and Expanded, Marcel Dekker, Basel, New York, 1987.



- [2] P. Schöberl, *Tenside Deterg.* 19 (1982) 329.
- [3] A. Szymanski, Z. Lukaszewski, *Analyst* 129 (1996) 1897.
- [4] A. Szymanski, Z. Lukaszewski, *Anal. Chim. Acta* 260 (1992) 25.
- [5] A. Szymanski, B. Wyrwas, Z. Lukaszewski, *Anal. Chim. Acta* 305 (1995) 256.
- [6] A. Szymanski, Z. Lukaszewski, *Anal. Chim. Acta* 231 (1990) 77.

## Speciation of selenite and selenate using living bacteria

L.C. Robles<sup>a</sup>, J.C. Feo<sup>a</sup>, B. de Celis<sup>b</sup>, J.M. Lumbreras<sup>b</sup>, C. García-Olalla<sup>a</sup>,  
A.J. Aller<sup>a,\*</sup>,<sup>1</sup>

<sup>a</sup> Department of Biochemistry and Molecular Biology, E-24071 León, Spain

<sup>b</sup> Department of Physics and Chemistry, E-24071 León, Spain

Received 7 September 1998; received in revised form 4 December 1998; accepted 8 December 1998

### Abstract

In this work, a reliable method is described for speciation of soluble inorganic selenium ions, Se(IV) and Se(VI), which combines an uptake process by using living bacterial cells and electrothermal atomic absorption spectrometry (ETAAS). A selective retention of either Se(IV) or Se(IV) plus Se(VI) can be carried out by using the uptake system made up of either *Pseudomonas putida* or *Escherichia coli* strains cultivated in a culture medium based on glucose (*P. putida*) and glucose plus dipotassium phosphate (*E. coli*) mixed together with the original sample solution containing the selenium species. Discrimination between inorganic selenium species is possible by combining the optimization of the bacterial cell, the growth conditions and the relative rates of their retention from the sample. In the general procedure, an equilibrium between the analyte in the solution and the uptake system is allowed to be established, and then the concentration of selenium is determined directly in the biomass by slurry sampling ETAAS. Nonetheless, a theoretical model is proposed to describe the retention process by the living bacterial cells, which also provides a feasible quantification of the extraction process before the adsorption equilibrium is reached and whenever the agitation conditions and the sampling time are under control. The detection limits for the inorganic selenium species at the best retention conditions are of 5.7 ng Se(IV) ml<sup>-1</sup> for *P. putida* and 6.1 ng Se(IV) ml<sup>-1</sup> and 6.3 ng Se(VI) ml<sup>-1</sup> for *E. coli*. The relative standard deviations of the adsorption/determination process are 2.9–6.3%. © 1999 Elsevier Science B.V. All rights reserved.

**Keywords:** Speciation; Electrothermal atomic absorption spectrometry; Inorganic selenium species; Living bacterial cells; Slurry sampling; Environmental analysis

### 1. Introduction

The relationship between the types of selenium species and its toxicological and nutritional importance has stimulated much research into the possibility of speciation of this element in biological and environmental samples [1]. In the majority of the environmental matrices, such as natural

\* Corresponding author. Tel.: +34-9-87-29-15-36; fax: +34-9-87-29-15-36.

E-mail address: dbbjaf@unileon.es (A.J. Aller)

<sup>1</sup> Presented at 6th SAS Symposium on Analytical Sciences, Valencia, Spain, 22–24 June, 1998.

water and fly ash, selenium is usually present as selenite, Se(IV), and selenate, Se(VI), because these oxidation states are the most environmentally mobile and geochemically important forms of this element. For this reason, most of the studies carried out so far on selenium speciation deal with these species.

Selenium species have occasionally been determined by making use of a few of its biological properties [2]; however, spectrometric techniques have been most often employed for speciation studies [3–17]. Among them, atomic absorption spectrometry (AAS) (flame AAS (FAAS) [3], quartz cuvette (QC) AAS [4–10]), atomic fluorescence [6,8], atomic emission (such as inductively coupled plasma atomic emission spectrometry (ICP-AES) [10,11]) and inductively coupled plasma mass spectrometry (ICP-MS) [10,12–16] have been largely employed. Nevertheless, electrothermal (ET) AAS has proved to be a very sensitive analytical tool for the determination of this metalloid [17]. Some important problems derived from both losses (due to vaporization at temperatures prior to atomization [18]) and interferences (spectral [19] and/or chemical [20]) have been successfully overcome, by using the chemical modifier approach joined together with the background corrections systems and/or separation/preconcentration procedures.

The thermal stabilization of selenium in a graphite atomizer is achieved by using a chemical modifier [21–26], palladium being the most generally accepted material [24–29]. Chemical modification with palladium is mainly carried out in combination with a reducing agent [30] in order to homogenize all the physico-chemical forms of palladium present in solution by transforming them into palladium metal. This elemental palladium seems to be the most effective form of this chemical modifier.

The chromatographic separation methods have been largely used for speciation of selenium. Hyphenated techniques using ion chromatography [4,12], ion-interchange resins [5] and mainly high performance liquid chromatography (HPLC) [3,8,10,13,14,16] have been the most popular, while flow injection (FI) systems [6,7,9] have also been recently incorporated in the analysis of these

selenium species. However, alternative separation methods, such as solvent or solid extraction procedures, seem to be more versatile and cheaper. Solid extraction using biological systems have received increasing interest [31,32], bacteria being some of the most recently used in the analytical applications. Thus, *Escherichia coli* (K-235) and *Pseudomonas putida* bacteria (living or dead) have proved to be very useful for the preconcentration of metals [33–36] and metalloids [36,37]. Recent research works also include speciation studies of inorganic [38,39] and organometalloid [40–42] species. The new capability of these biological systems for speciation studies frequently requires special attention to an increased selectivity of the uptake process. Increased selectivity of the bacterial cells can be achieved by modifying the composition of their outer membrane by an adequate selection of those variables affecting the growth of these living bacterial cells.

In this work, these parameters are optimized in order to increase the selectivity of the two living bacterial cells (*E. coli* and *P. putida*) used for speciation and preconcentration of Se(IV) and Se(VI). Then, selenium is determined by slurry sampling ETAAS after the addition of palladium as a chemical modifier. In order to test the precision and accuracy of the developed method, two National Institute of Standards and Technology (NIST) Standard Reference Materials were used.

## 2. Experimental

### 2.1. Apparatus and measurements

A Thermo Jarrel Ash atomic-absorption spectrophotometer (SH 11) equipped with a heated graphite atomizer (Model CTF-188), and the Smith–Hieftje background correction system were used for the measurements. The operating parameters used were as follows: wavelength, 196.0 nm; the selenium hollow cathode lamp, Visimax II, was used under the recommended conditions; slitwidth, 1 nm. Standard pyrolytic graphite-coated graphite cylindrical tubes were used. Argon (99.995% purity) served as the purge gas. The temperature program used is shown in

Table 1. The volume (10  $\mu\text{l}$ ) of the solution was manually injected into the atomizer at 150°C by using a syringe. At least, three replicate determinations based on the integrated absorbances were used for each measurement. An Epson 118 recorder was used.

A Mettler AE 240 semimicro analytical balance (sensitivity  $\pm 0.01$  mg) was used for weighing the samples. The slurry was maintained during sample introduction into the atomizer using a Branson sonicator (model B-5). A pH-meter (Crison model Digit 505) was used to measure the acidity of the aqueous phase.

## 2.2. Reagents and materials

Selenium stock solutions (1000  $\mu\text{g ml}^{-1}$  Se) were prepared by dissolving a suitable amount of each of the following compounds: selenium(IV) dioxide and sodium selenate(VI), in an appropriate volume of demineralized water. Working solutions were prepared by the appropriate dilution of the stock solutions immediately prior to their use. The stock solutions of interfering elements were prepared from pure nitrate or chloride salts, or as otherwise noted. The bacterial cells used were *E. coli* and *P. putida*. The nutritive solutions were standard growth media, such as tryptic soy agar (TSA) medium constituted by tryptic casein bios D (37.5% m/m), soy peptone (12.5% m/m), sodium chloride (12.5% m/m) and agar bios LL (37.5% m/m); and tryptic soy broth (TSB) medium constituted by tryptic casein bios D (56.7% m/m), soy peptone (10% m/m), sodium chloride (16.7% m/m) dipotassium phosphate (8.3% m/m) and glucose (8.3% m/m); as well as poor growth media like glucose; sodium chloride;

and/or sodium phosphate. All of the chemicals used in this study were of analytical reagent grade. Distilled, deionized water was used for the preparation of the samples and standards. The TSA growth medium and the selenium compounds were obtained from Merck and the TSB growth medium was from Biolife. The analytical possibilities and spiked studies were tested by analyzing the National Institute of Standards and Technology (NIST) Standard Reference Material (SRM), SRM 1643c Trace Elements in Water and SRM 1633a Coal Fly Ash. The solid sample, NIST SRM 1633a coal fly ash, was dissolved using a mixture of hydrofluoric acid, sulfuric acid, nitric acid, hydrochloric acid and hydrogen peroxide, as recommended elsewhere [43].

## 2.3. Procedures

Bacterial cells were first cultured in a solid medium TSA, (40 g  $\text{l}^{-1}$ ) (pH  $7.5 \pm 0.2$ ), harvested after 1 day and stored at 4°C until use. This constituted the bacterial reservoir. The temperature used in each cultivation stage was always of 37 (*E. coli*) and 30°C (*P. putida*). Sterilization was made by autoclaving at 120°C.

In the procedure used for speciation, the living bacterial cells were cultivated for 18 h under continuous stirring (200 rev  $\text{min}^{-1}$ ) in an adequate growth medium volume of 25 ml with the selenium species (pH  $7.5 \pm 0.2$ ). The seeding density of the bacterial cells suspension initially present in each flask was controlled by adding water as necessary in order to obtain the same optical density measured at  $\lambda = 600$  nm. Then, after taking off the Se-biomass solid phase by centrifugation, the slurry was treated with 4 ml of

Table 1  
Temperature programme conditions

Parameter	Dry	Pyrolysis 1	Pyrolysis 2	Atomization	Cleaning
Temperature (°C)	150	400	700	1500	2500
Ramp time (s)	2	20	10	0	–
Hold time (s)	0	0	0	4	0
Flow, position	Low	Medium	Medium	Off	High
Read on (s)	–	–	–	2.2	–

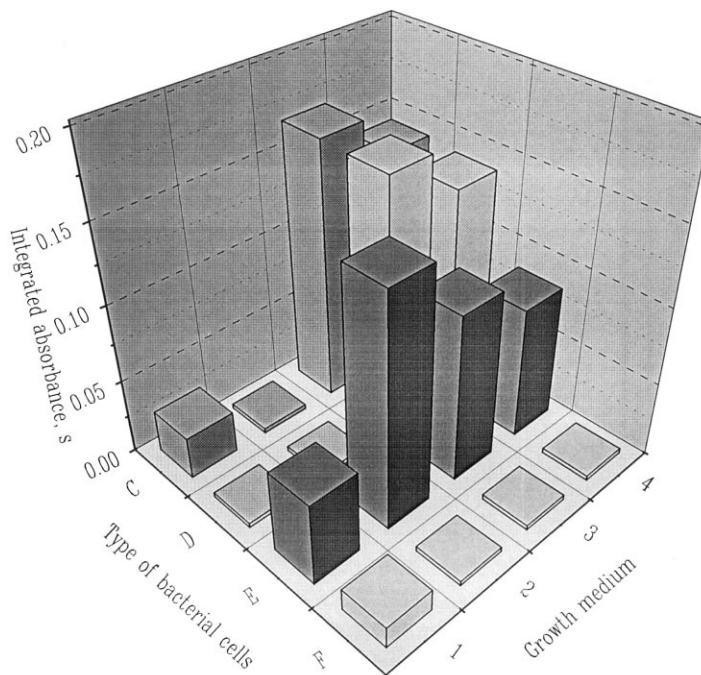


Fig. 1. A comparative response of *Escherichia coli* (C, D) and *Pseudomonas putida* (E, F) for the retention of Se(IV) ( $50 \text{ ng ml}^{-1}$ ) (C, E) and Se(VI) ( $50 \text{ ng ml}^{-1}$ ) (D, F) using four growth media. (1, tryptic soy broth (TSB); 2, glucose; 3, glucose plus dipotassium phosphate; 4, glucose + dipotassium phosphate + sodium chloride.)

a  $200 \mu\text{g ml}^{-1}$  Pd acidic (nitric) solution. Maintaining this slurry by sonication the amount of selenium was determined by slurry sampling ETAAS.

The concentration of selenium in the sample can be evaluated from a calibration graph prepared by treating selenium (Se(IV) and Se(VI)) standards in the same way as samples via bacterial preconcentration.

### 3. Results and discussion

#### 3.1. Selection of the uptake system

The optimization of the uptake system requires an adequate selection of the living bacterial cell (type and seeding density) as well as the growth medium (type and amount). A cross-study using two bacterial cells (*E. coli* and *P. putida*) was carried out with different types of growth media in order to obtain the highest Se ETAAS signal

(integrated absorbance). Thus, the optimized growth medium for *E. coli* and *P. putida* to recover Se(IV) ( $50 \text{ ng ml}^{-1}$ ) and/or Se(VI) ( $50 \text{ ng ml}^{-1}$ ), was selected by comparing the largest integrated absorbance of selenium obtained using various concentrations of the following growth media: (a) TSB, (b) glucose +  $\text{K}_2\text{HPO}_4$  + NaCl, (c) glucose +  $\text{K}_2\text{HPO}_4$ , and (d) glucose. A total of 25 ml of a growth medium was used, containing 2.25 g TSB, 0.1875 g glucose, 0.1875 g  $\text{K}_2\text{HPO}_4$  and 0.375 g NaCl each one. As shown in Fig. 1, the best results for the quantitative retention of the Se(IV) ions were found to be for the *P. putida* bacterium and using a growth medium based on glucose. On the other hand, the best way to separate Se(IV) and Se(VI) simultaneously was found for *E. coli* using a growth medium based on glucose plus dipotassium phosphate. The uptake capability of these bacterial cells has changed with the composition of the growth medium, in such a way that some selenium ions are not retained even for much higher concentrations. Thus, in Fig. 2

the retention response of the inorganic selenium species can be found using a TSB growth medium for different concentrations of the Se(IV) and Se(VI) ions, varying from 0 to 1000 ng ml<sup>-1</sup>. Changes in the uptake capability of the bacterial cells for the Se species using different culture media are the results of variations in the outer membrane composition, where the number and type of functional groups are modified.

The effect of the amount of glucose was studied for each of the Se species (Fig. 3). From the inserted figure of Fig. 3, which represents the

difference values between the lines A and B of this figure, the optimum amount of glucose 0.5 g l<sup>-1</sup> for the uptake of Se(IV) by *P. putida* and 3.0 g l<sup>-1</sup> for the uptake of Se(IV) and Se(VI) by *E. coli* can be derived.

The amount of cells initially seeded in the culture medium can also strongly affect the percentage of uptake. The results obtained for the selenium species studied are shown in Fig. 4. It can be seen that the optimum seeding density differs for each bacterial cell and for the Se compound. The values of 0.2 and 0.9 for the optical

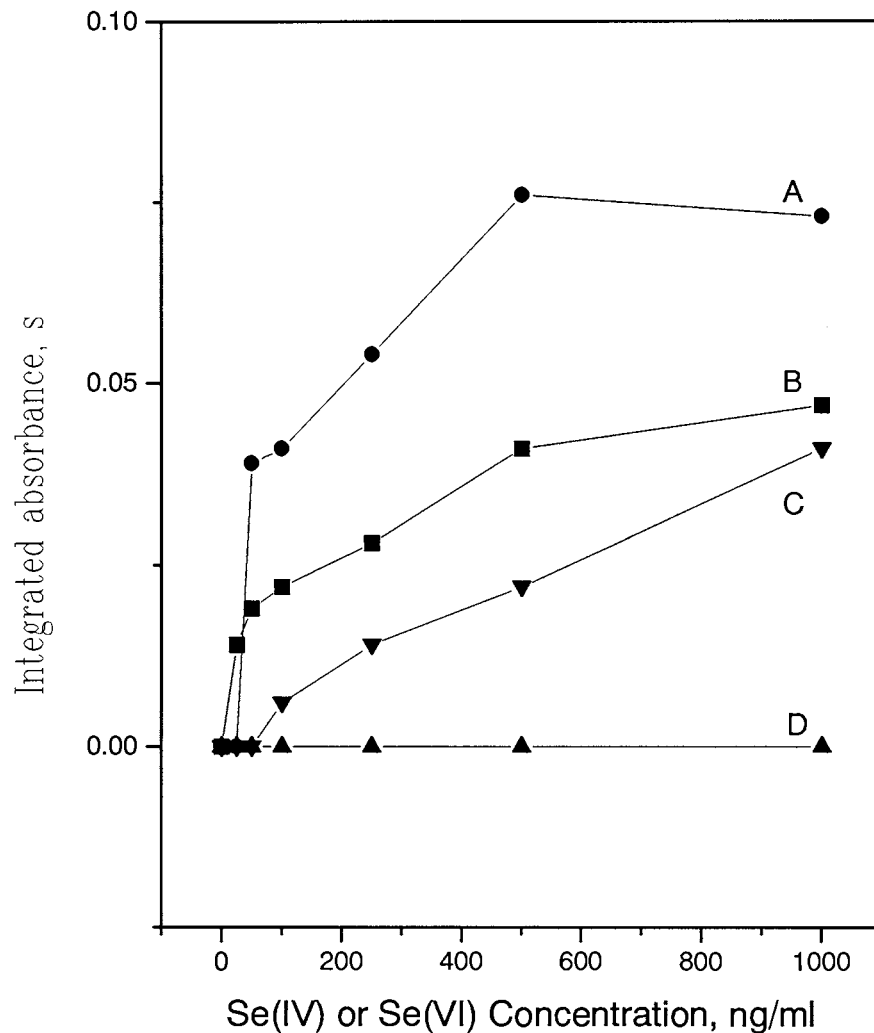


Fig. 2. A comparative response of *Escherichia coli* (B, D) and *Pseudomonas putida* (A, C) for the retention of different concentrations of Se(IV) (A, B) and Se(VI) (C, D) using tryptic soy broth (TSB) as a growth medium.

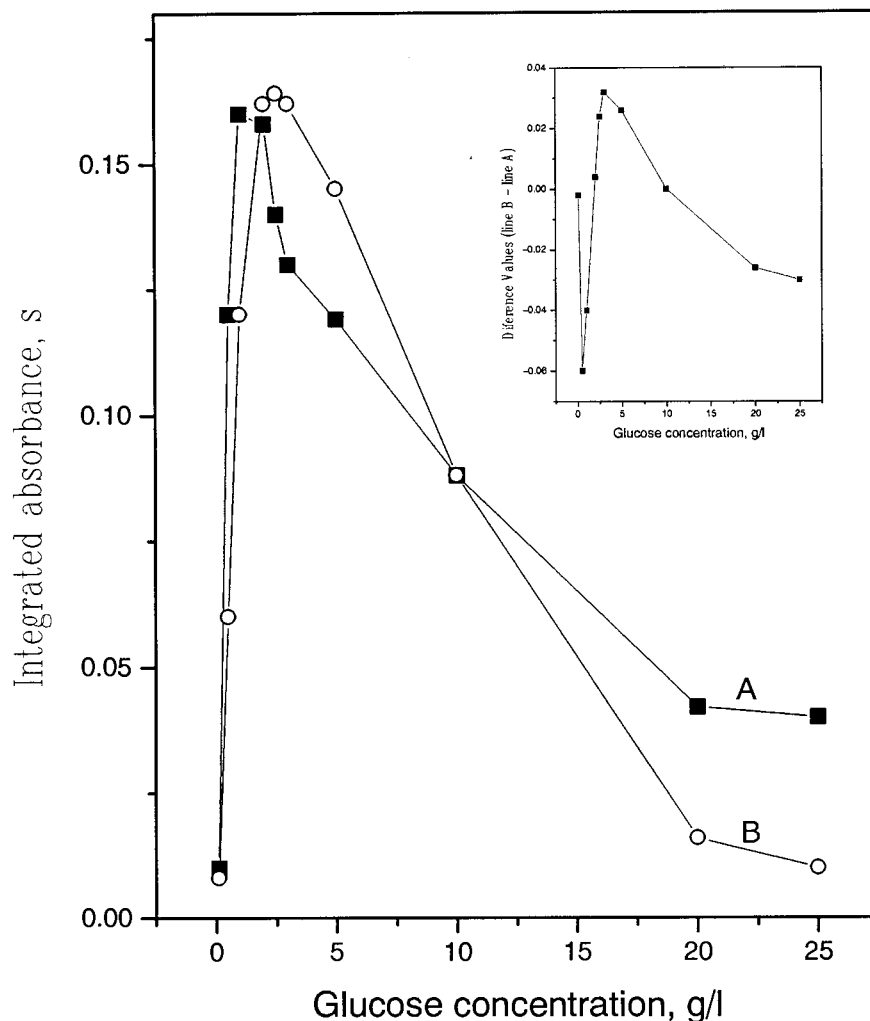


Fig. 3. Effect of the glucose concentration upon the retention of  $50 \text{ ng ml}^{-1}$  Se(IV) by the *Pseudomonas putida* bacterium (A) and Se(IV) or Se(VI) by the *Escherichia coli* bacterium (B) (measured as integrated absorbance of selenium from a Se-biomass slurry).

densities were selected as the optimum seeding densities of the bacterial cells *P. putida* and *E. coli*, respectively.

A way of distinguishing between Se(IV) and Se(VI) can be based on the fact that the *P. putida* bacterium can uptake quantitatively the Se(IV) ions but not Se(VI), while using the *E. coli* bacterium and a growth medium based on the mixture of glucose plus phosphate, a quantitative retention of the mixture of Se(IV) and Se(VI) is achieved (Fig. 1). The following studies were carried out in order to optimize the extraction system

and consequently to improve the analytical characteristics of the uptake process.

### 3.2. Optimization of the uptake process

#### 3.2.1. Uptake time

The effect of the uptake time for Se(IV) retained by *P. putida* was derived. In the same way, a similar study was carried out for Se(IV) and Se(VI) with *E. coli* and the optimum results obtained for both retention systems are shown in Table 2. A comparison between the results ob-

tained for the growth time of the bacterial cells (Table 2), provides the conclusion that there is good correlation between the time for the uptake at equilibrium of Se(IV) and the time for the maximum growth of the *P. putida* bacterium, but not for the uptake time of Se(IV) and Se(VI) and the growth time of *E. coli*. It can also be concluded from the results of Table 2 that the retention of selenium by *P. putida* was prolonged until the maximum time range for the cells grown. However, for Se(IV) and Se(VI) (for *E. coli*) this

uptake time finished much earlier than the maximum time of growth. It is also interesting to note that the best uptake time for Se(IV) and Se(VI) ends before the maximum growth time does. Selecting optimum conditions for each of the selenium species, it is possible to uptake selectively one of them in the presence of the other.

### 3.2.2. Uptake percentages

The uptake percentage was deduced by comparing the integrated absorbances of selenium

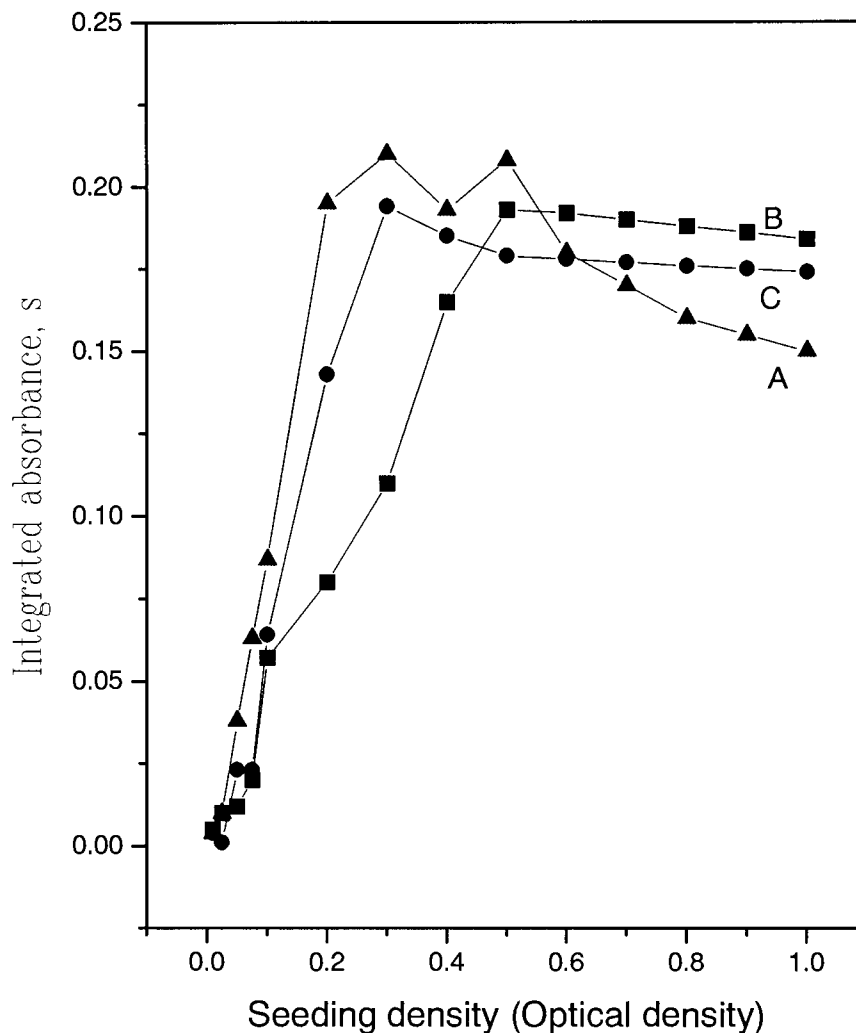


Fig. 4. Effect of the seeding density (measured as absorbance of the solution of cells) on the retention of  $50 \text{ ng ml}^{-1}$  Se(IV) by *Pseudomonas putida* (A) and  $50 \text{ ng ml}^{-1}$  Se(IV) (B) or Se(VI) (C) by *Escherichia coli* (B, C) (measured as integrated absorbance of selenium from a Se-biomass slurry).



Table 2

Minimum time for the highest growth of cells and the uptake at equilibrium of Se(IV) and Se(VI)

Parameter	<i>Pseudomonas putida</i>	<i>Escherichia coli</i>	
	Se(IV)	Se(IV)	Se(VI)
Growth time (h)	18	21	20
Uptake time (h)	18	3	4

from a Se-biomass pellet (*P. putida* or *E. coli*) prepared after applying the uptake/growth process with those derived from a Se-biomass obtained by adding selenium to a biomass pellet prepared by growing in the absence of selenium. The results obtained are shown in Table 3.

The uptake percentage of the inorganic selenium species was studied for various concentrations of the analytes in the range of 0–100 ng ml<sup>-1</sup>. The uptake percentage varies with the amount of analyte present in the sample solution. However, a different behaviour resulted for *P. putida* with Se(IV) compared with the results for *E. coli* for Se(IV) and Se(VI). For *E. coli*, the percentage of retention increases with the amount of analyte put in the sample solution; while the retention percentage lowers with the analyte concentration for *P. putida*. This means that saturation happens and consequently a small number of ligands are responsible of the uptake process for *P. putida*. It is obvious that the retention percentage increases with the amount of cells in the sample solution and, consequently, it is more interesting to find out the amount of the inorganic selenium ions retained by the weight of bacterial

cells. However, the amount of the bacterial cells grown depends on the density of the initial amount of cells seeded. So, a study of the influence of this parameter was carried out and a linearly direct relationship between the seeding density ( $x$ , absorbance of the solutions of cells) of the bacterial cells and the amount of biomass ( $y$ , mg) obtained was derived showing the following straight line equation,  $y = (-0.306 \pm 0.003) + (12.686 \pm 0.016)x$  with a correlation coefficient of  $r = 0.9999$ . Nonetheless, in the following studies the seeding densities of the solution of cells recommended in the previous sections are used.

An additional question, which comes from the use of the living bacterial cells as biosorbents, is that the growth of the bacterial cells might be affected by the concentration of selenium present in the growth medium. Thus, the amount of biomass decreases as the selenium concentration in the culture medium increases (Fig. 5). This negative effect on the growth process of the living bacterial cells is only important for the larger concentrations of selenium, while for concentrations of Se below 100 ng ml<sup>-1</sup> the growth process of the living bacterial cells is not really affected and the amount of biomass obtained is really constant ( $6.0 \pm 0.5$  mg).

### 3.2.3. Modelling of the uptake process

The uptake process was controlled by measuring the selenium content in the biomass as a function of the growth time. The results of the ETAAS response to time was modelled by using different mathematical expressions, fitting them by using Marquardt nonlinear regression techniques (MicroCal Origin™). Selecting the  $\chi^2$  and

Table 3

Extraction percentages for 50 ng ml<sup>-1</sup> of Se(IV) or Se(VI) in the original sample solution

Growth medium	% Extraction		
	Se(IV)- <i>Pseudomonas putida</i>	Se(IV)- <i>Escherichia coli</i>	Se(VI)- <i>Escherichia coli</i>
Glucose	94.4 ± 0.9	15.8 ± 1.5	14.6 ± 1.6
Glucose + dipotassium phosphate	72.2 ± 1.1	92.7 ± 1.0	93.1 ± 1.4
Glucose + dipotassium phosphate + sodium chloride	48.5 ± 2.3	90.5 ± 1.1	91.1 ± 1.2

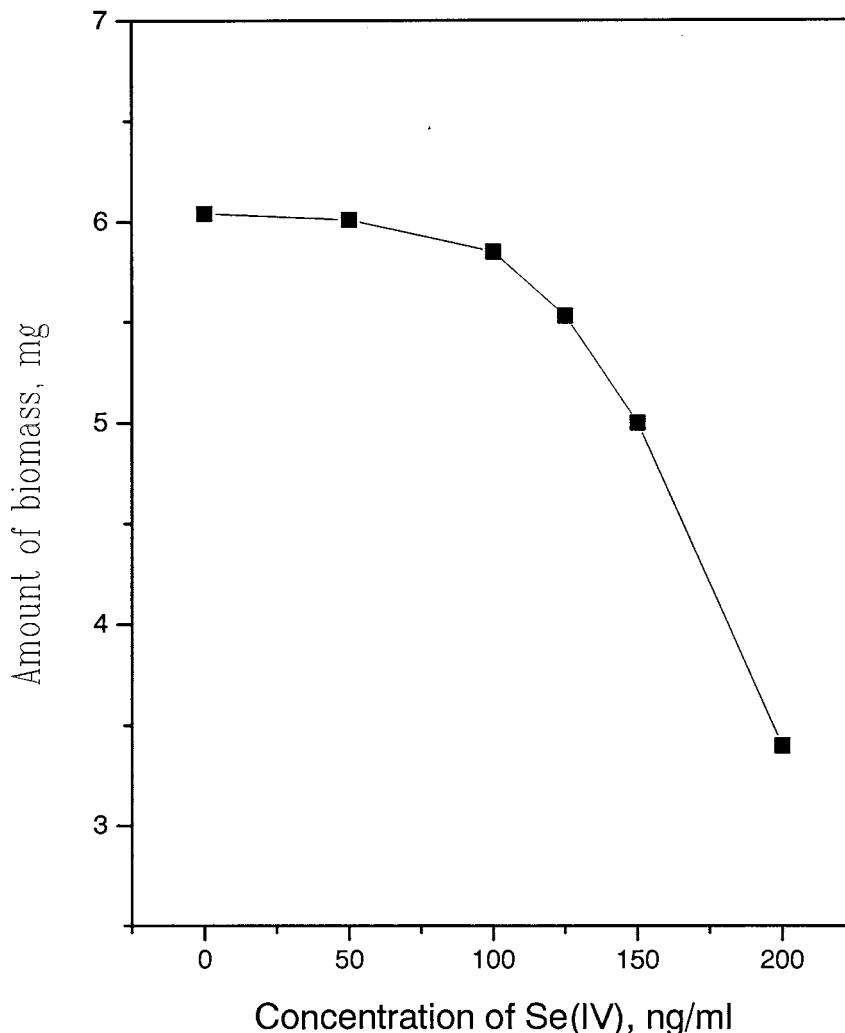


Fig. 5. Effect of the concentration of Se(IV) on the amount of biomass obtained after the growth stage of *Pseudomonas putida*.

the smallest relative error, shown by the values of the variables derived, as two parameters for the suitability of the fit of the models to the experimental data, the following exponential equation

$$n = a(1 - e^{-\gamma t}) \quad (1)$$

relating the amount of analyte retained,  $n$ , at any time,  $t$ , with the amount initially present in the sample solution,  $a$ , ( $\gamma$  is a constant) was found to be the best theoretical model to fit the experimental data (measured as Se ETAAS signals) of the uptake of Se(IV) and Se(VI) by the *E. coli* living

bacterial cells (Table 4). However, a sigmoidal model provided an appreciably better fit to the experimental data for the uptake of Se(IV) by *P. putida* (Table 4). The retention rate model can be considered to be a first order process, depending directly on the amount of cells,  $C_{\text{cells}}$ , and the amount of analyte,  $M_{\text{metal}}$ , in solution,

$$\frac{dM_{\text{m-b}}}{dt} = -\beta M_{\text{m-s}} C_{\text{cells}} \quad (2)$$

where,  $M_{\text{m-b}}$  and  $M_{\text{m-s}}$  are the analyte bound to biomass and in solution, respectively,  $\beta$  is a con-

stant, and  $C_{\text{cells}}$  is the concentration of cells used to uptake the analyte. Integrating Eq. (2) and applying neperians, it is possible to derive the following expression,

$$\ln \frac{M_{\text{initial}}}{M_{\text{final}}} = \beta C_{\text{cells}} t \quad (3)$$

where,  $M_{\text{initial}}$  and  $M_{\text{final}}$  are the amounts of free analyte before starting and at the end of the uptake process, respectively. From Eq. (3) it is possible to derive Eq. (1), from which the relationship between the two constants can be established,  $\gamma = \beta C_{\text{cells}}$ . Eq. (3) confirms that the retention percentage grows as the seeding density of cells increases. The growth rate of cells (*P. putida* and *E. coli*) in the presence of either Se(IV) or Se(VI) (measured as absorbance of a solution of cells) was fitted in well to a sigmoidal model (Table 4).

### 3.2.4. Uptake mechanism

A diffusion-controlled model, that is a two-step

process, can better describe the uptake of Se(IV) and Se(VI) by *E. coli* because the experimental uptake data (Table 4) are well fitted to a straight line. For two-step kinetics, the surface binding occurs quickly at first, and a pseudo equilibrium with the bacteria surface seems to be attained.

The uptake of Se(IV) by the *P. putida* bacterial cells seems to be fitted to one-step kinetics, because the experimental uptake data can be better described by a sigmoidal function (Table 4). For one-step kinetics, showing a non-parabolic diffusional model, the uptake mechanism requires an incubation period for as long as it depends on the growth rate of cells.

The pH variations obtained during the growth (and simultaneously the uptake) stage of the *E. coli* bacterial cells in the absence and in the presence of Se(IV) and Se(VI) at two concentration levels show that using *E. coli* the final pH is lower than that of the initial pH (Table 5). On the other hand, a final pH higher than that of the initial pH was obtained using the *P. putida* bacterium in the

Table 4

Experimental parameter values found for the mathematical modelling of both the uptake ( $n=f(t)$ ) of Se(IV) and Se(VI) and the growth ( $R=f(t)$ ) of the bacterial cells in the presence of either Se(IV) or Se(VI) with time<sup>a</sup>

Process	Se species and bacterial cells	Equation model	Parameters (U)	Values
Uptake $n=f(t)$	Se(IV) ( <i>Pseudomonas putida</i> )	Sigmoidal $n = \frac{A_0}{1 + b e^{-kt}}$	$A_0$ (s)	$0.184 \pm 0.008$
			$b$	$1.882 \pm 0.328$
			$k$ ( $\text{h}^{-1}$ )	$0.110 \pm 0.019$
			$\chi^2$	$2.9 \times 10^{-4}$
Growth $R=f(t)$	Se(IV) and Se(VI) ( <i>Escherichia coli</i> )	Exponential $n(t) = a(1 - e^{-\gamma t})$	$a$ (s)	$0.176 \pm 0.009$
			$\gamma$ ( $\text{h}^{-1}$ )	$0.113 \pm 0.018$
			$\chi^2$	$5.8 \times 10^{-4}$
			Uptake $n=f(t)$	Se(IV) ( <i>P. putida</i> )
$b$	$1.198 \pm 0.294$			
$k$ ( $\text{h}^{-1}$ )	$0.159 \pm 0.042$			
$\chi^2$	$5.5 \times 10^{-3}$			
Growth $R=f(t)$	Se(IV) and Se(VI) ( <i>E. coli</i> )	Sigmoidal $r = \frac{A'}{1 + b e^{-kt}}$	$A'$ (A)	$0.706 \pm 0.042$
			$b$	$2.597 \pm 0.769$
			$k$ ( $\text{h}^{-1}$ )	$0.137 \pm 0.029$
			$\chi^2$	$3.1 \times 10^{-4}$

<sup>a</sup>  $n$  is the integrated absorbance of selenium and  $R$  is the absorbance of the solution of cells at any time ( $t$ , in h) of the uptake of analyte and the growth process of the bacterial cells, respectively.  $A_0$  is the saturated integrated absorbance of selenium and  $A'$  is the saturated absorbance of the solution of cells after saturation of the uptake of analyte and the growth process of the bacterial cells, respectively.  $a$  (s),  $\gamma$  ( $\text{h}^{-1}$ ),  $k$  ( $\text{h}^{-1}$ ) and  $b$  (dimensionless) are constants.

Table 5  
Variation of pH of the growth solutions without and with two concentrations of analyte

Selenium species	Bacterial cells	Concentration of analyte	Total moles of the ions in the sample	pH <sub>i</sub>	pH <sub>f</sub>	$\Delta\text{pH} = \text{pH}_f - \text{pH}_i$	Absolute amount of protons interchanged
None	<i>Pseudomonas Putida</i>	0	0	5.25	5.35	0.1	$-1.16 \times 10^{-6}$
Se(IV)		100	$3.17 \times 10^{-8}$	4.30	5.25	0.95	$-4.45 \times 10^{-5}$
Se(IV)		400	$1.27 \times 10^{-7}$	3.15	5.35	1.50	$-1.37 \times 10^{-4}$
None	<i>Escherichia coli</i>	0	0	5.65	4.30	-1.35	$4.79 \times 10^{-5}$
Se(VI) <sup>a</sup>		100	$3.17 \times 10^{-8}$	5.00	4.15	-0.85	$6.08 \times 10^{-5}$
Se(VI) <sup>a</sup>		400	$1.27 \times 10^{-7}$		4.90	4.05	-0.85

<sup>a</sup> Similar results were obtained for Se(IV).

absence and in the presence of Se(IV). The results from Table 5 suggest that the overall behaviour of both bacterial cells is very different, supporting the existence of a different uptake mechanism for each bacterium type. The pH variations (Table 5), suggests that an ion interchange process (analyte/protons) could be behind the uptake of the selenium ions, or at least, this appears to be the case. The selenium ions, Se(VI) and Se(IV), seems to be retained by *E. coli* better than protons, because when the analyte ions are retained by the bacterial cells, a desorption of protons simultaneously occurs. As the variation of pH assessed is different for each ion and the amount of protons interchanged is much greater than that derived by a stoichiometric relationship (Table 5), it is possible to conclude that not only the analyte/protons interchange process occurs but other processes might also be implicated in the retention of these ions. Conformational and compositional changes in the membrane components make it possible for other functional groups to take part in the uptake process. Of course, a more thorough study would be necessary in order to better understand the interrelationship between the uptake process and the solution pH.

### 3.3. Speciation of Se(IV) and Se(VI)

The capability of these living bacterial cells for speciation of Se(IV) and Se(VI) was carried out by comparing the results obtained in the retention of one of the ions in the presence of the other. Thus, the effect of Se(VI) upon the uptake of 50 ng ml<sup>-1</sup> of Se(IV) by *P. putida* was studied for the concentration range of Se(VI) varying between 0 and 2000 ng Se(IV) ml<sup>-1</sup>. The results obtained are shown in Fig. 6 for three different growth media. From these results, it may deduced that Se(IV) can be quantitatively separated from Se(VI) using *P. putida* cultured in a growth medium based on glucose. The calibration line for Se(IV) is well fitted to the following straight line,  $y = (0.03 \pm 0.01) + (4.19 \pm 0.44) \times 10^{-4}x$  ( $r = 0.99714$ ), where  $y$  is the integrated absorbance of selenium and  $x$  is the concentration of analyte in ng ml<sup>-1</sup>. This means the extraction

of Se(IV) by *P. putida* is not dependent upon the presence of Se(VI). On the other hand, using the *E. coli* bacterium it was possible to separate (relative error < 5%) Se(IV) and Se(VI) simultaneously with similar sensitivity. Hence, the following straight lines were obtained for the retention of Se(IV),  $y = (0.005 \pm 0.003) + (4.07 \pm 0.33) \times 10^{-4}x$ , ( $r = 0.99702$ ), while for Se(VI) was,  $y = (0.007 \pm 0.001) + (3.89 \pm 0.38) \times 10^{-4}x$  ( $r = 0.99949$ ), and for a mixture of both selenium ions,  $y = (0.008 \pm 0.002) + (4.08 \pm 0.47) \times 10^{-4}x$  ( $r = 0.99624$ ). In conclusion, these results confirm the possibility of speciation of Se(IV) and Se(VI) by an adequate selection of the bacterial cell and the growth medium.

### 3.4. Determination of Se(IV) and Se(VI) by slurry ETAAS

The uptake process, adapted for speciation of Se(IV) and/or Se(VI), was enlarged to develop a procedure for the determination of Se(IV) and Se(VI) by slurry sampling ETAAS. In this stage, those factors affecting the atomic absorption signal of selenium were evaluated. These are the slurry characteristics (the washing acid concentration, the washing time and the concentration of slurry cells), interferences from other elements and some instrumental parameters.

#### 3.4.1. Slurry characteristics

Although, the Se-biomass pellet is introduced into the graphite tube as slurry, atomic absorption signals for Se dependent upon the slurry pH were found. So, different slurries were prepared by treating the Se-biomass pellet with nitric acid and sodium hydroxide solutions covering the pH range from 1 to 10 in order to obtain the best selenium atomic absorption signal. The best results (Fig. 7) were obtained using a nitric acid solution of pH 5 as a washing solution. This washing solution was used in all experiments.

The washing time over intervals of up to 10 h (using the optimum nitric acid washing solution every time) does not show a strong effect on the atomic absorption signal of selenium (50 ng ml<sup>-1</sup>) by ETAAS. Hence, a time interval of 10

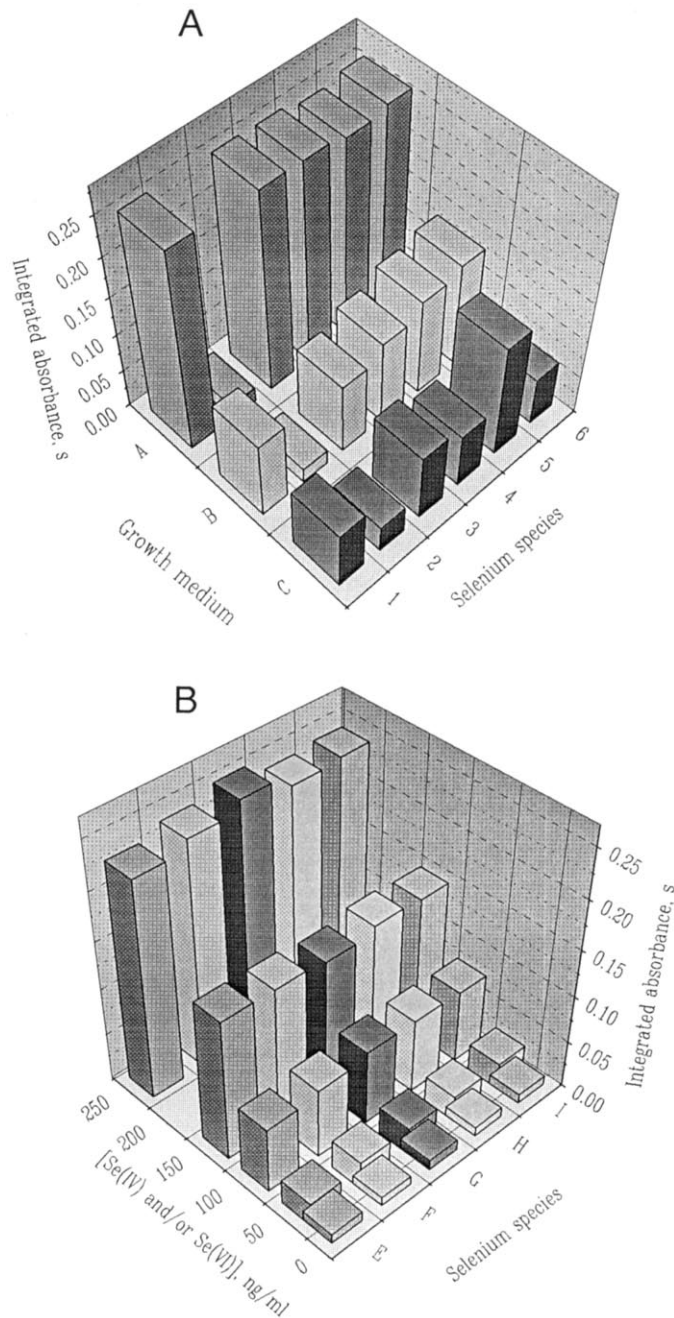


Fig. 6. (A) Speciation of Se(IV) in the presence of Se(VI) with *Pseudomonas putida* for three growth media (A, glucose; B, glucose + dipotassium phosphate; C, glucose + dipotassium phosphate + sodium chloride) (1, 50 ng ml<sup>-1</sup> Se(IV); 2, 50 ng ml<sup>-1</sup> Se(VI); 3, 50 ng ml<sup>-1</sup> Se(IV) + 250 ng ml<sup>-1</sup> Se(VI); 4, 50 ng ml<sup>-1</sup> Se(IV) + 500 ng ml<sup>-1</sup> Se(VI); 5, 50 ng ml<sup>-1</sup> Se(IV) + 1000 ng ml<sup>-1</sup> Se(VI); 6, 50 ng ml<sup>-1</sup> Se(IV) + 2000 ng ml<sup>-1</sup> Se(VI)). (B) Speciation of (Se(IV) + Se(VI)) with *Escherichia coli*. (E, Se(IV); F, Se(VI); G, Se(IV) + Se(VI) simultaneously at the 1:1 ratio; H, Se(VI) together with a fixed concentration, 50 ng ml<sup>-1</sup>, of Se(IV); I, Se(IV) together with a fixed concentration, 50 ng ml<sup>-1</sup>, of Se(VI)).

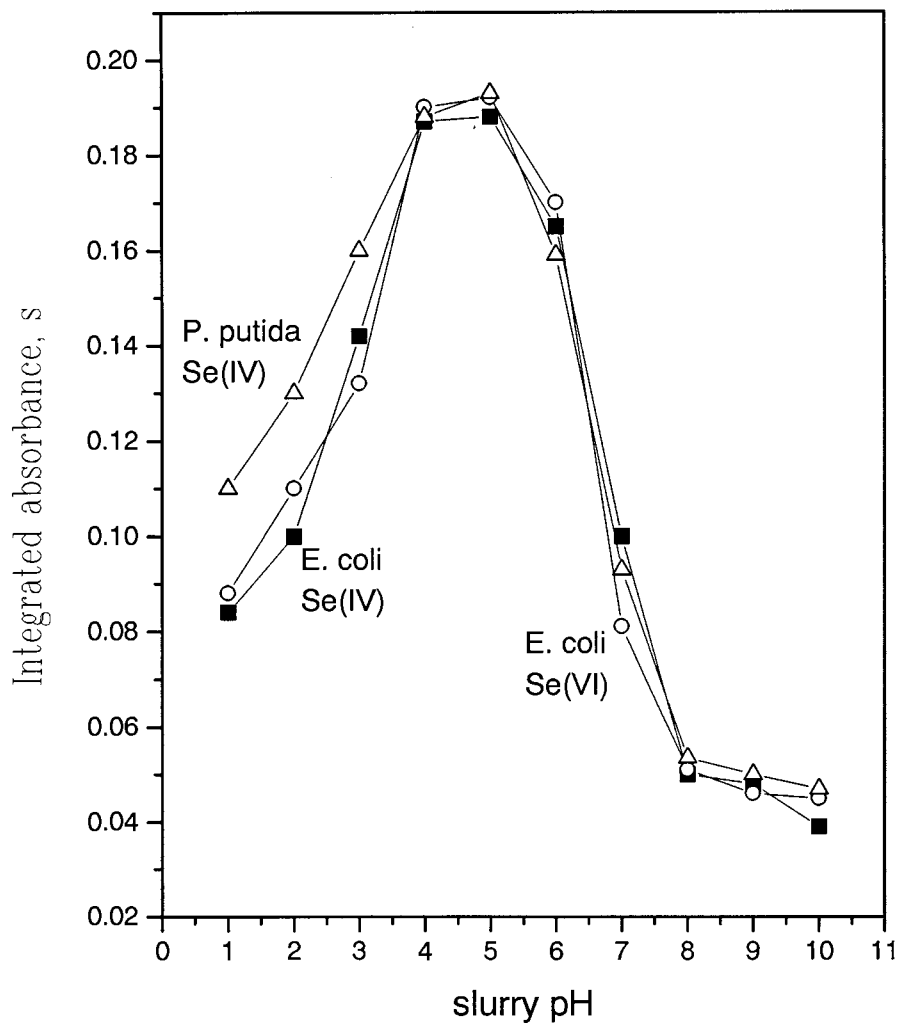


Fig. 7. Effect of the slurry pH on the atomic absorption signal (integrated absorbances) of Se(IV)-*Pseudomonas putida* biomass and Se(IV)- and Se(VI)-*Escherichia coli* biomass.

min was selected in all experiments. The possibility of determining Se in either the biomass pellet by the slurry sampling or in the supernatant after separation by centrifugation was also explored. However, higher absorbances for Se were obtained using the slurry sampling procedure, suggesting the participation of the biomass on the atomization of Se and/or that selenium is still bound to the biomass. A similar behaviour pattern for *E. coli* and *P. putida* was noted.

Although the selenium atomic absorbances gradually increase with the density of the bacterial

cells in the slurry volume, a bacterium concentration of above 10 mg of cells ml<sup>-1</sup> the atomic absorption signal of selenium decreases. This is probably due to the fact that the sample volume, and, consequently, the amount of selenium introduced into the graphite tube becomes lower as the amount of biomass increases, due to clogging of the syringe used. As a result of this, the maximum *effective* uptake capacity, defined as the amount of Se retained by mass unit of the bacterial cells corresponding to the maximum atomic absorption signal of Se when it is introduced as slurry, was

about 0.35 ng of selenium  $\text{mg}^{-1}$  of bacteria for both bacterium. This value represents an amount of Se a little lower than that derived from the Langmuir isotherm for the amount adsorbed at saturation (0.46 ng Se(IV)  $\text{mg}^{-1}$  bacterium and 0.41 ng Se(VI)  $\text{mg}^{-1}$  bacterium for *E. coli*, and 0.48 ng Se(IV)  $\text{mg}^{-1}$  bacterium for *P. putida*).

### 3.4.2. Effect of other elements

Elements usually found in environmental samples could compete with the inorganic selenium species on the uptake process showing interferent effects on the final stage of the determination of selenium by slurry ETAAS. Thus, a 50-fold concentration ( $2.5 \mu\text{g ml}^{-1}$ ) of the following ions [Ag(I) as ( $\text{NO}_3^-$ ), Be(II) as ( $\text{Cl}^-$ ), Ca(II) as ( $\text{NO}_3^-$ ), Cd(II) as ( $\text{NO}_3^-$ ), Ce(IV) as ( $\text{SO}_4^{2-}$ ), Co(II) as ( $\text{Cl}^-$ ), Cr(VI) as ( $\text{K}_2\text{Cr}_2\text{O}_7$ ), Fe(III) as ( $\text{NO}_3^-$ ), K(I) as ( $\text{Cl}^-$ ), Na(I) as ( $\text{Cl}^-$ ), Nb(IV) as ( $\text{Cl}^-$ ), Pd(II) as ( $\text{Cl}^-$ ), Sr(II) as ( $\text{NO}_3^-$ ), Te(IV) as ( $\text{Cl}^-$ ), Th(IV) as ( $\text{Cl}^-$ ), Tl(I) as ( $\text{NO}_3^-$ ), V(V) as ( $\text{VOCl}_3$ ), Zr(IV) as ( $\text{Cl}^-$ )] do not interfere ( $< 5\%$ ) on the preconcentration and slurry ETAAS determination of Se(IV) by *P. putida* and Se(IV) and Se(VI) by *E. coli*. Only, Al(III) as ( $\text{NO}_3^-$ ), Bi(III) as ( $\text{BiONO}_3$ ), Cu(II) as ( $\text{Cl}^-$ ), Hg(II) as ( $\text{NO}_3^-$ ), Mn(VII) as ( $\text{KMnO}_4$ ), and Zn(II) as ( $\text{Cl}^-$ ) slightly decreases, while Ti(III) as ( $\text{Cl}^-$ ) increases, the atomic absorption for Se. However, main interferent effects derived from concentrations of the interferent elements above  $2.5 \mu\text{g ml}^{-1}$ . Organo-selenium compounds, such as Se-methionine, Se-ethionine, and Se-cystamine at concentrations at least up to  $1.0 \mu\text{g ml}^{-1}$  do not interfere under recommended conditions.

### 3.4.3. Effect of some instrumental parameters on the atomization of selenium

**3.4.3.1. Aerosol versus liquid injection.** A comparative study of the sample introduction using an automatic aerosol sample introduction system (the Fastac system) and a manual introduction (syringe) was carried out. The results shown in Table 6 for three growth medium demonstrate the best suitability of the manual system.

**3.4.3.2. Stabilization and homogenization of Se(IV) and Se(VI).** Owing to the difficulties associated with the determination of selenium by slurry sampling ETAAS in a biological matrix, the use of a chemical modifier is a necessary requisite. The effect of different amounts of palladium on the stabilization of Se(IV) and Se(VI) in the graphite tube was elucidated. On the other hand, instrumental and operational conditions need also to be optimized when thinking in the optimization of the analytical characteristics. In order to find out the maximum allowable pyrolysis temperature for selenium, introduced as a Se(IV)- or Se(VI)-biomass slurry in the presence of palladium, a curve was derived from the analyte signal (integrated absorbance) and obtained at different temperatures for a pyrolysis step. The pyrolysis temperature was modified from 400 to  $1300^\circ\text{C}$  with ramp time (10 s) and hold time (0 s) constants. In each case, the same atomization temperature ( $1500^\circ\text{C}$ ) was used throughout. A second set of experiments exploring the relationship between the atomization temperature and the integrated absorbance of selenium (Se(IV) and Se(VI)) was also carried out. The pyrolysis and atomization curves obtained (Fig. 8) show that losses of selenium begin to occur at a pyrolysis temperature of around  $1100^\circ\text{C}$ , while an atomization temperature of about  $1500^\circ\text{C}$  using a fixed  $700^\circ\text{C}$  pyrolysis step shows the maximum atomic absorption signal of selenium (integrated ab-

Table 6

Comparison results of the integrated absorbances of selenium (average of five replicates) obtained by introducing the slurry sample (Se(IV)-biomass *Pseudomonas putida*) by two different introduction systems<sup>a</sup>

Growth medium	Introduction system	
	Manual	Aerosol
Glucose	$0.210 \pm 0.003$	$0.156 \pm 0.005$
Glucose + dipotassium phosphate	$0.190 \pm 0.004$	$0.128 \pm 0.003$
Glucose + dipotassium phosphate + sodium chloride	$0.168 \pm 0.004$	$0.135 \pm 0.005$

<sup>a</sup> The Se-biomass was obtained by extracting Se(IV) with *P. putida* using three different growth media.



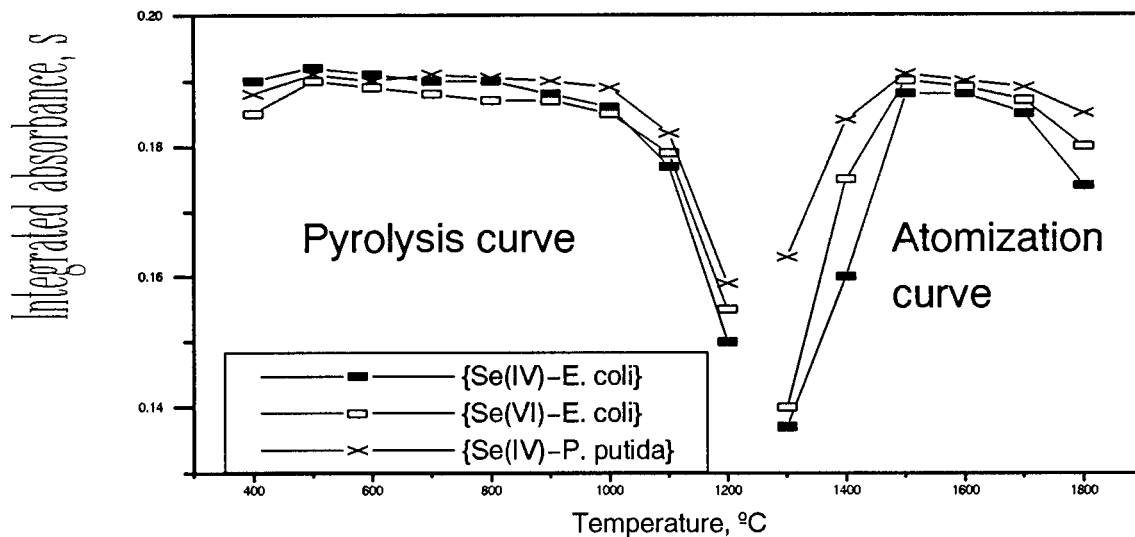


Fig. 8. Pyrolysis and atomization curves for the determination of 1 ng of Se(IV) and Se(VI) in a *Escherichia coli* biomass and Se(IV) in *Pseudomonas putida* from a Se-biomass slurry in the presence of 2.0  $\mu\text{g}$  of Pd (as  $\text{PdCl}_2$ ) by slurry sampling electrothermal atomic absorption spectrometry (ETAAS).

sorbances). From Fig. 8, it is also possible to see that homogenization and the stabilization of Se(IV) and Se(VI) occurs in the same way using an amount of palladium of 2.0  $\mu\text{g}$  Pd (as  $\text{PdCl}_2$ ). Other amounts of palladium produced smaller integrated signals for Se. The plots of Fig. 8 were obtained from a Se-biomass slurry after the retention of 50  $\text{ng ml}^{-1}$  of Se(IV) and Se(VI) by *P. putida* and/or *E. coli*. The amount of palladium added in the following experiments was 2.0  $\mu\text{g}$ . Using these atomization conditions completely removes the analyte from the surface of the graphite tube with no memory effects observed.

### 3.5. Analytical performances

If selenium species do not reach an adsorption equilibrium within a reasonable time (as in the case of *P. putida* for Se(IV)), from Eq. (1) it is possible to derive a (linearly) proportional relationship between the amount retained ( $n$ ) and the initial concentration ( $C_0$ ) of the selenium species in the aqueous solution at a particular uptake time before reaching the equilibrium conditions [42],

$$n = kC_0 \quad (4)$$

Consequently, it is not necessary to achieve the uptake equilibrium to perform a quantitative analysis if the uptake time and stirring conditions are maintained constant. This study was performed with Se(IV) and Se(VI), obtaining linear adsorption responses as a function of the concentration of the selenium species in the original sample solution maintaining the sampling time at 1 h. Applying Eq. (4) to sample volumes of 250 ml containing concentrations varying from 10 to 100  $\text{ng ml}^{-1}$  for the two analytes and the two bacterial cells, the following slopes of the calibration straight lines were found  $(9.3 \pm 0.4) \times 10^{-4}$ ,  $r = 0.99894$  and  $(9.5 \pm 0.4) \times 10^{-4}$ ,  $r = 0.99965$ , for the uptake of Se(IV) by *P. putida* and for the uptake of Se(IV) and Se(VI) by *E. coli*, respectively, obtained by plotting  $n$  versus  $C_0$  (from Eq. (4)). For the two bacterial cells, excellent linearity of the experimental data was obtained. These results confirm that the retained amount ( $n$ ) of analyte is linearly proportional to its initial concentration,  $C_0$ , in the aqueous sample (as described by Eq. (4)), showing the applicability of this equation to make quantitative analytical measurements.

A preconcentration factor was defined as the ratio between the volume of the initial sample (250 ml) and the final volume (4 ml) obtained after the extraction step. The AAS signal obtained with a direct injection of a selenium aqueous solution compared with that obtained with injection of a selenium pellet slurry of the same selenium concentration (50 ng ml<sup>-1</sup>) was named as the atomization factor. The atomization factor is the result of the positive contribution of the biomass on the atomization of Se (Table 7). The enhancement factor of Table 7 was derived by comparing the AAS signal obtained with a direct injection with that obtained after preconcentration and treatment with the appropriate volume and concentration of the nitric acid solution. The enhancement factors obtained were good for both bacterium.

Both high sensitivities and detection limits were obtained (Table 7). The sensitivity represents the

slope of the analytical calibration graph of absorbance versus concentration (in ng ml<sup>-1</sup>) obtained by linear regression, while the detection limit represents 3-fold the mean standard deviation of the background noise on 20 blanks. The sensitivity depends on the preconcentration factor as well as on the detector used. Thus, comparing the results which appear in Table 7 with those previously published using other detector systems, it can be seen that sensitive detectors, such as MS and AFS, provide the best detection limits. Thus, values in the range of (0.14–1.6) ng ml<sup>-1</sup> for MS [10,12,13] and (0.04–0.3) ng ml<sup>-1</sup> for AFS [6,8] have been obtained. However, for less-sensitive detectors, such as HGAAS, FAAS, ICP-AES, values in the range of (0.7–15), 0.8 and (2–30) ng ml<sup>-1</sup>, respectively, are usual [4,7,9–11]. The limits of detection in the slurry found in this paper (Table 7) are similar to or even better than those reported in other works for different extractants and detection systems. However, the limits of detection resulting for the original sample solution are obviously much better (Table 7, footnote). The time required to carry out a set of analysis is mainly spent on the preparation of the sample, usually being 4–5 h.

The repeatability varies from 2.9 to 6.3% for the selenium concentrations into the linear response range, but the best relative standard deviation was obtained for a Se concentration of 50 ng ml<sup>-1</sup> in the slurry for both bacterium (Table 7). The repeatability between bacterial batches was calculated using five harvested batches of bacteria, obtaining a similar value to those derived for analyses.

To demonstrate the applicability of the developed method, the accuracy of the extraction procedure was investigated by determining the recovery of Se(IV) and Se(VI) in spiked tap water samples. The results appear in Table 8, showing also that both the accuracy and precision are satisfactory. The accuracy of this procedure was also tested by replicate determinations of selenium in two standard samples (NIST SRM 1643c trace elements in water and NIST SRM 1633a coal fly ash). The measured selenium concentrations compared well with the certified values (Table 8). On the contrary, the solution procedure used to dis-

Table 7

Figures of merit for the determination of selenium by the developed analytical method using living bacterial cells

Parameter	Bacterium		
	<i>E. coli</i>		<i>P. putida</i>
	Se(IV)	Se(VI)	Se(IV)
Linear range <sup>a</sup> (ng ml <sup>-1</sup> )	6–100	4–80	4–90
Sensitivity (ng ml <sup>-1</sup> )	4.6	4.9	4.7
Limit of detection <sup>b</sup> (ng ml <sup>-1</sup> )	6.1	6.3	5.7
Preconcentration factor <sup>c</sup>	62.5	62.5	62.5
Atomization factor	2.4	2.1	2.3
Enhancement factor	150.0	131.2	143.7
R.S.D. <sup>d</sup> , 50 ng ml <sup>-1</sup> (%)	2.46	2.69	2.58

<sup>a</sup> The optimum linear range refers to the slurry sample and it was established over which the measured and predicted absorbances differed by less than 5%

<sup>b</sup> Limits of detection (in the slurry) represents three values of nine consecutive measurements of the signal from a blank. (These values correspond to an average equivalent detection limit in the original sample solution of 0.01 ng ml<sup>-1</sup> for both bacterium.)

<sup>c</sup> Using a sample volume of 250 ml.

<sup>d</sup> Relative standard deviation (R.S.D.) ( $n = 9$ ).

Table 8  
Recovery spiked studies and accuracy of the developed method using living bacterial cells ( $n = 5$ )

Bacterial cell	Analyte				
		Selenium species	Present (ng ml <sup>-1</sup> )	Found (ng ml <sup>-1</sup> )	Recovery (%)
<i>Pseudomonas putida</i>	Se(IV)		25	24.6	98.4
			50	50.3	100.6
			100	98.2	98.2
	Se(IV) <sup>a</sup> in water (SRM 1643c)	12.7	13.0 ± 0.4	102.4	
	Se(IV) <sup>a</sup> in coal fly ash (SRM 1633a)	10.3	9.9 ± 0.5	96.1	
<i>Escherichia coli</i>	Se(IV)		25	25.3	101.2
			50	50.4	100.8
			100	101.1	101.1
	Se(VI)		25	24.5	98.0
			50	49.5	99.0
			100	101.8	101.8
	Se(IV) <sup>a</sup> in water (SRM 1643c)	12.7	12.9 ± 0.4	101.6	
	Se(IV) <sup>a</sup> in coal fly ash (SRM 1633a)	10.3	10.1 ± 0.4	98.1	

<sup>a</sup> Values of the certified selenium are shown in ng ml<sup>-1</sup> for the water standard and in ng mg<sup>-1</sup> for the coal fly ash standard.

solve the other standard sample homogenizes the oxidation state of selenium as Se(IV). No standard samples are currently available with certified values for individual selenium species.

The blank level of Se from the biomass against water was of 0.005 AU and it was compensated for the determination of samples by setting 'zero' of the instrument against a biomass slurry without Se. The analytical blanks per single analysis procedure are below the detection limits of ETAAS.

#### 4. Conclusions

From this study it can be concluded that the bacteria *E. Coli* and *P. Putida* can be used for speciation of Se(IV) and Se(VI) in complex environmental samples. This approach coupled with the specific ETAAS detector provides a reliable method for characterizing different soluble forms of inorganic selenium at trace levels based on the differences in their relative sorption by the living bacterial cells. By selecting an adequate type of bacterial cell and modifying the growth conditions of the living bacterial cells, it is possible to alter appropriately the uptake mechanism of some analytes but not of others, allowing one to carry out an analytical discrimination between them. To the

extent that successful mathematical models can be developed for the uptake process, this approach can be used to estimate analyte species burdens in samples without having the complete retention. The uptake process for both bacterium shows higher efficiency, and the procedure for the retention/determination of Se exhibits good analytical sensitivity and excellent specificity.

#### Acknowledgements

We duly acknowledge the financial support of a Grant from the CICYT (Spain) under the project AMB96-0385. A part of this work was also financially supported by the Junta de Castilla y León under the project LE 33/96.

#### References

- [1] M.J. Blaylock, B.R. James, *J. Environ. Qual.* 22 (1993) 851.
- [2] I.G. Gokmen, E. Abdelgader, *Analyst (London)* 119 (1994) 703.
- [3] G. Kölbl, J. Lintschinger, K. Kalcher, K.J. Irgolic, *Mikrochim. Acta* 119 (1995) 113.
- [4] N. Ellend, C. Rohrer, H. Grasserbauer, J.A.C. Broekaert, *Fresenius J. Anal. Chem.* 356 (1996) 99.

- [5] U. Örnemark, Å. Olin, *Talanta* 41 (1994) 67.
- [6] D.W. Bryce, A. Izquierdo, M.D. Luque de Castro, *J. Anal. At. Spectrom.* 10 (1995) 1059.
- [7] M.G. Cobo Fernández, M.A. Palacios, C. Cámara, *Anal. Chim. Acta* 283 (1993) 386.
- [8] L. Pitts, A. Fisher, P. Worsfold, S.J. Hill, *J. Anal. At. Spectrom.* 10 (1995) 519.
- [9] J.M. González La Fuente, M.L. Fernández Sánchez, J.M. Marchante-Gayón, J.E. Sánchez Uría, A. Sanz-Medel, *Spectrochim. Acta Part B* 51B (1996) 1849.
- [10] J.M. González Lafuente, M.L. Fernández Sánchez, A. Sanz-Medel, *J. Anal. At. Spectrom.* 11 (1996) 1163.
- [11] J. Yang, T.S. Conner, J.A. Koropchak, *Anal. Chem.* 68 (1996) 4064.
- [12] N. Jakubowski, C. Thomas, D. Stuewer, Y. Dettlaff, J. Schram, *J. Anal. At. Spectrom.* 11 (1996) 1023.
- [13] M.A. Quijano, A.M. Gutierrez, M.C. Pérez-Conde, C. Cámara, *J. Anal. At. Spectrom.* 11 (1996) 407.
- [14] K. Takatera, N. Osaki, H. Yamaguchi, T. Watanabe, *Anal. Sci.* 10 (1994) 567.
- [15] D. Tanzer, K.G. Heumann, *Anal. Chem.* 63 (1991) 1984.
- [16] H.M. Crews, P.A. Clarke, D.J. Lewis, L.M. Owen, P.R. Strutt, A. Izquierdo, *J. Anal. At. Spectrom.* 11 (1996) 1177.
- [17] M. Deaker, W. Maher, *J. Anal. At. Spectrom.* 10 (1995) 423.
- [18] V. Krivan, M. Kückenwaitz, *Fresenius J. Anal. Chem.* 342 (1992) 692.
- [19] A.J. Aller, C. García-Olalla, *J. Anal. At. Spectrom.* 7 (1992) 753.
- [20] C. García-Olalla, L.C. Robles, A.J. Aller, *Anal. Sci.* 7 (1991) 611.
- [21] J. Alexander, K. Saced, Y. Thomassen, *Anal. Chim. Acta* 120 (1980) 377.
- [22] H.J. Robberecht, H.A. Deelstra, *Talanta* 31 (1984) 497.
- [23] J.-S. Blais, A. Huyghues-Despointes, G.M. Momplaisir, W.D. Marshall, *J. Anal. At. Spectrom.* 6 (1991) 225.
- [24] J.K. Johannessen, B. Gammelgaard, O. Jøns, S.H. Hansen, *J. Anal. At. Spectrom.* 8 (1993) 999.
- [25] F. Laborda, J. Viñuelas, J.M. Mir, J.R. Castillo, *J. Anal. At. Spectrom.* 8 (1993) 737.
- [26] B. Gammelgaard, O. Jøns, *J. Anal. At. Spectrom.* 12 (1997) 465.
- [27] L.M. Voth-Beach, D.E. Shrader, *J. Anal. At. Spectrom.* 2 (1987) 45.
- [28] C. García-Olalla, A.J. Aller, *Fresenius J. Anal. Chem.* 342 (1992) 70.
- [29] A.B. Volynsky, V. Krivan, *J. Anal. At. Spectrom.* 11 (1996) 159.
- [30] M.B. Knowles, K.G. Brodie, *J. Anal. At. Spectrom.* 3 (1988) 511.
- [31] C.A. Mahan, V. Majidi, J.A. Holcombe, *Anal. Chem.* 61 (1989) 624.
- [32] H.A.M. Elmahadi, G.M. Greenway, *J. Anal. At. Spectrom.* 9 (1994) 547.
- [33] L.C. Robles, C. García-Olalla, A.J. Aller, *J. Anal. At. Spectrom.* 8 (1993) 1015.
- [34] L.C. Robles, A.J. Aller, *J. Anal. At. Spectrom.* 9 (1994) 871.
- [35] L.C. Robles, A.J. Aller, *Talanta* 42 (1995) 1731.
- [36] L.C. Robles, A.J. Aller, *Quim. Anal.* 15 (1996) 21.
- [37] L.C. Robles, A.J. Aller, *Anal. Sci.* 12 (1996) 783.
- [38] A.J. Aller, J.M. Lumberras, L.C. Robles, G.M. Fernández, *Anal. Proc. Anal. Comm.* 32 (1995) 511.
- [39] A.J. Aller, J.M. Lumberras, L.C. Robles, G.M. Fernández, *Anal. Chim. Acta* 330 (1996) 89.
- [40] L.C. Robles, B. de Celis, J.M. Lumberras, A.J. Aller, *Anal. Commun.* 34 (1997) 409.
- [41] A.J. Aller, L.C. Robles, *J. Anal. At. Spectrom.* 13 (1998) 469.
- [42] A.J. Aller, L.C. Robles, *Analyst* 123 (1998) 919.
- [43] A.J. Aller, D. Bonilla, *Anal. Sci.* 6 (1990) 309.

# Determination of essential and potentially toxic trace elements in honey by inductively coupled plasma-based techniques

S. Caroli \*, G. Forte, A.L. Iamiceli, B. Galoppi

*Istituto Superiore di Sanità, Viale Regina Elena 299, 00161 Rome, Italy*

Received 7 September 1998; received in revised form 15 December 1998; accepted 18 December 1998

---

## Abstract

The mandate assigned by the European Union to the Community Reference Laboratory for residues at the Istituto Superiore di Sanità covers, among other things, the assessment of trace elements in living animals as well as their products. To better protect the health of the consumer, this task aims in particular at harmonizing the procedures in use at the National Reference Laboratories (NRLs) for residues of the Member States for such determinations as well as at developing new approaches wherever the need arises. In this context an investigation was undertaken to appraise the average levels of a number of key elements in several types of honey with special regard to the influence of the various processing steps. Instrumental methods of election for the analysis of this matrix turned out to be inductively coupled plasma atomic emission spectrometry (ICP-AES) and inductively coupled plasma mass spectrometry (ICP-MS) depending on the actual concentrations of the elements of interest. Dissolution of the samples for suitable presentation to the analytical systems could be easily achieved by gentle heating at ca. 50°C, sonication and addition of high-purity water. The ranges ascertained are as follows (in ng g<sup>-1</sup>): As, < 0.50–0.70; Cd, < 0.50–0.74; Cr, 1.03–3.93; Cu, 144–216; Fe, 191–651; Mn, 223–580; Ni, 17–49; Pb, 3.20–186; Pt, < 0.50; Sn, < 4–27; V, 1.22–1.94; and Zn, 565–1144. As a rule, concentrations of elements in honey from different beehives were similar. A few exceptions were noted for As, Cu, Fe, Ni and Zn. On the other hand, although data obtained with different analytical approaches for the same types of honey and beehive were generally in good agreement, yet some inconsistencies occurred, as in the case of Cu in freshly collected, extracted and ripened honey, Ni in extracted honey and Fe in ripened honey. These could not be traced back to specific procedural facts; rather, they should be ascribed to the inherent heterogeneity of the raw material. The experience gained with this exploratory study will be exploited to set up wider surveys and to plan the preparation of a new certified reference material in a matrix of honey to the benefit of NRLs for residues. © 1999 Elsevier Science B.V. All rights reserved.

*Keywords:* Honey; Trace elements; Inductively coupled plasma atomic emission spectrometry; Inductively coupled plasma mass spectrometry

---

\* Corresponding author. Tel.: +39-06-4990-2052; fax: +39-06-4990-2366.

*E-mail address:* caroli@iss.it (S. Caroli)

## 1. Introduction

Honey is a natural sticky material elaborated out of the nectar of flowers or of plant secretions in the honey sac of bees. The nectar is collected, transformed, combined with proper substances by bees and stored in honeycombs where ripening occurs. The chemical composition of nectar may depend on the botanical species, although the percentage amount of constituents is generally given by ca. 81% carbohydrates, ca. 18% water and ca. 1% proteins, aminoacids, vitamins, organic acids and minerals all together [1].

The high content of glucose and fructose makes honey one of the most digestible foodstuffs that can be consumed as it is, as a sugar substitute or in confectionery products. Moreover, the antimicrobial activity of honey against *Staphylococcus aureus* and *Escherichia coli* is well known [2]. Since 1970 honey has been proposed as an environmental indicator for the assessment of pollution in the area where beehives are placed [3]. An example is given by a study conducted in Sweden after the nuclear accident at Chernobyl to monitor the levels of radioactive Cs in a number of foodstuffs including honey [4]. In fact, bees in their research of food can carry, together with nectar, any other contaminant deposited on flowers.

In this study, samples of honey at different stages of production were collected in an uncontaminated area near Siena (Italy) and analyzed to determine their content in As, Cd, Cr, Cu, Fe, Mn, Ni, Pb, Pt, Sn, V and Zn. On the one hand, this work aims at ascertaining and quantifying inorganic contaminants in honey which are potentially hazardous to the environment and human health; on the other hand, the lack of certified reference materials (CRMs) for trace elements in a host matrix of honey prompted the investigation also in view of the possible launch of a certification campaign for the production of a new CRM based on this matrix [5,6].

## 2. Experimental

### 2.1. Sampling

Honey of sunflowers was collected at two different beehives, coded A and B respectively, located at Castelmuzio (Siena, Italy). The area is generally considered to be relatively unpolluted as it is far from large industrial plants and major railways and highways. Specimens were taken at different stages of honey processing. Four types of samples were considered useful for the purpose of this study, namely freshly collected, sealed, extracted and ripened honey. The so-called freshly collected honey is the nectar picked up by the bees, concentrated and enriched with enzymes from glandular secretions and stored in the hexagonal cells of the honeycomb. At this step the water content is around 70–80%. The ventilation produced by the beating of bee wings makes humidity decrease down to 17–18%. The cells are then capped with a thin layer of wax and the honey is now named sealed. The frames are subsequently withdrawn from the beehives, the wax removed and the honey inside collected after slow centrifugation and filtration (extracted honey). In the last phase the honey is stored in a steel container and kept a few days until complete maturation is achieved (ripened honey). During this period of time, the scattered exogenous particulate gets to the surface of honey and is afterward removed. Specimens of these four types of honey were bottled in previously decontaminated glass vessels and stored at room temperature until analysis.

### 2.2. Sample pretreatment

The physical state of the samples under test demanded thorough homogenization prior to any sub-sampling of aliquots for dissolution and analysis. To circumvent this difficulty, the containers with honey were gently heated at ca. 50°C and sonicated [7,8]. Aliquots of ca. 1 g of this mass were then transferred into teflon vessels and digested in a microwave (MW) oven after addition of 5 ml of a 4:1 HNO<sub>3</sub>–H<sub>2</sub>O<sub>2</sub> mixture. Instrumental parameters and settings are reported in Table 1.

Preliminary determinations of the elements of interest after this treatment clearly indicated that the 1-g portions significantly differed from each other, this pointing to a still unacceptable inhomogeneity of the raw mass. As a consequence of this and in order to obtain a more homogeneous and fluid material, samples of ca. 10 g of honey were instead taken, put into carefully decontaminated glass containers, precisely weighed and added with 5 g of high purity deionized water. This mixture was then heated up to 50°C and sonicated. Subsamples of ca. 1.8 g of this viscous solution were transferred into the MW teflon vessels, weighed and digested as described above. In order to check the possible release of analytes from the teflon containers, blanks were prepared following the same procedure adopted for the samples. For a given sample two different aliquots have been processed in two different runs, spaced by at least 1 day. After digestion samples were cooled at room temperature and made up to 25 ml with high purity deionized water in volumetric glass flasks.

### 2.3. Reagents and standards

Calibrants were prepared from 1000  $\mu\text{g ml}^{-1}$  stock solutions of As, Cd, Cr, Cu, Fe, Mn, Ni, Pb, Pt, Sn, V and Zn in 10%  $\text{HNO}_3$  (Spex Industries, Edison, NJ) by dilution with high purity deionized water produced by a Labconco system (Analytical Control, Milan, Italy). The same procedure was applied to prepare solutions of Rh which was chosen as the internal standard in the case of the mass spectrometric techniques (see below). The reagents used to digest samples were

high-purity concentrated  $\text{HNO}_3$  and  $\text{H}_2\text{O}_2$  (Merck, Darmstadt, Germany). In order to further decrease the blanks levels,  $\text{HNO}_3$  was sub-boiled prior to use with the subboiling distillation unit Duopur (FKV, Sorisole, Bergamo, Italy).

### 2.4. Sample analysis

Plasma-based techniques were employed in the determination of trace elements in honey samples, namely inductively coupled plasma atomic emission spectrometry (ICP-AES), quadrupole inductively coupled plasma mass spectrometry (Q-ICP-MS) and high resolution inductively coupled plasma mass spectrometry (HR-ICP-MS). These techniques can be applied to all possible matrices and analytes (provided that suitable dissolution procedures are resorted to), are characterized by extended dynamic concentration ranges (several orders of magnitude), are multielemental in nature and possess high sensitivity and appropriate detection power.

In particular, As, Cd, Cr, Ni, Pb, Pt, Sn and V were determined by Q-ICP-MS and HR-ICP-MS, Cu by the three methods, Fe by ICP-AES and HR-ICP-MS, and Mn and Zn by ICP-AES only. Instrumental characteristics and settings for the three techniques are summarized in Tables 2–4, respectively. The expected relatively high content of Cu, Fe, Mn and Zn of honey, along with the high sensitivity of ICP-AES for these metals makes the emission technique particularly suited for this type of analysis. In consideration of these two aspects, substantial aqueous dilution of the samples could be performed prior to analysis so that external calibration curves were more than adequate to quantify these elements.

In turn, ICP-MS is a well established and powerful analytical technique for the determination of trace and ultra-trace elements in a variety of environmental and biological samples [9]. However, the formation of spectral interferences originating from atomic and molecular ions produced in the plasma from argon and matrix constituents of the analytical solutions may sometimes seriously affect the quantification of several trace elements (e.g.  $^{40}\text{Ar}^{12}\text{C}$  vs  $^{52}\text{Cr}$ ,  $^{40}\text{Ar}^{16}\text{O}$  vs  $^{56}\text{Fe}$ ,  $^{40}\text{Ar}^{35}\text{Cl}$  vs  $^{75}\text{As}$ ) when no sufficient mass resolu-

Table 1  
Operative conditions for the microwave oven digestion<sup>a</sup>

Step	Power (W)	Time (min)
1	250	1
2	0	2
3	250	5
4	400	5
5	600	5

<sup>a</sup> Apparatus: MLS-1200 Mega (FKV, Sorisole, Bergamo, Italy).

Table 2

Instrumental conditions for inductively coupled plasma atomic emission spectrometry (ICP-AES)

Spectrometer	JY 70 VHR (Instruments S.A., Longjumeau, France)
RF generator	Durr-JY 3238; frequency, 56 MHz; power output, 1.2 kW
Induction coil	6 turns, o.d., 32 mm; height, 30 mm
Torch	INSA, demountable
Nebulizer	Meinhard pneumatic concentric with Scott chamber
Argon flows (l min <sup>-1</sup> )	Plasma, 16; auxiliary, 0.4; aerosol, 0.45
Monochromator	HR, 1000 M; focal length, 1 m; Czerny–Turner mounting, equipped with a 3600 grooves mm <sup>-1</sup> holographic plane grating; linear dispersion in the first order, 0.27 nm mm <sup>-1</sup> ; spectral range, 170–450 nm; entrance and exit slit widths, 40 μm
Spectral lines (nm)	Cu, 324.7; Fe, 238.2; Mn, 257.6; Zn, 213.8

tion ( $m/\Delta m$ ) power is available, as is often the case with Q-ICP-MS systems [10].

The use of high resolution magnetic sector field mass spectrometers allows many interference effects to be kept under control when a resolution higher than that afforded by Q-ICP-MS is needed. For the elimination of the most frequent polyatomic interferences an  $m/\Delta m$  value of 300, 3000 or even 7500 might become necessary [11]. Even only the first of these three modes can solve common interference problems more satisfactorily than the Q-ICP-MS system. With HR-ICP-MS the detection power is increased by about two orders of magnitude, primarily because of improved ion transmission as well as of lower detection noise (< 0.1 cps). Moreover, the use of an ultrasonic nebulizer in combination with both ICP-MS instruments instead of the more conventional pneumatic nebulizer generally increases the detection power by an additional order of magnitude.

Contrary to the approach adopted in the case of ICP-AES, calibration was carried out by the standard addition method for both Q-ICP-MS and HR-ICP-MS determinations. This is due to the fact that the quantification of the content of trace and ultra-trace elements with these two techniques is significantly affected by both matrix composition and acidity of the samples. On the other hand, unfortunately, digested samples could not be diluted more than 1:2 (v/v) because otherwise the expected concentrations of some analytes would be too close to the limits of detection of these techniques. In consideration of all this, the external calibration method obviously could not

be applied and it became necessary to resort to the standard addition approach. Solutions of Rh as the internal standard were added to the samples so as to reach a concentration of 0.5 ng ml<sup>-1</sup> of the metal.

### 3. Results and discussions

Tables 5–8 set forth the results of the determination of the elements of interest. Each value reported therein is the mean of two different sets of results, as explained under Section 2.2. In the

Table 3

Instrumental conditions for quadrupole inductively coupled plasma mass spectrometry (Q-ICP-MS)

Spectrometer	Sciex Elan 5000 (Perkin-Elmer, Norwalk, CT)
Nebulizer	Ultrasonic, U-5000 AT <sup>+</sup> (CETAC Technologies, Omaha, NB)
Interface	Sampler and skimmer cones in Pt–Rh alloy; i.d., 1 mm
RF generator	Power output, 1.0 kW
Argon flows (l min <sup>-1</sup> )	Plasma, 16; auxiliary, 0.9; aerosol, 1.0
Optimization	On masses <sup>24</sup> Mg, <sup>103</sup> Rh, <sup>207</sup> Pb and <sup>208</sup> Pb
Scanning conditions	Replicate time, 200 ms; dwell time, 100 ms; sweeps per reading, 4; readings per replicate, 3; number of replicates, 3
Scanning mode	Peak-hop transient
Vacuum	Interface, 133 Pa; analytical zone, < 1.33 10 <sup>-7</sup> Pa
Analytical masses (amu)	<sup>75</sup> As, <sup>114</sup> Cd, <sup>52</sup> Cr, <sup>65</sup> Cu, <sup>60</sup> Ni, <sup>204+206+207+208</sup> Pb, <sup>195</sup> Pt, <sup>120</sup> Sn, <sup>51</sup> V
Internal standard	<sup>103</sup> Rh



Table 4  
Instrumental conditions for high resolution inductively coupled plasma mass spectrometry (HR-ICP-MS)

Spectrometer	ELEMENT (Finnigan MAT, Bremen, Germany)
Geometry	Double focusing reverse Nier–Johnson
Resolution	$m/\Delta m = 300, 3000, 7500$
RF power	1.2 kW
Nebulizer	Ultrasonic, U-5000 AT <sup>+</sup> (CETAC Technologies, Omaha, NB)
Interface	Sampler and skimmer cones in Pt
Data acquisition ( $m/\Delta m = 300$ )	Electric scan; 4 runs; 10 passes; channels 6440
Data acquisition ( $m/\Delta m = 3000$ )	Electric scan; 5 runs; 10 passes; channels 12 500
Argon flows ( $l \text{ min}^{-1}$ )	Plasma, 13; auxiliary, 1.0; aerosol, 1.0
Analytical masses (amu) ( $m/\Delta m = 300$ )	<sup>75</sup> As, <sup>114</sup> Cd, <sup>208</sup> Pb, <sup>195</sup> Pt, <sup>120</sup> Sn, <sup>51</sup> V
Analytical masses (amu) ( $m/\Delta m = 3000$ )	<sup>52</sup> Cr, <sup>65</sup> Cu, <sup>56</sup> Fe, <sup>60</sup> Ni
Internal standard	<sup>103</sup> Rh

case of freshly collected and sealed honey, the paucity of raw material did not allow analyses by HR-ICP-MS to be also carried out. Table 9, in turn, gives information on the accuracy of measurements, which was tested by including in the analytical runs the Brown Bread BCR CRM 191, i.e. the only CRM available with a matrix of carbohydrates.

As mentioned in the previous section, the determination of As, Cd and V was attempted by both Q-ICP-MS and HR-ICP-MS ( $m/\Delta m = 300$ ). The expected levels of these analytes are in fact very

low. Their actual quantification was possible only with the HR-ICP-MS technique. It is also worth nothing that no more than slight variations occur in the concentrations of these three elements in extracted and ripened honey from the two beehives. In the case of As, the contribution of the <sup>40</sup>Ar<sup>35</sup>Cl interfering species to the signal at mass 75 seems to play only a modest role. This assumption is further supported by the As values obtained for the CRM, although the certification report gives only informative data for this element. There is in fact a satisfactory agreement between the concentration determined and the informative value, especially if one considers that this last was based on a completely different technique, i.e. hydride generation atomic absorption spectrometry (HG-AAS).

Results for Cu were obtained by all three techniques. Comparing the relevant sets of data, it is possible to conclude that, also in this case, there are no striking differences in the content of the analyte found in freshly collected, sealed, extracted and ripened honey samples as well as between the two beehives. A few discrepancies were found when results obtained by the three techniques for the same honey sample and beehive were compared. In particular, results obtained by Q-ICP-MS and HR-ICP-MS were slightly higher than those obtained by ICP-AES. A possible reason could be ascribed to the interference on mass 65 caused by the biatomic <sup>40</sup>Ar<sup>25</sup>Mg species.

A similar pattern was shown by Mn (for this element determinations were performed only by ICP-AES). Only in freshly collected honey of the hive A is the value of Mn much higher than in the other cases. In consideration of the great ability of

Table 5  
Results obtained in the analysis of freshly collected honey<sup>a</sup>

Technique	Hive	As	Cd	Cr	Cu	Fe	Mn	Ni	Pb	Pt	Sn	V	Zn
ICP-AES	A	na	na	na	163 ± 10	651 ± 7	580 ± 6	na	na	na	na	na	1144 ± 120
ICP-AES	B	na	na	na	166 ± 20	419 ± 21	301 ± 9	na	na	na	na	na	894 ± 5
Q-ICP-MS	A	<0.5	<0.5	74 ± 12	172 ± 6	na	na	23 ± 3	<4	<2	<4	<2	na
Q-ICP-MS	B	<0.5	<0.5	89 ± 8	182 ± 7	na	na	27 ± 5	<4	<2	<4	<2	na
HR-ICP-MS	A	na	na	na	na	na	na	na	na	na	na	na	na
HR-ICP-MS	B	na	na	na	na	na	na	na	na	na	na	na	na

<sup>a</sup> Concentration (ng g<sup>-1</sup>); na, not analyzed.

Table 6  
Results obtained in the analysis of sealed honey<sup>a</sup>

Technique	Hive	As	Cd	Cr	Cu	Fe	Mn	Ni	Pb	Pt	Sn	V	Zn
ICP-AES	A	na	na	na	146 ± 9	191 ± 7	223 ± 7	na	na	na	na	na	587 ± 29
ICP-AES	B	na	na	na	144 ± 15	262 ± 10	273 ± 3	na	na	na	na	na	647 ± 1
Q-ICP-MS	A	<0.5	<0.5	34 ± 5	167 ± 12	na	na	17 ± 1	<4	<2	<4	<2	na
Q-ICP-MS	B	<0.5	<0.5	67 ± 8	144 ± 15	na	na	23 ± 3	<4	<2	<4	<2	na
HR-ICP-MS	A	na	na	na	na	na	na	na	na	na	na	na	na
HR-ICP-MS	B	na	na	na	na	na	na	na	na	na	na	na	na

<sup>a</sup> Concentration (ng g<sup>-1</sup>); na, not analyzed.

plants to concentrate metals from soil, a possible explanation for this could be associated to the geochemical composition of the area where the bees of those two particular honeycombs feed [3,12].

Variability in the concentration of Fe and Zn (this last metal was determined only by ICP-AES) is in turn much higher when comparing all the values obtained for the two beehives and the four stages of production. Other authors ascribed this fact to the random presence of these two elements in the environment either as pollutants or as natural constituents of bees and flowers. [12,13].

The quantification of Fe was carried out also by HR-ICP-MS technique, but not by Q-ICP-MS. The latter technique, in fact, is not particularly suited to analyze this metal, as its most abundant isotope (mass 56, abundance 92%) is strongly affected by the overlapping biatomic <sup>40</sup>Ar<sup>16</sup>O species (abundance 99%). In principle, it would be possible to correct the signal of Fe at mass 56 with a mathematical equation based on the <sup>18</sup>O signal, but the huge amounts of Ar and O present in the plasma make this solution inapplicable. This problem can be solved by the HR-ICP-MS technique at a mass resolution of 3000. In fact, in order to separate the <sup>56</sup>Fe signal from that of <sup>40</sup>Ar<sup>16</sup>O one, a minimum theoretical resolution of 2503 is needed. The validity of this approach is further demonstrated by the satisfactory agreement of the two sets of data obtained by ICP-AES and HR-ICP-MS for extracted and ripened honey.

As regards Ni and Sn, the Q-ICP-MS results are in favour of an increase in element concentrations for extracted and ripened honey when com-

pared with the freshly collected and sealed material. The higher values of these two metals in extracted and ripened honey are also confirmed by the data obtained by HR-ICP-MS. In the case of Ni data, a slight difference between the two techniques was observed in that the results obtained by Q-ICP-MS were lower than those obtained by HR-ICP-MS. This could be due to the fact that the mathematical equation applied in the case of Q-ICP-MS actually overcorrects the interference caused by the <sup>44</sup>Ca<sup>16</sup>O double ion on <sup>60</sup>Ni.

In the case of Pb, the present findings show that ripened honey samples contain levels of Pb much higher than those measured in freshly collected, sealed and extracted honey. At present, no acceptable explanation could be found for this behaviour, although a possible reason can be postulated (Section 4). In the case of ripened honey, the data obtained by Q-ICP-MS and HR-ICP-MS show also some discrepancy. The only experimental difference between the two modes was that in the case of Q-ICP-MS analysis the four isotopes of Pb were measured and summed, whereas only the Pb mass at 208 was determined in the case of HR-ICP-MS. No convincing explanation could be found for this pattern, but for a possible malfunctioning of the Q-ICP-MS apparatus at the moment of the sample analysis.

For Cr it is quite evident that there is a substantial discrepancy between the two sets of data obtained by Q-ICP-MS and HR-ICP-MS, the former one being much higher. In this instance the use of the already mentioned CRM was of no avail as the concentration of the metal is given only as an informative figure in a wide range encompassing both experimental values. Most

Table 7  
Results obtained in the analysis of extracted honey<sup>a</sup>

Technique	Hive	As	Cd	Cr	Cu	Fe	Mn	Ni	Pb	Pt	Sn	V	Zn
ICP-AES	A	na	na	na	159 ± 13	277 ± 8	338 ± 13	na	na	na	na	na	567 ± 11
ICP-AES	B	na	na	na	169 ± 13	345 ± 25	334 ± 3	na	na	na	na	na	565 ± 33
Q-ICP-MS	A	<0.5	<0.5	39 ± 1	186 ± 15	na	na	28 ± 1	<4	<2	17 ± 1	<2	na
Q-ICP-MS	B	<0.5	<0.5	39 ± 7	185 ± 4	na	na	35 ± 4	<4	<2	18 ± 1	<2	na
HR-ICP-MS	A	0.50 ± 0.07	0.61 ± 0.01	1.03 ± 0.16	205 ± 10	301 ± 21	na	41 ± 1	3.97 ± 0.43	<0.5	22 ± 2	1.47 ± 0.12	na
HR-ICP-MS	B	0.70 ± 0.08	0.61 ± 0.10	1.38 ± 0.25	216 ± 9	276 ± 18	na	46 ± 8	3.20 ± 0.41	<0.5	21 ± 4	1.34 ± 0.23	na

<sup>a</sup> Concentration (ng g<sup>-1</sup>); na, not analyzed.

Table 8  
Results obtained in the analysis of ripened honey<sup>a</sup>

Technique	Hive	As	Cd	Cr	Cu	Fe	Mn	Ni	Pb	Pt	Sn	V	Zn
ICP-AES	A	na	na	na	158 ± 12	612 ± 41	387 ± 15	na	na	na	na	na	750 ± 43
ICP-AES	B	na	na	na	176 ± 9	598 ± 30	385 ± 8	na	na	na	na	na	698 ± 14
Q-ICP-MS	A	<0.5	<0.5	37 ± 4	196 ± 17	na	na	36 ± 3	110 ± 1	<2	23 ± 3	<2	na
Q-ICP-MS	B	<0.5	<0.5	28 ± 1	167 ± 10	na	na	35 ± 1	107 ± 3	<2	25 ± 2	<2	na
HR-ICP-MS	A	0.58 ± 0.06	0.74 ± 0.03	3.93 ± 0.50	208 ± 2	624 ± 78	na	40 ± 4	186 ± 6	<0.5	27 ± 2	1.22 ± 0.16	na
HR-ICP-MS	B	0.41 ± 0.02	0.70 ± 0.05	3.49 ± 0.42	211 ± 2	473 ± 23	na	49 ± 7	186 ± 4	<0.5	23 ± 1	1.94 ± 0.21	na

<sup>a</sup> Concentration (ng g<sup>-1</sup>); na, not analyzed.

likely, this can be traced back to the inadequacy of the mathematical equation used in the case of Q-ICP-MS to correct the interference caused by the  $^{40}\text{Ar}^{12}\text{C}$  double ion overlapping the peak of Cr at mass 52. The formation of this species is favoured by the high content of carbohydrates present in the honey matrix. In fact, it is well known that in order to minimize the formation of this interference, an essential prerequisite is the complete oxidation of the organic matrix to  $\text{CO}_2$  [14]. This drawback is entirely overcome by using the HR-ICP-MS technique because to obtain a complete separation between the  $^{52}\text{Cr}$  and  $^{40}\text{Ar}^{12}\text{C}$  signals a mass resolution of 3000 is more than sufficient. Thus, only HR-ICP-MS can be reliably used to quantify Cr. Unfortunately, no such data are available on freshly collected and sealed samples due to the shortage of the raw material. Consequently, no thorough correlation can be attempted between Cr levels and stages of production. What is rather apparent, instead, is that there is a noticeable difference in the content of Cr between extracted and ripened honey (1.03–1.38 vs 3.49–3.93  $\text{ng g}^{-1}$ ). This can be justified on the basis of the extraction of Cr from the stainless container where ripening takes place, obviously facilitated by honey acidity.

Finally, Table 10 reports a comparison between the concentration range spanned by each element for each type of honey tested and the levels of some of these elements in a commercial honey. Results show that there is no substantial difference between the two sets of data. Some discrepancy was observed only in the case of As, Fe and Ni. In fact, for the first two elements, the

levels found in the commercial honey were much higher than those obtained in the honey samples, whereas the content of Ni was slightly lower than those of the other specimens.

#### 4. Conclusions

On the basis of results obtained in this study, there is no doubt that a major difficulty in the obtainment of reliable data is the heterogeneity of the raw material, as also highlighted by the significant differences in concentrations noted when testing more subsamples from the same raw mass. Sample dissolution in water certainly mitigates such heterogeneity and facilitates manipulation, but does not succeed in completely overcoming the problem.

Moreover, contamination of honey from trace elements can occur in many different ways, not always easy to identify. A major contribution is due to the acidity of honey (pH 3.5–4). Under such conditions, metal release can occur during the centrifugation and ripening steps which are generally performed in stainless steel containers. This fact seems to be confirmed by the higher values of Pb in ripened honey samples found in this study, whereas it is almost undetectable in freshly collected and sealed honey. Similar considerations can be made in the case of Cr, detected at higher concentrations in ripened honey for the reason mentioned above, as well as in the case of Sn, the presence of which is to be traced back to the release of the metal from the lid of the glass

Table 9  
Results obtained in the analysis of the Brown Bread BCR CRM 191<sup>a</sup>

Concentration ( $\text{ng g}^{-1}$ )	As	Cd	Cr	Cu <sup>b</sup>	Fe <sup>b</sup>	Mn <sup>b</sup>	Ni	Pb	Zn <sup>b</sup>
Found (ICP-AES)	na	na	na	$2.3 \pm 0.2$	$43.0 \pm 1.8$	$22.1 \pm 1.2$	na	na	$21.2 \pm 1.5$
Found (Q-ICP-MS)	$26 \pm 3$	$29.5 \pm 1.3$	$374 \pm 32$	$2.3 \pm 0.2$	na	na	$381 \pm 32$	$185 \pm 11$	na
Found (HR-ICP-MS)	$29 \pm 4$	$29.4 \pm 1.4$	$147 \pm 12$	$2.7 \pm 0.1$	$40.0 \pm 2.0$	na	$352 \pm 30$	$190 \pm 15$	na
Certified	(23)	$28.4 \pm 1.4$	(68–360)	$2.6 \pm 0.1$	$40.7 \pm 2.3$	$20.3 \pm 0.7$	(406–510)	$187 \pm 14$	$19.5 \pm 0.5$

<sup>a</sup> na, not analyzed.

<sup>b</sup> Values in  $\mu\text{g g}^{-1}$ ; values within parentheses are not certified, but only informative.

Table 10

Comparison between element concentration ranges for the four types of honeys and the values measured for a commercial product<sup>a</sup>

Type of honey	As	Cd	Cr	Cu	Fe	Ni	Pb	Sn	V
Freshly collected	<0.5	<0.5	–	163–182	419–651	23–27	<4	<2	<2
Sealed	<0.5	<0.5	–	144–167	191–262	17–23	<4	<2	<2
Extracted	0.50–0.70	0.61–0.61	1.03–1.38	159–216	276–345	28–46	3.20–3.97	17–21	1.34–1.47
Ripened	0.41–0.58	0.70–0.74	3.49–3.93	158–211	473–624	35–49	107–186	23–27	1.22–1.94
Commercial	3.89 ± 0.27	0.70 ± 0.05	3.03 ± 0.28	121 ± 7	2320 ± 180	6.77 ± 0.52	23.9 ± 1.6	13.1 ± 0.7	3.83 ± 0.31

<sup>a</sup> Concentration (ng g<sup>-1</sup>).

pot where the extracted and ripened honey is stored [3,7].

Although more extended investigations are necessary, it can however be stated that in the light of these data the concentrations of trace elements in the honey samples investigated do not pose any serious concern to human health. Furthermore, with regard to the possible preparation of a honey-based multielemental CRM, this can be successfully undertaken once the difficulties caused by matrix heterogeneity are overcome.

### Acknowledgements

The Authors wish to thank the AMA (*Ape, Miele, Ambiente*, i.e. Bee, Honey, Environment) Project, supported by the Italian Ministry of Agricultural Policies for supplying the honey samples. A special word of thanks goes to Dr C. Porrini, whose continued support to this study is gratefully acknowledged.

### References

- [1] F. Belliardo, A. Martelli and G. Proserpio, I prodotti dell'alveare. Aspetti dietetico-alimentari, problematiche farmaco-tossicologiche, impieghi topico-cosmetici, Sinerga, Pero (MI), 1987, pp. 125.
- [2] D. Greenwood, Lancet 431 (1993) 90–91.
- [3] S.S.C. Tong, R.A. Morse, C.A. Bache, D.J. Lisk, Arch. Environ. Health 30 (1975) 329–332.
- [4] D. Mascanzoni, Sci. Total Environ. 67 (1987) 133–148.
- [5] B. Griepink, E.A. Maier, Ph. Quevauviller, H. Muntau, Fresenius J. Anal. Chem. 339 (1991) 599–603.
- [6] S. Caroli, Anal. Chim. Acta 283 (1993) 573–582.
- [7] K.C. Jones, Water, Air Soil Pollut. 33 (1987) 179–189.
- [8] P. Fodor, E. Molnar, Mikrochim. Acta 112 (1993) 113–118.
- [9] P. Boumans, J. Anal. At. Spectrom. 8 (1993) 767–780.
- [10] H. Vanhoe, J. Goossens, L. Moens, R. Dams, J. Anal. At. Spectrom. 9 (1994) 177–185.
- [11] N.M. Reed, R.O. Cairns, R.C. Hutton, Y. Takaku, J. Anal. At. Spectrom. 9 (1994) 881–896.
- [12] J.J. Bromenshenk, S.R. Carlson, J.C. Simpson, J.M. Thomas, Science 227 (1985) 632–634.
- [13] L. Leita, G. Muhlbachov, S. Cesco, R. Barbattini, C. Mondini, Environ. Monitor. Assess. 43 (1996) 1–9.
- [14] M.D. Mingorance, M.L. Pérez-Vazquez, M. Lachica, J. Anal. At. Spectrom. 8 (1993) 853–858.

# Colorimetric determination of copper in aqueous samples using a flow injection system with a pre-concentration poly(ethylenimine) column

Alberto N. Araújo<sup>a,\*</sup>, Rui C.C. Costa<sup>a</sup>, Julian Alonso-Chamarro<sup>b</sup>

<sup>a</sup> *CEQUP/Dep. Química-Física, Faculdade de Farmácia U.P., Rua Anibal Cunha, 164, 4050 Porto, Portugal*

<sup>b</sup> *Unidade de Química Analítica, Dep. de Química U.A.B., E-08193 Bellaterra, Spain*

Received 7 September 1998; received in revised form 8 December 1998; accepted 24 December 1998

## Abstract

A colorimetric flow injection-system for the determination of Cu(II) in waters based on complexation reaction with 4-(2-pyridylazo)-resorcinol, usually termed PAR, is described. Performing measurements in 0.25 mol l<sup>-1</sup> HNO<sub>3</sub> medium allowed improved selectivity of the analytical method. The lack of sensitivity deriving from the low complex absorption under acidic conditions was balanced by the insertion of an immobilised poly(ethylenimine) (PEI) column where Cu(II) pre-concentration in neutral media occurs. Using sample volumes ranging from 2 to 4 ml, sampling rates of 24 and 12 samples h<sup>-1</sup> within a detection limit of 25 and 13 µg l<sup>-1</sup>, respectively, were accomplished. Accuracy of the developed methodology was assessed by comparison with atomic absorption spectrometry being the relationship [FIA] mg l<sup>-1</sup> = 1.00 (± 0.03) × [AAS] mg l<sup>-1</sup> + 0.00 (± 0.02) obtained after analysing 15 samples. Precision was also evaluated using two samples of 0.05 and 0.5 mg l<sup>-1</sup> copper, and a relative standard deviation (R.S.D.) better than 3% was attained for both. © 1999 Elsevier Science B.V. All rights reserved.

**Keywords:** FIA; Copper; PAR; Poly(ethylenimine)

## 1. Introduction

Using colorimetry for the determination of copper and other transition metals in waters is advantageous both because it is easily operated and inexpensive, for instance, when compared to atomic absorption spectrometry (AAS). Another

important feature could lay on the possibility of having a reduced number of colour developing reagents whose selectivity and sensitivity would be easily adjusted to the species to be determined. Nevertheless, most of the analytical methods used require complex procedures for increasing selectivity or lack sensitivity imposing, therefore, the resorting to masking agents and pre-concentration strategies often fastidious and susceptible to contamination [1]. For example, 4-(2-pyridylazo)-resorcinol (PAR), which is a heterocyclic colour

\* Corresponding author. Tel.: +351-2-208-7132; fax: +351-2-200-3977.

E-mail address: anaraujo@mail.ff.up.pt (A.N. Araújo)

developing reagent forming hydrosoluble coloured chelates with different transition metals, has low selectivity in alkaline media. Under these conditions its application to speciation is conditioned by the sample matrix and might require complex and expensive sample treatments [2,3]. When in acidic conditions are employed, selective reactions with PAR can occur by adjusting the pH and the media composition, being the determination of copper(II) content in waters easily accomplished by promoting the selective reaction in weak acid nitric media. To the increase of selectivity in the Cu reaction with PAR is associated with a sensitivity decrease of the analytical determination since the PAR/metal complexes which are usually of the type 2:1 become 1:1 [4]. Sensitivity can still be improved if extraction or resin pre-concentration procedures are performed by means of continuous flow methods, which significantly decrease the total analysis time and contamination risk [5,6]. Based on the above mentioned considerations, the use of selective pre-concentration on polymers may be an advantageous alternative regarding simplicity as polymers selectivity can equally be adjusted by changing the pH media [7,8]. In this work, an immobilised poly(ethylenimine) (PEI) column that facilitates the selective concentration of Cu(II) in neutral media is proposed [7]. Forward elution of fixed Cu with weak nitric acid promotes the selective reaction with the colour developing reagent granting performances to the proposed procedure similar to those of the methods based on catalytic reactions [9,10] or specific reagents [11,12].

## 2. Experimental

### 2.1. Solutions and reagents

All solutions were prepared with deionised water (specific conductivity  $< 0.1 \mu\text{S cm}^{-1}$ ) and analytical grade reagents.

A stock copper solution in  $1000 \text{ mg l}^{-1}$  concentration was prepared by dissolving  $\text{Cu}(\text{NO}_3)_2 \cdot 3\text{H}_2\text{O}$  previously dried in about 400 ml of water and the volume made up to 500 ml in a volumetric flask. Calibrating copper solutions

were obtained from the stock solution by careful dilution with water.

The several phosphate buffer solutions used were prepared from two stock solutions of  $0.5 \text{ mol l}^{-1}$  in  $\text{KH}_2\text{PO}_4$  and  $2.0 \text{ mol l}^{-1}$  in  $\text{KOH}$ , respectively.

A  $0.25 \text{ mol l}^{-1}$  in  $\text{HNO}_3$  solution was used as an eluent.

The colour developing reagent solution was obtained by dissolving 0.0538 g of PAR in 100 ml of  $0.5 \text{ mol l}^{-1}$   $\text{HNO}_3$ .

PEI columns immobilised on silica gel granules in the size of 40–200 mesh (Aldrich, ref. 00920KZ) were prepared by filling up acrylic tubes of 1.6–2.9 mm internal diameter and with a length of 13–33 mm with an aqueous suspension of the polymer. To prevent the leakage of this polymer a small polyester sponge was placed in both ends of the tubes.

### 2.2. Instrumentation

In the proposed set-up (Fig. 1), solutions were propelled by two Gilson Minipuls 3 four-channel peristaltic pumps (Villiers-le-Bel, France), composed of PVC tubing of the same brand, ref. N03696, and with 1.2 mm internal diameter. PTFE tubing 0.8 mm internal diameter and two home-made acrylic confluences were used throughout. The 100 cm long reactor X was constructed by coiling the PTFE tubing around a plastic cylinder of 1 cm outer diameter.

Samples were injected through a 4-way Rheodyne 5020 injection valve. The column comprising the polymer provided the sampling loop of a Hamilton HVLX8-7 6-way valve (Hamilton, Reno, NV) electrically actuated. A Jenway 6300 colorimeter equipped with a Helma 178.311 QS flow cell of  $35 \mu\text{l}$  optical volume and connected to a Kipp and Zonen BD111 was used as a detector system.

A Pye Unicam SP9 flame atomic absorption spectrophotometer was used for the assessment of the quality of the results. When samples copper content was less than  $0.2 \text{ mg l}^{-1}$  a Perkin Elmer ZL4100 electrothermal atomisation spectrophotometer was also used.



### 2.3. Methods

A sample volume of 2 or 4 ml was inserted into a water continuous flow according to the pre-concentration treatment required (Fig. 1). The sample plug inserted merged with a phosphate buffer solution before reaching the immobilised PEI column. Afterwards, the 6-way valve was actuated until the copper collected by the column was carried by a nitric acid solution that flowed towards the column through another port of the valve. Then, the reaction of the Cu(II) eluted with PAR was promoted by adding a solution of the latter through the confluence positioned right before reactor X and the transient signal was measured at a 530 nm wavelength. During the pre-concentration step water instead of the nitric acid solution merged with the colour developing reagent solution.

The pH values providing the optimal copper retention by the immobilised polymer were estimated by inserting 2 ml solutions with  $5.00 \text{ mg l}^{-1}$  Cu at different pH values, which were attained by adding nitric acid or sodium hydroxide, into a water flow at a rate of  $0.8 \text{ ml min}^{-1}$ . Thus, a 13 mm long column with 1.6 mm internal diameter and filled with 15.7 mg PEI was used. While being pre-concentrated copper solutions flowed through the column towards the waste. When the 6-way valve was commutated a solution of  $0.25 \text{ mol l}^{-1}$  in  $\text{HNO}_3$  flowed into the column for 20 s and after collecting Cu merged with  $0.2 \text{ mmol l}^{-1}$  PAR solution.

To assess the minimum amount of the polymer used, 1 ml of a calibrating solution with  $1.00 \text{ mg l}^{-1}$  Cu was pre-concentrated under the optimal conditions previously described and using columns with lengths ranging from 13 to 33 and 1.6 to 2.9 mm of internal diameter.

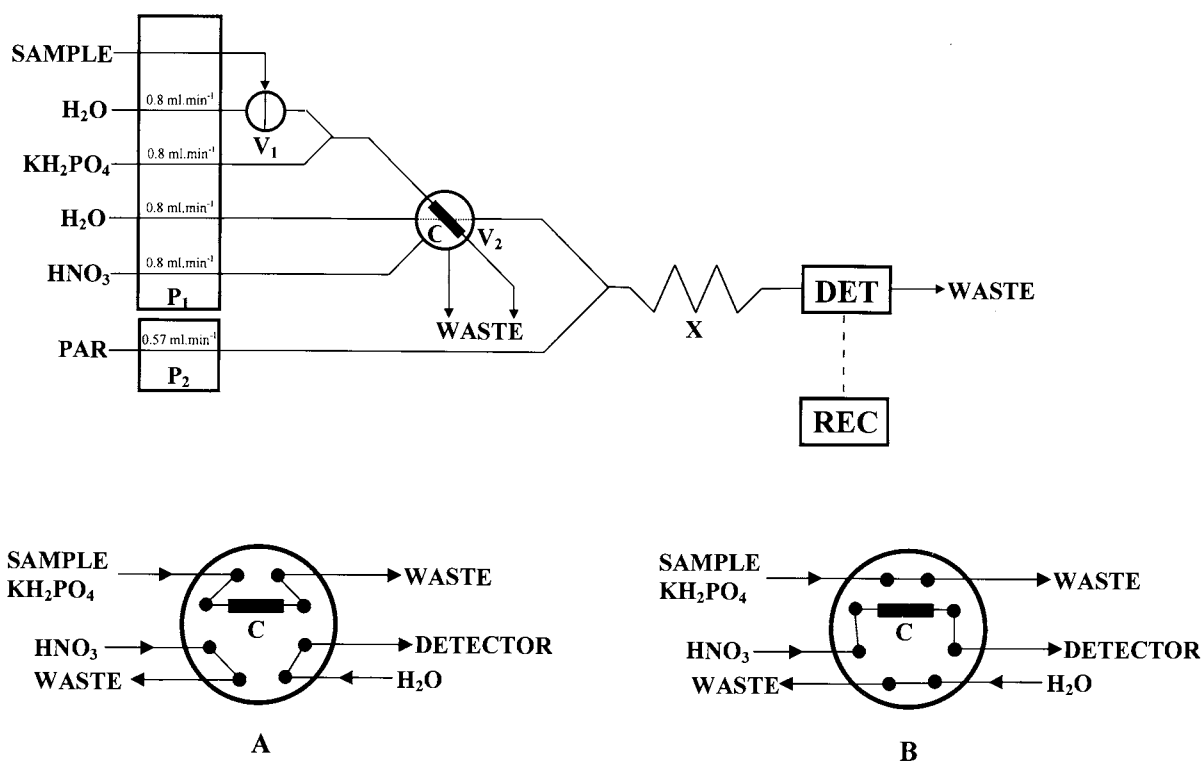


Fig. 1. Schematic representation of the developed FIA manifold. P<sub>1</sub>, P<sub>2</sub>, peristaltic pumps; V<sub>1</sub>, 4-way valve; V<sub>2</sub>, 6-way valve; C, PEI column; X, reaction coil; DET, spectrophotometer; REC, recorder. (A) Preconcentration step; (B) elution step.

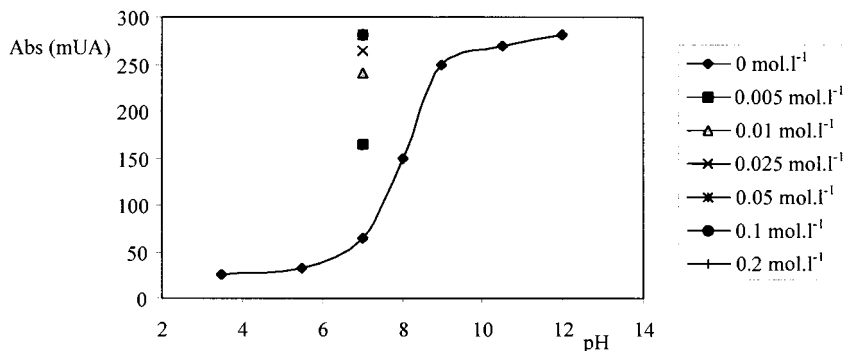


Fig. 2. pH effect of a  $5.00 \text{ mg l}^{-1}$  Cu(II) calibrating solution on the absorbance.

AAS was used as reference method [13]. Samples were formerly analysed by flame atomisation (FAAS), being aspirated to the flame without prior treatment and just after the conventional adjustment of the spectrophotometer. The absorption values attained were interpolated in a calibration curve that was obtained by analysis of the same calibrating solutions used in the proposed procedure. Samples presenting copper concentrations less than  $0.2 \text{ mg l}^{-1}$  were submitted to a replicate analysis by electrothermal atomisation (ETA-AAS). In this case, samples were diluted until copper content was found within the linear calibration interval ( $< 40 \text{ } \mu\text{g l}^{-1}$ ).

### 3. Results and discussion

#### 3.1. Selection of wavelength for univariate detection

The wavelength required for the measurements carried out under optimal sensitivity was set by depicting the spectrum of the coloured product formed from the mixture of equal volumes of PAR nitric solution and aqueous solutions of Cu(II). An absorption band was found between 470 and 600 nm, having a peak maximum at 530 nm. In acid media, particularly in acetic or sulphuric acid solutions, other metals can react with PAR, too [1]. Nevertheless, when performing similar experiments with ions such as Cd(II), Co(II), Mn(II), Pb(II) and Zn(II) that in acetic media promote the formation of colour complexes with

the proposed reagent, absorption bands within the range of 400–510 nm were found, which did not interfere with the determination procedure. A similar behaviour was observed for ions that in sulphuric media react with PAR, namely Bi(III), Pd(II), Ti(IV) and Zr(IV), and also for ions generally present in waters such as Al(III), Ca(II), Cr(VI), Fe(III), Mg(II) and Mo(IV). Therefore, the measurement of trace levels of copper at a 530 nm wavelength and based on the complex formed in nitric media allowed a selective determination, though restrained by the low molar absorption coefficient (about  $5.5 \times 10^3 \text{ l mol}^{-1} \text{ cm}^{-1}$ ).

#### 3.2. Optimisation of the system

To facilitate copper determinations in low concentrations a pre-concentration step consisting in the use of PEI, which is inexpensive and easily available on the market, was introduced. The selection of PEI was determined by the capacity of this polymer, when used in its soluble form, to collect Cu(II) with a 90% confidence level when the pH of the medium is raised to a neutral value [8]. As shown in Fig. 2 for pH values less than 6 uni retention was very low, whereas for 6 and 8 pH values a slight increase in retention was found. At the alkaline zone Cu was increasingly retained until a maximum retention corresponding to pH values higher than 10.5 was found, probably due to a filtration effect of the column over copper hydroxide precipitate. While performing these experiments a decrease of the pH was found for the column effluent during the pre-concentration step.

Therefore, the increase of Cu retention within the 6–8 pH range was tried by buffering the solutions. With this purpose an extra channel for the addition of the phosphate buffer solution was coupled to the system. It was found that when the concentration of the buffer increased copper retention increased as well (Fig. 2). The highest retention was accomplished by inserting a buffer solution with hydrogen phosphate concentrations from 0.05 up to 0.2 mol l<sup>-1</sup>.

The sampling rate achieved by the present manifold depended on the pre-concentration and elution times, i.e. the time required for the sample and the acid solution used as eluent to flow through the polymer column. Thus, the flow rates throughout these steps should be high enough to facilitate the highest sampling rate. The flow rate during retention was studied by propelling 2 ml of a calibrating solution with 5.00 mg l<sup>-1</sup> Cu at flow rates ranging from 0.4 to 3.2 ml min<sup>-1</sup>. The elution step consisted in the 270 µl of 0.25 mol l<sup>-1</sup> HNO<sub>3</sub> at a rate of 0.8 ml min<sup>-1</sup>. A gradual diminishing of the analytical signal intensity was found when the flow rate at the pre-concentration step increased (Fig. 3). The concentration efficiency (CE), defined as the result of the enrichment factor times the sampling rate (per min) [14], increased linearly within the same interval. A 1.6 ml min<sup>-1</sup> flow rate was selected as being the best compromise between sensitivity and sampling rate. The establishment of the flow rate at the elution step was also found to be of great importance as the

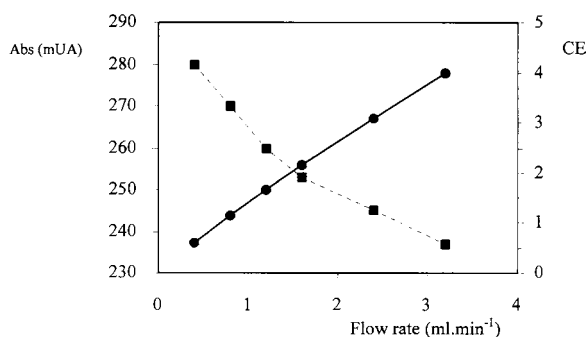


Fig. 3. Effect of the pre-concentration flow rate. The dark line plots the concentration efficiency (CE), whereas the outline represents the absorbance.

intensity of the analytical signal decreased about 15% due to the increase of the elution flow from 0.5 to 3.5 ml min<sup>-1</sup>. Using a slightly concentrated nitric acid solution facilitated the effective elution of the copper retained and therefore decreased copper dispersion through the eluent. It was found that the lowest concentration of nitric acid providing the highest analytical signal corresponded to 0.25 mol l<sup>-1</sup> and flowed through the column at a rate of 0.8 ml min<sup>-1</sup> for 9 s.

After selecting these conditions the PAR solution concentration and flow rate were studied in order to attain the lowest dilution of the sample when this merged with the PAR solution. The best results were registered with a PAR concentration of 2.5 mmol l<sup>-1</sup> prepared in 0.5 mol l<sup>-1</sup> HNO<sub>3</sub> and propelled towards the confluence at a 0.57 ml min<sup>-1</sup> flow rate. Lower flow rates were not tried since PAR could hardly be solubilised in concentrations higher than 2.5 mmol l<sup>-1</sup>.

In what column dimensions are concerned, it was found that the analytical signals intensity increased proportionally to the column length and inversely to the diameter. Using columns of the narrowest diameter and 35 mg PEI promoted the best compromise between signal intensity and amount of polymer. Higher amounts of PEI, led to the decrease of the analytical signal as a consequence of the dispersion effect originated by the column length.

PEI can also collect other metal species other than Cu, thus affecting the effectiveness of the pre-concentration step [8]. Hence, the performance of the PEI column selected regarding the cationic species previously referred to was assayed. The analytical signal attained using 3.8 ml of a calibrating solution presenting 1.00 mg l<sup>-1</sup> Cu did not decrease when the interferent species were present in concentrations lower than 2 mg l<sup>-1</sup> regarding transition metals, 50 mg l<sup>-1</sup> for Mg and 200 mg l<sup>-1</sup> for Ca.

The breakthrough capacity of the polymer, defined as the highest amount of the analyte retained per unit of the polymer mass [15], was assessed, also, under batch and flow conditions, being obtained values of 43.4 and 10.4 mg g<sup>-1</sup>,

Table 1  
Analytical performance of the developed flow injection analysis (FIA) set-up

Element	Volume (ml)	Detection limit <sup>a</sup> (mg l <sup>-1</sup> )	Quantification limit (mg l <sup>-1</sup> )	Upper limit (mg l <sup>-1</sup> )	Enrichment factor	Sampling rate (h <sup>-1</sup> )
Copper	2	0.025	0.083	0.8	5.6	24
	4	0.013	0.043	0.25	10.6	12

<sup>a</sup> Defined as  $3\sigma$  of the blank divided by the slope of the calibration plot.

respectively. Furthermore, some of the proposed set-up working characteristics regarding the insertion of 2 and 4 ml sample volumes, respectively, are presented on Table 1.

### 3.3. Application of the set-up to the analysis of residual and tap water samples

Considering that Cu(II) in residual waters could be present in amounts up to  $0.5 \text{ mg l}^{-1}$ , whereas those of tap water are rather lower, sample volumes of 2 and 4 ml were used respectively in the assay of real samples by the proposed method. These trials were carried out with ten samples of residual waters and five samples of tap water. The results obtained (Table 2) were compared to those given by FAAS for residual water samples and by ETA-AAS for tap water samples. A relationship  $[\text{FIA}] \text{ mg l}^{-1} = 1.00 (\pm 0.03) \times [\text{AAS}] \text{ mg l}^{-1} + 0.00 (\pm 0.02)$  presenting relative deviations less than 5% was obtained. At the 95% level of confidence, a value of 0.954 for the paired *t*-test was obtained showing that there is not a significant difference between the values obtained by the two methods.

Precision of the developed methodology was also evaluated by running ten replicate analyses of two samples with Cu concentrations of 0.05 and  $0.5 \text{ mg l}^{-1}$ , respectively, with a relative standard deviation less than 3% being obtained.

The procedure proposed in this work presents the advantage of being rather inexpensive since copper is determined in complex matrix samples using common techniques and reagents. Moreover, matrix interferences such as colour are easily eliminated, since its performance similar

when compared with other methodologies based on catalytic reactions or specific reagents.

### Acknowledgements

This work was carried out under the E-30/97-E-30/98 Portuguese–Spanish projects (CRUP). The authors acknowledge the financial support given by Fundação para a Ciência e Tecnologia through PBIC/C/QUI/2162/95 agreement and the Ph.D. grant (Praxis/BD/9544/96) conceded to one of us (R.C.C.C.).

Table 2  
Results ( $\text{mg l}^{-1}$ ) obtained in the determination of copper in waters<sup>a</sup>

Sample	AAS	FIA	Relative error (%)
<i>2 ml, residual water</i>			
1	$0.49 \pm 0.02$	$0.49 \pm 0.01$	-0.7
2	$0.78 \pm 0.02$	$0.80 \pm 0.01$	2.6
3	$0.44 \pm 0.02$	$0.45 \pm 0.01$	2.5
4	$0.251 \pm 0.01$	$0.245 \pm 0.006$	-2.6
5	$0.65 \pm 0.02$	$0.66 \pm 0.02$	0.5
6	$0.72 \pm 0.02$	$0.69 \pm 0.01$	-4.8
7	$0.187 \pm 0.008$	$0.184 \pm 0.005$	-1.7
8	$0.42 \pm 0.01$	$0.437 \pm 0.003$	3.3
9	$0.46 \pm 0.02$	$0.45 \pm 0.01$	-3.2
10	$0.551 \pm 0.02$	$0.569 \pm 0.006$	3.2
<i>4 ml, tap water</i>			
11	$0.126 \pm 0.002$	$0.124 \pm 0.001$	-1.6
12	$0.054 \pm 0.001$	$0.055 \pm 0.001$	2.0
13	$0.098 \pm 0.003$	$0.101 \pm 0.001$	3.1
14	$0.147 \pm 0.005$	$0.145 \pm 0.004$	1.4
15	$0.185 \pm 0.006$	$0.178 \pm 0.004$	-3.8

<sup>a</sup> The S.D. was obtained from three consecutive determinations. AAS, atomic absorption spectrometry; FIA, flow injection analysis.

## References

- [1] Z. Marczenko, *Separation and Spectrophotometric Determination of Elements*, Wiley, New York, 1985.
- [2] D.A. Roston, *Anal. Chem.* 56 (1984) 241.
- [3] A.A. Almeida, X. Jun, J.L.F.C. Lima, *Analyst* 123 (1998) 1283.
- [4] R.G. Anderson, G. Nickless, *Analyst* 92 (1967) 207.
- [5] L. Nord, B. Karlberg, *Anal. Chim. Acta* 145 (1983) 151.
- [6] J.L. Burguera, M. Burguera, P. Carrera, J. Marcano, C. Rivas, M.R. Brunetto, *J. Aut. Chem.* 17 (1995) 25.
- [7] K. Geckeler, G. Lange, H. Eberhardt, E. Bayer, *Pure Appl. Chem.* 52 (1980) 1883.
- [8] K. Geckeler, E. Bayer, V.M. Shkinev, B. Ya. Spivakov, *Fresenius Z. Anal. Chem.* 333 (1989) 763.
- [9] Z.X. Guo, *Fenxi Kexue Xuebao* 13 (3) (1997) 228.
- [10] S. Kawakubo, T. Katsumata, M. Iwatsuki, T. Fukasawa, T. Fukasawa, *Analyst* 113 (12) (1988) 1827.
- [11] S.W. Kang, T. Sakai, N. Ohno, K. Ida, *Anal. Chim. Acta* 261 (1–2) (1992) 197.
- [12] H. Wada, T. Ishizuki, G. Nakagawa, *Mikrochim. Acta III* (3–4) (1983) 235.
- [13] A.D. Eaton, L.S. Clesceri, A.E. Greenberg, *Standard Methods for the Examination of Water and Wastewater*, 19th Edition, 1995.
- [14] Z. Fang, *Flow Injection Separation and Pre-Concentration*, VCH, New York, 1993.
- [15] F. Helfferich, *Ion Exchange*, McGraw-Hill, New York, 1962.

# Optimisation and comparison of microwave-assisted extraction and Soxhlet extraction for the determination of polychlorinated biphenyls in soil samples using an experimental design approach

Olatz Zuloaga \*, Nestor Etxebarria, Luis A. Fernández, Juan M. Madariaga

*Kimika Analitikoaren Saila, Euskal Herriko Unibertsitatea, 644 P.K., E-48080 Bilbao, Spain*

Received 7 September 1998; received in revised form 29 December 1998; accepted 6 January 1999

## Abstract

Optimisation of microwave-assisted extraction (MAE) for the extraction of polychlorinated biphenyls (PCBs) from soil samples has been accomplished using an experimental design approach. Variables studied have been: percentage of acetone (v/v) in an acetone:*n*-hexane mixture, solvent volume, extraction time, microwave power and pressure inside the extraction vessel. Five samples of a certified soil (CRM 481) have been extracted under the optimum conditions of the developed method and the results have been compared to those obtained by Soxhlet extraction. Good recoveries (> 95%) have been obtained for all the PCBs studied. All extracts have been analysed by gas chromatography/mass spectrometry (GC/MS) and an optimum determination method for the electron impact mass spectrometric (EIMS) has also been developed. © 1999 Elsevier Science B.V. All rights reserved.

*Keywords:* Microwave-assisted extraction; Polychlorinated biphenyls; Soil samples; Experimental design

## 1. Introduction

Soils are crucial to life on earth. From ozone depletion to rain forest destruction to water pollution, the global ecosystem is impacted in far-reaching ways by the processes carried out in the soil. To great degree, soil quality determines the nature of plant ecosystems and the capacity of

land to support animal life and society. As human society becomes increasingly urbanised, fewer people have intimate contact with the soil, and individuals tend to lose sight of the ways in which they depend upon soils for their prosperity and survival [1].

Modern industrialised societies have developed thousands of synthetic organic compounds with different purposes. An enormous quantity of organic chemicals is manufactured every year [1]. Among these compounds, chlorinated biphenyls (CBs) have been manufactured since 1930 and

\* Corresponding author. Tel.: + 39-94-601-2707; fax: + 39-94-464-8500.

*E-mail address:* qabzuzuo@lg.ehu.es (O. Zuloaga)

Table 1  
Design matrix and response values in the central composite design for electron impact (EI) optimisation

Run no.	Data matrix			Responses									
	Electron energy (eV)	Splitless time (min)	Voltage gain (V)	CB-8	CB-28	CB-20	CB-52	CB-35	CB-101	CB-118	CB-153	CB-138	CB-180
1	35	1.25	94	457 292	256 245	193 855	110 600	252 431	71 715	74 208	76 714	47 905	46 460
2	45	1.25	94	596 003	328 403	243 142	138 401	322 048	91 027	90 311	97 079	61 591	59 171
3	35	2.75	94	459 631	245 554	182 861	118 115	236 056	81 178	77 712	84 196	52 637	48 849
4	45	2.75	94	553 240	291 617	213 436	136 198	278 316	93 174	88 339	96 146	60 446	54 881
5	35	1.25	307	830 008	491 672	363 331	257 567	462 616	203 812	190 113	214 476	136 454	119 475
6	42	1.25	307	1 186 534	623 493	462 059	315 475	575 333	233 929	218 818	242 643	152 618	136 448
7	35	2.75	307	913 844	483 791	358 104	255 153	452 271	207 313	18 9783	222 299	138 503	128 788
8	42	2.75	307	1 189 171	617 159	455 541	311 813	569 396	240 285	216 691	250 679	158 272	145 912
9	49	2.00	189	783 558	399 204	294 185	200 046	354 111	153 060	136 391	159 632	98 874	90 359
10	31	2.00	189	452 291	234 700	174 819	127 610	217 424	109 681	96 307	113 982	72 216	69 524
11	40	3.30	189	1 016 401	565 848	418 307	267 388	522 364	222 564	200 930	196 416	120 795	138 132
12	40	0.70	189	965024	533 336	398 575	255 034	488 501	212 681	183 937	188 058	117 557	133 920
13	40	2.00	402	2 112 856	1 181 354	884 995	569 647	1 092 704	478 078	413 942	419 950	272 644	299 922
14	40	2.00	0	417 247	225 331	165 840	106 013	203 364	90 139	75 904	80 834	49 731	58 966
15	40	2.00	189	890 315	496 969	369 202	236 448	454 937	202 707	173 053	182 724	112 303	130 524
16	40	2.00	189	892 158	498 193	367 550	238 203	451 933	201 879	168 920	181 959	112 908	128 196
17	40	2.00	189	873 617	485 226	360 034	231 999	438 973	198 829	160 336	177 734	110 256	127 545

Table 2

Values of parameters obtained for the central composite design for electron impact (EI)

	$\beta_0$	$\beta_1$	$\beta_2$	$\beta_3$	$\beta_{11}$	$\beta_{22}$	$\beta_{33}$	$\beta_{12}$	$\beta_{13}$	$\beta_{23}$	$\beta_{123}$	$r^2$
CB-8	$-7 \times 10^6$	$4 \times 10^5$	–	–	$-4 \times 10^3$	–	7.90	–	–	–	–	0.894
CB-52	$-2 \times 10^6$	$9 \times 10^4$	–	–	$-1 \times 10^3$	–	2.26	–	–	–	–	0.915
CB-180	$-1 \times 10^6$	$6 \times 10^4$	–	–	-740	–	1.15	–	–	–	–	0.855

production was stopped in 1983. They have been extensively used in electronic equipment like transformers and capacitors and as plasticisers in paint and rubber sealants. Large quantities of CBs have reached the environment through leakage, disposal, evaporation, etc. Due to their persistence the residence time in the environment is very long. In the aquatic environment CBs tend to accumulate in sediments and biota because of their hydrophobic character and consequent low solubility in water. Sediments act as a sink for CBs and are therefore important in pollution studies and monitoring [2].

The analysis of CBs in sediments and soils generally includes extraction with organic solvents, clean-up, removal of sulfur, column fractionation and gas chromatographic separation [2].

The procedures involved in the extraction of polychlorinated biphenyls (PCBs) from soil samples (e.g. Soxhlet) are usually lengthy and non-selective. Moreover, they entail a great deal of sample-handling, which adds to risk of errors [3]. Recently, microwave-assisted extraction (MAE) has become an important alternative for the extraction of organic pollutants from environmental matrices. Microwave energy is a non-ionising radiation that causes molecular motion by migration of ions and rotation of dipoles but does not induce changes in molecular structure. Rapid heating within an organic sample with a permanent dipole moment is brought about by alignment of molecules, followed by their rapid return to disorder [4]. MAE has been used for the extraction of PCBs [5,6], PAHs, [7,8], phenols [7,9] and organochlorine pesticides [7,10] in soils and sediments.

Nevertheless, the systematic optimisation of the extraction techniques is often missed in many works. In this work, a MAE method has been

developed for the extraction of PCBs in soil samples. The variables optimised have been: percentage of acetone in an acetone:*n*-hexane mixture, solvent volume, extraction time, microwave power and pressure inside the extraction vessel. The optimised method has been used for the extraction of PCBs from a certified soil (CRM 481) and the results have been compared to those obtained by Soxhlet extraction. All extracts have been analysed by gas chromatography/mass spectrometry (GC/MS) and an optimum determination method for the electronic impact mass spectrometric has also been developed.

## 2. Experimental section

### 2.1. MAE

MAE experiments were performed with a MDS-2000 closed microwave solvent extraction system (CEM, Mathews, NC) equipped with 12-sample tray and pressure feedback control. A 0.2 g aliquot of PCB polluted soil was accurately weighed, mixed with 2 g of anhydrous sodium

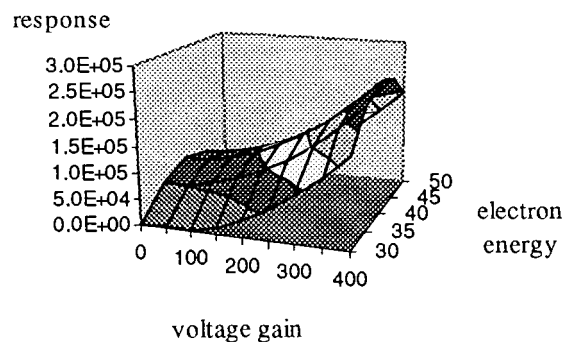


Fig. 1. Response surface for the optimisation of the gas chromatography/mass spectrometry (GC/MS) set-up.



Table 3  
Calibration statistical parameters for gas chromatography/mass spectrometry (GC/MS)

Parameters	CB-8	CB-28	CB-20	CB-52	CB-35	CB-101	CB-118	CB-153	CB-138	CB-180
Linear range(pg)	64–1920	40–1200	40–1200	40–1200	50–1488	28–840	31–936	28–840	26–792	22–648
$r^2$	0.999	0.998	0.999	0.998	0.993	0.994	0.997	0.998	0.999	0.998
Detection limit <sup>a</sup> (pg)	32	30	23	28	97	50	42	27	20	21
Between-injection R.S.D. (%) lowest point	2.9	4.6	6.6	5.6	3.7	4.6	6.7	5.9	4.7	3.6
Between-injection R.S.D. (%) highest point	6.6	5.4	6.5	4.8	7.3	4.6	5.3	5.4	6.8	6.7

<sup>a</sup> Detection limit was calculated as three times the total S.D. of the correlation curve.

Table 4

Design matrix and normalised values in the fractionated factorial design for microwave-assisted extraction (MAE) experiments

Run no.	Design matrix					Normalised values (%)			
	Pressure (psi)	Time (min)	Power (%)	Acetone (%)	Volume (ml)	CB-101	CB-153	CB-138	CB-180
1	16	16.5	44	30	30	-1.667	-1.343	-1.366	-1.567
2	26	16.5	44	70	15	-0.091	-0.761	-0.900	-0.774
3	16	33.5	44	70	15	-0.176	-0.237	-0.469	-0.382
4	26	33.5	44	30	30	-0.468	-0.447	-0.588	-0.538
5	16	16.5	70	70	30	-0.910	-0.910	-0.607	-0.604
6	26	16.5	70	30	15	-1.165	-0.342	-0.119	-0.522
7	16	33.5	70	30	15	-0.467	0.243	0.100	-0.097
8	26	33.5	70	70	30	0.449	-0.197	-0.249	-0.121
9	21	25	57	50	20	0.958	-0.379	-0.253	0.171
10	21	25	57	50	20	0.846	0.825	1.051	1.237
11	21	25	57	50	20	1.578	2.091	2.215	1.894

sulphate (which had been dried at 120°C overnight) and quantitatively transferred to the Teflon-lined extraction vessel. Sixty  $\mu\text{l}$  of a surrogate mixture of dibutyl chlorendate and 2,4,5,6-tetrachloro-*m*-xylene and the acetone:*n*-hexane mixture were then added to each sample and the extraction vessel was closed, after ensuring a new rupture membrane was used for each experiment. In this work, volume and percentage (v/v) of acetone in the acetone:*n*-hexane, as well as power, pressure and time in which extractions were performed were indicated by the experimental design. Extraction conditions were programmed in two stages. In the first stage, the system was allowed to reach the required pressure using full power; in the second stage, the pressure previously reached was kept constant and the power and the time were established according to the experimental design (see Tables 4 and 5). This way, samples stayed at the previously set pressure during the whole extraction process. When the irradiation period was complete, samples were removed from the microwave cavity and were allowed to cool in a water bath to room temperature before opening. The supernatant was filtered through glass wool prewashed with *n*-hexane–acetone and then combined with 7–10 ml acetone:*n*-hexane rinses of the extracted sample. The extract was concen-

trated to  $\sim 2$  ml using nitrogen evaporation with a Turbovap LV Evaporator (Zymark, Hopkinton, MA).

## 2.2. Clean-up

The extract was transferred on top of the Florisil<sup>®</sup> Cartridge which had been previously rinsed with 10 ml of *n*-hexane at flow rate of  $\sim 4$  ml  $\text{min}^{-1}$ . The extract was then eluted with 10 ml of *n*-hexane at flow rate of  $\sim 2$  ml  $\text{min}^{-1}$ . The eluate was concentrated under nitrogen blowdown, transferred into 5 ml calibrated flasks and dissolved in *n*-hexane. Extracts were kept in the fridge until analysis. For quantification, 200  $\mu\text{l}$  of the extract were diluted in *iso*-octane and transferred into injection vials for GC/MS analysis.

## 2.3. Soxhlet extraction

Soxhlet extractions were performed using 0.2 g of soil analytically weighed, mixed with 2 g of anhydrous sodium sulphate and transferred to the pre-rinsed paper thimble and 60  $\mu\text{l}$  of a surrogate mixture of dibutyl chlorendate and 2,4,5,6-tetrachloro-*m*-xylene were added. Samples were extracted under reflux (3 cycles  $\text{h}^{-1}$ ) with 200 ml of

acetone–hexane in the percentages and the time indicated by the experimental design. After cooling to room temperature,  $\sim 2$  ml of *iso*-octane were added prior to rotary evaporation [2] and the extract was concentrated to  $\sim 10$  ml at  $50^\circ\text{C}$  and reduced pressure. The last concentration step was performed by evaporation with a gentle stream of nitrogen. The sample extract was centrifugated for the elimination of the fine particulate matter caused by the paper thimble and then submitted to the clean-up step mentioned above.

#### 2.4. Reagents and chemicals

The PCBs–CEE–C mixture of 10 PCBs ( $2.7$ – $8 \mu\text{g ml}^{-1}$ ) was supplied by CromLab (Bar-

celona, Spain). EPA 8080/8270 Pesticide Surrogate Mix containing dibutyl chlorendate ( $1971.3 \mu\text{g ml}^{-1}$ ) and 2,4,5,6-tetrachloro-*m*-xylene ( $2000.1 \mu\text{g ml}^{-1}$ ) were supplied by Supelco (Bellefonte, PA). Weight loss of the standards was recorded during storage [2] and it never exceeded 1%. *n*-Hexane and acetone were purchased from LabScan (Dublin, Ireland) and purities were stated to be better than 95%. Anhydrous sodium sulphate (purissimum) was purchased from Panreac (Barcelona, Spain). Sep-Pak<sup>®</sup> Plus Florisil<sup>®</sup> Cartridges were purchased from Waters (Milford, MA). All solutions were stored at  $5^\circ\text{C}$  in the dark. All volumetric glassware was grade A and was calibrated at laboratory temperature.

Table 5

Design matrix and normalised values in the central composite design for microwave-assisted extraction (MAE) experiments

Run no.	Data matrix			Normalised values			
	Pressure (psi)	Time (min)	Acetone (%)	CB-101	CB-153	CB-138	CB-180
1	16	16.5	50	−0.630	−0.800	−0.801	−0.763
2	26	16.5	50	−1.314	0.798	0.658	0.944
3	16	33.5	50	0.382	−0.047	−0.223	−0.213
4	26	33.5	50	−0.116	−0.711	−0.854	−0.878
5	16	16.5	70	0.254	−0.103	−0.088	−0.052
6	26	16.5	70	1.982	2.216	2.201	2.351
7	16	33.5	70	1.562	1.575	1.665	1.546
8	26	33.5	70	0.401	0.279	0.320	0.581
9	30	25.0	60	0.031	0.099	0.185	0.165
10	13	25.0	60	−1.095	−1.161	−1.152	−0.927
11	21	40.0	60	0.942	0.623	0.640	0.319
12	21	10.0	60	−0.523	−0.748	−0.809	−0.923
13	21	25.0	77	0.228	−0.310	−0.323	−0.614
14	21	25.0	33	−1.922	−1.817	−1.687	−1.494
15	21	25.0	60	−0.089	0.169	0.192	0.015
16	21	25.0	60	−0.092	−0.063	0.077	−0.058

Table 6

Values of the parameters obtained for central composite design for microwave-assisted extraction (MAE) experiments

Compound	$\beta_1$	$\beta_2$	$\beta_3$	$\beta_{11}$	$\beta_{22}$	$\beta_{33}$	$\beta_{12}$	$\beta_{13}$	$\beta_{23}$	$\beta_{123}$	$r^2$
CB-101	−0.295	− <sup>a</sup>	−0.056	−	0.0039	−	−	0.0089	−	−0.00013	0.81
CB-153	−	−0.138	−0.175	−	−	−	−	0.0082	0.0086	−0.00029	0.81
CB-138	−	−0.143	−0.172	−	−	−	−	0.0081	0.0086	−0.00026	0.80
CB-180	−	−0.136	−0.169	−	−	−	−	0.0081	0.0083	−0.00028	0.80

<sup>a</sup> Empty values mean that the parameter was eliminated from the model.

Optimisation experiments were performed using a soil polluted with PCBs at an unknown concentration. Concentration of PCBs whose retention times and mass spectra matched with those of the standard mixture were measured (CB-101, CB-153, CB-138 and CB-180) and optimisation of both MAE and Soxhlet extraction was performed for these four PCBs. For evaluation of the efficiency of both extraction methods developed, CRM 481 industrial soil was purchased from BCR (Brussels, Belgium).

### 2.5. Analysis of the samples

Extracts were analysed on a Hewlett-Packard 5890 Series II GC interfaced to a Hewlett-Packard 5989 MS Engine mass spectrometer MS/DOS Chemstation (Avondale, PA) and equipped with a Hewlett-Packard 6890 Series autosampler. The samples were introduced via a 30-m  $\times$  0.25-mm i.d.  $\times$  0.25- $\mu$ m film thickness TRB-1701 (Tracer, Sant Cugat del Valles, Spain) fused-silica capillary open-tubular column. The column temperature was held at 80°C for 1 min and then increased at 25°C  $\text{min}^{-1}$  up to 170°C, and subsequently programmed at 3°C  $\text{min}^{-1}$  up to 260°C, where it was finally held for 7 min. The carrier gas was helium (N-50) at a flow rate of 2.07  $\text{ml min}^{-1}$  (52.9  $\text{cm}^{-1}$ ) and a pressure at column head of 20 psi. The injection volume was 1–3  $\mu\text{l}$  and the injection temperature was 270°C. Quantitative data were acquired operating the MS detector in selected ion monitoring mode (SIM) and the  $m/z$  values monitored were: CB-8 (222, 224), CB-28 (256, 258), CB-20 (256, 258), CB-52 (292, 220), CB-35 (256, 258), CB-101 (324, 326), CB-118 (324, 326), CB-153 (360, 362), CB-138 (360, 362) and CB-180 (394, 396). The instrument was tuned daily with perfluorotributylamine (PFTBA). In order to achieve the best response from the GC/MS set-up, an optimisation study of the variables splitless time (min), electron energy (eV) and optimum overpotential (V) was followed using a central composite design.

### 2.6. Optimisation of electron impact mass spectrometric (EIMS) determination of PCBs

Optimisation of the determination of PCBs by

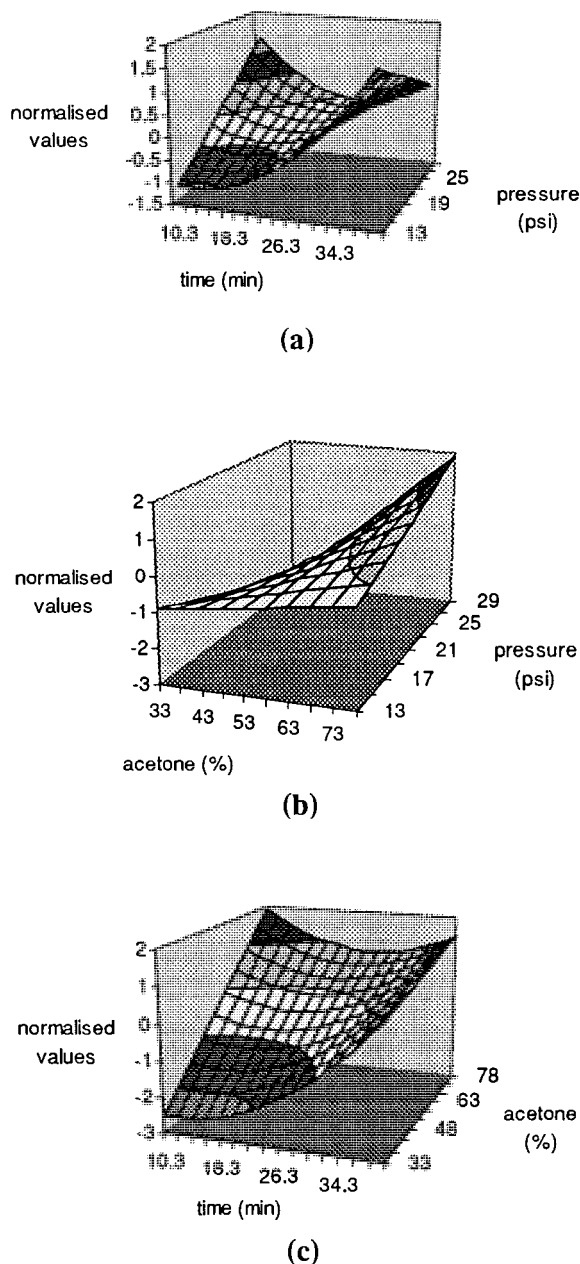


Fig. 2. Representation of the response surface for the central levels of percentage of acetone (%) (a), time (b) and pressure (c) for the central composite design for CB-101 for microwave-assisted extraction (MAE).

GC/EIMS was achieved by a central composite design approach. The variables studied were the energy of the electrons, splitless time and the

Table 7

Design matrix and normalised values in the complete factorial design for Soxhlet experiments

Run no.	Data matrix		Normalised values			
	Time (h)	Acetone (%)	CB-101	CB-153	CB-138	CB-180
1	8	25	-1.297	-1.420	-1.537	-1.484
2	24	25	-0.783	-0.897	-0.859	0.795
3	8	75	0.208	0.466	1.230	0.422
4	24	75	1.872	1.791	-0.299	1.924
5	16	50	0.279	0.353	1.105	0.349
6	16	50	0.473	-0.419	-0.119	-0.284
7	16	50	0.298	0.357	1.094	0.078

voltage gain applied over the optimum voltage value given by the tune of the mass spectrometer. A two-level factorial design plus star orthogonal composite design plus three central points was chosen. Table 1 gives the design matrix for those experiments and the responses obtained for each of the ten PCBs.

The data analysis of the results given in Table 1 was performed by the nonlinear regression analysis program (NLREG) [11]. Making use of this program, the response surface ( $Y$ ) was written as a second degree polynomial including all interactions. Eq. (1) shows the general polynomial function.

$$Y = \beta_0 + \sum_i \beta_i x_i + \sum_{ij} \beta_{ij} x_i x_j \quad (1)$$

$$U = \sum_i^n (Y_{\text{exp}} - Y_{\text{calc}})^2 \quad (2)$$

where  $Y$  is the response,  $x_i$  the variables considered for the optimisation of the extraction and  $\beta_i$  and  $\beta_{ij}$  the parameters to calculate. The estimation of the parameters ( $\beta_i$  and  $\beta_{ij}$ ) was achieved by the minimisation of the square sum of errors ( $U$ ) as given by Eq. (2). The analysis of the output was based on the evaluation of the  $\text{prob}(t)$  parameter associated to each  $\beta_i$  parameter, since  $\text{prob}(t)$  indicates the probability of  $\beta_i$  to be zero. Those parameters whose probability of being zero was greater than 10%, namely  $\text{prob}(t) > 0.1$ , were systematically eliminated.

Eq. (3) shows the most general function allowed for the central composite design:

$$Y = \beta_0 + \beta_1 x_1 + \beta_2 x_2 + \beta_3 x_3 + \beta_{12} x_1 x_2 + \beta_{13} x_1 x_3 + \beta_{23} x_2 x_3 + \beta_{11} x_1^2 + \beta_{22} x_2^2 + \beta_{33} x_3^2 + \beta_{123} x_1 x_2 x_3 \quad (3)$$

where  $x_1$  is the electron energy (eV),  $x_2$  the splitless time (min) and  $x_3$  the voltage gain. The results given by NLREG for CB-8, CB-52 and CB-180 are given in Table 2. The other PCBs had

Table 8

Values of the parameters obtained for complete factorial design for Soxhlet experiments

Compound	$\beta_1$	$\beta_2$	$\beta_{12}$	$r^2$
CB-101	-0.103	-0.017	0.0032	0.78
CB-153	-0.105	- <sup>a</sup>	0.0023	0.78
CB-138	-0.061	0.020	-	0.78
CB-180	-0.105	-	0.026	0.78

<sup>a</sup> Empty values mean that the parameter was eliminated from the model.

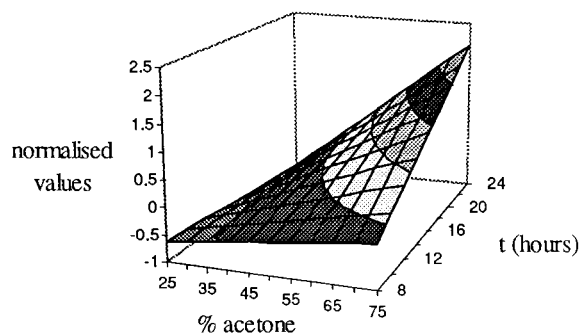


Fig. 3. Representation of the response surface for complete factorial design for CB-101 for Soxhlet extraction.

a similar behaviour. Fig. 1 shows the response surface obtained by the central composite design for EI.

To estimate the optimum GC/MS set-up conditions for the determination of PCBs the simplex [12] method implemented in the MultiSimplex [13] program was used. For this purpose, the parameters given in Table 2 were introduced in an EXCEL spreadsheet, where the responses for each of the PCBs were calculated under each of the experimental conditions suggested by MultiSimplex. On the other side, MultiSimplex suggested higher gain voltage values than the maximum value applied in the design matrix. The response is directly related to the gain voltage but no gain voltages higher than 400 V are recommended. On the other side, MultiSimplex suggested a value of 41–42 eV. Finally, the response was independent of the splitless time ( $\beta_2 = \beta_{22} = \beta_{123} = 0$ ) and therefore, the central value of the experimental design was chosen (2 min).

It could be concluded that for the analysis of PCBs by EI-MS the optimum conditions were: an electron energy of 41–42 eV, a splitless time of 2 min and a voltage gain of 400 V.

A 5-point standard calibration using standards at 37 and 418 ng ml<sup>-1</sup> and injecting different volumes (1–3  $\mu$ l) of the standards was performed daily to establish the GC/MS calibration curve. Each calibration standard and sample extract were injected in duplicate. After the injection of four sample extracts one of the calibration points and one blank sample were injected to verify that there were no memory peaks. Chromatographic peak areas were fitted by linear regression and the results are given in Table 3. For quantification, the average response factors obtained from the multilevel calibration were used.

### 3. Results and discussion

#### 3.1. Fractionated factorial design for MAE

The variables considered in the fractionated factorial design were pressure of extraction, percentage of microwave power, extraction time, volume of solvent and percentage (v/v) of acetone in

the acetone–hexane mixture. The aim of this design was to evaluate which of the variables were factors, that is, which of the variables had an influence on the extraction process and which ones did not. Due to the high number of experiments for a two-level factorial design (2<sup>5</sup>), two degrees of fractionality were introduced and the percentage of acetone and the volume of the solvent were defined as a combination of the other three variables (pressure, power and time) as shown in Eqs. (4) and (5).

$$\% \text{acetone} \equiv \text{Pressure} \times \text{Time} \times \text{Power} \quad (4)$$

$$\text{Volume} \equiv \text{Pressure} \times \text{Time} \quad (5)$$

Percentage of acetone and solvent volume were chosen for the fractionality since they were a priori the variables which least interacted with the other three (pressure, time and power). A two-level fractionated factorial design involving eight runs plus three central points was chosen. The concentration of those PCBs whose retention times and mass spectra matched with those of the calibration standards were followed (CB-101, CB-153, CB-138 and CB-180). As the true concentrations of the four PCBs were unknown, the data were normalised as shown in Eq. (6). The design matrix and the normalised results for the 11 runs are given in Table 4.

$$\text{Normalised value} = \frac{(x_i - \bar{x})}{s} \quad (6)$$

where  $x_i$  is the concentration value for one PCB and run number,  $\bar{x}$  is the mean value of all the concentration values obtained for one PCB in the eleven runs and  $s$  is the standard deviation of all the concentrations obtained for one PCB.

Eq. (7) shows the most general function allowed for the fractionated experimental design:

$$Y = \beta_1 x_1 + \beta_2 x_2 + \beta_3 x_3 + \beta_4 x_4 + \beta_5 x_5 + \beta_{13} x_1 x_3 + \beta_{23} x_2 x_3 \quad (7)$$

where  $x_1$  is the pressure in the extraction vessel,  $x_2$  is the extraction time,  $x_3$  is the percentage of microwave power,  $x_4$  is the % (v/v) of acetone and  $x_5$  is the solvent volume.  $\beta_0$  term was not included in Eq. (7) since the results had been previously normalised.  $\beta_{12}$  and  $\beta_{24}$  were not considered be-

Table 9

Concentrations ( $\mu\text{g g}^{-1}$ ) for 15 samples of each polychlorinated biphenyls (PCBs) extracted during 3 days by microwave-assisted extraction (MAE)

Sample no.	Day no. CB-101			Day no. CB-153			Day no. CB-138			Day no. CB-180		
	1	2	3	1	2	3	1	2	3	1	2	3
1	183	183	183	786	772	714	919	894	868	843	877	868
2	181	171	163	749	689	682	864	793	785	785	684	675
3	194	168	170	794	641	664	912	825	784	864	818	760
4	178	168	88	702	692	677	815	813	879	774	756	843
5	184	174	176	757	722	684	878	825	829	816	716	786

Table 10

Values for the residual standard deviations (microwave-assisted extraction, MAE)

Compound	R.S.D.% analysis	R.S.D.% within a day	R.S.D.% among days	Total R.S.D.%
CB-101	1.8	4.1	3.3	5.5
CB-153	1.2	3.4	5.6	6.6
CB-138	6.1	4.9	3.3	8.2
CB-180	5.1	8.2	3.0	9.8

cause they were equivalent to  $\beta_5$  and  $\beta_{13}$ , respectively. The reason for this equivalency lies on the confusion rules used to define  $x_4$  and  $x_5$  variables.

From the values obtained for the parameters for the fractionated factorial design it could only be concluded that power was the only variable which seemed not to have an influence in the extraction efficiency since  $\beta_3 = 0$  and  $\beta_{13}$  and  $\beta_{23}$  were of the same magnitude but opposite sign. The rest of the variables seemed to be factors for the extraction process of the four PCBs. Besides, the parameters were of the same sign and magnitude.

### 3.2. Central composite design for MAE

From the fractionated factorial design power could be fixed in the central value (57%). A second variable should be fixed to build a central composite design. It was first thought that percentage of acetone in the mixture acetone:*n*-hexane could be fixed at a high value of the percentage of acetone, since polar solvent mixtures are more efficient at the MAE [8,9] but when large volumes of solvent were used samples systematically dried. The reason for

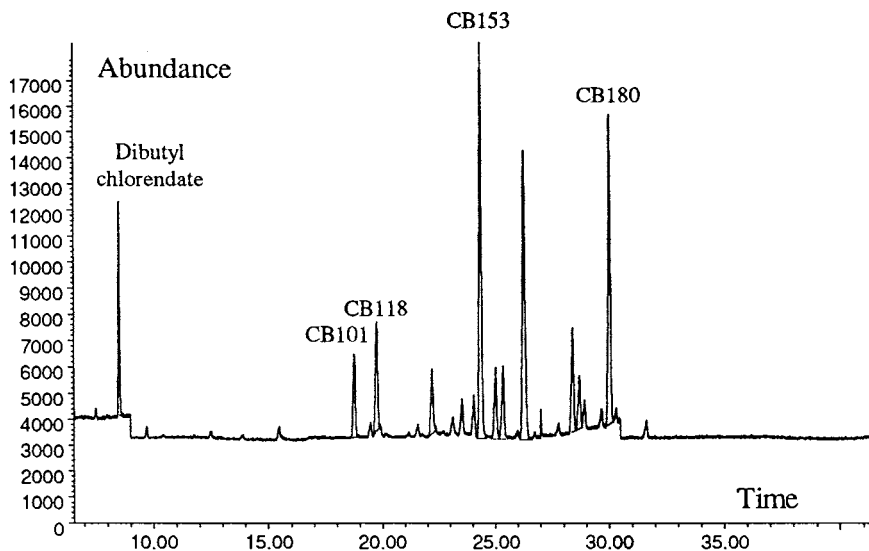
the fact might be the high ratio of total solvent volume versus solid sample when polar solvents are being used. In these cases, the microwave energy should be mostly absorbed by the supernatant rather than by the solid sample material [9]. Thus, volume of solvent was eventually fixed to a value of 15 ml. A central composite design was built using the other three variables: pressure inside the extraction vessel, extraction time and percentage of acetone (v/v) in the mixture acetone:*n*-hexane. A two-level factorial design plus star orthogonal composite design involving 14 runs plus two central points was chosen. Table 5 gives the design matrix for this experiment and the normalised concentrations obtained in each run.

The data in Table 5 were analysed by NLREG following the methodology mentioned above. Eq. (8) shows the most general function for central composite design:

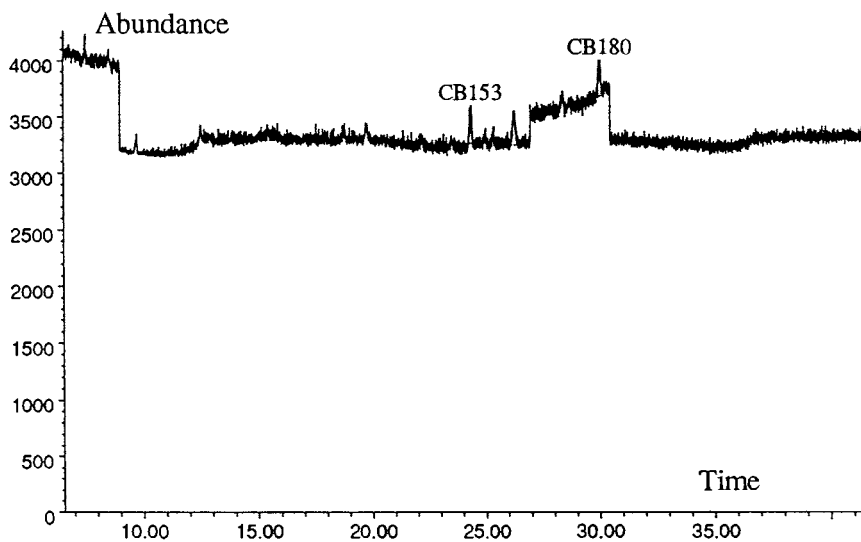
$$\begin{aligned}
 Y = & \beta_1 x_1 + \beta_2 x_2 + \beta_3 x_3 + \beta_{12} x_1 x_2 + \beta_{13} x_1 x_3 \\
 & + \beta_{23} x_2 x_3 + \beta_{11} x_1^2 + \beta_{22} x_2^2 + \beta_{33} x_3^2 \\
 & + \beta_{123} x_1 x_2 x_3
 \end{aligned} \quad (8)$$

where  $x_1$  is pressure inside the extraction vessel,  $x_2$  is the extraction time and  $x_3$  is the percentage of acetone (v/v) in the acetone:*n*-hexane mixture.  $\beta_0$  term was not included in Eq. (8) since the results had

been previously normalised. The results obtained by NLREG are given in Table 6. As for the fractionated factorial design, all parameters presented the same sign and magnitude for the four PCBs.



(a)



(b)

Fig. 4. Selected ion monitoring (SIM) chromatogram of microwave-assisted extraction (MAE) extract of the certified industrial soil CRM 481: (a) first extraction and (b) second extraction.



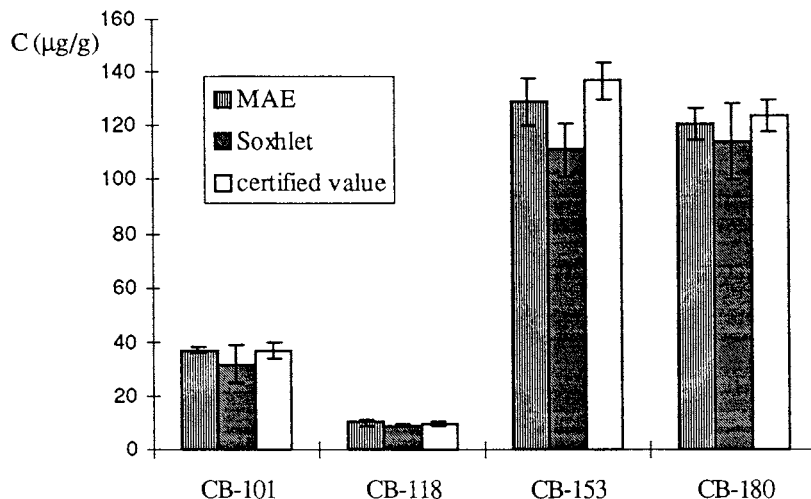


Fig. 5. Comparison of the results obtained for the extraction of the certified industrial soil CRM 481 by microwave-assisted extraction (MAE) and Soxhlet extraction with the certified values.

Three-dimensional representations keeping one of the variables at the central point value are presented in Fig. 2 for CB-101. It was observed that at constant time ( $t = 25$  min) better recoveries were obtained when both pressure and percentage of acetone in an acetone:*n*-hexane mixture increased (Fig. 2(b)). On the other hand, at pressure = 21 psi, Fig. 2(c), higher recoveries were obtained when both time and percentage of acetone in an acetone:*n*-hexane mixture increased. Finally, if percentage of acetone = 60% (Fig. 2(a)) higher recoveries were obtained for long extraction times and low pressures or high pressures and short extraction times. It could be concluded that the optimum conditions were a high pressure, long extraction time and a high percentage of acetone in an acetone:*n*-hexane (v/v) mixture. A similar behaviour was observed for the other three PCBs. The common optimum conditions were also estimated by the simplex method implemented in the MultiSimplex program. Optimum conditions obtained were a time of extraction of 40 min and a pressure inside the extraction vessel of 21 psi and for a percentage of acetone of 74%.

### 3.3. Complete factorial design for Soxhlet extraction

The variables considered in the complete facto-

rial design for Soxhlet extraction were the percentage of acetone in the mixture acetone–hexane and the extraction time. A two-level complete factorial design plus three central points involving seven runs was chosen. The design matrix and the results for the seven runs are given in Table 7.

Eq. (9) gives the most general function allowed for the complete factorial design carried out:

$$Y = \beta_0 + \beta_1 x_1 + \beta_2 x_2 + \beta_{12} x_1 x_2 \quad (9)$$

where  $x_1$  is extraction time and  $x_2$  is percentage (v/v) of acetone in the mixture acetone:*n*-hexane.

The results obtained by NLREG are given in Table 8. From the 3D plot for CB-101 shown in Fig. 3 it could be observed that long extraction times and high percentage of acetone in the acetone:*n*-hexane mixture gave the best recoveries. A higher content of polar solvent increases extraction potency [2]. A similar behaviour was observed for the other three PCBs.

### 3.4. Evaluation of the reproducibility for MAE

For evaluating the reproducibility of the measurements for MAE five aliquots of the sample were extracted each day and this procedure was repeated three times at the optimum conditions mentioned above (15 ml of a mixture acetone:hexane (74:26) (v/v) at 21 psi with a mi-

crowave power of 57% for 40 min). The results obtained during the 3 days are shown in Table 9.

The results were analysed by means of analysis of variance (ANOVA) of the set of experimental data in Table 9. It could be observed, for a degree of confidence of 95%, that there were no significant differences among samples extracted neither within a day nor among days for CB-101 and CB-138 ( $F_{CB101(\text{within a day})} = 0.76 < F_{\text{crit.}} = 3.84$ ,  $F_{CB101(\text{among days})} = 2.76 < F_{\text{crit.}} = 4.46$ ,  $F_{CB138(\text{within a day})} = 2.01 < F_{\text{crit.}} = 3.84$ ,  $F_{CB138(\text{among days})} = 2.93 < F_{\text{crit.}} = 4.46$ ) but there were significant differences for samples extracted within a day for CB-180 ( $F_{CB180(\text{within a day})} = 4.04 > F_{\text{crit.}} = 3.84$ ) and for samples extracted among days for CB-153 ( $F_{CB153(\text{among days})} = 7.46 > F_{\text{crit.}} = 4.46$ ).

As a consequence of these results it was decided to express the total variance of the measurements as the sum of the variance due to the analysis, the variance within days and the variance among days as indicated in Eq. (10):

$$s_{\text{tot}}^2 = s_{\text{a}}^2 + s_{\text{w.d}}^2 + s_{\text{a.d}}^2 \quad (10)$$

where  $s_{\text{tot}}^2$  is the total variance,  $s_{\text{a}}^2$  is the variance due to the analysis,  $s_{\text{w.d}}^2$  is the variance within days and  $s_{\text{a.d}}^2$  is the variance among days.

Table 10 gives the residual standard deviations for the analysis, for samples within a day, for samples among days and the total residual standard deviations. The percentage of relative standard deviation (R.S.D.%) values were good for the four PCBs.

### 3.5. Comparison of MAE and Soxhlet extraction

For the comparison of MAE and Soxhlet extraction five samples of the CRM 481 soil were extracted under the optimum conditions for MAE (15 ml of a mixture acetone:hexane (74:26) (v/v) at 21 psi with a microwave power of 57% and for 40 min) and three samples of the same soil were extracted under the best Soxhlet conditions (200 ml of a mixture acetone:hexane (75:25) (v/v) under reflux for 24 h). Samples extracted by MAE were reextracted under the same optimum conditions. SIM chromatograms of a sample of the CRM 481 soil extracted and reextracted under optimum condi-

tions for MAE are shown in Fig. 4. From the PCBs presented in the CRM 481 concentrations of CB-101, CB-118, CB-153 and CB-180 were worked out because these four PCBs were present in the calibration standards. The results obtained for MAE and Soxhlet extraction were compared with the certified values and it is shown in Fig. 5.

Results obtained by MAE are in good agreement with the certified values. As it can be seen in chromatogram (b) in Fig. 4 a second reextraction was not needed. Lower recoveries were obtained for Soxhlet extraction but the results are still comparable to those obtained by MAE.

### Acknowledgements

This research was supported by the Basque Government (project PIGV96/74). Olatz Zuloaga is grateful for the Scholarship granted to her by the Basque Government.

### References

- [1] N.C. Brady, R.R. Weil, Three Nature and Properties of Soils, 11th edition, Prentice-Hall, Engelwood Cliffs, NJ, 1996, p. 2.
- [2] F. Smedes, J. de Boer, Trends Anal. Chem. 16 (9) (1997) 503.
- [3] M.P. Llompart, R.A. Lorenzo, R. Cela, K. Li, J.M.R. Bèlanger, J.R.R. Paré, J. Chromatogr. A 774 (1997) 243.
- [4] S.P. Frost, J.R. Dean, K.P. Evans, K. Harradine, C. Cary, M.H.I. Camber, Analyst 122 (1997) 295.
- [5] V. Lopez-Avila, R. Young, W.F. Beckert, Environ. Sci. Technol. 29 (1995) 2709.
- [6] F.I. Onuska, K.A. Terry, J. High Resolut. Chromatogr. 18 (1995) 417.
- [7] V. Lopez-Avila, R. Young, W.F. Beckert, Anal. Chem. 66 (1994) 1097.
- [8] I.J. Barnabas, J.R. Dean, I.A. Fowles, S.P. Owen, Analyst 120 (1995) 1897.
- [9] M.P. Llompart, R.A. Lorenzo, R. Cela, J.R.J. Paré, Analyst 122 (1997) 133.
- [10] F.I. Onuska, K.A. Terry, Chromatographia 36 (1993) 191.
- [11] P.H. Sherod, NLREG—Nonlinear Regression Analysis Program, Nashville, 1995.
- [12] J.A. Nelder, R. Mead, Comput. J. 7 (1965) 308.
- [13] Bergström and Öberg, MultiSimplex (1.0 version), Gullberna Park, S-37154, Karlskrona, Sweden, 1997.

# Optimization of some instrumental factors in diffuse reflectance infrared Fourier transform spectroscopy

B. Azambre<sup>a,\*</sup>, O. Heintz<sup>a</sup>, M. Schneider<sup>b</sup>, A. Krzton<sup>c</sup>, J.V. Weber<sup>a</sup>

<sup>a</sup> *Laboratoire de Chimie Industrielle, Université de Metz, Rue Victor Demange, 57500 Saint-Avold, France*

<sup>b</sup> *Laboratoire de Chimie Organique, Université de Metz, Ile du Saulcy, 57045 Metz Cedex, France*

<sup>c</sup> *Institut de Carbochimie de l'Académie des Sciences, Sowinskiego 5, PL-44100 Gliwice, Poland*

Received 7 September 1998; received in revised form 29 December 1998; accepted 6 January 1999

## Abstract

The effects of some instrumental factors on infrared spectroscopy analysis were investigated in the case of diffuse reflectance infrared Fourier transform (DRIFT) mode. It is usually said that quantitative analysis is possible only if both particle size distribution and sample density are perfectly controlled. However, even if these conditions are checked, instrumental factors are of great interest for the goodness of a curve fitting procedure, which is often necessary in solid sample studies. A factorial design achieved on anthron made it possible to obtain major trends concerning the required values for one instrumental parameter (resolution) and two mathematical treatments (zero filling and Savitsky–Golay (S–G) smoothing). Resolution was found to have the greatest effect on measured responses. A value of  $2\text{ cm}^{-1}$  according to the corresponding aperture is sufficient to approach the real width of bands for powdered samples. The use of a zero filling factor (ZFF) improves the apparent resolution by data interpolation. The best values found for instrumental parameters were applied to an anthron–anthracen mixture. The optimization of spectral features made it possible to obtain semi-quantitative results quite easily, in good agreement with the data corresponding to each pure compound. © 1999 Elsevier Science B.V. All rights reserved.

*Keywords:* DRIFT; Instrumental parameters; Experimental design

## 1. Introduction

Fourier transform infrared spectroscopy (FTIR) has been used in transmission for many years to the qualitative and quantitative analysis of solid, liquid and gaseous samples. However, in

the specific domain of opaque materials or surface analysis, diffuse reflectance infrared Fourier transform spectroscopy (DRIFT) is better adapted. The information depth is assumed to be of the order of midinfrared wavelengths ( $\mu\text{m}$ ) for nonabsorbent samples and the scattering of light does not affect so much the baseline [1,2]. The preparation of the samples for DRIFT studies is fast: the sample is diluted in a nonabsorbent powdered material, like potassium bromide, which moreover minimizes the specular component [3–5].

\* Corresponding author. Tel.: +33-3-87-93-91-00; fax: +33-3-87-93-91-01.

E-mail address: bazambre@iut.univ-metz.fr (B. Azambre)

The Kubelka–Munk [6,7] theory predicts a linear relationship between the intensity  $f(R_\infty)$  of bands in a DR spectrum and the concentration  $C$  of absorbent materials in a nonabsorbing matrix ( $f(R_\infty) = [(1 - R_\infty)^2/2R_\infty] = (2.303aC)/s$ , where  $a$  is the absorptivity coefficient and  $s$  the scattering coefficient. Since  $s$  is a function of both particle size distribution and packing density [2,8], these parameters shall remain as constant as possible, if quantitative data are needed. In practice, it seems to be difficult [9,10] to avoid the variations of physical properties and this explains why quantitative analysis by DRIFT spectroscopy is often hazardous. However, even if these parameters are controlled, the quality of both the acquisition and the treatment of DR spectra has a great importance on quantitative results. Some of these acquisition parameters, like resolution, optical throughput, acquisition time and signal-to-noise ratio (SNR) [11,12] or apodization functions [13], have been largely studied. Nevertheless, these previous works only gave a theoretical significance to instrumental factors but no appropriate numerical values for DRIFT spectroscopy [14]. Moreover, the characterization by curve-fitting of each band in a mixture will be more accurate if these parameters are optimized, because of the induced effect on measured responses. This article deals with the contribution of some instrumental factors and mathematical treatments to the improvement of infrared spectra processing. Results were obtained to a great extent with the help of a factorial design achieved on anthron (polyaromatic hydrocarbon). This compound was chosen because of the presence of bands in the whole range of the midinfrared. Moreover, in order to avoid the great influence of physical properties, all acquisitions were made on the same sample during the factorial design. In the last section, improvement induced in curve-fitting initial estimates with the example of an anthron–anthracen mixture is shown.

## 2. Experimental

The spectrophotometer (BioRad FTS 185) and the optical accessory were already presented elsewhere [15].

The potassium bromide (spectronorm–Aldrich) was ground by hand and stored in a dessicator (for 24 h) heated at 110°C before use. The particle size distribution was checked to be of the same order that wavelenghts in the midinfrared (about 10  $\mu\text{m}$ ). Anthron (Aldrich, purity 96%) and anthracen (Aldrich, purity 98%) were not purified (the particle size distribution is centered around 10  $\mu\text{m}$  like KBr). The delay time for purging the compartment before each spectra recording was 240 s.

For each experimental part (the factorial design and the anthron–anthracen mixture), a single-beam spectrum of KBr was used as reference. The anthron sample was concentrated at 2.5 wt.% in KBr for the experimental design. Concerning the anthron–anthracen mixture, each compound was diluted at 2 wt.% in KBr. All samples were introduced in the sample cup without packing and were leveled with a glass blade.

Preliminary experiments and bibliography results have prevailed us to fix the following parameters for the factorial design: gain radius, undersampling ratio (UDR), apodization function and interferogram symmetry. In the case of solid materials analysis, the gain radius [12,16] has no effect on the intensities and the shape of bands. Concerning UDR [12,16], apodization [12,13,16,17] and interferogram symmetry [12,17], the optimal conditions of spectra processing are already known. It has been chosen to work with UDR = 40, triangular apodization and double-sided symmetry.

On the other hand, resolution ( $R$ ) [12] and zero filling factor (ZFF) [12,16] are factors for which the required values are rarely specified in bibliography, and no distinction is made according to the nature of infrared analysis. It has been chosen to test the instrumental parameter  $R$  and also two mathematical treatments, the zero filling and the Savitzky–Golay (S–G) smoothing [18–20], which is the more currently used for the removal of noise or undesirable features in IR spectra.

The number of scans was set arbitrary to 100. Since this instrumental parameter depends on both the concentration and the absorptivity of the sample, a standard value can not be attributed for all experiments.

Main effects of resolution  $R$ , ZFF and S–G smoothing and also interaction effects between these factors were studied in a factorial design of size 2 at two levels. Values and levels of the parameters are given in Table 1. (It should be noticed that the aperture is related with the resolution [2].)

Four experiments were found to be sufficient in order to evaluate the effects of three factors. A contrast [21] was carried out between the main effect of the third factor ( $E_3$ ) and the  $1 \times 2$  interaction ( $E_{12}$ ) (like between  $E_1$  and  $E_{23}$  and between  $E_2$  and  $E_{13}$ ). The three factors interaction was assumed to be too weak to be taken into account. The order of the experiments was

tossed. In order to compute the standard deviation  $\sigma_{n-1}$  corresponding to experimental errors, four central points were joined to the four tests on parameters (two blocks of four runs). All spectra of pure KBr were recorded with their respective parameters without removing the sample cup from the compartment, in order to eliminate the influence of the particle size and the density of the sample, and to focus the study on the influence of instrumental parameters. This procedure was repeated for the anthron sample. The responses criteria were the height, the full width at half-height (FWHH) and the valley between two adjacent bands. The measured noise was always too low to be considered.

Table 1  
Design matrix<sup>a</sup>

Experiment	Resolution ( $E_1$ )	S–G smoothing factor ( $E_2$ )	Zero filling factor ( $E_3$ )
1	+	–	–
2	–	–	+
3	–	+	–
4	+	+	+
Level –	$1 \text{ cm}^{-1}$	No smoothing	1
Level +	$4 \text{ cm}^{-1}$	3rd degree polynomial (7 points)	4
Central point	$2 \text{ cm}^{-1}$	No smoothing	2

<sup>a</sup> The effect of each factor is estimated between the measured responses at low level (–) and the measured responses at high level (+).

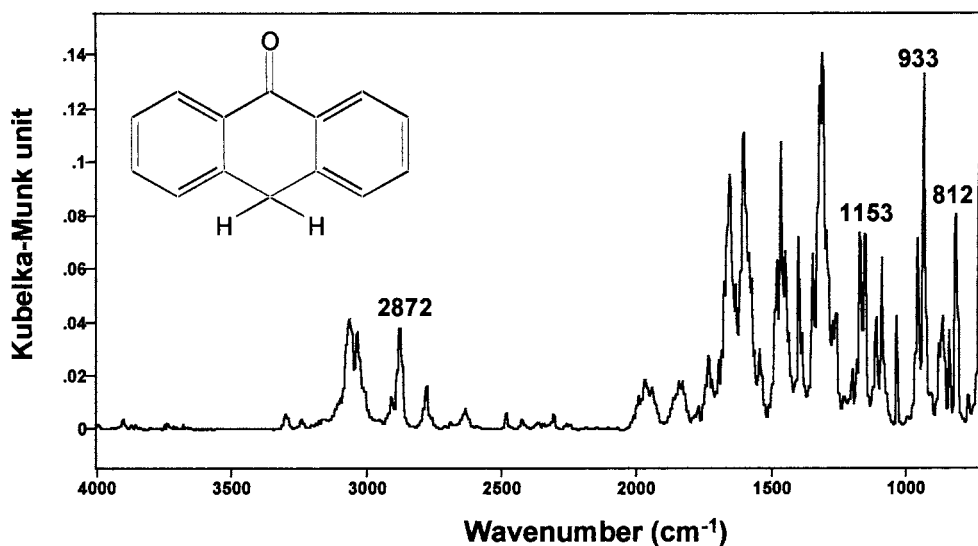


Fig. 1. Spectrum of anthron concentrated at 2.5 wt.% in KBr (the position of bands used for the factorial design is indicated in bold).

Table 2  
Results of the experimental design achieved on anthron<sup>a</sup>

Bands position (cm <sup>-1</sup> )		2872	1153	933	812
Height (K–M units) × 10 <sup>-4</sup>	Central point	364 ± 2.3	641 ± 1.5	1277 ± 1.5	750 ± 0.95
	E <sub>1</sub> +E <sub>23</sub>	-6.3 ± 1.5	-23.6 ± 0.8	-77.7 ± 0.8	-27.5 ± 0.5
	E <sub>2</sub> +E <sub>13</sub>	n.s.	n.s.	n.s.	2 ± 0.5
	E <sub>3</sub> +E <sub>12</sub>	-1.25 ± 1.5	n.s.	5.25 ± 0.8	5.5 ± 0.5
Width (cm <sup>-1</sup> )	Central point	21.05 ± 0.03		9.46 ± 0.04	12.35 ± 0.07
	E <sub>1</sub> +E <sub>23</sub>	0.48 ± 0.013		0.98 ± 0.02	0.37 ± 0.035
	E <sub>2</sub> +E <sub>13</sub>	-0.04 ± 0.013		0.03 ± 0.02	n.s. ± 0.035
	E <sub>3</sub> +E <sub>12</sub>	-0.11 ± 0.013		-0.02 ± 0.02	-0.065 ± 0.035
Valley (K–M units) × 10 <sup>-4</sup>	Central point	70.4 ± 0.25		1099 ± 1.3	
	E <sub>1</sub> +E <sub>23</sub>	-19.02 ± 0.13		-95.3 ± 0.65	
	E <sub>2</sub> +E <sub>13</sub>	0.92 ± 0.13		n.s.	
	E <sub>3</sub> +E <sub>12</sub>	0.67 ± 0.13		4.4 ± 0.65	

<sup>a</sup> The n.s. abbreviation is used when the effects of the factors are not significant (when it is inferior to the computed error  $\Delta E$ ).

### 3. Results and discussion

The spectrum of anthron is given in Fig. 1. The presence of some neighbored bands close to the 2872 cm<sup>-1</sup> (corresponding to the C–H aliphatic symmetric stretching vibration) and the 1153 cm<sup>-1</sup> (C–H aromatic asymmetric bending in plane) bands allows the measurement of the valley between the bands. The 933 cm<sup>-1</sup> isolated band (C–H aromatic symmetric bending in plane) and the 812 cm<sup>-1</sup> band (C–H aromatic bending out of plane) are well adapted to the evaluation of the effects on the widths at half-height.

Results of the factorial design are presented in Table 2.

#### 3.1. Effect of the resolution factor

The major effect on both heights, bandwidths and valleys was found for the resolution factor (according to the corresponding aperture). The improvement in resolution (when  $R$  decreases) increases the number of data points near the absorption maxima of the band and a gain in photometric accuracy occurs. Consequently, the measurement of intensities is also improved. The 933 cm<sup>-1</sup> isolated band is the most representative example to show the influence of resolution on bandwidths. When decreasing  $R$  from 4 to 1 cm<sup>-1</sup>, the FWHH of the band decreases by

about 10%. Working at upper resolutions (2 and 1 cm<sup>-1</sup>) is necessary to make deeper the separation between two adjacent bands, especially when they are close together. When changing the resolution value from 4 to 1 cm<sup>-1</sup>, an improvement of 27% can be observed for the height of the 2872 cm<sup>-1</sup> valley. In the case of solid samples where bandwidths are naturally broad, it would not be useful to increase indefinitely the resolution factor (according to the trading rules). A change in resolution from 2 to 1 cm<sup>-1</sup> does not affect the valley.

#### 3.2. Effect of the S–G smoothing factor

The parameters used for the S–G smoothing were a third degree polynomial applied to a window of seven points. This treatment is for almost responses not significant. The most important effect (1.31%) is observed for the 2872 cm<sup>-1</sup> valley, when the effect of the resolution factor is particularly strong (27%). A possible explanation, is that the effect of the S–G factor is measured simultaneously with the interaction effect between the first and third factor. In this particular case, it is thought that E<sub>13</sub> should be superior to E<sub>2</sub>. In conclusion, like the number of scans, the S–G treatment should be optimized in each particular case, in a specific wavenumber window. Its effect will obviously depend on the instrumental parameters and on the band width. Since smooth-

ing affects narrow bands first (a loss of resolution occurs), standard parameters shall not be estimated.

### 3.3. Effect of the ZFF

Its main effect is weak on band intensities. In opposition with the  $R$  factor that is related to the real resolution, zero filling improves the apparent resolution (by data interpolation). Moreover, this treatment has a more marked effect on intensity, when the band appears to be flat topped (when  $ZFF = 1$ ). Because of the increase of interpolated data points that ZFF induces by extending the

interferogram with zeros, the measured responses on both bandwidths and valleys shall be more consistent with their real values. Zero filling can also be obtained after the spectrum processing is over and a new interferogram is computed in the Fourier domain.

In conclusion, the best values found for the studied experimental parameters are (Fig. 2):

$$R = 2 \text{ cm}^{-1}$$

$$ZFF = 4$$

The S–G parameters must be adjusted in function of both the number and width of particular bands in a wavenumbers range.

### 3.4. Application of a least squares curve-fitting program to an anthron–anthracen blend

No attempt in this section was made to provide a mathematical method in order to analyse IR spectra of mixtures. This work was already carried out by other authors [22]. The aim was to improve the quality of DR spectra (according to the optimized results of the factorial design) before the application of a curve-fitting program.

The optimized parameters ( $R = 2 \text{ cm}^{-1}$ ,  $ZFF = 4$ ) were applied to the analysis of an anthron–anthracen mixture. All absorbance spectra were converted into K–M units after a local baseline correction. The curve-fitted region ranged from 1130 to 1200  $\text{cm}^{-1}$  and corresponds to the fingerprint of the compound (Fig. 2a–c). For more clarity, only data of two bands for each pure compound (co-added with the corresponding data values for the same bands in the mixture) are presented in Table 3. Concerning band positions, results appear to be in good agreement between the pure compounds and the mixture. For bandwidths, the obtained data seem also to be very close between pure anthron and the mixture. However, small deviations (of the order of 5%) can be observed for the  $A_1$  and  $A_2$  anthracen bands because they are overlapped to a great extent by some anthron bands. It is difficult to obtain accurate quantitative results, when the separation between bands is of the same order that the instrument line shape (ILS) [22] function.

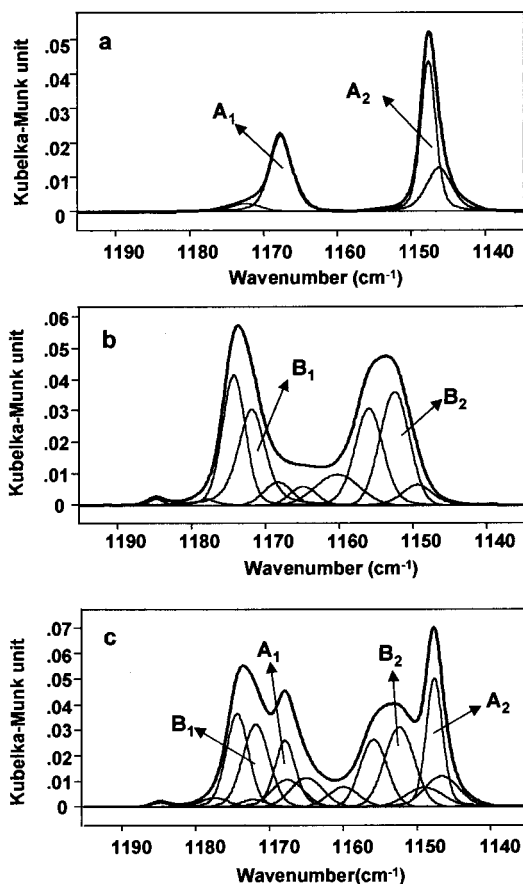


Fig. 2. Curve-fitting in the 1135–1195  $\text{cm}^{-1}$  domain. (a) Spectrum of anthracen concentrated at 2 wt.% in KBr. (b) Spectrum of anthron concentrated at 2 wt.% in KBr. (c) Spectrum of the anthron–anthracen experimental blend. Each compound is concentrated at 2 wt.% in KBr.

Table 3  
Results of the curve-fitting achieved on an anthron–anthracen blend<sup>a</sup>

Band	Compound	Position (cm <sup>-1</sup> )	Height (K–M units)	FWHH (cm <sup>-1</sup> )	Area (a.u.)	% Lorentzian <sup>b</sup>
A <sub>1</sub>	Anthracen	1167.6	0.022	3.54	0.096	37
	Blend	1167.9	0.026	3.3	0.103	30
A <sub>2</sub>	Anthracen	1147.6	0.044	2.41	0.129	35
	Blend	1147.6	0.05	2.59	0.153	25
B <sub>1</sub>	Anthron	1171.8	0.031	4.3	0.17	49
	Blend	1171.8	0.032	4.2	0.15	11
B <sub>2</sub>	Anthron	1152.5	0.036	4.7	0.182	0
	Blend	1152.4	0.031	4.73	0.156	0

<sup>a</sup> Comparison with the results obtained for pure compounds concentrated at 2 wt.% in KBr.

<sup>b</sup> Percentage of the Lorentzian fraction in respect with the Gaussian fraction.

Heights and areas can not be used in a direct way for quantitative analysis. Nevertheless, area measurements can be improved, if the sum of all the bands corresponding to an identical functional group is taken into account.

#### 4. Conclusions

Acquisition parameters values were optimized for DRIFT spectroscopy through a factorial design achieved on anthron. A resolution of 2 cm<sup>-1</sup> (according to an aperture of 2 cm<sup>-1</sup>) is adequate for accurate solid sample analysis, when bandwidths are broad. Zero filling seems very useful in order to improve the interpolation of the spectrum between two resolution points and to precise the initial estimates for the curve-fitting program. Concerning the number of scans and the smoothing factor, values should be optimized in each particular case. Moreover, even if the optimization of these parameters is important, it is essential to control perfectly the particle size and the density of the sample especially if the aim is quantitative analysis. The method described in this paper can be extended to a large number of infrared techniques and is no way restricted to DRIFT spectroscopy since required values of instrumental factors depend on intrinsic bandwidths and separation. For instance, in the case of IR analyses in gaseous phase, a further improvement of the resolution factor will bring a more accurate exploitation of

the spectra. These results will be applied to the semi-quantitative study of supported catalysts and functional groups on the surface of coal adsorbents.

#### References

- [1] P. Iwanski, P.R. Griffiths, *Energy Fuels* 4 (1990) 589–593.
- [2] T. Suzuki, K. Inoue, Y. Watanabe, *Energy Fuel* 2 (1988) 673–679.
- [3] M.P. Fuller, P.R. Griffiths, *Anal. Chem.* 50 (13) (1978) 1906–1910.
- [4] J.M. Chalmers, M.W. Mackenzie, *Appl. Spectr.* 39 (4) (1985) 634–644.
- [5] W. Yang, H.H. Montsch, F. Baudois, *Appl. Spectr.* 40 (7) (1986) 974–978.
- [6] P. Kubelka, F. Munk, *Z. Tech. Phys.* 12 (1931) 593.
- [7] P. Kubelka, *J. Opt. Soc. Am.* 38 (1948) 448.
- [8] I.M. Hamadeh, S.A. Yeboah, K.A. Tramball, P.R. Griffiths, *Appl. Spectr.* 38 (4) (1984) 486–491.
- [9] T. Burger, H.J. Ploss, J. Kahn, S. Ebel, J. Fricke, *Appl. Spectr.* 51 (9) (1997) 1323–1329.
- [10] A.A. Koukoulas, B.D. Jordan, *J. Pulp Paper Sci.* 23 (5) (1997) 224–232.
- [11] P.R. Griffiths, *Anal. Chem.* 44 (11) (1972) 1909–1913.
- [12] P.R. Griffiths, J.A. De Haseth, *Fourier Transform Infrared Spectrometry*, Wiley, New York, 1986.
- [13] J.K. Kauppinen, D.G. Moffat, D.G. Cameron, H.H. Mantsch, *Appl. Opt.* 20 (1981) 1866.
- [14] N.R. Smyrl, E.L. Fuller, G.L. Powell, *Appl. Spectr.* 37 (1) (1983) 38–44.
- [15] A. Krzton, O. Heintz, J. Petryniak, A. Koch, J. Machnikowski, T. Zimny, J.V. Weber, *Analisis* 24 (1996) 250–253.
- [16] P. Coleman, In: P.B. Coleman (Ed.), *Practical Sampling for Infrared Analysis*, CRC Press, London, 1993, ch. 8.



- [17] A. Reklat, W. Bessau, A. Kohl, *Mikrochim. Acta Suppl.* 14 (1997) 307–309.
- [18] H.H. Madden, *Anal. Chem.* 50 (9) (1978) 1383–1386.
- [19] A. Savitsky, M.J.E. Golay, *Anal. Chem.* 36 (8) (1964) 1627–1639.
- [20] P.D. Willson, S.R. Polo, *J. Opt. Soc. Am.* 71 (5) (1981) 599–603.
- [21] A. Goupy, *La méthode des plans d'expériences*, Dunod Ed, 1988.
- [22] J.A. Pierce, R.S. Jackson, K.W. Van Every, P.R. Griffiths, *Anal. Chem.* 62 (1990) 477–484.

# Validation of a high performance liquid chromatography analysis for the determination of noradrenaline and adrenaline in human urine with an on-line sample purification

Åse Marie Hansen \*, Jesper Kristiansen, Jeanet Løgsted Nielsen, Kirsten Byrialsen, Jytte Molin Christensen

*National Institute of Occupational Health, Department of Chemistry and Biochemistry, 105 Lersø Park allé, DK-2100 Copenhagen, Denmark*

Received 7 September 1998; received in revised form 2 December 1998; accepted 7 January 1999

---

## Abstract

A high performance liquid chromatography (HPLC) method with fluorescence detection including an on-line purification was established for determination of catecholamines in human urine. The method was evaluated using samples of pooled urine spiked with catecholamines and validated for measurements of catecholamines in urine of healthy individuals in a field study. The laboratory method evaluation study showed that the recovery of the method was 0.82 (confidence interval (CI): 0.79–0.86) and 0.92 (CI: 0.89–0.95) for noradrenaline and adrenaline, respectively. Thus, correction factors of  $0.82^{-1}$  and  $0.92^{-1}$  were applied to correct the measurement results for this systematic effect. Furthermore, an uncertainty budget was generated for the analytical method using the BIPM-approach recommended by the International Organization for Standardization. The relative uncertainty of the method was estimated to be 10–12%, which was consistent with the observed relative variability found in the method evaluation. The method was evaluated in accordance with EURACHEM Guidance Document No 1 concerning accreditation for chemical laboratories with respect to accuracy and precision. The field study showed that the standard deviation of the method was sufficiently low to distinguish between persons working with two different processes of garbage collection, i.e. collection using four wheeled containers versus collection using bins. © 1999 Elsevier Science B.V. All rights reserved.

*Keywords:* Catecholamines; HPLC; On-line sample purification; Human urine

---

## 1. Introduction

Endocrine factors have increased the understanding of the pathogenesis and adaptation phase of chronic diseases caused by the working

\* Corresponding author. Tel.: +45-39-165255; fax: +45-39-165201.

*E-mail address:* aamh@ami.dk (Å.M. Hansen)

environment. An intricate network of hormones and hormone-like activities is implicated in the psychophysiological response. Until now, neuroendocrine parameters, and in particular urinary catecholamine excretion, have been widely used to estimate the biological effects of stressors in field research [1,2]. An essential neuroendocrine response is the release of adrenaline from the chromaffin cells resulting in an increased production of noradrenaline and adrenaline. Some of the consequences of increased levels of urinary catecholamines are changes in heart rate and in blood pressure [3]. Urinary excretion of adrenaline and noradrenaline has been studied in relation to highly mechanized work processes in the Swedish Sawmill Industry. Excretion of catecholamines in urine was increased for the individuals with increased prevalence of psychosocial problems as insomnia, stomach and intestinal problems, and headache (150–250% of baseline level) compared to a control group [4]. Self-reported feelings of time pressure and pressure by demands were found to correlate positively with concentration of catecholamines in urine of male assembly line workers in a company manufacturing cars and trucks [5].

In order to use catecholamines to assess psychophysiological effects related to the working environment, the quality of an analytical method must fulfil several requirements. First, the measurement procedure must be described clearly and in sufficient detail in order to allow other laboratories to repeat the measurements [6]. Second, the method should be evaluated in order to document precision, accuracy, linearity, robustness [6], and other relevant performance parameters. Third, statistical and analytical control of measurement results must be documented by internal quality control (e.g. use of control charts [7–9]), analysis of certified reference materials, and external quality control (e.g. participation in interlaboratory comparisons) [10]. Fourth, measurement results should be reported together with an uncertainty, that allows the user to evaluate the reliability of the results [6].

Several high performance liquid chromatography (HPLC) methods with on-line purification have been described for use in analysis of cate-

cholamines in biological samples using either fluorescence detection [11,12], on-line chemical derivatization followed by fluorescence detection, [13] or electrochemical detection [14–16]. Validation of these methods included evaluation of the repeatability, reproducibility, and accuracy. The accuracy was estimated as the recovery of catecholamines added to buffer solutions. In general, the recovery of adrenaline was close to 100% in these studies and the recovery of noradrenaline was significantly lower, around 90%. The reason for the low recovery of noradrenaline was not discussed in the above mentioned studies [11–16]. Neither was it clear from the results, if a correction factor was applied to the results obtained for noradrenaline in urine samples as a consequence of the reduced recovery.

The purpose of the present study was:

- To develop a HPLC method for determination of adrenaline and noradrenaline in urine including an on-line purification and post column derivatization followed by fluorescence detection of the adrenochrome derivatives.
- To evaluate selected analytical performance parameters, i.e. reproducibility, linearity, accuracy, and limit of detection (LOD).
- To document the accuracy of the method by participation in external quality assessment scheme.
- To establish an uncertainty budget for the analytical method. The aim of the budget is to account for the contribution from all known uncertainty components.
- To demonstrate the applicability of the method with respect to reflection of work-related psychophysiological response in a preliminary field study.

## 2. Materials and methods

### 2.1. Study population of the preliminary field study

The study population consisted of six waste collectors in a rural Danish town. Information about the different work procedures was collected for each worker [17]. The waste collectors were

organized in two teams of three persons. One team collected waste in areas using four wheeled containers and the other team collected waste in areas with bins. The waste collectors were asked to deliver urine samples during a period of 4 working days. All workers were examined in August–September 1993.

## 2.2. Collection of urine samples

Urine samples were collected as spot samples during 24 h in bottles added 1.0 g citric acid per 50 ml of urine and analyzed separately. The samples were stored at  $-20^{\circ}\text{C}$  and analyzed within 2 months. Urinary creatinine [18] was used to standardize the results.

## 2.3. Apparatus

A HPLC system consisting of one isocratic and one gradient intelligent Merck Hitachi HPLC-pump series L 6200A, a Hitachi reaction pump model 655A-13 (Merck, Darmstadt, FRG) situated before a variable fluorescence detector model LS-4 (Perkin Elmer, Norwalk, CT), a WISP 710B autosampler for automatic injection and Millennium chromatography software (Waters Associates, Milford, US) was used for quantification. The analytical column was a LiChrospher<sup>®</sup> 100 column  $250 \times 4$  mm I.D. packed with RP C-18 (5  $\mu\text{m}$  particles). The guard column ( $4 \times 4$  mm) situated before the chromatographic column was packed with LiChrosorb RP-18, 5  $\mu\text{m}$  as well. The samples were purified automatically before injection on the analytical column by passing a catecholamine precolumn, packed with nitrophenylboronic acid on Co-polymer, 40–60  $\mu\text{m}$  (CA-precursor). All columns were from Merck, Darmstadt, FRG. A column thermostat L-5025 (Merck, Darmstadt, FRG) was used to keep the temperature at  $40^{\circ}\text{C}$  for the analytical column and the coils from the reaction pump (see Fig. 1).

## 2.4. Chemicals

Methanol, ammonia solution (25%), L(+)-ascorbic acid, di-ammoniumhydrogenphosphate,

sodium dihydrogenphosphate monohydrate, disodium hydrogenphosphate anhydrous, potassium hexacyanoferrate (III), phosphoric acid (85%) and sodium hydroxide pellets were analytical grade, hydrochloric acid (30%) was suprapur grade, and sodium azide was synthesis grade (Merck, Darmstadt, FRG). Sources of other chemicals were ethylenediaminetetraacetic acid–disodium-salt dihydrate (EDTA) (BDH Laboratory Supplies, UK), 1-octanesulfonic acid, sodium salt (98%) (Sigma, St. Louis, MO). Stock solutions were prepared in 1 mM hydrochloric acid using adrenaline hydrochloride (epinephrine hydrochloride) (purity  $>99\%$ ) and noradrenaline hydrochloride (norepinephrine hydrochloride) (purity  $>99\%$ ) (Aldrich, Milwaukee, US). Prior to dissolution of adrenaline 0.1 ml acetic acid was added. Lyphochek<sup>®</sup> quantitative urine control normal (1) and Lyphochek<sup>®</sup> quantitative urine control abnormal (2) (Bio-Rad Laboratories, Munich, FRG) were used as internal quality control samples. All solutions were prepared using ultra-pure water obtained by a Milli-Q water purification system (Millipore Waters, Taastrup, Denmark).

## 2.5. Mobile phase reagents

A precolumn buffer (0.2 M di-ammonium hydrogen phosphate, 10 mM EDTA, 1 mM sodium azide and adjusted to pH 8.7 with 25% ammonia solution) was used to apply the catecholamines to the precolumn. Milli-Q water was used to wash the precolumn before the next injection. The analytical eluent (0.1 M sodium dihydrogen phosphate, 5 mmol sodium-1-octane sulfonate, and 1 mM sodium azide, adjusted to pH 3 with 20% phosphoric acid and methanol (8:1)) eluted catecholamines from the precolumn and separated them on the analytical column. For the derivatization three solutions (A, B, and C) were used. Solution A contained 0.1 M sodium dihydrogen phosphate, 0.2 M disodiumhydrogen phosphate and 2 mM potassium hexacyanoferrate adjusted to pH 7. Solution B contained 1.5 mM ascorbic acid and 2.5 mM EDTA to stabilize the solution, and solution C contained 5 M sodium hydroxide (Fig. 1).

## 2.6. Preparation of standard solutions

Seven different calibration solutions were prepared in the range 0–480 nmol l<sup>-1</sup> for noradrenaline and 0–270 nmol l<sup>-1</sup> for adrenaline by serial dilution of stock solutions with the analytical eluent to give standards.

## 2.7. Preparation of method evaluation samples.

Samples for the method evaluation were prepared in the range 0–350 nmol l<sup>-1</sup> for noradrenaline and 0–180 nmol l<sup>-1</sup> for adrenaline by spiking pooled urine samples from white-collar workers with the stock solutions of noradrenaline and adrenaline in 1 mM hydrochloric acid. The background level of the pooled urine sample was 9 and 96 nmol l<sup>-1</sup> for adrenaline and noradrenaline, respectively. A recovery study was per-

formed using the same stock solutions added to eluent A.

## 2.8. Analytical procedure

Fig. 1 shows a flow diagram of the method. The HPLC procedure was performed according to Boos et al. [13,19] with improvements of the purification and derivatization steps. The eluents and solution B were degassed with helium. Degassing solution B makes it stable for 24 h. Filtered urine samples (0.45 µm) and standard solutions (100 µl) were applied directly to the precolumn with a flow rate of 1.0 ml min<sup>-1</sup> in 10 min by using the precolumn buffer. Noradrenaline and adrenaline were eluted from the precolumn with the analytical eluent and applied to the analytical column with a flow rate of 1.0 ml min<sup>-1</sup> in 3 min by changing flow direction auto-

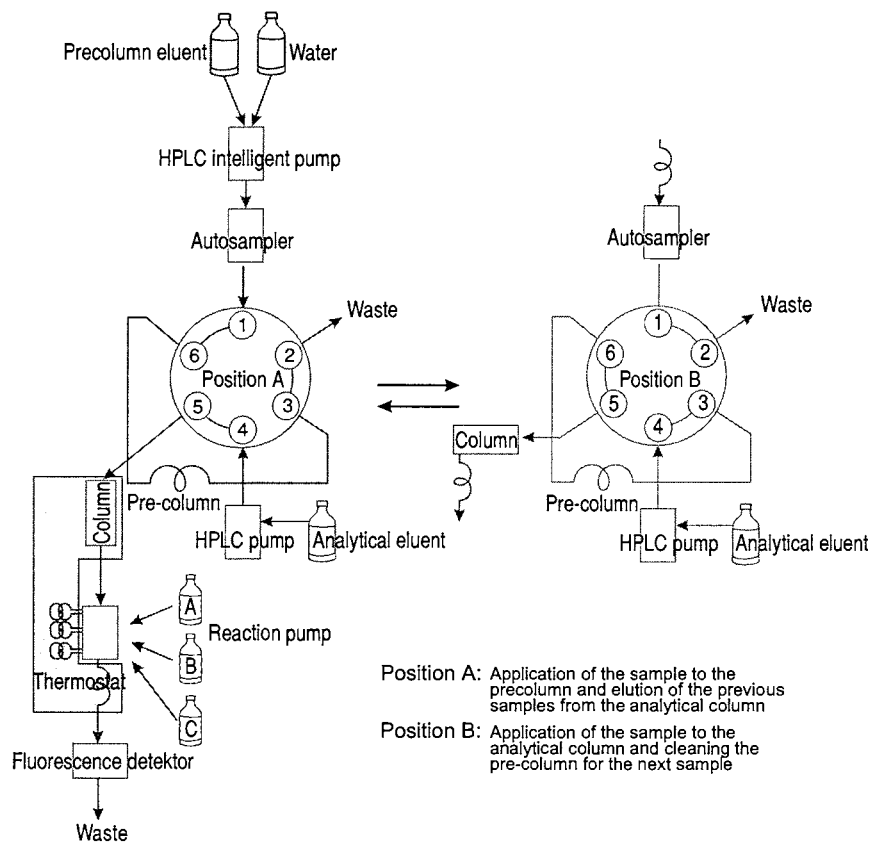


Fig. 1. Flow diagram of the method.

matically. Before fluorescence detection a post-column derivatization of noradrenaline and adrenaline to the corresponding trihydroxyindole derivatives was performed by adding solution A, B, and C with a flow rate of  $0.35 \text{ ml min}^{-1}$ . A Teflon coil of approximately 6 m was placed after addition of solution A–C to ensure that trihydroxyindole derivatives were generated. Maximum response of noradrenaline or adrenaline was found by combination of different flow rates of solution A, B, and C. During elution of catecholamines from the analytical column, the pre-column was washed for the next injection with 5.0 ml of water and primed with 6.9 ml of precolumn buffer.

Before each series of analyses, seven different calibration solutions of noradrenaline and adrenaline were injected to obtain a standard curve. Quality control samples were analyzed for every tenth sample. The calibration plots were found to be linear in the ranges of 0–480 and 0–270  $\text{nmol l}^{-1}$  for noradrenaline and adrenaline, respectively.

### 2.9. Uncertainty budget

An uncertainty budget for the analytical method was prepared using the BIPM-approach recommended by the International Organization for Standardization (ISO) et al. [20]. In this approach, type A uncertainty components are evaluated by statistical means, i.e. from replicate results, while type B uncertainty components are evaluated by non-statistical means, for example from information provided by a manual, a certificate or from literature [20]. After evaluating the standard uncertainty of all type A and B components, the standard uncertainty of the measurement result was calculated by combining the standard uncertainties of the components using the spreadsheet technique [21]. The model of the measurement procedure was a functional relationship between a measurement result and components of the measurement process. The model represents the relation between the ‘true’ concentration and the measured concentration with components of the measurement process as parameters [22]. For the measurement procedure

described above, the measured concentration ( $Y$ ) can be written as a simple function of the ‘true’ concentration ( $\mu$ ), the volume ( $V$ ) injected, the sensitivity of the method ( $\gamma$ , expressed as peak area per nmol catecholamine) and the slope of the calibration curve ( $b$ ):

$$Y = \frac{\lambda\mu V}{b} = \frac{A'}{b}$$

where  $A' = \gamma\mu V$  is the peak area.

This simple relationship does not, however, describe the influence of certain other components of the method. The influence of these components is incorporated in the expression as ‘correction factors’ and ‘correction terms’. For example, the stability of samples and reagents during analysis affects the ‘true concentration’ of the injected sample. This effect is incorporated by including a correction factor for the loss. In the same way, the peak area should be corrected for errors in establishing the baseline. With correction factors and terms included, the measurement model is expressed as

$$Y = f_3 f_4 \frac{A - \delta_1(A) - \delta_2(A)}{b}$$

where

$$A = f_1 f_2 \lambda \mu V f_1 f_2 A'$$

and

$$b = f_5 f_6 f_7 f_8 b_{\text{mean}}$$

In these expressions, correction factors and correction terms compensate for the effect of various essential method components as follows:  $f_1$ , catecholamine loss in samples during storage;  $f_2$ , catecholamine loss and reagent degradation during analysis;  $f_3$ , matrix effects on analytical performance;  $f_4$ , recovery as established in this study;  $f_5$ , purity of the compound (catecholamine) used to prepare the standards;  $f_6$ , preparation of standards;  $f_7$ , matrix effects on the calibration curve; and  $f_8$ , statistical estimation of the calibration curve. The correction terms  $\delta_1(A)$  and  $\delta_2(A)$  are correction terms for errors in establishing the baseline for peak integration and for the contribution from noise to the peak area, respectively. Each parameter was assigned a value and a stan-

standard uncertainty (corresponding to a standard deviation).

The parameters  $\gamma$  (sensitivity),  $\mu$  ('true' concentration) and  $b_{\text{mean}}$  (mean of calibration slopes) are parameters without uncertainty as the uncertainty of these parameters have already been accounted for by the correction terms.

### 2.10. Method evaluation

Detailed information on the statistical models for the employed method evaluation design has been described previously [23,24]. The method evaluation function (MEF) was estimated using a least square regression analysis of the measured concentration versus the true concentration of the analyte in the MEF-samples in the linear range of the components in the method. Significant deviations from the ideal slope ( $\beta = 1.00$ ) and intercept ( $\alpha = 0.00$ ) are expressions of the systematic effects. The standard deviation (S.D.<sub>y</sub>) of the distribution of the obtained results around the estimated MEF is an expression of the analytical variance of the method.

### 2.11. Evaluation of external quality control

The method performance was also evaluated by participation in the external quality assessment scheme UK National External Quality Assessment Schemes (UK NEQAS) for urinary catecholamines and metabolites. The specimens distributed in the scheme were acidified liquid urine. The target values used for evaluation of laboratory performance were calculated as method laboratory trimmed means of results obtained from HPLC analyses of the participating laboratories as outlined by UK NEQAS. The variance of the target values was estimated to be 10% divided by the square root of the number of participating laboratories (7.75 for  $N = 60$ ). Outliers were excluded prior to the calculation of the trimmed means. The evaluation of the laboratories was performed using the Variance Index Scoring System described by Bullock and Wilde [25]. In this study, the long-term laboratory performance was evaluated by comparing the designated values of the samples with the observed values.

The evaluation was performed by estimating the intercept ( $\alpha$ ) and the slope ( $\beta$ ) using the functional model  $E(Y_i) = \beta E(X_i) + \alpha$ , and calculating approximate standard deviations of the estimates [26]. The mathematical model was described as

$$\begin{aligned} X_i &= E(X_i) + \varepsilon_{X_i}; & Y_i \\ &= E(Y_i) + \varepsilon_{Y_i}; & \varepsilon_{X_i} \in N(0, \delta_1^2); & \varepsilon_{Y_i} \in N(0, \delta_2^2) \end{aligned}$$

where  $\varepsilon_{X_i}$  and  $\varepsilon_{Y_i}$  are constants. In order to estimate the functional model the ratio between the variance of the designated value ( $\delta_2^2$ ) and variance of our measurements ( $\delta_1^2$ ) =  $\delta_2^2/\delta_1^2$ , must be known [26].

## 3. Results

A representative chromatogram of a urine sample is presented in Fig. 2. The retention times for noradrenaline and adrenaline are 10 and 12 min, respectively. Within 8 min the baseline is stable and the system is ready for a new injection.

MEFs were estimated for noradrenaline and adrenaline in urine under reproducibility conditions. Since the S.D.<sub>y</sub> was a function of  $\mu$  (true value), it was necessary to perform a weighted regression analysis using the reciprocals of the concentrations as weights. The linearity of the MEFs was tested using a pure error lack of fit test, which was not significant at the 5% level. Thus demonstrating linearity (Fig. 3). The slopes of the MEFs were 0.82 (confidence interval (CI): 0.79–0.86) and 0.92 (CI: 0.89–0.95) for noradrenaline and adrenaline, respectively. The intercepts of the MEFs were not significantly different from zero. Therefore, the method was corrected for proportional errors of 0.82 and 0.92, respectively. The intercepts and slopes of the corrected MEFs are presented in Table 1. The LOD determined as 3 S.D. of 20 measurements of urine samples at low concentration level was 3.1 and 5.2 nmol l<sup>-1</sup> for adrenaline and noradrenaline, respectively. The estimated limits of detection based on the square root of relative mean squared error (R.M.S.E.<sup>1/2</sup>) [23,24] of the method evaluation in urine were 7.3 and 13.1 nmol l<sup>-1</sup>. The observed variability of the method (S.D.<sub>y</sub>) was given at the

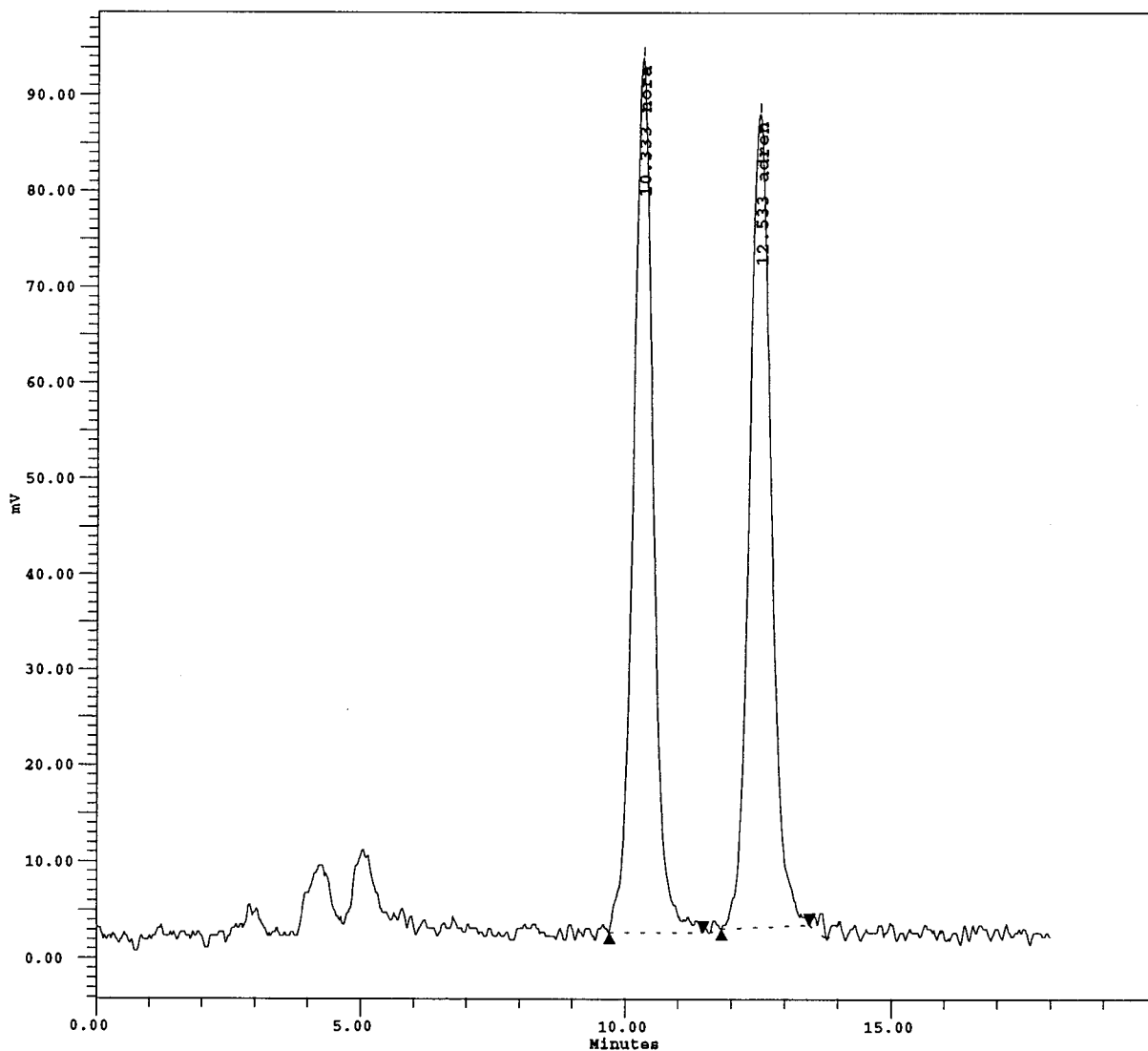


Fig. 2. A chromatogram of a human urine sample with levels of noradrenaline and adrenaline of approximately 301 and 156 nmol  $l^{-1}$ . On-line analysis of noradrenaline and adrenaline in human urine (1). Injection volume 100  $\mu$ l, eluent 0.1 M sodium dihydrogen phosphate, 5 mM octane-1-sulfonic acid, 1 mM sodium azide adjusted to pH 3.0 with phosphoric acid (20%) and methanol (11%), fluorescence detection  $e_x/e_m$  410 nm/520 nm, flow 1.0 ml  $min^{-1}$ , run time 30 min, data collection during 18 min.

lowest level of spiked samples approximately 44 nmol  $l^{-1}$  for noradrenaline and 22 nmol  $l^{-1}$  for adrenaline (including the level of the pooled urine levels were 140 and 31 nmol  $l^{-1}$ , respectively). The relative observed 'between run' variability was calculated to be 10.4% for noradrenaline and 10.1% for adrenaline. The recovery for adrenaline estimated from measurements of spiked samples

without the urine matrix (analytical buffer) was not significantly different from 100% (CI: 0.89–1.04%), and recovery for noradrenaline was estimated to be 91% (CI: 0.84–0.96).

The results of evaluation of uncertainty components are shown in Table 2. Details of the evaluation of each component are given below. The long-term stability was verified by following the



catecholamine content as a function of time of samples stored at  $-20^{\circ}\text{C}$ . Although no trends in the results were detected for the first 2 months, the variability of the results indicated a relative uncertainty of  $\pm 6\%$ , taken as the maximum deviation from 100% recovery (i.e.  $f_1 = 1$ ). This uncertainty was considered to be limits in a rectangular distribution. Hence, the standard uncertainty of long-term stability ( $u_{f_1}$ ) was  $0.06/\sqrt{3} = 0.017$ .

During automated analysis samples may stay in the sample tray for up to 24 h before injection. Neither the catecholamines nor the reagents (ascorbic acid in particular) are perfectly stable at room temperature, although stabilizing agents have been added. The time effect was evaluated by investigating pairs of control results (two levels) from ten analytical runs. Each pair consisted of control results from the start and end of the

Table 1

Method evaluation key parameters for adrenaline and noradrenaline in urine

	Adrenaline	Noradrenaline
Intercept ( $\alpha$ ) (nmol l <sup>-1</sup> )	-1.27	3.26
S.D. ( $\alpha$ )	0.82	3.15
Slope ( $\beta$ )	1.00	1.00
S.D. ( $\beta$ )	0.01	0.02
Pure test <sup>a</sup>	0.78 <sup>1</sup>	2.28 <sup>2</sup>
<i>N</i> -Score	0.97	0.99
S.D. <sub>y</sub> <sup>b</sup> (nmol l <sup>-1</sup> )	2.21	5.73
LOD <sup>c</sup> (nmol l <sup>-1</sup> )	7.30	13.1
LOD <sup>d</sup> (nmol l <sup>-1</sup> )	3.1	5.2

<sup>a</sup> 5% Table values: <sup>1</sup> 2.71, and <sup>2</sup> 3.295.

<sup>b</sup> Estimated S.D. on the method evaluation function.

<sup>c</sup> Limit of detection (LOD) is defined as the concentration resulting in  $\text{RMSE}^{1/2} = 33\%$ .

<sup>d</sup> LOD by using the definition of IUPAC, i.e. 20 measurements performed on a sample at a low concentration (22 nmol l<sup>-1</sup> for adrenaline and 44 nmol l<sup>-1</sup> for noradrenaline) under repeatability conditions.

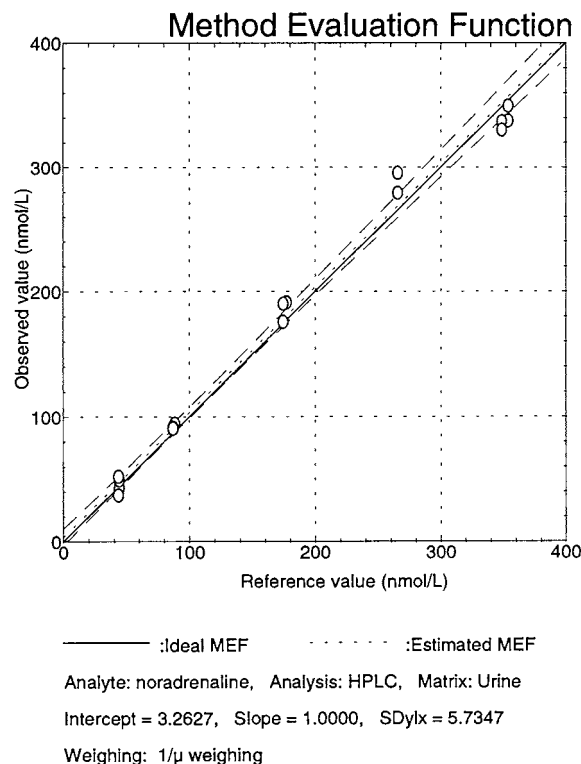


Fig. 3. Method evaluation function (MEF)-plot of noradrenaline in urine. The measured concentrations  $E(Y|\mu)$  of the 20 spiked urine samples plotted against the corresponding true concentration ( $\mu$ ).

run. From these results were estimated a standard uncertainty ( $u_{f_2}$ ) of 0.011 for the correction factor for the lack of short-term stability.

The injection volume was  $V = 100 \mu\text{l}$  with a standard uncertainty of  $u_v = 0.6 \mu\text{l}$ . The standard uncertainty was estimated from weightings.

The software calculates the peak area: a baseline is estimated by the software and the peak area calculated by integration. The software's choice of baseline can be changed manually. Occasionally the baseline chosen by the software is not satisfactory, which indicates that some uncertainty is involved in establishing the baseline. This uncertainty was evaluated by varying the baseline manually to give maximum and minimum peak areas that are acceptable by an experienced analyst. The standard uncertainty from this type B evaluation was found to be approximately linearly related to the peak area,  $u(\delta(A)) = 12885 \mu\text{VSL nmol}^{-1} + 0.005A$ , where  $A$  is the peak area).

The matrix may influence absorption and elution from the precolumn and the chemical reaction rate. The effect of matrix was evaluated from calibration functions based on standards prepared from different urine pools (and in eluent). The relative standard deviation of the slopes of the calibration functions were 7.3% ( $n = 5$ ). This was

taken as the standard uncertainty of the matrix influence ( $u_{f_3}, u_{f_7}$ ).

The uncertainty component from calibration (slope of the calibration curve) is composed of several uncertainty components: (1) the purity of the catecholamines, which were used to prepare the standards; (2) errors from the analytical balance and volumetric equipment used in preparing the standards; (3) the influence of the matrix on the measurement; (4) statistical estimation of the calibration function from the results; (5) non-linearity in the calibration function. The largest contribution to the uncertainty of calibration was the effect from the matrix (see above), accounting for approximately 90% of the variance of the calibration slope. The uncertainty contributions from the purity of the catecholamines ( $u_{f_3}$ ) were based on information in the Aldrich catalogue. The influence of the preparation of the standards on the uncertainty was estimated from the weighing data of volumetric equipment used ( $u_{f_5}$ ). The pooled standard deviations of the estimated slope of six calibration curves were taken as the uncertainty contribution from statistical estimation of the slope ( $u_{f_8}$ ). The calibration curve of each run is tested for linearity, and no deviations from linearity were observed. Hence, the uncertainty contribution from non-linearity was set to zero.

Finally, the parameters  $b_{\text{mean}}$ ,  $\lambda$  and  $\mu$  were estimated as follows:  $b_{\text{mean}}$  was estimated by taking the average of 22 calibration slopes,  $\gamma$  was estimated as  $b_{\text{mean}}/V$ , and  $\mu$  as the measured concentration (after correction of the result).

The results of the uncertainty estimation are shown in Fig. 4(a). The relative uncertainty is approximately constant (12.2–10.5% for noradrenaline, 11.3–10.5% for adrenaline) in the concentration range from the lowest to the highest standard. As expected, it increases rapidly when the concentration approaches the detection limit (Fig. 4(a)). The reason for the increase is seen from Fig. 4(b), where the relative contribution of the three most significant uncertainty components is shown. Only data for adrenaline are shown, but noradrenaline data reflect a similar trend. At concentrations higher than the lowest standard, only uncertainty components associated with matrix effects and with calibration are significant, each accounting for approximately 40–45% of the total variance. At concentrations between the lowest standard and the detection limit, the contribution to the variance from peak area determination increases dramatically. The influence of all other uncertainty components was insignificant.

Table 2

Method components, their values, their estimated standard uncertainties and type of uncertainty evaluation

PRIVATE Component	Value	Standard uncertainty	Type
Average calibration slope, $b_{\text{mean}}$ ( $\mu\text{VSL nmol}^{-1}$ )	$2 \times 10^{4a}$	0	–
Sensitivity, $\gamma$ ( $\mu\text{VS nmol}^{-1}$ )	$2 \times 10^{8a}$	0	–
Injection volume, $V$ ( $\mu\text{l}$ )	100	0.6	A
Correction factor long-term stability, $f_1$	1	0.017	B
Correction factor short-term stability, $f_2$	1	0.011	B
Correction factor for matrix effect, $f_3, f_7$	1	0.073	A
Correction factor for recovery, $f_4$	1.087 <sup>b</sup>	0.015	A
Correction factor for purity of catecholamine calibrator, $f_5$	1.01	0.006	B
Correction factor for preparation of standards, $f_6$	1	0.012	B
Correction factor for statistical evaluation of calibration slope, $f_8$	1	0.008 <sup>c</sup>	A
Baseline estimation correction, $\delta_1(A)$ ( $\mu\text{VSL nmol}^{-1}$ )	0	Variable ( $1.44 \times 10^4$ ) <sup>d</sup>	B
Peak integration correction, $\delta_2(A)$ ( $\mu\text{VSL nmol}^{-1}$ )	0	$0.34 \times 10^4$	B

<sup>a</sup> Adrenaline. Noradrenaline values:  $b_{\text{mean}} = 1.0 \times 10^4 \mu\text{VS nmol}^{-1}$ ,  $\gamma = 1.0 \times 10^8 \mu\text{VSL nmol}^{-1}$ ,  $f_{\text{recov}} = 0.82$ .

<sup>b</sup> Adrenaline. Noradrenaline values:  $f_4 = 1.22$ .

<sup>c</sup> Adrenaline. Noradrenaline value: 0.006.

<sup>d</sup> The uncertainty depends on the peak area (i.e. the concentration). The cited value is estimated at the lowest standard of adrenaline ( $19 \text{ nmol l}^{-1}$ ).

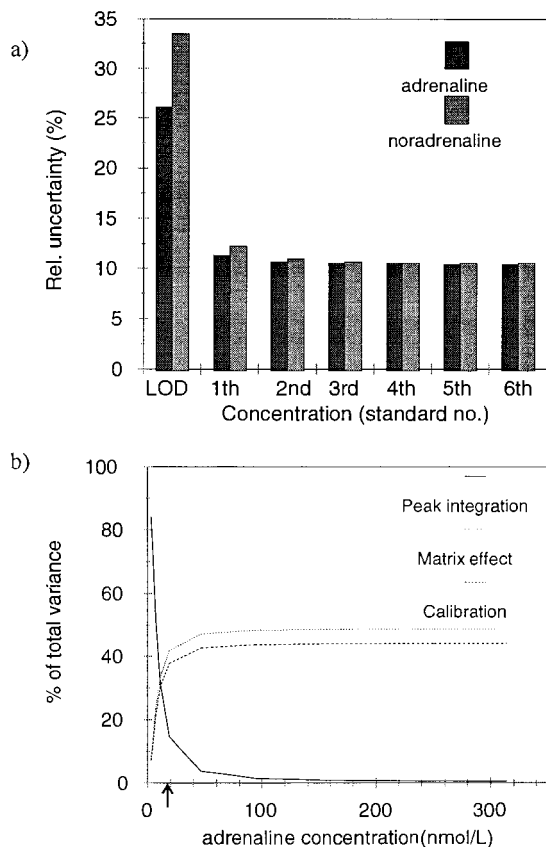


Fig. 4. Estimated relative uncertainty (a) and relative contribution to total uncertainty variance of adrenaline measurement results from selected uncertainty components (b). (a) Estimated relative uncertainty at the concentrations of standards 1–6 and at the detection limit. Limit of detection (LOD) = 3.1 nmol l<sup>-1</sup> (adrenaline) and 5.2 nmol l<sup>-1</sup> (noradrenaline). (b) The relative contribution from peak integration, matrix effects, and calibration to the total uncertainty (variance). The arrow indicates the concentration of the lowest standard.

The laboratory performance in the quality assessment scheme (UK NEQAS) in 1995–1997 with respect to urinary noradrenaline is presented graphically in Fig. 5 as plot of reported results versus designated values. The slope was estimated, by using the functional model, to be 1.27 (CI: 1.24–1.30) and the intercept to be zero (CI: -0.05–0.11).

Results from validation of the method used in a field study of the two teams of waste collectors are presented in Table 3. One team collected waste in areas using four wheel containers and

one team collected waste in areas with bins. The waste collectors delivered urine samples in a period of 4 working days in August–September 1993. The average age for the three waste collectors using four wheel containers was 31 years (21–50) and the mean urinary creatinine content was 20 mmol l<sup>-1</sup> (9.0–21.6). The average age for waste collectors collecting bins was 34 years (32–36) and the mean urinary creatinine content was 15.5 mmol l<sup>-1</sup> (8.0–33.3). A non-parametric test (Mann–Whitney) could not reveal any differences between the two teams at the 5% level with respect to age and creatinine content of urine. Mean levels of adrenaline and noradrenaline levels standardized with creatinine content were classified into groups of working process and time of collection of the urine sample, i.e. morning samples are samples before 06:00 h, working period from 06:00 to 14:00 h and night samples are after 19:00 h. A significant difference between morning levels of urinary noradrenaline and adrenaline of the two working processes was shown. No significant difference could be demonstrated between work and night levels of urinary noradrenaline and adrenaline. Excretion of urinary adrenaline and noradrenaline from morning level to work and night level were significantly higher for workers

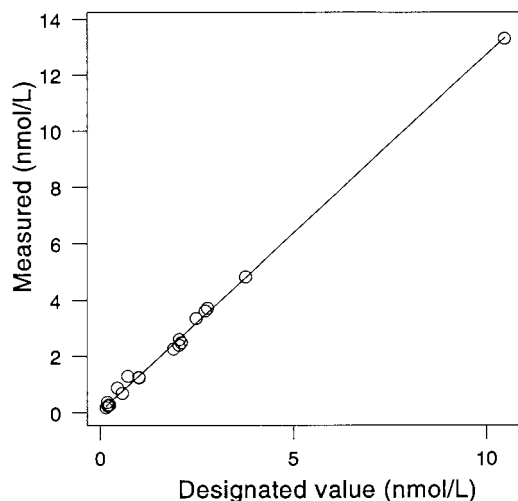


Fig. 5. Method performance in external quality control. Plot of results obtained from the present method of urinary noradrenaline and designated values from UK National External Quality Assessment Schemes (UK NEQAS).

Table 3  
Levels of adrenaline and noradrenaline in urine (nmol mol<sup>-1</sup> creatinine)

PRIVATE	Collecting four wheeled containers		Collecting bins	
	Adrenaline (nmol mol <sup>-1</sup> creatinine)	Noradrenaline (nmol mol <sup>-1</sup> creatinine)	Adrenaline (nmol mol <sup>-1</sup> creatinine)	Noradrenaline (nmol mol <sup>-1</sup> creatinine)
<i>Morning level</i>				
Mean	0.82	8.26	1.99	12.48
Range	0.77–0.88	7.10–10.39	1.00–3.20	7.75–21.20
<i>Work level</i>				
Mean	6.51	33.08	5.60	24.56
Range	2.79–10.03	29.17–36.57	5.00–6.09	15.71–32.47
<i>Night level</i>				
Mean	3.88	18.29	3.26	14.46
Range	0.65–8.85	11.46–27.30	2.33–5.10	13.95–15.33

using of four wheeled containers versus using bins ( $P = 0.02$ ).

#### 4. Discussion

Measurements of hormones or other metabolic biomarkers are well known in relation to diseases, i.e. following a disease in progress. In relation to diseases, several hormones show large variations. Biomonitoring of hormones contribute to an objective measurement, which may be useful for the assessment of occupational long-term health effects. However, small changes could be expected when measuring such hormones or other endocrine biomarkers. This implies that the quality of the analytical method, e.g. traceability of measurements and validation of the analytical method must be documented.

EURACHEM guidance Document No 1 [6] states that “the validation of standard methods should not be taken for granted—the laboratory should satisfy itself that the degree of validation of particular method is adequate for its purpose”. The validation includes analytical sensitivity and specificity demonstrated in our study using a separation of the components by HPLC and detection of specific derivatives of noradrenaline and adrenaline.

The method evaluation carried out on spiked urine samples indicated that the method was lin-

ear in the range up to 480 and 270 nmol l<sup>-1</sup> for noradrenaline and adrenaline, respectively. The distribution of the results could be approximated to a normal distribution, thus it was assumed that the method was in the state of statistical control [7]. The recovery was, however, significantly lower than 100% (82 and 92% for noradrenaline and adrenaline, respectively). In comparison, the recovery from spiked buffer samples was 91 (noradrenaline) and 100% (adrenaline). The difference in recovery reflects the vulnerability of the method to matrix effects. A method calibrated with standards prepared in aqueous buffer solutions will be particularly sensitive to this effect, and matrix effects will in general increase the uncertainty of the measurement results on unknown samples.

The estimated S.D., at the lowest concentration of  $\mu$  was 2.23 (10.1%) and 4.59 nmol l<sup>-1</sup> (10.4%) for adrenaline and noradrenaline, respectively, (Table 3) demonstrating, that the method had a good reproducibility even at low concentrations. A good accordance was observed between the estimated uncertainty and the observed variability, indicating that the method is in a state of statistical control [27]. The dominant uncertainty components were matrix variations, estimation of the calibration functions, and peak area determination. The matrix of urine is highly variable, and this may influence absorption and elution from the precolumn as well as the on-line trihydroxyindole derivatization. It is possible that the deriva-

tization is sensitive to the output of the pre-column, and in this way amplifies the effects of absorption and elution from the column. Similar effects may have caused the relatively high variability of the calibration curve, although the reasons for the matrix effects were not studied in detail. The uncertainty of peak area determination reflects the presence of noise in the measured signal. It consists of two contributions: (1) from establishing the baseline; and (2) from integration of the signal that is overlapped with random noise. The uncertainty of peak area determinations is approximately constant, and the relative uncertainty of peak area determination therefore increases as the concentration decreases (and, thus as the peak area decreases).

The uncertainty budget indicates how to improve the performance of the method. For example, the detection limit can be improved by increasing the signal-to-noise ratio (SNR) or by increasing the number of replicates. This will, however, have almost no effect on the uncertainty at concentrations above the lowest standard, because matrix effects are the major contributors to variability in this concentration range. In order to reduce the uncertainty at these levels, the variability caused by absorption to/elution from the pre-column and by the derivatization reaction must be reduced.

At present, no certified reference materials are available for urinary adrenaline and noradrenaline. Therefore, comparability of measurement results between different laboratories can only be obtained by means of interlaboratory intercomparisons. The performance evaluation in the external quality control showed a positive deviation from the designated values of 14 and 27% for adrenaline and noradrenaline, respectively. This deviation could be due to the fact that the reported results were corrected using the correction factors derived from the method evaluation. The deviation in the external quality control is relatively close to the correction factors derived from the method evaluation (adrenaline 8% and noradrenaline 18%).

A possible explanation for the deviation might be that the recovery of previous developed HPLC methods was determined using different buffer

solutions and not spiked urine solutions, or that measurement results obtained from these methods are not corrected for recovery. The true value of the samples in the external quality control scheme are calculated from the trimmed mean of the results from participating laboratories using HPLC as the analytical method. This might apply an error to the true result. Thus, the need for certified urine reference materials is obvious as the designation of the certified concentration values are based on several different analytical principles traceable to standard units (SI).

It is essential to be consistent with respect to the method evaluation, and therefore to continue using the correction factors. However, the method performance has to be followed carefully in order to explain poor performance. Besides, changes in the method have to imply a revision of the basis of the current method evaluation.

The evaluation of the method indicated that it has a reasonable low standard deviation and a good reproducibility. Furthermore, the short run time of the developed method (30 min—effectively 20 min due to the overlap of the purification step and separation step) makes it potentially applicable for large-scale surveillance of occupational exposure.

The analytical method was applied to measurements of catecholamines in urine from garbage collectors ( $N=6$ ) during 4 working days. The preliminary field study showed a significant increase in levels of both urinary noradrenaline and adrenaline when using four wheel containers versus collection using bins ( $P=0.02$ ). The preliminary results may indicate that increased levels of urinary catecholamines are useful to evaluate physiological responses to different occupational exposures, in this context different work procedure.

### Acknowledgements

The present study is part of the 1993–98 research program Waste Collection and Recycling, which is supported jointly by the Danish Ministry of the Environment and the Ministry of Labor. Duco Van Lelieveld is acknowledged for collec-

tion of samples. Anne Dorrit Meincke, Pia Birte Jeppesen, and Inger Margrethe Toxværd Larsen are acknowledged for technical assistance and data handling.

## References

- [1] G. Cesana, G. Panza, M. Ferrario, R. Zanettini, M. Arnoldi, A. Grieco, *J. Occup. Med.* 27 (5) (1985) 357.
- [2] E. Baulieu, P.A. Kelly (eds.), *Hormones: From Molecules to Disease*, Vol. 1, Herman, Paris, 1990, pp. 1–697.
- [3] A. Webber, I.A. MacDonald, *Baillière's Clin. Endocrinol. Metab.* 7 (2) (1993) 393.
- [4] G. Johansson, G. Aronsson, B.O. Lindström, Social psychological and neuroendocrine stress reactions in highly mechanized work, *Ergonomics* 21 (8) (1978) 583.
- [5] U. Lundberg, M. Granqvist, T. Hansson, M. Magnusson, L. Wallin, Psychological and physiological stress responses during repetitive work at an assembly line, *Work Stress* 3 (2) (1989) 143.
- [6] EURACHEM (ed.), EURACHEM Guidance Document No. 1. WELAC Guidance Document No WGD 2. Accreditation for Chemical Laboratories. WELAC, 1993, pp. 1–34.
- [7] J.M. Christensen, O.M. Poulsen, T. Anglov, H.G. Seiler, A. Sigel, H. Sigel (eds.), *Handbook on metals in clinical and analytical chemistry*. In: *Method Evaluation, Quality Control, and External Quality Assurance Systems of Analytical Procedures*, Vol. 4, Marcel Dekker, New York, 1994, pp. 45–61.
- [8] ISO (International Organization for Standardization) (ed.), *ISO 7870. Control Charts—General Guide and Introduction*. ISO, Geneva, Switzerland, 1993, pp. 1–9.
- [9] ISO (International Organization for Standardization) (ed.), *ISO 8258. Shewart Control Charts*. ISO, Geneva, Switzerland, 1991, pp. 1–29.
- [10] ISO (International Organization for Standardization) (ed.), *ISO 5725. Accuracy (Trueness and Precision) of Measurement Results, Part 1–6*. ISO, Geneva, Switzerland, 1994.
- [11] H. Tsuchiya, T. Koike, T. Hayashi, *Anal. Chim. Acta* 218 (1989) 119.
- [12] T. Seki, Y. Yanagihara, K. Noguchi, *J. Chromatogr.* 515 (1990) 435.
- [13] K.S. Boos, B. Wilmers, R. Sauerbrey, E. Schlimme, *Chromatographia* 24 (1987) 363.
- [14] C. Sarzanini, E. Mentasi, M. Nerva, *J. Chromatogr.* 671 (1994) 259.
- [15] K. Kemper, E. Hagemeyer, D. Ahrens, K.S. Boos, E. Schlimme, *Chromatographia* 19 (1984) 288.
- [16] G. Grossi, A. Bargossi, A. Lippi, R. Battistoni, *Chromatographia* 24 (1987) 842.
- [17] E.M. Nielsen, B.H. Nielsen, N.O. Breum, *Ann. Agric. Environ. Med.* 2 (1995) 53.
- [18] H. Bartels, M. Bohmer, *Clin. Chim. Acta* 32 (1971) 81.
- [19] K.S. Boos, B. Wilmers, E. Schlimme, R. Sauerbrey, *J. Chromatogr.* 456 (1988) 93.
- [20] ISO (International Organization for Standardization) and IUPAC (eds.), *Guide to the Expression of Uncertainty in Measurement*. BIMP, IEC, IFCC, ISO, IUPAC, IUPAP, OIML, Geneva, Switzerland, 1997, pp. 1–101.
- [21] J. Kragten, *Analyst* 119 (1994) 2161.
- [22] J. Kristiansen, J.M. Christensen, J.L. Nielsen, *Mikrochim. Acta* 123 (1996) 241.
- [23] J.M. Christensen, O.M. Poulsen, T. Anglov, *J. Anal. At. Spectrom.* 7 (1992) 329.
- [24] S.L. Christensen, J.T.B. Anglov, J.M. Christensen, E. Olsen, O.M. Poulsen, *Fresenius J. Anal. Chem.* 345 (1993) 343.
- [25] D.G. Bullock, C.E. Wilde, *Ann. Clin. Biochem.* 22 (1985) 273.
- [26] J. Mandel, *J. Qual. Technol.* 16 (1984) 1.
- [27] K. Heydorn, *Mikrochim. Acta* III (1991) 1.

# Use of ion-exchange chromatography coupled with TLC-laser scanning densitometry for the quantitation of fumonisin B<sub>1</sub>

R. Karuna, R.B. Sashidhar \*

Department of Biochemistry, University College of Science, Osmania University, Hyderabad 500 007, India

Received 9 November 1998; received in revised form 21 January 1999; accepted 26 January 1999

## Abstract

A simple TLC-Laser scanning densitometric (TLC-LSD) method was developed for the quantitation of fumonisin B<sub>1</sub> (FB<sub>1</sub>) isolated from solid media cultures (corn) and liquid media cultures of toxigenic *Fusarium moniliforme* strains (*F. moniliforme* MRC 826, *F. moniliforme* 4223 and *F. moniliforme* 2927)). FB<sub>1</sub> was isolated from the cultures by solvent extraction (methanol:water, 3:1) and purified in a single step by ion-exchange chromatography using Dowex-1. FB<sub>1</sub> in the purified extracts was detected by TLC analysis using *p*-anisaldehyde as a post-chromatographic derivatizing agent. The major toxin identified was FB<sub>1</sub> ( $R_f$  0.51) along with traces of FB<sub>2</sub> ( $R_f$  0.57) and FB<sub>3</sub> ( $R_f$  0.60) based on their comparison with the reference standard fumonisins. The sensitivity of the TLC-LSD method for the quantitation of FB<sub>1</sub> was found to be 500 ng g<sup>-1</sup>. The linear regression analysis performed for the quantitation of FB<sub>1</sub> by the TLC-LSD method showed a correlation coefficient ( $r$ ) value of 0.9. Spiking studies revealed the recovery of standard FB<sub>1</sub> (5 and 10 μg g<sup>-1</sup>) loaded on to Dowex-1 in the range of 87–96%. The purity of FB<sub>1</sub> purified from the cultures was determined by the two-dimensional TLC analysis. Two-dimensional TLC-analysis of the purified FB<sub>1</sub> revealed the purity to be greater than 85%. The method developed may find wide application in the environmental monitoring of the FB<sub>1</sub> contaminations in the various agricultural commodities and screening fumonisin producing toxigenic strains of *F. moniliforme*. © 1999 Elsevier Science B.V. All rights reserved.

**Keywords:** Fumonisins; Fumonisin B<sub>1</sub>; *Fusarium moniliforme*; TLC-laser scanning densitometry

## 1. Introduction

Fumonisins are a group of structurally related mycotoxins produced as secondary metabolites by several species of the genus *Fusarium*. The most

common and highest fumonisin-producing *Fusarium* species are *Fusarium moniliforme* and *Fusarium proliferatum* both of which are frequently found contaminating corn. The frequency of occurrence of *F. moniliforme* on corn is 90% higher than in other food grains, with 90% of the *F. moniliforme* producing fumonisins [1]. Fumonisins have been classified into four major series of mycotoxins, the A series, the B series, the C series

\* Correspondent author. Fax: +91-40-701-6868/701-9020.

and the P series. However the B series fumonisins (FB<sub>1</sub>, FB<sub>2</sub>, FB<sub>3</sub>, FB<sub>4</sub>) are the most predominant due to their abundance and toxicological effects in the various animal species. Among them FB<sub>1</sub> has been found to be produced in larger amounts (70–75% of the total fumonisins) followed by FB<sub>2</sub> and FB<sub>3</sub> [2]. Chemically, fumonisins are derivatives of 2-amino-12,16-dimethyl polyhydroxy icosane esterified at the C<sub>14</sub> and C<sub>15</sub> positions with tricarballic acid moieties. Differing hydroxyl substitutions accounts for different fumonisins within the B series. Fumonisin A<sub>1</sub> (FA<sub>1</sub>) and Fumonisin A<sub>2</sub> (FA<sub>2</sub>) are the *N*-acetyl derivatives of FB<sub>1</sub> and FB<sub>2</sub>, respectively [3] (Fig. 1). Upon alkaline hydrolysis, the basic structure of fumonisins cleaves into two products: the amino alcohols and the tricarballic acid moieties. However studies on the structure–activity relationships of fumonisins reported that the toxicity and carcinogenicity of fumonisins depends totally on the intact fumonisin molecules [4,5]. The natural occurrence of fumonisins in corn and corn-based products has been reported in the range of 0.3–330 ppm [1]. Ingestion of feed contaminated with fumonisins results in syndromes like equine leukoencephalomalacia in horses and porcine pulmonary edema in pigs, and induces hepato-car-

cinogenic and hepatotoxic effects in rats [6–8]. Consumption of corn contaminated with fumonisins has also been associated with high incidences and increased risk of human esophageal cancer in Transkei districts of South Africa, Linxian districts of China, North Eastern Italy and South Eastern regions of the USA [9–11]. The International Agency for Research on Cancer (IARC) Lyon, France, has classified FB<sub>1</sub> as possibly carcinogenic to humans (toxins derived from *F. moniliforme* as group 2B carcinogens) [12]. The biochemical and pathological basis of fumonisin toxicity is due to its structural similarities to sphingosine, which explains the epigenetic effect of the mycotoxin [13].

In view of the hazardous and toxic nature of FB<sub>1</sub> to both humans and animals, several attempts have been made to develop analytical procedures for the detection and quantitation of fumonisins in the high-risk commodities, such as corn and sorghum.

Analysis of mycotoxins typically involves extraction from the sample matrix followed by some preliminary clean-up, chromatographic separation and detection. A number of analytical methods for the evaluation of fumonisins in corn and corn products, including thin-layer chromatography

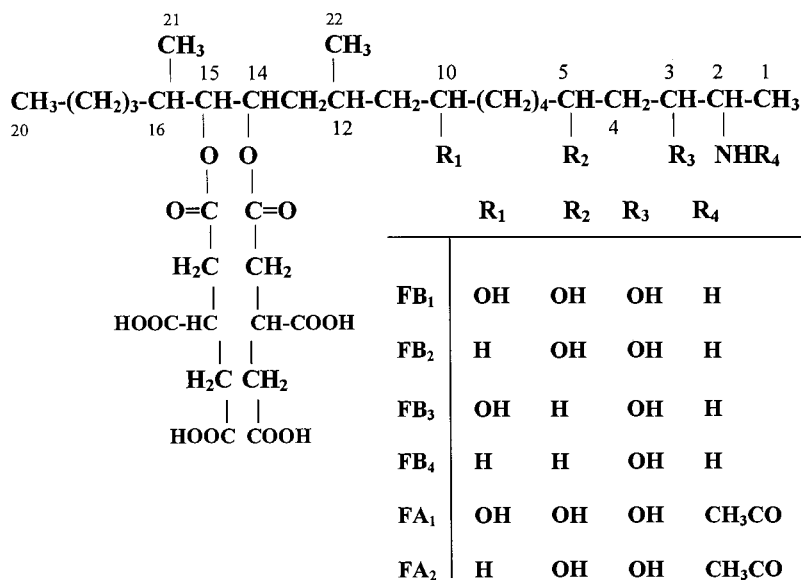


Fig. 1. Chemical structures of fumonisins.



(TLC), high-performance liquid chromatography (HPLC), gas chromatography–mass spectrometry (GC–MS), enzyme linked immunoassays (ELISA), and capillary zone electrophoresis (CZE), have been developed. TLC has only been used as a qualitative method of analysis to date. While the other methods are used for both the qualitative and quantitative analysis of fumonisins, they are also accompanied by major shortcomings, like extensive sample clean-up and pre-derivatization procedures of the fumonisins and subsequent analysis [14]. These derivatives are highly unstable with short retention time ( $R_t$ ) and are pH dependent [15]. In order to overcome the constraints of the unstable pre-column derivatization procedures, alternative approaches to separate intact fumonisins without derivatization, like fast atom bombardment–mass spectrometry (FAB–MS), ion pair chromatography and HPLC coupled with electrospray detection (ELSD), were also developed [16]. However, these methods require sophisticated and expensive instrumentation facilities. Apart from these methods, immuno-chemical methods like ELISA (based on polyclonal or monoclonal antibodies), fiber optic immunosensor method (based on monoclonal antibodies) and immuno-histochemical methods, have also been developed for the detection of fumonisins [17,18]. A major drawback of the immunoanalytical methods is that the antibodies raised against  $FB_1$  or hydrolysed  $FB_1$  cross-react with other fumonisin molecules. Comparative studies on the analytical procedures for  $FB_1$  contamination in corn samples conclude ELISA to be an unreliable method and may be applicable preferably as a screening method only [17]. Thus, a method of choice would be one which is simple, easy to perform and has least number of steps.

The objective of the present study was to develop and evaluate a simple TLC-densitometric method for the quantitation of  $FB_1$  in *F. moniliforme* culture extracts and in corn, a known high-risk agricultural commodity for fumonisin contamination. The methodology reported includes a single-step purification of  $FB_1$  from contaminated corn and culture extracts of toxigenic strains of *F. moniliforme* (*F. moniliforme* MRC

826, *F. moniliforme* 4223 and *F. moniliforme* 2927) on Dowex-1 ion-exchange resin followed by its separation on a TLC plate and post-chromatographic derivatization. The toxin was quantitated using a laser scanning densitometer.

## 2. Materials and methods

Fumonisin  $B_1$  ( $FB_1$ ), Fumonisin  $B_2$  ( $FB_2$ ) and Fumonisin  $B_3$  ( $FB_3$ ) reference standards were a kind gift from W.C.A. Gelderblom (MRC, Tygerberg, South Africa). Dowex-1 (ionic form:chloride, 8% cross-linked), *p*-anisaldehyde, pre-coated polyester silica gel-G (thickness, 250  $\mu$ m; particle size, 2–25  $\mu$ m) plates were purchased from Sigma (St. Louis, MO, USA). All other chemicals and reagents were of analytical grade.

### 2.1. Fungal strains

Toxigenic strain of *Fusarium moniliforme* MRC 826 was obtained from the South African Medical Research Council (MRC). *F. moniliforme* 4223 and *F. moniliforme* 2927 were obtained from the Indian Agricultural Research Institute (IARI), New Delhi. Corn was purchased from the local market.

### 2.2. Instrumentation

The environmental incubator used for incubating solid (stationary cultures) and liquid cultures (shake/submerged cultures) of *F. moniliforme* was purchased from Labline (IL, USA). The laser scanning densitometer used for the quantitation of  $FB_1$  was purchased from Biomed (CA, USA).

### 2.3. Production of $FB_1$ on corn cultures (solid media for $FB_1$ )

The solid media for the  $FB_1$  production was prepared by autoclaving (at 121°C and 21 kg/cm<sup>2</sup> pressure for 1 h) partially powdered corn (200 g) and 100 ml double distilled water in 1-l conical flasks, and leaving overnight.

### 2.3.1. Inoculation

A total of 5 ml of 0.1% Tween-20 solution was added to 8–10-day-old potato dextrose agar slants containing well grown toxigenic strains of *Fusarium moniliforme* (*F. moniliforme* MRC 826, *F. moniliforme* 4223 and *F. moniliforme* 2927) species and shaken gently to get the spore suspension. Spore suspension (equivalent to 50 000 spores/g corn) was inoculated into the flasks containing the solid media at room temperature under aseptic conditions. Different flasks in duplicate were maintained for the different toxigenic strains of *F. moniliforme*, which were then transferred into the Labline environmental incubator, set to 25°C. The fungus was allowed to grow for 7 weeks. At the end of the incubation period the corn cultures were then dried in the vacuum oven containing calcium chloride (fused), at  $45 \pm 3^\circ\text{C}$  for 2 days. Before inoculation the corn samples were screened for fumonisin contamination, and used for spiking studies.

### 2.4. Production of $\text{FB}_1$ in liquid cultures

A two-stage liquid medium (consisting of the first-stage medium and the second-stage medium) was used for the production of  $\text{FB}_1$  in liquid medium [19]. The nutrient composition of the media were as follows.

First stage medium:  $\text{NH}_4\text{Cl}$  (3 g),  $\text{FeSO}_4 \cdot 7\text{H}_2\text{O}$  (0.2 g),  $\text{MgSO}_4 \cdot 7\text{H}_2\text{O}$  (2 g),  $\text{KH}_2\text{PO}_4$  (2 g), peptone (2 g), yeast extract (2 g), malt extract (2 g) and glucose (20 g) per liter of double distilled water.

Second stage medium:  $(\text{NH}_4)_2\text{HPO}_4$  (1g),  $\text{KH}_2\text{PO}_4$  (3.0 g),  $\text{MgSO}_4$  (0.2 g),  $\text{NaCl}$  (5 g), sucrose (40 g) and glycerol (10 g) per l of double-distilled water. Initially the pH of both media were adjusted to 5, after which they were autoclaved at 21 kg/cm<sup>2</sup> pressure and 120°C temperature for 15 min.

### 2.4.1. Inoculation

The toxigenic strains of *F. moniliforme* (*F. moniliforme* MRC 826, *F. moniliforme* 4223 and *F. moniliforme* 2927) for the liquid culture studies were maintained on a 2% malt agar slant.

Slants containing 8–10-day-old cultures were taken and macerated in 25 ml of pyrogen-free and sterile double-distilled water. An aliquot of the macerate (2.5 ml) was then inoculated into 50 ml of the first stage medium, contained in 250-ml conical flasks for the growth of the fungus. The inoculation was done in triplicate, and the culture flasks were incubated in the environmental incubator at 25°C temperature and 150 rotations/min for 48 h. At the end of the incubation period the cultures were centrifuged at 10 000 rpm at 4°C (Hitachi SCR20 BA, Japan). Fifty percent of the supernatant was discarded, the pelleted mycelium was resuspended, and 3.5 ml of the suspension were added to 50 ml of the second stage medium contained in 250-ml conical flasks for the production of fumonisins. The cultures were then incubated under similar conditions used for first-stage medium for a period of 21 days. At the end of 21 days  $\text{FB}_1$  was isolated and purified from the liquid cultures.

### 2.5. Extraction of the toxin from corn cultures and liquid cultures

The dried contaminated corn culture (20 g) was powdered using a mechanical blender (1200 rpm) and subjected to ethylacetate extraction (20 ml) for 3–5 min. The extract was filtered through Whatman No. 1 filter paper, the residue was collected and dried for 1–2 h at 45–50°C. The dried residue was extracted with methanol:water (3:1; 20 ml) twice and filtered. The methanol:water extracts were pooled together and flash evaporated over a vacuum-based rotary evaporator at 40°C. The residue was re-dissolved in 8 ml of methanol:water (3:1) solvent and the pH was adjusted to 7.9.

The procedure for the extraction of  $\text{FB}_1$  from liquid cultures (50 ml) was similar to that of the corn cultures and was followed as illustrated in Fig. 2 (scheme for  $\text{FB}_1$  purification).

### 2.6. Purification of fumonisin $B_1$ by ion-exchange chromatography

Dowex-1 (25 g) was packed in a glass column (height, 20 cm; i.d., 1.5 cm). The packed resin

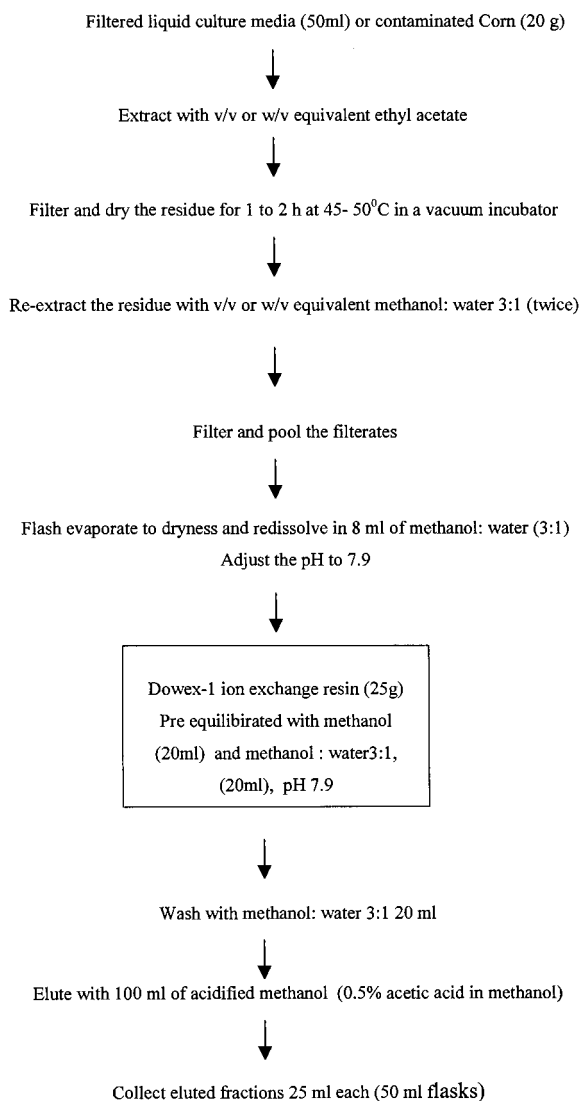


Fig. 2. Purification procedure for fumonisin B<sub>1</sub> (FB<sub>1</sub>).

was equilibrated with methanol (20 ml) followed by methanol:water (3:1; 20 ml), pH 7.9. The flow rate of the column was adjusted to 1 ml/min. The sample (solid/liquid culture extracts, pH 7.9) was then loaded on to the column. The column was washed with methanol:water (3:1) followed by methanol (20 ml). The toxin was eluted with 0.5% acetic acid in methanol (100 ml). Four separate fractions (25 ml each) were collected (Fig. 2).

## 2.7. Concentration of the samples

The acidified methanol fractions (0.5% acetic acid in methanol) used to elute the toxin were transferred into round-bottomed flasks (100 ml capacity) and evaporated to dryness. The residues were re-dissolved in 0.5–1.0 ml of acetonitrile:water (ACN:water, 1:1).

## 2.8. Qualitative analysis of FB<sub>1</sub> purified from corn cultures/liquid cultures

The residues re-dissolved in ACN:water (1:1) were spotted (spot volume, 5 µl) onto the polyester plates and the plates were developed in chloroform:methanol:acetic acid (6:3:1) solvent system. The plates were then air dried for 5–10 min and sprayed with the acidified *p*-anisaldehyde reagent (0.5 ml of *p*-anisaldehyde added to a mixture of 85 ml methanol, 10 ml glacial acetic acid and 8 ml concentrated sulphuric acid under ice-cold conditions) and heated at 130°C for 3 min to visualize the spots [17]. Reference standards FB<sub>1</sub>, FB<sub>2</sub> and FB<sub>3</sub> were also run along with the samples for comparison.

## 2.9. Quantitation of fumonisins by laser scanning densitometry

The fumonisin B<sub>1</sub> spots identified on the TLC plates were subjected to densitometric scans. The mode of detection was based on transmittance and brightness of the laser source.

## 2.10. Validation of laser scanning densitometry for the quantitation of FB<sub>1</sub>

Varying concentrations of standard FB<sub>1</sub> between 0.1, 0.25, 0.5, 1.0, 2.0, 2.5 and 3.0 µg were taken and subjected to TLC analysis as described above. Later the spots resolved were quantitated by laser scanning densitometry and a standard plot was established. A linear regression analysis was performed using concentration of FB<sub>1</sub> (µg) versus the peak area (cm<sup>3</sup>).

## 2.11. Validation of Dowex-1 for the purification of $FB_1$

### 2.11.1. Spiking studies

One gram of corn (pre-screened for fumonisins) was extracted with 5 ml of ethylacetate and filtered through a Whatman No. 1 filter. The residue was dried and re-extracted with 2 ml of methanol:water (3:1) and filtered (twice). The filtrates were pooled and evaporated to dryness. The residue was re-constituted in 750  $\mu$ l of methanol:water (3:1) (pre-adjusted to pH 7.9). The corn extracts were prepared in triplicate. To these extracts, standard  $FB_1$  was spiked individually at two levels (5 and 10  $\mu$ g  $g^{-1}$  corn). Glass columns (height, 125 mm; i.d., 10 mm) were packed with fresh Dowex-1 (2 g). The resin packed in the column was washed with double-distilled water. Later the columns were equilibrated with 1 ml of methanol followed by 1 ml of methanol:water (3:1), pH 7.9. The corn extracts spiked with the standard  $FB_1$  were then loaded on to the column. During the loading of the sample the flow rates of the column were maintained at 1 ml/min. The columns were washed with 1 ml of methanol:water (3:1) followed by 1 ml of methanol. Finally the toxin was eluted using 5 ml of 0.5% acetic acid in methanol. The acidified methanol eluent was collected in separate fractions (1 ml toxin fractions  $\times$  5) and evaporated to dryness in a 5-ml round-bottomed flask, and the residues re-dissolved in 100  $\mu$ l of acetonitrile:water. For further concentration, the toxin-containing fractions (100  $\mu$ l) were dried under nitrogen and the residues were re-dissolved in 25  $\mu$ l of ACN:water (1:1). These fractions were subjected to TLC analysis as described above and the standard  $FB_1$  recovered was quantitated using the laser scanning densitometer.

## 3. Results and discussion

### 3.1. Extraction and purification of $FB_1$

Dowex-1 was found to be useful in the single-step purification of fumonisin toxin as detailed

in Fig. 2. Earlier, several procedures have been established for the isolation and purification of  $FB_1$ . A preparative procedure for purification of  $FB_1$  was developed using Amberlite XAD-2, silica gel, and  $C_{18}$  with a purity of  $>90\%$ . Another procedure reported the separation and purification of  $FB_1$  using XAD-2 column chromatography; HPLC equipped with a  $C_{18}$  reversed-phase column. Using XAD-2 and repeated  $C_{18}$  LC steps,  $FB_1$  with a purity of  $>99\%$  was obtained.  $FB_1$  with a purity of 97% was obtained from liquid cultures of *F. moniliforme* strains by DEAE–Sephadex ion exchange, silica gel and gradient  $C_{18}$  LC.  $C_{18}$  and cyano partition LC was used for the purification of  $FB_1$  from solid rice cultures with a purity of  $>95\%$  [20]. Purification of fumonisins by immunoaffinity column technique has also been developed. The major problem associated with the immunoaffinity column with respect to  $FB_1$  is that it cannot be used for bulk purification. This method of purification can be applied to samples contaminated with less than 2  $\mu$ g  $g^{-1}$  of  $FB_1$ . The limitation of the method suggests that the immunoaffinity column technique can only be used as a screening tool and not for bulk purification of  $FB_1$  [21]. However, all these methods are lengthy and expensive as compared to the present single-step purification of  $FB_1$  on Dowex-1. The major advantage of Dowex-1 is that it can be regenerated using 2 N HCl and used repeatedly.

### 3.2. Qualitative analysis of the purified samples

TLC analysis of the purified sample extracts showed a major spot with  $R_f$  of 0.51 and two minor spots with  $R_f$  values of 0.57 and 0.60. The major spot was identified as  $FB_1$ , and minor spots were identified as  $FB_2$  and  $FB_3$  based on their comparison with  $R_f$  values of standard  $FB_1$ ,  $FB_2$  and  $FB_3$ . Fig. 3, gives the TLC separation profile of  $FB_1$  purified from liquid and solid culture media as compared with the reference standard. The two-dimensional analysis of the sample extracts revealed that the purity of  $FB_1$  to be  $>85\%$ .

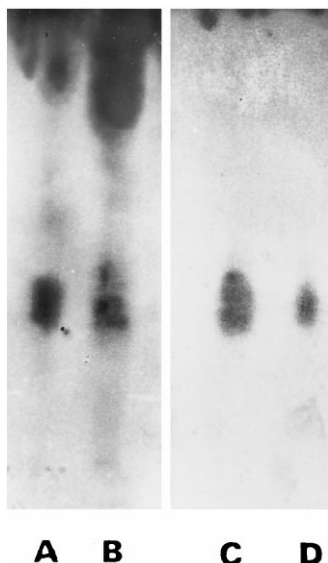


Fig. 3. TLC profile of separated fumonisin B<sub>1</sub>. (A) Corn sample no. 3; (B) corn sample no. 2; (C) liquid culture sample no. 4; and (D) reference standard of FB<sub>1</sub> (2.5 µg).

### 3.3. Validation of the method

The recovery studies for purification of FB<sub>1</sub> carried out at two levels of standard FB<sub>1</sub> (5 and 10 µg g<sup>-1</sup>), spiked to corn extracts showed recoveries in the range of 87–96%, Table 1. Earlier procedures for purification of FB<sub>1</sub> showed recoveries from a range of 80–90% only after two to three steps of column chromatographic purification [20].

Table 1  
Recovery of Standard FB<sub>1</sub> spiked to corn and subjected to Dowex-1 ion-exchange chromatography followed by TLC-laser scanning densitometry

Conc. of standard FB <sub>1</sub> spiked (µg g <sup>-1</sup> )	Total FB <sub>1</sub> recovered (µg)	% Recovery
5.0	4.4	87
10.0	9.6	96
10.0	8.8	88

Table 2  
Laser scanning densitometric response to various concentrations of standard FB<sub>1</sub>

Conc. Of standard FB <sub>1</sub> (µg)	Mean peak area ± S.D. (cm <sup>2</sup> )	Coefficient of variation <sup>a</sup> (%)
0.5	0.5 ± 0.10	20
1.0	1.0 ± 0.20	20
2.0	1.7 ± 0.07	4
2.5	1.8 ± 0.05	3
3.0	2.3 ± 0.03	1.3

<sup>a</sup> Based on five independent experiments.

### 3.4. Validation of TLC-laser scanning densitometry for the quantitation of FB<sub>1</sub>

*para*-Anisaldehyde was used as a post-chromatographic agent for the chemical confirmation of FB<sub>1</sub> on TLC to give a bluish green spot based on its reaction with the primary amine group in the fumonisin molecules. Earlier, a rapid, sensitive TLC procedure for the detection of FB<sub>1</sub> and FB<sub>2</sub> in corn and corn-based feed stuffs was developed using fluorecamine as the post-chromatographic derivatization agent for FB<sub>1</sub>. The method reported a detection limit of 0.1 µg g<sup>-1</sup> for fumonisins in corn [21]. However the above method has only been used for the qualitative analysis of fumonisins, while the present method shows the application of TLC as a quantitative method when coupled with the laser scanning densitometry. A range of concentrations of standard FB<sub>1</sub> (0.1, 0.25, 0.5, 1.0, 1.5, 2.0 and 3.0 µg) were subjected to TLC analysis followed by densitometric scanning. Concentrations of standard FB<sub>1</sub> below 0.5 µg were faintly detectable and the corresponding peak areas were not recordable. Concentration of standard FB<sub>1</sub> at 0.5 µg and above were easily detectable and the corresponding peak areas (cm<sup>2</sup>) showed a linear regression value of 0.9 ( $r = 0.9$ ), Table 2. Based on the laser scanning densitometric response the minimum detection limit of the method for the quantitation of FB<sub>1</sub> has been found to be 500 ng g<sup>-1</sup>, as compared to other methods like HPLC (50 ng g<sup>-1</sup>), GC-MS (100 ng g<sup>-1</sup>), ion pair chromatography (20 ng g<sup>-1</sup>), capillary zone electrophoresis (25 ng g<sup>-1</sup>), ELISA (200 ng g<sup>-1</sup>) and the fibre optic im-

Table 3

Determination of FB<sub>1</sub> in agricultural commodities (corn) contaminated with toxigenic strains of *F. moniliforme* (*F.m*) as determined by TLC-laser densitometry

Contaminated corn sample	Toxigenic strain used	FB <sub>1</sub> (µg g <sup>-1</sup> ) <sup>a</sup>
Sample 1	<i>F.m</i> MRC 826	380
Sample 2	<i>F.m</i> MRC 826	355
Sample 3	<i>F.m</i> 4223	761
Sample 4	<i>F.m</i> 2927	434

<sup>a</sup> Represents mean values.

munosensor method (10 ng ml<sup>-1</sup>) [17,18]. The major advantage of the method is that it facilitates separation of the other impurities and provides an on-line purification of the sample on the silica gel-coated TLC plates.

### 3.5. Application of the developed method

This method has been successfully used not only in detecting and quantitating the concentration of FB<sub>1</sub> in corn samples and liquid culture extracts contaminated with *F. moniliforme* MRC 826, but also in screening the toxigenic potentials of *F. moniliforme* 4223 and *F. moniliforme* 2927 on corn and in liquid cultures (Table 3 and Table 4).

## 4. Conclusions

The present paper reports the use of Dowex-1 as a single-step purification method for the isolation of fumonisin B<sub>1</sub>. Further, the quantitation of

Table 4

Determination of FB<sub>1</sub> in liquid Cultures inoculated with toxigenic strains of *F. moniliforme* (*F.m*) as determined by TLC-laser scanning densitometry

Liquid culture sample	Toxigenic strain used	FB <sub>1</sub> (µg ml <sup>-1</sup> ) <sup>a</sup>
Sample 1	<i>F.m</i> MRC 826	15 ± 1
Sample 2	<i>F.m</i> MRC 826	17 ± 2
Sample 3	<i>F.m</i> 4223	70 ± 20
Sample 4	<i>F.m</i> 2927	91 ± 14

<sup>a</sup> Represents mean value.

FB<sub>1</sub> based on TLC-laser scanning densitometry may find wide application in the environmental monitoring of FB<sub>1</sub> contaminations in various agricultural commodities and screening fumonisin producing toxigenic strains of *Fusarium moniliforme* grown in liquid cultures.

## Acknowledgements

The authors would like to thank Dr W.C.A. Gelderblom, South African Medical Research Council, Tygerberg, South Africa, for providing the *F. moniliforme* MRC 826 fungal strain. R. Karuna also wishes to thank the Council of Scientific and Industrial Research, New Delhi, for the research fellowship and the University Grants Commission, New Delhi, for providing instrumental facilities under the COSIST program in the department.

## References

- [1] C.W. Bacon, P.E. Nelson, *J. Food Prot.* 57 (1994) 514.
- [2] S.M. Musser, *J. Agric. Food Chem.* 45 (1997) 1169.
- [3] S.C. Bezuidenhout, W.C.A. Gelderblom, C.P. Gorst-Allman, R.M. Horak, W.F.O. Marasas, G. Spiteller, R. Vleggaar, *J. Chem. Soc. Chem. Commun.* (1988) 743.
- [4] W.C.A. Gelderblom, M.E. Cawood, S.D. Snyman, R. Vleggaar, W.F.O. Marasas, *Food Chem. Toxicol.* 36 (1993) 407.
- [5] T. Tanaka, H.K. Abbas, S.O. Duke, *Phytochemistry* 33 (4) (1993) 779.
- [6] W.F.O. Marasas, T. Kellerman, W.C.A. Gelderblom, J.A.W. Coltzer, J. Van der Lugt, *J. Vet. Res.* 55 (1988) 197.
- [7] L.R. Harrison, B.M. Colvin, J.J. Green, L.E. Newmaan, J.R. Cole, *J. Vet. Diagn. Invest.* 2 (1990) 217.
- [8] W.P. Norred, *J. Toxicol. Environ. Health* 38 (1993) 309.
- [9] W.C.A. Gelderblom, N.P.J. Kriek, W.F.O. Marasas, P.G. Thiel, *Carcinogenesis* 12 (1991) 1247.
- [10] T. Yoshizava, A. Yamashita, Y. Luo, *Appl. Environ. Microbiol.* 60 (1994) 1626.
- [11] S. Franceschi, E. Bidoli, A.E. Baron, C. LaVecchia, *J. Natl. Cancer Inst.* 82 (1990) 1407.
- [12] H. Vainio, E. Heseltine, J. Wilbourn, Report on IARC Group Meeting on Some Naturally Occurring Substances, vol. 53, 1993, p. 535.
- [13] R.B. Sashidar, R. Karuna, Mechanistic implications of fumonisins mycotoxin, in: C. Subramanyam, S.S. Singh

- (Eds.), *Molecular Mechanisms of Toxicity*, Department of Biochemistry, Osmania University Publication, 1997, p. 64.
- [14] A.E. Pohland, in: L.S. Jackson, J.W. De Vries, L.B. Bullerman (Eds.), *Fumonisin in Foods*, Plenum Press, New York, 1996, p. 19.
- [15] M. Miyahara, H. Akiyama, M. Toyoda, Y. Saito, J. *Agric. Food Chem.* 44 (1996) 390.
- [16] J.G. Wilkes, in: L.S. Jackson, J.W. De Vries, L.B. Bullerman (Eds.), *Fumonisin in Food*, Plenum Press, New York, 1996, p. 93.
- [17] F.S. Chu, in: L.S. Jackson, J.W. De Vries, L.B. Bullerman (Eds.), *Fumonisin in Food*, Plenum Press, New York, 1996, p. 123.
- [18] V.S. Thompson, C. Maragos, J. *Agric. Food Chem.* 44 (1996) 1041.
- [19] B.A. Blackwell, M.J. David, E.M. Savard, J. *Assoc. Anal. Chem.* 77 (1994) 506.
- [20] P.A. Murphy, C. Hawk, A. Clark, E. Hopmans, W.R. Dantzer, J. *Agric. Food Chem.* 44 (12) (1996) 3730.
- [21] G.E. Rottinghaus, C. Coatney, H.C. Minor, J. *Vet. Diagn. Invest.* 4 (1992) 326.

# FT-Raman and powder XRD analysis of the $\text{Ba}(\text{SO}_4)_x(\text{CrO}_4)_{1-x}$ solid solution

J.M. Alia <sup>a,\*</sup>, H.G.M. Edwards <sup>b</sup>, F.J. Garcia-Navarro <sup>a</sup>

<sup>a</sup> *E.U.I.T.A., Dpto. de Química Física, Universidad de Castilla-La Mancha, Ronda de Calatrava 5, E-13071 Ciudad Real, Spain*

<sup>b</sup> *Chemical and Forensic Sciences Department, University of Bradford, Richmond Road, Bradford BD7 1DP, UK*

Received 7 September 1998; received in revised form 1 February 1999; accepted 5 February 1999

## Abstract

The  $\text{Ba}(\text{SO}_4)_x(\text{CrO}_4)_{1-x}$  solid solution has been described in nature, forming the mineral Hashemite. From the geochemical point of view, however, anionic solid solutions have much interest because they are suitable systems to probe order–disorder phenomena. The solid solution analysed in the present study has, moreover, a special incentive in its possible use for the extraction from water, and immobilisation, of the pollutant Cr(VI) ion. The orthorhombic (space group Pnma) unit cell parameters of the solid solution change linearly with the mole fraction of both anions, decreasing with increase in the sulfate anion concentration. The vibrational spectroscopic study is centred on the behaviour of the anionic symmetric stretching band ( $\nu_1, A_1$ ), whose characteristics are examined in detail. While the chromate anion band retains its wavenumber along the full compositional range, the sulfate anion band is shifted toward lower wavenumbers with decrease in the corresponding mole fraction. The positional disorder induced by the random anionic substitution results in strong increase of the halfwidth in both bands, which becomes greatest in the central member of the series. © 1999 Elsevier Science B.V. All rights reserved.

*Keywords:* Mixed anions; Raman; Solid solutions

## 1. Introduction

Barium sulfate and barium chromate form a solid solution which is considered thermodynamically ideal [1] because the end member solubility products are very close, and both are isomorphous and crystallize in the spatial group Pnma. In nature, the existence of a mineral species named Hashemite that contains both of these

anions as the barium salt has been reported [2]. The environmental interest of this system has been stressed [3,4], because it could be possible to eliminate the strongly pollutant Cr(VI) ion from waters by a ‘sorption’ process over barium sulfate.

To the best of our knowledge, there is no available data on vibrational spectroscopy of this solid solution, except for the infrared study by Tarte and Nizet [5] in 1964, who studied some dilute solid solution samples obtained by precipitation, without reference to the corresponding anionic mole fractions. We have recently carried

\* Corresponding author. Fax: +34-926-295351.

E-mail address: jmalia@qifi-cr.uclm.es (J.M. Alia)



out [6] a FT-Raman study of some  $\text{Ba}(\text{SO}_4)_x(\text{CrO}_4)_{1-x}$  solid solution crystals grown by the counter-diffusion of  $(\text{CrO}_4^{2-}, \text{SO}_4^{2-})$  and  $\text{Ba}^{2+}$  ions through a porous silica gel transport medium [7].

In the present paper, 11 microcrystalline (precipitated) samples (the endmembers and nine intermediate compounds) are studied by means of powder X-ray diffraction and FT-Raman spectroscopy. The aim of this research is to provide some data that could help in the analytical characterisation of these materials.

## 2. Experimental

### 2.1. Solids

Solutions containing  $0.25 \text{ mol dm}^{-3}$  of  $\text{K}_2\text{SO}_4$ ,  $\text{K}_2\text{CrO}_4$  and  $\text{Ba}(\text{NO}_3)_2$  (Aldrich, A.C.S. reagents) in doubly distilled water were used in the precipitation of the solid solution samples. Appropriate volumes of potassium chromate and potassium sulfate solutions were made up to a final volume of 50 ml and heated to  $70 \pm 2^\circ\text{C}$ . Barium nitrate solution was added dropwise with vigorous stirring until it was in a slight excess (4–6%). On completion of the precipitation, the suspension was stirred for 1 h at the same temperature. Precipitates were separated from the mother liquor through  $0.65\text{-}\mu\text{m}$  Millipore filters, and washed repeatedly with doubly distilled water. Afterwards, solids were dried by heating at  $110^\circ\text{C}$  for 48 h.

Table 1  
Sulfur (%) content of the samples

$\chi \text{ SO}_4^{2-}$	% S (calc.)	% S (obs.)	$\sigma$
0.1	1.37	1.36	0.02
0.2	2.75	2.78	0.14
0.3	4.12	4.06	0.10
0.4	5.49	5.49	0.07
0.5	6.87	6.85	0.16
0.6	8.24	8.59	0.42
0.7	9.62	9.64	0.24
0.8	10.99	11.07	0.17
0.9	12.36	12.59	0.91
1	13.74	13.12	0.24

### 2.2. Chemical analysis

Sulfur content was evaluated with a CNS elemental analyser NA1500 (Carlo Erba Instrumentazione) using thiourea as standard. Table 1 shows the results of the elemental analysis. Each result is the average of five different runs.

### 2.3. Powder X-ray diffraction

X-ray diffraction was carried out using a Philips PW 1710 automatic diffractometer with Cu K $\alpha$  radiation (wavelength,  $1.54056 \text{ \AA}$ ) and graphite monochromator. Scanning rate for general identification (*qualitative*) diffractograms (from  $2\theta = 5\text{--}70^\circ$ ) was  $0.5^\circ \text{ min}^{-1}$ ; diffractograms used for unit cell parameter refinements (*quantitative*) and other detailed studies (from  $2\theta = 21\text{--}34^\circ$ ) were acquired in step-scan mode with 4.0 s preset time and steps of  $0.02^\circ$ . The diffractometer was calibrated using Si as an external standard. X-ray source conditions were 40 kV and 50 mA with 2200 W of power. The eight stronger reflections in the quantitative diffractograms were used in the unit cell parameter calculations.

### 2.4. FT-Raman spectra

FT-Raman spectra were excited at 1064 nm using an Nd:YAG laser and a Bruker IFS66 optical bench with a FRA 106 Raman accessory. Laser power was set at ca 100 mW and 1000 scans were accumulated with a resolution of  $2 \text{ cm}^{-1}$ . Powdered samples were lightly pressed in the Bruker powder holder and mounted with  $180^\circ$  scattering geometry.

The mathematical treatment of the spectra and diffractograms was carried out using the commercial software GRAMS/32<sup>®</sup> (Galactic Industries). Smoothing procedures or baseline correction routines were not applied in this work.

## 3. Results and discussion

### 3.1. Powder X-ray diffraction

Fig. 1 shows several *qualitative* powder diffractograms. The absence of any other solid phase

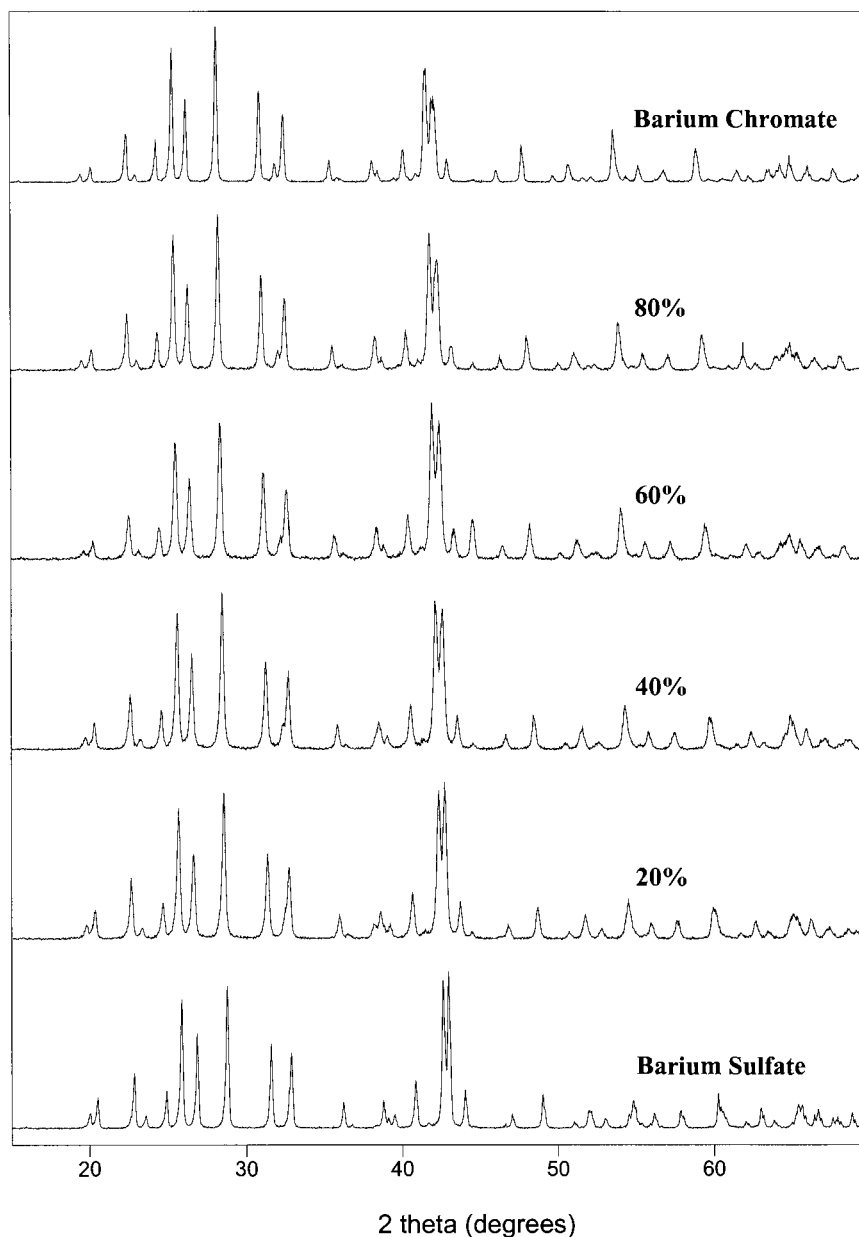


Fig. 1. Powder X-ray diffraction patterns (*qualitative*) of some samples of the studied solid solution. Percentages correspond to nominal mole fraction of barium chromate in the unit cell.

different from the solid solution phases is evident. Moreover, powder diffractograms demonstrate the existence of a true solid solution, i.e. not a simple mixture of endmembers,  $\text{BaCrO}_4$  and  $\text{BaSO}_4$ . The clear and continuous shift towards

lower  $2\theta$  angles when the chromate anion mole fraction increases is the result of the unit cell enlargement promoted by substitution of sulfate anion (ionic radius, 230 pm) by chromate anion (ionic radius, 240 pm) [8]. The presence of a small

feature close to  $44^\circ$ , particularly clear in the diffractogram corresponding to the 60% sample, and absent in both end-members could be explained as an effect of the local symmetry descent which would activate a formally absent diffraction line. The presence of an impurity can be ruled out

because no other extra band appears in none of the diffraction patterns. Fig. 2 shows the *quantitative* diffractograms of the endmembers and the central sample of the solid solution. The effect of the anionic substitution over the half-width and intensities of the diffraction peaks can be sum-

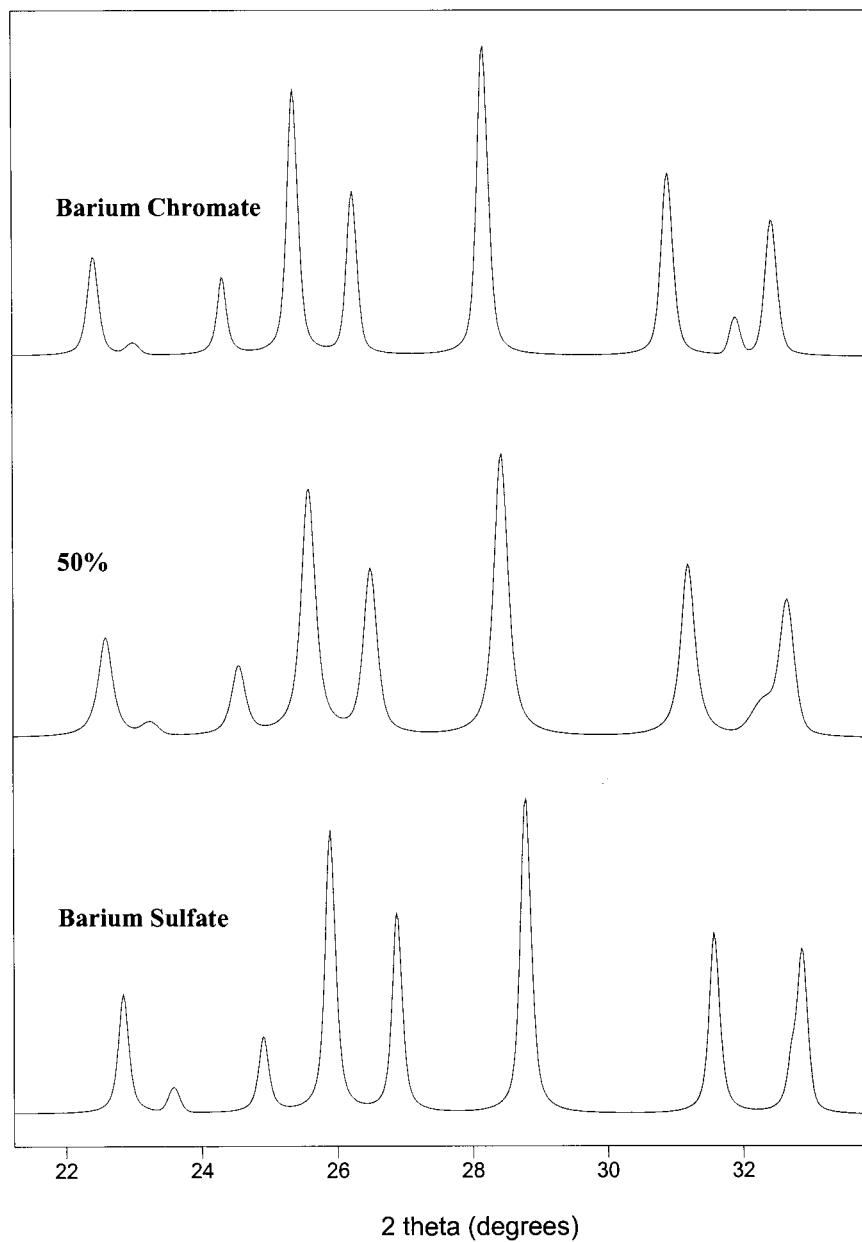


Fig. 2. Powder X-ray diffraction patterns (*quantitative*) used in the refinement of the unit cell parameters.

Table 2

Reflections used in the unit cell parameters refinement: Miller index and  $2\theta$  ( $^\circ$ ) values<sup>a</sup>

<i>hkl</i>	BaSO <sub>4</sub>	Exptl.	BaCrO <sub>4</sub>	Exptl.
	ASTM		ASTM	
111	22.807	22.812	22.348	22.402
004	24.892	24.869	24.251	24.303
410	25.862	25.868	25.316	25.347
104	26.861	26.855	26.171	26.230
411	28.770	28.762	28.131	28.168
114	31.546	31.559	30.821	30.903
901	32.743	32.721	31.904	31.916
040	32.817	32.884	32.318	32.396
Unit cell parameters ( <i>a</i> , <i>b</i> and <i>c</i> (Å); volume (Å <sup>3</sup> ))				
<i>a</i>	8.881	8.880 (0.022)	9.112	9.106 (0.024)
<i>b</i>	5.454	5.455 (0.018)	5.541	5.525 (0.021)
<i>c</i>	7.156	7.159 (0.005)	7.343	7.322 (0.004)
Volume	346.6	346.8 (0.9)	370.7	368.4 (0.6)

<sup>a</sup> Unit cell parameters: in brackets, standard error.

marised as follows. A general and progressive broadening affects all the diffraction peaks and reaches a maximum of ca 40% in the central sample. This observation can be interpreted as a result of the anionic positional disorder, which is a maximum in the central member of the solid solution. However, despite these differences in the peak half-widths, the intensity ratios calculated from the peak maxima as well as from the integrated intensities are independent of the anionic substitution, which means that the broadening is nearly the same in all the peaks of each diffractogram. This observation supports the previous interpretation of the peak broadening as arising from positional disorder, but not from differences in the crystallinity of the precipitates, which should influence the half-widths of the peaks in a differential and more selective way. The results obtained in the unit cell parameters refinement are given in Table 2. As can be observed, the differences with the corresponding ASTM reference data [9] are minimal, which must be pointed out taking into account the precipitate nature of the samples studied. When the unit cell parameters of the solid solution samples have been calculated, these can be plotted against the mole fraction of chromate ion to test Vegard's law fulfilment [10–12]. Such plots are shown in Fig. 3, where the good linear fit ob-

tained in every case can be appreciated. These results strongly support the ideal behaviour of the solid solution studied here because the chromate anion concentration plotted is the nominal (theoretical) mole fraction.

### 3.2. FT-Raman spectra

The sulfate anion symmetric stretching mode  $\nu_1(A_1)$  in barium sulfate and several of the solid solution samples studied is shown in Fig. 4. As the sulfate content is decreased, the band shifts towards lower wavenumbers, which could be justified considering that the unit cell volume increases with the same trend. The band half-width rises from the value corresponding to the barium sulfate spectrum, reaching a maximum relative increase of 22% in the central term of the series. This observation, already reported in other solid solutions [13–15], where the presence of two different cations disturbs the vibrational behaviour of the anion, can be understood in terms of positional disorder that impedes the intermolecular coupling. The bandshape does not change with the sulfate anion content. As can be observed in Fig. 5, bands corresponding to barium sulfate and the sample with least sulfate content (10%) are nearly identical once normalised and suitably transposed to higher wavenumber.

Fig. 6 shows the FT-Raman spectral region where the chromate anion symmetric  $\nu_1(A_1)$  and antisymmetric  $\nu_3(F_2)$  stretching modes appear. The stronger feature ( $863.0\text{ cm}^{-1}$ ) is the symmetric stretching band,  $\nu_1(A_1)$ , which appears at  $847\text{ cm}^{-1}$  in aqueous solution [16]. In the IR spectrum, the narrow band from this fundamental has been observed [5] at  $860\text{ cm}^{-1}$ . The bands grouped at higher wavenumbers should arise from the antisymmetric stretching mode,  $\nu_3(F_2)$ . The complexity of the antisymmetric fundamental and its changes with the chromate anion mole fraction

in the unit cell have been discussed elsewhere [6]. We will discuss here the characteristics corresponding to the symmetric stretching  $\nu_1(A_1)$ . The main difference with that observed in the equivalent fundamental of the sulfate anion is the stability of the wavenumber position (see Fig. 7) which does not change in the samples studied, despite the changes in the chromate anion mole fraction. This observation can be justified taking into account two aspects that differentiate the vibrational dynamics of the chromate and sulfate anions. Firstly, the chromate anion presents an

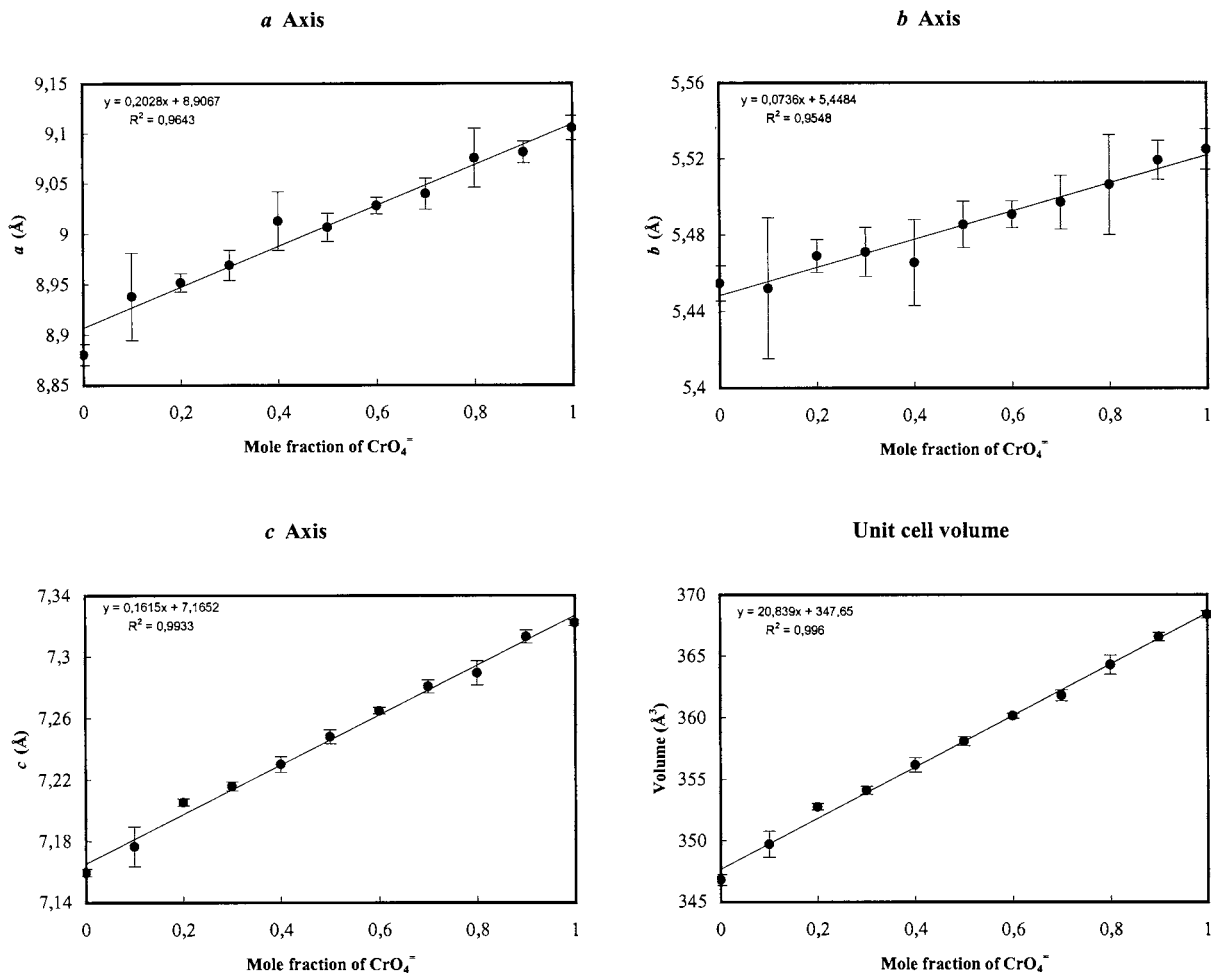


Fig. 3. Refined unit cell parameters of the solid solution samples plotted against the mole fraction of chromate ion. Error bars correspond to the standard error.

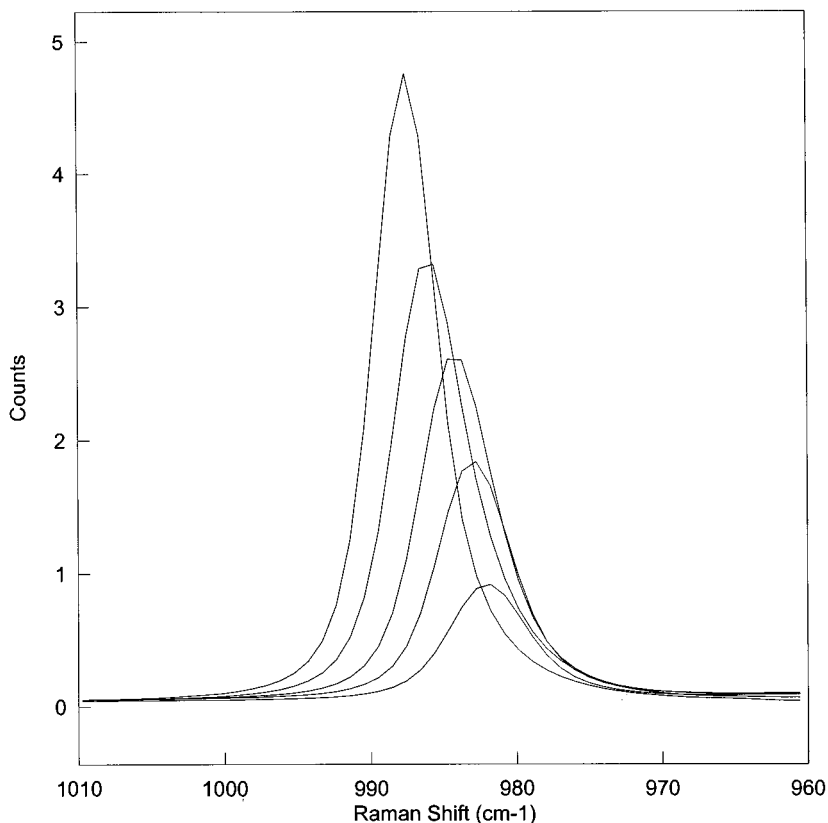


Fig. 4. Sulfate anion symmetric stretching  $\nu_1(A_1)$  band in some of the studied samples. From higher to lower intensity: barium sulfate, 80, 60, 40 and 20% of  $BaSO_4$ .

intense mechanical or kinematic intramolecular coupling [17] that is responsible for the small wavenumber difference ( $9\text{ cm}^{-1}$ ) observed between the symmetric and antisymmetric stretching bands, less than that noticed in the sulfate anion FT-Raman spectrum ( $96\text{ cm}^{-1}$ ). This high intramolecular coupling implies a low intermolecular coupling, which has been proposed [5] as one of the reasons that could promote changes in the band position when a different anion enters in the unit cell. Secondly, the stretching force constant, which is higher in the chromate anion ( $6.76\text{ mdyn}/\text{\AA}$ ) [16] than in the sulfate anion ( $6.27\text{ mdyn}/\text{\AA}$ ) [18], and the bigger mass of the central atom, would preserve the chromate anion from the influence of slight changes in the volume of the unit cell as the sulfate concentration increases. On the other hand, the evolution of the full-width at

half-height (FWHH) is parallel to that reported for the sulfate anion, even though its effect is stronger, since the FWHH observed in barium chromate is increased by about 46% in the sample with 50% of sulfate.

It is interesting to compare the relative intensities of the symmetric stretching bands because these data could be used for analytical purposes. As the integrated intensity of the  $\nu_1(A_1)$  FT-Raman band must be proportional to the relative concentration of the anion in the unit cell, the following equalities can be written:

$$I_C = \chi_C \cdot J_C$$

$$I_S = \chi_S \cdot J_S$$

where  $I_i$  are the integrated intensities of the chromate (C) and sulfate (S) symmetric stretching bands,  $\chi_i$  the corresponding mole fractions in the

unit cell and  $J_i$  are the proportionality constants, related to the Raman molar scattering coefficients. Combining the equalities:

$$\frac{I_C}{I_C + I_S} = \frac{\chi_C \cdot J_C}{(1 - \chi_C) \cdot J_S + \chi_C \cdot J_C}$$

where the mole fraction of sulfate anion ( $\chi_S$ ) has been substituted by  $(1 - \chi_C)$ . Inverting the previous equality:

$$\frac{I_S + I_C}{I_C} = \frac{J_S - \chi_C \cdot J_S + \chi_C \cdot J_C}{\chi_C \cdot J_C}$$

$$\frac{I_S}{I_C} + 1 = \frac{J_S}{J_C \cdot \chi_C} - \frac{J_S}{J_C} + 1$$

$$\frac{I_S}{I_C} = \frac{J_S}{J_C} \cdot \frac{1}{\chi_C} - \frac{J_S}{J_C}$$

The plot of the intensity ratio  $\frac{I_S}{I_C}$  against the inverse of the chromate anion mole fraction should give a straight line from whose slope or intercept the ratio between the Raman molar scattering coefficients can be calculated. With this representation, mole fractions can be obtained from intensity ratio data. Fig. 8 shows the plot. The linearity is good and the corresponding fitted parameters are: slope =  $0.2606 \pm 0.0047$ ; Y-axis intercept =  $-0.2814 \pm 0.0195$ ;  $r^2 = 0.9989$ ; standard error of the estimate = 0.0380. It can be concluded that the Raman molar scattering coefficient of the symmetric stretching band must be more than three times greater in chromate anion than in sulfate anion, in good qualitative correspondence with theoretical predictions [19,20].

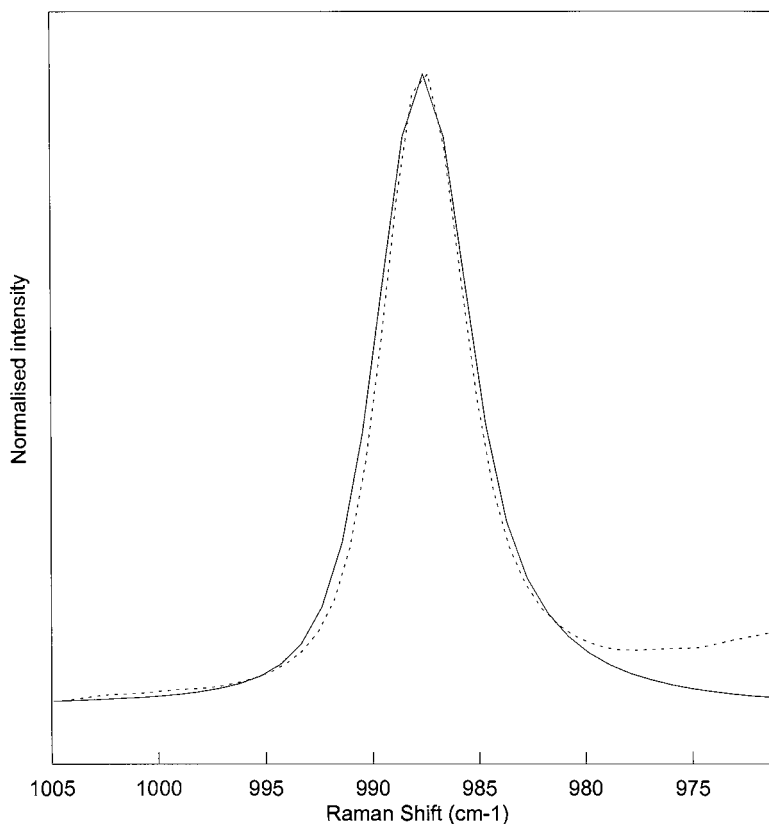


Fig. 5. Normalised sulfate anion symmetric stretching  $\nu_1(A_1)$  band in barium sulfate (full line) and in the 10% sulfate sample (dotted line). This band has been displaced towards higher wavenumber to coincide in position with the band of pure  $\text{BaSO}_4$ .

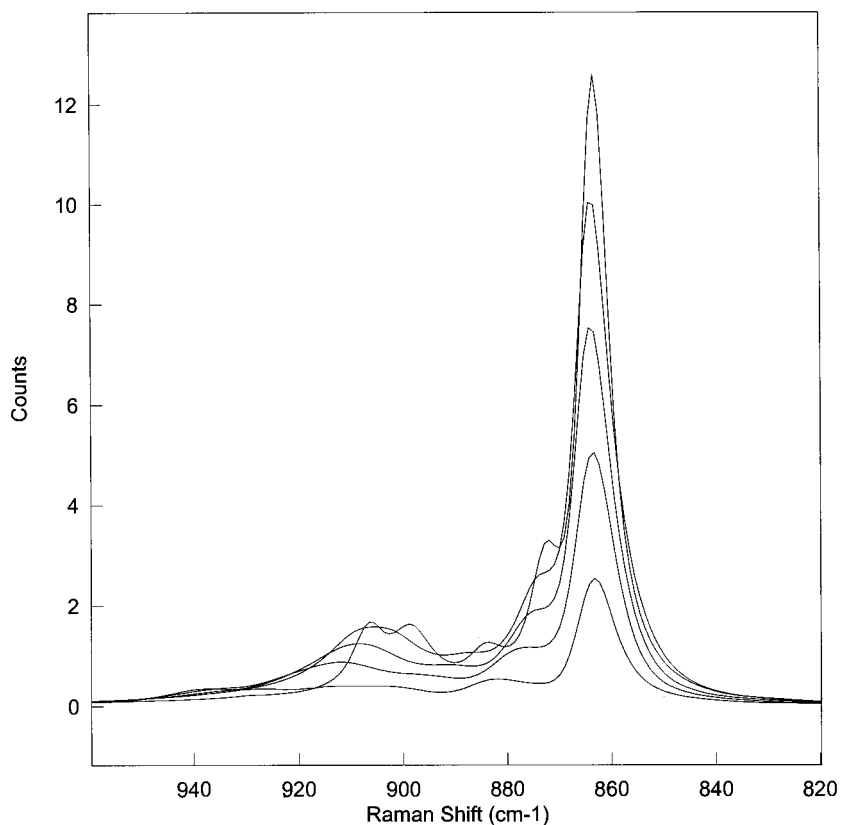


Fig. 6. Chromate anion symmetric stretching  $\nu_1(A_1)$  band ( $863\text{ cm}^{-1}$ ) and antisymmetric stretching  $\nu_3(F_2)$  group of bands in some of the studied samples. From higher to lower intensity: barium chromate, 80, 60, 40 and 20% of  $\text{BaCrO}_4$ .

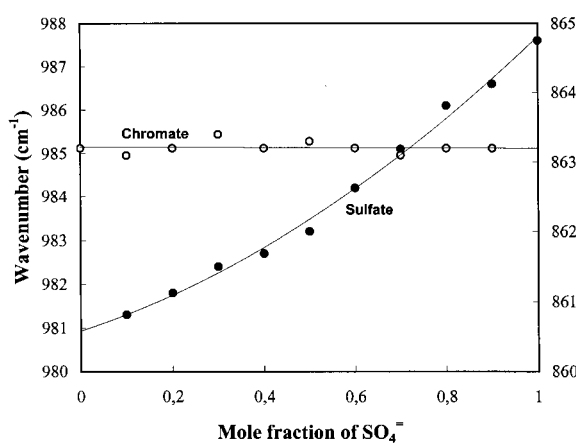


Fig. 7. Wavenumber position of the anion symmetric stretching  $\nu_1(A_1)$  bands in the solid solution. Right, Y-axis, chromate anion. Left, Y-axis, sulfate anion.

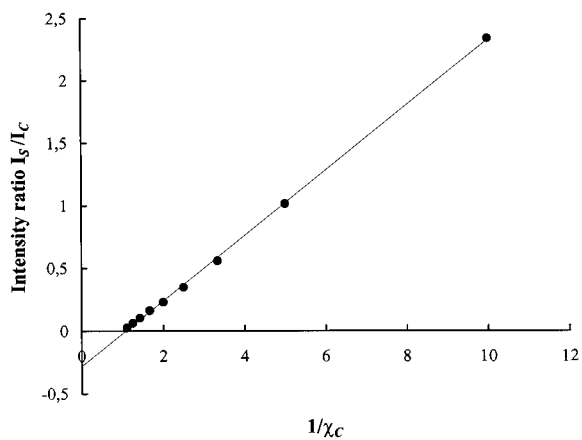


Fig. 8. Plot of the anion symmetric stretching  $\nu_1(A_1)$  bands intensity ratio  $I_S/I_C$  against the inverse of the chromate anion mole fraction,  $1/\chi_C$ .



## References

- [1] P.D. Glynn, E.J. Reardon, *Am. J. Sci.* 290 (1990) 164.
- [2] P.L. Hauff, E.E. Foord, S. Rosenblum, W. Hakki, *Am. Miner.* 68 (1983) 1223.
- [3] J.A. Davis, C.C. Fuller, A. Cook, *Geochim. Cosmochim. Acta* 51 (1987) 1660.
- [4] J.M. Zachara, C. Ciwan, C. Resch, *Geochim. Cosmochim. Acta* 55 (1991) 1549.
- [5] P. Tarte, G. Nizet, *Spectrochim. Acta Part A* 20 (1964) 503.
- [6] J.M. Alía, H.G.M. Edwards, A. Fernández, M. Prieto, *J. Raman Spectrosc.* 30 (1999) 105.
- [7] A. Putnis, L. Fernandez-Diaz, M. Prieto, *Nature (London)* 358 (1992) 743.
- [8] Y. Marcus, *Ion Properties*, Wiley, Chichester, 1998.
- [9] American Society for Testing Materials. Powder X-ray diffraction files, JCPDS-ASTM, Swarthmore, PA, 1980.
- [10] W.H. Casey, L. Chai, A. Navrotsky, P.A. Rock, *Geochim. Cosmochim. Acta* 60 (1996) 933.
- [11] I.A. Kiseleva, A.R. Kotelnikov, K.V. Martynov, L.P. Ogorodova, Ju.K. Kabalov, *Phys. Chem. Miner.* 21 (1994) 392.
- [12] L. Chai, A. Navrotsky, *Geochim. Cosmochim. Acta* 60 (1996) 4377.
- [13] B.E. Scheetz, W.B. White, *Am. Miner.* 62 (1977) 36.
- [14] W.D. Bischoff, S.K. Sharma, F.T. Mackenzie, *Am. Miner.* 70 (1985) 581.
- [15] J.M. Alía, Y. Díaz de Mera, H.G.M. Edwards, P. González-Martín, S. López-Andrés, *Spectrochim. Acta Part A* 53 (1997) 2347.
- [16] H. Stammreich, D. Bassi, O. Sala, *Spectrochim. Acta Part A* 12 (1958) 403.
- [17] P. Gans, *Vibrating Molecules. An Introduction to the Interpretation of Infrared and Raman Spectra*, Chapman and Hall, London, 1971.
- [18] M. Miyake, I. Minato, H. Morikawa, S.-I. Iwai, *Am. Miner.* 63 (1978) 506.
- [19] L.J. Basile, J.R. Ferraro, P. LaBonville, M.C. Wall, *Coord. Chem. Rev.* 11 (1973) 21.
- [20] N. Weinstock, H. Schulze, A. Müller, *J. Chem. Phys.* 59 (1973) 5063.

# Simple and rapid determination of the drug naproxen in pharmaceutical preparations by heavy atom-induced room temperature phosphorescence

Antonio Segura Carretero, Carmen Cruces-Blanco \*,  
M. Inmaculada Ramírez García, B. Cañabate Díaz,  
Alberto Fernández Gutiérrez

*Department of Analytical Chemistry, Faculty of Sciences, University of Granada, C/Fuentenueva s/n, 18071 Granada, Spain*

Received 7 September 1998; received in revised form 2 February 1999; accepted 5 February 1999

---

## Abstract

A simple, selective and sensitive heavy atom-induced room temperature phosphorimetric method (HAI-RTP) is described for the determination of naproxen (NAP) in pharmaceutical preparations. The phosphorescence signals are a consequence of intermolecular protection when analytes are, exclusively, in presence of a heavy atom salt and sodium sulfite as an oxygen scavenger to minimize RTP quenching. These variables selection constitute the basis of a HAI-RTP method for the determination of naproxen (detection limit  $17.6 \text{ ng ml}^{-1}$ ; 1.71% relative standard deviation at  $250 \text{ ng ml}^{-1}$ ). The method has been applied satisfactorily to the analysis of pharmaceutical preparations. © 1999 Elsevier Science B.V. All rights reserved.

*Keywords:* Heavy atom induced; Naproxen; Room temperature phosphorescence

---

## 1. Introduction

Naproxen [(+)-2-(6-methoxy-2-naphthyl)propionic acid or [(+)-2-(6-methoxy- $\alpha$ -methyl-2-naphthaleneacetic acid)] (NAP), is a non-steroidal anti-inflammatory drug with anti-inflammatory,

analgesic and antipyretic properties often preferred to acetylsalicylic acid (aspirin) because of its better absorption following oral administration and fewer adverse effects. Anti-inflammatory effects of naproxen are generally thought to be related to its inhibition of cyclo-oxygenase and consequent decrease in prostaglandin concentrations in various fluids and tissues [1]. Formulated in tablets or suppositories it is used in the treatment of rheumatoid arthritis and other rheumatic or musculoskeletal disorders, dysmenorrhea and acute gout.

---

\* Corresponding author. Tel.: +34-58-248594; fax: +34-58-243328.

*E-mail address:* mcruces@goliat.ugr.es (C. Cruces-Blanco)

The extensive use of naproxen formulations requires the development of a rapid, selective and accurate method that can be used in routine quality control. Naproxen in commercial formulations has been determined by coulometry [2,3], oscillometric titration [4], first- and second-derivative UV spectrophotometry [5] and high-performance liquid chromatography (HPLC) [6]. The United States Pharmacopeia XXI (1985) [7] and the Real Farmacopea Española (1997) [8] describes a UV spectrophotometric method for the assay of naproxen tablets and for a dissolution study and an acid–base titrimetric method with sodium hydroxide for the determination of the pure substance. Biological fluids can be analysed for naproxen using HPLC [9–11], GLC [12], fluorimetry [13], UV spectrophotometry [14] and mass fragmentography [15].

Although phosphorimetry is sensitive and more selective than fluorimetry for the analysis of many compounds, it has not been frequently used because of the time-consuming sample conditions required. Recently, different methodologies, such as sensitized room temperature phosphorescence (RTP), micelle-stabilized RTP or the use of cyclodextrins [16,17], combined with sodium sulfite as oxygen scavenger have allowed for development of RTP methods for numerous compounds in solution [18–23]. Only one phosphorimetric method has been proposed for this compound in micellar medium [24].

We have recently observed that it is possible, for some kinds of compounds, to observe phosphorescence signals in solution by using exclusively aqueous solutions of the analytes in presence of a heavy atom and salt sodium sulfite as oxygen scavenger, which is termed heavy atom-induced room temperature phosphorescence (HAI-RTP) [25,26].

The aim of this work is the development of the first application of heavy atom-induced room temperature phosphorimetric method in solution for the determination of naproxen in pharmaceutical preparations. The work presented here competes favorably in simplicity and detection limit with others methods proposed earlier in the literature.

## 2. Experimental

### 2.1. Apparatus

All recordings of uncorrected luminescence spectra and measurements of HAI-RTP intensities were carried out with an Aminco Bowman series 2 luminescence spectrometer equipped with a 7-W pulsed xenon lamp, required a personal computer with a 40-MB hard disk, 4 MB RAM memory, 3.5-inch 1.44-MB floppy disk drive, VGA colour monitor with VGA graphics adapter card, serial 2-button mouse, DOS 6.0, OS/2 version 2.0, and a GPIB(IEEE-524) interface card for computer instrument communication, equipped with a thermostated cell holder.

### 2.2. Reagents

Anhydrous sodium sulfite (Sigma) and reagent-grade thallium(I) nitrate (Sigma) were used as received. Aqueous solutions were made with doubly distilled water. The sodium sulfite solutions were prepared daily and kept in tightly stopped containers. Naproxen (Sigma) (see Fig. 1) was used without further purification. Stock solutions were prepared by dissolving 5 mg of NAP in 50 ml of water.

### 2.3. Basic procedure

A 100- $\mu$ l aliquot of the NAP stock solution, 8 ml of 0.25 M thallium(I) nitrate and 600  $\mu$ l of 0.1 M sodium sulfite were introduced into a 10-ml standard flask and made up to volume with water. Standard 10-mm fused-silica cells were filled with this analyte solution. Reagent blanks lacking naproxen were prepared and measured following the same procedure. The relative phosphorescence intensities (RPI) of the samples and the corre-

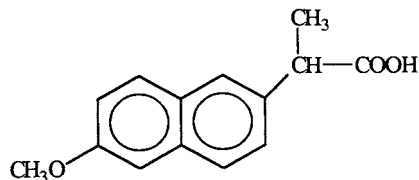


Fig. 1. NAP molecular structure.

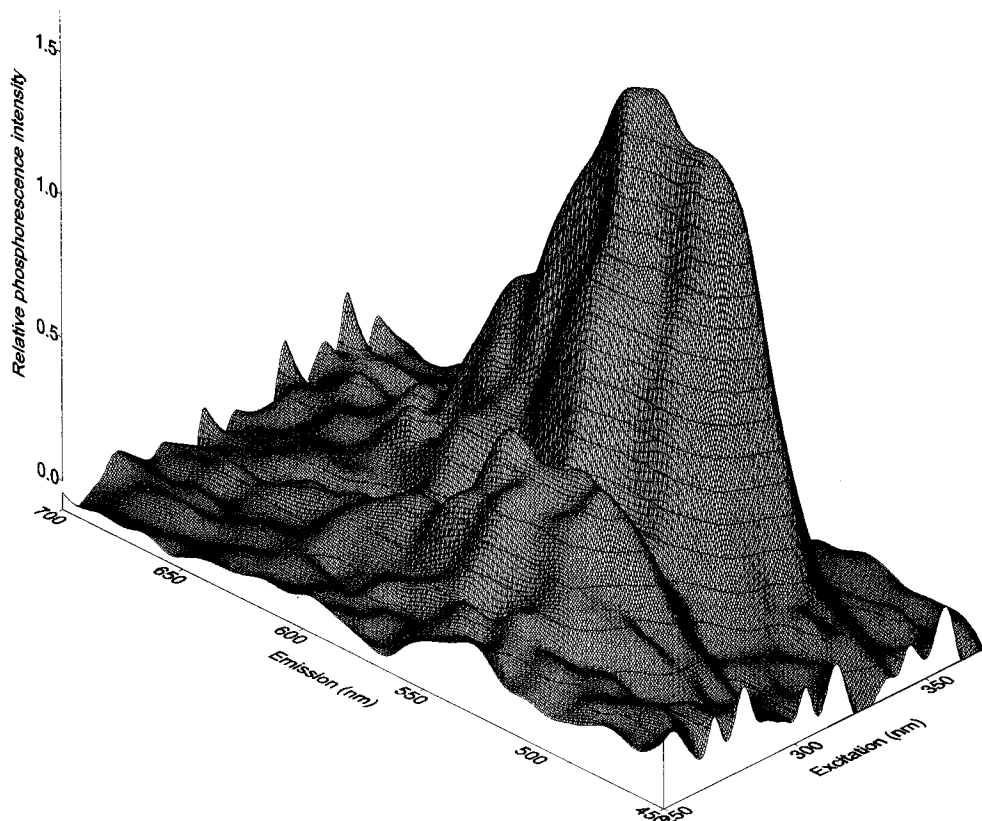


Fig. 2. Projected three-dimensional spectrum of NAP. [NAP] = 500 ng ml<sup>-1</sup>; [TiNO<sub>3</sub>] = 0.2 M; [Na<sub>2</sub>SO<sub>3</sub>] = 0.004 M. Emission, 450–700 nm; excitation, 250–350 nm; slits<sub>exc/em</sub>, 16/16 nm;  $t_d$  = 200  $\mu$ s;  $t_g$  = 400  $\mu$ s; detector sensitivity, 1000 V; and m.p.f., 5 ms.

sponding blanks were measured at phosphorescence wavelength maxima  $\lambda_{ex}/\lambda_{em}$  333/540 nm.

#### 2.4. Procedure for the pharmaceutical preparations

Two different commercial products were analyzed: Antalgin 550 (Sintex Latino, Madrid, Spain) with a nominal content of 673 mg g<sup>-1</sup> of naproxen and excipients and Naprosyn gel (Sintex Latino) with a nominal content of 100 mg g<sup>-1</sup> and also containing excipients, without indication of their concentration. For the analysis of Antalgin 550, the contents of five capsules were taken for analysis and the solid was powdered and homogenized. A portion of two products was dissolved in doubly distilled water and aliquots of

these solutions were treated as indicated under basic procedure.

### 3. Results and discussion

#### 3.1. Spectral characteristics

Fig. 2 shows the three-dimensional phosphorescence spectra of naproxen in an aqueous solution, obtained at 25°C in the presence of sulfite and Ti(I). NAP RTP spectra emit strong phosphorescence with maximum excitation and emission intensities at 334 and 540 nm, respectively, in aqueous solution and in presence of Ti(I) as a heavy atom with deoxygenation by Na<sub>2</sub>SO<sub>3</sub>. In the absence of either of these reagents the signal was

extinguished. The triplet lifetimes of naproxen under these conditions was determined as 1028  $\mu\text{s}$ .

Different instrumental parameters related to the luminescence technique could also affect the phosphorescence response, so they should be carefully selected. Slits of 16 nm, for the excitation and emission monochromators, a scan speed of 2 nm  $\text{s}^{-1}$ , with a delay time ( $t_d$ ) of 200  $\mu\text{s}$ , a gate time ( $t_g$ ) of 400  $\mu\text{s}$ , a detector sensitivity of 1000 V and a minimum period pulse (m.p.f.) or time between flashes of 5 ms were chosen. All these instrumental variables were kept constant for the rest of the experimental work.

The wavelength of maximum phosphorescence emission was red shifted by 207 nm with respect to the excitation wavelength and by 185 nm with respect to the wavelength of maximum fluorescence emission.

### 3.2. Effect of the heavy atom

Previous studies have already reported that heavy atom concentrations can affect the intensity of the HAI-RTP signal under certain conditions [25,26].

In this report, the following heavy atom salts have been studied: KI, NaI, KBr, NaBr, KCl,  $\text{TlNO}_3$ ,  $\text{Pb}(\text{NO}_3)_2$ , and  $\text{AgNO}_3$ .

$\text{Pb}(\text{NO}_3)_2$ , and  $\text{AgNO}_3$  precipitated in the presence of  $\text{SO}_3^{2-}$ , so they cannot be used.

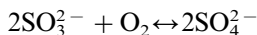
The basic vibrational structure of HAI-RTP emission spectra were not significantly altered by the presence of NaI, KBr, NaBr and KCl. This indicated that the heavy atom perturber did not significantly change the nature of the emitting species and the radiative process, while the concentration of the heavy atoms  $\text{TlNO}_3$  and KI could have significant influence on the HAI-RTP signal.

It has been proved that non-phosphorescence response of the analyte is obtained in the total absence of a heavy atom while, in general, the HAI-RTP intensity increased with increasing heavy atom concentration. Although the determination of an optimal concentration range was necessary. The best results were obtained using  $\text{TlNO}_3$  because the intensity is maxima, and a concentration of 0.2 M was selected for the rest of the experimental work (see Fig. 3).

### 3.3. Influence of sodium sulfite concentration and temperature

Sulfite ions can be used as an efficient  $\text{O}_2$  scavenger in the aqueous solution in HAI-RTP. This technical advance is a complement to using  $\text{N}_2$  purging to remove  $\text{O}_2$  from the solution. However, the concentration of  $\text{SO}_3^{2-}$  in the system is an important factor that affected the phosphorescence signal of NAP.

The method for sample deoxygenation is based on the redox reaction [18]:



These authors demonstrated that the temperature affects both the rate of oxidation of sulfite by the oxygen present in the solutions and the intensity of the phosphorescence signals. Increasing temperature accelerates the rate of oxidation of sulfite by oxygen. It was observed with naphthalene as the solute that at 15°C the oxygen was not effectively eliminated from the solutions and the phosphorescence signals were not reproducible, or the phosphorescence was even quenched. Consequently, it was considered necessary to eliminate the oxygen from the solutions by reaction with sulfite at room temperature and measure the phosphorescence signals at 18°C.

It should be taken into account that the solutions of the analytes were prepared in calibrated flasks where sulfite eliminated the oxygen, but subsequently the solutions were transferred into the phosphorimetric cells. After some time, the sulfite remaining in the solutions eliminated the oxygen in the cells.

The influence of sodium sulfite concentration was investigated by monitoring the RTP signal as a function of time until the HAI-RTP signal was stabilized for at least 5 min. Various amounts of sodium sulfite were added to a solution with a fixed amount of NAP and heavy atom salt while the concentration of sodium sulfite was varied from  $3.0 \times 10^{-5}$  to  $6.0 \times 10^{-3}$  M. The concentration of NAP was 500  $\text{ng ml}^{-1}$  and the concentration of  $\text{TlNO}_3$  was 0.2 M. They were transferred into a 10-ml flask, with the appropriate amounts of 0.1 M sodium sulfite stock solution to obtain the final desired concentration. The development

of the HAI-RTP emission was followed kinetically by monitoring at 540 nm with excitation at 334 nm.

Fig. 4 shows the influence of sodium sulfite concentration on the RTP emission from naproxen in presence of  $\text{TINO}_3$ . It has been observed that by increasing sodium sulfite concentration, the phosphorescence signal of the system decreased gradually and also the stabilization time ( $t$ ) or period of time necessary for RTP to reach stabilization increased, although diminishing sulfite concentration,  $t$  was considerably increased. A concentration of 0.004 M was selected in this work.

For obtaining the HAI-RTP signals of the three samples, a detailed study of temperature was carried out. The HAI-RTP intensities decrease almost linearly with an increase in temperature. This effect is markedly appreciate for the NAP– $\text{TINO}_3$  system, and this is mainly due to molecu-

lar motion and intermolecular energy conversion because of the collisional deactivation of the phosphors. A temperature of  $25 \pm 1^\circ\text{C}$  was selected for the rest of the experimental work.

### 3.4. Stability

The RPI signal of the system can reach stability instantaneously under the conditions of chemical deoxygenation, and remain stable for at least 1 h.

### 3.5. Validation of the method

The method was tested for linearity, precision, reproducibility and specificity. The phosphorescence response was linear in relation to the concentration of NAP over the range 0–500.0  $\text{ng ml}^{-1}$  calculated in the final solution. The regression equation was:

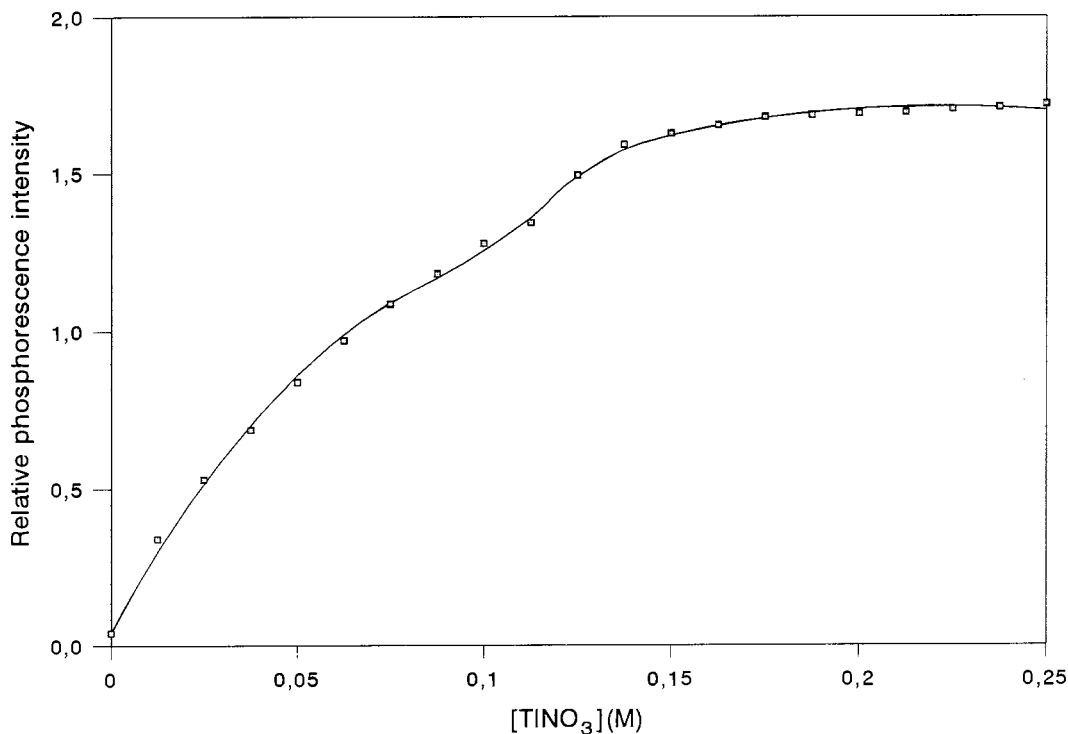


Fig. 3. Effect of heavy atom concentration.  $[\text{NAP}] = 500 \text{ ng ml}^{-1}$ ;  $[\text{Na}_2\text{SO}_3] = 0.004 \text{ M}$ ;  $\lambda_{\text{exc/em}} = 334/540 \text{ nm}$ ; slits $_{\text{exc/em}}$ , 16/16 nm;  $t_d = 200 \text{ } \mu\text{s}$ ;  $t_g = 400 \text{ } \mu\text{s}$ ; detector sensitivity, 1000 V; and m.p.f., 5 ms.

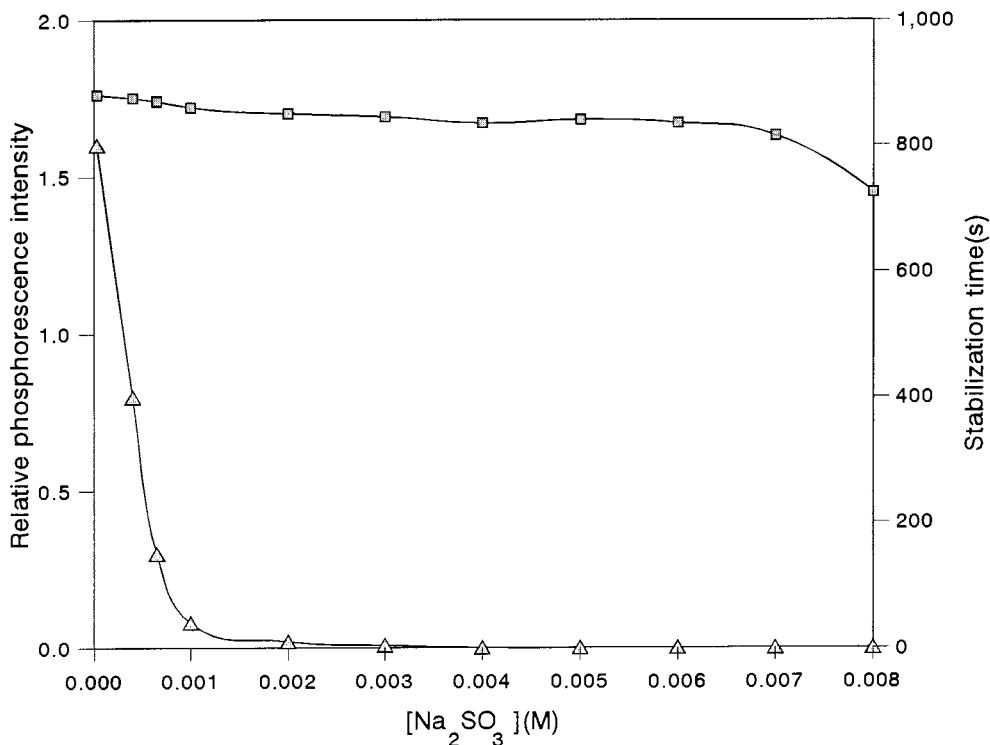


Fig. 4. Effect of  $\text{Na}_2\text{SO}_3$  concentration on RPI (■) and stabilization time (△).  $[\text{NAP}] = 500 \text{ ng ml}^{-1}$ ;  $[\text{TINO}_3] = 0.2 \text{ M}$ ;  $\lambda_{\text{exc/em}} = 334/540 \text{ nm}$ ;  $\text{slits}_{\text{exc/em}} = 16/16 \text{ nm}$ ;  $t_d = 200 \text{ } \mu\text{s}$ ;  $t_g = 400 \text{ } \mu\text{s}$ ; detector sensitivity, 1000 V; and m.p.f., 5 ms.

$$\text{RPI} = 0.02 + 0.034C$$

where  $C$  is the concentration of NAP in  $\text{ng ml}^{-1}$ .

The correlation coefficient ( $r = 0.999$ ,  $n = 7$ ), indicates good linearity. A detection limit [27] of  $17.6 \text{ ng ml}^{-1}$  was established.

The precision of the method was determined at two different concentrations. The relative standard deviation (RSD) ( $n = 7$ ) was 2.56 and 1.18% for concentrations of NAP of 200 and  $500 \text{ ng ml}^{-1}$ , respectively.

### 3.6. Applications

The proposed method was applied to the determination of naproxen in two pharmaceutical preparations, Antalgin 550 and Naprosyn gel. The samples did not require any previous treatment and were analysed using the phosphorimetric method described above.

The results obtained for the pharmaceutical preparations were compared with those obtained by the official method (an acid–base titrimetric method with sodium hydroxide for the determination of the pure substance) [8] for the same samples. Table 1 shows that the two methods provided equivalent results for the analysis of pharmaceutical preparations.

Table 1  
Results of the determination of naproxen in pharmaceutical preparations

Pharmaceutical preparations	Naproxen concentration ( $\text{mg g}^{-1}$ )	
	Proposed method	Official method
Antalgin 550	$633 \pm 24$	$673 \pm 45$
Naprosyn gel	$97 \pm 3$	$100 \pm 4$

#### 4. Conclusions

This paper presents an innovative way of obtaining RTP from naproxen in solution, without using any kind of organized media, which is a very important finding that opens the possibilities for room temperature phosphorescence measurements in solution in the future, and gives simple and good conditions to obtain some very attractive analytical characteristics. For the two kinds of commercial products tested, the statistical calculations of the assay results showed satisfactory precision of the phosphorimetric method proposed with no significant differences between the certified and experimental results, demonstrating that the heavy atom-induced room temperature phosphorimetry technique can enhance the sensitivity and selectivity for the analysis of small amounts of chemicals in real samples. The proposed method can be recommended for the routine determination of naproxen in aqueous solutions, as it is rapid and simple and the results obtained showed good precision.

#### Acknowledgements

The authors gratefully acknowledge the financed support of O.S.C. de UNICAJA.

#### References

- [1] P.A. Todd, S.P. Clissold, *Drugs* 40 (1990) 91.
- [2] Z. Cawrych, E. Szyszko, *Acta Pol. Pharm.* 36 (1979) 569.
- [3] G. Kanoute, E. Nivaud, B. Paulet, P. Boucly, *Talanta* 31 (1984) 144.
- [4] T. Pomazanska-Kolodziejska, *Acta Pol. Pharm.* 40 (1983) 357.
- [5] M.S. Mahrous, M.M. Abdel-Khakil, M.E. Abdel-Mamid, *J. Assoc. Off. Anal. Chem.* 68 (1985) 535.
- [6] J.W. Wainer, T.D. Doyle, *J. Chromatogr.* 284 (1984) 117.
- [7] United States Pharmacopeia XXI, National Formulary XVI, United States Pharmacopeial Convention, Rockville, MD, 1985, pp. 710 and 711.
- [8] Real Farmacopea Española, Ministerio de Sanidad y Consumo, Madrid, 1997, pp. 1346.
- [9] J.T. Slattery, G. Levy, *Clin. Biochem.* 12 (1979) 100.
- [10] D. Westerlund, A. Theodorsen, Y. Jaksch, *J. Liq. Chromatogr.* 2 (1979) 969.
- [11] R.A. Upton, J.N. Buskin, T.W. Guentert, D.L. Williams, S. Riegelman, *J. Chromatogr.* 190 (1980) 119.
- [12] S.H. Wan, S.B. Martin, *J. Chromatogr.* 170 (1979) 473.
- [13] A. Markku, *J. Pharm. Sci.* 66 (1977) 433.
- [14] M. Holzbecher, H.A. Ellerberger, J.M. Marsh, S. Bourdeau, *Clin. Biochem.* 12 (1979) 66.
- [15] H.E. Larsen, K. Marinelli, *J. Chromatogr.* 222 (1981) 482.
- [16] S. Scypinski, L.J. Cline Love, *Anal. Chem.* 56 (1984) 322.
- [17] S. Scypinski, L.J. Cline Love, *Anal. Chem.* 56 (1984) 331.
- [18] M.E. Díaz García, A. Sanz-Medel, *Anal. Chem.* 58 (1986) 1436.
- [19] A. Sanz-Medel, P.L. Martínez García, M.E. Díaz García, *Anal. Chem.* 59 (1987) 774.
- [20] R.J. Hurtubise, *Phosphorimetry. Theory, Instrumentation and Applications*, VCH, New York, 1990.
- [21] C. Cruces Blanco, A. Segura Carretero, A. Fernández Gutiérrez, *Anal. Chim. Acta* 318 (1996) 357.
- [22] A. Segura Carretero, C. Cruces Blanco, A. Fernández Gutiérrez, *Anal. Chim. Acta* 329 (1996) 165.
- [23] A. Segura Carretero, C. Cruces Blanco, A. Fernández Gutiérrez, *Anal. Sci.* 12 (1996) 653.
- [24] I. Rapado Martínez, R.M. Villanueva Camañas, M.C. García-Alvárez Coque, *Analyst* 119 (1994) 1093.
- [25] A. Segura Carretero, C. Cruces Blanco, B. Cañabate Díaz, A. Fernández Gutiérrez, *Anal. Chim. Acta* 361 (1998) 217.
- [26] A. Segura Carretero, C. Cruces Blanco, A. Fernández Gutiérrez, *J. Agric. Food Chem.* 46 (1998) 3683.
- [27] L. Cuadros Rodríguez, A.M. García Campaña, C. Jiménez Linares, M. Román Ceba, *Anal. Lett.* 26 (1993) 1243.



# An optimized sampling and GC–MS analysis method for benzene in exhaled breath, as a biomarker for occupational exposure

C. Plebani \*, G. Tranfo, A. Salerno, A. Panebianco, A.M. Marcelloni

*Department of Occupational Hygiene, National Institute for Prevention and Occupational Safety (ISPESL),  
Monteporzio Catone 00040 (RM), Italy*

Received 7 September 1998; received in revised form 3 February 1999; accepted 10 February 1999

---

## Abstract

Benzene is known to be toxic and carcinogenic: therefore, in case of exposure to benzene vapours, a reliable biological monitoring procedure is needed, particularly in the field of occupational hygiene. The determination of the concentration of benzene in the exhaled air 8 h after the exposure has been demonstrated to be a significant biomarker, even for low concentrations of airborne benzene vapours. This work presents a sampling and analysis method that optimizes previously described procedures: in the sampling phase, a double-step sample collection in Tedlar bags is used, in order to remove the breath moisture and to standardise the sample volumes. The analytical phase uses a cryogenic trap for the concentration of the air samples to be injected in the GC–MS, without the need for trapping materials, significantly reducing time and costs of the analysis and improving sensitivity. The presented method has been successfully applied to the biological monitoring of a mixed population (occupationally exposed and not exposed subjects, smokers and non-smokers), with a lower detection limit of 1.5 ng of benzene per litre of exhaled air, that is 1/200 of the biological exposure index recommended by the American Conference of Governmental Hygienists. © 1999 Elsevier Science B.V. All rights reserved.

*Keywords:* Benzene; Biological monitoring; Exhaled breath; GC–MS analysis

---

## 1. Introduction

Benzene is nowadays to be regarded as a ubiquitous pollutant, as its significant and widespread emission to the environment results from automobile traffic, heating and industrial plants [1]. A

minor contribution also comes from a fraction probably originating from fires of woods and natural resins [2]. The risk of benzene exposure is, therefore, not only an occupational risk, but the general population is involved; besides, a significant contribution to this non-occupational exposure is from cigarette smoke, specially to indoor air [3].

Benzene exposure has been linked to haematological problems in man [4] and is a class I human

---

\* Corresponding author. Tel.: +39-69-418-1429; fax: +39-69-419-453.

carcinogen according to the International Agency for Research on Cancer [5]. The American Conference of Governmental Hygienists (ACGIH) states (1996–97) a threshold limit value for the concentration of benzene in the air of working environments of  $32 \text{ mg/m}^3$ , and intends to reduce this value to  $1.6 \text{ mg/m}^3$  and to add the 'skin' notation [6], to outline that benzene cannot only be inhaled but is also absorbed by the skin [7]. For this reason environmental monitoring is not enough to assess the risk of exposure to benzene, but there is the need to perform also a biological monitoring of exposed subjects, by means of a biomarker sensitive also to low concentrations of benzene.

The biomarkers proposed and validated for exposure to benzene are phenol in urine and benzene in exhaled air, the latter being more specific for exposures to low concentrations [8], as phenol can be a final product also for the metabolism of endogenous substances [9,10].

The limits stated by the ACGIH, BEIs (biological exposure indexes) for the concentration of benzene in the exhaled air are 0.08 ppm for mixed air (total exhaled air) and 0.12 ppm for alveolar air (end exhaled air) [6], before the beginning of the following shift.

Several methods have been proposed for sampling and collecting exhaled air samples: glass tubes have been used for the sampling of alveolar air, and plastic bags mainly for the total air. From these, subsamples of the air are transferred to the analytical system directly [11,12] or through solid sorbents that are thermally desorbed [13]. All These methods make use of an external standard procedure for the quantitative analysis.

SPME has been also applied to analysis of human breath, but to date it is limited to compounds with relatively high concentrations in the breath [14].

This paper presents a sampling and analysis method optimized for the routine determination of benzene in mixed exhaled air, in which the samples are collected in Tedlar bags and benzene is analysed by gas chromatography and detected by single-ion monitoring mass spectrometry (GC–SIM-MS). The range of applicability is from 1.5 to 250 ng of benzene per litre of exhaled air, the latter corresponding to the BEI.

## 2. Experimental

### 2.1. Sampling devices

Tedlar bags of 1 and 3 l in volume have been used to collect the air samples, with both an opening valve and a septum. These bags were cleaned by filling them with pure nitrogen, and heating and emptying them several times before use.

For the storage of the standard atmospheres of benzene, 1-l glass bulbs have been used, with two glass stopcocks and a septum, cleaned as above.

### 2.2. Bags and bulbs blanks

An aliquot of the last washing air has been analysed according to the sample analysis procedure hereunder described. The resulting concentration of 'benzene' is the blank of the sampling and analysis procedure, and will be considered in the following samples analysis.

### 2.3. Sampling procedure

The subject breathes out normally into a 3-l Tedlar bag, collecting the volume of air of two or three complete breaths. The bag is then thermostated at  $40^\circ\text{C}$  for at least 30 min, and then part of its content is transferred, passing through a  $\text{CaCl}_2$  trap, to a 1-l bag filling it completely.

### 2.4. Internal standard introduction

Into each 1-l bag a known amount of perdeuterated benzene ( $\text{C}_6\text{D}_6$ ) is introduced, chosen as internal standard for the determination of the sample content of benzene. Perdeuterated benzene is stored in a glass bulb at a concentration of 0.95 mg/l in anhydrous nitrogen, thermostated at  $40^\circ\text{C}$ , from which 30  $\mu\text{l}$  are transferred by syringe to the sample bag.

### 2.5. Sample injection

Benzene determination is performed in a GC System equipped as follows: a thermal desorber

with cold trap (TCT) Chrompack; an HP 5890 gas chromatograph with 100% cross-linked dimethylpolysiloxane capillary column, 60 m length, 0.32 mm i.d., 1  $\mu\text{m}$  film thickness; an MSD HP 5790 mass detector, used in SIM for ions having  $m/z$  78 and 84.

A total of 100 ml of sample air is transferred from the Tedlar bags thermostated at 40°C to the cold trap, at an injection flow of about 100 ml/min. The cold trap is made from a fused-silica capillary (40 cm length, 0.53 mm i.d.) whose internal surface is covered by a cross-linked silicone film (thickness, 5  $\mu\text{m}$ ). Above this cold trap, instead of the sampling tube, a quartz tube containing  $\text{CaCl}_2$  is installed, kept at room temperature, in order to retain the possible sample residual moisture, which during the following gas chromatographic run will be dried at 170°C for 15 min, with a backflush of helium of 20 ml/min.

During the sample injection helium flows at 100 ml/min (desorption phase) through the TCT, having the trap cooled at  $-120^\circ\text{C}$  with liquid nitrogen. At the end of this step, the cold trap is flash heated (about 1 s) at 200°C and the components are injected onto the analytical column.

### 2.6. Gas chromatographic analysis

The elution of benzene is performed by means of a temperature gradient, as follows: (a) starting temperature 60°C for 5 min; (b) temperature increase of 5°C/min to 150°C, for 5 min; (c) temperature increase of 15°C/min to 240°C for 5 min. Under these conditions, the retention time for benzene was about 10 min.

Selected ion records are obtained at  $m/z = 78$  (the molecular ion of the analyte) and at  $m/z = 84$  (the molecular ion of the internal standard, D-6 benzene). The quantitation of benzene has been performed with the internal standard method; the calibration curve has been built on five points of benzene concentration, and the response linearity verified in the concentration range 1.5–250 ng of benzene per litre of air.

## 3. Results and discussion

### 3.1. Air sampling

The sampling procedure described, in which the mixed exhaled air is first collected in a 3-l bag and then transferred to a 1-l bag, makes possible to have an homogeneous aliquot from one or more complete breaths, standardising sample volume (1 l). Besides, if benzene concentration was too low to determine, it is always possible to repeat the analysis using a larger volume of sample.

In order to remove the moisture from the air samples, a  $\text{CaCl}_2$  trap could have been applied after the mouthpiece of the collecting bag, but this would have made it difficult to breath normally. Therefore, the  $\text{CaCl}_2$  trap has been applied between the 3- and 1-l Tedlar bags, while the possible residual moisture is retained by the  $\text{CaCl}_2$  in the quartz tube installed in the injection system.

### 3.2. Analytical method

In the proposed method the air samples are directly injected into the cryogenic trap, with the advantage of reducing the time of analysis, cost and complexity in comparison to the use of a sampling tube. A  $\text{CaCl}_2$  trap selectively retains the possible residual moisture of the exhaled air samples, which could compromise the efficacy of the cryogenic trap.

For the quantitative determination of benzene concentration an internal standard has been used, that is easier to use than the external standard technique. Perdeuterated benzene is injected into the 1-l Tedlar bag immediately after the sample transfer: this makes possible a storage of the bags before the analysis, without errors deriving from possible gas leaks, non-specific adsorption, incomplete freezing of the sample in the cryogenic trap. This results in a method particularly suitable for routine analysis.

Reproducibility, calculated as the variation coefficient of the results obtained analysing six times the same sample, is always better than 1.8% in the concentration range 1.5–250 ng/l.

As benzene is to be considered a ubiquitous pollutant, a 'blank' value has been determined for

the glass bulbs (less than 0.4 ng/l) and for the Tedlar bags (less than 0.9 ng/l), with a mean value of 0.7 ng/l (0.25 ng/l standard deviation).

The limit of applicability of this method (1.5 ng/l) has been calculated adding to the mean value of the bags blank three times its standard deviation.

### 3.3. Applications

The method described has been used to determine the benzene concentration of the exhaled air of a mixed population of 18 people representative of different situations: non-occupationally exposed non-smoker, non-occupationally exposed smoker, occupationally exposed non-smoker and occupationally exposed smoker.

The occupationally exposed subjects considered are workers employed in gas stations located in urban areas: the sample collection was performed 12 h after the end of the work shift, before the beginning of the following shift, in an environment far from the source of professional exposure. For the non-occupationally exposed subject, the sample collection was, instead, random.

The average benzene concentration found in the non-occupationally exposed non-smokers was 8 ng/l (range, 1.5–16); in the non-occupationally exposed smokers it was 45 ng/l (range, 36–70), although for smokers it has to be considered that the benzene concentration is strictly dependent from the time elapsed from the last cigarette smoked before the air sampling.

The values found for the occupationally exposed subjects are in the range 20–177 ng/l (average, 67 ng/l).

## 4. Conclusions

The analytical method described, compared to the methods more frequently applied, reduces the time and costs of the analysis, as it does not involve an enrichment step on solid adsorbents,

but the air samples can be injected directly into a cryogenic trap.

The lower applicability limit, 1.5 ng/l, that is 1/200 of the BEI, and the response linearity range of 1.5–250 ng/l, allow to perform biological monitoring also of subjects exposed to very low concentrations of benzene.

## References

- [1] R. Lauwerys, P. Hoet, *Industrial Chemical Exposure, Guidelines for Biological Monitoring*, second ed., Lewis Publishers, 1993, p. 108.
- [2] G. Pezzagno, Il problema benzene: fattori che influenzano i valori biologici della popolazione in generale, in: C. Minoia, P. Apostoli, E. Sabbioni, *Valori di riferimento di elementi in traccia e sostanze di interesse biotossicologico*, Morgan Edizioni Tecniche, Milano, 1994, p. 190.
- [3] *Documentation of TLVs and BEIs*. ACGIH Cincinnati, OH, 1991.
- [4] B.D. Goldstein, Hematotoxicity in humans, in: *Benzene Toxicity: a Critical Evaluation*, McGraw Hill, New York, 1977.
- [5] Benzene, IARC Monographs on the Evaluation of the Carcinogenic Risk of Chemicals to Human, vol. 29, IARC, Lyon, 1982, p. 99.
- [6] *Threshold Limit Values and Biological Exposure Indices*, ACGIH, Cincinnati, OH, 1996.
- [7] R. Lauwerys, in: *Industrial Health and Safety: Human Biological Monitoring of Industrial Chemicals Series, Benzene*, Luxembourg, Commission of the European Communities, 1983.
- [8] C.N. Ong, B.L. Lee, *J. Chromatography B* 660 (1994) 1–22.
- [9] L. Drummond, R. Luck, A.S. Afacan, H.K. Wilson, *Br. J. Ind. Med.* 45 (1988) 256–261.
- [10] L. Perbellini, G.B. Faccini, F. Pasini, F. Cazzoli, S. Pistoia, R. Rosellini, M. Valsecchi, F. Brugnone, *Br. J. Ind. Med.* 45 (1988) 345–352.
- [11] K. Pekari, S. Vainiotalo, P. Heikkila, A. Palotie, M. Luotamo, V. Riihmaki, *Scand. J. Work Environ. Health* 18 (1992) 317–322.
- [12] F. Brugnone, L. Perbellini, G.B. Faccini, F. Pasini, B. Danzi, G. Maranelli, L. Romeo, M. Gobbi, A. Zedde, *Am. J. Ind. Med.* 16 (1989) 385–399.
- [13] G.M. Ljungkvist, R.G. Nordlinder, *Am. Ind. Hyg. Assoc. J.* 56 (1995) 693–697.
- [14] C.Ph. Groto, J. Pavliszin, *Anal. Chem.* 69 (4) (1997) 587–596.

# Optimization of an extraction method of aroma compounds in white wine using ultrasound

Dolores Hernanz Vila <sup>a</sup>, Fco. José Heredia Mira <sup>b</sup>, Rafael Beltran Lucena <sup>a</sup>,  
M<sup>a</sup>Angeles Fernández Recamales <sup>a,\*</sup>

<sup>a</sup> *Dpto. Química y Ciencia de los Materiales. E.P.S. Universidad de Huelva, 21819 La Rabida, Spain*

<sup>b</sup> *Dpto. Nutrición y Bromatología, F. De Farmacia, Universidad de Sevilla, Sevilla, Spain*

Received 7 September 1998; received in revised form 2 January 1999; accepted 12 February 1999

## Abstract

A simple and rapid method is described for the extraction of wine volatile compounds. The procedure was based on the ultrasonic-assisted extraction using a mixing of *n*-pentane–diethylether (1:2) as solvent. Factorial designs have been used to optimize the sonication process. Factors such as sample volume, extraction time and solvent volume were considered. A statistical approach was used to find suitable conditions for the ultrasound extraction of aroma compounds of wine. A factorial design at two-level revealed that lower sample volume (100 ml instead of 125 ml) and solvent volume of 50 ml instead of 60 ml contributed to improve extraction efficiency. Performance of the method was evaluated, and the procedure applied to the analysis of aroma compound in white wines from ‘Condado de Huelva’ (Spain). © 1999 Elsevier Science B.V. All rights reserved.

*Keywords:* Aroma compounds; Ultrasound extraction; Wine

## 1. Introduction

Volatile compounds play an important role in the organoleptic characteristic of wines. It has been recognized that the aroma constituents of the wine have a leading contribution to its varietal character. Several hundred chemically different flavor compounds, such as alcohols, esters, or-

ganic acids, aldehydes, ketones, and monoterpenes, have been found in wines.

The flavor of a wine is extremely complex, due to the great number of compounds present which have different polarities, volatilities and, moreover, are found in a wide range of concentrations. Hence, sample preparation, especially, extraction and concentration of aroma compounds remains one of the critical areas in aroma volatiles analysis.

Continuous liquid–liquid extraction has been widely used in sample preparation for the determination of wine volatiles [1,2]. Other methods include liquid–liquid extraction, XAD-2 resin ex-

\* Corresponding author. Tel.: +34-9-59530213; fax: +34-9-59350962.

*E-mail address:* recamale@uhu.es (M. Fernández Recamales)

traction [3,4], supercritical fluid extraction [5] microwave extraction [6], sonication [7] and sorbent extraction [8].

In the present work, the factors (including choice of solvent and salt type) affecting efficiency extraction of volatiles from wines using sonication were investigated applying a factorial experimental design. The analytical performance of the rec-

ommended method, which has been applied to the analysis of a young white wine from 'Condado de Huelva' has also been studied.

## 2. Experimental procedures

### 2.1. Reagents

All the reagents used were of analytical grade. Solvents, ethanol, *n*-pentane, dichloromethane, diethylether were purchased from Romil (Cambridge, UK). The standards of aroma compounds, which ranged from 98 to 99% purity, were obtained from Chemservice (West Chester, PA) and Aldrich.

Two standard solutions, one in ethanol and another in an extractant mixture, of these compounds were prepared; Table 1 shows their concentrations. 2-Octanol was added at 316.8 mg/l to the standards and samples before extraction as internal standard.

A model wine solution was prepared with 1.15 g/l potassium bitartrate and at 0.7 g/l tartaric acid (pH 3.02) in 10.5% (v/v) aqueous ethanol solution [4].

### 2.2. Samples

Sixteen samples of wine were used in this study. These wines were manufactured with white grapes of the Zalema variety and were obtained from the wine cellar as representative examples of the young wines production from 'Condado de Huelva' during 1995 and 1996 harvests.

### 2.3. Sample preparation: ultrasonic extraction

The extraction procedure was optimized by applying a factorial experimental design at two levels (2<sup>3</sup>). The sample volume considered according to the level indicated in the respective trial (Tables 2 and 3) was extracted by means of ultrasound. The extraction time and amounts of extraction solvent were also optimized. A full 2<sup>3</sup> design would have required eight experiments which were duplicated in order to calculate the residual error. The knowledge of the pure error is required

Table 1  
Calibrated standard solutions

Compound	Concentration (mg/l)	
	In extractant	In ethanol
Acetaldehyde	531	423
Methyl acetate	1551	4490
Ethyl acetate	2129	5036
Methyl alcohol	2124	4395
Isopropyl alcohol	2417	3744
Ethyl propionate	2108	3776
Isobutyl acetate	828	227
<i>sec</i> -Butyl alcohol	892	4338
Ethyl butyrate	2849	5344
Propyl alcohol	2281	4303
Isobutyl alcohol	2168	5090
Isoamyl acetate	1401	615
<i>n</i> -Butyl alcohol	1352	4760
4-Methyl-2-pentanol	1692	4700
Isoamyl alcohol	2970	3997
Amyl alcohol	1255	3729
Hexyl acetate	1323	4736
Ethyl lactate	2610	3062
Ethyl octanoate	2262	3677
Heptyl alcohol	151	510
Linalool	1841	3529
Diethyl succinate	2244	3976
$\alpha$ -Terpineol	127	1178
Citronellol	880	5269
Nerol	1549	3432
Geraniol	560	3966
2-Phenylethyl alcohol	3472	4164

Table 2  
Factors and levels for the optimisation experiment

Notation	Factor	Level (-)	Level (+)
T	Time (min)	25	30
V	Sample volume (ml)	100	125
E	Extractant volume (ml)	50	60

Table 3  
Design matrix and the results as average recovery<sup>a</sup>

No.	V	T	E	Alcohols	Esters	Terpenes
1–9	–	–	–	73.550	47.120	47.265
2–10	+	–	–	51.680	21.955	39.380
3–11	–	+	–	62.745	47.590	49.205
4–12	+	+	–	63.610	26.725	43.285
5–13	–	–	+	50.045	45.380	44.235
6–14	+	–	+	53.065	27.160	43.405
7–15	–	+	+	50.725	52.795	43.045
8–16	+	+	+	54.815	19.775	46.86

<sup>a</sup> V, sample volume (ml); T, extraction time (min); E, extractant volume (ml).

Table 4  
Precision and linearity of chromatographic separation and retention times

Compound	$t_R$ (min)	$r$	% RSD
Methyl acetate	5.95	0.9995	4733
Ethyl acetate	6.98	0.9996	3810
Methyl alcohol	7.17	0.9971	4348
Isopropyl alcohol	7.90	0.9988	5150
Isobutyl acetate	8.82	0.9994	4475
sec-Butyl alcohol	10.76	0.9998	11 059
Ethyl butyrate	11.19	0.9999	23 419
Propyl alcohol	11.69	0.9991	4440
Isobutyl alcohol	13.88	0.9996	3339
Isoamyl acetate	15.40	0.9979	4525
n-Butyl alcohol	16.24	0.9993	3311
4-Methyl-2-pentanol	17.25	0.9977	4866
Isoamyl alcohol	18.97	0.9993	4633
Amyl alcohol	20.78	0.9996	3135
Hexyl acetate	21.80	0.9998	1640
Ethyl lactate	24.56	0.9993	2198
Ethyl octanoate	27.61	0.9997	2030
Heptyl alcohol	28.10	0.9990	3075
Linalool	30.47	0.9997	2643
Diethyl succinate	33.41	0.9998	6196
$\alpha$ -Terpineol	33.88	0.9997	2953
Citronellol	35.18	0.9985	14 017
Nerol	36.05	0.9905	35 136
2-Phenylethyl alcohol	39.53	0.9600	57 941

in order to check the significance of the calculated effects of the parameter. The experiments were performed in a randomized order to avoid any systematic error.

The procedure of extraction was repeated twice. The combined extracts were dried on an-

hydrous sodium sulphate, reduced in volume to 100  $\mu$ l in a vacuum rotatory evaporator, and then by a gentle stream of nitrogen. The extracts were stored in a refrigerator until the analysis by GC-FID.

#### 2.4. Gas chromatographic analysis

Analysis of extracts was carried out on a Varian Star Model 3400 CX gas chromatograph (Varian Ibérica, Madrid, Spain) equipped with a split/splitless capillary injection port and flame ionization detector. Separations were performed on a SGL-20 polyethylene glycol capillary column (50 m  $\times$  0.25 mm i.d., 0.25  $\mu$ m film thickness) from Sugelabor. The following conditions were used: injector temperature, 250°C; detector temperature, 300°C; carrier gas flow (N<sub>2</sub>), 1 ml/min. Injections were made in split mode (split ratio, 1:60; sample size, 1  $\mu$ l). The oven temperature was maintained at 40°C for 7 min, from 40 to 110°C at 4 °C/min, from 110 to 170°C at 10°C/min, then held 10 min.

A Star Chromatography Workstation version 4.0 was used for acquiring and processing the data. Measured retention times and peak areas represented at least triplicate injections. Identifications of volatile compounds were carried out by comparing retention times with standard compounds. Quantification was accomplished with 2-octanol as internal standard.

### 3. Results and discussion

The gas chromatographic conditions chosen allow the separation of most compounds studied, only the isopropyl alcohol and ethyl butyrate peaks overlap with the ethanol peak. Table 4 shows retention times of this compounds. The reproducibility and linearity of the chromatographic method was tested using the standard solution. For most of the compounds, precision (as %RSD) and linearity (as  $r$ , correlation coefficient) are very good, with RSD values lower than 6% and  $r$  values higher than 0.997.

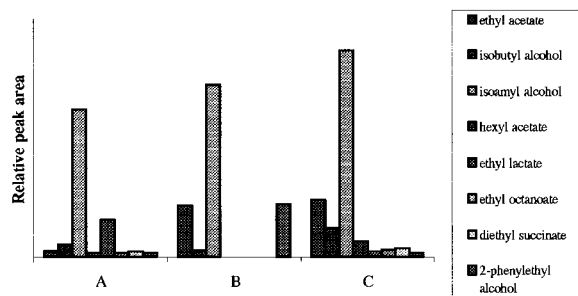
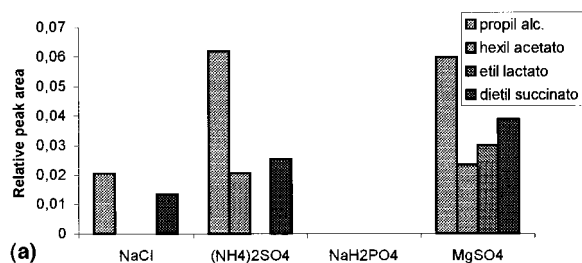


Fig. 1. Effects of different solvents. (A) Dichloromethane; (B) *n*-pentane–diethylether (2:1); (C) diethylether–*n*-pentane (2:1).

### 3.1. Effect of extraction solvent and type of salt

Initially, some preliminary experiments were performed in order to establish the most suitable extraction solvent and salt. Dichloromethane, and the mixtures *n*-pentane–diethylether (2:1) and diethylether–*n*-pentane (2:1) were studied. A synthetic wine was extracted by means of ultrasound according to the method described by Cocito et al. [7]. The results are presented in Fig. 1. Highest extraction efficiency of wine volatile compounds was obtained when diethylether–*n*-pentane (2:1) mixture was used as extractant.



Other parameters important to achieve a good extraction are the type and amount of salt. The experiments carried out with different salts are presented in Fig. 2. Better results are obtained with magnesium sulphate, an amount of 4 g being enough for high recoveries.

### 3.2. Optimization of the ultrasound extraction: factorial design

The operating variables such as sample volume, time of extraction and solvent volume were studied using a factorial design. Table 3 shows the experimental design matrix and the results obtained in each run expressed as average recovery for alcohols, esters and terpenes. The analysis of variance tables were constructed for testing the significance of the effects. Table 5 shows the *F* values and the direction of the effect of the factors on the average relative recoveries of the alcohols, esters and terpenes. The strength of the influence of a factor is indicated by the magnitude of the *F* value (variables with *F* values over 5.318 have a significant influence at the 5% significance level), while the direction of this influence is shown by the sign of the effect.

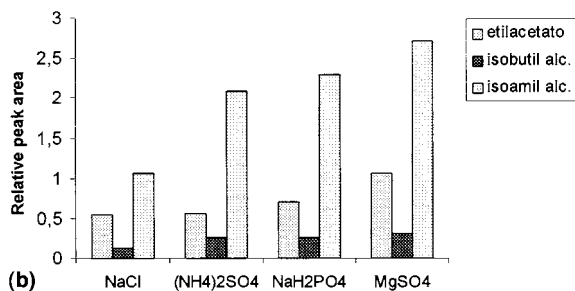


Fig. 2. (a) Effects of different salts; (b) effects of different salts.

Table 5  
*F*-Statistic and direction of the parameters of factorial design

Variable	Alcohols <i>F</i> value	Effect	Esters <i>F</i> value	Effect	Terpenes <i>F</i> value	Effect
Sample volume	0.854	–	56.996	–	7.258	–
Time	0.055	+	0.167	+	4.077	+
Extractant volume	8.165	–	0.017	+	0.156	–



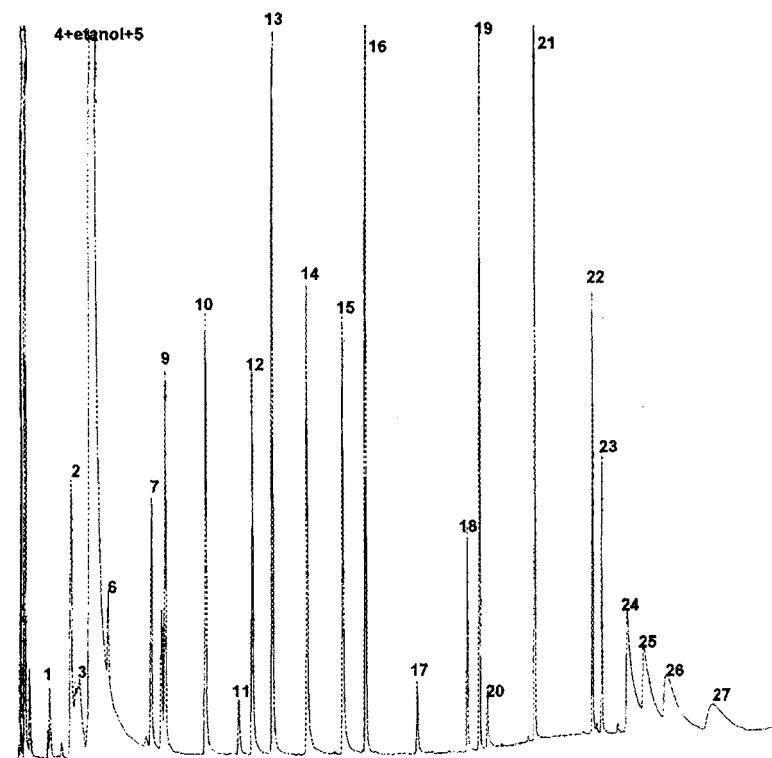


Fig. 3. Chromatogram of standard solution.

### 3.2.1. Alcohols

Only the extractant volumes were statistically significant and they were affected by a negative sign.

### 3.2.2. Esters

As depicted in Table 5, the sample volume has a strong negative effect on the recovery of these compounds. In other words, esters show higher recoveries with 50 ml of solvent than with 60 ml.

### 3.2.3. Terpenes

The main factor of influence is the sample volume and the interaction between sample volume and extractant volume.

Based on the previous results, the conditions for extraction of aroma compounds were chosen as follows: 100 ml as sample volume; extraction time, 30 min; diethylether-*n*-pentane (2:1, 50 ml) as extractant; and addition of magnesium sulphate (4 g) to achieve good salting out effect.

### 3.3. Analytical characteristics of the method

Fig. 3 shows the separation of 27 volatile compounds from a standard sample prepared in ethanol (Table 1) using the optimized extraction procedure. The performance of the method in terms of precision, linearity and accuracy is shown in Table 6.

The precision was studied as reproducibility and expressed as relative standard deviation for one wine sample which was extracted six times and injected in triplicate. Percent RSD values for peak area were less than 10%, only seven compounds show higher values.

Eight solutions containing 0.01, 0.05, 0.1, 0.2, 0.5, 1.0, 5.0 and 10.0 ml of the standard ethanol solution given in Table 1, and diluted to 100 ml with wine model solution were prepared, extracted following the proposed method, and analyzed by CG (injection in duplicate). The calibration curve for each analyte was created.

The linear correlation coefficients are higher than 0.994. This indicates that the linear range included at least the entire concentration range studied.

Table 6  
Analytical characteristics

No.	Compound	%RSD	Linearity
1	Methyl acetate	8.55	0.999
2	Ethyl acetate	9.58	0.994
3	Methyl alcohol	6.57	0.995
6	Isobutyl acetate	ND	0.999
7	<i>sec</i> -Butyl alcohol	11.38	0.999
8	Ethyl butyrate	14.01	0.999
9	Propyl alcohol	8.22	0.999
10	Isobutyl alcohol	21.50	0.999
11	Isoamyl acetate	6.63	0.999
12	<i>n</i> -Butyl alcohol	14.60	0.999
13	4-Methyl-2-pentanol	4.11	1.000
14	Isoamyl alcohol	15.16	0.999
15	Amyl alcohol	ND	0.999
16	Hexyl acetate	4.51	0.999
17	Ethyl lactate	15.29	0.999
18	Ethyl octanoate	5.98	0.999
19	Heptyl alcohol	ND	0.999
20	Linalool	ND	0.999
21	Diethyl succinate	5.31	0.999
22	$\alpha$ -Terpineol	ND	0.998
23	Citronellol	ND	0.999
24	Nerol	ND	0.997
25	Geraniol	ND	0.998
26	2-Phenylethyl alcohol	13.02	0.999

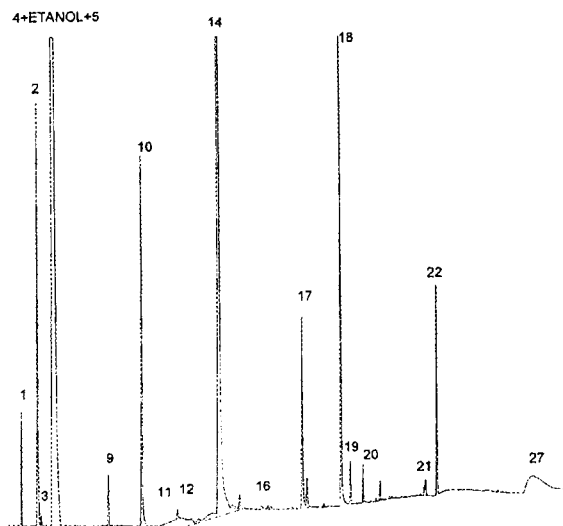


Fig. 4. Chromatogram of wine sample.

To verify the possible existence of matrix effects, known amounts of each aroma compound were added to the wine sample; this wine was extracted and analyzed by CG. The slope of the curve obtained was compared to that of a conventional calibration curve. The use of the Fisher's *F*- and Student's *t*-test for a confidence level of 95% showed that the slopes were not statistically different.

### 3.4. Application of the method to wine samples

In order to demonstrate the applicability of the method, it was applied to the determination of volatile compounds in wine samples. Fig. 4 shows the chromatogram corresponding to the analysis of the wine sample by the ultrasonic method. The results obtained on young white wines from different harvests are presented in Table 7. The aroma compound concentrations listed in this table correspond to an average of three samples of same wine.

When dealing with wine aroma, a distinction is made between primary or grape aroma which are found in the undamaged plant cells of the grape, and secondary grape aroma formed during the processing of the grapes (crushing, pressing) and by chemical, enzymatic–chemical and thermal reactions in grape must (fermentation and maturation bouquet) [9]. The wine studied shows high levels of isoamyl and isobutyl alcohols, compounds formed during fermentation process. The characteristic compounds of primary aroma are principally terpene compounds which are found in low concentrations in these samples. On the other hand, the rest of the compounds present levels according with those reported in other wines.

## 4. Conclusions

An ultrasound method for the extraction of aroma compounds from samples of white wine was developed and optimized for practical use, and has advantages over other extraction methods, such as higher reproducibility and the possibility of the simultaneous extraction of several

Table 7  
Volatile compounds (mg/l) identified in wine: (A) 1995 and (B) 1996

Compound	1	2	3	4	5	6	7	8
<i>(A) 1995</i>								
Methyl acetate	0.95 ± 0.59	0.13 ± 0.18	0.30 ± 0.26	0.70 ± 0.08	1.31 ± 0.38	0.94 ± 0.06	0.21 ± 0.09	0.35 ± 0.33
Ethyl acetate	43.94 ± 31.07	ND	3.41 ± 4.83	6.01 ± 1.03	34.95 ± 11.44	16.00 ± 9.43	ND	1.34 ± 1.90
Methyl alcohol	8.66 ± 6.03	4.4 ± 0.00	11.04 ± 2.07	14.39 ± 0.72	19.25 ± 0.26	4.4 ± 0.00	13.04 ± 3.37	8.76 ± 0.83
Isobutyl acetate	ND	ND	ND	ND	ND	ND	ND	ND
sec-Butyl alcohol	0.87 ± 1.23	2.03 ± 1.79	1.33 ± 0.80	1.04 ± 0.39	0.96 ± 0.28	5.85 ± 7.19	2.15 ± 1.16	ND
Ethyl butyrate	ND	0.08 ± 0.12	0.09 ± 0.13	ND	1.05 ± 1.49	0.87 ± 1.23	0.58 ± 0.82	ND
Propyl alcohol	6.03 ± 6.12	10.44 ± 10.80	4.20 ± 4.51	26.38 ± 4.46	15.82 ± 19.49	8.30 ± 9.19	6.53 ± 2.35	5.51 ± 3.98
Isobutyl alcohol	16.15 ± 7.06	21.44 ± 17.56	7.89 ± 7.76	31.07 ± 4.84	19.90 ± 9.54	16.18 ± 3.68	12.77 ± 2.08	28.04 ± 13.75
Isoamyl acetate	0.61 ± 0.58	1.21 ± 0.49	0.90 ± 0.98	1.15 ± 0.56	3.68 ± 2.18	0.68 ± 0.17	0.91 ± 0.68	0.23 ± 0.03
n-Butyl alcohol	0.62 ± 0.25	0.59 ± 0.09	1.89 ± 2.57	0.51 ± 0.20	0.87 ± 0.12	2.25 ± 2.51	0.83 ± 0.67	0.50 ± 0.17
4-Methyl-2-pentanol	ND	ND	ND	ND	ND	ND	ND	ND
Isoamyl alcohol	91.76 ± 30.56	100.72 ± 53.44	52.30 ± 19.98	159.58 ± 5.45	98.72 ± 40.01	87.29 ± 31.66	62.11 ± 3.44	168.97 ± 31.92
Amyl alcohol	ND	ND	ND	ND	ND	ND	ND	ND
Hexyl acetate	ND	ND	ND	0.11 ± 0.11	17.72 ± 16.11	ND	ND	ND
Ethyl lactate	ND	0.63 ± 0.03	0.09 ± 0.05	0.54 ± 0.07	4.30 ± 6.09	11.25 ± 4.31	0.50 ± 0.01	0.09 ± 0.05
Ethyl octanoate	0.22 ± 0.07	0.31 ± 0.07	0.18 ± 0.08	0.03 ± 0.05	0.19 ± 0.08	0.27 ± 0.28	0.13 ± 0.06	0.23 ± 0.00
Heptyl alcohol	0.03 ± 0.04	0.01 ± 0.02	ND	ND	0.89 ± 1.26	0.22 ± 0.07	0.37 ± 0.06	0.01 ± 0.00
Linalool	ND	ND	0.01 ± 0.01	ND	0.02 ± 0.03	ND	0.77 ± 1.09	0.02 ± 0.03
Diethyl succinate	0.02 ± 0.00	0.02 ± 0.00	0.01 ± 0.00	0.01 ± 0.02	0.01 ± 0.00	0.02 ± 0.02	0.03 ± 0.00	0.05 ± 0.02
α-Terpineol	ND	ND	ND	ND	ND	ND	ND	ND
Citronellol	ND	ND	ND	ND	ND	ND	ND	ND
Nerol	ND	ND	ND	ND	0.50 ± 0.71	0.44 ± 0.62	ND	ND
Geraniol	ND	n.d	ND	ND	ND	ND	ND	ND
2-Phenylethyl alcohol	8.23 ± 0.00	9.19 ± 0.26	8.70 ± 0.30	8.86 ± 0.42	8.78 ± 0.44	8.48 ± 0.35	9.06 ± 0.38	10.09 ± 2.63

Table 7 (Continued)

Compound	9	10	11	12	13	14	15	16
<i>(B) Volatile compounds identified in wine (1996) (mg/l)</i>								
Methyl acetate	0.74 ± 0.03	0.10 ± 0.01	0.32 ± 0.21	0.17 ± 0.08	0.56 ± 0.21	0.43 ± 0.22	0.13 ± 0.19	0.38 ± 0.25
Ethyl acetate	5.53 ± 3.15	ND	0.39 ± 0.55	ND	ND	ND	ND	ND
Methyl alcohol	11.40 ± 3.70	5.08 ± 0.96	8.73 ± 6.12	10.43 ± 8.53	10.63 ± 1.00	11.78 ± 5.60	4.40 ± 0.00	6.73 ± 3.30
Isobutyl acetate	ND	ND	ND	ND	ND	ND	ND	ND
sec-Butyl alcohol	1.26 ± 1.79	3.98 ± 3.81	2.96 ± 3.11	4.32 ± 3.32	2.88 ± 2.99	1.36 ± 0.84	2.81 ± 3.98	0.91 ± 0.20
Ethyl butyrate	0.65 ± 0.92	ND	0.19 ± 0.14	ND	0.91 ± 1.29	0.99 ± 1.40	ND	ND
Propyl alcohol	3.10 ± 1.75	26.00 ± 7.96	4.21 ± 2.33	18.14 ± 19.08	6.59 ± 3.14	10.42 ± 11.41	13.89 ± 7.02	3.50 ± 3.26
Isobutyl alcohol	14.88 ± 2.80	43.07 ± 16.39	7.85 ± 7.95	36.62 ± 25.52	10.80 ± 0.38	11.29 ± 11.63	32.76 ± 20.12	24.07 ± 9.05
Isoamyl acetate	1.39 ± 0.41	1.58 ± 1.47	0.58 ± 0.02	1.50 ± 1.57	0.54 ± 0.37	1.53 ± 1.10	1.99 ± 1.90	0.47 ± 0.01
n-Butyl alcohol	0.66 ± 0.04	0.83 ± 0.59	0.39 ± 0.05	1.41 ± 0.23	0.46 ± 0.29	0.42 ± 0.35	0.56 ± 0.35	0.53 ± 0.28
4-Methyl-2-pentanol	ND	ND	ND	ND	ND	ND	ND	ND
Isoamyl alcohol	94.37 ± 22.21	183.63 ± 30.91	74.10 ± 18.88	158.96 ± 65.80	84.87 ± 13.20	84.42 ± 45.59	102.77 ± 38.56	109.61 ± 27.86
Amyl alcohol	ND	ND	ND	ND	ND	ND	ND	ND
Hexyl acetate	0.44 ± 0.12	0.30 ± 0.42	ND	0.88 ± 0.39	0.19 ± 0.27	ND	ND	ND
Ethyl lactate	0.31 ± 0.20	0.78 ± 0.59	0.27 ± 0.07	0.66 ± 0.76	ND	ND	0.20 ± 0.08	0.28 ± 0.04
Ethyl octanoate	0.28 ± 0.07	0.15 ± 0.07	0.22 ± 0.03	0.10 ± 0.00	0.24 ± 0.15	0.28 ± 0.25	0.17 ± 0.06	0.17 ± 0.00
Heptyl alcohol	ND	0.03 ± 0.04	ND	ND	3.60 ± 5.01	0.10 ± 0.10	ND	0.05 ± 0.07
Linalool	0.01 ± 0.00	ND	ND	0.01 ± 0.00	0.02 ± 0.03	ND	ND	0.01 ± 0.01
Diethyl succinate	0.01 ± 0.00	0.01 ± 0.00	ND	0.01 ± 0.01	0.01 ± 0.00	ND	0.01 ± 0.00	0.01 ± 0.01
α-Terpineol	ND	ND	ND	ND	ND	ND	ND	ND
Citronellol	ND	ND	ND	ND	ND	ND	ND	ND
Nerol	ND	ND	ND	ND	ND	ND	ND	0.03 ± 0.04
Geraniol	ND	n.d	ND	ND	ND	ND	ND	ND
2-Phenylethyl alcohol	8.68 ± 0.47	8.46 ± 0.32	8.30 ± 0.09	9.06 ± 1.17	8.59 ± 0.18	8.23 ± 0.00	8.53 ± 0.41	8.53 ± 0.43

samples. The method proposed allows the quantification of 24 wine flavor compounds. The aroma constituents of wine have a leading contribution to its varietal character, and allow the differentiation of wines from other geographical areas. Therefore, this method is proposed as an interesting alternative for the analysis of wine flavor components.

## References

- [1] J. Diez, R. Cela, J.A. Perez-Bustamante, *Am. J. Enol. Vitic.* 36 (1) (1985).
- [2] C. De la Presa-Owens, R.M. Lamuela-Raventos, S. Buxaderas, M.C. De la Torre, *Am. J. Enol. Vitic.* 36 (1) (1985).
- [3] Y.Z. Gunata, C.L. Bayonove, R.L. Baumes, R.E. Cordonnier, *J. Chromatogr.* 331 (1985) 83–90.
- [4] Y. Zhou, R. Riesen, C.S. Gilpin, *J. Agric. Food Chem.* 44 (1996) 818–822.
- [5] G.P. Blanch, G. Reglero, M. Herraiz, *J. Agric. Food Chem.* 43 (1995) 1251–1258.
- [6] A. Razungles, E.H. Tarhi, R. Baumes, Z. Gunnata, C. Tapiero, C. Bayonove, *Sci. Aliments* 14 (6) (1994) 725–739.
- [7] C. Cocito, G. Gaetano, C. Delfini, *Food Chem.* 52 (1995) 311–320.
- [8] I. Moret, *Analyst* 120 (1995) 2561–2566.
- [9] A. Rapp, *Fresenius J. Anal. Chem.* 337 (1990) 777–785.

# SPME–HPLC analysis of *Allium* lacrymatory factor and thiosulfinates

B. Jaillais<sup>a,b</sup>, F. Cadoux<sup>a</sup>, J. Auger<sup>a,\*</sup>

<sup>a</sup> IRBI, Faculty of Sciences and Techniques, University F. Rabelais, Parc de Grandmont, 37200 Tours, France

<sup>b</sup> RP-Texel, Zone d'activité de Buxieres, B.P. 10, 86220 Dangé Saint-Romain, France

Received 7 September 1998; received in revised form 3 March 1999; accepted 3 March 1999

## Abstract

The commercial SPME–HPLC interface is investigated to improve the analysis of *Allium* volatiles. Volatiles trapped by liquid nitrogen were previously transferred to RP-HPLC by a classical injection. In this work we compare the results obtained with classical injection and SPME used in headspace mode. This SPME–HPLC interface can be used when it is important to spare the sample, but thiosulfinates are partially degraded. © 1999 Elsevier Science B.V. All rights reserved.

**Keywords:** *Allium*; HPLC; SPME; Thiosulfinates

## 1. Introduction

Analysis of *Allium* volatiles has to be improved as GC is not usable for these labile substances, and HPLC after cryo-trapping seems to be a good method for these compounds which could be responsible for the aromatic and medical properties of *Allium* plants.

When *Allium* plants are cut or crushed, enzymatic cleavage of *S*-alk(en)yl cysteine sulfoxides release sulfenic acids: R–S–OH, where R represents the groups: methyl (Me), *n*-propyl (Pr), 1-

propenyl (Pe) and allyl (Al). These sulfenic acids rearrange immediately  $2 \times 2$  to form the thiosulfinates (Ti): R–SO–S–R'; Pe sulfenic acid rearranges also preferentially to thiopropanol *S*-oxide, the lacrymatory factor (LF). Ti can persist in the environment of *Allium* [1] and represent the true odour of cut *Allium* [2]. Ti are, however, relatively reactive compounds and we demonstrated that RP-HPLC is the best technique for their analysis [2] if the sample is obtained by cryo-trapping isolation [3], compared to GC analysis where we see almost exclusively disulfides corresponding to Ti degradation [2]. But as Ti are very labile compounds, the aqueous samples cannot be concentrated or extracted and the sensitivity of this method cannot be improved.

\* Corresponding author. Tel./fax: +33-2-47-36-70-52.

E-mail address: auger@univ-tours.fr (J. Auger)

Consequently, from 50 g of fresh material, usually only one analysis can be performed which is a considerable drawback for statistical control of validity of the results and for analysis on very small quantities like those obtained from *in vitro* cultures.

The technique of solid-phase microextraction (SPME) has been investigated for the analysis of semi- and non-volatile organic compounds in water by HPLC [4] and it would be advantageous to use this sampling technique to provide a successful way of concentration and transfer of analytes directly into a narrow-bore HPLC column for further analysis.

A new SPME–HPLC interface developed recently by Supelco (Bellefonte, PA) can be used for both qualitative and quantitative analyses [5,6]. We tested this commercial interface with the available fiber coatings on *Allium* trapped volatiles.

The challenge of this application was to extract and desorb analytes completely with a minimum amount of solvent.

## 2. Experimental

### 2.1. Instrumentation

#### 2.1.1. Solid-phase microextraction

The SPME sampling technique based on adsorption is used to separate analytes from sample matrix and has been developed by Arthur and Pawliszyn [7]. The SPME device is a modified syringe. The plunger moves a fiber in and out of a metallic needle to protect the fiber coating. The fiber is coated with polydimethylsiloxane in different film thicknesses: 7  $\mu\text{m}$  (green), 30  $\mu\text{m}$  (yellow) and 100  $\mu\text{m}$  (red), with polyacrylate 85  $\mu\text{m}$  (white), or with Carbowax/templated resin 50  $\mu\text{m}$  (purple). These different types of coatings provide different adsorption properties for different kinds of analytes. They were purchased from Supelco (Bellefonte, PA).

The system consists of two independent parts: the SPME device and a desorption chamber (200  $\mu\text{l}$ ) placed instead the injection loop connected to a classical manual injection valve.

#### 2.1.2. HPLC separation and UV detection/identification

The HPLC equipment used included a Waters™ 616 gradient pump with the Waters™ 600 S controller and a Waters™ 996 Diode Array Detector. The separations were performed on an Adsorbosphere RP C<sub>18</sub> column (250 × 4.6 mm). The eluent was CH<sub>3</sub>OH/H<sub>2</sub>O (70/30, v/v) at a flow rate of 0.8 ml/min.

The detection was made by UV (250 nm) at a rate of 1 spec/s and chromatographic data were processed on a Digital personal computer equipped with Millennium™ (v2.15) program.

### 2.2. Sample preparation and transfer

#### 2.2.1. Plant material

The method was tested on cultivated species: *Allium cepa* (onion) and *A. sativum* (garlic), and wild species: *A. lineare*, *A. galanthum*. Wild species were maintained in the botanical garden of Institute of Plants Genetics and Crop Plants Research (IPK, Gatersleben, Germany) and cultivated species were purchased from the market.

#### 2.2.2. Reference compounds

Symmetrical thiosulfates (R = R' = Me, Al and Pr) were synthesized by oxidation of the corresponding disulfides [8]. Disulfides were supplied by Aldrich (Milwaukee, WI, USA).

#### 2.2.3. Cold trapping

Samples of wild and cultivated *Allium* were processed. A total of 50 g of leaves (wild species) or bulbs (cultivated species) were rapidly cut in a flask. The flask was fitted to another (10<sup>-1</sup> Torr) flask immersed in liquid nitrogen and connected to a vacuum pump. Headspace volatiles and water emitted were trapped during 20 min at room temperature. This frozen sample was allowed to warm until just thawing before transfer on fiber or injection in HPLC.

Volatiles were trapped on the SPME fiber to use the SPME–HPLC interface and the same aqueous sample (20  $\mu\text{l}$ , usually the totality) was further injected directly in HPLC, without concentration.

#### 2.2.4. Transfer by headspace SPME (HS-SPME)

After trapping, the extract was collected in a 2-ml vial closed by a septum. The septum was pierced with the metallic needle of the syringe and the fiber was pushed out into the gas phase (headspace mode). The conditioned fiber (30 min into the mobile phase) coated with 50  $\mu\text{m}$  Carbowax/templated resin was exposed to the water sample for 10 min under ultrasonic agitation.

Before transferring the fiber into the desorption chamber, the injection valve was placed in the load position. The fiber was then introduced into the desorption chamber. The union between the syringe and the chamber was closed tightly. Analytes were desorbed during 1 min (static mode desorption) into the chamber filled with eluent phase (methanol/water, 70/30, v/v). The valve was then switched to the injection position and analytes carried to the LC column. After 1 min of passage of solvent from HPLC pump through the desorption chamber, the valve was switched to the load position and fiber withdrawn.

### 3. Results and discussion

The first part of this study concerned optimizing SPME sampling conditions on dimethyl thiosulfinate (dimethyl Ti) before testing the method on natural samples.

#### 3.1. Choice of fiber

The different available fibers were tested with dimethyl Ti at a concentration corresponding to our application on *Allium* trappings or trapped volatiles. Good transfer of dimethyl Ti was observed with the purple fiber (Carbowax/templated resin, 50  $\mu\text{m}$ ) only.

#### 3.2. Optimal adsorption and desorption times

A kinetic study was performed to determine the optimal time to adsorb analytes on the fiber and the optimal time to desorb them with the mobile phase. The maximal response was obtained with 5 min of adsorption time (Fig. 1) and maintained with longer adsorption times. Thus, in all subse-

quent experiments we chose to expose the fiber for 10 min. For the desorption time (Fig. 2), the maximal response was observed for 2 min and the response decreased rapidly with longer times. Thus, in all subsequent experiments we chose to desorb for 1 min to be near the maximum.

#### 3.3. Level of desorption (for 1 min desorption)

We tested the level of residue on the fiber by making a second desorption of the same fiber. Compared to the first one, we found only 0.26% of Ti for the second desorption. In practice, the level of desorption is always superior to 99% ( $n = 6$ ). According to the supplier, the fibers can be used up to 50 times but we usually use them many more times without appreciable changes.

#### 3.4. Synthetic Ti results

Chromatograms of SPME and direct injection (DI) of the three synthetic thiosulfates presented a regular shape of peaks. The results are listed in Table 1. With DI of dimethyl Ti at various concentrations, we established a linear calibration curve corresponding to approximately to  $34 \times 10^6$  area units per 0.1  $\mu\text{mol}$ . Headspace SPME of dimethyl TI (1) at  $10^6$  area units correspond to  $3 \times 10^{-3}$   $\mu\text{mol}$  (Table 2).

The ratios DI/SPME of compounds are 30–100, respectively for TiMe<sub>2</sub> and TiPr<sub>2</sub>. This fact can be explained by the adsorption mode of the SPME from headspace which uses a small part of the sample, whereas DI uses all the sample. However, for our application the quantities of transferred thiosulfates by SPME–HPLC is generally sufficient.

Previous results of chromatographic analysis of synthetic thiosulfates (retention time, U.V. and mass spectra) allowed identification of different peaks in natural samples of *Allium*, which contained only Ti and LF [2,9].

#### 3.5. *Allium* results

Fig. 3a, b represent, respectively, HS-SPME and DI analysis of commercial garlic. All the peaks were present using the two methods but not



at the same level; however, proportions of different thioalkyl groups were preserved. In the garlic the only odour principles detected were thiosulfinates. Five compounds were identified and more particularly three peaks (3, 6, 7) with thioallyl group, the diallyl thiosulfinate (6) being the preponderant. This thioallyl group is characteristic of *A. sativum* and related wild species.

In the cultivated onion (Fig. 4a, b), the profile was very different from garlic, with one major peak corresponding to thiopropanol *S*-oxide (LF) (2) and a small amount of *trans*-2-hexenal (8), a general green leaf volatile. The LF is characteristic of onions as previously determined by HPLC/ESI/MS studies [2]. With SPME, LF is still widely preponderant but the relative quantity of *trans*-2-hexenal increases and we observe also the appearance of 2-methyl-2-pentenal (9), the LF degradation product.

The same results were obtained with *Allium galanthum* (Fig. 4c, d), a wild *Allium* species, i.e. an important peak of LF (2), a weak presence of (9) with, in addition, dimethyl Ti (1), dipropyl thiosulfinate (11) and the asymmetrical methyl-propyl thiosulfinate in the baseline (5). These compounds are well identified in DI but hardly detected in SPME, and tentatively identified. Because of the presence of LF and thiomethyl group, *A. galanthum* belongs to the onion species, the relative abundance of the methyl group being characteristic of wild species.

In the *A. lineare* chromatogram (Fig. 5), methyl, allyl, propenyl and propyl groups were all detected and dimethyl Ti (1) was the main component. To the thiomethyl compounds widely spread in *Allium* species, some thioallyl and particularly thio-1-propenyl compounds are added. Thus, *A. lineare* seems to be as garlic as an onion. Here, the use of SPME does not allow the identification of

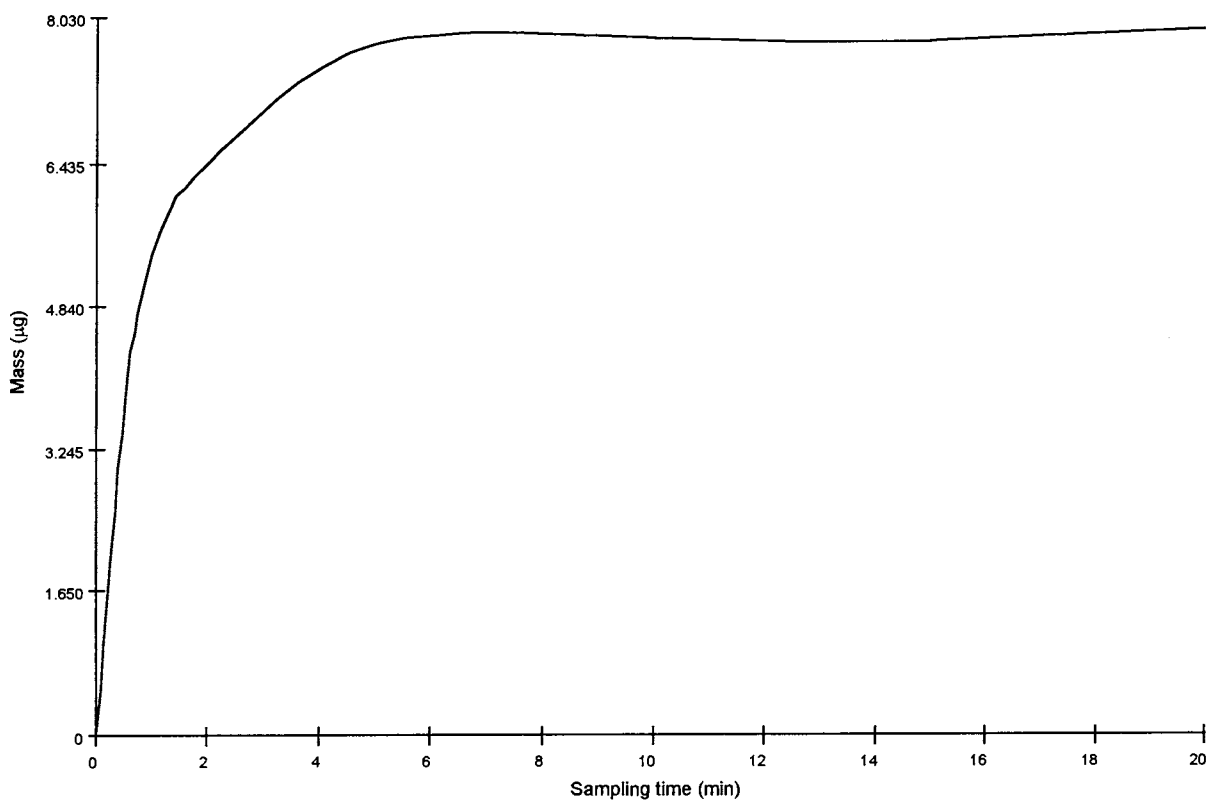


Fig. 1. Effect of sampling time on mass transfer of dimethyl Ti.

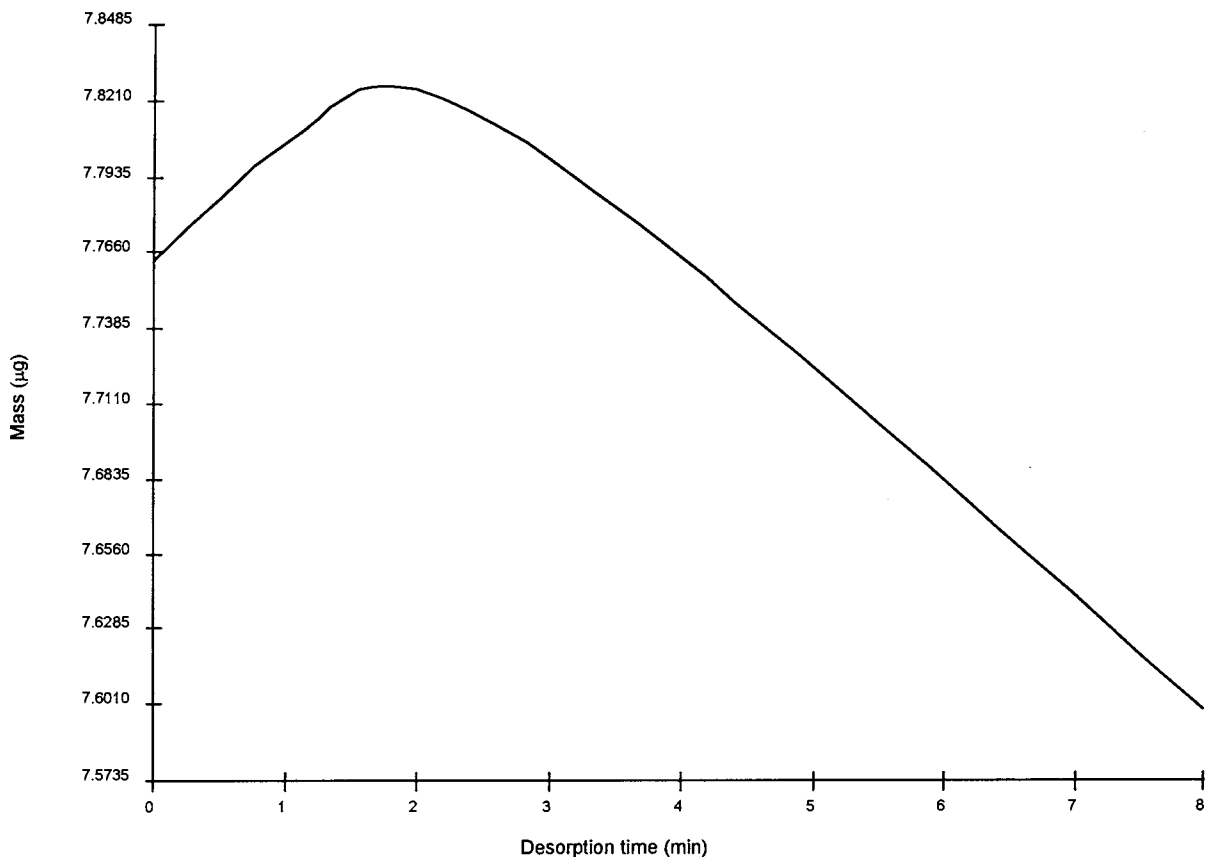


Fig. 2. Effect of desorption time on mass transfer of dimethyl Ti.

LF (2) and dipropyl thiosulfinate (11) and leads to an important variation for methyl compounds (1,4).

The study of the second part of the chromatogram (Fig. 3 and Fig. 5) shows some large peaks which are only present in the SPME injection mode, and we suppose that they are due to the decomposition on the fiber of allyl and methyl compounds.

#### 4. Conclusion

Usually, the limited quantities of fresh material from wild species (one bulb) does not allow the possibility to do many analyses by direct injection. Using the interface SPME–HPLC, we show that the analysis of low concentrated sample is

possible. Indeed, with headspace technique, we preserve sample for further analysis or other studies.

However, thiosulfates are very labile and SPME seems to produce their partial degradation,

Table 1  
Comparison between direct injection and headspace SPME on different thiosulfates analysis

Compounds	D.I. (µmol) <sup>a</sup>	SPME (µmol) <sup>b</sup>	Ratio DI/SPME
TiMe2	0.1	0.003	33
TiAl2	0.062	0.0007	89
TiPr2	0.2	0.0021	95

<sup>a</sup> The concentration corresponds to the injection of 20 µl.

<sup>b</sup> The concentration corresponds to an adsorption time of 10 mn and a desorption time of 1 mn.

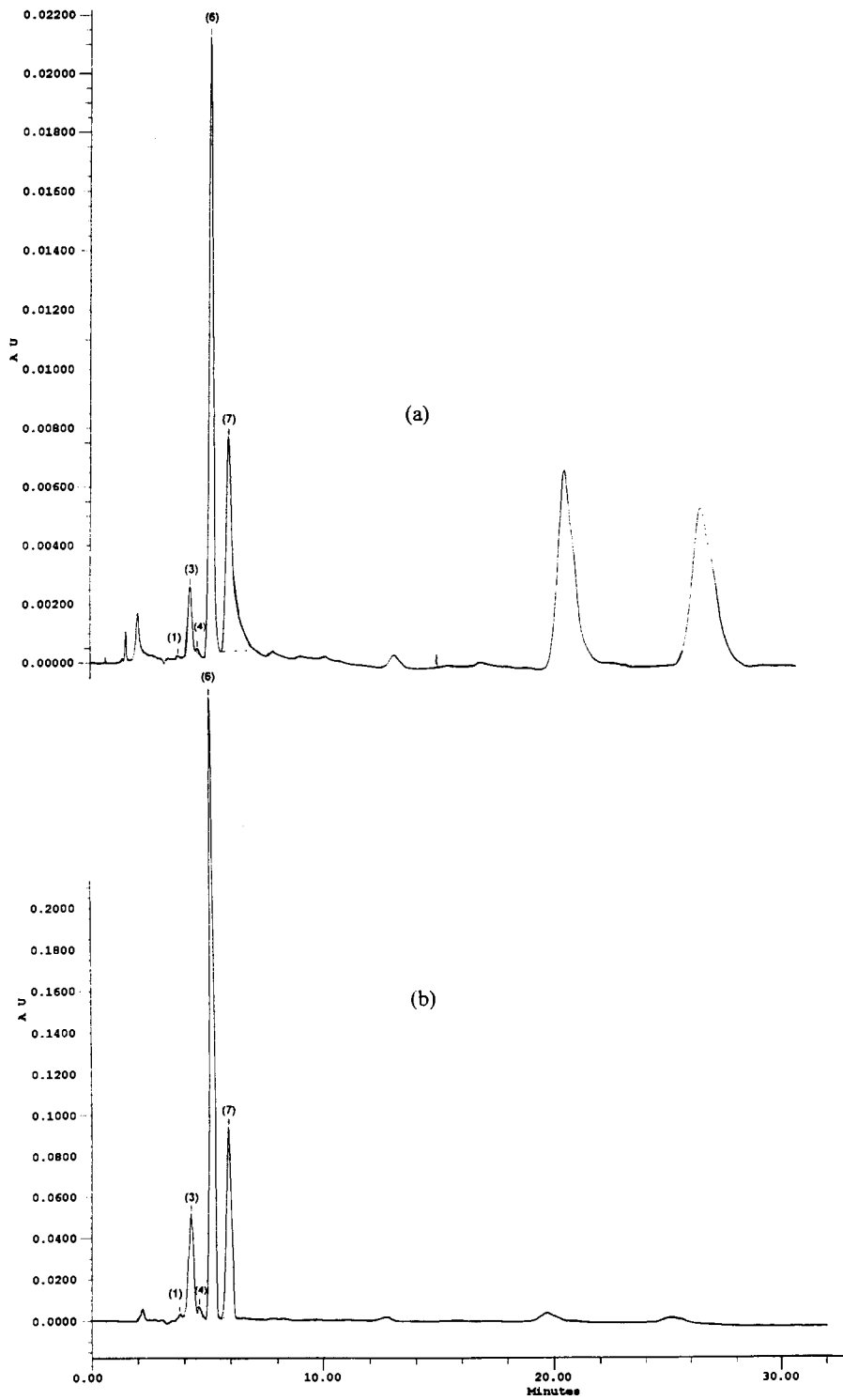


Fig. 3. HS-SPME (a) and DI (b) chromatogram of volatiles of commercial garlic.

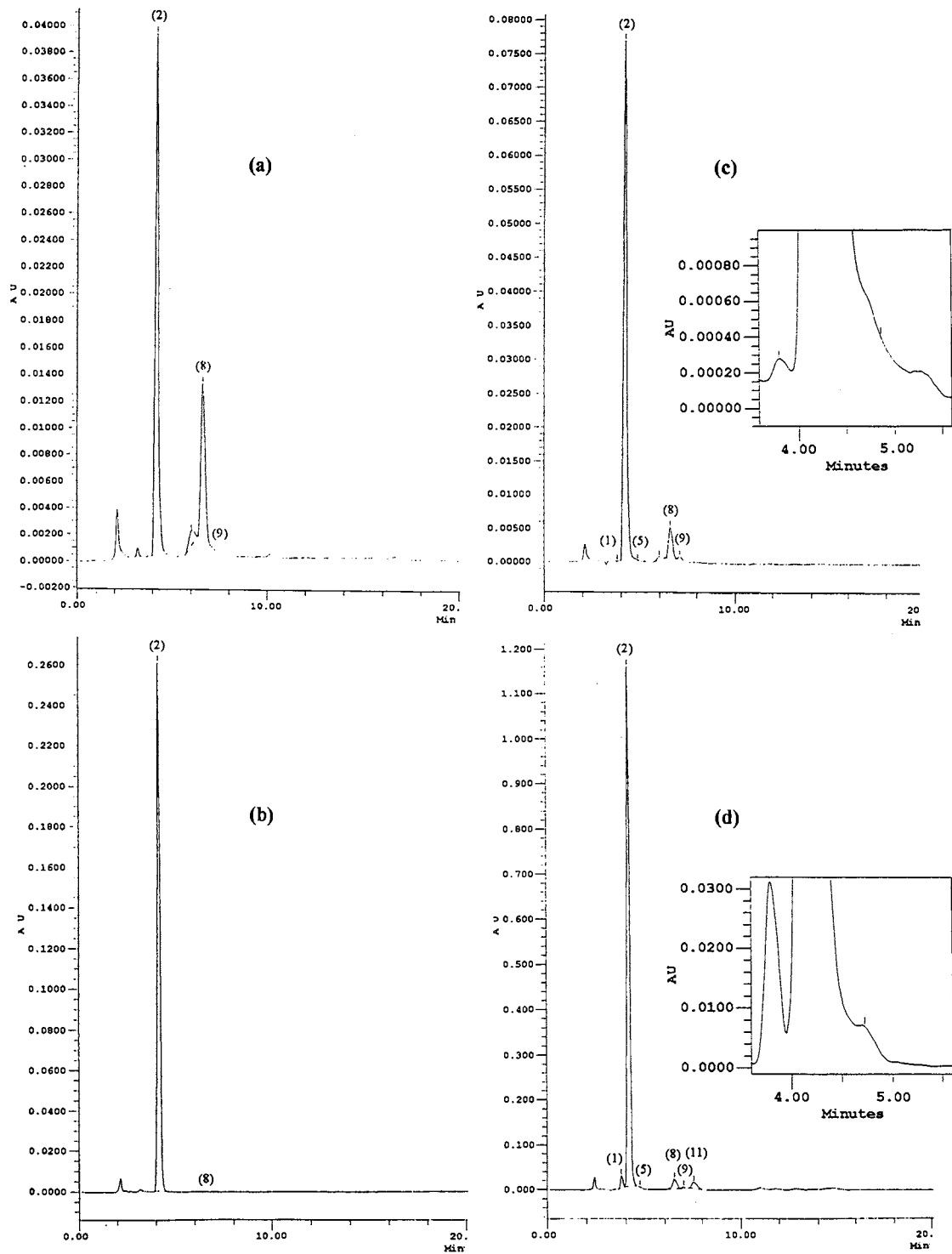


Fig. 4. HS-SPME (a), DI (b) chromatogram of volatiles of cultivated onion; HS-SPME (c), DI (d) chromatogram of volatiles of *A. Galanthum*.

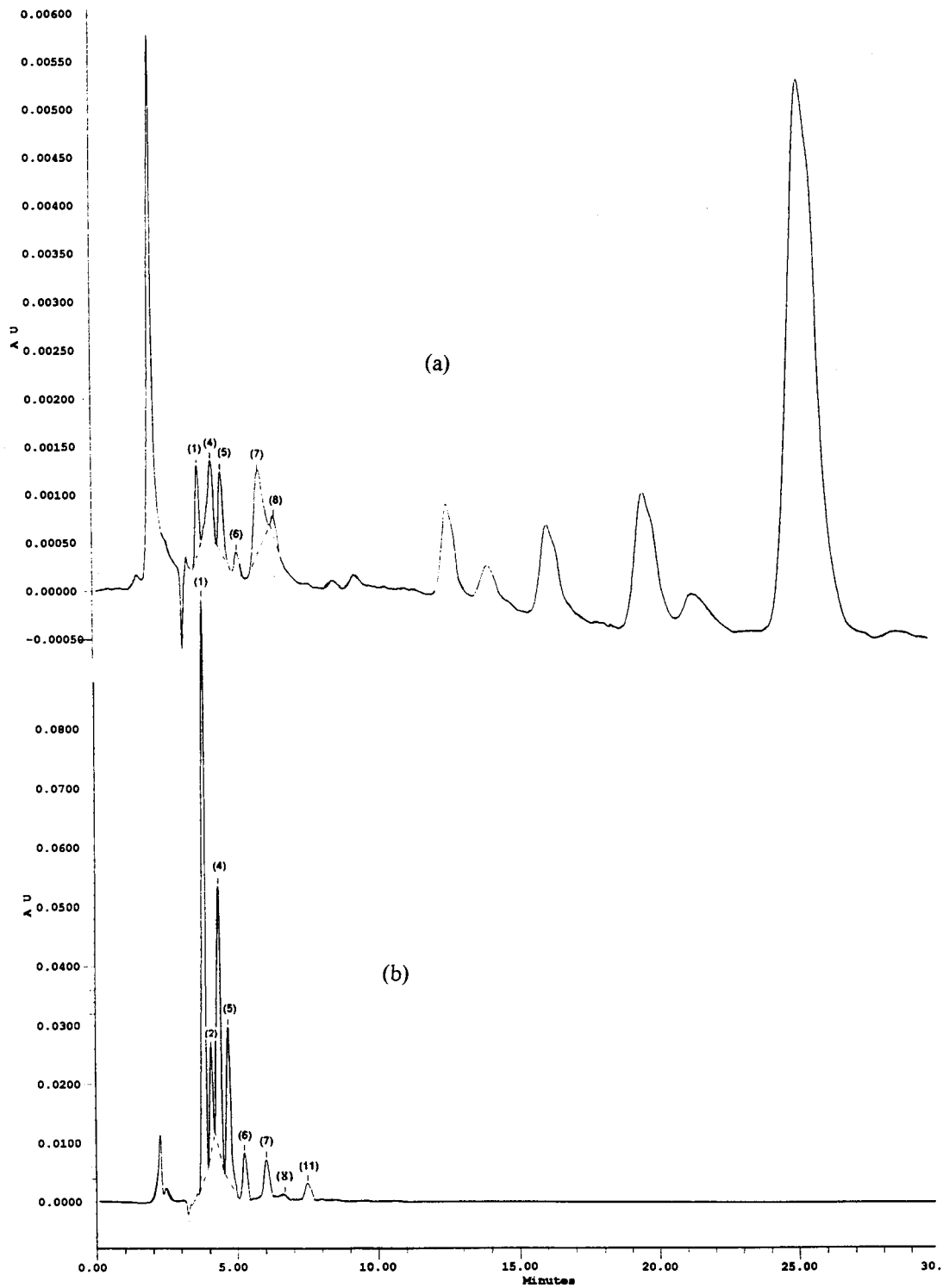


Fig. 5. HS-SPME (a) and DI (b) chromatogram of volatiles of *A. Lineare*.

Table 2  
Compounds identified in the odor of *Allium*

Peak no.	Compound
(1)	Dimethyl Ti
(2)	Lacrymatory factor
(3)	Methyl allyl Ti
(4)	Methyl propenyl Ti
(5)	Methyl propyl Ti
(6)	Diallyl Ti
(7)	Allyl propenyl Ti
(8)	<i>trans</i> -2-Hexenal
(9)	2-Methyl-2-pentenal
(10)	Propyl propenyl Ti
(11)	Dipropyl Ti

but less than during their SPME/GC/MS analysis [2].

Nevertheless, the advantage of sample conservation is important, especially for the analysis of rare endemic species of wild *Allium*.

Development of new SPME fibers or of low volume desorption chambers could improve our results.

## Acknowledgements

The financial support of EC (contract FAIR 95.465) is gratefully acknowledged. We acknowledge J. Keller from IPK for providing the wild species.

## References

- [1] J. Auger, F.X. Lalau-Keraly, C. Belinsky, *Chemosphere* 21 (1990) 837.
- [2] S. Ferary, J. Auger, *J. Chromatogr. A* 750 (1996) 63.
- [3] S. Ferary, J. Keller, J. Boscher, J. Auger, *Biomed. Chromatogr.* 12 (1998) 104.
- [4] J. Chen, J.B. Pawliszyn, *Anal. Chem.* 67 (1995) 2530.
- [5] T. Gorecki, M. Belkin, J. Caruso, J. Pawliszyn 34 (1997) 275.
- [6] Y. Liu, M.L. Lee, K.J. Hageman, Y. Yang, S.B. Hawthorne 69 (1997) 5001.
- [7] C.L. Arthur, J. Pawliszyn, *Anal. Chem.* 62 (1990) 2145.
- [8] J. Auger, E. Thibout, *CR Acad. Sci. Paris* 292 (1981) 217.
- [9] S. Ferary, E. Thibout, J. Auger, *Rapid Commun. Mass Spectrom.* 10 (1996) 1327.

# Trace metals analysis in estuarine and seawater by ICP-MS using on line preconcentration and matrix elimination with chelating resin<sup>☆</sup>

M. Nicolai<sup>a,\*</sup>, C. Rosin<sup>a</sup>, N. Tousset<sup>b</sup>, Y. Nicolai<sup>2</sup>

<sup>a</sup> *Laboratoire d'Hygiène et de Recherche en Santé Publique, INSERM U420,  
11 bis Rue Gabriel Péri F-54500 Vandœuvre-lès-Nancy, France*

<sup>b</sup> *L.S.E./L.C.P.E., UMR Université CNRS 7564, Faculté de Pharmacie, 5 Rue Albert Lebrun F-54000 Nancy, France*

Received 7 September 1998; received in revised form 10 March 1999; accepted 16 March 1999

## Abstract

The main difficulties of trace metals analysis in estuarine and seawater stem from their very low concentration ( $\mu\text{g/l}$  to sub- $\mu\text{g/l}$ ), and, by contrast, the high salt content (up to 38 g/l in the Mediterranean Sea). ICP-MS allows multi-elemental analysis and offers great sensitivity, but may be strongly affected by matrix effects induced by high salt contents ( $> 1 \text{ g/l}$ ). To perform trace metals analysis both in riverine, estuarine and seawater, we have developed a hyphenated method: ion chelation chromatography coupled on-line with ICP-MS. Iminodiacetate resin, Metpac CC-1 (Dionex), was used to concentrate most of the trace metals, and to separate them from alkaline and alkaline-earth metals. Behaviour of 17 elements (Pb, Cu, Cd, Ni, U, Cr, Mn, Al, Co, Ga, In, Zn, V, Tl, Bi, Ag and Sn) towards the resin was qualitatively investigated. A method validation, partly derived from AFNOR standard XPT 90-210, was carried out on 12 elements (Pb, Cu, Cd, Ni, U, Cr, Mn, Al, Co, Ga, Bi and In). Replicate measurements of multi-elemental standard solutions were used to check linearity, and to determine repeatability and detection limits. Method accuracy was then assessed by analysing two certified materials: a synthetic freshwater (SRM 1643d), and a natural filtered coastal seawater (NRCC CASS-3). An application assay of natural samples from the Rhône river (France) was eventually carried out, and the analytical results were found to be consistent with previous works. © 1999 Elsevier Science B.V. All rights reserved.

*Keywords:* Chelating resin; ICP-MS; Metals; Seawater

<sup>☆</sup> Paper presented at the Deauville Conference 98, 6th S.A.S., València, Spain, 22–24 June 1998

\* Corresponding author. Tel.: +33-383-50-36-36; fax : +33-383-57-90-75.

*E-mail address:* m.nicolai@wanadoo.fr (M. Nicolai)

<sup>1</sup> This paper is dedicated to my deceased brother Youri (1976–1998) forever in my heart.

<sup>2</sup> Deceased.

## 1. Introduction

There are at least two challenging areas in trace metals analytical chemistry: the speciation of organic and inorganic forms, and trace and ultra-trace determination in complex matrices, such as chemical reagents, biological fluids and tissues, environmental materials (biological and geological matter), oils, brines and seawater. In fact, most analytical techniques do not permit direct analysis of metals in such matrix samples. Hence recent researches reveal the spread of various pre-treatments, on-line and off-line, and of hyphenated methods [1]. In every case, the aim is the same: to concentrate the analyte in order to improve the detection limit and reduce the matrix content, and thereby enhance the analytical conditions.

Inductively coupled plasma (ICP-MS) is ideal for trace metals analysis, because it allows fast multi-elemental and isotopic analysis with high sensitivity (detection limit < 100 ng/l for most metallic elements), as well as a broad dynamic range (from D.L. to mg/l). Nevertheless, ICP-MS is extremely sensitive to matrix interferences induced by high salt contents (more than 1 g/l). These are from two main types: (1) spectral interferences, due to isobaric atomic or polyatomic species [2–7]; (2) matrix effects resulting in analytical signal variation, mainly suppression due to reduced ionisation efficiency, space charge effects, or clogging of tubes (e.g. nebuliser, torch) and cones [3–10], although signal enhancement has been reported elsewhere [7,10,11].

Sample pre-treatment (e.g. coprecipitation, solvent extraction) [12–14], calibration strategy development (internal standardisation, isotope dilution) [15–18], and alternative sample introduction (electrothermal vaporisation, hydride generation, flow injection, ultrasonic nebulisation, membrane desolvation, etc.) [4–6] are common ways to offset the ICP-MS lack of robustness. Other alternatives are available for spectral interferences: subtraction of interfering signal contribution by means of theoretical or empirical equations, and limitation of polyatomic species formation using ‘cold plasmas’ [5,13,19,20]. Different gas mixtures (e.g. addition of oxygen for

organic matrix) and various nebuliser and cone geometries were tried, to prevent clogging and to limit the sample volume introduced [4–6,21,22]. The development of hyphenated methods by coupling with chromatographic techniques appears to be one of the most promising avenues, for its many potentials applications, including speciation.

Among liquid chromatographic techniques, chelation by iminodiacetate resin has been largely investigated to achieve metals preconcentration and separation from seawater [23]. Chelex 100 has been the resin most studied [24–30], since its use was reported by Riley and Taylor in 1968 [31]. Recent researches have focused on another iminodiacetate resin Metpac CC-1, which is a highly cross-linked macroporous copolymer, and hence not liable to the large volume variations observed in Chelex 100 upon pH variations [11,32–34]. Thus Metpac CC-1 suits high-performance liquid chromatography (HPLC) and can withstand pressures up to 1500 psi [23,35].

The first step of our work was the on-line coupling of chelation ion chromatography with ICP-MS. We then conducted a method validation, partly derived from AFNOR Standard XPT 90-210 [36], on 12 elements (Cd, Pb, Cu, Mn, Ga, Ni, Cr, Co, Al, In, Bi and U) analysing standards and blanks. The behaviour of the 12 elements, plus Ag, Tl, Zn, Al and Sn, towards the resin, was qualitatively investigated. Method accuracy was then assessed by analysing two certified materials: a synthetic freshwater (SRM 1643d), and a natural filtered coastal seawater (NRCC CASS-3). A sampling campaign was finally run on the Rhône river estuary, as a preliminary study and in order to compare our method with environmental samples analyses.

## 2. Experimental

### 2.1. Reagents

All reagents used in this work were at least of analytical grade.

Ultrapure water used for all operations (cleaning, rinsing, preparation of solutions) was Milli-



Q + <sup>TM</sup> (Millipore), which has a resistivity of 18.2 MΩ/cm.

All vessels were acid cleaned with 10% nitric acid (65% Normatom), rinsed with ultrapure water and dried in a class 100 laminar flow hood before use.

Two eluents are used in the chromatographic device: 1.5 M nitric acid prepared by dilution of ultrapure nitric acid (69% HNO<sub>3</sub>, Carlo Erba), and 2 M ammonium acetate buffered to pH 5.4 ± 0.1, which is commercially available (Dionex).

Standard Reference Material 1643d Trace Elements in Water of the United States National Institute of Standards and Technology is a synthetic freshwater spiked with metals in different concentrations. It was diluted 10-fold prior to analysis, in order to obtain metallic concentrations closer to those found in riverine water.

CASS-3 Coastal Seawater from the National Research Council of Canada is a natural filtered seawater.

Standard solutions were obtained by diluting Spex 2 multi-elemental solution (Spex Certiprep), containing 10 mg/l of various metals.

## 2.2. Instrumentation

The instrument configuration is shown schematically in Fig. 1.

The chromatographic device consists of a four-way gradient pump (GP 40 from Dionex Corp.) and a six-way Rheodyne valve integrated in a temperature regulated oven (LC30 from Dionex). The chelating resin Metpac-CC1 is a macroporous (particle size about 20 μm) highly cross-linked (12%) polystyrene–divinylbenzene copolymer, functionalised by iminodiacetate. The resin is packed in a 5-cm column (4 mm i.d.) and presents a capacity of 0.9 meq/g (0.45 meq/column). Eluents are delivered by gradient pump from 2-l polyethylene bottles (GL 45 from Dionex), pres-

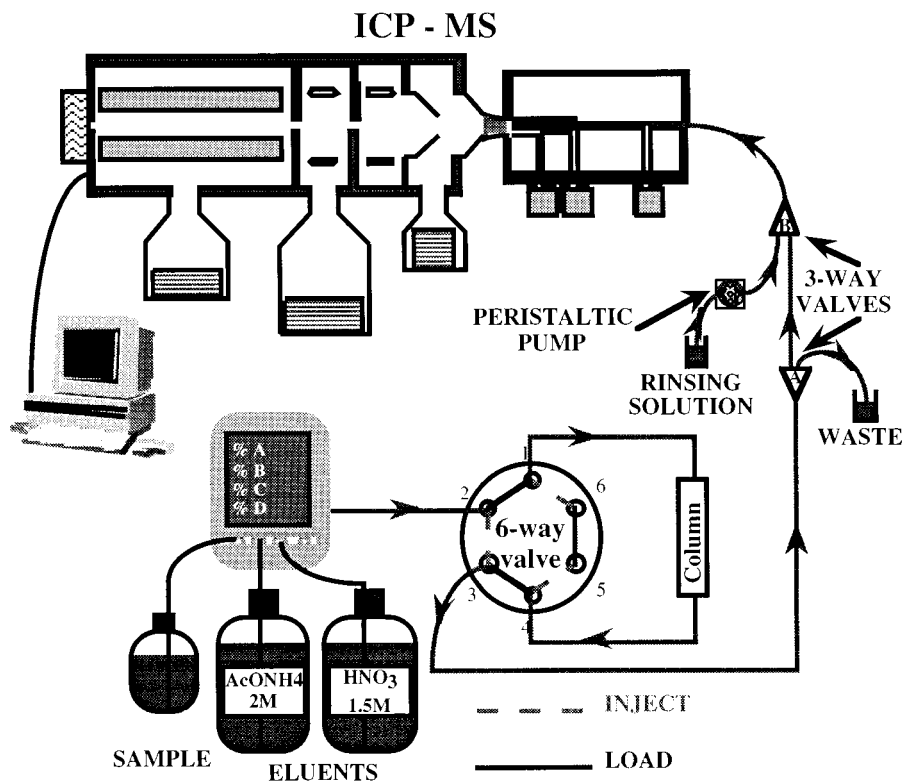


Fig. 1. On-line coupling of chelation chromatography with ICP-MS.

Table 1  
ICP-MS instrumental conditions

---

Cool flow: 15 l/min
Auxiliary flow: 1 l/min
Nebuliser flow: 0.865 l/min
Incident power: 1350 W
Acquisition mode: scan
Dwell time: 320 $\mu$ s
Channels/amu: 19
Time per sweep: 0.5 s
Acquisition time: 200 s
Chromatogram signal response: area

---

surised to 6 psi with helium. The gradient pump also pumps samples through the analytical column. The overall device allows mixing rates from 0.1 to 99.9% between samples and eluents, at flow-rates and pressures up to 4 ml/min and 1500 psi, respectively.

Connection to ICP-MS is provided by PTFE tubing and three-way Rheodyne valves (Rheodyne, Cotati, CA).

Trace elements are detected by an ICP-MS PQ2+ (VG elemental), monitored by a Pentium 200, under an OS2/Warp (IBM) operating system, and equipped with a Fassel torch, a Meinhard coaxial flow nebuliser, and a high-performance interface. ICP-MS rinsing is carried out by means of a peristaltic pump (Gilson, Minipuls 3). Data are acquired in time resolved analysis mode by means of PQ 4.3.1 software (VG elemental), before export to Mass Lynx 2.0 (VG Elemental) software (in Microsoft Windows environment) for further processing of the chromatograms obtained. ICP-MS instrumental conditions are summarised in Table 1.

### 2.3. Sampling and treatment of riverine, estuarine and seawater

Water from the Rhône estuary was sampled as described by Tousset et al. [37,38], in conformity with the conventional uses of marine samplings [39]. Samples were taken from a small rubber boat (motor stopped) by immersing capped, metal-free 5-l polypropylene bottles, 30 cm below the surface. The samples were stored at 4°C during transport to the laboratory. Six stations were set

along the salinity gradient of Rhône estuary, and two samples were taken by each station.

On arrival at the laboratory, the samples were acidified to under pH 2 by adding 1% Ultra-Pure nitric acid (69% HNO<sub>3</sub>, Carlo-Erba). Before analysis, samples were mineralised by adding 2% of Normapur hydrogen peroxide (20% H<sub>2</sub>O<sub>2</sub>, Pro-labo) and raised to 80°C for 1 h. By this procedure, most of the non-lithogenic colloidal and particulate matter was dissolved and the organic matrix was destroyed in order to avoid competition between organic ligands and the resin binding sites. Acidic pH, below 2, was maintained until sample analysis, to avoid depletion of metals concentration by precipitation and/or adsorption.

Analytical blanks were prepared with Milli-Q + <sup>TM</sup> water in the same way as environmental samples (addition of nitric acid and hydrogen peroxide before mineralisation).

### 2.4. Procedure

The operating procedure, described in Table 2, includes four main steps: sample loading, selective alkali and alkaline earth-metals elution, and resin regeneration.

Just before being passed through the cationic exchange column (in ammonium form) the water sample is buffered on-line by mixing with buffered 2 M ammonium acetate (pH 5.4  $\pm$  0.1) (Table 2). On-line buffering allows chelation at optimal pH (5.4  $\pm$  0.2) to separate metals from alkali and alkaline-earth metals, while maintaining an acidic pH, below 2, as long as possible. Heitmar et al. [11] also observed that a minimum buffering solution addition is necessary to prevent peak tailing. Hence we set the mixing rate at 20% AcONH<sub>4</sub>, inducing a residual buffer concentration of 0.4 M in the sample during chelation.

During sample loading, Metpac-CC1 resin retains not only trace metals but also alkaline-earth metals, and slightly alkaline metals. A specific elution of alkaline and alkaline-earth metals is therefore conducted by injecting ammonium acetate buffer.

The metals are then eluted with 1.5 M HNO<sub>3</sub>, by destruction of resin–metals complexes and chelates. The eluate is injected directly into ICP-

Table 2  
Ionic chelation operating programme

Time (min)	Mixing rate (%)			Flow-rate (ml/min)	Six-way valve position	Position three-way valves	Event
	Sample	HNO <sub>3</sub>	AcONH <sub>4</sub>				
Initial	80	0	20	2	Load	Waste	Start
0	80	0	20	3	Inject	Waste	Load sample
12.5	80	0	20	3	Inject	Waste	End loading
12.51	0	0	100	4	Inject	Waste	Elution start
13.70	0	0	100	4	Inject	Waste	Alkaline earth metal selective elution
13.80	0	100	0	4	Inject	Waste	Acid elution
14.0	0	100	0	2	Inject	ICP-MS	Metal elution, ICP-MS acquisition
17.00	0	100	0	2	Inject	ICP-MS	End ICP-MS acquisition
17.20	0	100	0	2	Inject	Waste	Column regeneration
17.30	0	0	100	3	Inject	Waste	
18.30	0	100	0	3	Inject	Waste	
19.30	0	0	100	3	Inject	Waste	
20.30	0	100	0	3	Inject	Waste	
21.30	0	0	100	3	Inject	Waste	Resin conditioning
22.40	0	0	100	0	Load	Waste	Stop

MS, which acts as a multi-elemental specific detector, and thus allows elution of all the analytes in a single step.

Resin cleaning and post-conditioning are carried out by successive flushes of nitric acid and ammonium acetate, rather than in a two-step way, in order to reduce the residual metals concentration, as described in Heitmar et al. [11].

### 2.5. Protocol

A standard solution containing 100 µg/l of indium was injected directly into ICP-MS after each analysis, in order to check the stability of the ICP-MS response. The signal obtained was read directly on the ICP-MS signal ratemeter, without computer processing.

Polyatomic species formation was investigated by comparing their relative contribution to the analytical signal at various  $m/z$  (i.e. mass/charge).

Qualitative observation of peak elution, in terms of shape and retention time, was conducted to evaluate the metals retention characteristics of the resin.

Calibrations were made with five concentration standards distributed in the range 0.05–10 µg/l. Student's parameter  $t$  was then calculated by Eq. (1) [36]:

$$t_{\text{calculated}} = \sqrt{\frac{r^2(N_1 - 2)}{1 - r^2}} \quad (1)$$

where  $r^2$  is the correlation coefficient and  $N_1$  the number of calibration points. Linearity is established if  $t_{\text{calculated}}$  is higher to  $t_{0.975}$  taken from the Student's law table.

The definition of AFNOR Standard XPT 90-210 was retained for determining detection limits (D.L.) [36]. D.L. are expressed as  $2\sqrt{2}t_{0.975}$  times the standard deviation observed analysing blanks in repeatability conditions.

Accuracy was evaluated by analysing two certified materials: a synthetic freshwater (NIST SRM 1643d), and a natural filtered coastal seawater (NRCC CASS-3).

Samples from the Rhône estuary were eventually analysed in order to assess the method efficiency on environmental samples.

## 3. Results and discussion

### 3.1. Removal of saline matrix interferences and signal stability

Signal stability was assessed using an indium standard solution passed after each sample. No suppression effect due to orifice clogging was observed after 10 h. Plasma stability appeared to be better than when analysing drinking water samples daily controlled in our laboratory. Such a good stability can primarily be attributed to the absence in eluates of matrix elements, such as Ca and humic acids, and to the short time of sample analysis, close to 3 min, compared with the long rinsing time of over 15 min.

Polyatomic ions consisting of two or three atoms may be responsible for signal overlap with analytes. The origins of polyatomic species are not yet fully elucidated, although previous works have highlighted incomplete dissociation in the plasma and recombination reactions as formation mechanisms. The main polyatomic interferences generate by high NaCl concentrations (until 1g/l), are  $^{35}\text{Cl}^{16}\text{O}^+$ ,  $^{37}\text{Cl}^{16}\text{O}^+$ ,  $^{40}\text{Ar}^{35}\text{Cl}^+$ ,  $^{40}\text{Ar}^{37}\text{Cl}^+$  and, to a lesser extent,  $^{23}\text{Na}_2^{16}\text{O}^+$  and  $^{40}\text{Ar}^{23}\text{Na}^+$ . They overlap the analytical signal respectively for  $^{51}\text{V}$ ,  $^{53}\text{Cr}$ ,  $^{75}\text{As}$ ,  $^{77}\text{Se}$ ,  $^{62}\text{Ni}$  and  $^{63}\text{Cu}$ . We found that all these interferences became insignificant after sample conditioning by the resin, as reported by Heitmar et al. [11].

Unfortunately, ion chelation chromatography is ineffective for reducing interferences resulting from combinations of argon with nitrogen and oxygen. Moreover, IC/ICP-MS magnified the matrix carbon content, due to the use of 2M  $\text{AcONH}_4$ . As a result, a black carbon deposit tended to appear on the sampler and even on the skimmer cone, which is likely to alter ion extraction. Another consequence was the formation of argides by combination between argon and carbon or carbonyl. Thus, the significant interferences we observed in detecting  $^{52}\text{Cr}$ ,  $^{53}\text{Cr}$  and  $^{68}\text{Zn}$  could be explained by the formation of  $^{40}\text{Ar}^{12}\text{C}^+$ ,  $^{40}\text{Ar}^{13}\text{C}^+$  and  $^{40}\text{Ar}^{12}\text{C}^{16}\text{O}^+$ . Heitmar et al. also reported a contribution of  $^{36}\text{Ar}^{12}\text{C}^+$  to the  $^{48}\text{Ti}$  analytical signal [11]. One way to reduce residual carbon concentration could be a further rinsing

with ultrapure water prior to nitric acid elution. Nevertheless, interferences induced by carbon matrix do not hinder isotope detection, because they are repeatable and contribute slightly to the analytical signal. The greatest interference signal contribution, is observed at  $m/z$  52, and is approximately equal to the signal obtained analysing a 5- $\mu\text{g/l}$  chromium standard.

After removing the salt matrix and assessing system stability, we investigated the behaviour of metals towards resin.

### 3.2. Behaviour of metals towards resin

Little previous work has been reported on Metpac CC-1 resin, so that it could be interesting to investigate its chelating properties towards metals. As a qualitative approach, we studied metal behaviour through peak shape and mean retention time observed on 19 standards (Table 3).

The resin is conditioned in a short column because Metpac CC-1 is designed for metal concentration rather than chromatographic separation. This physical characteristic and the resin's high affinity for metals, lanthanides and actinides are responsible of the narrow range of retention times observed for most metals (64.1–70.5 s). All the divalent transition metals (d group) display similar retention times, between 64.1 and 65.9 s. From our observations, other elements (Cr, V, In, Al, Ga, U, Sn and Bi) appear to exhibit longer retention times, probably related to higher cationic charge density ( $q/r^2$ , where  $q$  is the absolute charge and  $r$  the ionic radius), which may cause greater affinity for the resin. The ionic charge density is valence dependent and influences acidic properties [41].

The shift in retention time appears relatively insignificant for In and the two d group metals, Cr and V, but it is more significant for U and p group metals, Al and Ga. Two other p metals, Sn and Bi, which are known to form very acidic cations [41], obviously display distinctly longer retention times, and stand apart by tailing of the elution peak.

As reported by Dionex [35], silver and thallium are not efficiently concentrated by chelation on Metpac CC-1. This behaviour could be due to

their predominant monovalent cationic form in water and to their low charge density ( $\text{Tl}^+$  has no acidic properties in aqueous solution and silver hydroxide precipitates at about pH 8.5).

Conversely, chromium does not appear to have any particular behaviour upon retention characteristics observed, although it is claimed to be not quantitatively eluted [35].

### 3.3. Method validation

In order to evaluate method performance, we checked linearity, then we determined detection limits, before assessing accuracy and repeatability.

Standards and blanks were prepared with ultrapure water rather than with seawater treated for metals removal, assuming the same chelation efficiency in both media. In previous work on the same method, Bettinelli and Spezia observed close signal response (ratio from 0.85 to 1.05) of ICP-MS, between 1- $\mu\text{g/l}$  multi-elemental standard solutions prepared in deionised water and in synthetic seawater [34]. Moreover their blanks prepared in synthetic seawater treated with Chelex 100 iminodiacetate resin contained significantly higher concentrations of transition and heavy metals than blanks from ultrapure water.

Hence the preparation of standards in synthetic seawater for calibration or for evaluating method performances does not appear useful, particularly since this time-consuming step could cause analytical bias. However, evaluating method performances with standards that are so different from samples, requires assessment with appropriate certified materials.

Linearity was demonstrated for most elements (U, In, Co, Cd, Ga, Pb, V and Cu) in the range 0.05–10  $\mu\text{g/l}$ , with correlation coefficients better than 0.997 (five-point calibration). Peak tailing of Bi impaired repeatability and correlation coefficients were lower (down to 0.991). Relatively high blanks signal obtained on other elements (Ni, Mn, Zn and  $^{53}\text{Cr}$ ) shifted the linearity range towards higher concentrations.

Detection limits were determined by analysing blanks in repeatability conditions. The results, shown in Table 4, show good agreement, for most metals (Bi, U, In, Co, Cd, Ga, Pb, V and Cu),

Table 3  
Mean retention time, peak shape, valence and hydroxide precipitation pH

	Tl	Ag	Zn	Cd	Co	Pb	Cu	Mn	Ni	Cr	V	In	Al	Ga	U	Sn	Bi
Mean retention time (s) ( $n = 19$ )			64.1	64.1	64.7	64.8	65.2	65.3	65.9	66.5	66.6	66.7	70	70	70.5	85	94.2
S.D.			0.7	0.9	0.7	0.9	0.6	0.8	1.1	1.7	0.4	4.4	1.2	3.5	8.1	3.2	5.5
Peak shape <sup>a</sup>	N.P.	N.P.	R, I	R	R	R	R	R	R	R, I	R	R	R	R	R	T	T
Valence [41]	1	1	2	2	2	2	2	2	2	3	4–5	3	3	3	6	4	3–5
Hydroxide precipitation pH [41]	Strong base	8.5	6.5	8	7.5	7.5	5	8.5	7	5	4	2.5	3.9	3	4	0.5–2	1–2

<sup>a</sup> Peak shape: R, regular; I, interference; T, tailing; and N.P., no peak.

with those reported in previous works [11,34]. Others (Ni, Mn, Al and Zn) display comparatively high detection limits, which can be ascribed to contaminated blanks or materials. Better results could be obtained, since our laboratory and analytical instruments are not dedicated to ultra-trace (sub-ppb level) metals analysis. Moreover, Milli-Q + <sup>TM</sup> water, used for washing, dilution and as analytical blanks, may contain ultratraces of metals, which certainly impair detection limits. Pre-treatment of Milli-Q + <sup>TM</sup> water with Metpac CC-1 or another suitable resin, offers one way to improve analytical blanks and detection limits, as demonstrated by Boomer et al. with Ionpac CS-5 resin from Dionex [42].

As expected from peak observation, the detection limit achieved for chromium with isotope 50 does not set it apart. Conversely a much higher detection limit of 1739 ng/l was calculated for <sup>53</sup>Cr, whose detection is affected by <sup>40</sup>Ar<sup>13</sup>C<sup>+</sup> interference, and this isotope will be therefore discarded for quantification.

In our working conditions, all the elements except Zn display a sufficiently low detection limit for satisfactory seawater analysis.

Concentration levels in certified material SRM 1643d, which is a synthetic freshwater, are typical of drinking water. We therefore diluted SRM 1643d 10-fold before analysis to obtain matrix and analyte concentrations, approximating natural riverine water conditions. Accuracy was then

evaluated by repeat analyses of two certified materials, CASS-3 coastal seawater (salinity 35 g/l) and diluted SRM 1643d. In both cases, good recovery was obtained between certified and measured values for most metals investigated (Table 5). This demonstrates the robustness of the method and its suitability for successive analyses of samples as different as fresh and highly saline water.

The high detection limit obtained for Zn (Table 4), prevented its detection in CASS-3, although its concentration was accurately measured in SRM 1643d (Table 5).

IC/ICP-MS thus appears to be an ideal method for studying the salt/freshwater interface in an estuary, as it offers sufficiently low detection limits, is linear over the main range of metallic concentrations encountered, and is efficient in both riverine and saline matrices.

### 3.4. Environmental sample analysis

The analysis of environmental samples by ICP-MS requires attention to specific problems, such as isobaric interferences. Analysing Rhône estuary samples, we observed a significant overlap of major cadmium isotopes, i.e. <sup>112</sup>Cd and <sup>114</sup>Cd, by tin isotopes of the same atomic mass. Due to relative tin and cadmium concentrations, low salinity samples were more affected. Since the software provided by VG Elemental does not yet permit

Table 4  
Detection limits observed for each isotope (ng/l)

Isotope	Detection limit	Blank replicates	Isotope	Detection limit	Blank replicates
Bi 209	0.2	3	V51	34	4
U 238	0.5	4	Cu 63	42	6
In 115	1.0	5	Cu 65	72	5
Co 59	2	4	Cr 50	66	3
Ga 71	3	6	Ni 60	128	4
Ga 69	7	5	Ni 62	147	4
Cd 114	4	3	Ni 58	149	4
Cd 112	4	4	Mn 55	413	6
Cd 110	4	4	Al 27	762	4
Cd 111	5	6	Zn 64	1430	3
Pb 208	15	3	Zn 66	1720	4
Pb 206	18	4	Cr 53	1739	5
Pb 207	19	3	Zn 68	1773	4

Table 5  
Certified and measured concentrations of reference materials ( $\mu\text{g/l}$ )<sup>a</sup>

Element	NIST SRM 1643d (1/10)		NRCC CASS-3		
	Certified		Measured ( $n = 3$ )	Certified	Measured ( $n = 3$ )
Pb	1.815		$1.813 \pm 0.177$	$0.012 \pm 0.004$	$0.016 \pm 0.009$
Cd	0.647		$0.653 \pm 0.081$	$0.030 \pm 0.005$	$0.030 \pm 0.003$
Cu	2.05		$2.053 \pm 0.005$	$0.517 \pm 0.062$	$0.457 \pm 0.026$
Co	2.50		$2.50 \pm 0.19$	$0.041 \pm 0.009$	$0.047 \pm 0.005$
Ni	5.81		$5.88 \pm 0.53$	$0.386 \pm 0.062$	$0.418 \pm 0.038$
Bi	(1.3)		$1.63 \pm 0.17$	No data	–
Mn	3.766		$3.677 \pm 0.298$	$2.51 \pm 0.36$	$2.77 \pm 0.28$
Cr	1.853		$1.871 \pm 0.194$	$0.092 \pm 0.006$	$0.096 \pm 0.003$
Al	12.76		$12.61 \pm 0.58$	No data	–
Zn	7.248		$7.215 \pm 0.630$	$1.24 \pm 0.25$	<D.L.
V	3.51		$3.38 \pm 0.37$	No data	–
U	No data		–	(2.84)	$2.66 \pm 0.18$

<sup>a</sup> ( ) Indicative of non-certified values.

Table 6  
Metals concentration of Rhône estuary samples

	Salinity (g/l)	[Pb] ( $\mu\text{g/l}$ )	[Cd] ( $\mu\text{g/l}$ )	[Cu] ( $\mu\text{g/l}$ )	[Cr] ( $\mu\text{g/l}$ )	[Co] ( $\mu\text{g/l}$ )	[U] ( $\mu\text{g/l}$ )
S1	0.5	1.082	0.173	2.357	4.178	0.427	1.043
S2	7	0.620	0.164	2.320	1.593	0.367	1.441
S3	16	0.254	0.030	0.734	0.845	0.115	1.908
S4	25	0.251	0.018	0.561	0.600	0.119	2.473
S5	35	0.162	0.017	0.437	0.359	0.076	2.854
S6	38	0.162	0.019	0.410	0.390	0.025	3.203

the used of correction equations in time-resolved analysis, we have discarded both  $^{112}\text{Cd}$  and  $^{114}\text{Cd}$ , despite their greater abundance, in favour of isotopes 110 and 111. For the other elements, except chromium, every isotope has been taken into account to calculate the concentration.

Metals concentrations determined in Rhône estuary samples (Table 6) are consistent with those reported in previous works [40]. Trace metals analysed (Pb, Cd, Cu, Cr and Co) exhibit non-conservative behaviour typical of numerous salt–freshwater interfaces (e.g. estuary, salt marshes) [43]. In fact, metals flocculation and precipitation occurs upon wide variations in physico-chemical conditions (salinity, pH, turbidity, organic matter and particle concentration, oxido-reduction potential, etc.) [40,43–45]. Conversely, uranium displays conservative behaviour, as all the measured

concentrations can be placed on a theoretical dilution curve between the Rhône river and the Mediterranean Sea.

A more detailed study of metals behaviour and partitioning in the Rhône estuary [37] will be the topic of a subsequent paper [38]. To date, these early results confirm the ability of IC/ICP-MS to determine metals concentrations at sub- $\mu\text{g/l}$  levels, in an ‘analytically hostile’ environment like seawater.

#### 4. Conclusion

Chelation ion chromatography prior to ICP-MS detection appears to offer an efficient method for analysis of metals at ultra-trace level in complex matrices, such as seawater. The method is



also valid for lanthanides and actinides. Off-line sample pre-treatment is more cost effective, because it reduces working time in ICP-MS. Conversely, on-line coupling is fully automatable, enhances sensitivity, by reducing elution volume, and prevents subsequent sample contamination. The robustness of the coupling allows calibration with simple standards in deionised water, although working with standards so different from samples accentuates the need to introduce appropriate certified materials in analytical series.

The spreading use of ICP-MS as a chromatographic multi-elemental specific detector requires further improvements in data processing softwares in terms of capabilities, automation and userfriendliness.

### Acknowledgements

This research was undertaken in the framework of MAST-III-ELOISE European Union METRO-MED PROJECT (Dynamic of Matter Transfer and Biogeochemical Cycles: Their modelling in coastal systems of the Mediterranean Sea). We acknowledge the support of the European Commission's Marine Science Technology (MAST) Programme under contract CT 960049. We thank all the contributors and particularly J.C. Block, for his help and attention.

### References

- [1] K. Sutton, R.M.C. Sutton, J.A. Caruso, *J. Chromatogr. A* 789 (1997) 85.
- [2] B. Marin, M. Valladon, M. Polve, A. Monaco, *Anal. Chim. Acta* 342 (1997) 91.
- [3] J.W. Olesik, J.A. Kinzer, M.P. Dziewatkoski, Generation and transports of ions: ICP-MS from single drops and microsecond times scales to practical measurements in plasma source mass spectrometry: developments and applications, The Royal Society of Chemistry, Cambridge, 1997, pp. 1–12.
- [4] J.L.M. De Boer, Simultaneous reduction of polyatomic ion interferences in quadrupole ICP-MS using ultrasonic nebulisation and directed optimisation in plasma source mass spectrometry: developments and applications, The Royal Society of Chemistry, Cambridge, 1997, pp. 61–69.
- [5] N. Jakubowski & D. Stuever, New instrumental developments and analytical applications in ICP-MS in plasma source mass spectrometry: developments and applications, The Royal Society of Chemistry, Cambridge, 1997, pp. 218–312.
- [6] K.E. Jarvis, A.L. Gray, R.S. Houk, *Inductively Coupled Plasma Mass Spectrometry*, Blackie, New York, 1992.
- [7] C. Vandecasteele, C.B. Block, *Modern Methods for Trace Element Determination*, Wiley, Chichester, New York, Brisbane, Toronto, Singapore, 1993.
- [8] D.C. Gregoire, *Spectrochim. Acta* 42B (1987) 895.
- [9] J.A. Olivares, R.S. Houk, *Anal. Chem.* 58 (1986) 20.
- [10] D. Beauchemin, J.W. Mac Laren, S.S. Berman, *Spectrochim. Acta* 42B (1987) 467.
- [11] E.M. Heitmar, T.A. Hinnens, J.T. Rowan, J.M. Riviello, *Anal. Chem.* 62 (1990) 857.
- [12] S.L.C. Ferreira, A.S. Queiroz, M.D.A. Quorn, A.C.S. Costa, *Anal. Lett.* 30 (1997) 2251.
- [13] J. Wu, E.A. Boyle, *Anal. Chem.* 69 (1997) 2464.
- [14] P. Anderson, J. Ingrit, *Wat. Res.* 25 (1991) 617.
- [15] A.A. Specht, D. Beauchemin, *Anal. Chem.* 70 (1998) 1036.
- [16] D. Beauchemin, A.A. Specht, *Anal. Chem.* 69 (1997) 3183.
- [17] P.L. Lu, K.S. Huang, S.J. Jiang, *Anal. Chim. Acta* 284 (1993) 181.
- [18] A. Alimonti, F. Petrucci, S. Fioravanti, F. Laurenti, S. Caroli, *Anal. Chim. Acta* 342 (1997) 75.
- [19] D.E. Nixon, T.P. Moyer, *Spectrochim. Acta* 51B (1996) 13.
- [20] F. Pilon, D. Koller, A. Raith, The effect of high uranium matrix concentration on plasma screen torch: an evaluation of the improvement of iron analysis in actinide compounds in Plasma source mass spectrometry: developments and applications, The Royal Society of Chemistry, Cambridge, 1997, pp. 44–50.
- [21] G. Lespes, M. Potin-Gautier, A. Astruc, *Environ. Technol.* 13 (1992) 207.
- [22] H. Klinkenberg, S. Van Der Wal, C. De Koster, J. Bart, *J. Chromatogr. A* 794 (1998) 219.
- [23] C. Sarzanini, E. Mentasti, *J. Chromatogr. A* 789 (1997) 301.
- [24] H.M. Kingston, I.L. Barnes, T.J. Brady, T.C. Rains, M.A. Champs, *Anal. Chem.* 50 (1978) 2064.
- [25] R.R. Greenberg, H.M. Kingston, *Anal. Chem.* 55 (1983) 1160.
- [26] R.E. Sturgeon, S.S. Berman, J.A.H. Desaulniers, A.P. Mykytiuk, J.W. MacLaren, D.S. Russell, *Anal. Chem.* 52 (1980) 1585.
- [27] A. Miyazaki, R.A. Reimer, *J. Anal. Atomic Spectrom.* 8 (1993) 449.
- [28] W.W. Van Berkel, A.W. Oversbosh, G. Feenstra, F.J.M.J. Maessen, *J. Anal. Atomic Spectrom.* 3 (1988) 249.
- [29] F.M. Fernandez, J.D. Stripeikis, M.B. Tudino, O.E. Troccoli, *Analyst* 122 (1997) 679.
- [30] T.E. Florence, G.E. Batley, *Talanta* 22 (1975) 201.

- [31] J.P. Riley, D. Taylor, *Anal. Chim. Acta* 40 (1968) 479.
- [32] A. Siriraks, H.M. Kingston, J.M. Riviello, *Anal. Chem.* 62 (1990) 1185.
- [33] H. Lu, S. Mou, Y. Yan, S. Tong, J.M. Riviello, *J. Chromatogr. A* 800 (1998) 247.
- [34] M. Bettinelli, S. Spezia, *J. Chromatogr. A* 709 (1995) 275.
- [35] Dionex Corp., Technical Note 28, 1992
- [36] Afnor norm XPT 90-210, 1996
- [37] N. Tousset, M. Nicolai, A. Thill, J.Y. Bottero, J.C. Block, Communication to the 8th Annual Meeting of SETAC Europe, Bordeaux, 14–18 April 1998.
- [38] N. Tousset, M. Nicolai, A. Thill, J.Y. Bottero, J.C. Block, in preparation.
- [39] J.F. Chiffolleau, Aspect analytique du plomb en milieu marin, in: *Aspects analytiques du plomb dans l'environnement*, Technique & Document, 1996, pp. 14–87.
- [40] M. Dai, J.M. Martin, G. Cauwet, *Mar. Chem.* 51 (1995) 159.
- [41] G. Charlot, 1969. *Les réactions chimiques en solution*, L'analyse quantitative minérale, 6th ed., Masson & Cie, Paris, pp. 200–336.
- [42] D.W. Boomer, M.J. Powell, J. Hipfner, *Talanta* 37 (1990) 127.
- [43] A.R. Karbassi, S. Nadjafpour, *Environ. Pollut.* 93 (1996) 257.
- [44] A. Turner, *Mar. Chem.* 54 (1996) 27.
- [45] A.C.M. Bourg, *Continental Shelf Res.* 7 (1987) 1319.

# TURBISCAN MA 2000: multiple light scattering measurement for concentrated emulsion and suspension instability analysis

O. Mengual<sup>a,\*</sup>, G. Meunier<sup>a</sup>, I. Cayré<sup>a</sup>, K. Puech<sup>a</sup>, P. Snabre<sup>b</sup>

<sup>a</sup> *Formulation, 10 Av. de l'Europe, 31525 Ramonville Saint Agne, Toulouse, France*

<sup>b</sup> *I.M.P., CNRS BP5 66120, Font-Romeu, France*

Received 7 September 1998; received in revised form 1 April 1999; accepted 2 April 1999

---

## Abstract

Emulsion or suspension destabilisation often results from coalescence or particle aggregation (flocculation) leading to particle migration (creaming or sedimentation). Creaming and sedimentation are often considered as reversible, while coalescence and flocculation spell disaster for the formulator. Thus, it is of prime importance to detect coalescence or cluster formation at an early stage to shorten the ageing tests and to improve the formulations. This work mainly concerns the independent and anisotropic scattering of light from an emulsion or suspension in a cylindrical glass measurement cell, in relation with the optical analyser TURBISCAN MA 2000. The propagation of light through a concentrated dispersion can be used to characterise the system physico-chemical stability. Indeed, photons undergo many scattering events in an optically thick dispersion before escaping the medium and entering a receiver aperture. Multiple scattering thus contributes significantly to the transmitted and backscattered flux measured by TURBISCAN MA 2000. We present statistical models and numerical simulations for the radiative transfer in a suspension (plane or cylindrical measurement cells) only involving the photon mean path length, the asymmetry factor and the geometry of the light receivers. We further have developed an imaging method with high grey level resolution for the visualisation and the analysis of the surface flux in the backscattered spot light. We compare the results from physical models and numerical simulations with the experiments performed with the imaging method and the optical analyser TURBISCAN MA 2000 for latex beads suspensions (variable size and particle volume fraction). We then present a few examples of concentrated emulsion and suspension instability analysis with TURBISCAN 2000. It is shown that the instrument is able to characterise particle or aggregate size variation and particle/aggregate migration and to detect these phenomena much more earlier than the operator's naked eye, especially for concentrated and optically thick media. © 1999 Elsevier Science B.V. All rights reserved.

*Keywords:* Characterisation; Concentrated dispersion; Instability; Multiple light scattering

---

\* Corresponding author. Tel.: +33-561-28-5621; fax: +33-561-28-5677.

*E-mail address:* o.mengual@formulation.fr (O. Mengual)

## 1. Introduction

Colloids and dispersions are inherently unstable systems [1] which can be considered as kinetically stable if the destabilisation rate is enough small compared with the expected lifespan. The analysis of the dispersion instability is of prime importance for the formulator.

Two strategies are mainly conducted to get insight on the stability behavior:

1. Measurement of the zeta potential of the particle surface to predict the stability of the dispersion [1]. This predictive method is effective for relatively simple preparations, but is not suitable for complex industrial formulations. Indeed, the zeta potential cannot give information about the effects of the multiple components dissolved in the continuous phase on the flocculation behaviour of particles.
2. Ageing tests are often performed [2]. The products are stored under specific conditions (temperature, light, etc.) and submitted to regular analysis. The purpose of these ageing tests is to accelerate the destabilisation process in order to reduce the time needed for new products development.

The two major destabilisation phenomena affecting the homogeneity of dispersions are particle migration (creaming, sedimentation) and particle size variation or aggregation (coalescence, flocculation).

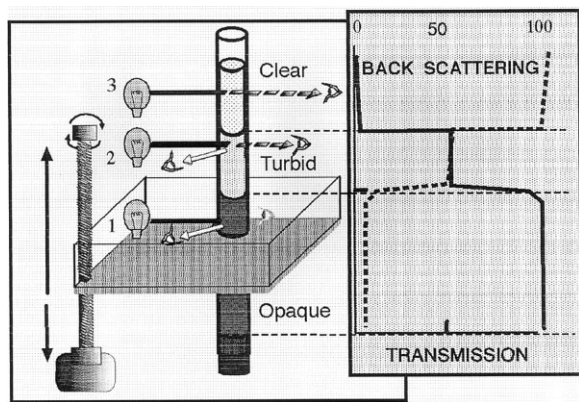


Fig. 1. TURBISCAN MA 2000 principle.

Techniques commonly used to detect physical destabilisation are either the naked eye or analytical instruments more accurate and reliable (particle size analysis, microscopy, spectroscopy [3]).

Most of dispersions are, however, quite concentrated and opaque and, as a result, fall outside the range of existing instruments. As a rule, dilutions have to be performed, reducing severely the accuracy and scope of these instruments.

A new instrument called TURBISCAN MA 2000 [4,5] has been developed to fill this gap and to allow the analysis of physical destabilisation of concentrated liquid dispersions (emulsions, suspensions).

In this paper, we first describe the measurement principle of the instrument. In the second part, we present principles and results concerning multiple scattering of light by a suspension in a cylindrical glass measurement cell. In the last section, we present examples of dispersion destabilisation detected by TURBISCAN MA 2000.

## 2. Measurement principle

The heart of TURBISCAN MA 2000 is a detection head which moves up and down along a flat-bottomed glass cylindrical cell (Fig. 1). The detection head is composed of a pulsed near infrared light source (wavelength  $\lambda = 850$  nm) and two synchronous detectors. The transmission detector receives the light which goes through the sample ( $0^\circ$  from the incident beam), while the backscattering detector receives the light scattered by the sample at  $135^\circ$  from the incident beam. The angle of  $135^\circ$  was chosen so as to be outside the coherent backscattering cone (the cone angle  $\theta_c$  of the coherent scattered intensity scales as  $\lambda/\lambda^*$  [13], where  $\lambda^*$  is the photon transport length, see Section 3.1).

The detection head scans the entire length of the sample (about 65 mm), acquiring transmission and backscattering data each  $40 \mu\text{m}$  (1625 transmission and backscattering acquisitions per scan). The measured fluxes are calibrated with a non-absorbing reflectance standard (calibrated polystyrene latex beads) and a transmittance standard (silicon oil).

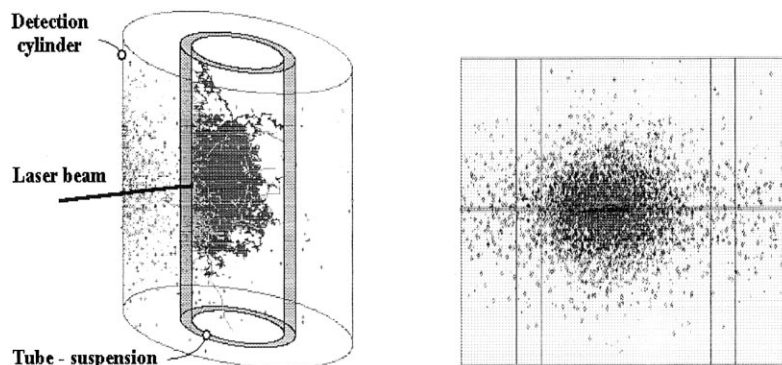


Fig. 2. 3D Monte Carlo simulation. Trajectory of photons (left) and backscattered spot light (right) for scatterers in a cylindrical cell.

The signal is first treated by a TURBISCAN MA 2000 current-to-voltage converter. The integrated microprocessor software handles data acquisition, analogue to digital conversion, data storage, motor control and computer dialogue.

### 3. Physical principles of multiple light scattering

#### 3.1. Definitions

The propagation of light in a random dispersed medium may be considered as independent or incoherent when the photon mean path length  $\lambda(\phi, d)$  is larger than the wavelength  $\lambda$  of the incident radiation [6,12,15]:

$$\lambda(\phi, d) = \frac{1}{n(\pi d^2/4)Q_e} = \frac{2d}{3\phi Q_e} \quad \text{and} \quad \phi = n \frac{\pi d^3}{6} \quad (1)$$

where  $n$  is the particle density,  $d$  the particle mean diameter,  $\phi$  the particle volume fraction and  $Q_e$  the extinction efficiency factor for scattering and absorption phenomena (ratio of the extinction cross-section to the geometrical cross-section). In this work, we only consider non-absorbing particles with an extinction efficiency factor  $Q_e$  equal to the scattering efficiency factor  $Q_s$ .

The anisotropic scattering of light by a particle can be characterised by the asymmetry factor  $g$  which is the average cosine  $\langle \cos \theta \rangle$  of the scattering angles weighted by the phase function or

scattering diagram  $P(\theta)$  of the scatterer ( $g = 0$  for isotropic Rayleigh scatterers and  $0 < g < 1$  for Mie scatterers of size larger than the wavelength) [6].

For anisotropic scatterers, we further define the photon transport length  $\lambda^* = \lambda/(1 - g)$  representing a decorrelation length above which the photon forgets both the direction of the incident beam and the scattering pattern of single particles [7,9].

Coherent light scattering due to a correlation increase among particles only occurs in concentrated media of particles smaller than the wavelength  $\lambda$  and results in a larger photon mean free path  $\lambda_c \approx \lambda(1 + 2\phi)^2/(1 - \phi)^4$  [14].

#### 3.2. Numerical simulation of independent multiple light scattering

We have developed a three-dimensional Monte carlo simulation of multiple light scattering from a random set of particles in a plane or cylindrical cell (Fig. 2) [7,8].

Numerical simulations of multiple light scattering consist in tracking individual photons while they leave the cell and reach a detector. From random numbers distributed in the range from 0 to 1 and cumulative distribution functions depending on the photon mean free path  $\lambda$  and the asymmetry factor  $g$ , we calculate the path length and the scattering angle between scattering events. The simulation further accounts for the boundary reflections (air/glass and glass/suspension interfaces) and the geometry of the light receivers.

### 3.3. Light flux in the backscattered spot light

We have developed an original imaging method to determine the flux in the two dimensional backscattered spot light resulting from the interaction of a collimated laser beam ( $\lambda = 0.6328 \mu\text{m}$ ) with a random dispersed medium. The backscattered spot light is visualised with a CCD video camera equipped with an electronic shutter (Figs. 3 and 4). We explore the different areas of the backscattered spot light by saving several images under variable shutter speed. The treatment of the images then gives the surface light flux in the backscattered spot light over more than  $10^6$  grey levels (Fig. 5). The flux calibration of the imaging system is performed with a non-absorbing reflectance standard (Labsphere).

Fig. 3 and Fig. 4 show the backscattered spot light for latex bead aqueous suspensions (average diameter  $d = 11.9 \mu\text{m}$  and  $d = 0.28 \mu\text{m}$ , particle volume fraction  $\phi = 1\%$ ) in a plane cell or a cylindrical measurement cell.

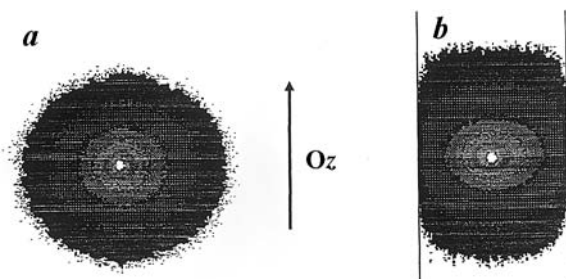


Fig. 3. Backscattered spot light for a latex suspension (mean particle diameter  $d = 11.9 \mu\text{m}$ , particle volume fraction  $\phi = 1\%$ ) in a plane cell (a) or a cylindrical cell (b).

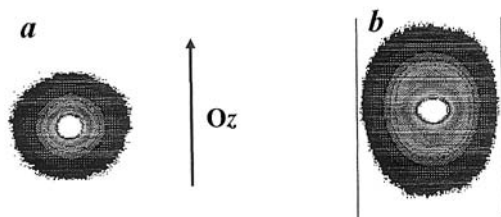


Fig. 4. Backscattered spot light for a latex suspension (mean diameter  $d = 0.28 \mu\text{m}$ , particle volume fraction  $\phi = 1\%$ ) in a plane cell (a) or a cylindrical cell (b).

For anisotropic scatterers such as particles larger than the wavelength ( $d \gg \lambda$ ), the spot light is quite large since the photons undergo many scattering events in the forward direction before escaping the cell (Fig. 3). The isotropic scattering of light by particles smaller than the wavelength ( $d \ll \lambda$ ,  $g \approx 0$ ) results in a smaller spot light much more luminous in the central part (Fig. 4). The geometry of the container (plane or cylindrical) weakly influences the light distribution in the central area of the backscattered spot light (Figs. 3 and 4). However, the curvature of the cell limits the lateral extension of the spot light and the boundary reflections further perturb the external area of the backscattering spot (Fig. 3b and Fig. 4b).

Fig. 5 shows the radial or axial dependence of the reduced surface flux  $F(r)\lambda^{*2}$  in a plane cell or  $F(z)\lambda^{*2}$  in a cylindrical cell for a latex bead aqueous suspension ( $d = 11.9 \mu\text{m}$ ,  $\phi = 1\%$ ). For long path photons (emitted at a large distance from the impact point of the laser), the reduced surface flux scales as  $(r/\lambda^*)^{-3}$  in plane geometry or  $(z/\lambda^*)^{-3}$  in cylindrical geometry in good agreement with Monte carlo simulations. The distribution of short path photons in the central part of the spot light obeys a different statistical law depending on the fine structure of the phase function. For a backward scattering probability  $P_b > 0.01 - 0.05$ , the reduced surface flux then scales as  $(r/\lambda^*)^{-1.4}$  in plane geometry or  $(z/\lambda^*)^{-1.4}$  in cylindrical geometry [7,9] (Fig. 5). The boundary reflections at air/glass and glass/suspension interfaces further result in a light ring at a distance of about  $2e$  from the spot center where  $e$  is the glass thickness.

The characteristic distance  $z^* \approx 4\lambda^*$  between the short path photon and long path photon regimes gives an estimation of the photon transport length  $\lambda^* = 2d/[3\phi(1-g)Q_s]$ . The values of the optical parameter  $(1-g)Q_s$  derived from the analysis of the backscattered spot light well agree with the predictions of the Mie theory.

The photon trajectory is equivalent to a random isotropic walk with an average step equal to the photon transport length  $\lambda^*(g)$ . For non-absorbing media, statistical models and numerical simulations lead to the following analytical expressions of the surface flux in the spot light [11]:

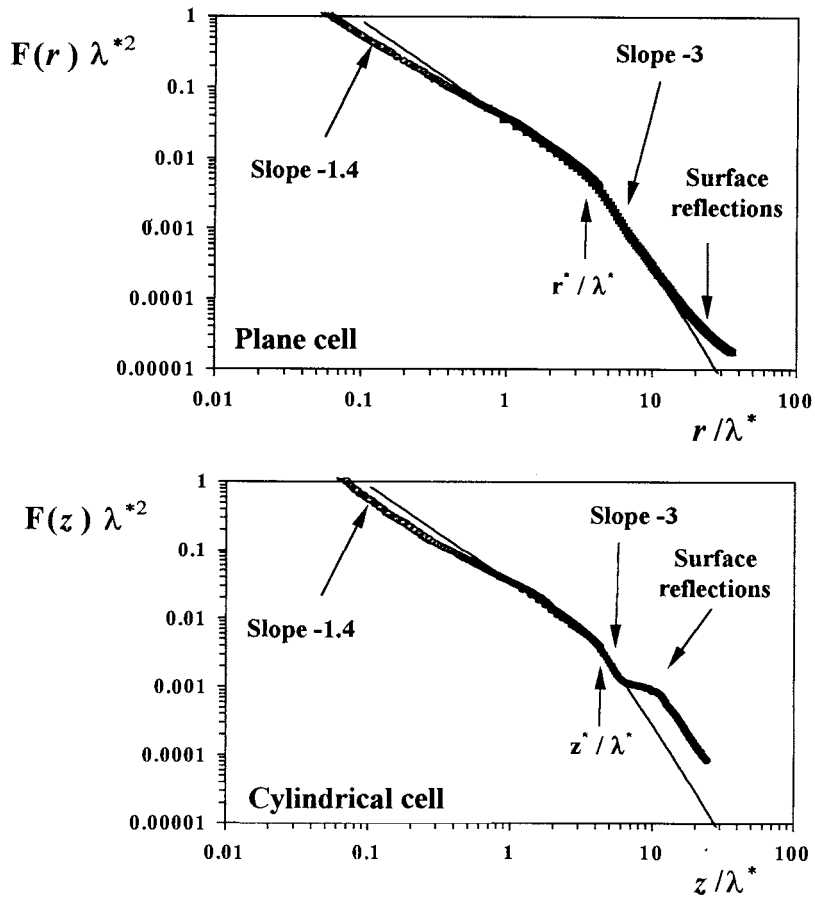


Fig. 5. Reduced light flux  $F(r/\lambda^*)\lambda^{*2}$  in a plane cell or  $F(z/\lambda^*)\lambda^{*2}$  in a cylindrical cell for a latex bead aqueous suspension ( $d = 11.9 \mu\text{m}$ ,  $\phi = 1\%$ ). Experiments (●) and numerical simulations (—) with  $(1-g)Q_s = 0.186$ .

$$F(z) \approx \frac{0.03}{\lambda^{*2}} \left(\frac{\lambda^*}{z}\right)^{1.4} = \frac{0.03}{z^{1.4}} \left(\frac{3\phi(1-g)Q_s}{2d}\right)^{0.6} \quad \text{for}$$

$$z > z^* \approx 4\lambda^* \frac{4\lambda}{1-g}$$

$$F(z) = \frac{\lambda^*}{\pi z^3} = \frac{1}{z^3} \frac{2d}{3\phi(1-g)Q_s} \quad \text{for } z < z^* \approx 4\lambda^* \quad (2)$$

3.4. Light flux measurement with the optical analyser TURBISCAN MA 2000

The optical analyser TURBISCAN MA 2000 detects the light flux backscattered at  $135^\circ$  by a

dispersed medium in a cylindrical cell. The light detector of relatively small aperture presents a rectangular cross-section (width  $\delta l$  and height  $\delta h < \delta l$ ). By integrating the surface flux given by Eq. (2) over the detection area (Fig. 6), then we derive an analytical expression for the diffuse reflectance  $R$  measured by TURBISCAN MA 2000.

$$R(\delta h, \delta l, \lambda^*) = \frac{\int_0^{\delta h} \int_0^{\delta l} F(x, y, \lambda^*) dx dy}{\int_0^{\delta h} \int_0^{\delta l} F_0(x, y, \lambda^*) dx dy} \quad (3)$$

The above relation takes the form:

$$R \approx \int_0^{\delta h/2} F(z) 2\pi z \, dz + 2 \int_{\delta h/2}^{z^*} F(z) \, dh \, dz + 2 \int_{z^*}^{\delta l/2} F(z) \, dh \, dz$$

with

$$\int_0^\infty F(z) 2\pi z \, dz = 1$$

From Eq. (2), the diffuse reflectance  $R$  then obeys:

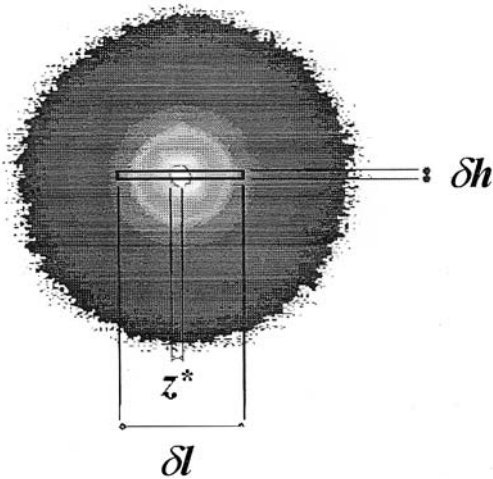


Fig. 6. Backscattered spot light and detection system of the optical analyser TURBISCAN MA 2000.

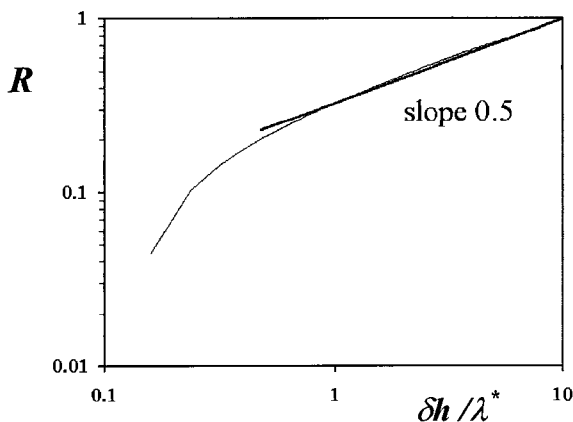


Fig. 7. Theoretical variation of the diffuse reflectance  $R$  with the dimensionless height  $\delta h/\lambda^*$  of the detector.

$$R \approx 0.2 \left( \frac{\delta h}{\lambda^*} \right)^{0.6} + \left[ 0.2 \left( \frac{\delta h}{\lambda^*} \right)^{0.6} - 0.09 \frac{\delta h}{\lambda^*} \right] + 0.02 \frac{\delta h}{\lambda^*} \left( 1 - \frac{64\lambda^{*2}}{\delta l^2} \right)$$

The variation of the diffuse reflectance  $R$  with the dimensionless detector height  $\delta h/\lambda^*$  (Fig. 7) shows a power law dependence  $R \approx (\delta h/\lambda^*)^{1/2}$  for  $\delta h > \lambda^*/2$  (Fig. 7) when long path photons mainly contribute to the detected scattered flux. The diffuse reflectance  $R$  then scales as:

$$R \approx \left( \frac{\delta h}{\lambda^*} \right)^{1/2} = \left( \frac{3\phi}{2} \delta h \frac{(1-g) Q_s}{d} \right)^{1/2} \quad \text{for}$$

$$0.2 < R < 0.9 \quad (4)$$

and  $\lambda^*/2 < \delta h < 8\lambda^*$  where  $\phi$  is the particle volume fraction,  $d$  the particle diameter,  $Q_s(d, A, n_p, n_f)$  the extinction efficiency factor and  $g(d, A, n_p, n_f)$  the asymmetry factor.

From the Lambert–Beer law, we further derive a simple theoretical expression of the transmittance  $T$  measured by TURBISCAN MA 2000:

$$T(\lambda, r_i) = T_0 e^{-\frac{2r_i}{\lambda}} = T_0 e^{-\frac{3r_i\phi Q_s}{d}} \quad (5)$$

where  $r_i$  is the internal radius of the TURBISCAN cylindrical measurement cell.

## 4. Experiments

### 4.1. Influence of particle volume fraction

Fig. 8 shows the experimental (TURBISCAN MA 2000) and theoretical (Monte Carlo simulations and transport models based on the photon diffusion approximation) variations of the diffuse reflectance  $R(\theta = 135^\circ)$  and the transmittance  $T(\theta = 0^\circ)$  versus particle volume fraction  $\phi$  for a latex bead aqueous suspension ( $d = 1.9 \mu\text{m}$ ).

In the diluted regime ( $\phi < \phi_c$ ), the transmittance  $T$  decreases exponentially with particle volume fraction in good agreement with the analytical expression Eq. (5) and the numerical predictions from the simulation. The high values of the diffuse reflectance  $R$  in the diluted regime results from the boundary reflections on the inner tube interface.



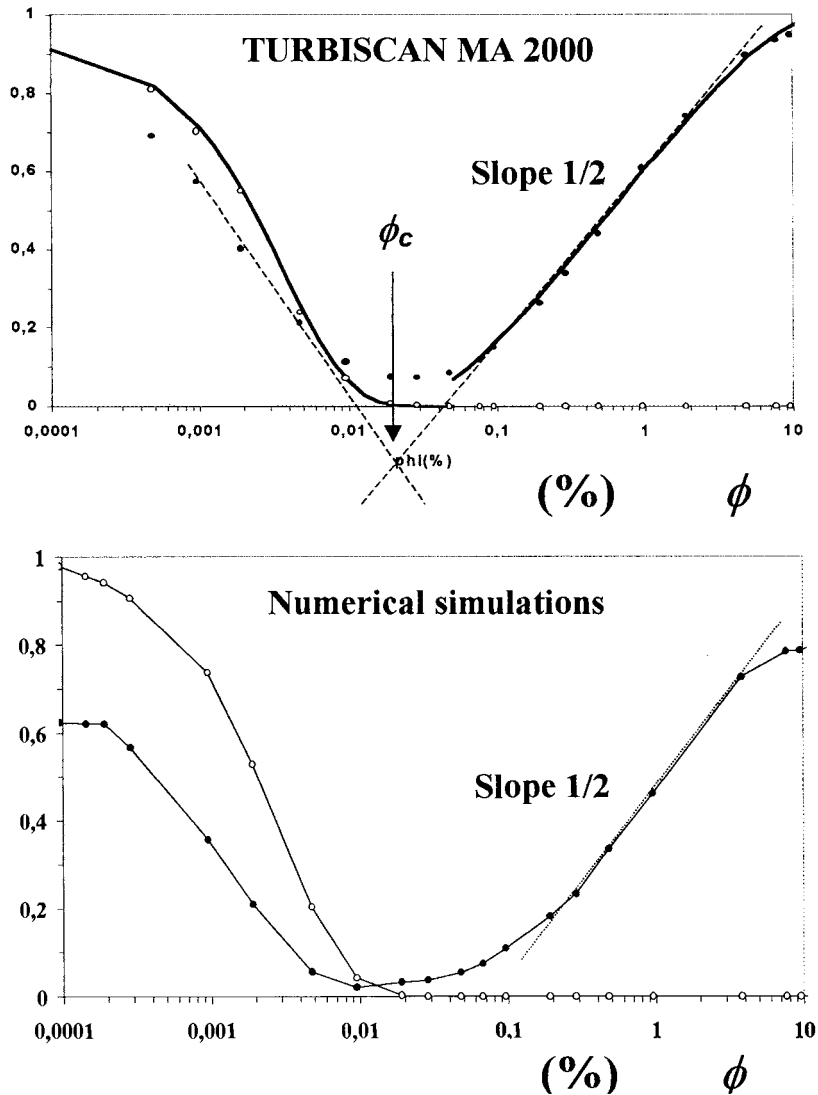


Fig. 8. Variation of the transmittance  $T(\theta = 0^\circ)$  and the diffuse reflectance  $R(\theta = 135^\circ)$  versus particle volume fraction for a latex beads aqueous suspension ( $d = 1.9 \mu\text{m}$ , wavelength  $\lambda = 0.85 \mu\text{m}$ ). Experiments (●) and physical models (—) for the top, numerical simulations (bottom).

In the concentrated regime ( $\phi > \phi_c$ ), both the numerical simulations, the transport model and the experiments show a zero transmission level and an increase of the diffuse reflectance with particle volume fraction before reaching a maximum. The diffuse reflectance  $R$  in the concentrated regime ( $\phi > \phi_c$ ) scales as  $\phi^k$  with  $0.42 < k < 0.56$  (Table 1) in good agreement with the relation Eq. (4).

The critical volume fraction  $\phi_c$  between diluted and concentrated regimes further corresponds to a photon transport length  $\lambda^*(\phi_c)$  equals to the tube diameter  $2r_i$  and may be expressed as:

$$\phi_c \approx \frac{d}{3r_i(1-g)Q_s} \quad (6)$$

From the transmission curve  $T(\phi)$  and the critical volume fraction  $\phi_c$ , then we may estimate

Table 1

Experimental values of the exponent  $k = d(\log R)/d(\log \phi)$  for latex bead aqueous suspensions ( $d = 11.9, 3.2, 1.9, 0.94$  and  $0.28 \mu\text{m}$ )

$d$ ( $\mu\text{m}$ )	$k$
11.9	0.50
3.189	0.54
1.923	0.56
0.944	0.61
0.280	0.42

the optical parameters  $Q_s/d$  and  $(1-g)Q_s/d$ . The values derived from the measurements performed with TURBISCAN MA 2000 are well correlated with the predictions of Mie theory (Table 2).

#### 4.2. Influence of particle mean diameter

Fig. 9 shows the particle diameter dependence of the diffuse reflectance  $R(\theta = 135^\circ)$  for aqueous suspensions of latex beads ( $\phi = 1\%$ ).

For small Rayleigh – Debye scatterers ( $d < d_c \approx 0.3 \mu\text{m}$ ), the diffuse reflectance  $R$  increases with particle diameter in good correlation with the transport model and the numerical simulations. On the other hand, the diffuse reflectance decreases with particle diameter for large anisotropic scatterers ( $d > d_c \approx 0.3 \mu\text{m}$ ).

Table 2

Experimental values of the optical parameters  $Q_s/d$  and  $(1-g)Q_s/d$  derived from the transmission curve  $T(\phi)$  and the critical volume fraction  $\phi_c$  for latex beads aqueous suspensions<sup>a</sup>

$d$ ( $\mu\text{m}$ )	$Q_s/d$ (Experimental, $\text{m}^{-1}$ )	$Q_s/d$ (Mie theory, $\text{m}^{-1}$ )
3.189	$8.40 \times 10^5$	$7.43 \times 10^5$
1.923	$1.99 \times 10^6$	$1.87 \times 10^6$
0.944	$1.88 \times 10^6$	$1.58 \times 10^6$
0.280	$2.68 \times 10^4$	$3.14 \times 10^4$
0.065	$5.69 \times 10^3$	$6.62 \times 10^3$

$d$ ( $\mu\text{m}$ )	$\phi_c$ (%)	$(1-g)Q_s/d$ (Experimental, $\text{m}^{-1}$ )	$(1-g)Q_s/d$ (Mie theory, $\text{m}^{-1}$ )
11.9	0.354	$1.52 \times 10^4$	$1.61 \times 10^4$
3.189	0.0479	$1.12 \times 10^5$	$9.38 \times 10^4$
1.923	0.0479	$1.12 \times 10^5$	$1.32 \times 10^5$
0.944	0.035	$1.10 \times 10^5$	$1.86 \times 10^5$
0.280	0.030	$1.79 \times 10^5$	$2.06 \times 10^5$

<sup>a</sup> Theoretical predictions from the Mie theory.

## 5. Applications

### 5.1. Qualitative understanding of concentrated dispersion destabilisation

The sample is a water in oil non-absorbing cosmetic emulsion (volume fraction  $\phi \approx 40\%$ , mean diameter  $d > 1 \mu\text{m}$  at time  $t = 0$ ).

Fig. 10 (left) shows a TURBISCAN MA 2000 screen page after 11.5 h time delay. The vertical axis represents the diffuse reflectance  $R$  (in %) normalized with respect to a non-absorbing standard reflector and the horizontal axis represents the sample height in mm ( $z = 0$  mm corresponds to the measurement cell bottom).

To follow the time evolution of the diffuse reflectance  $R(t, z)$ , the first diffuse reflectance profile  $R(t = 0, z)$  is subtracted from  $R(t, z)$  and the residual diffuse reflectance  $\Delta R = R(t, z) - R(t = 0, z)$  is plotted against sample height and time.

First, the coalescence of water droplets induces a diffuse reflectance fall over the whole height of the sample in good agreement with the theoretical model. Then, the droplets migrate from the top to the bottom of the sample (settling phenomenon), inducing a backscattering fall at the sample top (clarification) and a backscattering increase at the sample bottom (sediment formation and increase

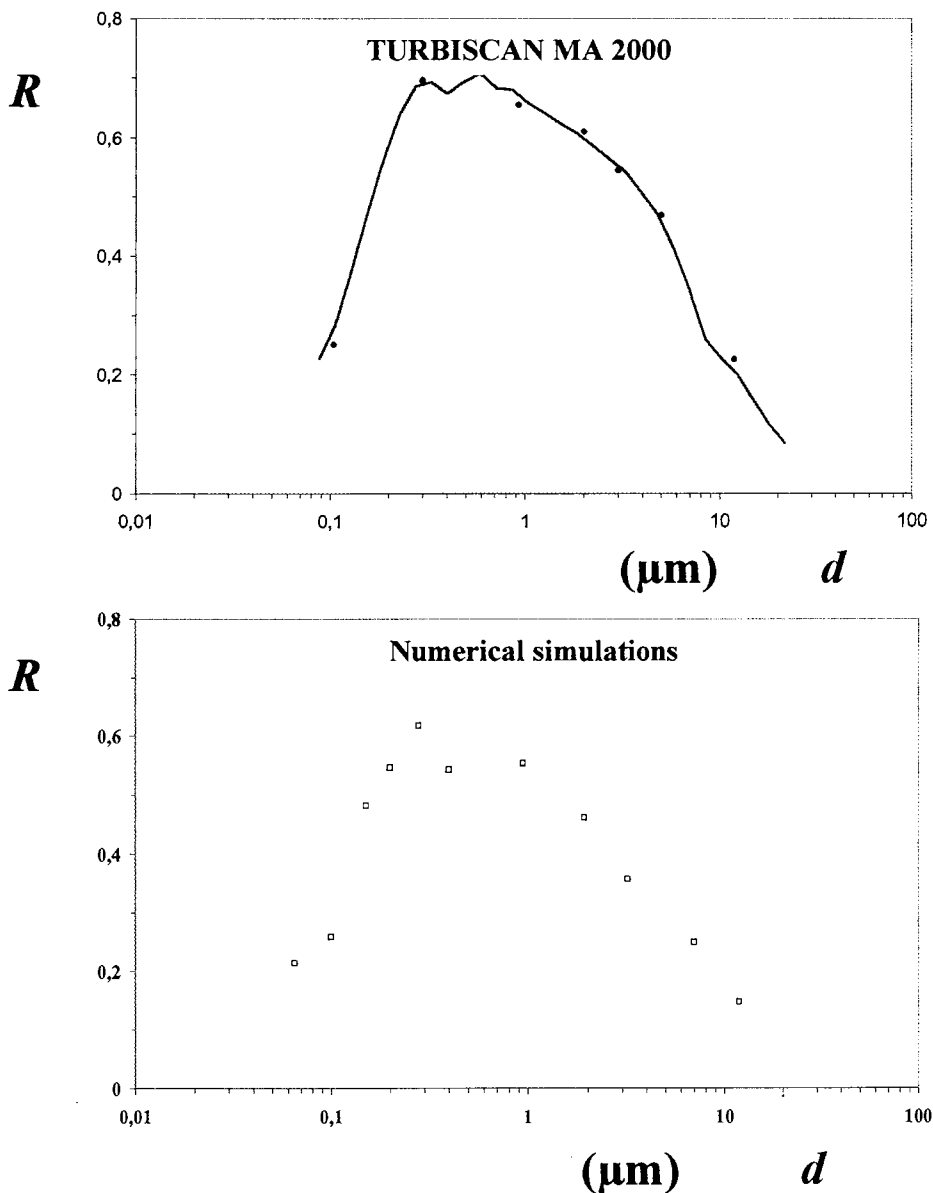


Fig. 9. Diffuse reflectance  $R(\theta = 135^\circ)$  versus particle mean diameter for latex bead aqueous suspensions ( $\phi = 1\%$ ,  $\lambda = 0.85 \mu\text{m}$ ). Experiments (●) and physical models (—) for the top, numerical simulations (bottom).

of scattering phenomena) in good agreement with the theoretical model.

The coalescence kinetic (time evolution of the diffuse reflectance at the sample middle) and clarification kinetic (time evolution of the diffuse reflectance at the sample top) seem to indicate that no particle size variation occurs while the

particles migrate from the top to the bottom of the sample.

It is interesting to notice that TURBISCAN MA 2000 allows the detection of the destabilisation at an early stage (coalescence detected after a few minutes) even though the medium is optically thick. With the naked eye, we would have had to

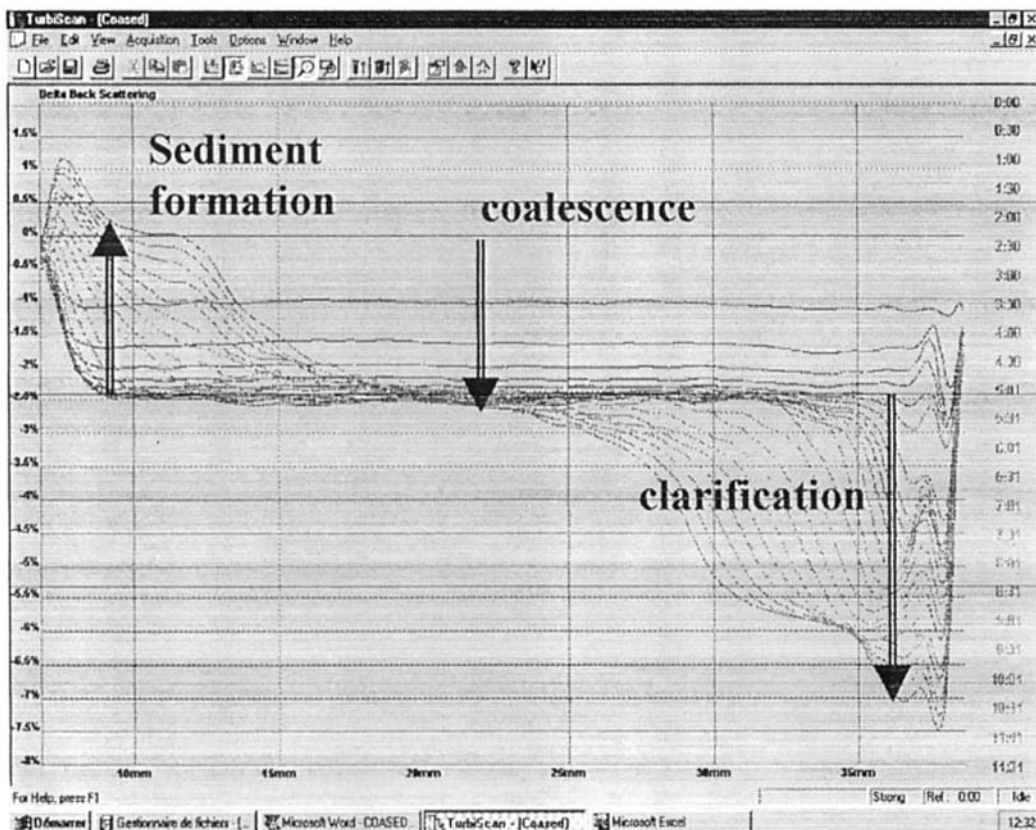


Fig. 10. Residual diffuse reflectance  $\delta R(h, t)$  versus sample height and time for the coalescence and the settling of a concentrated water/oil cosmetic cream. Particle mean diameter  $d > 1 \mu\text{m}$  at time  $t = 0$ , particle volume fraction  $\phi \approx 40\%$ . Experiment duration, 11.5 h.

have waited for the beginning of the phase separation before seeing anything.

Thus, the TURBISCAN MA 2000 is able to detect both particle size variation phenomena and particle migration phenomena.

### 5.2. Quantitative analysis of concentrated dispersion destabilisation

By measuring the diffuse reflectance  $R(\lambda^*)$  or the transmittance  $T(\lambda)$  of a homogeneous sample, the physical models allow to derive either the particle mean diameter from the knowledge of the particle volume fraction or the particle concentration from the particle size. We have calculated the mean diameter of concentrated polystyrene latex bead suspensions (Table 3) in good accordance with the manufacturer's data.

Thus, for non-absorbing suspensions or emulsions, TURBISCAN MA 2000 is able to predict quantitatively particle size changes.

The motorised vertical movement of both the infrared diode and the detectors along the cell axis makes possible the measurement of the migration rate of concentrated suspensions or emulsions.

Table 3

Time position  $z_0(t)$  and settling rate  $V(\phi, d)$  of a latex beads aqueous suspension ( $d = 3.189 \pm 0.054 \mu\text{m}$ ,  $\phi = 10\%$ ). Calculated values of the particle diameter  $d$

$t$ (s)	$z_0$ (cm)	$V$ (m/s)	$V_0$ (m/s)	$d$ ( $\mu\text{m}$ )
21675	0.405	$1.868 \times 10^{-7}$	$3.296 \times 10^{-7}$	3.157
28635	0.490	$1.711 \times 10^{-7}$	$3.018 \times 10^{-7}$	3.021

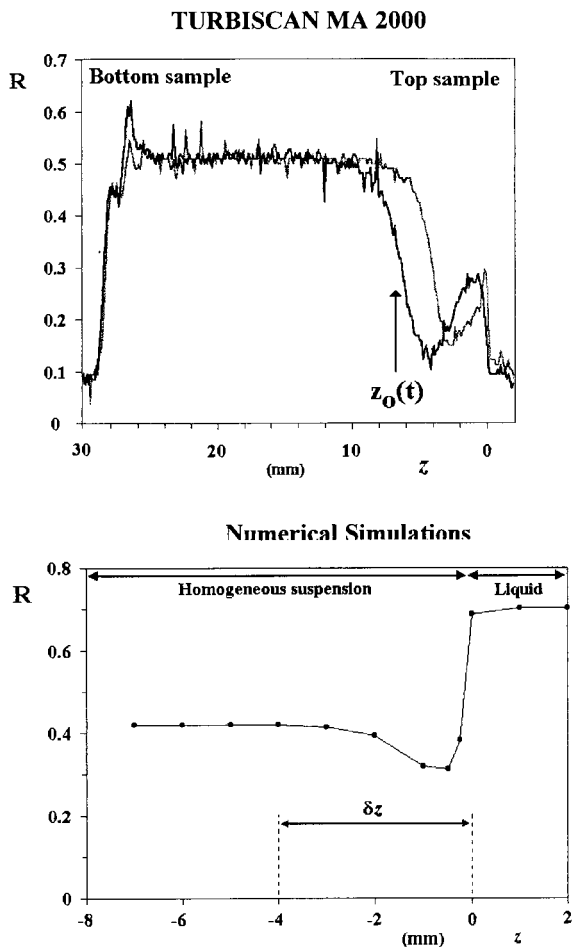


Fig. 11. Diffuse reflectance  $R(z)$  along the tube axis  $z$  for a  $3.2\text{-}\mu\text{m}$  latex bead aqueous suspension ( $\phi = 1\%$ ,  $\Lambda = 0.85\ \mu\text{m}$ ). Experiments (top) and Monte Carlo simulations (bottom).

Fig. 11 shows the experimental and the theoretical (Monte Carlo simulations) variations of the reflectance  $R(z)$  along the tube axis  $z$  during the

settling of a latex bead aqueous suspension ( $d = 3.2\ \mu\text{m}$ ,  $\phi = 1\%$ ). The distance  $z = 0$  corresponds to the air/suspension interface at the top of the sample.

Near the liquid/suspension interface, the numerical simulation shows a change of the diffuse reflectance over a distance  $\delta z \approx 5\lambda^* \approx 4\ \text{mm}$  since the interface disturbs the propagation of photons. Above the settling front, the backscattered flux strongly increases because the boundary reflections become predominant. The length  $\delta z = 5\lambda^* = 10d/[3\phi(1-g)Q_s]$  of the transition zone limiting the space resolution of the TURBISCAN MA 2000 scales as the photon mean free path and decreases with the particle volume fraction  $\phi$ .

By tracking the time position  $z_0(t)$  of a characteristic point of the diffuse reflectance profiles  $R(z, t)$ , we have determined the settling rate  $V(\phi, d) = \delta z_0(t)/t$  of latex bead aqueous suspensions (Table 4). From the sedimentation law proposed by Mills and Snabre in 1995 [10] for concentrated suspensions, we then derive a particle mean diameter very close from the manufacturer's data (Table 4).

$$V_0(d) = V(\phi, d) \frac{\left[1 + \frac{K\phi}{(1-\phi)^3}\right]}{1-\phi}$$

$$\text{with } V_0(d) = \frac{\delta\rho g d^2}{18\eta} \quad \text{and} \quad K = 4.6 \quad (7)$$

where  $V$  is the sedimentation velocity,  $d$  the particle diameter,  $\delta\rho$  the density difference between the solid and liquid phases,  $g$  the gravity acceleration and  $\eta$  the liquid dynamic viscosity.

By following the settling front for a concentrated flocculated suspension, the expression Eq.

Table 4

Calculated values of the particle mean diameter  $d$ , the photon transport length  $\lambda^*$  and the photon mean free path  $\lambda$  for two aqueous suspensions of polystyrene latex beads ( $d = 0.298 \pm 0.005\ \mu\text{m}$ ,  $n_p = 1.59$ ,  $n_r = 1.33$ ,  $\Lambda = 0.85\ \mu\text{m}$ ) and PMMA latex beads ( $d = 8.72 \pm 0.05\ \mu\text{m}$ ,  $n_p = 1.443$ ,  $n_r = 1.33$ ,  $\Lambda = 0.85\ \mu\text{m}$ )

$d$ (manuf.)	$n_p$	$n_r$	$R$ (%)	$T$ (%)	$\phi$ (%)	$\lambda^*$ ( $\mu\text{m}$ )	$\lambda$ ( $\mu\text{m}$ )	$d$ ( $\mu\text{m}$ )
0.3	1.59	1.33	97.8		11.4	83.6		0.29
0.3	1.59	1.33		88.9	0.00095		177833.0	0.32
8.7	1.443	1.33	66.6		16.7	406.9		7.6
8.7	1.443	1.33		78.9	0.01		35405.0	9.0

(7) giving the mean diameter of the sphere that settles with the same velocity as an aggregate may give an idea of the suspension flocculation level.

## 6. Conclusion

We have proposed physical models for the surface flux in the backscattered spot light and the diffuse reflectance measurement performed with the optical analyser TURBISCAN MA 2000.

Experiments lead to scaling laws in good agreement with the model and the Monte carlo simulations.

The diffuse reflectance measured by TURBISCAN MA 2000 mainly depends on the photon transport length and allows to detect destabilisation phenomena at a very early stage for concentrated dispersions.

Compared with other optical analytical methods such as microscopy, particle size and zeta potential analysis, the optical method presents the advantage of being a non-destructive tool (no sample dilution).

This instrument gives kinetic information on the process leading to phase separation. The TURBISCAN MA 2000 allows to detect two kinds of destabilisation phenomena: particle migration (creaming, sedimentation) which are often reversible by mechanical agitation and particle size variations (coalescence, flocculation). The monitoring of the sedimentation front in concentrated suspensions further yields an estimation of particle or aggregate size.

## References

- [1] P. Depraetere, Potentiel Zéta des émulsions, Galenica, Elsevier édition, 5, 1983, pp. 373–407.
- [2] Normes Experimentales, 1976, AFNOR, T73.409.
- [3] J.D. Stockman, R. Fochtamm, Particle Size Analysis, Ann Arbor Science, Ann Arbor, NY, 1978.
- [4] G. Meunier, Le TURBISCAN: un nouvel instrument de mesure de phénomènes naissants de démixtion dans les émulsions et les suspensions, Spectra Analyse 179 (1994) 53–58.
- [5] G. Meunier, O. Mengual, A new concept in stability analysis of concentrated colloidal dispersions (emulsions, suspensions, foams, gels) 4th World Surfactants Congress CESIO, vol. 4, 1996, pp. 301–313.
- [6] M. Kerker, The Scattering of Light, Academic Press, New York, 1969.
- [7] P. Snabre, A. Arhaliass, Heat Transfer Fluid Eng. 1037 (1996) 511–518.
- [8] A. Gandjbackche, P. Mills, P. Snabre, Appl. Optics 35 (7) (1995) 234–239.
- [9] P. Snabre, A. Arhaliass, Récents Prog. Génie Proc. 9 (41) (1995) 43–51.
- [10] P. Mills, P. Snabre, Europhysics Lett. 25 (9) (1995) 651–656.
- [11] P. Snabre, A. Arhaliass, Anisotropic scattering of light in random media. Incoherent backscattered spot light, Appl. Optics 37 (18) (1998) 211–225.
- [12] H.C. Van De Hulst, Multiple Light Scattering, vol. 1,2, Academic Press, New York, 1980, p. 2.
- [13] P.E. Wolf, G. Maret, E. Akkermans, R. Maynard, Optical coherent backscattering by random media: an experimental study, J. Phys. Fr. 49 (1988) 63–75.
- [14] A. Ishimaru, Wave Propagation and Scattering in Random Media, Academic Press, New York, 1978.
- [15] B.L. Drolen, C.L. Tien, Independent and dependent scattering in packed sphere systems, J. Thermophys. 1 (1987) 1.

# Determination of total chromium in tannery waste water by inductively coupled plasma-atomic emission spectrometry, flame atomic absorption spectrometry and UV–visible spectrophotometric methods

S. Balasubramanian \*, V. Pugalenti

*Education and Training Division, Central Leather Research Institute, Adyar, Chennai 600 020, India*

Received 9 September 1998; received in revised form 9 December 1998; accepted 28 January 1999

## Abstract

The determination of total chromium in different streams of tannery effluents were carried out by the digestion of samples in a  $\text{HNO}_3/\text{H}_2\text{SO}_4$  mixture followed by  $\text{KMnO}_4$  oxidation, which resulted in the complete conversion of Cr(III) to Cr(VI). The Cr(VI) ( $\text{Cr}_2\text{O}_7^{2-}$ ) species present in these samples were estimated by inductively coupled plasma-atomic emission spectrometry (ICP-AES), flame atomic absorption spectrometry (FAAS) and UV–visible spectrophotometry (1,5-diphenyl carbazide method). The results obtained from these methods were critically evaluated. UV–visible spectrophotometry was found to be better suited for this analysis when compared with the other two methods. Since these solutions contain relatively high concentrations of chromium (200–2400 mg/l), the need for preconcentration did not arise. The higher values obtained in the case of ICP-AES and FAAS methods can be attributed to the matrix effect arising out of high concentration of mineral acids and electrolytes. In addition, the values obtained in the latter methods (ICP-AES and FAAS) are comparable with each other, indicating that the interferences influence the results almost equally in both techniques. The statistical treatment of data indicates that the differences between the methods are within the acceptable range. © 1999 Elsevier Science B.V. All rights reserved.

*Keywords:* Inductively coupled plasma-atomic emission spectrometry; Flame atomic absorption spectrometry; UV–visible spectrometry; Total chromium; Statistical analysis

## 1. Introduction

The demand for rapid and sensitive analytical methods for the determination of chemical forms of toxic elements in environmental samples is increasing [1]. Chromium salts are used exten-

sively in several industrial processes, and enter water supplies through the discharge of effluents from corrosion inhibitors and water-cooled heat exchange systems, and also from electroplating, tanning, dyeing, textile, cement, and chemical industries [2–4].

Chromium (III) and chromium (VI) are the only significant oxidation states in natural waters,

\* Corresponding author.

the most probable species being  $\text{Cr}(\text{OH})^{2+} \cdot 4\text{H}_2\text{O}$  and  $\text{CrO}_4^{2+}$ . Cr(III) is more stable and exhibits a tendency to form inert complexes and is an essential trace nutrient for humans involved in glucose metabolism. This species is found to be a component of insulin cofactor and also shows lower toxicity in biological systems [5]. The anionic compounds of Cr(VI) ( $\text{CrO}_4^{2-}$ ,  $\text{Cr}_2\text{O}_7^{2-}$ ) are reported to have a toxic effect on the biological systems. Presently, Cr(VI) has been recognized as a probable agent of lung cancer, and it also produces gastrointestinal disorders, dermatitis and ulceration of skin in man [6].

The conventional tannery methods lead to discharge of solutions with chromium concentrations in the range of 1500–4000 mg/l. The specification for the discharge of chromium containing liquid wastes stipulates a range of 0.3–2 mg/l [21]. A recent estimate in India indicates that tanning salts equivalent to approximately 400 t of chromium are being discharged in the water streams, with an annual consumption of about 40 000 t of BCS salt.

Different instrumental techniques like differential-pulse polarography, X-ray spectrometry, neutron activation analysis, electrothermal atomic absorption spectrometry, inductively coupled plasma-mass spectrometry, UV-visible spectrophotometry and amperometry with various preconcentration techniques have been used to estimate chromium [1,6–10]. The methods employed are usually based on separation and preconcentration, acid digestion, co-precipitation, liquid-liquid extraction, and electrodeposition [2–4,11,12].

Simultaneous estimation of Cr(III) and Cr(VI) in aqueous solution by ion chromatography and chemiluminescence detection was carried out, and the results were compared with those of atomic absorption spectrometry (AAS). The simultaneous determination of total chromium and speciated Cr species in environmental samples using high-performance liquid chromatography (HPLC) combined with direct injection nebulization and inductively coupled plasma-mass spectrometry has been reported [13]. The precision of inductively coupled plasma-atomic

emission spectrometry (ICP-AES) was found to be inferior to that of flame atomic absorption spectrometry (FAAS) in the determination of Cr and six other elements in sewage sludge [14]. The determination of Cr(VI) in soil extracts by spectrophotometry, ion exchange chromatography and electrothermal AAS combined with reverse phase-HPLC (RP-HPLC) indicated the effect of organically complexed Cr(III) on the estimation of Cr(VI), and also the vulnerability of these methods to some types of interferences [15].

The present investigation aims at the comparative study of the three analytical techniques, namely ICP-AES, FAAS and UV-visible spectrophotometry for the determination of the total chromium content in tannery waste water after complete conversion of trivalent chromium to hexavalent chromium. The statistical treatment of data by *F*-test, paired *t*-test and analysis of variance (ANOVA) will also be made.

## 2. Experimental

### 2.1. Reagents and standards

The following chemicals were used as received without further purification: nitric acid,  $\text{HNO}_3$  (BDH, AR), sulfuric acid,  $\text{H}_2\text{SO}_4$  (Fischer, AR), methyl orange indicator solution (BDH), ammonium hydroxide,  $\text{NH}_4\text{OH}$  (Qualigens, LR), sodium hydroxide,  $\text{NaOH}$  (Qualigens, LR), potassium permanganate (Merck, AR) solution (5%), sodium azide (BDH, AR) solution (1%), argon (IOL, industrial grade), acetylene (IOL, AR), acetone (Fischer, AR), and water (double distilled).

#### 2.1.1. 1,5-Diphenylcarbazide solution

1,5-Diphenyl carbazide, 250 mg (SDs, AR), was dissolved in 50 ml acetone and stored in a brown bottle.

#### 2.1.2. Stock chromium solution

$\text{K}_2\text{Cr}_2\text{O}_7$ , 141.4 mg (BDH, AR), was dissolved in water and diluted to 1000 ml; 1.00 ml = 50.0  $\mu\text{g}$  Cr.



### 2.1.3. Standard chromium solution

Ten milliliters of stock chromium solution was diluted to 100 ml; 1.00 ml = 5.00  $\mu\text{g}$  Cr.

### 2.1.4. Calibration blank

Two milliliters of 1:1  $\text{HNO}_3$  and 10 ml 1:1 HCl were diluted to 100 ml with water, and was used to flush the system between standards and samples.

## 2.2. Sampling and sample preservation [16]

All containers were cleaned sequentially prior to use as follows: a detergent wash, tap water rinse, soaking in 2%  $\text{HNO}_3$  for 24 h, and distilled water rinse (six times). The samples were taken at different stages of leather processing and acidified with AR concentrated (conc.)  $\text{HNO}_3$  to  $\text{pH} < 2$ . Conc.  $\text{HNO}_3$  (2 ml) was added to 1 l of sample to prevent precipitation and adsorption of trace metals by container walls. The samples were kept in polyethylene containers and stored in a refrigerator at approximately 4°C to prevent change in volume due to evaporation.

## 2.3. Sample preparation

### 2.3.1. Digestion of the sample

Fifty milliliters of waste water sample was pipetted into a volumetric flask. The organic matter was destroyed using a 10 ml mixture of conc.  $\text{H}_2\text{SO}_4$  and conc.  $\text{HNO}_3$  (1:1). The solution was brought to a slow boil on a hot plate at 120°C and concentrated to half its original volume. The heating was discontinued, and 5 ml conc.  $\text{HNO}_3$  and 10 ml conc.  $\text{H}_2\text{SO}_4$  were added. The solution was evaporated on a hot plate at 120°C until dense white fumes of  $\text{SO}_3$  just appeared. If the solution was not clear, 10 ml conc.  $\text{HNO}_3$  was added and heated until excess  $\text{HNO}_3$  was removed. The heating was discontinued when the solution was clear and no brown fumes were observed. Fifty milliliters of water was added to the solution and boiled to dissolve any soluble salts, filtered, if necessary, and then Cr(III) was oxidized to Cr(VI) with 5%  $\text{KMnO}_4$  solution in an acidic medium.

### 2.3.2. Oxidation of Cr(III) to Cr(IV) by $\text{KMnO}_4$

The pH of the digested sample was adjusted with ammonium hydroxide solution until the sample was just basic to methyl orange, then acidified with 1:2  $\text{H}_2\text{SO}_4$  and heated to boiling on a hot plate for 10 min. The heating was discontinued and two drops of 5%  $\text{KMnO}_4$  was added until a faint pink color persisted, and the heating was continued on a steam bath for 20 min. If the color disappeared, 5%  $\text{KMnO}_4$  solution was added dropwise to maintain a slight pink color and boiled for another 2 min. One milliliter of 1% sodium azide solution was added dropwise to the boiling sample until the pink color of  $\text{KMnO}_4$  just disappeared. The sample was boiled again for 5 min, cooled and finally made up to 250 ml in a volumetric flask.

## 2.4. Inductively coupled plasma-atomic emission spectrometry

### 2.4.1. Analysis of samples [16,17]

Sample preparation, reagents and procedures for contamination were checked by the calibration blank. The entire flow system was rinsed with a mixture of dilute  $\text{HNO}_3/\text{HCl}$  for a minimum of 60 s between samples and blanks. After sample or blank was introduced, the system was equilibrated before starting signal integration. The calibration blank was examined and verified for each analysis so that no carry-over memory effect occurred. If carry-over was observed, the rinsing was repeated with a mixture of dilute  $\text{HNO}_3/\text{HCl}$  until proper blank values were obtained.

### 2.4.2. Calculation and corrections

**2.4.2.1. Blank correction.** The sample result was subtracted from the adjacent calibration blank to make a baseline drift correction.

**2.4.2.2. Dilution correction.** The sample result was multiplied by a dilution factor (DF) calculated as follows:

$$\text{DF} = \frac{\text{Final volume (ml)}}{\text{Initial volume (ml)}}$$

## 2.5. AAS-direct air-acetylene flame method [18]

### 2.5.1. Standardization

$K_2Cr_2O_7$  (AR) solution was used as a standard with five different concentrations. The blank was aspirated and the instrument was adjusted for zero. The standard solutions with different concentrations were aspirated in turn into flame and their absorbances were recorded. The calibration curve was prepared by plotting on a linear graph paper the absorbance of standards versus their concentrations.

### 2.5.2. Analysis of samples

The nebulizer was rinsed by aspirating an acidified solution which contained 1.5 ml conc.  $HNO_3/l$ . After the instrument was adjusted to zero, the blank and samples were atomized and their absorbances were recorded at 357.9 nm.

## 2.6. UV-visible spectrophotometry

### 2.6.1. Preparation of calibration curve

Chromium standard was treated by the same procedure as the sample to compensate the slight losses of chromium during digestion or other analytical operations. Accordingly, the standard chromium solution (5  $\mu g/ml$ ) was prepared ranging from 2.00 to 20.0 ml, to produce standard concentrations for 10–100  $\mu g$  Cr, into 50 ml volumetric flasks. After the development of color, a suitable portion of each solution was transferred to a 1-cm absorption cell, and the absorbance was measured at 540 nm. Distilled water was used as a reference. Absorbance readings were corrected by subtracting absorbance of a reagent blank carried through the method.

### 2.6.2. Color development and measurement

A 2 ml aliquot of the digested sample was neutralized with 5% NaOH solution and was pipetted into a 50 ml volumetric flask. It was then acidified with 3 ml 6 N  $H_2SO_4$ , 2 ml 0.25% 1,5-diphenyl carbazide solution was added, and it was made up to 50 ml. The solution was mixed thoroughly and kept for full color development for 5 min. After the development of color, the solution was transferred to a 1-cm absorption cell

and the absorbance was measured at 540 nm using distilled water as reference. Absorbance readings of samples were corrected by subtracting absorbance of a blank carried through the method. From the corrected absorbance, the amount of chromium was determined from the calibration curve.

## 3. Results and discussion

The waste water samples obtained from different streams as well as composite effluent from tanneries were used for the present investigation. The sampling was done according to the reported procedure [16]. The digestion of the sample was performed with a  $HNO_3/H_2SO_4$  acid mixture followed by  $KMnO_4$  oxidation, which ensures complete conversion of Cr(III) to Cr(VI) [16]. The clear yellow colored solutions thus obtained were analysed for chromium.

The conversion of trivalent chromium to hexavalent chromium is essential since the presence of both oxidation states in the samples pose serious problems in the determination of total chromium in the last two techniques. Even though estimation of chromium in trivalent states as well as hexavalent oxidation states by spectrophotometry has been reported [19,20] with different reagents, simultaneous determination has several limitations. The procedure adopted by different groups is either to reduce all of the species to Cr(III) or to oxidize them to Cr(VI). Similarly, in the case of FAAS, the determination of total chromium in hexavalent state has been recommended [18]. The choice of Cr(VI) for the determination of total Cr is important since dichromate solutions are stable for very long periods of time. Similarly, acidified solutions of  $K_2Cr_2O_7$  with  $H_2SO_4$ ,  $HClO_4$  or HCl are not reduced on long standing or boiling. The rate of reduction of dichromate solution is less when compared with that of  $KMnO_4$  solutions. Also, the reduction of Cr(VI) in biological samples as well as in waste water is much more difficult when compared with the oxidation of the sample, which not only results in the total conversion of Cr(III) to Cr(IV), but also completes destruction of the

organic matter, thereby facilitating the release of metal ion from the substrate.

The concentration of total chromium after its conversion to hexavalent state was determined in 25 different effluents collected from tanneries. They included composite samples, tan liquor samples and a rechrome sample. The composite sample is obtained where individual streams from various operations like soaking, liming, pickling, bating, tanning and finishing combine to form a mixture. Generally, this solution has high BOD and COD content in addition to fairly high total dissolved solids [21,22].

### 3.1. Inductively coupled plasma-atomic emission spectrometry

The estimation of total Cr from the oxidized samples was carried out on a JY24 sequential ICP spectrometer employing a high resolution

monochromator. The experimental conditions are provided in Table 1. The calibration of the instrument was done using a standard dichromate solution under the conditions already described. The correlation coefficient obtained for this standard graph was 0.9998 (Table 2).

The accuracy of the data obtained from the ICP also varies according to the experimental conditions. Similar to the procedure in AAS, each element has a series of wavelengths at which the analysis can be carried out. In the case of chromium, nearly 27 wavelengths have been employed, wherein the estimated detection limit varies over a wide range (4.1–300 µg/l) with both emission types (type 1 and 2) [17]. The wavelengths chosen for this investigation range from 185.21 to 428.972 nm. However, if the difference in the successive wavelengths is restricted to whole numbers, then 19 different wavelengths can be employed [17]. The present investigation with ICP

Table 1  
Operating conditions for ICP-AES, FAAS and UV-visible spectrophotometry

Operating conditions	ICP-AES	FAAS	UV-visible spectrophotometry
Instrument used	JOBIN YVON JY-24	PERKIN-ELMER AAS-3010	Double-beam spectrophotometer Shimadzu UV-150-02
Standard used	K <sub>2</sub> Cr <sub>2</sub> O <sub>7</sub> (AR)	K <sub>2</sub> Cr <sub>2</sub> O <sub>7</sub> (AR)	K <sub>2</sub> Cr <sub>2</sub> O <sub>7</sub> (AR)
Detection limit	4.7 µg/l (varies with the wavelength)	0.078 mg/l	5 µg/l
Wavelength used (nm)	283.563	357.9	540
	Radio frequency power, 1.0 kW	Air-acetylene flow rate, 4 l/min or 8.5 ft <sup>3</sup> /h	Source lamp, tungsten
	<i>Ar</i> gas	Grade of acetylene, welding grade	Normal lamp variation, 0.1 nm
	Central flow-nebulizing, ≈ 0.4 l/min ≈ 3 bars	Air-acetylene flame temperature, 2300°C	Cell Grade, special optical grade
	External flow (cooling), 12 l/min	Nebulizer	Design, open-top normal rectangular cell
	Auxiliary flow, 0 l/min	Normal uptake rate, 7–10 ml/min	Path length, 1 cm
	Aerosol flow, 0.3 l/min	By reducing the uptake rate, 4–6 ml/min	
	Sheath gas flow, 0.3 l/min (for multielement analysis of aqueous solution)	Burner head, 10 cm	
	Monochromator slits	Slit/spectral band width, 0.7 nm	
	Primary, 30 µm	Relative noise, 1.0	
	Secondary, 35 µm	Characteristic concentration check, 4.0 mg/ml	
	Plasma temperature, 10 000 K	Linear range, 5.0 mg/l	

Table 2

Calibration graph data for Cr(VI) determination by ICP-AES, FAAS and UV-visible spectrophotometric methods

Sl alignment, number	Method	Slope	Intercept	Correlation coefficient ( <i>r</i> )
1	ICP-AES	1226.23	28.4155	0.9998
2	FAAS*	0.016683	0.07734	0.9933
3	UV-visible spectrophotometry	0.070881	0.002785	0.9999

\* Slope and intercept for the best fit.

has been carried out at 283.563 nm, where the detection limit observed (4.7 µg/l) is very close to the minimum value reported in this series.

The oxidized sample contains Mn<sup>2+</sup> along with Cr<sup>6+</sup>, since the excess KMnO<sub>4</sub> used for the oxidation of Cr<sup>3+</sup> has been subsequently reduced with NaN<sub>3</sub>. Even though the emission wavelengths reported for Mn<sup>2+</sup> range from 172.65 to 279.827 nm with the estimated detection limit lying in the range 0.93–8000 µg/l, the interference from Mn<sup>2+</sup> for Cr<sup>6+</sup> estimation has not been reported earlier. So the presence of Mn<sup>2+</sup> in the sample is unlikely to contribute to any chemical interference in this estimation. The wavelength selected for the current estimation in ICP is 283.563 nm, which is almost 4 nm more than the highest wavelength indicated for manganese estimation[17].

Matrix interferences, especially from Cl<sup>-</sup> and SO<sub>4</sub><sup>2-</sup>, have been reported [23] in the determination of trace elements by ICP. Yoshimura et al. [24] have indicated that the presence of mineral acids decreases emission intensities of the atomic and ionic lines, when the acid concentration is high (≥ 1 M). The decrease in emission intensity by a reduced rate of sample uptake has been shown to be a dominant factor.

### 3.2. Flame atomic absorption spectrometry

The oxidized chromium solution has also been analyzed by atomic absorption spectrometry using an air-C<sub>2</sub>H<sub>2</sub> flame. The operating conditions maintained during this investigation have also been provided (Table 1). The calibration of the instrument was done using a standard dichromate solution. The correlation coefficient obtained for the calibration graph was 0.9933. The wavelength selected for the present investigation is 357.9 nm,

whose characteristic concentration is minimum [18].

The accuracy of the results also varies with the fuel gases employed [25]. The detection of Cr requires a fuel-rich air-C<sub>2</sub>H<sub>2</sub> flame (e.g. air-C<sub>2</sub>H<sub>2</sub>, N<sub>2</sub>O-C<sub>2</sub>H<sub>2</sub>, H<sub>2</sub>-O<sub>2</sub>, etc.). (The interferences during the estimation of Cr by FAAS in an air-C<sub>2</sub>H<sub>2</sub> flame are greater when compared with that of N<sub>2</sub>O-C<sub>2</sub>H<sub>2</sub>.) Even though the N<sub>2</sub>O-C<sub>2</sub>H<sub>2</sub> flame has been reported to reduce many chemical interferences, it considerably decreases the sensitivity. Similarly, the wavelength at which the absorption is measured also affects the accuracy of the results.

The interferences in the AAS method are relatively less and are classified into six categories: (a) chemical, (b) ionization, (c) matrix, (d) emission, (e) spectral, and (f) background absorption. The sensitivity and interferences are also related to the oxidation state of chromium [26,27], flame gas composition and the position of the burner. However, the problems are severe in the case of systems containing mixed oxidation states. In the present investigation, the burner position was automatically adjusted by the spectrometer itself. The non-specific absorption by concomitant species was eliminated by effective wash cycle as it removes the traces of residues from the earlier analysis.

The calibration graph for Cr using the air-C<sub>2</sub>H<sub>2</sub> flame in AAS is not a linear one, and it has been reported [28,29] that several inter-element and oxidation state effects in this flame cause such a deviation. The poor agreement between different laboratories observed in this method, especially when the concentration of Cr is above 2 µg/ml, is attributed to the oxidation states of the sample and standard [28,29]. Most of the AAS

standards contain Cr(VI), while in biological and environmental samples, Cr is predominantly available in the trivalent oxidation state. Hence, the sensitivity for Cr(III) is significantly different from that of Cr(VI), when it is determined by AAS. It has also been reported [3,30] that the preconcentration of Cr(III) is not as simple as in the case of Cr(VI), which is attributed to the kinetic inertness of Cr(III), resulting in poor sensitivity, low sampling frequency and incomplete recovery. If the solution is not strongly acidic or alkaline, the variation in pH can cause significant interference in the estimation due to  $\text{HCrO}_4^- \rightleftharpoons \text{CrO}_4^{2-}$  equilibrium. The importance of the valency state of Cr in its determination in  $\text{HClO}_4$  acid medium has been reported [31]. Also several methods are based on the determination of Cr(VI) and total chromium because Cr(III) is kinetically inert requiring conversions to higher oxidation states [32]. The factors discussed above, are taken into consideration while carrying out the present investigation, in which the entire chromium is converted to hexavalent state in acidic medium. Ajlec et al. [33] have reported that the cations present with Cr in the solution interfere in its estimation by FAAS, with either enhancing ( $\text{Al}^{3+}$ ,  $\text{Ca}^{2+}$ ,  $\text{Mg}^{2+}$ ) or depressing ( $\text{Fe}^{3+}$ ) effects, whereas both effects were observed with  $\text{Mn}^{2+}$ ,  $\text{K}^+$ ,  $\text{Na}^+$  and  $\text{Cu}^{2+}$ . However, in the present investigation, only enhancing effects have been observed.

### 3.3. UV-visible spectrophotometry

The spectrophotometric estimation involves the use of diphenyl carbazide as a reagent for Cr(VI) species, in which the Cr(III)-diphenyl dicarbazone formed has a maximum absorption at 540 nm. The concentrations of the samples were determined by carrying out identical measurements to those of the standard using the calibration graph. The standard  $\text{K}_2\text{Cr}_2\text{O}_7$  solution employed in the other two techniques has also been used as a standard in the present case. The experimental conditions are provided in Table 1. The correlation coefficient obtained in this case is 0.9999. In the case of spectrophotometric methods used for the determination of Cr(VI), the factors like tem-

perature, amount of reagent, order of addition and time allotted for the development of color should be maintained constant to achieve good reproducibility. When complex samples like that employed in the present study are used, then they have to be combined with a conversion step. Even though several reagents can be used to estimate chromium in the hexavalent state by spectrophotometry, the standard procedure recommended for the analysis of chromium makes use of diphenyl carbazide (DPC) [16]. The  $\text{Mn}^{2+}$  ion which is also present along with  $\text{Cr}^{6+}$  does not complex with DPC, and it also does not have any absorption around 540 nm. The relatively high acid concentration ensures the stability of Cr(VI) ion, which in turn reacts with diphenyl carbazide.

The relative standard deviation (% RSD) observed in the case of Cr(VI) determination has been reported to vary over a wide range according to the method employed. Peixoto et al. [34] report a value of 1.2–2.4 for the DPC method in natural water using a flow injection system, while the extraction of Cr(VI) with thiosemicarbazone, MIBK, etc. and its subsequent determination with AAS showed RSD in the range 1.5–22% [35]. However, the use of GAAS has indicated a value of 5.9–11 and 1–25% by two different groups [36].

The recovery experiments carried out with spiked water samples indicated a recovery of 99–100% in the case of spectrophotometry, while in the remaining two methods, the recovery rate is 95–98%.

### 3.4. Statistical analysis

The total chromium content in the samples evaluated from all three methods, namely ICP-AES, FAAS and UV-visible spectrophotometry, have been collected in Tables 3 and 4, along with their mean standard deviation (SD) and relative standard deviation (% RSD) values. The chromium content in these samples vary from 180 to 2400 mg/l in the first method, while the corresponding values in the second and third methods are 254–2350 and 205–1725 mg/l, respectively. One of the composite samples (A) has the least concentration, and one of tan liquors (B) shows

the maximum value. The trend slightly varies, if only the first two methods are taken into consideration. The percentage of relative standard deviation is less than 2 for samples (3), (4) and (5), while that of the remaining two varies from 13.88 to 24.11 when only the first two methods are considered. However, these values undergo a significant change when all the three methods are taken into consideration. Only the rechrome sample exhibits a value which is less than 2, while the remaining four samples exhibit values in the range 12.17–18.22. The overall difference is less when the first two methods are considered and it undergoes significant change when the values obtained from all the three methods are taken into consideration. Baudo et al. [38]

have reported a high RSD% while comparing the results obtained from AAS and UV–visible spectrophotometry for the determination of chromium. The results obtained from these three methods were also evaluated by the following statistical calculations [39]

#### 3.4.1. *F-Test*

The total number of samples analyzed in the present study is 15. Three samples from each category have been analyzed by all three methods and the mean values are presented in Table 3. The results obtained in all three methods are first compared by variance ratio test or, as popularly known, the *F*-test. *F* values are calculated according to the following equations.

Table 3  
Estimation of chromium in waste water by ICP-AES, FAAS and UV–visible spectrophotometric methods

Sl number	Sample	Concentration of chromium (mg/l)			Sample average	SD	RSD (%)
		ICP-AES <sup>a</sup>	FAAS <sup>b</sup>	UV–visible spectrophotometry <sup>c</sup>			
1	Tan liquor (A) ( <i>n</i> = 5)	900	1096	762	919.3	167.83	18.256
2	Composite (A) ( <i>n</i> = 5)	180	254	205	213	37.64	17.671
3	Tan Liquor (B) ( <i>n</i> = 5)	2400	2350	1725	2158.33	376.10	17.425
4	Rechrome ( <i>n</i> = 5)	575	560	562	565.66	8.144	1.439
5	Composite (B) ( <i>n</i> = 5)	525	533	425	494.33	60.17	12.172
Method average		916	958.6	735.8	870.124	–	–

<sup>a</sup> Uncertainty  $\pm 12$ .

<sup>b</sup> Uncertainty  $\pm 15$ .

<sup>c</sup> Uncertainty  $\pm 10$ .

Table 4  
Comparison of chromium concentration obtained by ICP-AES and FAAS methods

Sl number	Sample	Concentration of chromium (mg/l)		Mean	SD	RSD (%)
		ICP-AES	FAAS			
1	Tan liquor (A)	900	1096	998	138.59	13.886
2	Composite (A)	180	254	217	52.32	24.110
3	Tan Liquor (B)	2400	2350	2375	35.35	1.488
4	Rechrome	575	560	567.5	10.60	1.867
5	Composite (B)	525	533	529	5.65	1.068

Table 5  
ANOVA by range table

Source	Number of methods ( $k$ )	Number of samples ( $n$ )	Degrees of freedom ( $f$ )	Range ( $R$ )	Standard deviations of residual ( $S$ )
Between methods	3	5	–	222.8	–
Between samples	3	5	–	1945.33	–
Residual	3	5	7.4	472.796	241.22

$$F_1^1 = \frac{S_1^2}{S_2^2} = 1.739$$

$$F_2 = \frac{S_2^2}{S_3^2} = 2.0114$$

$$F_3 = \frac{S_1^2}{S_3^2} = 2.1713$$

$$S_i^2 = \frac{\sum(x_i - \bar{x})^2}{n_i - 1} \quad (i = 1, 2, 3, \dots)$$

where  $S_1$  is the standard deviation for the first method (ICP-AES),  $S_2$  that for the second method (FAAS), and  $S_3$  that for the third method (UV-visible).

The tabulated  $F$  value at the 0.05 ( $\alpha = 0.05$ ) level of significant difference, when the degrees of freedom is (4, 4), is 6.39. The calculated values ( $F_1$ ,  $F_2$  and  $F_3$ ) are much lower than this value and, hence, suggest that there is no significant difference between methods.

### 3.4.2. Paired $t$ -test

The results are further analyzed by paired  $t$ -test. The  $t$  values are calculated between any two methods. The calculated values as well as the value obtained from the table at 0.05 ( $\alpha = 0.05$ ) significance level are as follows:

$$t_1 = 0.9824$$

$$t_2 = 1.9244$$

$$t_3 = 1.4144 \quad t_{\text{tab}} = 2.776$$

where  $t_1$ ,  $t_2$  and  $t_3$  are calculated values, and  $t_{\text{tab}}$  is the tabulated value.

The fact that there is no significant variation between the results obtained from these methods is once again indicated by this calculation.

### 3.4.3. Analysis of variance

The tests of significance between samples as well as between methods have been carried out by the method known as analysis of variance by range (ANOVA by range). The relevant data are provided in Table 5. The calculated as well as the values obtained from the standard table from literature [39] ( $k = 3$  and  $n = 5$ ) are as follows:

1. between samples:  $q_{\text{cal}} = 18.032$

2. between methods:  $q_{\text{cal}} = 1.599$

The tabulated value for  $f = 7.4$  is  $q_{\text{tab}} = 4.16$  (at 0.05).

These values clearly show that there is significant difference between the samples, and the difference is not pronounced between methods.

The ANOVA by a two-way classification method is carried out to test the hypothesis whether there is any significant difference between samples and also between methods. The equation employed in this case is as follows:

$$F = \frac{\text{mean sum of squares (MSS)}}{\text{error sum of squares (ESS)}}$$

	Calculated value	Tabulated value (0.05)
$F_{(4, 8)}$	66.63	3.84
$= F_{(\text{col.}, \text{error})}$		
$F_{(2, 8)}$	2.669	4.46
$= F_{(\text{rows}, \text{error})}$		

This analysis also indicates that the difference is significant between samples and not between

methods, since  $F_{\text{cal}} > F_{\text{tab}}$  in the first case and  $F_{\text{cal}} < F_{\text{tab}}$  in the second case.

#### 4. Conclusions

The determination of chromium in different streams of tannery effluent was made after the complete conversion of Cr(III) to Cr(VI) by  $\text{KMnO}_4$  oxidation. The UV–visible spectrophotometric technique using 1,5-diphenylcarbazide has been found to be more suitable for this analysis when compared with ICP-AES and FAAS using an air–acetylene flame. The correlation coefficient obtained for the calibration graph in the case of UV–visible spectrophotometry is also high when compared with those of other two techniques. The matrix effects, especially due to the presence of relatively high acid content coupled with high concentration of electrolytes [37] ( $\text{Na}^+$ ,  $\text{Cl}^-$ ,  $\text{SO}_4^{2-}$ ), play a dominant role in influencing the results obtained in the latter two methods (ICP-AES and FAAS). The positive errors observed in the latter two techniques are comparable with each other, indicating that the interferences have almost similar impact in both methods. The %RSD of the results vary from 1.44 to 24.66, when FAAS and ICP-AES are considered, and the range changes to 1.48–18.44 while considering all the three methods, with only one sample showing below 2%, unlike the earlier case in which three samples indicated a RSD value less than 2%.

#### Acknowledgements

The financial support for this investigation from CLRI-AISHTMA project is gratefully acknowledged. The authors wish to thank the Director, CLRI for his encouragement and Anuradha, Chitra, Noorzahan and Vidya for their technical assistance.

#### References

- [1] S.D. Jadhar, Z.R. Turel, *J. Radioanal. Nucl. Chem.* 177 (1994) 185.
- [2] Y.S. Fung, W.C. Sham, *Analyst* 119 (1994) 1029.
- [3] M. Sperling, S. Xu, B. Welz, *Anal. Chem.* 64 (1992) 3101.
- [4] M.J. Powell, W.D. Boomer, D.R. Weiderrin, *Anal. Chem.* 67 (1995) 2474.
- [5] S. Deiana, C. Gessa, M. Usai, P. Piu, R. Seeber, *Anal. Chim. Acta* 248 (1991) 301.
- [6] J.R. Pretly, A.E. Blubaugh, A.J. Caruso, M.I. Davidson, *Anal. Chem.* 66 (1994) 1540.
- [7] K. Van den Broeck, L. Helsen, C. Vandacasteele, E. Van den Bulck, *Analyst* 122 (1997) 695.
- [8] F.J. Andrade, M.B. Tudino, O.E. Troccoli, *Analyst* 121 (1996) 613.
- [9] J. Wang, J. Wang, B. Tian, M. Jiang, *Anal. Chem.* 69 (1997) 1657.
- [10] I. Turyan, D. Mandlet, *Anal. Chem.* 69 (1997) 894.
- [11] K.S. Subramanian, *Anal. Chem.* 60 (1989) 11.
- [12] J. Obiols, R. Devesa, J. Garcia-Berro, J. Serra, *Int. J. Environ. Anal. Chem.* 30 (1987) 197.
- [13] M.I. Powell, D.W. Boomer, D.R. Wiederin, *Anal. Chem.* 67 (1995) 2474.
- [14] D.J. Hawke, A. Lioyd, *Analyst* 113 (1988) 413.
- [15] R. Milacic, I. Stupar, N. Kozuh, I. Korosin, *Analyst* 117 (1992) 125.
- [16] A.D. Eaton, L.S. Clesceri, A.E. Greenberg, (Eds.), *Standard Methods for the Examination of Water and Wastewater*, American Public Health Association, 19th edn., Washington, DC, 1995, pp. 3.58–3.60.
- [17] *The Spectrometer JY 24, Sequential ICP user's manual JY 24, part 3*, 1989.
- [18] *Analytical methods for Atomic Absorption Spectrometry*, Perkin Elmer, 1994.
- [19] Y. Shijo, K. Sakai, *Bull. Chem. Soc. Jpn.* 59 (1986) 1455.
- [20] S. Balasubramanian, S. Padmaja, *J. Soc. Leather Technol. Chem.* 81 (1997) 192.
- [21] M.C. Carre, A. Vulliermet, B. Vulliermet, *Environment and Tannery*, Centre Technique du Cuir, Lyon, France, 1983 p. 338.
- [22] S. Balasubramanian, V. Pugalenti, K. Anuradha, K. Chakradhar, *J. Environ. Sci. Health.* A34 (1999) 461.
- [23] A. Krushevska, S. Mointchilova, V. Gantcheva, C. Amarasirewaradana, *Analyst* 117 (1992) 1939.
- [24] E. Yoshimura, H. Suzuki, S. Yamazaki, S. Toda, *Analyst* 115 (1990) 167.
- [25] D.C. Harris, *Quantitative Chemical Analysis*, 4th ed, W.H. Freeman, New York, 1995 p. 603.
- [26] T. Maruta, M. Suzuki, T. Takeuchi, *Anal. Chim. Acta* 51 (1970) 381.
- [27] J. Kraft, D. Lidenberger, H. Beck, *Fres. Z. Anal. Chem.* 282 (1976) 119.
- [28] K.C. Thompson, *Analyst* 103 (1978) 1258.
- [29] J.A. Hurlbut, C.D. Chriswell, *Anal. Chem.* 43 (1971) 465.
- [30] A. Shah, S. Devi, *Anal. Chim. Acta* 236 (1990) 469.
- [31] M.S. Cresser, R. Hargitt, *Talanta* 23 (1976) 153.
- [32] P.T. Lynch, I.N. Kernoghan, N.I. Wilson, *Analyst* 109 (1984) 839.
- [33] R. Ajlec, M. Cop, J. Stupar, *Analyst* 113 (1983) 585.



- [34] C.R.M. Peixoto, Y. Gushikem, N. Baccan, *Analyst* 117 (1992) 1029.
- [35] T.K. Jan, D.R. Young, *Anal. Chem.* 50 (1978) 1250.
- [36] T. Nakamura, H. Oka, M. Ishii, J. Sato, *Analyst* 119 (1994) 1397.
- [37] P.R. Skidmore, S.S. Greetham, *Analyst* 108 (1983) 171.
- [38] R. Baudo, G. Galanti, P.G. Varini, *Analyst* 108 (1983) 722.
- [39] E.L. Bauer, *A Statistical Manual for Chemists*, Academic Press, New York, 1971.

# A sensitive and specific method for isoniazid determination based on selective adsorption using an isoniazid ion-selective piezoelectric sensor

Shouzhuo Yao <sup>a,\*</sup>, Weifeng Li <sup>b</sup>, Xiaoli Su <sup>b</sup>, Xingbing Zuo <sup>b</sup>, Wanzhi Wei <sup>b</sup>

<sup>a</sup> *Chemical Research Institute, Hunan Normal University, Changsha 410081, People's Republic of China*

<sup>b</sup> *College of Chemistry and Chemical Engineering, Hunan University, Changsha 410082, People's Republic of China*

Received 30 July 1998; received in revised form 18 March 1999; accepted 18 March 1999

## Abstract

A selective, sensitive and simple ion-selective piezoelectric (ISP) sensor was developed for the direct determination of isoniazid (INH) in body fluids. Based on sensitive mass response of piezoelectric quartz crystal and selective adsorption/desorption across the modified film, the ISP sensor was fabricated by coating a PVC film containing activant on one electrode of a thickness-shear mode piezoelectric quartz crystal. The observed frequencies of ISP sensor were found to decrease with the increase of the INH concentration in a 0.1 M NaNO<sub>3</sub> solution. In this paper, three activants, INH-phosphotungstate (I), INH-silicotungstate (II), and INH-[BiI<sub>4</sub>]<sup>-</sup> (III), were synthesized and investigated. Calibration graphs were linear from  $6 \times 10^{-8}$  to  $2 \times 10^{-3}$  M for I,  $2 \times 10^{-7}$  to  $2 \times 10^{-3}$  M for II and  $2 \times 10^{-7}$  to  $2 \times 10^{-3}$  M for III, with detection limits  $6 \times 10^{-8}$  M for I,  $2 \times 10^{-7}$  M for II and  $2 \times 10^{-7}$  M for III, in a 0.1 M NaNO<sub>3</sub> solution at pH 7.0 and 37°C. Recoveries were from 98% to 102% with R.S.D. up to 2%. Results for real samples obtained by the proposed method agreed well with those obtained by the conventional pharmacopeia method. © 1999 Elsevier Science B.V. All rights reserved.

**Keywords:** Isoniazid; ISP sensor; Pharmaceutical detection; Tuberculosis

## 1. Introduction

Recently, tuberculosis (TB) has been increasing and also been a hot topic in our life year by year. It is estimated that nearly one-third of the population are infected with tuberculosis fungus all over the world and 300 000 people died of tuberculosis

disease in 1995 [1]. Especially, the occurrence of multi-drug resistance (MDR-TB) brings new problems for the treatment of tuberculosis [2]. Isoniazid (INH), widely used together with rifampine and streptomycin, is an antitubercular drug which has been recommended as a first-line drug in spite of its toxicity [3].

Isoniazid is efficient in the treatment of pulmonary tuberculosis; on the other hand, poisoning accidents, even death, have sometimes

\* Corresponding author. Fax: +86-731-8865515.

E-mail address: xieqj@public.cs.hn.cn (S. Yao)

happened because of overdosage with INH [3]. Therefore, the assay of INH level in human body fluids is vital for clinical purposes, and the relatively small concentration difference between effectively therapeutic and toxic dosages makes it very necessary to develop rapid and specific methods for determining INH level in body fluids to aid the diagnosis of INH intoxication. Various analytical approaches to INH determination, including titrimetry [4], cyclic voltammetry [5], visible spectrophotometry [6], flow-injection analysis (FIA) with chemiluminescence [7], atomic absorption spectrophotometry [8], thin-layer chromatography (TLC) [3] and high-performance liquid chromatography (HPLC) [9], have been reported, but these methods required more sophisticated instrumentation or are more complex time-consuming procedures which are tedious and ideal sensitivity can not be obtained easily.

Selective adsorption/desorption processes of the component ions of insoluble salts at their solid/aqueous interface have been studied by several research groups and some fundamental characteristics of the adsorption mechanism of solid membranes were described. These theoretical results proved to agree well with experiments and applied to real samples [10–14]. In our work, three insoluble salts, INH–phosphotungstate, INH–silicotungstate and INH–[BiI<sub>4</sub>]<sup>−</sup> were synthesized and applied for the INH assay.

The bulk acoustic wave (BAW) technique has become a common method for real-time mass change monitoring, and has been used widely in interface processes [15]. It is based on the piezoelectric effect of quartz crystal. The resonant frequency of a BAW sensor can be affected by many factors, such as electrode mass, conductivity, density and viscosity of the oscillating medium. In recent years, many applications were based on these factors [16–18]. In our present work, the effects of the change of conductivity, density and viscosity of bulk solution can be neglected. The BAW sensor is used only to determine the change of electrode mass owing to selective adsorption on the modified film. This kind of sensor is also well known as an ion-selective piezoelectric (ISP) sensor. For AT-cut

quartz crystal, the relation between the shift in resonant frequency and mass change of the electrode can be expressed with the Sauerbrey equation [15]:

$$\Delta m = -K \cdot \Delta f \quad (1)$$

where  $\Delta f$  is the change in the resonant frequency of the crystal (in Hz) induced by the mass change,  $\Delta m$  is the mass change (in ng cm<sup>−2</sup>) and  $K$  is the proportionality constant and equal to  $(\mu_q \rho_q)^{1/2} / 2f_0^2$ , where  $f_0$  is the fundamental resonant frequency,  $\mu_q$  ( $= 2.947 \times 10^{11}$  g cm<sup>−1</sup>) is the shear modulus of quartz,  $\rho_q$  ( $= 2.648$  g cm<sup>−3</sup>) is the density of quartz and the minus symbol indicates that the resonant frequency of the modified quartz crystal oscillator will decrease when the mass of the modified membrane increases for the adsorption function [18]. According to Eq. (1), a minute of mass changes on the modified film can be expressed by the frequency shift. Compared with the conventional detection methods, as a mass response microgravimetry, ISP sensor possesses more sensitivity in mass change and has better frequency stability, rapid response, lower frequency–temperature coefficient. On the other hand, it is simple to fabricate and convenient to operate. It is not surprising that the BAW has been used so widely, for example for affinity-based chemical sensing in liquid phases [19], and recently for biochemical and physiological studies in life science [20,21].

On the basis of aforementioned principle, a novel all-solid-state isoniazid (INH) ion-selective piezoelectric sensor was fabricated and applied to real sample assay by exploiting a modified 9-MHz AT-cut piezoelectric quartz crystal.

## 2. Experimental

### 2.1. Reagents

All chemicals used were of analytical grade or chemical-pure grade. Isoniazid, obtained from Peking Medicine Factory (China), was of > 99.0% purity. Double-distilled water was used throughout.

## 2.2. Standard solution

A stock standard solution of INH was prepared by dissolving a suitable amount of INH powder in double-distilled water and adjusting to pH 7.0 with NaOH and HCl. The stock solution was diluted to a series of concentrations from 0.1 to  $10^{-6}$  M.

## 2.3. Preparation of body fluids

Artificial gastric juice was prepared by mixing 5 g pepsin with 8.2 ml dilute hydrochloride solution and diluting to 500 ml solution with double-distilled water [4]. The operation for artificial intestine juice preparation was performed similarly.

## 2.4. Apparatus

A schematic diagram of the proposed sensor device is illustrated in Fig. 1. The frequency changes caused by adsorption were measured by a universal frequency counter (Model SC-72001, Iwatsu, Japan). The thickness-shear mode piezoelectric quartz crystal (PQC) (JA-5, made in Peking Factory No. 707) used was a 9-MHz AT-cut crystal (12.5 mm diameter) having silver electrodes (6 mm diameter) on each side. As shown in Fig. 1, the quartz crystal was fixed to a detection cell made of PTFE, in which only one side of the quartz crystal was allowed to be in contact with the aqueous sample solutions. The crystal holder was directly connected to an IC-TTL oscillating circuit, whose design was given in a previous paper [21]. The oscillating circuit was supplied by a d.c. voltage regulator (JWY-30B Model, Shijiazhuang

Electronic Factory No. 4), and the i.c. working voltage was set at 5 V. A computer (Model 4192A, Hewlett-Packard) was used for data analysis, and temperature control ( $37 \pm 0.1^\circ\text{C}$ ) was achieved by using a constant-temperature water bath.

## 2.5. Preparation of ion-pair complexes

INH–phosphotungstate (INH–PPT) was prepared by mixing equal volumes of 0.01 M INH solution and 0.01 M phosphotungstate acid solution. The mixture was left overnight and then the precipitate was filtered off on a porosity-4 sintered glass crucible, washed several times with double-distilled water and dried under a vacuum (Fig. 2). The powder was stocked in a sealed brown container. INH– $\text{BiI}_4$  and INH–SCT ion-pair complexes were prepared in a similar manner.

## 2.6. Measurements of dissolution of ion-pair complexes

An appropriate amount of INH–PPT powder was added to 0.1 M  $\text{NaNO}_3$  solution with stirring for 30 min and kept standing for 2 h. The mixture was filtered with a disposable syringe filter and then the INH–PPT saturated solution was obtained for measurements of dissolution of INH–PPT by using INH ISP sensor. The same method was employed for the measurements of dissolution of INH–SCT and  $\text{INH}[\text{BiI}_4]^-$ . The results are given in Table 1.

## 2.7. Fabrication of the ISP sensor

The INH–PPT–PVC ISP sensor fabrication procedure in the present study for the surface modification of the Ag electrode on the PQC was as follows: 10 mg of INH–PPT ion-pair complex prepared by the aforementioned method, 0.5 ml of dibutyl phthalate and 200 mg poly(vinyl chloride) (PVC) powder were mixed completely and dissolved in 5 ml tetrahydrofuran. A minute of this solution was spread on one Ag electrode surface of a piezoelectric quartz crystal while it rotated rapidly. The tetrahydrofuran would slowly evaporate at room temperature from a mixture placed on the surface of the quartz crys-

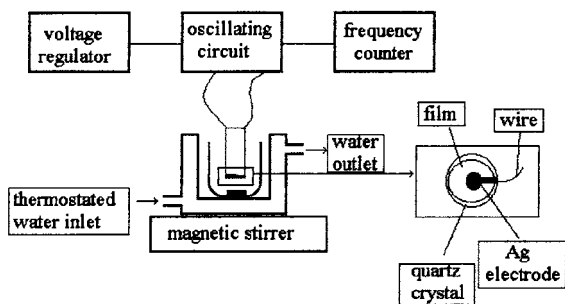
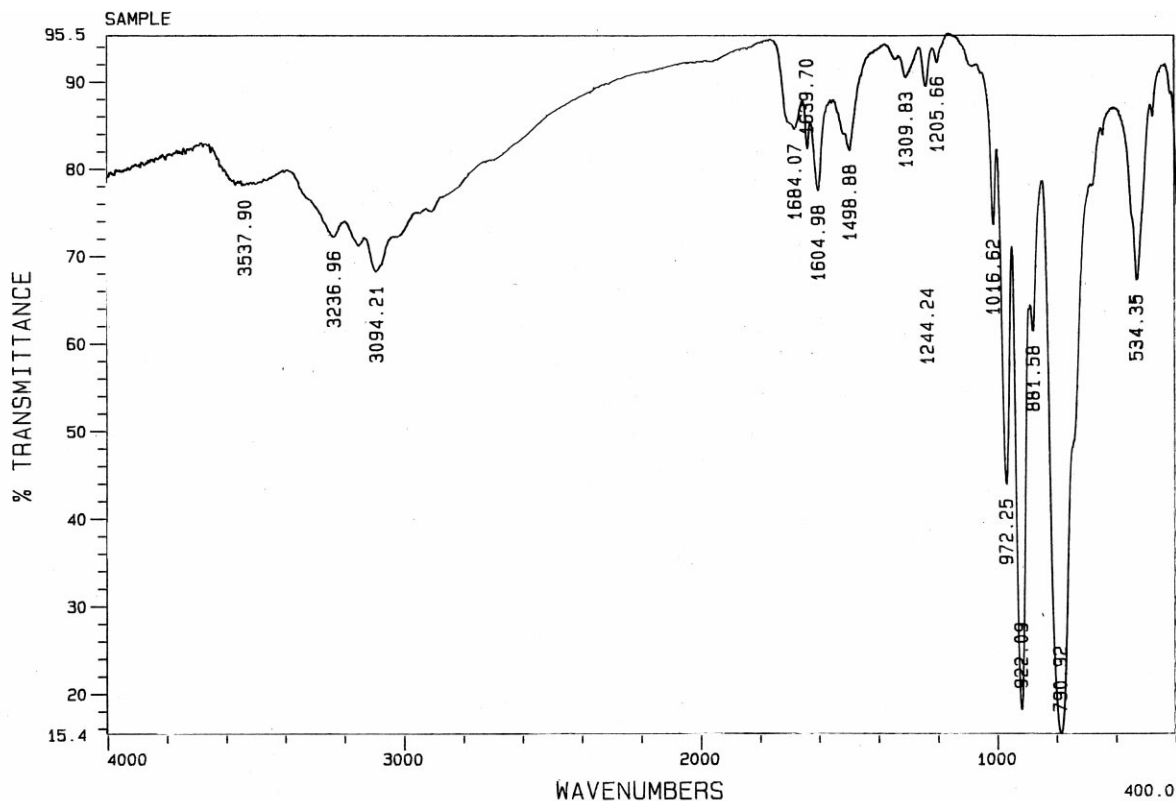


Fig. 1. Schematic diagram of the modified INH ISP sensor and detection system.



Nicolet Instrument  
Corporation

c27

SCANS: 32 RES: 4.0 TIME: 12/14/ 14: 54: 10

Fig. 2. Infrared spectrum of INH-PPT complex. IR characteristic bands (in  $\text{cm}^{-1}$ ): 3236.96 (N-H stretching); 3094.21 (=C-H stretching); 1684.07 (acrylamide carbonyl group, C=O stretching); 1604.98 (C=C stretching); 1498.88 (pyridine ring stretching); 1309.83 (C-N stretching + N-H bending vibration); 700–1100 (characteristic absorption peak for  $[\text{PW}_{12}\text{O}_{40}]^{3-}$ ).

Table 1

The solubility of ion-pair complexes for INH

Complex	Medium	pH	Temperature ( $^{\circ}\text{C}$ )	$[\text{INH}]^+$ (M)
INH-PPT	0.1 M $\text{NaNO}_3$	5.0	25	$2.7 \times 10^{-6}$
INH-SCT	0.1 M $\text{NaNO}_3$	5.0	25	$8.3 \times 10^{-5}$
INH-BiI <sub>4</sub>	0.1 M $\text{NaNO}_3$	5.0	25	$1.4 \times 10^{-5}$

tal. A transparent uniform membrane was formed on the crystal surface. The same procedures were carried out for INH-BiI<sub>4</sub>-PVC and INH-SCT-PVC ISP sensors. All ISP sensors made in this way can be stored in air when not in use.

### 2.8. Testing procedure of the INH using ISP sensors

In our work, a new method was developed to focus on application. So, the effect of the pH and

situations of human body have been taken into account: 0.1 M of  $\text{NaNO}_3$  solution was used as background electrolyte solution and pH 7.0 was chosen throughout; the temperature of the thermostatted cell was kept at  $37 \pm 0.1^\circ\text{C}$ , where the room temperature was  $18^\circ\text{C}$ . When modification

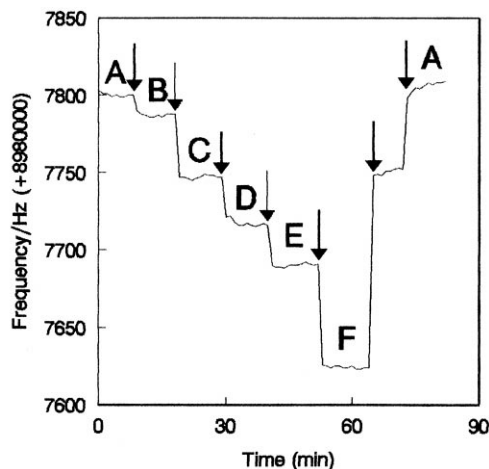


Fig. 3. Course of the observed frequency response of the INH-PPT modified ISP sensor with sample solution injections. Final concentration of INH: (A) 0 M, (B)  $6 \times 10^{-8}$  M, (C)  $2 \times 10^{-7}$  M, (D)  $2 \times 10^{-6}$  M, (E)  $2 \times 10^{-5}$  M, (F)  $2 \times 10^{-4}$  M, (G)  $2 \times 10^{-3}$  M (all containing 0.1 M  $\text{NaNO}_3$ , pH 7.0).

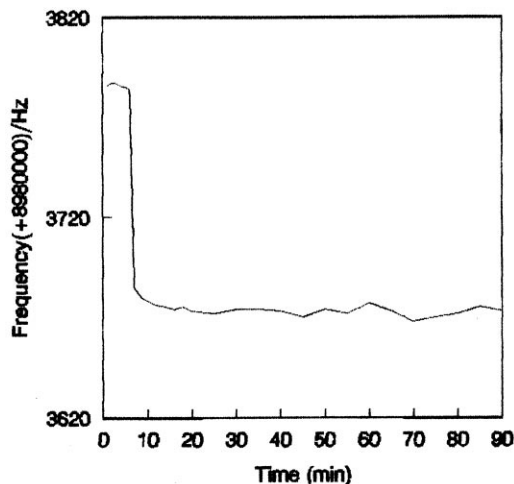


Fig. 4. The stability of the response in the proposed method was detected using the INH-PPT ISP sensor in  $1 \times 10^{-5}$  M INH solution containing 0.1 M  $\text{NaNO}_3$ .

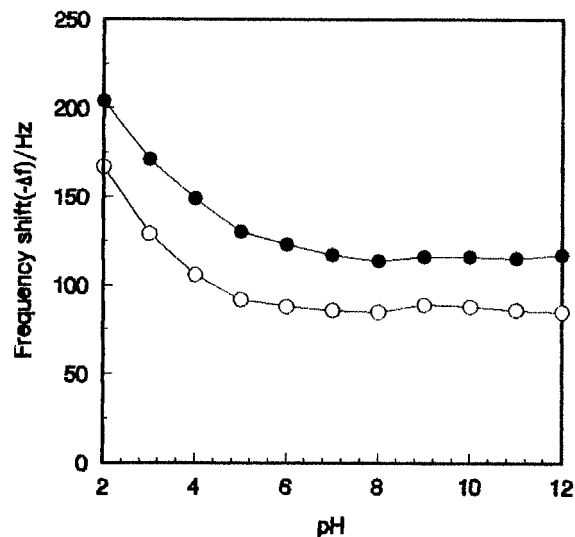


Fig. 5. Influence of the solution pH on the frequency response of the INH-PPT modified ISP sensor. (○)  $2 \times 10^{-5}$  M INH, (●)  $2 \times 10^{-4}$  M INH.

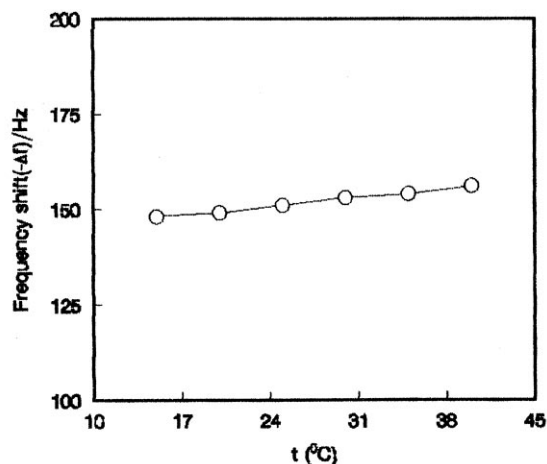


Fig. 6. Influence of temperature of the solution on the frequency response of the INH-PPT modified ISP sensor.

procedure on every quartz crystal oscillator was completed, the sensor should be immersed into  $1 \times 10^{-4}$  M INH solution (containing 0.1 M  $\text{NaNO}_3$  and pH 7.0) for 3 h in order to precondition before detection was carried out, and then washed with double-distilled water until the frequency returned to its original value (the frequency for the modified quartz crystal oscillator

in air,  $f_a$ ) nearby. To eliminate the effect of the membrane thickness and concentrations of activant, the same modified sensor was used repeatedly to complete a series of measurements and all experiments were carried out under strictly maintained similar measuring conditions.

A preconditioned ISP sensor was immersed into background electrolyte solution and a steady resonant frequency ( $f_1$ , the frequency shift less than 1 Hz in 3 min) was obtained. Then, a series of standard solution or sample solution from low to high concentration were injected in steps to raise the concentration of INH ion in the background solution. At constant time intervals, both the time and the frequency for the preconditioned ISP sensor were recorded until the frequency became stable ( $f_i$ ). The frequency shift for concentration of each solution was calculated as:

$$\Delta f = f_i - f_1 \quad (2)$$

Table 2  
Ion selectivity of the INH ISP sensor

Interfering ion	$k_{ij} = \Delta f_i / \Delta f_j^a$
Potassium chloride	No interference
Magnesium chloride	No interference
Barium chloride	0.00105
Copper chloride	0.0158
Urine	0.0052
Glucose	0.0316
Atropine sulfate	0.0217
Benzylamine	0.0211
Lactate	0.0316
Trimethoprim	0.0211
Tetramethylammonium bromide	0.0289
Ammonium chloride	0.0105
Quinine hydrochloride	0.0434
Theophylline	0.0486
Nicotinamide	0.0211
Morphine hydrochloride	0.0362

<sup>a</sup>  $\Delta f_i$  is the frequency response of the sensor to  $2.0 \times 10^{-4}$  M interfering ion;  $\Delta f_j$  is the frequency response of the sensor to  $2.0 \times 10^{-4}$  M INH ion.

### 3. Results and discussion

#### 3.1. Temporal course of the response to INH ion for the ISP sensor modified using INH–PPT–PVC

The present method is based on selective adsorption/desorption of INH ion across a INH–PPT–PVC, INH–BiI<sub>4</sub>–PVC or INH–SCT–PVC porous membrane. The selective adsorption/desorption of component ions will cause a mass change on the modified sensor which can be expressed by frequency shift. Fig. 3 shows a typical temporal course of the response of the ISP sensor modified with INH–PPT–PVC membrane. After conditioning in the 0.1 M NaNO<sub>3</sub> (pH 7.0) without any INH ion (plateau A, frequency  $f_0$ ), with increasing concentrations of INH ion, the frequency of the modified ISP sensor decreased rapidly. For each concentration of INH ion there is a corresponding plateau.

After completing a series of detection for different INH ion concentrations, the solutions were removed from the detection cell and double-distilled water was injected into it repeatedly, so the frequency of the ISP sensor would gradually increase. Finally, after renewing the background solution, the ISP sensor response ( $f_r$ ) was found to reach a value close to the steady oscillating frequency ( $f_0$ ) in the background solution obtained after the initial conditioning. Generally speaking, there is always a little difference between  $f_r$  and  $f_0$ , which is mainly due to the adsorption/desorption of INH ions at the sensor surface or probably the dissolution of activants in the renewed INH ion-free background solution. This slight frequency shift could be prevented by preconditioning the sensor in a certain INH concentration solution containing background solution until a steady baseline was obtained and the whole experiment was kept in the same situation. Our testing results indicate that the response of the presented ISP sensor was satisfactorily reversible over the range 0– $10^{-3}$  M INH ion in the background solution.

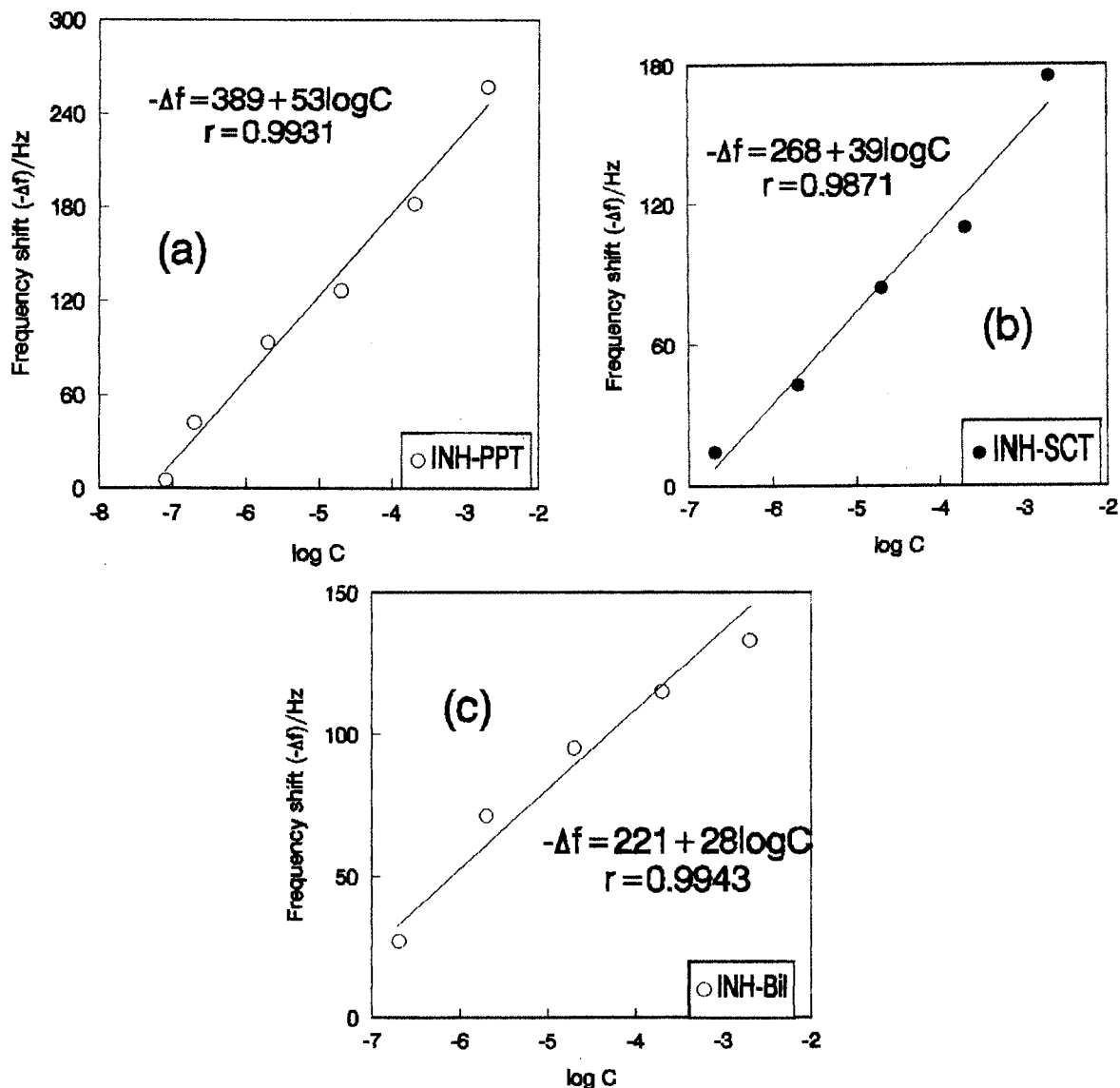


Fig. 7. Adsorption isotherms curve for INH ions using various ISP sensors modified using (a) INH-PPT-PVC, (b) INH-SCT-PVC, (c) INH-BiI<sub>4</sub>.  $r$  values are the respective correlation coefficients.

### 3.2. The stability of the response in the proposed method

Fig. 4 indicates that the stability of the response in the proposed method can be accepted.

Although there is a little frequency shift in the latter part of the curve resulting from outside factors, the frequency change around 10 min is small and can be neglected.

### 3.3. pH effect

Fig. 5 shows the pH effect on the response of the INH-PPT-PVC modified ISP sensor in the background solution containing various INH concentrations; the pH of solution was adjusted by adding appropriate amounts of hydrochloric acid or a sodium hydroxide solution using a 50- $\mu$ l microsyringe. The pH range where the frequency



Table 3  
Determination of INH using the INH ISP sensor

Artificial intestine juice					Artificial gastric juice				
Added (mg)	Found <sup>a</sup> (mg)	Recovery (%)	Mean recovery (%)	S.D.	Added (mg)	Found <sup>a</sup> (mg)	Recovery (%)	Mean recovery (%)	S.D.
9.3	9.2 ± 0.17	98.9			11.7	12.0 ± 0.21	102.6		
18.6	18.7 ± 0.38	100.5			21.3	21.2 ± 0.49	99.5		
24.5	24.9 ± 0.72	101.6	100.2	1.08	17.3	17.0 ± 0.60	98.3	100.0	1.6
33.6	33.4 ± 0.90	99.4			30.6	30.4 ± 1.05	99.3		
45.2	45.5 ± 1.35	100.7			41.4	41.6 ± 1.54	100.5		

<sup>a</sup> Values are given as mean ± S.D. (*n* = 3).

Table 4  
Determination of INH using the INH ISP sensor and the pharmacopoeia method

ISP sensor					UV spectrophotometry				
Added (mg)	Found <sup>a</sup> (mg)	Recovery (%)	Mean recovery (%)	S.D.	Added (mg)	Found (mg)	Recovery (%)	Mean recovery (%)	S.D.
8.4	8.6 ± 0.09	102.4			9.3	9.1	97.8		
11.9	11.6 ± 0.27	97.5			12.2	12.1	98.4		
16.7	16.3 ± 0.45	97.6	99.0	2.0	15.1	15.3	101.3	99.6	1.89
19.2	19.0 ± 0.66	99.0			18.7	18.4	98.4		
24.5	24.1 ± 0.81	98.4			21.6	22.0	101.9		

<sup>a</sup> Values are mean ± S.D. (*n* = 3).

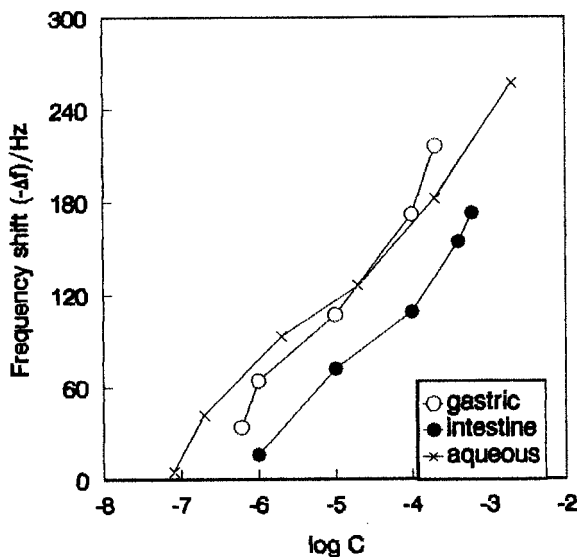
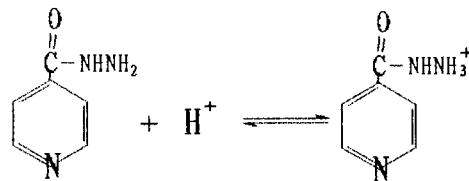


Fig. 8. Frequency shift ( $-\Delta f$ ) versus the logarithm of the concentration of INH ion plots for the INH-PPT modified ISP sensor. ( $\times$ ) in aqueous solution (containing a 0.1 M  $\text{NaNO}_3$  solution, pH 7.0), ( $\circ$ ) in artificial gastric juice, ( $\bullet$ ) in artificial intestine juice

shift remains constant is at  $\text{pH} > 6$ , while it decreases obviously at  $\text{pH} < 6$ . This is due to a shift of the equilibrium between INH and free INH ion in the solution:



Taking the situation of human body into account, pH 7.0 was adopted in this work.

### 3.4. Temperature effect

Fig. 6 shows that there is a little influence on the present sensor in a  $10^{-4}$  M INH concentration containing 0.1 M  $\text{NaNO}_3$  and pH 7.0. In order to keep the situation of human body,  $37^\circ\text{C}$  was adopted by using a constant-temperature water bath.

### 3.5. The effect of the membrane

By preconditioning and keeping the same detective situation for a ISP sensor, the effects due to the viscoelasticity of the coating could be neglected and the later testing results prove it is valid. The thickness of the membrane has significant effects on the response: An over-thick membrane leads to low sensitivity and instability, even non-oscillation of the sensor, while an over-thin

Table 5

Comparisons of the proposed method and other methods for the determination of INH

Method	Application	Calibration range	Detection limit	Recovery (%)	R.S.D. (%)	Reference
Cyclic voltammetry	In aqueous solution	0.4–2 mM		92	2.7 ( $n = 6$ )	[5]
HPLC	In serum	0.2–10 mg/l	0.02 mg/l	>99	1.2–3.5 ( $n = 10$ )	[9]
FIA chemiluminescence	In pharmaceuticals	0.1–10 $\mu\text{g}/\text{ml}$	30 ng/ml		<2 ( $n = 6$ )	[7]
AAS	In serum and tablets		0.29 g/ml	93.3–104		[8]
Spectrophotometry	In pharmaceuticals	2–5.6 $\mu\text{g}/\text{ml}$		99.0–101	0.85–1.1 ( $n = 5$ )	[6]
TLC	In serum	1–20 mg/l	0.5 mg/l	96.3–101.3	3.3–3.9	[3]
ISP sensor	In different media	$6 \times 10^{-8}$ – $2 \times 10^{-3}$ M	$6 \times 10^{-8}$ M	98–102	2.02 ( $n = 5$ )	This paper

membrane causes a long-time frequency shift as well as a narrow linear range. In our work, about a 10 000-Hz frequency shift, resulting from membrane, has usually been used.

### 3.6. Selectivity

All measurements were carried out in background electrolyte solution (containing 0.1 M NaNO<sub>3</sub> and the pH was adjusted to 7.0) which indicates that the sodium ion did not seriously interfere with the response of the present ISP sensors. At first, we define  $k_{ij} = \Delta f_i / \Delta f_j$  as the response-selectivity coefficient, where  $\Delta f_i$  is the frequency shift of the ISP sensor to  $1 \times 10^{-4}$  M of the interfering ion, and  $\Delta f_j$  is the frequency shift to  $1 \times 10^{-4}$  M of INH ion. Differences in the selectivity coefficient of more than 0.05 were considered to result from interferences. Table 2 gives the results of some interfering cations. It can be seen that there is no significant interference from potassium, barium, magnesium, copper, urea, glucose, atropine, benzydamine, lactate, trimethoprim, ammonium, theophylline, nicotinamide, tetramethylammonium, quinine and morphine cations.

### 3.7. Comparisons for various activants

As shown in Fig. 7, the plots of the decrease in the frequency versus the logarithm of the concentration of INH ion for the ISP sensors modified using each INH salt have a linear relationship. The ISP sensor modified using INH–PPT gives the widest linear range and highest sensitivity, which can be attributed to the differences in solubility products or solubilities for various activants [14].

### 3.8. Applications of the ISP sensor

In order to adapt the method to the assay of human body fluids, the suggested sensor was applied to a quantitative determination of INH in various samples. Fig. 8 shows the frequency shift of an ISP sensor modified using INH–PPT when the concentration of INH changed in artificial gastric juice and intestine juice. Obviously, the

frequency decrease in the gastric juice is greater than that in intestine juice. This is due to the acidity of the artificial gastric juice. The results listed in Tables 3 and 4 indicate that the results obtained by the present method agree well with those obtained by conventional methods.

## 4. Conclusions

The successful development of a method for the determination of INH and results obtained in a sample analysis confirm the usefulness of the proposed ISP for quantitative analysis, and indicate that this method might also find useful applications in the assay of other drugs.

For an overall evaluation of the proposed method, a comparison of this novel method with other methods (Table 5) has indicated that the ISP sensor provides a selective, sensitive and precise method for the determination of INH. The method proposed here has some advantages over other detection techniques; for example, the required reagents and instruments are simpler and cheaper than those required by the HPLC, FIA and spectrophotometry methods. Finally, the influence of the electrical properties of the modified membrane are negligible due to the mass response. Since no significant effect was caused by the background, good responses can easily be obtained. These advantages of the new method would make it an attractive alternative for the pharmaceutical assay compared to the other methods currently in use.

## Acknowledgements

This work was supported by the China Natural Science Foundation.

## References

- [1] J.P. Guo, H. Xu, *Chin. Pharm. J.* 33 (1998) 95.
- [2] D.H. Tu, *J. Tuberculosis Respir. Dis.* 21 (1998) 67 (Chinese).
- [3] K.M. Yuan, Y.Y. Wang, G.M. Li, *Chin. J. Pharm. Anal.* 172 (1997) 116.

- [4] Chinese Pharmacopoeia, vol. II, 1st ed., 1983.
- [5] J.A. Tong, X.J. Dang, H.L. Li, *Electroanalysis* 9 (1997) 165.
- [6] P. Nagaraja, K.C. Srinivasa Murthy, H.S. Yathirajan, *Talanta* 43 (1996) 1075.
- [7] F. Zhao, Y.Y. Wu, Z. Geng, H.X. Wang, *Fenxi Huaxue* 25 (1997) 927.
- [8] Z.Q. Zhang, Z.X. Cao, X.M. He, X.M. Li, Y.F. Li, *FenXi KeXue XueBao* 12 (1996) 52.
- [9] S. Nouredine, P. Nicole, D. Helene, D. Michel, *J. Chromatogr. B Biomed. Appl.* 675 (1996) 113.
- [10] E.G. Harsanyi, K. Tóth, L. Pólos, E. Pungor, *Anal. Chim. Acta* 152 (1983) 163.
- [11] T.R. Berube, R.P. Buck, E. Lindner, K. Tóth, E. Pungor, *Anal. Chem.* 63 (1991) 946.
- [12] K. Uosaki, Y. Shigematsu, H. Kita, Y. Umezawa, R. Souda, *Anal. Chem.* 61 (1989) 1980.
- [13] Y. Tani, Y. Umezawa, K. Chikama, A. Hemmi, M. Soma, *J. Electroanal. Chem.* 378 (1994) 205.
- [14] K. Iitaka, Y. Tani, Y. Umezawa, *Anal. Chim. Acta* 338 (1997) 77.
- [15] G. Sauerbrey, *Z. Phys.* 155 (1959) 206.
- [16] S.Z. Yao, Z.H. Mo, *Anal. Chim. Acta* 229 (1990) 205.
- [17] G.L. Hayward, G.Z. Chu, *Anal. Chim. Acta* 288 (1994) 179.
- [18] O. Melroy, K.K. Kanazawa, J.G. Gordon, D.A. Buttry, *Langmuir* 2 (1986) 697.
- [19] F.J. He, W.H. Zhu, Q. Geng, L.H. Nie, S.Z. Yao, *Anal. Lett.* 27 (1994) 555.
- [20] S.H. Si, D.Z. Shen, L.H. Nie, S.Z. Yao, *Bioelectrochem. Bioenerg.* 36 (1995) 161.
- [21] S.H. Si, Y.J. Xu, L.H. Nie, S.Z. Yao, *J. Biochem. Biophys. Methods* 31 (1995) 135.

# Optical fiber coupled light emitting diode based absorbance detector with a reflective flow cell

Sivakumar Jambunathan <sup>a</sup>, Purnendu K. Dasgupta <sup>a,\*</sup>, Duane K. Wolcott <sup>b</sup>,  
Graham D. Marshall <sup>b</sup>, Don C. Olson <sup>b</sup>

<sup>a</sup> *Department of Chemistry and Biochemistry, Texas Tech University, Lubbock, TX 79409-1061, USA*

<sup>b</sup> *Global FIA Inc., 3015 88th Ave. Ct. NW, Gig Harbor, WA 98335, USA*

Received 26 February 1999; received in revised form 12 April 1999; accepted 16 April 1999

## Abstract

We present a versatile, optical fiber coupled light emitting diode (LED) light source based flow-through optical absorbance detector. The LED source is readily changeable. Optical fibers are used to carry light from the electronics/display unit to a reflective flow-through cell and back. The cell can thus be located remotely from the electronics unit and the umbilical connection is not susceptible to electrical noise. The noise level of this detector with LEDs of different emission maxima were observed to be in the range of 3–20  $\mu$ AU under actual use conditions, with a maximum short term drift of 4  $\mu$ AU/min after the initial warm-up period. When the analyte absorbance is well matched with the source emission characteristics, the detector response is linear with concentration over at least two orders of magnitude. The liquid flow path through the cell is linear with a large exit aperture such that bubbles are not trapped in the optical path. The optical arrangement is such that the incident light crosses the liquid flow orthogonally and is reflected back by a rear mirror to the receiver fiber. This arrangement reduces the refractive index sensitivity by an order of magnitude relative to conventional Z-path flow cells. © 1999 Elsevier Science B.V. All rights reserved.

*Keywords:* Optical absorbance detectors; Optical fiber coupled light emitting diode; Reflective flow-through cell

## 1. Introduction

Measurement of optical absorbance is the most commonly used detection method for flow analyses, including high-performance liquid chromatography (HPLC), flow injection analysis

(FIA) and sequential injection analysis methods. There is continuing interest in developing miniaturized optical absorbance detection methods, down to the capillary scale [1]. Light emitting diodes (LEDs) are inexpensive, long life, high brightness, low noise, nearly monochromatic sources that are particularly attractive in conjunction with photodiodes for the fabrication of all solid-state flow-through photodetectors. Approaches to fabricating such photodetectors were

\* Corresponding author. Tel.: +1-806-742-3067; fax: +1-806-743-1289.

*E-mail address:* sandyd@ttu.edu (P.K. Dasgupta)

reviewed by Dasgupta et al. in 1993 [2]. At that time, the only true high brightness LEDs were available in the red (660 nm, AlGaAs emitters) and longer wavelengths. In the intervening years, major progress has been made towards the commercial availability of very high brightness LED sources in shorter wavelengths. GaN and InGaN based emitters in particular have led to very bright green, blue and even UV emitting LEDs with optical output powers at the milliwatt level (Nichia America Corporation, Mountville, PA, USA; [www.nichia.com](http://www.nichia.com)). Klipstein maintains a frequently updated information site on the web (LED main page at <http://www.misty.com/~don/ledx.html>) that is an excellent source of information on high brightness LEDs and where they can be purchased. Also in the intervening period, GaN based photodiodes have become commonly available that respond only in the UV and have no response to visible light (APA Optics, Inc., Blaine, MN, USA; [http://www.apaoptics.com/APAHome/html/GaN\\_Webpage.htm](http://www.apaoptics.com/APAHome/html/GaN_Webpage.htm)).

The interest in LED-based optical detectors is long standing [3–5]. Even multiwavelength photometers based on switch-selectable emitters have been made [6]. More recently, as capillary scale analytical methods, most notably capillary electrophoresis, are becoming popular, the use of LED based detectors for such studies is also increasing [7–11]. The use of capillary scale liquid core waveguides has permitted LED based fluorescence detectors with attomole detection limits [12].

Traditionally, whether capillary based or of conventional size, the light source and the photodetector are placed in close proximity to the detection cell. If the cell is not already within the electronics enclosure (an arrangement that has its own problems if there are any potential leaks) and must be remotely located (this is desirable in a variety of situations), the photodetector signal, typically in the nanoampere range, must be carried over signal cables. This greatly limits the length of the cables and even with short shielded cable connections the system is often susceptible to electrical/electromagnetic interference from the external environment.

One solution is to amplify the signal at the detection cell before it is transmitted. Phototransistors, rather than photodiodes, can be used for this purpose but the variety of available phototransistors is limited and the intrinsic noise level is often higher. A second solution is to use a low-noise operational amplifier in close proximity to the photodiode and transmit this amplified signal to the main electronics enclosure. When the light level is very small, as in capillary scale absorbance detectors, immediate amplification of the photodetector output is carried out before any other further processing to attain low noise. This is done even when the ‘cell’ and the processing electronics are located in the same enclosure [13]. To practice this with a cell remotely located from the detector electronics, the complexity of the umbilical connection increases significantly.

An alternative to electrical communication between the detection cell and the processing electronics is to use optical communication. The use of optical fibers to carry optical signals to and from an FIA detection cell was first proposed by Ruzicka and Hansen [14,15]. A fiber coupled detector can also be used in applications other than liquid phase measurements, such as reflection or transmission based measurements in microbead packed columns [16]. This concept, embodying in particular a sandwich construction where a membrane serves as a gas diffusion element between the two halves of a cell and also serves as an optical reflector, was elaborated subsequently by Pavon et al. [17]. Dasgupta et al. [18] suggested that, for uses other than gas diffusion etc., a more conventional reflector with a higher reflectivity than a membrane will increase light throughput and improve signal/noise (S/N). More importantly, they found that the reflective path cells have a lower refractive index sensitivity than conventional cells.

Most optical cells used for flow-through applications suffer from refractive index (RI) artifacts; this has been known for over two decades [3]. Common methods adopted to reduce the refractive index changes include imaging a source on the exit window with focusing optics and using tapered cell construction [19] or using a second wavelength as a reference [20,21]. In difficult sam-

ples, this can be such a vexing problem that one major advantage of monosegmented flow analysis in the multiple injection format is seen to be the introduction of a homogenized sample/reagent or sample/diluent aliquot and thus eliminate refractive index gradients [22]. This cannot, of course, eliminate static refractive index effects which leads to a variable degree of reflective light loss at the glass–liquid interface as the liquid refractive index varies. In a conventional Z-cell, the light path is collinear with the liquid flow path. In contrast, in the reflective cell design [17,18], the light path is orthogonal to the liquid flow path and the light is reflected back almost along the same path, reducing refractive index sensitivity substantially.

Finally, most flow-through optical absorbance detection cells in use today have various degrees of sensitivity to bubble or foreign particle entrapment problems. In HPLC, the detectors encounter only highly filtered samples and flow restrictors are often added to the cell exit to reduce bubble formation. The heritage of using HPLC type detectors from the early days of FIA has led to flow cells that have narrow entrance and exit bores and are particularly susceptible to bubble/particle entrapment, an important issue in process applications. Using the radial path across the flow conduit as the optical path provides a simple solution. In particular, the entrapment problems are vastly reduced for a linear flow path and a large exit bore. Normally this would result in a limited path length but reflective optics increases the path length to offset this disadvantage to a significant degree.

In the present work, we describe a low-cost fiber optic coupled detector/cell combination that permits rapid light source changeover, has very low refractive index susceptibility, does not trap bubbles and exhibits good signal/noise and drift performance.

## 2. Experimental

### 2.1. Flow cell

The design of the flow cell is shown in Fig. 1. The cell itself is composed of a (inside dimensions

$3 \times 3$  mm) square cross section glass or quartz tubing T (Vitrocom, Mountain Lakes, NJ) that has been tapered as shown on the entrance side to an inner diameter of  $\sim 0.7$  mm to match with the conduit inner diameters used in the flow manifold. The smooth taper provides a smooth flow transition and good washout profiles without leading to added flow noise. O-rings on both sides provide necessary liquid sealing. Fig. 1 shows an insert, I, into which two 1.5 mm core, jacketed technical grade acrylic optical fibers (Edmund Scientific, Barrington, NJ), F1 and F2, are push-fitted side by side. The fiber optic ends are cut flush with the insert end and polished for good light throughput. The insert fits snug into an appropriately drilled hole in the cell holder body, B. The fiber optic bearing insert is pushed flush to address the cell face and then fixed in place in the correct orientation with a retaining screw. On the opposite side of the cell, arrangements are made to reflect the launched light. In an initial design, a front surface concave mirror, C, was placed on the obverse face

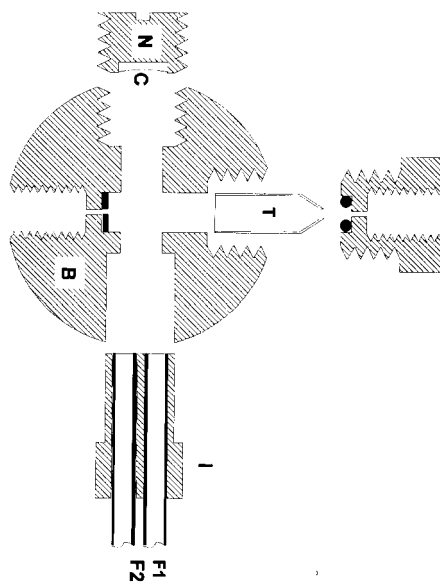


Fig. 1. Cell design. T, rectangular cross section glass/quartz cell, put in cell body, B, and sealed by O-ring seals on either side. IN/OUT connections are 1/4–28 threaded. Insert I carries fiber optics F1 and F2 that sit flush against the cell wall. Front surface concave mirror C is held by nut N on the obverse side of the cell; alternatively, the cell is silvered on all but the face addressed by the optical fibers.



of the cell with a retaining nut, N, as shown in Fig. 1. However, subsequent experiments showed that the simple expedient of silvering the outside of the cell body itself (Silvering Kit E-0060, Wilt Industries, Lake Pleasant, NY) provides the same results. In silvering, care should be taken to cover the entrance and the exit apertures of the cell to prevent the internal surface from being silvered. We find it expedient to silver the entire exterior of the cell and then remove the silver from the optically addressed face. The silver coating is protected by a clear acrylic spray coating. The results presented in this paper include data from either type of reflector design without distinction.

## 2.2. Light source and photodetector arrangements

The optical fiber LED/photodetector arrangement is shown in Fig. 2. On the electronics board, C, the reference and signal silicon photodiodes (S2007, Electronic Goldmine, Phoenix, AZ) are placed side by side on the circuit board on areas that are painted flat black to reduce stray light. Both detector diodes are covered with male SMA panel ‘hat’ connectors, S, that are also internally painted black. The details of the LED holder, H, constructed in three pieces, appear in the bottom panel of Fig. 2. The bottom of the LED holder contains spring-loaded electrical connector pins, P, and a polarity assuring alignment pin, A. The aperture on the bottom of this piece is 1/4–36 threaded so that it can be directly threaded into the SMA connector covering the reference photodiode. The middle piece of the LED holder, TFL is shaped like a stovepipe hat, with appropriately cut slots in the disk portion to accommodate the leads, E, of the LED, L, and an upper 1/4–28 threaded aperture through which the transmitting optical fiber, T, is affixed by a male nut and ferrule (used for retaining 1/8 inch o.d. tubes). The LEDs themselves were used after the excess plastic on the top of each LED was removed, rendering them flat. The epoxy top covering the emitter chip was largely removed, care being taken so that the bonding wire is not endangered. The top of the LED was polished using plastic buffing compound that was applied on the flannel buffs of a rotating wheel. The LED was then

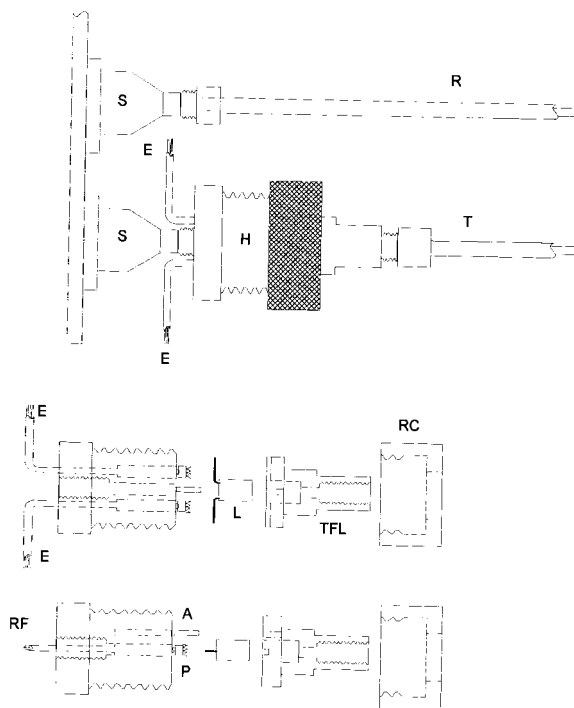


Fig. 2. Light detection arrangement. Top panel shows SMA style connectors, S, on circuit board, C, atop the photodiodes. The top one connects to the receiving fiber, R, carrying back light transmitted to the cell. The bottom SMA connector connects to the bottom of the LED holder, H, and receives the reference signal. The transmitting fiber, T, is connected to the top of H and this carries light to the cell. E, E are electrical leads connected to the LED. The two bottom panels show the details of the LED holder: L, flat-top LED; TFL, holder that holds the LED and the transmitter fiber optic; RC, retaining cap; A, LED polarity alignment pin; P, push-in electrical contacts to LED; RF, reference fiber optic to reference photodiode.

gently pressed against the face of the rotating wheels and buffing was conducted until the surface of the LED was shiny and free of scratches. Finally, the top part of the LED holder, the retaining cap RC holds the other two components together. The optical fiber carrying light back from the cell is fixed on the detector photodiode with the aid of a 1/8-inch tubing ferrule and using an SMA threaded female nut that is bored out to accommodate the large core optical fiber. The bottom two pieces of the LED holder H are constructed of opaque black plastic to eliminate stray radiation.

The light emission from the bottom of an LED is device dependent and depends both on the design of the cathode cup that holds the emitter chip [2] and the care taken to polish the top surface. For processing electronics that has a range of at least 2 absorbance units (AU), it is desirable that with water flowing through the cell the detector offset is able to provide readings of  $\pm 1$  AU. If there is to be departure from this, it should be remembered that most detection systems result in positive absorbance signals over a background rather than a negative absorbance signal from a high background. Consequently, the demand placed on the detector generally requires the capability of offsetting a high blank background. The direct placement of the bottom of the LED holder atop the reference diode SMA is often sufficient to accomplish this. If this results in too little light reaching the reference detector, a fiber cut to the right length is put in the space between the bottom of the LED holder and the photodetector. The best combination is generally achieved by having such a fiber but sanding down one end of the fiber to prevent too much light reaching the reference detector.

### 2.3. Electronic design

The present detector was based on a log ratio amplifier (LOG100JP, Burr-Brown Corp., Tucson, AZ). The photodiode outputs were connected directly to the amplifier input, which was operated at a fixed gain of 5 V/AU. User-selectable jumpers are provided on-board that allows selecting gains of 1 V/AU or 3 V/AU. User-switchable jumpers are also provided so that fixed current inputs can be substituted for the photodiode inputs. This allows operation as a single beam detector, checking temporal stability of the LED output and electronically checking the accuracy of the output per absorbance unit (and adjusting that, if desired). The amplifier output is available in analog form and is also registered on a 3-1/2 digit display, calibrated to read out in absorbance units. The only external control is the zero adjustment, this spans a maximum of  $\sim 2.7$  AU. The detector is commercially available from Global FIA (Gig Harbor, WA) or AnalTech (Lubbock, TX).

LEDs used in the present experiments displayed the following peak emission wavelengths (as measured by a calibrated high resolution photodiode array detector): 436 nm (C430-CB290-E1000, Cree Research, Durham, NC), 495 nm (590S, Nichia America Corp, Mountville, PA), 555 nm and 605 nm (HBG5566X and HAA5566X, respectively, Stanley Electric, Tokyo, Japan) and 658 nm (E184, Gilway Technical Lamp, Woburn, MA). All were used at a drive current of  $\sim 20$  mA.

### 2.4. Comparative experiments

As a comparison we used a previously described [2] log ratio amplifier based on a hybrid monolithic integrated circuit (757N, Analog Devices, Norwood, MA). The same photodiodes as used in the other detector were used. But these were located external to the electronics enclosure and connected to the latter by shielded cable and BNC connectors.

A bifurcated fiber cable with bundle diameters of 1.2 mm in the branched legs was also tested in place of the large core acrylic fibers.

All experiments were conducted in a FIA mode, with a single-line manifold constructed from 0.8 mm i.d. poly(ethylvinylacetate) tubing. The injection valve was equipped with a 75- $\mu$ l loop and the length of tubing connecting the injector and the detection cell was 28 mm. To avoid noise contributions from pump pulsations, gravity flow (0.80 ml/min) was used.

All chemicals were of reagent grade and were used without purification. Sodium tetraborate ( $\text{Na}_2\text{B}_4\text{O}_7 \cdot 10\text{H}_2\text{O}$ , EM Science), boric acid ( $\text{H}_3\text{BO}_3$ , Baker), bromthymol blue (BTB, Eastman), acid alizarin violet (Aldrich), methylene blue (Baker) were obtained as indicated. Nanopure deionized water (Barnstead) was used throughout. In FIA studies with bromthymol blue, the solution was made up in 10 mM borate buffer (pH  $\sim 8.9$ ). Borate buffer was also used as the carrier. Acid alizarin violet and methylene blue were prepared in deionized water and injected into a water carrier.

The detector output was acquired by a Keithley/Metrabyte DAS-1601 data acquisition board

housed in a personal computer with software written in-house. This software allowed the A/D card to sample at its maximum sampling rate of 100 K samples/s and averaged it on the fly to the indicated sampling period.

### 3. Results and discussion

#### 3.1. Noise and S/N characteristics

Fig. 3 shows the baseline traces obtained under different conditions. Traces a–c were obtained with a 605-nm emitter with data averaged over (a) 1 s and (b) 0.25 s. Trace c shows the 0.25-s data smoothed by a four-point running average routine in Microsoft Excel. Trace d shows similar data for the 495-nm emitter (which is much brighter than the 605-nm emitter and results in a  $12 \times$  greater photocurrent). Trace e shows data for the detector with a 430-nm LED operated in the single beam mode.

With a 1-s integration time, the p-p noise that is observed with either the 605 nm or the 495 emit-

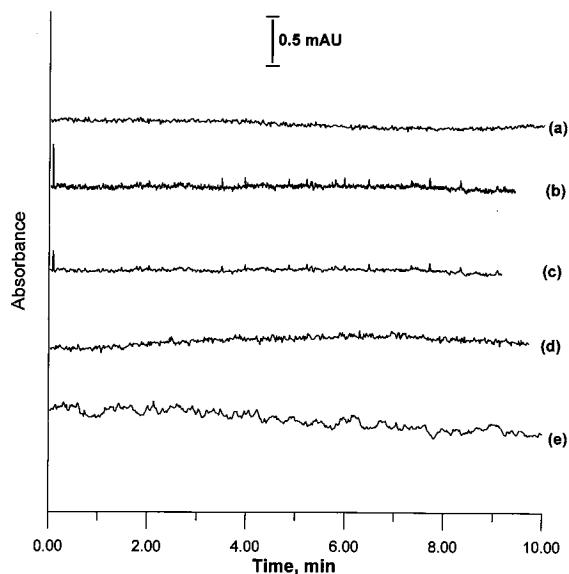


Fig. 3. Noise levels with water flowing through the cell, data averaging period 1 s except as stated: (a) 605 nm LED; (b) 605 nm LED, (0.25 s averaging); (c) data in b, smoothed by a four-point running average; (d) 495 nm LED; (e) 430 nm LED operated in a single beam mode.

ter is essentially the same, in the single digit  $\mu$ AU (all noise values quoted in this paper are p-p, measured over a period of 45 min). This suggests that the light intensity, at least between these two cases, is not a limiting factor in governing the noise. This, however, is a consequence of the use of the large core optical fibers with excellent light throughput. Under otherwise identical conditions, when the 605-nm emitter was tested with the much smaller numerical aperture bifurcated fiber, the noise level increased by 60%. With various different emitters and repeated runs over an extended period of study, our results show a noise level ranging from 3 to 20  $\mu$ AU. This is comparable to the best results reported for transmission based optical absorbance detectors, LED-based or otherwise. The maximum detector output drift rate was observed to be in the range of 1.3–4  $\mu$ AU/min. Detector baseline drift is largely dependent on temperature variations. In a laboratory environment, over a period of 1 h, the maximum base line excursion from the mean was observed to be  $\pm 50 \mu$ AU. Both drift and noise are clearly much worse when the detector is operated in the single beam mode (trace e; note that this LED produces a photocurrent larger than that elicited by the 605-nm emitter).

Regarding traces a and b in Fig. 3, in accordance with theoretical expectations, the observed noise increases approximately in proportion to the square root of the sampling rate. Averaging the data over the same interval of time thus results in comparable performance, as between traces a and c.

A typical chemical research laboratory is an electrically noisy environment. Large numbers of individual components with various power loads undergo changes in their power consumption. Carrying low levels of current to remotely located processing electronics invites induced noise. When the present cell and fibers were coupled to the older electronics and its externally located photodiodes (that were coupled to the fibers), the noise increased dramatically, by two orders of magnitude relative to the present detector, to  $\sim 1$  mAU. When the photocurrent was reduced further through the use of the smaller aperture fiber optic cable (which resulted in a light throughput reduc-

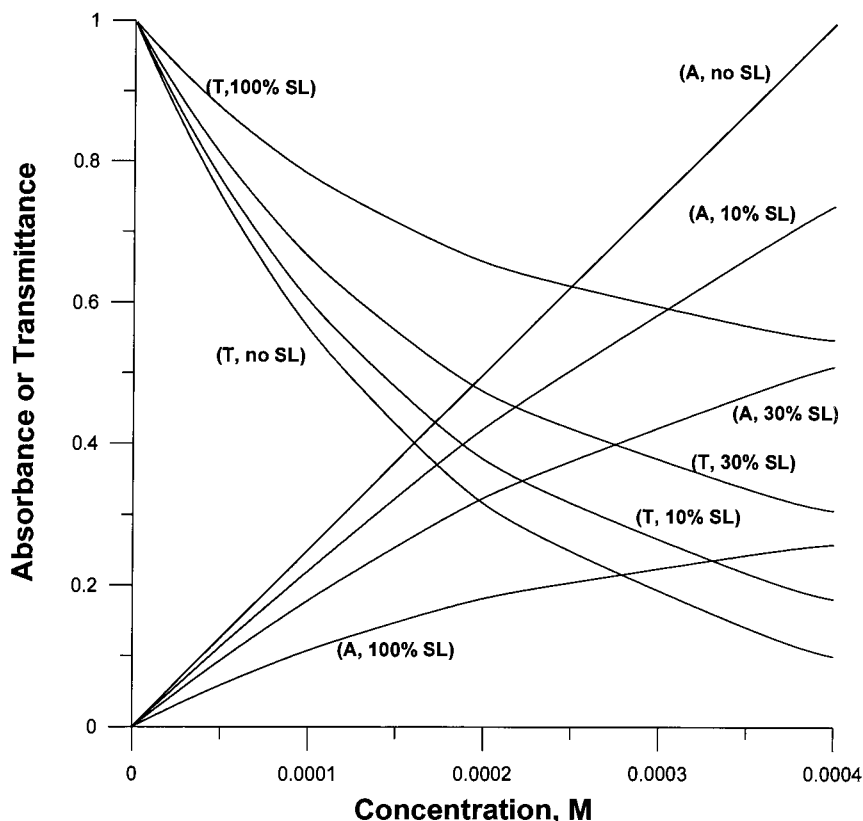


Fig. 4. Theoretically computed absorbance or transmittance values for a system with  $\epsilon = 5000 \text{ M}^{-1} \text{ cm}^{-1}$ , a pathlength of 5 mm and various levels of stray light.

tion of more than  $5 \times$ ), noise increased even further, to  $\sim 3 \text{ mAU}$ .

When the internal jumpers in the present detector was switched from monitoring photocurrents to fixed input currents, the noise level was found to be the same as that observed in the best case with the LEDs and the cell in operation. This suggests that the design performs at or near the limits of this electronics.

### 3.2. Linearity studies

Response linearity over a significant range of concentration is a desirable characteristic of any detector. Direct transmittance detection is an attractive option for capillary scale detectors because of the simplicity of the electronics and the fact that at very low absorbance values the rela-

tionship between concentration and transmittance is quite linear [2]. In the case of an LED-based detector, due to finite bandwidth and mismatch between analyte absorption and LED emission, the linear relationship between concentration and the observed absorbance can be significantly compromised. The net effects from limited monochromaticity is the same as that with stray light. In Fig. 4, this situation is graphically illustrated for transmittance and absorbance that are plotted for an analyte of molar absorptivity 5000 in a 5-mm cell for 0, 10, 30 and 100% stray light. The exact absorptivity and path length is unimportant, it is the overall absorbance that matters. Note the departure from linearity is marked at high stray light values and this is more so for the transmittance plots. For the present detector equipped with a 658-nm emitter LED, linearity was studied

with different concentrations of methylene blue which has an absorption maximum at 664 nm. The response of the detector to methylene blue was found to be linear ( $r^2 \geq 0.999$ ) with an intercept statistically indistinguishable from zero up to an absorbance of 0.65. For alkaline bromthymol blue detected with a 605 nm LED, the spectral match is poorer and strict linearity through zero (criteria as above) extends to 0.4 AU. An even poorer spectral match and a limit of strict linearity of 0.15 AU was observed for the 495-nm LED and acid alizarin violet. The limited monochromaticity/stray light issues are particularly important for capillary scale detectors and have been discussed in more detail in the literature [1].

### 3.3. Immunity to air bubbles

One of the important features of the present cell design is its relative immunity to air/gas bubbles

when the exit is pointed vertically upward. The rectangular cell cross section tapers to a circular bore at the entrance to reduce dispersion and flow noise. The response to purposely injected air bubbles at different durations is shown in Fig. 5. It is obvious that air bubbles pass through the cell completely and efficiently.

### 3.4. Refractive index effects

The reflective light path in the present flow cell is orthogonal to the flow direction. This causes the light beam entering the flow cell to essentially retrace its path upon reflection, thus greatly reducing the refractive index artifact. In Fig. 6 we show a situation where 50% methanol is injected into water for (a) a 5-mm path length Z-path cell [2] and (b) the present cell under otherwise identical conditions. A similar trace is shown when alkaline bromthymol blue (BTB) in borate buffer

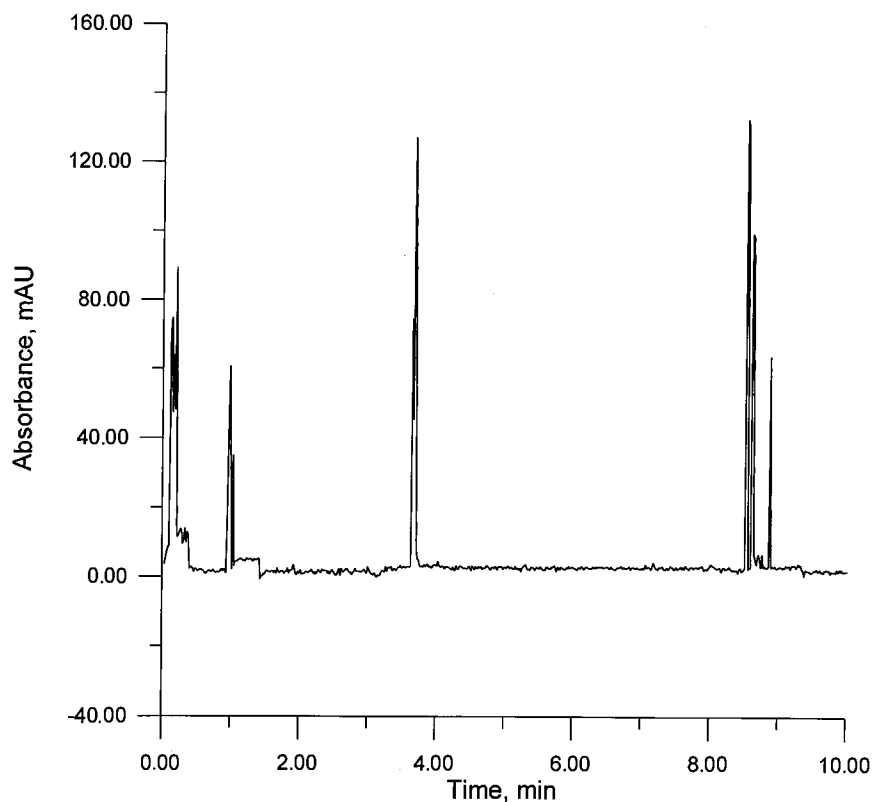


Fig. 5. Air bubbles were repeatedly injected deliberately in to the flow stream. In all cases, the bubbles pass through rapidly.

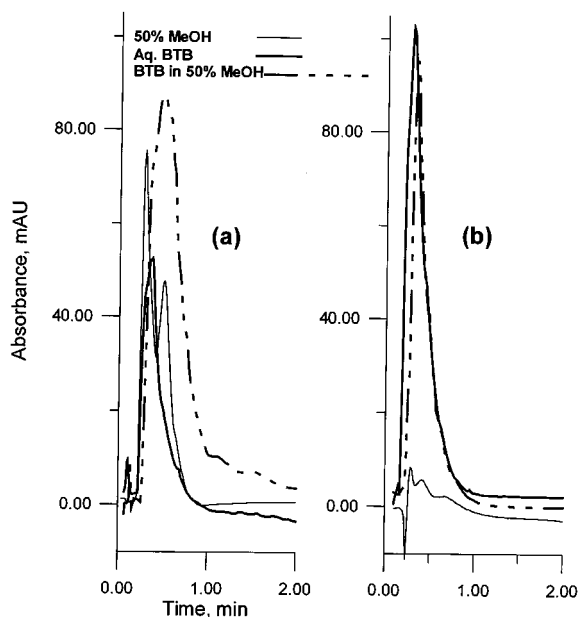


Fig. 6. In comparison with a Z-path cell (a), the present cell (b) shows remarkable immunity to refractive index effects; carrier is 10 mM borate in all cases. Samples: thin solid line, 50% methanol; thick solid line, aqueous bromthymol blue (BTB); thick dashed line, same concentration of alkaline BTB in 50% methanol.

and in 50% methanol is injected to a purely aqueous 10 mM borate buffer in the same two cells. The artifact absorbance response to methanol is very high in the conventional cell. Therefore, it is not surprising that in the conventional cell, when BTB is dissolved in methanol, the apparent response is very much higher than when it is dissolved in water. It should also be noted that the responses are not simply additive. Indeed, the practice of FIA with optical absorbance detection is likely more plagued with errors from refractive index mismatch between the sample and the calibrant than is commonly realized. This problem should be worse for capillary scale detectors. The extent of this problem is obviously very much less with the present detection cell.

In summary, we have presented here a sensitive and versatile low cost optical absorbance detector for FIA studies, with significant immunity to refractive index and air bubble induced

problems. The performance of the detector has been demonstrated to be comparable to the current state-of-the-art in commercial detectors. The detector design allows for the use of a variety of LEDs which can be rapidly exchanged.

## Acknowledgements

This work was supported in part by a grant from the Texas Tech University Leather Research Institute.

## References

- [1] C.B. Boring, P.K. Dasgupta, *Anal. Chim. Acta* 342 (1997) 123.
- [2] P.K. Dasgupta, H.S. Bellamy, H. Liu, J.L. Lopez, E.L. Loree, K. Morris, K. Petersen, K.A. Mir, *Talanta* 40 (1993) 53.
- [3] D. Betteridge, E.L. Dagless, B. Fields, N.F. Graves, *Analyst* 103 (1978) 897.
- [4] M. Trojanowicz, P.J. Worsfold, J.R. Clinch, *Trends Anal. Chem.* 7 (1988) 301.
- [5] M.N. Talib, R. Narayanaswamy, *Analyst* 120 (1995) 1617.
- [6] P.C. Hauser, T.W.T. Rupasinghe, C.C. Lucas, A. McClure, *Analyst* 120 (1995) 2635.
- [7] H. Liu, P.K. Dasgupta, H.J. Zheng, *Talanta* 40 (1993) 1331.
- [8] A.E. Bruno, F. Maystre, B. Krattiger, P. Nussbaum, E. Gassmann, *Trends Anal. Chem.* 13 (1994) 190.
- [9] W. Tong, E.S. Yeung, *J. Chromatogr. A* 718 (1995) 177.
- [10] M. Macka, P. Andersson, P.R. Haddad, *Electrophoresis* 17 (1996) 1898.
- [11] P.A.G. Butler, B. Mills, P.C. Hauser, *Analyst* 122 (1997) 949.
- [12] P.K. Dasgupta, Z. Genfa, J. Li, C.B. Boring, S. Jambunathan, R. Al-Horr, *Anal. Chem.* 71 (1999) 1400.
- [13] See for example, LINEAR UVIS 200 and similar instruments, Thermo Separation Products, Thermo Instrument Systems, Waltham, MA.
- [14] J. Ruzicka, E.H. Hansen, *Anal. Chim. Acta* 173 (1985) 3.
- [15] J. Ruzicka, E.H. Hansen, Method for non-segmented continuous flow analysis based on the interaction of radiation with a solid material situated in a flow-through cell. US Patent 4973,561, 27 November 1990.
- [16] P.S. Hodder, J. Ruzicka, *Anal. Chem.* 71 (1999) 1160.
- [17] J.L.P. Pavon, E.R. Gonzalo, G.D. Christian, J. Ruzicka, *Anal. Chem.* 64 (1992) 923.
- [18] P.K. Dasgupta, H.S. Bellamy, H. Liu, *Talanta* 40 (1993) 341.

- [19] J.E. Stewart, *Appl. Optics* 20 (1981) 654.
- [20] E.A.G. Zagatto, M.A.Z. Arruda, A.O. Jacintho, I.L. Mattos, *Anal. Chim. Acta* 234 (1990) 153.
- [21] H. Liu, P.K. Dasgupta, *Anal. Chim. Acta* 289 (1990) 347.
- [22] V.O. Brito, I.M. Raimundo Jr., *Anal. Chim. Acta* 371 (1998) 317.

# Optical sensor for sulfur dioxide based on fluorescence quenching

Taha M.A. Razek <sup>a,1</sup>, Michael J. Miller <sup>b</sup>, Saad S.M. Hassan <sup>c</sup>,  
Mark A. Arnold <sup>a,\*</sup>

<sup>a</sup> Department of Chemistry, University of Iowa, Iowa City, IA 52242, USA

<sup>b</sup> Department of Physics and Astronomy, University of Iowa, Iowa City, IA 52242, USA

<sup>c</sup> Department of Chemistry, Faculty of Science, Ain-Shames University, Cairo, Egypt

Received 22 February 1999; accepted 20 April 1999

## Abstract

A series of potential indicator dyes is evaluated for use in the development of optical sensors for measuring sulfur dioxide in gaseous samples. Rhodamine B isothiocyanate is selected on the basis of relative sensitivity to dynamic quenching by sulfur dioxide and oxygen. A solid-state fluorometer is described for monitoring the sulfur dioxide induced fluorescence quenching of sensing membranes composed of silicone and rhodamine B isothiocyanate. A modulated blue LED is coupled with the lock-in detection of a photodiode detector to provide high signal-to-noise ratios. The limit of detection is  $0.114 \pm 0.009\%$  for sulfur dioxide in a carrier stream of nitrogen gas. Selectivity measurements indicate no interference from several common gases (HCl, NH<sub>3</sub>, NO, and CO<sub>2</sub>). Oxygen alters the sensor response when comparing signals for sulfur dioxide in 0, 20 and 100% oxygen environments. © 1999 Elsevier Science B.V. All rights reserved.

*Keywords:* Optical sensor; Sulfur dioxide; Fluorescence quenching

## 1. Introduction

Sulfur dioxide is a primary air pollutant. Major sources of environmental sulfur dioxide include power plants that burn high-sulfur coal, the paper and pulp industries, petroleum refineries, roasting of non-metallic ores, and the incineration of solid

waste, particularly hazardous and medical waste [1,2]. The toxicity of sulfur dioxide is well recognized. Concentrations of 5–10 ppm in air are recommended threshold limits for human exposure [3] and 2 ppm is the recommended limit for working environments [4]. In addition, sulfur dioxide contributes significantly to acid rain, thereby adversely affecting the biotic nature of both soil and water resources and eroding historic man-made structures [1].

Many analytical methods are reported for measuring sulfur dioxide either continuously or dis-

\* Corresponding author. Fax: +1-319-3531115.

<sup>1</sup> On leave from the Department of Biological and Natural Sciences, Institute of Environmental Studies and Research, Ain-Shams University, Cairo, Egypt.



creetly [5–13]. Chemical sensors are under development for sulfur dioxide with the goal of generating devices capable of real-time, remote monitoring. Examples of chemical sensors include: high-temperature solid electrolyte sensors that are capable of process gas control [14–16]; sensors based on changes in the dielectric properties of silicone membranes [17], and gas-sensing potentiometric electrodes with anion-selective internal sensing elements [18].

Optical sensors are reported for various gaseous species, including oxygen [19–22], carbon dioxide [23], ammonia [24], hydrogen sulfide [1] and sulfur dioxide [25–30]. Many of these sensors operate on the basis of fluorescence quenching where the target analyte decreases the luminescence of an immobilized indicator dye. Dynamic quenching is measured and related to analyte concentration through the well-known Stern-Volmer relationship [31]. Molecular oxygen quenches many of these dyes and, as such, represents a serious interference that must be removed before the analytical measurement [32–34]. The need to deoxygenate a sample prior to the measurement drastically reduces the utility of a method for real-time, remote analytical sensing.

We are interested in developing an optical chemical sensor for measuring sulfur dioxide emission in smokestacks during incineration of biomedical waste. The first step is to identify dyes that are strongly quenched by sulfur dioxide, yet unaffected by molecular oxygen. An evaluation of several candidate dyes identifies rhodamine B isothiocyanate as a prime candidate. Findings from our initial screening experiment are detailed in this report. In addition, the analytical response characteristics are established for the corresponding sulfur dioxide optical sensor. This sensor consists of a dedicated solid-state fluorometer coupled with the rhodamine B isothiocyanate indicator.

## 2. Experimental

### 2.1. Apparatus

Fluorescence spectra were collected by using a SLM Aminco SPF 500C spectrometer equipped

with a 250 watt xenon arc lamp. An OLIS (Bogart, GA) modified Cary 14 double beam spectrometer was used to collect all absorbance spectra. Fluorescence signals from sensing membranes were measured with either the SLM Aminco spectrometer or the custom built fluorometer described below.

### 2.2. Chemicals, reagents and hardware

The following fluorescent dyes were purchased from the indicated supplier: (1) rhodamine B isothiocyanate (Sigma Chemical, St. Louis, MO); (2) pyrene isothiocyanate (Molecular Probes, Eugene, OR); (3) perylene (Fluka, Ronkonkoma, NY); (4) 2-ethoxynaphthalene (Pfaltz and Bauer, Waterbury, CT); and (5) 1-aminoanthroquinone (Pfaltz and Bauer, Waterbury, CT). All solvents were obtained from common suppliers. Oxygen (99.8%), nitrogen (99.9%), sulfur dioxide (99.9%), hydrogen chloride (99%), ammonia (99.99%), nitric oxide (99%) and carbon dioxide (99.98%) were purchased from Air Products and Chemicals (Allentown, PA). All commercially obtained chemicals were used as received without further purification. Type I, reagent grade water was obtained by passing house distilled water through a Milli-Q three-house purification unit.

Hardware components for the solid-state fluorometer were purchased from common suppliers. Interference and dichroic filters were purchased from Edmond Scientific (Barrington, NJ), blue LED's were obtained from Nichia (Japan) and the VTP-1250 photodiode detector was purchased from GE&E (St. Louis, MO). In general, individual circuit elements were obtained from Newark Electronics (Chicago, IL), although the OPA 121K operational amplifiers were from Insight Electronics (Milwaukee, WI). The model 506 Protek digital multi-meter was from Cole Palmer (Vernon Hill, IL) and the Omnibook 5500CS computer was from Hewlett Packard (Wilmington, DE).

### 2.3. Procedures

#### 2.3.1. Sensing membranes

1-Aminoanthraquinone, 2-ethoxynaphthalene, and perylene were immobilized in silicone mem-

branes by the procedure of Sharma and Wolfbeis [29]. Membranes with rhodamine B isothiocyanate and pyrene isothiocyanate were prepared from a casting solution prepared by first dispensing the dye in the silicone prepolymer, followed by adding toluene and mixing until the solution appeared homogeneous. In all cases, membranes were formed by dispensing a volume of casting solution onto the cleaned surface of a glass microscope slide. Solvent was allowed to evaporate under ambient conditions to produce sensing membrane layers with thicknesses on the order of 200 microns.

### 2.3.2. Membrane characterization

Glass slides with membranes were positioned along the diagonal inside a disposable polystyrene fluorescence cuvette. A two-hole rubber stopper was securely fitted into the top of the cuvette. Small glass tubes were placed in each hole to provide an inlet and outlet for flowing gases. For measurements taken with the SLM spectrofluorometer, the cuvette was mounted within the conventional cell holder which permitted surface fluorescence measurements from the sensing layer. For measurements taken with the custom fluorometer, the cuvette was mounted in a similar fashion as indicated schematically in Fig. 1.

Sensing membranes were characterized by monitoring the surface fluorescence as a function of time while exposing the immobilized fluorophore to different concentrations of selected gases. The required gas concentrations were obtained by mixing appropriate levels of the test gas with a nitrogen carrier gas. A Manostat 36-541-055 flow meter (New York, NY) was used to supply the correct amount of test gas to the nitrogen supply.

## 3. Results and discussion

Our development of a selective gas sensor for sulfur dioxide was carried out in two steps. First, a series of potential indicator dyes was screened with the goal of finding a dye that responds selectively for sulfur dioxide over oxygen. Results

from this screening experiment indicate that rhodamine B isothiocyanate is suitable for sulfur dioxide measurements. Secondly, the analytical response characteristics of membranes with rhodamine B isothiocyanate were established with the solid-state fluorometer described above.

### 3.1. Indicator screening

Seven unique indicator layers were evaluated as potential sensing chemistries for the selective measurement of sulfur dioxide over oxygen in gaseous samples. Five of these layers were composed of a single indicator, while two layers were composed of binary mixtures of indicators. Table 1 provides a listing of the tested indicator dyes along with the excitation and emission wavelengths used to monitor their luminescence. The excitation wavelengths correspond to absorbance wavelength maxima, which were taken directly from absorbance spectra. The emission wavelengths were taken from emission spectra collected with the SLM Aminco spectrofluorometer.

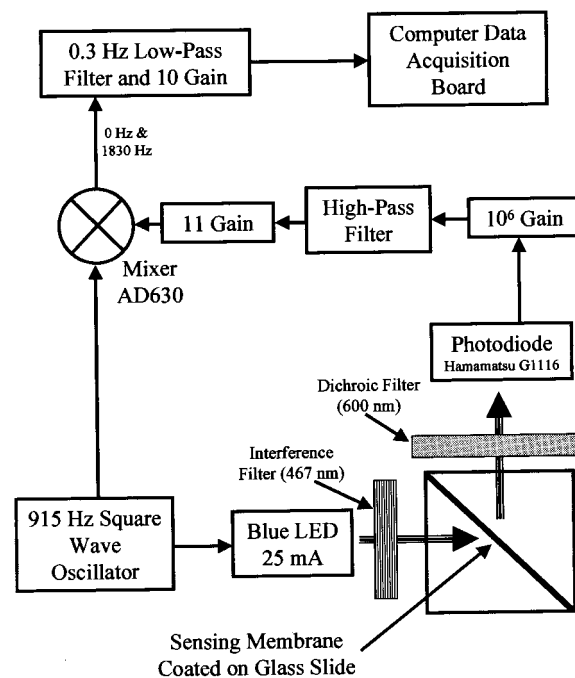


Fig. 1. Schematic representation of the solid-state fluorometer system, showing the sample holder configuration and a block diagram of the optic and electronic operation.

Table 1  
Indicator layers and wavelengths for luminescence measurements

Indicator	Excitation wavelength (nm)	Emission wavelength (nm)
Pyrene isothiocyanate	435	510
Rhodamine B isothiocyanate	466	607
Perylene	433	497
1-Aminoanthraquinone	479	594
2-Ethoxynaphthalene	300	356
Perylene and 1-aminoanthraquinone	419	464
Perylene and 2-ethoxynaphthalene	407	465

The selected indicator dyes were initially screened by comparing the degree of fluorescence quenching measured for sulfur dioxide and oxygen. These screening measurements were performed in the SLM Aminco spectrofluorometer and the surface fluorescence intensity was recorded continuously as a function of time. Initially, a baseline fluorescence reading was recorded by exposing the test membrane to a carrier stream of pure nitrogen. The membrane was then exposed sequentially to higher percentages of sulfur dioxide in the nitrogen carrier stream and the steady-state fluorescence signals were recorded at each step. The gas stream was switched back to pure nitrogen and a second baseline signal was recorded. Similarly, the test membrane was exposed sequentially to higher levels of oxygen in the nitrogen carrier stream. For sulfur dioxide, membranes were exposed to five concentration levels between the range of 0.3–6%. Concentration levels of oxygen were greater and ranged between 20 and 100%.

The resulting intensity values were plotted in a typical Stern-Volmer manner ( $(I_0/I - 1)$  versus percentage of the test gas). Linear regression analysis was used to compute the slopes (or Stern-Volmer constants) for these individual plots. Magnitude of the resulting Stern-Volmer con-

stants for sulfur dioxide and oxygen were taken as a measure of the relative sensitivity of the immobilized dye to sulfur dioxide and oxygen, respectively. The measured Stern-Volmer constants are tabulated in Table 2 for each of the tested indicator layers.

Sulfur dioxide quenched the fluorescence of each indicator layer. The highest degree of sulfur dioxide quenching was recorded for the combined mixture of perylene and 1-aminoanthraquinone. Unfortunately, the luminescence from this indicator layer was also quenched by oxygen, albeit to a much lesser extent. In fact, all the indicator layers that contained perylene responded to oxygen by essentially the same amount. Only layers composed of pyrene isothiocyanate, rhodamine B isothiocyanate, and 1-aminoanthraquinone demonstrate no response to oxygen under our experimental conditions. Of these, rhodamine B isothiocyanate possesses the highest sensitivity to sulfur dioxide. In addition, response and recovery times were rapid for the rhodamine B isothiocyanate layer and the preliminary Stern-Volmer plots were linear ( $r^2 = 0.995$ ). The limit of detection was estimated as  $0.52 \pm 0.02\%$  ( $S/N = 3$ ) from these plots. For this reason, all subsequent experiments were performed with rhodamine B isothiocyanate.

Table 2  
Stern-Volmer constants for the screened indicator dyes

Indicator	Stern-Volmer constant for sulfur dioxide ( $\%^{-1}$ )	Stern-Volmer constant for oxygen ( $\%^{-1}$ )
Pyrene isothiocyanate	0.100	0.000
Rhodamine B isothiocyanate	0.186	0.000
Perylene	0.250	0.007
1-Aminoanthraquinone	0.130	0.000
2-Ethoxynaphthalene	0.063	0.006
Perylene and 1-aminoanthraquinone	0.330	0.005
Perylene and 2-ethoxynaphthalene	0.250	0.005

### 3.2. Solid-state fluorometer

A solid-state fluorometer was built to facilitate data collection from the sensing membranes. This fluorometer is modeled after that reported by Hauser [35,36] and contains a modulated light emitting diode (LED) source and a solid-state photodiode detector. The schematic diagram in Fig. 1 illustrates the basic optical arrangement and general measurement configuration. In this design, the excitation radiation illuminates a portion of the sensing membrane by striking at a 45° angle relative to the membrane surface. The emitted luminescence is then detected 90° relative to the excitation beam. A 467 nm interference filter isolates the excitation radiation and a 600 nm dichroic filter isolates the emitted radiation before detection. This dichroic filter is attached directly to the detector housing to minimize stray source radiation from being detected. The source is a high intensity (1000 mcd) blue LED and the detector element is a Hamamatsu (G-1116) photodiode.

The basic circuitry to drive both the excitation and detection optics is taken from the work described by Hauser [35,36]. In our system, the LED source is modulated at a frequency of 915 Hz by using an LMC555 timer to generate a square-wave signal at 915 Hz. Output of the LMC555 drives a NPN transistor (2N3904) to switch the LED on and off. In addition, the LMC555 output is used as a reference signal for the multiplier circuit (AD630). Fluorescence from the sulfur dioxide sensitive membrane is detected by a photodiode and amplified by a transimpedance amplifier with a gain of 100 million. The signal is high pass filtered to remove any d.c. bias and amplified by an additional factor of eleven. The amplified signal is input into the AD630 where mixing occurs. The output of the AD630 provides signals at twice the input signal (1830 Hz) and d.c. A 0.3 Hz low-pass filter with a gain of ten provides the final output signal.

During normal operation, the fluorescence signal is continuously recorded as a function of time while gaseous samples are passed across the test membrane. The voltage is recorded by a Protek digital multi-meter interfaced with an Omnibook

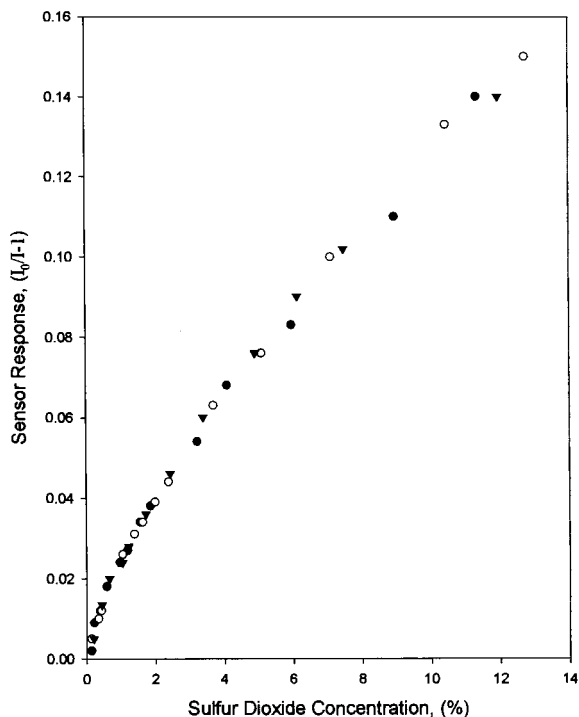


Fig. 2. Cumulative response curves for three sequential sensor responses to sulfur dioxide showing data for trial 1 (solid circles); trial 2 (open circles) and trial 3 (triangles).

portable computer. A typical signal-to-noise ratio (SNR) for the instrument was 6000 under baseline conditions. This SNR value corresponds to typical signal of  $3.704 \pm 0.0006$  volts (mean  $\pm 1$  standard deviation) with pure nitrogen as the carrier gas.

### 3.3. Solid-state sulfur dioxide sensor

Sulfur dioxide sensors were constructed by placing membranes with rhodamine B isothiocyanate in the custom-built fluorometer described above. Typical sensor response curves for sulfur dioxide are illustrated in Fig. 2. This figure shows computed responses for three sequential calibrations over a sulfur dioxide concentration range from 0.01 to 12.8%. Computed values correspond to the typical Stern-Volmer transformation (response =  $I_0/I - 1$ ) where  $I_0$  and  $I$  correspond to the measured steady-state intensities in the absence and presence of the quenching agent, re-

spectively. As the data in Fig. 2 demonstrate, this transformation of the data results in a non-linear curve with greater sensitivity at lower sulfur dioxide concentrations. Such non-linearity is common for optical sensors based on fluorescence quenching when the indicator is entrapped within a polymeric membrane [37–39]. Heterogeneity within the membrane matrix is thought to be responsible for such responses. Nevertheless, responses to sulfur dioxide are both sensitive and reproducible with rhodamine B isothiocyanate entrapped within silicone.

A portion of the data in Fig. 2 was used to estimate the limit of detection for this sensing configuration. Responses at low concentrations of sulfur dioxide are essentially linear. As such, the limit of detection was estimated from the pseudo-linear region from 0 to 0.67% sulfur dioxide. Responses from the three data sets were combined for this purpose. Linear regression analysis over this region for the combined data points indicates an  $r^2$  value of 0.9545 along with a slope of  $3.079 (\pm 0.002) \times 10^{-2} \%^{-1}$  and a  $y$ -intercept of  $-6.2 (\pm 9.6) \times 10^{-4}$ . The corresponding limit of detection (SNR = 3) is  $0.114 (\pm 0.009) \%$ .

Time-dependent response properties are presented in Fig. 3. This figure shows a series of raw data presented in a signal versus time format. In this experiment, the sensor is initially exposed to blank carrier gas. A brief initialization period is required to obtain a steady-state baseline signal. After an initial steady-state signal is achieved, sulfur dioxide is added to the nitrogen carrier stream to a final concentration of 0.28% while the response is monitored. After a steady-state signal is achieved, the level of sulfur dioxide is increased to 0.43%, and so on as indicated by the concentration values presented above the arrows in Fig. 3. The sensor response is continually recorded as sequentially higher sulfur dioxide levels are introduced. After the response to 10.94% sulfur dioxide, the sensing membrane is exposed to pure nitrogen carrier gas and the baseline intensity ( $I_0$ ) is measured. Finally, responses are presented while cycling the carrier gas from high to low sulfur dioxide levels.

The data in Fig. 3 demonstrate rapid response and recovery times for the rhodamine B isothio-

cyanate membranes. For both increases and decreases in the sulfur dioxide levels, steady-state responses were generally available within 30–60 s. In addition, the reproducibility of the baseline signal is illustrated by the data in this figure.

Selectivity of the rhodamine B isothiocyanate membrane was characterized in two ways. First, the membrane was exposed to varying levels of potentially interfering gases while monitoring sensor luminescence. Gases tested in this manner include hydrogen chloride, ammonia, nitric oxide and carbon dioxide. No changes in the luminescence signal of the rhodamine B isothiocyanate layer were noted for any of these gases. Hydrogen chloride, ammonia and nitric oxide were tested individually at levels up to 1%. Carbon dioxide was tested up to 12.4%. Again, none of these gases interferes with the signal.

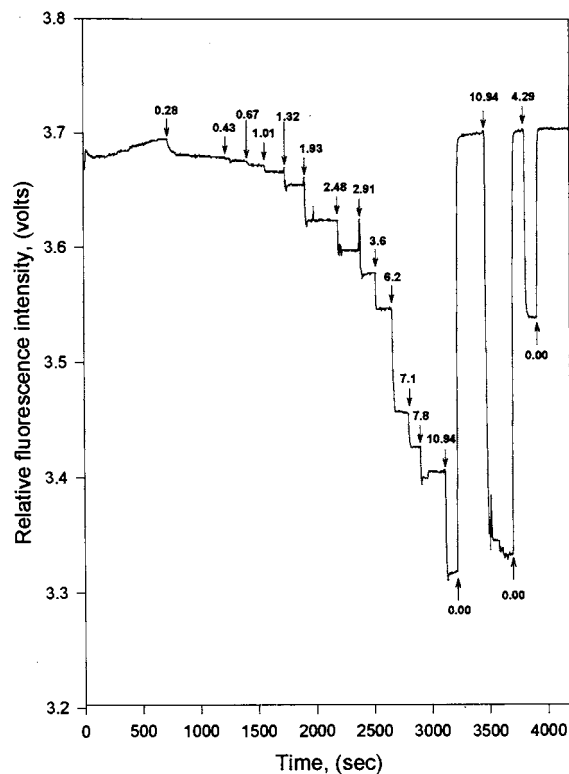


Fig. 3. Time profile showing dynamic response to different levels of sulfur dioxide. Arrows indicate point when the sulfur dioxide level was changed and the value associated with the arrow indicates the resulting level of sulfur dioxide in the nitrogen carrier gas.

Sensor selectivity was also tested by monitoring the sensor response to various levels of sulfur dioxide in the presence of oxygen. Responses to sulfur dioxide were recorded with air (20% oxygen) and 100% oxygen as the carrier gas and these responses were compared to those obtained with a pure nitrogen carrier gas. Although oxygen did not significantly quench the fluorescence in our initial screening experiment, subsequent results reveal a substantial effect by oxygen. Significantly lower responses are observed for a given sulfur dioxide level in the presence of oxygen. The extent of this interference can be judged by comparing Stern-Volmer constants computed for sulfur dioxide in the presence of 0, 20, and 100% oxygen in the carrier gas. Again, Stern-Volmer constants were computed over the pseudo-linear region from 0 to 1% sulfur dioxide, as discussed and identified above. The resulting values are  $0.031 \pm 0.002$ ;  $0.024 \pm 0.003$  and  $0.022 \pm 0.007\%^{-1}$  for 0, 20 and 100% oxygen in the carrier stream, respectively. These values indicate a significantly lower response in the presence of oxygen. No significant differences are indicated, however, between responses in 20 and 100% oxygen. These results suggest that the proposed sulfur dioxide sensors must be calibrated in the presence of the expected level of oxygen to avoid systematic errors. These findings also suggest that measurement accuracy is relatively insensitive to small differences in ambient oxygen levels (i.e. no difference between 20 and 100% oxygen). This second point may be critical, as oxygen-independent calibrations may be possible over a well-defined oxygen concentration range.

#### 4. Conclusions

Results from experiments described in this paper illustrate the feasibility of measuring sulfur dioxide levels in gaseous samples by fluorescence quenching. Membrane layers composed of rhodamine B isothiocyanate provide strong responses to sulfur dioxide even in the presence of high levels of molecular oxygen. The estimated limit of detection for sulfur dioxide is  $0.114 \pm 0.009\%$ . This level of performance is achieved by com-

bining rhodamine B isothiocyanate membranes with a dedicated solid-state fluorometer.

#### References

- [1] G.T. Miller Jr, Living in the Environment, Wadsworth Publishing Co, Belmont, CA, 1992.
- [2] B.L. Walker, C.D. Copper, J. Air Waste Manag. Assoc. 6 (1992) 784.
- [3] R.C. Weast (Ed.), Handbook of Chemistry and Physics, 55th edn., CRC Press, Cleveland, OH, 1975, p. D-90.
- [4] N.I. Sax, R. Lewis, Hazardous Chemical Desk Reference, Van Nostrand Publishers, New York, 1987.
- [5] J. Janak, Z. Vecera, Microchim. Acta 3 (1990) 29.
- [6] S.A. Al-Tamrarh, V. Townshend, A. Wheatley, Analyst 112 (1987) 883.
- [7] T.A. Arowolo, M.S. Cresser, Talanta 39 (1990) 1471.
- [8] J.P. Lodge, Methods of Air Sampling and Analysis, Lewis Publishers, New York, NY, 1989.
- [9] P.W. West, G.C. Gaeke, Anal. Chem. 28 (1956) 1816.
- [10] R.V. Nauman, P.W. West, F. Tron, G.C. Gaeke Jr, Anal. Chem. 32 (1960) 1307.
- [11] F.P. Scaringelli, B.E. Saltzman, S.A. Frey, Anal. Chem. 39 (1967) 1709.
- [12] G. Schiavon, G. Zotti, R. Toniolo, G. Bonempelli, Analyst 116 (1991) 797.
- [13] M.S. Black, R.P. Herbst, D.R. Hichcock, Anal. Chem. 50 (1978) 848.
- [14] J.M. Skaef, A.A. Dubreuil, Sensors and Actuators 10B (1993) 161.
- [15] Y. Yan, Y. Shimizu, N. Miura, N. Yamazoe, Chem. Lett. (1992) 635.
- [16] T. Maruyama, Mat. Sci. Eng. 146A (1991) 81.
- [17] H.-E. Enders, L.D. Mickle, C. Kosslinger, S. Dors, F. Hutter, Sensors and Actuators 6B (1992) 285.
- [18] M.E. Meyerhoff, D.M. Pranita, H.S. Kim, N.A. Chaniotakis, S.B. Park, ACS Symposium Series 403, Chemical Sensors and Microinstrumentation, 1989, pp. 26–43.
- [19] M.E. Cox, B. Dunn, SPIE 576 (1985) 60.
- [20] J.R. Bacon, J.N. Demas, Anal. Chem. 59 (1987) 278.
- [21] A. Sharma, O.S. Wolfbeis, Appl. Spectro. 42 (1988) 609.
- [22] C.A. Parker, W.T. Rees, Analyst 85 (1960) 587.
- [23] G. Orellana, M.C. Moreno-Bondi, E. Segova, D. Marazuela, Anal. Chem. 64 (1992) 2210.
- [24] A. Sharma, A. Zulfiquir, I. Higgins, SPIE 1637 (1992) 107.
- [25] M. Kuratli, E. Pretsch, Anal. Chem. 66 (1994) 85.
- [26] R.L. Cook, R.C. Macduff, A.F. Sammells, Anal. Chim. Acta 226 (1989) 153.
- [27] A. Sharma, O.S. Wolfbeis, Spectrochim. Acta B (1987) 1417.
- [28] A. Sharma, O.S. Wolfbeis, Anal. Chim. Acta 208 (1989) 53.
- [29] A. Sharma, O.S. Wolfbeis, SPIE 990 (1989) 8.
- [30] A. Sharma, A. Zulfiquir, D. McStay, SPIE 1637 (1992) 280.

- [31] J.D. Ingle Jr, S.R. Crouch, *Spectrochemical Analysis*, Chapter 12, Prentice Hall, Englewood Cliffs, NJ, 1988.
- [32] M.E. Rollie, C.N. Ho, I.M. Warner, *Anal. Chem.* 55 (1983) 2445.
- [33] M.E. Rollie, G. Patonay, I.M. Warner, *Anal. Chem.* 59 (1987) 180.
- [34] S. Matsuzawa, A. Wakisaka, M. Tamura, *Anal. Chem.* 62 (1990) 2654.
- [35] P.C. Hauser, S.S.S. Tau, *Analyst* 118 (1993) 991.
- [36] P.C. Hauser, C.L.C. Liang, B. Muller, *Meas. Sci. Technol.* 6 (1995) 1081.
- [37] E.R. Carraway, J.N. Demas, B.A. DeGraff, *Anal. Chem.* 63 (1991) 332.
- [38] J.N. Demas, B.A. DeGraff, *SPIE* 1981 (1992) 2.
- [39] J.N. Demas, B.A. DeGraff, W. Xu, *Anal. Chem.* 67 (1995) 1377.

# Poly(vinyl chloride)-based macrocyclic membrane sensors for magnesium

Seema Baniwal, S. Chandra, A. Panwar, A.K. Singh \*

*Department of Chemistry, University of Roorkee, Roorkee, 247 667 U.P., India*

Received 24 August 1998; received in revised form 19 April 1999; accepted 23 April 1999

## Abstract

Poly(vinyl chloride)-based membranes of macrocycles 4,11-dimethyl-2,4,9,11-tetraethyl-1,5,8,12-tetraaza cyclotetradeca-1,8-diene (I) and 4,11-dioxa-2,9-dimethyl-1,5,8,12-tetraaza cyclotetradeca-1,8-diene (II) with sodium tetrphenyl borate (STB) as an anion excluder and dibutyl phthalate (DBP), dioctyl phthalate (DOP), dibutylbutyl phosphonate (DBBP) and 1-chloronaphthalene (CN) as plasticizing solvent mediators were prepared and investigated as magnesium selective electrodes. The best performance was observed having the composition (II)-PVC-STB-DBP in the ratio 2:10:1:7, which works well over a wide concentration range ( $1.9 \times 10^{-6}$  to  $1.0 \times 10^{-1}$  M) with a Nernstian slope of 29 mV per decade of activity between pH 2.5 and 6.5. These electrodes have been found to be chemically inert showing a fast response time of 15 s and were used over a period of 3 months with good reproducibility ( $S = \pm 0.2$  mV). The selectivity coefficient values for mono-, di- and trivalent cations indicate excellent selectivity for  $Mg^{2+}$  over a large number of cations. The electrodes have also been used successfully in partially non-aqueous medium and as an indicator electrode in the potentiometric titration of  $Mg^{2+}$  with EDTA. Anions such as  $Cl^-$  and  $SO_4^{2-}$  do not interfere in the working of the electrode. The practical utility of the membrane sensor has also been observed in solutions contaminated with detergents (cetyltrimethyl ammonium bromide and sodium dodecyl sulphate). Above all, the membrane sensor has been very successfully used to analyse some babyfood products and soft drinks for the determination of  $Mg^{2+}$ . © 1999 Elsevier Science B.V. All rights reserved.

*Keywords:* Ion sensor; Macrocycle; Membrane sensor; Mg-selective electrodes

## 1. Introduction

The utility of ion-selective electrodes (ISEs) is being increasingly realised by analytical chemists in view of the rapid growth of industry and technology all over the world as they represent a

rapid, accurate and low-cost method of analysis. Moreover, analysis by these electrodes could be non-destructive and adaptable to small sample volumes. ISEs find application in various industrial and biological fields such as ion monitoring and in analysis of sea water, soils, food products, drinking water, industrial effluents, pharmaceutical compounds, etc. Although in the last few decades considerable efforts have been made for

\* Corresponding author. Fax: +91-1332-73560.

*E-mail address:* chemt@rurkiu.ernet.in (A.K. Singh)



the development of selective sensors for alkali and alkaline earth metals, very little work has been done on the development of ISEs for magnesium ions ( $Mg^{2+}$ ). Only a few electrodes are reported which show interference to other alkaline metal ions. Recently, an electrode prepared using a membrane of phenylene bis(ditolyl phosphine oxide) in poly(vinyl chloride (PVC) was reported as a  $Mg^{2+}$  sensor [1]. The electrode shows good selectivity towards  $Mg^{2+}$  over  $Ca^{2+}$  and works well in the concentration range  $6.0 \times 10^{-5}$  to  $1.0 \times 10^{-1}$  M. Rouilly et al. [2] described a dimethyl aspartamide neutral carrier (ETH 2220) with a measured selectivity of about 300, 200 and 400 for magnesium relative to calcium, potassium and sodium, respectively. There was strong interference by  $H^+$  ( $\log K_{Mg^{2+}, H^+}^{Pot} = 10.8$ ). Another magnesium selective carrier in a polymeric membrane electrode [3] was used to determine the concentration of free, ionized magnesium in undiluted blood serum. However, discrimination of calcium by the new ionophore membrane was not sufficient to keep calcium interference to less than 1%. O'Donnell et al. [4] have developed an electrode using various octamethylene bis(malonic acid diamides) and tris(malonic acid diamides) in PVC with 2-nitrophenyl octyl ether as solvent

mediator. The availability of ISEs with sufficient selectivity for  $Mg^{2+}$  has recently initiated a number of clinical investigations [5]. Recently, Siswanta et al. reported an optode-based sensor for  $Mg^{2+}$  [6].

With the availability of improved highly selective materials, the possibility of developing specific sensors has opened up. Efforts were initiated in this laboratory to develop selective electrodes for  $Mg^{2+}$  using macrocycles 4,11-dimethyl-2,4,9,11-tetraethyl-1,5,8,11-tetraaza cyclotetradeca-1,8-diene (I) and 4,11-dioxa-2,9-dimethyl-1,5,8,11-tetraaza cyclotetradeca-1,8-diene (II) as sensor material. These macrocycles occupied an intermediate position between crown ethers and cryptands. The former effect rapid and circular co-ordination of guest cations, while the latter form rigid and encapsulated complexes. These armed macrocycles, due to their characteristic structural features, not only bind metal cations with varying strength and serve as suitable electroactive materials for use in membrane electrodes but also exhibit kinetically fast complexation property of crown ethers and three-dimensional binding characteristic of cryptands [7]. The results presented in this paper show that the sensors developed using the above two materials as elec-

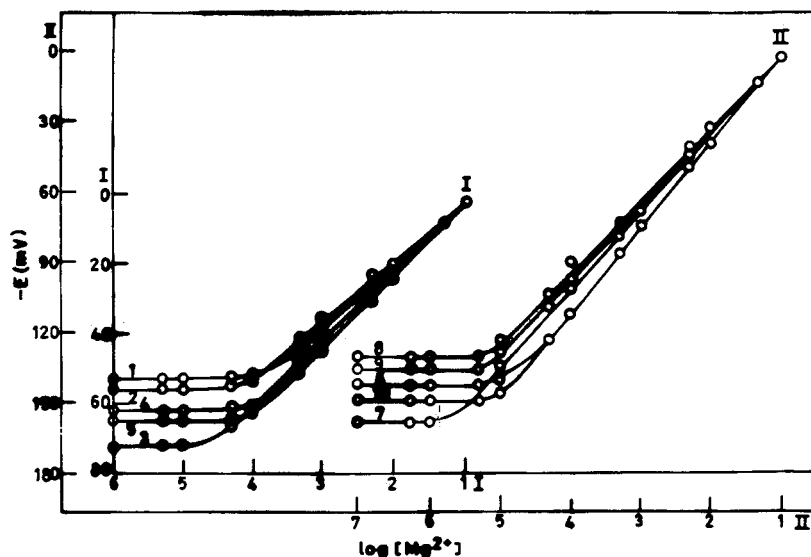


Fig. 1. Plots showing variation of membrane potentials of macrocycles I and II with concentration of  $Mg^{2+}$  (taken as magnesium nitrate).

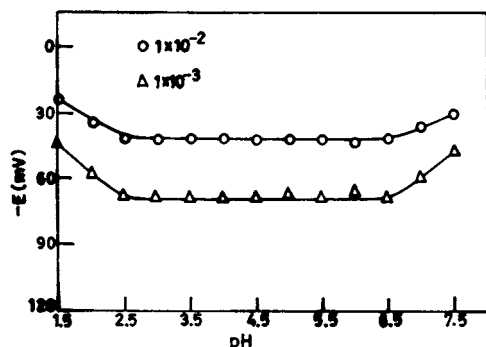


Fig. 2. Plots showing variation of membrane potentials with pH at  $1.0 \times 10^{-2}$  and  $1.0 \times 10^{-3}$  M  $Mg^{2+}$ .

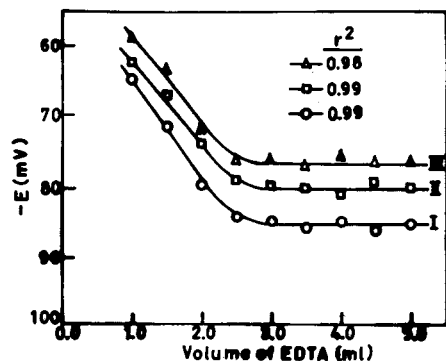


Fig. 3. Potentiometric titrations of 25 ml of  $1.0 \times 10^{-3}$  M  $Mg^{2+}$  solution (I),  $10^{-3}$  M  $Mg^{2+}$  +  $10^{-4}$  M  $Ca^{2+}$  (II) and  $10^{-3}$  M  $Mg^{2+}$  +  $10^{-4}$  M  $Ba^{2+}$  (III).

troactive phase in PVC matrix membranes are superior to those reported in the literature.

## 2. Experimental

### 2.1. Reagents

All reagents were of analytical reagent grade. Double-distilled water was used for the preparation of solutions of metal salts (nitrates) of different concentrations by diluting stock standard solutions (0.1 M). Sodium tetraphenyl borate (STB) from BDH (Poole, UK), dibutyl phthalate (DBP) and dioctyl phthalate (DOP) from Reidel (Hapur, India), dibutylbutyl phosphonate (DBBP) from Mobil (Richmond, VA, USA) and 1-

chloronaphthalene (CN) from Merck (Darmstadt, Germany) were used without further purification. High molecular mass PVC was obtained from Aldrich (Milwaukee, WI, USA).

### 2.2. Synthesis of macrocycles

#### 2.2.1. Macrocycle I

Macrocycle 4,11-dimethyl-2,4,9,11-tetraethyl-1,5,8,12-tetraaza cyclotetradeca-1,8-diene (I) was prepared by a reported method [8].  $C_{20}H_{40}N_4$ ; calculated, C 71.42, H 11.90, N 16.68; found, C 72.29, H 12.21, N 16.54.

The infrared (IR) spectrum of ligand I shows the  $\nu C=N$  band at  $1645\text{ cm}^{-1}$ . The spectra of ligand I also show the presence of a  $\nu-NH$  band at  $3350\text{ cm}^{-1}$ .

The paramagnetic resonance (PMR) spectra of ligand I show a singlet at 1.35 ppm which is due to the methyl component of the chiral ethyl groups. Occurrence of the singlet indicates that these groups are equivalent and are assigned a diequatorial configuration.

#### 2.2.2. Macrocycle II

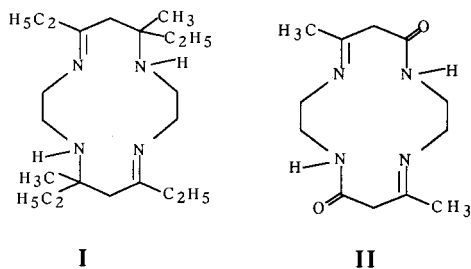
Macrocycle 4,11-dioxa-2,9-dimethyl-1,5,8,12-tetraaza cyclotetradeca-1,8-diene (II) was prepared by a reported method [9].  $C_{12}H_{20}N_4O_2$ ; calculated, C 57.1, H 7.9, N 22.4, O 12.6; found, C 57.4, H 8.2, N 21.6, O 12.1.

In the IR spectrum of ligand II the appearance of a strong absorption band in the region  $1635\text{--}1650\text{ cm}^{-1}$  corresponds to  $C=N$  stretching frequency. In addition, four amide bands have also been identified which appeared in the regions  $1695\text{--}1725$ ,  $1510\text{--}1530$ ,  $1250\text{--}1280$  and  $635\text{--}670\text{ cm}^{-1}$  and are assignable to amide I, amide II, amide III and amide IV vibrations, respectively. A single sharp band observed for the ligands in the region  $3310\text{--}3330\text{ cm}^{-1}$  corresponds to  $\nu N-H$  assigned for secondary amine. The absorption bands in  $2870\text{--}2960$  and  $1410\text{--}1465\text{ cm}^{-1}$  regions in all the ligands may reasonably correspond to CH stretching and CH bending vibration modes, respectively.

The  $^1H$  NMR spectra of ligand II show singlets at 1.55–1.60 and 2.05–2.28 ppm, corresponding to  $CH_3$  (6H) protons and  $CH_2$  (4H) protons of alkyl-

acetoacetate, respectively. The  $^1\text{H}$  NMR spectra of ligand II show a broad signal observed in the region 7.51–7.90 ppm, which may be assigned to amide protons (2H), and a singlet to  $\text{CH}_2$  (8H) protons of diaminoethane moiety.

The above data for both ligands are in good agreement and fit well to the following structures:



### 2.3. Preparation of membranes

Homogeneous membranes of the ligand using different binders and STB as an anion excluder were carried out as reported earlier [10]. Diluent

tetrahydrofuran (15 ml) was added to various amounts (20–100 mg) of macrocycles I and II. To these solutions an appropriate amount of PVC was added and in some cases anion excluder (STB) was also added. The stability of carrier complexes in membranes results from the electrostatic interaction between complexes and the surrounding membrane solvent [11]. Accordingly, for selecting the solvent mediator for magnesium-selective electrodes, we examined the solvents DBP, DOP, DBBP and CN. The effect of each solvent on the characteristics of  $\text{Mg}^{2+}$  ISEs based on the application of sensors I and II are given in Tables 1 and 2, respectively. After complete dissolution of the components and thorough mixing, the mixture was poured into glass casting rings resting on a smooth plate. The solution was then allowed to evaporate at ambient temperature. After 48 h, the transparent membranes of 0.4 mm thickness were obtained and a 6 mm diameter piece was cut away from the inner edge of the ring and glued to one end of a Pyrex glass tube with Araldite.

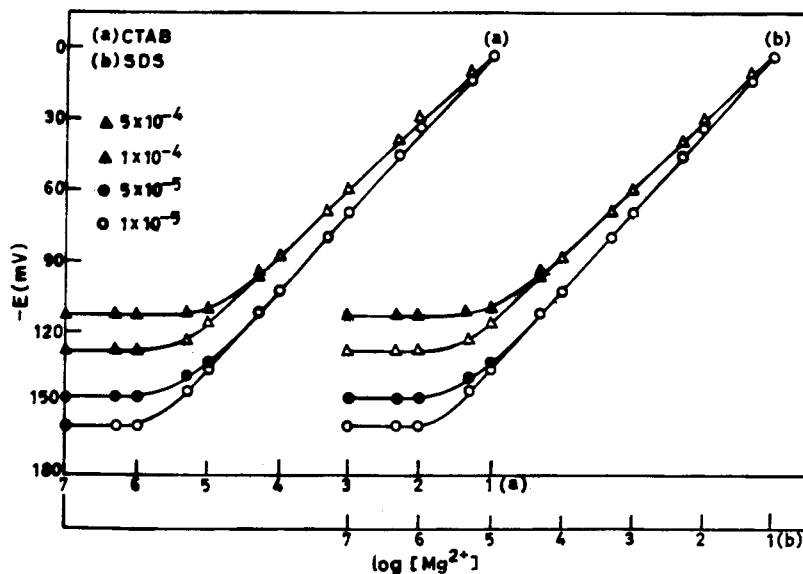


Fig. 4. Plots showing potential versus  $\log [\text{Mg}^{2+}]$  in the presence of (a) cetyltrimethyl ammonium bromide (CTAB) and (b) sodium dodecyl sulphate (SDS).

Table 1  
Composition of PVC-based membranes of macrocycle I and their performance characteristics as  $Mg^{2+}$  selective electrodes

Membrane number	Composition of membrane (%m/m)							Working concentration range (M)	Slope (mV/decade of activity)	Response time (s)
	Macrocycle I	PVC	STB	DBP	DOP	DBBP	CN			
1	10	80	10	–	–	–	–	$1.6 \times 10^{-4}$ – $1.0 \times 10^{-1}$	21	80
2	10	50	5	–	35	–	–	$1.0 \times 10^{-4}$ – $1.0 \times 10^{-1}$	17	20
3	10	50	5	35	–	–	–	$2.5 \times 10^{-5}$ – $1.0 \times 10^{-1}$	22	20
4	10	45	5	–	–	40	–	$1.0 \times 10^{-4}$ – $1.0 \times 10^{-1}$	21	30
5	10	45	5	–	–	–	40	$1.1 \times 10^{-4}$ – $1.0 \times 10^{-1}$	18	30

Table 2  
Composition of PVC-based membranes of macrocycle II and their performance characteristics as  $Mg^{2+}$  selective electrodes

Membrane number	Composition of membrane (%m/m)							Working concentration range (M)	Slope (mV/decade of activity)	Response time (s)
	Macrocycle II	PVC	STB	DBP	DOP	DBBP	CN			
6	10	80	10	–	–	–	–	$1.0 \times 10^{-5}$ – $1.0 \times 10^{-1}$	36	90
7	10	50	5	35	–	–	–	$1.9 \times 10^{-6}$ – $1.0 \times 10^{-1}$	29	15
8	10	50	5	–	35	–	–	$7.1 \times 10^{-6}$ – $1.0 \times 10^{-1}$	30	25
9	10	45	5	–	–	40	–	$5.6 \times 10^{-6}$ – $1.0 \times 10^{-1}$	30	30
10	10	45	5	–	–	–	40	$8.9 \times 10^{-6}$ – $1.0 \times 10^{-1}$	36	30

Table 3  
Selectivity coefficient values ( $K_{Mg^{2+},B}^{Pot}$ ) of electrodes 3 and 7 based on the membranes of macrocycles I and II, respectively

Interfering ion (B, 0.01 M)	Selectivity coefficient ( $K_{Mg^{2+},B}^{Pot}$ )	
	I	II
$NH_4^+$	$2.6 \times 10^{-1} \pm 0.12$	$2.1 \times 10^{-1} \pm 0.09$
$Li^+$	$2.2 \times 10^{-1} \pm 0.10$	$1.9 \times 10^{-1} \pm 0.11$
$Na^+$	$1.8 \times 10^{-1} \pm 0.08$	$1.0 \times 10^{-1} \pm 0.14$
$K^+$	$1.8 \times 10^{-1} \pm 0.12$	$1.0 \times 10^{-1} \pm 0.09$
$Rb^+$	$1.30 \times 10^{-2} \pm 0.07$	$1.21 \times 10^{-2} \pm 0.10$
$Cs^+$	$8.12 \times 10^{-3} \pm 0.18$	$7.94 \times 10^{-3} \pm 0.15$
$Co^{2+}$	$1.82 \times 10^{-2} \pm 0.12$	$1.77 \times 10^{-2} \pm 0.13$
$Hg^{2+}$	$1.82 \times 10^{-2} \pm 0.16$	$1.77 \times 10^{-2} \pm 0.17$
$Ca^{2+}$	$1.43 \times 10^{-2} \pm 0.15$	$1.34 \times 10^{-2} \pm 0.08$
$Zn^{2+}$	$1.43 \times 10^{-2} \pm 0.18$	$1.34 \times 10^{-2} \pm 0.12$
$Pb^{2+}$	$1.22 \times 10^{-2} \pm 0.09$	$1.12 \times 10^{-2} \pm 0.10$
$Cd^{2+}$	$9.92 \times 10^{-3} \pm 0.17$	$9.62 \times 10^{-3} \pm 0.04$
$Cu^{2+}$	$8.61 \times 10^{-3} \pm 0.10$	$8.91 \times 10^{-3} \pm 0.13$
$Ni^{2+}$	$8.61 \times 10^{-3} \pm 0.12$	$8.91 \times 10^{-3} \pm 0.06$
$Ba^{2+}$	$8.12 \times 10^{-3} \pm 0.16$	$7.94 \times 10^{-3} \pm 0.17$
$Sr^{2+}$	$3.68 \times 10^{-3} \pm 0.13$	$3.98 \times 10^{-3} \pm 0.11$
$Cr^{3+}$	$1.52 \times 10^{-3} \pm 0.04$	$1.47 \times 10^{-3} \pm 0.15$
$Fe^{3+}$	$1.41 \times 10^{-3} \pm 0.03$	$1.36 \times 10^{-3} \pm 0.09$
$Al^{3+}$	$1.19 \times 10^{-3} \pm 0.11$	$1.17 \times 10^{-3} \pm 0.06$

#### 2.4. Potential measurements

The membranes were equilibrated with 1.0 M magnesium nitrate solution for 4 days and the potentials across the membranes were measured with an ECIL Model pH 5662 digital pH/potentiometer and a Century CBM 301 microvoltmeter, in conjunction with saturated calomel electrodes (SCE) as reference electrodes. All measurements were made at constant temperature ( $25 \pm 0.1^\circ\text{C}$ ).

Response times were determined as follows: After the potential of one magnesium solution became constant, similar measurements were carried out in another solution of 100-fold concentration. The response time was defined by the time taken to reach a potential of 90% of the potential difference in the two measurements. Reproducibility was defined by the deviation

from the average potential value in the same three 'dip to read' measurements.

#### 2.5. Preparation of food samples and estimation of $Mg^{2+}$ in various soft drinks and some babyfood products

The dry ashing method [12] was used for preparing the samples for magnesium estimation.

##### 2.5.1. Soft drinks

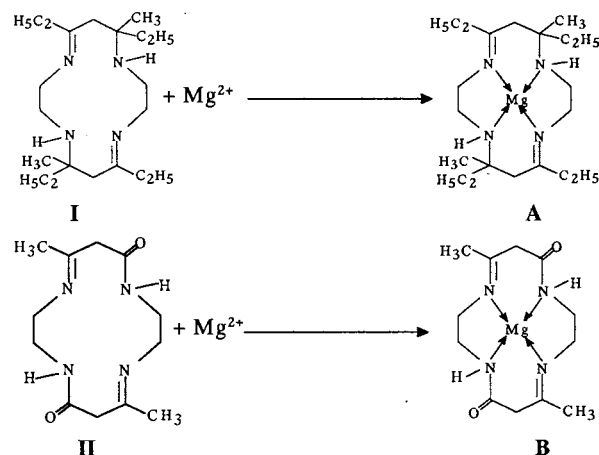
The solutions of the soft drinks (ready to drink) were prepared by the following method. Liquid soft drinks were first filtered to remove suspended materials. To an appropriate volume of the filtered soft drink, 2–3 ml of concentrated HCl was added. The volume was made up to 50 ml in a measuring flask with double-distilled water. The solutions were stored in tightly closed brown bottles and were used directly for analysis by atomic absorption spectrometry (AAS; Perkin Elmer AAS ICP 6500) and also by the sensor developed for the purpose after adjusting the pH of the samples using nitric acid and ammonia.

##### 2.5.2. Babyfood products

First a silica crucible was cleaned with concentrated  $HNO_3$  and water by boiling at  $400^\circ\text{C}$  until smoke no longer evolved. The dish was taken out, cooled and the ash was moistened with a few drops of concentrated  $H_2SO_4$ . Then the crucible was heated on a heating mantle until the fumes of  $H_2SO_4$  ceased. Again the crucible with ash was heated in a muffle furnace up to  $500\text{--}600^\circ\text{C}$  until the weight of the contents became constant. Then the ash was taken up by 2–3 ml of concentrated HCl and the volume was made up to 50 ml in a measuring flask by double-distilled water. These solutions were also stored in a tightly closed brown bottles and were used directly for AAS analysis and by the proposed sensor. The results reported are the average of a minimum of three determinations. Blank runs were also carried out and corrections made if required.

### 3. Results and discussion

The complexation of the macrocyclic ligands gave complexes of types A and B as shown below.



The optimal conditions for the best performance of the magnesium-selective electrode based on a membrane of macrocyclic ligands were investigated systematically.

#### 3.1. Response time and the effect of solvent mediators

The response time was recorded on an  $X-Y(t)$  recorder. Electrodes having membranes without solvent mediator gave a steady response time of about 90 s, whereas, after adding solvent mediators (DBP and DOP), the electrodes achieved an equilibrium response within 15–20 s over the whole concentration range. Potentials so obtained stayed constant for more than 5 min, after which a slow divergence was observed. Potentials were measured periodically; the S.D. of 20 identical measurements was  $\pm 0.2$  mV. The membranes were used over a period of 3 months without any significant change in potential. Whenever a drift in potential was observed, the membranes were re-equilibrated with 1.0 M  $Mg^{2+}$  for 2–3 days.

#### 3.2. Lifetime

The lifetime of electrodes based on ionophores

in solvent polymeric membranes depends on the distribution coefficient of the ionophore and the plasticizer between aqueous and membrane phases [13]. Thus, the lifetime of electrodes must depend on the components of the solution and the measured specimens with electrodes. The experimental results show that the lifetime of the present electrode was about 90 days. During this time, the detection limit and the slope of the electrode remained almost constant. After this time, the electrochemical behaviour of the electrode gradually deteriorated. This is attributed to ageing of the polymer (PVC), plasticizers and ionophore (macrocycles I and II). Further, the changes in membrane behaviour are due to the decrease in the quantity of the plasticizer and ionophore resulting in their migration from a PVC membrane into a PVC foil [13].

#### 3.3. Working concentration range and slope

The working concentration range and slope for all the membrane electrodes (numbers 1–10) are tabulated in Tables 1 and 2 (Fig. 1). The macrocycle-I-based membrane shows linearity in the concentration range  $1.6 \times 10^{-4}$ – $1.0 \times 10^{-1}$  with a slope of 21 mV per decade of activity without any solvent mediator. However, with the addition of solvent mediator DBP or DOP, the working concentration range improved to  $2.5 \times 10^{-5}$ – $1.0 \times 10^{-1}$  M and  $1.0 \times 10^{-4}$ – $1.0 \times 10^{-1}$  M with sub-Nernstian slopes of 22 and 17 mV/decade of activity, respectively, while the solvent mediators DBBP and CN did not improve the working concentration ranges and slopes significantly. Similar improvements in the working concentration range and slope were observed with the membrane of macrocycle II when DBP and DOP were used as solvent mediators. The best performance of all the membrane electrodes was exhibited by membrane 7 (Table 2) with macrocycle II, PVC, STB and DBP in the ratio 2:10:1:7 with a working concentration range of  $1.9 \times 10^{-6}$ – $1.0 \times 10^{-1}$  M, slope of 29 mV/decade of activity and a fast response time of 15 s. Thus, this particular membrane was studied in detail as a  $Mg^{2+}$ -selective electrode and as such

all further investigations were carried out with this particular membrane. Repeated monitoring of potentials (20 identical measurements) on the same portion of the sample gave a standard deviation of  $\pm 0.2$  mV.

### 3.4. Non-aqueous and pH effect

The practical utility of the proposed sensor was investigated in partially non-aqueous media using 15, 30 and 45% (v/v) water–methanol and water–ethanol mixtures. It was observed that the electrode assembly can only be used in non-aqueous medium when its content is not more than 30%, because a further increase in non-aqueous content causes a significant interference.

The pH dependence of the electrode potential was tested over the pH range 1.0–9.0 for  $1.0 \times 10^{-2}$  and  $1.0 \times 10^{-3}$  M  $\text{Mg}^{2+}$ . The pH was adjusted with nitric acid or ammonia solution. The potentials were independent of pH in the range 2.5–6.5 (Fig. 2) and the latter can be taken as the working pH range of the electrode assembly. Above and below these pH values sharp changes in potential are attributed to the hydrolysis of  $\text{Mg}^{2+}$  and  $\text{H}^+$  co-fluxing, respectively.

### 3.5. Potentiometric titration and effect of surfactant

The sensor assembly has been used as an indicator electrode in the potentiometric titration of  $\text{Mg}^{2+}$  with EDTA (Fig. 3). A 25-ml volume of  $1.0 \times 10^{-3}$  M solution of  $\text{Mg}^{2+}$  was titrated against  $1.0 \times 10^{-2}$  M EDTA solution. The addition of EDTA causes a decrease in potential as a result of the decrease in  $\text{Mg}^{2+}$  concentration due to its complexation with EDTA. The potentiometric titrations of  $\text{Mg}^{2+}$  could also be successfully carried out in the presence of  $\text{Ca}^{2+}$  and  $\text{Ba}^{2+}$  (Fig. 3). Thus, these plots demonstrate the usefulness of sensors developed for the potentiometric determination of  $\text{Mg}^{2+}$  in the presence of other metal ions.

The performance of the electrode assembly has also been observed in solutions contaminated with detergent material (Fig. 4). Small amounts

( $5.0 \times 10^{-5}$  M) of cetyltrimethyl ammonium bromide (CTAB) and sodium dodecyl sulphate (SDS) do not disturb the functioning of the membrane sensor, but higher concentrations ( $1.0 \times 10^{-4}$  M and beyond) can cause some problems.

### 3.6. Effect of anion excluder and PVC

Incorporation of salts consisting of a hydrophilic cation and a lipophilic anion (e.g. STB) in cation-selective membranes based on macrocyclic ligand has proved to be beneficial in many respects [14,15]. The additives reduce interferences by lipophilic anions in the sample, give rise to significant change in selectivity, are able to boost the cation sensitivity in the case of carriers with poor extraction capability and lower the electrical membrane resistance considerably [15,16]. The electrode prepared without STB is poorly sensitive and selective for  $\text{Mg}^{2+}$  owing to high resistance or a response to anions in the test solution. STB behaves as an ion-exchanger [17]; hence using STB leads to drastic changes in the slope of the electrode response and in the membrane selectivity. The effect of the content of PVC on the response and selectivity of the sensor was also studied. Construction of the membrane was difficult when the PVC content was less than 45 wt%. The optimum content of PVC was found to be 50%.

### 3.7. Potentiometric selectivity

The potentiometric selectivity coefficient was determined by the modified fixed interference method as suggested by Viteri and Diamond [18] at a  $1.0 \times 10^{-2}$  M concentration of interfering ions. The selectivity coefficient data (Table 3) indicate good selectivity for monovalent, divalent and trivalent cations. As such, these are not expected to interfere even at this higher concentration ( $10^{-2}$  M) of the interfering ions. A comparison of potentiometric selectivities (Table 3) shows that the electrode based on macrocycle II as the membranematerial is more selective for  $\text{Mg}^{2+}$  than electrodes based on membrane of macrocycle I.



Table 4  
Magnesium concentration in food products and soft drinks

Sample	Average magnesium concentration (ppm)	
	Proposed sensor	Atomic absorption spectrometry
1. Horlicks	2.08	2.10
2. Boosts	3.34	3.42
3. Cerelac	3.83	3.90
4. Bournvita	4.24	4.4
5. Citra	2.55	2.62
6. Lehar	4.75	4.78
Mirinda		
7 Lehar 7 Up	1.95	2.22
8. Lehar Pepsi	9.15	9.79
9. Teem	6.25	6.38
10. Soda	17.25	17.30

### 3.8. Estimation of $Mg^{2+}$ in soft drinks and baby-food products

The electrode has been successfully used for the estimation of  $Mg^{2+}$  in various soft drinks and babyfood products. No other treatment of the sample was necessary except the pH adjustments. The results (Table 4) indicate very good correspondence between the two values (one obtained by AAS and other by the proposed sensor under investigation). This also indicates the practical utility of the sensor.

## 4. Conclusions

The PVC-based membrane electrode of macrocycle II, with DBP as solvent mediator (membrane 7) is the best among all the membrane castings (1–10) prepared using macrocycles I and II as sensor material and DBP, DOP, DBBP and CN as solvent mediators in a PVC matrix. The sensor exhibited good reproducibility over a useful lifetime of 3 months. This electrode is superior to the existing electrodes with regard to working concentration range, slope, pH range,

response time and selectivity over a number of cations. Further, the electrode can be used to determine  $Mg^{2+}$  by both direct potentiometry and titration and can be successfully used in non-aqueous media. The proposed sensor is successful in estimating  $Mg^{2+}$  in real sample analysis, viz. in soft drinks (ready to drink) and babyfood products.

## Acknowledgements

S.B. and S.C. are grateful to the Council of Scientific and Industrial Research (CSIR), New Delhi, for providing Senior Research Fellowships. We also thank Prof. S.N. Tondon for his help.

## References

- [1] M.B. Saleh, J. Electroanal. Chem. 373 (1994) 89.
- [2] M.V. Rouilly, M. Badertscher, E. Pretsch, G. Suter, W. Simon, Anal. Chem. 60 (1988) 2013.
- [3] M.V. Rouilly, B. Rusterholz, U.K. Spichiger, W. Simon, Clin. Chem. 36 (1990) 466.
- [4] J. O'Donnell, B. Rusterholz, B. Aebersold, D. Ruegg, W. Simon, E. Pretsch, Mikrochim. Acta 113 (1994) 45.
- [5] B.M. Altura, B.T. Altura, Scand. J. Clin. Lab. Invest. 56 (1996) 251.
- [6] D. Siswanta, H. Hisamoto, S. Sato, Y. Matsumoto, Y. Koike, S. Yamamori, K. Suzuki, Anal. Sci. 13 (1997) 429.
- [7] H. Tsukube, Talanta 40 (1993) 1313.
- [8] A. Maheshwari, Ph.D. Thesis, University of Roorkee, 1987.
- [9] M. Shakir, S.P. Varkey, T.A. Khan, Ind. J. Chem. 34A (1995) 72.
- [10] W.E. Morf, The Principles of Ion-Selective Electrodes and Membrane Transport, Elsevier, Amsterdam, 1981.
- [11] S.K. Srivastava, H. Vardhan, M. Singh, G.N. Rao, S. Srivastava, Anal. Proc. Anal. Commun. 32 (1995) 173.
- [12] M.B. Jacob, The Chemical Analysis of Foods and Food Products, 2nd ed., D. Van Nostrand, New York, 1951, p. 182.
- [13] U. Oesch, W. Simon, Anal. Chem. 52 (1980) 692.
- [14] W.E. Morf, G. Kahr, W. Simon, Anal. Lett. 7 (1974) 9.
- [15] W.E. Morf, D. Ammann, W. Simon, Chimia 28 (1974) 65.
- [16] D. Ammann, W.E. Morf, P. Anker, P.C. Meier, E. Pretsch, W. Simon, Ion-Select. Electrode Rev. 5 (1983) 3.
- [17] P.C. Meier, W.E. Morf, M. Laubli, W. Simon, Anal. Chim. Acta 156 (1984) 1.
- [18] F.J. Saez de Viteri, D. Diamond, Analyst 119 (1994) 749.

# Frontal analysis of aqueous phenol solutions in amberlite XAD-4 columns

## Implications on the operation and design of solid phase extraction systems

Luz E. Vera-Avila <sup>a,\*</sup>, Jose Luis Gallegos-Perez <sup>a</sup>, Evangelina Camacho-Frias <sup>b</sup>

<sup>a</sup> *Departamento de Química Analítica, Facultad de Química, Universidad Nacional Autónoma de México, DF 04510, Mexico City, Mexico*

<sup>b</sup> *Instituto de Química, UNAM, DF 04510, Mexico City, Mexico*

Received 8 January 1999; received in revised form 20 April 1999; accepted 23 April 1999

---

### Abstract

Frontal analysis of aqueous phenol solutions in Amberlite XAD-4 columns was carried out at different experimental conditions. Operating variables such as the concentration, pH and ionic strength of the influent, the presence of competitor solutes, the fluid flow-rate and the column length were considered and their effects on the front profile, the phenol breakthrough volume and the equilibrium parameters were determined. The obtained results may explain some contradictory reported data concerning the recovery of hydrophilic compounds in solid phase extraction (SPE) systems using Amberlite XAD-2 or XAD-4 columns. Furthermore, it is demonstrated that the adsorption parameters derived from a frontal analysis in an XAD-4 column are directly transposable to columns of different sizes (at the analytical level). Therefore, the results of this study may also be used for prediction and/or design of a phenol SPE system adapted to a particular problem. © 1999 Elsevier Science B.V. All rights reserved.

*Keywords:* Frontal analysis; Amberlite XAD-4; Phenol; Solid phase extraction; Water analysis

---

### 1. Introduction

The use of columns packed with polymeric (styrene-divinylbenzene) adsorbents for the removal of organic compounds from aqueous ma-

trixes has been widely reported, either at the small (analytical) scale or in large-scale applications. The high hydrophobicity of these sorbents renders them particularly suitable for the extraction of hydrophilic solutes from water, which are indeed poorly retained in other popular sorbents as alkyl-bonded silicas. At the analytical level, solid phase extraction (SPE) is increasingly used for sample preparation (enrichment and/or sample cleanup), especially in the trace determination of pollutants

---

\* Corresponding author. Tel.: + 525-6223790; fax: + 525-6223723/6162010.

*E-mail address:* luzelena@servidor.unam.mx (L.E. Vera-Avila)

in environmental samples. Thus, polymeric sorbents packed in cartridges, precolumns or disks have been used for the off-line or on-line extraction and preconcentration of a wide variety of polar and medium polarity compounds (anilines, phenols, chlorophenoxy acid herbicides, carbamates, etc.) from aqueous samples [1–5].

Due to their macroporous structure, large surface areas and pore sizes, good rigidity and good hydraulic properties, the low cost Amberlite XAD-2 and XAD-4 adsorbents became very popular some years ago for the off-line SPE of organic micropollutants from water [6–9]. Although these sorbents were later displaced from many of their analytical applications by more efficient materials, some new application of functionalized XAD copolymers have been recently published for the off-line preconcentration of trace metals and organometallic compounds [10–12].

On the other hand, on-line SPE is generally carried out in modern pressure driven systems where stainless steel precolumns packed with high efficiency sorbents of small particle diameter (ca. PRP-1 or PLRP-S type copolymers) are coupled to a liquid chromatograph via switching valves. However, the application of on-line SPE has been actually extended to low pressure systems that still require the use of adsorbents with coarser particles. Thus, a recent work [13] reports the on-line coupling of an XAD-4 column with a flow injection analysis (FIA) manifold for the rapid enrichment and determination of phenols in water and wastewater.

Although there are many results in the literature that prove the effectiveness of the classical XAD-2 or XAD-4 adsorbents for the extraction and concentration of non-polar substances from water, the reported recoveries or the reproducibility obtained for more hydrophilic compounds are often contradictory or frankly disappointing [8,14,15]. This is probably due to the different experimental conditions used by the authors during the adsorption step, whose effect is not apparent with the strongly retained hydrophobic compounds but has a great impact on the recovery efficiency of the weakly retained substances. Therefore, in view of the renewed interest in the use of these materials for new applications, it

becomes necessary to carry out a systematic study of the influence of the main operational parameters on the adsorption of polar compounds.

This work presents the results obtained from the frontal analysis of phenol, used as model hydrophilic solute, in XAD-4 columns. The effect of several experimental parameters on the phenol breakpoint and on the front profile was determined and the impact of the results on the application of this adsorbent for the SPE of organic compounds from water is discussed.

### 1.1. Theoretical

The phenol fronts obtained at different experimental conditions and all the results derived from them are presented in normalized form to facilitate their comparison and analysis. Thus, the abscissa scale for all the curves is given in number of bed volumes of solution passed through the column and the ordinate scale is the relative concentration of phenol in the effluent with respect to its concentration in the influent (Eqs. (1) and (2)):

$$BV = V/(\Pi r^2 L) \quad (1)$$

$$\Phi = C/C_0 \quad (2)$$

Where, BV, is the number of bed volumes;  $V$ , is the volume of solution passed through the column (ml);  $r$ , is the internal column radius (cm);  $L$ , is the (wetted) bed length (cm);  $\Phi$ , is the relative concentration of phenol in the effluent;  $C$ , is the phenol concentration in the effluent at volume  $V$  ( $\text{mg l}^{-1}$ ) and  $C_0$  is the phenol concentration in the influent ( $\text{mg l}^{-1}$ ).

Flow-rates are expressed throughout in number of bed volumes per hour ( $\text{BV h}^{-1}$ ). The relation of these units with those commonly used in chromatography is given in Eq. (3):

$$\text{BV h}^{-1} = 60F/(\Pi r^2 L) = 3600v\varepsilon/L \quad (3)$$

where,  $F$ , is the volumic flow ( $\text{ml min}^{-1}$ ),  $v$ , is the linear velocity ( $\text{cm s}^{-1}$ ) and  $\varepsilon$ , is the bulk porosity of the bed.

Fig. 1 shows a typical front and its three most important points, the breakthrough point (b), the stoichiometric point (s) and the exhaustion or equilibrium point (e). The first one defines the

solute breakthrough volume ( $V_b$ ), which corresponds to the maximal allowable concentration of solute in the effluent for a given process. The second point defines the stoichiometric volume ( $V_s$ ), the vertical line passing through it (f–g) is known as the stoichiometric front. The volume,  $V_s$ , is a thermodynamical parameter (equivalent to the retention volume) representing the volume of influent that would ideally saturate the column if the adsorption kinetics were infinitely rapid. Finally, the exhaustion or equilibrium volume  $V_e$ , defined by the third point, corresponds to the real saturation of the adsorbent capacity. From this point, the solute concentration in the effluent equals its concentration in the influent ( $\Phi = 1$ ) and all the adsorbent bed is in equilibrium with the loading solution.

The area of the rectangle formed by tracing a vertical line through any point 'i' in the front (ca. the rectangle fghkf in Fig. 1 for the stoichiometric point, s) is proportional to the amount of solute contained in a volume  $V_i$  of the influent ( $V_s$  in our example). Inside this rectangle, the area over the curve (kbsghk in Fig. 1) is proportional to the amount of adsorbed solute and the area under the curve (bsfb) to the amount of non-retained solute. Therefore, the concentration of solute in the adsorbent when the point 'i' of the front exits the column can be evaluated by means of Eq. (4):

$$q_i = C_0 A'_{(i)} (V_i - V_0) [1 \text{ BV}] / (A_{r(i)} W) \quad (4)$$

where,  $A_{r(i)}$  is the area of the rectangle defined by the vertical line traced through point 'i' and  $A'_{(i)}$  is the area over the curve inside the rectangle (both in the same units);  $V_i$  is the volume of solution that has passed through the column at this point (in number of bed volumes, BV);  $V_0$  is the void volume (BV); [1 BV] is the volume occupied by the adsorbent bed (l);  $W$  is the mass of dry adsorbent in the column (g) and  $q_i$  is the solute concentration in the adsorbent ( $\text{mg g}^{-1}$ ). It is necessary to mention that for points with abscissa  $V_i < V_e$  the term 'concentration in the adsorbent' is not referred to an homogeneous concentration because in these conditions there is a fraction of unused bed in the column. However, to normalize all the parameters used in this work, it has been decided to relate the amount of adsorbed solute to the mass of dry adsorbent in the column.

At the breakthrough point, all the solute contained in the volume  $V_b$  of solution fed to the column has been adsorbed. Thus, the concentration of solute in the adsorbent at this point ( $q_b$ , in  $\text{mg g}^{-1}$ ) can be easily calculated by means of Eq. (5):

$$q_b = C_0 (V_b - V_0) [1 \text{ BV}] / W \quad (5)$$

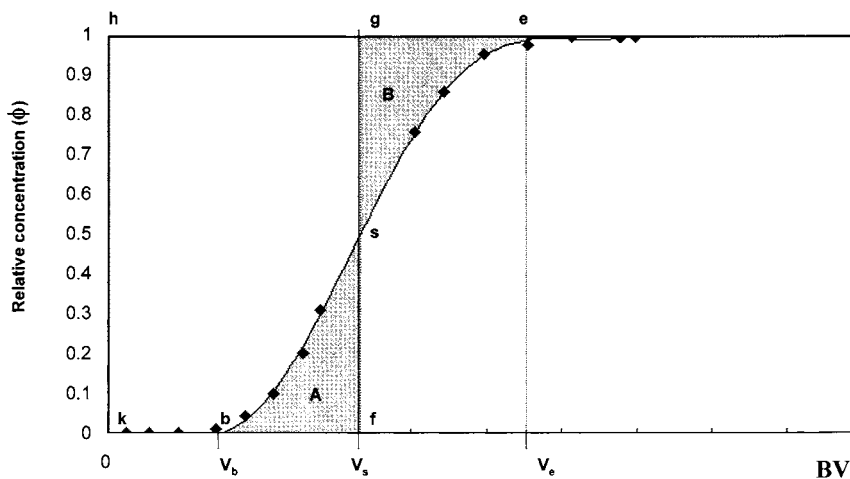


Fig. 1. Frontal analysis curve in normalized coordinates. BV, number of bed volumes;  $\Phi$ , solute concentration in the effluent with respect to its concentration in the influent; b, breakthrough point; s, stoichiometric point; e, exhaustion point;  $V_b$ , breakthrough volume;  $V_s$ , stoichiometric volume;  $V_e$ , exhaustion volume; f–g stoichiometric front.

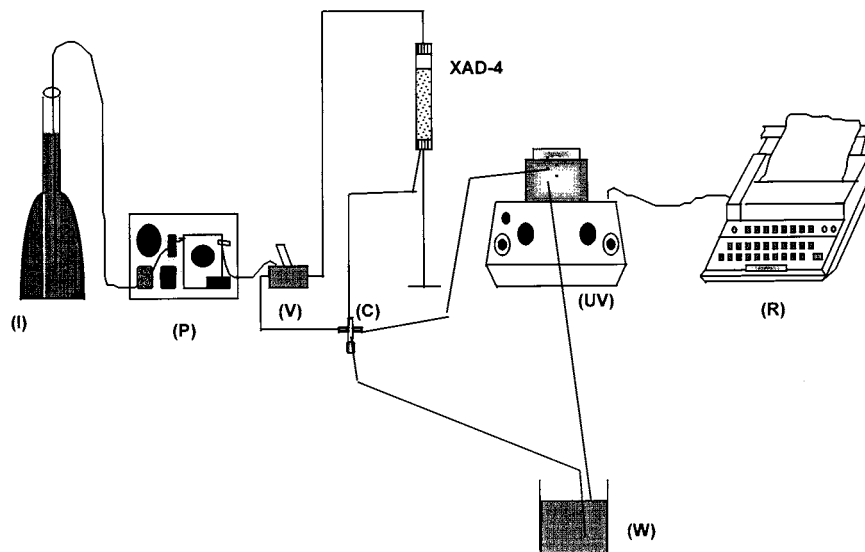


Fig. 2. Diagram of the experimental set-up. I, influent; P, peristaltic pump; V, selector valve; C, cross connector; UV, fixed-wavelength (254 nm) detector; XAD-4, glass column (1.50 cm I.D.) with piston to adjust the column length; W, waste; R, recorder.

On the other hand, the concentration of solute in the adsorbent at the exhaustion or equilibrium point ( $q_e$ , in  $\text{mg g}^{-1}$ ) can be calculated using the properties of the stoichiometric front instead of Eq. (4). The vertical line representing this front (f–g in Fig. 1) divides the real front in such a way that the area under the curve equals the area over the curve to the left and right of this line respectively (areas A and B in Fig. 1). Therefore, the amount of solute contained in the volume  $V_s - V_0$  is the same as the amount of solute adsorbed at exhaustion or saturation of the bed, and Eq. (6) can be used to determine  $q_e$ :

$$q_e = C_0(V_s - V_0)[1 \text{ BV}]/W \quad (6)$$

For any front, whatever its form and symmetry, the stoichiometric center is placed so that the vertical line traced through it forms a rectangle (fghkf in Fig. 1) equal in area to the total area over the breakthrough curve until the exhaustion point (area delimited by the points kbsehk in Fig. 1). When the front is perfectly symmetrical, the stoichiometric center, s, corresponds to the mid-height point of the curve ( $\Phi = 0.50$ ).

## 2. Experimental

### 2.1. Apparatus

A liquid chromatograph was used for the determination of phenol in the effluent samples collected from the frontal analysis experiments. It consisted of two Gilson model 305 and 306 pumps, a Gilson 805 manometric module, a Gilson 811B dynamic mixer and a Spectromonitor 3200 variable wavelength detector from Thermo Separation Products. Sample volumes of  $20 \mu\text{l}$  were injected by means of a 7125 Rheodyne valve in a  $150 \times 4.6 \text{ mm}$  I.D. Spherisorb (Phase Separations) ODS-2,  $5 \mu\text{m}$ , column. Chromatograms were recorded and integrated by a Hewlett-Packard 3396 Series II integrator. Quantitation was based on peak area measurements. Other conditions used throughout were: flow-rate  $1 \text{ ml min}^{-1}$ , detection wavelength  $270 \text{ nm}$  and detector sensitivity  $0.05 \text{ AU}$ .

Fig. 2 shows the diagram of the experimental setup used for the frontal analysis experiments. It consisted of a 55 rpm peristaltic pump with a 303 pumphead from Watson–Marlow, a three-way manual selector valve, a 15 mm I.D. glass column

with a slipping piston to vary the column length to a maximum of 15 cm and a model 153 fixed wavelength, 254 nm, UV detector from Beckman. The latter was used to follow the phenol desorption during the regeneration of the column. The Teflon tubing lines from the column outlet, the selector valve and the detector inlet were joined at a cross connector. The fourth hole of the cross was used for different purposes depending on the operation being performed. During the adsorption stage it remained opened and was used as the waste exit; effluent aliquots were thence collected for analysis. In the desorption stage and when the column was backwashed the hole was plugged. Besides, for the backwashing operation, the detector inlet tubing was disconnected from the cross and its corresponding hole was also plugged; simultaneously, the column inlet tubing was disconnected from the selector valve and became the waste exit. In fact, the selector valve and the cross connector controlled the direction of the flow at each stage of the experimental procedure. The pump flow was sent toward the upper column end during the adsorption and desorption operations, toward the lower column end for the backwashing of the column and directly toward the waste exit at the cross connector when the pump was purged with a new solution.

## 2.2. Chemicals

Analytical-reagent or HPLC-grade chemicals were used. Methanol, glacial acetic acid, perchloric acid, diethyl ether and ammonium hydroxide were purchased from Baker, acetonitrile was from Prolabo, phenol from Mallinckrodt, 4-chlorophenol from Merck and ammonium acetate from Productos Quimicos, Monterrey.

The spiked aqueous solutions and the mobile phases were prepared with type I reagent water obtained from a Nanopure (Barnstead Thermolyne) deionizer. The mobile phases for the HPLC determinations were acetonitrile–acetate buffer 0.01 M (pH 4.5) mixtures. The solvent proportions were, respectively, 25:75 (v/v) for the analysis of aliquots only containing phenol and 35:65 (v/v) for the samples containing phenol and 4-chlorophenol.

Rohm and Haas, Mexico kindly provided Amberlite XAD-4, as 20–60 mesh (500  $\mu\text{m}$  average) particles. The resin was first rinsed with water and then sequentially Soxhlet extracted with methanol, acetonitrile, diethyl ether and finally with methanol again. The extraction time for each solvent was 8 h. The purified adsorbent was stored in methanol.

## 2.3. Frontal analysis

A portion of the methanol slurried Amberlite XAD-4 was poured into the glass column and the piston was adjusted  $\sim 1.5$  cm above the adsorbent bed. Then, the column was backwashed with deionized water, beginning with a very slow flow and increasing it progressively until the resin beads occupied all the free space. Afterwards, the flow was stopped and when the resin beads were completely settled by gravity, the bed length was measured to determine the bed volume [1 BV].

For the experiments carried out in this work, two different bed lengths were used, 3.5 and 7.0 cm. The corresponding bed volumes calculated from the column dimensions were 6.19 and 12.4 ml, respectively. The mass of dry resin contained in each column was determined by collecting the adsorbent and drying it in a stove at 60°C until constant weight. The mean values resulting from three independent measurements of the adsorbent mass were 1.80 and 3.67 g for the 3.5 and 7.0 cm bed lengths, respectively.

Before each adsorption experiment, the column was conditioned in the normal downward flow direction with an aqueous solution of the same pH and composition as the one to be used later but without the solute(s) of interest; at this time the flow-rate was adjusted to the desired value. Then, the phenol solution to be studied was pumped through the column and effluent samples were collected periodically and analyzed. However, due to the long duration of the adsorption experiments (arriving in some cases to 36 h) and the slight variations of the flow provided by the peristaltic pump, the volume of solution passed through the column and the elapsed time were continuously monitored in order to calculate the mean flow-rate. At the end of each adsorption

experiment, the column was rinsed with deionized water, regenerated with an adequate volume of methanol and backwashed with water.

#### 2.4. Desorption study

The XAD-4 column (3.5 cm) was previously loaded with 2500 ml (404 BV) of a 10 mg l<sup>-1</sup> phenol solution at pH 2 using a flow-rate of 1.13 ml min<sup>-1</sup> (~ 11 BV h<sup>-1</sup>). From the results of the adsorption study these conditions correspond to a complete exhaustion of the bed and a phenol loading of about 17 mg. Desorption was carried out with methanol at different flow-rates or with different solvents (methanol, aqueous NaOH solutions at pH 10 and 12 or alkalinized methanol) at a fixed flow-rate. The column effluent was monitored by the fixed wavelength UV detector in the sensitivity range of 0.64 AU. First, the solvent was directly sent toward the detector in order to register the baseline absorbance and then, through the column for the elution of the adsorbed phenol. After the passage of the void volume, the absorbance abruptly increased, reached a plateau (probably due to detector saturation) and then, slowly decreased. Elution was considered to be complete at the point where the absorbance was 1% of the total range (0.0064 AU) higher than the baseline absorbance. The volume of solvent passed through the column from the beginning of the experiment to this point was taken as the desorption volume.

### 3. Results and discussion

The experimental data of phenol concentration in the effluent versus time were transformed to the normalized parameters,  $\Phi$  versus BV, and were numerically analyzed to adjust a mathematical expression representing the breakthrough curve or front. Using the Origin<sup>®</sup> program, the best fit for all the fronts was obtained with an exponential equation of the Boltzmann type.

In the SPE application of adsorbent columns, the most important parameter is the breakthrough volume because it defines the maximum volume of sample that can be loaded in a column for a

complete recovery of the solute of interest. In this work, the breakthrough point was arbitrarily defined for a phenol concentration in the effluent equal to 1% of the influent concentration. Thus, the breakthrough volumes at different experimental conditions were calculated with the adjusted equation of the respective front using the point of ordinate  $\Phi = 0.01$ ; the phenol concentration in the adsorbent at this point was calculated by means of Eq. (5), neglecting the void volume.

On the other hand, for the determination of the stoichiometric center it is necessary to have a complete and well-defined front, which was not the case for all the fronts obtained in this work. In some cases, the final part of the curve was not clearly defined, probably due to defects in the bed structure formed during the settling of the particles after the backwashing procedure. In other cases, the kinetic effects gave rise to incomplete fronts, tending asymptotically toward the limiting value at  $\Phi = 1$ . Therefore, it was decided to estimate the value of  $V_s$  from the volume corresponding to the mid-height point ( $\Phi = 0.50$ ) of the front and to use this value in Eq. (6), neglecting the void volume, for the evaluation of the phenol concentration in the adsorbent at equilibrium. Although the latter is only an approximation of the true equilibrium parameter, it can give a reasonably good appreciation of the effect of different operating conditions on phenol adsorption in Amberlite XAD-4.

#### 3.1. Reproducibility of the frontal analysis data

Five replicate adsorption experiments were carried out over a 6 month period using the same XAD-4 column. In the intermediate time between these experiments the column was used for other parts of the study; therefore, it was subjected to multiple adsorption–desorption cycles at different conditions.

Table 1 shows the experimental conditions used for the replicates and the results derived from the breakthrough curves presented in the chronological order in which the experiments were carried out. It is observed that the results don't show any tendency over the time, demonstrating that the column was not affected by the numerous experi-

Table 1

Reproducibility. Reagent water solutions spiked at  $10 \text{ mg l}^{-1}$  of phenol and acidified to pH 2 with perchloric acid were passed through a 1.50 cm I.D. glass column packed with Amberlite XAD-4 (1.80 g, dry adsorbent basis)<sup>a</sup>

Experiment	$V_b$ (BV)	$q_b$ (mg $\text{g}^{-1}$ )	$\hat{V}_s$ (BV)	$\hat{q}_e$ (mg $\text{g}^{-1}$ )
1	76.5	2.63	274	9.42
2	75.8	2.61	285	9.80
3	95.3	3.27	263	9.04
4	87.6	3.01	273	9.39
5	91.7	3.15	291	10.0
Mean	85.4	2.93	277	9.53
RSD (%)	10.3	10.3	3.95	3.95

<sup>a</sup> The height and volume of the bed embedded in water were 3.5 cm and 6.19 ml, respectively. The mean flow-rate in the five experiments was about  $11 \text{ BV h}^{-1}$ .  $V_b$ , breakthrough volume (in number of bed volumes);  $\hat{V}_s$ , estimated stoichiometric volume;  $q_b$ , phenol concentration in the adsorbent at the breakthrough point (in  $\text{mg g}^{-1}$  of dry adsorbent);  $\hat{q}_e$ , estimated phenol concentration in the adsorbent at equilibrium.

ments carried out in it during this period. From the statistical results, also reported in Table 1, it can be deduced that the frontal analysis data are reproducible with a precision of  $\sim 10\%$  for the parameters calculated from the breakthrough

point and a precision of  $\sim 4\%$  for those obtained from the stoichiometric point estimator

### 3.2. Effect of the phenol concentration in the influent

Fig. 3 shows the curves obtained from the frontal analysis of phenol at various concentrations in aqueous solutions. The characteristic parameters derived from the curves are reported in Table 2.

From these data it was possible to obtain the approximate adsorption isotherm of phenol in the system (Fig. 4) by relating the estimated equilibrium concentration in the adsorbent,  $\hat{q}_e$ , and the influent concentration,  $C_0$ . The analysis of the data demonstrated that the isotherm, of the Freundlich type, was represented by Eq. (7):

$$\log \hat{q}_e = 0.201 + 0.736 \log C_0 \quad (7)$$

(correlation coefficient = 0.997).

The convexity of the adsorption isotherm indicates that the distribution coefficient of phenol between the adsorbent and the fluid decreases as the concentration of the solute in the influent increases. As a result, the stoichiometric volume,

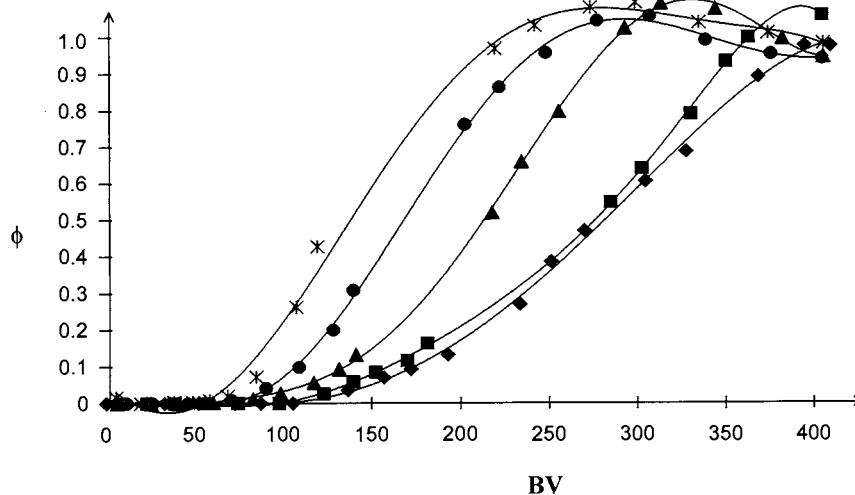


Fig. 3. Frontal analysis of phenol at different concentrations. Column: 1.50 cm I.D., packed with Amberlite XAD-4; 1.80 g (dry basis); bed volume 6.19 ml; bed height 3.5 cm. Influent: phenol in acidified (pH 2) water, ionic strength 0.01 M. Mean flow-rate:  $\sim 11 \text{ BV h}^{-1}$ . Phenol concentration:  $\blacklozenge$   $5 \text{ mg l}^{-1}$ ;  $\blacksquare$   $10 \text{ mg l}^{-1}$ ;  $\blacktriangle$   $20 \text{ mg l}^{-1}$ ;  $\bullet$   $40 \text{ mg l}^{-1}$  and  $*$   $80 \text{ mg l}^{-1}$ .



Table 2  
Effect of the phenol concentration<sup>a</sup>

$C_0$ (mg l <sup>-1</sup> )	$V_b$ (BV)	$q_b$ (mg g <sup>-1</sup> )	$\hat{V}_s$ (BV)	$\hat{q}_e$ (mg g <sup>-1</sup> )	$q_b/\hat{q}_e$ (%)
5	87.7	1.51	282	4.85	31
10	76.5	2.63	274	9.42	28
20	63.5	4.37	214	14.7	30
40	59.7	8.21	169	23.2	35
80	45.7	12.6	144	39.6	32

<sup>a</sup> Same conditions as in Table 1 except for the concentration of phenol in the influent ( $C_0$ ).

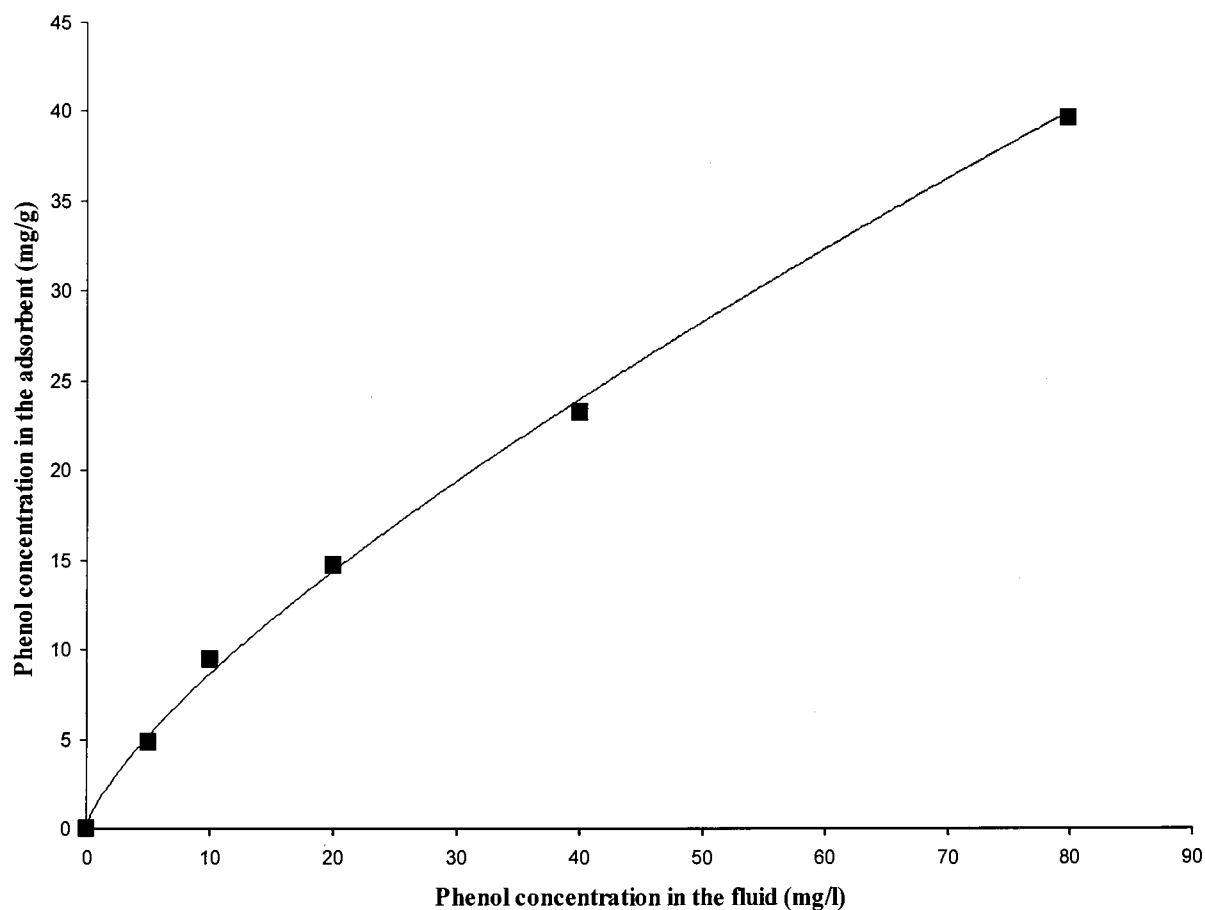


Fig. 4. Adsorption isotherm of phenol. Abscissa: phenol concentration of the influent,  $C_0$  (mg l<sup>-1</sup>); ordinate: phenol equilibrium concentration in the adsorbent,  $\hat{q}_e$  (mg g<sup>-1</sup>). The points represent the experimental data deduced from the frontal analysis curves at different concentrations. The continuous line corresponds to the equation of the Freundlich adsorption isotherm obtained from the regression analysis of the data.

being a measure of solute retention, also decreases with concentration. This can be clearly appreciated in the fronts of Fig. 3.

On the other hand, the breakthrough volume decreases with phenol concentration, but this decrease is lower, in volume units, than that of the

stoichiometric volume. The reason for this is that  $V_s$  only depends on the thermodynamics of the adsorption process while  $V_b$  is the result of thermodynamic and kinetic effects. In porous polymeric adsorbents, like Amberlite XAD copolymers, the rate-controlling factor is intraparticle diffusion (pore and surface diffusion); or, it has been reported [16,17] that the effective intraparticle diffusion coefficient increases with the concentration of adsorbed compound. Considering that the dispersion of the transition zone in the frontal analysis curves depends on the adsorption kinetics, it is to be expected that an increase in solute concentration will provoke a compression of the transition zone. Indeed, this is the effect observed in Fig. 3. Thus, as the phenol concentration in the influent increases, the fronts are sharpened and the breakthrough volume approaches the stoichiometric volume (Fig. 5).

For a given set of experimental conditions, the 'efficiency of an adsorption process' may be defined as the extent to which the adsorbent is loaded at the breakthrough point with respect to

its loading at saturation. From the data in Table 2 it can be seen that the combination of the thermodynamic and kinetic effects results in a rather constant process efficiency (measured by  $q_b/\hat{q}_e$ ) in the range of phenol concentrations studied.

Some practical considerations for the application of XAD-4 columns in the extraction of organic compounds from water may be derived from the results of this section. The most important is that the volume of sample that can be loaded in a given column (identified with  $V_b$ ) decreases when the concentration of the analyte in solution increases. However, if the adsorption isotherm is known and the breakthrough volume is determined for one concentration of the solute of interest, it is possible to predict the approximate breakthrough volumes for samples containing different concentrations. This is due to the constancy of the process efficiency with concentration but, as it will be shown in the next sections, other experimental conditions should be kept constant.

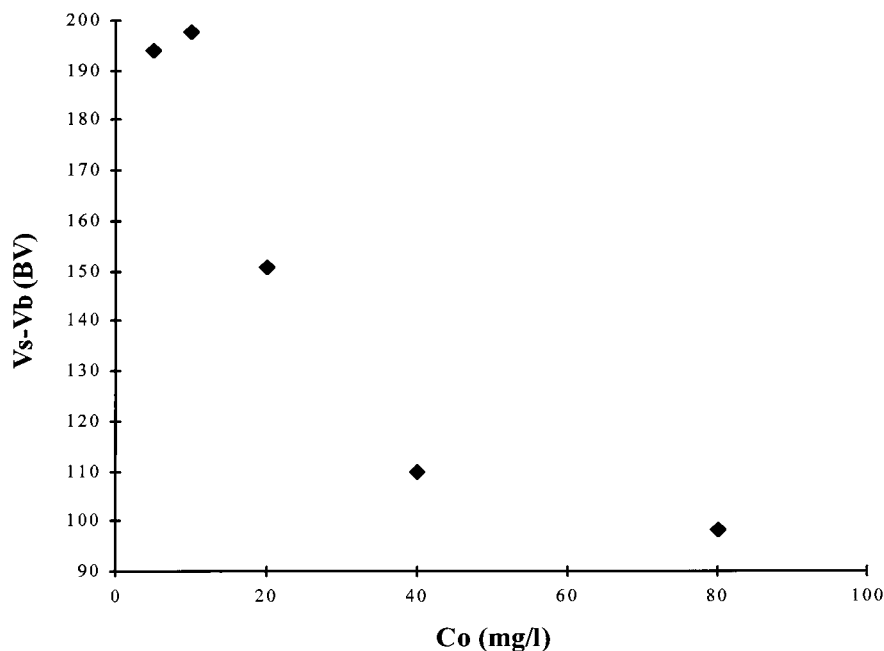


Fig. 5. Effect of the influent phenol concentration,  $C_0$ , on the dispersion of the transition zone in the fronts, evaluated from the difference between the stoichiometric volume,  $V_s$ , and the breakthrough volume,  $V_b$ .

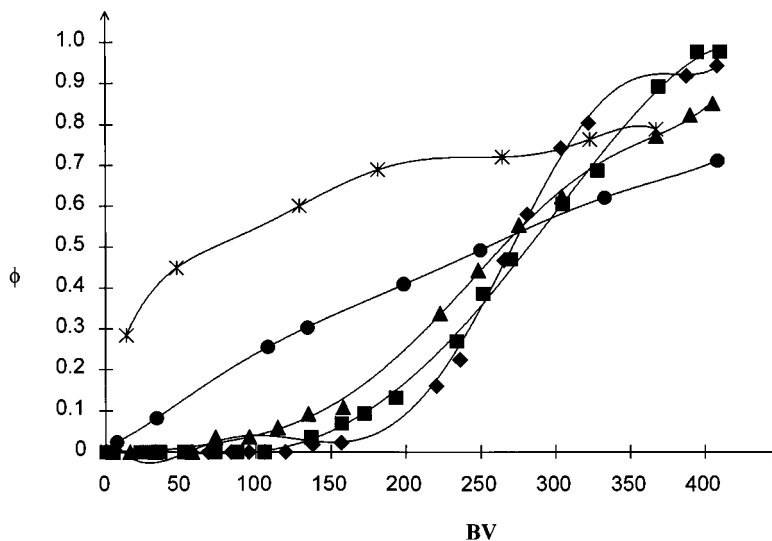


Fig. 6. Frontal analysis of phenol at different flow-rates of the mobile phase. Influent: phenol,  $5 \text{ mg l}^{-1}$ , in acidified (pH 2) water, ionic strength 0.01 M. Mean flow-rate:  $\blacklozenge$   $6.94 \text{ BV h}^{-1}$ ;  $\blacksquare$   $11.2 \text{ BV h}^{-1}$ ;  $\blacktriangle$   $21.8 \text{ BV h}^{-1}$ ;  $\bullet$   $94.4 \text{ BV h}^{-1}$  and  $*$   $346 \text{ BV h}^{-1}$ . Other conditions as in Fig. 3.

Table 3  
Effect of the fluid flow-rate<sup>a</sup>

Flow-rate ( $\text{BV h}^{-1}$ )	$V_b$ (BV)	$q_b$ ( $\text{mg g}^{-1}$ )	$\hat{V}_s$ (BV)	$\hat{q}_c$ ( $\text{mg g}^{-1}$ )
6.94	138	2.38	271	4.65
11.2	87.7	1.51	282	4.85
21.8	53.5	0.92	265	4.56
94.4	1.65	0.03	251	4.31
346	—	—	73	—

<sup>a</sup> Same conditions as in Table 1 but the influent phenol concentration was  $5 \text{ mg l}^{-1}$  and the fluid flow-rate was varied.

### 3.3. Effect of the flow-rate

The phenol fronts obtained at different flow-rates of the aqueous phase, from 6.9 to  $346 \text{ BV h}^{-1}$ , are presented in Fig. 6 and their characteristic parameters are reported in Table 3. The curves in Fig. 6 show that the front profile is very sensitive to the flow-rate, with a transition zone slope progressively decreasing as the flow-rate increases. Indeed, when the flow-rate approaches the value of  $100 \text{ BV h}^{-1}$ , the sigmoidal form of the front is completely lost and a very disperse transition zone, practically starting at the void volume, is obtained. For still higher flow-rates, a considerable fraction of phenol appears in the effluent from the beginning of the experiment.

The analysis of the front parameters is very interesting. Table 3 shows that for flow-rates lower than  $100 \text{ BV h}^{-1}$  the variation of the stoichiometric volume estimator is rather small, of the order of the experimental uncertainty. This is a confirmation of the thermodynamic nature of the stoichiometric point. Furthermore, it gives support to the choice of the mid-height point in the curve as a stoichiometric center estimator. The equilibrium phenol concentration in the adsorbent, calculated from  $\hat{V}_s$ , is thus practically identical in this range of flow-rates. From the experimental point of view, this represents a great advantage when the time required to obtain a complete front is very long because the results show that it is possible to evaluate the equilibrium

parameter,  $q_e$ , even from incomplete curves (ca. curve obtained at  $94.4 \text{ BV h}^{-1}$  in Fig. 6). On the other hand, the experiment performed at a flow-rate of  $346 \text{ BV h}^{-1}$  is completely different. Here a large fraction of the phenol molecules passed through the column without interacting with the adsorbent, therefore, the point of ordinate  $\Phi = 0.50$  in the curve does not have any particular meaning.

A completely opposite situation is found for the effect of flow-rate on the breakthrough point and the parameters derived from it. Table 3 shows that  $V_b$  and  $q_b$  dramatically decrease as the flow-rate of the aqueous phase increases. This effect is exclusively due to the kinetics of the adsorption process in Amberlite XAD-4. The slow diffusion of the solute in the polymeric network requires of very low fluid velocities in order to attain equilibrium between the mobile and the stationary phases. As the fluid velocity increases, the non-equilibrium phenomena become predominant and every point in the front, including the breakthrough point and the exhaustion point, moves away in volume units from the stoichiometric (or equilibrium) point. The result of this is the progressive spreading of the transition zone as the flow-rate increases. In fact, Fig. 6 shows that at flow-rates approaching  $100 \text{ BV h}^{-1}$ , the transition zone is approximately as long as the column and the breakthrough point emerges at the void volume. For higher flow-rates, the transition zone is not formed because the column is too small to contain it.

The results obtained in this section may explain some of the contradictory reported data concerning the solid phase extraction of hydrophilic compounds from water. A closer examination of several published works has permitted us to estimate that, in general, sample volumes from 100 to 1000 BV are loaded in XAD-2 or XAD-4 columns at flow-rates varying between 50 and  $1000 \text{ BV h}^{-1}$  for the SPE of organic pollutants from aqueous solutions. The great differences in operating conditions are reflected in the variability of the reported phenol recoveries, from 5% [8] to 100% [14], when this solute is present in the samples. In fact, the fronts of Fig. 6 demonstrate that when the aqueous samples are loaded in

XAD-4 columns at flow-rates higher than  $100 \text{ BV h}^{-1}$ , a non negligible fraction of phenol appears in the effluent from the void volume, resulting in low but not null solute recoveries. This is so because at these high flow-rates the transition zone is not formed and the saturation point is not reached; therefore, a fraction of the compound continues to be adsorbed during the passage of very large volumes of solution. Thus, depending on the flow-rate and the number of bed volumes of sample loaded in the column, large variations in solute recoveries might be observed. On the other hand, it must be mentioned that the highest reported phenol recovery [14] was obtained with a sample of  $\sim 150 \text{ BV}$  passed through the column at a flow-rate of about  $1000 \text{ BV h}^{-1}$ , but the column had been packed with XAD-4 beads previously ground and sieved. It is known that with a narrow size distribution of small adsorbent particles, the adsorption kinetics is considerably improved, the effect of flow-rate is minimized and the volume of sample that can be loaded in a SPE column without breakthrough of the analyte approaches the stoichiometric volume. Table 3 shows that the latter is indeed notably higher than 150 BV.

#### 3.4. Effect of the ionic strength and the pH of the influent

The characteristic parameters derived from the frontal analysis of phenol solutions containing different salt concentrations are reported in Table 4. The experimental conditions were identical to those used in the reproducibility study but sodium perchlorate was added as required to fix the ionic strength of the aqueous phase to the desired value. Besides, for the experiment carried out at zero ionic strength the solution was not acidified. It is observed that, in the range of ionic strength from 0 to 0.5 M, the parameters derived from the different experiments are very similar and don't show any tendency. In fact, they also are comparable to those obtained from the reproducibility experiments (Table 1). In the latter, the relative standard deviation (RSD) obtained from five replicates of the experiment at an ionic strength of 0.01 M was about 10% for the parameters derived

from the breakthrough point and about 4% for those derived from the stoichiometric point estimator. Considering that a similar RSD could be expected for the results of the experiments performed at other ionic strengths, it can be concluded that in the studied salt concentration range, this parameter does not have any influence on phenol adsorption.

An additional experiment was carried out at an ionic strength of 1 M. However, in this solution of high density the resin grains floated in the free space left at the upper end of the column and the bed was completely disturbed. As a consequence, the phenol breakthrough occurred from the begin-

ning of the experiment and the obtained curve was too dispersed.

Fig. 7 shows the fronts obtained from acid, neutral and basic phenol solutions. These curves reflect the acid–base behavior of phenol ( $pK_a = 9.9$ ); at pH 2 and 7 the fronts are practically identical because in these conditions phenol is completely in the molecular form and its retention in a reverse-phase adsorbent is maximal. On the other hand, at pH 10 a fraction of about 56% of phenol is ionized and this suffices to provoke a strong decrease of retention in the XAD-4 copolymer. Thus, the pH of the aqueous phase has a very important effect on the adsorption of com-

Table 4  
Effect of the ionic strength<sup>a</sup>

Ionic strength (M)	$V_b$ (BV)	$q_b$ (mg g <sup>-1</sup> )	$\hat{V}_s$ (BV)	$\hat{q}_c$ (mg g <sup>-1</sup> )
0	95.3	3.27	287	9.87
0.01	75.8	2.61	285	9.80
0.05	97.3	3.34	265	9.11
0.10	86.9	2.99	260	8.94
0.50	79.3	2.73	282	9.70
Mean	86.9	2.99	276	9.48
RSD (%)	10.9	10.8	4.5	4.5

<sup>a</sup> The required amount of sodium perchlorate was added to the aqueous phase to fix the ionic strength. Other conditions as in Table 1, except for the experiment at zero ionic strength where the solution was not acidified.

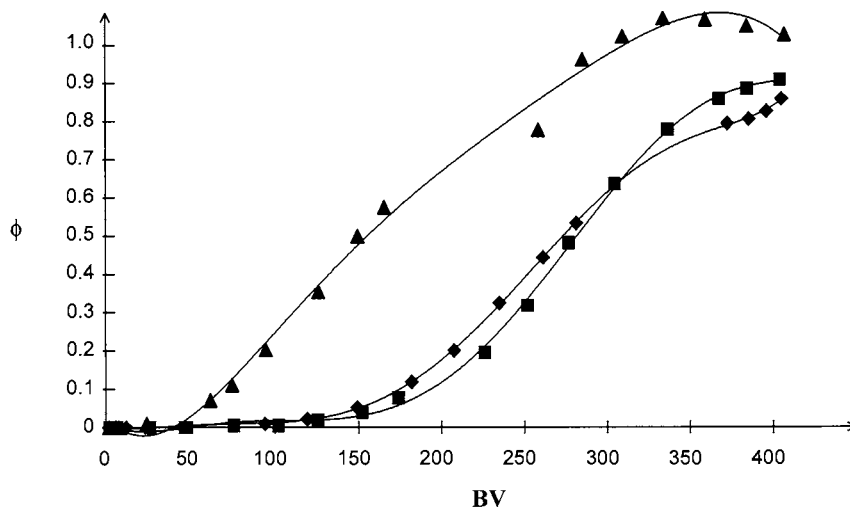


Fig. 7. Frontal analysis of phenol at different pH of the aqueous phase. Influent: phenol, 10 mg l<sup>-1</sup>, in aqueous solutions containing:  $\blacklozenge$  0.01 M perchloric acid (pH 2);  $\blacksquare$  0.01 M ammonium acetate (pH 7) and  $\blacktriangle$  0.01 M ammonium acetate with 0.013 M ammonia (pH 10). Other conditions as in Fig. 3.

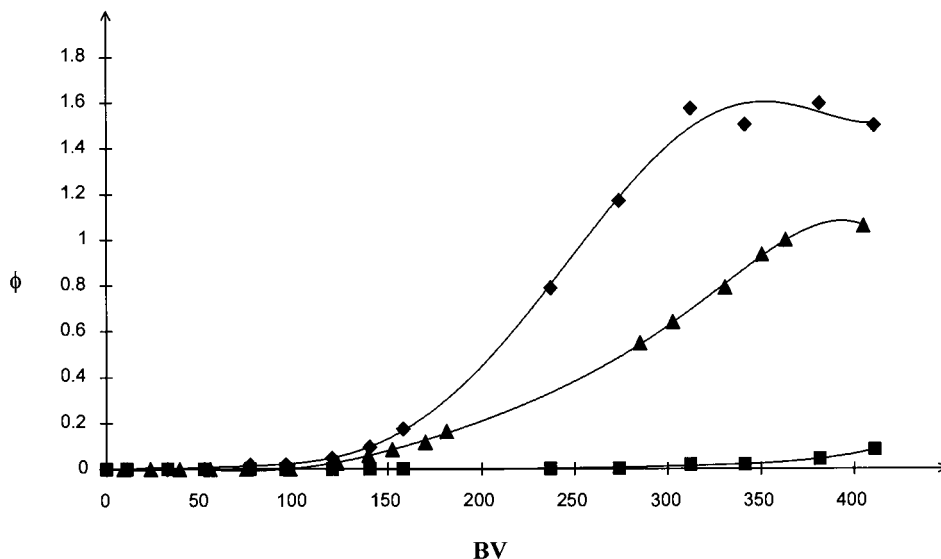


Fig. 8. Effect of a competitor solute on the phenol fronts. Frontal analysis curves of:  $\blacktriangle$  phenol,  $10 \text{ mg l}^{-1}$ , in an aqueous solution without competitor solutes;  $\blacklozenge$  phenol,  $10 \text{ mg l}^{-1}$ , in an aqueous solution containing  $50 \text{ mg l}^{-1}$  of 4-chlorophenol and  $\blacksquare$  beginning of the 4-chlorophenol front. Other conditions as in Fig. 3.

Table 5

Effect of a competitor solute. Same conditions as in Table 1, except that 4-chlorophenol ( $50 \text{ mg l}^{-1}$ ) was added to the influent in one of the experiments

	$V_b$ (BV)	$q_b$ ( $\text{mg g}^{-1}$ )	$\hat{V}_s$ (BV)	$\hat{q}_e$ ( $\text{mg g}^{-1}$ )
Without 4-chlorophenol	87.6	3.01	273	9.39
With 4-chlorophenol	62.1	2.13	210	–

pounds with acid–base properties but only when this parameter approaches the  $\text{p}K_a$  value of the solute. Indeed, the results obtained at pH 2 and 7 indicate that the pH of the influent does not have any influence on the adsorption of molecular solutes.

### 3.5. Effect of a competitor solute in the influent

A comparison of the phenol fronts obtained from a  $10 \text{ mg l}^{-1}$  solution of phenol alone and the same solution containing  $50 \text{ mg l}^{-1}$  of 4-chlorophenol is shown in Fig. 8. In the same figure is also shown the beginning of the breakthrough curve of the competitor solute. The characteristic parameters of the phenol curves are reported in Table 5.

It is observed that the presence of a compound more hydrophobic than phenol and more strongly retained on the XAD-4 adsorbent provokes a shift of the phenol front toward lower volumes. This indicates that the capacity of the column to adsorb the weak hydrophilic compounds is further reduced when the aqueous phase contains significant concentrations of other solutes that can advantageously compete for the adsorption sites. This fact must be considered in SPE applications of XAD copolymers. Thus, a method developed for the SPE of an hydrophilic compound from a ‘clean’ water sample (ca. tap water or potable water) should probably have to be modified for ‘dirty’ samples (wastewater or even river water).

Another interesting feature to be observed in Fig. 8 is a maximum in the phenol curve that

largely exceeds the limiting value at  $\Phi = 1$  when the influent contains 4-chlorophenol. Indeed, the height of this curve reaches a value of about 1.6, which means that the phenol concentration in the effluent arrives to be 60% higher than in the influent! Then, when the chlorophenol front begins to emerge from the column, the decline of the phenol curve also begins. In fact, Don DeVault predicted the 'excess concentration' of the less retained solute in the effluent since the 1940s [18] in his study of multicomponent adsorption. A simplified explanation of this phenomenon for a two-component system is given below.

The weakest adsorbate (phenol in our case), usually the most rapid from both the kinetic and the chromatographic points of view, arrives first to the adsorption sites where maximum adsorption occurs as if this compound was alone in the solution. When the slow strongest adsorbate (4-chlorophenol) reaches the active sites, it displaces some of the previously adsorbed weak solute provoking an increase of its concentration in the fluid. Thus, an excess concentration of the weak compound appears in the mobile phase migrating between the two fronts. As the adsorption of the strong solute progresses to its saturation point,

the displacement of the adsorbed weak solute decreases and so does its excess concentration in the fluid. Finally, both compounds reach the equilibrium state at the exhaustion point of the second (slower) front and their respective concentrations in the mobile phase equal their concentrations in the influent.

From the results obtained in this section it is not possible to ascertain whether our estimator of the stoichiometric volume, the point with ordinate  $\Phi = 0.50$ , may or may not be used to calculate the equilibrium concentration of phenol in the adsorbent when an excess concentration of this solute appears in the effluent. Therefore, for this case, the parameter  $\hat{q}_c$  is not reported in Table 5.

### 3.6. Comparison of results obtained in different bed sizes

A new column with twice the height, the bed volume and the weight of dry adsorbent, with respect to the previous experiments, was prepared. A phenol front was obtained in this 'long' column using the same normalized flow-rate ( $11 \text{ BV h}^{-1}$ ) and the same aqueous phase composition that were used in the reproducibility study with the

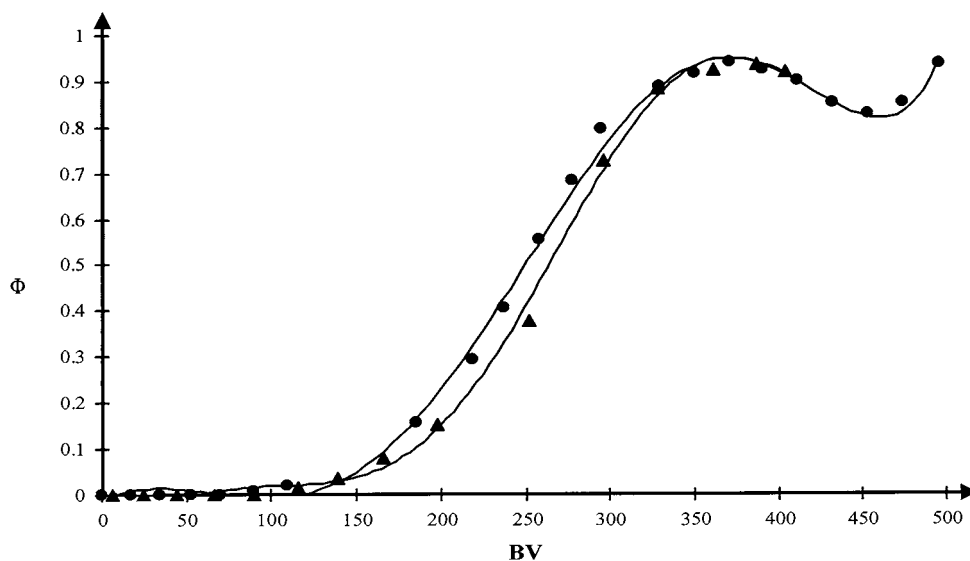


Fig. 9. Frontal analysis of phenol in columns of different size. Column: 1.50 cm I.D. packed with Amberlite XAD-4, ▲ 1.80 g (dry basis), bed volume 6.19 ml, bed height 3.5 cm and ● 3.67 g (dry basis), bed volume 12.4 ml, bed height 7.0 cm. Influent: phenol,  $10 \text{ mg l}^{-1}$ , in acidified (pH 2) water, ionic strength 0.01 M. Flow-rate  $\sim 11 \text{ BV h}^{-1}$ .

Table 6  
Adsorption in columns of different size<sup>a</sup>

	$V_b$ (BV)	$q_b$ (mg g <sup>-1</sup> )	$\hat{V}_s$ (BV)	$\hat{q}_e$ (mg g <sup>-1</sup> )
Short column	95.3	3.27	263	9.04
Long column	93.5	3.16	249	8.41

<sup>a</sup> Conditions: short column packed with Amberlite XAD-4 (1.80 g, dry basis); the height and volume of the wetted bed were 3.5 cm and 6.2 ml, respectively. Long column packed with Amberlite XAD-4 (3.67 g, dry basis), the height and volume of the wetted bed were 7 cm and 12.4 ml, respectively. The mean flow-rate in both columns was  $\sim 11$  BV h<sup>-1</sup>. Other conditions as in Table 1.

‘short’ column. For comparison Fig. 9 shows the fronts obtained with the two bed sizes and their characteristic parameters are reported in Table 6.

It is observed that the initial part of the two fronts is almost superimposed and the breakthrough volumes are practically identical when expressed in number of bed volumes. This indicates that the amount of phenol adsorbed in the column at the breakthrough point is directly proportional to the bed size. In other words, the concentration of phenol in the adsorbent at this point is independent of the bed size if the columns are loaded with the same influent and are operated at the same normalized flow-rate. Although this conclusion may seem too evident, it is important to note that the same normalized flow-rate (BV h<sup>-1</sup>) in columns of different length implicates that the fluid linear velocity (cm s<sup>-1</sup>) or the volumic flow-rate (ml min<sup>-1</sup>) is proportionally higher in the longer column. Or, it has been demonstrated in a previous section that  $V_b$  and  $q_b$ , strongly decreased when the flow-rate of the aqueous phase increased; however, in those experiments the variations in fluid velocity, volumic flow-rate and normalized flow-rate were all proportional because the column length was the same. Therefore, it seems that to compare and understand the real effect of variations in operating conditions for adsorption processes, it is advisable to normalize some parameters. In particular, fluid volume, effluent concentrations and volumic flow-rates (or linear velocities) should be transformed to number of bed volumes (BV), relative concentrations ( $\Phi$ ) and number of bed volumes per unit time (BV h<sup>-1</sup>), respectively.

The slight shift of the fronts observed in Fig. 9 can be attributed to a difference of bed structure

in the columns. Indeed, the settling and arrangement of the adsorbent particles after the back-washing procedure cannot be expected to be identical when the adsorbent amount and the column length are different. Nevertheless, within the experimental precision, the parameters derived from the curves, and expressed in normalized units, can be considered to be very similar for the two column lengths.

The results obtained in this section are very interesting for SPE applications. It has been demonstrated that the data derived from a frontal analysis in one column can be used to scale up or down the adsorption experiment as required by simply modifying the column length. If the normalized flow-rate is kept constant, the breakthrough volume (in number of bed volumes) will be the same whatever the column length.

### 3.7. Phenol desorption

Methanol, aqueous solutions of NaOH (10<sup>-2</sup> and 10<sup>-4</sup> M) and methanol solutions of NaOH (same concentrations) were tested as desorption solvents for the elution of phenol from the XAD-4 column. In all the experiments, the column (3.5 cm bed length) had been previously loaded to exhaustion using the same conditions, namely a flow-rate of  $\sim 11$  BV h<sup>-1</sup> and a 10 mg l<sup>-1</sup> aqueous phenol solution at pH 2. From the previous experiments (Table 1), these conditions during the adsorption stage correspond to the following mean parameters:  $V_b = 85.4$  BV;  $q_b = 2.93$  mg g<sup>-1</sup>;  $\hat{V}_s = 277$  BV and  $\hat{q}_e = 9.53$  mg g<sup>-1</sup>.

The solvent volumes required for the complete elution of phenol (desorption volumes) at the different conditions assayed are reported in Table



7. From these results, methanol is considerably more efficient for phenol desorption than the aqueous NaOH solutions. Indeed, the addition of NaOH to methanol does not appreciably change the eluent strength with respect to pure methanol. On the other hand, the solvent flow-rate also has an effect on the desorption efficiency; an increase in the flow-rate from  $\sim 3$  to  $\sim 50$  BV  $\text{h}^{-1}$  provokes an increase of about 1.8 times in the desorption volume. However, this effect is small by comparison with the effect of the flow-rate on the breakthrough volume during the adsorption process.

For the SPE application of XAD-4 columns, it is interesting to define a ‘concentration factor’ (CF) relating the phenol concentration in the desorption volume to its concentration in the aqueous sample loaded in the column (Eq. (8)):

$$\text{CF} = (q \times W) / (V_{\text{des}} \times [1 \text{ BV}] \times C_0) \quad (8)$$

where,  $V_{\text{des}}$  is the desorption volume (BV),  $C_0$  is the phenol concentration in the aqueous sample ( $\text{mg l}^{-1}$ ) and  $q$  is the phenol concentration in the adsorbent ( $\text{mg g}^{-1}$ ) corresponding to the operating conditions used during the adsorption. The ratio  $W/[1 \text{ BV}]$  (mass of dry adsorbent in the column/volume of the wetted bed, in  $\text{g l}^{-1}$ ) is expected to be practically constant for Amberlite XAD-4 columns.

For analytical applications, where a quantitative recovery of the analyte is required, the vol-

ume of sample loaded in the column is at most the breakthrough volume and  $q = q_b$ . For other applications, where quantitation is not a requirement, the column can be loaded to exhaustion and  $q = q_e$ . In this case, the result of Eq. (8) corresponds to the maximum concentration factor attainable in the SPE experiment for the operating conditions used during the adsorption–desorption cycle (desorption flow-rate and phenol concentration in the sample). It is important to note that the maximum CF is probably independent of the column length if the same normalized flow-rate is used for desorption.

For illustration, the last column of Table 7 gives the concentration factors for the experiments reported in this section. These results show that an hydrophilic compound as phenol cannot be concentrated from an aqueous sample containing  $10 \text{ mg l}^{-1}$  of this solute more than  $\sim 50$  times, when a XAD-4 column is used for the SPE of the sample and methanol is used for desorption. A somewhat higher concentration factor should be expected with a less polar desorption solvent, as acetonitrile, because  $V_{\text{des}}$  depends on the solvent strength. Besides, the maximum concentration factor must also be higher when the water sample contains lower phenol concentrations because, due to the convexity of the adsorption isotherm, the distribution coefficient ( $q_e/C_0$ ) increases as the concentration decreases.

Table 7  
Phenol desorption<sup>a</sup>

Desorption solvent	Flow-rate (BV $\text{h}^{-1}$ )	Desorption volume (BV)	Concentration factor
Methanol	2.96	5.3	52
Methanol	8.11	6.8	40
Methanol	13.6	7.1	39
Methanol	16.7	7.4	37
Methanol	26.4	8.3	33
Methanol	49.7	9.4	29
NaOH ( $10^{-4}$ M) in water	11.7	38	7
NaOH ( $10^{-2}$ M) in water	11.4	30	9
NaOH ( $10^{-4}$ M) in methanol	11.7	6.9	40
NaOH ( $10^{-2}$ M) in methanol	11.5	6.2	44

<sup>a</sup> Conditions: the Amberlite XAD-4 column (bed volume 6.19 ml) was previously loaded to exhaustion with a  $10 \text{ mg l}^{-1}$  aqueous phenol solution at pH 2 using a flow-rate of  $\sim 11$  BV  $\text{h}^{-1}$ . The elution of the analyte was carried out with different solvents and at different flow-rates.

It is interesting to notice that if the column is only loaded with the sample until the breakthrough point of the analyte, the concentration factor will decrease considerably with respect to its maximum value (more than three times in the case of the experiments reported in Table 7). The responsibility for this comes from the slow adsorption kinetics in Amberlite XAD-4. Thus, in order to improve the efficiency of an SPE system using XAD-4 columns for the extraction, concentration and quantitative recovery of hydrophilic compounds from water, it is essential to work at very low flow-rates, especially, during the adsorption stage. An alternative way to improve the efficiency would be the use of smaller XAD-4 beads to pack the column. In either case there is a price to be paid, a time-consuming operation in the former or more complex and expensive equipment due to the column pressure drop in the latter.

#### 4. Conclusions

The effect of the main operating conditions on the adsorption of a polar compound from water in Amberlite XAD-4 columns has been determined. The most important facts concerning the solid-phase extraction application of these columns are the following:

1. For an efficient adsorption of a compound in these columns, which means the largest possible breakthrough volumes, it is necessary to work at low flow-rates, preferably no more than about  $10 \text{ BV h}^{-1}$ . When the compound of interest is an hydrophilic one, as phenol, it is inadvisable to pass the influent through the column at flow-rates of the order of, or higher than,  $100 \text{ BV h}^{-1}$  because the solute will begin to emerge from the column at the void volume, even if its distribution coefficient predicts a higher retention.
2. The breakthrough volume (in number of bed volumes) of a compound in a particular sample is the same in columns of different sizes if, and only if, they are all operated at the same normalized flow-rate. This should permit to predict the size of the column required for a

particular application if one adsorption experiment is run in, for example, a small column. For the latter, it is not necessary to trace the whole adsorption curve, only the breakthrough volume at the chosen flow-rate has to be determined.

3. It was observed that, at a given flow-rate, the efficiency of the adsorption process was independent of the solute concentration in the sample. This means that the ratio of breakthrough volume to stoichiometric (or retention) volume is constant at constant flow-rate. Therefore, if the adsorption isotherm of the compound is known and its breakthrough volume at some concentration is determined, it is possible to predict the breakthrough volume at other concentrations.
4. The volume of eluent required to completely remove a compound adsorbed in an XAD-4 column depends on the flow-rate of the desorption solvent, although this parameter is not so critical as in the adsorption stage. Therefore, the concentration factor obtained for a compound during an adsorption–desorption cycle in these columns will be optimal if both stages are performed at low flow-rate.

It should be noted that the above conclusions were derived from columns packed with the commercial XAD-4 copolymer. For other polymeric adsorbents of small particle diameter or for the same XAD product previously ground and sieved, the effect of the flow-rate is considerably minimized but at the cost of an increase in the pressure drop of the column, which could be unacceptable for some applications (ca. on-line SPE-FIA). Nevertheless, besides the great effect of the flow-rate, all the conclusions derived from this work remain qualitatively valid regardless the particle diameter of the adsorbent.

On the other hand, this study demonstrates that, when the commercial XAD-4 sorbents are used for the SPE of polar compounds, a careful control of the flow-rate is necessary in order to obtain reproducible results and good recoveries. The common practice of rapidly passing the sample through the cartridge by means of a syringe is not adequate in these cases.

## Acknowledgements

The authors wish to thank the Dirección General de Asuntos del Personal Académico, Universidad Nacional Autónoma de México (project IN500197), for financial support and express their gratitude to Enrique Lemus from Rohm and Haas, Mexico who kindly provided the Amberlite XAD adsorbent.

## References

- [1] M.W.F. Nielen, U.A.Th. Brinkman, R.W. Frei, *Anal. Chem.* 57 (1985) 806.
- [2] M.-C. Hennion, P. Subra, V. Coquart, R. Rosset, *Fresenius J. Anal. Chem.* 339 (1991) 488.
- [3] L.E. Vera-Avila, R. Covarrubias, *Intern. J. Environ. Anal. Chem.* 56 (1994) 33.
- [4] L.E. Vera-Avila, P.C. Padilla, M.G. Hernandez, J.L.L. Meraz, *J. Chromatogr. A* 731 (1996) 115.
- [5] A.S. Warang, G. Eadon, *Intern. J. Environ. Anal. Chem.* 11 (1982) 167.
- [6] G.A. Junk, J.J. Richard, M.D. Grieser, et al., *J. Chromatogr.* 99 (1974) 745.
- [7] G.A. Junk, C.D. Chriswell, R.C. Chang, L.D. Kissinger, J.J. Richard, J.S. Fritz, H.J. Svec, *Fresenius Z. Anal. Chem.* 282 (1976) 331.
- [8] B. Wigilius, H. Boren, G.E. Carlberg, A. Grimvall, B.V. Lundgren, R. Svenhed, *J. Chromatogr.* 391 (1987) 169.
- [9] P.R. Musty, G. Nickless, *J. Chromatogr.* 89 (1974) 185.
- [10] A.M. Naghmush, M. Trojanowicz, E. Olbrych-Sleszynska, *J. Anal. At. Spectrom.* 7 (1992) 323.
- [11] V.K. Jain, S.S. Sait, P. Shrivastav, Y.K. Agrawal, *Talanta* 45 (1997) 397.
- [12] P. Bermejo-Barrera, G. Gonzalez-Campos, M. Feron-Novais, A. Bermejo-Barrera, *Talanta* 46 (1998) 1479.
- [13] W.L. Song, Z.L. Zhi, L.S. Wang, *Talanta* 44 (1997) 1423.
- [14] B. Gawdzik, J. Gawdzik, U. Czerwinska-Bil, *J. Chromatogr.* 509 (1990) 135.
- [15] I. Tolosa, J.W. Readman, L.D. Mee, *J. Chromatogr. A* 725 (1996) 93.
- [16] A.A. Aguwa, in: K.E. Noll, V. Gounaris, W.-S. Hou (Eds.), *Adsorption Technology for Air and Water Pollution Control*, Lewis Publishers, Chelsea, 1992, Ch. III, p. 49.
- [17] C. Arai, M.C. Yeh, in: K.E. Noll, V. Gounaris, W.-S. Hou (Eds.), *Adsorption Technology for Air and Water Pollution Control*, Lewis Publishers, Chelsea, 1992, Ch. VI, p. 100.
- [18] D. DeVault, *J. Am. Chem. Soc.* 65 (1943) 532.

# UV-spectrophotometric determination of beclomethasone dipropionate and phenylethyl alcohol in a nasal spray by inverse least-squares regression

M. Blanco <sup>a,\*</sup>, D. Serrano <sup>a</sup>, J.L. Bernal <sup>b</sup>

<sup>a</sup> *Departamento de Química, Unidad de Química Analítica, Facultad de Ciencias, Universidad Autónoma de Barcelona, E-08193 Bellaterra, Spain*

<sup>b</sup> *Departamento de Química Analítica, Facultad de Ciencias, Universidad de Valladolid, Prado de la Magdalena s/n, E-47005 Valladolid, Spain*

Received 7 December 1998; received in revised form 29 March 1999; accepted 28 April 1999

## Abstract

Inverse least-squares (ILS) regression was used for the simultaneous UV spectrophotometric determination of the active principle (beclomethasone dipropionate) and a solvent (phenylethyl alcohol) in a pharmaceutical preparation commercially available in nasal spray form. A factorial design was used to establish the calibration equations, which enables the construction of calibration models using a minimum number of samples. The operating wavelengths were chosen by first choosing that coinciding with the absorption maximum for the analyte to be determined and then adding terms, one at a time, following the stepwise-forward procedure until no significantly improved S.E. is obtained. Single calibration equations were found for both constituents that provide satisfactory results in absorbance mode. The ILS procedure was applied to five industrial preparations with highly satisfactory results. In all, coefficients of variation values were less than 2%. © 1999 Elsevier Science B.V. All rights reserved.

*Keywords:* Inverse least-squares regression; Experimental design; Beclomethasone dipropionate; Phenylethyl alcohol

## 1. Introduction

Beclomethasone dipropionate (BDP) is an active pharmaceutical principle with anti-inflammatory properties that can be administered in various forms. When it is applied as a nasal spray

it often includes a family of surfactants, i.e. benzalconium chloride (BKC), that act as emulsifiers and preservatives, and phenylethyl alcohol (PEA), that mainly works as a solvent.

Most methods reported for the determination of BDP in pharmaceutical preparations rely on a separation technique, such as HPLC [1–4], gas chromatography [5], capillary electrophoresis [4] and polarography [6]. On the other hand, spectrophotometric techniques have scarcely been used; the few available methods of this type for

\* Corresponding author. Tel.: +34-93581367; fax: +34-935812379.

*E-mail address:* iqan8@blues.uab.es (M. Blanco)

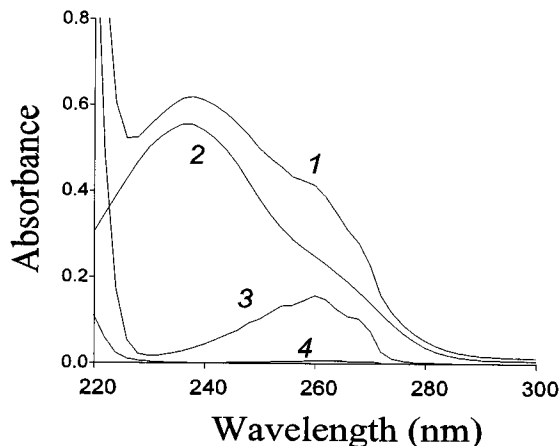


Fig. 1. UV-Vis absorbance spectra for (1) Béconase (diluted 1:25, w/v), (2) BDP ( $20 \mu\text{g ml}^{-1}$ ), (3) PEA ( $0.1 \mu\text{l ml}^{-1}$ ) and (4) BKC ( $9 \mu\text{g ml}^{-1}$ ).

BDP determination include two that involve univariate calibration [7,8] and one that uses classical least-squares regression [4].

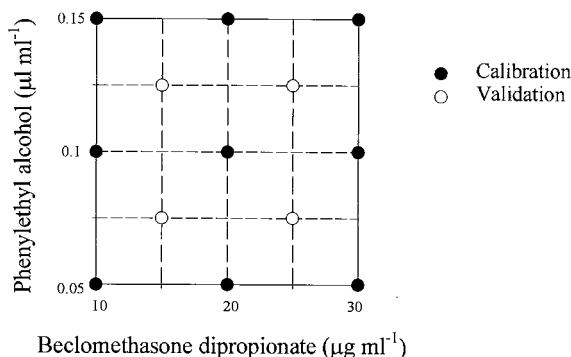


Fig. 2. Laboratory-made sample distribution within calibration and validation sets in the factorial design and its final concentration values in the measured solutions.

Table 1

Figures of merit and RSEP values for calibration of laboratory samples using the MW and the SW selection method

Analyte	Method		$b_0$	$b_1$	$b_2$	$b_3$	$R$	SEC	RSEPC (%)	RSEPP (%)
BDP ( $\mu\text{g ml}^{-1}$ )	SW, MW	$\lambda_1 = 240, \lambda_2 = 272$	-0.001	0.056	0.066	-	0.999	0.65	1.39	1.41
	SW	$\lambda_1 = 220, \lambda_2 = 226, \lambda_3 = 222$	-	-0.1	-0.4	0.6	0.992	7.83	2.12	5.10
PEA ( $\text{nl ml}^{-1}$ )	MW	$\lambda_1 = 260, \lambda_2 = 300, \lambda_3 = 258$	-	5.2	-0.4	-4.8	0.999	0.88	0.75	1.28

The literature abounds with applications of multivariate calibration (MC) procedures to the analysis of pharmaceutical preparations [9–12]. Most point out to the high potential of MC for the simultaneous determination of several absorbing components and the substantial time and economic savings derived from its use as a substitute for HPLC in routine control analyses. Among MC techniques one of the most useful and simple is the inverse least-squares (ILS) regression. The principles of ILS are well known and widely documented [13]. It is a very simple calibration procedure of wide use in near-infrared (NIR) spectroscopy since the 1970s [14] but scarcely employed in UV spectrophotometry to date. Essentially, ILS is a least-squares method that uses the inverse of Beer's law as its model. That is, concentration is modelled as a linear combination of absorbances. Two or three wavelengths are usually enough, so the ILS technique is specially well suited to filter instruments. The main problem with ILS lies in selecting the wavelengths to be used. A bad choice of them would imply elimination of useful information or an overfitting. However it can work successfully without knowing all the sample constituents and it is not affected by interactions between constituents, which are its main advantages over CLS.

Formal optimization techniques are often used to prepare sets of experiments in order to get the maximum information on the system with the minimum economic cost and waste of time in its preparation. One of the most used techniques are factorial designs [15,16] which rely on the

Table 2

Results obtained in the analysis of five production samples using the proposed ILS-MW and the standard addition methods

	Proposed		Standard addition		
	Average*	C.V. (%)	Concentration added**	Average	C.V. (%)
BDP ( $\mu\text{g ml}^{-1}$ )	0.49	1.44	0.12, 0.18, 0.24	0.50	1.79
PEA ( $\text{nl ml}^{-1}$ )	2.47	1.23	0.72, 1.02, 1.64	2.48	1.13

\* Labelled content:  $0.50 \mu\text{g ml}^{-1}$  for BDP and  $2.50 \text{nl ml}^{-1}$  for PEA.\*\*  $\mu\text{g ml}^{-1}$  For BDP and  $\text{nl ml}^{-1}$  for PEA.

availability of a mathematical description for identifying the optimum and carefully plans all the experiments prior to implementation.

The goal of this work was to find a simple, rapid and robust analysis method to determine BDP and PEA in a pharmaceutical preparation and compare it with the reference method, HPLC. BKC was excluded from the study due to its extremely low absorption values in front BPD and PEA absorption values at the level of pharmaceutical preparation contents. ILS was applied to simultaneous spectrophotometric determination of both constituents. The first wavelength included in the calibration equations are made to coincide with the maximum adsorption of the analyte to be determined and the others followed the forward stepwise wavelength selection procedure. The results thus obtained were compared with those provided by solely using the forward stepwise procedure, which is included in most statistical software.

### 1.1. Theoretical background

The ILS procedure is based on the relationship between concentration and absorbance values obtained at several selected wavelengths. As a rule, the concentration is expressed as a linear combination of the apparent absorbance at the different measurement wavelengths. The calibration equation thus obtained by using  $n$  different wavelengths is

$$c = b_0 + \sum_{i=1}^n b_i A_{\lambda_i} + e$$

where  $c$  is the concentration,  $A_{\lambda_i}$  is the absorbance at wavelength  $\lambda_i$ ,  $b_i$  is the regression coefficients

calculated by least-squares fitting during calibration, and  $e$  is the residual.

Choosing an appropriate wavelength in this context is pivotal to obtaining accurate results. In the forward stepwise selection procedure the wavelengths are chosen by first choosing that which is most highly correlated with the analyte concentration and then adding terms, one at a time, until no significantly improved S.E. is obtained.

## 2. Experimental

### 2.1. Samples and chemicals

The nasal spray Béconase as well as the standards of active ingredients and excipients were a gift from Glaxo Wellcome (Aranda de Duero, Burgos, Spain). Solvents used were methanol (for HPLC, Panreac, Montcada i Reixac, Spain) and acetonitrile (for HPLC, Carlo Erba, Rodano, Italy). The nominal content of BDP, PEA and BKC in the product are  $0.5 \mu\text{g mg}^{-1}$ ,  $2.5 \text{nl mg}^{-1}$  ( $2.55 \text{ng mg}^{-1}$ ) and  $0.22 \mu\text{g mg}^{-1}$ , respectively. Stock solutions were prepared for these com-

Table 3

Reproducibility values obtained for the determination carried out using ILS-UV spectroscopy and HPLC

Method	Reproducibility C.V. (%) ( $n = 5$ )	
	BPD	PEA
HPLC	2.45	2.65
UV-ILS	1.44	1.23

pounds and for all the substances that compose the excipient: cellulose microcrystalline, sodium carboxymethyl cellulose, glucose and polysorbate 80 (none presents UV absorption).

## 2.2. Sample preparation

The prepared stock solutions were used to make a set of 13 samples. The first nine were made according to a  $3^2$  whole factorial design comprising the two compounds, BDP and PEA, at three different concentration levels (viz. 10, 20 and  $30 \mu\text{g ml}^{-1}$  for BDP and 0.05, 0.1 and  $0.15 \mu\text{l ml}^{-1}$  for PEA, corresponding to 50, 100 and 150% of the nominal value after the proper dilution). The other four were made corresponding to four intermediate positions of the whole factor design. Accurately known and randomly chosen amounts close to the nominal values in the preparation for BKC and the excipients were added to the samples. These 13 samples were labelled laboratory samples (LS). In all, five production samples were used. This set was labelled production samples set (PS).

The sample treatment used was: 1 g of nasal spray Béconase was weighted and acetonitrile added to a final volume of 25 ml. The mixture was sonicated for 2 min and centrifuged at 3000 r.p.m. for 5 min. The spectrum for the supernatant solution was recorded between 190 and 350 nm against a blank consisting of acetonitrile.

## 2.3. Apparatus

UV spectra were recorded on a Hewlett-Packard HP 8452A diode array spectrophotometer equipped with an HP 7470 plotter, also from Hewlett-Packard, and connected to an IBM PC-AT compatible computer via an HP-IB interface. The software used, HP 89530 MS-DOS UV/VIS, includes modules for instrumental control and recording of UV-vis spectra. Absorbance spectra were recorded by using quartz cuvettes of 1 cm path length.

## 2.4. Data processing

First wavelength for ILS calibration was chosen

in two ways: the analyst selects those that correspond to the maximum absorption wavelength for the analyte to be determined (labelled manual wavelength selection method, MW) or by using the automatic forward stepwise selection method (SW) implemented in near infrared spectral analysis software (NSAS v. 3.20 software suite) (NIRSystems, Silver Spring, MD, USA). In both cases, the second wavelength was chosen following the automatic forward stepwise method, that is to say, those that leads to the lowest S.E. of calibration (SEC) from predicted samples used in the calibration set and the multiple correlation coefficient ( $R$ ) that was closest to unity. This procedure was successively repeated to add new terms to the equation until no significant improvement was obtained. The expression for SEC and  $R$  were thus as follows:

$$\text{SEC} = \sqrt{\frac{\sum_{i=1}^n (C_{\text{pre}_i} - C_{\text{ref}_i})^2}{n - m - 1}}$$

$$R = \sqrt{\frac{\sum_{i=1}^n (C_{\text{pre}_i} - \bar{C})^2}{\sum_{i=1}^n (C_{\text{ref}_i} - \bar{C})^2}}$$

where  $n$  is the number of samples used for calibration,  $m$  is the number of independent variables,  $\bar{C}$  is the average reference concentration, and  $C_{\text{pre}_i}$  and  $C_{\text{ref}_i}$  the predicted and reference concentration, respectively, for sample  $i$ . The precision with which the analyte was quantified in the whole prediction set was defined in terms of the relative standard error of prediction (RSEP):

$$\text{RSEP} (\%) = \sqrt{\frac{\sum_{i=1}^n (C_{\text{pre}_i} - C_{\text{ref}_i})^2}{\sum_{i=1}^n C_{\text{ref}_i}^2}}$$

where  $C_{\text{ref}_i}$  is the reference concentration,  $C_{\text{pre}_i}$  that calculated by the model and  $n$  the number of samples used. This value was expressed as RSEPC when referring to calibration samples and as RSEPP when applied to prediction samples—the latter where used to validate the calibration model.

### 3. Results and discussion

The preparation studied contained three absorbing components, viz. the active principle (BDP), a surfactant (BKC) and a solvent (PEA), but BKC had negligible absorption in front of the other two at the nominal concentration of the preparation. Therefore, we focused on the determination of BDP and PEA. Fig. 1 shows the UV spectra for BDP, BKC, PEA and Béconase at a concentration ratio identical to that in the preparation. As can be seen, BDP absorption was markedly stronger than PEA absorption and the two spectra extensively overlapped.

The predictive capacity of the proposed methods for the quantitation of BDP and PEA was assessed by constructing a calibration model from laboratory-made solutions. Calibration samples were prepared by using a factorial design  $3^2$ , consisting of two factors (BDP and PEA) and three concentration levels approximately corresponding to the nominal content in the pharmaceutical, 50 and 150%, respectively. This set was labelled calibration set (CS). The predictive capacity of the calibration models was evaluated by preparing four additional samples with concentration values within the previous concentration ranges. This set was labelled validation set (VS). Fig. 2 shows the laboratory-made sample distribution within both sets, CS and VS, and its concentration values after the proper dilution.

Table 1 shows the results (the wavelengths used, the coefficients for the corresponding calibration equations and the values of the statistics used) provided by an ILS calibration model using the MW described above, for BDP and PEA respectively. As can be seen, BDP needed an equation containing only two wavelengths (viz. 240 and 272 nm) to provide a good fit, with RSEP values below 1.5% for both prediction and calibration sets. On the other hand, PEA needed three wavelengths (viz. 260, 300 and 258 nm) to provide a good fit, with similar RSEP values. Correction terms at 300 and 258 nm were included in the calibration equation to correct baseline drifts due to scattering produced

by particles in suspension or the contributions of other compounds (BKC). Table 1 also shows the results obtained using SW. The results obtained for BDP were exactly the same, but for PEA the selected wavelengths changed. By SW three different wavelengths were used (viz. 220, 226 and 222 nm), but these led to a worse fit and RSEP values than those by fixing the first wavelength beforehand. The ILS-MW method was thus more suitable than the ILS-SW method and was chosen for calibration.

Once the optimum calibration model was established the proposed method was used to determine the PS set, composed of five manufacturing samples. The accuracy and reproducibility of the results were assessed by the standard addition method (three additions of both compounds corresponding to 4.7, 7.6 and 9.5  $\mu\text{g ml}^{-1}$  for BDP and 0.03, 0.04 and 0.06  $\mu\text{l ml}^{-1}$  for PEA after the properly dilution). Table 2 gives the average values for the five samples of the PS set using both methods. As shown, there was no significant differences between the proposed and the standard addition methods, either for BDP or for PEA. The coefficients of variation were less than 2% for both components which testifies to the reproducibility of the proposed method. Note the high consistency of the results provided by the proposed method. Table 3 shows the comparison between these results and those obtained by HPLC published by Bernal in a previous paper [4]. From the values in Table 3 it can be deduced that the UV-ILS-MW method renders slightly better values than HPLC (reference method).

### 4. Conclusions

The ILS method applied to UV spectrophotometric data is an effective tool to the simultaneous quantitation of beclomethasone dipropionate and phenylethyl alcohol in a pharmaceutical preparation. Although the complexity of the sample preparation is similar in both methods used, the total time per analysis is significantly shorter using the UV technique than that required when HPLC is employed.



The use of an experimental design allows the establishment of the calibration equation using a minimum of samples and assures the correct determination of samples with high deviations from the nominal values.

Manually choosing the first wavelength (that coinciding with the absorption maximum for the analyte to be determined) is an effective alternative to the automatic forward stepwise selection method, specially with analytes overlapped with other of higher absorption.

In summary, the UV-ILS method gives a faster and slightly better analysis than the reference HPLC method. The accuracy and precision of the UV method is slightly better than HPLC and these characteristics make this methodology suitable for a fast control analysis of the manufactured pharmaceuticals.

### Acknowledgements

This work was supported by a DGICYT Project (Project No. PB96-1180). The authors thank Glaxo Welcome S.A. (Aranda de Duero, Spain) for the donation of standards and spray samples, as well as for the information supplied about its pharmaceutical formulation.

### References

- [1] M. LeBelle, R.K. Pike, S.J. Graham, E.D. Ormsly, H.A. Bogard, J. Pham. *Biomed. Anal.* 14 (1996) 793.
- [2] J. Girault, B. Istin, J. Malgouyat, A.M. Brisson, J.B. Fourtillan, J. Chromatogr. *Biomed. Appl.* 102 (1991) 43.
- [3] D. De Orsi, L. Gagliardi, F. Chimenti, D. Tonelli, *Anal. Lett.* 28 (1995) 54.
- [4] J.L. Bernal, M.J. del Nozal, M.T. Martín, J.C. Diez-Masa, A.J. Cifuentes, *J. Chromatogr. A* 823 (1998) 423.
- [5] J. Girault, B. Istin, J.B. Fourtillan, *Biomed. Mass Spectrom.* 19 (1995) 295.
- [6] M.I. Walash, F. Belal, M.E.S. Metwally, M. Hefnawy, *Microchim. Acta* 112 (1994) 217.
- [7] N.M. Sanghavi, S. Mitra, *Indian Drugs* 30 (1993) 129.
- [8] E.R.M. Hackman, S.A. Benetton, M.I.R.M. Santoro, *J. Pharm. Pharmacol.* 43 (1991) 285.
- [9] G. Sala, S. Maspoch, H. Iturriaga, M. Blanco, V. Cerdà, *J. Pharm. Biomed. Anal.* 6 (1988) 765.
- [10] H. Ueda, R. Pereira-Rosario, C.M. Riley, J.H. Perrin, *J. Pharm. Biomed. Anal.* 7 (1989) 309.
- [11] M. Blanco, J. Coello, J. González, H. Iturriaga, S. Maspoch, X. Tomás, *Pharm. Biomed. Anal.* 12 (1994) 509.
- [12] M. Blanco, J. Coello, H. Iturriaga, S. Maspoch, S. Alaoui-ismaili, *Fresenius J. Anal. Chem.* 357 (1997) 967.
- [13] J.C. Sternberg, H.S. Stills, R.H. Schwendeman, *Anal. Chem.* 32 (1960) 84.
- [14] B.G. Osborne, *Near Infrared Spectroscopy in Food Analysis*, Longman, Harlow, 1986.
- [15] R. Carlson, *Design and Optimization in Organic Synthesis*, Elsevier, Amsterdam, 1992.
- [16] E. Morgan, *Chemometrics: Experimental Design*, Wiley, Chichester, 1991.

# Chemometric method to optimize chiral separation of imidazole derivatives by capillary electrophoresis

Yves Claude Guillaume\*, Eric Peyrin

*Laboratoire de Chimie Analytique, Faculté de Médecine Pharmacie, Place Saint Jacques 25030 Besançon Cedex, France*

Received 10 December 1998; received in revised form 13 April 1999; accepted 28 April 1999

## Abstract

A chemometric methodology was proposed to optimize the migration time, height equivalent to a theoretical plate and separation of a mixture of a series of imidazole compounds by capillary electrophoresis. The optimization process was based on a special polynomial from 9 or 18 preliminary experiments. This method connects a general simplex method to a computer. A simplex two or three optimization–capillary electrophoresis (STO-CE) method has been developed in our laboratory. The most efficient separation was achieved with acetonitrile–phosphate buffer, pH 4.70, (5.30 + 94.70 (v/v)) with a  $\beta$ -cyclodextrin concentration in the background electrolyte equal to 5.80 mM and a capillary temperature of 35°C. Similar results were obtained using simple step-wise scanning. The higher relative difference obtained for these values with these two methods (simplex and step-wise scanning) was 5% for the  $\beta$ -cyclodextrin concentration factor. © 1999 Elsevier Science B.V. All rights reserved.

*Keywords:* Chemometric methodology; Capillary electrophoresis;  $\beta$ -Cyclodextrin; Imidazole

## 1. Introduction

Cyclodextrin (CD) is a cyclic oligosaccharide containing six to eight glucopyranose units arranged in such a way as to create a cavity. This cavity can separate molecules on the basis of their size relative to the CD cavity and the stereoselectivity due to the optically active nature of the

carbohydrate units. Several papers have recently examined the nature of the chiral recognition mechanism for cyclodextrin mediated enantioseparation [1–7]. Optimization of these separations can be difficult due to the wide array of parameters and variables that must be controlled ( $\beta$ -CD concentration in the background electrolyte (BGE), temperature, etc.). Corstjens et al. [8] reviewed recent approaches for optimization of selectivity in CE, delineating statistical methods, fitting procedures, and practical optimization based on physico-chemical models of electromigration. Altria et al. [9] explored the various

\* Corresponding author. Tel: +33-81-66-55-46; fax: +33-81-66-55-27.

*E-mail address:* yves.guillaume@univ-fcomte.fr (Y.C. Guillaume)

chemometric experimental designs that have been utilized for systematic optimization of CE separations and methods. These authors concluded that implementation of these designs could facilitate the identification of optimal electrolyte composition as well as the critical parameters determining resolution and analysis. Chang and Yeung [10] thoroughly investigated the dynamic means, i.e. control of pH, temperature, application of external fields and field amplification, to improve resolution, analysis time and reproducibility and to reduce band broadening. Imidazole and triazole derivatives were used for the treatment of onychomycosis [11–13]. Nevertheless, these hydrophobic compounds had a weak penetration into hydrophilic human nail matrices. Their inclusion in apolar cyclodextrin could improve this penetration considering the hydrophilic character of the exterior of cyclodextrin, composed of a large number of hydroxyl groups. The aim of this paper was to investigate the chiral separation of a mixture of a series of imidazole compounds using a chemometric method. This method was used to provide an interrelationship between the migration time of an enantiomer, the resolution between two peaks, capillary plate height, ACN fraction in the BGE, capillary temperature, BGE pH and  $\beta$ -CD concentration in the BGE.

## 2. Experimental

### 2.1. Apparatus

CE separations were carried out using an automated CE apparatus (Beckman 550, Paris, France). The capillaries used were 57 cm (50 cm to the detector)  $\times$  75  $\mu$ m i.d. The following conditions were applied: voltage 30 kV; capillary thermostated at 25°C unless otherwise specified, UV detection at 230 nm; 2 s pressure injection of an imidazole derivative solution dissolved in the BGE.

### 2.2. Solvents and samples

Water was obtained from an Elgestat option I water purification system (Odil, Talant, France)

fitted with a reverse osmosis cartridge. The BGE buffer consisted of a mixture ACN–phosphate buffer with  $\beta$ -CD concentrations varying from 2 to 10 mmol l<sup>-1</sup> and the ACN fraction (v/v) from 0.02 to 0.1.  $\beta$ -CD was obtained from Roquette Laboratories (Lestrem, France). The phosphate buffer was composed of 0.05 M diammonium hydrogen phosphate and 0.05 M ammonium dihydrogen phosphate. The BGE pH were adjusted to values equal to 4.5 from 6.5 with ammoniac or phosphoric acid. The BGE at all pH values were stocked for 1, 2, and 4 h at ambient room temperature to study the accuracy of their pH values. No fluctuations were observed, the maximum relative difference of the pH value of the different mobile phase was always 0.5%. *R*- and *S*-bifonazole (1) *R*- and *S*-econazole (2), *R*- and *S*-sulconazole (3), *R*- and *S*-miconazole (4) obtained from Sigma (Saint Quentin, France), were dissolved in pure acetone to obtain a final concentration of 0.1 mmol l<sup>-1</sup>. The chemical structure of this compound is given in Fig. 1. Each solute or mixture of these was injected and the migration times were measured.

### 2.3. Temperature study

Compound migration times were determined at 20, 25, 30, 35 and 40°C. The electrophoretic system was equilibrated at each temperature for at least 1 h prior to each experiment. To study this equilibration, the compound migration time of the *R*-bifonazole was measured every hour for 7 h and again after, 22, 23 and 24 h. The maximum relative difference in the migration times of this compound between these different measurements was always 0.6% making the electrophoretic system sufficiently equilibrated for use after 1 h. All the solutes were injected in triplicate.

### 2.4. Chemometric methodology

The chemometric methodology was based on factorial designs. For two factors studied at two levels there are 2<sup>2</sup> combinations. The fitting of a first order model (linear model) to the data [14] was carried out using two level factorial designs [15] In general, central designs are constructed

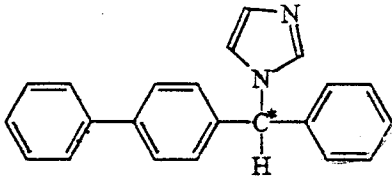
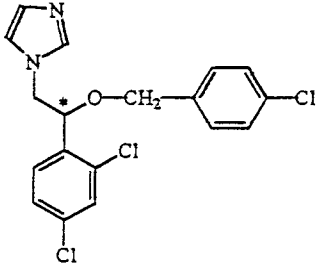
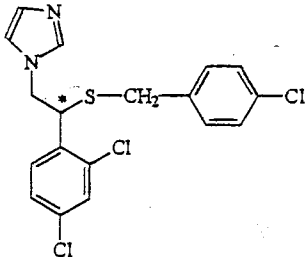
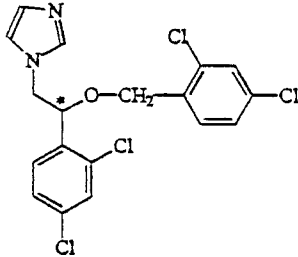
Compound n°	Name	Chemical structure
(1)	Bifonazole	
(2)	Econazole	
(3)	Sulconazole	
(4)	Miconazole	

Fig. 1. Imidazole derivative structures.

from a total of  $2^n + 2n + 1$  factor combinations, where  $n$  is the number of factors being studied [16]. Thus, the number of experiments required for two variables is nine. For four variables, the number is 25. As this was too high, an experimen-

Table 1  
Two-order experimental design for four factors

Experiment No.	$x_1$	$x_2$	$x_3$	$x_4$
1	1	1	1	-1
2	-1	1	1	1
3	-1	-1	1	1
4	1	-1	-1	1
5	-1	1	-1	-1
6	1	-1	1	-1
7	1	1	-1	1
8	-1	-1	-1	-1
9	0	0	0	0
10	-1	0	-1	1
11	1	-1	0	-1
12	-1	0	1	-1
13	1	0	1	1
14	0	-1	-1	0
13	0	-1	0	1
16	0	-1	1	-1
17	-1	-1	1	0
18	1	0	-1	-1

Table 2  
Results of the simplex process for the resolution (Rs) for the pair of peaks most difficult to resolve and two factors

Experiment No.	$T$ ( $^{\circ}\text{C}$ )	$[\beta\text{-CD}]$ ( $\text{mmol l}^{-1}$ )	Rs
1	30	2.00	0.28
2	27	2.01	0.27
3	38	6.40	0.42
4	32	6.04	0.51
2	25	7.01	0.61
6	33	8.02	0.72
7	40	6.02	0.82
8	38	5.02	0.64
9	20	7.07	0.68
10	28	5.15	0.61
11	32	6.12	0.60
12	25	6.24	0.88
13	20	4.24	1.10
14	22	7.12	1.12
15	24	7.14	1.11
16	25	7.15	1.18
17	25	7.14	1.16
18	25	7.19	1.18

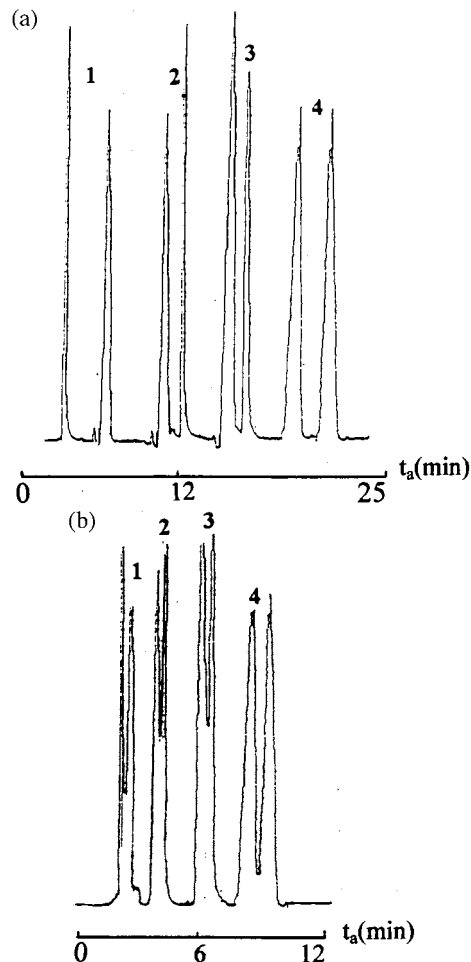


Fig. 2. Representative optimal electropherogram of chiral separation of a mixture of 6 imidazole and triazole derivatives controlled by two parameters: (A)  $\beta\text{-CD} = 7.2 \text{ mmol l}^{-1}$ ,  $T = 25^{\circ}\text{C}$ ; and (B)  $\beta\text{-CD} = 4.2 \text{ mmol l}^{-1}$ ,  $T = 34^{\circ}\text{C}$ . The *R* enantiomer was always eluted before *S* enantiomer. The number above the peaks refers to the six compounds, see Section 2.2.

tal design was developed that did not diverge from the optimal properties (i.e. the independence of effect estimations and the minimization of the bias errors of the model). The following design structure was adopted. The first design fraction was constructed with a factorial design at two levels (i.e. eight experiments). The second fraction was built up using one experiment in the center of the experimental design. The third fraction was developed by using the Fedorov exchange

Table 3  
Results of the simplex process for ERF for two factors

Experiment No.	<i>T</i> (°C)	[β-CD] (mmol l <sup>-1</sup> )	ERF
1	20	2.01	4.21
2	25	4.01	4.26
3	28	3.01	5.27
4	30	3.52	4.42
5	30	6.10	4.31
6	31	6.53	4.40
7	35	2.52	4.19
8	37	3.54	5.41
9	40	4.10	7.32
10	25	4.51	6.21
11	26	5.52	6.41
12	32	8.10	6.27
13	34	2.53	8.38
14	35	9.54	8.42
15	33	5.52	8.51
16	34	5.28	8.52
17	34	4.34	8.54
18	34	4.21	8.55
19	34	4.23	8.58
20	34	4.23	8.58

method. Among experiments with a complete factorial design at three levels, those which minimize the generalized variance of the chosen model parameters were selected. The previously determined points were fixed (i.e. nine experiments). The results of this construction are given in Table 1. The total number of experiments was 18. These two-order experimental designs provided sufficient data to fit a quadratic model to the data set. Regression analysis can be used with these models, e.g. for two factors, the model becomes:

$$Y = a_0 + a_1x_1 + a_2x_2 + a_{11}x_1^2 + a_{22}x_2^2 + a_{12}x_1x_2 \quad (1)$$

where *y* is the response and *x<sub>i</sub>* values are the logarithm of β-CD concentration in the BGE and temperature (for a two factor study) and ACN fraction and BGE pH (for a four factor study). The *a<sub>i</sub>*, *a<sub>ii</sub>* and *a<sub>ij</sub>* terms represent the parameters of the model. All variables were coded to have a variation range from  $-\sqrt{2}$  to  $+\sqrt{2}$  for two factors and from  $-1$  to  $+1$  for four factors.

Table 4  
Calculated and measured apparent electrophoretic mobility and capillary efficiency for *R*-sulconazole in 10 experimental conditions and four factors

Experiment No.	[β-CD] (mmol l <sup>-1</sup> )	<i>T</i> (°C)	pH	ACN (%)			
1	2	20	4.5	5			
2	2	20	6.5	8			
3	2	40	4.5	5			
4	2	40	6.5	8			
5	8	20	4.5	8			
8	8	40	6.5	8			
9	10	30	4.5	6			
10	10	30	6.5	6			
	$\mu_{app,m}$ (10 <sup>-8</sup> m <sup>2</sup> V <sup>-1</sup> s <sup>-1</sup> )	$\mu_{app,c}$	<i>e</i> % <sup>a</sup>	<i>H<sub>m</sub></i>	<i>H<sub>c</sub></i>	<i>e</i> % <sup>a</sup>	
1	1.85	1.82	1.6	3.28	3.31	0.9	
2	1.58	1.55	1.8	5.03	5.08	1.0	
3	2.08	2.12	1.9	2.80	2.88	2.8	
4	1.70	1.67	1.8	4.82	4.88	1.2	
5	1.46	1.43	2.0	4.92	5.04	2.3	
6	1.38	1.41	2.1	6.03	5.99	0.7	
7	1.72	1.75	1.7	5.82	5.79	0.5	
8	1.44	1.42	1.4	6.01	6.05	0.7	
9	1.78	1.75	1.7	3.84	3.82	0.5	
10	1.63	1.62	0.6	4.01	3.98	0.7	

<sup>a</sup> Relative difference between calculated and experimental values.

Table 5

Results of the simplex process for the resolution (Rs) for the pair of peaks most difficult to resolve and four factors

Experiment No.	<i>T</i> (°C)	[β-CD] (mmol l <sup>-1</sup> )	pH	ACN (%)	Rs
1	20	4.50	4.50	2.80	0.471
2	25	3.51	5.51	3.82	0.482
3	30	4.85	6.01	4.10	0.263
4	35	3.85	6.52	6.10	0.201
5	40	9.60	4.58	2.82	0.480
6	42	6.51	4.80	2.12	0.524
7	30	6.82	5.15	3.14	0.741
8	34	5.83	5.28	3.88	0.852
9	35	4.61	5.52	4.52	0.853
10	28	2.72	6.04	5.53	0.752
11	30	3.82	6.52	3.82	0.653
12	32	7.83	5.54	4.21	0.657
13	35	6.54	5.02	4.56	0.552
14	27	5.48	4.82	4.63	0.708
15	31	4.53	5.24	2.32	0.801
16	38	3.28	6.24	4.83	0.998
17	40	2.14	6.42	5.31	1.000
18	42	5.71	6.82	6.42	0.989
19	34	4.52	5.81	7.28	0.972
20	34	7.15	4.88	8.91	0.999
21	34	5.10	4.70	9.12	1.000
22	35	7.10	4.83	9.70	1.010
23	37	6.10	6.51	8.40	1.015
24	37	5.10	5.10	8.20	1.012
25	38	4.80	5.10	7.10	1.013
26	35	5.70	4.86	4.99	1.018
27	34	5.70	4.85	4.91	1.013
28	35	5.71	4.70	5.20	1.015
29	35	5.75	4.75	5.23	1.020
30	35	5.80	4.70	5.23	1.020

### 2.5. Simplex optimization process

To optimize the mathematical model ( $y$ ) given in the experimental design, a simplex method was used. The  $y$  value was calculated for  $m$  sets of starting conditions where  $m$  represented the number of factors to be optimized plus one. The point corresponding to the lowest value of  $y$  was then reflected in relation to the surface that was defined by the other points. A new set of starting conditions resulted. Once again, the point with the lowest value of  $y$  was reflected and the process repeated until the same conditions continued to be selected.

### 3. Results and discussion

The resolution Rs between two peaks is given by the equation:

$$Rs = \frac{1}{4} \frac{\Delta\mu_{app}}{\bar{\mu}_{app}} \sqrt{\frac{L}{H}} \quad (2)$$

where  $\Delta\mu_{app}$  is the difference in apparent electrophoretic mobility between two solutes,  $\bar{\mu}_{app}$  is the average apparent electrophoretic mobility of the two species,  $L$  the capillary length and  $H$  is the plate height. The BGE pH was kept at 5.5 and no ACN was added to the BGE. The effect of the β-CD concentration and temperature on elec-

trophoretic mobility and capillary efficiency were studied. The experimental  $H$  and  $\mu_{app}$  values for each compound were calculated from the nine electropherograms. All the experiments were repeated three times making 27 experiments. The variation coefficients of the  $H$  and  $\mu_{app}$  values were all less than 5% which indicated high reproducibility and good stability for the electrophoretic system. The results were processed by computer and the parameters of the  $\ln \mu_{app}$  and  $1/H$  models were obtained. The models fitted the results. All the correlation coefficients were greater than or equal to 0.98. The migration time for each compound is given by the equation:

$$t = \frac{lL}{V} \frac{1}{\exp(\ln \mu_{app})} \quad (3)$$

Where  $V$  is the applied voltage and  $l$  the detector position. Knowing the variation of  $\ln \mu_{app}$  with the two factors, the migration time for all solutes could be calculated. The observed agreement between predicted and experimental values showed the suitability of the models. For  $1/H$  models, Student's  $t$ -test showed that all factors were significant. Using Eq. (2), the resolution ( $R_s$ ) between two peaks for the different values of the

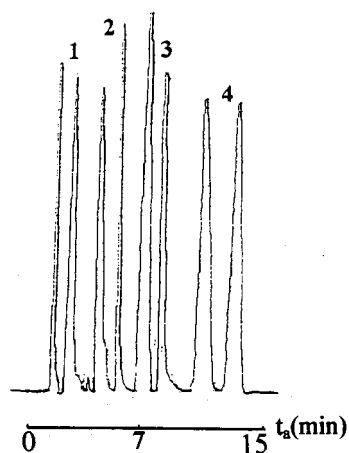


Fig. 3. Representative optimal electropherogram of chiral separation of a mixture of 6 imidazole and triazole derivatives controlled by four parameters:  $\beta$ -CD = 5.8 mmol l<sup>-1</sup>,  $T$  = 35°C, pH = 4.70, and ACN = 5.2%. R was always eluted before S enantiomer. Number above peaks refer to the four compounds, see Section 2.2.

two factors was calculated. With the simplex method, for the worst separated pair of peaks,  $R_s$  was found to be at a maximum (1.18) when the  $\beta$ -CD concentration was 7.2 mmol l<sup>-1</sup> and  $T$  = 25°C. The BGE pH was kept at 5.5 (Table 2). The analysis time was 25 min (Fig. 2A). To minimize the analysis time, an electrophoretic response function (ERF) derived from the chromatographic response function (CRF) [17–21] was used. This was defined as follows:

$$\text{ERF} = F_{obj} + n^a + b(t_A - t_L) \quad (4)$$

where  $F_{obj}$  is the objective function expressed in terms of the resolution ( $R_{sij}$ ) between two peaks  $i$  and  $j$ . In this application,  $F_{obj}$  is given by the following [22]:

$$F_{obj} = \sum \ln(1 + R_{sij}) \quad (5)$$

The sum extends to all the peak pairs on the electropherogram. In Eq. (4),  $n$  is the detected peak number,  $t_A$  is the maximum acceptable analysis time,  $t_L$  is the migration time of the last peak. The constants  $a = 1$ ,  $b = 0.5$  were determined empirically to give a function that sharply discriminated unsatisfactory separations from better separations.  $t_A$  Was set at 15 min. The optimum separation conditions were obtained when ERF reached its maximum in a short analysis time. The coefficient of multiple determination that corresponded to the ERF model was 0.98. The simplex optimization process resulted in a maximum ERF for the  $\beta$ -CD concentration = 4.20 mmol l<sup>-1</sup> and  $T$  = 34°C (Table 3). The corresponding analysis time was equal to 12 min and the worst resolution factor was 0.65. The electropherogram is given in Fig. 2B. If this separation had been proposed for only the qualitative determination of the compounds in the mixture, it would not have been necessary to obtain an optimal resolution. For a quantitative analysis this value of the resolution had to be increased. The separation was then carried out by studying the effect of two additional factors, i.e. BGE pH and the ACN fraction in the BGE which were parameters which are known to enhance chiral separation [23]. The effect of the four factors on solute migration time and capillary efficiency were assessed. The experi-



mental  $H$  and  $\mu_{\text{app}}$  values for each compound were calculated from the 18 electropherograms given by our constructed experimental design. All the experiments were repeated three times, making a total of 54 experiments. The variation coefficients of the  $H$  and  $\mu_{\text{app}}$  values were all less than 4%. As above, the results were processed by computer and the parameters of the  $\ln \mu$  and  $1/H$  models were obtained. The models agreed with the results. All the correlation coefficients were greater than or equal to 0.96. The Student's  $t$ -test confirmed that the  $\ln \mu_{\text{app}}$  and  $1/H$  values were dependent on the four factors. The apparent electrophoretic mobility  $\mu_{\text{app}}$  and  $H$  for the sulconazole were calculated for ten experimental conditions (Table 4). The observed agreement between predicted and experimental values showed the suitability of the models. Using Eq. (2), the resolution between two peaks was calculated for the different values of the four factors. The maximum  $R_s$  (1.01) was determined with the simplex method. The optimum separation was obtained in 15 min with a  $\beta$ -CD concentration equal to 5.80 mmol  $l^{-1}$ ,  $T = 35^\circ\text{C}$ ,  $\text{pH} = 4.70$ , and ACN fraction (v/v) = 0.052 (Table 5). The electropherogram is given in Fig. 3. Similar findings were obtained using simple step-wise scanning. The higher relative difference obtained for the optimized parameters (simplex and step-wise) was 5% for the  $\beta$ -CD concentration factor. These results confirmed the need to add organic modifier to the run buffer to enhance chiral recognition between the guest and host molecule in CE [23]. In summary, the results of this study demonstrate that this method can be used in CE to model solute migration time and chiral compound mixture separation. ACN can be used with  $\beta$ -CD to enhance enantioselectivity. This procedure reduces the number of experiments to be carried out and provides a rapid separation.

## References

- [1] F. Lelievre, P. Gareil, Y. Bahaddi, H. Galons, Anal. Chem. 69 (1997) 393.
- [2] F. Lelievre, P. Gareil, A. Jardy, Anal. Chem. 69 (1997) 385.
- [3] B.A. Ingelse, H.C. Claessens, S. Van der Wal, A.L.L. Duchateau, F.M. Everaerts, J. Chromatogr. A 745 (1996) 61.
- [4] G. Endresz, B. Chankvetadze, D. Bergenthal, G. Blaschke, J. Chromatogr. A 732 (1996) 133.
- [5] A. Petersen, J.P. Foley, J. Microcolumn Sep. 8 (1996) 427.
- [6] S. Surapaneni, K. Ruterbories, T. Lindstrom, J. Chromatogr. A 761 (1997) 249.
- [7] R.L. Williams, G. Vigh, J. Chromatogr. A 730 (1996) 273.
- [8] H. Corstjens, H.A.H. Billiet, J. Frank, K.C.A.M. Luyben, J. Chromatogr. A 715 (1995) 1.
- [9] K.D. Altria, B.J. Clark, S.D. Filbey, M.A. Kelly, D.R. Rudd, Electrophoresis 16 (1995) 2143.
- [10] H.T. Chang, E.S. Yeung, Electrophoresis 16 (1995) 2069.
- [11] M. Pedersen, M. Edelsten, V.F. Nielsen, A. Scarpellini, S. Skytte, C. Slot, Int. J. Pharm. 90 (1993) 247.
- [12] M. Pedersen, Drug Dev. Ind. Pharm. 19 (1993) 439.
- [13] H. Van Doorne, E.H. Bosch, C.F. Lerk, Pharm. Wkly. Sci. Ed. 10 (1998) 80.
- [14] A.F. Fell, T.A.G. Noctor, J.E. Mama, B.J. Clark, J. Chromatogr. A 434 (1988) 377.
- [15] G.E.P. Box, K.B. Wilson, J. Roy. Stat. Soc. B 13 (1951) 209.
- [16] W.G. Cochran, G.M. Cox, Experimental Designs, Wiley, New York, 1957.
- [17] S.L. Morgan, S.N. Deming, Chromatographia. 112 (1975) 267.
- [18] H.J.G. Debets, B.L. Bajema, D.A. Doornbos, Anal. Chim. Acta 151 (1983) 131.
- [19] H.J.G. Debets, B.L. Bajema, D.A. Doornbos, Anal. Chim. Acta 150 (1983) 259.
- [20] M.W. Watson, P.W. Carr, Anal. Chem. 51 (1979) 1835.
- [21] J.L. Glajch, J.J. Kirkland, K.M. Squire, J.M. Minor, J. Chromatogr. A 199 (1980) 57.
- [22] Y.C. Guillaume, C. Guinchard, J. Liq. Chromatogr. 17 (7) (1994) 1443.
- [23] T.J. Ward, M. Nichols, L. Sturdivant, C.C. King, Amino Acids 8 (1995) 337.

## Halide ion-selective electrode array calibration

M. Baret <sup>a</sup>, D.L. Massart <sup>b</sup>, P. Fabry <sup>c</sup>, C. Menardo <sup>a</sup>, F. Conesa <sup>a,\*</sup>

<sup>a</sup> Rhône-Poulenc Industrialisation, CRIT Décines, 24 Avenue Jean Jaurès, F-69153 Décines Charpieu Cedex, France

<sup>b</sup> Vrije Universiteit Brussel, Laarbeeklaan 103, B-1090 Brussel, Belgium

<sup>c</sup> L.E.P.M.I., Ecole Nationale Supérieure d'Electrochimie et d'Electrometallurgie de Grenoble, BP 75, F-38402 Saint Martin d'Hères Cedex, France

Received 10 December 1998; received in revised form 14 April 1999; accepted 28 April 1999

### Abstract

The calibration of several ions ( $\text{Cl}^-$ ,  $\text{Br}^-$ ,  $\text{F}^-$  and  $\text{OH}^-$ ) measured with an ion selective electrodes (ISE) array has been carried out in the presence of interferences using an experimental design and multivariate calibration methods. Partial least squares regression and principal component regression do not seem to improve the test set prediction compared to multivariate linear regression. In the case of very slight or no interference on the ISE, each ion can be determined using the corresponding ISE and univariate calibration methods, but the use of multivariate methods does not lead to worse results. © 1999 Published by Elsevier Science B.V. All rights reserved.

*Keywords:* Multivariate calibration; Univariate calibration; Ion-Selective electrodes; Interferences

### 1. Introduction

The measurement of several ion concentrations in solution in a reaction mixture, a final product or an industrial effluent can be a difficult problem. An interesting electrochemical technique is the use of ion selective electrodes (ISEs). This technique is non-destructive and the equipment is not expensive, but the main difficulty is the measurement of ionic concentrations in the presence of interfering ions because such sensors are not

perfectly selective. The aim of this work was the study of chemometric methods to monitor the concentrations of several ions in solution, using an array of ISEs. Since the 1980s some authors have been interested in the use of chemometrics to calibrate ISEs. Otto et al. [1] have shown the feasibility of an over-determined approach of the problem for multiple ion determination with  $\text{Ca}^{2+}$ ,  $\text{Mg}^{2+}$ ,  $\text{Na}^{2+}$  and  $\text{K}^+$ . The advantage of using sparingly selective electrodes in the array rather than highly selective electrodes was shown by Beebe et al. [2,3], using non linear multiple regression for  $\text{Na}^+$  and  $\text{K}^+$  analysis. The technique was improved by Forster et al. [4,5] to determine a low concentration of one cation ( $\text{Na}^+$ ,  $\text{K}^+$ , or  $\text{Ca}^{2+}$ ) in a medium where the other cations are present in large amount. They

\* Corresponding author. Tel.: +33-4-72-93-58-29; fax: +33-4-72-93-52-65.

E-mail address: francois.conesa@rhone-poulenc.com (F. Conesa)

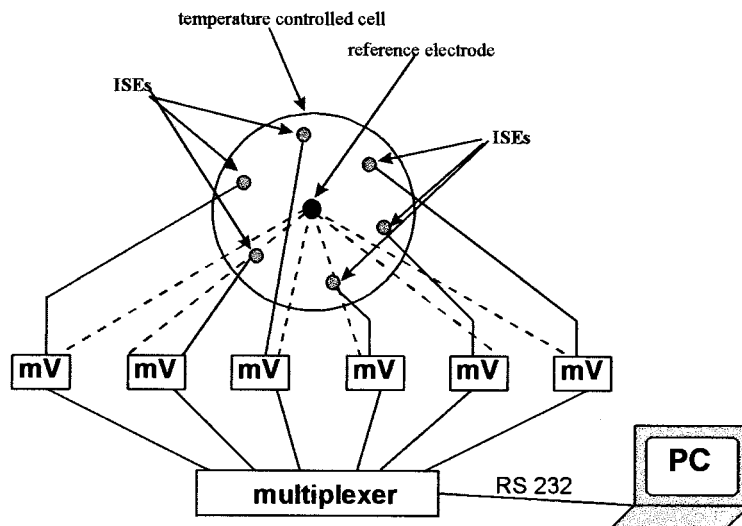


Fig. 1. Experimental set up. 'mV' are the millivoltmeters and 'PC' is the computer.

showed that the best results are obtained using a sparingly selective electrode associated with highly selective electrodes. More recently, Harnett and Diamond [6] presented the calibration of an array of cation ISEs by non linear multivariate methods determining the Nikolskii–Eisenman coefficient using a genetic algorithm and simplex optimisation.

The problem studied here is the calibration of an array of halide ISEs for the determination of chloride, bromide, fluoride and pH. Such an array does not seem to have been studied up to now

and, because the  $\text{Br}^-/\text{Cl}^-$  interferences can be very strong, this calibration is not simple. The aim was to see if measurements of these ions using an ISE array and chemometrics was possible in spite of interfering ions.

In a first study [7], univariate and multivariate chemometric methods were compared for the determination of ion concentrations measured with all or part of a 6-ISE array and the experimental conditions were chosen so that for most ion determinations ( $\text{Br}^-$ ,  $\text{F}^-$  and pH), the univariate methods investigated gave sufficiently good re-

Table 1  
Characteristics of the ISEs [12]<sup>a</sup>

ISE name	Reference	Nature	Primaryion	pX response range	Advised pH range	Interference
CL1	XS200	Polycrystalline	$\text{Cl}^-$	1–6	2–4	$\text{Br}^{-(S)}$ , $\text{OH}^{-(w)}$
CL2	XS210	Polycrystalline	$\text{Cl}^-$	1–5	2–14	$\text{Br}^{-(S)}$ , $\text{OH}^{-(w)}$
BR	XS22	Polycrystalline	$\text{Br}^-$	1–6	2–14	$\text{Cl}^{-(w)}$ , $\text{OH}^{-(w)}$
PF	XS270	Monocrystalline	$\text{F}^-$	1–6	0–8	$\text{OH}^{-(S)}$
PH	XG200	Glass	$\text{H}^+$	1–14	0–14	
SCN	XS250	Polycrystalline	$\text{SCN}^-$	1–6	0–14	$\text{Br}^{-(m)}$ , $\text{Cl}^{-(w)}$ , $\text{OH}^{-(w)}$

<sup>a</sup> The highest value of the pX response range corresponds to the detection limit.

<sup>(S)</sup> Strong interference.

<sup>(w)</sup> Weak interference.

<sup>(m)</sup> Medium interference.

Table 2  
pX levels for the calibration samples (pX unity)

Sample	1	2	3	4	5	6	7	8	9	10	11	12	13	14	15	16	17	18	19	20	21	22	23	24	25
pCl	2	3	1	1.5	2.5	1.5	2	2.5	1.5	2.5	1.5	2	2	2.5	2	1.5	2.5	1.5	2	2	2	2.5	2	2	2
pBr	4.5	4.5	4.5	3	6	6	4.5	3	4	5	5	3.5	4.5	4	5.5	4	5	5	4.5	3.5	4.5	4	5.5	4.5	4.5
pF	3	3	3	3	3	3	3	3	2	4	4	4	3	2	2	2.75	3.25	3.25	3	3.25	2.25	2.75	2.75	3.75	3
pH	6	6	6	6	6	6	6	6	6	6	6	6	6	6	6	7	5	5	6	5	5	7	7	7	6

Table 3  
pX levels for the test samples (pX unity)

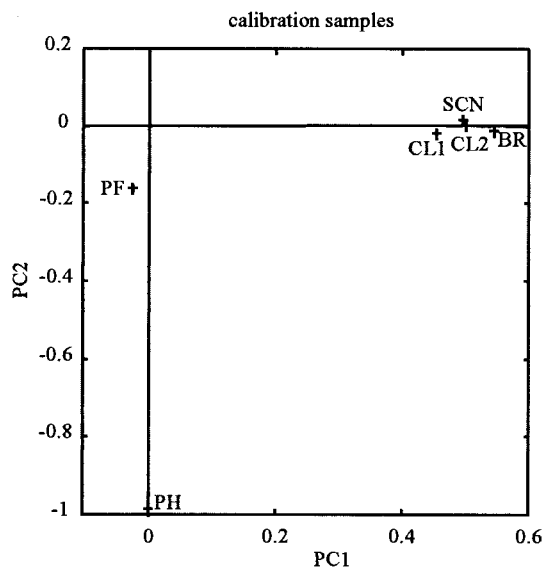
Sample	26	27	28	29	30	31	32	33	34	35	36	37	38	39	40	41	42	43	44	45	46	47	48	49	50
pCl	2	2.8	1.2	1.6	2.4	1.6	2	2.4	1.6	2.4	1.6	2	2	2.4	2	1.6	2.4	1.6	2	2	2	2.4	2	2	2
pBr	4.5	4.5	4.5	3.2	5.8	5.8	4.5	3.2	4.2	4.8	4.8	3.5	4.5	4.2	5.5	4.2	4.8	4.8	4.5	3.5	4.5	4.0	5.5	4.5	4.5
pF	3	3	3	3	3	3	3	3	2.2	3.8	3.8	3.8	3	2.2	2.2	2.8	3.2	3.2	3	3.2	2.4	2.8	2.8	3.6	3
pH	6	6	6	6	6	6	6	6	6	6	6	6	6	6	6	6.8	5.2	5.2	6	5.2	5.2	6.8	6.8	6.8	6

Table 4  
Correlation coefficients<sup>a</sup>

	CL1	CL2	BR	SCN	PF	PH
Correlation						
CL1		0.975	0.9266	0.9376	-0.0106	0.0192
CL2	0.975		0.9777	0.9843	-0.0191	-0.0055
BR	0.9266	0.9777		0.9818	-0.0394	0.0127
SCN	0.9376	0.9843	0.9818		-0.0334	-0.0242
PF	-0.0106	-0.0191	-0.0394	-0.0334		0.0254
PH	0.0192	-0.0055	0.0127	-0.0242	0.0254	
<i>P</i> -value						
CL1		0	0	0	0.9598	0.9272
CL2	0		0	0	0.9278	0.9793
BR	0	0		0	0.8515	0.9519
SCN	0	0	0		0.8741	0.9085
PF	0.9598	0.9278	0.8515	0.8741		0.9041
PH	0.9272	0.9793	0.9519	0.9085	0.9041	

<sup>a</sup> 0 denotes non significant values.

sults. In the present work the experimental conditions have been modified such that the  $\text{Br}^-/\text{Cl}^-$  interference occurs in a moderated way and at least for chloride and bromide, multivariate calibrations should lead to better results than univariate ones and we wanted to investigate if better methods can indeed be obtained.



## 2. Theory

### 2.1. Electrochemistry aspect

The electrochemical relationship between the ISE response (potential) and the ion concentration is given by the Nikolskii–Eisenman relationship [8]:

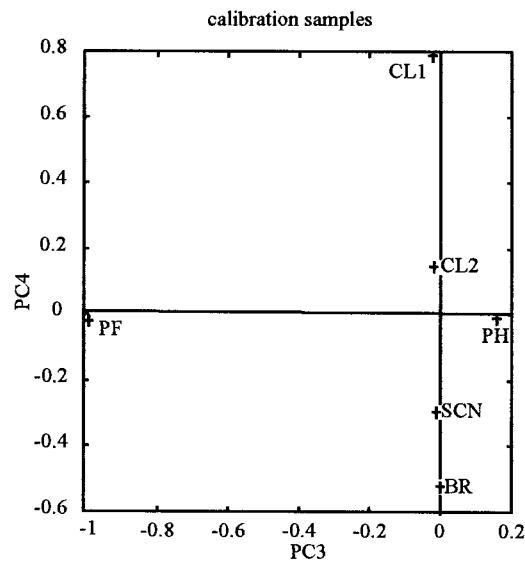


Fig. 2. Loading plots.

$$E_i = A + RT/(z_i F) \ln \left[ C_i + \sum_j K_{ij} (C_j)^{z_i/z_j} \right] \quad (1)$$

where  $E_i$  is the ISE potential versus the reference electrode,  $A$  is a constant representing the standardisation potential,  $R$  is the perfect gas constant,  $T$  is the temperature,  $F$  is the Faraday constant,  $C_i$  and  $z_i$  are the concentration and the charge of the primary ion,  $C_j$  and  $z_j$  are the concentration and the charge of the interfering ions and  $K_{ij}$  are the interference coefficients of the  $j$  interfering ions on the  $i$  ISE. For example, for a chloride selective electrode, Eq. (1) can be written:

$$E_{\text{Cl}} = A - RT/F \ln (C_{\text{Cl}^-} + K_{\text{Cl, Br}} C_{\text{Br}^-}) \quad (2)$$

where  $K_{\text{Cl, Br}}$  is about  $10^2$ , and for a bromide ISE:

$$E_{\text{Br}} = A - RT/F \ln (C_{\text{Br}^-} + K_{\text{Br, Cl}} C_{\text{Cl}^-}) \quad (3)$$

where  $K_{\text{Cl, Br}}$  is about  $10^{-2}$ .

In fact, the  $K_{ij}$  can vary with the concentrations of the various primary and interfering ions (see for example Ref. [9]). We have chosen not to use the Nikolskii relation but chemometric methods to be free of the determination of such coefficients that depend on the composition of the measured solution. This study will allow to

show the advantages and limitations of such chemometric methods for the present type of application.

The use of linear calibration methods leads us to use relations closer to the relation used by Iragashi et al. in case of ion selective field effect transistors (ISFET) [10]:

$$E_i = A + \sum_j k_{ij} \log C_j \quad (4)$$

where  $k_{ij}$  is a constant depending on the solution and on the  $i$  and  $j$  ions ( $k_{ij}$  must not be confused with  $K_{ij}$ ). If  $j = i$ ,  $C_j$  is the concentration of the primary ion ( $C_i$ ) and  $k_{ij} = 2.3 RT/z_i F$ .

In the two preceding relations, the assumption is made that the activities are equal to the concentrations as is the case in diluted solutions. In the following,  $-\log C_X$  will be written pX.

## 2.2. Chemometric methods

### 2.2.1. Calibration

First, univariate methods of calibration (classical and inverse) are compared briefly. Using the inverse calibration:  $\text{pX} = g(\text{potential})$ , we perform an estimation of the inverse of the  $f$

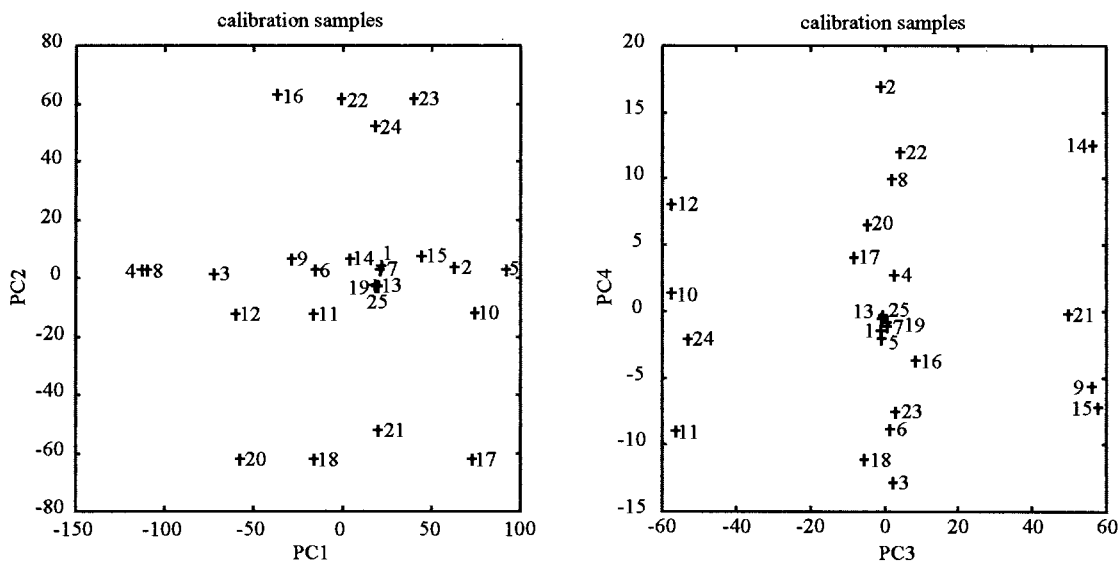


Fig. 3. Score plots. The figures represent the samples (see Table 2)

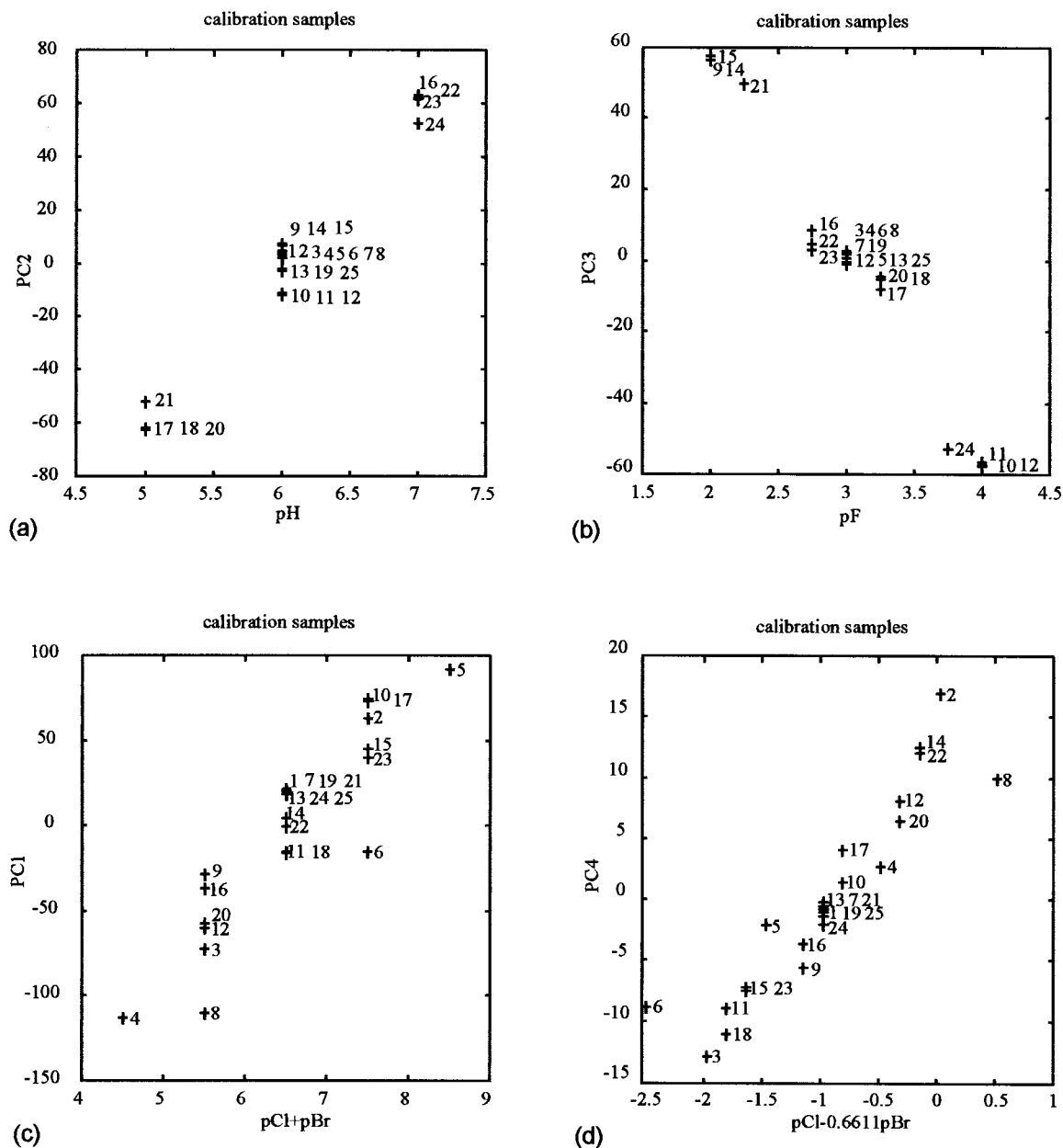


Fig. 4. Principle components from the PCA vs. pX.

classical regression function: potential =  $f(\text{pX})$  so that in fact  $g = \hat{f}^{-1}$ . The main difference results in the calculation of the errors: while the classical method minimises the squared residuals of the measurement values ( $y$ -values) towards the regression line, the inverse calibration minimises

them in the  $x$ -direction, i.e. the pX (or concentration).

Multivariate methods are also used to calibrate the different pX. These methods are multivariate linear regression (MLR), Principal component regression (PCR) and partial least squares regres-



Table 5  
Univariate calibration results

pX	Sensor	Method	Factors	RMSECV	RMSEC	RMSEP	Slope (mV/pX)
pCl	CL1	Inv. cal. <sup>a</sup>	CL1	0.3603	0.316	0.254	
pCl	CL1	Clas. reg. <sup>b</sup>	CL1		0.446	0.3665	39.03
pBr	BR	Inv. cal.	BR	0.4917	0.4614	0.377	
pBr	BR	Clas. reg.	BR		0.5744	0.462	30.14
pF	PF	Inv. cal.	PF	0.0256	0.02321	0.04933	
pF	PF	Clas. reg.	PF		0.0232	0.0495	57.80
pH	PH	Inv. cal.	PH	0.03909	0.0374	0.02864	
pH	PH	Clas. reg.	PH		0.0375	0.0296	-60.32

<sup>a</sup> Inv.cal., inverse calibration.

<sup>b</sup> Clas. reg., classical regression.

sion (PLS) [11]. They are based on inverse calibration.  $\mathbf{X}$  is the ( $n \times p$ ) matrix of the sensor responses ( $p$  columns corresponding to the sensors and  $n$  rows corresponding to the samples), and  $\mathbf{Y}$  is the ( $n \times q$ ) matrix of the pX values ( $q$  columns corresponding to the analytes and  $n$  rows corresponding to the samples). MLR is a regression of several  $x$  vectors of the  $\mathbf{X}$  matrix on one  $y$  variable of the  $\mathbf{Y}$  matrix. If only one vector is re-

gressed, MLR is reduced to univariate inverse regression. Performing the PCR, the  $x$  variables are reduced first to principal components and the scores on the PC's are used as  $x$  variables in MLR. PC's are orthogonal and therefore free from collinearity between variables. When performing PLS, the number of  $x$  variables is reduced as in PCR but the latent variables are built by maximising the covariance between  $\mathbf{X}$  and  $y$ .

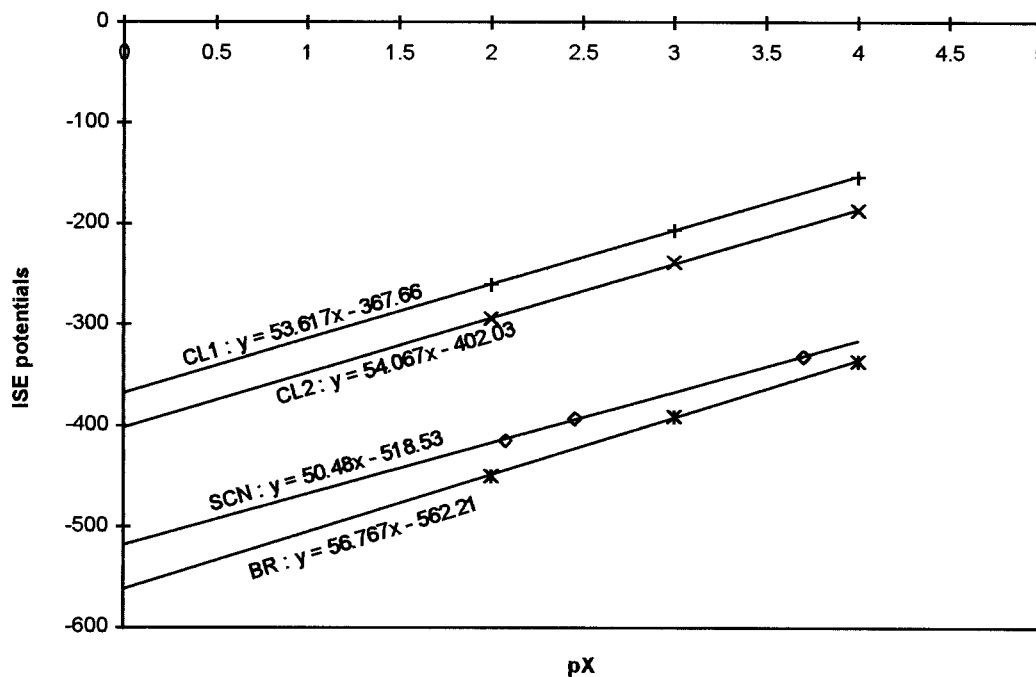


Fig. 5. Calibration plots in pure solutions (CL1 and CL2 potentials have been measured in  $\text{Cl}^-$  solutions, BR and SCN ones in  $\text{BR}^-$  and  $\text{SCN}^-$  solutions, respectively).

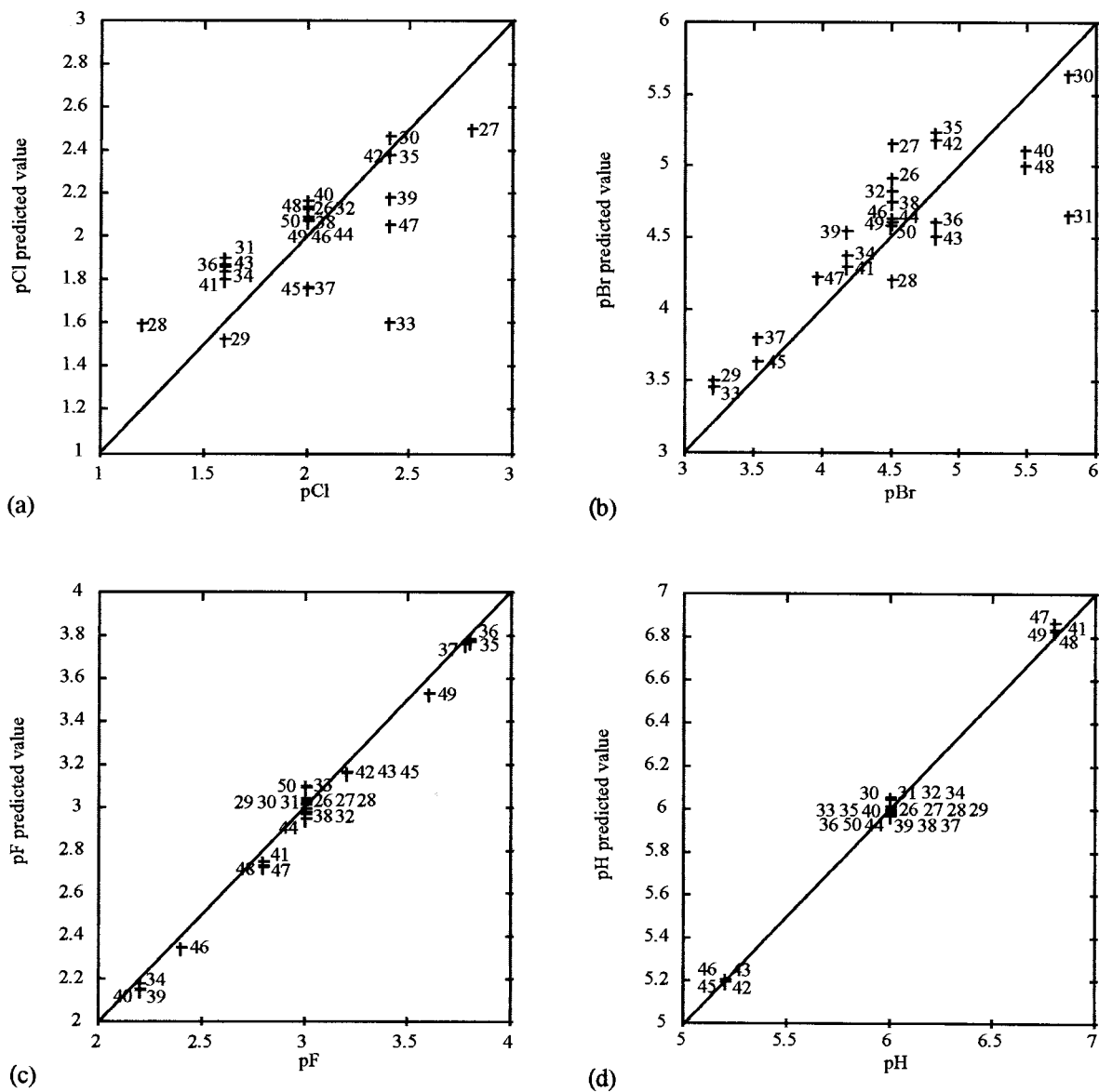


Fig. 6. Univariate inverse calibration results. (a) pCl inverse calibration with the CL1 electrode, RMSEP = 0.254. (b) pBr inverse calibration with the BR electrode, RMSEP = 0.377. (c) pF inverse calibration with the PF electrode, RMSEP = 0.0493. (d) pH inverse calibration with the PH electrode, RMSEP = 0.0286.

### 2.2.2. Validation

To validate the chemometric methods mentioned higher, we used cross-validation and test set validation. The leave-one-out cross-validation performs  $n$  times the calibration removing each time one row of the matrix of the training samples and predicts the sample left out with the calibration model based

on the  $(n - 1)$  remaining samples. The test set validation is an external validation which predicts the matrix of the test samples from the calibration model built from the training sample matrix. To compare the different models, the root mean square errors of cross-validation (RMSECV) and of prediction (RMSEP) are determined [11] as follows:

Table 6  
Multivariate calibration results<sup>a</sup>

pX	Sensors	Method	Factors	Training set RMSECV	Test set RMSEP	RMSECV*RMSEP
pCl	All	MLR	CL1, SCN	0.2003	0.1318	0.0264
pCl	All	PCR	PC4, PC1	0.2026	0.1534	0.0311
pCl	All	PLS	Two-factor	0.3901	0.144	0.0562
pCl	All	PLS	Three-factor	0.1861	0.1494	0.0278
pCl	4 ISEs	PCR	PC2, PC1	0.1853	0.1506	0.0279
pCl	4 ISEs	PLS	Two-factor	0.1841	0.1487	0.0274
pBr	All	MLR	BR, CL1	0.3487	0.3065	0.1069
pBr	All	PCR	PC1, PC4	0.3809	0.3039	0.1158
pBr	All	PLS	Three-factor	0.3816	0.3075	0.1173
pBr	4 ISEs	PCR	PC1, PC2	0.3723	0.3019	0.1124
pBr	4 ISEs	PLS	Two-factor	0.3654	0.3039	0.111
pF	All	MLR	PF, PH	0.02377	0.04874	0.0012
pF	All	MLR	PF	0.0256	0.04933	0.0013
pF	All	PCR	PC3, PC2	0.04988	0.04699	0.0023
pF	All	PLS	Two-factor	0.02781	0.0478	0.0013
pH	All	MLR	PH	0.03909	0.02864	0.0011
pH	All	PCR	PC2, PC3	0.05308	0.02812	0.0015
pH	All	PLS	Two-factor	0.0487	0.02795	0.0014

<sup>a</sup> 4 ISEs corresponds to CL1, CL2, BR and SCN.

$$\text{RMSECV} = \sqrt{\frac{1}{n} \sum_{i=1}^n (\hat{f}_{ij})^2} \quad (5)$$

$$\hat{f}_{ij} = y_{ij} - \hat{y}_{ij} \quad (6)$$

where  $n$  is the number of samples in the training set,  $\hat{f}_{ij}$  are the residuals towards the model and  $y_{ij}$  and  $\hat{y}_{ij}$  are, respectively, the true and the estimated values of  $y$  for the  $i$ th row and the  $j$ th column of the training set:

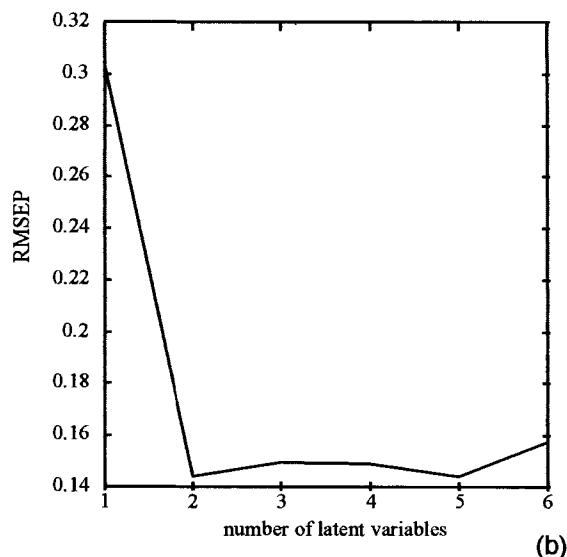
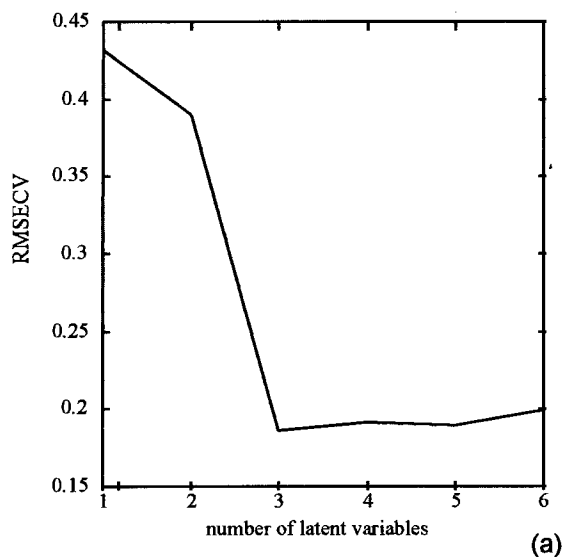


Fig. 7. RMSEP curves for pCl determination by PLS using 6 ISEs. (a) RMSECV curve: cross-validation on the calibration samples. (b) RMSEP curve: prediction on the test samples.

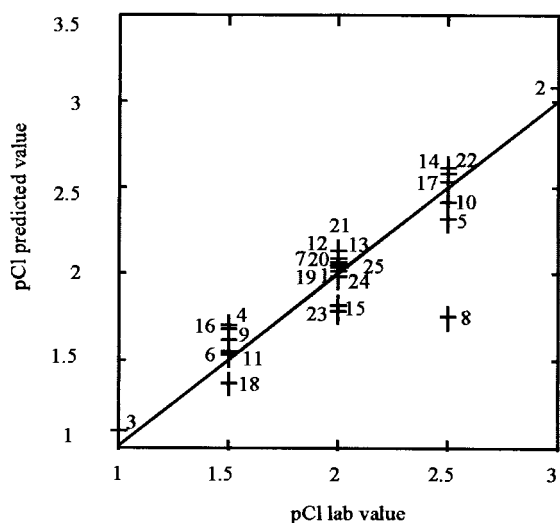


Fig. 8. pCl predicted for PSL three-factors model, cross-validation on the calibration samples.

$$\text{RMSEP} = \sqrt{\frac{1}{m} \sum_{i=1}^m (\hat{g}_{ij})^2} \quad (7)$$

$$\hat{g}_{ij} = y_{ij} - \hat{y}_{ij} \quad (8)$$

Table 7

Multivariate calibration results by extrapolation

pX	Array	Method	Factors	Test set RMSECV	Training set RMSEP	RMSECV*RMSEP
pCl	CL1	Inv. Cal <sup>a</sup>	CL1	0.286	0.3163	0.0905
pCl	All	MLR	CL1, SCN	0.1449	0.1671	0.0242
pCl	All	PCR	PC4, PC1	0.1764	0.178	0.0314
pCl	All	PLS	PLS1, 2, 3	0.1612	0.1753	0.0283
pCl	4 ISE	PCR	PC2, PC1	0.1601	0.1781	0.0285
pCl	4 ISE	PLS	PLS1, 2	0.1557	0.1718	0.0267
pBr	BR	Inv. cal	BR	0.3921	0.4697	0.1842
pBr	All	PCR	PC1, 4	0.3137	0.35	0.1098
pBr	All	PLS	PLS1, 2, 3	0.319	0.3493	0.1114
pBr	All	MLR	BR, CL1	0.3052	0.3354	0.1024
pBr	4 ISE	PCR	PC1, 2	0.3007	0.3482	0.1047
pBr	4 ISE	PLS	PLS1, 2	0.3016	0.3465	0.1045
pF	PF	Inv. cal	PF	0.0477	0.03136	0.0015
pF	All	MLR	PF	0.0477	0.03136	0.0015
pF	All	PCR	PC3, 2	0.0708	0.06632	0.0047
pF	All	PLS	PLS1, 2	0.05764	0.03198	0.0018
pH	PH	Inv. cal	PH	0.02532	0.04154	0.0011
pH	All	MLR	PH	0.02532	0.04154	0.0011
pH	All	PCR	PC2, 3	0.04012	0.05357	0.0021
pH	All	PLS	PLS1, 2	0.03052	0.04255	0.0013

<sup>a</sup> Inv.cal., inverse calibration.

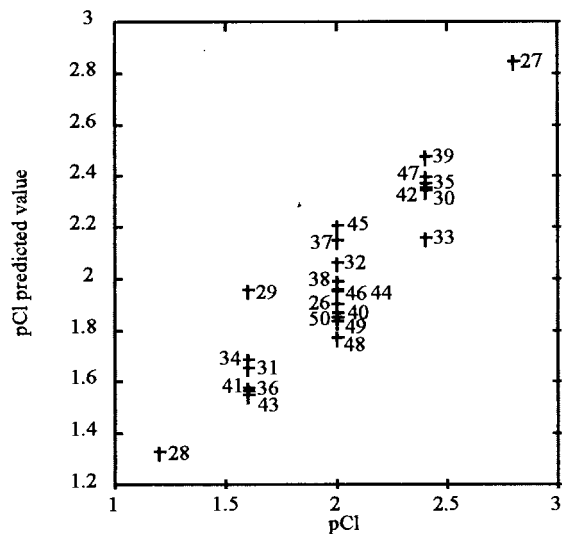


Fig. 9. pCl prediction of the test samples by the MLR model using CL1 and SCN variables.

where  $m$  is the number of samples in the test set,  $\hat{g}_{ij}$  are the residuals towards the model and  $y_{ij}$  and  $\hat{y}_{ij}$  are, respectively, the true and the estimated values of  $y$  for the  $i$ th row and the  $j$ th column of the test set.

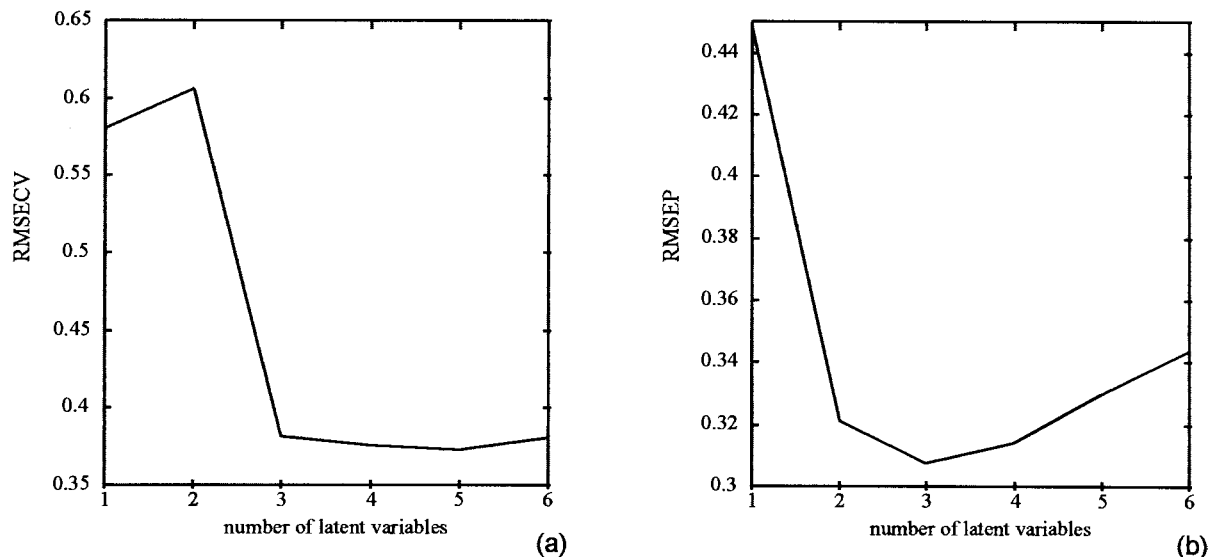


Fig. 10. RMSEP curves for pBr determination by PLS using 6 ISEs. (a) RMSECV curve: cross-validation on the calibration samples. (b) RMSEP curve: prediction on the test samples.

To compare the univariate methods the root mean square error of calibration (RMSEC) is also calculated:

$$\text{RMSEC} = \sqrt{\frac{1}{n} \sum_{i=1}^n (\hat{h}_{ij})^2} \quad (9)$$

$$\hat{h}_{ij} = y_{ij} - \hat{y}_{ij} \quad (10)$$

where  $n$  is the number of samples in the training set,  $\hat{h}_{ij}$  are the residuals towards the model and  $y_{ij}$  and  $\hat{y}_{ij}$  have the same signification as for the RMSECV.

### 3. Experimental

#### 3.1. Instrumentation and software

Fig. 1 shows a schematic view of the experimental set up. The cell used for the measurement is home made. The 6-ISEs are from Radiometer-Tacussel. Their characteristics are given in Table 1. The single reference electrode used for the whole array is a mercurous sulphate reference electrode  $\text{Hg}/\text{Hg}_2\text{SO}_4/\text{saturated K}_2\text{SO}_4$  (Tacussel reference TR 200). We have not used a calomel reference to avoid any con-

tamination by  $\text{Cl}^-$  anion. The cell used for the measurements is a temperature controlled glass cell ( $T = 25^\circ\text{C}$ ). The ISEs are placed around the reference electrode and are equidistant from it.

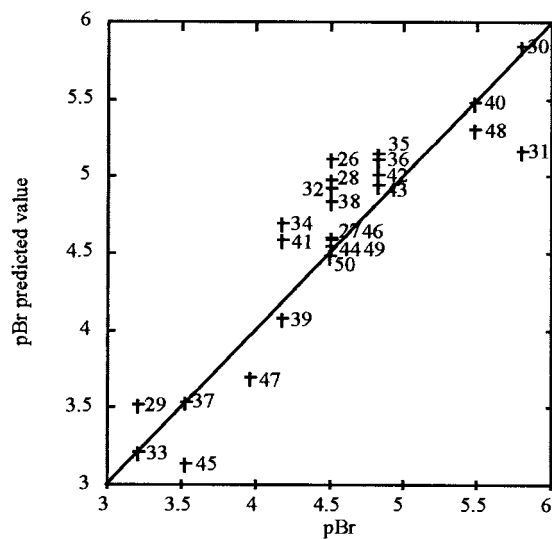


Fig. 11. pBr prediction of the test samples by the MLR model using BR and CL1 variables.

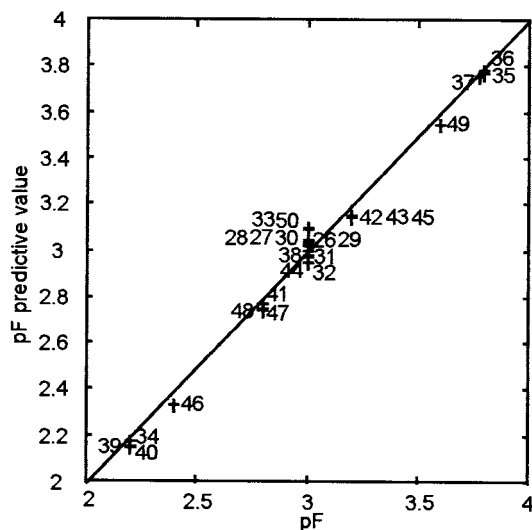


Fig. 12. pF prediction of the test samples by the MLR model using PF and PH variables.

Each electrode is connected to a high input impedance millivoltmeter (PHM220 model) from Radiometer-Tacussel. The millivolts are connected to a multiplexer (M4DAC model) from Bay-Tec driven by a computer (Compaq Prolinea 5100).

The software used for the data acquisition is home made. The software for the Pearson product moment correlations is Statgraphics version 3.1 from Manugistics. For the other data analysis, we used the Multivariate Calibration Toolbox from ChemoAC [13] working under MATLAB 4.0 software from The Math Works.

### 3.2. Measurement procedure

The sample is introduced into the temperature controlled cell ( $T=25^{\circ}\text{C}$ ) and the ISE array is steeped in the solution. The automatic acquisition of the ISE potentials is performed every 15 s: a scanning of each ISE response displayed by the millivoltmeter is sent to the computer and the temperature is recorded in the same file. A study of ISE responses allowed us to establish an experimental procedure. About 40 points are recorded, so that the measurement time (approximately 600 s) is sufficient to reach a stable temperature for the

sample and quasi stable ISE potentials. This length of time is a compromise between the stability of the response of the different ISEs and drifting of the ones subject to interference. Generally the response is stable at about 10 min after introducing the sensors into the solutions. To be able to use the procedure routinely we have chosen to fix the measurement time at 10 min for each sample and keep only the last points to exploit the data. When all the samples are measured, the file recorded on the computer is modified: for each sample only the five last points are kept and these points are averaged to keep only one mean potential value per ISE per sample.

### 3.3. Samples

The samples are synthetic aqueous solutions containing NaCl, NaBr, NaF and the supporting electrolyte is  $\text{K}_2\text{SO}_4$ . The pH buffer used is citric acid/citrate (0.01 M) and the pH values are adjusted in the supporting electrolyte by addition of solid NaOH and measuring the pH. The concentration levels have been set up according to a Doehlert experimental design with four factors (pCl, pBr, pF, pH), resulting in 25 calibration solutions including five central points. The Doehlert design has been chosen because it presents some advantages: its flexibility allows moving the design in one or another direction if the levels chosen are not the best possible. It is also possible to add a new factor by adding only a few experiments without starting again from the beginning. Table 2 shows the pX corresponding to the design. For the validation, we build another sample set according to the same theoretical Doehlert experimental design but with more restricted pX ranges (cf. Table 3), so that the test set is fully included in the calibration range.

The concentration ranges have been chosen so that there is no interference by  $\text{OH}^-$  on the fluoride selective electrode and that there are moderate interferences between  $\text{Cl}^-$  and  $\text{Br}^-$ . As previously mentioned, we wanted to work in a concentration range where moderate interferences are known to occur, so that we would be able to verify if chemometric methods allowed for calibrate under such circumstances.

## 4. Results and discussion

To study the bromide, chloride and fluoride concentrations, we use four ISEs (CL1, CL2, BR and SCN) which should respond to both  $\text{Cl}^-$  and  $\text{Br}^-$  and one (PF) which is known to respond to  $\text{F}^-$  very selectively without being perturbed by the other halides. This last electrode is only perturbed by  $\text{OH}^-$ , mainly when the  $\text{pH} < 8$ . For this reason a pH glass electrode (PH) was added. The array is then composed of two highly selective electrodes (PH and PF) and four sparingly selective electrodes.

### 4.1. Data examination

In the first step we investigated the correlation between the original variables which are the ISE responses. The Pearson product moment correlations between each pair of variables was calculated to give a measurement of the strength of their linear relationship. Table 4 shows these correlations and the corresponding  $P$ -values. Below  $P = 0.05$ , the correlation is considered statistically significant. From Table 4 we can conclude that, as expected, the four ISEs which respond to chloride and bromide ions are correlated while PF and PH are not correlated to any other electrode.

Principal component analysis should allow us to see the possibilities and the difficulties to be expected in the calibration of the different ions  $\text{pX}$  [7]. Principal component analysis on the calibration measurement data showed that four principal components (PC) describe 99.7% of the total variance of the calibration set. The first PC describes 55.3% of the variance for the calibration set. The loadings (Fig. 2) show that this PC represents a combination of mainly CL1, CL2, BR and SCN electrode responses. The second PC describes 23.4% of the variance for the calibration set and represents mainly the PH electrode variations and to a smaller extent the PF variations. PC3 explains 19.9% of the variance and represents the PF electrode response with a slight effect of PH. PC4 describes only 1.1% of the total variance for the calibration samples and represents responses of the four first electrodes with a positive influence of CL1 and CL2 electrodes and a nega-

tive influence of BR and SCN. This means that PC4 probably describes a combination of  $\text{pCl}$  and  $\text{pBr}$ . The score plots (Fig. 3) show that the repeatability of the measurements is quite good because the points representing the samples 1, 7, 13, 19 and 25, which have the same composition, are very close together.

When PC2 is plotted versus pH (Fig. 4a) we observe an obvious correlation between these two quantities. The same correlation is observed when PC3 is plotted versus pF (Fig. 4b). The correlation between PC1 or PC4 and  $\text{pCl}$  or  $\text{pBr}$  is less obvious. An observation of the loadings (Fig. 2) shows that PC1 is more or less equally influenced by the electrodes which should respond to  $\text{Br}^-$  and  $\text{Cl}^-$ . This could signify that PC1 is correlated to the sum of  $\text{pBr}$  and  $\text{pCl}$ . Fig. 4c shows that this hypothesis is correct.  $\text{pCl}$  and  $\text{pBr}$  should have an opposite influence on the loadings of PC4. To verify this hypothesis PC4 is related to, for example,  $\text{pCl} - \alpha \text{pBr}$ , where  $\alpha$  is the ratio between the PC4 loadings for BR and CL1 which are the two most influential electrodes on this PC (Fig. 4d). The relationship seems to be linear and the hypothesis verified.

We can conclude that principal component analysis indeed allows us to see the probable difficulties in determining  $\text{Cl}^-$  and  $\text{Br}^-$  because of the interferences and on the other hand the possibilities for fluorides and pH to be determined by univariate methods.

### 4.2. Univariate calibration

By linear regression of each ISE response on the different  $\text{pX}$ , it appears that, as was expected, four electrodes (BR, CL1, CL2 and SCN) respond to both chlorides and bromides. For these electrodes the best correlation is obtained for the  $\text{pCl}$  determination with the CL1 electrode and for the  $\text{pBr}$  with the BR electrode. Table 5 shows the results obtained by normal and inverse univariate calibration. Observing the slopes obtained for CL1 and BR in the case of normal regression on samples that contain both ions, one can realise that they are not nernstian. Such behaviour is normal since these electrodes are applied in a concentration range where  $\text{Br}^-/\text{Cl}^-$  interference

occurs. For further information the calibration plots for the electrodes in pure solutions is shown in Fig. 5 (we have observed some drift due to the interferences on such plots but the measurement procedure is done to minimise this effect). The results of both normal and inverse methods are equally good for the pF and the pH determinations, but for the pCl and pBr determinations the inverse calibration leads to better results than the classical regression. In both cases the prediction errors are, however, too large to make the calibration satisfactory for most applications (Fig. 6). Moreover in the case of  $\text{Br}^-$  the relationship is clearly not linear.

### 4.3. Multivariate calibration

Considering that univariate calibration is probably not the best method to calibrate the pCl and pBr, multivariate calibration was investigated with the aim of achieving better models. This can be expected because the use of different sensors can produce an averaging effect or a correction of the interference effects [1–5]. As in the present study, where the  $\text{Cl}^-$  and  $\text{Br}^-$  interferences have been chosen as important, we are mainly interested by the correction effect. As PLS is the most frequently applied of the multivariate chemometric methods, we will focus on this method to study its performances in the present context. The multivariate calibration results are shown in Table 6.

#### 4.3.1. pCl calibration

**4.3.1.1. PLS/6 ISEs.** In the first step the PLS method is considered for the pCl determination using all the sensors. The RMSEP curve for cross-validation of the calibration samples is shown in Fig. 7. PLS minimises the covariance within the  $y$  and the  $X$  data, i.e., respectively, the pCl and the responses of the 6 ISEs. Because the correlation part of the covariance dominates, such curves normally show a decrease in the RMSEP with the number of components included in the PLS model, until a minimum is reached. The number of components corresponding to the lowest RMSEP or the number of components where the RMSEP levels off is selected as optimal. Using

the PLS with a leave-one-out cross-validation method, the RMSEP curve shows its usual decreasing trend and leads to select a two-factor model. Although the RMSECV decreases dramatically from two to three factors (respectively, 0.3901 and 0.1861), the RMSEP increases only slightly: 0.144 for the two-factor model versus 0.149 for the three-factor one (Fig. 7). In Fig. 8 which shows the predicted pCl versus the laboratory value for the calibration samples, point 8 seems to be an outlier and has in fact an important leverage. This point corresponds to the sample for which the  $\text{Br}^-/\text{Cl}^-$  interferences are the most important. PLS does not seem to be able to model such an interference. For the second PLS component in the cross-validated model, the variance part of the covariance is important and leads to the inclusion of information on the PH and PF responses which are irrelevant for the measurement of pCl. The inclusion of noise due to the irrelevant information in the second PLS component leads only to a slight decrease in the RMSECV.

**4.3.1.2. PLS/4 ISEs.** In the second step we investigate what happens by retaining only the ISEs that are theoretically relevant for pCl and pBr, i.e. eliminating the PH and PF electrodes. Generally, the inclusion of irrelevant sensors in PLS is considered to have no influence on the quality of the prediction because these sensors should receive low weights in the final solution and therefore have little or no influence. On the other hand the inclusion of irrelevant measurement results could lead to worse results because of increasing noise.

When the PLS method is applied to the array consisting of CL1, CL2, BR and SCN ISEs, the best model is the two-factor one for both cross-validation and prediction. Compared to the errors obtained using the whole array, the results are equivalent: the RMSEP is 0.1487 versus 0.1494 for the three-factor PLS model using all the responses (Table 6). The elimination of the uninformative original variables leads to avoidance of the presence of an uninformative PLS-component in the model and to a decrease in the number of the selected factors, but the RMSEP and RMSECV of the retained model remain unchanged.



**4.3.1.3. MLR, PCR.** When selecting the original variables by stepwise MLR, the selected model is a two-factor one, using the CL1 and SCN responses. The RMSEP is 0.1318 compared to 0.1487 for the best PLS model whereas the RMSECV is 0.20 versus 0.1841. We observe that the first selected electrode is the best for the univariate calibration (i.e. the more selective electrode) and the other one is the ‘worst’, i.e. the one which gives most information about the interfering ions. This seems to confirm the conclusion by Forster and co-workers [4,5] that such problems can be treated by combining a highly and a sparingly selective electrode. It has been shown for spectroscopic data that when the test set is included within the calibration set, MLR is usually at least as good as PLS (D. Jouan-Rimbaud, F. Despagne, L. Pasti, R. Pappi, D.L. Messant, personal communication), which is also shown to be the case here. In an industrial problem extrapolation can be encountered in the test set, and as MLR is known to be less predictive than PCR or PLS when the test set contains extrapolations, the models were built with each method introducing extrapolation by inverting the calibration and test set. The results are shown in Table 7. In this case the results show that MLR is still the best choice for the calibration of pCl.

The PCR method is applied by selecting the principal components which describe the maximum correlation with pCl. Using the array of the 6 ISEs the minimum of both RMSECV and RMSEP are obtained for the two-factor model using PC4 and PC1. The RMSEP is 0.1534 versus 0.144 for the PLS model. Applying the method for the array of 4 ISEs (CL1, CL2, BR and SCN) the two-factor model again seems to be the best one and the RMSEP are comparable (0.1506 versus 0.1534 using the 6 ISEs) but the RMSECV is improved (0.1853 versus 0.2026).

#### 4.3.2. Conclusion for pCl

For the pCl determination, multivariate methods clearly lead to better results than univariate ones. The results by MLR, PLS and PCR are almost equivalent. The more sophisticated PLS, PCR method seem to bring no improvement in the prediction of the test set compared to MLR.

The RMSECV has the advantage, compared to the RMSEP, that the concentration domain investigated is larger. On the other hand it has the disadvantage that one does not validate the final model obtained, which is what is done with the RMSEP. It may then be useful to choose a composite criterion. When one could choose one model considering only the RMSECV (two-factor PLS model for the 4 ISE array) and another model considering only the RMSEP (MLR model on CL1 and SCN variables) the value of the product between the RMSECV and RMSEP values could help in the selection of the model. Using this criterion, the MLR model on the CL1 and SCN responses will be selected (Table 6). Fig. 9 shows the pCl predicted values using this model versus the true pCl value.

#### 4.3.3. pBr calibration

**4.3.3.1. PLS.** For the pBr calibration we proceed in the same way. Applying the PLS method on the 6 ISEs responses, the RMSECV indicates that three factors would be the best choice to build the model. As shown in Fig. 10, the RMSECV curve increases from one to two factors and then decreases dramatically until three factors. The method is then applied to only 4 ISEs: CL1, CL2, BR and SCN. The best model both in cross-validation and in prediction is now the two-factor model and RMSECV is 0.3654 versus 0.3816 for the three-factor PLS model built from the whole array and RMSEP is 0.3039 versus 0.3075.

**4.3.3.2. MLR.** Stepwise selection of the original variables leads to an MLR model with two factors, using BR and CL1. As for the pCl determination, the two electrodes retained are: (i) the one which is most selective, i.e. the one which gives the most information about the target ion ( $\text{Br}^-$ ), and (ii) the one which is the more sensitive to the interfering ion ( $\text{Cl}^-$ ). In this case the RMSEP (0.3065) is equivalent to that of the best PLS model (0.3039).

**4.3.3.3. PCR.** The PCR method using the array of the 6 ISEs leads to a two factor model on PC1 and PC4 and the results are equivalent or slightly better than the PLS ones for 6 ISEs. Using only

the 4 ISEs, the model again retained consists of two factors, namely PC1 and PC2 and the result (RMSEP is 0.3019) is comparable to the PLS model using 4 ISEs (0.3039).

#### 4.3.4. Conclusion for pBr

As in the pCl case, the results obtained by each multivariate method are equivalent (Table 7), and are better than those obtained by univariate calibration. It was also verified here whether extrapolation could change the results. Small extrapolation does not seem to influence the results. Since the lowest RMSEP is obtained by PCR and the lowest RMSECV is obtained by MLR (Table 6), the alternative criterion consisting of the product between the RMSECV and RMSEP values is applied and the MLR model is selected as the best one. Fig. 11 shows the pBr predicted value versus the true ones, using this MLR model.

As was observed for univariate calibration, there is a non-linearity. In principle multivariate methods are able to some extent to correct for this. It seems that in this case they do so, but not sufficiently.

#### 4.3.5. pF and pH calibration

**4.3.5.1. Multivariate calibration on the whole array.** For pF and pH, a good calibration was obtained by univariate calibration, but the question was whether multivariate methods would lead to as good a calibration or to worse results due to the introduction of uninformative variables. By applying the PLS method to the whole array for the determination of pF, the model selected is a two-factor one and the RMSEP (0.048) is very similar to the one obtained by inverse calibration on PF (0.049). In the case of pH determination, the PLS method on the whole array also leads to a two-factor model and the RMSEP is comparable to the inverse univariate method (0.0279 versus 0.0286). Stepwise MLR selects PF and PH as variables for the pF determination and only PH for the pH determination. MLR is, therefore, reduced to the univariate calibration in the pH case. For pF, the selection of both PF and PH leads to slightly better RMSECV

than the univariate calibration (0.0238 versus 0.0256 for the univariate method) but the RMSEP are comparable (0.0487 versus 0.0493 for the univariate method). Fig. 12 shows the pF prediction using the MLR model.

The PCR method described above for pF leads to a two-factor model using PC3 and PC2 and to a two-factor model using PC2 and PC3 for pH. The RMSEP are slightly but probably not significantly improved (0.047 versus 0.049 by the univariate method for pF and 0.0281 versus 0.0286 for pH). From the loading plots (Fig. 2) we know that PC2 is mainly influenced by PH but also to a smaller extent by PF and vice-versa for PC3. It seems logical that these two principal components are chosen to calibrate pF or pH. Using the alternative criterion, the model selected for the pF determination will be the MLR model using PF and PH variables and for the pH determination, the univariate inverse calibration on the PH variable.

#### 4.3.6. Conclusion on pF and pH

In the case of pF and pH calibration, multivariate calibration leads to results equivalent to the univariate inverse calibration ones but does not improve on them. Univariate methods are then preferred because they are easier to perform. The PH electrode is clearly not subject to interferences, but it has been verified that the PF electrode is subject to very slight interferences from pH in the chosen experimental conditions.

## 5. General conclusion

The calibration of several ions in the presence of interferences can be carried out using an experimental design and multivariate calibration methods. When the ISEs corresponding to the ion to be determined (primary ion) are subject to interference, multivariate methods allows for the establishment of a calibration which would not be possible by univariate methods. When there is no or only a slight interference on the ISEs, as in the pF or pH case in our study, each ion can be determined using the corresponding ISE and uni-

variate calibration methods. Multivariate methods are not needed, but do not lead to worse results.

Stepwise MLR is the best method to calibrate pCl and pBr. Indeed, methods more sophisticated than MLR do not seem to improve the prediction of the test set. This confirms results obtained in spectroscopy, which show that MLR is at least equally good as PCR and PLS when prediction is performed within the calibration range, i.e. when there is no extrapolation (D. Jouan-Rimbaud, F. Despagne, L. Pasti, R. Pappi, D.L. Massart, personal communication).

It should be noted that there is a clear non-linearity in the Br<sup>-</sup> case and perhaps, but less clearly so, in the Cl<sup>-</sup> case. This non-linearity which is due to the interference phenomenon is not completely eliminated by the multivariate approach. Therefore non-linear approaches (e.g. use of neural nets or non-linear regression using Eq. (1)) or local approaches such as local regression may be more appropriate. This is now being investigated. Another way to solve this problem is under study, namely the use of an exponential function of the potentials to directly determine the concentrations.

### Acknowledgements

We are grateful to G. Vallet from Rhône-Poulenc Industrialisation who made the data acquisition software and to D. Jouan-Rimbaud, V.

Centner and Q. Guo from the Vrije Universiteit Brussel (VUB) for their great help. MB also thanks J.R. Desmurs, G. Albert and M. Fraysse from Rhône-Poulenc Industrialisation for their support and their help. The authors also thank the Standard Measurement and Testing Project (CEE) and FWO for financial support.

### References

- [1] M. Otto, J.R.D. Thomas, *Anal. Chem.* 57 (1985) 2647.
- [2] K. Beebe, D. Uerz, J. Sandifer, B. Kowalski, *Anal. Chem.* 60 (1988) 66.
- [3] K. Beebe, D. Uerz, B. Kowalski, *Anal. Chem.* 60 (1988) 2273.
- [4] R. Forster, F. Regan, D. Diamond, *Anal. Chem.* 63 (1991) 8769.
- [5] R. Forster, D. Diamond, *Anal. Chem.* 64 (1992) 1721.
- [6] M. Hartnett, D. Diamond, *Anal. Chem.* 69 (1997) 1909.
- [7] M. Baret, P. Fabry, D.L. Massart, C. Menardo, M. Fraysse, *Analisis* 26 (1998) 267.
- [8] R.P. Buch, E. Lindner, *Pure Appl. Chem.* 66 (1994) 2527.
- [9] M. Cretin, P. Fabry, *Anal. Chim. Acta* 354 (1997) 291.
- [10] I. Igarashi, T. Ito, T. Taguchi, O. Tabata, H. Inagaki, *Sens. Actuators B* 1 (1990) 8.
- [11] H. Martens, T. Naes, *Multivariate Calibration*, Wiley, Chichester, 1989.
- [12] Radiometer-Tacussel, Monobloc Ion selective electrodes compacted polycrystalline or mixed crystal model of electrodes, Instruction manual, March 1993, Ref. DB12U113.
- [13] D. Jouan-Rimbaud, V. Centner, D.L. Massart, A toolbox for multivariate calibration, ChemoAC, Pharmaceutical Institute, Vrije Universiteit Brussel, Bruxelles, September 1996.

# Preconcentration of trace nickel with the ion pair of disodium 1-nitroso-2-naphthol-3,6-disulfonate and tetradecyldimethylbenzylammonium chloride on microcrystalline naphthalene or by the column method and determination by third derivative spectrophotometry

Mohammad Ali Taher \*

*Department of Chemistry, Shahid Bahonar University, Kerman, Iran*

Received 25 August 1998; received in revised form 9 April 1999; accepted 28 April 1999

## Abstract

Nickel is quantitatively retained by disodium 1-nitroso-2-naphthol-3,6-disulfonate (nitroso-R salt) and tetradecyldimethylbenzylammonium chloride (TDBA<sup>+</sup>Cl<sup>-</sup>) on microcrystalline naphthalene in the pH range 5.4–12.1 from large volumes of aqueous solutions of various alloys and biological samples. After filtration, the solid mass consisting of the nickel complex and naphthalene was dissolved with 5 ml of dimethylformamide (DMF) and the metal was determined by third derivative spectrophotometry. Nickel complex can alternatively be quantitatively adsorbed on tetradecyldimethylbenzylammonium–naphthalene adsorbent packed in a column and determined similarly. The detection limit is 10 ppb (signal to noise ratio 2) and the calibration curve is linear from 30 to  $5.4 \times 10^3$  ppb in dimethylformamide solution with a correlation coefficient of 0.9997 by measuring the distance  $d^3A/d\lambda^3$  between  $\lambda_1$  (537 nm) and  $\lambda_2$  (507 nm). Eight replicated determinations of 2.5  $\mu\text{g}$  of nickel in 5 ml of dimethylformamide solution gave a mean intensity (peak-to-peak signal between  $\lambda_1$  and  $\lambda_2$ ) of 0.339 with a relative standard deviation of  $\pm 0.87\%$ . The sensitivity of the method is 0.677 ml/ $\mu\text{g}$  found from the slope ( $d^3A/dnm^3$ ) of the calibration curve. Various parameters such as the effect of pH, volume of aqueous phase and interference of a number of metal ions on the determination of nickel has been studied in detail to optimize the conditions for nickel determination in various alloys and biological samples. © 1999 Elsevier Science B.V. All rights reserved.

*Keywords:* Alloys and biological samples; Derivative spectrophotometry; Nickel; Nitroso-R salt

## 1. Introduction

Disodium 1-nitroso-2-naphthol-3,6-disulfonate (nitroso-R salt) was introduced in 1921 by Van Klooster for the detection of cobalt [1]. Prelimi-

\* Tel.: +98-341-237001-9; fax: +98-341-232142.

E-mail address: taher@arg3.uk.ac.ir (M.A. Taher)

nary experiments indicated that metal ions such as  $\text{Ni}^{2+}$  also react with this reagent and form colored water-soluble anionic complex. This anionic complex in the presence of tetradecyldimethylbenzylammonium (TDBA) cation form a colored water-insoluble ion associated complex which can be easily adsorbed on microcrystalline naphthalene.

A survey of the literature reveals that nickel may be determined by zero order spectrophotometry using 1,10-phenanthroline disulfonate [2] 1,5-diphenylcarbohydrazide [3] di-2-pyridyl ketone benzoylhydrazone [4] and 2-pyridyl-decarboxaldehyde-5-nitropyridylhydrazone [5].

Derivative spectrophotometry offers the advantages of increased selectivity and sensitivity compared with normal spectrophotometry [6–12]. Spectrophotometers equipped with suitable derivative units enable not only the derivative spectra of the first and second orders to be obtained but also higher orders. The increased selectivity in derivative spectrophotometry results from the fact that bands which overlap in normal absorption spectra appear as separated bands in the derivative spectra. Derivative spectrophotometry can increase the sensitivity owing to the amplification of derivative signals and lowering of noise, and improvements in selectivity and in sensitivity are easier to obtain in instances where the bands in the normal absorption spectra are fairly sharp [13–15].

Solid-liquid separation after adsorption of metal chelates on microcrystalline naphthalene is rapid and convenient and can be applied to many types of metal complexes [16,17]. The only drawback is in the filtration and drying. A survey of the literature revealed that various adsorbents, such as thiol cotton [18], silanized glass beads [19],  $\text{C}_{18}$ -bonded silica gel [20], Amberlite XAD-4 resin [21], cellulose [22], silicagel [23], green tea leaves [24] and polythioether foam [25], have been tried for the preconcentration of metal ions. The desorption of the metal is carried out by a slow process of elution (probably the metal complex may be held by interior surfaces of the adsorbent and hence is not eluted easily), so the procedure is time-consuming.

In this paper, an efficient method for the preconcentration of nickel from a large volume of the

aqueous solutions of various standard reference materials with 1-nitroso-2-naphthol-3,6-disulfonate-TDBA-naphthalene adsorbent is described. The method is economical (all reagents are cheap compared with many other reagents used recently [26–28]), rapid (the metal complex simply adsorbs onto microcrystalline naphthalene) and sensitive (the solid mass can be dissolved in 2–5 ml of an organic solvent, and the whole of the solution may be used for the absorbance measurement). The solid mass, consisting of the metal ion associated complex and naphthalene (Ni-1-nitroso-2-naphthol-3,6-disulfonate-TDBA-naphthalene) can easily be dissolved with a suitable organic solvent such as dimethylformamide (DMF) and the nickel is determined by third derivative spectrophotometry. Various parameters for concentration measured by third derivative UV-Vis spectrophotometry were evaluated, and optimized conditions were utilized for the trace determination of nickel in various standard alloys and biological and environmental samples.

## 2. Experimental

### 2.1. Apparatus

A Shimadzu UV 160 spectrophotometer with a 1.0-cm quartz cell was used. A Beckman pH meter was employed for pH measurements. A funnel-tipped glass tube (60 × 7 mm i.d.) was used as a column. The column was plugged with polypropylene fibers and slurry-packed with the naphthalene material to a height of 1.0–1.2 cm, pushing lightly with a flat glass rod. All atomic absorption measurements were made with an atomic absorption spectrometer (Shimadzu AA 670). All glassware was washed with mixture of concentrated sulfuric acid and concentrated nitric acid (1 + 1) before use.

### 2.2. Reagents

All reagents were of analytical reagent grade. A standard nickel solution was prepared from nickel(II) nitrate (Merck) in distilled water and stan-

standardized [29]. Buffer solutions of pH 3–6, pH 6–8 and pH 8–11 were prepared by mixing an appropriate ratio of 0.5 M acetic acid and 0.5 M ammonium acetate, 0.1 M disodium hydrogen phosphate and 0.1 M potassium dihydrogen phosphate and 0.5 M aqueous ammonia and 0.5 M ammonium acetate, respectively. A 1% solution of tetradecyldimethylbenzylammonium chloride (TDBA) (Merck) and 0.1% 1-nitroso-2-naphthol-3,6-disulphonate acid (nitroso-R) (Fluka, Switzerland) were prepared in distilled water. A 20% solution of naphthalene was prepared in acetone. Solutions of alkali metal salts (1%) and various metal salts (0.1%) were used for studying the interference of anions and cations, respectively.

### 2.3. Preparation of nitroso-R–TDBA–naphthalene adsorbent

A solution of naphthalene was prepared by dissolving 20 g in 40 ml of acetone on a hot-plate stirrer at approximately 35°C. It was transferred into a beaker containing 1500 ml of distilled water and 0.9 g of nitroso-R salt in a fast stream with continuous stirring at room temperature. TDBA<sup>+</sup>Cl<sup>-</sup> (1.2 g, 0.0031 mole) was dissolved in 500 ml of distilled water by warming on a hot-plate. It was mixed with the above solution of naphthalene–acetone–nitroso-R salt in water. The yellow naphthalene material coprecipitated with TDBA and nitroso-R was stirred for about 2 h and then allowed to stand for another 2 h at room temperature. The supernatant solution was decanted off and the residue was washed twice with distilled water. The adsorbent in the form of a slurry was stored in a brown bottle for subsequent use.

### 2.4. General procedure for the column method

An aliquot of nickel solution containing 0.15–27 µg of nickel was taken in a 25-ml beaker. The pH of this solution was adjusted to 11 with the addition of 2 ml of buffer solution and diluted to about 15 ml with distilled water. The column loaded with the nitroso-R–TDBA–naphthalene adsorbent was conditioned to pH 11 with 2–3 ml of buffer and then the metal solution was passed through the

column at a flow rate of 1 ml min<sup>-1</sup>. The packing was washed with a small volume of water and then aspirated strongly for a few minutes, pushing down the naphthalene material with a flat glass rod to eliminate the excess water attached to the naphthalene. The solid mass, consisting of the metal complex along with naphthalene, was dissolved out the column with 5 ml of DMF. The third derivative spectrum of this solution was recorded from 400 to 550 nm against a reagent blank with  $\Delta\lambda = 9$  nm. The absorbances for standard amounts of nickel were measured and a calibration curve was constructed against a reagent blank prepared in a similar manner.

### 2.5. General procedure for microcrystalline naphthalene

An aliquot of nickel solution (containing 0.15–27 µg) was placed in a 100-ml Erlenmeyer flask with tightly fitting stopper. Then 1 ml of 0.1% of the reagent (nitroso-R) was added and the mixture was diluted to 30–40 ml with water. The pH was adjusted to 11 with 2 ml of the buffer and then 2 ml of 1% TDBA solution was added. The solution was mixed well and allowed to stand for few seconds. Then 2 ml of a 20% solution of naphthalene in acetone was added with continuous shaking. The solid mass so formed, consisting of naphthalene and metal complex, was separated by filtration on a Whatman filter paper (no. 1041). The residue was dried in the folds of a filter paper and transferred to the Erlenmeyer flask. The solid mass consisting of the metal complex along with naphthalene was dissolved with 5 ml of DMF. The third derivative absorption spectrum was recorded in the range 400 to 550 nm against a blank solution prepared in the same way. A calibration graph was prepared by taking various known amounts of nickel under the conditions given above.

## 3. Results and discussions

### 3.1. Spectral characteristics (zero order)

The absorption spectrum of the ion associated Ni–nitroso-R–TDBA in DMF against reagent

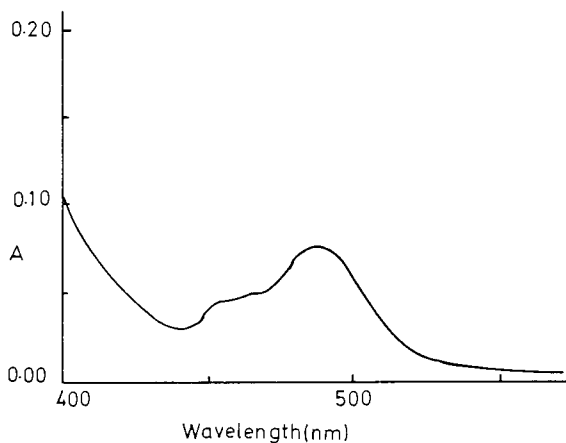


Fig. 1. Zero-order spectrum of the naphthalene–Ni–nitroso-R–TDBA complex. Ni, 2.5  $\mu$ g; buffer, 2 ml; pH 11; solvent, 5 ml DMF; reference, reagent blank.

blank prepared under similar conditions was recorded (Fig. 1); the first, second and third derivative spectra are shown in Fig. 2. Derivation of the spectra leads to sharper zero order bands and gives higher signal in the resolution spectra. The main instrumental parameters affecting the shape of the derivative spectra are the wavelength,

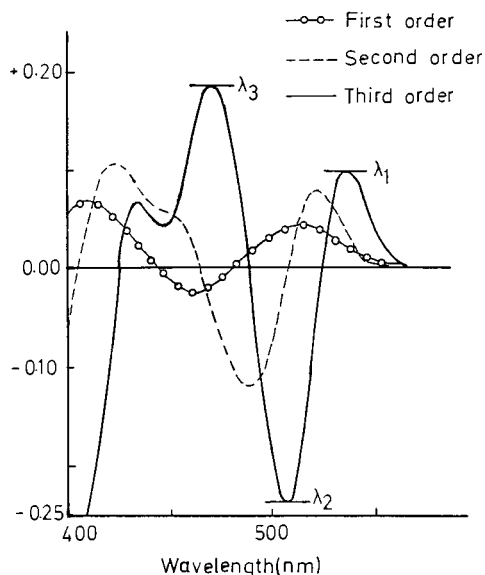


Fig. 2. First, second and third derivative spectra of the naphthalene–Ni(nitroso-R)–TDBA complex. For conditions see Fig. 1.

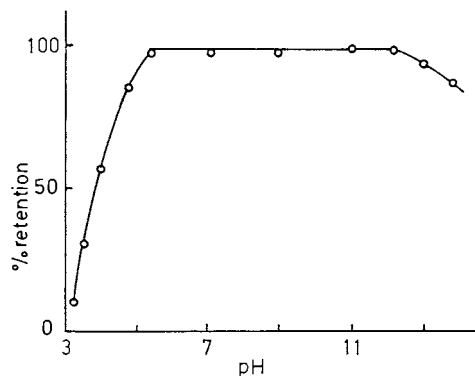


Fig. 3. Effect of pH. For conditions see Fig. 2.

scanning speed, the wavelength increment over which the derivative is obtained ( $\Delta\lambda$ ) and the response time. These parameters need to be optimized to give a well-resolved peak (better resolution) and thus good selectivity and higher sensitivity in a determination. Preliminary observations revealed that the best results were obtained from the third derivative (third derivative spectra from Fig. 2 leads to sharper and gives higher than first and second derivative spectra) with wavelength interval  $\Delta\lambda = 9$  nm. In the present work a peak-to-peak method between  $\lambda_1 = 537$  nm and  $\lambda_2 = 507$  nm was applied.

### 3.2. Reaction conditions

These were established using 2.5  $\mu$ g of nickel. The adsorption of nickel on this adsorbent was found to be maximum in the pH range 5.4–12.1 (Fig. 3). In a subsequent study, the pH was maintained at 11. Addition of 0.5–5.0 ml of the buffer (pH 11) did not affect the retention of nickel and use of 2.0 ml was recommended. Nickel was quantitatively adsorbed over the range 0.5–4.0 ml of the 0.1% of nitroso-R solution. Therefore, 1.0 ml of the reagent is recommended in the present study.

Various amounts of naphthalene (20% solution of naphthalene in acetone) were added to the sample solutions keeping other variables constant. It was observed that the signal height remained constant with the addition of 1.0–4.0 ml of 20% naphthalene solution. Therefore, 2.0 ml of 20%

naphthalene solution was used in subsequent studies. The effect of shaking time on the adsorption indicated that the signal height remained constant over a range of 0.5–7.0 min. Therefore, 1.0 min of shaking time was maintained in the present work.

For the column method, the flow rate was varied from 0.2 to 8 ml min<sup>-1</sup>. It was found that a flow rate of 0.2–5.0 ml min<sup>-1</sup> did not affect adsorption. A flow rate of 1 ml min<sup>-1</sup> was recommended in all experiments.

The volume of the aqueous phase was varied in the range of 10–700 ml under the optimum conditions, keeping other variables constant. It was observed that the signal height was almost constant up to 150 ml (preconcentration factor of 30). However, for convenience, all the experiments were carried out with 40 ml of the aqueous phase.

For the column method, peak height was almost constant up to an aqueous phase volume of 400 ml. Therefore, a preconcentration factor 80 can be achieved by the column.

### 3.3. Retention capacity of the adsorbent

The retention capacity of the adsorbent was determined by a batch method. The experiment was performed by taking 500 µg of nickel, 2 ml of buffer solution (pH 11) and 40 ml of water in a beaker. This solution was transferred into a separating funnel and then a suitable amount of the nitroso-R–TDBA–naphthalene adsorbent was added. The separating funnel was shaken vigorously on a mechanical shaker for 5 min. The solid mass was separated by filtration and nickel was determined from the filtrate by atomic absorption spectrometry (AAS). The solid mass on the filter paper was dried in an oven, kept in a desiccator and then weighed to determine the mass of the adsorbent. The maximum amount of nickel retained with 4.1 mg g<sup>-1</sup> of nitroso-R salt in the adsorbent. It was also noted that the retention capacity depends on the amount of TDBA and nitroso-R supported on naphthalene. The molar ratio of nitroso-R:TDBA<sup>+</sup> is 1:1; from the observations on the preparation of the adsorbent it was

found that with the use of nitroso-R (0.9 g) and TDBA<sup>+</sup> (1.2 g), a slight excess of nitroso-R and 20 g of naphthalene were sufficient for the complete retention of the metal ions.

### 3.4. Choice of solvent

A number of solvents were tried to dissolve the Ni–nitroso-R–TDBA–naphthalene. Since the solid mass was dissolved in a small volume (3–5 ml) of the solvent, it was essential to select a solvent in which the chelate is highly soluble and this results a high sensitivity for the spectrophotometry measurements. The solid material was found to be insoluble in ordinary organic solvents such as toluene, 1,2-dichloroethane, n-hexane, nitrobenzene, isoamyl alcohol, n-amyl alcohol, ethylacetate, methylisobutylketone, chloroform and dioxane, but soluble in dimethyl sulfoxide, dimethylformamide (DMF) and propylene carbonate. DMF was preferred due to the high solubility and stability. It was found that 3–5 ml of this solvent was sufficient to dissolve the mixture thus enhancing the sensitivity of the method. As only a small volume (3–5 ml) of the solvent was used to dissolve the complex and naphthalene, it was essential to study the effect of surplus water attached to naphthalene. It was noted that the surplus water decreased the absorbance by 12–15% and led to an error in the determination. Thus it was necessary to eliminate the water attached to the naphthalene.

### 3.5. Calibration

The calibration curve (Fig. 4) for the determination of nickel was prepared according to the general procedure under the optimum conditions developed above.

The detection limit was 10 ppb for nickel at the minimum instrumental setting (signal to noise ratio 2). The linearity was maintained in the concentration range of 0.03–5.4 ppm nickel with a correlation factor of 0.9997 and the relative standard deviation (R.S.D.) was found to be ± 0.87%.



### 3.6. Effect of diverse ions

Various salts and metal ions were added individually to a solution containing 2.5 µg of nickel and the general procedure was applied. The tolerance limit was set as the diverse ion required to cause  $\pm 3\%$  error in the determination of nickel. The results obtained are given in Table 1. Among the anions examined, large amounts of chloride, bromide, nitrate, acetate, carbonate and sulphate could be tolerated. Citrate, oxalate, orthophosphate, tartrate and EDTA interfered. Except EDTA, a relatively low amount of these anions could be tolerated. Obviously the stability constants of Ni–EDTA complex must be higher than of the Ni–nitroso-R complex. Of the metal ions examined, many did not interfere up to milligram levels, except Fe(III), Cu(II) and Ag(I). Fe(III) was masked with 3 ml of 5% NaF solution. Cu(II) and Ag(I) were masked with 3 ml of 1% Na<sub>2</sub>S<sub>2</sub>O<sub>3</sub> solution. Thus the proposed method is selective and can be used to determine nickel in standard alloys and biological samples without any prior separation.

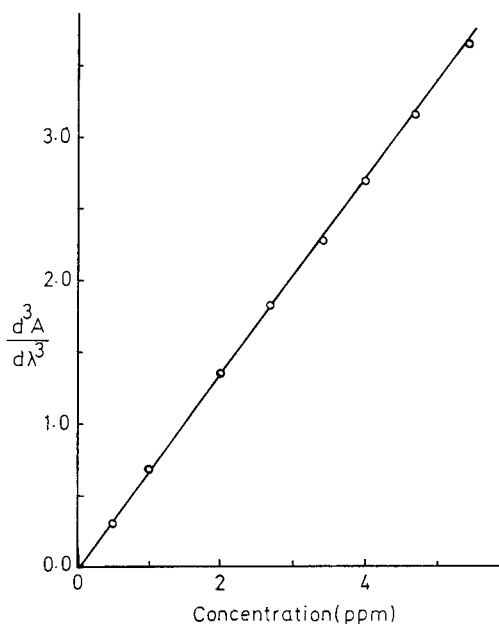


Fig. 4. Calibration curve for nickel by third derivative spectrophotometry from signal peak-to-peak measurements between  $\lambda_1$  and  $\lambda_2$ . For conditions see Fig. 2.

Table 1  
Effect of diverse salts and metal ions<sup>a</sup>

Salt or ion	Tolerance limit
CH <sub>3</sub> COONa·3H <sub>2</sub> O, KNO <sub>3</sub>	1 g
K <sub>2</sub> SO <sub>4</sub>	400 mg
KI, NaF	350 mg
Thiourea	250 mg
NH <sub>4</sub> Cl, Na <sub>3</sub> PO <sub>4</sub> ·12H <sub>2</sub> O, K <sub>2</sub> CO <sub>3</sub>	150 mg
Na <sub>2</sub> S <sub>2</sub> O <sub>3</sub>	100 mg
Sodium potassium tartrate	30 mg
KSCN	20 mg
Sodium oxalate	18 mg
Trisodium citrate	10 mg
Na <sub>2</sub> EDTA	20 µg
Mg(II)	300 mg
Ca(II)	90 mg
Pb(II)	10 mg
Cd(II)	7.0 mg
Sb(II)	6.0 mg
Ag(I)	70 µg, 2.5 mg <sup>b</sup>
Cu(II)	50 µg, 1.5 mg <sup>b</sup>
Mn(II), Ti(VI)	4.5 mg
Zn(II)	3.5 mg
Cr(VI), Cr(III)	3.0 mg
Se(VI), Ga(III)	2.5 mg
U(VI), Al(III)	1.5 mg
Mo(VI)	1.3 mg
Pd(II), Te(IV)	1.0 mg
Fe(III)	60 µg, 1.0 mg <sup>c</sup>
Os(VIII)	0.9 mg
Bi(III)	0.8 mg
Rh(III), V(V)	0.7 mg
Co(II), Ru(III)	0.5 mg
Hg(II)	0.3 mg

<sup>a</sup> Ni, 2.5 µg; pH 11; nitroso-R salt, 1–4 ml. Determination by third derivative spectrophotometry.

<sup>b</sup> Masked with 3 ml of 1% Na<sub>2</sub>S<sub>2</sub>O<sub>3</sub> solution.

<sup>c</sup> Masked with 3 ml of 5% NaF solution.

### 3.7. Analysis of nickel in standard alloys and steel samples

The proposed method was applied to the determination of nickel in Nippo Keikin-zoku Kogyo (NNK) CRM 916 and no. 920 aluminum alloy and NKK no. 1021 Al–Si–Cu–Zn alloy, and Japanese standards of iron and steel (JSS) CRM 651-7 and 653-7 stainless steel. A 0.1-g sample of the standard aluminum alloy or steel was completely dissolved in 6–14 ml of hydrochloric acid (1 + 1) by heating on a water-bath and then 1 ml

of 30% (v/v) hydrogen peroxide was added. The excess of peroxide was decomposed by heating the sample on a water-bath. The solution was cooled, filtered if needed and diluted to 100 ml with distilled water in a standard flask. An aliquot (1–2 ml) of this sample was taken in a 20-ml beaker and the general procedure was applied. The results obtained are given in Table 2. These results are in agreement with the certified values.

### 3.8. Analysis of nickel in biological samples

The accuracy and applicability of the proposed method has been applied to the determination of nickel in National Institute for Environmental Studies (NIES) No. 1 peppercorn, NIES No. 5 human hair and NIES No. 7 tea leaves. A 0.1-g sample was taken in a beaker and dissolved in concentrated nitric acid ( $\approx 5$  ml) with heating. The solution was cooled, diluted and filtered. The filtrate was made to 100 ml with water in a calibrated flask. NIES No. 8 vehicle exhaust particulates (1 g) was dissolved in 18 ml of concen-

trated nitric acid, 18 ml of concentrated perchloric acid and 2 ml of concentrated hydrofluoric acid in a 100-ml teflon beaker, evaporated to a small volume, filtered through a filter paper and made up to 100 ml with distilled water. An aliquot (10–50 ml) of the sample solution was taken individually and nickel was determined by the general procedure. The results are given in Table 3 and are in good agreement with the certified values.

## 4. Conclusion

A simple, economical and highly selective adsorbent has been generated simply by mixing aqueous solutions of nitroso-R salt and TDBA<sup>+</sup>Cl<sup>-</sup> with an acetone solution of naphthalene for the preconcentration of nickel from a large volume of aqueous solutions of alloys, biological and environmental samples. It is not possible to develop selective methods for metal ions using microcrystalline naphthalene or column

Table 2  
Analysis of nickel in standard alloys<sup>a</sup>

Sample	Composition (%)	Concentration (%)	
		Certified value	Found <sup>b</sup>
JSS 651-7 stainless steel	C, 0.047; Si, 0.072; P, 0.028; Cr, 18.60; S, 0.0063; Mo, 0.84; Al, 0.002; N, 0.0312; Co, 0.22; Mn, 1.72; Cu, 0.082	9.20	9.17 ± 0.04 <sup>c</sup>
JSS 653-7 stainless steel	C, 0.068; Si, 0.63; Cr, 22.53; Co, 0.35; Mn, 1.72; Cu, 0.030; N, 0.0276	13.91	13.83 ± 0.09 <sup>d</sup>
NKK no. 916 aluminum alloy	Si, 0.41; Fe, 0.54; Mg, 0.10; Cr, 0.05; Zn, 0.30; Ti, 0.10; Sn, 0.05; Pb, 0.04; Sb, 0.01; B, 0.0006; Zr, 0.05; Bi, 0.03; Co, 0.03; Mn, 0.11; Cu, 0.27; V, 0.02	0.06	0.059 ± 0.002 <sup>c</sup>
NKK no. 1021 Al-Si-Cu-Zn alloy	Si, 5.56; Fe, 0.99; Mg, 0.29; Cr, 0.03; Zn, 1.76; Ti, 0.04; Sn, 0.10; Pb, 0.18; Sb, 0.01; Zr, 0.01; Bi, 0.01; V, 0.007; Ca, 0.004; Mn, 0.11; Cu, 2.72	0.14	0.136 ± 0.005 <sup>c</sup>
NKK no. 920 aluminum alloy	Si, 0.78; Fe, 0.72; Mg, 0.46; Cr, 0.27; Zn, 0.80; Ti, 0.15; Sn, 0.20; Pb, 0.10; Sb, 0.10; Bi, 0.06; Ga, 0.05; Ca, 0.03; Co, 0.10; Mn, 0.20; Cu, 0.71; V, 0.15	0.29	0.284 ± 0.006 <sup>d</sup>

<sup>a</sup> 3 ml of 5% NaF solution and 3 ml of 1% Na<sub>2</sub>S<sub>2</sub>O<sub>3</sub> solution were added as masking reagents. Determination by third derivative spectrophotometry.

<sup>b</sup> Average of five determinations ± S.D.

<sup>c</sup> Column method.

<sup>d</sup> Microcrystalline naphthalene method.

Table 3  
Analysis of nickel in biological samples<sup>a</sup>

Sample <sup>b</sup>	Composition	Concentration ( $\mu\text{g g}^{-1}$ )	
		Certified value	Found <sup>c,d</sup>
NIES No. 1, pepperbush <sup>e</sup>	K, $1.51 \pm 0.06$ ; Mn, $0.203 \pm 0.107$ ; Mg, $0.408 \pm 0.020$ ; Ca, $1.38 \pm 0.07\%$ ; Cd, $6.7 \pm 0.5$ ; Cu, $12 \pm 1$ ; Fe, $205 \pm 17$ ; Co, $23 \pm 3$ ; Pb, $5.5 \pm 0.8$ ; Zn, $340 \pm 20$ ; Rb, $75 \pm 4$ ; Ba, $165 \pm 10$ ; Na, $106 \pm 13$ ; Sr, $36 \pm 4$ ; As, $2.3 \pm 0.3$ ; P, (1100); Cr, (1.3); Cs, (1.2); Tl, (0.13); Hg, (0.056) $\mu\text{g/g}$	$8.7 \pm 0.6$	$8.6 \pm 0.2^f$
NIES No. 5, human hair	Pb, 6.0; Cd, 0.20; Sb, 0.07; Zn, 169; Al, 240; Fe, 225; Mg, 208; Hg, 4.4; K, 34; Rb, 0.19; Sc, 0.05; Se, 1.4; Na, 26; Sr, 2.3; Ti, 3.2; Ca, 728; Cr, 1.4; Ba, 2.2; Cu, 16.3; Co, 0.10 $\mu\text{g/g}$	1.8	$1.75 \pm 0.05^f$
NIES No. 7, tea leaves	Pb, 0.80; Cd, 0.030; Sb, 0.014; Zn, 33; Cr, 0.15; Al, 775; Mg, 1530; Ba, 5.7; K, 18600; Sc, 0.011; Na, 15.5; Sr, 3.7; Ca, 3200; Cs, 0.221; Co, 0.12; Mn, 7.00; Cu, 7.0 $\mu\text{g/g}$	6.5	$6.52 \pm 0.04^g$
NIES No. 8, vehicle exhaust particulates <sup>e</sup>	K, $0.115 \pm 0.008$ ; Ca, $0.53 \pm 0.02$ ; Mg, $0.101 \pm 0.005$ ; Al, $0.33 \pm 0.02$ ; Zn, $0.104 \pm 0.005$ ; Na, $0.92 \pm 0.008\%$ ; Sr, $89 \pm 3$ ; Co, $3.3 \pm 0.3$ ; Cu, $67 \pm 3.5$ ; Cd, $1.1 \pm 0.1$ ; Pb, $219 \pm 9$ ; As, $2.6 \pm 0.2$ ; Cr, $25.5 \pm 1.5$ ; V, $17 \pm 2$ ; Sb, $6.0 \pm 0.4$ ; Cs, (0.24); Rb, (4.6); Sc, (0.055); La, (1.2); Br, (56); Ag, (0.2); Se, (1.3); Mo, (6.4); Ce, (3.1); Th, (0.35); Sm, (0.20); Eu, (0.05); Lu, (0.02) $\mu\text{g/g}$	$18.5 \pm 1.5$	$18.1 \pm 0.6^g$

<sup>a</sup> 3 ml of 5% NaF solution and 3 ml of 1% Na<sub>2</sub>S<sub>2</sub>O<sub>3</sub> solution were added as masking reagents.

<sup>b</sup> National Institute of Environmental Studies (NIES) reference materials.

<sup>c</sup> Average of five determinations  $\pm$  S.D.

<sup>d</sup> Standard addition method.

<sup>e</sup> Values in parentheses are approximate and not certified.

<sup>f</sup> Column method.

<sup>g</sup> Microcrystalline naphthalene method.

method since many metal–nitroso-R complexes absorb at close wavelengths. However, with the use of derivative spectrophotometry, this problem can be easily solved. Nickel may also be determined by directly aspirating the DMF solution of the metal complex after the preconcentration into the flame of the AAS or by pulse polarography. Although adsorption onto microcrystalline naphthalene is more rapid, the preconcentration factor is comparatively lower than with the column method.

## References

- [1] H.S. Van klooster, J. Am. Chem. Soc. 43 (1921) 746.
- [2] B.K. Pal, K.A. Singh, D. Chakraborty, Mikrochim. Acta 126 (1–2) (1997) 39.
- [3] Z. Tanwari, J. Pak. Sci. Res. 48 (3–4) (1996) 74.
- [4] S.A. Tarra, M. Encarnacion, V. Soares-Iha, Spectrosc. Lett. 30 (4) (1997) 625.
- [5] K.-W. Cha, C. Park, Y.-C. Jung, J. Korean Chem. 41 (6) (1997) 320.
- [6] T.C. Ohaver, G.L. Green, Anal. Chem. 48 (1976) 312.
- [7] G. Talsky, L. Mayring, H. Kreuzer, Angew. Chem. 90 (1978) 840.
- [8] G. Talsky, S. Gotz-Maler, H. Betz, Mikrochim. Acta II (1981) 1.
- [9] H. Ishii, K. Sotoh, Z. Frenius, Anal. Chem. 312 (1982) 114.
- [10] T.R. Griffiths, K. King, H.V. Hubbard, M.J. Schwing-Weill, J. Meullemeestre, Anal. Chim. Acta 143 (1982) 163.
- [11] M.A. Taher, B.K. Puri, Analyst 120 (1995) 1589.
- [12] M.A. Taher, Anal. Lett. 31 (12) (1998) 2115.
- [13] B. Morelli, Analyst 108 (1983) 870.
- [14] B. Morelli, Analyst 108 (1983) 1506.
- [15] H. Ishii, R.B. Singh, T. Odashima, Mikrochim. Acta III (1983) 149.
- [16] M.A. Taher, S. Puri, R.K. Bansal, B.K. Puri, Talanta 45 (1997) 411.

- [17] M.A. Taher, B.K. Puri, R.K. Bansal, *Microchem. J.* 58 (1998) 21.
- [18] M.Q. Yu, G.Q. Liu, *Talanta* 30 (1983) 265.
- [19] S. Taguchi, T. Yal, Y. Shimada, K. Goto, *Talanta* 30 (1963) 169.
- [20] H. Watanabe, K. Goto, S. Taguchi, J.W. Melaren, S.S. Berman, D.S. Russell, *Anal. Chem.* 53 (1981) 738.
- [21] Y. Saki, N. Mori, *Talanta* 33 (1986) 161.
- [22] P. Burba, P.G. Willmer, *Talanta* 30 (1983) 381.
- [23] M. Kubota, K. Matsumoto, K. Terada, *Anal. Sci.* 3 (1987) 45.
- [24] M. Kimura, H. Yamashita, J. Komada, *Bunseki Kagaku* 35 (1986) 400.
- [25] A.S. Khan, A. Chow, *Talanta* 33 (1986) 182.
- [26] M.J. Toral, P. Richter, L. Silva, *Talanta* 40 (1993) 1405.
- [27] M.A. Taher, B.K. Puri, *Talanta* 43 (1996) 247.
- [28] M.A. Taher, B.K. Puri, *Ann. Chim.* 85 (1995) 183.
- [29] A.I. Vogel, *A Text Book of Quantitative Inorganic Analysis*, 4th ed., Longmans, London, 1978.

# Reversed phase liquid chromatography with UV absorbance and flame ionization detection using a water mobile phase and a cyano propyl stationary phase

## Analysis of alcohols and chlorinated hydrocarbons

Wes W.C. Quigley, Scott T. Ecker, Paul G. Vahey, Robert E. Synovec \*

*Department of Chemistry, Center for Process Analytical Chemistry, University of Washington, Box 351700, Seattle, WA 98195, USA*

Received 21 January 1999; accepted 28 April 1999

### Abstract

The development of liquid chromatography with a commercially available cyano propyl stationary phase and a 100% water mobile phase is reported. Separations were performed at ambient temperature, simplifying instrumental requirements. Excellent separation efficiency using a water mobile phase was achieved, for example  $N = 18\,800$ , or  $75\,200\text{ m}^{-1}$ , was obtained for resorcinol, at a retention factor of  $k' = 4.88$  (retention time of 9.55 min at  $1\text{ ml min}^{-1}$  for a  $25\text{ cm} \times 4.6\text{ mm}$  i.d. column, packed with  $5\text{ }\mu\text{m}$  diameter particles with the cyano propyl stationary phase). A separation via reversed phase liquid chromatography (RP-LC) with a 100% water mobile phase of six phenols and related compounds was compared to a separation of the same compounds by traditional RP-LC, using octadecylsilane (ODS), i.e. C18, bound to silica and an aqueous mobile phase modified with acetonitrile. Nearly identical analysis time was achieved for the separation of six phenols and related compounds using the cyano propyl stationary phase with a 100% water mobile phase, as compared to traditional RP-LC requiring a relatively large fraction of organic solvent modifier in the mobile phase (25% acetonitrile:75% water). Additional understanding of the retention mechanism with the 100% water mobile phase was obtained by relating measured retention factors of aliphatic alcohols, phenols and related compounds, and chlorinated hydrocarbons to their octanol:water partition coefficients. The retention mechanism is found to be consistent with a RP-LC mechanism coupled with an additional retention effect due to residual hydroxyl groups on the cyano propyl stationary phase. Advantages due to a 100% water mobile phase for the chemical analysis of alcohol mixtures and chlorinated hydrocarbons are reported. By placing an absorbance detector in-series and preceding a novel drop interface to a flame ionization detector (FID), selective detection of a separated mixture of phenols and related compounds and aliphatic alcohols is achieved. The compound class of aliphatic alcohols is selectively and sensitively detected by the drop interface/FID, and the phenols and related compounds are selectively and sensitively detected by absorbance detection at 200 nm. The separation and detection of chlorinated hydrocarbons in a water sample matrix further illustrated the advantages of this methodology. The

\* Corresponding author. Fax: +1-206-6853478.

E-mail address: synovec@chem.washington.edu (R.E. Synovec)

sensitivity and selectivity of the FID signal for the chlorinated hydrocarbons are significantly better than absorbance detection, even at 200 nm. This methodology is well suited to continuous and automated monitoring of water samples. The applicability of samples initially in an organic solvent matrix is explored, since an organic sample matrix may effect retention and efficiency. Separations in acetonitrile and isopropyl alcohol sample matrices compared well to separations with a water sample matrix. © 1999 Elsevier Science B.V. All rights reserved.

*Keywords:* Liquid chromatography; Cyano propyl stationary phase; Water mobile phase; Phenol

## 1. Introduction

Reversed phase liquid chromatography (RP-LC) is a popular technique for both chemical analysis and preparative separations [1,2]. Traditionally, RP-LC is performed with a stationary phase such as octadecylsilane (ODS), i.e. C18, that is bonded to a silica substrate [3]. A timely separation with a C18 stationary phase often requires a significant amount of organic solvent, such as methanol or acetonitrile, in the aqueous mobile phase. While this practice of RP-LC has served chemical analysts well over the years, there is considerable interest and regulatory pressure to eliminate the use of organic solvent modifiers in the mobile phase [4]. Thus, the development of RP-LC without organic solvent modifiers is an important area of research, where the mobile phase can be as simple as 100% water, or water with a small amount of a more effective and less polluting modifiers, such as cyclodextrins [5,6].

There are three specific reasons for developing RP-LC with a 100% water mobile phase: the increasing pressure to reduce chemical waste and pollution resulting from chemical analysis procedures, the broadened scope and enhanced performance of detection, and the potential to develop LC into a technique that can be more readily adapted and applied for on-line and remote chemical analysis. With regard to each of these three issues, the organic solvent in the mobile phase is a limitation to the practice of RP-LC. Further development of RP-LC with a 100% water mobile phase, however, requires careful attention to the design of stationary phases, a subject that we will now consider.

In order to achieve a chemical separation in liquid chromatography, the correct balance of forces must be applied between two or more competing phases. In previous work, we have

shown that by carefully considering this balance of forces in RP-LC, a moderate to low polarity stationary phase of extremely low volume (in relation to the mobile phase volume within a column) could be synthesized that was effective in producing reasonable retention factors for hydrophobic analytes (benzene, toluene, ethyl benzene, etc.), with a 100% water mobile phase [7–9]. The stationary phases produced were relatively inefficient compared to commercial C18 phases. Possible causes for this relatively poor efficiency, are the difficulty in producing a uniform phase thickness over the substrate surface area, and the potential for slow mass transfer kinetics of the analytes transferring between a relatively hydrophobic phase and a 100% water mobile phase [10,11].

This manuscript presents results in which a separation of phenols and related compounds is achieved using a cyano propyl stationary phase bound to silica coupled with a 100% water mobile phase. These results are then compared to a separation of the same compounds by traditional RP-LC using C18 bound to silica with an acetonitrile modified aqueous mobile phase. The separations are performed at ambient temperature, instead of elevated temperatures [12,13], and are aimed at a broader range of analyte polarity than earlier work in the field [14]. The issues of analysis time, separation efficiency, and utility for chemical analysis are investigated. We report that excellent separation efficiency and excellent separation selectivity were both achieved using a 100% water mobile phase.

The benefit of having a 100% water mobile phase for novel chemical analysis strategies was also explored. In previous work [8] we described a novel drop interface that allowed volatile organic compounds, initially in water, to be selectively detected by a flame ionization detector (FID). By

placing an absorbance detector in-series but preceding the drop interface/FID, selective detection of a separated mixture of phenols and related compounds from aliphatic alcohols is achieved. The compound class of aliphatic alcohols is selectively and sensitively detected by the drop interface/FID, while the phenols and related compounds are selectively and sensitively detected by absorbance detection at 200 nm. The utility of this instrumental method is further illustrated by the separation and detection of chlorinated hydrocarbons in a water sample matrix, chlorinated hydrocarbons provide a signal for both the absorbance and FID channels. It will be shown that the sensitivity and selectivity of the FID signal for the chlorinated hydrocarbons is significantly better than absorbance detection, even at 200 nm. The use of RP-LC with a 100% water mobile phase and this combination of detectors is well suited to continuous and automated monitoring

of water samples. Another important issue is applicability to samples initially in an organic solvent matrix, since an organic sample matrix may effect retention and efficiency. This issue will be explored using host matrix solvents of acetonitrile and isopropyl alcohol. Separations of test analytes in these solvents will be compared to a separation with a water sample matrix.

## 2. Experimental

Test analytes used in this study were of analytical grade (J.T. Baker, Phillipsburg, NJ, USA, and Aldrich, Milwaukee, WI, USA), and are listed in Table 1 along with additional data and information that will be discussed later. The liquid chromatography hardware was routine, except for the drop interface/FID that will be described shortly. For RP-LC system with 100% water mobile

Table 1

List of analytes studied, the retention factor ( $k'$ ) measured, and log of the water:octanol partition coefficients ( $P_{ow}$ ) [15]. Retention factors were obtained using the RP-LC systems compared in Figs. 1 and 2

Compound class	Analyte	$k'^a$	$k'^b$	Log $P_{ow}$
<i>Phenols and related compounds</i>				
	Resorcinol	4.88	1.50	0.80
	Benzyl alcohol	5.56	3.52	1.10
	Phenol	5.96	4.91	1.46
	Phenethyl alcohol	9.28	5.79	1.36
	<i>o</i> -Cresol	11.28	9.74	1.95
	<i>p</i> -Cresol	12.52	10.91	1.94
<i>Aliphatic alcohols</i>				
	Methanol	0.95	–	–0.77
	Ethanol	1.21	–	–0.31
	1-Propanol	1.98	–	0.25
	1-Butanol	4.16	–	0.88
	<i>Tert</i> -amyl alcohol	6.46	–	0.89
	3-Pentanol	7.60	–	1.21
	Isopentanol	9.93	–	1.19
<i>Chlorinated hydrocarbons</i>				
	Methylene chloride	3.46	–	1.25
	Bromochloromethane	4.41	–	1.41
	1,2-Dichloroethane	6.24	–	1.48
	Chloroform	7.67	–	1.97

<sup>a</sup> Retention factors based upon a dead time of 1.57 min. for the nitrate ion using cyano propyl stationary phase and a 100% water mobile phase.

<sup>b</sup> Retention factors based upon a dead time of 1.51 min for the nitrate ion using C18 stationary phase and 25% acetonitrile:75% water mobile phase.

phase, distilled deionized water was used and was delivered by a syringe pump (LC2600, ISCO, Lincoln, NE, USA), while the traditional RP-LC system used a mobile phase composed of 25% acetonitrile:75% distilled deionized water (by volume), and was delivered by a piston pump (114M, Beckman, Berkeley, CA, USA). Pump selection was not a critical issue in this work and either could be used for both RP-LC systems. Six ports of a 10 port electrically actuated valve (EC10W, Valco Instruments, Houston, TX, USA) fitted with a 6  $\mu\text{l}$  sample injection loop made from 1/16" O.D.  $\times$  0.007" I.D. PEEK tubing (Upchurch, Oak Harbor, WA, USA) was used to inject samples with both systems. The two columns employed in this work were an Altex Ultrasphere ODS, 250  $\times$  4.6 mm, 5  $\mu\text{m}$  (Alltech, Deerfield, IL, USA) for the traditional RP-LC separation, and a Brownlee Spheri-5 non-end capped cyano propyl 250  $\times$  4.6 mm column (Perkin-Elmer, Norwalk, CT, USA) for 100% water mobile phase separations. A Dionex UV-Vis absorbance spectrometer (VDM-2, Dionex, Sunnyvale, CA, USA) with a 3.5  $\mu\text{l}$  cell and 0.5 cm path length was employed for absorbance detection at 200 nm with both systems. Additionally, only for the separations with a 100% water mobile phase, following the absorbance detector in-series was a novel drop interface coupled to a flame ionization detector that is within a gas chromatograph (Model 3600cx, Varian Analytical, Sugarland, TX, USA) [8]. With the drop interface, as eluent from the 100% water mobile phase separation forms drops at a fused silica capillary tip, helium flowing past the drop is enriched with the volatile components in each successive water drop. Flame ionization detection of the helium gas stream enriched in the vapor of volatile organic analytes is detected by the FID. The FID conditions were as follows: air flow at 300  $\text{ml min}^{-1}$ , hydrogen flow at 30  $\text{ml min}^{-1}$ , and helium carrier at 35  $\text{ml min}^{-1}$ . An earlier report [8] further discusses the design and investigated the performance of the drop head space interface/FID. PEEK tubing was used for all plumbing except where noted. Additionally, simultaneous UV absorbance detection for the 100% water mobile phase separations was shown to provide information about the non-volatile an-

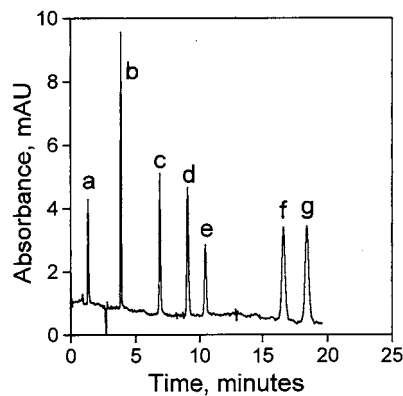


Fig. 1. Traditional RP-LC separation of six phenols and related compounds, 12 ng each dissolved in water injected, separated on C18 stationary phase, 4.6 mm  $\times$  250 mm column, with 25% acetonitrile:75% water mobile phase flowing at 1  $\text{ml min}^{-1}$ , and absorbance detection at 200 nm (1 mAU equals an absorbance of  $10^{-3}$ ). Analytes: (a) nitrate; (b) resorcinol; (c) benzyl alcohol; (d) phenol; (e) phenethyl alcohol; (f) *o*-cresol; (g) *p*-cresol.

alytes. Enhanced selectivity was obtained by utilizing these two complementary detectors in-series. Software written in-house controlled a data acquisition board (Model AT-MIO-16XE-50, National Instruments, Austin TX, USA) to acquire the absorbance detector and FID data at 1000 points per second and were boxcar averaged to two points per second.

### 3. Results and discussion

The commercial stationary phase based upon cyano propyl bound to silica, with the residual hydroxyl groups not end capped, has been evaluated and found compatible with a 100% water mobile phase. Traditional RP-LC with an organic modifier versus RP-LC with a 100% water mobile phase were compared using a test mixture of phenols and related compounds. Results are reported in Table 1 and shown in Figs. 1 and 2. These two figures show that baseline separation of a mixture of phenols and related compounds, was achieved, and that the overall analysis time is similar and identical elution order is achieved for both separations. Obtaining the same overall analysis time was accomplished by properly modi-



fying the mobile phase with an organic solvent for the traditional RP-LC separation on the C18 stationary phase, in order to match the retention time of the last eluting compound in the separation with the 100% water mobile phase. The similarity in the retention times and identical elution order of the analytes for the two separations demonstrates fair agreement in chemical selectivity between the two separations.

The cyano propyl stationary phase applied was not end capped to avoid high carbon loading and hydrophobic character that accompanies silica-based stationary phases end capped with trimethyl silane. The residual hydroxyl groups should contribute to retention, so retention factors were compared to octanol:water partition coefficients ( $P_{ow}$ ) in order to determine the extent to which analyte hydrophobicity and hydrogen bonding contributes to retention. Retention factors,  $k'$ , obtained for a variety phenols and related compounds, aliphatic alcohols and chlorinated hydrocarbons are listed in Table 1. In Fig. 3, the  $\log k'$  versus  $\log P_{ow}$  for these test analytes is plotted [15]. Two key observations can be made. First, there is indeed a strong correlation between  $\log k'$  and  $\log P_{ow}$ . Second, at a given  $P_{ow}$ , retention is shifted to a longer time for both compound classes that contain an alcohol group relative to

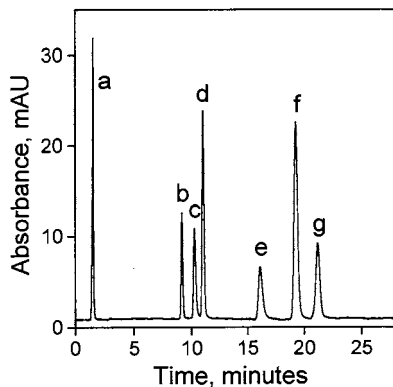


Fig. 2. RP-LC separation of six phenols and related compounds, 60 ng each dissolved in water injected, separated on cyano propyl stationary phase, 4.6 mm  $\times$  250 mm column, with 100% water mobile phase at 1 ml  $\text{min}^{-1}$ , and absorbance detection at 200 nm (1 mAU equals an absorbance of  $10^{-3}$ ). Analytes: same labels as in Fig. 1.

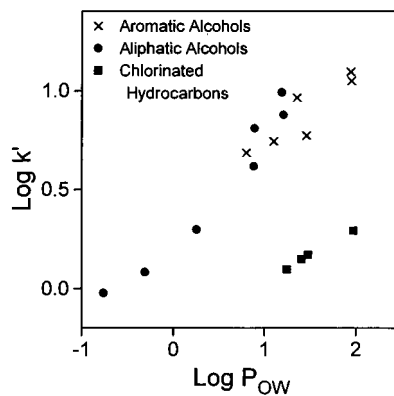


Fig. 3. Log of the retention factor,  $k'$ , versus the log of the octanol:water partition coefficient  $P_{ow}$  [15] for the analytes listed in Table 1, with the  $k'$  measured by RP-LC using the cyano propyl stationary phase and a 100% water mobile phase.

the chlorinated hydrocarbons. This effect is attributed to an additional retention mechanism probably due to hydrogen bonding between the hydroxyl group of the alcohols and the hydroxyl sites on the silica. There appears to be no significant difference in the correlation between the phenols and related compounds, and the aliphatic alcohols. The main point is that the separation follows a RP-LC pattern, with an additional retention effect due to the residual hydroxyl groups on the cyano propyl stationary phase column. Note that relatively small  $k'$  data are achieved with 100% water mobile phase at ambient temperature. This is in contrast to previous reports in which relatively large  $k'$  data were obtained, thus requiring the use of short columns to keep retention times reasonable [16,17].

An important issue for the development of RP-LC with a 100% water mobile phase is separation efficiency. A plot of the plate height  $H$  ( $\mu\text{m}$ ) versus the linear flow velocity (Fig. 4),  $u$  ( $\text{mm sec}^{-1}$ ), of the water mobile phase for resorcinol, using the cyano propyl column. Resorcinol was selected as a representative analyte, with data obtained from separations as shown in Fig. 2 at 1 ml  $\text{min}^{-1}$ , and a retention factor of  $k' = 4.88$  (Table 1). The  $H$  values plotted were determined by measuring the efficiency  $N$  using an empirical method that takes into account peak asymmetry

[18]. At  $1 \text{ ml min}^{-1}$  a respectable value of  $N = 18\,800$  was obtained for resorcinol with the 25 cm column filled with the cyano propyl stationary phase. Furthermore, at a flow rate of  $0.4 \text{ ml min}^{-1}$  ( $u = 1.1 \text{ mm s}^{-1}$ ), the  $H$  of  $10.9 \mu\text{m}$  corresponds to a reduced plate height of 2.2 (since the particle diameter was  $5 \mu\text{m}$ ). A reduced plate height of 2.2 indicates that the RP-LC system with a water mobile phase is operating in a high performance region with respect to separation efficiency [19]. In general, the narrow peak widths obtained (Fig. 2) further highlight the efficiencies possible with this commercial stationary phase applied with a water only mobile phase. We found the cyano propyl phase to be fairly robust, although continuous exposure to 100% water leads to faster hydrolysis, than if an organic modifier were present, and loss of the cyano propyl groups. It is reasonable that future developments in synthetic procedures, using zirconium based substrates for example, could readily lead to even more robust stationary phases for RP-LC with a 100% water mobile phase applications [20,21].

Using a 100% water mobile phase provides a low signal background under baseline conditions for many detection methods, such as absorbance, fluorescence, conductivity, as well as the flame ionization detector (FID), which is commonly applied in gas chromatography (GC). The low background leads to better detection limits and

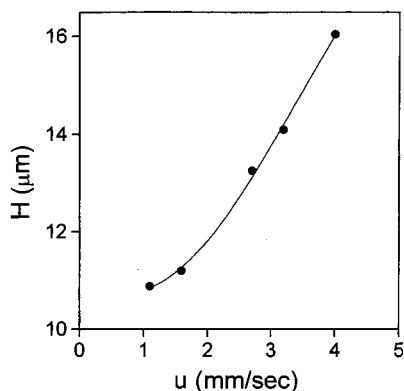


Fig. 4. Plot of plate height  $H$  ( $\mu\text{m}$ ) versus the mobile phase linear flow velocity  $u$  ( $\text{mm s}^{-1}$ ) for the test analyte resorcinol, retained with a  $k' = 4.88$  by using the cyano propyl stationary phase and a 100% water mobile phase.

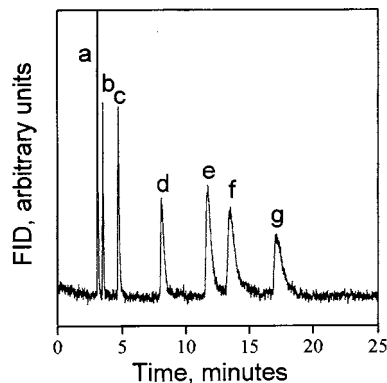


Fig. 5. Separation of seven aliphatic alcohols, 240 ng each in water injected, using the cyano propyl stationary phase,  $4.6 \times 250 \text{ mm}$  column, with 100% water mobile phase at  $1 \text{ ml min}^{-1}$  and FID detection using the drop interface [8]. Analytes: (a) methanol; (b) ethanol; (c) 1-propanol; (d) 1-butanol; (e) *t*-amyl alcohol; (f) 3-pentanol; (g) isopentanol. The aliphatic alcohols were selectively detected from a mixture of 13 phenols and related compounds and aliphatic alcohols. The six phenols and related compounds were selectively detected by absorbance at 200 nm, with resulting chromatogram identical to Fig. 2.

expanded applicability, and often simplifies the instrumentation. Since the FID offers excellent detection limits in GC, we have been developing RP-LC with a 100% water mobile phase with the intention to take advantage of the FID. RP-LC with a 100% water mobile phase was interfaced to a FID using a novel drop sampling device [8]. In work we report here, a mixture of 13 phenols and related compounds, and aliphatic alcohols was separated by RP-LC with a 100% water mobile phase, followed by absorbance detection in-series with the drop-interface/FID. This combination of detectors provided highly selective detection. The phenols and related compounds were selectively detected by absorbance at 200 nm, with the chromatogram virtually identical to Fig. 2. Concurrently, selective detection of volatile compounds, specifically the aliphatic alcohols was achieved, as seen in Fig. 5. The phenols and related compounds are not seen in Fig. 5 because they were not sufficiently volatile to be observed by the FID, while the aliphatic alcohols are not seen in Fig. 2 because they do not have a significant absorbance at 200 nm. Eliminating the need for a volatile organic solvent in the mobile phase was

essential to employing an FID with the drop sampling interface. A comparison of the band broadening between the aliphatic alcohols (Fig. 5) and the phenols and related compounds (Fig. 2) is warranted, since at a given retention time the observed band broadening for the aliphatic alcohols was somewhat higher. The higher band broadening is not due to the detector, since the earlier eluting peaks of methanol and ethanol exhibited quite narrow peak widths. The larger band broadening is most likely attributed to slower mass transfer kinetics for the aliphatic alcohols [10,11], yet a more detailed study is needed to confirm this possibility.

Additional applications further support the potential for this chemical analysis methodology. RP-LC with a 100% water mobile phase separation of four chlorinated hydrocarbons was coupled to the absorbance detector and drop interface/FID in-series. The resulting chromatograms are shown in Fig. 6. Note that analyte detectabilities are better with the FID than with absorbance at 200 nm. Again, a key application could be for routine water monitoring and testing in which in-situ analysis is needed, and when GC of water samples would require solvent extraction or solid phase extraction..

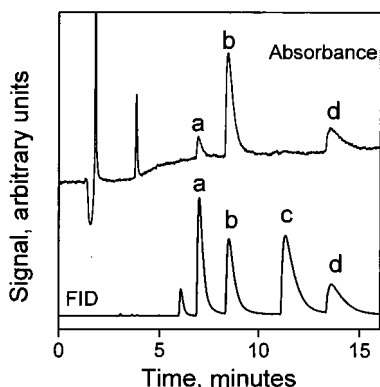


Fig. 6. Separation of four chlorinated hydrocarbons, 600 ng each in water injected, separated on cyano propyl stationary phase,  $4.6 \times 250$  mm column, with 100% water mobile phase at  $1 \text{ ml min}^{-1}$ . Absorbance detection at 200 nm and the drop interface/FID [8] are obtained in-series, providing dual channel data. Note the superior sensitivity and signal-to-noise ratio with the FID chromatogram. Analytes: (a) methylene chloride; (b) bromochloromethane; (c) 1,2-dichloroethane; (d) chloroform; (i) impurity or injection disturbance.

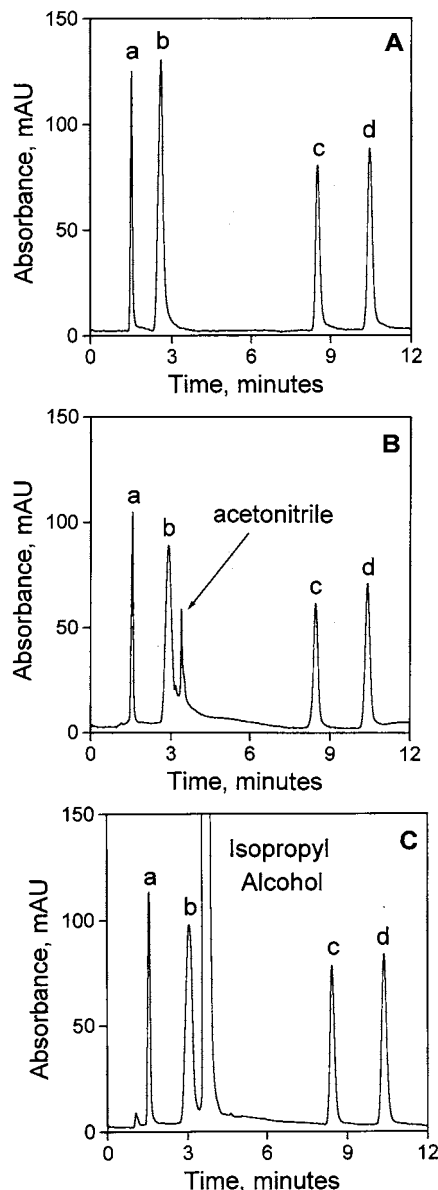


Fig. 7. Separations of analytes in various sample matrices, using cyano propyl stationary phase, with 100% water mobile phase at  $1 \text{ ml min}^{-1}$ , and absorbance detection at 200 nm ( $1 \text{ mAU}$  equals an absorbance of  $10^{-3}$ ). A volume of  $2 \mu\text{l}$  was injected at analyte concentrations of 5 ppm each (10 ng each) in (A) water sample matrix; (B) acetonitrile sample matrix; and (C) isopropyl alcohol sample matrix. Analytes: (a) nitrate; (b) benzaldehyde; (c) resorcinol; (d) phenol.

The use of RP-LC with a 100% water mobile phase for samples initially in an organic solvent matrix is an important application. RP-LC with a

100% water mobile phase should be amenable to samples originally in an organic solvent matrix, if one is careful to not inject too large of a sample volume. We addressed this issue by achieving and evaluating RP-LC with a 100% water mobile phase separations of test analytes dissolved in each of the following matrices: water, acetonitrile, and isopropyl alcohol, using the cyano propyl stationary phase and a water mobile phase (Fig. 7A, B, C). Comparison of these separations reveals that there are virtually no differences between the chromatograms, with the exception of the large solvent peak caused by the organic sample matrix in Fig. 7B and C, which appears to be the primary limitation.

Overall results of this work demonstrate that the future of RP-LC with a 100% water mobile phase is quite encouraging. Additional study and development are in order, including stationary phase development, experimental evaluation, and the theoretical study of RP-LC with a 100% water mobile phase separations. The present study has demonstrated that one can indeed obtain high efficiency separations via RP-LC with a 100% water mobile phase at room temperature using a commercially available column, and novel detection strategies can be applied.

### Acknowledgements

This work was supported by the Center for Process Analytical Chemistry (CPAC), a National Science Foundation initiated University/Industry Cooperative Research Center at the University of Washington.

### References

- [1] J.L. Glajch, J.J. Kirkland, L.R. Snyder, *J. Chromatogr.* 238 (1982) 269–280.
- [2] E. Grushka, *Preparative-Scale Chromatography*, Marcel Dekker, New York, 1989.
- [3] S.D. Fazio, S.A. Tomellini, H. Shih-Hsien, J.B. Crowther, T.V. Raglione, T.R. Floyd, R.A. Hartwick, *Anal. Chem.* 57 (1985) 1559–1564.
- [4] E.H. Smith, C. Davis, *J. Environ. Sci. Health A* 32 (1997) 171–193.
- [5] K. Fujimura, T. Ueda, M. Kitagawa, H. Takayanagi, T. Ando, *Anal. Chem.* 58 (1986) 2668–2680.
- [6] D.W. Armstrong, T.J. Ward, R.D. Armstrong, T.E. Beesley, *Science* 232 (1986) 1132–1135.
- [7] M.D. Foster, R.E. Synovec, *Anal. Chem.* 68 (1996) 2838–2844.
- [8] C.A. Bruckner, S.T. Ecker, R.E. Synovec, *Anal. Chem.* 69 (1997) 3465–3470.
- [9] T.E. Young, S.T. Ecker, R.E. Synovec, N.T. Hawley, J.P. Lomber, C.M. Wai, *Talanta* 45 (1998) 1189–1189.
- [10] J.H. Knox, M. Saleem, *J. Chromatogr. Sci.* 10 (1972) 80.
- [11] C. Horvath, H.J. Lin, *J. Chromatogr.* (1978) 43–70.
- [12] D.J. Miller, S.B. Hawthorne, *Anal. Chem.* 69 (1997) 623–627.
- [13] R.M. Smith, R.J. Burgess, *Anal. Comm.* 33 (1996) 327–329.
- [14] R.V. Vivilecchia, B.G. Lightbody, N.Z. Thimot, H.M. Quinn, *J. Chromatogr. Sci.* 15 (1996) 424–433.
- [15] C. Hansch, *Exploring QSAR*, American Chemical Society, in: A. Leon, D.H. Hoekman, Washington, DC, 1995.
- [16] M.M. Hsieh, J.G. Dorsey, *J. Chromatogr.* 631 (1993) 63–78.
- [17] P. Jandera, J. Kubat, *J. Chromatogr.* 500 (1990) 281–299.
- [18] J.P. Foley, J.G. Dorsey, *Anal. Chem.* 55 (1983) 730–737.
- [19] J.C. Giddings, *Unified Separation Science*, Wiley-Interscience, New York, 1991, pp. 274–278.
- [20] C. McNeff, P.W. Carr, *Anal. Chem.* 67 (1995) 3886–3892.
- [21] N. Tanaka, K. Kimata, Y. Midawa, K. Hosoya, T. Araki, Y. Ohtsu, Y. Shiojima, R. Tsuboi, H. Tsuchiya, *J. Chromatogr.* 535 (1990) 13–31.

# Determination of light hydrocarbons dissolved in seawater

Nobuo Tsurushima<sup>a,b,\*</sup>, Shuichi Watanabe<sup>b</sup>, Shizuo Tsunogai<sup>b</sup>

<sup>a</sup> *Department of Chemistry, Faculty of Fisheries, Hokkaido University, Hakodate 041-0821, Japan*

<sup>b</sup> *Laboratory of Marine and Atmospheric Geochemistry, Graduate school of Environmental Earth Science, Hokkaido University, Sapporo 060-0810, Japan*

Received 2 April 1998; received in revised form 23 April 1999; accepted 29 April 1999

## Abstract

A practical method for the on board determination of light (C1–C4) hydrocarbons dissolved in seawater has been developed. The gaseous hydrocarbons in seawater were extracted quickly with a vacuum sparge tower and determined gas chromatographically. By using two cryogenic columns at dry ice–ethanol temperature ( $-80^{\circ}\text{C}$ ) connected in series, it was possible to completely collect the hydrocarbons. The precision and sensitivity were comparable to that of previous methods. The analysis was completed within 45 min for one sample and the sample volume was 500 ml. The method was successfully applied to the northern North Pacific water collected in summer 1997. The concentrations of C2–C4 hydrocarbons in surface seawater ranged from several to several tens  $\text{pmol l}^{-1}$ , within the range of concentrations in previous studies. © 1999 Elsevier Science B.V. All rights reserved.

## 1. Introduction

Recently, oceanic emission of nonmethane hydrocarbons (NMHCs) have been identified as significant sinks of the OH radical for the remote marine atmosphere [1,2]. However, there is a lack of data from some ocean areas and a lack of time series data sets in the database of hydrocarbon concentrations in seawater at the present time [3]. Furthermore, most previous studies were focused on the measurement of concentrations of hydrocarbons in the surface seawater. Measurements of

concentrations in the water column and their seasonal variations in various marine environments also need to be investigated to determine the production and decomposition mechanisms of NMHCs.

Previous analysis methods of NMHCs in seawater are more or less based on that developed by Swinnerton and Linnenbom (1967) [4]. Their method was comprised of three processes: degassing, cryogenic concentration and pre-separation, and gas chromatographic determination. Stripping chambers have been used for the degassing of hydrocarbon gases from seawater, which requires at least 30 min and at least 870 ml of sample water for sensitive determination [5]. While dry ice was used as cryogen to trap the

\* Corresponding author. Fax: +81-11-7062247.

E-mail address: tsuru@ees.hokudai.ac.jp (N. Tsurushima)

extracted hydrocarbon gases in the early method of Swinnerton and Linnenbom (1967) [4], liquid nitrogen has been more recently used [2,5] because hydrocarbons are easier to trap at liquid nitrogen temperature. However, dry ice is more suitable, especially for the long term on board investigation, because it is cheaper, easily obtainable, and relatively easy to store.

In this study, we developed a method for on board determination of C1–C4 hydrocarbons in seawater, improving some areas of previous methods. We succeeded in reducing the sample volume to 500 ml and in using dry ice for the cryogen, keeping the sensitivity and precision at the same levels of previous methods. Furthermore, we attempted to apply a vacuum sparge tower for the rapid extraction of hydrocarbon gases dissolved in seawater. The method was successfully applied to obtain vertical profiles of NMHCs on board a vessel in the northern North Pacific Ocean.

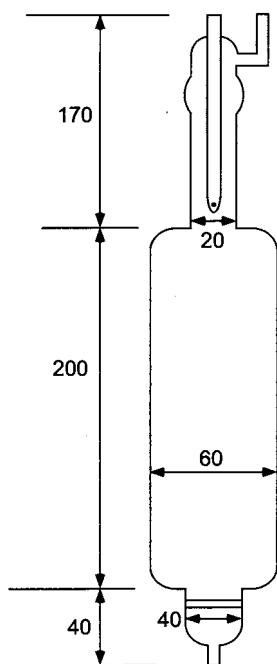


Fig. 1. Vacuum sparge tower used for extraction of hydrocarbon gases in seawater. This tower consisted of a glass cylinder with a coarse glass frit at the lower end. The size is shown in mm.

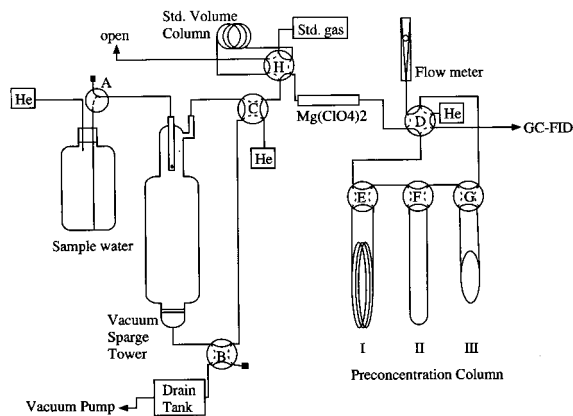


Fig. 2. Scheme of the degassing and pre-concentration apparatus.

## 2. Experimental

A schematic drawing of the apparatus used for degassing and concentration is shown in Figs. 1 and 2, and the various apparatus are listed in Table 1. Valves A to G (eight in total) in Fig. 2 are used to turn the pathway of carrier gas or sample water. In Fig. 1, the solid lines within the valves show the state before analysis. The dashed line shows a state of turning the valves. In this method, two concentration columns (column 1, 2 in Fig. 2) packed with Porasil C were used to collect all the hydrocarbons. The concentration of methane in seawater is generally one or more orders of magnitude greater than that of other hydrocarbons, which is apt to interfere with their gas chromatographic detection. Therefore, methane in seawater should be separated prior to detection by using another column packed with Unibeads C (column 3, Fig. 2) having a large retention volume for methane at dry ice–ethanol temperature as used by Tsurushima et al. (1996) [6]. A vacuum sparge tower (Fig. 1) developed by Law et al. (1994) [7] for determination of sulfur hexafluoride in seawater was modified and applied to this study for the rapid extraction of hydrocarbon gases dissolved in seawater.

Seawater samples for the determination of hydrocarbons were collected with samplers for

oceanographic use such as Niskin bottles. The sample water was drawn into a 500 ml sampling bottle through a rubber tube immediately after recovery of the Niskin bottles ensuring that no air bubbles entered the bottle. Sample bottles were over filled by >200 ml of sample water, and then capped without any air space. The samples were preserved in a cold (0–5°C), dark place for <24 h prior to analysis.

A gas chromatograph was conditioned as follows: carrier gas flowed with a rate of 30 ml min<sup>-1</sup>. The temperatures of the separation column, the vaporization unit, and the detector in the gas chromatograph were 40, 70, and 70°C, respectively.

To begin the operation, valve C was turned to replace the air in the sparge tower with helium gas flowing at 100 ml min<sup>-1</sup>. After several minutes, valve C was turned back to the original position and valve B opened to remove the helium gas in the sparge tower by evacuating

with a vacuum pump. For the first analysis of sample, this procedure was repeated twice to remove laboratory air inside the sparge tower. After attaining 5 torr or less within 3 min, valve B was turned back to the original position and valve A opened to transfer the sample water being gently pushed with helium gas. After 480 ml of the water had flowed into the sparge tower through small holes in its upper part, the dissolved gases in seawater were separated and accumulated in the upper part of the sparge tower.

The extracted gases were then allowed to flow through columns 1 and 3 (soaked in the dry ice–ethanol cryogen) by turning the valves in order of E, G, and C. After 20 min, when the extracted methane and ethane were trapped in column 3 and the other hydrocarbons were trapped in column 1, valves G, E, and C were turned back to the original position. Column 1 was then immersed in hot water (>90°C), and column 2 in dry ice–ethanol. Valves F and E were turned to transfer the hydrocarbon gases from column 1 to column 2. After 5 min, valves F and E were turned back to the original position. This procedure concentrated hydrocarbon gases to a smaller volume. To send the hydrocarbon gases to the gas chromatograph, column 2 was immersed in hot water and valves D and F turned. After the peak of 1-butene has passed through the GC, valve F was turned back to its original position. After immersing column 2 in the dry ice–ethanol cryogen and column 3 in hot water, valves F and G were turned in order to separate methane from ethane and send the methane to the gas chromatograph. Ethane was trapped with column 2. After 2 min, when the peak area of methane is counted, valves F and G were turned back to their original positions. Column 2 was immersed in hot water and valve F turned to send the ethane to the gas chromatograph. After measurement of ethane, valves F and D were turned back to their original positions. Valve B was then turned to drain the sample water from the sparge tower and finally, valve B was turned back to its original position.

Table 1  
Apparatus and reagents for the gas chromatographic analysis of C<sub>1</sub>–C<sub>4</sub> hydrocarbons in seawater

Gas chromatograph	Type GC-8A (Shimadzu)
Detector	Flame ionization detector (FID)
Separation column	Al <sub>2</sub> O <sub>3</sub> /KCL PLOT fused silica capillary column 0.53 mm i.d. × 25 m (Chrompak)
Carrier gas	Helium (99.9999%, Nippon Sanso)
Preconcentration columns	Stainless steel columns packed with
1 (2 mm i.d. × 100 cm)	Porasil-C, 80/100 mesh (Alltech Associates)
2 (2 mm i.d. × 20 cm)	Porasil-C, 80/100 mesh (Alltech Associates)
3 (3 mm i.d. × 20 cm)	Unibeads-C, 100/120 mesh (GL Sciences)
Standard gas	Several hundreds ppb hydrocarbons in nitrogen (Takachiho trading)
Vacuum pump	Oil rotary pump, type G-50S (Sinku Kiko)
Stripping chamber	Vacuum sparge tower shown in Fig. 1
Sample bottle	500 ml dark brown glass bottles
Desiccant	Magnesium perchlorate (GFS Chemicals)
Cryogen	Crushed lumps of dry ice in ethanol

Table 2

The reproducibility, recovery, and detection limits of this method for individual hydrocarbons

	Std. Gas reproducibility (%)	Recovery (%)	Actual seawater reproducibility (%)	Det. Limit (pmol l <sup>-1</sup> )
Methane	2.7	100	3.0	9.9
Ethane	2.9	95 ± 2	10	0.9
Propane	4.6	93 ± 2	11	0.8
n-Butane	3.3	64 ± 12	6.9	1.5
i-Butane	3.0	64 ± 12	6.9	1.3
Ethene	3.5	95 ± 2	4.5	0.9
Propene	2.7	93 ± 2	4.7	1.0
1-Butene	3.8	68 ± 13	13	3.9
Acetylene	7.8	–	–	–

The system was calibrated with a standard gas sample (every 10 to 20 samples) through a stainless steel column which had standard volume (0.2, 0.5 or 1 ml). Standard gas flowed into the standard volume column and introduced to the preconcentration columns by turning valve H.

In this study, we did not examine contamination from Niskin sampler. However, Lamontagne et al. (1974) [8] suggest that there was no significant contamination which could be ascribed to Niskin bottles. We confirm that the amounts of NMHCs in the seawater at 3000 m depth were not detectable or close to the detection limit in the northern North Pacific. This also suggests that significant contamination did not occur in the sampling procedure.

### 3. Results and discussion

#### 3.1. Reproducibilities and recoveries

The reproducibilities, recoveries, and detection limits of this method for respective hydrocarbons are listed in Table 2. The precision,  $1\sigma$  value obtained from the replicate determinations of a standard gas, was < 5% for each hydrocarbon except acetylene which was 8%.

The recoveries of the respective hydrocarbons depend on the retention times of the concentration columns and the extraction efficiencies at

the sparge vacuum tower. Due to the fact that the concentration columns were long enough to collect the hydrocarbons completely, the recoveries of the hydrocarbons depended largely on the extraction efficiencies at the sparge vacuum tower. The extraction efficiency was obtained by repeating the degassing experiments for one seawater sample and assuming that the extraction efficiencies were constant for all the subsequent degassing experiments. The equation for the extraction efficiency ( $r$ ) is given by:

$$r = 1 - (a_2/a_1)$$

where  $a_1$  and  $a_2$  are the amount of each hydrocarbon extracted in the first and second de-

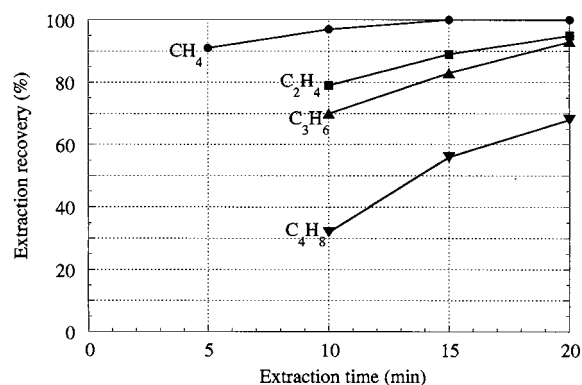


Fig. 3. Stripping efficiency corresponding to the stripping time for determination of methane, ethene, propene, and 1-butene in the actual seawater.



Table 3

Sampling date, time, and location in the cruise of T/S Ohoro Maru in the northern North Pacific as well as surface sea temperature and wind speed

Station no.	Date	Time (local time)	Latitude	Longitude	Depth (m)	SST (°C)	Wind speed (m s <sup>-1</sup> )
193	1997.8.7	16:57	53°30' N	177°00' W	3781	9.3	5.0
194	1997.8.10	15:29	48°59' N	174°56' W	5456	10.3	3.2
200	1997.8.11	20:35	49°00' N	180°00' W	5275	10.1	6.0
204	1997.8.11	8:26	47°00' N	180°00' W	1745	10.8	4.5
208	1997.8.12	21:23	45°00' N	180°00' W	5645	12.1	5.0

gassing processes, respectively. The efficiencies for methane were > 90% even for 5 min extraction (Fig. 3). The extraction efficiency decreased with an increasing molecular weight of hydrocarbon. The extraction efficiencies of C1–C3 hydrocarbons for the 20 min degassing time were > 90%. These values were comparable to those in previous studies. The extraction efficiencies of C4 hydrocarbons were 60–70%, lower than those of previous methods. For instance, in the method of Plass et al. [5] extraction efficiencies of C4 hydrocarbons were 91% after 30 min of helium gas purge with a normal stripping chamber. Although low extraction efficiency induced large uncertainties for determination of C4 hydrocarbons, the absolute errors were not much larger than those for C1–C3 hydrocarbons, because the concentrations and the variabilities of C4 hydrocarbons in the ocean were generally smaller than those of C1–C3 hydrocarbons. Thus, although the sparge vacuum tower may be not effective for hydrocarbons heavier than C4, it is sufficiently practical for the determination of C1–C4 hydrocarbons in seawater.

The 1 $\sigma$  values obtained from the replicate determinations of actual seawater samples were < 15%, except for acetylene. The detection limits of NMHCs have been calculated by measuring the baseline noise and extrapolating the sample sizes to where they would have signal-to-noise ratios of three. They were < 3 pmol l<sup>-1</sup>. These reproducibility and detection limits were also almost the same as those in the previous studies. Acetylene was not detected in the open ocean water used in this experiment.

### 3.2. Concentrations of hydrocarbons in seawater

Measurements were made at five stations in the northern North Pacific (Table 3) during the period August 6–12, 1997 by T/S Oshoro Maru. The concentrations of hydrocarbons in the surface water are listed in Table 4 and vertical profiles are shown in Fig. 4.

The concentration of methane in the surface water was  $2.50 \pm 0.10$  nmol l<sup>-1</sup> ( $n = 5$ ) in the northern North Pacific. This value was not different from  $2.78 \pm 0.46$  observed in the western North Pacific (36–40°N, 165°E) surface water in 1991 [9]. Furthermore, the vertical profiles were also similar to those in the previous study, having the maximum concentration (> 2.5 nmol l<sup>-1</sup>) at depths below 50 m (Fig. 4a).

Table 4

Mean concentration of methane (in nmol l<sup>-1</sup>) and the other light hydrocarbons (in pmol l<sup>-1</sup>) in the surface water as well as its standard deviation ( $\pm 1\sigma$ )<sup>a</sup>

	This study	Previous studies*
CH <sub>4</sub>	$2.50 \pm 0.10$	( $2.78 \pm 0.46$ )
C <sub>2</sub> H <sub>6</sub>	$6.7 \pm 2.3$	$22 \pm 44$
C <sub>2</sub> H <sub>4</sub>	$62.2 \pm 7.6$	$134 \pm 95$
C <sub>2</sub> H <sub>2</sub>	–	$14 \pm 10$
C <sub>3</sub> H <sub>8</sub>	$10.0 \pm 3.1$	$11 \pm 14$
C <sub>3</sub> H <sub>6</sub>	$31.0 \pm 3.9$	$59 \pm 36$
T-C <sub>4</sub> H <sub>10</sub>	$4.3 \pm 1.3$	$7.4 \pm 12$
C <sub>4</sub> H <sub>8</sub> -1	$15.6 \pm 0.5$	$37 \pm 29$

<sup>a</sup> T-C<sub>4</sub>H<sub>10</sub> (total butane) showed the sum of the concentration of n-C<sub>4</sub>H<sub>10</sub> and 1-C<sub>4</sub>H<sub>10</sub>.

\* Mean concentration of methane at the surface in the western North Pacific (Watanabe et al., 1995 [9]) and of other hydrocarbons determined by in situ measurements in various marine environments (compiled by Plass-Dülmer et al., 1995 [3]).

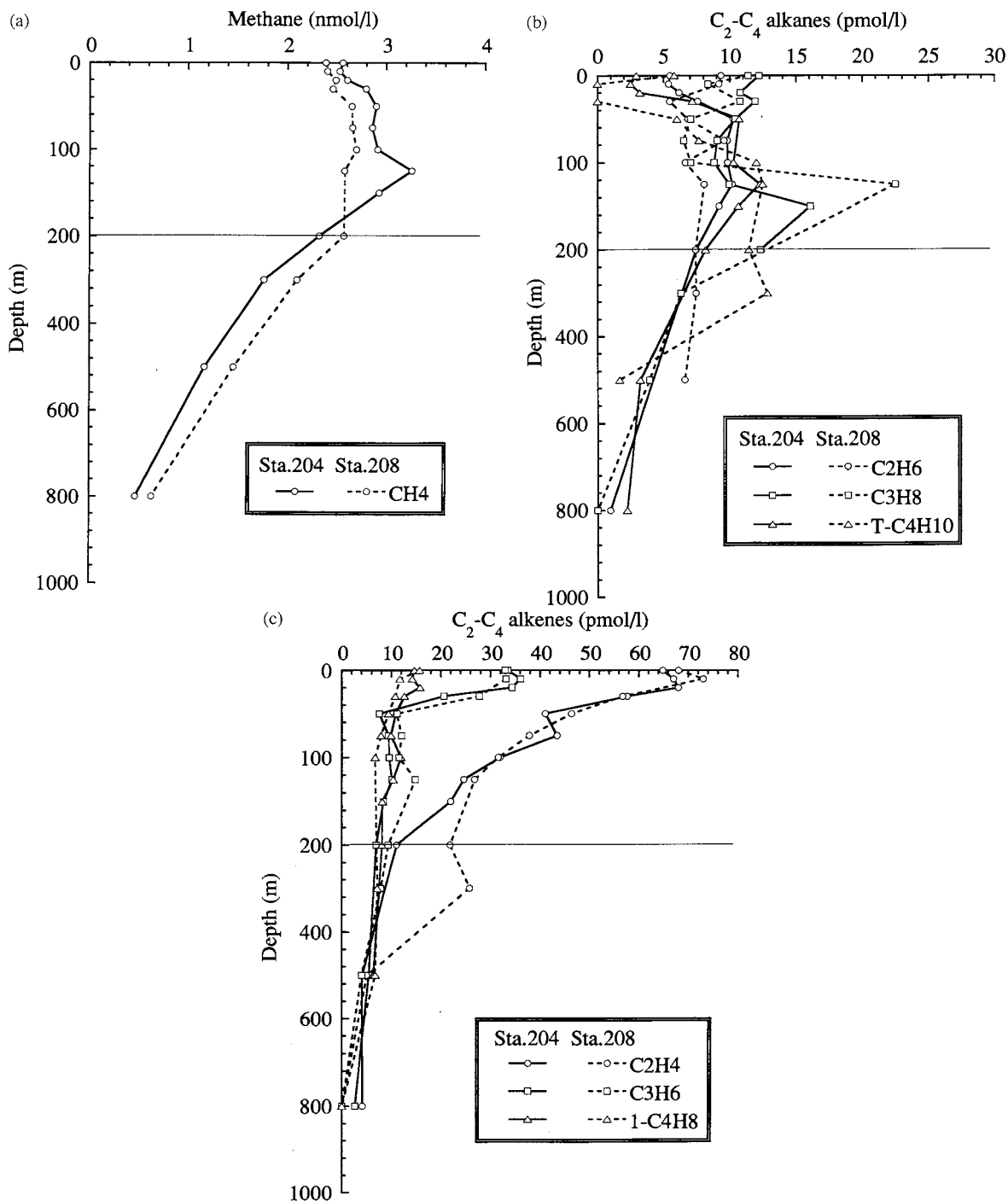


Fig. 4. The vertical profiles of methane (a), C<sub>2</sub>-C<sub>4</sub> alkanes (b) and C<sub>2</sub>-C<sub>4</sub> alkenes (c) at station 204 (solid line) and 208 (broken line) in the northern North Pacific. T-C<sub>4</sub>H<sub>10</sub> (total butane) means sum of the concentration of n-C<sub>4</sub>H<sub>10</sub> and i-C<sub>4</sub>H<sub>10</sub>.

The mean concentrations of NMHCs in the surface water determined in this study were nearly half of those previously reported (Table 4), although the wide ranges make the differences insignificant. The concentrations of alkenes were greater than those of alkanes, and the concentration of alkenes decreased with increasing carbon number. These characteristics agree with results obtained in previous studies.

The concentrations of alkenes had maxima at the surface and decreased with depth (Fig. 4c). While the concentration of propene decreased rapidly in the layer below 50 m, that of ethene decreased more gradually with depth. The concentrations of alkanes, except methane, were < 30 pmol l<sup>-1</sup>. The maximum concentrations of C2–C4 alkanes were not at the surface, and their concentrations decreased with depths below 200 m (Fig. 4b).

#### 4. Summary

The described method allows shipboard measurement of C1–C4 hydrocarbons in seawater. Only dry ice was used to cryofocus. The sample volume and degassing time were somewhat smaller than for previous methods. Sparge vacuum tower was effective for the extraction of C1–C3 hydrocarbons from seawater. The method employed in this study is somewhat complicated to operate and not suitable for continuous measurement because there are many valves and cryofocusing traps. However, this

method can be automated for easier operation using automatic valves.

#### Acknowledgements

We would like to thank our colleagues in the Laboratory of Analytical Chemistry and the Laboratory of Marine and Atmospheric Geochemistry, Hokkaido University for their cooperation throughout this study. We wish to thank the captain and crew of T/S Oshoro Maru and R/V Ushio Maru of Hokkaido University for their help with sampling. We also thank Dr P.P. Murphy for helpful comments. This study was supported by Grant-in-Aid for JSPS Fellows.

#### References

- [1] N.M. Donahue, R.G. Prinn, *J. Geophys. Res.* 95 (1990) 18387.
- [2] N.M. Donahue, R.G. Prinn, *J. Geophys. Res.* 98 (1993) 16915.
- [3] C. Plass-Dülmer, R. Koppman, M. Ratte, J. Rudolph, *Global Biogeochem. Cycles* 9 (1995) 79.
- [4] J.W. Swinnerton, V.J. Linnenbom, *Science* 156 (1967) 1119.
- [5] C. Plass, R. Koppmann, J. Rudolph, *Fres. J. Anal. Chem.* 339 (1991) 746.
- [6] N. Tsurushima, S. Watanabe, S. Tsunogai, *J. Oceanogr.* 52 (1996) 221.
- [7] C.S. Law, A.J. Watson, M.I. Liddicoat, *Mar. Chem.* 48 (1994) 57.
- [8] R.A. Lamontagne, J.W. Swinnerton, W.J. Linnenbom, *Tellus* 26 (1974) 71.
- [9] S. Watanabe, N. Higashitani, N. Tsurushima, S. Tsunogai, *J. Oceanogr.* 51 (1995) 39.

# Determination of protein by its enhancement effect on the Rayleigh light scattering of carboxyarsenazo

Gang Yao, Ke An Li\*, Shen Yang Tong

*Department of Chemistry, Peking University, Beijing 100871, PR China*

Received 28 December 1998; received in revised form 27 April 1999; accepted 29 April 1999

## Abstract

This is the first report on the determination of proteins based on the interaction with carboxyarsenazo (CAA) by Rayleigh light scattering (RLS). At pH 4, the weak RLS of CAA can be enhanced greatly by the addition of proteins, resulting in three characteristic peaks. Based on this, the interactions of CAA with nine kinds of proteins were studied and a new quantitative determination method for proteins has been developed. This method is very sensitive ( $0.10\text{--}15.3\ \mu\text{g ml}^{-1}$  for bovine serum albumin (BSA)), rapid ( $< 2\ \text{min}$ ), simple (one step), tolerant of most interfering substances, and gives a close value to that of the Coomassie brilliant blue (CBB) method in the determination of proteins in human serum. Thus, the CAA assay can be useful for routine analytical purposes and may overcome some of the limitations of other currently employed methods. Mechanism studies show that the three RLS peaks correspond to the absorption valleys of the CAA–protein complex. © 1999 Elsevier Science B.V. All rights reserved.

*Keywords:* Rayleigh light scattering; Carboxyarsenazo; Protein determination

## 1. Introduction

Although the quantitative determination of proteins is a basic requisite in biochemistry (as it is often used as a reference for the measurements of other components in biological systems), the widely used methods have their disadvantages. The Lowry method can only assay protein concentration greater than  $10\ \mu\text{g ml}^{-1}$  [1]. The silver staining method suffers multiple steps, high background and toxicity of formaldehyde [2]. As for the Coomassie brilliant

blue (CBB) assay, ‘There is a slight nonlinearity in the response pattern’ [3]. This intrinsic nonlinearity compromises the sensitivity and accuracy, and only a narrow range of relatively high protein concentrations,  $2\text{--}10\ \mu\text{g ml}^{-1}$  BSA, is used for assay and construction of the calibration graph [4].

Since organic dyes can serve as effective probes of the structures and functions of biological macromolecules, interest has been raised in the study of the interaction of dyes with proteins or nucleic acids in recent decades. Various new dye binding methods have been put forward for protein analysis by spectrophotometric and fluorometric methods [5–7].

\* Corresponding author. Fax: +86-10-62751408.

*E-mail address:* likn@chemms.chem.pku.edu.cn (K.A. Li)

Rayleigh light scattering (RLS) from both small and large molecules in the various states of matter has been extensively studied and applied for many years [8–11]. This technique however, traditionally regarded as suffering from the disadvantages of low signal levels and lack of selectivity, had not been applied in quantitative analysis until Huang etc. [12] first used it for the determination of nucleic acids with  $\alpha,\beta,\gamma,\delta$ -tetra-(4-trimethyl-ammoniumphenyl) porphyrin (TAPP). They chose the incident light wavelength in the absorption band envelope of TAPP, and its scattering intensity could be enhanced by nucleic acids. That phenomenon is considered as resonance enhanced Rayleigh light scattering or resonance light scattering. The first study of this technique from molecules in solution was a study of diphenyl-polyenes by Bauer [9], which was followed by Miller's theoretical treatment [13] of macroscopic fluctuation theory, and by Anglister and Steinberg's experimental studies [14] of intensities and depolarization ratios.

According to Pasternack [10], a particle, assumed to be spherical, absorbs and scatters light depending on its size, shape and refractive index relative to the surrounding medium. The intensity of RLS was calculated by Anglister [14] to be

$$R(90^\circ) = (4000\pi^2 n^2 C / \lambda^4 N_A) [(dn/dC)^2 + (dk/dC)^2] \quad (1)$$

where  $R(90^\circ)$  is the Rayleigh ratio for the incident beam and total scattered light at  $90^\circ$ ,  $n$  is the refractive index of the medium,  $\lambda$  is the wavelength of incident light,  $N_A$  is Avogadro constant,  $C$  is the molarity of the scattering particle,  $dn/dC$  and  $dk/dC$  are the increment in the real and imaginary components, respectively, of the refractive index of the solution due to the scattering particles. So when analytical conditions such as wavelength, pH and dye concentration are fixed,

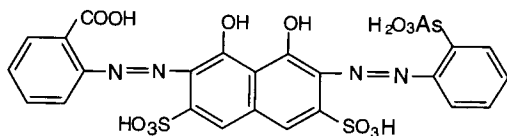


Fig. 1. Structure of CAA.

the RLS intensity is only proportional to the concentration of scattering particles.

The present work is aimed at developing Rayleigh light scattering, not resonance light scattering, as a tool for analytical chemistry. Unlike Huang, who chose the wavelengths in the absorption bands, we set the incident and emission wavelengths in the absorption valley of the BSA–dye complex. A new determination method with high sensitivity for proteins has been developed in our group based on the interaction of proteins with CAA (Fig. 1). By spectroscopic data, we got a regression equation at pH 1.9 between the absorption and the concentration of protein. But the low sensitivity (Sandell's sensitivity was  $0.25 \mu\text{g cm}^{-2}$  and detection limit was  $1.9 \mu\text{g ml}^{-1}$  for BSA) prevented it from microanalysis of protein. We report in this paper that at pH 4.00, the RLS intensity of CAA can be highly enhanced by proteins, and the intensity of RLS enhancement is proportional to the concentration of proteins.

## 2. Experimental

### 2.1. Reagent

All chemicals were of analytical reagent grade or the best grade commercially available in China. All stock solutions were prepared in doubly deionized water. The Britton–Robinson buffer was used to control pH of the tested solutions.

CAA was obtained from E. Merck, and CBB G-250 was obtained from Fluka. Trypsin, haemoglobin, lysozyme, bovine serum albumin (BSA), human serum albumin (HSA) and human  $\gamma$ -globin ( $\gamma$ -G) were obtained from Sigma. Egg albumin,  $\alpha$ -chymotrypsin and pepsin were obtained from Shanghai Biochemistry Institute (PR China).

The protein concentrations were determined spectrophotometrically at 280 nm with the  $\epsilon^{1\%}$  value for: BSA 6.6 [15], HSA 5.3 [15],  $\gamma$ -G 13.8 [16], lysozyme 26.04 [16], egg albumin 7.5 [16]. And the concentration of haemoglobin, trypsin, pepsin and  $\alpha$ -chymotrypsin were determined as [17]: protein concentration =  $144 (A_{215} - A_{225})$ , where  $A_{215}$  and  $A_{225}$  were absorbance at 215 and 225 nm measured with 1 cm cell.

Fresh human serum was bought from Peking University Hospital and diluted by doubly deionized water.

## 2.2. Apparatus

In the most parts, a Hitachi model RF-540 spectrofluorometer (Japan), equipped with a xenon lamp, a recorder, dual monochromator and a 1-cm quartz cell, was used to record the RLS spectra and intensity. A Shimadzu model UV-265 spectrophotometer (Japan) was used to obtain absorption spectra in a 1-cm quartz cell. In the part of spectral calculation, a Shimadzu model F-4500 spectrofluorometer (Japan) and a Varian model Cary 1E spectrophotometer (Australia) were used to record, respectively, the RLS and absorption spectrum, which were converted to ASCII format by the software equipped to these spectrometers for further computation. A WH-861 vortex mixer (Huangjing Instrumental Co., Jiangsu, PR China) was used to blend the solutions in volumetric flasks, and a model 821 pH meter (Zhongshan University, PR China) was used to measure pH of the solution.

## 2.3. Method

In a 10 ml flask, CAA, buffer and protein or sample solution were added in order in different ratios, then diluted to 10 ml with water. The mixture was stirred after each addition. The RLS spectrum was obtained by scanning simultaneously the excitation and emission monochromators of the RF-540 spectrofluorometer from 250 to 700 nm. The RLS intensity was measured with the excitation and emission wavelength at 370 nm. Both the slits of excitation and emission were 5 nm. The sensitivity and ordinate of the spectrofluorometer were all one if not specially mentioned.

## 3. Result and discussion

### 3.1. Spectrum characteristics

Fig. 2 shows the light scattering spectra and

absorption spectra of both CAA and CAA–BSA complex at pH 4.23. It can be seen that light scattering intensity of CAA is very small in the above wavelength regions. However, enhanced light scattering can be observed when CAA coexists with BSA. Unlike the resonance light scattering spectra whose peaks are situated at the absorption bands envelope, the peaks of this light scattering spectra of the complex were located at the minimum absorption, while the valleys of the light scattering spectra was located at the peaks of the absorption spectra. This difference can be explained as follows: according to the theory about resonance light scattering, the intensity increases due to the increase of the refractive index of the solution in the optical absorption region. Usually this increase is masked by the absorption. However, when dye aggregates are formed this effect can be strongly enhanced as the resonance light scattering intensity is proportional to the square of the scattering particle volume [11]. So the resonance light scattering bands are expected for large aggregates with the wavelength where the molar absorption coefficient is large, such as porphyrin whose light scattering peak appeared nearby its solet band [10]. In the system of this paper, no enhancement was found at the absorption band envelope. It can hence be concluded that no resonance light scattering occurred. The peaks and valleys of the light scattering spectra were because the complex absorbed the RLS intensity. That the complex absorbed the RLS intensity caused not only the peaks and valleys of the light scattering spectra, but also the symmetry of the RLS spectra and the absorption spectra.

### 3.2. Stability

The reaction between CAA and protein occurs rapidly at room temperature (< 2 min). Scattering intensity is stable for at least 3 h (data not shown). Thus, this assay does not require crucial timing.

### 3.3. Addition sequence

Two types of mixing sequence were investigated. One was to mix CAA and buffer first, then

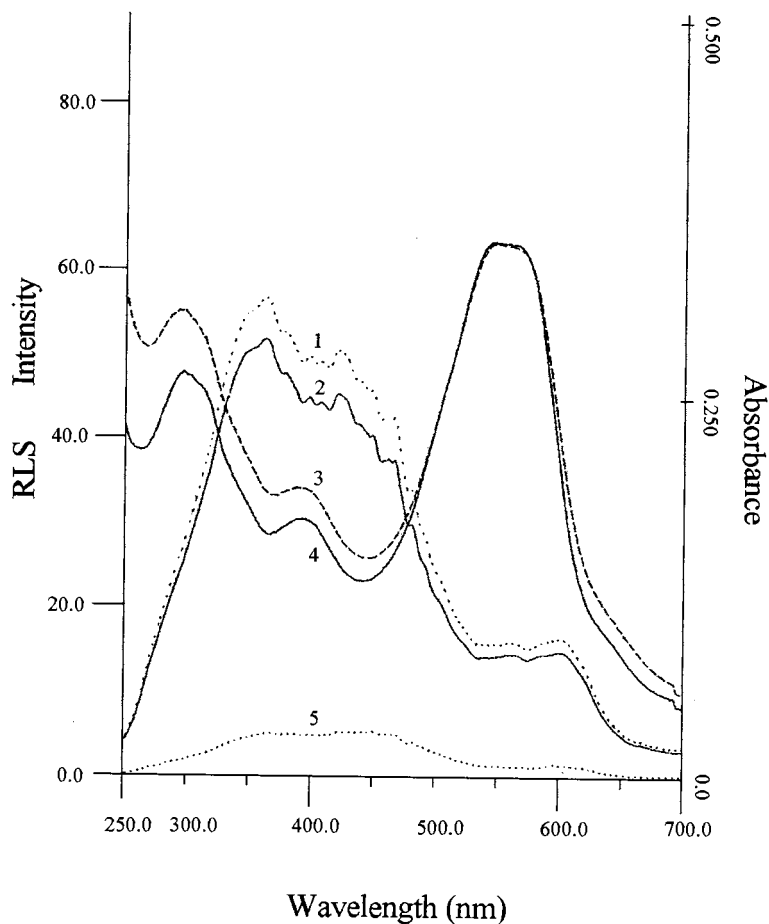


Fig. 2. RLS spectra and absorption spectra at pH 4. (1) Absorption spectrum of CAA-BSA; (2) absorption spectrum of CAA; (3) RLS spectrum of CAA-BSA; (4) the difference RLS spectrum of CAA-BSA and CAA; (5) RLS spectra of CAA. CAA, 10.0  $\mu\text{M}$ ; BSA, 10.0  $\mu\text{g ml}^{-1}$ , pH 4.

BSA solution was added. The other was adding buffer to the mixture of CAA and BSA. The RLS of the two sequences were measured at the same assay condition. The results show that the addition sequence greatly effected RLS intensity (data not shown). Mixing of CAA and buffer first can get a higher RLS intensity, compared to mixing CAA and protein first. This can show that the electronic coupling makes CAA bind to protein. After being mixed with buffer (pH 4.00), CAA was negatively charged ( $\text{p}K_1$  2.67 [18]), so that it would be easy to bind to positively charged BSA

(pI 4.8–4.9). If CAA was mixed with BSA first at neutral condition (pH  $\sim$  7), the negatively charged dye would be hard to bind to the negatively charged BSA.

#### 3.4. Acidity

Fig. 3 shows that the scattering intensity of the CAA-BSA complex was affected greatly by pH. The highest intensity was obtained at pH 4, so this pH was chosen for the assay. The effect of pH can be interpreted as follows: With the pH

increased, the greater negative charge on CAA would enhance the interaction between dye and positively charged BSA. On the other hand, an increase in pH also causes an increase in the negative charge on the protein, which would weaken the binding of dye to BSA. These two opposing effects of pH resulted in the strongest binding and hence the maximum RLS intensity at pH 4. We have tested the optimum pH for some other proteins and found that each optimum pH was between  $pK_1$  of CAA and  $pI$  of the protein, where CAA was negatively charged and protein was positively charged.

### 3.5. Effect of CAA concentration

The concentration of CAA affects the RLS sensitivity and intensity. As shown in Fig. 4, when the concentration of CAA was as low as 5.0  $\mu\text{M}$ , the linear range was narrow and the calibration curve bent to a platform at a BSA concentration of 8.98  $\mu\text{g ml}^{-1}$ . At this concentration, all available CAA was bound so that further protein addition cannot lead to further CAA–protein interaction. It can also be seen from Fig. 4 that the

highest sensitivity and intensity was reached at a CAA concentration of 5.0  $\mu\text{M}$ , above which the slopes of the calibration curves decreased with the increase of the dye concentration. This phenomenon is owing to the higher concentration of the free dye that resulted in a higher absorbance and thus less enhancement of the scattering. Meanwhile, higher CAA concentration means higher concentration of bound BSA, which would give a longer linear range. So CAA concentration was chosen to be 10.0  $\mu\text{M}$  for this assay in order to get a higher sensitivity and a better linear range.

### 3.6. Variation between proteins

Individual responses of various proteins determined in the assay at pH 4 are carried out. The equations of RLS intensity against the concentration of several proteins are listed in Table 1. A satisfactory linear relationship with high regression coefficient and a wide linear range are obtained.

It was reported early [11,19] that the intensity of enhanced RLS signals appeared to depend on

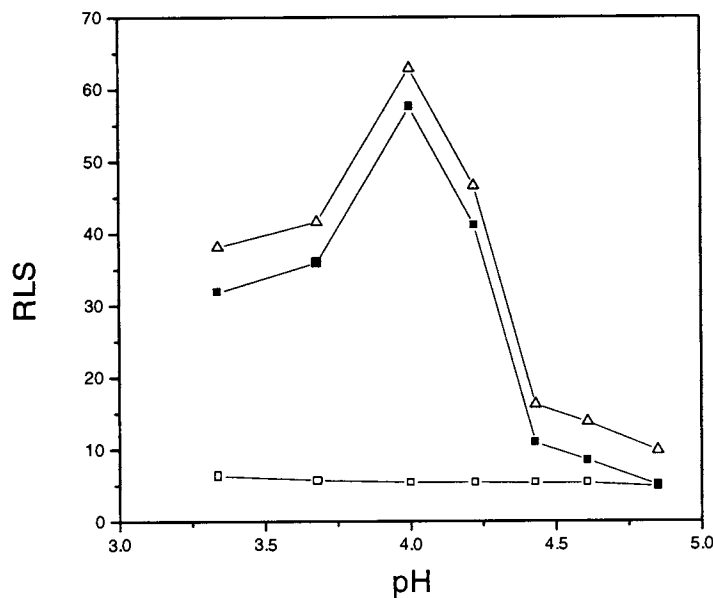


Fig. 3. Effect of pH on RLS intensity of 10.0  $\mu\text{M}$  CAA ( $\square$ ), the mixture of 10.0  $\mu\text{M}$  CAA and 10.0  $\mu\text{g ml}^{-1}$  BSA ( $\triangle$ ) and the difference between sample and blank ( $\blacksquare$ ).



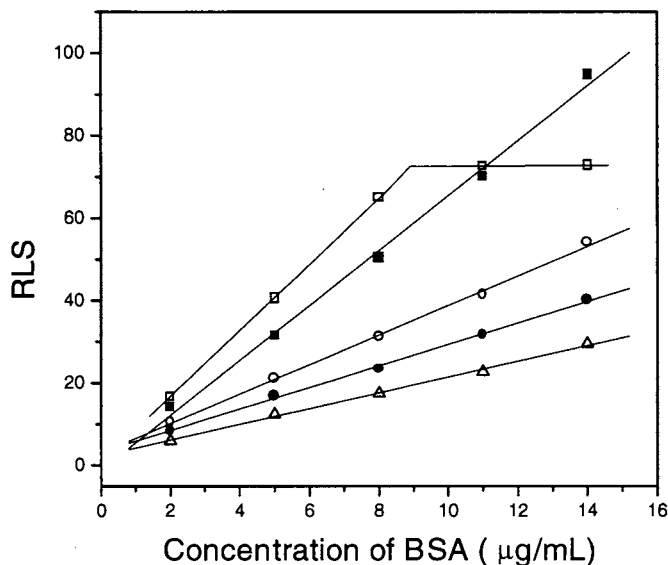


Fig. 4. Effect of CAA concentration on this assay at pH 4.00. CAA concentration: 5.0  $\mu\text{M}$  ( $\square$ ); 10.0  $\mu\text{M}$  ( $\blacksquare$ ); 20.0  $\mu\text{M}$  ( $\circ$ ); 30.0  $\mu\text{M}$  ( $\bullet$ ); 40.0  $\mu\text{M}$  ( $\triangle$ ).

the electronic properties of the individual chromophores, the extent of the electric coupling among chromophores, and the size of the aggregate thus formed. The sizes of various proteins differ, and so do the binding strengths between a dye and different kinds of proteins. Hence the protein-to-protein variability cannot be avoided with RLS technique. It can be seen from Table 1 that the RLS sensitivities increase roughly, but not strictly, with the increase of iso-electric points

( $pI$ ) of proteins. So we can conclude that electronic coupling plays the main, but not the only role in the formation of protein–CAA complex.

### 3.7. Interfering substances

The influence of coexisting substances such as irons, amino acids and detergents Fig. 5 were tested at 10.0  $\mu\text{g ml}^{-1}$  BSA, which was in the middle of the linear range. As shown in Table 2,

Table 1  
The equation of RLS intensity and protein concentration<sup>a</sup>

Protein	$pI$	Equation	Linear range ( $\mu\text{g ml}^{-1}$ )	$r$
Protamin sulfate	10–12	$I = 2.86 + 24.2C$	0.060–3.03	0.9951
Lysozyme	11.0–11.2	$I = 5.68 + 9.24C$	0.023–10.1	0.9985
HAS	4.7	$I = 2.71 + 5.71C$	0.097–14.5	0.9955
BSA	4.8–4.9	$I = 4.02 + 5.29C$	0.10–15.3	0.9968
Haemoglobin	6.9	$I = 5.95 + 4.75C$	0.012–9.62	0.9984
$\gamma$ -G	5.8–6.6	$I = 7.51 + 3.42C$	0.016–14.0	0.9950
Egg albumin	4.6–4.7	$I = 5.69 + 3.02C$	0.018–3.57	0.9921
$\alpha$ -Chymotrypsin	8.1	$I = 7.69 + 1.18C$	0.046–7.58	0.9955
Trypsin	5.0–8.0	$I = 5.72 + 0.63C$	0.88–9.39	0.9936
Pepsin	1.0	N <sup>b</sup>		

<sup>a</sup> Concentration of CAA 10.0  $\mu\text{M}$ , pH 4, average of three measurements.

<sup>b</sup> No RLS enhancement of CAA was observed by addition of protein at pH 4.

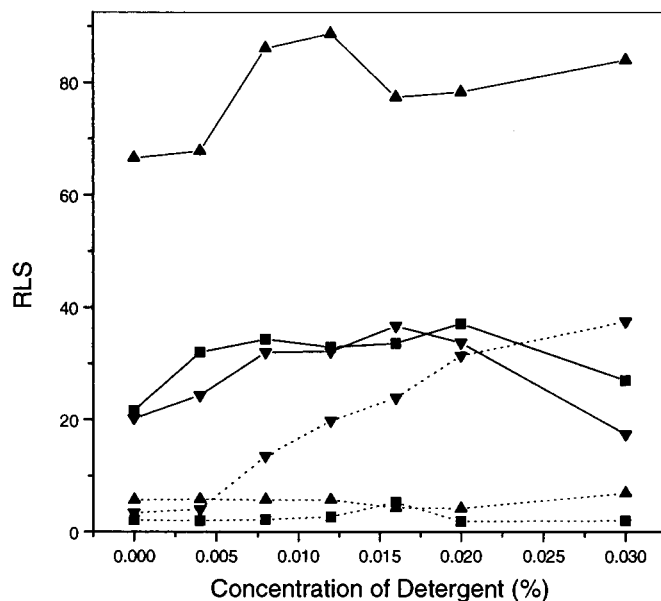


Fig. 5. Effect of detergents on the RLS intensity of 10.0  $\mu\text{M}$  CAA (...), the mixture of 10.0  $\mu\text{M}$  CAA and 10.0  $\mu\text{g ml}^{-1}$  BSA (—) at pH 4. SDS (▲) with sensitivity 1 and ordinate 1; CTAB (▼) and Triton X-100 (■) with sensitivity 2 and ordinate 6 in measurement.

few ions interfere with this assay, while 0.4 M urea has a negative effect. Table 3 shows that this assay is not affected by amino acids. The effects of detergents are shown in Fig. 6. SDS and Triton X-100 did not affect the RLS intensity of CAA while CTAB increased that of the dye. This may be due to the binding of positively charged CTAB with the negatively charged CAA. As for the complex of CAA and BSA, the effect of the detergents can be divided into two parts: first, the refractive index of the solution increased with the addition of the detergents, which, according to Eq. (1), raised the RLS intensity. Then, when the concentration of detergents was above a value, the electronic coupling of dye with CTAB and protein with SDS prevented the interaction of CAA and BSA, which surpassed the effect of the increase of refractive index, and resulted in a decrease of RLS intensity.

### 3.8. Measurement of sample

Although the CBB method is widely used because of its ease performance, rapidity, relative sensitivity, and specificity for proteins, however,

as stated in the abstract, the CBB method has some disadvantages. By using our method and choosing HSA as the standard, proteins in sam-

Table 2

Effect of interfering substances<sup>a</sup>

Interfering substance <sup>b</sup>	Change (%)	Interfering substance	Change (%)
K <sup>+</sup> , chloride	-3.4	Cu <sup>2+</sup> , nitrate	-7.8
Ca <sup>2+</sup> , chloride	1.4	Pb <sup>2+</sup> , nitrate	1.9
Al <sup>3+</sup> , chloride	2.1	Zn <sup>2+</sup> , chloride	-5.0
Mg <sup>2+</sup> , chloride	0.1	Cd <sup>2+</sup> , chloride	-3.7
Fe <sup>3+</sup> , chloride	1.4	Hg <sup>2+</sup> , sulfate	-1.6
Co <sup>2+</sup> , chloride	0.1	EtOH (5%)	6.4
Ni <sup>2+</sup> , chloride	-2.1	Glucose (0.4 mg ml <sup>-1</sup> )	0.2
Cr <sup>3+</sup> , chloride	2.3	Urea (0.4 M)	-7.7
Mn <sup>2+</sup> , chloride	-6.1		

<sup>a</sup> Concentration of CAA 10.0  $\mu\text{M}$ , BSA 10.0  $\mu\text{g ml}^{-1}$ , pH 4.00, average of three measurements.

<sup>b</sup> Concentration of interfering substance was 20.0  $\mu\text{M}$  if not mentioned.

Table 3  
Effect of amino acids<sup>a</sup>

Amino acid	Change (%)	Amino acid	Change (%)
L-Gly	-2.5	L-His	1.6
L-Leu	0.3	L-Tyr	2.3
L-Asp	-4.1	L-Try	-4.6
L-Phen	-3.8	L-Ser	0.1
L-Lys	-1.2	L-Ala	-2.4
L-Arg	-4.5	L-Cys	-1.6
L-Pro	0.2	L-Glu	0.8

<sup>a</sup> Concentration of CAA 10.0  $\mu\text{M}$ , BSA 10.0  $\mu\text{g ml}^{-1}$ , amino acid 20  $\mu\text{g ml}^{-1}$ , pH 4, average of three measurements.

ples of human serum were measured. The results were compared with those assayed by the CBB method. All results are satisfactory and shown in Table 4.

Compared to the CBB method, the CAA assay has many advantages: (1) CBB was easy to stain to the cell but hard to clean away, while CAA has no such dyeability; (2), the CBB method was performed in a high acidic solution (1.4 M  $\text{H}_3\text{PO}_4$ ) which cannot ensure all proteins dissolve well, but the CAA method was in a moderate surrounding (pH 4); (3) the CAA method has a much better linearity than the CBB method; (4) the CBB method was effected by time, but the CAA method has a good stability; and (5) Although the reported linear range for the CBB method was 2–10  $\mu\text{g ml}^{-1}$ , the commonly used range was 0.01–1.0  $\text{mg ml}^{-1}$  [19]. This sensitivity was much lower than that of the CAA method (0.10–15.3  $\mu\text{g ml}^{-1}$ ).

### 3.9. Mechanism of the formation of RLS peaks

To clarify the RLS spectrum, a Hitachi model F-4500 spectrofluorometer (Japan) was used to record these RLS spectra. It can be seen that the RLS spectra obtained from this spectrofluorometer (Fig. 7); were not the same as those from RF-540 (Fig. 2). The main difference was located in the range of 250–300 nm, where the signal magnitude obtained from F-4500 was higher than that obtained from RF-540. The shapes of these two spectra in the range of 300–700 nm are almost the same. This phenomenon, we believe

comes mainly from the different optical systems of these two spectrometers, especially the detector and/or light source intensity difference.

According to Rayleigh's Law, the light scattering intensity of pure water should depend on the wavelength as  $1/\lambda^4$ . The difference between Rayleigh's Law and the measured spectrum is due to the dependence of the spectrofluorometer sensitiv-

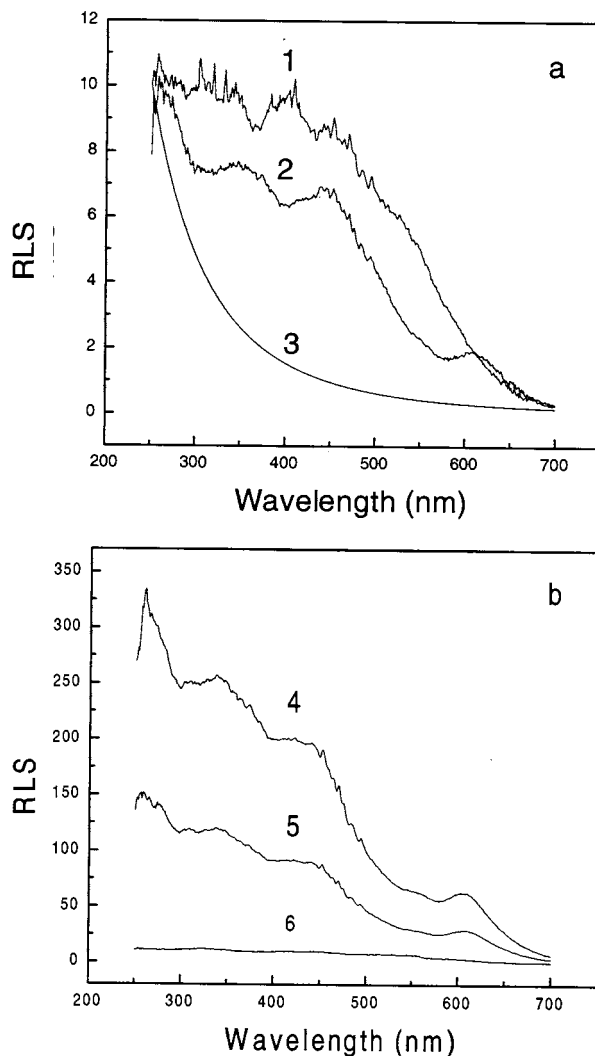


Fig. 6. RLS spectra obtained from F-4500. (a) 1, RLS spectrum of pure water; 2, RLS spectrum of 10.0  $\mu\text{M}$  CAA; 3, Rayleigh curve; (b) 4, RLS spectrum of the mixture of 10.0  $\mu\text{M}$  CAA and 10.0  $\mu\text{g ml}^{-1}$  BSA; 5, RLS spectrum of the mixture of 10.0  $\mu\text{M}$  CAA and 5.0  $\mu\text{g ml}^{-1}$  BSA; 6, RLS spectrum of buffer solution.

Table 4  
Analytical results of protein in human serum<sup>a</sup>

Sample	This method (mg ml <sup>-1</sup> )	CBB method (mg ml <sup>-1</sup> )
No. 1	75.0	75.2
No. 2	85.0	82.5
No. 3	89.2	83.7
No. 4	94.7	92.1

<sup>a</sup> Each result was the average of four measurements.

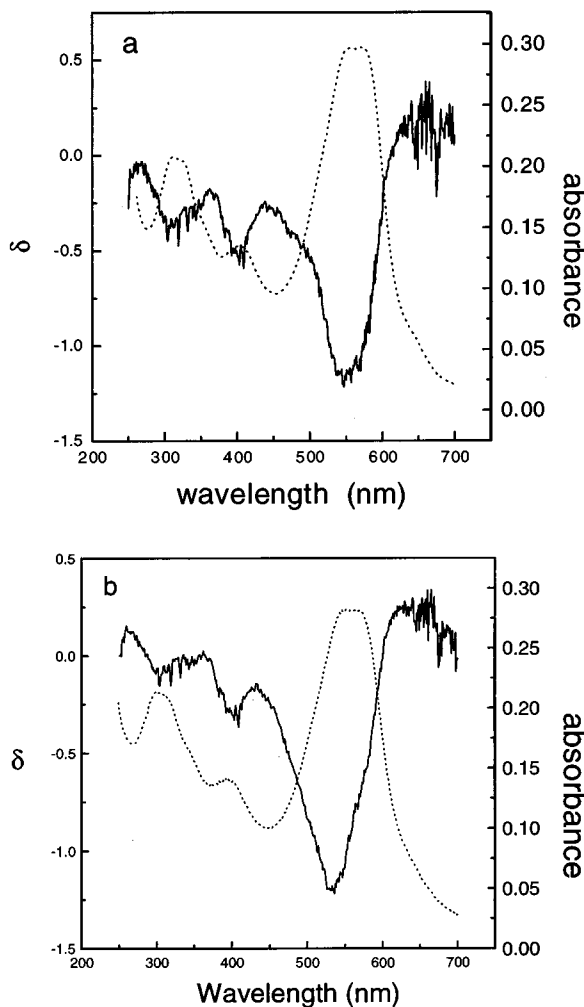


Fig. 7. Spectra calculated as  $\delta = (I_{\text{cal}} - R)/I_{\text{cal}}$  (—) and absorption spectra (---) at pH 4. (a) 10.0  $\mu\text{M}$  CAA; (b) 10.0  $\mu\text{M}$  CAA and 10.0  $\mu\text{g ml}^{-1}$  BSA.

ity on the wavelength of the incident light. We can define here the instrument sensitivity  $S$  as

$$S = I_w + R_w \quad (2)$$

where  $I_w$  is the measured intensity of pure water and  $R$  is the Rayleigh spectrum normalized to unity by the value of  $I_w$  at 250 nm ( $R_w = (250/\lambda)^4 I_{w, 250 \text{ nm}}$ ). Hence, we will calculate the corrected light scattering intensity ( $I_{\text{cal}}$ ) from the measured light scattering intensity ( $I_{\text{exp}}$ ) as

$$I_{\text{cal}} = I_{\text{exp}}/S \quad (3)$$

and Rayleigh curve normalized by  $I_{\text{cal}}$  at 250 nm as

$$R_c = (250/\lambda)^4 I_{\text{cal, cal, 250 nm}} \quad (4)$$

With statistical treatment, we can only find a slight difference between  $I_{\text{cal}}$  and  $R_c$ . What's more, we find no obvious difference of  $I_{\text{cal}}$  in the region of CAA or CAA–BSA complex absorption (resonance light scattering effect). So it can be concluded that no CAA aggregation was formed in the presence of BSA, and this scattering was not resonance light scattering but Rayleigh light scattering.

In order to see the difference clearly between  $I_{\text{cal}}$  and  $R_c$ , we defined  $\delta$  as

$$\delta = (I_{\text{cal}} - R_c)/I_{\text{cal}} \quad (5)$$

and put the  $\delta$ – $\lambda$  curve together with the absorption spectrum, we can see also clearly from Fig. 7. that the decrease of light scattering is due to the absorption of exciting and scattered light of the dye or dye–protein complex.

#### 4. Conclusion

CAA exists in anions at pH 4 and can only exhibit weak RLS signals. But it can interact with positively charged BSA mainly through electrostatic binding, which results in an enhancement of RLS intensity. Based on this observation, a novel means for determination of proteins that can be done on a commonly used spectrofluorometer was provided. This new method has the advantage of simplicity, high sensitivity, convenience and tolerance of most interfering substances. Spectral computation elucidated that this light scattering was not resonance light scattering but Rayleigh light

scattering. The RLS peaks are attributed to the absorption of dye or dye–protein complex.

It should be taken in mind that the CAA method has its own limitation. Because some proteins produced responses that varied significantly, this method cannot be used for the determination of total protein without separation, except in serum where albumin has almost the same response to  $\gamma$ -globin.

### Acknowledgements

This work was supported by the National Natural Science Foundation of China, and all the authors express their deep thanks.

### References

- [1] O.H. Lowry, N.J. Rosebrough, A.L. Farr, R.J. Randall, *J. Biol. Chem.* 193 (1951) 265–275.
- [2] K.K. Oshawa, N. Ebata, *Anal. Biochem.* 135 (1983) 409–415.
- [3] M.M. Bradford, *Anal. Biochem.* 72 (1976) 248–254.
- [4] V.S. Gasparov, V.G. Degtyra, *Biochem. Mosc.* 59 (1994) 563–572.
- [5] H.S. Soedjak, *Anal. Biochem.* 220 (1994) 142–148.
- [6] P.A.E. Piuno, U.J. Krull, *Anal. Chem.* 67 (1995) 2635–2643.
- [7] N. Li, K.A. Li, S.Y. Tong, *Anal. Biochem.* 233 (1996) 151–155.
- [8] A. Einstein, *Ann. Phys.* 33 (1910) 1275–1298.
- [9] D.R. Bauer, B. Hudson, R. Prcora, *J. Chem. Phys.* 63 (1975) 588–589.
- [10] R.F. Pasternack, C. Bustamante, P.J. Collings, A. Gianetto, E.J. Gibbs, *J. Am. Chem. Soc.* 115 (1993) 5393–5399.
- [11] R.F. Pasternack, P.J. Collings, *Science* 269 (1995) 935–939.
- [12] C.Z. Huang, K.A. Li, S.Y. Tong, *Anal. Chem.* 68 (1996) 2259–2263.
- [13] G.A. Miller, *J. Phys. Chem.* 82 (1978) 616–618.
- [14] J. Anglister, I.Z. Steinberg, *Chem. Phys. Lett.* 65 (1979) 50–54.
- [15] G.D. Fasman, *Proteins*, in: *CRC Practical Handbook of Biochemistry and Molecular Biology*, vol. 2, CRC, Boca Raton, FL, 1976.
- [16] J.B. Murphy, M.W. Kies, *Biochem. Biophys. Acta* 45 (1960) 382.
- [17] B. Budesinsky, *Talanta* 16 (1969) 1277–1288.
- [18] A. Muk, S.B. Savvin, *Anal. Chim. Acta* 44 (1969) 59–65.
- [19] R.F. Pasternack, K.F. Schaefer, P. Hambright, *Inorg. Chem.* 33 (1994) 2062–2065.

# Flow injection determination of bromide ion in a developer using bromide ion-selective electrode detector

Takashi Masadome <sup>a,\*</sup>, Yasukazu Asano <sup>b</sup>, Takashi Nakamura <sup>c</sup>

<sup>a</sup> Department of Chemical Science and Engineering, Ariake National College of Technology, Omuta, Fukuoka 836-8585, Japan

<sup>b</sup> Laboratory of Chemistry, Department of General Education, Ariake National College of Technology, Omuta, Fukuoka 836-8585, Japan

<sup>c</sup> Ashigara Research Laboratories, Fuji Photo Film Co. Ltd., Minamiashigara, Kanagawa 250-0193, Japan

Received 21 January 1999; received in revised form 23 April 1999; accepted 29 April 1999

## Abstract

A potentiometric flow injection determination method for bromide ion in a developer was proposed, by utilizing a flow-through type bromide ion-selective electrode detector. The sensing membrane of the electrode was  $\text{Ag}_2\text{S-AgBr}$  membrane. The response of the electrode detector as a peak-shape signal was obtained for injected bromide ion in a developer. A linear relationship was found to exist between peak height and the concentration of the bromide ion in a developer in a concentration range from  $1.0 \times 10^{-3}$  to  $1.0 \times 10^{-2}$  mol l<sup>-1</sup>. The relative standard deviation for 10 injections of a  $6 \times 10^{-3}$  mol l<sup>-1</sup> bromide ion in a developer was 1.3% and the sampling rate was ca 17–20 samples h<sup>-1</sup>. The present method was free from the interference of an organic reducing reagent, an organic substance in a developer sample solution for the determination of bromide ion in a developer. © 1999 Published by Elsevier Science B.V. All rights reserved.

**Keywords:** Bromide ion; Bromide-selective electrode detector; Developer; Flow injection analysis

## 1. Introduction

Recently, we can obtain many kinds of films for taking photos. The films, which have different film form, based on the sensitivity of ISO 100, 200, 400, 800, and 1600 are supplied from many manufacturers. Furthermore, there are many kinds of the films, depending on the kinds of cameras and exposure condition. When we de-

velop so many kinds of films in the same developer, the concentration of bromide ion in the developer is often changed by the kinds of films, film form, exposure condition, and processing technique. The changes of the concentration of bromide ion in the developer have an influence on photo quality such as sharpness and brightness of photos. Therefore, it is very important to control precisely the concentration of bromide ion in the developer in film developing laboratory.

The concentration of bromide ion in a developer is usually determined by potentiometric titra-

\* Corresponding author. Fax: +81-944-531-361.

E-mail address: masadome@ariake-nct.ac.jp (T. Masadome)

tion [1]. In this method, an analyst must determine optimal analytical conditions by examining the concentration of  $\text{AgNO}_3$  as a titrant and the titration speed, and so on, because the optimal analytical condition depends on the concentration level of the bromide ion and the kind of coexisting substances in a developer. The determination of optimal analytical conditions is generally time-consuming and needs a skilled technique. Furthermore, the titration procedure is also time-consuming. The sampling rate of the potentiometric titration is only ca. four samples  $\text{h}^{-1}$ . Ion chromatography (IC) is often used in the determination of bromide ion in a developer. However, the durability of the ion exchange column is limited and IC is not cost-effective. The sampling rate of IC for the determination of bromide ion in a developer is also only ca. five samples  $\text{h}^{-1}$ . On the other hand, potentiometry utilizing bromide ion-selective electrodes (ISEs) is promising method for the determination of the bromide ion in a developer. However, bromide ion in a developer could not be determined by batchwise method using the conventional solid-state bromide ISE because an organic reducing reagent in a developer interferes with the potential response of the bromide ISE, and as the result, the potential response of the bromide ISE has no reproducibility.

A flow injection analysis (FIA) with an ISE detector represents a very advantageous analytical method because of its ease of handling, high reproducibility, high sampling rate, and its ease of control of chemical reactions [2–11]. Therefore, a FIA method using  $\text{Br}^-$ -ISE detector would be expected to be the promising technique for determination of  $\text{Br}^-$  ion in a developer. If a developer is highly diluted in a FIA system, the concentration of an organic reducing agent which interferes with the potential response of the  $\text{Br}^-$ -ISE detector will decrease. As a result, it is expected that interference from an organic reducing agent for the determination of bromide ion in a developer decreases by using the FIA system.

In this paper, we applied FIA system using a bromide ISE detector to the determination of the bromide ion in a developer in order to develop simpler and faster determination method of bro-

midide ion in a developer. As the results, we found that the bromide ion in a developer can be determined by FIA using a bromide ISE detector.

## 2. Experimental

### 2.1. Chemicals

An organic reducing reagent in a developer was received from Fuji Photo Film Co. Ltd., Kanagawa, Japan. All other chemicals of analytical reagent grade were used.

### 2.2. Flow injection analysis

Fig. 1 shows a schematic diagram of the FIA system for the  $\text{Br}^-$  ion. The flow system is composed of a double plunger pump equipped with a sample injector (DMX-2300T, Sanuki Industry Co., Tokyo, Japan), a flow-through type ISE detector (FLC-11, Denki Kagaku Keiki, DKK, Tokyo, Japan), an ion-meter (DKK, COM-20R), and a strip chart recorder (LR 4120, Yokogawa Co., Tokyo, Japan). The flow-through type  $\text{Br}^-$  ISE detector consists of the solid-state type  $\text{Br}^-$  ISE based on a  $\text{Ag}_2\text{S-AgBr}$  membrane (DKK, 7041) and a reference electrode (DKK, 4401L). A sample solution (a developer) was injected into a water stream (carrier: CS). This stream was subsequently merged with a reagent solution (RS) stream of mixed solution of  $1 \times 10^{-1} \text{ mol l}^{-1} \text{ KNO}_3$  and  $5 \times 10^{-4} \text{ mol l}^{-1} \text{ KBr}$  adjusted to pH

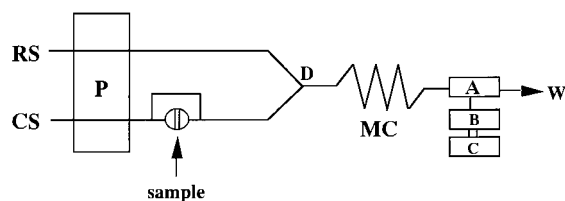


Fig. 1. Flow diagram for determination of  $\text{Br}^-$  ion. CS, carrier solution (distilled and deionized water,  $1.0 \text{ ml min}^{-1}$ ); RS, reagent solution (a mixed solution of  $1 \times 10^{-1} \text{ M KNO}_3$  and  $5 \times 10^{-4} \text{ M KBr}$  adjusted to pH 5.0 by  $0.1 \text{ mol l}^{-1} \text{ CH}_3\text{COOH/CH}_3\text{COONa}$  buffer,  $1.0 \text{ ml min}^{-1}$ ); MC, mixing coil (i.d.  $0.5 \text{ mm} \times 80 \text{ m}$ ); A, flow-through type  $\text{Br}^-$ -selective electrode detector; B, ion-meter; C, recorder; D, confluence point; P, pump; W, waste; sample volume;  $20 \mu\text{l}$ .

Table 1  
Effect of KBr concentration on the sensitivity of the Br<sup>-</sup>-selective electrode detector

Concentration of KBr in the reagent solution/mol l <sup>-1</sup>	Sensitivity (mV/decade)	
	Concentration range	
	10 <sup>-3</sup> –10 <sup>-2</sup> mol l <sup>-1</sup> KBr	10 <sup>-2</sup> –10 <sup>-1</sup> mol l <sup>-1</sup> KBr
1 × 10 <sup>-5</sup>	51	52
1 × 10 <sup>-4</sup>	47	52
1 × 10 <sup>-3</sup>	44	51

5.0 by a 0.1 mol l<sup>-1</sup> CH<sub>3</sub>COOH/CH<sub>3</sub>COONa buffer. KNO<sub>3</sub> was added as a supporting electrolyte to the RS to minimize streaming potential, which affects the response of the electrode detector. The flow rates of the streams of CS and RS were 1.0 ml min<sup>-1</sup>. The potential difference between the Br<sup>-</sup> ISE and the reference electrode was measured using the ion-meter and the peak-shaped response signals of the detector were fed to the strip-chart recorder.

### 3. Results and discussion

#### 3.1. Effect of KBr concentration in a reagent solution on the sensitivity of the electrode detector

At first, the effect of KBr concentration in a RS on the sensitivity of the electrode detector to the KBr solution was examined when the length of the mixing coil (MC) and the sample volume were 100 cm and 100 μl, respectively. The results were shown in Table 1. When the KBr concentration in a RS is 1 × 10<sup>-5</sup> and 1 × 10<sup>-4</sup> mol l<sup>-1</sup>, the electrode detector showed the Nernstian response to the KBr solution in the concentration range more than 1 × 10<sup>-3</sup> mol l<sup>-1</sup>. When the KBr concentration in a RS is 5 × 10<sup>-4</sup> mol l<sup>-1</sup>, the electrode detector showed the sub-Nernstian response to the KBr solution in the concentration range from 1 × 10<sup>-3</sup> mol l<sup>-1</sup> to 1 × 10<sup>-2</sup> mol l<sup>-1</sup>. In this case, the sensi-

tivity of the electrode detector (peak height) was found to be linear against the concentration of KBr solution. In general, the calibration curve which is linear against the concentration of an objective substance in a sample solution is more desirable than that is linear against logarithmic concentration of an objective substance in a sample solution for the determination of an objective substance. Therefore, from the results, the RS containing 5 × 10<sup>-4</sup> mol l<sup>-1</sup> KBr was used in subsequent experiments.

#### 3.2. Effect of the organic reducing agent in a developer on the sensitivity of the electrode detector

A developer contains masking agents (diethylenetriamine pentaacetic acid and 1-hydroxyethane-1,1-diphosphonic acid), salts for adjusting pH, KBr, KI and an organic reducing agent (4-(N-ethyl-N-β-hydroxyethylamino)-2-methyl aniline, sulfate salt). When the batchwise method using bromide ISE is used for the determination of Br<sup>-</sup> ion in a developer, an organic reducing agent interferes with the potential response of the bromide ISE and the potential response of the bromide ISE has no reproducibility. The mechanism of interfering with the potential response of bromide ISE by an organic reducing agent may be as follows:

Based on the silver ion conduction mechanism, the potential of the bromide ISE is known to be determined by silver ion at the surface of the Ag<sub>2</sub>S/AgBr membrane, which is related to the precipitation equilibrium shown in Eq. (1).



If an organic reducing agent reduces Ag<sup>+</sup> at the surface of the membrane of the bromide ISE to Ag<sup>0</sup>, the activity of the silver ion at the surface of the electrode membrane decreases. Hence, the bromide ion activity at the surface of the bromide ISE in the presence of an organic reducing agent are estimated to be higher than that in case of absence of an organic reducing agent. This means that the slope of the potential change against the concentration of bromide ion



for bromide ISE in the presence of an organic reducing agent is much smaller than that in the absence of an organic reducing agent.

Therefore, the effect of an organic reducing agent in a developer on the sensitivity of the electrode detector to the KBr in a developer was examined in the FIA system, when the length of the MC and the sample volume were 100 cm and 100  $\mu\text{l}$ , respectively. The results were shown in Table 2. The sensitivity of the electrode detector to the KBr in a developer containing all substances other than an organic reducing agent was 90% for that to the KBr solution. This may be a result of the interference from iodide ion in a developer. On the other hand, the sensitivity of the electrode detector to the KBr in a developer containing an organic reducing agent was only 25% for the sensitivity of the electrode detector to the KBr in a developer containing all substances other than an organic reducing agent. This result shows that an organic reducing agent in a developer seriously interferes the potential response of the  $\text{Br}^-$  ISE in the FIA system.

### 3.3. Effect of length of mixing coil and sample volume on the sensitivity of the electrode detector

The effect of the dilution of the developer in the FIA system was examined by changing the length of the MC and the sample volume because it is expected that the dilution of the developer decreases the interference from an organic reducing agent for the determination of KBr in a developer. At first, effect of the sample volume on the sensitivity of the electrode

Table 2

Effect of the organic reducing reagent on the sensitivity of the  $\text{Br}^-$ -selective electrode detector to KBr in the concentration range from  $10^{-3}$  to  $10^{-2}$  mol  $\text{l}^{-1}$

Sample	Sensitivity (mV/decade)
KBr solution	44
A developer containing all substances other than an organic reducing agent	39
A developer	11

Table 3

Effect of the length of mixing coil on the sensitivity of  $\text{Br}^-$ -selective electrode detector to KBr in the concentration range from  $10^{-3}$  to  $10^{-2}$  mol  $\text{l}^{-1}$

Mixing coil length/m	Sensitivity (mV/decade)
1	11
20	22
40	24
60	27
80	28

detector to KBr in a developer was examined. When the sample volume was changed from 100 to 20  $\mu\text{l}$ , the sensitivity of the electrode detector slightly increased. Subsequent experiments were performed using the sample volume 20  $\mu\text{l}$ . Table 3 shows the effect of the length of MC on the sensitivity of the electrode detector to KBr in a developer. When the length of MC and the sample volume was 80 m and 20  $\mu\text{l}$ , respectively, the sensitivity of the electrode detector seriously increased from 10 mV decade $^{-1}$  to 30 mV decade $^{-1}$  compared with the case that the length of MC and the sample volume was 1 m and 100  $\mu\text{l}$ , respectively. As shown in Table 3, the maximum sensitivity was obtained, when the length of MC was 80 m. Subsequent experiments were performed using the MC (80 m).

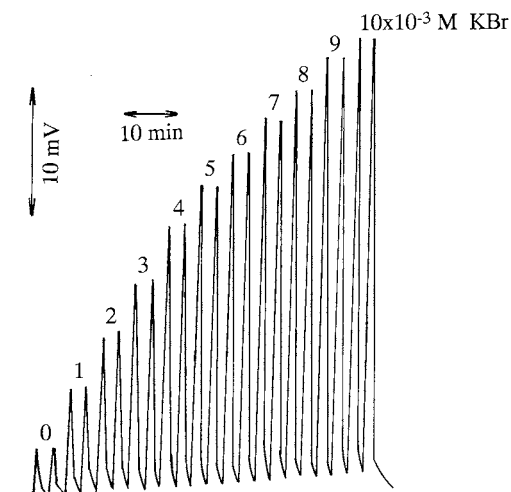


Fig. 2. Typical calibration peaks for KBr in a developer. Experimental conditions are identical to those in Fig. 1.

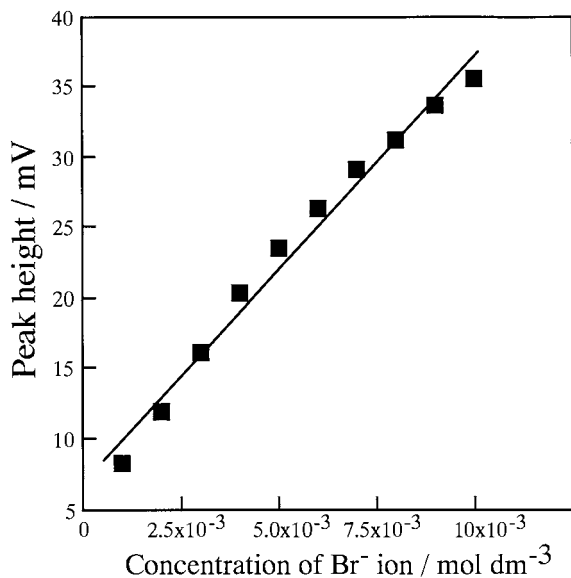


Fig. 3. Typical calibration curve for KBr in a developer obtained by the Br<sup>-</sup>-selective electrode detector. Regression line,  $y = 3035.2x + 6.9$ ; correlation factor, 0.992.

#### 3.4. Calibration curve

Fig. 2 shows the calibration peaks for bromide ion in a developer obtained using the flow system shown in Fig. 1. When the length of MC and the sample volume was 80 m and 20  $\mu$ l, respectively, a linear relationship was found to exist between peak heights obtained from the calibration peaks of Fig. 2 and the concentration of the bromide ion in a developer in a concentration range from  $1.0 \times 10^{-3}$  to  $1.0 \times 10^{-2}$  mol l<sup>-1</sup>, as shown in Fig. 3. The calibration equation is  $y = 3035.2x + 6.9$ ;  $r = 0.992$  where  $y$  is peak height obtained by the Br<sup>-</sup>-selective electrode detector and  $x$  the concentration of KBr. The relative standard deviation for 10 injections of a  $6 \times 10^{-3}$  mol l<sup>-1</sup> bromide ion in a developer was 1.3% and the sampling rate was ca 17–20 samples h<sup>-1</sup>.

#### 3.5. Correlation between the FIA method and the conventional potentiometric titration method

The relationship between concentration of KBr obtained by the present method and that by po-

tentiometric titration method for the determination of KBr in a developer sample is shown in Fig. 4. The calibration equation is  $y = 0.963x + 0.209$ ;  $r = 0.989$  where  $y$  is concentration of KBr obtained by the present method and  $x$  the concentration of KBr obtained by the conventional potentiometric titration method. From the result, we concluded that the present method is applied to the determination of KBr in a developer.

#### 4. Conclusion

The present method allows for the precise and fast determination of bromide ion in a developer by using a very long MC (80 m) in the FIA system in order to decrease the interference from an organic reducing agent in a developer. The present method is a useful alternative to conventional potentiometric titration method for the determination of bromide ion in a developer.

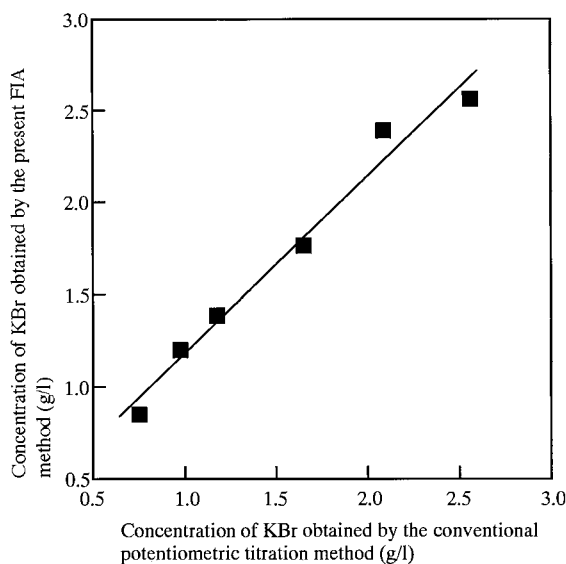


Fig. 4. Correlation between the FIA method and the conventional potentiometric titration method for the determination of KBr in a developer. Regression line,  $y = 0.963x + 0.209$ ; correlation factor, 0.989.

**References**

- [1] I. Sasaki, K. Nakashima, H. Ueno, *Jpn. Photo Soc.* 14 (1951) 17.
- [2] J. Alonso, J. Baró, J. Bartrolí, J. Sánchez, N. del Valle, *Anal. Chim. Acta* 308 (1995) 115.
- [3] C.W. Dowle, B.G. Cooksey, J.M. Ottaway, W.C. Campbell, *Analyst* 113 (1988) 117.
- [4] T. Masadome, T. Imato, N. Ishibashi, *Bunseki Kagaku* 40 (1991) 1.
- [5] T. Masadome, T. Imato, N. Ishibashi, *Anal. Sci.* 6 (1990) 605.
- [6] T. Masadome, T. Imato, N. Ishibashi, *Bunseki Kagaku* 39 (1990) 519.
- [7] E. Pungor, Z. Feher, G. Nagy, K. Toth, *CRC Crit. Rev. Anal. Chem.* 14 (1983) 175.
- [8] H. Wada, T. Ogawa, G. Nakagawa, Y. Asano, S. Ito, *Anal. Chim. Acta* 211 (1988) 213.
- [9] A. Sakai, A. Hemmi, H. Hachiya, F. Kobayashi, S. Ito, Y. Asano, T. Imato, Y. Fushinuki, I. Taniguchi, *Talanta* 45 (1998) 575.
- [10] T. Masadome, T. Imato, N. Ishibashi, *Bunseki Kagaku* 40 (1991) 7.
- [11] T. Masadome, T. Imato, S. Itoh, Y. Asano, *Fresenius, J. Anal. Chem.*, 357 (1997) 901.

# Estimation of trace impurities in reactor-grade uranium using ICP-AES

R.K. Malhotra \*, K. Satyanarayana

*Chemical Laboratory, Atomic Minerals Directorate for Exploration & Research, Department of Atomic Energy, Government of India, Begumpet, Hyderabad-500 016, India*

Received 9 February 1999; received in revised form 27 April 1999; accepted 29 April 1999

## Abstract

Estimation of impurities in reactor grade uranium is important from the point of view of neutron economy. For chemical separation, ion exchange and solvent extraction techniques have been employed although the latter is generally preferred. Amongst various extractants TBP (tri-n-butyl phosphate), TBP-TOPO (tri-n-octyl phosphine oxide), or TOPO only (in CCl<sub>4</sub>, xylene, dodecane) is most often used. New reagents like Cyanex-923 (mixture of 4 tri-alkyl phosphine oxides)/TEHP (tri-ethylhexyl phosphoric acid) are also being used. This communication reports chemical separation of uranium by precipitation using 1,2-diaminocyclohexane NNN'N'-tetra acetic acid (CyDTA)/ammonium hydroxide in presence of 1,10-phenanthroline and estimation of impurities in the filtrate by ICP-AES. Quantitative separation of U, a high spectral interferer in plasma and recovery of impurities have been achieved. Recovery of Cd has been improved by using 1,10-phenanthroline. The method is accurate and precise, offering a relative standard deviation ranging from less than 4% (3.8% for Eu at the 10 μg g<sup>-1</sup> level) to 12.9% (for Ce at the 2.5 μg g<sup>-1</sup> level) for all the elements studied. © 1999 Elsevier Science B.V. All rights reserved.

*Keywords:* Reactor-grade uranium; Impurities; Chemical separation; Inductively coupled plasma atomic emission spectrometry

## 1. Introduction

The presence of common elements like B, Cd, Hf and some of the rare earth elements (REE) such as Sm, Eu, Gd and Dy in reactor-grade uranium fuel even at ultra trace levels is detrimental to the efficient functioning of a nuclear reactor. The concentrations of the metallic im-

purities in the fuel must be below the maximum permissible levels specified to obtain the required density for the pellets and also to reduce the loss of neutrons by the high neutron absorption cross-section elements. Quantitative determination of these elements in nuclear-grade uranium is therefore necessary prior to its use as a nuclear fuel. About 35 trace elements have been listed in the C 787 specification issued by the ASTM for UF<sub>6</sub> [1] and needed six or more techniques to determine all these impurities [2].

\* Corresponding author. Tel.: +91-040-7766603/7767101 (O), 3730535 (R); fax: +91-040-7762940.

*E-mail address:* amdhyd@ap.nic.in (R.K. Malhotra)

Different instrumental techniques have been reported [3–7] for the estimation of trace metallic impurities in uranium. Carrier distillation emission spectrography [7] has been widely used for the determination of trace metal impurities in uranium, for quality control of U-fuels. While Cd, Co, Cr, Cu, Fe, Mn, Ni etc. have been determined by carrier distillation technique, the REEs were determined after separation from uranium [8–11]. Boron in uranium has been determined spectrophotometrically with curcumin after separation by distillation as methyl borate [12] and after solvent extraction with 2-ethylhexane-1,3-diol [13]. This laboratory has reported [14] the estimation of boron in uranium-rich samples by inductively coupled plasma atomic emission spectrometry (ICP-AES) after separation of boron from the matrix by fusing the samples with potassium hydroxide (KOH) and nebulization of the aqueous leach filtrate into the plasma. The separation and pre-concentration of the REEs has been performed either by ion-exchange column chromatography or by solvent extraction. Separation and preconcentration of some of these trace elements from high-purity uranium has also been carried out on Chelex-100, prior to their estimation by graphite furnace atomic absorption spectrometry [15]. An ICP-AES method has also been reported [16] for the determination of 23 metallic impurities including some REEs in nuclear-grade uranium dioxide, after separation of the uranium by TOPO-CCl<sub>4</sub> extraction prior to their determination in the raffinate. Methods have also been reported to separate uranium from the trace metallic impurities, using Cyanex-923 (mixture of four tri-alkyl phosphine oxides)/TBP-TOPO [17,18]. Overall, it has been observed that almost all the instrumental techniques used for the determination of trace elements in uranium require the prior separation of analytes from uranium for obtaining accurate values. No single technique appears to be ideally suited to estimate all the metallic impurities, particularly at ultra-trace levels as far as the power of detection, precision and accuracy and number of elements that can be determined as concerned and

which are an important criteria for the choice of a method.

Inductively coupled plasma atomic emission spectrometry (ICP-AES) has been established itself as a powerful multi-element analytical technique in many laboratories [19–21], as it provides superior detection limits for a many number of elements as compared to flame atomic absorption spectrometry (FAAS).

This communication reports separation of uranium by precipitation with ammonium hydroxide in presence of 1,2-cyclohexane diamine tetra acetic acid (Cy DTA). Trace impurities like Ce, Sm, Eu, Gd, Dy, Cd, Cr, Cu, Ni, Mn, Fe, Ti, Hf, etc. remain in the filtrate and after adjusting acidity (with regard to HCl, 5% v/v), the same are estimated by ICP-AES using suitable emission lines. Using the above method, the recovery of added Cd was only about 60%. This was enhanced by adding 1,10-phenanthroline and this resulted in quantitative recoveries of Cd also. The method is simple, fast and precise as number of stages for uranium separation is limited to one only. In a comparative evaluation of ethylene diamine tetra acetic acid (EDTA), CyDTA and diethylene triamine penta-acetic acid (DTPA), CyDTA was found most suitable in terms of recovery of trace elements and quantitative separation of uranium respectively.

## 2. Experimental

### 2.1. Instrumentation

All ICP-AES measurements were performed on a LABTAM (now GBC, Melbourne, Australia) Model-8410 Plasmascan sequential instrument equipped with a computer-controlled rapid-scanning monochromator (focal length, 750 mm) Model-750 series, with a ruled grating of 1800 grooves/mm and a Czerny–Turner mounting system. A more detailed description of the equipment is given in our earlier publications [22–24]. All analyses were carried out under vacuum conditions. The details of instrumental parameters and other operating conditions used are given in Table 1.

Table 1  
ICP-AES instrumental parameters and operating conditions

Instrument	LABTAM Model-8410	
Rf Generator	Plasmascan	
Rf Coil	27.12 MHZ (crystal-controlled)	
Plasma torch	Three turn gold plated-copper coil, with water cooling system	
Pump	Demountable type, DMT-2000 (GBC, Australia)	
Nebulizer	Peristaltic, ten-roller, Gilson Minipuls-2	
Operating power	G.M.K. (V-grove, modified Babington type)	
Reflected power	1200 W	
Viewing height	<5 W	
Argon gas flow rates	15 mm above load coil	
	Coolant	14 l min <sup>-1</sup>
	Auxiliary	1.0 l min <sup>-1</sup>
	Sample	0.8 l min <sup>-1</sup>
PMT voltage	1000 V	
Integration time	3 s ( <i>n</i> = 3)	
Solution uptake rate	3.5 ml min <sup>-1</sup>	
Sample flush time	10 s	
Entrance slit	20 μm and 3 mm height (fixed)	
Exit slit	40 μm (adjustable)	
Peak search window width	0.12 nm	

All flame AAS measurements were made by Varian Model Spectr AA-20 atomic absorption spectrophotometer (Melbourne, Australia) using the operation conditions as listed in Table 2.

Table 2  
Flame AAS operating conditions

Element	Wavelength (nm)	Slit width (nm)	Lamp current (mA)	Type of flame	Flame stoichiometry
Cd <sup>a</sup>	228.8	0.5	4	Air/C <sub>2</sub> H <sub>2</sub>	Oxidizing
Cr	357.9	0.2	7	Air/C <sub>2</sub> H <sub>2</sub>	Reducing
Cu	324.7	0.5	4	Air/C <sub>2</sub> H <sub>2</sub>	Oxidizing
Ni <sup>a</sup>	232.0	0.2	4	Air/C <sub>2</sub> H <sub>2</sub>	Oxidizing
Mn	279.5	0.2	5	Air/C <sub>2</sub> H <sub>2</sub>	Oxidizing
Fe <sup>a</sup>	248.3	0.2	5	Air/C <sub>2</sub> H <sub>2</sub>	Oxidizing

<sup>a</sup> All absorbance measurements in case of Cd, Ni and Fe are obtained after applying deuterium background correction method.

## 2.2. Reagents

All reagents used were prepared from analytical-grade/specpure (Johnson Matthey, UK) chemicals.

## 2.3. Standard solutions

The standard stock solutions of the elements (1000 μg ml<sup>-1</sup>) were prepared as follows: All single-element REE-stock solutions were prepared by dissolving specpure rare earth oxides in hydrochloric acid maintaining an overall acidity of 5% v/v. However, CeO<sub>2</sub> was dissolved in a mixture of HNO<sub>3</sub> and H<sub>2</sub>O<sub>2</sub> and then converted to HCl medium maintaining 5% v/v HCl acidity, and the remaining standards as follows:

For Cd: 0.2856 g cadmium oxide in 250 ml of 5% HCl; for Cr: 0.7072 g of potassium dichromate in 250 ml of 5% HCl; for Cu: 0.2500g of copper turnings, initially in minimum volume of 50% v/v HNO<sub>3</sub> and finally in 250 ml of 5% HCl; for Ni: 0.5056 g of nickel carbonate, initially in minimum volume of 5% HCl and finally to 250 ml volume maintaining an overall acidity of 5% v/v HCl; for Mn: 0.2500 g of manganese metal pieces/dust in 250 ml of 5% HCl; for Fe: 0.3574g of ferric oxide, initially in little aquaregia and finally in 250ml of 5% HCl; for Ti: 0.250g of titanium metal wire, initially in few drops of hydrofluoric acid and after evaporation with HCl, in 250 ml of 5% HCl; for Hf: 0.2948g of hafnium oxide, initially in few drops of hydrofluoric acid, and after evaporation with HCl, in 250ml of 5% HCl. All the standard materials (metals/oxides/carbonates)

used were specpure chemicals from Johnson Mathey, UK.

The working calibration standards of  $1 \mu\text{g ml}^{-1}$  (for Eu) and  $10 \mu\text{g ml}^{-1}$  (for all other elements) were single element solutions in 5% (v/v) HCl, prepared by serial dilutions of the respective stock solutions in presence of 20 ml of 0.2M CyDTA (plus 0.50g of 1,10-phenanthroline per 100 ml volume) and all measurements were made using a minimum point background correction method.

#### 2.4. Procedure

A 2.3585 g of specpure uranium oxide,  $\text{U}_3\text{O}_8$  (Johnson Mathey) sample (equivalent to 2.0000g of uranium metal) was dissolved in minimum volume of 50% v/v  $\text{HNO}_3$  by keeping on hot water bath, evaporated to dryness and finally dissolved in about 50 ml of 5% v/v HCl. The solutions were prepared in triplicate and the solutions so obtained were cooled and known amounts of 5, 10 and 20  $\mu\text{g}$  each of the studied elements were added into three solutions and kept aside. To all these solutions 10 ml each of 0.2M (7.28 g/100 ml) 1,2-diaminocyclohexane NNN'N'-tetra acetic acid (CyDTA) and 0.25 g of 1,10-phenanthroline were added and  $\text{NH}_4\text{OH}$  precipitation was carried out while hot by keeping on water bath. The uranium hydroxide precipitate was cooled and filtered through Whatman No. 540 (15 cm) filter paper. The precipitate was thoroughly washed twice with a solution of 5% v/v  $\text{NH}_4\text{OH}$  in 0.01 M CyDTA, and the precipitate was then discarded. The filtrate was acidified with 50% v/v HCl and finally brought to a volume of 50 ml maintaining an overall acidity of 5% v/v HCl for measurement. A reagent process blank was also prepared in the same way. These solutions were aspirated into the plasma and Ce (418.660 nm); Sm (442.434 nm); Eu (381.967 nm); Gd (364.619 nm); Dy (353.170 nm); Cd (228.802 nm); Cr (267.716 nm); Cu (324.754 nm); Ni (221.647 nm); Mn (257.610 nm); Fe (259.940 nm); Ti (334.941 nm); and Hf (277.336 nm) were determined after calibrating the instrument at their respective emission lines.

### 3. Results and discussion

The three most sensitive emission lines for the REEs and the other elements as listed in the Atlas of spectral lines [25] were scanned thoroughly. Based on the detection limits, possible elemental concentrations, the matrix interferences, and the precision and accuracy, the emission lines cited above are recommended in this type of matrix. The statistically evaluated analytical data viz: the peak counts ( $I_p$ ), background counts ( $I_b$ ), background equivalent concentration (*BEC*), detection limits and net line to background intensity ratios for all the elements studied in 5% v/v HCl, obtained at their respective emission lines are presented in Table 3. On the basis of these above observations and on 10 times the detection limits (*LOD*), the minimum determinable concentration (*LOQ*) of the analytes starting with 2.0g (uranium or equivalent  $\text{U}_3\text{O}_8$  and analytes in 50 ml final volume) using the proposed method works out as ( $\mu\text{g g}^{-1}$ ), Ce:1.8; Sm: 1.0; Eu:0.1; Gd: 1.2; Dy: 0.30; Cd: 0.25; Cr 0.35; Cu:0.30; Ni:0.75; Mn:0.20; Fe:0.30; Ti: 0.50; and for Hf: 1.0.

As the standard reference materials of uranium samples are not available, specpure uranium oxide powder after dissolution in  $\text{HNO}_3/\text{HCl}$  acid solutions and after doping with known amounts (5–20  $\mu\text{g}$ ) of the analyte concentrations were processed using the proposed method. The results obtained are shown in Table 4 along with their percent relative standard deviations of the respective elements for the added concentrations. The method is accurate and precise, offering a relative standard deviation ranging from less than 4% (3.8% for Eu at the  $10 \mu\text{g g}^{-1}$  level) to 12.9% (for Ce at the  $2.5 \mu\text{g g}^{-1}$  level) for all the elements studied. The percent recovery of all the elements studied was greater than 90% and therefore, it was concluded that there was no significant loss in the sample preparation steps using the proposed method.

The sample solutions were also monitored for some of the studied elements viz. Cd, Cr, Cu, Ni, Mn and Fe by ICP-AES and FAAS, as these were reported to be most sensitive by both the techniques, and the results are compared in Table 5. Both sets of results are in excellent agreement.

Table 3

Detection limits (DLs) and background equivalent concentrations (BECs) of the studied trace elements in 5% v/v HCl medium with peak integration time of 3 s ( $n = 3$ ).  $I_p$ , peak intensity;  $I_b$  = blank intensity

Element	Wavelength (nm)	Concentration ( $\mu\text{g ml}^{-1}$ )	$I_p$	$I_b$	BEC <sup>a</sup> ( $\mu\text{g ml}^{-1}$ )	D.L. <sup>b</sup> ( $\mu\text{g ml}^{-1}$ )	$I_p - I_b / I_b$
Ce	418.660	10	2477	58	0.2398	0.0072	41.7
Sm	442.434	10	3576	47	0.1332	0.0040	75.1
Eu	381.967	1.0	3343	47	0.0143	0.0004	70.1
Gd	364.619	10	2118	36	0.1729	0.0052	57.8
Dy	353.170	10	14070	52	0.0371	0.0011	269.6
Cd	228.802	10	18406	60	0.0327	0.0010	305.8
Cr	267.716	10	15066	68	0.0453	0.0014	220.6
Cu	324.754	10	10406	43	0.0415	0.0012	241.0
Ni	221.647	10	8267	82	0.1002	0.0030	99.8
Mn	257.610	10	127108	256	0.0202	0.0006	495.5
Fe	259.940	10	14748	58	0.0395	0.0012	253.3
Ti	334.941	10	9663	57	0.0593	0.0018	168.5
Hf	277.336	10	3804	47	0.1251	0.0037	79.9

<sup>a</sup> BEC is calculated from: Concentration ( $\mu\text{g ml}^{-1}$ )  $X I_b / I_p - I_b$ .

<sup>b</sup> D.L. is calculated based on three times the standard deviation of the blank at 1% RSD ( $D.L. = BEC \times 0.03$ ).

Table 4

Analytical values for some REEs and other trace elements in synthetic uranium samples using the proposed method (data in  $\mu\text{g}$ )

Element	Wavelength (nm)	SYN-1 <sup>a</sup>			SYN-2 <sup>a</sup>			SYN-3 <sup>a</sup>		
		Added	Found	RSD (%)	Added	Found	RSD (%)	Added	Found	% RSD
Ce	418.660	5.0	4.7	12.9	10.0	9.6	7.1	20.0	19.4	5.2
Sm	442.434	5.0	4.8	11.2	10.0	9.7	6.5	20.0	19.5	4.8
Eu	381.967	5.0	5.1	8.9	10.0	10.1	5.2	20.0	19.9	3.8
Gd	364.619	5.0	4.9	10.5	10.0	9.7	6.4	20.0	19.7	4.6
Dy	353.170	5.0	5.2	9.6	10.0	10.2	6.2	20.0	20.2	4.5
Cd	228.802	5.0	4.7	9.1	10.0	9.5	6.0	20.0	19.1	4.7
Cr	267.716	5.0	4.9	9.8	10.0	9.8	6.3	20.0	19.7	4.4
Cu	324.754	5.0	4.9	9.5	10.0	9.7	5.9	20.0	19.5	4.5
Ni	221.647	5.0	5.1	10.2	10.0	10.2	6.5	20.0	20.2	5.0
Mn	257.610	5.0	4.9	9.7	10.0	9.8	6.2	20.0	19.7	4.9
Fe	259.940	5.0	4.8	10.4	10.0	9.7	5.8	20.0	19.5	4.8
Ti	334.941	5.0	4.8	10.1	10.0	9.7	6.1	20.0	19.6	4.7
Hf	277.336	5.0	5.1	11.4	10.0	10.2	6.4	20.0	20.1	5.0

<sup>a</sup> SYN-1/SYN-2/SYN-3, all synthetic solutions prepared by doping known amounts of the analytes to 2.0 g uranium solutions, and analyzed after processing the solutions using the proposed method and made upto a volume of 50 ml. The results presented are average of five values.

Values for the remaining elements at these low levels of concentrations could not be measured by FAAS, due to their least sensitive in nature by this technique.

Further, the decontamination of uranium (2.0 g) was so high that the concentration level of the uranium present in the final volume (50 ml) was

not more than 10–15  $\mu\text{g ml}^{-1}$ , after single precipitation, which did not cause any spectral/matrix interference at the selected emission lines of the analytes, at above concentration. However, in case of Cd, without the addition of 1,10-phenanthroline, the recovery was found to be not more than 60% and the same was improved to more



than 90% in presence of this special reagent. The enhancement in recovery of cadmium in presence of 1,10-phenanthroline was due to formation of a stable 1:2 complex with the reagent thus facilitating quantitative separation from uranium [26]. Therefore, it is understood that  $\text{Cd}^{++}$  also be-

has similarly to  $\text{Fe}^{++}$  in the formation of a very stable complex with 1,10-phenanthroline.

Some of the other procedures reported for decontamination of uranium from the analyte elements using  $\text{H}_2\text{O}_2$ -NaOH system/ $\text{H}_2\text{O}_2$ - $\text{Na}_2\text{CO}_3$  systems [10]/anion-exchange separation system

Table 5

Comparison of analytical results for some of the studied elements (Cd, Cr, Cu, Ni, Mn and Fe) by ICP-AES and FAAS (data in  $\mu\text{g}$ )<sup>a</sup>

Element	SYN-1		SYN-2			SYN-3			
	Added	Found		Added	Found		Added	Found	
		A	B		A	B		A	B
Cd	5.0	4.7	4.6	10.0	9.5	9.5	20.0	19.1	19.0
Cr	5.0	4.9	4.8	10.0	9.8	9.7	20.0	19.7	19.5
Cu	5.0	4.9	4.8	10.0	9.7	9.6	20.0	19.5	19.3
Ni	5.0	5.1	5.0	10.0	10.2	10.1	20.0	20.2	20.3
Mn	5.0	4.9	4.8	10.0	9.8	9.7	20.0	19.7	19.5
Fe	5.0	4.8	4.7	10.0	9.7	9.6	20.0	19.5	19.6

<sup>a</sup> A, Values obtained by ICP-AES; B, values obtained by FAAS.

Table 6

Comparison of different separation systems, for isolation and estimation of the studied trace elements in uranium sample solutions (values are presented in  $\mu\text{g}$ )<sup>a</sup>

Element	$\text{H}_2\text{O}_2$ -NaOH System <sup>b</sup>		$\text{H}_2\text{O}_2$ - $\text{Na}_2\text{CO}_3$ System <sup>c</sup>		Anion-exchange separation System <sup>d</sup>	
	Added	Found	Added	Found	Added	Found
Ce	20	19.2	20	8.2	20	19.1
Sm	20	19.1	20	2.8	20	19.3
Eu	20	19.7	20	2.0	20	19.8
Gd	20	19.5	20	N.D	20	19.4
Dy	20	19.9	20	N.D	20	20.2
Cd	20	N.D	20	8.1	20	N.D
Cr	20	N.D	20	N.D	20	19.2
Cu	20	15.8	20	7.2	20	N.D
Ni	20	19.2	20	11.6	20	19.8
Mn	20	19.3	20	19.6	20	16.6
Fe	20	19.4	20	19.5	20	4.2
Ti	20	2.5	20	N.D	20	19.5
Hf	20	6.0	20	N.D	20	19.3

<sup>a</sup> N.D, not detected.

<sup>b</sup> Separation of the added trace elements was carried out by precipitating as insoluble hydroxides/carbonates in presence of Yttrium as carrier, and dissolution in 5% v/v HCl acid after complexing uranium as peroxocomplex/carbonate complex and double precipitations.

<sup>c</sup> Separation was carried out by replacing NaOH with  $\text{Na}_2\text{CO}_3$  in presence of  $\text{H}_2\text{O}_2$ .

<sup>d</sup> Anion-exchange separation of the added trace elements from uranium was carried out by loading the mixed solution (50 ml of 6 M HCl) onto a column of Amberlite IRA-400 (chloride form), of length 20 cm and I.D. 1 cm and elution with 50 ml of 6 M HCl.

[27], and the results are presented in Table 6. In case of  $\text{H}_2\text{O}_2$ – $\text{NaOH}$  separation system, the recovery of Cd, Cr, Ti and Hf was very poor while using  $\text{H}_2\text{O}_2$ – $\text{Na}_2\text{CO}_3$  separation system, the recovery of all the studied elements was negligible except in case of Mn and Fe when quantitative recoveries were obtained. Similarly, in case of anion-exchange separation system, the recovery of Cd, Cr and Fe was found to be negligible and incomplete recovery in case of Mn. But no single system offered quantitative recovery of all the studied elements, except the proposed method in presence of CyDTA plus 1,10-phenanthroline and  $\text{NH}_4\text{OH}$  precipitation.

Thus Table 6 gives a comparative evaluation of other separation procedures for uranium-either as precipitate or in solution. It is obvious that the CyDTA– $\text{NH}_4\text{OH}$  precipitation of uranium offers quantitative separation of uranium and quantitative recoveries of various elements listed above. As reported in literature [28] CyDTA generally forms somewhat more stable complexes than EDTA does while precipitating out uranium quantitatively with consequential advantages in the present investigations. Further, by using EDTA–DTPA, major amounts of uranium were found to be accompanied the trace elements, causing severe spectral–matrix interferences and thus making impossible the measurement of trace values. Thus, the simplicity and fastness of the procedure further recommends itself.

#### 4. Conclusion

The procedure described in this work offers a fast, accurate and an effective separation method for the rare earth elements and the various other trace elements from uranium, which need to be separated from the matrix for quality/process control and characterization of various uranium fuels to be used in nuclear-reactors. The simplicity of precipitative separation of uranium and quantitative recoveries of analytes investigated, recommends the process in the most eminent manner.

#### Acknowledgements

Grateful thanks go to Shri D.C. Banerjee, Director, AMD for impetus in thrust areas of R&D, and to Shri G.V. Ramanaiah for continued support and fruitful discussions.

#### References

- [1] J.P. Howe, *The Metal Thorium*, American Society of Metals, Chap. 1, in: H.A. Wilhem (Ed.), Cleveland, OH, 1958.
- [2] M.A. Floyd, R.W. Morrow, R.B. Farrar, *Spectrochim. Acta*, Part B 8 (1983) 303.
- [3] V.L. Ribeiro Salvador, K. Imakuma, *Anal. Chim. Acta*. 188 (1986) 67.
- [4] P.S. Murthy, R.M. Barnes, *J. Anal. At. Spectrom.* 1 (1986) 145.
- [5] T.K. Seshagiri, Y. Babu, M.L. Jayanth Kumar, A.G.L. Dalvi, M.D. Sastri, B.D. Joshi, *Talanta* 31 (1984) 773.
- [6] M.D. Palmieri, J.S. Fritz, J.J. Thomson, R.S. Bouk, *Anal. Chim. Acta* 184 (1986) 187.
- [7] A.G.I. Dalvi, C.S. Deodhar, T.K. Seshagiri, M.S. Khalap, B.D. Joshi, *Talanta* 25 (1978) 665.
- [8] J.G. Crock, F.E. Lichte, G.O. Riddle, C.L. Beech, *Talanta* 33 (1986) 610.
- [9] K. Satyanarayana, G. Srinivasan, R.K. Malhotra, B.N. Tikoo, *Exploration and Research for Atomic Minerals* 2 (1989) 235.
- [10] G.V. Ramanaiah, *Talanta* 46 (1998) 533.
- [11] K. Satyanarayana, *At. Spectrosc.* 17 (1996) 69.
- [12] M.R. Hayes, J. Metcalfe, *Analyst* 87 (1962) 956.
- [13] K.R. Betty, G.T. Day, *Analyst* 3 (1986) 455.
- [14] K. Satyanarayana, G.V. Ramanaiah, G. Srinivasan, R.K. Malhotra, *At. Spectrosc.* 16 (1995) 235.
- [15] N. Raje, S. Kayasth, T.P.S. Ansari, S. Gangadharan, *Anal. Chim. Acta* 290 (1994) 371.
- [16] B. Gopalan, *Proceedings of the Fifth National Symposium on Analytical Spectroscopy including Hyfenated Techniques*, ISAS, Hyderabad, 1988, p. 197.
- [17] M.J. Kulkarni, A.A. Argekar, J.N. Mathur, A.G. Page, M.D. Sastry, *Proceedings of XIII ISAS National Symposium on Analytical Techniques-2001*, Bangalore, India, November 1998, p. 293.
- [18] B. Rajeswari, B.A. Dhawale, M.J. Kulkarni, M.K. Bhide, T.K. Seshagiri, T.R. Bangia, A.G. Page, M.D. Sastry, *Proceedings of XIII ISAS National Symposium on Analytical Techniques-2001*, Bangalore, India, November 1998, p. 297.
- [19] P.W.J.M. Bourmans (Ed.), *Inductively Coupled Plasma Emission Spectroscopy, Part I-Methodology, Instrumentation, Performance*, Wiley-Interscience, New York, 1987, pp. 584.

- [20] P.W.J.M. Bourmans (Ed.), *Inductively Coupled Plasma Emission Spectroscopy, Part II-Applications and Fundamentals*, Wiley-Interscience, New York, 1987, pp. 486.
- [21] A. Montaser, D.W. Golightly, *Inductively Coupled Plasma in Analytical Atomic Spectrometry*, VCH, New York, 1987, p. 660.
- [22] K. Satyanarayana, S. Durani, G.V. Ramanaih, *Anal. Chim. Acta* 376 (1998) 273.
- [23] K. Satyanarayana, K. Subramanyam, A.V. Raghunath, G.V. Ramanaih, *Analyst* 121 (1996) 825.
- [24] K. Satyanarayana, M.A. Nayeem, *At. Spectrosc.* 14 (1993) 180.
- [25] R.K. Winge, V.A. Fassel, G.J. Peterson, M.A. Flyod, *Inductively Coupled Plasma—Atomic Emission Spectroscopy-Atlas of Spectral Information Physical Sciences Data* 20, Elsevier, Amsterdam, 1985.
- [26] F. Vydra, K. Stulik, *Chemist—Analyst* 54 (1965) 77.
- [27] J. Brody, J. Faris, R. Buchanan, *Anal.Chem.* 30 (1909) 1958.
- [28] G. Schwarzenback, H. Flaschka, *Complexometric titrations*, Methuen & Co. Ltd, London, 1969, p. 10.

# Differential pulse polarographic determination of trace selenium(IV) and molybdenum(VI) using the catalytic hydrogen wave

Recai İnam, Güler Somer \*

*Gazi Üniversitesi, Fen-Edebiyat Fakültesi, Kimya Bölümü, 06500 Ankara, Turkey*

Received 23 December 1998; received in revised form 20 April 1999; accepted 3 May 1999

## Abstract

In the presence of selenium(IV) and molybdenum(VI) a new polarographic peak appears which corresponds to a hydrogen catalytic wave. By differential pulse polarography a single, sharp peak at about  $-1.1$  V is obtained, allowing trace determination of selenium(IV) and molybdenum(VI) in the range  $1 \times 10^{-6}$ – $5.0 \times 10^{-9}$  M with a linear calibration and a detection limit of  $1.5 \times 10^{-9}$  M. The optimum conditions are found to be 0.1 M  $\text{KNO}_3$  and a pH of about 3.2 (Britton–Robinson buffer). There is no serious interference from some ions when present at 1.0–40 times that of molybdenum. At higher amounts of interfering ions the interference is eliminated by the addition of EDTA. © 1999 Elsevier Science B.V. All rights reserved.

*Keywords:* Catalytic hydrogen wave; Differential pulse polarography; Molybdenum(VI); Selenium(IV)

## 1. Introduction

In our selenium determination studies in the presence of some ions using polarographic or voltammetric techniques, some interference does occur. During anodic stripping voltammetric (ASV) studies [1] in the presence of copper ion, a new peak appeared which was due to the reduction of a CuSe intermetallic compound. This intermetallic compound formation was confirmed by our cyclic voltammetric (CV) studies [2]. A

similar behaviour was reported to occur [3] between selenium and copper during the anodic and cathodic stripping voltammetric determination of selenium. During differential pulse polarographic (DPP) studies we observed that selenite and some ions, such as cadmium, lead and copper, diminished the peaks of each other, and new peak formations at more positive potentials for the corresponding ions appeared. This observation was attributed to the formation of an intermetallic compound between selenium and the ions present [4]. It was shown that corrections had to be made during quantitative determination of these ions by taking into account the interferences.

\* Corresponding author. Tel.: +90-312-212-2900; fax: +90-312-212-2279.

*E-mail address:* gsomer@quark.fef.gazi.edu.tr (G. Somer)

In our present study using DPP we found a different type of interference between molybdenum and selenium. Here a new peak appeared at fairly high negative potentials in contrast to our former studies where new peaks were formed at more positive potentials. Molybdenum(VI) showed two polarographic peaks at about pH 3.0, one of which corresponded to the reduction of Mo(VI) to Mo(V) ( $E = -0.38$  V) and the second Mo(V) to Mo(III) ( $E = -0.50$  V). It is known that molybdenum exhibits a catalytic wave in the presence of perchloric acid [5] and nitric acid [6]. These catalytic waves have been used for its determination [7,8] by DPP. The determination of molybdenum using polarographic methods has advantages of accuracy, sensitivity and simplicity [9–11]. Molybdenum in soil and plants has been determined using the catalytic wave of adsorbed complex of Mo(VI)–cupferron [12]. The sensitivity for molybdenum was improved by the use of catalytic adsorptive stripping voltammetry and it was claimed that an extremely low detection limit of 1.7 pM was obtained [13,14].

In the present study the peak which is only observed when selenium and molybdenum are present together should be of a different nature than those reported previously. This new peak appears when a trace amount of molybdenum is added to the solution containing selenite ion or vice versa. It must be a catalytic hydrogen peak since it is formed at about 100 mV more positive potentials than the hydrogen reduction peak. A catalytic effect of this kind was first observed in the presence of proteins [15]. Similar catalytic hydrogen currents have been observed in the presence of alkaloids [16] and of pyridine and its derivatives [17]. These kinds of waves are also produced in the presence of both cobalt and nickel [18], molybdenum(VI) and metatungstate [19] as well as by platinum complexes with ethylenediamine [20] or formazone [21]. This paper describes an extremely sensitive and highly selective catalytic adsorptive polarographic procedure for the simultaneous determination of selenium and molybdenum in the same sample.

## 2. Experimental

### 2.1. Apparatus

A PAR Model 174 A polarographic analyser system, equipped with a PAR mercury drop timer, was used. A Kalousek electrolytic cell with reference saturated electrode (SCE), separated by liquid junction, was used in a three-electrode configuration. The counter electrode was platinum wire. The natural drop time of the mercury electrode was in the range 2–3 s (2.37 mg/s). The polarograms were recorded with a Linseis LY 1600 *X*–*Y* recorder. DP polarograms were recorded under the conditions of a drop life of 1 s, a scan rate of 5–10 mV/s and a pulse amplitude of 50 mV.

### 2.2. Reagents

All chemicals,  $\text{SeO}_2$ ,  $(\text{NH}_4)_2\text{Mo}_7\text{O}_{24}\cdot 4\text{H}_2\text{O}$ ,  $\text{KNO}_3$ ,  $\text{HCl}$  (37%),  $\text{HNO}_3$  (65%),  $\text{HClO}_4$  (60%),  $\text{H}_2\text{SO}_4$  (98%),  $\text{H}_3\text{PO}_4$  (85%),  $\text{H}_3\text{BO}_3$ ,  $\text{NaOH}$ , glacial  $\text{CH}_3\text{COOH}$ , were reagent grade chemicals (Merck, Darmstadt). Triple-distilled water was used in preparation of all solutions. The 0.1 M stock solutions of Se(IV) and Mo(VI) were prepared by dissolving  $\text{SeO}_2$  and  $(\text{NH}_4)_2\text{Mo}_7\text{O}_{24}\cdot 4\text{H}_2\text{O}$  in 100 ml of water;  $1.0 \times 10^{-3}$ ,  $1.0 \times 10^{-4}$ ,  $1.0 \times 10^{-5}$  M working solutions were prepared by daily dilution.

Britton–Robinson (B-R) buffer solution was prepared in such a way that 2.3 ml glacial acetic acid, 2.7 ml phosphoric acid and 2.4720 g boric acid dissolved by dilution with water to 1.0 l; 50.0-ml portions of this solution were taken and the pH was adjusted between 2.0 and 5.0 by addition of the appropriate amount of 2.0 M  $\text{NaOH}$ .

### 2.3. Procedure

A 10.0-ml volume of acid solution or B-R buffer solution (pH 2.0–5.0) and 0.5 ml of 2.0 M  $\text{KNO}_3$  in the polarographic cell was de-aerated by a stream of nitrogen gas (99.999%) for 3.0 min, then, according to the need, 50  $\mu\text{l}$  of  $1.0 \times 10^{-2}$ – $1.0 \times 10^{-6}$  M Se(IV) and 50  $\mu\text{l}$  of  $1.0 \times 10^{-2}$ –

$1.0 \times 10^{-6}$  M Mo(VI) solutions were added. Polarograms were taken by scanning the potential in the negative potential direction from 0.0 V to about 1.5 V at a scan rate of 5–10 mV/s.

### 3. Results and discussion

The direct current (d.c.) and differential pulse polarograms of Mo(VI) in the presence of Se(IV) ion exhibit a well-defined polarographic wave that appeared at about  $-1.1$  V with a characteristic peak shape in d.c. polarography (Fig. 1). This wave occurred only in the presence of selenite ion at sufficiently high concentrations. In DPP, Mo(VI) ion showed different behaviour in different supporting electrolytes. While it has one peak in 0.1 M HCl,  $\text{HNO}_3$  and  $\text{HClO}_4$  solutions at

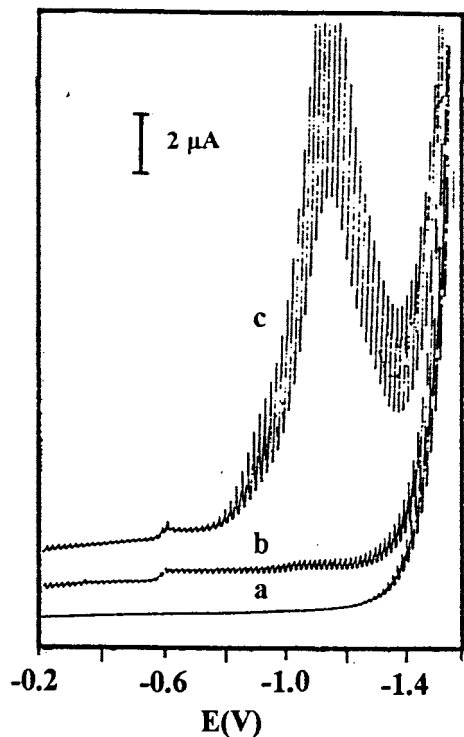


Fig. 1. The catalytic d.c. polarographic wave observed for Mo–Se. (a) 10 ml B-R buffer, pH 3.24, 0.1 M  $\text{KNO}_3$ ; (b)  $5.0 \times 10^{-5}$  M Se(IV); (c)  $5.0 \times 10^{-5}$  M Se(IV),  $5.0 \times 10^{-6}$  M Mo(VI). Drop time 3.2 s,  $t = 2.37$  mg/s,  $h = 85$  cm, scan rate 5 mV/s.

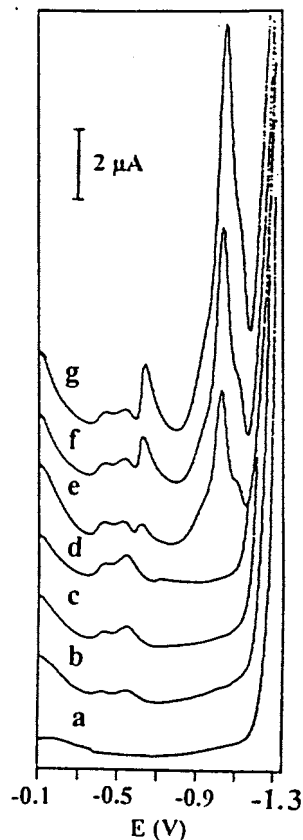


Fig. 2. Formation of catalytic peak by the addition of selenium onto molybdenum. (a) 10 ml B-R buffer, pH 2.94, 0.1 M  $\text{KNO}_3$ ; (b)  $1 \times 10^{-5}$  M Mo(VI); (c)  $2 \times 10^{-5}$  M Mo(VI); (d)  $3 \times 10^{-5}$  M Mo(VI); (e)  $5 \times 10^{-6}$  M Se(IV); (f)  $1 \times 10^{-5}$  M Se(IV); (g)  $1.5 \times 10^{-5}$  M Se(IV). Drop time 1.0 s, scan rate 5.0 mV/s, pulse amplitude 50 mV.

about  $-0.28$  V, it showed two peaks at pH values of 2–3, the first being at  $-0.38$  V and the second at  $-0.50$  V. It has been shown [12] that Mo(VI) is first reduced to Mo(V) and then to Mo(III).

During our polarographic studies by the addition of Se(IV) ion to Mo(VI) solutions a new peak appeared at about  $-1.1$  V which is 100 mV more positive than the hydrogen evolution peak and also a peak for Se(IV) reduction at about  $-0.62$  V. The new peak at  $-1.1$  V and the peak for selenite ion at  $-0.62$  V increased with increased selenite ion concentrations (Fig. 2). This behaviour was observed in various electrolyte solu-

tions, such as 0.1 M HCl, 0.1 M HNO<sub>3</sub>, 0.1 M HClO<sub>4</sub> and in B-R buffer solutions at pH values higher than 2.

As can be seen from Fig. 2, while the peaks for Mo(VI) are not sensitive enough for determination of traces of that ion, the peak at about -1.1 V showed a large increase in sensitivity for both Se(IV) and Mo(VI) ions. There is a linear relationship between the height of this peak and the concentration of these ions.

The DPP peak potential shifted to more negative potentials with increasing pH (at pH 1.0,  $E_p = -0.93$  V; at pH 4.5,  $E_p = -1.30$  V) and maximum current height was obtained at about pH 3.2 (Fig. 3). Since at pH values larger than 2, B-R buffer solutions were used and since the maximum current was obtained at these pH values, it had to be shown that it was not because of phosphate buffer which was present in B-R buffer solution. For this purpose a pH 3.70 solution was prepared using acetic acid–acetate buffer solution and the same result was obtained, excluding the effect of phosphate. Addition of nitrate ion (0.1 M KNO<sub>3</sub>) increased the catalytic peak current at all pH values, as can be observed in Fig. 3.

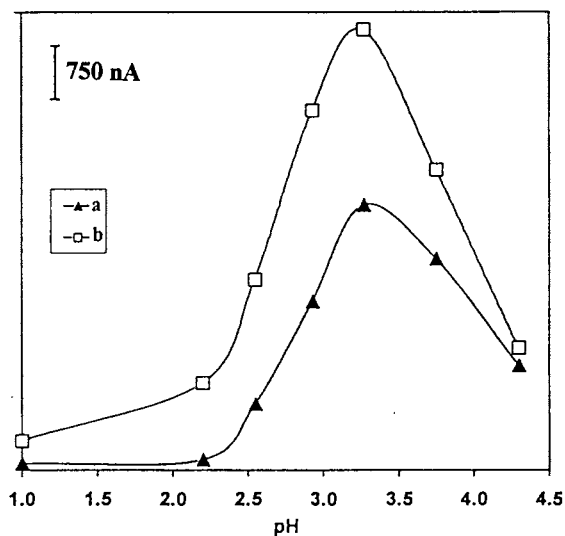
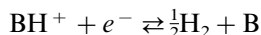
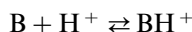
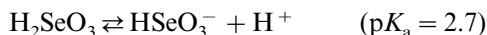


Fig. 3. Effect of pH on the catalytic peak current in the presence and absence of nitrate ion [ $5.0 \times 10^{-5}$  M Se(IV),  $2.5 \times 10^{-6}$  M Mo(VI)]. (a) without nitrate; (b) with 0.1 M NO<sub>3</sub><sup>-</sup>. Drop time 1.0 s, scan rate 5.0 mV/s, pulse amplitude 50 mV.

According to the pH dependence (Fig. 3) the following mechanism can be suggested:



Here, B may be a heteropolyacid formed in the presence of HSeO<sub>3</sub><sup>-</sup> and Mo(VI).

The decrease of current with pH at the right-hand side of the maximum (Fig. 3) is expected from catalytic hydrogen wave. However, the increase of current with pH between 2 and 3.2 can be explained with the formation of HSeO<sub>3</sub><sup>-</sup> (at pH 2.7, H<sub>2</sub>SeO<sub>3</sub> and HSeO<sub>3</sub><sup>-</sup> concentrations are equal). At very low pH values, on the other hand, HSeO<sub>3</sub><sup>-</sup> is not present in significant amounts, resulting in a very low current.

The effect of drop time on the peak current was investigated for a solution of  $2.5 \times 10^{-6}$  M Mo(VI) and  $5.0 \times 10^{-5}$  M Se(IV) in 0.1 M KNO<sub>3</sub> solution at a fixed column height ( $h$ ) of 80 cm using d.c. polarography. The d.c. peak current ( $i_p$ ) was linearly dependent on drop time between 0.5 and 3.3 s at a constant mercury flow rate, an indication of the involvement of an adsorption step in the electrode process.

There is a linear relationship between the DPP peak current ( $I$ ) and Mo(VI) concentration ( $C$ ) between  $5.0 \times 10^{-9}$  and  $5.0 \times 10^{-6}$  M (Se(IV) =  $5.0 \times 10^{-6}$  M) with a correlation coefficient of 0.9986 ( $I = 21.0C + 1.0 \times 10^{-8}$ ;  $I$  in ampere,  $C$  in molarity). A linear relationship is obtained for Se(IV) also in the same concentration range (Mo(VI)  $5.0 \times 10^{-6}$  M) under the conditions of pH 3, B-R buffer, 0.1 M KNO<sub>3</sub> ( $r = 0.9989$ ,  $I = 12.1C + 2.0 \times 10^{-9}$ ). Some of the results are given with their S.D. in Tables 1 and 2 for molybdenum and selenium, respectively. Differential pulse polarograms for the determination of  $5.0 \times 10^{-8}$  M Mo(VI) and of  $5.0 \times 10^{-7}$  M Se(IV) are given in Fig. 4.

Investigation in unbuffered solutions of strong acids indicates that the sensitivity of the peak

Table 1  
Determination of Mo by using the catalytic peak<sup>a</sup>

Synthetic sample (M)	Mo found (M)	% Error	R.S.D. <sup>b</sup> (%)
$4.95 \times 10^{-7}$ Mo, $3.96 \times 10^{-6}$ Se	$(4.9 \pm 0.4) \times 10^{-7}$	-1.0	8.2
$4.95 \times 10^{-7}$ Mo, $4.95 \times 10^{-6}$ Se	$(5.0 \pm 0.3) \times 10^{-7}$	+1.0	6.0
$4.93 \times 10^{-8}$ Mo, $4.95 \times 10^{-6}$ Se	$(5.3 \pm 0.3) \times 10^{-8}$	+7.5	5.6
$4.98 \times 10^{-9}$ Mo, $1.0 \times 10^{-5}$ Se	$(5.2 \pm 0.8) \times 10^{-9}$	+4.4	15.3

<sup>a</sup> pH 3.0 (B-R solution).

<sup>b</sup> R.S.D., relative standard deviation.

Table 2  
Determination of Se by using the catalytic peak<sup>a</sup>

Synthetic sample (M)	Se found (M)	% Error	R.S.D. <sup>b</sup> (%)
$4.83 \times 10^{-6}$ Se, $2.89 \times 10^{-5}$ Mo	$(4.6 \pm 0.3) \times 10^{-6}$	-4.8	6.5
$0.98 \times 10^{-6}$ Se, $4.93 \times 10^{-6}$ Mo	$(1.05 \pm 0.06) \times 10^{-6}$	+7.1	5.7
$4.92 \times 10^{-8}$ Se, $4.95 \times 10^{-6}$ Mo	$(4.7 \pm 0.5) \times 10^{-8}$	-4.5	10.6

<sup>a</sup> pH 3.0 (B-R solution).

<sup>b</sup> R.S.D., relative standard deviation.

depends on the nature of the acid present and its concentration. For this purpose, HCl, HClO<sub>4</sub>, HNO<sub>3</sub>, H<sub>2</sub>SO<sub>4</sub> and HNO<sub>3</sub> are used at different concentrations changing from 0.1 M to 1.5 M. With increased acid concentrations the current became smaller (Fig. 5). The current had its highest value in HClO<sub>4</sub>. But even the largest current obtained in this acid was ten times smaller than that obtained at pH 3. In HNO<sub>3</sub>, on the other hand, because of the reaction of HNO<sub>3</sub> with mercury, no peak could be observed. The nature and concentrations of added electrolyte were also investigated. As can be seen from Fig. 6, 0.1 M KNO<sub>3</sub> gives the largest current. With increasing nitrate concentration the hydrogen reduction is shifted to more positive potentials so that the

catalytic hydrogen peak becomes a shoulder, making its observation difficult.

As the optimum working conditions, 0.1 M KNO<sub>3</sub> and pH 3.2 were selected. The detection limit (signal-to-noise ratio, S/N = 3) of the method for Mo (VI) and for Se (IV) is  $1.5 \times 10^{-9}$  M. For the determination of one of these ions, the second ion concentration has to be about 10<sup>2</sup>–10<sup>3</sup> times higher than the other ion under investigation. However, at concentrations higher than 10<sup>-6</sup> M, this ratio may be 1:1.

The effect of possible interferences from some metal ions, such as Pb(II), Cd(II), Cu(II), Ni(II), Cr(III), Zn(II) and Tl(I), were investigated at a concentration of  $5.0 \times 10^{-6}$  M Se(IV) and  $5.0 \times 10^{-8}$  M Mo(VI). The co-existing ions were taken

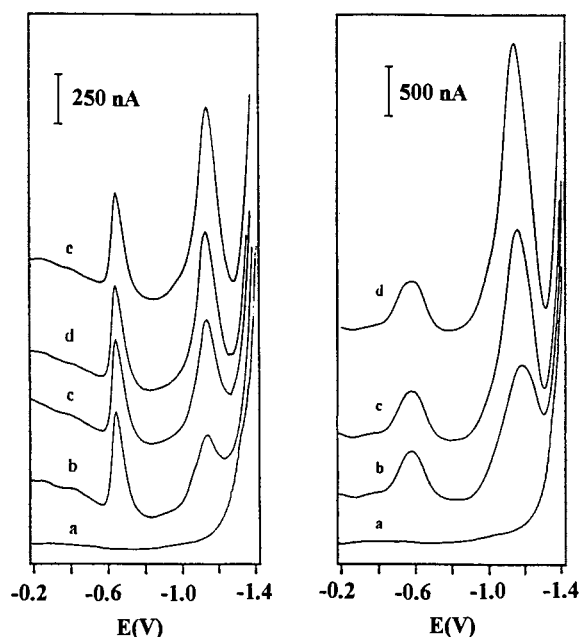


Fig. 4. (Panel a) Determination of  $5.0 \times 10^{-8}$  M Mo by the catalytic peak current. (a) 10 ml B-R buffer, pH 3.20, 0.1 M KNO<sub>3</sub>; (b)  $5 \times 10^{-6}$  M Se(IV),  $5 \times 10^{-8}$  M Mo(VI); (c)  $1 \times 10^{-7}$  M Mo(VI); (d)  $1.5 \times 10^{-7}$  M Mo(VI); (e)  $2 \times 10^{-7}$  M Mo(VI). Drop time 1.0 s, scan rate 5.0 mV/s, pulse amplitude 50 mV. (Panel b) Determination of  $5.0 \times 10^{-7}$  M Se by the catalytic peak current. (a) 10 ml B-R buffer, pH 3.20, 0.1 M KNO<sub>3</sub>; (b)  $5 \times 10^{-6}$  M Mo(VI),  $5 \times 10^{-7}$  M Se(IV); (c)  $1 \times 10^{-6}$  M Se(IV); (d)  $1.5 \times 10^{-6}$  M Se(IV). Drop time 1.0 s, scan rate 5.0 mV/s, pulse amplitude 50 mV.



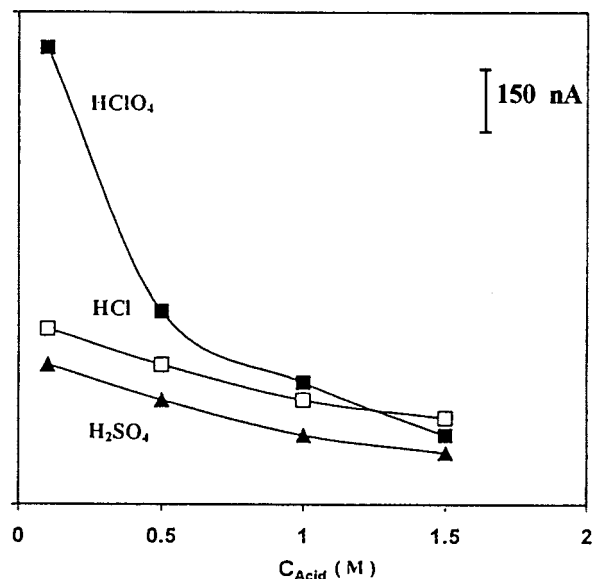


Fig. 5. Effect of different kinds of acids on the catalytic peak [ $5.0 \times 10^{-5}$  M Se(IV),  $2.5 \times 10^{-6}$  M Mo(VI), 0.1 M  $\text{KNO}_3$ ].

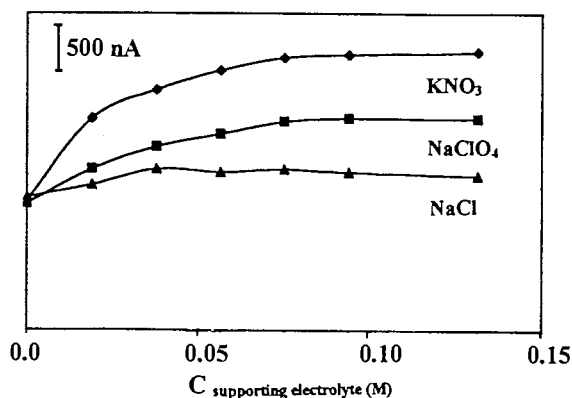


Fig. 6. Effect of different kinds of supporting electrolytes [B-R buffer, pH 3.24,  $5.0 \times 10^{-5}$  M Se(IV),  $5.0 \times 10^{-7}$  M Mo(VI)].

at the same concentration, and at ten, 20 and 40 times the amount of Mo(VI). The results are summarized in Table 3. The values show the ratio of the peak currents in the presence of the co-existing ions to that in their absence (by percentage). According to the results 20-fold higher amounts of Pb(II), Cd(II), Cu(II), Zn(II) and Tl(I) exert nearly no interference in the determination of Se and Mo. However, at higher concentrations of

co-existing ions some interference was observed. In our former studies we had explained the interactions between Se and some ions such as Cd, Cu and Pb [4] and we used this behaviour for the determination of Se and Pb in blood [22]. Since these ions interact with selenium the catalytic peak observed here diminishes by the addition of these interfering ions. The inhibition effect of these ions on the catalytic peak has been eliminated by the addition of a very small amount of EDTA. As can be seen from Fig. 7, by the addition of EDTA in nearly the same concentration as the interfering ion, the interference is

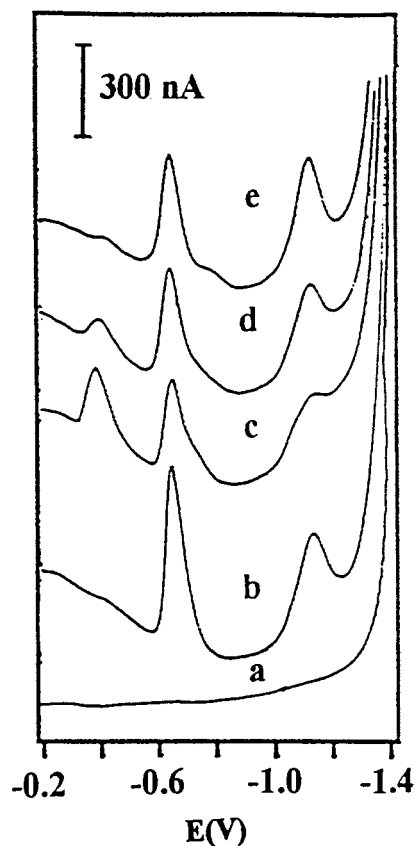


Fig. 7. Elimination of interference by EDTA. (a) 10 ml B-R buffer, pH 3.24, 0.1 M  $\text{KNO}_3$ ; (b)  $5 \times 10^{-6}$  M Se(IV),  $5 \times 10^{-8}$  M Mo(VI); (c)  $2 \times 10^{-6}$  M Pb(II); (d)  $2 \times 10^{-6}$  M EDTA; (e)  $4 \times 10^{-6}$  M EDTA. Drop time 1.0 s, scan rate 5.0 mV/s, pulse amplitude 50 mV.

Table 3

Influence of co-existing ions on the catalytic peak current and elimination of interference by EDTA<sup>a</sup>

Concentration of co-existing ions	Co-existing ions and their influence on signal ratio (%)						
	Pb(II)	Cd(II)	Cu(II)	Ni(II)	Cr(III)	Zn(II)	Tl(I)
$5.0 \times 10^{-8}$	100	97	103	100	97	97	100
$5.0 \times 10^{-7}$	94	97	94	100	75	94	103
$1.0 \times 10^{-6}$	93	92	88	116	63	94	105
$2.0 \times 10^{-6}$	76	80	80	125	54	–	106
$2.0 \times 10^{-6}$	98 <sup>b</sup>	97 <sup>b</sup>	100 <sup>b</sup>	–	–	–	–

<sup>a</sup>  $5.0 \times 10^{-6}$  M Se(IV) and  $5.0 \times 10^{-8}$  M Mo(VI). pH 3.24 (B-R buffer solution).<sup>b</sup> In the presence of  $4.0 \times 10^{-6}$  M EDTA.

effectively eliminated. The results obtained in the absence and in the presence of EDTA are given in Table 3. At too high concentrations of EDTA, however, the catalytic current peak is also affected, because of the formation of a Mo–EDTA complex. In practice, in a solution containing these interfering ions, EDTA has to be added until the catalytic peak reaches its maximum value.

### 3.1. Application to real samples

The present method has been applied to garlic samples in order to determine the selenium content. For this purpose 5.0 g of dried garlic are digested in HNO<sub>3</sub>:HClO<sub>4</sub> (1:1) acid mixture [23]. After addition of buffer and KNO<sub>3</sub>, pulse polarogram is taken. From the catalytic peak obtained after the addition of  $5 \times 10^{-6}$  M Mo(VI), the selenium content was determined by standard additions of selenite solution. As a result  $508 \pm 36$  ng/g selenium was determined with an R.S.D. of 7.1%. The same garlic sample was analysed by cathodic stripping voltammetry [23] and  $485 \pm 35$  ng/g Se was obtained in our previous work, which demonstrates the validity of the new method.

## 4. Conclusion

It is shown in this work that the catalytic hydrogen wave of Mo–Se can be detected with improved sensitivity and resolution by DPP. The

single sharp peak obtained by DPP is suitable for the trace determination of selenium and molybdenum simultaneously in the  $10^{-6}$ – $10^{-9}$  M range. There is no need for separation and preconcentration methods which are tedious, time-consuming and also polluting. This method could be applied directly for the determination of selenium in garlic and the results were consistent with those obtained by cathodic stripping voltammetry. The proposed method can be applied safely for many biological samples.

## Acknowledgements

This work was supported by the Gazi University Research Fund.

## References

- [1] H. Aydın, G. Somer, Anal. Sci. 5 (1989) 89.
- [2] G. Somer, M.S. Karacan, Electroanalysis 6 (1994) 527.
- [3] S.B. Adeloju, A.M. Bond, H.C. Hughes, Anal. Chim. Acta 148 (1983) 59.
- [4] R. İnam, G. Somer, Anal. Sci. 14 (1998) 399.
- [5] G.P. Haight, Anal. Chem. 23 (1951) 1505.
- [6] M.G. Johnson, R.J. Robinson, Anal. Chem. 24 (1952) 366.
- [7] G.D. Christian, J.L. Vandenbalck, G.J. Patriarche, Anal. Chim. Acta 108 (1979) 149.
- [8] B. Stach, K. Schoere, Microchim. Acta 2 (1977) 565.
- [9] T.E. Edmonds, Anal. Chim. Acta 116 (1986) 323.
- [10] C.M.G. Van den Berg, Anal. Chem. 57 (1985) 1532.
- [11] B. Magyar, S. Wanderli, Microchim. Acta III (1985) 223.
- [12] K. Jiao, W. Jin, H. Metzner, Anal. Chim. Acta 260 (1992) 35.

- [13] K. Yokoi, C.M.G. Van den Berg, *Anal. Chim. Acta* 257 (1992) 293.
- [14] Z. Gao, K.S. Siow, *Talanta* 43 (1996) 719.
- [15] F. Herles, A. Vancura, *Rozpr. II Tr. Ces. Acad.* 42 (21) (1932) 4.
- [16] J. Pech, *Coll. Czech. Chem. Commun.* 6 (1934) 126.
- [17] E. Knobloch, *Coll. Czech. Chem. Commun.* 12 (1947) 406.
- [18] A. Calușaru, *J. Electroanal. Chem.* 15 (1967) 269.
- [19] M. Lamache, P. Souchay, *J. Electroanal. Chem.* 21 (1969) 509.
- [20] P.W. Alexander, R. Hoh, L.E. Smyth, *Talanta* 24 (1977) 543.
- [21] Z. Zhao, H. Freiser, *Anal. Chem.* 58 (1986) 1498.
- [22] R. Ínam, G. Somer, *Talanta* 46 (1998) 1347.
- [23] R. Ínam, G. Somer, *Food Chem.* (in press).

# Transversely illuminated liquid core waveguide based fluorescence detection

## Fluorometric flow injection determination of aqueous ammonium/ammonia

Jianzhong Li, Purnendu K. Dasgupta \*, Zhang Genfa

*Department of Chemistry and Biochemistry, Texas Tech University, Lubbock, TX 79409-1061, USA*

Received 7 April 1999; received in revised form 4 May 1999; accepted 4 May 1999

### Abstract

The analytical performance of a new type of fluorescence detector, based on a transversely illuminated liquid core waveguide (LCW), has been investigated using the determination of  $\text{NH}_3/\text{NH}_4^+$  as the 1-sulfonatoisindole. With a very inexpensive combination of a miniature Hg blacklight as an excitation source, a colored plastic sheet as the emission filter, and an integrated blue sensitized photodiode-operational amplifier as the detector (totaling < \$100 in hardware cost), we were able to achieve a limit of detection (LOD) of 35 nM (1.6 pmol)  $\text{NH}_3$  with a linear dynamic range up to 60  $\mu\text{M}$   $\text{NH}_3$ . Details of detector construction and performance are given. © 1999 Elsevier Science B.V. All rights reserved.

*Keywords:* Fluorescence detector; Liquid core waveguide

### 1. Introduction

The literature reports several studies in which the optical path length in liquid phase absorption measurements has been extended by using a reflective cell, either through the use of a physically reflective wall, or ensuring conditions in which the liquid has a refractive index (RI) greater than that of the conduit material and the

assembly therefore exhibits total internal reflection, i. e. it behaves as a liquid core waveguide (LCW) [1–3]. Until recently, due to the unavailability of any convenient material that has a RI value less than that of water, LCW applications has been largely limited to high RI organic solvents like carbon disulfide [4], or mixed aqueous solvents that contain large amounts of alcohol [2] or glycol [5], limiting the number of practical analytical applications.

Recently, a fluoropolymer based on 2,2-bistrifluoromethyl-4,5-difluoro-1,3-dioxole was introduced [6]. It is available as a copolymer with

\* Corresponding author. Tel.: +1-806-7423067; fax: +1-806-7421289.

*E-mail address:* sandyd@ttu.edu (P.K. Dasgupta)

tetrafluoroethylene and carriers the trade name Teflon® AF. Teflon AF is an amorphous, glassy, perfluorinated copolymer with the important characteristic that throughout the 200–2000 nm wavelength range, it is essentially transparent with a RI (1.29) lower than that of water (1.33). Thus, when such a tube is filled with water, it behaves as an LCW and can efficiently transfer the light launched at one end to another. This unusual and useful property of such tubes has been exploited in long pathlength absorbance spectroscopy [7–10].

Fujiwara et al. were among the pioneers in LCW based absorbance spectroscopy. The first use of LCW for fluorometric measurements was also reported by these authors [11,12]. They used a laser source to excite the fluorophore in an LCW axially and read the fluorescence axially from the other terminus of the tube. With this geometry, very effective means of rejecting the excitation light are required. A further disadvantage of the axial excitation scheme is that low wavelength laser sources necessary for fluorescence excitation are expensive and can not provide excitation over a broad wavelength range. They also used a 'side-view cell' to overcome the excitation rejection problem. In this geometry, the plane of a spirally shaped tubular flow cell is placed next to the photosensitive window of an 'end-on' type photomultiplier tube (PMT). The excitation light is launched axially into the spiral. The fluorescence signal is said to be linearly dependent on the refractive index of the solution. In this case, an expensive large window PMT must be used and a higher background, resulting from leaking of the excitation light from the spiraled LCW, is expected.

We propose an altogether different geometry for an LCW based fluorescence detector. An inexpensive linear light source illuminates the LCW from the side (transverse illumination). Light incident orthogonal to the axis of a wave guide is efficiently rejected. Thus, the exciting radiation does not proceed down the lumen of the LCW. We have measured that about 1 out of  $10^6$  incident photons actually traverses down the lumen (this occurs, presumably, from scattering by particles in the aqueous phase or from surface imper-

fections in the tube) [13]. In any case, this degree of rejection is better than what many monochromators can provide. On the other hand, if scattering or fluorescent species are present in the solution, a significant portion of the scattered/emitted radiation [the exact extent depends on the numerical aperture (NA) of the LCW] undergoes total internal reflection and proceeds down the lumen of the fiber. This light can be efficiently coupled to a high NA conventional optical fiber placed at the end of the LCW. Because the light is now already available in a optical fiber coupled format (without any focusing optics), detection by a small area inexpensive photodiode detector is facile. There is no great problem associated with rejection of the excitation light as exists in the axial excitation schemes. As a result, neither excitation nor emission monochromators are essential in this unique fiber optic coupled transversely illuminated LCW based flow-through fluorescence detection scheme. For highest sensitivity applications, a simple filter can be incorporated on the emission side to further reject any residual broadband excitation light that propagates down the lumen. The system also has the advantage that illumination can be provided over a large surface area but the resulting luminescence becomes available as a point source.

Fundamental studies related to the dependence of the  $S/N$  to the illumination length and illumination volume are discussed in our first report of such a detector. In the present paper we focus on testing the performance of such a detector in an application important to our laboratory, the determination of trace levels of  $\text{NH}_3\text{-N}$ .

Ammonia is the principal atmospheric base responsible for the neutralization of atmospheric acidity [14]. Ammonium salts are typically the principal constituents of the inhalable fraction of the atmospheric particulate matter and are widely believed to be the primary responsible agents for the degradation of atmospheric visibility [15]. Sensitive and affordable methods for determining  $\text{NH}_3\text{-N}$  are essential to improve the time resolution of atmospheric measurements. Traditionally, the indophenol blue reaction [limit of detection (LOD)  $\sim 0.6 \mu\text{M}$ ] and Nessler's reaction (LOD  $1.2 \mu\text{M}$ ) have been used [16]. In 1971, Roth [17]

discovered the ternary reaction of *o*-phthalaldehyde (OPA), a ‘reducing agent’ [borohydride or mercaptoethanol (ME)], and ammonia or primary amino acids, to produce intensely fluorescent products and described its analytical usefulness. Many studies have been done on this fluorometric reaction. The OPA–sulfite–NH<sub>3</sub> fluorometric detection system in particular was developed in this laboratory [18] and has the advantage over the corresponding ME-based detection system that the use of malodorous thiol compounds is avoided and the reaction is much more selective for ammonia compared to amino acids. In the present work, we have used this reaction for testing the detector performance.

## 2. Experimental

### 2.1. Reagents

Reagents were prepared as previously reported [18]. Briefly, standard grade *o*-phthalaldehyde (P-1378, Sigma, St. Louis, MO) was used without further purification. The OPA solution (10 mM) was prepared by dissolving 268 mg OPA in 50 ml methanol and diluting with water to 200 ml. The solution can be stored in the refrigerator for 1 week.

Phosphate buffer (0.1 M) was made by dissolving 14.2 g of analytical reagent grade Na<sub>2</sub>HPO<sub>4</sub> in 900 ml water, adjusting pH with 2 M NaOH and diluting to 1 l. Sodium sulfite solution (3.0 mM) was prepared daily in the phosphate buffer. Ammonium standards were prepared from a 0.1000 M NH<sub>4</sub>Cl stock. Dilute solutions were prepared just prior to use by successive dilution.

All chemicals used were of analytical reagent grade, and freshly deionized water was used throughout all experiments.

### 2.2. Liquid core waveguide based fluorescence detector

The detector is schematically shown in Fig. 1. It consists of a Teflon® AF tube (BioGeneral, San Diego, CA, 0.84 mm i.d., 1.04 mm o.d.,

~115 mm long) that constitutes the LCW flow cell. As shown, at the bottom end it butts up against a large NA fiber optic (1 mm core fused silica, Polymicro Technologies, Phoenix, AZ), at the center of an opaque tee fitting composed of PEEK (P-713, Upchurch Scientific, Oak Harbor, WA). An appropriate length of a stainless steel tubing (5.2 mm o.d., 4.4 mm i.d., ~85 mm long, HTX-6, Small Parts, Miami Lakes, FL) is taken and the terminal ends are carefully deburred to remove all sharp edges. The tube is polished inside with a pipe cleaner and tooth paste until the inside is highly reflective. The tube fits in snug into the head of the nut in the tee fitting, as shown in the figure. On the other side of the tube, a  $\frac{1}{4}$ -28-to-10-32 male–male

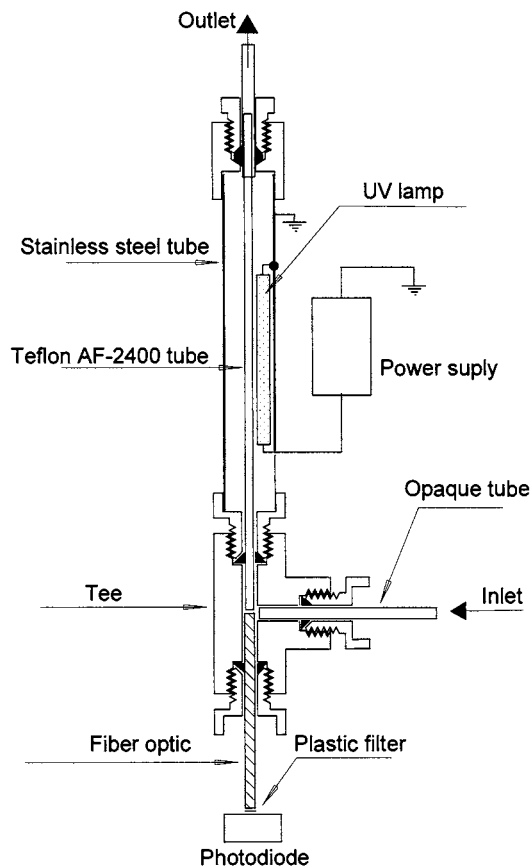


Fig. 1. The liquid–core waveguide fluorescence detector schematically shown. Teflon AF-2400 LCW length 115 mm, 0.84 mm i.d.

chromatography style union is used (P/N 42806, Dionex, Sunnyvale, CA). The  $\frac{1}{4}$ -28 threaded side is bored out with an appropriately sized drill bit to snugly accommodate the stainless steel tube. The through hole in this union is drilled out to 1.5 mm bore. Two small holes are drilled through one side of the stainless steel tube,  $\sim 55$  mm apart, to provide exits for the leads to the light source.

The light source is a miniature Hg black light tube ( $3 \times 50$  mm, P/N BF 350-UV1, Digi-Key, Thief River Falls, MN), that is operated by a miniature high voltage power supply (P/N BXA-502, JKL Component Corp., Pacoima, CA) with the primary input supply being 5 V. The total input power to the power supply is 250 mW without the lamp being connected and 950–1000 mW with the lamp connected. The optical lamp output flux is 200–300  $\mu\text{W cm}^{-2}$  at a distance of 1 cm from the lamp. The axial leads of the lamp are cut short to only  $\sim 1$  mm length. Kynar-coated lead wires are inserted through the holes in the stainless steel tube such that both comes out of one end of the tube. These protruding ends are then soldered on to the lamp leads. The lamp is then pushed inside the tube, and the lead wires suitably withdrawn. The insulation is removed from one of the lead wires and it is wrapped around the stainless steel shell and cemented in place with electrically conductive epoxy adhesive to provide a grounded end. The other lead wire is also wrapped around the shell a few turns and the turns epoxied in place with ordinary non conductive epoxy adhesive to secure the lamp firmly in place. The lead wire is connected to the high voltage end of the power supply. The power supply ground is connected to the shell. (Our standard practice is to also provide a third aperture in the stainless steel shell, slightly larger than the other two apertures and located approximately equidistant from the other two. A photodiode is cemented on this hole and can be used to monitor the lamp intensity. No explicit use of this has been made in the present work.)

Because the lamp consumes little power, there are no problems associated with excessive heat-

ing of the lamp or the AF tube; the latter is, of course, also cooled by the flowing fluid.

With the Teflon<sup>®</sup> AF tube and the silica fiber optic already connected to the tee, the lamp-bearing stainless steel shell is guided over the AF tube and firmly inserted into the head of the nut. The AF tube now protrudes out of the free end of the stainless steel shell and the union fitting is now pushed over the end of the AF tube to securely connect to the stainless steel shell. The length of the AF tube is such that it protrudes  $\sim 2$  mm beyond the central partition of the union. An opaque 1/16 in PTFE tube is taken and the terminal end is bored out with a drill bit so that the AF tube can fit in to this end. This is then slipped over the end of the AF tube and secured in place with a 10–32 nut and ferrule. A small disk of blue plastic sheet (No. 856, P/N 60403, Edmund Scientific, Gloucester, NJ) was cemented by UV-Cure adhesive (optical adhesive type 81, Norland Products, New Brunswick, NJ) to the free end of the silica fiber optic. After the disk fully adheres to the optic, it is trimmed to the fiber diameter with a sharp surgical knife.

The photodetector used in the present work is a blue-sensitive integrated photodiode-operational amplifier available in a TO-99 (OPT-301, Burr-Brown, Tucson, AZ) metal can. We used an opaque chromatography style bulkhead fitting with a  $\frac{1}{4}$ -28 threaded flat bottom female port on both sides (P/N 38654, Dionex). One side is bored out and the photodetector is securely cemented therein. The bulkhead fitting is secured to the faceplate of the electronics enclosure. In use, the silica fiber optic passes through the through hole of the bulkhead fitting and is secured in place by a  $\frac{1}{4}$ -28 nut and a flat bottom ferrule.

The electronic circuit for the detector is shown schematically in Fig. 2. The OPT-301 photodetector/amplifier output signal produces increasing positive outputs with increasing light input. A dual BIFET operational amplifier (TL 082) is used to provide offset and further gain to the primary output. The first stage functions as a summing inverting amplifier. The two 100 K 10-turn potentiometers connected to the first

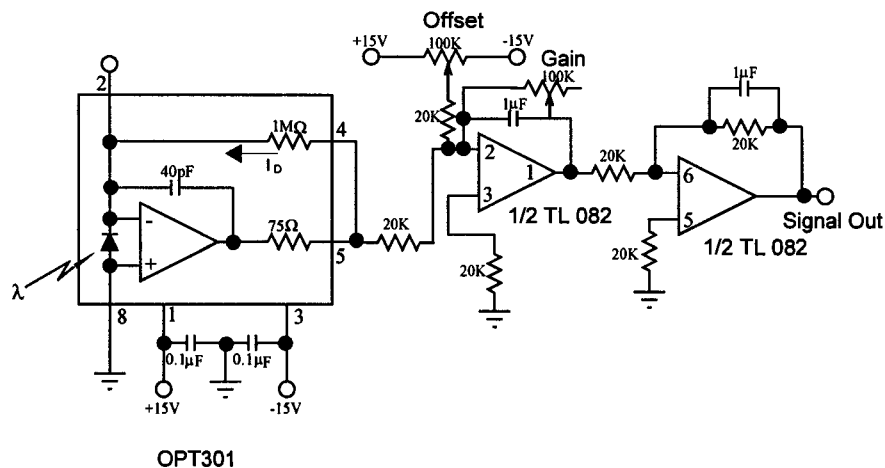


Fig. 2. Electronic schematic for the detector.

stage of the TL 082 IC, respectively provides adjustable offset and variable gain (up to  $5 \times$ ) functions. Since this stage also inverts the signal, the second stage is operated simply as a unity gain inverting amplifier so that the final output is a positive signal that increases with increasing light input. The detector is commercially available from AnalTech (Lubbock, TX).

### 2.3. Analytical system

The flow system is schematically shown in Fig. 3. A peristaltic pump P (Rabbit, RAININ, Instrument, Emeryville, CA) was used to pump water (W) as carrier at  $50 \mu\text{L min}^{-1}$  through an electropneumatically actuated six-port rotary valve V (type 5020P, Rheodyne, Cotati, CA) equipped with a  $46 \mu\text{L}$  volume sample loop. The sample S was aspirated by the pump through the valve. The carrier stream mixed with the OPA reagent stream O ( $50 \mu\text{L min}^{-1}$ ) at a low-volume tee. This was followed by a knotted mixing coil M1 ( $0.3 \times 250 \text{ mm}$ ), and merged again with the buffered sulfite reagent stream B ( $50 \mu\text{L min}^{-1}$ ). The next mixing coil M2 ( $0.3 \times 1000 \text{ mm}$ ) was followed by a Teflon reaction coil R ( $0.3 \times 1200 \text{ mm}$ ) kept in a water bath thermostated at  $85 \pm 1^\circ\text{C}$ . Finally, the fluorescence is detected by the LCW cell; a silica capillary ( $7\text{--}10 \text{ cm}$  long,  $100 \mu\text{m}$  i.d.) is connected to the cell exit to apply backpressure.

## 3. Results and discussion

### 3.1. Excitation source

The maximum excitation wavelength of the fluorescent product from OPA-sulfite- $\text{NH}_3$  system is  $365 \text{ nm}$  in the pH 11.0 phosphate buffer. A miniature blacklight type Hg line source emitting at  $365 \text{ nm}$  is perfectly matched for this application. In operation, the lamp appears to be stable such that ratioing the fluorescence signal versus the lamp intensity was not found to be necessary.

### 3.2. Prevention of bubbles

In a flow system heated as much as  $85^\circ\text{C}$ , there is a high likelihood of bubble formation unless

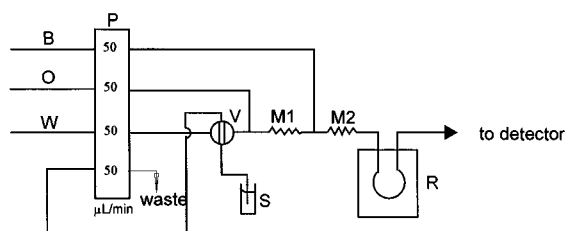


Fig. 3. Flow injection manifold for the determination of  $\text{NH}_3/\text{NH}_4^+$ . P, peristaltic pump; B, phosphate buffered sulfite; O, *o*-phthalaldehyde; W, water; V, rotary loop injection valve; S, sample; M1, 2, knotted mixing coils; R, heated reactor, thermostated at  $85^\circ\text{C}$ .



preventive measures are taken. The presence of a bubble in an LCW cell causes serious problems in much the same way bubbles are problematic in any other optical detection system. It is interesting to note however, that the precise effect of a bubble in the present detector system depends on the position of the bubble. When the bubble is located in the illuminated region of the LCW, it can scatter the excitation light directly to the light detector and thus result in a large background signal. When the bubble is located between the illuminated zone and the silica fiber, the bubble blocks the transmission of the emitted light and a low signal level is observed. For proper operation, the detector cell is built without any dead volume as far as practicable. The cell is positioned vertically with the exit on the top to prevent bubble entrapment. Most importantly, sufficient back pressure is placed at the cell exit to prevent bubble formation in the first place. Occasionally, a small bubble will stick nevertheless on the walls of the LCW tube or the connecting section of AF tube and fiber optics, causing a baseline shift. Such bubbles can be effectively removed by washing the cell with a low surface tension solvent like methanol.

### 3.3. Performance

The fluorescence intensity was linear with ammonia concentration between the range of 0.2–60  $\mu\text{M}$  with a linear  $r^2$  value of 0.9993. System output for 0.2–1.0  $\mu\text{M}$   $\text{NH}_4^+$  is shown in Fig. 4. The relative standard deviation at the 200 nM level was 1.7% ( $n = 11$ ). Repeated measurements at the 100 nM level are shown in Fig. 5. The baseline oscillations at this level are significant and we therefore conservatively estimate the  $S/N = 3$  LOD to be 35 nM. The cause of the baseline variability at this level is not detector noise, but specific contributions from other sources could not be ascertained. Nevertheless, this performance is very comparable to the best LOD of 20 nM obtained with a commercial fluorometer with an optimized long-pass emission filter and a photomultiplier tube detector [18].

In conclusion, dedicated fluorescence detectors based on a transversely illuminated LCW consti-

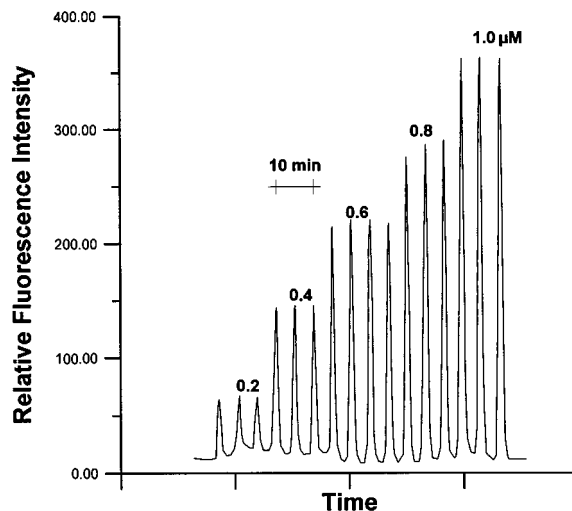


Fig. 4. Typical chart output for  $\text{NH}_3/\text{NH}_4^+$  determination. The  $\text{NH}_3/\text{NH}_4^+-\text{N}$  concentration of the sample in  $\mu\text{M}$  is indicated.

tute simple, sensitive, miniature affordable instruments that are especially amenable to portable and flow-through applications. It is remarkable that this photodiode based detector, with a hardware cost more than an order of magnitude less than that of a commercial filter fluorometer, can provide almost the same performance.

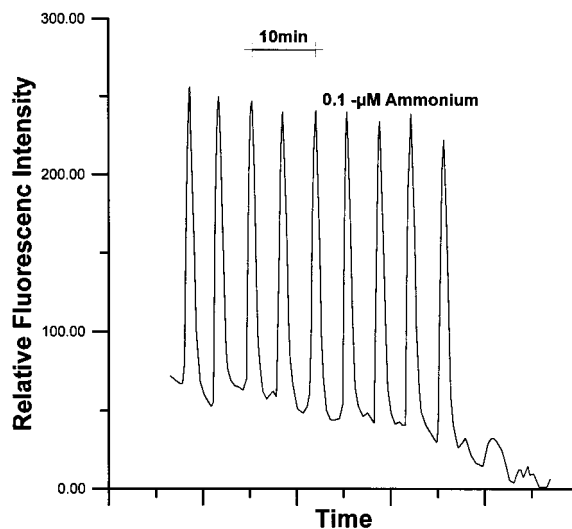


Fig. 5. Typical system output for 0.1  $\mu\text{M}$  ammonium and the background noise level.

## References

- [1] P.K. Dasgupta, *Anal. Chem.* 56 (1984) 1401–1403.
- [2] K. Tsunoda, A. Nomura, J. Yamada, S. Nishi, *Appl. Spectrosc.* 44 (1990) 163–165.
- [3] K. Fujiwara, T. Nakamura, T. Kashima, *Appl. Spectrosc.* 44 (1990) 1084.
- [4] K. Fuwa, W. Lei, K. Fujiwara, *Anal. Chem.* 56 (1984) 1640–1644.
- [5] K. Hong, L.W. Burgess, *Proc. SPIE* 2293 (1994) 71–79.
- [6] Dupont Fluoroproducts, AF Teflon amorphous fluoropolymers technical information, Dupont Fluoroproducts, Wilmington, DE, February, 1997.
- [7] R.D. Waterbury, W. Yao, R.H. Byrne, *Anal.Chim. Acta* 357 (1997) 99.
- [8] W. Yao, R.H. Byrne, R.D. Waterbury, *Environ. Sci. Technol.* 32 (1998) 2646.
- [9] P.K. Dasgupta, Z. Genfa, S.K. Poruthoor, S. Caldwell, S. Dong, S.-Y. Liu, *Anal. Chem.* 70 (1998) 4661.
- [10] W. Yao, W.R.H. Byrne, *Talanta* 48 (1999) 277.
- [11] K. Fujiwara, S. Ito, *Trends Anal. Chem.* 10 (1991) 184.
- [12] K. Fujiwara, S. Ito, R.-E. Kojyo, H. Tsubota, R.L. Carter, *Appl. Spectrosc.* 46 (1992) 1032.
- [13] P.K. Dasgupta, Z. Genfa, J. Li, C.B. Boring, S. Jambunathan, R. Al-Horr, *Anal. Chem.* 71 (1999) 1400.
- [14] National Academy of Science, Ammonia, University Park Press: Baltimore, MD, 1979.
- [15] R.L. Poirot, P.R. Wishinski, *Atmos. Environ.* 20 (1986) 1457.
- [16] Standard Methods for examination of Water and Wastewater, 16th ed., American Public Health Association, Washington DC, 1985.
- [17] M. Roth, *Anal.Chem.* 43 (1971) 880.
- [18] Z. Genfa, P.K. Dasgupta, *Anal. Chem.* 61 (1989) 408.

# Adsorption and thermodynamic characteristics of Hg(II)-SCN complex onto polyurethane foam

Mohammad Mufazzal Saeed \*, Syed Moosa Hasany, Munir Ahmed

*Nuclear Chemistry Division, Pakistan Institute of Nuclear Science and Technology, PO Nilore, Islamabad, Pakistan*

Received 30 November 1998; received in revised form 04 May 1999; accepted 06 May 1999

## Abstract

The sorption of Hg(II) in the presence of sodium thiocyanate solution onto polyurethane (PUR) foam, an excellent sorbent, has been investigated in detail. Maximum sorption of Hg(II) is achieved from 0.1 M hydrochloric acid solution containing  $7.5 \times 10^{-2}$  M sodium thiocyanate in 5 min. The sorption data followed both Freundlich and Langmuir adsorption isotherms. The Freundlich constants  $1/n$  and sorption capacity,  $C_m$ , are evaluated to be  $0.44 \pm 0.02$  and  $(3.86 \pm 0.89) \times 10^{-3}$  mol g<sup>-1</sup>. The saturation capacity and adsorption constant derived from Langmuir isotherm are  $(6.88 \pm 0.28) \times 10^{-5}$  mol g<sup>-1</sup> and  $(5.6 \pm 0.37) \times 10^4$  dm<sup>3</sup> mol<sup>-1</sup> respectively. The mean free energy ( $E$ ) of Hg(II)-SCN sorption onto PUR foam computed from D–R isotherm is  $12.4 \pm 0.3$  kJ mol<sup>-1</sup> indicating ion-exchange type mechanism of chemisorption. The variation of sorption with temperature yields thermodynamic parameters of  $\Delta H = -30.7 \pm 1.2$  kJ mol<sup>-1</sup>,  $\Delta S = -70.1 \pm 4.1$  J mol<sup>-1</sup> K<sup>-1</sup> and  $\Delta G = -9.86 \pm 0.77$  kJ mol<sup>-1</sup> at 298 K. The negative value of enthalpy and free energy reflects the exothermic and spontaneous nature of sorption. On the basis of the sorption data, sorption mechanism has been proposed. © 1999 Elsevier Science B.V. All rights reserved.

*Keywords:* Hg(II)-SCN; Adsorption; Thermodynamic characteristics; Polyurethane foam

## 1. Introduction

Mercury and its compounds are hazardous for humans, plants and animals [1]. Mercury metal, its vapours, and most of its organic and inorganic compounds are protoplasmic poisons. The tolerance limit of inorganic mercury in aqueous solution is 1 µg l<sup>-1</sup>. The major sources of mercury

poisoning are its mining and recovery and its usage in a variety of products, industrial waste and its accumulation in human body via food chain. Mercury has a tendency to absorb and adhere or amalgamate to various surfaces which are in immediate contact with it. It is capable to form complexes with many inorganic ligands and reagents [2,3].

The low level of mercury in environmental and biological samples, makes it necessary to preconcentrate these samples before their actual determination. A number of solid/liquid preconcentration

\* Corresponding author. Fax: +92-51-9290275.

*E-mail address:* pinstech@paknet2.ptc.pk (M. Mufazzal Saeed)

systems have been used for mercury in off-line procedures such as activated carbon [4,5], inorganic metal oxides [6], ion exchange resins [7,8], etc., and with immobilised reagents such as diethyl dithiocarbamate [9], 8-hydroxyquinoline [10] and dithizone [11], etc., onto solid supports.

Polyurethane foam, an excellent sorbent for the separation and preconcentration of trace metal ions, reflects its potential in the environmental and analytical chemistry prior to the instrumental analyses. In last two decades, polyurethane (PUR) foam is widely used for the separation and preconcentration of trace metal ions. The unloaded and reagent loaded PUR foam provides a cheap, simple and fast sorbent for the separation and preconcentration based on solid-liquid contact [12,13]. The uptake of different divalent metal ions from thiocyanate media onto PUR foam has been reported [14–19]. A number of different mechanisms such as ion-exchange, solvent extraction, ligand addition, ion-association, surface sorption, etc., have been reported by different workers depending upon the nature of the chemical species sorbed and the conditions of sorption [20–23].

The mass transfer of metal complexes of thiocyanate from the bulk solution to the surface of PUR foam and from its outer surface to the interior surface is not well established. The surface of the PUR foam is heterogeneous, in surface structure and in the distribution of surface energy. During sorption, first molecules arrive at the bare surface and preferentially adsorb where their potential energy will be minimum. Several adsorption models in batch technique can be used for the description of randomly distributed sites of unequal energy in which Freundlich and Langmuir adsorption isotherms are most commonly used [3,24–28].

In previous investigations [29–31], the uptake mechanism of Co(II) and Fe(III) on 2-thenoyl-trifluoroacetone loaded PUR foam indicated that the sorption of trace metal ions had clearly followed the adsorption phenomena. In the present study, the uptake conditions of mercuric ions from aqueous thiocyanate solution have been worked out in terms of the nature of the transport of the mercuric ions from the bulk solution to the

surface of the ether type PUR foam using different adsorption isotherms. The adsorption mechanism is also proposed on the basis of thermodynamic studies, and the nature of Hg(II)-SCN species.

## 2. Experimental

All the reagents used in this work were of Analar grade. The buffer solutions of pH 1–2.5 and 3–6 were prepared by mixing appropriate amounts of 0.2M solutions of HCl and KCl, and of CH<sub>3</sub>COOH and CH<sub>3</sub>COONa solutions respectively. However, buffer solutions of pH 6.5–8 and 8.5–10 were prepared by mixing different volumes of 0.2 M solutions of NaH<sub>2</sub>PO<sub>4</sub>, NaOH and H<sub>3</sub>BO<sub>3</sub>. The ionic strength of the solutions was kept at 0.1 M with deionised water and stability was checked periodically.

The radiotracer of <sup>203</sup>Hg was prepared by the irradiation of specpur HgO in PARR-I reactor of this institute at a flux density of  $5 \times 10^3 \text{ n cm}^{-2} \text{ s}^{-1}$ . The irradiated oxide was dissolved in concentrated HCl, heated to near dryness and the residue was dissolved in 10 ml of 0.2 M HCl solutions and kept as a stock solution for further use. The radionuclidic purity was checked on 4k series of 85 Canberra multichannel analyser coupled with a 25 cm<sup>3</sup> Ge(Li) detector.

### 2.1. Preparation of PUR foam

Open pore polyether type PUR foam with a bulk density of 22 kg m<sup>-3</sup> was characterised and used as a sorbent. The foam was cut into small cylindrical plugs of 5 mm dia × 10 mm length with the help of a borer for batch shaking purpose. The foam plugs were washed thoroughly to remove the organic and inorganic contaminants in the following order:

1. The cylindrical foam plugs were first squeezed in acetone for 30 min to open the pores of the foam, washed with deionised water and dried in an oven at 80°C.
2. The dried foam plugs were soaked in 2 M HCl solution for two hours to remove all the inorganic impurities. The foam plugs were thor-

oroughly washed with deionised water till the washings were acid free and neutral. The washed foam plugs were dried at 80°C in an oven.

- The dried foam plugs were again soaked in acetone for 30 min in order to remove all organic impurities present in the foam. The foam was pressed between filter paper sheets to remove the excess acetone present in the foam and dried at 80°C and stored in a plastic bottle for further use.

## 2.2. Procedure

Five millilitre aqueous solution of known pH or acid concentration was taken in a glass culture tube with a polythene cap. The known concentration of  $^{203}\text{Hg}$  radiotracer was added in tubes and mixed thoroughly. An aliquot of 1 ml was taken out for gross gamma counts ( $A_0$ ). The remaining solution was shaken with washed ether type PUR foam plugs ( $\sim 29$  mg) for 5 min on a wrist-action shaker. After phase separation, 1 ml aliquot ( $A_e$ ) was assayed radiometrically on a Tenelec gross gamma counter equipped with a 30 cm<sup>3</sup> well-type Na(Tl) crystal.

The sorbed concentration of  $^{203}\text{Hg}$  at equilibrium was calculated by the difference in the activity of the aliquots drawn before ( $A_0$ ) and after ( $A_e$ ) shaking. The gross gamma activity of  $^{203}\text{Hg}$  radiotracer used in the aqueous solution for equilibration was in the range of 55 000–60 000 cpm ml<sup>-1</sup>. The percentage sorption (% sorption) and distribution coefficient ( $K_d$ ) are calculated as

$$\% \text{ sorption} = \frac{A_0 - A_e}{A_0} \times 100$$

and

$$K_d = \frac{\text{amount of metal in foam}}{\text{amount of metal in solution}} \times \frac{\text{volume of solution (V)}}{\text{weight of dry foam (W)}} = (\text{cm}^3 \text{ g}^{-1})$$

The percent sorption and  $K_d$  can be correlated by the following equation:

$$\% \text{ sorption} = \frac{100K_d}{K_d + (V/W)}$$

All experiments were performed at least in triplicate at  $23 \pm 2^\circ\text{C}$  or as specified otherwise. The linear regression computer programme with one independent variable was used for slope analysis and for the statistical treatment of the data [29]. The correlation coefficient ( $r$ ) for all regression analyses was in the range of 0.9914–0.9958. The results are the average of at least triplicate independent measurements and precision in most cases was  $\pm 3\%$ .

## 3. Results and discussion

The sorption of  $1.2 \times 10^{-4}$  M solution of Hg(II) ions in the presence ( $7.5 \times 10^{-2}$  M) and absence of sodium thiocyanate on unloaded PUR foam was carried out from aqueous solutions having a pH in the range of 1–10. The variation of percent sorption with pH is shown in Fig. 1. The maximum sorption is observed at pH 1 in the presence of sodium thiocyanate. The sorption of Hg(II) ions in the absence of thiocyanate ions increases with an increase in the pH and attains a constant value around pH 3 ( $> 50\%$ ). However, the adsorption profile of Hg-SCN complex decreases with increasing pH and becomes almost

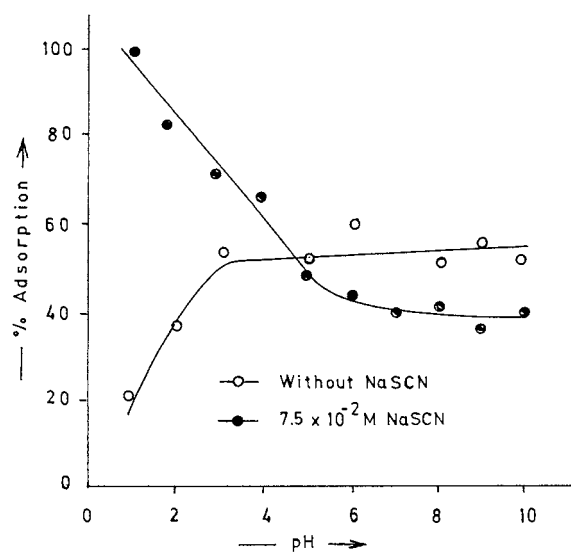


Fig. 1. Variation of percent adsorption of Hg(II) metal ion on PUR foam with pH.

Table 1

Variation of distribution coefficient ( $K_d$ ) and percent sorption of Hg(II)-SCN complex with acid concentration on polyurethane foam

HCl (M)	$K_d$ ( $\text{cm}^3 \text{g}^{-1}$ )	Adsorption (%)
0.01	814	85
0.05	2050	93
0.1	13208	99
0.5	5720	97
1.0	5057	97
1.5	3931	96
2.0	2770	96

constant ( $\geq 42\%$ ) in neutral to alkaline range up to pH 10. The decrease in the sorption of Hg(II)-SCN complex with pH is attributed to the instability of Hg(II)-SCN complex at higher pH and subsequent hydrolysis of Hg(II) metal ions. The sorption of Hg(II) is also studied from 0.01–2.0 M HCl solution in the presence of 0.08 M NaSCN and results are tabulated in Table 1. This indicates that 0.1 M was optimum acid concentration, the distribution coefficient ( $K_d$ ) decreases with an increase in the HCl concentration beyond 0.1 M but percent adsorption remains almost constant. The influence of sodium thiocyanate from 0.005 to 0.15 M in 0.1 M HCl solution on the adsorption of  $1.2 \times 10^{-4}$  M solution of Hg(II) ions on PUR foam is shown in Fig. 2. This figure shows that the maximum sorption occurred at 0.08 M solution of NaSCN which was kept constant for subsequent experiments.

The shaking time from 5 to 30 min at an interval of 5 min on the retention of Hg(II) metal ions on PUR foam under the optimum conditions of 0.1 M HCl and 0.08 M NaSCN was varied. The data indicate that the maximum equilibrium is attained within 5 min contact time and remained constant on further increase in the shaking time. However, for higher Hg(II) metal ion and lower NaSCN concentration, an increase in shaking will be needed to attain maximum adsorption.

The variation of the amount of PUR foam on the distribution coefficient ( $K_d$ ) of Hg(II) from 0.1 M HCl solution containing sodium thiocyanate ( $7.5 \times 10^{-2}$  M) is shown in Fig. 3. This figure

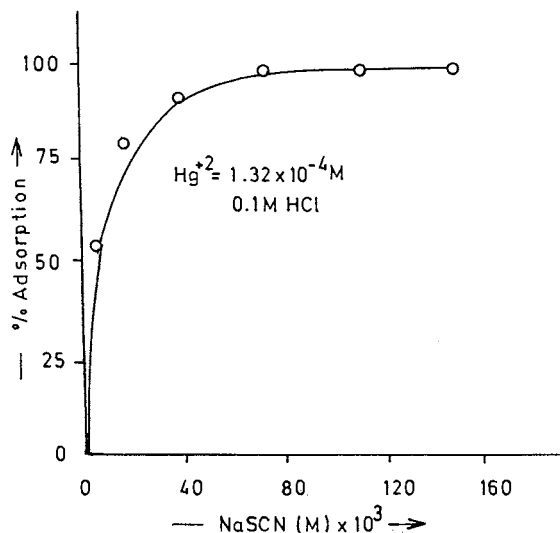


Fig. 2. Dependence of percentage adsorption of Hg(II)-SCN complex on sodium thiocyanate concentration.

depicts that maximum  $K_d$  is achieved at  $13.5 \text{ mg ml}^{-1}$  of PUR foam. On further increase in PUR foam amount,  $K_d$  showed a decrease. For further experiments  $\sim 29 \text{ mg}$  of PUR foam is used for 4 ml aqueous solution.

In order to check the sensitivity of PUR foam for the pre-concentration of Hg(II)-SCN complex on PUR foam, the influence of different anions under the optimum conditions was evaluated. The addition of foreign ions in the sorptive medium may change environment around the central metal

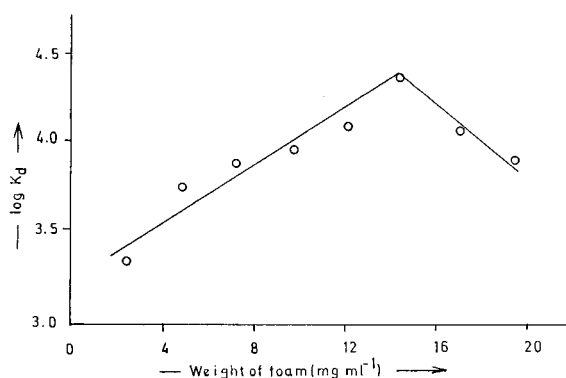


Fig. 3. Distribution coefficient of  $1.32 \times 10^{-3}$  M solution of Hg(II)-SCN complex as a function of the amount of adsorbent from 0.1 M HCl solution.

Table 2  
Effect of different anions on the sorption of Hg(II)-SCN complex on polyurethane foam from aqueous solution of 0.1 M HCl

Anion	Compound added	$K_d$ ( $\text{cm}^3 \text{g}^{-1}$ )	Adsorption (%)
Nil	–	13208	99
Ascorbate	$\text{C}_6\text{H}_8\text{O}_6$	13178	99
Citrate	$\text{C}_6\text{H}_8\text{O}_7 \cdot \text{H}_2\text{O}$	9845	98
Iodide	NaI	6182	98
Sulphate	$\text{Na}_2\text{SO}_4 \cdot 2\text{H}_2\text{O}$	2814	96
Tartrate	$\text{Na}_2\text{C}_6\text{H}_4\text{O}_6 \cdot 2\text{H}_2\text{O}$	2141	94
Oxalate	$\text{Na}_2\text{C}_2\text{O}_4$	2100	93
Phosphate	$\text{NaH}_2\text{PO}_4$	2054	95
EDTA	$\text{Na}_2\text{C}_{10}\text{H}_{18}\text{N}_2\text{O}_{10}$	1398	91
Nitrate	$\text{NaNO}_3$	1028	91
Perchlorate	$\text{NaClO}_4$	740	84
Chloride	NaCl	444	81
Fluoride	NaF	381	73
Acetate	$\text{CH}_3\text{COONa}$	193	58
Bromide	NaBr	185	64
Molybdate	$\text{Na}_2\text{MoO}_4 \cdot 2\text{H}_2\text{O}$	40	22
Cyanide	KCN	<1	<1
Thiosulphate	$\text{Na}_2\text{S}_2\text{O}_3$	<1	<1
Thiourea	$\text{H}_2\text{NCSNH}_2$	<2	<2

ion and subsequently its solution chemistry and sorption behaviour. The sorption was measured in the presence of these ions and results are listed in Table 2. This table indicates that on addition of different electrolytes, the  $K_d$  and percent sorption decrease due to the formation of more stable metal complexes with added ions than Hg(II)-SCN complex. The reduction in the sorption of mercury thiocyanate complex on PUR foam in the presence of cyanide, chloride, fluoride, bromide, acetate and molybdate anions may be due to the formation of more stable complexes of mercury with these ions and their very low affinity towards the sorbent. Cyanide completely reduces the sorption (< 1%) while other anions register a decrease in the sorption of mercury in the range of 81–22%. However, thiosulphate and thiourea reduce the Hg(II) ions [32] which or its anionic complexes with these anions may not sorb on the PUR foam surface at all, subsequently reducing the

sorption of mercury on PUR foam. The effect of different cations under investigation on the adsorption of Hg(II)-SCN complex is comparatively small except in case of Fe(III) as shown in Table 3. The Cd(III), Co(II), Sr(II), Mn(II) and Fe(II) partially suppressed the sorption while Fe(III) completely masks. This is attributed to the formation of more stable Fe(III)-SCN complex as compared to the Hg(II)-SCN complex.

### 3.1. Adsorption isotherms

The mass transfer of Hg(II)-SCN complex from bulk aqueous solution onto PUR foam can be expressed in the form of its diffusion and thermodynamic behaviour. The sorption of Hg(II)-SCN complex on PUR foam is very rapid and >95% of Hg(II)-SCN complex is sorbed within 5 min shaking time as described earlier. This indicates that the film diffusion, i.e. diffusion of the solute through a hypothetical ‘film’ or hydrodynamic boundary layer takes place in the sorption phenomena [24]. The film diffusion is governed by molecular diffusion and considered to be very rapid and generally occurs at the macropores of the sorbent [3,28].

Table 3  
Influence of different cations on the sorption of Hg(II)-SCN complex on polyurethane foam from 0.1 M HCl aqueous solution<sup>a</sup>

Cation	$K_d$ ( $\text{cm}^3 \text{g}^{-1}$ )	Adsorption (%)
Nil	13208	99
Ni(II)	2127	99
Cd(II)	1803	92
Ce(III)	1444	91
Al(III)	1236	91
Ba(II)	1090	89
Cr(III)	1036	90
Mg(II)	915	90
Cd(II)	757	84
Co(II)	609	85
Sr(II)	549	85
Mn(II)	289	73
Fe(II)	256	71
Fe(III) <sup>b</sup>	34	19

<sup>a</sup> All cations added as chloride.

<sup>b</sup> As nitrate.

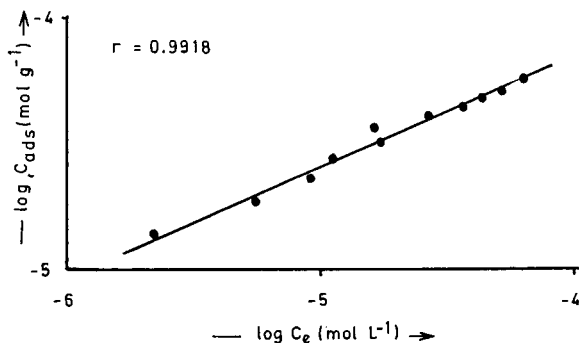


Fig. 4. Freundlich adsorption profile of  $[\text{Hg}(\text{SCN})_4]^{2-}$  complex on PUR foam.

For thermodynamic consideration in terms of adsorption isotherms, a series of experimental points for the adsorption of Hg(II)-SCN complexes on PUR foam were plotted. Three commonly used mathematical expressions to describe the adsorption equilibria, i.e. Freundlich, Langmuir and Dubinin–Radushkevich (D–R) isotherm models were tested with the experimental data.

The Freundlich isotherm [33], most widely used mathematical description of adsorption, usually fits the experimental data over a wide range of concentration. This isotherm gives an empirical expression encompassing the surface heterogeneity and the exponential distribution of active sites and their energies. The Freundlich model is expressed as

$$C_{\text{ads}} = K_{\text{F}} C_{\text{e}}^{1/n} \quad (1)$$

where  $C_{\text{ads}}$  = amount of Hg(II) adsorbed ( $\text{mol g}^{-1}$ ),  $C_{\text{e}}$  = amount of Hg(II) in solution ( $\text{mol l}^{-1}$ ),  $K_{\text{F}}$  and  $1/n$  are characteristic constants.

The linearised form of Eq. (1) is

$$\log C_{\text{ads}} = \log K_{\text{F}} + \frac{1}{n} \log C_{\text{e}} \quad (2)$$

The plot of  $\log C_{\text{ads}}$  vs  $\log C_{\text{e}}$  is shown in Fig. 4 which facilitates to determine the Freundlich constants  $1/n$  and  $K_{\text{F}}$  from the slope and intercept of the plot. The numerical value of adsorption capacity ( $K_{\text{F}}$ ) and  $1/n$  indicating the energy and intensity are  $(3.86 \pm 0.89) \times 10^{-3} \text{ mol g}^{-1}$  and  $0.44 \pm 0.02$  respectively. The numerical value of

$1/n < 1$  indicates that sorption capacity is only slightly reduced at lower equilibrium concentrations. Freundlich adsorption isotherm does not predict any saturation of the solid surface of the adsorbent by the adsorbate, thus infinite surface coverage is predicted mathematically.

The Langmuir model [34] was originally developed to represent chemisorption on a set of well defined localised adsorption sites having same sorption energy, independent of surface coverage and no interaction between adsorbed molecules. Maximum sorption is noticed when surface of the sorbent is covered with a monolayer of adsorbate. The familiar form of Langmuir isotherm based on the kinetic consideration is expressed as:

$$\frac{C_{\text{e}}}{C_{\text{ads}}} = \frac{1}{K_{\text{L}} b} + \frac{C_{\text{e}}}{K_{\text{L}}} \quad (3)$$

where  $C_{\text{e}}$  = equilibrium concentration of Hg(II) in solution ( $\text{mol l}^{-1}$ ),  $C_{\text{ads}}$  = amount of Hg(II) adsorbed on PUR foam ( $\text{mol g}^{-1}$ ),  $K_{\text{L}}$  = constant related to maximum amount of solute adsorbed,  $b$  = constant related to the binding energy of solute.

For testing the curve fit of the Langmuir model to experimental data involves plotting of  $C_{\text{e}}/C_{\text{ads}}$  against  $C_{\text{e}}$  as shown in Fig. 5. The model parameters  $K_{\text{L}}$  and  $b$  obtained from the slope and intercept of the plot are  $(6.88 \pm 0.28) \times 10^{-5} \text{ mol g}^{-1}$  and  $(5.6 \pm 0.37) \times 10^4 \text{ dm}^3 \text{ mol}^{-1}$  respectively. The value of  $K_{\text{L}}$  corresponding to the monolayer coverage and independent of temperature, while the sorption coefficient  $b$  is related to the enthalpy of adsorption and should vary with temperature.

To distinguish between physical and chemical adsorption, the data were applied to D–R isotherm model [35]. The sorption is postulated within a adsorption ‘space’ close to adsorbent surface. This model features the heterogeneity of energies over the surface. The linear form of D–R isotherm is:

$$\ln C_{\text{ads}} = \ln K_{\text{DR}} - B\varepsilon^2 \quad (4)$$

where  $C_{\text{ads}}$  is the amount of metal ions adsorbed per unit mass of the PUR foam,  $K_{\text{DR}}$  is the maximum amount of Hg(II)-SCN complex adsorbed,  $B$  is a constant with dimensions of energy and Polanyi potential ( $\varepsilon$ ) =  $RT \ln(1 + (1/C_{\text{e}}))$



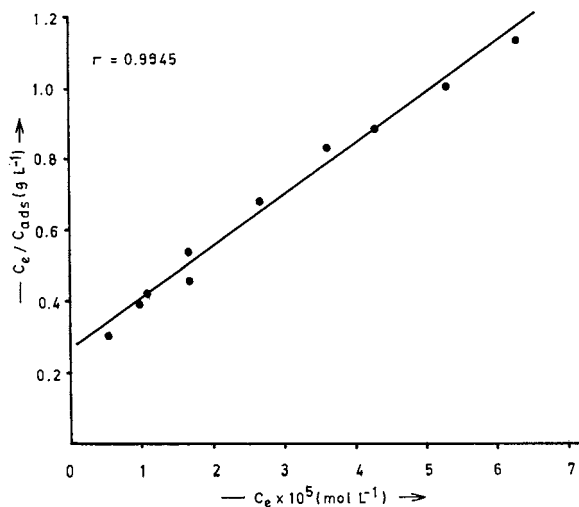


Fig. 5. Langmuir adsorption plot of  $[\text{Hg}(\text{SCN})_4]^{-2}$  complex on PUR foam.

where  $R$  is a gas constant in  $\text{kJ K}^{-1} \text{mol}^{-1}$  and  $T$  is temperature in Kelvin.

The plot of  $\ln C_{\text{ads}}$  vs  $\epsilon^2$  shown in Fig. 6 is a straight line. The computed values of  $B$  and  $K_{\text{DR}}$  from the slope and intercept are  $-0.003266 \pm 0.000146 \text{ kJ}^2 \text{ mol}^{-2}$  and  $(3.36 \pm 0.34) \times 10^{-4} \text{ mol g}^{-1}$ , respectively. If the surface is heterogeneous and an approximation to a Langmuir isotherm is chosen as a local isotherm for all sites that are energetically equivalent then the quantity  $B^{1/2}$  can be related to the mean sorption energy ( $E$ ) as:

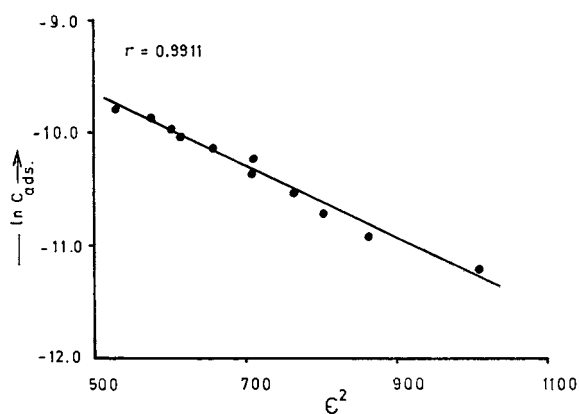


Fig. 6. Dubinin-Radushkevich isotherm of  $[\text{Hg}(\text{SCN})_4]^{-2}$  complex on PUR foam.

$$E = \frac{1}{\sqrt{-2B}} \quad (5)$$

which is the free energy of the transfer of 1 mol of solute from infinity to the surface of PUR foam. The numerical value of  $E$  evaluated from the Eq. (5) is  $12.4 \pm 0.26 \text{ kJ mol}^{-1}$  which reflects the chemical absorption based on ion exchange.

### 3.2. Thermodynamic studies

The dependence of sorption with temperature have been evaluated using the following equations:

$$\log K_c = \frac{-\Delta H}{2.303RT} + \frac{\Delta S}{2.303R} \quad (6)$$

$$\Delta G = \Delta H - T\Delta S \quad (7)$$

$$\Delta G = -RT \ln K_c \quad (8)$$

$$K_c = \frac{F_c}{1 - F_c} \quad (9)$$

where  $\Delta H$ ,  $\Delta S$ ,  $\Delta G$  and  $T$  are the enthalpy, entropy, Gibbs free energy and temperature in K, respectively,  $R$  is the gas constant ( $8.3143 \text{ J mol}^{-1}$ ) and  $K_c$  is the equilibrium constant depending upon the fractional attainment ( $F_c$ ) of the sorption of  $\text{Hg}(\text{II})\text{-SCN}$  complex at equilibrium [29]. The plot of  $\log K_c$  vs  $1/T$  gives the numerical values of  $\Delta H$  and  $\Delta S$  from slope and intercept respectively. The values of  $K_d$  and  $K_c$  measured at different temperatures are given in Table 4 which are decreasing with an increase in temperature. The numerical values of  $\Delta G$  from Eq. (7) and Eq. (8) and  $\Delta H$  and  $\Delta S$  obtained from the slope and intercept of Fig. 7 are given in Table 4.

The increase in the numerical value of  $\Delta G$  with temperature may be due to spontaneous nature of sorption and more favourable at low temperature confirming exothermic chemisorption. Similarly, the negative value of  $\Delta H$  may be interpreted as the exothermic chemisorption process, while negative change in the entropy may be indicative of the faster adsorption of the  $\text{Hg}(\text{II})\text{-SCN}$  complex onto active sites of the ad-

Table 4  
Thermodynamic functions of Hg(II)-SCN sorption on Polyurethane foam

Temperature (K)	Distribution coefficient $K_d$ ( $\text{cm}^3 \text{g}^{-1}$ )	Equilibrium constant $K_c$	$\Delta G$ ( $\text{kJ mol}^{-1}$ )	$\Delta H$ ( $\text{kJ mol}^{-1}$ )	$\Delta S$ ( $\text{J mol}^{-1} \text{K}^{-1}$ )
288	8886	85.53			
293	6392	61.53			
298	5534	53.27	$-9.86 \pm 0.77$	$-30.7 \pm 1.2$	$-70.1 \pm 4.1$
303	4805	46.25			
308	3720	35.81			
313	3159	30.40			
323	2079	20.01			

sorbent [36]. This appears to be in agreement with the observation that Hg(II)-SCN complex sorbed on PUR foam attains an equilibrium within five minutes. This can further be explained on the basis of the high energy of the PUR foam sorption sites for Hg(II)SCN complex provided by an increase in temperature may prevent stable interaction between the sorption sites and metal ions, resulting a lower adsorption at higher temperature. The exothermic nature of sorption may be explained in terms of solvation type bond formation between metal ion and solid surface based on hydrogen and/or ionic bonding comprising ion exchange or ion association interaction [17,37–39].

The data obey the Freundlich and Langmuir adsorption isotherms indicating the transfer of Hg(II)-SCN complex from aqueous solution to the surface of the PUR foam following the adsorption rather than absorption. According to D–R isotherm the interaction between the solute and solvent and between other solutes in solution are reflected in their solubilities. The experimental adsorption isotherm is independent of temperature. It does not refer to the adsorption by specific surface groups. Strong adsorption may be due to chemisorption whereas weak adsorption is limited to London forces. Neither constituent is likely to adsorb unless the net energy of adsorption is sufficient to overcome the negative entropy changes associated with condensation to the saturation concentration. The bond formation between Hg(II) metal ion and PUR foam may be chemical in nature as predicted by Langmuir and D–R isotherms.

The step wise intermediate complexes of thiocyanate ions of Hg(II) are  $[\text{Hg}(\text{SCN})]^+$ ,  $[\text{Hg}(\text{SCN})_2]$ ,  $[\text{Hg}(\text{SCN})_3]^-$  and  $[\text{Hg}(\text{SCN})_4]^{-2}$  and their stability constants are  $10^{16.8}$ ,  $10^{17.6}$ ,  $10^{20.4}$  and  $10^{21.23}$  respectively [40]. Under the optimum conditions of acid concentration, sodium thiocyanate and metal ion, the concentration of the  $[\text{Hg}(\text{SCN})_4]^{-2}$  species is  $> 99.9\%$  responsible for the sorption on PUR foam. The geometric configuration of  $[\text{Hg}(\text{SCN})_4]^{-2}$  complex is four co-ordinated tetrahedral [41].

The negative value of enthalpy shows that the inner sphere of  $[\text{Hg}(\text{SCN})_4]^{-2}$  complex is likely to be partially disrupted indicating the similar nature of the species sorbed on PUR foam and

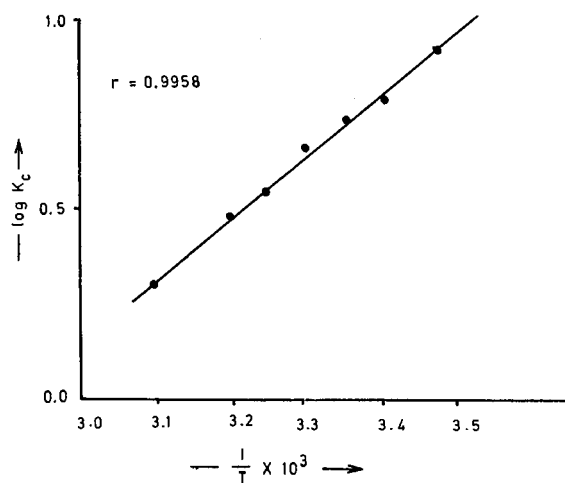
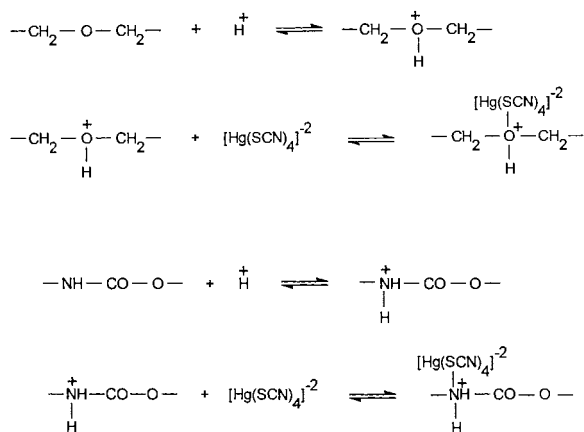


Fig. 7. Variation of equilibrium constant of  $[\text{Hg}(\text{SCN})_4]^{-2}$  complex on PUR foam with temperature.

formed in aqueous solution before sorption. The negative entropy may be viewed due to the ordering of ionic charges without a compensatory disordering of the inner sphere of the  $[\text{Hg}(\text{SCN})_4]^{-2}$  complex sorbed on PUR foam. The bond formation between  $[\text{Hg}(\text{SCN})_4]^{-2}$  and PUR foam may proceed via the neutralisation of negatively charged  $[\text{Hg}(\text{SCN})_4]^{-2}$  species followed by the accumulation through chemisorption [42].

The possible mechanism derived on these bases envisages the solvation/ion association type interaction of PUR foam and  $[\text{Hg}(\text{SCN})_4]^{-2}$  complex similar to the solvent extraction mechanism of  $[\text{FeCl}_4]^-$  and  $[\text{AuCl}_4]^-$  in diethyl ether [42,43] and cation–chelation mechanism [22]. The lone pair of electrons on nitrogen atom of isocyanate (amine) group and oxygen atom of ether group of PUR foam, have the ability to take hydronium ion ( $\text{H}^+$ ) from 0.1 M aqueous solution of HCl in order to neutralise the charge of  $[\text{Hg}(\text{SCN})_4]^{-2}$  complex in adsorption process. However, metal ion in  $[\text{Hg}(\text{SCN})_4]^{-2}$  species may not be bonded directly to the active sites of PUR foam but may exist as an entity like quaternary ammonium salt. The possible reactions of the chemisorption of  $[\text{Hg}(\text{SCN})_4]^{-2}$  complex on PUR foam in acidic solutions are:



The tetrahedral anionic  $[\text{Hg}(\text{SCN})_4]^{-2}$  complex has the ability to neutralise its charge with other associated active sites of PUR foam like solvation due to its exothermic nature of ad-

sorption and to support the cation–chelation mechanism. The large decrease in the entropy is indicative of the minimal freedom of  $[\text{Hg}(\text{SCN})_4]^{-2}$  complex in the PUR foam reflecting in acidic solution, minimum extent of solvation process as compared to the ion-exchange chemisorption. The  $\text{p}K_a$  value of the protonation of the oxygen atom of ether group and nitrogen atom of the amine group are  $-3$  and  $-6$  respectively [44,45]. This shows that at low acid concentration, the ether group can easily be protonated in 0.1 M HCl and the interaction of  $[\text{Hg}(\text{SCN})_4]^{-2}$  complex appears to be stronger and greater than the amine group interaction. However, the intensity of sorption is also dependent on the nature of the species to be sorbed onto PUR foam. The maximum sorption energy ( $E$ ) from D–R isotherm  $12.4 \pm 0.3 \text{ kJ mol}^{-1}$  indicates the ion association interaction among the metal ion and PUR foam. Hence, the  $[\text{Hg}(\text{SCN})_4]^{-2}$  complex appears to be quite stable and reactive to neutralise its charge by association with the protonated ether group in acidic media. The pH dependence curve (Fig. 1) also supports this phenomena because at higher pHs, the low concentration of hydronium ions decreases the extent of protonation of the ether group and subsequently decreases the sorption of  $[\text{Hg}(\text{SCN})_4]^{-2}$  complex on PUR foam.

#### 4. Conclusions

1. The accumulation of  $\text{Hg}(\text{II})\text{-SCN}$  complex onto PUR foam follows Langmuir, Freundlich and D-R adsorption isotherms.
2. The temperature variation has been used to compute the values of  $\Delta G$ ,  $\Delta H$  and  $\Delta S$ . The negative values of  $\Delta H$  and  $\Delta G$  indicate exothermic and spontaneous nature of sorption respectively.
3. The value of adsorption energy,  $E$ , gives an idea of the nature of sorption.
4. The sorption mechanism has been postulated on the basis of experimental data and theoretical models.
5. Thiourea, thiosuphate, cyanide and  $\text{Fe}(\text{III})$  reduce the sorption significantly.

## References

- [1] E. Niboer, D.H.S. Richardson, *Environ. Pollut. Ser. B* 1 (1980) 3.
- [2] J. Versieck, R. Cornelis, *Anal. Chim. Acta* 116 (1980) 217.
- [3] S.D. Faust, O. Aly, *Adsorption Processes of Water Treatment*, Butterworths, Boston, 1986.
- [4] C.P. Huang, D.W. Blankenship, *Water Res.* 18 (1984) 37.
- [5] G. Mcbay, J.B. Murad, *J. Chem. Technol. Biotechnol.* 37 (1987) 81.
- [6] M.A. Rauf, S.M. Hasany, M.T. Hussain, *J. Radioanal. Nucl. Chem.* 132 (1989) 397.
- [7] E.A. Novikov, L.K. Shpigum, A.Y. Zolotov, *Anal. Chim. Acta* 230 (1990) 157.
- [8] N.S.C. Becker, R.J. Eldrige, *Reactive Polym.* 21 (1993) 5.
- [9] S. Arpadjan, L. Vuchkova, E. Kostadinova, *Analyst* 122 (1997) 243.
- [10] M.N. Abbas, N.B. El-Assy, S.H. Moniem, *Anal. Letts.* 22 (1989) 2575.
- [11] V. Porta, O. Abollino, E. Mentalti, C. Sarzanini, *J. Anal. At. Spectrom.* 6 (1991) 119.
- [12] T. Braun, J.D. Navratil, A.B. Farag, *Polyurethane Foam Sorbents in Separation Science*, CRC Press, Boca Raton, 1985.
- [13] S. Palagyi, T. Braun, in: Z.B. Alfassi, C.M. Wai (Eds.), *Preconcentration Techniques for Trace Elements*, CRC Press, Boca Raton, 1992, pp. 363.
- [14] T. Braun, M.N. Abbas, *Anal. Chim. Acta* 134 (1982) 321.
- [15] T. Braun, M.N. Abbas, A. Elek, L. Bakkos, *J. Radioanal. Chem.* 67 (1981) 359.
- [16] T. Braun, A.B. Farag, *Anal. Chim. Acta* 98 (1978) 133.
- [17] R.F. Hamon, A. Chow, *Talanta* 31 (1984) 963.
- [18] S.J. Al-Bazi, A. Chow, *Talanta* 29 (1982) 507.
- [19] S.J. Al-Bazi, A. Chow, *Talanta* 30 (1983) 487.
- [20] S.J. Al-Bazi, A. Chow, *Anal. Chem.* 55 (1983) 1094.
- [21] A. Chow, S.L. Ginsberg, *Talanta* 30 (1983) 620.
- [22] R.F. Hamon, A.S. Khan, A. Chow, *Talanta* 29 (1982) 313.
- [23] L. Jones, F. Nel, K.R. Koch, *Anal. Chim. Acta* 182 (1986) 61.
- [24] W.J. Weber, in: F.L. Slejko (Ed.) *Principles of adsorption and adsorption process*, vol. 19, Marcel Dekker Inc, New York, 1985, pp. 16.
- [25] M.S. El-Shahawi, A.B. Farag, M.R. Mostafa, *Sep. Sci. Technol.* 29 (1994) 289.
- [26] M.S. El-Shahawi, *Talanta* 41 (1994) 1481.
- [27] H.D. Gesser, B.M. Gupta, *J. Radioanal. Nucl. Chem.* 132 (1989) 37.
- [28] W.J. Weber, S. Liang, *Environ. Prog.* 2 (1983) 167.
- [29] M.M. Saced, A. Rusheed, N. Ahmed, J. Tölggyessy, *Sep. Sci. Technol.* 29 (1994) 2143.
- [30] M.M. Saced, A. Rusheed, N. Ahmed, *J. Radioanal. Nucl. Chem. Art.* 211 (1996) 283.
- [31] M.M. Saced, A. Ghaffar, *J. Radioanal. Nucl. Chem. Art.* 232 (1998) 171.
- [32] H. Freundlich, *Colloid and Capillary Chemistry*, Methuen, London, 1926.
- [33] I. Langmuir, *J. Am. Chem. Soc.* 40 (1918) 136.
- [34] M.M. Dubinin, L.V. Radushkevich, *Proc. Acad. Sci., USSR Phys. Chem. Soc.* 55 (1947) 331.
- [35] K.P. Yadava, B.S. Tyagi, V.N. Singh, *J. Chem. Tech. Biotechnol.* 51 (1990) 47.
- [36] C. Luo, S. Huang, *Sep. Sci. Technol.* 28 (1993) 1253.
- [37] P.S. Lawson, R.M. Sterritt, J.N. Lester, *J. Chem. Tech. Biotech.* 34B (1984) 253.
- [38] S. Aksoyoglu, *J. Radioanal. Nucl. Chem. Art.* 140 (1990) 301.
- [39] L.G. Sillen, A.E. Martell, *Stability Constants of Metal-Ion Complexes*, Suppl. 1, The Chemical Society, London, 1971, pp. 179.
- [40] F.A. Cotton, G. Wilkinson, *Advance Inorganic Chemistry*, third ed, Interscience Publishing, New York, 1972, p. 519.
- [41] G.R. Choppin, W.F. Strazik, *Inorg. Chem.* 4 (1965) 1250.
- [42] T. Sekine, Y. Hasegawa, *Solvent Extraction Chemistry*, Marcel Dekker, Inc, New York, 1977, p. 272.
- [43] R.M. Diamond, D.G. Tuck, *Prog. Inorg. Chem.* 2 (1960) 109.
- [44] G.M. Loudon, *Organic Chemistry*, Addison-Wesley, Reading, MA, 1984, p. 1187.
- [45] K. Rzeszutek, A. Chow, *Talanta* 46 (1998) 507.

# Determination of theophylline in tea and drug formulation using a Nafion<sup>®</sup>/lead–ruthenium oxide pyrochlore chemically modified electrode

Jyh-Myng Zen <sup>a,\*</sup>, Tung-yue Yu <sup>a</sup>, Ying Shih <sup>b</sup>

<sup>a</sup> Department of Chemistry, National Chung-Hsing University, Taichung 402, Taiwan, ROC

<sup>b</sup> Department of Applied Cosmetology, Hung-Kuang Institute of Technology, Taichung 433, Taiwan, ROC

Received 17 December 1998; received in revised form 7 May 1999; accepted 7 May 1999

## Abstract

Square-wave voltammetry was used for the determination of trace amounts of theophylline in tea and drug formulation at a Nafion<sup>®</sup>/lead–ruthenium oxide pyrochlore chemically modified electrode. This chemically modified electrode exhibits a marked enhancement of the current response compared to a bare glassy carbon electrode. The calibration graph for the determination of theophylline was linear up to 100  $\mu\text{M}$  in 0.1 M, pH 3 phosphate solution with a detection limit ( $S/N = 3$ ) of 0.1  $\mu\text{M}$ . The results of 15 successive repetitive measurement-regeneration cycles showed a relative standard deviation of 1.3% for 10  $\mu\text{M}$  theophylline indicating that the electrode renewal gives a good reproducible surface. Quantitative analysis was performed by the standard addition method for the theophylline content in commercially available tea and drug. © 1999 Elsevier Science B.V. All rights reserved.

**Keywords:** Theophylline; Tea; Drug formulation; Chemically-modified electrode

## 1. Introduction

Theophylline (1,3-dimethyl-1*H*-purine-2,6-dione) is a xanthine derivative with diuretic, cardiac stimulant, and smooth muscle relaxant activities. Accurate and rapid method is required for the determination of soluble theophylline in tea and tea products because the stimulating effect of tea beverage is due to the presence of purine bases, such as, caffeine, theobromine, and

theophylline. Meanwhile, theophylline has been widely used for the treatment of asthma and bronchospasm in adult [1]. The efficiency and toxicity of this drug can be modified by many factors [2]. Thus, in order to adapt dosing and to verify compliance, therapeutic drug monitoring is necessary. Previous approaches used for the determination of theophylline include high-performance liquid chromatography (HPLC) and gradient capillary HPLC [3–7], spectrophotometry [8], enzyme immunoassay [9], capillary electrophoresis [10], frit-fast atom bombardment mass spectrometry (LC-frit-FAB-MS) [11], and electro-

\* Corresponding author. Fax: +886-4-2862547.

E-mail address: jmzen@mail.nchu.edu.tw (J.-M. Zen)

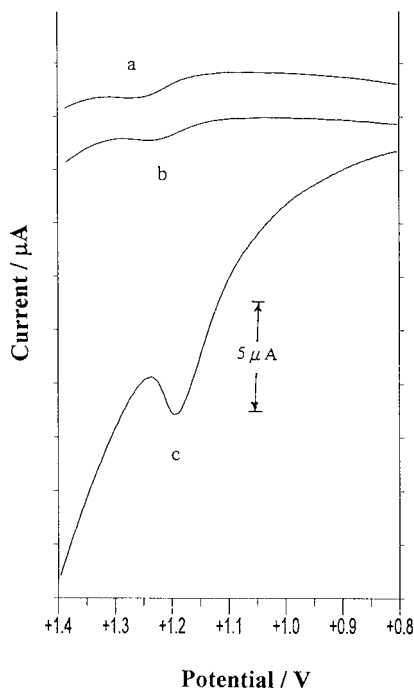


Fig. 1. SW voltammograms for 20  $\mu\text{M}$  theophylline in 0.1 M phosphate solution (pH 3) at a bare GCE (a), the Nafion<sup>®</sup>-coated GCE (b), and the CME (c). SW amplitude, 25 mV; SW frequency, 15 Hz; step height, 4 mV.

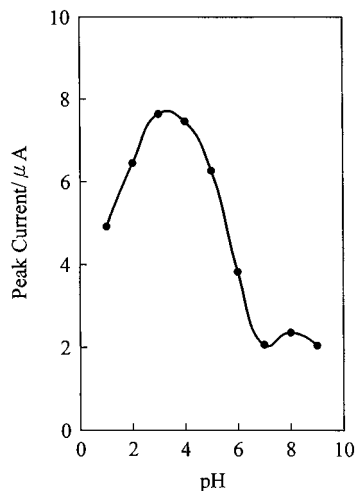


Fig. 2. Dependence of the anodic peak current on pH in SW voltammetry for 20  $\mu\text{M}$  theophylline at the CME. SW parameters are as in Fig. 1.

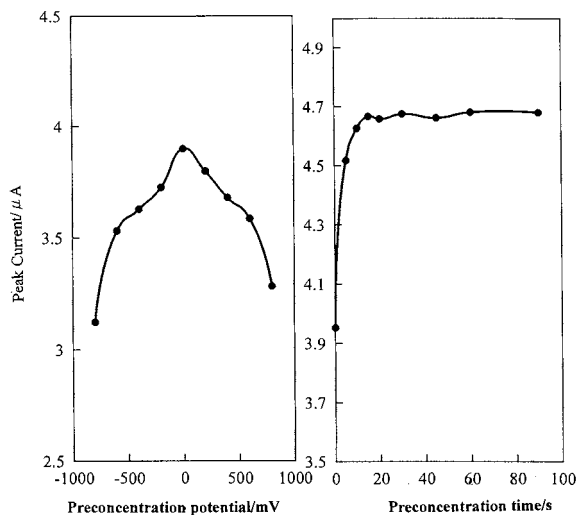


Fig. 3. The effects of preconcentration potential (a) and the preconcentration time (b) on the SW response for 20  $\mu\text{M}$  theophylline at the CME. Other conditions are as in Fig. 1.

chemical method [12]. Compare to the electrochemical method, the HPLC method is time consuming and the LC-frit-FAB-MS is not suitable for routine analysis. Enzyme immunoassay procedures are often used in therapeutic controls in hospital. The main prospect of this study is therefore to develop a good alternative method for this purpose.

The previous electrochemical method used adsorptive cathodic stripping voltammetry for the determination of trace amount of theophylline at a hanging mercury drop electrode [12]. There is an interference problem from some purine compounds and metal ions. We report here a relatively rapid and selective electrochemical method for the determination of theophylline using a Nafion<sup>®</sup>/lead–ruthenium oxide pyrochlore chemically modified electrode (CME). This work describes a combined catalytic–adsorbing interface layer to modify an electrochemical electrode surface to measure theophylline in tea and tablet formulations. The optimal experimental conditions were thoroughly investigated. Practical analytical utility was illustrated by selective measurements of theophylline in commercially available drug (ampoule of aminophylline for i.v. injection) and tea.

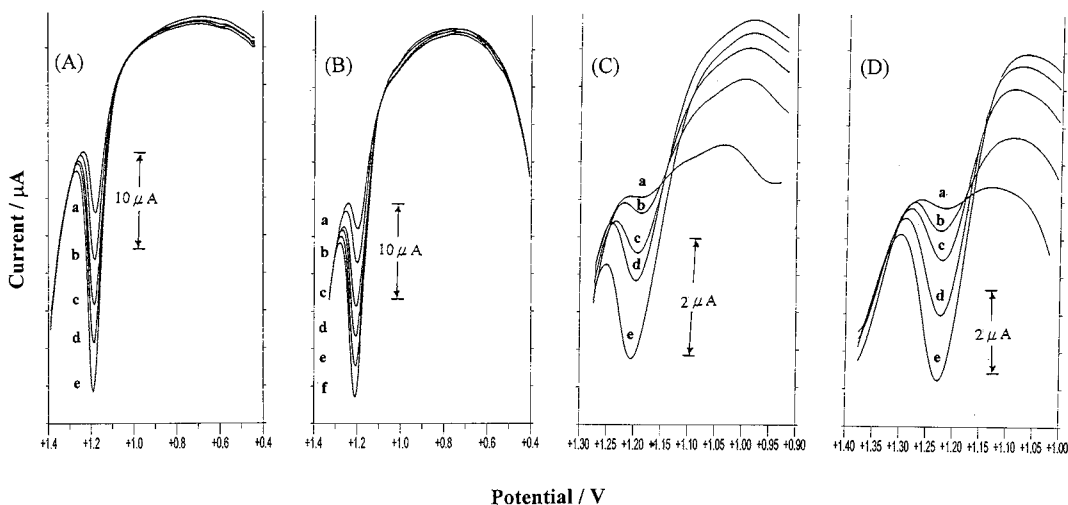


Fig. 4. Typical SW voltammetry responses for the determination of theophylline in (A) ampoule, (B) tablet, (C) black tea, and (D) green tea with spiking theophylline concentrations of (a) 0, (b) 20, (c) 40, (d) 60, (e) 80, (f) 100  $\mu\text{M}$ . Other conditions are as in Fig. 1.

## 2. Experimental

Nafion<sup>®</sup> perfluorinated ion-exchange powder, 5 wt% solution in a mixture of lower aliphatic alcohols and 10% water, was obtained from the Aldrich (Milwaukee, WI, USA). Theophylline (Aldrich) and all the other com-

pounds (ACS-certified reagent grade) were used without further purification. Aqueous solutions were prepared with doubly distilled deionized water.

Electrochemistry was performed on a Bioanalytical Systems (West Lafayette, IN, USA) BAS-50W electrochemical analyzer. A BAS VC-2

Table 1

Determination of theophylline in tea beverages\* and pharmaceutical formulation\* with the CME

	Original value ( $\mu\text{M}$ )	Spike ( $\mu\text{M}$ )	Detected value after spike ( $\mu\text{M}$ )	Recovery (%)
<i>Ampoule</i> <sup>a</sup>	40.48 $\pm$ 0.23	20	60.93 $\pm$ 0.43	102.25 $\pm$ 2.44
		40	78.33 $\pm$ 0.41	94.60 $\pm$ 1.18
		80	115.60 $\pm$ 0.67	93.90 $\pm$ 0.89
<i>Tablet</i> <sup>a</sup>	38.73 $\pm$ 0.39	40	79.23 $\pm$ 0.54	101.25 $\pm$ 1.68
		60	98.66 $\pm$ 0.78	99.90 $\pm$ 1.45
		80	118.03 $\pm$ 0.91	99.10 $\pm$ 1.24
<i>Black tea</i> <sup>b</sup>	9.20 $\pm$ 0.15	40	48.67 $\pm$ 0.68	98.68 $\pm$ 1.75
		60	67.42 $\pm$ 0.89	97.00 $\pm$ 1.50
		80	89.65 $\pm$ 1.15	100.60 $\pm$ 1.45
<i>Green tea</i> <sup>b</sup>	7.32 $\pm$ 0.15	40	45.45 $\pm$ 0.79	95.32 $\pm$ 2.00
		60	66.17 $\pm$ 0.95	98.10 $\pm$ 1.60
		80	86.16 $\pm$ 1.21	98.60 $\pm$ 1.50

<sup>a</sup> Dilution factor: 6/1000.

<sup>b</sup> Dilution factor: 1/20.

\* Number of samples assayed, 3.

electrochemical cell was employed in these experiments. The three-electrode system consisted of either a glassy carbon electrode (GCE) or a Nafion<sup>®</sup>/lead–ruthenium oxide pyrochlore CME working electrode, an Ag–AgCl reference electrode (Model RE-5, BAS), and a platinum wire auxiliary electrode. Since dissolved oxygen did not interfere with the anodic voltammetry, no deaeration was performed.

The Nafion<sup>®</sup>/lead–ruthenium oxide pyrochlore CME was prepared as follows. In brief, the GCE was first polished with the BAS polishing kit and rinsed with deionized water, then further cleaned ultrasonically in 1:1 nitric acid and deionized water successively. Nafion<sup>®</sup>, polymer was spin-coated onto a cleanly polished GCE. Lead-ruthenium oxide pyrochlore particles were then synthesized in the Nafion<sup>®</sup> matrix by treatment of Ru<sup>3+</sup>, Pb<sup>2+</sup>-exchanged polymer in alkaline aqueous solution with purging of O<sub>2</sub>. Electrode were prepared with the optimum coating solution of 1.25 wt% Nafion<sup>®</sup> at a 3000 rpm spin-coating rate. The CME was equilibrated in the test solution containing theophylline before measurement. Square-wave (SW) voltammograms were obtained by scanning the potential from +0.6 to +1.4 V (vs. Ag–AgCl) at a SW frequency of 45 Hz and SW amplitude of 30 mV. At a step height of 4 mV, the effective scan rate is 180 mV s<sup>-1</sup>. The theophylline quantitation was achieved by measuring the oxidation peak current after background subtraction.

A stock solution was prepared by dissolving 180.17 mg of theophylline in 100 ml of water. An aliquot was diluted to the appropriate concentrations with 0.1 M, pH 3.0 phosphate solution before actual analysis. Pharmaceutical samples were prepared by dissolving 2.0 ml ampoule or 1.0 g tablet in 100 ml water. They were then diluted by a factor of 6/1000 (v/v) for detection. Tea was prepared by infusion, using a tea-bag (2.0 g) immersed in 100 ml of boiling water for 3 min. It was then diluted by a factor of 1/20 (v/v). The standard addition method was used to evaluate the content of theophylline in real samples.

### 3. Results and discussion

#### 3.1. Voltammetric behavior

Fig. 1 demonstrates the catalytic function of the CME in the determination of theophylline by SW voltammetry. On scanning from +0.4 V toward a positive potential at a bare GCE, only a much smaller anodic peak at +1.26 V was observed for 20 μM theophylline (curve a). A slightly increase in anodic peak at +1.24 V was observed when a Nafion<sup>®</sup>-coated GCE was used (curve b). Whereas, a large increase in the peak current at +1.17 V was observed when the CME was used (curve c). The enhancement in current response and the shift in oxidation potential are clear evidences of the catalytic effect of the CME toward theophylline oxidation. Further investigation was made to the transport characteristics of theophylline in the CME. The linear scan voltammetry current response obtained at the CME was found linearly proportional to the scan rate, which illustrated that the process was adsorptive-controlled. More evidences for the adsorption behavior of theophylline was demonstrated by the following experiment. When the CME was switched to a medium containing only supporting electrolyte after being used in measuring a theophylline solution, the same voltammetric signal was observed.

#### 3.2. Analytical characterization

Both the electrode and the detection aspects should be considered to arrive at the optimum conditions for theophylline determination. As to the electrode aspect, the optimum conditions generally follow those used in previous studies [13–18]. The effect of pH on the voltammetric response of the CME was studied first and the results for 20 μM theophylline is shown in Fig. 2. As can be seen, the CME shows an optimum performance around pH 3. A 0.1 M, pH 3 phosphate solution is therefore used in subsequent studies. The effects of pre-concentration potential and the pre-concentration time on the SW response for theophylline were studied next. The results obtained are shown in Fig. 3(A) and Fig.



3(B), respectively. As can be seen in Fig. 3(A), the peak current increases as the potential of the electrode becomes more negative in the experimental range. This behavior is explained by the fact that theophylline bears a positive charge in pH 3 environment; as a result, the accumulation of theophylline is favoured at more negative potentials. However, the peak current drops rapidly when the potential is less than  $-0.2$  V. The decrease in the current at potentials below  $-0.2$  V is evidently caused by competition from adsorption of hydrogen. This is another evidence that the analyte is pre-concentrated by adsorption. A pre-concentration potential of  $0$  V was therefore chosen in all the subsequent work. As to the effect of the pre-concentration time, for  $20$   $\mu\text{M}$  of theophylline, the peak current increases as the pre-concentration time increases and starts to level off at around  $15$  s as shown in Fig. 3(B). It takes longer time for the peak current to level off for a lower concentration of theophylline. This phenomenon is as expected and further confirms the adsorption-controlled behavior of the CME. Therefore, in order to increase the sensitivity of detection, a longer time is needed for the lower concentration of theophylline. A pre-concentration time of  $15$  s was used in most of the subsequent work.

The peak current obtained in SW voltammetry depends on various instrumental parameters such as SW amplitude, SW frequency, and step height. These parameters are interrelated and effect the response, but here only the general trends will be examined. It was found that these parameters had little effect on the peak potential. When the SW amplitude was varied in the range of  $10$ – $50$  mV, the peak currents were increased with increasing amplitude until  $30$  mV. However, when the amplitude was greater than  $30$  mV the peak width increase at the same time. Consequently,  $30$  mV was chosen as the SW amplitude. The step height together with the frequency defines the effective scan rate. Hence, an increase with either the frequency or the step height results in an increase in the effective scan rate. The response for theophylline increases with SW frequency; however, above  $45$  Hz the peak current was unstable and obscured by a large residual current. By

maintaining the frequency as  $45$  Hz, the effect of step height was studied. At a step height of  $4$  mV, the response is more accurately recorded. Overall, the optimized parameters can be summarized as follows: SW frequency,  $45$  Hz; SW amplitude,  $30$  mV; step height  $4$  mV. The effective scan rate is  $180$   $\text{mV s}^{-1}$ .

Under optimal conditions, the SW voltammetric current response is linearly dependent on the concentration of theophylline between  $0$  and  $100$   $\mu\text{M}$  in pH 3 phosphate solution with slope ( $\mu\text{A}/\mu\text{M}$ ), and correlation coefficient of  $0.110$  and  $0.999$ , respectively. The detection limit ( $S/N=3$ ) is  $0.1$   $\mu\text{M}$ . To characterize the reproducibility of the CME, repetitive measurement-regeneration cycles were carried out in  $10$   $\mu\text{M}$  theophylline. The electrode was removed from the test solution after measurement, washed thoroughly and introduced into buffer solution and potential sweep were carried out in the same potential window several times until the original background current was regained. The results of  $15$  successive measurements show a coefficient of variation of  $1.34\%$ . Thus, the electrode renewal gives a good reproducibility surface.

### 3.3. Sample analysis

The CME was applied to the measurement of theophylline in commercially available drug and tea and typical results are shown in Fig. 4. The accuracy of the method was determined by its recovery during spiked experiments. A commercial drug of theophylline was spiked with theophylline standard solution at a concentration of  $20$   $\mu\text{M}/\text{spike}$  or  $40$   $\mu\text{M}/\text{spike}$ . The recoveries of theophylline from the drug matrices and tea matrices were satisfactory with values ranging from  $94$  to  $102\%$  and  $95$  to  $101\%$ , respectively. Confirming those quantitative and reproducible results can be obtained with this method (Table 1).

This study has demonstrated that the CME can be applied to the detection of theophylline in pharmaceutical formulation and tea with excellent sensitivity and selectivity by SWV. The CME can be easily regenerated and the detection can be achieved without deoxygenating. Significant advantages have been achieved by combining the

electrocatalytic function of the catalyst with charge exclusion and preconcentration features of Nafion<sup>®</sup>. The reliability and stability of the CME offers a good possibility for extending the technique in routine analysis of theophylline.

### Acknowledgements

The authors gratefully acknowledge financial support from the National Science Council of the Republic of China under Grants NSC 88-2113-M-005-019 and NSC 88-2113-M-005-020.

### References

- [1] J.E.F. Reynolds, Martindale: The Extra Pharmacopoeia, 29th ed., Pharmaceutical Press, London, 1989.
- [2] C. Pham Huy, B. Degez, M. Postaire, A. Vassault, M. Hamon, *Ann. Falsif. Expert Chim.* 904 (1992) 9.
- [3] D. Habel, S. Guermouche, M.H. Guermouche, *Analyst* 118 (1993) 1511.
- [4] E. Tanaka, *J. Chromatogr.* 575 (1992) 311.
- [5] J.D. Davis, L. Aarons, J.B. Houston, *J. Chromatogr.* 621 (1993) 105.
- [6] P. Dobrocky, P.N. Benett, L.J. Notarianni, *J. Chromatogr. B* 652 (1994) 104.
- [7] J. Moncrieff, *J. Chromatogr.* 465 (1989) 315.
- [8] M.L. Estelles, R.M. Saez, M.D.S. Ciges, *Talanta* 43 (1996) 1589.
- [9] Z.Y. Zhang, M.J. Fasco, L.S. Kaminsky, *J. Chromatogr. B* 665 (1995) 201.
- [10] D.A. Palmer, T.E. Edmonds, N.J. Seare, *Analyst* 117 (1992) 1679.
- [11] Y. Hieda, S. Kashimura, K. Hara, M. Kageura, *J. Chromatogr. B* 667 (1995) 241.
- [12] R.M. Shubietah, A.Z. Abu Zuhri, A.G. Fogg, *Analyst* 119 (1994) 1967.
- [13] J.-M. Zen, C.-B. Wang, *J. Electroanal. Chem.* 368 (1994) 251.
- [14] J.-M. Zen, J.-S. Tang, *Anal. Chem.* 67 (1995) 208.
- [15] J.-M. Zen, J.-S. Tang, *Anal. Chem.* 67 (1995) 1892.
- [16] J.-M. Zen, Y.-S. Ting, *Anal. Chim. Acta* 342 (1997) 175.
- [17] J.-M. Zen, I.-L. Chen, *Electroanalysis* 9 (1997) 537.
- [18] J.-M. Zen, Y.-S. Ting, Y. Shih, *Analyst* 123 (1998) 1145.

# Spectroscopic and chemical characterizations of molecular size fractionated humic acid

Hyun-Shang Shin, Jean Marc Monsallier, Gregory R. Choppin \*

*Department of Chemistry, The Florida State University, Tallahassee, FL 32306, USA*

Received 11 January 1999; received in revised form 4 May 1999; accepted 7 May 1999

## Abstract

A sample of humic acid was divided by ultrafiltration into five fractions of different molecular size (F1; 300 000: F2; 100 000–300 000: F3; 50 000–100 000: F4; 10 000–50 000: F5; 1000–10 000 daltons). Characterization by IR, and CPMAS C-13 NMR spectroscopy indicated that the molecules of the fraction of  $\geq 100\,000$  daltons were primarily aliphatic, while the smaller molecules of the  $\geq 10\,000$  dalton fraction were predominantly aromatic. Titration (pH) data were consistent with an increase in the number of carboxylate groups per unit mass as molecular size became smaller. A comparative study with unpurified and purified (by treatment with ion exchange elution, acid precipitation and alkaline dissolution) humic acid samples showed chemical alteration with some loss of carboxyl groups in the humic acid. © 1999 Elsevier Science B.V. All rights reserved.

*Keywords:* Humic acid; Aliphatic; Aromatic; Carboxyl groups

## 1. Introduction

Humic acids are heterogeneous mixtures of oxidized organic material having various molecular moieties and functional groups. The molecular sizes of humic acids are reported to range from several hundred to several hundred thousand daltons, and the chemical structures show no repetitive pattern [1,2]. Studies performed to characterize and compare various properties of the size-fractionated humic acids have found wide variation in structural features, in acidities and in binding properties for different metal ions [3–7].

It has been proposed that the aliphatic character and the apparent surface potential [4,5] increase as the molecular weight increases. The building of metal ions with different molecular sized humic acid has been investigated spectroscopically and the binding constant was shown to increase with the molecular size even though such fractions have smaller carboxylate ( $\text{meq g}^{-1}$ ) capacity [8]. These results may reflect differences in the nature of metal binding sites in different molecular size fractions and effects of changes in the three dimensional structure of the humic acid [9]. Such substantial differences among the humic acid fractions of different molecular sizes indicate the value of characterizing properly the size fractions in order to better interpret the measurements of

\* Corresponding author. Tel.: +1-850-6448277.

E-mail address: choppin@chem.fsu.edu (G.R. Choppin)

metal ion binding and transport by natural humic acids in different aqueous media.

In this work, a commercially available humic acid was fractionated, without purification to remove metal ions, into different nominal molecular size ranges using ultrafiltration. These size-fractionated humic acids were characterized using both chemical and spectroscopic methods. Emphasis was given to the identification of differences in chemical structures and functional groups in the humic acids. We also compared the characterization data (IR and NMR) of the unpurified humic acid with that of a purified humic acid from the same source. The purification of the humic acid was achieved by acid–base precipitation procedures. Comparison of the characterization data of unpurified and purified HA provides insight into chemical alteration effects of the humic acid molecules by the purification process.

## 2. Experimental

A sample of humic acid (from Aldrich Chemical Company) was fractionated into different molecular size groups by ultrafiltration [10,11] by a procedure similar to that described previously [8]. Five liters of the humic acid solution (200 mg l<sup>-1</sup> in 0.1 M NaClO<sub>4</sub> pH ≈ 7) were filtered through membranes (Diafla<sup>®</sup>, Amicon) using an Amicon Model, (8050) ultrafiltration cell, beginning with the membrane of largest pore size (nominal molecular weight cut-off: 300 000 daltons). When the volume of solution retained by the membrane was reduced to about 20 ml, filtration was stopped. The solution, containing the HA fraction with molecular weight nominally greater than 300 000 daltons was removed from the cell and the filtrate returned to the reservoir. The filtration was repeated with membranes of successively reduced pore size (molecular weight cut-offs of 100 000, 50 000, 10 000 and 1 000 daltons) to obtain humic acid fractions with different nominal molecular size which were classified as: F1, larger than 300 000; F2, 100 000–300 000; F3, 50 000–100 000; F4, 10 000–50 000; F5, 1000–10 000 daltons. The separated fractions of the humic acid were freeze-dried, weighed and stored in a desiccator prior to use.

A second sample of the original unfractionated humic acid was purified by contact with ion exchange resin and repetitive precipitation and dissolution [12]. Following the dissolution of the original sample of unfractionated HA in 0.1 M NaOH, the solution was shaken for 24 h in a polyethylene bottle with Dowex 50W-X12 (40–100 mesh), in Na<sup>+</sup> form, to remove any bound metal ions. The resin was filtered and washed with distilled water to remove the soluble humic acid. This supernatant humic acid was precipitated slowly by acidification with a solution of HClO<sub>4</sub> and, after separation by centrifugation, the solid humic acid was washed repeatedly with distilled water to remove perchlorate ions. The purified humic acid was freeze-dried, and stored in the dark until it was fractionated and characterized by the same procedures used for the unpurified HA.

The humic acid fractions were characterized by solid-state C-13 NMR measurement using the technique of cross-polarization with magic angle spinning [13]. The spectrum was collected using an IBM/Brucker WP 200SY spectrometer at a magnetic field of 50.325 MHz with a 90° pulse width of a 4.5 μs and a contact time of 1 ms. The spin rate was 4.0 kHz and the delay between pulses was 3 s. The chemical shift was measured relative to an external standard of *p-t*-butyl benzene with the shift of the methyl carbons (31 ppm relative to tetramethyl silane) assigned as 0 ppm. Infrared spectra of the humic acid fractions were recorded using samples in KBr pellets (1 mg of humic acid per 100 mg of KBr) with a Nicolet 520 FT-IR spectrometer. The KBr (FT-IR grade, Aldrich Co.) was dried by heating and was kept under vacuum in a desiccator prior to use.

All humic acid fractions were characterized by potentiometric titration, in which the carboxylate group equivalence of a sample was determined by pH measurements. About 40–50 mg of each humic acid fraction was dissolved with a sufficient amount of 0.1 M (carbonate free) NaOH in a jacketed titration cell maintained at 25°C by circulation of water from a constant-temperature bath. Nitrogen gas was passed over the solution to avoid absorption of atmospheric carbon dioxide during the titration of the HA sample from a pH of about 11.5 to one of about 2.3 with 0.04 M

HClO<sub>4</sub> at total ionic strength of 0.1 M. The titration was performed by an automatic titrator, consisting of a model 950 Accumet Fisher digital pH-meter, a model 665 Metrohm digital autoburette and a glass electrode (Corning) filled with saturated NaCl.

### 3. Results and discussion

Table 1 lists the percent by weight of the five humic acid samples obtained from the fractionation process for both the unpurified HA and purified HA. The yields of the fractions with molecules of large size (more than 100 000 daltons) was reduced in the purification process. In an additional experiment, a sample of the F1 fraction of unpurified Ha was purified using the acid–base precipitation procedure with ultrafiltration through a membrane of 300 kDa pore size (mwco: 300 000 daltons). The result was that  $\approx 85\%$  of this purified HA passed through the filtering membrane. This suggests that some of the molecules on the original fraction  $> 300$  kDa were degraded, possibly by rupture of hydrogen bonds, to the molecules of smaller size during the purification procedure of acid–base precipitation which is commonly used to isolate and purify humic acid from soil and water [14]. The size–fractionation of humic acid samples has been shown to be related to the ionic medium [1]; accordingly, these data are related to 0.10 M NaClO<sub>4</sub> solutions.

Fig. 1 shows the IR spectra of the five humic acid fractions of different nominal molecular size and of unfractionated, unpurified humic acid. Absorption bands characteristic of humic acid [15]

Table 1

Size fraction (kDa)	Unpurified HA (wt%)	Purified HA (wt%)
F1 (>300 kDa)	19.9	14.0
F2 (100–300 kDa)	14.1	10.0
F3 (50–50 kDa)	4.2	5.7
F4 (10–50 kDa)	34.3	42.2
F5(1–10 kDa)	27.5	28.3

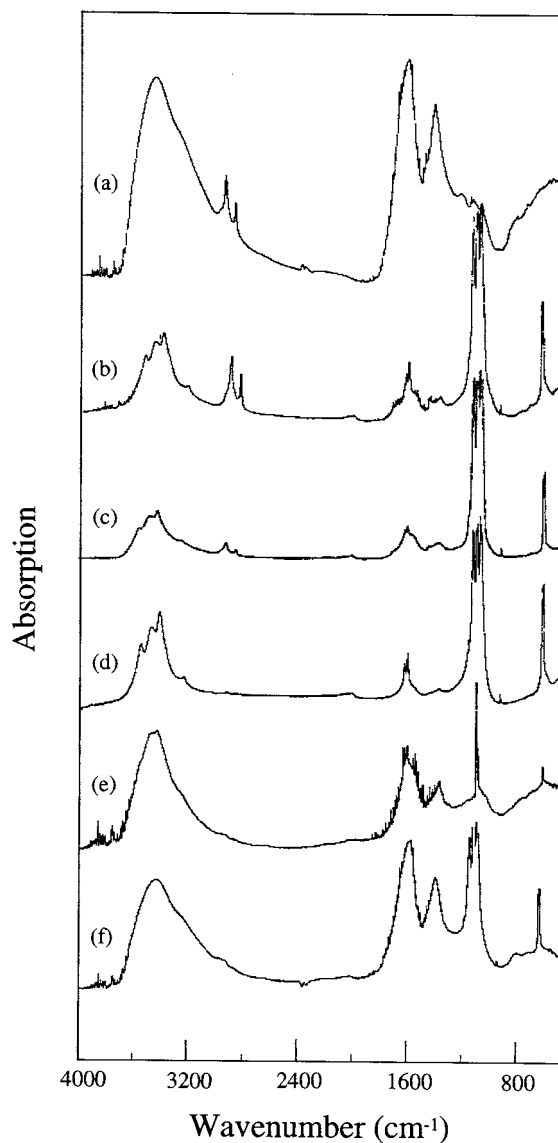


Fig. 1. Infrared spectra of unpurified humic acids of different molecular size ranges. (a) Unfractionated, (b) F1 (> 300 kDa), (c) F2 (100–300 kDa), (d) F3 (50–100 kDa), (e) F4 (10–50 kDa), (f) 1–10 kDa.

are observed in the IR spectra in the regions of 3400 cm<sup>-1</sup> (H-bonded OH stretching of carboxyl, phenol and alcohol), 2900 cm<sup>-1</sup> (aliphatic C–H stretching), 1600–1650 cm<sup>-1</sup> (C=O stretching of COO<sup>-</sup>, ketonic C=O and aromatic C=C conjugated with COO<sup>-</sup>), 1400 cm<sup>-1</sup> (aliphatic C–H

bending and  $\text{COO}^-$  asymmetric stretching). The relative peak intensities, reflecting the relative amount of each functional group differ for the different samples. The spectra of the F1 and F2 fractions (Fig. 1b–c) showed that bands centered around  $1620\text{ cm}^{-1}$  and  $3400\text{ cm}^{-1}$  (carboxylate groups and aromatic rings) are considerably lower in relative intensity while the bands around  $2910\text{ cm}^{-1}$  (aliphatic groups) is relatively stronger. In contrast, the spectra of the F4 and F5 fractions of smaller size (Fig. 1e–f) have relatively strong bands around  $1620\text{ cm}^{-1}$  and very weak bands at  $2910\text{ cm}^{-1}$ . These results are consistent with a greater aliphatic nature for the humic acid fractions of larger molecular size, whereas the content of aromatic and carboxylate groups are relatively higher in the smaller size fractions. A band centered around  $1050\text{--}1150\text{ cm}^{-1}$  was observed in all the spectra of the fractionated humic acids, but was not in the spectrum (Fig. 1a) of the unfractionated humic acid. This band may reflect the presence of Si–O bonds due to contamination during the ultrafiltration procedures in which the

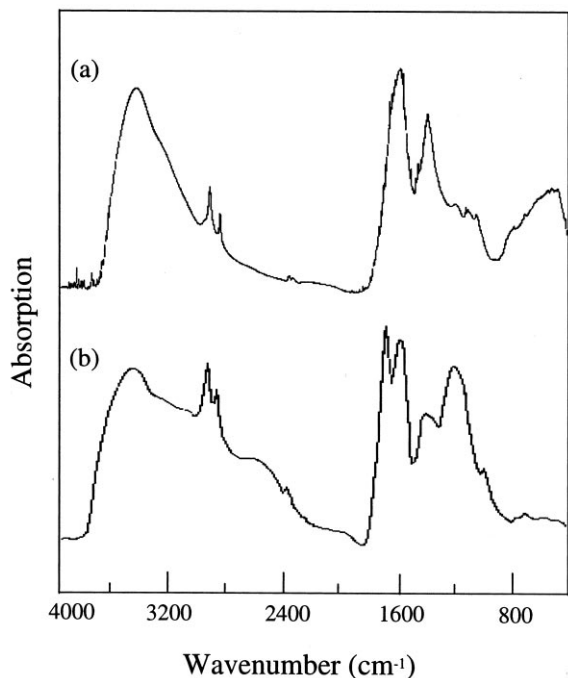


Fig. 2. Infrared spectra of the unfractionated humic acid: (a) unpurified (same as Fig. 1a); (b) purified.

solutions of humic acid were in the fiberglass reservoirs of the filtration unit for several days.

The IR spectra of unfractionated samples of purified HA and unpurified HA are shown in Fig. 2 for comparison. The carboxylate band at  $1610\text{ cm}^{-1}$  of unpurified HA is shifted in frequency to  $1720\text{ cm}^{-1}$  indicating that the carboxylate groups are protonated. The two bands from carbonyl groups at  $1720$  and  $3400\text{ cm}^{-1}$  in the spectrum of purified HA are decreased in intensity, indicating that the purified humic acid molecules contain a lower relative concentration of carboxyl groups than those of unpurified HA.

The solid-state C-13 NMR spectra of the five humic acid fractions and of unfractionated, unpurified HA are shown in Fig. 3. These spectra of the humic acids contain strong peaks at  $0\text{--}90\text{ ppm}$  (aliphatic carbons), broad peaks at  $110\text{--}160\text{ ppm}$  (aromatic carbons) and  $160\text{--}190\text{ ppm}$  (carboxyl carbons) [16,17]. This suggests that the bulk properties of the carbon functionalities of each humic acid fraction are similar to one another. However, the relative intensities of the different carbon shifts in the spectra differ significantly in the humic fractions. The spectral data of the humic acids were analyzed quantitatively, according to the manner described in the literature [13], which divides these spectra into three regions as in Table 2. Such division of the spectra into three regions is somewhat arbitrary, and the absence of well defined line shapes in some cases results in estimated uncertainties of  $\pm 8\%$  from three replicate measurements. The averaged values are presented in Table 2 as is the ratio of aromatic versus aliphatic carbon. These values indicate that the F1 and F2 fractions with molecules of large size contain humic molecules which are predominantly aliphatic with small amounts of aromatic and carboxyl carbons. By contrast, the F4 and F5 fractions with molecules of much smaller size have much higher contents of aromatic and carboxyl carbons and lower levels of aliphatic carbons. These findings agree with the results obtained from the IR spectra and the HA fractions.

Fig. 4 shows the CPMAS C-13 NMR spectra of the unfractionated humic acids of both unpurified and purified HA. The results of quantitative anal-

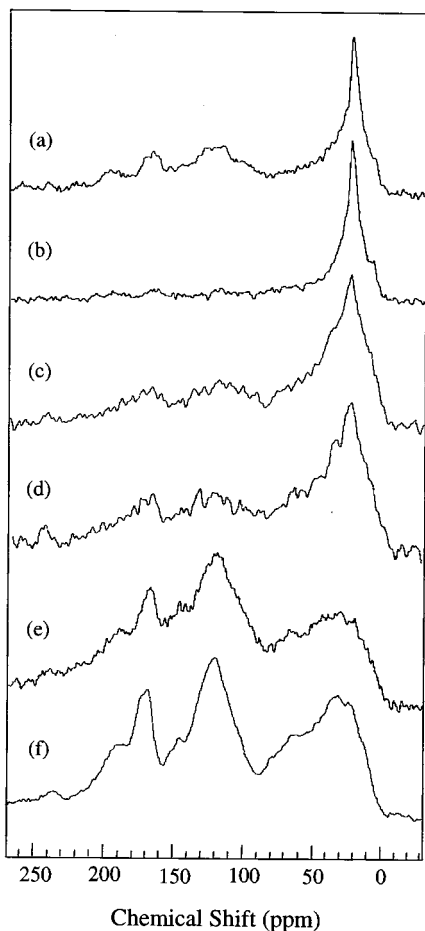


Fig. 3. Solid state C-13 NMR spectra of unpurified humic acids of different molecular size ranges. (a) unfractionated; (b) F1 (> 300 kDa), (c) F2 (100–300 kDa), (d) F3 (50–100 kDa), (e) F4 (10K5–50 kDa), (f) K5 (1–10 kDa).

ysis of these spectra was listed in Table 2. Compared with unpurified HA, the intensity of the

Table 2

The relative intensities of different type carbons in humic acids determined by solid state C-13 NMR spectroscopy

Humic acid	Size fraction (kDa)	C <sub>aliphatic</sub> (0–90 ppm)	C <sub>aromatic</sub> (110–160 ppm)	C <sub>carboxyl</sub> (160–190 ppm)	C <sub>arom</sub> /C <sub>alip</sub>
Unpurified HA	Unfractionated	55 ± 2	31 ± 2	14 ± 1	0.56
	F1 (> 300 kDa)	89 ± 2	7 ± 2	4 ± 1	0.08
	F2 (100–300 kDa)	71 ± 2	20 ± 2	9 ± 1	0.28
	F3 (50–100 kDa)	66 ± 2	23 ± 2	10 ± 1	0.33
	F4 (10–50 kDa)	43 ± 2	41 ± 2	16 ± 2	0.95
Purified HA	F5 (1–10 kDa)	43 ± 2	40 ± 2	17 ± 1	0.93
	Unfractionated	57 ± 2	34 ± 2	9 ± 1	0.60

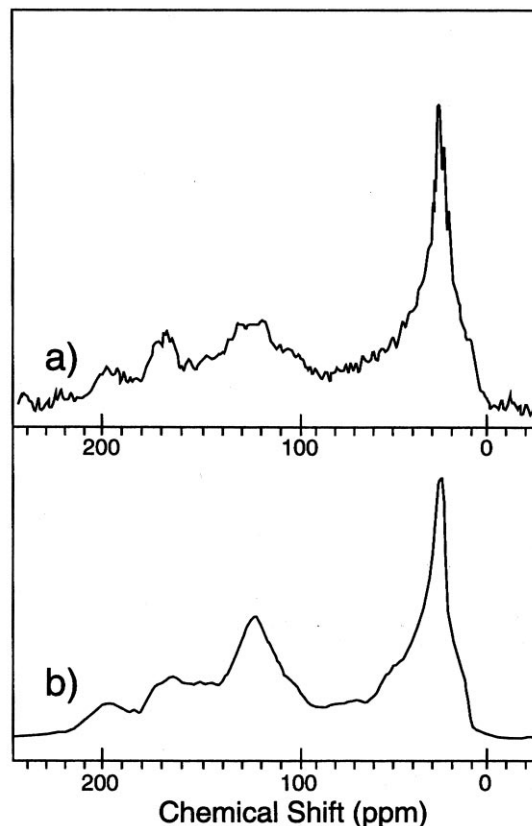


Fig. 4. Solid-state C-13 NMR spectra of unfrac-tionated humic acid: (a) unpurified (same as Fig. 1a); (b) purified HA.

carboxyl carbons of purified HA was considerably reduced (13 vs. 9%). This could indicate that some portion of the carboxyl carbons in unpurified HA were dissociated and removed during the purification procedure [3,18]. Such a loss of carboxyl carbons during purification is also consistent

with the differences in the results in the IR spectra.

From the first derivative plots of the pH titration curves, the carboxylate group equivalencies and  $pK_a$  values of the five fractions of purified HA were determined. The  $pK_a$  values were found to be dependent on the degree of ionization ( $\alpha$ ) of the carboxylic acid groups in the humic acids. Table 3 lists the calculated equivalencies of carboxylate groups and their  $pK_a$  values at  $\alpha = 0.5$  for the humic acids (the uncertainties are estimated from the titration curve analysis). As the molecular sizes of HA in the fractions decrease, the carboxylate group equivalencies are seen to increase while the average  $pK_a$  values decrease. Thus, the humic acids molecules of smaller size have a higher content of carboxyl groups and are stronger acids. The IR and C-13 NMR data and reports from other studies [4,8] agree with these observations.

#### 4. Conclusion

In this work, we have conducted chemical and spectroscopic characterizations of a commercial humic acid (Aldrich) fractionated into different molecular size ranges by ultrafiltration, and have identified certain differences between the fractions with molecules of larger size ( $> 100$  kDa) and the fractions with molecules of smaller size ( $< 10$  kDa). One such difference is that the fractions are comprised of molecules of larger size and more aliphatic in nature, while the frac-

tions with molecules of smaller size are more aromatic and have a higher content of carboxyl groups. Such differences in the structural characteristics and functional group contents of the humic acids affect their solubility and binding ability for metal ions. We have also observed that humic acid undergoes certain chemical change during purification procedures using acid–base precipitation. These results suggest that a milder method is needed to isolate humic materials from soil and water in order to purify them with minimal or no alteration.

#### Acknowledgements

This research was supported by F.S.U. by a grant from the USDOE-OBES Division of Chemical Sciences. H.S.S. is grateful for a Fellowship from the Korea Science and Engineering Foundation (KOSEF). The assistance of D. Gormin and B. van de Burgt with the luminescence measurements is gratefully acknowledged.

#### References

- [1] R.S. Swift, Humic substances in soil, sediment and water, in: G.R. Aiken, D.M. McKnight, R.L. Wershaw, P. McCarthy (Eds), Wiley, New York, 1985, p. 387.
- [2] F.J. Stevenson, Humus Chemistry, Genesis, Compostion, Reactions, Wiley, New York, 1994, p. 285.
- [3] N.A. Marley, J.S. Gaffney, K.A. Orlandini, K.C. Picel, G.R. Choppin, Sci. Total Environ. 113 (1992) 159.
- [4] M. Fukushima, S. Tanaka, H. Nakamura, S. Ito, Talanta 43 (1996) 383.
- [5] S.A. Green, F.M.M. Morel, N.V. Blogh, Environ. Sci. Technol. 26 (1992) 294.
- [6] H.S. Shin, S.W. Rhee, B.H. Lee, H. Moon, Org. Geochem. 24 (1996) 523.
- [7] H. Zunino, J.P. Martin, Soil Sci. 123 (1977) 188.
- [8] K. Rao, G.R. Choppin, Radiochim. Acta. 69 (1995) 87.
- [9] G.R. Choppin, S.B. Clark, Marine Chem. 36 (1991) 27.
- [10] J. Buffle, P. Deladdy, W. Haerdi, J. Inorg. Nucl. Chem. 35 (1973) 4255.
- [11] P. Burba, V. Shkinev, B.Y. Spivakov, Fresenius J. Anal. Chem. 351 (1995) 74.
- [12] K.L. Nash, G.R. Choppin, J. Inorg. Nucl. Chem. 42 (1978) 1045.

Table 3  
Carboxyl group concentrations and  $pK_{a(\text{avg})}$  ( $\alpha = 0.5$ ) values for HA fractions

Size fraction (kDa)	-COOH (meq g <sup>-1</sup> HA)	Average $pK_{a(\text{avg})}$ ( $\alpha = 0.5$ )
Unfractionated	4.38 ± 0.05	4.26 ± 0.03
F1 (>300 kDa)	2.50 ± 0.11	5.04 ± 0.10
F2 (100–300 kDa)	3.31 ± 0.05	4.67 ± 0.03
F3 (50–100 kDa)	3.68 ± 0.04	4.61 ± 0.03
F4 (10–50 kDa)	4.77 ± 0.02	4.40 ± 0.01
F5 (1–10 kDa)	5.75 ± 0.05	3.67 ± 0.03



- [13] R.L. Wershaw, M.A. Mikita, *NMR of Humic Substances and Coal*, Lewis Publishers, Michigan, 1987.
- [14] E.M. Thurman, R.L. Malcolm, *Environ. Sci. Technol.* 15 (1981) 463.
- [15] F.J. Stevenson, K.M. Goh, *Geochem. Cosmochim. Acta* 35 (1971) 471.
- [16] M.A. Wilson, P.F. Barron, A.H. Gillan, *Geochem. Cosmochim. Acta* 45 (1981) 1743.
- [17] K.A. Throne, *Humic Substances in the Susewanee River, Georgia; Interactions, Properties, and Proposed Structures*, in: R.C. Avertt, J.A. Leenheer, D.M. McKnight, K.A. Throne, (Eds.), *US Geological Survey Open-File Report 87–557*, Colorado, 1989, p. 251.
- [18] F.J. Stevenson, *Humus Chemistry, Genesis, Composition, Reactions*, Wiley, New York, 1994, p. 24.

# Simultaneous determination of Cu, Cd and Pb in drinking-water using W-Coil AAS

Arthur Salido, Bradley T. Jones \*

*Department of Chemistry, Wake Forest University, Winston-Salem, NC 27109-7486, USA*

Received 21 January 1999; accepted 7 May 1999

## Abstract

An inexpensive, multi-element, W-coil atomic absorption spectrometer has been developed. Atomization occurs on W-coils extracted from commercially available slide projector bulbs. The system has minimal power requirements, 120 ACV and 15 A. A small, computer controlled CCD spectrometer is used as the detector. A multi-element Cu, Cd and Pb hollow cathode lamp is used as the source. 20  $\mu\text{l}$  volumes are deposited on the coil and atomized at 6.7 A or approximately 2200°C. Cu, Cd and Pb were simultaneously determined in tap water, drinking water and a quality control sample. The instrument detection limits are 0.8, 0.2 and 3.0  $\mu\text{g/l}$  for Cu, Cd and Pb, respectively. © 1999 Elsevier Science B.V. All rights reserved.

*Keywords:* W-Coil atomic absorption spectrometer; Multi-element Hollow Cathode Lamp; Drinking water

## 1. Introduction

### 1.1. Drinking water analysis

The Safe Drinking Water Act of 1974 was established as a means to ensure the safety of the public drinking water supply [1]. It was amended in 1986, and it requires the EPA to establish regulations for 83 drinking water contaminants including Pb, Cu and Cd [2]. For each chemical, the EPA develops a maximum contaminant level goal (MCLG) based purely on the health effects of the contaminant. An enforceable standard,

called the maximum contaminant level (MCL), is established as close to the MCLG as possible. The MCL takes into account other factors such as economic impact and analytical capabilities [3].

The current MCL's for Pb, Cu and Cd are 0.015, 1.3 and 0.005 mg/l, respectively. In the area of atomic spectroscopic analysis, a variety of techniques have been proposed that are capable of determining the three elements at their respective MCL's. For instance, flame atomic absorption spectrometry (FAAS) has been used in conjunction with preconcentration procedures that offer detection limits in the sup-ppb range [4,5]. Additionally, FAAS without preconcentration has been used with the result of slightly higher detection limits [6,7]. Inductively coupled plasma

\* Corresponding author. Tel.: +1-336-7585512; fax: +1-336-7583889.

*E-mail address:* jonesbt@wfu.edu (B.T. Jones)

atomic emission spectrometry (ICP-AES) has also been utilized, with detection limits similar to those found with FAAS [6,8,9]. Inductively coupled plasma mass spectrometry (ICP-MS) has proven to be a powerful technique with detection limits of approximately 10 ng/l [9,10]. Of these methods, graphite furnace AAS (GFAAS) may be the most ubiquitous when it comes to trace determinations in a variety of samples. Detection limits for most metals generally lie in the 0.1–15 pg [6,11] range and with preconcentration, these detection limits can be reduced substantially [12]. GFAAS systems can often produce the same signal as ICP-MS for a given solution using a much smaller sample volume. The graphite furnace is capable of analyzing very small (10  $\mu$ l) discrete sample volumes. In most cases, the other techniques require volumes on the order of ml.

However, there are several limitations to all techniques mentioned in terms of system cost and complexity. For example, a typical ICP-MS instrument can cost over \$100 000. Graphite furnace instruments are less expensive (\$50 000) but still may be prohibitively costly. Cost may be a concern for small water supply companies wishing to analyze their own water instead of hiring an outside source. An inexpensive instrument would be well-suited for a small company wishing to perform in-house analyses. With respect to system complexity, an instrument without elaborate sample treatment methods, especially those requiring preconcentration columns, may keep system costs down and reduce the number of variables to address. More importantly, several of the mentioned techniques require a separate analysis for each element. This can drastically increase analysis time, which may be severe when each element requires unique operating parameters. The development of an inexpensive GFAAS system for the simultaneous determination of Pb, Cu and Cd is unlikely for three reasons. First of all, GFAAS has long been considered a single-element technique. Currently available systems employ single-element lamps and single photomultiplier tube detectors. Secondly, the graphite furnace atomization system is inherently expensive, requiring a high current power supply. Finally, current GFAAS systems are very complex, due to the

transient nature of the signal and the sophisticated background correction techniques that must be employed.

## 1.2. Multi-element AAS

Traditional AAS lamps are single-element light sources. To perform the determination of more than one element requires the positioning of different lamps into the optical train. To accommodate this necessity, some commercial instruments have rotating carousels that may hold as many as 16 different lamps. A different lamp can be positioned into the light path, and a new analytical wavelength can be selected by the detector/monochromator in as little as 3 s [13]. With a flame atomizer, 16 elements can be determined in less than 1 min. Unfortunately, such an approach is not feasible when furnace atomization is required due to the transient nature of the furnace atomizer signal.

During the past 20 years several research groups have explored the possibility of using continuum sources, such as the xenon arc lamp, for simultaneous multi-element GFAAS measurements [14–16]. While this approach is feasible and projected instrument costs are low, it has not become commercially available. A relatively inexpensive high resolution echelle monochromator can be used to fully resolve the atomic absorption profile. Any light falling on the detector outside of the absorption profile will behave as stray light and will cause reduced sensitivity and deviation from Beer's law [17], but this effect can be corrected. Light throughput using a continuum source is equal to or better than that for a hollow cathode lamp, and the continuum sources are priced only about 2–3 times more than an HCL. But the question is one of economics: most instrument companies forecast that any new sales generated by multi-element continuum source AAS systems would not cover their development costs.

In view of the multi-lamp and continuum source limitations listed above, the ideal emission source for simultaneous Pb, Cu and Cd determinations by AAS might well be a multi-element line source. In this case, a single source would emit radiation at several different analytical wave-

lengths. Also, since this source will produce narrow line spectra, rather than the broad band emitted by continuum sources, a high resolution monochromator will not be necessary.

Multi-element hollow cathode lamps have been available commercially for some time [18]. These sources are useful for certain combinations of metals which can form an alloy. As many as six elements may be present in a single lamp. For lead, copper and cadmium, a multi-element lamp consisting of Pb/Cu/Cd/Zn is available. There are several disadvantages of multi-element lamps. Some metal combinations are not available, intensities are not uniform, and every multi-element lamp (at a set current) will have a reduced intensity due to the reduced mass of each metal in the cathode. Increased intensities can be achieved with greater lamp currents at a cost of sensitivity (broadened emission lines) and reduced lamp life. These disadvantages are compensated in the current system: (1) only a single set of elements is required for the dedicated system, and that set is available in a multi-element HCL; (2) intensities are 'equalized' for each element using an absorbing filter solution; and (3) intensities are increased by using a high throughput detection system in combination with normal lamp currents.

The simultaneous determination of Pb, Cu and Cd by atomic absorption spectrometry will require the use of a multi-channel detector. Several types of multi-channel detectors have recently been employed in atomic absorption spectrometry. They include multiple photomultiplier tube (PMT) systems [14,15], the photodiode array (PDA) detector [16], the charge injection device (CID) detector [19], and the charge-coupled device (CCD) detector [20]. Until the recent availability of a CCD detector mounted on a PC card, each of these detectors required a separate power supply and controller that added expense and complexity to the system. The proposed system will be small and capable of performing simultaneous determination of Pb, Cu and Cd by using a multi-element hollow cathode lamp along with the CCD detector mounted on a PC card.

### 1.3. *W-Coil AAS*

Conventional atomic absorption spectrometers employ either the graphite furnace or an acetylene flame as the sample atomizer. Neither furnace nor flame AA is feasible in a compact instrument: the furnace requires a large, expensive power supply, and the flame requires large amounts of flammable gases. The feasibility of an inexpensive, small, portable instrument depends upon the availability of a low cost, low power atomizer with sensitivity approaching that of the graphite furnace.

A low-cost W coil atomizer which uses the filament originally produced with high precision from the halogen bulbs of photo-projectors was first demonstrated by Berndt and Schladach, and has since been described in several articles [21–26]. These filaments are produced in mass to very strict optical specifications, and they require a simple 150 W power supply. For example, at 15 V and 10 A the filament reaches a temperature of 3000°C, well above the normal atomization temperatures for Pb, Cu and Cd. The atomizer is applicable to most elements that can be determined by the graphite furnace, but there are some limitations. Most non-volatile elements (V, Ta, Mo) are difficult to determine because of contamination in the coil or because, at high temperature, they form amalgams with the coil. The coil has also been highly subject to matrix interferences, and it has been most successful with relatively pure solutions (like drinking water). In addition, the analytical signals are often very rapid (with a half-width less than 0.5 s) requiring fast detector electronics. Nevertheless, for the more volatile elements, such as Pb, sensitivities better than those reported for GFAAS have been observed [25,26]. One would therefore expect detection limits for these metals to be on the order of 0.2 µg/l, well below the MCL for Pb in water. Sample volumes up to 50 µl can be atomized by the filament. Using the W-coil atomizer, better than 95% accuracy was found for the elements in water, bovine liver, pig kidney, rice flour, and blood [21,22,24,26]. With the proposed system, W-coil atomization is adapted for simultaneous Pb, Cu and Cd determinations in drinking water.

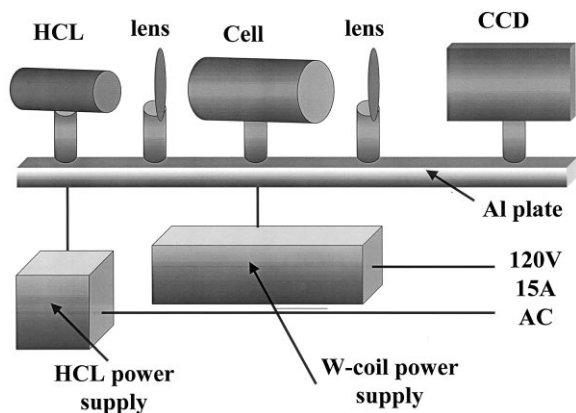


Fig. 1. W-Coil atomic absorption spectrometer schematic (personal computer and PC-connections not shown).

## 2. Experimental

### 2.1. Apparatus

The major components and electrical organization of the W-coil atomic absorption spectrometer are represented by Fig. 1. A multi-element Pb, Cu and Cd hollow cathode lamp operated at 12 mA serves as the light source. The HCL radiation is

focused through a 2.5 cm (5 cm focal length) fused silica lens to a point 2 mm above the W-coil which is housed in an ACE glass cell (Vineland, NJ part # 7488-383). After exiting the cell, light is focused through another fused silica lens to a 10  $\mu\text{m}$  entrance slit of an Ocean Optics S2000 Spectrometer. The spectrometer plugs into a PC or notebook computer PCMCIA slot using a DAQ-700 card. All the components pictured are mounted on a 35 cm optical rail.

The multi-element lamp emission signal warranted a modification before analyses could commence. The Cu line emission intensity is ten times or greater than the Pb and Cd lines. Thus, keeping the Cu line on the spectrometer scale severely reduces the Pb and Cd intensities. It is vital to maximize the signal level since the signal to noise (S/N) ratio increases with the square root of source intensity in a shot noise limited system. It is beneficial to equalize the peak intensities and maximize their signals as much as possible. Thus, a cuvette containing a filter solution (approximately  $5 \times 10^{-7}$  M 6-(dimethylamino)fulvene in acetonitrile) was placed in the light path in front of the detector. The filter solution absorbs UV light strongly in the 324 nm Cu region and weakly

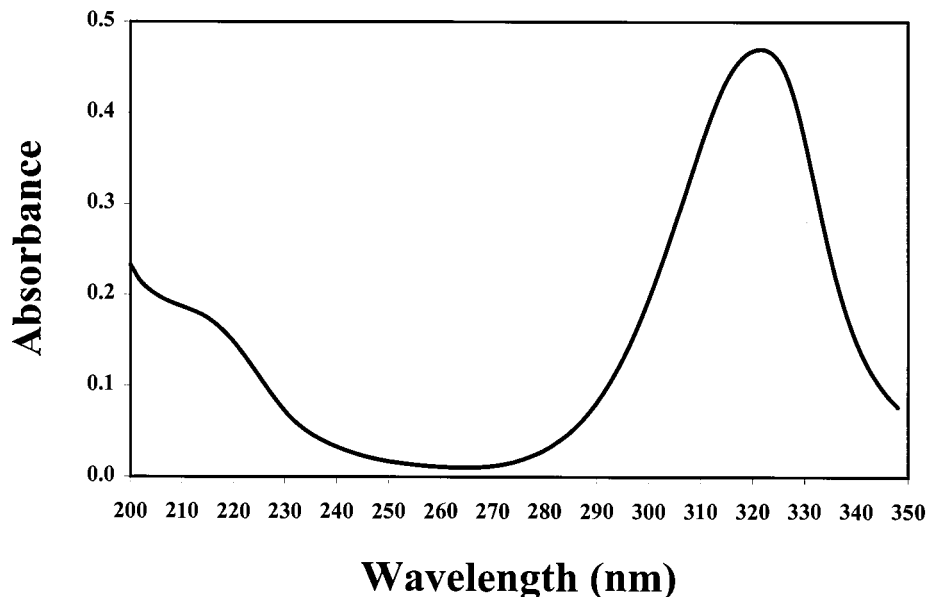


Fig. 2. UV-Vis spectrograph of a filter solution containing approximately  $5 \times 10^{-7}$  M 6-(dimethylamino)fulvene in acetonitrile.

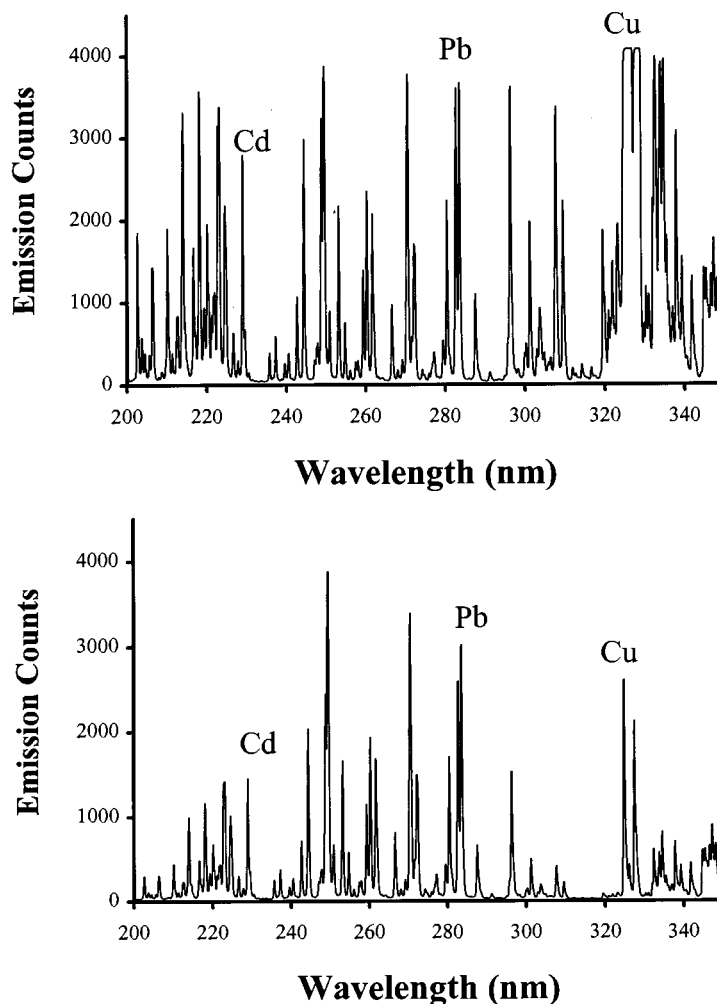


Fig. 3. Top, HCL spectrum without the filter solution in front of the detector slit; bottom, HCL spectrum after insertion of the filter solution.

in the Pb 283 and Cd 228 nm region. Fig. 2 shows a transmission profile of a filter solution (Hewlett Packard UV–Vis Diode Array Spectrophotometer) comparable to that used in the AA experiments. The lamp emission profile before and after insertion of the cuvette is pictured in Fig. 3. The plots show that the Pb, Cu and Cd signals have been nearly equalized.

#### 2.1.1. Atomization cell

The atomization cell schematic is pictured in Fig. 4. The cell is sealed on both ends with quartz windows contained in # 25 sized nylon bushings

which screw into each end of the cell. The W-coils are procured by breaking the glass exterior of a common slide projector bulb, leaving the bulb base intact. Typically, Osram BRJ or General Electric EVB bulbs are used. The bulbs are rated at 15 V and 150 W and are capable of a temperature of 3000°C at full power. The W-coil fits into a ceramic bulb mount (diameter = 19 mm, Gray Supply Company, Chicago, IN part # ORX6350) which is epoxied into an Al cylinder (2.5 × 5 cm) along with a 3 mm o.d. segment (45 cm) of polyethylene (PE) tubing. A continuous 10% $H_2$ /Ar purge (50 ml/min) is introduced through the

PE tubing to prevent coil oxidation and to maintain a reducing environment during atomization. The Al cylinder containing the coil mount and purge tubing fit snugly into a #25 sized nylon bushing that screws into the bottom of the cell perpendicular to the light path. The glass atomization cell also contains a 10/18 ground glass joint 120° from the cell mount. This port enables sample introduction and gas exhaust.

### 2.1.2. Power control

The W-coil power supply consists of a line filter (Vicor, Andover, MA part #07818), harmonic attenuator module (part VI-HAM, Vicor) and a current source module (part BatMod, Vicor). These three components are mounted in a separate case (dimensions of 10 × 20.5 × 30 cm) which weighs less than 1 kg. The case contains connections for computer control input, coil output and 120 ACV external power. The incoming 120 ACV is passed through the line filter to the harmonic attenuator module which converts the 120 AC line voltage to 240 DCV. The voltage is reduced to 12 DCV using the current source module. Using a Computer Boards 2 channel D/A converter, a range of 0–5 DCV is sent from the computer to the current source module which adjusts the output current to the coil and subsequently adjusts the temperature. A Qbasic program was written

to control the DAC outputs. An ammeter placed between the current source module output and the coil displays the coil current. The second channel of the DAC sends out 5 V to trigger the spectrometer data acquisition. A 250 DCV power supply (Acopian, 8 × 9 × 13 cm, model #U420Y10) powers the HCL. A rheostat (Ohmite, part #PFE5K6R80) adjusts the HCL current. An ammeter displays the HCL operating current which is typically 12 mA.

An Ocean Optics S2000 CCD spectrometer is the most compatible detector for the system since it is small (12.5 × 15 × 2.5 cm) and inexpensive. The CCD covers a spectral range of 200–350 nm. It is configured with an 1800 lines/mm grating which yields an optical resolution of about 0.6 nm (FWHM) and a relative linear dispersion of 8.8 nm/mm. The detector requires 128 mA of current at 5 DCV so it is conveniently powered by the PC. The current system uses a 500 KHz DAQ-700 A/D card which plugs into a PCMCIA slot as mentioned previously. The maximum possible detector integration time, without saturation of the detector at 4000 counts, is 30 ms (Fig. 3). To improve S/N, three 30 ms spectra are averaged for a final integration time of 90 ms. In this manner, eleven data points are collected per s (Fig. 5). Data was collected using the manufacturer's software.

Data files were stored and later opened using an Excel macro written in Visual Basic. The macro imports raw data and plots the absorption profile of the Pb 283.3; Cu 324.7 and Cd 228.8 nm lines, calculates the integrated absorbance ( $A_i$ ) and copies the  $A_i$  value of all samples to a separate sheet.

### 2.2. GFAAS Comparison

A GBC 902 D<sub>2</sub>-corrected graphite furnace spectrophotometer was used to monitor W-Coil AAS performance. Pyrolytically coated tubes and platforms were used for Pb and Cd determinations. For Cu, better results were obtained without platforms. Background correction was used with all samples (20 µl volume).

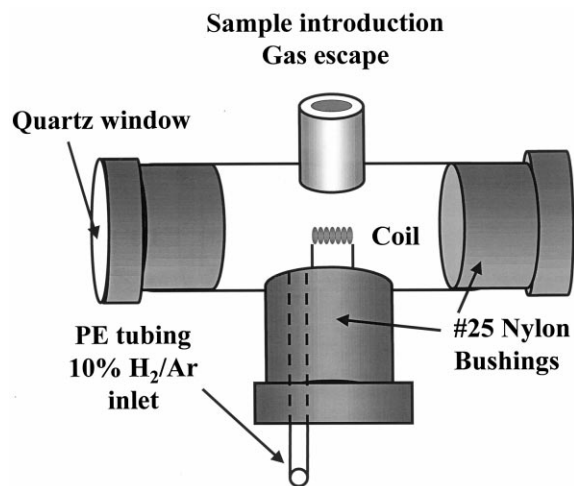


Fig. 4. Atomization cell schematic.

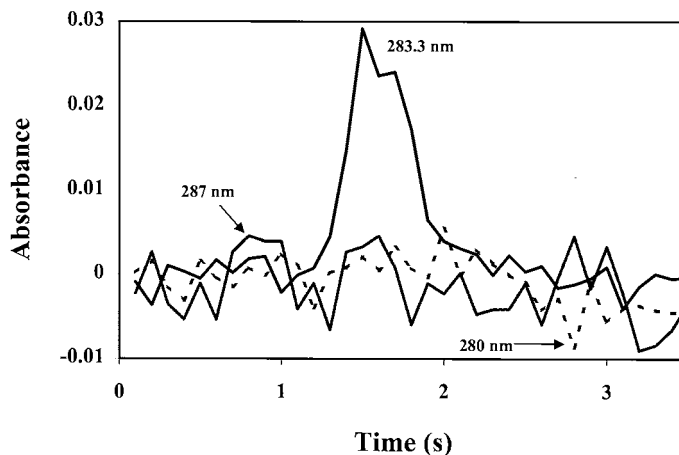


Fig. 5. Pb absorption of a 40  $\mu\text{g/l}$  spiked tap-water sample at the 283.3 nm analytical line and two non-absorbing Pb lines (280 and 287 nm).

### 2.3. Sample preparation

Spex Plasma standard solutions were diluted with distilled de-ionized (DDI) water to prepare calibration standards. Spiked tap-water was obtained from a normal tap dispenser. The tap water was collected in the morning after sitting in the pipes overnight. The tap was opened at full flow and was emptied into an acid-washed Nalgene 1 l flask. Tap water was spiked with diluted Spex standard solution for final concentrations of 40 (Pb), 15 (Cu) and 5 (Cd)  $\mu\text{g/l}$ . This collection–spike process was repeated a total of three times. ‘Primary drinking water metals’ sample for Cd and Pb (High Purity Standards, Charleston SC, Cat. #DWPS) and ‘secondary drinking water metals’ for Cu (High Purity Standards, Charleston, SC, Cat. #DWSS) were mixed 1:1 and diluted with DDI water to concentrations appropriate for GFAAS and W-coil determination. This procedure was repeated three times. Three ‘ULTRA-check metals sample’ (QCI-701, ULTRA Scientific, North Kingston, RI) were diluted according to manufacturer’s directions and further diluted to fit the instrument linear dynamic range.

### 2.4. Heating programs

20  $\mu\text{l}$  of each sample were deposited on the W-coil or in the furnace and subjected to the programs listed in Table 1. The W-coil programs were longer than GFAAS in order to prevent sample sputtering during the dry step. Typically, the samples were dried at 2.2 A for 3 min. At higher currents, the temperature was approximated by [27]:

$$T = 309 (I) + 325$$

where the temperature ( $T$ ) in Kelvin is related to the applied coil current ( $I$ ) displayed by the ammeter. It should be noted that this relationship is valid for currents between 4.5 and 8 A. During the drying step, while liquid is on the coil, the temperature–coil relationship does not hold, and it is estimated that the sample temperature is near the boiling point of water. Prior to atomization, the coil current was reduced to 0.0 A for 10 s, and then the current was stepped immediately to 6.7 A. Sharper peaks were observed when this step was employed. During sample atomization, a higher temperature is optimum for Cu whereas a lower temperature suits Cd atomization, so a compromise at 6.7 A was used corresponding to a temperature slightly greater than 2200°C. Tung-



Table 1  
Graphite furnace and W-coil heating programs

GFAAS														
Pb					Cd					Cu (no platform)				
<i>T</i>	Ramp	Hold	Ar	Read	<i>T</i>	Ramp	Hold	Ar	Read	<i>T</i>	Ramp	Hold	Ar	Read
(°C)	(s)	(s)	(l/min)		(°C)	(s)	(s)	(l/min)		(°C)	(s)	(s)	(l/min)	
200	20	75	2.6		200	20	50	2.6		100	20	50	2.6	
20	1	2	0		20	1	2	0		20	1	2	0	
2000	1	2	0	On	1800	1	2	0	On	2300	1.1	2	0	On
2300	0.1	2	2.6		2300	0.1	2	2.6		2500	0.1	2	2.6	
W-Coil AAS														
					Current (A)	<i>T</i> (°C)	Hold (s)	Ar/H <sub>2</sub> (l/min)	Read					
					2.2	100*	190	50						
					0.0	20	10	50						
					6.7	2200	5	50	On					

\* Approximate temperature only.

sten coil heating rates have been reported in the range 2–4 K/ms [26], but no attempt was made to measure the rate for the current instrument. The combination of heating rate, and relatively low atomization temperature resulted in atomization profiles having half-widths of about 0.5 s (Fig. 5). Thus, each profile was sampled approximately ten times at 11 spectra per s. Higher sampling rates resulted in lower S/N, and lower rates would result in under-sampling the profile.

### 2.5. Background correction

Background correction is commonly used in most metal determinations. In the case of GFAAS, two major modes of background correction are involved: D2 correction and Zeeman background correction. In order to have a small, bench-top, possibly portable drinking-water Pb, Cu and Cd analyzer, background correction is unwanted unless near-line correction is used [21]. With the proposed system, background correction was unnecessary, due to the relatively clean nature of the samples. For example, Fig. 5 shows Pb absorbance profiles for a 40  $\mu\text{g/l}$  spiked tap water sample at the Pb 283, 280 and 287 nm lines. Absorption occurs only at the Pb 283.3 nm analytical line.

## 3. Results

### 3.1. Analytical figures of merit

Fig. 6 shows the calibration curves for Cu, Cd and Pb acquired with W-coil AAS. In each case, the absorption profiles were integrated for 1 s under the peak. It should be noted that values for all three elements were obtained simultaneously. Table 2 lists the figures of merit for the W-coil system. The results approach those acquired with GFAAS in the single element mode. Tungsten coil detection limits (3s, based on peak area measurements) of 3, 0.8 and 0.2  $\mu\text{g/l}$  were determined for Pb, Cu and Cd, respectively. The blank noise in absorbance-seconds was 0.02 (Pb); 0.005 (Cu); and 0.01 (Cd). W-coil detection limits obtained with this system fall below the EPA's MCL for each element.

### 3.2. Sample results

Table 3 lists results determined by GFAAS and W-coil AAS for spiked tap water, 'primary drinking water metals', 'secondary drinking water metals' and 'ULTRAcHECK metals sample'. The spiked tap-water results reflect the recovered value minus blank tap water values for each element.

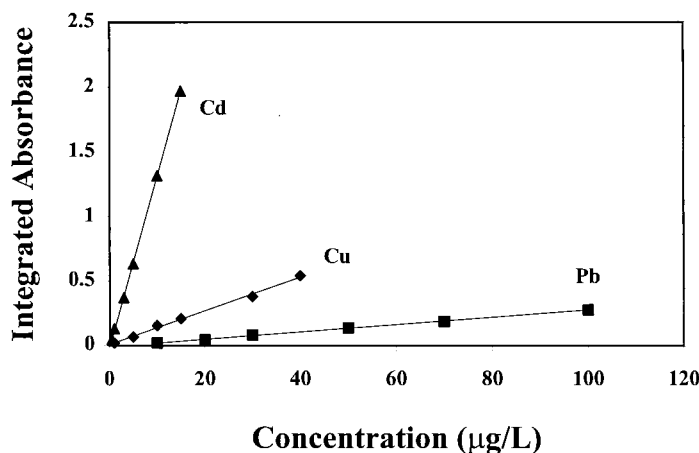


Fig. 6. Cd, Pb and Cu calibration curves.

Table 2  
Analytical figures of merit

	GFAAS			W-coil		
	Pb	Cu	Cd	Pb	Cu	Cd
Detection limit $3\sigma$ (pg, $\mu\text{g/l}$ )	4, 0.2	6, 0.3	0.8, 0.04	60, 3	16, 0.8	4, 0.2
Characteristic mass (pg)	1.0	2.1	0.03	1.6	0.34	0.03
Linear dynamic range (orders of magnitude)	2.4	1.7	2.1	2.5	2.7	2.9

The % recovery for all samples analyzed with the W-coil range from 94 to 105. The average %RSD of all samples is 2.7. Background correction was not used with W-coil AAS.

#### 4. Conclusion

This work shows the feasibility of an inexpensive, bench-top, multi-element, W-coil AAS spectrometer for simultaneous Pb, Cu and Cd determinations in drinking water. The system is small, light-weight and has minimal power requirements. The system figures of merit are comparable to GFAAS figures of merit but without the larger, costlier equipment required to operate a GFAAS instrument. Additionally, multi-ele-

ment determinations save extra time necessary for sequential measurements. The W-coil instrument meets the demands established by the EPA in regard to metal MCL's. Background correction is unnecessary.

#### Acknowledgements

This work was supported by Leeman Labs, Inc. (Hudson, NH) and by grants from the NIH-STTR Program (grant # 1R41RR13245-01) and the NSF-GOALI Program (grant # CHE-9710218).

#### References

- [1] Safe Drinking Water Act, 42 U.S.C., (1974) 300f.
- [2] Safe Drinking Water Act Amendments of 1986, P.L. (1986) 99-339.
- [3] US Environmental Protection Agency, Risk Assessment, Management and Communication of Drinking Water Contamination, US EPA 625/4-89/024, Washington, DC, 1989.
- [4] Z. Fang, G. Tiezheng, B. Welz, Talanta 6 (1991) 613.
- [5] R. Saran, T. Basu Baul, P. Srinivas, D. Khathing, Anal. Letts. 25 (8) (1992) 1545.
- [6] W. Slavin, Anal. Chem. 58 (1986) 589A–597A.
- [7] S.J. Haswell (Ed.), Atomic Absorption Spectrometry: Theory, Design, and Applications, Elsevier, New York, 1991.
- [8] A. Varma, CRC Handbook of Inductively Coupled Plasma Atomic Emission Spectroscopy, CRC Press, Boston, MA, 1991.
- [9] A. Montaser, D.W. Golightly (Eds.), Inductively Coupled Plasmas in Analytical Atomic Spectrometry, VCH Publishers, New York, 1992.
- [10] R.S. Houk, S.C.K. Shum, D.R. Wiederin, Anal. Chim. Acta 250 (1991) 61–70.
- [11] D. Littlejohn, J.N. Egila, R.M. Gosland, U.K. Kunwar, C. Smith, X. Shan, Anal. Chim. Acta 250 (1991) 71–84.

Table 3  
Results

	W-coil ( $\mu\text{g/l}$ (%RSD))	GFAAS ( $\mu\text{g/l}$ (%RSD))	Expected value
<i>Spiked tap water</i>			
Pb	39 [0.9]	40 [2.8]	40 $\mu\text{g/l}$
Cu	15 [2.1]	15 [2.4]	15 $\mu\text{g/l}$
Cd	5 [4.2]	5 [3.1]	5 $\mu\text{g/l}$
<i>'Primary' and 'secondary' drinking water mix</i>			
Pb	104 842 [2.2]	100 952 [5.6]	100 000 $\mu\text{g/l} \pm$ 0.5%
Cu	49 293 [5.3]	49 027 [0.7]	50 000 $\mu\text{g/l} \pm$ 0.5%
Cd	51 028 [4.1]	50 174 [1.6]	50 000 $\mu\text{g/l} \pm$ 0.5%
<i>'Ultra check metals' water</i>			
Pb	160 [2.8]	149 [2.3]	150 $\mu\text{g/l} \pm 2$ ( $2\sigma$ )
Cu	725 [1.3]	701 [1.6]	700 $\mu\text{g/l} \pm 7$ ( $2\sigma$ )
Cd	94 [1.7]	100 [1.5]	100 $\mu\text{g/l} \pm 1$ ( $2\sigma$ )

- [12] M. Sperling, X. Yan, B. Welz, *Spectrochim. Acta B* 51 (1996) 1891.
- [13] Analyte 16 Spectrometer Systems, Manufacturer's Literature, Leeman Labs, Inc., Lowell, MA, 1994.
- [14] T.C. O'Haver, *Analyst* 109 (1984) 211.
- [15] J.M. Harnly, *Anal. Chem.* 58 (1986) 933A.
- [16] R. Fernando, C.P. Calloway Jr, B.T. Jones, *Anal. Chem.* 64 (1992) 1556.
- [17] T.C. O'Haver, *Anal. Chem.* 63 (1991) 164.
- [18] S.J. Haswell, *Atomic Absorption Spectrometry: Theory, Design, and Applications*, Elsevier, New York, 1991 Chapters 2 & 3.
- [19] C. Hsieh, S.C. Petrovic, H.L. Pardue, *Anal. Chem.* 62 (1990) 1983.
- [20] K.P. Schmidt, H. Becker-Ross, S. Florek, *Spectrochim. Acta* 45B (1990) 1203.
- [21] J. Batchelor, S. Thomas, B. Jones, *Appl. Spectr.* 52 (8) (1998) 1086.
- [22] C. Bruhn, F. Ambiado, H. Cid, R. Woerner, J. Tapia, R. Garcia, *Anal. Chim. Acta* 306 (1995) 183.
- [23] F. Krug, M. Silva, P. Oliveira, J. Nobrega, *Spectrochim. Acta* 50B (1995) 1469.
- [24] P. Parsons, H. Qiao, K. Aldous, E. Mills, W. Slavin, *Spectrochim. Acta* 50B (1995) 1475.
- [25] H. Berndt, G. Schaldach, *J. Anal. At. Spectrom.* 3 (1988) 709–712.
- [26] M.F. Gine, F.J. Krug, V.A. Sass, B.F. Reis, J.A. Nobrega, H. Berndt, *J. Anal. At. Spectrom.* 8 (1993) 243–245.
- [27] K. Levine, K. Wagner, B.T. Jones, *Appl. Spec.* 52 (9) (1998) 1165.

# Determination of acetylsalicylic acid by FIA-potentiometric system in drugs after on-line hydrolysis

Lauro Tatsuo Kubota <sup>a,\*</sup>, Julio Cesar Bastos Fernandes <sup>a</sup>, Laércio Rover Jr. <sup>a</sup>,  
Graciliano de Oliveira Neto <sup>b</sup>

<sup>a</sup> Instituto de Química—UNICAMP, PO Box 6154, 13083-970 Campinas, SP, Brazil

<sup>b</sup> Faculdade de Farmácia—USF, 12900-000, Bragança Paulista, SP, Brazil

Received 16 February 1999; received in revised form 4 May 1999; accepted 7 May 1999

## Abstract

A potentiometric flow injection (FI) system was developed for the acetylsalicylic acid (ASA) determination in drugs, without previous treatment. The tubular potentiometric electrode for salicylate (SA) was based on tricapyryl-trimethyl-ammonium-salicylate (aliquat-salicylate) as the ion-exchanger, supported on poly(ethylene-co-vinyl-acetate) (EVA) matrix and applied directly onto a conducting support. The standards and samples were freshly prepared in ethanol solution ( $0.10 \text{ mol l}^{-1}$  Tris- $\text{SO}_4$  buffer, pH 8.0, containing  $0.25 \text{ mol l}^{-1}$   $\text{Na}_2\text{SO}_4$  and 8.0% v/v ethanol) to facilitate the dissolution of ASA and were injected directly into the system. The SA formed due to the on-line alkaline hydrolysis of alcoholic ASA solution, with  $0.50 \text{ mol l}^{-1}$  NaOH (coil, 50 cm length), was monitored by the tubular electrode after neutralization with  $0.25 \text{ mol l}^{-1}$   $\text{H}_2\text{SO}_4$ . A solution of  $0.10 \text{ mol l}^{-1}$  Tris- $\text{SO}_4$  buffer (pH 8.0), containing  $0.25 \text{ mol l}^{-1}$   $\text{Na}_2\text{SO}_4$  was employed as carrier. In optimized conditions (flow rate of  $2.1 \text{ ml min}^{-1}$  and volume of injection of  $150 \mu\text{l}$ ), the tubular electrode showed a linear response to ASA in the concentration range between  $4.0 \times 10^{-3}$  and  $4.0 \times 10^{-2} \text{ mol l}^{-1}$ . A conversion factor of ASA to SA of 85% occurs in these conditions with an increase of about 130% in the signal to the system with on-line hydrolysis (three-channel) in comparison to the system without (one-channel). The response time of the electrode was about 5 s with an analytical frequency of 28 samples per h and a relative standard deviation (R.S.D.) of 2.1% for 30 successive injections. Determinations of ASA in tablet samples by the proposed method exhibited relative differences of 1.0–3.5%, compared to the official method of the British Pharmacopoeia. The useful lifetime of the sensor was greater than 1 month, in continuous use. © 1999 Elsevier Science B.V. All rights reserved.

**Keywords:** Acetylsalicylic acid determination; Salicylate tubular electrode; On-line alkaline hydrolysis

## 1. Introduction

Acetylsalicylic acid is widely employed in pharmaceutical formulations for the relief of headaches, fever, muscular pains and inflamma-

\* Corresponding author. Fax: +55-19-7883023.

E-mail address: kubota@iqm.unicamp.br (L.T. Kubota)

tion due to arthritis or injury. The high consumption of this substance in the world [1–3] shows the importance of the development of new analytical methodologies for its determination. The main metabolite resulting from ASA hydrolysis is salicylate (SA) and in general this is used to monitor indirectly the ASA through of acid–base titration [4] or spectrophotometric method [5]. Few applications in pharmaceutical analysis have been reported utilizing FIA combined with electrochemical methods, the majority of these procedures being associated with amperometric detection [6–8]. Other methods for ASA and SA determination have been made by column-switching liquid chromatography (HPLC) using on-line solid-phase extraction and on-line post-column photochemical derivatization [9,10]; however, these methods require sophisticated and expensive equipment. A recent paper reported the application of an FIA spectrophotometric method for ASA determination using microwave-assisted hydrolysis, but the system was very complex [11]. The official method [4] for ASA quantification is simple, but requires sample heating over reflux before sample analysis and takes time.

Some papers describe the construction of tubular electrodes [12–14] for several ions based on ion exchangers or ionophores using poly(vinyl-chloride) (PVC) [15,16]. In a previous paper [12], the use of a tubular electrode with an aliquat-salicylate anion exchanger occluded in EVA polymeric membrane was described. The principal advantage of the electrode used in this system was the preparation of the sensing membrane without plasticizing solvent, because the EVA polymer presents lower glass transition temperature than PVC. The sensor presented high stability and lifetime, however the hydrolysis of the ASA was realized in a batch system, before injecting the sample in a FIA system, increasing the total analysis time.

The aim of this paper is develop a potentiometric FI-system for direct ASA monitoring in pharmaceutical samples using on-line alkaline hydrolysis in order to minimize the time of analysis, without loss of precision and accuracy in the analysis. For this purpose, the potentiometric method was chosen using a tubular salicylate

ion-selective electrode due to low cost of the equipment, simple preparation and good selectivity of the sensing membrane. The most important analytical parameters that affect the on-line ASA hydrolysis were studied in the FIA system, such as coil-length of reaction and alkali concentration.

## 2. Experimental

### 2.1. Reagents and materials

The ASA tablets were obtained in a local drug-store. Sodium sulfate, sodium salicylate, sulfuric acid and ethanol were purchased from Merck. Tris buffer, EVA-40% polymer and anion-exchanger (aliquat-chloride) were acquired from Aldrich. All other reagents were of analytical grade.

The ASA standard solutions were prepared in the concentration range of  $2.0 \times 10^{-3}$  to  $4.0 \times 10^{-2}$  mol l<sup>-1</sup>. These solutions were diluted with 0.10 mol l<sup>-1</sup> Tris-SO<sub>4</sub>, pH 8.0, containing 0.25 mol l<sup>-1</sup> Na<sub>2</sub>SO<sub>4</sub> to adjust the ionic strength and 8.0% (v/v) ethanol to aid ASA dissolution. The ASA tablet samples were prepared in a similar manner. The tablets were pulverized and dissolved in the same buffer solution. All solutions of ASA were prepared freshly before analysis. For the alkaline hydrolysis, 0.50 mol l<sup>-1</sup> sodium hydroxide solution was used as well as a 0.25 mol l<sup>-1</sup> sulfuric acid solution to neutralize the base excess after hydrolysis.

### 2.2. Apparatus and FIA manifold

The EVA membrane and tubular electrodes based on graphite/epoxy were fabricated according to the studies described elsewhere [12,13,17]. The membrane composition was 40.0 wt.% aliquat-salicylate, 59.5 wt.% EVA and 0.5 wt.% potassium tetrakis(4-chloro-phenyl) borate. Before use, the electrodes were conditioned in 0.1 mol l<sup>-1</sup> sodium salicylate aqueous solution for 1 day.

The measurements of potential difference were performed with an OP-271 pH/ion analyser (P). As reference electrode (RE), a double junction

OP-0820P electrode of Ag/AgCl with  $1.0 \text{ mol l}^{-1}$   $\text{LiNO}_3$  filling solution was used and for pH measurements, an OP-808P glass electrode. All these appliances were manufactured by Radelkis (Hungary). The employed FIA system (Fig. 1) used  $0.10 \text{ mol l}^{-1}$  Tris- $\text{SO}_4$  buffer, pH 8.0, as carrier solution, conducted by a peristaltic pump (PP) (Ismatec model IPC-8 from Switzerland), through the tubular electrode (ISE). A manual injector (IV) was used to insert ASA solutions into the carrier solution. An XY recorder ECB, model RB-101 (Brazil) (R) was employed to register the potentiometric signals. The Tygon™ and polyethylene tubes for the connections were of 0.80 mm i.d. The pump uses two more channels through which sodium hydroxide (NaOH) and sulfuric acid ( $\text{H}_2\text{SO}_4$ ) solutions were injected into the FIA system.

The parameters chosen for the flow system were a flow-rate of  $2.1 \text{ ml min}^{-1}$ , injection volume of  $150 \mu\text{l}$  and a coil length of 50 cm (B). The response time to the system was considered as the time since the injection until the signal return to baseline, while to the electrode this time was determined from start on peak up to the maximal signal. The standard method of the British Pharmacopoeia [4] for ASA determination in pharmaceutical samples was utilized to compare the results obtained with the system. This method consists of a back acid–base titration, where an excess of  $0.1 \text{ mol l}^{-1}$  NaOH solution is added to the ASA sample and heated over reflux for 15 min. Then, the NaOH that did not react with the ASA is titrated with  $0.1 \text{ mol l}^{-1}$  HCl solution. The NaOH solution was standardized against potassium hydrogen phthalate using phenolph-

thalein as indicator and HCl solution with sodium carbonate using bromocresol green as indicator.

### 3. Results and discussion

In general, ASA analysis is not realized directly, and a previous hydrolysis is necessary, converting ASA to salicylate for its determination [4,12,13]. This hydrolysis is carried out by sodium hydroxide solution [4], but no on-line alkaline hydrolysis with potentiometric detection is described in the literature to our knowledge. One procedure for on-line hydrolysis using microwave digestion has been described [11], where salicylate is spectrophotometrically monitored after complex formation with Fe(III). This procedure heats the sample and the solution needs cooling before analysis generating bubbles in the FIA system; moreover colored samples can give interference with this method.

Thus, a methodology with potentiometric detection may be an alternative for colored samples; however, the potentiometric sensor cannot support a heated solution. A good alternative for this problem is the alkaline hydrolysis and subsequent neutralization for salicylate detection with an ion selective electrode coupled to the flow system. However, the ASA stability in solution is poor, being slowly converted to SA and acetic acid [18]. Thus, the use of a microwave-oven is not necessary to aid in the procedure of sample digestion. On the other hand, ASA solubility in water is not very high, it being necessary to add alcohol, in general methanol or ethanol, to facilitate its dissolution [18,19]. Thus, 8% (v/v) of ethanol was used to prepare the standards and sample solutions.

Based on this, a tubular electrode selective for SA was employed to monitor this anion formed during the hydrolysis of ASA. Initially, the FIA system was optimized using one-channel with Tris- $\text{SO}_4$  as the carrier and SA standard solution at a concentration of  $5 \times 10^{-3} \text{ mol l}^{-1}$ . In this case, it was observed that the injection volume significantly affected the response of the system. An injection volume of  $150 \mu\text{l}$  was chosen because under these conditions, the FIA system exhibited a greater height to width ratio of the signal (Fig.

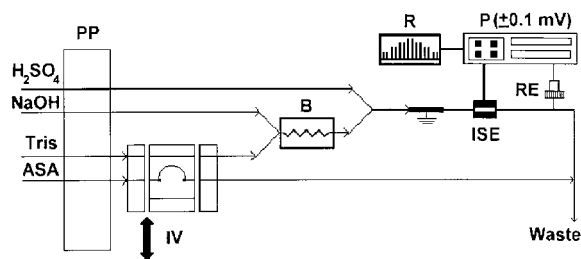


Fig. 1. Schematic diagram of the FI-system used for ASA potentiometric determination.

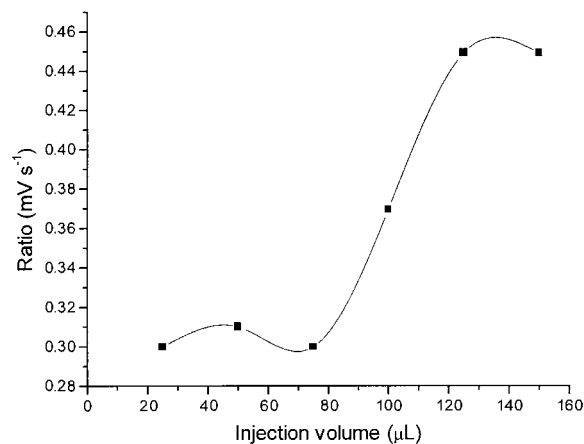


Fig. 2. Graphic showing the ratio between the signal produced and the washing time obtained as a function of the injected volume.  $[SA] = 5 \times 10^{-3} \text{ mol l}^{-1}$ ; flow rate =  $2.1 \text{ ml min}^{-1}$ .

2). The flow-rate also affects the signal, increasing up to  $3 \text{ ml min}^{-1}$ , but this effect is not significant for the system, being almost constant. Therefore,  $2.1 \text{ ml min}^{-1}$  was chosen as the flow rate considering the compromise between the analytical frequency and the reagents being consumed. These conditions were used in the three-channel system.

The two most important factors that affect the FIA three-channel system are the coil length and base concentration, because these are directly responsible for the degree of hydrolysis of ASA. The block diagram clearly shows the effect of the coil length and the base concentration on the response signal and analytical frequency (Fig. 3). The signal decreases with lowering of the base concentration and the coil length, while the analytical frequency is the inverse. Considering the sensitivity and speed of the system for drug analyses, the concentration of sodium hydroxide was fixed at  $0.50 \text{ mol l}^{-1}$  and the coil length at 50 cm.

An FIA manifold using one channel was used to determine the hydrolysis degree of an ASA solution at  $4 \times 10^{-2} \text{ mol l}^{-1}$ , injected into the line-carrier containing  $0.1 \text{ mol l}^{-1}$  Tris- $\text{SO}_4$  buffer. In comparison with the injection of SA solution at the same concentration, only 27% of ASA was converted to SA in this system, which is not enough to give the sensitivity to detect salicylate in the concentration range of interest. Using

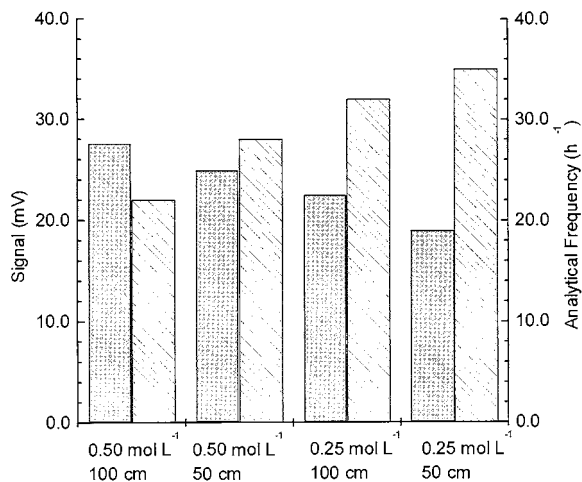


Fig. 3. Graphic of the interaction between results for signal (mV) and number of injections per hour relative to the FI-potentiometric system for ASA determination. Under the x-axis are the parameters studied in the system: NaOH concentrations, 0.50 and  $0.25 \text{ mol l}^{-1}$ ; coil lengths of reactor, 100 and 50 cm; injected volume,  $150 \mu\text{l}$ ;  $[ASA] = 2 \times 10^{-2} \text{ mol l}^{-1}$ . Grey blocks, potentiometric signal; striped blocks, analytical frequency. Average values for three sequential injections. All solutions were freshly prepared.

the three-channel FIA system, the hydrolysis degree was greater than 83% (Fig. 4). It is important to mention that though the dispersion is major

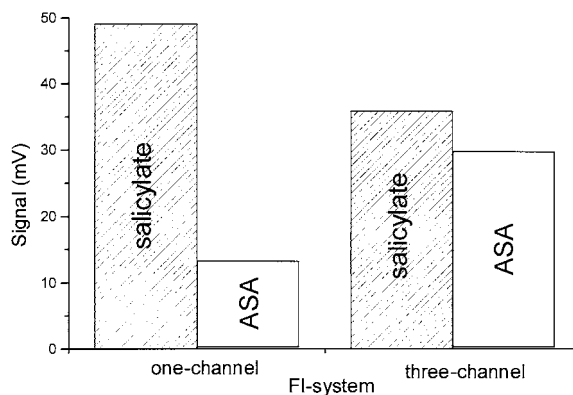


Fig. 4. Graphic showing the signals for SA and ASA with and without on-line hydrolysis employing FI potentiometric system: with Tris- $\text{SO}_4$  carrier solution (one-channel) and with NaOH carrier solution to promote the ASA hydrolysis in the system (three-channel). Injected volume,  $150 \mu\text{l}$ ; flow rate,  $2.1 \text{ ml min}^{-1}$ ;  $[ASA] = 4 \times 10^{-2} \text{ mol l}^{-1}$ . Average values for three sequential injections. All solutions were freshly prepared.



Table 1  
Evaluation of tubular electrode lifetime for FI-potentiometric ASA determination<sup>a</sup>

Time (days)	Slope (V decade <sup>-1</sup> ) <sup>b</sup>	Correlation coefficient ( <i>r</i> )
0	0.034 ± 0.001	0.9993
7	0.034 ± 0.001	0.9994
14	0.035 ± 0.001	0.9998
21	0.035 ± 0.002	0.9971
28	0.033 ± 0.001	0.9988
35	0.032 ± 0.002	0.9938

<sup>a</sup> All solutions were freshly prepared.

<sup>b</sup> Relative slopes for the ASA calibration curves in the range between 2.0 and 40.0 mmol l<sup>-1</sup> obtained for the evaluated period.

(diminution in the signal to salicylate) in the three-channel system, the on-line hydrolysis compensates this deficiency in the three-channel system, where the signal to ASA solution increases by about 130%.

The linear range of the electrode response for alcoholic solution of ASA was similar to that observed for SA aqueous solution, between  $4.0 \times 10^{-3}$  and  $4.0 \times 10^{-2}$  mol l<sup>-1</sup>. On the other hand, the sensitivity of the sensor for ASA alcoholic solution decreased to about 40% of the initial value in SA aqueous solution (0.058 V decade<sup>-1</sup>), giving a slope of 0.035 V decade<sup>-1</sup>. This behavior was assigned to the necessity of using ethanol for ASA dissolution, changing the dielectric constant of the medium and affecting the sensitivity of the membrane. Moreover, the alcohol probably attacks the EVA membrane causing leaching out of the aliquat-salicylate to the solution from the electrode surface. However, the stability of the sensor in the experimental condition was not critical, giving the same performance during 35 days of continuous use (Table 1). Although the sensor may be used for a longer time, indicating that leaching out is not significant, its great advantage is the facility and rapidity for sensing membrane preparation [12], where the active material, aliquat-salicylate is stable after preparation when kept under refrigeration.

A typical calibration curve obtained for ASA (Fig. 5) with the tubular electrode showed good correlation ( $r = 0.9971$ ) for  $n = 5$ , fit by the

equation:

$$\Delta E = (0.085 \pm 0.004) + (0.035 \pm 0.002) \log [\text{ASA}]$$

where  $\Delta E$  (V) is the potentiometric signal.

The interfering anions for the salicylate electrode based on aliquat exchanger were described previously and are iodide > bicarbonate > nitrate > ascorbate [12]. Iodide and nitrate are not significant interfering anions because these ions are not present in the drug formulation of ASA. Therefore, bicarbonate and ascorbate are the

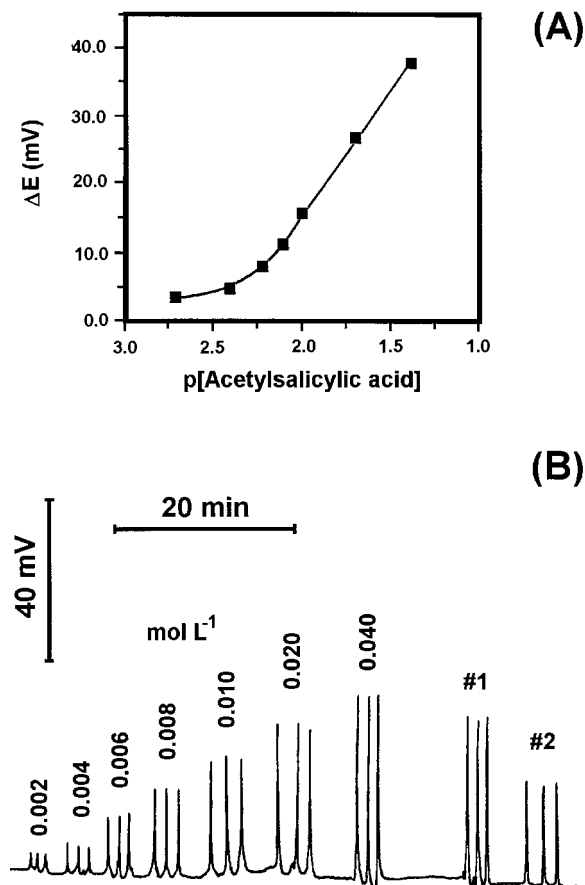


Fig. 5. (A) Potentiometric calibration curve of the ISE for ASA solutions. (B) Transient potentiometric signals obtained for ASA standards and sample solutions of tablets. From left to right: triplicate signals for seven reference solutions (2.0–40.0 mmol l<sup>-1</sup>) followed by three consecutive signals for two commercial samples. Injected volume, 150  $\mu$ l; coil length, 50 cm; NaOH concentration, 0.50 mol l<sup>-1</sup>; flow rate, 2.1 ml min<sup>-1</sup>. All solutions were freshly prepared.

Table 2

Results obtained by the proposed (FIA-potentiometric) and official method (British Pharmacopoeia) for the assay of ASA in some drug tablets<sup>a</sup>

Sample	Label	Acetylsalicylic acid (values in mg per tablet)		
		FIA-potentiometric		British Pharmacopoeia
		With on-line hydrolysis	Without on-line hydrolysis	
#1	85	86 ± 1 <sup>b</sup>	79 ± 3 <sup>b</sup>	83 ± 1 <sup>b</sup>
#2	500	518 ± 1	495 ± 2	513 ± 2

<sup>a</sup> All solutions were freshly prepared.

<sup>b</sup> Average for three sequential injections with respective standard deviation estimate.

most important interfering anions as they are ingredients in some pharmaceutical formulations, but these anions are unstable in acid and alkaline media, respectively and could be attenuated by adjustment of the acid and base line carriers.

The experiments carried out to verify the reliability of the system in real samples showed good accuracy and precision in the ASA determination in drug samples (Table 2), with a repeatability for 30 successive injections of 2.1% (R.S.D.) to  $2.0 \times 10^{-2} \text{ mol l}^{-1}$ . The results obtained by the FIA-potentiometric system with and without on-line hydrolysis were similar to those using the official method of the British Pharmacopoeia. The relative difference for sample analysis between the average value obtained by the official and the proposed method, with on-line hydrolysis, varied between 1.0% (sample # 2) and 3.5% (sample # 1). The main difference between the methodologies was the analytical frequency, which in the optimized conditions for the FIA systems was 28 and 100 samples per h, with and without on-line hydrolysis, respectively. However, the better analytical frequency obtained in the system without on-line hydrolysis does not take into consideration the time required for the preparation of samples, in general of 15 or 20 min due to the necessity for the samples to hydrolyze out of the system. Considering this time, the official method of the British Pharmacopoeia and the FIA system without on-line hydrolysis presented an analytical frequency of three or four samples per hour. Then, the FIA system with on-line hydrolysis has

the advantage of lower total analysis time.

An important aspect that should be mentioned here is the necessity to prepare the standards and samples of ASA freshly and during analysis to avoid differences in the possible decomposition of ASA to SA in the solution. Finally, is interesting to point out that the Trinder method (red complex between SA and  $\text{Fe}^{3+}$ ) is not a convenient methodology to determine ASA in sample # 1, because this sample has a red dye in its formulation. All these facts show the advantages of proposed FIA-potentiometric system with on-line hydrolysis.

In conclusion, the ASA determination using a salicylate-sensitive tubular ion-selective electrode is useful in analysis of real samples, particularly considering the linear range and selectivity. The association of the electrode in an FIA system with on-line hydrolysis enhances the use of this sensor, when repeated analyses are required allowing a rapid, sensitive and accurate method for routine procedures.

### Acknowledgements

The authors thank FAPESP (Fundação de Amparo à Pesquisa do Estado de São Paulo) CNPq (Conselho Nacional de Desenvolvimento Científico e Tecnológico), and CAPES (Coordenação de Aperfeiçoamento de Pessoal de Nível Superior) for financial support.

## References

- [1] J.J. Thiessen, in: H.J.M. Barnett, J. Hirsh, J.F. Mustard (Eds.), *Acetylsalicylic Acid: New Uses for an Old Drug*, Raven Press, New York, 1992, pp. 49–61.
- [2] T.M. Brown, A.T. Dronsfield, P.M. Ellis, J.S. Parker, *Educ. Chem.* 35 (1998) 47.
- [3] P. Nietsch, *Therapeutic Applications of ASPIRIN®*, Bayer, Germany, 1989, pp. 7–34.
- [4] *British Pharmacopoeia*, HMSO, London, 1980, 733 pp.
- [5] P. Trinder, *Biochem. J.* 57 (1954) 301.
- [6] M. Neumayr, O. Friedrich, G. Sontag, F. Pittner, *Anal. Chim. Acta* 273 (1993) 469.
- [7] M. Ehrendorfer, G. Sontag, F. Pittner, *Fresenius J. Anal. Chem.* 356 (1996) 75.
- [8] J.M.P.J. Garrido, J.L.F.C. Lima, C. Delerue-Matos, V.V.M. Meijden, *Port. Electrochim. Acta* 15 (1995) 335.
- [9] A.M. DiPietra, R. Gatti, V. Andrisano, V. Cavrini, *J. Chromatogr. A* 729 (1996) 355.
- [10] G.P. McMahon, M.T. Kelly, *Anal. Chem.* 70 (1998) 409.
- [11] A.V. Pereira, C. Aniceto, O.F. Filho, *Analyst* 123 (1998) 1011.
- [12] L. Rover Jr., C.A.B. Garcia, G.O. Neto, L.T. Kubota, F. Galembeck, *Anal. Chim. Acta* 366 (1998) 103.
- [13] J.L.F.C. Lima, M.C.B.M. Montenegro, A.M.R. Silva, *J. Flow Injection Anal.* 7 (1990) 19.
- [14] J.A. Chamarro, J. Bartrolí, S. Jun, J.L.F.C. Lima, M.C.B.M. Montenegro, *Analyst* 118 (1993) 1527.
- [15] M.N.M.P. Alçada, J.L.F.C. Lima, M.C.B.M. Montenegro, *J. Pharm. Biomed. Anal.* 1 (10/12) (1992) 757.
- [16] S. Jun, J.L.F.C. Lima, M.C.B.M. Montenegro, *J. Trace Elem. Electrolytes Health Dis.* 8 (1994) 93.
- [17] L. Rover Jr., G.O. Neto, J.L.F.C. Lima, M.C.B.M. Montenegro, *Quím. Nova* 19 (1996) 549.
- [18] *The Merck Index—An Encyclopedia of Chemicals, Drugs and Biologicals*, 12th edn., Merck, 1996, 144 pp.
- [19] D. Ivanovic, M. Medenica, E. Nivaud-Guernet, M. Guernet, *Spectrosc. Lett.* 28 (1996) 557.

# Determination of tungsten in niobium–tantalum, vanadium and molybdenum bearing geological samples using derivative spectrophotometry and ICP-AES

V. Padmasubashini, M.K. Ganguly, K. Satyanarayana, R.K. Malhotra \*

*Chemical Laboratory, Atomic Minerals Directorate for Exploration and Research, Department of Atomic Energy, Begumpet, Hyderabad-500 016, India*

Received 29 December 1998; received in revised form 14 May 1999; accepted 14 May 1999

## Abstract

Two different procedures, one using derivative spectrophotometry and another using inductively coupled plasma atomic emission spectrometry (ICP-AES) have been developed for the determination of tungsten in niobate–tantalates, tin slag samples, ores, concentrates and vanadium and molybdenum bearing geological materials. In the first method involving derivative spectrophotometry, 0.05–0.5 g of the sample is fused with sodium hydroxide, the tungsten is extracted by leaching the melt with distilled water and estimated as thiocyanate using a second derivative spectrophotometric method in the presence of interferents, i.e. Nb, Mo and V, without separating them. Mixtures of tungsten with V, Nb and Mo are used for standardizing the various parameters like zero-crossing wavelength, wavelength range, etc. Tolerance limits for V, Nb and Mo have also been evaluated. In the second method involving ICP-AES, 0.05–0.5 g of sample is fused with  $\text{KHSO}_4$  to a clear melt and dissolved in ammonium oxalate solution. Ammonium hydroxide precipitation is then carried out to separate Nb and Ta as hydroxides and the filtrate is boiled with nitric acid to destroy the oxalates before aspiration into the plasma for measurement of tungsten values by ICP-AES using the 207.911 nm emission line. Both methods have been applied to niobate–tantalate and tin slag samples and the results obtained are reported in this paper. The values obtained by both methods are in good agreement with each other. The proposed methods have also been applied to the determination of tungsten in two Canadian Certified Reference Standards (CT-1 and MP-2) and the values obtained are in good agreement with the certified values and the R.S.D.% in case of the ICP-AES method varied from 1–2% at  $> 1000 \mu\text{g g}^{-1}$  level to 9.4% at the  $20 \mu\text{g g}^{-1}$  level whereas the R.S.D.% in case of the derivative method varied from 1 to 7.8%. © 1999 Elsevier Science B.V. All rights reserved.

*Keywords:* Tungsten; Niobate–tantalates; Geological materials; Derivative spectrophotometry; Inductively coupled plasma atomic emission spectrometry

\* Corresponding author. Tel.: +91-40-7767101; fax: +91-40-7762940.  
E-mail address: amdhyd@ap.nic.in (R.K. Malhotra)

## 1. Introduction

Accurate and rapid analysis of tungsten in various types of geological samples like minerals, ores, concentrates and beneficiation products has become necessary in order to render support to the exploration and evaluation programmes which have been initiated to meet the increasing demand for tungsten from the defence, space and industrial sectors. Various instrumental methods are now available for the determination of tungsten including: spectrophotometry [1–8], flame atomic absorption spectrometry (FAAS) [9,10], inductively coupled plasma atomic emission spectrometry (ICP-AES) [11–13], inductively coupled plasma mass spectrometry (ICP-MS) [14], X-ray fluorescence (XRF) [15], and neutron activation analysis (NAA) [16]. The sensitivity for tungsten by FAAS is poor even when a nitrous oxide–acetylene flame is used. ICP-AES offers good sensitivity and better detection limits for tungsten. Methods for estimating tungsten in a variety of matrices, i.e. water samples (after a preconcentration step) [17,18], alloys, steels, ores and concentrates, have been reported using ICP-AES. A method for direct determination of tungsten in geological samples by ICP-AES has been reported from this laboratory [19]. The method has now been applied to niobium–tantalum bearing samples and the results obtained are reported in this

paper. Interference encountered due to tantalum in niobate–tantarate and tin slag samples with a high tantalum to tungsten ratio has been eliminated by precipitating out the interferent using ammonium oxalate and ammonium hydroxide.

Spectrophotometric methods offer the best alternative for routine analysis of tungsten in the absence of ICP-AES. Various chromogenic agents like thiocyanate and dithiol are available. Amongst them, the thiocyanate method is the most preferred method for routine analysis of geological samples owing to its rapidity and moderate sensitivity. However, vanadium, molybdenum and niobium interfere. In order to eliminate this interference, various methods based on the separation of tungsten from the interferents using different techniques have been reported in the literature [5–8]. In this context, second derivative spectrophotometry has been utilized by us to improve the tolerance limits of the interferents, vanadium, niobium and molybdenum, in order to enable the estimation of tungsten in their presence without having to separate them. The results obtained on the application of this method to niobium–tantalum bearing samples are also reported in this paper.

## 2. Experimental

### 2.1. Instrumentation

An ICP-AES model Plasmascan 8410 (LAB-TAM, now GBC, Australia) with a computer controlled rapid scanning monochromator and a Shimadzu model UV-2100 UV–visible spectrophotometer were used for the measurements. The operating conditions and instrumental parameters for the ICP-AES are given in Table 1. For the proposed derivative spectrophotometric method, a second derivative zero-crossing method was used [20] owing to its better signal to noise values. The absorbance spectra were recorded at a scan rate of 700 nm min<sup>-1</sup> at 0.5 nm wavelength intervals versus a reagent blank. The second derivative spectra were obtained by digital differentiation using the Golay–Savitzky convolution method.

Table 1  
ICP-AES operating conditions and instrumental parameters

R.F. generator frequency	27.12 MHz, crystal controlled
Forward power	1200 W
Reflected power	<5 W
Observation height	14 mm above load coil
PMT voltage	1000 V
Integration time	3 s ( <i>n</i> = 3)
Entrance slit	20 μm and 3 mm height (fixed)
Exit slit	40 μm (adjustable)
Sample flush time	10 s
<i>Argon gas flow rates (l min<sup>-1</sup>)</i>	
Coolant	14
Auxiliary	1.0
Sample	0.8
Solution uptake rate	3.0 ml min <sup>-1</sup>

## 2.2. Reagents and standards

All reagents and standards were prepared from analytical grade chemicals. Standard stock solution of tungsten ( $1 \text{ mg ml}^{-1}$ ) was prepared by dissolving sodium tungstate (0.4485 g) in distilled water, diluting to 250 ml and the lower standards were prepared by successive dilutions. For the interference studies, niobium standard stock solution ( $1 \text{ mg ml}^{-1}$ ) was prepared by fusing niobium oxide with  $\text{KHSO}_4$  and dissolving the melt in 3% citric acid. Ammonium vanadate and ammonium molybdate were used to prepare vanadium and molybdenum standards, respectively. Matrix matching was done with respect to  $\text{KHSO}_4$  for the ICP-AES method and with respect to NaOH for the derivative method.

## 2.3. Procedure

### 2.3.1. Determination of tungsten by derivative spectrophotometry

For spectrophotometric measurements, 0.05–0.5 g of the sample (–200 mesh) was weighed (depending on the anticipated tungsten content) into a nickel crucible containing 2 g solid NaOH, fused to a red-hot melt, leached with distilled water, filtered and made up to 100 ml volume in a plastic volumetric flask (Tarson's make). From this solution 5 ml was taken in a 25 ml flask, 10 ml of hot 10% (w/v)  $\text{SnCl}_2$  solution in concentrated HCl was added (acidity maintained at 7.5 M of HCl), boiled in a hot water bath and cooled. Then 1 ml of freshly prepared 20% (w/v) KSCN solution was added, diluted to the mark with distilled water and the absorbance measured after 30 min.

### 2.3.2. Determination of tungsten by ICP-AES

For measurements by ICP-AES, 0.05–0.5 g of sample (–200 mesh) was weighed (depending on the anticipated tungsten content) in a silica crucible, fused with 4–8 g of  $\text{KHSO}_4$  to a clear melt, dissolved in citric acid and made up to the mark in a 100 ml flask (3% w/v citric acid). This solution was directly aspirated into the plasma. In the case of silica containing samples, the sample was weighed into a platinum crucible and hy-

drofluoric acid along with a few drops of sulphuric acid was added and the silica fumed off. The residue was then fused with  $\text{KHSO}_4$  and the cooled melt was dissolved in 3% (w/v) citric acid as above.

For separation of tungsten from niobium–tantalum the samples, after fusion with  $\text{KHSO}_4$ , were dissolved in 3% (w/v) ammonium oxalate followed by precipitation with  $\text{NH}_4\text{OH}$ , digested on a hot water bath for about 15 min and filtered. The precipitate was washed twice with dilute 2% (v/v)  $\text{NH}_4\text{OH}$  solution. The filtrate was diluted to 100 ml volume for aspiration into the plasma after removing the oxalate from it by boiling with nitric acid (final concentration of 10% v/v  $\text{HNO}_3$ ).

## 3. Results and discussion

### 3.1. Determination of tungsten as thiocyanate by derivative spectrophotometry

The method of fusing the samples with NaOH, followed by extraction of the melt with distilled water as described earlier was applied to various types of geological samples for the determination of tungsten and good results have been obtained [21–23]. However, during NaOH fusion and the subsequent water leaching and filtration of the samples, tungsten gets separated from most elements like calcium, magnesium, iron, titanium and manganese and most of the niobium as well but molybdenum, vanadium and significant amounts of niobium accompany tungsten into the solution, thereby causing interference in conventional thiocyanate spectrophotometry. In this context, the scope for application of a derivative method to minimise the interference due to niobium, molybdenum and vanadium was investigated by the authors and a second derivative zero-crossing method was opted for. Standard solutions of tungsten, vanadium, niobium and molybdenum in the range of a few  $\mu\text{g ml}^{-1}$  to  $100 \mu\text{g ml}^{-1}$  as well as mixtures of tungsten with the interferents vanadium, molybdenum and niobium in ratios ranging from 1:1 to 1:50 were taken and the various parameters, i.e. wavelength scan range, scan speed, differentiation step, etc., were

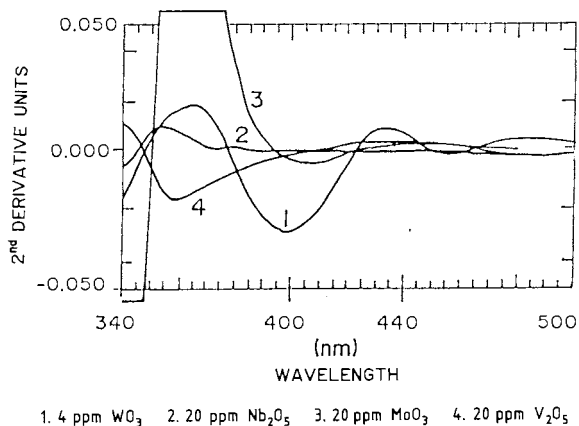


Fig. 1. Second derivative curves for thiocyanates of tungsten, niobium, molybdenum and vanadium

optimised to attain a maximum second derivative value with minimum noise and stability of zero crossing wavelengths. Fig. 1. shows the second derivative curves for the tungsten thiocyanate complex along with those of vanadium, niobium and molybdenum. It can be seen that the second derivative curve of vanadium complex shows a zero-crossing at 401 nm at which the second derivative of tungsten shows a maximum value. The second derivative values of niobium and molybdenum complexes are negligible at 401 nm up to 1250  $\mu\text{g}$  niobium in presence of 60  $\mu\text{g}$  tungsten and up to 250  $\mu\text{g}$  for molybdenum in presence of 50  $\mu\text{g}$  tungsten. Hence, 401 nm was selected as the wavelength for determining tung-

sten in presence of vanadium, niobium and molybdenum. Linearity was obtained up to 13  $\mu\text{g ml}^{-1}$  of tungsten. The proposed derivative method was found to have tolerance ratios of 1:5, 1:10 and 1:20 for molybdenum, vanadium and niobium in the final solution. The zero point wavelength was confirmed using mixtures of tungsten with niobium, molybdenum and vanadium by the point of intersection method and there was no decrease in the derivative amplitude of tungsten at the zero point wave length within the tolerance limits given earlier. This method was applied to two standard reference materials (SRM's) issued by CANMET: CT-1 and MP-2 (CT-1 is a scheelite ore whereas MP-2 is a tungsten–molybdenum ore and their compositions are given in Table 2). The results obtained are given in Table 2. It can be seen from the table that the values obtained in presence of the interferences based on the normal absorbance values at 400 nm show considerable error whereas the values obtained using the derivative method and also the values obtained by ICP-AES, both direct as well as after separation, are in good agreement with the certified values. The results obtained on the application of this method to niobate–tantarate samples are given in Table 3 along with those obtained by ICP-AES. Even when the ratio of tungsten to niobium is higher than the tolerance limit in some of the samples given in Table 5, the ratio in the final solution comes within the favourable tolerance ratio of the derivative method

Table 3  
Tungsten values in niobium–tantalum bearing samples

Sample No.	A <sup>a</sup> (%)		B <sup>a</sup> (%)		C <sup>a</sup> (%)	
	$WO_3^b$	R.S.D.	$WO_3^b$	R.S.D.	$WO_3^b$	R.S.D.
CHEM-1	1.20	3.3	0.98	4.6	0.98	3.7
CHEM-2	1.87	2.7	1.62	4.9	1.60	3.7
CHEM-3	0.41	5.0	0.34	4.0	0.32	4.3
CHEM-4	1.99	3.8	1.71	1.0	1.76	5.4
CHEM-5	1.51	2.3	1.20	1.0	1.23	3.9
CHEM-6	0.78	6.6	0.67	4.1	0.74	2.8

<sup>a</sup> A, normal spectrophotometric method; B, proposed derivative method; C, direct determination by ICP-AES using the tungsten(II) 207.911 emission line.

<sup>b</sup> Mean of five replicate measurements.

Table 2  
Tungsten values in Certified Reference Standards by derivative spectrophotometry/ICP-AES

Sample	Interferent	Amount added <sup>a</sup>	A <sup>b</sup> (%)		B <sup>b</sup> (%)		C <sup>b</sup> (%)		D <sup>b</sup> (%)		WO <sub>3</sub> certified value [23] (%)
			WO <sub>3</sub> <sup>c</sup>	R.S.D.	WO <sub>3</sub> <sup>c</sup>	R.S.D.	WO <sub>3</sub> <sup>c</sup>	R.S.D.	WO <sub>3</sub> <sup>c</sup>	R.S.D.	
CT-1 <sup>d</sup>	–	–	1.33	1.1	1.29	4.4	1.30	2.1	1.36	2.6	1.31
CT-1 <sup>d</sup>	Nb <sub>2</sub> O <sub>5</sub>	325	1.66	3.4	1.27	2.3	1.28	1.0	1.26	3.7	1.31
CT-1 <sup>d</sup>	MoO <sub>3</sub>	325	1.93	3.6	1.36	6.1	1.29	1.4	1.29	2.8	1.31
CT-1 <sup>d</sup>	V <sub>2</sub> O <sub>5</sub>	325	2.38	2.9	1.36	4.3	1.29	1.0	1.28	1.8	1.31
MP-2 <sup>e</sup>	–	–	0.89	8.7	0.81	2.6	0.80	1.8	0.79	3.4	0.82
MP-2 <sup>e</sup>	Nb <sub>2</sub> O <sub>5</sub>	200	1.01	2.1	0.78	7.8	0.82	1.0	0.77	4.3	0.82
MP-2 <sup>e</sup>	MoO <sub>3</sub>	200	1.23	5.5	0.86	7.5	0.82	1.3	0.78	2.0	0.82
MP-2 <sup>e</sup>	V <sub>2</sub> O <sub>5</sub>	200	1.48	4.6	0.86	6.9	0.83	1.0	0.79	4.1	0.82

<sup>a</sup> Amount in  $\mu\text{g}$  added to a 5 ml aliquot from solutions of CT-1 and MP-2 (0.1 g/100 ml), maintaining WO<sub>3</sub>: interferent ratio = 1:5.

<sup>b</sup> A, by normal spectrophotometry; B, by proposed derivative method; C, direct determination by ICP-AES (at W(II) 207.911 nm emission line); and D, Proposed determination by ICP-AES, after ammonium oxalate/ammonium hydroxide separation.

<sup>c</sup> Mean of five replicate measurements.

<sup>d</sup> CT-1 is a scheelite ore containing (in percent):  $1.04 \pm 0.017$  W, 17.5 Fe, 17.2 Si, 12.2 Cu, 8.2 S, 2.9 Al, 2.0 Mg, 1.7 C, 0.7 Mn, 0.7 K, 0.2 Na, 0.2 Ti, and 0.03 Mo (40% pyroxene, 18% quartz, 12% pyrrhotite, 10% amphibole, 80% calcite, 5% mica and 2% each of feldspar and dolomite).

<sup>e</sup> MP-2 is a tungsten–molybdenum ore containing (in percent):  $0.65 \pm 0.02$  W,  $0.281 \pm 0.01$  Mo,  $0.245 \pm 0.007$  Bi,  $0.043 \pm 0.002$  Sn,  $4.9 \pm 0.3 \mu\text{g g}^{-1}$  Ag, 76.1 SiO<sub>2</sub>, 5.4 Al, 4.1 F, 3.7 Fe, 2.7 Ca, 0.9 Cu, 0.7 S, 0.4 Zn, 0.2 As, 0.043 Sn, 0.04 Mg, 0.04Pb, 0.02C, and  $<0.1 \text{ H}_2\text{O}$  (105°C)



Table 4

Tungsten values in tantalum-rich samples By ICP-AES using the tungsten(II) 207.911 nm emission line

Sample No.	A <sup>a</sup> (%)		B <sup>a</sup> (%)		C <sup>a</sup> (%)		D <sup>a</sup> (%)	
	WO <sub>3</sub> <sup>b</sup>	R.S.D.	WO <sub>3</sub> <sup>b</sup>	R.S.D.	WO <sub>3</sub> <sup>b</sup>	R.S.D.	WO <sub>3</sub> <sup>b</sup>	R.S.D.
CHEM-7	0.13	5.7	0.12	6.2	0.20	7.4	0.13	3.4
CHEM-8	0.22	3.1	0.11	6.1	0.40	1.4	0.10	7.4
CHEM-9	<0.02	–	<0.05	–	0.24	6.1	0.008	5.7
CHEM-10	0.03	5.0	<0.05	–	0.38	3.3	0.002	9.4

<sup>a</sup> A, normal spectrophotometric method(W-SCN); B, proposed derivative method; C, direct determination by ICP-AES; and D, proposed determination by ICP-AES after ammonium oxalate/ammonium hydroxide separation.

<sup>b</sup> Mean of five replicate measurements.

as tungsten gets separated from the major amount of niobium as stated earlier. Tungsten values obtained using the derivative method are in good agreement with those obtained using the ICP-AES, whereas the values obtained by normal spectrophotometry are much higher due to interference from niobium.

### 3.2. Determination of tungsten by ICP-AES

For determination of tungsten in niobium–tantalum samples as stated earlier [19], the most sensitive 207.911 nm line was chosen as only zinc has been found to interfere causing a direct overlap with an interference coefficient of 1.752  $\mu\text{g ml}^{-1}$  tungsten for 100  $\mu\text{g ml}^{-1}$  zinc. The results obtained in niobium–tantalum containing geological samples are given in Table 3 along with those obtained by the derivative method and there is good agreement between the values obtained by both methods as stated earlier. However, it was observed that the tantalum 207.930 nm line which lies within 0.02 nm of the tungsten line causes spectral interference of wing overlap type. This leads to enhanced tungsten values especially for low tungsten contents in high tantalum bearing samples. In order to eliminate this interference, we propose that the samples after fusion with KHSO<sub>4</sub>, are dissolved in 3% ammoniacal oxalate followed by precipitation with NH<sub>4</sub>OH and filtration. The filtrate was diluted to 100 ml volume for aspiration into the plasma after removing the oxalate by boiling it with nitric acid. By this method tungsten is separated from niobium and

tantalum making the line interference free. Values obtained with and without the separation of tantalum from tungsten in some high tantalum and low tungsten bearing samples are given in Table 4. It can be seen from this Table that ammonium oxalate separation is efficient for the separation of tantalum from tungsten, thereby giving values which are in good agreement with those values obtained by the derivative method. The major matrix elemental compositions of the niobate–tantalate samples studied are given in Table 5. Three synthetic niobate–tantalate samples, prepared by doping known amounts of tungsten (1000  $\mu\text{g}$ ), were also studied using the proposed ammonium oxalate and ammonium hydroxide separation method and the results obtained are presented in Table 6. Almost quantitative recoveries (94–95%) were observed in all the synthetic cases thus establishing no hold up of tungsten values in the precipitate.

## 4. Conclusion

The normal thiocyanate spectrophotometric method used for determination of tungsten in minor and major amounts can tolerate only low amounts of vanadium and molybdenum. Hence it becomes essential to separate the interferents from tungsten. The proposed second derivative method for estimation of tungsten as thiocyanate improves the tolerance limits of interferents vanadium, molybdenum and niobium thus enabling

Table 5  
Major matrix composition of niobate-tantalate samples

Sample No	Matrix composition (%)						
	Nb <sub>2</sub> O <sub>5</sub>	Ta <sub>2</sub> O <sub>5</sub>	TiO <sub>2</sub>	FeO	Fe <sub>2</sub> O <sub>3</sub>	MnO	SnO <sub>2</sub>
CHEM-1	66.4	8.8	1.8	12.9	0.6	6.7	<0.1
CHEM-2	58.9	13.6	3.8	11.3	1.6	5.3	0.3
CHEM-3	29.8	31.4	1.8	6.8	1.7	7.1	10.4
CHEM-4	33.8	37.2	1.2	11.8	<0.1	5.3	0.1
CHEM-5	20.2	46.1	4.4	6.6	2.4	6.3	5.8
CHEM-6	3.3	62.3	1.5	2.0	0.8	9.2	9.1
CHEM-7	4.6	14.3	1.3	10.0	<0.1	1.3	15.1
CHEM-8	6.9	21.4	1.3	<0.1	14.6	3.3	18.4
CHEM-9	20.5	42.9	1.6	<0.1	1.3	<0.1	15.4
CHEM-10	33.4	35.2	4.0	10.4	1.5	7.0	0.3

Table 6  
Tungsten values in synthetic niobate-tantalate samples by ICP-AES using the tungsten(II) 207.911 nm emission line

Sample	Amount added (mg)					Tungsten (μg) <sup>a</sup>		Recovery (%)
	Nb <sub>2</sub> O <sub>5</sub> <sup>b</sup>	Ta <sub>2</sub> O <sub>5</sub> <sup>b</sup>	TiO <sub>2</sub>	Fe	Mn	Added	Found <sup>c</sup>	
SYN-1	350	50	25	25	25	1000	954	95.4
SYN-2	50	350	25	25	25	1000	938	93.8
SYN-3	200	200	25	25	25	1000	945	94.5

<sup>a</sup> Proposed determination by ICP-AES after ammonium oxalate/ammonium hydroxide separation.

<sup>b</sup> Standard Nb<sub>2</sub>O<sub>5</sub>/Ta<sub>2</sub>O<sub>5</sub> stock solutions are prepared by fusing with KHSO<sub>4</sub> and dissolution in ammonium oxalate.

<sup>c</sup> Mean of five replicate measurements.

determination of tungsten in molybdenum, vanadium and niobium bearing samples without having to separate them. The method has been applied to niobium rich samples and has been found to give good results. Determination of tungsten in minor, major as well as trace levels in niobate-tantalate samples by ICP-AES is feasible using the proposed separation method at all levels of niobium and tantalum contents. Thus the proposed method offers good recoveries for tungsten values from niobium and tantalum in different types of niobate-tantalate samples using ICP-AES.

### Acknowledgements

The authors profusely thank Shri G.V. Ra-

maniah for his constant encouragement and support extended during the course of these investigations. Thanks are also due to Shri D.C. Banerjee, Director, AMDER, for his kind permission to publish these findings.

### References

- [1] J. Topping, *Talanta* 25 (1978) 61.
- [2] E.P. Welsch, *Talanta* 30 (1983) 876.
- [3] V.A. Nazarenko, V.P. Antonovich, N.A. Vesichkova, *Talanta* 34 (1987) 215.
- [4] Z. Fan, L. Zhang, H. Zhou, *Anal. Chim. Acta* 270 (1992) 267.
- [5] A.G. Fogg, D.R. Marriot, D.T. Burnes, *Analyst* 95 (1970) 848.
- [6] G.S. Reddi, C.R.M. Rao, H.S. Muralidhar, *Talanta* 40 (1993) 1433.

- [7] P. Chattopadhyay, P. Mistry, Fresenius J. Anal. Chem. 360 (1) (1998) 38.
- [8] X. Wu, Fenxi Shiyanshi 10 (2) (1991) 22.
- [9] S. Raoot, S.V. Athavale, T.H. Rao, Analyst 111 (1986) 115.
- [10] R.K. Malhotra, D.S.R. Murthy, G. Srinivasan, K. Satyanarayana, At. Spectrosc. 8 (1987) 161.
- [11] G. Wunsch, Talanta 26 (1979) 291.
- [12] I.B. Brenner, S. Elrich, Appl. Spectrosc. 38 (1984) 887.
- [13] G.E.M. Hall, J.C. Pelchat, K.N. Desilva, Analyst 112 (1987) 631.
- [14] J.E.M. Hall, C.J. Park, J.C. Pelchat, J. Anal. At. Spectrom. 2 (1987) 189.
- [15] V.I. Smolnikov, X-Ray Spectrom. 23 (4) (1994) 183.
- [16] K.W.W. Sims, E.S. Gladney, Anal. Chim. Acta 251 (1991) 297.
- [17] J.E.M. Hall, C.W. Jefferson, F.A. Michel, J. Geochem. Explor. 30 (1988) 63.
- [18] X. Luo, Z. Su, W. Gao, G. Zhan, X. Chang, Analyst 117 (1992) 145.
- [19] K. Satyanarayana, D.S.R. Murthy, M.K. Ganguly, R.K. Malhotra, in: Proc. of 6th Natl. Symp. on Earth Sciences, Shillong, India, 276, 1988.
- [20] T.C. O'Haver, G.L. Green, Anal. Chem. 48 (2) (1976) 312.
- [21] M.K. Ganguly, D.S.R. Murthy and R.K. Malhotra, in: Proc. Natl. Workshop on Tungsten Resources Development, Bhubaneswar, India, 139, 1989.
- [22] S. Bhattacharjee, L.P. Pandey, S.N. Jha, K.K. Gupta, Spectrosc. Eur. 4 (5) (1993) 26.
- [23] W.S. Bowman, CANMET Certified Reference Materials, CCRMP90-1E, 63, 1990.

# Flow-injection determination of trace amounts of dopamine by chemiluminescence detection

Lihe Zhang, Norio Teshima<sup>1</sup>, Takashi Hasebe, Makoto Kurihara, Takuji Kawashima \*

Laboratory of Analytical Chemistry, Department of Chemistry, University of Tsukuba, Tsukuba 305-8571, Japan

Received 15 March 1999; received in revised form 17 May 1999; accepted 17 May 1999

## Abstract

A flow-injection analysis (FIA) for the determination of dopamine has been developed. The method is based on the inhibition effect of dopamine on the iron(II)-induced chemiluminescence (CL) of 10,10'-dimethyl-9,9'-biacridinium dinitrate (lucigenin). The presence of a non-ionic surfactant, polyoxyethylene (23) lauryl ether (Brij 35), caused an increase in the inhibition effect. The present method allows the determination of dopamine over the range  $1 \times 10^{-8}$ – $2 \times 10^{-7}$  mol dm<sup>-3</sup>. The relative standard deviation was 0.7% for eight determinations of  $6 \times 10^{-8}$  mol dm<sup>-3</sup> dopamine. The detection limit ( $S/N = 3$ ) was  $2 \times 10^{-9}$  mol dm<sup>-3</sup> with the sampling rate of 40 samples h<sup>-1</sup>. The effect of other catecholamines and compounds of similar structure on the lucigenin CL reaction was studied: quinone, hydroquinone, norepinephrine, pyrocatechol and L-dopa suppressed the CL intensity. © 1999 Elsevier Science B.V. All rights reserved.

*Keywords:* Chemiluminescence; Dopamine; Flow-Injection; Lucigenin

## 1. Introduction

Catecholamines, of which dopamine is a typical compound, are the sympathetic neurotransmitter. In addition, catecholamines play an important role in the metabolism of sugar, lipid and so on. Dopamine, in particular, has relation to the ex-

trapyrnidial functions. Recently, dopamine has become of interest in the relation to Parkinson's syndrome [1]. Hence the determination of catecholamines is extremely important in the elucidation of nervous function, the diagnosis of diseases and the development of pharmaceuticals [2]. The concentration of these compounds in biological matrices is rather low and they are metabolized quickly in certain cases. The methods of determination for these compounds should be of high sensitivity and of rapid measurement.

For the determination of catecholamines in biological matrices, HPLC/fluorometry [2–6] and

\* Corresponding author. Tel.: +81-298-53-6521; fax: +81-298-53-6503.

*E-mail address:* kawashima@staff.chem.tsukuba.ac.jp (T. Kawashima)

<sup>1</sup> Present address: Department of Applied Chemistry, Aichi Institute of Technology, Toyota 470-0392, Japan.

HPLC/electrochemical analysis [7,8] are frequently used. With HPLC/fluorometry, a picomolar level of dopamine in rat plasma was determined [3]. Electrochemical methods using modified electrodes are also used, in particular for in vivo measurement [9–11]. Although these methods are highly sensitive, they need laborious

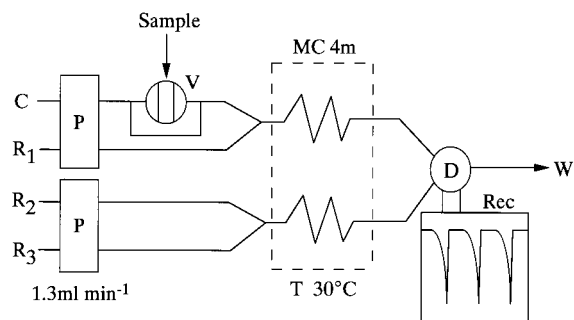


Fig. 1. Flow diagram for the CL determination of dopamine. C, water; R<sub>1</sub>,  $1.2 \times 10^{-5} \text{ mol dm}^{-3}$  iron(II); R<sub>2</sub>, mixture of  $1.0 \times 10^{-5} \text{ mol dm}^{-3}$  lucigenin and 0.1 wt% Brij 35; R<sub>3</sub>,  $0.5 \text{ mol dm}^{-3}$  NaOH; P, micro pump ( $1.3 \text{ ml min}^{-1}$ ); V, injection valve (sample volume 355  $\mu\text{l}$ ); MC, mixing coil; T, thermostated bath ( $30^\circ\text{C}$ ); D, CL detector; Rec, recorder; W, waste.

Table 1

Effect of surfactants on the CL intensity for  $1 \times 10^{-6} \text{ mol dm}^{-3}$  of dopamine solution injected<sup>a</sup>

Surfactant <sup>b</sup>	Relative CL intensity (%)
None	-100
<i>Anionic:</i>	
SDS	-13.3
<i>Nonionic:</i>	
Brij 35	-187
Tween-20	-95
Tween-80	-106
Triron X-100	-184
<i>Cationic:</i>	
CPC	-9.5
DTAC	-347
CTAC	-184

<sup>a</sup> R<sub>1</sub>,  $1.0 \times 10^{-5} \text{ mol dm}^{-3}$  iron(II); R<sub>3</sub>,  $0.75 \text{ mol dm}^{-3}$  NaOH; T, room temperature; flow rate,  $2.0 \text{ ml min}^{-1}$ . Other conditions as in Fig. 1.

<sup>b</sup> The concentrations of all surfactants used were ten times the critical micellar concentration.

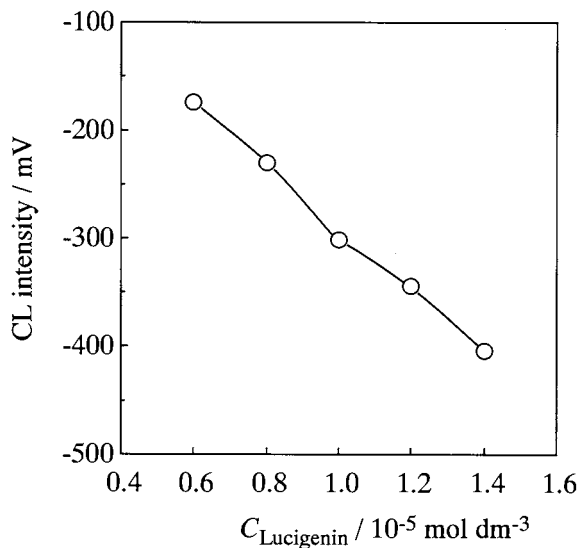


Fig. 2. Effect of lucigenin concentration on the CL intensity for  $1 \times 10^{-7} \text{ mol dm}^{-3}$  of dopamine solution injected. R<sub>1</sub>,  $1.0 \times 10^{-5} \text{ mol dm}^{-3}$  iron(II); flow rate,  $1.6 \text{ ml min}^{-1}$ . Other conditions as in Fig. 1.

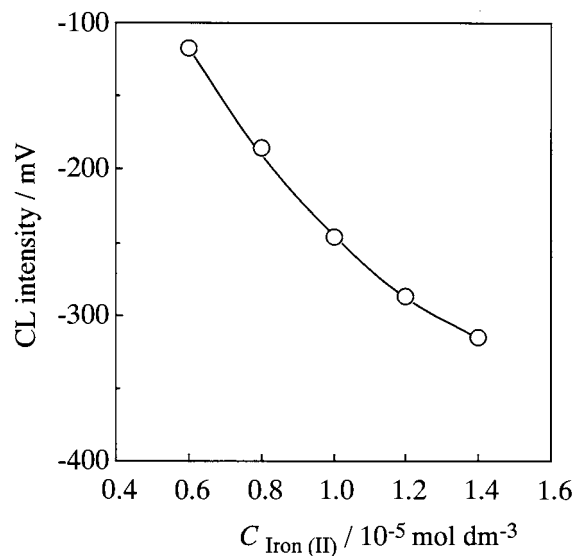


Fig. 3. Effect of iron(II) concentration on the CL intensity for  $1 \times 10^{-7} \text{ mol dm}^{-3}$  of dopamine solution injected. Flow rate,  $1.6 \text{ ml min}^{-1}$ . Other conditions as in Fig. 1.

sequence of treatments such as extraction, column separation, on-column fluorogenic derivatization, post-column chemiluminescent reaction and detection.

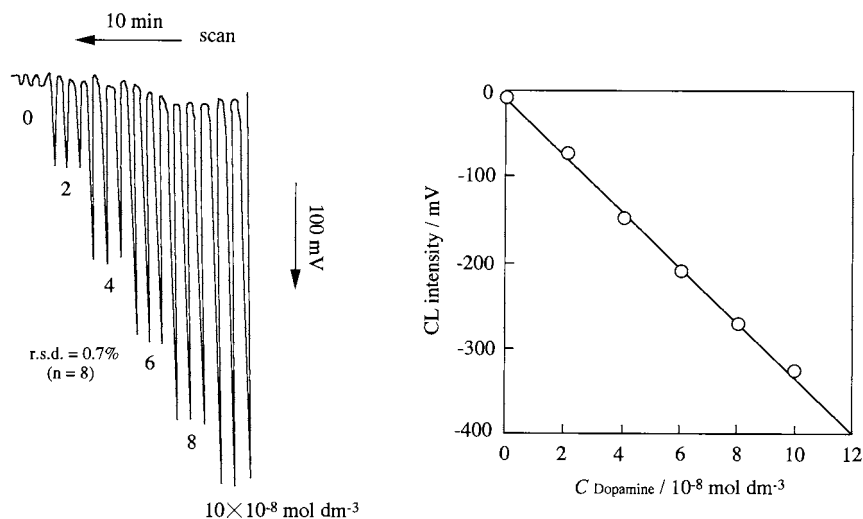


Fig. 4. Typical flow pattern and calibration curve for dopamine. Conditions as in Fig. 1.

On the other hand, flow injection analysis (FIA) method enables us rapid analysis. The determination of dopamine using the FIA method has been reported [12–14], in which the output signal of a biosensor system [12], the absorption of UV light [13] and the amperometric response of a wall jet cell [14] are used for detection. Especially, the FIA method consisting of an immobilized tyrosinase bioreactor and an oxygen electrode detector with L-ascorbic acid as a reduc-

ing agent is highly sensitive, and the detection limit of dopamine is  $2 \times 10^{-9} \text{ mol dm}^{-3}$  [12].

The chemiluminescence (CL) method is also of high sensitivity and is easily combined with the FIA to provide a rapid and sensitive method of determination. However, the use of the FIA/CL method for the determination of catecholamines is rather rare [15,16]. Deftereos et al. utilized chemiluminogenic oxidation of catecholamines with potassium permanganate in acidic medium, and

Table 2

Effect of coexisting foreign ions and compounds on the determination of  $1 \times 10^{-7} \text{ mol dm}^{-3}$  dopamine<sup>a</sup>

Foreign ions and compounds	Relative CL intensity (%)	Foreign ions and compounds	Relative CL intensity (%)
None	–100	Ascorbic acid	–93
Sorbitol	–94	Fructose	–96
Glucose	–98	Valine	–100
Lysine	–98	Leucine	–98
Histidine	–97	Tryptophan	–99
Serine	–99	L-Glutamine	–100
Glutamic acid	–105	L-Cystine	–106
L-Aspartic acid	–104	Galactose	–123
L-Alanine	–113	Sodium urate	–51
Cl <sup>–</sup>	–95	SO <sub>3</sub> <sup>2–</sup>	–88
PO <sub>4</sub> <sup>3–</sup>	–102		
Na <sup>+</sup>	–95	K <sup>+</sup>	–104
Mg <sup>2+</sup>	–104	Ca <sup>2+</sup>	–109
Cu <sup>2+</sup>	–485		

<sup>a</sup> These foreign ions and compounds ( $1 \times 10^{-6} \text{ mol dm}^{-3}$ ) were mixed in the solution of dopamine. Conditions as in Fig. 1.

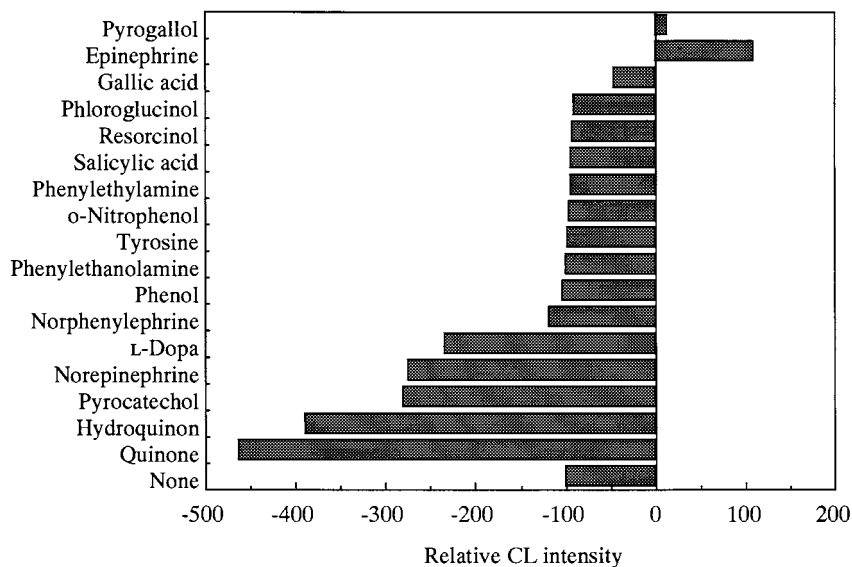


Fig. 5. Effect of coexisting organic compounds with similar structure to dopamine on the determination of  $1 \times 10^{-7}$  mol dm $^{-3}$  dopamine. These compounds were mixed in the solution of dopamine with the concentration of  $1 \times 10^{-6}$  mol dm $^{-3}$ . Conditions as in Fig. 1.

the method can determine 0.05–1.0  $\mu\text{g cm}^{-3}$  of epinephrine and L-dopa and 0.1–1.0  $\mu\text{g cm}^{-3}$  of norepinephrine and dopamine with a sampling rate of 80 samples h $^{-1}$  [15]. Lucigenin chemiluminescence was used by Al-Warthan et al. for the FIA determination of isoprenaline, and the logarithmic calibration curve was linear over the range  $10^{-7}$ – $10^{-4}$  mol dm $^{-3}$  [16].

We have developed FIA methods for the determination of ascorbic acid by iron(III)-catalyzed lucigenin CL in a micellar system [17]. We found that dopamine strongly interferes with the CL reaction of the iron(II)–lucigenin system in basic solution. The degree of this interfering effect depends on the concentration of dopamine and can be used to determine dopamine. In this paper, we describe a new FIA method utilizing lucigenin CL for the determination of dopamine. Using the present method, determination of  $1 \times 10^{-8}$ – $2 \times 10^{-7}$  mol dm $^{-3}$  dopamine with a relative standard deviation of 0.7% is possible. The detection limit ( $S/N=3$ ) is  $2 \times 10^{-9}$  mol dm $^{-3}$ , and the sampling rate is 40 samples h $^{-1}$ . The proposed method was successfully applied to the determination of dopamine in pharmaceuticals.

## 2. Experimental

### 2.1. Reagents

All of the reagents were of analytical grade and were used without further purification. The water used to prepare the solutions was purified with a Milli-Q PLUS water system (Millipore).

A stock solution of lucigenin ( $1.0 \times 10^{-3}$  mol dm $^{-3}$ ) was prepared by dissolving 0.102 g of 10,10'-dimethyl-9,9'-biacridinium dinitrate (Tokyo Kasei) in 200 ml of water. A stock solution of dopamine ( $1.0 \times 10^{-2}$  mol dm $^{-3}$ ) was prepared by dissolving 0.190 g of 3,4-dihydroxyphenethylamine hydrochloride (Wako Pure Chemical) in water and diluting to 100 ml. A stock solution of NaOH ( $1.0$  mol dm $^{-3}$ ) was prepared by dissolving 40.0 g of sodium hydroxide (Wako) in 1000 ml of water. A stock solution of iron(II) ( $1.0 \times 10^{-2}$  mol dm $^{-3}$ ) was prepared by dissolving 1.961 g of ammonium iron(II) sulfate hexahydrate in  $1 \times 10^{-2}$  mol dm $^{-3}$  hydrochloric acid and diluting to 500 ml with the same acid. The dissolved oxygen in the stock solution of iron(II) was removed by bubbling nitrogen gas. Working solu-

tions were prepared by appropriate dilution of the stock solutions. A solution of Brij 35 (0.1 wt%) was prepared by dissolving 0.20 g of polyoxyethylene(23) lauryl ether (Wako) in 200 ml of a lucigenin solution ( $1.0 \times 10^{-5}$  mol dm<sup>-3</sup>).

## 2.2. Apparatus

A schematic diagram of the flow system for the determination of dopamine is shown in Fig. 1. Two double-plunger micro-pumps (Sanuki Kogyo, DMX-2000) and a six-way injection valve (Sanuki Kogyo, SVM-6M2) were used to assemble the system. The flow lines were made from Teflon tubing (0.5 mm i.d.). A CL detector equipped with a spiral flow-cell (100  $\mu$ l) (Soma Optics, S-3400) was used for the measurement of CL intensities. The output of the detector was recorded on a recorder (Chino, EB 22005). The reaction temperature was maintained at 30°C by circulating water from a constant temperature bath (TAITEC, DX-100).

## 2.3. Procedure

In the flow system (Fig. 1), water as a carrier solution (C), a  $1.2 \times 10^{-5}$  mol dm<sup>-3</sup> iron(II) solution (R<sub>1</sub>), a mixed solution of  $1.0 \times 10^{-5}$  mol dm<sup>-3</sup> lucigenin and 0.1% (w/v) Brij 35 (R<sub>2</sub>) and a 0.5 mol dm<sup>-3</sup> NaOH (R<sub>3</sub>) were pumped at a flow rate of 1.3 ml min<sup>-1</sup>. A 355- $\mu$ l sample solution was injected into the carrier stream. The CL reaction of lucigenin with iron(II) suppressed in the spiral flow-cell, and the intensities decreased with an increase in the concentration of dopamine. Thus a negative peak, whose height corresponds to the concentration of dopamine, was monitored and recorded.

Table 3  
Determination of dopamine in pharmaceutical preparation<sup>a</sup>

Calibration method <sup>b</sup>	19.6 $\pm$ 0.7 mg ml <sup>-1</sup>
Standard addition method <sup>b</sup>	19.4 $\pm$ 0.9 mg ml <sup>-1</sup>
Reference value	20 mg ml <sup>-1</sup>

<sup>a</sup> The sample was diluted two million times with water.

<sup>b</sup> Average of three determinations.

## 3. Results and discussion

### 3.1. Inhibition effect of dopamine on the iron(II)-catalyzed lucigenin CL reaction

In a basic solution, lucigenin is reduced by iron(II) to excited *N*-methylacridon, which then emits fluorescence [18,19]. It was found that the presence of dopamine causes an inhibition of this CL reaction. Since the degree of inhibition depends on the concentration of dopamine present in sample solution, it is possible to determine the concentration of dopamine from the decrease in the CL intensity.

Dopamine has two absorption maxima at 280 and 340 nm. However, an absorption maximum of 340 nm disappeared by adding iron(II). This suggests that there exists some interaction between them. This interaction would hamper iron(II) from reducing lucigenin, and the CL reaction of the lucigenin–iron(II) system would be inhibited [20,21].

### 3.2. Optimization of the flow system

#### 3.2.1. Effects of surfactants

For the application of the CL reaction of lucigenin to the FIA system, there is one major problem concerning the solubility of reaction products: *N*-methylacridon produced precipitates in the flow system, and this affects the reproducibility of the measurement. In order to solve this problem, and also to improve the sensitivity, we have examined the effects of some surfactants on the performance of the system. The surfactants examined were as follows: an anionic surfactant, sodium dodecylsulfate (SDS); nonionic surfactants, Brij 35, Tween 20, Tween 80 and Triton X-100; cationic surfactants, cetylpyridinium chloride (CPC), *n*-dodecyltrimethylammonium chloride (DTAC) and cetyltrimethylammonium chloride (CTAC). Each surfactant was dissolved in the lucigenin solution at the concentration of ten times the critical micellar concentration (CMC), and the solution was pumped from reservoir R<sub>2</sub> (Fig. 1). The relative CL intensities obtained from these surfactants are shown in Table 1. The negative peak height for dopamine remark-



ably increased in the presence of Brij 35, Triton X-100, DTAC and CTAC. However, the baseline intensity in the absence of dopamine also increased in the presence of these surfactants except Brij 35, and it led to an unstable baseline. As the baseline was relatively stable in the case of Brij 35, it was used for the procedure. The effect of the Brij 35 concentration over the range 0.01–1.0% (w/v) was thus examined. The negative peak height increased with increasing the concentration of Brij 35 up to 1.0% (w/v). However, at concentrations higher than 0.1 wt%, a stable baseline was not obtained and the reproducibility of the peaks became poorer. Thus a 0.1% (w/v) Brij 35 concentration was selected for the procedure.

### 3.2.2. Effect of lucigenin

When lucigenin concentrations higher than  $1.6 \times 10^{-5}$  mol dm<sup>-3</sup> were pumped, the baseline heavily fluctuated, and reproducible measurement was impossible. The effect of the lucigenin concentration was examined over the range  $6.0 \times 10^{-6}$ – $1.4 \times 10^{-5}$  mol dm<sup>-3</sup>. The results are shown in Fig. 2. In this concentration range, the negative peak height increased with increasing concentration of lucigenin. A  $1.0 \times 10^{-5}$  mol dm<sup>-3</sup> lucigenin concentration was selected taking into account the stability of baseline and the reproducibility of the peak height.

### 3.2.3. Effect of iron(II)

The effect of iron(II) concentration was examined over the range  $6.0 \times 10^{-6}$ – $1.4 \times 10^{-5}$  mol dm<sup>-3</sup>. The results are shown in Fig. 3. The higher the iron(II) concentration, the more negative intense peak was obtained. By considering the stability of baseline and the reproducibility of the peak height, a  $1.2 \times 10^{-5}$  mol dm<sup>-3</sup> iron(II) concentration was chosen for the procedure.

### 3.2.4. Effect of sodium hydroxide

The effect of the sodium hydroxide concentration was examined over the range 0.1–1.0 mol dm<sup>-3</sup>. The negative peak height increased with increasing sodium hydroxide concentration up to 0.5 mol dm<sup>-3</sup>, and a maximum and constant peak height was obtained at concentrations higher than 0.5 mol dm<sup>-3</sup>. Thus, a 0.5-mol dm<sup>-3</sup> sodium hydroxide concentration was chosen.

### 3.2.5. Effect of temperature

The effect of reaction temperature was examined over the range 25–40°C. The negative CL intensities became larger as the temperature increased up to 40°C. However, the stability of the baseline became poorer at higher temperatures. Thus, a temperature of 30°C was selected for the procedure.

### 3.2.6. Effect of flow rate

The negative CL intensities became larger with increasing the flow rate up to 1.6 ml min<sup>-1</sup>. Beyond 1.3 ml min<sup>-1</sup>, however, the baseline became unstable, so that the flow rate of each stream was set at 1.3 ml min<sup>-1</sup>.

### 3.2.7. Effect of injection volume

The effect of the injection volume of dopamine was examined over the range 130–590 µl. The sensitivity of dopamine was maximum and almost constant beyond 355 µl. Thus, a 355-µl of dopamine solution was used for the procedure.

## 3.3. Calibration graph

A calibration curve for  $10^{-8}$  mol dm<sup>-3</sup> levels of dopamine was obtained by using the optimized flow system mentioned above. A typical flow pattern and a calibration graph are shown in Fig. 4. The calibration graph is linear over the range  $1 \times 10^{-8}$ – $2 \times 10^{-7}$  mol dm<sup>-3</sup> dopamine concentration. The relative standard deviation was 0.7% for eight determinations of  $6 \times 10^{-8}$  mol dm<sup>-3</sup> dopamine. The detection limit ( $S/N = 3$ ) was  $2 \times 10^{-9}$  mol dm<sup>-3</sup> with the sampling rate of 40 samples h<sup>-1</sup>.

## 3.4. Interferences

The interference effects of coexistence of substances which are expected to present in the biological matrices or the pharmaceutical preparation were examined. The concentration of the coexisting substance was ten times that of dopamine. The results are summarized in Table 2. Ascorbic acid, sorbitol and iron(III) did not show interference effect. Galactose, L-alanine and sodium sulfite gave a little interference. Cop-

per(II) and sodium urate markedly interfered with the determination of dopamine. Hence these interference effects should be considered when a real sample is analyzed.

Effects of coexisting organic compounds with similar structure of dopamine, such as epinephrine, quinone, etc., on the determination of  $1 \times 10^{-7}$  mol dm $^{-3}$  dopamine were also examined. The results are shown in Fig. 5, where the peak height for  $1 \times 10^{-7}$  mol dm $^{-3}$  dopamine (without coexistent organic compounds) is set to –100. Each organic compound ( $1 \times 10^{-6}$  mol dm $^{-3}$ ) shown in Fig. 5 was mixed in the solution of dopamine. It is shown that the coexistence of quinone, hydroquinone, norepinephrine and catechol markedly interferes with the determination of dopamine. Hence, a separation process by using an ion-exchange column would be recommended before determination [22]. On the contrary, these compounds may be determined in a similar manner as dopamine.

As shown in Fig. 5, regardless of similar structures between epinephrine and norepinephrine, epinephrine gives a positive signal and norepinephrine shows the negative. As described in Section 3.1, inhibition effect of dopamine on the CL reaction is attributable to the interaction between dopamine and iron(II). Similar interaction was also observed for norepinephrine, but not epinephrine. Thus, the interaction of these compounds except epinephrine with iron(II) caused negative interference on the CL reaction, while epinephrine with no interaction gave a positive signal.

### 3.5. Determination of dopamine in a pharmaceutical preparation

The concentration of dopamine in an injection as a pharmaceutical preparation was determined by the present method. A sample was diluted two million times with water before measurement. The

results are shown in Table 3. The values obtained by the calibration method, as well as the standard addition method are in excellent agreement with the reference value.

## References

- [1] L. Stryer, *Biochemistry*, 3, W.H. Freeman, San Francisco, New York, 1988.
- [2] I.J. Kopin, Plasma level of catecholamines and dopamine- $\beta$ -hydroxylase, in: U. Trendelenburg, N. Weiner (Eds.), *Catecholamines II*, Springer, Berlin, 1989.
- [3] S. Higashidate, K. Imai, *Analyst* 117 (1992) 1863.
- [4] C.A. Marsden, M.H. Joseph, Z.L. Kurk, N.T. Maidment, R.D. O'Neill, J.O. Schenk, J.A. Stamford, *Neuroscience* 25 (1988) 389.
- [5] S. Lennart, C.W.H. Peter, J. Kenn, E.A. Joergen, *Brain Res.* 609 (1993) 36.
- [6] N.R. Wrightman, J.B. Zimmermann, *Brain Res. Rev.* 15 (1990) 135.
- [7] S.A. McClintock, W.C. Purdy, *Anal. Chim. Acta* 166 (1984) 171.
- [8] N.R. Musso, C. Vergassola, A. Pende, G. Lotti, *J. Liq. Chromatogr.* 14 (1991) 3695.
- [9] R.D. O'Neill, *Analyst* 119 (1994) 766.
- [10] Z. Gao, B. Chen, M. Zi, *Analyst* 119 (1994) 459.
- [11] Y. Hasebe, T. Hirano, S. Uchiyama, *Sensors Actuators B* 24/25 (1995) 94.
- [12] Y. Hasebe, K. Takamori, S. Uchida, *Anal. Chim. Acta* 282 (1993) 363.
- [13] J.J.B. Nevados, J.M.L. Gallego, P.B. Laguna, *J. Pharm. Biomed. Anal.* 14 (1996) 571.
- [14] E.M. Garrido, J.L.F.C. Lima, C.D. Matos, *J. Pharm. Biomed. Anal.* 15 (1997) 845.
- [15] N.T. Deftereos, A.C. Calokerinos, C.E. Efstathiou, *Analyst* 118 (1993) 627.
- [16] A.A. Al-Warthan, S.A. Al-Tamrah, A.A. Al-Akel, *Anal. Sci.* 10 (1994) 449.
- [17] T. Hasebe, T. Kawashima, *Anal. Sci.* 12 (1996) 773.
- [18] J.R. Totter, *Photochem. Photobiol.* 22 (1975) 203.
- [19] R. Maskiewicz, D. Sogah, T.C. Bruice, *J. Am. Chem. Soc.* 101 (1979) 5355.
- [20] A.K. Babko, H.M. Lukovskaya, *Ukr. Khim. Zh.* 35 (1969) 1060.
- [21] A.A. Al-Warthan, S.A. Al-Tamrah, A.A. Akel, *Anal. Chim. Acta* 292 (1994) 201.
- [22] T. Kitahashi, Y. Ohba, Y. Sawada, H. Suzuki, *Rinsho Kagaku* 20 (1991) 24.

## Book Review

***Modern Derivatization Methods for Separation Sciences* by Toshimasa Toyo'oka (editor), Wiley, Chichester, 1999, xiv + 298 pp. ISBN 0-471-98364-0; £80.00**

This book is written by sixteen Japanese chemists from mainly analytical and pharmaceutical backgrounds. In 298 pages the multi-author team describes the choice, the handling and some applications of many important derivatization reactions in analytical chemistry with the emphasis on the detection of organic compounds using high performance liquid chromatography (HPLC) and capillary electrophoresis (CE).

Six chapters guide the reader from pretreatment of real samples to more detailed descriptions of the most important derivatization methods. Applications in the first chapter are subdivided into three different areas: pharmaceutical, agrochemical and environmental. This chapter, which contains information about more problem-oriented subjects such as air sampling, is very useful for teaching. It offers a good survey of the different kinds of derivatization reagents have been used for particular classes of compounds. The following chapters are more purpose oriented: derivatization methods for UV-detection, fluorescence and chemiluminescence detection, as well as electrochemical detection for HPLC and CE. The description of the most popular procedures for separation and mainly detection of listed classes of compounds includes useful data about performance of the method such as detection limits along with the operational parameters. Furthermore, molecular structures of the derivatizing

reagents and chromatograms are given. However, it can be quite time consuming to compare the different methods for one particular analytical problem.

The last chapter is devoted to the separation of chiral compounds. It is the most comprehensive essay in this book and contains detailed descriptions of useful derivatization reactions for all aspects of separation which includes gas chromatography as well as HPLC and CE.

In general the title of the book '...methods for separation sciences' is a bit misleading; more than three quarters of the described methods are for HPLC and CE detection. Very little information is available about applications for gas chromatography, i.e. reaction for the formation of volatile compounds, e.g. by using silylation for carbohydrates or hydride generation and ethylation for organometallic compounds such as TBT. The book is also lacking information on derivatization reactions used for liquid-liquid separation, volatilization, or condensation reactions. In fact the chapter of derivatization methods used for environmental samples is disappointing. It is short and does not contain any detailed information about the methods themselves.

I would recommend this book to everyone who would like to use it for teaching purposes. For research it is useful as a guide for derivatization methods used to enhance the detectability of organic compounds after liquid chromatography or capillary electrophoresis.

J. Feldmann

## Book Review

***Analytical Chemistry by Open Learning—Mass Spectrometry. 2nd Edition. By D. J. Ando (editor), Wiley, Chichester, 1999, 509 pp. ISBN 0-471-96762-9; £37.50.***

This ACOL volume on mass spectrometry is an extensively updated version of the previous edition written by Reginald Davis and Martin Frearson in 1987. I had studied the first edition in my undergraduate years and later returned to it to brush-up on mass spectroscopy as my PhD viva approached. Unfortunately, I found that many advances had been made and my old volume had become outdated. When this book arrived on my desk to review I was delighted to find it had been reorganised and extensively up-dated with new developments in mass spectroscopy.

The basic theory of ion formation and behaviour, instrumentation and interpretation of spectra are well presented and the reader's participation in the learning process is constantly challenged by self-assessment questions. The answers to which, at the back of the text, are well explained and easily understood. Recent developments in sample ionisation such as laser desorption and matrix-assisted laser desorption ionisation techniques have been introduced.

The chapter on typical fragmentation patterns of common functional groups has been expanded to include the analysis of biomolecules—in particular that of proteins. The inclusion of this small but relevant section allows the student to appreciate, to some extent, the analytical power of mass spectroscopy in protein sequencing.

I was very impressed with the chapter on hyphenated mass spectral techniques which is currently a very dynamic area of interest with respect

to separation analysis. The section on LC/MS has been completely updated and gives a very comprehensive overview of the various interfaces that are available such as electrospray, ionspray, particle-beam and atmospheric-pressure chemical ionisation. Although tandem MS/MS was included, it perhaps warranted more than the three pages that were allocated to it. Examples of published reports utilising MS/MS would have more fully shown the potential of this technique.

The use of computers in structure elucidation and data acquisition and processing is also included and reflects their integral part in modern mass spectroscopy. This updated edition also contains a small appendix which includes isotopes in ascending mass order and isotopic abundances for compositions of C, H, O and N for the student to appreciate a 'hands on' interpretation of spectra.

The final chapter in this book describes the principles of operation of some common methods in inorganic mass spectroscopy and applies this to the analysis of surfaces, bulk solids and solutions. The student is not only tutored in their advantages but also in their limitations.

The addition of an index will be welcomed by all who study using ACOL. Even more so by those returning for a quick reference. In comparison to the first edition, there is greater breakdown of the chapters into smaller, more specific, sections. These are listed in the contents which is of benefit to the more casual reader.

To conclude this book is a much awaited revision and expansion of the previous edition of 1987. It will be of great use to students and provides a working knowledge of mass spectroscopy.

A.S. Low

## Book Review

***Stereoselectivity in Synthesis* by Tse-Lok Ho, Wiley, Chichester. 1999, xv + 333 pp. ISBN 0-471-32922-3; £61.50.**

The title of the book, '*Stereoselectivity in Synthesis*', encompasses such a wealth of organic chemistry that it is difficult to envisage how the subject may be explained in a logical context. In this respect, Professor Tse-Lok Ho has done remarkably well by subdividing the material into nine chapters. Each of which has an informative title, several subheadings, numerous clear diagrams, a good reference section and has been appropriately indexed.

I enjoyed reading the opening chapter, where the basis of stereochemical induction and nomenclature are succinctly, yet immaculately, described. The brief explanations at the beginning of the various topics throughout the book were also a delight to read, but the predominance of target-

orientated examples that followed them made me wonder if the phrase 'natural products' should have appeared in the title. Although this volume provides an edifying review of the asymmetric synthesis of natural products, it focused slightly too much on exemplifying, rather than explaining, techniques for obtaining stereocontrol in the synthesis of organic compounds. By doing so, the author has limited the appeal of the book to the more advanced reader. In addition, parts of the text would benefit from some editorial attention and occasionally the rationale behind the stereoselectivity was not to my liking. Nonetheless, the abundance of chemistry contained within Ho's latest contribution has been presented in an educational and engaging manner, which should appeal to many in the chemical community.

M.F. Ward

## Book Review

***Electroanalysis* by C.M.A. Brett and A.M.O. Brett, OUP, Oxford, 1998, 88 pp. ISBN 0-19-854816-8; £5.99**

Older readers may remember the very useful series of OUP paperbacks that came out in the 1970s. I must admit I found them particularly useful as a supplement to the main recommended textbooks in the three branches of chemistry, in particular for the more specialist courses one finds in the final year of British undergraduate chemistry courses. Now we have a new series with the same philosophy, and with a very reasonable cover price, thanks to a subsidy from Zeneca. It is a delight to see the series blossoming into so many titles; it is a wonderful showcase for chemistry topics from the (mostly) British undergraduate perspective. Having said that, the authors of the book in question teach at Coimbra University, Portugal. Hard-pressed students might consider buying these books if their main text-book is not very helpful. This particular title is a case in point, covering electroanalytical methods which you would not find in a physical chemistry text book such as Atkins, but analytical chemistry majors might find this material in their analytical chemistry book (e.g. Skoog and West). The book begins with a rather rapid discussion of electrochemical principles, topics which incidentally are covered in two other books in the series. (I would also strongly recommend Derek Pletcher's book on electrode processes and Bryn Hib-

bert's book on electrochemistry.) Inevitably, given the space constraints—less than 90 pages—many techniques in the following chapters are described without much explanation of the key equations associated with each technique. However, the diagrams are very good and the text is very clearly written and accurate. In my own experience, I have found that lecturing a list of techniques to students can be unrewarding unless accompanied by computer simulation of the techniques and a short laboratory course. Modern instruments are perfectly capable of carrying out a repertoire of the techniques mentioned in this book. There is not much in the book on biosensors, which is rather a pity as this is a topic that students find very interesting, and there are no problems. The last chapter is the most disappointing, since it is on applications, but the opportunity has been missed to enthuse students with research case studies with a few interesting diagrams and key references. However, overall, I would recommend this inexpensive book to accompany (or even to help write!) a short course, on electroanalytical techniques, but students should be referred to other books for detailed understanding and for derivations. Incidentally, a mechanical problem with the old books was that their pages easily fell out: there should be no such problems with this new series.

J. Crayston

Preface

## Special Issue Methodologies for wastewater quality monitoring

The European Community has decided in 1991 to oblige all the Member States to be equipped with wastewater treatment plants for all the cities whose wastewater organic loads is greater than 15 000 equivalent-inhabitants (before 31 December 2000) and 2000 equivalent-inhabitants (before 31 December 2005). The quality of the treated wastewater must be better than reference values for some parameters such as BOD (biological oxygen demand), COD (chemical oxygen demand), TSS (total suspended solids), global nitrogen and total phosphorus. Unfortunately, the usual monitoring procedure is not very satisfying because the chosen parameters are not easy to measure without sampling, storage and laboratory analysis.

The only way to reach the Community levels fixed in 1991 for the wastewater treatment is to ensure that the plants are able to work with a great reliability, which implies that monitoring should be performed for the characterisation of raw and treated wastewaters and for the control of the plant itself. In this perspective, on-line measurement is more relevant than sampling and laboratory analysis.

A better management of wastewater treatment and monitoring implies a close collaboration among industrialists, municipalities, legislators and research organisations. To respond to the need of strengthening links between various organisations, the Standards, Measurements and

Testing Programme of the European Commission decided to launch a workshop on ‘Methodologies for Wastewater Quality Monitoring’ which was organised by the Ecole des Mines (Alès, France) and was held in Nîmes (France) on 29–30 October 1998. The scientific committee of the workshop was chaired by Professor O. Thomas (Ecole des Mines d’Alès, France) and composed by Professor Victor Cerda (University of Balearic Islands, Spain), Dr Ph. Quevauviller (European Commission, Belgium) and Dr A. Lynggard-Jensen (VKI, Denmark); the local organising committee was coordinated by Dr M.-F. Pouet and Dr E. Touraud (Ecole des Mines d’Alès, France). The workshop aimed to stimulate partnership between industry, research organisations, universities, environmental control laboratories, SMEs, regulatory bodies and wastewater treatment plants for the identification of possible actions to be undertaken in the sector of wastewater monitoring. Several topics were debated in round-table during the workshop attended by 25 experts from 12 European countries, namely: (1) applications; (2) trends in methodologies; and (3) technical solutions and validation; the background of the discussions focused on the research and end user’s needs, the advantages and drawbacks of existing methodologies and the validation of methods for different applications (e.g. sewer measurement, wastewater treatment plant control, treated wastewater survey, etc.).

This special issue of *Talanta* contains selected (peer reviewed) papers covering the expertise of the group of participants. Highlights of the issue are reviews on flow techniques in water analysis and trends in wastewater monitoring, discussion papers describing the regulatory background (EC Directive on wastewater) and costs related to on-line instrumentation, and original papers describing methodologies for wastewater characterisation (e.g. of heterogeneous fractions, mineral sulphide, TOC and nitrogen and phosphorus). The issue also contains a summary paper giving the conclusions of the round-table discussions.

The editors gratefully acknowledge all the participants for the fruitful discussions which guaranteed the success of the workshop. A special thanks goes to the chair persons and rapporteurs of the round-tables, and to the local organisers for their efficient work and dedication.

O. Thomas

*Ecole des Mines, d'Alès, France*

M.-F. Pouet

*Ecole des Mines, d'Alès, France*

Ph. Quevauviller

*European Commission, Brussels, Belgium*



## Flow techniques in water analysis

V. Cerdà <sup>a,\*</sup>, J.M. Estela <sup>a</sup>, R. Forteza <sup>a</sup>, A. Cladera <sup>a</sup>, E. Becerra <sup>b</sup>,  
P. Altimira <sup>c</sup>, P. Sitjar <sup>c</sup>

<sup>a</sup> *Department of Chemistry, University Illes Balears, E-07071, Palma de Mallorca, Spain*

<sup>b</sup> *IMRE, Universidad de la Habana, Habana, Cuba*

<sup>c</sup> *Crison Instruments, S.A., Alella, Spain*

### Abstract

In the present work the main flow techniques for the analysis and monitoring of several parameters of interest in the quality control of different types of waters are reviewed. Firstly, a review involving the advantages and disadvantages of flow techniques, from those currently out-dated, such as segmented flow analysis (SFA), to the most modern techniques, such as flow injection analysis (FIA), sequential injection analysis (SIA) and multi-commutation techniques (MCFA), is carried out. On the other hand, a new technique, the multi-syringe flow analysis (MSFA) is hereby described for the first time as both a fast and robust alternative. Its possibilities, limitations and potential advantages when using this technique either on its own or coupled to SIA, which carries out a previous sample handling, are outlined. © 1999 Elsevier Science B.V. All rights reserved.

*Keywords:* Quality control; Waters; Syringe

### 1. Introduction

The acceptance of the existence of a correlation between environmental preservation and standard of living has led to the need of a vigilance and continuous control of a large number of environmental parameters. In this way new analytical methods — fast, robust and whenever possible multiparametric — capable of undergoing analysis of a large number of samples within a short period of time have been set up.

One of the current trends in the analysis of environmental parameters involves avoiding sam-

pling in which all the samples are required to be carried to the laboratory. Thus, the use of screening methods, which may not be very selective, allow, however, the detection of alarm situations and, therefore, the most complete analyses are only carried out in those samples where eventually analysis is required.

Having to dispose of methods applicable to measurements in the open country, implies a change of the analyst's mentality, excessively used to very sophisticated and expensive techniques, their use being difficult to adapt outside the laboratory. On the other hand, this problem requires the use of robust techniques without demanding the continuous presence of the analyst, especially if they are applied to a continuous monitoring and/or

\* Corresponding author. Tel.: +34-971-173426.

E-mail address: vcerda@p01.uib.es (V. Cerdà)

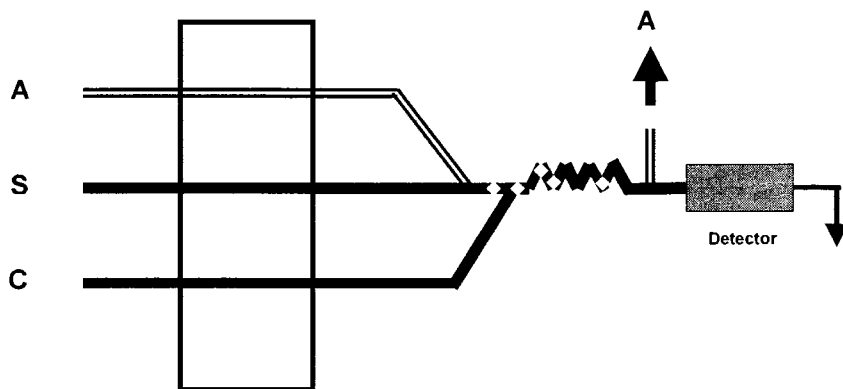


Fig. 1. Segmented flow system.

with very frequent measurements, in which, besides, reagent consumption for the performance of the analytical essays is not required or minimized. In order to be consistent with the aim of an environment quality improvement these reagents should be also environment-friendly.

Although for the analysis of certain environmental samples all the above-mentioned objectives are difficult to be achieved in a completely automatic way, aqueous samples are especially well adapted to be analysed by flow techniques. The advantages and disadvantages of each of the former techniques are reviewed below.

The importance and interest of these flow techniques regarding the study of water quality is reflected by numerous reviews which have been carried out within this field [1–18] either with a general approach, or in the case of their application to the determination of certain parameters. A vast majority of these works are referred to the application of flow injection analysis (FIA), which has been -by large- imposed during the last decades over the remaining techniques. There are hardly any bibliographical reviews worth to be mentioned regarding the other techniques, because of the fact that either they are no longer in use (SFA) or they have not been sufficiently developed yet (MCFA and MSFA). The only bibliographical review on SIA which we are aware of has been very recently published [19].

## 2. Techniques

### 2.1. Segmented flow analysis (SFA)

Segmented flow analysis was one of the first techniques widely imposed in the laboratories requiring a large volume of analysis, such as hospitals and oceanographic laboratories. The continuous segmented flow analysis methods (SFA), commercialized by the trade Technicon by the name Autoanalysers, are the classic methods described by Skeggs in 1957 [20] (Fig. 1).

Samples are sequentially aspirated and between them air bubbles are located which separate (segmentate) the flow established, including a washing cycle. Usually, the air bubbles are eliminated before reaching the detector flow cell. They frequently consist in multichannel techniques, in which there is an individual detector for each

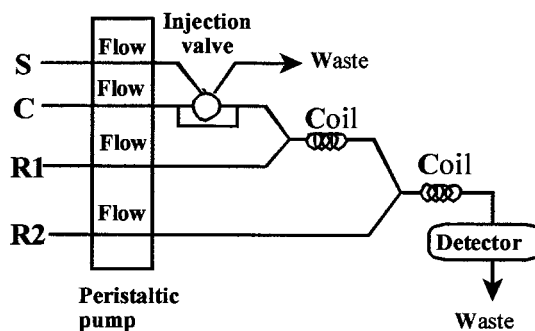


Fig. 2. Flow injection system.

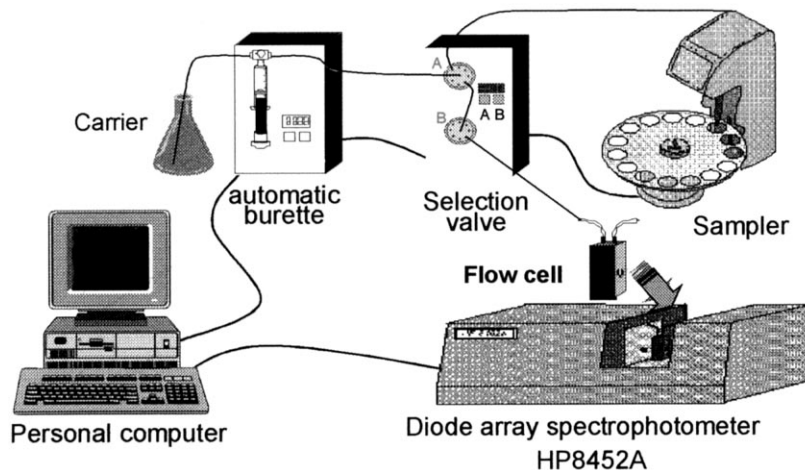


Fig. 3. Sequential injection system.

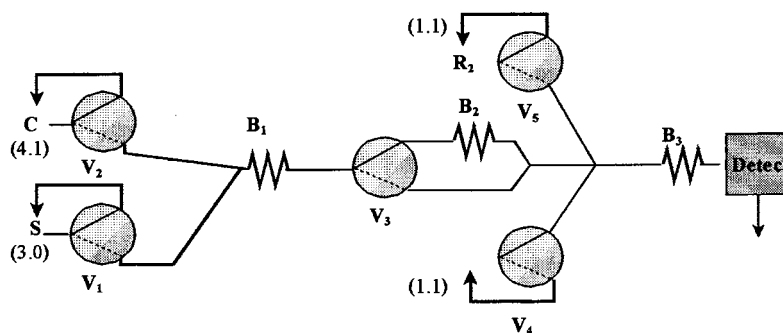


Fig. 4. Flow diagram of a multicommutation system for automatic single stage dilutions.

parameter to be determined, and therefore are usually expensive, although they offer good possibilities of working capacity. They have been designed to simultaneously determine even more than 20 parameters. These systems were gradually phased out by discontinuous automatic systems, until flow injection analysis (FIA) was introduced (Fig. 2).

Among the technical characteristics of SFA are the following: aspirated sample volumes 0.2–2 ml; response time 2–30 min; tube diameters 2 mm; detection in homogeneous equilibrium state; sampling frequency of up to 80 samples  $\text{h}^{-1}$ , precision of 1–2%, high reagent consumption and

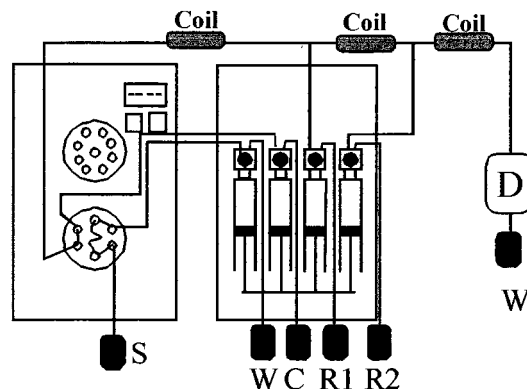


Fig. 5. Multisyringe flow system.

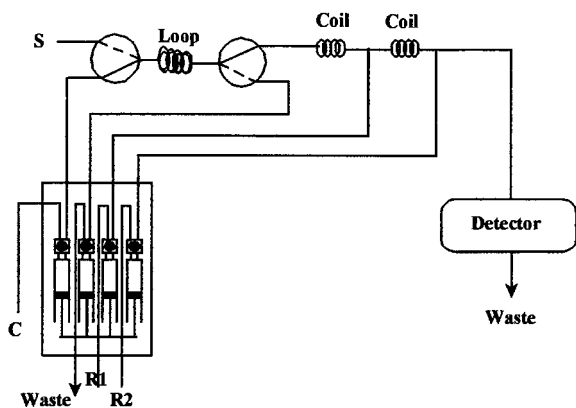


Fig. 6. Improved multisyringe flow system with sampling set up.

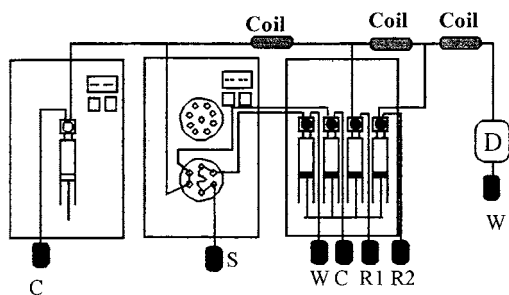


Fig. 7. Multisyringe flow system with additional burette.

essential washing cycle. More recently, microsegmented techniques for water analysis have been proposed [21–23].

## 2.2. Flow injection analysis (FIA)

The designation of flow injection analysis (FIA) [24,25] was proposed in 1975 by J. Ruzicka and E. Hansen. The inclusion of the term ‘injection’ in the name of this technique is due to more a historical aspect rather than the present situation. In the beginning of the former technique a syringe was used to inject a sample through a septum into a flow of reagents. Nowadays, rotation valves which insert the sample into a flow of reagents, rather than injecting the sample, are used.

Although schematically and conceptually FIA and SFA may appear to be very similar, however, the differences in practice are remarkable. In the first place, in FIA, samples are not segmented by air bubbles and tubes are considerably narrower (of the order of 0.5–0.7 mm of i.d.), through which the flow pattern is of the laminar type. The injected sample volume in SFA is considerably larger than that of FIA, in which only volumes of the order of 10–100 ml are used. The response time is of 3–60 s, the frequency may well be of 120 samples  $h^{-1}$ , a similar precision to that of SFA (1–2%) is achieved, reagent consumption

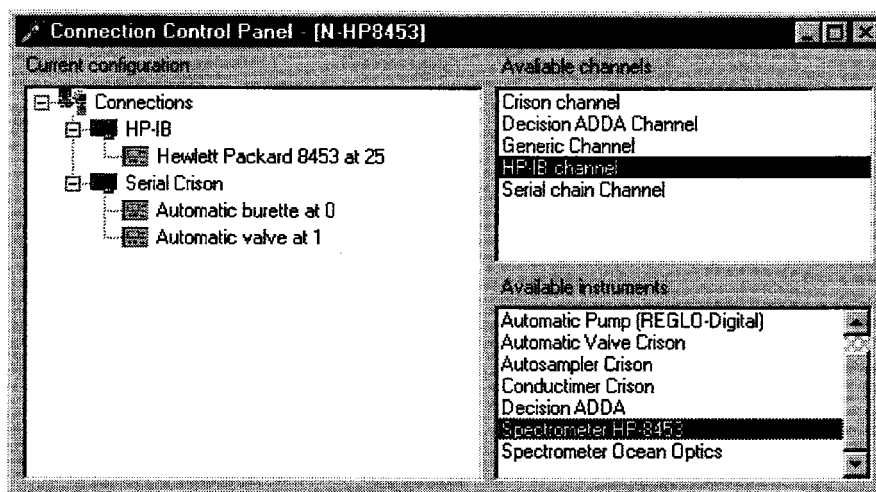


Fig. 8. Connection control panel for the AUTOANALYSIS program.

Table 1  
Devices which can be controlled with the AUTOANALYSIS program

Device	Function	Model	Firm
A/D 14 bits	16 channels	Super ADDA 14	Decision
A/D 8 bits Card with automatic gain adjustment	4 channels	SilMon Scope	Silmon
A/D 12 bits	8 channels	DASH8	Keithley
A/D 12 bits	8 channels, progr. Gain	DAS 801/CE	Keithley
I/O digital Card	48 lines 3 counters 16 bits 8255–8253		Decision
I/O digital Card			Flytec
I/O Card	16 Photo 16 reels	Industrial Smat-Lab	Decision
Peristaltic pump	Direct and reverse control, 4 channels	Reglo-Digital	Ismatec
SIA system	2 burettes, 2 analogic inputs, 1 selection valve + autosampler	Compact Titrator	Crison
Automatic burette	5000 steps	Microbur 2031	Crison
Automatic burette	1000 steps	Modelo 738	Crison
Automatic burette	4 syringes + 2 commutation valves		Crison
Valves module	2 selection valves, 8 channels each	Pump 2060	Crison
Valves module	1 selection valve 8 channels, 1 injection valve 6 canales	Pump 2060	Crison
Valves module	1 selection valve 6 channels, 1 injection valve 6 canales		Sciware
Autosampler	40 samples	Microsampler 2040	Crison
Autosampler	15 samples		Crison
Microwaves oven	Needs DASH8 or DAS801 card	Maxidigest	Prolabo
Conductimeter		Digilab 517	Crison
Conductimeter		Modelo 525	Crison
Conductimeter		GLP 32	Crison
pH meter	Only pH	517	Crison
pH meter	pH and temperature	MicropH 2002	Crison
pH meter	pH and temperature	GLP22	Crison
Diode array spectrophotometer	190–800 nm	HP8452A	Hewlett-Packard
Diode array spectrophotometer	190–1100 nm	HP8453	Hewlett-Packard
CCD array fiber optic spectrophotometer	Master	PC1000	Ocean Optics
CCD array fiber optic spectrophotometer	Master	PC2000	Ocean Optics
CCD array fiber optic spectrophotometer	Slave	PC2000	Ocean Optics
Fluorimeter	Flurimetry for single point, synchronous, variable angle spectra	LS50	Perkin Elmer
Fluorimeter	Flurimetry for single point, synchronous, variable angle spectra	LS5	Perkin Elmer
Atomic fluorescence	Hydrides generator	Excalibur	PSA Analytical
SIA system	2 burettes, 1 selection valve, 2 A/D inputs	Compact Titrator	Crison

drastically decreases, the washing cycle is not required and the application of kinetic methods is feasible, with or without stopped-flow. The numerous advantages of FIA justified the fact that

at that moment the continuous flow analysis methods were revitalized. However, undoubtedly, perhaps the major advantage is the great reproducibility in the results obtained by one

technique which can be set up without excessive difficulties and at very low cost of investment and maintenance. These advantages have led to an extraordinary development of FIA, not comparable to that of any other technique.

Nevertheless, to the former advantages a series of disadvantages are opposed, which are especially evident when used in the monitoring of environmental parameters. Undoubtedly, the Achilles' heel of this technique is the use of peristaltic pumps. The flexible tubing which these pumps require imply a change in both the sample and reagent flows in the short or long term due to tube squashing, which in turn implies a recalibration of the system. These tubes become especially vulnerable when management of relatively aggressive reagents is required, such as moderately concentrated acids or bases, or — especially — when handling organic solvents to improve solubilization of compounds or carrying out extraction processes. On the other hand, although several methods which allow the simultaneous determination of different parameters have been developed, the FIA technique is basically monoparametric, being also relatively limited when carrying out

sample pre-treatments. In any case, FIA is one of the most preferred techniques in the determination of a parameter in a set of a large number of samples.

### 2.3. Sequential injection analysis (SIA)

Sequential injection analysis has been also proposed by J. Ruzicka et al. in 1990 [26] (Fig. 3). It consists in a conceptually simple technique and was initially proposed as a possible alternative to FIA. In practice, it has been proved that it offers very different possibilities, with a series of advantages and disadvantages in relation to the former. Initially, the use of sinusoidal propelling pumps difficult to program was proposed, however, subsequently, other alternatives have been introduced such as the same peristaltic pumps used in FIA [27], or the burettes used in automatic titrations [28]. The latter were initially limited by the still high rates at which they performed even at their lowest range rates (values  $> 2 \text{ ml min}^{-1}$ ). Subsequent modifications in the firmware introduced by the manufacturer have allowed to solve the problem. Automatic burettes as an advantage elimi-

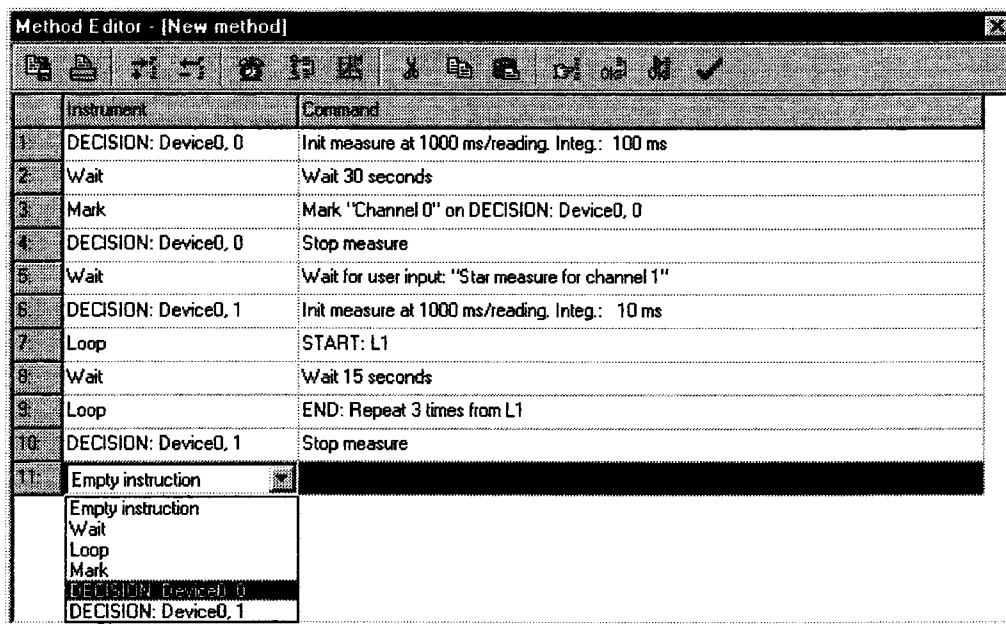


Fig. 9. Editor of the analytical methods of the AUTOANALYSIS program.

nate the use of the flexible tubing in peristaltic pumps, thus making the use of aggressive solvents or reagents more feasible.

Among the advantages of SIA in the first place it should be mentioned the fact that the manifold is more simple and universal than that of FIA. Thus, although in the latter technique the residence time in the reactors is fixed according to the tubing length, in SIA the manifold can remain fixed and control of the reaction times can be carried out by means of a computer internal timer. This device fixes the circulation of the liquids in the different directions, being able to stop the flows whatever time required. In SIA the use of peristaltic pumps can be completely eliminated, being replaced by glass syringes to which usually neither the samples nor the different reagents reach. In this way, SIA becomes a very robust technique from the point of view of the setting-up of monitoring systems of environmental parameters, since these systems do not tend to present a faulty calibration, they can easily manage aggressive reagents and/or solvents, which are at all times only in contact with glass or PTFE tubes. On the other hand, in FIA the peristaltic pump is usually permanently in movement, the analytical measurements -being or not carried out, giving rise to an inadequate reagent consumption, whereas in SIA the system only performs when measurements are required, thus, the reduction in consumption of both samples and reagents is drastic in relation to FIA. Thus, e.g. for a week in monitoring processes a consumption of  $\approx 10$  l of reagent per channel is required in FIA, whereas the former consumption is being reduced to 1.5 l in SIA. However, in spite of these advantages, SIA presents a series of disadvantages against FIA, the analysis frequency being the most important. FIA can be considered a technique in parallel, in which both the sample and the different reagents are simultaneously propelled by the peristaltic pump. However, SIA on its own account (and as stated by its name) operates by aspirating sample and reagents one after the other, which introduces two major critical aspects: a considerably decrease in the sampling rate (it is easily reduced to half as much in relation to FIA) and

major difficulties in the mixture of sample and reagents.

Other of the inconvenients of SIA is the almost compulsory control of the whole system by incorporating a computer which imposes the performance of the instruction sequence in well defined periods of time in order to achieve a reproducible process. On the other hand, it is responsible for data acquisition and treatment (in FIA potentiometric recorders are more widely used, which allow the use of manual systems, although inconvenients in data treatment and storage are introduced). The hardly any presence up to present in the market of commercialized software of a general approach for SIA explains the fact that the development of the former technique has been considerable slower than that of FIA. Although being a major disadvantage, since setting-up of an automated SIA on one's own involves evident difficulties (there is no point in using manual SIA), however, it constitutes one of the advantages of SIA against FIA, especially when applying stop-flow techniques.

In spite of the above-mentioned disadvantages against FIA, SIA has finally presented a series of additional advantages initially not taken into account. Firstly, SIA has proved to possess an exceptional capacity in relation to previous sample handling, allowing to circulate the sample and reagents through several channels, to reverse flows, to handle aliquots, etc. On the other hand, SIA has proved to be a technique which can be designed to operate in a multiparametric way, which is of special interest when considering the design of environmental monitors. Usually, these monitors do not require a considerable sample frequency; at times carrying out measurements every 15 min or even at less frequencies is sufficient. Since the sample and the different reagents can be placed around the selection valve, the programming of the computer work for the determination of successive parameters which will characterise the sample quality becomes immediate. Thus, a monitor of waste water has been proposed with which the DQO, DBO, ammonium, nitrate, nitrite, total nitrogen, orthophosphate, total phosphorus, detergents, etc. can be sequentially determined every 15 min [29].

#### 2.4. Multicommutation flow analysis (MCFA)

Multicommutation is a novel approach in flow analysis which can be implemented by using discrete commutation devices, such as three way solenoid valve. The approach has been used to perform binary sampling [30], making feasible the reduction of reagent consumption, sequential determinations [31,32] and sequential management of incompatible reagents in single line manifolds [32]. This technique has been proposed to significantly widen the determination ranges [33,34] (Fig. 4).

#### 2.5. Multisyringe flow analysis (MSFA)

It is in fact a technique which is hereby described for the first time [35]. It has arisen with the aim to transfer the robustness of the SIA methods based on the use of syringes, to the FIA technique and, thus, solve the problem of using peristaltic pumps together with the inconveniences related to flexible tubing which their use is based on. As shown in Fig. 5, in both MSFA and SIA, liquids are only in contact with the glass or PTFE tubing, which makes the use of aggressive reagents and solvents feasible. In order to make this technique competitive from an economic point of view against the remaining techniques, the first prototypes have been assembled adapting a typical burette of automatic titrations (like those used in SIA) to simultaneously enable the movement of four syringes, which can be of different capacity, allowing the different channels to perform at a different flow. In this technique the use of solenoid valves employed in the multicommutation techniques has been also incorporated to eliminate the critical aspects of the use of rotary motors. Thus, the problem of the detection of positions is solved and, besides, the rate in the selection of channels is increased.

The first prototype was constructed by incorporating only four syringes with their corresponding solenoid valves. In order to apply the system, this module should be used together with an injection valve. In the filling position of the burettes the injection valve is placed in the loading position and the samples aspirated by one of the syringes

(W), whereas the remaining syringes aspirate the reagents which will be required in the analytical method. By commuting the valve in the injection position and using one of the syringes of the system to propel the sample (C) and using the remaining two to propel the reagents (R1 and R2), the device operates the same as FIA. However, the difference lies in the fact that reagent consumption is carried out only when a measurement is required, being independent from time and, therefore, being only dependent on the sampling frequency.

The incorporation of two additional commutation valves in the subsequent prototypes has increased the possibilities within the system, allowing to use the same module for the development of the multicommutation techniques. However, in this case flows are originated by liquid propelling and not by aspiration, thus reducing the risk from formation of undesirable bubbles.

On the other hand, the use of the two additional valves which operate replacing the injection valve is feasible (Fig. 6), thus, simplifying and decreasing the cost of the system even more.

#### 2.6. Hyphenated techniques

The combination of the different flow techniques above mentioned is of great interest.

Thus, the advantages offered by the SIA technique can be of great use in relation to the previous sample handling, and subsequently, once the samples happen to be under appropriate conditions they can be injected following the criterion of other techniques. The determination of iron in water by carrying out its pre-concentration by SIA on a Chelex 100 column has been described [36]. The pre-concentrated iron is eluted with nitric acid, converging the eluate with another thiocyanate flow according to the traditional FIA approach, to determine the red complex formed by spectrophotometric detection.

A simple combination which has led to excellent results is that of coupling the multisyringe technique to another normal burette (Fig. 7). The process is initiated by loading the sample as described in the corresponding MSFA section. Subsequently, the sample is injected and mixed with



other reagents, also as previously described. The additional syringe is used to end the passing of the remainder liquid through the detector, whereas, simultaneously the multisyringe starts a new cycle of reagent filling and sample loading, the analytical process being subsequently repeated. The extra syringe is filled with carrier when the multisyringe is performing the injection process. Thus, an alternative balance multisyringe-additional syringe takes place, which allows to achieve frequencies of up to 180 injections  $\text{h}^{-1}$ , with the robustness of MSFA, since no flexible tubes are used at any moment and the liquids are only in contact with glass or teflon.

Good results are also achieved by the coupling of SIA to MSFA, which has been applied to the determination of acidity in the lixiviates in the treatment of minerals [37].

Although this combination could be considered as a coupled technique, this terminology is applied when the flow technique is coupled to another different technique, such as gas chromatography, capillary electrophoresis [38] or mass spectrometry [39]. On some occasions the use of this terminology has been exaggerated, being extended to the cases in which the very expensive or sophisticated detectors have been used such as ICP. If the former inclusion was accepted almost all the proposed flow methods should be included within this group, since the connection the former flow system with one detection method or another takes place.

### 3. Software

One of the major difficulties which has retarded the development of the most modern flow techniques has been the availability of the programs which manage the system. As mentioned before one of the major advantages of FIA which has allowed an explosive development of publications is its feasibility in being assembled in the laboratory without requiring the use of a computer to control the system.

On the other hand, it is hardly unthinkable the application of the SIA, MCA and MSFA techniques together with their combined use without

involving a computer, since residence times and other characteristics of the systems are directly controlled by computer. Until a few years ago software had to be developed by the users themselves, which explains the fact that the development of SIA, in spite of its advantages, has not been as spectacular as that of FIA. Likewise we believe that the generalization of MCA and MSFA techniques will be also delayed.

At present there are several commercialized programs or programs available for the SIA users, some of which have been already mentioned, cited by J.F. van Standen in a recent SIA review published in LRA [40], FlowTEK [41], DARRAY [42] and FIALab [43].

Frequently, one of the major limitations of these programs is the fact that they have been designed for excessively specific purposes and should be modified when requiring either the development of other applications or the change of the types of detectors. In order to avoid the former critical aspects, the program AUTOANALYSIS has been recently developed [44] to work under Windows of 32 bits. The design has been carry out to operate in four different layers, with their corresponding DLLs, being the first and fourth interconnected with the intermediate ones, however, at the same time the former layers remain isolated between them. This allows the developed analytical methods to be independent from the instrumentation used, being the incorporation of new instrumental modules feasible with only the development of the corresponding DLLs which will allow them to be controlled from the main module.

In Fig. 8 the menu of the AUTOANALYSIS program is shown. In the left window it can be noticed the communication channels opened for the connection of the different elements. In those to the right it can be observed how the HP-IB communication channel is selected (top window), to which a diode spectrophotometer is hung (bottom window).

Working at 32 bits implies a multiarea program making simultaneously feasible the application of developed flow methods, data treatment with the same program, document edition with other commercial programs, etc. The program has been

thought to work under the conception of laboratory unitary operations, with which the implementation of individual flow (FIA, SIA, MCA, MSFA) or coupled techniques (SIA-FIA, SIA-MSFA, etc.) is feasible. In Table 1 the different types of instruments and apparatus which can be controlled by the AUTOANALYSIS program and may be used for the configuration of automatic systems are specified.

In Fig. 9 the edition of an analysis method by the AUTOANALYSIS program is depicted.

#### 4. Applications

Flow techniques have been widely used in the analysis of environmental parameters, and, especially, in water analysis, to which they are particularly adapted. In the E.Hansen [45] database, which may be accessed to by internet, more than 750 citations related to water analysis are found, most of which are based on the use of FIA. In the review of the former applications several types of waters, such as natural, residual, drinking, marine, estuary, salty, superficial, underground, refrigeration, energy co-generation waters, etc. are found.

##### 4.1. Monitoring

Although many techniques have been developed to be used in the laboratory, being water a fluid easy to handle, one of the major possibilities of flow techniques is that of their application in the monitoring of parameters of interest, especially in on-line mode, which has given rise to several reviews [46–57] and even EPA regulations have been established [58,59].

#### Acknowledgements

The authors acknowledge the financial support of the CICyT through project PETRI 95-0139-OP, and the University and AEST through a sabattical grant to EB.

#### References

- [1] A.R. Rios, M.D. Luque de Castro, M. Valcárcel, *Analyst* 110 (1985) 277.
- [2] K. Toei, *J. Flow Inject. Anal.* 1 (1984) 2.
- [3] H. Casey, S. Smith, *Anal. Chem.* 4 (1985) 256.
- [4] Y. Baba, *J. Flow Inject. Anal.* 4 (1987) 36.
- [5] T. Korenaga, *Bunseki* 4 (1987) 245.
- [6] T. Greatorex, P.B. Smith, *J. Inst. Water Eng. Sci.* 39 (1985) 81.
- [7] J.A. Nobrega, A.A. Mozeto, R.L. Bozelli, *Cienc. Cult.* 40 (1988) 1118.
- [8] S. Motomizu, M. Oshima, *Nippon Kaisui Gakkaishi* 50 (1996) 363–377.
- [9] W. Zimmermann, J.K. Reichert, W. Maurer, *Mater. Landesumweltamt Nordrhein-Westfalen* (1996), Volume Date 1995.
- [10] M. Kunimatsu, T. Kuroishi, K. Harada, Y. Setsu, K. Imai, K. Tsukada, C. Maekoya, *Kokai Tokkyo Koho, Pat. No.:* 95260796 (Hitachi), 1995.
- [11] F. Oshima, *Fukuoka Kyoiku Daigaku Kiyo, Dai-3-bun-satsu: Sugaku, Rika, Gijyutsuka Hen;* 44 (1995) 45–51.
- [12] P. Maccarthy, R.W. Klusman, S.W. Cowling, J.A. Rice, *Anal. Chem.* 67 (1995) R525–R582.
- [13] M. Agudo, A. Rios, M. Valcárcel, *TRAC Trends Anal. Chem.* 13 (1994) 409.
- [14] J.S. Cosano, M.D. Luque de Castro, M. Valcárcel, *J. Autom. Chem.* 15 (1993) 147.
- [15] S. Kado, *Shigen Kankyo Taisaku* 28 (1992) 1119.
- [16] W. Frenzel, M. Selan, *GIT Fachz. Lab.* 36 (1992) 1239.
- [17] A. Mueller, J. Petrowsky, T. Kraemer, W. Kopprasch, H. Mitschick, *Acta Hydrochim. Hydrobiol.* 19 (1991) 573.
- [18] Y. Asano, S. Itoh, *Kogyo Yosui* 395 (1991) 80.
- [19] R.E. Taljaard, J.F. van Staden, *Lab. Robot. Autom.* 10 (1998) 325–337.
- [20] L.T. Skeggs, *Am. J. Clin. Pathol.* 28 (1957) 311.
- [21] M.R. Straka, *Am. Environ. Lab.* 1 (1989) 60.
- [22] M.R. Straka, *Int. Lab.* 20 (1990) 33.
- [23] P. Serizot, *Analisis* 19 (1991) 127.
- [24] M. Valcárcel, M.D. Luque de Castro, *Flow-Injection Analysis. Principles and Applications*, Ellis Horwood Series in Analytical Chemistry, Ellis Horwood, Chichester, England, 1987.
- [25] J. Ruzicka, E. Hansen, *Flow Injection Analysis*, J. Wiley, New York, 1988.
- [26] J. Ruzicka, G.D. Marshall, *Anal. Chim. Acta* 237 (1990) 329.
- [27] A. Ivaska, J. Ruzicka, *Analyst* 118 (1993) 885–889.
- [28] A. Cladera, C. Tomás, E. Gómez, J.M. Estela, V. Cerdà, *Anal. Chim. Acta* 302 (1995) 297–308.
- [29] O. Thomas, F. Theraulaz, V. Cerdà, D. Constant, P. Quevauviller 16 (1997) 419–424.
- [30] B.F. Reis, M.F. Giné, E.A.G. Zagatto, J.L.F.C. Lima, R.A. Lapa, *Anal. Chim. Acta* 293 (1994) 129.
- [31] P.B. Martelli, B.F. Reis, E.A.M. Kronka, H. Bergamin, M. Korn, E.A.G. Zagatto, J.L.F.C. Lima, A.N. Araujo, *Anal. Chim. Acta* 308 (1995) 397.

- [32] E.A.M. Kronka, B.F. Reis, M. Korn, H. Bergamin, *Anal. Chim. Acta* 334 (1996) 287.
- [33] F.R.P. Rocha, P.B. Martelli, R.M. Frizzarin, B.F. Reis, *Anal. Chim. Acta* 366 (1998) 45–53.
- [34] J.A. Vieira, B.F. Reis, E.A.M. Kronka, A.P.S. Paim, M.F. Giné, *Anal. Chim. Acta* 366 (1998) 251–255.
- [35] V. Cerdà, J.M. Estela, R. Forteza, unpublished results.
- [36] E. Rubí, R. Forteza, V. Cerdà, *Lab. Robot. Autom.* 8 (1996) 149–156.
- [37] F. Albertús, A. Cladera, V. Cerdà, unpublished results.
- [38] L. Arce, A. Rios, M. Valcárcel, *J. Chromatogr. A* (1997) 791.
- [39] H.F. Schroeder, *Water Sci. Technol.* (1996).
- [40] R.E. Taljaard, J.F. van Staden, *Lab. Robot. Autom.* 10 (1998) 325–337.
- [41] G.D. Marshall, J.F. van Staden, *Anal. Instrum.* 20 (1992) 79.
- [42] A. Cladera, C. Tomás, E. Gómez, J.M. Estela, V. Cerdà, *Anal. Chim. Acta* 302 (1995) 297.
- [43] P.J. Baxter, G.D. Christian, J. Ruzicka, *Analyst* 119 (1994) 1807.
- [44] E. Becerra, A. Cladera, V. Cerdà, *Lab. Robot. Autom.* 11 (1999) 131.
- [45] E.Hansen. <http://www.flowinjection.com/search.html>
- [46] J.R. Clinch, P.J. Worsfold, H. Casey, *Anal. Chim. Acta* 200 (1987) 523.
- [47] K.N. Andrew, N.J. Blundell, D. Price, P.J. Worsfold, *Anal. Chem.* 66 (1994) 916.
- [48] M. Trojanowicz, R.L. Benson, P.J. Worsfold, *Trac. Trends Anal. Chem.* 10 (1991) 11.
- [49] W. Zimmermann, J.K. Reichert, W. Maurer, *GIT Fachz. Lab.* 39 (1995) 964–968.
- [50] B. Winter, *Gewaesserschutz Wasser Abwasser* 102 (1988) 209.
- [51] Y. Kondo, H. Shimomura, M. Katoh, *Boshoku Gijutsu* 36 (1987) 234.
- [52] Z. Zhou, J. Shi, S. Ye, *Huanjing Wuran Yu Fangzhi* 12 (1990) 43.
- [53] R. Rumelfanger, K.J. Salamon, *Off. Proc. Int. Water Conf.* 56 (1995) 30–36.
- [54] Y.S. Li, *Bunseki Kagaku* 45 (1) (1996) 107–108.
- [55] Y. Li, Z. Wang, *Lab. Rob. Autom.* 7 (1995) 229–238.
- [56] Y. Li, Y. Narusawa, *Bunseki Kagaku* 41 (1992) 463.
- [57] P.W. Alexander, L.T. Di Benedetto, T. Dimitrakopoulos, D.B. Hibbert, J.C. Ngila, M. Sequeira, D. Shiels, *Talanta* 43 (1996) 915–992.
- [58] C.B. Ranger, *Proc. Water Qual. Technol. Conf.* 15 (1988) 499.
- [59] C.B. Ranger. *Am. Lab.* 20(9) (1988) 42. NIPDWR Monitoring of Waters and Wastes *Amer. Lab.*, 20(9) (1988) 42.

# Trends in monitoring of waste water systems

Anders Lynggaard-Jensen \*

VKI, Science Park Aarhus, Gustav Wieds Vej 10, DK-8000 Aarhus C, Denmark

## Abstract

A review of the trends in monitoring of waste water systems is given — with the focus on the use of sensors for on-line real-time monitoring and control. The paper formed a basis for discussion at the workshop on Methodologies for Wastewater Quality Monitoring, Nîmes, 29–30 October 1998, organised by the European Commission and Ecoles des Mines d'Alès. The basic structure of the typical organisation of monitoring and control based on sensors and the handling of the sensor data are discussed and the different types of sensors are classified according to the method used for their introduction into the structure. Existing and new sensor technologies are briefly described, and the possibilities of how standardisation of on-line in-situ sensors can encourage further developments and use of sensors are presented. © 1999 Elsevier Science B.V. All rights reserved.

*Keywords:* Waste water systems; Semi-micro mechanics; Sewer systems

## 1. Structure of monitoring and control

The automation of waste water systems (sewer systems and waste water treatment plants — municipal as well as industrial) is not as developed as other process industries mostly due to the very hostile environment where sensors have to be located. There has simply been a lack of proper sensors, which can be used for on-line real-time monitoring/control.

However, recent years have shown use of classical sensors as pH, dissolved oxygen, redox, turbidity, etc, and also the development and use of analyser systems for nutrients and organic matter have reached a level of practical use. Furthermore, new technologies are introduced, most of these

using the real time calculation capabilities of microprocessor systems located directly in the sensors.

The typical structure used for introduction of these sensors into waste water systems for monitoring or even control is shown in Fig. 1.

At the lowest level sensor data are collected in data loggers or PLCs and transmitted to a SCADA system main station. If the sensor data only are used for simple monitoring the timeseries may be displayed to the operators at this level, but if the sensor data are used for decision support or real time control, it is now more common to transmit these further on to a superior system, which is using the SCADA system as a front end as described by Lynggaard-Jensen in Ref. [1].

These superior systems are also more and more frequently connected to each other, if the monitored/controlled areas are connected in the real world (e.g. sewer system and treatment plants in

\* Fax: +45-861-975511.

the same catchment area) giving the possibilities of exchanging data and information of preferred set points.

Furthermore, these superior systems can be connected as information providers to the administrative level, giving condensed information to create an overview of the operative levels.

The data handling in the superior systems is typically organised as shown in Fig. 2. An extremely important feature of these systems (which in time might be added to the SCADA system functionalities) is the sensor data validation. Even with more and more reliable sensors the sensor data should before direct use for other than monitoring be validated.

The figure also indicates a new paradox: ‘the more sensors available, the more timeseries to be followed in real time — which is impossible for the operators, who then will want less timeseries’.

The paradox demands that software on the superior systems is capable of turning a huge amount of sensor data into reliable information, which can either be over looked by operators or used directly for closed loop real-time control. This type of software is now known as data fusion software. An example of an implemented system based on classical sensors and analysers and the system structure described is given by Lynggaard-Jensen et al. in Ref. [2].

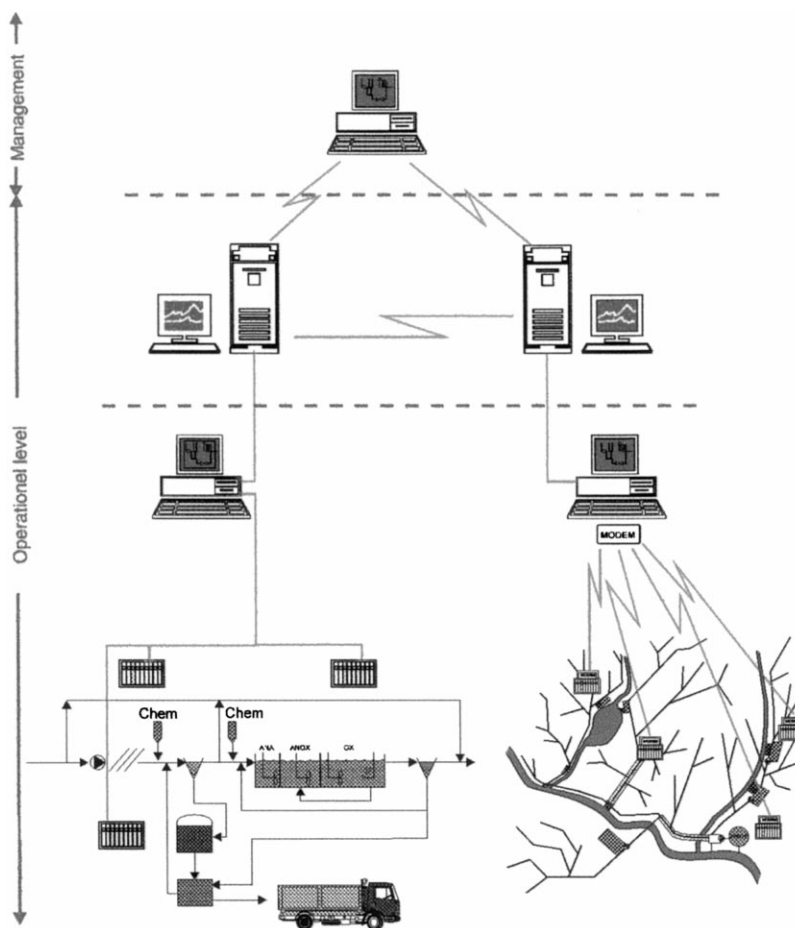


Fig. 1. Typical information flow in a waste water system.

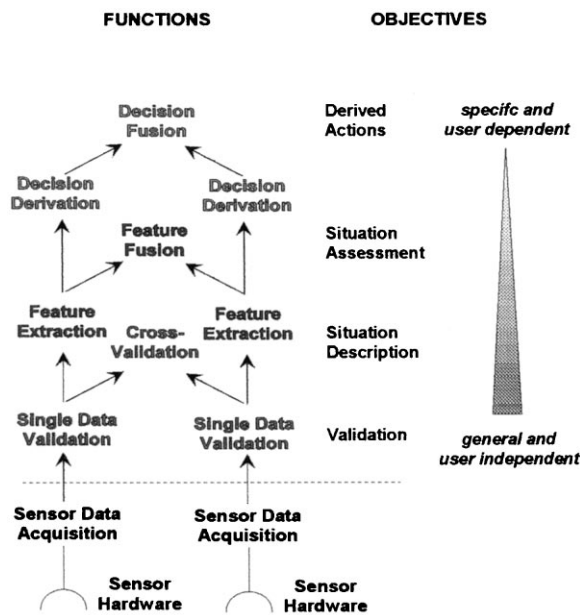


Fig. 2. The data fusion hierarchy.

Table 1  
Sensor properties

Property	Example
1 Placement of sensor	In-situ, at-line, in-line; on-line, off-line
2 Principle of sampling	External sampling, no external sampling
3 Principle of filtration	Filtration, no filtration
4 Principle of sample treatment	Continuous, batch
5 Principle of measurement	Photometric, colorimetric, enzymatic, titrimetric
6 No. measurands	Single parameter, multi parameter
7 Need for supplies	Consumeables, no consumeables
8 Service intervals	Long intervals, medium intervals, short intervals

## 2. Sensor classification

Existing sensors and analysers can be divided into classes after their respective properties. Table 1 shows eight different sensor/analyser properties, which all should be taken into account before

installation of these. First of all the placement of the sensor is important, e.g. in which environment shall the sensor operate and shall data be available in real time.

Equally important are sampling and filtration of the sample. Are these procedures acceptable for the measurement in question, and if so, is it acceptable to do this batchwise? The principle of the measurement itself is important in order to take known interfering substances into account, and of course it is important if one sensor can give information of more than one measurerand.

The need for supplies is of course a cost parameter and also influence the service intervals, which also include cleaning, calibration, etc. Table 2 shows a sensor classification, which suggests that sampling, filtration and the number of measurands are the most important properties to take into account when looking at existing and known to-come/sensors analysers for waste water systems.

Table 2  
Sensor classes

	Single parameter	Multi parameter
External sampling	Class 1	Class 2
External sampling and filtration	Class 3	Class 4
No external sampling	Class 5	Class 6

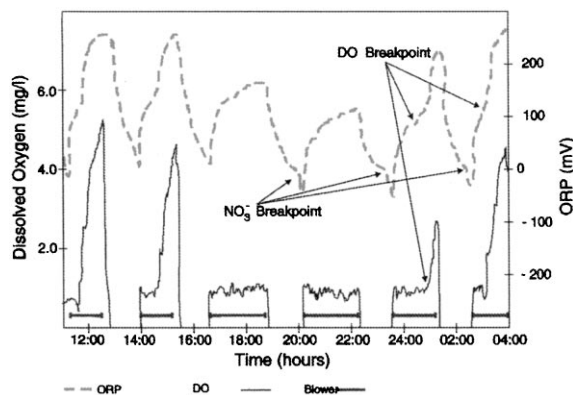


Fig. 3. Use of simple classical sensors for process control.

### 3. Existing and new sensor technologies

The classical sensor type — ‘a small probe measuring directly in the water and giving a continuous signal’ — is in fact according to the above classification, a class 5 sensor and therefore by the definition an attractive technology. Well known classical sensors are temperature, pH, conductivity, oxidation reduction potential (ORP or redox potential) and (to a lesser degree) dissolved oxygen. Apart from the DO these sensors are physical–chemical sensors, and in that sense not giving specific information of a certain substance. However, with the correct maintenance and a little bit of real time computing these sensors can be used for rather complex process control, as already documented by Wouters-Wasiak [3] in 1994 and shown in Fig. 3. The figure shows the measurements of ORP and the DO concentration together with the operation of the blower in an intermittent aerated waste water treatment plant with nitrogen removal.

The nitrate breakpoint measured by ORP indicates the end of the denitrification period (anoxic to anaerobic conditions), whereas the DO breakpoint indicates the end of the nitrification period. The rapid increase in the DO shows the smaller oxygen consumption due to the fact that all ammonium has been oxidised.

Measuring nutrients (ammonium, nitrate and phosphate) are very important in waste water systems, and a lot of effort have been used in order to develop sensors/analysers for this. Table 3 shows the most common commercial available systems — most of these based on well-known colorimetric reactions automated in analysers.

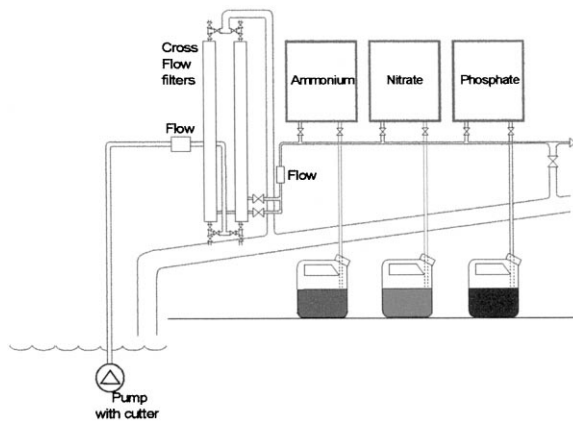


Fig. 4. Sampling and filtration system for nutrient analysers.

However, these analysers require external sampling and most of these also filtration (class 1 and 3). Fig. 4 shows the set-up with these analysers.

The filtration of the sample is often done using cross flow filtration. The typical system is using a main stream provided by a submersible pump mounted with a cutter system and giving  $10 \text{ m}^3 \text{ h}^{-1}$  to the cross flow filtration unit based on

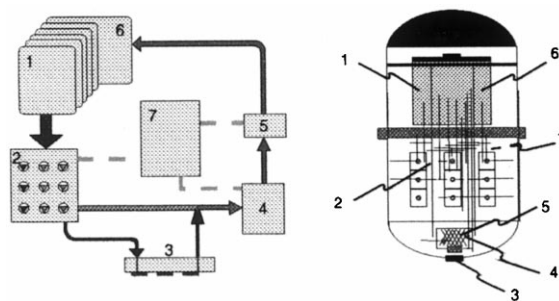


Fig. 5. Micro continuous flow analysis.

Table 3  
Nutrient analysers — the chemical method and the alternative(s)

Measurand	Chemical method	Alternative
Ammonium	Indophenol Blue	Increase pH and measure $\text{NH}_3$ with a gas sensitive electrode
Nitrate	Reduction to nitrite followed by formation of a purple Di-Azo complex	Absorbance at 205 nm or ion-selective electrode
Phosphate	Molybdenum blue	None

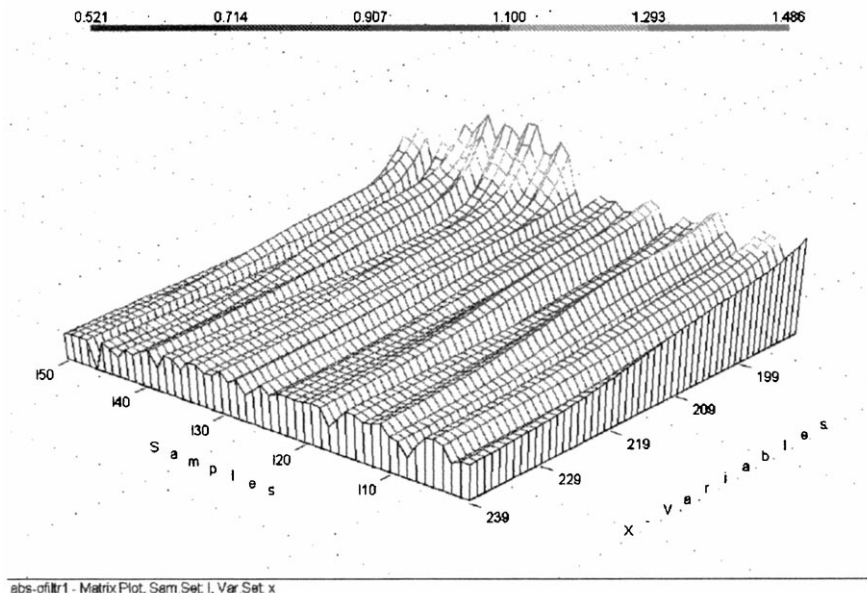


Fig. 6. Absorbance spectra-waste water (activated sludge).

ceramic tubes with a pore size of 20  $\mu\text{m}$ . The unit is typically providing a filtrate of 10  $\text{l h}^{-1}$  down to 2  $\text{l h}^{-1}$  before cleaning. The operating time between cleanings is 2–3 weeks. A solution of NaOCl is typically used for cleaning.

Although the described analyser systems are used during normal operations as standard equipment, they require a good deal of maintenance in order to be reliable — a fact described by many experienced users (Londong and Wachtl [4], Schlegel and Baumann [5], Thomsen and Kisbye [6], Nyberg et al. [7]). Furthermore, the installation costs can be considerable, and the long response times (10–25 min) cause difficulties in incorporating them in standard feed-back process control loops.

Thus, the need for new principles for sensors for real-time on-line process control seems obvious, and some of the major demands to the development work have been and are to design sensors, which can be placed directly in the waste water systems (no sampling and filtration) and measure the right measurands within appropriate ranges with a fast response time (less than 5 min) and continue to do that with maintenance only once a month.

Several well known measuring principles can be used to comply with these demands if the principles are used together with technology now available (possibilities for fast and big computations, optical standard components, membrane technology and micro-mechanic designs). Some of these principles include:

- Colorimetry combined with semi-micro mechanics and membrane technology.
- Absorbance using photodiode-arrays for spectral information
- Fluorescence with multi excitation and scanning for emissions
- Bio-sensors based on immobilised bacteria

Colorimetry combined with semi-micro mechanics and membrane technology have been assembled in a concept called micro continuous flow analysis ( $\mu\text{CFA}$ ), which is described by Lynggaard-Jensen et al. in Ref. [8], and briefly shown in Fig. 5. The figure shows the functions and how these have been built into the sensor. Reagents and clean water are stored in bags (1) and transported around the sensor with pumps mounted on a transportation manifold (2). A carrier (clean water) is pumped to the membrane device (3) and flows in a track on one side of the membrane. The



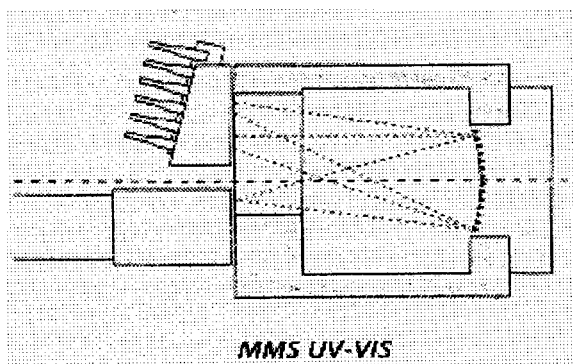


Fig. 7. Example of micro-scale spectrophotometer (Zeiss).

other side of the membrane is exposed to the activated sludge/wastewater, and the carrier is enriched with ions passing through the membrane. The enriched carrier is mixed with reagents and pumped to the reaction area (4) and further on to the photometer for detection (5) — both of these are heated to a constant temperature. From the photometer all liquid is pumped to the waste bag (6). All functions are supervised and controlled by a microcomputer (7).

The sensor design, which can be used for virtually any ion with a known and stable colori-

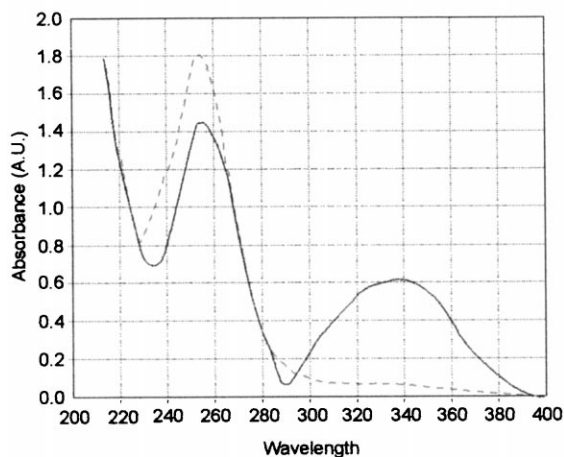


Fig. 8. Single channel fluorimeter for the measurement of NADH in activated sludge.

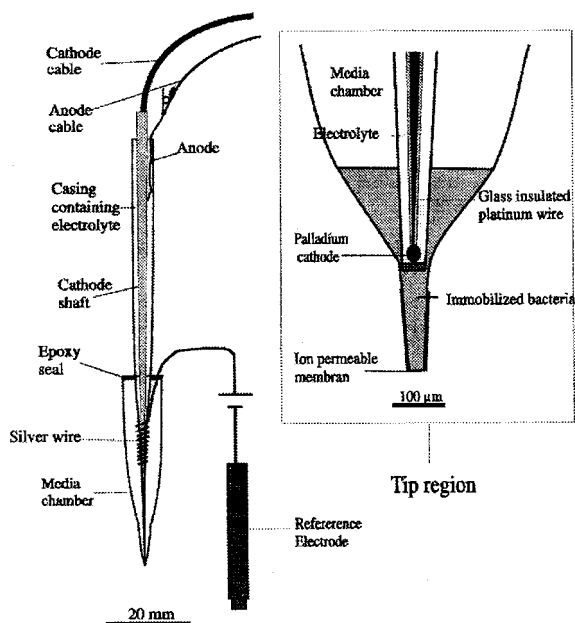
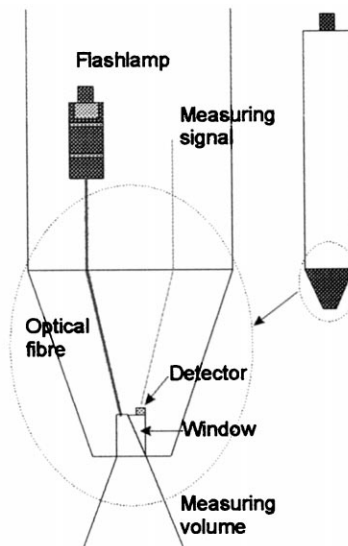


Fig. 9. Bio-sensor based on immobilised bacteria.

metric reaction, demonstrates that it is possible to design and construct real-time on-line in-situ closed loop sensors (without the need for a preceding cross flow filtration and without spill of chemicals) with response times less than 5 min,



a maintenance period of 1 month is possible due to a very low consumption of chemicals (less than 3 l month<sup>-1</sup>), an effective auto-calibration system and no fouling of the membranes used. The principle has been applied to sensors for ammonium, nitrate and phosphate respectively. These three sensors have been tested for wastewater treatment plant applications and are commercially available on the market.

Absorbance using photodiode-arrays for spectral information gives the possibility to construct low cost multiparameter sensors. Whereas the sensors presented in the previous section measures absorbance at a specific wavelength determined by the developed colour, it is also possible to measure the absorbance spectrum — with or without adding chemicals. The spectral information represents a composite and complex picture of information of the absorbance of all substances which have molecular energy levels which are able to absorb the light used.

Absorbance measurements are usually used in the ultraviolet and visible light (UV-VIS) region. The region has a lower limit due to the strong absorbance of water itself below 200 nm. Nitrate is a good example of a strong specific absorbance (205 nm), but unfortunately this is in waste water often hidden in the strong absorbances from organic substances. However, nitrate analysers based on absorbance at 205 nm are available on the market — all of these trying to compensate for the organic substances by calculations using absorbances from other wavelengths in the spectrum.

Fig. 6 shows an example of 50 absorbance spectra of samples of activated sludge at different times during the cycle of a bio-denitro waste water treatment plant. The absorbance spectra are recorded in the laboratory with an HP8453 UV-VIS spectrophotometer. If the same samples are analysed for different substances, it is possible to carry out a multivariate calibration of the spectra to the analysed values. This calibration can then be used with spectra recorded at a later time giving the concentrations of the substances without any need for analyses.

The principle is clearly demonstrated for nitrate by Karlsson [9], who also is able to measure

Table 4  
Performance characteristics of on-line in-situ sensors/analysers<sup>a</sup>

Performance characteristics	Laboratory test	Field test
Linearity (range)	✓	
Lowest detectable change	✓	
Selectivity	✓	
Limit of detection	✓	
Limit of quantification	✓	
Response times	✓	✓
Dead (lag) time	✓	
Rise and fall times	✓	
Ruggedness	✓	
Trueness/bias	✓	✓
Repeatability	✓	
Reproduceability	✓	
Up time		✓
Drift		✓
Memory effects	✓	

<sup>a</sup> Accuracy: trueness/bias (systematic error) and precision (random error). Precision: repeatability and reproduceability

total-P, total-N, ammonium and iron simultaneously with the nitrate. The methodology used is also known as chemometrics, and together with the development of stable micro-scale spectrophotometers (diodearrays) — as the one shown in Fig. 7 — it will be possible to develop small integrated multiparameter absorbance sensors.

The application of UV-spectrophotometry for industrial waste waters has been exploited by Thomas [10], who uses the combination of spectral measurements and multivariate calibration for rapid determination/estimation of nitrate, TOC, COD and anionic surfactants. The results are generated by an on-line real time analyser and used for incident detection/diagnosis, process control and waste water characterisation. The analyser is now commercially available.

Fluorescence with multi excitation and scanning for emissions produces a 3-dimensional spectrum — each excitation wavelength might give a fluorescence which is a function of the emission wavelength. A prerequisite for the generation of fluorescence is of course that the substance can absorb the light at the excitation wavelength and that the energy is released again through emission of light. This light is the fluorescence and it has a

specific wavelength for a given substance. The fluorescence will always have a longer wavelength than the light absorbed, because some of the energy release always will happen through vibration and rotation in the molecules.

The oldest and best known sensors based on fluorescence are fluorimeters for chlorophyll and oil, respectively. Most of these are single channel fluorimeters, meaning that a specific wavelength of light is used for excitation of the molecules and the resulting fluorescence is measured at one specific and somewhat longer wavelength. The advantages of fluorescence to absorbance are the more specific measurement and lower detection limits.

A typical design of a single channel fluorimeter is described in Nørgaard [11] and shown in Fig. 8. This fluorimeter measures NADH, which is an important proton transporter for the processes inside the bacteria. NADH fluorescence is measured at 460 nm (excitation at 340 nm). Because the corresponding oxidised state, NAD<sup>+</sup>, is non-fluorescent at 460 (does not absorb at 340), it is possible to measure biological activity expressed by the concentration of NADH, a fact that has been well known within fermentation industry for several years.

Isaacs [12] shows that the NADH fluorescence can be used to detect the end of the denitrification in an alternating activated sludge plant and also reports some correlation between fluorimeter output and the peak oxygen uptake rate. These results are confirmed by Nørgaard [11], who also describes a theory for the fluorimeter output and how this can be used for a process control strategy for nitrogen removal.

As mentioned fluorescence can also be measured as a 3-dimensional spectrum. Multichannel fluorimeters for detection of different PAHs have been developed — most of these with one excitation wavelength only and therefore producing a 2-dimensional spectrum, but very little has been done on waste water treatment plants on measurement of real spectras combined with chemometrics. After faster electronic chips have become available work has also been done to make the fluorescence measurements even more selective by incorporating the time response for the fluores-

cence (typically in the order of 5–100 ns depending on the substance). This also produces a 3-dimensional spectrum with the fluorescence as a function of emission wavelength and time, as reported by Eisum [13].

Bio-sensors based on immobilised bacteria are now starting to be commercially available for operational use. Larsen [14] reports the results obtained with a micro-scale nitrate sensor used in sediments, which was able to work for 2–4 days. This sensor has now been improved to work in activated sludge by the attachment of an ion permeable membrane to the tip of the sensor (Fig. 9), and has been tested to work without calibration for at least 1 month (personal communication, paper in preparation).

The distance from the tip to the traditional N<sub>2</sub>O microelectrode (Revsbech [15]) constitutes the reaction chamber containing a strain of denitrifying bacteria lacking the enzyme N<sub>2</sub>O reductase. The bacteria are then only able to reduce the NO<sub>3</sub><sup>-</sup> coming through the membrane to N<sub>2</sub>O, which in turn is measured electrochemically by the N<sub>2</sub>O microelectrode.

The electron donors and other nutrients are supplied via diffusion from the media chamber, which is so big compared to the bacterial consumption rate making the reservoir virtually inexhaustible. The bacteria oxidise organic matter from the media chamber using oxygen and nitrate as electron acceptors. The bacteria closest to the membrane reduce all incoming oxygen, which leaves most of the immobilised bacteria in an anoxic environment making denitrification the only possible metabolism.

#### 4. Standardisation

As described above sensor development can be seen to exploit very different technologies and routes towards the target: reliable continuous measurements without too much maintenance and at an affordable price. However, this somewhat soft formulation is not good enough when sensors are going to be used in real life for process control, compliance control, etc. In this case the performance characteristics of the actual sensor

must be known. Therefore, clear definitions of performance characteristics and how to test/measure these become very important and call for a common guideline, a guideline which should not limit but rather encourage further developments and use of sensors. Jacobsen [16] describes work along these lines, a work which now has led to the formation of a working group under ISO called TC147 WG2, on-line in-situ sensors/analysers. The driving forces for the working group are:

- Users want clear and documented specifications
- Producers want clear and documentable specifications
- Authorities want documented performance and the target is to produce a horizontal standard/guideline which is non-specific for any instruments, does not favour a certain technology, support new developments and can document performance in the laboratory and in the field. The scope of the work is to:
  - standardise the description of technical specifications of on-line in-situ sensors/analysers.
  - standardise the performance test giving actual values to the technical specifications of online in-situ sensors/analysers.
  - standardise the operational procedures and checks that will secure reliable results of online in-situ sensors/analysers when operated in real applications.

Jacobsen [16] describes how it is possible to establish a validation procedure in the form of a standardised performance test which can be used in two situations: in the laboratory for documentation of the instrumentation according to the performance claimed by the producers and in-situ during operation for documentation of the reliability of results obtained by the user. Table 4 lists the defined performance characteristics and in which case they are tested.

## 5. Conclusions

In general, the sensors are the weakest part of the chain in real time monitoring and control of sewer systems and waste water treatment plants.

Compared to computer technology — hardware and software products — the sensor technology is far behind, but the effort put into sensor development during the recent years has demonstrated that it is possible to develop and market sensors which can produce reliable continuous measurements without too much maintenance and at an affordable price. However, the sensors now available are only capable of measuring a very limited number of the determinants that should be measured in real time, which means that sampling and subsequent laboratory analyses still in the foreseeable future will be the most common source of data — with its well known limitations — for monitoring and control of waste water systems.

## References

- [1] A. Lynggaard-Jensen, Status for on-line sensors and automated operation of wastewater treatment plants. Proceedings of Nordic Seminar: Nitrogen Removal from Municipal Wastewater, 23–25 January 1995, Espoo, Finland, pp. 174–186. Nordic Council of Ministers, Copenhagen.
- [2] A. Lynggaard-Jensen, A. Billington, A. Mpe, T. Wittig, M.A. Rovira, B. Schmidt, WaterNet-distributed water quality monitoring using sensor networks. Waste-Decision 98, International Workshop on Decision and Control on Wastes Bio-Processing, Narbonne, February 25–27, 1998.
- [3] K. Wouters-Wasiak, A. Héduit, J.M. Audic, F. Lefèvre, Real-time control of nitrogen removal at full-scale using oxidation reduction potential, *Wat. Sci. Tech.* 30 (4) (1994) 207–210.
- [4] J. Londong, P. Wachtl, Six years of practical experience with the operation of on-line analyzers, *Wat. Sci. Tech.* 33 (1) (1996) 159–164.
- [5] S. Schlegel, P. Baumann, Requirements with respect to on-line analyzers for N and P, *Wat. Sci. Tech.* 33 (1) (1996) 139–146.
- [6] H.A. Thomsen, K. Kisbye, N and P on-line meters: requirements, maintenance and stability, *Wat. Sci. Tech.* 33 (1) (1996) 147–157.
- [7] U. Nyberg, B. Andersson, H. Aspegren, Experiences with on-line measurements at a wastewater treatment plant for extended nitrogen removal, *Wat. Sci. Tech.* 33 (1) (1996) 175–182.
- [8] A. Lynggaard-Jensen, N.H. Eisum, I. Rasmussen, H.S. Jacobsen, T. Stenström, Description and test of a new generation of nutrient sensors, *Wat. Sci. Tech.* 33 (1) (1996) 25–35.

- [9] M. Karlsson, B. Karlberg, R.J.O. Olsson, Determination of nitrate in municipal waste water by UV spectroscopy, *Anal. Chim. Acta* 312 (1995) 107–113.
- [10] O. Thomas, F. Theraulaz, C. Agnel, S. Suryani, Advanced UV examination of wastewater, *Environ. Technol.* 17 (1996) 251–261.
- [11] P. Nørgaard, K. Helmo, E.W. Sørensen, Treatment process for nitrogen removal controlled by NADH, *Vand. Jord.* 3 (3) (1996) 125–129 In Danish.
- [12] S. Isaacs, M. Henze, Fluorescence monitoring of an alternating activated sludge process, *Wat. Sci. Tech.* 30 (4) (1994) 229–238.
- [13] N.H. Eisum, A. Lynggaard-Jensen, The development of a fluorimeter using laser induced single-shot fluorescence lifetime spectroscopy. International Congress on Optical Science and Engineering, 12–15 March 1990, The Hague, Netherlands. SPIE Proceedings, vol. 1269, Environment and Pollution Measurement Sensors and Systems, pp. 167–174, 1990.
- [14] L.H. Larsen, T. Kjær, N.P. Revsbech, A microscale  $\text{NO}_3^-$  biosensor for environmental applications, *Anal. Chem.* 69 (17) (1997) 3527–3531.
- [15] N.P. Revsbech, L.P. Nielsen, P.B. Christensen, J. Sørensen, Combined oxygen and nitrous oxide microsensor for denitrification studies, *Appl. Environ. Microbiol.* 54 (9) (1988) 2245–2249.
- [16] H.S. Jacobsen, A. Lynggaard-Jensen, On-line measurement in waste water treatment plants: sensor development and assessment of comparability of on-line sensors. Proceedings of the Workshop on Standards, Measurement and Testing for the Monitoring of Water Quality. The Contribution of Advanced Technologies, Nancy, France, 29–31 May, 1997).

# Compliance assessment for the 91/271/EEC directive and an end-user's view on potentials for further on-line monitoring and control at wastewater treatment plants

Bo N. Jacobsen

*Avedore Wastewater Services Company, Kanalholmen 28, DK-2650 Hvidovre, Denmark*

---

## Abstract

This paper provides an introduction to the workshop on methodologies for wastewater quality monitoring, Nîmes, 29–30 October 1998, organised by the European Commission and Ecoles des Mines d'Alès. It highlights some overall aspects for the potential uses of on-line instrumentation related to wastewater management and focuses on relations to the urban wastewater treatment directive (91/271/EEC). Some potentials for further developments and actions related to the EU Directive are proposed. © 1999 Elsevier Science B.V. All rights reserved.

*Keywords:* Urban; Wastewater; Treatment

---

## 1. Introduction

Why monitor wastewater quality? There are three main reasons:

- compliance assessment;
- wastewater treatment plant design and operation;
- research and development;

Compliance assessment is important for both plant operators and the environmental authorities as this provides the judgement for success or failure in relation to the legal requirements. Monitoring influent wastewater quality and quantity is essential for treatment plant design and monitoring for process control needed for the operation. The ability to monitor certain parameters for improving process understanding, and for experimental work is essential in research and development (R&D).

Traditionally, a situation of non-compliance will lead to a demand for new or improved, wastewater treatment plant (WWTP) design and operation, and observed problems during operation will lead to a priority for development of improved process lay-outs, instrumentation, and control routines, etc. In modern management, however, the influence should just as well go the other way. New R&D findings should give inspiration for novel plant design and operation, including automated on-line monitoring, and process control. Such new features will soften the meaning of plant capacity since this will not only depend on tank volumes and power of machinery but just as much of process efficiency. Furthermore, new opportunities for on-line monitoring of environmentally relevant parameters should give influence to the way compliance criteria are formulated and interpreted. These traditional and

potential routes in decision making are illustrated in Table 1.

The EU directive on urban wastewater treatment (91/271/EEC) [1] puts all three reasons into perspective; the implementation of this directive will require substantial actions by the EU member states involving a wide range of stakeholders — the plant owners, the environmental authorities, as well as designing engineers, contractors and instrument suppliers. In particular for tertiary treatment plants, there is a high potential for advanced process monitoring and control. A schematic diagram for the various conditions and time deadlines included in the directive is shown in Fig. 1. It should be noted for inspiration to legislators that such diagrams are very illustrative.

It also apparent from Fig. 1 that WWTPs > 10000 PE with discharges to sensitive areas shall meet effluent standards corresponding tertiary treatment before year 1999 — this is now!

## 2. Compliance assessment

Wastewater quality monitoring for compliance assessment includes three main elements:

- sampling;
- analysis;
- assessment method;

An overview of the methods typically used in the 15 EU Member States and five other european countries has been prepared by European Water

Pollution Control Association (EWPCA) [3]. For larger WWTPs, flow proportional 24 h composite samples are typically used, however, the grab sampling method is used in Germany and the UK. For analysis all countries use nationally or internationally recognised standard methods. There is a trend in the direction of accepting quick test methods; but at present, online instrumentation is not used for compliance assessment.

An often overlooked aspect is the assessment method. The methods typically used in the 15 EU member states range from the very strict interpretation, that all results from all samples shall meet the standard value, to the less stringent interpretations where the arithmetic average for the sample population shall meet the standard, EWPCA [3,4]. The effluent standards in the directive are shown in Table 2. For the chemical oxygen demand (COD), biochemical oxygen demand (BOD) and suspended solids parameters, two assessment methods are included, namely the so-called look-up table (III), for how many samples are allowed to fail as well as a multiply of the standard, + 100 and + 150%, respectively, should not be exceeded by any sample (*I*). It is evident that a direct comparison of a certain criterion, e.g. 25 mg BOD l<sup>-1</sup> which either relates to a maximum never to be exceeded, to an annual average or something in between — is meaningless. The numerical effluent standard value, the sampling method, analytical method, and assessment method should be regarded as integrated elements — not to be regarded separately.

On-line instrumentation, providing continuous data rather than discrete daily composite samples, and may eliminate the errors of sampling and minimise uncertainty of the assessment method—provided that the analysis is reliable!

## 3. Problems and challenges

Today, neither the EU directive nor the national standards in European countries regard on-line measurements as valid for compliance assessment. This may result in a limited user interest, purchase, and installation of on-line instruments in WWTP for effluent analysis, unless

Table 1  
Traditional and potential routes in decision making

Traditional route	Potential route
	Compliance assessment
Standard design ↓	↑ Integrated approach and environmentally sound management
	WWTP design and operation
Trouble shooting ↓ R&D priority	↑ Plant specific optimisation
	Research and Development

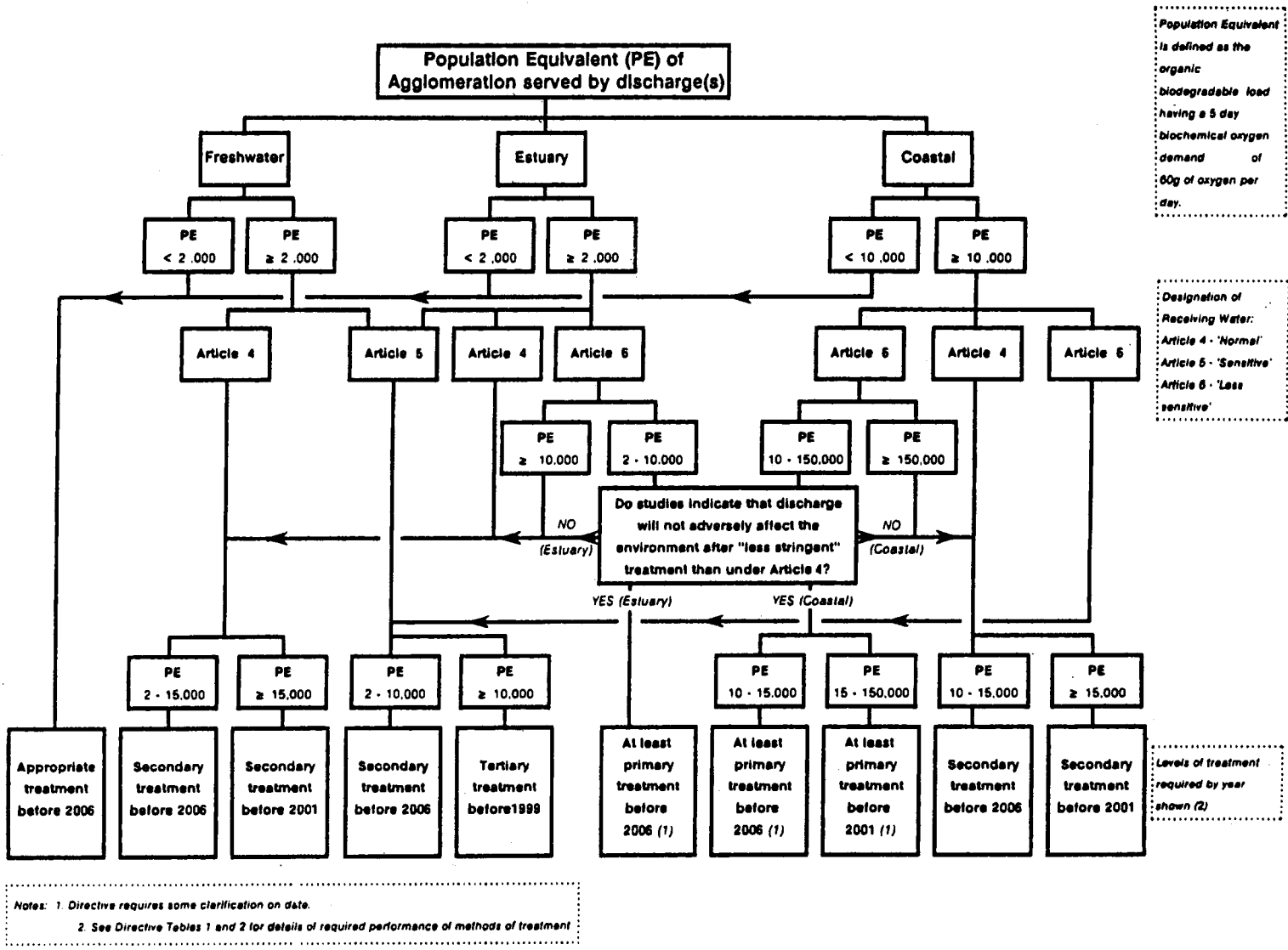


Fig. 1. Overview of the level of urban wastewater treatment according to the EU Directive (91/271/EEC); (Wright [2]).



Table 2  
Overview of compliance criteria, EU Directive (91/271/EEC)<sup>a</sup>

Parameter	WWTP size 1000 PE	Normal conditions		Sensitive areas		Assessment method <sup>b</sup>
		mg l <sup>-1</sup>	% reduction	mg l <sup>-1</sup>	% reduction	
COD	>2	125	75	125	75	III <sup>e</sup> , I(+100%) <sup>c</sup>
BOD	>2	25	70–90	25	70–90	III <sup>e</sup> , I(+100%) <sup>c</sup>
SS	>2	35	90	35	90	III <sup>e</sup> , I(+150%) <sup>d</sup>
Total (N)	10–100			15	70–80	IV <sup>f</sup>
	>100			10	70–80	IV <sup>f</sup>
Total (P)	10–100			2	80	IV <sup>f</sup>
	>100			1	80	IV <sup>f</sup>

<sup>a</sup> Sampling is based on 24 h composites, Unusual situations, such as heavy rain, are excluded.

<sup>b</sup> Codes for assessment methods.

<sup>c</sup> I(+100%) Each sample shall meet 2.0 K.

<sup>d</sup> I(+150%) Each sample shall meet 2.5 K.

<sup>e</sup> III A variable number of the samples shall meet K (Annex I, Table 3).

<sup>f</sup> IV The arithmetic average of the sample values shall meet K.

this is justified for process control alone. The acceptance by the environmental authorities for compliance assessment may be regarded as a bottleneck for future applications in WWTP effluent analysis.

This situation has actually been foreseen in the EU directive, so no change in this legal document is needed. The Annex I, D on reference methods for monitoring and evaluation of results include the paragraph “Alternative methods ... may be used provided that it can be demonstrated that equivalent results are obtained.” This may, according to Article 15.5 be formulated by the so-called ‘Article 18 Committee’ which assists the EC in implementing the directive. Therefore, convincing documentation should be provided that on-line instruments — meeting certain standards for precision and repeatability — may be accepted for monitoring of compliance assessment.

One problem is that such standard test procedures do not exist today. It is therefore crucial that initiatives for development and maintenance of such procedures be supported. Currently, the ISO/TC147/WG2 ‘On-line in-situ sensors/analyzers for water — specifications, performance tests and possible accreditation procedures’ is highly relevant in overcoming the above bottleneck.

The assessment method should be included when proposing on-line measurements as an op-

tion for compliance assessment. Strictly speaking, for the type I<sup>1</sup> method of assessment (Table 2) the presence of continuous data series rather than, e.g. 12–24 daily composite samples per year will increase the probability that a certain concentration be exceeded; this would result in an apparent non-compliance. Such stringent evaluation of maximum concentrations of a given effluent should be prevented. This problem could be over-

Table 3  
Current on-line instrumentation at WWTPs

Traditional	
–	Liquid level
–	Dissolved oxygen (DO)
–	Suspended solids (MLSS, effluent SS)
–	Substrate (TOC)
–	pH, redox potential (ORP), temperature,..
Novel	
–	Nutrients (NO <sub>3</sub> -N, NH <sub>4</sub> -N, PO <sub>4</sub> -P, total P)
–	Sludge blanket level and profile, sludge rheology
–	Total oil content
Forth coming	
–	Specific biosensors

<sup>1</sup> Each sample shall meet the standard value, K.

come, e.g. by using 50% percentile value of on-line data equivalent to the arithmetic average (method IV<sup>2</sup>) and 95% percentile values for extreme values (method I). By selecting proper percentile values, it should be possible to obtain an interpretation of on-line data for effluent concentration which would be neutral with respect to the EU directive. The challenge will be to have this accepted by the 'Article 18 Committee'.

#### 4. Operator's (or customer's) view on on-line instruments

First of all, an on-line instrument must be able to provide data for a relevant parameter; whether this parameter is measured directly in the same way as a corresponding standard analytical method, or via an indirect measure, is not a key issue for the operator. The instrument should meet certain requirements for precision, stability, and dynamics depending on the specific use.

For process control, the operator would often have high requirements on stability, and dynamics, probably compromising on the precision of the instrument to achieve this. On the other hand for compliance assessment, the requirements will typically be higher on precision and stability rather than on dynamics, furthermore, the environmental authorities may here prefer measurements based on the same analytical method as the effluent standard rather than measurements based on indirect measures (surrogate parameters).

As for all other equipment in a WWTP, the operator will give priority to instruments which are easy and not too time-consuming to maintain — and the price for capital costs, operation, and maintenance should be affordable.

The situations where on-line instruments will be cost-effective are, if extra capacity for the treatment may be facilitated as a result of better process understanding and control, or if savings in power consumption and/or chemicals will be the achieved.

#### 5. Current on-line instrumentation at WWTPs

Table 3 gives a brief overview of current on-line instrumentation at WWTPs. More comprehensive state-of-the-art overview is available, e.g. from the IAWQ Specialist Group on this topic [5].

Today, several modern WWTPs have been automated to a degree where they can be operated without attendance, e.g. during the weekend. This is due to the rapid development in relatively cheap and reliable sensors and controllers for industrial applications. Automatic control based on measurements of liquid levels, dissolved oxygen (DO), suspended solids (MLSS), pH, redox potential (ORP), etc. is considered to be standard.

Novel sensors, e.g. for control of biological nutrient removal have been available for about 10 years, with the latest developments, it is now possible to have sensor installation directly in the aeration tanks which has improved sensor dynamics significantly.

A new promising area is the application of specific biosensors, e.g. for specific organic compounds or heavy metals. Subscription to the Newsletter service from the ongoing concerted action BIOSET [6] can be recommended to scientists and companies working in this area.

#### 6. Potentials for further developments

Although significant progress has been made within the last two decades for automation of WWTPs there is still a high potential for further developments and improvements. Table 4 highlights some topics; a review by Olsson and Newell [7] gives some general reflections, too.

The performance and economy of existing instruments may be further improved. Product development on the basis of life cycle analysis may lead to increased lifetime of instruments, better use of resources, and handling of waste, including return systems for chemicals. Proven documentation of reliability may further expand the market from large to medium-sized WWTPs; according to EWPCA [3] (there are about 500 WWTP with capacity > 150 000 PE in the EU member States and about 4000 in the range 15 000–150 000 PE).

---

<sup>2</sup> The arithmetic average of the sample values shall meet K.

Table 4  
Some potentials for further developments

Existing instruments	
–	Improved reliability, dynamics, maintenance and price
–	Advanced interpretation of results (process rates)
New instruments	
–	Substrate fractions
–	Viable biomass and specific fractions
–	Activated sludge flocculation (sedimentation and thickening)
–	Dewatering properties
–	Xenobiotic compounds
–	Inhibition/toxicity
–	Hygienic parameters
New concepts	
–	Automatic adjustment of setpoints
–	Grey-box modelling and forecasting
–	Total WWTP and catchment area versus unit operations
–	Man-machine interfaces

Also, a more advanced interpretation of results, e.g. estimation of respiration in an aeration tank on the basis of on-line DO data, may increase the use of existing instruments.

The intense development of mathematical models for wastewater treatment processes has led to an increased demand for rapid measurements or estimations of various fractions of substrates (e.g. COD fractions) in the wastewater and WWTP reactors and similar fractionation's of the biomass (viability, specific activity and specific degraders). Various methodologies have been developed for research purposes but there is a potential for simplifying some of these for practical field applications. Also the physical separation processes need new instruments for optimisation of secondary clarifier performance as well as sludge dewatering; this contributes towards R&D purposes for improved understanding of flocculation mechanisms as well as process control at the plants. Increased public attention and priority to xenobiotic compounds calls for new instruments for field applications, not only for measuring concentrations of certain compounds but also the

biological responses in terms of inhibition of treatment processes, e.g. nitrification, and toxicity to aquatic organisms in the receiving water; the sensitivity of the methods here are considered a major problem as concentration levels are often in the  $\mu\text{g l}^{-1}$  range. The growing globalisation of the tourist industry leads to a much faster and widespread import of diseases from overseas destinations, rapid methods for detection of other pathogenic micro-organisms than the indicator *Escherichia coli* are needed for increasing confidence to the control of recreational waters.

New concepts are also under development for the automated control of WWTP processes. The existing closed control loops for unit process areas are being linked to supervisory control with wider frames for the optimisation; this includes more holistic approaches where simplified (grey-box) models are used in the on-line control of not only the WWTP but also the catchment area sewerage system with the objective of minimising overall receiving water impacts.

Wastewater treatment plants should be regarded as complex production facilities aiming at making clean water effluents and re-usable by-products out of the ever-changing mixture called wastewater, as the raw material. The organisations, production facilities, and methods will develop as in any other industry in our modern societies.

## 7. Summary

The situation may be summarised as follows:

- relevant instrumentation may save energy consumption, improve process performance and treatment capacity, and increase knowledge and understanding;
- traditional and novel on-line instruments have been on the market for several years and are considered reliable for WWTP process control;
- there is a high potential for further development and use of on-line measurements in wastewater quality monitoring for both R&D, process control and compliance assessment;
- actions should be taken to allow on-line measurements as an option for compliance assess-

ment in national emission standards and the 91/271/EEC directive;

- new concepts and methods for signal processing and interpretation should have a high priority for R&D and implementation.

## References

- [1] European Commission, Council directive of 21 May concerning urban waste water treatment, in: (91/271/EEC), EEC, 1991.
- [2] P. Wright, *J. IWEM* 6 (1992) 675–689.
- [3] European Water Pollution Control Association (EWPCA), The Comparability of Quantitative Data on Waste Water Collection and Treatment, Final report to the EC DG XI B1, CEC Study Contract no. B4/3040/93/000924/JS/B1.
- [4] B.N. Jacobsen, B.M. Petersen, J.E. Hall, *Eur. Water Pollut. Control* 7 (1997) 19–24.
- [5] IAWQ, Instrumentation, control and automation of water and wastewater treatment and transport systems, *Water Sci. Tech.* 37 (1997) 1998 R. Briggs (editor).
- [6] EU Concerted Action, BIOSET: Biosensors for Environmental Technology, Newsletter, Editor: S. Alcock, Cranfield University. E-mail: s.alcock@cranfield.ac.uk
- [7] G. Olsson, R. Newell, *Water Sci. Tech.* 37 (1998) 397–401.

# Methodologies for wastewater quality monitoring, Nîmes, October '98 Cost of ownership of on-line instrumentation

Michael Scott \*

*SWIG, 27 West Green, Barrington, Cambridge, CB2 5RZ, UK*

## 1. Introduction

It is a reasonable assumption that, over the next few years, the regulators in Europe will demand more and better information about the activities of the Water and Waste Treatment (W&WT) industry. This will put pressure on both the quality and the costs of the data used to generate the required information. Although there has been some recent improvement, there is a considerable lack of confidence in the data produced by on-line monitoring. This unhappy situation arises because the elements which make up the life time cost, sometimes called cost of ownership, are not usually an integral part of the purchasing considerations. There are many anecdotal stories to support this assertion.

Both users and suppliers have produced sufficient evidence to show that operating costs (OPEX) often exceed the cost of acquiring the monitor (CAPEX) by an order of magnitude ( $\times 10$ ). The problem is that CAPEX is usually dealt with by procedures and departments which are not directly connected with the procedures and departments responsible for setting OPEX budgets and resources.

## 2. Cost of ownership

There are many components which add up to the life time cost of ownership of on-line monitoring and some of these are summarised in Table 1.

Each component may include several elements such as manhours, travel, reagent consumption etc. The costs of each of these components should be estimated and the total used to generate a net present value of owning and using the on-line monitor. This cost should then be compared to the estimated business benefits. The consequence of not generating detailed costings is that appropriate budgets and responsibilities are not allocated, with the inevitable detrimental affects on monitor performance.

Table 1  
Cost of ownership considerations

---

Design costs
Purchase price
Installation costs
Operation costs
Calibration costs
Reagents and other consumables
Spares cost and availability
Power requirement
Training costs
Depreciation and replacement costs

---

\* Tel./fax: +44-1223-870967.

E-mail address: michaeljscott@compuserve.com (M. Scott)

Table 2  
Yorkshire Water investment in on-line monitoring

Parameter	Number of instruments
Quality	1860
Flow	2646
Level	2664
Other	1599
Total	8769

Instrumentation specialists in a number of UK Water Companies are well aware of the importance of OPEX and have developed such mechanisms as Framework agreements and compliant supplier lists to steer purchasing to those instruments which are likely to provide the least life time cost for the largest business benefit. Estimating the actual costs of the elements which make up OPEX is extremely difficult but North West Water and, more recently Yorkshire Water, have put estimates of cost of ownership of on-line monitors into the public domain via SWIG Workshops.

For example they have both estimated that an on-line pH measurement costs around £1200 per year to own. Such an instrument costs considerably less than £1000 to purchase but for the purposes of discussion let us assume that the installed cost is £1200. The normal planned life of an instrument in the W&WT industry is 10 years so we have the position that OPEX is an order of magnitude greater than CAPEX.

This has, of course, very important implications for any industrial company and the scale of this is shown by the following two charts derived from information put into the public domain by Yorkshire Water at the SWIG Conference in June '98 (Table 2).

With nearly 9000 on-line instruments and, as can be seen, OPEX costs exceeding amortised CAPEX by a considerable margin there is a need to understand and control the elements that contribute to OPEX; especially as inadequate budgets for elements such as reagents, consumables and calibration will make the difference between useful data and unreliable or no data.

### 3. CAPEX

Capital expenditure should include the total cost of the components required to purchase and install the instrument. CAPEX should also include the cost of designing the installation so that the instrument 'sees' the process in a manner which ensures that the data generated truly represents the process. However the purchase, whether as part of a larger contract or for an extension, is normally via a purchasing department which has the responsibility of achieving least purchasing price for the instrument. Only where an experienced and knowledgeable 'champion' is available for the whole design, purchase, commissioning cycle will there be sufficient information available to consider the cost of ownership issues.

The supplier has an interest in the difficulties in helping to organise a full consideration of the elements of life time cost since both margins and reputation are threatened. Narrow margins caused by cutting the price so as to gain the order often leave nothing left to support the instrument once it reaches the commissioning stage. If the supplier does not support the instrument the resulting poor data may harm the product image and prejudice future orders.

### 4. OPEX

A full understanding of the operating costs of an on-line instrument is vital to establishing confidence in the data it generates. Without that understanding the appropriate budgets do not get allocated and the appropriate responsibilities are not assigned. This, of course, is not unique to on-line monitoring and some water companies have assigned every asset to an individual 'asset manager'. Unfortunately instrument assets are of very low value compared to other process plant assets and the notional financial gains from detailed support seem small in the context of the larger picture. The significant business benefits to be gained by high quality data are rarely balanced against the OPEX costs.

Several suppliers have recognised the logistical problems that the water companies face in sup-

porting widely distributed, high technology, but low value, assets and are offering to sell the measurement to the user; taking care of every thing else. One leading European supplier offers a multi-parameter on-line measurement for around £2250 per annum which looks an attractive proposition when Table 3 is reviewed.

## 5. What is needed?

The user's, regulators and suppliers all need to have an increased confidence in the data generated. It is suggested that this might be achieved by taking a different approach to meeting the needs. The technology is usually the dominant topic when on-line monitoring is being discussed and, it is suggested, this can lead to the wrong conclusions. Perhaps the business needs should be the starting point:

- operating costs must be < £1000 per year. We do not maintain our televisions or the sensors on our cars; why do we need to give so much attention to industrial sensors? The scale of production is of course a factor but not the complete answer to the differences in operating costs.
- The capital cost must be < £2000 for all measurands and the instrument must be a 'thing' which is inserted into the process via standard valves or other readily available probe technology; plug and play.
- Aggregate measurements into one insertion into the process.

Table 3  
Yorkshire Water, costs of ownership

Parameter	Amortised CAPEX pa	Revenue pa	Total £ pa
Aluminium	1685	4333	6018
Manganese	1685	3170	4855
Colour	1516	2324	3850
Iron	1685	4382	6067
Temperature	72	176	248
Phosphate	1782	5139	6921
Nitrate	1422	3242	4664
Pressure	89	58	172

- Understand the calibration trail to the nearest point of excellence. Do we really need high accuracy?
- Forget the science-understand the need.
- Radio costs are dropping rapidly; telemeter everything back to the supplier.

### 5.1. The supplier

The supplier has a problem in meeting the needs of the W&WT industry because the market is rather small and the purchasing widely spread. It is interesting to note that the user often has as much difficulty finding the supplier as the supplier has in finding the user with a current need. This of course imposes costs on both which, in the case of the user, is almost certainly not budgeted.

An aspect of the cost of ownership for on-line monitoring in the W&WT industry which is almost completely ignored by the users is the fact that the CAPEX must include the cost of developing and marketing the instrument in the modest sized. For example one leading supplier estimated that it would cost £350 000 to take demonstrable technology of an single measurand optical instrument to the market. A selling price of £2000–3000 would be ambitious and the market need in Europe, because of the current activity to deal with cryptosporidium, might be an ambitious 700–1000 units annual sales; probably achievable over 3–4 years by a new product. After that there might be sales of, say, 100 units per annum. It does not need an business analyst to see that even obtaining a positive cash flow from the project is open to question.

If the W&WT industry is to obtain the high quality on-line monitors it needs for its wide range of measurands some mechanism must be established so that the inventors, developers and suppliers have a mutually supportive understanding of the total market and each must obtain a proper return on their investments.

## 6. Ownership of the monitoring

Confidence must be generated in the data provided by on-line monitors and one way to achieve

this is to establish widespread ‘ownership’ of the data. In some way or other there are often several ‘clients’ for each piece of data. The ‘clients’ may range from the local operator through to an affect on consolidated reports to the shareholders. For example Thames Water have a major installation programme of magnetic flowmeters underway in London; aiming to provide more and better data about the process with bi-directional data and information transmission via a radio transmitter which is built into a purpose designed roadside bollard. The integration of the data is the key issue and there are big advantages in communicating directly with an instrument. The fast response of this particular system quickly uncovered new features of activity in the distribution system. The ability to look directly at each valve, on-line flowmeter or monitor, allowed the organisation of maintenance from anywhere to anywhere; which was very valuable when there are so few experts about. A wireless data network was used to avoid the high cost incurred in laying telephone wires, and to provide quick and easy installation. The connection costs are relatively low, and surprisingly, the ‘line rental’ and call charges are lower

than a normal telephone line. The bi-directional information flow to these widely distributed assets has significantly increased confidence. In this case both CAPEX and OPEX are down but confidence in the data is up and the effect on leakage is already pleasing both the regulator and the shareholders.

## 7. Summary

The problem is that the user is being presented with ‘packets’ of high technology choices without the structure, time or skills available to integrate these packets of technology excellence. There should be more emphasis on why measurements are made and on the life time cost of making those measurements. This may automatically lead to an emphasis on generating confidence in the data which is being used by an increasing range of clients. The probability is that there will need to be an emphasis on an integrated approach to the development, purchase and use of on-line monitors.



# Methodology for the characterisation of heterogeneous fractions in wastewater

Sabine Vaillant, Marie-Florence Pouet \*, Olivier Thomas

*Laboratoire Génie de l'Environnement Industriel, Ecole des Mines d'Alès, 6 Avenue de Clavières, 30 319 Alès Cedex, France*

---

## Abstract

A better knowledge of colloidal and particulate matter of urban wastewater is necessary for the optimisation of the wastewater treatment. This paper presents a methodology based on the study of each granular fraction (settleable, supracolloidal, colloidal and soluble matter) separated by different techniques of liquid-solid separation and analysed by non specific parameters (chemical oxygen demand, total suspended solids, UV spectra). The application of this methodology to a storm event allows to explain the quality variation observed during this period. © 1999 Elsevier Science B.V. All rights reserved.

*Keywords:* Wastewater; Fractionation; Colloids; Particulate pollution; UV spectrophotometry; Isosbestic point

---

## 1. Introduction

The European Directive of 21st May 1991 sets the criteria for an efficient drainage and sewer treatment. It recommends in particular the implementation of a reliable self-monitoring for wastewater quality survey, and for treatment control. Several technical solutions can be envisaged but, unfortunately, there is a lack of relevant and reliable methods for the characterisation of heterogeneous fractions such as suspended solids. This reality is due, on one hand to the poor knowledge of colloidal and particulate phases generally considered as easily removable, and, on

the other hand, to the technical difficulty related to their characterisation.

Most of the time, turbidity measurement is proposed for on-line estimation of total suspended solids (TSS), but this parameter is actually very sensitive to the granular distribution and thus to the colloidal fractions limiting its use to constant quality of wastewater.

The knowledge of colloidal and particulate phases of wastewater is very important in case of urban storm runoffs because of the variability of particle size influencing strongly the efficiency of treatment processes [1].

In case of dry and wet weather effluents, the main problem is the difficulty to classify clearly two weather situations and to characterise accurately each size fraction (settleable, colloidal and soluble) enable to influence the treatment. Most studies concerning urban wet weather discharges

---

\* Corresponding author. Tel.: +33-4-66782728; fax: +33-4-66782701.

*E-mail address:* mfpouet@ensema.fr (M.-F. Pouet)

have focused on particulate and colloidal fractions greater than  $0.45\ \mu\text{m}$  [2]. However, the treatment which can be applied to these effluents is strongly influenced by the size ranges of their contaminants. Therefore, a more complete fractionation (from settleable to soluble matter) has been designed for a better knowledge of the smallest fractions. This work presents the methodology used to characterise urban wastewater in dry and wet weather conditions and the results obtained on a storm event.

## 2. Methodology

### 2.1. General procedure

The methodology is presented on Fig. 1. It is based on a liquid-solid separation by different techniques such as settling, centrifugation and filtrations.

### 2.2. Materials and methods

#### 2.2.1. Analysis and spectrophotometric measurement

Chemical oxygen demand (COD) was analysed with HACH test tube method using a spectrophotometer DR/2000 (Hach).

TSS (total suspended solids) were measured according to the European Standard CEN872 with glass fibre filters [3].

For UV spectra acquisition, the spectrophotometer used was a S1000 (Secomam) of 2 nm bandwidth, with a quartz cell of 10 mm path-length. The selected scan speed ( $1800\ \text{nm}\ \text{min}^{-1}$ ) was chosen with respect to the presence of suspended solids in samples. General work on spectra was achieved with DATHELIE PC software (Secomam).

The first method of exploitation of UV spectra is a semi-quantitative one. It consists of calculating the areas defined by the sum of absorbance

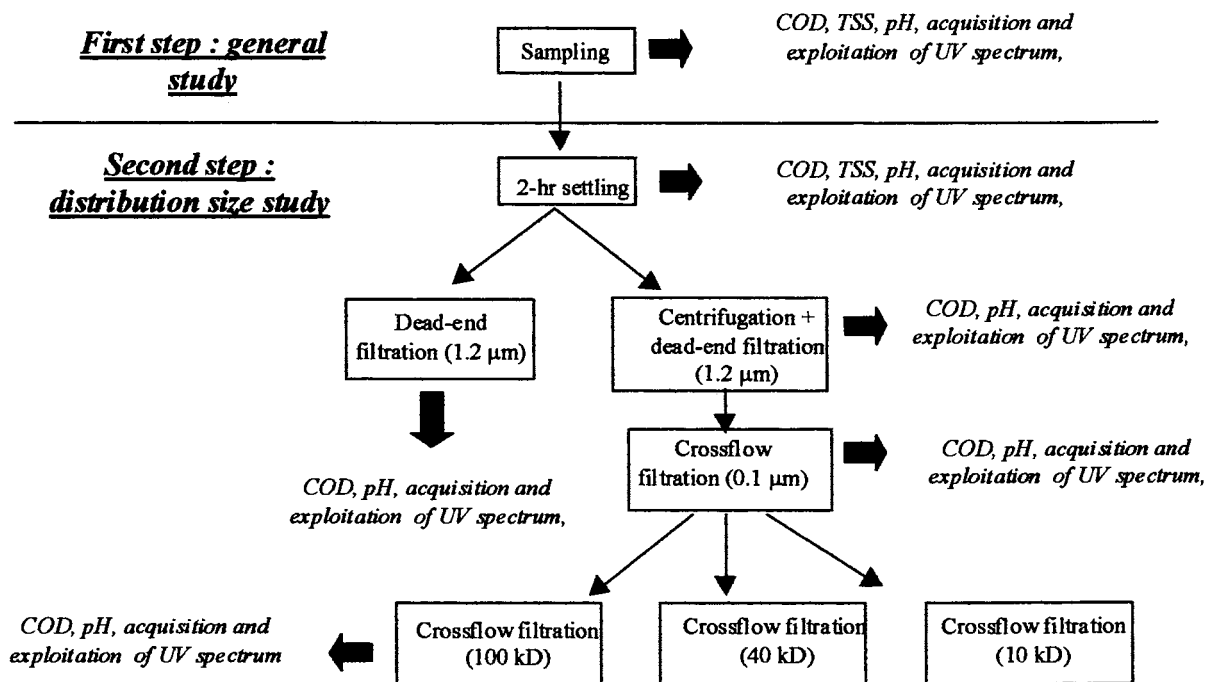


Fig. 1. Methodology of characterisation of wastewater.

values between 200 and 350 nm (measured every 1 nm). Contrary to the use of absorbance values at a single wavelength, it takes into account all the absorbing species and will be compared to non specific parameter values (COD).

The second method is the normalisation of UV spectra. Generally, dilute spectra are flattened with reduced shoulders and slopes. In order to compare spectra shape in a pure qualitative way, it is necessary to restrict dilution effects. Normalised spectra have the same area, i.e. the total sum of absorbance values between 200 and 350 nm.

### 2.2.2. Fractionation technique

- The settleable fraction was assessed by 2-h settling in an Imhoff tank.
- Supracolloids were separated by filtering with glass fibre filters ( $\approx 1.2 \mu\text{m}$ ).
- Colloids were fractionated up to the soluble part by crossflow microfiltration ( $0.1 \mu\text{m}$ ) followed by various ultrafiltrations (100, 40, 10 kD).

To avoid membrane fouling and the corresponding information loss, a pretreatment was applied to the settled samples prior to microfiltration: centrifugation (80 ml, 15 min, 8000 rpm,  $9600 \times g$ , GR4.11 JOUAN centrifuge) followed by filtration with glass fibre filters.

Moreover, in order to restrict the material loss resulting from adsorption on membranes, only microfiltration ( $0.1 \mu\text{m}$ ) was used before any ultrafiltration.

Crossflow filtration was carried out with a flat apparatus PLEIADE RAYFLOW  $\times 100$  (Tech-Sep) with two membranes of  $100 \text{ cm}^2$ . It was operated in a batch mode at 105 Pa transmembrane pressure. Continuous feed was provided with a  $2.5 \times 10^{-5} \text{ m}^3 \text{ s}^{-1}$  flow and retentate was fully recycled. Four organic membranes were used:  $0.1 \mu\text{m}$ , 100, 40, 10 kD.

The ultrafiltration cut off points correspond approximately to the following pore size diameters: 0.01, 0.004 and  $0.001 \mu\text{m}$ .

## 3. Application: study of wastewater quality variation during a storm event

### 3.1. Experimental

The methodology has been tested on real effluents. All samples were influents of the wastewater treatment plant of Alès (France). The sampler used was an ISCO 3710. The samples are time or flow proportional.

Dry weather samples were taken after the grit chamber (sample 1) and wet weather samples collected at the overflow of the main sewer leading to the treatment plant. They are numbered from the beginning of the rain (sample 2) to the end (sample 6) with time. Studied events are presented in Table 1.

### 3.2. Analytical results and interpretation

The first step of the procedure is based on a direct comparison between evolution of UV spectra and non specific parameter values.

Graph from Fig. 2a shows the evolution of non specific parameter values (COD and TSS) during the storm event, compared to the ones of dry weather sewage (sample 1). The results obtained with UV spectrophotometry is given in Fig. 2 (b).

The analysis of the five wet weather samples shows that the first sample (sample 2) is heavily

Table 1  
Sample characteristics and sampling methods

Sample number	Sample nature	Storm event and sampling method
1	Dry weather	24-h proportional time composite: one sample every 15 min
2	Wet weather	first 1270 $\text{m}^3$ : one sample every 16 $\text{m}^3$
3	Wet weather	5340 $\text{m}^3$ covered: one sample every 100 $\text{m}^3$
4	Wet weather	2740 $\text{m}^3$ covered: 1 sample every 50 $\text{m}^3$
5	Wet weather	7800 $\text{m}^3$ covered: one sample every 50 $\text{m}^3$
6	Wet weather	920 $\text{m}^3$ covered: one sample every 50 $\text{m}^3$

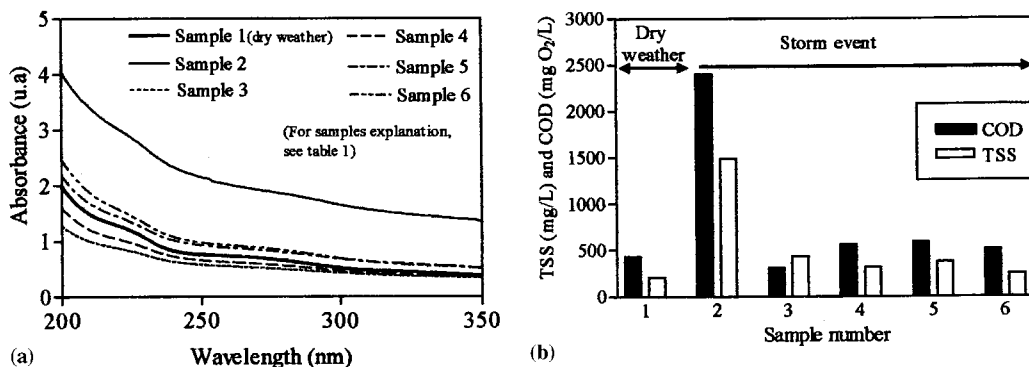


Fig. 2. (a) and (b): Study of a storm event: evolution of non specific parameters and UV spectra (dilution  $\frac{1}{2}$ ).

loaded in terms of COD. The following is diluted (sample 3). It has a lower COD than dry weather sample (sample 1), but still has a higher TSS concentration. After the heaviest part of the storm event (samples 4–6), COD and TSS values become closer to the ones corresponding to dry weather conditions.

All these characteristics change progressively during the storm event to correspond to the ones of dry weather sample (sample 1) at the end of the rain (sample 6). The set of spectra allows to visualise the storm event effect:

- the set of spectra presents the same evolution, representative of the phenomenon,
- quantitatively, UV spectrophotometric results thus follow the same trend as COD and TSS values: at the beginning of the rain (sample 2),

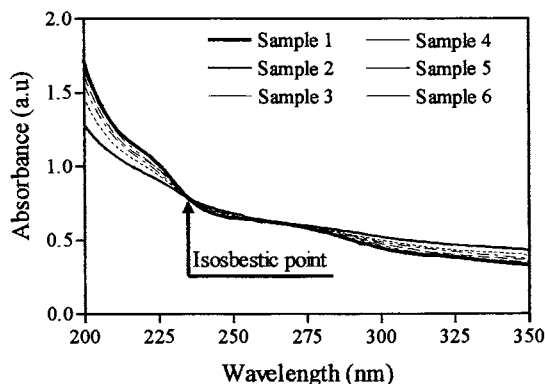


Fig. 3. Study of the evolution of a storm event with normalised UV spectra.

the load of absorbing contaminants is almost twice as high as the one of dry weather flow. Immediately after this first step, the effluent is diluted. At the end of the storm event (sample 6), absorbance values are slightly higher than the ones of dry weather sewage (sample 1).

Qualitative information can also be deduced from spectra shape. A scale effect between the more and less concentrate (usually flattened) samples would lead to flawed conclusions for a qualitative comparison of spectra shape. Therefore, the spectra must be normalised.

### 3.3. Exploitation of UV spectra by normalisation procedure

As specified in Section 2.2, the normalisation procedure of UV spectra consists of giving the same area to each spectrum. The set of spectra presented on Fig. 3 has been normalised in order to obtain a relative area of  $100 \text{ au nm}^{-1}$ .

Several remarks can be made:

- as a whole, wet weather discharges have more monotonous spectra than dry weather sample (sample 1). At the beginning of the rain (sample 2) the shape is diffuse: the slope varies gently from 200 to 350 nm without any sharp change, whereas a more structured shape is shown for dry weather sewage (sample 1). Progressively, the slope between 200 and 240 nm becomes steeper while the absorbance above 250 nm decreases. Finally, the two mixture proportions vary according to weather condi-

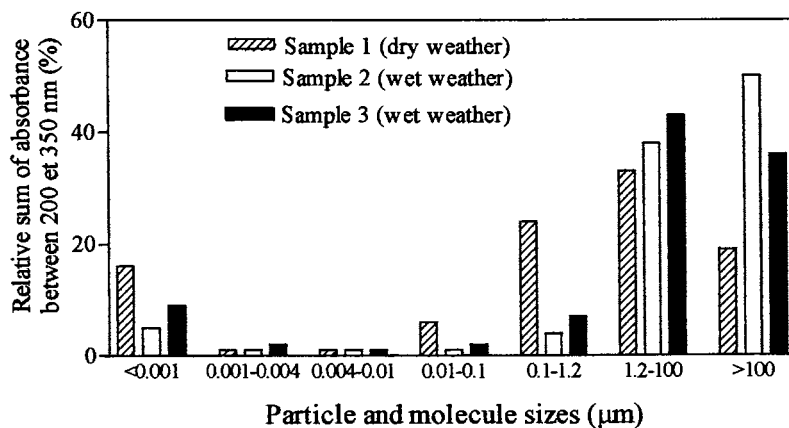


Fig. 4. Size distributions of organic pollution (% absorbance) of samples 1, 2, and 3.

tions: suspended solids predominate at the beginning of the rain, whereas dissolved matter is preponderant in dry weather flows. One can also notice that as characteristics get closer to the ones of dry weather flows, the two shoulders (around 223 and 270 nm) corresponding to anionic surfactants [4] and benzoic cycles [5] appear gradually with time, leading to a more structured spectrum shape.

- These two phenomena take place around one isosbestic point ( $\approx 234$  nm) where the whole set of spectra shows a same intersection point. The presence of such an isosbestic point is very important to note: indeed, it means that two mixtures in the effluent have a fixed relationship between their concentration [6].

When an isosbestic point is visible without normalisation, it is possible to establish a mass balance. In this case, the isosbestic point revealed after normalisation does not prove a mass balance but the water quality conservation, which is an important point in terms of treatment.

#### 3.4. Fractionation study

Urban wastewater is a mixture of organic and mineral pollutants whose size distribution is very wide. Two reasons explain the necessity to establish and to identify the organic pollution size distribution:

- The implement of a monitoring tool based on UV spectrophotometry for wastewater treatment plant management asks for a better knowledge of colloidal and particulate fractions that influence strongly the UV spectra shapes.
- Effluent size distribution has a great effect on its treatability.

UV spectra obtained after each filtration have been exploited according to the first method described in Section 2.2 (calculation of area). For example, Fig. 4 presents the evolution of UV spectra area with size distribution for sample 1, 2, and 3.

Observing size distributions in terms of absorbance for the two wet weather samples of the storm event (samples 2, and 3), one can see that TSS (matter above 1.2  $\mu\text{m}$ ) represent from 79 to 88% of raw urban wet weather discharge absorbance whereas they are only 52% of raw sewage absorbance.

On the contrary, the large colloids (0.1–1.2  $\mu\text{m}$ ) are responsible for a lower absorbance during wet weather conditions. Moreover, dissolved materials represent a small contribution to total absorbance  $\leq 10\%$  for the two wet weather samples, while they reach 16% for dry weather sample.

These phenomena could be explained according to the following reasons:

- The relative decrease observed in the soluble population cannot be a result of a shift towards larger molecules except for the case of adsorption, which would probably not be sufficient enough to explain the decrease from 16 to  $\leq 10\%$  of the contribution of soluble matter to total absorbance. It could be as a result of dilution by rainwater. However, the comparison of the absolute absorbance values (200–350 nm) would show that only sample 3 is dilute. Therefore, the relative decrease in the soluble population is likely to be due to the large contribution of SS in sample 2 proceeding almost like a dilution, and to a dilution by rainwater for sample 3.
- Concerning large colloids (0.1–1.2  $\mu\text{m}$ ), their decrease seems too important to be due to these phenomena. Therefore, they could have been trapped with the large amount of settleable solids and flocculated with them [7]. Indeed, Chebbo and Bachoc [2] found that SS of urban storm runoffs flocculate and settle more easily.

In conclusion, this step of fractionation associated with UV spectrophotometry is interesting because it allows the explanation of the general shape of the UV spectra obtained during a storm event presented in Fig. 2(b). Some results of the comparison between COD and UV absorbance in terms of organic matter size distribution are given in Table 2

One can see that settleable fraction is underestimated by the calculation of spectrum areas since it corresponds to 29% of COD, but only 19% of total absorbance. On the contrary, large colloids (0.1–1.2  $\mu\text{m}$ ) and soluble matter (< 10 kD) are overestimated since they represent 19 and 9% of COD, respectively, but 24% and 16% of total absorbance respectively. The same conclusions can be made for wet weather samples.

The fact that spectra areas are not exactly proportional to COD is not surprising since suspended solids and colloids represent the major absorbance and their absorbance is diffuse. It does not follow Beer–Lambert law and is not likely to be proportional to concentration in the same way as absorbance of the lowest fractions.

Nevertheless, when TSS (including settleable and supracolloidal matter) are considered all together, absorbance result (52%) is rather close to COD value (60%). This last point is important because it means that the UV estimation of TSS is possible even if the difference between settleable matter and supracolloids is difficult to establish.

#### 4. Conclusion

A methodology of urban wastewater characterisation based on fractionation of heterogeneous fractions is studied and applied to the differentiation of two weather conditions.

A semi-quantitative approach after a fractionation of samples by settling, microfiltration and ultrafiltration showed that organic matter distribution is different in urban storm runoffs than in dry weather flow. Urban wet weather discharges have a high suspended solid load and a lower content of large colloids (0.1–1.2  $\mu\text{m}$ ). These colloids could have been trapped with the large amount of easily settleable suspended solids and flocculated with them.

A qualitative approach studied a storm event from the beginning till the end using normalised UV spectra to release them from dilution hiding effect. An isobestic point appeared, i.e. the whole set of spectra had the same intersection point. It can be assumed that combined sewage is a mixture of two complex mixtures (suspended solids and ‘soluble’ matter) whose proportions vary according to weather conditions with a fixed relation between their concentration.

Thanks to a semi-deterministic procedure using reference spectra, a quantitative estimation of non specific parameters could be achieved from the use of a UV spectrophotometer and a multicomponent software [8]. Indeed, ultraviolet spectrophotometry has proved to be a valuable tool to monitor wastewater treatment [9] and to estimate some non specific parameters [10,11,8]. This would be the following step for the elaboration of a tool for diagnosis and control of sewage in different weather conditions.

Table 2  
 COD values of cumulative fractions and contribution of each fraction to total COD and total absorbance for sample 1 (dry weather)

Sample	Raw	2-h settled	1.2 ( $\mu\text{m}$ )	0.1 ( $\mu\text{m}$ )	100 (kD)	40 (kD)	10 (kD)
COD ( $\text{mg l}^{-1}$ )	430	305	170	88	58	48	37
Fraction	Settleable (> 100 $\mu\text{m}$ )	Supracolloidal (10 <sup>2</sup> –1.2 $\mu\text{m}$ )	Colloidal (1.2–0.1 $\mu\text{m}$ )	Colloidal (<0.1 $\mu\text{m}$ > 100 kD)	Colloidal (100–40 kD)	Colloidal (40–10 kD)	Soluble (<10 kD)
COD (%)	29	31	19	7	2	3	9
Abs. (%)	19	33	24	6	1	1	16

## Acknowledgements

We would like to thank Laetitia Fabre, technician student and the staff of Ales wastewater treatment plant who helped with analysing and sampling the effluents.

## References

- [1] A.D. Levine, G. Tchobanoglous, T. Asano, J. WPCF 57 (1985) 805.
- [2] G. Chebbo, A. Bachoc, *Water Sci. Technol.* 25 (1992) 171.
- [3] European Standard EN 872, AFNOR T91K, Brussels, Feb. 1996.
- [4] F. Theraulaz, L. Djellal, O. Thomas, *Tenside. Surf. Detect.* 33 (1996) 1.
- [5] R.M. Silverstein, G.C. Bassler, *Identification spectrométrique des composés organiques*, Masson, Paris, 1968.
- [6] S. Gallot, O. Thomas, *Fresenius J. Anal. Chem.* 346 (1993) 976.
- [7] Vaillant S, Pouet M-F, Thomas O. Innovative Technologies in Urban Storm Drainage, in: *Proceedings of the Novatech Third International Conference*, Lyon, France, 1998, p. 39.
- [8] O. Thomas, F. Theraulaz, C. Agnel, S. Suryani, *Environ. Technol.* 17 (1996) 251.
- [9] N. Matsché, K. Stumwöhler, *Water Sci. Technol.* 33 (1996) 211.
- [10] S.K.E. Brookman, *Water Res.* 31 (1997) 372.
- [11] G.V. Korshin, C.-W. Li, M.M. Benjamin, *Water Res.* 31 (1997) 946.



# An alternative method for the measurement of mineral sulphide in wastewater

F. Pouly <sup>a,\*</sup>, E. Touraud <sup>a</sup>, J.-F. Buisson <sup>b</sup>, O. Thomas <sup>a</sup>

<sup>a</sup> *Laboratoire Génie de l'Environnement Industriel, Ecole des Mines d'Alès, 6 Avenue de Clavières, 30319 Alès Cedex, France*

<sup>b</sup> *Total Raffinage Distribution, Raffinerie de Provence, La Mède, 13220 Chateaufort-les-Martigues, France*

## Abstract

A simple and rapid procedure for sulphide measurement in crude oil refinery wastewater has been developed. This method is based on the knowledge of the UV response of sulphur compounds and the mathematical deconvolution of the sample spectrum using reference spectra (specific compounds or aggregate spectra). The detection limit of the method is  $0.5 \text{ mg l}^{-1}$  for a quartz cell pathlength of 10 mm. The range is up to  $15 \text{ mg l}^{-1}$ . The method has been validated for crude oil refinery wastewater. Compared to conventional methods, the UV determination is quicker and easier to run. © 1999 Elsevier Science B.V. All rights reserved.

*Keywords:* Total sulphide; UV spectrophotometry; Industrial wastewater

## 1. Introduction

Sulphur occurs in wastewater in various forms. Most of the time, anoxic conditions in urban sewers lead to the production of hydrogen sulphide but, more often, the presence of sulphur compounds is related to industrial discharges, mainly from refineries or petrochemical plants. Some petroleum contains elemental sulphur and sulphur can occur as hydrogen sulphide ( $\text{H}_2\text{S}$ ) and carbonyl sulphide (COS). Sulphur is also present in a wide range of hydrocarbons, largely in the form of mercaptans, organic sulphides and thiophene derivatives [1].

Sulphur compounds tend to be concentrated in the higher boiling fractions of petroleum and are

generally corrosive to metals and may poison various catalysts. Stripping water is responsible for the presence of sulphide and mercaptans in crude oil refinery wastewater.

Sulphide in dissolved  $\text{H}_2\text{S}$  form is toxic to fish and other aquatic organisms [2] and can be responsible of the decrease in wastewater treatment plants efficiency. Hence, its concentration needs to be controlled, especially in crude oil refineries wastewater.

Sulphide can be determined in different media, using various techniques [3–5], unfortunately often complex or non robust (interferences). The aim of this paper is to propose a simple and fast method based on UV spectrophotometry for estimating the concentration of sulphide in wastewater, even high concentrations as in crude oil refineries wastewater.

\* Corresponding author. Fax: +33-466-782-701.

## 2. Inorganic sulphide standard methods

From an analytical point of view, total sulphide includes dissolved  $\text{H}_2\text{S}$  and bisulphide ion  $\text{HS}^-$  which are in equilibrium with hydrogen ions. The conditional ionization constant, which is valid for usual temperature and ionic strength, is  $\approx 10^{-7}$ . The  $\text{S}^{2-}$  form is negligible, amounting to  $< 0.5\%$  of the dissolved sulphide at pH 12.

Three main methods are commonly used for the determination of sulphide in solution (Table 1)

- the colorimetric method, the methylene blue method, is based on the reaction of sulphide, ferric chloride and dimethyl-*p*-phenylenediamine to produce methylene blue which absorbs at 664 nm [2],
- the iodometric method based on the oxidation of sulphide by iodine in acidic solution followed by a back titration with sodium thiosulphate solution,
- the potentiometric method using a selective silver electrode.

The use of UV spectrophotometry is proposed as an alternative method for determination of inorganic sulphide in industrial wastewater. The potentiometric method will be chosen as reference for the validation of the procedure.

## 3. Experimental

### 3.1. Material

UV spectra have been acquired with a UV-Visible spectrophotometer Anthelie, Secomam

(suprasil quartz cell; pathlength, 10 mm; scan speed,  $1800 \text{ nm min}^{-1}$ ).

The potentiometric titration is carried out in alkaline conditions with a Mettler DL 40 GP Memotitrator using a sulphided Ag electrode Mettler DM 141 SC.

### 3.2. Reagents

- Silver nitrate solution 0.05 N (Merck).
- Sodium sulphide nonahydrate (Prolabo Normapur AR).
- Sulphuric acid 95% (Prolabo Rectapur).
- Nitric acid 68% (Prolabo).
- Sodium hydroxide (solid, Prolabo Rectapur).
- 2-Naphtol (Merck).
- *p*-Chlorophenol (Merck).
- Sodium chloride (Prolabo Normapur AR).
- Sodium sulphate (Prolabo Normapur AR).
- 1-Propanthiol (Acros).
- RBS 25 (Traitements chimiques de surfaces–F-59236 Frelinghien).

For the potentiometric method, an alkaline solution (100 ml for 400 ml of sample) is prepared by adding 20 ml of ammonia min. 28% (Prolabo Normapur) to 1000 ml of 1 M sodium hydroxyde (Merck) solution.

### 3.3. Sampling

Effluents from crude oil refinery were sampled before the biological treatment, in tightly closed bottles in order to avoid any contact with gaseous phase so as to keep sulphides in solution. As raw samples have a pH between 7.5 and 8, pH correction is needed. Samples are immediately analysed.

Table 1  
Standard methods for inorganic sulphide determination

Method	Detection limit ( $\text{mg l}^{-1}$ )	Advantages	Drawbacks
Methylene blue	0.1	Flow techniques available	Interferences (strong reducing substances)
Iodometric	0.1	Simple	Not valid for complex samples such as industrial wastewater
Potentiometric	0.03	Unaffected by any interference (except humic substances)	Needs sample pretreatment and specific equipment

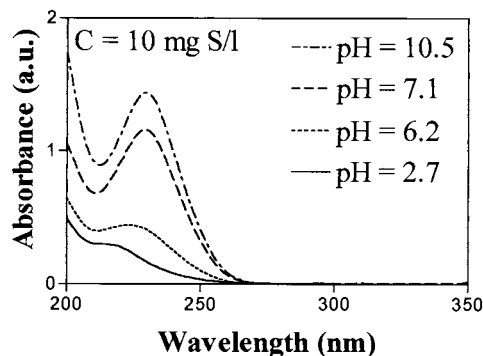


Fig. 1. UV spectra of inorganic sulphide.

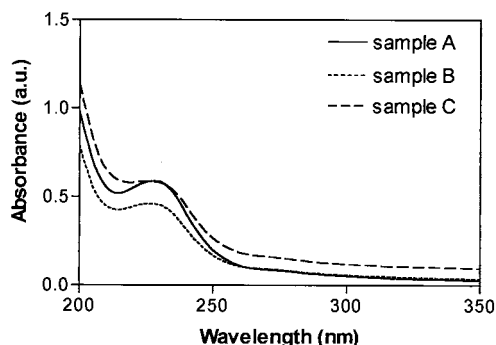


Fig. 2. Refinery wastewater UV spectra.

## 4. UV spectrophotometry of inorganic sulphide

### 4.1. Standard solutions

The sulphide ion absorbs UV light which promotes the excitation of the unshared electrons  $n$  of sulphur atom ( $n \rightarrow \pi^*$ ) and Fig. 1 shows UV spectra of inorganic sulphide, according to the pH medium.

For pH higher than 7,  $\text{HS}^-$  is the predominant form and absorbs with a maximum at 231 nm.

At lower pH, an hypsochromic shift and hypochromic effect are observed due to the apparition of the hydrogen sulphide form (volatile).

### 4.2. Wastewater samples

Fig. 2 shows the UV spectra of refinery wastewater containing mineral sulphide. Sample pH is basic (pH 9.3). The characteristic peak of the

bisulphide ion appears clearly on the UV spectra (231 nm), despite the matrix sample.

### 4.3. Quantitative determination

For quantitative estimation, the exploitation of UV spectra is needed. Several methods have been proposed using either a mono-wavelength approach, either derivative spectra or mathematical modelling of interference [6–8,10]. Some limits occur in their applications due to interference matrix nature.

Starting from a statistical knowledge of spectra, a semi-deterministic method using a mathematical deconvolution of the sample UV signal is proposed [9]. This approach is based on the additivity of Beer–Lambert's law and on the fact that an unknown UV spectrum can be substituted as a linear combination of a number of reference spectra (specific compounds or aggregate spectra). The calculation of spectra contribution is carried out using the following relation

$$S_w = \sum_{i=1}^p a_i \cdot \text{REF}_i \pm r$$

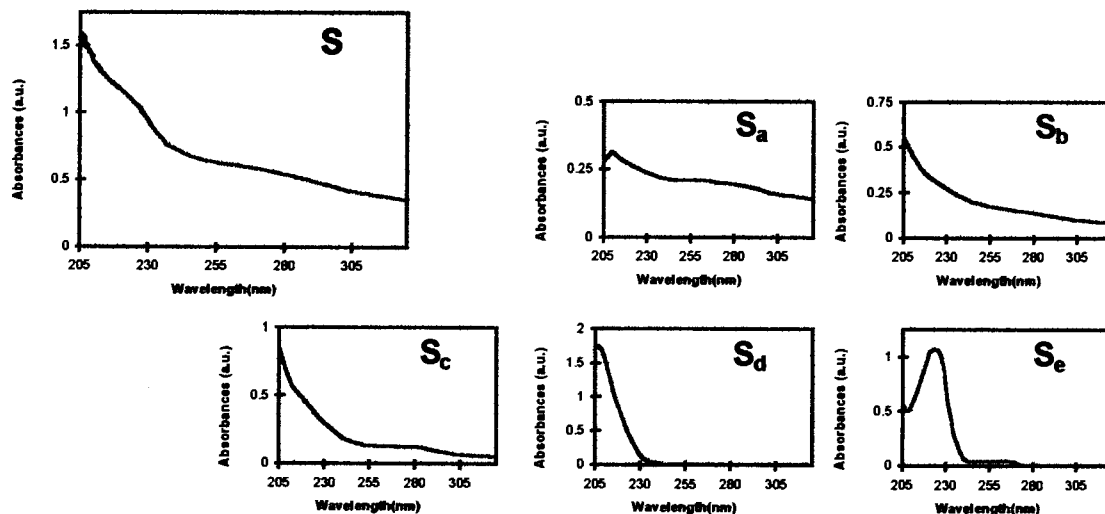
where  $S_w$  is the sample spectrum,  $a_i$ , the contribution coefficient of the  $i$ th reference spectra  $\text{REF}_i$ ,  $p$ , the number of reference spectra and  $r$ , the quadratic error.

Spectral deconvolution is illustrated in Fig. 3. In this case, the unknown UV spectrum ( $S$ ) has been decomposed by using five reference spectra

- $S_a$ , total suspended solids UV spectrum (aggregate spectrum);
- $S_b$ , colloids UV spectrum (aggregate spectrum);
- $S_c$ , dissolved organic matter (aggregate spectrum);
- $S_d$ , nitrate spectrum (specific compound);
- $S_e$ , surfactant (DBS) spectrum (specific compound).

Compared to multicomponent procedure even including a mathematical modelling of interference, the use of aggregate reference spectra allows a better fit of interference signal. The choice of reference spectra depends on

- the knowledge of the composition of effluents (compounds expected to be present),



$$\mathbf{S} = 1.7356 \cdot \mathbf{S}_a + 1.4112 \cdot \mathbf{S}_b + 0.2506 \cdot \mathbf{S}_c + 0.0000 \cdot \mathbf{S}_d + 0.1150 \cdot \mathbf{S}_e$$

Fig. 3. Spectral deconvolution.

- the shape of raw samples UV spectra (presence of peaks or shoulders),
- the value and distribution of the error (the optimisation is aimed for an error value lower than 1% and a regular distribution all over the wavelength range).

The quantification was carried out between 205 and 320 nm. Raw samples were diluted four times to prevent the UV signal saturation for a 10 mm quartz cell. Sulphide ( $\text{HS}^-$ ) concentration is given by the product of the contribution coefficient of sulphide reference spectrum (replacing nitrate in the previous set) and the corresponding concentration, affected by the dilution factor.

## 5. Results and discussion

### 5.1. Calibration

Calibration has been performed using standard solutions of sodium sulphide nonahydrate ( $\text{Na}_2\text{S} \cdot 9\text{H}_2\text{O}$ ) (pH close to 9.5). Fig. 4 shows a good agreement between UV determination and theoretical concentrations

The regression line is  $y = 0.95x + 0.17$  with a  $R^2$  value of 0.99.

### 5.2. Validation

About 40 real refinery wastewater samples have been used for the validation of the UV method. Fig. 5 shows a good linear adjustment between the measured concentration by potentiometric method and UV determination of sulphide.

The regression line is  $y = 0.87x + 0.15$  with a  $R^2$  value of 0.95.

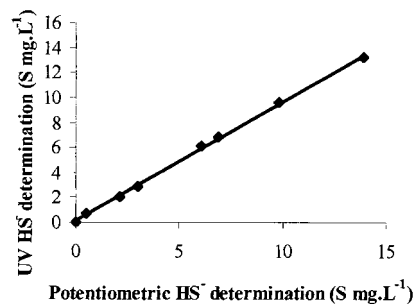


Fig. 4. Calibration of UV determination with standard solutions of sodium sulphide.

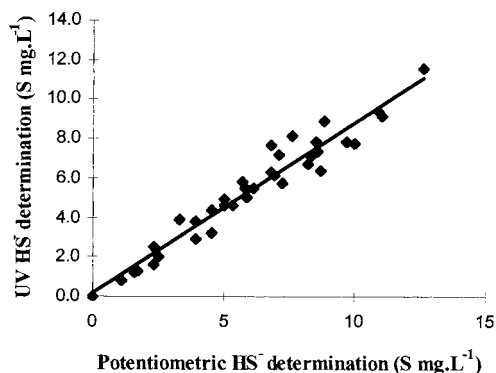


Fig. 5. Validation of UV determination of  $\text{HS}^-$ .

Table 2  
Characteristics of the UV method

Detection limit	$0.5 \text{ mg l}^{-1}$
Range (without sample dilution)	$0.5\text{--}15 \text{ mg l}^{-1}$
Precision (for an average value of $4.5 \text{ mg l}^{-1}$ )	2.2%

The characteristics of the UV method are summarised in Table 2.

### 5.3. Interferences study

Some compounds absorbing close to 231 nm may be present in raw samples and thus may interfere with sulphide spectra. The following organic compounds have been tested

- 2-naphtol (absorption at 225 nm),
- *p*-chlorophenol (absorption at 227 nm),

- anionic surfactant, RBS (absorption at 223 nm),
- 1-propanthiol (absorption at 239 nm).

The effect of the salinity was studied, too, with  $\text{Cl}^-$  and  $\text{SO}_4^{2-}$  ions. The results are presented in Table 3.

The results show low interference values for the studied compounds. The most important interfering component is the anionic surfactant leading to an error of 4.3%. Notice that the concentration of RBS used for the study is rather high.

## 6. Conclusions

The alternative UV method for the determination of sulphide in wastewater is a quick and simple procedure. The method has been validated for refinery wastewater with a standard method (potentiometric method). This method presents the following advantages

- can be run with any PC controlled UV spectrophotometer (only 2 min for acquisition and exploitation of UV spectra),
- unaffected by interference (salinity, suspended matter, tested organic compounds),
- no pre-treatment for samples with  $\text{pH} > 7.5$ ,
- may be used even by non analytical person.

This method can be considered as an alternative way for wastewater sulphide determination, namely for a self survey procedure (laboratory or on-line measurement) required for the monitoring of industrial wastewater.

Table 3  
Interference study

Interfering compound	Concentration ( $\text{mg l}^{-1}$ )	$\text{HS}^-$ ( $\text{mg l}^{-1}$ ) without interfering compound	$\text{HS}^-$ ( $\text{mg l}^{-1}$ ) in presence of interfering compound	Error (%)
2-Naphtol	20	6.0	6.0	0.0
<i>p</i> -Chlorophenol	20	12.1	11.9	1.7
Surfactant <sup>a</sup>	200	11.5	12.0	4.3
1-Propanthiol	13	12.4	12.1	2.4
Chloride	1000	11.6	11.6	0.0
Sulphate	500	11.8	11.7	0.8

<sup>a</sup> Anionic surfactant (commercial name: RBS).

## References

- [1] D.W. Connell, *Basic Concepts of Environmental Chemistry*, Lewis, New York, 1997.
- [2] A.D. Eaton, L.S. Clesceri, A.E. Greenberg, *Standard Methods for the Examination of Water and Wastewater*, 19 ed., American Public Health Association, Washington, 1995.
- [3] R. Al Farawati, C.M.G Van Den Berg, The determination of sulphide in seawater by flow-analysis with voltametric detection, *Marine Chem.* 57 (3–4) (1997) 277–286.
- [4] J.L. Wilcox, R. Del Delumyea, Determination of sulphide using reflectance analysis and its applicability to sediment samples, *Anal. Lett.* 27 (14) (1994) 2805–2811.
- [5] A.G. Howard, C.Y. Yeh, Sulphide measurement by flow injection analysis with flame photometric detection, *Anal. Chem.* 70 (22) (1998) 4868–4872.
- [6] S. Gallot, O. Thomas, State of the art for the examination of UV spectra of water and wastewater, *Inter. J. Envir. Anal. Chem.* 52 (1993) 149–158.
- [7] S. Gallot, O. Thomas, Fast and easy interpretation of a set of absorption spectra: theory and qualitative applications for UV examination of water and wastewater, *Fresenius J. Anal. Chem.* 346 (1993) 976–983.
- [8] O. Thomas, S. Gallot, Ultraviolet multiwavelength absorptiometry, *Fresenius J. Anal. Chem.* 338 (1990) 234–244.
- [9] O. Thomas, F. Theraulaz, M. Domeizel, C. Massiani, UV spectral deconvolution: a valuable tool for waste water quality determination, *Environ. Technol.* 14 (1993) 1187–1192.
- [10] O. Thomas, ed., *Métrologie des eaux résiduaires*, CEBEDOC sprl, Liège, 1995.

# TOC versus UV spectrophotometry for wastewater quality monitoring

O. Thomas <sup>a,\*</sup>, H. El Khorassani <sup>a</sup>, E. Touraud <sup>a</sup>, H. Bitar <sup>b</sup>

<sup>a</sup> *Laboratoire Génie de l'Environnement Industriel, Ecole des Mines, 6 avenue de Clavières 30319, Alès Cedex, France*

<sup>b</sup> *Laboratoire, Faculté des Sciences, avenue Normandie Niemen, 13013, Marseille, France*

---

## Abstract

Total organic carbon (TOC) is one of the most important parameter for the knowledge of water and wastewater quality, because it concerns theoretically all organic compounds. Unfortunately, some restrictions with respect to TOC measurement must be considered, explaining that alternative procedures have been envisaged, among which UV spectrophotometry. Starting from a comparison of results between high temperature digestion and UV photo-oxidation techniques for some specific compounds and real wastewater samples, the work shows the complementary interest of using UV spectrophotometry either directly (with multiwavelength procedures) or after UV photo-oxidation. © 1999 Elsevier Science B.V. All rights reserved.

*Keywords:* TOC; UV spectrophotometry; Wastewater; Monitoring

---

## 1. Introduction

Total organic carbon (TOC) is the most relevant parameter for the global determination of organic pollution of water and wastewater. It has been proposed in the 1970s namely for automatic survey because of problems related to the field use of BOD and COD. Actually, the organic carbon is used for that purpose or for the completion of the knowledge of organic pollution, as old parameters quantify its main effect, the oxygen consumption. It is the reason why TOC is often considered as the 'true' parameter. Unfortunately, some problems exist with the use of TOC measurement for wastewater due to technical or

metrological consideration. TOC measurement seems to give a specific information (the organic carbon content of the sample) but only leads to a global aggregate response.

The aim of this work is to test the TOC availability from several experiments on wastewater and to propose a complementary approach, based on the use of UV spectrophotometry, in order to complete the knowledge of wastewater quality and to bring some explanation to the composition of organic matrix.

## 2. TOC availability

TOC measurement can be performed by using two main techniques for the conversion of organic

---

\* Corresponding author.

Table 1  
Comparison of TOC values for different analysers

TOC meter type	Number of instruments	Measurement type	Average value of series (ppm)	Mean difference (%)
High temperature	2	Laboratory	37.2	8.5
High temperature	2	Laboratory	354.1	16.1
UV persulfate + high temperature	1	Laboratory	318.7	30.2
UV persulfate	2	On line	222.8	26.2

carbon into carbon dioxide. The first one involves a UV photo-oxidation at low temperature with a persulfate solution, after stripping of the mineral fraction, and the second one uses a catalytic oxidation at high temperature (650–900°C). This last technique is chosen for wastewater as the conversion yield is more efficient for anthropogenic organic matter. Both technologies use a NDIR detector for the final measurement of carbon dioxide. Other techniques are proposed either for the oxidation step improvement or for the final determination of carbon dioxide, but these latter lead to more fragile instruments than the basic techniques [1,2]. Unfortunately, as the cold technique is more easy to run, TOC on line analysers (actually off line) are often built around this procedure.

A comparison between the two techniques has been carried out in a petrochemical site. Four TOC analysers, two on site (off line) and two in laboratory have been tested. The analysers were identical for each purpose (cold technique — Seres — off line, and high temperature — Shimadzu — in laboratory) as well as the technical team for experiments and maintenance. Fresh standard solutions used for calibration were also identical. Several samples of raw and treated wastewater, characterised by a low concentration of suspended solids, were simultaneously analysed with two TOC analysers depending on the experiment. More than 20 samples have been considered for each experiment. Table 1 presents the different results and some observations can be done:

- for a same technique, the mean difference between the results obtained from two high-temperature laboratory instruments is 8.5 and 16.1%, respectively for samples with about 40

and 350 mg l<sup>-1</sup> of TOC. For two UV-persulfate on line analysers, the mean difference is 26.2% for about 220 mg l<sup>-1</sup> of TOC.

- For the two techniques, the mean difference between two laboratory instruments is 30.2% for about 220 mg l<sup>-1</sup> of TOC. Fig. 1 shows the distribution of results.

The observed difference between the set of results can be explained by several reasons among which, a best efficiency of high temperature instruments for industrial wastewater containing refractory anthropogenic organic matrix or the heterogeneity of sampling (for on line instruments).

One important point is the availability of the measure, it means the frequency during which the user gets an acceptable result without any trouble of the instrument. For a year and the four instruments of the petrochemical site, the percentage of the mean availability is about 80% of the time with good efforts for maintenance, representing each year about 50% of the investment cost of the analysers.

In conclusion, even if these observations seem to be penalizing for TOC, this parameter remains the most relevant and its measurement is rather fast.

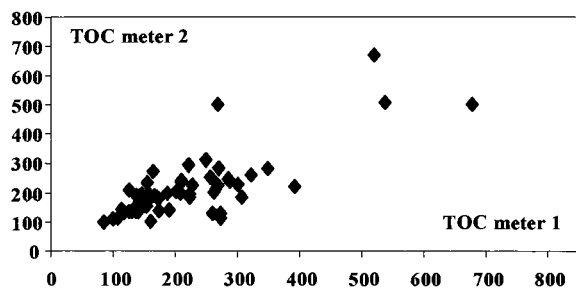


Fig. 1. Dispersion of results, expressed in mg l<sup>-1</sup> of TOC, for two on line analysers.



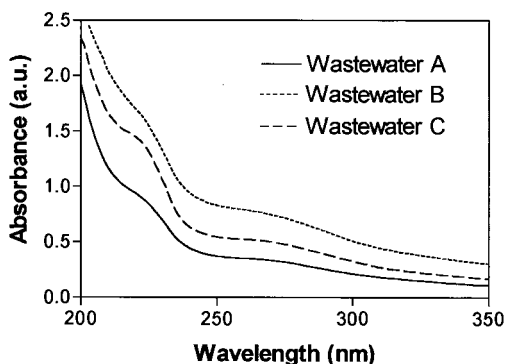


Fig. 2. UV spectra of wastewater samples ( $\text{TOC} = 57 \text{ mg l}^{-1}$ ).

### 3. Interest of UV spectrophotometry for TOC explanation

The interest of the explanation of TOC is evident as it is important to know the stability degree of organic matter in water. In raw wastewater, the fresh organic pollution will be degraded, first slowly in sewers and then, more efficiently in a biological treatment plant for example. This evolution is depending on the presence of microorganisms and oxygen. After the treatment plant, the residual TOC is very low and can be accepted by water body.

In some cases, a better knowledge of the organic matrix corresponding to a given value of TOC could be useful. For example, for a given organic pollution load, there is a difference between one wastewater sample from urban origin with a wide variety of organics and another one characterised by the presence of a major pollutant coming from an industrial discharge in sewer. In the last case, the diagnosis of the presence of a potential toxicity is important. On the other hand, two samples with low content of TOC could be either a treated effluent or a diluted raw sample. For the environment, the effects of both water are obviously not similar. Another example given in Fig. 2 shows UV spectra of different wastewater samples with a same value of TOC ( $57 \text{ mg l}^{-1}$ ).

The spectra shape can be explained by the difference of composition of the organic matrix in the aqueous, colloidal and solid phases. For this purpose, the COD values would be of poor inter-

est meanwhile the results of BOD could be probably useful. Unfortunately, its experimental conditions are not acceptable for an efficient control. Other parameters as total hydrocarbons, anionic surfactants or phenol index could be used but with a very low probability to give relevant results. Analytical procedures as chromatographic methods could also be considered if samples composition has already be studied. Otherwise, it is not realistic to use separation techniques.

UV spectrophotometry is regularly proposed and used for water and wastewater quality control for 50 years [3], either from urban [4,5] or industrial origin [6,7]. Its main quantitative application concerns the estimation of aggregate parameters (TOC, COD, TSS, anionic surfactants, ...) [8–11] and the determination of specific compounds (nitrate, chromium VI, phenol, ...) [12,13] namely by the robust exploitation of spectra [14,15] using direct multiwavelength procedures [16,17]. Other quantitative applications of UV spectrophotometry concern the estimation of PAH in soils [18] or of biodegradable dissolved organic carbon (BDOC) [19]. The use of UV spectrophotometry is possible because of the basic interaction between UV light and unsaturated ionic or molecular structures (chromophores). Moreover a simple UV photo-oxidation step can be proposed for the estimation of reduced nitrogen forms (TKN and ammonia). In this technique, called UV/UV, a final UV determination of nitrate is included [20].

On the other hand, UV spectrophotometry can give relevant qualitative information as for example for the study of treated wastewater discharges [21], for the detection of incidents in industrial context [7] or for the treatability study of industrial wastewater [22].

Table 2 presents the TOC and UV responses of several organic compounds families.

The study of TOC and UV responses of organic compounds shows obviously that saturated molecules do not absorb even in the UV region. Moreover, small molecules like simple carboxylic acids or aldehydes absorb in the far UV region ( $< 200 \text{ nm}$ ), showing only the tail of their spectra. TOC is generally more efficient for organic compounds characterisation but can be limited for the study of some molecules. The detection of these

latter can be envisaged either directly (S compounds) or after photo-oxidation (ketones, amines) with UV spectrophotometry.

Before considering some applications for wastewater quality monitoring, an attempt to compare the advantages and drawbacks of the two techniques can be proposed (Table 3). From this comparison, it is obvious that the two techniques are complementary.

Table 2  
TOC and UV responses of organic compounds<sup>a</sup>

Compounds	TOC	UV	UV/UV
Saturated compounds	Y	N	–
Aliphatic unsaturated hydrocarbons	Y	P	–
Aromatic compounds	Y	Y	–
Acids	Y	P	–
Aldehydes, ketones	P	P	Y
Alcohols	Y	N	Y
Phenolic compounds	Y	Y	–
Aliphatic amines	P	N	Y
Aromatic amines	Y	Y	–
N unsaturated heterocycles	Y	Y	–
S unsaturated heterocycles	P	Y	–
Humic like substances	P	Y	–

<sup>a</sup> Y: 90–100% of conversion or high absorption or absorption after photo-oxidation; P: partially converted or some absorbing compounds; N: non absorbing compounds.

Table 3  
Comparison of TOC and UV spectrophotometry: advantages and drawbacks

	TOC	UV
<i>Advantages</i>	Aggregate parameter Reference Quick measurement	Simple, fast, not expensive Qualitative information Other parameters (NO <sub>3</sub> <sup>-</sup> , CrVI, . . .)
<i>Drawbacks</i>	Some refractory organics Suspended solids Measure availability Chloride	Saturated hydrocarbons Low MW compounds Sensitivity, selectivity but dilution often needed

## 4. Applications

### 4.1. Variations of raw wastewater quality

TOC monitoring is often used for the monitoring of industrial wastewater quality. Fig. 3 presents the TOC variation with time (during 3 months) monitored at the inlet of a wastewater treatment plant of a petrochemical site. For each TOC measurement (every 3 h), a UV spectrum has been acquired. Considering that the maximum admitted value for the protection of the biological reactor of the plant is 500 mg l<sup>-1</sup> of TOC, three peaks of pollution have been detected.

The study of the corresponding UV spectra and a comparison with the one of regular wastewater shows that these three incidents are related to three different accidental discharges in sewer. Moreover, the study of UV spectra shows that incidents 1 and 3 are characterised by the presence of a few concentrated pollutants. Starting from this information, and after a more complete study, a UV monitor has been installed close to the main source of the potential accidental discharge.

### 4.2. Treatment plant control

TOC and UV measurements can also be used for the control of wastewater treatment plant. If the treatment efficiency is the major goal of an industrial wastewater treatment plant in term of TOC yield for example (Fig. 4), other objectives are more and more considered as the nitrogen removal possibility for urban treatment plant (Fig. 5).

Some complementary observations can be made from the UV spectra shape of Figs. 4 and 5. The closeness of the shape of raw samples spectra is not so evident taking into account the position of the 220–240 nm shoulders and the relative absorbance values around 230 and 270 nm. On the other hand, the spectrum of the outlet 1 (Fig. 5) is characterised by a high residual absorption after 300 nm related to the presence of suspended solids. Moreover, the increase of absorbance values around 210 nm seen on some spectra, is due to the appearance of nitrate in wastewater.

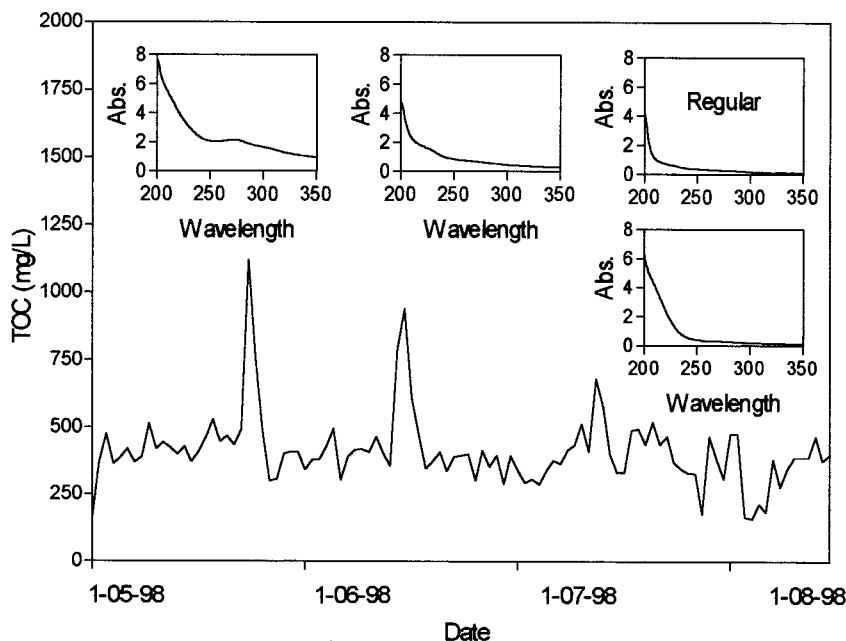


Fig. 3. TOC and UV monitoring of petrochemical wastewater (the absorbance values are for a 1 cm optical pathlength quartz cell).

#### 4.3. Discharge survey

UV spectrophotometry can be used when TOC measurement is very difficult to carry out (high concentration of chloride). Fig. 6 displays the different spectra acquired for a dispersion study of treated wastewater discharge in sea water. The set of spectra shows an isobestic point due to the mixing of wastewater with sea water, the spectrum of which presenting a sharp absorbance at 205 nm due to chloride (notice that the difference between spectra of nitrate and chloride solutions is chemometrically easy to exploit). After 100 m, the impact of the discharge is difficult to see.

### 5. Conclusion

The study of characteristics of TOC measurement and UV spectrophotometry shows that both techniques are complementary for the monitoring of wastewater quality. These techniques can be used for regulation applications but also for process control including the detection of incidents (early warning). On line TOC meters and UV

monitors (diode array systems) are available for the purpose. Moreover, several developments of UV analysers are interesting to consider in order to complete the on line monitors, such as field portable spectrophotometers, immersed sensors, simple kit for NTK and ammonia estimation.

Thus, the best available solution for wastewater monitoring nowadays is the choice of a TOC analyser equipped with a TSS kit, completed by a

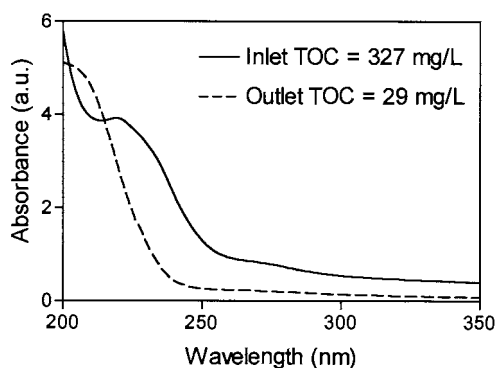


Fig. 4. Treatment plant efficiency for petrochemical wastewater (removal of 91% of TOC — measured — and 85% of TOC — estimated with a UV deconvolution procedure [8]).

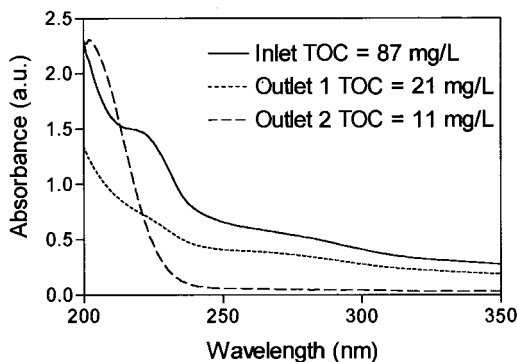


Fig. 5. Efficiency of urban wastewater treatment plant (outlet 1 and 2, respectively without and with nitrification step).

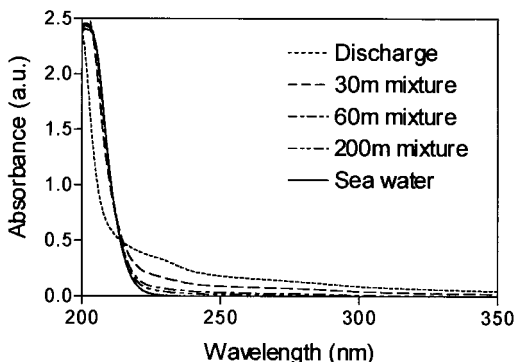


Fig. 6. Discharge of treated industrial wastewater in sea water: set of UV spectra.

UV detector including a NTK kit. In some cases, namely for industrial application, the measurement of conductivity and pH could be useful. If possible an autosampler should be coupled with the chosen on line systems.

### Acknowledgements

The authors wish to acknowledge Caroline Lhospitallier and Pierre Trébuchon from Naph-tachimie for their contribution.

### References

- [1] R.W. Matthews, M. Abdullah, G.K.C. Low, Photocatalytic oxidation for total organic carbon analysis, *Anal. Chim. Acta* 233 (1990) 171–179.
- [2] J. Qian, K. Mopper, Automated high-performance, high-temperature combustion total organic carbon analyzer, *Anal. Chem.* 68 (1996) 3090–3097.
- [3] R.C. Hoater, Application of spectrophotometry in the examination of water, *Wat. Treat. Exam.* 2 (1952) 9–19.
- [4] R.A. Dobbs, R.H. Wise, R.B. Dean, The use of ultraviolet absorbance for monitoring the Total Organic Carbon content of water and wastewater, *Water Res.* 6 (10) (1972) 1171–1180.
- [5] M. Mrkva, Automatic U.V.-control system for relative evaluation of organic water pollution, *Water Res.* 9 (1975) 587–589.
- [6] E. Naffrechoux, N. Mazas, O. Thomas, Identification rapide de la composante industrielle d'une eau résiduaire, *Envir. Technol.* 12 (1991) 325–332.
- [7] H. El Khorassani, P. Trébuchon, H. Bitar, O. Thomas, Petrochemical wastewater management assistance, *Water Sci. Technol.*, to be published, 1999.
- [8] O. Thomas, F. Théraulaz, C. Agnel, S. Suriyani, Advanced UV examination of wastewater, *Envir. Technol.* 17 (1996) 251–261.
- [9] F. Théraulaz, L. Djellal, O. Thomas, Simple LAS determination in sewage using advanced UV spectrophotometry, *Tenside Surf. Det.* 6 (1996) 447–451.
- [10] O. Thomas, F. Théraulaz, V. Cerda, D. Constant, P. Quevauviller, Wastewater quality monitoring, *Trends Anal. Chem.* 16 (7) (1997) 419–424.
- [11] B. MacCraith, K.T.V. Grattan, D. Connolly, R. Briggs, W.J.O. Boyle, M. Avis, Results of a cross-comparison study: optical monitoring of total organic carbon (TOC) of a limited range of samples, *Sensors Actuators B* 22 (1994) 149–153.
- [12] A.R. Hawthorne, S.A. Morris, R.L. Moody, R.B. Gamme, Duvas as a real time, field portable wastewater monitor for phenolics, *J. Envir. Sci. Health A19* (1984) 253–266.
- [13] H. El Khorassani, G. Besson, O. Thomas, Direct UV visible determination of chromium VI in industrial wastewater, *Quimica Anal.* 16 (1997) 239–242.
- [14] S. Gallot, O. Thomas, State of the art for the examination of UV spectra of water and wastewater, *Intern. J. Envir. Anal. Chem.* 52 (1993) 149–158.
- [15] S. Gallot, O. Thomas, Fast and easy interpretation of a set of absorption spectra: theory and qualitative applications for UV examination of water and wastewater, *Fresenius J. Anal. Chem.* 346 (1993) 976–983.
- [16] O. Thomas, S. Gallot, Ultraviolet multiwavelength absorptiometry, *Fresenius J. Anal. Chem.* 338 (1990) 234–244.
- [17] O. Thomas, F. Théraulaz, M. Domeizel, C. Massiani, UV spectral deconvolution: a valuable tool for wastewater quality determination, *Envir. Technol.* 14 (1993) 1187–1192.
- [18] E. Touraud, M. Crône, O. Thomas, Rapid diagnosis of polycyclic aromatic hydrocarbons (PAH) in contaminated soils with the use of ultraviolet detection, *Field Anal. Chem. Technol.* 2 (1998) 221–229.

- [19] O. Thomas, N. Mazas, C. Massiani, Determination of biodegradable dissolved organic carbon in waters with the use of UV absorptiometry, *Envir. Technol.* 14 (1993) 487–493.
- [20] B. Roig, C. Gonzalez, O. Thomas, Measurement of dissolved total nitrogen in wastewater by UV photo-oxidation with peroxodisulfate, *Anal. Chim. Acta*, accepted for publication.
- [21] H. El Khorassani, F. Théraulaz, O. Thomas, Application of UV spectrophotometry to the study of treated wastewater discharges in rivers, *Acta Hydrochim. Hydrobiol.* 26 (1998) 296–299.
- [22] O. Thomas, H. El Khorassani, L. Castillo, UV treatability test for chemical and petrochemical wastewater, *Water Sci. Technol.*, to be published, 1999.

# Simple UV/UV-visible method for nitrogen and phosphorus measurement in wastewater

B. Roig \*, C. Gonzalez, O. Thomas

*Laboratoire Génie de l'Environnement Industriel, Ecole des Mines d'Alès, 6 avenue de Clavières, 30319, Alès Cedex, France*

## Abstract

A simple UV/UV-visible method is described for the determination of global nitrogen and total phosphorus in wastewater. This method includes two steps: first, the photo-oxidation of nitrogen and phosphorus forms into nitrate and orthophosphate ions, and their quantification by UV-visible spectrophotometry. Potassium peroxodisulfate is used as oxidant. The developed system consists of on-line association of UV photo-oxidation reactor with UV-visible detector. The conversion yields vary between 80 and 100% for both nitrogen compounds (ammonium, urea, aminoacids, and others N-containing compounds), and phosphorus compounds (ADP, ATP, and others P-containing compounds). The time requires for nitrogen and phosphorus forms determination is no longer than 20 min. © 1999 Elsevier Science B.V. All rights reserved.

*Keywords:* Global nitrogen; Oxidant; Phosphorus

## 1. Introduction

Nitrogen and phosphorus compounds occur in wastewater under various forms among which reduced ones are predominant. For nitrogen, organic compounds and ammonium nitrogen are present in wastewater, whereas nitrate and nitrite appear with biodegradation as oxidised forms. On the contrary, the phosphorus compounds of wastewater concern not only some organic forms but also orthophosphate ion and acid hydrolysable phosphate (polyphosphate) mainly due to surfactants.

Standard methods (AFNOR [1]) used for the determination of global nitrogen and total phosphorus include several steps (Table 1).

In a first step, nitrogen and phosphorus oxidised forms ( $\text{NO}_3^-$ ,  $\text{NO}_2^-$ ,  $\text{PO}_4^{3-}$ ) are determined by colorimetry, ion chromatography or spectrophotometry (UV). Then a chemical digestion followed by the determination of resulting species ( $\text{NH}_4^+$  or  $\text{PO}_4^{3-}$ ) allowed the measurement of organic nitrogen and phosphorus forms. Procedures are time-consuming (more than 5 h) and require strong conditions (acidic medium, high temperature, catalyst). Some improvements have been proposed such as the use of photo-oxidation as an alternative to chemical digestion, as it has been successfully used for similar applications (Armstrong [2], Henriksen [3], Goossen [4], Shkil

\* Corresponding author. Tel.: +33-4-66782769; fax: +33-4-66782701.

*E-mail address:* benoit.roig@ema.fr (B. Roig)

Table 1  
General procedure for global nitrogen and total phosphorus determination

	Oxidised forms determination	Organic compounds digestion	Determination of converted forms
Nitrogen	$\text{NO}_3^-$ , $\text{NO}_2^-$	Organic (Norg)	$\text{NH}_4^+$
Phosphorus	Orthophosphate ( $\text{PO}_4^{3-}$ )	Organic and hydrolysable (Porg, Phyd)	Orthophosphate ( $\text{PO}_4^{3-}$ )

[5]). In order to minimize the photo-oxidation time, the UV light source (high, medium or low pressure mercury lamp) can be associated with oxidants (hydrogen peroxide or potassium peroxodisulfate). Generally, the converted forms (nitrate, orthophosphate) are determined by off-line analysis but can also be measured by flow injection or sequential injection analysis (McKelvie [6], Thomas [7]).

This work presents a simple procedure based on the use of an on-line association of UV photo-oxidation reactor (low pressure mercury lamp and potassium peroxodisulfate) with a UV-visible spectrophotometer. For nitrogen, the photo-oxidation is carried out in alkaline or acidic medium and leads to the speciation of organic, inorganic and oxidised forms. In the same way, phosphorus forms (orthophosphate, organic and hydrolysable phosphorus) could be also differentiated.

## 2. Experimental

### 2.1. Material

Experiments are carried out with a photochemical reactor shown in Fig. 1. It is composed of a UV source surrounded by a synthetic quartz (suprasil) coil. The sample circulates in a 20 ml closed circuit and the determination is carried out with a UV-visible spectrophotometer.

A low pressure mercury lamp (Pen Ray® UV-P) is used as irradiation source. The length of the radiant part of the lamp is 22.9 cm and the external diameter is 0.95 cm. The nominal 254 nm emission power is  $42 \mu\text{W cm}^{-2}$  at 30 cm and the delivered electric current is 18 mA. The emission spectrum shows that 90% of the energy is related to the 254 nm ray and the remaining 10% for the 185, 313, 365, 405, 436 nm rays (Fig. 2). The

lifetime given by the supplier is more than 5000 h. The jacket of the lamp is made of synthetic quartz as well as the quartz coil in order to use the 185 nm radiation.

Assuming that the emission can be considered as monochromatic (90% of energy at 254 nm), the photonic flux has been determined at 254 nm. Chemical actinometry has been carried out with

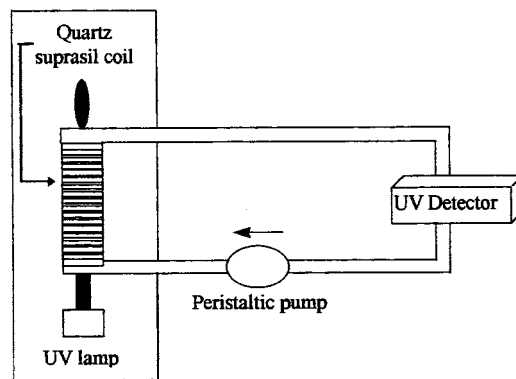


Fig. 1. UV photochemical reactor.

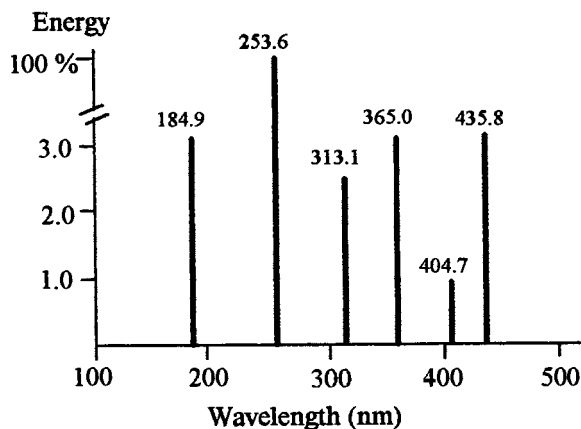


Fig. 2. Emission spectrum of a low pressure mercury lamp.

potassium ferrioxalate (Harris [8]) and the photonic flux was found as  $2.3 \times 10^{-7}$  einstein  $s^{-1}$ .

The UV-visible detector is an Anthelie (Secmam) UV-visible spectrophotometer controlled by Dathelie software version 4.1f. The pathlength of the suprasil quartz cell is either 2 mm (for nitrate measurement) or 40 mm (for orthophosphate determination) and the scan speed is 1800 nm  $min^{-1}$ .

## 2.2. Reagents and compounds

Two main reagents are used as oxidant for the conversion step or complexant for orthophosphate: potassium peroxodisulfate,  $K_2S_2O_8$  (Aldrich) as oxidising agent and ammonium molybdate  $(NH_4)_6Mo_7O_{24} \cdot 4H_2O$  (Carlo Erba) as complexing agent.

Depending on compounds determination, the photo-oxidation is carried out under basic or acidic conditions. The pH of alkaline photo-oxidation (pH 9) is adjusted with a buffer solution prepared as follows: dissolve 38 g of sodium tetraborate decahydrate (Aldrich) in 800 ml of ultra-pure water. Add 30 ml of a 2.5 M sodium hydroxide (Carlo Erba) solution and dilute to 1000 ml of ultra-pure water.

Acidic photo-oxidation (pH 2) is carried out using sulphuric acid 20% (Carlo Erba 96%).

N-containing model compounds have been studied: urea, ammonium chloride, glycine, 4-nitrophenol, atrazine, 4-aminophenol (Riedel de Haen), *N*-acetyl-glucosamine, glutamic acid, 3-aminophenol, aniline, 3-toluidine (Merck), EDTA (Carlo Erba), 2-nitrophenol (Fluka).

Phosphorus compounds analysed have been chosen among pesticides as mevinphos, dichlorvos or dibrom (Riedel de Haën), synthetic organic monophosphate as tris (2-chloroethyl) phosphate and N (phosphonomethyl) glycine (Aldrich) or natural polyphosphate like  $\alpha$ -D-glucose-1-phosphate dipotassium salt dihydrate, adenosine-5'-monophosphate (AMP), adenosine-5'-diphosphate disodium salt hydrate (ADP), adenosine-5'-triphosphate diphosphate disodium salt hydrate (ATP, Acros).

Solutions of standard compounds are prepared in ultra-pure water.

## 2.3. Principles of determination

The measurement of nitrogen and phosphorus in wastewater consists of the conversion of nitrogen and phosphorus compounds respectively in nitrate and orthophosphate. The determination of these ions is possible with UV-visible spectrophotometry by using a spectrum deconvolution method (Thomas [9]).

The principle of the spectrum deconvolution method is to consider the UV absorption spectrum as a linear combination of a few reference spectra which are related either to specific analytes (nitrate for example) or aggregate constituents (generally considered as interferences). The calculation of spectra contribution is carried out by using the following relation:

$$S_w = \sum_{i=1}^p a_i \cdot REF_i \pm r$$

where  $S_w$  is the sample spectra,  $a_i$  the contribution coefficient of the  $i^{\text{th}}$  reference spectra  $REF_i$ ,  $p$  the number of reference spectra used and  $r$  the quadratic error.

For nitrate determination, a base of reference spectra has been proposed with spectra corresponding to residual matrix, suspended solids, colloids, nitrate and oxidant. The quantification is carried out between 205 and 335 nm. Nitrate concentration is given by the product of nitrate coefficient by the concentration of the corresponding reference spectrum.

Orthophosphate concentration is calculated from the phosphomolybdate complex formation. A base of reference spectra has been used with spectra corresponding to molybdate solution ( $2.4 \text{ g l}^{-1}$ ) and to the phosphomolybdate complex obtained from  $10 \text{ mg l}^{-1}$  of orthophosphate. Notice that in this case the use of a simple multi-component procedure may be sufficient. The quantification is carried out between 380 and 450 nm. Orthophosphate concentration is given by the product of phosphomolybdate complex coefficient by the concentration of the corresponding reference spectrum.

The general procedure (Fig. 3) includes two main steps: direct ( $NO_3^-$ ,  $NO_2^-$ ) or indirect ( $PO_4^{3-}$ ) UV-visible measurement and photo-oxidation



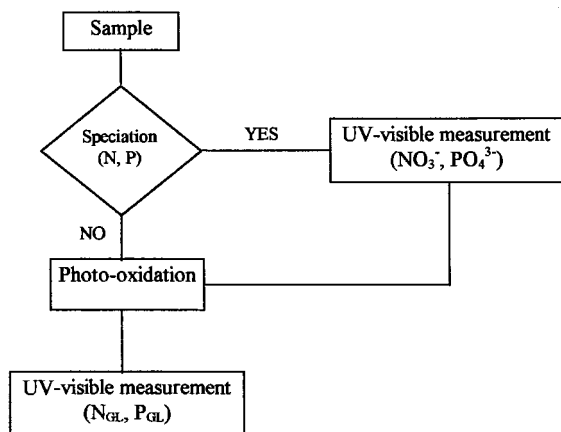


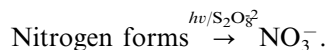
Fig. 3. General scheme for N and P speciation.

( $N_{GL}$ ,  $P_{GL}$ ) followed by the UV-visible measurement.

#### 2.4. Nitrogen forms determination

The method for N compounds determination earlier described (Roig [10]) consists of firstly, the determination of inorganic oxidised nitrogen forms ( $NO_3^-$ ,  $NO_2^-$ ) by direct UV spectrophotometry.

Notice that the deconvolution method for spectra exploitation can be replaced by classical methods for the estimation of nitrate (Standard Method [11]). Secondly the oxidant solution (potassium peroxodisulfate  $K_2S_2O_8$ ) is added to the sample for the photo-conversion of organic and inorganic nitrogen forms into nitrate determined by UV spectrophotometry (Thomas [9]).



The photo-oxidation carried out under different pH conditions allows to convert specifically the nitrogen reduced forms. Indeed, in acidic conditions, only organic nitrogen is converted into nitrate whereas in alkaline medium, all the reduced nitrogen forms (organic and ammonium) are converted, giving the global nitrogen measurement. Fig. 4 shows the general procedure.

The procedure allows the measurement of the oxidised forms ( $N_{OX} = NO_2^- + NO_3^-$ ), global nitrogen ( $N_{GL}$ ) and aggregate organic forms ( $N_{ORG}$ ).

The calculation of Kjeldahl nitrogen ( $TKN = N_{GL} - N_{OX}$ ) and of the ammonium form ( $NH_4^+ = TKN - N_{ORG}$ ) is then possible.

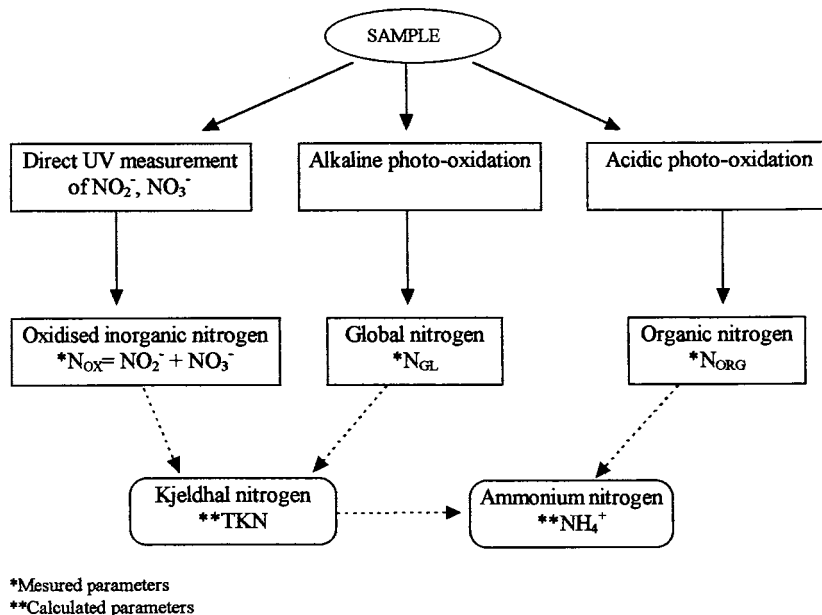


Fig. 4. Speciation of nitrogen in wastewater.

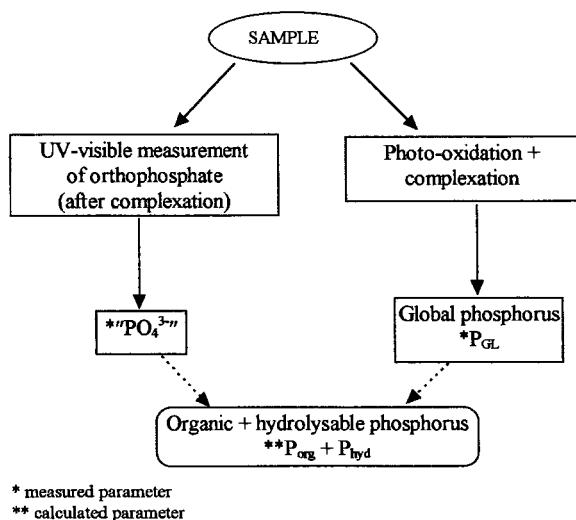
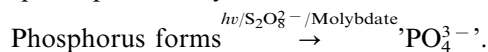


Fig. 5. Speciation of phosphorus in wastewater.

### 2.5. Phosphorus forms determination

As previously mentioned, phosphorus compounds are commonly classified into orthophosphates ( $\text{PO}_4^{3-}$ ), acid-hydrolysable phosphates and organic phosphates. It must be notice that acid-hydrolysable phosphates (as pyrophosphates) are neglectible in sewage (Jolley [12]). The determination of phosphate consists of firstly the determination of orthophosphates by spectrophotometric measurement of a phosphomolybdate complex (formed with addition of 1.5 ml of ammonium molybdate  $40 \text{ g l}^{-1}$ ) using the spectrum deconvolution method. Then, an oxidant solution (2 ml of  $40 \text{ g l}^{-1}$  potassium peroxodisulfate  $\text{K}_2\text{S}_2\text{O}_8$ ) is

added to the sample for the photo-conversion (15 min irradiation time) of the organic phosphorus forms into orthophosphates. Orthophosphates are then determined by UV-visible spectrophotometry.



The general procedure is illustrated in Fig. 5.

The procedure allows the measurement of orthophosphate ( $\text{PO}_4^{3-}$ ) and global phosphorus ( $\text{P}_{\text{GL}}$ ). The determination of the sum of organic and hydrolysable phosphorus ( $\text{P}_{\text{ORG}} + \text{P}_{\text{hyd}} = \text{P}_{\text{GL}} - \text{PO}_4^{3-}$ ) is then possible.

## 3. Results

### 3.1. Conversion yields from model compounds

#### 3.1.1. Nitrogen compounds

Table 2 displays the results for the determination of the nitrogen concentration from various N-containing compounds. The conversion into nitrate from all compounds is quantitative whatever the concentration, with a very short conversion time are (around 3 min).

#### 3.1.2. Phosphorus compounds

Table 3 displays the results for the determination of the orthophosphate concentration from the photo-oxidation of various P-containing compounds. The molybdate solution (1.5 ml) is introduced in the reactor in order to follow the phosphomolybdate complex formation. The con-

Table 2  
Conversion yields obtained from nitrogen compounds (Roig [10])

Compounds <sup>a</sup>	Conversion yields <sup>b</sup>	Compounds <sup>a</sup>	Conversion yields <sup>b</sup>
Urea	100	Glycine	95
$\text{NH}_4\text{Cl}$	100	EDTA	90
<i>N</i> -acetyl-glucosamine	100	Atrazine	90
4-Aminophenol	100	3-Toluidine	90
2-Nitrophenol	100	Aniline	80
4-Nitrophenol	100	Glutamic acid	80
3-Aminophenol	100		

<sup>a</sup> Concentrations between 5 and  $50 \text{ mg N l}^{-1}$ .

<sup>b</sup> 3 min irradiation time.

Table 3

Conversion yields obtained from phosphorus compounds

Compounds <sup>a</sup>	Conversion yields <sup>b</sup>	Compounds <sup>a</sup>	Conversion yields <sup>b</sup>
N(phosphonomethyl) glycine	100	Glucose-1-phosphate	100
Mevinphos	100	AMP	90
Dichlorvos	100	ADP	90
Dibrom	100	ATP	85
Tris(2chloroethyl) phosphate	90		

<sup>a</sup> Concentration between 1 and 10 mg P l<sup>-1</sup>.<sup>b</sup> 10–15 min irradiation time.

version yields are quantitative using irradiation time no longer than 15 min.

### 3.2. Conversion yields from raw effluents

#### 3.2.1. Nitrogen: TKN measurement

Fifty samples of urban and industrial wastewaters were analysed with both Kjeldahl method and UV oxidation (Fig. 6). A good adjustment can be observed between the results.

#### 3.2.2. Phosphorus: total phosphorus measurement

The UV/UV-visible method was applied for the determination of total phosphorus from raw effluents. The results were compared with those obtained by atomic absorption analysis (Fig. 7).

This comparison showed a good correlation ( $R^2 = 0.991$ ). Notice that others samples may be analysed in order to obtained a more suitable comparison.

### 3.3. Measurement validation

#### 3.3.1. Nitrogen

The nitrogen forms are determined by UV spectrophotometry measurement of the nitrate (present before and after photo-oxidation). The estimation of nitrate concentration by UV deconvolution was first compared with theoretical concentration of standard solutions and secondly with the estimation of the concentration by capillary electrophoresis (Fig. 8A and B).

The good correlation obtained by these comparison allows to justify the use of this UV method for nitrate estimation.

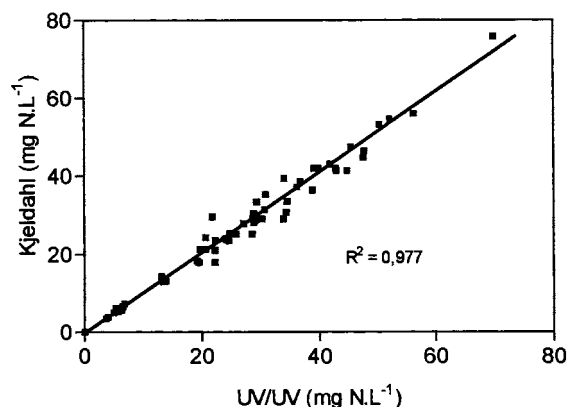


Fig. 6. Nitrogen measurement by the Kjeldahl method and the UV/UV one.

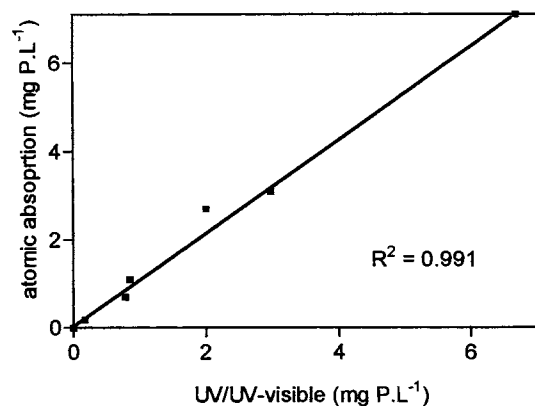


Fig. 7. Total phosphorus measurement by the atomic absorption analysis and the UV/UV-visible one.

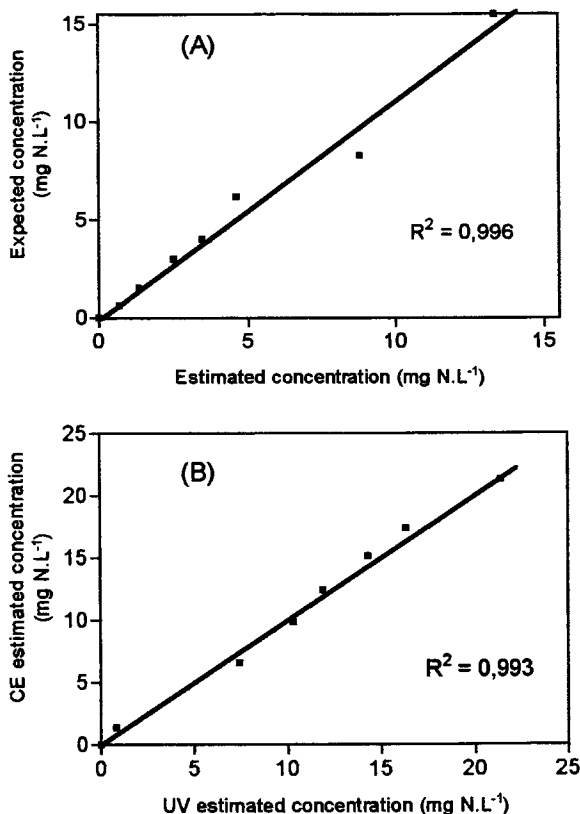


Fig. 8. between the nitrate concentration estimated by UV and the expected one (A) or the concentration measured by capillary electrophoresis (B).

### 3.4. Phosphorus

The UV-visible deconvolution estimation of phosphomolybdate complex is firstly compared with the expected concentration of standard added solutions (Fig. 9A). Moreover, orthophosphate concentration in wastewater has been estimated both by UV deconvolution and by ascorbic acid colorimetry (Fig. 9B).

In the two cases, UV estimated concentrations are in a great agreement with expected concentrations and then can be used as an alternative to the standardised method.

## 4. Discussion

The determination of the nitrogen and phosphorus forms in wastewater could be carried out by direct (UV measurement) or indirect (photo-oxidation + UV measurement) spectrophotometry. Moreover, a complexation step can be added to the procedure when compounds have not an absorption in UV region (Table 4).

It must be noticed that the determination of all parameters (nitrogen and phosphorus compounds) is no longer than 30 min.

## 5. Conclusion

The photo-oxidation/UV system has been described as an efficient method for the measurement of nitrogen and/or phosphorus in

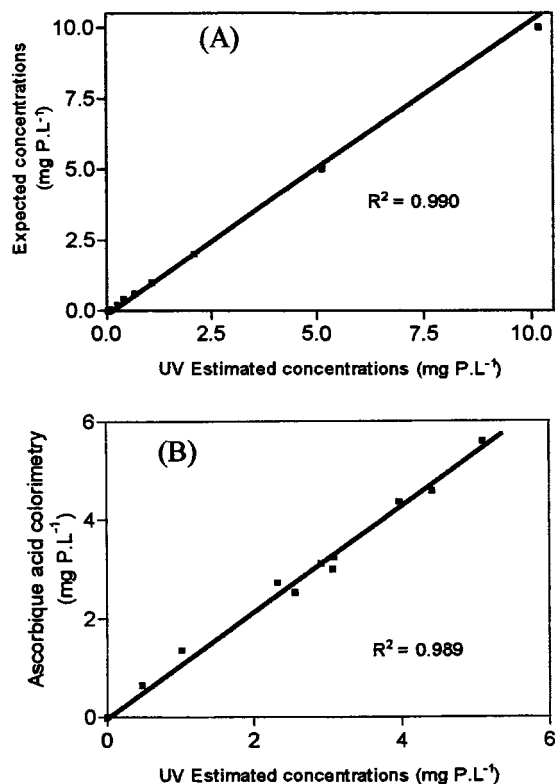


Fig. 9. Comparison between the UV estimation of orthophosphate concentration and the expected one (A) or the standardised estimation one (B).

Table 4  
Principle of determination of nitrogen and phosphorus forms

Parameters	Principle	Reagent	Complexant
NO <sub>2</sub> <sup>-</sup>	UV measurement	N	N
NO <sub>3</sub> <sup>-</sup>	UV measurement	N	N
N <sub>GL</sub>	Alkaline photo-oxidation	Y	N
N <sub>ORG</sub>	Acidic photo-oxidation	Y	N
TKN	Calculation	Y	N
NH <sub>4</sub> <sup>+</sup>	Calculation	Y	N
PO <sub>4</sub> <sup>3-</sup>	UV-visible measurement	N	Y
P <sub>GL</sub>	Acidic photo-oxidation	Y	Y
P <sub>org</sub> + P <sub>hyd</sub>	Calculation	Y	Y

wastewater. Compared with the standardised method, this simple UV/UV-visible method presents some advantages especially for time consuming which is six times lower. Moreover, this procedure minimises the consumption of reagents and is realised in softer conditions. On the other hand, this system could be carried out either for laboratory analysis or for field measurement.

According to experimental conditions of photo-oxidation or UV measurement, it will be possible to evaluate the major part of nitrogen and phosphorus forms (oxidised, organics, inorganics, hydrolysable) and also global nitrogen and total phosphorus. This method is very suitable for treatment plants.

## References

- [1] AFNOR: Recueil de normes française. Qualité de l'eau, 1997, 2<sup>e</sup> éd., Paris.
- [2] F.A.J. Armstrong, S. Tibbitts, *J. Mar. Biol. Ass. U.K.* 48 (1968) 143–152.
- [3] A. Henriksen, *Analyst* 95 (1970) 601–608.
- [4] L.T.H. Goosen, J.G. Kloosterboer, *Anal. Chem.* 50 (6) (1978) 707–711.
- [5] A.N. Shkil, A.V. Krasnushkin, I.T. Gavrilov, *J. Anal. Chem. USSR* 45 (8) (1990) 1165–1171.
- [6] I.D. McKelvie, B.T. Hart, *Analyst* 114 (1989) 1459–1463.
- [7] O. Thomas, F. Theraulaz, V. Cerda, D. Constant, P. Quevauviller, *Trends Anal. Chem.* 16 (7) (1997) 419–424.
- [8] G.D. Harris, M. Asce, V.D. Adams, W.M. Moore, D.L. Sorensen, *J. Environ. Eng.* 1133 (1987) 612–627.
- [9] O. Thomas, F. Theraulaz, C. Agnel, S. Suryani, *Environ. Technol.* 17 (1996) 251–261.
- [10] B. Roig, C. Gonzalez, O. Thomas, *Anal. Chem. Acta* 389 (1999) 267–274.
- [11] Standard Methods for the Examination of Water and Wastewater, nineteenth ed., APHA, Washington, 1995.
- [12] D. Jolley, W. Maher, P. Cullen, *Water Res.* 32 (3) (1998) 711–716.

Review

# Methods of analysis of 4-quinolone antibacterials

F. Belal \*, A.A. Al-Majed, A.M. Al-Obaid

*Department of Pharmaceutical Chemistry, College of Pharmacy, King Saud University, P.O. Box 2457, Riyadh 11451, Saudi Arabia*

Received 26 November 1998; received in revised form 20 April 1999; accepted 28 April 1999

## Abstract

A comprehensive review with 270 references for the analysis of the members of an important class of drugs, 4-quinolone antibacterials, is presented. The review covers most of the methods described for the analysis of these drugs either per se, in dosage forms or in biological fluids. © 1999 Elsevier Science B.V. All rights reserved.

*Keywords:* 4-Quinolones; Fluoroquinolones; Dosage forms; Biological fluids

## 1. Introduction

Following the discovery of nalidixic acid in 1962 by Leshner et al. [1], numerous structural modifications have been made in the quinoline nucleus to increase antimicrobial activity and improve pharmacokinetic performance. A major advance occurred during the 1980s with the discovery that a fluorine atom at position 6 conferred broad and potent antimicrobial activity, e.g. norfloxacin, but still with relatively less activity for gram-positive and anaerobic organisms than gram-negative bacteria. Subsequent developments produced quinolones with further improvements, predominantly in either solubility (e.g.

ofloxacin), antimicrobial activity (e.g. ciprofloxacin) or prolonged serum half-life (e.g. pefloxacin). Recent modifications have attempted to achieve an optimal blend of favorable properties together with potential for undesirable side effects [2]. A good guide to the pharmacology, spectrum of activity, pharmacokinetics, clinical efficacy and adverse effects of the next generation of fluoroquinolones, recently approved by FDA, is found in the review written by Ernst et al. [3].

During the past 15 years the 4-quinolone antibacterials have been progressed from relative obscurity to a highly visible and intensely studied class of compounds. The zeal for developing and marketing newer fluoroquinolones closely parallels that of the cephalosporins for the past 20 years. All of these newer agents have similar mechanism of action, but numerous derivatives of the basic 4-quinolone structure have been synthe-

\* Corresponding author. Tel.: +966-1-4676383; fax: +966-1-4677348.

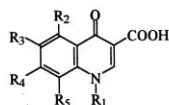
*E-mail address:* ffbelal@ksu.edu.sa (F. Belal)

sized in an effort to enhance the antimicrobial spectrum and pharmacological properties of these antimicrobials.

The increasing interest in this class of compounds led us to review the methods reported for their analysis in pure form, their formulations and biological fluids, animal and fish feed, etc.

## 2. Chemistry

Large numbers of analogs and derivatives of the basic 4-quinolone structure have been synthesized over the past 35 years (Fig. 1). Prototype quinolone antibacterials, such as nalidixic acid (naphthpyridine nucleus) and cinoxacin (cinoline nucleus) and piperimidic acid (pyridopyrimidine ring) differ in structure from the parent com-



A. Quinolone ring

Name	R <sub>1</sub>	R <sub>2</sub>	R <sub>3</sub>	R <sub>4</sub>	R <sub>5</sub>
Oxolinic acid	-C <sub>2</sub> H <sub>5</sub>	H	-O-	CH <sub>2</sub> -O-	H
Norfloxacin	-C <sub>2</sub> H <sub>5</sub>	H	F		H
Pefloxacin	-C <sub>2</sub> H <sub>5</sub>	H	F		H
Amifloxacin	-NHCH <sub>3</sub>	H	F		H
Ciprofloxacin		H	F		H
Fleroxacin	-C <sub>2</sub> H <sub>2</sub> F	H	F		F
Temafloxacin		H	F		H
Ofloxacin	$\begin{matrix} \text{CH}_3 \\   \\ -\text{C}_2\text{H}_5-\text{R}_5 \end{matrix}$	H	F		O-
Lomefloxacin	-C <sub>2</sub> H <sub>5</sub>	H	F		F
Danofloxacin		H	F		H

pound by the incorporation of an additional nitrogen atom into the quinoline nucleus. The early antibacterials have limited spectrum of activity, and newer compounds were sought to improve their antimicrobial spectrum. For the most part, the newer drugs have a structure similar to the parent 4-quinolone first isolated from the synthesis of chloroquine and they possess halogen atom on the non-nitrogenated ring. A fluorine residue at position 6 is present on all of the newer agents. The addition of piperazinyl ring at position 7 was found to extend the spectrum of activity leading to broad-spectrum fluoroquinolones. The fluoroquinolones are small molecules with weights between 300 and 500 Da. Many of these compounds are Zwitterions and exhibit different solubility characteristics with changes in pH. These agents are quite stable in both oral and parenteral

Difloxacin		H	F		H
Sparfloxacin		-NH <sub>2</sub>	F		F
Enrofloxacin		H	F		H
Sarafloxacin		H	F		H
Miloxacin	-OCH <sub>3</sub>	H	-O-	-CH <sub>2</sub> -O-	H
Flumequine		H	F	H	-CH <sub>2</sub> -
Rufloxacin	-CH <sub>2</sub> -CH <sub>2</sub> -	H	F		-S-

Fig. 1. List of the structures of the quinolone antimicrobials.

dosage forms at or below 30°C. They have been shown to be stable in reconstituted serum and urine for several weeks, but they have chelation potential for transition metal ions, such as copper, lead, zinc and magnesium. The compounds are sensitive to strong light and should be protected from light for long-term storage to prevent loss of activity.

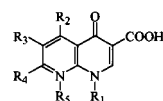
### 2.1. Official and compendial methods of analysis

Ciprofloxacin and its hydrochloride salt, nalidixic acid, cinoxacin and norfloxacin are the subjects of monographs in the United States Pharmacopoeia [4], while only nalidixic acid is official in the British Pharmacopoeia [5]. High-performance liquid chromatography (HPLC) method is recommended for the assay of ciprofloxacin and its preparations [4]. As for nalidixic acid and norfloxacin, they are assayed by non-aqueous titration depending on the presence of carboxylic group, while their preparations are analysed spectrophotometrically [4,5]. Cinoxacin, on the other hand, is assayed by HPLC, and its capsules are analysed spectrophotometrically [4]. The details of these methods will be mentioned later.

Monographs in the 'Analytical Profile of Drug Substances', series, were also published for nalidixic acid [6], norfloxacin [7] and lomefloxacin [8]. A comprehensive book dealing with clinical antimicrobial assays, including a chapter on 4-quinolones, was recently published [259]. A review with 86 references on the application of HPLC to the pharmacokinetic analysis of antibiotics was recently presented [270].

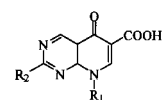
Among drugs administered to food-producing animals, antimicrobials are the most important. Drug residues may be present in slaughter animals that have been treated during the fattening period, and numerous chemical methods exist to detect these residues in meat or offal [260]. The European Community (EC) reference Laboratory in Fougères recommends the use of the 4-plate test on muscle tissue to detect residual amounts of antibacterial in slaughter animals [261]. The accepted Maximum Residue Limit (MRL) for enrofloxacin and ciprofloxacin in muscle, liver and kidney is 30  $\mu\text{g kg}^{-1}$  [262]. Residues of

fluoroquinolones in tissues of food-animals are of concern because of reports that humans have developed antibacterial resistance to these drugs, the FDA has recently banned the extralable use of these drugs in food-producing animals [263,264]. Sarafloxacin and enrofloxacin are approved for use in Poultry in the United States (US-FDA, Green Book) [265]. Enrofloxacin is approved in the US, for non-food animals, it is used extensively in Europe [266]. A peer-verified liquid chromatographic method was described for the simultaneous determination of residues of flumequine, nalidixic acid, oxolonic acid and piromidic acid in catfish muscle [267].



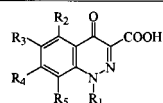
B. Naphthyridine Ring

Name	R <sub>1</sub>	R <sub>2</sub>	R <sub>3</sub>	R <sub>4</sub>	R <sub>5</sub>
Nalidixic acid	-C <sub>2</sub> H <sub>5</sub>	H	CH <sub>3</sub> -		
Enoxacin	-C <sub>2</sub> H <sub>5</sub>	F			



C. Pyridopyrimidine ring.

Name	R <sub>1</sub>	R <sub>2</sub>
Pipermidic acid	-CH <sub>2</sub> CH <sub>3</sub>	



D. Cinnoline Ring

Name	R <sub>1</sub>	R <sub>2</sub>	R <sub>3</sub>	R <sub>4</sub>	R <sub>5</sub>
Cinoxacin	-C <sub>2</sub> H <sub>5</sub>	H	-O-	-CH <sub>2</sub> -O	H

### 2.2. Pharmacokinetics

The pharmacokinetic properties of 4-quinolones have been reviewed by Brown and Reeves [268]. Table 1 summarizes the properties of some of them. They are orally absorbed (some also have parenteral formulations), have large volume of distribution, and are, with the exception of some of the newer agents, eliminated



Table 1  
Physico-chemical and pharmacokinetic properties of 4-quinolones

Drug	Mol. Wt.	pK <sub>a</sub>	Dosage forms	Elimination half-life (h)	Protein binding (%)	Metabolites	Urinary excretion
<i>Naphthyridines</i>							
Clinafloxacin	365.78		Hydrochloride	5.2	50	Glucuronide	> 50%, mostly unchanged
Enoxacin	320.32	6.2, 8.8	3/2 Hydrate	3–6	35	Oxo	60% 10–15% as oxo
Nalidixic Acid	232.2	6.7		1.5	93	Glucuronide, hydroxy	> 80%, mostly metabolites
Tosufloxacin	404.33		Tosilate	6–7	37		30–35%
Trovafloxacin	416.36	5.87, 8.09	L-Ala-L-Ala mesylate	9–13	70	Glucuronide, <i>N</i> -acetyl	< 10%
<i>Quinolines</i>							
Ciprofloxacin	331.3	6.0, 8.8	Lactate or hydrochloride	3–4	20–40	Sulpho, oxo, formyl, desethyl	50–70%, ≈ 10% metabolites.
Fleroxacin	369	5.5, 8.0		9–12	23	Desmethyl, <i>N</i> -oxide	> 50%, with < 11% as metabolites
Grepafoxacin hydrochloride	395.86		Hydrochloride sesquihydrate	8–15	50	Glucuronide, sulphate open-ring	≈ 10%
Levofloxacin	361.37	7.9	Hemihydrate	3–7	30	<i>N</i> -oxide, desmethyl	> 75%, < 10% as metabolites
Lomefloxacin	351.37			7–8	15	Glucuronide	> 60%, 5–10% as metabolite
Moxifloxacin hydrochloride	437.9			10–12	50		≈ 20%
Norfloxacin	319.3	6.2–6.4, 8.7–8.9		3–4	15	Formyl, oxo, desethyl, etc.	35%, with 10% as metabolites
Ofloxacin	361.37	7.9	Hydrochloride	3–7	30	<i>N</i> -oxide, desmethyl	> 75%, < 10% as metabolites
Pefloxacin	333.37		Mesylate dihydrate	8–13	20–30	As norfloxacin plus desmethyl	> 60%, mostly as metabolites
Sparfloxacin	380.38			15–20	37	Glucuronide	< 10% mostly as metabolite

mainly by renal excretion and, to a greater or lesser extent depending on the compound, metabolic conversion. Within this generalization, there are quite large differences between the different compounds.

### 3. Reported methods of analysis

#### 3.1. Titrimetric methods

The British Pharmacopoeia [5] recommends a titrimetric assay for nalidixic acid. The drug is dissolved in  $\text{CH}_2\text{Cl}_2$ /isopropanol, then titrated with ethanolic sodium hydroxide and detecting the end point potentiometrically using glass/silver–silver chloride electrode system. Nalidixic acid was also titrated in DMF against lithium methoxide using thymolphthalein as indicator [4]. A similar method, using ethylenediamine or DMF–methanol mixture as a solvent, and sodium methoxide as the titrant and thymol blue as an indicator, was reported for nalidixic acid [9]. Bachrata [10] titrated nalidixic acid with sodium borohydride, the detection of the end point was accomplished potentiometrically or using thymol blue indicator. In another report, Bachrata et al. [11] titrated nalidixic acid alkalimetrically in non-aqueous medium. Norfloxacin, on the other hand, was titrated in glacial acetic acid with perchloric acid, the detection of the end point was accomplished potentiometrically [4]. Ciprofloxacin was titrated in pyridine with tetrabutyl ammonium hydroxide in methanol/isopropanol, the end point being detected potentiometrically using combined glass electrode [13]. An acid-dye biphasic titrimetric method was described for ciprofloxacin. The sample was dissolved in water, mixed with phosphate/citrate buffer of pH 7, chloroform was then added. The mixture was titrated with 0.4 mM bromothymol blue to a light blue colour in the aqueous layer [14].

For the analysis of ofloxacin, the drug was dissolved in ethanol and titrated with 0.046 M NaOH, the end point was detected either potentiometrically or conductometrically [15]. Belal et al. [256] described a conductimetric titration method for ofloxacin, norfloxacin and nalidixic

acid based on the use of NaOH,  $\text{AgNO}_3$  or tetrabutylammonium hydroxide.

#### 3.1.1. Direct potentiometry using ion-selective electrode

Avsec and Gomiscek [12] described the preparation of ciprofloxacin PVC-coated wire ion-selective electrode based on quinolin-4-ones. The useful pH range was 4.5–7 and the response was rectilinear for 0.1–10 mM. Li et al [16] described the preparation and application of poly (vinyl chloride) membrane selective electrode for norfloxacin. The Nernstian response of the electrode was linear over the range 18–63 mM. In another contribution, Guo et al. [17] used sodium tetraphenylborate to prepare the electroactive substance, the response of the electrode was linear from 10  $\mu\text{M}$  to 10 mM.

#### 3.2. Ultraviolet spectroscopic methods

The quinolone derivatives are highly absorbing light in the ultraviolet region of the spectrum, therefore, numerous methods were developed based on measuring their absorbance at that region. For example, norfloxacin was determined in capsules by measuring the absorbance of its solution in 0.4% NaOH at 273 nm [18]. A simultaneous spectrophotometric method was described for the estimation of norfloxacin and tinidazole by measuring the absorbance of their solution in DMF at 275.6 and 317.8 nm or measuring the difference in their absorbance from 275.6 to 353.6 nm and from 317.8 to 254.2 nm for norfloxacin and tinidazole, respectively [19]. A similar method was described for the same mixture [20]. The absorbance of the solution of the two drugs in 0.01 M acetic acid was scanned from 400 to 200 nm using two sampling points of 227 and 316 nm.

Ciprofloxacin HCl was determined in tablets by differential spectrophotometry [21]. The absorbance of the sample in dil HCl was measured at 283 nm against a reference sample treated with dil. NaOH. The calibration curve was linear from 3 to 15  $\text{mg l}^{-1}$ . Ciprofloxacin was also determined in 0.1 M HCl at 227 nm [22]. The latter method was further utilized for its determination in ophthalmic solutions [23]. The excretion of

ciprofloxacin in urine was estimated by measuring its absorbance in 0.01 M NaOH at 335 nm [24]. Ofloxacin was determined in urine after passing on Amberlite XAD-2 activated with methanol/water/acetone, the elute was measured at 293 nm [25]. El-Yazbi [26] proposed a spectrophotometric method for the determination of ofloxacin in tablets by measuring the absorbance of two equal portions in 0.1 M NaOH and 0.1 M HCl in the zero-order, first and second derivative modes. Ofloxacin was determined in granules by direct UV-spectrophotometry at 293 nm [27], and in tablets and ointments by second derivative spectroscopy with  $\Delta\lambda$  6 nm and measurement of the peak–trough amplitude between 303 and 315 nm [31].

Norfloxacin was determined in tablets by second-derivative UV-spectroscopy [28]. A stability-indicating derivative spectrophotometric method was described for the determination of norfloxacin in tablets [29]. The first derivative measurements at 264 nm were applied for the quantitation of norfloxacin without interference from its 3-decarboxylated derivative. UV spectrophotometric measurements of norfloxacin at 276 nm were used for its determination in the presence of different antacids (derivatives of Al and Mg) [30].

The application of ultraviolet spectroscopy to the determination of nalidixic acid has been reported by many workers [32–34]. The determination of nalidixic acid and its hydroxy metabolite is based on the fact that in aqueous solutions, both compounds absorb UV strongly at 336 nm but hardly at all at 370 nm. The difference in absorbance at these two wavelengths gives a highly specific measure of the total amount of the two compounds [33]. A difference spectrophotometric method was described for the determination of lomefloxacin in tablets whereby the absorbance of the solution in acetate buffer of pH 3.8 and the solution in phosphate buffer of pH 7.2 was measured at 259.4 and 292.2 nm, respectively [35].

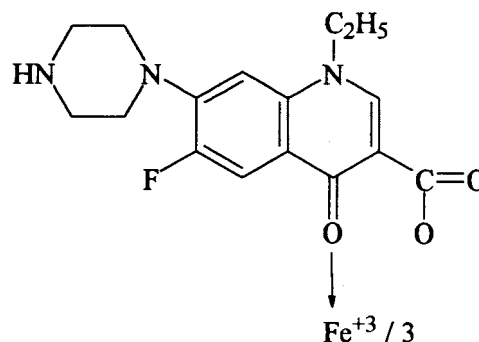
### 3.3. Visible spectrophotometric methods

The reaction of 4-quinolones with metal ions to produce coloured complexes was exhaustively utilized by many authors to develop methods for

their determination. The complexation behavior of fluoroquinolones was studied. The absorption, fluorescence and IR spectra of these drugs with Fe (III) were recorded. The formation constant of the 1:1 complexes was determined spectrophotometrically using Bjerum's method and scratched plots, the optimum pH for complexation was 3.8. The complexes were stable for 1 h. It was found Ni (II), Co (II), Mg (II) and Zn (II) did not interfere, but Cu (II) did [36].

The detection of fluoroquinolones in urine of patients with Tuberculosis could be achieved by the change of color of a paper impregnated with FeCl<sub>3</sub> [37].

Ferric chloride reacts with norfloxacin, ciprofloxacin, cinoxacin and nalidixic acid in DMSO/methanol producing orange colors peaking at 440, 442, 490 and 430 nm, respectively, the corresponding optimum ranges were: 50–125; 40–100; 4–100 and 40–100  $\mu\text{g ml}^{-1}$ . The reaction-product with ciprofloxacin is proposed to be as follows [38]:



Ciprofloxacin was determined in pharmaceuticals through its reaction with ferric chloride and measuring the produced colour at 430 nm [22]. Raman-Rao et al. [39] described two spectrophotometric methods for ciprofloxacin, the first involved the use of 0.2% FeCl<sub>3</sub>/0.5 M HCl, while the second was based on the use of 3-methylbenzothiazolin-2-one hydrazone/ceric sulphate. Ferric nitrate was also used for the determination of ciprofloxacin, a yellow–orange colour peaking at 435 nm was obtained in 1% nitric acid [40], while a yellow colour peaking at 370 nm was produced in neutral medium [41]. Ofloxacin—on the other hand—could be determined through its yellow

colour with Cu (II) at pH 4.5 ( $\lambda_{\max}$  360 nm) [42] or with Fe (III) ( $\lambda_{\max}$  410 nm) [43]. Flumequine was similarly determined in pharmaceuticals depending on the use of FeCl<sub>3</sub> [44]. As for nalidixic acid, several methods have been reported for its determination depending on its complexation with Fe (III). A yellow colour peaking at 419 nm at pH 3 over the concentration range 0.5–4.0 ppm, was developed [45]. At pH 7, a yellow colour with  $\lambda_{\max}$  430 nm was obtained, the working range was 10–200  $\mu\text{g ml}^{-1}$  [46]. Similar methods based on measuring the yellow colour at 410 nm were reported [47,48]. A spectrophotometric method was proposed for ciprofloxacin and norfloxacin based on ternary complex-formation with eosin and Pd (II) in acetate buffer pH 4 or 4.2 and measuring the produced colour at 545 nm over the range 3–10  $\mu\text{g ml}^{-1}$  [49]. A spectrophotometric method for lomefloxacin based on reduction of Folin–Ciocalteu reagent to produce molybdenum blue peaking at 770 nm, was reported [50].

Charge-transfer complexation between 4-quinolones as electron donors and certain  $\pi$ -acceptors formed the basis of several spectrophotometric methods. Amin et al. [51] used each of 1,3-dichloro-5,6-dicyano-*p*-benzoquinone (DDQ), 7,7,8,8-tetracyanoquinodimethane (TCNQ), *p*-chloranil (CL) or chloranilic acid (CLA) as  $\pi$ -acceptors to give highly coloured species, peaking at 460, 843, 550 and 531 nm, respectively, the concentration range is 10–400  $\mu\text{g ml}^{-1}$ . Zhou et al. [52] used each of DDQ, *p*-benzoquinone (BQ), tetrachlorobenzoquinone (TCB) or tetrabromobenzoquinone (TBB) for the same purpose. Ciprofloxacin was determined using BQ at pH 7.8,  $\lambda_{\max}$  was 495 nm [53]. The same reagent was used by Al-Khamees [54] to determine norfloxacin in tablets,  $\lambda_{\max}$  was 495 nm, the working range was 15–40  $\mu\text{g ml}^{-1}$ . A similar method involving the use of TCB was reported for ciprofloxacin,  $\lambda_{\max}$  was 376 nm and the working range 0.9–25  $\mu\text{g ml}^{-1}$ . [55]. Recently, *p*-nitrophenol was described for the determination of pipemidic acid, norfloxacin and ciprofloxacin in aqueous medium to produce complexes peaking at 404, 407 and 403 nm, respectively [257], the linear ranges were 0.1–12, 0.3–16 and 0.1–18  $\mu\text{g ml}^{-1}$ , respectively. The method was applied to dosage forms.

Ion-pair complex-formation was successfully utilized for the determination of this class of compounds. Fluoroquinolones were determined through their reaction with supracene violet 3B and measuring the orange colour at 485 nm [56]. Ciprofloxacin was determined using either bromocresol purple or bromophenol blue, the yellow colour produced was measured at 410 nm [57]. A similar method involving the use of methyl orange or bromothymol blue for ciprofloxacin was described, the absorbance was measured at 425 nm or 410 nm, respectively, the working range was 3–25  $\mu\text{g ml}^{-1}$  [58]. Sulphophthalein dyes (bromophenol blue, bromothymol blue and bromocresol purple) were used for the determination of ofloxacin and lomefloxacin, [59],  $\lambda_{\max}$  was 410, 415 and 410 nm, respectively. The working ranges were 5–25, 2–15 and 2–20  $\mu\text{g ml}^{-1}$ , respectively. Similarly, lomefloxacin was determined using bromothymol blue, bromophenol blue, bromocresol purple and bromocresol green [60]. An extractive spectrophotometric method was described for norfloxacin based on oxidation with ceric sulphate/ammonium sulphate. The yellow colour produced is measured at 350 nm. The working range is 10–1000  $\mu\text{g ml}^{-1}$  [61].

### 3.4. Spectrofluorimetric methods

The 4-quinolone derivatives are characterized by their high native fluorescence, therefore, several methods were developed for their determination based on this fact; yet, many other methods were introduced based on chemical derivatization, whereby more intense fluorophores were obtained. Norfoxacin was determined in capsules after dissolving in 0.05 M HCl and measuring its fluorescence at 440 nm (excitation 280 nm), the concentration range was 0.1–0.36  $\mu\text{g ml}^{-1}$  [62]. Similarly raxofloxacin was determined in capsules and serum by measuring its fluorescence at 440 nm (excitation 360 nm) in 0.05 M H<sub>2</sub>SO<sub>4</sub>. The detection limit was 0.3  $\mu\text{g ml}^{-1}$  [63]. A similar method was described for enrofloxacin in poultry tissues after extraction with CH<sub>2</sub>Cl<sub>2</sub>, the fluorescence was measured in buffered solution (pH 3.5) at 445 nm after excitation at 282 nm [64]. Ofloxacin in tablets was determined either in ac-

etate buffer pH 3.5 or in 0.1 M HCl, the fluorescence of the solution was measured at 500 nm (excitation at 292 nm), the recovery was 98.7–99.5% [65]. In the same manner, El-Yazbi could determine ofloxacin in tablets by measuring its fluorescence in 0.1 N H<sub>2</sub>SO<sub>4</sub> at 512 nm (excitation 298 nm), the concentration range was 0.2–1.2 µg ml<sup>-1</sup> [26]. The dissolution of norfloxacin tablets in gastric juice in presence of antacids was studied spectrofluorimetrically by measuring the fluorescence at 445 nm (excitation 330 nm), the calibration curve was linear over the concentration range 1–10 µg ml<sup>-1</sup> with limit of detection of 0.58 µg ml<sup>-1</sup>. Nalidixic acid was determined in biological fluids after extraction with ethylacetate: chloroform and measuring its fluorescence at 350/435 nm [66]. A similar method involving extraction with chloroform and measuring its fluorescence at 325/408 nm, was reported [67]. Recently, Moras et al. [68] reported on the simultaneous determination of nalidixic acid and 7-hydroxy-derivative by partial least squares calibration based on measuring the fluorescence of these compounds in the presence of cyclodextrin at 357 nm, exciting at 314 nm. Matrix isopotential synchronous spectrofluorimetry was applied to the determination of nalidixic acid in urine without prior separation, working concentration range was 25–1000 ng ml<sup>-1</sup> [69]. Lizondo et al. [70] studied the fluorescence characteristics of enrofloxacin in different solvents, H<sub>2</sub>O, acetate buffer of pH 4.7 methanol, ethanol and chloroform.

Complexation with metals has been utilized by several workers for the development of fluorimetric methods for the determination of these compounds. The complexation of scandium with fluoroquinolones at pH 4.2 was utilized for their determination by measuring the fluorescence at 430 or 480 nm (excitation 280 nm) [71]. The calibration graphs were linear up to 1.0 µM and the limit of detection was about 0.6 µM. Norfloxacin was determined in serum through complexation with Al (III) over the range 0.001–2 µg ml<sup>-1</sup>, λ<sub>max</sub> was 440 nm (excitation 320 nm) [72]. The same complexation reaction was utilized for the determination of norfloxacin in pharmaceuticals and urine [73], the complex was measured at 423 nm (excitation 339 nm) over the range 0.003–

6.8 µg ml<sup>-1</sup>. Tb (III) was also used to determine norfloxacin in serum [74]. The complex was measured at 545 nm (excitation 325 nm) over the range 0.05–1 µg ml<sup>-1</sup>. Similarly, ciprofloxacin and norfloxacin were determined in pharmaceuticals through ternary complex-formation with PdCl<sub>2</sub>/eosin at pH 4 and measuring the fluorescence at 540 nm (excitation 310), the calibration curves were linear over the ranges 35–70 and 25–50 µg ml<sup>-1</sup>, respectively [49].

As for nalidixic acid, several fluorimetric methods were reported: the ternary-complex formation of nalidixic acid with Tb (III) in presence of hexamine (pH 7.2) was exploited for its determination in formulations and biological fluids [75]. The working range was 0.1–2.4 µg ml<sup>-1</sup> with limit of detection of 2 ng ml<sup>-1</sup>, the complex was measured at 490/310 nm. A similar method was described for the determination of nalidixic acid in bovine serum, complexation was affected using Eu (III) or Tb (III) [76]. Terbium-sensitized fluorescence was reported for the determination of fluoroquinolone antibacterials in serum at pH 5.5, λ<sub>max</sub> 546/333 nm [77]. The fluorescence characteristics of norfloxacin–Mguanylic acid reaction product and its quenching by Fe (III) or Cu (II) was utilized for its determination [78]. The host–guest complexation of 4-quinolones with cyclodextrins formed the basis of many fluorimetric methods. Nalidixic acid formed 1:1 complex with γ-cyclodextrin [79], a fluorimetric method was developed based on measuring the fluorescence of the complex at 357/314 nm over the range 0.1–2 µg ml<sup>-1</sup>. The method was applied to urine and pharmaceuticals. A similar method was reported for nalidixic acid in biological fluids [80]. Norfloxacin was determined in veterinary preparations by measuring its fluorescence at pH 2.6 in the presence of β-cyclodextrin [81]. The entrapment rate of ofloxacin liposomes was determined spectrofluorimetrically at pH 7.2 by measuring the fluorescence at 467.2 nm (excitation at 288 nm) over the range 54–513 µg l<sup>-1</sup> [82].

### 3.5. Voltammetric methods

Voltammetry and polarography are becoming increasingly important in the determination of

pharmaceutical compounds. These methods are sufficiently sensitive and selective, and are suitable for the analysis of trace materials in complicated systems, such as dosage forms, biological fluids, etc. The presence of carbonyl group attached to the quinolone or naphthpyridine nucleus, in conjunction with carboxylic acid groups initiated several polarographic studies for this class of compounds. A differential-pulse polarographic (DPP) method was described for the determination of norfloxacin in tablets based on measuring the single DP peak in 2 M HCl in the range  $-0.95$  to  $-1.05$  V versus C or the peak that appears in the range  $1.79$  to  $-1.95$  in base electrolyte of  $\text{pH} \geq 7.5$  [83]. An oscillographic titration method was applied to the determination of norfloxacin in capsules [84], the drug was precipitated as its tetraphenylborate and the filtrate was titrated with thallos sulphate using an ac voltage from 6 V 50 Hz to 0.25 V, the dc voltage to  $-0.79$  V. A similar method was described for norfloxacin in pharmaceuticals [85], after precipitation with tetraphenylboron, the filtrate was titrated with the same titrant using an ac voltage of 2.3 V and dc voltage of  $-1.5$  V. Wang et al. [86] applied the same technique for norfloxacin in capsules, the working voltages were dc voltage at  $-9$  to  $-1$  V and ac voltage at  $-5.8$  to 6 V. The average recovery was 99.6%. Adsorptive stripping voltammetry (ASV) was reported for the determination of norfloxacin in eye drops [87], the peak potential of the reductive wave at  $-1.52$  V was measured in ammonia buffer of  $\text{pH} 7.49$ . The same technique (ASV) was utilized for norfloxacin in tablets [88], the accumulation time was 60–300 s and the scan rate was 2–10  $\text{mV s}^{-1}$ . The polarographic behaviour of nalidixic acid has been studied by Staroscik et al. [89]. The  $\text{pH}$  range was 2.9–11 in 20% DMF. Nalidixic acid was polarographically determined in urine after extraction with  $\text{CHCl}_3$ . The DP peak is measured in phosphate buffer  $\text{pH} 3$  over the range 0.4–100  $\mu\text{M}$  [90]. Ciprofloxacin was determined in formulations by oscillography with measurement of the reductive peak potential at  $-1.51$  V versus SCE in phosphate buffer of  $\text{pH} 6.9$  [91]. Single sweep polarography was performed for ciprofloxacin dosage forms with measurement of

the peak potential of the second-derivative wave at  $-1.49$  V versus SCE [92]. Ciprofloxacin was determined in urine after passing on  $\text{C}_{18}$  cartridge then recording the stripping curve in BRb of  $\text{pH} 6.3$  after accumulation for 60 s. with use of either Hanging mercury drop electrode or a carbon paste electrode versus Ag/AgCl electrode [93]. Differential pulse polarography (DPP) was applied to the determination of ciprofloxacin in serum at  $\text{pH} < 10$  (0.1 M LiOH) measuring the peak at  $-1.87$  V versus SCE [94,95]. Ofloxacin was determined in tablets and in blood adopting single sweep polarography by measuring the reduction peak produced in phosphate buffer of  $\text{pH} 6$  at  $-1.55$  V versus SCE [96]. An ASV method was described for ofloxacin in tablets [97]. The stripping peak produced in BRb of  $\text{pH} 6$  was measured at  $-1.675$  V versus Ag/AgCl after preconcentration for 60 s. The concentration range was 0.08–197.5  $\mu\text{g ml}^{-1}$  with minimum detectability of 1  $\text{ng ml}^{-1}$ . Ofloxacin was also determined polarographically in BRb of  $\text{pH} 4$  [98]. Rizk et al. [99] applied DPP to determine ofloxacin in pharmaceuticals and biological fluids by measuring the peak in BRb of  $\text{pH} 8.36$  at  $-1.4$  V versus Ag/AgCl over the range 0.01–0.1 mM. In addition, ofloxacin was determined by DPP through its complex with Cu (II) [42]. Tamer [100] applied DPP to the determination of pipemidic acid and its metabolites (acetyl, formyl and oxo-pipemidic acid) in BRb of  $\text{pH} 1.7$ . At 13  $\mu\text{M}$ , the coefficients of variation ranged from 1.2 to 1.7% for all compounds. Belal and Sharaf-El-Din [101] described a polarographic method for the determination of flumequine in dosage forms based on measuring the DPP peak in BRb of  $\text{pH} 8$  containing 40% methanol, the  $E_{1/2}$  was  $-1.48$  V versus Ag/AgCl electrode, the diffusion-current constant was 1.57 (RSD = 2.48%). Cinoxacin is assayed in capsules, urine and plasma by using ASV at  $\text{pH} 4.5$  after applying a preconcentration potential of  $-0.45$  V for 55 s [102]. Pipemidic acid was determined in tablets by differential pulse adsorptive anodic-stripping voltammetry, the drug was concentrated in the carbon fibre indicator electrode at 100 mV for 30 s and determined by anodic-stripping between 0 and  $+1.3$  V [269].

Table 2  
HPLC methods for the simultaneous determination of different members quinolone antibacterials<sup>a</sup>

Drugs	Material	Column	Mobile phase	Detection	Ref.
Nor., dif., cipro., sara.	Fish feed	Alltech C <sub>18</sub> , 10 μm	Sodium citrate-citric acid, pH 2.4/acetonitrile (13:7)	UV, 280 nm	[116]
Several quinolones	Fish and animal tissues	Nucleosil C <sub>18</sub> , 5 μm	0.02 M H <sub>3</sub> PO <sub>4</sub> in acetonitrile/THF (1:1)	Fluor. 336 and 375 nm	[117]
OA, NA, fl., POA, beno., dano., ofl.	Fish and meat	Wakosil IIS, C <sub>18</sub> HG	Phosphate buffer, pH 2.5/acetonitrile (65:35)	UV, 280 nm and Fluor. 325/365 nm	[118]
Cipro, enox, fero., nor, ofl, PMA	Raw material	Lichrosphere 100 C <sub>18</sub> , 5 μm	Tetrabutylammonium bromide in H <sub>3</sub> PO <sub>4</sub> , pH 3.89/acetonitrile (93:7)	Potentiometry	[119]
Cipro., ofl., pef. +PMA, NA, cino.	Dosage forms	Cosmosil 5, C <sub>18</sub>	Methanolic SDS/Phosphate buffer/acetonitrile (5:11:4)	UV, 257 nm	[120]
Fluoroquinolones	Human plasma	C <sub>18</sub>	Acetonitrile/Phosphate buffer pH 2	Fluor.	[121]
Fluoroquinolones	Clinical specimens	Lichrosorb C <sub>18</sub> , 10 μm	Acetonitrile/0.4 M citric acid (1:5)	Fluor. 275, 340 nm	[122]
Fluoroquinolones + theophylline	Plasma	Spherisorb 5 ODS 2	15% Acetonitrile in phosphate buffer pH 3 containing tetrabutyl ammonium hydrogen sulphate	UV, 280 nm	[123]
Quinolonic and cinolonic acid derivatives	Urine	Nova Pack C <sub>18</sub>	Acetonitrile/0.4% acetic acid (7:18)	UV, 265 nm	[124]
Four quinolones	Raw material	Lichrosphere 100, C <sub>18</sub> , 5 μm	Acetonitrile/H <sub>3</sub> PO <sub>4</sub> adjusted to pH 3.09 with tetrabutyl ammonium hydroxide (7:93)	UV	[125]
-Eno. + ofl. + nor., cipro. + pef. + enro.	Dosage forms	Shimpack CLC-ODS	Tetrabutylammonium hydroxide/acetonitrile (9:1)	UV, 280 nm	[126]
-Lome. + ofl. + pef. + enro.	Dosage forms	Shadex C <sub>18</sub> , 5 μm	0.025 M H <sub>3</sub> PO <sub>4</sub> /acetonitrile (17:3)	UV, 278 or 285 nm	[127]
-Nor. + cipro. + lome. + pef. + ofl. + ami.	Pharmaceuticals	Lichrosorb C <sub>18</sub> , 5 μm	Methanol/Phosphate buffer (1:1)	UV, 254 nm	[128]
-Enro. + cipro.	Bovine milk and plasma	Spherisorb, 3 μm	0.05 μ SDS in: water/acetonitrile/ methanol/triethylamine/ H <sub>3</sub> PO <sub>4</sub> (1623:180:180:9:8)	UV, 230–330 nm	[129]
-Benro. + enro. + dano. + ofl.	Chicken tissues	Wakosil II 5 C <sub>18</sub>	Phosphate buffer pH 2.4/acetonitrile (4:1)	Fluor. 245, 455 nm	[130]
-Pef. + nor.	Human serum	Novapak C <sub>18</sub> , 4 μm	14% Acetonitrile in buffer solution containing triethylamine	Flour. 330, 440 nm	[131]
-Cipro. + norf.	Tablets	Bondapak C <sub>18</sub>	Acetonitrile/methanol/acetic acid 10.01 M KH <sub>2</sub> PO <sub>4</sub> (15:12:0.3:73)	UV	[132]
-Tema. + sara. + dif.	Dosage forms	Nucleosil C <sub>18</sub> , 5 μm	Citrate buffer pH 2.4/Acetonitrile (13:7)	UV, 280 nm	[133]
-Cipro. + ofl. + nor.	Human hair	Tsk gel-ODS-80Ts, 5 μm	Acetonitrile/phosphoric acid adjusted to pH 3 with tetrabutylammonium hydroxide (1:19)	Fluor.	[134]
-Ofl. + cipro. + nor. + pef.	Biological fluids	Nucleosil, C <sub>18</sub> , 5 μm	H <sub>2</sub> O/85% H <sub>3</sub> PO <sub>4</sub> /tetrabutyl ammonium iodide/methanol (7000:19:14:3000)	UV, 278 or 294 nm	[135]
-Enro. + cipro., sara + difl.	Milk	Inertsil phenyl	Acetonitrile/2% acetic acid (15:85)	Fluor. 278 and 450 nm	[136]
-NA + OA + PMA	Fish	Inertsil ODS-2	0.1 M ammonium acetate buffer pH 4.5/acetonitrile (3:2)	MS	[168]

Table 2 (Continued)

Drugs	Material	Column	Mobile phase	Detection	Ref.
–NA+OA+POA	Fish	Nucleosil, C8, 7 $\mu$ m	Methanol/0.1 M; citric acid/ acetonitrile (2:2:1)	UV, 254 nm	[171]
Miloxacin, OA, NA, fl. PMA	Fish and meat	ODS	0.05 M NaH <sub>2</sub> PO <sub>4</sub> /acetonitrile (3:2)	Fluor. 325, 365 nm	[173]
Cipro. enro.+sara. dif.	Catfish muscle	Inertsil phenyl, 5 $\mu$ m	2% Formic acid /acetonitrile (86+14)	MS	[175]
–NA+OA POA	Fish	Kaisersorb LC ODS 300-5	0.005 M NaH <sub>2</sub> PO <sub>4</sub> /acetonitrile (3:2)	Flor. and UV, 280 nm	[164]
–Fl, NA, OA, POA	Salmon and shrimp	PLRP-S, 5 $\mu$ m	0.02 M H <sub>3</sub> PO <sub>4</sub> /acetonitrile THF (18:4:3)	Flor. and UV	[176]

<sup>a</sup> Abbreviations: nor, norfloxacin; NA., nalidixic acid; ofl., ofloxacin; cino., cinoxacin; dif., difloxacin; fl., flumequine; pef., pefloxacin; fluor., fluorometrically; cipro., ciprofloxacin; PMA: pipemidic acid; OA, oxolonic acid; sara, sarafloxacin; beno., benofloxacin; dano., danofloxacin; POA, piromidic acid; eno, enoxacin; enro, enrofloxacin; tema: temafloxacin; ami: amifloxacin; lome: lomefloxacin.

### 3.6. Chromatographic methods

#### 3.6.1. Gas chromatographic methods

Takatsumki [103] described a gas chromatographic (GC)-MS method for the determination of oxolonic acid, nalidixic acid and piromidic acid in fish. The method involved extraction of the drugs from the homogenized sample, reduction with NaBH<sub>4</sub> and analysis by GC on a fused silica column of DB-S with H<sub>2</sub> as a carrier gas, the concentration range was 0.2–20 ng. A derivatization GC method using pentafluorobenzylbromide was described for the determination of nalidixic acid in tablets [104] Pentafluorobenzyl bromide was used for derivatization, and N as carrier gas. GC was used to study the stability of nalidixic acid as reference sample [105]. A similar derivatization GC method was used for the determination of cinoxacin in capsules [106],  $\alpha$ -bromopentafluorotoluene was the derivatizing agent. The column was OV-1 on chromosorb W AW-DMCS operated at 255°C. A GC method was also described for the determination of cinoxacin in pharmaceuticals [107].

#### 3.6.2. Thin layer chromatography

Nalidixic acid was determined in pharmaceuticals by thin layer chromatography (TLC) after irradiation from a high pressure mercury lamp then applying to silica gel 60 F<sub>254</sub> high pressure

thin layer chromatography (HPTLC) plates with CH<sub>3</sub>OH/H<sub>2</sub>O/NH<sub>3</sub> (18:12:1) as a mobile phase and screening at 257 nm [108]. A similar method was described for its determination in plasma [109]. Nalidixic acid was also determined in the presence of metronidazole using the same plates and ethylactate/CHCl<sub>3</sub>/CH<sub>3</sub>OH/NH<sub>3</sub> (5:5:3:1) as a mobile phase and measurement at 370 nm [110]. TLC technique was also used to study the stability of nalidixic acid [107]. Lomefloxacin was determined in tablets adopting HPTLC using silica gel 60 F<sub>254</sub>, HPTLC plates with CH<sub>3</sub>OH/H<sub>2</sub>O/NH<sub>3</sub> (18:12:1) as a mobile phase and scanning at 286 nm [60]. Oxolonic acid residues were determined in fish using HPTLC [111]. TLC was also proposed for the simultaneous determination of norfloxacin, pefloxacin and ciprofloxacin in urine and serum, silica gel plates impregnated with EDTA and a mobile phase consisting of CHCl<sub>3</sub>/CH<sub>3</sub>OH/CH<sub>2</sub>Cl<sub>2</sub>/toluene/NH<sub>3</sub> (27:46:5:17:5) were used, the determination was affected spectrophotometrically or spectrofluorometrically [112].

HPTLC was also recommended for the simultaneous determination of norfloxacin and tinidazole in pharmaceutical preparations. Silica gel 60 F<sub>254</sub> HPTLC plates and a mobile phase consisting of C<sub>4</sub>H<sub>4</sub>OH/C<sub>2</sub>H<sub>5</sub>OH/12.5% NH<sub>3</sub> (20:5:11) were used, the determination was affected densitometrically at 293 nm [113]. Ciprofloxacin was determined in pharmaceuticals by HPTLC after



Table 3  
Application of HPLC to the determination of ciprofloxacin

Material	Column	Mobile phase	Detection	Ref.
Pharmaceuticals	Inertsil ODS 2	THF/acetonitrile/hexane sulphometa (2:1:17)	UV, 254 nm	[137]
Human aqueous humor	Novapak C <sub>18</sub> cartridge	Methanol/acetonitrile/0.4 M citric acid (3:1:10)	Fluor. 278 nm, 450 nm)	[138]
Body fluids	5 µm PLRP-S	0.02 M TCA/acetonitrile/methanol (37:11:2)	Fluor. 277 nm (418 nm)	[139]
Formulations	10 µm C <sub>18</sub>	Methanol/H <sub>2</sub> O/acetic acid (840:159:1)	UV, 254 nm	[140]
Biological materials	Inertsil OSD-2, 5 µm	50% Aqueous methanol of pH 2.5	Flo. 320,, 545 nm	[141]
Plasma	CLC-Shim pack ODS, 5 µm	Methanol: 0.2 M ammonium acetate (8:17)	UV, 280 nm	[142]
Plasma and chinchilla middle ear effusion	Hypersil C <sub>18</sub> , 5 µm	NaH <sub>2</sub> PO <sub>4</sub> + triethylamine+SDS of pH 3/acetonitrile (3:2)	Fluor. 278 nm; 456 nm	[143]
Serum	Bondapak C <sub>18</sub>	Methanol/acetonitrile/phosphate buffer pH 2.8 (5:4:11)	Fluor. 338 nm; 455 nm	[144]
Urine, serum, saliva	Spheri-5-OD-5A	0.1 M KH <sub>2</sub> PO <sub>4</sub> /acetonitrile (1:1)	UV, 280 nm	[145]
Serum	KYWG-C <sub>18</sub> , 10 µm	KH <sub>2</sub> PO <sub>4</sub> /methanol/acetonitrile (56:33:11).	Fluor. 280, 455 nm	[146]
Serum	Nucleosil C <sub>18</sub> , 3 µm	KH <sub>2</sub> PO <sub>4</sub> /H <sub>2</sub> O/tetrabutylammonium bromide /acetonitrile (12:6:1:1)	UV, 277 nm	[147]
Brain and CSF	Wakosil 5 C <sub>18</sub>	Sodium dodecylsulphonate in methanol/0.02 M KH <sub>2</sub> PO <sub>4</sub> (3:2, adjusted to pH 2.5)	Fluor. 277, 445 nm	[148]
Plasma micro samples	MB C <sub>18</sub> Radial Pak, 10 µm	(NH <sub>4</sub> ) <sub>2</sub> HPO <sub>4</sub> (0.1 M)/acetonitrile/methanol (80/13/7)	Fluor. 277, 453 nm	[149]

irradiation by mercury lamp and applying to silica gel 60 F<sub>254</sub> HPTLC plates using CH<sub>3</sub>CN/NH<sub>3</sub> and scanning in the absorbance/reflectance mode at 283 nm [114]. Recently, HPTLC was applied to the screening of quinolone residues in pig muscles using silica gel 60 HPTLC plates and CH<sub>3</sub>OH/NH<sub>3</sub> solution (17:3) as a mobile phase. The detection was affected at 312 nm before and after spraying with terbium chloride [115].

### 3.6.3. High-performance liquid chromatographic methods

HPLC is the most frequently applied technique to the determination of the 4-quinolones whether in formulations biological, fluids, fish and fish feed, etc.

Table 2 abridges the reported methods for the simultaneous determination of a group of these compounds. Tables 3–7 show the reported methods for ciprofloxacin ofloxacin, norfloxacin, nalidixic acid and flumequine, respectively. Table

8 is concerned with the reported methods for the other compounds of this class.

### 3.7. Microbiological methods

Ciprofloxacin, enrofloxacin, oxolinic acid and flumequine were analysed in fish by diffusion on agar plates with *E. coli*. The limit of detection was 0.0009–2 µg l<sup>-1</sup> [234]. A bacterial inhibition test was described for the detection of ciprofloxacin, enrofloxacin and flumequine in meat. The test strain was *E. coli* [235]. Enrofloxacin was determined in tissue fluid, serum and secretions by a microbial method utilizing *E. coli* [236], Nash et al. [237] reported a microbiological method for the determination of cinoxacin in plasma and compared it to a fluorimetric method. A bacteriological assessment of the activity of sparfloxacin, ofloxacin, levofloxacin and other fluoroquinolones was studied using listeria monocytogens adopting time-kill kinetic methodology [238]. Klopman et

al. [239] determined the Minimum Inhibitory Concentrations (MICs) of 63 quinolones against 14 references and clinical strains of the *Mycobacterium avium*–*Mycobacterium intracellulare* complex. Korsrud et al. [240] reviewed the bacterial inhibition tests used to screen for antimicrobial veterinary drug residues in slaughtered animals. Microbiological determination of nalidixic acid in

pharmaceutical preparations was early reported by Moniciu et al. [241]. A diffusimetric method using *E. coli* was adopted. A similar method was reported for nalidixic acid and its hydroxy derivative in biological samples [242]. Norfloxacin was assayed in body fluids by a microbiological method using *E. coli* NIHJ JC-2 and modified Muller–Hinton medium with a detection limit of

Table 4  
Application of HPLC to the determination of ofloxacin

Material	Column	Mobile phase	Detection	Ref.
Aqueous humor	Novapak C <sub>18</sub> , 4 μm	0.4 M citric acid/methanol/acetonitrile (10:3:1)	Fluor. 290, 500 nm	[150]
Human saliva	Develosil (C <sub>18</sub> ), 5 μm	0.06 M sodium acetate of pH 2.5/acetonitrile (21:4).	UV, 300 nm	[151]
Human plasma	Separon SGX C <sub>18</sub> 7 μm	5.5% THF in 0.06 M KH <sub>2</sub> PO <sub>4</sub> of pH 2.6	Fluor. 282, 450 nm.	[152]
Human scalp hair	ODS 120-T, 5 μm	KH <sub>2</sub> PO <sub>4</sub> pH 2.6/acetonitrile (41:9)	Fluor. 290, 460 nm	[153]
Plasma and lung tissue	Ultrabase RP8, 5 μm	Citrate buffer of pH 4.8/acetonitrile (17:3)	Fluor. 280, 500 nm	[154]
Hair	TSK gel ODS-120 T, 5 μm	Phosphate buffer of pH 2.6/acetonitrile (41:9)	Fluor. 290, 460 nm	[155]
Dosage forms	Anion exchange vydac, 10 μm	0.05 M phosphate buffer pH 7/acetonitrile (1:4)	UV, 297 nm.	[31]
Human serum	Develosil ODS-5, 5 μm	0.5% Sodium acetate pH 2.5/acetonitrile (87:13)	UV, 300 nm	[156]
Serum	Develosil CN, 5 μm	0.04 M NaH <sub>2</sub> PO <sub>4</sub> /0.04 M H <sub>3</sub> PO <sub>4</sub> /methanol (2:5:3)	UV, 300 nm	[157]
Body fluids	Nucleosil 5, C <sub>18</sub>	Acetonitrile/0.005 M tetrabutylammonium phosphate pH 2 (7:43)	Fluor. 295, 418 nm	[158]
Body fluids	Nucleosil 5, C <sub>18</sub>	Acetonitrile/0.05 M H <sub>3</sub> PO <sub>4</sub> containing triethylamine, pH 2.8 (9:41)	Fluor. 310, 487 nm	[159]

Table 5  
Application of HPLC to the determination of norfloxacin

Material	Column	Mobile phase	Detection	Ref.
Serum	C <sub>18</sub> , 5 μm	10 mM triethylamine phosphate in 55% acetonitrile of pH 4.8	UV, 226 nm	[160]
Dosage forms	C <sub>18</sub> , 5 μm	0.2% H <sub>3</sub> PO <sub>4</sub> , pH 2/acetonitrile (87:13)	UV, 275 nm	[161]
Serum	Spheri-3, C <sub>18</sub> , 3 μm	11% acetonitrile in 0.01 M NaH <sub>2</sub> PO <sub>4</sub> , pH 2.5 containing 0.001 M triethylamine	UV, 279 nm	[162]
Blood	Zorbax C <sub>18</sub> , 5 μm	Methanol/TFA, 0.01% (1:3)	Fluor. 280, 418 nm	[163]
Tablets	Micropak-NH <sub>2</sub> -10, 10 μm	Acetonitrile/tetrabutylammonium hydroxide/ <i>o</i> -phosphoric acid/water (10:1.5:0.167:100)	UV, 278 nm	[174]

Table 6  
Application of HPLC to the determination of nalidixic acid

Material	Column	Mobile phase	Detection	Ref.
Formulations	Machery–Nagel RP8, 5 $\mu$ m	H <sub>2</sub> O/acetonitrile/triethylamine (680:320:1)	UV, 310 nm	[165]
Pharmaceuticals	Alltech Anion R, 10 $\mu$ m	0.001 M TbCl <sub>3</sub> and 0.005 M heptanesulphonate in acetic acid pH 6.8/methanol (11:9)	Fluor. 318, 545 nm	[166]
Serum, brain, CSF	Wakosil 5C <sub>18</sub> , 5 $\mu$ m	CH <sub>3</sub> OH/acetonitrile/0.015 M KH <sub>2</sub> PO <sub>4</sub> containing sodium lauryl-sulphate (3:2:5)	UV, 255 nm	[167]
Formulations	Hypersil, C <sub>18</sub>	Water/acetonitrile/Triethylamine (600:400:1)	UV, 254 nm	[169]
Cultured fish	Nucleosil, C <sub>18</sub>	THF/acetonitrile/H <sub>3</sub> PO <sub>4</sub> /H <sub>2</sub> O (29:1:0.06:69.94)	UV, 260 nm	[170]
Fish	Nucleosil 3 C <sub>18</sub> 3 $\mu$ m	Acetonitrile/methanol/0.01 M oxalic acid of pH 3 (3:1:6)	UV, 290 nm	[172]

Table 7  
Application of HPLC to the determination of flumequine

Material	Column	Mobile phase	Detection	Ref.
Cat fish	PLRP-S, 5 $\mu$ m	0.02 M H <sub>3</sub> PO <sub>4</sub> /acetonitrile/THF (18:4:3)	Fluor. And UV	[177]
Fish tissues	PLRP-S, 5 $\mu$ m polymer column	0.02 M H <sub>3</sub> PO <sub>4</sub> /acetonitrile/THF (13:4:3)	Fluor. 325, 350 nm	[178]
Fish silage	PLRP-S, 5 $\mu$ m	0.002 M H <sub>3</sub> PO <sub>4</sub> /acetonitrile/THF (68:17:15)	Fluor. 325, 360 nm	[179]
Fish tissues	Lichrosorb RP-8, 5 $\mu$ m	0.025 M oxalic acid pH 3.2/acetonitrile (17:8)	Fluor. 327 $\mu$ m and 369 nm	[180]
Drug delivery system	PLRP-S, 5 $\mu$ m	0.02 M H <sub>3</sub> PO <sub>4</sub> /acetonitrile/THF (13:4:3)	UV, 336 nm	[181]
Plasma	Cp-Spher-C8	DMF-acetonitrile-0.6% H <sub>3</sub> PO <sub>4</sub> (3:3:14)	UV, 320 nm	[182]
Fish tissues	PLRP-S, 5 $\mu$ m	0.002 M H <sub>3</sub> PO <sub>4</sub> /acetonitrile/THF (64:21:15)	Fluor. 260, 380 nm	[183]
Fish liver	PLRP-S, 5 $\mu$ m	0.02 M H <sub>3</sub> PO <sub>4</sub> /acetonitrile/THF (33:10:7)	Fluor. 325, 365 nm	[184]
Fish extracts	PLRP-S, 5 $\mu$ m	Acetonitrile/THF/0.02 M H <sub>3</sub> PO <sub>4</sub> (4:3:13)	Fluor. 325, 365 nm	[185]
Salmon plasma	PLRP-S, 15 $\mu$ m	Acetonitrile/THF/0.02 M H <sub>3</sub> PO <sub>4</sub> (9:7:24)	Fluor. 262, 380 nm	[186]
Fish tissues	PLRP-S, 5 $\mu$ m	0.002 M H <sub>3</sub> PO <sub>4</sub> /acetonitrile/THF (13:4:3)	Fluor. 260, 380 nm	[187]
Fish	Hypersil ODS, 5 $\mu$ m	0.1 M citric acid/methanol/acetonitrile/THF (12:6:1:1)	Fluor. 324, 363 nm	[188]
Biological fluids and meat	RP-8, 4 $\mu$ m	Acetonitrile/0.025 M H <sub>3</sub> PO <sub>4</sub> (7:3)	Fluor. 320, 380 nm	[189]
Pharmaceutical preparations	Nucleosil 5, C <sub>18</sub>	Mixture of acetonitrile and 0.05 M H <sub>3</sub> PO <sub>4</sub> – dioxan (99:1)	UV, 323 nm	[190]
Urine and plasma	Lichrosorb RP-C <sub>18</sub>	0.01 M KH <sub>2</sub> PO <sub>4</sub> /methanol (9:11, pH 3).	UV, 254 nm.	[191]
Sheep tissues	Lichrospher RP, 5 $\mu$ m	Phosphoric acid /DMF/acetonitrile (54:28:48).	Fluor. 320 nm, 365 nm.	[192]

Table 8  
Application of HPLC to the determination of the new generation of 4-quinolones

Drug	Material	Column	Mobile phase	Detection	Ref.
Sparfloxacin	Human plasma	Novapak, C <sub>18</sub> 4 μm	5% Acetic acid/acetonitrile/methanol (14:3:3)	Spec. 364 nm	[193]
Sparfloxacin	Serum and urine	Nucleosil 100SA, 5 μm	Acetonitrile/0.1 M H <sub>3</sub> PO <sub>4</sub> (3:1)	Fluor. 295, 525 nm	[194]
Trovafloxacin	Serum and urine	Novapak C <sub>18</sub> 4 μm	0.04 M H <sub>3</sub> PO <sub>4</sub> /acetonitrile/tetrabutylammonium hydroxide/0.005 M dibutylamine phosphate, pH 3 (83: 16.85:0.05:0.1)	UV 275 nm	[195]
Eurofloxacin	Tablets	Bondapak C <sub>18</sub>	Acetonitrile/H <sub>2</sub> O/triethylamine (700:300:1)	UV 282 nm	[196]
Eurofloxacin	Milk and meat	PLRP-S, 5 μm	Heptanesulphonate in: 0.02 M H <sub>3</sub> PO <sub>4</sub> /acetonitrile/methanol (65:27:8)	Fluor. 278, 440 nm	[197]
Eurofloxacin	Meat and fish	ODS	0.05 M NaH <sub>2</sub> PO <sub>4</sub> /acetonitrile (7:3)	Fluor. 285, 445 nm	[198]
Eurofloxacin	Fish serum and tissues	PLRP-S, 5 μm	Methanol/1.0 M H <sub>3</sub> PO <sub>4</sub> /methanol (39:11 to 41:9)	Fluor. 278, 440 nm	[199]
Eurofloxacin	Fish tissues	PLRP-S, 5 μm	0.02 M H <sub>3</sub> PO <sub>4</sub> /acetonitrile/methanol (73:19:8)	Fluor. 278, 440 nm	[200]
+ sarafloxacin					
Danofloxacin	Cattle and chicken tissue	Inertsil C8, 5 μm	0.05 M phosphate buffer pH 3.5 containing 12% acetonitrile	Fluor. 280, 440 nm	[201]
Danofloxacin	Cattle and chicken liver	Keystone BDS Hypersil C <sub>18</sub>	Acetonitrile/0.1% trifluoroacetic acid (4:1)	EIMS	[202]
Difloxacin	Plasma	Shinapak CLC-ODS	Methanol/ammonium acetate of pH 2.7 (19:31)	UV 280 nm	[203]
Difloxacin	Biological matrices	Adsorbosphere C <sub>18</sub> HS 7 μm	0.05 M Sodium phosphate/SDS/acetonitrile	UV 280 nm or Fluor. 280, 389 nm	[204]
Sarafloxacin	Fish serum	PLRP-S, 5 μm	0.02 M H <sub>3</sub> PO <sub>4</sub> /acetonitrile/methanol (18:5:2)	Fluor. 278, 440 nm	[205]
Sarafloxacin	Cat fish tissues	ODS-A, C <sub>18</sub> , 5 μm	0.02 M ammonium acetate pH 3.5/acetonitrile (7:3)	Tandem MS	[206]
Sarafloxacin	Cat fish tissues	ODS-5 μm	Acetonitrile/methanol (3:2)	Fluor. 280, 384 nm	[207]
Levofloxacin	Blood	YWG-C <sub>18</sub>	0.01 M KH <sub>2</sub> PO <sub>4</sub> /0.01 M tetrabutylammonium bromide/acetonitrile/triethylamine (45:44:10:1)	UV, 295 nm	[208]
Levofloxacin	Plasma and urine	Inertsil ODS2, 5 μm	0.005 M CuSO containing methanolic 87.5% isoleucine	UV, 330 nm	[209]
Oxolonic acid	Shells of blue mussel	Lichrospher 100, RP-18E	Acetonitrile/0.02 M H <sub>3</sub> PO <sub>4</sub> (6:19)	UV 262 nm	[210]
Oxolonic acid	Turbot serum	Supelcosil ABZt	Acetonitrile/THF/0.001 M H <sub>3</sub> PO <sub>4</sub> (11:5:34)	Fluor. 360 372 nm	[211]
Oxolonic acid	Fish	Regis Pinkerton GFF, 5 μm	0.1 M KH <sub>2</sub> PO <sub>4</sub> /acetonitrile (9:1)	UV, 254 nm	[212]
Oxolonic acid	Fish silage	MOS Hypersil, C8, 3 μm	0.025 M oxalic acid/acetonitrile/methanol/THF (160:5:30:5)	Fluor. 325, 360 nm	[213]
Oxolonic acid	Seabass plasma	Lichrospher 5 μm	Acetonitrile/0.02 M H <sub>3</sub> PO <sub>4</sub> , pH 2.3/DMF (1:6:3)	UV, 340 nm	[214]
Oxolonic acid	Chicken plasma	Nucleosil, C8, 5 μm	Methanol/0.1 M citric acid/acetonitrile (6:7:1)	UV, 260 nm	[215]
Oxolonic acid	Fish serum	Novapak C <sub>18</sub> , 4 μm	Methanol/phosphate buffer, pH 8.2 (2:3)	UV, 258 nm	[216]
Euoxacin	Rat plasma	Chemcosorb 5, ODS-H	Methanol/0.005 M SDS (2:1) pH 2.5	UV, 275 nm	[217]
Temafloxacin	Scalp hair	TSK gel, ODS-80 TM	Acetonitrile/0.05 M citric acid/1 M ammonium acetate (22:78:1)	Fluor. 280, 406 nm	[218]
Temafloxacin	Bulk drug	Nucleosil C <sub>18</sub> , 5 μm	Phosphate buffer (pH 2.4)/acetonitrile/THF	UV, 325 NM	[219]

Table 8 (Continued)

Drug	Material	Column	Mobile phase	Detection	Ref.
Temafloxacin	Biological fluids	Zorbax Sil	Hexane/methylacetate/methanol/ammonia water (150:100:10:1)	UV, 280 nm	[220]
Amifloxacin	Plasma and urine	Bondapak C X Corasil, 37.5 $\mu\text{m}$	0.3 M $\text{KH}_2\text{PO}_4$ (pH 2.2)/acetonitrile (7:1)	UV, 280 nm	[221]
Fleroxacin	Plasma and urine	TSK-Gel-ODS, 5 $\mu\text{m}$	0.005 M tetrabutylammonium hydrogen sulphate/methanol (79:21)	Fluor. 290, 450 nm	[222]
Fleroxacin	Rat plasma	Shim-pack CLC-ODS, 5 $\mu\text{m}$	Methanol/tetrabutylhydrogen phosphate in $\text{NaH}_4\text{PO}_4$ (93:7)	Fluor. 290, 450 nm	[223]
Fleroxacin	Plasma	Zorbax RX-C8	Acetonitrile/0.05 M potassium phosphate pH 2.7 (9:41)	UV, 287 nm	[224]
Fleroxacin	Plasma	Zorbax ODS, 5 $\mu\text{m}$	0.025 M $\text{H}_3\text{PO}_4$ /methanol/acetonitrile (88:11:11)	Fluor. 281, 470 nm	[225]
Fleroxacin	Plasma and urine	Nucleosil 5, $\text{C}_{18}$	0.01 M tetrabutylammonium hydrogen sulphate + 0.05 M $\text{KH}_2\text{PO}_4$ /methanol (18:7)	Fluor. 290, 450 nm	[226]
Fleroxacin	Serum and urine	Bondapak $\text{C}_{18}$	Phosphate buffer pH 3/acetonitrile/methanol (34:3:3)	Fluor. 290, 470 nm	[227]
Lomefloxacin	Biological fluids	Bondapak $\text{C}_{18}$	Sodium acetate-citrate buffer pH 4.8/acetonitrile (800:230)	Fluor. 280, 340 nm	[228]
Lomefloxacin	Injections	Spherisorb $\text{C}_{18}$ , 5 $\mu\text{m}$	Citric acid/acetonitrile, pH 4.0 (4:1)	UV, 258 nm	[229]
Lomefloxacin	Human serum	Lichrosorb RP18, 10 $\mu\text{m}$	Methanol/phosphate buffer pH 2.3/tetrabutyl ammonium iodide (31:58:11)	UV, 288 nm	[230]
Lomefloxacin	Human plasma	Novapak, 4 $\mu\text{m}$	Hexane/ $\text{CHCl}_3$ /methanol (129:66:5)	Fluor. 280, 470 nm	[231]
Lomefloxacin	Human plasma	Vydac, anion exchange, 10 $\mu\text{m}$	Phosphate buffer pH 7/acetonitrile (9:1)	UV, 280 nm	[232]
Lomefloxacin	Human plasma	Nucleosil, $\text{C}_{18}$ 7 $\mu\text{m}$	Phosphate buffer/methanol/tetrabutylammonium bromide (75:30:4)	UV, 254 nm	[233]

0.05  $\mu\text{g ml}^{-1}$  adopting disk-diffusion method [243]. To assay norfloxacin in serum, tissues and urine, *Klebsiella pneumoniae* ATCC 10031 was used, the assay sensitivity was 0.2  $\mu\text{g ml}^{-1}$  [244]. Leigh et al. [245] reported on the microbiological determination of lomefloxacin using the disc susceptibility test. They adopted this method to study the stability of lomefloxacin in serum. A modified 4-plate test was used to screen antibiotics and antibacterials residues in meat samples from retail outlet using three media seeded with *Bacillus subtilis* [246]. The antibacterial activity of balofloxacin was studied using isolates from patients with bacterial enteritis, the MIC was 0.39  $\mu\text{g ml}^{-1}$  [247]. Lomefloxacin was measured in biological fluids by the standard agar diffusion

method using *E. coli* ATCC 1346 as the test organism [228].

### 3.8. Miscellaneous methods

The application of capillary electrophoresis for the analysis of quinolones in pharmaceutical preparations, biological fluids and foods was reviewed [248]. The separation of 14 quinolone antibacterials by capillary electrophoresis was reported [251]. The method involved the use of fused silica column at 30 KV with a background electrolyte of pH 7.3 and detection at 260 nm. Sultan and Suliman [249] described a flow-injection method for the determination of ciprofloxacin based on injecting the drug sample

into a carrier stream of Fe (III)/H<sub>2</sub>SO<sub>4</sub> and measuring the brown red complex formed at 447 nm [249]. A stopped flow kinetic determination of nalidixic acid and norfloxacin in serum based on lanthanide-sensitized fluorescence was reported [253]. A fluorine-19 NMR study of lomefloxacin in human erythrocytes and its interaction with haemoglobin was conducted. Separate resonances for intra and extracellular F were observed [250]. Nuclear magnetic resonance was described for the determination of ofloxacin [252]. Nalidixic acid could be determined in tablets and suspensions by applying PM spectroscopy, the integral of the methyl group protons at 2.56 ppm was compared to that of the singlet of a known amount of hexamethylcyclotrisilazane at 0.000 ppm [254]. Laser desorption fourier transform ion cyclotron resonance mass spectrometry was applied to the determination of flumequine [255]. An optical immunobiosensor assay was developed for the determination of enrofloxacin and ciprofloxacin in bovine milk [258].

## References

- [1] G.Y. Leshner, E.D. Froelich, M.D. Gruet, J.H. Bailey, R.P. Brudage, *J. Med. Pharm. Chem.* 5 (1962) 1068.
- [2] A. Percival, *J. Antimicrob. Chemother.* 28 (Suppl. C.) (1991) 1.
- [3] M.E. Ernst, E.J. Ernst, M.E. Klepser, *Am. J. Health. Sys. Pharm.* 54 (1997) 2569.
- [4] The United States Pharmacopoeia XXIII and NF 18, US Pharmaceutical Convention, MD, 1995, pp. 374, 375, 1047, 1104.
- [5] The British Pharmacopoeia, vol. I and II, Her Majesty Stationary Office, London, 1993, pp. 438 and 1019.
- [6] P.E. Grubb, in: K. Florey (Ed.), *Analytical Profile of Drug Substances*, vol. 8, Academic Press, NY, 1979, p. 371.
- [7] C. Mazuel, in: K. Florey (Ed.), *Analytical Profile of Drug Substances*, vol. 20, Academic Press, NY, 1991, p. 557.
- [8] Y.D. Sanzgiri, S.R. Knaub, C.M. Riley, in: H.G. Britain (Ed.), *Analytical Profile of Drug Substances and Exceptions*, vol. 23, Academic Press, NY, 1994, p. 321.
- [9] V. Ignat, H. Beral, *Rev. Chim. (Bucharest)* 17 (1966) 50. *Thro Chem. Abstr.* 64 (1966) 17360h.
- [10] M. Bachrata, *Pharmazie* 19 (1964) 724.
- [11] M. Bachrata, M. Blesova, Z. Bezakova, *Farm. Obz.* 52 (1983) 195. *Anal. Abstr.* 45 (1983) 5E27
- [12] H. Avsec, S. Gomiscek, *Anal. Chim. Acta* 268 (1992) 307.
- [13] E. Kilic, F. Koseoglu, M.A. Akay, *J. Pharm. Biomed. Anal.* 12 (1994) 347.
- [14] S.F. Zhang, Z.X. Sun, Z.L. Sun, *Yaowu-Fenxi Zazhi* 16 (1996) 402; *Anal. Abstr.* 59 (1997) 5653.
- [15] M. Tuncel, Z. Atkosar, *Pharmazie* 47 (1992) 642.
- [16] D.H. Li, M. Wang, V.D. Ding, *Fenxi-Huaxue* 24 (1996) 931; *Anal. Abstr.* 59 (1997) 1G 32.
- [17] L. Guo, Y.Z. Wang, J. Lin, *Fenxi-Huaxue* 24 (1996) 308; *Anal. Abstr.* 58 (1996) 8 G46.
- [18] Y.H. Tang, Z.X. Zhao, *Guangpuxue-Yu-Guangpu-Fenxi* 16 (1996) 120; *Thro. Anal. Abstr.* 59 (1997) 7 G 31.
- [19] G.K. Srinivasa, M.S. Bhatia, D.K. Jain, P. Trivedi, *Indian Drugs* 34 (1997) 190.
- [20] P.P. Dahibhate, O.D. Chandwani, S.S. Kadam, S.R. Dhaneshwar, *Indian Drugs* 34 (1997) 48.
- [21] L.T. Zhang, Z.F. Yuan, R.H. Chen, Z.X. Zhou, Y.M. Zhou, A.H. Zhang, W.N. Liu, Z.H. Zhang, *Yaowu-Fenxi Zazhi.* 17 (1997) 33; *Anal. Abstr.* 59 (1997) 8 G 62.
- [22] R.L. Liu, J.R. Xu, Y.G. Liu, Z. Yao, *Yaowu-Fenxi-Zazhi.* 14 (1994) 45; *Anal. Abstr.* 56 (1994) 7 G 47.
- [23] J. Su, Z. Yuan, Z. Zhao, X. Wang, T. Li, G. Sun, *Zhongguo-Yiyuan-Yaoxue-Zazhi.* 13 (1993) 198; *Anal. Abstr.* 56 (1994) 2 G 17.
- [24] H. Zhang, Q. Zhang, Q. Feng, *Zhongguo-Yiyuan-Yaoxue-Zazhi.* 13 (1993) 116; *Anal. Abstr.* 56 (1994) 1G 46.
- [25] C.V.S. Subrahmanyam, S.E. Reddy, M.S. Redd, *Indian Drugs* 33 (1996) 76.
- [26] F.A. El-Yazbi, *Spectrosc. Lett.* 25 (1992) 279.
- [27] H. Zhang, Y.C. Hong, C. Yu, D.K. Li, Z.F. Qui, *Yaowu-Fenxi-Zazhi.* 16 (1996) 9; *Anal. Abstr.* 58 (1996) 7 G 27.
- [28] M. Stankov, D. Stankov, Z.M. Milicevic, D. Veselinovic, P. Djurdjevic, *Spectrosc. Lett.* 26 (1993) 1709.
- [29] K.A. Al-Rashood, E.M. Abdel-Moety, O.A. Al-Deeb, A.A. Khalil, N.A. Khattab, *Sci. Pharm.* 62 (1994) 225.
- [30] M. Cordoba-Borrego, M. Cordoba-Diaz, I. Bernabe, D. Cordoba-Diaz, *J. Pharm. Biomed. Anal.* 14 (1996) 977.
- [31] G. Carlucci, P. Mazzeo, T. Fantozzi, *Anal. Lett.* 26 (1993) 2193.
- [32] E.F. Salim, I.S. Shupe, *J. Pharm. Sci.* 55 (1966) 128.
- [33] R.S. Andrews, C.G. Nicol, in: D.S. Reches, J. Phillips, J.D. Williams, R. Wise (Eds.), *Laboratory Methods in Antimicrobial Chemotherapy*, Churchill Livingstone, Edinburgh, 1978, pp. 254–264.
- [34] M.J.J.V. da Silva, M.T.C. Nagueiva, *Prev. Port. Pharm.* 15 (1966) 290.
- [35] J. Baswaraj, S. Ravisankar, B. Suresh, R. Dube, *Indian Drugs* 33 (1996) 130.
- [36] D.S. Lee, H.J. Han, K. Kim, W.B. Park, J.K. Cho, J.H. Kim, *J. Pharm. Biomed. Anal.* 12 (1994) 157.
- [37] C.Y. Chan, D.S. Isang, T.L. Chan, W.W. Yew, S.W. Cheung, A.F. Cheng, *Chemotherapy* 44 (1998) 7.

- [38] S.K. Bhowal, T.K. Das, *Anal. Lett.* 24 (1991) 25.
- [39] G. Ramana Rao, A.B. Avadhanulu, D.K. Vatsa, *Indian Drugs* 27 (1990) 532.
- [40] L. Fratini, E.E.S. Shapoval, *Int. J. Pharm.* 127 (1996) 279.
- [41] K.P.R. Chowdary, Y.V. Rama-Prasad, *Indian Drugs* 31 (1994) 277.
- [42] V. Kapetanovic, L. Milovanovic, M. Erceg, *Talanta* 43 (1996) 2123.
- [43] S.C. Mathur, Y. Kumar, N. Murugesan, Y.K.S. Rathore, P.D. Sethi, *Indian Drugs* 29 (1992) 376.
- [44] F.M. Abdel-Gawad, F.M. Abou-Attiya, *Microchem. J.* 50 (1994) 106.
- [45] P.B. Issopoulos, *Acta Pharm. Jugosl.* 39 (1989) 267.
- [46] K.P.R. Chowdary, P. Venkateshwara-Rao, *Indian Drugs* 28 (1991) 569.
- [47] N. Murgu, *Pharmazie* 19 (1964) 724.
- [48] I. Dick, N. Murgu, *Prev. Chim. (Bucharest)* 15 (1964) 757; *Thro. Chem. Abstr.* 62 (1965) 15600h.
- [49] A.F.M. El-Walily, S.F. Belal, R.S. Bakry, *J. Pharm. Biomed. Anal.* 14 (1996) 561.
- [50] K.P.R. Chowdary, G.D. Rao, *Indian Drugs* 34 (1997) 107.
- [51] A.S. Amin, G.O. El-Sayed, Y.M. Issa, *Analyst* 120 (1995) 1189.
- [52] X.G. Zhou, Y.J. Wang, Y.Q. Zhang, L. Feng, N. Zhang, *Fenxi-Huaxue* 24 (1996) 1186; *Anal. Abstr.* 59 (1997) 4 G 30.
- [53] S. Shanbag, P.P. Thampi, C.S. Thampi, *Indian Drugs* 28 (1991) 279.
- [54] H.A. Al-Khamees, *Anal. Lett.* 28 (1995) 109.
- [55] C.S. Xuan, S.C. Ren, J.L. Song, Z.Y. Wang, *Yaowu-Fenxi-Zazhi*, 16 (1996) 164; *Anal. Abstr.* 58 (1996) 10 G 43.
- [56] C.S.P. Sastry, K. Rama-Rao, D.S. Prasad, *Talanta* 42 (1995) 311.
- [57] S. Tosunoglu, N. Savci, *Acta Pharm. Turc.* 35 (1993) 1; *Anal. Abstr.* 56 (1994) 3 G 49.
- [58] Z. Bilgic, S. Tosunoglu, N. Buyuktimkin, *Acta Pharm. Turc.*, 33 (1991) 19; *Anal. Abstr.* 53 (1991) 11 G 43.
- [59] Y.M. Issa, F.M. Abdel-Gawad, M.A. Abou-Table, H.M. Hussein: *Anal. Lett.*, 30 (1997) 2071.
- [60] R.A. Sodhi, J.L. Chawla, R.T. Sane, *Indian Drugs* 34 (1997) 512.
- [61] P.V. Bharat, G. Rajani, *Indian Drugs* 34 (1997) 78.
- [62] J. Jin, *Yaowu Fenxi Zazhi*, 10 (1990) 362; *Anal. Abstr.* 53 (1991) 5 G 39.
- [63] A. Farina, *J. Pharm. Biomed. Anal.* 7 (1989) 1579.
- [64] T.B. Waggoner, M.C. Bowman, *J. Assoc. Off. Anal. Chem.* 70 (1987) 813.
- [65] N. Murugesan, S.C. Mathur, Y. Kumar, Y.K.S. Rathore, P.D. Sethi, *East Pharm.* 35 (1992) 117.
- [66] E.W. McChesney, E.J. Froelich, G.Y. Leshner, A.V.R. Croim, D. Rossi, *Toxicol. Appl. Pharmacol.* 6 (1964) 292.
- [67] R.S. Browning, E.L. Pratt, *J. Assoc. Off. Anal. Chem.* 53 (1970) 464.
- [68] I.D. Moras, A. Munoz de La Pena, M.I.R. Caceres, F.S. Lopez, *Talanta* 45 (1998) 899.
- [69] J.A.M. Pulgarin, A.A. Molina, P.F. Lopez, *Talanta* 43 (1996) 431.
- [70] M. Lizondo, M. Pons, M. Gallardo, J. Esterlich, *J. Pharm. Biomed. Anal.* 15 (1997) 1845.
- [71] A.I. Drakopoulos, P.C. Ioannou, *Anal. Chim. Acta* 354 (1997) 197.
- [72] P.T. Djurdjevic, M. Jelikic-Stankov, D. Stankov, *Anal. Chim. Acta* 300 (1995) 253.
- [73] T. Perez-Ruiz, C. Martinez-Lozano, V. Tomas, J. Carpena, *Analyst* 122 (1997) 705.
- [74] Z.Y. Huang, R.X. Cai, K. Zhang, H.P. Huang, Y.N. Zeng, *Anal. Lett.* 30 (1997) 1531.
- [75] M. Rizk, F. Belal, F.A. Aly, N.M. El-Enany, *Anal. Lett.* 30 (1997) 1897.
- [76] Y. Xu, H.X. Shen, H.G. Huang, *Fenxi Huaxue*, 25 (1997) 423; *Anal. Abstr.* 59 (1997) 11 G 48.
- [77] C.J. Veipoulou, P.C. Ioannou, E.S. Lianidou, *J. Pharm. Biomed. Anal.* 15 (1997) 1839.
- [78] Y. Xu, H.X. Shen, H.G. Huang, *Fenxi-Huaxue* 25 (1997) 419; *Anal. Abstr.* 59 (1997) 11 G 47.
- [79] I. Duran-Meras, A. Munoz-de-La-Pena, F. Salinas, I. Rodriguez-Caceres, *Analyst* 119 (1994) 1215.
- [80] I. Duran-Meras, A. Munoz-de la Pena, F. Salinas, I. Rodriguez-Caceres, *Appl. Spectrosc.* 51 (1997) 684.
- [81] L. Xu, Z.Y. Huang, Z.H. Chen, *Fenxi-Kexue-Xuebao* 11 (1995) 72; *Anal. Abstr.* 58 (1996) 3 G 28.
- [82] S.D. Ma, M.C. Li, *Yaowu Fenxi Zazhi* 17 (1997) 179; *Anal. Abstr.* 60 (1998) 4 G 48.
- [83] A.M.Y. Jaber, A. Lounici, *Anal. Chim. Acta* 291 (1994) 53.
- [84] X.L. Wang, S.M. Zhang, W.W. Zhaug, Q.H. Cai, *Anal. Lett.* 29 (1996) 131.
- [85] X.L. Wang, S.M. Zhang, W.W. Zhang, W.S. Wu, *Fenxi Huaxue* 23 (1995) 1189.
- [86] Y.H. Wang, W. Wang, Y.T. Wu, R.L. Ma, *Yaowu Fenxi Zazhi*. 17 (1997) 198; *Anal. Abstr.* 60 (1998) 4 G 50.
- [87] X.J. Liu, G.N. Chen, E.C. Xie, S.J. Wang, R.Q. Zhang, L.Z. Ding, L. Ming, *Yaowu Fenxi Zazhi*. 15 (1995) 30.
- [88] A.M.Y. Jaber, A. Lounici, *Analyst* 119 (1994) 2351.
- [89] R. Staroscik, J. Prochowska, J. Sulkowska, *Pharmazie* 29 (1974) 387.
- [90] W.J. Van Oort, R.H.A. Sorel, D. Brussee, S.G. Schulman, P. Zuman, J. Den-Hartigh, *Anal. Chim. Acta* 149 (1983) 175.
- [91] J.W. Di, M. Jin, *Fenxi-Shiyanshi*. 14 (1995) 33; *Anal. Abstr.* 57 (1995) 11 G 34.
- [92] Y. Chen, F.M. Han, Z.B. Yuan, *Fenxi Kexue Xuebao*. 11 (1995) 55; *Anal. Abstr.* 57 (1995) 11G 33.
- [93] P. O'Dea, A. Costa-Garcia, A.J. Miranda-Ordieres, P. Tunon-Blanco, M. Smyth, *Electroanalysis* 3 (1991) 337.
- [94] P. O'Dea, A. Costa-Garcia, A.J. Miranda-Ordieres, P. Tunon-Blanco, M.R. Smyth, *Electroanalysis* 2 (1990) 637.

- [95] L. Tekstor, M. Veber, M. Marlot-Gomiscek, S. Gomiscek, *Vestn-Slov-Kem. Drus.* 36 (1989) 25; *Anal. Abstr.* 52 (1990) 6 E 56.
- [96] S.M. Zhang, C.X. He, X. Yu, X.L. Wang, *Fenxi Huaxue.* 23 (1997) 1177; *Anal. Abstr.* 60 (1998) 5 G 63.
- [97] A. Tamer, *Anal. Chim. Acta* 231 (1990) 129.
- [98] G.O. Zhou, J.H. Pan, *Anal. Chim. Acta* 307 (1995) 49.
- [99] M. Rizk, F. Belal, F.A. Aly, N.M. El-Enany, *Talanta* 46 (1998) 83.
- [100] A. Tamer, *Acta Pharm. Turc.* 32 (1990) 141; *Anal. Abstr.* 53 (1991) 10 G 46.
- [101] F. Belal, M. Sharaf-El-Din, *Microchem. J.* 42 (1990) 300.
- [102] P. Gratteri, S. Furlanetto, S. Pinzuti, R. Leardi, P. Corti, *Electroanal.* 7 (1995) 1161.
- [103] K. Takatsumki, *J. Assoc. Off. Anal. Chem. Int.* 75 (1992) 982.
- [104] S.M. Wu, H.L. Wu, S.H. Chen, *J. Chin. Chem. Soc.* 34 (1987) 7.
- [105] C.R. Gutierrez, A. Garzon, *Rev. Soc. Quim-Mex.* 23 (1979) 129; *Anal. Abstr.* 40 (1981) 2E2.
- [106] K.J. Wang, S.H. Chen, S.J. Lin, H.L. Wu, *J. Chromatogr.* 360 (1986) 443.
- [107] H.L. Wu, S.J. Lin, C.Y. Hsu, *J. Chin. Chem. Soc.* 28 (1981) 59.
- [108] H. Salomies, S. Koski, *J. Planar. Chromatogr-Mod-TLC.* 9 (1996) 103.
- [109] H.K.L. Hundt, E.C. Barlow, *J. Chromatogr. Biomed. Appl.* 12 (1981) 165.
- [110] A.P. Argekar, S.V. Raj, S.U. Kapadia, *Indian Drugs* 33 (1996) 167.
- [111] M. Vega, G. Rios, R. Saelzer, E. Herlitz, *J. Planar-Chromatogr-Mod-TLC.* 8 (1995) 378.
- [112] P.L. Wang, Y.L. Feng, L.A. Chen, *Microchem. J.* 56 (1997) 229.
- [113] A.P. Argekar, S.U. Kapadia, S.V. Raj, *J. Planar-Chromatogr-Mod-TLC.* 9 (1996) 208.
- [114] S. Tammilehto, H. Salomies, K. Torniainen, *J. Planar. Chromatogr-Mod-TLC.* 7 (1994) 368.
- [115] M. Juhel-Gaugain, J.P. Abjean, *Chromatographia* 47 (1998) 101.
- [116] J.F. Bauer, S. Howard, A. Schmidt, *J. Chromatogr.* 514 (1990) 348.
- [117] R. Charriere, W. Leiser, R. Dousse, *Mitt. Geb. Lebensmittellunters. Hyg.* 87 (1996) 223.
- [118] M. Horie, K. Saito, N. Nose, H. Nakazawa, *Shokuhin-Eiseigaku-Zasshi.* 36 (1995) 62; *Anal. Abstr.* 57 (1995) 10 G 316.
- [119] J. Barbosa, R. Berges, V. Sanz-Nebot, *J. Chromatogr.* 719 (1996) 27.
- [120] Y.P. Chen, C.Y. Shaw, B.L. Chang, *Yaowu-Shipin-Fenxi.* 4 (1996) 155; *Anal. Abstr.* 59 (1997) 1 G 39.
- [121] A. Nangia, F. Lam, C.T. Hung, *J. Pharm. Sci.* 79 (1990) 998.
- [122] C.Y. Chan, A.W. Lam, G.L. French, *J. Antimicrob. Chemother.* 23 (1989) 597.
- [123] J.D. Davis, L. Aarou, J.B. Houston, *J. Chromatogr. B* 132 (1993) 105.
- [124] I. Duran Meras, T. Galeano Diaz, M.I.R. Caceres, F.S. Lopez, *J. Chromatogr.* 787 (1997) 119.
- [125] J. Barbosa, R. Berges, V. Sanz-Benot, *J. Liquid Chromatogr.* 18 (1995) 3445.
- [126] R. Jain, C.L. Jain, *LC. GC.* 10 (1992) 707.
- [127] A.P. Argekar, S.U. Kapadia, S.V. Raj, S.S. Kunjir, *Indian Drugs* 33 (1996) 261.
- [128] Z. Budvari-Barany, G. Szasz, K. Takacs-Novak, I. Hermez, A. Lore, *J. Liquid Chromatogr.* 14 (1991) 3411.
- [129] K.L. Tyczkowska, R.D. Voyksner, K.L. Anderson, M.G. Papich, *J. Chromatogr. B* 658 (1994) 341.
- [130] M. Horie, K. Saito, N. Nose, H. Nakazawa, *J. Chromatogr. B* 653 (1994) 69.
- [131] N. Abanmi, I. Zaghoul, N. El-Sayed, K.I. Al-Khamis, *Ther. Drug Monit.* 18 (1996) 158.
- [132] J. Parasrampur, V. Das-Gupta, *Drug Dev. Indian Pharm.* 16 (1990) 1597.
- [133] J.F. Bauer, L. Elrod, J.R. Fornnarino, D.E. Heathcote, S.K. Krogh, C.L. Linton, B.J. Norris, J.E. Quick, *Pharm. Res.* 7 (1990) 1177.
- [134] A. Mizuno, T. Uematsu, M. Nakashima, *J. Chromatogr. B* 653 (1994) 187.
- [135] A.J.N. Groeneveld, J.R.B.J. Brouwers, *Pharm. Weekbl. Sci. Ed.* 8 (1986) 79.
- [136] J.E. Roybal, A.P. Pfenning, S.B. Turnipaseed, C.C. Walker, J.A. Hurlbut, *J. Assoc. Off. Anal. Chem. Int.* 80 (1997) 982.
- [137] P.M. Lacroix, N.M. Curran, R.W. Sears, *J. Pharm. Biomed. Anal.* 14 (1996) 641.
- [138] N.E. Basci, A. Bozkurt, D. Kalayci, S.O. Kayaalp, *J. Pharm. Biomed. Anal.* 14 (1996) 353.
- [139] G.J. Krol, G.W. Beck, T. Benham, *J. Pharm. Biomed. Anal.* 14 (1995) 181.
- [140] S. Husain, S. Khalid, V. Nagaraju, R. Nageswara-Rao, *J. Chromatogr. A* 705 (1995) 380.
- [141] A. Rieutord, L. Vazquez, M. Soursac, P. Prognon, J. Blais, P. Bourget, *Anal. Chim. Acta* 290 (1994) 215.
- [142] Z.W. Li, P. Guo, Q. Guo, *Yaowu-Fenxi-Zazhi.* 14 (1994) 16; *Anal. Abstr.* 56 (1994) 10 G 63.
- [143] M. Lovdhal, J. Steury, H. Russlie, D.M. Canafax, *J. Chromatogr. B* 128 (1993) 329.
- [144] H. Sun, L. Zhang, S. Xie, Z. Sun, *Zhongguo-Yaoxue Zazhi* 28 (1993) 285; *Anal. Abstr.* 55 (1993) 12 G55.
- [145] G. Mack, *J. Chromatogr. B* 120 (1992) 263.
- [146] B. Yao, H. Yu, *Yaowu-Fenxi-Zazhi* 12 (1992) 270; *Anal. Abstr.* 55 (1993) 8G 116.
- [147] L. Pou-Clave, F. Campos-Barreda, C. Pascual-Mostaza, *J. Chromatogr. B* 101 (1991) 211.
- [148] Y. Katagiri, K. Naora, N. Ichikawa, M. Hayashibara, I. Iwamoto, *Chem. Pharm. Bull.* 38 (1990) 2884.
- [149] A. El-Yazigi, S. Al-Rawithy, *Ther. Drug Monit.* 12 (1990) 378.
- [150] N.E. Basci, S. Hanioglu-Kargi, H. Soysal, A. Bozkurt, S.O. Kayaalp, *J. Pharm. Biomed. Anal.* 15 (1997) 663.



- [151] T. Ohkubo, M. Suno, M. Kudo, T. Uno, K. Sugawara, *Ther. Drug Monit.* 18 (1996) 598.
- [152] J. Macek, P. Ptacek, *J. Chromatogr. B* 673 (1995) 316.
- [153] T. Uematsu, K. Kosuge, S.I. Araki, M. Ishiye, Y. Asai, M. Nakashima, *Ther. Drug Monit.* 17 (1995) 101.
- [154] D. Fabre, F. Bressolle, J.M. Kinowski, O. Bouvet, F. Paganin, M. Galtier, *J. Pharm. Biomed. Anal.* 12 (1994) 1463.
- [155] N. Miyazawa, T. Uematsu, A. Mizuno, S. Nagashima, M. Nakashima, *Forensic Sci. Int.* 51 (1991) 65.
- [156] T. Ohkubo, M. Kudo, K. Sugawara, *J. Chromatogr. B* 111 (1992) 289.
- [157] T. Ohkubo, M. Kudo, K. Sugawara, *Anal. Sci.* 7 (1991) 741.
- [158] K. Borner, H. Hartwig, H. Lode, G. Hoeffken, *Fresenius Z. Anal. Chem.* 324 (1986) 355.
- [159] E. Kraas, A. Hirle, *Fresenius Z. Anal. Chem.* 324 (1986) 354.
- [160] J.W. Holladay, M.J. Dewey, S.D. Yoo, *J. Chromatogr. B* 704 (1997) 259.
- [161] S.K. Ghosh, M. Banerjee, *Indian Drugs* 33 (1996) 127.
- [162] S.G. Wallis, B.G. Charles, L.R. Gahan, *J. Chromatogr. B* 674 (1995) 306.
- [163] M.S. Hussain, V. Chukwumaeze-Obiajunwa, R.G. Micetich, *J. Chromatogr. B* 663 (1995) 379.
- [164] M. Horie, K. Saito, Y. Hoshino, N. Nose, E. Mochizuki, H. Nakazawa, *J. Chromatogr.* 402 (1987) 301.
- [165] A.P. Argekar, S.J. Shah, *Indian Drugs* 34 (1997) 520.
- [166] T.J. Wenzel, K. Zomlefer, S.B. Rapkin, R.H. Keith, *J. Liquid Chromatogr.* 18 (1995) 1473.
- [167] N. Ichikawa, K. Naora, M. Hayashibara, K. Iwamoto, *J. Pharm. Biomed. Anal.* 11 (1993) 993.
- [168] M. Horie, K. Saito, N. Nose, M. Tera, H. Nakazawa, *J. Liquid Chromatogr.* 16 (1993) 1463.
- [169] U.P. Halkar, S.H. Rane, N.P. Bhandari, *Indian Drugs* 34 (1997) 302.
- [170] N. Nose, Y. Hoshino, Y. Kikuchi, M. Horie, K. Saitoh, T. Kawachi, H. Nakazawa, *J. Assoc. Off. Anal. Chem.* 70 (1987) 714.
- [171] S. Horii, C. Yasuoka, M. Matsumoto, *J. Chromatogr.* 388 (1987) 459.
- [172] Y. Ikai, H. Oka, N. Kawamura, M. Yamada, K.I. Harada, M. Suzuki, H. Nakazawa, *J. Chromatogr.* 477 (1989) 397.
- [173] M. Horie, K. Saito, N. Nose, H. Nakazawa, *Shokuhin-Eiseigaku-Zasshi* 33 (1992) 442; *Anal. Abstr.* 55 (1993) 8H 347.
- [174] E.M. Abdel-Moety, O.A. Al-Deeb, M.A. Abounassif, S.R. Al-Zaben, *Boll. Chim. Farmaceutico* 134 (1995) 497.
- [175] S.B. Turnipseed, C.C. Walker, J.E. Roybal, A.P. Pfenning, J.A. Hurlbut, *J. Assoc. Off. Anal. Chem. Int.* 81 (1998) 554.
- [176] A.P. Pfenning, R.K. Munns, S.B. Turnipseed, J.E. Roybal, D.C. Holland, A.R. Long, S.M. Plakas, *J. Assoc. Off. Anal. Chem. Int.* 79 (1996) 1227.
- [177] R.K. Munns, S.B. Turnipseed, A.P. Pfenning, J.E. Roybal, D.C. Holland, A.R. Long, S.M. Plakas, *J. Assoc. Off. Anal. Chem. Int.* 78 (1995) 343.
- [178] V. Hormazabal, M. Yndestad, *J. Liquid Chromatogr.* 17 (1994) 2911.
- [179] V. Hormazabal, M. Yndestad, *J. Liquid Chromatogr.* 17 (1994) 2901.
- [180] J.M. Degroodt, B. Wyhowski-de-Bukanski, S. Srebrnik, *J. Liquid Chromatogr.* 17 (1994) 1785.
- [181] A. Rogstad, B. Weng, *J. Pharm. Sci.* 82 (1993) 518.
- [182] T.B. Vree, E.W.J. Van-Ewijk-Beneken-Kolmer, J.F.M. Nouws, *J. Chromatogr. B* 117 (1992) 131.
- [183] I. Steffenak, V. Hormazabal, M. Yndestad, *J. Liquid Chromatogr.* 14 (1991) 61.
- [184] A.T. Andresen, K.E. Rasmussen, *J. Liquid Chromatogr.* 13 (1990) 4051.
- [185] H.H. Thanh, A.T. Andresen, T. Agasoster, K.E. Rasmussen, *J. Chromatogr. B* 97 (1990) 363.
- [186] K.E. Rasmussen, F. Toennesen, Hoang-Huu-Thanh, A. Rogstad, A. Aanesrud, *J. Chromatogr. B* 88 (1989) 355.
- [187] A. Rogstad, V. Hormazabal, M. Yndestad, *J. Liquid Chromatogr.* 12 (1989) 3073.
- [188] O.B. Samuelsen, *J. Chromatogr. B* 89 (1989) 355.
- [189] L. Ellerbroek, M. Bruhn, *J. Chromatogr. B* 87 (1989) 314.
- [190] W. Backe, *Arch. Pharm.* 320 (1987) 1093.
- [191] D. Decolin, A. Nicolas, G. Siest, *J. Chromatogr. B* 58 (1987) 499.
- [192] J.M. Delmas, A.M. Chapel, P. Sanders, *J. Assoc. Off. Anal. Chem. Int.* 81 (1998) 519.
- [193] Y.M. El-Sayed, *Anal. Lett.* 28 (1995) 279.
- [194] K. Borner, E. Borner, H. Lode, *J. Chromatogr. B* 117 (1992) 285.
- [195] R. Teng, T.G. Tensfeldt, T.E. Liston, G. Foulds, *J. Chromatogr. B* 675 (1996) 53.
- [196] V.M. Shinde, P.B. Shetkar, *Indian Drugs* 33 (1996) 230.
- [197] V. Hormazabal, Y. Yndestad, *J. Liquid Chromatogr.* 17 (1994) 3775.
- [198] M. Horie, K. Saito, N. Nose, H. Nakazawa, *Shokuhin-Eiseigaku-Zasshi.* 34 (1993) 289; *Anal. Abstr.* 56 (1994) 8H 194.
- [199] A. Rogstad, V. Hormazabal, M. Yndestad, *J. Liquid Chromatogr.* 14 (1991) 521.
- [200] V. Hormazabal, A. Rogstad, I. Steffenak, M. Yndestad, *J. Liquid Chromatogr.* 14 (1991) 1605.
- [201] T.J. Strelevitz, M.C. Linhares, *J. Chromatogr. B* 675 (1996) 243.
- [202] R.P. Schneider, J.F. Ericson, M.J. Lynch, G. Fouda, *Biol. Mass. Spectrom.* 22 (1993) 595.
- [203] P. Guo, Z. Li, T. Wu, Yaowu-Fenxi-Zazhi. 12 (1992) 1; *Anal. Abstr.* 55 (1993) 5G 200.
- [204] G.R. Granneman, L.T. Sennello, *J. Chromatogr. B* 57 (1987) 199.
- [205] I. Steffenak, V. Hormazabal, M. Yndestad, *J. Liquid Chromatogr.* 14 (1991) 1983.
- [206] J.B. Schilling, S.P. Cepa, S.D. Menacherry, L.T. Bavda, B.M. Heard, *Anal. Chem.* 68 (1996) 1905.

- [207] J.R. Meinertz, V.K. Dawson, W.H. Gingerich, B. Cheng, M.M. Tubergen, *J. Assoc. Off. Anal. Chem. Int.* 77 (1994) 871.
- [208] J.C. Lei, R.H. Zhang, S.D. Luo, H.S. Cai, Y. Xiang, *Yaowu Fenxi Zazhi* 17 (1997) 295; *Anal. Abstr.* 60 (1998) 5G 80.
- [209] F.A. Wong, S.J. Juzwin, S.C. Flor, *J. Pharm. Biomed. Anal.* 15 (1997) 765.
- [210] H. Pouliquen, D. Gouelo, M. Larhantec, N. Pilet, L. Pinault, *J. Chromatogr. B* 702 (1997) 157.
- [211] H. Pouliquen, F. Armand, F. Loussouarn, *J. Liquid Chromatogr. Relat. Technol.* 21 (1998) 591.
- [212] H.V. Bjorklund, *J. Chromatogr. B* 95 (1990) 75.
- [213] O.B. Samuelsen, *J. Chromatogr. B* 655 (1994) 311.
- [214] S. Loussouarn, H. Pouliquen, F. Armand, *J. Chromatogr. B* 698 (1997) 251.
- [215] K. Hamamoto, *J. Chromatogr. B* 54 (1986) 453.
- [216] S.O. Hustvedt, R. Salte, T. Benjaminsen, *J. Chromatogr. B* 86 (1989) 335.
- [217] K. Yoshihiro, N. Kohji, I. Nobuhiro, H. Masakazu, I. Kikuo, *Byoin-Yakugaku* 15 (1989) 292; *Anal. Abstr.* 52 (1990) 12D 106.
- [218] T. Uematsu, K. Kondo, S. Yano, T. Yamaguchi, K. Umemura, M. Nakashima, *J. Pharm. Sci.* 83 (1994) 42.
- [219] L. Elrod, C.L. Linton, B.P. Shelat, C.F. Wong, *J. Chromatogr.* 519 (1990) 125.
- [220] M. Matsuoka, K. Banno, T. Sato, *J. Chromatogr. B* 766 (1996) 117.
- [221] B.P. Cawner, J.A. Cook, R.R. Brown, *J. Chromatogr. B* 95 (1990) 407.
- [222] D. Dell, C. Partos, R. Portmann, *J. Liquid Chromatogr.* 11 (1988) 1299.
- [223] N. Hobarra, H. Kameya, N. Hokama, S. Ohshiro, M. Sakanashi, *J. Chromatogr. B* 703 (1997) 279.
- [224] A.J. Szuna, R.W. Blain, *J. Chromatogr. B* 131 (1993) 211.
- [225] E. Brunt, J. Limberg, H. Derendorf, *J. Pharm. Biomed. Anal.* 8 (1990) 67.
- [226] P. Heizmann, D. Dell, H. Eggers, R. Gora, *J. Chromatogr. B* 92 (1990) 91.
- [227] W.M. Awni, J.A. Maloney, K.L. Heim-Duthoy, *Clin. Chem.* 34 (1988) 2330.
- [228] A.M. Shibl, A.K. Tawfik, S. El-Houfy, F.J. El-Shammary, *J. Clin. Pharm. Ther.* 16 (1991) 353.
- [229] Y. Guo, H.M. An, *Yaowu-Fenxi Zazhi* 18 (1998) 25; *Anal. Abstr.* 60 (1998) 6G 79.
- [230] M. Peng, *Yaowu-Fenxi-Zazhi* 15 (1995) 39; *Anal. Abstr.* 58 (1996) 2G 66.
- [231] R.T. Foster, R.A. Carr, F.M. Pasutto, J.A. Longstreth, *J. Pharm. Biomed. Anal.* 13 (1995) 1243.
- [232] G. Carlucci, A. Cilli, M. Liberato, P. Mazzeo, *J. Pharm. Biomed. Anal.* 11 (1993) 1105.
- [233] L. Tan, D. Xu, Y. Diao, Y. Yuan, *Yaowu-Xuebao* 28 (1993) 286; *Anal. Abstr.* 56 (1994) 1G 49.
- [234] P. Diez, J.A. Berenguer, V. Calderon, J. Gonzalez, P. Gordo, *Alimentaria (Madrid)* 240 (1993) 45; *Thro. Anal. Abstr.* 55 (1993) 11 H 229.
- [235] L. Ellerbroek, *Fleischwirtschaft* 71 (1991) 187; *Thro. Anal. Abstr.* 54 (1992) 5H 292.
- [236] W. Unglaub, *Fleischwirtschaft* 75 (1995) 1441.
- [237] J.F. Nash, M.K. Brunson, J.W. Lamb, J.S. Welles, *Can. J. Pharm. Sci.* 14 (1979) 84.
- [238] C.E. Cherubin, C.W. Stratton, *Diagn-Microbiol. Infect. Dis.* 20 (1994) 21.
- [239] G. Klopman, D. Fercu, T.E. Renau, M.R. Jacobs, *Antimicrob. Agents Chemotherap.* 40 (1996) 2637.
- [240] G.O. Korsrud, J.O. Boison, J.F.M. Nouws, J.D. McNeil, *J. Assoc. Off. Anal. Chem. Int.* 81 (1998) 21.
- [241] D. Monciu, et al., *Farmacia (Bucharest)* 20 (1972) 459.
- [242] W. Goss, W. Deitz, *Bacteriol. Proc.* (1963) 93.
- [243] Y. Oomori, et al., *Chemotherapy* 29 (1981) 91.
- [244] J. Bland, et al., *Eur. J. Clin. Microbiol.* 2 (1983) 249.
- [245] D.A. Leigh, C.A. Harris, S. Tait, B. Walsh, P. Hancock, *J. Antimicrob. Chemother.* 27 (1991) 655.
- [246] L. Okerman, J. Van Hoof, W. Debeuckelaere, *J. Assoc. Off. Anal. Chem. Int.* 81 (1998) 51.
- [247] M. Fukuyama, K. Kawakami, O. Suda, Y. Imagawa, *Kansenshogaku-Zasshi* 69 (1995) 987.
- [248] C.L. Flurer, *Electrophoresis* 18 (1997) 2427.
- [249] S.M. Sultan, F.E.O. Suliman, *Analyst* 117 (1992) 1523.
- [250] S.R. Knaub, M.J. Priston, M.D. Morton, J.D. Slechta, D.G. Vander-Velde, C.M. Riley, *J. Pharm. Biomed. Anal.* 13 (1995) 1225.
- [251] S.W. Sun, L.Y. Chen, *J. Chromatogr. A* 766 (1997) 215.
- [252] G. Fardella, P. Barbetti, I. Chiappini, G. Grandolini, *Int. J. Pharm.* 121 (1995) 123.
- [253] S. Panadero, A. Gomez-Hens, D. Perez-Bendito, *Anal. Chim. Acta* 303 (1995) 39.
- [254] H.Y. Aboul-Enein, K.A. Al-Rashood, H.M. El-Fataty, *Chem. Biomed. Environm. Instrum.* 10 (1980) 237.
- [255] C. Masselon, G. Krier, J.F. Muller, S. Nelieu, J. Einhorn, *Analyst* 121 (1996) 1429.
- [256] F. Belal, M. Rizk, F. Aly, N. El-Enany, *Chem. Anal.* (in press).
- [257] C.S. Xuan, Z.Y. Wang, J.L. Song, *Anal. Lett.* 31 (1998) 1185.
- [258] C. Mellgren, A. Sternesjo, *J. Assoc. Off. Anal. Chem. Int.* 81 (1998) 394.
- [259] L.O. White, C.M. Tobin, A.M. Lovering, J.M. Andrews, in: D.S. Reeves, R. Wise, J.M. Andrews, L.O. White (Eds.), *Clinical Antimicrobial Assays*, Oxford University Press, Oxford, UK, 1999, pp. 149–175.
- [260] H. Oka, H. Nakazawa, K.I. Harada, J.D. MacNeil (Eds.), *Chemical Analysis of Antibiotics Used in Agriculture*, AOAC International, Arlington, VA, 1995.
- [261] R.J. Heitzman (Ed.), *Veterinary Drug Residues: Residues in Food-Producing Animals and Their Products—Preference Materials and Methods*, Blackwell Scientific Publications, Oxford, UK, 1994.
- [262] C. Mellgers, A. Sternesjo, *J. AOAC Int.* 81 (1998) 394.
- [263] *Food Chemicals News*, August, 12 (1996) 36.
- [264] *Fed. Regist. May* 22, 1997.
- [265] Year-in review, in: *Food Chemicals News*, 1995, pp. 55–57.

- [266] P. Haumer, W. Heeschen, *Milchwissenschaft* 50 (1995) 513.
- [267] K. Munns, S.B. Turnipseed, A.P. Pfenning, J.E. Roybal, D.C. Holland, A.R. Long, *J. Assoc. Off. Anal. Chem. Int.* 81 (1998) 825.
- [268] M.E. Brown, D.S. Reeves, A monograph on Quinolones, in: F. O'Gredy, H.P. Lambert, R.G. Fince, O. Greenwood (Eds.), *Antibiotics and Chemotherapy* 7th ed., Churchill Livingstone, Edinburg, 1997, pp. 419–452.
- [269] Y.N. He, H.Y. Chen, *Electroanalysis* 9 (1997) 1426.
- [270] L.D. Marzo, *Bo. J. Chromatogr.* 812 (1998) 17.

# Coulometric determination of $\text{NAD}^+$ and $\text{NADH}$ in normal and cancer cells using LDH, RVC and a polymer mediator

F. Torabi <sup>a</sup>, K. Ramanathan <sup>b</sup>, P.-O. Larsson <sup>b</sup>, L. Gorton <sup>c</sup>, K. Svanberg <sup>d</sup>,  
Y. Okamoto <sup>e</sup>, B. Danielsson <sup>b</sup>, M. Khayyami <sup>a,\*</sup>

<sup>a</sup> TMS CHEM AB, Ideon, S-223 70, Lund, Sweden

<sup>b</sup> Department of Pure and Applied Biochemistry, Center for Chemistry and Chemical Engineering, Lund University, S-221 00 Lund, Sweden

<sup>c</sup> Department of Analytical Chemistry, Center for Chemistry and Chemical Engineering, Lund University, S-221 00 Lund, Sweden

<sup>d</sup> Department of Oncology, Lund University Hospital, S-221 00 Lund, Sweden

<sup>e</sup> Department of Chemistry, Polytechnic University, Brooklyn, NY 11201, USA

Received 10 September 1998; received in revised form 22 January 1999; accepted 11 February 1999

## Abstract

An electrochemical method for the measurement of  $\text{NAD}^+$  and  $\text{NADH}$  in normal and cancer tissues using flow injection analysis (FIA) is reported. Reticulated vitreous carbon (RVC) electrodes with entrapped L-lactate dehydrogenase (LDH) and a new redox polymer containing covalently bound toluidine blue O (TBO) were employed for this purpose. Both  $\text{NAD}^+$  and  $\text{NADH}$  were estimated coulometrically based on their reaction with LDH. The latter was immobilized on controlled pore glass (CPG) by cross-linking with glutaraldehyde and packed within the RVC. The concentrations of  $\text{NAD}^+$  and  $\text{NADH}$  in the tissues, estimated using different electron mediators such as ferricyanide (FCN), meldola blue (MB) and TBO have also been compared. The effects of flow rate, pH, applied potential (versus  $\text{Ag}/\text{AgCl}$  reference) and adsorption of the mediators have also been investigated. Based on the measurements of  $\text{NAD}^+$  and  $\text{NADH}$  in normal and cancer tissues it has been concluded that the  $\text{NADH}$  concentration is lower, while the  $\text{NAD}^+$  concentration is higher in cancer tissues. Amongst the electron mediators TBO was found to be a more stable mediator for such measurements. © 1999 Elsevier Science B.V. All rights reserved.

**Keywords:**  $\text{NAD}^+$  and  $\text{NADH}$ ; Normal and cancer tissues; Flow injection analysis (FIA)

## 1. Introduction

Sensing of  $\text{NADH}$  has formed the basis of several reports in electrochemical biosensing [1]. A recent review on amperometric biosensors exhaus-

\* Corresponding author. Tel.: +46-46-2862190; fax: +46-46-2862191.

E-mail address: masoud.khayyami@tms.ideon.se (M. Khayyami)

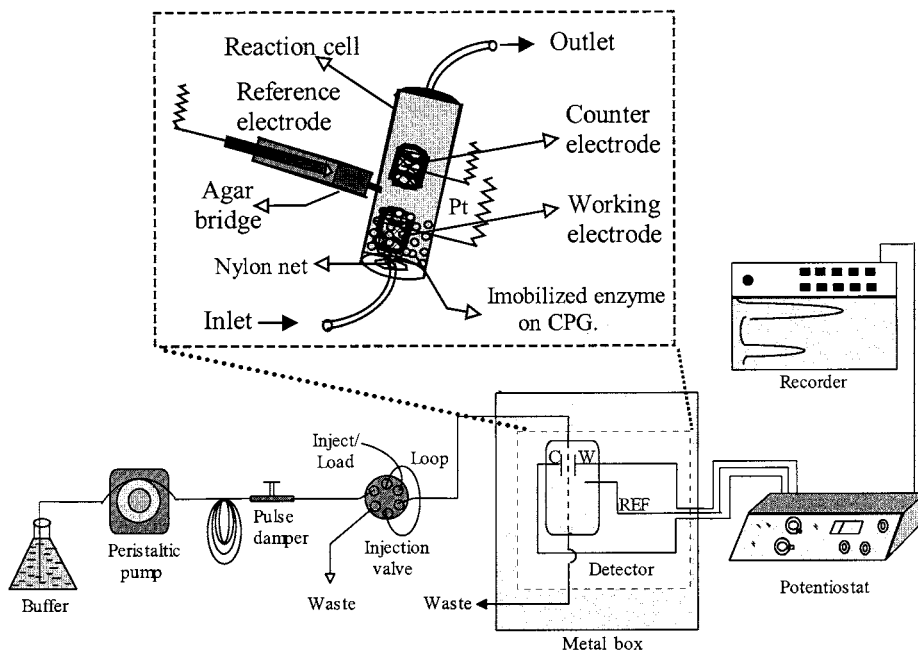


Fig. 1. Schematic of the flow injection set-up with the various components appropriately labelled. The flow injection cell is enlarged and indicates the placement of the RVC cylinder and the platinum contact made through the polyacrylate block.

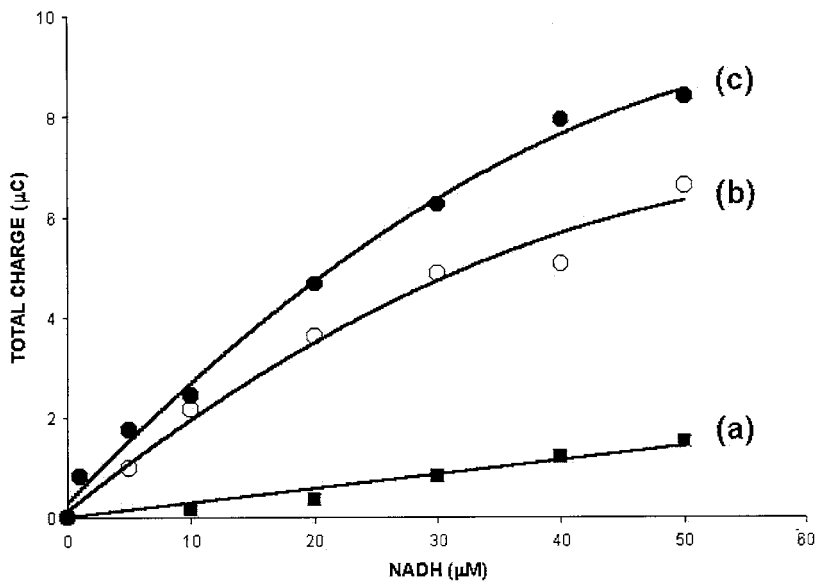


Fig. 2. The coulometric response of (a) MB; (b) TBO; and (c) FCN to varying NADH concentrations between 1 and 50  $\mu\text{M}$  in buffer. Mediator concentration is  $2.8 \text{ mg l}^{-1}$ . Flow rate  $0.5 \text{ ml min}^{-1}$ .

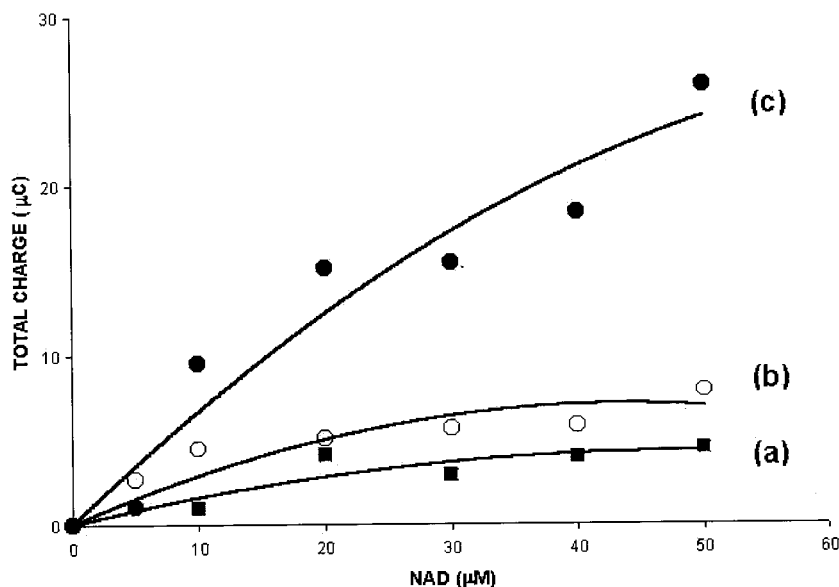


Fig. 3. The coulometric response of (a) MB; (b) TBO; and (c) FCN to varying  $\text{NAD}^+$  concentrations between 1 and 50  $\mu\text{M}$  (co-injected with 50 mM lactate) in the presence of LDH ( $7.5 \text{ U mg}^{-1}$ ) immobilised CPG packed within the RVC. Flow rate  $0.5 \text{ ml min}^{-1}$ .

tively covers several classes of  $\text{NAD}^+/\text{NADH}$  based dehydrogenases and their application in biosensors [2,3]. Both amperometric and coulometric approaches have been employed for the sensing process. Either, the direct oxidation of  $\text{NADH}$  to  $\text{NAD}^+$  at a suitable potential [4] or, coupling of  $\text{NADH}/\text{NAD}^+$  with suitable mediators were investigated [5]. Amongst the dehydrogenases, LDH has been extensively used with  $\text{NADH}/\text{NAD}^+$  as its natural cofactor for sensing of pyruvate/lactate.

Lactate monitoring is useful in intensive care units, during cardiac surgery, foetal distress, lactic acidosis, diabetes mellitus, leukemia, glycogen storage disease and ethanol ingestion [6–9]. In this context, the coupling of LDH reaction with fast electron transfer mediators [10] enabled more specific and sensitive assays [11]. Although initially the  $\text{Fe}^{+3}/\text{Fe}^{+2}$  couple was employed, later, other mediators with well characterised reaction mechanisms, e.g. ferrocene and its derivatives, were applied. Other phenoxazinium ring compounds [12], fulvalene and its derivatives [13] have also been tested. Implementing novel mediators has also enabled lowering of the redox potential

from 350 mV (for  $\text{Fe}^{+3}/\text{Fe}^{+2}$  couple) to much below 0.0 mV, leading to more selective measurements of analytes in physiological fluids. Especially, the interference by ascorbic acid, acetaminophen, uric acid, urea and salicylic acid [14] were overcome by this approach.

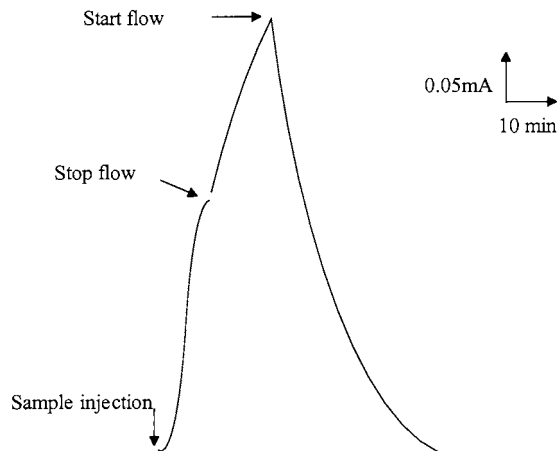
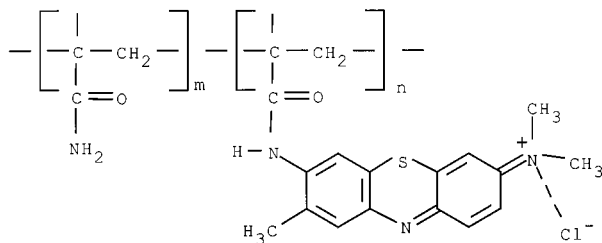
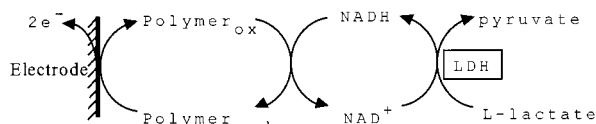


Fig. 4. The trace depicts a stop flow assay. The buffer was stopped after 14 min for 11 min and restarted. Circulation medium: buffer containing  $2.8 \text{ mg ml}^{-1}$  TBO. Injection solution: 50 mM lactate and  $30 \mu\text{M}$   $\text{NAD}^+$ .



Scheme 1. Structure of the TBO mediator.

The synergy of coulometry/amperometry with FIA has been demonstrated earlier for ethanol measurements [15]. The theory elucidating the mechanism of electrolysis in flowing solutions on a porous electrode has also been discussed in an earlier report [16]. RVC has also been employed for analysis of ascorbic acid, epinephrine and L-dopa, both in coulometric and amperometric modes [17]. These studies pointed out that RVC was a suitable material [18] for electrode construction and applications to sensing of biomolecules. The principle

Scheme 2. The reaction scheme for conversion of L-lactate to pyruvate in the presence of LDH,  $\text{NAD}^+$  and TBO on the RVC surface.

advantage of RVC is its excellent electrical conductivity ( $10^{-4} \Omega \text{ cm}^{-1}$ ) with minimum flow resistance in the FIA mode. However, the application of such porous materials [19] to detection of analytes in cancer tissues is as yet less exploited.

The motivation for the present investigations was derived from the hypothesis (based on fluorimetric studies on cancer cells) that there was a difference in the NADH content in normal and cancerous tissues [20,21]. Other investigations [22,23] have indicated the presence of NADH oxidase specifically in the serum of cancer patients. These and other studies suggested that there is a need for

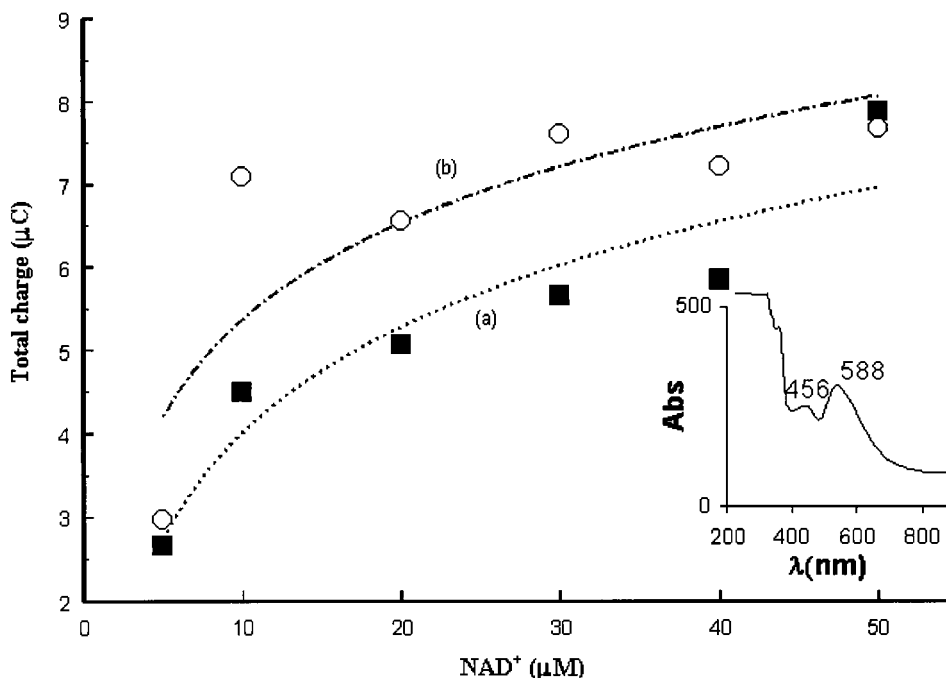


Fig. 5. The coulometric response of adsorbed (□) and circulating (○) TBO.  $2.8 \text{ mg l}^{-1}$  of TBO in buffer was circulated. Injection solution:  $5\text{--}50 \mu\text{M NAD}^+$  co-injected with  $50 \text{ mM lactate}$ . Inset: the spectrum of  $2.8 \text{ mg l}^{-1}$  solution of TBO between 200 and 900 nm, recorded at  $120 \text{ nm min}^{-1}$  scan speed.

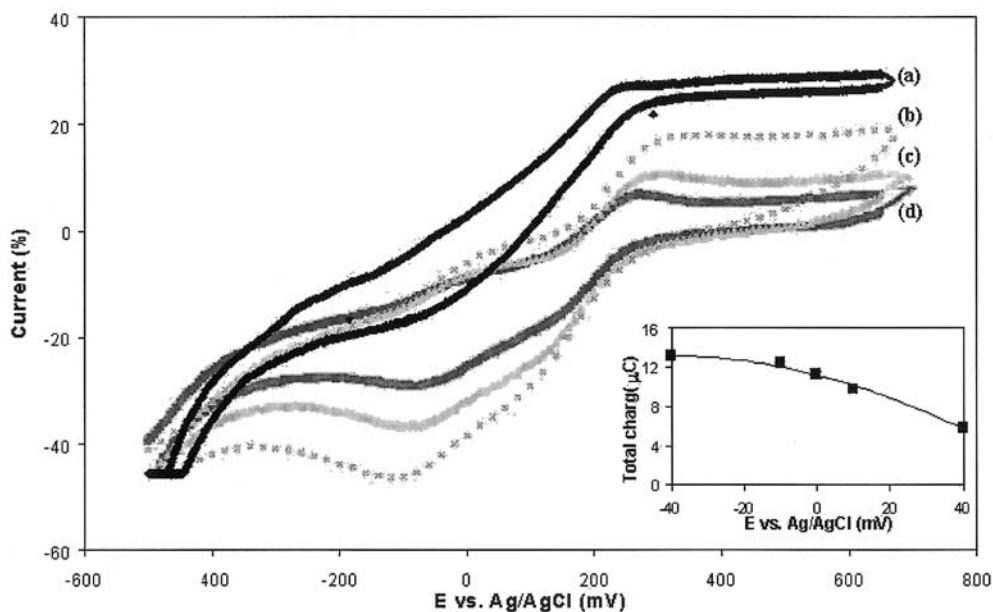


Fig. 6. CV of TBO (in buffer) adsorbed on RVC surface ( $2.54 \times 10^{-7}$  mol  $\text{cm}^{-2}$ ) at varying scan speeds, ( $\bullet$ ) 10; ( $\square$ ) 20; ( $\triangle$ ) 40; and ( $\times$ ) 50  $\text{mV s}^{-1}$ . Inset: the response of adsorbed TBO to  $\text{NAD}^+$  between 1 and 50  $\mu\text{M}$  co-injected with 50 mM lactate.

alternative detection techniques for  $\text{NADH}/\text{NAD}^+$  in normal and cancer tissues.

In the present studies a coulometric measurement technique for  $\text{NAD}^+/\text{NADH}$  using RVC, in the presence of FCN/MB/TBO-derivative is reported (Scheme 2). Structurally the TBO has a polymeric backbone with an amino functionality [24–26]. Earlier reports demonstrated the successful application of TBO as a mediator with a glassy carbon electrode [24,27] or carbon wax electrode [28] and horse-radish peroxidase, for the detection of hydrogen peroxide. Although, in principle, an amperometric analysis would provide a faster detection; a coulometric approach was used to provide a better estimate of the  $\text{NAD}^+$  and  $\text{NADH}$  concentrations in the normal and cancer tissues. During the investigations the mediators were either adsorbed on RVC and/or circulated in the flow buffer. The reaction of  $\text{NAD}^+$  with L-lactate in the presence of LDH was used for quantifying  $\text{NAD}^+$  while  $\text{NADH}$  was directly estimated. The application of a flow through cell using TBO modified RVC for the estimation of  $\text{NAD}^+$  and  $\text{NADH}$  in normal and cancer lung tissues is reported.

## 2. Experimental details

### 2.1. Chemicals

$\text{Na}_2\text{HPO}_4$ ,  $\text{NaH}_2\text{PO}_4$ , KCl and Glutaraldehyde (25% solution) were from Merck, Germany.  $\text{K}_4\text{Fe}(\text{CN})_6$ ,  $\text{K}_3\text{Fe}(\text{CN})_6$  and MB (dye content 90%) were obtained from Aldrich chemicals. The TBO was a generous gift from Okamoto's laboratory. L-lactate,  $\text{NADH}$  and  $\text{NAD}^+$  (98% purity) were from Sigma. Ultrapure water 18.2  $\text{M}\Omega$  resistance was from Elgastat maxima, Sweden. L-lactate dehydrogenase (EC 1.1.1.27) from bovine heart was from Boehringer Mannheim, Germany.

Table 1

Comparison between cyclic voltammetric investigations of TBO adsorbed on carbon paste and RUC electrode (see also Fig. 6)

	TBO — Polymer adsorbed on the electrode surface			
	A1	A2	C1	C2
Carbon paste	-100	+125	-60	+190
RVC	0	300	-100	+85



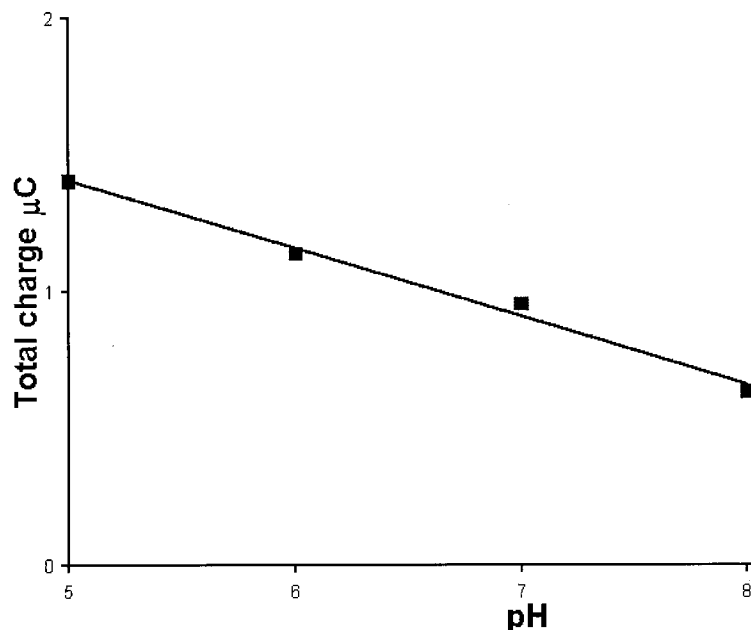


Fig. 7. Effect of buffer pH on response of adsorbed TBO to 30  $\mu\text{M}$   $\text{NAD}^+$  coinjecting with 50 mM lactate.

Table 2

A comparison of the coulometric response obtained for NADH and  $\text{NAD}^+$  concentration in normal and cancer cells, using potassium ferricyanide, meldola blue and TBO-polymer as mediators

Mediators	Normal cell			Cancer cell		
	NADH ( $\mu\text{M}$ )	$\text{NAD}^+$ ( $\mu\text{M}$ )	NADH+NAD <sup>+</sup> ( $\mu\text{M}$ )	NADH ( $\mu\text{M}$ )	$\text{NAD}^+$ ( $\mu\text{M}$ )	NADH+NAD <sup>+</sup> ( $\mu\text{M}$ )
Ferricyanide	52	8.5	60.5	47	22	69
Meldola blue	19	3	22	15	18	33
TBO-P	5	1	6	4	1	5

## 2.2. Materials

The RVC (80–110 pores  $\text{inch}^{-1}$  and  $10^{-4} \Omega \text{ cm}^{-1}$  conductivity) was from ERG Inc., California.  $\gamma$ -amino-propyl triethoxysilanised. Controlled pore glass 100–200  $\mu\text{m}$  diameter with 50 nm pore size occupying a volume of  $954.92 \text{ mm}^3 \text{ g}^{-1}$  and surface area of  $67.53 \text{ m}^2 \text{ g}^{-1}$  were obtained from Trisoperl, Germany. A platinum foil ( $3 \times 10 \text{ mm}^2$ ) was used as the counter electrode for recording cyclic voltammograms while a platinum wire (0.5 mm diameter and 10 mm long) was used to connect the RVC to the potentiostat.

## 2.3. Apparatus

The peristaltic pump was from Ventur, Sweden. Disposable filters 0.2  $\mu\text{m}$  from Filtron, Germany. A polyacrylate (5 mm thick) flow through cell, was fabricated in the local workshop. A potentiostat model MA 5410 was from Iskra Elektronika, Yugoslavia. The output from the potentiostat was recorded on a strip chart recorder from Kipp and Zonen, at a sensitivity of  $0.3 \mu\text{A}$  and a chart speed of  $1 \text{ cm min}^{-1}$ . The cyclic voltammetry (CV) program was operated in Qbasic using a personal computer equipped with an analog to

digital converter card. The electrochemical cell for recording the CV consisted of RVC (working electrode), platinum foil (counter electrode) and Ag/AgCl as the reference electrode. A Shimadzu spectrophotometer model UV 120 was used for enzyme activity measurements. A homogeniser (ultraturax 1KA) for extraction of the cellular contents from the normal and cancerous tissues was from Janke Kunkel, Germany.

#### 2.4. The flow injection set-up

The set-up is depicted in Fig. 1. It consists of RVC as the working and counter electrode. A Ag/AgCl reference electrode was connected using an agar salt bridge. Holes of 0.8 mm diameter were drilled through the body of the polyacrylate cell to insert 0.5 mm diameter platinum wire establishing contact with the RVC cylinder within the cell. The porous nature of the RVC with 97% void volume was used to pack the CPG with immobilised LDH. During the experiments the pulsation from the peristaltic pump (LKB, Sweden) was minimised by using a pulse damper in the flow stream. The entire setup was enclosed in a 1 mm thick iron container to prevent electromagnetic interference.

#### 2.5. Methods

Preparation of the RVC electrodes: RVC was washed with buffer for 16 h. The size of the electrode (12 mm<sup>2</sup> cylinder) was optimised to fit snugly into the cell. Mechanical fracture of the RVC was avoided during insertion into the cell.

Buffers, standard solutions and immobilisation of LDH: phosphate buffer 0.1 M and pH 7.0 was used in all the experiments. The buffer solution was de-gassed for 30 min prior to use. The de-gassed buffer was also employed for suspending 60 mg of the normal and cancer tissues for homogenisation. Standard solutions 1–50  $\mu$ M of NAD<sup>+</sup>, NADH and L-lactate were prepared in this buffer. LDH was cross-linked using glutaraldehyde on CPG by a method described in an earlier report [29].

Flow injection operation: The buffer was continuously circulated at 0.5 ml min<sup>-1</sup> and samples

were introduced (six samples per h) through a six port injection valve (type 50, Rheodyne, California) using a 150  $\mu$ l sample loop. Stop flow measurements were performed by stopping the pump exactly at 9 min after sample injection and restarting after 13 min. The mediator solutions in buffer (2.8 mg l<sup>-1</sup>) were either continuously circulated or they were circulated for 10 min followed by circulation of pure buffer.

Extraction of cellular contents: 60 mg of normal/cancerous tissues (wet weight) were suspended in 1 ml degassed buffer and homogenised at 24 000 rpm for 1 min. The buffer temperature was between 0–4°C during extraction or storage. Fresh homogenates were prepared prior to all experiments.

The coulometric studies: Within the polyacrylate cell the RVC (working and counter) and Ag/AgCl reference were connected to the potentiostat. The desired potentials were applied on the working electrode versus Ag/AgCl reference. The current passing through the working and counter were recorded on a strip chart recorder with a chart speed of 1 cm min<sup>-1</sup>. The area under the current time curve (total charge) was integrated manually. All potentials (mV) were applied versus Ag/AgCl reference electrode.

### 3. Results and discussion

#### 3.1. Physical characteristics of the measurement cell

The measurement cell shown in Fig. 1 had several operational advantages. The highly porous RVC (97% void volume) allowed unhindered flow of the circulating buffer. The close packing of CPG within RVC permitted efficient diffusion of products (LDH reaction) to the RVC surface. The LDH was not affected by the heavy metal impurities [30] present on RVC. The enzyme activity was retained for at least 200 assays. The flow rate of 0.5 ml min<sup>-1</sup> was optimised to avoid bouncing of the CPG within the RVC matrix as observed with a flow rate of 1 ml min<sup>-1</sup>. The presence of a pulse damper in the flow stream was useful in reducing the noise from pulsations of the peristaltic pump.

### 3.2. Detection of NADH

Fig. 2 shows the plot of charges ( $\mu\text{C}$ ) produced with injections of varying NADH concentrations, between 0 and 50  $\mu\text{M}$ , respectively. Curves a–c correspond to the data obtained with MB, TBO and FCN as mediators, facilitating the oxidation of NADH at varying applied potentials. Both MB and TBO were operated at an applied potential of 0.0 mV while FCN was operated at 350 mV. It was observed that the response in all three cases were linear up to 20  $\mu\text{M}$  prior to reaching a plateau. The dynamic range for TBO and MB were low while the magnitude of response was higher in case of TBO compared to MB (curves b and a). Although the response with FCN (curve c) was highest, its operation at 350 mV made it less suitable for application to tissue extracts. The diminished response of both TBO and MB compared to FCN may be attributed to a combined effect of adsorption on RVC and the replenishment of the mediators from the circulating buffer. In all cases the data shows an average of five measurements with an r.s.d of  $\pm 10\%$ .

### 3.3. Detection of $\text{NAD}^+$ in the presence of LDH

Fig. 3 shows the plot of the charges ( $\mu\text{C}$ ) produced with injections of varying  $\text{NAD}^+$  concentrations (between 0 and 50  $\mu\text{M}$ ) and 50 mM L-lactate into the cell packed with CPG containing the immobilised LDH. The curves a–c correspond to the presence of MB, TBO and FCN in the circulating buffer during the measurement. In comparison to NADH measurement, the magnitude of the total charge in the case of  $\text{NAD}^+$  injections were much higher (25  $\mu\text{C}$  compared to 8  $\mu\text{C}$  in case of NADH). This indicated a signal amplification in the case of LDH catalysed reaction of  $\text{NAD}^+$ . The magnitude of response with TBO (curve b) was 20% higher compared to MB (curve a). Although higher magnitude of charges were obtained with TBO and FCN (curves b and c) as compared to MB, the signal was non linear and less reproducible compared to MB. In the case of FCN the applied potential of 350 mV the surface impurities on the RVC [30] may intro-

duce non-linear effects during measurements. In the regard,  $\text{Fe}(\text{CN})_6^{3-}$  is a one electron mediator and will introduce NAD which will produce major interfering effects. However, the non linearity with TBO is not clear. The higher response of TBO with LDH compared to MB could be attributed to the efficient oxidation of NADH (produced locally on the CPG due to the LDH reaction) by TBO in close proximity of the RVC surface. In contrast, in the case of direct oxidation of NADH the proximity to the electrode is very poor. However, under a similar situation the oxidation by MB is very poor due to inefficient electron transfer on the RVC surface.

### 3.4. Stopped flow assay

In order to investigate signal amplification in the presence of LDH a stopped flow assay was performed. This concept had been exploited earlier for enzyme assays [31]. Fig. 4 illustrates the profile of the stopped flow assay in the presence of LDH in the FIA mode. On stopping the flow there was a sharp rise in the current and the slope of this rise was approximately 0.024  $\mu\text{A min}^{-1}$ . This value denotes a zero or pseudo-zero order rate of conversion of L-lactate to pyruvate or  $\text{NAD}^+$  to NADH by LDH. As the flow was stopped at the peak, the entire substrate injected into the flow stream had reached the cell and reacted continuously with LDH leading to a signal amplification. The theory for the stopped flow assay was proposed in the initial work of Ruzicka [32,33]. Based on our results the dispersion coefficient ( $D_t$ ) was calculated to be 3.7 according to the following equation.

$$D_t = C_o/C = 2\pi^{3/2}r^2L^{1/2}F^{1/2}\delta^{1/2}\tau^{1/2}S_v^{-1}$$

where  $r$ , radius of the cell;  $L$ , the length;  $F$ , mean linear flow velocity of solution;  $\tau$ , mean residence time;  $S_v$ , injected sample volume and  $\delta = D_f/L_v$ , where  $D_f$  is the axial dispersion coefficient, and  $\delta = 1/8[(8\sigma^2 + 1)^{1/2} - 1]$ , for a non gaussian curve. Here  $\sigma^2$  was the variance [34]. If the carrier stream ceased to move then the dispersion of the sample zone would stop and  $D_t$  would thus remain a constant independent of time.

### 3.5. Characteristics of the TBO mediator

It was observed that continuous circulation of the TBO provides a stable response. During the circulation the mediator continuously adsorbed on the RVC surface and was found to saturate by 3 min. The electroactivity was maintained for at least 100 assays. However, adsorbed MB was inactivated after ten assays, suggesting the suitability of TBO for  $\text{NAD}^+$  and NADH estimations. These findings suggested that the coulometric response shown in Figs. 2 and 3 were a combined effect of adsorption and regeneration of the mediator on the RVC surface. This behaviour of TBO could perhaps be attributed to the presence of free  $-\text{CH}_3$  and carboxyl groups on the acrylamide portion of the polymer [35] forming Schiff base like complexes, enabling physisorption and chemisorption to occur. The adsorption might have also been enhanced by hydrophobic interaction with the  $-\text{CH}_3$  groups. In addition the sparingly soluble nature of TBO in water coupled to its affinity to the carbon within RVC may also favour adsorption. A similar approach had been adopted to adsorb TBO on hydrophobic carbon paste employed in the amperometric studies on peroxide [28] (Scheme 1).

### 3.6. Effect of adsorption versus circulation of the TBO mediator

A comparison of the coulometric response (Fig. 5) of adsorbed (curve a) versus circulating (curve b) TBO mediator revealed that the profiles were similar between the  $\text{NAD}^+$  concentration of 0 and 50  $\mu\text{M}$  coinjected with 50 mM lactate. However, in the case of adsorbed TBO ( $2.54 \times 10^{-7}$  mol  $\text{cm}^{-2}$ ) the saturation in the response was observed at a  $\text{NAD}^+$  concentration of 20  $\mu\text{M}$ , although the response at lower concentrations was much better. This may be attributed to the lack of regeneration of TBO on the RVC surface, thereby limiting the response. In case of the circulating TBO this barrier is overcome by the constant replenishment of the mediator on the RVC surface. Similar findings on MB adsorbed on carbon surface had been reported earlier [36]. During the studies on adsorbed TBO there was no loss of the

mediator due to desorption or leakage from the RVC surface. This was verified by monitoring absorbance (Fig. 5, inset) of the eluted buffer at 588 nm (the absorbance maxima of TBO in buffer).

### 3.7. Electroactivity of the TBO on RVC

Cyclic voltammetric investigations of TBO adsorbed on RVC (Fig. 6) revealed that the potentials of the oxidation and reduction of TBO coincided well with those reported [24] for TBO on carbon paste electrodes (Table 1). The reproducibility of the response (for at least ten cycles) at varying scan speeds between 10–50  $\text{mV s}^{-1}$  also confirmed a stable and electroactive TBO on RVC surface. However, the oxidation and reduction peaks of TBO on RVC were much broader compared to those reported on glassy carbon surface. This may be attributed to the cylindrical geometry of the electrodes leading to variation in the diffusion path length and thereby affecting the charge distribution along the surface. Based on the CV the amount of mediator adsorbed on the RVC surface [30] was calculated to be  $2.54 \times 10^{-7}$  mol  $\text{cm}^{-2}$ . This calculation method and the final value conformed well with similar studies performed earlier [24].

### 3.8. Effect of applied potential on TBO response

In order to verify the suitability of employing TBO below 0 mV, the response of TBO between  $-40$  and  $+40$  mV was carried out. The plot (Fig. 6, inset) did not indicate a substantial increase at  $-40$  mV compared to  $+40$  mV for identical injections of 50  $\mu\text{M}$   $\text{NAD}^+$  and 50 mM lactate. Between  $-40$  and 0 mV the response was almost unchanged. Thus, 0 mV was used as the applied potential for all response measurements with TBO in the present investigations.

### 3.9. Effect of pH on TBO response

Earlier reports on MB [36] had indicated higher reaction rates for NADH at low pH. However, in the case of TBO the reaction rate or the overall response did not increase substantially in the pH

range 5–8 as shown in Fig. 7. Hence, pH 7 was adopted for all further investigations with this mediator.

### 3.10. Detection of NADH/NAD<sup>+</sup> in normal and cancer tissues

Our attempts to apply the mediator based coulometric studies to measurement of NAD<sup>+</sup> and NADH in normal/cancer tissue extracts is summarized in Table 2. Each value is an average of three independent injections of freshly extracted samples (diluted ten times) in degassed buffer, without any pre-treatment. From Table 2 it is seen that the NADH content in cancer cells is less than in normal cells, as measured with either of the mediators. Similarly the NAD<sup>+</sup> content in cancer cells is equal or higher than in normal cells (with an r.s.d of  $\pm 10\%$ ). This points out to the existence of a biochemical reaction leading to depletion of NADH in cancer cells and their subsequent conversion to NAD<sup>+</sup>. These results agree with the recent reports [22,23] on the presence of NADH oxidase, predominantly in cell membrane and serum of cancer tissues. Our findings also add valuable information to the earlier hypotheses [20,21] on changes in NADH content in cancer tissues. These results indicate the suitability of the electrochemical approach for measurement of NAD<sup>+</sup> and NADH in biological samples, especially in the presence of the novel TBO based mediators.

## 4. Conclusions

The RVC based LDH catalysis is useful in estimation of NAD<sup>+</sup> and NADH in normal and cancer tissues. NADH content in cancer tissues are lower than in normal tissues while NAD<sup>+</sup> content shows the reverse trend. Amongst the mediators, adsorbed TBO exhibits a more stable and reproducible electroactivity on RVC surface for measurement of biological samples. The operation of TBO at 0 mV enables much reduced interference while employing normal and cancer tissue extracts. Following this preliminary report, in depth analysis on the use of TBO for estima-

tion of other analytes in clinical samples would be attempted.

## Acknowledgements

We wish to thank the referee (for useful suggestions), Professor G. Johansson, Dr Nii Djohan and Dr M.O. Månsson for their help. The authors gratefully acknowledge the financial support from the Swedish Institute. Financial support from TMS CHEM AB is acknowledged.

## References

- [1] H.K. Chenault, G.M. Whitesides, *Appl. Biochem. Biotechnol.* 14 (1987) 147.
- [2] I. Katakis, E. Domínguez, *Mikrochim. Acta* 126 (1997) 11.
- [3] M.J. Lobo, A.J. Miranda, P. Tuñón, *Electroanalysis* 9 (1997) 191.
- [4] M. Beley, J.P. Collin, *J. Mol. Catal.* 79 (1993) 133.
- [5] A. Bardea, E. Katz, A.F. Bückmann, I. Willner, *J. Am. Chem. Soc.* 119 (1997) 9114.
- [6] G. Marrazza, M. Mascini, J.D. Newman, G. Palleschi, A.P.F. Turner, in: S.J. Alcock, A.P.F. Turner (Eds.), *In-Vivo Chemical Sensors-Recent Developments*, Cranfield press, UK, 1993.
- [7] H.-C. Shu, H. Håkansson, B. Mattiasson, *Anal. Chim. Acta.* 300 (1995) 277.
- [8] A. Silber, C. Brauchle, N. Hampp, *Sens. and Act. B* 18–19 (1994) 235.
- [9] F. Scheller, N. Siegbahn, B. Danielsson, K. Mosbach, *Anal. Chem.* 57 (1985) 1740.
- [10] P.N. Bartlett, P. Tebbutt, R.P. Whitaker, *Progr. React. Kinet.* 16 (1991) 55.
- [11] M.F. Cardosi, A.P.F. Turner, in: A.P.F. Turner, I. Karube, G.S. Wilson (Eds.), *Biosensors: Fundamentals and Applications*, Oxford University Press, New York, 1987.
- [12] S.A. Wring, J.P. Hart, *Analyst* 117 (1992) 1215.
- [13] A.P.F. Turner, *Advances in Biosensors*, Suppl. 1, 2, 3, JAI Press, London, 1991–1994.
- [14] S. Sampath, O. Lev, *J. Electroanal. Chem.* 426 (1997) 131.
- [15] W.J. Blaedel, J. Wang, *Anal. Chem.* 52 (1980) 76.
- [16] R.E. Sioda, *Electrochim. Acta* 15 (1970) 783.
- [17] A.N. Strohl, D.J. Curran, *Anal. Chem.* 51 (1979) 353.
- [18] J. Wang, *Electrochim. Acta* 26 (1981) 1721.
- [19] W.J. Blaedel, J. Wang, *Anal. Chem.* 52 (1980) 1426.
- [20] W. Lohmann, F. Hugo, *Naturwissenschaften* 77 (1989) 476.

- [21] W. Lohmann, S. Kunzel, J. Musmann, C. Hoersch, *Naturwissenschaften* 77 (1990) 476.
- [22] D.J. Morre, T. Reust, *J. Bioenerg. Biomemb.* 29 (1997) 281.
- [23] D.J. Morre, S. Caldwell, A. Mayorga, L.Y. Wu, D.M. Morre, *Arch. Biochem. Biophys.* 342 (1997) 224.
- [24] S. Paradowski, Masters' dissertation, Department Analytical Chemistry, Lund University, Sweden, 1996.
- [25] A. Heller, *J. Phys. Chem.* 96 (1992) 3579.
- [26] J.-M. Laval, C. Bourdillon, J. Moiroux, *J. Am. Chem. Soc.* 106 (1984) 4701.
- [27] E. Dominguez, H.L. Lan, Y. Okamoto, P.D. Hale, T.A. Skotheim, L. Gorton, *Biosens. Bioelec.* 8 (1993) 167.
- [28] V. Rajendran, E. Csöregi, Y. Okamoto, L. Gorton, *Anal. Chim. Acta* (1999) in press.
- [29] F. Torabi, Diploma work, Department of Analytical Chemistry, Lunds University, Sweden.
- [30] Notes on RVC, Energy Research and Generation, Inc., 900, Stanford Ave., Oakland, CA 94608, USA
- [31] J. Ruzicka, E.H. Hansen, *Anal. Chim. Acta.* 106 (1979) 207.
- [32] E.H. Hansen, J. Ruzicka, B. Rietz, *Anal. Chim. Acta.* 89 (1977) 241.
- [33] A. Ramsing, J. Ruzicka, E.H. Hansen, *Anal. Chim. Acta.* 114 (1980) 165.
- [34] E.H. Hansen, Doctor Technices, dissertation, Technical University of Denmark, Denmark, 1986.
- [35] R.D. Bongard, M.P. Merker, R. Shundo, Y. Okamoto, D.L. Roerig, J.H. Linehan, C.A. Dawson, *Am. J. Physiol. (Lung Cell. Mol. Physiol.)* 13) 269 (1995) L78.
- [36] L. Gorton, A. Torstensson, H. Jaegfeldt, G. Johansson, *J. Electroanal. Chem.* 161 (1984) 103.

## An automatic flow-injection analysis system for determining phosphate ion in river water using pyruvate oxidase G (from *Aerococcus viridans*)

Hideaki Nakamura<sup>a</sup>, Hiroko Tanaka<sup>b</sup>, Mami Hasegawa<sup>c</sup>, Yuzo Masuda<sup>b</sup>,  
Yoshiko Arikawa<sup>c</sup>, Yoko Nomura<sup>a</sup>, Kazunori Ikebukuro<sup>a</sup>, Isao Karube<sup>a,\*</sup>

<sup>a</sup> Research Center for Advanced Science and Technology, University of Tokyo, 4-6-1 Komaba, Meguro-ku, Tokyo 153-8904, Japan

<sup>b</sup> Department of Industrial Chemistry, Faculty of Engineering, Science University of Tokyo, 1-3 Kagurazaka, Shinjuku-ku, Tokyo 162-8601, Japan

<sup>c</sup> Department of Chemical and Biological Sciences, Faculty of Science, Japan Women's University, 2-8-1 Mejirodai, Mejiro-ku, Tokyo 112-0015, Japan

Received 17 November 1998; received in revised form 24 February 1999; accepted 24 February 1999

### Abstract

An automated flow-injection system combining a pyruvate oxidase reaction and chemiluminescence for the detection of phosphate ion in river water has been developed. In this research, we used pyruvate oxidase G (PyrOxG), from *Aerococcus viridans*, immobilizing it on *N*-hydroxysuccinimidimido beads without a cross-linker. In this sensor system, which was constructed as a trial system of desktop type, the temperature was precisely controlled. After the sensor system was optimized, a calibration curve was obtained with a detection limit of 96 nM phosphate ion, a range between 96 nM and 32 μM phosphate ion, and a relative standard deviation of 2.3% ( $n = 5$ ) at 25°C. The sensitivity of this sensor was sufficient to determine the maximal permissible phosphate-ion concentration in the environmental waters of Japan (0.32 μM). In addition, the sensor could determine the calibration curves between 0.16 and 32 μM phosphate ion (five points,  $n = 3$ ; averaged correlation,  $r = 1.00$ ) for at least 2 weeks, demonstrating enough stability for practical use. Furthermore, we investigated the influence on the sensor response of dissolved substances in river water such as metal ions, heavy metal ions, inorganic ions, and organic compounds. Treatment with activated carbon could improve the response of the sensor when inhibited by dissolved substances in river water, except for manganese ion and uric acid. The sensor system could determine the concentrations of phosphate ion in various samples of river water from the Tone River. The results obtained by this sensor system and the modified molybdenum blue method were compared, and good correlation ( $r = 0.94$ ) was obtained. © 1999 Elsevier Science B.V. All rights reserved.

**Keywords:** Phosphate ion; Chemiluminescence; Pyruvate oxidase G; *Arthromyces ramosus* peroxidase; *N*-Hydroxysuccinimidimido gel; Flow-injection analysis; Activated carbon treatment; River water

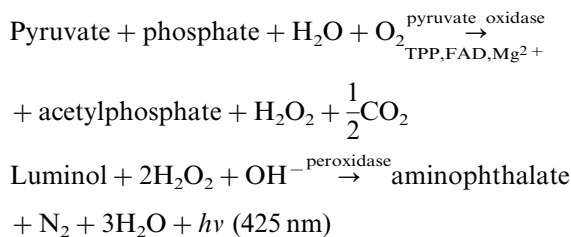
\* Corresponding author. Tel.: +81-3-5452-5220; fax: +81-3-5452-5227.

E-mail address: karube@bio.rcast.u-tokyo.ac.jp (I. Karube)

## 1. Introduction

Increases of phosphate-ion concentration lead to the eutrophication of river waters [1], which in turn affects human health by the excessive intake of the phosphate [2]. Therefore, monitoring of phosphate-ion concentrations is very important to maintain the quality of environmental drinking water. Conventional methods for phosphate-ion determination are available [3]. However, these methods have poor selectivity, are tedious, and require the use of heavy metal ion, which affects the environment. Biosensors are expected to be simple, selective, economical, and ecologically sound methods.

Highly sensitive biosensors have been developed for the determination of phosphate ion [4–8]. However, these sensors cannot be used to measure phosphate-ion concentration in various environmental waters. We have previously reported a phosphate-ion sensor for on-site monitoring of dam water for drinking [7]. Such a sensor could only measure the phosphate-ion concentration of pure water and was affected by dissolved substances in the dam water. This sensor system, which employs flow-injection analysis (FIA), combines pyruvate oxidase (PyrOx) (EC 1.2.3.3, from *Pediococcus* sp.) reaction and luminol chemiluminescence catalyzed by *Arthromyces ramosus* peroxidase (ARP) (EC 1.11.1.7). The reaction scheme of PyrOx is as follows (TPP, thiamine pyrophosphate; FAD, flavin adenine dinucleotide):



In the study mentioned [7], the effects on the sensor response of inhibitors dissolved in normal environmental water were not investigated. The effects of coexisting substances must be eliminated for the determination of phosphate ion in various environmental waters.

In our present study, we constructed a trial sensor system of desktop type for practical use. This system was controlled by a precise temperature control system. Pyruvate oxidase G (PyrOxG), from *Aerococcus viridans* [9], was used as a practical enzyme; it was purified from recombinant *Escherichia coli* by a simple purification process and had better stability and higher activity than PyrOx. After the sensor system was optimized, the influences of coexisting substances on both the chemiluminescence and the PyrOxG reaction were investigated. The treatment methods to remove inhibitors in the water samples were examined. The phosphate-ion concentrations of various treated environmental waters were determined and compared with the results obtained by an analyzer (DR/2000; Hach Company, USA) employing a modified molybdenum blue method.

## 2. Experimental

### 2.1. Materials

PyrOxG was kindly donated by Asahi Chemical Industry (Shizuoka, Japan). ARP was purchased from Nacalai Tesque (Kyoto, Japan). Sodium pyruvate, TPP, FAD, 3-aminophthaloylhydrazine (luminol), monopotassium phosphate, hydrogen peroxide (H<sub>2</sub>O<sub>2</sub>), and activated carbon of grain were purchased from Wako Pure Chemicals (Osaka, Japan). All other chemicals used were of analytical grade.

The PyrOxG reaction mixture, prepared prior to the measurements, contained 0.4 mM pyruvate, 30 μM TPP, 3 nM FAD, and 10 mM MgCl<sub>2</sub>·6H<sub>2</sub>O in 0.02 M *N*-2-hydroxyethylpiperazine-*N'*-2-ethanesulfonic acid (HEPES) buffer (pH 7.0). A stock solution of 100 nM FAD was prepared in 0.02 M HEPES buffer (pH 7.0) and stored at 4°C.

A stock solution of luminol was prepared according to previously reported methods [10,11]. Ten millimolar luminol was dissolved in 0.5 M potassium borate buffer (pH 11.0) and stored at 4°C for 3 days for its stabilization in a light-protected bottle. The chemiluminescence reaction mixture contained 70 μM luminol and 6250 U l<sup>-1</sup>



ARP in 0.8 M carbonate buffer (pH 10.0;  $pH_{\text{mix}}$  10.1). The solvent was left for at least 1 h in a light-protected bottle at ambient temperature for stabilization.

## 2.2. Preparation of immobilized enzyme

PyrOxG was immobilized onto a *N*-hydroxy-succinimidimido (NHS) (porous cellulose beads, diameter 44–125  $\mu\text{m}$ ; kindly donated by Chisso, Japan) gel containing activated ester. The NHS gel in solvent was washed with water three times to remove isopropanol. One milliliter of NHS gel was suspended in 0.8 ml of 0.1 M HEPES buffer (pH 8.0) containing 200 U of PyrOxG, and rotated slowly for 2 h at 4°C. The gel was then treated with 0.1 M Tris–HCl buffer (pH 8.0) containing 1 M NaCl for blocking residual ester groups for 1 h, and finally washed three times with 0.1 M HEPES buffer (pH 8.0) for 15 min each time. The PyrOxG immobilized on the NHS gel was stored in 0.02 M HEPES buffer (pH 7.0) containing 100 nM FAD at 4°C until use.

The PyrOxG immobilized on NHS gel was then packed into stainless-steel columns (length 35 mm, inner diameter 2 mm, 20  $\mu\text{m}$  polyethylene filter).

## 2.3. Measurement and apparatus

The automatic sensor system used is depicted in Fig. 1. This system was constructed as a trial

system in an attempt to realize automatic phosphate detection in various environmental waters in collaboration with the Water Resources Environment Technology Center, the Association of Electrical Engineering, and Hiranuma Co. Ltd. The system was held in a light-protected box, and its inside temperature was precisely controlled. Such a temperature control was necessary to keep the high reproducibility of sensor responses obtained by PyrOxG-catalyzed and subsequent ARP-catalyzed luminol chemiluminescence reactions.

The homoisothermal system in this sensor consisted of a heat sink (Model A6063SS-T5; Unitus, Japan), two fans (Model MDS510-24; Oriental Motors, Japan) and two thermocouples (SY11S-SUS; Sigma Controls, Japan). The fans were used for circulating the inside atmosphere, and the thermocouples were used as thermometers for the precise control of atmospheric temperature. The homoisothermal system could change and maintain the temperature; for example, terms for changing to  $\pm 5^\circ\text{C}$  at ambient temperature (20–30°C) were within 20 min.

As already mentioned, this sensor system consists of a PyrOxG reaction and a luminol chemiluminescence reaction. The sample passed through a 500  $\mu\text{l}$  sample loop by a sampling pump at a flow rate of 12  $\text{ml min}^{-1}$  for 15 s. The PyrOxG mixture was delivered to an immobilized PyrOxG column by a peristaltic pump. The peristaltic pump simultaneously delivered the solutions for

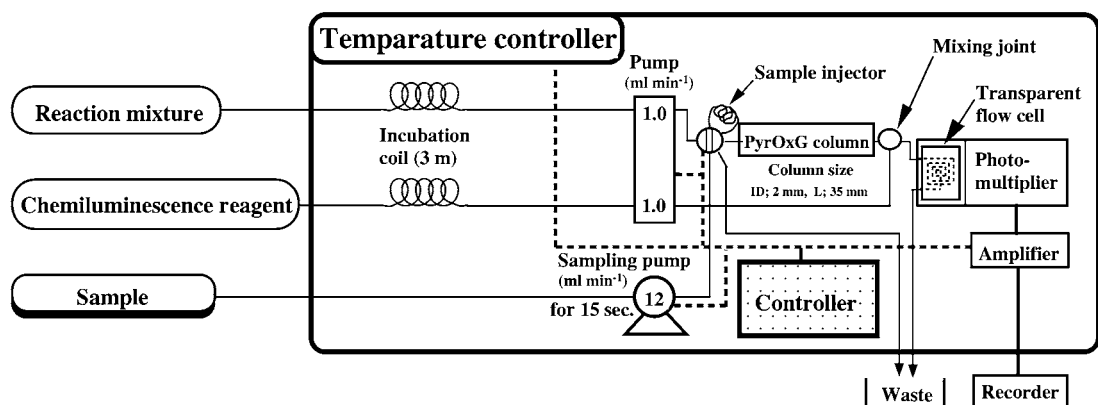


Fig. 1. Schematic diagram of the automatic phosphate-ion measuring system with precisely controlled temperature.

the luminol chemiluminescence reaction mixture and the PyrOxG reagent at a flow rate of 1.0 ml min<sup>-1</sup>. The sample was automatically injected into an eight-way valve by an integrated controller and delivered to the immobilized PyrOxG column.

The hydrogen peroxide generated by the PyrOxG reaction in the column was mixed with the luminol chemiluminescence reaction mixture at a mixing joint, and the resulting chemiluminescence was measured in a transparent spiral tube by a neighboring photomultiplier (PMT) (Hamamatsu Photonics, Japan). Its signal was then amplified and recorded (Model SP-J5C; Riken Densi Kogyo, Japan).

The measurement of phosphate ion in this system was performed by handling an operating panel on the sensor box. The integrated controller regulated the timing for the next injection by reading the output of the previous peak from the detector. One measurement took approximately 2 min from sampling back to baseline after the peak as a sensor response. All measurements were performed at 25 ± 0.1°C.

### 3. Results and discussion

#### 3.1. Optimization of the sensor system

##### 3.1.1. Comparison between PyrOx and PyrOxG

To realize the phosphate-ion sensor for the determination of phosphate ion in various environmental waters, we chose PyrOxG instead of PyrOx for practical purposes. To compare the activity of free PyrOx with PyrOxG, the sensor responses to 0.32 μM phosphate ion using each enzyme were compared using the sensor system shown in Fig. 1 with previously optimized conditions without a column [7]. The experimental condition was as follows: the buffer for enzyme reaction contained 0.4 mM pyruvate, 40 nM FAD, 0.24 mM TPP, and 20 mM Mg<sup>2+</sup> in 0.02 M HEPES buffer. The chemiluminescence reaction mixture contained 12.5 μM luminol and 1250 U l<sup>-1</sup> ARP in 0.2 M carbonate buffer (pH 9.0) with a flow rate of 1.0 ml min<sup>-1</sup>. The measurements were performed three times, respectively.

The response obtained with PyrOxG was twice as high as that with PyrOx.

##### 3.1.2. Comparison of the immobilization methods

Subsequently, PyrOxG was immobilized on Chitopearl BCW 2601 beads using a covalent bonding method [7]. However, the PyrOxG activity after immobilization decreased. Considering it possible that the enzyme activity had been lost because of conformation changes of the enzyme by cross-linking using glutaraldehyde, we employed NHS gel, which can immobilize the enzymes without a cross-linker. As a result, PyrOxG activity was kept after immobilization onto the NHS gel (data not shown). Accordingly, NHS gel was used as the enzyme support in this study.

##### 3.1.3. Optimization of the PyrOxG reaction mixture

To optimize the component of the PyrOxG reaction mixture, a previously optimized PyrOx mixture was used at the beginning of the experiment, as already mentioned [7]. The optimal concentrations of pyruvate, FAD, TPP, and Mg<sup>2+</sup>, and the pH of the 0.02 M HEPES buffer were investigated by measuring sensor responses to 16 μM phosphate ion. Each optimization experiment was performed five times. Results showed that the optimum condition of the PyrOxG mixture was 0.4 mM pyruvate, 3 nM FAD, 30 μM TPP, and 10 mM Mg<sup>2+</sup> in 0.02 M HEPES buffer with a pH of 7.0. This component of the PyrOxG reaction mixture was used in the subsequent experiments.

##### 3.1.4. Optimization of the chemiluminescence reaction mixture

In the previous study using PyrOx, we chose a chemiluminescence reaction mixture containing 12.5 μM luminol and 1250 U l<sup>-1</sup> ARP in 0.2 M carbonate buffer with a pH of 9.0 in consideration of enzyme stability. However, we found that ARP was stable even at pH 10.0. Subsequently, we carefully investigated the relationship between that composition and stability using eight kinds of chemiluminescence reaction mixtures. We found that the most stable composition of the chemiluminescence reagent was 70 μM luminol and 6250 U l<sup>-1</sup> ARP in 0.8 M carbonate buffer (pH 10.0;

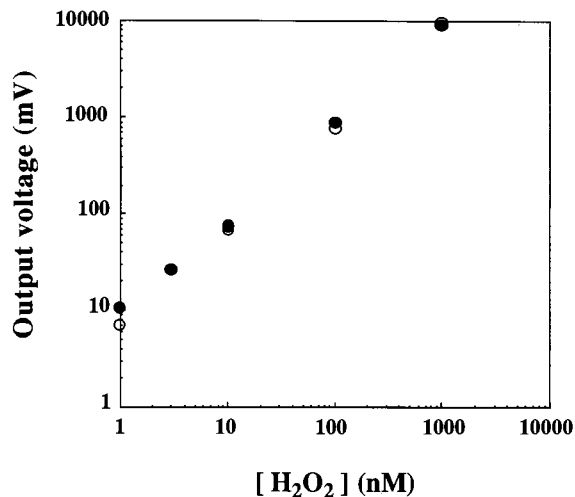


Fig. 2. Stability of the chemiluminescence reaction mixture from the first day (○) until 2 weeks later (●).

$\text{pH}_{\text{mix}}$  10.1). This result is shown in Fig. 2. In this figure, the sensor responses ( $n=3$ ) to 1, 3, 10, 100, and 1000 nM  $\text{H}_2\text{O}_2$  were almost similar from the first day until 2 weeks later. Therefore, that composition of the chemiluminescence reaction mixture was used in the subsequent experiments.

### 3.1.5. Optimization of the FIA system

Using the optimal condition of the PyrOxG- and ARP-catalyzed luminol chemiluminescence reaction, the optimizations of temperature and flow rate in this system were examined. Each of these experiments was performed five times. The temperature was examined at 20, 25, and 30°C. Results indicated that the sensor responses to 16  $\mu\text{M}$  phosphate ion tended to increase with increases in temperature (data not shown). For indoor use and maintenance of PyrOxG and ARP activity, we chose a measuring temperature of  $25 \pm 0.1^\circ\text{C}$ .

The flow rates were examined at 0.70, 0.82, 1.00, 1.16, 1.33, and 1.50  $\text{ml min}^{-1}$ . The highest sensor response to 16  $\mu\text{M}$  phosphate ion was obtained at 1.0  $\text{ml min}^{-1}$ . The flow rate of 1.0  $\text{ml min}^{-1}$  was used in the subsequent experiments.

### 3.1.6. Calibration curve for phosphate-ion concentration

A calibration curve for phosphate-ion concentration under the optimized condition of the sensor system was obtained (Fig. 3). A linear response was observed from 96 nM to 32  $\mu\text{M}$  with a correlation coefficient of 0.999, and correlative variance averaging sensor responses was approximately 2.3% (average of each five measurements). The signal-to-noise ratio was over 20 at 96 nM phosphate ion, and measurement time was approximately 2 min. All parameters obtained in this system showed improvement as compared with previously reported sensor systems using PyrOx [7]. Our system could detect 0.16  $\mu\text{M}$  phosphate ion for at least 2 weeks.

### 3.2. Influences of coexisting substances

To examine the influences on the sensor response of coexisting substances in environmental water, we investigated the inhibitors of luminol chemiluminescence and PyrOxG reactions, as pre-

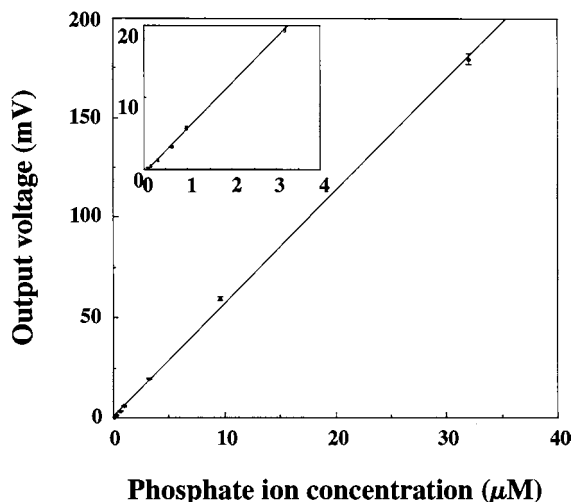


Fig. 3. Calibration curve for phosphate-ion concentration. The PyrOxG reaction mixture contained 0.4 mM pyruvate, 3 nM FAD, 30  $\mu\text{M}$  TPP, and 10 mM  $\text{MgCl}_2$  in 0.02 M HEPES buffer (pH 7.0). The luminol chemiluminescence reaction mixture contained 70  $\mu\text{M}$  luminol and 6250  $\text{U ml}^{-1}$  ARP in 0.8 M sodium carbonate buffer (pH 10.0;  $\text{pH}_{\text{mix}}$  10.1). The flow rate was 1.0  $\text{ml min}^{-1}$ , the temperature was  $25 \pm 0.1^\circ\text{C}$ , and the injection volume was 500  $\mu\text{l}$ .

Table 1

Rate of inhibition to chemiluminescence or PyrOxG reaction and effectless concentration of inhibitor on sensor response<sup>a</sup>

Coexisting substance	Concentration of inhibitor (mg l <sup>-1</sup> )	Sensor response to chemiluminescence (%)	Sensor response to PyrOxG (%)	Effectless concentration of inhibitor on sensor response (mg l <sup>-1</sup> )
<i>Metal ion</i>				
Na <sup>+</sup>	100	98.7	<b>55.5</b>	≤5.0
K <sup>+</sup>	10	99.6	97.5	>10
Mg <sup>2+</sup>	10	97.0	95.5	>10
Ca <sup>2+</sup>	50	98.7	96.9	>50
<i>Heavy metal ion</i>				
Zn <sup>2+</sup>	1.0	101	102	>1.0
Fe <sup>3+</sup>	1.0	97.8	<b>47.3</b>	≤0.05
Cr <sup>3+</sup>	1.0	<b>44.6</b>	<b>25.8</b>	≤0.05
Cu <sup>2+</sup>	1.0	<b>0</b>	–	≤0.005
Mn <sup>2+</sup>	1.0	<b>0</b>	–	≤0.001
<i>Inorganic ion</i>				
S <sup>2-</sup>	1.0	104	<b>52.8</b>	≤0.01
F <sup>-</sup>	10	99.4	<b>90.5</b>	≤5.0
NH <sub>4</sub> <sup>+</sup>	1.0	99.0	99.0	>1.0
NO <sub>2</sub> <sup>-</sup>	1.0	98.8	96.0	>1.0
NO <sub>3</sub> <sup>-</sup>	30	99.4	<b>64.4</b>	≤1.0
SO <sub>4</sub> <sup>2-</sup>	500	99.0	<b>56.9</b>	≤10
<i>Organic compound</i>				
Urea	1.0	99.2	98.6	>1.0
Uric acid	1.0	<b>0</b>	–	≤0.001
LAS	10	102	97.1	>10
Cellulose	10	100	95.8	>10
Humic acid	10	<b>71.0</b>	<b>70.6</b>	≤0.1
Lignin	1.0	<b>0</b>	–	≤0.01

<sup>a</sup> Bold numbers indicate influenced substances at that concentration on sensor response.

viously reported [9,10,12]. The maximum values of dissolved substances in the Tone River observed by the Ministry of Construction were investigated. After selecting 21 kinds of chemical substances of metal ions, heavy metal ions, inorganic ions, and organic compounds as dissolved substances in the environmental water, we examined their influences using each substance at higher concentrations than the maximal value observed in the Tone River. In this experiment, the influences on either luminol chemiluminescence or PyrOxG reaction were examined comparing the sensor responses obtained by 100 nM H<sub>2</sub>O<sub>2</sub> or 16 μM phosphate ion as controls. The results are shown in Table 1. Luminol chemiluminescence

reactions were affected by 1 mg l<sup>-1</sup> Cr<sup>3+</sup>, Cu<sup>2+</sup> and Mn<sup>2+</sup>, 1 and 10 mg l<sup>-1</sup> humic acid, and 1 mg l<sup>-1</sup> lignin; and the PyrOxG reactions were affected by 100 mg l<sup>-1</sup> Na<sup>+</sup>, 1 mg l<sup>-1</sup> Fe<sup>3+</sup>, Cr<sup>3+</sup> and S<sup>2-</sup>, 10 mg l<sup>-1</sup> F<sup>-</sup>, 30 mg l<sup>-1</sup> NO<sub>3</sub><sup>-</sup>, and 500 mg l<sup>-1</sup> SO<sub>4</sub><sup>2-</sup> in addition to those substances affecting the chemiluminescence reaction. Additionally, we investigated levels of concentration of these inhibitors at which no effect on the sensor response was observed (Table 1).

### 3.3. Treatment methods

To remove these inhibitors, we examined several methods using two kinds of chelate resins, a

chelate agent, and activated carbon. The treatment using every chelate resin (Chelex 100, imino-2-acetic acid; Bio-Rad Laboratories, USA; or CT-03, aromatic carboxyl group; Fuji Spinning, Japan) caused a chemiluminescence reaction by substances eluted from the resin in spite of thorough wash by an acid–base treatment. Ethylenediaminetetraacetic acid (EDTA) was used as a chelate agent. The addition of 1 mM EDTA did not affect the sensor response to 16  $\mu\text{M}$  phosphate ion. It was more effective to remove 1  $\text{mg l}^{-1}$   $\text{Cu}^{2+}$  and  $\text{Mn}^{2+}$  than  $\text{Cr}^{3+}$  and  $\text{Fe}^{3+}$ . These experiments were performed three times.

Next, we investigated the effects of treatment with activated carbon. After being thoroughly washed by pure water, the activated carbon was poured into a column until filling it. Distilled water and the solution containing the inhibitor were treated by being passed through the activated carbon. Distilled water was used as a control for the measurement. The solution containing the inhibitor was treated by the same procedure. The effects of treatment were evaluated in the same way as for the investigation of the influences of inhibitors. These experiments were also performed three times. The influence of inhibitors on the sensor response decreased, except for 1  $\text{mg l}^{-1}$   $\text{Mn}^{2+}$  and uric acid (Table 2). These inhibitors are able to remove with EDTA treatment

or combined enzyme reaction with uricase and catalase.

In this experiment, we investigated the influences of excess concentrations of each inhibitor. Our results indicated that it was possible to remove the effects of inhibitors by treatment with activated carbon.

### 3.4. Determination of phosphate ion in environmental water

For the determination of phosphate ion in environmental water, we obtained river and marsh waters from the Tone River and the Ara River with the help of the Kanto Engineering Laboratory, the Ministry of Construction. These samples were filtered with 0.45  $\mu\text{m}$  hydrophilic membrane to measure dissolved phosphate ion.

The determination of phosphate ion after EDTA treatment of environmental water was performed by using seven samples from the Tone River and the Ara River. One millimolar EDTA was added to the standard solutions and samples. The results obtained were unsatisfactory. The Py-rOxG reaction was affected by some dissolved substances in the environmental water. These results indicated the necessity of a treatment method which could remove the dissolved substances effectively.

Table 2  
Effect of treatment using activated carbon

Inhibitor	Concentration of inhibitor ( $\text{mg l}^{-1}$ )	Sensor response (%) <sup>a</sup>	Sensor response after treatment (%)
$\text{Na}^+$	100	55.5	104
$\text{Fe}^{3+}$	1.0	47.3	111
$\text{Cr}^{3+}$	1.0	25.8	39.5
$\text{Cu}^{2+}$	1.0	0	14.7
$\text{Mn}^{2+}$	1.0	0	0
$\text{S}^{2-}$	1.0	52.8	82.3
$\text{F}^-$	10	90.5	99.1
$\text{NO}_3^-$	30	64.4	97.0
$\text{SO}_4^{2-}$	500	56.9	82.2
Uric acid	10	0	0
Humic	10	70.6	75.9
Lignin	1.0	0	19.7

<sup>a</sup> These values were from Table 1.

Table 3

Measurements of phosphate ion in environmental water by treatment using activated carbon

The source of sample	Phosphate ion sensor ( $\mu\text{M}$ phosphate ion)	DR/2000 ( $\mu\text{M}$ phosphate ion)	BOD ( $\text{mg l}^{-1}$ )	pH
The Watarase River	1.45 (0.138 $\text{mg l}^{-1}$ )	1.6 (0.15 $\text{mg l}^{-1}$ )	1.41	7.1
	2.48 (0.236 $\text{mg l}^{-1}$ )	2.6 (0.25 $\text{mg l}^{-1}$ )	2.39	7.5
	4.10 (0.389 $\text{mg l}^{-1}$ )	5.2 (0.49 $\text{mg l}^{-1}$ )	2.77	7.5
The Ayase River	2.97 (0.282 $\text{mg l}^{-1}$ )	2.9 (0.28 $\text{mg l}^{-1}$ )	5.07	7.6
The Naka River	2.90 (0.276 $\text{mg l}^{-1}$ )	2.9 (0.28 $\text{mg l}^{-1}$ )	4.48	7.6
	2.00 (0.190 $\text{mg l}^{-1}$ )	2.3 (0.21 $\text{mg l}^{-1}$ )	5.30	7.3
	2.87 (0.273 $\text{mg l}^{-1}$ )	2.6 (0.25 $\text{mg l}^{-1}$ )	4.27	7.5

Subsequently, we examined the treatment with activated carbon by measuring seven samples from the Tone River. First, we investigated the differences of phosphate concentrations in the samples before and after treatment with activated carbon. For the measurements of phosphate concentration, we used a commercially available water-quality measurement system (DR/2000; Hach Company, USA) based on a modified molybdenum blue method. However, the results indicated no differences of phosphate concentration by the treatment with activated carbon (Table 3). In these results, the measurements by this method were not affected by the dissolved substances in various environmental waters containing 1.41–5.30  $\text{mg l}^{-1}$  BOD.

### 3.5. Comparison between our phosphate-ion sensor and a commercial method

The results obtained by the phosphate-ion sensor (treatment with activated carbon) and by the commercial sensing system (DR/2000) were compared (Table 3). Both results showed good agreement. Fig. 4 shows the relationship between both results. The correlation coefficient for these results was 0.94. The concentration of phosphate ion obtained by the commercial sensing system were slightly lower than that obtained by our sensor due to the higher detection limit of our sensor.

## 4. Conclusions

We have constructed a trial sensor system for the measurement of phosphate ion in environmen-

tal water. In this system, PyrOxG was used, and the optimized sensor system proved to be highly sensitive (96 nM phosphate ion). It had a wide calibration range from 96 nM to 32  $\mu\text{M}$ , high reproducibility, and good stability (2 weeks for 0.16  $\mu\text{M}$  phosphate ion) at precisely controlled temperature. We investigated the effects of coexisting substances in environmental water on sensor response, decreasing the effects by treatment with activated carbon. By means of this treatment, we realized a highly sensitive detection of phosphate ion in environmental water. The comparison of the results between our phosphate-ion sensor and the commercial method showed good agreement and a correlation coefficient of 0.94.

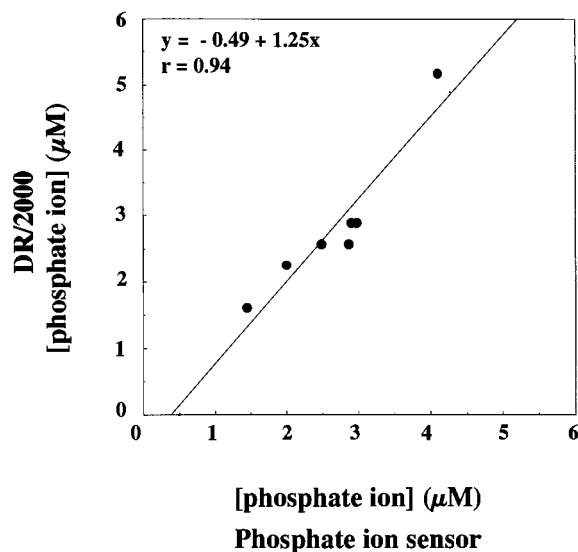


Fig. 4. Comparison between our phosphate-ion sensor and a commercial method.

Our phosphate-ion sensing system would be available in the near future as a simple, economical, and harmless method for the detection of phosphate ion.

### Acknowledgements

The authors gratefully acknowledge the financial support for this work from the Water Resources Environment Technology Center and the Association of Electrical Engineering, and the supply of samples of environmental water from the Kanto Engineering Laboratory, the Ministry of Construction.

### References

- [1] L.L. Keup, *Water Res.* 2 (1968) 373.

- [2] E. Watanabe, H. Endo, K. Toyama, *Biosensors* 3 (1988) 297.
- [3] APHA AWWA WPCF, 14th ed. 1976, p. 466.
- [4] U. Wollenberger, F. Schubert, W.F. Scheller, *Sensors Actuators B* 7 (1992) 412.
- [5] N. Conrath, B. Grundig, K. Huwel, K. Cammann, *Anal. Chim. Acta* 309 (1995) 47.
- [6] K. Ikebukuro, R. Nishida, H. Yamamoto, Y. Arikawa, H. Nakamura, M. Suzuki, I. Kubo, T. Takeuchi, I. Karube, *J. Biotechnol.* 48 (1996) 67.
- [7] H. Nakamura, H. Yamamoto, I. Kubo, M. Suzuki, K. Hayashi, S. McNiven, K. Ikebukuro, I. Karube, *Biosens. Bioelectron.* 12 (1998) 959.
- [8] M. Suzuki, H. Kurata, Y. Inoue, H. Shin, I. Kubo, H. Nakamura, K. Ikebukuro, I. Karube, *Denki Kagaku* 66 (1998) 579.
- [9] H. Misaki, Y. Horiuchi, K. Matsuura, Japanese Patent, 58-40465, 1983.
- [10] K. Tabata, T. Murachi, I. Imai (Ed.), Hirokawa Publishing, Tokyo, 1989, pp. 242–248 [in Japanese].
- [11] K. Hayashi, S. Sasaki, K. Ikebukuro, I. Karube, *Anal. Chim. Acta* 329 (1996) 127.
- [12] S.G. Schulmann, *Molecular Luminescence Spectroscopy: Methods and Applications—Part 1*, Wiley, New York, 1985, p. 463.

# Complexation and determination of palladium (II) ion with *para*-Cl-phenylazo-R-acid spectrophotometrically

Wageih Georgy Hanna \*

Chemistry Department, Faculty of Science, Ain Shams University, Abbassia, Cairo 11566, Egypt

Received 24 November 1998; accepted 5 March 1999

## Abstract

The complexation of *para*-Cl-phenylazo-R-acid azo dye with Pd(II) has been studied spectrophotometrically. Protonation constant ( $pK_a$ ) of the ligand has been calculated and the stability conditional constants of *para*-Cl-phenylazo-R-acid ligand with palladium ion has been determined at a constant temperature (25.0°C), where the molar ratio of this complex is 1:1 (metal:ligand) with  $\log \beta_1 = 3.75$ , and 1:2 with  $\log \beta_2 = 8.55$ . Solid complex of *para*-Cl-phenylazo-R-acid has been prepared and characterized on the basis of elemental analysis and FTIR spectral data. A procedure for the spectrophotometric determination of Pd(II) using *para*-Cl-phenylazo-R-acid as a new azo chromophore is proposed where it is rapid, sensitive and highly specific. Beer's law was obeyed in the range 0.50–10.00 ppm at pH 5.0–6.0 to form a violet–red complex ( $\epsilon = 7.7 \times 10^4 \text{ l}^{-1} \text{ mol}^{-1} \text{ cm}^{-1}$  at  $\lambda_{\text{max}} = 560 \text{ nm}$ ). Metal ions such as Cu(II), Cr(III), La(III), Yb(III), Y(III), and Rh(III) interfere with the complex. Ammonium salt of trimellitic acid is used to precipitate some of the interfering ions and a scheme for separation of Pd(II) from a synthetic mixture similar in composition to platinum ore or deposit was made. © 1999 Elsevier Science B.V. All rights reserved.

**Keywords:** Palladium; Spectrophotometry; *para*-Cl-phenylazo-R-acid

## 1. Introduction

R-salt (2-hydroxy-naphthalene-3,6-disulphonic acid, disodium salt) is used for the production of azo dyes which apply for many purposes, e.g. as dyeing sausage casings [1,2], pharmaceutical preparations [3], and tissue cultures [4]. Issa et al. [5] studied absorption spectra of mono azo com-

pounds in organic solvents of varying pH. The UV, and visible spectra of these compounds were examined and the  $pK_a$  values were determined via the pH dependence of the absorbency.

Extensive studies of the composition of the metal complexes of hydroxyazo compounds were carried out by Pfeiffer et al. [6] and Snaveley et al. [7]. Azo derivatives possessing one-hydroxy group yield 1:2 complexes, but those with dihydroxy substituents produce 1:1 complexes. Bis azo

\* Tel.: +20-2-484-3118; fax: +20-2-483-1836.



derivatives of chromotropic acid were used successfully as photometric reagents for palladium over a wide range of acidity below pH 5.0 without interference from other platinum metals [8]. In acid medium suitable for the formation of Pd(dithizone)<sub>2</sub> ( $\epsilon = 3.55 \times 10^4 \text{ l}^{-1} \text{ mol}^{-1} \text{ cm}^{-1}$  at  $\lambda_{\text{max}} = 635 \text{ nm}$ ), other noble metals {Au(III), Pt(II), Ag(I), Hg(II), and Cu(II)} also react with dithizone. Palladium and platinum can be determined successively with dithizone in SnCl<sub>2</sub>, silver is masked by chloride while iodide masks interfering gold and mercury [9]. PAR {4-(2-pyridylazo)-resorcinol} is used for spectrophotometric determination of Pd(II) at pH 4.0 or 10.5 ( $\epsilon = 1.8 \times 10^4 \text{ l}^{-1} \text{ mol}^{-1} \text{ cm}^{-1}$  at  $\lambda_{\text{max}} = 510 \text{ nm}$ ) [10], sulphochlorophenolazorhodanine [11], and palladiazole ( $\epsilon = 5.7 \times 10^4 \text{ l}^{-1} \text{ mol}^{-1} \text{ cm}^{-1}$  at  $\lambda_{\text{max}} = 640 \text{ nm}$ ) [12]. Other compounds also proposed for determining palladium(II) include Arsenazo III [13], 2-pyridylhydrazone [14], 2,2'-dipyridyl-2-pyridylhydrazone [15], and substituted formazans [16], 3-(5'-tetrazolylazo)-2,6-diaminotoluene ( $\epsilon = 5.2 \times 10^4 \text{ l}^{-1} \text{ mol}^{-1} \text{ cm}^{-1}$  at  $\lambda_{\text{max}} = 536 \text{ nm}$ ) [17], 5-(5-nitro-2-pyridylazo)-2,4-diaminotoluene ( $\epsilon = 1.25 \times 10^5 \text{ l}^{-1} \text{ mol}^{-1} \text{ cm}^{-1}$  at  $\lambda_{\text{max}} = 592 \text{ nm}$ ) where the sensitivities of some typical reagents for palladium is included [18]. Chromo Azurol S was used as an indicator for spectrophotometric determination of Pd(II) in acetate buffer solution [19]. Also determination of Pd(II) with tin(II) chloride and Rhodamine 6G after flotation was been made [20]. Complexation of R-acid azo dye derivatives with some trivalent lanthanide has been studied potentiometrically by the author [21].

From the foregoing literature survey it was found that there was no work available on the R-acid azo dye complexes especially on palladium ion in solution, so this work is devoted to determine the ionization constant ( $\text{p}K_{\text{a}}$ ) of *para*-Cl-phenylazo-R-acid ligand spectrophotometrically and their use as a new azochromophoric reagent for the determination of Pd(II). Further insight on the possible structure of [*para*-Cl-phenylazo-R-acid: Pd] complex has been investigated by elemental analysis {C, H, N, S, and Pd}, and FTIR, also the stability constants of

the complex have been determined. Determination of Pd(II) from a synthetic mixture similar in composition to platinum ore or deposit has been made and the procedure was applied for determination of Pd(II) in the real samples taken from ultramafic rocks of the Bird River Sill, SE Manitoba, Canada.

## 2. Experimental

### 2.1. Materials

The palladium chloride used was AR grade and their solution was prepared by dissolving the calculated amount in the least amount of concentrated HCl (to prevent hydrolysis) and diluted with carbonate free-double distilled water up to the appropriate volume. The solution was standardized by potentiometric back titration of excess iodide with standard mercury(II) solution using silver amalgam as the indicator electrode [22]. Azo dye was prepared by coupling the diazotized corresponding amines with R-acid in sodium hydroxide solution [23], the resulting precipitate was recrystallized by the method of Mehata et al. [24].

### 2.2. Universal buffer solutions

A series of buffer solutions covering the range of pH values 2.0–12.0 were prepared as recommended by Britton [25], the pH of buffer solutions were checked with the aid of a Beckman pH-meter fitted with a combined glasscalomel electrode where it's accurate to  $\pm 0.05$  pH unit.

### 2.3. Spectral measurements

The visible spectra of the compounds investigated were obtained at a constant temperature (25.0°C) using thermostatically a Spekol S spectrophotometer and a Beckman DK2 spectrophotometer.

## 2.4. FTIR spectra

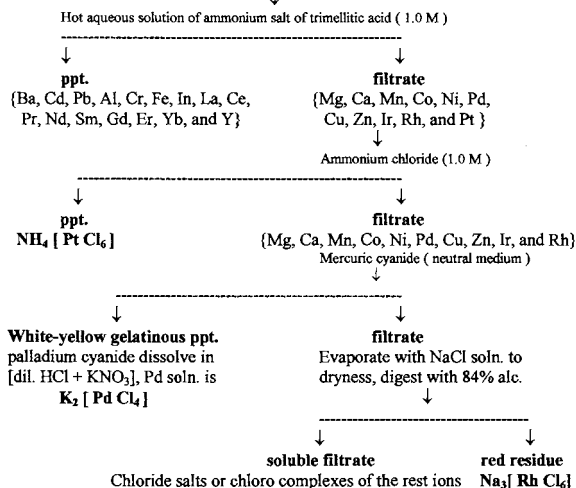
The infrared spectra was obtained by the aid of a MATTSON 1000 FTIR spectrometer from 4000 to 400  $\text{cm}^{-1}$  using KBr disc technique.

## 2.5. Absorption spectra in buffer solutions

The absorption spectra of the azo dye under investigation was studied in a buffer solution of varying pH values. For this purpose a known volume (0.3–0.8 ml  $\times 10^{-3}$  M) of the aqueous solution of the azo compound was added to 8.0 ml of the buffer solution in a 10.0 ml volumetric flask dropwise with continuous shaking. The mixture was then made to the mark with the buffer solution. The present spectral measurements were confined to the visible region. The study carried out in this part considers mainly two points viz. the effect of pH on absorption spectra and the determination of the acid dissociation constants of the –OH group using different methods of calculation: (i) half height method [26]; (ii) limiting absorbance method [26].

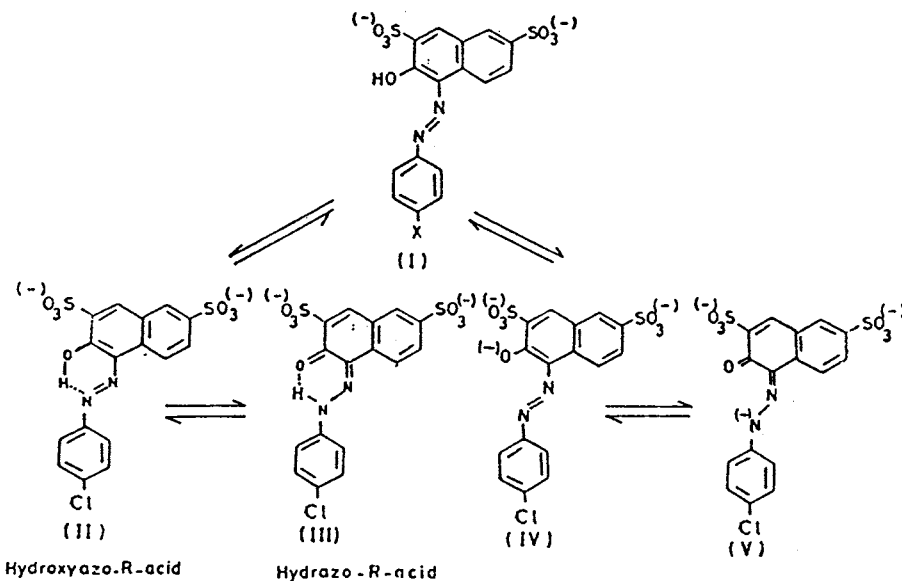
## 2.6. Scheme for separation of palladium from platinum ore or deposit

{ Mg(II), Ca(II), Ba(II), Mn(II), Fe(II), Co(II), Ni(II), Pd(II), Cu(II), Zn(II), Cd(II), Pb(II), Al(III), Cr(III), Fe(III), In(III), Ir(III), Rh(III), La(III), Ce(III), Pr(III), Nd(III), Sm(III), Gd(III), Er(III), Yb(III), Y(III), and Pt(IV) }



## 2.7. Procedure

To a 1.0 ml solution containing (0.50–10.00 ppm) of  $\text{Pd}^{2+}$ , add 2.0 ml ( $10^{-5}$  M) ligand, 5.0 ml buffer plus 1.5 ml isopropyl alcohol, complete with water up to 10.0 ml, and measure the absorbance at 560–570 nm against a blank contain-



ing the same ingredients except  $\text{Pd}^{2+}$ . Compute the concentration of  $\text{Pd}^{2+}$  by extrapolation from a standard calibration curve prepared in the same manner. The present method is simple, rapid, reliable, reproducible, and highly selective. Analysis of Pd(II) ion shows an average recovery of 100.025% with a standard deviation (S.D.) equal to 0.05%, in the presence of interfering ions {Al(III), Cr(III)} the average recovery was 99.950% with a S.D. equal to 0.06%, in presence of non interfering ions {Fe(II), Mn(II), Ca(II), Pt(IV)} the average recovery was 100.160% with a S.D. equal to 0.06%, and in presence of all ions {Al(III), Cr(III), Fe(II), Mn(II), Ca(II), Pt(IV)} the average recovery was 99.840% with a S.D. equal to 0.06% (four concentrations of Pd(II), each one determined three times) indicating the reproducibility of the present method (Table 1).

### 2.8. Analysis of a synthetic mixture similar in composition to platinum ore

Dissolve separately the following salts (in 0.01 g scale) {Mg(II), Ca(II), Ba(II), Mn(II), Fe(II), Co(II), Ni(II), Pd(II), Cu(II), Zn(II), Cd(II), Hg(II), Pb(II), Al(III), Cr(III), Fe(III), In(III), Ir(III), Rh(III), La(III), Ce(III), Pr(III), Nd(III), Sm(III), Gd(III), Er(III), Yb(III), Y(III), and Pt(IV)} (as chloride or nitrate form) in small amounts of water and then mix together. Then add 50 ml of hot 0.50 M trimellitic acid, ammonium salt, and the resulting mixture is then subjected to strong stirring for 30 min, cooled, filtered and washed with water several times. The precipitate contains the following ions {Cd, Hg, Ba, Pb, Al, In, Fe, Cr, La, Ce, Pr, Nd, Sm, Gd, Er, Yb, and Y} as trimellitate residues [27], while the filtrate contains the rest of the ions {Mg, Ca, Mn, Co, Ni, Pd, Cu, Zn, Ir, Rh, and Pt}. The resulting solution was boiled till dryness and 5.0 ml of concentrated [(HCl:HNO<sub>3</sub>); 1:1 v/v] are added to decompose and evaporate any volatile matters, then cooled and diluted to 50.0 ml with H<sub>2</sub>O. Add 20.0 ml of 0.50 M NH<sub>4</sub>Cl, stir for 10 min, filter and wash with water several times. The precipitate is ammonium chloroplatinate while the filtrate contains the remaining ions in the chloride forms. This filtrate is stirred with 0.10 M mercuric

cyanide in neutral medium for 10 min, a white–yellow gelatinous precipitate (palladium cyanide) was separated, washed carefully, and dissolved with dilute HCl + KNO<sub>3</sub> in a fuming-cupboard where the resulting solution is K<sub>2</sub>[Pd Cl<sub>4</sub>], which is ready for analysis by *para*-Cl-phenylazo-R-acid. The filtrate resulting from the cyanide treatment is subjected to evaporation with saturated NaCl solution to dryness to drive off hydrogen cyanide, the residues were digested with 84% ethyl alcohol (sp.gr. 0.837) to extract the chloride salts or chloro complexes of {Mg, Ca, Mn, Co, Ni, Cu, Hg, and Ir}, which pass into the solution while chlororhodate remains as a dark-red powder. By this modified scheme (Wollaston's process), Pd(II) can be separated from any platinum ore or deposit and subjected for determinations using the above procedure. This scheme was tested for Pd(II) concentration range from 10<sup>-4</sup> to 10<sup>-1</sup> g, and all results are very reliable, reproducible, highly selective, and simple.

### 2.9. Application

As an application of the scheme and procedure given above for determination of Pd in a real sample, palladium and platinum in ultramafic rocks of the Bird River Sill, SE Manitoba, Canada [28], have been determined, where the major elements in the crackle zone (93–121 m) are, SiO<sub>2</sub> (38.0–37.1%), Al<sub>2</sub>O<sub>3</sub> (7.06–5.03%), CaO (3.56–2.61%), MgO (30.0–32.3%), Fe<sub>2</sub>O<sub>3</sub> (5.68–7.49%), MnO (0.16–0.17%), the concentration of palladium increases up to 84.0 ppb and fluctuates between 70 and 300 ppb throughout most of the remainders of this zone. Platinum closely follows the enrichment pattern of Pd but at 1/3 to 1/4 concentration. In the thin periodic unit zone (37–48 m) a slightly elevated concentration of S (0.40–1.00%), Cr<sub>2</sub>O<sub>3</sub> (0.30–1.90%) and a significant Pd and Pt concentration increase up to 350 ppb and fluctuates between 300 and 500 ppb, Pt closely follows the pattern of Pd but at 1/2 to 1/3 concentration. The major elements present in the above sample are Si, Mg, Al, Ca, Fe, while the minor elements are Mn, Cr, Pt, and Pd, when subjected to separation by ammonium salts of trimellitic acid, it precipitates Al, Cr, Fe, and Si, while Mn,

Table 1  
Spectrophotometric determination of Pd(II) using para-Cl-phenylazo-R-acid in presence of different interfering ions\*

Metal ion	Concentration taken (ppm)	Concentration found (ppm)	Recovery (%)	S.D. (%)
Pd(II)	4.00, 4.00, 4.00	4.00, 4.00, 4.00	100.000	0.05
	6.00, 6.00, 6.00	6.00, 6.00, 6.00	100.000	
	8.00, 8.00, 8.00	8.00, 8.00, 8.00	100.000	
	10.00, 10.00, 10.00	10.01, 10.00, 10.02	100.100	
Pd(II) + Al(III)	4.00, 4.00, 4.00	4.00, 4.00, 4.00	100.000	0.12
	6.00, 6.00, 6.00	6.01, 6.00, 6.02	100.160	
	8.00, 8.00, 8.00	8.00, 8.00, 8.00	100.000	
	10.00, 10.00, 10.00	9.99, 10.00, 9.98	99.900	
Pd(II) + Cr(III)	4.00, 4.00, 4.00	4.00, 4.00, 4.00	100.000	0.08
	6.00, 6.00, 6.00	6.01, 6.00, 6.02	100.160	
	8.00, 8.00, 8.00	8.01, 8.00, 8.02	100.125	
	10.00, 10.00, 10.00	10.00, 10.00, 10.00	100.000	
Pd(II) + Al(III) + Cr(III)	4.00, 4.00, 4.00	3.99, 4.00, 3.98	99.750	0.17
	6.00, 6.00, 6.00	6.01, 6.00, 6.02	100.160	
	8.00, 8.00, 8.00	8.00, 8.00, 8.00	100.000	
	10.00, 10.00, 10.00	9.99, 10.00, 9.98	99.900	
Pd(II) + Fe(II)	4.00, 4.00, 4.00	4.00, 4.00, 4.00	100.000	0.05
	6.00, 6.00, 6.00	6.00, 6.00, 6.00	100.000	
	8.00, 8.00, 8.00	8.00, 8.00, 8.00	100.000	
	10.00, 10.00, 10.00	10.01, 10.00, 10.02	100.100	
Pd(II) + Mn(II)	4.00, 4.00, 4.00	4.00, 4.00, 4.00	100.000	0.08
	6.00, 6.00, 6.00	6.02, 6.00, 6.01	100.160	
	8.00, 8.00, 8.00	8.00, 8.00, 8.00	100.000	
	10.00, 10.00, 10.00	10.00, 10.00, 10.00	100.000	
Pd(II) + Ca(II)	4.00, 4.00, 4.00	4.01, 4.02, 4.00	100.250	0.10
	6.00, 6.00, 6.00	6.01, 6.00, 6.02	100.160	
	8.00, 8.00, 8.00	8.01, 8.02, 8.00	100.125	
	10.00, 10.00, 10.00	10.00, 10.00, 10.00	100.000	
Pd(II) + Pt(IV)	4.00, 4.00, 4.00	4.00, 4.00, 4.00	100.000	0.08
	6.00, 6.00, 6.00	6.01, 6.02, 6.00	100.160	
	8.00, 8.00, 8.00	8.00, 8.00, 8.00	100.000	
	10.00, 10.00, 10.00	10.01, 10.00, 10.02	100.100	
Pd(II) + Fe(II) + Mn(II) + Ca(II) + Pt(IV)	4.00, 4.00, 4.00	4.01, 4.00, 4.02	100.250	0.06
	6.00, 6.00, 6.00	6.01, 6.02, 6.00	100.160	
	8.00, 8.00, 8.00	8.01, 8.01, 8.01	100.125	
	10.00, 10.00, 10.00	10.01, 10.01, 10.01	100.100	
Pd(II) + Al(III) + Cr(III) + Fe(II) + Mn(II) + Ca(II) + Pt(IV)	4.00, 4.00, 4.00	3.99, 4.00, 3.98	99.750	0.06
	6.00, 6.00, 6.00	5.99, 6.00, 5.98	99.833	
	8.00, 8.00, 8.00	7.99, 7.99, 7.99	99.875	
	10.00, 10.00, 10.00	9.99, 10.00, 9.98	99.900	

\* Thirty fold concentration of different interfering metal ions {Al(III), Cr(III)} and non-interfering metal ions {Fe(II), Mn(II), Ca(II), Pt(IV)} were added to the Pd(II) ion and were separated according to the scheme of separation.

Ca, Mg, Pt, and Pd remain in solution, when this solution is treated with ammonium chloride,

Pt is separated as  $\text{NH}_4[\text{PtCl}_6]$  and is recovered, while the rest of the solution is treated with

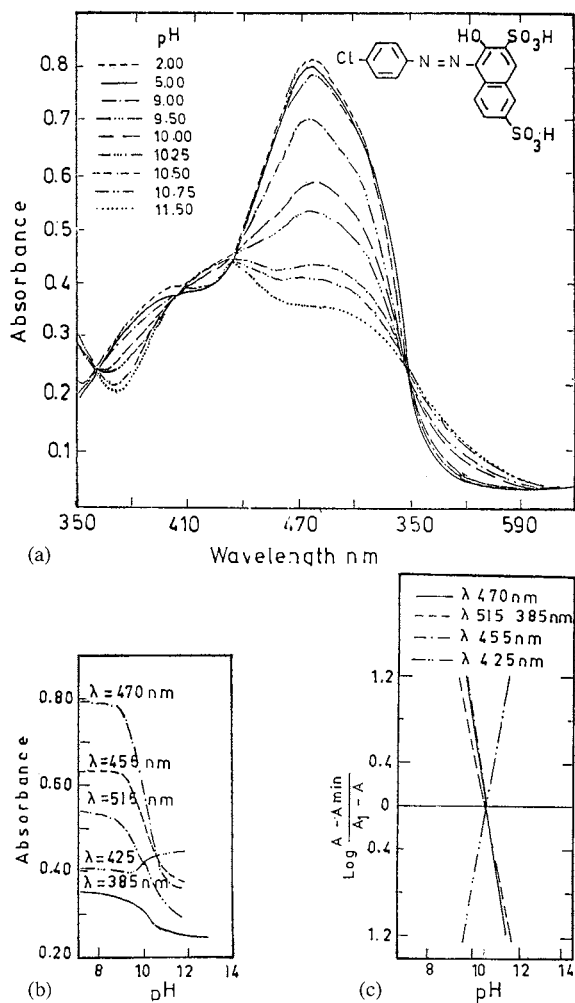


Fig. 1. (a) Absorption spectra of  $4 \times 10^{-5}$  M of *p*-Cl-phenylazo-R-acid in aqueous solution of varying pH values. (b) Absorbance-pH curves (half height method). (c)  $\text{Log}(A - A_{\text{min}})$ -pH curves (limiting absorbance method).

$\text{Hg}(\text{CN})_2$  to precipitate Pd as  $\text{Pd}(\text{CN})_2$  and is recovered.

### 3. Results and discussion

The absorption of some *para*-Cl-phenylazo-R-acid was studied in aqueous buffer solutions in the visible region (Fig. 1a). The azo compounds display mainly a broad band in the visible region which was assigned as  $n-\pi^*$  transition within the

azo linkage influenced by intramolecular charge transfer. The band was observed in the R-acid azo dye investigated in the range 460–490 nm and a shoulder located at longer wavelength and this was attributed to the participation of the hydrazoquinone tautomerism before neutralization (structure I and II) and to the oscillation of the negative charge between the phenolic oxygen and the azo group after neutralization (structure IV and V). This band was greatly affected by the  $[\text{H}^+]$  concentration as the -OH group undergoes ionization which leads to a hypochromic effect, such variation was used in calculating the ionization constant ( $\text{p}K_a$ ) of the hydroxyl group.

A secondary band was observed in the range 380–410 nm which is assigned as  $\pi-\pi^*$  transition with the hydrogen chelate ring. This is confirmed by the disappearance of this band in alkaline solutions due to the ionization of the -OH group and the rupture of the hydrogen bond ring. Clear isosbestic points are observed in the spectra of azo-compound under investigation in buffer solutions indicating the existence of an equilibrium between the non-ionized and ionized -OH group,

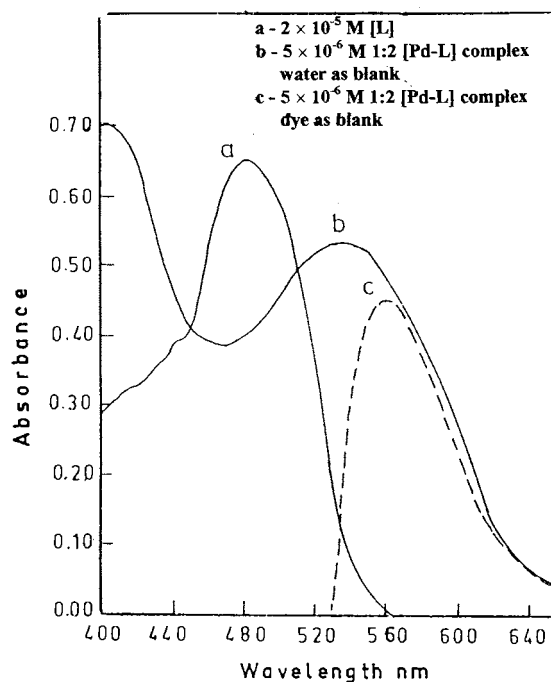


Fig. 2. Absorption spectra of [Pd-L] complex in universal buffer at pH 6.0.

i.e. an acid–base equilibrium where the neutral species (II and III) are predominated in solution of the lower pH values and the ionized species (IV and V) are existing in solution at high pH values.

The ionization constant value ( $pK_a$ ) of naphthalenic –OH group in the present investigation has been determined by two methods; (i) half height method [26], which is represented in Fig. 1(b), and the  $pK_a = 10.67$ , and (ii) limiting absorbance method [26], which represented in Fig. 1(c) and the  $pK_a = 10.68$ .

The results obtained are comparable to those derived from 1-(6-quinolinoyl-azo)-2-naphthol [29] which are determined spectrophotometrically, and with the result of the R-acid azo dye which are determined potentiometrically [21]. The ionization of the strong sulphonic groups takes place at lower pH values and the ionization constants values ( $pK_a$ s) are in the order of magnitude of 4 [30]. Moreover such ionization does not cause any spectral changes due to the ionizable proton in the sulphonic groups which is not directly attached to the  $\pi$  system of the molecule.

### 3.1. Spectrophotometric studies of [palladium(II);para-Cl-phenylazo-R-acid] complex

Palladium forms a violet-red coloured complex with ligands using a universal buffer at pH 6.0,

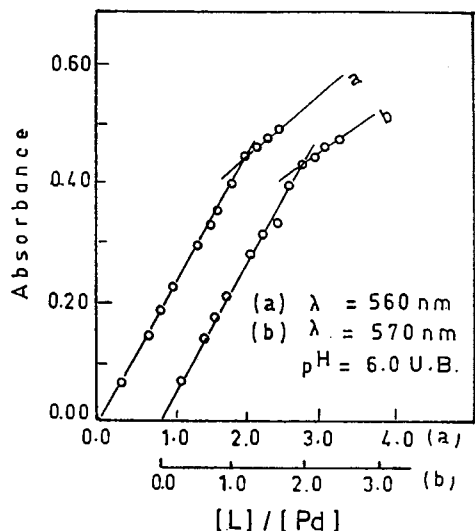


Fig. 3. Molar ratio method of [Pd-L] complex.

where  $\lambda_{\text{max}} = 560 \text{ nm}$  which was selected as the optimum wavelength to be used for studying other factors influencing the formation of the complex, Fig. 2. The effect of some common organic solvents (methyl alcohol, ethyl alcohol, isopropyl alcohol, and acetone) on the color intensity of the complex showed that, 15% of isopropyl alcohol is the best in presence of universal buffer (pH 6.0), where optical density (OD) = 0.44. Under the optimum conditions stated above it was found that a minimum of 0.50 ppm of Pd(II) can be determined with fair accuracy and precision, indicating high sensitivity. The influence of the sequence of addition on the complex was found that, dye  $\rightarrow$  buffer  $\rightarrow$  metal  $\rightarrow$  and solvent.

The complex is completely formed after 3 min and remains stable for 24 h in all recommended media. The stability of the complex ( $5 \times 10^{-6} \text{ M}$ ) indicates that boiling has no effect on its stability.

### 3.2. Molar ratio of complex [M:L ratio]

#### 3.2.1. The molar ratio method [31]

The optical density-molar ratio relationship indicates that the probable formation of one complex having the composition 1 Pd:2 L where  $\log \beta_2 = 8.27$ , Fig. 3.

#### 3.2.2. The continuous variation method [32]

A plot of the optical densities against the mole fraction of Pd(II) indicates that the probable formation of one complex having the composition 1 Pd: 2 L, where  $\log \beta_2 = 8.85$ .

#### 3.2.3. The limiting logarithmic method [33]

The results obtained by this method show that the probable existence of two types of complexes 1 Pd:1 L and 1 Pd:2 L, where  $\log \beta_1 = 3.75$ , and  $\log \beta_2 = 8.55$ .

### 3.3. Abeyance of Beer's law

The optical densities of complexes formed at  $\lambda_{\text{max}} = 560 \text{ nm}$  with universal buffer (pH = 6.0), acetate buffer (pH = 5.0), and 0.1 N sodium acetate show a straight line passing by the origin, i.e. obeying Beer's law and the value of the molar absorption coefficients ( $\epsilon$ ) amount to  $7.7 \times 10^4$ ,

$6.7 \times 10^4$ , and  $6.3 \times 10^4 \text{ l}^{-1} \text{ mol}^{-1} \text{ cm}^{-1}$  respectively.

By the aid of the [Pd:L] complex formed we can determine Pd(II) is in range 0.50–10.0 ppm.

### 3.4. Influence of foreign ions

The data led to the conclusion that up to thirty fold of  $\{\text{Na}^+, \text{K}^+, \text{Tl}^+, \text{Ag}^+, \text{Cl}^-, \text{Br}^-, \text{I}^-, \text{VO}_4^{3-}, \text{Mg}^{2+}, \text{Ca}^{2+}, \text{Sr}^{2+}, \text{Zn}^{2+}, \text{Cd}^{2+}, \text{Hg}^{2+}, \text{Mn}^{2+}, \text{Fe}^{2+}, \text{Co}^{2+}, \text{Ni}^{2+}, \text{ZrO}^{2+}, \text{UO}_2^{2+}, \text{Pt}^{2+}, \text{SO}_4^{2-}, \text{B}_4\text{O}_7^{2-}, \text{WO}_4^{2-}, \text{MoO}_4^{2-}, \text{Bi}^{3+}, \text{Au}^{3+}, \text{Ce}^{3+}, \text{Pt}^{4+}, \text{and Th}^{4+}\}$ , ions do not interfere. On the other hand  $\text{CN}^-, \text{Cu}^{2+}, \text{Pb}^{2+}, \text{Al}^{3+}, \text{Cr}^{3+}, \text{La}^{3+}, \text{Yb}^{3+}, \text{Y}^{3+}, \text{Rh}^{3+}$ , and  $\text{EDTA}^{2-}$  ions do interfere.

### 3.5. Infrared spectra study

The FTIR spectra of the *para*-Cl-phenylazo-R-acid, disodium salt [HL] ligand, Fig. 4(a), and

$\text{Na}_4[\text{Pd}(\text{L})_2 \cdot 2\text{H}_2\text{O}]$  complex Fig. 4(b) are recorded in the solid state as KBr discs which illustrate the different bands arising from the functional groups in these compounds and are analyzed in a way similar to that given by Looker et al. [34]. Each region of the spectrum will be compared with the corresponding one of azo-dye ligand.

### 3.6. Absorption in the 4000–2600 $\text{cm}^{-1}$ region

This region involves the bands of –OH, –NH, and –SO<sub>3</sub>H groups as well as those of the C–H phenyl and C–H aliphatic and associated water molecules in the ligand [35,36]. The spectrum of [HL] contains a band at  $3480 \text{ cm}^{-1}$  which is a composite band showing the stretching frequencies of C–H and strongly the –OH stretching frequency of R-acid, this band is shifted to the lower wavelength when the chelate with Pd(II) forms [Pd:L] and it appears at  $3439 \text{ cm}^{-1}$ .

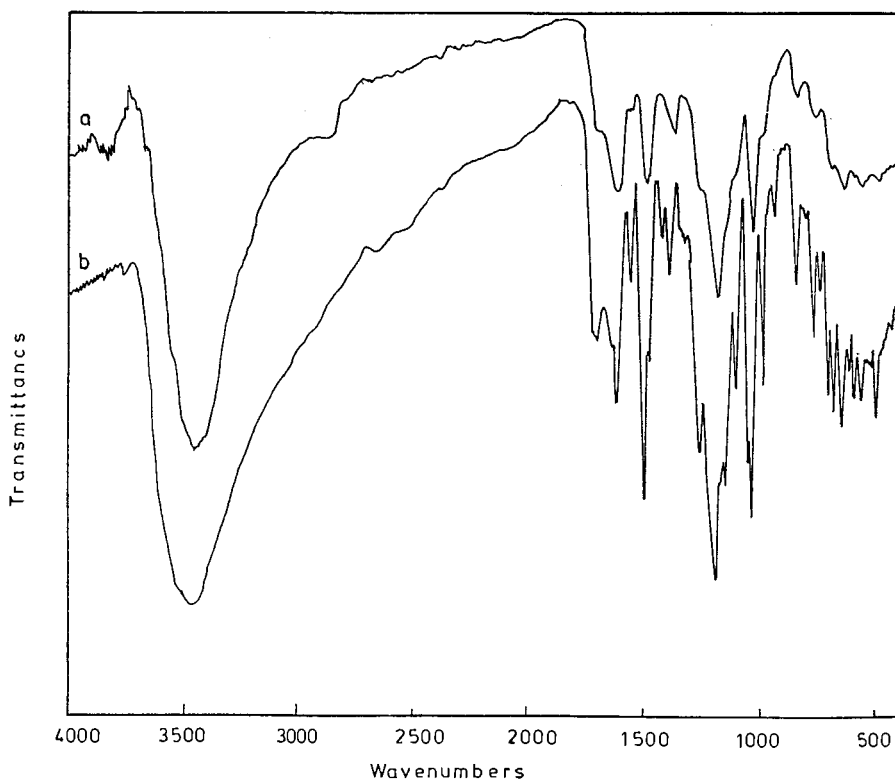


Fig. 4. FTIR spectra of *para*-Cl-phenylazo-R-acid [HL] (a), and the  $[\text{PdL}_2 \cdot 2\text{H}_2\text{O}]$  complex (b).

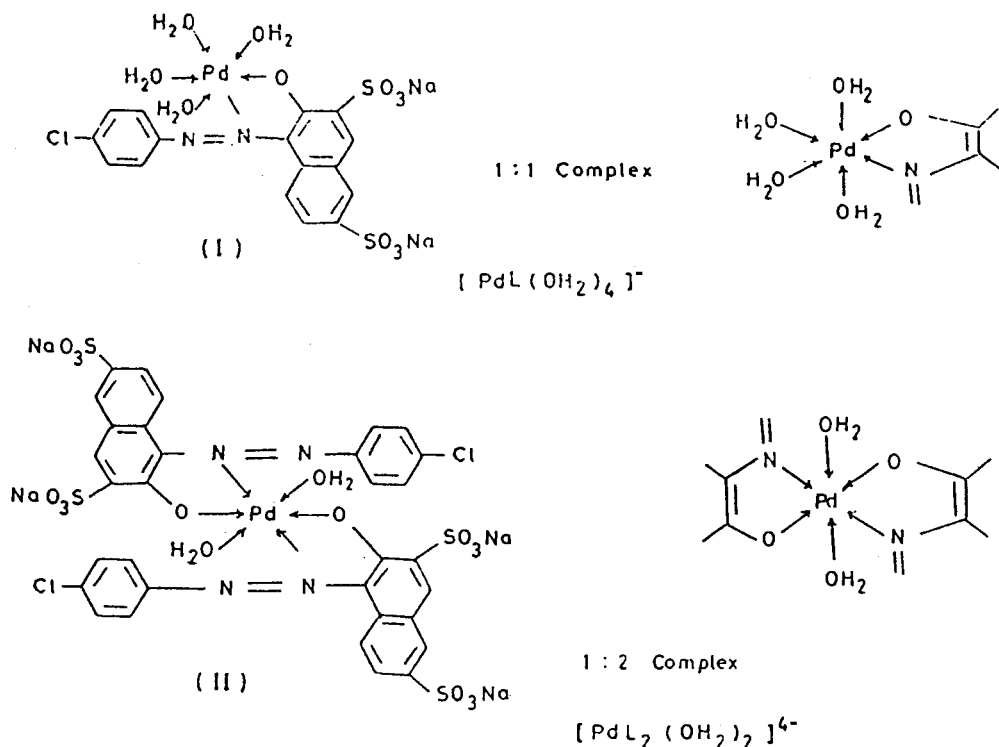


Fig. 5. Structure of  $[PdL(OH_2)_4]^-$  (1:1 complex), and  $[PdL_2(OH_2)_2]^{4-}$  (1:2 complex).

### 3.7. Absorption in the 2600–1400 $cm^{-1}$ region

This region is interesting, since it contains bands of  $>C=O$ ,  $>S=O$ ,  $HN=N^-$ , and  $>C=C<$ . The [HL] shows bands at 1616  $cm^{-1}$  which is assigned to the  $HN=N^-$  vibration which is coupled with  $C=C$  vibration and it is slightly affected by complexation to 1611  $cm^{-1}$ . Other bands which appear in this region are at 1493 and 1389  $cm^{-1}$  which can be assigned to the  $\sigma_{NH}$  and in-plane deformation of aliphatic and aromatic  $C-H$  which generally overlap with the  $\nu_{C-C}$  vibration are slightly affected by complexation and change to 1503 and 1391  $cm^{-1}$ .

### 3.8. Absorption in the 1400–1000 $cm^{-1}$ region

This region involves other bands such as the aromatic  $C-H$  in plane deformation vibration,  $C-N$  stretching vibration and  $C-C$  stretching vibration. Two bands were noticed at this region—one at 1200  $cm^{-1}$  which changes to 1198

$cm^{-1}$  while the other band at 1046  $cm^{-1}$  changes to 1040  $cm^{-1}$ . The vibration spectra of the complex showed two new bands at this region at 1271  $cm^{-1}$  which would involve an appreciable  $C-O$  stretching vibration and at 997  $cm^{-1}$  which is assigned to  $\{\sigma_{(C-O)} + \nu_{(M-O)}\}$ .

### 3.9. Absorption in the 1000–400 $cm^{-1}$ region

At this region the out of plane deformation frequencies of aromatic  $C-H$  band are expected where it is observed at 846  $cm^{-1}$  and slightly change to 843  $cm^{-1}$  on complexation while the band at 642  $cm^{-1}$  changes to 646  $cm^{-1}$  which is assigned to  $\{\text{ring}_{\text{def}} + \nu_{(C-O)}\}$ . At this region three new bands were noticed at 774  $cm^{-1}$  which were assigned as  $\{\text{ring}_{\text{def}} + \nu_{(M-OH_2)}\}$ , i.e. coordinate water molecule in this complex, another band at 571  $cm^{-1}$  which was assigned as  $\nu_{(M-N)}$ , while the third band is at 496  $cm^{-1}$  which was assigned as  $\nu_{(M-O)}$  [37,38]. From these results, the author can propose the mode of coordination of the Pd(II)



with different *para*-substituted-phenylazo-R-acid that are 1:1 and 1:2 complex which are represented in Fig. 5.

#### 4. Conclusion

This method for the determination of palladium ion ( $\text{Pd}^{2+}$ ) as a [*para*-Cl-phenylazo-R-acid]:Pd complex is simple, rapid, reliable, reproducible, and highly selective, where the S.D. for determination of 5.00 ppm Pd(II) amounts to 0.0025 indicating the reproducibility of the present method. Even though the molar absorption coefficients ( $\epsilon$ ) =  $7.7 \times 10^4 \text{ l}^{-1} \text{ mol}^{-1} \text{ cm}^{-1}$  is not high but due to the simple preparation of the ligand, cheap chemicals, and the easy way for determination it was recommended for rapid routine analysis. A comparison between the ( $\epsilon$ ) value for this complex and any other azo chromophoric reagent, the author found that ( $\epsilon$ ) is higher than the Palladiazoreagent which is sensitive and selective to Pd(II). Also the author has made a comparison between the complex formed with this new ligand and dithizone reagent and he found that the new ligand is selective to Pd(II) and not to the other noble metals such as Pt(II), Ag(I), and Au(III) which are always present in any noble metal ore. From elemental analysis and FTIR spectra of [HL], and  $\text{Na}_4[\text{Pd}(\text{L})_2 \cdot 2\text{H}_2\text{O}]$ , the author concluded that the metal–nitrogen and metal–oxygen stretching frequencies of this complex are very interesting and Pd(II) coordinates with azo dye-R-acid to form five member chelating rings with benzenoid type resonance through the  $\sigma$  coordinate bonding from the ligand to metal [39,40].

#### References

- [1] B. Winkler, Ger. Offen 2 (1973) 212–399.
- [2] B. Winkler, Appl. 15 Mar. (1972) 5, 22, 399.
- [3] J. Chistian, Soc. Tech. Pharm. 2 (1973) 117.
- [4] G.Z. Grigoraghvili, D.G. Merabishvili, S.D. Taktakishvili, M.A. Bokuchava, Soobshch Akad. Nauk. Gruz. USSR 66 (1972) 445.
- [5] I.M. Issa, R.M. Issa, M.S. El-Ezaby, Z. Physik Chem. (Leipzig), 242 (1969) 169; 244 (1970) 155; 253 (1973) 289.
- [6] P. Pfeiffer, T. Hesse, H. Pfitzner, H. Thelert, J. Prakt. Chem. 149 (1973) 217.
- [7] A. Snavey, W.C. Fernellus, R.E. Douglas, J. Soc. Dyers Colour 73 (1975) 492.
- [8] B. Budesinsky, B. Menclove, Talanta 15 (1968) 986.
- [9] Z. Marczenko, S. Kus, M. Mojski, Talanta 31 (1984) 959.
- [10] H. Flaschka, J. Hicks, Microchem. J. 11 (1969) 517.
- [11] S.B. Savvin, R.F. Propistsova, Yu.G. Rozovskill, Zh. Analit. Khim. 27 (1972) 1554.
- [12] J.A. Perez-Bustramante, Talanta 22 (1975) 769.
- [13] S.B. Savvin, R.F. Propistsova, A.L. Okhanova, Talanta 16 (1969) 423.
- [14] P.W. Beaupre, W.J. Holland, R.A. Sieler, Mikrochim. Acta II (1979) 479.
- [15] J.A. Stratis, A.N. Anthemidis, G.S. Vasilikiotis, Analyst 109 (1984) 373.
- [16] A. Kettrup, M. Grotee, Z. Anal. Chem. 293 (1978) 155.
- [17] O. Hernandez, A.I. Jimenez, J.J. Arias, J. Havel, Talanta 41 (1994) 775.
- [18] H. Yang, G. Zhang, L. Zhang, G. Liu, X. Zhang, Talanta 43 (1996) 747.
- [19] R. Ishida, Bull. Chem. Soc. Jpn. 42 (1969) 1011.
- [20] K. Kalinowski, Z. Marczenko, Anal. Chim. Acta 186 (1986) 331.
- [21] M. Zaky, W.G. Hanna, A.L. Ansary, M.M. Moawad, S.L. Stefan, Oriental J. Chem. 4 (1988) 26.
- [22] H. Khalifa, M.F. Kotry, Microchem. J. 13 (1968) 705.
- [23] M.I. Ishibashi, S. Hiashi, Jpn. Analyst 4 (1955) 14.
- [24] C.D. Mehata, K.H. Shan, Indian J. Appl. Chem. 29 (1966) 122.
- [25] H.T.S. Britton, Hydrogen Ions, 4th edition, Chapman and Hall, London, 1952.
- [26] R.M. Issa, A.H. Zewail, J. Chem. U.A.R. 14 (1971) 461.
- [27] W. Brzyska, W. Blaszezak, W. Hulicki, Mat.-Fiz.-Chem. 21 (1979) 3.
- [28] P. Theyer, Miner. Deposita 26 (1991) 165.
- [29] Y.M. Issa, R.M. Issa, and F.M. Issa, Egypt J. Chem. 18 (1975) 403, 427, 801.
- [30] G. Schwarzenbach, H. Flaschka, Complexometric Titrations, 2nd edition, Methuen, London, 1969.
- [31] J.H. Yoe, A. Jones, Indust. Eng. Chem. Analyst Ed. 16 (1944) 14.
- [32] W.C. Vosburgh, G.R. Cooper, J. Am. Chem. Soc. 63 (1941).
- [33] B. Bent, F. French, J. Am. Chem. Soc. 63 (1941) 568.
- [34] J.R. Looker, W.W. Hennerman, J. Org. Chem. 27 (1962) 381.
- [35] K. Nakamoto, The Infrared Spectra of Inorganic and Coordination Compounds, 2nd edition, Wiley Interscience, New York, 1969.
- [36] L.J. Bellamy, The Infrared Spectra of Complex Molecules, Champan and Hall, London, 1973.
- [37] E.P. Powell, N. Sheppard, Spectro. Chim. Acta 17 (1961) 68.
- [38] E.P. Powell N. Sheppard, J. Chem. Soc. (1961) 1112.
- [39] R.G. Wikins, Kinetics and Mechanism of Reaction of Transition Metal Complexes, 2nd edition, VCH, Weinheim, 1991.
- [40] A.V. Zelewsky, Stereochemistry of Coordination Compounds, Wiley, Chichester, 1996.

# Spectrophotometric determination of nitrite and nitrate using phosphomolybdenum blue complex

Nidal A. Zatar \*, Maher A. Abu-Eid, Abdullah F. Eid

*Chemistry Department, An-Najah N. University, P.O. Box 7, Nablus, Palestine, Israel*

Received 15 February 1999; received in revised form 26 April 1999; accepted 3 May 1999

## Abstract

A method for spectrophotometric determination of nitrite and nitrate is described. This method is based on the reduction of phosphomolybdic acid to phosphomolybdenum blue complex by sodium sulfide. The obtained phosphomolybdenum blue complex is oxidized by the addition of nitrite and this causes a reduction in intensity of the blue color. The absolute decrease in the absorbance of the blue color or the rate of its decrease is found to be directly proportional to the amount of nitrite added. The absorbance of the phosphomolybdenum blue complex is monitored spectrophotometrically at 814 nm and related to the concentration of nitrite present. The effect of different factors such as acidity, stability of the complex, time, temperature, phosphate concentration, molybdenum concentration, sodium sulfide concentration and the tolerance amount of other ions have been reported. Maximum absorbance is at 814 nm. The range of linearity using the conventional method is 0.5–2.0 ppm with molar absorptivity of  $1.1 \times 10^4$  l mol<sup>-1</sup> cm<sup>-1</sup>. and a relative standard deviation of 2.6% for five measurements. The range of linearity using the reaction rate method is 0.2–3.6 ppm with a relative standard deviation of 2.4% for five measurements. The method is applied for determination of nitrite and nitrate in water, meat products and vegetables. © 1999 Elsevier Science B.V. All rights reserved.

*Keywords:* Nitrate; Nitrite; Phosphomolybdenum blue; Spectrophotometry

## 1. Introduction

Nitrite is a characteristic pollutant [1]. It can react with secondary amines present in the body resulting in the formation of carcinogenic nitrosoamines [2–4]. On the other hand, when present at high concentration in blood nitrite can react

with iron(III) of the hemoglobin, forming methemoglobin which has no oxygen-carrying ability. This fatal disease is called methemoglobinemia. Nitrate also at high concentrations can be considered as pollutant since it can be reduced to nitrite. Therefore, food and drinking water with high concentration of nitrate are also dangerous. The reduction of nitrate to nitrite is possible in the stomach of infants, where the low acidity allows the growth of nitrite-reducing microorganisms.

\* Corresponding author. Tel.: +972-9-2370042; fax: +972-9-2387982.

*E-mail address:* nidalz@najah.edu (N.A. Zatar)

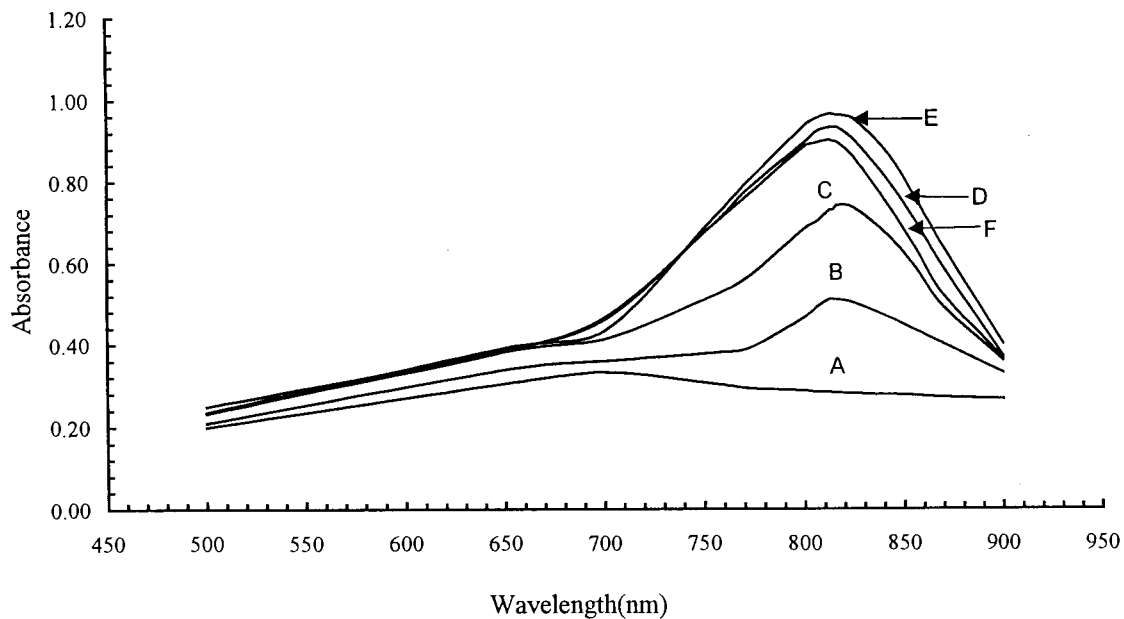


Fig. 1. Absorption spectra of phosphomolybdenum blue complex as a function of hydrochloric acid concentration: (A) 0.02 M, (B) 0.20 M, (C) 0.50 M, (D) 1.0 M, (E) 1.46 M, (F) 2.0 M. Conditions: [phosphate] =  $3.0 \times 10^{-3}$  M, [molybdenum(VI)] =  $9.0 \times 10^{-3}$  M, [sodium sulfide] =  $3.0 \times 10^{-4}$ %, temperature = 25°C, time = 30 min after mixing.

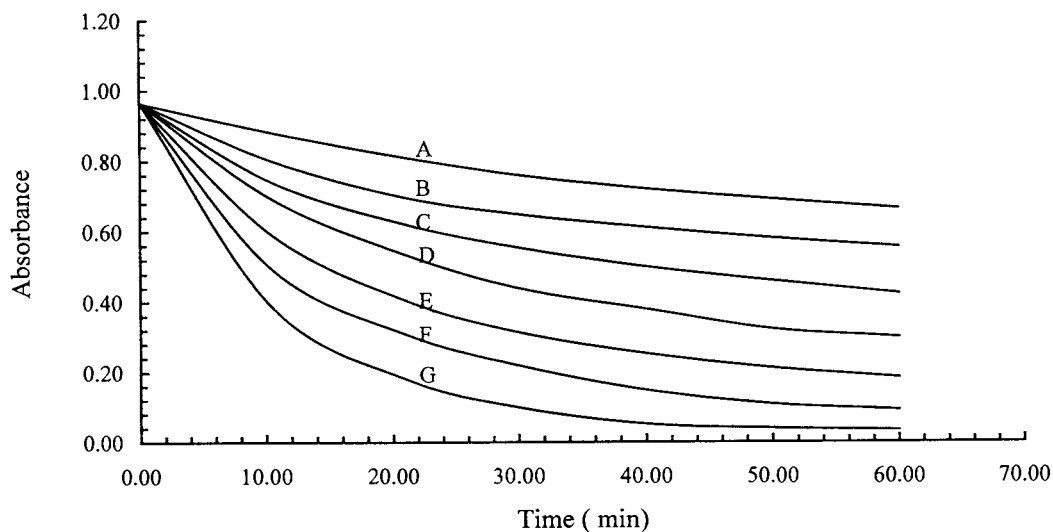


Fig. 2. Recorded absorbance–time curve for the reaction between nitrite and phosphomolybdenum blue complex. Nitrite concentration: (A)  $1.1 \times 10^{-5}$  M, (B)  $2.0 \times 10^{-5}$  M, (C)  $3.0 \times 10^{-5}$  M, (D)  $4.0 \times 10^{-5}$  M, (E)  $5.0 \times 10^{-5}$  M, (F)  $6.0 \times 10^{-5}$  M, (G)  $7.0 \times 10^{-5}$  M. Conditions: [phosphate] =  $3.0 \times 10^{-3}$  M, [molybdenum(VI)] =  $9.0 \times 10^{-3}$  M, [sodium sulfide] =  $3.0 \times 10^{-4}$ %,  $\lambda = 814$  nm, temperature = 25°C.

Table 1

Calculated molar absorptivity and range of linearity as a function of time after mixing for absorbance measurement, using the conventional method

Time of measurement (min)	Molar absorptivity ( $l \text{ mol}^{-1} \text{ cm}^{-1}$ )	Range of linearity (ppm)
10	$0.70 \times 10^4$	0.50–4.20
20	$1.00 \times 10^4$	0.50–3.70
30	$1.10 \times 10^4$	0.50–3.00
40	$1.20 \times 10^4$	0.50–2.90
50	$1.24 \times 10^4$	0.50–2.50
60	$1.25 \times 10^4$	0.50–2.40

Many methods have been reported for quantitative determination of nitrite and nitrate, including kinetic [5–8], chromatographic [9–11], potentiometric [12,13], amperometric [14], flow injection [15,16] and spectrophotometric [17–20] methods. Among the spectrophotometric methods that are adopted as an AOAC official method of analysis for nitrite and nitrate determination is its reaction with *N*-(1-naphthyl)ethylenediamine·2HCl and sulfanilamide [20]. This method requires careful control of acidity for each step of the process and causes a carcinogenic effect [21].

In the present work, a new method is proposed for the determination of nitrite and nitrate. It is based on the reduction of phosphomolybdic acid to phosphomolybdenum blue complex by sodium sulfide. The obtained phosphomolybdenum blue complex is oxidized by the addition of nitrite causing a reduction in intensity of the blue color. The decrease in the absorbance of the blue color is directly proportional to the amount of nitrite added. The absorbance of the phosphomolybdenum blue complex is monitored spectrophotometrically at 814 nm and related to the concentration of nitrite. The main advantage of the proposed method over the other methods is related to the short analysis time and the low detection limit.

## 2. Experimental

### 2.1. Chemicals

Unless otherwise stated, all chemicals and solvents used were of analytical reagent grade. Molybdenum(VI) solution 0.1 M was prepared by

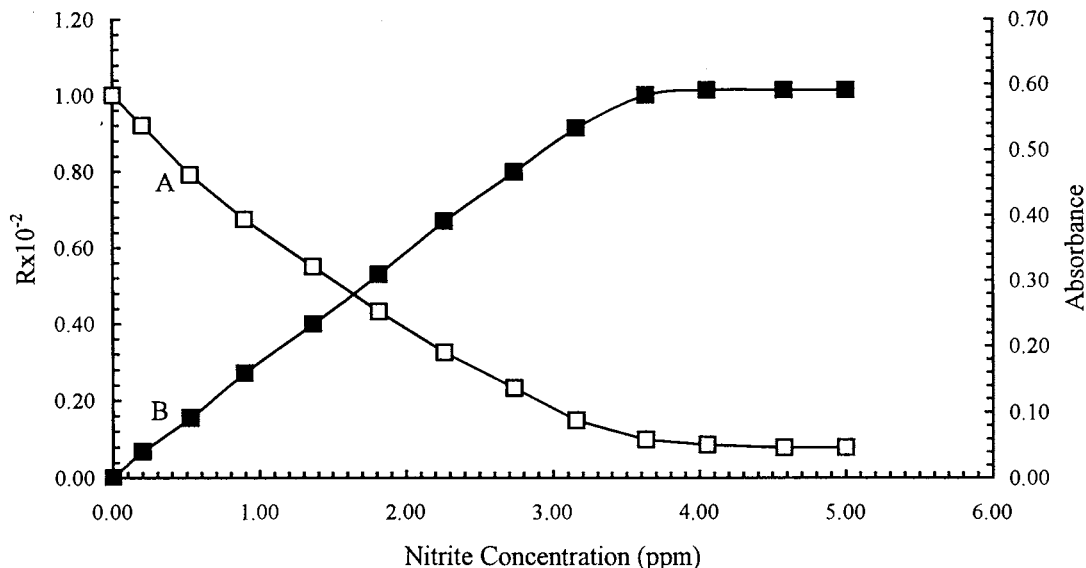


Fig. 3. Calibration curves for nitrite determination using (A) the conventional method and (B) the reaction rate method. Conditions: [phosphate] =  $3.0 \times 10^{-3}$  M, [molybdenum(VI)] =  $9.0 \times 10^{-3}$  M, [sodium sulfide] =  $3.0 \times 10^{-4}$  (w/v),  $\lambda = 814$  nm, temperature = 25°C. Absorbance was measured at  $t = 30$  min (conventional method) and  $t = 5$  min (reaction rate method).

Table 2

Interference effect of other ions on the determination of 2.1 ppm of nitrite using the proposed method

Foreign ion	Nitrite:foreign ion mole ratio	Concentration of foreign ion <sup>a</sup> (ppm)	Error <sup>b</sup> (%)
Pb <sup>2+</sup>	1:20	207.0	+20.0
Pb <sup>2+</sup>	1:10	103.0	+9.0
Pb <sup>2+</sup>	1:2	20.7	+5.0
Fe <sup>+3</sup>	1:7	20.6	-8.0
Fe <sup>+3</sup>	1:5	14.7	-1.0
Fe <sup>2+</sup>	1:5	14.7	-12.0
Fe <sup>2+</sup>	1:3	8.9	-5.5
Zn <sup>2+</sup>	1:4	13.0	-11.0
Zn <sup>2+</sup>	1:3	9.8	-6.0
Cu <sup>2+</sup>	1:8	25.4	+10.0
Cu <sup>2+</sup>	1:4	12.7	+6.0
Ni <sup>2+</sup>	1:11	32.5	-9.0
Ni <sup>2+</sup>	1:5	17.7	-4.0
Sn <sup>2+</sup>	1:10	59.5	-11.0
Sn <sup>2+</sup>	1:6	35.7	-6.0
Co <sup>2+</sup>	1:11	32.0	-12.0
Co <sup>2+</sup>	1:3	8.8	-5.0
Ag <sup>+</sup>	1:9	48.0	-10.0
Ag <sup>+</sup>	1:5	26.7	-6.0
I <sup>-</sup>	1:7	44.5	-25.0
I <sup>-</sup>	1:4	25.5	-7.0
I <sup>-</sup>	1:1	6.3	-3.5
NO <sub>3</sub> <sup>-</sup>	1:20	62.0	+9.0
Cl <sup>-</sup>	1:1000	1720.0	±3.0
Br <sup>-</sup>	1:1000	4000.0	±3.0
CH <sub>3</sub> COO <sup>-</sup>	1:1000	2950.0	±3.0

<sup>a</sup> Final concentration of foreign ion in the reaction solution.<sup>b</sup> +, positive interference, causing decrease in absorbance at 814 nm (oxidation of PMBC to PMA); -, negative interference, causing increase in the absorbance at 814 nm (reduction of PMA to PMBC); ±, no interference.

weighing accurately 1.44 g of MoO<sub>3</sub> and dissolving it in 40 ml of 1 M NaOH; the volume was completed to 100 ml with water. Potassium dihydrogen phosphate solution 0.10 M was prepared by weighing accurately 1.33 g of KH<sub>2</sub>PO<sub>4</sub> and dissolving it in water in a 100-ml volumetric flask. Sodium sulfide solution 0.01% (w/v) was prepared by weighing accurately 1.0 g of Na<sub>2</sub>S and dissolving it in water in a 100-ml volumetric flask. Nitrite solution 0.10 M was prepared by dissolving exactly 0.69 g of NaNO<sub>2</sub> in water in a 100-ml volumetric flask; working solutions were prepared by diluting volumes of the stock solution to known volumes with water. Nitrate standard solution 0.10 M was prepared by dissolving exactly 0.85 g of NaNO<sub>3</sub> in water in a 100-ml volumetric flask; working solutions were pre-

pared by diluting volumes of the stock solution to known volumes with water. Other solutions used for the interference study were prepared by dissolving the corresponding salt in water. Modified Jones reductor was prepared as described in the AOAC official methods of analysis [20].

## 2.2. Apparatus

All spectrophotometric measurements were carried out using a UV-2, Unicam UV-vis spectrophotometer. Constant temperature cell holder was used for absorbance measurements. The cells used for absorbance measurements were 1 × 1 cm glass cells. A Hanna 8521 model pH meter was used for pH measurements.

Table 3  
Published methods for spectrophotometric determination of nitrite

Reaction system <sup>a</sup>	Range of linearity (ppm)	Reference
Sulfanilamide	10–1000	[20]
+ NED		
PCPH + BrO <sup>3-</sup>	40–920	[5]
Thionine	0.3–55	[6]
+ BrO <sup>3-</sup>		
Prochlorperazine	0.8–70	[25]
+ BrO <sup>3-</sup>		
Bindschler's Green + Br <sub>2</sub>	50–400	[26]
PCA + DAP	0.002–0.008	[27]
TAPP	0.00018–0.0018	[15]
Chlorpromazine	3–1500	[8]
+ H <sub>2</sub> O <sub>2</sub>		
PMBC	0.5–2.0	Proposed conventional method
PMBC	0.2–3.6	Proposed initial rate method

<sup>a</sup> NED, *N*-(1-naphthyl)ethylenediamine; PCA, *p*-chloroaniline; PCPH, pyridine-2-carbalddehyde-2-pyridylhydrazone; PMBC, phosphomolybdenum blue complex; TAPP, 5,10,15,20-tetrakis(4-aminophenyl)prophine.

### 3. Procedures

#### 3.1. Preparation of phosphomolybdenum blue complex

A 30-ml volume of 0.1 M molybdenum(VI) solution is transferred into a 100-ml volumetric flask, then 10 ml of 0.10 M potassium dihydrogen

phosphate solution is added, followed by 10 ml of 0.01% (w/v) sodium sulfide solution and 13 ml of 11.2 M HCl, in that order. The volume is completed with water. The absorbance of the solution is measured after 30 min at 814 nm against water as a blank in a thermostatted bath at 25 ± 0.2°C.

#### 3.2. Spectrophotometric determination of nitrite

An aliquot of solution containing nitrite ions in the range 4.60–36.00 ppm is transferred into a 10-ml volumetric flask. Then 3.0 ml of phosphomolybdenum blue complex is added and the volume is completed with water. A portion of the solution was placed in the cell and the absorbance–time curve was recorded at 814 nm against water as a blank in a thermostatted bath at 25 ± 0.2°C. The concentration of nitrite can be calculated either by measuring the absorbance of the solution after exactly 30 min at 814 nm against water as a blank, or, in a different approach, by measuring the slope  $dA/dt$  of the reaction curve at 5 min after initiating the reaction.

#### 3.3. Spectrophotometric determination of nitrate

A 5-ml portion of solution containing an amount of nitrate in the range 10.00–100.00 ppm is transferred into the modified Jones reductor where the flow rate is adjusted to 3–5 ml/min. The reductor is then washed with 5 ml of water. The nitrite solution obtained from the reductor is treated as described in the above procedure for spectrophotometric determination of nitrite.

Table 4  
Analytical results of nitrite and nitrate determination in water, meat and vegetables

Sample analyzed	Nitrite found (ppm, average ± S.D.) <sup>a</sup>		Nitrate found (ppm, average ± S.D.) <sup>a</sup>	
	Proposed method	AOAC official method [20]	Proposed method	AOAC official method [20]
Well water	None	None	9.9 ± 0.1	8.1 ± 0.2
Corned beef	24.2 ± 0.2	24.4 ± 0.1	13.1 ± 0.5	12.0 ± 0.7
Fresh tomato	None	None	10.2 ± 1.0	9.3 ± 0.5
Fresh cucumber	None	None	75.5 ± 2.0	80.5 ± 1.8

<sup>a</sup> Average of three separate measurements.

### 3.4. Preparation of real samples for analysis

For water samples, an appropriate volume of water is treated using the above procedure for the determination of nitrite and nitrate.

For meat samples, about 25 g of meat are weighed out accurately, minced and transferred into a 250-ml beaker. Then 50 ml of water is added and the mixture is heated to 80°C for 15 min and then transferred into a 250-ml volumetric flask. Enough hot water is added to bring the volume to about 200 ml. The flask is transferred to a steam bath for 2 h with occasionally shaking. The solution is cooled to room temperature. The volume is completed to 250 ml with water, filtered and centrifuged to clear. The concentration of nitrite and nitrate are determined following the procedures given above.

For vegetable samples, about 100 g of vegetable are weighed out accurately and blended into 400 ml of water for about 5 min. The solution is filtered and the above procedures are followed for the determination of nitrite and nitrate content.

## 4. Results and discussion

It was found that the reduction of phosphomolybdic acid to phosphomolybdenum blue by sodium sulfide and the oxidation of phosphomolybdenum blue by nitrite are affected by many factors. In the present work each of these factors is studied carefully in order to optimize the conditions for spectrophotometric determination of nitrite and nitrate.

### 4.1. Absorption spectra of phosphomolybdenum blue complex

Different workers [22–24] have reported different absorption spectra with a different wavelength of maximum absorbance for the phosphomolybdenum blue complex. In the present work it was found that when sodium sulfide is used as a reducing agent for phosphomolybdic acid and by the addition of hydrochloric acid an intense blue color is developed. The shape of the absorption spectra and the wavelength of maximum ab-

sorbance are found to vary by changing the concentration of hydrochloric acid in the solution. Fig. 1 shows the absorption spectra as a function of hydrochloric acid concentration in the solution. Comparison among these spectra show that maximum absorbance for the solution containing 0.02 M hydrochloric acid is obtained at 700 nm. A new absorption peak develops at 814 nm upon increasing the concentration of hydrochloric acid. On the other hand, increasing the acidity causes a gradual increase in the absorbance at 814 nm, while the absorbance at 700 nm remains almost fixed. The absorbance at 814 nm reached its maximum value at hydrochloric acid concentration of 1.46 M (Fig. 1) beyond which any further increase in the acidity caused a decrease in the absorbance. The results obtained suggested an absorbance wavelength of 814 nm and a hydrochloric acid concentration of 1.46 M as optimum for further work.

### 4.2. Effect of changing phosphate to molybdenum mole ratio on the absorbance of phosphomolybdenum blue complex

The effect is studied for solutions which contained  $9.0 \times 10^{-3}$  M molybdenum and various concentrations of phosphate. The solutions were prepared as described in the general procedure. The results obtained showed that increasing the concentration of phosphate leads to an increase in the absorbance, up to phosphate to molybdenum mole ratio of 1:3. Any further increase in the phosphate concentration affects a gradual decrease in the absorbance.

### 4.3. Effect of sodium sulfide concentration on the absorbance of phosphomolybdenum blue complex

The effect is studied for solutions containing fixed concentrations of molybdenum, phosphate and hydrochloric acid and various amounts of sodium sulfide. The solutions are prepared as described in the general procedure under the preparation of phosphomolybdenum blue complex. The results obtained showed that increasing the concentration of sodium sulfide results to an increase in the absorbance up to a concentration of  $5.0 \times 10^{-3}\%$  (w/v), beyond which a brown precipitate is formed.

#### 4.4. Effect of time on formation of phosphomolybdenum blue complex

The effect of time on the absorbance of phosphomolybdenum blue complex is studied for solution containing  $9.0 \times 10^{-3}$  M molybdenum,  $3.0 \times 10^{-3}$  M phosphate,  $3.0 \times 10^{-4}$  M sodium sulfide and 1.46 M hydrochloric acid. The solution is prepared as described in the general procedure and the results obtained showed that the absorbance increases gradually as a function of time and reached its maximum value after 30 min. The intensity of the color remained constant for at least 24 h after preparation of the sample.

#### 4.5. Effect of time on the reaction between nitrite and phosphomolybdenum blue complex

The reaction between nitrite and phosphomolybdenum blue complex is studied as a function of time for solutions containing different amounts of nitrite and prepared as described in the general procedure. The results obtained (Fig. 2) showed that the absorbance of the solutions decreases gradually with time due to oxidation of phosphomolybdenum blue complex by nitrite. The reaction is slow and is attained after 60 min. It can be seen from the Fig. 2 that the sensitivity of the method is inversely proportional to time of reaction. In order to obtain maximum sensitivity the absorbance should be measured after 60 min. This can be considered as time-consuming. For the method to be more convenient for quantitative analysis the absorbance is measured after exactly 30 min.

#### 4.6. Effect of temperature

The effect of temperature on the absorbance of two solutions prepared as described in the recommended procedure was studied. Solution A contained phosphomolybdenum blue complex and solution B contained nitrite and phosphomolybdenum blue complex. The results obtained showed that the absorbance for both solutions decreases gradually by increasing the temperature. Increasing the temperature above  $70^\circ\text{C}$  caused a color change from blue to light green. This change

in color and the decrease in the absorbance of the solution could be due to the decomposition of the phosphomolybdenum blue complex. In the present work all measurements were carried out in a thermostatted bath at  $25 \pm 0.2^\circ\text{C}$ .

#### 4.7. Calibration curves and sensitivity

##### 4.7.1. Using the conventional method

From the investigation of the variables that effect the absorbance, the conditions for the color development and the absorbance measurements were selected. Following the recommended procedure, reciprocal dependence was obtained between nitrite concentration and the corresponding absorbance. The range of linearity, the sensitivity and the calculated molar absorptivity were found to vary with the time of measurement (Table 1). It can be seen (Table 1) that the sensitivity and the molar absorptivity increase as the time of measurements increase while the linearity of the calibration curve is decreased. In order to simplify the method, the measurements were taken at 30 min, at which the linearity was in the range 0.5–2.0 ppm and the detection limit was 0.2 ppm, as shown in Fig. 3. The molar absorptivity was calculated to be  $1.1 \times 10^4 \text{ l mol}^{-1}$  and the relative standard deviation (R.S.D.) was 2.6% for five measurements. Higher sensitivity can be achieved by measuring the absorbance at 60 min.

The reaction rate method has been applied for determination of nitrite by plotting  $\Delta A (A_0 - A_t)$  against concentration of nitrite. The results obtained (Fig. 3) show that the linearity of the calibration curve using the reaction rate method is in the range 0.2–3.6 ppm with a detection limit of 0.2 ppm. The R.S.D. was 2.4% for five measurements.

It can be concluded from the results that the linearity of the calibration curve and the time of analysis using the reaction rate method is much better than that using the conventional method. Also it can be seen from Fig. 3 that the absorbance of phosphomolybdenum blue complex decreases until the signal has stabilized with nitrite concentration, indicating that the reaction is stoichiometrically dependent on the nitrite concentration.



#### 4.8. Interference studies

The effect of other ions on the determination of nitrite using the proposed method is studied for solutions containing 2.1 ppm nitrite and prepared as described in the general procedure. The results obtained are presented in Table 2. Passing the sample through a cation exchanger in the hydrogen form (such as Amberlite IR-120) before the general determination procedure is carried out can eliminate the interference from the cations.

#### 4.9. Comparison with other published methods

Table 3 compares the results obtained for the determination of nitrite using the proposed method with that of published methods. The proposed method competes well from sensitivity, precision and interference of other ions with most of the published methods.

#### 4.10. Applications

The proposed method is applied successfully to the determination of nitrite and nitrate in water samples, meat product and vegetables. The results obtained (Table 4) are compared with those obtained using the AOAC official method of analysis [20].

### References

- [1] BIBRA Working Group, Toxicity profile, BIBRA Toxicol. Int. 12 (1990).
- [2] J.K. Hurst, S.V. Lumar, Chem. Res. Toxicol. 10 (1997) 804–809.
- [3] K.J. Reszka, Z. Matuszak, C.F. Chignell, Chem. Res. Toxicol. 10 (1997) 1325–1330.
- [4] C.J. Wang, H.P. Huang, T.H. Tseng, Y.L. Lin, S.J. Shiow, Arch. Toxicol. 70 (1995) 5–10.
- [5] M.A. Kupparis, K.M. Walczol, H.V. Malmstadt, Analyst 107 (1983) 1309–1314.
- [6] R. Montes, J.J. Laserna, Talanta 34 (1987) 1021–1026.
- [7] A.A. Ensafi, M. Saminifar, Talanta 40 (1993) 1375–1378.
- [8] B. Liang, M. Iwatsuki, T. Fukasawa, Analyst 119 (1994) 2113–2117.
- [9] W. Shotyck, J. Chromatogr. 640 (1993) 309–316.
- [10] K. Ohta, K. Tanaka, Bunseki Kagaku 43 (1994) 471–474.
- [11] S.F. Mou, T.H. Wang, Q.J. Sun, J. Chromatogr. 640 (1993) 161–165.
- [12] J.Z. Li, X.C. Wa, R. Yuan, H.G. Lin, R.Q. Yu, Analyst 119 (1994) 1363–1366.
- [13] U. Schaaler, E. Bakker, E. Spichiger, E. Pretsch, Talanta 41 (1994) 1001–1005.
- [14] M. Bertotti, D. Pletcher, Anal. Chim. Acta 337 (1997) 49–55.
- [15] A. Kojlo, E. Gorodkiewicz, Anal. Chim. Acta 302 (1995) 283.
- [16] M.J. Ahmed, C.D. Stalikas, S.M. Tzouwarakarayanni, M.I. Karayannis, Talanta 43 (1996) 1009–1018.
- [17] T. Kawakami, S. Igrashi, Anal. Chim. Acta 333 (1996) 175–180.
- [18] A. Cerda, M.T. Oms, R. Forteza, V. Cerda, Analyst 121 (1996) 13–17.
- [19] Q.Q.F. Wu, P.F. Liu, Talanta 30 (1983) 374–376.
- [20] AOAC, Method 36.1.21, in: Official Methods of Analysis, 16th ed., AOAC, 1995, pp. 8–9.
- [21] S.E. Allen, Chemical Analysis of Ecological Material, Blackwell, Oxford, 1974, p. 203.
- [22] R.P. Sims, Analyst 86 (1961) 584–590.
- [23] S.J. Lyle, N.A. Zatar, Anal. Chim. Acta 135 (1982) 327–332.
- [24] S.Z. Qureshi, T. Hasan, Acta Pharm. Jugosl. 38 (1988) 183–187.
- [25] A.A. Mohamed, M.F. El-shahat, T. Fukasawa, M. Iwatsuki, Analyst 121 (1996) 8992.
- [26] T. Okutani, A. Sakuragawa, S. Kamikura, M. Shimura, S. Azuchi, Anal. Sci. 7 (1991) 793.
- [27] J. Lawrence, M. Dombroski, J.E.J. Pratt, Anal. Chem. 44 (1972) 2268–2272.

# Estimation of microscopic, zwitterionic ionization constants, isoelectric point and molecular speciation of organic compounds

S.H. Hilal<sup>a,\*</sup>, S.W. Karickhoff<sup>a</sup>, L.A. Carreira<sup>b</sup>

<sup>a</sup> *Environmental Research Laboratory, US Environmental Protection Agency, Athens, GA 30605, USA*

<sup>b</sup> *Department of Chemistry, University of Georgia, Athens, GA 30605, USA*

Received 7 December 1998; accepted 4 May 1999

## Abstract

Mathematical models based on structure–activity relationships and perturbed molecular orbital theory have been developed to calculate the ionization  $pK_a$ s for a large number of organic molecules. These models include resonance, direct and indirect electrostatic field effects, sigma induction, steric effects, differential solvation and hydrogen bonding. The thermodynamic microscopic ionization constants,  $pK_i$ , of molecules with multiple ionization sites and the corresponding complex speciation as a function of pH have been determined using these chemical reactivity models. For a molecule of interest SPARC (SPARC performs automated reasoning in chemistry) calculates all of the microscopic ionization constants and the fraction of each species as a function pH along with the titration (charge) curve. The system has been tested on several biologically and environmentally important compounds. © 1999 Published by Elsevier Science B.V. All rights reserved.

*Keywords:* Ionization equilibrium constant; Microscopic ionization constants; pH;  $pK_a$ ; SAR; SPARC; Speciation; Zwitterionic equilibria

## 1. Introduction

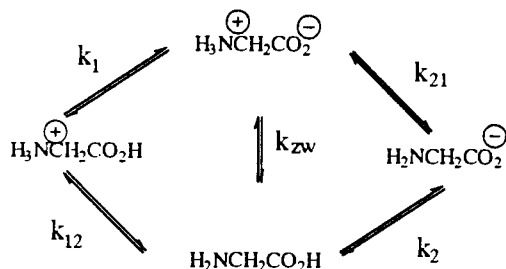
Determination of microscopic constants and zwitterionic ratios has played an important part in understanding the ionic composition of many biologically active molecules, particularly since all proteins fall into this class. The chemical and biological activity of these substances would be

expected to vary with the degree of ionization. For this reason, accurate knowledge of the ionization constants for zwitterionic substances is a prerequisite to an understanding of their mechanism of action in both chemical and biological processes.

Unfortunately, microscopic ionization constants have been determined for less than 100 compounds and only for a very few of these molecules has the zwitterionic constant been determined or calculated [1–4]. Moreover, determi-

\* Corresponding author. Fax: +1-706-542-9454.

E-mail address: said@sunlc2.chem.uga.edu (S.H. Hilal)



Scheme 1.

nation or calculation of the fraction of the various microscopic species as a function of the pH has been reported in the literature for less than a dozen molecules. Most of these measurements were restricted to aliphatic amino acid derivatives and only for simple, two ionization site molecules such as glycine and cysteine (where the  $\text{CO}_2\text{H}$  is already ionized). Benesch and Benesch [2] calculated the relative concentration of the four microscopic forms for cysteine where the carboxylic acid group was ionized in all the forms. He found that the concentration ratio of the  $^-\text{S-R-NH}_3^+$

species to the  $\text{HS-R-NH}_2$  species at any given pH is approximately 2:1 rather than 1:1 as suggested by Grafius and Neilands [3]. This discrepancy indicates the order of magnitude of the uncertainty involved in the various approximations which have been made to calculate the microscopic constants and relative concentration of the different species. In addition, only a very few of the total number of microconstants needed to characterize the equilibria have been measured or calculated. For example, only two microconstants have been determined for molecules with four ionizable sites such as dihydroxyphenylalanine (DOPA) and epinephrine [4]. Estimation or measurement of the microscopic constants and relative concentration of the various species is an extremely difficult task.

The object of this study is to use the SPARC  $\text{pK}_a$  calculator to estimate the microscopic constants for almost any molecule of interest strictly from molecular structure. Hence, the microscopic ionization constants, the zwitterionic constant and the fraction of the various microscopic species as function of the pH can be estimated without approximations such as limiting the number of

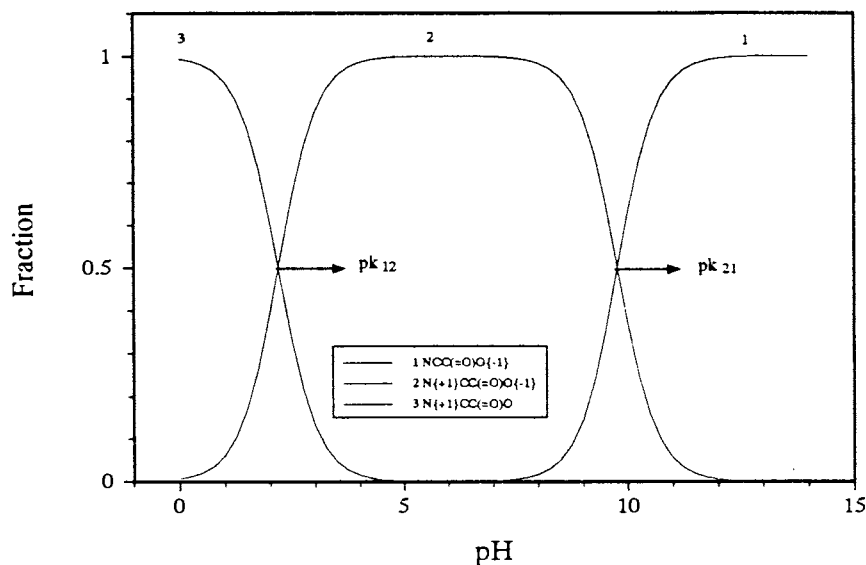


Fig. 1. Fraction of the major microscopic species of glycine as a function of pH. The two macroscopic  $\text{pK}_a$ s are far apart and are equal to the microscopic constants ( $\text{pK}_{12}$  and  $\text{pK}_{21}$ ). The number on the top of each curve corresponds to the microscopic species shown in the inset.

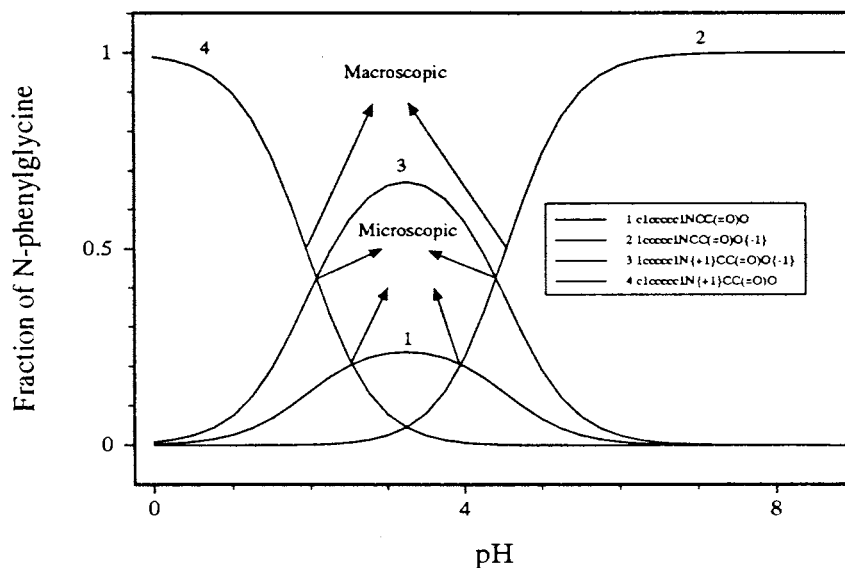


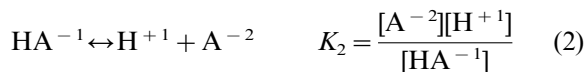
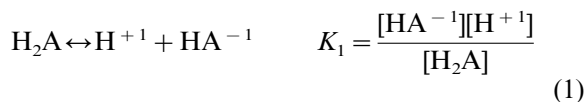
Fig. 2. Fraction of the major microscopic species of *N*-phenylglycine as a function of pH. Both the microscopic/macroscopic  $pK_a$ s are shown in the plot. The number on the top of each curve corresponds to the microscopic species shown in the inset.

species considered. The titration curves (charge versus pH) can be calculated using the same reactivity models.

## 2. Calculation of macroconstants

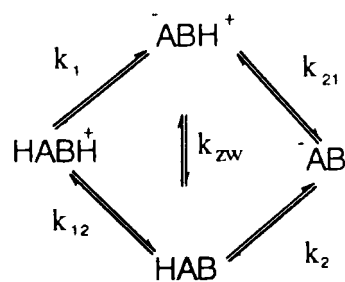
A Brønsted acid is defined as a proton donor and a base as a proton acceptor. The acid–base ionization properties in solution are generally expressed in terms of ionization constants ( $pK_a$ ) which describe the tendency for an acid to give up a proton to a solvent or the affinity of a base for a hydrogen ion. The strength of an acid in a solvent S is measured by the ionization constant for the reaction. Many molecules of great importance in chemistry and biochemistry contain more than one acidic or basic site and some macromolecules such as amino acids, peptides, proteins and nucleic acids may contain hundreds of such groups. These molecules may exist in a great number of distinct ionization states. The acidic groups are uncharged in strongly acidic solutions and negatively charged in sufficiently alkaline solutions. The basic groups are positively charged (protonated) in a strongly acidic solution and are

uncharged in sufficiently alkaline solution. For a bifunctional acidic, compound the ionization equilibria are usually written as:



where the constant concentration of the solvent has been absorbed in  $K$ . The  $pK_1$  and  $pK_2$  ( $pK_a = -\log K_a$ ) are commonly evaluated from a pH titration or spectroscopic measurement. These measured  $pK_a$ s are termed macroscopic constants because they often only describe a composite of the processes which are actually occurring in solution. The actual donor sites where the protons reside are not specified and may not be unique. Thus a solution ‘species’ such as  $H_2A$  may in fact consist of several  $H_2A$  species with proton occupying a different basic site in each of the species. On the other hand, microconstants are the equilibrium constants for equilibria involving individual species in solution. These microconstants may or may not be capable of being measured or determined distinctly.

Table 1

Observed (Obs.) versus SPARC-calculated (Calc.) values for the microscopic  $pK_{a,s}$  for two or more ionizable sites

Molecule	$pK_{zw}$		$pK_1$		$pK_{12}$		$pK_{21}$		$pK_2$	
	Obs.	Calc.	Obs.	Calc.	Obs.	Calc.	Obs.	Calc.	Obs.	Calc.
Glycine [15]	-5.6	-5.60	2.35	2.15	8.00	7.8	9.80	9.70	4.43	4.20
Phenylglycine [16]	-0.26	-0.58	2.03	2.15	2.29	2.67	4.22	4.60	3.96	3.95
<i>m</i> -NO <sub>2</sub>	-	1.35	-	2.00	0.06	0.50	-	2.50	3.75	3.80
<i>m</i> -CN	-	1.10	-	2.00	0.28	0.80	-	2.70	3.78	3.80
<i>m</i> -Cl	0.90	0.40	2.01	2.12	1.10	1.63	2.99	3.55	3.90	3.86
<i>m</i> -COMe	0.85	0.07	2.03	2.11	1.20	1.90	3.05	3.87	3.87	3.87
<i>p</i> -Cl	0.36	0.05	1.99	2.10	1.61	1.95	3.51	3.88	3.89	3.86
<i>m</i> -OMe	-0.21	0.27	2.09	2.16	1.89	2.33	3.74	4.26	3.95	3.90
<i>m</i> -Me	-0.32	-0.70	2.06	2.15	2.38	2.83	4.43	4.76	4.00	3.96
<i>p</i> -Me	-0.70	-0.90	2.05	2.16	2.75	3.00	4.77	4.90	4.07	3.95
<i>p</i> -OMe	-1.00	-0.94	2.12	2.19	3.11	3.10	5.07	5.00	4.07	3.98
Niflumic acid [28]	1.24	1.36	2.28	1.81	3.52	3.13	3.18	2.82	4.42	4.31
<i>p</i> -Aminobenzoic acid [17]	0.93	0.87	3.40	3.71	2.47	2.83	3.90	3.80	4.83	4.61
<i>p</i> -Dimethylaminobenzoic [17]	0.62	0.42	3.28	3.74	2.66	2.98	4.28	4.39	4.9	4.51
<i>m</i> -Aminobenzoic acid [18]	0.43	0.72	3.22	3.40	3.65	4.00	4.66	4.79	4.23	4.02
Picolinic acid [19]	-1.15	-1.2	1.04	1.37	2.21	2.67	5.29	5.28	4.12	4.12
Nicotinic acid [19]	-1.00	-1.18	2.11	2.42	3.13	3.46	4.77	4.87	3.75	3.52
Isonicotinic acid [19]	-1.40	-1.12	1.86	2.61	3.26	3.56	4.84	4.78	3.44	3.48
Tyrosine ethyl ester <sup>a</sup> [4]	-	1.59	9.63	9.10	7.33	7.3	-	8.35	-	9.75
5-Thiomethylimidazole [20]	1.15	2.0	7.72	8.51	6.57	5.91	8.36	8.34	9.51	9.91
2-Thiomethylimidazole [20]	-0.46	0.25	6.50	6.81	6.96	6.91	9.13	9.31	8.67	8.70
1-Methyl-2-thiomethylimidazole [20]	-0.36	0.37	6.47	6.80	6.83	6.90	8.75	9.40	8.39	8.70
Tyramine [21]	-0.4	-0.76	9.58	9.43	-	9.97	10.68	11.02	-	10.09
<i>N,N</i> -Dimethyltyramine [21]	-0.09	-0.35	9.03	9.4	-	9.56	10.31	10.68	-	10.07
<i>m</i> -Hydroxyphenethyl dimethylamine [21]	-0.07	-0.30	8.9	9.20	-	9.48	10.27	10.73	-	9.950
<i>m</i> -Hydroxyphenethyl methylamine [21]	0.778	-0.11	9.30	9.29	-	10.9	11.06	11.56	-	9.950
DOPA [4]	-	-	8.97	9.10	9.62	9.61	9.17	9.15	9.40	9.42
Dopamine [4]	-	-	8.90	8.86	-	-	10.1	9.93	-	-
Norepinephrine [4]	-	-	8.92	8.83	-	-	9.18	9.10	-	-
Epinephrine [4]	-	-	8.88	8.73	-	-	9.51	9.40	-	-

<sup>a</sup> The CO<sub>2</sub>H is replaced by an ester so 1 corresponds to ionization of the OH not the CO<sub>2</sub>H.

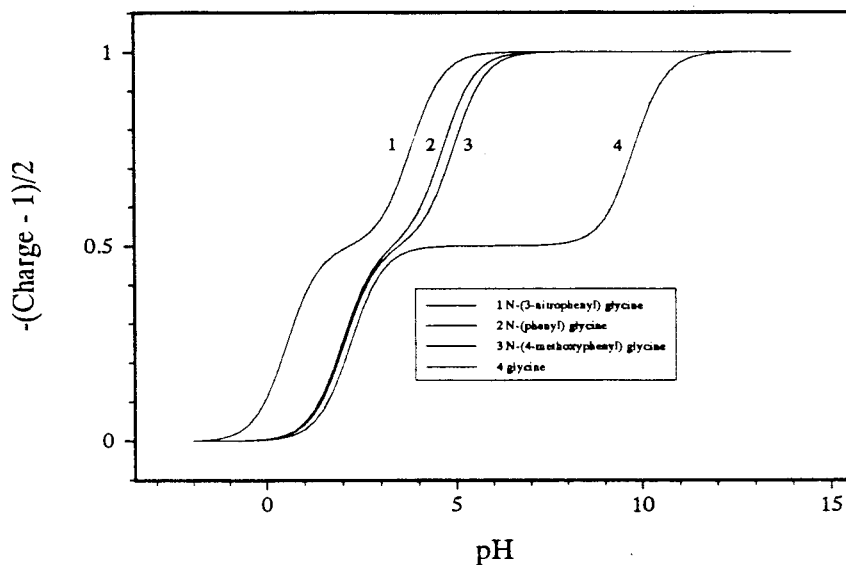


Fig. 3. Titration curves for *N*-(*m*-nitrophenyl)glycine, *N*-(phenyl)glycine, *N*-(*m*-methoxyphenyl)glycine and glycine as function of pH.

### 3. $pK_a$ computational procedure

SPARC does not do ‘first principles’ computation, but seeks to analyze chemical structure relative to a specific reactivity query in much the same manner in which an expert chemist would do so. For chemical properties, molecular structures are broken into functional units with known chemical properties. Reaction centers with known intrinsic reactivity are identified and the impact on reactivity of appended molecular structures quantified by perturbation theory. As we described previously in detail [5–8], molecular structures are broken into functional units called the reaction center and the perturber. The reaction center, C, is the smallest subunit that has the potential to ionize and lose a proton to a solvent. The perturber, P, is the molecular structure appended to the center (denoted C). The perturber structure (denoted P) is assumed to be unchanged in the reaction. The  $pK_a$  of the reaction center is adjusted for the molecule in question using the mechanistic perturbation models. The  $pK_a$  for a molecule of interest is expressed in terms of the contributions of both the perturber and the reaction center as:

$$pK_a = (pK_a)_c - \delta_p(pK_a)_c \quad (3)$$

$(pK_a)_c$  describes the ionization behavior of the reaction center, and  $\delta_p(pK_a)_c$  is the change in ionization behavior brought about by the perturber structure. SPARC computes reactivity perturbations,  $\delta_p(pK_a)_c$ , which are then used to ‘correct’ the ionization behavior of the reaction center for the compound in question in terms of potential ‘mechanisms’ for interaction of P and C as:

$$\delta_p(pK_a)_c = \delta_{\text{ele}}pK_a + \delta_{\text{res}}pK_a + \dots \quad (4)$$

where  $\delta_{\text{res}}pK_a$  and  $\delta_{\text{ele}}pK_a$  describe the differential resonance and electrostatic interactions of P with the protonated and unprotonated states of C, respectively. Electrostatic interactions are derived from local dipoles or charges in P interacting with charges or dipoles in C.  $\delta_{\text{ele}}pK_a$  represents the difference in the electrostatic interactions of the P with the two states of the reaction center. Direct electrostatic effects (field effect) are manifested by ‘fixed’ dipoles or charges in a substituent and transmitted directly from S to C. The substituent can also ‘induce’ electric fields in R that can interact electrostatically with the reaction center. This indirect interaction is called the ‘mesomeric field effect’. In addition, electrostatic

Table 2

Observed (Obs.) versus SPARC-calculated (Calc.) values for the microscopic  $pK_s$  for molecules with three ionizable sites

	Tyrosine [14]		Cysteine [2]		Cysteine glycine [22]		Cysteine ethyl ester <sup>a</sup> [22]	
	Obs.	Calc.	Obs.	Calc.	Obs.	Calc.	Obs.	Calc.
$pK_1$	2.21	2.00	1.71	1.80	–	3.17	–	–
$pK_{21}$	2.61	2.30	2.79	2.40	–	3.40	–	–
$pK_{31}$	4.37	3.90	3.80	3.80	–	3.50	–	–
$pK_{231}$	4.77	4.20	4.74	4.40	–	3.71	–	–
$pK_2$	9.31	9.30	7.45	7.80	–	7.10	7.45	7.08
$pK_{12}$	9.71	9.60	8.53	8.20	7.87	7.40	–	–
$pK_{32}$	9.91	10.0	9.50	9.09	–	8.90	9.09	8.88
$pK_{132}$	10.3	10.3	10.0	10.0	9.45	9.20	–	–
$pK_3$	7.19	7.30	6.77	6.70	–	6.50	6.77	6.29
$pK_{13}$	9.35	9.60	8.86	8.60	7.14	6.88	–	–
$pK_{23}$	7.79	8.40	8.41	8.60	–	8.43	8.41	8.38
$pK_{123}$	9.95	10.6	10.4	10.5	8.75	8.80	–	–
	Lysine [25]		Ornithine [25]		2,3-Diaminopropanoic acid [25]		Glutamic acid [24]	
	Obs.	Calc.	Obs.	Calc.	Obs.	Calc.	Obs.	Calc.
$pK_1$	–	1.90	–	1.89	–	1.26	2.15	2.13
$pK_{21}$	–	3.91	–	3.85	–	3.75	2.62	2.30
$pK_{31}$	–	2.20	–	2.20	–	1.95	4.30	4.10
$pK_{231}$	–	4.16	–	4.15	–	4.10	4.74	4.20
$pK_2$	–	7.30	–	7.00	–	4.6	3.85	4.20
$pK_{12}$	9.27	8.96	8.89	8.61	7.02	6.61	4.32	4.30
$pK_{32}$	–	8.18	–	8.10	–	7.28	4.65	4.60
$pK_{132}$	9.79	9.79	9.79	9.73	9.12	9.21	5.09	4.80
$pK_3$	–	9.58	–	9.28	–	6.6	7.04	7.87
$pK_{13}$	10.15	9.95	9.53	9.71	7.07	7.29	9.19	9.50
$pK_{23}$	–	10.19	–	10.1	–	9.06	7.84	8.40
$pK_{123}$	10.68	10.56	10.43	10.5	9.16	9.69	9.96	10.0

<sup>a</sup> For cysteine ethyl ester, the acidic group  $CO_2H$  is replaced by an ester group; hence the microscopic constants may be correlated with  $pK_2$ ,  $pK_3$ ,  $pK_{23}$  and  $pK_{32}$ .

Table 3

Observed (Obs.) versus SPARC-calculated (Calc.) microscopic ionization constants for glutathione [26]

$pK_{ijk}$	$CO_2H$ (1)		$pK_{ijk}$	$CO_2H$ (2)		$pK_{ijk}$	SH (3)		$pK_{ijk}$	$NH_3^+$ (4)	
	Obs.	Calc.		Obs.	Calc.		Obs.	Calc.		Obs.	Calc.
$pK_1$	2.09	1.92	$pK_2$	3.12	3.26	$pK_3$	–	7.94	$pK_4$	–	7.04
$pK_{21}$	2.33	1.98	$pK_{12}$	3.36	3.31	$pK_{13}$	–	8.14	$pK_{14}$	–	8.65
$pK_{31}$	–	2.06	$pK_{32}$	–	3.50	$pK_{23}$	–	8.21	$pK_{24}$	–	7.31
$pK_{41}$	–	3.84	$pK_{42}$	–	3.35	$pK_{43}$	–	8.24	$pK_{34}$	–	7.64
$pK_{241}$	–	3.91	$pK_{132}$	–	3.56	$pK_{123}$	8.93	8.37	$pK_{124}$	9.13	8.88
$pK_{231}$	–	2.12	$pK_{142}$	–	3.41	$pK_{243}$	–	8.49	$pK_{134}$	–	9.26
$pK_{341}$	–	4.10	$pK_{342}$	–	3.60	$pK_{143}$	–	8.43	$pK_{234}$	–	7.86
$pK_{3421}$	–	4.10	$pK_{1342}$	–	3.65	$pK_{1243}$	9.08	8.91	$pK_{1234}$	9.28	9.50

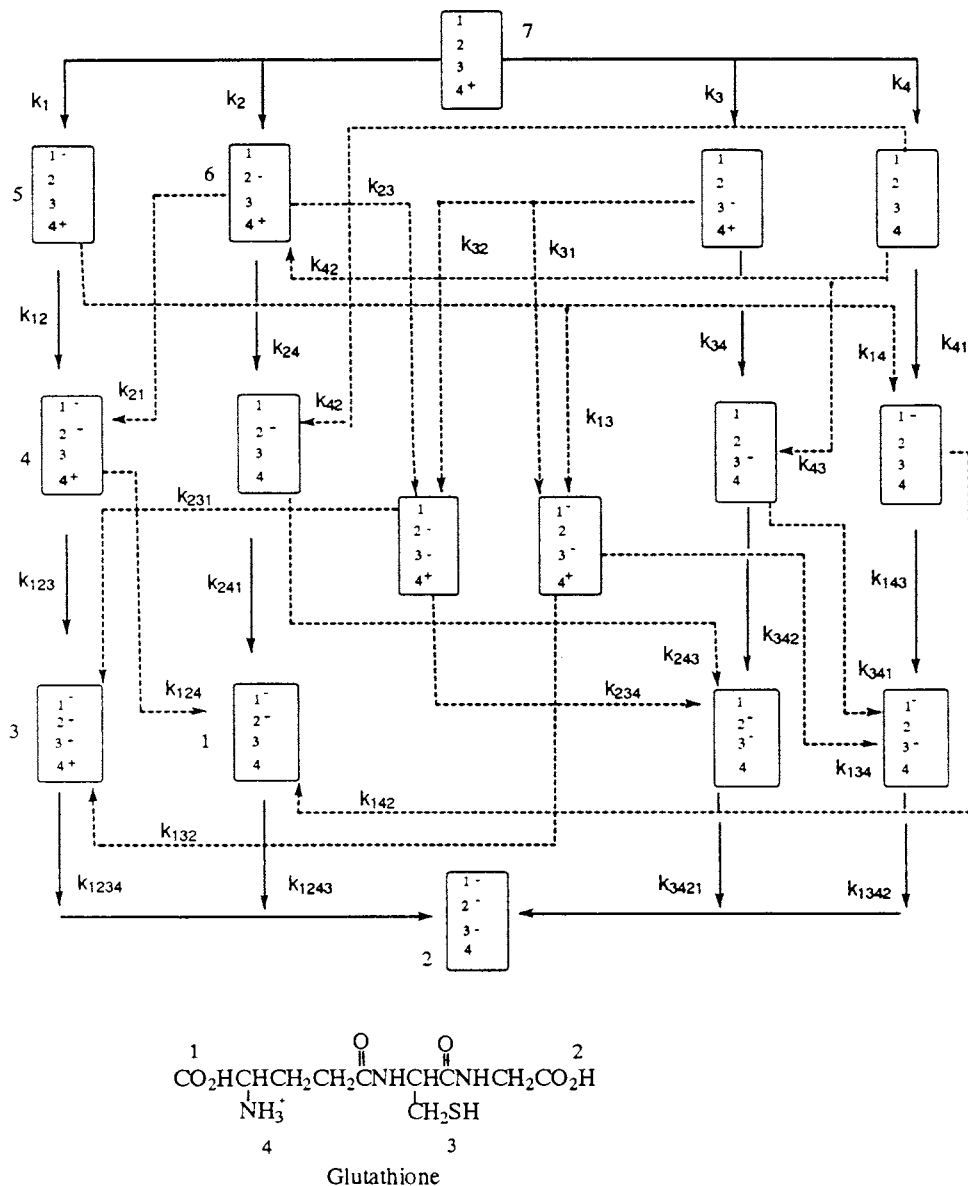


Fig. 4. The 16 microscopic states of glutathione and the 32 microscopic ionization constants which interrelate them. The numbers beside the species boxes correspond to the microscopic species in Fig. 5. See text for more details.

effects derived from electronegativity differences between the reaction center and the substituent are termed sigma induction. These effects are transmitted progressively through a chain of  $\sigma$ -bonds between atoms.  $\delta_{\text{res}}pK_a$  describes the change in the delocalization of  $\pi$  electrons of the two states due to P. This delocalization of  $\pi$

electrons is assumed to be into or out of the reaction center. Additional perturbations include direct interactions of the structural elements of P that are contiguous to the reaction center such as hydrogen bonding interactions or steric blockage of solvent access to C. (For more details see [8,9].)



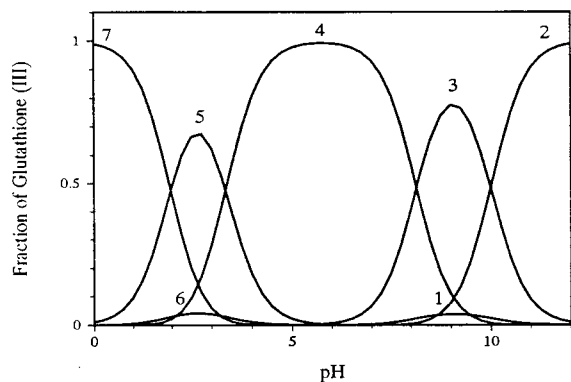


Fig. 5. Fraction of the major microscopic species of glutathione as a function of pH. The number on the top of each curve corresponds to the microscopic species labeled by the same number beside the species boxes in Fig. 4.

The microscopic ionization constants for a molecule of interest can be calculated using the SPARC program. The SPARC  $pK_a$  calculator was tested on 4338  $pK_a$ s for more than 3685 compounds spanning a range of over 31  $pK_a$  units [7]. The system was tested for multiple ionizations up to the sixth (simple organic molecules) and eighth ionization (azo dyes) for multiple ionization sites molecule [6]. The root mean square

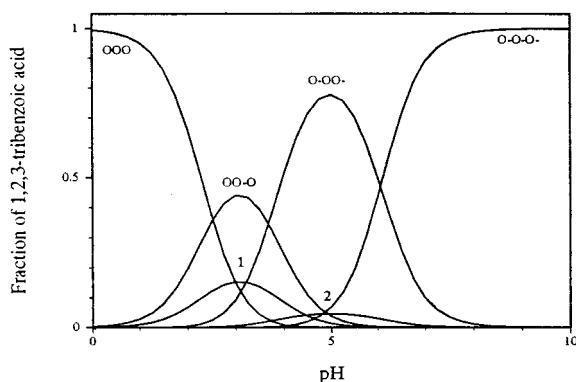


Fig. 7. The calculated fraction of the eight microscopic species of 1,2,3-tribenzoic acid versus pH. Four of the microscopic species are shown on the top of the corresponding graph. Curves 1 and 2 show the other four microscopic species. Each graph has two different symmetrical species lying on the top of each other:  $O^-OO/OO^-$  and  $O^-O^-O/OO^-$ , respectively.

(RMS) deviation for this large set of compounds was found to be 0.37  $pK_a$  units. SPARC presently predicts ionization  $pK_a$  [5–8], electron affinity [10] and numerous physical properties [11–13] such as distribution coefficients between immiscible solvents, solubilities, vapor pressure, boiling points, gas-chromatographic (GC) retention times, etc.

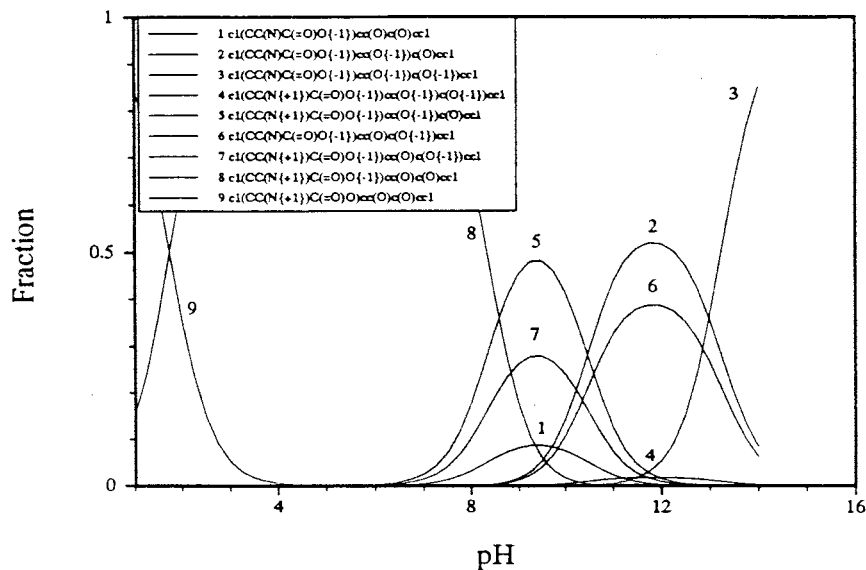


Fig. 6. Fraction of the major microscopic species of DOPA. The number on the top of each curve corresponds to the microscopic species shown in the inset.

#### 4. Zwitterionic equilibria: microscopic constant calculation

Many molecules contain both acid and base functionality but these sites are not able to ionize simultaneously. These molecules are usually referred to as amphoteric. Amino phenols are good examples of amphoteric molecules. When the pH is very low the cationic species predominates while at high pH the anionic species predominates. At intermediate pHs the molecule exists in the neutral form. Other substances contain both acid and base functionality where both the base and the acid sites may be simultaneously ionized to form an internal salt. These substances are referred to as zwitterionic or dipolar ions [14–18]. The amino acids are an example of molecules that

can exist as zwitterions. At low pH and high pH the cationic species and the anionic species predominate, respectively, as in the case of the amino phenol. But unlike the amphoteric amino phenol, the internal salt predominates as an intermediate over a wide range of pH. Actually the zwitterion and the isomeric uncharged molecule are in equilibrium in aqueous solutions. The nature of this equilibrium depends on the acid and the base strength of the ionizing groups involved. For a molecule with two ionizable sites this process can be represented diagrammatically as in Scheme 1.

Each ionizable group has two microscopically different ionization pathways ( $k_1$  and  $k_{12}$  for loss of the first hydrogen, and  $k_2$  and  $k_{21}$  for loss of the second hydrogen). Each group has two constants associated with its ionization, one when the

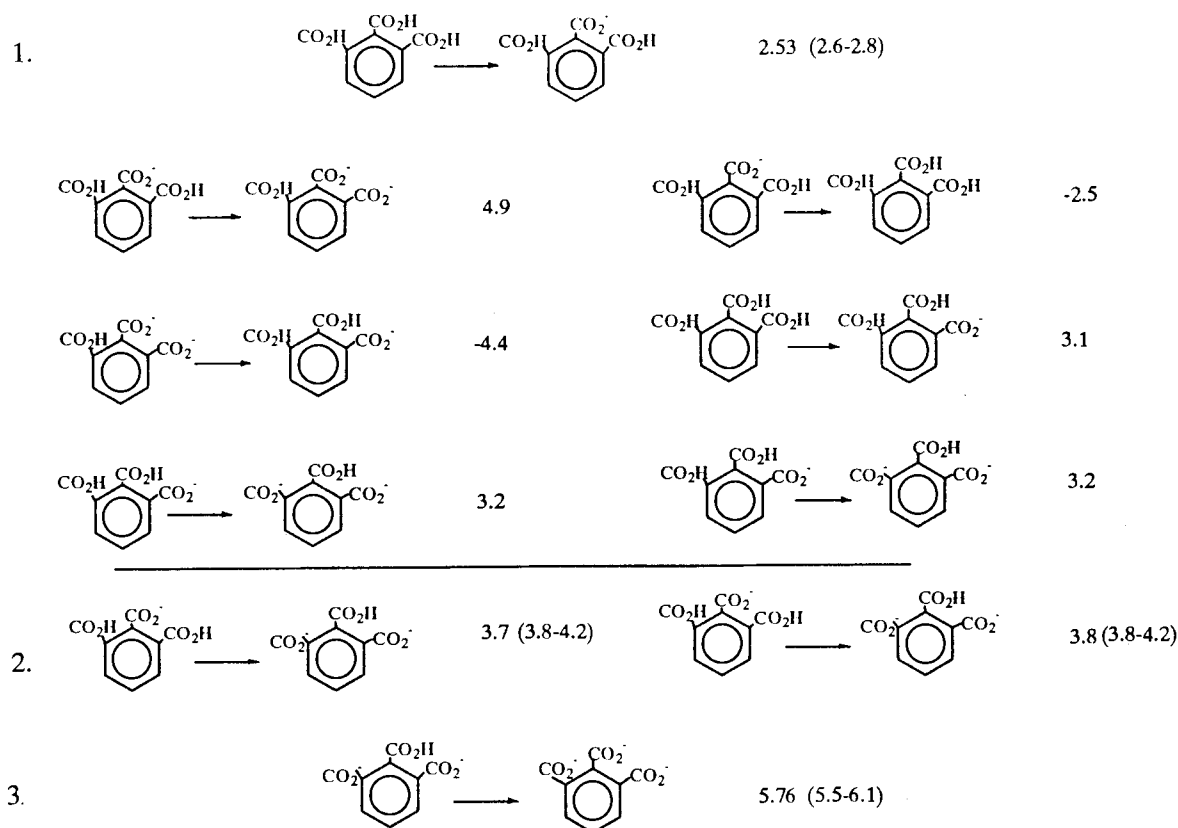


Fig. 8. The three ionization macroscopic  $pK_a$ s for hemimellitic acid. The second macroscopic ionization  $pK_a$  involves three different microscopic constants which are shown to the side of each step. Paths (a) and (b) are calculated within 0.1 of each other. The observed macroscopic are the number between the brackets other are SPARC-calculated  $pK_a$ s.

Table 4  
SPARC-calculated isoelectric points

Molecule	Observed	Calculated
Glycine [22]	6.0	5.8
Cysteine [27]	5.1	5.0
Lysine [22]	10	9.8
Glutamic acid [22]	3.2	3.2
Penicillamine [27]	4.9	5.0
Phenylglycine <sup>a</sup>	3.1	3.2
<i>m</i> -NO <sub>2</sub>	1.9	2.0
<i>m</i> -CN	2.0	2.1
<i>m</i> -Cl	2.5	2.6
<i>m</i> -COMe	2.5	2.6
<i>p</i> -Cl	2.7	2.8
<i>m</i> -OMe	2.9	3.0
<i>m</i> -Me	3.2	3.3
<i>p</i> -Me	3.4	3.4
<i>p</i> -OMe	3.6	3.4
Thiazolidine-4-carboxylic acid [27]	3.9	4.4
2-Methyl	4.4	4.6
2,2-Dimethyl	4.2	4.7
5,5-Dimethyl	4.3	4.4
2,5,5-Trimethyl	4.1	4.5
2,2,5,5-Tetramethyl	4.2	4.7
2-Ethyl-2-methyl	5.3	4.7
2-Ethyl-2,5,5-trimethyl	5.2	4.7
Niflumic acid [28]	3.3	3.1

<sup>a</sup> The observed values are calculated from  $\text{pH}_1 = (\text{p}K_1 + \text{p}K_2)/2$  for the phenylglycine derivative; see [22].

other group is ionized and one when the other group is not ionized.

When the  $\text{p}K_a$ s of the ionizing groups are arithmetically far apart (as those of glycine shown in Fig. 1), knowledge of the two macroscopic constants,  $K_1$  and  $K_2$ , is enough to calculate speciation as a function of pH. When the two  $\text{p}K_a$  values lie within 3  $\text{p}K_a$  units of one another, such as in the case of *N*-phenylglycine (as shown in Fig. 2), a more detailed survey of the problem becomes necessary. In such a case, the two macroscopic constants,  $K_1$  and  $K_2$ , cannot fully describe the equilibria denoted by the four microscopic constants,  $k_1$ ,  $k_{12}$ ,  $k_{21}$  and  $k_2$ , and the zwitterionic constant,  $k_{zw}$ . However, the macroscopic and microscopic equilibrium constants are closely related by the following equations:

$$K_1 = k_1 + k_{12} \quad (5)$$

$$\frac{1}{K_2} = \frac{1}{k_{21}} + \frac{1}{k_2} \quad (6)$$

The four microscopic ionization constants ( $k_i$ ) involving the individual, microscopically distinct species describe precisely the acid–base chemistry of a such system at the molecular level while the two macroscopic  $\text{p}K_a$ s provide an incomplete specification of the equilibria. It should be noted that the four constants are not independent but are subject to the relation  $k_1 k_{12} = k_{21} k_2$  [14,18]. In order to calculate molecular speciation as a function of pH,  $k_{zw}$  must be calculated.  $k_{zw}$  may be determined using the left or the right path of Scheme 1. Since both thermodynamic paths give the zwitterion product,  $k_{zw}$  may be expressed as function of the microscopic constants within any loop as:

$$k_{zw} = \frac{k_1}{k_{12}} = \frac{k_2}{k_{21}} \quad (7)$$

The integrity of the  $\text{p}K_a$  calculator can be checked by calculating  $k_{zw}$  using the two different loops. The RMS deviation in  $\text{p}k_{zw}$  for the cases tested is 0.5  $\text{p}K_a$  units. This value is what one would expect from a calculation requiring two  $\text{p}K_a$  calculations ( $0.37 * \sqrt{2}$ ). Values of  $k_{zw}$  calculated from different thermodynamic paths are averaged over the number of thermodynamic paths.

## 5. Results and discussion

### 5.1. Two ionizable sites

In the pH range 4–10, more than 99% of glycine in solution exists in a zwitterionic form where both the carboxylic and the amine groups are simultaneously charged. Over a wide pH range only three microscopic species have significant concentrations, as shown in Fig. 1. The concentration of the fourth species (neutral) is negligible (below 1%) over the entire pH range. The ratio of the zwitterionic concentration to the neutral concentration is about  $4 * 10^5$ . The macroconstants in a figure such as Fig. 1 occur when the fraction of the ionizing group of interest is reduced to 50%. So, the left- and the right-hand sides where the fraction is equal to 50% are the

macroscopic  $pK_{\text{CO}_2\text{H}}$  and the  $pK_{\text{NH}_2}$ , respectively. The microconstants interconnecting the species of interest occur where the species curves intersect. In the case where the two macroconstants are very far apart, the two macroconstants  $pK_1$  and  $pK_2$  are equal to the microconstants  $pk_1$  and  $pk_{21}$ , respectively, as shown in Fig. 1. Hence, the two macroconstants can satisfactorily describe the equilibrium. On the other hand, *N*-phenyl substitution of glycine substantially lowers the macroscopic constant of the amine group due to resonance contributions. As a result the amine and the carboxylic acid will have comparable hydrogen ion affinities and both functional groups would make important contributions to the hydrogen ion concentration (i.e. appreciable concentrations of the acidic and the basic forms of both functional groups would be present in solution simultaneously). Their macroconstants become more nearly equal (within 2  $pK_a$  units) and the ratio of the zwitterionic species to the neutral species in solution will decrease as indicated in Table 1. In this case the macroconstants are not equal to the microconstants (as shown in Fig. 2) and the equilibrium cannot be satisfactorily described by  $pK_1$  and  $pK_2$ . Substituents with a large dipole moment such as a nitro or cyano group will further decrease the zwitterionic ratio due to electrostatic and/or resonance effects [16,18]. For example, *m*-nitro- and *m*-cyano-phenylglycines exist in aqueous solution predominantly in the non-zwitterionic form due to the large electrostatic effect of the dipolar group. Weaker dipole substituents such as methyl- and methoxyphenylglycines exist largely in the zwitterionic form. Substituent effects on  $pK_a$  are illustrated for glycine, *N*-(phenyl)glycine, *N*-(*m*-nitrophenyl)glycine and *N*-(*m*-methoxyphenyl)glycine where the charge lost in the molecule as function of the pH is shown in Fig. 3. The zwitterion ratio  $k_{zw}$  is very dependent on the nature of the substituent in these molecules. The proportion of zwitterions in aqueous solution is governed by the effect of the substituent on the  $pK_a$ s and can vary substantially as shown in Table 1. Table 1 shows the observed versus SPARC-calculated microscopic ionization constants  $pk_{ij}$  and zwitterionic constants  $pk_{zw}$  for two ionizable site systems.

## 5.2. Multiple ionization sites

Martin et al. [14] have measured the 12 microscopic constants for tyrosine. They used various approximations to estimate the fraction of all the tyrosine species present in which the hydroxy group was ionized. They assumed that the macroscopic constant,  $K_1$ , was equal to the microscopic constant,  $k_1$ , for the  $\text{CO}_2\text{H}$  and that the ionization of the hydroxy group was completely independent of the ammonium group. In addition, they assumed that the molar extinction coefficients for some species were identical. Martin [4] also used this approach to calculate the speciation of DOPA, where the phenolic groups are ionized, as a function of pH. To the best of our knowledge, estimation of all the different microscopic species for molecules having four or more ionizable sites has not been reported.

For a molecule that has  $N$  ionizable sites, there are  $N$  macroscopic ionization constants which can be measured. There are, however,  $2^{N-1} * N$  microscopic ionization constants and  $2^N$  microscopically different species or states. For example, tyrosine in a strongly acid solution contains three ionizable protons attached to the carboxyl, aromatic hydroxyl and the ammonium group. Since each of the three groups may exist in either of two states, tyrosine may exist in eight ( $2^3$ ) microscopically different forms. The most positive of these eight states is the cation, with net charge  $Z = 1$ ; the most negative is the divalent anion, with  $Z = -2$ . Each of the two intermediate states of net charge  $Z = 0$  and  $Z = -1$ , respectively, may have three microscopically different forms. Each of the ionizable groups in tyrosine is characterized by four microconstants, because the tendency of each group to accept or donate a proton depends on the ionization state of the other two groups. Hence, there are 12 ( $3 \times 2^2$ ) microscopic ionization constants connecting the eight species. Three macroscopic ionization constants ( $K_1$ ,  $K_2$ ,  $K_3$ ) have been determined experimentally from titration and spectroscopic data [14].

For tyrosine only five of the eight species ever have appreciable concentration [7]. The fraction of each of the microscopic species formed by a molecule with three ionizable sites (e.g. tyrosine or

cysteine) can be expressed as function of pH in terms of the microconstants. If we start from the neutral species (uncharged species) rather than from the positively charged species, the fraction of any microscopic species for a molecule having  $N$  ionizable sites can be expressed in general as  $D_{ij\dots k}/D$  where  $D$  can be expressed as:

$$D = \frac{1}{0!} + \frac{\sum_i k_i [\text{H}]^{L_i}}{1!} + \frac{\sum_{i \neq j} \sum k_i k_j [\text{H}]^{L_{ij}}}{2!} + \dots + \frac{\sum_{i \neq j} \sum \dots \sum_{k \neq ij\dots} k_i k_j \dots k_{ij\dots k} [\text{H}]^{L_{ij\dots k}}}{N!} \quad (8)$$

and  $L_{ij\dots k}$  is the charge of the final state ( $ij\dots k$  state). The factorial is the number of different thermodynamic paths that lead to the  $ij\dots k$  state and  $D_{ij\dots k}$  is one of terms in the denominator. For example, the fraction of neutral species would be  $1/D$  and the fraction of a singly ionized species would be  $k_i^*[\text{H}]^{L_i}/D$ .

The fraction of any distinct species as function of pH (fraction–species curve) can be determined from Eq. (8). Whenever the total net charge of two (or more) charged species are equal, the maximum of the corresponding fraction–species curves will occur at the same pH (see Figs. 2, 5 and 6). This can be shown by estimating the ratio of the fraction of any two equally charged species using Eq. (8). The H ion dependence will cancel and the ratio of the two fractions will be totally independent of pH. In addition, the titration curve (charge curve) can be determined by multiplying the fraction–species curve by the charge on the species and summing over all species as shown in Fig. 3. The macroscopic  $pK_a$ s can be determined directly from these plots by taking the first derivative of the titration curve [7]. Table 2 shows the observed versus SPARC-calculated microscopic constants for several systems containing three ionizable sites. The notation for the macroconstants follows the scheme first proposed by Hill [23] and used later by Martin et al. [14]. The ionizing group of interest is indicated in the microscopic  $pK$  by the last number in the subscript. Any number preceding this in the subscript denotes another specified group in the molecule

which already exists in the basic form when the ionization under consideration is taking place. Thus  $pK_{32}$  denotes the  $pK$  value for the ionization of the OH group when the  $\text{NH}_3^+$  group has already been converted to the conjugate base  $-\text{NH}_2$ . Since the number 1 does not appear in the subscript 32, its absence denotes that group 1, the carboxyl, is still in the un-ionized form during the reaction corresponding to the  $pK$  value in question.

Table 3 shows the observed versus the SPARC-calculated microscopic  $pK$ s for glutathione where two  $\text{CO}_2\text{H}$  groups, an SH and a  $\text{NH}_3^+$  can be ionized simultaneously in solution. Because each of the four groups may exist in either of two states (acidic or basic), the molecule may exist in  $2^4$  states. To describe the population of the 16 microscopic species, 32 microscopic ionization constants are required [7] (see Fig. 4). However, only eight of these constants have been measured. In general, for  $N$  ionizable sites in a molecule there are  $NI$  microconstants that lead to a state of ionization of  $S$ , where  $S$  is the number ( $\leq N$ ) of sites that are ionized.  $NI$  may expressed as:

$$NI = \frac{N!}{(S-1)!(N-S)!} \quad (9)$$

For example, in the glutathione case  $N=4$  and there are four microscopic constants leading to both one ( $S=1$ ) and four ionized sites ( $S=4$ ) and 12 microconstants for each of the two and three ( $S=2$  and 3) ionized species. Only seven microscopic species have an appreciable concentration between pH 0 and 14 as shown in Fig. 5. The complete scheme for glutathione is illustrated in Fig. 4. The notation for the microscopic constants is similar to the notation used for a three site system such as tyrosine while Fig. 6 shows the fraction of the major species as a function of pH for DOPA.

Hemimellitic acid (1,2,3-benzenetricarboxylic acid) presents unusual ionization behavior. The micro constants and the observed macroscopic constants are not identical. The first ionization step favors leaving the molecule ionized at the 2 position and is stabilized by hydrogen bonding with the carboxylic groups in positions 1 and 3. The second step is more complicated. Here the

most stable di-anion is the species ionized at positions 1 and 3. This minimizes electrostatic interactions. Going from the molecule ionized at the 2 position to a di-anion ionized at the 1 and 3 positions is not a simple one proton loss. This process involves three protons as shown in Fig. 7. The thermodynamic steps for two different paths, the SPARC-calculated results for each step (the micro constants), and the first and the final step (the observed macro constant) are shown in Fig. 8.

## 6. Calculation of isoelectric points

Many molecules such as amino acids, peptides and proteins contain both acidic and basic groups. The acidic sites for these molecules are uncharged in strongly acidic solutions and negatively charged in sufficiently alkaline solutions. The basic groups are positively charged in strongly acid solution, and the conjugate bases are uncharged in sufficiently alkaline solution. In an electric field such a molecule migrates as a cation in strongly acid solution and as an anion in strongly alkaline solution. At some intermediate pH value, therefore, the mean net charge,  $Z$ , must attain the value zero, and the molecule will remain stationary in an electric field. The pH value at which this occurs is known as the isoelectric point. Edsall and Wyman [22] point out, “for most simple ampholytes of this type, such as glycine or phenylglycine,  $pK_1$  and  $pK_2$  are so far apart that there is not merely an isoelectric point, but a broad zone of pH values in which the ampholyte is practically isoelectric”. However, they show that the isoelectric point for two ionizable sites system such as those mentioned above can be given as:

$$pH_I = \frac{pK_1 + pK_2}{2} \quad (10)$$

For polyvalent ampholytes, Edsall and Wyman show that, for molecules containing only three ionizing groups where one of the macroscopic  $pK_a$ s is far apart from the other two  $pK_a$ s, a reasonable approximation can be made to calculate the isoelectric point [22]. Unfortunately, for

more complicated systems, a very rough approximation has to be made. In SPARC, the isoelectric point can be estimated by plotting the fraction of neutral or zwitterionic species versus pH (e.g. Figs. 1, 2 and 5). The pH at the middle of the zwitterionic (or any other species where the total net charge in molecule is zero) range is the isoelectric point. The observed versus SPARC-calculated isoelectric points for several molecules are shown in Table 4.

## 7. Conclusion

The SPARC chemical reactivity models, which were used to estimate both ionization  $pK_a$  and electron affinity, can also predict zwitterionic and microscopic ionization constants,  $pK_i$ , of organic molecule with multiple ionization sites that are as reliable as most experimental measurements. The corresponding complex speciation for these molecules as a function of the pH and the titration curve can be estimated using the same models without any modification.

## Acknowledgements

We gratefully acknowledge the financial support provided by the National Research Council and the US Environmental Protection Agency.

## References

- [1] A.E. Martell, R.J. Motekaities, *The Determination and Use of Stability Constants*, VCH, Weinheim, 1988.
- [2] R.E. Benesch, R. Benesch, *J. Am. Chem. Soc.* 5877 (1955) 77.
- [3] M.A. Grafius, J.B. Neilands, *J. Am. Chem. Soc.* 3389 (1955) 77.
- [4] R.B. Martin, *J. Phys. Chem.* 2657 (1971) 75.
- [5] S.H. Hilal, Y. El-Shabrawy, L.A. Carreira, S.W. Karickhoff, S.S. Toubar, M. Rizk, *Talanta* 607 (1996) 43.
- [6] S.H. Hilal, L.A. Carreira, C.M. Melton, G.L. Baughman, S.W. Karickhoff, *J. Phys. Org. Chem.* 122 (1994) 7.
- [7] S.H. Hilal, L.A. Carreira, S.W. Karickhoff, *Quant. Struct.-Act. Relatsh.* 14 (1995) 345.
- [8] S.H. Hilal, L.A. Carreira, S.W. Karickhoff, in: P. Polizer, J.S. Murray (Eds.), *Theoretical and Computational*

- Chemistry: Quantitative Treatment of Solute/Solvent Interactions, vol. 1, Elsevier, Amsterdam, 1994.
- [9] M.J.S. Dewar, R.C. Dougherty, *The PMO Theory of Organic Chemistry*, Plenum Press, New York, 1975.
- [10] S.H. Hilal, L.A. Carreira, C.M. Melton, S.W. Karickhoff, *Quant. Struct.-Act. Relatsh.* 12 (1993) 389.
- [11] S.H. Hilal, L.A. Carreira, C. Melton, S.W. Karickhoff, *J. Chromatogr.* 662 (1994) 269.
- [12] S.H. Hilal, L.A. Carreira, C.M. Melton, S.W. Karickhoff, *Proc. Solute/Solvent Interact.* 257 (1992).
- [13] Hilal S.H., Carreira L.A., Karickhoff, S.W. (in preparation).
- [14] R.B. Martin, J.T. Edsall, D.B. Wetlaufer, B.R. Hollingworth, *J. Biol. Chem.* 1429 (1958) 233.
- [15] P. Haberfield, *J. Chem. Educ.* 346 (1980) 57.
- [16] A. Bryson, N.R. Davies, E.P. Serjeant, *J. Am. Chem. Soc.* 1933 (1963) 85.
- [17] B. van de Graf, A.J. Hoefnagel, B.M. Wepster, *J. Org. Chem.* 653 (1981) 46.
- [18] A. Albert, E.P. Serjeant, *The Determination of Ionization Constants*, 3rd ed., Chapman and Hall, New York, 1984.
- [19] R.W. Green, H.K. Tong, *J. Am. Chem. Soc.* 4896 (1956) 78.
- [20] K.I. Skorey, R.S. Brownm, *J. Am. Chem. Soc.* 4070 (1985) 107.
- [21] R.B. Barlow, *J. Pharmacol.* 503 (1982) 75.
- [22] J.T. Edsall, J. Wyman, *Biophysical Chemistry*, vol. 1, Academic Press, New York, 1958.
- [23] T.L. Hill, *J. Phys. Chem.* 101 (1944) 48.
- [24] A. Neuberger, *Biochem. J.* 2085 (1936) 30.
- [25] R. Griffith Jr., L. Pillai, M.S. Greenberg, *J. Solut. Chem.* 601 (1979) 8.
- [26] D.D. Perrin, *Dissociation Constants of Organic Bases in Aqueous Solution*, Butterworth, London, 1965.
- [27] H.E. Howard-Lock, C.J.L. Lock, M.L. Martinsm, *Can. J. Chem.* 1721 (1991) 69.
- [28] K. Takacs-Novak, A. Avdeef, K.J. Box, B. Podanyi, G. Szasz, *J. Pharm. Biomed. Anal.* 12 (1994) 1369.

# Sequential injection spectrophotometric assay of bromazepam complexed with iron(II) in hydrochloric acid with chemometric optimization

Salah M. Sultan \*, Yousif A.M. Hassan, Kamal E.E. Ibrahim

*Chemistry Department, King Fahd University of Petroleum and Minerals, KFUPM Box 2026, Dhahran 31261, Saudi Arabia*

Received 15 March 1999; received in revised form 3 May 1999; accepted 4 May 1999

## Abstract

A sequential injection spectrophotometric method for the assay of bromazepam anxiolytic drug has been reported. The method is based on the complexation reaction of bromazepam with iron(II) in hydrochloric acid media and spectrophotometrically measuring the product at  $\lambda_{\max} = 585$  nm. A comprehensive chemometrical optimization treatment was successfully utilized for determining the proper optimum operating conditions for both the system and the chemical variables. The experimental design approach was employed and a  $2^k$  factorial design was run for studying the interaction effects of four factors namely, hydrochloric acid concentration, iron(II) concentration, delay time and flow rate. The super modified simplex algorithm was utilized for optimizing the three highly interacting factors which were, hydrochloric acid, iron(II), and delay time. The conditions obtained were  $150 \mu\text{l}$   $0.110 \text{ mol l}^{-3}$  hydrochloric acid,  $75 \mu\text{l}$   $0.328 \text{ mol l}^{-3}$  iron(II), 1200 s delay time and  $40 \mu\text{l s}^{-1}$  flow rate. The method was found to be suitable for the determination of Bromazepam in pharmaceutical preparations and the results obtained for the assay of the compound in proprietary drugs indicate that the method suffers no interference from excipients. © 1999 Published by Elsevier Science B.V. All rights reserved.

*Keywords:* Bromazepam; Iron(II); Hydrochloric acid; Sequential injection analysis; Chemometrics

## 1. Introduction

Bromazepam is chemically known as 7-bromo-1,3-dihydro-5-(2-pyridyl)-2H-1,4-benzodiazepin-2-one. It is medically used as a psychotropic drug that acts on psychic function, behaviour or experi-

ence. It alters the mental state by affecting the neurophysiological and biochemical activity of the functional units of the CNS. It is formerly known as a tranquilizer commonly used to reduce pathological anxiety, tension, agitation and depression [1–4].

Bromazepam has been determined by various methods, each with its advantages and disadvantages, including chromatography [3,5–15] electrochemistry [16–18] spectrophotometry [19–24] and

\* Corresponding author. Tel.: +966-3-860-2111; fax: +966-3-860-5534.

*E-mail address:* smsultan@kfupm.edu.sa (S.M. Sultan)



still no official method, either in the BP or in the USP monographs, has been reported.

Few flow injection analysis (FIA) methods [25–27] for the determination of this compound have been reported in the literature including two by the first author [1,2]. One is a FIA stopped flow method [1] that lacks automation and requires high precision in measuring the delay time in the reaction coil. The other is a sequential injection analysis (SIA) kinetic method [2] with the conditions of the determination based on the kinetic data and lacks validation and full chemometrical optimization [25–28] for the experimental variables.

Since numerous methods are inevitably time dependent and primarily follow the kinetic methods of analysis such as the fixed-time and the fixed-concentration methods, computer controlled sophisticated equipment such as SIA is found to be mandatory. Not only that but thorough investigation of the experimental operating conditions has to be performed and the chemometrical optimization approach is found to be essential and extremely useful for such reactions. This work comprises both methodologies for the spectrophotometric determination of bromazepam after its complexation with iron(II) in hydrochloric acid media.

## 2. Experimental

### 2.1. Apparatus

An Alitea USA/FIALab 3000 (Medina, WA USA) has been used in this study. The apparatus consists of a syringe pump, a multi-position valve, a spectrophotometer, XY recorder and a PC. The syringe pump is a 24 000 steps syringe pump with an optical encoder feedback; 1.5 s to 20 min per stroke of 5.0 ml size. It has > 99% accuracy at full stroke. The multi-position valve has eight (8) ports with a standard pressure of 250 psi (gas)/600 psi (liquid); zero dead volume; chemically inert; and port selection by manual or software control. The spectrophotometer is a Spectronic Mini 20 spectrophotometer used as a detector with a 20  $\mu$ l ultra-micro flow-through cell having a path length

of 1.0 mm and connected to a Cole-Parmer (Chicago, IL, USA) model 0555 single-channel strip-chart recorder with the speed adjusted to 1  $\text{cm min}^{-1}$ . The pump tubing, 0.30 in. i.d. Teflon type supplied by Upchurch Scientific (Oak Harbor, WA, USA), was used for connecting the different units, making the holding coil (200 cm long) and the reaction coil (50 cm long).

### 2.2. Software packages

Alitea FIALab software has been used for programming and controlling the SIA system. Sigmaplot, version 1.02 (Jandel Scientific, Erkrath, Germany) was employed for data handling calculations and constructing graphs. The 'Chemometric Optimization by Simplex' (COPS) program was obtained from Elsevier Scientific, The Netherlands, and utilized for the optimization of variables using a compatible IBM personal computer.

### 2.3. Reagents and stock solutions

Double-distilled de-ionized water was used through out for the preparation of the following solutions and all other dilutions.

#### 2.3.1. Iron(II) standard solution (0.410 $\text{mol dm}^{-3}$ )

A stock solution of dried ANALAR di-ammonium iron(II) sulfate 6-hydrate ( $(\text{NH}_4)_2\text{SO}_4 \cdot \text{FeSO}_4 \cdot 6 \text{H}_2\text{O}$ ) (BDH) was prepared by dissolving (exactly) 80.386 g in 500 ml 0.0150 M hydrochloric acid solution.

#### 2.3.2. Hydrochloric acid (1.0 $\text{mol dm}^{-3}$ )

This was prepared by diluting analytical-reagent grade concentrated acid, other working solutions were prepared by further dilution.

#### 2.3.3. Bromazepam ( $3.229 \times 10^{-3}$ $\text{mol dm}^{-3}$ )

A stock solution was prepared by dissolving exactly 0.1166 g of the pure compound (Hoffmann-La Roch, Basel, Switzerland), in about 30  $\text{cm}^3$  0.02  $\text{mol dm}^{-3}$  hydrochloric acid. The mixture was stirred for 25 min, then the volume was made up to 100  $\text{cm}^3$  with the same acid. Working solutions were prepared from this stock solution.

### 2.3.4. Lexotanil tablets (389 ppm bromazepam)

Five tablets of the proprietary drug lexotanil (Hoffman-La Roche, Basel Switzerland) each claimed to contain 3 mg bromazepam were crushed and weighed out. A solution of 389 ppm bromazepam was prepared by dissolving an amount of the powder equivalent to a certain mass of the drug in  $0.02 \text{ mol dm}^{-3}$  hydrochloric acid solution.

### 2.4. Manifold and procedure

Fig. 1 illustrates the different components of the computer controlled SIA manifold used in this study. Various commands were fed into the program and the steps are summarized as follows:

1. With the valve position in, the syringe pump was filled at a flow rate of  $250 \text{ l s}^{-1}$ .
2. With the valve position out the following steps were carried out.
3. The carrier solution ( $1200 \mu\text{l}$  water) was dispensed at a flow rate of  $250 \mu\text{l s}^{-1}$  through port 1 of the selector valve. This step was performed to adjust the absorbance of the spectrophotometer to zero and to insure complete clearance of any residual solutions.
4. Iron(II) and bromazepam solutions ( $150 \mu\text{l}$  each) were aspirated at a flow rate of  $100 \mu\text{l s}^{-1}$  through ports 4 and 5, respectively, with

their appropriate solutions. The excess was discarded by dispensing  $500 \mu\text{l}$  at the same flow rate through port 7.

5. Iron(II) ( $75 \mu\text{l}$ ) was aspirated at a flow rate of  $150 \mu\text{l s}^{-1}$  through port 4.
6. With the same flow rate as above,  $150 \mu\text{l}$  Bromazepam was aspirated through port 5.
7. The reagents were delayed for  $1200 \text{ s}$  in the holding coil to guarantee completion of the reaction.
8. Finally,  $1200 \mu\text{l}$  of the reaction mixture was dispensed at a flow rate of  $40 \mu\text{l s}^{-1}$  through port 1 and the absorbance was recorded.

## 3. Results and discussion

### 3.1. Chemical system and optimization:

The present SIA method is based [1] on the complexation reaction of bromazepam with iron(II) in hydrochloric acid media and spectrophotometrically measuring the stable pink–violet product that absorbs at the maximum wavelength  $\lambda_{\text{max}} = 585 \text{ nm}$ . The reaction kinetics and the stoichiometry of this system has been well studied and documented and the reaction was found to take place only under specific conditions depending mainly on the acid concentration, with the absorbance of the complex increasing as time passes, thus indicating the slowness of the reaction [2].

The following equation illustrates the complexation reaction scheme: Scheme 1

As a result of previous [1,2] investigations carried out on this reaction which revealed complex reaction conditions depending on acid concentration and the low sensitivity of the product, it was decided to perform a full chemometrical optimization for the experiment for both the system and the chemical operating variable conditions. The experimental design approach [28] was employed and a  $2^k$  factorial design was run where 2 stands for variable levels considering the higher and lower values and  $k$  is the number of factors studied. Four factors were chosen, i.e. hydrochloric acid and iron(II) concentrations, delay time and flow rate variables. The highest and lowest

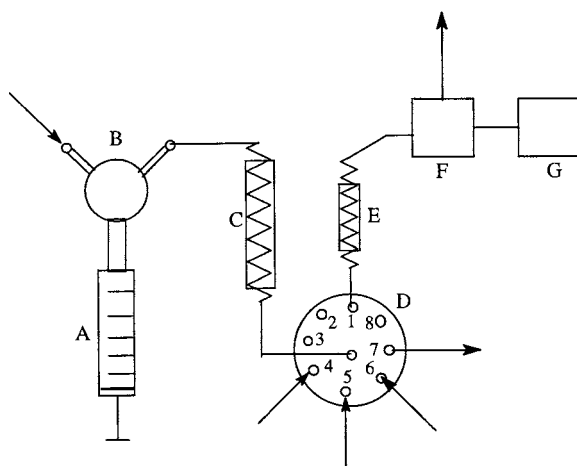
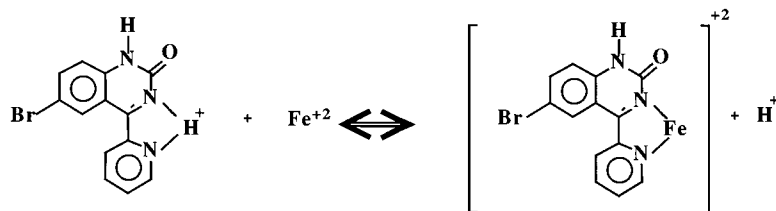


Fig. 1. SIA manifold comprised of; (A) 5 ml syringe pump; (B) two-way valve; (C) holding coil; (D) eight ports selector valve; (E) reaction coil; (F) spectrophotometer; and (G) recorder.



Scheme 1.

Table 1

Full treatment combinations in both their original and coded levels along with the responses obtained by injecting  $75 \mu\text{l}$   $3.229 \times 10^{-3} \text{ mol dm}^{-3}$  bromazepam prepared in  $0.02 \text{ M}$  hydrochloric acid and  $150 \mu\text{l}$   $4.1 \times 10^{-1} \text{ mol dm}^{-3}$  iron(II) prepared in the appropriate acid

Experiment No.	[HCl] (M)	[Iron(II)] (M)	Time (s)	Flow rate ( $\mu\text{l s}^{-1}$ )	Response (mm)
1	0.0080	0.0050	60	20	1.0
2	0.10	0.0050	60	20	1.0
3	0.0080	0.15	60	20	3.0
4	0.10	0.15	60	20	2.0
5	0.0080	0.0050	600	20	5.5
6	0.10	0.0050	600	20	2.0
7	0.0080	0.15	600	20	8.0
8	0.10	0.15	600	20	5.5
9	0.0080	0.0050	60	50	1.0
10	0.10	0.0050	60	50	1.0
11	0.0080	0.15	60	50	3.0
12	0.10	0.15	60	50	2.0
13	0.0080	0.0050	600	50	5.5
14	0.10	0.0050	600	50	2.0
15	0.0080	0.15	600	50	8.0
16	0.10	0.15	600	50	5.5
1	-1	-1	-1	-1	1.0
2	+1	-1	-1	-1	1.0
3	-1	+1	-1	-1	3.0
4	+1	+1	-1	-1	2.0
5	-1	-1	+1	-1	5.5
6	+1	-1	+1	-1	2.0
7	-1	+1	+1	-1	8.0
8	+1	+1	+1	-1	5.5
9	-1	-1	-1	+1	1.0
10	+1	-1	-1	+1	1.0
11	-1	+1	-1	+1	3.0
12	+1	+1	-1	+1	2.0
13	-1	-1	+1	+1	5.5
14	+1	-1	+1	+1	2.0
15	-1	+1	+1	+1	8.0
16	+1	+1	+1	+1	5.5

values were determined and assigned +1 and -1 coded levels, respectively, and both shown in Table 1. For hydrochloric acid, the highest con-

centration was 0.2 and the lowest was  $0.02 \text{ mol l}^{-3}$ ; for iron(II), the highest was 0.20 and the lowest was 0.01. Beyond these concentrations the

reaction does not take place and no coloured complex exists. For the delay time, the highest was 1200 and the lowest was 60 s; below this delay time, the peak absorbance was not significant. For the flow rate, the highest was 50 and the lowest was 20  $\mu\text{l s}^{-1}$  as a reasonable system

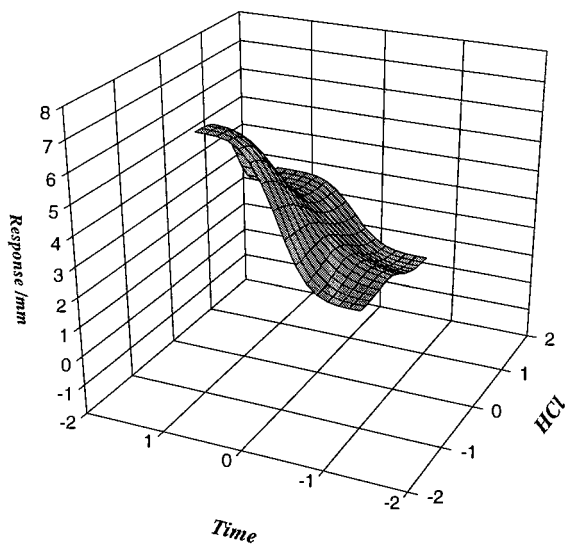


Fig. 2. Surface plot of the response in mm vs. time and hydrochloric acid levels.

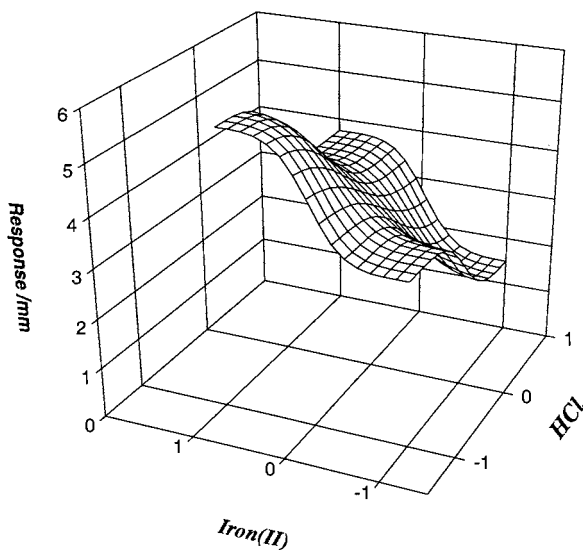


Fig. 3. Surface plot of the response in mm vs. iron(II) and hydrochloric acid levels.

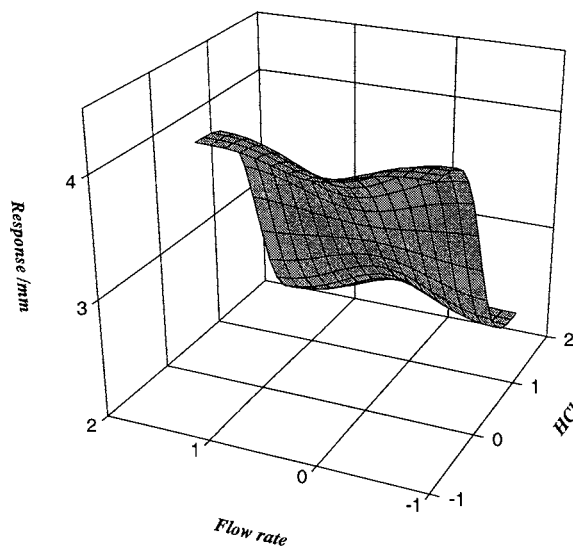


Fig. 4. Surface plot of the response in mm vs. flow rate and hydrochloric acid levels.

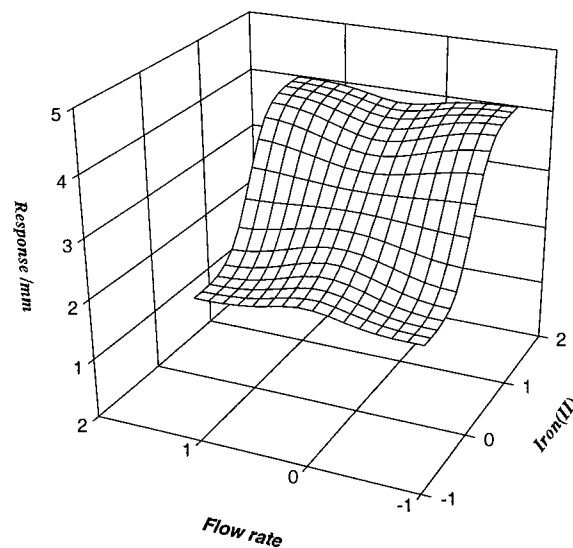


Fig. 5. Surface plot of the response in mm vs. flow rate and iron(II) levels.

variable. Sixteen experiments were arranged and the equivalent response function, measured as peak height in mm, was recorded as in Table 1. The results were treated by the Sigmaplot Software and every two factors were considered for a 3D response surface plot thus producing six plots

as in Figs. 2–7. Fig. 2 shows the response surface as a function of delay time and hydrochloric acid levels, indicating the significant effect of the delay time compared to the effect of the acid which shows a small increase and a decrease as its concentration increases. Fig. 3 shows the response surface as a function of iron(II) and hydrochloric

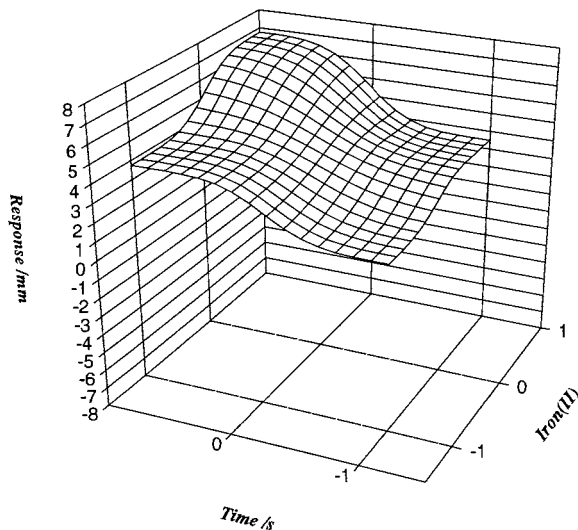


Fig. 6. Surface plot of the response in mm vs. time and iron(II) levels.

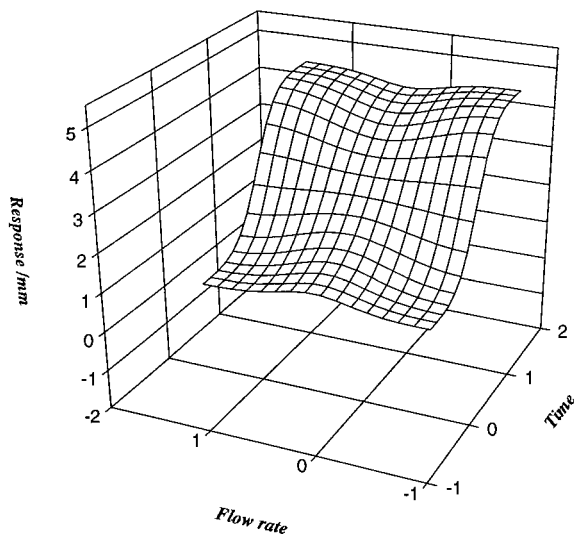


Fig. 7. Surface plot of the response in mm vs. flow rate and time levels.

acid levels, indicating the significant effect of iron(II) compared to the effect of the acid which shows a small increase and a decrease to confirm the above observation. Fig. 4 shows the response surface as a function of the flow rate and hydrochloric acid levels indicating no effect of the former and a sharp decrease on the effect of the acid as it increases. Fig. 5 shows the response surface as a function of flow rate and iron(II) levels confirming the negligible effect of the flow rate and a sharp positive effect of iron(II) as its concentration increases. Fig. 6 shows the response surface as a function of delay time and iron(II) levels confirming the positive effect of both variables at their higher levels. Fig. 7 shows the response surface as a function of flow rate and delay time levels confirming the negligible effect of the flow rate and a sharp effect at higher delay time.

Multiple regression analysis was run on the data obtained and the interaction effects of all possible combinations of the variables were calculated as shown in Table 2. The sum of squares (SS) due to the regression as a percentage of the total sum of squares is 89.6%, showing that a reasonably large proportion of the variance is explained by the regression equation. The variance ratio of the regression mean square (MS) to the residual mean square gives a value of 23.6, indicating that the regression equation accounts for a reasonable proportion of the variance in the responses at a probability level of  $P = 0.0001$ . The main effect of the delay time was found to be the highest and the zero main effect of the flow rate justifies keeping it constant and is not necessary to be included in optimization. The interactive effect of time was also found to be more significant with both hydrochloric acid and iron(II). It is interesting to note that the zero interactive effect of hydrochloric acid with iron(II) is the reason for reducing the overall interactive effect of time with both variables.

The above indicates that the graphical representations and the computation results are in good agreement and clearly justifies fixing the flow rate parameter at  $40 \mu\text{l s}^{-1}$  and not including it in further optimization treatments. The super modified simplex algorithm [29–31] was per-

Table 2  
Analysis of variance

Source of variation	Degree of freedom	Sum of squares	Mean square	Variance ratio
Regression	4	81.5	20.375	
Residual	11	9.5	0.864	23.6
Total	15	91.00	6.067	
<i>Main effect</i>				
HCl	= -1.75			
Iron(II)	= 2.25			
Time	= 3.625			
Flow rate	= 0			
<i>Interactive effects</i>				
HCl × iron(II)	= 0			
HCl × time	= -1.25			
Iron(II) × time	= 0.75			
HCl × iron(II) × time	= 0.5			

formed to obtain the exact optimum experimental conditions for the variables, iron(II), delay time and flow rate. The highest and lowest levels for the three factors of the same values for the factorial design experiment above were again used, except for the delay time which was adjusted to 1200 s. The step values for hydrochloric acid, iron(II) and delay time were  $0.05 \text{ mol l}^{-3}$ ,  $0.07 \text{ mol L}^{-3}$  and 300 s, respectively. Bromazepam ( $150 \mu\text{l}$  of 900 ppm) prepared in  $0.02 \text{ mol l}^{-3}$  hydrochloric acid mixed with  $75 \mu\text{l}$  iron(II) prepared in the appropriate acid were taken as fixed values to run the simplex. Twenty-two experiments (Table 3) were conducted by the simplex, starting with experiment 1, fed to the computer as the initial experiment as found by previous investigations. Fig. 8 shows the smooth progress of the simplex by experiment number that indicates a significant and convincing success of the procedure and a considerable increase in the sensitivity compared to the initial simplex experiment. The steps clearly indicate that peak absorbance increases at lower acid concentration, higher iron(II) concentration and longer delay time. This result is in good agreement with the reaction scheme presented above which indicates that decreasing the acidity and increasing iron(II) concentration favors the formation of the complex. The hydrogen proton as a product in the reaction

verifies the experimental findings that the reaction should be carried out in low acidic media, but not to the extent of being basic as iron hydrolyses and the complex becomes unstable. The simplex performed nine reflections and a maximum response value was obtained by experiment 17 and 18 for optimum conditions of  $150 \mu\text{l}$   $0.110 \text{ mol l}^{-3}$  hydrochloric acid,  $75 \mu\text{l}$   $0.328 \text{ mol l}^{-3}$  iron(II) and 1200 s delay time. Again the same peak height was obtained at vertex 18 with exactly the above conditions.

### 3.2. Analytical appraisals

With the above optimum conditions,  $0.110 \text{ mol l}^{-3}$  hydrochloric acid,  $0.328 \text{ mol l}^{-3}$  iron(II) and 1200 s delay time and following the procedure stated above, a series of bromazepam standard solutions were prepared and run. Absorbance measurements were plotted versus bromazepam concentrations and the following calibration equation was obtained:

$$A = -0.001444 + 0.00005865C$$

where  $C$  is the concentration of bromazepam in ppm.

The above calibration equation was found to be linear over the concentration range 300–1100 ppm with a correlation coefficient of 0.988 with a relative S.D. of 0.33% for three injections.

### 3.3. Application

Under the above stated optimized conditions the method was applied to the determination of bromazepam in lexotanil proprietary drug in its tablet form. The above standard calibration equation was computed and the results obtained were found to be highly precise with a relative S.D. of not less than 0.3. A percentage recovery of 99.89% of the claimed content of bromazepam was obtained indicating the higher degree of accuracy. The results obtained also showed that no interference from excipients, usually added to the drug in tablet form, were encountered, thus rendering the method suitable for determination of this drug in pharmaceutical preparations.

### 4. Conclusion

A successful comprehensive chemometrical optimization treatment for the operating system and

chemical variables has resulted in obtaining the proper conditions and higher sensitivity for the product than that obtained previously [1], thus validating the method. The molar absorptivity was calculated to be  $731.6 \text{ l mol}^{-1} \text{ cm}^{-1}$  in the present work compared to  $504.85 \text{ l mol}^{-1} \text{ cm}^{-1}$  previously [1]. The agreement in both graphical representations and computation results for the behavior of the parameters investigated is considered positive and justifies conducting such a useful study for such a complicated system.

By using a SIA instrument equipped with a syringe pump rather than a peristaltic pump, more accurate and precise uptake of the drug and precise monitoring of the delay time could be attained. Automation is considered novel and inevitable for kinetically controlled reactions, thus overcoming the drawback of the delay time and reducing the errors encountered in monitoring reaction rates and measurements employing the fixed time method. In this respect the present method is considered superior relative to the FIA method earlier reported [1].

Table 3

Super-modified simplex optimization progress obtained by injecting  $150 \mu\text{l}$  900 ppm bromazepam prepared in 0.02 M hydrochloric acid and  $75 \mu\text{l}$  iron(II) prepared in the appropriate acid<sup>a</sup>

Vertex No.	Iron(II)	HCl	Time (s)	Response (mm)
1	0.08	0.05	120	2.00
2	0.146	0.061	190.7	3.00
3	0.096	0.097	190.7	2.00
4	0.146	0.061	402.8	4.00 R
5	0.179	0.097	402.8	4.30
6	0.184	0.0121	544.26	5.5 R
7	0.206	0.065	567.83	6.00
8	0.175	0.058	695.72	6.50 R
9	0.181	0.098	880.51	7.00
10	0.281	0.106	1017.15	8.00 R
11	0.314	0.128	1077.92	9.50
12	0.265	0.14	1200	11.00 R
13	0.265	0.09	1200	11.00
14	0.230	0.085	1200	11.00 R
15	0.239	0.095	899.83	9.50
16	0.328	0.110	995.25	10.00
17	0.328	0.110	1200	14.00
18	0.328	0.110	1200	14.00 R
19	0.176	0.078	1079.62	10.00
20	0.286	0.109	790.5	8.30 R
21	0.239	0.111	1148.8	11.50
22	0.358	0.151	1169.28	12.30 R

<sup>a</sup> The flow rate was fixed at  $40 \mu\text{l s}^{-1}$ . R, reflected vertex.

### Bromazepam simplex Curve

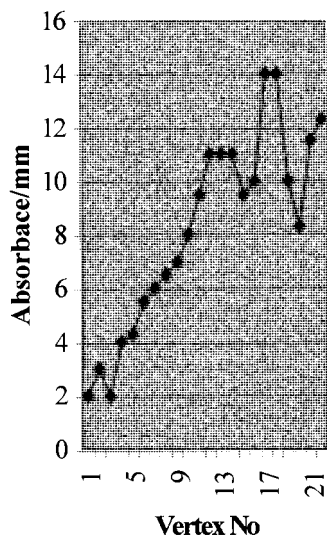


Fig. 8. Response function progress of the simplex.

### Acknowledgements

Thanks is due to F. Hoffman-La Roche Ltd., Basel, Switzerland for the gift of the bromazepam generic sample. Yousif A.M. Hassan wishes to thank KFUPM for allowing him to use their facilities at the Chemistry Department. Thanks is also due to KFUPM for allowing the first author to present this paper at the 10th International Conference on Flow Injection Analysis (IC-FIA99), Prague, Czech Republic, 20–25 June 1999.

### References

- [1] S.M. Sultan, *Analyst* 117 (1992) 773.
- [2] S.M. Sultan, F.O. Suliman, *Analyst* 121 (1996) 617.
- [3] S.M. Sultan, A.H. El-Mubarak, *Talanta* 43 (1996) 569.
- [4] The Extra Pharmacopeia, 28th edn., Martindale, London, 1982.
- [5] S.J. Mules, G.A. Casella, *J. Anal. Toxicol.* 13 (1989) 179.
- [6] H. Friedman, H. Greenblatt, E.S. Burstein, H.R. Ochs, *J. Chromatogr.* 51 (1986) 1.
- [7] W.D. Hooper, J.A. Roome, A.R. King, M. Smith, T. Eadie, R.G. Dickinson, *Anal. Chim. Acta* 117 (1985) 267.
- [8] A.C. Tas, J. Van der Greef, M.C. Ten Noever, et al., *J. Anal. Toxicol.* 10 (1986) 46.
- [9] C.E. Jones, F.H. Wians, L.A. Martinez, G.J. Merritt, *Clin. Chem.* 35 (1989) 1394.
- [10] J.P. Chovan, J.D. Vermeulen, *J. Chromatogr.* 86 (1989) 413.
- [11] M. Sunzel, *J. Chromatogr.* 83 (1989) 455.
- [12] H. Shutz, V. Westenberger, *J. Chromatogr.* 169 (1979) 409.
- [13] S. Barazi, M. Bonini, *J. Chromatogr.* 202 (1980) 473.
- [14] M.I. Gonzales Martin, C. Gonzales Perez, J. Hernandez Mendex, *Anal. Quim.* 82 (1986) 71.
- [15] C. Violon, L. Pessemier, A. Vercruysee, *J. Chromatogr.* 236 (1982) 157.
- [16] L. Hernandez, A. Zapardiel, J.A. Perezlopez, E. Bermejo, *Talanta* 35 (1988) 287.
- [17] L. Valdeon, E.M. Sevilla, H.L. Hernandez, *Analyst* 112 (1987) 1365.
- [18] E. Ruiz Zarobe, B.M. Hernandez, E. Lorenzo Abad, L. Hernandez, *Anal. Quim.* 84 (1988) 120.
- [19] A.F. Fartushnyi, E.B. Muzhanovskii, A.P. Sukhin, A.I. Sedov, E.B. Kvasov, *Pharm. Zh.* 5 (1986) 47.
- [20] C. Caille, J. Braun, S.A. Mockle, *Can. J. Pharm. Sci.* 5 (1970) 78.
- [21] A. Hernandez, P. Gutierrez, J. Thomas, *Farmaco* 41 (1986) 300.
- [22] P. Fiearra, A. Villari, R. Ficarra, G. Mondio, *Farmaco* 42 (1987) 241.
- [23] M.A. Abounassif, *J. Pharm. Belg.* 44 (1989) 329.
- [24] D. Lorenzo, M. Hernandez, L. Hernandez, *Microchem. J.* 37 (1988) 257.
- [25] D. Parada, E. Lorenzo Abad, M. Hernandez, L. Hernandez, *Microchem. J.* 37 (1988) 257.
- [26] R.E. Santelli, M. Gallego, M. Valcarcel, *Talanta* 38 (1991) 1241.
- [27] M. Valcarcel, M. Gallego, R. Montero, *J. Pharm. Biomed. Anal.* 8 (1990) 655.
- [28] E.D. Morgan, *Chemometrics: Experimental Design*, Wiley, Chichester, 1991.
- [29] W. Spendley, G.R. Hext, F.R. Himsworth, *Technometrics* 4 (1962) 441.
- [30] J.A. Nedler, R. Mead, *Comput. J.* 7 (1965) 308.
- [31] S.M. Deming, S.L. Morgan, *Anal. Chem.* 45 (1973) 278A.



# A passive sampler–GC/ECD method for analyzing 18 volatile organohalogen compounds in indoor and outdoor air and its application to a survey on indoor pollution in Shizuoka, Japan

Olansandan, Takashi Amagai \*, Hidetsuru Matsushita

*Division of Environmental Health Sciences, Graduate School of Nutritional and Environmental Sciences, University of Shizuoka, 52-1 Yada, Shizuoka 422-8526, Japan*

Received 11 February 1999; received in revised form 19 May 1999; accepted 19 May 1999

## Abstract

A simple and reliable method was developed for analysis of 18 volatile organohalogen compounds (VOHCs) both indoors and outdoors, consisting of VOHC collection by a passive sampler, extraction with toluene by mechanical shaking, and automatic separation analysis by capillary gas-chromatography with electron capture detector (GC/ECD). The passive sampler is a porous polytetrafluoroethylene (PTFE) tube ( $30.30 \pm 0.37$  mm net collection length, 5.0 mm inside diameter, 0.990 g weight) uniformly packed with activated charcoal ( $194.4 \pm 3.8$  mg). The procedure was applied to a field survey on indoor and outdoor VOHC pollution in Shizuoka, Japan. Ten VOHCs, including trichloroethylene, tetrachloroethylene, chloroform, carbon tetrachloride, and *p*-dichlorobenzene, were detected from indoor and outdoor air samples. The ratios of maximum to minimum VOHC concentrations, both outdoors and indoors, were large. The indoor and outdoor concentrations of 1,1-dichloroethylene, dichloromethane, 1,1,1-trichloroethylene, carbon tetrachloride and trichloroethylene were found to be similar. Indoor concentrations of trihalomethanes, *p*-dichlorobenzene and tetrachloroethylene were higher than those of outdoors. © 1999 Elsevier Science B.V. All rights reserved.

*Keywords:* Volatile organohalogen compounds; Indoor pollution; Passive sampler

## 1. Introduction

In recent years, the interest in and necessity of evaluating indoor air pollution have grown substantially. Indoor air is polluted not only by penetration of outdoor substances, but also by emissions from various indoor sources, such as heating, cooking, smoking, other human activities

\* Corresponding author. Tel.: +81-54-2645798 fax: +81-54-264-5798.

*E-mail address:* amagai@smail.u-shizuoka-ken.ac.jp (T. Amagai)

and building materials [1–3]. Therefore, levels of personal exposure to such compounds cannot be estimated from their outdoor concentrations alone. The target chemicals in this study, volatile organohalogen compounds (VOHCs), have received special attention as indoor air pollutants. These chemicals have widely been used in insect repellents [4], washing clothes and dishes, cleaning car engines [5], dry cleaning, and a dry cleaned clothes [6,7]. Trihalomethanes are generated from tap water when we shower and bath, etc. [8]. The VOHCs include various suspected carcinogens, for example, trichloroethylene and tetrachloroethylene have been classified as probable human carcinogens (class 2A) by IARC [9,10]. Because most people spend the greater part of their time indoors [11–14], it is useful to develop a simple and highly sensitive analytical method to determine the sources and types of VOHCs emitted indoors and to quantify the emission rates of these compounds. However, there are few data on the occurrence in indoor air, mainly due to the lack of inexpensive and reliable monitoring methods.

Recently, our knowledge in the field of indoor air quality has been increasing steadily [15–18]. Traditional integrative sampling methods for outdoor and personal exposure monitoring are usually based on active sampling techniques, which need expensive equipment, a power source and a skilled staff; thus, they are unsuitable for large field studies. The passive sampler was originally designed to monitor elevated concentrations in working areas, and has been adopted in the last years to low-concentration monitoring. Although a passive sampler for indoor air measurements at environmental concentrations was previously developed, it used 2-week passive sampling methodology [19], and day-to-day variations could not be determined. Another approach included a passive sampler and thermal desorption gas-chromatography (GC) analysis [20,21]. This system, however, needed expensive apparatus.

In this paper, an analytical method for measurement of outdoor and indoor VOHC concentrations over 24 h is described. The method consists of VOHC collection by a passive sampler (a polytetrafluoroethylene tube uniformly packed

with activated charcoal), extraction with toluene by mechanical shaking, and separation analysis by capillary GC with an electron capture detector.

## 2. Experimental

### 2.1. Reagents

The 18 VOHCs investigated were dichloromethane, chloroform, bromodichloromethane, chlorodibromomethane, bromoform, 1,1-dichloroethylene, 1,1,1-trichloroethane, carbon tetrachloride, 1,2-dichloroethane, trichloroethylene, tetrachloroethylene, 1,1,1,2- and 1,1,2,2-tetrachloroethane, *o*-, *m*- and *p*-dichlorobenzenes, and hexachloro-1,3-butadiene. Standard compounds of the highest available purity were obtained from Wako Pure Chemical Industries, and were not further purified. The solvent for extraction of VOHCs was HPLC grade toluene (> 99.8%, Wako Pure Chemical Industries). Immediately before use, the solvent was checked by GC to confirm it free of VOHC contamination.

Stock standards solution were made by dissolving the following amounts of VOHCs in 50 ml of toluene: 4.715 g for 1,1-dichloroethylene; 5.274 g for dichloromethane; 0.5865 g for chloroform; 0.6453 g for 1,1,1-trichloroethane; 0.4702 g for carbon tetrachloride; 1.045 g for 1,2-dibromomethane; 0.7588 g for bromodichloromethane; 0.9426 g for chlorodibromomethane; 0.4869 g for trichloroethylene; 0.4869 g for bromoform; 0.5729 g for 1,1,1,2-tetrachloroethane; 0.7786 g for 1,1,2,2-tetrachloroethane; 0.4118 g for hexachloro-1,3-butadiene and 3.681, 3.810, 9.118 g for *o*-, *m*- and *p*-dichlorobenzenes, respectively. Relative concentrations of the VOHCs in the environment were considered in preparing the standard solutions.

### 2.2. Passive samplers

The passive sampler used was an improved type of passive gas tube (8015-066) from Shibata Scientific Technology, consisting of granular activated charcoal packed inside of porous polyte-

trafluoroethylene (PTFE) tubes. The net collection length and the amount of absorbent were standardized at  $30.30 \pm 0.37$  mm and  $194.4 \pm 3.8$  mg, respectively. Fig. 1 shows the structure of the passive sampler. To avoid external contamination, each sampler was put in an aluminum bag and sealed. Twelve such bags were put in another, large aluminum bag and sealed again. The passive samplers were taken from the bag just before the sampling and exposed to the air for 24 h to collect the target compounds. After sampling, the sampler was returned to same aluminum bag. The inside air was removed, and the bag was zippered, sealed with cellophane tape and stored at  $-45^{\circ}\text{C}$  until analysis.

### 2.3. Extraction

The extraction method of the VOHCs was as follows: The activated charcoal in the passive sampler was transferred to a glass test tube containing 2 ml of toluene, and stoppered tightly. The test tubes were shaken mechanically ( $115 \text{ min}^{-1}$ ) at room temperature for 2 h. They were centrifuged for 10 min at  $4^{\circ}\text{C}$ , 3000 rpm, and 1 ml of supernatant was then transferred into autosampler vials for analysis by GC with electron capture detector (ECD).

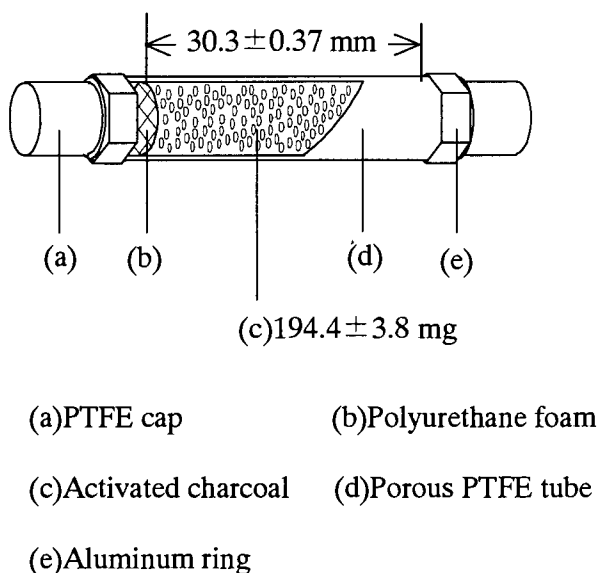


Fig. 1. Structure of the passive sampler used.

### 2.4. Gas chromatography analysis

The apparatus was composed of a Hewlett-Packard 5890 series II GC/ECD, an HP 7637 automatic injector and an HP Chem Station system. The column used was a VOCOL™ Fused Silica Capillary Column (60 m in length, 0.32 mm i.d., and film thickness of  $3.00 \mu\text{m}$ ) from Supelco. The carrier gas was helium ( $> 99.995\%$ ), and the make-up gas was highly pure nitrogen ( $> 99.9999\%$ ). The GC conditions were as follows: the flow rates of carrier gas and make-up gas were 4.0 and  $50 \text{ ml min}^{-1}$ , respectively. Injection volume was  $1.0 \mu\text{l}$ . The initial temperature of the column was  $40^{\circ}\text{C}$ , and was increased to  $210^{\circ}\text{C}$  by  $4^{\circ}\text{C min}^{-1}$  and held at 15 min. After the oven cooled to the initial temperature, the next sample was injected automatically. The analytical cycle was almost one hour. The temperature of the injector was  $240^{\circ}\text{C}$  and that of detector was  $280^{\circ}\text{C}$ .

Compound identification was performed by comparing the retention times of the peaks of the sample solution with those of the standards solution. In the peak identification, permissible variation in retention time was set within  $\pm 0.2\%$  for each peak. Before every measurement of samples, calibration curves were obtained from the VOHC concentrations and peak areas, using standards solution.

### 2.5. Recovery (desorption efficiency)

For recovery test, one of the PTFE caps of the passive sampler was removed, and a small amount of VOHC standard solution was injected directly into the activated charcoal using a micro syringe. Ten samples were treated together. After capping and keeping them for 30 min in clean air, 10 spiked samples and two blank samples (not spiked) were extracted and analyzed as described above.

### 2.6. Reproducibility

A small amount of standard compound was evaporated and diffused homogeneously in a room ( $75 \text{ m}^3$ ) in building. Then, 10 passive sam-

plers were simultaneously exposed for 24 h to the air in the room. These samples were extracted and analyzed as described above.

### 2.7. Storage of the samples

Loss of VOHCs during storage of samples was also investigated. The 18 VOHCs were evaporated and diffused homogeneously in a room in building. Then, eight passive samplers were exposed to the air in the room for 24 h. Half of the samples were analyzed immediately. The rest were packed separately into aluminum bags, the air in the bags was removed, and each bag was zippered, sealed, and put into another larger aluminum bag. They were stored at  $-45^{\circ}\text{C}$  for 1 month.

### 2.8. Calculation of air concentration of volatile organohalogen compounds from the amount collected by passive sampler

To calculate the concentrations of the VOHCs in the air, active and passive samplings were performed simultaneously, and the results were compared with each other. The active sampler was a custom-made charcoal tube from Shibata Scientific Technology, connected to a personal pump (PAS-500; Shibata Scientific Technology). The charcoal tube had two separate layers of activated charcoal: the front layer contained 150 mg of activated charcoal; and the rear layer contained 50 mg; the latter provided a check for any breakthrough of VOHC. The flow rate of the pump ( $50\text{ ml min}^{-1}$ ) was measured before and after the sampling period, and the average was used to calculate the VOHC concentrations. These simultaneous measurements were performed 32 times under various conditions.

The extraction procedure of the actively-collected samples was as follows: the activated charcoal in the active sampler was put into the test tube containing 3.0 ml of toluene for the front layer and 1.0 ml of toluene for the rear layer. After they were shaken mechanically ( $115\text{ times min}^{-1}$ ) at room temperature for 2 h, the target VOHCs were separated and analyzed by the GC/ECD described above. As the adsorption amount by the activated charcoal was proportional to air

concentration, the efficiencies were calculated from the ratio of the collection amount by the front layer of active sampler to that of the rear layer, according to the literature [22]. The collection efficiencies were at least 96.4%. The amounts collected by passive sampling were then compared with the air concentration obtained by active sampling.

### 2.9. Effect of wind velocity, temperature and relative humidity

The experiment to compare the amounts of VOHCs collected by passive samplers with their concentration in the air, as described above, was performed under various wind velocity, temperature and relative humidity conditions. To confirm the effect of high relative humidity, additional experiments were performed during the rainy season, when several 24-h samples were taken in residences ( $22\text{--}24^{\circ}\text{C}$ , relative humidity 87–98%) on rainy days.

### 2.10. Application to a field survey

Indoor pollution in Shizuoka was surveyed during the summer season of 1996. The Shizuoka city is located in the middle of Japan and has a population of  $\approx 470\,000$ . Sampling for 24 h was carried out in the living room, kitchen, bedroom, bathroom and outdoors of 70 residences.

Field blank sample was taken at every 10 samples (every two households).

## 3. Results and discussion

### 3.1. Passive sampler

Sampling of indoor and outdoor volatile organic compounds (VOC), including VOHCs, has often been performed using active samplers containing polymer beads such as Tenax TA as the collection media. The passive sampler has advantages when personal exposures are determined in daily life, because the passive sampler is small, light and noiseless, etc. Collection tubes of the active samplers have been used for passive sam-

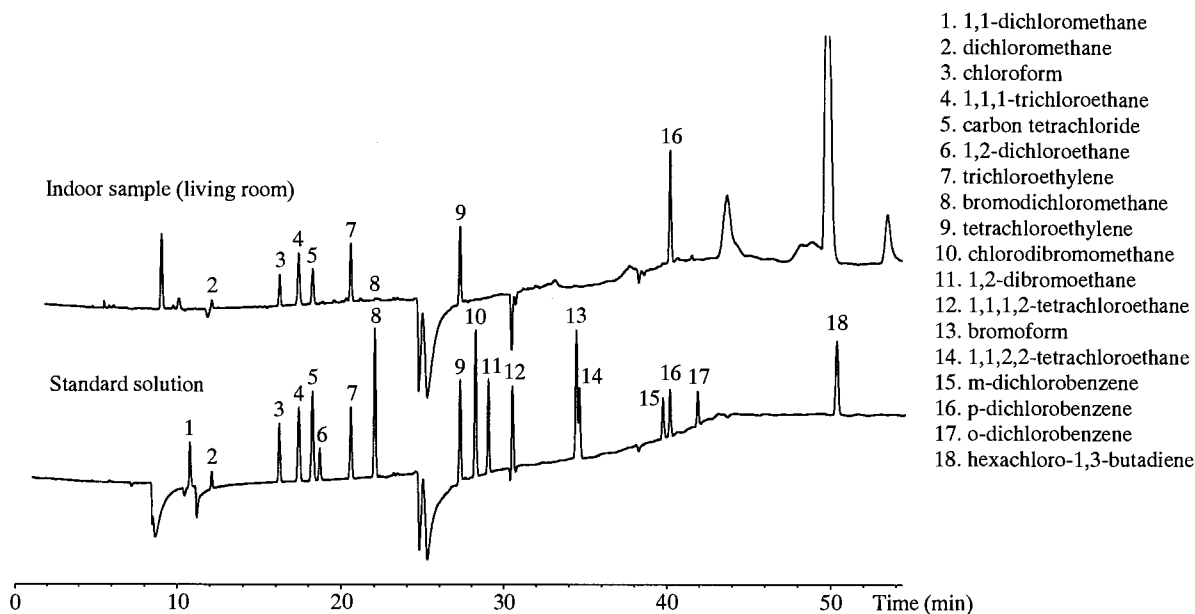


Fig. 2. Gas chromatograms of volatile organohalogen compounds.

pling [19,20], but sampling rates of these samplers are low; sample collection took 1–4 weeks. For example, the sampling rate of Perkin Elmer type sampling tubes is about  $0.5 \text{ ml min}^{-1}$  for some VOCs, and the sampling duration required 4 weeks. Furthermore, the analytical instruments and thermal description/GC system are expensive, and their operation is complicated. Diffusive badges such as the Organic Gas Monitor (3M), have high sampling rates ( $20\text{--}40 \text{ ml min}^{-1}$ ) [23]. Therefore, large amounts of analytical compounds can be collected and the sampling duration can be decreased (to about 24 h). However, a field survey needing many samples would be expensive. The Passive Gas Tube (Shibata), which consists of activated charcoal and a porous PTFE tube, is cheap and has a high sampling rate (about  $50 \text{ ml min}^{-1}$ ). This tube had been used in the field of industrial hygiene, but it had precision problems when used in an environment with low concentrations of VOCs. In the present study, the net collection length of the sampler and amount of activated charcoal in passive Gas Tube were improved and standardized. And then the precision of analysis in the environment was improved to CV (coefficient of variation) of 1.7–7.8% for all

the compounds tested except dichloromethane (11%). This method is therefore, simple, cheap, highly sensitive and precise for determination of 24-h average VOHC concentrations.

### 3.2. Gas chromatography analysis

Fig. 2 shows gas chromatograms of the 18 VOHC standard solutions and indoor samples using this method. All peaks were well separated from each other, and eluted within 51 min. When standards solution were analyzed 10 times consecutively, CV of the peak areas were in the range 0.29–1.03%. The retention time was more precise, with CV values  $< 0.034\%$ .

### 3.3. Recovery (desorption efficiency)

Table 1 shows the results of the recovery, in which small and known amounts of VOHC standards solution were spiked on the activated charcoal of the passive sampler, and the VOHCs were extracted and analyzed by the above method. When the amounts of spiked VOHCs were in the range  $1.27 \mu\text{g}$  (*o*-dichlorobenzene) to  $8.35 \mu\text{g}$  (*p*-dichlorobenzene), recoveries of the 18 VOHCs

ranged from 90.8% (carbon tetrachloride) to 104.0% (dichloromethane). The recoveries of 14 out of 18 compounds were more than 95%. This shows that the 18 VOHCs were extracted effectively by the present method, though these values were known to over-predict values as compared with those by a method using a standard gas.

### 3.4. Reproducibility

When 10 passive samplers were simultaneously exposed for 24 h to indoor air into which a small quantity of standard compounds had been evaporated and homogeneously diffused, the reproducibility of the analytical values was shown in Table 2. CV values of the VOHC concentrations ranged from 1.7% (hexachloro-1,3-butadiene) to 7.8% (1,1-dichloroethylene), except for dichloromethane (11%), suggesting that the 18 VOHCs can be analyzed precisely in indoor air using this

method. The determination limits were also shown in Table 2, and were in the range 4.1 pg (hexachloro-1,3-butadiene) to 12 pg (trichloroethylene), except for 1,1-dichloroethylene (90 pg), dichloromethane (117 pg), 1,2-dichloroethane (200 pg), and *m*-, *p*- and *o*-dichlorobenzene (72, 131, and 106 pg, respectively) that have only two chlorine atoms in the molecule. Clearly, the method is highly sensitive.

### 3.5. Storage of the samples

Table 3 shows the variations in the analytical values of the 18 VOHCs after freezer storage ( $-45^{\circ}\text{C}$ ) for 1 month. the resulting concentrations were 85.7% (chloroform) to 97.6% (1,1,2,2-tetrachloroethane) of those measured immediately after sampling. Therefore, the samplers can be stored for at least 1 month, if sealed and frozen as described earlier.

Table 1  
Recovery of volatile organohalogen compounds (VOHCs) collected by passive sampler<sup>a</sup>

Compounds	VOHC spiked (A) ( $\mu\text{g}$ )	VOHC recovered (B) ( $\mu\text{g}$ )	VOHC blank (C) ( $\mu\text{g}$ )	VOHC recovery $(B - C)/A \times 100$ (%)
1,1-Dichloroethylene	2.36	2.30	0.00	97.4
Dichloromethane	5.25	5.46	1.69	104.0
Chloroform	1.45	1.33	0.26	91.4
1,1,1-Trichloroethane	1.30	1.25	0.03	96.1
Carbon tetrachloride	1.59	1.44	0.03	90.8
1,2-Dichloroethane	6.15	6.07	0.00	98.7
Trichloroethylene	1.45	1.37	0.00	94.5
Bromo- dichloromethane	1.93	1.91	0.00	98.9
Tetrachloroethylene	1.60	1.57	0.00	98.1
Chloro- dibromomethane	2.39	2.41	0.00	101.0
1,2-Dibromoethane	5.44	5.24	0.00	96.3
1,1,1,2-Tetra- chloroethane	1.51	1.50	0.00	99.2
Bromoform	2.84	2.78	0.00	97.8
1,1,1,2,2-Tetra- chloroethane	1.57	1.56	0.00	99.6
<i>m</i> -Dichlorobenzene	1.28	1.23	0.00	96.1
<i>p</i> -Dichlorobenzene	8.35	8.33	0.00	99.8
<i>o</i> -Dichlorobenzene	1.27	1.24	0.00	97.3
Hexachloro-1,3-buta- diene	2.06	1.99	0.00	96.5

<sup>a</sup> Number of the samples was 10.

Table 2  
Reproducibility of analysis using passive samplers<sup>a</sup>

Compounds	Concentration in the air ( $\mu\text{g m}^{-3}$ )			Determination limit (pg; $S/N = 10$ )
	Mean	SD	CV (%)	
1,1-Dichloroethylene	86.6	9.6	7.8	90
Dichloromethane	175	13.6	11.2	117
Chloroform	326	15.5	4.7	5.8
1,1,1-Trichloroethane	235	15.6	6.7	5.1
Carbon tetrachloride	161	8.4	5.2	3.1
1,2-Dichloroethane	278	15.2	5.5	200
Trichloroethylene	167	7.6	4.5	9.4
Bromodichloromethane	143	9.4	6.6	5.3
Tetrachloroethylene	103	2.6	2.5	2.8
Chlorodibromomethane	196	4.7	2.4	5.0
1,2-Dibromoethane	228	11.2	4.9	6.4
1,1,1,2-Tetrachloroethane	144	5.9	4.1	8.4
Bromoform	300	7.5	2.5	6.8
1,1,2,2-Tetrachloroethane	150	3.7	2.4	8.5
<i>m</i> -Dichlorobenzene	84.8	3.6	4.2	72
<i>p</i> -Dichlorobenzene	189	7.2	3.8	131
<i>o</i> -Dichlorobenzene	68.5	3.4	5.0	106
Hexachloro-1,3-butadiene	127	2.1	1.7	4.1

<sup>a</sup> Number of the samples was 10.

Table 3  
Stability of volatile organohalogen compounds in passive sampler during storage at  $-45^{\circ}\text{C}$ <sup>a</sup>

Compounds	Average concentration ( $\mu\text{g m}^{-3}$ )		Recovery (%)
	Measured immediately (average $\pm$ SD)	Measured after 11 month (average $\pm$ SD)	
1,1-Dichloroethylene	125 $\pm$ 12	109 $\pm$ 5.6	87.2
Dichloromethane	1409 $\pm$ 120	1288 $\pm$ 56	91.4
Chloroform	40.7 $\pm$ 2.3	34.9 $\pm$ 1.7	85.7
1,1,1-Trichloroethane	6.77 $\pm$ 0.54	6.00 $\pm$ 0.32	93.1
Carbon tetrachloride	4.40 $\pm$ 0.04	4.10 $\pm$ 0.05	93.2
Trichloroethylene	7.78 $\pm$ 0.21	7.29 $\pm$ 0.12	93.7
Bromodichloromethane	5.97 $\pm$ 0.52	5.16 $\pm$ 0.12	86.5
Tetrachloroethylene	3.83 $\pm$ 0.31	3.63 $\pm$ 0.15	94.7
Chlorodibromomethane	8.79 $\pm$ 0.81	7.70 $\pm$ 0.31	87.6
1,2-Dibromoethane	7.90 $\pm$ 0.76	6.44 $\pm$ 0.49	90.8
1,1,1,2-tetrachloroethane	5.18 $\pm$ 0.53	4.82 $\pm$ 0.13	93.1
Bromoform	9.48 $\pm$ 0.91	8.38 $\pm$ 0.59	88.4
1,1,2,2-Tetra- chloroethane	3.57 $\pm$ 0.03	3.48 $\pm$ 0.28	97.6
<i>m</i> -Dichlorobenzene	24.4 $\pm$ 2.1	22.1 $\pm$ 1.8	90.3
<i>p</i> -Dichlorobenzene	41.3 $\pm$ 3.4	37.9 $\pm$ 3.3	91.8
<i>o</i> -Dichlorobenzene	47.5 $\pm$ 6.5	41.4 $\pm$ 3.6	87.2
Hexachloro-1,3-butadi- ene	1.48 $\pm$ 0.01	1.41 $\pm$ 0.04	95.3

<sup>a</sup> Number of each sample was 4.

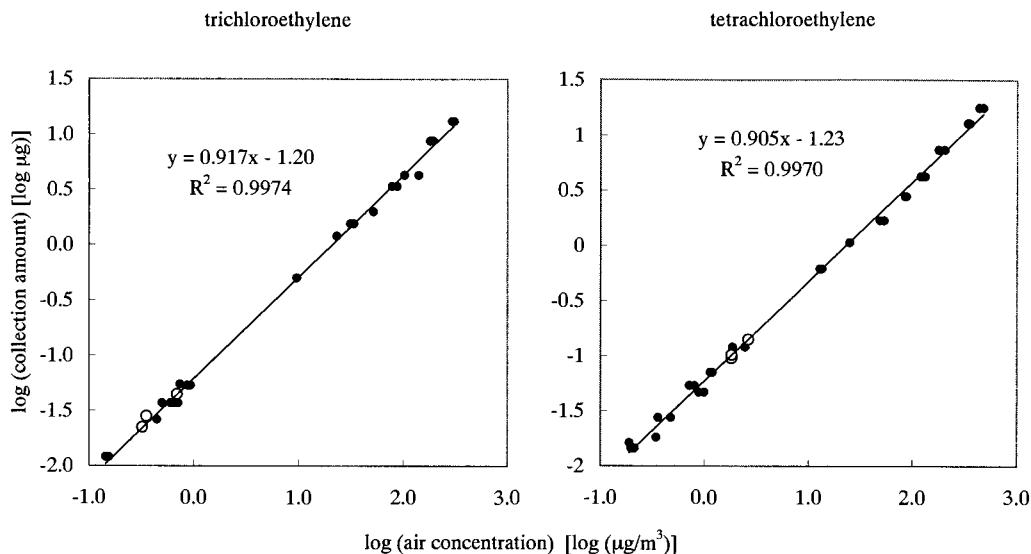


Fig. 3. Relation between logarithms of the amount collected and those of concentrations in the air.

### 3.6. Conversion of volatile organohalogen compounds quantities into concentration in the air

VOHC concentration in the air was calculated from the amount collected by the passive sampler using a conversion equation derived from the

results of simultaneous measurements with passive and active samplers. Linear correlation was found between the logarithms of the amounts of VOHC collected by the passive samplers and those of the concentrations in the air measured by active sampling over a wide concentration range

Table 4

Equation constants for calculation of VOHC concentrations in the air from amounts collected by the passive sampler<sup>a</sup>

Compounds	Concentration range ( $\mu\text{g m}^{-3}$ )	$1/n$	$\log(a)$
1,1-Dichloroethylene	8.9 ~ 2500	$0.991 \pm 0.008$	$-1.21 \pm 0.02$
Dichloromethane	19 ~ 8200	$0.911 \pm 0.028$	$-1.20 \pm 0.06$
Chloroform	6.1 ~ 7400	$0.903 \pm 0.029$	$-1.11 \pm 0.07$
1,1,1-Trichloroethane	1.0 ~ 310	$0.901 \pm 0.014$	$-1.23 \pm 0.02$
Carbon tetrachloride	0.50 ~ 360	$0.921 \pm 0.014$	$-1.26 \pm 0.02$
1,2-Dichloroethane	11 ~ 120	$0.953 \pm 0.013$	$-1.15 \pm 0.02$
Trichloroethylene	0.14 ~ 310	$0.920 \pm 0.009$	$-1.21 \pm 0.01$
Bromodichloromethane	0.48 ~ 370	$0.908 \pm 0.019$	$-1.21 \pm 0.02$
Tetrachloroethylene	0.19 ~ 480	$0.904 \pm 0.009$	$-1.23 \pm 0.01$
Chlorodibromomethane	0.77 ~ 430	$0.911 \pm 0.023$	$-1.23 \pm 0.03$
1,2-Dibromoethane	0.21 ~ 110	$0.966 \pm 0.011$	$-1.26 \pm 0.01$
1,1,1,2-tetrachloroethane	0.72 ~ 260	$0.892 \pm 0.018$	$-1.24 \pm 0.03$
Bromoform	0.44 ~ 590	$0.906 \pm 0.016$	$-1.23 \pm 0.03$
1,1,1,2,2-Tetrachloroethane	0.067 ~ 260	$0.879 \pm 0.014$	$-1.27 \pm 0.02$
<i>m</i> -Dichlorobenzene	2.0 ~ 190	$0.815 \pm 0.034$	$-1.13 \pm 0.05$
<i>p</i> -Dichlorobenzene	2.6 ~ 1300	$0.799 \pm 0.015$	$-0.983 \pm 0.03$
<i>o</i> -Dichlorobenzene	1.9 ~ 220	$0.837 \pm 0.038$	$-1.15 \pm 0.05$
Hexachloro-1,3-butadiene	0.025 ~ 5.0	$0.977 \pm 0.013$	$-1.41 \pm 0.01$

<sup>a</sup> Number of each sample was 32.



(< 1  $\mu\text{g m}^{-3}$  to 100 or 1000  $\mu\text{g m}^{-3}$ ) for all VOHCs, which was different from normal diffusive samplers. The linear correlations of trichloroethylene and tetrachloroethylene are given as examples in Fig. 3; the concentration range of the simultaneous measurements is shown in Table 4. For trichloroethylene, a linear correlation was found in the range from 0.14 to 310  $\mu\text{g m}^{-3}$ , and for tetrachloroethylene, a linear correlation was found in the range from 0.19 to 480  $\mu\text{g m}^{-3}$ .

$$\log(\Gamma) = a \log(c) + b \quad (1)$$

$$c = 10^{(\log(\Gamma) - b)/a} \quad (2)$$

where:  $c$  is the concentration of VOHC in air;  $\Gamma$  is the amount collected by the passive sampler, and  $a$  and  $b$  are constants.

Using Eq. (2), VOHC concentrations were calculated from the VOHC amount collected by passive sampler. Table 4 shows the values of the constants  $a$  and  $b$  of each compound.

The amount collected by passive sampler and active sampler were almost the same. Since the flow rate of the active sampler used was 50  $\text{ml min}^{-1}$ , the sampling rate of the passive sampler was estimated to be  $\approx 50 \text{ ml min}^{-1}$ .

### 3.7. Effect of wind velocity, temperature and humidity

The principle of VOHC collection by the passive sampler is based on molecular diffusion, thus, wind velocity and ambient temperature affected the collection amount [24–27]. The effect of wind velocity, however, can be minimized by indoor sampling or sheltering the sampler. Porous PTFE tube also acts to minimize the effect of wind velocity. The effect of temperature can be ignored theoretically under Japanese climatic conditions (Fick's law).

It was reported that the collection amount was affected by relative humidity because water vapor adsorbed on the activated carbon [24,25,28–32]. In the present study, the simultaneous measurements of passive and active samplers were performed in rainy season to estimate the effect of relative humidity. Then the results show that data taken in the rainy season (at the end of June),

shown as open circles in Fig. 3, did not vary from the regression lines of the plots of logarithms of amounts collected by the passive sampler against those of concentration in the air. This suggests that the amount of VOHC collected by the passive samplers were not affected by relative humidity.

### 3.8. Application to a field survey

A field survey of indoor and outdoor pollution by VOHCs in 70 residences in Shizuoka was carried out in order to confirm the usefulness of this method. Eight VOHCs, including 1,1-dichloroethylene, dichloromethane, chloroform, 1,1,1-trichloroethane, carbon tetrachloride, trichloroethylene, tetrachloroethylene and *p*-dichlorobenzene, were detected in all residences. Bromodichloromethane and chlorodibromomethane were detected from several houses as shown in Fig. 4.

Among the target 18 VOHCs, eight VOHCs were not detected in this survey. 1,2-Dichloroethane is produced in large quantities as a raw material for polyvinyl chloride, etc. [33]. (Annual production in Japan in 1995 was 2.93 million tonnes for 1,2-dichloroethane, whereas that of trichloroethylene was 0.08 million tonnes and tetrachloroethylene was 0.06 million tonnes). Concentrations of 1,2-dichloroethane in the outdoor environment in Japan range from 0.005 to 14.4  $\mu\text{g m}^{-3}$  with a geometric mean of 0.30  $\mu\text{g m}^{-3}$  [34], but the detection limit ( $S/N = 2$ ) of the present method for this compound is 6.1  $\mu\text{g m}^{-3}$ . This compound was not detected in Shizuoka, because it is a relatively clean city. We selected 1,1,2,2-tetrachloroethane and hexachloro-1,3-butadiene, since they are highly toxic and the production of them has been prohibited. We also selected 1,2-dibromoethane, 1,1,1,2-tetrachloroethane and *o*-, *m*-dichlorobenzene because they are analogs of 1,2-dichloroethane, 1,1,2,2-tetrachloroethane and *p*-dichlorobenzene, respectively. These three compounds were not detected in Shizuoka since they are seldom produced there for industrial use. Bromoform is one of the trihalomethane. Unlike bromodichloromethane and chlorodibromomethane, bromoform was not de-

tected perhaps because bromoform concentration was usually lower than those of bromodichloromethane and chlorodibromomethane [35]. Therefore, monitoring of these compounds thought to be important.

The distributions of VOHC concentrations were found to be almost log-normal. Table 5 shows the number of samples, geometric mean concentration, maximum and minimum concentration, 95th percentile concentration and the ratio of maximum and minimum concentration. When the geometric mean concentration was calculated, data below detection limit were replaced to the value of the half of detection limit.

The ratios of maximum to minimum outdoor concentration of VOHCs were more than 31.3 except for carbon tetrachloride (2.65). These results suggest that VOHC concentrations outdoors have large regional differences.

The ratios of maximum to minimum indoor VOHC concentration were larger than those of outdoors. The ratios for dichloromethane, chloroform and *p*-dichlorobenzene were more than 900. Maximum concentration of dichloromethane and chloroform were found in the houses of chemists (staffs of the university) that used these chemicals in the work place. On the other hand, the ratio of maximum to minimum concentration for 1,1,1-

trichloroethane ranged from 14.8 to 87.5. The ratios varied largely between compounds. These data suggest that VOHC concentrations indoors were significantly affected by lifestyle. Especially, since there are differences between maximum and 95 percentile concentrations for all VOHCs, VOHC concentrations of one or two out of 70 houses were found to be very high.

Indoor concentrations of 1,1-dichloroethylene, dichloromethane, 1,1,1-trichloroethane, carbon tetrachloride and trichloroethylene were almost the same as those outdoors. No significant differences were found by ANOVA (analysis of variance) between indoor and outdoor concentrations of these compounds ( $P < 0.05$ ). This suggests that indoor concentrations of these five VOHCs were predominantly affected by outdoor VOHC pollution levels.

Correlations among outdoor concentrations of the 10 VOHCs were not significant except for that between 1,1,1-trichloroethane and trichloroethylene ( $P < 0.01$ ). This may due to their use together in e.g. cleaning fluid.

Although geometric mean concentrations of trihalomethanes, tetrachloroethylene and *p*-dichlorobenzene in a certain type of room were higher than those of outdoors, no significant differences were observed between the geometric

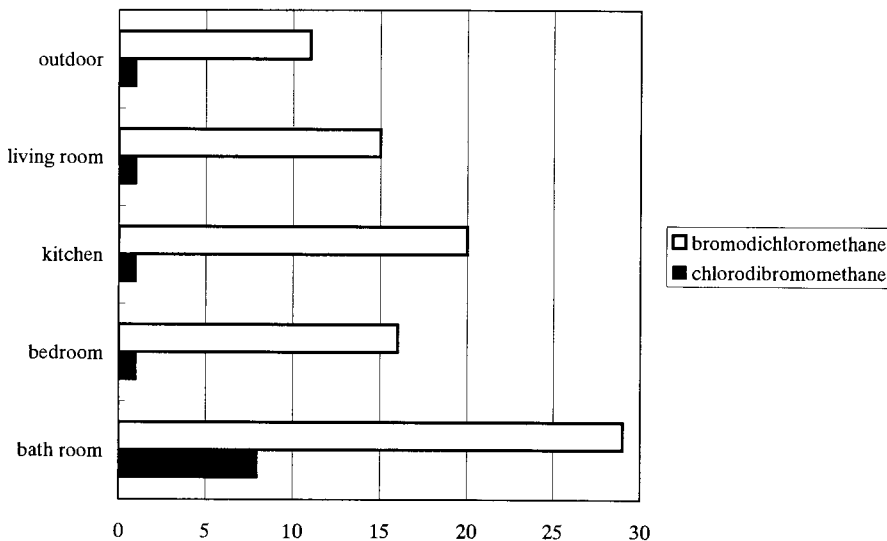


Fig. 4. Numbers of households in which bromodichloromethane and chlorodibromomethane were detected.

Table 5

Indoor and outdoor VOHC levels in Shizuoka, Japan—geometric mean (GM), standard deviation (GSD), range (Min.–Max.), 95th percentile (P95) and Max/Min ratio, and number of samples (*N*)<sup>a</sup>

Compounds	GM ( $\mu\text{g}/\text{m}^3$ )	GSD ( $\mu\text{g}/\text{m}^3$ )	Min.–Max. ( $\mu\text{g}/\text{m}^3$ )	P95 ( $\mu\text{g}/\text{m}^3$ )	Max/Min	<i>N</i>
<i>1,1-Dichloroethylene</i>						
Outdoor	0.374	2.34	<0.29–23.7	3.74	>82	70
Living room	0.340	2.10	<0.29–28.3	1.72	>98	60
Kitchen	0.360	2.51	<0.29–28.8	1.84	>99	69
Bedroom	0.341	2.27	<0.29–41.6	1.15	>140	65
Bathroom	0.365	2.29	<0.29–20.7	2.41	>70	68
<i>Dichloromethane</i>						
Outdoor	9.04	6.70	<0.36–15 400	251	42 700	65
Living room	17.9	6.61	<0.36–10 500	173	29 100	57
Kitchen	14.1	7.11	<0.36–11 400	202	31 600	66
Bedroom	13.1	7.56	<0.36–8580	554	23 800	65
Bathroom	4.89	7.94	<0.36–23 000	66.1	64 000	61
<i>Chloroform</i>						
Outdoor	2.53	4.40	0.117–97.7	22.4	838	55
Living room	3.10	4.56	0.111–101	70.6	909	52
Kitchen	2.62	5.19	0.122–169	76.1	1383	60
Bedroom	2.31	4.81	0.024–347	30.3	14 300	62
Bathroom	2.52	4.98	0.245–113	26.8	462	60
<i>1,1,1-Trichloroethane</i>						
Outdoor	0.911	1.71	0.341–10.6	2.39	31.2	70
Living room	1.05	1.70	0.388–5.76	2.61	14.8	60
Kitchen	1.05	1.83	0.479–22.5	2.55	47.0	70
Bedroom	1.16	2.00	0.365–31.5	3.95	87.5	70
Bathroom	0.843	1.80	0.357–17.3	1.91	48.1	70
<i>Carbon tetrachloride</i>						
Outdoor	0.740	1.21	0.514–1.35	1.01	2.65	70
Living room	0.784	1.36	0.489–4.28	1.08	8.73	60
Kitchen	0.791	1.36	0.527–3.52	1.21	6.64	70
Bedroom	0.790	1.34	0.556–3.19	1.41	5.70	70
Bathroom	0.704	1.36	0.442–2.58	1.37	5.86	70
<i>Trichloroethylene</i>						
Outdoor	0.392	2.71	<0.024–4.43	2.10	>180	70
Living room	0.330	2.82	<0.024–4.48	1.94	>190	60
Kitchen	0.371	2.65	<0.024–4.03	1.90	>170	70
Bedroom	0.353	2.82	<0.024–4.58	1.75	>190	70
Bathroom	0.362	2.90	<0.024–11.8	1.87	>490	70
<i>Bromodichloromethane</i>						
Outdoor	0.027	1.52	<0.012–0.215	0.066	>18	70
Living room	0.029	1.65	<0.012–0.149	0.12	>13	60
Kitchen	0.030	1.75	<0.012–0.236	0.14	>20	70
Bedroom	0.028	1.55	<0.012–0.177	0.091	>15	70
Bathroom	0.042	2.63	<0.012–0.879	0.35	>70	70
<i>Tetrachloroethylene</i>						
Outdoor	0.245	2.34	0.014–3.38	1.16	241	70
Living room	0.301	2.56	0.035–5.44	3.44	155	60

Table 5 (Continued)

Compounds	GM ( $\mu\text{g}/\text{m}^3$ )	GSD ( $\mu\text{g}/\text{m}^3$ )	Min. – Max. ( $\mu\text{g}/\text{m}^3$ )	P95 ( $\mu\text{g}/\text{m}^3$ )	Max/Min	N
Kitchen	0.279	3.00	<0.006–5.41	1.33	>900	70
Bedroom	0.384	2.64	0.091–15.4	2.74	169	70
Bathroom	0.241	2.86	<0.006–3.07	1.92	>620	70
<i>Chlorodibromomethane</i>						
Outdoor	0.006	1.19	<0.012–0.051	0.012	>4.0	70
Living room	0.006	1.33	<0.012–0.109	0.012	>9.0	60
Kitchen	0.006	1.28	<0.012–0.092	0.012	>8.0	70
Bedroom	0.006	1.25	<0.012–0.080	0.012	>19	70
Bathroom	0.015	1.92	<0.012–0.233	0.068	>67	70
<i>p-Dichlorobenzene</i>						
Outdoor	2.80	3.32	<0.21–49.5	28.7	>230	70
Living room	12.1	9.62	1.15–13 800	2060	12 000	60
Kitchen	9.35	9.06	0.961–3130	768	3260	70
Bedroom	71.6	11.1	1.69–16 000	3460	9510	70
Bathroom	10.4	7.67	<0.21–1760	375	>8300	70

<sup>a</sup> When the geometric mean was calculated, data below detection limit was replaced to the value of half the detection limit.

means of indoor concentrations and those of outdoor concentrations except for *p*-dichlorobenzene. Numbers of households in which bromodichloromethane and chlorodibromomethane were detected were shown in Fig. 4. These compounds could be detected more frequently in bathroom and kitchen. Bathroom concentrations of these two compounds were significantly higher ( $P < 0.01$ ) than those of other rooms. These suggest that the primary emission sources of trihalomethanes are tap water, showers and baths. But, differences among the concentrations of chloroform in each room type were not significant ( $P < 0.05$ ) due to large variations. Bedroom concentrations of tetrachloroethylene were higher than those in other rooms, and significantly higher ( $P < 0.01$ ) than in bathrooms. Since tetrachloroethylene is used as dry-cleaning fluid, the primary indoor emission source was thought to be dry-cleaned clothes. The geometric mean concentration of *p*-dichlorobenzene in bedroom was  $71.6 \mu\text{g m}^{-3}$ , which is about 26 times higher than that outdoors (Table 5), and was significantly higher ( $P < 0.01$ ) than in outdoors, kitchen and bathrooms, as well as significantly higher ( $P < 0.05$ ) than that in living rooms. This compound has been widely used as an insect repellent in closets

that were usually found in bedroom, in Japan. Then, this compound was emitted indoors, especially in bedroom. The maximum concentrations of *p*-dichlorobenzene found in our survey reached  $16\,000 \mu\text{g m}^{-3}$ .

#### 4. Conclusions

The laboratory and field survey results clearly demonstrate the usefulness of the passive sampler–GC/ECD method for the determination of VOHC concentrations in indoor and outdoor air. In the field survey, we found that trihalomethanes were emitted from tap water, showers and baths; the indoor concentration of tetrachloroethylene was associated with dry-cleaned clothes; and the primary emission source of *p*-dichlorobenzene was insect repellents in closets.

#### Acknowledgements

This work was supported partly by grants from Environment Agency and Smoking Research Foundation.

## References

- [1] B. Seifert, Sampling and analysis of ambient and indoor air, in: L. Fishbein, I.K. O'Neill (Eds.), *Environmental Carcinogens—Methods of Analysis and Exposure Measurement*, IARC Science Publications No 85, 1988, pp. 165–178.
- [2] I. Turiel, *Indoor Air Quality and Human Health*, Stanford University Press, Stanford, California, 1985.
- [3] L.A. Wallace, E.D. Pellizzari, B. Leaderer, H. Zelon, L. Sheldon, *Atmos. Environ.* 21 (1987) 385–393.
- [4] S. Suzuki, S. Nagano, S. Sato, *Jpn. Soc. Air. Pollut.* 21 (1986) 419–427.
- [5] L.A. Wallace, E.D. Pellizzari, T.D. Hartwell, V. avis, L.C. Michael, R.W. Whitmore, *Environ. Res.* 50 (1989) 37–55.
- [6] E.D. Pellizzari, K.W. Thomas, D.J. Smith, K. Perritt, M. Morgan, *Total Exposure Assessment Methodology: 1987 Study in New Jersey*, vol. I. Prepared for the U.S. EPA, Office of research and development, Washington, DC, 1988.
- [7] B.A. Tichenor, L.E. Sparks, M.D. Jackson, Z.G. Guo, M.A. Mason, C.M. Plunket, S.A. Rasor, *Atmos. Environ.* 24A (1990) 1219–1229.
- [8] T.E. Mckone, *Environ. Sci. Technol.* 21 (1987) 1194–1201.
- [9] IARC, Overall Evaluations of Carcinogenicity, An Updating of IARC Monographs, Suppl. 7, IARC, Lyon, 1987.
- [10] IARC, IARC Monographs on the Evaluation of Carcinogenic Risks to Humans, vol. 63, Dry Cleaning, Some Chlorinated Solvents and Other Industrial Chemicals, IARC, Lyon, 1995.
- [11] D.J. Moschandreas, *Bull. N.Y. Acad. Med.* 57 (1981) 845–859.
- [12] World Health Organization (WHO). *Indoor Air quality Research, EURO Reports and Studies 103*. WHO Regional Office for Europe, Copenhagen, 1986.
- [13] T. Mori, M. Yoshikawa, H. Matsushita, *J. Jpn. Soc. Air Pollut.* 21 (1986) 446–454.
- [14] H. Matsushita, K. Tanabe, *Exposure Monitoring of Nitrogen Dioxide. An International Pilot Study Within the WHO/UNEP Human Exposure Assessment Location (HEAL) Programme*, WHO and UNEP, Nairobi, 1991.
- [15] B. Seifert, W. Mailahn, C. Schulz, D. Ullrich, *Environ. Int.* 15 (1989) 397–408.
- [16] L.A. Wallace, W.C. Nelson, R. Ziegenfus, D. Westerdahl, *J. Exp. Anal. Environ. Epidemiol.* 1 (1991) 37–72.
- [17] R.A. Field, J.L. Phillips, M.E. Goldstone, J.N. Lester, R. Perry, *Environ. Technol.* 13 (1992) 391–408.
- [18] L.H. David, T.M. Walter, W.O. Michael, *Environ. Int.* 21 (1995) 3–21.
- [19] C. Krause, W. Mailahn, R. Nagel, C. Schulz, B. Seifert, D. Ullrich, Occurrence volatile organic substances in the air of 500 homes in the Federal Republic of Germany, in: B. Seifert, H. Esdorn, M. Fischer, H. Rüdén, J. Wegner (Eds.), *Indoor Air '87*, 1987, pp. 17–21.
- [20] V.M. Brown, D.R. Crump, D. Gardiner, *Environ. Technol.* 13 (1992) 367–375.
- [21] A.M. Laurent, A. Person, B. Festy, *Publ. R. Soc. Chem.* 108 (1992) 384–386.
- [22] T. Amagai, Olansandan, H. Matsushita, *J. Jpn. Soc. Atmos. Environ.* 31 (1996) 191–202.
- [23] 3M, 3M 3500/3520 Organic Vapor Monitor Sampling and Analysis Guide, 1996.
- [24] D.W. Gosselink, D.L. Braun, H.E. Mullins, S.T. Rodriguez, A New Personal Organic Vapor Monitor With in-situ Sample Elution, Occupational Health and Safety Products Division, 3M, 1978.
- [25] W.J. Lautenberger, R.B. Kring, J.A. Morello, *Am. Ind. Hyg. Assoc. J.* 41 (1980) 737–747.
- [26] B. Sasami, L. Falbo, *Am. Ind. Hyg. Assoc. J.* 44 (1983) 402–408.
- [27] K. Lee, Y. Yanagisawa, J.D. Spengler, I.H. Billick, *J. Expos. Anal. Epidem.* 2 (1992) 207–219.
- [28] L.A. Jonas, E.B. Sansone, T.S. Farris, *Am. Ind. Hyg. Assoc. J.* 46 (1985) 20–23.
- [29] G.O. Wood, *Am. Ind. Hyg. Assoc. J.* 48 (1987) 622–625.
- [30] L.B. Adams, C.R. Hall, R.J. Holms, R.A. Newton, *Carbon* 26 (1989) 451–459.
- [31] K. Tamakawa, K. Kuchida, K. Tohkai, M. Chiba, T. Kato, T. Seki, *J. Environ. Chem.* 3 (1993) 709–716.
- [32] K. Kawamoto, N. Sakaji, *J. Environ. Chem.* 5 (1995) 450–451.
- [33] MITI, The Annual report on Japanese Chemical Industries, Ministry of International Trade and Industry, Japan, 1997.
- [34] JESC, The Report on the Health Effect by Hazardous Air Pollutants, Japan Environmental Sanitation Center, 1994.
- [35] Olansandan, T. Amagai, H. Matsushita, A survey on indoor pollution by halogenated hydrocarbons in Tokyo using passive sampler, in: *Proceedings of The Thirty-sixth Annual Meeting of the Japan Society for Atmospheric Environment*, Tokyo, 1995, p. 379.

# Determination of Ag(I), Hg(II) and Pb(II) by using silica gel loaded with dithizone and zinc dithizonate

O. Zaporozhets \*, N. Petruniok, V. Sukhan

*Department of Analytical Chemistry, Taras Shevchenko Kyiv University, 64 Volodymirska Street, Kyiv 252033, Ukraine*

Received 1 December 1998; received in revised form 26 May 1999; accepted 27 May 1999

## Abstract

The modified sorbents with dithizone and zinc dithizonate adsorbed on the silica surface were obtained. The adsorption of heavy metal ions from aqueous solutions onto loaded silicas was studied. Color scales for Ag(I), Hg(II) and Pb(II) visual test detection were worked out. The modified silica gels were established to be applicable to semi-quantitative determination of these metal ions in buttermilk, natural, mineral and waste water. © 1999 Elsevier Science B.V. All rights reserved.

*Keywords:* Dithizone; Zinc dithizonate; Modified silica gel; Metal ions determination

## 1. Introduction

Dithizone ( $H_2Dz$ ) is known to be one of the effective chelating reagent for a lot of metal ions extraction-spectrophotometric determination [1]. But these methods require the use of toxic organic solvents. The extraction of metal ions from solutions by sorbents modified with analytical reagents is one of the most promising methods of their determination, especially in environmental objects [2]. It is caused by two main reasons. Firstly, such methods permit to combine the recovery of metal ions from dilute solutions with their visual or spectroscopic detection on the sor-

bent surface. Secondly, as the loss of analytical reagent from the sorbent surface into the aqueous phase is low, the influence on the original equilibrium of different forms of metal ions in real systems is not significant.  $H_2Dz$  immobilized on polymer membrane filled with cation exchanger was used for mercury (II) visual and spectrophotometric determination in natural and waste water [3]. The cross-linked polystyrene gel with  $Zn(HDz)_2$  impregnated was used for mercury (II) preconcentration [4]. It is known [5] that the application of highly dispersed silicas offers some distinct advantages over the use of organic polymer supports: short time for equilibration, excellent swelling resistance in different solvents, possibility of surface modification with analytical reagents by different methods. The  $H_2Dz$  impregnated silica gel was proposed for Pb(II) determi-

\* Corresponding author. Tel.: + 380-44-2210211; fax: + 380-44-2244188.

*E-mail address:* smyk@akcecc.kiev.ua (O. Zaporozhets)

nation using low-temperature luminescent method [6]. The preparation of modified silicas via reagent adsorption is rather simple, and their chemical-analytical properties do not markedly differ from those of the sorbent with covalent grafted reagent [7]. As far as we know, no modification of silicas with  $H_2Dz$  and its complexes adsorption has been reported.

In the present work we have studied the adsorption of  $H_2Dz$  and  $Zn(HDz)_2$  from organic solvents onto silica surface, and established the usefulness of modified sorbents in the visual test determination of  $Ag(I)$ ,  $Hg(II)$  and  $Pb(II)$  in water and buttermilk.

## 2. Experimental

### 2.1. Reagents

Water was purified according to Ref. [8]. Hexane and chloroform were purified by flowing over metallic sodium. Stock  $Ag(I)$ ,  $Pb(II)$  and  $Hg(II)$  solutions were prepared as nitrates dissolved in  $0.01 \text{ mol l}^{-1}$  nitric acid and standardized by complexometry. The standard metal salts solutions were acidified with sulfuric or nitric acid and further diluted as required. Sodium chloride ( $4.0 \text{ mol l}^{-1}$ ), and thiosulfate ( $0.5 \text{ mol l}^{-1}$ ) aqueous solutions were prepared by dissolving the appropriate substances in water. Ammonia buffer with pH 8.5 was prepared according to Ref. [9].  $H_2Dz$  (Merck, Germany) was purified by recrystallization from chloroform [1]. Solution of  $H_2Dz$  in hexane ( $1 \cdot 10^{-5} \text{ mol l}^{-1}$ ), chloroform ( $2 \cdot 10^{-3} \text{ mol l}^{-1}$ ) and acetone ( $2.4 \cdot 10^{-4} \text{ mol l}^{-1}$ ) were obtained by dissolving the appropriate amount of substance.  $Zn(HDz)_2$  chloroform solution was obtained by extraction the appropriate amount of  $Zn(II)$  from aqueous solution at pH 6.3 with  $H_2Dz$  chloroform solution [1]. This solution was used for preparation of  $Zn(HDz)_2$  hexane–chloroform mixtures with different solvents ratio. Saturated solutions of diphenylcarbazone (DPHC) in ethanol, *p*-dymethylaminobenzyliden-erhodanine (BRh) in acetone and pyridylazoresorcinol (PAR) in water were obtained by dissolving the appropriate amount of substances

(Merck, Germany). All chemicals were of analytical reagent grade. Silica gel L 40/100 (SG) and Silpearl UV 254 (SP) for chromatography (Chemapol, Prague, Czech Republic) was digested in hydrochloric acid, washed with purified water and dried at  $180^\circ\text{C}$  for 18 h.

### 2.2. Apparatus

The absorbance spectra of solutions and diffusion reflectance spectra (DRS) of sorbents were recorded with a UV/Vis spectrophotometer Specord M-40 (Carl Zeiss Jena, Germany). Flame atomic absorption (FAAS) measurements were recorded on a model Saturn atomic absorption spectrometer (Severodonetsk, Ukraine) equipped with a standard burner for air–propane–butane flame. Standard hollow-cathode lamps were applied as a light source for  $Ag$  and  $Zn$  determination. A potentiometer model EV-74 with glass electrode (Gomel, Belarus) was used for pH measurements.

### 2.3. Procedures

The batch technique has been used for studying  $H_2Dz$  and  $Zn(HDz)_2$  adsorption onto unloaded silicas and metal ions adsorption onto modified sorbents. The reagent desorption from surface of modified silicas into aqueous solutions at different pH was studied by the same technique, too.

#### 2.3.1. Adsorption of $H_2Dz$ and $Zn(HDz)_2$ onto silicas surface from organic solvents

The weighed amount ( $0.01$ – $0.5 \text{ g}$ ) of silicas was stirred with  $10 \text{ ml}$  of  $H_2Dz$  hexane solution or  $Zn(HDz)_2$  chloroform:hexane (1:9) solution. The  $H_2Dz$  and  $Zn(HDz)_2$  residues in solutions were controlled spectrophotometrically by their own absorbance at  $440$  and  $526 \text{ nm}$ , respectively. The amount of modifying agent adsorbed was calculated as:  $a = (C_0 - C) \cdot V/m$ , where  $C_0$ ,  $C$  were the initial and equilibrium adsorbate concentrations in solution in  $\text{mol l}^{-1}$ , respectively;  $V$  was the volume of solution in liters;  $m$  was the sorbent mass in grams.

### 2.3.2. Adsorption of Ag(I), Hg(II) and Pb(II) from aqueous solutions onto modified sorbents surface

The weighed amount (0.01–0.2 g) of sorbents modified with H<sub>2</sub>Dz (H<sub>2</sub>Dz-SP, H<sub>2</sub>Dz-SG) and Zn(HDz)<sub>2</sub> (Zn(HDz)<sub>2</sub>-SP) was stirred with 5–500 ml of aqueous solution of metal salts for 1–60 min. Ag(I), Hg(II) and Pb(II) equilibrium concentration in solution was controlled by FAAS, spectrophotometrically by the absorbance of HgI<sub>4</sub><sup>2-</sup> at 320 nm [10] and extraction-spectrophotometrically with H<sub>2</sub>Dz [1], respectively. The amount of metal ions adsorbed onto the silica surface was determined as mentioned above. Sorbents with metal ions adsorbed were separated and dried at room temperature for 24 h or at 60°C for 1 h and analyzed using DRS.

### 2.3.3. Desorption of H<sub>2</sub>Dz and Zn(HDz)<sub>2</sub> from modified silicas surface into aqueous solution at different pH

For these purposes SG containing 40 μmol g<sup>-1</sup> and SP containing 46 μmol g<sup>-1</sup> of H<sub>2</sub>Dz or 8 μmol g<sup>-1</sup> of Zn(HDz)<sub>2</sub> were used. The aqueous solution (5–100 ml) at the desired pH (0–9) was stirred for 1–60 min with the weighed amount (0.01–0.1 g) of modified sorbents. The amount of Zn(II) removed from surface into solution was determined by FAAS. The residue of H<sub>2</sub>Dz on the surface was determined by DRS.

### 2.3.4. Impregnation of BRh from acetone solution onto H<sub>2</sub>Dz-SP with Ag(I) adsorbed

The portion (10 ml) of Ag(I) standard solution was stirred with 0.02 g of H<sub>2</sub>Dz-SP at pH 1.0 for 10 min. The sorbent was separated and treated with 40 μl of BRh solution in acetone.

### 2.3.5. Impregnation of DPhC from ethanol solution onto H<sub>2</sub>Dz-SG with Hg(II) adsorbed

The portion (25 ml) of Hg(II) aqueous solution containing 1.0 mmol l<sup>-1</sup> sodium chloride was stirred with 0.02 g of H<sub>2</sub>Dz-SG at pH 4.5 for 5 min. The sorbent was separated and treated with 40 μl of DPhC solution in ethanol.

### 2.3.6. Impregnation of PAR from aqueous solution onto H<sub>2</sub>Dz-SG with Pb(II) adsorbed

The portion (10 ml) of Pb(II) aqueous solution was mixed with 0.1 ml of sodium thiosulfate (0.1 mol l<sup>-1</sup>), 1.0 ml of ammonia buffer solution (pH 8.5) and stirred with 0.02 g of H<sub>2</sub>Dz-SG for 30 min. The sorbent was separated, washed with 5.0 ml of 1.0 mmol l<sup>-1</sup> sodium thiosulfate and treated with 40 μl of PAR aqueous solution.

## 3. Results and discussion

### 3.1. Dithizone adsorption onto silica surface

The adsorption of H<sub>2</sub>Dz onto SG and SP from chloroform, toluene, hexane and their mixtures was studied. The best reagent adsorption was observed in the case of hexane. The kinetics experiments have shown that the equilibrium of H<sub>2</sub>Dz adsorption onto SG and SP (0.02 g) surface from hexane solution (10 ml) was reached in 15 and 30 min, respectively. The isotherms are represented in Fig. 1. The values of H<sub>2</sub>Dz maximum adsorption onto SP and SG were 46 and 40 μmol g<sup>-1</sup>, respectively. In the present work H<sub>2</sub>Dz-SG and H<sub>2</sub>Dz-SP with this reagent content on the surface were used.

### 3.2. Zn(HDz)<sub>2</sub> adsorption onto SP surface

The adsorption of Zn(HDz)<sub>2</sub> onto SP surface from chloroform and its mixtures with hexane was studied. The best complex adsorption was observed in the case of mixture with the ratio chloroform:hexane = 1:9. The kinetics experiments have shown that the equilibrium of Zn(HDz)<sub>2</sub> adsorption onto SP (0.01 g) surface from this mixture (5 ml) was reached in 5 min. The shape of isotherm of zinc dithizonate adsorption (Fig. 1(b)) testifies the stronger complex binding with the SG surface, in contrast to H<sub>2</sub>Dz. It is caused probably by its plane fixation [11]. In the present work SP containing 8 μmol g<sup>-1</sup> Zn(HDz)<sub>2</sub> was used.



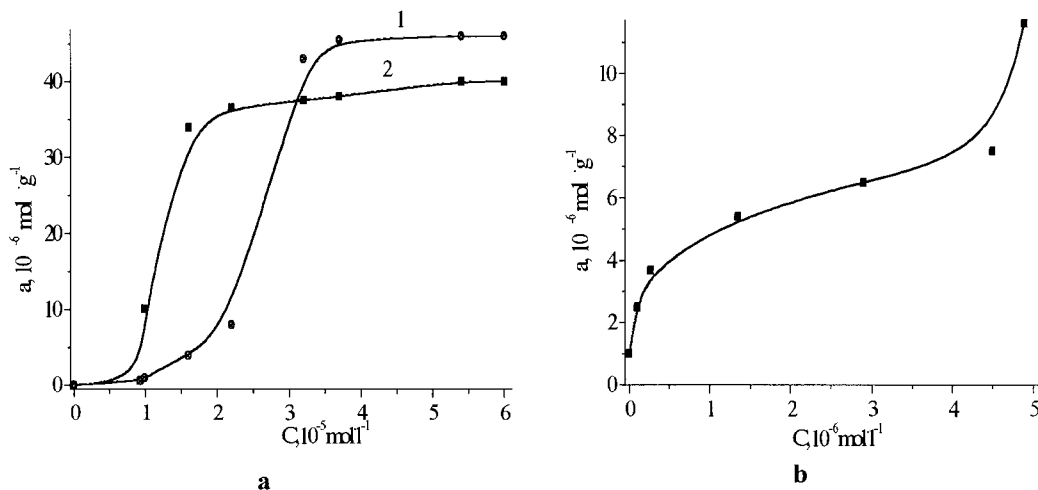


Fig. 1. Isotherms of adsorption of  $\text{H}_2\text{Dz}$  (a) onto SP (1), SG (2) and  $\text{Zn}(\text{HDz})_2$  (b) onto SP.  $V = 10 \text{ ml}$ ,  $m = 0.01 \text{ g}$ ,  $T = 293.0 \pm 0.5 \text{ K}$ .

### 3.3. Desorption of $\text{H}_2\text{Dz}$ and $\text{Zn}(\text{HDz})_2$ from modified silicas surface into aqueous solution at different pH

To establish the possibility of new solid-phase reagents application to analytical practice, reagent desorption from  $\text{H}_2\text{Dz-SG}$  and  $\text{H}_2\text{Dz-SP}$  surfaces as a function of solution pH was studied. The data obtained has shown that  $\text{H}_2\text{Dz}$  desorption at pH 0–9 was less than or equal to 5% (sorbent mass  $\geq 0.01 \text{ g}$ , aqueous solution volume  $\leq 100 \text{ ml}$ , time of phases contact  $\leq 60 \text{ min}$ ).

Zinc dithizonate immobilized on the surface was found to be destroyed when contacted with an aqueous solution at pH  $< 3.5$ . The loss of  $\text{Zn}(\text{II})$  into solution under these conditions was confirmed by FAAS. The desorption of dithizone remaining on the surface at pH  $< 3.5$  was similar to that from  $\text{H}_2\text{Dz-SP}$  surface. So,  $\text{Zn}(\text{HDz})_2\text{-SP}$  at pH 0–3.5 may be applied to determine the metal ions forming more stable complexes with  $\text{H}_2\text{Dz}$  than  $\text{Zn}(\text{II})$ .

### 3.4. Metal ions adsorption onto silicas with $\text{H}_2\text{Dz}$ immobilized

$\text{H}_2\text{Dz}$  forms colored chelate complexes with several metal ions [1]. Adsorption of  $\text{Zn}(\text{II})$ ,

$\text{Ag}(\text{I})$ ,  $\text{Cd}(\text{II})$ ,  $\text{Hg}(\text{I, II})$ ,  $\text{Mn}(\text{II})$ ,  $\text{Pb}(\text{II})$ ,  $\text{Cu}(\text{II})$ ,  $\text{Ni}(\text{II})$  and  $\text{Co}(\text{II})$  onto  $\text{H}_2\text{Dz-SG}$  and  $\text{H}_2\text{Dz-SP}$  was studied. It was found, that only  $\text{Ag}(\text{I})$ ,  $\text{Hg}(\text{II})$ ,  $\text{Pb}(\text{II})$ ,  $\text{Zn}(\text{II})$  interact with immobilized  $\text{H}_2\text{Dz}$  under optimal conditions of complex formation in chloroform solution.

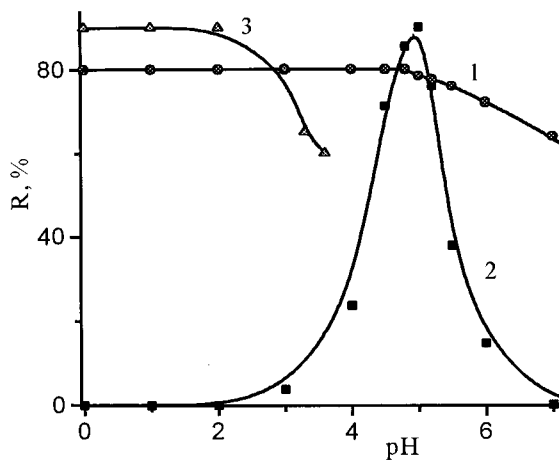


Fig. 2. The pH dependencies of  $\text{Ag}(\text{I})$  adsorption onto  $\text{H}_2\text{Dz-SP}$  (1) and  $\text{Hg}(\text{II})$  adsorption onto  $\text{H}_2\text{Dz-SG}$  (2) and  $\text{Zn}(\text{HDz})_2\text{-SP}$  (3), respectively.  $a$  ( $\mu\text{mol g}^{-1}$ ): 46 (1), 40 (2), 8 (3);  $C_{\text{NaCl}} = 1.0 \text{ mmol l}^{-1}$ (2);  $m = 0.02 \text{ g}$ ;  $V = 10 \text{ ml}$ ;  $\tau = 10 \text{ min}$ .

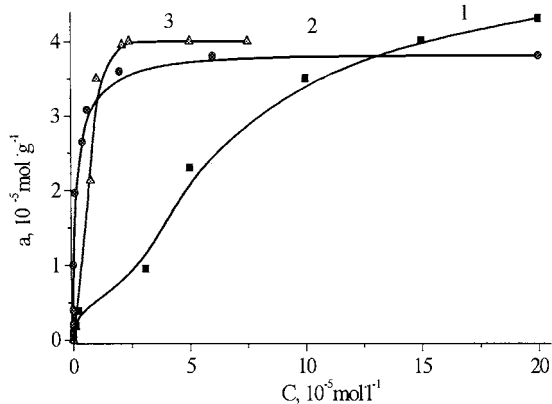


Fig. 3. Isotherms of adsorption of Ag(I) onto H<sub>2</sub>Dz-SP (1), Hg(II) (2) and Pb(II) (3) onto H<sub>2</sub>Dz-SG. *a* ( $\mu\text{mol g}^{-1}$ ): 46 (1) and 40 (2, 3).  $V = 10$  ml,  $m = 0.02$  g,  $T = 293.0 \pm 0.5$  K.

#### 3.4.1. Ag(I) adsorption onto H<sub>2</sub>Dz-SP

The pH dependence of Ag(I) adsorption is represented in Fig. 2. The kinetics experiments have shown that equilibrium was reached at pH 1.0 in 10 min. The sorbent mass and solution volume dependencies of Ag(I) adsorption onto H<sub>2</sub>Dz-SP were studied. The maximum concentration factor was found to be  $2500 \text{ ml g}^{-1}$  at volume of solution 50 ml and mass of sorbent 0.02 g.

The isotherm of Ag(I) adsorption (Fig. 3, curve 1) may be characterized as H-type and testified about chemical interaction between metal ion and immobilized reagent. The chelating capacity of H<sub>2</sub>Dz-SP was  $44 \mu\text{mol g}^{-1}$  Ag(I) for  $46 \mu\text{mol g}^{-1}$  dithizone. That may point to a surface complex with the ratio Ag(I):H<sub>2</sub>Dz = 1:1. The similarity of absorbance spectrum of AgHDz chloroform solution and diffusion reflectance spectrum of H<sub>2</sub>Dz-SP with Ag(I) adsorbed (Fig. 4) confirmed this supposition. It was found that Ag(I) was not adsorbed onto unloaded silica from aqueous solution under such conditions.

The possibility of H<sub>2</sub>Dz-SP application to the determination of silver traces has been studied. The DRS method for its determination was developed. The calibration equation was:  $R_{480} = 8 \times 10^{-3} \cdot C(\mu\text{g l}^{-1})$  at  $V = 50$  ml,  $m = 0.02$  g. The calibration graph was linear in the range 5–200  $\mu\text{g l}^{-1}$  and detection limit was  $2.5 \mu\text{g l}^{-1}$ .

#### 3.4.2. Hg(II) adsorption onto H<sub>2</sub>Dz-SG

As well known [1] Hg(II) forms HgDz in chloroform solution at pH > 4.0. To avoid difficulties with soluble hydroxide formation of Hg(II) under these conditions of adsorption, sodium chloride was added. Its necessary concentration was calculated from the solubility products and stability constants of correspondent complexes [12,13]. The optimum concentration of sodium chloride was greater than  $1.0 \text{ mmol l}^{-1}$ . The pH dependence of Hg(II) adsorption (Fig. 2) has shown that its maximum value was reached at pH 4.4–5.1. The kinetics experiments have shown that equilibrium under optimal conditions was reached in 5 min. The sorbent mass and solution volume dependencies of Hg(II) adsorption onto H<sub>2</sub>Dz-SP were studied. The maximum concentration factor was found to be  $2500 \text{ ml g}^{-1}$  at volume of solution 50 ml and mass of sorbent 0.02 g.

The isotherm of Hg(II) adsorption (Fig. 3) may be characterized as H-type. Chelating capacity of H<sub>2</sub>Dz-SG was  $38 \mu\text{mol g}^{-1}$  Hg(II) for  $40 \mu\text{mol g}^{-1}$  reagent. This fact and the similarity of the spectra shown in Fig. 5 (curves 1, 3) confirmed the formation of the complex with the ratio Hg:H<sub>2</sub>Dz = 1:1 on the surface.

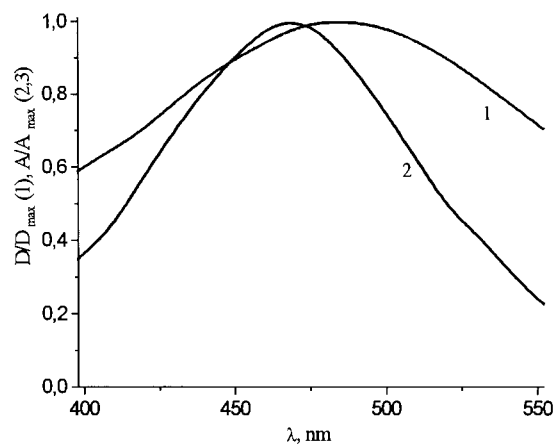


Fig. 4. Standardized diffusion reflectance spectra of H<sub>2</sub>Dz-SP with Ag(I) adsorbed (1) and absorbance spectra of AgHDz solution in chloroform (2).

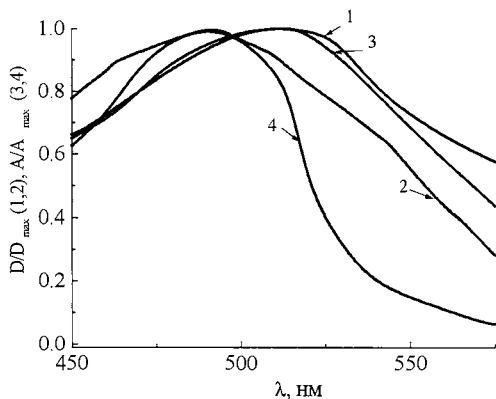


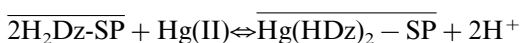
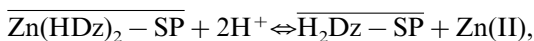
Fig. 5. Standardized diffusion reflectance spectra of H<sub>2</sub>Dz-SG (1) and Zn(HDz)<sub>2</sub>-SP (2) with Hg(II) adsorbed and absorbance spectra of HgDz (3) and Hg(HDz)<sub>2</sub> (4) solutions in chloroform.

### 3.4.3. Hg(II) adsorption onto Zn(HDz)<sub>2</sub>-SP

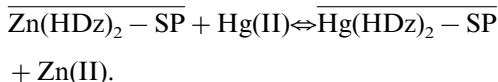
The formation of Hg(HDz)<sub>2</sub> in solution is known to be more preferable than HgDz [1]. But interaction of metal ions with more than one molecule of immobilized reagent is difficult [14]. The optimal dithizone molecules disposition for Hg(HDz)<sub>2</sub> formation on the surface may be obtained by Zn(HDz)<sub>2</sub> fixing.

The pH dependence of Hg(II) adsorption onto Zn(HDz)<sub>2</sub>-SP (Fig. 2, curve 3) has shown that the maximum of its value was arrived at pH 0–3.5. The kinetics experiments have shown that the adsorption of Hg(II) on the surface of Zn(HDz)<sub>2</sub>-SP under optimal conditions is rather complete and rapid. The equilibrium was arrived in 10 min (for 0.02 g of loaded sorbent and 10 ml of solution). The maximum concentration factor was 2500 ml g<sup>-1</sup> at volume of solution 50 ml and mass of sorbent 0.02 g.

The chelating capacity of Zn(HDz)<sub>2</sub>-SP was 9 μmol g<sup>-1</sup> Hg(II) for 8 μmol g<sup>-1</sup> Zn(HDz)<sub>2</sub>. Spectrophotometrically it was found (Fig. 5, curves 2, 4) that Hg(HDz)<sub>2</sub> was formed on the surface under optimal conditions. So, the interface transformations at pH < 3.5 may be represented by the following equations:



or



### 3.4.4. Pb(II) adsorption onto H<sub>2</sub>Dz-SG

Pb(II) adsorption onto H<sub>2</sub>Dz-SG from aqueous solution was studied under optimal conditions of its extraction with H<sub>2</sub>Dz chloroform solution: pH 7–9 (ammonia buffer) in the presence of the sodium thiosulphate [1]. The kinetics experiments have shown that the equilibrium was reached in 5 min at pH 8.5 and 1.0 mmol l<sup>-1</sup> Na<sub>2</sub>S<sub>2</sub>O<sub>3</sub>. The sorbent mass and solution volume dependencies of Pb(II) adsorption onto H<sub>2</sub>Dz-SG were studied. The maximum concentration factor was found to be 500 ml g<sup>-1</sup> at volume of solution 10 ml and mass of sorbent 0.02 g.

As well known [1] only Pb(HDz)<sub>2</sub> is formed in organic solutions. The spectra represented in Fig. 6 have shown that the surface complex of Pb(II) was different from Pb(HDz)<sub>2</sub>. The isotherm of Pb(II) adsorption onto H<sub>2</sub>Dz-SG from Na<sub>2</sub>S<sub>2</sub>O<sub>3</sub> solution is represented in Fig. 3. The chelating capacity of H<sub>2</sub>Dz-SG was 39.5 μmol g<sup>-1</sup> Pb(II) for 40 μmol g<sup>-1</sup> dithizone. That may point to a surface complex with the ratio Pb(II):H<sub>2</sub>Dz = 1:1. The interaction between Pb(II) and H<sub>2</sub>Dz immobilized was not studied in detail. Pb(II) was also found to be adsorbed onto unloaded SG, but it

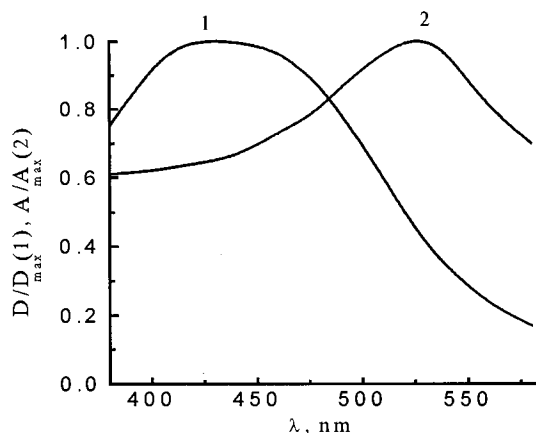


Fig. 6. Standardized diffusion reflectance spectra of H<sub>2</sub>Dz-SG with Pb(II) adsorbed (1) and absorbance spectra of Pb(HDz)<sub>2</sub> solution in chloroform (2).

was easily removed from the surface by 1.0 mmol  $l^{-1}$   $Na_2S_2O_3$  solution.

### 3.5. The interference from foreign ions

Ag(I) determination with  $H_2Dz$ -SP is rather selective. No interference was observed for alkaline, alkaline-earth metals and heavy metal ions at  $pH \leq 1.0$ .

It was found that among natural water components only Hg(II), Cu(II) and Fe(III) are adsorbed by  $H_2Dz$ -SG at pH 4.5 in the presence of 1.0 mmol  $l^{-1}$  NaCl. But Cu(II) and Fe(III) at a concentration of less than or equal to 0.6 mg  $l^{-1}$  do not interfere with Hg(II) determination by using  $H_2Dz$ -SG; Hg(II) determination with  $Zn(HDz)_2$ -SP was found to be more selective. Cu(II) and Fe(III) at a concentration of less than or equal to 30 mg  $l^{-1}$  do not influence Hg(II) determination with this sorbent at  $pH \leq 1.0$ .

Pb(II), Cu(II) and Zn(II) were adsorbed onto  $H_2Dz$ -SG at pH 8–9. But Cu(II) and Zn(II) may be easily removed from the surface by 1.0 mmol  $l^{-1}$   $Na_2S_2O_3$  solution.

### 3.6. Application of $H_2Dz$ immobilized to Ag(I), Hg(II) and Pb(II) visual test determination

The results obtained testified that the adsorption of Ag(I), Hg(II) and Pb(II) on the surface of loaded silicas is rather complete and rapid. But the surface complexes are colored too light and could not be used for visual detection. It is well known, that BRh, DPhC and PAR form colored complexes with these ions correspondingly [15]. So, the possibility of application of these reagents to the preparation of color scales was studied. The results obtained have shown their usefulness for this purpose.

The color of  $Zn(HDz)_2$ -SP with Hg(II) adsorbed was brightly orange. This sorbent was used for visual test scale preparation without any treatment.

#### 3.6.1. The color scale for Ag(I) visual test determination

The color scale on the base of  $H_2Dz$ -SP for Ag(I) visual test determination in the range of

0–50  $\mu g$  per sample was obtained. It was prepared by stirring of 0.02 g of  $H_2Dz$ -SP with 10 ml of standard solution containing 0, 2.5, 5.0, 7.5, 10, 25, and 50  $\mu g$  of Ag(I) at pH 1.0. The sorbents were separated and colored by 40  $\mu l$  of BRh acetone solution. The color changing was light yellow/red–orange.

#### 3.6.2. The color scale for Pb(II) visual test determination

The color scale for lead ions detection was prepared by Pb(II) adsorption onto 0.02 g of  $H_2Dz$ -SG from 10 ml of 1 mmol  $l^{-1}$  sodium thiosulfate solution, buffered to pH 8.5 with ammonia buffer solution, containing 0, 5, 10, 20, 40, and 100  $\mu g$  of Pb(II) for 30 min. The sorbents were separated, washed with 5 ml of 1.0 mmol  $l^{-1}$  sodium thiosulfate solution and colored by 40  $\mu l$  of PAR aqueous solution. The color changing was yellow/orange–red.

#### 3.6.3. The color scale for Hg(II) visual test determination with $H_2Dz$ -SG

The scale was obtained by stirring of 0.02 g  $H_2Dz$ -SG with 25 ml of 1.0 mmol  $l^{-1}$  chloride solution containing 0, 5, 10, 25, 50, and 100  $\mu g$  of Hg(II) at pH 4.5. Sorbents were separated. Damp sorbents were colored by 40  $\mu l$  of DPhC ethanol solution. The color changing was pink–brown/violet.

Unfortunately the scales mentioned above were only stable for 1 h. That is why we applied the imitation of scales which has been computer generated using Microsoft Power Point program.

#### 3.6.4. The color scale for Hg(II) visual test determination with $Zn(HDz)_2$ -SP

The color scale on the basis of  $Zn(HDz)_2$ -SP for Hg(II) visual test determination in the range of 0–20  $\mu g$  per sample was obtained. It was prepared by stirring 0.02 g of modified SP with 10 ml of standard solution containing 0, 0.5, 1.0, 2.0, 5.0, 10, and 20  $\mu g$  of Hg(II) at pH 0. The color changing was light–violet/orange. The color scale, in contrast to the one used with  $H_2Dz$ -SG, has been stable for more than 1 month.

The data represented in Table 1 show that the developed visual test method is more sensitive than known ones.

Table 1  
Comparative description of visual test methods of Ag(I), Hg(II) and Pb(II) determination

Ion	Sorbent	Detection range, mg l <sup>-1</sup> (V, ml)	Reference
Hg(II)	H <sub>2</sub> Dz-polymer membrane	1.0–3.0 (10)	[3]
	<i>p</i> -Phenolazo-3-aminorhodanine—polymer membrane	0.02–0.4 (25)	[18]
	H <sub>2</sub> Dz-SG	0.1–2.0 (50)	Proposed
	Zn(HDz) <sub>2</sub> -SP	0.01–0.4 (50)	Proposed
Ag(I)	Fixing bath Test Merckoquant (Merck)	(0.5–10)·10 <sup>3</sup>	[19]
	Polymer fibers filled with KU-2 ion-exchanger	0.02–0.2 (20) <sup>a</sup>	[18]
	H <sub>2</sub> Dz-SP	0.05–2.0 (50)	Proposed
		0.005–0.2 (50) <sup>a</sup>	
Pb(II)	Lead Test Merckoquant (Merck)	20–500	[19]
	H <sub>2</sub> Dz-SG	0.5–10 (10)	Proposed

<sup>a</sup> DRS detection.

### 3.7. The visual test determination of Ag(I), Hg(II) and Pb(II) in real objects

The sorbents obtained were applied to lead, mercury and silver ions visual test determination in buttermilk, natural, mineral and waste water.

*Ag(I) determination* in mineral water ‘Cyljushcha’. The sample of mineral water (10 ml) was acidified to pH 1.0 and stirred with 0.02 g of

H<sub>2</sub>Dz-SP. Sorbent was separated and colored with 40 μl of BRh acetone solution.

*Hg(II) determination* in synthetic solutions of waste of chlorine manufacturing by mercury method. For this purpose H<sub>2</sub>Dz-SG (0.02 g) was stirred for 5 min with a portion (50 ml) of waste water prepared according to Ref. [16] and acidified to pH 4.5. Damp sorbent was colored with 40 μl of DPhC ethanol solution.

Table 2  
The results of Ag(I), Hg(II) and Pb(II) visual-test determination in real objects (*n* = 3, *P* = 0.95)

Ion	Type of sorbent	Sample	Amount (μg/sample)	
			Added	Found
Ag(I)	H <sub>2</sub> Dz-SP	Standard solution	5.0	5.0 ± 1.3
		Standard solution	25	25 ± 5
		Mineral water	5.0	5.0 ± 1.3
		Mineral water	5.0	5.0 ± 0.5 <sup>a</sup>
Pb(II)	H <sub>2</sub> Dz-SG	Standard solution	15	15 ± 5
		Standard solution	20	20 ± 5
		Buttermilk	10	10 ± 2.5
		Buttermilk	10	9.5 ± 0.5 <sup>a</sup>
Hg(II)	H <sub>2</sub> Dz-SG	Standard solution	10	12 ± 3
		Standard solution	25	25 ± 5
		Synthetic solution <sup>b</sup>	15	20 ± 5
	Zn(HDz) <sub>2</sub> -SP	Standard solution	0.75	0.75 ± 0.25
		River water	0.50	0.50 ± 0.25
		Synthetic solution <sup>c</sup>	10	10 ± 2.5

<sup>a</sup> Determined by FAAS.

<sup>b</sup> Concentration, g l<sup>-1</sup>: NaCl—300, V(V)—1 × 10<sup>-4</sup>, Cr(III)—5 × 10<sup>-6</sup>.

<sup>c</sup> Concentration, g l<sup>-1</sup>: NaCl—300, V(V), Fe(III)—1 × 10<sup>-4</sup>, Cr(III)—5 × 10<sup>-6</sup>.

*Zn(HDz)<sub>2</sub>-SP* was applied to *Hg(II)* determination in natural and waste water containing 0.1 mg l<sup>-1</sup> of Fe(III). The portion (10 ml) of river water or (50 ml) of waste was acidified to pH 0 and stirred with 0.02 g of *Zn(HDz)<sub>2</sub>-SP* for 10 min. The sorbents were separated.

*Pb(II)* determination in buttermilk. Buttermilk was digested with 20% trichloroacetic acid solution for proteins separation [17]. Then the portion of solution obtained (10 ml) was buffered with ammonia buffer to pH 8.5, mixed with 0.1 ml of 0.1 mol l<sup>-1</sup> Na<sub>2</sub>S<sub>2</sub>O<sub>3</sub> and stirred with 0.02 g of H<sub>2</sub>Dz-SG for 30 min. Sorbent was separated, washed with 10 ml of 1.0 mmol l<sup>-1</sup> Na<sub>2</sub>S<sub>2</sub>O<sub>3</sub> and colored with 40 μl of PAR aqueous solution.

The color of the sorbents was compared with the corresponding standard scales. The data obtained are represented in Table 2. The accuracy results of Ag(I) and Pb(II) determination were controlled by FAAS method (Table 2). The relative standard errors did not exceed 0.3. The data confirm the usefulness of the proposed sorbents for the semi-quantitative determination of mentioned ions in real objects.

### Acknowledgements

This work was partly supported by the International Soros Science Education Program through grants N SPU073063; N APU073033.

### References

- [1] G. Iwantscheff, *Das Dithizon Und Seine Anwendung* in der Mikro- und Spurenanalyse, Verlag Chemie, GMBH, Weinheim/Bergstr, 1958, 450 pp. (in German).
- [2] R.E. Clement, G.A. Eiceman, C.J. Koester, *Anal. Chem. Applic. Rev.* 67 (1995) 221R.
- [3] S.B. Savvin, T.G. Dzherayan, T.V. Petrova, A.V. Mikhailova, *Zh. Anal. Khim.* 52 (1997) 154 (in Russian).
- [4] T. Yano, Sh. Ide, Y. Tobeta, H. Kobayashi, K. Uenu, *Talanta* 23 (1976) 457.
- [5] M.A. Marshall, H.A. Mottola, *Anal. Chem.* 57 (1985) 729.
- [6] D.V. Bol'shoi, Z.M. Topilova, N.V. Rusakova, S.B. Meshkova, *Zh. Anal. Khim.* 52 (1997) 387 (in Russian).
- [7] O.A. Zaporozhets, O.M. Gawer, V.V. Sukhan, *Russ. Chem. Rev.* 66 (1997) 637.
- [8] *Methods of Analysis of Pure Chemical Reagents*, Khimija, Moscow, 1984, 384 pp. (in Russian).
- [9] Yu.Yu. Lur'e, *Handbook of Analytical Chemistry*, Khimia, Moscow, 1984, 48 pp. (in Russian).
- [10] V.P. Gladishev, G.A. Levitskaya, L.M. Fillipova, *Analytical Chemistry of Mercury*, Nauka, Moscow, 1974, 228 pp. (in Russian).
- [11] C.H. Gilles, T.N. MacEwan, S.H. Nakhwa, D. Smith, *J. Chem. Soc.* (1960) 3973.
- [12] L.G. Sillen, A.E. Martell, *Stability Constants of Metal-Ion Complexes*, Special Publication, London, 1971.
- [13] G.F. Baes, R.E. Mesmer, *The Hydrolysis of Cations*, New York, London, Sydney, Toronto, 1973.
- [14] A.G.D. Brykina, D.O. Marchenko, O.A. Shpygun, *Zh. Anal. Khim.* 50 (1995) 484 (in Russian).
- [15] Z. Marzenko, *Kolorymetryczne Oznaczanie Pierwiastkow*, Wydawnictwa Naukowo-Techniczne, 1968, 505 pp. (in Polish).
- [16] A.T. Pilipenko, O.A. Zaporozhets, *Ukr. Khim. Zh.* 56 (1990) 1177 (in Russian).
- [17] H. Tadashi, T. Motohiro, T. Kazuhiko, *Bull. Chem. Soc. Jpn.* 57 (1994) 289.
- [18] R.V. Gur'eva, S.B. Savvin, *Zh. Anal. Khim.* 52 (1997) 247 (in Russian).
- [19] *Chemicals reagents*, Merck, KGaA, Darmstadt, 1999/2000.

# Determination of selenium in nutritional supplements and shampoos by flow injection-hydride generation-atomic fluorescence spectrometry

L. Gámiz-Gracia, M.D. Luque de Castro \*

*Analytical Chemistry Division, Faculty of Sciences, University of Córdoba, E-14004 Córdoba, Spain*

Received 29 March 1999; received in revised form 18 May 1999; accepted 27 May 1999

## Abstract

A method for the determination of Se in pharmaceutical samples (nutritional supplements and shampoos) is proposed. The method involves two steps: (1) digestion of the samples and reduction of all forms of Se to Se<sup>IV</sup>, which is complete in only 10 min by the use of a focused microwave digester; and (2) continuous derivatisation (hydride formation) and spectrometry detection by atomic fluorescence. The method can be applied over a wide range of concentrations (0.3–1300 ng ml<sup>-1</sup> of Se) with good repeatability (RSD values lower than 4.6%). The method has been applied successfully to a reference material, and two different types of pharmaceuticals (namely, five different nutritional supplements—with Se present as sodium selenite and Se-methionine—and two shampoos, with selenium sulphide), in agreements with the certified and nominal values, respectively. Yields ranged between 86.5 and 104.8%, and good precision (RSD values lower than 4.2%) were obtained in all instances. © 1999 Elsevier Science B.V. All rights reserved.

*Keywords:* Selenium; Atomic fluorescence; Flow injection; Microwave digestion

## 1. Introduction

Selenium is an oligoelement with an ambivalent behaviour: it is essential at low concentrations but toxic at high concentrations, with a relatively small difference between these values. It is an essential nutrient for animals [1], and for human health in the range 0.8–1.7 μmol l<sup>-1</sup>, but toxic

above this value [2]. The essential role of the Se is due to its presence in the active sites of some enzymes (namely glutathione peroxidase and iodotironine-5'-deiodinase) [3] and the catalytic effect of selenium compounds on the reactions of intermediate metabolism and inhibition of the toxic effect of heavy metals [4]. It has been established that diets with deficit in Se are associated with some human diseases [5], but diets with Se contents higher than 5 mg kg<sup>-1</sup> are toxic and causes important symptoms in humans and animals [6,7]. All these factors, together with the fact

\* Corresponding author. Tel.: +34-957-218615; fax: +34-957-218606.

*E-mail address:* qallucam@uco.es (M.D. Luque de Castro)

that the concentration levels are extremely low, call for sensitive and accurate methods for the determination of this element. Selenium has been previously determined in nutritional supplements (or other pharmaceuticals) by voltammetry [8–11], colorimetry methods [12], spectrophotometry [13] and atomic spectrometry, with [14,15] or without [16] hydride generation, but it has been scarcely determined by hydride generation-fluorescence spectroscopy [17]. In the methods previously reported, the pre-treatment of the nutritional supplements (digestion of the sample and reduction of the forms of Se to  $\text{Se}^{\text{IV}}$ ) takes between 45 min to more than 2 h, so in the present research a faster pre-treatment step was sought. Selenium is also employed in the pharmaceutical industry, as selenium sulphide, in medicated shampoos used for the treatment of dandruff and as antiseborrhoeic agent. It has been usually determined spectrophotometrically [18–25], although isotope dilution [26], HPLC [27], molecular fluorescence [28] and gravimetric [29] methods have also been reported. All these methods involve tedious derivatisation steps, with detection limits higher than those obtained by atomic spectroscopy.

## 2. Experimental

### 2.1. Apparatus

An Excalibur atomic fluorescence detector (PS Analytical, UK) fitted with a boosted discharge hollow cathode lamp for Se (Photron, Australia), and a specific ultraviolet filter to allow transmis-

sion of the Se atomic fluorescence spectrum in conjunction with a solar blind photomultiplier was used. A Microdigest 301 focused microwave system (Prolabo, France), with a maximum irradiation power of 200 W, was used. A Minipuls-3 peristaltic pump (Gilson, USA); a Rheodyne 5041 injection valve and teflon tubing of id of 0.5 mm were used in order to construct the FI manifold in Fig. 1. A Knauer recorder (Germany) was used in order to record the signals.

### 2.2. Reagents and solutions

All reagents were of analytical-reagent grade. Ultrapure water obtained from a Milli-Q system (Millipore, USA) was used throughout. Hydrochloric acid  $3 \text{ mol l}^{-1}$  (Merck, Germany), 2%  $\text{NaBH}_4$  solution (Sigma–Aldrich, Germany) in  $0.1 \text{ mol l}^{-1}$  NaOH solution (Merck) were used in the FI system. Sixty-five percent of Nitric acid (Merck), 33% hydrogen peroxide (Panreac, Spain) and  $6 \text{ mol l}^{-1}$  hydrochloric acid were used in the digestion step. A  $\text{Na}_2\text{SeO}_3$  (Merck) stock solution of  $1 \text{ g l}^{-1}$  was prepared in Milli-Q water. Working solutions were prepared daily by appropriate dilution in  $3 \text{ mol l}^{-1}$  hydrochloric acid. A few drops of dibutyl phthalate (Sigma–Aldrich) were placed in the gas–liquid separator in order to avoid foam formation. Argon (Carburros Metálicos, Spain) was used in order to flush the hydride formed to the detector.

### 2.3. Procedure

#### 2.3.1. Digestion/reduction step

An appropriate amount of pharmaceutical (1.5 or 2.5 ml for nutritional supplements and 0.05 g

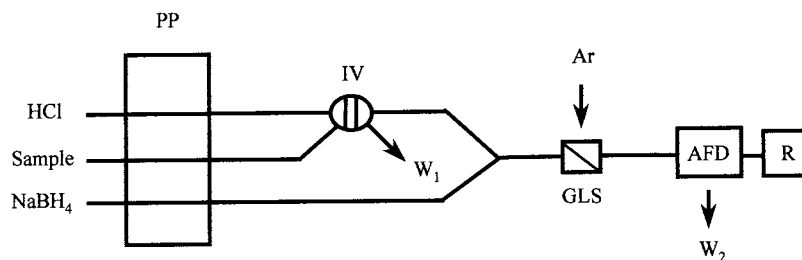


Fig. 1. FI manifold. PP, peristaltic pump; IV, injection valve; GLS, gas–liquid separator; AFD, atomic fluorescence detector; W, waste; R, recorder.



for shampoos) or reference material (0.1 g) was placed in the digestion vessel. 5 ml of nitric acid and 2 ml of hydrogen peroxide are added and the mixture subjected to microwave (MW) irradiation (25% power, 5 min) in order to digest the sample. After this, 10 ml of 6 mol l<sup>-1</sup> hydrochloric acid is added and the mixture is MW irradiated (75% power, 5 min) in order to reduce all Se to Se<sup>IV</sup>. The mixture is then transferred to a 25-ml volumetric flask and made up to volume with Milli-Q water.

### 2.3.2. Determination step

The treated sample is injected into the HCl carrier. After merging with the NaBH<sub>4</sub> stream, the volatile hydride is formed and swept out of the gas–liquid separator by an Ar stream into a chemically generated hydrogen diffusion flame. The flame is maintained by the excess of hydrogen produced in the reaction between NaBH<sub>4</sub> and HCl. The hydride is then atomised in the flame and the atoms are detected by fluorescence spectrometry.

## 3. Results and discussion

### 3.1. Optimisation

The optimisation of the overall method was developed in two steps: first, the detection of Se<sup>IV</sup> and the FI system were studied. Then, the digestion of the samples and the reduction step were optimised, being the main purpose to carry out them in the shortest time. Table 1 shows the studied ranges and optimum values for all the variables. The univariate method was used in both instances.

#### 3.1.1. Determination step

For the optimisation of this step the FI variable studied was the flow rates, and the chemical variables were the NaBH<sub>4</sub> and HCl concentrations. As a compromise between sensitivity, signal-to-noise ratio and sampling frequency, a flow rate of 4.5 and 2.15 ml min<sup>-1</sup> were chosen for the carrier and reagent, respectively. A concentration of 2% m/v of NaBH<sub>4</sub> (in 0.1 mol l<sup>-1</sup> NaOH solution)

Table 1  
Optimisation of the method

	Studied range	Optimal value
<i>Digestion step</i>		
[HNO <sub>3</sub> ] (%)	6–65	65
HNO <sub>3</sub> (ml)	2–10	5
H <sub>2</sub> O <sub>2</sub> (ml)	0–5	2
MW power (%)	15–50	25
MW irradiation time (min)	2–20	5
<i>Reduction step</i>		
[HCl] (mol l <sup>-1</sup> )	3–12	6
HCl (ml)	5–15	10
MW power (%)	25–100	75
MW irradiation time (min)	2–10	5
<i>Determination step</i>		
Flow rate of HCl (ml min <sup>-1</sup> )	0.65–5.0	4.5
Flow rate of NaBH <sub>4</sub> (ml min <sup>-1</sup> )	0.65–4.5	2.15
[HCl] (mol l <sup>-1</sup> )	1.5–8	3
[NaBH <sub>4</sub> ] (% m/v)	0.5–2	2

was selected as optimum, as concentrations lower than that were not enough to maintain the hydrogen flame as insufficient hydrogen was formed. The concentration of HCl had a minimal effect on the analytical signal and a value of 3 mol l<sup>-1</sup> was chosen, which provided enough acidic medium for hydride generation.

#### 3.1.2. Digestion/reduction step

Different oxidant reagents were tested in the digestion step, namely hydrobromic acid-bromine [30], sodium peroxodisulfate [31,32] and nitric acid. Finally, nitric acid was chosen and the addition of hydrogen peroxide was necessary in order both to complete the process and maintain oxidising conditions throughout the digestion [33]. Once the volumes of the reagents had been optimised, the MW power was studied, and 25% of the nominal value (50 W) was selected. The MW irradiation time was 5 min as this interval was the minimum necessary to complete the digestion in the selected conditions. Once the sample had been digested, the concentration and volume of HCl necessary to reduce the Se was studied. The more

Table 2  
Features of the determination method<sup>a</sup>

	Calibration 1	Calibration 2
Equation <sup>b</sup>	$Y = 4.11 + 4.94 C$	$Y = -4.38 + 0.15 C$
$r^2$ (%)	98.53	98.21
Calibration range (ng ml <sup>-1</sup> )	0.30–40	40–1300
%RSD ( $n = 7$ )	4.6 (at 15 ng ml <sup>-1</sup> )	2.86 (at 750 ng ml <sup>-1</sup> )
Detection limit (ng ml <sup>-1</sup> ) <sup>c</sup>	0.4	–
Quantification limit (ng ml <sup>-1</sup> ) <sup>d</sup>	1.4	–

<sup>a</sup> All concentration are expressed as Se.

<sup>b</sup>  $Y$  is expressed in arbitrary fluorescence unit and  $C$  in ng ml<sup>-1</sup>.

<sup>c</sup> As three time SD (IUPAC).

<sup>d</sup> As ten times SD (IUPAC).

diluted the acid, the longer the irradiation time necessary to complete the reduction. Finally, 10 ml of 6 mol l<sup>-1</sup> HCl was selected as reductant, as more concentrated acid did not accelerate the process. Once more, the MW power and irradiation time were optimised in order to provide a complete reduction in the shortest time, and 75% (150 W) and 5 min, respectively, were chosen.

Table 3  
Validation and applications of the method

Sample	Nominal (or certified) value (ng ml <sup>-1</sup> of Se)	Found value ( $n = 3$ ) (ng ml <sup>-1</sup> of Se)	$t^a$	%Yield
CRM CRR 278	$1.66 \pm 0.04$	$1.61 \pm 0.05$	1.73	$97.0 \pm 3.0$
<i>Nutritional supplements</i>				
1	50	$52 \pm 1$	3.41	$104.8 \pm 2.4$
2	65	$62 \pm 2$	2.59	$94.6 \pm 3.4$
3	70	$67 \pm 3$	1.70	$96.1 \pm 4.0$
4	101.7	$102 \pm 2$	0.13	$99.8 \pm 2.3$
5	100	$97 \pm 4$	1.24	$97.4 \pm 3.6$
<i>Shampoos<sup>b</sup></i>				
1	25	$21.4 \pm 0.3$	24.94	$86.5 \pm 1.2$
2	25	$25.4 \pm 0.4$	1.78	$101.5 \pm 1.5$

<sup>a</sup>  $t$  (0.05, 2 degrees of freedom) = 4.30.

<sup>b</sup> Concentration expressed as g l<sup>-1</sup> of selenium sulphide.

### 3.2. Features of the method

Two calibration curves were run using standard solutions of Se<sup>IV</sup> (injected in triplicate), changing the sensitivity of the detector in order to cover a wide range of concentrations, from 0.3 to 40 ng ml<sup>-1</sup> (Calibration 1) and from 40 to 1300 ng ml<sup>-1</sup> (Calibration 2). Table 2 shows the characteristics of both calibration curves, limit of detection and the repeatability of the method expressed as RSD ( $n = 7$ , injected in triplicate), with good results in all instances. The sample throughput was ca. 5 samples h<sup>-1</sup> for the pre-treatment step and ca. 50 samples h<sup>-1</sup> for derivatisation-detection.

### 3.3. Validation of the method

The method was applied to a reference material of mussel tissue (CRM CRR 278), using the Calibration 1 and the result is shown in Table 3. The agreement of the certified and found values and the good precision of the method, make it an advantageous alternative for the determination of selenium in pharmaceutical samples.

### 3.4. Applications

The method was applied to two kinds of pharmaceuticals: five liquid nutritional supplements

with different concentrations of Se, and two shampoos. The nutritional supplements, kindly supplied by Reina Sofia Hospital (Córdoba, Spain), are the following: (1) Dietgrif (Lab. Gri-fols, Spain), with Se present as Se-methionine; (2) Ensure HN (Lab. M&R, Holland), with Se present as sodium selenite; (3) Enrich (Lab. M&R, Holland); (4) Nepro (Lab. Abbott, Spain); and (5) Edanec (Lab. Abbott, Spain). In samples (3), (4) and (5) the Se-compound was not specified. For samples (1) and (2), 2.5 ml of liquid sample was taken for the application of the method, while in all the rest, the analysis was carried out using 1.5 ml. Each pharmaceutical was analysed three times, and injected in triplicate. Calibration 1 was used in all instances. The results obtained are shown in Table 3, with yields ranging between 96.1 and 104.8, and good precision. The shampoos were acquired in local pharmacies, and were as follows: (1) Bioselenium (Lab. J. Uriach & Cia., Spain); and (2) Abbott Selsun (Lab. Abbott, Spain). Approximately 0.05 g of shampoo was accurately weighted and subjected to the treatment described in Section 2. 0.25 ml of the final solution was taken, diluted to 10 ml with 3 mol l<sup>-1</sup> HCl, and analysed. Calibration 2 was used for these samples. The results thus obtained are shown in Table 3. As can be seen, a good agreement between nominal and found values was obtained for one of the samples, but not for the other, although the precision was excellent in both instances.

#### 4. Conclusions

A new method for the analysis of pharmaceutical samples (nutritional supplements and shampoos) has been developed and validated, and good results have been obtained in almost all the cases. The digestion and reduction steps are quite short (only 10 min), as compared with other recently described in the literature. It could be applied to other kind of matrices (as different foods or other pharmaceuticals), although it should be optimised in each case. The derivatisation-detection method is very sensitive, covering a wide range of concentrations with good linearity,

reproducibility and excellent sampling frequency. This is also the first time that FI-HG-AFS is applied to this kind of samples. The method reported here follows the trend of increasing automation in the pharmaceutical field.

#### Acknowledgements

The Spanish Comisión Interministerial de Ciencia y Tecnología (CICYT) is thanked for financial support (Project No. PB95-1265).

#### References

- [1] W. Maher, M. Deaker, D. Jolley, F. Krikowa, B. Roberst, *Appl. Organomet. Chem.* 11 (1997) 313.
- [2] M. Albert, C. Demesmay, J.L. Rocca, *Fres. J. Anal. Chem.* 351 (1995) 426.
- [3] B.A. Zachara, *J. Trace Elem.* 6 (1992) 137.
- [4] P.B. Moser-Veillon, A. Reeds Mangels, K.Y. Patterson, C. Veillon, *Analyst* 117 (1992) 559.
- [5] O.A. Levander, *Am. Diet. Assoc.* 91 (1991) 1572.
- [6] I.S. Krull, in: J.K. Lawrence (Ed.), *Liquid Chromatography in Environmental Analysis*, Humana Press, Clifton, NJ, 1983.
- [7] R.S. Shamberger, *Trace Elem. Med.* 3 (1986) 105.
- [8] W. Holak, J.J. Specchio, *Analyst* 119 (1994) 2179.
- [9] Z. Fijalek, K. Sarna, P. Suchocki, B.A. Fitak, *Chem. Anal. (Warsaw)* 43 (1998) 833.
- [10] A. Lozak, Z. Fijalek, *Chem. Anal. (Warsaw)* 43 (1998) 1.
- [11] Z. Fijalek, A. Lozak, K. Sarna, *Electroanalysis* 10 (1998) 846.
- [12] J.A. Hurlbut, R.G. Burkepile, C.A. Geisler, *J. AOAC Int.* 75 (1992) 269.
- [13] G.A. Milovanovic, R.B. Petronijevic, M.M. Cakar, *Mikrochimica Acta* 128 (1998) 43.
- [14] C.P. Hanna, G.R. Carnrick, S.A. McIntosh, L.C. Guyette, D.E. Bergemann, *At. Spectrosc.* 16 (1995) 82.
- [15] K.A. Anderson, B. Isaacs, *J. AOAC Int.* 76 (1993) 910.
- [16] E.H. Larsen, J. Ekelund, *Analyst* 114 (1989) 915.
- [17] J. Zou, P. Zhang, Z.G. Yang, X.Y. Lai, *Fenxi-Shiyanshi* 17 (1998) 84.
- [18] A.S. Amin, M.N. Zareh, *Anal. Lett.* 29 (1996) 2177.
- [19] A. Safavi, A. Afkhami, *Anal. Lett.* 28 (1995) 1095.
- [20] A.A. Ensafi, G.B. Dehaghi, *Anal. Lett.* 28 (1995) 335.
- [21] M.N. Pathare, A.D. Sawant, *Anal. Lett.* 28 (1995) 317.
- [22] A. Ramesh, T.V. Ramakrishna, M.S. Subramanian, *Bull. Chem. Soc. Jpn.* 67 (1994) 2121.
- [23] A. Afkhami, A. Safavi, A. Massoumi, *Talanta* 39 (1992) 993.
- [24] J. Sanz, F. Gallarta, J. Galban, J.R. Castillo, *Analyst* 113 (1988) 1387.

- [25] M.F. Mousavi, A.R. Ghiasvand, A.R. Jahanshahi, *Talanta* 46 (1998) 1011.
- [26] A. Ramesh, K. Raghuraman, M.S. Subramanian, T.V. Ramakrishna, *Analyst* 119 (1994) 2067.
- [27] M.Y. Khuhawar, R.B. Bozdar, M.A. Babar, *Analyst* 117 (1992) 1725.
- [28] G. Alfthan, *Clin. Chem.* 31 (1985) 500.
- [29] D. Bertini, V. Nuti, G. Linari, *Boll. Chim. Farm.* 121 (1982) 535.
- [30] A. D'ulivo, L. Lampugnani, I. Sfetsios, R. Zamboni, C. Forte, *Analyst* 119 (1994) 663.
- [31] M.G. Cobo-Fernández, M.A. Palacios, D. Chakraborti, P. Quevauviller, C. Cámara, *Fresenius J. Anal. Chem.* 351 (1995) 438.
- [32] C. Rico Varadé, M.D. Luque de Castro, *J. Anal. Atom. Spectrom.* 13 (1998) 787.
- [33] D.W. Bryce, A. Izquierdo, M.D. Luque de Castro, *Analyst* 120 (1995) 2171.

# Flow-injection fluorimetric determination of mercury(II) with calcein

A.G. Lista, M.E. Palomeque, B.S. Fernández Band \*

*FIA Laboratory, Department of Chemistry and Engineering Chemistry,  
Universidad Nacional del Sur. Av. Alem 1253-8000 Bahía Blanca, Argentina*

Received 19 January 1999; received in revised form 1 June 1999; accepted 1 June 1999

## Abstract

A flow-injection spectrofluorimetric method for the determination of Hg(II) is described. The method is based on the complex that is formed between Hg(II) and calcein at pH 11–12. This reagent was not used before for determining Hg(II). The excitation wavelength is 324 nm and the emission wavelength is 522 nm. The calibration graph shows a linear range between 7.7 and 128  $\mu\text{g l}^{-1}$  (relative standard deviation 2.0%), the sampling rate was 90  $\text{h}^{-1}$ . The effect of several interferents has been examined. Trace mercury in natural waters were determined satisfactorily using a modified manifold, which has an EDTA stream in order to minimize the calcium and magnesium interference. © 1999 Elsevier Science B.V. All rights reserved.

*Keywords:* FIA; Hg; Fluorimetric determination; Calcein

## 1. Introduction

The determination of traces of heavy metals in natural waters is becoming increasingly interesting in environmental analysis. The Hg(II) is considered a chemical pollutant and for low concentration its toxicity can be dangerous hence its importance in the detection of mercury.

There are well-established laboratory methods such as atomic absorption spectrometry [1,2], with cold vapor [3,4], ICP emission spectrometry coupled with mass spectroscopy [5,6]. They are char-

acterized by their high sensitivity but at present the easier, faster and inexpensive analysis for monitoring Hg(II) in natural waters is becoming important.

The aim of the present paper is to develop a simple and fast method which can be considered as a screening flow injection analysis (FIA) method for a fluorimetric determination of Hg(II) based on the Hg(II)-calcein complex formation in alkaline medium. The literature contains no report of quantitative determination of Hg(II) by using this reagent. For this purpose, a manifold was designed and optimized. The proposed method has reached a linear range of Hg(II) concentration that turned out to be wider than the fluorimetric determination of Hg(II) by using

\* Corresponding author. Fax: +54-291-4595160.

*E-mail address:* usband@criba.edu.ar (B.S. Fernández Band)

an optochemical sensor [7] or the fluorimetric flow-injection method applied in soil samples [8].

## 2. Experimental

### 2.1. Apparatus

An Aminco Bowman Serie 2 luminescence spectrophotometer equipped with a Hellma 176752-QS flow cell with an inner volume of 25  $\mu\text{l}$  and 1.5 mm light path. All the reaction coils were made of PTFE tubing (i.d. 0.5 mm). A Gilson Minipuls-3 peristaltic pump and Rheodyne 5041 injection valve were used.

### 2.2. Reagents

Calcein stock solution: a stock solution of 1000  $\mu\text{g ml}^{-1}$  calcein was prepared by dissolving 0.25 g of calcein (Hopkin & Williams) in 250 ml of 0.6 M potassium hydroxide (Mallinckrodt). This solution was stored in a plastic bottle and kept in a refrigerator.

Calcein working solution: the reagent working solution of 30  $\mu\text{g ml}^{-1}$  was prepared daily, by the dilution of 3 ml of calcein stock solution to 100 ml with 0.6 M potassium hydroxide.

Mercury standard solution: a solution of 0.01 M Hg(II) was prepared, by dissolving 0.6785 g of  $\text{HgCl}_2$  (Sigma) in 250 ml of bidistilled water.

Mercury working solution: the reagent working solution of  $8 \times 10^{-4}$  M Hg(II) was prepared daily. More dilute solutions were prepared as required.

Disodium ethylenediamine tetraacetate (EDTA) (Mallinckrodt): an aqueous solution  $4 \times 10^{-4}$  M was prepared.

### 2.3. General procedure

The configuration showed in Fig. 1 was designed and optimized for the application of the proposed method.

The sample was injected into bidistilled water as a carrier that merged with the alkaline calcein reagent, the complex was formed along the reactor and its fluorescence was monitored as it

passed through the flow cell. Fluorescence intensities were measured at 522 nm (excitation wavelength 324 nm). The baseline was adjusted while the calcein reagent was continuously flowing through the system.

## 3. Results and discussion

### 3.1. Optimization of variables

#### 3.1.1. Chemical variables

The pH required for the formation of the binary complex was 11–12. At  $4 < \text{pH} < 10$  there was an important interference owing to the enhancement of the fluorescence of the baseline by calcein reagent.

The effect of reagent concentration was studied, with a concentration of potassium hydroxide fixed at 0.6 M the calcein concentration was varied from 15 to 120  $\mu\text{g ml}^{-1}$ . Calcein concentration (30  $\mu\text{g ml}^{-1}$ ) gave the greatest slope of the calibration curve.

The potassium hydroxide concentration was studied with a fixed calcein concentration of 30  $\mu\text{g ml}^{-1}$ , it was varied between 0.2 and 1.0 M, the slopes of the calibration curves only changed slightly with the increase of the potassium hydroxide concentration. The optimum concentration was 0.6 M.

#### 3.1.2. FIA variables

**3.1.2.1. Manifold configuration.** For designing the manifold we have considered three types: two- and three-channel systems, and a double injection system.

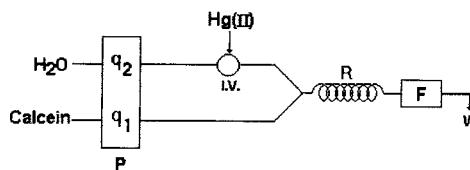


Fig. 1. Flow injection manifold for the fluorimetric determination of Hg(II). F, spectrofluorimeter; I.V., injection valve; P, peristaltic pump, R, reaction coil; W, waste.

Table 1  
Optimization of FIA variables

Variable	Studied range	Optimum value
Reactor length	10–200 cm	100 cm
Sample volume	50–300 $\mu\text{l}$	200 $\mu\text{l}$
Reagent flow rate ( $q_1$ )	0.8–2.6 ml/min	1.5 ml/min
Carrier flow rate ( $q_2$ )	1.3–3.2 ml/min	2.6 ml/min

1. In the two-channel system, the sample was injected into bidistilled water, then it merged with the calcein reagent and the binary complex was formed inside the reaction coil.
2. In the three-channel system, the sample was injected into bidistilled water, it merged with 0.6 M of potassium hydroxide solution into a reaction coil, then it merged with calcein reagent into a second reaction coil to form the complex.
3. In a double injection system, the sample and the calcein reagent were both injected into their carriers, bidistilled water as a carrier for the sample and 0.6 M potassium hydroxide as a carrier for the calcein.

The two-channel system was the manifold selected because the fluorescence signal of the sample increased sharply and it was obtained more sensitivity for the lower mercury (II) concentration.

The double injection system produced a high peak for the blank reagent and a consequent loss of sensitivity when low concentration of mercury (II) was measured.

The range of the FIA variables studied and their optimum values are listed in Table 1.

The calibration curve was linear over the range 7.7–128  $\mu\text{g l}^{-1}$  (Fig. 2) and the regression equation is:  $y = 0.036 (\text{Hg}^{2+}, \mu\text{g l}^{-1}) + 1.0$ ,  $r^2 = 0.996$ . The relative standard deviation after 11-fold triplicate processing of 77  $\mu\text{g l}^{-1}$  Hg(II) solution was estimated as 2.0%. The sampling throughput was 90  $\text{h}^{-1}$ .

### 3.2. Interferences

A systematic study of potential interferents in the determination of 80  $\mu\text{g l}^{-1}$  mercury was per-

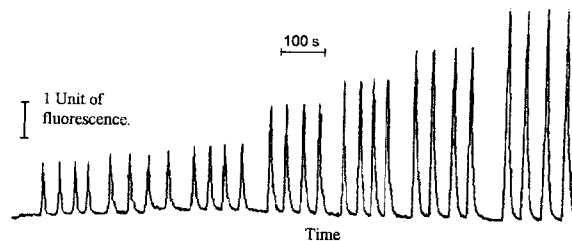


Fig. 2. Flow injection response of standard solutions with 7.7, 16, 26, 51, 77, 102 and 128  $\mu\text{g l}^{-1}$  by working with the optimized FIA system which is shown in Fig. 1

formed. The tolerance limits shown in Table 2 were obtained by considering that foreign ions do not cause interference if its signal is not different than 3% of the analyte signal.  $\text{Ca}^{2+}$ ,  $\text{Mg}^{2+}$  caused the greatest interference. Good tolerance to most of the species commonly found in waters was observed.

### 3.3. Determination of Hg(II) in real samples

The flow injection manifold above presented, was modified by incorporating an EDTA stream to minimize the calcium and magnesium interference.

Table 2  
Interferences

Interferences	Tolerance limits (mg/l)
$\text{Mn}^{2+}$	12.0
$\text{Cu}^{2+}$	11.6
$\text{Mg}^{2+}$	Interfere
$\text{Ca}^{2+}$	Interfere
$\text{Ni}^{2+}$	12.0
$\text{Fe}^{3+}$	2.3
$\text{Na}^+$	120
$\text{F}^-$	6.0
EDTA	372.2
Citrate	2.0
Oxalate	30
$\text{NO}_3^-$	10
$\text{Cl}^-$	100
$\text{SO}_4^{2-}$	120

Table 3  
Hg(II) determination in real samples

Samples <sup>a</sup>	Hg(II) added ( $\mu\text{g/l}$ )		Hg(II) found ( $\mu\text{g/l}$ )		% Recovery	
1	12.8		13.5		105	
2	12.8		13.0		101.5	
3	17.6	35.2	17.9	35.0	101.7	99.41
4	17.6	35.2	17.8	35.6	101.1	101.1

<sup>a</sup> Water samples obtained from different places of the Casa de Piedra lake. (Lat. 38° 10' S, Long. 67° 20' W, Colorado River, Argentine).

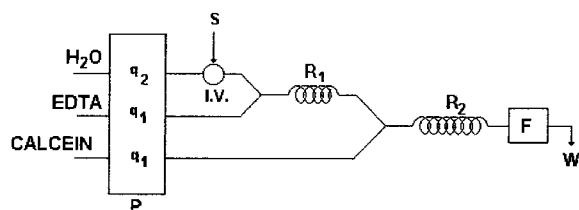


Fig. 3. Flow-injection manifold for the fluorimetric determination of Hg(II) in real water samples. F, spectrofluorimeter; I.V., injection valve; P, peristaltic pump;  $q_1$ , 1.5 ml/min;  $q_2$ , 2.6 ml/min;  $R_1$ , reaction coil (30 cm,  $\Phi = 0.5$  mm);  $R_2$ , reaction coil (100 cm,  $\Phi = 0.5$  mm); S, sample; W, waste.

The sample volume is injected into a carrier stream merging with the EDTA stream inside the first reactor ( $R_1$ ). Then it merges with the reagent stream inside the reactor  $R_2$ . Fig. 3 shows the optimized system.

The total  $\text{Ca}^{2+}$  and  $\text{Mg}^{2+}$  concentration in water samples were determined by the titrimetric method [9], therefore the EDTA concentration to be used in the FI manifold was calculated, keeping in mind that EDTA does not interfere in a concentration up to  $1 \times 10^{-3}$  M (Table 2).

The real samples showed that Hg was not present in them, so they were spiked with standard mercury solution and then the samples were analyzed by standard addition method.

The greatest concentration of  $\text{Ca}^{2+}$  and  $\text{Mg}^{2+}$  in real samples tested was 210 mg  $\text{CO}_3\text{Ca/l}$ . As the addition standard method involves a sample dilution for preparing the

spiked samples, an appropriate sample volume was taken and in agreement with this dilution, a  $4 \times 10^{-4}$  M EDTA solution was used in the above FIA system, so the interference of  $\text{Ca}^{2+}$  and  $\text{Mg}^{2+}$  was minimized.

The obtained results were shown in Table 3.

#### 4. Conclusion

A new, fast and simple fluorimetric FIA method for the determination of Hg(II) has been developed. Given the simplicity of the system and the easily instrumentation availability it can be a useful method to control effluents that may have a certain content of Hg(II) as a screening method.

In order to determine Hg(II) in real samples, it requires the incorporation of an EDTA stream in the FIA system to minimize the calcium and magnesium interference. This fluorimetric method is an alternative to other methodologies and provides good results in terms of accuracy and precision ( $\text{RSD}\% = 2\%$ ) and a sample throughput of  $90 \text{ h}^{-1}$ .

#### Acknowledgements

The authors thank the CONICET (Consejo Nacional de Investigaciones Científicas y Técnicas de la República Argentina) for financially supporting this work.



**References**

- [1] S. Landi, F. Fagioli, *Anal. Chim. Acta* 298 (1994) 363.
- [2] K. Bulska, W. Kandler, P. Paslawski, A. Hulanicki, *Mikrochim. Acta* 119 (1995) 137.
- [3] I. Karadjova, *J. Anal. At. Spectrom.* 10 (1995) 1065.
- [4] J.L. Manzoori, M.H. Sorouraddin, A.M. Shabani, *J. Anal. At. Spectrom.* 13 (1998) 673.
- [5] N. Mickelli, M.O. Amato, *At. Spectrosc.* 18 (1997) 186.
- [6] P. Canada, J.M. Cano, A. García de Torres, F. Sanchez, *Fresenius J. Anal. Chem.* 352 (1995) 615.
- [7] M. Plaschke, R. Czolk, H.J. Ache, *Anal. Chim. Acta* 304 (1995) 107.
- [8] D. Narinesingh, R. Mungal, T. Ngo, *Anal. Chim. Acta* 292 (1994) 185.
- [9] *Standard Methods for the Examination of Water and Wastewater*, 15th ed. American Public Health Association, 1981.

# Spectrophotometric determination of ceterizine hydrochloride with Alizarin Red S

K. Basavaiah \*, SriLatha, J. Manjunatha Swamy

*Department of Studies in Chemistry, University of Mysore, Manasagangotri, Mysore 570 006, India*

Received 1 June 1999; accepted 2 June 1999

## Abstract

A simple, rapid and sensitive spectrophotometric method has been developed for the assay of ceterizine hydrochloride (CTZH) in bulk drug and its pharmaceutical preparations. This method is based on the ion-pair complex reaction between CTZH and Alizarin Red S in Clarks–Lubs buffer. The chromogen being extractable with chloroform, could be measured quantitatively at 440 nm. All variables were studied to optimise the reaction conditions. Regression analysis of Beer's Law plot showed good correlation in the concentration range 2.5–22  $\mu\text{g ml}^{-1}$ . The method has a detection limit of 0.1328  $\mu\text{g ml}^{-1}$ . The proposed method has been successfully applied for the analysis of the bulk drug and its dosage forms such as tablets and syrups. No interference was observed from common pharmaceutical adjuvants. © 1999 Elsevier Science B.V. All rights reserved.

*Keywords:* Ceterizine hydrochloride; Ion-pair complex; Spectrophotometric method

## 1. Introduction

Ceterizine hydrochloride, CTZH, (2-(4-(4-chlorophenyl) phenylmethyl)-1-piperazinyl)-ethoxy)-acetic acid dihydrochloride is a new antihistaminic drug [1–3], currently marketed in India under the trade names cetzine, zyncet, zyrtec, cetrizet and cetiriz. It is indicated for the treatment of perennial and seasonal allergic rhinitis and also for chronic urticaria. Currently, CTZH and its formulations are not to be found in any pharmacopoeia. Only two gas-chromato-

graphic methods [4,5] and three high performance liquid chromatography (HPLC) methods [6–8] have been described for the determination of ceterizine in biological materials. Recently [9], El-Walily et al. have reported derivative spectrophotometric and HPLC methods for the determination of CTZH in pharmaceutical tablets. No methods based on colour formation have been reported for CTZH.

This paper describes a spectrophotometric method based on ion-association complex formation between CTZH and the acid dye, Alizarin Red S in Clarks–Lubs buffer of pH 3.2 (Fig. 1). The proposed method is simple, sensitive and the complex formed is stable for more than 24 h.

\* Corresponding author. Tel.: +91-821-421-263; fax: +91-821-520-600.

## 2. Experimental

### 2.1. Apparatus

An Elico Model SL 171 digital spectrophotometer with 1-cm matched glass cells was used for the absorbance measurements. pH measurements were made with an Elico Model L1-120 digital pH meter, calibrated with buffer solution (pH  $4 \pm 0.05$ ).

### 2.2. Chemicals and reagents

All chemicals and reagents were of analytical grade. CTZH 99.62% purity (UNI-UCB, Mumbai, India) was used as the working standard. Alizarin Red S ARS (s.d. Fine Chemicals) was 0.05% w/v in Clarks–Lubs buffer of pH 3.2. Clarks–Lubs buffer of pH 3.2 was prepared by mixing 125 ml of 0.1 M potassium hydrogen phthalate and 36.75 ml of 0.1 M HCl and diluting

to 250 ml. Spectroscopic grade chloroform was used.

Dosage forms used in this investigation were: cetizine tablets and syrup (Glaxo Lab); cetirizine tablets and syrup (Alchem Labs); zyncet tablets and suspension (Unichem India); cetirizet-D tablets (Sunpharm); alerid tablets and syrup (Cipla); Zyrtec tablets (UNI-UCB) and zirtin tablets (Torrent Pharm).

### 2.3. Preparation of standards

Twenty mg of CTZH, accurately weighed, were transferred into a 100 ml volumetric flask, dissolved in water and completed to volume with the same solvent. This solution was diluted appropriately to get a working solution of  $50 \mu\text{g ml}^{-1}$ .

### 2.4. Assay procedure

Aliquots of solution containing  $2\text{--}22 \mu\text{g ml}^{-1}$  of CTZH were transferred into a series of 125 ml of separating funnels; then 5 ml of Clarks–Lubs buffer of pH 3.2 and 2 ml of 0.05% ARS were added. The total volume was adjusted to 15 ml by adding distilled water. Chloroform (10 ml, accurately measured) was added to each separating funnel and the contents were shaken for exactly 1 min. The two phases were allowed to separate and the chloroform layer was passed through anhydrous sodium sulphate and the absorbance was measured at 440 nm against the reagent blank. The reagent blank was prepared exactly like the procedure described above, but in the absence of CTZH. A calibration graph was drawn or regression equation calculated.

### 2.5. Assay procedure for tableted dosage

Tablets: twenty tablets were weighed and powdered. An amount of the powder equivalent to 20 mg of antiallergic drug was weighed into a 100 ml volumetric flask, 60 ml of distilled water were added and shaken thoroughly for about 20 min. The contents were diluted to the mark, mixed well and filtered through a quantitative filter paper (Whatman 40) to remove the insoluble matter remaining. Twenty five ml of this filtrate was

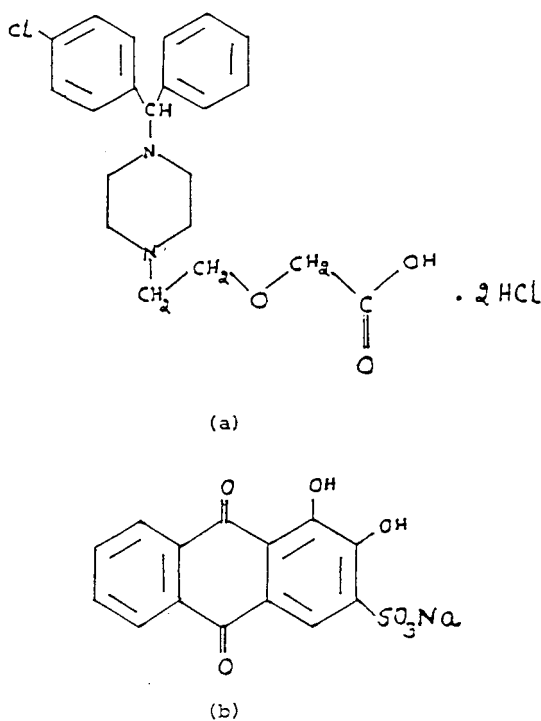


Fig. 1. Structure of (a) ceterizine dihydrochloride; (b) Alizarin Red S.

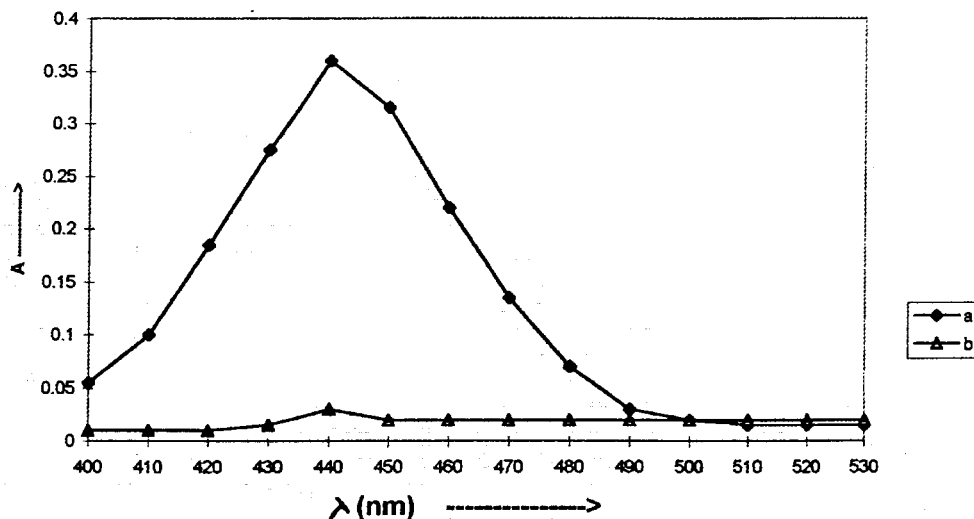


Fig. 2. Absorption spectra of (a) ceterizine (CTZ)-ARS complex; (b) reagent blank.

diluted to 100 ml and a suitable aliquot was taken for analysis using the procedure described earlier.

### 2.6. Syrup and suspension

In respect of syrup and suspension, 20 ml equivalent to 20 mg of drug were transferred into a 250 ml separator. The sample was rendered alkaline to litmus with 6 N ammonia solution and 1 ml in excess was added. The mixture was then extracted with  $3 \times 15$  ml portions of chloroform, the chloroform extracts were evaporated to dryness and the residue was dissolved in 0.1 N HCl and made upto 100 ml with distilled water. This solution was diluted to get  $50 \mu\text{g ml}^{-1}$  of drug and an aliquot was analysed as above.

## 3. Results and discussion

Ion-pair extraction spectrophotometry has received considerable attention for quantitative estimation of many pharmaceutically important compounds [10–14]. CTZH reacted with ARS in an acidic buffer to form a yellow ion-pair complex which was extracted into chloroform. This complex has an absorption maximum at 440nm against reagent blank, hence this wavelength was

used for all subsequent measurements. Under the same experimental conditions the reagent blank gave negligible absorbance (Fig. 2).

### 3.1. Optimum conditions for complex formation

The optimum conditions for quantitative determination of the associated ion-pair formed were established via a number of preliminary experiments. The effect of pH was studied by extracting the coloured complex formed in the presence of various buffers of different acidic pH values. Of the various buffers tried, Clark-Lubs (pH 2.2–3.8) was found to be more suitable compared to Walpole or Sorenson buffer in terms of sensitivity. In order to establish the optimum pH range, CTZH was mixed with ARS in selected buffer of pH 2.2–3.8, and the absorbance of the ion-associated complex was measured. Fig. 3 shows that the absorbance increases and reaches a maximum and a constant value at 3.0–3.4 pH range. At pH values greater than 3.4, the decrease in absorbance of the complex and increase in absorbance of the blank were observed. Hence, a pH of 3.2 was used in all subsequent experimental work. The shape of the absorption spectrum and maximum position did not vary with pH, so, it was concluded that only one complex was formed in this pH range.

The optimum volume of the dye used was also studied. Fig. 4 revealed an increase in the absorbance readings with the increase of volume of ARS upto 3.0 ml. However, a significant increase in the absorbance value of the blank was observed at volumes larger than 3 ml. Therefore, 3 ml of 0.05% w/v ARS was found to be quite adequate

in a total volume of 15 ml of aqueous phase. Several organic solvents were tried to provide an effective extraction of the drug-dye complex from the aqueous phase and chloroform was preferred for its selective extraction. A ratio of 3:2 of aqueous to chloroform phases was required for efficient extraction of the coloured species. Shak-

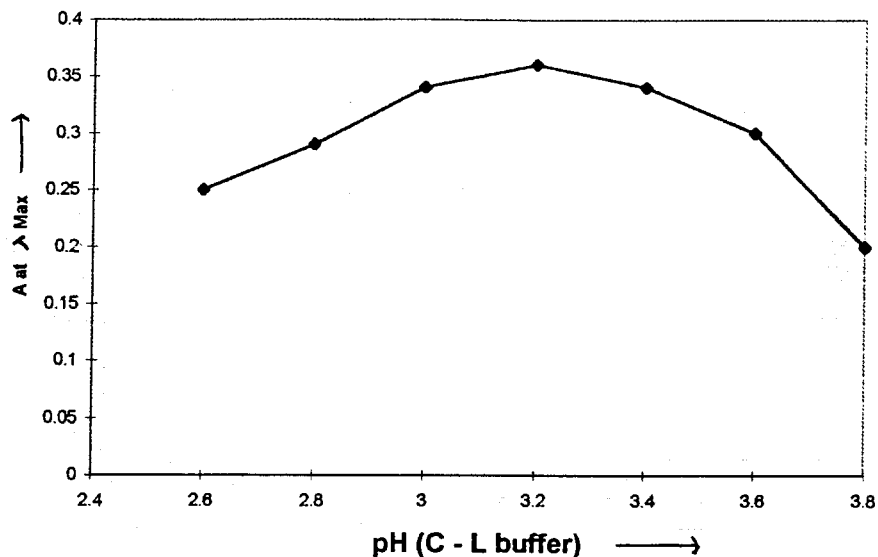


Fig. 3. Effect of pH on the absorbance of the ceterizine hydrochloride (CTZH)-ARS complex (final concentration of CTZH was  $10 \mu\text{g ml}^{-1}$ ).

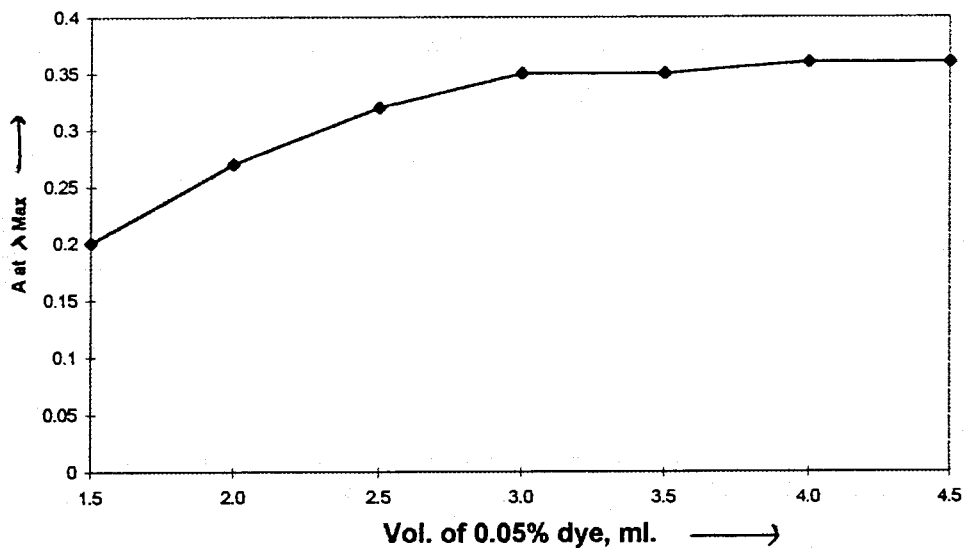


Fig. 4. Effect of concentration of ARS (final concentration of ceterizine hydrochloride, CTZH, was  $10 \mu\text{g ml}^{-1}$ ).

Table 1

Analysis of pharmaceutical preparations containing ceterizine hydrochloride (CTZH) by the proposed method

Preparation*	Label claim (mg tablet <sup>-1</sup> or ml <sup>-1</sup> )	Recovery by the proposed method (%)	RSD (%)
Ceterzine tablets <sup>a</sup>	10	97.58	1.32
Cetzine syrup <sup>a</sup>	1	103.26	0.84
Cetiriz tablets <sup>b</sup>	10	98.35	1.06
Cetiriz syrup <sup>b</sup>	1	97.64	0.95
Zyncet tablets <sup>c</sup>	10	102.14	0.72
Zyncet suspension <sup>c</sup>	1	96.58	0.64
Cetirizet-D tablets <sup>d</sup>	10	98.42	0.26
Alerid tablets <sup>e</sup>	10	97.95	0.52
Alerid syrup <sup>e</sup>	1	98.12	0.75
Zyrtec tablets <sup>f</sup>	10	101.54	0.68
Zirtin tablets <sup>g</sup>	10	98.73	1.26

\* Marketed by: a, Glaxo Lab; b, Alchem; c, Unichem; d, Sun Pharmaceuticals; e, Cipla; f, UNI-UCB; g, Torrent Pharmaceuticals.

ing times of 0.5–5 min produced a constant absorbance, and hence a shaking time of 1 min was used throughout. Only one extraction was adequate to achieve a quantitative recovery of the complex. Absorbances of the separated extracts were stable for more than 24 h. The drug-dye ratio as evaluated from the slope-ratio method was 1:2.

### 3.2. Quantification

A linear correlation was found between absorbance and concentration of CTZH in the range 2–22  $\mu\text{g ml}^{-1}$ . The equation for one representative calibration curve is:

$A_{440} = (0.0115 + (0.035)C)$ , where  $A$  and  $C$  correspond to absorbance and CTZH concentration in  $\mu\text{g ml}^{-1}$ , respectively. The correlation coefficient,  $r = 0.9995$  ( $n = 8$ ), indicates excellent linearity. The molar absorptivity coefficient was  $1.60 \times 10^4 \text{ l mol}^{-1} \text{ cm}^{-1}$ , and Sandell sensitivity was  $0.3019 \text{ ng cm}^{-2}$ . The method has a detection limit of  $0.1328 \mu\text{g ml}^{-1}$ .

The precision of the proposed method was excellent as indicated from the relative standard deviation (S.D. < 1%) calculated from eight replicate analysis of  $10 \mu\text{g ml}^{-1}$  of pure CTZH.

### 3.3. Application

The applicability of the method to the assay of dosage forms was examined by analysing tablets,

syrups and suspension marketed under different trade names. Table 1 shows the quantities obtained by the proposed method and labelled amount. The relative S.D.s are lower than 1% indicating good precision and the independence of the matrix effect over the absorbance. The method is simple and inexpensive as compared to the currently available methods [4–9] which are tedious and involve expensive experimental set-up which ordinary laboratories cannot afford.

### Acknowledgements

The authors thank M/s UNI-UCB Ltd., Mumbai, India, for gifting pure sample of ceterizine hydrochloride.

### References

- [1] E. Balter, J. de Lannoy, R.L. Rodriguez, Eur. Pat. Appl. EP 58146 A, Aug 18, 1982.
- [2] J.P. Rihoux, C. De Vos, E. Balter, J. de Lannoy, Ann. Allergy 55 (1985) 392.
- [3] C. De Vos, M.R. Malleux, E. Balter, J. Gobert, Ann. Allergy 55 (1985) 396.
- [4] B. Eugene, C. Rene, B. Leon, G. Jean, J. Chromatogr. 430 (1988) 149.
- [5] E. Balter, R. Coupez, L. Browsers, J. Gobert, J. Chromatogr. 430 (1988) 74.
- [6] M.T. Rossel, R.A. Lefebvere, J. Chromatogr. 561 (1991) 504.
- [7] J. Moncrieff, J. Chromatogr. 583 (1992) 128.

- [8] M.V. Suryanarayana, B.P. Reddy, G.L.D. Krupadanam, S. Venkataraman, C.S.P. Sastry, *Indian Drugs* 29 (1992) 605.
- [9] A.F.M. El Walily, M.A. Korany, A. El Gindy, M.F. Bedair, *J. Pharm. Biomed. Anal.* 17 (1998) 435.
- [10] C.S.P. Sastri, K. Rama Rao, D. Siva Prasad, *Talanta* 42 (1995) 311.
- [11] J.C. Botello, G. Perez-Caballero, *Talanta* 42 (1995) 105.
- [12] K. Basavaiah, G. Krishnamurthy, *Talanta* 46 (1998) 665.
- [13] O.H. Abdelmageed, P.Y. Khashava, *Talanta* 40 (1993) 1289.
- [14] Tadao Sakai, Noriko Ohno, *Talanta* 33 (1986) 415.

# Flow injection kinetic spectrophotometric determination of ascorbic acid based on an inhibiting effect

Jing Fan \*, Cunling Ye, Suling Feng, Guien Zhang, Jianji Wang

*Department of Chemistry, Henan Normal University, Xixiang, Henan 453002, People's Republic of China*

Received 3 December 1998; received in revised form 2 June 1999; accepted 3 June 1999

## Abstract

A rapid and sensitive flow-injection kinetic spectrophotometric method is proposed for the determination of ascorbic acid. The procedure is based on the inhibiting effect of ascorbic acid on the enhancing effect of oxalate on the potassium dichromate-potassium iodide/rhodamine 6G system. The detection limit and linear ranges are 0.08 and 0.10–4.00  $\mu\text{g/ml}$ , respectively. The relative standard deviation of 11 replicate measurements is less than 2.0%. This method has been successfully used to determine ascorbic acid in pharmaceuticals, tomatoes and oranges. © 1999 Elsevier Science B.V. All rights reserved.

*Keywords:* Flow injection; Kinetic spectrophotometric method; Ascorbic acid; Rhodamine 6G

## 1. Introduction

Ascorbic acid (Vitamin C) is an essential vitamin and participates in many different biological processes. It occurs naturally in most fruit juices and vegetables. The content of Vitamin C in vegetables and fruits is a maturity index and its determination in such samples is of special interest in quality control. Therefore, numerous methods have been established for the determination of ascorbic acid based on its reducing property. These methods have been recently reviewed [1,2].

Flow injection analysis (FIA) has been applied to the determination of ascorbic acid with detec-

tion techniques such as spectrophotometry [3–10], amperometry [11–13], potentiometry [14], coulometry [15], spectrofluorimetry [16] and chemiluminescence [17,18]. The big advantage of FIA is a short analysis time and a reduced human participation in operations. The kinetic spectrophotometric method is one of the most attractive approaches for trace determination of some species because of its high sensitivity. Therefore, flow-injection kinetic spectrophotometric analysis combines the advantages of both FIA and kinetic spectrophotometric analysis. However, few investigations have been reported for the flow-injection kinetic spectrophotometric determination of ascorbic acid [5,6,9,10]. To the best of our knowledge, no inhibitory system has been reported for the kinetic spectrophotometric determination of this analyte.

\* Corresponding author. Fax: +86-373-3383145.  
E-mail address: wjjly@public.zz.ha.cn (J. Fan)



In this work, a new flow-injection kinetic spectrophotometric method is developed for the determination of ascorbic acid. The procedure is based on the inhibiting effect of ascorbic acid on the enhancing effect of oxalate on the potassium dichromate-potassium iodide/rhodamine 6G system. A controlled and weighted centroid simplex method has been used to optimize the operating conditions. The suggested method is rapid and sensitive. It has been applied for the determination of ascorbic acid in pharmaceuticals, tomatoes and oranges with satisfactory results.

## 2. Experimental

### 2.1. Apparatus

A schematic diagram of the flow-injection system used is outlined in Fig. 1. The manifold consisted of 0.7 mm i.d. polytetrafluoroethylene (PTFE) tubing which was cut to the required lengths and wound around a 15-mm o.d. glass tube. The following equipment also formed part of the flow-injection analysis system: a six-channel peristaltic pump (Shanghai Instrument Factory) fitted with Tygon pump tubing was used for propulsion of fluids; sample solutions were introduced into the flow-line by a valve fitted with a by-pass coil; a spectrophotometer (Model 722, Shanghai No.3 Analytical Instrument Factory)

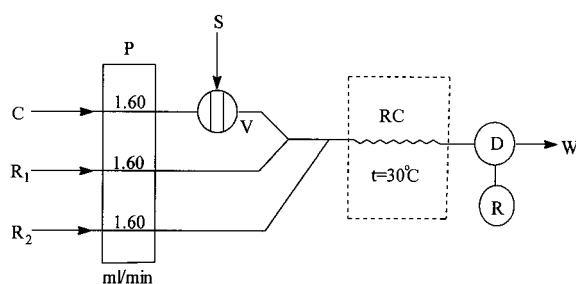


Fig. 1. Manifold used for the determination of ascorbic acid. C, water carrier; D, spectrophotometric cell; P, peristaltic pump; R, recorder; R<sub>1</sub>, rhodamine 6G solution; R<sub>2</sub>, a mixed solution of potassium dichromate and sulfuric acid; RC, reaction coil in a water bath at 30°C; S, sample or standard solutions (potassium iodide + sodium oxalate + ascorbic acid); V, injection valve; W, waster.

with a 10-mm flow-through cell was used as the detector; the signal output of the detector was recorded with a recorder (XWT-204, Shanghai Dahua Instrument Factory); the reaction coil was immersed in a circulating thermostated bath (Model 501, Chongqing Instrument Factory).

### 2.2. Reagents

All reagents were of analytical or guaranteed grade, and all solutions were prepared using distilled-deionized water.

Ascorbic acid stock solution (1.0 mg/ml) was prepared freshly before measurement by dissolving 0.1000 g of ascorbic acid in 100 ml of water. The stock solution must be stored in a refrigerator when not used. Working solutions were prepared by suitable dilution. Oxalate stock solution ( $1.14 \times 10^{-3}$  mol/l) was prepared by dissolving 0.1532 g of sodium oxalate in 100 ml of water. Rhodamine 6G stock solution ( $1.0 \times 10^{-3}$  mol/l) was prepared by dissolving 0.1194 g of rhodamine 6G into 250 ml of water. Solutions of lower concentration were prepared by dilution of the stock solution with water. Dichromate stock solution ( $2.0 \times 10^{-2}$  mol/l) was prepared by dissolving 0.5884 g of potassium dichromate in 100 ml of water. Potassium iodide solution (0.5 mol/l) was prepared by dissolving 8.3 g of potassium iodide in 100 ml of water. Sulfuric acid solution, 1.0 mol/l.

### 2.3. Treatment of samples

#### 2.3.1. Vitamin C tablets

Several tablets of vitamin C drug were accurately weighed, ground and powdered. An amount of this powder equivalent to about 50 mg of ascorbic acid was transferred into a 100-ml volumetric flask. Water was added up to the mark. The content of the flask was shaken for about 5 min. Then it was filtered and the first portion of the filtrate was rejected. This solution was further diluted with water to adjust the concentration to meet the requirement of the experimental conditions adopted.

### 2.3.2. Vitamin C injection

A known volume of vitamin C injection equivalent to about 50 mg of ascorbic acid was transferred into a 100-ml volumetric flask. Water was added up to the mark and the mixture was well mixed. This solution was further diluted for determination.

### 2.3.3. Tomatoes and oranges

Tomatoes and oranges were squeezed, respectively. The juice obtained was diluted quantitatively with water for determination.

## 2.4. Manifold and procedure

Fig. 1 shows the FIA system used to implement the method. Carrier solution (water), rhodamine 6G solution and a mixed solution of potassium dichromate and sulfuric acid, are each pumped into the analytical lines at the same flow rate. The sample solution, premixed with potassium iodide and sodium oxalate solutions, was introduced into the carrier stream by a loop-valve injector when the absorbance of rhodamine 6G was maximum and stable, and then merged with the reagent solutions. The reaction takes place in a reaction coil immersed in the thermostated bath at  $30.0 \pm 0.1^\circ\text{C}$ . The absorbance ( $A$ ) at 528 nm was monitored and the peak height measured. At least three injections were made for every sample solution. A blank containing no ascorbic acid was treated in the same way as the sample, and used to obtain the absorbance ( $A_0$ ) and the corresponding peak height. Concentration of the analyte can be found from the calibration curves of  $\Delta A$  ( $= A - A_0$ ) versus ascorbic acid concentration obtained from standards under the same working conditions.

A calibration curve was obtained by injecting 0.00, 0.10, 0.50, 1.00, 2.00, 3.00, 4.00  $\mu\text{g/ml}$  ascorbic acid standard solutions. These standard solutions were prepared by adding 1.25 ml of 0.5 mol/l potassium iodide and 3.2 ml of  $1.14 \times 10^{-3}$  mol/l sodium oxalate solution into 25 ml flasks, and diluting to the mark with water. Three injections were also made for the standard solutions.

## 3. Results and discussion

Rhodamine 6G is one of the triphenylmethane dyes. It was widely used in analytical chemistry. For example, it has been used as an indicator in titration analysis and a chelating agent in the extraction-spectrophotometric and extract-spectrofluorimetric determinations of metal ions and non-metal ions.

It is observed in the experiment that the reaction between potassium dichromate and potassium iodide was accelerated by oxalate; the reaction product ( $\text{I}_2$ ) reacts with rhodamine 6G to form a colorless compound. The reaction rate of this system can be inhibited by ascorbic acid. In other words, a maximum peak (negative peak) was obtained in the absence of ascorbic acid. The presence of ascorbic acid caused a decrease in the analytical signal. This difference in absorbance intensity of rhodamine 6G is proportional to the ascorbic acid concentration. Based on this fact, a new flow-injection kinetic spectrophotometric method is proposed for the determination of ascorbic acid, although the detailed reaction mechanism is not clear. The kinetic curves [19] of ascorbic acid reaction at different concentrations are displayed in Fig. 2.

### 3.1. Optimization of variables

Flow-injection and chemical variables were optimized for the proposed flow-injection method. This was carried out by the controlled and weighted centroid simplex method [20]. The optimum flow-injection and chemical variables chosen were those that yielded the maximum absorbance difference ( $\Delta A$ ) between the blank and the sample.

#### 3.1.1. Simplex optimization of variables

A univariate method was conducted over a wide range of values for each factor. The experimental factors include the best dose of different reagents, temperature and physical parameters of FIA.

On the basis of the results of the univariate, the controlled and weighted centroid simplex method [20] was used to achieve the maximum absorbance

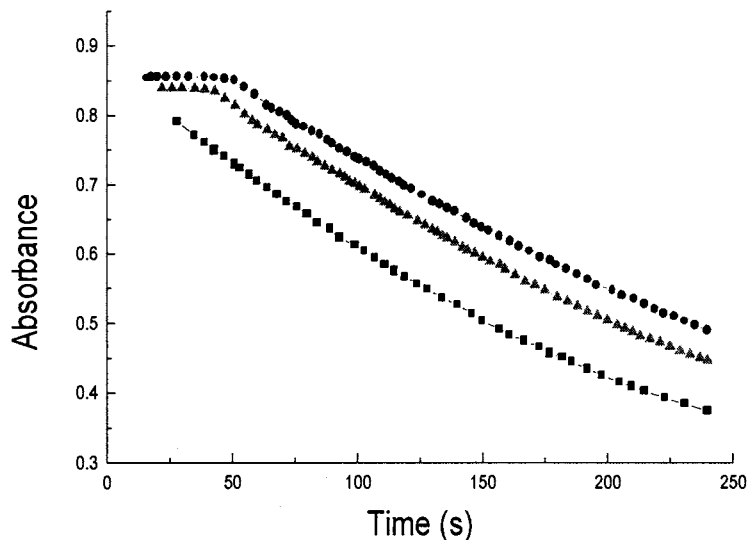


Fig. 2. Progress curves when ascorbic acid is at concentrations of: ---■---, 0 µg/ml; ---▲---, 1 µg/ml; and ---●---2 µg/ml.

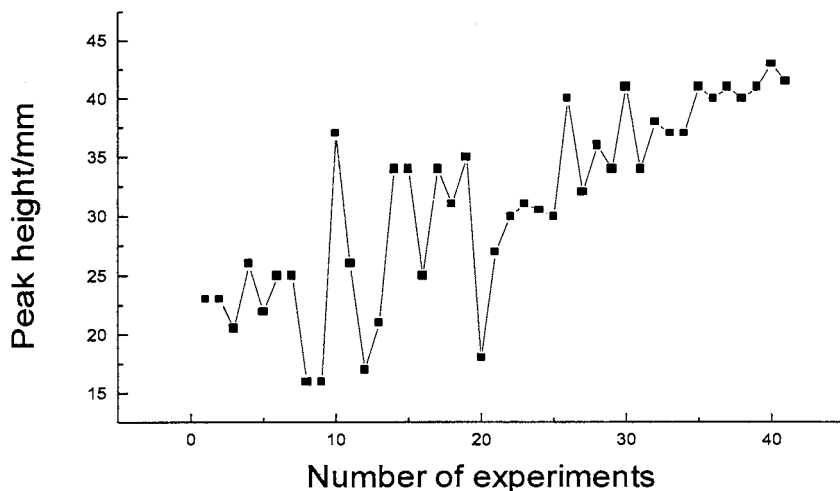


Fig. 3. Response function progress of the simplex.

difference. The factors chosen each affect the absorbance of the system. The simplex was halted after 41 vertexes. The progress of the simplex is shown in Fig. 3, indicating a gradual improvement in peak height. The centroid (the mean of ten retention points) was taken as the optimum operating conditions. Table 1 lists the optimal values obtained for each of the nine factors investigated.

### 3.1.2. Choice of medium

The following media have been tried in the proposed experiments: sulfuric acid, phosphoric acid, hydrochloric acid, potassium hydrogen phthalate-hydrochloric acid and Britton–Robinson buffer solutions. It was found that the sensitivity of reaction is very low in phosphoric acid, potassium hydrogen phthalate-hydrochloric acid and Britton–Robinson buffer solutions; and the

inhibiting effect of ascorbic acid is strong in sulfuric acid and hydrochloric acid solutions. But the sensitivity is higher and the reproducibility is bet-

ter only in sulfuric acid solution. Therefore, sulfuric acid was selected as the best reaction medium.

Table 1

Optimal conditions for the determination of ascorbic acid obtained by the controlled and weighted centroid simplex method

Operating parameters	Simplex optimum
Coil length (cm)	100
Sample volume ( $\mu\text{l}$ )	193
Flow rate (ml/min)	1.60
$\text{H}_2\text{SO}_4$ (mol/l)	$4.1 \times 10^{-2}$
Rhodamine 6G (mol/l)	$5.4 \times 10^{-5}$
$\text{K}_2\text{Cr}_2\text{O}_7$ (mol/l)	$9.9 \times 10^{-4}$
KI (mol/l)	$2.5 \times 10^{-2}$
$\text{C}_2\text{O}_4^{2-}$ (mol/l)	$1.45 \times 10^{-4}$
Temperature ( $^\circ\text{C}$ )	30.0

Table 2

Comparison of the methods of flow-injection kinetic spectrophotometric analysis for ascorbic acid

Reference	Beer's law range	Sampling frequency (per hour)
[5]	10.6–29.9 mg/ml	36
[6]	100–400 $\mu\text{g/ml}$	100
[9]	17.6–1761 $\mu\text{g/ml}$	60
[10]	0.02–0.09 $\mu\text{g/ml}$	—
This work	0.10–4.00 $\mu\text{g/ml}$	100

Table 3

Influence of foreign ions

Ion added	Ratio (ion/ascorbic acid)
$\text{Br}^-$ , $\text{Cl}^-$ , $\text{K}^+$ , $\text{NO}_3^-$ , Urea	400–600
Vitamin B <sub>1</sub> , Vitamin B <sub>6</sub> , $\text{Na}^+$ , Citric acid	100–200
$\text{ClO}_3^-$ , $\text{SO}_4^{2-}$ , $\text{PO}_4^{3-}$	70
$\text{F}^-$ , Glucose, $\text{Mg}^{2+}$	40
$\text{CH}_3\text{COO}^-$ , Glycine, Fructose, Sodium bitartrate	20
$\text{Ni}^{2+}$ , Starch, $\text{Mn}^{2+}$	10
Vitamin B <sub>12</sub> , $\text{Ca}^{2+}$ , $\text{Cd}^{2+}$ , $\text{Pb}^{2+}$	2
$\text{NO}_2^-$	1

### 3.2. Features of the method

A series of standard solutions were injected into the manifold under the optimized conditions to test the linearity of the calibration graph. A linear relationship between  $\Delta A$  and ascorbic acid concentration was obtained in the range of 0.10–4.00  $\mu\text{g/ml}$ . The calibration equation obtained by the least-squares method is given by:

$$\Delta A = 0.0124 + 0.0746C \quad (r = 0.9979, n = 6)$$

Where  $C$  is the concentration of ascorbic acid in  $\mu\text{g/ml}$  and  $r$  is the linear correlation coefficient. The detection limit was 0.08  $\mu\text{g/ml}$ . The relative standard deviations of 0.50 and 3.00  $\mu\text{g/ml}$  ascorbic acid solutions were 2.0% ( $n = 11$ ) and 1.2% ( $n = 11$ ), respectively. The analysis can be performed at a rate of 100/h.

A comparison of the proposed method with the flow-injection kinetic spectrophotometric analysis methods for Vitamin C reported in the literature [5,6,9,10] is shown in Table 2. Obviously, the suggested method in this work has higher sensitivity and sampling frequency.

### 3.3. Effect of foreign ions

The effects of foreign ions on the determination of 2.00  $\mu\text{g/ml}$  ascorbic acid were investigated. When the permitted relative deviation from  $\Delta A$  is less than  $\pm 5\%$ , the interferences are listed in Table 3.

### 3.4. Applications to real samples

The proposed method was applied to the determination of ascorbic acid concentrations in Vitamin C tablet, Vitamin C injection, tomatoes and oranges by using the procedure described in the experimental section. The results were statistically compared with those obtained by iodimetry [21] in Table 4. It is evident from the calculated  $t$ -test values that our results for ascorbic acid in Vitamin C tablet, Vitamin C injection, tomatoes and oranges were in good agreement with those ob-

Table 4

Comparison of ascorbic acid concentrations determined by the proposed FIA and by iodimetry

Sample	Iodimetry <sup>a</sup>	Proposed method <sup>b</sup>	<i>t</i> <sup>c</sup>
Tablet (mg/tablet)	97.7 ± 0.3	97.1 ± 0.6	2.24
Injection (mg/ml)	192.2 ± 0.3	191.9 ± 0.5	1.34
Tomato (mg/100 ml)	25.1 ± 0.4	24.9 ± 0.3	1.49
Orange (mg/100 ml)	39.9 ± 0.5	39.6 ± 0.4	1.68

<sup>a</sup> Average of three determinations.

<sup>b</sup> Mean ± standard deviation of five determinations.

<sup>c</sup> Theoretical value = 2.78, *n* = 5 with 95% confidence limits.

tained by iodimetry. This confirms the validity of the method proposed in this work.

#### 4. Conclusions

A new reaction system for the flow-injection kinetic spectrophotometric determination of ascorbic acid was suggested. The main features of the proposed method are rapid, simple and sensitive. These facts encourage the application of this method in routine analysis of ascorbic acid in pharmaceuticals, vegetables and fruits.

#### References

- [1] P.W. Washko, R.W. Welch, K.R. Dhariwal, Y. Wang, M. Levine, *Anal. Biochem.* 204 (1992) 1.
- [2] S.M. Sultan, E. Bishop, *J. Pharm. Biomed. Anal.* 8 (1990) 345.
- [3] J.M. Alamo, A. Maquieira, R. Puchades, S. Sagrado, *Fresenius' J. Anal. Chem.* 347 (1993) 293.
- [4] T. Yamane, T. Ogawa, *Bunseki Kagaku* 36 (1987) 625.
- [5] S.M. Sultan, *Talanta* 40 (1993) 593.
- [6] S.M. Sultan, A.M. Abdennabi, F.E.O. Suliman, *Talanta* 41 (1994) 125.
- [7] F. Lazaro, A. Rios, M.D. Luque de Castro, M. Valcarcel, *Analyst* 111 (1986) 163.
- [8] J.A. Nobrega, G.S. Lopes, *Talanta* 43 (1996) 971.
- [9] M.A. Koupparis, P. Anagnostopoulou, H.V. Malmstadt, *Talanta* 32 (1985) 411.
- [10] M. Tabata, H. Morita, *Talanta* 44 (1997) 151.
- [11] L.E. Leon, *Talanta* 43 (1996) 1275.
- [12] A. Strohl, D. Curran, *Anal. Chem.* 51 (1979) 1045.
- [13] G.M. Greenway, P. Ongomo, *Analyst* 115 (1990) 1297.
- [14] B. Karlberg, S. Thelander, *Analyst* 103 (1978) 1154.
- [15] D.J. Curran, T. Tougas, *Anal. Chem.* 56 (1984) 672.
- [16] H. Huang, R. Cai, Y. Du, Y. Zeng, *Anal. Chim. Acta* 309 (1995) 271.
- [17] A.A. Alwarthan, *Analyst* 118 (1993) 639.
- [18] T. Perez-Ruiz, C. Martinez-Lozano, A. Sanz, *Anal. Chim. Acta* 308 (1995) 299.
- [19] M. Zhu, X. Hung, J. Li, H. Shen, *Anal. Chim. Acta* 357 (1997) 261.
- [20] G. Zhang, D. Cheng, S. Feng, *Talanta* 40 (1993) 1041.
- [21] M.Z. Barakat, S.K. Shehab, N. Darnish, A. El-Zoheivy, *Anal. Biochem.* 53 (1973) 245.

# Flow injection spectrophotometric determination of reducing sugars using a focalized coiled reactor in a domestic microwave oven

André Fernando Oliveira, Orlando Fatibello-Filho \*

*Grupo de Química Analítica, Departamento de Química, Centro de Ciências Exatas e de Tecnologia, Universidade Federal de São Carlos, Caixa Postal 676, CEP 13560-970 São Carlos, SP, Brazil*

Received 4 December 1998; received in revised form 2 June 1999; accepted 3 June 1999

## Abstract

A flow injection (FI) spectrophotometric procedure for determining reducing sugars content in sugar cane juices using a focalized PTFE coiled reactor positioned at the output antenna of a domestic microwave oven at 700 W is proposed. In this system, sample solution converge to  $1.0 \text{ mol l}^{-1}$  NaOH and  $5.2 \text{ mmol l}^{-1}$   $\text{K}_3\text{Fe}(\text{CN})_6$  solutions previously mixed and the decrease of hexacyanoferrate(III) concentration was monitored at 420 nm. Under best analytical conditions, there was a direct relationship between absorbance decrease and reducing sugar content (fructose plus glucose concentrations) in the concentration range from 50 to  $1200 \text{ } \mu\text{mol l}^{-1}$  with a detection limit of  $15 \text{ } \mu\text{mol l}^{-1}$ . The relative standard deviations (rds) were less than 1.4% for ten injection of 400 and  $800 \text{ } \mu\text{mol l}^{-1}$  fructose solution and the analytical frequency was  $70 \text{ h}^{-1}$ . A paired *t*-test showed that all results obtained for sugar cane juices using this FI procedure and the Somogyi–Nelson batch procedure agree at the 95% confidence level. © 1999 Elsevier Science B.V. All rights reserved.

*Keywords:* Flow injection spectrophotometric; Reducing sugars; Coiled reactor; Domestic microwave oven

## 1. Introduction

The frequent determination of reducing sugars content (glucose plus fructose concentrations) in raw material, final products and during the fermentation in industrial bioprocess, such as wine, hydrated alcohol, penicilins production is very important [1–3].

Several analytical procedures using chemical oxidation of reducing sugar have been proposed in the literature [4,5]. However, these procedures need a time consuming heating step, before the reducing sugars content determination. Several flow injection procedures for determining reducing sugars content have been employing a hot water batch [6–10].

Microwave ovens have been largely used as an energy source in the mineralization of samples for metals, Kjeldahl nitrogen, COD and total phos-

\* Corresponding author. Fax: +55-16-2608350.

E-mail address: bello@dq.ufscar.br (O. Fatibello-Filho)

phorus determinations [11–14]. Flow injection systems using microwave ovens have been also proposed for the determination of several substances and the distribution of radiation in the oven cavity has been studied only on its floor, or simply, the coil was centered inside the microwave oven cavity [15–17].

In this work, a fast and efficient heating of the reaction medium was obtained by positioning strategically a flow-coiled reactor at the output antenna of a domestic microwave oven. With this heating form, a flow injection system with a microwave oven coupled is proposed to reducing sugars content determination by decolorization of hexacyanoferrate(III) in alkaline medium, without the need of the employment of colorimeters compound to improved the procedure sensitivity, such as ferroin or prussian blue formations [8].

## 2. Experimental

### 2.1. Apparatus

The flow injection manifold is shown in Fig. 1. An eight-channel Ismatec (Zurich, Switzerland)

Model 7618-40 peristaltic pump supplied with Tygon pump tubing was used for the propulsion of fluids. All flow tubes used inside the microwave oven cavity were 0.8-mm i.d. PTFE. Spectrophotometric measurements were carried in a Micronal (São Paulo, Brazil) Model B342II spectrophotometer with a Hellma flow-through cell (optical path 1.0 cm) at 420 nm coupled to a Cole Parmer (Nile, IL, USA) Model 12020000 two channel strip-channel recorder. Sample and reagents were inserted into the carrier stream using a Micronal (São Paulo, Brazil) Model B352 automatic proportional-comutator.

A Panasonic (Manaus, Brazil) Model Junior domestic microwave oven equipped with a magnetron of 700 W at 2.45 GHz was used. PTFE coiled reactor was used strategically positioned onto the output antenna localized in one wall of the oven cavity, allowing thus a focused microwave radiation. The turning plate and its motor were removed to allow the passage of tubings for the circulation of tap water at a flow rate of *c.* 500 ml min<sup>-1</sup> in two 500 ml glass closed vessels (CV<sub>1</sub> and CV<sub>2</sub>) attained in series. The aim of the use these vessels, was for attenuation of radiation excess not absorbed by fluids in the coiled reactor, i.e. a dummy load.

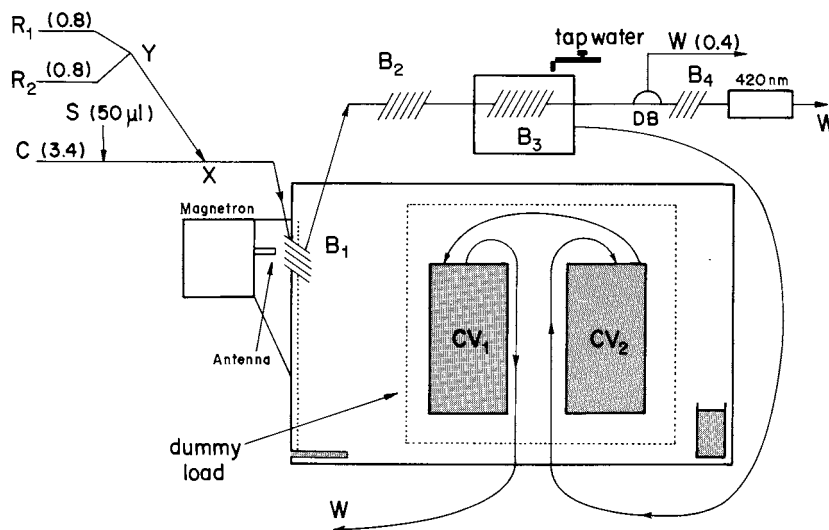


Fig. 1. Schematic manifold FI system for spectrophotometric determination of reducing sugar contents determination. B<sub>1</sub>–B<sub>4</sub> indicates 100, 200, 150 and 25 cm coil lengths, respectively; C, water carrier (3.4 ml min<sup>-1</sup>); CV<sub>1</sub> and CV<sub>2</sub>, 500 ml glass closed vessels supplied with tap water at flow rate of *c.* 450 ml min<sup>-1</sup>; D, detector, DB, debubbler; R<sub>1</sub>, 5.2 mmol l<sup>-1</sup> hexacyanoferrate(III) solution (0.8 ml min<sup>-1</sup>); R<sub>2</sub>, 1.5 mol l<sup>-1</sup> sodium hydroxide solution (0.8 ml min<sup>-1</sup>); S, sample loop (50 µl); W waste.

## 2.2. Reagents and solutions

All reagents used were of analytical reagent-grade. All solutions were prepared with water from Millipore (Bedford, MA, USA) Model UV Plus Ultra-Low Organics Water Milli-Q System.

Glucose, fructose or sucrose stock sugar solution was prepared by dissolution of sugar from Sigma (St. Louis, MO, USA) in water and the solution was kept at 4°C. The reference solutions were prepared daily from each stock solutions, before use.

The potassium hexacyanoferrate(III) solutions were prepared by dissolution of appropriated mass of  $K_3Fe(CN)_6$  (Riedel) in a 500-ml volumetric flask and diluting to volume with water.

## 2.3. Methods

### 2.3.1. Analysis of sugar cane juice samples

Aliquots of sugar cane juices varying from 0.5 to 2 ml were filtered through four layers of cheese-cloth and diluted with water to 100 ml. Then, a volume of 50  $\mu$ l of diluted sample was rapidly inserted in the flow injection system.

### 2.3.2. Reference methods

In order to compare the results obtained by flow injection (FI) procedure, the Somogyi–Nelson batch procedure used in the Brazilian alcohol industry [3] was carried out with minor modifications. An aliquot of 1.0 ml of diluted sample with 1.0 ml of Somogyi reagent was heated in a boiling water bath for 2 min. This solution was quickly cooled, and 1.0 ml of Nelson reagent and 7.0 ml of water were then added. After 15 min, the absorbance of the colored solution was measured at 720 nm.

### 2.4. Study of radiation distribution in microwave oven cavity

The distribution of radiation in the oven cavity was realized similarly to a literature procedure [18], but in three different heights (bottom, middle and top of oven cavity). On a Perspex plate, 16 plastic flasks containing 10 g of water were introduced simultaneously into the oven cavity and heated for 2 h in 20% of total power to avoid the

water boiling. The relative mass loss in each position was then calculated. This same procedure was repeated in triplicate in other two heights.

## 2.5. Flow injection procedure

Fig. 1 shows the FI system used. Milli-Q water at a flow rate of 3.4 ml min<sup>-1</sup> was used as carrier. A sample solution contained in the sample loop (50  $\mu$ l) was transported by the carrier. At point X, R<sub>1</sub> and R<sub>2</sub> solutions (previously mixed at point Y) were introduced so that the reducing sugar oxidation by potassium hexacyanoferrate(III) proceed in the PTFE coiled reactor B<sub>1</sub> (100 cm; 0.8 mm i.d.). As can be seen, the reactor B<sub>1</sub> was placed at the output antenna of microwave oven turn on at maximum power level (700 W) where the stream is heating and partially volatilized. For safety reasons, these PTFE tubes were passed through the walls the microwave oven using the external oven air vents. The oxidized samples passed through a PTFE coil B<sub>2</sub> (200 cm; 0.8 mm i.d.) and then, the vapor was condensed in a PTFE coil B<sub>3</sub> (150 cm; 0.8 mm i.d.) immersed in a 450-ml circulated tap water batch. The remainder bubbles produced by dissolved gases were removed with a T-shaped glass debubbler DB at an aspiration rate of 0.4 ml min<sup>-1</sup>. The residual potassium hexacyanoferrate(III) concentration in the sample zone was measured at 420 nm in a spectrophotometer cell after passing through a coiled reactor B<sub>4</sub> (25 cm; 0.8 mm i.d.). The height of the recorded transient signal was proportional to the reducing sugar content in the sample. To avoid damage in the magnetron two 500-ml closed vessels (CV<sub>1</sub> and CV<sub>2</sub>) were placed inside the microwave oven cavity. These two vessels attained in series were supplied with tap water at a flow rate of *c.* 500 ml min<sup>-1</sup>.

## 3. Results and discussions

### 3.1. Study of radiation distribution in a microwave oven cavity

A proposed schematic profile of radiation for the microwave oven used was present in Fig. 2. As



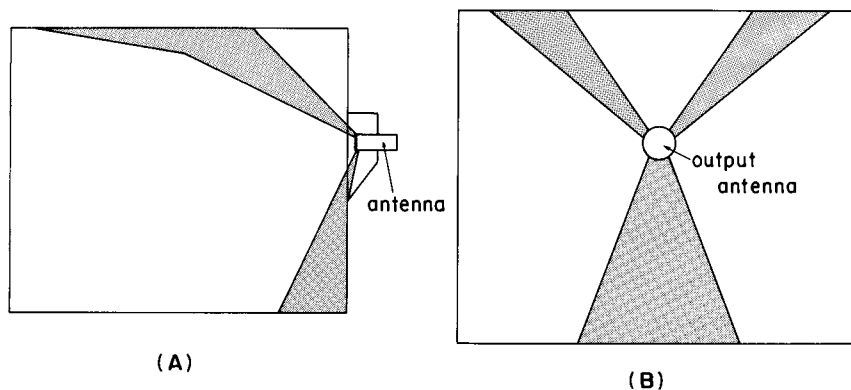


Fig. 2. Profile of microwave radiation emitted by the antenna of magnetron: (A) frontal view; and (B) lateral view of the microwave oven. The shading regions represent the main ways of microwave radiation. This drawing is not to scale.

can be seen in this figure, the point where the microwave energy is more intense was in the output antenna, so the coil  $B_1$  was localized in this point. With the manifold used, the zone sample stayed inside the coil by *c.* 6 s, time enough for boiling NaOH solutions at the concentrations equal to or higher than  $0.1 \text{ mol l}^{-1}$ . This system has a high elevation temperature rate, once a partial volatilization of the carrier was observed after an irradiation time of 4–6 s. This volatilization also increased the total linear velocity owing to the increase of pressure.

The maximum power is chosen, once the relative high oven cycling time of 11 s when the microwave oven is operated in other power levels led to a decrease of the repeatability.

### 3.2. Study of chemical parameters

The oxidation rate of sugar by potassium hexacyanoferrate(III) in FI system depends on the temperature and also on  $\text{K}_3[\text{Fe}(\text{CN})_6]$  and NaOH concentrations. Mattos et al. [8] reported that the glucose peak height was always lower than the fructose peak height at the same concentration when the temperature of water bath was less than  $75^\circ\text{C}$ , emphasizing the differences in the fructose and glucose rates. At temperatures higher than  $90^\circ\text{C}$ , this difference was not relevant when more concentrated reagents ( $2.0 \text{ mol l}^{-1}$  NaOH and  $1\%$  m/v potassium hexacyanoferrate(III)) were used.

In order to attained a high temperature a PTFE coiled reactor ( $B_1$ ) was placed at the output antenna of a domestic microwave oven turned on at the maximum power level (700 W).

The effect of potassium hexacyanoferrate(III) ( $R_1$ ) concentration ranged from  $1.3$  to  $6.4 \text{ mmol l}^{-1}$  on the analytical signal for  $800 \text{ } \mu\text{mol l}^{-1}$  fructose solution and  $1.5 \text{ mol l}^{-1}$  NaOH solution was initially evaluated using the FI manifold presented in Fig. 1. The absorbance increased with increasing  $\text{K}_3[\text{Fe}(\text{CN})_6]$  solution concentration, but the  $5.2 \text{ mmol l}^{-1}$  potassium hexacyanoferrate(III) concentration was selected as the maximum baseline absorbance, once in this procedure a decolorimetric reaction was exploited.

The increase of NaOH concentration ( $R_2$  reagent) can increase both the fructose and glucose oxidation rates and the absorption of microwave radiation. Thus, the effect of NaOH concentration in the concentration range from  $0.5$  to  $1.5 \text{ mol l}^{-1}$  for  $5.2 \text{ mmol l}^{-1}$  potassium hexacyanoferrate(III) and  $800 \text{ } \mu\text{mol l}^{-1}$  fructose and  $800 \text{ } \mu\text{mol l}^{-1}$  glucose solutions were studied, respectively. As can be seen in Fig. 3, the variation of absorbance ( $\Delta A$ ) for fructose and glucose increase with the increase of NaOH concentration and reached a similar value at a NaOH concentration equal to or higher than  $1.1 \text{ mol l}^{-1}$ . As discussed before, a similar sensitivity to both analytes is necessary, aiming to obtain an accurate reducing sugar content that represents the sum of

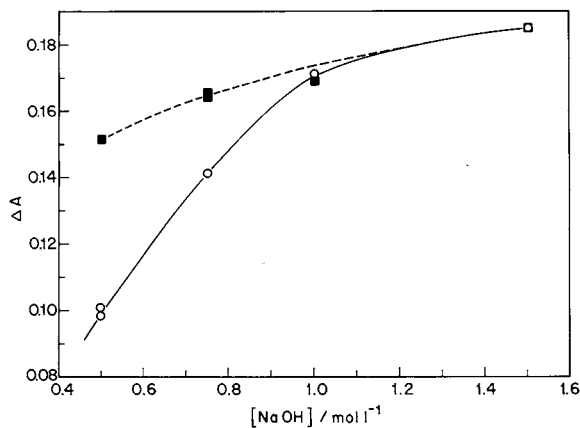


Fig. 3. Effect of the NaOH concentration on the oxidation of ○○○: glucose and ■■■ fructose using  $5.2 \text{ mmol l}^{-1}$  potassium hexacyanoferrate(III) and  $800 \text{ } \mu\text{mol l}^{-1}$  of each sugar.

these analyte concentrations. Sodium hydroxide concentration higher than  $1.8 \text{ mol l}^{-1}$  cannot be used due to the higher back-pressure that arises in the FI system. Thus, a  $1.5\text{-mol l}^{-1}$  NaOH solution was used in further experiments.

### 3.3. System characteristics and applications

In the study of repeatability (Fig. 4), the relative standard deviations were less than 1.4% for at least eleven  $50\text{-}\mu\text{l}$  insertions of  $400$  and  $800 \text{ } \mu\text{mol l}^{-1}$

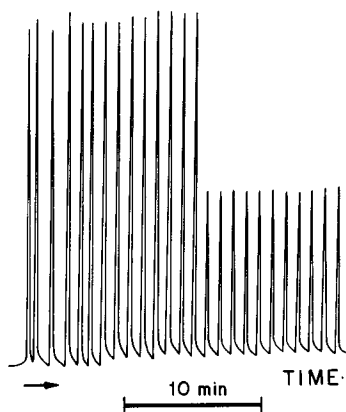


Fig. 4. Repeatability of the FI system. A,  $800$  and B,  $400 \text{ } \mu\text{mol l}^{-1}$  fructose solutions. The direction of measurements in from left to right and the experimental conditions were the same of Fig. 1

$1^{-1}$  fructose solutions. Recoveries varying from 97.5 to 102.1% fructose from three sugar cane juices ( $n = 6$ ) were obtained using the FI spectrophotometric procedure under experimental conditions of Fig. 1. In this study,  $100$ ,  $200$  and  $500 \text{ } \mu\text{mol l}^{-1}$  fructose were added to each sample. This is a good evidence of absence of matrix effects.

Several potential interferents such as sucrose, polysaccharides and inorganic salts were evaluated at concentration levels equal to or higher than that normally found in sugar cane juices. In this study,  $400 \text{ } \mu\text{mol l}^{-1}$  fructose containing  $100 \text{ mmol l}^{-1}$  sucrose, 1% m/v starch (in the place of polysaccharides) and  $1.0 \text{ mol l}^{-1}$  NaCl (in the place of the electrolytes) solutions, respectively, were inserted in the FI system and no interference was observed.

Triplicate signals for five reference fructose solutions and quadruplicate signals for four sugar cane juice sample solutions demonstrate good precision and baseline stability (Fig. 5). Under the experimental conditions shown in Fig. 1, there was a direct relationship between absorbance decrease and reducing sugars concentration (fructose) in the concentration range from  $50$  to  $1200 \text{ } \mu\text{mol l}^{-1}$  with a detection limit of  $15 \text{ } \mu\text{mol l}^{-1}$  and an analytical frequency of  $70 \text{ h}^{-1}$ . Table 1 presents the results obtained using the Somogyi–Nelson [3] and the proposed FI procedures. Applying *t*-test to the results obtained by either procedure, it was found that all results were in agreement at the 95% confidence level. Due the high sensitivity of this FI procedure, very little sugar cane juice volume was used in the reducing sugar determination without the need of removing the previous color and/or sample treatment. Moreover, the manifold of the proposed FI procedure is much more sensitive and simple than those described earlier [7–9] and/or does need the use of colorimeters compound to improve the procedure sensitivity [7–9] and thermostatic bath with temperatures varying from  $50$  to  $95^\circ\text{C}$ . Also, the procedure presented here is precise, inexpensive and rapid and it may be suitable for routine analysis.

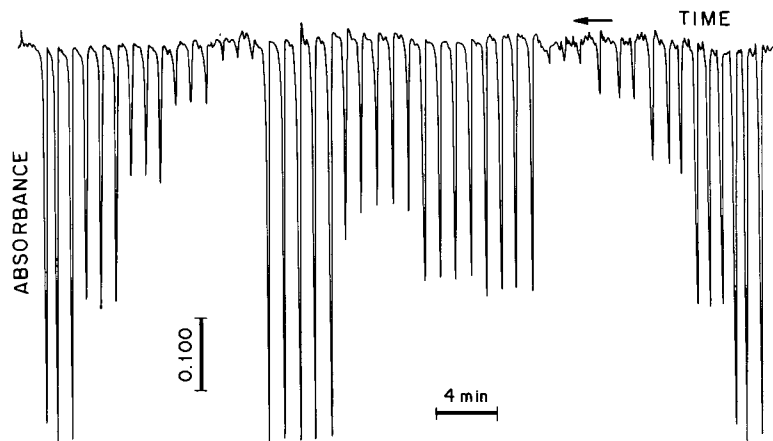


Fig. 5. Triplicate transient signals for five reference fructose solutions and quadruplicate transient signals for four sugar cane juice samples solutions (A, B, C and D) and reference solutions again.

Table 1

Determination of reducing sugars content in sugar cane juice samples using Somogyi–Nelson [4] and the proposed FI spectrophotometric procedures ( $n = 4$  or  $5$ , 95% confidence level)

Sample	Reducing sugar/% m/v		
	Somogyi –Nelson	FI proposed	Relative error (%)
A	$1.48 \pm 0.02$	$1.42 \pm 0.03$	–4.0
B	$1.32 \pm 0.02$	$1.36 \pm 0.02$	3.0
C	$2.28 \pm 0.04$	$2.27 \pm 0.02$	–0.4
D	$1.04 \pm 0.05$	$1.07 \pm 0.01$	2.9

## References

- [1] R.W. Swartz, in: M.Y. Murray (Ed.), *Penicillins—Comprehensive Biotechnology—The Principles, Applications and Regulations of Biotechnology in Industry, Agriculture and Medicine*, vol. 3, Pergamon, Oxford, 1985, pp. 7–47.
- [2] J.D. Camhi, *Brasil Açucareiro* 34 (1979) 14 (in Portuguese).
- [3] E.A. Zago, H.V. Amorim, L.C. Basso, L.E. Gutierrez, A.J. Oliveira, *Analytical Methods for the Control of Alcohol Production, Fermentec/ESALQ-USP, Piracicaba, 1989* (in Portuguese), p. 51.
- [4] G. Ashwell, in: S.P. Colowick, N.O. Kaplan (Eds.), *Methods in Enzymology*, Academic Press, New York, 1957, pp. 73–105.
- [5] S. Willians (Ed.) *Official Methods of Analysis*, AOAC, 14th ed., Arlington, 1984.
- [6] A. Maqueira, M.D. Luque de Castro, M. Valcárcel, *Analyst* 112 (1987) 1569.
- [7] E.A.G. Zagatto, I.L. Mattos, A.O. Jacintho, *Anal. Chim. Acta* 204 (1988) 259.
- [8] I.L. Mattos, E.A.G. Zagatto, A.O. Jacintho, *Anal. Chim. Acta* 214 (1988) 247.
- [9] J. Michalowski, A. Kojlo, M. Trojanowicz, B. Szostek, E.A.G. Zagatto, *Anal. Chim. Acta* 271 (1993) 239.
- [10] T.I.M.S. Lopes, A.O.S.S. Rangel, J.L.F.C. Lima, M.C.B.S.M. Montenegro, *Anal. Chim. Acta* 308 (1995) 122.
- [11] M. De La Guardia, A. Salvador, J.L. Burguera, M. Burguera, *J. Flow Inject. Anal.* 5 (1988) 121.
- [12] H.M. Kingston, S.J. Haswell (Eds.), *Microwave-Enhanced Chemistry—Fundamentals, Sample Preparation and Applications*, ACS, Washington DC, 1997.
- [13] H.M. Kuss, *J. Fresenius Anal. Chem.* 343 (1992) 788.
- [14] J.L. Burguera, M. Burguera, *J. Anal. At. Spectrom.* 8 (1993) 235.
- [15] A.V. Pereira, C. Aniceto, O. Fatibello-Filho, *Analyst* 123 (1998) 1011.
- [16] R.L. Benson, I.D. McKelvie, B.T. Hart, *Anal. Chim. Acta* 291 (1994) 233.
- [17] V. Karanassios, F.H. Li, B. Liu, E.D. Salin, *J. Anal. At. Spectrom.* 6 (1991) 457.
- [18] A. Morales-Rubio, J. Cerezo, A. Salvador, M. De la Guardia, *Microchem. J.* 47 (1993) 270.

# Solid–liquid extraction of copper from slurried samples using high intensity probe sonication for electrothermal atomic absorption spectrometry

J.L. Capelo, A.V. Filgueiras, I. Lavilla, C. Bendicho \*

*Departamento de Química Analítica y Alimentaria, Facultad de Ciencias (Química), Universidad de Vigo, As Lagoas-Marcosende s/n., 36200 Vigo, Spain*

Received 31 March 1999; received in revised form 2 June 1999; accepted 11 June 1999

## Abstract

A fast and simple method is proposed for determination of copper by electrothermal atomic absorption spectrometry in biological samples. Pulverized solid samples were placed in autosampler cups, slurried in an acidic diluent and subsequently treated by sonication under optimized conditions. Parameters influencing extraction such as sonication time, ultrasound amplitude, acid concentration and particle size were optimized so that quantitative copper recovery could be achieved. Quantitative recoveries for copper in mussel tissue were obtained using a 3 min sonication time, a 60% ultrasound amplitude, a 3% V/V HNO<sub>3</sub> concentration along with a particle size of the solid particles less than 50 µm. Under these extraction conditions, quantitative recovery of copper was also seen to be achieved for several certified reference materials such as BCR 278 mussel tissue, NRCC DORM-2 dogfish muscle and BCR CRM 60 (*Lagarosiphon major*) aquatic plant. The LOD of copper in the biological samples was 0.16 µg g<sup>-1</sup> when a sample mass of 10 mg were slurried in a volume of 1.5 ml. When comparing within- and between-batch precision values no significant differences occurred, hence indicating good homogeneity at the 10 mg mass level. Potential advantages of the method proposed over conventional slurry sampling such as an improved precision, since the representative subsample is the whole mass weighed in the autosampler cup, a decreased build-up of carbonaceous residues inside the graphite tube and the removal of volumetric and sedimentation errors can be anticipated. © 1999 Elsevier Science B.V. All rights reserved.

*Keywords:* Solid–liquid extraction; Ultrasound; Copper determination; Electrothermal-AAS

## 1. Introduction

Slurry sampling has emerged as a reliable technique for trace metal determination by electrothermal atomic absorption spectrometry (ETAAS), being implemented in many laboratories in order to avoid intensive sample pretreat-

\* Corresponding author. Tel.: +34-986-812281; fax: +34-86-812382.

E-mail address: bendicho@uvigo.es (C. Bendicho)

ment (i.e. wet or dry ashing procedures) [1]. Successful slurry analysis requires characterization of a number of variables, e.g. sample homogeneity, slurry mixing, grinding and sieving, addition of stabilizing and wetting agents, slurry diluent and particle size. Application of slurry sampling is not free from some drawbacks. Thus, sedimentation and volumetric errors are reported to be present when a slurry of the finely ground material is used for sampling [2,3]. In spite of the simplicity inherent to the slurry technique, good accuracy and precision are only achieved provided that a homogeneous slurry is maintained during the time required for sample introduction into the atomizer [1].

So far, several workers have observed the extraction of analyte in some extent when developing slurry methods [4–6]. Partial extraction of the analyte into the liquid medium of the slurry provides some advantages in the slurry technique, mainly concerning precision. When quantitative analyte extraction (i.e. solid–liquid extraction) occurs, the representative sub-sample is the whole amount of solid material weighed in the cup, which is much larger than the amount of solid material introduced into the furnace, and the precision should approach to that achieved with a liquid sample.

Miller-Ihly reported quantitative extraction of Cu and Mn in some biological samples such as rice, spinach leaves and bovine liver when using ultrasonic slurry sampling [5,7]. In a few papers addressed to achieving solid–liquid extraction from slurried samples some controversial results arise, quantitative metal recoveries being apparently dependent on both the analyte-to-matrix interaction in the solid and the performance of the ultrasonic processor. For instance, Takuwa et al. [6] found that a Co, Cu and Ni remained partly occluded into the solid particles when using ultrasonic slurry sampling. However, Minami et al. [8] reported quantitative extraction of Cd, Cu, Pb and Mn from several biological samples.

In a previous paper the authors showed that quantitative ultrasound-assisted extraction of Cd from slurried biological samples could be reached provided that a high intensity ultrasonic processor was used along with optimized extraction conditions [9].

In this work, a high intensity ultrasonic processor is employed for extraction of Cu from biological and environmental slurried samples prepared in autosampler cups for the subsequent determination by ETAAS. Variables such as ultrasound amplitude, sonication time, particle size, acid concentration and sample mass are optimized so that complete extraction of Cu can be achieved. Sonochemical extraction of the analyte from slurried samples should be advantageous over slurry sampling since the representative sub-sample is the whole amount of solid material weighed in the cup, the build-up of carbonaceous residues inside the furnace diminishes, and more importantly, there is no need to maintain a homogeneous slurry, hence eliminating this source of variability.

## 2. Experimental

### 2.1. Apparatus

An Unicam Solar 939 atomic absorption spectrometer (Cambridge, UK) was used in combination with an Unicam GF-90 graphite furnace and an Unicam FS 90 autosampler. Pyrolytically coated graphite tubes with pyrolytic platforms were used throughout. The spectrophotometer was equipped with a CCD camera so that sample introduction into the furnace could be monitored. An Unicam hollow cathode lamp of Cu operated at 8 mA and a deuterium background corrector were used. The resonance line at 324.8 nm and 0.5 nm slit width were used. Peak area measurements was used for signal quantitation. The graphite furnace operating conditions are shown in Table 1. A MM-2000 Retsch micro-mill (Haan, Germany) was employed to obtain a ground sample from an unknown mussel tissue. Sieves made of nylon with mesh-sizes of (50  $\mu\text{m}$ , (100  $\mu\text{m}$ , (150  $\mu\text{m}$  and (200  $\mu\text{m}$  were used to study the influence of particle size on recovery. A 100 W, 20 kHz VC-100 Sonics and Materials ultrasonic processor (Danbury, CT, USA) equipped with a 3 mm titanium microtip was used for sonochemical extraction. A 45 ml capacity Parr reactor was used together with a 1000 W domestic microwave oven (Samsung, Korea) for acid digestion of an un-

known mussel tissue sample. Autosampler cups made of polyethylene were used for ultrasonic treatment of slurried samples.

## 2.2. Reagents

All reagents used were of analytical reagent-grade. Ultrapure water of Milli-Q quality (18.3 M $\Omega$ ) was used throughout the work; the stock solution of Cu (1000  $\mu\text{g ml}^{-1}$ ) was obtained by dissolving the appropriate amount of Cu metal (Merck, Darmstadt, Germany) with 65% v/v nitric acid (Merck). Calibration standards were obtained by suitable dilution of the stock solution; magnesium nitrate (Merck) at a 1600  $\mu\text{g ml}^{-1}$  concentration was used as matrix modifier. Diluted nitric acid solutions used as extractants were prepared from the concentrated acid by suitable dilution. The following reference certified materials were employed for validation of the method: BCR 278 mussel tissue BCR 60 (*Lagarosiphon major*) aquatic plant, supplied by the Community Bureau of Reference, and NRCC DORM-2 dogfish muscle supplied by the National Research Council of Canada.

## 2.3. Sample pretreatment

About 50 mussels (*Mytilus edulis*) were collected from the Ria de Vigo (Galician, Spain). Once in the laboratory, samples were homogenized using a mixer and dried for 48 h in an oven at 40°C to constant weight. Then, they were ground in the vibrational agate ball mill for 5 min. The powdered samples were sieved so that

separation in several fractions with different particle size could be achieved. Powdered samples were stored in capped polypropylene flasks at 4°C. CRMs were used as received and no additional grinding was performed.

## 2.4. Sonochemical extraction

Slurries of the different powdered samples were prepared by accurate weighing an amount of the solid material (typically 10–20 mg) in 2 ml capacity autosampler cups and adding 1.5 ml of diluted nitric acid. Slurries were subjected to sonication for a time at a preselected ultrasound amplitude, placed in the autosampler tray and left without further stirring. Experiments showed that sedimentation of the disrupted solid particles was very fast so that centrifugation was unnecessary.

## 2.5. Microwave digestion

Cu concentration in the unknown mussel tissue was determined after microwave digestion. Approximately 100 mg of sample and 4 ml of nitric acid 65% m/m were placed in a PTFE vessel and capped. The vessel was put into a Parr reactor and closed. The reactor was irradiated for 150 s at 400 W. After cooling to ambient temperature, it was opened and 1 ml of 30% m/m hydrogen peroxide was added. The reactor was irradiated again for 60 s at 400 W. After cooling, the resultant solution was transferred into a 10 ml calibrated flask and diluted to volume with ultrapure water.

Table 1  
Thermal program for Cu

	Stage Dry	Dry	Ash	Ash	Atomize*	Clean-up
Temperature (°C)	150	225	300	1300	2500	2800
Ramp	20	15	25	100	0	300
Hold time (s)	20	15	12	12	5.5	2
Read	–	–	–	–	Yes	–

\* The purge gas flow-rate was 300 ml min<sup>-1</sup> in all stages excepting the atomization stage, where stop-flow was used.

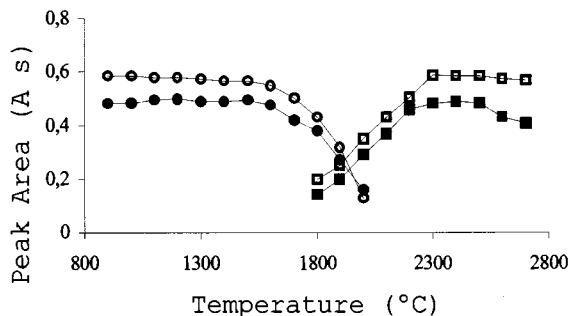


Fig. 1. Ashing and atomisation curves for Cu in an aqueous standard (●, ashing curve; ■, atomisation curve) (500 pg Cu mass) and a supernatant obtained after sonication of a mussel tissue slurry (○, ashing curve; □, atomisation curve) (600 pg Cu mass).

### 3. Results and discussion

#### 3.1. Ash–atomize curves

In order to evaluate the behaviour of Cu from a supernatant obtained upon sonication of a slurry as compared to an aqueous standard, ash/atomize curves were performed (Fig. 1). The solid material chosen for this experiments was the unknown mussel tissue after determination of its Cu content following microwave digestion. Around 10 mg of sample (particle size less than 50  $\mu\text{m}$ ) were slurried with 1.5 ml of 3% v/v  $\text{HNO}_3$  and subsequently sonicated for 5 min at 40% amplitude. 10  $\mu\text{l}$  of the resulting supernatant and 5  $\mu\text{l}$  of Mg nitrate modifier (1600 ppm as salt) were injected into the graphite furnace. Monitoring of the drying and ashing steps by means of the CCD camera allowed to observe that some boiling occurred when only a drying step was used. The use of an additional ashing step was also seen to be convenient in order to avoid some sputtering of sample. Maximum ashing temperatures for Cu in both the supernatant obtained after sonication and a Cu aqueous standard was 1300 and 1500°C, respectively, when using matrix modifier. Maximum ashing temperatures achieved without matrix modifier were the same as compared to the use of matrix modifier, meaning that the matrix modifier was unnecessary. In all cases, the optimum atomization temperature was 2300°C.

#### 3.2. Extraction conditions

Ultrasonic treatment of slurries for ETAAS applications has been shown to cause metal extraction as a result of the acoustic cavitation and the consequent disruption action caused by ultrasound [1]. However, the percentage of extraction depends of factors such as analyte-to-matrix interaction and the capability of the ultrasonic processor used to dissipate ultrasound. Thus, quantitative extraction was reported for biological matrices but it is more difficult for typical inorganic matrices. Likewise, the use of high intensity ultrasonic processors should be attempted in order to achieve good performance for extraction [10].

Optimization of the following variables was performed in order to assess the extraction capability of probe sonication for Cu extraction: (i) sonication time; (ii) ultrasound amplitude; (iii) acid concentration; (iv) sample mass; and (v) particle size. Unlike slurry sampling where a surfactant (e.g. Triton X-100) is recommended as wetting agent in order to prevent the solid particles to float on the top of the liquid, addition of surfactants in sonochemical extraction might cause the intensity to decrease. Furthermore, the use of wetting agents such as Triton X-100 could be unnecessary due to the capability of ultrasound in wetting particles as well as dispersing solids. Therefore, the addition of a wetting agent was omitted for sonochemical extraction from slurries.

The study was carried out with the unknown mussel tissue after separation in different particle size fractions. Microwave digestion of the mussel tissue yielded a Cu concentration of  $8.96 \pm 0.35 \mu\text{g g}^{-1}$  for three different digestions.

#### 3.3. Effect of acid concentration

Previous work carried out in slurry sampling using ultrasonic stirring has demonstrated the importance of adding an acidic diluent so that analyte extraction is facilitated [5]. The use of an acidic diluent combined with the ultrasonic action makes the solid particles more flocculent hence helping the extraction process. Among the acids employed as diluents,  $\text{HNO}_3$  shows an enhanced performance due to its oxidant properties. In this study, the  $\text{HNO}_3$  concentration was varied from 0

to 5% v/v. From Fig. 2 (A), it can be concluded that a 3% v/v acid concentration is at least necessary for quantitative extraction. This acid concentration is close to that typically employed for slurry sampling in ETAAS [5].

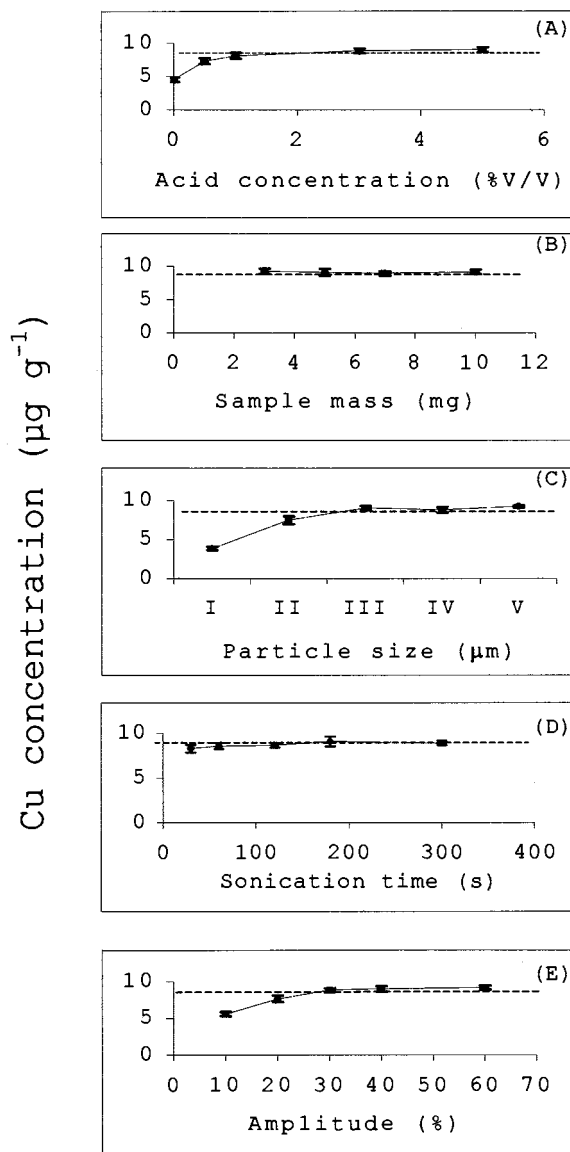


Fig. 2. Optimisation of the variables that influence Cu extraction from mussel tissue. (A) Acid concentration (% v/v); (B) sample mass (mg); (C) particle size ( $\mu\text{m}$ ); (D) sonication time (s); (E) ultrasound amplitude (%). The dashed line indicates the average Cu concentration ( $\mu\text{g g}^{-1}$ ) found as determined by ETAAS after microwave digestion.

### 3.4. Effect of sample mass and particle size

Slurry concentration can usually be varied in a large extent for slurry sampling applications [1], the limiting factors being the insufficient number of particles in the liquid medium when using very diluted slurries or difficulties in pipeting when the slurry is too concentrated. When solid–liquid extraction is pursued, the influence of slurry concentration should be carefully established. Fig. 2 (B) shows that no influence of sample mass slurried in 1.5 ml on extraction efficiency in the range of 3–10 mg. Lower sample mass caused the precision to worsen as a result of the increased influence of inhomogeneity. Particle size showed a remarkable influence at values higher than 150  $\mu\text{m}$  (Fig. 2 (C)).

### 3.5. Effect of sonication time

In contrast to ultrasonic baths, the use of high intensity ultrasonic processors can drastically accelerate extraction of analytes from solid samples [10]. In this study, sonication times between 30 s and 5 min were attempted. The remaining variables affecting extraction efficiency were fixed as follows: a 60% ultrasound amplitude; a 3% v/v  $\text{HNO}_3$  concentration; a 10 mg sample mass and a particle size less than 50  $\mu\text{m}$ . As can be observed in Fig. 2 (D), quantitative extraction takes place even using very short sonication times which is advantageous for expeditious extraction of Cu.

### 3.6. Effect of ultrasound amplitude

The amplitude control of the ultrasonic processor allows the ultrasonic vibrations at the probe tip to be set to any desired level.

Extraction efficiency should increase with increasing ultrasound amplitude. Fig. 2 (E) shows the influence of this variable on Cu extraction using the remaining variables at the values fixed above. The curve obtained indicates that at least a 30% amplitude is necessary for quantitative extraction. With the 100 W ultrasonic processor used in combination with the 3 mm microtip, amplitude values higher than 60% should be avoided so as to prevent the slurry to come out the cup.



Table 2  
Between-batch and within-batch precision for Cu

Sample	Between-batch precision (RSD, %)	Within-batch precision (RSD, %)	$F_{\text{exp}}^*$	$F_{\text{crit}}^*$
Unknown mussel tissue	3.60	0.90	0.9	2.78
BCR CRM 278 Mussel tissue	7.21	2.50	9	4.30
NRCC DORM-2 Dogfish muscle	3.20	3.53	1	4.30
BCR CRM 60 Aquatic plant	2.61	1.47	1.4	4.30

\*  $F_{\text{exp}}$  is the ratio between  $s^2$  (between-batch,  $n-1$  freedom degrees) and  $s^2$  (within-batch,  $m-1$  freedom degrees) where  $n$ ,  $m$  = number of determinations and  $s$  is the standard deviation.  $F_{\text{crit}}$  is the tabulated  $F$ -ratio for the same freedom degrees. The two-sided  $F$ -test was used [11]. Significant differences ( $P = 0.95$ ) occur when  $F_{\text{exp}} > F_{\text{crit}}$ .

### 3.7. Analytical figures of merit

The equation for the linear range of the Cu calibration graph was the following:

$$Y = 8.2(10^{-3} X + 8.3(10^{-2}))$$

where  $Y$  is integrated absorbance (A.s) and  $X$  is Cu concentration ( $\mu\text{g l}^{-1}$ ). The regression coefficient was 0.998. Characteristic mass for Cu was 5.37 pg. The LOD was defined as  $3 \sigma/m$ , where  $s$  is the standard deviation corresponding to ten blank injections and  $m$  is the slope of the calibration graph. The LOD for Cu was  $0.16 \mu\text{g g}^{-1}$  when 10 mg of solid sample were slurried in 1.5 ml of diluent. The LOQ, defined as  $10 \sigma/m$ , was  $0.55 \mu\text{g g}^{-1}$ . When within- and between-batch precision (RSD) were compared (Table 2), no significant differences were found ( $P = 0.95$ ) with exception of Cu determination in BCR CRM 278 mussel tissue which means that an inhomogeneous distribution

of Cu in this material occurs at the 10 mg mass level.

Identical absorption profiles were obtained for Cu atomised from a standard, a slurry (unknown mussel tissue; particle size less than  $50 \mu\text{m}$ ) and a supernatant obtained after sonication (unknown mussel tissue; particle size less than  $50 \mu\text{m}$ ), which suggests the absence of matrix effects.

### 3.8. Analytical results

Table 3 shows the Cu concentration found in three CRMs and the unknown mussel tissue sample. Extraction conditions used in all cases were: a 60% ultrasound amplitude; a 3 min sonication time; a 10 mg sample mass; a 3% v/v  $\text{HNO}_3$  concentration (1.5 ml volume). The particle size used for the unknown mussel tissue was  $50 \mu\text{m}$  whereas CRMs were used as provided without further grinding. Certificates for CRMs ensured a particle size less than  $125 \mu\text{m}$ . Concentration values found for Cu

Table 3  
Analytical results for Cu as determined in slurries after solid-liquid extraction using probe sonication

Sample	Found <sup>a</sup> concentration ( $\mu\text{g g}^{-1}$ ) ( $x \pm ts/\sqrt{n}$ )	Certified value ( $\mu\text{g g}^{-1}$ ) ( $x \pm$ $ts/\sqrt{n}$ )	Recovery (%)	$t_{\text{crit}}$	$t_{\text{exp}}$
Unknown mussel tissue	$8.96 \pm 0.35$	$9.24 \pm 0.30^{\text{b}}$	$103.16 \pm 1.30$	2.78	2.64
BCR CRM 278 Mussel tissue	$7.91 \pm 1.41$	$9.60 \pm 0.16$	$82.39 \pm 5.94$	4.30	5.13
NRCC DORM 2 Dogfish muscle	$2.18 \pm 0.15$	$2.34 \pm 0.15$	$93.16 \pm 3.00$	4.30	3.95
BCR CRM 60 Aquatic plant	$52.40 \pm 3.40$	$51.4 \pm 1.90$	$102.35 \pm 2.68$	4.30	1.52

<sup>a</sup> Average value of three different extractions. Results are expressed as mean  $\pm$  confidence interval ( $P = 0.95$ ).

<sup>b</sup> Average value  $\pm$  confidence interval ( $P = 0.95$ ) for three different digestions.

were expressed as average value  $\pm$  confidence interval ( $P = 0.95$ ), for  $n = 3$  different extractions. The Cu concentration in the unknown mussel tissue was also determined after microwave digestion according to the procedure pointed out above. Recovery was calculated as the ratio between the found value and the certified one, expressed as percentage. As can be observed, recoveries ranged from 82 to 103%. In order to ascertain whether there were significant differences between the found and certified concentration values for Cu, the  $t$ -test was applied. As can be observed,  $t_{\text{exp}}$  was usually less than  $t_{\text{crit}}$  for  $P = 0.95$ , hence meaning that the null hypothesis can be retained.

### Acknowledgements

This work was financially supported by the Galicia Government (Xunta de Galicia) in the framework of the project XUGA38301B96.

### References

- [1] C. Bendicho, M.T.C. de Loos-Vollebregt, *J. Anal. At. Spectrom.* 6 (1991) 353.
- [2] J.A. Holcombe, V. Majidi, *J. Anal. At. Spectrom.* 4 (1989) 423.
- [3] V. Majidi, J.A. Holcombe, *Spectrochim. Acta Part B* 45 (1990) 753.
- [4] M.S. Epstein, G.R. Carnrick, W. Slavin, N.J. Miller-Ihli, *Anal. Chem.* 61 (1989) 1414.
- [5] N.J. Miller-Ihli, *J. Anal. At. Spectrom.* 9 (1994) 1129.
- [6] D.T. Takuwa, G. Sawula, G. Wibetoe, W. Lund, *J. Anal. At. Spectrom.* 12 (1997) 849.
- [7] N.J. Miller-Ihli, *Fresenius J. Anal. Chem.* 337 (1990) 271.
- [8] H. Minami, T. Honjyo, I. Atsuya, *Spectrochim. Acta Part B* 51 (1996) 211.
- [9] J.L. Capelo, I. Lavilla, C. Bendicho, *J. Anal. At. Spectrom.* 13 (1998) 1285.
- [10] S. Mamba, B. Kratochvil, *Intern. J. Environ. Anal. Chem.* 60 (1995) 295.
- [11] J.C. Miller, J.N. Miller, *Estadística para Química Analítica*, 2nd Edition, Addison-Wesley Iberoamerican, Wilmington, Delaware, 1993.

Short communication

# Rapid test methods for minor components analysis of hydraulic cement. Spectrophotometric determination of manganese oxide content of Portland cement and cement raw meal

K.A. Idriss <sup>a,\*</sup>, H. Sedaira <sup>a</sup>, M.S. Abdel-Aziz <sup>b</sup>, H.M. Ahmad <sup>b</sup>

<sup>a</sup> *Chemistry Department, Faculty of Science, Assiut University, Assiut, Egypt*

<sup>b</sup> *Assiut Cement Company, Assiut, Egypt*

Received 8 February 1999; received in revised form 19 May 1999; accepted 11 June 1999

## Abstract

A rapid, sensitive and highly selective spectrophotometric method for the determination of manganese oxide content of Portland cement and cement raw meal is developed. The method is based on the reaction of manganese(II) with 1,2,4 trihydroxyanthraquinone (purpurin, PURP) in 50% v/v ethanol–water solution at pH 8.5. The solution equilibria of manganese chelates are demonstrated and characterized for delineating optimal conditions of the complexation reaction and analytical aspect of the Mn–PURP system. The analysis of cement materials of variable manganese content is feasible over the concentration range 1.67–8.13  $\mu\text{g ml}^{-1}$  Mn, the limit of detection (at the 95% confidence level) of the method is 68  $\text{ng ml}^{-1}$  for manganese. Under optimum conditions, the use of first derivative spectrophotometry has the advantage of high sensitivity than normal spectrophotometric method and allows the determination of 0.5  $\mu\text{g ml}^{-1}$  of manganese. © 1999 Elsevier Science B.V. All rights reserved.

*Keywords:* Manganese(II) determination; Portland cement analysis; Spectrophotometry; Complexation equilibria

## 1. Introduction

The hydraulic cement is a cement that sets and hardens by chemical interaction with water and that is capable of doing so under water. One of the minor components of hydraulic cement (usu-

ally below 0.5% each) is manganese oxide. The standard methods applied for manganese content analysis of cements are complicated and time consuming [1]. The continuing need for better methods for the determination of minor components of hydraulic cement, cement clinker and raw mixes has led to several investigations. The authors of this work have recently presented data

\* Corresponding author. Fax: +20-88-312564.

from their newly developed spectrophotometric test method [2] for the analysis of titanium(IV) as a minor component of Portland cement to ASTM subcommittee of cement compositional analysis.

Several instrumental methods for cement analysis are fairly common such as AAS, XRF, ICP-AS, NAA and absorption spectrophotometry. The common availability and low cost instrumentation, the simplicity of the procedures and the accuracy of the technique make spectrophotometry advantageous for several determinations. It was the main objective of this work to make use of spectrophotometry in the determination of manganese oxide content of Portland cement and raw meal.

The majority of the spectrophotometric procedures applied for the determination of manganese was based on the oxidation of an organic reagent by hydrogen peroxide, catalyzed by manganese(II) [3–7]. Use of a selective reagent for direct spectrophotometric determination of manganese is particularly difficult and several methods have the draw-back of interference from many cations and anions. Much work has been discussed for overcoming these interferences [7].

In this paper, complexation reaction of manganese(II) with purpurin (1,2,4 trihydroxyanthraquinone) is described and a method for the direct spectrophotometric determination of manganese oxide content of Portland cement is proposed. No studies have yet been reported demonstrating the solution equilibria of Mn with purpurin or the use of this reagent for the analysis of cement matrices. The validity of the proposed method was thoroughly examined by using several NIST SRM Portland cement samples and variety of Portland cement materials.

## 2. Experimental

### 2.1. Chemicals and solutions

All chemicals were of analytical–reagent grade and doubly distilled water (or pure ethanol) was used for the preparation of solutions.

Manganese stock standard solution: a  $5 \times 10^{-3}$  mol  $l^{-1}$  stock solution was prepared using

AnalaR manganese(II) chloride and standardized with EDTA, it was diluted as required, just before use.

Purpurin (PURP)–Aldrich-stock solution:  $10^{-3}$  mol  $l^{-1}$  stock solution in absolute ethanol was prepared by dissolving an accurately weighed amount of the purified reagent. More dilute solutions were obtained by appropriate dilution.

Iron(III) chloride stock solution: a stock solution of iron(III) (1 ml = 0.675 mg iron) was prepared using AnalaR iron(III) chloride in 0.05 mol  $l^{-1}$  HCl and standardized as recommended.

Buffer solution: a pH 8.5 buffer solution was prepared from 2 mol  $l^{-1}$  ammonium chloride and 2 mol  $l^{-1}$  ammonia solutions.

Other solutions included sodium citrate (0.5 mol  $l^{-1}$ ), sodium perchlorate (1 mol  $l^{-1}$ ), standard solutions of sodium hydroxide and perchloric acid. Solutions of diverse ions used for interference studies were prepared from AnalaR products of chlorides or nitrates of the metal ions and potassium or sodium salts of the anions to be tested. The ionic strength of solutions was maintained at a constant value of  $I = 0.1$  mol  $l^{-1}$  ( $NaClO_4$ ). All measurements were made in 50% (v/v) ethanol at 25°C.

### 2.2. Cement samples

NIST standard reference materials (SRM): 1880, 1881, 1885 and 1889 were used as Portland cement matrix in this study. Precautions for handling and use were taken in accordance with the instructions [8] on the NIST data sheet and certificate of analysis of percent constituents. Other real samples of cement, clinker, clay and raw meal were analysed using XRF spectrometry by F.L. Smidth and Co. A/S (Copenhagen; Denmark)

### 2.3. Apparatus

A Perkin–Elmer (M Lambda 40) double beam spectrophotometer was used for ordinary and first derivative spectral measurements using 1 cm matched quartz cells. pH values were measured using a radiometer pH meter (M 210) equipped with a radiometer combined glass electrode. The pH-values in water–ethanol medium were corrected as described elsewhere [9].

#### 2.4. Spectrophotometric determination of manganese (procedure A)

Into a 25-ml standard flask transfer 6.5 ml of  $10^{-3}$  mol  $l^{-1}$  PURP solution and 6 ml of pure ethanol to ensure a final ethanol content 50% v/v. Add 6 ml of pH 8.5 buffer solution and suitable volume of manganese(II) solution containing 45–280  $\mu$ g of manganese. Dilute to volume with re-distilled water and measure the absorbance of the solution at 590 nm against a reagent blank as the reference.

#### 2.5. First-derivative spectrophotometry (procedure B)

Operate as described above, but use a volume of manganese(II) solution containing 14–130  $\mu$ g of manganese. Record the first derivative spectrum from 750 to 500 nm against a reagent blank at a scan-speed of 240 nm  $min^{-1}$  and slit width of 2 nm. A calibration curve covering the range from 0.5 to 5.2  $\mu$ g  $ml^{-1}$  of manganese(II) was established.

#### 2.6. Manganese oxide content analysis of Portland cement

Weigh accurately 1.0 g of the sample (dried at 110°C, for  $\approx$  2 h) into a beaker and dissolve it in the minimum volume of hydrochloric acid. Heat to dryness, add 25 ml of HCl (6 mol  $l^{-1}$ ) to the residue, digest and filter the insoluble residue into 100 ml calibrated flask and then dilute to volume with redistilled water. Transfer 5–7.5 ml aliquot of the sample solution into a 25-ml calibrated flask, add 6.5 ml of PURP ( $10^{-3}$  mol  $l^{-1}$ ), 2.5 ml of sodium citrate (0.25 mol  $l^{-1}$ ), and 6 ml of pure ethanol. Adjust the pH to 8.5 and dilute to volume while keeping final ethanol content of 50% v/v. Measure the absorbance of the solution at 590 nm against a reagent blank as the reference. If the first-derivative spectrophotometric method is used take a smaller aliquot of the sample solution (2.0–4.0 ml) and prepare the test solution as given but without addition of citrate.

### 3. Results and discussion

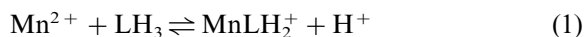
In 50% v/v ethanol–water medium and in the pH range 2.5–10.5, the reagent PURP exists in four different acid–base forms depending on the acidity of the medium, these forms include the cationic ( $LH_4^+$ ), neutral ( $LH_3$ ), monoanionic ( $LH_2^-$ ) and dianionic ( $LH^{2-}$ ) species. Further proton dissociation of reagent seems to be difficult under the given conditions. The pH-dependence of the absorption spectrum of PURP in mixed aqueous solvents has been discussed earlier [10]. In this work, the variation of absorbance with pH was re-examined through a systematic study of the acid–base equilibria of reagent and solution equilibria of its manganese(II) complexes. Refined values of acidity constants of PURP were evaluated by a general least squares method, treating the original data [ $A = f(\text{pH})$ ] and calculated the estimated standard deviation concerning scattering of experimental data [11]. The values of  $pK_{a_1}$  ( $LH_4^+/LH_3$ ),  $pK_{a_2}$  ( $LH_3/LH_2^-$ ),  $pK_{a_3}$  ( $LH_2^-/LH^{2-}$ ), as determined in this work were found to be  $5.18 \pm 0.02$ ,  $7.65 \pm 0.01$  and  $10.27 \pm 0.03$ , respectively.

#### 3.1. Complexation reaction of manganese(II) with PURP

We studied the complexation reaction of manganese(II) with PURP spectrophotometrically in solutions containing 50% v/v ethanol over the pH range 5–10.5. The solution spectra, measured within the wavelength range 400–750 nm, exhibit primarily a low intensity band at 540 nm in the pH range 5.4–6.6. At higher pH values, the spectra revealed a new absorption band at  $\sim$  590 nm which continuously increased in height with rise of pH. The maximum intensity of this band was attained at pH 8–8.7, above which a gradual decrease of absorbance was observed. The absorbance versus pH graphs at  $\lambda = 590$  nm, for solutions of different component ratio, show the ranges of formation of Mn complexes which indicate the existence of two chelate equilibria within the pH range 5.5–9.0. The addition of the cationic surfactant cetyltrimethyl ammonium bromide ( $5 \times 10^{-3}$  mol  $l^{-1}$ ) causes an insignificant

change of the absorbance values of Mn–PURP complex, but prevents the decrease of absorbance at higher pH values. The absorbance versus pH graphs were interpreted using the relationships derived by Voznica et al. [12] and Idriss et al. [13] and by the generalized approach described previously [14,15].

The analysis of the absorbance versus pH graphs of Mn–PURP system (containing a preponderance of reagent) proved the existence of equilibrium (Eq. (1)) at pH 5.5–6.7 and formation of Mn(LH<sub>2</sub>)<sub>2</sub> complex at pH 7.0–8.5.



The analysis of the descending branch of the graphs (in the pH range 9.0–10.5) confirmed the existence of a hydrolytic reaction of the Mn(LH<sub>2</sub>)<sub>2</sub> complex. The stoichiometry of Mn–PURP chelates was further verified by the method of continuous variation. A component ratio of 1:2 (metal to ligand) was obtained at pH 8.5. The calculated values of the apparent equilibrium con-

stant ( $\log {}^*K$ ), stability constant ( $\log \beta$ ) and molar absorptivity of the Mn(LH<sub>2</sub>)<sub>2</sub> complex are given in Table 1.

### 3.2. Effect of matrix elements

Owing to the existence of high concentrations of other (accompanying) elements such as, Al<sup>3+</sup>, Fe<sup>3+</sup>, Ca<sup>2+</sup>, Mg<sup>2+</sup>, Sr<sup>2+</sup>, Ti<sup>4+</sup> in cement matrices, a systematic interference study of these elements and many other cations and anions on the determination of manganese was performed. Solutions containing 0.14 mg of Mn<sup>2+</sup> per 25 ml and varying concentrations of each ion to be tested were prepared. The manganese was then determined as Mn(LH<sub>2</sub>)<sub>2</sub> complex under the optimum conditions as described in the given procedure of normal spectrophotometry. The tolerance criterion for a given ion was taken as the deviation of the absorbance values by more than +2% from the value expected for manganese alone. The results of this work indicate that the presence of

Table 1

Mean values of equilibrium constants ( $\log {}^*K$ )<sup>a</sup>, stability constants ( $\log \beta$ ) and molar absorptivities of manganese(II) and iron(III) complexes with PURP, 50% v/v ethanol,  $I = 0.1$ , 25°C. Values in parentheses were obtained in presence of CTAB  $5 \times 10^{-3}$  mol l<sup>-1</sup>

Equilibrium <sup>b</sup>	Constant	Log constant	Molar absorptivity (l mol <sup>-1</sup> cm <sup>-1</sup> )
Manganese–PURP complexes [Mn (LH <sub>2</sub> )][H]/[Mn][LH <sub>3</sub> ]	$*K_1$	$-3.72 \pm 0.02$ (–2.70+0.02)	$3.85 \times 10^3$ ( $4.12 \times 10^3$ ) $\lambda = 590$ nm
[Mn (LH <sub>2</sub> ) <sub>2</sub> ][H]/[Mn (LH <sub>2</sub> )] [LH <sub>3</sub> ]	$*K_2$	$-3.54 \pm 0.03$ (–2.55 ± 0.02)	
[Mn (LH <sub>2</sub> ) <sub>2</sub> ]/[Mn] [LH <sub>2</sub> ]	$\beta_1$	3.93 (4.08)	
[Mn (LH <sub>2</sub> ) <sub>2</sub> ]/[Mn] [(LH <sub>2</sub> ) <sup>2</sup> ]	$\beta_2$	8.04 (8.31)	
$(\beta_1 = *K_1 K_{a_2}^{-1}, \beta_2 = \beta_1^* K_2 K_{a_2}^{-1})$			
Iron(III)–PURP complexes			
[Fe (LH <sub>3</sub> )][H]/[Fe] [LH <sub>4</sub> ]	$*K_1$	$0.6 \pm 0.01$ (0.95 ± 0.01)	
[Fe (LH <sub>2</sub> )][H]/[Fe (LH <sub>3</sub> )]	$*K_{1H}$	$-3.85 \pm 0.03$ (–2.85 ± 0.02)	
[Fe (LH <sub>2</sub> ) <sub>2</sub> ][H]/[Fe (LH <sub>2</sub> )] [LH <sub>3</sub> ]	$*K_2$	$-3.68 \pm 0.04$ (–2.90 ± 0.03) <sup>c</sup>	$1.5 \times 10^4$ ( $7.2 \times 10^3$ ) $\lambda = 600$ nm
[Fe (LH <sub>3</sub> )]/[Fe] [LH <sub>3</sub> ]	$\beta_1$	5.78 (5.91)	
[Fe (LH <sub>2</sub> )]/[Fe] [LH <sub>2</sub> ]	$\beta_{1H}$	9.57 (9.84)	
[Fe (LH <sub>2</sub> ) <sub>2</sub> ]/[Fe] [LH <sub>2</sub> ] <sup>2</sup>	$\beta_2$	13.54 (13.72)	
$\beta_1 = *K_1^* K_{a_1}^{-1}, \beta_{1H} = \beta_1^* K_1^* K_{a_2}^{-1}$ $\beta_2 = \beta_{1H}^* K_2^* K_{a_2}^{-1}$			

<sup>a</sup> From the absorbance–pH graphs.

<sup>b</sup> Charges of the species are omitted.

<sup>c</sup> In the presence of excess reagent.

~ 12 mg each of alkali metal or alkaline-earth ions ( $\text{Mg}^{2+}$ ,  $\text{Ca}^{2+}$ ,  $\text{Sr}^{2+}$ ,  $\text{Ba}^{2+}$ ),  $\text{Al}^{3+}$ ,  $\text{Ti}^{4+}$ ,  $\text{Cr}^{3+}$ ,  $\text{NH}_4^+$ ,  $\text{Cl}^-$ ,  $\text{Br}^-$ ,  $\text{PO}_4^{3-}$ ,  $\text{SO}_4^{2-}$ ,  $\text{NO}_3^-$ ,  $\text{B}_4\text{O}_7^{2-}$ ,  $\text{SO}_3^{2-}$ ,  $\text{ClO}_4^-$  had no effect on the procedure. The determination of manganese was also possible in the presence of  $\text{V}^{+5}$ ,  $\text{Zn}^{2+}$ ,  $\text{Mo}^{6+}$ ,  $\text{Ag}^+$ ,  $\text{Cd}^{2+}$ ,  $\text{Pb}^{2+}$  (~ 8 mg each), and  $\text{Co}^{2+}$ ,  $\text{Ni}^{2+}$ ,  $\text{Cu}^{2+}$ ,  $\text{Zr}^{4+}$ ,  $\text{Hg}^{2+}$  (5 mg). Using the present experimental conditions, it was observed that  $\text{Mn}^{2+}$  could not be determined in the presence of EDTA,  $\text{CN}^-$  or  $\text{F}^-$  ions. Although the determination of manganese using the given procedure was not affected by the commonly associated elements in cement matrix, iron(III), normally present in Portland cement and cement raw meal, was found to be seriously interfered by absorbing very close to the wavelength of measurement. For this reason, the effect of iron(III) on the determination of manganese(II) was specially investigated.

Our preliminary results indicated that iron(III) and manganese(II) were analogously reacted with PURP, we felt that it would be of interest to investigate the complexation reaction between iron(III) and the reagent used. The solution spectra of  $\text{Fe}^{3+}$ –PURP binary system with reagent blank as reference were characterized by an absorption band with  $\lambda_{\text{max}}$  at ~ 600 nm in the pH range of 6.0–9.5. The band was broadened, shifted

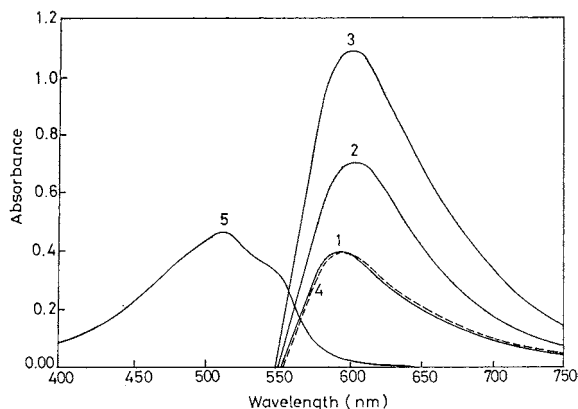


Fig. 1. Absorption spectra of (1) Mn–PURP complex; (2) Fe–PURP complex; (3) mixture of  $\text{Mn}^{2+}$  and  $\text{Fe}^{3+}$  complexes; (4) the same mixture as (3) in the presence of  $0.025 \text{ mol l}^{-1}$  citrate; (5) PURP solution  $5 \times 10^{-5} \text{ mol l}^{-1}$ . ( $C_L = 2.5 \times 10^{-4} \text{ mol l}^{-1}$ ;  $C_{\text{Mn}} = C_{\text{Fe}} = 10^{-4} \text{ mol l}^{-1}$ ,  $[\text{CTAB}] = 5 \times 10^{-3} \text{ mol l}^{-1}$ ; pH 8.5, 50% v/v ethanol).

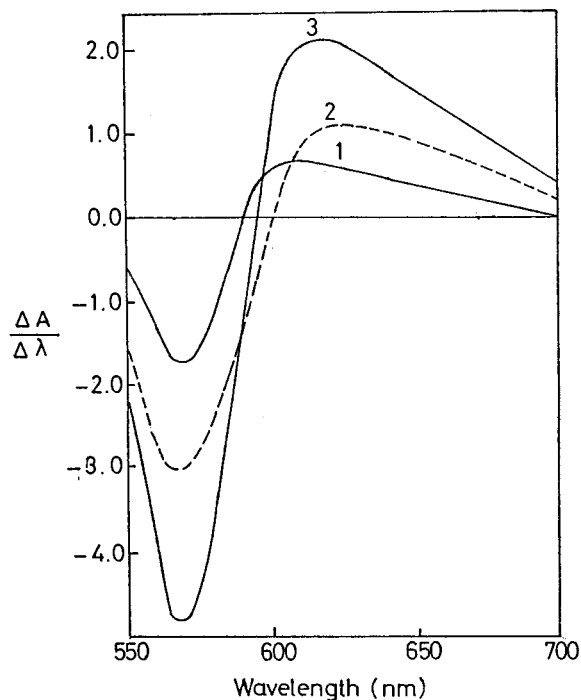


Fig. 2. First derivative absorption spectra of (1) manganese(II) complex,  $[\text{Mn}] = 2.75 \text{ } \mu\text{g ml}^{-1}$ ; (2) iron(III) complex,  $[\text{Fe}] = 2.8 \text{ } \mu\text{g ml}^{-1}$ ; (3) mixture of manganese(II) and iron(III) complexes  $[\text{Mn}] = 5.5 \text{ } \mu\text{g ml}^{-1}$ ;  $[\text{Fe}] = 2.8 \text{ } \mu\text{g ml}^{-1}$ . ( $C_L = 2.5 \times 10^{-4} \text{ mol l}^{-1}$ ,  $[\text{CTAB}] = 5 \times 10^{-3} \text{ mol l}^{-1}$ ; pH 8.5, 50% v/v ethanol).

to shorter wavelengths and became of lower intensity at higher acidity. The study of the spectral changes as a function of pH for solutions containing equimolar concentrations of components or an excess of ligand or metal ion have led us to conclude that the initial  $\text{Fe}^{3+}$ –PURP complex formed at  $\text{pH} < 3.5$  was deprotonated in the pH range 4–5.5 and a bis-binary complex was formed at  $\text{pH} 7.5$ –8.5. When the absorbance versus pH graphs for the  $\text{Fe}^{3+}$ –PURP system were interpreted by direct and logarithmic analysis using transformations given elsewhere [12,13,16], the complexation equilibria involving formation of  $\text{Fe}(\text{LH}_3)^{3+}$ ,  $\text{Fe}(\text{LH}_2)^{2+}$  and  $\text{Fe}(\text{LH}_2)_2^+$  complexes were established. In solutions containing excess iron(III), the  $\text{Fe}(\text{LH}_2)_2^+$  was proved to be the predominate species at  $\text{pH} 6$ –9.5. The basic characteristics of the iron–PURP complexes were determined and listed in Table 1.

Table 2

Application of the PURP-spectrophotometric method to the direct determination of  $\text{Mn}_2\text{O}_3$  in some Portland cement materials

Material	Manganese determination <sup>c</sup> (% $\text{Mn}_2\text{O}_3$ ) (normal procedure)			XRF $\text{Mn}_2\text{O}_3$ (%)	
	Sample <sup>a</sup>	Statistical term <sup>b</sup>			
		$\bar{x}$	<i>S</i>		95% <i>CL</i>
Clay	1	0.168	$2.73 \times 10^{-2}$	$\bar{x} \pm 0.029$	0.17
	2	0.254	$4.47 \times 10^{-2}$	$\bar{x} \pm 0.047$	0.24
Raw meal	1	0.105	$9.1 \times 10^{-2}$	$\bar{x} \pm 0.096$	0.11
	2	0.125	$4.66 \times 10^{-2}$	$\bar{x} \pm 0.049$	0.13
Clinker		0.088	$3.9 \times 10^{-2}$	$\bar{x} \pm 0.041$	0.09
Cement	1	0.148	$2.97 \times 10^{-2}$	$\bar{x} \pm 0.084$	0.16
	2	0.340	$5.19 \times 10^{-2}$	$\bar{x} \pm 0.055$	0.35
	3	0.380	$8.88 \times 10^{-2}$	$\bar{x} \pm 0.093$	0.39
NIST standard cement <sup>d</sup>	(SRM)				
	1889	0.236	$6.02 \times 10^{-2}$	$\bar{x} \pm 0.063$	0.23
	1885	0.115	$6.52 \times 10^{-2}$	$\bar{x} \pm 0.071$	0.12
	1881	0.258	$9.34 \times 10^{-2}$	$\bar{x} \pm 0.098$	0.25
	1880	0.075	$8.53 \times 10^{-2}$	$\bar{x} \pm 0.090$	0.07

<sup>a</sup> Number of determinations for each sample ( $n$ ) = 5.<sup>b</sup>  $\bar{x}$  = Mean recovery (%  $\text{Mn}_2\text{O}_3$ ); *S* = standard deviation (%); *CL* = confidence limit (%).<sup>c</sup> Test solutions of the samples investigated contained 50–75 mg of cement material per 25 ml.<sup>d</sup> Certified amounts (%  $\text{Mn}_2\text{O}_3$ ), SRM 1889 (0.24); 1885 (0.12); 1881 (0.26); 1880 (0.08).

To try out the reliability of the proposed method for manganese determination in cementitious systems, we analysed mixtures of varying proportions of manganese(II) and iron(III) together with appropriate amounts of other elements frequently found in cement matrices. In the ordinary spectrophotometric procedure, the only interfering ion was iron(III) and could be eliminated by sodium citrate ( $0.025 \text{ mol l}^{-1}$ ) (Fig. 1). On the other hand, manganese(II) could be determined in the presence of iron(III) without using masking agent by measuring the first-derivative spectral signal at 600 nm (zero-crossing point of iron(III)). The precision (RSD, five determinations) was 0.85% for manganese in mixture containing  $3.72 \mu\text{g ml}^{-1}$  of manganese and  $18 \mu\text{g ml}^{-1}$  of iron(III).

The first-derivative spectrum of Mn(II)–PURP complex was shown in Figs. 1 and 2. Effects of the scan speed and slit width on the measurement of the first-derivative signal were examined. The change of the scan speed from 120–480  $\text{nm min}^{-1}$  did not affect the value of the signal. A scan speed of 240  $\text{nm min}^{-1}$  was chosen for the

measurements. There was also no significant difference in sensitivity among various slit widths, a slit of 2 nm was selected to perform the measurements.

### 3.3. Calibration graph, precision and accuracy

In the ordinary spectrophotometric method, Beer's law was obeyed over the range 1.37–12.36  $\mu\text{g ml}^{-1}$  of manganese with a molar absorptivity of  $4.1 \times 10^3 \text{ l mol}^{-1} \text{ cm}^{-1}$  at 590 nm. A Ringbom plot showed that the optimum working range for manganese determination was 1.75–11.2  $\mu\text{g ml}^{-1}$ . The calibration graph for the first-derivative spectrophotometric method was linear in the manganese concentration range of 0.5–5.2  $\mu\text{g ml}^{-1}$ . The calibration sensitivity of the method ( $2.21 \text{ ml } \mu\text{g}^{-1}$ ) was higher than that of the normal spectrophotometric method ( $0.074 \text{ ml } \mu\text{g}^{-1}$ ).

To assess the reliability of the method for manganese oxide content analysis of Portland cement, several samples of certified NIST SRM [8] were used to analyse their manganese content which normally expressed as manganese trioxide. The



analysis of samples of cement materials containing various proportions of manganese was feasible over the concentration range 1.67–8.13  $\mu\text{g ml}^{-1}$  Mn. The calculated detection limit was found to be 68  $\text{ng ml}^{-1}$  for Mn using normal method and 42  $\text{ng ml}^{-1}$  using first derivative spectrophotometry. Some results obtained for the analysis of cement materials were given in Table 2.

#### 4. Conclusion

The proposed purpurin spectrophotometric method for the determination of manganese oxide content of Portland cement has proved to be reliable, sensitive and highly selective. The method is efficient and precise enough and has the potential to be used as a rapid test method for cement analysis.

#### Acknowledgements

The authors acknowledge the financial support of Assiut Cement Company (Assiut, Egypt). They are grateful to the company for providing the facilities which made it possible to undertake this work.

#### References

- [1] Annual Book of ASTM Standards, Cement. Lime Gypsum (C-114), Vol. 0401, American Society for Testing and Materials, PA, USA, 1997, pp. 116 & 118.
- [2] H. Sedaira, K.A. Idriss, M. Abdel-Aziz, *Analyst* 121 (1996) 1079.
- [3] D. Bendito-Perez, M. Valcarcel, M. Ternero, F. Pino, *Anal. Chim. Acta* 94 (1977) 405.
- [4] T. Saro Raya, D. Bendito-Perez, *Analyst* 108 (1983) 857.
- [5] A. Moreno, M. Silva, D. Bendito-Perez, M. Valcarcel, *Talanta* 30 (1983) 107.
- [6] S. Rubio, A. Gomez, M. Valcarcel, *Analyst* 109 (1984) 717.
- [7] B. Chiswell, G. Rauchile, *Talanta* 37 (1990) 237.
- [8] Certificate of Analysis, Standard Reference Materials, US Department of Commerce, National Institute of Standards and Technology, (NIST) USA (1989).
- [9] G. Douheret, *Bull. Soc. Chim. Fr.* (1967) 1412.
- [10] I.M. Issa, R.M. Issa, K.A. Idriss, A. Hammam, *Ind. J. Chem.* 13 (1975) 136.
- [11] N.V. Nalimov, *The application of Mathematical Statistics to Chemical Analysis*, Pergamon Press, London, 1963, p. 65.
- [12] P. Voznica, J. Havel, L. Sommer, *Collect. Czech. Chem. Commun.* 45 (1980) 54.
- [13] K.A. Idriss, M. Seleim, H. Saleh, M. Abu-Bakr, H. Sedaira, *Analyst* 113 (1988) 1643.
- [14] L. Sommer, V. Kuban, J. Havel, *Folia Fac. Sc. Univ. Brno* 11 (1) (1970) 33.
- [15] L. Sommer, M. Langova, V. Kuban, *Collect. Czech. Chem. Commun.* 41 (1976) 1317.
- [16] K.A. Idriss, M. Saleh, *Analyst* 118 (1993) 223.

Review article

# Pushing the detectability of voltammetry: how low can we go?

Myung-zoon Czae <sup>a,\*</sup>, Joseph Wang <sup>b</sup>

<sup>a</sup> Department of Chemistry, Hanyang University, Seoul 133-791, South Korea

<sup>b</sup> Department of Chemistry and Biochemistry, NMSU, Las Cruces, NM 88003, USA

Received 8 January 1999; received in revised form 29 June 1999; accepted 8 July 1999

---

## Abstract

The coupling of adsorptive accumulation with catalytic reactions results in remarkably low (sub-picomolar) detection limits. This review assesses various strategies for attaining such dual-amplification effects, that lead to the most sensitive voltammetric technique, adsorptive-catalytic stripping voltammetry (AdCtSV). © 1999 Elsevier Science B.V. All rights reserved.

*Keywords:* Detection limits; Adsorptive-catalytic stripping voltammetry; Electrocatalysis; Trace metals

---

## 1. Introduction

The significance of ultratrace levels of metal ions in environmental, industrial or clinical samples has led to continued efforts for enhancing the sensitivity of analytical methods. Various advances during the past 50 years have ‘pushed’ the detectability of voltammetric techniques from the submicromolar level for pulse voltammetric techniques to the subpicomolar level in connection to adsorptive-catalytic stripping voltammetry (Ad-

CtSV). These efforts and related progress have been discussed elsewhere [1–5].

The purpose of this review is to assess the state of the art of adsorptive-catalytic stripping voltammetry, trying to account for earlier results and to elucidate the factors which may be important in guiding further improvements in detectability. The focus is on approaches to increase the signal (S) for enhancing the signal-to-noise ratio (S/N) with the aim of attaining extremely low detection limits (DL). Some instrumental or methodological approaches to reduce the noise (N, capacitive current, for example) in electrochemical analysis have been reviewed by Galus [6].

---

\* Corresponding author. Fax: +82-2-2299-0762.

E-mail address: mzczae@email.hanyang.ac.kr (M.-z. Czae)

## 2. Amplification factors

There are many levels of electrodic (electrochemical) complexity that contribute to the enhancement of the voltammetric signal, including accumulation, adsorption, catalysis (including enzyme-related), and/or recycling. The recycling or repetition occurs naturally in the catalytic processes as a chain reaction or catalyst regeneration. Coupling several of these gives the overall gain  $G$ , an amplification factor in detectability, as

$$G = \kappa\alpha\beta\gamma \quad (1)$$

where  $\alpha$ , accumulation factor;  $\beta$ , adsorption effect;  $\gamma$ , catalytic effect; and  $\kappa$ , a factor contributing to change in DL due to improvements in signal measuring (analytical instrumentation) and in signal (chemometric) processing. The estimated values,  $a$ ,  $b$ , and  $c$  of  $\alpha$ ,  $\beta$ , and  $\gamma$  respectively, which denote the effects of electrodic processes may have variations due to the differences in practical procedures or protocols used for estimating the DL. Hence it is helpful to express the effects properly; an adjusting factor  $K$  may be introduced as:

$$\alpha = Ka, \beta = Kb, \gamma = Kc$$

The literature shows that  $K$  may vary between 1 and 5 depending on the differences in target analyte and their reversibility, schemes used, wave forms in stripping mode, preconcentration period, electrode variation (MFE vs HMDE), etc. All the factors have a value of 1, i.e. no improvement in DL is observed when the corresponding process is not operative. The significance of adsorption factor,  $b$ , in distinction from accumulation factor,  $a$ , deserves to be discussed and understood at this point. The factor  $a$  refers to the effect of prolonged time in the preconcentration on the response by whatever route it may be electrolytic or nonelectrolytic in connection with or without a faradaic process. Adsorption is also a preconcentration process (nonelectrolytic). Being an interfacial (surface) process, however, besides its enrichment effect, the adsorption (of metal-chelate) may exert many favorable effects to en-

hancing the detectability. Effective collection, change in peak shape (the sharper, the more the peak height increases), and increase in faradaic current as a result of simultaneous reduction of the bound ligand (Ref. [7] for examples), may account for most of the effect,  $b$ .

We can estimate an empirical value for each factor ( $a-c$ ) by surveying the literature.

From Fig. 1 [8–27] the amplification factor for catalysis,  $c$ , is estimated to be about 20-fold for common metals (Table 1) and more than several thousands for platinum and rhodium which can be detected at the lowest detection limit.

The accumulation factor,  $a$ , can be estimated by comparing the detection limit obtained by differential pulse polarography (DPP) (i.e. no accumulation) with that obtained in stripping voltammetry (SV) (i.e. after accumulation). Accumulation factors of 100 and 120 have been observed for platinum using the formazone [22,28] and formaldoxime [29,30] systems, respectively. For nickel,  $a$  is calculated to be about 340 [31,7].

The adsorption factor,  $b$ , can be estimated from the detection limit or current difference between those obtained in the presence and absence of a complexing ligand. Flora et al. [31] have found that the detection limit of DPP measurement of nickel can be lowered by ca 15-fold in the presence of DMG (dimethylglyoxime). In stripping voltammetry,  $b$  corresponds to the ratio of detection limits of ASV to that of AdSV. Some values of  $b$  are: 20 for Bi-cupferron [32], 10 for Bi-(5-Br-PADAP) (5'-bromo-2'-pyridylazo)-5-diethylamino-phenol) [33], 50 for Co-DMG system [11] and 100 for Zn-APDC system [34]. The remarkably low detection limit for mercury attained by anodic stripping voltammetry on glassy carbon electrode [27] without any further apparent complexity, may be ascribed to the strong adsorption of the atomic (gaseous state) mercury generated under UPD (underpotential deposition) conditions [35]. Hence we included it in the category of AdSV in Fig. 1. The adsorptive accumulation is characterized by the restrictions imposed upon detection limits, hence it will not be discussed here.

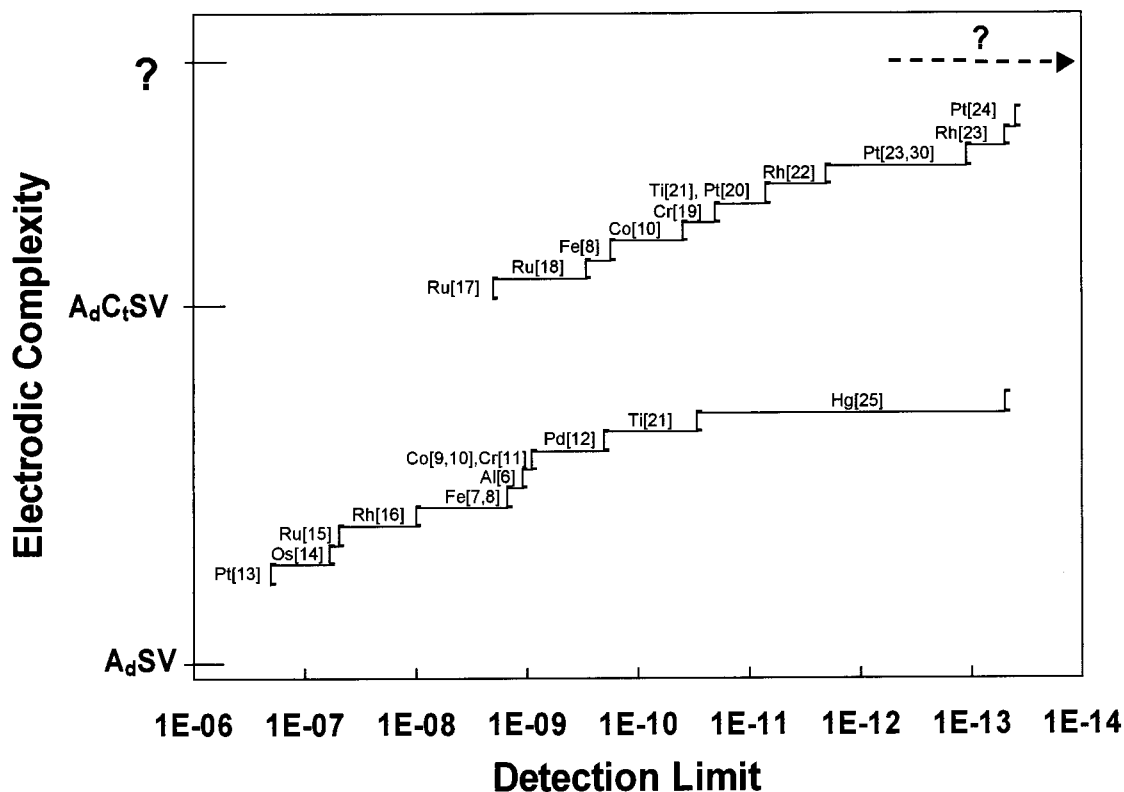


Fig. 1. Survey of the target metals with their detection limits achieved by the method expressed on the ordinate.

### 3. Catalysis

Catalysis refers to the reaction rate amplification as a response to the catalyst input to a chemical system. Exploiting the catalytic effect for enhancing the detectability relies on the catalytic action of the catalysts that are of three general types: mediator catalysts, electrocatalysts and enzymes (biocatalysts).

#### 3.1. Mediator catalysts

If in a redox reaction (Eq. (2)), the so-called indicator reaction [36]:



can be accelerated by a catalyst,  $Ct^{ox}$ , then the rate increment is a measure of the catalyst (target analyte) concentration. In this (catalytic) kinetic method of analysis the catalyst always acts as a

mediator, that is, it shuttles electron from the electron source,  $R_2$  (for a reduction process), to substrate  $O_1$  (Fig. 2Ab). The catalytic amplification of the reaction rate to be produced by a

Table 1  
Survey of the catalytic systems that enhance the sensitivity

Substrate	Catalyst/ analyte	Amplification factor <sup>a</sup>	Reference
Bromate	Ti-EDTA	20	[47]
Chlorate	Ti-mandelic acid	20	[23]
Cupferron	Cr-Cupferron	45	[13,21]
Hydrogen peroxide	Fe-BHA	23	[10]
Hydroxy- lamine	Ru-NH <sub>2</sub> OH	–	[20]
Nitrite	Co-DMG	20	[12]

<sup>a</sup> Amplification factor denotes the ratio of the current in the presence and absence of substrate.

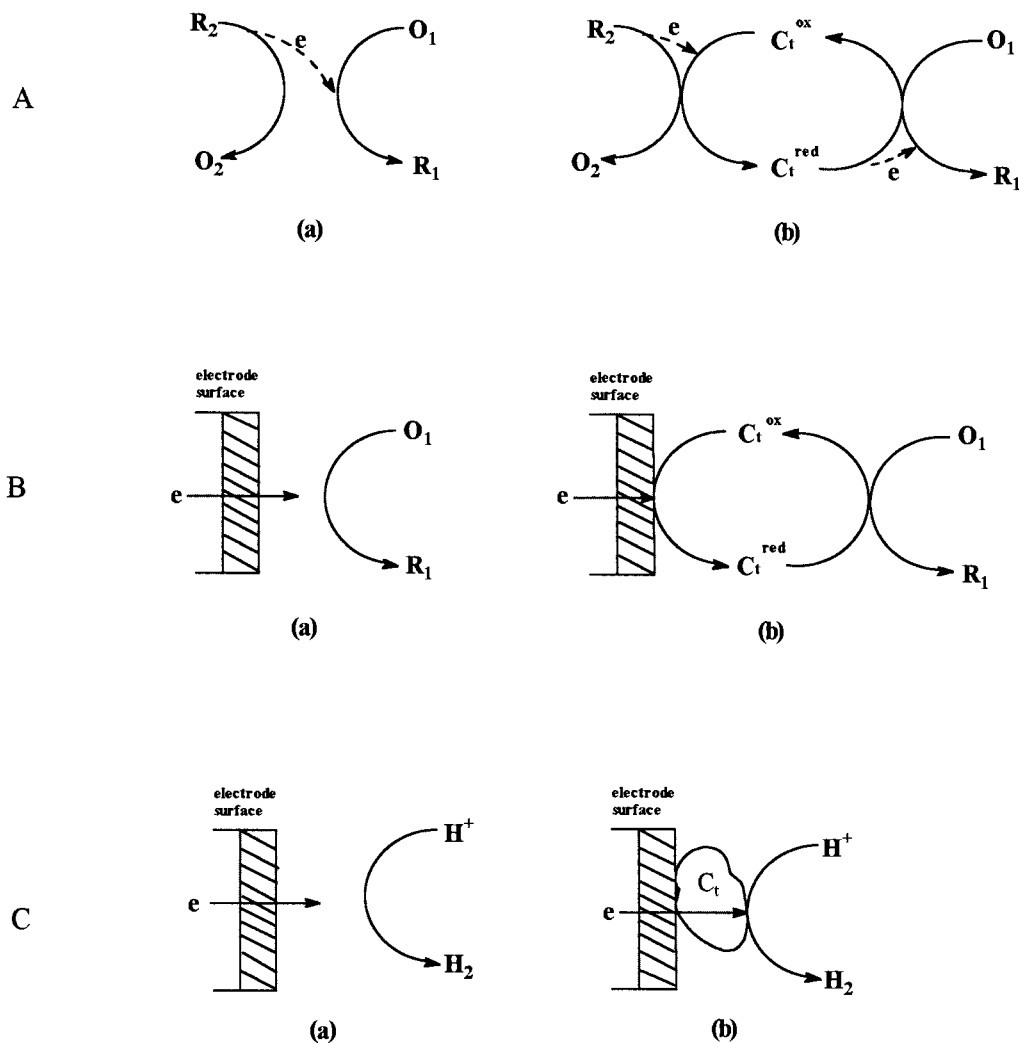


Fig. 2. Schematic representation of the catalytic action for the reduction of  $O_1$  (A, B) and  $H^+$  (C) utilized in (A) kinetic method; (B,C) voltammetry; (a) uncatalyzed, (b) catalyzed reaction for the determination of a catalyst (analyte). (Aa) depicts the indicator reaction used to determine catalyst,  $C_t^{ox}$ , a target analyte, showing the difficulty of electron transfer to  $O_1$  from the electron source  $R_2$  in the absence of catalyst. (B) shows the role of analyte  $C_t^{ox}$  as an electron mediator. In B, the electron source is changed to an electrode, as in usual voltammetry and the mediating process results in catalytic current in EC'. (C) depicts the electrocatalytic process. In C, substrate (an enzyme terminology) is a proton, not  $O_1$ . The proton receives an electron from the electrode directly via  $C_t$ , an electrocatalyst which consists of reduced (to metallic state) analyte complexes, evolving as hydrogen gas (Cb).

catalyst, the standard redox potential ( $E_{ct}^0$ ) of it should lie between those ( $E_1^0$  for  $O_1/R_1$  and  $E_2^0$  for  $O_2/R_2$  couple) of the components of the catalyzed reaction:

$$E_2^0 < E_{ct}^0 < E_1^0 \quad (3)$$

Transition metals, especially platinum group metals that exhibit many different oxidation states, can exert a powerful catalytic effect on many reactions. Ultrasensitive procedures for determining the metal catalyst can thus be devised by monitoring the reaction rate [37].

### 3.2. EC' processes

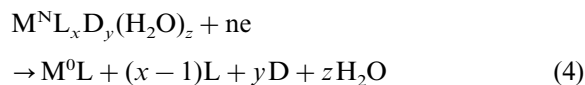
In an electrochemical reaction, the electron source is an electrode instead of  $R_2$  (Fig. 2B), and the current is simply a measure of the rate. In these processes, electrochemically produced mediator  $Ct^{red}$  passes electron from electrode to the substrate  $O_1$ . Therefore, the activation of the catalyst is electrodic but the coupled overall process, the transformation of the substrate, is a redox chemical reaction. A catalytic action to be produced in voltammetry (Eq. (3)) must be satisfied, namely the substrate  $O_1$  should be a stronger oxidant than a mediator catalyst,  $Ct^{ox}$ . Moreover, the  $O_1/R_1$  couple must be irreversible so that substrate  $O_1$  can be reduced at a more negative potential than  $Ct^{ox}$  reduction whose couple should be reversible. Catalytic systems that meet these two requirements (EC' processes) are summarized in Table 1. All substrates are rather the strong oxidants but the amplification factors are less than 50. The 'catalytic' for common metals means the EC' process. It is evident that detection limits lower than  $10^{-11}$  M cannot be achieved by utilizing the EC' process regardless of the target.

### 3.3. Mediatorless processes

Beside EC', there is another type of catalytic process in which the substrate receives electrons (discharge) directly from the electrode without mediator. A system in which the proton ( $H^+$ ) is the substrate (Fig. 2Cb) yields catalytic hydrogen currents. It is well known that many O-, N-, or S-containing organic compounds themselves [38] or in the presence of some metals (e.g. Co), yield a voltammetric (polarographic) catalytic hydrogen signal known as the Brdicka current (BC) [39]. Two types of mediatorless catalytic processes are possible for the proton reduction to molecular hydrogen. One is a catalytic chain reaction (BC type) and the other is electrocatalysis depending on whether the ligand site (Eq. (5)) or metal site (Eq. (6)) is activated in the protonation step.

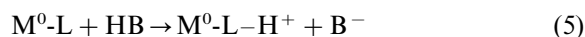
The metal complex (precatalyst),  $M^N L_x D_y (H_2O)_z$  (M denotes the central metal ion with oxidation number N, L is  $\pi$ -complexing ligands, D is any hard ligand from the buffer or

supporting electrolyte) is preconcentrated by adsorption and reduced to the catalyst,  $M^0-L$ , by electronation:

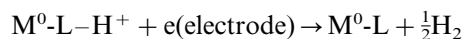


Eq. (4), which initiates the catalytic chain reaction, followed by a protonation step, as in Eq. (5).

### 3.4. BC process



↑-----↓ propagation



and/or



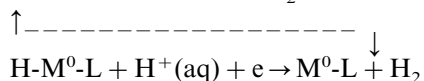
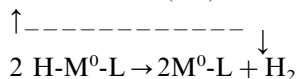
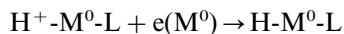
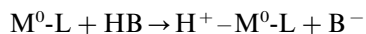
It has been observed that the ruthenium-hydroxylamine/hydrazine system yields this type of hydrogen catalytic currents [19,20]. The catalytic effect in these systems was not so large that the system was misunderstood as an EC' process. When the catalyst (Ru) concentration, however, is high enough, the evolution of hydrogen gas can be visually observed. From the analytical (trace metal) point of view, the BC type catalytic effect is not very helpful for improving the detectability.

### 3.5. Electrocatalysis

If the protonation step follows Eq. (6) instead of Eq. (5), the following step is the hydrogen evolution reaction on the metal ( $M^0$ ) electrode, a typical example of electrocatalysis, which is among the most intensively studied and the mechanism is well established [40]. It is typical of electrocatalytic reactions that the rates depend strongly on the electrode material and on the composition of the electrode-solution interface.

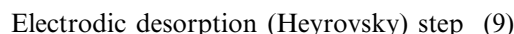
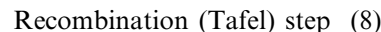
In the case of hydrogen evolution, the electrocatalytic effects on platinum and rhodium (Eq. (7) and following steps) can be attained as large as  $10^9$ -fold [41] to which the large catalytic effects for platinum and rhodium can be ascribed. This large

value comes from the difference in  $-\log i_0$  (exchange current density for the hydrogen-evolution reaction in  $\text{amp cm}^{-2}$ ) on mercury (12.3) and on platinum (3.1) and rhodium (3.6) electrodes.



Electrocatalysts depend on the rate-determining step of the reaction concerned. We can see that the rate-determining step is the discharge step (Eq. (7)) for common metals and chemical desorption (Eq. (8)) or diffusion of molecular hydrogen away from the catalyst surface for platinum and rhodium [41]. Czae et al. [42] demonstrated that the inverted peak (observed only with the rhodium–formaldehyde system) is due to the rate determining electrochemical desorption step (Eq.

(9)). This inverted peak may be attributed to a strong M–H bond and a stable organometallic formyl complex with the strong back bonding of rhodium. It suggests a new strategy for enhancing



the sensitivity for rhodium measurement by accumulation of the intermediate, M–H. As a conclusion, we summarize our discussions in Table 2.

#### 4. Biocatalysis–accumulation

Ultrasensitive measurements can also be achieved by coupling efficient biocatalytic reactions with preconcentration processes. Of particular interest, in this context, is the enzyme AP (alkaline phosphatase), a biological catalyst, which is known to be determined with the lowest detection limit to date,  $4 \times 10^{-16}$  M [43]. AP is one of the most commonly used labels in affinity sensing methods (e.g. immunoassays), due to its high turnover number and broad substrate specificity. Remarkable sensitivity (with subfemtomolar detection limits) could be achieved with the proper choice of substrate/product couples and accumulation of the cationic electroactive product onto cation-exchanger (Nafion) film covering a screen-printed electrode.

#### 5. Towards a femtomolar level

How far can we go? What are the limits? Can we go into a femtomolar, attomolar, or even further into the zeptomolar ( $10^{-21}$  M) regime without any limit in the concentration detection limit? This question leads to other interrelated questions: first, is there a theoretical limit in detectability? Second, are we fully exploiting the various factors for analytical purpose? Various

Table 2

Factors that exert profound effects on the reaction rate amplification

Factor	Amplification/ fold	Examples utilized (DL reached /M)
Accumulation	$a \approx 100$	Most of the metals ( $10^{-10}$ ) Mercury ( $5 \times 10^{-14}$ )
Adsorption	$b \approx 20$	
Catalysis		
Analyte as a catalyst:		
EC'	$c \approx 20$	Common metals ( $10^{-11}$ )
BC	$c \approx 10$	Ruthenium ( $10^{-10}$ )
Electro- catalysis	$c \geq 10^3$	Pt ( $4 \times 10^{-14}$ ), Rh ( $5 \times 10^{-14}$ )
Affinity assays	$c \geq 10^4$	AP (alkaline phosphatase enzyme) ( $4 \times 10^{-16}$ ) [43]
Analyte as a substrate (EC')		Uranium ( $10^{-8}$ ) [48]
Kinetic method		Ru, Os ( $3 \times 10^{-12}$ ) Mn ( $5 \times 10^{-11}$ ) by chaotic process [44]

advances answer ‘yes’ to the first question, suggesting it to be 0.1 fM. Detecting one (0.6) molecule means yoctomole ( $10^{-24}$  mol, amount not concentration!) detection limit. If the sample volume can be reduced to nanoliters (nl volumes are becoming routine), one (0.6) molecule corresponds to 0.1 femtomolar ( $10^{-16}$  M) which is the detectable concentration limit. Bagel et al. [43] achieved this limit ( $4 \times 10^{-16}$  M for alkaline phosphatase) by an affinity assay technique that consists of all types of contributing factors (Table 2). Yatsimirskii et al. [44] showed the theoretically attainable detection limit to be  $10^{-15}$  M for Mn(II) by a catalytic kinetic method based on the chaotic process in the Belousov–Zhabotinskii reaction.

Estimations for the gain  $G$  (Eq. (1)) from Table 2 show  $4 \times 10^4$  (with  $k = 1$ ) and  $1 \times 10^{6 \sim 8}$  for EC' and electrocatalysis factors in the coupled Ad-CtSV, respectively. By taking the micromolar level as the detection limit of standard linear scan voltammetry, we can obtain the detection limits as  $10^{-11}$  M for common metals (EC') and  $10^{-12 \sim 14}$  M for Pt and Rh by current AdCtSV.

As a conclusion, we are not fully exploiting the great advantages of the electrocatalysis (enzyme-like) process, using only a small fraction, say 0.01% (maximum  $10^5$  out of  $10^9$ ) for the metal target. Various chemical and instrumental approaches have been used to reduce the concentration detection limits. ASV with collection at IDA (interdigitated array) microelectrode [45], especially with redox cycling [46] is, in principle, analogous to AdCtSV, the most integrated electroodic complexity (due to its unique ability to regenerate the analyte).

So far we have focused on various means for enhancing the current signal in connection to adsorptive catalytic stripping voltammetry. Since the overall detectability is determined by the signal-to-noise (S/N) characteristics, proper attention needs to be given to advanced means for compensating the various components of the background current (faradaic and non-faradaic) and minimizing the associated noise (in connection with signal averaging). In addition to ad-

vanced microprocessor-controlled baseline fitting and noise-filtration strategies, attention should be given to the minimization of contamination risks through proper laboratory practice (expected for ultratrace work).

## 6. Concluding remarks

Voltammetric techniques have advanced very rapidly during the second half of the 20th century. The judicious combination of effective preconcentration and catalytic processes has opened the door to remarkably sensitive protocols, suitable for centralized and in situ detection of trace metals. The judicious design and coupling of proper methodologies should further lower the detection limits to the ppq (femtomolar) regime.

## References

- [1] J. Wang, in: A.J. Bard (Ed.), *Electroanalytical Chemistry*, vol. 16, Marcel Dekker, New York, 1989, pp. 1–88.
- [2] C.M.G. van den Berg, *Anal. Chim. Acta* 250 (1991) 265.
- [3] M.G. Paneli, A. Voulgaropoulos, *Electroanalysis* 5 (1993) 355.
- [4] D.W.M. Arrigan, *Analyst* 119 (1994) 219.
- [5] M.A. Cousino, T.B. Jarbawi, H.B. Halsall, W.R. Heineman, *Anal. Chem.* 69 (1997) 544A.
- [6] Z. Galus, *Fundamentals of Electrochemical Analysis*, 2nd edn, Ellis Horwood, Chichester, UK, 1994.
- [7] B. Pihlar, P. Valenta, H.W. Nürnberg, *Fresenius Z. Anal. Chem.* 307 (1981) 337.
- [8] J. Wang, J. Lu, R. Setiadji, *Talanta* 40 (1993) 351.
- [9] M. Czae, K. Kim, Y. Kwon, *J. Korean Chem. Soc.* 39 (1995) 186.
- [10] J. Lu, J. Wang, C. Yarnitzky, *Electroanalysis* 7 (1995) 79.
- [11] F.G. Bodewig, *Microchim. Acta (Wien)* 111 (1989) 75.
- [12] A. Bobrowski, A.M. Bond, *Electroanalysis* 4 (1992) 975.
- [13] J. Lu, W. Jin, S. Wang, T. Sun, *J. Electroanal. Chem.* 291 (1990) 49.
- [14] J. Wang, K. Varughese, *Anal. Chim. Acta* 199 (1987) 185.
- [15] K. Kritsotakis, H.J. Tobschall, *Fresenius Z. Anal. Chem.* 320 (1985) 156.
- [16] Y. Kwon, S. Kim, M. Czae, *Anal. Sci. Technol. (Seoul)* 10 (1997) 114.
- [17] R. Pallaniapan, T.A. Kumar, *Analyst* 118 (1993) 293.
- [18] J. Wang, Z. Taha, *Talanta* 38 (1991) 489.
- [19] T. Hong, Y. Kwon, M. Czae, *Anal. Sci. Technol. (Seoul)* 10 (1997) 119.
- [20] M. Czae, Y. Kwon, S. Kim, *J. Korean Chem. Soc.* 41 (1997) 246.



- [21] J. Wang, J. Lu, *Analyst* 117 (1992) 1913.
- [22] J. Wang, J. Zadeii, M.S. Lin, *J. Electroanal. Chem.* 237 (1987) 281.
- [23] K. Yokoi, C.M.G. van den Berg, *Anal. Chim. Acta* 245 (1991) 167.
- [24] T. Hong, M. Czae, C. Lee, Y. Kwon, M. Hong, *Bull. Korean Chem. Soc.* 15 (1994) 1035.
- [25] C. Leon, H. Emons, P. Ostapczuk, K. Hoppstock, *Anal. Chim. Acta* 356 (1997) 99.
- [26] C.M.G. van den Berg, G.S. Jacinto, *Anal. Chim. Acta* 211 (1988) 129.
- [27] S. Meyer, F. Scholz, R. Trittler, *Fresenius Z. Anal. Chem.* 356 (1996) 247.
- [28] Z. Zhao, H. Freiser, *Anal. Chem.* 58 (1986) 1498.
- [29] M. Czae, S. Lee, K. Chung, D. Lee, *J. Korean Chem. Soc.* 36 (1992) 616.
- [30] J. Wang, M. Czae, J. Lu, M. Vuki, *Microchem. J.* 62 (1999) 121.
- [31] C.J. Flora, E. Nieboer, *Anal. Chem.* 52 (1980) 1013.
- [32] J. Wang, J. Lu, R. Setiadji, *Electroanalysis* 5 (1993) 319.
- [33] J. Zhao, W. Jin, *J. Electroanal. Chem.* 256 (1988) 181.
- [34] C.M.G. van den Berg, *Talanta* 31 (1984) 1069.
- [35] M. Lovric, F. Scholz, *Electroanalysis* 9 (1997) 1189.
- [36] M. Kopanica, V. Stara, in: G. Svehla (Ed.), *Comprehensive Analytical Chemistry*, vol. XVIII, Elsevier, Amsterdam, 1983, pp. 33–125.
- [37] K.B. Yatsimirskii, L.P. Tikhonova, *Analyst* 34 (1987) 69.
- [38] S.G. Mairanovskii, *J. Electroanal. Chem.* 6 (1963) 77.
- [39] I.M. Kolthoff, P. Madar, *Anal. Chem.* 42 (1970) 1762.
- [40] S. Trasatti, in: H. Gerischer, C.W. Tobias (Eds.), *Advances in Electrochemical Science and Engineering*, vol. 2, VCH, Weinheim, 1992, pp. 1–85.
- [41] J.O'M. Bockris, A.K.N. Reddy, *Modern Electrochemistry*, vol. 2, Plenum, New York, 1972, pp. 1231–1251.
- [42] M. Czae, Y. Kwon, K. Im, Annual Meeting of the Korean Electrochemical Soc. P10, Oct. 9, 1998, Seoul, South Korea.
- [43] O. Bagel, B. Limoges, B. Schollhorn, C. Degrand, *Anal. Chem.* 69 (1997) 4688.
- [44] K.B. Yatsimirskii, P.E. Strizhak, T.S. Ivashenko, *Talanta* 40 (1993) 1227.
- [45] J. Wang, D. Luo, T. Horiuchi, *Electroanalysis* 10 (1998) 107.
- [46] F.F. Fan, J. Kwak, A.J. Bard, *J. Am. Chem. Soc.* 118 (1996) 9669.
- [47] Y. Yamamoto, K. Hasebe, T. Kambara, *Anal. Chem.* 55 (1983) 1942.
- [48] K.-H. Lubert, M. Schnurrbusch, *Anal. Chim. Acta* 186 (1986) 57.

# Determination of calcium, magnesium and strontium in soils by flow injection flame atomic absorption spectrometry

Zikri Arslan, Julian F. Tyson \*

*Department of Chemistry, University of Massachusetts, Box 34510, Amherst, MA 01003-4510, USA*

Received 15 March 1999; received in revised form 24 May 1999; accepted 24 May 1999

## Abstract

Several procedures for the determination of Ca, Mg and Sr in soils have been compared on the basis of the accuracy of analysis of two NIST reference materials (Montana Soils SRM 2710 and SRM 2711). Samples were dissolved in a mixture of hydrofluoric and nitric acids in sealed vessels in a microwave oven and in teflon beakers on a hot plate. The digests obtained from both dissolution methods were evaporated to dryness in an attempt to remove silicon. Boric acid was added to prevent the precipitation of the lanthanum releasing agent (as lanthanum fluoride) and potassium was added as an ionization buffer. Determinations were made by flame atomic absorption spectrometry with both the nitrous oxide–acetylene flame and the air–acetylene flame, with calibration either by standard additions or against external standards matrix matched with respect to nitric acid, boric acid, lanthanum and potassium. The silicon remaining in the solution was also determined by external calibration. A single-line flow injection manifold was used to overcome any problems due to the presence of high dissolved solids. A volume of 300  $\mu\text{l}$  was injected into a water carrier stream flowing at 8  $\text{ml min}^{-1}$ . To determine Ca in the air–acetylene flame, it was necessary to remove silicon. Magnesium was determined in either flame without complete removal of the silicon, however, for the determination of Sr, it was necessary to remove the silicon and use the nitrous oxide–acetylene flame. The indicative value for Sr in SRM 2710 was too low: the value determined was  $360 \pm 30 \mu\text{g g}^{-1}$ . © 1999 Elsevier Science B.V. All rights reserved.

*Keywords:* Calcium; Magnesium; Strontium determination; Soil dissolution; Silicon removal; Flow injection; Flame atomic absorption spectrometry

## 1. Introduction

As part of an on-going study of the uptake of elements by marine phytoplankton, it has been

necessary to devise validated methods for the determination of major and minor components by a number of different procedures. Although the main emphasis of our study has been on the use of plasma source mass spectrometry, methods involving flame atomic absorption spectrometry, and gas chromatography (following derivatization) with microwave induced plasma atomic

\* Corresponding author. Tel.: +1-413-545 0195; fax: +1-413-545-4846.

*E-mail address:* tyson@chem.umass.edu (J.F. Tyson)

emission detection are also under development. As there are, at present, no standard reference marine plankton materials available, suitable alternative materials for use in the method validation have been sought. We considered that soil would be a suitable surrogate reference material in this study as, to a first approximation, phytoplankton consist of a silicate skeleton together with plant-like organic material. Part of the study of plankton concerns whether it is necessary to dissolve the skeletal material to obtain information on the total elemental composition or whether an acid leaching procedure would be satisfactory. Initial experiments were conducted, in which the total elements (selected as those which could be readily determined by flame atomic absorption spectrometry) were determined following complete dissolution.

A critical stage in silicate analysis is the complete dissolution of siliceous materials. The conventional methods used are based on attacking the material with strong oxidizing acids or the use of fusion methods. The use of acids has advantages compared with fusion methods since it not only provides lower concentrations of dissolved salts, but also allows the removal of silicon by volatilization as fluoride [1]. Various workers have described methods for the complete dissolution of silicates using hydrofluoric/perchloric/nitric acids [2,5–7] hydrofluoric/sulphuric/nitric acids [2] and hydrofluoric/hydrochloric/nitric acids [2–4,6,8] in polytetrafluoroethylene (PTFE)-lined pressure vessels. However, great care must be taken if perchloric acid is used due to the risk of explosion.

Although atomic absorption spectrometry is practically free from spectral interferences, chemical interferences have to be taken into account in the development of new methods. The effect of chemical interferences and the steps needed to avoid or to compensate for, these effects have been well studied in flame atomic absorption spectrometry (FAAS). Silicon, aluminum and phosphate suppress the absorption signals of calcium, magnesium and strontium in the air–acetylene flame through the formation of stable compounds. These effects can be reduced by the addition of releasing agents such as lanthanum or

vanadium [4,7]. However, the addition of lanthanum to sample solutions containing fluoride results in the precipitation of lanthanum fluoride. Therefore, it is necessary to complex the excess hydrofluoric acid with boric acid prior to the addition of lanthanum [4,6,8]. However, it has been reported that for the determination of calcium by FAAS, it was necessary to use the nitrous oxide–acetylene flame and to matrix match with respect to silicon and aluminum since the lanthanum–fluoroborate–boric acid matrix did not completely eliminate the chemical interferences of silicon and aluminum [9].

Roos and Price [4] described the determination of calcium, magnesium and strontium in cement samples. However, they used the air–acetylene flame emission technique for calcium and magnesium, and determined strontium by absorption in the nitrous oxide–acetylene flame to eliminate the chemical interferences, despite the addition of boric acid and lanthanum.

Langmyhr et al. [6] used the bomb technique for decomposition of inorganic siliceous materials, and added saturated boric acid solution to the sample solutions. The authors recommended the nitrous oxide–acetylene flame for the determination of calcium and magnesium. EDTA was first used by Adams and Passmore [7] as a chelating agent to increase the effectiveness of lanthanum as a releasing agent in the air–acetylene flame. They reported that the pH of the solution was critical and should be adjusted to alkaline with ammonium hydroxide before final dilution to avoid subsequent precipitation of lanthanum fluoride.

Córdoba et al. reported the determination of calcium and magnesium in cements [10], soils [11], vegetables [12] and other samples with high silica content [13] with slurry nebulization flow injection flame atomic absorption spectrometry (FI-FAAS). Hydrochloric/hydrofluoric and nitric/hydrofluoric acids were used as suspension media. The major problems reported were nebulizer clogging and poor reproducibility due to the large particle size and instability of the suspensions, respectively. Thus, it was necessary to further grind the materials for approximately 30 min prior to preparation of slurries. A T-piece was also placed between the FI manifold and the

nebulizer to overcome the clogging problem observed for conventional FI sample introduction. Air sucked up through the T-piece allowed the introduction of the slurries in a discrete manner to the nebulizer [10,13]. For the vegetable samples, a precalcination step in a muffle furnace was also performed and the slurries made from the ground ash to overcome the clogging problems [12]. Soil slurries were heated in a microwave cavity for approximately 2 min to promote extraction of species into the suspension medium [11]. Various reagents such as glycerol [10] and Triton X-100 [12] were used to increase the stability of suspensions with continuous magnetic stirring during the introduction of slurries to the FI manifold.

David [14] described the determination of strontium in soils and plants by FAAS with an air–acetylene flame. An anion-exchange column was used to eliminate the interference of phosphate, and the standard additions method was used for calibration. Gutteridge et al. [15] reported a method for the determination of strontium in serum, in which strontium was coprecipitated with calcium oxalate. The precipitate was dissolved in hydrochloric acid and lanthanum was added. Recently, Lin and co-workers [16] have reported a continuous co-precipitation dissolution procedure for the determination of strontium in silicate rocks. In this method, samples were dissolved by hydrofluoric/perchloric/hydrochloric acid and followed by the co-precipitation of strontium with lead sulphate with dissolution in hot EDTA.

The advantages of flow injection sample introduction in atomic spectrometry over the conventional methods are well documented [17–21]. The major advantages can be summarized as the use of reduced sample volume without loss of sensitivity, reduced analysis time due to the high sample throughput (typically in the range of 100–120 samples  $\text{h}^{-1}$ ), improved precision (carrier solution is continuously introduced keeping the spray chamber saturated and the burner temperature constant). Another important advantage is the higher tolerance to the dissolved solids content, since a small volume of sample solution is introduced to the carrier stream, and the nebulizer-

burner system is continuously flushed with the carrier solution, which minimizes the blockage of nebulizer orifice and burner slot, as well as transport interferences and solute volatilization interferences.

We have developed a method for the determination of calcium, magnesium and strontium in silicates, based on dissolution in a mixture of hydrofluoric and nitric acids in which the depressive effect of silicon on the subsequent FAAS analysis was removed by the volatilization of silicon as the tetrafluoride. To minimize the problems associated with the build up of salts on the burner head, sample solutions were introduced to the spectrometer by a single-line FI manifold. Two methods of dissolution were evaluated. Dissolution in PTFE beakers on a hot plate was found to be preferable to dissolution of the samples in closed vessels in a microwave field.

## 2. Experimental

### 2.1. Apparatus

All measurements were made with a Perkin–Elmer (Norwalk, CT, USA) Model 1100 B atomic absorption spectrometer equipped with an Epson Model LQ-850 printer. Two types of interchangeable burner heads were used, a single-slot solid titanium air–acetylene burner with 100 mm path length and a nitrous oxide–acetylene burner with a 50 mm path length. Intensitron (Perkin–Elmer) hollow cathode lamps were used for the determination of Sr and Si. A multi-element (Ca, Mg and Zn) hollow-cathode lamp was used for Ca and Mg. Instrumental and operational parameters are given in Table 1. For the microwave digestion of the samples a CEM (Indian Trail, NC, USA) Model MSD-81D oven providing  $630 \pm 70$  W output power at 100% power setting was used. The 12-vessel turntable drive system rotates the samples  $360^\circ$  within the microwave field at 6 rpm. The vessel body and the cap are made of polyetherimide (Ultem), and the liner, cover and the rupture membrane are made of Teflon<sup>®</sup> perfluoroalkoxy (PFA). The vent screw is constructed of PTFE. The volume of the liner is 100 ml. The

Table 1

Instrumental parameters used for determination of Ca, Mg, Sr and Si by FI-FAAS

Element	Wavelength (nm)	Slit width (nm)	Lamp current (mA)	Air–acetylene flame characteristics (l min <sup>-1</sup> )		Nitrous oxide–acetylene flame characteristics (l min <sup>-1</sup> )	
				Air	Acetylene	Nitrous oxide	Acetylene
Ca	422.7	0.7	7	8	2.5	7	6.5
Mg	285.2	0.7	4	8	2.5	7	6.5
Sr	460.7	0.4	15	8	2.5	7	6.5
Si	251.6	0.2	40	–	–	7	6.5

digestion power and time were adjusted from the operation control panel, and displayed during the operation. A single line flow injection manifold was used. A pump (IsmaTec sa MS-REGLO) was used with Tygon pump tubes 1.5 mm internal diameter (i.d.) delivering a water carrier stream 8 ml min<sup>-1</sup>. Samples were introduced by a six-port rotary flow injection valve with a 300- $\mu$ l sample loop. All connecting tubing and the sample loop were made from 0.8 mm i.d. PTFE tubing. To minimize the dispersion, the length of tubing connecting the valve to the nebulizer was the minimum (300 mm).

### 2.2. Data collection and processing

The peak absorbance was measured at a 10 Hz data collection frequency. Five replicate measurements were made. The absorbance value for each replicate was displayed on the screen of the spectrometer. After five replicates, the mean peak height absorbance, the standard deviation and the relative standard deviation (RSD) of data were calculated and displayed by the instrument, and then printed by the printer. The calibration data for each element was processed on a personal computer using a graphics software (Cricket Graph Version 1.3.2) to construct the calibration curve and to obtain the equation of the calibration curve. Visual inspection of all scatter plots indicated that the external calibration and standard additions calibration plots were linear over the concentration range used. Correlation coefficients ( $r$ ) ranged from 0.998 to 1.00.

### 2.3. Reagents and standard solutions

All reagents used were of analytical grade unless specified otherwise. High-purity deionized distilled water with a resistivity of 18 M $\Omega$  cm was used to prepare all standard and sample solutions. A boric acid stock solution (2% m/v) was prepared from high purity solid boric acid (Alfa) by dissolving 5 g of the solid boric acid in 250 ml of deionized water. Standard working solutions of Ca, Mg, Sr and Si were prepared from 1000  $\mu$ g ml<sup>-1</sup> stock standard solutions by one-stage dilution with 4 ml of concentrated HNO<sub>3</sub> (Fisher), 30 ml of 2% m/v H<sub>3</sub>BO<sub>3</sub> and diluting to 100 ml with water. Lanthanum nitrate (Aldrich) and KNO<sub>3</sub> (Fisher) were added to all standards to yield the concentrations of 0.5% m/v and 1% m/v for lanthanum and KNO<sub>3</sub>, respectively.

Standard and sample solutions were stored in polyethylene bottles which had been soaked in 5% v/v nitric acid and rinsed with water before use.

### 2.4. Method development

An alternating variable search procedure was used to investigate the effect of operating parameters and to select suitable values for these. As the variables studied were not interactive to any great extent, this procedure is satisfactory and has the advantage (over a multivariate procedure) of providing useful information about the effect of a particular parameter on the method performance.

The flow injection variables were optimized to obtain the greatest peak height sensitivity for a 5  $\mu$ g ml<sup>-1</sup> calcium standard solution. The flow rate of carrier was varied from 2 to 14 ml min<sup>-1</sup>. The

volume of the sample loop was varied from 50 to 1000  $\mu\text{l}$ .

For the studies of the various other parameters (reagent concentration, heating program, and calibration procedure) the figure of merit was accuracy in the analysis of the standard reference materials. The concentration of  $\text{KNO}_3$  added to standard and sample solutions as ionization suppressor was varied from 0 to 2% m/v. The volume of concentrated hydrofluoric acid required for complete dissolution of samples was varied from 1 to 12 ml. For dissolution of samples on a hot plate, the temperature of the hot plate was varied from 100 to 180°C. For microwave-assisted digestion, the applied power of microwave system was varied from 20 to 60%. Preliminary experiments were performed to investigate the effect of the addition of lanthanum and boric acid sequence to the sample solutions.

### 2.5. Procedures

Two different methods were used to dissolve the soil samples. One was a microwave assisted digestion (Method 1), the other involved the digestion on a hot plate in PTFE beakers (Method 2). For determination of calcium and magnesium, approximately 100 mg of sample, 7 ml concentrated  $\text{HNO}_3$  and 3 ml concentrated HF were placed in the PTFE vessels of the microwave digestion system. The vessels were tightly capped and irradiated at 40% power for 10 min with continuous monitoring. At the end of the program, the vessels were removed and allowed to cool for 2–3 min in a fume hood and the pressure inside the vessels slowly released. After re-tightening, the vessels were irradiated for a further 10 min. This step was repeated three times altogether. At the end of the third time, the vessels were cooled to room temperature and opened to check if the complete dissolution, yielding colorless solutions, had been accomplished. In cases of incomplete dissolution, the microwave program was continued until the sample had dissolved. The vessels were then loosely capped and irradiated almost to dryness (30–40 min). After cooling, the residue was dissolved in 4 ml concentrated  $\text{HNO}_3$ ; and diluted to 100 ml in a calibrated flask with

water after the addition of 30 ml of 2% m/v  $\text{H}_3\text{BO}_3$ , lanthanum nitrate (0.5% m/v as La) and potassium nitrate (1% m/v). For the determination of strontium, approximately 150 mg of the sample was treated with the same digestion procedure, but the final dilution was made to 50 ml after the addition of 2 ml of  $\text{HNO}_3$  and 15 ml of 2% m/v  $\text{H}_3\text{BO}_3$ , lanthanum nitrate (0.5% m/v as La) and potassium nitrate (1% m/v).

In Method 2, the same volumes of HF and  $\text{HNO}_3$  and sample masses as for Method 1 were placed in PTFE beakers. The beakers were covered with PTFE covers and heated on a hot plate at 140°C (measured with a mercury in glass thermometer) for 3–4 h under the fume hood. After complete dissolution, the solutions were heated at the same temperature until all acid was removed. The temperature was decreased to 70°C and the solid residue was heated on the hot plate for 4–5 min to remove all volatile silicon tetrafluoride. The dried samples were dissolved by warming with 4 ml of concentrated  $\text{HNO}_3$  and the solutions were transferred to 100-ml calibrated flasks for calcium and magnesium determinations. For strontium, 2 ml concentrated  $\text{HNO}_3$  was added to dissolve the residue by warming, and the solution was transferred to a 50-ml calibrated flask. Boric acid, lanthanum and potassium were added as for the Method 1.

In both digestion methods, two reagent blank solutions were also prepared with the particular digestion procedures. One was diluted to 100 ml for Ca and Mg determinations, the other to 50 ml for Sr determination. The concentrations of  $\text{HNO}_3$ , La,  $\text{KNO}_3$  and  $\text{H}_3\text{BO}_3$  were all matched with those of the sample solutions.

The concentrations of Si remaining in the solutions after evaporation were determined, for SRM 2710, with the nitrous oxide–acetylene flame using the optimized flow injection parameters.

### 2.6. Method validation and calibration procedures

Two NIST reference materials were used for method validation, SRM 2710 Montana Soil (Highly Elevated Traces) and SRM 2711 Montana Soil (Moderately Elevated Traces). The concentration of Ca, Mg and Sr are similar in both

samples, but only SRM 2711 is certified for the Sr content. All three elements were determined in the SRM 2710, whereas only Sr was determined in SRM 2711. Four replicate analyses were made for each SRM.

Calibration was carried out by both external and standard additions methods. For external calibration, a blank and four standards containing 4% v/v HNO<sub>3</sub>, 0.5% m/v La, 1% m/v KNO<sub>3</sub> and 30 ml of 2% m/v H<sub>3</sub>BO<sub>3</sub>, were used. The external standards were 0.5, 1.0, 2.0 and 5.0 µg ml<sup>-1</sup> for Ca and Sr, and 0.1, 0.2, 0.4, and 0.6 µg ml<sup>-1</sup> for Mg. For the determination calcium and magnesium by external calibration, original solutions were diluted 5-fold by measuring 20 ml aliquots from the original sample solutions and diluting to 100 ml with a solution of 4% v/v HNO<sub>3</sub>, 0.5% m/v La, 1% m/v KNO<sub>3</sub> and 30 ml of 2% m/v H<sub>3</sub>BO<sub>3</sub>. Strontium was directly determined from the original (50 ml) solutions.

In the standard additions method, the data for one unspiked and three spiked sample solutions were used to construct the calibration curve. For the determination of Ca and Mg, 24 ml portions of the five-fold diluted sample solution was transferred to a 25-ml calibrated flask by using 20-ml and 2-ml bulb pipettes. The solution was spiked with either 25, 50 or 125 µl of the 1000 µg ml<sup>-1</sup> Ca standard solution, and either 5, 10 or 25 µl of the 1000 µg ml<sup>-1</sup> Mg standard solution. For the determination of Sr, 9 ml portions of the original sample solution were transferred to a 10-ml calibrated flask by a 10-ml graduated pipette and spiked with either 10, 20 or 50 µl of 1000 µg ml<sup>-1</sup> Sr standard solution. All spiked sample solutions were then diluted to volume with a 100 ml solution of 4% v/v HNO<sub>3</sub>, 0.5% m/v La, 1% m/v KNO<sub>3</sub> and 30 ml of 2% m/v H<sub>3</sub>BO<sub>3</sub>.

For the determination of Si, only external calibration was performed with a blank and three aqueous standard solutions, 20, 50 and 100 µg ml<sup>-1</sup>, which contained 4% v/v HNO<sub>3</sub>, 0.5% m/v La, 1% m/v KNO<sub>3</sub> and 30 ml of 2% m/v H<sub>3</sub>BO<sub>3</sub>.

Five replicate measurements were made for each solution, and the mean peak height absorbances calculated. To calculate the concentration of each analyte, the mean peak height absorbances for the samples from the analysis

solutions were substituted into the appropriate calibration equation. In the determination of the elements by the standard additions method, the concentrations of analytes were directly calculated by dividing the intercept on the absorbance axis by the slope of the calibration curve. The quotient was then corrected for the appropriate dilution factor.

### 3. Results and discussions

The optimum flow rate of the carrier stream was 8 ml min<sup>-1</sup>. The optimum sample loop volume was 300 µl. For injection volumes greater than 300 µl, there was no significant increase in the absorbance signal compared with that for direct aspiration. The optimum concentration of KNO<sub>3</sub> was 1% m/v. For the concentrations lower than 1% m/v, the recoveries of the analytes from the soils were significantly low due to the ionization interference which produced high absorbance values for the standards. The effect of volume of HF added into the digestion vessel is shown in Fig. 1 in terms of relative recoveries of Ca and Mg obtained from the N<sub>2</sub>O–C<sub>2</sub>H<sub>2</sub> and air–C<sub>2</sub>H<sub>2</sub> flames, respectively. The results indicated that 1

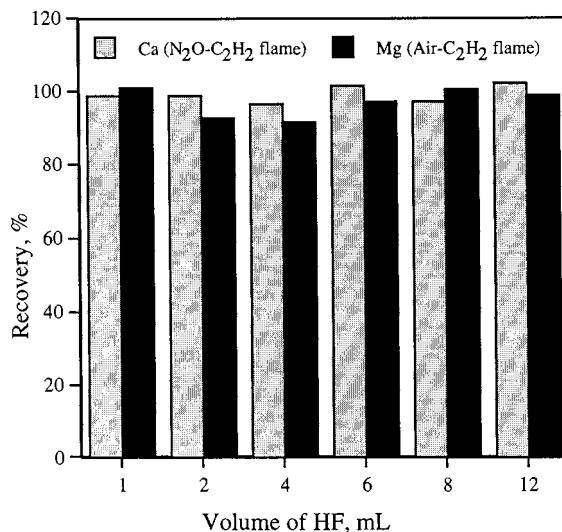


Fig. 1. The effect of concentrated hydrofluoric acid volume on the dissolution of silicate structure of soils (SRM 2710).

Table 2

Ca, Mg and Sr content of the samples solutions obtained by Method 1 in the air–acetylene and nitrous oxide–acetylene flames by FI-FAAS<sup>a</sup>

Sample	Element	Air–acetylene flame		Nitrous oxide–acetylene flame		Certified value
		By aqueous standards	By standard additions	By aqueous standards	By standard additions	
SRM 2710	Ca (%)	1.01 ± 0.05	1.30 ± 0.06	1.19 ± 0.05	1.28 ± 0.11	1.25 ± 0.03
	Mg (%)	0.876 ± 0.035	–	0.809 ± 0.073	0.813 ± 0.011	0.853 ± 0.042
	Sr (µg g <sup>-1</sup> )	214 ± 15	350 ± 11	348 ± 21	367 ± 27	240 <sup>b</sup>
SRM 2711	Sr (µg g <sup>-1</sup> )	135 ± 2.4	241 ± 15	245 ± 14	248 ± 33	245.3 ± 0.7

<sup>a</sup> Results are given as mean ± 95% confidence interval for four separate analyses.

<sup>b</sup> Indicative value.

ml of concentrated HF was sufficient to dissolve the samples. However, 3 ml was added to all soil samples to avoid any possible incomplete dissolution. The optimum hot plate temperature was 140°C. At higher temperatures, distortion of the bottom of the PTFE beakers was observed. The optimum power for the microwave oven was 40%, which gave a digestion time of 1–2 h. At lower power settings, not only did the digestion take longer, but did not completely dissolve some samples. A rapid increase in pressure inside the vessels occurred at higher power settings. For safety reasons, these values were not used.

A white precipitate of LaF<sub>3</sub> was rapidly formed for method 1 solutions, when lanthanum (0.5% m/v) was added prior to the H<sub>3</sub>BO<sub>3</sub> solution (30 ml v/v of 2% m/v H<sub>3</sub>BO<sub>3</sub>), which did not dissolve on the addition of up to 2 ml of concentrated HNO<sub>3</sub>. For the solutions digested by method 2, a faint turbidity was observed, indicating that some fluoride was still present, which dissolved slightly in 2 ml of concentrated HNO<sub>3</sub>. No precipitation occurred if the boric acid solution was added prior to the lanthanum solution. Thus, the boric acid solution was added first throughout the preparation of all standard and sample solutions to avoid any possible precipitation.

The concentrations of Ca, Mg and Sr obtained from the soil solutions are given in Tables 2 and 3 for methods 1 and 2, respectively. It is clear from the results of the standard additions analyses that complete dissolution of the soil samples were achieved in both digestion methods. Although the

magnesium results were unaffected by the digestion method and flame conditions, those of calcium and strontium from method 1 were significantly lower than those for method 2 when the air–acetylene flame was employed. The magnesium results are in agreement with those of Oguma et al. [22], who determined magnesium (only) in silicate rock by FI-FAAS after fusion with lithium carbonate and boric acid. Interferences were overcome by the addition of lanthanum. It was thought that the depression of the calcium signals was due to the incomplete removal of silicon by method 1. The certified concentration of silicon in SRM 2710 is 28.97 ± 0.18% (m/m). Thus, the concentration of silicon would be approximately 300 µg ml<sup>-1</sup> for Ca and Mg solutions and 900 µg ml<sup>-1</sup> for Sr solutions if silicon was not removed by evaporation. The silicon content of the solutions from method 1 varied from 10 to 50 µg ml<sup>-1</sup> whereas for those of method 2 it was less than 1 µg ml<sup>-1</sup>. These results indicated that for complete removal of Si, heating to dryness is necessary. Although the majority of Si was also removed in Method 1 by irradiating almost to dryness, the remaining one or two drops of liquid residue at the bottom of the digestion vessel, due to the equilibrium of evaporation and condensation process, contained a significant amount of Si. This could not be removed by evaporation to complete dryness, as for method 2, because of possible damage to the vessel body and liner by microwave radiation. The addition of lanthanum to the sample solutions did



Table 3

Ca, Mg and Sr content of the samples solutions obtained by Method 2 in the air–acetylene and nitrous oxide–acetylene flames by FI-FAAS<sup>a</sup>

Sample	Element	Air–acetylene flame		Nitrous oxide–acetylene flame certified		Certified value
		By aqueous standards	By standard additions	By aqueous standards	By standard additions	
SRM 2710	Ca (%)	1.29 ± 0.03	1.36 ± 0.11	1.22 ± 0.14	1.35 ± 0.12	1.25 ± 0.03
	Mg(%)	0.858 ± 0.039	—	0.856 ± 0.065	0.848 ± 0.062	0.853 ± 0.042
	Sr (µg g <sup>-1</sup> )	304 ± 14	377 ± 17	377 ± 27	381 ± 25	240 <sup>b</sup>
SRM 2711	Sr (µg g <sup>-1</sup> )	204 ± 15	275 ± 14	262 ± 26	286 ± 25	245.3 ± 0.7

<sup>a</sup> Results are given as mean ± 95% confidence interval for four separate analyses.

<sup>b</sup> Indicative value.

not, therefore, completely compensate for the suppression of silicon on calcium and strontium in the air–acetylene flame. However, the suppression was eliminated by use of the hotter nitrous oxide–acetylene flame.

In the case of strontium, it appears that the indicative value of 240 µg g<sup>-1</sup> for SRM 2710 is inaccurate. It is also apparent from the results for SRM 2711 that even with the removal of silicon, inaccurate results are obtained with the air–acetylene flame. However, the results of the standard additions method in the air–acetylene flame agreed with those of both external and standard additions methods in the nitrous oxide–acetylene flame. It is thought that the suppression of the Sr signal in the air–acetylene flame is due to the interference of other species such as aluminum and phosphate which are present at 6.44, and 6.53% for Al and 0.106, and 0.086 µg g<sup>-1</sup> for P in SRMs 2710 and 2711, respectively.

The slopes of the calibration curves of the standard additions methods for Sr in the air acetylene flame were 0.152 and 0.208 for methods 1 and 2, respectively, and they were significantly lower than that of the external method (0.239). This result also supports the hypothesis that there is a significant suppression of the Sr signal in the air–acetylene flame despite the removal of silicon.

The concentration of total dissolved solids in 100 ml diluted analysis solutions was around 2% m/v due to the addition of lanthanum (0.5% m/v),

KNO<sub>3</sub> (1% m/v) and 30 ml of 2% m/v H<sub>3</sub>BO<sub>3</sub>. No blockage of nebulizer and burner was observed with the air–acetylene flame due to the flow injection introducing 300 µL of 2% m/v sample solutions, and analysis was performed at approximately 60–70 h<sup>-1</sup> sampling frequency with manual injection. However, with the hotter nitrous oxide–acetylene flame, depositions were observed on the burner slot possibly due to the melting of metals and salts, which were frequently removed by a spatula to prevent the subsequent flame noise.

The absorbance data obtained from the air–acetylene flame were more precise than those for the nitrous oxide–acetylene flame. The relative standard deviation (RSD) in the peak height absorbance for five replicate measurements varied in the range of 0.8–3.1% for calcium, 1.0–4.1% for magnesium, 1.2–3.6% for strontium. The major problem during the measurements with the hotter and fast-burning nitrous oxide–acetylene flame was the substantial flame noise caused by the freezing of nitrous oxide at the cylinder outlet. Although the gas supply line was electrically heated at the outlet, it was not possible to control the temperature closely. Thermostatic heating is necessary to avoid any possible change in the flame conditions. Thus, the relative standard deviation (RSD) in the peak height absorbance in the nitrous oxide–acetylene flame was significantly higher than that of the air–acetylene flame and varied from 2.5–8.5% for calcium, 2.8–7.4% for magnesium, 2.7–7.4% for strontium.

#### 4. Conclusion

It is concluded that a mixture of hydrofluoric and nitric acids can completely dissolve the silicate materials in soils without the need for perchloric or hydrochloric acids, thus minimizing reagent contamination. The calibration by standard additions method requires further treatment of the analysis solutions, which increases the total analysis time and also the risk of contamination. Thus, external calibration is recommended provided that matrix matched standard solutions are used. Calcium can be determined accurately with the nitrous oxide–acetylene flame without complete removal of silicon, while the removal of the silicon is necessary for the accurate determination in the air–acetylene flame. It is not necessary to remove the silicon to obtain accurate analyses for magnesium determination, both air–acetylene and nitrous oxide–acetylene flames can be used, but the former is twice as sensitive as the latter. Considering the problems associated with the operation and the lower precision, however, the use of fast-burning nitrous oxide–acetylene flame is not recommended for calcium or for magnesium determination. For the determination of strontium, it is concluded that the removal of silicon is not sufficient to perform accurate analysis in the air–acetylene flame despite the addition of lanthanum as a releasing agent and potassium as an ionization suppressor. Thus, the nitrous oxide–acetylene flame should be used to eliminate the interferences (possibly due to aluminum and phosphates) on strontium.

It is thought that the indicative value of strontium in SRM 2710 reported by NIST is inaccurate. This hypothesis has been confirmed<sup>1</sup>.

#### Acknowledgements

The authors gratefully acknowledge Marmara

University (Turkey) for financial support for Zikri Arslan during the course of this study. This paper is funded in part by a grant from the National Oceanic and Atmospheric Administration (NOAA). The views expressed herein are those of the authors and do not necessarily reflect the views of NOAA or any of its sub-agencies.

#### References

- [1] M.S. Cresser, in: N.W. Barnett (Ed.), *Flame Spectrometry in Environmental Analysis. A Practical Guide*, The Royal Society of Chemistry, Cambridge, 1994, pp. 62–65.
- [2] C. Marqueda, J.L. Perez Rodriguez, J. Angel, *Analyst* 111 (1986) 1107.
- [3] B. Bernas, *Anal. Chem.* 40 (1968) 1682.
- [4] J.T.H. Roos, W.J. Price, *Analyst* 94 (1969) 89.
- [5] C.B. Belcher, K.A. Brooks, *Anal. Chim. Acta* 29 (1963) 202.
- [6] P.B. Adams, W.O. Passmore, *Anal. Chem.* 38 (1966) 630.
- [7] F.J. Langmhyr, P.E. Paus, *Anal. Chim. Acta* 43 (1968) 397.
- [8] C. Marqueda, E. Morillo, *Fresenius J. Anal. Chem.* 338 (1990) 253.
- [9] R.W. Lee, N. Guven, *Chem. Geol.* 16 (1975) 53.
- [10] M.A. Baustista, C.P. Sirvent, I.L. García, M.H. Córdoba, *Fresenius J. Anal. Chem.* 350 (1994) 359.
- [11] I.L. García, M.S. Merlos, M.H. Córdoba, *At. Spectrosc.* 17 (1996) 107.
- [12] P. Vinas, N. Campillo, I.L. García, M.H. Córdoba, *Anal. Chim. Acta* 283 (1993) 393.
- [13] I.L. García, J.A. Cortez, M.H. Córdoba, *Talanta* 40 (1993) 1677.
- [14] D.J. David, *Analyst* 87 (1962) 576.
- [15] D.C. Curnow, D.H. Gutteridge, E.D. Horgan, *At. Abs. Newsl.* 7 (1968) 45.
- [16] S. Lin, C. Zheng, H. Zu, *Talanta* 42 (1995) 1143.
- [17] J.F. Tyson, *Analyst* 110 (1985) 419.
- [18] J.F. Tyson, *Spectrochim. Acta Rev.* 14 (1991) 169.
- [19] J.F. Tyson, S.R. Bysouth, E.A. Grzeszczyk, E. Debrah, *Anal. Chim. Acta* 261 (1992) 75.
- [20] B. Welz, M. Sperling, *Pure Appl. Chem.* 65 (1993) 2465.
- [21] Z. Fang, *Flow Injection Atomic Absorption Spectrometry*, Wiley, New York, 1995, pp. 45–104.
- [22] K. Oguma, T. Nara, R. Kuroda, *Bunseki Kagaku.* 35 (1986) 690.

<sup>1</sup> R.L. Watters, Personal Communication.

# A study of the effect of proteins and endogenous cations on a lipophilic $\beta$ -cyclodextrin-based potentiometric lidocaine sensor using discrete solution and flow-injection analysis

Ritu Katakay<sup>a,\*</sup>, Klara Toth<sup>b</sup>, Simon Palmer<sup>a</sup>, Zsafia Feher<sup>b</sup>

<sup>a</sup> Department of Chemistry, University of Durham, Durham, DH1 3LE, UK

<sup>b</sup> Technical University of Budapest, Institute of General and Analytical Chemistry, Szent Gellert tér 4, H-1111 Budapest, Hungary

Received 19 May 1999; accepted 11 June 1999

## Abstract

2,6 Didodecyl  $\beta$  cyclodextrin (2,6dd $\beta$ CD) modified ion-selective electrodes (ISEs) were used in discrete solutions and in a flow injection analysis manifold for monitoring the local anaesthetic lidocaine hydrochloride (lignocaine) in the presence of endogenous cations and proteins. Membrane matrices comprised of either high molecular weight poly (vinyl chloride) (PVC) or polyurethane (Tecoflex SG 80) were compared. The behaviour of these electrodes in the presence of bovine serum albumin (BSA),  $\alpha_1$  acid glycoprotein (AAG) and human serum (HS) indicate that the Tecoflex-based membrane matrices are preferable to PVC as the drift induced by proteins on baseline lines and peak height reproducibility was considerably reduced in the former. Interference from 'serum' levels of sodium, potassium and calcium ( $145 \text{ mmol dm}^{-3} \text{ Na}^+$ ,  $1.26 \text{ mmol dm}^{-3} \text{ Ca}^{2+}$ ,  $4.30 \text{ mmol dm}^{-3} \text{ K}^+$ ) was negligible ( $-\text{Log } K_{ij}^{\text{POT}}$  (overall)  $\geq 4.0$ ). The major organic interferents were molecules of similar size and structure, which caused reduced slope and drift in baseline potentials, at equimolar concentration levels. A reduction in interferent concentration by a factor of 10 negated these effects. © 1999 Elsevier Science B.V. All rights reserved.

**Keywords:** Lidocaine; Ion-selective electrodes; Proteins; Cyclodextrins

## 1. Introduction

Several commonly used local anaesthetics consist of an aromatic moiety linked via an ester or amide group to a basic side chain. The molecules are weak bases (the  $\text{p}K_a$  of lidocaine, Fig. 1.2, is

8.2) so that they are partially ionised at physiological pH. In extra cellular fluids they are present as 'protein-bound' and 'free' fractions. The proteins, to which drugs most commonly bind, are albumin and  $\alpha_1$  acid glycoprotein (AAG). The acidic drugs, (e.g. barbiturates), in the main, bind to albumin and the more basic drugs (e.g. lidocaine) bind to AAG [1]. AAG is also called the acute phase or 'stress' protein. Approximately 65% of lidocaine is bound by AAG and this percentage

\* Corresponding author. Tel.: +44-191-3747391; fax: +44-191-3844737.

E-mail address: ritu.katakay@durham.ac.uk (R. Katakay)

can increase as the concentration of AAG in serum increases, for example after surgery or myocardial infarction.

Lidocaine not only acts as effective local anaesthetic but also as an antidysrhythmic drug. The normal therapeutic plasma range is  $4 \times 10^{-6}$ – $2 \times 10^{-6}$  mol dm<sup>-3</sup>, although in some patients, concentrations of up to  $2.0 \times 10^{-5}$  mol dm<sup>-3</sup> may be required to prevent arrhythmias [2].

Several analytical methods have been described for the detection of local anaesthetics. These include colorimetry [3,4], gas–liquid chromatography (GLC) [5–9] and high pressure liquid chromatography (HPLC) combined with UV detection [10–13] or electrochemical detection [14]. Ion-selective electrodes (ISEs) reported for lidocaine [15–17] are all based on ion pairing. All electrodes produced a Nernstian response in aqueous solutions, however, few interference studies were performed and no protein interference effects were studied. In a previous publication [18], lipophilic cyclodextrins were reported as the first neutral ionophores for local anaesthetics [19] with excellent selectivities over charge dense cations and several endogenous cations.

In this study 2,6 didodecyl  $\beta$  cyclodextrin (2,6dd $\beta$ CD; Fig. 1.1) based electrodes were incorporated in a flow injection manifold and the effects of proteins and endogenous cations were monitored in discrete solutions and flow-injection analysis (FIA) experiments.

## 2. Experimental procedures

### 2.1. Reagents

Lidocaine hydrochloride, bovine serum albumin (BSA) and AAG were obtained from Sigma (Poole, Dorset, UK). Fresh human serum (HS; without anticoagulants) was obtained from willing blood donors at Dryburn Hospital, Durham. These samples were used within 24 h. High relative molecular mass poly (vinyl chloride) (PVC), *o*-nitrophenyl octyl ether (*o*NPOE), dioctyl sebacate (DOS) and potassium tetraphenyl chloroborate (KTpClB) were obtained from Fluka (Buchs, Switzerland). The polyurethane Tecoflex SG 80 was obtained from Thermedics, USA. The ionophore 2,6 didodecyl  $\beta$  cyclodextrin was synthesised in Durham [19]. Sodium and potassium chloride of analytical grade were obtained from BDH (Merck House, Poole, Dorset). All standard solutions were prepared in de-ionised water.

#### 2.1.1. Electrodes

The electroactive membranes were prepared as 1.2% ionophore, 65.6% *o*NPOE (or DOS), 32.8% PVC (or TECOFLEX SG 80) and 0.4% KTpClB. These membranes were mounted in Philips IS (561) electrode bodies (Philips Analytical, Eindhoven, The Netherlands), with an inner filling solution of  $10^{-3}$  ammonium chloride solution. The electrodes were conditioned for 12 h in  $10^{-3}$  mol dm<sup>-3</sup> analyte solutions prior to use.

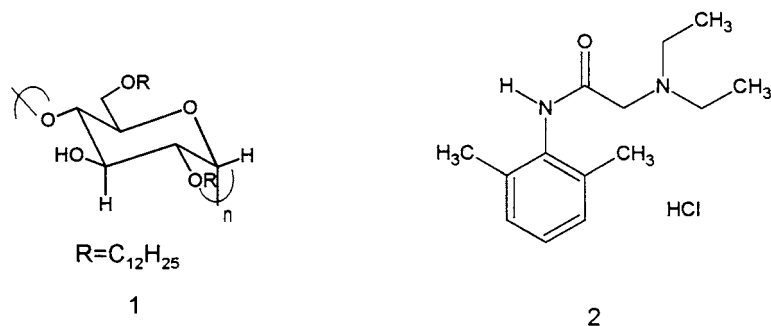


Fig. 1. Structures of the ionophore and analyte: 1, 2,6dd $\beta$ CD; and 2, lidocaine hydrochloride.

## 2.2. Flow-injection analysis manifold

The flow-injection manifold comprised an injector, dispersion coil, detector and peristaltic pump. Samples and carrier solutions were introduced into the flow system by a six-port manual injector with a sample loop volume of 250  $\mu\text{l}$  (Omnifit). The dispersion coil consisted of 1 m Teflon tubing. The detector cell [20] configuration was a macro wall jet system comprising a Philips IS-560 electrode body (Philips Analytical, Eindhoven, The Netherlands) and a single junction calomel electrode (ATI, Russell, Fife, Scotland, UK) with the ceramic frit fitted into the detector cell body. The reference electrolyte (0.1 mol  $\text{dm}^{-3}$  KCl) flowed continuously around the reference electrode frit, forming a thin film of flowing solution around the ion-selective as it entered the reservoir. The carrier stream impinged directly on the ISE membrane surface through a capillary.

The ISE and reference electrodes were connected to a buffer amplifier (Molspin, Newcastle, UK) with a voltage gain of three. The amplifier was connected to a digital multimeter (METEX M4650CR) and the results analysed using Microcal Origin. Measurements were made at ambient temperature. The flow rate of the system was 4  $\text{ml min}^{-1}$ .

## 2.3. Discrete solutions measurements

PVC and TECOFLEX based lidocaine selective electrodes were transferred back and forth between aqueous solutions containing a simulated clinical electrolyte background (145 mol  $\text{dm}^{-3}$   $\text{Na}^+$ , 4.3 mol  $\text{dm}^{-3}$   $\text{K}^+$  and 1.3 mol  $\text{dm}^{-3}$   $\text{Ca}^{2+}$ ) and electrolyte solutions that contained BSA (40 g  $\text{dm}^{-3}$ ), AAG (0.55 g  $\text{dm}^{-3}$ ) or pooled HS (40 g  $\text{dm}^{-3}$ ). The ISE and reference electrodes were placed, first in the aqueous analyte solution and the potential difference recorded after 20 min. The electrodes were then put into the protein containing solution and the potentials recorded after 20 min. This is a standard method for measuring protein-induced asymmetry potentials in calcium ISEs [21,22].

All calibration measurements were made at 298 K using a continuous dilution method described

Table 1  
 $\text{p}K_{\text{a}}$  and  $\text{p}I$  values of lidocaine and some endogenous cations studied as interferents

Compound	$\text{p}K_{\text{a}}$ (298 K)	Isoelectric point ( $\text{p}I$ )
Lidocaine	8.2	–
Glycine	9.60, 2.34	5.97
Vitamin B <sub>1</sub>	4.8, 9.2	–
Histidine	9.28, 6.17, 2.22	7.59
Nicotinamide	3.4 (pyridinium)	–

previously [23]. The fixed interference method (FIM) as defined by IUPAC (International Union of Pure and Applied Chemistry) [24] was used for selectivity coefficient determinations.

## 3. Results and discussions

### 3.1. Discrete solutions measurements

#### 3.1.1. Calibration and interferences

Calibration of an electrode comprising 2,6dd $\beta$ CD/Tecoflex/*o*NPOE/KTpClB at 298 K gave a marginally super-Nernstian response of 61.0 mV decade<sup>-1</sup> with a limit of detection  $1.58 \times 10^{-7}$ , whereas the equivalent PVC matrix electrode gave a slope of 55 mV decade<sup>-1</sup> and a limit of detection  $1.58 \times 10^{-5}$ . The linear relationship was maintained and excellent selectivity coefficients ( $-\log K_{ij}^{\text{POT}}$ , overall = 4.2) were obtained in a background of ‘serum’ levels of  $\text{Na}^+$ ,  $\text{K}^+$  and  $\text{Ca}^{2+}$  (145 mmol  $\text{dm}^{-3}$  NaCl, 4.3 mmol  $\text{dm}^{-3}$  KCl and 1.26 mmol  $\text{dm}^{-3}$   $\text{CaCl}_2$ ). This corroborates the preferential inclusion of the hydrophobic aryl moiety and/or the amine portion of the local anaesthetic preventing interference from hydrophilic alkali and alkaline earth cations.

Interferences from various organic endogenous organic substances such as vitamin B<sub>1</sub>, histidine, glycine and nicotinamide (Table 1) were studied using both PVC and Tecoflex based membranes (Fig. 2(a, b)). A selectivity coefficient was calculated for vitamin B<sub>1</sub>, which has a  $\text{p}K_{\text{a}}$  value of 4.8 and hence is ionic at the physiological pH. For the other organic interferents, glycine, histidine and nicotinamide results have not been reported

as selectivity coefficients as the interferences are primarily non-ionic at physiological pH (Table 1). The isoelectric point for glycine, for example, is 5.97. However, only 1% is in the cationic or anionic form at pH values between 4.3 and 7.7 [24,25]. For histidine, only 1.2% is ionised at pH 7.4, and 17.4% at pH 6.8. Any interferent effect would be attributable to a blockage of the ionophore or electrode fouling rather than a competition between the interferent and analyte for charge induced membrane transport. A major interferent for the lidocaine selective electrode was

10 mmol dm<sup>-3</sup> histidine which reduced the slope of the PVC electrode to 41.7 mV decade<sup>-1</sup> and increased the slope of the Tecoflex electrode to 67.4 mV decade<sup>-1</sup>. A 10-mmol dm<sup>-3</sup> nicotinamide background also interfered, the interference manifesting as a continuous drift of the baseline over 2–3 h. Vitamin B<sub>1</sub> (10 mmol dm<sup>-3</sup>) interfered with selectivity coefficients of  $-\log K_{ij}^{\text{POT}} = 2.4$  and 2.1 for PVC and Tecoflex membrane matrices, respectively (Table 2). These observations suggest that the major interferents are molecules of similar size and structure to the

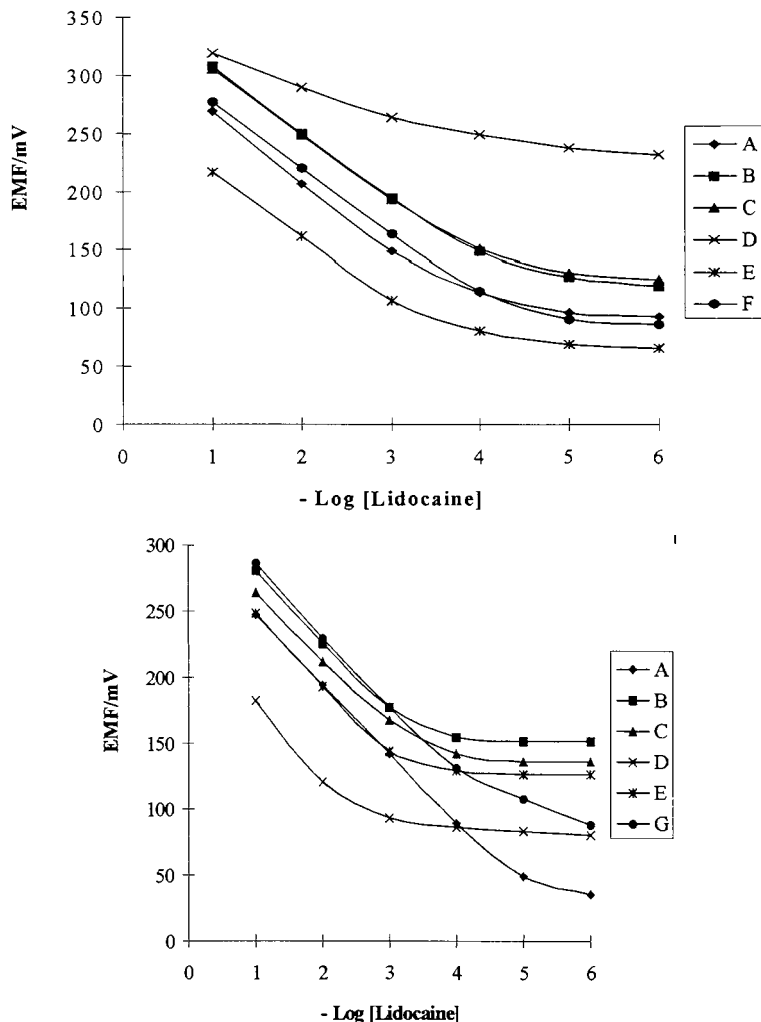


Fig. 2. Response curves for calibration and interferents for: (a) PVC; and (b) TECOFLEX membranes. A: aqueous; B: 145 mmol dm<sup>-3</sup> Na<sup>+</sup>, 4.3 mmol dm<sup>-3</sup> K<sup>+</sup>, 1.26 mmol dm<sup>-3</sup> Ca<sup>2+</sup>; C: 10 mmol dm<sup>-3</sup> Glycine; D: 1 mmol dm<sup>-3</sup> Nicotinamide; E: 10 mmol dm<sup>-3</sup> Vitamin B<sub>1</sub>; and F: 10 mmol dm<sup>-3</sup> L-histidine

Table 2  
Membrane matrices comprising of either PVC or Tecoflex were compared

Membrane matrix	PVC (interferent)		TECOFLEX (interferent)	
	'Serum cations'	Vitamin B <sub>1</sub>	'Serum cations'	Vitamin B <sub>1</sub>
Gradient (mV decade <sup>-1</sup> )	58.0	56.4	55.7	56.8
Selectivity Coeff., $-\log K_{ij}^{\text{POT}}$	4.2	2.4	4.2	2.1

primary ion. The interaction of lidocaine with  $\beta$ -CD may involve aryl inclusion strengthened by hydrogen bonding interactions either between the protonated amino group or the amido-NH and the glycosidic oxygen. Thus the major competitive binders are aryl molecules of similar size with pendant amino groups. Glycine being much smaller than lidocaine, does not compete for inclusion in the cyclodextrin cavity. However interference was removed when the concentration of nicotinamide background was reduced to 1.0 mmol dm<sup>-3</sup>. The physiological ranges of the endogenous organic interferents studied are: glycine, 1.46E-04–3.52E-04; histidine, 7.3E-05–1.25E-04; vitamin B<sub>1</sub>, 1.28E-08–5.9E-08; and nicotinamide, 3.3E-05–7.7 E-05 mol dm<sup>-3</sup>. This implies that whilst at such low concentration levels, substantial interference from these ions is unlikely.

### 3.1.2. Protein effects

Protein effects in discrete solutions were studied using established methods for calcium reference cells [21,22]. Three sets of graphs, corresponding to BSA, HS and AAG effects, were obtained (Fig. 3(a–c)) by switching PVC and Tecoflex based electrodes between aqueous electrolyte (containing 'serum' levels of Na<sup>+</sup>, K<sup>+</sup> and Ca<sup>2+</sup>) and electrolyte solution with added protein. Each set of graphs was comprised of two pairs corresponding to aqueous and protein-containing solutions for PVC and Tecoflex based membranes.

In BSA and HS containing electrolyte solutions, the Tecoflex-based membrane showed an initial drop in potential (pts. 1 and 2 in Fig. 3(a, b)). This effect was more pronounced for BSA containing solutions. Following this initial drop, the potentials returned to their original  $E^0$  values

(in aqueous solutions of 145 mmol dm<sup>-3</sup> Na<sup>+</sup>, 4.3 mmol dm<sup>-3</sup> K<sup>+</sup> and 1.26 mmol dm<sup>-3</sup> Ca<sup>2+</sup> consistently). With the PVC-based membranes, the recovery in  $E^0$  values after exposure to BSA and HS was scattered. This observation is consistent with a report by D'Orazio et al. [21,22] which indicates a scatter in protein induced calibration shifts for PVC-based Ca<sup>2+</sup> ISEs. Furthermore, the induced  $E^0$  shift resulting from the switching between aqueous and protein-containing solutions was higher for pooled HS (approximately 20 mV) compared to BSA (approximately 8 mV).

Basic drugs such as lidocaine tend to bind, preferentially, to the protein AAG (reference range in plasma; 0.55–1.4 g dm<sup>-3</sup>). Measurements in 'serum' levels of AAG in a background of 'serum' levels of Na<sup>+</sup>, K<sup>+</sup> and Ca<sup>2+</sup> indicated that the effect of AAG on protein induced  $E^0$  shifts was very small at the relative concentration ratios of analyte and AAG used in this study (Fig. 3(c)).

With all three proteins the slope of the electrode was checked (between 10<sup>-2</sup> and 10<sup>-3</sup> mol dm<sup>-3</sup> solutions) after washing the membrane with 2 mol dm<sup>-3</sup> NaCl solutions. Nernstian response was maintained despite the shift in  $E^0$  values as discussed above.

## 3.2. Flow-injection-analysis

### 3.2.1. Aqueous calibrations

Calibrations with various combinations of 2,6dd $\beta$ CD, polymer matrix, plasticiser and anionic additive in a carrier solution of 1.0 mmol dm<sup>-3</sup> lidocaine hydrochloride and 0.1 mol dm<sup>-3</sup> NaCl at ambient temperature showed that the Tecoflex based membranes produced Nernstian slopes whereas the PVC-based membrane was

sub-Nernstian (slope, 54.5 mV decade<sup>-1</sup>). Responses to the analyte at concentrations greater than that of the carrier solution (1.0 mmol dm<sup>-3</sup> lidocaine) were evident as positive peaks and responses to concentrations less than 1.0 mmol dm<sup>-3</sup> lidocaine as negative peaks.

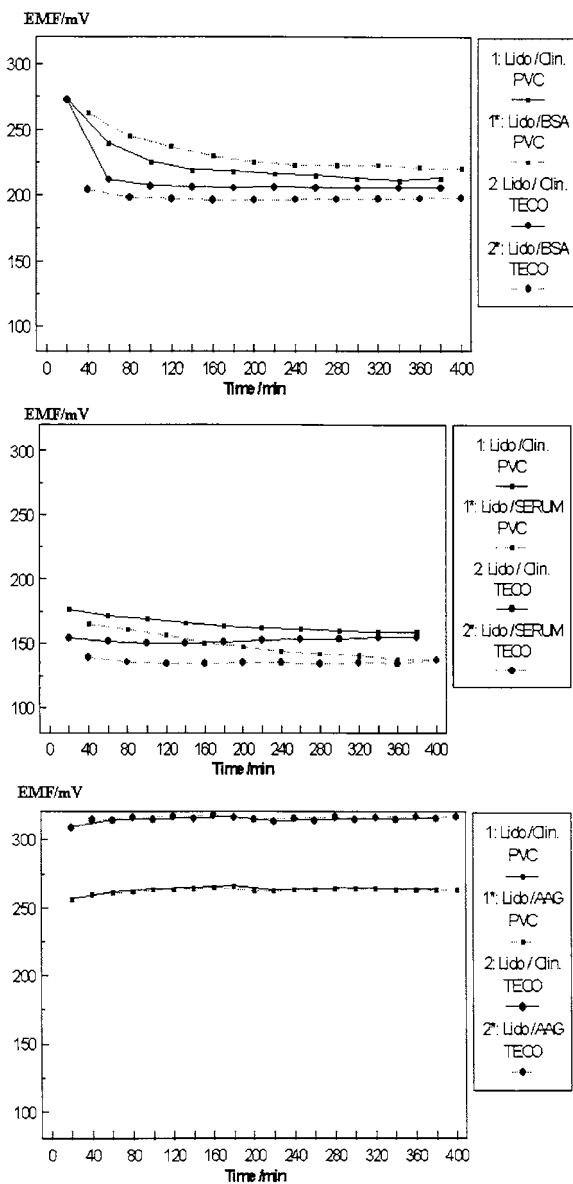


Fig. 3. Potentiometric response for PVC and Tecoflex membranes in presence of proteins in a background of 145 mmol dm<sup>-3</sup> Na<sup>+</sup>, 4.3 mmol dm<sup>-3</sup> K<sup>+</sup>, 1.26 mmol dm<sup>-3</sup> Ca<sup>2+</sup>: (a) 40 g dm<sup>-3</sup> BSA; (b) 40 g dm<sup>-3</sup> pooled HS; and (c) 0.55 g dm<sup>-3</sup> AAG.

### 3.2.2. Calibrations in protein based solutions

Corroborating observations in discrete solutions measurements, the Tecoflex-based membranes showed a superior Nernstian response and stable baseline (Fig. 4) compared to PVC based membranes with electrolyte solutions containing 40 g dm<sup>-3</sup> BSA. The drift was not apparent in solutions containing serum levels of AAG (0.55 g dm<sup>-3</sup>). However, fresh HS doped with 10<sup>-5</sup> mol dm<sup>-3</sup> lidocaine caused a baseline drift with Tecoflex based membranes compared to an aqueous electrolyte solution containing 'serum' levels of Na<sup>+</sup>, K<sup>+</sup> and Ca<sup>2+</sup> and doped with the same amount of lidocaine (Fig. 5). This may be attributable to the fact that the fresh HS samples were not thoroughly separated from whole blood resulting in membrane fouling by corpuscles. Another possibility is that proteins adhere to the membrane resulting in a systematic drift. In order to verify this possibility, a solution of 5% pepsin in 0.1 mol dm<sup>-3</sup> hydrochloric acid, known to remove proteins from electrodes, was injected alternately with the fresh HS samples. A dramatic reduction in base line drift was observed (Fig. 5) rendering this procedure suitable for analysis in undiluted HS.

Calibrations of Tecoflex/2,6ddβCD/DOS/KTp-CIB membranes in backgrounds of 'serum' levels of cations, 0.55 g dm<sup>-3</sup> AAG, 40 g dm<sup>-3</sup> BSA and HS doped with 10<sup>-1</sup>–10<sup>-7</sup> mol dm<sup>-3</sup> lidocaine hydrochloride were plotted using average peak heights of the injected solutions for each concentration (Fig. 6). A linear Nernstian response was maintained with the AAG and BSA containing solutions down to approximately 10<sup>-5.5</sup> mol dm<sup>-3</sup> analyte. In aqueous solutions, the limit of detection was extended to approximately 10<sup>-6</sup> mol dm<sup>-3</sup> while in fresh HS solutions the limit of detection was reduced to 10<sup>-5</sup> mol dm<sup>-3</sup>.

In conclusion, a study of the effect of proteins and endogenous cations (exemplified using lidocaine hydrochloride) on the measurements of 'onium' ion drugs on modified cyclodextrin based ISEs leads to the following outcome. Interference is only observed with equivalent concentrations of



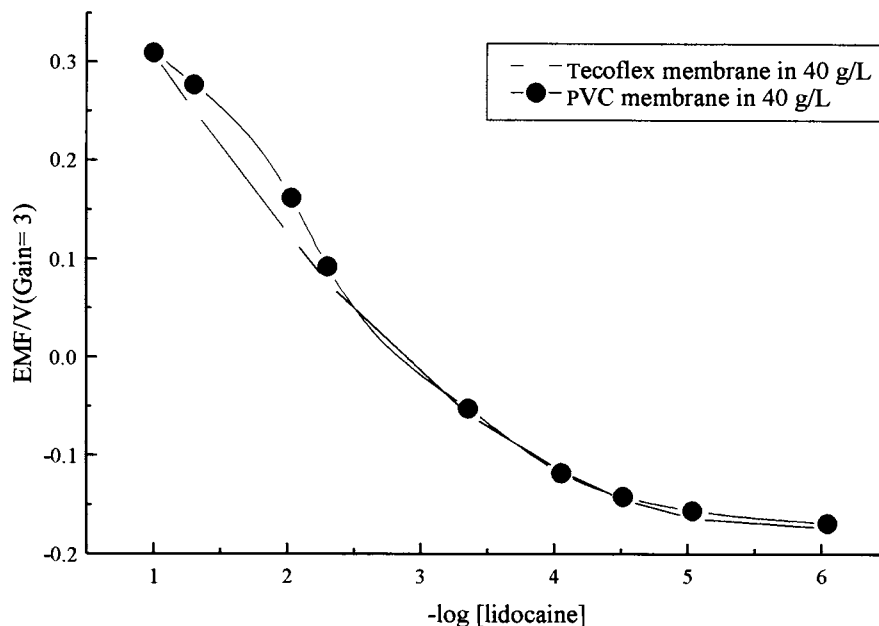


Fig. 4. Comparison of the effect of electrode calibration in FIA using a PVC and Tecoflex membrane matrix in a background of  $40 \text{ g dm}^{-3}$  BSA,  $145 \text{ mmol dm}^{-3}$   $\text{Na}^+$ ,  $4.3 \text{ mmol dm}^{-3}$   $\text{K}^+$ ,  $1.26 \text{ mmol dm}^{-3}$   $\text{Ca}^{2+}$ .

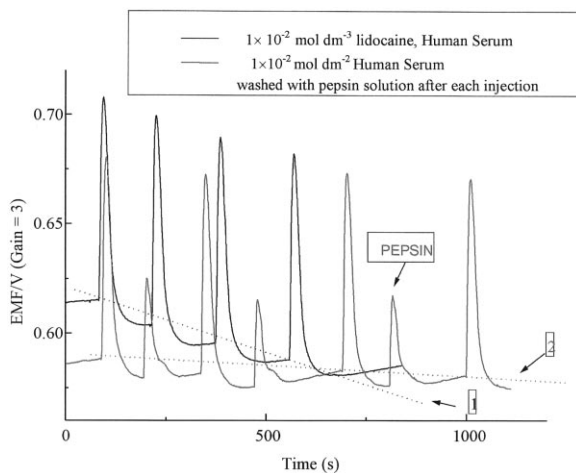


Fig. 5. Response of a Tecoflex matrix electrode to fresh HS doped with  $10\text{-mmol dm}^{-3}$  lidocaine hydrochloride (1). Reduction in baseline drift after intermittent washing with pepsin (2).

endogeneous cations of similar structure and charge. For calibrations in protein containing solutions FIA using Tecoflex SG80 based membrane matrices with intermittent washing using pepsin gives the minimum drift in base line and the lowest detection limit.

### Acknowledgements

We thank Professor David Parker (Department of Chemistry, Durham University) for synthesis of the cyclodextrin ionophores and discussions and Professor A.K. Covington (Emeritus Professor, University of Newcastle) for discussions on standard protein interference measurements and selectivity coefficient measurements. We also thank the British Council and the Hungarian Academy of Science for funding the collaboration between Durham University (UK) and the Technical University of Budapest (Hungary).

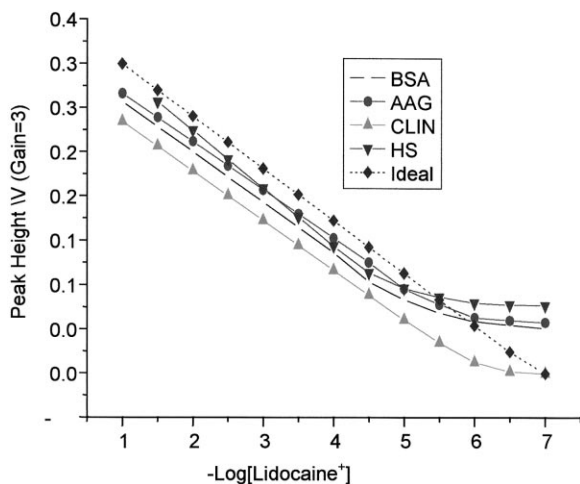


Fig. 6. Calibration of a Tecoflex matrix membrane electrode in: 1, 40 g dm<sup>-3</sup> BSA + CLIN; 2, 0.55 g dm<sup>-3</sup> AAG + CLIN; 3, CLIN: 145 mmol dm<sup>-3</sup> Na<sup>+</sup>; 4.3 mmol dm<sup>-3</sup> K<sup>+</sup>, 1.26 mmol dm<sup>-3</sup> Ca<sup>2+</sup>; 4, HS + CLIN; and 5, Ideal Nernstian response.

## References

- [1] C.J. Hall, S.A. Feldmann, W. Paton, S. Scurr, *Mechanisms of Drugs in Anaesthesia*, 2nd ed., Edward Arnold, London, 1993, chapter 5.
- [2] H.P. Rang, M.M. Dale, J.M. Ritter, *Pharmacology*, 3rd ed., Churchill Livingstone, London, 1995, chapter 34.
- [3] A. Cruz, M. Lopez-Rivadulla, A.M. Bermejo, I. Sanchez, P. Fernandez, *Anal. Lett.* 27 (14) (1995) 2663–2675.
- [4] G.A. Saleh, H.F. Askal, *Anal. Lett.* 28 (15) (1995) 2663–2671.
- [5] C.A. Di-Fazio, R.E. Brown, *Anesthesiology* 34 (1) (1971) 86–88.
- [6] L.J. Lesko, J. Ericson, *J. Chromatogr. Biomed. Appl.* 182 (1980) 226–231.
- [7] J.D. Hawkins, R.R. Bridges, T.A. Jennison, *Ther. Drug Monit.* 4 (1982) 103–106.
- [8] K.K. Adjepon-Yamaoh, L.F. Presscott, *J. Pharm. Pharmacol.* 26 (1974) 889–893.
- [9] H. Hattori, S. Yamamoto, T. Yamada, O. Suzuki, *J. Chromatogr. Biomed. Appl.* 564 (1991) 278–282.
- [10] H. Arimoto, K. Shiomi, T. Fujii, *J. High Res. Chromatogr.* 14 (1991) 672–675.
- [11] R.L.P. Lindberg, J.H. Kanto, K.K. Phlajamki, *J. Chromatogr. Biomed. Appl.* 382 (1992) 357–364.
- [12] H. Kastrissios, M. Hung, E.J. Triggs, *J. Chromatogr. Biomed. Appl.* 577 (1992) 103–107.
- [13] I. Murillo, J. Costa, P. Salva, *J. Lig. Chromatogr.* 16 (16) (1993) 3509–3514.
- [14] M.K. Halbert, R.O. Baldwin, *J. Chromatogr. Biomed. Appl.* 306 (1984) 269–277.
- [15] M.S. Ionescu, A.A. Abrutis, N. Radulescu, G.E. Baiulescu, V.V. Cosofret, *Analyst* 110 (1985) 929–931.
- [16] S.S.M. Hassam, M.-A. Ahmed, *J. Assoc. Off. Anal. Chem.* 69 (4) (1986) 618–621.
- [17] A.S. Kureichuck, V.I. Pantsurkin, E.V. Ptukha, K.D. Potemkin, *Zhurnal Analiticheskoi Khimii* 45 (3) (1990) 569–574.
- [18] R. Kataký, S. Palmer, *Electroanalysis* 8 (6) (1996) 585–590.
- [19] P.S. Bates, R. Kataký, D. Parker, *J. Chem. Soc. Perkin Trans. 2* (1994) 669.
- [20] J. Jenny, K. Toth, E. Linder, E. Pungor, *Microchem. J.* 45 (1992) 232–247.
- [21] P. D’Orazio, M.F. Burnett, S.F. Sena, *Proc. Blood Gas and Other Critical Analytes: the Patient, the Measurement and the Government Conf., Electrolyte and Blood Gas Division of AAC, Chatham, Massachusetts*. 17–20, May, 1992, vol. 114, p. 21.
- [22] P. D’Orazio, *Methodology and Clinical Applications of Blood Gases, pH, Electrolytes and Sensor Technology, IFCC symposium proceedings, Monterey, USA, 12 (1990) 373.*
- [23] R. Kataký, P.E. Nicholson, D. Parker, A.K. Covington, *Analyst* 116 (1991) 135.
- [24] *Recommendations for Nomenclature of Ion-Selective Electrodes*, *Pure Appl. Chem.* 48 (1975) 129.
- [25] E.J. Cohn, J.T. Edsall, *Proteins, Amino Acids and Peptides*, Reinhold, New York, 1943, p. 84.

# Determination of manganese in grain by potential titration with catalytic end-point indication

Dong Xuezhi \*, Li Deliang, Chen Chunshan, Zhang Jingwei

*Department of Chemistry, Henan University, Kaifeng, Henan 475001, People's Republic of China*

Received 9 December 1998; received in revised form 10 June 1999; accepted 15 June 1999

## Abstract

A method of catalytic potential titration for the determination of trace manganese by using crystal violet ion selective electrode is reported in this paper. It is based on the catalytic effect of manganese (II) on the oxidation of crystal violet by potassium periodate in the presence of nitrilotriacetic acid (NTA). The experiments indicated that this technique showed high sensitivity and high accuracy. The results of determination of trace manganese in grain could be compared with the results obtained by means of atomic absorption spectrometry. © 1999 Elsevier Science B.V. All rights reserved.

*Keywords:* Catalytic potential titration; Manganese; Grain; Crystal violet; Ion selective electrode

## 1. Introduction

Manganese is one of the important trace elements for human body. It functions in haematogenous organs, acts on the organic oxidizing process, and takes part in the activating of oxidase and dipeptidase. Furthermore, it is useful to the synthetical process of thiamine and ascorbic acid [1]. Grain is an important source of Mn that human body needs. So the determination of Mn in grain is quite necessary.

However, it is not easy to determine Mn owing to its less content in grain. The potential titration

with catalytic end-point indication proposed in this paper exhibited high sensitivity and high accuracy comparing to the normal analytical method. The apparatus used this method is very simple and the operation is rather easy.

The theory and application of the titrimetric methods with catalytic end-point indication have been reported [2–6]. However, in the recent years these titrations have gradually declined in number [7,8]. The investigation of trace Mn(II) determination, which is based on the catalytic effect of Mn(II) on the oxidation of crystal violet (CV) by potassium periodate in the presence of NTA, was carried out in our laboratory. The reactions are described as follows:

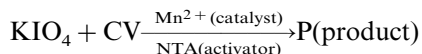
Titration reaction:



\* Corresponding author.

E-mail address: jingfangzhou@371.net (D. Xuezhi)

Indicator reaction:



This method has been applied for the determination of Mn in rice and millet. The results are in good agreement with the results obtained by atomic absorption spectrometry method.

## 2. Experimental

### 2.1. Reagents and apparatus

#### 2.1.1. Reagents

EDTA standard solution: 0.01 M EDTA standard solution was prepared from the sodium ethylene diamine tetracetate and was standardized with ZnO by conventional method. Working standard solutions ( $1 \times 10^{-6}$ – $1 \times 10^{-3}$  M) were prepared by suitable dilution.

Mn(II) standard solution: The solution (0.01 M) was prepared from the  $\text{MnSO}_4$  and was standardized with EDTA standard solution by conventional method. Working standard solution ( $1 \times 10^{-6}$ – $1 \times 10^{-3}$  M) were prepared by suitable dilution.

Other solutions were prepared by conventional method. All of the chemicals used in the experiments were of analytical-reagent grade. Double distilled water was used in the experiments.

#### 2.1.2. Apparatus

Model ZD-2 (Shanghai, China) automatic electric potential titration meter;

Model 180-60 (Japan) atomic absorption spectrometer;

Model 501 (Chongqing, China) thermostat;

CV ion selective electrode was prepared by the authors [9].

### 2.2. Procedure

The schematic diagram of apparatus is described in Fig. 1.

All the solutions used were thermostated at  $41 \pm 0.5^\circ\text{C}$  in the thermostat before use. The reaction temperature in titration process was main-

tained at  $41 \pm 0.5^\circ\text{C}$  with water flowing from the thermostat. The proper amount of Mn (II) sample solution and a known excess of EDTA standard solution were added into the thermostated titration cell under magnetic stirring. Subsequently, 1.5 ml of  $1 \times 10^{-3}$  M CV, 1 ml of  $5 \times 10^{-3}$  M NTA, 2 ml of  $1 \times 10^{-2}$  M potassium periodate ( $\text{KIO}_4$ ) and 2 ml of pH, 4 buffer were added into the titration cell one by one, then the solution was diluted to 25 ml with water. A CV ion selective electrode (ISE) and a saturated calomel electrode were immersed into the solution, The two electrodes were linked with an automatic electric potential titration meter and a recorder. Finally, the Mn (II) standard solution was added into the titration tube. Then began to titrate and the variance of the cell potential with consumed volume of the Mn(II) standard solution was recorded simultaneously. Before the end-point of the titration arrives, the indicator reaction rate is slow, accordingly the potential of CV ISE varies very slowly. While the end-point of the titration arrives, a excess drop of Mn(II) catalyzes the indicator reaction immediately, so the potential of CV ISE varies considerably. In the titration curve, the

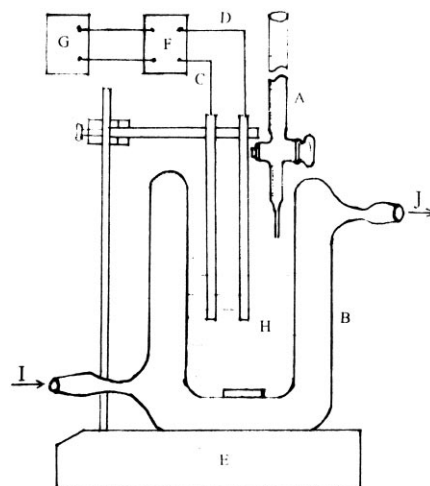


Fig. 1. The schematic diagram of apparatus. A: titration tube; B, titrated cell; C, CV ion selective electrode; D, saturated calomel electrode; E, magnetic stirrer; F, automatic electrical potential titration meter; G, recorder; H: solution to be titrated; I, thermostated water inlet; J, thermostated water outlet.

point where the cell potential varies considerably with consumed volume of the Mn(II) standard solution is used to locate the end-point of the titration reaction. The content of Mn in the sample can be calculated by the difference between EDTA standard solution added and Mn(II) standard solution consumed at the end-point of the titration.

### 3. Results and discussion

#### 3.1. Choice of the experimental conditions

The temperature and other variables were kept constant during the titrating.

In the following experiments, except the conditions to be chosen, the other conditions were the same as which mentioned in the procedure. We use 3 ml  $1.012 \times 10^{-4}$  M EDTA, which was titrated with  $8.096 \times 10^{-5}$  M Mn(II) standard solution.

The concentration of reagents is meant their concentration in the solution (its volume is 25 ml) before the titrating.

##### 3.1.1. Choice of concentrations of CV and $KIO_4$

The concentration of CV chosen is  $6 \times 10^{-5}$  M in this work. It is based on that the CV ISE exhibits a Nernstian response over the concentration range from  $2 \times 10^{-6}$  M to  $2 \times 10^{-4}$  M.

During the titrations, the concentration of potassium periodate must be kept at a rather large level in order to ensure that the rate of the indicator reaction is independence of it. The effect of the concentration of periodate on the titration curve has been investigated in the range of  $4 \times 10^{-4}$ – $1.6 \times 10^{-3}$  M. The results were shown in Fig. 2. It can be seen that the variations of the cell potential at the end-point of the titrations increases with the concentration of periodate increasing, and the end-points of these titrations are all remarkable and are in agreement each other. The concentration of periodate chosen is  $8 \times 10^{-4}$  M.

##### 3.1.2. Influence of NTA concentration

The effect of NTA concentration was investigated in the range of  $0$ – $2 \times 10^{-3}$  M. The experi-

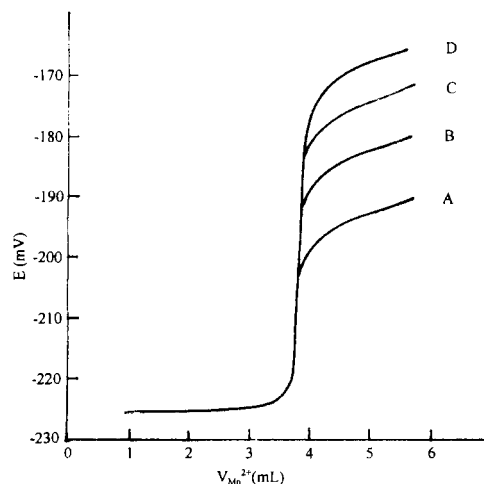


Fig. 2. Effect of potassium periodate concentration on the titration curve. A,  $4 \times 10^{-4}$  M  $KIO_4$ ; B,  $8 \times 10^{-4}$  M  $KIO_4$ ; C,  $1.2 \times 10^{-3}$  M  $KIO_4$ ; D,  $1.6 \times 10^{-3}$  M  $KIO_4$ .

ments showed that NTA can increase the catalytic effect of Mn(II). When NTA is absent, the cell potential at the end-point of the titration varied so slow that the end-point of the titration cannot be located. The end-point became remarkable gradually with the concentration of NTA increasing. When the concentration of NTA is in the range of  $1 \times 10^{-4}$ – $5 \times 10^{-4}$  M, the end-point can be remarkably observed, and the reproducibility of the titration is much better, because NTA is not amenable to complexometric titration with the catalytic end-point indication reported here. However, when the concentration of NTA is too high (higher than  $1 \times 10^{-3}$  M), the reproducibility of the titration is not good. It is possibly ascribed to the formation of trace of Mn-NTA complex, and the further investigation is necessary for this question. The chosen concentration of NTA is  $2 \times 10^{-4}$  M. On the other hand, NTA can react with other metal ions to form stable complexes under the chosen experimental condition. So NTA can mask these metal ions from EDTA to increase the selectivity of the method.

##### 3.1.3. Effect of pH value on titrating behavior

The influence of pH value on the titration curve was investigated in the range of 2.5–11.0. The results were shown in Fig. 3. The experiment

showed that when the pH value of the solution was lower than 3, the end-point of the titration was not evident because the reaction of the Mn(II) complexes with EDTA was not complete. When the pH was in the range of 3.2–6.0, the end-point was very evident and the accuracy of the titration was very high. When the pH was higher than 7.0, the sensitivity of the end-point gradually decreases with the rising of the pH. This is due to that high pH values would decrease selectivity and increase the possibility of competing hydroxo-complexes or precipitation of hydrated oxides in the vicinity of the end-point. When the pH was 9.8, the end-point of the titration could not be located. If the pH was higher than 10.5, the CV would precipitate before the titration. The suitable range of pH is 3.2–6.0, so pH of 4 is chosen in this work.

### 3.1.4. Effect of reaction temperature

The effect of temperature on the indicator reaction has been investigated specially. The comparison experiments between the catalyzed and the uncatalyzed reactions were investigated at 20, 25, 30, 35, 37, 39, 40, 41, 43, 45, 50, 55, and 60°C, respectively. The experiments showed

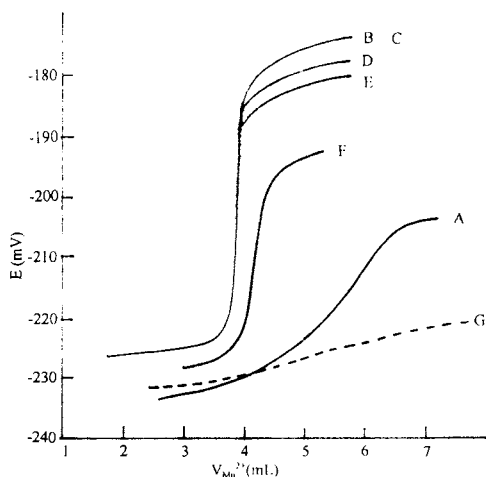


Fig. 3. The influence of pH on titrating behavior. A: pH, 2.5; B: pH, 3.2; C: pH, 4; D: pH, 5; E: pH, 6.0; F: pH, 7.5; G: pH, 9.8.

that when temperature is lower than 30°C, the catalyzed reaction is so slow that it is difficult to determine the difference between the catalyzed and uncatalyzed reaction rates. When the temperature is in the range of 30–43°C, the difference between the two reaction rates will increase with the temperature rising. When the temperature is higher than 50°C, the difference will decrease with the temperature rising. The largest difference appeared in the temperature range of 39–43°C.

The effect of temperature on the titration reaction was investigated also in the range of 35–50°C. The experiments indicated that the sensitivity of the end-point of the titration reaction increases with the temperature increasing up to 45°C. When the temperature is higher than 45°C, the sensitivity of the end-point decreases gradually with the temperature increasing. The suitable range of temperature is 39–43°C, so 41°C was used in this work.

In this work, the reaction temperature is controlled by thermostated water.

### 3.1.5. Effect of titration rate

The effect of the titration rate on the titration was investigated in the range of 0.8–1.3 ml·min<sup>-1</sup>. The experiments showed that the end-points of these titrations are all remarkable. Thus 1 ml·min<sup>-1</sup> is used in this work.

### 3.2. Effect of the concentration of Mn(II) standard solution as titrant

The effect of the concentration of Mn(II) on the titration curve was investigated in the range of  $1 \times 10^{-6}$ – $1 \times 10^{-3}$  M under the chosen experimental conditions. 3 ml EDTA standard solution was titrated with Mn(II) standard solution that had the same concentration as EDTA. The results were shown in Fig. 4. The experiments showed that the sensitivity of the end-points and the accuracy of titration are all high when the concentration of Mn(II) standard solution is not lower than  $8 \times 10^{-5}$  M. Thus the suitable range of the concentration of the titrant is very wide.

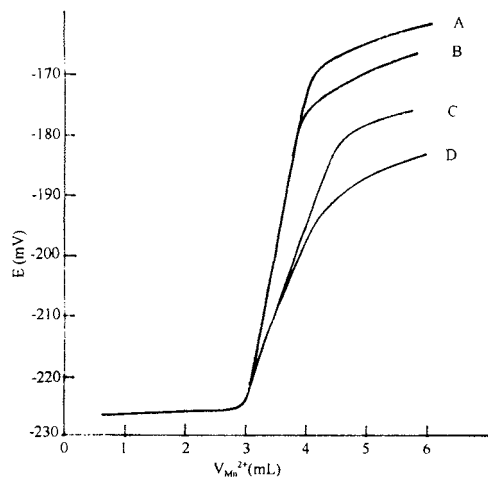


Fig. 4. Effect of the concentration of Mn(II) on the titration curve. A,  $1.012 \times 10^{-3}$ ; B,  $6.072 \times 10^{-4}$ ; C,  $1.626 \times 10^{-4}$ ; D,  $8.310 \times 10^{-5}$ .

### 3.3. Interference of coexistence ions

#### 3.3.1. Interference in the indicator reaction

Under the experimental conditions, the interference test in the indicator reaction has been investigated in the solution containing Mn(II) 1  $\mu\text{g}/25$  ml. The experiments showed that the following ions at the 300-fold level did not show interference:  $\text{Ca}^{2+}$ ,  $\text{Sr}^{2+}$ ,  $\text{Cd}^{2+}$ ,  $\text{Co}^{2+}$ ,  $\text{VO}_2^+$ ,  $\text{Zn}^{2+}$ ,  $\text{Al}^{3+}$ ,  $\text{Cu}^{2+}$ ,  $\text{Li}^+$ ,  $\text{K}^+$ ,  $\text{Na}^+$ ,  $\text{Pb}^{2+}$ ,  $\text{Fe}^{3+}$ ,  $\text{NH}_4^+$ ,  $\text{Ni}^{2+}$ ,  $\text{NO}_3^-$ ,  $\text{SO}_4^{2-}$ , and  $\text{Cl}^-$ . However the  $\text{PO}_4^{3-}$  and  $\text{AsO}_4^{3-}$  ions showed remarkable positive interference on the catalytic effect of Mn(II), so they must be masked or separated from the Mn(II) when Mn is determined by direct catalytic kinetic method. But in the back-titration with catalytic end-point indication, the  $\text{PO}_4^{3-}$  and  $\text{AsO}_4^{3-}$  ions in sample don't interfere with the determination of Mn, so the mask or separation them from Mn is unnecessary.

#### 3.3.2. Interference in the titration reaction

The interference in the titration reaction mainly comes from the metal ions that can react with EDTA to form stable complex under the chosen experimental conditions. Two steps were taken to dispel the interference in this work. Firstly the most of the  $\text{Fe}^{3+}$ ,  $\text{Al}^{3+}$  etc. metal ions were

separated from the Mn(II) by the precipitating in the sample treatment. After the sample was burned to ash and digested with hydrochloric acid, the sample solution was adjusted to pH 6, with diluted NaOH solution. Many metal ions as  $\text{Fe}^{3+}$ ,  $\text{Al}^{3+}$  are precipitated form hydroxides and are separated from the sample solution by the filtering. The second step is to mask the trace  $\text{Fe}^{3+}$ ,  $\text{Al}^{3+}$  etc. interference ions remained in the solution by adding a small amount of sodium tartrate triethanolamine and sulfourea solution. Moreover, the NTA also can mask some interference ions as described above. So the selectivity of this method is high.

### 3.4. Accuracy of the method

The accuracy of the method was studied by analyzing a Mn(II) standard solution which was prepared from the metal Mn of Guarantee reagent (G.R). The average value for ten parallel experiments is  $6.046 \times 10^{-4}$  M, the relative standard deviation is 0.6%. The standard value of the concentration of Mn(II) solution is  $6.035 \times 10^{-4}$  M, the relative error is 0.18%.

## 4. Sample analysis and recovery

### 4.1. The determination of Mn in grain

#### 4.1.1. Sample treatment

A mass of 20 g of rice and millet was weighed accurately, then burnt to ashes at  $700^\circ\text{C}$  for 3 h, respectively. The powder was cooled and digested with the appropriate amount of 6 M hydrochloric acid and heated gently until near to dryness. The procedure was repeated once. Finally, the solid residue was dissolved with double distilled water and the solution was neutralized to pH 6, with 1% NaOH solution. The solution was poured into a 100 ml volumetric flask and diluted to the mark of flask with distilled water. Filtering the solution and throw 10–20ml of the first filtered solution. Collect the rest of the filtered solution as the sample for further determination.

Table 1  
Comparisons of results with two methods

Sample	Catalytic titration			AAS ( $n = 6$ )	
	Parallel determined ( $\mu\text{g} \cdot \text{g}^{-1}$ )	Average ( $\mu\text{g} \cdot \text{g}^{-1}$ )	RSD (%)	Average ( $\mu\text{g} \cdot \text{g}^{-1}$ )	RSD (%)
Millet	23.71	23.82	23.46	23.38	4.6
	23.50	22.80			
Rice	15.44	16.31	16.24	16.17	5.1
	16.75	16.44			

Table 2  
The recovery<sup>a</sup>

Mn <sup>2+</sup> added ( $\mu\text{mol}$ )	Mn <sup>2+</sup> determined ( $\mu\text{mol}$ )	Recovery (%)
1.619	1.606	99.20
2.429	2.392	98.48
3.238	3.226	99.63
4.048	4.100	101.28

<sup>a</sup> The average recovery is 99.65%, the relative standard deviation is 1.2%.

#### 4.1.2. Determination of sample solution

The proper amount of the sample solution, 1 ml of  $1 \times 10^{-3}$  M sodium tartrate, 1 ml of  $1 \times 10^{-3}$  M triethanolamine and 1 ml of  $5 \times 10^{-4}$  M sulfourea were added into the titration cell. Then the determinations were done according to the procedure. Moreover, the determination was followed for the same sample by atomic absorption spectrometry (AAS). The results obtained by these two methods were shown in Table 1. It can be seen that there is good agreement between the results of these two methods.

#### 4.2. Recovery

According to the procedure the recovery of this

method was determined with the standard addition procedure. The result measured is shown in Table 2.

#### Acknowledgements

The authors gratefully acknowledge Professor Li Qinglin, Zhang Zhongyi, Liu Hailan, Zi Mingxian and Liu Xiuhua for their sincere help.

#### References

- [1] Ye Shibo, The Guide to Physical Testing and Chemical Analysis of Food, Beijing University Press, Beijing, 1991, p. 63.
- [2] F.F. Gaal, B.F. Abramovic, Talanta 31 (1984) 987.
- [3] H.A. Mottola, Anal. Chem. 42 (1970) 630.
- [4] S. Pantel, H. Weiszl, Anal. Chim. Acta 202 (1987) 1.
- [5] F.F. Gaal, Analyst 112 (1987) 739.
- [6] B.F. Abramovic, K.S. Horvath, F.F. Gaal, Analyst 118 (1993) 899.
- [7] H.A. Mottola, D. Perez-Bendito, Anal. Chem. 68 (1996) 257R.
- [8] S.R. Crouch, T.F. Cullen, A. Scheeline, E.S. Kirkor, Anal. Chem. 70 (1998) 53R.
- [9] Dong Xuezhi, Yejin Fenxi 16 (5) (1996) 7.



# Determination of oxalic acid in urine by co-electroosmotic capillary electrophoresis with amperometric detection

Chonggang Fu <sup>a,\*</sup>, Lixin Wang <sup>a</sup>, Yuzhi Fang <sup>b</sup>

<sup>a</sup> Department of Chemistry, Liaocheng Teacher's College, Shandong, 252059, People's Republic of China

<sup>b</sup> Department of Chemistry, East China Normal University, Shanghai, 200062, People's Republic of China

Received 14 April 1999; received in revised form 14 June 1999; accepted 16 June 1999

## Abstract

Co-electroosmotic capillary electrophoresis with amperometric detection at a Cobalt phthalocyanine (CoPC) modified carbon paste electrode was evaluated for the determination of oxalic acid in urine. The running buffer consisted of 10 mM phosphate (pH = 5.70) and 0.25 mM Cetyltrimethylammonium bromide. Under the optimum conditions, a detection limit of 0.12  $\mu\text{M}$  was achieved for oxalic acid. The response was linear between 0.5 and 1000  $\mu\text{M}$  with a correlation coefficient of 0.9995. Applications of the method to real urine samples were described. © 1999 Elsevier Science B.V. All rights reserved.

**Keywords:** Co-electroosmotic capillary electrophoresis; Amperometric detection; Oxalic acid; Urine

## 1. Introduction

Based on the pioneering work of Wallingford and Ewing [1], capillary electrophoresis with amperometric detection (CE-AD) has made essential progress [2]. The number of analytes accessible to CE-AD has been largely increased. In addition to electroactive species such as catecholamines [3], sugars [4–6] and phenols [7], a wide range of difficult-to-electrolyze or even non-electroactive species also become amenable to CE-AD via employment of various chemically modified electrodes (CMEs) [8–11] or indirect electrochemical detection mode [12]. The use of normal size elec-

trodes [5] or on-capillary electrodes (OCE) [13,14], as well as on-chip microband array electrochemical detector [15] made the electrode-capillary alignment more convenient and reproducible than before. Recently, CE-AD technique has attracted a great deal of interest in clinical and medical field for several reasons. Firstly, the extremely high separation efficiency and high sensitivity of CE-AD allows for the determination of a trace amount of components in a complex matrix with only minimum sample preparation. Secondly, the extremely small sample volume requirement of CE-AD has a great significance in some cases such as the single cell analysis and living body analysis. Thirdly, CE separation typically can be accomplished in a relatively short time. As application examples, the determinations of cysteine

\* Corresponding author. Tel: +86-635-8238613.  
E-mail address: anal@lctu.edu.cn (C. Fu)

[16] and uric acid [17,18] in urine, tryptophan and kynurenine in brain tissue [19] and L-dopa in blood [20] by CE-AD have been reported. New applications of CE-AD still need to be explored. The urinary level of oxalic acid has long been recognized as an important indicator for the diagnosis of renal stone formation. A number of methods have been suggested for the determination of oxalic acid such as enzymatic spectrophotometry [21], enzymatic amperometry [22], chemiluminescence [23], gas chromatography (GC) [24] and liquid chromatography (LC) with UV-absorption [25] or electrochemical detection [26,27]. But each method has often suffered from diverse disadvantages with regard to cost-ineffectiveness, insufficient selectivity, essential derivatization for sensitive detection, and time-consuming process of sample wash-up to prevent deteriorating chromatographic columns. Recently, a CE-based method with indirect UV-absorption detection was proposed for the determination of oxalic acid and other anions in urine [28], but the method suffered from insufficient selectivity and sensitivity.

In this paper, we described a CE-AD method for the determination of oxalic acid and established the optimal separation and detection conditions. Its applicability was demonstrated by determining the urinary oxalic acid.

## 2. Experiment

### 2.1. Apparatus

The CE-AD system used was laboratory-built and has been described in detail elsewhere [4,29]. In brief, Electrophoresis in capillary was driven by a high-voltage power supply (Shanghai Institute of Atomic Nucleus Research, China). Separations were performed in a 75 cm  $\times$  25  $\mu$ m I.D.  $\times$  360  $\mu$ m O.D. fused silica capillary (Polymicro Technologies, Phoenix, AZ, USA). Detection was carried out in the end-column amperometric mode using a conventional three-electrode configuration, with a CoPC-modified carbon paste working electrode (I.D. 200  $\mu$ m, prepared according to Ref. [8]), an Ag/AgCl reference elec-

trode and a platinum auxiliary electrode. The working electrode was positioned directly in front of a capillary outlet at a distance of approximately 10  $\mu$ m with the help of a microscope. Potential control and current output was provided by a BAS LC-3D amperometric detector (Bioanalytical System, West Lafayette, IN, USA). Electropherograms were recorded using a strip-chart recorder (Model XWT-204, Shanghai Dahua Instrument Factory, China). Cyclic voltammetry experiments were performed with a BAS-100B electrochemical analyzer.

### 2.2. Reagent

Cobalt phthalocynine, cetyltrimethylammonium bromide (CTAB) and uric acid were purchased from Sigma (St. Louis, MO, USA). Ascorbic acid and oxalic acid were obtained from First Chemical Reagent Factory (Shanghai, China). All other chemicals were analytical reagent grade. All solutions were prepared in deionized water and passed through a 0.45- $\mu$ m cellulose acetate filter (Xinya Purification Factory, Shanghai, China). Standard solutions of all analytes were prepared daily. Running buffer consisted of 10 mM phosphate and 0.25 mM CTAB, and was adjusted to the desired pH with sodium hydroxide just before use.

### 2.3. Sample preparation

Urine samples were obtained from healthy volunteers, filtered by passing a 0.45- $\mu$ m cellulose acetate filter, and diluted 200-fold with run buffer. The diluted samples were immediately used for CE analyses.

### 2.4. Procedures

Each new capillary was prerinsed with 1 M HCl and 1 M NaOH both for half an hour. Before each run, the capillary was sequentially rinsed using a self-made washing system with 0.1 M HCl for 3 min, distilled water for 3 min and running buffer for 10 min. That was necessary for obtaining reproducible results. Sample introduction was carried out by electromigration at  $-21$  kV for 3 s.

### 3. Results and discussion

#### 3.1. Electrochemical behavior of oxalic acid

The electrochemical behavior of oxalic acid was studied using cyclic voltammetry. Fig. 1(A) shows a cyclic voltammogram obtained for oxalic acid at an unmodified electrode. It exhibited a single oxidation peak around 1.2 V vs. Ag/AgCl, but no corresponding reduction peak was seen under the conditions employed. This indicated that oxalic acid could be only irreversibly oxidized at the unmodified electrode. In this case, the needed detection potential of oxalic acid with CE-AD could not be lower than 1.2 V vs. Ag/AgCl in order to obtain enough sensitivity. However, the detection limit and selectivity of amperometric detection was affected at the extremely positive potential. One approach to overcome this problem was the use of CMEs to reduce overpotentials. The CoPC-modified carbon paste electrode was one type of the most commonly used CMEs. It possessed the advantages of easy preparation and high reproducibility, and has been used for the detection of a variety of analytes including thiols [8], hydrazine [30] and carbohydrate [31]. As shown in Fig. 1(B), the electrocatalytic oxida-

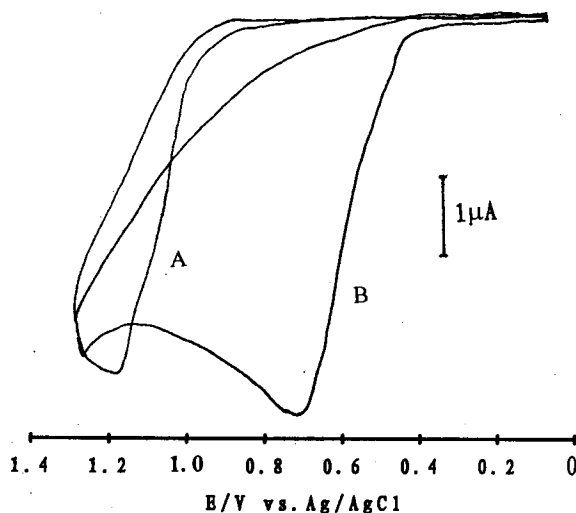


Fig. 1. Cyclic voltammograms of oxalic acid (100  $\mu\text{M}$ ) at unmodified (A) and CoPC-modified (B) carbon paste electrode in 10 mM phosphate buffer (pH = 5.70), scan rate: 50 mV/s.

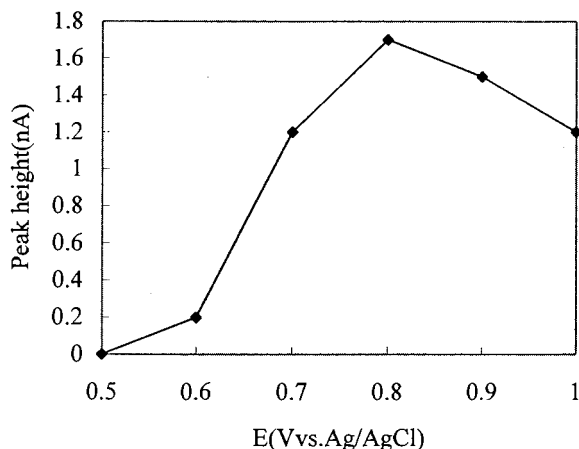


Fig. 2. Hydrodynamic voltammogram of oxalic acid (100  $\mu\text{M}$ ) in CE-AD system. Sample injection:  $-21$  kV for 3 s; separation voltage:  $-21$  kV; electrophoretic medium: 10 mM phosphate buffer (pH = 5.70) + 0.25 mM CTAB.

tion of oxalic acid using this electrode is also apparent. There is a substantial increase in the oxidation peak current along with an obvious negative shift in the peak potential (*c.* 0.75 V vs. Ag/AgCl). Moreover, the peak currents were proportional to the concentration of oxalic acid and the square root of potential scan rate employed (up to 200 mV/s). This is characteristic of a typical diffusion-limited process. Another observation was that the electrocatalytic effect was enhanced by the addition of CTAB to the electrolyte. The catalytic current increased as the CTAB concentration increased, but it was leveled off when the CTAB concentration was over 0.25 mM, at which the catalytic current increased 30% compared with that without CTAB. Probably, this is due to the adsorption of CTAB onto the electrode surface by hydrophobic attraction to form a positively charged layer, facilitating the oxidation of ionized oxalic acid. Similar effects have been observed for other species [4]. Fig. 2 shows the hydrodynamic voltammograms (HDVs) obtained for oxalic acid by capillary electrophoretic amperometric detection at a CoPC-modified electrode. After each change in applied potential, about 10 min of stabilization time was allowed prior to injection of the sample. Each point in the hydrodynamic voltammetric curve

represented an average of three separate injections. As shown in Fig. 2, a peak-shaped HDV was obtained with a maximum response at 0.8 V vs. Ag/AgCl. A decrease in electrocatalytic activity was observed as the potentials increased over 0.8 V vs. Ag/AgCl. Moreover, the decreased electrocatalytic activity cannot be restored once the applied potential exceeds 1.1 V vs. Ag/AgCl. Probably this arose from the further oxidation and decomposition of phthalocyanine or irreversible complexation of the Co(III) center. As a result, a detection potential of 0.8 V vs. Ag/AgCl was chosen for subsequent studies.

### 3.2. Separation conditions

Uric acid and ascorbic acid are customary urine components. They are electroactive at the selected detection potential and potentially interfere with the determination of oxalic acid in urine. Therefore, a synthetic sample from oxalic acid, uric acid and ascorbic acid was employed to select the optimum separation conditions. In view of the urine samples having weak acidity and the  $pK_a$  values of the analytes studied being in the range of 1.27–5.40, several weakly acidic buffer solutions (phosphate pH 4.5–6.5) were investigated as separation media. However, oxalic acid could not be detected together with ascorbic acid and uric acid at the cathode end using the conventional CE mode. The reason is that oxalic acids ( $pK_{a1} = 1.27$ ,  $pK_{a2} = 4.27$ ) are almost completely dissociated under these pH conditions, thus having a large charge-to-mass ratio, accordingly a large anodically oriented electrophoretic mobility. Therefore, oxalic acids migrate toward the anode against the cathodically oriented electroosmotic flow (EOF) and make it undetectable at the cathode end. This problem can be overcome by use of co-electroosmotic capillary electrophoretic mode. In this mode, the electroosmotic and electrophoretic mobility share one direction. In case of negatively charged analytes, the EOF is toward the anode, injection is carried out at the cathodic end and detection at the anodic end. Co-electroosmotic conditions can be established via the addition of CTAB to the carrier electrolyte [32]. In

order to determine the optimum separation electrolyte, a series of electrolytes having different pH values (4.5–6.5) and CTAB concentrations (0.10–0.50 mM) were examined. It was found that the CTAB concentration was a crucial parameter. A lower CTAB concentration displayed an irreproducible EOF and a longer separation time, while a greater CTAB concentration resulted in a noisy baseline. The pH values of electrolytes are relatively insignificant in the examined range, because in most cases satisfactory separation could be obtained. As a best compromise with respect to resolution, reproducibility, baseline noise and separation time, an electrolyte composed of 0.25 mM CTAB and 10 mM phosphate buffer (pH = 5.70) was used for subsequent works. Fig. 3 shows a typical electropherogram of a synthetic sample from oxalic acid, uric acid and ascorbic acid under the optimized conditions.

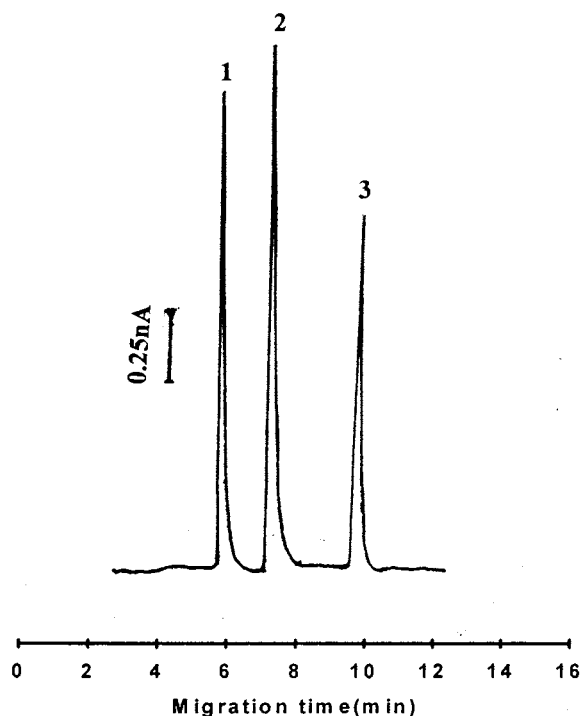


Fig. 3. Electropherogram of a mixture composed of: (1) oxalic acid; (2) ascorbic acid; and (3) uric acid. Concentrations: 10  $\mu$ M for each compound. Detection potential: 0.8 V vs. Ag/AgCl; conditions as in Fig. 2.

Table 1  
Linearity and detection limit

Analytes	Migration time (min)	Concentration range ( $\mu\text{M}$ )	Regression equation $I$ (nA), $C$ ( $\mu\text{M}$ )	$r^a$	Detection limit ( $\mu\text{M}$ ) <sup>b</sup>
Oxalic acid	5.8	0.5–1000	$I = 0.113C + 0.050$	0.9995	0.12
Ascorbic acid	7.2	0.5–1000	$I = 0.181C + 0.042$	0.9986	0.10
Uric acid	9.4	0.5–1000	$I = 0.102C + 0.045$	0.9993	0.13

<sup>a</sup>  $n = 8$ .

<sup>b</sup> Based on three times ratio of signal-to-noise.

### 3.3. Analytical characterization

Under the optimized conditions, the linearity and detection limit of the method was evaluated. The results are summarized in Table 1. As shown in Table 1, a good linear relationship between peak heights and concentrations were observed with correlation coefficients better than 0.9986 ( $n = 8$ ) for each analyte studied in the range of 0.5–1000  $\mu\text{M}$ . Because the main concern of this paper is about the determination of oxalic acid, the short-term reproducibility expressed as relative standard derivation (R.S.D.) was evaluated for ten consecutive injections of 5  $\mu\text{M}$  oxalic acid. It was found that R.S.D. was 4.2% for the peak heights and 1.0% for the migration times. The long-term stability was also investigated by a week period of consecutive run. The electrode response remained almost constant, indicating that no apparent electrode fouling took place. A detection limit of 0.12  $\mu\text{M}$  was obtained for oxalic acid, which was considerably improved compared to those reported with indirect UV detection [28,33] ( $c$  10 and 41.6  $\mu\text{M}$ , respectively).

### 3.4. Analytical application

The practical utility of the CE-AD system with a CoPC-modified electrode was demonstrated for the analysis of urinary oxalic acid from healthy volunteers. Fig. 4 shows a typical electropherogram of a 200-fold diluted urine sample, a well-defined oxalic acid peak can be clearly identified from the background of the urine by matching of the migration time with that of standard substance. The results obtained are presented in Table 2. It was found that the urinary oxalic acid

concentrations determined by this method fell in the normal range (160 ~ 550  $\mu\text{M}$  [34]) expected from healthy persons. The reliability of the method was established by the recovery test of spiked samples. The results are given in Table 3, which indicate that better than 94.7% recoveries were obtained.

## 4. Conclusion

Co-electroosmotic CE-AD technique has been successfully used for the determination of oxalic acid in urine. The co-electroosmotic mode permitted rapid and efficient separation of oxalic acid from the urine background, while the amperomet-

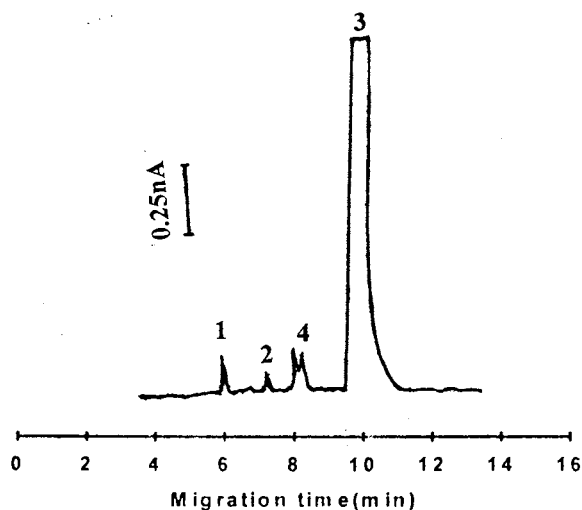


Fig. 4. Electropherogram of a diluted urine sample. Peaks: (1) oxalic acid; (2) ascorbic acid; (3) uric acid; and (4) unknown. Conditions as in Fig. 3.

Table 2  
Determination of oxalic acid in urine

Sample	Concentration of oxalic acid (average value $\pm$ standard deviation) <sup>a</sup>	
	Diluted urine ( $\mu\text{M}$ )	Original urine ( $\mu\text{M}$ )
1	1.15 $\pm$ 0.04	230 $\pm$ 8
2	2.30 $\pm$ 0.05	460 $\pm$ 10
3	2.40 $\pm$ 0.04	480 $\pm$ 8
4	1.87 $\pm$ 0.05	374 $\pm$ 10
5	2.18 $\pm$ 0.04	436 $\pm$ 8

<sup>a</sup> Results for triplicate determinations.

Table 3  
Recovery of oxalic acid from spiked urine sample

Added ( $\mu\text{M}$ )	Found ( $\mu\text{M}$ ) <sup>a</sup>	R.S.D. (%)	Recovery (%)
1.0	0.95	3.4	95.0
1.5	1.42	4.1	94.7
2.0	1.94	3.8	97.0
2.5	2.40	3.0	96.0
3.0	2.95	4.3	98.3

<sup>a</sup> Average value for triplicate determinations.

ric detection mode employed provided enhanced selectivity and sensitivity for oxalic acid.

## References

- [1] R.A. Wallingford, A.E. Ewing, *Anal. Chem.* 59 (1987) 1762.
- [2] L.A. Holland, S.M. Lunte, *Anal. Commun.* 35 (1998) 1H.
- [3] T.M. Olefirowicz, A.G. Ewing, *Anal. Chem.* 62 (1990) 1872.
- [4] C. Fu, L. Song, Y. Fang, *Anal. Chim. Acta* 371 (1998) 81.
- [5] J. Ye, R.P. Baldwin, *Anal. Chem.* 65 (1993) 3525.
- [6] J. Ye, W. Jin, X. Zhao, Y. Fang, *Chem. J. Chin. Univ.* 19 (1998) 31.
- [7] C.D. Gaitonde, P.V. Pathak, *J. Chromatogr.* 514 (1991) 389.
- [8] T.J. O'Shea, S.M. Lunte, *Anal. Chem.* 66 (1994) 307.
- [9] X. Huang, W.Th. Kok, *J. Chromatogr.* 707 (1995) 335.
- [10] W. Zhou, L. Xu, M. Wu, E. Wang, *Anal. Chim. Acta* 299 (1994) 189.
- [11] J. Zhou, T.J. O'Shea, S.M. Lunte, *J. Chromatogr.* 680 (1994) 271.
- [12] T.M. Olefirowicz, A.E. Ewing, *J. Chromatogr.* 499 (1990) 713.
- [13] P.D. Voegel, W. Zhou, R.P. Baldwin, *Anal. Chem.* 69 (1997) 951.
- [14] M. Zhong, S.M. Lunte, *Anal. Chem.* 69 (1996) 2488.
- [15] J.M. Slater, E.J. Watt, *Analyst* 119 (1994) 2303.
- [16] J. Zhou, T.J. O'Shea, S.M. Lunte, *J. Chromatogr.* 680 (1994) 271.
- [17] D. Xu, L. Lin, Z. Man, H. Chen, *J. Chromatogr. B. Biomed. Appl.* 694 (1997) 461.
- [18] J. Hong, R.P. Baldwin, *J. Cap. Elec.* 4 (1997) 461.
- [19] M.A. Malone, H. Zuo, S.M. Lunte, M.R. Smyth, *J. Chromatogr.* 700 (1995) 73.
- [20] T.J. O'Shea, M.W. Telting-Diaz, S.M. Lunte, C.E. Lunte, M.R. Smyth, *Electroanalysis* 4 (1992) 463.
- [21] M.F. Laker, A.F. Hofman, B.J.D. Meeuse, *Clin. Chem. (Winston-Salem N.C.)* 26 (1980) 827.
- [22] S.M. Reddy, S.P. Higson, P.M. Vadgama, *Anal. Chim. Acta* 343 (1997) 59.
- [23] I. Rubinstein, C.R. Martin, A.J. Bard, *Anal. Chem.* 55 (1983) 1580.
- [24] E.J. Jellum, *J. Chromatogr. B. Biomed. Appl.* 143 (1977) 427.
- [25] M. Gaffney, N. Morrice, M. Cooke, *Anal. Proc.* 21 (1984) 434.
- [26] L.M. Santos, R.P. Baldwin, *Anal. Chem.* 58 (1986) 848.
- [27] A.G. Fogg, R.M. Alonso, M.A. Fernandez-Arciniega, *Analyst* 111 (1986) 249.
- [28] B.J. Wildman, P.E. Jackson, W.R. Jones, P.G. Alden, *J. Chromatogr.* 546 (1991) 459.
- [29] C. Fu, A. Wang, J. Ye, Y. Fang, *Chem. J. Chin. Univ.* 19 (1998) 53.
- [30] K.M. Korfhage, K. Ravichandran, R.P. Baldwin, *Anal. Chem.* 56 (1984) 1514.
- [31] L.M. Santos, R.P. Baldwin, *Anal. Chem.* 59 (1987) 1766.
- [32] C.A. Lucy, R.S. Underhill, *Anal. Chem.* 68 (1996) 300.
- [33] R.P. Holmes, *Clin. Chem.* 41 (1995) 1297.
- [34] R.K. Kobos, T.A. Rammsey, *Anal. Chim. Acta* 121 (1980) 111.

# Spectrophotometric detection of arsenic using flow-injection hydride generation following sorbent extraction preconcentration

José Anchieta Gomes Neto \*, Ronaldo Montes, Arnaldo A. Cardoso

*Departamento de Química Analítica, Instituto de Química, Universidade Estadual Paulista, P.O. Box 355, 14801-970, Araraquara SP, Brazil*

Received 16 February 1999; received in revised form 8 June 1999; accepted 17 June 1999

## Abstract

An automated system with a C<sub>18</sub> bonded silica gel packed minicolumn is proposed for spectrophotometric detection of arsenic using flow-injection hydride generation following sorbent extraction preconcentration. Complexes formed between arsenic(III) and ammonium diethyl dithiophosphate (ADDP) are retained on a C<sub>18</sub> sorbent. The eluted As-DDP complexes are merged with a 1.5% (w/v) NaBH<sub>4</sub> and the resulting solution is thereafter injected into the hydride generator/gas–liquid separator. The arsine generated is carried out by a stream of N<sub>2</sub> and trapped in an alkaline iodine solution in which the analyte is determined by the arsenomolybdenum blue method. With preconcentration time of 120 s, calibration in the 5.00–50.0 µg As l<sup>-1</sup> range and sampling rate of about 20 samples h<sup>-1</sup> are achieved, corresponding to 36 mg ADDP plus 36 mg ammonium heptamolybdate plus 7 mg hydrazine sulfate plus 0.7 mg stannous chloride and about 7 ml sample consumed per determination. The detection limit is 0.06 µg l<sup>-1</sup> and the relative standard deviation ( $n = 12$ ) for a typical 17.0 µg As l<sup>-1</sup> sample is ca. 6%. The accuracy was checked for arsenic determination in plant materials from the NIST (1572 citrus leaves; 1573 tomato leaves) and the results were in agreement with the certified values at 95% confidence level. Good recoveries (94–104%) of spiked tap waters, sugars and synthetic mixtures of trivalent and pentavalent arsenic were also found. © 1999 Elsevier Science B.V. All rights reserved.

*Keywords:* Spectrophotometry; Hydride generation; Flow-injection analysis; Ammonium diethyl dithiophosphate; Arsenic

## 1. Introduction

Arsenic compounds are used as fungicide, herbicide, insecticide, algacide, wood preservative and defoliant in cotton fields. In the manufacture

of products, they also improve hardening and corrosion resistance of alloys of copper and lead. The use of arsenic in semiconductor technology, in pigments, in anti-fouling paints, in therapeutic and veterinary medicine [1,2] is also related. As arsenic may accumulate in agricultural and horticultural soils and plants [3], its accurate determination is of considerable importance owing to the

\* Corresponding author. Tel.: +55-16-2227932.

E-mail address: anchieta@iq.unesp.br (J.G. Neto)

toxicity of this element and its related compounds [4,5].

Several analytical techniques have been used for arsenic determination at trace levels, such as atomic absorption spectrometry [6], atomic fluorescence spectrometry [7], ICP mass spectrometry [8] and ICP atomic emission spectrometry [9]. Regarding spectrophotometry, the molybdenum blue (MB) method has been described among the Official Methods of Analysis of AOAC International [10] for arsenic determination in food, plant and water samples. Up to this time, only two flow spectrophotometric procedures based on MB have been proposed for determination of arsenic in real samples [11,12]. However, a serious limitation of the MB method for most samples routinely analyzed is interference caused by phosphate and silicate, which also form blue complexes. A flow procedure using an anion exchanger packed minicolumn to remove phosphate and silicate prior to the selection of the sample aliquot to be injected has been described [11]. The shortcoming of this procedure is that small variations in the acidity of samples seriously affect the separation process. The matrix separation and arsenic concentration can be efficiently performed by using solid-phase extraction (SPE) technique based on a  $C_{18}$  reversed-phase packed minicolumn [13].

Dithiophosphates have been proposed to perform separation and determination of different oxidation states of arsenic by graphite furnace atomic absorption spectrometry after sorption on solid supports [13,14] or liquid–liquid extraction with organic solvent [15,16]. Little attention has been given to the use of ammonium diethyl dithiophosphate (ADDP) for the determination of arsenic by spectrophotometry. Likewise, procedures involving SPE and hydride generation coupled to flow-injection spectrophotometry are lacking in the literature.

This study reports on a flow-injection hydride generation spectrophotometric procedure for the determination of trace inorganic arsenic in real samples by using the arsenomolybdenum blue method. In-line complex formation with ADDP and sorption on a  $C_{18}$  bonded silica gel packed minicolumn were exploited for sensitivity en-

hancement and to remove potential interfering ions (of the hydride generation and complex formation processes) occurring at concentration higher than the analyte in workable samples. The performance of the proposed procedure was checked after analyzing plant digests, sugar and tap water.

## 2. Experimental

### 2.1. Reagents, analytical solutions and samples

All solutions were prepared with pro analysi chemicals and distilled–deionized water (Milli-Q system, Millipore). Hydrochloric and nitric acids used were Suprapur (Merck).

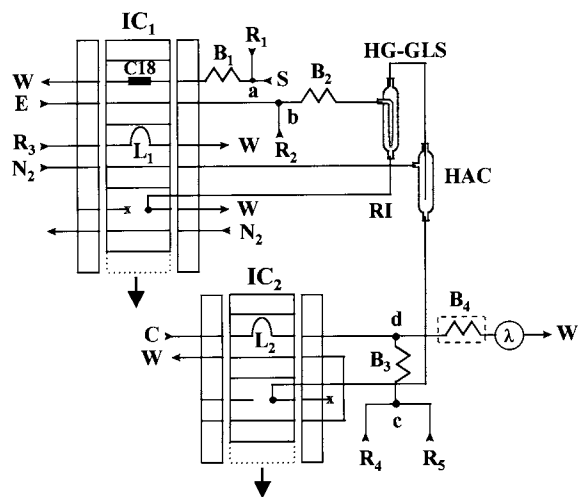


Fig. 1. Flow diagram of the system for arsenic determination. IC<sub>1</sub>, IC<sub>2</sub>: injector-commutators; C<sub>18</sub>: minicolumn (20 × 3 mm); S: sample (3.2 ml min<sup>-1</sup>); R<sub>1</sub>: 0.1% w/v ADDP solution (1.2 ml min<sup>-1</sup>); R<sub>2</sub>: 2% w/v NaBH<sub>4</sub> solution (1.2 ml min<sup>-1</sup>); R<sub>3</sub>: 0.04% w/v KI plus 0.025% w/v I<sub>2</sub> in 0.1 M NaHCO<sub>3</sub> (2.0 ml min<sup>-1</sup>); C: water (2.5 ml min<sup>-1</sup>); R<sub>4</sub>: 1% w/v (NH<sub>4</sub>)<sub>6</sub>Mo<sub>7</sub>O<sub>24</sub> in 0.5 M H<sub>2</sub>SO<sub>4</sub> (1.2 ml min<sup>-1</sup>); R<sub>5</sub>: 0.2% w/v hydrazine sulfate plus 0.02% w/v SnCl<sub>2</sub> in 0.5 M H<sub>2</sub>SO<sub>4</sub> (1.2 ml min<sup>-1</sup>); E: 4% v/v HCl (3.2 ml min<sup>-1</sup>); N<sub>2</sub>: carriers (20 ml min<sup>-1</sup>); W<sub>i</sub>: wastes; L<sub>1</sub>: 750 μl; L<sub>2</sub>: 500 μl; RI: reversed-intermittent flow; HG-GLS: hydride generator/gas–liquid separator; HAC: hydride absorbing chamber; B<sub>1</sub>–B<sub>4</sub>: coiled reactors (30, 30, 30, and 100 cm; 0.7 mm i.d.); λ: detector (840 nm). The downward arrows indicate the movement of the central part of IC<sub>1</sub> and IC<sub>2</sub>.



A 1.0% (w/v) ADDP solution ( $R_1$ , Fig. 1) was prepared weekly by dissolving 1.00 g of the ammonium salt (Aldrich) in about 5 ml of ethanol and diluting up to 100 ml with water. This solution was purified by passing it through a  $C_{18}$  bonded silica packed column and kept in a refrigerator.  $R_2$  reagent was a 2% (w/v)  $NaBH_4$  solution in 0.05 M NaOH. Absorbing solution ( $R_3$  reagent) was prepared by dissolving 0.04 g KI, 0.025 g  $I_2$  and 0.42 g  $NaHCO_3$  in 100 ml water.  $R_4$  reagent was prepared by dissolving 1.0 g  $(NH_4)_6Mo_7O_{24} \cdot 4H_2O$  in 100 ml 0.5 M  $H_2SO_4$  and  $R_5$  consisted of 0.5 M  $H_2SO_4$  solution containing 0.02% (w/v)  $SnCl_2$  plus 0.2% (w/v) of hydrazine sulfate. It should be commented that ammonium molybdate in the presence of sulfuric acid may precipitate as molybdic acid in a few days. So its a good practice to prepare the reagent  $R_4$  daily.

Arsenic(III) stock standard solution ( $1000 \text{ mg l}^{-1}$ ) was prepared by dissolving 1.320 g  $As_2O_3$  in about 20 ml 1.0 M NaOH. To this solution 50 ml 0.5 M HCl were added and the volume was completed to 1000 ml with water. Arsenic(V) stock standard solution ( $1000 \text{ mg l}^{-1}$ ) was prepared by dissolving 1.533 g  $As_2O_5$  in 1000 ml water. Trivalent or pentavalent arsenic working standards ( $5.00\text{--}50.0 \text{ } \mu\text{g l}^{-1}$ ) were daily prepared by appropriate dilution of the stock standards.

The minicolumn was prepared by packing  $C_{18}$  bonded silica gel (Waters Division of Millipore Corp., part no. 51910, 50–100  $\mu\text{m}$ ) into a  $20 \times 3$  mm i.d. hole drilled into a perspex block [17]. A polyethylene screen was placed at each end of the packed column in order to avoid sorbent losses during system operation.

The standard reference materials (1572 citrus leaves and 1573 tomato leaves from the National Institute of Standards and Technology, Gaithersburg, MD) were mineralized in triplicate with nitric acid and hydrogen peroxide [18].

Sugar samples were supplied by Copersucar (sugar-cane, alcohol and sugar fabricator association of São Paulo State, Brazil) and were collected from different Brazilian industries. 10 g sugar samples were dissolved in about 35 ml of 10% v/v HCl. The hydrolysis was carried out at  $40^\circ\text{C}$  overnight. Thereafter the volume was completed to 50 ml with the same acid solution.

Tap water was collected at the Analytical Chemistry Department of São Paulo State University (UNESP), Brazil. This water was used without previous treatment.

## 2.2. The flow system

The system comprised two IPC-8 Ismatec peristaltic pumps furnished with Tygon<sup>®</sup> pumping tubes, two electronically operated injector-commutators ( $IC_1, IC_2$ ), a 482 Femto spectrophotometer with a U-shaped flow cell (10 mm optical path;  $\approx 100 \text{ } \mu\text{l}$  lighted volume), a 111 Kipp and Zonen strip chart recorder, a hydride generator and gas-liquid separator (HG-GLS), a hydride absorber chamber (HAC), an IL 60714a Cole Parmer flowmeter, a  $C_{18}$  minicolumn, a TE 184 Micronal thermostatic water bath, polyethylene tubing (i.d. 0.7 mm), coiled reactors and accessories. The flow diagram of the system with the  $C_{18}$  bonded silica gel packed minicolumn acting as a sampling loop is shown in Fig. 1. The operation of the injector-commutator  $IC_1$  comprises two steps: pre-concentration in the position specified in the figure and elution in the next position. Samples or analytical solutions (S) merge at the confluent point a with an acidic ADDP solution ( $R_1$ ). The As-DDP complexes are formed inside the reactor  $B_1$  and reach the  $C_{18}$  minicolumn where they are retained. Phosphate, silicate, arsenate and other potential interferents, if present, pass through the minicolumn and are discharged ( $W_1$ ). During the preconcentration,  $750 \text{ } \mu\text{l}$  of absorbing solution ( $R_3$ ) are selected by the loop  $L_1$  and the residual solution inside the chamber HG-GLS is removed by the reversed-intermittent flow RI. After the pre-set concentration time, the injector-commutator  $IC_1$  is switched and the selected volume of absorbing solution is injected into the chamber HAC. The minicolumn is placed in line with channel E, and the eluent enters the minicolumn displacing the analyte. The established sample zone merges with reagent  $R_2$  (point b) and the resulting solution is mixed inside reactor  $B_2$  and afterwards injected into the chamber HG-GLS. The arsine generated is carried by a nitrogen flow to the chamber HAC and bubbled through the absorbing solution for 30 s. There-

after, IC<sub>1</sub> and IC<sub>2</sub> are simultaneously switched. The absorbing solution containing arsenate is then pumped by the intermittent flow I, filling the sampling loop L<sub>2</sub>. When IC<sub>2</sub> is switched back to the position specified in Fig. 1, arsenate is injected into the sample carrier stream C. The established sample zone merges with previously mixed reagents R<sub>4</sub> and R<sub>5</sub> at the confluence d. Arsenate species react under acidic conditions with ammonium heptamolybdate and stannous chloride forming the arsenomolybdenum blue complex inside the heated reactor B<sub>4</sub>. Details of the chemistry involved are given elsewhere [19]. Passage of the colored complex through the flow cell of spectrophotometer (840 nm) results in a transient absorbance which is recorded as a peak with height proportional to the arsenic content in the sample. After peak maximum measurement, another cycle can be started.

### 2.3. Procedure

With the system in Fig. 1, influence of the main parameters such as timing, flow rates, concentration and order of addition of reagents, composition and concentration of acid, temperature and effects of potential interferents, on the processes of preconcentration, hydride generation and blue complex formation, were investigated.

Arsenic complex formation was investigated by varying the ligand concentration [0.02–0.5% (w/v) ADDP], the nature and concentration of acid [0.10–10% (v/v) HNO<sub>3</sub> or HCl] and the time of interaction between arsenic and ligand (0.2–30 min).

Influence of sample volume on column loading was studied at sample flow rates within 0.9 and 3.2 ml min<sup>-1</sup>. Different column lengths (5–30 mm, i.d. = 3 mm) were also tested. Elution conditions were investigated by varying the flow rate of E (0.5–3.2 ml min<sup>-1</sup>) and the eluent composition. This study was carried out with an extra peristaltic pump in order to maintain the flow rates of S and R<sub>1</sub>.

Generation of arsine was investigated by varying the reducing agent concentration [0.25–4.0% (w/v) NaBH<sub>4</sub>], the concentration of hydrochloric acid [1.0–10% (v/v) HCl] and the flow rate of the

arsine carrier stream (25–100 ml min<sup>-1</sup> N<sub>2</sub>). The solutions 1.0 10<sup>-4</sup> M KMnO<sub>4</sub> in 0.5 M H<sub>2</sub>SO<sub>4</sub>, 1.0 10<sup>-4</sup> M KMnO<sub>4</sub> = 1% (w/v) (NH<sub>4</sub>)<sub>2</sub> Mo<sub>7</sub>O<sub>24</sub>·4H<sub>2</sub>O in 0.5 M H<sub>2</sub>SO<sub>4</sub> or 0.4% (w/v) KI = 0.25% (w/v) I<sub>2</sub> in 0.1 M NaHCO<sub>3</sub> were tested for trapping arsine.

Ammonium molybdate and stannous chloride concentrations were investigated in the 0.1–1.0 and 0.005–0.05% (w/v) ranges, respectively. Interaction time between these reagents was studied by varying the length of the coil B<sub>3</sub> from 5 to 250 cm. For each particular concentration, the reagents were prepared in HNO<sub>3</sub> or H<sub>2</sub>SO<sub>4</sub> solutions in the 0.05–5.0 M range.

Influence of flow rate of the carrier C on peak height was investigated within 0.8 and 3.0 ml min<sup>-1</sup>. The influence of temperature on signal measurements was also investigated by immersing the reactor B<sub>4</sub> in a thermostatic water bath and by varying the temperature within 25 and 70°C.

After the parameters had been selected, the proposed procedure was applied to arsenic determination in digests of plant materials, sugar and tap water. In addition, arsenite and arsenate recovery tests were also carried out on tap water and sugar samples.

### 3. Results and discussion

Initial experiments dealing with in-line preconcentration and arsine generation were carried out without the injector-commutator IC<sub>2</sub>. After bubbling and trapping arsine, an aliquot of the absorbing solution was manually removed from the HAC chamber and transferred to a quartz cuvette (10 × 10 mm) in which arsenic was assayed by the molybdenum blue method in batch mode. In this way, influence of ADDP, NaBH<sub>4</sub> and HCl concentrations, flow rates, reaction time and nature of eluent and absorbing solution were investigated. After optimization of these variables, the injector IC<sub>2</sub> was coupled to the system and the concentration and order of addition of spectrophotometric reagents, the length of sampling loop and the temperature were investigated. The whole procedure could then be automated.

Preliminary experiments revealed high blank values when 100 and 250  $\mu\text{g As l}^{-1}$  were processed in the flow system, owing to contamination of the ADDP reagent. The acidic ADDP stock solution was then purified by passing it through a  $50 \times 10 \text{ mm C}_{18}$  column in further experiments.

The flow system for arsenic determination depicted in Fig. 1 was designed to obtain high sensitivity since arsenic ions are usually found at trace levels in agroindustrial samples. Preliminary experiments were carried out with 0.2% (w/v) ADDP solution, to guarantee the displacement of the chemical equilibrium towards  $\text{As(DDP)}_3$  formation, and preconcentration time of 60 s was chosen. Sodium borohydride ( $R_2$ ) and hydrochloric acid (E) were 1% (w/v) and 2% (v/v) solutions, respectively.

The first parameter investigated was the influence of the nature of the liquid absorption media for trapping arsine. No signal was detected when acidic permanganate was used as  $R_3$  reagent, even in the presence of molybdate. The best results were obtained with 0.04% (w/v)  $\text{KI} = 0.025\%$  (w/v)  $\text{I}_2$  in 0.1 M  $\text{NaHCO}_3$ , and this combined solution was selected for further experiments.

The reaction between arsenic and ADDP is highly dependent on the nature of the acid used. Nitric and sulfuric acids must be avoided since arsenite may be converted to arsenate, which is not complexed by ADDP nor retained in the  $\text{C}_{18}$  minicolumn. Indeed, for speciation purposes, the original  $\text{As}^{3+}/\text{As}^{5+}$  ratio of the samples should be maintained. Thus, hydrochloric acid was chosen to maintain acidic conditions. The As-DDP complex formation is highly dependent on HCl concentration. Higher analytical signals for 50.0  $\mu\text{g As l}^{-1}$  were obtained as HCl was increased to 4% (v/v), whereas higher acid concentrations changed the signals only slightly. Hence, the analytical solutions and the eluent were prepared in 4% (v/v) HCl in subsequent experiments.

With regards to ADDP concentration, increased peak heights for an analytical solution containing 50  $\mu\text{g As l}^{-1}$  were obtained up to 0.1% (w/v) ADDP, then fell continuously as ADDP concentration rose further to 0.5% (w/v). Concentrations higher than 1.0% (w/v) were not investigated due to difficulties of ligand solubilization.

Further experiments were then conducted with 0.1% (w/v) ADDP in 4% (v/v) HCl as  $R_1$ .

No significant difference in signals were observed when the interaction time between arsenic and ADDP was varied from 0.2 to 30 min. Hence, the complex formation could be carried out in-line and the length chosen for the reactor  $B_1$  was 30 cm.

The length of the  $\text{C}_{18}$  minicolumn could not be increased at will because high back-pressure may cause leakage of the flowing solutions. For columns longer than 30 mm, leakage of the sample and eluate was observed for flow rates of S in the 0.9–3.2  $\text{ml min}^{-1}$  range. Columns shorter than 5 mm were not tested owing to the distance between two connecting points located in the central part of the injector-commutator. So, a  $20 \times 3 \text{ mm}$  column was chosen.

Flow rates of sample (S) and eluent (E) through the minicolumn are important parameters, as they relate to sampling rate, sensitivity, linearity of the calibration curve, elution efficiency and back-pressure. As the total flow rates of S or E (F) was increased from 0.9 to 3.2  $\text{ml min}^{-1}$ , the absorbance signal observed for 50  $\mu\text{g As l}^{-1}$  increased according the following equation:  $A = 1.7 \times 10^{-3} + 3.6 \times 10^{-3}F + 2.7 \times 10^{-3}F^2$ ;  $R^2 = 0.99649$ ). Flow rates = 3.2  $\text{ml min}^{-1}$  resulted in solution leakage at the inlet of the column. As a compromise between system stability, sensitivity and sampling rate, 3.2  $\text{ml min}^{-1}$  was selected. It should be noted that when a flow procedure involving in-line complexation with ADDP and sorption onto  $\text{C}_{18}$  column was studied to evaluate elimination of interference in ICP-MS [20], ethanol, nitric and hydrochloric acid were found to be suitable eluents for arsenic. By contrast, Pb-DDP, Bi-DDP, Cu-DDP, Fe-DDP Ni-DDP, Co-DDP were efficiently eluted only by ethanol or methanol. Consequently, metals that usually inhibit the generation of arsine (e.g. Cu, Ni, Co, Cr, Fe) can be separated from the matrix during the elution step. The removal of these metals from the  $\text{C}_{18}$  minicolumn was achieved by aspirating a small volume of ethanol at the channel S immediately before an analytical cycle. When flow rate E was slower than 0.5  $\text{ml min}^{-1}$ , elution and washing times were too long. Good

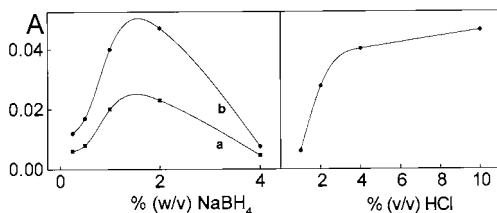


Fig. 2. Influence of NaBH<sub>4</sub> (A) and HCl (B) concentrations. Curves a and b correspond to 25.0, and 50.0 μg As l<sup>-1</sup>, respectively. Preconcentration time: 60 s. R<sub>1</sub>: 0.1% w/v ADDP in 1–10% v/v HCl; R<sub>3</sub>: 0.1M NaHCO<sub>3</sub> containing 0.04% w/v KI = 0.025% w/v I<sub>2</sub>. The studies in (B) were carried out with 1.5% w/v NaBH<sub>4</sub>.

elution and column rinsing were achieved at 1.2 ml min<sup>-1</sup>, the flow rate of E selected for further experiments. In order to avoid problems related to the transport of analyte through the mini-column, elution in a reversed flow was adopted.

Commutation time is a relevant parameter too since it relates to column loading time. Better sensitivities were obtained with loading times higher than 180 s, but the efficiency was poor and few samples could be processed per hour. For longer times, sensitivity approached a limiting value owing to the saturation of the column. Since the choice was among sensitivity, preconcentration efficiency and sampling rate, a time of 120 s was set as a good compromise. In this situation, tenfold enrichment was obtained.

The extent of reduction to arsenite is highly dependent not only on concentrations of KI, ascorbic acid, and hydrochloric acid, but also on reaction time. These variables have already been studied [13] and fixed at 2% (w/v) KI and ascorbic acid, 4% (v/v) HCl and 30 min reaction time. It should be stressed that this waiting time was extremely long for in-line reduction in the flow system. Thus, the reduction was carried out off-line.

Regarding the influence of sodium borohydride concentration, as the reagent R<sub>2</sub> was varied from 0.25 to 1.5% (w/v), the analytical signals corresponding to 25 and 50 μg l<sup>-1</sup> As(III) or As(V) increased about five times. At higher concentrations the signals fell (Fig. 2a). Analytical curves linear up to 50 μg As l<sup>-1</sup> were always obtained when R<sub>2</sub> was 1.5% (w/v) NaBH<sub>4</sub> and E was 4%

(v/v) HCl (Fig. 2b), so these were the solutions selected for further experiments. Different acidic medium showed in Fig. 2b were attained by varying the HCl concentration of eluent E.

Metals that inhibit arsine generation and are generally present in food and environmental samples [21,22] were tested as interferents. For the most serious interfering metals (M: Fe, Cu, Ni, Co, Cr) at the M/As ratio 100, 50, 10, 10, and 10, respectively, no measurable modifications in the analytical signals were found. In the elution conditions used in this work (4% (v/v) HCl as eluent and ethanol as washing solution), arsine formation occurs in the presence of practically negligible amounts of these potential interferents.

The flow set up in Fig. 1 was then used in the studies of arsenomolybdenum blue formation. The flow system was based on that of Frenzel et al. [11]. The reagents R<sub>4</sub> and R<sub>5</sub> were pre-mixed because the peak heights for 50.0 μg l<sup>-1</sup> increased by about 25% if compared with those obtained with sequential addition.

It should be stressed that when R<sub>4</sub> and R<sub>5</sub> reagents were prepared in nitric acid, peak heights were typically twice those obtained in sulfuric acid. However, the baseline changed from 0.015 A (H<sub>2</sub>SO<sub>4</sub>) to 0.1 A (HNO<sub>3</sub>), generating a very unstable system. The chemical reaction development time is highly dependent on the sulfuric acid concentration, faster reactions being observed at lower acidity. Sulfuric acid solutions = 1 M inhibited the reaction and no measurable signals were observed. Solutions = 0.2 M acid increased the rate of uncatalyzed reaction resulting in high baseline. As the carrier C is alkaline, the reagents R<sub>4</sub> and R<sub>5</sub> were prepared in 1.0 M H<sub>2</sub>SO<sub>4</sub> in order to obtain a good yield in the formation of heteropolyacid.

The concentration of R<sub>4</sub> and R<sub>5</sub> reagents are also important parameters to be considered in the system design. When R<sub>4</sub> was varied from 0.2 to 1.0% (w/v) NH<sub>4</sub>-molybdate, analytical signals of 25.0 μg As l<sup>-1</sup> increased ( $A = -0.0058 + 0.0458[R_4] - 0.02[R_4]^2$ ,  $R^2 = 1.000$ ). For higher concentrations, the uncatalyzed reaction increased and, consequently, the baseline. When the stannous chloride concentration (R<sub>5</sub>) increased up to 0.02% (w/v), higher signals were obtained. As the

signals did not vary for  $R_5 = 0.02\%$  (w/v), this was the concentration selected in this work. When hydrazine sulfate was added to this reagent at several concentrations in the 0.2–1.0% (w/v) range, no significant variation in the peak heights was observed. Reagent  $R_5$  was therefore 0.02% (w/v)  $\text{SnCl}_2$  plus 0.2% (w/v) of hydrazine sulfate in 0.5 M  $\text{H}_2\text{SO}_4$ .

With regards the length of loop  $L_2$ , signals increased with the injected sample volume. With  $L_2 = 100$  cm a limited dispersion [23] was obtained. As a compromise between sensitivity and sampling rate, this was the loop length selected.

Regarding the influence of temperature on blue complex development, better recorded signals were obtained at higher temperatures. However, when reactor  $B_4$  was immersed in a thermostatic water bath at  $T = 70^\circ\text{C}$ , air bubbles were observed in the analytical line and flow cell. Consequently, the system was operated at  $70^\circ\text{C}$  in subsequent experiments as a compromise between system stability and sensitivity.

After parameters had been chosen, analytical solutions within the 5.00–50.0  $\mu\text{g l}^{-1}$  range were injected in triplicate and calibration curves with good linearity ( $R^2 = 0.9997$ ) were consistently obtained. Accuracy was assessed by analyzing plant

certified materials from the NIST (Table 1). The results obtained with the proposed procedure were not statistically different from the certified values at 95% confidence level ( $t$ -test). For 120 s pre-concentration time and 30 s arsine bubbling, a throughput of about 20 samples  $\text{h}^{-1}$  can be attained, corresponding to 36 mg ADDP plus 36 mg  $(\text{NH}_4)_6\text{Mo}_7\text{O}_{24}$  plus 7 mg of hydrazine sulfate plus 0.7 mg  $\text{SnCl}_2$  and about 7 ml sample consumed per determination. The sensitivity can be improved since the column loading time is related to the arsenic content in the sample to be processed. The relative standard deviation was estimated as 6% for 17  $\mu\text{g As l}^{-1}$  after twelve sequential analyses of typical samples. In addition, recoveries within 94 and 104% of spiked tap water, sugars and synthetic mixtures of trivalent and pentavalent arsenic were found.

The usual methods involving hydride generation coupled to spectrometric techniques such as atomic absorption spectrometry [24], inductively coupled plasma atomic emission spectrometry [25] and inductively coupled plasma mass spectrometry [26] are very attractive for arsenic determination due to their high sensitivity and low detection limit. On the other hand, they require more sophisticated instrument which make these coupling

Table 1

Results for arsenic ( $n = 3$ ) in tap water, sugar and plant material (SRM1: 1572 citrus leaves<sup>a</sup>; SRM2: 1573 tomato leaves<sup>a</sup>) with the FIA system in Fig. 1

Sample	Certified value, $\mu\text{g g}^{-1}$	Spiked, $\mu\text{g l}^{-1}$		Recoveries, $\mu\text{g l}^{-1}$	
		As(III)	As(V)	As(III)	As(V)
Water 1		–	–	n.d.	n.d.
Water 2		5.00	–	$5.20 \pm 0.21$	–
Water 3		10.0	10.0	$10.6 \pm 0.3$	$12.1 \pm 0.4$
Water 4		25.0	–	$24.7 \pm 0.2$	–
Water 5		50.0	50.0	$49.3 \pm 0.5$	$49.1 \pm 0.4$
Sugar 1		–	–	$0.29 \pm 0.02$	–
Sugar 2		5.00	–	$5.20 \pm 0.26$	–
Sugar 3		10.0	10.0	$9.92 \pm 0.59$	$12.4 \pm 0.7$
Sugar 4		25.0	–	$25.5 \pm 0.5$	–
Sugar 5		50.0	50.0	$50.2 \pm 0.3$	$49.2 \pm 0.4$
SRM1	$3.1 \pm 0.3$			$2.9 \pm 0.1$	
SRM2	$0.27 \pm 0.05$			$0.29 \pm 0.04$	

<sup>a</sup> National Institute of Standards and Technology, Gaithersburg, MD; n.d.: not detected.

difficult to be used for most commercial laboratories. Although the proposed procedure in this work comprises sorbent extraction, hydride generation and liquid phase trapping, high selectivity, low reagent consumption, rapidity, low detection limit and other favorable analytical characteristics were obtained for determining arsenic at trace levels in spectrophotometry due to repetitive and automated operation of all separation steps. With some adaptations, the described system can be applied to the determination of low levels of arsenic in other matrices.

### Acknowledgements

The authors thank the FAPESP (Project 97/5108-0) and FUNDUNESP (Project 009/98) for financially supporting this work and the CNPq for the fellowships for J.A.G.N. and A.A.C.

### References

- [1] G.E. Batley, Trace Elements Speciation: Analytical Methods and Problems, CRC Press, Boca Raton, FL1989, p. 350.
- [2] A. Vercruyse, (Ed.), Hazardous Metals in Human Toxicology, Elsevier, New York, 1984, p. 337.
- [3] FDA Homepage, Center for food safety and applied nutrition <http://vmcfsan.fda.gov/~frf/guid-as.html>
- [4] G.F. Vandergrift, D.T. Reed, I.R. Tasker (Eds.), Environmental Remediation. Removing Organic and Metal Ion Pollutants, American Chemical Society, Washington, DC, 1992, p. 275.
- [5] J.K. Irgolic, A.E. Martel, Environmental Inorganic Chemistry, VCH, New York, 1985, 654.
- [6] B.S. Chana, J.N. Smith, Anal. Chim. Acta 197 (1987) 177.
- [7] Á. Woller, Z. Mester, P. Fodor, J. Anal. At. Spectrom. 10 (1995) 609.
- [8] J. Wang, M.J. Tomlinson, J.A. Caruso, J. Anal. At. Spectrom. 10 (1995) 601.
- [9] J.M. Costa-Fernández, F. Junzer, R. Pereiro-García, A. Sanz-Medel, J. Anal. At. Spectrom. 10 (1995) 1019.
- [10] P. Cunniff (Ed.), Official Methods of Analysis of AOAC International, sixteenth ed., vol. 1, Arlington, AOAC International, 1995. pp. 3.13, 9.9, 11.23.
- [11] W. Frenzel, F. Titzenthaler, S. Elbel, Talanta 41 (1994) 1965.
- [12] P. Linares, M.D. Luque de Castro, M. Valcárcel, Anal. Chem. 58 (1986) 120.
- [13] D. Pozebon, V.L. Dressler, J.A. Gomes Neto, A.J. Curtius, Talanta 45 (1998) 1167.
- [14] M. Sperling, X. Yin, B. Welz, Spectrochim. Acta 46B (1991) 1798.
- [15] H. Bode, W. Arnswald, Z. Anal. Chem. 185 (1962) 179.
- [16] P. Bermejo-Barrera, M.C. Barciela-Alonso, M. Ferrón-Novais, A. Bermejo-Barrera, J. Anal. At. Spectrom. 10 (1995) 247.
- [17] B.F. Reis, M.F. Giné, M.M. Santos Filha, N. Bacan, J. Braz. Chem. Soc. 3 (1992) 80.
- [18] J.A. Gomes Neto, H. Bergamin Filho, R.P. Sartini, E.A.G. Zagatto, Anal. Chim. Acta 306 (1995) 343.
- [19] S.R. Crouch, H.V. Malmstadt, Anal. Chem. 39 (1967) 1084.
- [20] V.L. Dressler, D. Pozebon, A.J. Curtius, Spectrochim. Acta 53B (1998) 1527.
- [21] W.W. Ding, R.E. Sturgeon, Anal. Chem. 69 (1997) 527.
- [22] J. Dedina, D. Tisalev, Hydride Generation Atomic Absorption Spectrometry, John Wiley & Sons, New York, 1995, p. 526.
- [23] J. Ruzicka, E.H. Hansen, Flow Injection Analysis, second ed., John Wiley & Sons, New York, 1988, p. 498.
- [24] X. Yin, E. Hoffman, C. Ludke, Fresenius J. Anal. Chem. 355 (1996) 324.
- [25] L. Vuchkova, S. Arpadjan, Talanta 43 (1996) 479.
- [26] M. Huang, S. Jiang, C. Hwang, J. Anal. At. Spectrom. 10 (1995) 31.

# Determination of cadmium and lead in mussels by tungsten coil electrothermal atomic absorption spectrometry

C.G. Bruhn <sup>a,\*</sup>, N.A. San Francisco <sup>a</sup>, J.Y. Neira <sup>a</sup>, J.A. Nóbrega <sup>b</sup>

<sup>a</sup> *Departamento de Análisis Instrumental, Facultad de Farmacia, Universidad de Concepción, P.O. Box 237, Concepción, Chile*

<sup>b</sup> *Departamento de Química, Universidade Federal de Sao Carlos, Caixa Postal 676, 13565-905, Sao Carlos, SP, Brazil*

Received 1 March 1999; received in revised form 8 June 1999; accepted 17 June 1999

## Abstract

In this work it was evaluated the determination of Cd and Pb in mussels by tungsten coil electrothermal atomic absorption spectrometry (TCA-AAS). A critical and comprehensive study of the effects caused by Pd, Mg, ascorbic acid, and binary mixtures of these compounds on the atomization of Cd and Pb in acid digested solutions of mussels was performed. Palladium and mixtures containing it were useful to increase sensitivity and thermal stability of Cd and Pb. Additionally, the coil lifetime was increased and the background signals were decreased in these modifiers. All these favorable effects were analytically exploited to determine Cd and Pb in samples of mussels. The proposed methodology was validated using two certified reference materials (oyster tissue and mussel). No statistical difference was observed between determined and certified values at a 95% confidence level. Cadmium and Pb in Chilean bivalve mussels were determined by TCA and by graphite furnace-AAS. Again, the results showed statistical agreement. © 1999 Elsevier Science B.V. All rights reserved.

*Keywords:* Cadmium; Lead; Tungsten coil electrothermal atomizer; Mussels; Chemical modifiers

## 1. Introduction

The use of a tungsten coil as an electrothermal atomizer (TCA) is attractive due to its low cost and simplicity. However, there are some obstacles for the dissemination of this atomizer as an alternative to the well-established graphite furnace atomic absorption spectrometry (GFAAS). After one decade of the revival of the TCA by Berndt and Schaldach [1] and despite several further pa-

pers published in the literature [2–13] in which a niche is recognized for this atomizer, there is no commercial device available yet. Though, recent progress was made in developing a simple, low-cost, multi-element atomic absorption spectrometer with a tungsten coil atomizer [9] which is in the beta test stage of commercialization. However, its outcome as a marketable device remain still uncertain. Hence, the lack of a commercial device clearly hinders the spreading of this technique. Additionally, the TCA is strongly affected by matrix interferences and most of the published applications relied on matrix matching approach

\* Corresponding author. Fax: +56-41-231903.

E-mail address: cbruhn@udec.cl (C.G. Bruhn)

[5,13], matrix separation [10], or standard additions method [4,11,12,14] for proper quantification. Despite of the feasibility of these procedures and their easy implementation, the sample manipulation is somewhat increased and contamination can become a problem.

The state of the art of the TCA may be regarded similar to the situation observed for the GFAAS before the establishment of the stabilized temperature platform furnace (STPF) conditions [15]. To aggravate the current development status of the TCA, the knowledge coming from decades of research with the GFAAS cannot be easily transferred to the TCA owing to the intrinsic characteristics of this latter atomizer, such as the fast heating rate (20 to 30 K ms<sup>-1</sup>) and the non-isothermal ambient [11].

One possible alternative to reduce or eliminate interferences is the use of chemical modifiers to change the thermal behavior of the analyte in a medium containing the sample matrix. The main difficulty for adopting this strategy is the lack of systematic studies related to the performance of chemical modifiers in metallic atomizers. Recently it was showed that most interferences on Cd and Pb atomization in the TCA for hair and blood samples seem to occur in condensed phase and affect the atomization appearance temperature and the sensitivity [11,12]. Therefore the use of chemical modifiers could alter condensed phase processes and could improve the efficiency of atomization. Also, it should be remarked that for most elements investigated in the TCA the atomization occurs predominantly through chemical processes which are critically dependent on the presence of the hydrogen in the purge gas and the thermal processes are less operative. This can be understood considering the intense gradient of temperature between the gaseous phase and the coil surface [16]. The atomization processes in a tungsten tube atomizer are different because this system is essentially an isothermal furnace, and according to Krakovská [17] volatile analytes are evaporated in their oxides forms which are reduced with hydrogen or tungsten. However, even for volatile elements in this isothermal furnace the atomization also proceeds through evaporation of their metallic form previously formed via hydrogen reduction in condensed phase [17].

In spite of the difficulties for an increase of analytical applications using the TCA, this device remains as a promising low-cost alternative for trace analysis in developing countries. Additionally, the development of dedicated instruments is also an interesting route for this atomizer, as proposed by Jones et al. [7–9], originally, as a portable atomic absorption spectrometer for the determination of Pb in blood [7] and Cd in environmental and biological samples [8], and more recently, as a simple multielement atomic absorption spectrometer with a TCA [9].

The effect of chemical modifiers is practically unknown in the TCA [11]. To our knowledge, Shan et al. made pioneering studies on the performance of Pd [18] and ascorbic acid [19] as chemical modifiers in a transversely heated tungsten tube atomizer (e.g. WETA-90 [20]) which is an isothermal atomizer. In the TCA, which is an open and non isothermal atomizer, only recently were described the effects of phosphates and Pd modifiers on the atomization of Cd and Pb in hair and blood samples [11,12]. The use of Pd was effective to improve the sensitivity and to increase the thermal stabilization, mainly for Pb. This observation was consistent with the effect of Pd on Pb absorbance described previously in the tungsten tube atomizer by Shan et al. [18]. Additionally, the Pd modifier improved the background signal correction and extended the coil lifetime by 20% (i.e., from 300 to 360 heating cycles). All these favorable effects in Pd modifier lead to improvements in accuracy and precision. Phosphates caused a negative interference on Cd atomization and this impaired its use [12].

In the present work it was investigated the determination of Cd and Pb in bivalve mussels by tungsten coil electrothermal atomic absorption spectrometry. Mussels are known to collect (or extract) heavy metals like Cd from their natural water environment. These specimens were chosen because they are regular food items included in the Chilean diet and only limited information is available about the levels of heavy metals in mussels.

The effect of chemical modifiers, i.e. Pd, Mg, ascorbic acid and its binary mixtures, on the atomization of Cd and Pb in mussel samples was



systematically evaluated. In a previous work involving the effect of chemical modifiers on Cr determination in acid-digested solutions of mussels and non-fat milk powder were shown favorable effects caused by mixtures of ascorbic acid and Mg [14]. The organic modifier seems to generate reducing compounds (C and CO) during its thermal decomposition and to increase the reducing character of the medium, which is essential for chemical atomization of most elements in the TCA [16]. The effect of these modifiers and their mixtures on Cd and Pb atomization in the non isothermal TCA is unknown.

## 2. Experimental

### 2.1. Apparatus

The TCA was installed on a vertical–transversal alignment system adapted to the basis of a laboratory-made quick-change mount system, and was aligned in the optical beam of a Perkin–Elmer (PE) model 1100 atomic absorption spectrometer (Überlingen, Germany) [1]. The limiting time resolution of the spectrometer was 0.02 s, which is sufficient to measure the fast signals of the TCA as was demonstrated by the reasonably low variation coefficient attained for both analytes in the within-run reproducibility study (see Section 3). The conditions used for Cd and Pb were according to manufacturers recommendations: resonance lines 228.8 nm (Cd) and 283.3 nm (Pb) with the spectrometer slit in 0.7 nm (low); the hollow cathode lamps were operated with 4 mA (Cd) and 8 mA (Pb), respectively, and deuterium arc background correction was used throughout. The signal measurement time was 0.7 s for both elements except in the study of atomization voltage in which 2 s was necessary at low atomization voltages (1–5 V) to enable full record of the delayed absorption signal. The TCA was heated by a programmable power supply with voltage feedback control and run with a PC computer. A mixture of Ar (90%)-H<sub>2</sub> (10%) was used as purge gas. Sample aliquots of 10 µl were delivered into the coil by means of a PE AS-40 autosampler attached to the quick-change mount

system and coupled to the TCA. A special interface and software was used for synchronous control of the autosampler and TCA power supply [21]. A graphite furnace with autosampler was used to check for method accuracy.

All samples were acid digested under pressure in a Milestone MLS-1200 MEGA Microwave system (Bergamo, Italy) using a Milestone MDR-300-S/10 TFM rotor, TFM vessels, and a standard cooling system for the MDR rotor. A MCR-6-E rotor with an acid scrubber unit was used for evaporation of digested samples. The graphite furnace (HGA-700) was used with pyrolytic graphite-coated tubes (Part No. B3001254) and pyrolytic graphite platforms (Part No. B3001256). The matrix modifier was NH<sub>4</sub>H<sub>2</sub>PO<sub>4</sub> (0.02 mg PO<sub>4</sub><sup>3-</sup> in a 10 µl aliquot) and the heating programs for Cd and Pb were identical to those previously used [11,12].

The absorbance signals were measured in peak height mode due to the short residence time (ca. 0.2 s) caused by the fast heating rate and fast atoms removal from the TCA [12]. As was demonstrated by Krakovská [17,22] for the tungsten tube atomizer it is more advantageous to work with peak height absorbance due to the signal sampling frequency and short duration of the signals. This criteria becomes more evident on the open TCA in which the high rate of generation of free atoms and fast atoms removal occurs in non isothermal conditions.

### 2.2. Reagents, materials and samples

All reagents were of analytical-reagent grade (Merck, Darmstadt, Germany), except for HNO<sub>3</sub> which was further purified in a quartz sub-boiling still and stored in quartz. Ultrapure water (18 MΩ-cm) was used throughout. Cadmium and Pb stock and reference solutions were prepared as described elsewhere [11,12].

Cadmium and Pb in acid digested solutions of mussel were subjected to a preliminary study to establish the appropriate concentration of each chemical modifier. This study included four concentrations of each chemical modifier: 0.5; 5.0; 50; and 100 mg l<sup>-1</sup>. The concentration range to be studied for each modifier was based on the ther-

mal behavior observed for Cd and Pb in the pyrolysis curves, the magnitude and shape of the absorption signals, the magnitude of the background absorption signal and the sensitivity. The atomization curves were obtained with and without the optimum modifier concentrations at the respective optimum pyrolysis voltages. The HNO<sub>3</sub> concentration in the acid digested solutions was 2% v/v. The following chemical modifiers and binary combinations were studied: Pd (as Pd(NO<sub>3</sub>)<sub>2</sub>), Mg (as Mg(NO<sub>3</sub>)<sub>2</sub>), ascorbic acid, Pd-Mg, Pd-ascorbic acid and Mg-ascorbic acid.

The optimization studies were performed in lyophilized powdered samples of the bivalve mussel 'navajuelas chilenas' (*Tagelus dombeii*) collected in the Arauco Gulf (Eighth Region, Chile). The samples of bivalve mussels were 'almejas' (*Semelle sólida*) and 'navajuelas chilenas', prepared from fresh samples collected in natural banks of the Chilean coast and classified by size [23].

The sample masses for Cd was 100 mg and for Pb was 250 mg of lyophilized mussel powder and was digested in 4 ml HNO<sub>3</sub> + 1 ml H<sub>2</sub>O<sub>2</sub> (30%). The samples were digested following a 6-steps program (25 min): 2 min — 250 W; 2 min — 0 W; 6 min — 250 W; 5 min — 400 W; 5 min — 650 W, 5 min-vent. The acid digests were subsequently evaporated in a MCR-6-E rotor using an acid scrubber unit. The optimized evaporation program used was implemented in 36 min: 2 min — 250 W; 2 min — 350 W; 2 min — 450 W; 5 min — 500 W, 20 min — 600 W, 5 min-vent. The dry residue was carefully dissolved in 7 ml 1 mol l<sup>-1</sup> HNO<sub>3</sub>, transferred into 25 ml volumetric flasks and diluted with ultrapure water. Blank solutions of the acid digestion were prepared likewise.

### 2.3. Procedure

Based on previous work with the TCA for Cd and Pb the pyrolysis step was studied between 300–860°C, and the atomization step was studied between 760–1860°C [11,12]. The coil temperature was estimated by voltamperometric measurements according to the procedure previously described [12]. Based on the experience achieved

in the aforementioned studies, the pyrolysis and atomization times were 10 s and 1 s throughout, respectively. The other steps were also optimized but experimental details were not included here. A mixture of 90% argon plus 10% hydrogen flowing at 1.0 and 1.5 l min<sup>-1</sup> for Cd and Pb, respectively, was used as the purge gas. This optimum flow rate was previously established [4], is comparatively higher than the gas flow rate used in an enclosed TCA [2,7], and is required to protect the coil from oxidation while providing reasonable sensitivity. The reducing atmosphere is necessary to increase tungsten coil lifetime considering the effects caused by air diffusion in the open TCA [1].

Using optimized thermal programs (Table 1) for Cd and Pb in mussel matrix medium with the selected chemical modifiers, the analytical figures of merits were assessed including the linear working range, the reciprocal sensitivity and characteristic mass, the repeatability, the reproducibility and the method detection limits (3 s<sub>blank</sub>/slope). The methodology was validated employing certified reference materials (CRMs): Oyster tissue (SRM 1566a, National Institute of Science and Technology, NIST, USA) and mussel (GBW 08571, National Research Centre for Certified Reference Materials, NRCRM, China) and by addition–recovery experiments. The methodology was applied to the determination of Cd and Pb in mussel samples of 'navajuelas chilenas' and 'almejas'. The results for samples were validated by GFAAS under STPF conditions.

Table 1  
Thermal program for the determination of Cd (in 35 µg ml<sup>-1</sup> Pd) and Pb (in 100 µg ml<sup>-1</sup> Pd + 50 µg ml<sup>-1</sup> ascorbic acid) in mussels with selected chemical modifiers by electrothermal AAS with a tungsten coil atomizer

Step	Time (s)	Temperature (°C)	Read
1	65 (80 <sup>a</sup> )	275	No
2	10	325	No
3	10	430 (670 <sup>a</sup> )	No
4	10	0	No
5	0.2	0	Yes
6	1	1670 (1730 <sup>a</sup> )	No
7	2	1850	No

<sup>a</sup> For Pb.

### 3. Results and discussion

As mentioned, the first study was related to the effect of different chemical modifiers on the thermal behavior of Cd and Pb in acid-digested mussel solutions. This study included the verification of the chemical-modifier concentration effect (optimum modifier concentration), and the investigation of the optimum pyrolysis and atomization temperatures.

#### 3.1. Cd atomization in the TCA: study of chemical modifiers

The evaluation of the effect of chemical modifiers on Cd atomization was performed in 1 + 1 v/v acid digested mussel solution with and without each one of the chemical modifiers, i.e. Pd, Mg, and ascorbic acid, and their binary combinations in study. The Cd concentration in the diluted solution was  $8 \mu\text{g l}^{-1}$ .

In Fig. 1a are shown the pyrolysis curves obtained in each individual modifier and binary combinations of modifiers at the optimum modifier concentration. Taking into account the thermal stability and the absorbance sensitivity, the best condition was attained for Cd in Pd modifier at an atomization temperature of  $1770^\circ\text{C}$  (12.0 V). The concentration of Pd was more favorable from 0.5 to  $50 \mu\text{g ml}^{-1}$ , and within this range the optimum Pd concentration was  $35 \mu\text{g ml}^{-1}$ . It provided thermal stabilization of Cd up to a pyrolysis temperature of  $500^\circ\text{C}$  (1.10 V) and higher absorbance sensitivity compared to thermal losses evidenced beyond  $330^\circ\text{C}$  in the curve without chemical modifier. However, the binary combinations including  $100 \mu\text{g ml}^{-1}$  Pd plus  $50 \mu\text{g ml}^{-1}$  Mg or  $100 \mu\text{g ml}^{-1}$  Pd plus  $5 \mu\text{g ml}^{-1}$  ascorbic acid also provided similar effects attributed to Pd. Considering that the use of a single chemical modifier reduces the possibility of contamination of the sample solution, Pd was selected as modifier in this case. The optimum pyrolysis temperature for Cd in Pd was  $430^\circ\text{C}$  (0.90 V).

The atomization curves obtained for Cd in acid digested solution of mussel 'navajuelas' with the three chemical modifiers containing Pd and with-

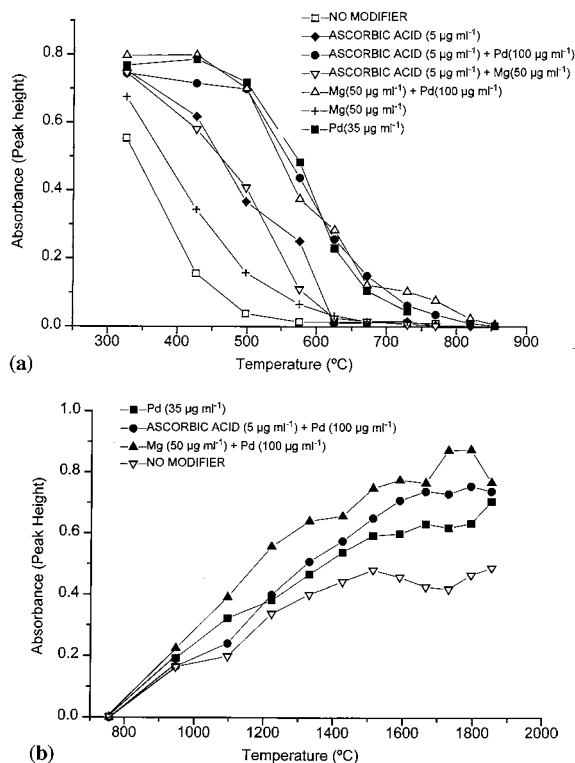


Fig. 1. Pyrolysis (1a) and atomization (1b) curves for Cd ( $8.0 \mu\text{g l}^{-1}$ ) in acid digested solutions of mussel (*Tagelus Dombeyi*) with and without chemical modifiers by TCA-AAS

out addition of chemical modifiers are shown in Fig. 1b. The pyrolysis temperature was fixed at  $430^\circ\text{C}$  or  $330^\circ\text{C}$  for solutions with and without chemical modifiers, respectively. The optimum atomization temperature for Cd with  $35 \mu\text{g ml}^{-1}$  Pd modifier in this mussel solution was  $1670^\circ\text{C}$  (10.0 V).

It can be concluded that the Pd modifier and its mixtures with Mg or ascorbic acid were effective in increasing both the thermal stabilization and the absorbance sensitivity of Cd in a mussel matrix solution. The effect of these modifiers in the elimination of interferences will be discussed later on.

#### 3.2. Pb atomization in the TCA: study of chemical modifiers

This study was performed in 1 + 1 v/v acid digested mussel solution spiked with  $50 \mu\text{g l}^{-1}$

Pb, with and without Pd, Mg, or ascorbic acid and their combinations. The Pb spike was necessary due to the low concentration of this analyte in the acid digested mussel solution.

In Fig. 2a are shown the pyrolysis curves obtained in individual and binary combinations of the modifiers at the optimum concentration. Once again, Pd and both Pd binary combinations with Mg or ascorbic acid showed a pronounced thermal stabilization of Pb compared to the curve without modifier. Considering thermal stabilization and absorbance sensitivity, the best condition was attained with the binary combination containing  $50 \mu\text{g ml}^{-1}$  Pd plus  $100 \mu\text{g ml}^{-1}$  ascorbic acid at an atomization temperature of  $1770^\circ\text{C}$  (12.0 V). It provided thermal stabilization of Pb up to a pyrolysis temperature of  $670^\circ\text{C}$  (1.70 V) and a significant enhancement in absorbance sensitivity. It can be seen that without chemical modifier and at  $670^\circ\text{C}$ , Pb is nearly quantitatively

lost during the pyrolysis step. When Pd was used without ascorbic acid, the thermal stabilization is slightly lower (ca.  $100^\circ\text{C}$ ) but the absorbance sensitivity is still better. Comparing to the no use of modifier, the pyrolysis temperature was increased from  $430$  to  $580^\circ\text{C}$  or  $670^\circ\text{C}$  in Pd or Pd + ascorbic acid, respectively with significant enhancement of absorbance sensitivity. The thermal stabilization reached in this latter medium was the most pronounced effect observed in all experiments. As previously indicated, the most pronounced effects were caused by Pd.

The atomization curves obtained for Pb in acid digested solution of mussel ‘navajuelas’ with the three chemical modifiers containing Pd and without modifier are shown in Fig. 2b. The pyrolysis temperature used in this study was  $540^\circ\text{C}$  (1.20 V) in Pd,  $580^\circ\text{C}$  (1.30 V) in Pd + Mg and  $670^\circ\text{C}$  (1.70 V) in Pd + ascorbic acid media. Without modifier the pyrolysis temperature was fixed at  $430^\circ\text{C}$  (0.90 V). The optimum atomization temperature for the mussel solution containing Pb in Pd + ascorbic acid modifier was  $1730^\circ\text{C}$  (11.0 V).

Although thermal stabilization by Pd and Mg modifiers is well known and described for these and other analytes in GFAAS, to our knowledge, the thermal stabilization effects achieved in this work for Cd and Pb in the acid digested solutions of mussels have no precedent in this open TCA.

### 3.3. Analytical application and figures of merit

After optimizing the pyrolysis and atomization temperatures for Cd and Pb in acid digested mussel solution, the calibration curves and linear working ranges were established and are reported in Table 2. For Cd the best sensitivity was reached in Pd ( $35 \mu\text{g ml}^{-1}$ ) and for Pb, in the presence of Pd ( $50 \mu\text{g ml}^{-1}$ ) + ascorbic acid ( $100 \mu\text{g ml}^{-1}$ ). In comparison with the sensitivity achieved in previous work for Cd and Pb in Pd modifier at a lower concentration ( $15 \mu\text{g ml}^{-1}$ ) [11,12], in the present work this figure was comparable for Pb and slightly lower for Cd, and the linear working ranges were comparable for Cd and slightly shorter for Pb.

In Table 3 are shown the analytical figures of merits obtained for Cd and Pb in the selected

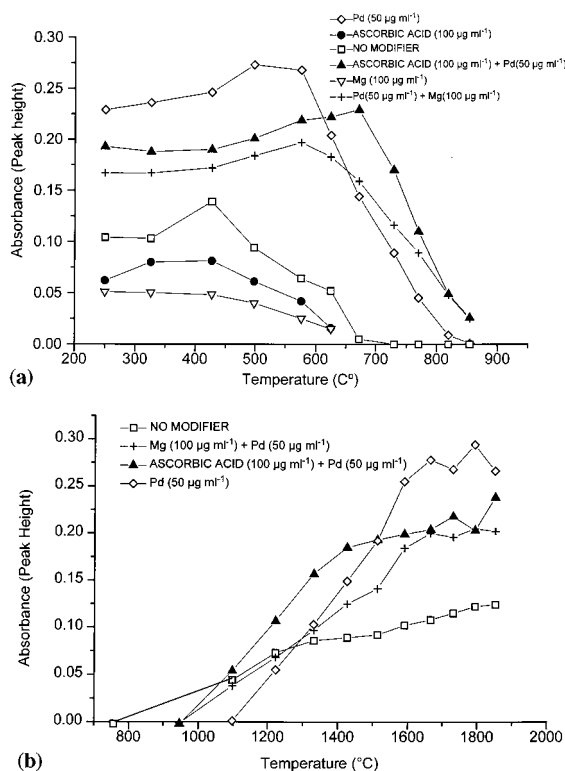


Fig. 2. Pyrolysis (2a) and atomization (2b) curves for Pb ( $50 \mu\text{g l}^{-1}$ ) in acid digested solutions of mussel (*Tagelus Dombeyi*) with and without chemical modifiers by TCA-AAS

Table 2  
Calibration graphs<sup>a</sup> for Cd and Pb in 0.1% v/v HNO<sub>3</sub> and selected chemical modifiers obtained with the TCA-AAS<sup>b</sup>

	Cadmium	Lead
Chemical modifier	35 µg ml <sup>-1</sup> Pd	50 µg ml <sup>-1</sup> Pd + 100 µg ml <sup>-1</sup> ascorbic acid
Calibration range (µg l <sup>-1</sup> )	0.3–3.0	2.5–100
Slope ± s	0.1300 + 0.0044	0.00464 + 0.00011
Intercept ± s	0.0027 + 0.0072	0.00542 + 0.00729
Standard error (n = 6)	0.0105	0.00853
Correlation coefficient	0.998	0.999

<sup>a</sup> Linear regression ( $A = mC + b$ ) representative of  $n = 6$  for each data point.

<sup>b</sup> Obtained with 7-steps thermal programs (Table 1).

modifiers. Previous data obtained without using modifiers are also included for comparison. The reciprocal sensitivity for Cd was somewhat better in Pd (35 µg ml<sup>-1</sup>), and for Pb was 100% higher in Pd (50 µg ml<sup>-1</sup>) + ascorbic acid (100 µg ml<sup>-1</sup>). The repeatability for Cd in Pd (35 µg ml<sup>-1</sup>) was satisfactory and comparatively better than without modifier; for Pb in the selected binary mixture this figure was similar and significantly better than without modifier. The between-day reproducibility of measurements showed similar figures indicating that the intralaboratory variability was small at least for reference solutions of both analytes in the selected modifiers. Considering the relatively high sensitivity and low variation coefficient in the repeatability study obtained for both

analytes, the limiting time resolution of the spectrometer was satisfactory for fast signal measurement. The instrumental detection limits ( $3 s_{\text{blank}}/\text{slope}$ ) for Cd and Pb were reasonably low, being slightly better for Cd in Pd (35 µg ml<sup>-1</sup>) and at least 4-fold better for Pb in the selected modifiers compared to the measurements without the modifier. In general, these detection limits for Cd and Pb in the selected modifiers are somewhat better than the ones obtained for both analytes either without modifier or in phosphate modifiers [11,12].

The method detection limit by TCA-AAS was assessed for mussel sample matrix and selected modifiers, and for Cd is 0.009 µg g<sup>-1</sup> and for Pb is 0.07 µg g<sup>-1</sup>. The quantification limit for Cd is 0.03 µg g<sup>-1</sup> and for Pb is 0.21 µg g<sup>-1</sup>. These values are comparable for Cd and somewhat better for Pb than the ones found by Jones et al. [9] in oyster tissue sample matrix by AAS with an enclosed TCA, and very near to those typically found by GFAAS.

The analytical methodology including the sample digestion procedures and the determination by TCA-AAS was validated for Cd and Pb by the determination of both in two CRMs: oyster tissue and mussel. The quantification was performed by the standard additions method because matrix effects were not fully corrected by the employ of the selected chemical modifiers. The same quantification method was required by Jones et al. [9] too in the determination of Cd and Pb in oyster tissue by AAS with an enclosed TCA. It should be pointed out that the maximum pyrolysis temperatures without losses of analytes even in the pres-

Table 3  
Analytical figures of merits obtained for Cd and Pb in selected chemical modifiers by TCA-AAS

	Cd 0.2% v/v HNO <sub>3</sub>	Cd in Pd	Pb 0.2% v/v HNO <sub>3</sub>	Pb in Pd + ascorbic acid
Chemical modifier concentration (µg ml <sup>-1</sup> )	–	35	–	50 + 100
Reciprocal sensitivity µg l <sup>-1</sup>	0.05	0.04	2	1
Characteristic mass (pg)	0.5	0.4	20	10.1
Linear working range (µg l <sup>-1</sup> )	0.3–3.0	0.3–3.0	10–125	2.5–100
Within-run reproducibility CV%	3.6	2.4	6.3	2.3
Reproducibility CV%	–	2.7	–	2.9
Detection limit (µg l <sup>-1</sup> )	0.10	0.09	3	0.63

Table 4

Determined and certified values of Cd and Pb ( $\mu\text{g g}^{-1}$ , dry weight)<sup>a</sup> in certified reference materials (CRMs) by TCA-AAS

CRM	Cd determined	Cd certified	Pb determined	Pb certified
1566a oyster tissue	$4.05 \pm 0.12$	$4.15 \pm 0.38$	$0.36 \pm 0.04$	$0.371 \pm 0.014$
08571 mussel	$4.32 \pm 0.05$	$4.5 \pm 0.5$	$1.88 \pm 0.13$	$1.96 \pm 0.09$

<sup>a</sup> Mean  $\pm$  standard deviation for triplicate determinations.

ence of the modifiers are not enough for complete thermal remotion of severe interferences, such as the alkaline and alkaline-earth elements [24]. However, the use of the selected modifiers enabled a significant enhancement in the sensitivity for the determinations of both analytes. Additionally, a marked decrease of background absorption and an increase in the coil lifetime were also observed. The effect of ascorbic acid on the tungsten surface (0.01% m/v ascorbic acid solution) in the presence of Pd is not enough to cause a decrease in coil lifetime due to formation of tungsten carbide. On the other hand, the generation of hydrogen is probably useful to protect the coil from oxidation. In fact, the coil lifetime in the presence of Pd and ascorbic acid enabled at least between 320 and 360 heating cycles before a coil change became necessary. The Cd and Pb results for CRMs are shown in Table 4. A *t*-test showed no statistical difference at a 95% confidence level between the results obtained by TCA-AAS and the certified values of oyster tissue and mussel. By TCA-AAS in these CRMs the mean relative percent error ( $E_{\text{rel}}\%$ ) for Cd was 3.2% (2.4–4.0%) and for Pb was 3.6% (3.0–4.1%), and the relative standard deviation (RSD) for Cd was 2.1% (3.0–1.2%) and for Pb was 8.9% (11.1–6.7%). These higher RSD values for Pb can be attributed to the relatively low Pb concentration found in the oyster tissue SRM.

Recovery studies were performed for Cd and Pb in blanks as well as in a sample of 'navajuelas' with known concentrations of Cd and Pb, and spiked with  $5 \mu\text{g l}^{-1}$  Cd and  $50 \mu\text{g l}^{-1}$  Pb before the acid digestion procedure (Table 5). The mean recoveries obtained in blanks of mussel were  $95.1 + 4.0\%$  ( $n = 3$ ) and  $98.8 + 6.1\%$  ( $n = 4$ ), and in the sample of 'navajuelas',  $102.2 + 3.7\%$  ( $n = 3$ ) and  $97.5 + 2.8\%$  ( $n = 3$ ) for Cd and Pb, respec-

tively. Mean recoveries varied from 95.1 to 102.2% and mean RSD was 3.2 and 4.1% for Cd and Pb, respectively.

The TCA was applied to the determination of Cd and Pb in five samples of lyophilized Chilean mussels: 'almejas' and 'navajuelas chilenas'. Cadmium and Pb were also determined by GFAAS for comparison. No statistically significant differences were established by Student *t*-test between the results obtained in mussels by both analytical methods. The mean  $E_{\text{rel}}\%$  was 4.8% (0.2–12.7%) and 3.9% (0–11.4%) and the mean RSD was 7.8% (4.5–12%) and 21% (10.3–31.5%) for Cd and Pb, respectively. The Cd levels were significantly higher than the Pb levels (i.e. 10 to 20-fold higher). The relatively high mean RSD obtained for Pb in mussel samples was attributed to the concentration levels close to the method quantification level in three samples. The levels of Cd in two samples of 'almejas' collected in the same coastal area were quite different, with one of them significantly higher, whereas in 'navajuelas' the Cd levels were similar in two samples from the same coastal area which receives industrial waste waters, and somewhat lower in one sample from a different bay which receives two river courses, one of them carrying domestic wastes.

#### 4. Conclusion

The TCA with the appropriate chemical modifiers can be applied for the accurate and precise determination of Cd and Pb in freeze-dried mussel samples. Despite the only partial correction of interferences due to its incomplete thermal removal at the adopted pyrolysis temperatures, the Pd modifiers and mixtures of it with Mg or ascorbic acid were operative to increase

Table 5

Determination of Cd and Pb ( $\mu\text{g g}^{-1}$ , dry weight)<sup>a</sup> in Chilean bivalve mussels by TCA-AAS and by GFAAS

SAMPLE	CD TCA-AAS	CD GFAAS	PB TCA-AAS	PB GFAAS
Almejas 1 (Ancud Gulf)	5.99 ± 0.32	5.87 ± 0.26	0.34 ± 0.08	0.34 ± 0.02
Almejas 2 (Ancud Gulf)	2.58 ± 0.19	2.81 ± 0.10	0.39 ± 0.09	0.35 ± 0.02
Navajuelas 1 (Arauco Gulf)	4.49 ± 0.45	4.50 ± 0.20	0.29 ± 0.05	0.29 ± 0.02
Navajuelas 2 (Arauco Gulf)	4.64 ± 0.21	4.59 ± 0.14	0.19 ± 0.06	0.18 ± 0.05
Navajuelas 3 (Corral Bay)	2.74 ± 0.33	3.14 ± 0.29	0.39 ± 0.04	0.40 ± 0.02

<sup>a</sup> Mean ± standard deviation for triplicate determinations.

thermal stability and the sensitivities of Cd and Pb, to increment coil lifetime, and to decrease background absorption. All these favorable effects make attractive the use of these modifiers and could extend the analytical applications of the TCA.

### Acknowledgements

We are grateful to Fondo Nacional de Desarrollo Científico y Tecnológico (FONDECYT, Research Grant No. 1960664), European Commission (Contract CII-CT94-014) and Dirección de Investigación of the Universidad de Concepción (DIUC research grant N° 95.71.01-4) for financial support; to Dr Harald Berndt for providing the TCA unit through the agreement of cooperation between the Institute für Spektrochemie und angewandte Spektroskopie (ISAS) Dortmund, Germany, and the Facultad de Farmacia, Universidad de Concepción; and to the Centro EULA-Chile of the Universidad de Concepción for allowing the use of their PE-1100B atomic absorption spectrometer with HGA-700 graphite furnace and AS-70 autosampler.

### References

- [1] H. Berndt, G. Schaldach, *J. Anal. At. Spectrom.* 3 (1988) 709.
- [2] M.F. Giné, F.J. Krug, V.A. Sass, B.F. Reis, J.A. Nóbrega, H. Berndt, *ibid.*, 8 (1993) 243.
- [3] M.M. Silva, R.B. Silva, F.J. Krug, J.A. Nóbrega, H. Berndt, *ibid.*, 9 (1994) 861.
- [4] C.G. Bruhn, F.E. Ambiado, H.J. Cid, R. Woerner, J. Tapia, R. García, *Anal. Chim. Acta* 306 (1995) 183.
- [5] F.J. Krug, M.M. Silva, P.V. Oliveira, J.A. Nóbrega, *Spectrochim. Acta Part B* 50 (1995) 1469.
- [6] P. Parsons, H. Qiao, K.M. Aldous, E. Mills, W. Slavin, *ibid.*, 50 (1995) 1475.
- [7] C.L. Sanford, S.E. Thomas, B.T. Jones, *Appl. Spectrosc.* 50 (1996) 174.
- [8] J.D. Batchelor, S.E. Thomas, B.T. Jones, *ibid.*, 52 (1998) 1086.
- [9] K.A. Wagner, K.E. Levine, B.T. Jones, *Spectrochim. Acta Part B* 53 (1998) 1507.
- [10] M.M. Silva, F.J. Krug, P.V. Oliveira, J.A. Nóbrega, B.F. Reis, D. Penteado, *Spectrochim. Acta Part B* 51 (1996) 1925.
- [11] C.G. Bruhn, J.Y. Neira, G.D. Valenzuela, J.A. Nóbrega, *J. Anal. At. Spectrom.* 13 (1998) 29.
- [12] C.G. Bruhn, J.Y. Neira, G.D. Valenzuela, J.A. Nóbrega, *Talanta* 48 (1999) 537.
- [13] P.O. Lucas, J.A. Nóbrega, P.O. Olivera, F.J. Krug, *Talanta* 48 (1999) 695.
- [14] C.G. Bruhn, J.Y. Neira, M.I. Guzmán, M.M. Darder, J.A. Nóbrega, *Fresenius J. Anal. Chem.* 364 (1999) 273.
- [15] W. Slavin, D.C. Manning, G.R. Carnrick, *At. Spectrosc.* 2 (1981) 137.
- [16] P.V. Oliveira, Atomization mechanisms of Ba, Cd, Cr, and Pb by atomic absorption spectrophotometry with tungsten coil. Ph.D. Thesis, Universidade Federal de São Carlos, Brazil, 1997.
- [17] E. Krakovská, *Spectrochim. Acta Part B* 52 (1997) 1327.
- [18] X.-q. Shan, B. Radziuk, B. Welz, V. Sychra, *J. Anal. At. Spectrom.* 7 (1992) 389.
- [19] X.-q. Shan, B. Radziuk, B. Welz, O. Vyskocilová, *J. Anal. At. Spectrom.* 8 (1993) 409.
- [20] V. Sychra, J. Dolezal, R. Hlavác, L. Petros, O. Vyskocilová, D. Kolihová, *J. Anal. At. Spectrom.* 6 (1991) 521.
- [21] J.Y. Neira, C.G. Bruhn, J.L. Vega, G.D. Valenzuela, J.A. Nóbrega, *Quím. Nova* 21 (1998) 490.
- [22] E. Krakovská, P. Pulis, *Spectrochim. Acta Part B* 51 (1996) 1271.
- [23] I. De Gregori, D. Delgado, H. Pinochet, et al., *Sci. Tot. Environ.* 111 (1992) 201.
- [24] Z. Queiróz, Thermal behavior of Na, K, Ca, and Mg in a tungsten coil atomizer. M.Sc. Dissertation, Universidade de São Paulo, 1997.

# Anodic stripping voltammetric determination of bismuth(III) using a Tosflex-coated mercury film electrode

Hao-Yun Yang, Wen-Yin Chen, I-Wen Sun \*

*Department of Chemistry, National Cheng-Kung University, Tainan, 70101, Taiwan, ROC*

Received 5 March 1998; received in revised form 14 June 1999; accepted 18 June 1999

## Abstract

A Tosflex–mercury film electrode (TMFE) was prepared by spin-coating a solution of the perfluorinated anion exchange polymer Tosflex onto a glassy carbon electrode surface followed by electrodeposition of mercury film on this electrode. This electrode was used for the determination of trace bismuth(III) which was preconcentrated onto the TMFE as anionic bismuth(III) complexes with chloride in a chloride medium. The preconcentration was carried out at a potential of  $-0.2$  V, and the preconcentration of the bismuth(III) was enhanced significantly by the anion-exchange feature of Tosflex. The accumulated bismuth(III) was then determined by anodic square-wave stripping voltammetry (SWSV). Various parameters influencing the determination of bismuth(III) were examined in detail. With 2 min accumulation, the analytical signal versus concentration dependence was linear up to 50 ppb, and the detection limit was 0.58 ppb. This modified electrode showed good resistance to the interferences from surface-active compounds and common ions. © 1999 Elsevier Science B.V. All rights reserved.

*Keywords:* Bismuth; Stripping voltammetry; Electroanalysis; Tosflex

## 1. Introduction

Anodic stripping voltammetry is a sensitive technique for the determination of traces of bismuth(III) in aqueous media [1–4]. For example, ng of Bi(III) could be detected using a glassy carbon rotating disk electrode with square-wave anodic stripping voltammetry [4]. This method, however, is time-consuming: a 20 min preconditioning procedure was required before a 5 min (or 20 min) accumulation and stripping of Bi(III) could

be carried out. Extensive efforts have been devoted to improve the anodic stripping voltammetric determination of Bi(III). Several carbon paste chemically modified electrodes containing a complexing reagent with chemical affinity for Bi(III) have been developed for the determination of Bi(III) [5–9]. These procedures, however, do not achieve the detection limit obtained with mercury electrode.

The applicability of stripping analysis can be improved by the use of ion-exchange polymer modified electrodes. The ion-exchange polymer modified electrode exhibit enhanced preconcentration efficiency for analytes, and is less subject to

\* Corresponding author. Fax: +886-06-2740552.

*E-mail address:* iwsun@mail.ncku.edu.tw (I.-W. Sun)



interferences from surface-active compounds. Numerous examples on the use of cation-exchanger, Nafion, modified electrodes for the determination of cations have been published [10,21,22]. While most species of analytical interest exist in the form of cations in sample solutions, Bi(III) is mostly present in anionic forms. Apparently, an anion-exchange polymer modified electrode would be particularly appealing for the determination of anionic Bi(III). Zen et al. [11] have developed a poly(4-vinylpyridine)–mercury film modified glassy carbon electrode (PVP–MFE) to determine bismuth in the form of  $[\text{BiCl}_4]^-$ . Although the PVP–MFE exhibits good resistance to interferences from surface-active compounds and a good detection limit, the use of PVP–MFE presents some problems. Because PVP dissolves easily in acidic solution, a cross-link agent was required to stabilize the PVP film and the PVP coated electrode needed to be heated at 90°C for about 2 h for the cross-link process to complete [12]. Moreover, the PVP–MFE is effective only in fairly acidic solution because the PVP polymer is protonated more completely in more acidic solutions [13]. Relatively recently, a new class of perfluorinated anion-exchange polymer named Tosflex (Tosoh Soda) has become commercially available [14]. Similar to Nafion, Tosflex exhibits very good stability and is easy to use. Thus, Tosflex can be an ideal alternative to PVP for the determination of anions. However, reports on the employment of Tosflex film modified electrodes for the determinations of trace metal ions are relatively limited. Only several examples including copper(I), mercury(II), thallium(III) and tellurium(IV) have been demonstrated recently [15–18].

This paper describes a square-wave stripping voltammetric (SWSV) procedure for the determination of bismuth(III) by using a Tosflex–mercury film modified electrode (TMFE). Anionic bismuth(III) chloride complex is first accumulated on the electrode surface by the ion exchange feature of the TMFE and followed by anodic SWSV measurement. Various factors influencing the determination of bismuth(III) were investigated.

## 2. Experimental

### 2.1. Apparatus

All electrochemical experiments were performed with a Bioanalytical Systems BAS CV-50W electrochemical analyzer in conjunction with a BAS model C-2 electrochemical cell. The three-electrode system consisted of a glassy carbon disk working electrode (BAS, 3 mm diameter) coated with Tosflex and mercury, a saturated Ag–AgCl reference electrode (BAS), and a platinum spiral auxiliary electrode. All glassware was cleaned with 1:1 nitric acid and rinsed with deionized water.

### 2.2. Chemicals and reagents

The Tosflex membrane, denoted IE-SA 48, was obtained from Tosoh Soda, Japan. Sodium perchlorate, sodium nitrate and nitric acid were of analytical grade from Riedel-de Haen (RDH). Standard metal solutions (1000 ppm) of Zn(II), Ge(IV), Cr(VI), Cu(II), and Cd(II) were from Fisher. Standard solutions (1000 ppm) of Se(IV) and bismuth(III) were from Mallinckrodt. Hg(II) standard solution (1000 ppm) was from Merck. The nonionic surfactant Triton X-100 was received from Lancaster. All the preparation and dilution of solutions were made with deionized water.

### 2.3. Preparation of Tosflex–mercury film electrode and sample solution

The dissolution of Tosflex membrane was carried out according to the procedure described in the literature [14]. About 2.5 g of finely cut dry membrane and 10 ml of water–methanol–2-propanol aqueous–alcoholic solution was heated to the boiling point at atmospheric pressure under reflux and stirring for 20–50 h. After cooling, the undissolved membrane was separated by centrifugation and a clear, yellowish solution was collected. The concentration of the dissolved polymer was determined gravimetrically from an evaporated portion of the solution. The coating solution was brought to a final concentration of 1.2 wt% by dilution with methanol.

After being polished with a polishing cloth to a shiny surface, the glassy carbon electrode (GCE) was rinsed with deionized water and then cleaned ultrasonically in 1:1 nitric acid and deionized water. Then, 4  $\mu\text{l}$  of Tosflex coating solution was spin-coated onto the GCE at a spin rate of 3000 rpm. A uniform thin film was formed by evaporating the solvent after about 3 min of spinning.

Mercury was electrodeposited on the Tosflex coated GCE from 5 ml of 10 ppm mercury(II) solution containing 0.1 M sodium chloride at an applied potential of  $-0.8$  V versus Ag–AgCl for 4 min with stirring.

The sample solution medium contained bismuth(III) and proper amounts of KCl as the supporting electrolyte. The solution pH was adjusted with 0.05 M  $\text{HNO}_3$  and 0.05 M NaOH.

Groundwater and tap water were collected from the campus of National Cheng-Kung University. Seawater was collected from the beach of Tainan, Taiwan. All water samples, except seawater, were added with 0.5 M KCl as the supporting electrolyte. All sample were passed through the # 1 filter paper and then adjusted to the pH 1.4 by nitric acid. Urine samples were obtained from laboratory personnel. After being passed through a filter with 0.45 mm pore size, the urine solutions were further treated by centrifugation at 12 000 rpm for 20 min.

#### 2.4. Procedure for voltammetric measurement

In the voltammetric measurement, 5 ml of the sample solution was placed in the voltammetric cell. The solution was deaerated with argon for 5 min, and then a preconcentration potential was applied to the freshly prepared TMFE while the solution was stirred. After the preconcentration period, the stirring was stopped, and after 10 s the Osteryoung square-wave stripping voltammogram was recorded by applying a positive-going scan.

### 3. Results and discussion

#### 3.1. Electrochemical behavior of bismuth(III) on the Tosflex modified electrodes

When a mercury film modified glassy carbon electrode (MFE) is dipped in a 10 ppm bismuth

(III) solution containing 0.5 M KCl and nitric acid as the supporting electrolyte, the Osteryoung square wave stripping voltammogram (OSWSV) shown in Fig. 1(a) is obtained. In this figure, a stripping peak was observed at  $-80$  mV. Fig. 1(b), on the other hand, shows the OSWSV for the same solution recorded on the TMFE. In this figure the stripping peak shifts to  $-110$  mV. As can be clearly seen in Fig. 1, the response of Bi(III) on the TMFE is significantly higher than that on the MFE. This fact implies that bismuth can be accumulated more efficiently on the TMFE than on the MFE, and thus, the TMFE is more suitable for the determination of bismuth.

Fig. 2 shows the cyclic voltammograms of bismuth on the TMFE in different supporting electrolytes. As can be seen in this figure, the bismuth response detected by the TMFE in a medium containing nitrate ion is much smaller than that detected in a medium containing chloride ion

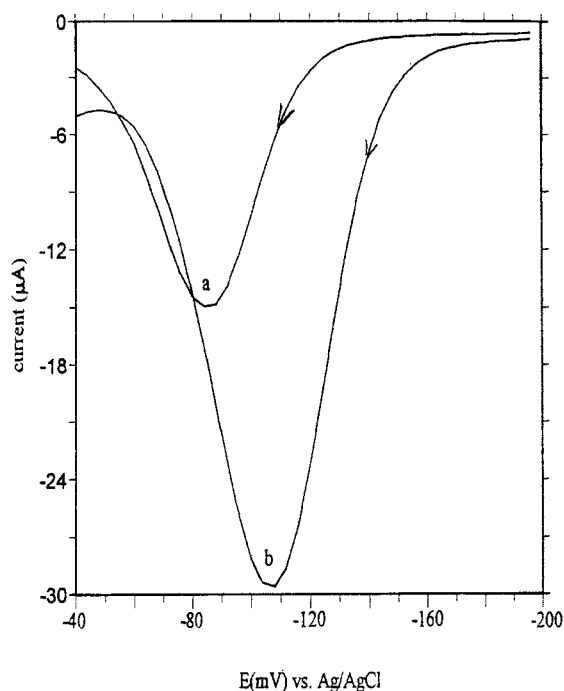


Fig. 1. Osteryoung square wave voltammogram for a 10 ppm bismuth(III) solution containing 0.5 M KCl, (a) at a mercury film coated glassy carbon disk electrode; (b) at the Tosflex-mercury film electrode (TMFE). SWSV parameters, modulation amplitude 20 mV; modulation frequency 120 Hz.

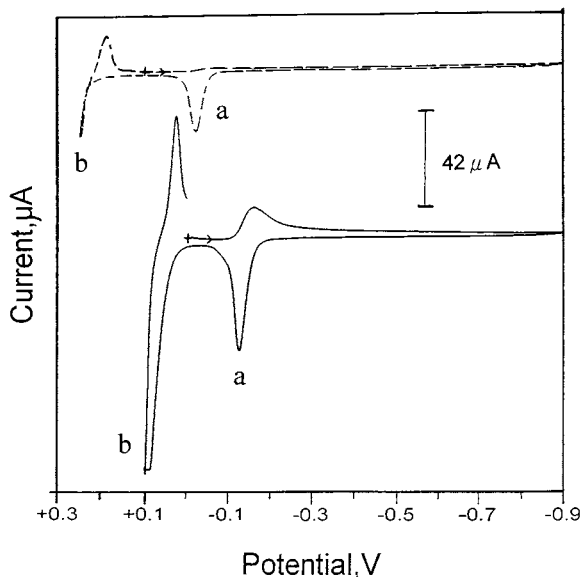


Fig. 2. Cyclic voltammograms for 10 ppb bismuth(III) in 0.05M HNO<sub>3</sub> (dashed line) and 0.5M KCl and 0.05M HNO<sub>3</sub> (solid line) on TMFE. Scan rate was 100 mV s<sup>-1</sup>.

(wave a in Fig. 2). Apparently, in the nitrate medium, the bismuth (III) ion is in the cationic form and thus, cannot be effectively accumulated by the anionic exchanger, Tosflex, of the TMFE during the preconcentration step. In contrast, anionic bismuth (III) complexes, are formed in the chloride medium and can be effectively accumulated into the TMFE during the preconcentration step. Moreover, the bismuth stripping peak obtained in the chloride media occurs at a potential more negative than that obtained in the nitrate media. As shown in Fig. 2, this potential shift was similar to what was observed for the oxidation of mercury (wave b in Fig. 2) which also had been described in the literature [19].

### 3.2. Factors affect the performance of the TMFE

The thickness of the Tosflex film directly affects the electrode performance since it controls the diffusion process and the maximum loading of the bismuth(III) chloride anions in the TMFE. The film thickness was varied by preparing the electrodes with different spin-coating rate. The bis-

mut stripping peak current was found to increase with the spin-coating rate, until 3000 rpm, which is the limit spin rate of the instrument. Electrodes prepared with the coating solution of 1.2 wt% of Tosflex at a 3000 rpm spin-coating rate for 3 min were therefore used in all subsequent experiments.

The amount of mercury electrodeposited on to the Tosflex coated GCE is dependent on the deposition time. The effect of mercury deposition on the electrode performance was evaluated with 10 ppm mercury (II) standard solutions. The results showed that the bismuth stripping peak current increased upon increasing the mercury deposition time and reached a maximum after 4 min. Therefore, a mercury deposition time of 4 min was used in the subsequent works.

### 3.3. Effect of solution pH

The dependence of the bismuth stripping peak current on the pH was studied by maintaining the chloride concentration at 0.1 M and the results obtained show that the bismuth stripping peak current gradually increases with decreasing the pH and starting level off when the pH is 1.4. This behavior suggests that the formation of bismuth(III) chloride is more favorable in an acidic environment. As a result, solutions with pH 1.4 were used in the subsequent experiments. It is worth to note that at this pH value Tosflex film was still very stable.

### 3.4. Effect of chloride ion concentration

The detection of bismuth with TMFE relies on the effective formation of the bismuth(III) chloride anions. Fig. 3 presents the effect of changing the chloride ion concentration on the bismuth stripping peak current. The optimum concentration range of chloride ion is found to be around 0.5 M. Lowering the chloride ion concentration results in lower signals, indicating that a reasonable excess of chloride ions is required for converting the bismuth (III) into its chloride complexes. The decrease of the stripping peak

current at chloride concentration higher than 0.5 M might be attributed to failures in permselectivity, which were previously observed at high ionic strengths also for Nafion coated electrode [20]. A 0.5 M concentration of chloride ion was therefore employed in the subsequent experiments.

### 3.5. Effect of square-wave parameters

The square-wave parameters that were investigated were the pulse height and the frequency. These parameters together affect the peak shape and peak current of the bismuth response. The peak current of bismuth increases with square-wave pulse height up to 20 mV, and further increase in the pulse height decreases and broadens the bismuth stripping peak. Meanwhile, considerable increase in the background current is also observed when the pulse height exceeds 20 mV. Increases in the square-wave frequency up to 120 Hz results in a substantial increase in the

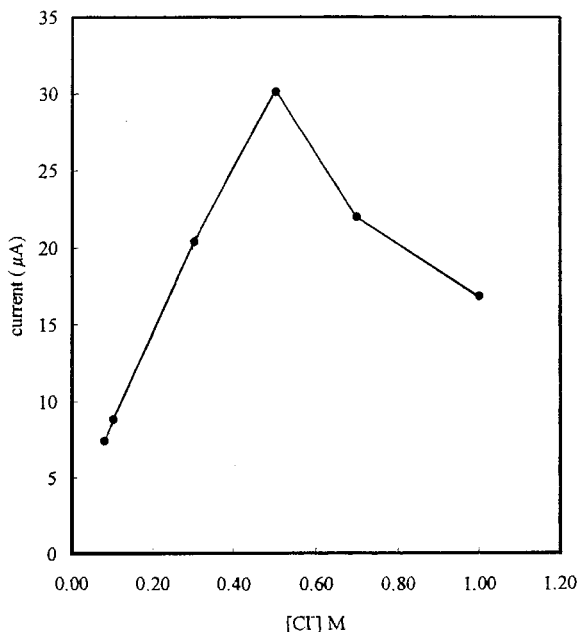


Fig. 3. Effect of chloride ion concentration on the SWSV response for 10 ppb bismuth(III) obtained on TMFE.  $E_d = -0.2$  V;  $t_d = 120$  s; pH = 1.4.

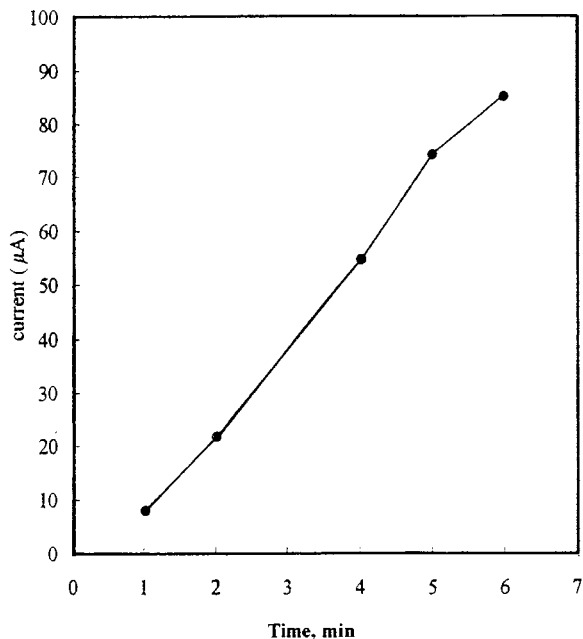


Fig. 4. Effect of preconcentration time on the SWSV response for 10 ppb bismuth(III) obtained on TMFE.  $E_d = -0.2$  V s; KCl = 0.5 M; pH = 1.4.

response for bismuth. Overall, the optimum pulse height and frequency selected for SWSV were 20 mV and 120 Hz, respectively.

### 3.6. Effect of preconcentration potential and time

The dependence of the bismuth stripping peak current on the preconcentration potential is studied and the results show that the peak current increases as the preconcentration potential becomes more negative between  $-0.15$  and  $-0.4$  V and starts to level off as the preconcentration potential becomes more negative than  $-0.4$  V. Because a more negative preconcentration potential would increase the possibility of co-deposition of interfering species, a preconcentration potential of  $-0.2$  V was chosen in the subsequent work.

The effect of preconcentration time on the SWSV response of bismuth was studied, and the results are displayed in Fig. 4. The peak current increases with increasing preconcentration time up to 6 min. This phenomenon indicates that the

ion-exchange process between Tosflex and bismuth(III) chloride anions is very good. Although this figure shows that higher sensitivity for the detection of lower bismuth concentration can be achieved by increasing the preconcentration time, a preconcentration time of 2 min was chosen for the construction of the calibration curve in this study.

### 3.7. Calibration

A calibration graph was constructed from data taken for bismuth(III) solutions following 2 min preconcentration under optimum experimental conditions described above. Fresh sample solutions were used for each individual bismuth(III) concentration and at least three independent determinations were made for each data point. The calibration plot thus obtained showed a linear behavior between 0 and 50 ppb of bismuth(III) with slope (mA/ppb), and correlation coefficient of 2.99, and 0.995, respectively. The detection limit ( $S/N = 3$ ) is 0.58 ppb. An even lower detection limit could be achieved for bismuth(III) provided that the preconcentration time is longer than 2 min.

### 3.8. Interferences

The influences of various metal ions on the determination of bismuth were examined. The results obtained for 10 ppb bismuth with 2 min preconcentration time are summarized in Table 1. This table shows that over 1000-fold wt. excess concentrations of zinc(II), germanium(IV), tellurium(IV), lead(II), cadmium(II) and 500-fold excess of copper(II) and 100-fold excess of chromium(VI), antimony(III) only slightly interfere with the bismuth response. The only major interfering ion among the ions studied was selenium(IV).

It is well documented that surface-active compounds can often adsorb on the electrode surface and reduce the analytical response of the analyte in a stripping analysis using a bare mercury electrode. Coating the electrode with Tosflex can circumvent such interferences. The Tosflex membrane coated on the electrode surface can prevent

Table 1

Influence of other ions on the response of Bi(III) at TMFE<sup>a</sup>

Ions	Concentration excess	Contribution (%)
	Over Bi(III)	( $i_{\text{Bi(III)}} = 100\%$ )
Pb(II)	1000 ×	−2
Cd(II)	1000 ×	−3
Te(IV)	1000 ×	−6
Zn(II)	1000 ×	+3
Ge(IV)	1000 ×	+7
Cu(II)	500 ×	−17
Sb(III)	100 ×	+16
Cr(VI)	100 ×	+3

<sup>a</sup> (Bi(III)) = 10 ppb;  $E_p = -0.2$  V;  $t_p = 120$  s; pH, 1.4; KCl = 0.5 M.

the organic interferences from reaching the interface at which the deposition and stripping of bismuth takes place. In this study, the nonionic surfactant Triton X-100 was used to exemplify the effect of a typical surfactant. As shown in Fig. 5, for 10 ppb bismuth(III), the detection was found to tolerate the presence of Triton X-100 for at least up to 10 ppm with the TMFE. Compared to the same experiments performed with a bare MFE

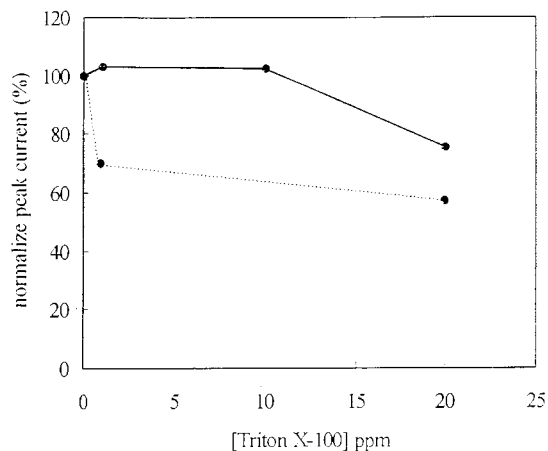


Fig. 5. Effect of the surfactant Triton X-100 at different concentrations on the stripping response for 10 ppb bismuth(III) with the TMFE (solid line) and the bare MFE (dashed line). KCl = 0.5 M, pH = 1.4,  $t_d = 120$  s,  $E_d = -0.2$  V. Normalised peak currents are calculated as the ratio between signals recorded in the presence and in the absence of surfactant.

Table 2

Determination of Bi(III) in sea water, tap water, ground water, and urine samples<sup>a</sup>

	Sea water	Tap water	Ground water	Urine <sup>b</sup>
Detected value original	ND	ND	ND	ND
Spiked (ppb)	4	1	2	5
Detected value after spike (ppb)	3.88 ± 0.04	1.02 ± 0.02	1.99 ± 0.03	5.04 ± 0.12
Recovery (%)	97	102	99	101

<sup>a</sup> Number of samples assayed = 3.<sup>b</sup> Deposition potential = -0.6 V.

(Fig. 5), the TMFE shows a much better resistance towards surfactant interference.

### 3.9. Determination of bismuth in real water samples

The analytical utility of the TMFE for the determination of bismuth(III) was assessed by applying it to the determination of bismuth(III) in sea water, tap water, groundwater, and urine samples. No bismuth(III) was detected in all the four original water samples so they were spiked with appropriate amounts of bismuth(III). The results collected in Table 2 are those for the original and spiked water samples. As can be seen, the recovery of the spiked bismuth(III) is very good for all the four water samples, indicating that the proposed procedure is feasible for the determination of bismuth(III) in various water samples. Note that the amount of bismuth(III) in natural water is typically very low, and this is indeed the case in this study. The amount of bismuth(III) in the original urine samples assayed in this study can not be detected by the proposed procedure with 2 min preconcentration at a potential of -0.2V. Nevertheless, it was found that the spiked 5 ppb bismuth(III) stripping peak could be actually seen for these samples with a preconcentration potential of -0.6 V, and the amount of bismuth(III) in these original water samples was therefore believed to be well below 5 ppb.

## 4. Conclusion

The application of the TMFE for the determination of trace bismuth(III) is evident from the

above results. The presence of Tosflex polymeric coating improves the efficiency and selectivity of the preconcentration step, as well as the mechanical stability of the mercury film. Compared to the PVP-MFE procedure reported earlier [11], the TMFE offers some advantages in addition to better resistance to the interferences from common ions and organic surface-active compound. Because of the intrinsic stability of Tosflex, the preparation of the TMFE does not require any cross-linking agent nor the heating process, and thus, the time for preparing the working electrode is greatly reduced. Consequently, the TMFE would be an ideal substitute for the PVP-MFE.

## Acknowledgements

The authors gratefully acknowledge the financial support of the National Science Council of the Republic of China (Taiwan) under Grants NSC87-2815-C-006-073M.

## References

- [1] T.M. Florence, J. Electroanal. Chem. 35 (1972) 237.
- [2] T.R. Gilbert, D.N. Hume, Anal. Chim. Acta 65 (1973) 451.
- [3] T.M. Florence, J. Electroanal. Chem. 49 (1974) 255.
- [4] S. Komorsky-Lovric, Anal. Chim. Acta 204 (1988) 161.
- [5] J. Lexa, K. Stulik, Talanta 32 (1985) 1027.
- [6] K. Kalcher, Fresenius Z. Anal. Chem. 325 (1986) 186.
- [7] K.L. Dong, L. Kryger, J.K. Christensen, K.N. Thomsen, Talanta 38 (1991) 101.
- [8] I. Svancara, K. Vytras, Anal. Chim. Acta 273 (1993) 195.
- [9] C. Wang, Q. Sun, H. Li, Electroanalysis 9 (1997) 645.
- [10] D.W.M. Arrigan, Analyst 119 (1994) 1953.
- [11] J.M. Zen, M.J. Chung, Anal. Chim. Acta 320 (1996) 43.

- [12] B. Lindholm, M. Sharp, *J. Electroanal. Chem.* 198 (1986) 37.
- [13] J.M. Zen, M.J. Chung, *Anal. Chem.* 67 (1995) 3571.
- [14] L. Dunsch, L. Kavan, J. Weber, *J. Electroanal. Chem.* 280 (1990) 313.
- [15] P. Ugo, L.M. Moretto, G.A. Mazzocchin, *Anal. Chim. Acta* 273 (1993) 229.
- [16] P. Ugo, L.M. Moretto, G.A. Mazzocchin, *Anal. Chim. Acta* 305 (1995) 74.
- [17] T.-H. Lu, I.-W. Sun, *Electroanalysis* 10 (1998) 1052.
- [18] H.-Y. Yang, I.-W. Sun, *Electroanalysis* 11 (1999) 195.
- [19] L.M. Moretto, G.A. Mazzocchin, P. Ugo, *J. Electroanal. Chem.* 427 (1997) 113.
- [20] R. Nagegeli, J. Redepenning, F.C. Anson, *J. Phys. Chem.* 90 (1986) 6227.
- [21] P. Ugo, L.M. Moretto, *Electroanalysis* 7 (1995) 1105.
- [22] H.-Y. Yang, I.-W. Sun, *Anal. Chim. Acta* 358 (1998) 285.

# Surface water preparation procedure for chromatographic determination of polycyclic aromatic hydrocarbons and polychlorinated biphenyls

L. Wolska<sup>a</sup>, K. Galer<sup>a</sup>, T. Górecki<sup>b</sup>, J. Namieśnik<sup>a,\*</sup>

<sup>a</sup> Department of Analytical Chemistry, Chemical Faculty, Technical University of Gdańsk, 11/12 Narutowicz Str, 80-952, Gdańsk, Poland

<sup>b</sup> Department of Chemistry, University of Waterloo, Ont., Canada

Received 27 October 1998; received in revised form 30 March 1999; accepted 24 June 1999

## Abstract

A new sample preparation procedure for the analysis of polycyclic aromatic hydrocarbons (PAHs) and polychlorinated biphenyls (PCBs) in water containing suspended particulate matter (SPM) has been developed. A specially designed filtration vessel coupled directly to an SPE cartridge was used for this purpose. SPM separation and analyte isolation/concentration were carried out in a single step. Both the SPE cartridge and the suspended matter collected on the filter were solvent extracted, and analyte recoveries were determined. Analyte recoveries from the filtrate ranged from 64 to 100% of the spiked amount for PAHs with the highest aqueous solubilities, and did not exceed 20% for those with the lowest solubilities. Total recoveries of PAHs from surface water containing  $21 \text{ mg l}^{-1}$  SPM ranged from 65 to 121%. PCB recoveries from the particulate matter reached over 10% of the spiked amount, while those from the filtrate ranged from 20 to 57%. Total PCBs recoveries ranged from 34 to 69%. © 1999 Elsevier Science B.V. All rights reserved.

**Keywords:** Filtration; Suspended particulate matter; Surface water; Polycyclic aromatic hydrocarbons; Polychlorinated biphenyls

## 1. Introduction

Suspended matter present in surface waters in a wide range of concentrations makes reliable determination of polycyclic aromatic hydrocarbons (PAHs) and polychlorinated biphenyls (PCBs) a very difficult task. Analytical and technical prob-

lems caused by the suspended matter affect both accuracy and precision of analyte determination in the dissolved phase.

Suspended particulate matter (SPM) consists of organic and inorganic particles, floating in water. For practical purposes, SPM is defined as particles stopped by a  $0.45 \mu\text{m}$  filter [1]. Surface characteristics of the SPM can vary significantly, from particles of small specific surface area (e.g. sand) to particles of very well developed surfaces (e.g. particulates originating from combustion).

\* Corresponding author. Fax: +48-58-3472694.

E-mail address: chemanal@pg.gda.pl (J. Namieśnik)



Because of their low solubility and hydrophobic character, both PAHs and PCBs are easily adsorbed by SPM, as well as absorbed by humic and fulvic acids, lipids and proteins, forming dissolved organic matter (DOM) [2]. Concentration differences between SPM and solution due to preferential adsorption can reach a factor of  $10^5$  or more. In addition, the results obtained by Readman et al. [3] indicate that the PAHs in the Tamar Estuary are not in equilibrium between the aqueous and the particulates phases, and that they are considerably enriched in the particulates. It has been also demonstrated that the presence of SPM during sample transport and storage can reduce PAH recoveries by 20–70% [4].

Because of their very poor aqueous solubility, PCB and PAH concentration levels in water are typically very low ( $\text{ng l}^{-1}$  or lower), which makes it necessary to incorporate a concentration step in the analytical procedure. This step is often combined with matrix exchange to one that is more compatible with the final determination method (usually GC or LC). Liquid–liquid extraction (LLE) [5,6], solid-phase extraction (SPE) [7–10] and its modification, Empore disk technique are most often used for this purpose. In the recent years, a new sampling/sample preparation method, solid phase microextraction (SPME) [11], has been used increasingly often for this purpose as well. SPME is based on analyte partitioning between the sample and a stationary phase coated on a fused silica fibre. Research is also conducted on the application of membrane techniques for PCB and PAH analysis [12].

The result of extraction carried out in the presence of SPM depends on the combination of several processes:

- sorption equilibrium of the analytes between the aqueous phase and the suspension during sample transport and storage;
- efficiency of analyte extraction from the aqueous phase;
- efficiency of analyte extraction from the suspended matter (when extracting the aqueous phase).

In any case, the result of determination of PAH and PCB concentration in water always depends on the SPM properties and SPM content of a sample.

Apart from analytical, also technical problems can occur, including plugging of the SPE cartridges and disks, which can make the extraction last several hours, or even render it impossible.

Filtration under gravity, by applying vacuum or pressure, as well as centrifugation, are typically used to eliminate SPM from the samples [1]. Glass fibre or Teflon [13] filters with 0.45 or 0.7  $\mu\text{m}$  pore sizes are usually used for filtration [14–18]. Recently, application of polycarbonate screen filters (Nucleopore 0.4  $\mu\text{m}$ ) [19] and cellulose ester filters (Millipore, 0.45  $\mu\text{m}$ ) [20] was reported. Clogging [1,2], analyte adsorption on the filter [1] and on the layer of particulate matter formed on the filter [13,21] are the main problems encountered during filtration. Clogging can be a problem also with Empore disks when analyte isolation and preconcentration are carried out from large volumes of samples with high SPM content. Application of high density glass beads (filter aid 400) instead of a filter has been proposed to overcome this problem [13,22].

An alternative method to filtration is centrifugation. Also this method is not problem-free. Particles with density equal to or lower than water are not removed, and hydrophobic organic compounds undergo accumulation on them.

Van Noort and Wandergem [21] indicate that PAHs dissolved in water can be sorbed on the surfaces of the filter and probably on the layer of suspended matter formed during filtration. It seems that removal of SPM by filtration or centrifugation may change the distribution of the analytes between the aqueous phase and the suspension. Thus, the results of determination of PAHs in the filtrate do not necessarily reflect the true concentrations of the analytes dissolved in water containing the SPM. Similarly, PAH concentrations in the particulate matter stopped on the filter do not necessarily correspond to true concentrations in the SPM before the filtration.

In conclusion, the presence of suspended matter in samples analyzed for PAHs and PCBs affects the results of determination of those compounds in water independently of the extraction technique used. The results can be artificially high compared to the true concentration of the dissolved analytes in water when LLE is used [5], since analytes can

be extracted both from the aqueous phase and from the suspension (yielding a result close to the total content of the analyte in the sample). In contrast, lower results can be expected when using SPE with cartridges and Empore disks because of analyte sorption on filters and probably on the layer of particulate matter formed on them. Also, the conditions of analyte desorption from the SPM during elution are far from optimal in SPE [5]. The significance of the phenomena described above increases with decreasing solubility and volatility of the analytes.

In spite of all these reservations, it seems almost certain that the procedure for PAH and PCB determination in surface waters should include SPM isolation. Without this step, it is virtually impossible to extract all the analytes from the particulate matter. In LLE, the organic solvent cannot effectively contact the particles surrounded by water. In SPE, the contact time between the particulate matter trapped in the cartridge or on the filter and the solvent is too short for effective extraction. In order to achieve quantitative analyte recoveries from the SPM, it is necessary to isolate the particulate matter, remove water from it and extract it with a solvent under optimized conditions (e.g. assisted by sonication, microwaves, or high temperature and pressure, as in ASE). In addition, separation of SPM eliminates many technical problems, including cartridge plugging. Optimally, particulate matter separation should be carried out during sampling.

When the concentration of free PAHs and PCBs in the aqueous phase is of primary interest, SPME can be particularly useful. Poerschmann et al. successfully used this technique to study partitioning of organic compounds between water and dissolved organic polymers with properties similar to those of humic organic matter (HOM) [23].

The paper presents the design of a special filtration vessel enabling simultaneous isolation of SPM and preconcentration of the analytes on an SPE cartridge. The particulate matter stopped on the filter is freeze-dried, weighed and extracted with dichloromethane using sonication. Analyte content can be determined independently for the two phases involved (particulate matter and the solution), or the total content can be determined

in one run by combining the extracts obtained. The design of the vessel is based on the experience of the authors and other researchers.

## 2. Material and methods

### 2.1. Reagents and materials

High-purity, HPLC-grade dichloromethane (DCM) and methanol were purchased from Merck (Germany). US EPA certified standard containing 16 PAHs (2000  $\mu\text{g ml}^{-1}$  of each compound in DCM) and US EPA certified standard containing 7 PCBs (10  $\mu\text{g ml}^{-1}$  of each compound in isooctane) were from Restek Corporation (USA). Certified Naphtalene-d8 (2000  $\mu\text{g ml}^{-1}$  in DCM) and Benzo(a)anthracene-d12 (2000  $\mu\text{g ml}^{-1}$  in DCM) standards were from Supelco (USA). Certified PCB 209 (Decachlorobiphenyl) standard was from Dr Ehrenstorfer GmbH (Germany). Milli-Q ultrapure water was used for preparation of aqueous standards (Millipore, Austria). SPE columns filled with octadecyl-bonded silica  $\text{C}_{18}$  (300 mg) were from J.T. Baker (Germany). Silanized glass wool was purchased from Alltech Associates (England). Empore filter aid 400 high-density glass beads were from 3M (J.T. Baker, USA). Glass-fibre filters used were Whatman GF/F (0.7  $\mu\text{m}$ ) (Germany).

### 2.2. Sampling

A 20 l sample of water from the Vistula River (Kiezmak region, northern Poland) was collected in the spring of 1997. Average suspended particulate matter concentration in this water was 21  $\text{mg l}^{-1}$  (triplicate measurements). The SPM content was determined using Whatman 0.7  $\mu\text{m}$  filters.

### 2.3. Isolation and enrichment

A filtration vessel whose design is presented in Fig. 1 was used for the investigations. The vessel consists of a glass tube (1); equipped with two Teflon end covers (2); sealed with silicone O-rings (3). The glass tube presses a Teflon screen (4) against the bottom end cover. A Whatman GF/F

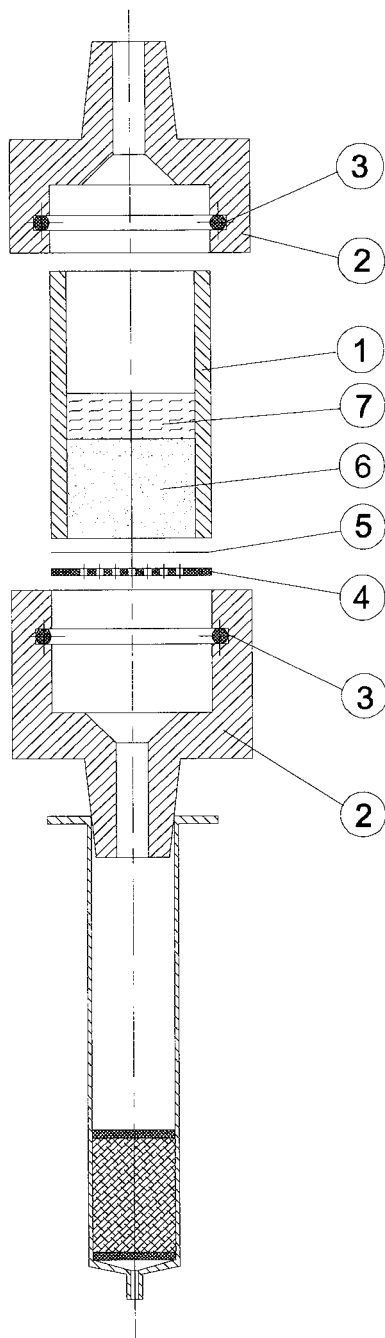


Fig. 1. A home-made filtration vessel directly connected with SPE cartridge: glass tube (1); Teflon end covers (2); silicone O-rings (3); Teflon screen (4); Whatman GF/F glass fibre filter (0.7  $\mu\text{m}$ ) (5); high density glass beads (Empore 3M, Filter Aid 400) (6); glass wool (7).

glass fibre filter (0.7  $\mu\text{m}$ ) (5) is placed on top of the screen. Tube (1) contains also  $\sim 4$  g of high density glass beads (6) (Empore 3M, Filter Aid 400) kept in place with glass wool (7).

SPE cartridges ( $\text{C}_{18}$ ) were washed with 2 ml dichloromethane, followed by activation with methanol ( $2 \times 3$  ml) and water (3 ml). Filtration vessels were mounted on top of conditioned cartridges and 0.5 l samples of water spiked with 16 PAHs ( $40 \text{ ng l}^{-1}$ ), 7 PCBs ( $20 \text{ ng l}^{-1}$ ), naphthalene-d8 and benzo(a)anthracene-d12 were passed through each of them under vacuum. Filtration time for surface water samples was  $\sim 3$  h, with an average sample flow rate of  $2.8 \text{ ml min}^{-1}$ . The cartridges and the filtration vessels were subsequently freeze dried in a lyophilising cabinet (Lab-conco, USA) for  $\sim 6$  h. Analytes trapped by the SPE cartridges were extracted with dichloromethane ( $2 \times 2$  ml) and the extract was gently evaporated under nitrogen to 0.3 ml.

The contents of the filtration vessels (filter, glass beads and glass wool) were transferred to reaction vials and extracted with two portions of dichloromethane in an ultrasonic bath (3 ml for 30 min, followed by 2 ml for 10 min). The two extracts were combined and evaporated under nitrogen to 0.3 ml. The concentrated extracts from the SPE cartridges and filtration vessels were analysed by GC separately.

#### 2.4. Analytical procedure

The extracts were analysed by GC/MS, using a GC-8000 gas chromatograph and an MD-800 quadrupole mass spectrometer, both from Fisons Instruments. A 2  $\mu\text{l}$  sample was injected using a cold on-column injector with secondary cooling, activated for 20 s. A  $30 \text{ m} \times 0.25 \text{ mm} \times 0.25 \mu\text{m}$  SPB-5<sup>TM</sup> GC column (Supelco, Bellefonte, USA) was used with helium as the carrier gas (70 kPa). The following oven temperature program was applied:  $40^\circ\text{C}$  for 0.5 min, ramped at  $40^\circ\text{C min}^{-1}$  to  $120^\circ\text{C}$ , then at  $5^\circ\text{C min}^{-1}$  to  $280^\circ\text{C}$ , held for 15 min. Transfer line temperature was  $300^\circ\text{C}$ . The MS was operated in selected ion monitoring (SIM) mode.

Analyte recoveries from the filtrate and the particulate matter were determined by subtracting

background concentrations from the results obtained for spiked samples (mean of three determinations).

### 3. Results and discussion

The filtration vessel presented in Fig. 1 enables easy separation of suspended matter from water samples. The vessel was tested on 0.5 l surface water samples (containing  $21 \text{ mg l}^{-1}$  SPM) spiked with standard mixtures of PAHs (final concentration of  $40 \text{ ng l}^{-1}$ ) and PCBs (final concentration of  $20 \text{ ng l}^{-1}$ ), using SPE for analyte isolation and preconcentration from filtrate.

Table 1 presents the recoveries of the individual PAHs from the filtrate and the suspended matter, as well as total recoveries. The data clearly show that more soluble PAHs prevailed in the filtrate (64–100% of the spike), while those characterized by lower solubilities and volatilities were mainly trapped on the filter (84–96% of the spike). Total PAH recoveries from surface water samples obtained using the method described were high, ranging from 81 to 121% (except for acenaphthylene).

Phenomena different from the ones described above were observed for PCBs (Table 1). While aqueous solubilities of PCBs are similar to the solubilities of PAHs ranging from benzo(a)anthracene to benzo(ghi)perylene, different trends in recovery were observed for the former. Analyte recoveries from the particulate matter reached more than 10% of the spike, while those from the filtrate ranged from 20 to 57%. Total PCB recoveries from surface water containing  $21 \text{ mg l}^{-1}$  SPM ranged from 48 to 70% (except for PCB 180).

Table 1 also includes the statistical analysis of the results obtained for surface water samples spiked with PAH and PCB standards. Relative standard deviations (%RSD) for PAHs did not exceed 50%, while for PCBs ranged from 53 to 96% in filtrate and from 28 to 42% in the SPM. This indicates that the repeatability of the results was adequate to the low analyte concentration levels.

Lower PCB recoveries can probably be attributed to analyte losses through sorption on the additional elements of the apparatus (e.g. tubes connecting the sample flasks with the filtration vessel). Further research using standard solutions containing PCBs at other, and especially lower, concentration levels is necessary to confirm this assumption.

The proposed design has two main advantages. First, it enables a one-step isolation of the SPM and preconcentration of the analytes from the same volume of the sample. Second, it makes it possible to achieve optimum recoveries of the analytes from the SPM, as the particulate matter is isolated and dried prior to solvent extraction, which can additionally be assisted, e.g. by sonication. Separation of SPM and analyte preconcentration can be performed easily under field conditions.

The use of high density glass beads (filter aid 400) prevents the possible clogging of the filter and SPE cartridge when SPM levels in the samples are high. The difference between the masses of the vessel after drying and before filtration yields the SPM content of the sample.

The vessel can also be used in combination with Empore disks. It has a simple design, using materials recommended for trace analysis of organic compounds (glass, PTFE) and is very easy to use.

One of the downsides of the technique proposed is the long time required to filter the sample and concentrate the analytes (3 h for a 0.5 l sample). This drawback can be overcome by using large volume injection (LVI) for the extracts [24,25]. LVI makes it possible to introduce much larger volumes of the extracts into the column than on-column injection (up to  $100 \mu\text{l}$ , compared to  $\sim 2 \mu\text{l}$ ). Consequently, sample volume required to achieve the sensitivity desired can be reduced by at least an order of magnitude, and the filtration/extraction time can be shortened to  $< 30$  min. Alternatively, LVI can be used to achieve much lower detection limits (20–50 times) with unchanged sample volumes.

Table 1  
Analyte recovery and precision of the proposed procedure for the analysis of PAHs and PCBs in surface water

Compounds	b.p. (°C)	Solubility (mg l <sup>-1</sup> ) at 25°C	Background		Surface water sample spiked with PAHs and PCBs								
			Average concentration		Filtrate				Suspension				Total recovery
			Filtrate (ng l <sup>-1</sup> )	Suspension (ng · l <sup>-1</sup> )	Average concen- tration (ng · l <sup>-1</sup> )	Recovery (%)	n	RSD (%)	Average concen- tration (ng · g <sup>-1</sup> )	Recovery (%)	n	RSD (%)	
<i>PAHs</i>													
Naphthalene	217.9	30	13	112	48	89	6	20	170	6	5	43	95
Acenaphthylene	265–275	16	5	21	30	64	9	49	36	1	9	54	65
Acenaphthene	279	3.93	18	144	58	100	5	24	170	3	6	20	103
Fluorene	298	1.81	22	78	61	98	5	39	170	9	7	16	107
Phenanthrene	340	1.6	85	1734	112	66	3	13	2000	21	7	13	87
Anthracene	342	1.24	7	267	40	84	8	44	350	4	8	27	88
Fluoranthene	~375	0.2–0.26	43	1802	78	87	8	34	2000	24	6	21	111
Pyrene	393	0.15	36	1413	69	83	6	16	1800	38	7	19	121
Benzo(a)anthracene	435	0.009–0.014	15	751	28	32	6	38	1300	49	7	26	81
Chrysene	448	0.0006	10	888	25	37	8	40	1400	54	9	25	91
Benzo(b)	398	0.001	ND	766	13	33	7	42	1600	87	6	13	120
fluoranthene													
Benzo(k)	480	0.043	ND	975	13	32	7	46	1800	84	7	31	116
fluoranthene													
Benzo(a)pyrene	495	0.004 (27°C)	9	569	14	11	5	16	1500	91	5	23	102
Indeno(1,2,3-cd)	536	0.062	10	717	15	10	5	13	1600	90	9	31	100
pyrene													
Dibenzo(a,h)	524	0.0005 (27°C)	4	90	11	17	7	47	1000	93	7	40	110
anthracene													
Benzo(ghi)perylene	>500	0.00026	11	640	12	ND	9	45	1600	96	9	42	96
<i>PCBs</i>													
PCB 28		–	1	4	12	54	8	53	110	10	8	38	64
PCB 52		0.029	2	58	14	57	7	49	150	12	10	28	69
PCB 101		0.010	2	117	11	45	8	90	210	16	10	37	61
PCB 118		0.0021	4	175	14	52	7	89	230	15	7	36	67
PCB 138		0.0018	1	92	8	31	6	77	230	17	8	36	48
PCB 153		0.00091	1	177	10	44	8	96	230	13	6	35	57
PCB 180		0.00063	ND	12	4	20	3	58	150	14	6	42	34

#### 4. Conclusions

The work reported here presents the design of a special filtration vessel enabling simultaneous isolation of the particulate matter and preconcentration of the analytes from the filtrate by means of SPE. Optimal analyte recoveries from the particulate matter can be achieved owing to the fact that it is processed independently of the liquid sample after the initial isolation step. Total recoveries of PAHs and PCBs spikes from SPM containing surface waters achieved with the procedure described were high, ranging from 81 to 121% (except for acenaphthylene) and 48–69% (except for PCB 180), respectively. Further investigations on the optimization of the design and operation of the filtration vessel are under way.

#### Acknowledgements

This study was partially supported by the German Federal Ministry of Education and Research and the Foundation of Polish–German Cooperation.

#### References

- [1] G. Font, J. Mañes, J.C. Moltó, Y. Picó, *J. Chromatogr. A* 733 (1996) 449.
- [2] G.J. Stroomberg, I.L. Freriks, F. Smedes, W.P. Cotino, VCH, Weinheim, 1995, p. 51. Chapter 3.
- [3] J.W. Readman, R.F.C. Mantoura, M.M. Rhead, *Fresenius Z. Anal. Chem.* 319 (1984) 126.
- [4] The determination of 6 specific PAH, Materials for the Examination of Waters and Associated Materials, Her Majesty's Stationery Office, London, 1985.
- [5] E. Manoli, C. Samara, *Chromatographia* 43 (1996) 135.
- [6] EPA, U.S. EPA Environmental Protection Agency, Method 550, Cincinnati, Ohio, 1990, p. 117.
- [7] U.A.T. Brinkman, T. Hankemeier, J.J. Vreuls, *Chem. Anal.* 40 (1995) 495.
- [8] L.A. Berrueta, B. Gallo, F. Vicente, *Chromatographia* 40 (7/8) (1995) 474.
- [9] E.R. Brouwer, E.A. Struys, J.J. Vreuls, U.A.T. Brinkman, *Fresenius Z. Anal. Chem.* 350 (1994) 487.
- [10] E.R. Brouwer, A.N.J. Hermans, H. Lingeman, U.A.T. Brinkman, *J. Chromatogr. A* 669 (1994) 45.
- [11] J. Pawliszyn, *Solid Phase Microextraction — Theory and Practice*, Wiley-VCH, New York, 1997.
- [12] J.A. Lebo, J.L. Zajicek, J.N. Huckins, J.D. Petty, P.H. Peterman, *Chemosphere* 25 (5) (1992) 697.
- [13] T.A. Albanis, D.G. Hela, *J. Chromatogr. A* 770 (1995) 283.
- [14] M. Martinez, D. Barcelo, *Chromatographia* 42 (1,2) (1996) 72.
- [15] M. Ahel, K.M. Erans, P.W. Fileman, R.F.C. Mantoura, *Anal. Chim. Acta* 268 (1992) 195.
- [16] M.T. Meyer, M.S. Mills, E.M. Thurman, *J. Chromatogr.* 629 (1993) 55.
- [17] I. Hammond, K. Moore, H. James, C. Watts, *J. Chromatogr.* 474 (1989) 175.
- [18] E.M. Thurman, M. Meyer, M. Pomes, C.A. Perry, A.P. Schwab, *Anal. Chem.* 62 (1990) 2043.
- [19] D.J. McMillin, J.C. Means, *J. Chromatogr. A* 754 (1994) 169.
- [20] J. Namieśnik, Z. Jamrógiewicz, M. Pilarczyk, L. Torres, [L]Chemia i Inżynieria Ekologiczna S1 (1997) 3.
- [21] P.C.M. van Noort, E. Wandergem, *Anal. Chim. Acta* 172 (1985) 335.
- [22] G. Michor, J. Carron, S. Bruce, D.A. Cancilla, *J. Chromatogr. A* 732 (1996) 85.
- [23] J. Poerschmann, Z. Zhang, F.D. Kopinke, J. Pawliszyn, *Anal. Chem.* 69 (1997) 597.
- [24] H.G.J. Mol, H.-G.M. Janssen, C.A. Cramers, J.J. Vreuls, U.A.T. Brinkman, *J. Chromatogr. A* 703 (1995) 277.
- [25] J. Staniewski, in: *Proceedings of the Sixteenth International Symposium on Capillary Chromatogr.*, Riva del Garda, 1994, Hüthig, Heidelberg, 1994, p. 1071.

# On the acid behaviour of the alcoholic group of serine

Emilio Bottari \*, Daniele Cellulosi, Maria Rosa Festa

*Dipartimento di Chimica, Università 'La Sapienza', P. le A. Moro 5, 00185 Rome, Italy*

Received 1 February 1999; received in revised form 17 June 1999; accepted 24 June 1999

## Abstract

The behaviour of L-serine in strongly alkaline solution was studied at 25°C and in 3.00 mol/l NaClO<sub>4</sub>, as a constant ionic medium, to obtain quantitative information about the eventual dissociation of its alcoholic group. A spectrophotometric method was employed to measure the free concentration of hydrogen ions. Two indicators, methyl thymol blue and eriochrome blue type R, were used. Their values as protonation constants and absorbance coefficients were determined in advance. The method here proposed has been validated beforehand by applying it to D-mannite and glycerine and by comparing results so obtained with those previously provided by literature. The investigation showed weak acid properties of the –OH of serine and its dissociation constant was determined. Polynuclear species or further dissociation were not observed. © 1999 Elsevier Science B.V. All rights reserved.

*Keywords:* L-Serine; Alcoholic group dissociation; D-Mannite; Glycerine

## 1. Introduction

The complex formation between cations and ligands can be studied when the protolytic behaviour of the ligand is already known, because equilibria are often investigated by using competitive reactions involving hydrogen ions.

Serine is an important ligand towards cations and its properties were previously studied towards cadmium(II), calcium(II), cobalt(II), copper(II), lead(II), magnesium(II) and nickel(II) [1–3]. For this purpose protonation of the aminic and carboxylic groups of serine were previously studied

[1] and no evidence was found for the dissociation of the –OH group present in the same compound, even in strongly alkaline solution.

On the other hand, a few researchers showed that other compounds, containing alcoholic groups, for instance polyols, have a behaviour similar to that of very weak acids.

Michaelis [4] found these properties in galactitol, D-mannite and glucitol by means of electromotive force (e.m.f.) measurements. Souchay et al. [5] estimated the value of the dissociation constant of glycerine, D-mannite and D-glucitol from  $\Delta T$  measurements of saturated solutions of Na<sub>2</sub>SO<sub>4</sub>, whereas Thames [6] obtained the value of the constant of D-glucitol at 18°C from e.m.f. measurements. Long et al. [7] explained the conductivity decrease of NaOH solutions due to the

\* Corresponding author. Tel.: +39-6-49913643; fax: +39-6-490631.

E-mail address: bottari@axrma.uniroma1.it (E. Bottari)

addition of glycerine, by assuming an acid behaviour for glycerine and calculated its dissociation constant. Also the dissociation of the two –OH of tartrate was studied polarimetrically in idroalcoholic solutions at very high NaOH or KOH concentration (7 mol/l) by Beck et al. [8] who found the values of the constants. In 1971 Gut et al. [9], by studying methanolic solutions of 1 mol/l in LiCl or N(CH<sub>3</sub>)<sub>4</sub>Cl, estimated the acid constant of methanol, by means of e.m.f. measurements with a H<sub>2</sub> electrode. Several papers [10–13], treating equilibria between cations and hydroxyacids, showed loss of protons, perhaps from the –OH of the ligand, involved in the complex formation.

Vicedomini [14] in 1981 estimated the acid constants of some polyhydroxylate compounds (D-glucitol, galactitol, mesoinositol and D-mannitol) in strongly alkaline solution at 25°C and 3.00 mol/l NaCl as a constant ionic medium, by means of e.m.f. measurements with a H<sub>2</sub> electrode. On the other hand, we were not able to determine the acid properties of –OH of citrate with the same procedure [15].

A calorimetric method had been used to study the acid behaviour of glycerine and the acid dissociation constant ( $10^{-14.76}$ ) was determined at 25°C and in 3.00 mol/l NaClO<sub>4</sub> [16].

The aim of our research was to investigate the properties of the –OH group of serine in strongly alkaline solution and at high concentration of serine. Since it was necessary to study a wide range of reagent concentration, without any remarkable change of the activity coefficients, the constant ionic medium method, proposed by Biedermann and Sillén [17], was adopted. These authors proved experimentally that by substituting up to 15–20% of the ions of the ionic medium with those of the reagents, activity coefficients do not vary remarkably.

Investigation on the acid properties of the –OH group of serine was carried out at 25°C and 3.00 mol/l NaClO<sub>4</sub>. In this way it was possible to substitute activities with concentrations in all the calculations.

A colorimetric method of investigation dependent on the change of optical absorbance of alkaline solutions containing a suitable indicator and

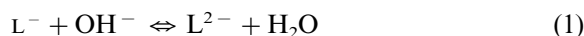
L-serine was performed. Before use the method was validated by applying it on known compounds and by comparing our results with the ones in the literature. The calorimetric method was not used because the presence of aminic and carboxylic groups could interfere in the determination. The e.m.f. method was considered not suitable, because of the very weak acid properties expected for the –OH of serine, comparable with those of citrate and glycerine. Finally the proposed procedure seems to be only slightly manipulative.

## 2. Experimental

### 2.1. Method

To avoid writing the summary formula here and in the following, the fully protonated serine is indicated as H<sub>2</sub>L<sup>+</sup>, the zwitterion as HL and the compound with the deprotonation also of the hydroxyl group as L<sup>2-</sup>.

To study the dissociation of the –OH group of L-serine, two hypotheses were formulated a priori. The absence of polynuclear species and the loss of only one proton per mole were supposed. On this basis, the acid properties of L-serine could be represented by means of the following equilibrium:



with the relative equilibrium constant  $\beta_{SR}$ , defined as follows:

$$\beta_{SR} c_{SR} c_{OH} = c_{SR^{2-}}, \quad (2)$$

where SR = L<sup>-</sup> and SR<sup>-</sup> = L<sup>2-</sup>. The hypotheses supporting Eqs. (1) and (2) will be confirmed a posteriori. In Eq. (2),  $c_x$  indicates the free concentration of the generic species  $x$ , while  $C_x$  will represent the total concentration of  $x$ . By introducing  $K_w$  (the ionic product of water), Eq. (2) can be written, as follows:

$$\beta'_{SR} = c_{SR} - c_H / c_{SR} = \beta_{SR} K_w. \quad (3)$$

To investigate Eq. (1) and to obtain  $\beta_{SR}$  and  $\beta'_{SR}$ , it was necessary to determine  $c_{OH}$ , the free concentration of OH<sup>-</sup>. By adding each test solu-



tion of an indicator HJ,  $c_{\text{OH}}$  can be determined, if the protonation of  $\text{J}^-$  and the absorbance coefficients of HJ and  $\text{J}^-$  are known in the same experimental conditions.

The development of the method involves different steps. After the choice of the indicator (with its dissociation constant value  $K$ , similar to the  $c_{\text{H}}$  range to be investigated) and the estimation of its protonation constant and the absorbance coefficients of its species  $x$ ,  $\epsilon_x$ , the indicator was used to obtain  $c_{\text{H}}$  values in already studied systems, so that the method could be validated. Finally the method was applied to L-serine. The compounds D-mannite (MN) and glycerine (GLY) were selected as test systems, to validate the proposed method. For these two compounds equilibria similar to Eq. (1) can be formulated:



with the constants, respectively:

$$\beta'_{\text{MN}} = \beta_{\text{MN}} K_w = K_w c_{\text{MN}^-} / (c_{\text{MN}} c_{\text{OH}})$$

$$= c_{\text{MN}^-} c_{\text{H}} / c_{\text{MN}} \quad (2 \text{ bis})$$

and

$$\beta'_{\text{GLY}} = \beta_{\text{GLY}} K_w = K_w c_{\text{GLY}^-} / (c_{\text{GLY}} c_{\text{OH}})$$

$$= c_{\text{GLY}^-} c_{\text{H}} / c_{\text{GLY}} \quad (3 \text{ bis}).$$

The problem of  $-\log c_{\text{H}}$  measurements in strong basic solution was studied firstly by Schwarzenbach and co-workers [18,19] in the 1930s and 1940s. For the here investigated  $-\log c_{\text{H}}$  range, two indicators were used for the application of the method. Eriochrome blue type R = 1-(2-hydroxy-naphthylazo)-2-naphthol 4-sulfonic acid (CC) was used in all three systems, whereas in the case of MN, also methyl thymol blue = 3,3' bis-(( $N,N'$ -dicarboxymethyl)-amino-methyl)-thymolsulphonftalein (MTB) could be applied.

### 2.1.1. Protonation of MTB (Y) and CC (C)

Protonation constants of MTB and CC were determined at 25°C and 3.00 mol/l  $\text{NaClO}_4$ , as constant ionic medium. In the same experimental

conditions, the  $\epsilon_x$  values were also estimated for all their species.

From literature data [20], it could be deduced that the first three protonations of MTB and the first one of CC fall in alkaline solution and the relative constants had to be determined in this concentration range. By indicating with C the deprotonated CC, its protonation constant  $K'_1$  can be defined by the following relationship:

$$K'_1 = c_{\text{HC}} / (c_{\text{C}} c_{\text{H}}). \quad (4)$$

The  $K'_1$  value can be determined if  $C_{\text{C}}$  and  $\epsilon_{\text{HC}}$  are known and  $c_{\text{H}}$  is experimentally measured.

By recording spectra of solutions where only the species HC is present (in the range  $11 \leq -\log c_{\text{H}} \leq 12$ ), a maximum of absorbance,  $A$ , was remarked at  $\lambda = 631 \text{ nm}$ . From the measurement of  $A$  of solutions at increasing CC, using the Lambert–Beer law, the value of  $\epsilon_{\text{HC}}$  at same  $\lambda$  could be obtained. Analysis of solutions where HC and C were contemporarily present gave  $K'_1$  by means of Eq. (4). For such solutions, it could be assumed that, in the investigated  $c_{\text{H}}$  range,  $C_{\text{OH}} \cong c_{\text{OH}}$ , because the concentration of CC was negligible respect to  $C_{\text{OH}}$ . It was not necessary to determine  $K'_2$  for  $\text{H}_2\text{C}$  and  $K_n$  with  $n > 2$  for MTB, because  $\text{H}_2\text{C}$  and  $\text{H}_n\text{Y}$  (with  $n > 2$ ) do not exist in the investigated  $c_{\text{H}}$  range.

Therefore, from preliminary measurements, it could be deduced that  $\text{H}_2\text{Y}$  (where Y is MTB deprotonated) was formed in moderately alkaline solution, whereas Y and HY contemporarily exist only in strongly alkaline solution. To obtain  $K_2$  ( $K_2 = c_{\text{H}_2\text{Y}} / (c_{\text{HY}} c_{\text{H}})$ ) a method similar to that applied for CC, was used.

To have  $c_{\text{H}}$ , e.m.f. of the following cell was measured:



where R.E. is the reference electrode and G.E. a glass electrode. From e.m.f. measurements of (I),  $c_{\text{H}}$  values could be obtained as previously described [1–3]. Solution S had the following general composition:  $C_{\text{H}}$  mol/l;  $C_{\text{H}_2\text{Y}}$  mol/l;  $C_{\text{HY}}$  mol/l;  $(3 - C_{\text{H}}) \text{ mol/l}$  in  $\text{Na}^+$ ; 3 mol/l in  $\text{ClO}_4^-$ .  $C_{\text{H}_2\text{Y}}$  and  $C_{\text{HY}}$  were between  $10^{-4}$  and  $10^{-5}$  mol/l.

At first, spectra of Solution S were recorded at  $\lambda = 604 \text{ nm}$  by increasing  $C_{\text{H}_2\text{Y}}$  in the absence of  $\text{H}_3\text{Y}$ . In this way,  $\epsilon_{\text{H}_2\text{Y}}$  could be obtained, whereas

$c_H$  could be obtained from e.m.f. measurements of cell (I).

A different procedure had to be followed in the case of the existence of HY and Y in the same  $c_H$  range.

The absorbance,  $A$ , of a solution containing the species  $H_nY$  can be expressed according to Lambert–Beer, as follows:

$$A = b \left( c_Y \sum_n \beta_n c_H \varepsilon_n + c_H \varepsilon_H \right) = b (C_{H_nY} \varepsilon + c_H \varepsilon_H) \quad (5)$$

where  $b$  is the optical path,  $\beta_n = K_1 K_2 \dots K_n$  and  $\varepsilon = \sum_n \varepsilon_n \alpha_n$  where  $\alpha_n$  represents the molar ratio of the indicator present as  $H_nY$ .

When only two species (for instance HY and Y) are present, Eq. (5) can be written, as follows:

$$A = b(\varepsilon_1 K_1 c_H c_Y + c_Y \varepsilon_0 + c_H \varepsilon_H) \\ = b(\varepsilon_1 K_1 c_H c_Y + c_Y \varepsilon_0) = b C_{H_nY} \varepsilon \quad (6)$$

because  $\varepsilon_H = 0$ , in the studied  $\lambda$  range.

As the  $\varepsilon$  values can be obtained from measurements of  $A$  at known  $b$  and  $C_{H_nY}$ , from Eq. (6), the following relationship can be written:

$$\varepsilon = A / (b C_{H_nY}) = (\varepsilon_1 K_1 c_H + \varepsilon_0) / (1 + K_1 c_H) \quad (7)$$

If  $c_H$  and alternatively  $\varepsilon_1$  or  $\varepsilon_0$  are known, the value of  $K_1$  can be obtained by elaborating Eq. (7) in the following way:

$$(\varepsilon - \varepsilon_0) / c_H = \varepsilon_1 K_1 - K_1 \varepsilon. \quad (8)$$

In the plot  $(\varepsilon - \varepsilon_0) / c_H$  versus  $\varepsilon$ , the slope and intercept are  $-K_1$  and  $K_1 \varepsilon_1$ , respectively.

This method will be applied to determine  $K_1$ ,  $K_2$ , and  $\varepsilon_0$ ,  $\varepsilon_1$ , after the determination of  $\varepsilon_{H_2Y}$ , as described in Section 3.

## 2.2. Materials and analysis

$\text{NaClO}_4$ ,  $\text{HClO}_4$  and  $\text{NaOH}$  were prepared and analysed as previously described [21]. D-mannite was a C. Erba p.a. reagent, recrystallized from hydroalcoholic (1:1) solution and dried at  $110^\circ\text{C}$ . Absence of electroactive species in the purified product was checked by polarographic analysis. L-serine was from Fluka p.a., twice recrystallized from bidistilled water and dried at  $110^\circ\text{C}$ . Solutions of D-mannite and L-serine were prepared by

dissolving a weighed amount in the ionic medium. Glycerine, from C. Erba or Baker p.a., used to validate the proposed method, was purified as described by Ciavatta et al. [22]. The use of both products brings to the same results. Solutions of GLY were prepared at known concentration according to Bosard and Snoddy [23]. MTB and CC, from Fluka p.a. and C. Erba p.a., respectively, were used without further purification.

## 2.3. Details on measurements

Absorbance measurements were performed by using a UV–visible spectrophotometer Unicam model PU 8720 with printer plotter and quartz vessels with  $b = 1$  cm. To check indicators stability in alkaline solution, their spectrum was recorded for the time necessary to perform the relative measurement. HCC absorbance recorded for 15 minutes at  $\lambda = 631$  nm, proves its stability. During 15 min, absorbance remains constant within  $\pm 0.001$ .

E.m.f. measurements were carried out by means of models 605 and 654 Metrohom electronic voltmeters equipped with glass electrodes from the same firm. The reference electrode, R.E., was prepared according to Brown [24]. The salt bridge was similar to that described by Forsling et al. [25]. Values of  $-\log c_H$  obtained by measuring the e.m.f. of cell (I) could be taken as correct only up to  $-\log c_H \leq 9$  in the selected experimental conditions, as previously demonstrated [26].

A stream of hyperpure  $\text{N}_2$  from cylinder, bubbled through alkaline solutions to prevent the absorption of  $\text{CO}_2$ .  $\text{N}_2$  was further purified by passing it through 10%  $\text{NaOH}$ , 10%  $\text{H}_2\text{SO}_4$  and 3.00 mol/l  $\text{NaClO}_4$ .

## 3. Results

The results of this research are described in different sections. At first, the values of  $K_n$  and  $K'_1$  of MTB and CC, respectively and those of the relative  $\varepsilon_x$  are presented. A second section reports on the application of the method to the test compounds (i.e. D-mannite and glycerine) and a third one shows the results obtained for L-serine.

### 3.1. MTB and CC protonation

Although, as below described, only the indicator CC will be used to study the acid dissociation of the –OH group of L-serine, it seems interesting to report also the results obtained for the protonation of MTB, because it was applied to the study of system D-mannite, used for the validation of the method.

#### 3.1.1. Protonation of MTB

For the application of the proposed method, it was necessary to know only  $K_2$ ,  $K_1$  and  $\varepsilon_{H_2Y}$ ,  $\varepsilon_{HY}$  and  $\varepsilon_Y$ . The determination of  $K_2$  and  $\varepsilon_{H_2Y}$  was carried out easily, while those of  $K_1$  and  $\varepsilon_{HY}$  and  $\varepsilon_Y$  had to be performed by elaborating absorbance measurements,  $A$ , according to Eq. (8).

From preliminary measurements and literature data [20], it could be deduced that the only species present in the range  $9 \leq -\log c_H \leq 10$ , was  $H_2Y$  giving a spectrum with a maximum of absorbance at  $\lambda = 604$  nm. For such  $\lambda$ , the value  $\varepsilon_{H_2Y} = 1.75 \times 10^4$  mol/l/cm could be calculated.

Absorbance measurements obtained in the range  $9.5 \leq -\log c_H \leq 11$  were carried out to obtain  $K_2$  and  $\varepsilon_{HY}$  according to Eq. (8), by knowing  $c_H$  and  $\varepsilon_{H_2Y}$  at the same  $\lambda$ .

Experimental data are plotted in Fig. 1 in the form  $-(\varepsilon - \varepsilon_{H_2Y})c_H$  versus  $\varepsilon$ . All the points of

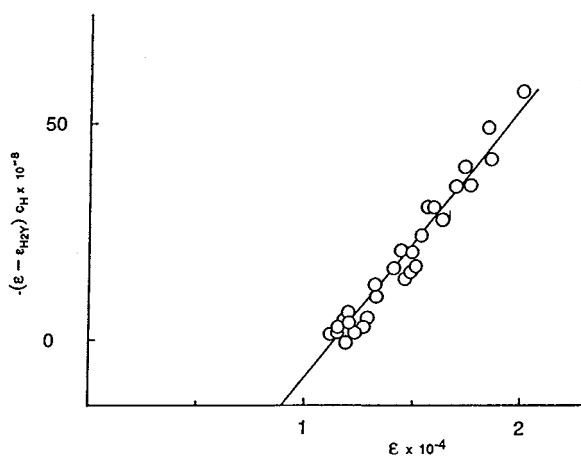


Fig. 1. Determination of  $-K_2$  (slope) and  $K_2\varepsilon_{HY}$  (intercept) from absorbance measurements. The experimental points are well approximated with a straight line.

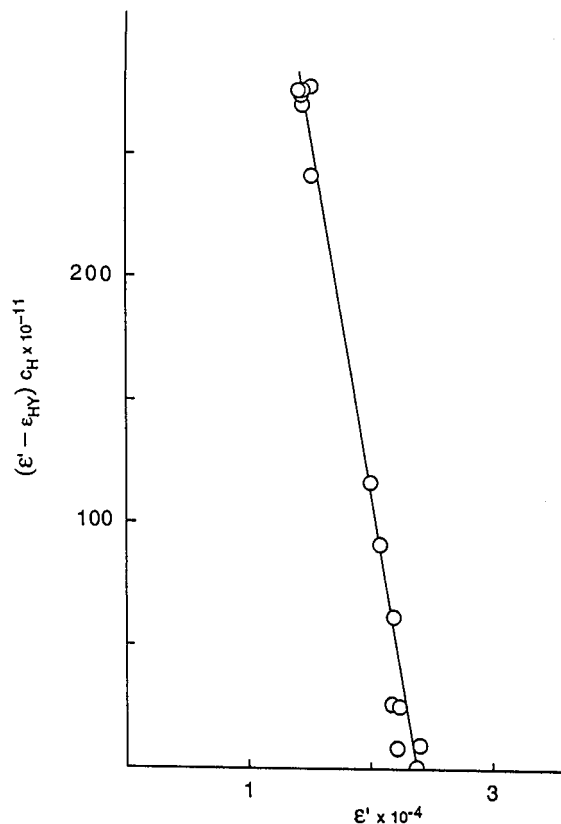


Fig. 2. Determination of  $-K_1$  (slope) and  $K_1\varepsilon_Y$  (intercept) from absorbance measurements. The experimental points are well approximated with a straight line.

Fig. 1 fall on a straight line with slope  $-K_2^{-1}$  and intercept  $\varepsilon_{HY}K_2^{-1}$ . The values obtained are  $\log K_2 = 11.2 \pm 0.1$  and  $\varepsilon_{HY} = 1.12 \times 10^5$ . The same procedure was applied successively for data of absorbance obtained from solutions at  $-\log c_H \geq 11$ , to calculate  $K_1$  and  $\varepsilon_Y$ . Since for all the investigated solutions in this range  $C_{MTB} \leq 0.02 C_{OH}$ , the  $-\log c_H$  values could be well approximated as  $c_H \cong c_H$  without loss of accuracy. Fig. 2 shows the plot  $(\varepsilon' - \varepsilon_{HY})c_H$  versus  $\varepsilon'$ , where, in this case  $\varepsilon'$  is the ratio  $A/C_{MTB}$  for solutions in the range  $-\log c_H \geq 11$ . Also in this case, experimental points can be well approximated with a straight line. From its slope and intercept on ordinate, the values  $-K_1^{-1}$  and  $\varepsilon_Y K_1^{-1}$  could be obtained, respectively. To calculate the protonation constants, the value  $-\log K_w = 14.24$  previ-

ously obtained in the same experimental conditions [26] had to be taken into account.

The protonation constant  $K_1$  and  $\varepsilon_Y$ , obtained for the MTB species, were:  $\log K_1 = 12.22 \pm 0.08$  and  $\varepsilon_Y = 2.21 \times 10^4$ .

### 3.1.2. Protonation of CC

From preliminary measurements, it could be deduced that only the form HC was present at  $-\log c_H = 10$ . At  $\lambda = 631$  nm its maximum  $A$  value was obtained and  $\varepsilon_{HC}$  was calculated. The  $A$  values of solutions at  $-\log c_H \geq 13$  and different  $C_{CC}$  were recorded, where  $C_H \cong c_H$  could be assumed, because in all the investigated solutions  $C_{CC} \leq 0.01 C_{OH}$ .

From the spectra and from the knowledge of  $C_{CC}$ ,  $c_H$  and  $\varepsilon_{HC}$ , the  $K'_1$  value could be calculated. The average values  $\log K'_1 = 13.65 \pm 0.09$  and  $\varepsilon_{HC} = 1.32 \times 10^4$  are obtained. The  $K'$  value agrees well with that proposed by Schwarzenbach et al. [27] and Hildebrand et al. [28], even if these authors operated at very low ionic strength.

Our values obtained for MTB only partially agree with those of Körbl et al. [20]. Only  $K_3$  and  $K_2$  values are similar to those of Körbl, while our  $\log K_1$  is lower than that of Ref. [20]. This disagreement is probably due to the different experimental conditions, because Körbl et al., disregarding activity coefficients, calculated  $c_{OH}$ , by assuming  $-\log K_w = 14.00$  (i.e.  $\text{pH} = 14 + \log C_{OH}$ ).

### 3.2. Validation of the proposed method

The method was applied to D-mannite and glycerine, to investigate on the acid dissociation of their  $-\text{OH}$  groups. Several series of solutions with known  $C_{MN}$ ,  $C_{OH}$  and  $C_{CC}$  were analysed to obtain the corresponding spectra and the  $A$  values at  $\lambda = 631$  nm. From the knowledge of  $\varepsilon_{HC}$  at the same  $\lambda$ , the values of  $-\log c_H$  could be obtained for each solution.

From the material balance of  $C_{OH}$  and  $C_{MN}$ , the formation function  $Z_{MN}$  could be calculated, as follows:

$$Z_{MN} = (C_{OH} - c_{OH})/C_{MN}.$$

The same procedure, applied to glycerine, allowed to calculate  $Z_{GLY}$ , as follows:

$$Z_{GLY} = (C_{OH} - c_{OH})/C_{GLY}.$$

The results relative to D-mannite and glycerine will be presented and discussed in two following sections.

#### 3.2.1. D-mannite

As described below, the acid dissociation of D-mannite is stronger than that of L-serine and glycerine, so that the  $-\log c_H$  values of solutions of mannite could be found by using either CC or MTB.

Solutions with total concentration of D-mannite,  $C_{MN} = 0.050, 0.100, 0.200, 0.300, 0.400, 0.500$  and  $0.600$  mol/l and in the range  $5.0 \times 10^{-3} \leq C_{OH} \leq 0.800$  mol/l were investigated. From the material balance of  $C_{MN}$  and  $C_{OH}$  and from the  $c_H$  values obtained by using CC and alternatively MTB, couples of values  $Z_{MN}$  and  $-\log c_{OH}$  could be obtained.

Fig. 3 shows the plot  $Z_{MN}$  versus  $-\log c_{OH}$ . Points obtained by using CC or MTB fall on the same curve, hence the method is independent of the used indicator. Furthermore,  $Z_{MN}$  is independent of  $C_{MN}$ , because all the points obtained at different  $C_{MN}$  fall together on the same curve. Polynuclear species in D-mannite are not present in appreciable quantity. Since low values of  $Z_{MN}$  ( $Z_{MN} < 1$ ) are reached in Fig. 3, it seems reasonable to assume that only a proton per mannite is dissociated. The two hypotheses formulated a priori by writing from Eq. (1) and the constant  $\beta_{1,MN}$  (Eq. (2)) are confirmed. On this basis, the formation function  $Z_{MN}$ , can be written as follows:

$$Z_{MN} = \beta_{1,MN} c_{OH} / (1 + \beta_{1,MN} c_{OH}). \quad (9)$$

Eq. (9) can be normalized, according to Sillén [29], in the form  $y = u/(1 + u)$ , where  $u = \beta_{1,MN} c_{OH}$ . In the position of best fit between curve and points and using the value  $-\log K_w = 14.24$ , as previously found [26], the value  $-\log \beta'_{1,MN} = 13.7 \pm 0.1$ , shown in Table 2, was obtained. Fig. 3 shows that the points and curve agree well, supporting the validity of the procedure.

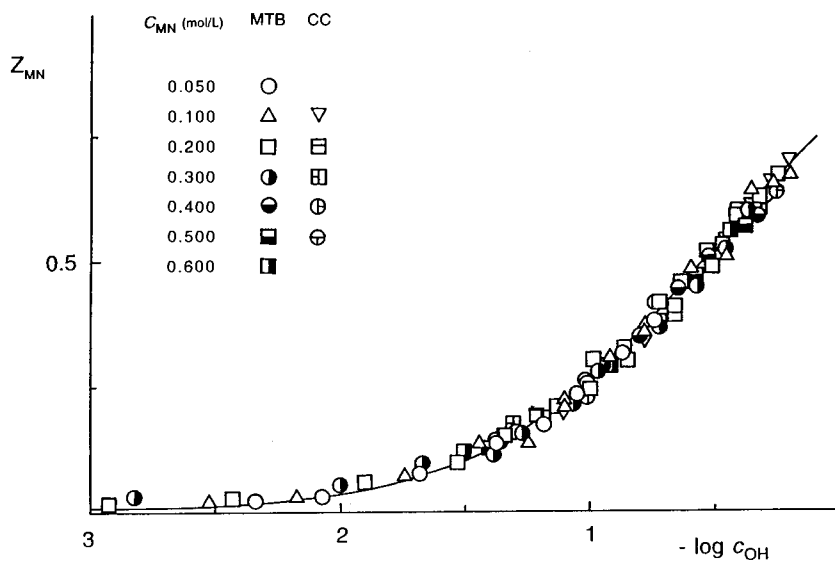


Fig. 3. Formation function of D-mannite. The curve is the normalized one in the position of best fit.

### 3.2.2. Glycerine

Only CC was used in the case of glycerine, because of its acid properties are weaker than those of D-mannite and probably of L-serine. MTB has a  $\log K_1$  value too low to give an accurate  $-\log c_H$  value in very alkaline solutions ( $-\log c_H \geq 13$ ).

Solutions with total concentration of glycerine,  $C_{GLY} = 0.300, 0.600$  and  $1.00$  mol/l, in the range  $0.300 \leq C_{OH} \leq 0.900$  mol/l were analysed, in the presence of known concentrations of CC. From the absorbance at  $\lambda = 631$  nm and by knowing  $\epsilon_{HC}$ , the value of  $-\log c_{OH}$  for each solution could be obtained. From the material balance of glycerine and the knowledge of  $c_{OH}$ , the formation function  $Z_{GLY}$  could be calculated. As in this case  $Z_{max} \cong 0.15$ , it was preferred to calculate  $\beta_{1,GLY}$  directly from each pair of values  $Z_{GLY}$  and  $-\log c_{OH}$ . Also in the case of glycerine the hypotheses of only one dissociation without appreciable formation of polynuclear species were confirmed. The value of the constant was obtained from the expression  $\beta_{1,GLY} = Z_{GLY}/(c_{OH} - Z_{GLY}c_{OH})$ . By using  $K_w$ , as previously determined [26], the average value  $-\log \beta'_{1,GLY} = 14.9 \pm 0.1$ , reported in Table 1, was obtained.

Table 1

Survey of experimental data, obtained at 25°C and in 3.00 mol/l NaClO<sub>4</sub> as a ionic medium, to calculate  $-\log \beta'_{1,GLY}$ <sup>a</sup>

Glycerine = 0.300 mol/l

$C_{OH}, A, -\log c_{OH}, Z:$  0.302, 0.090, 0.547, 0.060; 0.400, 0.083, 0.420, 0.066; 0.500, 0.100, 0.322, 0.081; 0.601, 0.056, 0.245, 0.110; 0.700, 0.083, 0.177, 0.117; 0.801, 0.080, 0.122, 0.152; 0.900, 0.087, 0.070, 0.160.

Glycerine = 0.600 mol/l

$C_{OH}, A, -\log c_{OH}, Z:$  0.302, 0.102, 0.565, 0.050; 0.400, 0.102, 0.446, 0.070; 0.500, 0.100, 0.348, 0.086; 0.600, 0.107, 0.270, 0.105; 0.700, 0.120, 0.200, 0.113; 0.799, 0.101, 0.146, 0.141; 0.901, 0.091, 0.085, 0.132.

Glycerine = 1.00 mol/l

$C_{OH}, A, -\log c_{OH}, Z:$  0.299, 0.121, 0.613, 0.055; 0.400, 0.117, 0.475, 0.065; 0.501, 0.082, 0.373, 0.077; 0.600, 0.156, 0.291, 0.088; 0.701, 0.101, 0.221, 0.099; 0.799, 0.095, 0.162, 0.111; 0.900, 0.094, 0.109, 0.122.

<sup>a</sup> The average value  $-\log \beta'_{1,GLY} = 14.9 \pm 0.1$  can be calculated. The error limit of the constant is not the S.D., but only the difference between minimum and maximum of the calculated values.

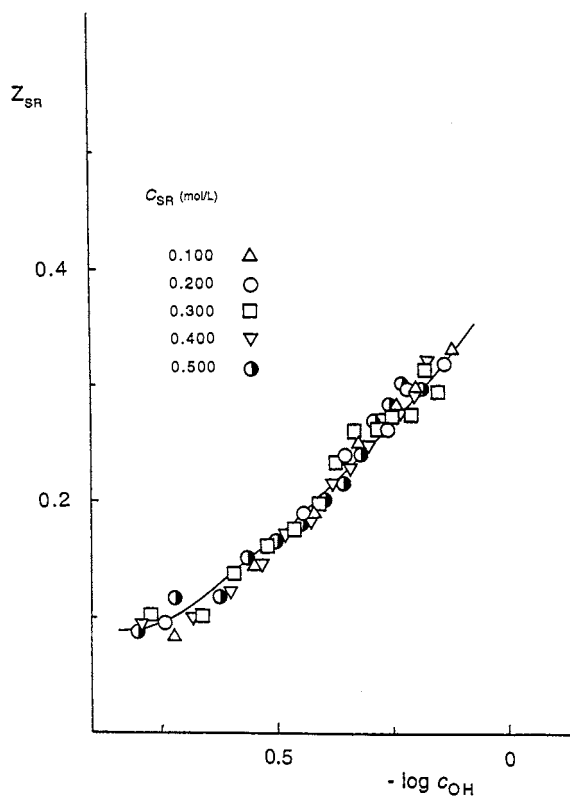


Fig. 4. Formation function of L-serine. The curve is the normalized one in the position of best fit.

Table 2

Proposed values (at 25°C and in 3.00 mol/l NaClO<sub>4</sub> as a ionic medium) for the dissociation constants ( $-\log \beta'_{1,x}$ ) of the investigated compounds<sup>a</sup>

Compound	$-\log \beta'_{1,x}$
D-mannite	$13.7 \pm 0.1$
L-serine	$14.4 \pm 0.1$
Glycerine	$14.9 \pm 0.1$

<sup>a</sup> The symbol *x* indicates alternatively D-mannite, L-serine or glycerine. The error limit of the constants is not the S.D., but only the difference between minimum and maximum of the calculated values.

### 3.3. Application of the procedure to L-serine

Since the results obtained for D-mannite and glycerine agree with the literature data, as indicated in the Section 4, the proposed method of

investigation is validated and it can be applied to L-serine. By supposing that L-serine could show acid properties stronger than glycerine, but weaker than D-mannite, only CC was used to obtain  $-\log c_H$  from the recorded spectra of solutions at  $C_{SR} = 0.100, 0.200, 0.300, 0.400,$  and  $0.500$  mol/l, where  $C_{OH}$  varied from 0.200 to 0.800 mol/l. From the knowledge of  $\epsilon_{HC}$  at  $\lambda = 631$  nm and from the  $A$  values measured for each solution, the value of  $c_{OH}$  could be obtained. The material balance of  $C_{SR}$  and  $C_{OH}$  was used to calculate the formation function in the following form:

$$Z_{SR} = (C_{OH} - c_{OH})/C_{SR}.$$

Experimental points are plotted in Fig. 4, in the form  $Z_{SR}$  as a function of  $-\log c_{OH}$ . It can be seen that points obtained for different  $C_{SR}$  fall together. Since  $Z_{SR}$  is not a function of  $C_{SR}$ , polynuclear species in L-serine are not present in appreciable amount. As expected,  $Z_{SR}$  never overtakes 1 ( $Z_{max} \cong 0.4$ ) so that only one proton per serine can be loss. The two hypotheses assumed in the formulation of Eqs. (1) and (2) are confirmed and the formation function can be expressed in the form

$$Z_{SR} = \beta_{1,SR} c_{OH} / (1 + \beta_{1,SR} c_{OH}).$$

As previously described for D-mannite, the normalized curves method [29] can be applied and the value of the constant was obtained in the position of best fit. Fig. 4 shows the good agreement between points and normalized curve, supporting the validity of the procedure. In Table 2, the value  $-\log \beta'_{1,SR} = 14.4 \pm 0.1$  is reported.

## 4. Discussion

The values of  $-\log \beta'_{1,MN}$ ,  $-\log \beta'_{1,SR}$  and  $-\log \beta'_{1,GLY}$  are collected in Table 2. Together with  $K_n$  of MTB and CC, also the  $\epsilon$  values of the considered forms of the two studied indicators are reported. Results obtained for the test systems, D-mannite and glycerine, must be compared with relative literature data to validate the proposed method.

The acid behaviour of D-mannite had been already shown [4, 5 and 14], but the literature data disagree each other. A few authors [4,5] explain their data by assuming the dissociation of only one proton per D-mannite, while another [14] attributes weak acid properties also to a second proton. In our paper, experimental data can account for the dissociation of only one proton with a constant of the same order of magnitude of those found previously [4,5,14]. For the first dissociation, Vicedomini [14] proposed  $-\log \beta'_{1,MN} = 13.1$ , while Michaelis [4] proposed 13.5 and we propose 13.7. Although our value was obtained under different experimental conditions, it agrees better with that proposed by Michaelis, while it is rather higher than that proposed by Vicedomini.

A better comparison can be effected for glycerine, because data obtained in the same experimental conditions are available. From calorimetric measurements carried out at 25°C and in 3.00 mol/l NaClO<sub>4</sub>, the value  $-\log \beta'_{1,GLY} = 14.76 \pm 0.06$  was obtained [16]. The value obtained here  $14.9 \pm 0.1$  agrees well with the calorimetric method, within the experimental error. The validation of the proposed method is fully verified.

The method was successful for L-serine. Although complicated equilibria are not involved, it would be hard to put into evidence the acid properties of the –OH group of L-serine, because the dissociation takes place at very high  $-\log c_H$  values, where many difficulties arise for e.m.f. measurements of  $c_H$ , even with a H<sub>2</sub> electrode. The use of a suitable indicator, in this case CC, was necessary to overtake the difficulty of the determination of  $c_H$  at equilibrium.

The found value  $-\log \beta'_{1,SR} = 14.4$  shows that L-serine behaves as an acid, even in the form SR, but it is weaker than D-mannite. As disagreeing results were obtained for D-mannite, by means of e.m.f. measurements, it would be not possible to obtain information for L-serine in this way. On the other hand, L-serine shows stronger acid properties than glycerine as supported by the values of the constants in Table 2.

On the basis of the adopted ionic method [17], it can be assumed that the activity coefficients of the reagents do not vary remarkably because the substitution of ClO<sub>4</sub><sup>-</sup> does not exceed 15–20%.

At  $-\log c_H$  lower than the here investigated values, the –OH group of both L-serine and glycerine does not behave as an acid and only protolytic effects due to aminic and carboxylic groups of L-serine can be observed.

## 5. Conclusion

This paper gives a contribution to the quantitative knowledge of the acid properties of the –OH group of L-serine.

A method, different with respect to the e.m.f. measurement, was described for the determination of the free hydrogen ion concentration in strongly alkaline solutions. The method was validated by applying it to two systems already studied (D-mannite and glycerine) and here obtained results that agree in both cases with the literature data. For glycerine the value obtained here agrees within the experimental error.

Colorimetric  $-\log c_H$  determination involved the knowledge of the behaviour of two indicators (MTB and CC) used for developing this method. Their protonation constants and the absorbance coefficients were also determined under the same experimental conditions.

The application of the method is favoured by the high values of  $\varepsilon$  of the species of indicators involved. It can be alternative to calorimetric measurements for the determination of very low values of acid dissociation constants.

The  $-\log \beta'_{1,SR}$  value is particularly important in the investigation on the complex formation between cations and L-serine in alkaline solutions. At high  $-\log c_H$ , cations could be bound by the carboxylic and aminic groups together with the –OH group, with contemporary loss of protons.

## Acknowledgements

This work was supported by the Consiglio Nazionale delle Ricerche (CNR) and by the Ministero dell'Università e della Ricerca Scientifica e Tecnologica (MURST) of Italy.

**References**

- [1] E. Bottari, M.R. Festa, R. Jasionowska, *Ann. Chim. (Rome)* 77 (1987) 837.
- [2] E. Bottari, M.R. Festa, R. Jasionowska, *J. Coord. Chem.* 17 (1988) 245.
- [3] E. Bottari, R. Porto, *Ann. Chim. (Rome)* 75 (1985) 393.
- [4] L. Michaelis, *Berl. Deutch. Chem. Ges.* 46 (1913) 3683.
- [5] P. Souchay, R. Scool, *Bull. Soc. Chim. Fr.* 819 (1950).
- [6] J. Thamsen, *Acta Chem. Scand.* 6 (1952) 270.
- [7] F.A. Long, F. Bullinger, *Electrolytes Proc. Int. Symp. Trieste (I)* 64 (1959) 152.
- [8] M.T. Beck, B. Csiszar, P. Szarvas, *Nature* 188 (1960) 846.
- [9] R. Gut, E. Schmid, J. Serrallach, *Helv. Chim. Acta* 54 (1971) 593.
- [10] E. Bottari, M. Vicedomini, *J. Inorg. Nucl. Chem.* 33 (1971) 1463.
- [11] E. Bottari, M. Vicedomini, *Gazzetta* 102 (1972) 902.
- [12] E. Bottari, A. Liberti, M. Vicedomini, *Gazzetta* 103 (1973) 859.
- [13] E. Bottari, M. Vicedomini, *Gazzetta* 104 (1974) 523.
- [14] M. Vicedomini, *Ann. Chim. (Rome)* 71 (1981) 213.
- [15] E. Bottari, M. Vicedomini, *J. Inorg. Nucl. Chem.* 35 (1973) 1657.
- [16] E. Bottari, P. Ippoliti, R. Porto, *Ann. Chim. (Rome)* 73 (1983) 473.
- [17] G. Biedermann, L.G. Sillén, *Ark. Kem.* 5 (1953) 425.
- [18] G. Schwarzenbach, G.H. Ott, *Helv. Chim. Acta* 20 (1937) 627.
- [19] G. Schwarzenbach, R. Sulzbereger, *Helv. Chim. Acta* 27 (1944) 248.
- [20] J. Körbl, B. Kakac, *Coll. Czech. Chem. Commun.* 23 (1958) 889.
- [21] E. Bottari, *Ann. Chim. (Rome)* 66 (1976) 139.
- [22] L. Ciavatta, G. Nunziata, M. Vicedomini, *Ric. Sci.* 35 (1965) 1096.
- [23] L.W. Borsart, A.O. Snoddy, *Ind. Eng. Chem.* 20 (1928) 1377.
- [24] A.S. Brown, *J. Am. Chem. Soc.* 56 (1934) 646.
- [25] W. Forsling, S. Hietanen, L.G. Sillén, *Acta Chem. Scand.* 6 (1952) 901.
- [26] E. Bottari, R. Jasionowska, *Ann. Chim. (Rome)* 69 (1979) 597.
- [27] G. Schwarzenbach, W. Biedermann, *Helv. Chim. Acta* 31 (1948) 678.
- [28] G.P. Hildebrand, C.N. Reilley, *Anal. Chem.* 29 (1957) 258.
- [29] L.G. Sillén, *Acta Chem. Scand.* 10 (1956) 186.



# Spectrophotometric determination of cysteine and/or carbocysteine in a mixture of amino acids, shampoo, and pharmaceutical products using *p*-benzoquinone

Dimas A.M. Zaia <sup>a,\*</sup>, Kelly C.L. Ribas <sup>a</sup>, Cássia T.B.V. Zaia <sup>b</sup>

<sup>a</sup> Departamento de Química-CCE, Universidade Estadual de Londrina, 86051-990, Londrina, PR, Brazil

<sup>b</sup> Departamento de Ciências Fisiológicas, Universidade Estadual de Londrina, 86051-990, Londrina, PR, Brazil

Received 28 January 1999; received in revised form 22 June 1999; accepted 28 June 1999

## Abstract

A simple, sensitive, and selective method has been developed for determination of cysteine (Cys) or carbocysteine (carboCys) in pharmaceutical products, shampoos and a mixture of amino acids. The results showed the reaction between *p*-benzoquinone (PBQ) and Cys occurs through the sulfhydryl group. Previous derivatization or extraction is not necessary before the assay is carried out. The method is based on the fact that the product of reaction between PBQ and Cys absorbs at 352 and 500 nm or PBQ and carboCys absorbs at 500 nm. Beer's law is followed in the range 0–40 µg/ml for Cys and 0–150 µg/ml for carboCys. The product of reaction PBQ-Cys is stable for 2 h with absorption bands at 352 and 500 nm. In the presence of amino acids, PBQ is highly selective to Cys. Several substances such as amino acids, urea, salts, and dipeptide did not interfere with the proposed method. A recovery of about 100% is observed for both Cys and carboCys, when the method is applied to determine Cys in a mixture of amino acids resembling blood plasma, shampoo, and pill food as well as carboCys in pharmaceutical products. © 1999 Elsevier Science B.V. All rights reserved.

**Keywords:** *p*-Benzoquinone; Spectrophotometry; Cysteine; Carbocysteine; Pharmaceutical products

## 1. Introduction

Cysteine (Cys) plays an important role in several biological processes [1]; Cys or compounds of Cys are widely used in many pharmaceutical products. Determinations of Cys or compounds of Cys are commonly used in clinical investigation, pharmaceutical industry, and research.

Among the many methods for determination of Cys [2,3] or compounds of Cys, chromatographic methods are widely used. In spite of HPLC [4–6] or gas-chromatographic methods [7,8] which are very popular with equipment easily available in many laboratories, several disadvantages can be cited. In all chromatographic methods, the samples should pass through derivatization and extraction of the products of reaction before their microinjection into the column. Those methods

\* Corresponding author. Fax: +55-43-328-4440.

E-mail address: zaiazaia@sercomtel.com.br (D.A.M. Zaia)

use expensive reagents and equipment, and a significant period of time for whole assay.

In a previous paper [9], the use of *p*-benzoquinone (PBQ) for simultaneous determination of total proteins and amino acids was reported. It was observed that the spectrum of the product of reaction between Cys and PBQ (PBQ-Cys) was very different from the other proteic amino acids. An investigation of the reaction PBQ-Cys was undertaken and it was possible to obtain a specific reaction medium in which PBQ was selective for Cys in a mixture of amino acids.

The present paper describes the utilization of PBQ for spectrophotometric determination of Cys using the absorption bands at 352 and 500 nm, in pill food, shampoo, and a mixture of amino acids resembling blood plasma [10], as well as determination of carbocysteine (carboCys) using the absorption band at 500 nm in two pharmaceutical products (Mucoflux and Mucolitic). In all samples analysed, a good agreement between the nominal values and assay values was obtained.

## 2. Materials and methods

### 2.1. Materials

Ultraviolet and visible spectrophotometry were carried out on Varian DMS-80 and Shimadzu UV-1203 spectrophotometers.

All reagents were of analytical reagent grade. The pill food and shampoo were purchased from Calendola Pharmacy. Mucoflux (Merck) and Mucolitic (Laboratory Wyeth-Whitehall Ltda.) were purchased at a pharmacy in Londrina city (PR, Brazil). CarboCys and *N*-acetyl-cysteine (analytical reagent grade) were a gift from Dr João R.F. Teixeira of Merck and Dr Marta Y.Y. Satake of Zambon Laboratórios Farmacêuticos Ltda, respectively.

#### 2.1.1. *p*-Benzoquinone (Sigma)

PBQ was purified by sublimation and a 0.1 M solution in DMSO was prepared, kept in an airtight flask and used for 5 days after its preparation.

#### 2.1.2. Cysteine (CAAL) and carbocysteine

Cys and carboCys solutions (1.5 g/l) were prepared with distilled, deionized water and used as standards in all assays.

#### 2.1.3. Buffer

The following 0.1 M solutions were used as buffer: Na<sub>2</sub>B<sub>4</sub>O<sub>7</sub>-H<sub>3</sub>BO<sub>3</sub>, pH 8.0; Na<sub>2</sub>HPO<sub>4</sub>-NaH<sub>2</sub>PO<sub>4</sub>, pH 6.0 and 7.0; CH<sub>3</sub>COONa-CH<sub>3</sub>COOH, pH 3.0, 4.0 and 5.0.

#### 2.1.4. Mixture of amino acids

An amino acid solution was prepared that contained a mixture of amino acids (Ala, Arg, Asn, Glu, Gln, Gly, Hys, Ile, Lys, Met, Pro, Ser, Tre, Tyr, Val) in proportions similar to those observed in blood plasma [10]. This solution was separated in aliquots and stored at -20°C.

### 2.2. Sample preparations

#### 2.2.1. Standard samples

2.2.1.1. *Cysteine*. By dilution of the 1.5 g/l standard solution of Cys, a calibration curve was constructed using the following concentrations: 0.0, 7.5, 15.0, 22.5 and 30.0 µg/ml, and the volume was adjusted to 4.8 ml with acetate buffer, pH 3.0.

2.2.1.2. *Cysteine with sodium dodecyl sulfate (SDS)*. Cysteine with SDS was used for assay of Cys in shampoo. The calibration curve was obtained as above and SDS was added to all tubes until the final concentration was 160 µg/ml.

2.2.1.3. *Carbocysteine*. By dilution of the 1.5 g/l standard solution of carboCys, a calibration curve was constructed using the following concentrations: 0.0, 30.0, 60.0, 90.0 and 120.0 µg/ml; the volume was adjusted to 4.8 ml with phosphate buffer, pH 7.0.

#### 2.2.2. Pill food

A pill was ground and dissolved in 100 ml of distilled, deionized water. A 100-µl aliquot of this solution was transferred to a test tube, and the volume was adjusted to 4.8 ml with acetate buffer, pH 3.0.

### 2.2.3. Shampoo

A 200- $\mu$ l aliquot of shampoo was transferred to a 5.0-ml volumetric flask and the volume was made up with distilled, deionized water. A 100- $\mu$ l aliquot of this solution was transferred to a test tube, and the volume was adjusted to 4.8 ml with acetate buffer, pH 3.0.

### 2.2.4. Amino acids mixture

To 250  $\mu$ l of the amino acids mixture, 710  $\mu$ l of acetate buffer, pH 3.0 were added.

### 2.2.5. Mucoflux or Mucolitic

A 100- $\mu$ l aliquot of Mucoflux or Mucolitic was transferred to a test tube and the volume was made up to 1.0 ml with distilled, deionized water. A 75- $\mu$ l aliquot of this solution was transferred to a second test tube, and the volume was adjusted to 4.8 ml with phosphate buffer, pH 7.0.

### 2.3. Cys standard curve and Cys assay

To each tube of sample of pill food, shampoo, and standard Cys was added 200  $\mu$ l of 0.1 M of PBQ, and for the sample of amino acids mixture, 40  $\mu$ l of 0.1 M PBQ was added. The tubes were shaken, incubated at 37°C for 5 min, cooled to room temperature, and the absorbances at 352 and 500 nm were read against the blank.

### 2.4. CarboCys standard curve and carboCys assay

To each tube of sample of Mucoflux, Mucolitic, and standard carboCys was added 200  $\mu$ l of 0.1 M of PBQ, shaken and incubated at 37°C for 10 min. The tubes were then cooled to room temperature and the absorbances at 500 nm were read against the blank.

## 3. Results and discussion

The reaction between quinones and amines, amino acids or proteins has sometimes been reported as a charge transfer complex [11,12] or substituted quinone compounds [13–16]. These discrepancies could be attributed to differences in the reaction conditions employed.

Table 1 shows that the reaction between PBQ and a pool of amino acids or PBQ and carbocysteine occurs when the pH is increased; in this case, the nitrogen of amino group is probably involved in the reaction as observed by several authors [11–16]. As pointed out by Ratajczak and Orville-Thomas [12], first a charge transfer complex is formed, then depending on conditions of reaction a mono- or di-substituted compound is formed. Several authors [13,14,16] obtained mono- or di-

Table 1

Maximum absorbance of the products of the reaction between *p*-benzoquinone (PBQ) and cysteine, pool of amino acids<sup>a</sup> (pool AAs) or carbocysteine (carboCys) at various pH values

PH	Maximum absorbance (nm)		
	Cys (30 $\mu$ g/ml) <sup>b</sup>	Pool Aas <sup>b</sup> (30 $\mu$ g/ml each)	CarboCys <sup>c</sup> (22.5 $\mu$ g/ml)
8.0 <sup>e</sup>	–	461–373	495–385 <sup>d</sup>
7.0 <sup>f</sup>	291	500–357–279	500–350 <sup>d</sup>
6.0 <sup>f</sup>	507 <sup>d</sup> –343 <sup>d</sup> –289	500–279	495 <sup>d</sup>
5.0 <sup>g</sup>	516–327 <sup>d</sup> –284	275	–
4.0 <sup>g</sup>	513–355–293	288	–
3.0 <sup>g</sup>	500–352–293	288	–

<sup>a</sup> AAs used: Trp, Tre, Ser, Lys, Leu, Phe, Tyr, Val.

<sup>b</sup> Samples heated at 37°C for 20 min with 2.0 mM PBQ.

<sup>c</sup> Samples heated at 37°C for 10 min with 4.0 mM PBQ.

<sup>d</sup> Bands not well defined.

<sup>e</sup> Boric acid/borax buffer (0.1 M).

<sup>f</sup> Monobasic/dibasic sodium phosphate buffer (0.1 M).

<sup>g</sup> Acetic acid/acetate buffer (0.1 M).

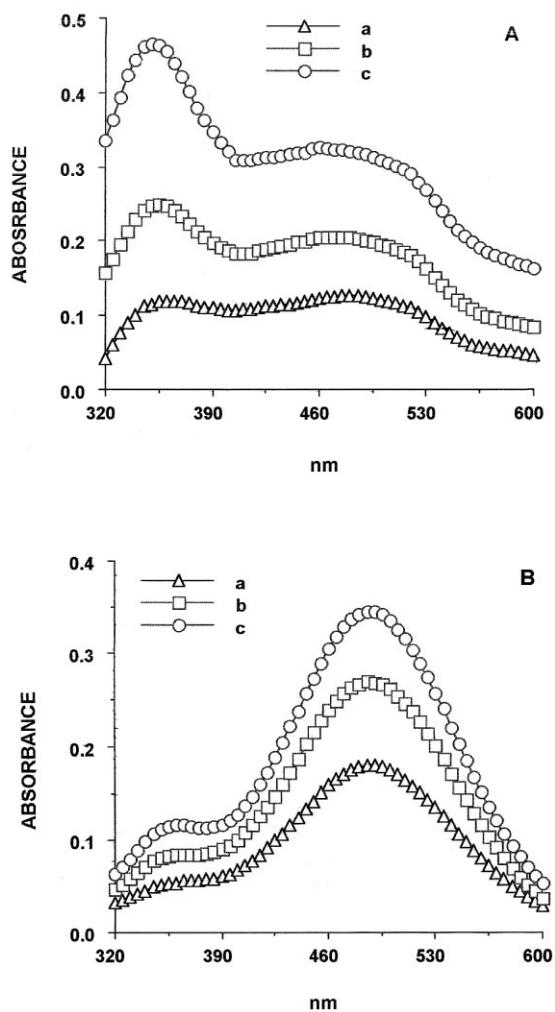


Fig. 1. (A) Absorbance spectra of the product of reaction between 7.5 (a); 15.0 (b) or 22.5 (c)  $\mu\text{g/ml}$  cysteine and 4.0 mM *p*-benzoquinone (PBQ); 5 min of heating at 37°C in acetate buffer 0.1 M, pH 3.0. (B) Absorbance spectra of the product of reaction between 60 (a); 90 (b) or 120 (c)  $\mu\text{g/ml}$  carbocysteine and 4.0 mM PBQ; 10 min of heating at 37°C in phosphate buffer 0.1 M, pH 7.0.

substituent compounds as the product of reaction between amines/amino acids and PBQ. Iskander and Medien [16] obtained a mono-substituent compound when an excess of PBQ reacts with Gly, which showed strong absorption at 500 nm and weak absorption at 340 nm. On the other hand, when an excess of Gly reacts with PBQ, the product of reaction had a strong absorption at

340 nm. As the product of reaction carboCys-PBQ (with an excess of PBQ) showed a strong absorption at 500 nm we probably also obtained a mono-substituent compound. The reaction between PBQ and Cys occurs when the pH is decreased probably because the sulfhydryl group is involved. We also tested carboCys (Table 1) and *N*-acetyl-cysteine (data not shown); for *N*-acetyl-cysteine, we observed the same behavior as observed for Cys, since the amino group is blocked by acetyl, thus the reaction was through the sulfhydryl group; for carboCys, we also observed the same behavior as observed for the pool of amino acids, since the sulfhydryl group is blocked by carboxy, then the reaction was through the amino group. At moderate temperatures in acidic solution with a high ratio of quinone/thio compounds (Cys, thiourea,  $\beta$ -thiopropionic acid), several authors [17] obtained mono-substituent compounds with the sulfhydryl group attached to the ring of the quinone. As our blocking experiments showed, reaction between PBQ and Cys/*N*-acetyl-cysteine was through the sulfhydryl group, thus we probably also obtained a mono-substituent compound. The buffer components and the pH used here did not interfere with the reaction PBQ-pool of aas/carboCys/Cys. However, when borate buffer was used with pH higher than 9.0, polymerization of PBQ occurred interfering with the method.

Fig. 1 shows the absorbance spectra of the product of reaction between Cys or carboCys and PBQ. For the product of reaction between Cys and PBQ, there are two bands, one at 352 nm and another at 500 nm, both bands follow Beer's law in the range 0–40  $\mu\text{g/ml}$  Cys (Table 2) and therefore both can be used for analytical purposes. In this case, the reaction PBQ-Cys occurred through the sulfhydryl group. On the other hand, the product of reaction between carboCys and PBQ shows one band at 500 nm that followed Beer's law in the range 0–150  $\mu\text{g/ml}$  carboCys (Table 2) and can be used for analytical purposes. The reaction carboCys-PBQ occurred through the amino group.

Table 2 shows the straight line equations and range of linearity for the products of reaction between PBQ and Cys or carboCys in various

Table 2

Straight line equations and range of linearity (Beer's Law) for the products of reaction between *p*-benzoquinone (4.0 mM) and cysteine or carbocysteine in various media<sup>a</sup>

Medium	Straight line equation ( $Y$ (absorbance) = $mX$ ( $\mu\text{g}/\text{ml}$ ) + $b$ )	Range of linearity ( $\mu\text{g}/\text{ml}$ )
<i>Cysteine</i> <sup>b</sup>		
Acetate buffer 0.1 M, pH 3.0 (with 160 $\mu\text{g}/\text{ml}$ of SDS)	$Y = 0.01029X + 0.025$ at 500 nm (6) $Y = 0.01558X - 0.016$ at 352 nm (7)	0–40
Acetate buffer 0.1 M, pH 3.0	$Y = 0.01230X + 0.013$ at 500 nm (25) $Y = 0.02180X - 0.045$ at 352 nm (25)	0–40
Acetic acid 1.0 M	$Y = 0.01530X - 0.021$ at 500 nm (2) $Y = 0.02200X - 0.113$ at 352 nm (2)	0–40
Acetic acid 0.5 M	$Y = 0.01510X + 0.078$ at 500 nm (2) $Y = 0.02550X - 0.019$ at 352 nm (2)	0–40
Acetic acid 0.1 M	$Y = 0.00920X - 0.063$ at 500 nm (2) $Y = 0.01770X - 0.053$ at 352 nm (2)	0–40
Acetic acid 0.01 M	$Y = 0.00770X + 0.006$ at 500 nm (2) $Y = 0.01750X - 0.085$ at 352 nm (2)	0–40
Hydrochloric acid 0.5 M	$Y = 0.00290X + 0.008$ at 500 nm (2) $Y = 0.00820X + 0.009$ at 352 nm (2)	0–40
Hydrochloric acid 0.1 M	$Y = 0.00870X + 0.114$ at 500 nm (2) $Y = 0.01470X + 0.034$ at 352 nm (2)	0–40
Hydrochloric acid 0.01 M	$Y = 0.01390X + 0.104$ at 500 nm (2) $Y = 0.01840X - 0.045$ at 352 nm (2)	0–40
<i>Carbocysteine</i> <sup>c</sup>		
Borax buffer 0.1 M, pH 8.0	$Y = 0.00952X + 0.001$ at 500 nm (3)	0–40
Phosphate buffer 0.1 M, pH 7.0	$Y = 0.00266X + 0.018$ at 500 nm (7)	0–150

<sup>a</sup> Number of experiments in parentheses.

<sup>b</sup> Samples heated at 37°C for 5 min.

<sup>c</sup> Samples heated at 37°C for 10 min.

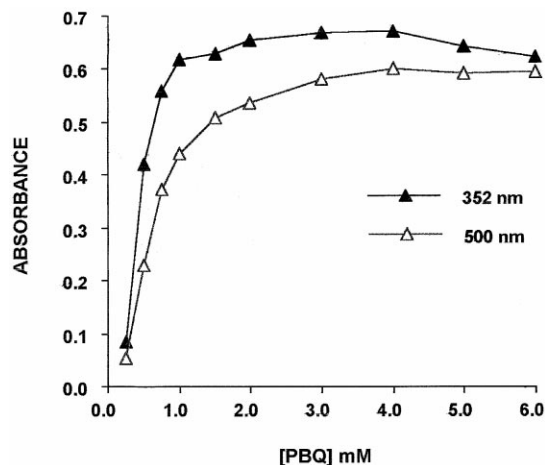


Fig. 2. Dependence of absorbance on the concentration of *p*-benzoquinone (PBQ). The samples of cysteine (30  $\mu\text{g}/\text{ml}$ ) were heated with different amounts of PBQ in acetate buffer, pH 3.0, at 37°C for 20 min.

media. For determination of Cys in the samples with absorbances at 352 and 500 nm, acetate buffer 0.1 M (pH 3.0) was used because one of the best specific absorbances and the best correlation coefficient of the straight line were obtained with that medium. Higher specific absorbances for Cys, shown in Table 2, were obtained in the pH range 2–3. The samples with 0.01 M acetic acid and 0.5 and 0.1 M hydrochloric acid were out of that range and their specific absorbances were lower. Only one buffer medium (0.1 M acetic acid) showed specific absorbance as low as the media buffer outside the good range. In spite of 0.1 M phosphate buffer (pH 7.0) showing minor specific absorbance at 500 nm, when compared with borax buffer pH 8.0 at 500 nm (Table 2), it was used for determination of carboCys, because the product of reaction was more stable at pH 7.0 than at pH 8.0 and the straight line equations were better. For the reaction PBQ-carboCys, an increase in specific absorbance was obtained when the pH was increased because the amino group is free. The correlation coefficients for all the straight lines shown in Table 2 were at least 0.98.

Fig. 2 shows the effect of different concentrations of PBQ on the absorbance of Cys. For both absorption bands (352 and 500 nm), the absorbance increased almost linearly with the in-

crease in PBQ concentration up to 1.0 mM. Above 3.0 mM, there is only a small increase in absorbance. Shifts of 352 or 500 nm bands were not observed at any of the PBQ concentration tested (data not shown). PBQ (4.0 mM) was used which gave a ratio of 16 of PBQ/Cys in mol for the curve with the highest concentration of Cys. This concentration seems to be sufficient because Beer's law was followed up to 30  $\mu\text{g/ml}$  of Cys.

We also tested the effect of heating time at 37°C on absorbance of products of reaction between PBQ (4.0 mM) and Cys or carboCys (data not shown). The temperature was standardized at 37°C because on cold days (15°C), the reaction is slow. Heating at 37°C provide an easier way to control and to standardize the time of reaction. It was observed that there was only a small increase in absorbance for Cys after 5 min of heating; for carboCys heating, it should last for 10 min.

After heating, the absorbance at 352 nm of the product of reaction between PBQ and Cys showed a smaller increase up 20 min and after that, the stability lasted for 2 h (Fig. 3). At 500 nm, a slight decrease in the absorbance was observed after 30 min of heating (Fig. 3). Thus, time after heating is not a critical factor for the mea-

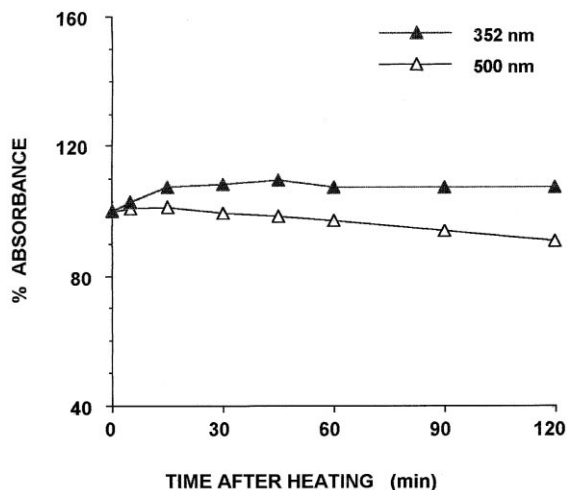


Fig. 3. Stability of the absorbance of the products of reaction between *p*-benzoquinone (PBQ) and cysteine (30  $\mu\text{g/ml}$ ). The samples were heated at 37°C for 5 min in 0.1 M acetate buffer, pH 3.0, with 4.0 mM PBQ and their absorbances at zero time were taken as 100%.

surement of Cys with PBQ at 352 or 500 nm. On the other hand, the product of reaction between PBQ and carboCys was not as stable as the PBQ-Cys product (data not shown), so after heating, the absorbance must be measured promptly.

Table 3 shows the effect of selected potential interfering compounds on Cys determination. For both bands (352 or 500 nm), Cys determination with PBQ was not susceptible to interference by the pool of amino acids (7.5  $\mu\text{g/ml}$ ), salts (30 mM), cystine, dipeptide, glucose and urea (30 mM). Fatty acids, triglycerides, and cholesterol did not react with PBQ but they seriously interfered with Cys assay because they increased the turbidity of the solution, so these substances should be removed before Cys assay is carried out.

The absorbance spectra of 160  $\mu\text{g/ml}$  SDS plus 4.0 mM PBQ and 4.0 mM PBQ, using buffer pH 3.0 as blank, showed a decrease in the absorbance of PBQ with SDS (data not shown). Although PBQ seems to be consumed by SDS, there are not differences between the spectrum of PBQ with or without SDS. This consumption of PBQ by SDS could explain why the Cys recovery shown at Table 3 is low. Thiourea was also studied (Table 3). It was shown to interfere with the Cys assay at concentrations higher than 11.4  $\mu\text{g/ml}$  because the product of reaction between PBQ and thiourea shows two bands, one strong at 275 nm and other at 420 nm.

This method using PBQ was applied to the determination of Cys in pill food, shampoo and a mixture of amino acids resembling blood plasma [10], as well as carboCys in Mucoflux and Mucolitic (Table 4). The results show that determination of Cys can be carried out with the band at 352 nm as well as at 500 nm, because the results shown in Table 4 for both bands are not statistically different. It was necessary to add SDS to the standard curve for determination of Cys in shampoo, because it interferes with the Cys assay. In all samples studied (Table 4), the results showed a good agreement between the nominal and assay value using the proposed method. The recoveries are from 97.0 to 104.4% for all results shown in Table 4.

Table 3  
Effect of selected potential interfering compounds on cysteine determination<sup>a</sup>

Cys (150 µg)+interfering compounds	Addition	Absorbance at 352 nm as percentage of control	Absorbance at 500 nm as percentage of control
Cysteine	Buffer	100.0 ± 3.2	100.0 ± 3.2
KNO <sub>3</sub>	300 mM	124.2 ± 0.4	145.6 ± 0.5
	30 mM	101.7 ± 1.2	103.5 ± 1.6
MgCl <sub>2</sub>	300 mM	130.0 ± 0.2	105.8 ± 4.5
	30 mM	105.4 ± 0.6	111.1 ± 1.5
NaCl	300 mM	126.3 ± 3.1	121.0 ± 2.7
	30 mM	100.0 ± 4.1	103.2 ± 1.6
CaCl <sub>2</sub>	30 mM	101.4 ± 0.3	106.7 ± 0.5
BSA	600 µg/ml	75.1 ± 1.5	76.0 ± 0.9
	60 µg/ml	82.8 ± 1.3	84.4 ± 2.1
Amino acids <sup>b</sup>	75 µg/ml	93.4 ± 1.3	83.0 ± 0.9
	7.5 µg/ml	102.5 ± 1.6	101.7 ± 1.7
Glucose	150 mM	96.0 ± 2.5	101.2 ± 1.8
	15 mM	91.6 ± 4.1	96.8 ± 3.7
Fatty acids <sup>c</sup>	1000 µg/ml	271.8 ± 1.0	542.5 ± 0.9
	100 µg/ml	187.9 ± 0.4	186.5 ± 0.6
Triglycerides	100 µg/ml	142.0 ± 0.2	117.1 ± 1.0
	10 µg/ml	120.5 ± 0.4	98.9 ± 1.9
Cholesterol	200 µg/ml	365.1 ± 0.8	407.2 ± 0.6
	20 µg/ml	205.4 ± 0.8	130.3 ± 1.1
TEA	10 mM	209.8 ± 0.2	24.9 ± 2.1
	1.0 mM	77.5 ± 3.1	66.6 ± 3.1
Ethanol 100%	100 µl/ml	87.6 ± 1.0	90.4 ± 0.6
	10 µl/ml	103.7 ± 1.4	101.7 ± 1.7
Ascorbic acid	1000 µg/ml	–	7.9 ± 3.1
	100 µg/ml	108.0 ± 3.7	94.5 ± 3.2
EDTA	100 µg/ml	95.5 ± 0.3	89.3 ± 0.8
	10 µg/ml	100.9 ± 3.2	98.2 ± 3.8
Sodium tungstate	135 mg/ml	274.6 ± 2.2	65.0 ± 3.8
	13.5 mg/ml	288.7 ± 6.6	86.3 ± 2.9
Glycylglycine	100 µg/ml	103.3 ± 1.0	95.5 ± 0.7
	10 µg/ml	102.5 ± 2.9	101.6 ± 2.9
Cystine	100 µg/ml	99.9 ± 2.6	96.7 ± 3.3
	10 µg/ml	103.9 ± 3.1	101.7 ± 3.4
Urea	300 mM	88.1 ± 2.2	90.7 ± 1.5
	30 mM	95.5 ± 1.7	99.5 ± 2.5
Sodium dodecyl sulfate	160 µg/ml	89.8 ± 5.2	79.2 ± 4.7
Thiourea	11.4 µg/ml	105.3 ± 4.0	78.1 ± 6.6
	114.0 µg/ml	247.4 ± 2.5	87.4 ± 1.1

<sup>a</sup> The results are presented as mean ± S.E.M. of four determinations. Each well contained 150 µg of cysteine and the indicated concentration of the addition in a total volume of 5.0 ml.

<sup>b</sup> The concentration of each of the proteic amino acids.

<sup>c</sup> Pool of oleic and palmitic acids.

#### 4. Conclusion

The results show that the reaction between PBQ and Cys occurs through the sulfhydryl group, the product of reaction PBQ-Cys is stable,

and PBQ is highly selective to Cys in a mixture of amino acids. The proposed method is sensitive for most applications, is not interfered with by many substances, and is not expensive. The proposed method for determination of Cys or carboCys is

Table 4

Determination of cysteine or carbocysteine in pharmaceuticals, shampoo or a mixture of amino acids<sup>a</sup>

Sample	Source	Nominal value (mg)	Found (mg)	
			500 nm	352 nm
Pill food <sup>b</sup>	Calendola Pharmacy	80.0	77.8 ± 2.0 (4)	78.6 ± 3.3 (4)
Shampoo <sup>b</sup>	Calendola Pharmacy	25.0	24.7 ± 0.6 <sup>d</sup> (6)	25.1 ± 0.5 <sup>d</sup> (6)
Mixture of amino acids <sup>b</sup> (10 <sup>-3</sup> ) –		40.0	21.6 ± 0.7 <sup>e</sup> (7)	20.9 ± 0.6 <sup>e</sup> (7)
Mucoflux <sup>c</sup>	Merck S.A.	50.0	39.0 ± 1.4 (6)	38.8 ± 0.8 (7)
Mucolitic <sup>c</sup>	Laboratory Wyeth-Whitehall Ltda.	50.0	51.5 ± 1.4 (5)	–
			52.2 ± 2.0 (6)	–

<sup>a</sup> The samples were heated at 37°C with 4.0 mM of p-benzoquinone. The results are presented as mean ± S.E.M. Number of assays in parentheses. Composition of the samples: Pill food: methionine, 200 mg; cysteine, 80 mg; cystine, 25 mg; collagen, 25 mg; calcium pantothenate, 25 mg; vitamin B-6, 10 mg; vitamin B-2, 1 mg; vitamin E, 3 mg; biotin, 0.2 mg and excipients. Shampoo: cysteine, 25 g; sodium dodecyl sulfate, 200 g and 1 l of water. Mixture of amino acids (Ala, Arg, Asn, Glu, Gln, Gly, Hys, Ile, Lys, Met, Pro, Ser, Tre, Try, Tyr, Val) with composition and concentration similar to blood plasma [10]. Mucoflux: carbocysteine, 250 mg; excipients and water 5 ml. Mucolitic: carbo-cysteine, 250 mg; excipients and water 5 ml.

<sup>b</sup> Acetate buffer 0.1 M, pH 3.0, 5 min of heating.

<sup>c</sup> Phosphate buffer 0.1 M, pH 7.0, 10 min of heating.

<sup>d</sup> Standard curve with 160 µg/ml of sodium dodecyl sulfate.

<sup>e</sup> Standard curve without sodium dodecyl sulfate.

simple to carry out, because it is not necessary to perform any derivatization or extraction as occurs in chromatographic methods [4–8] and good recoveries were obtained in all applications.

### Acknowledgements

This research was supported by CPG/UEL (N° 259.207/92). C.T.B.V. Zaia was recipient of a fellowship from CNPq (N° 524096/96-1). K.C. Ribas was recipient of a fellowship from PIBIC/CNPq/UEL. The authors are grateful to Dr João R.F. Teixeira of Merck S.A. for the gift of carbocysteine and Dr Marta Y.Y. Satake of Zambon Laboratórios Farmacêuticos Ltda, for the gift of *N*-acetyl-cysteine.

### References

- [1] W.F. Ganong, Review of Medical Physiology, Prentice-Hall, Englewood Cliffs, NJ, 1997.
- [2] F. Blasco, M.J. Medina-Hernandez, S. Sagrado, Anal. Chim. Acta 348 (1997) 151–159.
- [3] N. Radic, J. Komljenovic, Lab. Robot. Autom. 10 (1998) 143–149.
- [4] H. Birwé, A. Hesse, Clin. Chim. Acta 199 (1991) 33–42.
- [5] R.A. Sherwood, J. Neurosci. Methods 34 (1990) 17–22.
- [6] D.W. Jacobsen, V.J. Gatautis, R. Green, Clin. Chem. 40 (1994) 873–881.
- [7] H. Kataoka, H. Tanaka, A. Fujimoto, I. Noguchi, M. Makita, Biomed. Chromatogr. 8 (1994) 119–124.
- [8] H. Kataoka, K. Takagi, M. Makita, J. Chromatogr. B 664 (1995) 421–425.
- [9] D.A.M. Zaia, W.J. Barreto, N.J. Santos, A.S. Endo, Anal. Chim. Acta 277 (1993) 89–95.
- [10] R. Montgomery, T.W. Conway, A.A. Spector, Bioquímica: uma abordagem dirigida por casos, Livraria e Editora Artes Médicas, São Paulo, 1994, p. 475.
- [11] J.B. Birks, M.A. Slifkin, Nature 197 (1963) 42–45.
- [12] M.A. Slifkin, in: H. Ratajczak, W.J. Orville-Thomas (Eds.), Molecular Interactions, vol. 2, Wiley, New York, 1980, pp. 271–304.
- [13] M. Morrison, W. Steele, D.J. Danner, Arch. Biochem. Biophys. 134 (1969) 515–523.
- [14] S.S.M. Hassan, M.L. Iskander, N.E. Nashed, Talanta 32 (1985) 301–305.
- [15] L.M. Rzepecki, J.H. Waite, Anal. Biochem. 179 (1989) 375–381.
- [16] M.L. Iskander, H.A.A. Medien, Microchem. J. 41 (1990) 172–182.
- [17] K.T. Finley, in: S. Patai (Ed.), Chemistry of The Quinonoid Compounds, Part 2, Wiley, Chichester, 1974, pp. 889–892.



# Trace analysis of aluminum in natural waters with rubeanic acid by adsorption chronopotentiometry

Shuping Bi <sup>a,\*</sup>, Xianlong Wang <sup>a</sup>, Lei Ye <sup>a</sup>, Ning Gan <sup>a</sup>, Gongwei Zou <sup>a</sup>,  
Hongzhen Liang <sup>b</sup>, Lemei Dai <sup>b</sup>, Mi Cao <sup>b</sup>, Yijun Chen <sup>b</sup>

<sup>a</sup> Department of Chemistry, Nanjing University, Nanjing, 210093, People's Republic of China

<sup>b</sup> Modern Analytical Center, Nanjing University, Nanjing, 210093, People's Republic of China

Received 29 July 1998; received in revised form 19 June 1999; accepted 28 June 1999

## Abstract

The determination of trace levels of aluminum in natural waters with rubeanic acid (RA) by adsorption chronopotentiometry is developed in this paper. Optimum experimental conditions include an accumulation potential of  $-0.40$  V, accumulation time of 60 s, and a RA concentration of  $6 \times 10^{-6}$  M in 0.2 M NaAc–HAc buffer solution (pH 4.6). The response is linear over the  $1 \times 10^{-8} \sim 4 \times 10^{-7}$  M concentration range. The detection limit is  $5.6 \times 10^{-9}$  M and the relative S.D. (at the  $3 \times 10^{-7}$  M level) is 2.6%. Possible interferences are evaluated. The method has been applied to the determination of trace levels of Al in various real samples. Direct determination of toxic forms of Al in surface waters by this technique is also explored. © 1999 Elsevier Science B.V. All rights reserved.

*Keywords:* Aluminium; Rubenic acid; Toxic; Natural water; Adsorption chronopotentiometry

## 1. Introduction

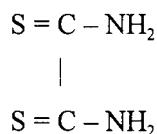
There is considerable concern over the environmental and ecological significance of aluminum. It is reported that elevated Al concentrations associated with the acid deposition in natural waters are toxic to aquatic organisms and plants [1]. Since the concentration of Al is low ( $10^{-7} \sim 10^{-5}$  M) in natural waters and the toxicity depends on its speciation present in solution, research work has been carried out in the last decade in two aspects:

(1) developing ultra-sensitive analytical techniques for determining trace levels of Al and (2) speciating Al in real waters to fraction toxic forms and non-toxic species [2]. Electrochemical method has been recognized as a very useful technique to determine Al in aquatic environment in recent years, in which the adsorption stripping voltammetry seems to be most attractive [3]. It is based on the adsorption of complex of organic dyes with Al on the electrode surface yielding the sensitive polarographic peak. The usually used organic dyes are: (a) anthraquinone dye (DASA); (b) di-o-hydroxyazo dye (SVRS) and (c) triphenylmethane dye (PCV) [4–6]. In this paper,

\* Corresponding author. Fax: +852-23649932.

E-mail address: bisp@nju.edu.cn (S. Bi)

we will report the use of another dye, rubeanic acid (RA), in the adsorption chronopotentiometric determination of trace levels of Al in natural waters. RA (or thiamide of oxalic) is identified with dithio-oxamide as it results from the sulphhydrolysis of cyanogena [7]. Its structure can be represented as:



It has been used in the spectrophotometric determination of various metal ions. In 1974, Fukushi studied the linear-sweep oscillographic polarographic behavior of Al with RA, but the analytical sensitivity is not high (only determined  $10^{-4} \sim 10^{-3}$  M Al) [8]. The aim of this paper is to set up a novel and sensitive electroanalytical approach for the analysis of Al by RA. Adsorption chronopotentiometry is utilized as the electrochemical scan mode. Accumulation is achieved by controlled adsorption of the Al–RA complex on the static mercury drop electrode. Constant reduction current stripping gives two peaks at  $-0.64$  and  $-1.00$  V, corresponding to the redox reactions of Al–RA complex and RA, respectively. The peaks were well resolved. The peak height of the Al–RA complex increased with increasing Al concentration in solution. The linear working range is  $1 \times 10^{-8} \sim 4 \times 10^{-7}$  M. The detection limit is  $5.6 \times 10^{-9}$  M and the relative S.D. (at the  $3 \times 10^{-7}$  M level) is 2.6%. The proposed method has been applied to the practical analysis of Al in natural waters and the results were compared with ICP-AES method. In addition, direct determination of the toxic forms of Al (labile Al, mainly in inorganic Al forms) in surface waters by this method was also investigated. The accuracy has been verified by the classic ion exchange technique.

## 2. Experimental

### 2.1. Reagents

Aluminum standard stock solution  $1 \times 10^{-2}$  M, prepared by dissolving 0.0675 g of high-purity Al

metal powder in 20 ml of 1:4 HCl solution and then diluting it with water to 250 ml. Standard Al solutions were prepared by dilution of stock solution with water.

RA stock solution  $1 \times 10^{-2}$  M, prepared by dissolving the necessary amount of the dye in alcohol and then diluting it with alcohol to 100 ml. RA solution ( $1 \times 10^{-3}$  M) was prepared by diluting the above solution in 100 ml flask with water, and was used throughout the experimental.

The aqueous stock pH buffer solution prepared was a 2 M NaAc-HAc (pH 4.6). Addition of this buffer to give a concentration of 0.2 M in test solution produced a pH of 4.6.

All reagents were of analytical-reagent grade and the water was doubly distilled from quartz. All laboratory glassware and plasticware were acid washed and rinsed with water before each experiment.

### 2.2. Apparatus

The apparatus used for adsorption chronopotentiometry were the same as used previously [9]. A 180-80 atomic absorption spectrometer (Hitachi Company, Japan) and a 1100 ICP-AES spectrometer (Jarrell-Ash Company, USA) were used to determine total Al. The experiment was carried out at 25°C.

### 2.3. Procedures

Solutions for analysis were prepared by successive addition of 3 ml 2 M NaAc-HAc (pH 4.6), 180  $\mu\text{l}$   $1 \times 10^{-3}$  M RA and adequate amounts of standard Al solution into the cell, and then filled up to total volume of 30 ml with water. The solution was deaerated for 15 min with pure  $\text{N}_2$ . The measurements were performed after an accumulation step in which the solution was stirred for 60 s at an accumulation potential  $E_a$  of  $-0.40$  V. Following a 30 s rest time period, the potentiostatic circuitry was disconnected, a constant reduction current  $i_0$  (20  $\mu\text{A}$ ) was passed through the cell, and the  $dt/dE$  vs.  $E$  curve was recorded.

### 3. Results and discussion

#### 3.1. Adsorption chronopotentiogram of rubeanic acid and Al–RA complex

Fig. 1 shows the adsorption chronopotentiogram of RA and Al–RA complex. In the absence of Al, there is a large and broad peak  $P_1$  occurred at the potential of  $-1.00$  V. It reflects the adsorption reaction of RA on the surface of HMDE. After adding trace amount of Al, a new peak  $P_2$  appears at  $-0.64$  V which is corresponding to the redox reaction of the Al–RA complex. This  $P_2$  peak is linear to the Al concentration and can be quantitatively used in Al analysis.

#### 3.2. Optimization of variables

Experimental parameters were optimized. It was established experimentally that the best electrolyte was  $0.2$  M NaAc-HAc buffer, pH 4.6, at which the peak height was maximum. The other optimization variables are: accumulation potential  $E_a = -0.40$  V, accumulation time  $t_a = 60$  s and  $6 \times 10^{-6}$  M of RA. See Fig. 2.

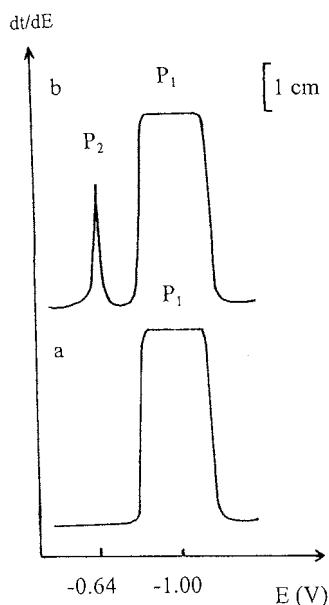


Fig. 1. Adsorption chronopotentiogram of RA (a) and Al–RA complex (b)  $a$ –RA =  $6 \times 10^{-6}$  M,  $E_a = -0.40$  V,  $t_a = 60$  s, pH = 4.6  $b$ – $a$  +  $3 \times 10^{-7}$  M Al.

#### 3.3. Linear range, detection limit and relative standard deviation

Under the optimum conditions, the linear working range is  $1 \times 10^{-8} \sim 4 \times 10^{-7}$  M (see Fig. 3). The detection limit is  $5.6 \times 10^{-9}$  M (estimated for the signal-to-noise characteristics of the response for  $3 \times 10^{-8}$  M Al) and the relative S.D. (at the  $3 \times 10^{-7}$  M level) is 2.6% ( $n = 10$ ).

#### 3.4. Interference of foreign ions

The interference of foreign ions on the determination of Al in waters was investigated experimentally. The results showed that in the presence of  $3 \times 10^{-7}$  M aluminum, large amounts of Co(II), Mn(II), Ce(IV),  $\text{Cl}^-$ ,  $\text{PO}_4^{3-}$ ,  $\text{NO}_3^-$ ,  $\text{NO}_2^-$ , Si(IV) and Sr(II), 1000-fold excess of Ni(II), Zn(II), Ca(II), Tl(I), Mg(II), Sn(II),  $\text{F}^-$ , citrate and  $\text{NH}_4^+$ , 500-fold excess of Cd(II) or Ge(IV), 250-fold excess of Pb(II), Ba(II), In(III), Ga(III) and  $\text{SO}_3^{2-}$ , 100-fold of Bi(III), Fe(II), Zr(IV) and tartrate, 50-fold of Fe(III) and oxalate did not interfere in the determination of aluminum. A 10-fold of Mo(VI) or  $\text{Br}^-$ , 5-fold of EDTA and 1-fold of Cu(II) or  $\text{I}^-$  did interfere. Possible interference by surface active materials has also been tested. It was indicated that 2 mg/l of polyethylene glycol, 1 mg/l of ( $n\text{-C}_{16}\text{H}_{33}$ )- $\text{N}(\text{CH}_3)_3\text{Br}$ , 0.3 mg/l Triton X-100 or  $(\text{C}_2\text{H}_5)_4\text{NBr}$ , 0.2 mg/l of  $(n\text{-C}_3\text{H}_7)_4\text{NBr}$  and 0.1 mg/l of  $(\text{CH}_3)_4\text{NBr}$  did not interfere. A linear calibration can still be obtained for Al in the presence of surface active materials, but the sensitivity is reduced. Analysis by standard addition calibration would be valid in the presence of surface active agents. Too large an amount of surface active materials may distort the chronopotentiogram greatly and completely masked the peak  $P_2$ .

#### 3.5. Practical analysis of trace levels of Al in natural waters

The proposed method has been applied to the practical analysis of Al concentrations in natural waters. No. 1–6 are the market-sold drinking

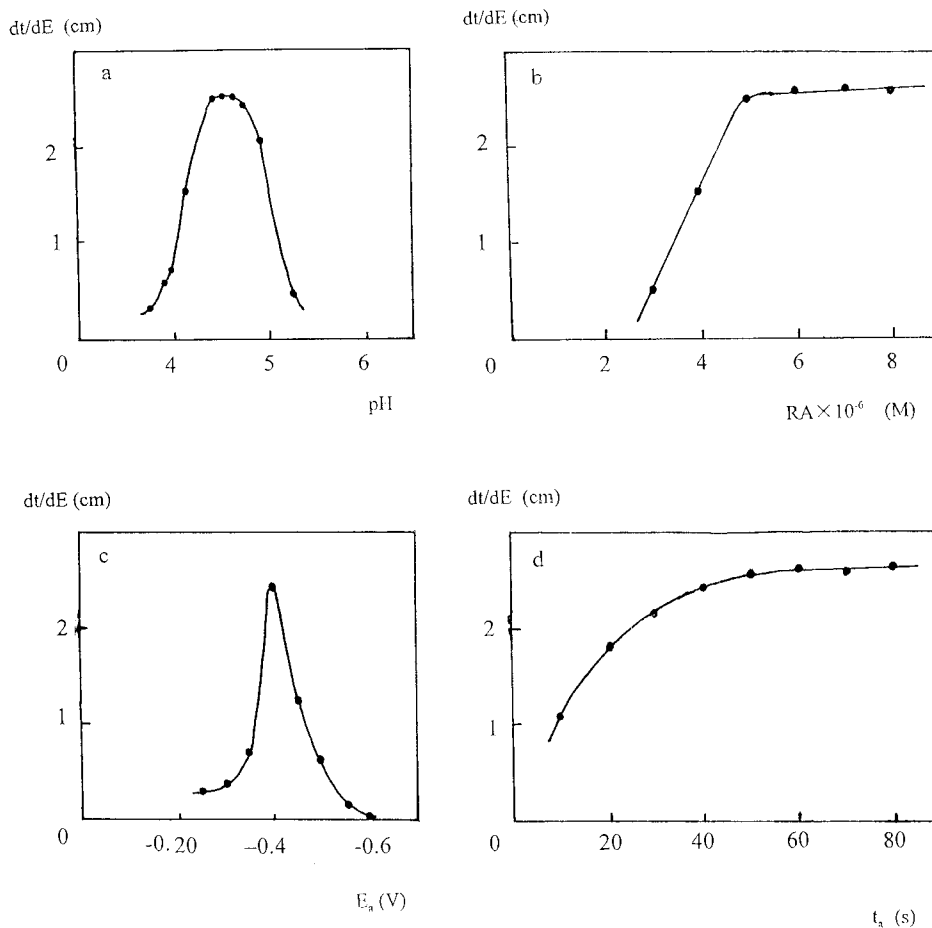


Fig. 2. Optimization of the variables ( $3 \times 10^{-7}$  M Al) (a) dependence of peak height  $P_2$  on pH ( $RA = 6 \times 10^{-6}$  M,  $E_a = -0.40$  V,  $t_a = 60$  s) (b) dependence of peak height  $P_2$  on RA concentration ( $E_a = -0.40$  V,  $t_a = 60$  s, pH = 4.6) (c) dependence of peak height  $P_2$  on the accumulation potential  $E_a$  ( $RA = 6 \times 10^{-6}$  M, pH = 4.6,  $t_a = 60$  s) (d) dependence of peak height  $P_2$  on the accumulation time  $t_a$  ( $RA = 6 \times 10^{-6}$  M,  $E_a = -0.40$  V, pH = 4.6).

mineral waters. No. 7–12 are the surface water samples collected from the lake and rivers in the vicinity of Nanjing. The surface waters were passed through a glass-core filter to remove the impurities. Ultraviolet irradiation of some surface samples containing high levels of organic was performed as suggested by Van Den Berg et al. [4] for determining total Al. The general procedure for determining Al in real waters is: an adequate volume of water sample solution is pipetted into the 50-ml flask, then 300  $\mu$ l of  $1 \times 10^{-3}$  M RA is added, followed by 5 ml 2 M NaAc-HAc buffer solution (giving pH 4.6), and diluted to volume

with water to bring them within the recommended concentration range for Al analysis ( $1 \times 10^{-8} \sim 4 \times 10^{-7}$  M). Then it is transferred to the cell and degassed with nitrogen for 15 min, and the chronopotentiogram of Al-RA is recorded. The standard addition method is used in all instances. The results were compared with those obtained by ICP-AES. Table 1 shows that both results were in good agreement. This indicates this method is accuracy and acceptable. Table 2 lists the water quality data, it indicates that the amount of the interference ions present in samples [such as Cu(II) and Fe(III)] are so low compared with Al

that in practice they do not interfere with the determination.

### 3.6. Direct determination of toxic forms of Al in surface waters

It was reported that inorganic monomeric Al is the toxic form in natural water, including free  $\text{Al}^{3+}$  plus Al hydroxide, Al-fluoride and Al-sulfate complexes [10]. Any study of the aluminum toxicity of water would be helpful if one could detect the inorganic forms of Al directly rather than just the total aluminum. We explore the direct electrochemical measurement of toxic forms of Al in surface waters. Under the acidic condition (pH 4.6), the bound organic Al complexes may not be measured by this method. The Al-RA electrochemical signal only responds to inorganic Al forms [11,12]. Thus, the proposed method can be employed to determine inorganic forms of Al concentrations in surface waters polluted by organic substances. The experimental results demonstrate that this assumption is correct and reasonable. Table 3 indicates that results obtained by the proposed method are in agreement with the results by the 8-hydroxyquinoline

Table 1

Determination of total Al concentrations in natural waters ( $\mu\text{M}$ ) ( $n = 4$ )

No.	Samples	This method	ICP-AES
1	Kang-Shi-Fu mineral water	0.35	<0.37
2	Tian-Yu-Di mineral water	5.94	5.92
3	Jiu-Zai-Gou mineral water	5.48	5.48
4	Xia-Lu mineral water	3.45	3.41
5	Cheng-De mineral water 2	4.37	4.44
6	Cheng-De mineral water 3	6.59	6.67
7	Xuan-Wu lake	5.89	5.93
8	Nan-Hang river	11.5	11.9
9	Dan-Yang river	5.48	5.50
10	Zhen-Zhu river	4.52	4.56
11	Qing-Huai river 1	4.79	4.81
12	Qing-Huai river 2	5.44	5.56

$dt/dE$  (cm)

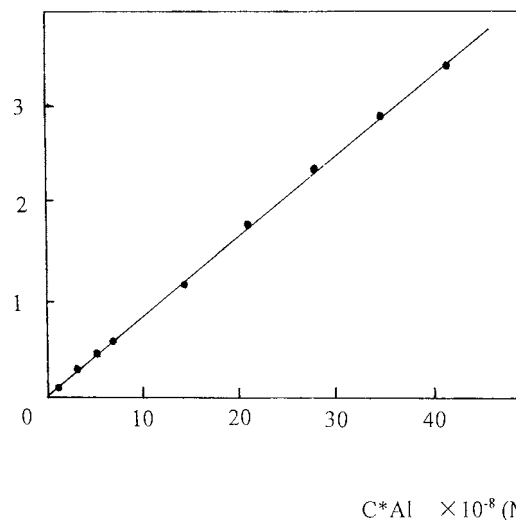


Fig. 3. Calibration curve. Other conditions are the same as Fig. 1.

extraction/ion exchange method [13,14]. (In our experiment, a 732 cation-exchange resin was used. The cation exchange column was 1 cm in diameter and contained 10 ml of prepared resin).

## 4. Conclusions

We conclude that adsorption chronopotentiometric determination of aluminum using RA is promising provided the copper and iron levels are low. Besides the merits described before (high sensitivity, inexpensive instrumentation and simple manipulations) [15], the proposed technique still possesses some distinct advantages: (1) unique electrochemical characteristics. The Al-RA peak occurs at the potential more positive than that of RA, yielding the better resolution over 360 mV. It is completely different from that observed in using other dyes. Due to the complicated complex reaction between Al and RA [16], we do not attempt to elucidate its electrochemical redox mechanism in this paper. (2) Direct determination of toxic forms of Al in natural waters. Although this method is somewhat rough, it still can be easily employed in field to evaluate the inorganic Al

Table 2  
The water quality data (mg/l)

	1	2	3	4	5	6	8	9	10	12
Ca	<10	19 800	69 700	40 300	71 500	12 3000	41 300	60 200	52 000	50 700
Mg	<10	4300	13 100	9740	6400	15 100	7900	11 700	10 500	80 500
Ba	<1	4	13	66	20	70	10	28	38	33
Sr	<1	20	538	215	190	480	150	200	215	230
Si	<10	4040	2280	1850	8400	12 400	4900	11 300	50 600	6790
Na	180	29 300	1900	33 500	10 100	18 400	24 500	42 600	29 200	49 100
K	800	5200	<300	3700	<300	<300	4800	20 300	69 400	8700
Cu	<2	<2	<2	<2	<2	<2	<2	<2	<2	<2
Zn	<4	<4	6	<4	150	40	<4	<121	<1	
Pb	<25	–	<25	<25	<25	<25	–	<25	<25	<25
Cd	<2	–	<2	<2	<2	<2	–	<2	<2	<2
Fe	<15	<15	<15	<15	<15	<15	20	40	<15	30
Mn	<1	<1	<1	<1	3	4	60	70	2	110
Co	<3	<3	<3	<3	<3	<3	<3	<3	<3	<3
Ni	<10	<10	<10	<10	<10	<10	<10	<10	<10	<10
Cr	<5	<5	<5	<5	<5	<5	<5	<5	<5	<5
Mo	<5	–	<5	<5	<5	<5	–	–	–	–
F <sup>-</sup>	–	300	600	200	–	–	2600	100	200	300
Cl <sup>-</sup>	600	19 900	1800	20 600	5700	52 300	15 000	31 000	28 700	38 200
NO <sub>3</sub> <sup>-</sup>	–	3200	2200	4400	22 200	96200	700	900	58 500	2200
SO <sub>4</sub> <sup>2-</sup>	–	30 600	47 800	57 200	4100	14600	1100	38 900	37 200	6400
PO <sub>4</sub> <sup>3-</sup>	–	24 300	900	1400	–	–	8700	7000	5200	4300

Table 3  
Comparison of the proposed method with the 8-HQ extraction/ion exchange for determining inorganic forms of Al concentrations in surface waters ( $\mu\text{M}$ ) ( $n = 4$ )<sup>a</sup>

No.	This method	8-HQ extraction/ion exchange
7	2.40 (40.5%)	2.85 (48.1%)
8	8.13 (68.3%)	7.70 (66.0%)
9	4.41 (80.2%)	4.30 (74.5%)
10	3.45 (75.7%)	3.50 (76.8%)
11	3.45 (71.7%)	3.10 (64.4%)
12	1.34 (24.1%)	1.30 (23.4%)

<sup>a</sup> Numerical values in brackets are the percentages of the inorganic Al in the total Al concentration.

speciation in natural waters, as an effective alternative to the ion exchange method.

### Acknowledgements

This project is supported by the research funding of the Electrochemistry Open Laboratory of

Changchun Applied Chemistry Institute, Chinese Academy of Sciences, National Natural Science Foundations of China (key project of Nos. 49831005 and 29777013) and research funding of the Modern Analytical Center of Nanjing University. The authors would like to express their best thanks to Professors Guoliang Gi, Tianren Yu and Hongyuan Chen for their support and help during this work.

### References

- [1] T.E. Lewis, *Chemistry and Toxicity of Aluminum*, Lewis Publishers, Chelsea, 1989.
- [2] G. Sposito, *The Environmental Chemistry of Aluminum*, second ed., CRC Press, Boca Raton, FL, 1995.
- [3] J. Wang, J.M. Liu, R. Setiadji, *Talanta* 40 (1993) 351.
- [4] C.M.G. Van Den Berg, K. Murphy, J.P. Riley, *Anal. Chim. Acta* 188 (1986) 177.
- [5] J. Wang, P.A.M. Farias, J.S. Mahmoud, *Anal. Chim. Acta* 172 (1985) 57.
- [6] Q.L. Li, J.L. Xing, *Chem. J. Chin. Univ.* 7 (1986) 15.
- [7] P. Ray, J. Xavier, *J. Ind. Chem. Soc.* 38 (1961) 15.

- [8] N. Fukushi, *Jpn. J. Anal. Chem.* 24 (1975) 471.
- [9] S.P. Bi, J. Yu, *Electroanalysis* 9 (1997) 1369.
- [10] S.P. Bi, *Analyst* 120 (1995) 2033.
- [11] D.V. Vukomanovic, J.A. Page, G.W. Vanloon, *Can. J. Chem.* 69 (1991) 1418.
- [12] K.E. Johnson, A.K. Brichta, K.L. Holter, *Can. J. Chem.* 66 (1988) 139.
- [13] C.T. Driscoll, *Int. J. Environ. Anal Chem.* 16 (1984) 267.
- [14] R.B. Barnes, *Chem. Geol.* 15 (1976) 177.
- [15] S.P. Bi, M.J. Song, D. Xu, *Anal. Lett.* 31 (1998) 1937.
- [16] T. Halder, W. Schwarz, J. Weilein, P. Fischer, *J. Organometal. Chem.* 246 (1983) 29.

# Monitoring fermentation media by ion-chromatography with a double chamber bulk acoustic wave detector

You-tao Xie, Hong-shan Zeng, Shou-zhuo Yao, Wan-zhi Wei \*

*Chemistry and Chemical Engineering College, Hunan University, Hunan, Changsha 410082, People's Republic of China*

Received 24 March 1999; accepted 28 June 1999

## Abstract

A reliable ion-chromatographic (IC) method with a novel double chamber bulk acoustic wave (DCBAW) detector was developed for monitoring five important inorganic cations ( $\text{Na}^+$ ,  $\text{K}^+$ ,  $\text{NH}_4^+$ ,  $\text{Ca}^{2+}$ ,  $\text{Mg}^{2+}$ ) in biological culture media. A Shimpack IC-C1 analytical column with 5 mM hydrochloric acid and 2 mM acetonitrile as mobile phase was used. All investigated inorganic cations could be detected and qualified in the range of 0.1–100 mg/l. Results showed that the consumption velocities of  $\text{Mg}^{2+}$  and  $\text{K}^+$  are related to the growth of the cells and decrease fastest during the first 2–5 h. Mg became a growth limiting factor at concentration below 0.1 mg/l. The concentrations of the other cations stayed nearly constant during the whole fermentation process. The simple sample preparation, short analytical time and accurate results made it a useful tool for the on-line monitoring, controlling and optimization of the fermentation process. © 1999 Elsevier Science B.V. All rights reserved.

*Keywords:* Ion-chromatography; Double chamber bulk acoustic wave detector; Monitor; Fermentation

## 1. Introduction

Inorganic cations are essential for the cellular growth and fulfill specific metabolic and structural roles. Therefore, improvements may be achieved by a supply of the culturae media with inorganic nutrients. The concentration of some cations must be very low to satisfy cellular growth needs [1], although these levels are rarely manifest. The optimal concentrations vary depending upon species and cellular density.

In industrial fermentation, a high cellular den-

sity fermentation is often required, and so the media composition becomes a critical factor in achieving a successful high cellular density process. A rapid and conventional analytical tool for the determination and monitoring concentrations of inorganic species in fermentation media during the whole cultural process is essential for the development of suitable industrial culture media. Atomic absorption [2] and colorimetric [3] assays, flow injection chemiluminescence and HPLC [4,5] were used for the analysis of inorganic cations and metals in biological samples. Moreover, HPLC analysis was applied to monitor cations and trace elements of fermentation broths. Bell [6] used HPLC to analyze ashed fermentation sam-

\* Corresponding author.



ples for ten cations highlighting the importance of micronutrient cations in industrial antibiotic fermentation. Ion-chromatography (IC) is a widely used versatile separation technique. Joerqensen [7] reported an IC method to quantitate anions, cations and transition metals present in a methanotropic bacterial fermentation, and used IC as a tool for optimization and control of fermentation process. R.S. Robin Robinett [8] described an IC method with conductivity detection for the analysis of some inorganic cations in fermentation broth.

Due to the high sensitivity, low cost, and conceptual simplicity, piezoelectric quartz crystals (PQC) were used widely as detectors in a variety of commercial and research analysis. After T. Nomura [9] first used PQC in HPLC, the use of series piezoelectric quartz crystal (SPQC) as an alternative detector in IC was reported by Chen Po [10]. In our laboratory, a novel double chamber bulk acoustic wave (DCBAW) sensor was developed [11] and used in single column ion-chromatography. One chamber of the DCBAW detector is used to adjust the frequency responses of the crystal to the other. In this paper, an IC separation technique with a DCBAW detector was used to monitor the five common inorganic cations in the fermentation media for *Escherichia coli* (*E. coli*).

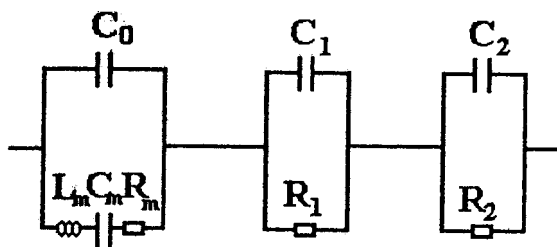


Fig. 1. A electric equivalent circuit model of a DCBAW detector ( $C_m$  is the capacitance of the crystal,  $C_1$ ,  $C_2$  are the solution capacitance in the adjusting and detection chamber,  $C_0$  is the static capacitance of the structure,  $R_m$  is the resistance of the crystal,  $R_1$ ,  $R_2$  are the solution resistance in the adjusting and detection chamber.  $L_m$  is the motional inductance of the crystal.)

## 2. Theory bases of the detector

Fig. 1 shows the equivalent circuit of the DCBAW detector. The impedance of a DCBAW can be expressed as the following equation:

$$Z = R + jX \quad (1)$$

where  $R$  is the real part of  $Z$ , the resistive part,  $X$  is the imaginary part of  $Z$ , the reactance and  $j = \sqrt{-1}$ . For the circuit shown in Fig. 1, the motional resistance  $R_m$  can be ignored for simplification as its value is very small compared with the reactance part of the crystal, then the real part and the imaginary part of the total impedance of the DCBAW can be expressed as follows:

$$R = \frac{G_1}{G_1^2 + 4\pi^2 F^2 C_1} + \frac{G_2}{G_2^2 + 4\pi^2 F^2 C_2} \quad (2)$$

$$X = \frac{2\pi F L_m - 1/(2\pi F C_m)}{1 + C_0/C_m - 4\pi^2 F^2 L_m C_0} - \frac{2\pi F C_1}{G_1^2 + 4\pi^2 F^2 C_1} - \frac{2\pi F C_2}{G_2^2 + 4\pi^2 F^2 C_2} \quad (3)$$

where  $F$  is the oscillating frequency,  $C_0$  is the static capacitance of the structure,  $C_m$ ,  $L_m$  are the motional capacitance and motional inductance of the quartz crystal,  $C_1$ ,  $C_2$  are the capacitance of the adjusting chamber and detection chamber,  $G_1$ ,  $G_2$  are the solution conductivity in the adjusting and detection chambers.

Because the DCBAW is the feedback network of an integrated circuit (IC)-TTL oscillator, two conditions must be satisfied for the DCBAW to maintain a stable oscillation in a aqueous media, the phase shift around the loop should be zero and the loop gain should be unity. The oscillation equation can be simplified as Eq. (4):

$$\frac{\omega L_m - 1/(\omega C_m)}{1 + C_0/C_m - \omega^2 L_m C_0} - \frac{G_1 \tan \theta + \omega C_1}{G_1^2 + \omega^2 C_1^2} - \frac{G_2 \tan \theta + \omega C_2}{G_2^2 + \omega^2 C_2^2} = 0 \quad (4)$$

where  $\theta$  is the oscillator's coherent shift and  $\omega = 2\pi F$ . The above equation is a quadratic function of frequency. It yields the necessary frequency of the quartz crystal to satisfy the phase shift need of the detector. This is the theoretical basis of the DCBAW detector. Solving Eq. (4) with the numerical solution method, we know that the fre-

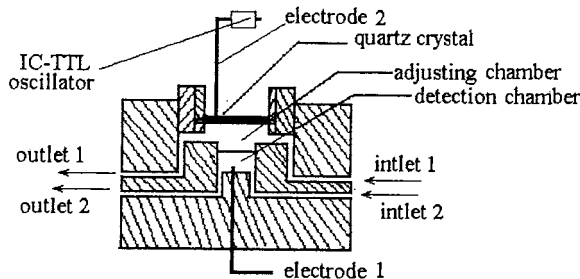


Fig. 2. Schematic diagram of a DCBAW detector.

quency shift of the quartz crystal is only related to the change of the solution conductivity and permittivity in the detection chamber when the background conductivity and background capacitance are constant. In this work, only aqueous dilute solution was used and the permittivity variation can be negligible.

### 3. Experimental

#### 3.1. Preparation of inorganic cation standard solution

All inorganic cation standards were prepared from chloride (analytical-reagent grade) at a concentration of 1 mg/ml for NaCl, KCl, MgCl<sub>2</sub>, NH<sub>4</sub>Cl, CaCl<sub>2</sub>. All solutions were prepared with doubly distilled, chemically purified water and filtered through a 0.45 μm filter membrane (Milipore, USA)

#### 3.2. Preparation of fermentation media

The fermentation media used for this study had following composition: 20 g/l glucose, 20 g/l glutamic acid, 1.1 g/l MgSO<sub>4</sub> · 7H<sub>2</sub>O, 1.35 g/l CaCl<sub>2</sub>, and 0.05 g/l FeCl<sub>3</sub> · 6H<sub>2</sub>O, 0.5 g/l K<sub>2</sub>HPO<sub>4</sub>, 1.28 g/l KH<sub>2</sub>PO<sub>4</sub>, 1.65 g/l Na<sub>2</sub>HPO<sub>4</sub> · 7H<sub>2</sub>O, 0.17 g/l NH<sub>4</sub>Cl.

#### 3.3. Incubation of *E. coli*

A 100 ml volume of the fermentation media was placed in a 150 ml sterilized fermentor and four loops of *E. coli*. on slant agar were inocu-

lated with an inoculating loop. The optimum grown temperature is 37°C or parasitic in human and warm-blooded animals, therefore the inoculated media was incubated at 37°C. Five milliliters of fermentation media was obtained from the fermentor regularly and centrifuged at 4000 × g for 15 min to remove bacterial cells (biomass). The supernatant (dilution of 1:10) was filtered through a 0.45 μm filter membrane and 20 μl filtrate was injected into the IC system for analysis.

#### 3.4. DCBAW detector

The schematic diagram of a DCBAW detector is illustrated in Fig. 2. The quartz crystal was mounted on the top of a Teflon column with one side facing liquid. The two opposite electrodes inducing an alternating electrical field across the crystal were separated by two flow-through conductivity chambers, chamber 1 and 2. Chamber 2 was connected to the IC system with a 0.5 mm diameter inlet and outlet and the platinum electrodes in chamber 2 were retreated with 6 mM HNO<sub>3</sub> first, then by water and acetone. The constant of chamber 1 can be adjusted by changing the position of the PTEF column with the crystal device. However, during one experiment the chamber constant of chamber 1 and 2 were kept unchanged to provide stable experimental conditions. The DCBAW detector was connected to a laboratory-made integrated circuit (IC)-TTL oscillating circuit, and the frequency signals were transferred to a C-R4A chromatographic workstation (Shimadzu, Japan) by a frequency to voltage converter (made in this laboratory) [10], where the data were processed.

#### 3.5. Chromatographic system

Chromatographic separations were carried out on a Shimadzu IC-6A IC system (Shimadzu corporation, Japan) with a LP-6A liquid delivery pump, a SLC-6B system controller, a SIL-6B autoinjector and a CTO-6AS column oven, and a Shim-pack IC-C1 (5 mm i.d. × 15 cm) stainless cation-exchange column and a Shim-pack IC-GC1 guard column.

Table 1  
Effect of temperature on noise and response drift

$t$ (°C)		20	25	30	35	40	45	50	55
DCBAW	Noise (Hz)	8	5	2	1	1	4	6	9
	Drift(Hz/h)	9	6	3	3	4	5	7	10
ESPC	Noise (Hz)	12	9	6	5	6	8	10	14
	Drift (Hz/h)	15	13	10	7	6	11	13	16

## 4. Results and discussion

### 4.1. Optimization of the DCBAW

The phase angle of the crystal can be shifted by a change in conductance,  $G_1$ , in chamber 1. The sensitivity of the DCBAW was studied at different background conductances,  $G_1$  and  $G_2$ . It shows that the proportion conductance/sensitivity of the DCBAW detector is independent of background  $G_2$  in the range of 7.2–2500  $\mu\text{S}$  at  $G_1$  about 600  $\mu\text{S}$ .

As conductance and capacitance of the solution are dependent on the chamber constant, these both important parameters affect the sensitivity of the detector. Optimum chamber constants  $K_1$  and  $K_2$  were found as the best compromise between the sensitivity and the work region. In this experiment,  $K_1 = 1.0$  cm,  $K_2 = 0.85$  cm were selected.

### 4.2. Dependence of the DCBAW on the temperature

Detector temperature greatly influences the baseline, noise, and hence limit of the conventional conductivity method. The behavior of the DCBAW detector as a function of the temperature is shown in Table 1. It can be seen that the DCBAW detector, however, depends slightly on the temperature in the range of 30–45°C. Results show that noise level and baseline drift of the DCBAW detector are very small in comparison to the ESPC detector and are independent of the change in viscosity and density of the chromatographic flow because the crystal is not in direct contact with the mobile phase in chamber 2. In our work, the detector temperature as well as the column were maintained at 35°C.

### 4.3. Detection limit, regression equation

A typical chromatogram of a mixture of inorganic cation standards is shown in Fig. 3, using 5 mM hydrochloric acid and 2 mM acetonitrile at 1.2 ml/min as mobile phase and other condition as mentioned. In this experiment, protein bound on the column material irreversibly reduced the retention time of the inorganic ions and hindered the separation of their peaks. Protein adsorption did increase the pressure drop across the column as well. It was not possible to regenerate these column materials. So, how to remove the protein was a problem. B. Green et al. [13] used a automatic membrane dialysis instrument to minimize

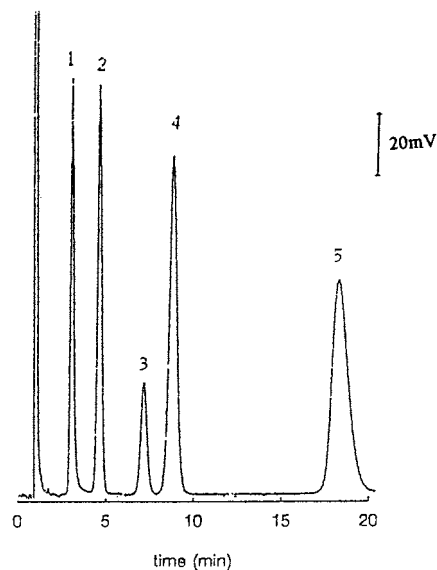


Fig. 3. A typical chromatogram of a mixture of inorganic cation standards (peaks: 1,  $\text{Na}^+$  10 mg/l; 2,  $\text{NH}_4^+$  10 mg/l; 3,  $\text{K}^+$  5 mg/l; 4,  $\text{Mg}^{2+}$  5 mg/l; 5,  $\text{Ca}^{2+}$  5 mg/l).

Table 2

Detection limits, regression equation and linear range of the five cations (mg/l)

Species	Limits <sup>a</sup>	Regression equation <sup>b</sup>	Range	Corr.
Na <sup>+</sup>	0.05	$y = 7.437 + 11.256C$ <sup>d</sup>	0.1–25	0.989
K <sup>+</sup>	0.1	$y = 5.687 + 6.263C$	0.5–50	0.991
NH <sub>4</sub> <sup>+</sup>	0.05	$y = 7.447 + 11.055C$	0.1–25	0.995
Ca <sup>2+</sup>	0.05	$y = 6.444 + 11.111C$	0.1–50	0.992
Mg <sup>2+</sup>	0.05	$y = 8.081 + 18.384C$	0.1–50	0.995

<sup>a</sup> Limits were calculated by signal-to-noise = 3.

<sup>b</sup> Regression equations were obtained by nine injections results ( $n = 9$ ).

<sup>c</sup> 'y' highness of the peak.

<sup>d</sup> 'C' concentration of the sample.

the influence of the protein. A large factor dilution was necessary for dialysis and this decreased the sensitivity and accuracy of the assays. In order to develop the accuracy of the analysis, minimizing sample dilution was a good idea. In this experiment, a minor range setting (1:10) was used for the DCBAW detector. Centrifugation at  $4000 \times g$  for 15 min to remove bacterial cells followed by a filtration through a  $0.45 \mu\text{m}$  membrane were sufficient for the analysis.

Precision measurements were established using 5 mg/l standard aqueous solution species detected parallel ten times, coefficients of variation were all less than 8%. Detection limits, linear range, calibration lines were also obtained using inorganic ions in water. The results were illustrated in Table 2.

#### 4.4. Monitoring inorganic cations in the fermentation process

Changes in the concentration of the five inorganic cations were monitored during the whole fermentation process. Fig. 4a shows the consumption of Mg during the whole fermentation. Magnesium in a microorganism can stabilize plasmalemma and nucleic acid, is also an activator of some important enzymes. It is especially necessary for the activation of the transphosphate enzyme. Some researchers tried to use EDTA for removing Mg and found that the plasmalemma was first destructed and the growth stopped at the

end. D.W. Tempezt [12] tried Mg as a control factor in the cells culture and found that the concentration of Mg in the culture media is linear with the gross biomass. This experiment showed that the concentration of Mg decreased with the cultural time and fastest during the first 2–5 h, during which the cells are in an exponential growth state. The experiments also proved that the concentration of Mg in fermentation media has to be above 0.1 mg/l to maintain optimum growth conditions. The growth of the bacteria will cease if the Mg concentration is lower than 0.1 mg/l.

Fig. 4b showed the change in concentration of potassium (K). The biological roles of K is that it activates respiration and erythrocyte, protein synthesis, acetylcholine synthesis and controls the osmotic pressure of cells and Na is reversed. It inhibits these metabolic processes. Potassium is present in a much higher concentration than Na inside a cell and that the relative concentration is reversed outside the cell and so the consumption of K in the media is large and the concentration of Na kept nearly constant. At the end of the fermentation, the concentration of K showed a little increase. This may due to the disappearance of the concentration gradient between inside and outside of the cells when the cells died. Fig. 4c shows that the concentrations of Na<sup>+</sup>, NH<sub>4</sub><sup>+</sup>, Ca<sup>2+</sup> were nearly constant during the whole process, although a wider variety of biological functions they perform. It is perhaps the requests of the cell growth are very low for Na and Ca. For NH<sub>4</sub><sup>+</sup>, on one hand, the cell growth consumed some NH<sub>4</sub><sup>+</sup>, on the other hand, the decomposition of glutamic acid produced some. In this experiment, the concentration of NH<sub>4</sub><sup>+</sup> kept constant during the whole fermentation process. It might due to the similar velocities of the consumption and production that the concentration of NH<sub>4</sub><sup>+</sup> remains constant during the whole fermentation.

#### 4.5. Advantages of the DCBAW detector

DCBAW can adjust the quartz crystal's frequency response on the detection chamber conductivity by changing the resistance of the adjusting chamber. When  $G_1 = 600 \mu\text{S}$ , DCBAW

is nearly independent with the background conductivity. Experiments show that it has a satisfactory frequency response to conductance change at backgrounds from 10 to 2700  $\mu\text{S}$ , which covers the normal eluant conductance region of single-column IC. Moreover, the frequency stability and frequency-temperature coefficient of a DCBAW detector are improved greatly. The DCBAW detector also has several advantages compared to conventional conductivity

detectors. In conventional conductivity detectors, electric double layer capacitance and Faraday impedance are problematic. These phenomena change the effective potential applied to the detector chamber, and hence hamper precise measurement. This limitation can be overcome by a multi-electrode technique or by applying electrodes with alternating potential, but the apparatus becomes more complex. With the DCBAW detector, a high frequency (9 MHz)

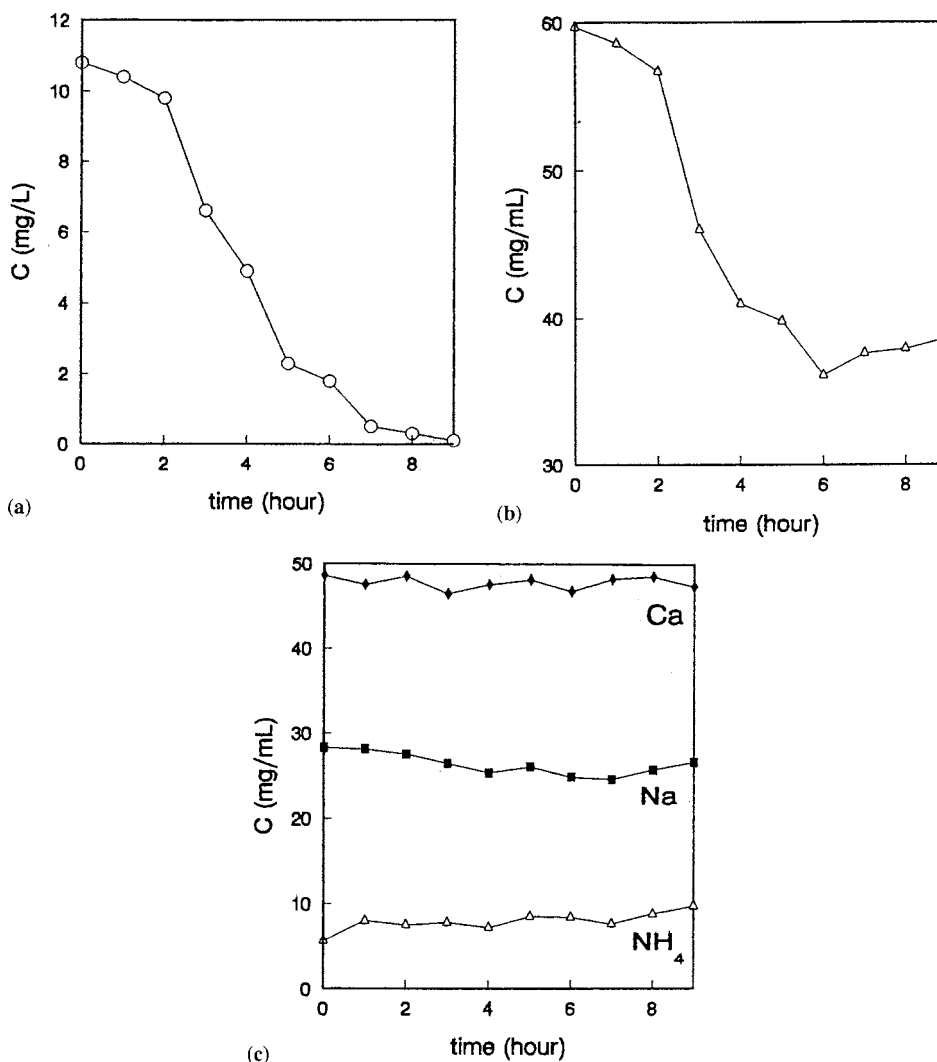


Fig. 4. Changes in the concentration of (a)  $\text{Mg}^{2+}$ , (b)  $\text{K}^+$ , (c)  $\text{Na}^+$ ,  $\text{NH}_4^+$ ,  $\text{Ca}^{2+}$  during the fermentation process.

alternating electric field is applied to the electrodes, and thus the influence of the electrical double layer capacitance can be ignored. Furthermore, the small potential difference between the electrode couples is not enough to cause electrolysis.

## 5. Conclusion

High resolution of the exchange-chromatography combined with good sensitivity and wide working range of the DCBAW detector was tested to be a reliable, rugged method for monitoring inorganic cations in chemically defined fermentation. This method was also evaluated for broth and other complex fermentation media and was shown to be useful for various microbial and cell culture media. The simple preparation of samples, accurate results, the simultaneous detection and quantitation of various cations and short analytical times make this method a potentially useful tool for on-line monitoring and optimization of fermentation processes. The monitoring results show that the inorganic nutrients are essential for cells culture. It also can control the fermentation process by controlling the concentration of some inorganic nutrients.

## Acknowledgements

This work was supported by the National Natural Science Foundation and the Education Commission Foundation of China.

## References

- [1] B. Atkinson, F. Mavituna, *Biochemical Engineering and Biotechnology Handbook*, The Nature Press, New York, 1983, pp. 221–225.
- [2] R.P. Jones, *Process Biochem.* 21 (1986) 183.
- [3] J. Huth, S. Werner, H.G. Müller, *J. Basic Microbiol.* 30 (1990) 8.
- [4] P. Vila, J.L. Corchero, A. Benito, A. Villaverde, *Biotechnol. Prog.* 10 (1994) 648.
- [5] Z. Yi, G. Zhuang, P. Brown, *J. Liq. Chromatogr.* 16 (1993) 3133.
- [6] R.G. Bell, *Chromatography* 546 (1991) 251.
- [7] L. Joergensen, A. Weimann, *J. Chromatogr. A* 602 (1992) 179.
- [8] R.S. Robin Robinett, W.K. Herber, *J. Chromatogr. A* 671 (1994) 315.
- [9] T. Nomura, T. Yanagihara, T. Nitsuo, *Anal. Chim. Acta* 248 (1992) 329.
- [10] P. Chen, L.H. Nie, S.Z. Yao, *J. Chromatogr. Sci.* 33 (1995) 268.
- [11] K. Chen, P. Chen, L.H. Nie, S.Z. Yao, *J. Chromatogr. A* 753 (1996) 1.
- [12] D.W. Tempezt, *Symp. Soc. Gen. Microbiol.* 19 (1969) 87.
- [13] B. Green, J.D.H. Cooper, D.C. Turnell, *Ann. Clin. Biochem.* 26 (1989) 361.

# Micellar effects on the electrochemistry of dopamine and its selective detection in the presence of ascorbic acid

Xiao-Lin Wen, Yun-Hua Jia, Zhong-Li Liu \*

National Laboratory of Applied Organic Chemistry, Lanzhou University, Lanzhou, Gansu 730000, China

Received 23 November 1998; received in revised form 24 June 1999; accepted 29 June 1999

## Abstract

The electrochemistry of dopamine (3-hydroxytyramine) was studied by cyclic voltammetry at a glassy carbon electrode in the presence of cetyltrimethylammonium bromide (CTAB) and sodium dodecyl sulfate (SDS) micelles at different pH. The anodic peak potential ( $E_{pa}$ ) and peak current ( $I_{pa}$ ) were found to be remarkably dependent on the charge and the concentration of the surfactant. The  $E_{pa}$  and  $I_{pa}$  change abruptly around the critical micellar concentration (CMC) of the surfactants and reach a plateau above the CMC. The  $E_{pa}$  at the plateau shifts to more positive values in the cationic CTAB micellar solution, e.g. from 180 mV vs SCE in aqueous solution at pH 6.8 to 410 mV in CTAB micelle, whilst it shifts to less positive values in the anionic SDS micellar solution, e.g. 150 mV at pH 6.8. Therefore, the overlapped anodic peaks of dopamine and ascorbic acid in the mixture of the two compounds in aqueous solutions can be separated in CTAB micelles since the micelle shifts the  $E_{pa}$  of ascorbic acid to less positive values. The two peaks are separated by ca. 400 mV at pH 6.8 in CTAB micelle, hence dopamine can be determined in the presence of 100 times excess of ascorbic acid. In SDS micelle and in the presence of ascorbic acid, the  $I_{pa}$  of dopamine is greatly enhanced due to the catalytic oxidation of the latter that enables quantitative determination of both compounds. © 1999 Elsevier Science B.V. All rights reserved.

**Keywords:** Cyclic voltammetry; Glassy carbon electrode; Dopamine; Ascorbic acid; Micellar effect

## 1. Introduction

Micellar effects in electrochemistry is a subject of substantial current interest [1]. Adsorption of surfactants on electrodes and solubilization of electrochemically active compounds in micellar aggregates might significantly change the redox potential, charge transfer coefficients and diffu-

sion coefficients of electrode processes, as well as change the stability of electrogenerated intermediates and electrochemical products [1–15]. For example, Rusling [1] has successfully used micelles and other surfactant microstructures to catalyze the electrochemical dehalogenation of organic halides. Kaifer and colleagues [2,3] reported significant changes in the redox potential and peak current of methylviologen in sodium dodecyl sulfate (SDS) micellar solution. Davidovic et al. [4] found that the rate of electrochemical reduction

\* Corresponding author. Fax: +86-931-8625657.  
E-mail address: liuzl@lzu.edu.cn (Z.-L. Liu)

of *p*-nitrosodiphenylamine decreased in the presence of cetyltrimethylammonium bromide (CTAB) micellar solution. We [5,6] have found recently that the oxidation potential, electron-transfer rate constant and diffusion coefficient of ascorbic acid and its lipophilic derivatives are significantly influenced by CTAB and SDS micelles. Surfactants have also been employed as selective masking agents to improve selectivity and sensitivity of electrochemical analysis [1,7,8]. In addition, micellar systems are considered to be primitive model systems for biological membranes [9]. Rusling [1] and others [10–12] have suggested that micelle-bound catalytic systems are attractive candidates for future design of surfactant assemblies that may mimic redox events in biological membranes.

Dopamine (3-hydroxytyramine) is an important neurotransmitter in mammalian central nervous systems [16]. Intensive effort has been devoted to *in vitro* and *in vivo* electrochemical determination of dopamine and other catecholamines [17–19]. A major problem in the determination is the lack of resolving power between dopamine and coexisting ascorbic acid whose concentration is much higher than dopamine. At most solid electrodes, ascorbic acid is oxidized at potentials close to that of the dopamine, resulting in an overlapping voltammetric response. Therefore, a number of chemically modified electrodes have been developed to separate the electrochemical response of dopamine and ascorbic acid [20–24]. For example, self-assembled monolayers of  $\omega$ -mercapto-carboxylic acid and stearic acid deposited on a gold electrode [17] and on a graphite paste electrode [23], respectively, were used to move the oxidation potential of ascorbic acid towards a more positive value, hence separating its anodic peak from that of dopamine.

Here we describe a cyclic voltammetric study of dopamine in cationic CTAB and anionic SDS micellar systems both in the absence and presence of ascorbic acid. Since the two compounds exhibit opposite micellar effect their overlapped anodic peaks can be separated in the micellar solution, hence dopamine can be determined in the presence of ascorbic acid.

## 2. Experimental

A conventional single-compartment, three-electrode cell thermostatted at 20°C and kept under an argon atmosphere was used for all experiments. The electrochemical instrumentation consisted of a PAR model 173 potentiostat coupled with a PAR model 175 universal programmer, and a Houston Instruments model 2000 X-Y recorder. An electrochemical analyzer (BAS-100B) was used for the differential pulse voltammetric determination. The acidity of buffer solutions was determined by a PH-2 pH-meter (Shanghai). A glassy carbon electrode (4.5 mm in diameter) employed as a working electrode was carefully polished with 0.05 nm alumina slurry on a flat surface and sonicated immediately before use. A platinum wire was employed as an auxiliary electrode. All potentials were recorded relative to a saturated calomel electrode (SCE) reference electrode.

L-Dopamine and L-ascorbic acid were from Fluka and Xian Chemicals respectively and used as received. The surfactants CTAB and SDS were recrystallized from acetone–water (9:1 v/v) and ethanol respectively. Dopamine and/or ascorbic acid solutions were prepared with triply distilled water and deaerated thoroughly with argon immediately before use.

## 3. Results and discussion

### 3.1. Surfactant effect

L-Dopamine (DA) showed a quasireversible cyclic voltammogram in aqueous phosphate buffer solution. Addition of the cationic surfactant cetyltrimethyl ammonium bromide (CTAB) to the solution shifted the anodic peak potential,  $E_{pa}$ , to more positive values and the cathodic peak potential,  $E_{pc}$ , to less positive values, and decreased both peak currents,  $I_{pa}$  and  $I_{pc}$ , significantly. The anionic surfactant sodium dodecyl sulfate (SDS) influenced the voltammetric behavior in an opposite way. It decreased  $E_{pa}$  a small amount, increased  $I_{pa}$  significantly, and increased  $E_{pc}$ , but did not appreciably influence  $I_{pc}$ . The



reversibility of the electrochemical process was reduced when the solution acidity was decreased, and the cathodic peak totally disappeared at pH 9.4. In addition, the electrochemical behavior of DA was surfactant concentration-dependent. The

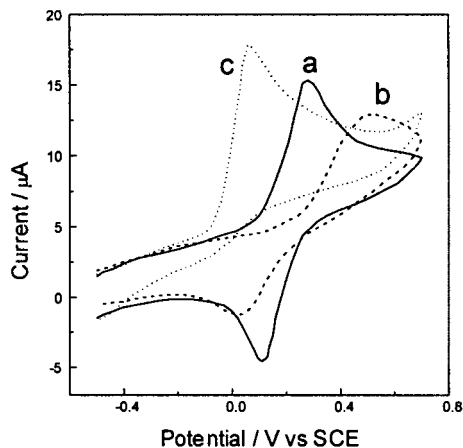


Fig. 1. Cyclic voltammograms of dopamine (0.26 mM) recorded at a glassy carbon electrode in 0.1 M phosphate buffer. The potential was scanned from  $-0.5$  to  $+0.7$  V with a scan rate of  $0.1 \text{ V s}^{-1}$ : (a) in aqueous solution, pH 4.3; (b) in 3.0 mM CTAB micelles, pH 4.3; (c) in 3.0 mM SDS micelles, pH 9.4.

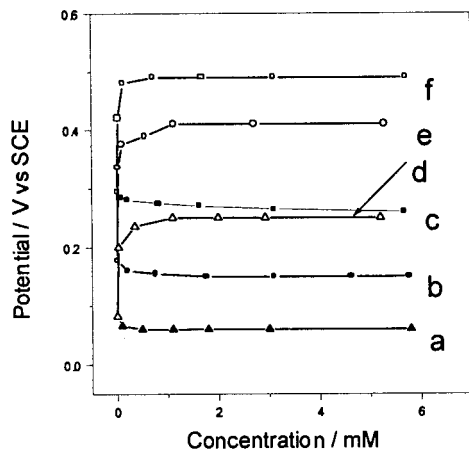


Fig. 2. Variation of oxidation potential ( $E_{pa}$ ) of dopamine at a glassy carbon electrode with surfactant concentrations ( $C$ ) and pH. Experimental conditions were the same as indicated in the legend of Fig. 1: (a) in SDS, pH 9.4; (b) in SDS, pH 6.8; (c) in SDS, pH 4.3; (d) in CTAB, pH 9.4; (e) in CTAB, pH 6.8; (f) in CTAB, pH 4.3.

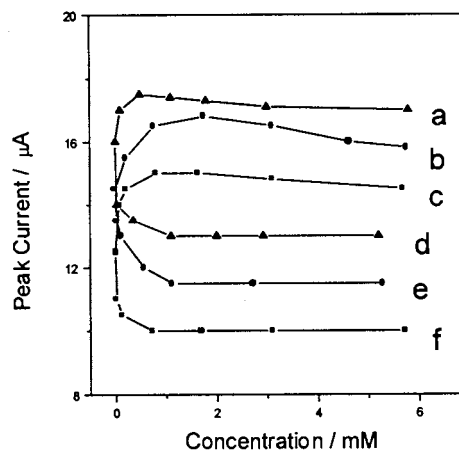


Fig. 3. Variation of peak current ( $I_{pa}$ ) of dopamine at a glassy carbon electrode with surfactant concentrations ( $C$ ) and pH. Experimental conditions were the same as indicated in the legend of Fig. 1: (a) in SDS, pH 9.4; (b) in SDS, pH 6.8; (c) in SDS, pH 4.3; (d) in CTAB, pH 9.4; (e) in CTAB, pH 6.8; (f) in CTAB, pH 4.3.

Table 1

Potentials (mV) of dopamine in aqueous solution and in micelles<sup>a</sup>

	pH 4.3		pH 6.8		pH 9.4	
	$E_{pa}$	$E_{pc}$	$E_{pa}$	$E_{pc}$	$E_{pa}$	$E_{pc}$
In water	295	110	180	44	86	–
In CTAB	490	16	410	–50	240	–
In SDS	275	135	150	80	53	–

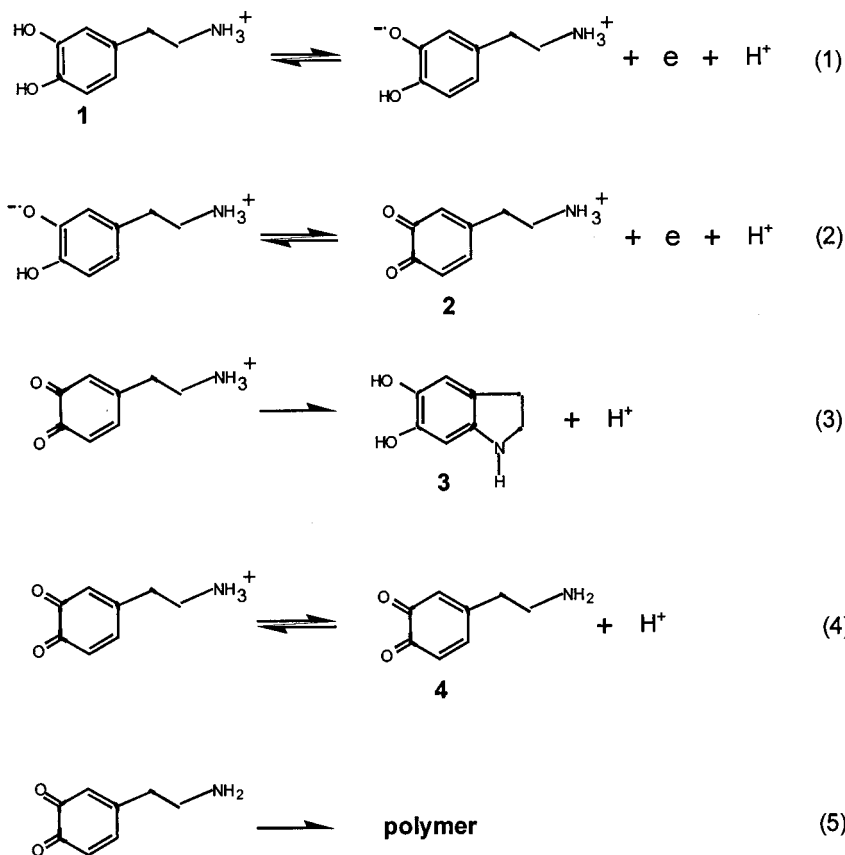
<sup>a</sup> All determinations were made in 0.1 M phosphate buffer. All values in mV. Potentials were recorded with reference to saturated calomel electrode (SCE) and scanned from  $-0.5$  to  $+1.7$  V with a scan rate of  $0.1 \text{ V/s}$ . The concentration of CTAB and SDS were 3.0 mM.

peak potential and peak current changed abruptly at very low surfactant concentrations and reached a plateau around the critical micellar concentration (CMC) of the surfactant. Representative cyclic voltammograms are shown in Fig. 1, and the surfactant concentration-dependence of  $E_{pa}$  and  $I_{pa}$  are illustrated in Figs. 2 and 3 respectively. Electrode potentials at the plateau are listed in Table 1.

The electrochemical oxidation of dopamine has been suggested to be an ECC process as shown in Scheme 1 [19,25,26]. Two consecutive one electron transfer from protonated dopamine **1** ( $pK_a = 8.92$ ) [25] produces the dopamine ortho-quinone **2** as the primary intermediate. Upon losing a proton **2** undergoes intramolecular cyclization producing 5,5-dihydroxyindoline **3** and/or forming an aminochrome **4**. The latter polymerizes readily to melanin-like products on the electrode surface, thus inhibits the electron transfer reaction. Since the cyclization reaction (Scheme 1, Eq. 3) involves deprotonation and its rate decreases remarkably upon increasing the solution acidity in the pH range of 2–6 [26], high acidity should prevent the cyclization reaction and the polymerization reaction, and hence increase the reversibility of the electron transfer reaction. The pH-dependence of

our cyclic voltammetric results is consistent with this mechanism. That is,  $E_{pa}$  and  $E_{pc}$  decrease and  $I_{pa}$  increases with increasing pH (Figs. 2 and 3), whilst  $I_{pc}$  decreases with increasing pH and the cathodic peak disappeared at pH 9.4.

The significant shift of the oxidation potential and change of the peak current upon addition of CTAB and SDS surfactants can be rationalized by the adsorption of the surfactant at the electrode surface which may alter the overvoltage of the electrode and influence the rate of electron transfer, and by the formation of micellar aggregates which may influence the mass transport of electroactive species to the electrode. It is well established that surfactants can be adsorbed on solid surfaces to form surfactant films [7,10]. In the present case, adsorption of the anionic surfactant SDS at the electrode surface may form a



Scheme 1.

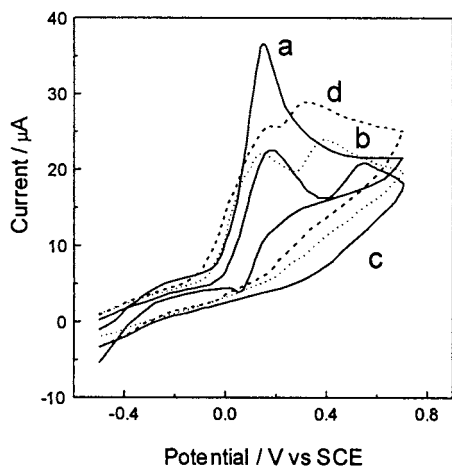


Fig. 4. Cyclic voltammograms of mixtures of dopamine (0.2 mM) and ascorbic acid (1.0 mM) recorded at a glassy carbon electrode in 0.1 M phosphate buffer. The potential was scanned from  $-0.5$  to  $+0.7$  V with a scan rate of  $0.1 \text{ V s}^{-1}$ : (a) in aqueous solution, pH 6.8; (b) in 3.0 mM CTAB, pH 6.8; (c) same as (b), pH 4.3; (d) same as (b), pH 9.4.

negatively charged hydrophilic film on the electrode with the polar head group directing to the bulk water phase. This negatively charged hydrophilic layer increases the concentration of the protonated dopamine **1** on the electrode surface via electrostatic interaction, and stabilizes the ortho-quinone cation **2**, hence the overvoltage is reduced and the electron transfer rate is increased. Therefore, the oxidation of dopamine is facilitated by SDS. On the other hand, the adsorption of the cationic CTAB prevents the dopamine cation from approaching the electrode surface, hence the reac-

Table 2

The potential difference of dopamine (DA) and ascorbic acid (AA) in CTAB micelles<sup>a</sup>

	pH 4.3	pH 6.8	pH 9.4
$E_{\text{pa}}$ (AA) (mV)	80	10	-65
$E_{\text{pa}}$ (DA) (mV)	490	410	240
$\Delta E_{\text{pa}}$ (mV)	410	400	315

<sup>a</sup> All determinations were made in 0.1 M phosphate buffer. All values in mV. Potentials were recorded with reference to saturated calomel electrode (SCE) and scanned from  $-0.5$  to  $+1.7$  V with a scan rate of  $0.1 \text{ V/s}$ . The concentration of CTAB was 3.0 mM.

tion is retarded. This micellar effect on the anodic oxidation of dopamine is basically an electrostatic interaction between the surfactant film adsorbed on the electrode and the protonated dopamine. The plateau in the plot of  $E_{\text{pa}}$  or  $I_{\text{pa}}$  versus the surfactant concentration (Figs. 2 and 3) demonstrates saturation of the adsorption of the surfactant at the electrode, because after complete coverage of the electrode surface the surfactant would form micelles in the bulk water and would no longer affect the electrode oxidation process. It has been well established that the saturated adsorption of surfactants on solid surfaces generally coincides with the CMC of the surfactant [7], and cyclic voltammetry has been suggested as a method for estimating the CMC of surfactants [2,3,13,14]. The slight decrease of  $I_{\text{pa}}$  with increasing SDS concentrations above its CMC (Fig. 3, lines a and b) is probably due to the binding of the dopamine cation **1** with the anionic micelle by electrostatic interaction that may decrease the diffusion coefficient of the substrate.

### 3.2. Selective detection of dopamine and ascorbic acid in CTAB micellar solution

Since the anodic peak potential of dopamine in aqueous solution (180 mV at pH 6.8) is very close

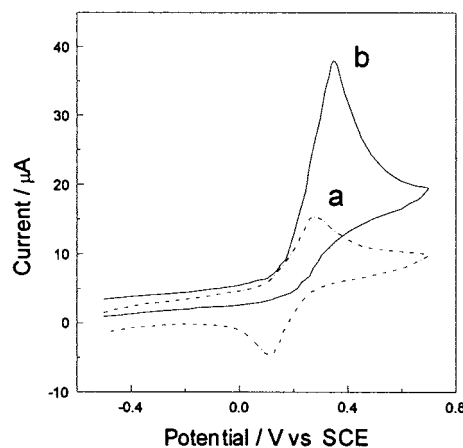
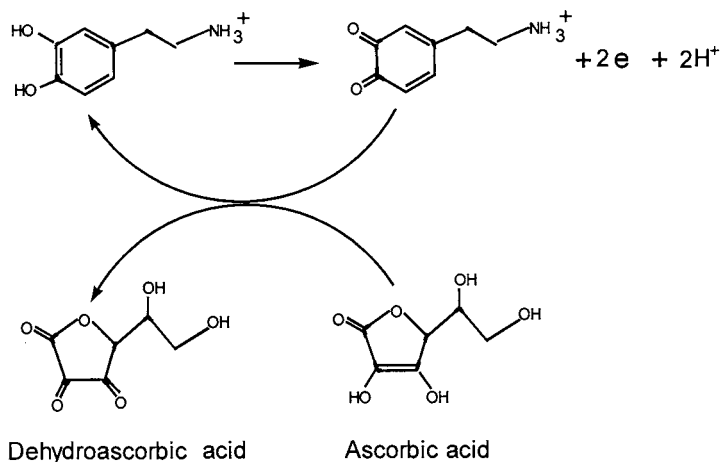


Fig. 5. Cyclic voltammograms of dopamine recorded at a glassy carbon electrode in 0.1 M phosphate buffer (pH 4.3) and 3.0 mM SDS. The potential was scanned from  $-0.5$  to  $+0.7$  V with a scan rate of  $0.1 \text{ V s}^{-1}$ : (a) 0.2 mM dopamine; (b) 0.2 mM dopamine and 1.0 mM ascorbic acid.



Scheme 2.

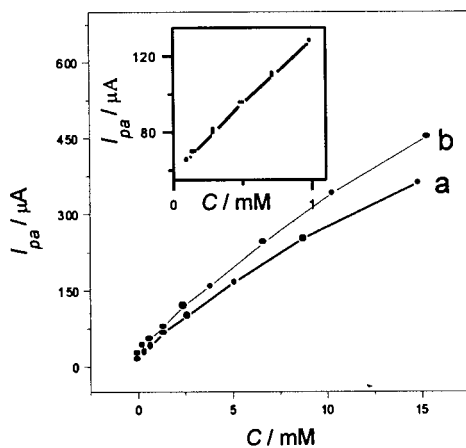


Fig. 6. Dependence of the catalytic anodic peak current ( $I_{pa}$ ) of dopamine with the concentration ( $C$ ) of ascorbic acid and dopamine in 3.0 mM SDS (pH 6.8). Experimental conditions were the same as indicated in the legend of Fig. 1: (a) 0.37 mM dopamine with different concentrations ( $C$ ) of ascorbic acid; (b) 0.74 mM ascorbic acid with different concentrations ( $C$ ) of dopamine. The inset shows the low concentration part of line b.

to that of ascorbic acid (200 mV at pH 6.8) [5], cyclic voltammetric determination of a mixture of dopamine and ascorbic acid showed only a single peak (Fig. 4a). However, taking advantage of the opposite micellar effect on the anodic oxidation of dopamine, which is positively charged in neutral and acidic solutions, and ascorbic acid, which is negatively charge, it should be possible to

separate the two anodic peaks in ionic micelles. Indeed, addition of CTAB surfactant to the mixture of dopamine and ascorbic acid shifts the anodic peak of the former to positive values and that of the latter to negative values, hence makes the two anodic peaks well separated (Fig. 4). The acidity of solution exerts a similar effect on the anodic peak potential of the two substrates, i.e.  $E_{pa}$  increases with increase of the acidity, but the effect is more pronounced for dopamine than for ascorbic acid (compare Fig. 2 in this paper and Fig. 2 in our previous paper [5]). The potential difference between dopamine and ascorbic acid in CTAB micelles is 410, 400 and 315 mV at pH 4.3, 6.8 and 9.4 respectively (Table 2), that is more than enough to allow selective detection of the two compounds. Indeed, dopamine could be quantitatively determined by differential pulse voltammetry in CTAB micelle at pH 4.3 in the concentration range of  $5 \times 10^{-6}$ – $3 \times 10^{-4}$  M with a detection limit of  $3 \times 10^{-6}$  M in the presence of 100 times excess of ascorbic acid. Uric acid is oxidized at 370 mV at pH 4.3 which does not interfere with the determination.

### 3.3. Catalytic oxidation of ascorbic acid in the presence of dopamine in SDS micelles

It seems that a similar anodic peak separation should also be achieved in SDS micellar solutions since the anionic surfactant decreases the anodic

peak potential of dopamine, whilst it increases that of ascorbic acid. For example, the  $E_{pa}$  of dopamine and ascorbic acid are 150 and 460 mV, respectively, vs SCE<sup>4</sup> in 1.0 mM SDS micelles at pH 6.8. However, a cyclic voltammogram of dopamine in the presence of ascorbic acid in SDS micellar solutions showed a dramatically enhanced anodic peak of dopamine accompanied by the disappearance of its cathodic peak, and the anodic peak of ascorbic acid was not observed (Fig. 5). Since in SDS micelles dopamine is electrooxidized before ascorbic acid, this result suggests a catalytic EC' process as shown in Scheme 2. That is, the dopamine ortho-quinone **2** formed by the electrochemical oxidation is reduced back to dopamine by ascorbic acid, resulting in an enhanced anodic current of dopamine. This process implies that ascorbic acid can serve as an antioxidant to prevent the oxidation of dopamine, hence possibly may prevent melanin formation in biological systems.

Chronoamperometric determination of this reaction gave the catalytic rate constant,  $k'$ , as 7.6, 4.1 and  $3.7 \times 10^2 \text{ M}^{-1} \text{ s}^{-1}$  at pH 4.3, 6.8 and 9.4 respectively. A similar catalytic effect has been observed previously at a stearic acid modified carbon paste electrode [27]. Quantitative determination demonstrates that the oxidation peak current increases approximately linearly with increasing concentration of both dopamine and ascorbic acid in the concentration range of 0.1–5 mM (Fig. 6). Therefore, this catalytic peak current of dopamine can be used to determine the concentration of either dopamine or ascorbic acid in their mixtures if one could be determined by other methods, e.g. by selective determination of dopamine in CTAB micelles (vide supra).

In conclusion, this study demonstrates a significant micellar effect on the electrochemical behavior of dopamine. Taking advantage of the opposite micellar effect of dopamine and ascorbic acid, the two bioactive compounds can be simultaneously determined in the ionic micelles CTAB or SDS. In addition, the presence of ascorbic acid in SDS micelles greatly enhances the electrochemical response of dopamine via a catalytic EC' process that can be used for a sensitive determination of dopamine.

## Acknowledgements

We are grateful to the National Natural Science Foundation of China and the Department of Education of China for financial support.

## References

- [1] J.F. Rusling, *Acc. Chem. Res.*, 24 (1991) 24, 75.
- [2] A.E. Kaifer, A.J. Bard, *J. Phys. Chem.* 89 (1985) 4876.
- [3] D.A. Ouiatela, A. Diaz, A.E. Kaifer, *Langmuir* 4 (1988) 663.
- [4] A. Davidovic, I. Tabakovic, D. Davidovic, L. Duic, *J. Electroanal. Chem.* 280 (1990) 371.
- [5] X.L. Wen, Z.X. Han, A. Rieker, Z.L. Liu, *J. Chem. Res. (S)*, 1997, 108.
- [6] X.L. Wen, Z.X. Han, A. Rieker, Z.L. Liu, *J. Chem. Soc. Perkin Trans. 2* (1998) 905.
- [7] T.F. Connors, J.F. Rusling, A. Owlia, *Anal. Chem.* 57 (1985) 170.
- [8] M. Stadlober, K. Kalcher, G. Raber, C. Neuhold, *Talanta* 43 (1996) 1915.
- [9] S. Tascioglu, *Tetrahedron* 52 (1996) 11113.
- [10] G.N. Kamau, T. Leipert, S. Shukla, J.R. Rusling, *J. Electroanal. Chem.* 233 (1987) 173.
- [11] J.F. Rusling, A.E.F. Nassar, *J. Am. Chem. Soc.* 115 (1993) 11891.
- [12] U. Sivagnam, M. Palaniandavar, *J. Electroanal. Chem.* 410 (1996) 43.
- [13] A.B. Mandal, B.U. Nair, *J. Phys. Chem.* 95 (1991) 9008.
- [14] D.O. Wipf, R.M. Wightman, *Anal. Chem.* 60 (1988) 2460.
- [15] N.C. Sarada, I.A.K. Reddy, K.M. Rao, *J. Indian Chem. Soc.* 71 (1994) 729.
- [16] R.M. Wightman, C. Amatore, R.C. Engstrom, P.D. Hale, E.W. Kristensen, W.G. Kubr, L.J. May, *Neuroscience* 25 (1988) 513.
- [17] K. Takehara, H. Takemura, M. Aihara, M. Yoshimura, *J. Electroanal. Chem.* 404 (1996) 179.
- [18] S. Cosnier, C. Innocent, L. Allien, S. Poitry, M. Tsacopoulos, *Anal. Chem.* 69 (1997) 968.
- [19] R.F. Lane, A.T. Hubbard, *Anal. Chem.* 48 (1976) 1287.
- [20] D.M. Zhou, H.X. Ju, H.Y. Chen, *J. Electroanal. Chem.* 408 (1996) 219.
- [21] J. Wang, A. Walcarius, *J. Electroanal. Chem.* 407 (1996) 183.
- [22] T.F. Kang, G.L. Shen, R.Q. Yu, *Talanta* 43 (1996) 2007.
- [23] M. Franck, M. Daniel, *Anal. Chem.* 65 (1993) 37.
- [24] B.G. Mark, D.J. Curran, *Anal. Chem.* 58 (1986) 1028.
- [25] M.D. Hawley, S.V. Tatawawadi, S. Piekarski, R.N. Adams, *J. Am. Chem. Soc.* 89 (1967) 447.
- [26] E. Rodenas, S. Vera, *Tetrahedron* 42 (1986) 143.
- [27] M.A. Dayton, A.G. Ewing, R.M. Wightman, *Anal. Chem.* 52 (1980) 2392.

# Slurry sampling graphite furnace atomic absorption spectrometry: determination of trace metals in mineral coal

Márcia M. Silva \*, Maria Goreti, R. Vale, Elina B. Caramão

*Instituto de Química, Universidade Federal do Rio Grande do Sul, P.O. Box 15003, Av. Bento Gonçalves, 9500 CEP 91501-970, Porto Alegre, RS, Brazil*

Received 2 February 1999; received in revised form 24 June 1999; accepted 29 June 1999

## Abstract

A procedure for lead, cadmium and copper determination in coal samples based on slurry sampling using an atomic absorption spectrometer equipped with a transversely heated graphite tube atomizer is proposed. The slurries were prepared by weighing the samples directly into autosampler cups (5–30 mg) and adding a 1.5 ml aliquot of a diluent mixture of 5% v/v HNO<sub>3</sub>, 0.05% Triton X-100 and 10% ethanol. The slurry was homogenized by manual stirring before measurement. Slurry homogenization using ultrasonic agitation was also investigated for comparison. The effect of particle size and the use of different diluent compositions on the slurry preparation were investigated. The temperature programmes were optimized on the basis of pyrolysis and atomization curves. Absorbance characteristics with and without the addition of a palladium–magnesium modifier were compared. The use of 0.05% m/v Pd and 0.03% m/v Mg was found satisfactory for stabilizing Cd and Pb. The calibration was performed with aqueous standards. In addition, a conventional acid digestion procedure was applied to verify the efficiency of the slurry sampling. Better recoveries of the analytes were obtained when the particle size was reduced to < 37 µm. Several certified coal reference materials (BCR Nos. 40, 180, and 181) were analyzed, and good agreement was obtained between the results from the proposed slurry sampling method and the certificate values. © 1999 Elsevier Science B.V. All rights reserved.

*Keywords:* Slurry sampling; Coal analysis; Copper; Lead; Cadmium; Graphite furnace atomic absorption spectrometry

## 1. Introduction

In Brazil, mineral coal reserves represent about 60% of the total non-renewable energy sources.

Total consumption of coal burned in coal-fired power plants and steamer boiler is around  $3.7 \times 10^6$  tons year<sup>-1</sup>. The content of trace elements in coal can give valuable information about its origin, and even more importantly, on the environmental impact of its processing and use. Despite its importance to Brazil's economy, and environment, there are only a very few studies concerning that subject [1].

\* Corresponding author. Tel.: +55-51-3166278; fax: +55-51-3191499.

E-mail address: mmsilva@if.ufrgs.br (M.M. Silva)

It is well known that coal is difficult to bring into solution, therefore the elimination of the dissolution step is highly desirable as this would greatly reduce the costly and time-consuming sample preparation stage, as well as the associated risk of contamination. A potential alternative to wet digestion is the direct analysis of solid samples by graphite furnace atomic absorption spectrometry (GFAAS). Problems resulting from high background, calibration difficulties, weighing errors, sample inhomogeneity, etc. must however be considered [2]. Slurry sampling combines the benefits of solid and liquid sampling, and permits for example the use of conventional liquid sample handling apparatus such as autosamplers. Slurries may also be diluted similar to solutions, although precision is degrading with increasing dilution [3]. For coal, slurry concentrations down to about  $10^{-4}\%$  (m/v) have been reported [4,5]. Slurry preparation does not require special tools or equipment and can be done in advance using almost any amount of the original sample material [6]. On the other hand, GFAAS is particularly well suited for solids and slurry analyses because, unlike nebulization techniques, it does not suffer significantly from particle size effects since it offers long residence times with a correspondingly high atomization efficiency [7]. Several groups have reported quantitative analyte recovery for particle sizes of up to  $40\ \mu\text{m}$  [3,5,8]. The success of slurry analysis, however, depends on several factors such as sample homogeneity, material density, slurry concentration, diluent, mixing, and homogenization technique [3,9]. A homogenous slurry can be obtained by manual, mechanical or ultrasonic agitation, or by passing a gas stream through the sample [10].

A slurry can be stabilized using a highly viscous liquid medium. Such stabilizing agents are particularly useful when an autosampler is used, as the slurry can be left in the sampling cups for extended periods of time without further homogenization [3]. Viscalex [4,11], glycerol [11,12], non-ionic surfactants, and organic solvents are mentioned in the literature as stabilizing agents for slurries. Triton X-100 has been widely used to disperse solid particles that could float on top of the liquid [6,8,12,13]. Moreover, Triton X-100

does not cause problems with the reproducibility of pipetting, such as reported for Viscalex and glycerol [6,12,14,15]. The poor precision could be attributed to sample adhering to the outside of the autosampler capillary. The use of ethanol as a wetting agent has also been reported by several authors [4,8,16]. The presence of nitric acid in the diluent solution leads to a partial extraction of analytes into the liquid phase of the slurry. Miller-Ihli [9] reported that 75–90% of lead were extracted into the liquid phase of sediment slurries, and that the precision approached that obtainable with liquid digests when a high percentage of the analyte was in the liquid phase.

The objective of the present study, was to establish a simplified slurry sampling method for the determination of lead, cadmium, and copper in coal samples by GFAAS. The main focal points were the factors of interest in optimizing slurry sampling analyses such as particle size, diluent composition, and the effect of the agitation technique, as well as the influence of chemical modifiers and the optimization of the furnace temperature programme. Trueness and precision of the slurry method using aqueous standards for calibration were evaluated by the analysis of coal standard reference materials and by comparison with a conventional acid digestion method.

## 2. Experimental

### 2.1. Apparatus

A Zeiss AAS5 EA atomic absorption spectrometer (Analytik Jena, Germany), equipped with a transversely heated graphite tube atomizer and an MPES autosampler, was employed for the majority of this work. Deuterium arc background correction was used throughout. Pyrolytically coated graphite tubes were employed exclusively. Platform atomization was used for cadmium and lead, and wall atomization for copper. Argon was used as the purge gas, with a rate of  $300\ \text{ml}\ \text{min}^{-1}$  during all stages, except for atomization, where the flow was stopped. The spectrometer was interfaced to an IBM PC/AT compatible micro-computer.

For comparison, part of the work was carried out in a different laboratory (CENA-USP, Piracicaba, S.P.), using a Perkin–Elmer 4100ZL atomic absorption spectrometer with Zeeman-effect background correction, furnished with a transversely heated graphite tube atomizer (THGA) and an AS-71 autosampler, and a USS-100 ultrasonic probe mixer.

Optimization of pyrolysis and atomization temperatures was carried out according to the procedure proposed by Welz [17]. Calibration was performed by the standard calibration technique using aqueous standards under the same experimental conditions. Coal standard reference materials were analyzed in the same way. Integrated absorbance (peak area) measurements were used exclusively for all determinations. The instrumental parameters are summarized in Table 1.

## 2.2. Reagents

Analytical grade reagents were used throughout. The nitric acid (Merck) used to prepare the slurries, the aqueous calibration standards, and also for the conventional acid digestion, was further purified by subboiling distillation in a quartz apparatus. All containers and glassware were soaked in 3 mol l<sup>-1</sup> nitric acid for at least 24 h, and rinsed three times with deionized water before use. Distilled, deionized water, 18 MΩ cm<sup>-1</sup> specific resistivity, from a Millipore water purifier

system, was used for the preparation of the samples and standards.

The chemical modifier for lead and cadmium determinations was a mixture of 0.05% m/v Pd and 0.03% m/v Mg solutions, both as the nitrates (Merck).

Lead, cadmium, and copper stock solutions (1000 mg l<sup>-1</sup> in 0.014 mol l<sup>-1</sup> nitric acid) were prepared from Pb(NO<sub>3</sub>)<sub>2</sub>, Cd(NO<sub>3</sub>)<sub>2</sub>, and CuSO<sub>4</sub> (Merck), respectively. The working standards were prepared by serial dilution of stock solutions with the slurry diluent medium.

## 2.3. Coal samples

The coal sample used in this study was collected at the Candiota mine, Rio Grande do Sul, Brazil (density, 1.18 g cm<sup>-3</sup>). The coal sample was first ground in a ball mill and passed through a 60 mesh polyester sieve. In order to reduce the particle size further, an agate mortar and different mesh-size polyester sieves were used. This way, four sets of particle sizes were obtained: (a) 250–74 μm; (b) 74–44 μm; (c) 44–37 μm; and (d) < 37 μm.

The following certified reference materials were used in this work: coal-BCR No. 40 (particle size 60–90 μm); gas coal BCR no. 180 (particle size 63–212 μm), coking coal-BCR No. 181 (particle size 63–212 μm). To reduce the particle size to < 37 μm these reference materials were submitted

Table 1  
Instrumental and graphite furnace parameters for the Zeiss AAS 5EA, used for slurry sampling (sample size 20 μl)

Parameters	Element		
	Pb	Cd	Cu
Wavelength: (nm)	283.3	228.8	324.8
Furnace program steps			
Pre-heating (°C)	80	80	80
Drying: (°C); ramp (s); hold (s)	180; 20; 20	180; 20; 20	180; 20; 20
Pyrolysis: (°C); ramp (s); hold (s)	900; 10; 30	700; 10; 40	1000; 10; 30
Cooldown: (°C); ramp (s); hold (s)	200; NP <sup>a</sup> ; 3	200; NP <sup>a</sup> ; 3	200; NP <sup>a</sup> ; 3
Atomize: (°C); ramp (s); hold (s)	1800; FP <sup>b</sup> ; 5	1500; FP <sup>b</sup> ; 4	2000; FP <sup>b</sup> ; 5
Clean: (°C); ramp (s); hold (s)	2600; 2; 5	2600; 3; 5	2600; 2; 5
Modifier	Pd + Mg	Pd + Mg	–

<sup>a</sup> No power.

<sup>b</sup> Full power.



to an additional grinding and sieving process, as described above.

#### 2.4. Acid digestion

Finely ground powdered coal samples, average particle sizes: (a) 250–74  $\mu\text{m}$ ; and (b)  $< 37\mu\text{m}$ , and the certified reference standard materials, as received, were dried in an oven at 105°C until constant weight was reached, and stored over silica gel in a desiccator.

A 1.0 g portion of dried samples was accurately weighed in a porcelain crucible and subject to a mild calcination step in a muffle furnace at 450°C, for about 1 week. The acid digestion of the residual ashes was carried out under pressure in a 50 ml PTFE bomb (Berghof system) in two steps. The ashes (0.250 g) were first treated with 2 ml of nitric acid (67%) and then, with additional 2 ml of hydrofluoric acid (Merck, 49%). Both steps were carried out at 160°C over a period of 4 h. The resulting solution was then diluted to 50 ml with 0.014 mol  $\text{l}^{-1}$  nitric acid in a calibrated polypropylene flask.

#### 2.5. Slurry preparation

The slurries were prepared by weighing the sample directly into polyethylene autosampler cups, using quantities of 5–30 mg of coal, and weighing to an accuracy of 0.1 mg. A volume of 1.5 ml of diluent was added to the cups, resulting in slurry concentrations of 0.33–2% (m/v). Slurry concentrations  $> 2\%$  (m/v) resulted in excessive buildup of residues in the graphite tube and were avoided. The slurries were homogenized for 60 s, either manually or with an ultrasonic probe. If necessary, although not practised in this work, this slurry can be further diluted for the determination of higher analyte concentrations. Prior to pipetting, the slurry was homogenized one more time, either manually or by sonication at  $\approx 8 \text{ W}$ , for  $\approx 5 \text{ s}$ . In order to avoid possible sedimentation errors, the autosampler capillary was immersed 9 mm below the surface of the liquid. Then, 20  $\mu\text{l}$  of slurry were taken up automatically and delivered into the atomizer.

To prepare the diluent, nitric acid, Triton X-100 surfactant (Union Carbide) and ethanol (Merck) were used, and different compositions were tested: (a) 5% v/v  $\text{HNO}_3$  + 0.05% v/v Triton X-100; (b) 5% v/v  $\text{HNO}_3$  + 10% v/v ethanol; and (c) 5% v/v  $\text{HNO}_3$  + 0.05% v/v Triton X-100 + 10% v/v ethanol.

The fraction of analyte extracted into the diluent phase during the preparation of the slurry was determined by allowing the slurry to settle and adjusting the autosampler tip so that only the solvent phase was sampled.

### 3. Results and discussion

#### 3.1. Furnace program and chemical modifier for the determination of Pb, Cd, and Cu

Accuracy and reproducibility of determinations by GFAAS with the slurry-sampling technique depend, among other things, on appropriate temperature programmes, and on the use of chemical modifiers. The introduction of a cooling step, before the atomization, has been proposed by several authors as a way of avoiding interferences and enhancing the sensitivity [9,11,18–21]. Experiments were carried out to determine the optimum temperatures, and times for drying, pyrolysis, and atomization, for aqueous solutions, and coal slurries.

In Figure 1, (a) and (b), the pyrolysis, and atomization curves for lead from an aqueous solution of 50  $\mu\text{g l}^{-1}$  Pb and from a 0.5% m/v coal sample slurry with and without the addition of the palladium–magnesium modifier are shown. The influence of the modifier on the pyrolysis and atomization temperatures is obvious for the aqueous solution (Fig. 1 (a)). However, the modifier did not further stabilize lead in the coal slurries during pyrolysis, but it increased the optimum atomization temperature to 1400°C, as can be seen in Figure 1 (b). This behavior has been observed previously by Qiao and Jackson [18], who suggested that the slurry particle itself acts as a modifier, stabilizing the analyte during the pyrolysis. Furthermore, Hinds and Jackson [22] established that the use of a chemical modifier

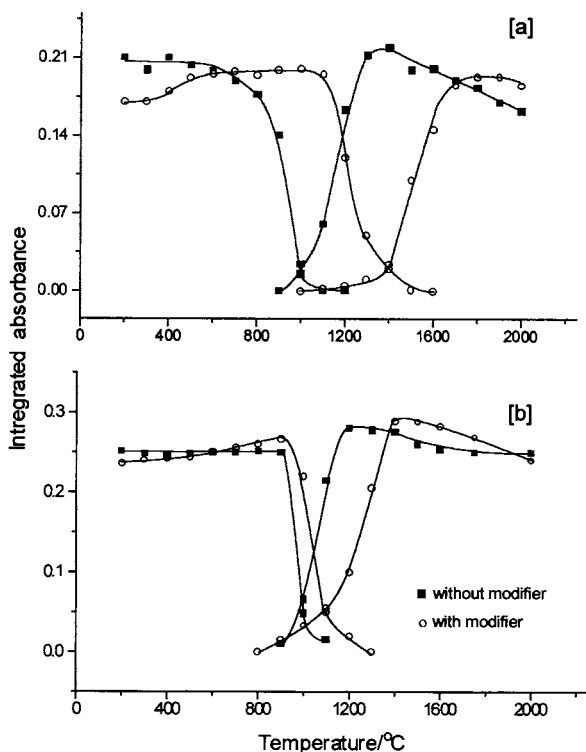


Fig. 1. Pyrolysis and atomization curves of lead in absence and presence of palladium–magnesium modifier. (a)  $50 \mu\text{g Pb l}^{-1}$  (5% v/v  $\text{HNO}_3$  + 0.05% v/v Triton X-100 + 10% v/v ethanol); (b) 0.5% m/v coal slurry sample (particle size  $< 37 \mu\text{m}$ ).

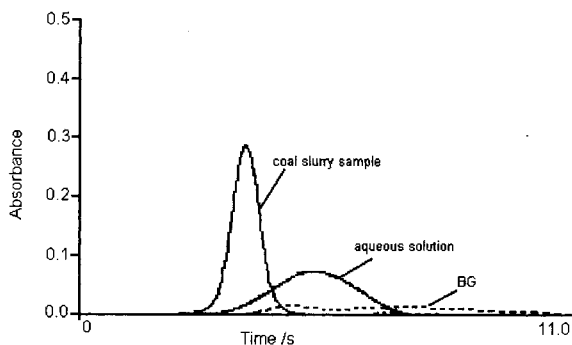


Fig. 2. Absorbance profiles for lead in aqueous solution ( $50 \mu\text{g Pb l}^{-1}$  in 5% v/v  $\text{HNO}_3$  + 0.05% v/v Triton X-100 + 10% v/v ethanol) and coal slurry sample (0.5% m/v) measured with the Zeiss AAS5 EA. The furnace parameters are shown in Table 1. BG, background absorbance.

causes solutions and slurries to behave almost identically. The atomization pulses for lead in an

aqueous solution and in a coal slurry are shown in Figure 2, however, it indicates that this is not the case for the samples investigated in this work. The atomization pulse for lead in the slurry sample is significantly narrower than for the aqueous solution indicating a faster release of lead atoms from the coal matrix. This might be as a result of the different chemical form in which lead is present in the coal and/or the reducing action of the coal matrix. It should also be mentioned that, due to the faster atomization, the introduction of a cooldown step before the atomization proved to be very useful in this case. It should, however be noted that the significantly different peak shapes had no influence on the accuracy of the results obtained with the standard calibration technique when integrated absorbance (peak area) was used for signal evaluation, this is of some analytical importance.

Similar effects were also observed for cadmium, as can be seen in Figure 3, (a) and (b); where the pyrolysis and atomization curves for cadmium from an aqueous solution of  $2.0 \mu\text{g l}^{-1}$  Cd, and from a 2.0% m/v coal slurry with and without the addition of the palladium–magnesium modifier are shown. Again, the presence of the chemical modifier increased the optimum atomization temperature by  $200^\circ\text{C}$ .

In the case of Cu there were no practical advantages of using a chemical modifier, since the profiles of the pyrolysis and atomization curves without modifier were similar for an aqueous solution of  $30 \mu\text{g l}^{-1}$  Cu and a 0.33% m/v coal slurry (Fig. 4).

Other parameters of the graphite furnace temperature programme, such as ramp and hold times for the pyrolysis, atomization stages, drying, cooling, and cleaning steps, were also investigated, the optimum values being shown in Table 1.

### 3.2. Optimization of slurry preparation

A number of preliminary experiments were performed in order to optimize the slurry preparation. For this purpose lead was chosen as the test element since its concentration in the Candiota coal sample and in the reference materials is most suitable for this type of measurement.

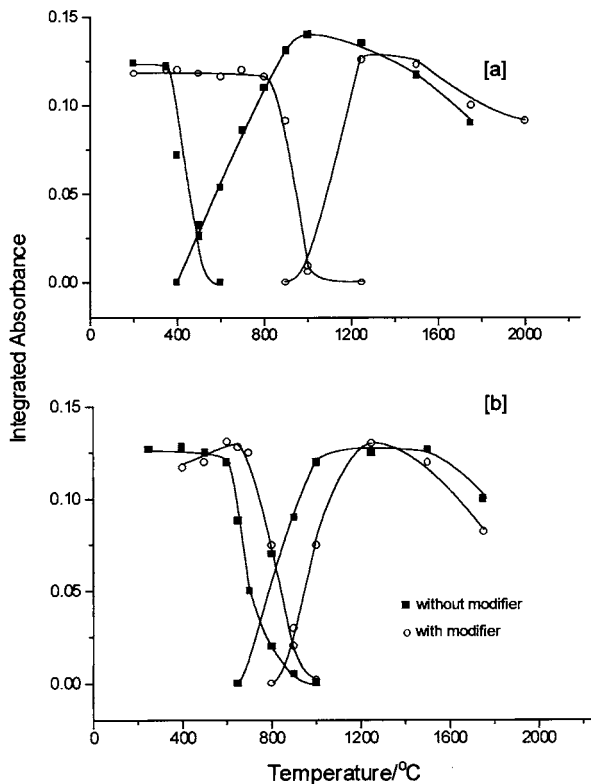


Fig. 3. Pyrolysis and atomization curves of cadmium in absence and presence of palladium/magnesium modifier. (a)  $2.0 \mu\text{g Cd l}^{-1}$  ( $5\% \text{ v/v HNO}_3 + 0.05\% \text{ v/v Triton X-100} + 10\% \text{ v/v ethanol}$ ); (b)  $2.0\% \text{ m/v}$  coal slurry sample (particle size  $< 37 \mu\text{m}$ ).

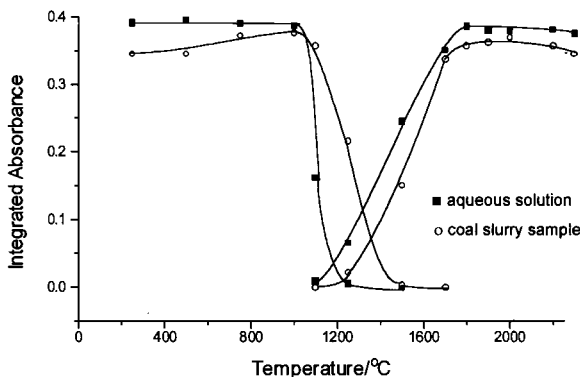


Fig. 4. Pyrolysis and atomization curves of copper in aqueous solution ( $30 \mu\text{g Cu l}^{-1}$  in  $5\% \text{ v/v HNO}_3 + 0.05\% \text{ v/v Triton X-100} + 10\% \text{ v/v ethanol}$ ) and in coal slurry sample ( $0.33\% \text{ m/v}$ ; particle size  $< 37 \mu\text{m}$ ).

Table 2

Effect of diluent composition on integrated absorbance and precision ( $n = 10$ ) of the Pb signal obtained from  $0.5\% \text{ m/v}$  coal slurry sample (particle size  $< 37 \mu\text{m}$  and  $0.05\% \text{ m/v Pd} + 0.03\% \text{ m/v Mg}$ )

Diluent	Integrated absorbance Relative Standard Deviation (RSD) (%)	
	Manual agitation <sup>a</sup>	Ultrasonic agitation <sup>b</sup>
$5\% \text{ v/v HNO}_3 + 0.05\% \text{ v/v Triton}$	0.209 (5.4)	0.141 (2.7)
$5\% \text{ v/v HNO}_3 + 10\% \text{ v/v ethanol}$	0.210 (5.1)	0.152 (3.6)
$5\% \text{ v/v HNO}_3 + 0.05\% \text{ v/v Triton} + 10\% \text{ v/v ethanol}$	0.221 (3.1)	0.156 (2.3)
Aqueous solution $50 \mu\text{g Pb l}^{-1}$ $5\% \text{ v/v HNO}_3$	0.137 (1.7)	0.098 (1.5)

<sup>a</sup> Zeiss AAS5 EA.

<sup>b</sup> Perkin-Elmer 4100ZL.

The precision and trueness of determinations using the slurry technique depend basically on the particle size of the solid material, the sample homogenization, the slurry stability, the liquid medium employed to prepare the slurry, and the slurry concentration ( $\% \text{ m/v}$ ). Based on the data published in the literature, Triton X-100,  $\text{HNO}_3$  and ethanol were chosen as diluent media and the effect of different diluent compositions were investigated by determining the within-run precision [relative standard deviation (RSD)] for ten replicate measurements of a single sample ( $< 37 \mu\text{m}$ ) as shown in Table 2. The choice of the best diluent composition was made according to the lowest RSD. Hence the  $5\% \text{ v/v HNO}_3 + 0.05\% \text{ v/v Triton X-100} + 10\% \text{ v/v ethanol}$  was found to be optimum with respect to a good stabilizing effect, sensitivity and precision. For comparison, there are also the corresponding data for an aqueous solution of  $50 \mu\text{g l}^{-1}$  Pb in  $5\% \text{ v/v HNO}_3$  given in Table 2, indicating that the precision deteriorates by less than a factor of two, compared with a pure solution, when a slurry is analyzed in a proper diluent.

Table 2 also shows a comparison between manual and ultrasonic mixing, which was carried out in different laboratories using different instru-

ments and graphite furnaces (see Section 2.1). In general the two mixing techniques provided comparable precision for all diluents studied, although the values for ultrasonic mixing tend to be somewhat better. The difference in sensitivity between the two sets of data is as a result of the different atomizer tube dimensions used in the two different laboratories, a fact that is well documented in the literature [23,24].

The particle size of the solid material used to make a slurry can influence the stabilization and atomization efficiency of the slurries [5], which in turn can influence both trueness and precision. The influence of particle size was studied by measuring the integrated absorbance signals for lead

with different slurries prepared from the same coal sample but with different particle sizes, for both manual and ultrasonic agitation. In addition, the degree of extraction of lead into the liquid phase of the slurry was investigated by allowing the solids in the slurry to settle and analyzing the supernatant liquid. Figure 5 shows a significant decrease in the integrated absorbance with increasing particle size for both ultrasonic and manual mixing, although, the change of absorbance with particle size is less pronounced for ultrasonic mixing, and the fractions  $< 37 \mu\text{m}$  and  $37\text{--}44 \mu\text{m}$  give essentially the same analytical results with the latter technique. The difference in the integrated absorbance values between the two curves is again as a result of the different atomizer tube dimensions used in the two sets of the experiment, as discussed earlier. Interestingly enough, the amount of analyte extracted into the liquid phase is almost independent of the particle size for both agitation techniques. It should also be noted that the degree of analyte partitioning in slurries was similar (about 45% for  $< 37 \mu\text{m}$ ), for both mixing techniques.

### 3.3. Evaluation of the method

The slurry method was applied to the determination of lead in one coal sample and three certified reference materials using both manual and ultrasonic agitation. All data are summarized in Table 3. The results for the unknown coal sample were compared with those obtained after a conventional acid digestion. In order to verify its reliability, the same acid digestion procedure was also applied to analyze the BCR reference material No. 40, and the result obtained ( $22.1 \pm 0.7 \mu\text{g g}^{-1}$ ) indicated good agreement with the certified value ( $24.2 \pm 1.7 \mu\text{g g}^{-1}$ ).

It can be seen that the contents of lead in the unknown coal sample obtained for both agitation techniques, were in good agreement when the particle size was  $< 37 \mu\text{m}$ . However, as expected from earlier experiments, the concentration values measured for larger particle size samples were about 40% low with manual agitation, and about 20% low for ultrasonic agitation. As shown in Table 3, satisfactory results were obtained for the

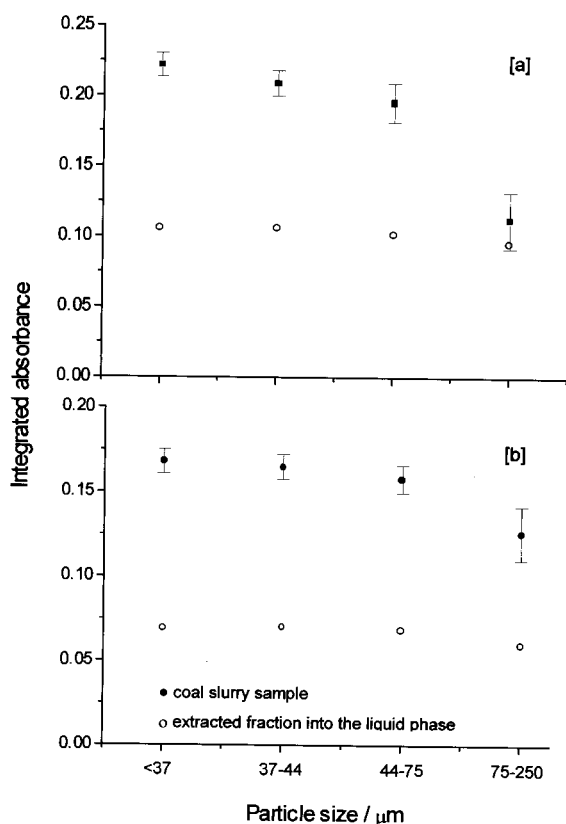


Fig. 5. Effect of the particle size on the integrated absorbance signal and the extracted fraction of lead in 0.5% m/v coal slurry sample (particle size  $< 37 \mu\text{m}$ ). (a) Manual agitation, Zeiss AAS5 EA; (b) Ultrasonic agitation, Perkin Elmer 4100ZL. The lower sensitivity in (b) compared to (a) is as a result of the shorter atomizer tube length of the 4100ZL.

Table 3

Determination of Pb in coal sample and reference materials by slurry sampling and conventional digestion ( $n = 3$ )

Coal Sample	Conventional digestion $\mu\text{g g}^{-1} \pm \text{SD}$	Manual agitation <sup>a</sup> $\mu\text{g g}^{-1} \pm \text{SD}$	Ultrasonic agitation <sup>b</sup> $\mu\text{g g}^{-1} \pm \text{SD}$
Candiota Mine (<37 $\mu\text{m}$ )	$13.9 \pm 0.6$	$14.7 \pm 1.3$	$15.1 \pm 0.6$
Candiota Mine (74–250 $\mu\text{m}$ )	$13.3 \pm 0.8$	$7.9 \pm 0.8$	$12.2 \pm 1.2$
Reference Material	Cert. Value $\mu\text{g g}^{-1} \pm \text{SD}$	Manual agitation <sup>a</sup> $\mu\text{g g}^{-1} \pm \text{SD}$	Ultrasonic agitation <sup>b</sup> $\mu\text{g g}^{-1} \pm \text{SD}$
BCR No.180 (<37 $\mu\text{m}$ )	$17.5 \pm 0.5$	$19.3 \pm 1.3$	$15.9 \pm 0.7$
BCR No.180 (63–212 $\mu\text{m}$ )	$17.5 \pm 0.5$	$16.7 \pm 1.3$	$15.4 \pm 1.4$
BCR No.40 (<37 $\mu\text{m}$ )	$24.2 \pm 1.7$	$20.3 \pm 0.6$	$22.9 \pm 1.0$
BCR No.40 (60–90 $\mu\text{m}$ )	$24.2 \pm 1.7$	$17.2 \pm 0.6$	$17.8 \pm 1.7$
BCR No.181 (<37 $\mu\text{m}$ )	$2.59 \pm 0.16$	$2.69 \pm 0.23$	$2.50 \pm 0.11$
BCR No.181 (63–212 $\mu\text{m}$ )	$2.59 \pm 0.16$	$1.13 \pm 0.16$	$1.68 \pm 0.32$

<sup>a</sup> Zeiss AAS5 EA.<sup>b</sup> Perkin–Elmer 4100ZL.

three certified reference materials when particle sizes were reduced to < 37  $\mu\text{m}$ . Application of a common t-test revealed that there were no significant differences between manual and ultrasonic agitation. For the majority of the samples, however, low results were obtained with larger particle sizes, i.e. when the samples were analyzed without further grinding and sieving, even when ultrasonic mixing was applied. Therefore it appears to be generally advisable to reduce the particle size to < 37  $\mu\text{m}$  for slurry sampling, independent of the agitation technique used, which is in good agreement with the particle size of < 40  $\mu\text{m}$  reported by other groups [3,5,8].

The results for cadmium and copper in the coal sample and in the reference materials, which were measured with the manual mixing technique only, are listed in Table 4. Statistical evaluation indi-

cated that the results of the proposed slurry sampling procedure are comparable to those of the traditional acid digestion and certified values. Certified values for copper are not available for the BCR reference materials, so that only the digestion method could be applied for comparison. The analytical figures of merit, of the proposed slurry sampling method, using manual agitation, are summarized in Table 5 for all three elements investigated.

#### 4. Conclusion

In coal slurry analysis, the palladium–magnesium modifier had little effect in stabilizing cadmium and lead during pyrolysis, but it increased the optimum atomization temperature for both

Table 4

Determination of Cd and Cu in coal by slurry sampling with manual agitation and acid digestion using the Zeiss AAS5 EA only ( $\mu\text{g g}^{-1} \pm \text{SD}$ ,  $n = 3$ ; particle size < 37  $\mu\text{m}$ )

Coal Sample	Cd			Cu	
	Slurry sampling	Acid digestion	Certified value	Slurry sampling	Acid digestion
Candiota mine	$0.081 \pm 0.009$	$0.085 \pm 0.002$	–	$11.0 \pm 0.9$	$11.9 \pm 0.52$
BCR No. 180	$0.239 \pm 0.012$	–	$0.212 \pm 0.011$	–	–
BCR No. 40	$0.12 \pm 0.01$	–	$0.11 \pm 0.02$	–	–
BCR No. 181	$0.048 \pm 0.005$	–	$0.051 \pm 0.003$	–	–

Table 5

The analytical figures of merit of the proposed slurry sampling method (Zeiss AAS5 EA)

Element	Concentration of slurry (%m/v)	Average slope (s ng <sup>-1</sup> )	Detection limit µg g <sup>-1</sup> (3σ)	Characteristic mass pg (0.0044s) <sup>-1</sup>	Concentration of high STD (ng)
Pb	0.5	0.152 ± 0.002	0.3	42	2.0
Cd	2.0	2.29 ± 0.02	0.005	2.2	0.12
Cu	0.33	0.481 ± 0.005	0.1	6.9	1.0

elements. Apparently the coal matrix itself had a stabilizing effect on these elements in the pyrolysis stage. The results obtained in this work have shown that slurry sampling is a very rapid and economic alternative to conventional acid digestion procedures for coal analysis. Sample preparation and the analysis can be performed in about 15 min, and only very small amounts of reagents are required. The low risk of contamination, the simple handling, and the possibility to use the standard calibration technique with aqueous standards are very favorable for a routine application. Finally, when particle size is reduced to < 37 µm, both, manual and ultrasonic agitation gave good trueness and precision so that manual agitation may be considered an attractive low-cost approach.

### Acknowledgements

The authors gratefully acknowledge the assistance of Dr Francisco J. Krug (CENA-USP, Piracicaba, S.P.) and Dr Bernhard Welz (Depto. de Quimica, UFSC, Florianópolis, S.C.) who have helped making this work possible. The FAPERGS and CNPq are acknowledged for financial support.

### References

- [1] Informativo anual da indústria carbonífera. Departamento Nacional de Produção Mineral—DNPM. Brasília. Ano XII, 1994.
- [2] M.C. Carneiro, R.C. Campos, A.J. Curtius, *Talanta* 40 (1993) 1815.
- [3] C. Bendicho, M.T.C. Loos-Vollebregt, *J. Anal. At. Spectrom.* 6 (1991) 353.
- [4] L. Ebdon, H.G.M. Parry, *J. Anal. At. Spectrom.* 2 (1987) 131.
- [5] L. Ebdon, H.G.M. Parry, *J. Anal. At. Spectrom.* 3 (1988) 131.
- [6] N.J. Miller-Ihli, *J. Anal. At. Spectrom.* 3 (1988) 73.
- [7] N.J. Miller-Ihli, *Spectrochim. Acta* 50B (1995) 477.
- [8] U. Schäffer, V. Krivan, *Spectrochim. Acta* 51B (1996) 1211.
- [9] N.J. Miller-Ihli, *J. Anal. At. Spectrom.* 9 (1994) 1129.
- [10] A. Carlosena, M. Gallego, M. Valcárcel, *J. Anal. At. Spectrom.* 12 (1997) 479.
- [11] P. Bermejo-Barrera, A. Moreda-Piñero, T. Romero-Barbeito, J. Moreda-Piñero, A. Bermejo-Barrera, *Talanta* 43 (1996) 1099.
- [12] P. Bermejo-Barrera, A. Moreda-Piñero, J. Moreda-Piñero, A. Bermejo-Barrera, *Anal. Chim. Acta* 296 (1994) 181.
- [13] R. Dobrowolski, J. Mierzwa, *Fresenius J. Anal. Chem.* 346 (1993) 1058.
- [14] P. Bermejo-Barrera, C. Barciel-Alonso, M. Aboal-Somoza, A. Bermejo-Barrera, *J. Anal. At. Spectrom.* 9 (1994) 469.
- [15] S.C. Stephen, D. Littlejohn, J.M. Ottaway, *Analyst* 110 (1985) 1147.
- [16] X-q. Shan, W. Wang, B. Wen, *J. Anal. At. Spectrom.* 7 (1992) 761.
- [17] B. Welz, M. Sperling, *Atomic Absorption Spectrometry*, third ed., Wiley, Weinheim, New York, Chichester, Toronto, Brisbane, Singapore, 1999, p. 367.
- [18] H. Qiao, K.W. Jackson, *Spectrochim. Acta* 47B (1992) 1267.
- [19] N.J. Miller-Ihli, *Fresenius J. Anal. Chem.* 345 (1993) 482.
- [20] P. Bermejo-Barrera, A. Moreda-Piñero, J. Moreda-Piñero, A. Bermejo-Barrera, *Anal. Chim. Acta* 310 (1995) 355.
- [21] M.W. Hinds, M. Katyal, K.W. Jackson, *J. Anal. At. Spectrom.* 3 (1988) 83.
- [22] M.W. Hinds, K.W. Jackson, *J. Anal. At. Spectrom.* 3 (1988) 997.
- [23] W. Slavin, G.R. Carnrick, *Spectrochim. Acta* 39B (1984) 271.
- [24] B.V. L'vov, V.G. Nikolaev, E.A. Norman, L.K. Polzik, M. Mojica, *Spectrochim. Acta* 41B (1986) 1043.

# Novel calibration of a dynamic surface tension detector: flow injection analysis of kinetically-hindered surface active analytes

Keith E. Miller<sup>a</sup>, Kristen J. Skogerboe<sup>b</sup>, Robert E. Synovec<sup>a,\*</sup>

<sup>a</sup> Center for Process Analytical Chemistry, Department of Chemistry, Box 351700, University of Washington, Seattle, WA 98195-1700, USA

<sup>b</sup> Department of Chemistry, Seattle University, Seattle, WA 98122, USA

Received 12 April 1999; received in revised form 30 June 1999; accepted 1 July 1999

## Abstract

First, a novel technique for calibration of a dynamic surface tension detector (DSTD) is described. The DSTD measures the differential pressure as a function of time across the liquid–air interface of growing drops that repeatedly form and detach at the end of a capillary tip. The calibration technique utilizes the ratio of pressure signals acquired from the drop growth of two separate solutions, i.e. a standard solution and a corresponding mobile phase, such as water, both of which have a known surface tension. Once calibrated, the dynamic surface tension of an analyte is obtained from the ratio of the pressure signals from the analyte solution to that of the mobile phase solution. Thus, this calibration technique eliminates the need to optically image the radius of the expanding drop of liquid. Accurate dynamic surface tension determinations were achieved for aqueous sodium dodecyl sulfate (SDS) solutions over a concentration range of 0.5–5.4 mM. The measured surface tensions for these SDS solutions range from 70.3 to 46.8 dyne/cm and were in excellent agreement with the literature. A precision of 0.2 dyne/cm (1 S.D.) was routinely obtained. Second, the DSTD with this calibration technique was combined with flow injection analysis (FIA) for the study of model protein solutions and polymer solutions. The kinetic surface tension behavior of aqueous bovine serum albumin (BSA) solutions as a function of concentration and flow rate is presented. Evaluation of the dynamic surface tension data illustrates that a protein such as BSA initially exhibits kinetically-hindered surface tension lowering, i.e. a time dependence, as BSA interacts with the liquid–air interface of an expanding drop. FIA/DSTD is then shown to be an effective tool for the rapid study of kinetically-hindered surfactant mixtures. It was found that mixtures of SDS and the polymeric surfactant Brij<sup>®</sup>-35 (lauryl polyoxyethylene ether with an average molecular weight of 1200 g/mol) result in essentially an additive lowering of the surface tension. Mixtures of polyethylene glycol (PEG), with an average molecular weight of 1470 g/mol, and Brij<sup>®</sup>-35, however, result in a competitive (non-additive) surface tension with the Brij<sup>®</sup>-35 dominating the response. © 1999 Elsevier Science B.V. All rights reserved.

\* Corresponding author. Fax: +1-206-685-8665.

E-mail address: synovec@chem.washington.edu (R.E. Synovec)

*Keywords:* Dynamic surface tension detector (DSTD); Flow injection analysis; Kinetically-hindered surface active analytes

---

## 1. Introduction

The commercial use of surfactants is widespread [1], and a wide variety of analytical techniques that measure the dynamic surface tension of surfactant solutions has been reported [2,3]. These include methods utilizing the maximum bubble pressure [4,5], drop volume [6,7], growing drop [8–11], and pulsating bubble methods [12,13]. Many of these techniques require large volumes or focus on repeatedly perturbing a single drop or bubble, thus making them impractical for flow-based analytical applications such as liquid chromatography or flow injection analysis.

The development of a dynamic surface tension detector (DSTD) for use in flow injection analysis (FIA) and high performance liquid chromatography (HPLC) applications is a continuing focus of our research [14–18]. Our efforts in this area are aimed at the development of a detector that requires small volumes of sample and is amenable to HPLC and FIA. The DSTD is a capillary-based detector that senses the surface tension properties of liquid drops that repeatedly form at a capillary tip.

We have recently reported modifications to earlier designs of the DSTD based on measuring the differential pressure across the liquid–air interface of growing drops as a function of time [17,18]. While this new configuration offers many advantages, the multi-dimensional nature of the signal necessitates improvements in calibration and data analysis in order to extract more fully the kinetic information of the surface tension lowering process. Related surface tension measurements based upon the growing drop technique have been reported [8,9]. In this work, the dynamic surface tension at either the liquid–air or liquid–liquid interface was obtained by fitting the measured pressure inside growing drops at a constant flow rate to a modified Young–Laplace equation. The authors reported that while the drop maintained a spherical shape during the first third of drop growth, the drop elongates due to hydrostatic forces acting on the mass of the drop during the

remaining growth. To compensate for the effects of drop elongation, the radius of the drop was also measured throughout drop growth, and corrections were made to the corresponding pressure signal to obtain an accurate dynamic surface tension. The method [8,9] focused on the elongation and subsequent correction of the pressure signal within one drop, i.e. for a given sample solution. Thus, a radius correction derived from optically imaging the drop was required to obtain the dynamic surface tension information from the measured pressure signal.

We present a novel calibration technique for the measurement of surface tension that eliminates the need for drop imaging. The calibration technique utilizes the ratio of pressure signals acquired from the drop growth of two separate solutions, i.e. a standard solution and a corresponding mobile phase, such as water, both of which have a known surface tension. Once calibrated, the dynamic surface tension of an analyte is obtained from the ratio of the pressure signals from the analyte solution to that of the mobile phase solution. Essentially, within a reasonably wide range of surface tension, each solution's drop exhibits a similar degree of elongation as a function of time. Using these time-dependent pressure measurements from individual drops, which are hereon referred to as drop profiles, we present a technique that provides a rapid calibration of the DSTD without the use of cumbersome optical methods. We confirm, by using a laser-based optical measurement, that an acceptably small error is introduced. Once calibrated, the DSTD is shown to provide an accurate dynamic surface tension measurement throughout nearly the entire growth of each drop. We use the new calibration technique to advantage with the application of the DSTD as a 'multi-channel' detector for FIA. Our previous work was limited in signal-to-noise ratio (S/N) and response time to using the pressure data at the pressure maximum of each drop [18]. In this work, we determined that use of a pressure sensor with a considerably faster response and a syringe pump with a steady, low-



noise pump flow rate enabled the use of the nearly complete pressure data for each drop. Thus, the measurement of interesting kinetic surface tension behavior of surface active proteins, such as bovine serum albumin (BSA), and polymer mixtures are presented, where the molecular structure and size of the surface active analytes significantly inhibit the diffusion to, and molecular orientation at, the liquid–air interface during the growth of a drop. The effect of solution viscosity is examined and the time-dependent surface tension lowering is shown to be not due to solution viscosity. In addition, the ability to examine additive and competitive effects on surface tension of individual surface active components in surfactant mixtures is presented.

## 2. Theory

The DSTD relies on a pressure sensor mounted in the side arm off the main flow of a capillary (not shown for brevity, see Fig. 1 in Ref. [17]). A constant flow is maintained to the DSTD resulting in the repeated formation and detachment of drops. Each drop is considered an individual sample, with the DSTD providing a vector of pressure data, i.e. *drop profile*, over each drop's lifetime. The drops are approximately spherical for a significant portion of their growth. Thus, the surface tension at the liquid–air interface of the drop can be related to the Young–Laplace equation [19] by

$$P = 2\gamma/r \quad (1)$$

where  $P$  is a measure of the differential pressure across the drop interface relative to atmospheric pressure,  $\gamma$  is the surface tension at the liquid–air interface, and  $r$  is the radius of a static drop. Since the radius of the drop is constantly changing as a function of time,  $t$ , Eq. (1) is modified to

$$P(t) = 2\gamma(t)/r(t) \quad (2)$$

The measured pressure signal consists not only of changes in surface tension occurring at the liquid–air interface in the growing drop, but also from viscosity, drop elongation and instrumental contributions. Therefore, Eq. (2) must, in practice [8], be modified to account for these contributions such that

$$P(t) = 2\gamma(t)/r(t) + P_{\text{VIS}}(t) + P_{\text{INST}} - P_{\text{ELONG}}(t) \quad (3)$$

where  $P_{\text{VIS}}(t)$  accounts for the viscosity induced pressure drop in the capillary tubing,  $P_{\text{INST}}$  accounts for pressure offset due to differences in the relative position of the pressure sensor from the capillary tip, and  $P_{\text{ELONG}}(t)$  accounts for drop elongation due to gravity acting on the drop's mass. MacLeod and Radke [8] previously defined the elongation contribution

$$P_{\text{ELONG}}(t) = \rho g(z_{\text{T}}(t) - z_{\text{E}}(t)) \quad (4)$$

where  $\rho$  is the density of the solution forming a drop and  $g$  is the gravitational constant. The distances defined as  $z_{\text{T}}(t)$  and  $z_{\text{E}}(t)$ , correspond to the vertical diameter of a growing drop and the vertical distance from a drop's apex to the equator, respectively (see Ref. [8] for a complete discussion).  $P_{\text{ELONG}}(t)$  accounts for a hydrostatic pressure difference contribution that provides an additional downward force opposing the liquid–air surface tension force of the drop at the capillary tip.

While  $P_{\text{ELONG}}(t)$  is an important contributor to the total signal, we show that it is not necessary to determine this factor for accurate surface tension measurements. It is possible to calibrate by relying on the condition that for a limited, but useful range of  $\gamma(t)$ , the  $P_{\text{ELONG}}(t)$  and  $P_{\text{VIS}}(t)$  contributions to the measured pressure signal in Eq. (3) are essentially negligible, and  $P_{\text{INST}}$  is essentially constant. Indeed, the capillary tip can and has been designed to minimize the viscosity contribution [17]. Thus, the additional pressure contributions can be reduced to a single, time-independent constant,  $P_{\text{C}}$ , allowing Eq. (3) to be modified such that

$$P(t) = 2\gamma(t)/r(t) + P_{\text{C}} \quad (5)$$

Furthermore, the drop growth function,  $r(t)$ , while not truly radial due to elongation, is approximately equivalent at any given time during drop growth when comparing two separate drops to each other. By this we mean that at a given volumetric flow rate, the *effective* radius of the growing drop will be approximately the same at a given time,  $t$ , for both a drop containing only the

mobile phase, M, and a drop containing either a surface active standard or analyte, A. This condition is consistent with treatment of the radius function by MacLeod and Radke [8] where they approximate the  $r(t)$  as the mean radius of the drop at any given instant in time. This is the key to the calibration method. Using this approximation,  $r(t)_A = r(t)_M$ , and Eq. (5), a surface tension ratio can be obtained, effectively removing the radius term,

$$\gamma(t)_A/\gamma_M = (P(t)_A - P_C)/(P(t)_M - P_C) \quad (6)$$

where  $\gamma_M$  replaces  $\gamma(t)_M$  since the surface tension of the mobile phase is constant. By taking the ratio in this fashion, essentially all of the effects due to drop elongation are cancelled and the need for the optical measurement of drop radius can be avoided. The surface tension ratio defined in Eq. (6) is, from this point forward, referred to as a dynamic surface tension ratio (DST ratio). Note that a DST ratio is obtained for each drop over the course of a FIA or HPLC run that will contain many DST ratios. Thus, the data are processed very much like one would process full absorbance spectra, with a matrix of data produced for each run. Here, the time interval of the FIA or HPLC run is determined by keeping track of the drop time interval and running time of each DST ratio [18]. While the drop time interval also contains other interesting information regarding the behavior of surfactants, such as adhesion [17], we do not make use of the drop time interval data for this purpose in the current study.

Detector calibration is accomplished by measuring the drop profile data,  $P(t)$  as defined in Eq. (5), for both an aqueous standard and a suitable aqueous mobile phase, generally water or a buffer, each with known surface tensions. It is critical that the selected standard and mobile phase each possess surface tension characteristics that are time-independent. That is,  $\gamma(t)$  for the calibration substances must be essentially constant throughout the growth of a drop. By using the drop profiles,  $P(t)$ , of these calibrating solutions, and establishing a condition that the surface tension ratio,  $\gamma(t)_A/\gamma_M$ , must be both constant and accurate, the correct constant,  $P_C$ , as defined in Eq. (6) is readily obtained. For the results pre-

sented here, aqueous acetic acid solutions are selected as calibration standards for the detector since acetic acid is a small molecule that is expected to rapidly obtain an equilibrium surface concentration throughout drop growth. Thus, the  $\gamma(t)_A/\gamma_M$  for acetic acid should be constant throughout the growth of the drop, and is assumed so for the purpose of determining  $P_C$ .

Once the DSTD is calibrated by determining  $P_C$ , the DST ratio of an analyte solution can be measured and then converted to absolute dynamic surface tension  $\gamma(t)_A$ , if the surface tension  $\gamma_M$  for the mobile phase is known and constant, by the following relationship:

$$\gamma(t)_A = \gamma(t)_A/\gamma_M \times \gamma_M \quad (7)$$

using  $P_C$  following Eq. (6) to determine  $\gamma(t)_A/\gamma_M$  for the analyte from  $P(t)$  data. For analytes that exhibit a known and constant  $\gamma(t)_A$ , Eq. (7) can be applied to evaluate the validity, i.e. accuracy, of the calibration procedure. Furthermore, once the DSTD has been calibrated, Eqs. (6) and (7) can be applied to a variety of analyte systems to examine the kinetic dependence of  $\gamma(t)_A$ . We explore both of these applications.

### 3. Experimental

#### 3.1. Materials

Sodium salt of dodecyl sulfate (SDS) (98%) and Brij<sup>®</sup>-35 (lauryl polyoxyethylene ether with an average molecular weight of 1200 g/mol) were obtained from Aldrich (Milwaukee, WI). Bovine serum albumin (BSA) (greater than 97% purity) was obtained from Sigma (St Louis, MO). Polyethylene glycol (PEG) with an average molecular weight of 1470 g/mol ( $M_p = 1470$ ,  $M_w/M_n = 1.02$ ) was obtained from Polymer Laboratories (Amherst, MA). All other chemicals were reagent grade quality and obtained from J.T. Baker (Phillipsburg, NJ): acetic acid (glacial), glycerol (anhydrous), disodium hydrogen phosphate and potassium diphosphate. All chemicals were used as received without further purification. Deionized (DI) water, demineralized to greater than 18 M $\Omega$  with a Millipore system (Millipore,

Bedford, MA), was used in the preparation of all sample solutions and buffer solutions. The water was degassed prior to use. A phosphate buffer solution (0.016 M  $\text{KH}_2\text{PO}_4$ , 0.062 M  $\text{Na}_2\text{HPO}_4$ , pH 7.4) and protein samples prepared in this buffer were refrigerated when not in use. All results reported here were obtained within 48 h of sample preparation.

### 3.2. Instrumentation

#### 3.2.1. FIA experiments

A schematic of the DSTD configuration, not shown here for brevity, is shown in Fig. 1 of Ref. [17]. A syringe pump (Isco  $\mu\text{LC}$ -500, Lincoln, NE) was used to deliver the mobile phase (DI water) to the DSTD during FIA experiments. Samples were introduced via a six-port injection valve (Rheodyne 7125, Cotati, CA). Injection volumes of 85 and 200  $\mu\text{l}$  were used for FIA experiments conducted at 120  $\mu\text{l}/\text{min}$  and below. For experiments conducted at 200  $\mu\text{l}/\text{min}$ , a 360- $\mu\text{l}$  injection volume was used. Sample loop injection volumes were adjusted by varying the length of poly(etheretherketone) (PEEK) tubing (Upchurch, Oak Harbor, WA). Sufficient volume was injected so that, even for the samples in phosphate buffer, the center of the detected sample plug was not diluted by the water mobile phase. Thus, the sample size injected in the FIA experiments was selected such that the analyte signal reached a steady state (i.e. constant concentration) response during the measurement.

The DSTD configuration is identical to that detailed in previous work [17] with the important exception of the sensitivity and response time of the sensing membrane. The pressure sensor (Validyne P305D-20-2369, Northridge, CA) was configured with a sensing membrane (Validyne diaphragm 3-36, Northridge, CA) that optimized the response time of the DSTD for measurements of interfacial kinetics, without sacrificing too much sensitivity, although it was 40-fold less sensitive than in our previous work [17,18].

All data were collected at 10 kHz with a personal computer (150 MHz Pentium<sup>®</sup>, Intel, Santa Clara, CA) equipped with a data acquisition card (DAC) (MIO-16B, National Instruments, Austin,

TX). The data were averaged down to 100 points/s prior to saving. Data collection and drop profile extraction were completed using LABVIEW (Version 5, National Instruments, Austin, TX) programs written in-house. Subsequent data manipulation and calculations, including a 10-point, moving boxcar smooth, were performed with MATLAB 4 (MathWorks, Natick, MA) and Excel (Microsoft, Redmond, WA) software applications.

#### 3.2.2. Optical measurement of drop effective radius

For some experiments, additions to the FIA apparatus were made to optically probe the growing drop radius. The DSTD and a laser diode at 670 nm (5 mW, Model PL-0, Laser Devices, Monterey, CA) were each mounted on separate X-Y-Z translational stages (Newport, 460 X-Y-Z, Fountain Valley, CA). Modifications to earlier configurations were made [15,16] in order to measure the change in the elongated drop radius as a function of time, for drops of different surface tension. The laser diode beam was positioned along the same axis and near the tip of the capillary, thus probing the growth of a given drop in the vertical plane, prior to impinging on the photodiode. The signal from the photodiode was amplified and collected simultaneously with the pressure signal from the DSTD. A calibration curve was obtained by adjusting the vertical position of the diode laser with the X-Y-Z translational stage. This change in position was then related to a relative change in the elongated drop radius. The difference in the elongated radius of two drops of differing surface tension was obtained as a function of drop growth time.

## 4. Results and discussion

### 4.1. Detector calibration

Representative raw data obtained using FIA/DSTD is shown in Fig. 1(A). Individual drop profiles for both the analyte and water are extracted from the raw data and used in the calibration procedure. The extracted drop profiles,

corresponding to the analyte and water, are shown in Fig. 1(B). Selected time regimes of the drop profiles were removed before commencing with the calibration procedure to eliminate portions of the drop profile that were dominated by an artifact from the pressure sensing membrane. As previously described [17,18], there exists a finite ‘loading’ time of the sensor membrane as the pressure builds to a pressure maximum. This loading time, identified in Fig. 1(B) as the initial portion of the drop profile that rises rapidly, is subsequently followed by an ‘unloading’ of the sensor membrane. The loading and unloading time has been significantly minimized, reduced from our previous configuration by the selection of a 40-fold more rigid membrane. With the cur-

rent sensor membrane, the unloading time was estimated to be equal in duration to that of the loading period. Thus, only  $P(t)$  data collected after twice the loading period within each drop were used. For example, from Fig. 1(B), the time interval neglected was the first 1.5 s of each  $P(t)$  drop profile. After this time interval, the volume and effective radius of any given growing drop is approximately equal. At higher flow rates, the neglected time interval will be proportionately less. Alternatively, a pressure sensor based upon a piezoelectric transducer can be considered. Previous reports indicate that the piezoelectric pressure sensors also exhibit a finite response time [8,9] similar to the response time observed with our current design. Additional study into the information content in the sensor ‘loading’ and ‘unloading’ time is warranted, since surface elasticity information is also present in this region of the drop profile data.

Calibration of the DSTD according to Eq. (6) was applied as follows. Drop profiles for 2.5 and 5.0% (w/w) acetic acid solutions, similar to those shown in Fig. 1(B), were used to obtain DST ratios,  $\gamma(t)_A/\gamma_M$ , at each concentration. Since surface tension lowering for acetic acid is essentially constant throughout drop growth, the scatter of the DST ratio data about a line with zero slope, i.e. variance, should be at or near zero when the correct  $P_C$  is selected. In addition, the predicted surface tensions of the acetic acid solutions should be accurate since they are used as standards. The calibration constant,  $P_C$ , is determined by iterative calculation until the variance of the predicted DST ratio,  $\gamma(t)_A/\gamma_M$ , was minimized, as shown in Fig. 2(A) for 5.0% acetic acid in water. The importance of minimizing the variance about  $\gamma(t)_A/\gamma_M$  for the 5.0% acetic acid solution is shown in Fig. 2(B). When a  $P_C$  corresponding to the minimum variance [point b in Fig. 2(A)] psi was selected, the slope of the 5.0% acetic acid DST ratio in Fig. 2(B) was essentially zero and the predicted surface tension of 62.7 dyne/cm was in excellent agreement with the literature [20]. If an incorrect value of  $P_C$  is selected, the slopes of the DST ratios were not zero [points a and c in Fig. 2(B)] and the predicted surface tension values were not accurate, thus failing to meet the zero

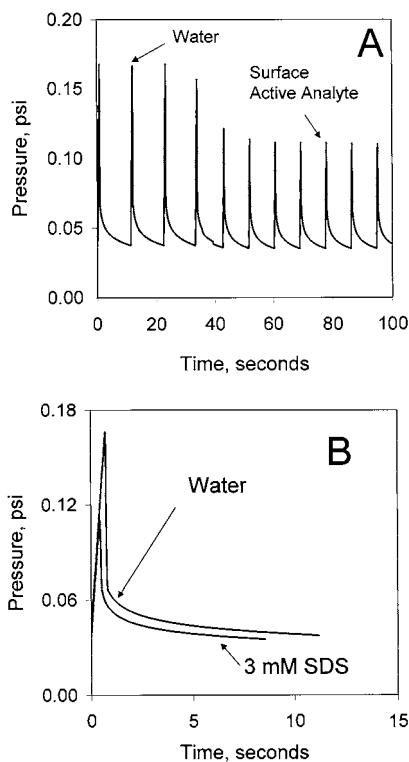


Fig. 1. (A) Raw pressure data using FIA/DSTD: A representative DSTD pressure signal,  $P(t)$ , for a 3 mM SDS sample eluted in water at 40  $\mu\text{l}/\text{min}$ . Each drop produces a maximum and a minimum pressure during drop growth. As the SDS solution is eluted, the maximum pressure signal is lowered, indicating the lowering of surface tension of the sample. (B) Drop profiles: An overlay of individual drop profiles of water and 3 mM SDS extracted from the  $P(t)$  data shown in (A).

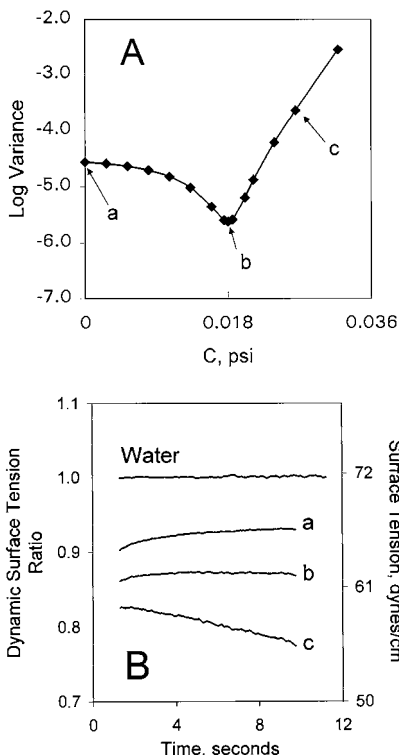


Fig. 2. Calibration of the DSTD at 40  $\mu\text{l}/\text{min}$ . (A) Log of the variance of the surface tension ratio versus calibration constant,  $P_C$ , using 5.0% acetic acid solution and water. The point at which the variance is minimized, b, is selected as the calibration constant. (B) DST ratios and absolute surface tension after application of Eq. (7) of 5.0% acetic acid solutions, shown in relation to water, using the calibration constants indicated in (A). Note how only the  $P_C$  corresponding to point b (0.018 psi) in (A) meets both the zero slope and surface tension accuracy criteria. By application of Eq. (6), the radius dependence of drop profiles similar to those shown in Fig. 1(B) is removed.

slope and accuracy criteria of the calibration procedure. These DST ratios are representative, and are shown for one acetic acid solution drop relative to one water drop for the 5.0% acetic acid standard. The DST ratio for one water drop relative to another water drop results in a value nominally at 1.00.

The calibration constant ( $P_C = 0.018$  psi) was found to be the same for both acetic acid solutions. The detector was calibrated by this procedure each day it was used, since  $P_C$  is flow rate and temperature-dependent. Note that a  $P_C$  of 0.018 psi at 40  $\mu\text{l}/\text{min}$  water, when added to the

predicted minimum pressure due to surface tension (0.019 psi) accounts for essentially all of the vertical offset of the raw data in Fig. 1(A,B). This is strong evidence that the pressure contributions due to  $P_{\text{ELONG}}(t)$  (hydrostatic pressure) and  $P_{\text{VIS}}(t)$  (viscosity) can be neglected. We now turn our attention to investigating whether or not the calibration constant and Eq. (7) can be applied to accurately measure surface tension.

#### 4.2. Assessment of calibration accuracy with sodium dodecyl sulfate (SDS) solutions

Following calibration, the DST ratios over a range of SDS concentrations were determined, with representative results shown in Fig. 3(A). Each DST ratio in Fig. 3(A) represents the application of Eq. (6) to one SDS drop profile and one water drop profile. Next, all DST ratios for each SDS solution were converted to absolute, dynamic surface tensions by Eq. (7), using a surface tension for water of 72.1 dyne/cm at 24°C (temperature corrected surface tension obtained from Ref. [21]). Note that at the flow rate applied, the DST ratios for each SDS solution in Fig. 3(A) are nearly constant (zero slope). Thus, an average of the DST ratio was calculated over the lifetime of the drop for each SDS solution presented in Fig. 3(A) to determine an average surface tension. To assess the accuracy of the calibration procedure, the average dynamic surface tension for each SDS solution was compared to literature values reported by Mysels [22]. In this reported work, the surface tensions over a concentration range of SDS solutions were fit to a second-order function. The comparison between methods is graphically presented in Fig. 3(B). Dynamic surface tensions reported in Fig. 3(B) were obtained by calculating the mean from the drop profiles of five separate aqueous SDS solutions and five water drops. The drop profiles were paired such that 25 surface tension profiles at each concentration were determined. The relative standard deviation (R.S.D.) at each SDS concentration was 0.2 dyne/cm. With this R.S.D., the error bars associated with each measurement are too small to be graphically depicted in Fig. 3(B). The surface tensions obtained by our method are in good agreement with litera-

ture values [22]. Based on these results, the assumptions made in the derivation of Eqs. (5)–(7) and the calibration procedure are supported. To examine the issue of reproducibility and long-term accuracy, additional SDS dynamic surface tensions, obtained from a subsequent experiment, are also shown in Fig. 3(B). A comparison of the dynamic surface tensions obtained from our two experiments (conducted over 2 months apart) shows excellent reproducibility.

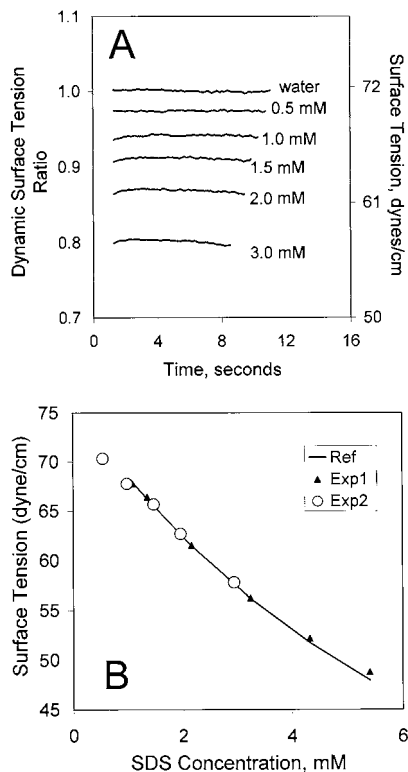


Fig. 3. Assessment of calibration accuracy using SDS solutions. (A) The DST ratios and absolute surface tension after application of Eq. (7) of SDS solutions ranging in concentration from 0.5 to 3.0 mM. Measurements were made at 40  $\mu$ /min using the calibration constant determined from Fig. 2. (B) Comparison of surface tensions obtained with the calibrated DSTD (Exp. 1 and Exp. 2) with those reported in the literature [22]. For comparison purposes, the calculated mean of the dynamic surface tension over the lifetime of the drops shown in (A) is used. Average surface tensions for two separate experiments (Exp. 1 and Exp. 2), conducted 2 months apart, are shown covering a range of SDS concentrations of 0.5–5.4 mM.

#### 4.3. Examination of the assumptions in the calibration procedure

To further confirm the validity of the calibration procedure, additional measurements were performed to determine to what extent the assumptions made in the derivation of Eqs. (5)–(7) are valid. Specifically, drop size was measured to determine the significance of equating the time-dependent radius functions for drops of differing surface tension. Secondly, the effect of sample viscosity on the measured pressure signal and subsequent calibration procedure was also evaluated.

The change in the elongated drop radius as surface tension is lowered was examined using the optical arrangement described in Section 3. The vertical dimension of a growing drop was optically measured as a function of drop time. The change in the elongated drop radius between a 2.5% acetic acid solution ( $\gamma = 65$  dyne/cm) and water ( $\gamma = 72$  dyne/cm) as a function of drop time was measured, but not shown for brevity. The increase in the elongated radius for the 2.5% acetic acid solution was observed to be from 1.5 to 5  $\mu$ m throughout the first 95% of drop growth. While this change in the elongated radius does not directly correspond to a change in the *effective mean* radius of the drop, we made this conservative assumption for the purposes of the following discussion; that is, the change in the elongated radius corresponds to a change in the effective mean radius. Assuming the effective mean radius of the drop began at about 125  $\mu$ m and detached with an effective mean radius of about 1.1 mm, the error in equating the effective radius at a given time ranges from about 1.5% as the drop just emerges, to less than 1% error just prior to detachment. These optical measurements are supported by theory. At drop detachment, Eq. (2) yields a water drop pressure of 0.019 psi for a 1.1 mm radius drop. Using Eq. (4) coupled with Fig. 6 in Ref. [8], the  $P_{\text{ELONG}}(t)$  for the water drop at the moment of detachment is estimated to be 0.0002 psi. Thus, the  $P_{\text{ELONG}}(t)$  contribution, which is the most significant at the moment of detachment, is only about 1% of the drop pressure due to liquid–air surface tension, and we accept this error.

It must be noted that confidence in our optical measurement of drop elongation during the last 5% of drop growth was limited due to rapid elongation, or ‘necking’, just prior to drop detachment. While this phenomenon has been observed and reported by others [7], the apparent contribution to the measured pressure is minimal. Evidence for this assertion is that the DST ratios in Fig. 2(B) and Fig. 3(A) are well behaved up to and including the moment of drop detachment, and surface tension measurements are accurate.

The assessment of the contribution of sample viscosity to the DSTD signal was evaluated by measuring the relative viscosity of the surface active sample solutions analyzed in this study. The relative viscosity measurements were made with a viscometer built in-house using aqueous glycerol solutions as standards [21]. The relative viscosity of all the surface active samples reported here are considerably closer to the viscosity of water than that of a 10% glycerol solution. In addition to viscosity measurements, DST ratios for selected glycerol solutions were obtained with the DSTD. A 10% glycerol yielded a time-independent DST ratio of 0.99 relative to water. Thus, the 10% glycerol solution exhibits only a slight reduction in surface tension relative to water, about a 0.8 dyne/cm decrease, as is expected at this concentration. Thus, based on the results of the viscosity measurements and the evaluation of the DST ratios of the glycerol solutions (not shown for brevity), it was concluded that the viscosity contribution to the DSTD signal at and below the level of viscosity exhibited by 10% glycerol can be neglected in the current configuration for the surface active samples analyzed. The error introduced increases with flow rate, but we found the error was still less than 1% at 200  $\mu\text{L}/\text{min}$  for a sample with a relative viscosity at or below 1.05, such as a 1 mg/ml BSA solution.

#### 4.4. Kinetic surface tension behavior of proteins and surfactant mixtures

The results presented above include only those from solutions with surface active analytes that show negligible kinetic hindrance. By this we mean surface active analytes whose molecular

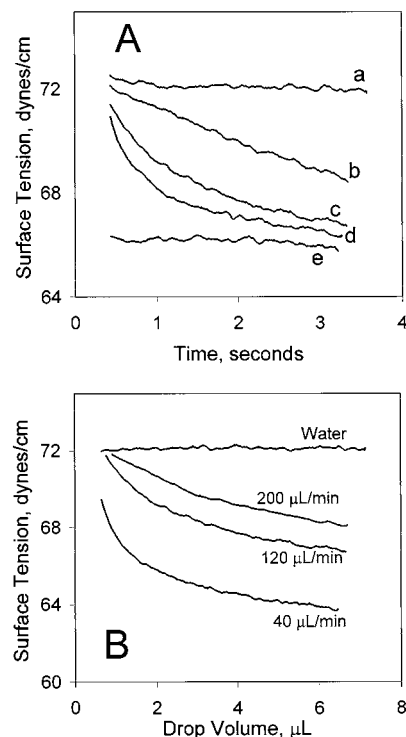


Fig. 4. Dynamic surface tension plots showing the kinetic behavior of BSA solutions in phosphate buffer at 0.10 ionic strength, pH = 7.4, 24°C, and 120  $\mu\text{L}/\text{min}$ . (A) Protein concentration dependence: (a) water; (b) 0.5 mg/ml BSA; (c) 1.0 mg/ml BSA; (d) 1.5 mg/ml BSA; (e) 1.25 mM SDS shown for reference. (B) Flow rate dependency of a 1.0 mg/ml BSA solution, normalized to drop volume (drop time/flow rate).

structure do not significantly inhibit the diffusion to, and molecular orientation at, the liquid–air interface. Many proteins and polymers are known to lower surface tension of aqueous solutions, and due to their molecular size, structure and behavior, their ability to lower liquid–air surface tension is kinetically hindered [23–25]. Fig. 4(A) depicts this kinetic dependence in the dynamic surface tension plots of BSA solutions, a globular protein. The dynamic surface tension plots of BSA are bracketed by water and a 1.5 mM SDS solution. The dynamic surface tension plot for the buffer was essentially identical to that of water, but not shown for brevity. As shown in Fig. 4(A), the surface tension of BSA begins with a relatively high surface tension early in drop growth. This is likely due to the difficulty BSA molecules have in

keeping up with the rapid change in the surface area/volume of the growing drop. The surface tension then decreases as the surface area/volume ratio decreases during drop growth, allowing BSA molecules to more readily orient themselves at the liquid–air interface. Thus, the FIA/DSTD instrument can be used to examine in real-time the self-assembly of kinetically-hindered surface active analytes into a sub-monolayer at the drop liquid–air interface. As expected, Fig. 4(A) illustrates that as the bulk concentration of BSA is increased, the concentration of oriented BSA molecules in the surface layer is also increased. This is characterized by more rapid decrease in the surface tension early in drop growth and by a lower minimum surface tension at drop detachment.

The effect of flow rate as a tuning variable for examining the kinetic behavior is illustrated in Fig. 4(B) where the dynamic surface tensions of a 1 mg/ml BSA sample are obtained at various flow rates. By tuning the flow rate, selectivity of the method for the study of various analytes can be enhanced. The dynamic surface tensions for BSA at each flow rate are plotted as a function of drop volume instead of drop time for clearer comparison. Note that as the flow rate is decreased, surface tension lowering is enhanced. Selection of the correct flow rate for the analysis and characterization of a protein such as BSA requires considering both the protein's concentration range of interest as well as the degree of sensitivity in observing the protein's kinetic behavior. For example, if BSA concentrations up to 1 mg/ml are to be analyzed, a flow rate of 40  $\mu\text{l}/\text{min}$  should be applied to utilize the full range of surface tension response. Analysis of higher BSA concentrations would thus be accomplished at a higher flow rate, while lower BSA concentrations would require a slower flow rate to maintain optimum sensitivity and selectivity. Similar kinetic behavior of BSA solutions was observed when the FIA experiments were repeated with a sensor tip composed of PEEK, indicating that interactions at the solid–liquid interface probably make a negligible contribution to the observed kinetic behavior. In addition, it is clear from the viscosity experiments previously described that the kinetic effect for

BSA is not directly due to viscosity, but rather the molecular dynamics of the BSA molecules at the liquid–air interface. This conclusion is supported by the similarity in the kinetic behavior of BSA reported here and that reported by static drop measurements [24].

Because the DSTD has demonstrated selectivity when a kinetic effect is observed as in Fig. 4, it is likely indicative of a specific protein or other macromolecule. This attribute can be applied to the identification and study of surface active materials. Furthermore, the kinetic behavior of a specific surface active analyte is sensitive to the solution matrix. Thus, the DSTD may provide valuable information regarding the chemical environment in which the surface active analyte finds itself.

The potential for using FIA/DSTD for studying interactions of surfactant mixtures was also investigated, with representative results presented. Mixtures of the polymeric surfactant Brij<sup>®</sup>-35 with either SDS or PEG 1470 were analyzed by FIA/DSTD. By tuning the FIA/DSTD with flow rate, the ability to distinguish between contributions of individual surface active components in mixtures was possible. In Fig. 5 are shown the dynamic surface tension plots obtained from representative drop profile data for solutions of 1.0 mM SDS, 100 ppm Brij<sup>®</sup>-35, and a mixture of 1.0

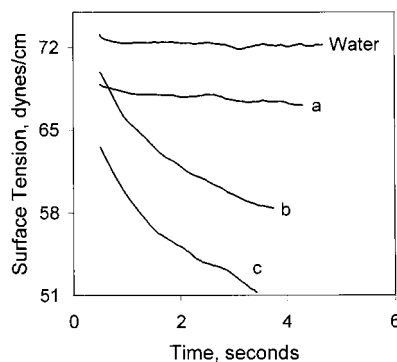


Fig. 5. Additive effects in surfactant mixtures. The dynamic surface tension plots from representative drop profile data using FIA at 100  $\mu\text{l}/\text{min}$ : (a) 1.0 mM SDS sample; (b) 100 ppm Brij<sup>®</sup>-35 sample; (c) 1.0 mM SDS and 100 ppm Brij<sup>®</sup>-35 sample. Note how the individual surfactants act collectively in the mixture, in contrast to the mixture shown in Fig. 6.



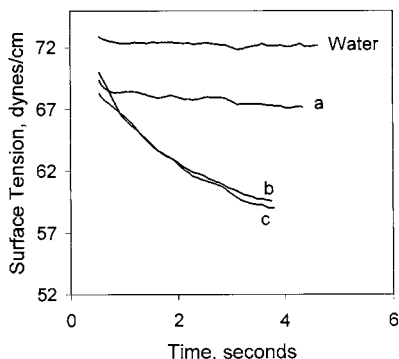


Fig. 6. Non-additive effect in surfactant mixtures. The dynamic surface tension plots from representative drop profile data using FIA at 100  $\mu$ l/min: (a) 50 ppm polyethylene glycol (PEG) 1470 sample; (b) 100 ppm Brij<sup>®</sup>-35 sample; (c) 50 ppm PEG 1470 and 100 ppm Brij<sup>®</sup>-35 sample. Note how the individual surfactants appear to be competing for surface coverage in the mixture with the resulting surface tension of the mixture resembling that of Brij<sup>®</sup>-35 alone.

mM SDS and 100 ppm Brij<sup>®</sup>-35. Notice how the individual components, SDS and Brij<sup>®</sup>-35, exhibit an additive effect, acting collectively when combined in the mixture. This additive interaction in mixed surfactant systems has been well documented [26,27] in steady-state surface tension measurements. The degree of interaction between SDS and Brij<sup>®</sup>-35 is dependent on the compatibility of their hydrophobic chains and hydrophilic head groups. Both the hydrophobic chains of SDS and Brij<sup>®</sup>-35 are lauryl groups, allowing the molecules to form a regular packing arrangement at the drop liquid–air interface. In addition, Brij<sup>®</sup>-35 polyoxyethylene ether head groups shield the anionic head group of SDS molecules from one another, thereby minimizing the electrostatic repulsion forces in the mono-layer assembly formed at the drop liquid–air interface [26]. Both of these contributions are important in the collective response of the SDS-Brij<sup>®</sup>-35 shown in Fig. 5. FIA/DSTD can also elucidate when mixtures of surfactants compete for drop surface coverage. In Fig. 6 are shown the dynamic surface tension plots of 50 ppm PEG 1470, 100 ppm Brij<sup>®</sup>-35, and a mixture of 50 ppm PEG 1470 and 100 ppm Brij<sup>®</sup>-35. In Fig. 6, the individual surface active components appear to compete for coverage at the surface of the growing drop, with the resulting

surface tension dominated by Brij<sup>®</sup>-35. This response is readily explained when the molecular structure is considered. Unlike Brij<sup>®</sup>-35, PEG 1470 molecules do not have nearly as distinct hydrophobic and hydrophilic regions. Indeed, the hydrophilic portion of Brij<sup>®</sup>-35 and PEG 1470 are derived from the same monomer (ethylene glycol). Thus, when Brij<sup>®</sup>-35 and PEG 1470 are placed together in solution, the hydrophobic tail (lauryl group) of Brij<sup>®</sup>-35 dominates the mono-layer formation at the liquid–air interface.

This ability to study the dynamic surface tension behavior of mixed surfactant systems has only recently been demonstrated [28] with the maximum bubble pressure method, a technique that is not ideally suited for surface tension measurements of flowing samples like FIA/DSTD. Thus, a clear advantage of our DSTD is that it can be combined with FIA. With a properly tuned DSTD, the magnitude of slight compositional variations on the overall behavior of a surfactant mixture can potentially be assigned to individual components. Thus, the ability to selectively examine these additive and non-additive (competitive) contributions with FIA/DSTD shows promise for rapidly studying formulation processes.

## 5. Conclusions

A novel calibration procedure for the DSTD is presented that facilitates application to FIA/DSTD. The DSTD provides kinetic information in the ca 100 ms to 10 s time regime for the surface active protein BSA and the polymeric surfactant Brij<sup>®</sup>-35. Additive and competitive interactions for surfactant mixtures can be readily studied by FIA/DSTD, thus opening up broad opportunities for studying surfactant chemistry of mixtures. Thus, FIA/DSTD has promise as an investigative tool for the study of complex biological and industrial samples. The kinetic information provided by the DSTD can be obtained when coupled with HPLC. We are currently working on instrumental modifications to couple the DSTD to the separation of surface active proteins and polymers by aqueous size-exclusion chromatography.

## Acknowledgements

We thank the Center for Process Analytical Chemistry (CPAC), a National Science Foundation University/Industry Cooperative Research Center at the University of Washington, for financial support, and Max J. Kopp of the Validyne Corporation for technical support through the donation of the pressure sensor used in this work. We thank Carsten A. Bruckner and Bryan J. Prazen for their assistance in developing data acquisition programs for this work.

## References

- [1] A.H. Turner, J.H. Houston, in: D.R. Karsa (Ed.), *Industrial Applications of Surfactants III*, Royal Society of Chemistry, Cambridge, 1992, pp. 3–19.
- [2] D.C. Cullum, *Introduction to Surfactant Analysis*, Blackie, Glasgow, 1994.
- [3] S.S. Dukhin, G. Kretschmar, R. Miller, in: D. Mobius, R. Miller III (Eds.), *Studies in Interface Science*, Elsevier, Amsterdam, 1995, pp. 140–201.
- [4] T.H. Iliiev, C.D. Dushkin, *Colloid Polym. Sci.* 270 (1992) 370–376.
- [5] V.B. Fainerman, R. Miller, P. Joos, *Colloid Polym. Sci.* 272 (1994) 731–739.
- [6] R. Miller, K.-H. Schano, A. Hofmann, *Colloids Surf. A* 92 (1994) 189–196.
- [7] R. Miller, S.A. Zhlob, A.V. Makievski, P. Joos, V.B. Fainerman, *Langmuir* 13 (1997) 5663–5668.
- [8] C.A. MacLeod, C.J. Radke, *J. Colloid Interface Sci.* 160 (1993) 435–448.
- [9] C.A. MacLeod, C.J. Radke, *J. Colloid Interface Sci.* 166 (1994) 73–88.
- [10] R. Nagarajan, D.T. Wasan, *J. Colloid Interface Sci.* 159 (1993) 164–173.
- [11] J.M. Soos, K. Koczo, E. Erdos, D.T. Wasan, *Rev. Sci. Instrum.* 65 (1994) 3555–3562.
- [12] G. Enhorning, *J. Appl. Physiol.* 43 (1977) 198–203.
- [13] C.-H. Chang, K.A. Coltharp, S.Y. Park, E.I. Frances, *Colloids Surf. A* 114 (1996) 185–197.
- [14] L.R. Lima III, D.R. Dunphy, R.E. Synovec, *Anal. Chem.* 66 (1994) 1209–1216.
- [15] L.R. Lima III, R.E. Synovec, *J. Chromatogr. A* 691 (1995) 195–204.
- [16] T.E. Young, R.E. Synovec, *Talanta* 43 (1996) 889–899.
- [17] N.A. Olson, R.E. Synovec, W.A. Bond, D.M. Alloway, K.J. Skogerboe, *Anal. Chem.* 69 (1997) 3496–3505.
- [18] N.A. Olson, K.J. Skogerboe, R.E. Synovec, *J. Chromatogr. A* 806 (1998) 239–250.
- [19] A.W. Adamson, A.P. Gast, *Physical Chemistry of Surfaces*, 6th edn, Wiley-Interscience, New York, 1996.
- [20] E. Alvarez, G. Vazquez, M. Sanchez-Vilas, B. Sanjurjo, J.M. Navaza, *J. Chem. Eng. Data* 42 (1997) 957–960.
- [21] R.C. Weast, *Handbook of Chemistry and Physics*, 66th edn, CRC Press, Boca Raton, FL, 1986.
- [22] K.J. Mysels, *Langmuir* 2 (1986) 423–428.
- [23] B.C. Tripp, J.J. Magda, J.D.J. Andrade, *Colloid Interface Sci.* 173 (1995) 16–27.
- [24] G. Serrien, G. Geeraerts, L. Ghosh, P. Joos, *Colloid Surf.* 64 (1992) 219–233.
- [25] A.V. Makievski, V.B. Fainerman, M. Bree, R. Wustneck, J. Kragel, R. Miller, *J. Phys. Chem. B* 102 (1998) 417–425.
- [26] D.L. Chang, H.L. Rosano, in: J.F. Scamehorn (Ed.), *Phenomena in Mixed Surfactant Systems*, American Chemical Society, Washington, DC, 1986, pp. 117–132.
- [27] K. Tsujii, *Surface Activity: Principles, Phenomena, and Applications*, Academic Press, San Diego, CA, 1998.
- [28] V.B. Fainerman, R. Miller, *Langmuir* 13 (1997) 409–413.

# Differential scanning potentiometry: surface charge development and apparent dissociation constants of natural humic acids

Silvia B. Ceppi <sup>a,\*</sup>, Manuel I. Velasco <sup>a</sup>, Carlos P. De Pauli <sup>b</sup>

<sup>a</sup> *Depto. de Recursos Naturales, Facultad de Ciencias Agropecuarias, Universidad Nacional de Córdoba, CC 509, 5000 Córdoba, Argentina*

<sup>b</sup> *INFIQC, Depto. de Fisicoquímica, Facultad de Ciencias Químicas, Universidad Nacional de Córdoba, 5000 Córdoba, Argentina*

Received 7 April 1999; accepted 2 July 1999

## Abstract

Humic acids (HA) are the main components of soil organic matter which can form complexes with metal ions and other soil and/or water contaminants. Here, we focus on their acid–base properties. HA were extracted from two different soils (Typic Ustifluent and Entic Haplustoll) with different vegetation. In this study we use a simple method, differential scanning potentiometry (DSP), to determine HA buffer capacity distribution, apparent dissociation constant values and surface charge development. © 1999 Elsevier Science B.V. All rights reserved.

*Keywords:* Humic acids; Differential scanning potentiometry

## 1. Introduction

Humic substances are polyfunctional macromolecules, widely spread in soils, sediments and water. Humic acids (HA) behave as weak polyelectrolytic acids and can be investigated by analytical techniques. Most of the acidity in the HA is due to the carboxylic, OH phenolic and/or enolic groups which dissociate to develop negative charges. The imide groups (=NH<sub>2</sub>), secondary and even tertiary amines, among others, can be proto-

nated to develop positive charges at very low pH. The degree to which these groups are ionized or protonated at the environmental pH value and their abundance and distribution influence the interaction between humic substances and soil contaminants [1].

Because of their high content of acidic functional groups (ionized or protonated), HA show great reactivity for binding soil particles through metal ion interaction. Thus, they have more resistance to microbiological decay [2] and they are the best cementing agents in soil microaggregates [3–5]. Another important property of HA is their relatively high buffer capacity in a wide pH range. Although their exact contribution to the soil

\* Corresponding author. Tel.: + 54-351-4334116/17; fax: + 54-351-4334118.

*E-mail address:* sceppi@agro.uncor.edu (S.B. Ceppi)

buffer capacity is not well known, in general, soils rich in humic substance are well buffered [6].

Quantitative analysis of HA interactions requires detailed data on: (1) types, (2) abundance, and (3) strength of humic acid functional groups. Thus, studies have been undertaken to subdivide the total acidity in the main components (i.e. carboxyls and hydroxyls) with methods based on the  $pK_a$  values (apparent dissociation constants) rather than on macromolecular structure. Potentiometric titrations are widely used to understand the combined effect of the polyelectrolytic nature and functional group heterogeneity of humic acids [7–15].

Full elucidation of the proton equilibria of humic acids is a complicated issue due to the chemical complexity of the macromolecule [16–21]. The buffer capacity distribution of the HA is also useful to understand the acid–base properties of humic acids [1].

Conventional methods of potentiometric acid–base titration have limitations mainly when a mixture of weak acids and bases or polyelectrolyte

substances are titrated, as a result of overlap of equivalent points (inflection points) of titration. Due to this overlapping the calculation of the dissociation constant values of the groups involved becomes difficult. Another hindrance is the presence of interfering substances when the concentration of titrating substances is low.

Some of these problems can be overcome by differential scanning potentiometry (DSP) which enhances the sensitivity about quantity rather than quality (acid or basic strength) of these groups when polyelectrolytic macromolecules are titrated [22].

The analytical responses are, in this case (DSP), areas rather than inflection points. A plot of  $\Delta pH$  vs  $V$  (volume of titrating base) can be obtained, where  $\Delta pH$  is defined as the pH difference between the blank titration and the HA titration [22,23]. When  $\Delta pH$  vs  $V$  is plotted, a profile is obtained which depends on the amount and acid–base nature of the problem substance (Fig. 1). The values of the negative and/or positive areas are related to the titrated mass and to the number of groups involved (acid and basic respectively) in the macromolecule.

The DSP technique can be used to titrate small quantities of compounds slightly soluble in aqueous medium without mixing different types of solvents and thus evaluate the number of ionised groups (acid or basic) as well as the positive or negative charges [22,23].

In this study we use a simple method, differential scanning potentiometry (DSP), to determine the acid–base properties of HA. The buffer capacity distribution of HA solutions, the apparent dissociation constant of their acidic groups and the surface charge development of soil humic acids are investigated.

## 2. Experimental

### 2.1. Materials

All the solutions were prepared with tridistilled water and chemicals were of analytical grade. Natural humic acids were extracted and purified according to the technique proposed by Chen et

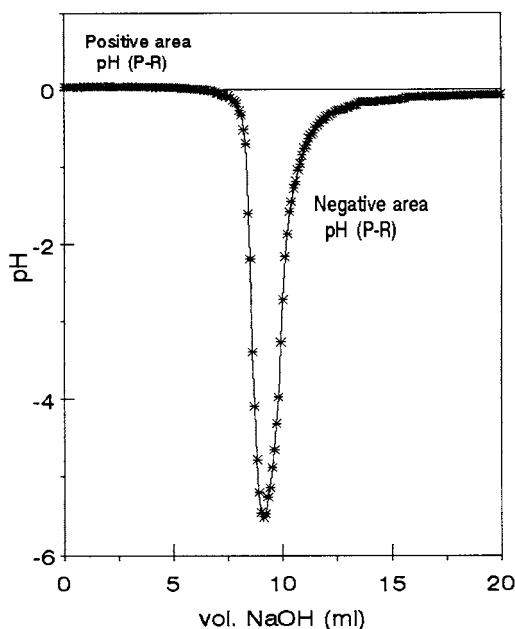


Fig. 1. Negative and positive area calculated from experimental data (DSP). Desmonte HA: mass, 15.01 mg; negative area, 10.37; positive area, 0.18.

Table 1

The amount of COOH and phenolic OH expressed in mequiv./g humic acid determined by the calcium acetate and Ba(OH)<sub>2</sub> methods

Humic acids	Total acidity (mequiv./g)	COOH groups (mequiv./g)	Phenolic OH (mequiv./g)
Algarrobo	9.16	4.08	5.08
Desmonte	10.80	5.49	5.03
Gramma	9.00	4.20	4.80
Pastizal	9.70	4.68	5.02

al. [24] from two different soils covered with different vegetation: (a) Typic Ustifluent: one with *Prosopis* sp. (Algarrobo HA) and another which was logged Desmonte HA and (b) Entic Haplustoll: one with *Gramma Rhodes* (Gramma HA) and another with native grassland (Pastizal HA).

The acidic group content was obtained according to the technique proposed by Schnitzer and Gupta [25] and is shown in Table 1.

### 3. Methods

#### 3.1. Differential scanning potentiometry

##### 3.1.1. Titration of the sample

An aliquot (10 ml) of sulphuric acid solution (approximately  $5 \times 10^{-2}$  N) plus an aliquot of HA with a known HA mass was titrated with sodium hydroxide solution (approximately  $5 \times 10^{-2}$  N).

##### 3.1.2. Reference or blank titration

An aliquot (10 ml) of sulfuric acid solution (approximately  $5 \times 10^{-2}$  N) was titrated with sodium hydroxide solution (approximately  $5 \times 10^{-2}$  N).

The titrated amount for each humic acid was about 15 mg except for Algarrobo HA which was of 2.8, 4.7, 6.6, 10.6 and 15.4 mg in order to evaluate the variation of the buffer capacity with HA concentration. All titrations were performed in absence of the background electrolyte ( $I=0$ ). Sodium hydroxide and sulfuric acid concentrations were the same for all experiments.

The DSP was performed with an automatic burette Schott Gerate T80/20, at a titration rate of 0.1 ml/40 s. This rate was chosen taking into consideration that the variation of the pH values should range between 0.02 and 0.04 pH units.

The pH values were measured with an Orion Research 901 pH meter equipped with a glass combined electrode Orion 9113.

### 4. Results and discussion

Table 2 shows the results of area values and the HA negative surface charges estimated using DSP. The negative area values, which are proportional to the group content with ability to develop negative charges, show the following increasing order for charge development: Desmonte > Pastizal > Algarrobo > Gramma. The calculated values

Table 2

Negative areas and negative surface charges obtained from differential scanning potentiometry (DSP) calculated with potassium biphthalate as standard

	Titred mass (mg)	Negative area	Negative charge (mequiv./100 g)
Algarrobo HA	15.46	10.51	988
Desmonte HA	15.58	17.16	1600
Pastizal HA	15.51	10.71	1037
Gramma HA	15.38	8.87	838

are in agreement with those corresponding to the total acidity obtained by another chemical method (barium hydroxide method) (Table 1).

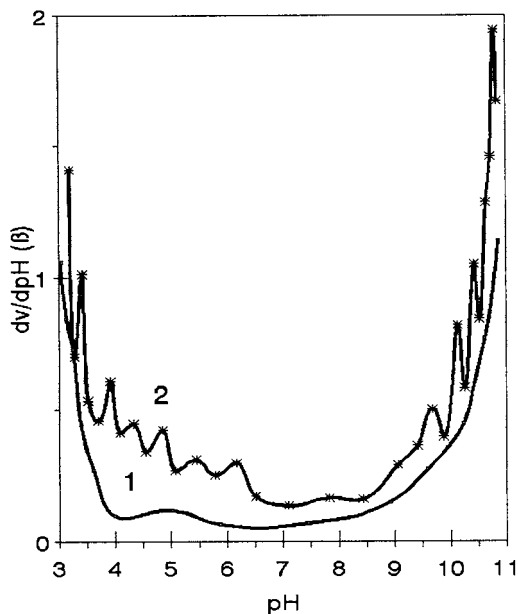


Fig. 2.  $\beta$  ( $dV/dpH$ ) vs pH plot for HA Algarrobo. AH mass: (1) 1.90 mg and (2) 15.45 mg.

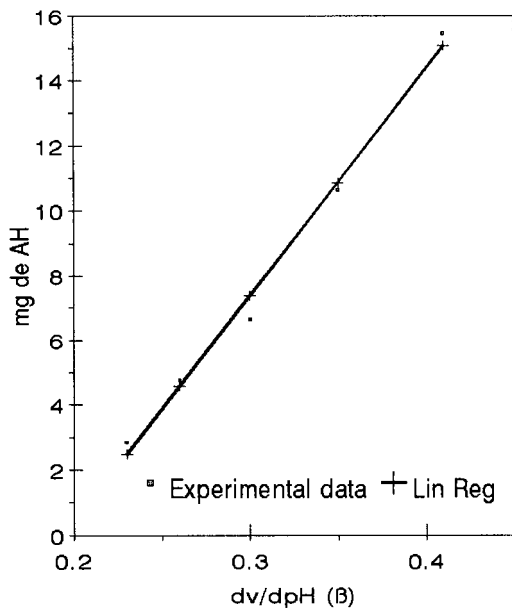


Fig. 3. The relationship between Algarrobo HA mass (mg) vs  $dV/dpH$  ( $\beta$ ) at pH value approximately 5.

The values of the positive areas were null for the Algarrobo and Desmorte HA. For the Pastizal and Grama HA they ranged between 0.18 and 0.15 respectively, showing a very low or almost negligible content of the groups that can develop positive charges. These results are in agreement with the nitrogen content found in the elemental analysis (0.8–1.5% for Algarrobo HA and Desmorte HA and approximately 2% for the Pastizal HA and Grama HA).

#### 4.1. Buffer capacity of the humic acids

Fig. 2 shows buffer capacity vs pH curves for two different mass values of Algarrobo HA. It can be noted that several  $\beta$  maxima can be obtained depending on the mass value. The dependence of these  $\beta$  maxima at approximately pH 5 with the HA mass is shown in Fig. 3. Under the concentration range studied, the good linear relationship confirms the presence of an ionised functional group. This behavior validates the use of  $\beta$  for locating the HA buffer capacity maxima and consequently the ionised acidic functional groups and their apparent dissociation constant values.

All titrations were performed with increasing amounts of HA until a good profile of the first derivative (buffer capacity) was generated, where the maxima corresponding to a particular acidic functional group or a set of ionised acidic functional groups were clearly observed. Since the buffer capacity of an acid–base system is directly proportional to the concentration of the groups (acids or basic), if the height of a maximum obtained from the first derivative of the titration curve increases with the amount of HA titrated, the presence of a particular acidic functional group is confirmed.

At relatively low mass values ( $\sim 2$  mg) (Fig. 2), the curves profiles ( $dV/dpH$ ) showed three wide maxima at around pH 3–4, 5–5.5 and 9–11. Increasing HA mass, the shoulders observed in the  $\beta$  vs pH curve in the pH region lower than 4 and higher than 9, appear more distinctly, and like separated maxima at a HA mass value of approximately 15 mg. The broad maximum between pH 4.5 and 5.5 gets narrower ending in two separate narrow and more distinct clear maxima.

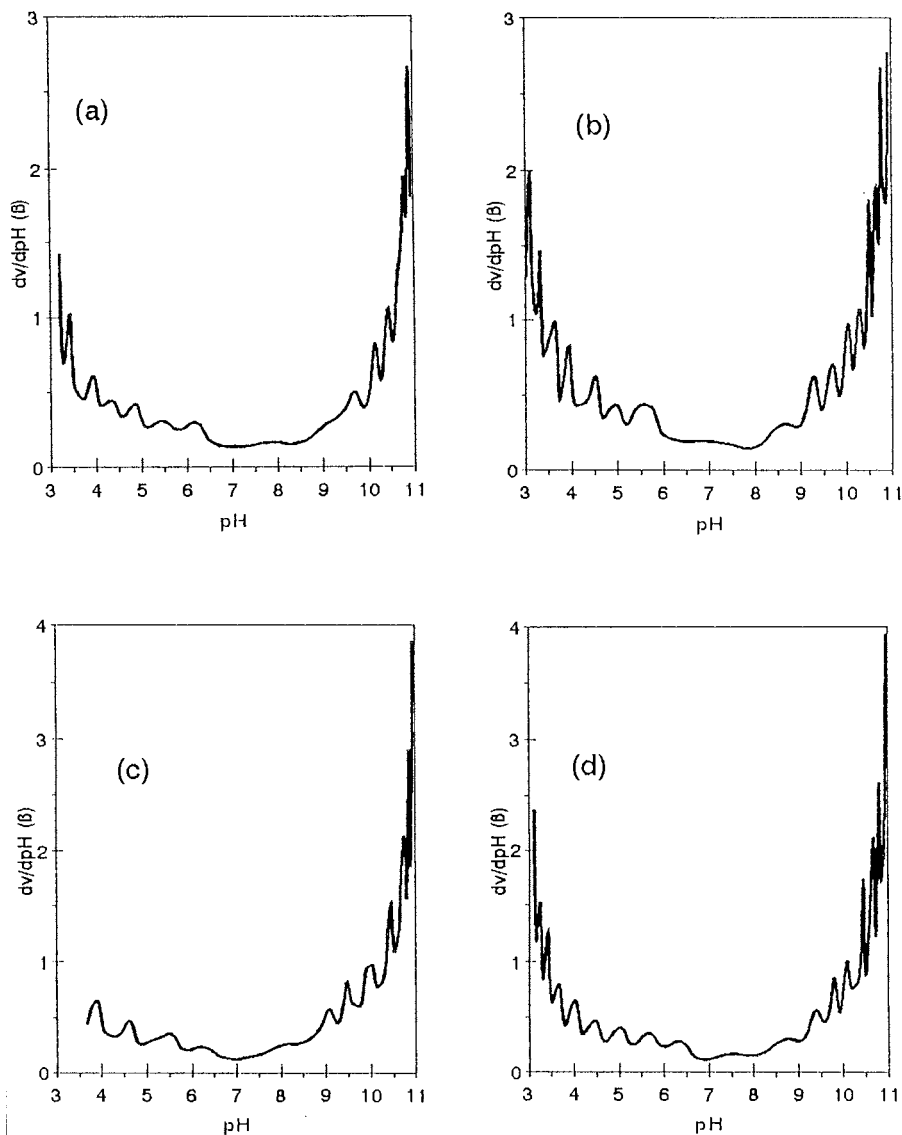


Fig. 4.  $dV/dpH (\beta)$  vs pH curve for different HA. (a) Algarrobo HA: mass, 15.45 mg. (b) Desmonte HA: mass, 15.58 mg. (c) Grama HA: mass, 14.38 mg. (d) Pastizal HA: mass, 15.01 mg.

From the experimental data performed with HA masses between 14 and 15 mg, the plots of  $dV/dpH (\beta)$  vs pH (Fig. 4a–d) show similar profiles for the different HA studied. Small maxima are observed between pH 3 and 6–7 and between 8–8.5 and 11. In all cases, the buffer capacity minima occur at pH 6–7. This region is assigned to the transition from carboxylic to phenolic groups [1]. To calculate the  $pK_a$  values from

experimental data we have used a value of  $\Delta pK_a = 1$ , based on that used by Westall et al. [16] who reported that there is considerable flexibility in the way that the spectrum is selected. Then, the  $pK_a$  values can be associated with a known group as a check on the physical plausibility of the method; however, this comparison cannot be regarded as a reliable method for assessing humic acid structure.

Table 3

Values for the apparent dissociation constants of HA ( $K_a$ ) obtained by differential scanning potentiometry (DSP)

Humic acid	$K_{a1}$ ( $pK_a$ )	$K_{a2}$ ( $pK_a$ )	$K_{a3}$ ( $pK_a$ )	$K_{a4}$ ( $pK_a$ )	$K_{a5}$ ( $pK_a$ )	$K_{a6}$ ( $pK_a$ )
Algarrobo	$3.2 \times 10^{-4}$ (3.5)	$5.0 \times 10^{-5}$ (4.3)	$6.3 \times 10^{-6}$ (5.2)	$3.2 \times 10^{-8}$ (7.5)	$1.9 \times 10^{-10}$ (9.7)	$3.2 \times 10^{-11}$ (10.5)
Desmonte	$2.9 \times 10^{-4}$ (3.5)	$5.1 \times 10^{-5}$ (4.3)	$3.5 \times 10^{-6}$ (5.5)	$1.6 \times 10^{-9}$ (8.8)	$2.8 \times 10^{-10}$ (9.5)	$3.56 \times 10^{-11}$ (10.4)
Pastizal	$3.4 \times 10^{-4}$ (3.5)	$4.6 \times 10^{-5}$ (4.3)	$3.3 \times 10^{-6}$ (5.5)	$2.9 \times 10^{-7}$ (6.5)	$2.1 \times 10^{-10}$ (9.7)	$2.4 \times 10^{-11}$ (10.6)
Grama	$2.9 \times 10^{-4}$ (3.5)	$1.9 \times 10^{-5}$ (4.7)	$3.0 \times 10^{-6}$ (5.5)	$3.2 \times 10^{-7}$ (6.5)	$5.5 \times 10^{-10}$ (9.2)	$3.3 \times 10^{-11}$ (10.5)

Differences in the magnitude of the buffer capacity are observed in  $\beta$  vs pH plots (Fig. 4). This magnitude is higher for Grama and Pastizal HA (Fig. 4c,d) in the whole pH range, and especially at the ends ( $pH < 3$  and  $pH > 10$ ), than those observed for Algarrobo and Desmonte HA (Fig. 4a,b). This could be due to the different soils (Entic Haplustoll and Typic Ustifluent) from which the HA were extracted. This difference in the source of the HA implies differences in the humification process. The HA of Entic Haplustoll are more humified and exhibit higher buffer capacity with a higher contribution to the total soil buffer capacity than those extracted from a Typic Ustifluent.

The height of the maxima in the  $\beta$  vs pH plot around pH 5 ( $pK_a$  of typical carboxylic groups) can be used to compare qualitatively the relative amount of this type of acidic group between, for example, Algarrobo and Desmonte HA. In this way, the latter has more acidic groups of this type because it presents a higher value of  $\beta$  and a higher amount of separate peaks around this pH value than Algarrobo HA. This is in agreement with the amount of this group obtained by the Calcium Acetate technique (Table 1).

On the other hand, the second derivative ( $d^2V/dpH^2$ ) with respect to pH of HA titration can be used to find the apparent  $pK_a$  values. The HA apparent dissociation constants values obtained in this way ( $d^2V/dpH^2$ ) are shown in Table 3.

The apparent dissociation constant values can be assigned to different acidic functional groups  $K_{a1}$ ,  $K_{a2}$  and  $K_{a3}$  corresponding to carboxylic groups,  $K_{a4}$  and  $K_{a5}$  to secondary or tertiary amines titrated, probably, together with phenolic groups or other weak acidic functional groups [9,16,26]. The  $K_{a6}$  values can be assigned to phe-

nolic groups whereas the  $K_{a1}$  value can be assigned to carboxylic sites like  $\alpha$ -COOH which have a strong acid behaviour.

It should be noted that the values of the dissociation constants obtained by differential scanning potentiometry are average values of apparent dissociation constants of a set of acidic sites involved in a range of pH like  $\Delta pH = 1$ .

## 5. Conclusions

Differential scanning potentiometry (DSP) can be quantitatively and/or comparatively applied to estimate the HA charge development in the full range of pH and in a simple way. The technique allows determination of HA buffer capacity distribution and calculation of apparent dissociation constants of the acidic functional groups or the set of acidic functional groups.

The surface charge development of the studied HA shows the following increasing order: Desmonte > Pastizal > Algarrobo > Grama.

The value of positive areas were null for Algarrobo and Desmonte HA, and for Pastizal and Grama HA were 0.18 and 0.15 respectively, showing a very low content of groups that can develop positive charges.

Finally, DSP offers an easy approach to estimate both charge development and apparent dissociation constants.

## Acknowledgements

CONICET, CONICOR and SECyT-UNC are gratefully acknowledged for financial support.



## References

- [1] M.L. Machesky, *Sci. Technol.* 27 (1993) 1182–1188.
- [2] A. Piccolo, S.C. Mbagwu, *Soil Sci. Soc. Am. J.* 58 (1994) 950–955.
- [3] J.M. Tisdall, J.M. Oades, *J. Soil Sci.* 33 (1982) 141–163.
- [4] A. Piccolo, J.S.C. Mbagwu, *Plant Soil* 123 (1990) 27–37.
- [5] K. Chaney, R.S. Swift, *J. Soil Sci.* 37 (1986) 337–343.
- [6] F.J. Stevenson, *Humus Chemistry Genesis—Composition—Reactions*, Wiley-Interscience, New York, 1982.
- [7] D.S. Gamble, *Can. J. Chem.* 48 (1970) 2662–2669.
- [8] D.S. Gamble, *Can. J. Chem.* 50 (1972) 2680–2690.
- [9] O.K. Borggaard, *Acta Chem. Scand.* 28 (1974) 121–122.
- [10] G. Sposito, K.M. Holtzclaw, C.S. LeVesque-Madore, *Soil Sci. Soc. Am. J.* 43 (1979) 1148–1155.
- [11] J. Ephraim, S. Alegret, A. Mathuthu, M. Bicking, R.L. Malcom, J.A. Marinsky, *Environ. Sci. Technol.* 20 (1986) 354–366.
- [12] J. Ephraim, M. Reid, J.A. Marinsky, in: B. Allard, H. Boren, A. Grimvall (Eds.), *Humic Substances in the Aquatic and Terrestrial Environment*, Springer, Berlin, 1991.
- [13] J.A. Marinsky, T. Miyajima, E. Högfeldt, M. Muhammed, *Reactive Polym.* 11 (1989) 279–289.
- [14] A. Maes, J. Tits, G. Mermans, A. Dierckx, *J. Soil Sci.* 43 (1992) 669–677.
- [15] P. Dubach, N.C. Metha, T. Jakab, F. Martin, N. Routlet, *Geochim. Cosmochim. Acta* 28 (1964) 1567–1578.
- [16] J.C. Westall, J.D. Jones, G.D. Turner, J.M. Zachara, *Environ. Sci. Technol.* 29 (1995) 951–959.
- [17] S.J. Marshall, S.D. Young, K. Gregson, *Eur. J. Soil Sci.* 46 (1995) 471–480.
- [18] J.C.M. De Wit, W.H. Van Riemsdijk, L.K. Koopal, *Environ. Sci. Technol.* 27 (1993) 2005–2014.
- [19] J.C.M. De Wit, W.H. Van Riemsdijk, L.K. Koopal, *Environ. Sci. Technol.* 27 (1993) 2015–2022.
- [20] M.M. Nederlof, J.C.M. De Wit, W.H. Van Riemsdijk, L.K. Koopal, *Environ. Sci. Technol.* 27 (1993) 846–856.
- [21] E. Tipping, A. Fitch, F.J. Stevenson, *Eur. J. Soil Sci.* 46 (1995) 95–101.
- [22] R.H. Manzo, E. Luna, *Anal. Chem.* 58 (1986) 1055–1057.
- [23] E. Luna, Ph.D. Thesis, 1989.
- [24] V. Chen, N.F. Senesi, M. Schnitzer, *Geoderma* 20 (1978) 87–104.
- [25] M. Schnitzer, U.C. Gupta, *Soil Sci. Soc. Am. Proc.* 29 (1965) 274–280.
- [26] L.M. Aleixo, O.E.S. Godinho, W.F. Da Costa, *Anal. Chim. Acta* 257 (1992) 35–39.

# Studies on the liquid-liquid extraction of iron(III) and titanium(IV) with 3-phenyl-4-benzoyl-5-isoxazolone

J. Saji, T. Prasada Rao, T.R. Ramamohan, M.L.P. Reddy \*

*Regional Research Laboratory (CSIR), Trivandrum 695 019, India*

Received 1 June 1999; accepted 2 July 1999

## Abstract

The extraction behaviour of iron(III) and titanium(IV) from acidic chloride solutions has been investigated using 3-phenyl-4-benzoyl-5-isoxazolone (HPBI) in xylene as an extractant. The results demonstrate that these metal ions are extracted into xylene as  $\text{Fe(PBI)}_3$  and  $\text{TiO(PBI)}_2$ . The equilibrium constants of the extracted complexes have been deduced by non-linear regression analysis by taking into account complexation of metal ion with inorganic ligands in the aqueous phase and all plausible complexes extracted into the organic phase. IR and proton NMR ( $^1\text{H}$  NMR) spectra were used to further clarify the nature of complexes extracted into organic phase. The effect of the nature of the diluent on the extraction of iron(III) and titanium(IV) has been studied and correlated with dielectric constants. The extraction behaviour of titanium(IV) has also been compared with that of other metal ions, viz. magnesium(II), vanadium(V), chromium(VI), iron(III), manganese(II), zinc(II) and zirconium(IV), which are associated with the titanium in waste chloride liquors of the titanium-mineral-processing industry. © 1999 Elsevier Science B.V. All rights reserved.

*Keywords:* Extraction; Separation; Iron(III); Titanium(IV); 3-Phenyl-4-benzoyl-5-isoxazolone; Chemically based model

## 1. Introduction

Efficient separation and recovery of metal ions from industrial wastes as well as from raw materials are gaining more importance because of the increasing demand for high purity products and also due to environmental concerns. For example, waste acid solutions from  $\text{TiO}_2$  production contain appreciable quantities of iron along with other metals such as titanium, magnesium, man-

ganese, chromium, vanadium, zirconium, and zinc. Solvent extraction is one of the common techniques used for the recovery of valuable metals from the waste chloride liquors [1,2].

A survey of the literature showed that a large number of reagents have been used for the extraction of both iron(III) and titanium(IV). Organophosphorus acid derivatives such as di-2-ethylhexyl phosphoric acid (DEHPA) and 2-ethylhexyl phosphonic acid mono-2-ethylhexyl ester (EHEHPA) have been used by several investigators [3–6]. Amines extract both iron(III) and titanium(IV) efficiently from acidic chloride solutions

\* Corresponding author. Fax: +91-471-490186/491712.

E-mail address: reddy@csrrlrd.ren.nic.in (M.L.P. Reddy)

[7–9]. Neutral organophosphorus compounds such as tributyl phosphate (TBP) and trioctyl phosphine oxide (TOPO) have also been used for extraction of these metals [10,11]. Cyanex 923, a mixture of trialkyl phosphine oxides has been recently used in our laboratory, as an extractant for separating iron and titanium from acidic chloride solution [12,13].

Besides the above well-known reagents, pyrazolone derivatives have also been used for the selective extraction of iron from acidic aqueous solutions. Generally, 4-acyl-5-pyrazolones extract metal ions at lower pH than open chain  $\beta$ -diketones because of their lower  $pK_a$  values (2.5–4.0) [14,15]. 3-Phenyl-4-benzoyl-5-isoxazolone, HPBI has been recently explored in our laboratory as a chelating agent for the extraction of trivalent lanthanides and actinides from acidic aqueous solutions and better extraction efficiency has been achieved compared to 4-acyl pyrazolones [16]. The acid dissociation constant of HPBI is 1.23, lower than that of the corresponding pyrazolones, because of the electron delocalisation induced by the isoxazolone group. This property makes the isoxazolones an interesting class of  $\beta$ -diketones with potential application as reagents for extraction of metal ions from complexing strong acid media. Hence in the present study the extraction behaviour of iron(III) and titanium(IV) from hydrochloric acid solutions using HPBI as an extractant has been investigated. The extraction behaviour of some of the associated elements in the waste chloride liquors of the titanium minerals processing industry has also been studied.

## 2. Experimental

### 2.1. Apparatus

A Hitachi (Tokyo, Japan) 220 double beam microprocessor controlled spectrophotometer was used for measuring absorbances. An Orion (MA, USA) ion analyser was used for the pH measurements.

### 2.2. Reagents

HPBI was synthesised in our laboratory by the benzoylation of 3-phenyl-5-isoxazolone (Aldrich WI, USA) following the method of Korte and Storiko [17]. Elemental analysis calculated for recrystallised  $C_6H_{11}NO_3$ : C, 72.45; H, 4.18; N, 5.28; found: C, 70.27; H, 4.18; N, 5.17%; melting point 146°C. All other chemicals and solvents used were of AR grade.

Iron(III) stock solution was prepared by dissolving 8.11 g of ferric chloride in 20 ml of concentrated hydrochloric acid and diluted to 1 l with distilled water. Titanium(IV) stock solution was prepared by dissolving 18.4 g of potassium titanyl oxalate and 5 g of ammonium sulphate in 100 ml of concentrated hydrochloric acid and diluted to 1 l with distilled water. Stock solutions of chromium(V) magnesium(II), manganese(II), zinc(II) and zirconium(IV) were prepared by dissolving 14.71 g of potassium dichromate, 12.32 g of  $MgSO_4 \cdot 7H_2O$ , 8.45 g of  $MnSO_4 \cdot H_2O$ , 14.38 g of  $ZnSO_4 \cdot 7H_2O$  and 11.65 g of  $ZrCl_4$  in 1 l each of distilled water, respectively. Vanadium(V) stock solution was prepared by dissolving 5.85 g of ammonium monovanadate in 20 ml of concentrated hydrochloric acid and diluted to 1 l with distilled water. Suitably diluted stock solutions of the above mentioned metal ions were used in the extraction and analytical studies. All organic phase solutions were prepared by dissolving weighed amounts of HPBI in xylene which were diluted to required volume.

### 2.3. Extraction and analytical procedure

Liquid-liquid extractions were carried out by shaking equal volumes of aqueous and organic phases for the required time in a glass stoppered vial using a mechanical shaker at  $303 \pm 1K$ . After phase separation, the concentration of the particular metal ion left in the aqueous phase was determined using standard procedures. Thus titanium(IV) [18], iron(III) [18], chromium(VI) [18], magnesium(II) [18] vanadium(V) [19], and zirconium(IV) [20] were analysed spectrophotometrically using hydrogen peroxide; 1,10-phenanthroline, diphenyl carbazide; Eriochrome black-T; oxine;

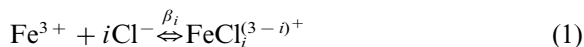
and Alizarin red-S, respectively. Zinc(II) and manganese(II) were analysed by titration with EDTA [21]. The concentration of the metal ion in the organic phase was then obtained from a material balance. The distribution ratio,  $D$  was taken as the ratio of the concentration of the metal ion in the organic phase to that present in the aqueous phase. All the computer programs were written in FORTRAN 77 and executed on a 32 bit mini-computer (HCL HORIZON III).

#### 2.4. Preparation of solid complexes

The metal complexes were prepared by following the general procedure: the stoichiometric amount of ferric chloride was added gradually to a well stirred solution of HPBI in xylene and then mixed well for 5 h, to ensure completion of the reaction. The precipitate formed was filtered, washed with diethyl ether and dried in a desiccator over fused calcium chloride. Loading of HPBI with titanium(IV) was carried out by repeated contact of fresh portions of metal solution for 1 h. The loaded phase was then subjected to evaporation of xylene at room temperature to yield yellowish Ti-HPBI complex, which was dried in an oven at 50°C for 48 h. The Nicolet (WI, USA) impact 400D IR spectrometer using potassium bromide was used to obtain IR spectra and the Bruker (MA, USA) 300 MHz NMR spectrometer was used to obtain the proton NMR ( $^1\text{H}$  NMR) spectra of complexes in  $\text{CDCl}_3$  solvent. The solutes studied were HPBI,  $\text{Fe}(\text{PBI})_3$  and  $\text{TiO}(\text{PBI})_2$ .

### 3. Theoretical

The trivalent iron in the aqueous phase forms a variety of complexes in the presence of chloride ions. However, under the present experimental conditions, we have assumed the formation of the first two complexes were defined by



where  $i = 0, 1, 2$  and  $\beta_i$  is the stability constant for the corresponding complex formation. Then the total metal ion in the aqueous phase is given by

$$\begin{aligned} [\text{Fe}^{3+}]_{\text{total}} &= [\text{Fe}^{3+}] + [\text{FeCl}^{2+}] + [\text{FeCl}_2^+] \\ &= [\text{Fe}^{3+}](1 + \beta_1[\text{Cl}^-] + \beta_2[\text{Cl}^-]^2) \end{aligned} \quad (2)$$

The values of the stability constant  $\beta_1 = 4.26$  and  $\beta_2 = 5.62$  were taken from the literature [22].

The extraction equilibrium of iron(III) from hydrochloric acid solutions with HPBI in xylene can be written as



The distribution ratio,  $D$  of iron(III) can be written from (Eq. (1)) to (Eq. (3)) as

$$D = \frac{K_{\text{Fe}}[\text{HPBI}]^3}{[\text{H}^+]^3(1 + \beta_1[\text{Cl}^-] + \beta_2[\text{Cl}^-]^2)} \quad (4)$$

Titanium(IV) in the aqueous phase forms a variety of complexes in the presence of chloride ions. Then the total Ti(IV) concentration can be expressed as

$$\begin{aligned} [\text{Ti}^{4+}]_{\text{Total}} &= [\text{TiO}^{2+}] + [\text{TiOCl}^+] + [\text{TiOCl}_2] \\ &= \text{TiO}^{2+}(1 + \beta_1[\text{Cl}^-] + \beta_2[\text{Cl}^-]^2) \end{aligned} \quad (5)$$

where  $\beta_1$  and  $\beta_2$  are stability constants of the following reactions



The values of stability constants,  $\beta_1 = 3.55$  and  $\beta_2 = 1.41$  were obtained from literature [23].

The extraction equilibrium of titanium(IV) with HPBI can be written as



The distribution ratio,  $D$  for titanium(IV) can be written from Eqs. (7) and (8) as

$$D = \frac{K_{\text{Ti}}[\text{HPBI}]^2}{[\text{H}^+]^2(1 + \beta_1[\text{Cl}^-] + \beta_2[\text{Cl}^-]^2)} \quad (9)$$

### 4. Results and discussion

#### 4.1. Effect of phase contact time

The distribution ratios for extracting iron(III) from 0.5 mM  $\text{Fe}^{3+}$  solution containing 0.2 M HCl with 0.0075 M HPBI in xylene have been measured at different phase contact times (Fig. 1).

It is found that the distribution ratio increases with increasing phase contact time up to 120 min and after that the curve levels off. It is concluded that the equilibrium time for this system is 2 h. Hence in the subsequent experiments 3 h were allowed to ensure equilibration. On the other hand, the extraction equilibria of titanium(IV) (2.5 mM) from acidic chloride (0.072 M HCl) solutions using 0.01 M HPBI are found to be faster and an equilibrium is achieved within 5 min.

#### 4.2. Effect of HPBI concentration

The effect of HPBI concentration on the extraction of iron(III) and titanium(IV) has been studied.

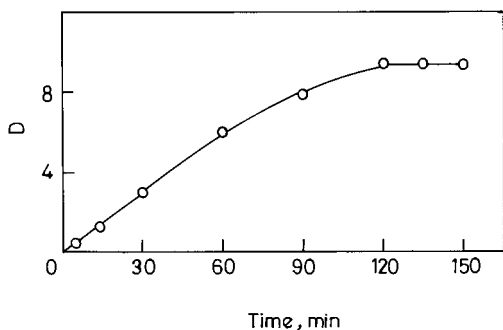


Fig. 1. Dependence of distribution ratio on phase contact time:  $[\text{Fe}^{3+}]$ , 0.5 mM; HCl, 0.2 M; HPBI, 0.0075 M.

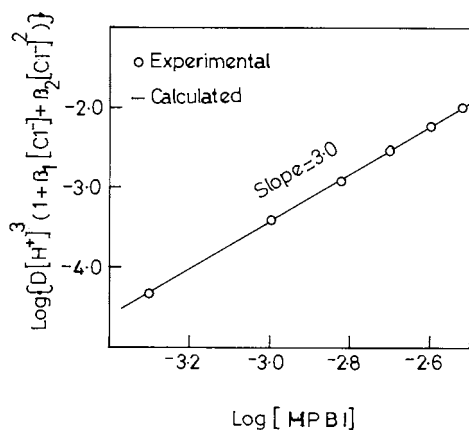


Fig. 2. Effect of HPBI concentration on the extraction of iron(III):  $[\text{Fe}^{3+}]$ , 0.5 mM; HCl, 0.1 M.

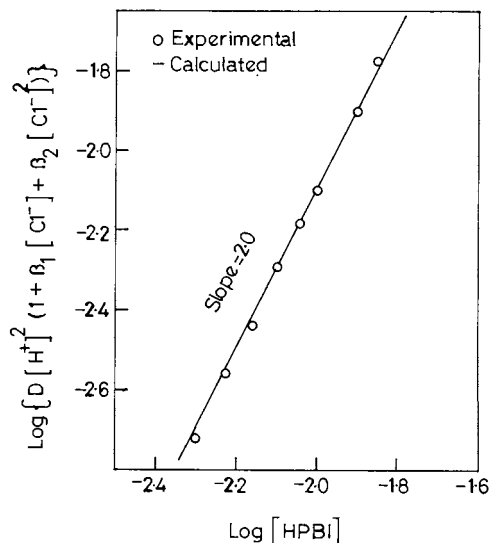


Fig. 3. Effect of HPBI concentration on the extraction of titanium(IV):  $[\text{Ti}^{4+}]$ , 2.5 mM; HCl, 0.07 M.

ied by keeping metal and acid concentrations constant and the results are shown in Figs. 2 and 3. It is clear from the figures that the extraction of both iron(III) and titanium(IV) increases with increasing concentrations of HPBI. The log–log plots gave slopes of 3.0 for iron(III) and 2.0 for titanium(IV) indicating the extraction of complexes  $\text{Fe}(\text{PBI})_3$  and  $\text{TiO}(\text{PBI})_2$ .

#### 4.3. Effect of acidity

The extraction of iron(III) and titanium(IV) with HPBI in xylene as a function of hydrogen ion concentration has been studied. In both cases, the extraction behaviour shows an inverse dependence with acidity. The plots (Figs. 4 and 5) of  $\log D(1 + \beta_1[\text{Cl}^-] + \beta_2[\text{Cl}^-]^2)$  versus  $\log [\text{H}^+]$  for iron(III) and titanium(IV) gave slopes of  $-3.0$  and  $-2.0$ , respectively, confirming the formation of simple metal chelates.

The formation of the above simple metal chelates was further confirmed by analysing the equilibrium data (presented in Figs. 2–5) using Eq. (4) for iron(III) and Eq. (9) for titanium(IV). The equilibrium constants for the above extracted complexes were determined by non-linear regression analysis as described in our earlier publica-

tion [24] and are found to be  $\log K_{\text{Fe}} = 5.57 \pm 0.02$  for iron(III) and  $\log K_{\text{Ti}} = 1.91 \pm 0.03$  for titanium(IV).

It is clear from these equilibrium constant values that  $K_{\text{Fe}}$  is about  $4 \times 10^3$  fold higher than  $K_{\text{Ti}}$ . This clearly shows the superior extractability of iron(III) compared to titanium(IV) with HPBI. The equilibrium constants thus calculated refer only to concentration quotients, calculated on the assumption that the activity coefficients of the

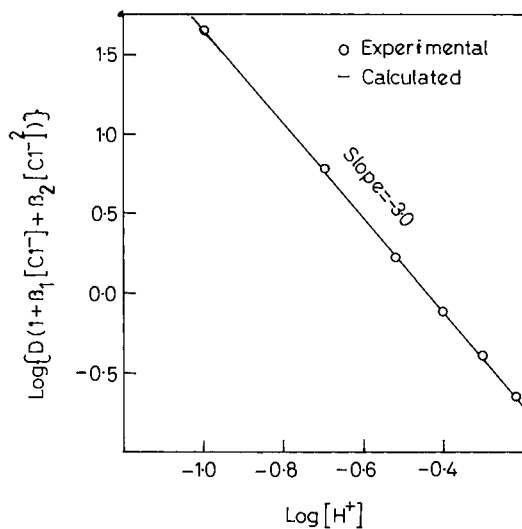


Fig. 4. Effect of hydrogen ion concentration on the extraction of iron(III):  $[\text{Fe}^{3+}]$ , 0.5 mM; HPBI, 0.005 M.

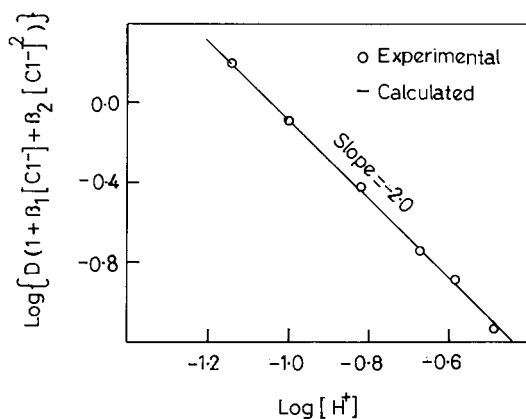


Fig. 5. Effect of hydrogen iron concentration on the extraction of titanium(IV):  $[\text{Ti}^{4+}]$ , 2.5 mM; HPBI, 0.01 M.

Table 1

Equilibrium constant values for various  $\beta$ -diketones used in the extraction of iron(III)

Extractant	$\text{p}K_{\text{a}}$	$\text{Log } K_{\text{Fe}}$
Dibenzoylmethane	9.35	-1.93 [25]
Acetyl acetone	8.82	-1.39 [25]
Benzoyl acetone	8.73	-0.50 [25]
1-Phenyl-3-methyl-4-(2-ethylhexanoyl)5-pyrazolone	6.89	0.74 [14]
1-Phenyl-3-methyl-4-(butanoyl)5-pyrazolone	5.97	3.98 [14]
3-Phenyl-4-benzoyl-5-isoxazolone	1.23	5.57

species involved do not change significantly under the experimental conditions. Table 1 gives the equilibrium constant values for various  $\beta$ -diketones comparing with HPBI for the extraction of Iron(III). It can be concluded from these comparisons that  $\log K_{\text{Fe}}$  values increase as the  $\text{p}K_{\text{a}}$  value decreases.

#### 4.4. Spectra of solid complexes

##### 4.4.1. IR spectra

The IR spectra of the extracted complexes show that the stretching frequency of the C=O group in HPBI has shifted from 1701 to 1607  $\text{cm}^{-1}$  in the  $\text{Fe}(\text{PBI})_3$  complex and to 1620  $\text{cm}^{-1}$  in  $\text{TiO}(\text{PBI})_2$  complex. This indicates that the carbonyl group is involved in bonding during complex formation.

##### 4.4.2. $^1\text{H}$ NMR spectra

In the  $^1\text{H}$  NMR spectra of  $\text{Fe}(\text{PBI})_3$  and  $\text{TiO}(\text{PBI})_2$  the disappearance of the peak at  $\delta = 12.22$  ppm as a result of the enolic-OH proton of HPBI indicates the ionisation of the enolic OH group and involvement of the oxygen of the hydroxyl group in chelation.

#### 4.5. Dependence of extraction on the nature of diluent

The extraction of iron(III) (0.5 mM) from 0.23 M HCl solutions with 0.005 M HPBI and titanium(IV) (2.5 mM) from 0.072 M HCl solutions with 0.01 M HPBI using various diluents has been studied and the results are shown in Table 2.

Table 2

Dependence on the nature of diluent on the extraction of iron(III) and titanium(IV)

Diluent	Dielectric constant ( $\epsilon$ ) [26]	Percentage of extraction	
		Iron(III)	Titanium(IV)
Methyl isobutyl ketone	13.11	34	8
Chloroform	4.90	27	17
Benzene	2.28	63	47
Xylene	2.26	60	51
Toluene	2.24	60	45
Carbon tetrachloride	2.21	75	75

These results clearly demonstrate that diluents such as benzene, xylene, toluene and carbon tetrachloride having low dielectric constants, show higher extraction for both iron(III) and titanium(IV). On the other hand, diluents having higher dielectric constants such as chloroform and MIBK give poor extraction.

#### 4.6. Comparison of extraction behaviour of iron(III) and titanium(IV) with other associated metal ions

The effect of hydrochloric acid concentration on the extraction of iron(III) (0.5 mM), titanium(IV) (1.25 mM), magnesium(II) (0.5 mM), chromium(VI) (0.5 mM), manganese(II) (1.0 mM), zinc(II) (1.0 mM), vanadium(V) (0.5 mM), and zirconium(IV) (1.25 mM) has been studied using 0.005 M HPBI with xylene as the solvent and the results are shown in Fig. 6. It is clear from the results that the percentage extraction of iron(III) decreases drastically from 99 to about 4% with increasing HCl concentration from 0.1 to 0.6 M.

On the other hand, titanium(IV) was found to be moderately extracted (23% at 0.07 M HCl; 1% at 0.3 M HCl) from 0.1 to 0.2 M HCl solutions. However, under the present experimental conditions, the extraction of magnesium(II), vanadium(V), chromium(VI), manganese(II), and zinc(II) was found to be negligible. The extraction of zirconium(IV) was found to be almost quantitative when extracted from 0.1 to 1.0 M hydrochloric acid solution. Thus, these results clearly indicate that it is possible to separate iron(III) from titanium(IV), vanadium(V), magnesium(II), manganese(II), zinc(II) and chromium(VI) using HPBI as an extractant by controlling the aqueous acidity.

Thus, these results clearly indicate that it is possible to separate iron(III) from titanium(IV), vanadium(V), magnesium(II), manganese(II), zinc(II) and chromium(VI) using HPBI as an extractant by controlling the aqueous acidity.

## 5. Conclusion

The extraction equilibrium of iron(III) and titanium(IV) from hydrochloric acid solutions with HPBI has been investigated. HPBI was found to be a powerful extractant for iron(III) owing to its strong acidity as compared to other  $\beta$ -diketones such as 4-acyl-5-pyrazolones. The results clearly

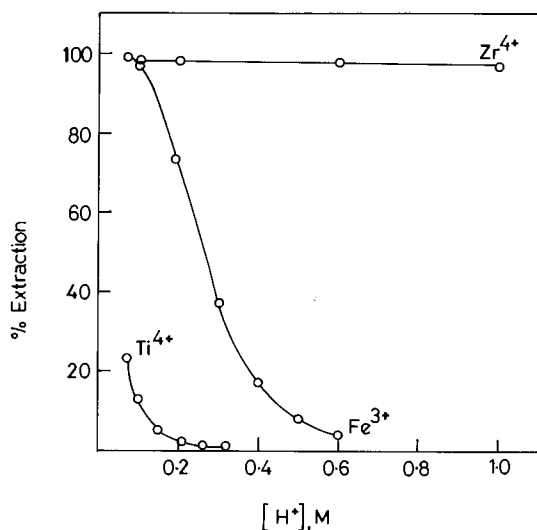


Fig. 6. Effect of HCl concentration on the extraction of iron(III), titanium(IV) and zirconium(IV) with HPBI: [Fe<sup>3+</sup>], 0.5 mM; [Ti<sup>4+</sup>], 2.5 mM; [Zr<sup>4+</sup>], 1.25 mM; HPBI = 0.005 M.

demonstrate the superior extraction of iron(III) over other associated multivalent metal ions when extracted with HPBI. Hence such a system could be of practical value for the extraction and separation of iron(III) from other metal ions present in the waste chloride liquors of the titanium-mineral-processing industry.

### Acknowledgements

This work was supported by Science, Technology and Environment Department, Government of Kerala. The authors wish to thank Dr G.D. Surender, Head of the Mineral Process Engineering Division and Dr G. Vijay Nair, Director of the Regional Research Laboratory, Trivandrum for their constant encouragement.

### References

- [1] H. Kodama, Jpn. Kokai Tokkyo Koho JP0 388 (1989) 718.
- [2] T. Yamamura, Y. Omote, S. Sato, T. Hiyama, Ger Offen. 112 (1947) 1970.
- [3] T. Sato, K. Sato, T. Yukio, Proceedings of the Symposium on Solvent Extraction, CA # 116: 239155e (1991), p. 339.
- [4] X. Kislik, A. Eyal, Solvent Extr. Ion Exch. 11 (1993) 259.
- [5] R.K. Biswas, D.A. Begum, Hydrometallurgy 49 (1998) 263.
- [6] K.K. Sahu, R.P. Das, Met. Mater. Trans. B 28B (1997) 181.
- [7] N.M. Sundaramurthi, V.M. Shinde, Analyst 114 (1989) 201.
- [8] F. Islam, R.K. Biswas, C.M. Mustafa, Hydrometallurgy 13 (1985) 365.
- [9] F.J. Algnacil, S. Amer, A. Luis, Hydrometallurgy 18 (1987) 65.
- [10] B.R. Reddy, B.P.V.R. Sarma, Hydrometallurgy 43 (1996) 299.
- [11] K.M. Allal, D. Hauchord, M. Stambouli, D. Pareau, D. Durand, Hydrometallurgy 45 (1997) 113.
- [12] J. Saji, T. Prasada Rao, C.S.P. Iyer, M.L.P. Reddy, Hydrometallurgy 49 (1998) 289.
- [13] K. Saji John, J. Saji, M.L.P. Reddy, T.R. Ramamohan, T.P. Rao, Hydrometallurgy 51 (1999) 9.
- [14] W. Mickler, A. Reich, E. Uhlemann, Sep. Sci. Tech. 33 (1998) 359.
- [15] M.O.C. Ogwuehbu, N.C. Oforika, Hydrometallurgy 34 (1994) 359.
- [16] M.L.P. Reddy, R. Luxmi Varma, T.R. Ramamohan, T. Prasada Rao, C.S.P. Iyer, A.D. Damodaran, J.N. Murali, R.H. Iyer, Radiochim. Acta 69 (1995) 55.
- [17] F. Korte, K. Storiko, Chem. Ber. 94 (1961) 1956.
- [18] A.I. Vogel, A Textbook of Quantitative Chemical Analysis, fifth ed., ELBS, Longman, UK, 1989, pp. 686–696.
- [19] G.H. Morrison, H. Freiser, Solvent Extraction in Analytical Chemistry, Wiley, New York, 1957, p. 244.
- [20] F.D. Snell, C.T. Snell, Colorimetric methods of analysis, third ed. vol. 2A, p.332, D. Van Nostrand, New Jersey.
- [21] A.I. Vogel, A Text Book of Quantitative Chemical Analysis, fifth ed., ELBS, Longman, UK, 1989, p. 329.
- [22] R.M. Smith, A.E. Martell, Critical Stability Constants, vol. 4, Plenum Press, New York, 1976.
- [23] S. Kotrly, Handbook of Chemical Equilibria in Analytical Chemistry, Ellis Harwood, Chichester, UK, 1985, p. 414.
- [24] P.B. Santhi, M.L.P. Reddy, T.R. Ramamohan, A.D. Damodaran, Talanta 41 (1994) 9.
- [25] J. Stary, E. Hladky, Anal. Chim. Acta 28 (1963) 227.
- [26] T. Sekine, Y. Hasegawa, Solvent Extraction Chemistry, Fundamentals and Applications, Marcel Dekker, New York, 1997, p. 48.



# High resolution spectrophotometry for identification of chlorine dioxide in concentrated chlorine solutions

R.D. Gauw<sup>a</sup>, G.L. Emmert<sup>a</sup>, B. Bubnis<sup>b</sup>, G. Gordon<sup>a,\*</sup>

<sup>a</sup> Department of Chemistry, Miami University, Oxford, OH 45056, USA

<sup>b</sup> Novatek, A Division of EBB Inc., Oxford, OH 45056, USA

Received 31 December 1998; received in revised form 6 July 1999; accepted 7 July 1999

## Abstract

Electrolyzed salt brine generators hold great promise for water disinfection in small communities and remote locations. Electrolysis cell liquors have been reported to contain chlorine, chlorine dioxide and ozone. High resolution spectrophotometry was used to observe the presence (or absence) of a unique spectral absorbance pattern present in solutions containing 1–2 mg/l chlorine dioxide. © 1999 Elsevier Science B.V. All rights reserved.

*Keywords:* High resolution spectrophotometry; Chlorine dioxide

## 1. Introduction

Chlorine ( $\text{Cl}_2$ ,  $\text{HOCl}$ ,  $\text{OCl}^-$ ) is the most widely used chemical for water disinfection in the United States. Because chlorine gas transportation raises safety concerns and liquid bleach storage may not be an alternative, a number of utilities are investigating the use of small salt brine electrolysis systems to produce chlorine at the point of use. It has been suggested [1–5] that electrolyzed salt brine liquors can contain chlorine, chlorine dioxide ( $\text{ClO}_2$ ) and ozone ( $\text{O}_3$ ). If this is true, it provides a reasonable basis to infer that the presence of  $\text{ClO}_2$  or  $\text{O}_3$  might lead to enhanced microbiological inactivation or reduced levels of

trihalomethanes (THMs) compared to chlorine gas in finished water. This work was undertaken to bring clarity to this issue with respect to  $\text{ClO}_2$ .

It is well recognized that the distribution of chlorine species in solution is pH-dependent. This is not the case for  $\text{ClO}_2$ . Dissolved chlorine dioxide does not undergo hydrolysis [6] to any appreciable extent ( $K = 1.2 \times 10^{-7}$  at 20°C) and is relatively stable over a wide pH range in low demand waters. In other words, unreacted  $\text{ClO}_2$  molecules are present in solution as a dissolved gas.

It is well known that the  ${}^2\text{B}_1-{}^2\text{A}_2$  electronic transition of  $\text{ClO}_2$  demonstrates vibrational structure. In the gas phase, these transitions appear as a series of sharp absorbance maxima [7,8] over the 320–400 nm region. In solution, the absorbance maxima are also observed [9], however they are

\* Corresponding author. Fax: +1-513-523-0005.

E-mail address: gordong@muohio.edu (G. Gordon)

typically broad and less defined. The existence of the absorbance fine structure means that the  $\text{ClO}_2$  molar extinction coefficient can vary depending on the quality of the spectrophotometer used for measurement.

## 2. Experimental section

All solutions were prepared using double distilled deionized water (DDW) unless otherwise noted. All chemicals were used without further purification. Fresh  $\text{ClO}_2$  (45–60 mg/l) was prepared using technical grade sodium chlorite (16 g/100 ml) mixed with potassium persulfate (8 g/200 ml) in a gas wash bottle [10–12]. Nitrogen gas was slowly passed into the gas wash bottle to displace  $\text{ClO}_2$  into chilled DDW.

Chlorine dioxide stock solutions were standardized using a Milton Roy Spectronic 3000 Array UV–Visible spectrophotometer where the  $\text{ClO}_2$  molar absorptivity was determined to be  $1225 \text{ M}^{-1} \text{ cm}^{-1}$  at 360 nm. The  $\text{ClO}_2$  stock solution was stored in a shrinking bottle [13]. The shrinking bottle is a zero headspace syringe attached to a calibrated screw. The apparatus is capable of

delivering a highly reproducible ( $\pm 0.005 \text{ ml}$ ) defined volume.

Electrolyzed brine solutions were freshly generated prior to each experiment according to the manufacturer's specifications [14,15].

An OLIS-Cary 14 high resolution (0.1 nm) spectrophotometer was used to record  $\text{ClO}_2$  absorbance spectra. A spectral resolution of 0.1 nm was employed to ensure accurate reproduction of the vibronic structure of the absorption spectrum.

## 3. Results and discussion

The high resolution spectrum presented in Fig. 1 clearly shows the presence of the unique  $\text{ClO}_2$  absorbance pattern over the 320–400 nm region. When a 10-cm measuring cell is used, the absorbance fine structure can be observed in solutions containing 1–2 mg/l  $\text{ClO}_2$ . Fig. 2 shows the absorbance and first derivative spectra for a 1.9 mg/l  $\text{ClO}_2$  solution over the 345–375 nm region. The first derivative spectrum helps to define the distance between the observed absorbance maxima and can be an important tool for confirmation of the presence of  $\text{ClO}_2$  in complicated solutions (i.e. electrolyzed salt brine liquors).

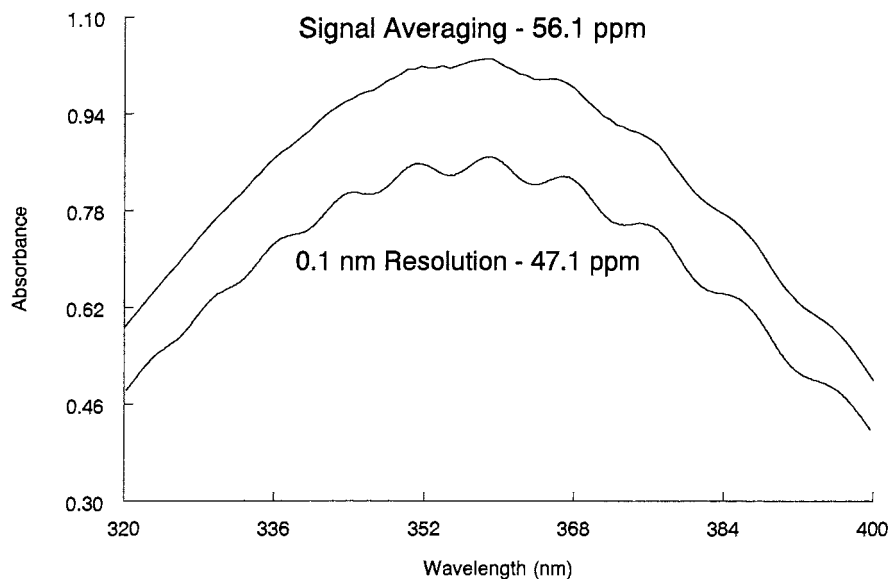


Fig. 1. Signal averaging vs 0.1 nm resolution.

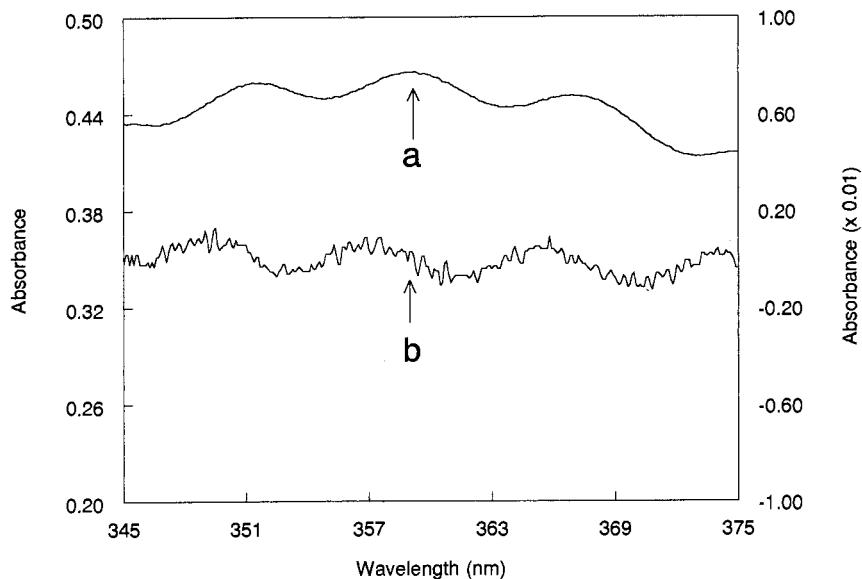


Fig. 2. (a) 1.9 mg/l  $\text{ClO}_2$  in solution; (b) first derivative spectra of 1.9 mg/l  $\text{ClO}_2$  in solution.

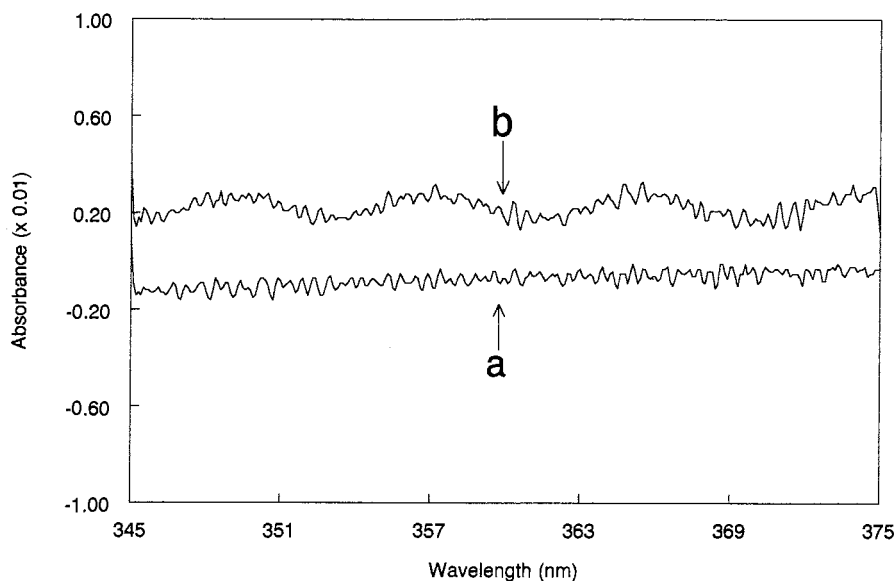


Fig. 3. (a) First derivative spectra of electrolyzed brine; (b) first derivative spectra of brine spiked with 1.9 mg/l  $\text{ClO}_2$ .

### 3.1. Evaluation of electrolyzed brine liquors for chlorine dioxide

The cell liquor from two salt-brine electrolysis systems (a bench top laboratory generator and a

full scale utility-size generator) were evaluated. In each case, the  $\text{ClO}_2$  'fingerprint' was not observed. We re-confirmed our ability to observe the presence of mg/l concentrations of  $\text{ClO}_2$  in cell liquors by spiking the full scale liquor with 1.9 mg/l  $\text{ClO}_2$ .

Fig. 3 shows the first derivative spectra of the unspiked (spectrum a) and spiked (spectrum b) liquors. These data are unambiguous and confirm that electrolyzed brine solutions contain  $< 2$  mg/l  $\text{ClO}_2$  within minutes of electrolysis.

Subsequent studies were designed to observe cell liquors spiked with  $\text{ClO}_2$  over long periods of time. Two water sources were used to prepare the starting brine solutions. Laboratory distilled water was used for the laboratory generator experi-

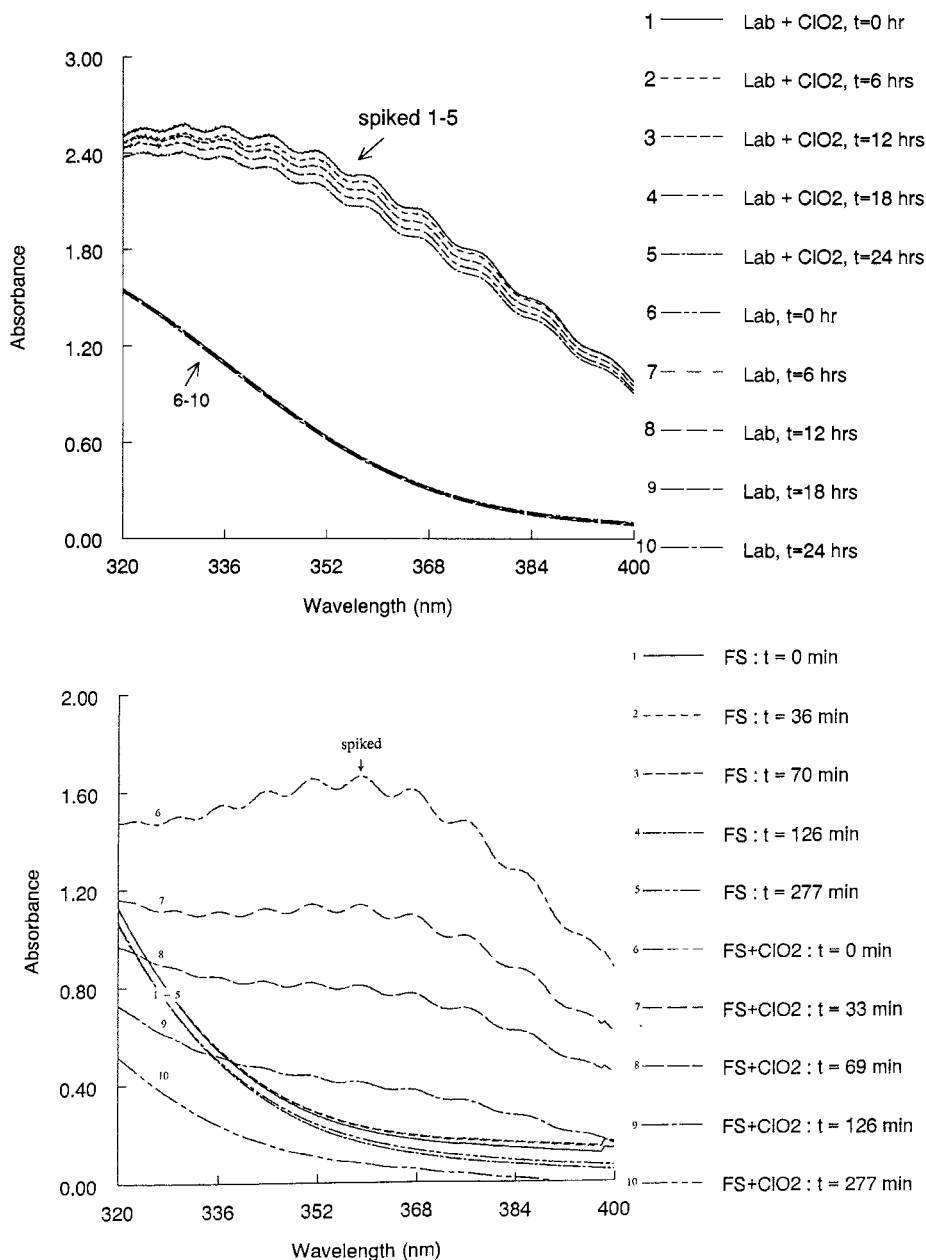


Fig. 4. (a) Laboratory unit electrolyzed brine solution and electrolyzed brine solution spiked with 10 mg/l  $\text{ClO}_2$  for 24 h; (b) full-scale electrolyzed brine solution and full-scale electrolyzed brine solution spiked with 10 mg/l  $\text{ClO}_2$  for  $\sim 4.5$  h.

ments while a treated surface water was used to prepare the brine solution for the full-scale system. Laboratory and full-scale cell liquors were spiked with 10 mg/l  $\text{ClO}_2$  and spectra recorded periodically over 24 h (Fig. 4a Fig. 4b respectively). The bottom series of absorbance spectra are of freshly prepared cell liquors. Liquors from both generators show no indication of the presence of  $\text{ClO}_2$  immediately following electrolysis.

The upper series of spectra are of the same cell liquors spiked with 10 mg/l  $\text{ClO}_2$ . The spectra of the laboratory generator liquor (Fig. 4a) clearly show an absorbance shoulder in the 360-nm region. The spectra also shows that there is a small decrease in  $\text{ClO}_2$  concentration over the analysis period. The full-scale cell liquor was prepared at the USEPA Testing and Evaluation (T&E) facility in Cincinnati, OH using Mill Creek potable water. The interesting aspect of this data set is that after  $\sim 4.5$  h, the spiked  $\text{ClO}_2$  is not observable. The spectra show that  $\sim 25\%$  of the original spiked  $\text{ClO}_2$  reacts in the first 33 min. After this initial reaction period,  $\text{ClO}_2$  continues to react at a slower rate.

These observations indicate that the initial demand for  $\text{ClO}_2$  in electrolysis cell liquors is to some degree dependent on the water used to prepare the starting brine solution. A second more important implication of these studies is that if an appreciable concentration of  $\text{ClO}_2$  were present in freshly prepared cell liquors (i.e. a  $\text{ClO}_2$  concentration that satisfies the demand), the cell liquors would not expect to exhibit a  $\text{ClO}_2$  demand following the addition of spiked  $\text{ClO}_2$  because  $\text{ClO}_2$  would be present in excess of the demand. The absence of the  $\text{ClO}_2$  fine structure in the absorbance spectra of freshly prepared electrolyzed salt brine liquors indicates that  $\text{ClO}_2$  is not present at concentrations exceeding 1–2 mg/l.

#### 4. Conclusions

High resolution spectrophotometry can be used to observe the  $\text{ClO}_2$  fine structure in the

absorbance spectra of solutions containing 1–2 mg/l  $\text{ClO}_2$ . Although it has been speculated that salt brine electrolysis cell liquors contain  $\text{ClO}_2$ , our studies show that the  $\text{ClO}_2$  fine structure cannot be observed in the absorbance spectra of these solutions. These data are strong and unambiguous evidence that  $\text{ClO}_2$  is not present in freshly prepared electrolysis liquors.

#### Acknowledgements

The authors are indebted to the cooperation and participation of the following organizations that are involved in this research; United States Environmental Protection Agency Contract No. 68-C5-0039 (Jim Goodrich, Ben Lykins and Roy Haught), IT Corporation (E. Radha Krishnan) and Miami University.

#### References

- [1] MIOX literature, Alternative Comparison for Important Features in Municipal Plants and Wells, MIOX Corporation, circa 1995.
- [2] United States Patent No. 4,761,208, Electrolytic Method and Cell for Sterilizing Water, 2 August 1988.
- [3] United States Patent No. 5,308,507, Method and Apparatus for Removing Organic Contaminants, 3 May 1994.
- [4] United States Patent No. 5,316,740, Electrolytic Cell for Generating Sterilization Solutions Having Increased Ozone Content, 31 May 1994.
- [5] United States Patent No. 5,385,711, Electrolytic Cell for Generating Sterilization Solutions Having Increased Ozone Content, 31 January 1995.
- [6] E.M. Aieta, J.D. Berg, *J. Am. Waterworks Assoc.* 78 (6) (1986) 62–72.
- [7] V. Vaida, E. Richard, *J. Chem. Phys.* 94 (1) (1991) 153.
- [8] V. Vaida, E. Richard, *J. Chem. Phys.* 94 (1) (1991) 163.
- [9] R. Dunn, B. Flanders, V. Vaida, J. Simon, *Spectrochim. Acta* 48A (9) (1992) 1293.
- [10] G.H. Cady, *Inorganic Synthesis*, vol. 5, McGraw-Hill, New York, 1957.
- [11] L.C. Adam, Analysis of the Decomposition of Hypochlorous Acid in the pH 6 to 8 Region, M.S. Thesis, Miami University, Oxford, OH, 1991, p. 74.

- [12] I. Nagypál, G. Peintler, I.R. Epstein, *J. Phys. Chem.* 94 (1990) 2954–2958.
- [13] R.A. Silverman, G. Gordon, *Anal. Chem.* 46 (1) (1974) 178.
- [14] MIOX<sup>®</sup> Brine Pump System Installation and Operation Manual.
- [15] MIOX<sup>®</sup> SAL-20, SAL-30, SAL-40 Installation and Operation Manual.

# Cathodic and anodic stripping voltammetry: simultaneous determination of As–Se and Cu–Pb–Cd–Zn in the case of very high concentration ratios<sup>☆</sup>

Clinio Locatelli \*, Giancarlo Torsi

*Department of Chemistry 'G. Ciamician', University of Bologna, Via Selmi 2, I-40126 Bologna, Italy*

Received 2 February 1999; received in revised form 6 May 1999; accepted 7 July 1999

## Abstract

Arsenic(III), selenium(IV), copper(II), lead(II), cadmium(II) and zinc(II) are determined in environmental matrices. The voltammetric measurements were carried out using a conventional three-electrode cell and the ammonia–ammonium chloride buffer pH 9.3 as supporting electrolyte. The analytical procedure was verified by the analysis of the standard reference materials Estuarine Sediment BCR-CRM 277 and River Sediment BCR-CRM 320. The precision, expressed as relative standard deviation ( $s_r$ ), and the accuracy, expressed as relative error, were, in all cases, less than 5%; the detection limits, for each element and in the experimental conditions employed, were around  $10^{-9}$  M. The standard addition technique significantly improved the resolution of the voltammetric method, even in the case of very high metal concentration ratios. © 1999 Elsevier Science B.V. All rights reserved.

*Keywords:* Voltammetry; Trace determination; Interferences; Sediments

## 1. Introduction

The voltammetric methods are a valid and effective option in the multicomponent analysis of metals, since the high sensitivity of the voltammetric method [1–3] can be associated with the considerable selectivity especially if the second harmonic alternating current technique is em-

ployed [4–6]. The sensitivity and selectivity have further been improved also by the introduction of new types of electrodes [7,8].

In the field of multicomponent determinations multiple-element schemes, coupling anodic stripping and cathodic stripping voltammetry, were reported by Adeloju et al. [9], while Gil and Ostapczuk [10] have developed an interesting potentiometric stripping analysis approach which considers the concentration ratios of the interfering elements.

The present work examines the simultaneous determination of As(III), Se(IV), Cu(II), Pb(II), Cd(II) and Zn(II) by differential pulse cathodic

<sup>☆</sup> Work presented at the 49th ISE Meeting, Kitakyushu, Japan, September 13–18, 1998.

\* Corresponding author. Tel.: +39-2099-456-51; fax: +39-20099-450-51.

*E-mail address:* clinio@ciam.unibo.it (C. Locatelli)

(DPCSV) and anodic (DPASV) stripping voltammetry in environmental matrices like estuarine and river sediments.

The above mentioned elements, frequently simultaneously present in matrices of this type and in the supporting electrolyte commonly used for the voltammetric measurements, interfere with one another [11–16]. For this reason a new speedy, precise and accurate method for their simultaneous determination is proposed and applied also in the case of very high element concentration ratios, employing the standard addition method.

## 2. Experimental

### 2.1. Apparatus

Voltammetric measurements were carried out with an AMEL (Milan, Italy) Model 433 Multipolarograph, employing a stationary mercury electrode as working electrode, while an Ag/AgCl, KCl satd. electrode and a platinum wire were used as reference and auxiliary electrode, respectively.

The voltammetric cell was kept at  $20.0 \pm 0.5^\circ\text{C}$ .

The solutions were deaerated with pure nitrogen for 15 min prior to the measurements, while a nitrogen blanket was maintained above the solution during the analysis. The solutions were deaerated for 2 min after each standard addition.

### 2.2. Reagents and reference solutions

All solutions were prepared with deionized water (Millipore, Milli Q), and all reagents were 'suprapure' grade.

Ammonia–ammonium chloride buffer solution (pH 9.3) was prepared by mixing an appropriate amount of hydrochloric acid and ammonia solution.

Aqueous stock solutions of As(III), Se(IV), Cu(II), Pb(II), Cd(II) and Zn(II) were prepared by dilution of the respective standard  $1000 \text{ mg l}^{-1}$  solutions (BDH, UK).

The Teflon voltammetric cell was rinsed every day with suprapure concentrated nitric acid to minimise potential contamination.

The following standard reference materials were chosen for the analyses: Estuarine Sediment BCR-CRM 277 and River Sediment BCR-CRM 320.

### 2.3. Sample preparation

For the voltammetric measurements, Estuarine Sediment BCR-CRM 277 and River Sediment BCR-CRM 320 were mineralised as follows.

Approximately 0.5–0.8 g of sediment, accurately weighed in a Pyrex digestion tube calibrated at 25 and 50 ml were dissolved in 4 ml of 37% ( $\text{m m}^{-1}$ ) hydrochloric acid, and 5 ml of 69% ( $\text{m m}^{-1}$ ) nitric acid were successively added. The tube was inserted in the cold home-made block digester, the temperature of which was gradually raised through a heating plate up to  $130\text{--}150^\circ\text{C}$ , maintaining the temperature constant until the red nitrous fumes stopped. After cooling 3 ml of 60% ( $\text{m m}^{-1}$ ) perchloric acid were added, raising the temperature again up to  $130\text{--}150^\circ\text{C}$ . The solution was slowly boiled, evaporated almost to dryness and, after cooling, the soluble salts were dissolved in 250 ml of ammonia–ammonium chloride buffer solution (pH 9.3). Finally, the solutions so obtained were analysed by voltammetric technique.

The same procedure was employed for the mineralization of sediments sampled in the Goro Bay zone.

## 3. Results and discussion

### 3.1. Influence of pH on $i_p$

At first, the analytical procedure has been set up using the aqueous reference solutions in order to optimise all the analytical parameters like sensitivity, detection limit, precision and accuracy, and successively verifying the validity of the method by means of the standard reference materials. The experimental conditions of the voltammetric analytical procedure and the experimental peak potentials are reported in Table 1. All the parameters were chosen in order to optimise the instrumental signal.



The solution pH affects the peak height of each element; the pH versus  $i_p$  behaviours of As(III), Se(IV) employing DPCSV (Fig. 1a), and Cu(II), Pb(II), Cd(II), Zn(II) employing DPASV (Fig. 1b) show that the best pH value compromise for all the elements is 9.3, since the peak currents, for all the elements, are generally higher at this pH value.

Aqueous reference solutions were used to determine the analytical calibration functions for all the elements by differential pulse cathodic and anodic stripping voltammetry (Tables 2 and 3). In all cases, the correlation coefficients are good ( $r > 0.9990$ ), while the precision of the method, expressed as residual standard deviation, was found to be satisfactory ( $s_r < 5\%$ ). Tables 2 and 3 report also the detection limits for each element.

Once calculated the analytical calibration functions of each element, the problem of simultaneously determining the metals has been considered.

Table 1

Experimental conditions for the determination of As(III)–Se(IV) and Cu(II)–Pb(II)–Cd(II)–Zn(II) by differential pulse cathodic (DPCSV) and anodic stripping voltammetry (DPASV)<sup>a,b</sup>

	As(III)–Se(IV) (DPCSV)	Cu(II)–Pb(II)–Cd(II)–Zn(II) (DPASV)
$E_d$	–1.100	–1.250
$E_r$	–1.650	–0.200
$t_d$	210	120
$t_r$	10	10
$dE/dt$	10	10
$\Delta E$	50	50
$\tau$	0.065	0.065
$\nu$	0.250	0.250
$r$	600	600

<sup>a</sup> Supporting electrolyte: ammonia–ammonium chloride buffer (pH 9.3).

<sup>b</sup>  $E_d$ , deposition potential (V/Ag, AgCl, KCl sat.);  $E_r$ , final potential (V/Ag, AgCl, KCl sat.);  $t_d$ , deposition time (s);  $t_r$ , delay time before the potential sweep (s);  $dE/dt$ , potential scan rate ( $\text{mV s}^{-1}$ );  $\Delta E$ , amplitude of pulse superposed (mV);  $\tau$ , pulse duration (s);  $\nu$ , pulse repetition (s);  $r$ , stirring rate (r.p.m.). Experimental peak potentials (V/Ag, AgCl, KCl sat.):  $-1.323 \pm 0.005$  [As(III)],  $-1.415 \pm 0.010$  [Se(IV)],  $-0.469 \pm 0.010$  [Cu(II)],  $-0.596 \pm 0.005$  [Pb(II)],  $-0.750 \pm 0.005$  [Cd(II)],  $-1.035 \pm 0.010$  [Zn(II)].

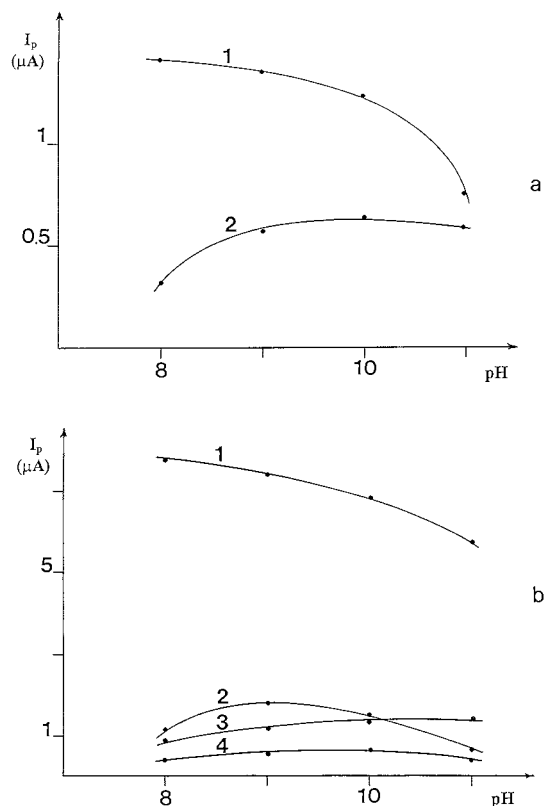


Fig. 1. Behaviours ( $i_p$  vs pH) in ammonia–ammonium chloride buffer as supporting electrolyte. (a) As(III) (curve 1) and Se(IV) (curve 2). Voltammetric technique: DPCSV. (b) Cd(II) (curve 1), Zn(II) (curve 2), Cu(II) (curve 3) and Pb(II) (curve 4). Voltammetric technique: DPASV.  $c = 2.3 \times 10^{-7}$  M for all the elements. Experimental conditions are given in Table 1.

### 3.2. Monivariate and bivariate analysis

The simultaneous determinations of As(III)–Se(IV) and Cu(II)–Pb(II)–Cd(II)–Zn(II) were studied in a wide range of concentration ratios, in the concentration ranges corresponding to the respective calibration functions.

The element concentration ratios, within which each single element could be determined without mutual interferences, were investigated. To a fixed, but very small, concentration of the element of interest, standard additions of the interfering element were added in such a way as to change their concentration ratios.

The peak current values of the elements in the various mixtures were compared to those calculated by using the respective calibration curves.

The errors of these data, relevant to the As(III)–Se(IV), Cu(II)–Pb(II) and Pb(II)–Cd(II) couples, as a function of the concentration ratios are shown in the curves of Fig. 2a and b. It is apparent that, at the confidence level of 95%, the determination of the metals is possible, within a maximum random error of 5%, in the following concentration ratio ranges:  $55:1 > c_{\text{As}}:c_{\text{Se}} > 1:49$ ,  $58:1 > c_{\text{Cu}}:c_{\text{Pb}} > 1:62$ ,  $69:1 > c_{\text{Pb}}:c_{\text{Cd}}:1:77$ .

The experimental data were also confirmed by monovariate and bivariate statistical analysis [17–19]. Mono- and bivariate analyses permitted reliable decision on the presence or not of interferences: in monovariate analysis the interference from the second element is neglected; it is considered, however, in bivariate analysis. In fact, the interference is excluded, as in the present work, according to the model relevant to the bivariate analysis (Tables 2 and 3), when the slopes of the calibration function of a given element in the mixture are found to be equal to that observed in the absence of the other element, and, particularly, when the second term of the model of the analytical calibration function related to the interfering element is negligible.

The same Tables 2 and 3 report also the detection limits, the precision, expressed as the residual standard deviation  $s_r$ , and the accuracy, expressed as the relative error  $e$ .

In the supporting electrolyte employed, the determination of Zn(II) did not show interference problems. In fact the peak of Zn(II) is well separated from that of Cd(II) ( $\Delta E_p \text{Zn-Cd} = 285 \text{ mV}$ ). For this reason the Zn(II) determination was carried out using its analytical calibration function (Table 3).

#### 4. Usefulness of standard addition method in the case of mutual interferences

However, the interesting aspect of the work is evidently the possibility of determining, in the mixture, the metal having the lower concentration and an unfavourable concentration ratio as to the neighbouring element. In such a case the standard addition method permitted the extension of the analysis beyond the concentration ratio intervals within which the mutual interferences did not exceed the accepted error level of 5%.

In this situation, bringing the concentration ratio within the interval valid for mono- and

Table 2

Analytical calibration functions<sup>a</sup> and relative mono and bivariate analysis (differential pulse cathodic stripping voltammetry, DPCSV)

	Calibration functions of the single element	Monovariate analysis*	Bivariate analysis*
As(III)	$i_p = (0.02 \pm 0.02) + (5.77 \pm 0.09) \times 10^6 c$ $r = 0.9990^b$ $s_r = 2.7\%^c$ D.L. = $1.73 \times 10^{-9} \text{ M}^d$	$i_p = (0.01 \pm 0.02) + (5.52 \pm 0.10) \times 10^6 c$ $r = 0.9989$ $s_r = 2.5\%$ $e = -4.3\%^c$ D.L. = $1.81 \times 10^{-9} \text{ M}$	$i_p = (0.01 \pm 0.01) + (6.01 \pm 0.10) \times 10^6 c_{\text{As}} + (4.9 \pm 0.1) \times 10 c_{\text{Se}}$ $r = 0.9988$ $s_r = 3.9\%$ $e = +4.2\%$ D.L. = $1.66 \times 10^{-9} \text{ M}$
Se(IV)	$i_p = (0.01 \pm 0.02) + (2.69 \pm 0.08) \times 10^6 c$ $r = 0.9991$ $s_r = 3.1\%$ D.L. = $3.72 \times 10^{-9} \text{ M}$	$i_p = (0.02 \pm 0.03) + (2.55 \pm 0.09) \times 10^6 c$ $r = 0.9992$ $s_r = 3.7\%$ $e = -5.2\%$ D.L. = $3.92 \times 10^{-9} \text{ M}$	$i_p = (0.02 \pm 0.02) + (2.58 \pm 0.08) \times 10^6 c_{\text{Se}} + (6.9 \pm 0.3) \times 10 c_{\text{As}}$ $r = 0.9989$ $s_r = 4.3\%$ $e = -4.1\%$ D.L. = $3.88 \times 10^{-9} \text{ M}$

<sup>a</sup> The errors correspond to a probability of 95%;  $i_p$  = peak current ( $\mu\text{A}$ );  $c$  = concentration of the electroactive species (M).

<sup>b</sup>  $r$  = correlation coefficient.

<sup>c</sup>  $s_r$  = mean standard residual deviation.

<sup>d</sup> Limit of detection (D.L.) is expressed according to IUPAC [22] and corresponds to a probability of 99% [23].

<sup>e</sup> Relative error.

\* In monovariate analysis interferences from neighbouring elements are neglected; it is considered, however, in bivariate analysis [17–19].

Table 3

Analytical calibration functions<sup>a</sup> and relative mono and bivariate analysis (differential pulse anodic stripping voltammetry, DPASV)

	Calibration functions of the single element	Monovariate analysis*	Bivariate analysis*
Cu(II)	$i_p = (0.02 \pm 0.01) + (5.69 \pm 0.10) \times 10^6 c$ $r = 0.9988^b$ $s_r = 4.0\%^c$ D.L. = $1.76 \times 10^{-9}$ M <sup>d</sup>	$i_p = (0.01 \pm 0.01) + (5.87 \pm 0.13) \times 10^6 c$ $r = 0.9990$ $s_r = 3.6\%$ $e = +3.2\%^c$ D.L. = $1.70 \times 10^{-9}$ M	$i_p = (0.02 \pm 0.02) + (5.95 \pm 0.11) \times 10^6 c_{Cu} + (8.9 \pm 0.3) \times 10 c_{Pb}$ $r = 0.9989$ $s_r = 3.1\%$ $e = +4.6\%$ D.L. = $1.68 \times 10^{-9}$ M
Pb(II)	$i_p = (0.01 \pm 0.02) + (2.63 \pm 0.08) \times 10^6 c$ $r = 0.9990$ $s_r = 2.4\%$ D.L. = $3.80 \times 10^{-9}$ M	$i_p = (0.02 \pm 0.02) + (2.72 \pm 0.09) \times 10^6 c$ $r = 0.9991$ $s_r = 2.5\%$ $e = +3.4\%$ D.L. = $3.68 \times 10^{-9}$ M	$i_p = (0.01 \pm 0.02) + (2.50 \pm 0.09) \times 10^6 c_{Pb} + (6.5 \pm 0.2) \times 10 c_{Cu}$ $r = 0.9993$ $s_r = 2.8\%$ $e = -4.9\%$ D.L. = $4.00 \times 10^{-9}$ M $i_p = (0.02 \pm 0.03) + (2.49 \pm 0.11) \times 10^6 c_{Pb} + (7.7 \pm 0.1) \times 10 c_{Cd}$ $r = 0.9991$ $s_r = 3.8\%$ $e = -5.3\%$ D.L. = $4.02 \times 10^{-9}$ M
Cd(II)	$i_p = (0.02 \pm 0.03) + (3.21 \pm 0.07) \times 10^7 c$ $r = 0.9994$ $s_r = 2.0\%$ D.L. = $0.31 \times 10^{-9}$ M	$i_p = (0.01 \pm 0.02) + (3.08 \pm 0.08) \times 10^7 c$ $r = 0.9992$ $s_r = 2.3\%$ $e = -4.0\%$ D.L. = $0.32 \times 10^{-9}$ M	$i_p = (0.02 \pm 0.02) + (3.35 \pm 0.12) \times 10^7 c_{Cd} + (5.9 \pm 0.3) \times 10 c_{Pb}$ $r = 0.9995$ $s_r = 1.8\%$ $e = +4.4\%$ D.L. = $0.30 \times 10^{-9}$ M
Zn(II)	$i_p = (0.01 \pm 0.02) + (7.69 \pm 0.09) \times 10^6 c$ $r = 0.9988$ $s_r = 3.9\%$ D.L. = $1.30 \times 10^{-9}$ M	–	–

<sup>a</sup> The errors correspond to a probability of 95%;  $i_p$  = peak current ( $\mu$ A);  $c$  = concentration of the electroactive species (M).<sup>b</sup>  $r$  = correlation coefficient.<sup>c</sup>  $s_r$  = mean standard residual deviation.<sup>d</sup> Limit of detection (D.L.) is expressed according to IUPAC [22] and corresponds to a probability of 99% [23].<sup>e</sup> Relative error.

\* In monovariate analysis interferences from neighbouring elements are neglected; it is considered, however, in bivariate analysis [17–19].

bivariate analysis by adding the standard solution of the metal with the lower concentration was enough to allow the determination of the metal itself. In fact, the peak current versus concentration plot of the element having the lower concentration in the mixture was non-linear after the initial standard additions, owing to the peak overlappings; linearity was, however, attained as soon as the concentration ratio of the metals was within the validity range of mono- and bivariate analysis. The extrapolation of the linear portion of the curve permitted the evaluation of the concentration of the element present at the lower concentration. Fig. 3a and b shows as examples the As(III) and Pb(II) determinations in the pres-

ence of a large excess of Se(IV) and Cu(II), respectively.

The As(III) ( $2.3 \times 10^{-8}$  M) and Pb(II) ( $1.2 \times 10^{-8}$  M) concentrations were increased by standard addition of the same metals. The  $i_p$  versus concentration behaviours were non linear as long as the concentration ratios were higher than the non interference values previously reported ( $c_{Se}:c_{As} = 49$ ;  $c_{Cu}:c_{Pb} = 58$ ), becoming linear for lower concentration ratio values. So applying the procedure described above, and statistically evaluating the limit within which linearity prevails according to the method of Liteanu et al. [20] using the  $t$ -test criterion (probability of 99%), the metal concentrations were easily determined.

#### 4.1. Application of the method to the standard reference materials

The experimental conditions for determining the metals in Estuarine Sediment BCR-CRM 277 and River Sediment BCR-CRM 320 were identical with those employed in the case of the aqueous reference solution (Table 1).

Table 4 shows the slopes and merits of the

analytical calibration functions calculated in the standard reference materials for all the elements: the slope comparisons with those determined in the aqueous reference solutions (Tables 2 and 3) emphasise that, in all cases, no matrix interferences were present, not having the analytical sensitivities differences at 5% error level, considering such a value reasonably within the experimental errors.

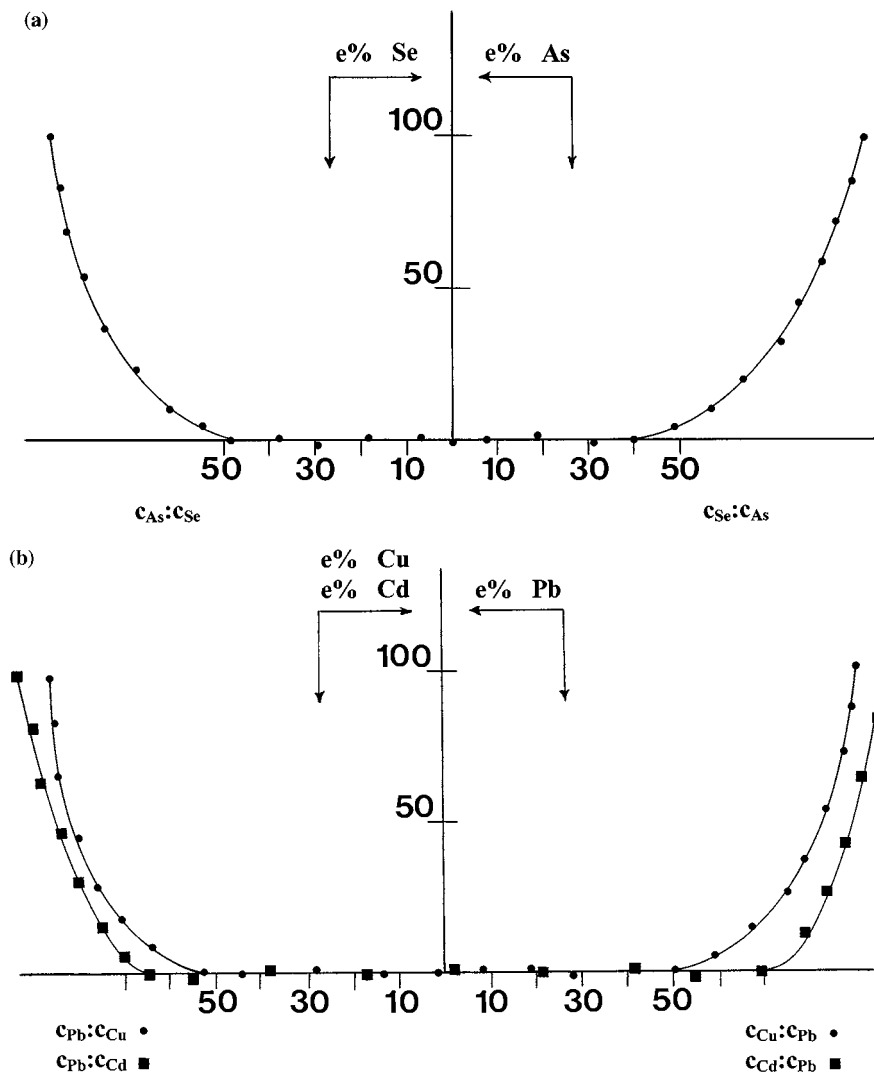


Fig. 2. (a) Relationship between the metal concentration ratios As(III)/Se(IV) and the relative errors in the determination of the element present at the lowest concentration. Supporting electrolyte: ammonia–ammonium chloride buffer pH 9.3. Voltammetric technique: DPCSV. (b) Relationship between the metal concentration ratios Pb(II)/Cu(I) and Pb(II)/Cd(II) and the relative errors in the determination of the element present at the lowest concentration. Supporting electrolyte: ammonia–ammonium chloride buffer pH 9.3. Voltammetric technique: DPASV.

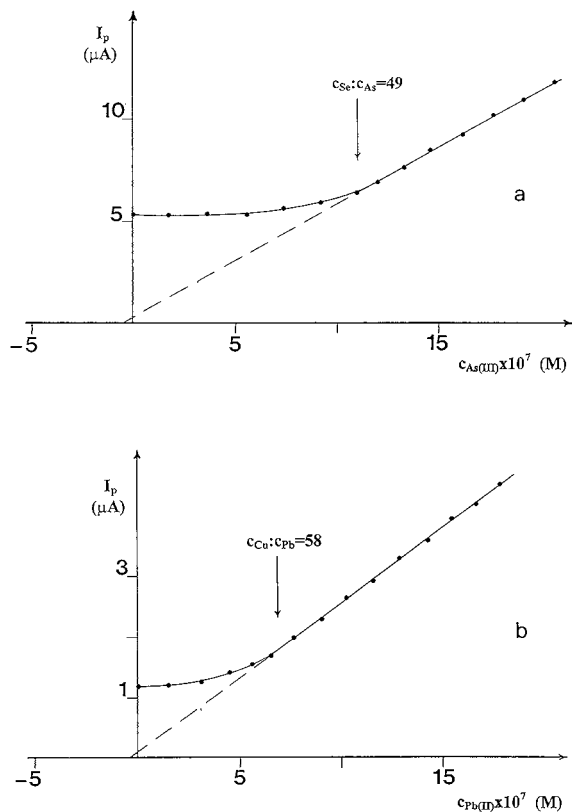


Fig. 3. (a) Differential pulse cathodic (DPCSV) stripping voltammetric determination of As(III) in ammonia–ammonium chloride buffer pH 9.3 by standard addition method in the presence of Se(IV) excess. Concentrations:  $c_{\text{Se}} = 1.8 \times 10^{-6}$  M;  $c_{\text{As}} = 2.3 \times 10^{-8}$  M;  $c_{\text{Se}}:c_{\text{As}} = 78.3$ . (b) Differential pulse anodic (DPASV) stripping voltammetric determination of Pb(II) in ammonia–ammonium chloride buffer pH 9.3 by standard addition method in the presence of Cu(II) excess. Concentrations:  $c_{\text{Cu}} = 8.3 \times 10^{-7}$  M;  $c_{\text{Pb}} = 1.2 \times 10^{-8}$  M;  $c_{\text{Cu}}:c_{\text{Pb}} = 69.2$ . Experimental conditions are given in Table 1.

Furthermore, always on the standard reference materials, the non-interference concentration ratio intervals have been also evaluated by adding, during the digestion procedure, the single metals; their comparison with those calculated in the aqueous reference solution shows no significant differences, being  $57:1 > c_{\text{As}}:c_{\text{Se}} > 1:52$ ,  $60:1 > c_{\text{Cu}}:c_{\text{Pb}} > 1:65$ ,  $68:1 > c_{\text{Pb}}:c_{\text{Cd}} > 1:74$ .

In the case of Estuarine Sediment BCR-CRM 277 As(III) and Se(IV) are simultaneously determined by the relevant analytical calibration functions, in fact the concentration ratio  $c_{\text{As}}:c_{\text{Se}}$  is

$47.3:2.04 = 23.2$  (concentration expressed in  $\text{mg kg}^{-1}$ ) with molar concentration ratio equal to 24.5, then less than the interference limit  $c_{\text{As}}:c_{\text{Se}} = 57$ .

The analytical results are listed in Table 5.

The case of River Sediment BCR-CRM 320, where the concentration ratio  $c_{\text{As}}:c_{\text{Se}}$  is  $76.7:0.214 = 358.4$  (concentration expressed in  $\text{mg kg}^{-1}$ ) with a molar concentration ratio equal to 376.5, shows a very strong interference. However, also in this case, the simultaneous determination of the two elements is equally obtained, with acceptable accuracy.

The element with the higher concentration, As(III), was calculated by its analytical calibration function, while the element with the lower concentration, Se(IV), was determined employing the standard addition procedure and the analytical results are listed in Table 5.

In the case of Cu(II), Pb(II), Cd(II) Zn(II) determinations, for both standard reference materials, the metal concentration ratios in the sample digestion solution did not exceed the values of the reciprocal interferences at the 5% error level reported above: each element was so determined by the respective analytical calibration functions, employing the standard addition method and the analytical results are reported in Table 5.

The experimental data reported in Table 5 show that the precision and the accuracy are good; in fact, in all cases, the precision, expressed as relative standard deviation ( $s_r$ ), and the accuracy, expressed as relative error ( $e$ ), were less than 5%.

#### 4.2. Application to the Goro Bay zone, Po river delta (Italy)

The analytical procedure, so set up on the standard reference materials, was transferred to real samples: the sediments sampled inside the Po river delta in the 'Goro Bay' zone, a very important area devoted to the fishing and breeding of mussels and clams for food. Sampling have been carried out in three positions: the internal, where flows the Po river branch, the central and near the connection with the Adriatic sea, in order to have a sufficiently realistic situation of the ecosystem pollution.

The sediments were dried, powdered and finally mineralised with the  $\text{HNO}_3\text{--HCl--HClO}_4$  acidic mixture, following the same analytical procedure employed in the case of the standard reference materials and previously reported.

The results are listed in Table 6. These values, if compared with those found in the sediments sampled in different ecosystems [21] show to be, for selenium and arsenic, of the same order of magnitude and in substantial agreement, but, on the contrary, in the case of copper, lead, cadmium and zinc, pollution seems general, uniform and in some cases very high.

It can be concluded that, if the supporting electrolyte is accurately chosen, voltammetry together with the standard addition method is cer-

tainly a valid analytical method (good selectivity and, especially, sensitivity) for simultaneously determining elements having very similar half-wave potentials and, consequently, very strong interference problems. Then the proposed procedure is certainly suitable for metal determinations in multicomponent complex matrices like, for example, all the environmental samples, since it does not need enrichment steps or particular sample treatments.

### Acknowledgements

The work was supported by Funds for Selected Research Topics of the University of Bologna (Italy).

Table 4

Analytical sensitivities ( $\mu\text{A M}^{-1}$ ) and merits of the analytical calibration functions<sup>a</sup> in the standard reference materials

	Estuarine Sediment BCR-CRM 277	River Sediment BCR-CRM 320	Analytical calibration function*
As(III)	$(5.91 \pm 0.11) \times 10^6 c$ $r = 0.9989^b$ $s_r = 4.1\%^c$ $e = +2.4\%^c$ D.L. = $1.69 \times 10^{-9}$ M <sup>d</sup>	$(5.99 \pm 0.10) \times 10^6 c$ $r = 0.9991$ $s_r = 3.7\%$ $e = +3.8\%$ D.L. = $1.67 \times 10^{-9}$ M	$(5.77 \pm 0.09) \times 10^6 c$ $r = 0.9990$ $s_r = 2.7\%$ D.L. = $1.73 \times 10^{-9}$ M
Se(IV)	$(2.83 \pm 0.08) \times 10^6 c$ $r = 0.9990$ $s_r = 4.1\%$ $e = +5.2\%$ D.L. = $3.53 \times 10^{-9}$ M	$(2.57 \pm 0.10) \times 10^6 c$ $r = 0.9989$ $s_r = 4.0\%$ $e = -4.5\%$ D.L. = $3.89 \times 10^{-9}$ M	$(2.69 \pm 0.08) \times 10^6 c$ $r = 0.9991$ $s_r = 3.1\%$ D.L. = $3.72 \times 10^{-9}$ M
Cu(II)	$(5.48 \pm 0.09) \times 10^6 c$ $r = 0.9991$ $s_r = 3.8\%$ $e = -3.7\%$ D.L. = $1.82 \times 10^{-9}$ M	$(5.45 \pm 0.12) \times 10^6 c$ $r = 0.9988$ $s_r = 4.1\%$ $e = -4.2\%$ D.L. = $2.22 \times 10^{-9}$ M	$(5.69 \pm 0.10) \times 10^6 c$ $r = 0.9988$ $s_r = 4.0\%$ D.L. = $1.76 \times 10^{-9}$ M
Pb(II)	$(2.49 \pm 0.10) \times 10^6 c$ $r = 0.9990$ $s_r = 2.8\%$ $e = -5.3\%$ D.L. = $4.02 \times 10^{-9}$ M	$(2.75 \pm 0.09) \times 10^6 c$ $r = 0.9988$ $s_r = 3.2\%$ $e = +4.6\%$ D.L. = $3.64 \times 10^{-9}$ M	$(2.63 \pm 0.08) \times 10^6 c$ $r = 0.9991$ $s_r = 2.4\%$ D.L. = $3.80 \times 10^{-9}$ M
Cd(II)	$(3.35 \pm 0.11) \times 10^7 c$ $r = 0.9993$ $s_r = 1.5\%$ $e = +4.4\%$ D.L. = $0.30 \times 10^{-9}$ M	$(3.39 \pm 0.12) \times 10^7 c$ $r = 0.9994$ $s_r = 1.7\%$ $e = +5.6\%$ D.L. = $0.29 \times 10^{-9}$ M	$(3.21 \pm 0.07) \times 10^7 c$ $r = 0.9994$ $s_r = 2.0\%$ D.L. = $0.31 \times 10^{-9}$ M
Zn(II)	$(7.42 \pm 0.13) \times 10^6 c$ $r = 0.9988$ $s_r = 3.6\%$ $e = -3.5\%$ D.L. = $1.35 \times 10^{-9}$ M	$(7.37 \pm 0.11) \times 10^6 c$ $r = 0.9990$ $s_r = 3.1\%$ $e = -4.2\%$ D.L. = $1.36 \times 10^{-9}$ M	$(7.69 \pm 0.09) \times 10^6 c$ $r = 0.9988$ $s_r = 3.9\%$ D.L. = $1.30 \times 10^{-9}$ M

<sup>a</sup> The errors correspond to a probability of 95%;  $i_p$  = peak current ( $\mu\text{A}$ );  $c$  = concentration of the electroactive species (M).

<sup>b</sup>  $r$  = correlation coefficient.

<sup>c</sup>  $s_r$  = mean standard residual deviation.

<sup>d</sup> Limit of detection (D.L.) is expressed according to IUPAC [22] and corresponds to a probability of 99% [23].

<sup>e</sup> Relative error.

\* In monovariate analysis interferences from neighbouring elements are neglected; it is considered, however, in bivariate analysis [17–19].

Table 5  
Analytical results obtained in the standard reference materials\*

Element		Estuarine Sediment BCR-CRM 277	River Sediment BCR-CRM 320
As(III)	Certified (mg kg <sup>-1</sup> )	47.3 ± 1.6	76.7 ± 3.4
	Determined (mg kg <sup>-1</sup> )	49.6 ± 2.5	79.3 ± 2.8
	<i>e</i> (%)**	+4.9	+3.4
	<i>s<sub>r</sub></i> (%)**	3.7	2.8
Se(IV)	Certified (mg kg <sup>-1</sup> )	2.04 ± 0.18	0.214 ± 0.034
	Determined (mg kg <sup>-1</sup> )	2.13 ± 0.19	0.223 ± 0.021
	<i>e</i> (%)	+4.4	+4.2
	<i>s<sub>r</sub></i> (%)	3.1	3.9
Cu(II)	Certified (mg kg <sup>-1</sup> )	101.7 ± 1.6	44.1 ± 1.0
	Determined (mg kg <sup>-1</sup> )	106.9 ± 5.3	43.0 ± 1.9
	<i>e<sub>r</sub></i> (%)	+5.1	-2.5
	<i>s<sub>r</sub></i> (%)	4.7	2.3
Pb(II)	Certified (mg kg <sup>-1</sup> )	146 ± 3	42.3 ± 1.6
	Determined (mg kg <sup>-1</sup> )	149 ± 5	40.1 ± 2.8
	<i>e</i> (%)	+2.1	-5.2
	<i>s<sub>r</sub></i> (%)	2.9	4.6
Cd(II)	Certified (mg kg <sup>-1</sup> )	11.9 ± 0.4	0.533 ± 0.026
	Determined (mg kg <sup>-1</sup> )	11.6 ± 0.4	0.523 ± 0.013
	<i>e</i> (%)	-2.5	-1.9
	<i>s<sub>r</sub></i> (%)	2.7	3.0
Zn(II)	Certified (mg kg <sup>-1</sup> )	547 ± 12	142 ± 3
	Determined (mg kg <sup>-1</sup> )	569 ± 25	149 ± 8
	<i>e</i> (%)	+4.0	+4.9
	<i>s<sub>r</sub></i> (%)	3.2	4.1

\* Number of samples, 5.

\*\* *e*, relative error; *s<sub>r</sub>*, relative standard deviation.

Table 6  
Determination of As(III), Se(IV), Cu(II), Pb(II), Cd(II) and Zn(II) in the superficial sediments (0–10 cm), sampled in the Goro Bay (Ferrara, Italy)\*

Sampling time	April, 1997			October, 1997		
	A	B	C	A	B	C
As(III)	55.2 ± 0.3 <i>s<sub>r</sub></i> = 3.5%	41.7 ± 0.5 <i>s<sub>r</sub></i> = 2.8%	21.2 ± 0.2 <i>s<sub>r</sub></i> = 1.9%	59.7 ± 0.5 <i>s<sub>r</sub></i> = 4.0%	47.8 ± 0.4 <i>s<sub>r</sub></i> = 4.2%	20.5 ± 0.5 <i>s<sub>r</sub></i> = 3.8%
Se(IV)	0.69 ± 0.07 <i>s<sub>r</sub></i> = 2.7%	0.75 ± 0.08 <i>s<sub>r</sub></i> = 3.4%	0.49 ± 0.09 <i>s<sub>r</sub></i> = 3.5%	1.47 ± 0.07 <i>s<sub>r</sub></i> = 2.7%	1.63 ± 0.10 <i>s<sub>r</sub></i> = 3.1%	1.03 ± 0.06 <i>s<sub>r</sub></i> = 4.7%
Cu(II)	66.3 ± 2.1 <i>s<sub>r</sub></i> = 3.1%	53.8 ± 1.8 <i>s<sub>r</sub></i> = 4.5%	45.2 ± 2.6 <i>s<sub>r</sub></i> = 2.8%	74.8 ± 4.4 <i>s<sub>r</sub></i> = 3.2%	65.9 ± 3.1 <i>s<sub>r</sub></i> = 1.8	58.8 ± 2.6 <i>s<sub>r</sub></i> = 4.7%
Pb(II)	45.4 ± 1.1 <i>s<sub>r</sub></i> = 5.1%	36.7 ± 1.6 <i>s<sub>r</sub></i> = 3.8%	15.6 ± 0.9 <i>s<sub>r</sub></i> = 4.2%	51.3 ± 2.1 <i>s<sub>r</sub></i> = 4.3%	35.4 ± 1.8 <i>s<sub>r</sub></i> = 3.7%	28.3 ± 1.5 <i>s<sub>r</sub></i> = 4.9
Cd(II)	0.516 ± 0.015 <i>s<sub>r</sub></i> = 3.8%	0.311 ± 0.037 <i>s<sub>r</sub></i> = 4.3%	0.123 ± 0.010 <i>s<sub>r</sub></i> = 4.6%	0.609 ± 0.023 <i>s<sub>r</sub></i> = 3.9%	0.435 ± 0.032 <i>s<sub>r</sub></i> = 4.7%	0.169 ± 0.019 <i>s<sub>r</sub></i> = 3.5
Zn(II)	365.2 ± 15.3 <i>s<sub>r</sub></i> = 2.7%	429.0 ± 16.7 <i>s<sub>r</sub></i> = 4.0%	269.4 ± 11.2 <i>s<sub>r</sub></i> = 3.7%	443.5 ± 21.2 <i>s<sub>r</sub></i> = 5.0%	438.3 ± 19.6 <i>s<sub>r</sub></i> = 3.4%	296.8 ± 16.9 <i>s<sub>r</sub></i> = 4.9%

\* Concentration, mg kg<sup>-1</sup>. The residual standard deviation *s<sub>r</sub>* is determined on five independent measurements. Sampling site: A (internal), B (central), C (near the connection with Adriatic sea).

## References

- [1] G.P. Thomas, L.C. Goldstone, *Int. Lab.* 24 (1994) 13.
- [2] J. Wang, *Stripping Analysis-Principles, Instrumentation and Applications*, VCH, Deerfield Beach, FL, 1985, ch. 4 and 5.
- [3] A.M. Bond, *Modern Polarographic Methods in Analytical Chemistry*, Marcel Dekker, New York, 1980.
- [4] A. Bobrowski, A.M. Bond, *Croatica Chem. Acta* 66 (1993) 499.
- [5] A.M. Bond, R.J. O'Halloran, I. Ruzic, D.E. Smith, *Anal. Chem.* 48 (1976) 872.
- [6] C. Locatelli, F. Fagioli, C. Bigli, T. Garai, *Talanta* 34 (1987) 529.
- [7] J.K. Christensen, L. Kryger, N. Pind, *Anal. Chim. Acta* 141 (1982) 131.
- [8] E. Wang, W. Sun, Y. Yang, *Anal. Chem.* 56 (1984) 1903.
- [9] S.B. Adeloju, A.M. Bond, M.H. Briggs, H.C. Hughes, *Anal. Chem.* 55 (1983) 2076.
- [10] E.P. Gil, P. Ostapczuk, *Anal. Chim. Acta* 293 (1994) 55.
- [11] H. Robberecht, R. Van Grieken, *Talanta* 29 (1982) 823.
- [12] T. Ferri, P. Sangiorgio, *Anal. Chim. Acta* 321 (1996) 185.
- [13] S. Caroli, *Element Speciation in Bioinorganic Chemistry*, Wiley, New York, 1996, ch. 13.
- [14] R.W. Andrews, D.C. Johnson, *Anal. Chem.* 47 (1975) 294.
- [15] R.A. Zingaro, W.C. Cooper, *Selenium*, Van Nostrand Reinhold, New York, 1974, p. 594.
- [16] W. Holak, *Anal. Chem.* 52 (1980) 2189.
- [17] A. Hald, *Statistical Theory with Engineering Applications*, Wiley, London, 1952.
- [18] H.L. Youmans, *Statistical for Chemistry*, Charles E. Merrill, Columbus, OH, 1973, ch. 10.
- [19] F. Fagioli, T. Garai, J. Devay, *Ann. Chim. (Rome)* 64 (1974) 633.
- [20] C. Liteanu, I.C. Popescu, E. Hopirtean, *Anal. Chem.* 48 (1976) 2010.
- [21] E. Merian, *Metals and their Compounds in the Environment-Occurrence, Analysis and Biological Relevance*, VCH, Weinheim, 1991.
- [22] IUPAC, *Spectrochim. Acta Part B* 33B (1978) 241.
- [23] J.C. Miller, J.N. Miller, *Statistics for Analytical Chemistry*, Ellis Horwood, Chichester, 1984, ch. 4, paragraphs 4.5, 4.7.



# High performance liquid chromatography method for determination of methyl-5-benzoyl-2-benzimidazole carbamate (mebendazole) and its main degradation product in pharmaceutical dosage forms

Z. Al-Kurdi <sup>a</sup>, T. Al-Jallad <sup>a</sup>, A. Badwan <sup>a</sup>, A.M.Y. Jaber <sup>b,\*</sup>

<sup>a</sup> *The Jordanian Pharmaceutical Manufacturing and Medical Equipment Co. Ltd., P.O. Box 94, Naor 11710, Jordan*

<sup>b</sup> *Department of Chemistry, King Fahd University of Petroleum and Minerals, Dharam 31261, Saudi Arabia*

Received 6 November 1998; received in revised form 30 March 1999; accepted 8 July 1999

## Abstract

Methyl-5-benzoyl-2-benzimidazole carbamate (mebendazole) is a drug used as an anthelmintic. A high performance liquid chromatography method has been developed in this study to determine mebendazole and its degradation product in the pharmaceutical dosage forms (tablets and suspension). The expected major degradation product of mebendazole in the dosage forms has been prepared, and identified as 2-amino-5-benzoylbenzimidazole. The proposed HPLC assay was found to be selective, accurate (% recoveries were in the range of 99.9–100.9) for both, mebendazole and the degradation product, repeatable and reproducible (replicate measurements for short and long term measurements showed % RSD of  $\leq 1.4$ ). The methodology could be considered as a stability indicating method for mebendazole in pharmaceutical dosage forms. © 1999 Elsevier Science B.V. All rights reserved.

*Keywords:* Mebendazole; HPLC; Degradation; Pharmaceutical dosage forms

## 1. Introduction

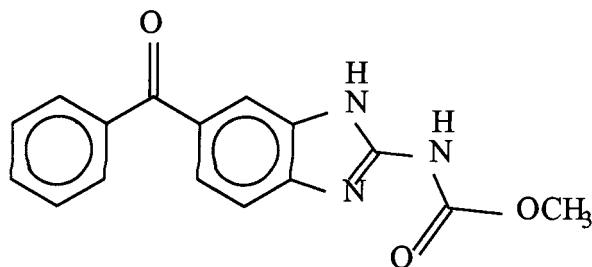
Methyl-5-benzoyl-2-benzimidazole carbamate (mebendazole) is used as an anthelmintic. The drug is known to act through the irreversible inhibition of glucose uptake in the parasite, leading to the depletion of glycogen store. This results in a decrease in adenosine triphosphate activity.

Only 5–10% of the ingested drug are absorbed from the human gastrointestinal tract. The drug is known to be dysmorphogenic in experimental animals [1]. Mebendazole starting material and tablet dosage forms are both included in the USP 23 monographs [2], while the oral suspension is listed in the second supplement [3] of USP 23 (Scheme 1).

Different analytical methods are reported in literature for the assay of mebendazole in dosage forms and in biological fluids. High performance

\* Corresponding author. Tel.: +966-3-860-2611; fax: +966-3-860-4277.

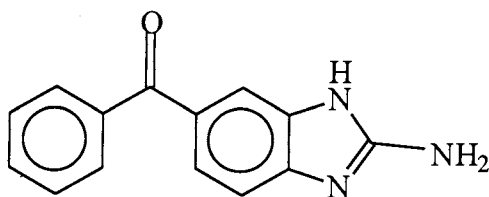
*E-mail address:* amjaber@kfupm.edu.sa (A.M.Y. Jaber)



Scheme 1. Mebendazole.

liquid chromatography [4–9] has been extensively used for the determination of mebendazole in various drug formulations and biological fluids such as whole blood, plasma and serum. Other methods have also been used, such as infrared spectroscopy [10], proton NMR [11], differential pulse polarography [12], mass spectrometry [13], fluorescence [14,15] and phosphorescence [16] spectrophotometry. The assay of mebendazole is made by a potentiometric titration in the European Pharmacopoeia [17], by spectrophotometric measurement in the UV region for

the oral suspension in the USP 23 [2], and by HPLC for the tablets formulation in the USP 23 [18]. Most of these methods deal with the determination of the intact mebendazole molecule. Very little attention has been directed to identify the major degradation impurity in the dosage formulations. However, HPLC methods based on UV detection [19] at 254 nm and coulometric detection [7] were utilized for estimation of low levels of mebendazole and its metabolites in human sera after an extraction procedure in which the sample was passed through a Sep Pak C18 cartridge. Determination of mebendazole in combination with one of



Scheme 2. 2-Amino-5-benzoylbenzimidazole.

its major degradation products in the pharmaceutical formulations has been investigated in this study by using HPLC technique with UV detection.

## 2. Experimental

### 2.1. Materials

Mebendazole USP grade supplied by the Jordanian Pharmaceutical Manufacturing Co., Jordan, JPM, was used. Mebendazole dosage forms (bendazole, the JPM brand name for mebendazole) manufactured by JPM was also used. All the matrix ingredients were of pharmaceutical grade, and all other chemical reagents used were of HPLC grade from Merck.

### 2.2. Instrumentation

A Beckman Gold system liquid chromatograph, equipped with a 116 pump, a Rheodyne 7010 injection valve (20  $\mu$ l loop size) and a 166 UV spectrophotometric detector set at 290 nm, was used for the HPLC studies. A Perkin-Elmer 16F PC FT-IR spectrophotometer, a JEOL JNM-LA500 ET NMR system, and a JEOL JMS-XX 100 mass spectrometer were used for the identification of the degradation product.

### 2.3. Standard, sample, and matrix solutions

Mebendazole stock solutions of 1 mg ml<sup>-1</sup> were prepared in 0.1 M methanolic hydrochloric acid. Standard solutions were freshly prepared from the stock solution by dilution with mobile phase.

Sample solutions of bendazole tablets were prepared from 20 tablets, which were finely powdered and well mixed. A bendazole quantity equivalent to 100 mg of mebendazole was weighed and dissolved in 100 ml of 0.1 M methanolic hydrochloric acid, shaken for 15 min and centrifuged. Five ml of this solution were diluted to 50 ml with mobile phase.

Sample solutions of bendazole suspension were prepared by dissolving a volume equivalent to 100

mg of mebendazole in 100 ml of 0.1 M methanolic hydrochloric acid, shaking for 10 min and centrifuging for 15 min. Five mL of the supernatant were diluted to 50 ml with the mobile phase.

A solution of the matrix used for bendazole tablets was prepared from the following components: maize starch, colloidal anhydrous silica, sunset yellow, peppermint flavor, povidone K29-32, sodium starch glycolate, and magnesium stearate. One hundred and thirty mg of this preparation were dissolved and diluted the same as the sample of bendazole tablets.

A solution of the matrix used for bendazole suspension was prepared from the following materials: glycerol, sucrose, polysorbate 80, xanthan gum, colloidal anhydrous silica, butyl hydroxybenzoate, propyl hydroxybenzoate, anhydrous citric acid, sodium citrate and banana flavor TR 6232. All these materials were suspended into purified water. Ten ml of this matrix component was dissolved and diluted to 50 ml the same as above.

#### 2.4. Preparation of the degradation product

Mebendazole raw material was dissolved in 1 M NaOH solution, heated to boiling under reflux for 30 min, cooled and neutralized with 1 M HNO<sub>3</sub>. The resulting solution was evaporated to dryness and purified by recrystallization from an ethanolic solution.

#### 2.5. Preparation of solutions for selectivity studies

Samples of mebendazole standard (50 mg), bendazole tablets (quantity equivalent to 100 mg mebendazole), bendazole suspension (quantity equivalent to 100 mg mebendazole), matrix used for tablets (130 mg), or matrix used for suspension (10 ml), were treated separately with 10 ml methanolic hydrochloric acid, and 5 ml of 1 M NaOH, 5 ml of 1 M HCl or 5 ml of 3.3% H<sub>2</sub>O<sub>2</sub>. The resultant solutions were refluxed for 30 min, cooled and diluted to 100 ml with 0.1 M methanolic hydrochloric acid. Five ml of the final solution was diluted to 50 ml with the mobile phase.

#### 2.6. Chromatographic conditions

The chromatographic separation was carried out using a stainless steel column (250 × 4.6 mm), from WATERS, packed with 5 μm Spherisorb S5 ODS 1. The mobile phase was 0.05 M KH<sub>2</sub>PO<sub>4</sub>: methanol: acetonitrile (5:3:2, v/v) at a flow-rate of 1 ml min<sup>-1</sup>. All measurements were made at room temperature. Twenty μl of standard, sample, matrix and degradation product solutions were injected into the chromatographic system.

### 3. Results and discussion

Preliminary HPLC runs for bendazole dosage forms showed two chromatographic peaks, the

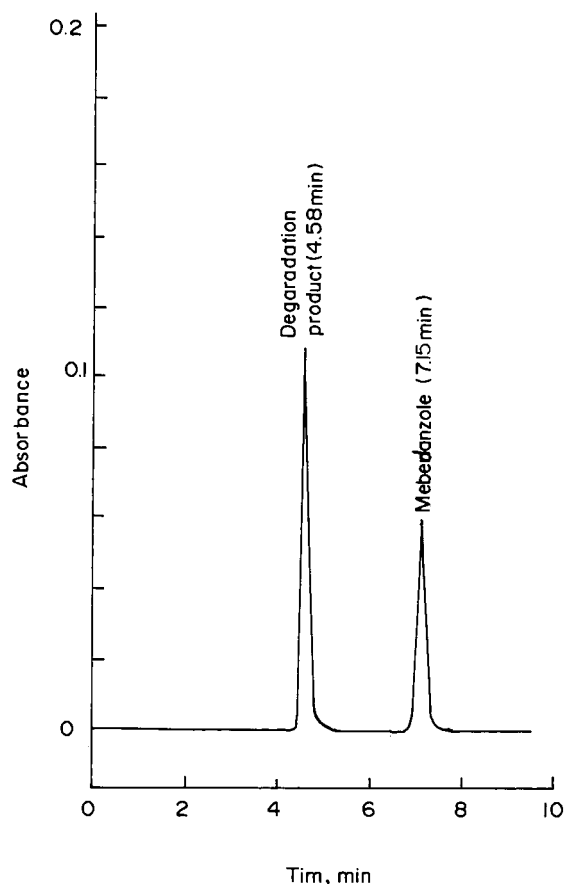


Fig. 1. A chromatogram for methyl-5-benzoyl-2-benzimidazole carbamate (mebendazole) and its degradation product.

Table 1  
Linearity of calibration plots for methyl-5-benzoyl-2-benzimidazole carbamate (mebendazole) standards prepared in different matrices and diluted by the mobile phase

Solution	Concentration range (mg 100 ml <sup>-1</sup> )	Correlation coefficient	Intercept	95% Confidence intervals of the intercept	Slope	95% Confidence intervals of the slope	LOD (mg 100 ml <sup>-1</sup> )	LOQ (mg 100 ml <sup>-1</sup> )
Mebendazole standards in 0.1 M methanolic HCl	4–16	0.9999	0.491	±2.181	7.032	±0.203	0.243	0.810
Mebendazole standards in the matrix used for tablets	4–16	0.9998	1.055	±2.608	7.098	±0.241	0.288	0.959
Mebendazole standards in the matrix used for suspension	4–16	0.9993	0.927	±3.400	4.817	±0.303	0.553	1.843
Degradation product standards in methanolic HCl	0.04–0.2	0.9999	0.00485	±0.00950	5.827	±0.0762	0.00152	0.00504
Degradation product standards in the matrix used for suspension	0.04–0.2	0.9994	-0.0170	±0.0105	6.079	±0.0648	0.0124	0.0292

main one belongs to mebendazole and the other appeared at the same retention time as that obtained after alkaline treatment of mebendazole. Thus, the other peak was attributed to the degradation product (Fig. 1) mentioned above.

Various HPLC trials have been attempted to determine mebendazole in the bendazole dosage forms, together with its degradation product. When a ratio of 5:3:2 (v/v) water:methanol:acetonitrile was used as the mobile phase, the tailing factor appeared to be high. A total of 0.05 M  $\text{KH}_2\text{PO}_4$  was used in the aqueous portion of the mobile phase which gave good resolution, reliable retention times, low tailing factor (not greater than 3.0), good column efficiencies (not less than 3000 theoretical plates), good repeatabilities (RSD of less than 2.0% for six replicates)

when applied to standard solutions. Also, good resolution between the drug excipients, degradation product and mebendazole has been observed. The spectrophotometric detector was set to 290 nm, since mebendazole and its degradation product show a maximum absorbance at this wavelength.

### 3.1. Identification of the degradation product

Infrared spectrum of the degradation product showed a double peak at  $3402\text{ cm}^{-1}$  which may be assigned to a primary amine group rather than the secondary amine group in mebendazole. The peak at  $2752\text{ cm}^{-1}$  in the mebendazole spectrum assigned to a methyl group has disappeared in the spectrum of the degradation product.

Table 2

Accuracy of HPLC determination of methyl-5-benzoyl-2-benzimidazole carbamate (mebendazole) and its degradation product in synthetic solutions containing the matrix used for either tablets or suspension

Material and matrix	Quantity added (mg 100 ml <sup>-1</sup> )	Quantity found (mg 100 ml <sup>-1</sup> )	Recovery <sup>a</sup> (%)	Bias <sup>b</sup> (%)
Mebendazole in the matrix used for tablets	4.016	4.110	102.3	2.3
	8.032	8.062	100.4	0.4
	10.04	10.097	100.6	0.6
	12.048	12.223	101.5	1.5
	16.064	15.998	99.5	0.5
Average % recovery			100.9	–
%RSD of recovery			1.1	–
Mebendazole in the matrix used for suspension	4.168	4.136	99.2	–0.8
	8.336	8.420	101.0	1.0
	10.420	10.463	101.2	1.2
	12.048	12.457	100.4	0.4
	16.672	16.355	98.1	–1.9
Average % recovery			100.0	–
% RSD of recovery		1.3	–	–
Degradation product in the matrix used for suspension	0.043	0.0419	97.5	–2.5
	0.064	0.0637	99.5	–0.5
	0.112	0.113	101.0	1.0
	0.146	0.144	98.7	–1.3
	0.195	0.200	102.7	2.7
Average % recovery			99.9	–
%RSD of recovery			2.0	–

$$^a \text{ \%Recovery} = \frac{\text{sample response}}{\text{standard response}} \times \frac{\text{conc. of standard}}{\text{conc. of sample}} \times 100$$

$$^b \text{ \%Bias} = \text{ \%recovery} - 100.$$

NMR spectra for the degradation product of mebendazole showed a disappearance of the peak at 3.774 ppm indicating the loss of  $-\text{OCH}_3$  group. The peak observed at 8.756 ppm was not present in the spectrum of mebendazole; this peak may be assigned to an  $-\text{NH}$  group or a change in the environment of the secondary amine group in mebendazole. C-13 NMR for the degradation product indicated the presence of 12 unequivalent carbon atoms.

Low resolution mass spectrometry showed that the degradation product has a molar mass of 237. However, high resolution mass spectrometry indicated that a compound of molar mass 237.0987 exists in the degradation product, although some other compounds may also exist, in a much lower extension.

In conclusion, all the above evidences indicate that the degradation product could be 2-amino-5-benzoylbenzimidazole (Scheme 1). This compound was reported to be one of the major decomposition products when mebendazole is heated [20] to about 235°C, and was among the mebendazole metabolites separated from the human serum using Sep Pak C18 cartridge and determined by HPLC [7,19] (Scheme 2). 2-Amino-

5-benzoyl benzimidazole was, also, one of three mebendazole metabolites isolated from the bile of rat [21]. Liver and kidney were found to contain the highest levels of mebendazole metabolites [22], however, the highest levels of parent compound were found in fat. Mebendazole and its hydroxy metabolites were eliminated within 5 days from the muscle and skin whereas mebendazole amino metabolite was still detectable on day 14 following the end of the treatment period. Consequently, mebendazole aminometabolite should be taken as a compound of interest in studying the toxicity or the withdrawal time for mebendazole. Different compendia are not taking this degradation product into consideration thus, it may be beneficial to have it listed in mebendazole monographs and to take it into account when mebendazole is assayed.

### 3.2. Selectivity

When the matrix used for tablets or suspension was chromatographed, a complete absence of interference effect was observed. The degradation in sample solutions of mebendazole standards, benzazole tablets and suspension, and the matrix

Table 3

HPLC response for freshly prepared and stored standard and synthetic methyl-5-benzoyl-2-benzimidazole carbamate (mebendazole) solutions

Mebendazole solutions	Mebendazole added (mg 100 ml <sup>-1</sup> )	Mebendazole found (mg 100 ml <sup>-1</sup> )		<i>D</i> <sup>a</sup> (%)
		Fresh solutions	Stored solutions (24 h)	
Mebendazole in standard solutions	4.00	4.129	4.047	2.0
	10.00	10.00	9.985	0.2
	16.00	16.201	15.960	1.5
Mebendazole in the matrix used for tablets	4.00	4.073	4.117	-1.1
	10.00	9.946	9.845	1.0
	16.00	15.591	15.162	2.8
Mebendazole in the matrix used for suspension	4.168	4.118	4.143	-0.6
	10.420	10.498	10.541	-0.4
	16.672	16.278	16.469	-0.7

$${}^a \%D = \frac{\text{amount found (fresh)} - \text{amount found (stored)}}{\text{amount found (fresh)}} \times 100.$$

used for both tablets and suspension was induced by treating each of these products separately with 1 M HCl, 1 M NaOH or 3.3% H<sub>2</sub>O<sub>2</sub> solutions (Section 2.5). The possibility of decomposition and interference from the degradation products in the HPLC response was investigated by chromatographing each of these sample solutions. The matrix used for tablets or suspension did not show any HPLC response after a treatment with any of the three reagents and refluxing for 30 min. When HCl was used no degradation of mebendazole was observed in the standards nor in the mebendazole tablets or suspension and an almost 100% recovery was

observed. However, mebendazole in standard, tablets or suspension solutions, was partially degraded after treatment with H<sub>2</sub>O<sub>2</sub> (77.5% was recovered for standards, 53.4% for tablets and 77.5% for suspension) and almost completely after treatment with NaOH (about 0.3–0.5% was recovered for standards, tablets or suspension).

Moreover, degradation experiments in 0.1 M NaOH as a function of the degradation time showed that another chromatographic peak, different from that of mebendazole, has appeared and showed an increase with time, whereas the peak of mebendazole decreased with time.

Table 4

Repeatability and reproducibility of the HPLC response for methyl-5-benzoyl-2-benzimidazole carbamate (mebendazole) in the matrix used for suspension

Analyst no.	Trial no.	Mebendazole added (mg 100 ml <sup>-1</sup> )	Response (peak area)	Recovery (%)
1	1	10.361	51.017	100.2
	2	10.341	51.544	101.4
	3	10.281	51.487	101.9
	4	10.460	50.907	99.0
	5	10.136	55.932	101.2
	6	10.420	51.818	101.2
Average % recovery	–	–	–	100.8
% RSD	–	–	–	1.0
	Standard	10.340	50.823	–
2	1	10.062	49.620	100.4
	2	10.241	50.907	101.2
	3	10.281	51.018	99.3
	4	10.182	49.396	98.7
	5	10.122	50.569	101.7
	6	10.102	50.778	102.3
Average % recovery	–	–	–	100.6
% RSD	–	–	–	1.4
	Standard	10.340	50.823	–
3	1	10.080	50.670	101.3
	2	10.102	51.109	101.9
	3	10.241	51.299	100.9
	4	10.281	51.128	100.2
	5	9.396	49.842	100.9
	6	10.321	51.633	100.9
Average % recovery	–	–	–	101.0
% RSD	–	–	–	0.6
	Standard	10.202	50.617	–
Overall % recovery	–	–	–	100.8
Overall % RSD	–	–	–	1.0

### 3.3. Assay of mebendazole and its degradation products

#### 3.3.1. Linearity of calibration plots

The calibration linearity was checked for a series of mebendazole standards within a concentration range of 4–16 mg mebendazole 100 ml<sup>-1</sup>. Furthermore, the calibration linearity was also checked for mebendazole standards prepared in the matrix used for the tablets or that used for the suspension (concentration range of 4–16 mg 100 ml<sup>-1</sup>) and for the degradation product prepared in the matrix for the suspension formulation (concentration range of 0.04–0.2 mg 100 ml<sup>-1</sup>). In all cases, the correlation coefficients for the calibration plots in all matrices studied were better than 0.999 (Table 1).

The confidence intervals for the slope and the intercept have been estimated using the equations:  $b \pm t_{s_b}$  and  $a \pm t_{s_a}$  respectively, where  $t$ -value is taken at 95% confidence level and  $n - 2$  degrees of freedom,  $b$  and  $a$  are the slope and the intercept of the regression line,  $s_b$  and  $s_a$  are the standard deviations of the slope and the intercept, respectively [23]. The limit of detection, LOD, has been calculated based on the definition that, it is the analyte concentration giving a signal equal to the blank signal (the values of the intercept of the calibration line on the  $y$ -axis was used as an estimate of the blank signal [23]), plus 3 S.D. of the blank (the S.D. of the  $y$ -residuals on the regression line was used as the S.D. of the blank signal [23]). The limit of quantitation, LOQ, has been calculated based on the same definition used for LOD but using a value of 10 S.D. of the blank [23] rather than a value of 3. The 95% confidence intervals for the intercepts and the slopes of calibration lines and both LOD and LOQ have been calculated for the different calibration plots and listed in Table 1.

#### 3.3.2. Accuracy

Mebendazole and its degradation product already prepared in 0.1 M methanolic hydrochloric acid and the mobile phase were diluted by the matrix used for either the tablets or the suspension formulations to give certain nominal concentrations. The solutions were chromatographed

and the concentrations assessed with respect to a 10 mg mebendazole 100 ml<sup>-1</sup> standard solution. Table 2 shows the percentage recoveries, the bias, and the percent relative standard deviations (% RSD) for these measurements. It is obvious that the average percentage recoveries are in the range of 99.9–100.9, the bias is  $\leq 2.7$ , and the % RSDs are  $\leq 2$ . Thus, the method of analysis is accurate for both mebendazole and its degradation product.

#### 3.3.3. Stability of standard and synthetic mebendazole solutions

Stability of mebendazole in standard solutions, and in the matrix used for tablets and that used for suspension, was investigated for certain mebendazole concentrations (4, 10, and 16 mg 100 ml<sup>-1</sup>). After a storage of 24 h, the variations of mebendazole concentration were in all cases less than 3.0% (Table 3). This indicates that mebendazole solutions (standards or synthetic matrices) are stable within 24 h and can be used without having any significant effect on the results.

#### 3.3.4. Repeatability and reproducibility

HPLC measurements were carried out by three analysts over a day (tests made by each analyst) or different days (tests made by the three analysts) periods, thus the long and short term precisions have been estimated. Table 4 represents precisions for various mebendazole quantities prepared in a synthetic matrix used for the suspension formulation. It is obvious from Table 4, that the % RSDs for the measurements made by each analyst and for the overall measurements are 1.0, 1.4, 0.6 and 1.0, respectively. The % recoveries for the measurements made by each analyst and the overall % recovery are 100.8, 100.6, 101.0 and 100.8, respectively. When the experiments were repeated for mebendazole in a matrix used for tablets, better % RSD and % recoveries were obtained. The %RSD's for the measurements made by each analyst on mebendazole in the matrix used for tablets and that for the overall measurements were 0.9, 0.5, 0.4 and 0.6 respectively; however, the corresponding % recoveries were 100.3, 99.8, 99.8 and 99.9, respectively. These results indicate



that the method proposed for the determination of mebendazole in the tablet and suspension formulations is precise and accurate allowing the major degradation product to be determined at the same assay time.

### Acknowledgements

JPM and KFUPM are thanked for the support of this research project.

### References

- [1] J.E.F. Reynolds (Ed.), Martindale, The Extra Pharmacopoeia, 31st edition, The Royal pharmaceutical Society, London, 1996, p. 118.
- [2] US Pharmacopoeia 23 NF, Official monographs, 1995, p. 934.
- [3] US Pharmacopoeia 23 NF, Official Monographs, Second supplement, 1997, p. 2651.
- [4] S. Ramanathan, N.K. Nair, S.M. Mansor, V. Navaratnam, J. Chromatogr. B Biomed. Appl. 655 (1994) 269.
- [5] M.E.C. Valois, O.M. Takayanagui, P.S. Bonato, V.L. Lanchote, D. Carvalho, J. Anal. Toxicol. 18 (1994) 86.
- [6] S. Ramanathan, N.K. Nair, S.M. Mansor, V. Navaratnam, J. Chromatogr. B Biomed. Appl. 126 (1993) 303.
- [7] P. Betto, M. Gianbenedetti, F. Ponti, R. Ferretti, G. Settmij, M. Gargiulo, R. Lorenzini, J. Chromatogr. B Biomed. Appl. 563 (1991) 115.
- [8] Z. Zeng, Z. Chen, Z. Yuan, Yaowu Fenxi Zazhi 10 (1990) 202.
- [9] G.S. Sadana, G.G. Parikh, Indian Drugs 24 (1987) 533.
- [10] Z. Sha, W. Sun, H. Gao, Zhongguo Yaoxue Zazhi 24 (1989) 932.
- [11] H.A. Al-Khamees, B.E.D.M. El-Shazly, Analyst 113 (1988) 599.
- [12] A. Temizer, N. Ozaltin, M.T. Orbey, T. Ozecan, J. Pharm. Belg. 4 (1987) 247.
- [13] N.M. Sanghavi, V. Tandel, Indian Drugs 30 (1993) 136.
- [14] W. Baeyens, F. Abdel Fattah, P. DeMoerloose, Pharmazie 41 (1986) 636.
- [15] W. Baeyens, F. Abdel Fattah, P. DeMoerloose, J. Pharm. Biomed. Anal. 3 (1985) 397.
- [16] W. Baeyens, F. Abdel Fattah, P. DeMoerloos, Anal. Lett. 18 (B17) (1985) 2105.
- [17] European Pharmacopoeia, 3rd edition, Council of Europe, Strasbourg, 1997, p. 1151.
- [18] US Pharmacopoeia 23, Official Monographs, seventh supplement, 1997, p. 3903.
- [19] R.J. Allan, H.T. Goodman, T.R. Watson, J. Chromatogr. B Biomed. Appl. 183 (1980) 311.
- [20] M. Himmelreich, B.J. Rawson, T.R. Watson, Aust. J. Pharm. Sci. 5 (1997) 125.
- [21] P.A. Braithwaite, M.S. Roberts, R.J. Allan, T.R.E. Warson, Eur. J. Clin. Pharmacol. 22 (1982) 161.
- [22] E.G. Iosifidou, N. Haagsma, M. Olling, J.H. Boon, M.W. Tanck, Drug Metab. Dispos. 25 (1997) 327.
- [23] J.C. Miller, J.N. Miller, Statistics for Analytical Chemistry, vol. 22, Ellis Horwood, Chichester, 1984, p. 82.

# The use of dansyl chloride in the spectrofluorimetric determination of the synthetic antioxidant butylated hydroxyanisole in foodstuffs

C. Cruces-Blanco \*, A. Segura Carretero, E. Merino Boyle,  
A. Fernández Gutiérrez

*Department of Analytical Chemistry, Faculty of Sciences, University of Granada, C/Fuente Nueva s/n 18071, Granada, Spain*

Received 9 March 1999; received in revised form 30 June 1999; accepted 8 July 1999

## Abstract

A sensitive method is presented for the determination of the synthetic antioxidant butylated hydroxyanisole (BHA) based on the dansylation process of the phenolic hydroxy group. The fluorescence developed can be measured directly without previous extraction or chromatographic separation of the labelled fluorescent compound. It is shown the effect of numerous experimental variables affecting the fluorescence intensity and the signal-to-noise ratio of the dansyl derivative. The compound was determined over the range  $0.05\text{--}5\ \mu\text{g ml}^{-1}$ , with a relative S.D. of 3.8% ( $300\ \text{ng ml}^{-1}$ ) and a detection limit of  $52\ \text{ng ml}^{-1}$ . The selectivity conferred by the dansylation reaction has permitted to avoid the interference of normally accompanying antioxidants, such as butylated hydroxytoluene (BHT), due to steric impediment. The stability of the DNS-derivative is well suited for the analysis of different foodstuffs. © 1999 Elsevier Science B.V. All rights reserved.

*Keywords:* Butylated hydroxyanisole (BHA); Dansyl chloride labelling; Food analysis; Fluorimetry

## 1. Introduction

Butylated hydroxyanisole (BHA) is a synthetic phenolic antioxidant which has been added to foods for decades to retard the autooxidation of lipids that leads to rancidity [1]. It is numbered as E-320 in the International Food Codex and its content in foods has been ruled in almost every country [2].

With respect to the safety of this kind of compounds, there are numerous studies suggesting that BHA is a useful additive with a possible role in cancer chemoprevention, inhibiting the induction of this disease by a wide variety of chemical carcinogens and radiation at many target sites in mice, rats, hamsters and man [3]. In other studies, this food additive has been shown to induce gastrointestinal hyperplasia in rodent by an unknown mechanism, while the relevance of this observation for human risk assessment is not clear [4,5]. For such a reason, the amount of these additives

\* Corresponding author. Tel.: +34-958-243326.

E-mail address: mcruces@goliat.ugr.es (C. Cruces-Blanco)

present in a particular food is limited. For example, in United States, only 200 mg kg<sup>-1</sup> in fats, oils and chewing-gum and 50 mg kg<sup>-1</sup> in breakfast cereals or dehydrated soups are permitted. So, antioxidants, either singly or in combination needs analytical control based on sensitive and selective methods.

In the literature, many UV absorption methods are presented because they provide an excellent way to quantify phenolic antioxidants [6,7] but the lack of specificity in food analysis has promoted the application of different methodologies, such as partial least square models (PLS) [8] or approaches as first, second or fourth derivative of the absorption spectra [9,10], which have shown to be very useful in many types of multicomponent trace analysis [11–13].

Also, chromatography in all forms, such as thin-layer [14], supercritical fluid [15], liquid [16–18] and gas [19,20] have been previously applied. Recently, a comparison between HPLC and capillary electrophoresis demonstrated the excellent resolution and efficiency of the latter [21]. Electrochemical methods have found few applications in the determination of antioxidants [22,23].

Methods involving fluorescence spectrometry have been widely applied to analytical problems which require highly sensitive detection. The availability of a number of fluorogenic reagents capable of reacting with specific functional groups of non or poorly fluorescent compounds has permitted the development of analytical methods which combine the sensitivity of fluorimetry with the selectivity of a separation technique [24–26]. Due to the weak fluorescence of BHA, there is only one fluorescence method for its determination [27] presenting very poor sensitivity and selectivity.

5-Dimethylaminonaphthalene sulfonylchloride (dansyl chloride, DNS-Cl) [28,29] is an important and widely used fluorescence reagent, reacting with amino, phenolic and active hydroxyl groups under suitable experimental conditions. Many studies concerning DNS-Cl have been carried out in the literature [30–35].

The aim of this work was to demonstrate the use of the potent fluorescent labelling reagent DNS-Cl as an excellent tool to establish sensitive

and selective determination of analytes with weak or no native fluorescence without further separation techniques. The only compound, frequently found in foodstuffs accompanying BHA is BHT and, due to a steric impediment, despite a phenolic hydroxy group is also presented, makes the dansylation reaction specific for BHA, so the principal interference that normally appear in this type of analysis, have demonstrated to be avoided.

## 2. Experimental

### 2.1. Instruments and apparatus

Relative fluorescence intensity (R.F.I.) measurements were carried out on a Perkin-Elmer Model MPF-66, equipped with a xenon arc lamp (150 W) and 1 × 1 cm path-length quartz cells. The spectrofluorometer was operated in the computer-controlled mode via the R-928 photomultiplier interfaced by a Perkin-Elmer Model 7600 Professional microcomputer and a printer PR 210. Instrumental control and data acquisition were achieved by using the commercially available Perkin-Elmer software (C-646-0280). When fluorescence spectra were recorded, both slits widths were set at 3 nm. To obtain the three dimensional spectra and contour maps of the corresponding fluorescence spectra, an Aminco Bowman series 2 luminescence spectrometer equipped with a continuous xenon lamp (150 W) and a pulse lamp (7 W), and were recorded with a personal computer. A GPIB (IEEE-488) interface card for computer-instrument communication was used.

Cell-compartment was thermostatically controlled at 25 ± 0.5°C with a water bath circulator (S-383 Fritigerm). An electric shaker (Selecta model Vibromatic-384) with speed selection between 2 and 20 vib min<sup>-1</sup> and automatic temporizer, was used for extraction procedures.

### 2.2. Reagents and solutions

BHA, BHT, ethyl paraben, sorbic acid, biphenyl, benzoic acid, n-propylgallate, tartrazine

and DNS-Cl were supplied by Sigma (Madrid, Spain), while amaranth was supplied by Aldrich (Madrid, Spain) and sodium carbonate and bicarbonate were from Merck (Darmstadt, Germany). All solvents were of analytical reagent grade (Merck) and demineralized water was used throughout the experiment.

Acetone stock solutions of BHA ( $1000 \mu\text{g ml}^{-1}$ ) were prepared weekly and stored in glass-stopped bottles at  $4^\circ\text{C}$ . Working standard solutions were prepared daily from these stock solutions by appropriate dilution.

The DNS-Cl solution ( $500 \mu\text{g ml}^{-1}$ ) was prepared in dried acetone and kept into the refrigerator until used. Working solutions of  $250 \mu\text{g ml}^{-1}$  ( $9.3 \times 10^{-4} \text{ M}$ ) were prepared every two days. Sodium carbonate was prepared at a concentration  $0.02 \text{ M}$  in demineralized water.

### 2.3. Procedures

#### 2.3.1. Labelling procedure

In a  $10 \text{ ml}$  volumetric flask,  $300 \text{ ml}$  of BHA in acetone ( $1000 \mu\text{g ml}^{-1}$ ) was placed and taken to final volume with  $0.02 \text{ M}$  sodium carbonate. Different volumes of this working solution were placed in  $15 \text{ ml}$  test tubes to obtain final BHA concentrations between  $90$  and  $600 \text{ ng ml}^{-1}$ .  $18 \text{ ml}$  of a solution of dansyl chloride in acetone ( $250 \mu\text{g ml}^{-1}$ ) was added and the tubes were loosely stopped and heated in a water-bath at  $45^\circ\text{C}$ . The labelling time was  $10 \text{ min}$ . Then, the tubes were allowed to cool to room temperature and a  $3 \text{ ml}$  volume of cyclohexane was added and the tubes were shaken for  $1 \text{ min}$ . Afterwards, the samples were allowed for both layers to clearly separate.

#### 2.3.2. Fluorescence measurements

The cyclohexane layer containing the BHA-DNS derivative was measured at an excitation wavelength of  $341 \text{ nm}$  with the emission monochromator installed at  $482 \text{ nm}$ . A labelling blank was prepared at the same time by reaction with cyclohexane and DNS-Cl under the same experimental conditions. The three dimensional spectra and contour maps were obtained at emission  $410\text{--}600 \text{ nm}$  with an excitation between  $250$  and  $428 \text{ nm}$  and at a scanning speed of  $2 \text{ nm s}^{-1}$ .

#### 2.3.3. Procedure for commercial powdered soup

The samples of commercial dehydrated soup (Sopistant-Consomé al jerez, Gallina Blanca, Spain) were placed in a mortar and ground to a fine mesh. A portion of  $20\text{--}30 \text{ g}$  of the resulting powder was placed in a separatory funnel and mixed with  $25 \text{ ml}$  of acetone and shaken vigorously for  $5 \text{ min}$ . The solution was placed in an ultrasonic bath for  $5 \text{ min}$  to favour the solubilization of BHA in acetone and, afterwards, filtered through a ground glass funnel No. 4 and taken to a final volume of  $10 \text{ ml}$  with acetone in a volumetric flask. Five millilitres of this solution were placed in a  $10 \text{ ml}$  volumetric flask and taken to the final volume with  $0.04 \text{ M}$  sodium carbonate, so the final concentration of  $\text{Na}_2\text{CO}_3$  would be the optimum  $0.02 \text{ M}$ . Then the procedure described under Labelling procedure was carried out.

#### 2.3.4. Procedure for chewing-gum

A commercial chewing-gum (Sportlife, Dulciora, Spain) was analyzed. A portion of  $5 \text{ g}$  was chopped and was placed in and  $250 \text{ ml}$  erlenmeyer flask and  $50 \text{ ml}$  ethylacetate were added. The mixture was shaken magnetically for  $12 \text{ h}$  and afterwards introduced in a refrigerator for  $2 \text{ h}$  to allow the polymer components which normally accompany the analyte to precipitate. The mixture was filtered in a Büchner funnel and after through a ground glass funnel No. 4. An aliquot of  $10 \text{ ml}$  was placed in a test tube and evaporated to dryness with nitrogen and subsequently  $10 \text{ ml}$  acetone was added to dissolve the residue.  $5 \text{ ml}$  of this solution was placed in a  $10 \text{ ml}$  volumetric flask and taken to final volume with  $0.04 \text{ M}$  sodium carbonate, so the final concentration of  $\text{Na}_2\text{CO}_3$  would be the optimum  $0.02 \text{ M}$ . Then the procedure described under Labelling procedure was carried out.

## 3. Results and discussion

### 3.1. Fluorescence properties

An aqueous solution containing pure BHA was measured, in order to determine its excitation and emission wavelengths. As it is observed in Fig. 1,

this compound shows a weak native fluorescence at 368 nm when excited at 267 nm.

Dansyl chloride reacts with the phenolic group of BHA to form a highly fluorescent derivative. The mechanism of dansylation reaction may be interpreted as shown in Scheme 1. BHA is first hydrolyzed in an alkaline aqueous solution to the corresponding phenolate which then reacts with DNS-Cl at an interface to form a fluorescent dansylated product which is extracted into an organic phase to avoid the inter-

ference of the highly fluorescent dansyl hydroxyde formed.

The fluorescence spectra obtained for the fluorophor, under the final experimental conditions, are also shown in Fig. 1. As expected, a considerable increase on the fluorescence intensity was observed and, also, a marked bathochromic shift of both excitation and emission maxima (341 and 482 nm, respectively), was observed. Both observations will be of great interest to increase both sensitivity and selectivity of the analytical determination.

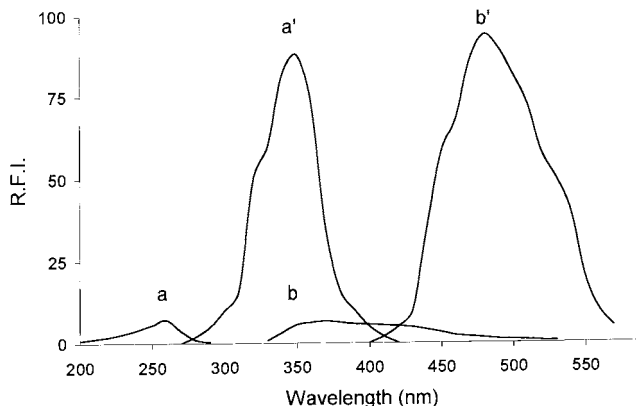
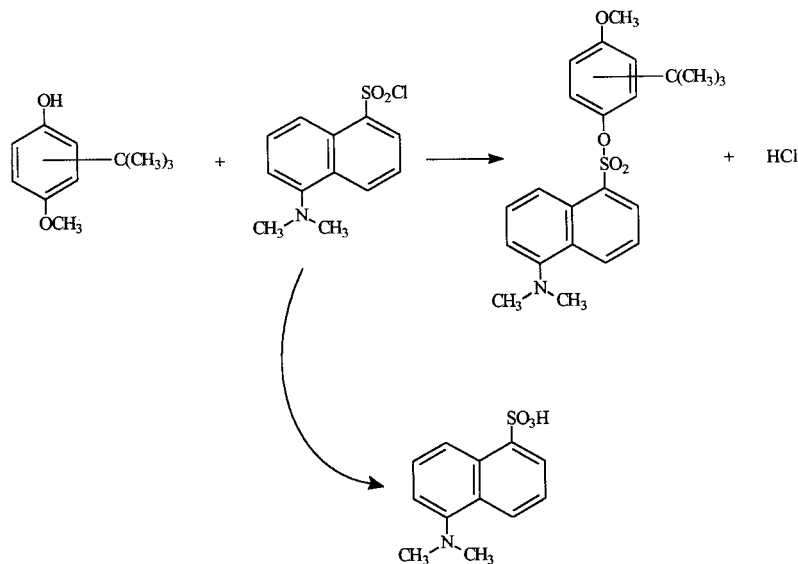


Fig. 1. Excitation (a,a') and emission (b,b') of unlabelled (a,b) and labelled (a',b') [BHA] = 2  $\mu\text{g ml}^{-1}$ , [DNS-Cl] = 5  $\mu\text{g ml}^{-1}$ .



Scheme 1. The mechanism of dansylation reaction.

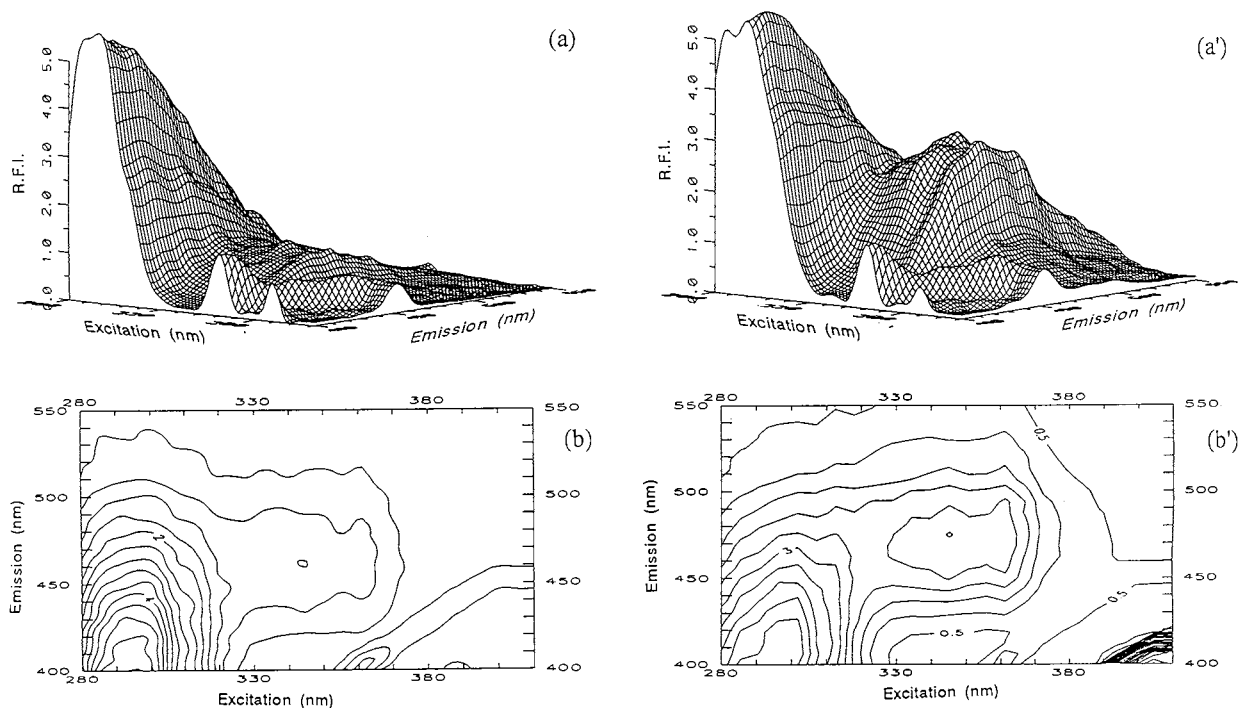


Fig. 2. Three-dimensional spectra (a,a') and the corresponding contour maps (b,b') of DNS-Cl (a,b) and DNS-Cl-BHA (a',b'). [BHA] = 300 ng ml<sup>-1</sup>; [DNS-Cl] = 1.5 µg ml<sup>-1</sup>.

### 3.2. Optimization of the derivatization reaction

#### 3.2.1. Influence of pH and solvent

Because hydrochloric acid is released during the dansylation reaction (see Scheme 1), buffering of the solution is always required.

Dansylation of BHA was performed in acetone with different concentrations of sodium carbonate solution between 0.01 and 0.1 M. Using the above procedure, the pH of the reaction mixture was found to be 10. We chose pH 10 as the optimum for dansylation because labelling of most phenols has been found to be optimal at pH 9.5–10.5 [36]. In this connection, it is interesting to note that the velocity of the dansylation process increases with increasing pH, but the reaction is paralleled by an increased hydrolytic rate of DNS-Cl into dansyl sulphonic (see Scheme 1) which is strongly fluorescent and hence seriously interferes in the determination. The maximum fluorescence differences between the labelled compound and its corresponding blank was obtained with a 0.02 M

sodium carbonate solution, which was used throughout the experimental work.

To check that the surplus DNS-Cl is hydrolyzed with transfer of the hydrolysis product to the aqueous phase, a blank test was performed without BHA and the three dimensional and corresponding contour maps are recorded and compared (see Fig. 2).

Due to the fact that the labelling reagent has to be dissolved in an organic solvent such as acetone, the dansylation was performed in mixture acetone–0.02 M sodium carbonate. To observe the influence of other solvents in the reaction medium, dilution with water, acetonitrile and dimethylformamide (DMF) was carried out. Very weak fluorescence was observed with acetonitrile and DMF but a great increase was observed when water was employed. The increase in the fluorescence intensity when using water may be attributed to lowering of the fluorescence of the reagent and was used throughout.

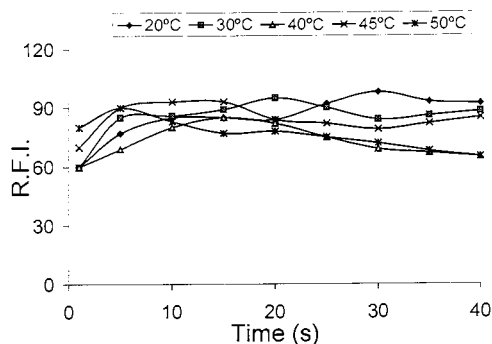


Fig. 3. Influence of temperature and time on the dansylation reaction of BHA.  $[BHA] = 2 \mu\text{g ml}^{-1}$  and  $[DNS\text{-}Cl] = 5 \mu\text{g ml}^{-1}$ .

### 3.2.2. Influence of dansyl chloride concentration

The influence of the reagent concentration selected for the recommended method was studied by carrying out the fluorimetric procedure using  $2 \mu\text{g ml}^{-1}$  of the drug and varying the reagent concentration, hence different ratios reagent: BHA were tested. In order to reduce the fluorescence of the blank to a minimum, but still guarantee a quantitative derivatization, a 0.3–20-fold molar excess of DNS-Cl was tested.

Changing the concentration of DNS-Cl over this molar proportion, it was shown that a final two-fold molar excess in the measured solution was necessary for highest fluorescence intensity to be obtained. The emission spectrum of the dansylated product formed between DNS-Cl and BHA at this molar proportion was measured at 5-min intervals in the cyclohexane organic phase during 12 h. From the results obtained, no decrease in the fluorescence intensity was observed, allowing the measurement to be carried out in a wide time.

### 3.2.3. Influence of temperature and time

Fig. 3 shows the influence of different temperatures at reaction times in the dansylation reaction of BHA. The curves were corrected for blank fluorescence. When using a concentration of  $2 \mu\text{g ml}^{-1}$  BHA, maximum fluorescence develops within 10 min at a  $45^\circ\text{C}$ .

At 30, 40 and  $50^\circ\text{C}$ , maxima are reached at 20 and 15 min, respectively, but the derivatives are quite unstable. However, using a temperature of  $45^\circ\text{C}$ , the fluorescence intensity remains constant between 1 and 15 min, choosing a 10 min reaction time for BHA to be completely derivatized. These temperatures and time periods are considerably smaller than previously published for this kind of derivatization reaction [37,38].

### 3.2.4. Choice of organic solvent and time for the extraction procedure

As it was indicated previously, the dansylated derivative of BHA is to be extracted into an organic solvent to avoid the interference of the strongly fluorescent dansyl hydroxyde formed in the dansylation reaction (see Scheme 1).

Different solvents such as benzene, cyclohexane, hexane, toluene and chloroform were examined for the extraction of DNS-Cl-BHA. As it is observed in Table 1, maximum fluorescence intensity was observed with cyclohexane, which presents a zero dipolar moment and a very similar dielectric constant as benzene, cyclohexane is however very much more preferable because its lower threshold limit value (TLV) related to benzene.

It is observed from this study that solvents such as chloroform with the highest solubility in water gave worse results due to the higher blank signal

Table 1  
Study of extraction solvent

Solvent	$\mu$ ( $25^\circ\text{C}$ )	$\varepsilon$ ( $25^\circ\text{C}$ )	Solubility in water ( $20^\circ\text{C}$ )	Threshold limit values ( $\mu\text{g ml}^{-1}$ )	$\lambda_{\text{exc}}$ (nm)	$\lambda_{\text{em}}$ (nm)	R.F.I.
Benzene	0	2.27	0.180	10	348	505	62
Cyclohexane	0	2.02	0.010	300	343	488	93
Hexane	0.08	1.88	0.001	100	342	487	77
Toluene	0.31	2.38	0.051	200	350	505	61
Chloroform	1.15	4.81	0.815	25	347	512	55

Table 2  
Analytical figures of merit<sup>a</sup>

Detection limit (ng ml <sup>-1</sup> )	Quantitation limit (ng ml <sup>-1</sup> )	Linear range (µg ml <sup>-1</sup> )		Sensitivity (ng ml <sup>-1</sup> )		Linearity (%)		Relative S.D. (%)	
		Curve 1	Curve 2	Curve 1	Curve 2	Curve 1	Curve 2	Curve 1 300 ng ml <sup>-1</sup>	Curve 2 3 µg ml <sup>-1</sup>
59	174	0.05–0.5	1–5	18	140	97	98	3.8	2.7

<sup>a</sup> Curve 1. Slits 3/3 nm; Curve 2. Slits 2/2 nm.

because of interference from dansyl hydroxide. As a result, for extraction of the derivatives, cyclohexane was found to be most suitable.

Different shaking times (1–240 s) were proved to observe differences in the relative fluorescence intensity between labelled BHA and the corresponding DNS-Cl blank. No differences were observed when more than 30 s were employed, so an extraction time of 1 min was chosen to assure the effectiveness of the extraction procedure.

### 3.3. Analytical performance

The dependence of the signals for BHA on the concentration was determined under the optimum experimental and instrumental conditions. Two analytical curves for standard solutions containing different concentrations of BHA from 1 to 5 µg ml<sup>-1</sup> and from 100 to 500 ng ml<sup>-1</sup> were obtained by plotting the R.F.I. against the analyte concentration. The analytical figures of merit obtained, for the two calibration curves, are summarised in Table 2. The analytical characteristics of the proposed method have been carried out by the model proposed by Cuadros Rodríguez et al. [39] where the precision of the method is obtained from the calibration curve data and the detection limit ( $\alpha = 0.05$ ,  $\beta = 0.05$ ) has been calculated taken into account false positive and false negative error, according to the criterium of Clayton [40]. As observed in Table 2, the precision of the method, expressed as relative S.D. ranged from 2.7 to 3.8%.

### 3.4. Interference

Different substances commonly accompanying the synthetic antioxidant BHA such as the antioxidants BHT (E-321), propyl gallate (E-310) and ascorbic acid (E-300), preservatives such as sorbic acid (E-200), biphenyl (E-230), benzoic acid (E-210) and ethyl paraben (E-214) and colorants such as tartrazine (E-102) and amaranth (E-123) were tested in order to check their interference with the BHA signals. Under the experimental conditions described for the determination of BHA and a concentration of 300 ng ml<sup>-1</sup>, a concentration 100:1 (interferent:BHA) was the maximum ratio tested.

The tolerance criteria was a S.D. of students *t* plus the relative S.D. of 300 ng ml<sup>-1</sup> BHA for seven replicates. For the three acids analyzed, negative signals were observed due to their acid character that modifies the pH of the media. This can be avoided controlling the pH and the maximum ratio tested was allowed. Ethyl paraben and propyl gallate gave positive interferences, due to the fact that dansylation reaction takes place with these compounds but a proportion of 5:1 could be present. No interference was observed from the two colorants and from BHT.

The most important conclusions on the above interference study are the results related to the absence of interference in the determination of BHA in presence of BHT, being a major problem in their simultaneous determination, due to the fact that similar chemical structures are present in both compounds (see Scheme 2), as it is demonstrated in the numerous publications related to the determination of BHA in the presence of



BHT. At first, a great interference from BHT on the determination of BHA was expected as a result of labelling reaction with dansyl chloride. On the other hand, as can be observed in Fig. 4, the BHT contour map shows no fluorescence at the same wavelength maxima characteristics of dansylated products, so it could be concluded that the reaction does not take place. The reason to justify the behaviour of BHT in presence of a labelling reagent characteristic of phenolic hydroxy groups is that the dansylation reaction does not take place because of a steric impediment between the substituent of BHT and the big DNS-Cl molecule so a selective determination of BHA in the presence of

BHT could be carried out, without need of any separation step.

### 3.5. Determination of BHA in foodstuffs

The proposed method was applied to the determination of BHA in two foodstuffs that usually contain BHA in presence of other additives, such as dehydrated soup and chewing-gum; samples were pre-treated as described under Section 2.3.

The composition of the dehydrated soup was: maltodextrin, sugar, salt, yeast, meat extract, gelatine, jerez wine, aromas, vegetable extracts, flavour potential (621), colorant caramel and the antioxidant BHA and for the chewing-gum: sorbitol, xilitol, aromas, the sweetener sacharin, colorant (E-171) and the antioxidant BHA were present.

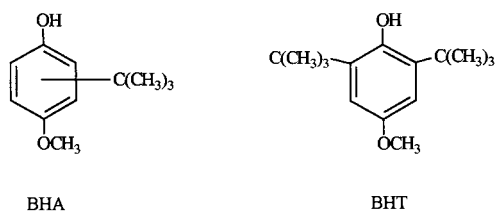
To verify the trueness of the proposed method for the determination of BHA, a calibration method standard additions (SAM) was performed for both samples [39,41]. By using the standard addition method, three calibration lines, standard calibration (SC), Youden curve (YC) and standard addition (AC) were carried out, for each sample.

The SC was obtained from the analytical signal set for replicates of BHA standard solutions containing 0, 100, 200, 300, 400 and 500 ng ml<sup>-1</sup>. Solutions of pre-treated sample with a concentration of 160 mg ml<sup>-1</sup> (for dehydrated soup) and 21 mg ml<sup>-1</sup> (for chewing-gum), were prepared.

To establish the Youden curve, sample solutions of 0.5, 1.0, and 1.5 mg ml<sup>-1</sup> for both dehydrated soup (YC<sup>1</sup>) and chewing-gum (YC<sup>2</sup>) were prepared.

Finally, the standard addition curves (AC) were constructed adding volumes of analyte to obtain final concentrations of 0, 100, 200 and 300 ng ml<sup>-1</sup> to the same concentrations of sample solution, 333 µg ml<sup>-1</sup> for dehydrated soup (AC<sup>1</sup>) and 42 µg ml<sup>-1</sup> for chewing-gum (AC<sup>2</sup>), respectively.

The results are presented in Table 3. Also, the parameters of five calibration curves are shown in Table 4. *t*-Student test [42] shows that the three slopes compared ( $b_{SC}$ ,  $b_{AC}^1$ ,  $b_{AC}^2$ ) are not significantly different (*P*-value of 0.92 and 0.88) for AC<sup>1</sup> and AC<sup>2</sup>, respectively. This means that a proportional systematic error does not exist, be-



Scheme 2. Chemical structures of BHA and BHT.

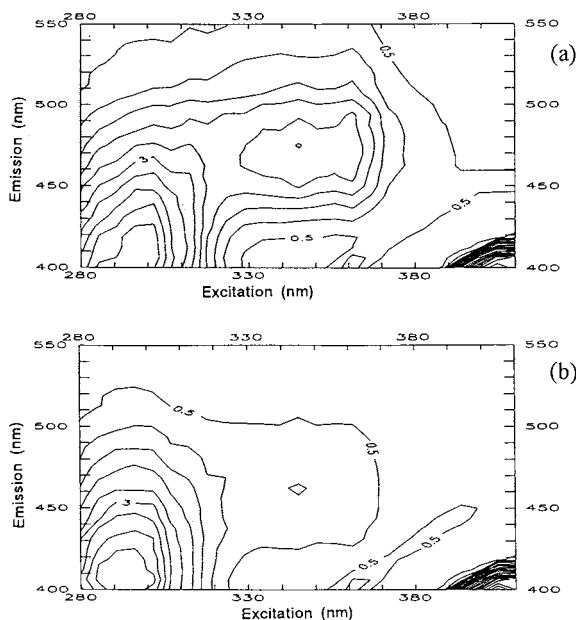


Fig. 4. Contour maps of reaction products of BHA (a) and BHT (b) in presence of dansyl chloride. [BHA] = [BHT] = 300 ng ml<sup>-1</sup>; [DNS-Cl] = 1.5 µg ml<sup>-1</sup>.

Table 3

Analytical signals obtained to establish standard calibration (SC), standard additions calibrations (AC<sup>1</sup> and AC<sup>2</sup>), and Youden calibration (YC<sup>1</sup> and YC<sup>2</sup>)

Calibration	Concentration of std analyte solution added, ng ml <sup>-1</sup>	Concentration of sample solution added, µg ml <sup>-1</sup>	Analytical signal
SC	0	0	19
	100	0	31
	200	0	42
	300	0	54
	400	0	66
	500	0	76
AC <sup>1</sup>	0	333	36
	100	333	46
	200	333	55
	300	333	71
YC <sup>1</sup>	0	500	52
	0	1000	61
	0	1500	69
AC <sup>2</sup>	0	84	19
	100	84	31
	200	84	43
	300	84	54
YC <sup>2</sup>	0	500	44
	0	1000	48
	0	1500	54

Table 4

Parameters for SC, AC<sup>1</sup>, YC<sup>1</sup>, AC<sup>2</sup>, and YC<sup>2</sup> calibrations<sup>a</sup>

Parameter	SC	AC <sup>1</sup>	YC <sup>1</sup>	AC <sup>2</sup>	YC <sup>2</sup>
<i>N</i>	15	4	3	4	3
<i>A</i>	19.6	35	44	21.2	39
<i>B</i>	0.114	0.113	0.017	0.117	0.010
<i>S</i>	3.6	2.31	0.4	0.39	0.46
<i>R</i>	0.999	0.992	0.999	0.999	0.98

<sup>a</sup> *N*, number of measurements used, *A*, intercept; *B*, slope; *S*, regression S.D.; *R*, correlation coefficient.

ing possible to determine the BHA content, in these real samples, from the standard calibrations.

The content of BHA in the dehydrated soup and in chewing-gum, obtained from the AC<sup>1</sup> and AC<sup>2</sup> calibrations are 287 and 585 µg g<sup>-1</sup>, respectively.

From this study, it may be concluded that the BHA content, in this type of sample can be determined directly by using the standard addition calibration method. In all cases, the Youden blank must be eliminated from all measurements.

This rapid and sensitive fluorimetric method may be suitable for the determination of BHA in commercial products both in the absence and in the presence of normally accompanying compounds such as BHT or propyl gallate.

## References

- [1] B.D. Page, C.F. Charbonneau, J. Assoc. Off. Anal. Chem. 72 (1989) 259.

- [2] T.E. Furia (Ed.), CRC Handbook of Food Additives, second ed., vol. II, CRC Press, FL, USA, 1980.
- [3] T.J. Slaga, Crit. Rev. Food Sci. Nutr. 35 (1995) 51.
- [4] P.A.R.L. Schilderman, E. Rhijnsburger, I. Zwingmann, J.C.S. Kleinjans, Carcinogenesis 16 (1995) 507.
- [5] H. Yamazaki, T. Yamaguchi, A. Yamauchi, Y. Kakiuchi, Chemosphere 29 (1994) 1293.
- [6] M.E. Komaitis, M. Kapel, J. Am. Oil Chem. Soc. 62 (1985) 1371.
- [7] C.S.P. Sastry, S.G. Rao, B.S. Sastry, J. Food Sci. Technol. 29 (1992) 101.
- [8] A. Espinosa Mansilla, F. Salinas, M. del Olmo, I. de Orbe Paya, Appl. Spectrosc. 50 (1996) 449.
- [9] A.G. Cabanillas, T.G. Díaz, F. Salinas, Analisis 19 (1991) 262.
- [10] D. Ivanovic, M. Medenica, E. Nivaudguernet, M. Guernet, Spectrosc. Lett. 28 (1995) 557.
- [11] F. García Sánchez, C. Cruces Blanco, Int. J. Environ. Anal. Chem. 31 (1987) 23.
- [12] C. Cruces Blanco, F. García Sánchez, Analisis 17 (1989) 80.
- [13] C. Cruces Blanco, A.M. García Campaña, F. Alés Barrero, Talanta 43 (1996) 1019.
- [14] M. Guldborg, Fresenius J. Anal. Chem. 309 (1981) 117.
- [15] A. Staby, C. Borch-Jensen, S. Balchen, J. Mollemp, J. Am. Oil Chem. Soc. 71 (1994) 355.
- [16] W.P. King, J. Kissinger, J. Assoc. Off. Anal. Chem. 63 (1980) 137.
- [17] D. Ivanovic, M. Medenica, E. Nivaud-Guernet, M. Guernet, Chromatographia 40 (1995) 652.
- [18] L. Bianchim, M.A. Colivicchi, L. Dellacorte, M. Valoti, G.P. Sgaragli, P. Bechi, J. Chromatogr. B 694 (1997) 359.
- [19] K. Helrich (Ed.), Official Methods of Analysis of the Association of Official Analytical Chemists, 15th ed., Association of Official Analytical Chemists, Arlington, VA, 1990.
- [20] S. Kmostak, D.A. Kurtz, J. AOAC Int. 76 (1993) 735.
- [21] C.A. Hall, A. Zhu, M.G. Zeece, J. Agr. Food Chem. 42 (1994) 919.
- [22] P. Yañez Sedeño, J.M. Pingarrón, L.M. Polo Diez, Anal. Chim. Acta 252 (1991) 153.
- [23] M. Gonzalez, E. Ballesteros, M. Gallego, M. Valcárcel, Anal. Chim. Acta 359 (1998) 47.
- [24] F. García Sánchez, C. Cruces Blanco, Anal. Chem. 58 (1986) 73.
- [25] F. García Sánchez, A. Aguilar Gallardo, C. Cruces Blanco, Talanta 39 (1992) 1195.
- [26] C. Cruces Blanco, A. Segura Carretero, A. Fernández Gutiérrez, M. Román Ceba, J. Pharm. Biomed. Anal. 13 (1995) 1019.
- [27] K. Robards, S. Dilli, Analyst 102 (1977) 201.
- [28] G. Weber, Biochem. J. 51 (1952) 155.
- [29] W.R. Gray, B.S. Hartley, Biochem. J. 89 (1963) 59.
- [30] M. Ayad, M.H. Abdel-Hay, Analyst 109 (1984) 1431.
- [31] W. Baeyens, B. Lin, V. Corbisier, Analyst 115 (1990) 359.
- [32] C. Cruces Blanco, F. García Sánchez, Analyst 116 (1991) 851.
- [33] A.J. Tong, Y.G. Wu, L.D. Li, Talanta 43 (1996) 1429.
- [34] P. Clausing, L.G. Rushing, G.D. Newport, J.F. Bowyer, J. Chromatogr. B. 692 (1997) 419.
- [35] R.M. Linares, J.H. Ayala, A.M. Afonso, V. González, Analyst 123 (1998) 725.
- [36] N. Seiler, Methods Biochem. Anal. 18 (1970) 259.
- [37] J. Lawrence, C. Renault, R.W. Frei, J. Chromatogr. 121 (1976) 343.
- [38] S. Traore, J.J. Aaron, Talanta 28 (1981) 765.
- [39] L. Cuadros Rodríguez, A.M. García Campaña, F. Alés Barrero, C. Jiménez Linares, M. Román Ceba, JAOAC Inter. 78 (1995) 471.
- [40] C.A. Clayton, J.W. Hines, P.D. Elkins, Anal. Chem. 59 (1987) 2506.
- [41] J.M. Bosque-Sendra, L. Cuadros Rodríguez, A.M. García Campaña, Recent Res. Devol. Pure Appl. Anal. Chem. 1 (1998) 115.
- [42] A. Martín Andrés, J.B. Luna del Castillo, Bioestadística para las Ciencias de la Salud, Norma, Madrid, 1990.

# Speciation of arsenic by hydride generation–atomic absorption spectrometry (HG–AAS) in hydrochloric acid reaction medium

Amjad Shraim <sup>a,\*</sup>, Barry Chiswell <sup>a</sup>, Henry Olszowy <sup>b</sup>

<sup>a</sup> Department of Chemistry, The University of Queensland, St. Lucia, Qld 4072, Australia

<sup>b</sup> Queensland Health Scientific Services, 39 Kessels Rd., Coopers Plains, Qld 4108, Australia

Received 31 March 1999; received in revised form 7 July 1999; accepted 15 July 1999

## Abstract

The effects on the absorbance signals obtained using HG–AAS of variations in concentrations of the reaction medium (hydrochloric acid), the reducing agent [sodium tetrahydroborate(III); NaBH<sub>4</sub>], the pre-reducing agent (L-cysteine), and the contact time (between L-cysteine and arsenic-containing solutions) for the arsines generated from solutions of arsenite, arsenate, monomethylarsonic acid (MMA), and dimethylarsenic acid (DMA), have been investigated to find a method for analysis of the four arsenic species in environmental samples. Signals were found to be greatly enhanced in low acid concentration in both the absence (0.03–0.60 M HCl) and the presence of L-cysteine (0.001–0.03 M HCl), however with L-cysteine present, higher signals were obtained. Total arsenic content and speciation of DMA, As(III), MMA, and As(V) in mixtures containing the four arsenic species, as well as some environmental samples have been obtained using the following conditions: (i) total arsenic: 0.01 M acid, 2% NaBH<sub>4</sub>, 5% L-cysteine, and contact time < 10 min; (ii) DMA: 1.0 M acid, 0.3–0.6% NaBH<sub>4</sub>, 4.0% L-cysteine, and contact time < 5 min; (iii) As(III): 4–6 M acid and 0.05% NaBH<sub>4</sub> in the absence of L-cysteine; (iv) MMA: 4.0 M acid, 0.03% NaBH<sub>4</sub>, 0.4% L-cysteine, and contact time of 30 min; (v) As(V): by difference. Detection limits (ppb) for analysis of total arsenic, DMA, As(III), and MMA were found to be 1.1 (*n* = 7), 0.5 (*n* = 5), 0.6 (*n* = 7), and 1.8 (*n* = 4), respectively. Good percentage recoveries (102–114%) of added spikes were obtained for all analyses. © 1999 Elsevier Science B.V. All rights reserved.

**Keywords:** Arsenic; Arsenite; Arsenate; Monomethylarsonic acid; Dimethylarsenic acid; Speciation; L-cysteine; Hydride generation; Selective reduction

## 1. Introduction

Arsenic, which is potentially toxic to humans, animals, and plants [1–4] and according to recent reports [5–8] may be carcinogenic to humans, occurs naturally in many chemical forms. Arsenic

\* Corresponding author. Fax: +61-7-33653839.

E-mail address: a.shraim@chemistry.uq.edu.au (A. Shraim)

poisoning is a major public health problem, especially in countries such as Bangladesh, where the soil is high in arsenic compounds and the well water may contain as much as 300–4000  $\mu\text{g L}^{-1}$  of arsenic [9].

The toxicity of arsenic varies widely, ranging from highly hazardous inorganic arsenicals (arsine, arsenite, and arsenate) to relatively harmless organic species (monomethylarsonate and dimethylarsenate) [10–14]. Indeed some organo-arsenicals, such as arsenobetaine and arsenocholine, are effectively non-toxic towards living organisms [15]. Therefore, determination of total arsenic content in a sample does not reflect the level of hazard of the element actually present, and it is increasingly important that the various forms of arsenic be determined in biological and environmental samples to provide a much clearer view of the risk associated with exposure to arsenic in the environment. Reported arsenic concentrations in some parts of Australia range up to 36 000  $\text{mg kg}^{-1}$  in surface soils and 300  $\text{mg kg}^{-1}$  in ground water [16]; the current ANZECC/NHMRC arsenic guideline for soil is 100  $\text{mg kg}^{-1}$ , while the NHMRC drinking water guideline has recently been reduced from 50 to 7  $\mu\text{g/l}$  [16].

Speciation of arsenic in environmental samples usually involves several steps including derivitization, separation, and detection; hydride generation (HG), initially developed by Braman and Foreback in 1973 [17], coupled to one of several separation and detection systems has been found to be one of the most common techniques used for derivitization of arsenic. A number of detection systems have been used in arsenic analysis, of which the most popular and preferred one in terms of simplicity, sensitivity, precision, speed, and cost is AAS.

Our aim in the work described here was to develop a simple, rapid, and inexpensive technique for the speciation of the most commonly occurring species in environmental samples, viz. As(III), As(V), monomethylarsonic acid (MMA), and dimethylarsenic acid (DMA) using hydride generation–atomic adsorption spectrometry (HG–AAS), i.e. a derivitization and detection technique only, without the need for a separation

step such as HPLC and cryogenic trapping, which we believe has caused many complications and resulted in lengthy analytical techniques. To compensate for the absence of a separation step in our method, a selective–reduction concept is employed to generate hydrides of each arsenic species.

Critical evaluation of the existing literature, showed that some work has been done on the use of HG–AAS for the speciation of arsenic [18–21], and much of this work dealt with the use of thiol-containing ligands, such as L-cysteine, L-cystine, and thioglycerol, to obtain identical response from all four arsenic species. These thiols have been used as pre-reducing agents before the addition of  $\text{NaBH}_4$ , and have been shown to enhance the arsine signals in low acid concentration and to reduce the effects of interferences [20,22–24].

In this study, the effect of HCl as a reaction medium on the arsine generation from the four arsenic species has been investigated. Control of the concentrations of the reaction medium (HCl), of the reducing and hydride generating agent ( $\text{NaBH}_4$ ), and of the pre-reducing agent (L-cysteine) when used, and the employment of HG–AAS has resulted in methods for the analysis and speciation of the four arsenic species in environmental samples.

## 2. Experimental

### 2.1. Equipment

A Vapour Generation Accessory (VGA-76, Varian) connected to an Atomic Absorption Spectrometer (Spectra 300, Varian) was used in this study, and operated according to manufacturer's instructions; instrument parameters used are summarised in Table 1. In this system, arsenic-containing solutions were pumped into a mixer and reacted with sodium tetrahydroborate(III) solution; generated arsines were swept to a gas–liquid separator using nitrogen gas and then to a heated T-shaped absorption cell.

## 2.2. Reagents and solutions

### 2.2.1. General

All chemicals were of analytical-reagent grade unless otherwise specified. All glassware was soaked in 4 M HNO<sub>3</sub> for a minimum of 12 h and washed with distilled water and finally rinsed with Milli-Q reagent water before use. All water used was obtained from a Milli-Q reagent system (Millipore), resistivity 18 MΩ cm. L-cysteine (minimum 98%, TLC) was obtained from Sigma (St. Louis, MO), sodium tetrahydroborate(III) from Merck and Alfa, As(III) atomic absorption standard solution (1 mg ml<sup>-1</sup>) and As(V) (As<sub>2</sub>O<sub>5</sub>, 99.999%) from Acros, MMA (disodium methylarsenate, 99%) from Chem Service, and DMA (cacodylic acid, 98%) was obtained from Aldrich. Various concentrations of NaBH<sub>4</sub> solution stabilised with NaOH were used; the concentration of NaOH was maintained at 0.5% in experiments where NaBH<sub>4</sub> concentrations exceeded 0.6%. While both reagents were kept at the same concentration when NaBH<sub>4</sub> was used at concentration levels < 0.6%.

### 2.2.2. Arsenic stock solutions

The arsenic stock solutions were prepared as follows: 1000 ppm As(III): arsenic(III) atomic absorption standard solution (1 mg ml<sup>-1</sup> As in 2% potassium hydroxide).

1000 ppm As(V): 0.03835 g of arsenic(V) oxide (As<sub>2</sub>O<sub>5</sub>) was dissolved in a minimum volume of 4.0 M NaOH, neutralised by a same volume of 4.0 M HCl, and the final volume was adjusted to 25 ml with Milli-Q water.

1000 ppm MMA: 0.09844 g of disodium methylarsenate (CH<sub>3</sub>AsO(ONa)<sub>2</sub>·6H<sub>2</sub>O) was dissolved in 25 ml Milli-Q water.

1000 ppm DMA: 0.04699 g of cacodylic acid (CH<sub>3</sub>)<sub>2</sub>AsO(OH) was dissolved in 25 ml of Milli-Q water. Cacodylic acid is the commercial name for DMA, the acronym used in this work.

The stock solutions of As(V), MMA, and DMA were prepared monthly and stored in glass volumetric flasks wrapped with aluminum foil and kept refrigerated at 4°C to prevent any change in speciation. The As(III) stock solution was also kept refrigerated at 4°C. All arsenic solutions were found to be stable under these conditions when tested after 1 month.

### 2.3. Analytical procedures

Solutions were prepared as required by appropriate dilution of stock solutions and additions of the required volumes of hydrochloric acid and L-cysteine solutions to achieve the required concentrations. Solutions were then rapidly mixed. When using L-cysteine, measurement of contact time was commenced upon addition of L-cysteine and stopped at the beginning of the analysis. Throughout this study contact time refers to the time that has been allowed for L-cysteine to react with the arsenic-containing solutions before the commencement of the introduction of solutions to HG–AAS.

## 3. Results and discussion

To understand the role of NaBH<sub>4</sub> as a reducing and HG agent in the analysis of arsenic, the following mechanism has been proposed [25,26]:

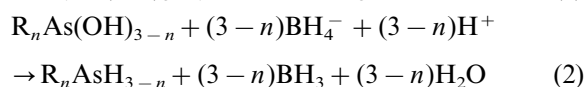
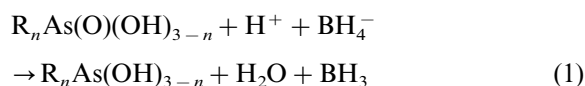


Table 1  
Operating conditions of the HG–AAS system

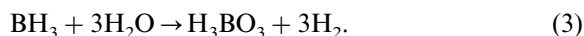
Instrument mode	Absorbance
Calibration mode	Concentration
Measurement mode	Integration
Slit width (nm)	0.5
Slit height	Normal
Wavelength (nm)	193.7
Flame	Air–acetylene
Sample introduction	Normal
Delay time (s)	40
Time constant	0.05
Measurement time (s)	2.0
Replicates	3
Background correction	On
Sample flow rate (ml min <sup>-1</sup> )	7
NaBH <sub>4</sub> flow rate (ml min <sup>-1</sup> )	1

Table 2

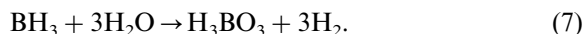
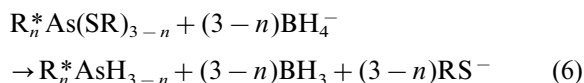
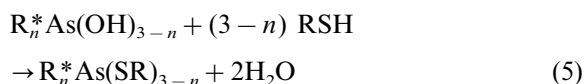
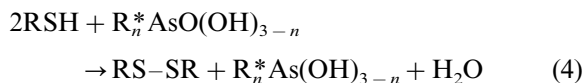
Steps followed for the analysis of arsenic species<sup>a</sup>

Steps	HCl concentration	NaBH <sub>4</sub> concentration	L-cysteine concentration	Contact time
Step 1	V	C	0	NA
Step 2	C	V	0	NA
Step 3	V	C	C	C
Step 4	C	V	C	C
Step 5	C	C	C	V

<sup>a</sup> V = varied; C = constant; 0 = zero; NA = not applicable.



While in the presence of L-cysteine the proposed mechanism is shown below [23,25,27]:



We have used these proposed mechanisms to develop a method for the speciation of arsenic using the steps shown in the Table 2.

### 3.1. Effect of HCl concentration when using 0.6% NaBH<sub>4</sub> solution in the absence of L-cysteine

The effect of using 0.001–9.6 M HCl on the absorbance signals in the absence of L-cysteine is shown in Fig. 1. The absorption signals of As(III), MMA, and DMA sharply increase with increase in acid concentration over a range of 0.01–0.10 M, while the increase in the As(V) absorption signal is much slower. Further increase in the acid concentration results in:

(a) a sharp decrease in the DMA signal up to an acid concentration of 1.0 M, then a slow decrease to negligible values beyond 4.0 M,

(b) a broad maximum for MMA over an acid concentration range of 0.2–1.0 M, and a slow decrease thereafter to a negligible signal at 9.60 M,

(c) a slow increase in the As(III) signal up to an

acid concentration of 2.0 M and a very broad plateau afterwards, and

(d) a much slower increase in the As(V) signal, when compared to the As(III) signal, up to an acid concentration of 4 M, and a broad plateau thereafter. Our results are similar to those obtained by workers who used similar instrumentation and analytical procedure. For example Anderson et al. [18] and Hakala and Pyy [28] used a HG–AAS and a HCl concentration of up to 5.0 M and reported similar results. However, changes in experimental conditions may cause major differences in results, as shown in the work of Rude and Puchelt [19], who used flow injection analysis (FIA)–HG–AAS and HCl concentrations of up to 5.0 M, and found the following:

1. at HCl concentration of > 1.0 M, they obtained an increasing response with a linear function ( $r = 0.995$ ) for As(III) which disagrees with our and the findings of others [18,20,29], in which As(III) showed a constant response. This increasing linear response is most probably caused by incomplete generation of arsine, which is due to the use of a low KBH<sub>4</sub> concentration (0.2%). As reported below, results obtained by us when using low NaBH<sub>4</sub> concentrations are similar to those of Rude and Puchelt [19];
2. the low KBH<sub>4</sub> concentration used by Rude and Puchelt [34] yielded a negligible As(V) absorbance across the whole acid concentration range;
3. MMA has an almost identical response to DMA over the whole acid range (0.0–5.0 M) covered by the study of Rude and Puchelt [19], and both MMA and DMA showed a negligible response in 2.0 M and higher HCl concentrations.

Further examination of Fig. 1, shows the following:

1. the sharp increase in the absorption signals of the arsenic species, especially As(III), MMA, and DMA, with increase in the acid concentration over the low range (0.1–0.6 M), suggests that an investigation into the use of higher  $\text{NaBH}_4$  concentrations may be warranted to determine whether this condition might increase the signal of As(V) and produce identical responses from all four arsenic species and thus enable the determination of total arsenic;
2. at low acid concentration (0.01–0.1 M), DMA shows higher signals when compared to the other three species. An investigation into the use of  $\text{NaBH}_4$  concentrations seemed appropriate and suggested that a low acid and low  $\text{NaBH}_4$  concentrations could result in a condi-

tion where all species signals, except that of DMA, are reduced to negligible values, thus leading to the speciation of DMA in the presence of the other three species,

3. the observation that the DMA and MMA response signals decrease to negligible levels at high HCl concentrations whilst As(III) and As(V) essentially provide a constant positive response prompted another investigation where an As(III) speciation might be possible, with the As(III) signal retained, by use of low  $\text{NaBH}_4$  concentration at high acid concentrations.

To address the above-mentioned points the effect of  $\text{NaBH}_4$  concentration over the range 0.02–2.0% when using low (0.005–0.1 M) and moderate to high acid concentrations (2.0–8.0 M) has been investigated.

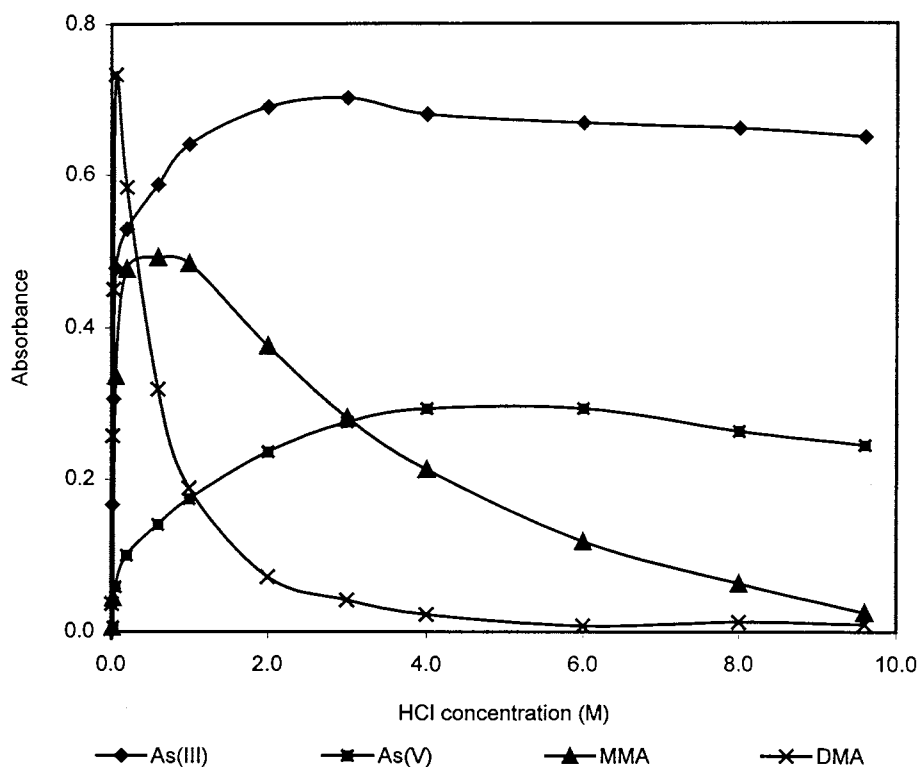


Fig. 1. Effect of HCl concentration on the absorption signals of As(III), As(V), MMA, and DMA (40 ppb As each) when using 0.6%  $\text{NaBH}_4$ , in the absence of L-cysteine.



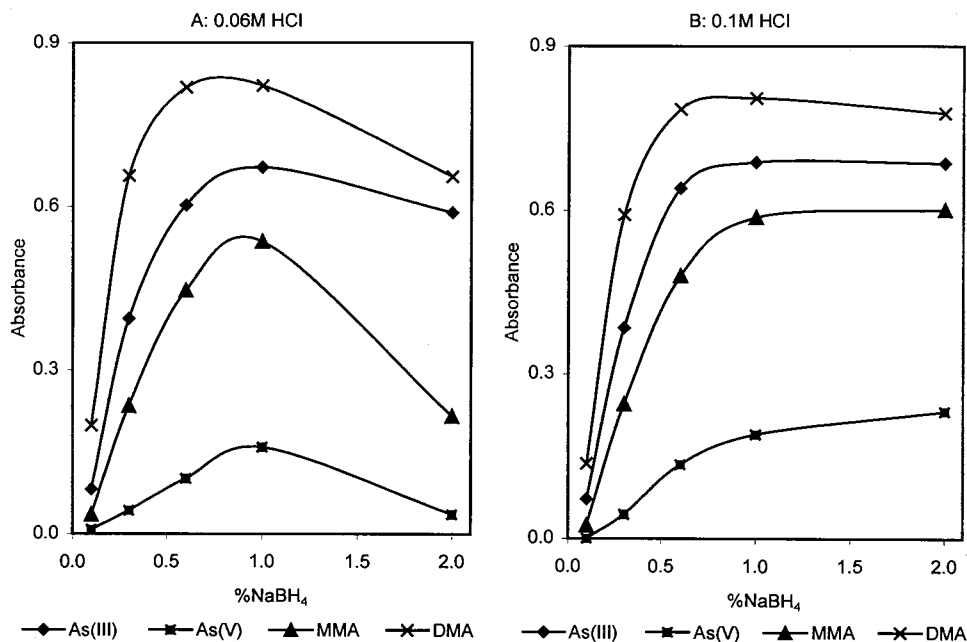


Fig. 2. Effect of NaBH<sub>4</sub> concentration on the absorption signals of As(III), As(V), MMA, and DMA (40 ppb As each) when using 0.06 M HCl (A) and 0.10 M HCl (B) in the absence of L-cysteine.

### 3.2. Effect of NaBH<sub>4</sub> concentration in the absence of L-cysteine

#### 3.2.1. Use of low concentrations of HCl

The effect of using 0.1–2.0% NaBH<sub>4</sub> and low acid concentrations (0.06 and 0.1 M) on the absorption signals of the four arsenic species is shown in Fig. 2. The use of NaBH<sub>4</sub> concentrations up to 2.0% failed to produce identical signals from the four arsenic species, and thus under these conditions, determination of a total arsenic signal is not possible. Further increase in NaBH<sub>4</sub> concentrations up to 4.0% was found to cause large instability in the signals, and could not be used to check possible increases in signal responses. This instability may be caused by either or both of the following two reasons:

1. it was observed that the preparation of NaBH<sub>4</sub> solutions with concentrations > 1.0% results in cloudy solutions (an indication of undissolved particles) which settle down with time and become clear. The settled particles tend to dissolve when mixed with acid solution inside reaction tubes, producing a non-homogeneous

reaction mixture with localised cells of NaBH<sub>4</sub> concentrations thus causing the signal instability. Filtering the solution, or leaving it to settle and withdrawing clear portions partially reduced this instability;

2. The use of high concentrations of NaBH<sub>4</sub> may result in a vigorous production of arsines, as well as the production of large quantities of H<sub>2</sub> gas, where both can cause large signal instability. Several droplets of solution were observed at the top of the gas-liquid separator when using high NaBH<sub>4</sub> concentrations, which support this assumption.

It is also clear from Fig. 2 that the use of NaBH<sub>4</sub> concentrations of < 0.6% has resulted in a decrease in the signals of the four arsenic species. Fig. 2A and B show that DMA still yields a relatively large signal, whereas the signals of the other three species are reduced to lower values. Nevertheless the signals of As(III), As(V), and MMA effectively result in a total interference of 60–70% in the DMA signal. In order to reduce this interference, the use of lower acid concentrations has been investigated; results are shown in Fig. 3.

Fig. 3A and B show that the use of low  $\text{NaBH}_4$  concentrations, when using 0.03 and 0.01 M acid, resulted in a high DMA signal with low interference from As(III) and negligible signals for both As(V) and MMA. On the other hand, at a  $\text{NaBH}_4$  concentration of 2.0% in 0.01 M HCl (Fig. 3B), DMA showed a reduced response, but with no interference from the other three species. Further decrease in acid concentration to 0.005 M eliminated all the inter-

ferences and produced significant signals from DMA at  $\text{NaBH}_4$  concentrations of  $< 0.6\%$  (Fig. 3C).

To eliminate the interference of As(III) in the DMA signal when using 0.01 M acid (see Fig. 3B), the use of  $\text{NaBH}_4$  concentrations of lower than 0.1% has been investigated; as shown in Fig. 3D, this approach has eliminated the interference of As(III) in the DMA signal when  $\text{NaBH}_4$  concentrations of 0.02–0.075% are used.

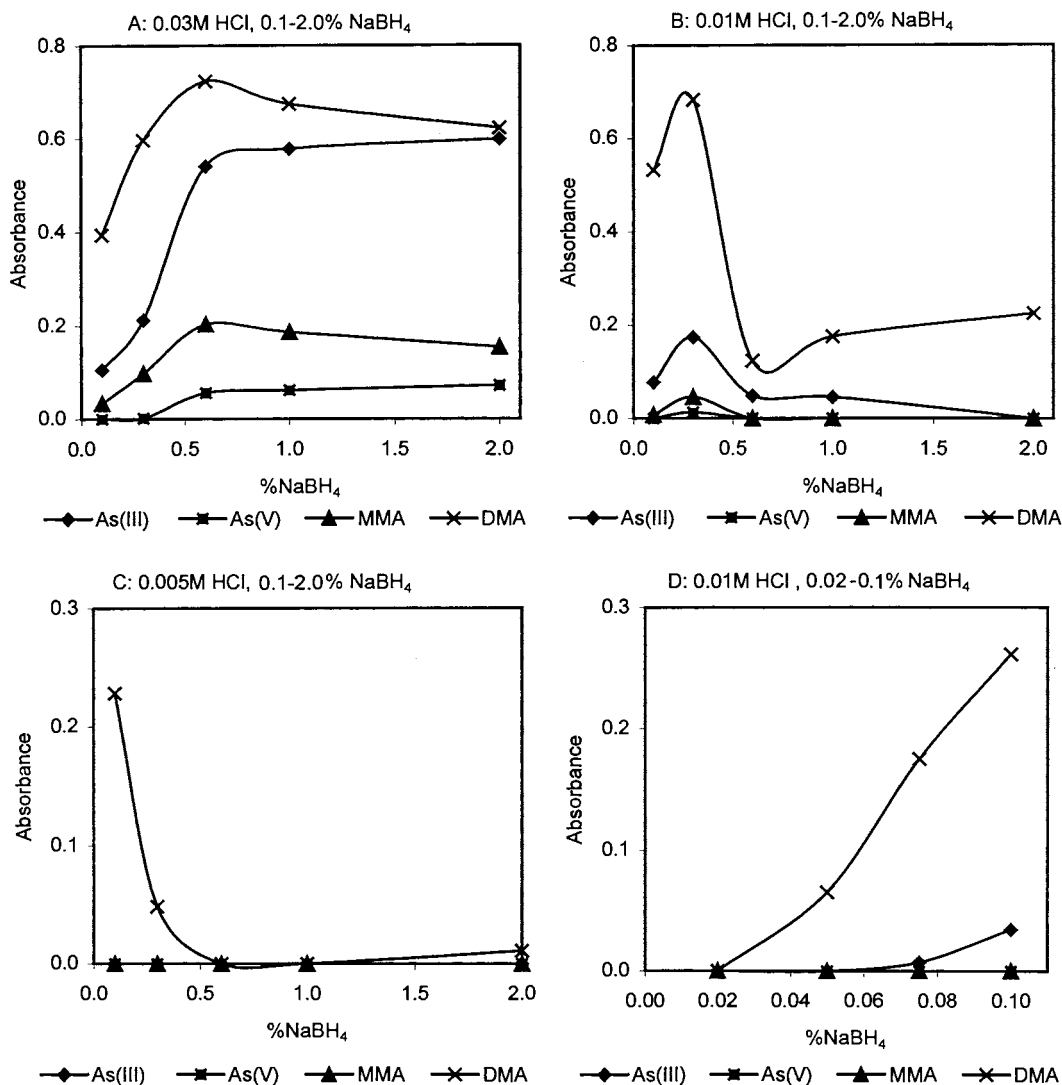


Fig. 3. Effect of  $\text{NaBH}_4$  concentration on the absorption signals of As(III), As(V), MMA, and DMA (40 ppb As each) when using A: 0.03; B: 0.01; C: 0.005 and D: 0.01 M HCl in the absence of L-cysteine.

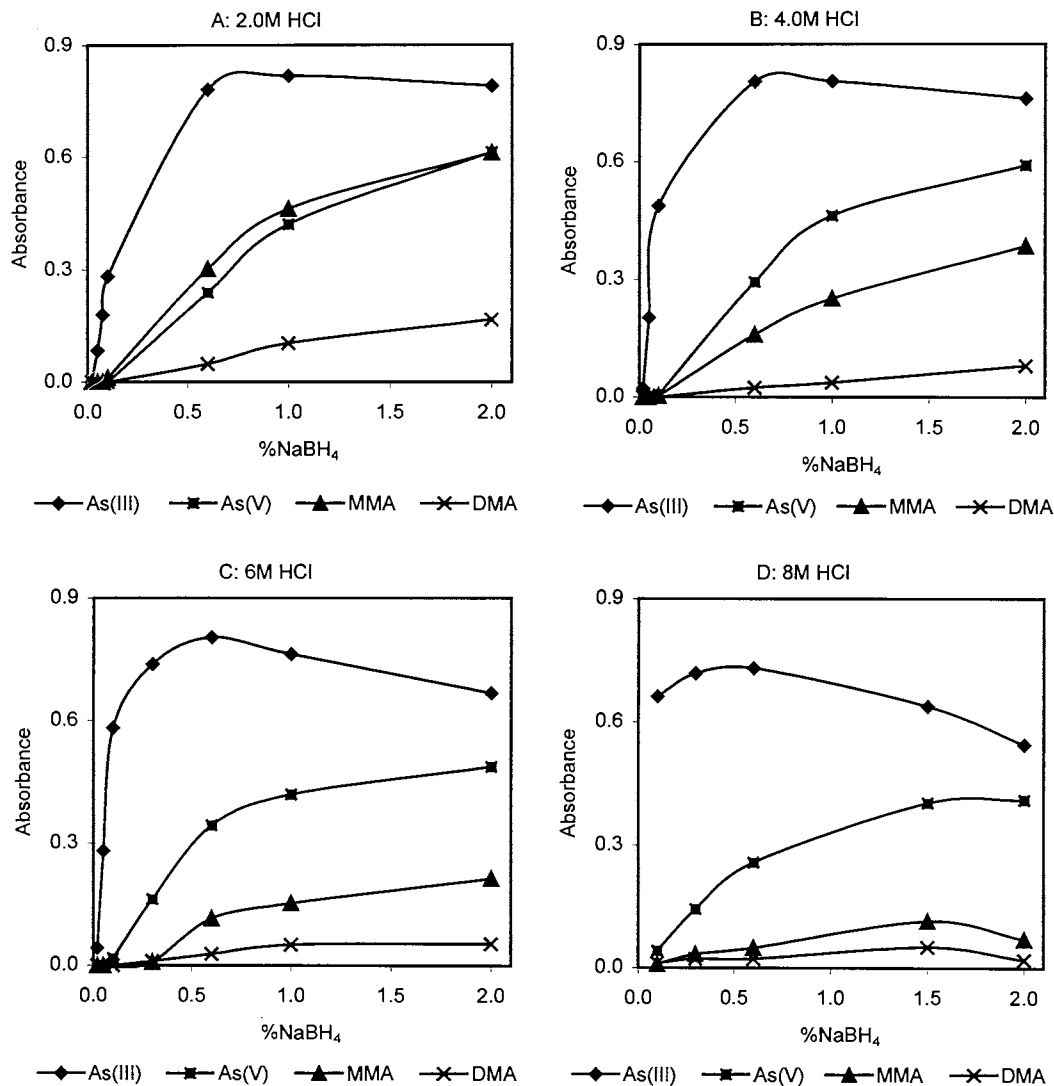


Fig. 4. Effect of NaBH<sub>4</sub> concentration on the absorption signals of As(III), As(V), MMA, and DMA (40 ppb As each) when using A: 2; B: 4; C: 6; and D: 8 M HCl in the absence of L-cysteine.

The use of 0.005 M HCl and 0.1% NaBH<sub>4</sub> in the absence of L-cysteine has produced excellent results for the speciation of DMA in a mixture containing all four arsenic species (Table 3A).

On the other hand the use of 0.07 and 2.0% NaBH<sub>4</sub> with 0.01 M HCl yields very large errors. Although the other three arsenic species show no signals when analysed separately (see Fig. 3B and D), they yielded a combined interference of 27.3

and 56.3% when NaBH<sub>4</sub> concentrations of 0.07 and 2.0%, respectively were used.

### 3.2.2. Use of moderate to high concentrations of HCl

The effect of using 0.02–2.0% NaBH<sub>4</sub> and moderate to high acid concentrations (2, 4, 6, and 8 M) on the absorption signals of the four arsenic species is shown in Fig. 4; the results indicate that the use of NaBH<sub>4</sub> concentrations of ≤ 0.1% at any acid concentration produces high signals from

Table 3  
Experimental conditions for speciation of arsenic in mixtures containing the four arsenic species

No.	Species <sup>a</sup>	[HCl], M	% L-cysteine	<i>T</i> <sup>b</sup>	%NaBH <sub>4</sub>	As used <sup>c</sup>	<i>N</i> <sup>d</sup>	Avg <sup>e</sup>	%Err <sup>f</sup>	$\delta$ <sup>g</sup>	Equation <sup>h</sup>	<i>R</i> <sup>2i</sup>	LWR <sup>j</sup>	DL <sup>k</sup>
A	DMA	0.005	0.0	N/A	0.1	80	7	20.2	0.8	0.46	$y = 0.005408x$	0.9987	0–40	0.9
B	As(III)	4.0	0.0	N/A	0.05	80	7	20.0	0.1	0.59	$y = 0.005587x$	0.9928	0–80	0.6
		6.0	0.0	N/A	0.05	80	8	19.7	–1.6	0.36	$y = 0.009332x$	0.9963	0–40	0.8
C	TAs	0.01	4.0	10	1.0	40	3	39.6	–1.0	0.82	$y = 0.030760x$	0.9986	0–20	1.0
		0.01	5.0	5	2.0	40	7	40.8	1.9	0.72	$y = 0.032440x$	0.9913	0–10	1.1
D	DMA	1.0	4.0	4	0.6	80	5	21.7	8.7	0.56	$y = 0.012853x$	0.9961	0–20	0.5
E	MMA	4.0	0.4	30	0.03	80	4	20.4	2.2	0.56	$y = 0.005693x$	0.9952	0–80	1.8

<sup>a</sup> Species for which analysis was undertaken.

<sup>b</sup> Contact time after which the first reading was taken.

<sup>c</sup> Total arsenic in the mixture solution, equal concentrations of each of the four arsenic species were added (ppb).

<sup>d</sup> Number of readings taken for each speciation analysis.

<sup>e</sup> Average concentration of arsenic species found (ppb).

<sup>f</sup> Percentage error from the average.

<sup>g</sup> S.D. (ppb).

<sup>h</sup> Equation of calibration curve.

<sup>i</sup> *R*<sup>2</sup> value of calibration curve.

<sup>j</sup> Linear working range of calibration curve (ppb).

<sup>k</sup> Detection limit (ppb) calculated from three times the S.D. of the replicated blanks.

As(III) only and negligible signals from the other three species. The increase in acid concentration from 2 to 8, when using  $\text{NaBH}_4$  concentrations of 0.02–2.0%, slightly increased the As(V) signal, but has little effect on the As(III) signal, while the signals of the organic arsenicals decrease with increase in the acid concentration.

From the results shown in Fig. 4, it appears likely that a signal for As(III) only can be obtained when acid concentrations of 2–8 M and low concentrations of  $\text{NaBH}_4$  are used. To check this, the analysis of arsenic solution mixtures using 4 and 6 M HCl and 0.05%  $\text{NaBH}_4$  has been carried out and found to yield excellent results (see Table 3B).

Controlling the concentrations of acid and  $\text{NaBH}_4$  in the absence of L-cysteine has resulted in methods for the speciation of DMA and As(III). To find methods for the speciation of the other species and the analysis of total arsenic, the use of L-cysteine has been introduced.

### 3.3. Effect of HCl concentration when using 0.4% L-cysteine, 0.6% $\text{NaBH}_4$ solutions, and constant contact time

The effect of HCl concentration (0.001–9.2 M) and 0.6%  $\text{NaBH}_4$  in the presence of 0.4% L-cysteine, on the absorption signals of the four arsenic species is shown in Fig. 5. The presence of L-cysteine produces a very rapid increase in the signals for the four arsenic species with increase in acid concentration over a lower and narrower range of 0.001–0.03 M HCl compared to the signals obtained in the absence of L-cysteine (see Fig. 1). The four species showed similar maxima at an acid concentration 0.03–0.06 M with very similar absorption signals for As(III), As(V), and DMA and a lower signal for MMA (Fig. 5B). As discussed later, improvements in the MMA signal and production of similar signals from all four species have been achieved by using more concentrated solutions of L-cysteine and  $\text{NaBH}_4$  allowing the determination of total arsenic content.

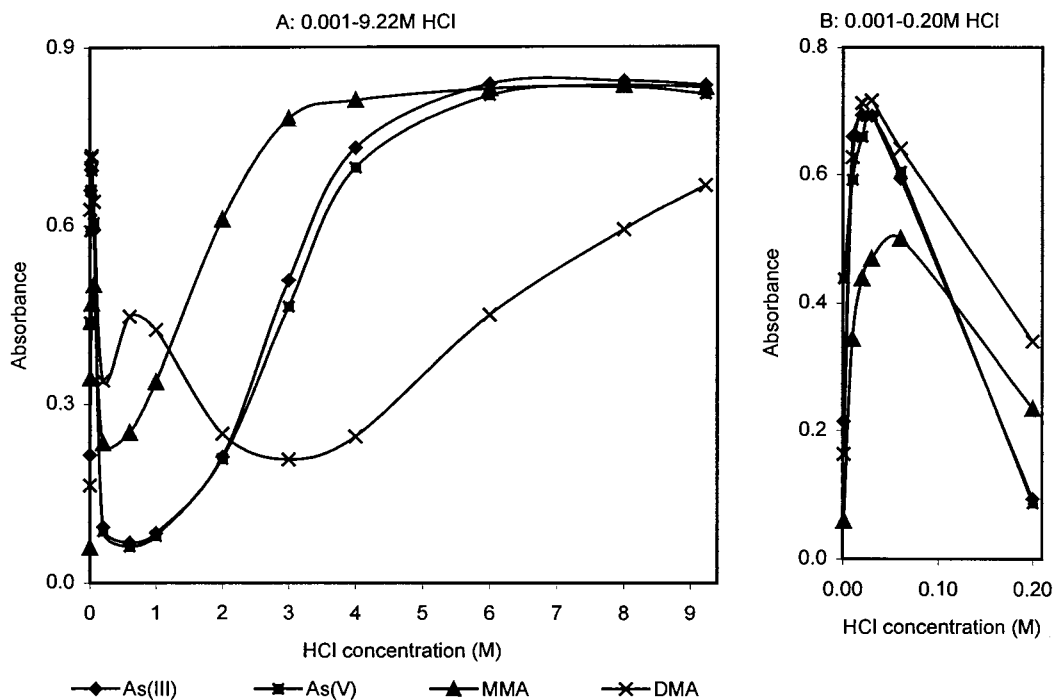


Fig. 5. Effect of HCl concentration on the absorption signals of As(III), As(V), MMA, and DMA (40 ppb As each) when using 0.6%  $\text{NaBH}_4$  and 0.4% L-cysteine after a contact time of 2 h.

Chen et al. [23] used a HG–DCP–AES to study the effect of low concentrations of HCl and HNO<sub>3</sub> (0.002–0.1 M) on the arsine generation from As(III) and As(V) only, in the absence and the presence of L-cysteine. In agreement with our findings, they reported that the As(III) signal, in the presence of L-cysteine, was increased by more than 75% when using an acid concentration of  $\approx 0.02$  M. They also reported that the reduction of As(V) to As(III) in the presence of L-cysteine is slow and time-dependent. Our results showed identical responses from both As(III) and As(V) over the entire HCl concentration range (0.001–9.2 M) in the presence of 0.4% L-cysteine.

Le et al. [20] have also studied the effect of HCl concentration (> 0.0–4.0 M) on the arsine generation from As(III), As(V), MMA, and DMA in the presence and the absence of many pre-reducing agents, such as L-cysteine and methionine, using a FIA–HG–AAS with 2.5% NaBH<sub>4</sub>. They obtained maximum and identical responses from the four arsenic species when using 0.3–0.7 M HCl after 10–20 min of contact with 2.5% L-cysteine. These results are different to ours and to the work of Anderson et al. [18] in which very similar responses from the four arsenic species were obtained when using much lower and narrower acid concentration ranges of 0.01–0.03 M HCl and 0.06–0.1 M mercaptoacetic acid, respectively. Reasons behind these differences are unclear, but the use of high concentrations of L-cysteine and NaBH<sub>4</sub> may be responsible. Also, the reported results for the determination of MMA and DMA in acid concentration above 1 M are inconsistent; thus Le et al. [20] found that DMA gave a higher signal than MMA, whereas our results show the opposite. The increase in the As(III) and As(V) signals at > 2 M acid was also much slower than that found by us. The use of high concentrations of L-cysteine and NaBH<sub>4</sub> by Le et al. [20] may be responsible for these differences.

Further examination of Fig. 5 shows the following:

1. the use of high acid concentrations of  $\geq 6.0$  M produces similar signals from all species, except DMA, which showed a lower signal; we have been unsuccessful in our attempts to increase the DMA signal,
2. obtaining a signal for only DMA at an acid concentration of  $\approx 0.6$  M is possible if the interferences of MMA, As(III), and As(V) signals are eliminated,
3. obtaining an MMA signal at an acid concentration of 2–3 M is also possible, if the interference of the other three species is also eliminated,
4. the presence of L-cysteine produces similar signals from both As(III) and As(V) over the whole acid concentration range, supporting the proposed mechanism shown in Eqs. (4)–(7).

Based on these observations, we proceeded to study the effect of using NaBH<sub>4</sub> and L-cysteine concentrations other than 0.6 and 0.4%, respectively in 0.01, 0.6, and > 2.0 M HCl.

### 3.4. Effect of NaBH<sub>4</sub> concentration

#### 3.4.1. Effect of NaBH<sub>4</sub> concentration on obtaining a total arsenic signal when using 0.01 M HCl, 2.5% L-cysteine, and constant contact time

The effect of NaBH<sub>4</sub> concentration when using 0.01 M HCl, 2.5% L-cysteine over a contact time of 50–70 min is shown in Fig. 6. The MMA signal has been enhanced and similar signals from the four arsenic species have been produced, when a minimum NaBH<sub>4</sub> concentration of 0.6% is employed; this allows for determination of a total arsenic signal. A long contact time has been used to make sure that the reduction of arsenic(V) species to arsenic(III) analogues, and subsequent generation of arsine is complete. Fig. 6 also indicates that increase in NaBH<sub>4</sub> concentration up to 0.6% results in sharp increase in absorption signals of all four arsenic species; no more increase is observed with increase in NaBH<sub>4</sub> concentration beyond 0.6%.

#### 3.4.2. Effect of NaBH<sub>4</sub> concentration on obtaining a sole signal for DMA when using 0.6 M HCl, 0.4% L-cysteine, and constant contact time

Fig. 5 indicates that at an acid concentration of  $\approx 0.6$  M, obtaining a signal for only DMA may be possible if the signals for the other three spe-

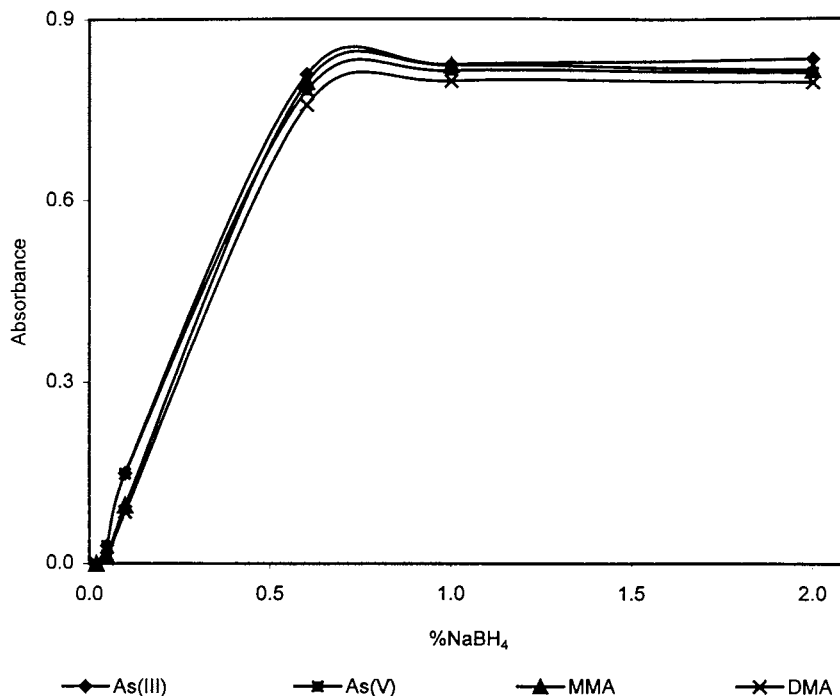


Fig. 6. Effect of  $\text{NaBH}_4$  concentration on the absorption signals of As(III), As(V), MMA, and DMA (40 ppb As each) when using 0.01 M HCl and 2.5% L-cysteine after a contact time of 50–70 min.

cies are reduced to negligible values. Based on this, the effect of  $\text{NaBH}_4$  concentrations of 0.02–2.0% and 0.4% L-cysteine at a contact time of about 2 h has been investigated as shown in Fig. 7. It is evident that a DMA signal, although low, can be obtained if  $\text{NaBH}_4$  concentrations between 0.05 and 0.1% are employed. The use of  $\text{NaBH}_4$  concentrations of  $>0.6\%$  will significantly increase the signals of the other species and therefore increase their interference with the DMA signal.

#### 3.4.3. Effect of $\text{NaBH}_4$ concentration on obtaining a sole MMA signal when using low to medium HCl concentrations, 0.4% L-cysteine, and constant contact time

The effect of  $\text{NaBH}_4$  concentrations of 0.02–2.0% and 0.4% L-cysteine at a contact time of about two h when using 1.5–6.0 M acid, has been investigated as shown in Fig. 8. The use of low concentrations of  $\text{NaBH}_4$  ( $<0.03\%$ ) when using 3–4 M acid (Fig. 8B and C) produces a high

signal only from MMA with negligible interference from the other three species. The use of an acid concentration of  $<3$  M (Fig. 8A) has increased the interference caused by DMA, while the use of acid concentrations of  $>4$  M (Fig. 8D) has increased the As(III) and As(V) interferences with the MMA signal.

### 3.5. Effect of contact time

#### 3.5.1. Effect of contact time on obtaining a total arsenic signal when using 0.01 M HCl, 4.0% L-cysteine, and 1.0% $\text{NaBH}_4$

In an attempt to find a short analysis time for determination of total arsenic signal when using the experimental conditions described in Section 3.4.1, but with an L-cysteine concentration increased to 4%, the effect of contact time of 1–20 min on the absorption signals of solutions containing single arsenic species was investigated. It was found that a minimum of 5–10 min was needed before obtaining similar signals from all

four species. It was also noticed that signals of all species were largely increased with increase in contact time from 1 to 5 min, except for As(III), where the signal reached a maximum from the beginning and remained so until the end of the analysis time.

To confirm these results, the analysis of total arsenic in a solution mixture containing 40 ppb as total arsenic (10 ppb each of the four species) using the above-mentioned experimental conditions was investigated. The reduction of arsenic species was found to be complete after 8–10 min under these experimental conditions, and very good results for total arsenic were achieved. However the use of higher concentrations of L-cysteine (5%) and NaBH<sub>4</sub> (2.0%) reduces the reduction time to 5 min; very good results for total arsenic were also obtained (Table 3C). Therefore the use of 0.01 M HCl under these experimental conditions can be used for the determination of total arsenic.

Low concentrations of HCl and HNO<sub>3</sub> in the presence L-cysteine, have been used in literature for the determination of total arsenic content [20,22–24], and two techniques similar to ours have been employed in these studies e.g. FIA–HG–AAS [20,22] and HG–Direct Current Plasma–AES [23,24]. Le et al. [20] allowed 10–20 min as a contact time between the sample and L-cysteine when using FIA–HG–AAS for the determination of total arsenic in urine samples. For each 10 ml sample in 2% L-cysteine, the concentration and the flow rate of the HCl and the NaBH<sub>4</sub> were 0.5 M and 3.4 ml min<sup>-1</sup>, and 0.65 M and 3.4 ml min<sup>-1</sup>, respectively. In comparison, our results have shorter contact time (5–10 min) when using lower acid concentration (0.01 M), and NaBH<sub>4</sub> concentrations of 1.0–2.0% at a higher L-cysteine concentration (4.0%).

In the study by Yin et al. [22], the contact time allowed for the determination of total inorganic arsenic when using FIA–HG–AAS was much longer than ours; they found that the reduction of

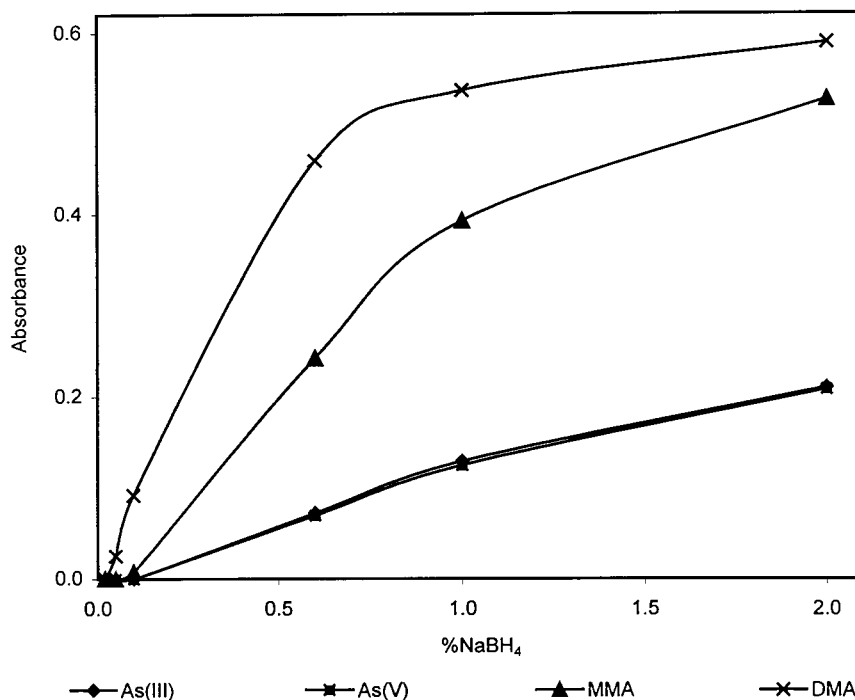


Fig. 7. Effect of NaBH<sub>4</sub> concentration on the absorption signals of As(III), As(V), MMA, and DMA (40 ppb As each) when using 0.60 M HCl and 0.40% L-cysteine after a contact time of 2 h.



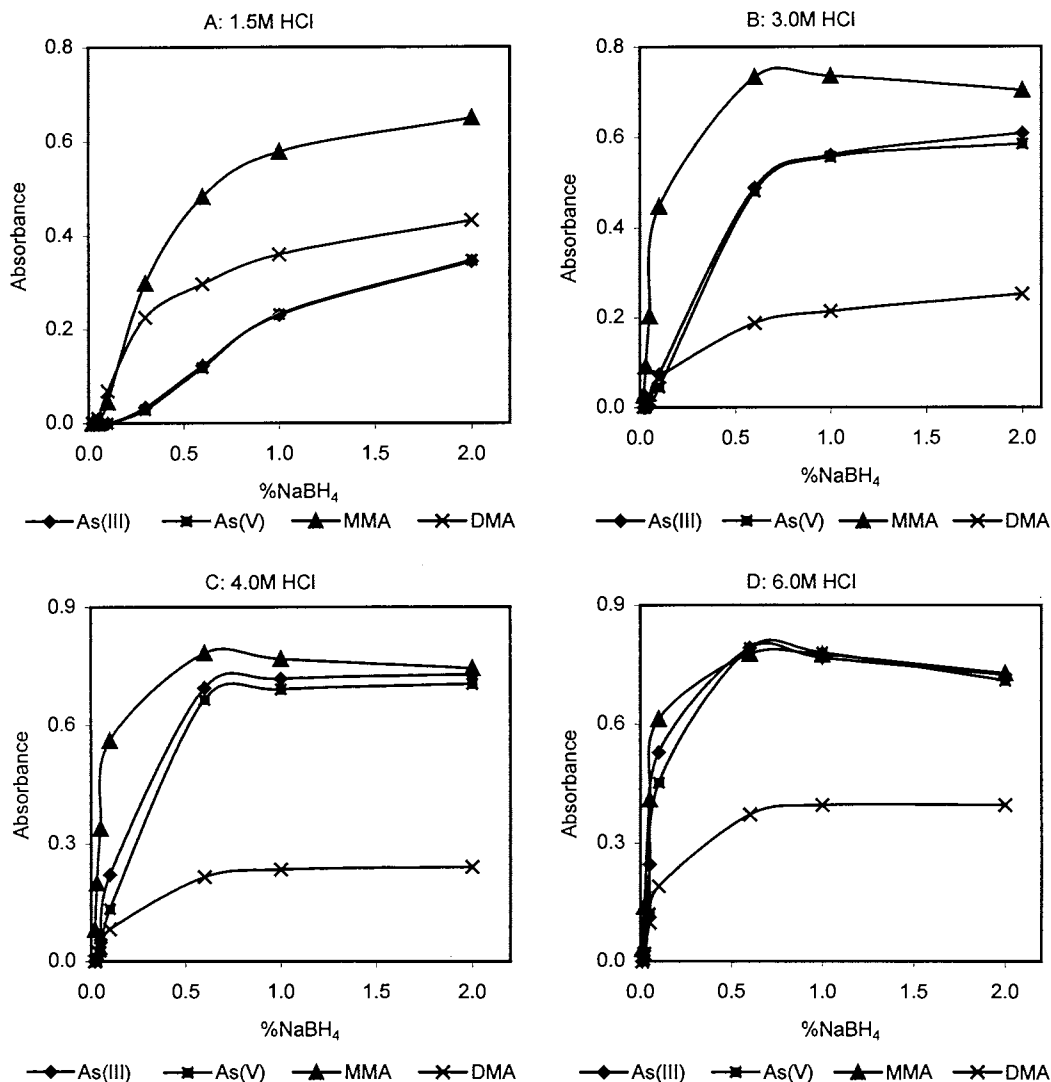


Fig. 8. Effect of NaBH<sub>4</sub> concentration on the absorption signals of As(III), As(V), MMA, and DMA (40 ppb As each) when using A: 1.5; B: 3; C: 4 and D: 6 M HCl and 0.4% L-cysteine after a contact time of 2 h.

As(V) (500  $\mu$ l of 2 ppb As) to As(III) was completed within 60, 40, and 20 min when using 0.04, 0.08, and 1.6 M, respectively of L-cysteine in 0.024 M HCl (or 0.029 M HNO<sub>3</sub>) and 0.5% NaBH<sub>4</sub>. Flow rates of acid and NaBH<sub>4</sub> were 7.8 and 5.4 ml min<sup>-1</sup>, respectively. In the present study, the As(V) reduction was completed in < 10 min compared to 40 min in their work.

In the other two studies [23,24], the reduction of As(V) required a longer time to complete, but

when the sample and L-cysteine were boiled for a short time before the introduction of NaBH<sub>4</sub>, the reduction was immediate.

In the work of Chen et al. [23], 0.01 M HCl (or HNO<sub>3</sub>) has been employed to determine the total inorganic arsenic using HG-DCP-AES. The As(V) content was determined as follows: 1 ml of 2% L-cysteine was injected into a 5 ml sample (the final L-cysteine concentration was 0.33%), followed by 0.5% NaBH<sub>4</sub>. No As(V) signal was

detected when the  $\text{NaBH}_4$  was added just after the addition of L-cysteine, but when the reaction was given 5 min before the addition of  $\text{NaBH}_4$ , a small signal was detected, which increased with increase in contact time. The As(V) reduction was complete within 35, 60, and 135 min when 1.0, 0.5, and 0.25 g, respectively of L-cysteine were added to 100 ml of 50 ppb As(V) when using 0.02 M acid. But when the solution was heated in boiling water for 5 min, As(V) was completely reduced to As(III). We have been able to obtain complete reduction of As(V) at room temperature in a much shorter time ( $< 10$  min) when using 4.0% L-cysteine.

In the other study, Brindle et al. [24] have achieved an immediate and complete reduction of As(V) to As(III) after mixing the sample solution with L-cysteine and  $\text{NaBH}_4$  under the following conditions: in a continuous flow HG–DCP–AES the sample ( $10 \text{ ml min}^{-1}$ ), L-cysteine (0.7%,  $1.6 \text{ ml min}^{-1}$ ), and  $\text{HNO}_3$  (0.02 M,  $10 \text{ ml min}^{-1}$ ) were mixed and heated, online to  $95\text{--}98^\circ\text{C}$ ,

cooled to room temperature, and reacted with  $\text{NaBH}_4$  (0.5%,  $1.6 \text{ ml min}^{-1}$ ).

It is evident from the last two studies [23,24], that the introduction of a heating step has eliminated any delay and spontaneously and completely produced arsine from As(V). We will consider this in future work.

### 3.5.2. Effect of the contact time on obtaining a DMA signal when using 0.6 M HCl, 4.0% L-cysteine, and 0.1 and 0.6% $\text{NaBH}_4$

Use of 0.6%  $\text{NaBH}_4$  and applying the same experimental conditions of Section 3.4.2 (0.6 M HCl, 0.4% L-cysteine), results in negligible signals from all species including DMA, even after the application of contact time of 40 min. As a result the L-cysteine concentration was increased to 4.0% to obtain a high DMA signal within reasonable contact times. The effect of contact time, under the new experimental conditions is shown in Fig. 9, which shows high DMA signals with negligible signals from the other three species up

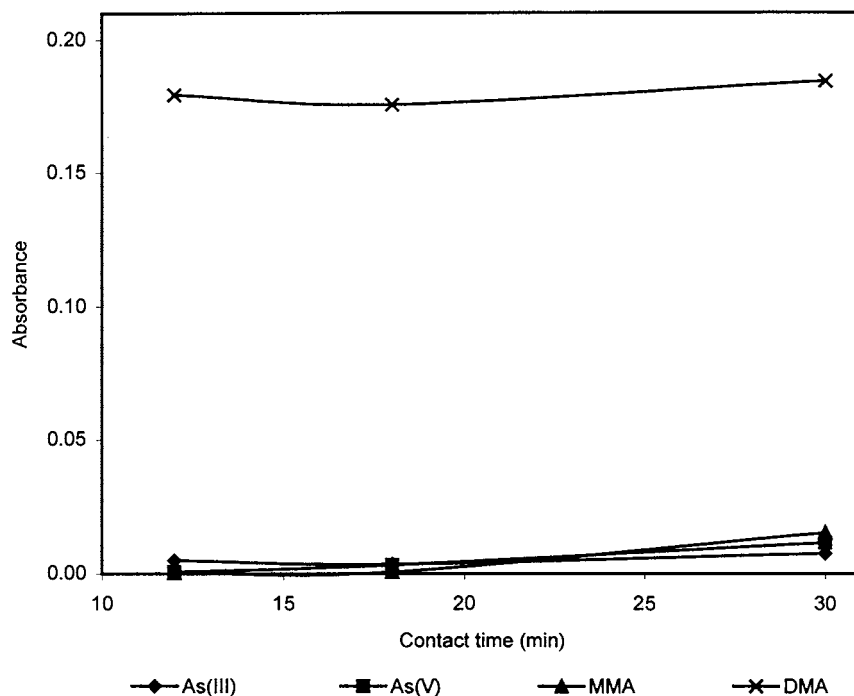


Fig. 9. Effect of contact time on the absorption signals of As(III), As(V), MMA, and DMA (40 ppb As each) when using 0.60 M HCl, 4.0% L-cysteine, and 0.60%  $\text{NaBH}_4$ .

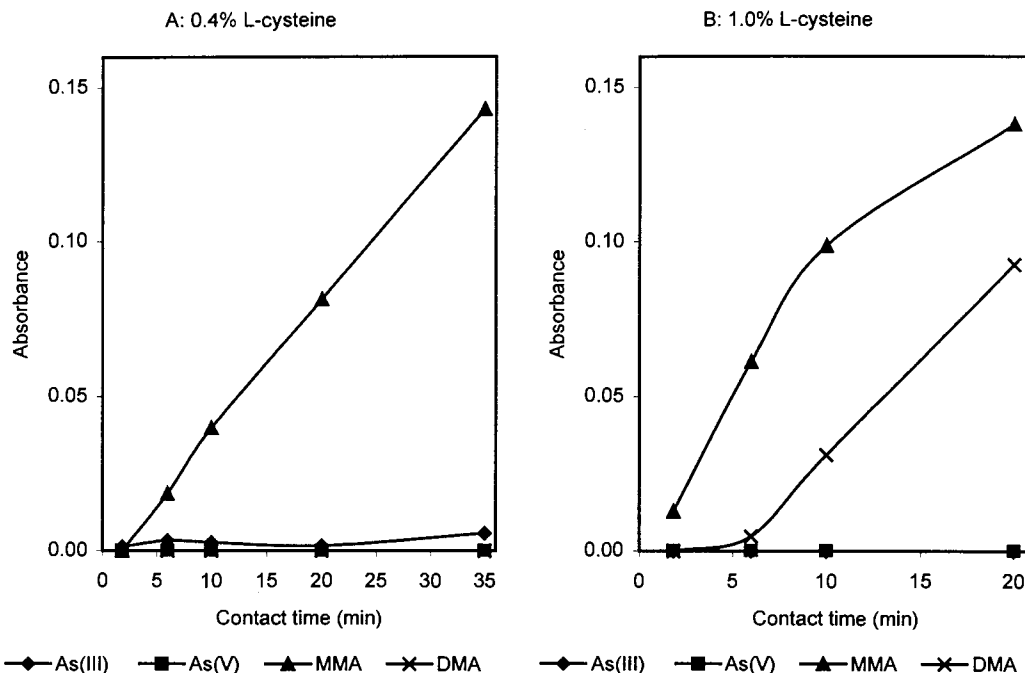


Fig. 10. Effect of contact time on the absorption signals of As(III), As(V), MMA, and DMA (40 ppb As each) when using 4.0 M HCl, 0.03% NaBH<sub>4</sub>, and A: 0.4% and B: 1% L-cysteine.

to a contact times < 18 min. It is also clear from Fig. 9 that a maximum of 12 min (the lowest time tried) can be safely used to obtain a signal for DMA only, in the presence of the other three species; shorter times can also be used.

Even though no interferences from the other three species on the DMA signals were found when solutions of single arsenic species were analysed (see Fig. 9), the use of 0.6 M HCl, 0.6% NaBH<sub>4</sub>, and 4.0% L-cysteine for the analysis of a mixture of the four arsenic species has produced huge errors (70%) in the DMA analysis. The increase in HCl concentration to 1 M, under the above experimental conditions, has significantly reduced the interferences and produced very good results after a contact time of only 4 min (Table 3D). By comparison, the use of 0.005 M HCl, 0.1% NaBH<sub>4</sub> in the absence of L-cysteine has produced better results with an error of only 0.81%. However, the analysis of actual environmental samples will decide which method is more appropriate for DMA speciation.

### 3.5.3. Effect of contact time on obtaining a sole MMA signal when using 4.0 M HCl, 0.2, 0.4, and 1.0% L-cysteine, and 0.03% NaBH<sub>4</sub>

Attempts to study the effect of contact time on speciation of MMA was undertaken using 4.0 M HCl, 0.4 and 1.0% L-cysteine, and 0.03% NaBH<sub>4</sub>, and results are shown in Fig. 10. Use of 0.2% L-cysteine after a contact time of 20 min was also examined and found to result in negligible signals from all species. Increasing the concentration of L-cysteine to 0.4% results in a linearly increasing signal for MMA with increase in contact time from 1.8 to 35 min, while the other three species exhibited negligible signals (Fig. 10A). Therefore, under these conditions, an MMA signal can be obtained with good intensity and little interference from the other three species after a contact time of around 20 min. However, the sole MMA signal may also be obtained in a shorter contact time, but with less intensity. On the other hand, the use of L-cysteine concentrations of > 0.4% (1.0% as shown in Fig. 10B), under the above-mentioned conditions, yields a higher MMA sig-

nals over shorter contact times; however the DMA signal starts to appear after 6 min, and consequently interferes with the MMA signal. Therefore, the best conditions, under these circumstances, for obtaining a sole signal for MMA with minimal interference from the other three species, are 4.0 M HCl, 0.03% NaBH<sub>4</sub>, and 0.4% L-cysteine after any contact time between 10 and 35 min.

The speciation of MMA in a solution mixture containing all four arsenic species has been achieved by using 4 M HCl, 0.4% L-cysteine, and 0.03% NaBH<sub>4</sub>, but a minimum contact time of 30 min should be provided to obtain good reproducible results (see Table 3E).

### 3.6. Calibration curves

Using appropriate conditions developed in this study, five different calibration curves were constructed for the speciation analysis. Arsenic species used to construct a calibration curve were the same ones for which the speciation analysis was

undertaken. Although any species could be used for TAs analysis, As(III) was used in this study.

### 3.7. Analysis of environmental samples

Two environmental water samples were obtained from Coen dam, Queensland, Australia; a dam close to gold mining activities. The first sample was taken before water treatment purification (BWT), while the other one was taken after treatment (AWT). Using experimental conditions shown in Table 3, five sub-samples of each water sample were analysed; the first was used for the analysis of TAs in the presence of L-cysteine, the second two sub-samples were used for the speciation of DMA and As(III) in the absence of L-cysteine, and the last two sub-samples were used for the speciation of DMA and MMA in the presence of L-cysteine. Details of the results and experimental conditions applied to obtain the results are summarised in Table 4.

The AWT water sample was found, as expected, to contain much less TAs when compared

Table 4  
Results and details of experimental conditions used for the analysis of water samples

Sample ID	Analysis	[HCl]	%L-cyst	T <sup>a</sup> (, min	%NaBH <sub>4</sub>	Arsenic (ppb)			
						Found <sup>b</sup>	Added <sup>c</sup>	Total <sup>d</sup>	%Recovery <sup>e</sup>
BWT <sup>f</sup>	TAs	0.01	5.0	5	2.0	38.9	8.0	47.5	107.5
AWT <sup>g</sup>						2.8	16.0	19.1	101.9
BWT <sup>f</sup>	DMA	0.005	0.0	N/A	0.1	0.8	80.0	18.3	87.5
AWT <sup>g</sup>						4.9	80.0	25.4	102.5
BWT <sup>f</sup>	As(III)	4.0	0.0	N/A	0.05	0.2	80.0	21.3	105.5
AWT <sup>g</sup>						0.0	80.0	21.9	109.5
BWT <sup>f</sup>	DMA	1.0	4.0	5	0.6	0.3	80.0	21.0	103.5
AWT <sup>g</sup>						0.0	80.0	20.6	103.0
BWT <sup>f</sup>	MMA	4.0	0.4	45	0.03	1.6	80.0	23.8	111.0
AWT <sup>g</sup>						0.1	80.0	22.8	113.5
BWT <sup>f</sup>	As(V) <sup>h</sup>					36.8			
AWT <sup>g</sup>						2.7			

<sup>a</sup> Contact time (min).

<sup>b</sup> Total arsenic concentration found (ppb) in unspiked sample.

<sup>c</sup> Total arsenic concentration added (ppb) to spike the sample, equal quantities of each of the four arsenic species were added.

<sup>d</sup> Total arsenic concentration found (ppb) in spiked sample.

<sup>e</sup> %Recovery of added spike.

<sup>f</sup> Water sample before water treatment.

<sup>g</sup> Water sample after water treatment.

<sup>h</sup> Calculated by difference, i.e. As(V) = [TAs – {As(III) + MMA + DMA}].

to the BWT sample; TAs concentration of 2.8 ppb was found which represents the arsenic residue left after water treatment.

Two methods for the speciation of DMA were applied; the first one in the absence of L-cysteine, while the second method was in the presence of L-cysteine. The first method yielded a DMA value of 0.8 ppb for the BWT sample, while a much larger value of 4.9 ppb was obtained for the AWT sample. The second method gave DMA values of 0.3 and 0.0 ppb for BWT and AWT samples respectively. The DMA value obtained for the AWT sample when using the first method appears to be unrealistically high and was rejected.

As expected, As(V) was the main species found in both samples; its concentration  $\geq 95\%$  of TAs. The pH value of each sample was found to be  $\approx 6.5$ , and as the dominancy of the inorganic arsenic species in natural and ground waters is controlled by the pH values and the oxidising or reducing conditions of such waters, it would be expected that As(V) would be the most dominant species in oxygenated natural waters, as it is the most thermodynamically stable species under these conditions [30–33]. Results for other natural water samples, which have been analysed for their arsenic species concentration by various workers, confirm these predictions; As(V) was found to be the predominant species in these studies [30,34–36] with values of greater than 90% of total arsenic.

Initial attempts to assess the accuracy of the methods developed in this work were undertaken using the standard addition method. Table 4 indicates that very good recoveries were obtained (101.9–113.5%); equal concentrations from all four arsenic species were added to each of the two water samples, ie. for the speciation of As(III), 20 ppb of each of the four species was added to give a total arsenic concentration of 80 ppb. From these samples 21.1 and 21.9 ppb As(III) for the BWT and AWT samples, respectively were recovered; these results represent percentage recoveries of 105.5 and 109.5% for the BWT and AWT samples, respectively.

## 4. Conclusions

The results reported in this paper, for the analyses and speciation of arsenic using methods developed in this work employing the selective-reduction–HG–AAS technique, show that these analyses can be quickly and accurately undertaken using this simple and inexpensive technique. The only exception is the analysis of MMA, which needs a minimum of 30–45 min to provide reliable results. The reduction of contact time in case of MMA may be achieved if different suitable experimental conditions such as a heating step are introduced to this system.

There is no doubt that a much more comprehensive analysis program of environmental samples from a wide variety of sources has to be undertaken before the usefulness of these methods can be accurately assessed.

## Acknowledgements

The authors would like to thank Claire Moore and Ron Sumner of the Queensland Health Scientific Services for their help in operating the HGAAS.

## References

- [1] J.P. Gustafsson, G. Jacks, *Appl. Geochem.* 10 (1995) 307.
- [2] A.R. Marin, P.H. Masscheleyn, W.H. Patrick, *Plant Soil* 152 (1993) 245.
- [3] J.R. Abernathy, Role of Arsenical chemicals in agriculture, in: W.H. Lederer, R.J. Fentsterheim (Eds.), *Arsenic: Industrial, Biomedical, Environmental Perspective's*, VNR, New York, 1983, pp. 57–62.
- [4] K. Ringwood, *Arsenic in the Gold and Base-Metal Mining Industry*, Australian Minerals and Energy Environment Foundation (AMEEF), Melbourne, Australia, 1995, pp. 1–33.
- [5] M. Piscator, *Life Sci. Res. Rep* 33 (1986) 59.
- [6] M. Buat-Menard, P.J. Peterson, M. Havas, E. Steinnes, D. Turner, Group Report: Arsenic, in: T.C. Hutchinson, K.M. Meema (Ed.), *Lead, Mercury, Cadmium Arsenic in the Environment*, SCOPE 31, Pub. John Wiley and Sons, Chichester, England, 1987, pp. 43–48.
- [7] G. Stohrer, *Arch. Toxicol.* 65 (1991) 525.
- [8] C. Hopenhayn-Rich, M.L. Biggs, A.H. Smith, D.A. Kalman, L.E. Moore, *Environ. Health Perspect.* 104 (1996) 620.

- [9] J. Beard, L. Cruces, *New Sci.* 28 (1998) 10.
- [10] R.W. Whitcare, C.S. Pearse, *Miner. Ind. Bull.* 17 (1974) 1.
- [11] G.M.P. Morrison, G.E. Batley, T.M. Florence, *Chem. Brit.* 25 (1989) 791.
- [12] B. Amran, F. Lagrade, M.J.F. Leroy, A. Lamotte, M. Olle, M. Albert, G. Rauret, J.F. Lopez-Sanchez, *Tech. Instr. Anal. Chem.* 17 (1995) 285.
- [13] W.R. Cullen, K.J. Reimer, *Chem. Rev.* 89 (1989) 713.
- [14] J.M. Wood, *Science* 183 (1974) 1049.
- [15] S. Caroli, F.L. Torre, F. Petrucci N. Violante, *Arsenic speciation and Health Aspects*, in: S. Caroli (Ed.), *Element Speciation in Bioinorganic Chemistry*, John Wiley and Sons, New York, 1996, pp. 445–463.
- [16] A. Hinwood, R. Bannister, A. Shugg, M. Sim, *Water* 25 (4) (1998) 34.
- [17] R.S. Braman, C.C. Foreback, *Science* 182 (1973) 1247.
- [18] R.K. Anderson, M. Thompson, E. Culbard, *Analyst* 111 (1986) 1143.
- [19] T.R. Rude, H. Puchelt, *Fresenius Z. Anal. Chem.* 350 (1994) 44.
- [20] X.C. Le, W.R. Cullen, K.J. Reimer, *Anal. Chim. Acta* 285 (1994) 277.
- [21] I.D. Brindle, X.C. Le, *Anal. Chem.* 61 (1989) 1175.
- [22] X. Yin, E. Hoffmann, C. Ludke, *Fresenius Z. Anal. Chem.* 355 (1996) 324.
- [23] H. Chen, I.D. Brindle, X.C. Le, *Anal. Chem.* 64 (1992) 667.
- [24] I.D. Brindle, H. Alarabi, S. Karshman, X.C. Le, S. Zheng, H. Chen, *Analyst* 117 (1992) 407.
- [25] A.G. Howard, *J. Anal. At. Spectrom.* 12 (1997) 267.
- [26] J. Aggett, A.C. Aspell, *Analyst* 101 (1976) 341.
- [27] A.G. Howard, C. Salou, *Anal. Chim. Acta* 333 (1996) 89.
- [28] E. Hakala, P. Lauri, *J. Anal. At. Spectrom.* 7 (1992) 191.
- [29] P.H. Masscheleyn, R.D. Delune, W.H. Patrick, *J. Envir. Qual.* 20 (1991) 96.
- [30] Battelle, *A Report: Speciation of Selenium and Arsenic in Natural Waters and Sediments. Vol. 2: Arsenic Speciation*, No. EPRI EA-4641, Pacific Northwest Laboratories, Sequim, Washington, 1986.
- [31] L.E. Hunt, A.G. Howard, *Mar. Pollut. Bull.* 28 (1994) 33.
- [32] H. Hasegawa, Y. Sohrin, M. Matsul, M. Hojo, M. Kawashima, *Anal. Chem.* 66 (1994) 3247.
- [33] J. Stummeyer, B. Harazim, T. Wippermann, *Fresenius Z. Anal. Chem.* 354 (1996) 344.
- [34] P. Thomas, K. Sniatecki, *J. Anal. At. Spectrom.* 10 (1995) 616.
- [35] C.J. Hwang, S.J. Jiang, *Anal. Chim. Acta* 289 (1994) 205.
- [36] R.J.A. Van Cleuvenbergen, W.E. Van Mol, F.C. Adams, *J. Anal. At. Spectrom.* 3 (1988) 169.

Short communication

# A method for the determination of potentiometric selectivity coefficients of ion selective electrodes in the presence of several interfering ions

Farzad Deyhimi \*

*Department of Chemistry, Shahid Beheshti University, Evin-Tehran, 19839, Iran*

Received 29 January 1998; received in revised form 7 May 1999; accepted 24 June 1999

## Abstract

In this work a new method is reported for the determination of potentiometric selectivity coefficients of ion-selective electrode in which, similar to real samples, several interfering ions are simultaneously present in test solutions and where the electrode shows its practical behavior. In order to illustrate this method, the potentiometric selectivity coefficients of a commercial liquid membrane ammonium selective electrode is determined for biologically important interfering ions:  $\text{Li}^+$ ,  $\text{Na}^+$  and  $\text{K}^+$ . © 1999 Elsevier Science B.V. All rights reserved.

*Keywords:* Potentiometric selectivity coefficient; Interfering ions; Ion-selective electrode (ISE); Ammonium ion-selective electrode

## 1. Introduction

The non ideal behavior of a liquid membrane ion-selective electrode (ISE) is usually described by potentiometric selectivity coefficients ( $K_{i,j}^{\text{Pot}}$ ), defined in semiempirical Nikolsky–Eisenman equation.  $K_{i,j}^{\text{Pot}}$  coefficients is used to express, generally, the ability of the electrode to distinguish between the desired ion ( $i$ ) and the interfering one ( $j$ ). Different experimental methods were proposed in the past [1–3] and two specialized IUPAC commissions were held concerning the

determination of potentiometric selectivity coefficients [4,5]. In the first IUPAC commission held in 1975 [4], the separate solution method (SSM) was recommended only if the electrode exhibits Nernstian response, but it was considered less desirable compared to the fixed interference method (FIM), because it does not represent as well the actual conditions under which the electrodes are used. In 1995, faced with a few limitations and inconveniences of these coefficients such as: values found for ions of unequal charges, non Nernstian behavior of interfering ions and activity dependence of  $K_{i,j}^{\text{Pot}}$ , the second IUPAC commission on methods for reporting  $K_{i,j}^{\text{Pot}}$  coefficients

\* Tel.: +98-21-2401765; fax: +98-21-2403041.

[5], recommended the matched potential method (MPM) which is independent of Nikolsky–Eisenman equation [6]. Clearly, IUPAC recommended MPM when ions of unequal charges are involved or when interfering ions and/or the primary ion (even with equal charges) do not satisfy the Nernstian behavior. However, this problem still remained subject of debate and discussion and several new propositions and methods were also presented [7–14]. In fact, the limitations of the MPM for the determination of potentiometric selectivity coefficients for ions of unequal charges, have first been shown by Macca [15] and later by others (e.g. [12,13]). For describing the response behavior for ions of different charge and selectivity coefficients of liquid and solvent polymeric ISE, Bakker et al. [7,14] proposed a theoretical treatment, different from Nikolsky–Eisenman equation. A new conditioning method have also been proposed by Bakker [8,9], in which the ISE is first placed in the solution of discriminated ion in order to eliminate the so called biased value for selectivity coefficient, due to the difficulty that interfering ion has in displacing the preferred ion from the membrane in the test solution. However, the disadvantage of the SSM and Bakker variation on it [8,9] was pointed out later by Kane and Diamond [12], just as an unrealistic representation of the ‘practical behavior of the electrode’ in the absence of both primary and interfering ions. Reviewing critically the other earlier regression methods, Kane and Diamond [12] mentioned their inconveniences such as the lack of information, like numerical or graphical data, or implementing approach. These authors proposed a method of determining potentiometric selectivity coefficients, in which, the experimental data obtained by FIM are fitted to an appropriate model by a non-linear least-squares regression. Surprisingly, better statistical results were obtained, with their particular data, for ion of unequal charge applying Nikolsky–Eisenman equation compared to the formalism proposed by Bakker et al. [7]. Recently, using a liquid membrane magnesium ISE, Spichiger and coworkers [13] showed also explicitly, several drawbacks and problems arising in the application of MPM for the determination of selectivity of the ISEs. Based on Nikolsky–

Eisenman equation and SSM, these authors defined mathematically a consistent selectivity coefficient which is designed to bypass the above mentioned inconsistencies and which could be conveniently used for a primary and an interfering ion of unequal charge number. The emergence of these different opinions and the variety of the proposed methods, in recent years, show clearly the absence of unanimity regarding the determination of potentiometric selectivity coefficients. Although, the determination of selectivity coefficients in a mixture of several interfering ions were also investigated, in particular cases e.g. [10,16], however, the most widely used determining methods of selectivity coefficients use simple solutions, in which only one or two different ions (primary and/or interfering) are present in the test solution. In this work a new method is proposed in which the determination of  $K_{i,j}^{\text{Pot}}$  coefficients is performed in mixed solutions, similar to the environment and the ionic strength of real samples. This method is based on the extension of FIM method where the presence of several interfering ions, and the mixed ion response or the ‘practical behavior of the electrode’ in the test solutions, are taken into account. To illustrate the principle of this method, the  $K_{i,j}^{\text{Pot}}$  coefficients of a commercial liquid membrane ammonium ISE, containing monactin/nonactin ionophores, are determined for biologically important interfering ions:  $\text{Li}^+$ ,  $\text{Na}^+$ , and  $\text{K}^+$  (in normal concentration ranges found in human serum). The obtained values compared relatively well with the previously reported SSM values [17,18].

## 2. Experimental

### 2.1. Instrumentation

The experimental electrochemical cell used in all these experiments consisted of an ammonium liquid membrane ion-selective electrode (QSE 334), a double liquid junction reference calomel electrode (E8094), both from EDT Instrument (UK) and an Orion ion meter (SA 720, USA) with automated temperature correction control.



## 2.2. Materials

Different solutions of primary and interfering ions were prepared in doubly distilled water from their chloride salts, which were all of analytical grade from Merck (Germany) and covering the physiological ionic concentration range. For the determination of each  $K_{i,j}^{\text{Pot}}$  coefficient, i.e. for  $i = \text{NH}_4^+$  and  $j = \text{K}^+$ , two series of solutions were prepared. In the first series (solutions I), the concentration of all four interfering ions ( $\text{Li}^+$ ,  $\text{Na}^+$ ,  $\text{K}^+$  and  $\text{Mg}^{2+}$ ) were fixed but the concentration of the primary ion ( $i = \text{NH}_4^+$ ) was varied. The fixed concentration of interfering ions used were:  $[\text{Li}^+] = 1.15 \times 10^{-3} \text{ M}$ ,  $[\text{Na}^+] = 0.15 \text{ M}$ ,  $[\text{K}^+] = 4.5 \times 10^{-3} \text{ M}$  and  $[\text{Mg}^{2+}] = 8.2 \times 10^{-4} \text{ M}$ , which were chosen to be within their range in normal human serum. In the second series (solutions II), the primary ion ( $i = \text{NH}_4^+$ ) was absent and the concentration of the interfering ions ( $\text{Li}^+$ ,  $\text{Na}^+$  and  $\text{Mg}^{2+}$ ) were the same as in the first series, but a varying concentration of the desired interfering ion ( $j = \text{K}^+$ ) was used. The measurements were performed using solutions under stirring conditions at  $T = 25 \pm 2^\circ\text{C}$ . The calibration of the ammonium ISE was controlled before and after each series of measurements.

## 3. Principle of method

For the determination of each selectivity coefficient, the plotted  $E$  (mV) versus  $a_i$  (using solutions I) curve was used. Applying Nikolsky–Eisenman equation for the first solution series (solutions I), we have:

$$E_1 = E' + s \log[a_i + K_{i,j}^{\text{Pot}}(a'_j)^{\frac{z_i}{z_j}} + D] \quad (1)$$

$E_1$  is the experimental potential of the corresponding solution,  $E'$  is the cell constant potential,  $a_i$  is the varying activity of the primary ion,  $a'_j$  is the known fixed activity of the interfering ion whose selectivity coefficient has to be measured,  $z_i$  and  $z_j$  are integers with sign and magnitude corresponding respectively to the charge of the primary ( $i$ ) and interfering ions ( $j$ ) to be measured and  $s = 2.303RT/Z_iF$  is the slope of the electrode.

$D$  represents the contribution to potential of all interfering ion species with known fixed activities other than ( $j$ ):

$$D = \sum_l K_{i,l}^{\text{Pot}}(a_l)^{\frac{z_i}{z_l}} \quad (2)$$

The extrapolation of the linear portions of the curve (generated with solutions I) will intersect at a point, which gives the value of  $a_i$ , to be used for the calculation of  $K_{i,j}^{\text{Pot}}$  from the equation:

$$a_i = K_{i,j}^{\text{Pot}}(a'_j)^{\frac{z_i}{z_j}} + D \quad (3)$$

$D$  can be evaluated by plotting the curve  $E$  (mV) versus  $a_j$  (using solutions II). Applying Nikolsky–Eisenman equation again for the second solutions series (solutions II), we have:

$$E_2 = E' + s \log[K_{i,j}^{\text{Pot}}(a_j)^{\frac{z_i}{z_j}} + D] \quad (4)$$

Once again, the extrapolation of the linear portions of the curve will intersect at a point, which gives the value of  $D$  from the equation:

$$D = K_{i,j}^{\text{Pot}}(a'_j)^{\frac{z_i}{z_j}} \quad (5)$$

Substituting  $D$  in Eq. (3) gives:

$$K_{i,j}^{\text{Pot}} = \frac{a_i}{(a_j)^{\frac{z_i}{z_j}} + (a'_j)^{\frac{z_i}{z_j}}} \quad (6)$$

where, for ions of equal charge,  $K_{i,j}^{\text{Pot}}$  will be independent of the charges and we have:

$$K_{i,j}^{\text{Pot}} = \frac{a_i}{a_j + a'_j} \quad (7)$$

Using Eq. (7),  $K_{i,j}^{\text{Pot}}$  can be determined by substituting the known fixed value of  $a'$  (in solutions I) and the values of  $a_i$  and  $a_j$  extracted from the plotted curves.

## 4. Results and discussion

The experimental values of  $K_{i,j}^{\text{Pot}}$  for the commercial ammonium ISE used in this work, for the primary and interfering ion of equal charge ( $i = \text{NH}_4^+$  and  $j = \text{Li}^+$ ,  $\text{Na}^+$ ,  $\text{K}^+$ ), which were determined by the mixed ion response method described above, are summarized in Table 1. As the selectivity coefficients depend on the mem-

brane composition (which was not indicated by the supplier), these coefficients were first determined by the traditional SSM for this electrode in order to make possible the comparison with the published SSM data for ammonium ISEs with known compositions. All these results are included in Table 1. The published SSM values illustrate the order of magnitude of the selectivity coefficients for such ISEs. A typical membrane composition (wt%) [18] is: 4.6% of the mixture of nonactin (72%) and monactin (28%), tris(2-ethylhexyl)-phosphate (68.9%) and PVC (26.5%). For the (primary and interfering) ion of equal charge, the already published SSM data and those obtained in this work by the traditional SSM are very close to each other. The  $\log K_{i,j}^{\text{Pot}}$  coefficients for all interfering ions: ( $\text{Li}^+$ ,  $\text{Na}^+$  and  $\text{K}^+$ , found by the proposed method are very close, i.e. show little more negative values (better selectivity), compared to all traditional SSM data, showing that the simultaneous presence of other ions does

not mask the mixed ion response of the electrode, and consequently, the proposed method could not be considered worse than the traditional SSM or FIM. As, with exception [12], Nikolsky–Eisenman equation is not recommended for the determination of selectivity coefficient when (primary and interfering) ions of unequal charge are involved [5,7,14], the  $\log K_{i,j}^{\text{Pot}}$  values found for interfering ion  $\text{Mg}^{2+}$  were not reported in the table. However, if these values could not be practically useful, they could at least be used for comparison with the similar earlier published data. The corresponding  $\log K_{i,j}^{\text{Pot}}$  values for  $\text{Mg}^{2+}$  interfering ion, were successively: ( $-2.5$ ) found by the proposed method, ( $-5$  and  $-4.2$ ) earlier published SSM data [18] and ( $-4$ ) obtained in this work by the traditional SSM for this commercial ISE. With the proposed method, in which several interfering ions are simultaneously present, a less negative  $\log K_{i,j}^{\text{Pot}}$  value for  $\text{Mg}^{2+}$  is found compared to the single ion SSM. The activ-

Table 1  
Potentiometric selectivity coefficients of ammonium ISE<sup>a,f</sup>

Reference <sup>b</sup>	Method	$a_{\text{NH}_4^+}^c$	$a_{\text{Li}^+}$	$\text{Log } K_{\text{NH}_4^+, \text{Li}^+}^{\text{Pot}}$	$a_{\text{Na}^+}$	$\text{Log } K_{\text{NH}_4^+, \text{Na}^+}^{\text{Pot}}$	$a_{\text{K}^+}$	$\text{Log } K_{\text{NH}_4^+, \text{K}^+}^{\text{Pot}}$
[24]	SSM <sup>d</sup>	0.1	0.1	-2.7	-	-	-	-
[117]	SSM	0.1	0.1	-2.4	-	-	-	-
This work	SSM	7.6E-2	7.6E-2	-2.8	-	-	-	-
This work	EFIM <sup>d</sup>	8.9E-4	8.4E-1	-3.0	-	-	-	-
[24]	SSM	0.1	-	-	0.1	-2.7	-	-
[117]	SSM	0.1	-	-	0.1	-2.7	-	-
[118]	SSM	? <sup>e</sup>	-	-	?	-2.8	-	-
This work	SSM	0.1	-	-	0.1	-2.6	-	-
This work	EFIM	8.9E-4	-	-	3.2E-1	-2.7	-	-
[24]	SSM	0.1	-	-	-	-	0.1	-0.8
[116]	SSM	?	-	-	-	-	?	-1
[117]	SSM	0.1	-	-	-	-	0.1	-0.9
[118]	SSM	?	-	-	-	-	?	-0.8
This work	SSM	0.1	-	-	-	-	0.1	-0.8
This work	EFIM	8.9E-4	-	-	-	-	5.0E-3	-1.0

<sup>a</sup> Selectivity coefficients determined by SSM (this work) and by the proposed method (EFIM) for the commercial ISE are compared to those reported before for different ammonium ISE membranes.

<sup>b</sup> Reference numbers cited in [18].

<sup>c</sup> Activity ( $a_i$ ) of ion species ( $i$ ) in mol/l.

<sup>d</sup> Separate solution method (SSM) and extended fixed interference method (proposed method: EFIM).

<sup>e</sup> Experimental conditions not specified (?).

<sup>f</sup> Ammonium membrane compositions (in wt%) [18]: 4.6 % of the mixture of nonactin (72%) and monactin (28%), tris(2-ethylhexyl)-phosphate (68.9%) and PVC (26.5 %) for the membrane [24]; nonactin (0.3%) in dibutyl sebacate for the filter paper membrane [116]; saturated solution of tris(2-ethylhexyl)-phosphate in the mixture of nonactin (72%) and monactin (28%) for the filter paper membrane [117]; unknown composition membrane [118].

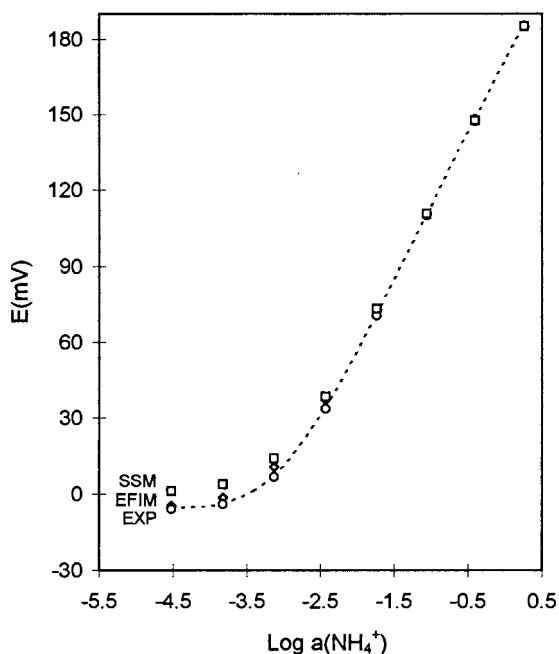


Fig. 1. Comparison of experimental and calculated potential response curve for a commercial ammonium liquid membrane ISE ( $E$  (mV) vs.  $\log a(\text{NH}_4^+)$ ). EXP-curve: experimental ISE potential response, EFIM and SSM-curves: calculated potential ISE responses using Nikolsky–Eisenman equation with  $K_{i,j}^{\text{Pot}}$ , determined respectively by the present method and those determined in this work by SSM. A varying concentration of  $\text{NH}_4^+$  and a fixed concentration of all interfering ions:  $[\text{Li}^+] = 1.15 \times 10^{-3}$  M,  $[\text{Na}^+] = 0.15$  M,  $[\text{K}^+] = 4.5 \times 10^{-3}$  M and  $[\text{Mg}^{2+}] = 8.2 \times 10^{-4}$  M were used in test solution.

ity of the primary and interfering ion, used in this work (in EFIM), were generally less than those used in the determination of previous SSM published data (see Table 1). The occurrence of the Nernstian slopes for each ion was checked in single ion solution for the used commercial ammonium electrode at  $T = 20 \pm 2^\circ\text{C}$ . The electrode showed a typical Nernstian slope for  $\text{NH}_4^+$  (58.12 mV),  $\text{K}^+$  (56.94 mV, in the log of the tested activity range:  $-4.295$  to  $-1.381$ ) and  $\text{Na}^+$  (55.5 mV, in the log of the tested activity range:  $-2.428$  to  $-1.110$ ). However, sub-Nernstian slopes were obtained for  $\text{Mg}^{2+}$  (21.57 mV, in the log of the tested activity range:  $-6.089$  to  $-2.337$ ) and for  $\text{Li}^+$  (28.39 mV, in the log of the tested activity range:  $-2.04$  to  $-5.002$ ). However, according to Umezawa et al. [5] only a few

electrodes respond in a Nernstian manner to all primary and interfering ions (e.g.  $\text{K}^+$  valinomycin liquid membrane ISE). Note that with the Bakker conditioning method, once the membrane is exposed to the most preferred ion, the electrode will no longer respond in a Nernstian manner to the extremely discriminated ions. Unfortunately, this conditioning method could only be once used for a given membrane and practically only by those who fabricate their own ISE membranes themselves [19]; consequently, it is not of practical use for such commonly used commercial electrodes. On the other hand, the present method could be applied for a solution mixture containing any number of interfering ions as long as the use of Nikolsky–Eisenman equation is permitted. However, in this case the contribution of ions of unequal charge is negligible because of the very low concentration and selectivity coefficient of  $\text{Mg}^{2+}$ . Using the selectivity coefficients values (SSM, in this work) and those obtained by the present method (EFIM), potentials were calculated by Nikolsky–Eisenman equation and compared to the experimental values measured by the commercial ammonium ISE. The test solutions were with varying concentrations of ammonium but each containing the same fixed values of all interfering ions. The fixed concentration of the interfering ions were within their range in normal human serum (with values indicated in Section 2.2). The results are shown graphically in Fig. 1.  $K_{i,j}^{\text{Pot}}$  values determined by this method (EFIM) and those determined by SSM generate two potential curves, the former corresponding closer than the latter to the experimental curve. The best fit found by the values obtained by the method presented in this work (EFIM), could be due to the competitive effective response mechanism of the ISE membrane to the several ions simultaneously present in the test solution (in the proposed method), as compared to the single ion solution used in SSM.

## References

- [1] K. Srinivasan, G.A. Rechnitz, Anal. Chem. 41 (1969) 1203.

- [2] G.J. Moody, J.D.R. Thomas, *Lab. Practice* 20 (1971) 307.
- [3] G.J. Moody, J.D.R. Thomas, *Selective Sensitive Electrodes*, Merrow, England, 1971.
- [4] G.G. Guibault, R.A. Durst, M.S. Frant, H. Freiser, E.H. Hansen, T.S. Light, E. Pungor, G.A. Rechnitz, N.M. Rice, T.J. Rohm, W. Simon, J.D.R. Thomas, *Pure Appl. Chem.* 48 (1976) 127.
- [5] Y. Umezawa, K. Umezawa, H. Sato, *Pure Appl. Chem.* 67 (1995) 507.
- [6] V.P.Y. Gadzekpo, G.D. Christian, *Anal. Chim. Acta* 164 (1984) 279.
- [7] E. Bakker, R.K. Meruva, E. Pretsch, E. Meyerhoff, *Anal. Chem.* 66 (1994) 3021.
- [8] E. Bakker, *J. Electrochem. Soc.* 143 (1996) L83.
- [9] E. Bakker, *Anal. Chem.* 69 (1996) 1061.
- [10] R.J. Forster, D. Diamond, *Anal. Chim. Acta* 276 (1993) 75.
- [11] F.J. Saez de Viteri, D. Diamond, *Electroanalysis* 6 (1994) 9.
- [12] P. Kane, D. Diamond, *Talanta* 44 (1997) 1847.
- [13] W. Zhang, A. Fakler, C. Demuth, U.E. Spichiger, *Anal. Chim. Acta* 375 (1998) 211.
- [14] M. Nagele, E. Bakker, E. Pretsch, *Anal. Chem.* 71 (1999) 1048.
- [15] C. Macca, *Anal. Chim. Acta* 321 (1996) 1.
- [16] R. Eugster, B. Rusterholz, A. Schmid, U.E. Spichiger, *Clin. Chem.* 39 (1993) 855.
- [17] R.P. Sholler, W. Simon, *Chimia (Switzerland)* 24 (1970) 372.
- [18] P.C. Meier, D. Ammann, W.E. Morf, W. Simon, in: J. Koryta (Ed.), *Medical and Biological Applications of Electrochemical Devices*, Wiley, New York, 1980, p. 13.
- [19] E. Bakker, *Anal. Chem.* 69 (1997) 1061.

Short communication

## pH-Metric method for acid number determination in hydraulic oils without titration

E. Strochkova, Ya.I. Tur'yan, I. Kuselman \*

*The National Physical Laboratory of Israel, Givat Ram, Jerusalem 91904, Israel*

Received 26 February 1999; received in revised form 14 June 1999; accepted 24 June 1999

### Abstract

A heptane-mediated extraction of acids from hydraulic oils is proposed for pH-metric acid number determination without titration. The acids are extracted in the reagent consisting of triethanolamine and potassium nitrate dissolved in water and isopropanol. The use of heptane allows us to overcome the influence of additives in the hydraulic oil on the glass electrode. Simultaneously the extraction of acids from the oil into the water–isopropanol phase is simplified. The method is validated and suitable metrological characteristics of the acid number determination are obtained. Published by Elsevier Science B.V.

*Keywords:* Acid number; pH-Metry; Hydraulic oils; Metrological parameters

### 1. Introduction

For elimination of the known drawbacks of the standard titration method for acid number (AN) determination in oils alternative pH-metric without titration methods have been developed [1–4]. The methods developed are based on the use of special reagents extracting acids from vegetable [2,3] or some petroleum [4] oils in the isopropanol–water phase. The sum of the acids is detected in this phase by the pH-metric sensor.

Since AN values in hydraulic oils (AN > 0.3 mg KOH/g [5]) are significantly larger than in transformer, white or basic oils [4], the reagent for the pH-metric AN determination should contain, in this case, a stronger base in higher concentration. Therefore, the reagent for vegetable oils [2,3] consisted of triethanolamine (TEA) and potassium nitrate in the mixed solvent of water and isopropanol was used in the present study. This reagent can not be used directly for hydraulic oils [5] which have a number of additives (antioxidants, corrosion inhibitors, viscosity index improvers and others [6]) influencing both the glass electrode and the process of the acid extraction. For example, hydraulic oils specified by symbols

\* Corresponding author. Tel.: +972-2-6536534; fax: +972-2-6520797.

*E-mail address:* kuselman@netvision.net.il (I. Kuselman)

H or HL (discussed below) have corrosion-inhibiting additives [7] such as salts of nitrogenous molecules with carboxylic acids, nitrogen quaternaries, polyoxylated amines, amides and imidazolines, and nitrogen heterocyclics [8].

In the present work a heptane-mediated extraction of acids from the oil is proposed to combine properties of the previously developed triethanolamine–potassium nitrate–isopropanol–water reagent and heptane. The last component dissolves the oil and its additives and allows us to overcome their interference, i.e. to overcome the matrix effect.

## 2. Experimental

### 2.1. Apparatus

The 632 Metrohm titroprocessor (Metrohm Ltd., Herisau, Switzerland) was used as the pH-meter with a  $\pm 0.01$  pH scale and a 6.0133.100 glass indicator electrode and a 6.0726.100 aqueous Ag/AgCl reference electrode.

### 2.2. Reagents

TEA, potassium nitrate, potassium chloride, sulfuric acid and potassium hydroxide were purchased from Merck (Darmstadt, Germany), isopropanol and toluene from Frutarom (Haifa, Israel), *n*-heptane were from Riedel-de Haën (Seelze, Germany), and the buffers were from BDH (Poole, UK).

Hydraulic oils (original Heliar H-24 by standard [5] and used once) were obtained from Sonol (Haifa, Israel). Fortified samples of these oils were prepared by the addition of naphthenic acid as

described previously [4]. Naphthenic acid (EEC No 2156628) was purchased from Fluka (Buchs, Switzerland).

Reagent for the analysis consisted of 0.2 M TEA + 0.01 M KNO<sub>3</sub> in the solvent of 50% water–50% isopropanol (vol.%). The initial conditional  $\text{pH}'_0 = 11.30 \pm 0.02$  of the reagent was adjusted by addition of KOH traces [2,3].

### 2.3. Procedures

About 50 ml of the reagent for the analysis (see Section 2.2) were put into the pH-metric cell, 20 ml of heptane were added and then the oil test portion was introduced (Table 1). The stirrer was turned on to provide good mixing of components. The electrodes were introduced into the cell and the conditional  $\text{pH}'_1$ , which should be stable after approximately 3 min was read. If  $\text{pH}'_1 > \text{pH}'_0 - 0.5$  at the max weight of the test portion (5 g),  $\text{AN} < 0.1$ , i.e. the AN value is smaller than the limit of quantitation by the technique. If  $\text{pH}'_1 < \text{pH}'_0 - 0.5$ , a certain volume of the standard 0.1 N H<sub>2</sub>SO<sub>4</sub> solution is added while stirring (Table 1) and again the conditional  $\text{pH}'_2$ , which should be stable for 1 min, was read. The optimal  $\Delta\text{pH}' = \text{pH}'_1 - \text{pH}'_2 \approx 0.25 - 0.35$  should be adjusted.

The AN calculation is carried out according to the following expression [2–4]:

$$\text{AN} = 56.11 N_{\text{st}} V_{\text{st}} / m (10^{\Delta\text{pH}'} - 1) \quad (\text{mg KOH/g oil}) \quad (1)$$

where 56.11 is the molecular mass of KOH,  $N_{\text{st}}$  is the concentration of the standard H<sub>2</sub>SO<sub>4</sub> solution in eqv/l,  $V_{\text{st}}$  is the volume of added standard H<sub>2</sub>SO<sub>4</sub> solution in ml, and  $m$  is the mass of the oil sample (g).

The  $V_{\text{st}}$  volume (Table 1) should be considerably less than the volume of the water–isopropanol phase (50 ml) [2–4].

The experiment for evaluation of the metrological parameters consisted of  $n_s = 10$  replicate AN determinations by the standard titration method [9] during a day and of  $n_p = 20$  determination by the proposed new method, four replicates per day over five days [3].

Table 1  
Mass of a test portion

Expected AN	Mass of test portion for analysis (g)	Addition of 0.1 N H <sub>2</sub> SO <sub>4</sub> ( $V_{\text{st}}$ ) (ml)
0.2–1	5–1.5	0.2–0.3
1–3	1.5–0.5	0.3–0.6
>3	<0.5	<0.3

Table 2

Parameters of the regression analysis of the dependence  $\text{pH}'$  vs.  $\log N_a$  for 50 ml of the reagent: 0.2 M TEA+0.01 M  $\text{KNO}_3$  in the solvent of 50% isopropanol–50%  $\text{H}_2\text{O}$  in the presence of heptane<sup>a</sup>

Amount of heptane (ml)	<i>A</i>	<i>B</i>	<i>r</i> <sup>2</sup>
0	$7.212 \pm 0.012$	$0.995 \pm 0.010$	0.999
5	$7.173 \pm 0.012$	$1.008 \pm 0.010$	0.999
10	$7.214 \pm 0.016$	$0.999 \pm 0.013$	0.999
20	$7.215 \pm 0.014$	$0.998 \pm 0.011$	0.999

<sup>a</sup> *a* is the intercept, *b* is the slope, and *r* is the correlation coefficient.

### 3. Results and discussion

Eq. (1) is derived from the following dependence [1,2]:

$$\text{pH}' = A - \log N_a, \quad (2)$$

where *A* is a constant for the given pH-sensor, reagent and temperature;  $N_a$  is the concentration of the sum of acids in the reagent in eqv/l.

The linear dependence  $\text{pH}'$  versus  $\log N_a$  in the range  $N_a = 2 \times 10^{-4} \div 6 \times 10^{-3}$  eqv/l for different amounts of heptane added to 50 ml of the isopropanol–water reagent is characterized in Table 2 (*b* is the slope). The values of  $N_a$  correspond to the concentrations of  $\text{H}_2\text{SO}_4$  added to the reagent (eqv/l) in the water–isopropanol phase only. The parameters shown in Table 2 confirm Eq. (2). The independence of these parameters from the amount of added heptane means that the salt of TEA and the acid ( $\text{H}_2\text{SO}_4$ ) are practically in the water–isopropanol phase. It should be noted that the contact of the water–isopropanol and heptane phases their volumes and composition are insignificantly changed. For example, from data [10] at the initial water–isopropanol volume 50 ml (50% water and 50% isopropanol, vol.%) and heptane volume 20 ml equilibrium volume of the water–isopropanol phase is 49 ml and its composition is 47% water, 51% isopropanol and 2% heptane. However, the heptane phase volume is 21 ml, the composition is 90% heptane, 9.5% isopropanol and 0.5% water. The reagent volume is not important in the pH-metric AN determination in Eq. (1) [2–4].

In the attempt to determine AN in hydraulic oils with the water–isopropanol reagent without heptane the results were significantly lower than by the standard method. A possible reason is the additives contained in the hydraulic oils. The additives can cause both glass electrode poisoning and incomplete extraction of the acids from the oil. Heptane dissolves them and supports the correct AN determination.

It was shown in Ref. [2] (in the absence of heptane) that the dependence  $\text{pH}'$  versus  $\log N_a$  (Eq. (2)) remains linear up to a minimal  $N_a$  value of  $2 \times 10^{-4}$  eqv/l. Since, up to 20 ml of heptane added to  $V = 50$  ml of the water–isopropanol phase do not influence this dependence, such as the addition of up to  $m = 5$  g of the oil test portion, the minimal  $N_a$  value can also be used here for calculation of the minimal AN which is determined correctly by the method  $\text{AN}_{\min}$ . Therefore,  $\text{AN}_{\min} = 56.11 N_a (V/m) = 56.11 \times 2 \times 10^{-4} \times 50/5 = 0.1$  mg KOH/g. This value is sufficient for the characterization of hydraulic oils. Note, formally  $\text{AN}_{\min}$  is not a limit of quantitation (LOQ) as a precision linked value [11,12], but it is helpful as the LOQ preliminary assessment or prediction.

Table 3 shows the average results obtained by the standard  $\text{AN}_s$  and proposed  $\text{AN}_p$  methods, corresponding S.D.s of the replicates,  $S_s$  and  $S_p$  with  $f_s = n_s - 1 = 9$  and  $f_p = n_p - 5 = 15$  numbers of degrees of freedom, Fisher's ratio  $F = S_p^2/S_s^2$  and the Student's ratio  $t = |\text{AN}_s - \text{AN}_p| / [(S_s^2/n_s) + (S_p^2/n_p)]^{0.5}$ .

The critical value for Fisher's ratio is 2.60 at the 0.95 level of confidence and the numbers of degrees of freedom 9 and 15. For Student's ratio, the critical value is 2.06 at the 0.95 level of confidence and  $f_s + f_p = 9 + 15 = 24$  degrees of freedom. From the comparison of these *F*-data with the critical value, it follows that the difference between the repeatability of the results obtained by the standard and the new method is insignificant (all *F*-values are less than the critical one). The accuracy of the standard and new methods is approximately the same because the differences between  $\text{AN}_p$  and  $\text{AN}_s$  are insignificant in comparison with the S.D. of replicates: all *t*-values are less than the critical value (2.06).

Table 3

Comparison of the results of AN determination by the standard titration method and those obtained by the proposed method<sup>a</sup>

No.	Oil Sample	Standard titration		Proposed method		<i>F</i>	<i>T</i>
		AN <sub>s</sub> (mg KOH/g)	<i>S</i> <sub>s</sub>	AN <sub>p</sub> (mg KOH/g)	<i>S</i> <sub>p</sub>		
1	New	0.553	0.0106	0.551	0.0126	1.41	0.46
2	Used	0.611	0.0160	0.600	0.0146	0.84	1.92
3	Fortified 1	1.215	0.0314	1.203	0.0218	0.48	1.13
4	Fortified 2	2.488	0.0413	2.508	0.0586	2.01	1.05

<sup>a</sup> AN<sub>s</sub> and AN<sub>p</sub> are the average results obtained by the standard and new methods, respectively; *S*<sub>s</sub> and *S*<sub>p</sub> are the S.D.s for these replicates; *F* is the Fisher's ratio; *t* is the Student's ratio.

Table 4

Determination of recovery for fortified samples<sup>a</sup>

Sample number	AN <sub>i</sub> (mg KOH/g)	<i>G</i> (g)	<i>Q</i> (g)	AN <sub>avg</sub> (mg KOH/g)	Recovery (%)	Norm of recovery (%)
1	0.55	444.52	1.2990	1.20	98.38	95–105
2	0.55	458.81	4.0512	2.51	98.18	95–105

<sup>a</sup> AN<sub>i</sub> is the AN of the initial oil sample; *G* and *Q* are the masses of the initial oil test portion and naphthenic acid added; AN<sub>avg</sub> is the average acid numbers for fortified samples.

The recovery (Table 4) was determined for all fortified samples in accordance to the following formula:

$$R(\%) = (\text{AN}_f - \text{AN}_i)GM_{\text{NA}} / (Q\text{AN}_{\text{NA}}), \quad (3)$$

where AN<sub>f</sub> and AN<sub>i</sub>, mg KOH/g, are the average acid numbers for fortified and initial samples, correspondingly, determined by pH-metric method; *G* and *Q*, g, are the masses of the initial oil sample and the naphthenic acid added, correspondingly; *M*<sub>NA</sub> = 100 is the molecular mass of naphthenic acid; AN<sub>NA</sub> is the average acid number of naphthenic acid determined by titration (226.1 mg KOH/g). Values of the recovery (Table 4) satisfy the requirements of the AOAC Peer-Verified Methods Program [3]: the norms shown in Table 4 are taken for the contents of acids in oils equivalent to the corresponding AN values.

Hence, the estimated metrological characteristics of the pH-metric method are sufficient for the quality control of hydraulic oils. Advantages of the new method are the following: low time and labor consumption, the technique including automation is simple and inexpensive.

## Acknowledgements

The authors would like to express their gratitude to Professor E. Shoenberger for helpful discussion.

## References

- [1] O.Y. Berezin, Y.I. Tur'yan, I. Kuselman, A. Shenhar, *Talanta* 42 (1995) 507.
- [2] Y.I. Tur'yan, O.Y. Berezin, I. Kuselman, A. Shenhar, *J. Am. Oil Chem. Soc.* 73 (1996) 295.
- [3] I. Kuselman, Y.I. Tur'yan, O.Y. Berezin, L. Kogan, A. Shenhar, *J. AOAC Int.* 81 (1998) 873.
- [4] Y.I. Tur'yan, E. Strochkova, O.Y. Berezin, I. Kuselman, A. Shenhar, *Talanta* 47 (1998) 53.
- [5] DIN 51 524. Hydraulic oils, Beuth Verlag GmBH, Berlin, Germany, 1985.
- [6] K.H. Altgelt, T.H. Gouw (Eds.), *Chromatography in Petroleum Analysis*. Chromatographic Science Series, vol. 11, Marcel Dekker, New York, 1979, pp. 260–262.
- [7] DIN 8659, Part 1. Identification of lubricating points on machine tools. Beuth Verlag GmBH, Berlin, Germany, 1980.
- [8] P.H. Ogden (Ed.), *Chemicals in the Oil Industry: Developments and Applications*. The Proceedings of the International Symposium, The Royal Society of Chemistry, London, 1991, pp. 218–222.



- [9] Standard test method for acid number of petroleum products by semi-micro color indicator titration. An American National Standard D3339-87, 1987.
- [10] A.I. Vorob'eva, M.K. Karapet'yants, *Russian J. Phys. Chem.* 41 (1967) 1061.
- [11] A.D. Eaton, L.S. Clesceri, A.E. Greenberg (Eds.), *Standard Methods for the Examination of Water and Wastewater*, 19th edn, 1995.
- [12] CITAC Guide 1. International guide to quality in analytical chemistry. An aid to accreditation. 1st edn. 1995.

# Determination of bisphenol A (BPA) in the presence of phenol by first-derivative fluorescence following micro liquid–liquid extraction (MLLE)

M. del Olmo, A. Zafra, A.B. Jurado, J.L. Vilchez \*

*Department of Analytical Chemistry, University of Granada, C/Fuentenueva, E-18071 Granada, Spain*

Received 21 January 1999; received in revised form 20 May 1999; accepted 11 June 1999

## Abstract

Bisphenol A (BPA) in the presence of phenol is determined using a method based on first-derivative spectrofluorimetry. The proposed method involves a micro liquid–liquid extraction of sodium chloride saturated water samples with diethyl ether followed by direct fluorimetric analysis of extracts. The excitation spectra of both compounds in diethyl ether are recorded between 200 and 290 nm, with the emission wavelength at 306 nm. The first-derivative spectra were calculated, measuring the analytical signal for BPA at 239 nm. The concentration range over which the method was applied was 0.5–10.0  $\mu\text{g}\cdot\text{l}^{-1}$  of BPA with relative standard deviations of 2.9% for a concentration of 4.0  $\mu\text{g}\cdot\text{l}^{-1}$  of BPA. The detection limit was 0.07  $\mu\text{g}\cdot\text{l}^{-1}$ . The proposed method was applied satisfactorily to the determination of BPA in synthetic mixtures and water samples from different sources previously spiked with different amounts of these chemicals. Recovery values ranging from 93% to 112% were obtained for water samples. © 2000 Elsevier Science B.V. All rights reserved.

*Keywords:* Bisphenol A (BPA); Micro liquid–liquid extraction; Derivative fluorescence; Water analysis

## 1. Introduction

Bisphenol A (BPA) is a monomer used in the manufacture of epoxy, polycarbonate and corrosion-resistant unsaturated polyester-styrene resins [1,2]. Its industrial name indicates preparation from two molecules of phenol and one of acetone. It can be found in a diverse range of products including the interior coatings of cans and drums

[3], reinforced pipes, adhesives, flooring, water main filters, artificial teeth, nail polish, food packaging materials, dye developers, etc. [4]. Global production of bisphenol A is well over a million tonnes per year, with an estimated European annual production of 504 000 tonnes [5].

The worry is that exposure to BPA and to other man-made oestrogenic substances which act through the oestrogen receptor [6] might be a factor in the decreasing sperm count in males, the increasing rates of breast cancer in women, the increase in other hormone-linked diseases, as well

\* Corresponding author. Tel.: +34-958-243-326; fax: +34-958-243-328.

as the increase in certain abnormalities of the human reproductive system [7]. Due to the widespread human exposure to BPA, there is a need to monitor the presence of BPA in the environment [5].

BPA shows native fluorescence in organic solvents but its fluorescence intensity in aqueous medium is too low to be directly analysed. To address this problem, a change in the chemical environment of the analyte by forming  $\beta$ -cyclodextrin inclusion complexes was applied to determine trace levels of bisphenol A in aqueous solution by spectrofluorimetry [8]. To increase the sensitivity of the method, an adequate preconcentration step is required. This may be by liquid or solid-phase extraction. In most methods the solvent phase requires further concentration which may cause serious losses of the analyte. Thus, methods of analyses which avoid the solvent concentration step are preferable for the recovery of organic traces in water [9,10]. In addition, the use of micro methods in which the amount of organic solvents is very small reduces the damage to the environment and the handling of the samples which reduces the analysis time.

When phenol is present together with BPA in the same sample their similar spectral features and extraction behaviour make free interference determination of only one of them difficult. Derivative spectrofluorimetry using zero-crossing method proposed by Savitzky and Golay [11] can be a useful technique for resolving the samples without previous separation step [12,13].

Micro liquid–liquid extraction is commonly applied as a preconcentration step in GC [14,15]. In the present work, for the first time, a micro method for extracting organic residues from water samples is used in conjunction with derivative spectrofluorimetric determination.

## 2. Experimental

### 2.1. Apparatus

Fluorescence spectra were obtained with a Perkin Elmer LS-50 spectrofluorimeter equipped with a Xenon discharge lamp (20 kW), Monk–

Gillieson monochromators, a Quantic Rhodamine 101 counter to correct the excitation spectra and a Gated photomultiplier. The luminescence spectrometer was interfaced with a Mitac MPC 3000F-386 microcomputer supplied with FL Data Manager Software for spectral acquisition. The excitation and emission slits were both maintained at 5 nm. The scan rate of the monochromators was maintained at 240 nm min<sup>-1</sup>.

All measurements were performed in a 10 mm quartz cell with a 2 mm width (Hellma 1 115F QS), maintained at 10 ± 0.5°C through the use of a thermostatic cell holder and a Braum Melsungen Thermomix 1441 thermostat.

The micro liquid–liquid extraction procedure was carried out using a laboratory-made equipment designed for solvents with density lower than water [16]. An IKA Labortechnik Eurostar basic stirrer was used to shake the samples mechanically into a separation funnel.

### 2.2. Reagents

All reagents were of analytical reagent grade unless stated otherwise.

Stock solutions of bisphenol A (Aldrich) and phenol (Aldrich) containing 100.0 µg ml<sup>-1</sup> were prepared in 100 ml volumetric flasks, by dissolving 10.0 mg of these compounds in ethanol 99% (v/v) (Panreac). The solutions were stored in dark bottles at 4°C, remaining stable for at least six months. These solutions were used to spike the water samples. Sodium chloride and diethyl ether (Panreac) were used for the micro-extraction procedure.

### 2.3. Treatment of water samples

Water samples were filtered through a cellulose acetate filter (0.45 µm pore size, Millipore HAWP 04700) and collected in dark glass bottles previously cleaned with hydrochloric acid and washed with deionized water. No losses of BPA were observed on filtration. The samples were stored at 4°C until analysis, which was performed with the minimum possible delay [17].

Spectral acquisition and calculation were performed in the same manner as for the analytical procedure.

Table 1  
Fluorescent characteristics of BPA in different media

Solvent	$\lambda_{\text{ex}}$ (nm)	$\lambda_{\text{em}}$ (nm)	$R^a$
Methanol	274	297	2.14
Ethanol	275	306	0.67
Diethyl ether	278	305	0.42
Hexane	278	305	0.29
Dimethyl sulfoxide	282	309	0.20
Ethyl acetate	279	305	0.10
Water	276	306	0.02
$\beta$ -cyclodextrin in water	276	306	0.28

<sup>a</sup>  $R$ , fluorescence intensity/[BPA]  $\mu\text{g}\cdot\text{l}^{-1}$ .

#### 2.4. Analytical procedure

Seventy-five grams of NaCl was added to 250 ml water samples containing between 0.5 and 10.0  $\mu\text{g}\cdot\text{l}^{-1}$  of BPA and up to 20.0  $\mu\text{g}\cdot\text{l}^{-1}$  of phenol and stirred until completely dissolved. The solutions were transferred to separatory funnels and 2.5 ml of diethyl ether was added. The mixtures were mechanically shaken for 1 min at 1700 rpm. The separatory funnel was attached using a teflon tube to a vessel filled with deionized water saturated with NaCl. Upon raising this vessel the supernatant organic phase rises to the bottleneck. Then, the extracts were collected with a Pasteur pipette

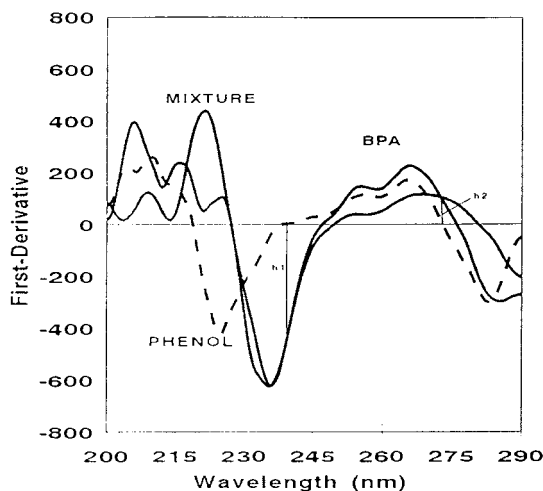


Fig. 1. Excitation and emission spectra of BPA (8.0  $\mu\text{g}\cdot\text{l}^{-1}$ ) and phenol (12.0  $\mu\text{g}\cdot\text{l}^{-1}$ ) in diethyl ether recorded at  $\lambda_{\text{em}} = 306$  nm and  $\lambda_{\text{ex}} = 278$  nm, respectively.

and transferred to a 10 mm quartz cell with 2 mm of inside width and a volume of 400  $\mu\text{l}$  being then ready for spectrofluorimetric measurements. A blank solution was prepared and treated in the same way as the sample.

The excitation spectra of the mixtures in diethyl ether are recorded at  $10.0 \pm 0.5^\circ\text{C}$  between 200 and 290 nm, with the emission wavelength at 306 nm. The spectra were corrected for the blank signal and the first-derivative spectra were calculated using 15 nm intervals. The first-derivative analytical signal was measured as the vertical distance from the first-derivative spectrum at 239 nm to the base line.

A calibration graph was constructed in the same way with BPA solutions of known concentrations.

### 3. Results and discussion

#### 3.1. Spectral features

Bisphenol A shows two excitation maxima at 212–226 nm and 272–278 nm and one emission maximum located between 297 and 308 nm in non-aqueous solvents with a wide range of polarities. The maximum fluorescent signal is obtained in polar organic solvents such as methanol or ethanol but in water the signal decreases markedly as shown in Table 1. A method for analysing BPA directly in water samples by enhancement of the fluorescent signal through the formation of BPA- $\beta$ -cyclodextrin inclusion complexes was previously proposed [8]. In order to improve the sensitivity, a preconcentration procedure was tested, selecting microliquid–liquid extraction (MLLE). Among the different organic solvents tested, diethyl ether was selected as the most adequate for use in micro liquid–liquid extraction of bisphenol A from water samples and for the direct measurement of the fluorescent BPA signal.

Although phenol can be directly analysed in water due to its native fluorescence in this medium, it is extracted together with BPA in diethyl ether and shows a fluorescent signal twice as high as in water.

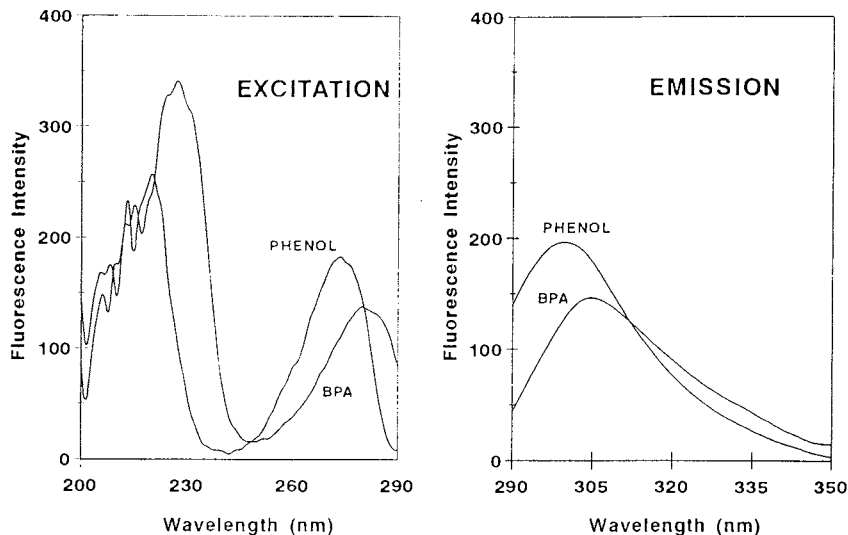


Fig. 2. First-derivative excitation spectra of BPA, phenol and a mixture of both compounds in diethyl ether.

Fig. 1 shows the excitation and emission spectra of BPA and phenol in diethyl ether. The excitation spectra are both characterized by two maxima at 225 and 278 nm for BPA and 219 and 273 nm for phenol and one emission maximum at 306 nm for BPA and 302 nm for phenol. Because of the large overlap of the excitation and emission spectra, the determination of BPA in the presence of phenol is subject to considerable difficulties. This overlap can be resolved by taking the first-derivative of the spectra in both cases.

The technique used to choose a suitable wavelength to make measurements proportional to the BPA concentration was 'zero crossing'. Using this technique, two possible  $h$  values ( $h_1 \lambda = 239$  nm and  $h_2 \lambda = 273$  nm) may be chosen from the first-derivative excitation spectrum of BPA (Fig. 2) and one from the first-derivative emission spectrum at  $\lambda = 299$  nm where the phenol signal is null. Finally, the height  $h_1$  located at  $\lambda = 239$  nm in the first-derivative excitation spectrum of BPA was selected because it exhibits a sensitivity four times higher than the height located at the other wavelengths.

### 3.2. Other experimental variables

In order to decrease the aqueous solubility of the organic solvent, the ionic strength was kept

constant by using NaCl saturated solutions in all cases.

An important advantage of the MLLE, provided that an adequate organic solvent volume is selected, is the potential increase in sensitivity with an increase in the sample volume analysed. To recover the necessary final organic volume to fill the cell (400  $\mu$ l) different aqueous volume/organic solvent ratios were tested. The appropriate volume of organic phase was respectively 1.5 ml for 100 ml of water sample, 2.5 ml for 250 ml and 5.0 ml for 500 ml.

The dependence of the fluorescence intensity on temperature was studied over the range 5.0–30.0°C. The fluorescent signal decreased when the temperature of the system was increased and the effect was reversible. Although the increase in sensitivity is not great, there is a significant increase in the precision of the system. It has been shown that the loss of diethyl ether is greater at 20°C than at 10°C and so the temperature of the measurement cell was fixed at 10°C to prevent a loss of organic solvent due to its high volatility.

The effect of the agitation time in a separatory funnel using a mechanical stirrer was monitored through agitation times ranging from 15 to 180 s.

One minute appeared to be suitable, since the fluorescent signal increases with the agitation time up to 1 min, remaining constant for longer agitation times.

The optimum agitation speed necessary for maximum fluorescence signal development was 1500 rpm in the case of 100 ml sample volume and 1700 rpm for 250 and 500 ml sample volume; higher agitation speeds did not result in any improvement.

The effect of pH was studied using sodium hydroxide and hydrochloric acid for adjustment. The results obtained showed that the extraction efficiency remained constant and maximum for pH values lower than 10.3 for BPA, decreasing sharply for higher values. This meant adjustment of the sample pH was unnecessary.

### 3.3. Analytical parameters

In order to test the independence of the analytical signal for BPA, i.e. to show that  $h$  is independent of phenol concentration, four calibration graphs were obtained for an aqueous volume of 100 ml containing between 1.0 and 20.0  $\mu\text{g}\cdot\text{l}^{-1}$  of BPA in the presence of 0.0, 5.0, 10.0 and 20.0

$\mu\text{g}\cdot\text{l}^{-1}$  of phenol respectively from the height measurements. The  $t$ -test was applied to check the similarity between the values of the slope for each calibration [18] obtained in the absence and in the presence of phenol. Firstly, it was necessary to compare the variances estimated as  $S^2$  by means of an  $F$ -test. The calculated  $F$ -values (13.9 for 5  $\mu\text{g}\cdot\text{l}^{-1}$  of phenol, 7.37 for 10  $\mu\text{g}\cdot\text{l}^{-1}$  and 18.43 for 20  $\mu\text{g}\cdot\text{l}^{-1}$ ) were higher than the critical  $F$ -value (6.39) for a significant level of 5% for the three phenol concentrations tested. Consequently, the calculated  $t$ -value is obtained with the following equation:

$$t_{\text{cal}} = (b_1 - b_2) / (S_{b_1}^2 + S_{b_2}^2)^{1/2}$$

where  $b_1$ ,  $b_2$ ,  $S_{b_1}^2$  and  $S_{b_2}^2$  are the slopes of the calibrations in absence and presence of phenol and their respective variances. These values are compared with a theoretical  $t$ -value furnished by:

$$t = (t_1 S_{b_1}^2 + t_2 S_{b_2}^2) / (S_{b_1}^2 + S_{b_2}^2)$$

where  $t_1$  and  $t_2$  are the tabulated values for a significant level of 5% and  $n_1 - 2$  and  $n_2 - 2$  degrees of freedom. The calculated  $t$ -values obtained were 0.36 for 5  $\mu\text{g}\cdot\text{l}^{-1}$  of phenol, 0.75 for 10  $\mu\text{g}\cdot\text{l}^{-1}$  and 0.06 for 20  $\mu\text{g}\cdot\text{l}^{-1}$  which are lower than the theoretical  $t$ -value of 2.78 and so show no significant differences in the slopes. From this we can conclude that there is no phenol effect on the BPA determination. The confidence intervals of the slopes calculated from  $(b \pm t_{\alpha, n-2} \cdot S_b)$  were  $65.3 \pm 7.3$   $\text{l}\ \mu\text{g}^{-1}$  in absence of phenol,  $64.9 \pm 3.0$   $\text{l}\ \mu\text{g}^{-1}$  for a phenol concentration of 5.0  $\mu\text{g}\cdot\text{l}^{-1}$ ,  $65.9 \pm 2.2$   $\text{l}\ \mu\text{g}^{-1}$  for 10.0  $\mu\text{g}\cdot\text{l}^{-1}$  and  $65.2 \pm 3.5$   $\text{l}\ \mu\text{g}^{-1}$  for a phenol concentration of 20.0  $\mu\text{g}\cdot\text{l}^{-1}$ .

The analytical parameters were also obtained for 250 and 500 ml and compared in Table 2 with those corresponding to 100 ml in the absence of phenol. The precision was determined for a BPA concentration of 10.0  $\mu\text{g}\cdot\text{l}^{-1}$  for 100 ml of water sample and 4  $\mu\text{g}\cdot\text{l}^{-1}$  for 250 and 500 ml by performing ten independent measurements. The IUPAC detection limit [19] ( $k = 3$ ), the quantification limit [20] ( $k = 10$ ) and the analytical sensitivities were calculated for 100, 250 and 500 ml sample volumes.

Table 2  
Analytical parameters

Parameters	Sample volume (ml)		
	100	250	500
Slope ( $\text{l}\ \mu\text{g}^{-1}$ )	65.5	135	138
$S_b$	2.65	0.91	0.47
Intercept	0.56	14.9	14.0
$S_a$	0.29	3.76	1.94
Determination coefficient % ( $R^2$ )	99.8	99.9	99.9
Linear dynamic range ( $\mu\text{g}\ \text{l}^{-1}$ )	1.0–20.0	0.5–10.0	0.5–10.0
Detection Limit ( $\mu\text{g}\cdot\text{l}^{-1}$ )	0.14	0.07	0.07
Quantification limit ( $\text{g}\cdot\text{l}^{-1}$ )	0.48	0.23	0.23
Relative standard deviation (%)	2.37	2.92	2.86
$S_{y/x}$	3.92	5.56	2.86

Table 3  
Effect of foreign species on the determination of 10.0  $\mu\text{g}\cdot\text{l}^{-1}$  of BPA

Foreign species	Tolerance ( $\text{mg l}^{-1}$ )	Foreign species	Tolerance ( $\text{mg l}^{-1}$ )
$\text{CO}_3^{2-}$	> 200	$\text{Hg}^{2+}$	> 200
$\text{CO}_3\text{H}^-$	> 200	$\text{Zn}^{2+}$	> 200
$\text{SO}_4^{2-}$	> 200	$\text{Be}^{2+}$	> 200
$\text{SO}_3^-$	> 200	$\text{Ca}^{2+}$	> 200
$\text{NO}_3^-$	> 10	$\text{Mg}^{2+}$	> 200
$\text{NO}_2^-$	> 10	$\text{Cr}^{3+}$	> 200
$\text{PO}_4^{3-}$	> 200	$\text{Al}^{3+}$	> 200
$\text{SiO}_3^{2-}$	> 200	$\text{Fe}^{3+}$	> 200
$\text{Cl}^-$	> 200	Dichlone <sup>a</sup>	> 0.10
$\text{Br}^-$	> 200	Morestan <sup>a</sup>	> 0.26
$\text{ClO}^-$	0.80 $\mu\text{g l}^{-1}$	Bentazone <sup>a</sup>	> 1.00
$\text{Pb}^{2+}$	> 200	Warfarine <sup>a</sup>	> 2.00
$\text{Mn}^{2+}$	> 200	Benomyl <sup>a</sup>	> 4.00
$\text{Cd}^{2+}$	> 200	Carbaryl <sup>a</sup>	> 120
$\text{Cu}^{2+}$	> 200	<i>o</i> -phenylphenol <sup>a</sup>	> 700

<sup>a</sup> Saturation levels in water.

Increasing the sample volume can enhance the sensitivity in these methods. This increase can be calculated from the slope of the calibration graphs. The values of the sensitivity ratio for samples analysed in this study were calculated to be  $S_{250/100} = 2.03$  and  $S_{500/250} = 1.03$  where the subscripts represent the sample volume. These values show that the sensitivity increases markedly from 100 to 250 ml of sample volume while the increase in the case of 250–500ml is almost imperceptible.

It is worthy of note that the increase in the sensitivity obtained with the proposed method in comparison to that previously obtained using BPA- $\beta$ -cyclodextrin inclusion complexes [8] is  $S_{250/\beta\text{-cyclodextrin}} = 47.01$ . Moreover, the detection limit obtained in this case is one order of magnitude lower.

### 3.4. Interference study

To evaluate method selectivity, a systematic study of the effect of foreign species usually present in water samples on the determination of BPA at 10  $\mu\text{g}\cdot\text{l}^{-1}$  was carried out. Tolerance level was defined as the amount of foreign species which produces an error not exceeding  $\pm 5\%$  in the determination of the analyte. Potentially inter-

fering species were tested at different concentration levels depending on their normal concentrations in the waters analysed. If interference occurred, the ratio was progressively reduced until interference ceased. The results obtained are shown in Table 3.

Interference due to cations or anions at higher levels than is usual in water (1  $\text{mg l}^{-1}$ ) was not detected. The most serious interference was due to the presence of chlorine with a tolerance of 0.8  $\mu\text{g}\cdot\text{l}^{-1}$ ; this level is lower than the level usually present in tap water.

The presence of phthalates and the fluorescent pesticides carbaryl, dichlone, morestan, *o*-phenylphenol, bentazone, warfarin and benomyl, commonly used in agriculture, did not cause interference at saturation levels in water.

### 3.5. Applications of the method

The proposed method was applied to the determination of BPA in several synthetic mixtures of BPA and phenol in different ratios for an aqueous volume of 250 ml. Table 4 summarizes the results calculated from the calibration graph.

To check the accuracy of the proposed method, a recovery study was carried out on various types of water samples. River water from Loja

Table 4  
Determination of BPA in presence of phenol<sup>a</sup>

[BPA]/[Phenol]	Taken ( $\mu\text{g}\cdot\text{l}^{-1}$ )		BPA <sup>b</sup>		
	BPA	Phenol	Found ( $\mu\text{g}\cdot\text{l}^{-1}$ )	Recovery (%)	RSD (%)
1:1	4.0	4.0	4.10	102.0	0.5
1:2	4.0	8.0	3.92	98.0	0.3
1:4	4.0	16.0	3.89	97.3	0.9
2:1	8.0	4.0	8.31	103.9	1.1
1:1	8.0	8.0	7.69	96.1	1.2
1:2	8.0	16.0	8.02	100.2	1.4
3:1	12.0	4.0	11.50	95.8	0.5
1.25:1	12.0	8.0	12.30	102.5	0.6
1:1.25	12.0	16.0	10.98	91.5	0.4
4:1	16.0	4.0	15.64	97.8	1.3
2:1	16.0	8.0	15.25	95.3	0.8
1:1	16.0	16.0	16.80	105.0	0.9

<sup>a</sup> Data referred to sample volumes of 250 ml.

<sup>b</sup> Data based on the average obtained from three determinations.

(Granada, Spain), seawater from Motril (Granada) and underground water from a well in the aquifer of the fertile plain of Granada were analysed after adequate additions of BPA. The sample volume used was 250 ml in all instances.

The results are summarized in Table 5 and show that the recoveries are acceptable. Fortunately, prior to our deliberate spiking with BPA, these waters are apparently free of this pollutant within the low detection limit obtained by our method.

#### 4. Conclusions

In this work, for the first time, a micro method for extracting organic residues from water samples is used in conjunction with first-derivative fluorimetric determination. The detection limit obtained ( $70 \text{ ng l}^{-1}$ ) is lower than the actual European Community tolerance level for organic pollutants in water ( $100 \text{ ng l}^{-1}$ ). The method was applied satisfactorily to the analysis of waters from different sources with good recoveries in all cases.

Table 5  
Recovery study of bisphenol A in water

Water sample <sup>a</sup>	Added ( $\mu\text{g}\cdot\text{l}^{-1}$ )	Found <sup>b</sup> ( $\mu\text{g}\cdot\text{l}^{-1}$ )	Recovery (%)	RSD <sup>b</sup> (%)
River water	1.00	0.93	93.0	1.2
	4.00	4.12	103.0	0.3
	8.00	7.83	97.9	0.9
Seawater	1.00	1.12	112.0	1.1
	4.00	3.87	96.7	1.7
	8.00	8.09	101.1	0.5
Underground water	1.00	1.05	105.0	1.2
	4.00	4.06	101.5	1.5
	8.00	7.89	98.6	0.8

<sup>a</sup> Data referred to sample volumes of 250 ml.

<sup>b</sup> Data based on the average obtained from three determinations.



## Acknowledgements

This work was supported by the Interministerial Commission of Science and Technology of Spain (CICYT) (Project no. PB96-1404).

## References

- [1] M. Jaeger, F. Hurtado, *Revista de Plásticos Modernos*, Marzo 73 (1997) 253.
- [2] L.A. O'Neil, C.P. Cole, *J. Appl. Chem.* 6 (1956) 356.
- [3] P.A. Tice, J.D. McGuinness, *Food Additives and Contaminants* 4 (1987) 267.
- [4] E.N. Doyle, *The Development and Use of Polyester Products*, McGraw Hill, New York, 1969.
- [5] Oslo and Paris Convention for the Prevention of Marine Pollution Working Group on Concentrations (SIME). World Wide Fund for Nature, Ostend 3–7, February 1997.
- [6] R.E. Morrissey, J.D. George, C.J. Price, R.W. Tyl, M.C. Marr, C.A. Kimmel, *Fundam. Appl. Toxicol.* 8 (1987) 571.
- [7] A. Atkinson, D. Roy, *Environ. Mol. Mutag.* 26 (1995) 60.
- [8] M. del Olmo, A. Zafra, A. Gonzalez-Casado, J.L. Vilchez, *Intern. J. Environ. Anal. Chem.* 69 (1998) 99.
- [9] H. Steinwandter, Fresenius J. Anal. Chem. 348 (1994) 688.
- [10] A. Zapf, R. Heyer, H.J. Stan, *J. Chromatogr. A* 694 (1995) 453.
- [11] A. Savitzky, M.J.E. Golay, *Anal. Chem.* 36 (1964) 1627.
- [12] L.F. Capitán-Vallvey, R. Avidad Castañeda, M. del Olmo Iruela, J.L. Vilchez Quero, *Mikrochim. Acta* 112 (1993) 55.
- [13] L. Fermín-Capitán-Vallvey, M. Ignacio de Orbe, C. Valencia, J.J. Berzas-Navado, *Mikrochim. Acta* 111 (1993) 223.
- [14] A. Fernández-Gutiérrez, J.L. Martínez-Vidal, F.J. Arrebola-Liébanas, A. González-Casado, J.L. Vilchez, *Fresenius J. Anal. Chem.* 360 (1998) 568.
- [15] J.L. Vilchez, P. Espinosa, F.J. Arrebola, A. Gozález-Casado, *Anal. Sci.* 13 (1997) 817.
- [16] M. del Olmo, A. Zafra, N.A. Navas, J.L. Vilchez, *Analyst* 124 (1999) 385.
- [17] American Public Health Authority, American Water Works Association and Water Pollution Control Federation, in: Díaz de Santos (Ed.) *Standard Methods For the Examination of Water and Wastewater*, seventeenth ed., 1992.
- [18] R. Cela, *Avances en Quimiometría Práctica*, Universidad de Santiago de Compostela, Servicio de Publicaciones e Intercambio Científico, Santiago de Compostela, 1994.
- [19] IUPAC, *Spectrochim. Acta Part. B At. Spectrosc.* 33 (1978) 242.
- [20] Analytical Methods Committee, *Analyst* 112 (1987) 199.

# Determination of protein–dye association by near infrared fluorescence-detected circular dichroism

Frederick Meadows<sup>a</sup>, Nara Narayanan<sup>b</sup>, Gabor Patonay<sup>a,\*</sup>

<sup>a</sup> Department of Chemistry, Georgia State University, University Plaza, Atlanta, GA 30303, USA

<sup>b</sup> Biotechnology Division, LI-COR Incorporated, 4308 Progressive Avenue, Lincoln, NE 68504, USA

Received 19 April 1999; accepted 1 July 1999

## Abstract

Near-infrared (NIR) squarylium dye spectral properties were evaluated by absorption, fluorescence, circular dichroism (CD), and fluorescence-detected circular dichroism (FDCD). Substituents of the two NN dyes differed at R<sub>1</sub> and R<sub>2</sub>, located symmetrically on the chromophore. The side chains of NN525 are R<sub>1</sub> = hexanoic acid, R<sub>2</sub> = butyl sulfonate and R<sub>1</sub> = R<sub>2</sub> = ethyl for NN127. FDCD signals were first confirmed by denaturing BSA with 2–8 M urea showing a diminution of dye FDCD peaks, but no change occurred in spectral properties of the dyes in urea. This indicated that the observed cotton effects occurred by noncovalent interactions with the secondary structure of the protein. The average BSA–dye association constants found by fluorescence, absorbance, and FDCD were  $1.27 \times 10^6$  ( $n = 1$ ) and  $3.3 \times 10^6 \text{ M}^{-1}$  ( $n = 1$ ) for NN127 and NN525 respectively. These values were in good agreement when calculated by the three spectroscopic methods validating the use of NIRFDCD for optical parameter calculations. These results are useful to describe NIR squarylium dye labeling of BSA. © 2000 Elsevier Science B.V. All rights reserved.

*Keywords:* Squarylium dye; Circular dichroism (CD); Bovine serum albumin

## 1. Introduction

In vivo, albumins act as carrier molecules and bind to a number of ligands, both natural and synthetic [1]. Owing to their nearly indiscriminate binding capacity, a plethora of ligand studies have led to the discovery of protein structure–function

relationships. Binding modes for biological ligands, drugs, and synthetic dyes have been identified [1–3]. Much of the information gathered on albumin has occurred through the use of optical spectroscopic methods.

Traditionally, transmission circular dichroism (CD) has been used to examine conformations of proteins and bound ligands. However a valuable tool for conformational studies, CD is contributed to by all chromophores exhibiting cotton effects at a particular wavelength. This creates

\* Corresponding author. Tel.: +1-404-651-3856; fax: +1-404-651-1416.

E-mail address: cheggp@panther.gsu.edu (G. Patonay)

difficulties when attempting to extrapolate quantitative information of a single contributing chromophore. These band overlaps are a major source of the background interferences in proteins that contain multiple optically active centers limiting the use of CD in the ultraviolet/visible region.

Useful alternatives have been reported to circumvent problems associated with traditional CD analysis. Sophianopoulos et al. reported the use of near infrared (NIR) squarylium fluorophores as noncovalent probes capable of exhibiting induced cotton effects [3]. This approach is particularly attractive since dyes that possess NIR spectral properties elude matrix interferences from biomolecules that exhibit cotton effects at shorter wavelengths. Secondly, the use of fluorescence-detected circular dichroism (FDCD) which measures the contributions of only fluorescent molecules to CD has been reported [4–9]. One drawback of using short wavelength FDCD in protein analysis is the existence of chiral fluorophores in the ultraviolet/visible region. For instance, fluorescence energy transfer can occur between tyrosine and tryptophan requiring subtraction methods to measure contributions from tryptophan alone. The absence of band overlaps prevents fluorescence energy transfer from the protein fluorophores to NIR acceptors simplifying optical determinations. If the advantages of NIR measurements are coupled with those of FDCD, a powerful technique arises for measuring CD. Since NIR optically-active fluorescent biomolecules are nearly non-existent, NIR fluorophores are, for all practical purposes, the only contributors to NIRFDCD signals. Therefore, common tasks associated with transmission CD measurements are minimized.

We have combined the advantages of NIR spectroscopy and FDCD for obtaining selective and sensitive CD measurements. In this work, the chirality induced by BSA on two inoptically-active NIR squarylium dyes was measured. Fluorescence, absorbance, FDCD and CD were used to confirm dye–protein interactions. The objective was to explore the use of NIRFDCD for obtaining CD of fluorophores bound to BSA.

## 2. Experimental

### 2.1. Sample preparation

Stock fatty-acid free bovine serum albumin (Sigma, St Louis, MO) was prepared in deionized distilled water at a concentration of 0.1 mM. NN127 (prepared in our laboratories) and NN525 (a gift from LI-COR, Lincoln, NE) solutions were prepared by solubilizing solid dye in a minimal amount of HPLC grade methanol (Sigma, St Louis, MO) (usually 3% of final volume) and brought to a final concentration of 0.1 mM in deionized distilled water. Sodium dihydrogen phosphate buffer (0.1 M) was prepared at approximately pH 7.0 and was used as the solvent for samples.

In binding studies solutions containing BSA and NN dyes were prepared in a total of 15 ml of phosphate buffer. BSA was added to make final concentrations ranging from 0.1 to 10  $\mu$ M. Dye concentrations were held constant usually between 0.1 and 2  $\mu$ M. Mixtures containing dye and BSA were incubated at room temperature for 1 h. A stock solution of 10 M urea was prepared for denaturation studies and working solutions were prepared by diluting in 15 ml of deionized distilled water to make 2–8 M final concentrations. Protein and dye concentrations were held constant.

### 2.2. Spectrophotometric measurements

Fluorescence measurements were made with an ISS-K2 multifrequency phase fluorometer (Champaign, IL). Absorbance measurements were taken with a Perkin-Elmer Lambda 20 UV/vis/NIR spectrophotometer (Norwalk, CT). CD and FDCD measurements were made with a Jasco 710 spectropolarimeter equipped with a NIR photo-multiplier tube and a model 309 FDCD attachment (Easton, MD). All cells were quartz with 1-cm pathlengths.

### 2.3. Data analysis

Several models have been proposed representing macromolecules interacting with small ligands.

The equations used in these studies are based on the Scatchard model assuming  $n$  ligands binding with equal affinities. The modification of these equations for NIR squarylium dye–BSA association analysis has been presented previously [3] and is presented here as they are also pertinent in these studies. The association constant ( $K_a$ ) representing the complex formed between proteins ( $P$ ) and dyes ( $D$ ) can be described by Eq. (1):

$$K_a = \frac{[PD]}{[P] \cdot [D]} \quad (1)$$

where  $[PD]$  represents the concentration of the protein–dye complex. Varying the protein concentration and holding the dye constant, Eq. (2) the protein–dye complex concentration divided by the total amount of dye is represented as

$$v' = \frac{[PD]}{[D]_T} = \frac{n \times K_a \times [P]}{1 + K_a + [P]} \quad (2)$$

When proteins bind to dyes, there are  $n$  possible binding sites occupied on the dye. At the concentrations used in these studies it is most probable that only one protein binds a single dye molecule. Conversely, more than one binding site may exist for dyes in proteins. Therefore,  $n \leq 1$  indicates one or more dyes binding to the protein.

Two equations were solved by linear least-squares in data analyses. An analogue of the Scatchard equation is [10]

$$\frac{v'}{[P]} = (n \times K_a) - (K_a \times v') \quad (3)$$

A plot of  $v'/[P]$  versus  $v'$  yields values for  $K_a$  and  $n$  where the slope is  $-K_a$  and the  $y$ -intercept is  $nK_a$ . Similarly the variables  $n$  and  $K_a$  can be measured using [11]

$$\frac{[P]}{v'} = \frac{1}{(n \times K_a)} + \frac{[P]}{n} \quad (4)$$

#### 2.4. Determination of association using FDCD

In order to express the bound dye in terms of the measured CD, equations relating molecular ellipticity  $[\theta]$  to the association constant ( $K_a$ ) were described by Sophianopolous et al. [3]. They are presented as they are also pertinent to these stud-

ies. As in induced absorbance circular dichroism, the unbound dyes used in these studies contribute minimally to the observed FDCD signal. Ignoring pathlengths and the contribution of the protein to CD in the NIR region, the quantity  $v'$  can be related to the FDCD signal by

$$v' = \frac{[PD]}{[D]_T} = \frac{\left[ \frac{\Theta_{\text{exp}}}{[D]_T} - [\Theta]_D \right]}{[\Theta]_{PD} - [\Theta]_D} = \frac{[\Theta]_{\text{upper}}}{[\Theta]_{\text{lower}}} \quad (5)$$

where  $\theta_{\text{exp}}$ ,  $[\theta]_D$ , and  $[\theta]_{PD}$  are the experimental ellipticity, molecular ellipticity of dye, and complex molecular ellipticity, respectively. Substitution of  $v'$  into Eqs. (3) and (4) leads to two new equations (Eqs. (6) and (7)):

$$\frac{[\Theta]_{\text{upper}}}{[P]} = (n \times K_a \times [\Theta]_{\text{lower}}) - (K_a \times [\Theta]_{\text{upper}}) \quad (6)$$

$$\frac{[PD]}{[\Theta]_{\text{upper}}} = \frac{1}{(n \times K_a \times [\Theta]_{\text{lower}})} + \frac{[P]}{(n \times K_a \times [\Theta]_{\text{lower}})} \quad (7)$$

Solving either equation leads to the value of  $[\theta]_{PD}$ , the molecular ellipticity of the complex.

### 3. Results and discussion

#### 3.1. Squarylium dye properties

In these studies we evaluated the binding parameters of two squarylium dyes using FDCD. These dyes share the same chromophoric back-

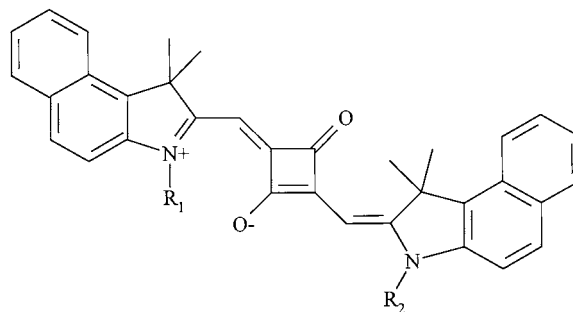


Fig. 1. Structure of squarylium dyes used. Both have a common squarylium backbone with  $R_1$  and  $R_2$  varying.  $R_1 = R_2 = C_2H_5$  (ethyl) for NN127.  $R_1 = C_6H_{11}O_2$  (hexanoic acid) and  $R_2 = C_4H_9SO_3$  (butyl sulfonate) for NN525.

Table 1  
Spectral properties of NN squarylium dyes in different solvents

Dye	Solvent	Molar absorptivity, $\times 10^5$ ( $\text{cm}^{-1} \text{M}^{-1}$ )	Absorbance, $\lambda_{\text{max}}$ (nm)	Fluorescence, $\lambda_{\text{max}}$ (nm)	FDCD, $\lambda_{\text{max}}$ (nm)
NN127	Water	0.5	670	663	–
NN127	Methanol	2.0	663	669	–
NN127	BSA <sup>a</sup>	1.0	680	685	680
NN525	Water	2.0	662	670	–
NN525	Methanol	1.0	666	671	–
NN525	BSA <sup>a</sup>	10	680	685	680

<sup>a</sup> 0.2–2.0  $\mu\text{M}$  dye in 1 mM BSA in phosphate buffer pH 7.0.

bone, but have different side chains (Fig. 1). Previous studies with NN127 showed that a large induced CD was exhibited when bound to BSA [3]. We measured the same binding parameters here for NN127 and NN525 using FDCD.

It was suggested that these squarylium dyes occupy a common hydrophobic binding site on BSA. When bound in environments of different polarities molar absorptivities, fluorescence and absorbance maxima changes occur. This trend is seen for NN dyes in water, methanol and BSA (Table 1). Additionally, when the concentration of BSA is increased holding the dye concentration constant, an increase in fluorescence intensity is observed as seen in Fig. 2.

### 3.2. Confirmation of FDCD

As in normal fluorescence measurements, increases in FDCD signals are indicative of an increased number of bound fluorophores. In this case, interactions with the protein causes asymmetrical perturbations in fluorophores creating an induced CD. A decrease in FDCD is indicative of quenching, disassociating dyes, and/or protein denaturation resulting in fluorophores without induced chirality. In instances where optical impurities exist, as with some sample cells or lenses, FDCD signals can indicate optical activity in an inoptically active sample.

The NIR dyes used in these studies have nearly immeasurable optical activity in solvents. Only when bound in the asymmetric environment of proteins will a substantial FDCD signal occur.

Thus, the optical activity of the bound dye diminishes when the secondary structure of the protein is disrupted. In order to evaluate false induced circular polarization in NIR dyes, proteins were denatured in up to 10 M urea which is known to weaken hydrophobic and hydrogen bonding interactions [1]. Therefore, induced chirality in these dyes will be weakened and optical activity diminished. The FDCD signal was found to decrease as the urea concentration increased (Fig. 3). This indicates that the observed FDCD signal occurs as a result of the dye interacting with the three-dimensional arrangement of the protein, unless CD is observed in the presence of urea alone. The absence of CD and FDCD of dyes in urea ruled out the formation of either fluorescent or non-fluorescent optically active complexes that could interfere with these FDCD measurements.

### 3.3. Instrumental stability

FDCD measurements were made for seven replicates of NN dye–albumin samples to determine the variability in the methods used in binding studies. These values were found to be  $-44 \pm 2$  mdeg for NN525/BSA and  $-16 \pm 1$  mdeg for equimolar (2  $\mu\text{M}$ ) NN127/BSA. Similarly, the instrumental variability was determined by making repeated measurements with the same sample removing cuvettes intermittently. The instrumental variability was found to fluctuate by  $\pm 1$  mdeg using seven replicate measurements with each type of NN dye/protein sample used in these studies.

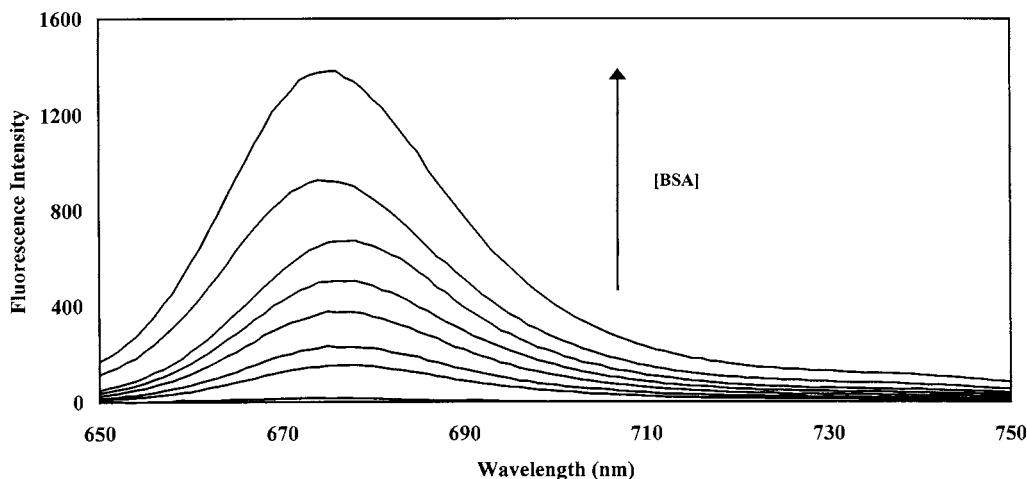


Fig. 2. Representative fluorescence spectra of NN127 showing an enhancement in the intensity at 675 nm as a function of increasing BSA concentration (0.17–1.5  $\mu\text{M}$ ). The dye concentration was kept constant at 1.5  $\mu\text{M}$ .

### 3.4. Method sensitivity

One of the advantages of using FDCD to obtain CD information is the increase in sensitivity. This enhancement is observed as a result of fluorescence being measured against zero background. Comparison of the sensitivities of CD and FDCD measurements is illustrated for NN127 in Fig. 4. At least a 100-fold improvement in sensitivity was found for FDCD over CD using a signal-to-noise ratio of three as a reference. CD signals were immeasurable at lower BSA concentrations (0.02  $\mu\text{M}$ ). FDCD was still measurable at the same concentrations. A similar experiment was performed for NN525 showing a 10-fold improvement in sensitivity in FDCD versus CD. In instances where experimental error may be ruled out, these differences in sensitivities may account for discrepancies in quantities derived from the measured CD, such as the association constant and molecular ellipticity. The higher concentrations needed in absorbance CD measurements can also affect the measured complex concentration since secondary intermolecular and intramolecular interactions such as dye aggregation can have induced chirality and contribute to the total CD signal. Induced chirality in squarylium dye aggregates has been discussed previously

[12,13]. Due to the lower concentration needed in FDCD these types of interactions can be minimized. Therefore, FDCD measurements should better approximate simple dye–protein interactions.

### 3.5. Dye–protein association

Previous studies showed that different squarylium side chains affected the extent of binding to BSA [3]. The binding stoichiometries for these studies were found to be 1:1 for both dye–protein complexes using Scatchard analysis (Fig. 5). The association constants were calculated using Eqs. (3) and (4), but Eq. (4) exhibits the least

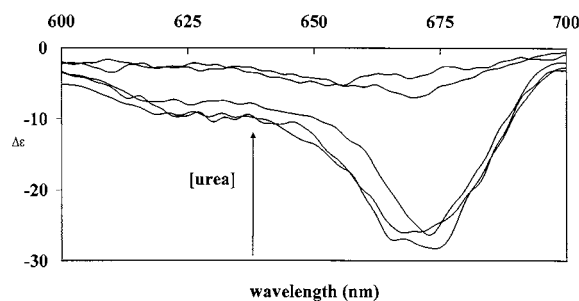


Fig. 3. Diminution of NN525 FDCD signal as the urea concentration is increased from 2 to 10 M.

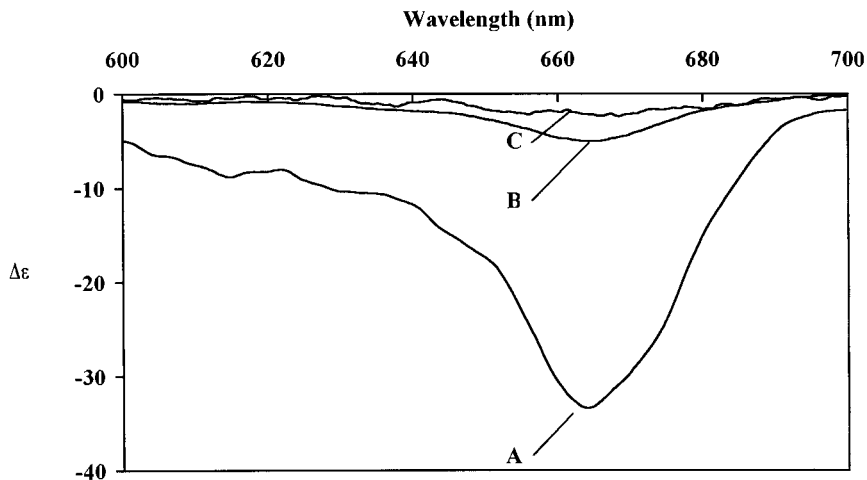


Fig. 4. Representative FDCD and CD spectra of equimolar NN127 and BSA. (A) FDCD at 1.7  $\mu\text{M}$ ; (B) CD of NN127 at 1.7  $\mu\text{M}$  ( $S/N = 3$ ); (C) FDCD at 0.02  $\mu\text{M}$  ( $S/N = 3$ ).

amount of noise for the concentrations used. This bias was found for calculations with fluorescence, absorbance, and FDCD data. The equilibrium constants calculated using these different optical methods were in good agreement (Table 2).

The equilibrium constants calculated for NN127 were twice the value of those reported earlier [3]. These discrepancies can be due to the differences in the sensitivities of the methods or in experimental conditions used. Therefore, the equilibrium constant may vary. The value of the parameters calculated for the bulkier NN525 were higher than those of NN127. While it is beyond the scope of this paper, it is noteworthy to mention that NN525's side chains, possessing a negative charge at neutral pH, can enhance electrostatic interactions with positively-charged amino acids and impose asymmetry in the bound dye. These same electrostatic interactions are not prevalent in NN127 resulting in a lower molecular ellipticity and association constant. Although electrostatic forces can also serve to enhance non-covalent interactions, hydrophobic forces appear to be the main mode of NN dye binding to BSA. Reversible binding studies will allow for the location and nature of the binding sites to be determined. These and other topics will be discussed in the future.

#### 4. Conclusion

At least four advantages exist in favor of using NIRFDCD for CD measurements. As in fluorescence, FDCD is measured against a zero background; therefore, the sensitivity is greater than in absorbance CD measurements. Secondly, signal changes occur as a result of changes in the microenvironment of only fluorophores making FDCD more selective than normal absorbance CD. Biomolecular background interferences and scattering are minimal in the NIR region that further increases the sensitivity of the FDCD technique. Sensitivity can also be enhanced by laser excitation. Commercially available laser diodes are suitable for squarylium dye excitation

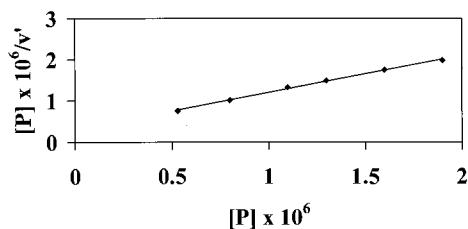


Fig. 5. Representative Scatchard plot of NN525 (2  $\mu\text{M}$ ) bound to BSA (0.6–2.0  $\mu\text{M}$ ).

Table 2  
Association parameters for NN dyes and BSA

Dye	$K_a \times 10^6 \text{ M}^{-1}$ (absorbance, %)	$K_a \times 10^6 \text{ M}^{-1}$ (fluorescence, %)	$K_a \times 10^6 \text{ M}^{-1}$ (FDCD, %)	$[\theta] \times 10^5$ (deg cm <sup>2</sup> /dmol)
NN127	$1.40 \pm 8.7$	$1.30 \pm 8.1$	$1.10 \pm 9.0$	1.10
NN525	$3.40 \pm 7.2$	$2.50 \pm 6.5$	$4.0 \pm 8.3$	3.70

in the NIR [14]. Synovec and Yeung used ultraviolet laser excitation in FDCD [9].

In our studies, there is a 10- to 100-fold greater sensitivity in FDCD than in CD. This sensitivity improvement allows smaller sample concentrations to be used minimizing secondary molecular interactions that may produce interferences. Hence, the optical activity measured with FDCD more accurately reflects that of simple protein–dye association. When impeding molecular interactions such as dye aggregation do not exist, FDCD can be used in conjunction with CD affording optical determinations over a wide range of concentrations. The squarylium dyes used in our studies have absorbance and fluorescence properties suitable for using smaller concentrations. Furthermore, these properties are enhanced when bound to BSA making their detection even simpler.

Contributing to their detection in either transmission or fluorescence-detected circular dichroism is the ability of these dyes to undergo conformational changes. These optical properties make squarylium fluorophores useful in NIRFDCD.

## Acknowledgements

Solvay Pharmaceuticals are sincerely thanked for their financial support.

## References

- [1] T. Peters, All about Albumins, Biochemistry, Genetics, and Medical Applications, Academic Press, New York, 1996.
- [2] K. Hansen, Biochem. J. 273 (1991) 641.
- [3] A.J. Sophianopoulos, J. Lipowski, N. Narayanan, G. Patonay, Appl. Spectrosc. 51 (1997) 1511.
- [4] M.P. Thomas, G. Patonay, I.M. Warner, Anal. Biochem. 164 (1987) 466.
- [5] D.H. Turner, I.J. Tinoco, J. Am. Chem. Soc. 96 (1974) 4340.
- [6] K. Wu, L. Geng, M.J. Joseph, L. McGown, Anal. Chem. 65 (1993) 2339.
- [7] L. Geng, L.B. McGown, Appl. Spectrosc. 48 (1994) 167.
- [8] P.L. Christensen, E.S. Yeung, Anal. Chem. 61 (1989) 1344.
- [9] R.E. Synovec, E.S. Yeung, J. Chromatogr. 368 (1986) 85.
- [10] G. Scatchard, Ann. N. Y. Acad. Sci. 51 (1949) 660.
- [11] J.A. Sophianopoulos, A.J. Sophianopoulos, W.C. McMahon, Arch. Biochem. Biophys. 223 (1983) 350.
- [12] H. Chen, K.Y. Law, J. Perlstein, D.G. Whitten, J. Am. Chem. Soc. 117 (1995) 7257.
- [13] H. Chen, M.S. Farahat, K.Y. Law, D.G. Whitten, J. Am. Chem. Soc. 118 (1996) 2584.
- [14] E. Terpetschnig, H. Szmecinski, J.R. Lakowicz, Anal. Chim. Acta 282 (1993) 633.



# Potentiometric determination of hydrogen peroxide at MnO<sub>2</sub>-doped carbon paste electrode

Xingwang Zheng \*, Zhihui Guo

*Department of Chemistry, Shaanxi Normal University, Xi'an 710062, People's Republic of China*

Received 23 November 1998; received in revised form 20 May 1999; accepted 16 July 1999

## Abstract

A novel hydrogen peroxide (H<sub>2</sub>O<sub>2</sub>) potentiometric sensor, made with a MnO<sub>2</sub>-doped carbon paste electrode (CPE), is reported. Under optimum conditions, the electrode gives a Nernstian response for H<sub>2</sub>O<sub>2</sub> in the concentration range  $3.00 \times 10^{-7}$ – $3.63 \times 10^{-4}$  mol/l, with a slope of 21–19.4 mV/pH<sub>2</sub>O<sub>2</sub> and a detection limit of  $1.2 \times 10^{-7}$  mol/l H<sub>2</sub>O<sub>2</sub>. In addition, this sensor offers some analytical characteristics such as sensitivity, good reproducibility and a simple preparation procedure. The effects of both the components of the electrode and other conditions on the potential response of the sensor, as well as the possible response mechanism, are discussed. © 2000 Elsevier Science B.V. All rights reserved.

*Keywords:* Hydrogen peroxide; Manganese dioxide; Modified carbon paste electrode; Potentiometric sensor

## 1. Introduction

Chemically modified electrodes [1–3] as useful analytical tools have been widely used in different research fields since more analytical possibilities [4–7] are offered by electrode manufacture. However, only a few analytical applications have employed chemically modified electrodes as potentiometric sensors [8–13], and the modified methods of the electrodes often involve covalent attachment and polymeric films to the surface of based electrodes [14–16], so the preparation of these potentiometric sensors often suffers from the complex preparation process of the based-

electrodes and are time-consuming. Compared with these methods, the fabrication of chemically modified carbon paste electrodes (CPE) made with liquid paraffin oil as the gluing material are simple and cheap, these modified carbon paste electrodes are often applied for this purpose and many CPE-based potentiometric sensors have been reported in the literature [17–19], but these CPE-based sensors often have poor stability and poor reproducibility since the carbon powder on the face of the CPE is easy to be omitted.

Recently, some CPE-based potentiometric sensors prepared with solid paraffin oil as the gluing material have been reported [20,21], these new types of CPE-based electrodes have presented some advantages, such as good stability and reproducibility.

\* Corresponding author. Tel.: +86-29-5235570.

Hydrogen peroxide ( $\text{H}_2\text{O}_2$ ) is a very important intermediate in environmental and biological reactions. The monitoring of  $\text{H}_2\text{O}_2$  with a reliable, rapid and economic method is of great significance for numerous processes. Several analytical techniques have been employed for its determination [22–24], including the manganese dioxide-modified CPE amperometric sensor [25], but most suffer from interference, complex instrumentation and expensive reagents [26–28].

The potentiometric analytical method has been found to be more suitable for determination of many analytes since it possesses advantages such as rapid, simple instrumentation and a wide linear range. But until now, to the best of our knowledge, a potentiometric method for the determination of  $\text{H}_2\text{O}_2$  has not been reported.

In this paper, by doping the CPE with  $\text{MnO}_2$  and using solid paraffin as gluing material, a new CPE-based electrode was prepared and it was found that this CPE-based electrode presented the Nernstian response for  $\text{H}_2\text{O}_2$ . Based on this observation, a new potentiometric sensor for the determination of  $\text{H}_2\text{O}_2$  was proposed and factors which affected the analytical performance of this sensor such as the components of paste and condition time were studied. At the same time, the possible response mechanism of the sensor is discussed. This sensor has been used to detect  $\text{H}_2\text{O}_2$  in rain water samples and it has some advantages such as simple instrumentation, simple preparation procedures and good stability and reproducibility.

## 2. Experimental

### 2.1. Reagents

All reagents were of analytical-reagent grade or better and water doubly-distilled in a fused-silica apparatus was used throughout the experiment. A stock solution of  $\text{H}_2\text{O}_2$  (0.100 mol/l) was prepared by diluting 5.5 ml of 30% v/v  $\text{H}_2\text{O}_2$  (Shanghai Chemical Reagents Plant) to 500 ml with water. The solution was standardized

by titration with potassium permanganate. Test standard solutions were prepared daily by appropriate dilution of the stock solution. A 0.10 mol/l  $\text{NH}_4\text{Cl}$  solution was prepared by dissolving 5.5 g of  $\text{NH}_4\text{Cl}$  (Xi'an Chemical Reagents Plant) in 1 l of water and a 0.10 mol/l  $\text{NH}_3\text{--H}_2\text{O}$  solution was prepared by diluting an appropriate volume of saturated  $\text{NH}_3$  solution (Xi'an Chemical Reagents Plant) in 1 l of water.

### 2.2. Apparatus

The potentials were measured with a PHX-215 ION-meter (Shanghai Second Analytical Instrument Plant, China). The reference electrode was a saturated calomel electrode (SCE) and the 0.10 mol/l  $\text{NH}_3\text{--NH}_4\text{Cl}$  buffer solution (pH 8.50) was stirred with a Teflon-coated magnetic bar during measurement. The electrochemical cell used can be represented by  $\text{Cu}|\text{MnO}_2\text{-modified carbon paste}|\text{sample solution (0.10 mol/l, pH 8.50, NH}_4^+\text{--NH}_3\text{ buffer solution)}||\text{SCE}$ .

### 2.3. Construction of the sensor

A Teflon rod (11 mm o.d.) with a hole at one end (7 mm diameter, 3.5 mm deep) for the carbon paste filling served as the electrode body. Electrical contact was made with a copper wire through the centre of the rod. Unmodified carbon paste was prepared by adding 1.58 g of solid paraffin oil to 5.00 g of spectral carbon powder. Modified carbon paste was prepared by replacing corresponding amounts of the carbon powder (2.5, 5, 10, 15 and 20% m/m) with manganese dioxide and then adding the solid paraffin oil. The mixtures were homogenized carefully by heating on an electric hot-plate and then the hot carbon paste was packed into the hole of the electrode; after a shorted cooling time, the carbon paste was smoothed onto paper until it had a shiny appearance. Before using the modified paste for potentiometric measurements, the electrode was preconditioned in 0.10 mol/l  $\text{NH}_3\text{--NH}_4\text{Cl}$  buffer solution for 72 h until a steady potential response was obtained.

## 2.4. EMF measurement and selectivities

The electrode potential was measured in 50 ml of sample or standard hydrogen peroxide solutions (pH 8.50, 0.10 mol/l  $\text{NH}_3\text{-NH}_4^+$  buffer) with stirring at 28°C, and potentiometric measurement of the steady-state response was carried out in the usual manner. After each measurement, the  $\text{H}_2\text{O}_2$  sensor was washed free of residual  $\text{H}_2\text{O}_2$  and pH buffer solution with water until a stable blank potential was obtained. The selectivity coefficients of the electrode for  $\text{H}_2\text{O}_2$  with respect to other ions were quantified using the mixed solution method [29].

## 3. Results and discussion

### 3.1. Electrode response

A typical calibration curve of the electrode response for  $3.00 \times 10^{-8}$ – $3.60 \times 10^{-3}$  mol/l  $\text{H}_2\text{O}_2$  shows that the linear range of electrode response is  $3.00 \times 10^{-7}$ – $3.63 \times 10^{-4}$  mol/l  $\text{H}_2\text{O}_2$  and the electrode gives a near-Nernstian response of 19.4 mV/p $\text{H}_2\text{O}_2$  and a detection limit of  $1.20 \times 10^{-7}$  mol/l  $\text{H}_2\text{O}_2$ . The calibration curve is presented in Fig. 1.

### 3.2. Choice of the modifier on the sensor

The composition of the electrode is an important aspect to be considered for the analytical

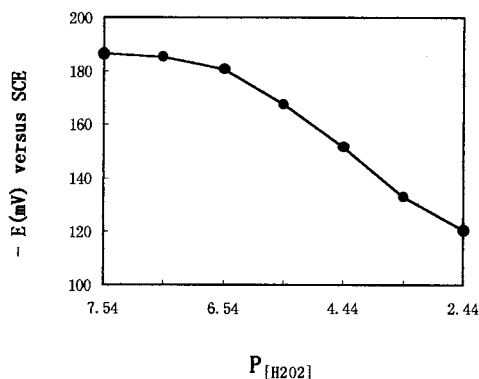


Fig. 1. Typical calibration graph for the  $\text{H}_2\text{O}_2$  sensor.

performance of this sensor. The initial testing showed that an unmodified carbon paste electrode did not have any potential response to  $\text{H}_2\text{O}_2$ . In order to improve the analytical characteristics of the CPE electrode, different metal oxide microparticles of  $\text{MnO}_2$ ,  $\text{NiO}$ ,  $\text{Co}_2\text{O}_3$  and  $\text{TiO}_2$  were employed as modifiers. Of these modified electrodes, the CPE modified with  $\text{MnO}_2$  showed a stable Nernstian response to  $\text{H}_2\text{O}_2$ , the sensor doped with  $\text{Co}_2\text{O}_3$  gave an unstable potential response to  $\text{H}_2\text{O}_2$ , and sensors prepared with other modifiers did not show any Nernstian response to  $\text{H}_2\text{O}_2$ . Thus  $\text{MnO}_2$  was selected as the modifier for preparing the  $\text{H}_2\text{O}_2$  potentiometric sensor.

### 3.3. Effect of the amount of $\text{MnO}_2$ in CPE on the response

The effect of the amount of  $\text{MnO}_2$  on the potential response of the sensor for  $\text{H}_2\text{O}_2$  was investigated by altering the ratio of  $\text{MnO}_2$  to graphite powder in the mixture. The results showed that the potential response increased with increasing amounts of  $\text{MnO}_2$  up to 4.0% and it decreased above 7%. Thus, an electrode modified with 4%  $\text{MnO}_2$  was employed in further work.

### 3.4. Effect of electrode conditioned time on the response

The  $\text{MnO}_2$ -doped carbon paste electrode gave a stable response to  $\text{H}_2\text{O}_2$  after conditioning for a sufficient period of time in 0.10 mol/l  $\text{NH}_4\text{Cl-NH}_3$  aqueous buffer medium. The response of a newly made electrode drops rapidly with time, but becomes stable after conditioning for 72 h; Fig. 2 shows the response curves after different conditioning times. The response is also more rapid (< 3 min) than that of a conventional electrode, owing to the low resistance. Fig. 1 shows that the response of this electrode conditioned for > 72 h is Nernstian.

### 3.5. Effect of pH on the response

Based on the preliminary testing results, none of the other acid or basic buffer solutions investi-

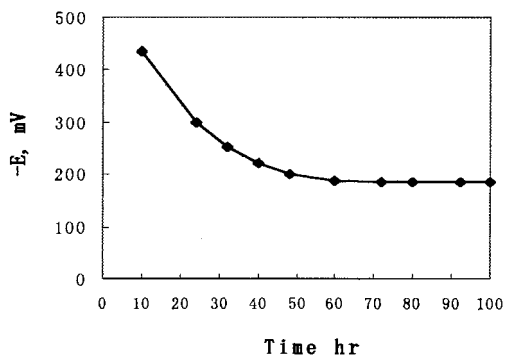


Fig. 2. Effect of conditioning time of the sensor for 10.0  $\mu\text{mol/l}$   $\text{H}_2\text{O}_2$  (pH 8.50, 0.10 mol/l  $\text{NH}_4^+ - \text{NH}_3$  solution).

Table 1  
Interferences of various ions for the  $\text{H}_2\text{O}_2$  sensor

Interfering ions	
$\text{C}_2\text{O}_4^{2-}$	$7.2 \times 10^{-3}$
$\text{Co}^{2+}$	$3.0 \times 10^{-2}$
$\text{CO}_3^{2-}$	$2.4 \times 10^{-4}$
$\text{PO}_4^{3-}$	$1.1 \times 10^{-2}$
$\text{SO}_4^{2-}$	$1.6 \times 10^{-4}$
$\text{SO}_3^{2-}$	$3.0 \times 10^{-4}$
$\text{NO}_2^-$	$2.5 \times 10^{-4}$

gated, such as  $\text{H}_2\text{SO}_4$ ,  $\text{HCl}$ ,  $\text{NaOH}$ ,  $\text{NaHCO}_3$  and  $\text{N}_2\text{B}_4\text{O}_7$  (their concentrations were 0.10 mol/l, respectively), proved to be better than 0.10 mol/l  $\text{NH}_4^+ - \text{NH}_3$  buffer solution for  $\text{H}_2\text{O}_2$  determination. So the  $\text{NH}_4^+ - \text{NH}_3$  buffer solution was chosen for controlling the pH values of sample solutions.

The effect of pH values of sample solutions on the potential readings of the  $\text{H}_2\text{O}_2$  sensor was

Table 2  
Results of examination of the sensor reproducibility<sup>a</sup>

Number of repeats for determination of $\text{H}_2\text{O}_2$ response	$1.00 \times 10^{-6}$ mol/l $\text{H}_2\text{O}_2$	$1.00 \times 10^{-5}$ mol/l $\text{H}_2\text{O}_2$
1	-183.2	-163.9
2	-182.6	-164.1
3	-182.5	-163.8
4	-183.1	-164.0

<sup>a</sup> Results are given in mV.

checked by recording the e.m.f. of a standard cell  $\text{Cu}|\text{MnO}_2$  chemically modified CPE| $1.00 \times 10^{-5}$  mol/l  $\text{H}_2\text{O}_2$ ,  $\text{NH}_4^+ - \text{NH}_3$  buffer solution|SCE and varying the acidity by the addition of small volumes of  $\text{HCl}$  and/or ammonium solution (1.0 mol/l of each); the concentration of  $\text{H}_2\text{O}_2$  was  $1.00 \times 10^{-5}$  mol/l. The results showed that while the pH changed in the range 7.0–8.0, the potential response increased with increasing pH; this results may be related to the enhancing of oxidizing ability of  $\text{H}_2\text{O}_2$  when pH changed in this range. For pH values in the range 8.0–9.0, the response was almost constant; Above pH 9.0, the potential response dropped, possibly because it is difficult to oxidize  $\text{MnO}^{2+}$  to its higher oxidation state when  $\text{pH} > 9.0$ . So the potential response dropped. Thus, pH 8.50  $\text{NH}_4^+ - \text{NH}_3$  buffer solution was selected for the further experiments.

### 3.6. Selectivity of the electrode

The selectivity of the sensor was evaluated by the mixed solution method. The results are presented in Table 1 and show that the sensor offered a good selectivity for  $\text{H}_2\text{O}_2$ , and that many potentially interfering ionic species, excepting  $\text{Co}^{2+}$  and  $\text{PO}_4^{3-}$ , do not interfere in the determination of  $\text{H}_2\text{O}_2$ .

### 3.7. The performance of the sensor

#### 3.7.1. The response time

When the hydrogen peroxide concentration was above  $1.00 \times 10^{-5}$  mol/l, the response time was shorter than 3 min; when the  $\text{H}_2\text{O}_2$  concentration was  $3.00 \times 10^{-7}$  mol/l, the response time was 5 min.

#### 3.7.2. The reproducibility of the sensor

The reproducibility of the sensor was examined using the reference method [30]. The results are shown in Table 2 and reveal that the sensor had a good reproducibility for determination of  $\text{H}_2\text{O}_2$ .

#### 3.7.3. The life time of the sensor

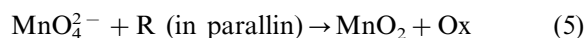
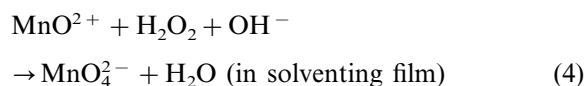
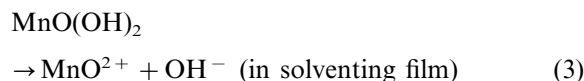
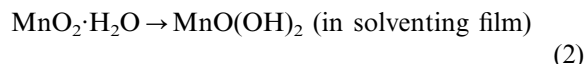
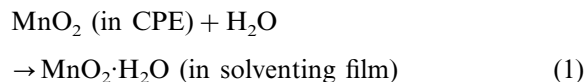
After the new sensor had been conditioned for a given time, it showed a stable response for  $\text{H}_2\text{O}_2$  when it was used continually for 20 days; the

response slope and linear range of the sensor for  $\text{H}_2\text{O}_2$  kept from any obvious various. The sensor appeared the poor stability and long response time after it was continually used over such a long time as 30 days; at the same time, the response linear range of the sensor for  $\text{H}_2\text{O}_2$  was also poor. But the sensor regained its good response performance after it was smoothed and conditioned when it was first prepared.

### 3.8. Discussion on the possible response mechanism of the sensor

When the sensor was conditioned in 0.10 mol/l  $\text{NH}_3\text{-NH}_4^+$  buffer solution, the e.m.f. increased with time at first and then gave a constant response over a long time. While a few of  $\text{H}_2\text{O}_2$  presented in the testing buffer solution, the response of this sensor was faster than that of blank testing buffer solution. Based on those experimental phenomena and some of  $\text{MnO}_2$  chemically properties, we proposed the possible response mechanism of this sensor as follows. First, a few of the solvated  $\text{MnO}_2$  was formed on the face of the sensor when the sensor was inserted in the testing solution. Second,  $\text{H}_2\text{O}_2$  can oxidize  $\text{MnO}_2$  to produce  $\text{MnO}_4^{2-}$  [31], so the sensor appeared response for  $\text{H}_2\text{O}_2$ . Third, the response results showed that the e.m.f. became more positive with increasing  $\text{H}_2\text{O}_2$  concentration and the sensor regained its blank e.m.f. response after it was again inserted in the blank solution (not contained  $\text{H}_2\text{O}_2$ ). The possible reason is that the organic materials which existed in parallin oil reduced the

$\text{MnO}_4^{2-}$  to produce  $\text{MnO}_2$ . So the possible response mechanism of this sensor is attributed to the following procedures and reactions:



So the potentiometric response of this sensor may be a mixture redox potential between the  $\text{MnO}_4^{2-}$  and  $\text{MnO}^{2+}$ ; at the same time, the ratio of  $[\text{MnO}_4^{2-}]/[\text{MnO}^{2+}]$  (in the solvent film) is adjusted by the concentration of  $\text{H}_2\text{O}_2$  in buffer solution, so the electrode gives the Nernstian response for the  $\text{H}_2\text{O}_2$ .

### 3.9. The sample analysis

The utility of this sensor was checked by using it for the quantitative determination of  $\text{H}_2\text{O}_2$  in rainwater samples collected on different days (in Xi'an, China) and comparing the results with that of the chemiluminescence (CL) method [32]. The results (shown in Table 3) clearly show that the proposed method performs exceptionally well and the results obtained are in agreement with the CL method.

Table 3  
Analytical concentrations (mol/l) of  $\text{H}_2\text{O}_2$  in rainwater samples

Sample	Concentration as determined by proposed method <sup>a</sup>	Concentration as determined by CL method <sup>b</sup>
1	$(2.5 \pm 0.3) \times 10^{-6}$	$2.6 \times 10^{-6}$
2	$(3.7 \pm 0.4) \times 10^{-6}$	$3.6 \times 10^{-6}$
3	$(0.8 \pm 0.4) \times 10^{-6}$	$0.8 \times 10^{-6}$
4	$(0.9 \pm 0.3) \times 10^{-6}$	$0.9 \times 10^{-6}$

<sup>a</sup> Mean of four determinations ( $\pm$  R.S.D., %).

<sup>b</sup> Mean of three replications.

## References

- [1] R.A. Durst, A.J. Baumner, R.W. Murray, R.P. Buck, C.P. Andrieux, *Pure Appl. Chem.* 69 (1997) 1317–1323.
- [2] J.A. Cox, M.E. Tess, T.E. Cummings, *Rev. Anal. Chem.* 15 (1996) 173–223.
- [3] T.E. Mallouk, H.-N. Kim, P.J. Ollivier, S.W. Keller, in: G. Alberti, T. Bein (Eds.), *Comprehensive Supramolecular Chemistry*, Elsevier, Oxford, 1996, pp. 189–217.
- [4] I.G. Casella, M.R. Guascito, A.M. Salvi, E. Desimoni, *Anal. Chim. Acta* 354 (1997) 333–341.
- [5] P.V.A. Pamidi, J. Wang, *Electrolysis* 8 (1996) 244–247.
- [6] J. Liu, W. Zhou, T. You, F. Li, E. Wang, S. Dong, *Anal. Chem.* 68 (1996) 3350–3353.

- [7] M.E.G. Lyons, *Analyst* 119 (1994) 805–826.
- [8] J. Kankare, L.A. Vinokurov, *Anal. Chem.* 69 (1997) 2337–2342.
- [9] Y.B. Shim, D.E. Stilwell, S.M. Park, *Electrolysis* 3 (1991) 31–36.
- [10] J.M. Teresa, A. Lewenstam, *Anal. Chim. Acta* 322 (1996) 141–149.
- [11] R.K. Meruva, M.E. Meyerhoff, *Anal. Chim. Acta* 341 (1997) 187–194.
- [12] H.S. Yim, M.E. Meyerhoff, *Anal. Chem.* 64 (1992) 1777–1784.
- [13] R.K. Meruva, M.E. Meyerhoff, *Electrolysis* 7 (1995) 1020–1027.
- [14] G.G. Guibaultt, R.A. Durst, M.S. Frantt, H. Freiser, E.H. Hansen, T.S. Light, E. Pungor, G.A. Rechnitz, X.M. Rice, T.J. Bohm, W. Simon, J.D.R. Thomas, *Pure Appl. Chem.* 48 (1976) 127.
- [15] S. Dong, Z. Sun, Z. Lu, *Analyst* 113 (1988) 1525.
- [16] S. Dong, Z. Sun, Z. Lu, *Analyst* 113 (1988) 1525.
- [17] X.-Y. Hu, Z.-Z. Leng, *Anal. Proc.* 32 (1995) 12.
- [18] X.-Y. Hu, Z.-Z. Leng, *Fenxi Huaxue* 24 (5) (1996) 595–598.
- [19] X.-Y. Hu, Z.-Z. Leng, *Anal. Lett.* 28 (13) (1995) 2263–2274.
- [20] Q.-L. Mao, S.-G. Wu, H.-C. Zhang, *Fenxi Huaxue* 23 (6) (1995) 648–651.
- [21] J.-P. Li, B.-B. Liu, B.-G. Wu, *Fenxi Huaxue* 26 (3) (1998) 279–282.
- [22] A.A. Karyakin, O.V. Gitelmacher, E.E. Karyakina, *Anal. Chem.* 67 (1995) 2419.
- [23] Q. Chin, S. Dong, *Anal. Chim. Acta* 310 (1995) 429.
- [24] Yuji, M., Junko, M., Kenichi, M., Sanae, I., *Anal. Chim. Acta* (in press).
- [25] K. Schachl, H. Alemu, K. Kalcher, J. Jezkova, *Analyst* 122 (1997) 985–989.
- [26] A.L. Vogel, *Textbook of Inorganic Analysis*, 4th ed., Longman, New York, 1981, p. 381.
- [27] C. Matsubura, N. Kawamoto, K. Takamura, *Analyst* 117 (1992) 1781.
- [28] W. Oungpipat, P. Alexander, P. Southwell-Kelly, *Anal. Chim. Acta* 309 (1995) 35.
- [29] P.-D. Hong, Z.-P. Sheng, G.-L. Wu, *The Application and Principle of ISO*, New Time Press, Beijing, 1982, p. 51.
- [30] P.-D. Hong, Z.-P. Sheng, G.-L. Wu, *The Application and Principle of ISE*, New Time Press, Beijing, 1982, p. 64.
- [31] Beijing Normal University, *Inorganic Chemistry*, 2nd ed., High Education Press, Beijing, 1986.
- [32] C. Niu, J. Li, *Environ. Chem.* 00 (1988) 634–638.

# Simultaneous quantitative analysis of overlapping spectrophotometric signals using wavelet multiresolution analysis and partial least squares

Shouxin Ren \*, Ling Gao

*Department of Chemistry, Inner Mongolia University, 010021 Huhehot, Inner Mongolia, China*

Received 30 December 1998; received in revised form 9 July 1999; accepted 16 July 1999

## Abstract

The mathematical bases and program algorithms of discrete wavelet transform (DWT), multiresolution and Mallat's pyramid algorithm were described. The multiresolution analysis (MRA) based on Daubechies orthogonal wavelet basis was studied as a tool for removing noise and irrelevant information from spectrophotometric spectra. After wavelet MRA pre-treatment, eight error functions were calculated for deducing the number of factors. A partial least squares based on wavelet MRA (WPLS) method was developed to perform simultaneous spectrophotometric determination of Fe(II) and Fe(III) with overlapping peaks. Data reduction was performed using wavelet MRA and principal component analysis (PCA) algorithm. Two programs, SPWMRA and SPWPLS, were designed to perform wavelet MRA and simultaneous multicomponent determination. Experimental results showed the WPLS method to be successful even where there was severe overlap of spectra. © 2000 Elsevier Science B.V. All rights reserved.

*Keywords:* Simultaneous quantitative analysis; Overlapping spectrophotometric signals; Wavelet multiresolution analysis; Partial least squares

## 1. Introduction

During the last few years a new and very versatile technology named wavelet analysis has been developed. Wavelets are a powerful tool with a very rich mathematical content and great potential for application [1–3]. Many scientists are interested in this field and applied its algorithm in the areas of data compressing, denoising, image processing, acoustics and fluid mechanics. In this

rapidly developing field, even the meaning of wavelet analysis keeps changing to incorporate new ideas. Wavelet theory is still developing at a rapid pace. Wavelets are functions generated from one basic function by dilations ( $W(X) \rightarrow W(2X)$ ) and translations ( $W(X) \rightarrow W(X + 1)$ ). Projection of a signal onto wavelet basis functions is called wavelet transform (WT). A wavelet transform resembles the familiar sines and cosines in a Fourier transform (FT) in some respects. FT utilizes just a single set of basis function, but WT have versatile basis functions to be selected due to

\* Corresponding author. Fax: +86-471-4951761.

the type of signal analyzed. A Fourier transform is localized in frequency but not in time, WT has dual localization both in scale (frequency) and in position (time). Wavelet transform is a linear operation, thus, the signals of each component obtained from wavelet transform decomposition maintain their linearity. Wavelet analysis represent relatively recent mathematical developments, and they have not found many application in chemistry yet. In 1992, Bos and Hoogendau firstly applied WT to analytical chemistry for evaluation of peak intensities in a flow injection analysis [4]. Other scientists used WT in pattern recognition of near infrared spectra [5], electroanalytical chemistry [6], chromatography [7] and removing the influence of complex backgrounds of infrared spectra [8].

Today the multivariate calibration techniques such as multiple linear regression (MLR), principal component regression (PCR), partial least squares (PLS) regression have frequently been used in multicomponent analysis without a prior separation, however, these approaches have been scarcely used in combination with wavelet analysis. Although denoising and data compression from an analytical signal were performed routinely by finite impulse response (FIR) and infinite impulse response (IIR) digital filters [9], in practice, denoising and data compression of analytical data using wavelets were rarely explored. Information about the speciation of metals in natural water is important in studies of the toxicity of metals for aquatic organisms. The speciation of iron as Fe (II)–Fe(III) was required to control the concentration of both oxidized states of iron, which is important in investigations of environmental pollution and in power plant due to their erosive action on the surface of turbine blades [10]. In this paper, a partial least squares based on wavelet MRA (WPLS) method was used to perform simultaneous quantitative analysis of Fe (II) and Fe (III).

## 2. Theory

### 2.1. The continuous wavelet transform (CWT) [11,12]

Given a time-varying signal  $f(t)$ , wavelet transforms consist of computing coefficients, which are

inner products of the signal and a family of wavelets. In a continuous wavelet transform, the wavelet corresponding to scale  $a$  and time location  $b$  can be written in terms of the mother wavelet:

$$\psi_{a,b}(t) = \frac{1}{\sqrt{|a|}} \psi\left(\frac{t-b}{a}\right), \quad \text{with } a, b \in R, \quad a \neq 0 \quad (1)$$

where  $R$  is the domain of real numbers. The continuous wavelet transform (CWT) of  $f(t)$  is given by:

$$\begin{aligned} \text{CWT}\{f(t); a, b\} &= \int_{-\infty}^{\infty} f(t)\psi_{ab}^*(t) dt \\ &= \langle f(t), \psi_{a,b} \rangle \end{aligned} \quad (2)$$

where the superscript \* represents the complex conjugate.  $\langle f(t), \psi_{a,b} \rangle$  is a notation used for inner products or the projection of function  $f(t)$  onto the wavelet function  $\psi_{a,b}$ . Suppose that the wavelet  $\psi$  satisfies the admissibility condition

$$\int_{-\infty}^{+\infty} \frac{|\hat{\psi}(\omega)|^2}{\omega} d\omega < \infty \quad (3)$$

where  $\hat{\psi}$  denotes the Fourier transform

$$\hat{\psi}(\omega) = \frac{2}{\sqrt{2\pi}} \int e^{i\omega t} \psi(t) dt \quad (4)$$

then continuous wavelet transform  $\text{CWT}(a, b)$  is invertible on its range, and an inverse transform is given by the relation

$$f(t) = \frac{1}{c} \int_{-\infty}^{\infty} \int_{-\infty}^{\infty} \text{CWT}(a, b) \psi_{a,b} \frac{da db}{a^2} \quad (5)$$

Therefore, by using Eq. (5) the original signal can be reconstructed from  $\psi_{a,b}$ .

### 2.2. The discrete wavelet transform DWT [11,13]

The DWT has been recognized as a natural wavelet transform for discrete time signals. Both time and scale parameters are discrete. This means that the possible  $(a, b)$  values are chosen as follows:

$$a = a_0^j, \quad b = kb_0 a_0^j \quad (6)$$

where  $k, j$  are members in the set of all possible negative and positive integers. The choice of  $a_0 =$



2 and  $b_0 = 1$  is called dyadic dilations and translations. The DWT is a basis transformation, i.e. it calculates the coordinates of a data vector in the so called wavelet basis. The wavelet basis is generated by stretching out the wavelet to fit different scales of the signal and by moving it to cover all parts of the signal. The DWT can give a time–frequency analysis of signals.

A DWT is a linear operation that decomposes a signal  $f(t)$  into a weighted sum of basis function  $\psi_{j,k}(t)$ :

$$f(t) = \sum_j \sum_k C_{j,k} \psi_{j,k}(t) \quad j, k \in \mathbb{Z} \quad (7)$$

where  $\mathbb{Z}$  means the set of integers. The  $\psi_{j,k}(t)$  are generated from a single mother wavelet  $\psi(t)$  by dilations and translations:

$$\psi_{j,k}(t) = 2^{-j/2} \psi(2^{-j}t - k) \quad (8)$$

where  $j$  is the dilation scale index, and  $k$  is the translation index. The empirical wavelet coefficients  $C_{j,k}$  are found by projecting the signal  $f(t)$  onto the wavelet basis set  $\psi_{j,k}(t)$  i.e.

$$C_{j,k} = \langle f, \psi_{j,k} \rangle \quad (9)$$

Several families of wavelet exist such as Daubechies, Symmlet, Coiflet and Beylkin wavelets etc. [14,15]. The Daubechies family was found to be highly successful in terms of speed, compression and dynamic response. These are orthonormal basis of compactly supported wavelets. That means the wavelets are non-zero over a finite interval and zero elsewhere.

### 2.3. Multiresolution analysis (MRA) [11,13,16]

The basic idea of wavelet analysis is that of multiresolution. The multiresolution is known as the simultaneous appearance of a signal on multiple scales. This concept of the multiresolution was introduced by Meyer and Mallat [17,18], and provides a powerful framework to understand wavelet decomposition.

A multiresolution analysis of  $L^2(\mathbb{R})$  is defined as a sequence of closed subspace  $V_j$  of  $L^2(\mathbb{R})$ ,  $j \in \mathbb{Z}$  with the following properties.

1.  $\dots \subset V_2 \subset V_1 \subset V_0 \subset V_{-1} \subset V_{-2} \dots$
2.  $f(t) \in V_j \Leftrightarrow f(2t) \in V_{j+1}$
3.  $f(t) \in V_0 \Leftrightarrow f(t+1) \in V_0$
4.  $\cup_{j \in \mathbb{Z}} V_j$  is dense in  $L^2(\mathbb{R})$  and  $\cap_{j \in \mathbb{Z}} V_j = \{0\}$
5. A function  $\phi \in V_0$  such that  $\{\phi(t-k)\}_{k \in \mathbb{Z}}$  is an orthonormal basis for  $V_0$

The function  $\phi$  is called the scaling function for the analysis, and  $V_j$  is called the  $j$ th scale space. By defining  $W_j$  as an orthogonal complement of  $V_j$  in  $V_{j-1}$ ,

$$V_{j-1} = V_j \oplus W_j, \quad W_j \perp V_j \quad (10)$$

the space  $L^2(\mathbb{R})$  is represented as direct sum

$$L^2(\mathbb{R}) = \bigoplus_{j \in \mathbb{Z}} W_j \quad (11)$$

where  $\bigoplus$  represents direct sum. On each fixed scale  $j$ , the wavelets  $\{\psi_{j,k}(t)\}_{k \in \mathbb{Z}}$  form an orthonormal basis of  $W_j$  and the functions  $\{\phi_{j,k}(t) = 2^{-j/2} \phi(2^{-j}t - k)\}_{k \in \mathbb{Z}}$  form an orthonormal basis of  $V_j$ . In other words, the final requirement for multiresolution concerns a basis for each space. The basis functions for the approximation space are known as scaling functions  $\phi$ . The basis function for wavelet spaces are known as wavelets  $\psi$ .

S. Mallat exploited the attractive features of multiresolution analysis to construct a efficient algorithm for decomposing a signal into its wavelet coefficients and reconstructing the signal from the coefficients.

### 2.4. The quadrature mirror filter (QMF) and Mallat's pyramid algorithm

Wavelet coefficients calculated by DWT are related to the basis wavelet. The particular basis wavelets are specified by a set of numbers, called wavelet filter coefficients. Once a specific wavelet has been chosen, one can use its coefficients to define two filters, the low-pass (scaling) filter and the high-pass (wavelet) filter. Both types of filters use the same set of wavelet filter coefficients, but with alternating sign and in reversed order, For the Daubechies 4-coefficient family the coefficients of the low-pass scaling filter are  $C_0, C_1, C_2,$

and  $C_3$  where  $C_0 = (1 + \sqrt{3})/4$ ,  $C_1 = (3 + \sqrt{3})/4$ ,  $C_2 = (3 - \sqrt{3})/4$  and  $C_3 = (1 - \sqrt{3})/4$ . The coefficients of the high-pass wavelet filter are  $C_3$ ,  $-C_2$ ,  $C_1$ , and  $-C_0$ , respectively [19,20]. In the field of signal processing, the pair of filters is known as the quadrature mirror filters (QMF). These filters are used to construct the filter matrices, denoted as  $L$  and  $H$ . Taking the Daubechies 4-coefficient family as an example, if the signals only contain eight data points, the  $L$  and  $H$  matrices have the following structure:

$$L = \begin{bmatrix} C_0 & C_1 & C_2 & C_3 & 0 & 0 & 0 & 0 \\ 0 & 0 & C_0 & C_1 & C_2 & C_3 & 0 & 0 \\ 0 & 0 & 0 & 0 & C_0 & C_1 & C_2 & C_3 \\ C_2 & C_3 & 0 & 0 & 0 & 0 & C_0 & C_1 \end{bmatrix} \quad (12)$$

$H =$

$$\begin{bmatrix} C_3 & -C_2 & C_1 & -C_0 & 0 & 0 & 0 & 0 \\ 0 & 0 & C_3 & -C_2 & C_1 & -C_0 & 0 & 0 \\ 0 & 0 & 0 & 0 & C_3 & -C_2 & C_1 & -C_0 \\ C_1 & -C_0 & 0 & 0 & 0 & 0 & C_3 & -C_2 \end{bmatrix} \quad (13)$$

Once the filters have been defined, one applied the Mallat's pyramid algorithm to perform the recursive decomposition [11,12,19].

While the  $N$  input data is passed through the scaling and the wavelet filters, the output of the filters consists of two sets of  $N/2$  coefficients. The high-pass and low-pass filtered data are detail  $d^1$  and approximation coefficients  $a^1$  of the WT at first level of resolution. The approximation coefficients  $a^1$  can be used as the data input for the QMF to generate sets of  $N/4$  of detail  $d^2$  and approximation coefficients  $a^2$  at the second level of resolution. This process is iterated as many times as wanted. If the original signals were taken as the approximation of signals at the lowest resolution level 0, i.e.

$$a_0 = f(t) \quad (14)$$

then  $a^j$  and  $d^j$  are computed via the following decomposition equation:

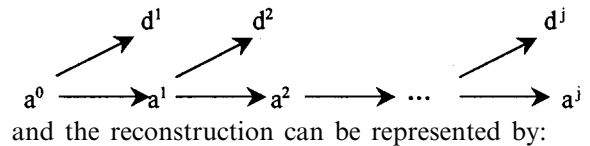
$$a^j = La^{j-1} \quad (15)$$

$$d^j = Ha^{j-1} \quad (16)$$

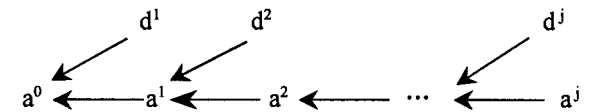
where  $j$  denotes the resolution level and  $j = 0, 1, \dots, J-1$ . To reconstruct the signal from its wavelet decomposition is just to run the recursion algorithm in the reverse with conjugates of  $H$  and  $L$ . The reconstruction algorithm is therefore also a pyramid algorithm, using the same filter coefficients as the decomposition. Signal reconstruction can be presented as follows:

$$a^{j-1} = L^*a^j + H^*d^j \quad (17)$$

where  $L^*$  and  $H^*$  represent the conjugates of the  $L$  and  $H$  matrices. Schematically, the decomposition can be represented by:



and the reconstruction can be represented by:



### 2.5. The partial least squares based on wavelet MRA (WPLS) method [12,13]

In the method, wavelet MRA is used as a tool for removing noise and irrelevant information from original data. The denoising cutoff is fulfilled by choosing the optimal wavelet transform depth  $j$ . The denoising is applied to the wavelet domain, prior to back-transforming it to signal domain. The reconstructed matrices from standard and unknown mixtures were obtained for further PLS operation. The PLS algorithm is built on the properties of the nonlinear iterative partial least-squares (NIPALS) algorithm by calculation one latent vector at a time. The NIPALS-PLS

algorithm is shown in table 1 of ref. [21]. The calibration with use of the PLS approach is done by decomposition of both the concentration and absorbance matrix into latent variables,  $D = TP^T + E$  and  $C = UQ^T + F$ . The regression coefficients are expressed as  $B = W(P^TW)^{-1}Q^T$ , where  $W$  is a weight matrix.

According to these algorithms, two programs called SPWMRA and SPWPLS were designed to perform wavelet MRA, data compression and denoising as well as simultaneous determination.

### 3. Experimental

#### 3.1. Apparatus

A Shimadzu UV-240 spectrophotometer with optional model OPI-2 was used for all experiments. A Legend pentium 120 microcomputer was used for all the calculations.

#### 3.2. Reagents

All reagents were of analytical reagent grade. Doubly distilled and deionized water was used. Stock standard solutions of Fe(II) and Fe(III) were prepared by dissolving  $\text{Fe}(\text{NH}_4)_2(\text{SO}_4)_2 \cdot 6\text{H}_2\text{O}$  and  $\text{FeNH}_4(\text{SO}_4)_2 \cdot 12\text{H}_2\text{O}$ , respectively, in  $0.05 \text{ mol l}^{-1}$  sulphuric acid and standardized according to generally accepted procedures.  $0.05 \text{ mol l}^{-1}$  1,10-phenanthroline (phen) solution and  $0.05 \text{ mol l}^{-1}$  sulphosalicylic acid (SSA) solution were used.

#### 3.3. Procedures

A series of mixed standard solutions containing various ratios of the Fe(II) and Fe(III) ions was prepared in 50 ml standard flasks, 2 ml  $0.05 \text{ mol l}^{-1}$  SSA and 2 ml  $0.05 \text{ mol l}^{-1}$  Phen were added, the pH was adjusted to 3.0 with  $\text{HNO}_3$  and NaOH, ionic strength was adjusted to  $0.001 \text{ mol l}^{-1}$  with  $\text{KNO}_3$ , then diluted with distilled water to the mark. Cuvettes with a path length 1 cm were used and the blank absorbance due to distilled water was subtracted. Spectra were recorded between 440 and 560 nm at 2 nm intervals by the

mode named 'data print out at wavelength intervals' of the Shimadzu UV-240 spectrophotometer. An absorption matrix OD was built up from these data. According to the same procedures an absorption matrix for unknown mixtures ODU was built up. All the experimental operations were performed at room temperature ( $19\text{--}20^\circ\text{C}$ ).

## 4. Results and discussion

Although there exist a very large number of possible wavelet basis, in this paper we limited ourselves to the Daubechies family of orthogonal wavelets. After test, the Daubechies 12-coefficient wavelets were used in all work.

#### 4.1. Wavelet multiresolution analysis of the absorption matrix and denoising operation

Because wavelet analysis possesses the property of localized time-frequency, DWT decomposes a signal into localized contributions labeled by a scale and a position parameter. Here, we selected the mean spectrum of OD matrix as the original signals. After DWT, the signals were described by wavelet transform coefficients. The mean spectrum and its wavelet transform coefficient (on a normal and a log scale) are presented in Fig. 1. The presented set of wavelet coefficients shown in Fig. 1b contains exactly the same information contents of the mean spectrum, but the basis of the spectrum presentation is changed. From Fig. 1c, it is fairly obvious that the spectrum presentation is sparse. This sparseness means that there are many wavelet transform coefficients with very small amplitude, the coefficients due to representing unimportant details can be omitted without substantially affecting the information content. Thus, denoising can be done in the wavelet domain.

A series of  $a^j$  and  $d^j$  were obtained for the mean spectrum. Fig. 2 shows the plots of the  $a^j$  and  $d^j$  vectors with  $j = 1\text{--}4$ . The figure indicates that the waveforms have a positive part for the approximation but a positive and negative part for the details. Both approximation,  $a^1$  and  $a^2$  are similar to the original signal. However, when  $a^1$

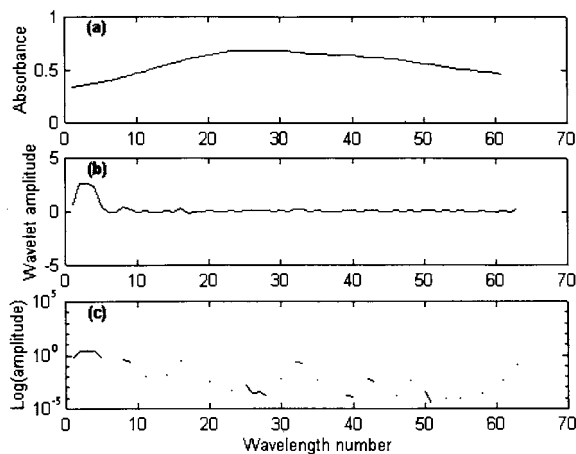


Fig. 1. The mean spectrum and its wavelet transform coefficient (on a normal and a log scale). (a) The mean spectrum of OD matrix. (b) The wavelet transform coefficients of the mean spectrum. (c) The wavelet transform coefficients of the mean spectrum on a logarithmic scale.

was converted to  $a^2$ , the lost information was stored in the detail signal  $d^2$ . In other words, the difference in the information contained in the approximation  $a^{j-1}$  and  $a^j$  was contained in the detail  $d^j$ .

Where to place the denoising cutoff is how to judicious choice of wavelet transform depth  $j$  and

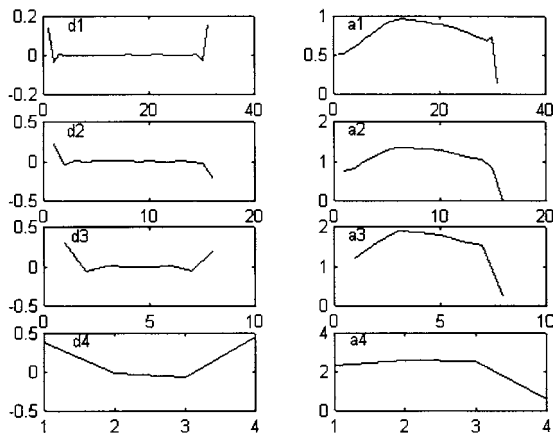


Fig. 2. Plots of the approximations  $a^j$  and details  $d^j$  vectors with  $j=1-4$  obtained from the Daubechies 12-coefficient DWT on the mean spectrum. (a) Left: the details  $d^j$  on  $j=1-4$  from top graph to bottom. (b) Right: the approximations  $a^j$  on  $j=1-4$  from top graph to bottom.

length  $m$ . If a lower  $j$  is utilized the more noise in the original signal will be retained, whereas while a higher  $j$  is utilized, the more information will be removed. If the length of original signals is  $N$ , the wavelet transform length  $m$  will be  $N/2^j$ . When the optimum  $j$  was selected, the  $m$  wavelet coefficients will be retained and the others will be eliminated. Thus, this approach can be used to remove noise and irrelevant information from the original signals in the wavelet domain. Denoising removes small-amplitude components occurring in the wavelet domain regardless of position. After denoising the spectra will be reconstructed from the compressed data. The MRA decomposition and reconstruction of a discrete signals can be accomplished with Mallat's pyramid algorithm.

How to choose the optimum  $j$  and  $m$  without a priori knowledge of the noiseless signals is very important. Ideally, the spectrum reconstructed from the compressed data is identical to the original one. In practice, this is not true for the reason that cutoff and computational error. The relative mean square difference (RMSD) between the original spectrum  $f$  and the reconstructed spectrum  $a$  was used to judge the validity of choice of  $f$  and is defined by:

$$\text{RMSD} = \text{norm}(f - a) / \text{norm}(f)$$

where norm means the Euclidean norm and

$$\text{norm}(f) = \|f\|_2 = \left( \sum_{j=1}^n |f_j|^2 \right)^{1/2}$$

In this paper, the optimum compression or cutoff is that which gives the smallest RMSD. The RMSD values of the mean spectrum for  $j=1-4$  were 0.0535, 0.0828, 0.1354, and 0.1988, respectively, thus, we chose  $j=1$  as optimum and only retained 31 wavelet coefficients in the following operation. Of course as one can notice that the RMSD is not relative mean square error (RMSR). Because the noise-free spectrum does not exist, so the RMSR cannot be calculated from the raw experimental spectrum. Theoretically, the optimum cutoff is that which give the smallest RMSR. Fig. 3 shows the original and reconstructed mean spectrum as well as their estimated difference. It can be seen that the reconstructed

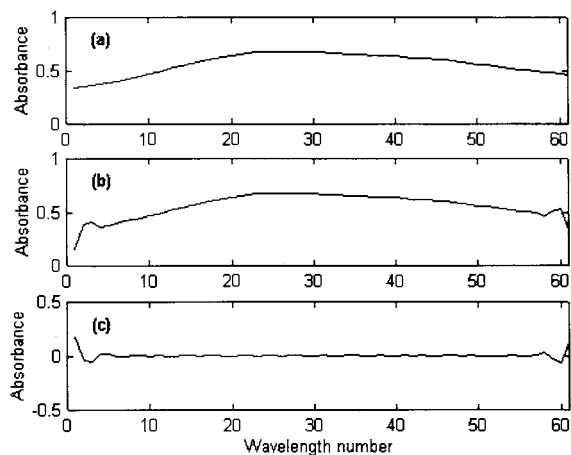


Fig. 3. The original and reconstructed mean spectrum as well as their estimated difference (a) the original; (b) the reconstructed; (c) the difference.

spectrum is similar to the experimental mean spectrum except in the two edge regions, where the absorption intensities are low. Thus, the original spectra were replaced with the reconstructed spectra in next experimental procedure.

With DWT one can treat each spectrum individually i.e. one by one row of the data matrix. Therefore, in the same way each row vector of matrix OD and ODU was decomposed, denoised at  $j=1$  and reconstructed by applying wavelet MRA. Wavelet transformation is a linear operation, thus, the dataset after DWT preserves the important property of the Lambert–Beer relationship. The reconstructed spectrum after denoising observes this relationship too. The reconstructed matrix D and DU obtained from original matrix OD and ODU by applying wavelet MRA were used in the SPWPLS operation. Three-dimensional plots of the matrix ODU and DU presented in Figs. 4 and 5. In the Fig. 5, the irrelevant information and noise was removed from the matrix ODU. Both three-dimensional plots, Figs. 4 and 5, show an obvious difference to a certain degree. What degree of the difference was depend on the denoising cutoff, i.e. the choice of the wavelet transform depth  $j$ .

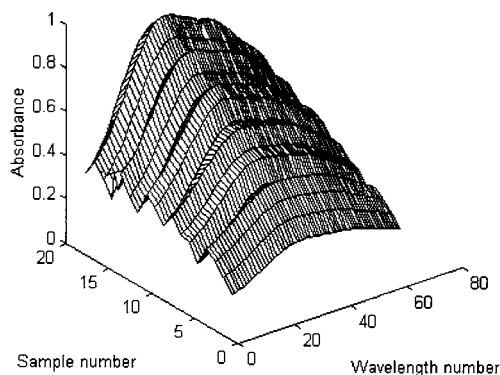


Fig. 4. Three-dimensional plots of ODU.

#### 4.2. Estimating the number of factors after the wavelet MRA pre-treatment

In a first step of multivariate statistical methods, the number of independent factors is determined by principal component analysis (PCA). These techniques require the rank of the absorbance matrix to be equal to the number of independent factors. The essence of the techniques is the pseudorank determination of an experimental data matrix. The pseudorank means the mathematical rank in absence of noise [22,23]. However, experimental spectra are often complicated by noise, which may be due to physical and chemical processes and imperfections in the experimental apparatus or other reasons. In this case as a first step the wavelet MRA pre-treatment was taken to eliminate the noise. Eight criteria were

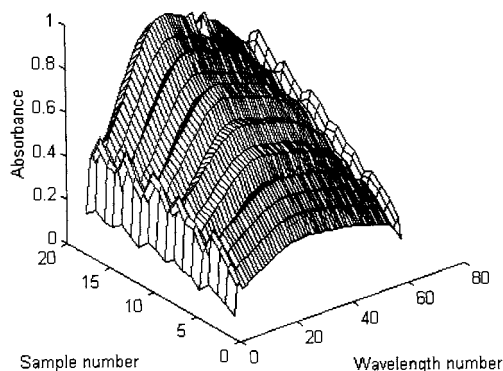


Fig. 5. Three-dimensional plots of DU.

Table 1  
Result of PCA on the matrix Du after MRA pre-treatment

<i>t</i>	EV	RE	IND	XE	IE	ER	REV	Frac
1	3.8582e+2	1.8571e-2	6.4259e-5	1.8048e-2	4.3772e-3	1.1662e+3	3.5138e-1	9.9907e-1
2	3.3082e-1	5.2415e-3	2.0475e-5	4.9418e-3	1.7472e-3	1.4672e+1	3.2434e-4	8.5667e-4
3	2.2548e-2	2.1593e-3	9.5968e-6	1.9711e-3	8.8152e-4	7.6795e+0	2.3886e-5	5.8388e-5
4	2.9361e-3	1.2480e-3	6.3672e-6	1.1006e-3	5.8830e-4	2.3794e+0	3.3749e-6	7.6031e-6
5	1.2340e-3	3.4803e-4	2.0593e-6	2.9577e-4	1.8343e-4	3.2193e+1	1.5464e-6	3.1954e-6
6	3.8331e-5	2.8081e-4	1.9501e-6	2.2928e-4	1.6213e-4	1.8227e+0	5.2652e-8	9.9257e-8
7	2.1030e-5	2.3384e-4	1.9326e-6	1.8280e-4	1.4583e-4	1.6929e+0	3.1864e-8	5.4457e-8
8	1.2422e-5	1.9946e-4	1.9946e-6	1.4867e-4	1.3298e-4	1.5943e+0	2.0913e-8	3.2167e-8
9	7.7919e-6	1.7324e-4	2.1388e-6	1.2250e-4	1.2250e-4	1.7222e+0	1.4702e-8	2.0177e-8
10	4.5244e-6	1.5650e-4	2.4454e-6	1.0434e-4	1.1665e-4	1.4682e+0	9.6675e-9	1.1716e-8
11	3.0816e-6	1.4414e-4	2.9416e-6	8.9886e-5	1.1268e-4	1.3973e+0	7.5529e-9	7.9797e-9
12	2.2054e-6	1.3495e-4	3.7487e-6	7.7916e-5	1.1019e-4	1.2939e+0	6.3018e-9	5.7110e-9
13	1.7045e-6	1.2754e-4	5.1016e-6	6.7220e-5	1.0839e-4	1.2391e+0	5.7977e-9	4.4139e-9
14	1.3757e-6	1.2122e-4	7.5765e-6	5.7146e-5	1.0691e-4	1.0304e+0	5.7319e-9	3.5622e-9
15	1.3351e-6	1.1090e-4	1.2322e-5	4.5274e-5	1.0123e-4	1.2687e+0	7.1015e-9	3.4572e-9
16	1.0523e-6	9.9105e-5	2.4776e-5	3.3035e-5	9.3437e-5	1.5329e+0	7.6254e-9	2.7249e-9
17	6.8646e-7	9.1598e-5	9.1589e-5	2.1590e-5	8.9017e-5	1.3413e+0	7.6273e-9	1.7776e-9
18	5.1180e-7						1.1632e-8	1.3253e-9

used to estimate the number of factors [24]. The results for the reconstructed matrix DU produced by the wavelet MRA pre-treatment are shown in Table 1. From this calculated results the numbers of optimal factors were determined. The magnitude of the first two eigenvalues (EV) were larger than those of the others. The reduced eigenvalues (REV) of the first two were also larger than those of the others. The Frac function showed a sharp drop from the first to third eigenvectors and then they stabilized. The IND function show a sharp drop between first and second eigenvectors and they level off. RE, IE and XE functions show a sharp drop between first and second eigenvectors and they level off. In order to support the particular choice of model dimensionality, we present results for the relative standard error of prediction (RSEP). The values for factors 1–4 were 20.9854, 3.1183, 3.1568, and 3.4226%, respectively. The definition of RSEP will be described in Section 4.3 of this paper. From these results, it was concluded that two factors were optimum choice.

PCA is used to decompose the raw data matrix into its most dominant factors. The essence of wavelet MRA is similar to the PCA. The PCA eliminate the irrelevant PCs, which associated

with the insignificant eigenvalues. The wavelet MRA pre-treatment can eliminate the noise before PCA. From Table 1 we can find that only two PCs can capture almost all the variance in this case.

#### 4.3. The partial least squares based on wavelet MRA (WPLS) method

Fig. 6 shows the absorption spectra of Fe(II), Fe(III) and their mixed solution with phen and SSA as reagents. The maximum absorption wavelengths of complexes of Fe(II)-Phen and Fe(III)-SSA were 510.6 and 499.2 nm, respectively. Their absorption maximums were 0.658 and 0.861, respectively. The absorption spectra of their mixture are severe overlap. A training set of 18 samples formed by Fe(II) and Fe(III) mixture was designed. Spectra were measured between 440 and 560 nm at 2 nm distances, giving values at 61 wavelengths for 18 standard samples. A spectra matrix OD was built up. A set of 18 synthetic 'unknown' samples were measured in same way as the training set. The reconstructed matrix D and DU were obtained by applying wavelet MRA. Using SPWPLS program, the concentration of

Fe(II) and Fe(III) were calculated with two factors. Actual concentration and recoveries of Fe(II) and Fe(III) are listed in Table 2. All the values measured were means of three replicate. The experimental results showed that this method gave satisfactory results for simultaneous determination of Fe(II) and Fe(III) mixture with severely overlapping spectra. In this case the overlap is so severe that for mixed solution only one peak can be recognized, though with a slightly skewed shape indicating two constituents. In fact, the two individual components spectra were not similar enough and their difference of maximum absorption wavelengths was 11.4 nm. As a consequence of peak overlapping, the quality of analytical information is lower than derived from individual peaks, the extent of the loss depends on the extent of overlap. Therefore, this method has its limitations, if the degree of overlap is too high, erroneous analytical results will be occur. Some work will be done on the quantitative relationship between analytical errors and the degree of overlap of two close signals by means of simulation method, its further discussion in detail will be reported in other paper.

For comparison of the performance of the techniques, a criterion of the goodness of fit must be chosen. Standard error of prediction (SEP) and the relative standard errors of prediction (RSEP)

were considered, For a single component, the SEP is given by the expression:

$$SEP = \sqrt{\frac{\sum_{j=1}^m \{C_{ij} - \hat{C}_{ij}\}^2}{m}}$$

The SEP for the all components is given by the expression:

$$SEP = \sqrt{\frac{\sum_{i=1}^n \sum_{j=1}^m \{C_{ij} - \hat{C}_{ij}\}^2}{nm}}$$

The RSEP is given by:

$$RSEP = \sqrt{\frac{\sum_{i=1}^n \sum_{j=1}^m \{C_{ij} - \hat{C}_{ij}\}^2}{\sum_{i=1}^n \sum_{j=1}^m C_{ij}^2}}$$

Where  $C_{ij}$  and  $\hat{C}_{ij}$  are the actual and estimated concentrations for  $i$ th component in the  $j$ th mixture,  $m$  is the number of mixture and  $n$  is the number of components.

The two methods with and without wavelet resolution were compared quantitatively. The SEP and RSEP for the WPLS and PLS are given in Table 3. From Table 3, it can be seen that WPLS method give better prediction results than PLS method.

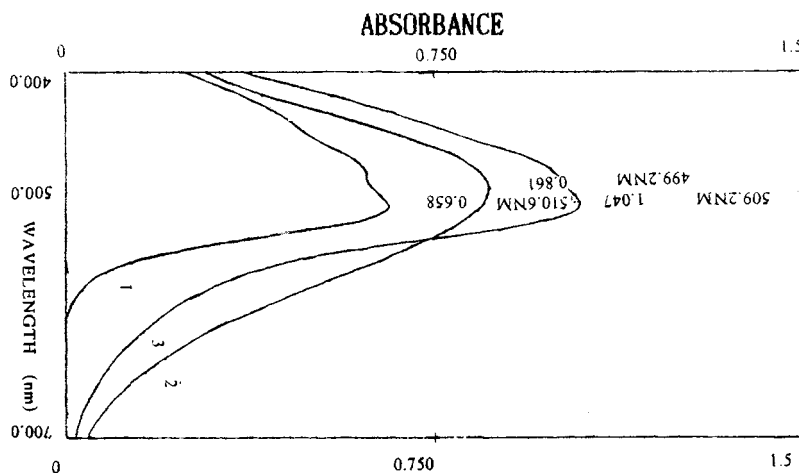


Fig. 6. Absorption of spectra of Fe(II), Fe(III) and their mixed solution with Phen and SSA as reagents. 1,  $2.05 \times 10^{-5} \text{ mol l}^{-1}$  Fe(II) +  $2.03 \times 10^{-4} \text{ mol l}^{-1}$  Phen; 2,  $4.03 \times 10^{-4} \text{ mol l}^{-1}$  Fe(III) +  $1.93 \times 10^{-4} \text{ mol l}^{-1}$  SSA; 3, mixed solution of 1 and 2.

Table 2  
Actual concentration and percentage recovery of the unknowns

Sample number	Actual concentration ( $10^{-5}$ mol l $^{-1}$ )		Recovery (%)	
	Fe(II)	Fe(III)	Fe(II)	Fe(III)
1	1.2000	8.0000	86.7936	93.6847
2	1.2000	12.0000	88.9890	97.8856
3	1.2000	15.0000	90.8046	101.3490
4	1.2000	18.0000	95.9246	100.3708
5	2.2000	10.0000	99.4427	94.8003
6	2.2000	15.0000	100.8466	98.4032
7	2.2000	16.0000	100.5552	99.2999
8	2.2000	20.0000	100.7902	101.7151
9	3.2000	14.0000	101.4775	97.5522
10	3.2000	18.0000	102.7340	101.6999
11	3.2000	20.0000	103.1490	102.6147
12	4.2000	12.0000	101.7520	95.2028
13	4.2000	15.0000	102.1363	98.1117
14	4.2000	20.0000	96.8619	104.2500
15	5.2000	10.0000	96.3275	110.5280
16	5.2000	14.0000	102.7763	97.3707
17	5.2000	18.0000	101.2461	102.1157
18	5.8000	12.0000	102.2183	95.6291

## 5. Conclusions

A set of original spectral data was decomposed into the approximation signal part and the detail signal part by means of DWT. The approximation signal concentrates most energy of the source signal, while the detail signal represents the change in the source signal. As most coefficients of the detail signal are close to zero, only very few large value coefficients are needed to store. Sparse representation of a signal in the wavelet domain allows for its significant compression and denoising. Wavelet MRA is studied as a tool for removing noise and irrelevant information from spectrophotometric spectra. The denoising cutoff is fulfilled by choosing the optimal wavelet transform depth  $j$  and length  $m$  according to the values of RMSD. The denoising method is applied to the wavelet domain, prior to back-transforming it to signal domain. Both the decomposed and reconstructed technique of spectra are based on the Mallat's pyramid algorithm.

An optimal choice of model dimensionality in the multivariate system is very important for a

successful quantitative analysis. Here, we use the wavelet MRA as pre-treatment step before doing a PCA. Eight error functions were calculated for deducing the number of factors. DWT can decompose the overlapping signal into localized contributions of different frequency. Each of these contributions keeps its linearity, which ensures that quantitative results can be obtained from the decomposed signals or reconstructed signals. A partial least squares based on wavelet MRA

Table 3  
SEP and RSEP values for Fe(II)–Fe(III) system by WPLS and PLS method

Method	SEP		RSEP (%)	
	Fe(II)	Fe(III)	Fe(II)	Fe(III)
WPLS	0.1019	0.4776	2.8927	3.1299
	Total 0.3453		Total 3.1183	
PLS	0.1149	0.8532	3.2615	5.5918
	Total 0.6088		Total 5.4976	



(WPLS) method was developed to perform simultaneous spectrophotometric determination with overlapping peaks. The method was proved to be a convenient and efficient method. The method can be used to analyze the whole spectra rather than just picking out a few characteristic values. Data compression was performed using wavelet MRA and PCA, thus, the method can be considered as a powerful tool for efficient compression of raw data matrix and applied for the rapid simultaneous multicomponent determination.

### Acknowledgements

The authors would like to thank the National Natural Science Foundation of China for financial support.

### References

- [1] L. Andersson, N. Hall, B. Jawerth, G. Peters, Wavelet on closed subsets of the real line, in: L.L. Schumaker, G. Webb (Eds.), *Recent Advances in Wavelet Analysis*, Academic Press, San Diego, CA, 1994, pp. 1–64.
- [2] S.D. Casey, D.F. Walnut, *SIAM Rev.* 36 (1994) 537.
- [3] M.L. Hilton, R.T. Ogden, *IEEE Trans. Signal Processing* 45 (1997) 496.
- [4] M. Bos, E. Hoogendan, *Anal. Chim. Acta* 267 (1992) 73.
- [5] B. Walczak, B. Bogaert, D.L. Massart, *Anal. Chem.* 68 (1996) 1742.
- [6] X. Zou, J.Y. Mo, *Anal. Chim. Acta* 340 (1997) 115.
- [7] X. Shao, W. Cai, P. Sun, M. Zhang, G. Zhao, *Anal. Chem.* 69 (1997) 1722.
- [8] M. Bos, J.A.M. Vrieling, *Chemom. Intell. Lab. Syst.* 23 (1994) 115.
- [9] B.V.D. Bogaert, H.F.M. Boelens, H.C. Smit, *Chemom. Intell. Lab. Syst.* 25 (1994) 297.
- [10] M. Novic, M. Novic, J. Zupan, N. Zafran, B. Pihlar, *Anal. Chim. Acta* 348 (1997) 101.
- [11] I. Daubechies, *Commun. Pure Appl. Math.* XLI (1998) 909.
- [12] B. Jawerth, W. Sweldens, *SIAM Rev.* 36 (1994) 377.
- [13] G. Beylkin, *SIAM J. Num. Anal.* 6 (1992) 1716.
- [14] I. Daubechies, *SIAM J. Math. Anal.* 24 (1993) 499.
- [15] A. Cohen, I. Daubechies, *SIAM J. Math. Anal.* 24 (1993) 520.
- [16] C.E. Heil, D.F. Walnut, *SIAM Rev.* 31 (1989) 628.
- [17] Y. Meyer, *Wavelet Operator*, vol. 1, Herrman, Paris, 1990.
- [18] S. Mallat, *Trans. Am. Math. Soc.* 315 (1989) 69.
- [19] G. Strang, *SIAM Rev.* 31 (1989) 614.
- [20] W.H. Press, S.A. Toukolsky, W.T. Vetterling, B.P. Flannery, *Numerical Recipes in C: The Art of Scientific Computing*, Cambridge University Press, New York, 1992, p. 591.
- [21] L. Gao, S. Ren, *J. Autom. Chem.* 20 (1998) 179.
- [22] K. Faber, B.R. Kowalski, *Anal. Chim. Acta* 337 (1997) 57.
- [23] K. Faber, B.R. Kowalski, *J. Chemom.* 11 (1997) 53.
- [24] S. Ren, L. Gao, *Microchem. J.* 58 (1998) 156.

# Development of wavelet transform voltammetric analyzer

Xueguang Shao \*, Chunyan Pang, Shouguo Wu, Xiangqin Lin

*Department of Chemistry, University of Science and Technology of China, Hefei, Anhui, 230026, People's Republic of China*

Received 1 February 1999; received in revised form 7 July 1999; accepted 16 July 1999

## Abstract

An on-line wavelet transform algorithm and development of voltammetric analyzer with the on-line wavelet transform (WT-voltammetric analyzer) are described. Because the on-line wavelet transform decomposes the sampled signal simultaneously with the progress of sampling, the WT-voltammetric analyzer gives all the components contained in the sampled voltammogram. Applications of the WT-voltammetric analyzer in linear sweep voltammetric analysis of mixtures of Pb(II) and Tl(I) and in square wave voltammetric analysis of mixture of Cd(II) and In(III) were investigated. Results showed that the overlapping peaks of Pb(II) and Tl(I) can be separated easily, and the peak position after the on-line wavelet transform does not change. The linearity of the calibration curves for Cd(II) and In(III) in the overlapping square wave voltammetric curves were kept after the on-line wavelet transform. Quantitative determination of Cd(II) and In(III) in mixture samples were investigated. The recoveries are between 92.5 and 107.1%. © 2000 Elsevier Science B.V. All rights reserved.

*Keywords:* Cd(II); In(III); On-line analysis; Pb(II); Tl(I); Voltammetric analyzer; Wavelet transform

## 1. Introduction

Wavelet transform (WT) is a high performance signal processing technique developed from the Fourier transform (FT). Applications of the technique in analytical chemistry have been reported in recent years [1–3], such as data compression [3–5], de-noising [5–7], baseline correction [8], and the resolution of multi-component overlapping chromatograms [9,10]. The main characteristic of the wavelet transform is that it decomposes a signal into localized contributions labeled by a

scale and a position parameter. Each of the contributions represents the information of different frequency contained in the analyzing signals. But all these applications are accomplished off-line, i.e. to obtain the experimental data and then to conduct the wavelet transform, which in some cases makes it inconvenient to use the technique.

In this paper, an on-line algorithm for wavelet transform is proposed. Because the on-line wavelet transform decomposes the sampled signal simultaneously with the progress of sampling, a WT-voltammetric analyzer was developed, which gives all the components contained in the sampled voltammogram. Applications of the WT-voltammetric analyzer in linear sweep and square wave

\* Corresponding author. Fax: +86-551-3631760.  
E-mail address: xshao@ustc.edu.cn (X. Shao)

voltammetric analysis were investigated. It was shown that overlapping peaks can be resolved by the method and recoveries for quantitative determination are between 92.5 and 107.1%.

## 2. Theory and algorithm

Grossmann and Morelet [11] defined the WT by decomposing a signal into a family of functions which are the translation and dilation of a basic function  $\psi(x)$ . For a function  $f(t) \in L^2(R)$ , its WT can be written as:

$$Wf(a, b) = \langle f(t), \psi_{a,b}(t) \rangle \\ = \frac{1}{\sqrt{a}} \int_{-\infty}^{+\infty} f(t) \overline{\psi\left(\frac{t-b}{a}\right)} dt \quad (1)$$

where  $a$  and  $b$  are, respectively, the scale parameter and the translation parameter.

The discrete wavelet transform is commonly used, which can be obtained by defining  $a = a_0^j$ ,  $b = kb_0$ ,  $j, k \in \mathbb{Z}$ , and generally  $a_0 = 2$ ,  $b_0 = 1$ . Therefore, Eq. (1) becomes:

$$Wf(j, k) = \langle f(t), \psi_{j,k}(t) \rangle \\ = 2^{-j/2} \int_{-\infty}^{+\infty} f(t) \overline{\psi(t - 2^{-j}k)} dt \quad (2)$$

In practical calculation, the multi-resolution signal decomposition (MRSD) proposed by Mallat [12,13] is commonly used. MRSD method decomposes a signal  $f(t)$  into two parts: one part can be represented by wavelet functions  $\psi_{j,k}(t) = 2^{-j/2} \psi_{2^j}(t - 2^{-j}k)$  and the other part can be represented by scaling functions  $\phi_{j,k}(t) = 2^{-j/2} \phi_{2^j}(t - 2^{-j}k)$ , which correspond to the wavelet functions. Due to the properties of  $\psi_{j,k}(t)$  and  $\phi_{j,k}(t)$ , by mathematical proofs, Mallat [13] obtained the following equations:

$$A_{2^j}f(n) = \sum_{k=-\infty}^{+\infty} h(k) A_{2^{j+1}}f(n - 2^{-j-1}k) \quad (3)$$

$$D_{2^j}f(n) = \sum_{k=-\infty}^{+\infty} g(k) A_{2^{j+1}}f(n - 2^{-j-1}k) \quad (4)$$

where  $A_{2^j}f(n)$  is called the discrete approximation,  $D_{2^j}f(n)$  is called the discrete detail,  $j \in -J \cdots -1$  is the scale of decomposition,

$h(k) = \langle \phi_{2^{-j-1}}(u), \phi(u-k) \rangle$  and  $g(k) = \langle \psi_{2^{-j-1}}(u), \phi(u-k) \rangle$  are discrete filters corresponding to  $\psi(t)$  and  $\phi(t)$ .

If we replace  $j$  with  $-j$ ,  $A_{2^j}f(n)$  and  $D_{2^j}f(n)$  with  $C^{(j)}(n)$  and  $D^{(j)}$ , then Eqs. (3) and (4) become:

$$C^{(j)}(n) = \sum_{k=-\infty}^{+\infty} h(k) C^{(j-1)}(n - 2^{j-1}k) \quad (5)$$

$$D^{(j)}(n) = \sum_{k=-\infty}^{+\infty} g(k) C^{(j-1)}(n - 2^{j-1}k) \quad (6)$$

If  $C^{(0)}(n)$ ,  $n \in \mathbb{Z}$ , denotes a signal obtained from an experiment, the decomposition can be described as:

$$\begin{array}{ccccccccccc} C^{(0)} & \rightarrow & C^{(1)} & \rightarrow & C^{(2)} & \rightarrow & \dots & \rightarrow & C^{(j-1)} & \rightarrow & C^{(j)} \\ \downarrow & & \downarrow & & \downarrow & & & & \downarrow & & \\ D^{(1)} & & D^{(2)} & & & & \dots & & & & D^{(j)} \end{array} \quad (7)$$

where  $J$  is the highest scale of decomposition, and as to  $C^{(0)}$ ,  $C^{(j)}$  is the low frequency part of the signal with the frequency lower than  $2^{-j}$ , and  $D^{(j)}$  is the high frequency part with the frequency between  $2^{-j}$  and  $2^{-j+1}$ .

In order to conduct on-line decomposition of the wavelet transform for a signal from an analytical instrument, an alteration was made to the MRSD algorithm. We doubled the number of data points of the filters by inserting  $2^{j-1} - 1$  zeros into the every adjacent item of  $\{h(k)\}$  and  $\{g(k)\}$  ( $k = 1 \cdots L$ ,  $L = 2^{j-1}L_0$ ,  $L_0$  is the number of points of the original filters) to prepare and , and rewrote Eqs. (5) and (6)) as [14,15]:

$$C^{(j)}(n) = \sum_{k=1}^L h(k)^{(j)} C^{(j-1)}(n - k) \quad (8)$$

$$D^{(j)}(n) = \sum_{k=1}^L g(k)^{(j)} C^{(j-1)}(n - k) \quad (9)$$

But this is still an off-line algorithm, because  $C^{(j)}$  and  $D^{(j)}$  must be calculated one by one from  $C^{(0)}$  to  $C^{(1)}$ ,  $D^{(1)}$ , from  $C^{(1)}$  to  $C^{(2)}$ ,  $D^{(2)}$  and so on. For an on-line wavelet transform, all of the  $C^{(j)}(n)$  and  $D^{(j)}(n)$  for  $j = 1 \cdots J$  should be calculated simultaneously with the progress of sampling from  $n = 1$  to  $N$  ( $N$  is the data point number of an experiment result). That is, whenever a data

point was sampled, the corresponding  $C^{(j)}$  and  $D^{(j)}$  should be calculated. Therefore, the following program was proposed for the on-line wavelet transform:

```

/* preset the necessary parameters and variables, such as the number of decomposition, the filters and , etc. */
while (! Stop-sampling)
/* wait until elapsed time equals to the sampling time interval */
/* sampling to get  $C^{(0)}(n)$  */
for ( $j = 0; j < J; j + +$ )
 $\{C^{(j)}(n) = \sum_{l=1}^L h_l^{(j)} C^{(j-1)}(n-l)$  /* set  $C^{(0)}$  to zeros out any values not yet known. */
 $D^{(j)}(n) = \sum_{l=1}^L g_l^{(j)} C^{(j-1)}(n-l)$ 
}
 $n = n + 1$ 
end of while

```

For a voltammogram, the frequency of the signals at the position of peaks will be higher than that of the signals at the overlapping valleys or baseline. Therefore, by means of the above calculation, each component of signals (noise, information at peak position and that at non-peak

position) contained in a voltammogram will be separated into the contributions of different scale, and then useful information can be obtained [9,10].

### 3. Experimental

#### 3.1. Construction of the WT-voltammetric analyzer

Fig. 1 shows the construction of the WT-voltammetric analyzer. It is mainly composed of a microcomputer, a digital-to-analog converter (DAC), an analog-to-digital converter (ADC) and a potentiostat.

In this study, a Pentium PC microcomputer with software written in the C language was used. The desired waveforms were generated by the DAC under the control of the microcomputer, which is filtered and applied to the potentiostat's input.

The data-collecting system is composed of an amplifier, the ADC and the microcomputer. The response signal is amplified by a proper amplification, then converted to a digital signal by the ADC after filtering the noise. At the same time, the wavelet transform is performed and the  $C^{(j)}$  and  $D^{(j)}$  ( $j = 1 \dots J$ ) obtained will be displayed on the screen of the computer.

A 12-bit DAC and a 12-bit ADC were used. There is an operational amplifier in front of the ADC, with which 1, 10 and 100 can be selected as the amplification factor according to the magnitude of signal. The conversion rate of the ADC is 25  $\mu$ s and the DAC is 1  $\mu$ s.

Using the WT-voltammetric analyzer, several voltammetric techniques such as linear sweep voltammetry, differential pulse voltammetry and square wave voltammetry can be performed. Furthermore, sophisticated routines for subtracting baselines, comparing responses with those from standard, calculating unknown concentrations, identifying peaks, and plotting rescaled results, ect. are incorporated as standard software.

The discrete filters of Daubechies ( $N = 4$ ) [16], i.e.  $h(k) = \{0.4830, 0.8365, 0.2241, -0.1294\}$  and  $g(k) = \{0.4830, -0.8365, 0.2241, 0.1294\}$ , were used.

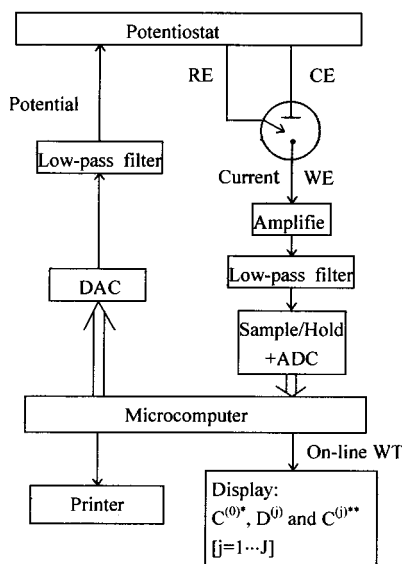


Fig. 1. Construction of the WT-voltammetric analyzer. WE, working electrode; RE, reference electrode; CE, counter electrode. \* $C^{(0)}$ , the normal voltammogram; \*\* $D^{(j)}$ ,  $C^{(j)}$ , discrete details and discrete approximations obtained by on-line wavelet transform.

Table 1  
Concentration of the mixture of Pb(II) and Tl(I)<sup>a</sup>

Number	Pb(II)	Tl(I)
1	8.2	7.6
2	2.0	9.6
3	1.0	1.0

<sup>a</sup> Concentration unit:  $1.0 \times 10^{-5} \text{ mol l}^{-1}$ .

Table 2  
Concentration of the mixture of Cd(II) and In(III)<sup>a</sup>

Number	Cd(II)	In(III)
1	0.6	0.5
2	1.6	1.3
3	1.8	1.8
4	2.6	2.9
5	4.2	4.8
6	5.2	5.9
7	2.2	2.4
8	3.4	3.6
9	4.8	4.2

<sup>a</sup> Concentration unit:  $1.0 \times 10^{-5} \text{ mol l}^{-1}$ .

### 3.2. Chemicals and samples

Stock solutions of  $2.0 \times 10^{-2} \text{ mol l}^{-1}$  Pb(II), Tl(I), Cd(II) and In(III) were prepared using Pb(II) nitrate, Tl(I) nitrate, cadmium (GR), and In(III) oxide, respectively. Pb(II) nitrate and Tl(I) nitrate were prepared by dissolving in double distilled water acidified with  $2 \text{ mol l}^{-1}$  concentrated nitric acid, cadmium and In(III) oxide were dissolved in double distilled water acidified with  $2 \text{ mol l}^{-1}$  concentrated hydrochloric acid. All of salts used were of analytical-reagent grade. Diluted solutions were also acidified. Tables 1 and 2 show the samples prepared for the experiment.

Table 3  
Experimental conditions used for LS and SW at hanging mercury drop electrode

Parameter	LS	SW
Initial potential (V)	-0.8	-0.35
Final potential (V)	-0.2	-0.65
Scan rate ( $\text{mV s}^{-1}$ )	20	
SW amplitude (mV)		15
Frequency (Hz)		6.25

A solution containing  $0.1 \text{ mol l}^{-1} \text{ KNO}_3$  was used as the supporting electrolyte.

### 3.3. Experiment and procedure

Linear sweep (LS) and square wave (SW) voltammetric measurements were obtained from the WT-voltammetric analyzer described above. A hanging mercury drop electrode (HMDE) is used as the working electrode with area of about  $0.01 \text{ mm}^2$ , while the auxiliary electrode is platinum wire. The reference electrode is Ag/AgCl in  $2 \text{ mol l}^{-1} \text{ KCl}$ . The instrumental settings used in the linear sweep and square wave voltammetric measurements are summarized in Table 3.

An appropriate volume of sample and 10 ml of the potassium nitrate electrolyte were placed in a 10-ml voltammetric vessel. The solution was purged for 20 min with high purity nitrogen. Then the experiment was performed under the selected conditions. For the qualitative determination of Pb(II) and Tl(I) and the quantitative determination of Cd(II) and In(III), linear sweep and square wave voltammogram were respectively obtained according to the experimental condition listed in Table 3. An appropriate volume of each sample was added with a micropipette each time, purged for 2 min and the curve was again obtained.

All voltammetric measurements were done in triplicate, and all experiments were performed at  $20^\circ\text{C}$ . The vessel was immersed with 20% nitric acid for 24 h and washed thoroughly with double distilled water before the experiment.

## 4. Results and discussion

### 4.1. Qualitative analysis

Fig. 2 is the linear sweep (anodic) voltammograms of Pb(II), Tl(I) and their mixture (sample 1 in Table 1). Because the difference in their peak potential is only about 50 mV, serious overlapping exists in the voltammograms for the mixtures. Therefore, it is difficult to detect the position of the peaks.

As mentioned above, the wavelet transform is able to decompose an overlapping voltammogram

into contributions of different frequency. Figs. 3–5 are respectively the linear sweep (anodic)

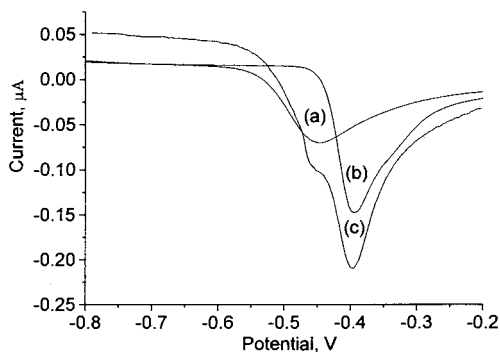


Fig. 2. Linear sweep (anodic) voltammograms of Pb(II), Tl(I), and their mixture. (a) Tl(I) ( $C_{\text{Tl}^+} = 7.60 \times 10^{-5} \text{ mol l}^{-1}$ ). (b) Pb(II) ( $C_{\text{Pb}^{2+}} = 8.20 \times 10^{-5} \text{ mol l}^{-1}$ ). (c) Mixture of Pb(II) and Tl(I) ( $C_{\text{Tl}^+} = 7.60 \times 10^{-5} \text{ mol l}^{-1}$ ,  $C_{\text{Pb}^{2+}} = 8.20 \times 10^{-5} \text{ mol l}^{-1}$ ).

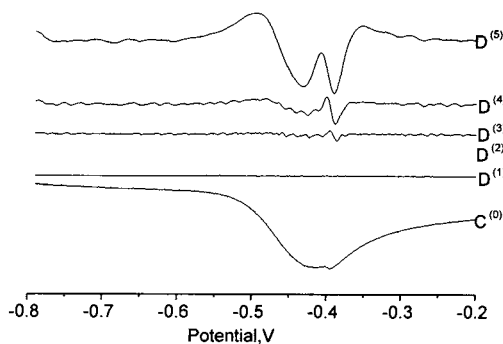


Fig. 3. Linear sweep (anodic) voltammograms  $C^{(0)}$  and decomposed details  $D^{(1)} \dots D^{(5)}$  of sample 1 in Table 1.

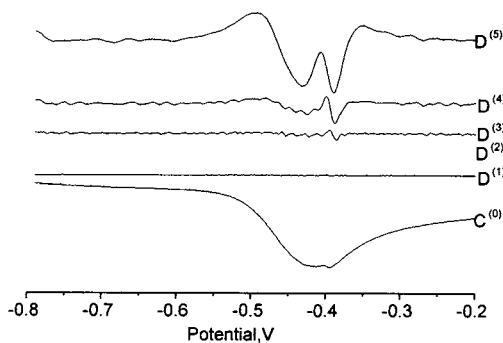


Fig. 4. Linear sweep (anodic) voltammograms  $C^{(0)}$  and decomposed details  $D^{(1)} \dots D^{(5)}$  of sample 2 in Table 1.

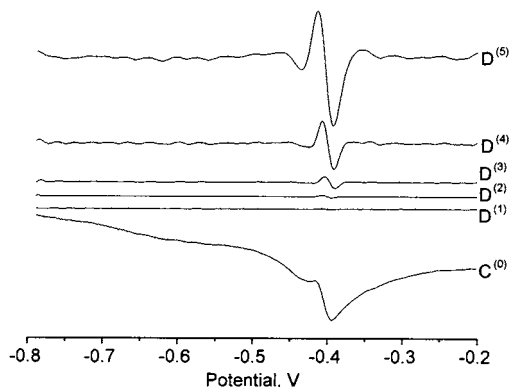


Fig. 5. Linear sweep (anodic) voltammograms  $C^{(0)}$  and decomposed details  $D^{(1)} \dots D^{(5)}$  of sample 3 in Table 1.

voltammograms  $C^{(0)}$  and the decomposed details  $D^{(1)} \dots D^{(5)}$  of samples 1–3 obtained with the WT-voltammetric analyzer. The resolution level  $J$  for the wavelet transform is 5.

From Fig. 3 it can be seen that the first three  $D^{(j)}$  ( $j = 1, 2, 3$ ) are mainly composed of noise (the magnitude of noise is very small so that the  $D^{(1)}$  looks like a straight line). The line  $D^{(4)}$  is similar to line  $D^{(5)}$ , but the magnitude of voltammetric signals in line  $D^{(4)}$  is comparatively small. The line  $D^{(5)}$  is composed of mainly voltammetric signals of the components. In line  $D^{(5)}$ , the two peaks are separated entirely. Comparing with  $C^{(0)}$ , the shape of peaks gets sharper and clearer.

Fig. 4 and Fig. 5 are respectively output results of the samples 2 and 3 in Table 1. From the figure, it also can be seen that the two peaks are separated entirely in line  $D^{(5)}$ . The position of peaks after the on-line wavelet transform did not change, but, comparing with the normal voltammograms, the position of peaks can be identified easily. Therefore, the WT-voltammetric analyzer will give better information for qualitative analysis.

## 4.2. Quantitative determination

### 4.2.1. The linearity of the voltammograms with on-line wavelet transform processing

Fig. 6 shows the square wave voltammograms of Cd(II), In(III) and their mixture. The peak potentials of Cd(II) and In(III) are, respectively,

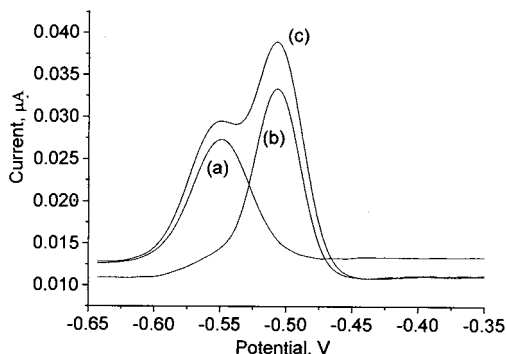


Fig. 6. Square wave voltammograms of Cd(II), In(III) and their mixture. (a) Cd(II) ( $C_{\text{Cd}^{2+}} = 0.6 \times 10^{-5} \text{ mol l}^{-1}$ ). (b) In(III) ( $C_{\text{In}^{3+}} = 0.5 \times 10^{-5} \text{ mol l}^{-1}$ ). (c) Mixture of Cd(II) and In(III) ( $C_{\text{Cd}^{2+}} = 0.6 \times 10^{-5} \text{ mol l}^{-1}$ ,  $C_{\text{In}^{3+}} = 0.5 \times 10^{-5} \text{ mol l}^{-1}$ ).

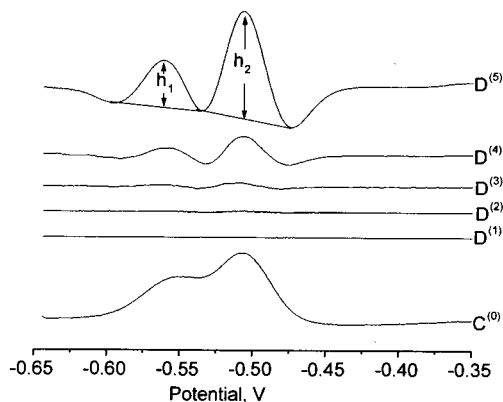


Fig. 7. Square wave voltammograms  $C^{(0)}$  and decomposed details  $D^{(1)} \dots D^{(5)}$  of sample 1 in Table 2.

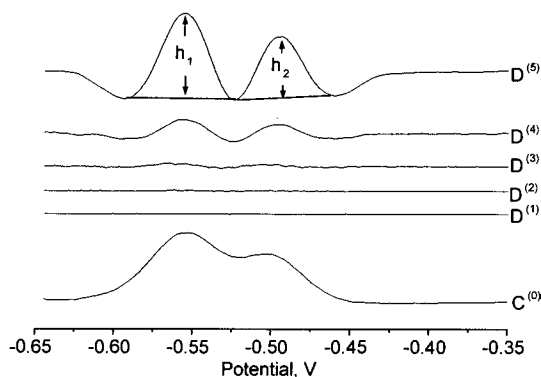


Fig. 8. Square wave voltammograms  $C^{(0)}$  and decomposed details  $D^{(1)} \dots D^{(5)}$  of sample 2 in Table 2.

at  $-0.549$  and  $-0.507$  V (versus Ag/AgCl/2 mol  $\text{l}^{-1}$  KCl). Therefore, overlapping exists in the voltammograms for the mixtures.

Because the wavelet transform is a linear operation, the voltammograms after decomposition should keep the linear relationship between the peak current and the concentration of the components. Six samples, samples 1–6 in Table 2, were measured with the WT-voltammetric analyzer. Fig. 7 is the square wave voltammogram and decomposed details  $D^{(1)} \dots D^{(5)}$  of sample 1 in Table 2. From the  $C^{(0)}$  signal, it is evident that the peaks of Cd(II) and In(III) are overlapping. It is difficult to detect the position of the peaks and to determine the concentration of each component. From the signal  $D^{(4)}$  and  $D^{(5)}$ , it is obvious that there are two peaks, which are, respectively, corresponding to the reduction peaks of Cd(II) and In(III).  $D^{(5)}$  consists mainly of voltammetric signals. Therefore,  $D^{(5)}$  is chosen for quantitative determination. In the  $D^{(5)}$ ,  $h_1$  and  $h_2$  respectively denote the peak current of Cd(II) and In(III) after wavelet transform.

Fig. 8 shows the square wave voltammogram and decomposed details  $D^{(1)} \dots D^{(5)}$  of sample 2 in Table 2. The result is similar to that of sample 1, the resolved information can be easily separated from the overlapping peaks by wavelet transform decomposition.

Fig. 9 is the calibration curves obtained from the line  $D^{(5)}$  (decomposed detail by on-line wavelet transform) with the samples 1–6 in Table 2. The correlation coefficients with the on-line wavelet transform processing, the lines (a) and (b), are respectively 0.998 for Cd(II), 0.996 for In(III). It is obvious that the linear relationship between the peak current and the concentration of each component remained in the decomposed details.

#### 4.2.2. Quantitative determination of mixed samples

Three mixed samples, samples 7–9 in Table 2, were measured at the same experimental condition using the WT-voltammetric analyzer. Table 4 shows the results of the quantitative determination calculated from the  $D^{(5)}$  signals given by the WT-voltammetric analyzer using the calibration curves in Fig. 9. From the Table 4, it can be seen

Table 4

Calculated results of the mixture of Cd(II) and In(III) with on-line wavelet transform<sup>a</sup>

Sample number	Added	Calculated/recovery (%)			Average/recovery (%)
7	Cd 2.2	2.25/102.3	2.17/98.6	2.07/94.1	2.16/98.2
	In 2.4	2.57/107.1	2.22/92.5	2.43/101.3	2.41/100.4
8	Cd 3.4	3.25/95.6	3.26/95.9	3.17/93.2	3.23/95.0
	In 3.6	3.37/93.6	3.47/96.4	3.51/97.5	3.45/95.8
9	Cd 3.8	3.74/98.4	3.94/103.7	3.61/95.0	3.76/98.9
	In 4.2	4.32/102.9	4.49/106.9	4.34/103.3	4.38/104.3

<sup>a</sup> Concentration unit:  $1.0 \times 10^{-5}$  mol l<sup>-1</sup>.

that the recoveries are between 92.5 and 107.1%. The result indicated that simultaneous quantitative determination of Cd(II) and In(III) in overlapping voltammogram can be obtained with the on-line wavelet transform.

## 5. Conclusion

In this study, an on-line wavelet transform algorithm is proposed and WT-voltammetric analyzer is developed based on the algorithm. Because the on-line wavelet transform decomposes the sampled signal simultaneously with the progress of sampling, the WT-voltammetric analyzer gives all the components contained in the sampled voltammogram. Applications of WT-voltammetric analyzer in linear sweep and square wave voltammetric analysis were investigated. Results showed that the overlapping peaks of Pb(II)

and Tl(I) can be separated easily and the peak position after the on-line wavelet transform does not change. Because wavelet transform does not affect the linearity of the instrumental signals, the quantitative determination can be done by the decomposed signals. Quantitative determination of Cd(II) and In(III) in mixture samples were investigated. The recoveries are between 92.5 and 107.1%. It is demonstrated that the WT-voltammetric analyzer provides a convenient and efficient method of on-line processing instrumental signals.

## References

- [1] M. Bos, J.A.M. Vrieling, *Chemometr. Intell. Lab. Syst.* 23 (1994) 115.
- [2] D. Jouan-Rimbaud, B. Walczak, R.J. Poppi, O.E. de Noord, D.L. Massart, *Anal. Chem.* 69 (1997) 4317.
- [3] F.T. Chau, T.M. Shih, J.B. Gao, C.K. Chan, *Appl. Spectrosc.* 50 (1996) 339.
- [4] B. Walczak, D.L. Massart, *Chemometr. Intell. Lab. Syst.* 36 (1997) 81.
- [5] V.J. Barclay, R.F. Bonner, I.P. Hamilton, *Anal. Chem.* 69 (1997) 78.
- [6] C.R. Mittermayr, S.G. Nikolov, H. Hutter, M. Grasserbauer, *Chemometr. Intell. Lab. Syst.* 34 (1996) 187.
- [7] L.M. Shao, B. Tang, X.G. Shao, G.W. Zhao, S.T. Liu, *Chin. J. Anal. Chem.* 25 (1997) 15.
- [8] Z.X. Pan, X.G. Shao, H.B. Zhong, W. Liu, H. Wang, M.S. Zhong, *Chin. J. Anal. Chem.* 24 (1996) 149.
- [9] X.G. Shao, W.S. Cai, P.Y. Sun, M.S. Zhang, G.W. Zhao, *Anal. Chem.* 69 (1997) 1722.
- [10] X.G. Shao, P.Y. Sun, W.S. Cai, M.S. Zhang, *Chin. J. Anal. Chem.* 25 (1997) 671.
- [11] A. Grossmann, J. Morelet, *SIAM J. Math. Anal.* 15 (1984) 723.
- [12] S.G. Mallat, *Trans. Am. Math. Soc.* 315 (1989) 69.

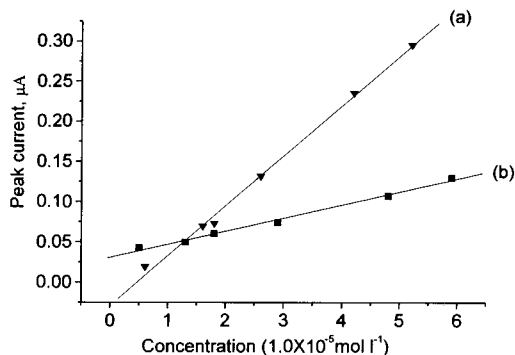


Fig. 9. The calibration curves of (a) Cd(II) and (b) In(III) from the details by WT-voltammetric analyzer.



- [13] S.G. Mallat, IEEE Trans. Pattern Anal. Machine Intell. 11 (1989) 674.
- [14] X.G. Shao, W. Li, G. Chen, Q.D. Su, Fresenius J. Anal. Chem. 363 (1999) 215.
- [15] X.G. Shao, W.S. Cai, Rev. Anal. Chem. XVII (1998) 235.
- [16] G. Liu, S. Di, Wavelet Analysis and Its Application, Press of University of Electronic Science and Technology of Xi'an, Xi'an, 1992, p. 57.

# Electrochemistry and electrocatalysis with myoglobin in biomembrane-like surfactant-polymer $2C_{12}N^+PA^-$ composite films

Yujiao Hu, Naifei Hu \*, Yonghuai Zeng

*Department of Chemistry, Beijing Normal University, Beijing, 100875, PR China*

Received 17 February 1999; received in revised form 2 July 1999; accepted 16 July 1999

## Abstract

Biomembrane-like polyionic complex,  $2C_{12}N^+PA^-$ , was prepared by reacting sodium polyacrylate ( $Na^+PA^-$ ) with didodecyldimethylammonium bromide ( $2C_{12}N^+Br^-$ ). Stable thin films made from  $2C_{12}N^+PA^-$ , with incorporated myoglobin (Mb), on pyrolytic graphite (PG) electrodes were then characterized by electrochemistry and other techniques. Cyclic voltammetry of Mb- $2C_{12}N^+PA^-$  films showed a pair of well-defined quasi reversible peaks for MbFe(III)/Fe(II) couple at about  $-0.19$  V versus SCE in pH 5.5 buffers. The electron transfer rate between Mb and PG electrodes was greatly facilitated in the microenvironment of  $2C_{12}N^+PA^-$  films. Square wave voltammetry data were used to estimate the apparent heterogeneous electron transfer rate constants by nonlinear regression analysis using a model featuring dispersion of formal potentials. Positions of Soret absorption bands suggested that Mb keeps its secondary structure similar to its native state in  $2C_{12}N^+PA^-$  films at the medium pH. The results of differential scanning calorimetry and X-ray diffraction suggest that synthesized  $2C_{12}N^+PA^-$  lipid films have an ordered multibilayer structure and the incorporated Mb does not disturb this structure. Oxygen was catalytically reduced by Mb- $2C_{12}N^+PA^-$  films with a significant decrease in the electrode potential. MbFe(I), a highly reduced form of Mb, was also produced in Mb- $2C_{12}N^+PA^-$  films at about  $-1.09$  V, and could be used to catalytically reduce organohalide pollutants such as perchloroethylene (PCE) and trichloroethylene (TCE). The catalytic reduction peak currents had linear relationships with concentrations of PCE and TCE in a range of  $10$ – $100$   $\mu$ M. The potential applications of the film electrode as a sensor for detecting organohalides are discussed. © 2000 Elsevier Science B.V. All rights reserved.

*Keywords:* Myoglobin; Surfactant-polymer multibilayer composite films; Didodecyldimethylammonium polyacrylate; Electrocatalysis

## 1. Introduction

In living organisms, biomembranes are made up of roughly 40% lipids and 60% proteins, and

generally exist in a partly fluid, selectively permeable state [1,2]. The lipids are arranged in bilayers, and proteins can be adsorbed onto the surface or imbedded into the bilayer. Some synthesized water-insoluble surfactants can be introduced onto surface of electrodes by various methods, such as adsorption, casting, covalent bonding, or transfer-

\* Corresponding author. Fax: +86-10-62200567.  
E-mail address: hunafei@bnu.edu.cn (N. Hu)

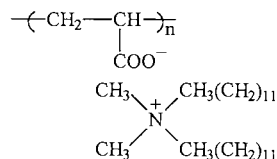
ring of Langmuir–Blodgett films. By self-assembling, the surfactant molecules can form ordered bilayers with properties similar to biomembranes [3–7]. Thus, the direct electrochemistry of redox proteins in these biomembrane-like films may provide a good model for the study of redox processes in biological systems. Some recent papers have demonstrated the effectiveness of the electrochemical approach for the study of proteins using modified electrodes with biomembrane-mimetic structures and properties [8–19]. In addition to fundamental studies, films containing functional proteins may also have applications in biosensors and biocatalysis.

Myoglobin (Mb) is a heme protein which can store and transport oxygen in muscle cells in mammals. It contains a single polypeptide chain with an electroactive iron heme as prosthetic group [20]. Although Mb does not function physiologically as an electron carrier, it is an ideal model molecule for the study of electron transfer reactions of heme proteins or enzymes. Early electrochemical investigations of Mb focused on polarographic reduction of Mb, showing that Mb could be reduced irreversibly on dropping mercury electrodes [21]. Because of slow rates of electron transfer between Mb and solid electrodes, great efforts have been made to facilitate the electron transfer of Mb by using mediators, promoters or special electrode materials [22–24]. Rusling et al. recently reported that in lamellar surfactant films on pyrolytic graphite (PG) electrodes, direct electron transfer was greatly enhanced for Mb [13–18]. This may provide a general way to make protein films, in which incorporated redox proteins can reside in a bilayer, biomembrane-like microenvironment and improve their electrochemical properties [25]. However, the Mb-surfactant films were subject to mechanical damage in stirred electrolytic reactors [19]. Thus, making Mb films with well behaved electrochemistry and also good stability which are amenable to a variety of electrochemical and other experiments is one of our main goals for the present work. Once useful films are developed using Mb, they might then be applied to other proteins.

Surfactant–clay or surfactant–polymer composite films showed similar biomembrane-like bi-

layer structure to simple surfactant films, but demonstrated advantages over the latter in mechanical stability because of the introduction of clay or polymer backbones [26–32]. The clay or polymer backbone may provide better structure and solidity to films containing proteins, and may be more useful for practical applications. Various types of surfactant–polymer composite films have been developed by Kunitake [28–30] and Okahata [31,32] groups.

The polyionic complex,  $2C_{12}N^+PA^-$ , synthesized by reacting anionic polymer sodium polyacrylate ( $Na^+PA^-$ ) with cationic bilayer forming surfactant didodecyldimethylammonium bromide ( $2C_{12}N^+Br^-$ ), is most probably one of those materials for making multibilayer composite films. Its chemical structure is shown below. With a shorter hydrocarbon chain,  $2C_{12}N^+PA^-$  has similar structure to  $2C_{18}N^+PA^-$  which was studied previously by Kunitake and believed to form ordered bilayer films by self-assembling [28]. Thus, we expect that  $2C_{12}N^+PA^-$  films should also have multibilayer structure and similar properties to lipid membranes. No electrochemistry of heme proteins in either  $2C_{12}N^+PA^-$  or  $2C_{18}N^+PA^-$  films have been reported to our knowledge.



Organohalides are recognized as widespread environmental pollutants arising from various industrial as well as smaller scale sources [33,34], such as pesticides and solvents. A simple, general-purpose organohalide sensor that can directly detect the carbon-halogen bond could be of important significance. Mb in cast films of  $2C_{12}N^+Br^-$  on PG electrode could reductively catalyze dehalogenation of some organohalide pollutants with high efficiency [13,15,35]. We thus expect the potential application of Mb- $2C_{12}N^+PA^-$  film electrode as a sensor for determining these pollutants.

In this paper, Mb incorporated in  $2C_{12}N^+PA^-$  films were characterized by electrochemistry, UV-

Vis spectroscopy and other surface analysis techniques. The catalytic reductions of some organohalides, as well as oxygen, at Mb- $2C_{12}N^+PA^-$  film electrodes were also discussed.

## 2. Experimental

### 2.1. Chemicals

Horse heart myoglobin (Mb) from Sigma was used as received without further purification. Dodecyltrimethylammonium bromide ( $2C_{12}N^+Br^-$ ) was from Kodak. Sodium polyacrylate ( $Na^+PA^-$ , wt.% = 30%, MW 4500) was a gift from Institute of Chemistry, Academia Sinica. Perchloroethylene (PCE) and trichloroethylene (TCE) were from Beijing Yili Fine Chemicals, China. All other chemicals were reagent grade.

The supporting electrolyte was usually 0.1 M sodium acetate buffer at pH 5.5 containing 0.1 M KBr. Other buffers were 0.05 M sodium dihydrogen phosphate, 0.05 M boric acid or 0.05 M citric acid, all containing 0.1 M KBr. The pH was regulated with HCl or KOH solutions. 10 mM PCE and TCE stock solutions were prepared by dissolving them in solvent of acetonitrile/water (V/V = 1:4), respectively. Aliquots of these solutions were added to the final volume of aqueous buffers for electrochemical experiments. Twice distilled water was used for all experiments.

### 2.2. Preparation of Mb- $2C_{12}N^+PA^-$ films

The powder of polyionic complex,  $2C_{12}N^+PA^-$ , was synthesized by reacting  $Na^+PA^-$  with  $2C_{12}N^+Br^-$ . 3 ml of 30%  $Na^+PA^-$  solution was mixed with 10 ml of 50 mM aqueous dispersion of  $2C_{12}N^+Br^-$  at room temperature. A white precipitate of  $2C_{12}N^+PA^-$  was formed immediately. After centrifuging, washing and drying, the pure and dry solid powder of  $2C_{12}N^+PA^-$  was collected. A total of 75 mg of  $2C_{12}N^+PA^-$  powder was then dissolved in 10 ml chloroform.

Prior to coating, basal plane pyrolytic graphite (PG, gifts from Chinese Geologic Academy of Science, geometric area 0.26 cm<sup>2</sup>) electrodes were abraded with metallographic SiC sand paper, and

then polished on a clean Buehler billiard cloths (No. 40-7308) with pure water. Electrodes were sonicated in pure water for 30 s after each polishing step.

A volume of 5  $\mu$ l of 7.5 mg ml<sup>-1</sup>  $2C_{12}N^+PA^-$  in chloroform was spread evenly onto a freshly abraded PG electrode with a microsyringe. A small tube was fit tightly over the electrode to serve as a closed evaporation chamber so that chloroform evaporated more slowly and the films were formed more uniformly. After about 1 h, the films were dried completely. Ten microlitres of 0.15 mM Mb solution was then spread onto the  $2C_{12}N^+PA^-$  film surface. A small tube was placed onto the electrode for a few hours so that water evaporated slowly. The Mb- $2C_{12}N^+PA^-$  films were then dried in air overnight at room temperature.

### 2.3. Apparatus and procedures

A CHI 660 electrochemical workstation (CH Instruments) was used for cyclic voltammetry (CV) and square wave voltammetry (SWV). A three-electrode cell was used with a saturated calomel electrode (SCE) as reference, a platinum wire as counter electrode, and a PG disk with films as working electrode. All electrochemical experiments were done at temperature of  $25 \pm 2^\circ C$ .

Voltammetry on electrodes coated with Mb- $2C_{12}N^+PA^-$  films was done in buffers containing no Mb. Buffers were purged with highly purified nitrogen for about 20 min before a series of experiments. A nitrogen environment was then kept over solutions in the cell during the experiment. In the experiment with oxygen, measured volumes of air were injected through solutions via a syringe in a sealed cell which had been previously degassed with purified nitrogen.

UV-Vis absorption spectroscopy was done with a UV-250 spectrophotometer (Shimadzu). Sample films for spectroscopy were prepared by first depositing 40  $\mu$ l of 7.5 mg ml<sup>-1</sup>  $2C_{12}N^+PA^-$  in chloroform onto indium tin oxide coated slides (ITO, from Delta Technologies). After the films became dry in 1 h, 30  $\mu$ l of 0.30 mM Mb solution was put onto the  $2C_{12}N^+PA^-$  film surface, and the films stood in a chamber overnight for drying.

Differential scanning calorimetry (DSC) was performed with a DSC-30 differential scanning calorimeter (Mettler) to examine the phase transition of the synthetic lipid  $2C_{12}N^+PA^-$  samples with and without Mb incorporated.  $2C_{12}N^+PA^-$  samples were prepared by casting their chloroform solutions onto glass slides and drying in air. Mb- $2C_{12}N^+PA^-$  samples were prepared with the same way as that of Mb- $2C_{12}N^+PA^-$  films for spectroscopy described above. About 28 mg of  $2C_{12}N^+PA^-$  and 41 mg of Mb- $2C_{12}N^+PA^-$  samples were hermetically sealed in aluminum pans, respectively, after addition of a few drops of pure water. The heating rate was  $5^\circ\text{C min}^{-1}$ .

X-ray diffraction studies were done with a D/MAX-RB powder diffractometer (Rigaku) using a Cu K $\alpha$  source at 40 kV and 100 mA. Scan rate was  $2^\circ \text{min}^{-1}$ . Composite films of  $2C_{12}N^+PA^-$  for X-ray diffraction were prepared by casting their chloroform dispersions onto glass microscope slides and drying in air. Mb- $2C_{12}N^+PA^-$  films were prepared by the same way as that of Mb- $2C_{12}N^+PA^-$  films for spectroscopy.

### 3. Results

#### 3.1. Cyclic voltammetry (CV)

Steady state CVs for Mb- $2C_{12}N^+PA^-$  films at  $0.1 \text{ V s}^{-1}$  in pH 5.5 buffers containing no Mb (Fig. 1b) showed two pairs of well defined and near reversible cathodic-anodic peaks. The first pair centered near  $-0.19 \text{ V}$  versus SCE, characteristic of MbFe(III)/Fe(II) redox couple [13,14].

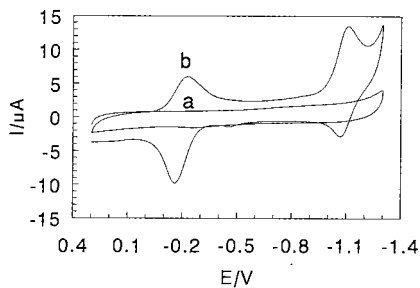


Fig. 1. Cyclic voltammograms at  $0.1 \text{ V s}^{-1}$  in pH 5.5 buffers for (a)  $2C_{12}N^+PA^-$  films and (b) Mb- $2C_{12}N^+PA^-$  films.

The second pair centered at about  $-1.09 \text{ V}$ , which was also reported at Mb- $2C_{12}N^+Br^-$  film electrodes previously and was considered to be probably attributed to MbFe(II)/Fe(I) redox couple [35]. The formal potential at  $-1.09 \text{ V}$  is similar to values of  $-1.03$  to  $-1.06 \text{ V}$  for Fe(II)/Fe(I) couple of tetraphenylporphyrin iron (TPPFe) in weakly complexing solvents containing  $Br^-$  [36,37]. In contrast, blank  $2C_{12}N^+PA^-$  films in pH 5.5 buffers showed no CV signal at all in the potential range of  $0.3 \text{ V}$  to  $-1.3 \text{ V}$  (Fig. 1a). Since the first redox couple is better known and understood in Mb electrochemistry, the following experiments were mainly focused on this pair of peaks.

When a Mb- $2C_{12}N^+PA^-$  film electrode was placed into pH 5.5 buffer solutions containing no Mb, the first pair of peaks increased slowly with soaking time at first, and then reached to the steady state in a few hours. Thus, most of the following electrochemical experiments with Mb- $2C_{12}N^+PA^-$  films were done at the steady state except for where otherwise indicated.

The first redox peak pair had an approximately symmetric peak shape and nearly equal heights of cathodic and anodic peaks. The cathodic peak current increased linearly with scan rate from  $0.1$  to  $2 \text{ V s}^{-1}$ , which is characteristic of thin layer electrochemical behavior [38]. Integration of peaks at different scan rates gave nearly constant charge ( $Q$ ) values, from which the surface concentration of electroactive Mb in the films,  $\Gamma^*$ , could be estimated [39]. The average  $\Gamma^*$  value was  $(3.7 \pm 0.3) \times 10^{-10} \text{ mol cm}^{-2}$  with scan rates from  $0.1$  to  $2 \text{ V s}^{-1}$ , which accounted for about 6.5% of the total Mb deposited on the electrode.

For comparison, blank  $2C_{12}N^+PA^-$  films on PG electrodes were placed into pH 5.5 buffers containing  $0.15 \text{ mM}$  Mb, and CVs were run periodically to test the possibility of Mb entering the films. CV scans at different soaking times revealed the growth of the first pair of peaks, accompanied by a little negative shift of peak potentials (Fig. 2). Increasing of peak currents with time suggests increasing amounts of Mb entering the  $2C_{12}N^+PA^-$  films. CVs representing films fully loaded with Mb was obtained in about 60 h. The CV peak potentials of  $2C_{12}N^+PA^-$  films fully loaded

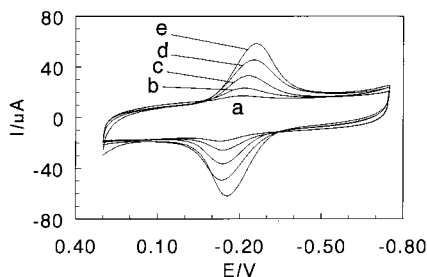


Fig. 2. Cyclic voltammograms at  $0.2 \text{ V s}^{-1}$  for  $2\text{C}_{12}\text{N}^+\text{PA}^-$  films immersed in pH 5.5 buffers containing  $1.5 \times 10^{-4} \text{ M Mb}$  for: (a) 5 min; (b) 5 h; (c) 36 h; (d) 48 h and (e) 60 h.

with Mb centered at about  $-0.19 \text{ V}$  (Fig. 2e), similar to those of cast  $\text{Mb-}2\text{C}_{12}\text{N}^+\text{PA}^-$  films in blank buffers. But its peak currents were about 2.7 times larger than those of cast  $\text{Mb-}2\text{C}_{12}\text{N}^+\text{PA}^-$  films. When a fully loaded  $\text{Mb-}2\text{C}_{12}\text{N}^+\text{PA}^-$  film electrode was transferred from the Mb solution into a blank buffer at the same pH, its CV responses maintained identical to the CVs in Mb solutions.

Both cast and immersing methods showed very similar peak positions for  $\text{Mb-}2\text{C}_{12}\text{N}^+\text{PA}^-$  films, but the former was more convenient and quantitative, and thus was used for preparing  $\text{Mb-}2\text{C}_{12}\text{N}^+\text{PA}^-$  films for the following studies.

The stability of  $\text{Mb-}2\text{C}_{12}\text{N}^+\text{PA}^-$  films was tested by CV with two different methods. In the solution studies, a PG electrode coated with  $\text{Mb-}2\text{C}_{12}\text{N}^+\text{PA}^-$  films was stored in buffers all the time, and CVs were run periodically. Alternatively,  $\text{Mb-}2\text{C}_{12}\text{N}^+\text{PA}^-$  films were dried in air for most of the storing time and CVs were run periodically after returning the dry electrode into buffer solutions. With both methods,  $\text{Mb-}2\text{C}_{12}\text{N}^+\text{PA}^-$  films showed similar and very good stability. For instance, after storing in buffers for 1 month, the  $\text{Mb-}2\text{C}_{12}\text{N}^+\text{PA}^-$  films showed only 10% decrease in their CV response compared with their initial steady state peak currents.

Visible absorption spectroscopy was used to check the possible leaching of Mb out  $\text{Mb-}2\text{C}_{12}\text{N}^+\text{PA}^-$  films. A PG electrode coated with  $\text{Mb-}2\text{C}_{12}\text{N}^+\text{PA}^-$  films had been stored in a small cuvette filled with pH 5.5 buffers for several days, the external solution was then checked with the

characteristic and sensitive Soret band of Mb at about 408 nm by spectroscopy. No indication of leaching Mb was observed from the external solutions, which is consistent with the CV results showing  $\text{Mb-}2\text{C}_{12}\text{N}^+\text{PA}^-$  films had extreme stability.

### 3.2. Square wave voltammetry (SWV)

Square wave voltammetry has advantages of better signal-to-noise ratio and resolution than CV [40] and was used here to estimate the average formal potential ( $E^{\circ}$ ) and the apparent heterogeneous electron transfer rate constant ( $k_s$ ). The procedure employed nonlinear regression analysis for SWV forward and reverse curves, as described in detail previously [18,41].

Since the SWV model of a single electroactive species with thin-layer electrochemical behavior [42] did not fit the experimental voltammograms for  $\text{Mb-}2\text{C}_{12}\text{N}^+\text{PA}^-$  films, we used a model which combines dispersions of formal potentials with the single-species SWV model [18,41]. Thus, the SWV current ( $I$ ) can be expressed as:

$$I = \sum_{j=1}^p I_j \quad (1)$$

where  $I_j$  is the contribution of the  $j$ th of  $p$  classes of redox centers with formal potential  $E_j^{\circ}$  to the total current.

It is important to realize that the  $k_s$  value obtained by the above fitting method is not a real measure of only electron transfer rate. Any physical or chemical factors which might influence the SWV curve shape are embodied in this 'apparent'  $k_s$ . Thus, the  $k_s$  value is probably best interpreted as a measure of rate of overall electron transfer process dependent on film and electrode properties. It is suitable for between-film comparison only.

Preliminary studies showed that the  $E^{\circ}$  dispersion model with  $p = 5$  gave a reasonable compromise between acceptable goodness of fit, consistency of parameters, and time of computation. A similar conclusion was found for SWV data on Mb-AQ [19] and Mb-surfactants films [18,41].

Table 1

Apparent heterogeneous electron transfer rate constants and formal potentials for myoglobin films on PG electrodes in pH 7.0 buffers containing no myoglobin

Films <sup>a</sup>	av. $k_s$ , s <sup>-1</sup>	av. $E^{o'}$ vs. SCE		Ref. <sup>b</sup>
		CV	SWV	
Mb-2C <sub>12</sub> N <sup>+</sup> PA <sup>-</sup>	11 ± 1	-0.231	-0.212	tw
Mb-2C <sub>12</sub> N <sup>+</sup> Br <sup>-</sup>	31 ± 3	-0.228	-0.240	[18]
Mb-DMPC	59 ± 9	-0.326	-0.342	[18]
Mb-DLPC	50 ± 8	-0.329	-0.343	[18]
Mb-2C <sub>12</sub> N <sup>+</sup> Br <sup>-</sup> -Nafion	40 ± 6	-0.193	-0.202	[19]
Mb-AQ	52 ± 6	-0.362	-0.340	[19]

<sup>a</sup> 2C<sub>12</sub>N<sup>+</sup>PA<sup>-</sup>, didodecyldimethylammonium polyacrylate; 2C<sub>12</sub>N<sup>+</sup>Br<sup>-</sup>, didodecyldimethylammonium bromide; DMPC, dimyristoyl phosphatidylcholine; DLPC, dilauroyl phosphatidylcholine, AQ, Eastman AQ38.

<sup>b</sup> tw, this work, reporting average values for analysis of six SWVs at frequencies of 30–50 Hz, amplitudes of 30–45 mV, and a step height of 4 mV.

The analysis of SWV data for Mb-2C<sub>12</sub>N<sup>+</sup>PA<sup>-</sup> films showed goodness of fit of the model over a range of amplitudes and frequencies. The average apparent heterogeneous electron transfer rate constant ( $k_s$ ) obtained from fitting SWV data at pH 7.0 was 11 s<sup>-1</sup> (Table 1), and the average  $E^{o'}$  was -0.212 V versus SCE. Values obtained by the same method for Mb in different films are listed in Table 1 for comparison.

### 3.3. Influence of pH on voltammetry

CV peak potentials of the first peak pair for Mb in 2C<sub>12</sub>N<sup>+</sup>PA<sup>-</sup> films shifted negatively with increasing pH, accompanied by the decrease of peak currents and change of peak shape (Fig. 3). CV data were also used to investigate the pH dependence of the formal potentials ( $E^{o'}$ ), which were estimated as the average of cathodic and anodic peak potentials of MbFe(III)/Fe(II) redox couple.  $E^{o'}$  had a linear relationship with pH from pH 4.0 to 9.0 with a slope of -27 mV pH<sup>-1</sup> (Fig. 4), nearly half of the theoretical value of -59 mV pH<sup>-1</sup> at 25°C for a reversible proton-coupled single electron transfer [43,44]. An inflection point appeared at pH 4.0 in the  $E^{o'}$ -pH plot. At pH < 4.0,  $E^{o'}$  values changed much slower with changing pH (Fig. 4).

The changes in CV peak potentials and currents with pH were reversible between pH 4 and 8. For example, CVs for Mb-2C<sub>12</sub>N<sup>+</sup>PA<sup>-</sup> films in pH 7

buffers were reproduced after soaking the film in pH 5.5 buffers and then returning it to the pH 7 buffers again.

The surface concentration ( $\Gamma^*$ ) of electroactive Mb in the films estimated by integration of CV reduction peak decreased significantly with increasing pH at pH > 6, which indicates that pH significantly influences the amount of electroactive Mb in the films at pH > 6.

### 3.4. UV-Vis spectroscopy

Positions of the Soret absorption band of iron heme provide information about possible denaturation of Mb [45]. Solution spectrum has Soret band at 408 nm for Mb at pH 5.5 [16]. Both dry films cast from Mb and Mb-2C<sub>12</sub>N<sup>+</sup>PA<sup>-</sup> on transparent ITO slides showed Soret bands at 408

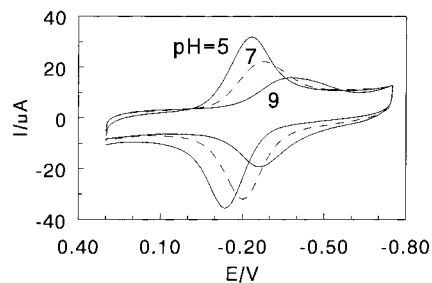


Fig. 3. Cyclic voltammograms at 0.5 V s<sup>-1</sup> for 2C<sub>12</sub>N<sup>+</sup>PA<sup>-</sup> films in buffers at different pH.

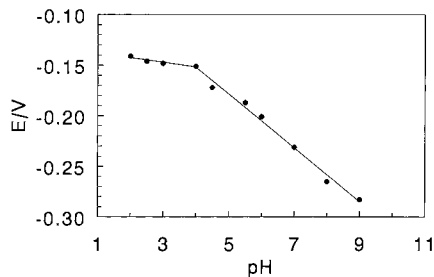


Fig. 4. Influence of pH on CV formal potentials for Mb- $2C_{12}N^+PA^-$  films at  $0.5 \text{ V s}^{-1}$ .

nm (Fig. 5a and b), suggesting that Mb in dry  $2C_{12}N^+PA^-$  films has a secondary structure similar to the native state of Mb in dry Mb films alone. The dependence of the Soret band position on external solution pH was tested when Mb- $2C_{12}N^+PA^-$  films were placed into buffers with different pH. At pH 5.5 and 7.0, the Soret band appeared at 406 nm (Fig. 5d and e), indicating that at the medium pH range, Mb almost keeps its native conformation in  $2C_{12}N^+PA^-$  film environment. When  $\text{pH} < 5.5$ , the Soret band began to shift blue and tended to be more broad. At pH 3.5, the Soret band almost disappeared (Fig. 5c), suggesting the possible denaturation of most Mb in the films. When  $\text{pH} > 7$ , the Soret band slightly shifted blue. For example, at pH 9.0, the Soret band was observed at 404 nm, and it shifted to

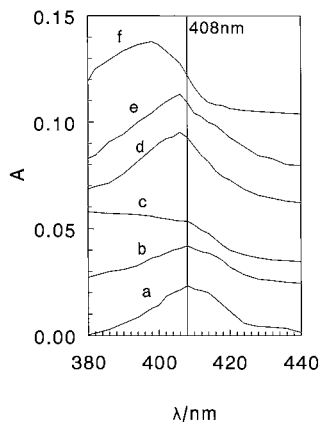


Fig. 5. UV-Vis spectra of Mb and Mb- $2C_{12}N^+PA^-$  films on indium tin oxide (ITO) slides for (a) dry Mb films; (b) dry Mb- $2C_{12}N^+PA^-$  films and Mb- $2C_{12}N^+PA^-$  films in different pH buffers: (c) pH 3.5; (d) pH 5.5; (e) pH 7.0; (f) pH 11.0.

Table 2

Gel-to-liquid crystal phase transition temperatures measured by DSC for films of lipids and Mb-lipids

Films	$T_c$ (°C)	Ref.
$2C_{12}N^+Br^-$	11	[14]
Mb- $2C_{12}N^+Br^-$ (pH 5.5)	12	[13]
Mb- $2C_{12}N^+Br^-$ (pH 7.0)	15	[13]
Clay- $2C_{12}N^+Br^-$	15	[26]
$2C_{12}N^+PA^-$	18	This work
Mb- $2C_{12}N^+PA^-$	20	This work

402 nm at pH 11.0 (Fig. 5f). The Mb- $2C_{12}N^+PA^-$  films showed considerable stability on ITO slides. But they did not adhere to ITO slides as strongly as to PG electrodes. The films peeled off ITO slides in  $< 1$  day.

### 3.5. Differential scanning calorimetry (DSC)

Evidence for surfactant assembly into bilayers in surfactant-polymer composite films can be obtained by observing gel-to-liquid crystal phase transition with DSC. This phase transition is related to the onset of fluidity of the surfactant hydrocarbon tails arranged in bilayers [13,14].  $2C_{12}N^+PA^-$  films demonstrated a major phase transition temperature ( $T_c$ ) at  $18^\circ\text{C}$ , while Mb- $2C_{12}N^+PA^-$  films showed  $T_c$  at  $20^\circ\text{C}$  (Table 2). These results indicate that  $2C_{12}N^+$  surfactants are arranged in bilayers in both films. The similar  $T_c$  values for  $2C_{12}N^+PA^-$  and Mb- $2C_{12}N^+PA^-$  films suggest the presence of protein does not seem to influence the bilayer structure of  $2C_{12}N^+PA^-$  films. The  $T_c$  values of some other synthetic lipids and Mb-lipid films are also listed in Table 2 for comparison.

### 3.6. X-ray diffraction

The lowest reflection angle  $2\theta$  of X-ray diffraction for polyionic complex films can be used to obtain the inter-layer basal spacing of the films through Bragg's law [46,47]. This small angle peak was observed for both  $2C_{12}N^+PA^-$  and Mb- $2C_{12}N^+PA^-$  composite films in  $1-10^\circ$  region of  $2\theta$  (Fig. 6a and b). Similar patterns and almost the same peak positions were observed in X-ray



diffraction experiments for both films. For  $2C_{12}N^+PA^-$  films, the peak at  $2.92^\circ$  gave the  $PA^-$  basal spacing of  $30.3 \text{ \AA}$ , while for Mb- $2C_{12}N^+PA^-$  films, the peak at  $2.96^\circ$  showed a basal spacing of  $29.9 \text{ \AA}$ . This indicates the intercalation of macromolecule Mb does not expand the inter-layer spacing of  $2C_{12}N^+PA^-$  films. Rather sharp  $2\theta$  peaks suggest well-defined layer orders in both films.

### 3.7. Catalytic reactivity

Electrocatalytic reduction of oxygen by Mb- $2C_{12}N^+PA^-$  films was examined by cyclic voltammetry. When certain volume of air was passed through a pH 5.5 buffers by a syringe, compared to the reduction peak of the first redox pair for Mb- $2C_{12}N^+PA^-$  films without oxygen present (Fig. 7c), a significant increase in reduction peak at about  $-0.19 \text{ V}$  was observed (Fig. 7d). This increase in reduction peak was accompanied by the disappearance of the oxidation peak for MbFe(II) because MbFe(II) had reacted with oxygen. An increase in the amount of oxygen in the solution increased the reduction peak current (Fig. 7e). For  $2C_{12}N^+PA^-$  films with no Mb

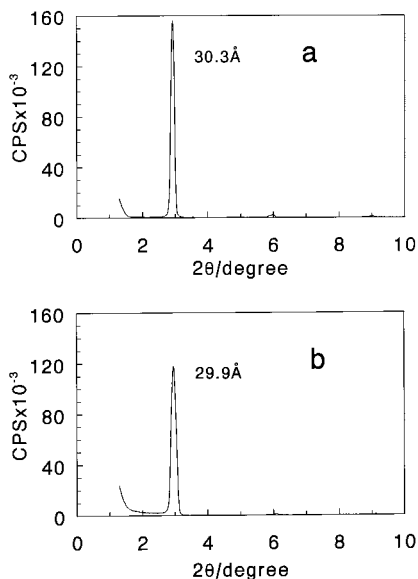


Fig. 6. X-ray diffraction patterns for (a)  $2C_{12}N^+PA^-$  and (b) Mb- $2C_{12}N^+PA^-$  films.

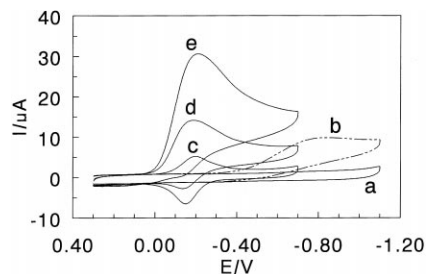


Fig. 7. Cyclic voltammograms at  $0.1 \text{ V s}^{-1}$  in 5 ml of pH 5.5 buffers: (a)  $2C_{12}N^+PA^-$  films with no oxygen present; (b)  $2C_{12}N^+PA^-$  films after 40 ml of air was injected into a sealed cell; (c) Mb- $2C_{12}N^+PA^-$  films with no oxygen present; (d) Mb- $2C_{12}N^+PA^-$  films after 40 ml of air was injected; (e) Mb- $2C_{12}N^+PA^-$  films after 80 ml of air was injected.

incorporated, the peak for direct reduction of oxygen was observed at about  $-0.75 \text{ V}$  (Fig. 7b), far more negative than the catalytic peak potential. Catalytic efficiency expressed as the ratio of reduction peak current of MbFe(III) in the presence ( $I_c$ ) and absence of oxygen ( $I_d$ ),  $I_c/I_d$ , decreased with increasing scan rate. All of these results are characteristic of reduction of oxygen by electrochemical catalysis with Mb- $2C_{12}N^+PA^-$  films [39].

The electrochemical catalysis of reduction of PCE by Mb- $2C_{12}N^+PA^-$  films was also tested by CV. The results showed that the catalytic reduction peak of PCE was not observed at the potential of the first peak pair for Mb- $2C_{12}N^+PA^-$  films without PCE in solution, but at the potential of the second one. When PCE was added into a pH 5.5 buffer solution, an increase in the MbFe(II) reduction peak at  $-1.1 \text{ V}$  was observed (Fig. 8c), compared to the reduction peak for the films without PCE present (Fig. 8b). This increase in reduction peak for Fe(II) was accompanied by the disappearance of the MbFe(I) oxidation peak. The reduction peak current increased with increasing the concentration of PCE in the solution (Fig. 8d). These results indicate reaction of MbFe(I) with PCE in a catalytic cycle, presumably resulting in the reductive dechlorination of PCE. For  $2C_{12}N^+PA^-$  films with no Mb incorporated, the direct reduction peak of PCE would appear at the potential more negative than  $-1.8 \text{ V}$  (Fig. 8a). The catalytic efficiency ( $I_c/I_d$ ) de-

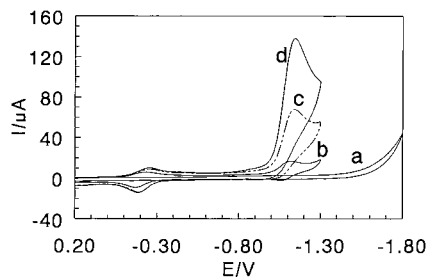


Fig. 8. Cyclic voltammograms at  $0.1 \text{ V s}^{-1}$  in pH 5.5 buffers: (a)  $2\text{C}_{12}\text{N}^+\text{PA}^-$  films in buffers containing  $40 \mu\text{M}$  PCE; (b)  $\text{Mb-}2\text{C}_{12}\text{N}^+\text{PA}^-$  films in buffers containing no PCE; (c)  $\text{Mb-}2\text{C}_{12}\text{N}^+\text{PA}^-$  films in buffers containing  $40 \mu\text{M}$  PCE; (d)  $\text{Mb-}2\text{C}_{12}\text{N}^+\text{PA}^-$  films in buffers containing  $120 \mu\text{M}$  PCE.

creased with increasing of scan rate (Fig. 9), which is also characteristic of electrocatalytic reduction of PCE by  $\text{Mb-}2\text{C}_{12}\text{N}^+\text{PA}^-$  films [39].

The catalytic reduction of PCE by  $\text{Mb-}2\text{C}_{12}\text{N}^+\text{PA}^-$  films was used to detect and determine PCE in solution. Fig. 10a shows the calibration curve for the system. The reduction peak height of PCE on  $\text{Mb-}2\text{C}_{12}\text{N}^+\text{PA}^-$  films had a linear relationship with PCE concentration in a range of  $10\text{--}100 \mu\text{M}$  with a correlation coefficient of 0.999 and detection limit of  $2 \mu\text{M}$ . The level-off of the peak currents was observed when the concentration of PCE was above  $100 \mu\text{M}$ .

The electrocatalysis of other organohalides with  $\text{Mb-}2\text{C}_{12}\text{N}^+\text{PA}^-$  films were also studied. For instance, TCE showed similar electrocatalytic behaviors to PCE. The catalytic reduction peak current of TCE had a linear relationship with its concentration between  $10\text{--}100 \mu\text{M}$  ( $r = 0.997$ )

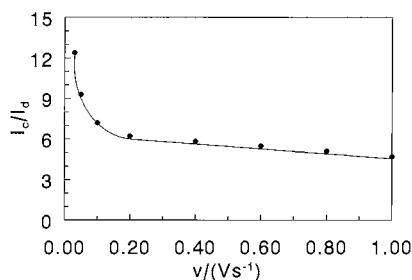


Fig. 9. Influence of scan rate on catalytic efficiency,  $I_c/I_d$ , for  $\text{Mb-}2\text{C}_{12}\text{N}^+\text{PA}^-$  films in pH 5.5 buffers, where  $I_d$  is the CV reduction peak current in buffers without PCE and  $I_c$  is the CV reduction peak current in buffers containing  $40 \mu\text{M}$  PCE.

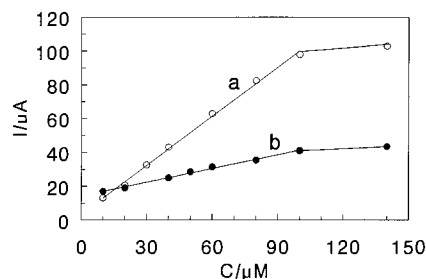


Fig. 10. Calibration curves of  $\text{Mb-}2\text{C}_{12}\text{N}^+\text{PA}^-$  films in pH 5.5 buffers at CV scan rate of  $0.1 \text{ V s}^{-1}$  for (a) PCE and (b) TCE systems.

with detection limit of  $2 \mu\text{M}$  (Fig. 10b). However, trichloroacetic acid (TCA) did not show any catalytic behavior at the  $\text{Mb-}2\text{C}_{12}\text{N}^+\text{PA}^-$  films at all, indicating the films have some selectivity to the substrates. All of these results demonstrate the potential application of the stable  $\text{Mb-}2\text{C}_{12}\text{N}^+\text{PA}^-$  films as a sensor for detecting some organohalide pollutants.

## 4. Discussion

### 4.1. Electrochemical properties

Nearly reversible cyclic voltammograms for Mb were obtained when  $\text{Mb-}2\text{C}_{12}\text{N}^+\text{PA}^-$  films were placed in blank buffers (Fig. 1b), indicating direct electron transfer between Mb and PG electrode in  $2\text{C}_{12}\text{N}^+\text{PA}^-$  films. Electron transportation was much faster for  $\text{Mb-}2\text{C}_{12}\text{N}^+\text{PA}^-$  films in buffers than for Mb in solution on bare PG [13,15], on which little evidence of electron transfer was observed for Mb. Thus,  $2\text{C}_{12}\text{N}^+\text{PA}^-$  films must have great effect on kinetics of electrode reaction for Mb. The role of the films in enhancing Mb electron transfer is probably because the films inhibit adsorption of the macromolecules from Mb solution including denatured Mb on the electrodes, which could otherwise block electron transfer to Mb [15]. The films allow an 'opened path' for the electrons between Mb and underlying electrodes. Another possibility is the orientation of Mb in  $2\text{C}_{12}\text{N}^+\text{PA}^-$  films or its interactions with surfactant  $2\text{C}_{12}\text{N}^+$  may be more

favorable to the electron transfer. For Mb- $2C_{12}N^+PA^-$  films, the value of apparent heterogeneous electron transfer rate constant ( $k_s$ ) is smaller than that for  $2C_{12}N^+Br^-$  and other films (Table 1). The exact reasons for this has not yet been very clear. It is probably because the introduction of layered polyions between surfactant bilayers increases the distance between redox center of Mb and underlying PG, and also increases the resistance of electron transfer for Mb. But all of them are in the same order.

The formal potential ( $E^\circ$ ) of MbFe(III)/Fe(II) couple in  $2C_{12}N^+PA^-$  films is very similar to that in  $2C_{12}N^+Br^-$  films, but slightly more negative than that in  $2C_{12}N^+Br^-$ -Nafion films and more positive than those in DMPC, DLPC and AQ films (Table 1). This confirms a specific influence of film environment on  $E^\circ$  of heme proteins which had been reported previously [18,19,41]. Film components may shift formal potentials through interactions with the protein or by their influence on the electrode double-layer [18,41]. Similar  $E^\circ$  values for Mb- $2C_{12}N^+PA^-$  and Mb- $2C_{12}N^+Br^-$  films suggest  $2C_{12}N^+PA^-$  films most probably have the similar surfactant multibilayer structure to that of  $2C_{12}N^+Br^-$  films, which was confirmed previously [13].

The linear relationship between cathodic peak current and scan rate for Mb- $2C_{12}N^+PA^-$  films, combined with nearly constant surface concentration for electroactive Mb in the films at different scan rates, suggests the surface or thin-layer electrochemical behavior [38] for Mb in  $2C_{12}N^+PA^-$  films. That is, almost all electroactive MbFe(III) in the films has been reduced to MbFe(II) on the forward scan to more negative potentials, with full conversion of MbFe(II) back to MbFe(III) on the reverse positive scan.

Electrochemical experiments for Mb in  $2C_{12}N^+PA^-$  films verify that pH influences the CV formal potential ( $E^\circ$ ) (Figs. 3 and 4), which is similar to that for Mb- $2C_{12}N^+Br^-$  and Mb-PC films [18], as well as Mb-AQ films [19]. However, the slope of  $-27 \text{ mV pH}^{-1}$  for linear plot of  $E^\circ$  versus pH at pH between 4 and 9 for Mb- $2C_{12}N^+PA^-$  films is far below the theoretical value of  $-59 \text{ mV pH}^{-1}$  at  $25^\circ\text{C}$  for a reversible, proton-coupled single electron transfer [43,44]. The expla-

nation on this has yet been unclear and needs to be further studied. But one thing for sure is that the electron transfer of MbFe(III)/Fe(II) couple in  $2C_{12}N^+PA^-$  films is accompanied by proton transportation.

When Mb- $2C_{12}N^+PA^-$  films were placed into buffers at pH between 5.5 and 7.0, the Soret band at 406 nm was close to that of dry Mb- $2C_{12}N^+PA^-$  films at 408 nm, as well as that of dry Mb films alone. This indicates that Mb essentially retains its conformation of native state in the medium pH range. Soret bands of Mb in  $2C_{12}N^+PA^-$  films shifted blue from 406 nm when the pH changed towards acidic direction from 5.5, and became a broad band around 390 nm at pH 3.5 (Fig. 5c). This suggests at least the partial denaturation of Mb in  $2C_{12}N^+PA^-$  films at  $\text{pH} < 4$ , as observed previously in aqueous solutions [45,48,49] and in surfactant films [18].

A partly unfolded form of MbFe(III) called a molten globule predominates in solution at about pH 5–3.5 [50]. A conformer of Mb similar to this molten globule may be formed in cast surfactant films at pH 4.8–3, and accepts electron from the electrode more readily than the native form [18]. Thus, the existence of a partly unfolded conformer similar to the molten globule in  $2C_{12}N^+PA^-$  films at  $\text{pH} < 4$  seems a reasonable suggestion. The relative pH-independence of  $E^\circ$  in this pH range indicates that this form may be reduced directly in  $2C_{12}N^+PA^-$  films. It is of interest that the pH below which Mb unfolding occurs as shown by spectroscopic studies and the inflection point in  $E^\circ$  versus pH plots is a bit lower in  $2C_{12}N^+PA^-$  films (pH 4.0) than in  $2C_{12}N^+Br^-$  films (pH 4.9) [18]. Fully folded Mb conformations may be more stable in  $2C_{12}N^+PA^-$  films by interactions with the components of the films.

#### 4.2. Stability and structural factors

$2C_{12}N^+PA^-$  could take up Mb from its solution at pH 5.5. The CV peak currents grew with soaking time until getting to the fully loaded state in about 60 h (Fig. 2). The CV peak potentials of fully loaded  $2C_{12}N^+PA^-$  films with Mb in blank pH 5.5 buffers are similar to those of casting

Mb- $2C_{12}N^+PA^-$  films in the same buffers at the same scan rate. The polyions  $PA^-$  with negative charges on their backbones can combine positively charged surfactants  $2C_{12}N^+$  by Coulombic attraction and form neutral precipitation of  $2C_{12}N^+PA^-$ . Thus, the polyions complex composite films of  $2C_{12}N^+PA^-$  on PG surface are essentially neutral. At pH 5.5, with its isoelectric point (pI) at pH 6.8 [51,52], Mb shows positive surface charges. The driving force for Mb to enter into  $2C_{12}N^+PA^-$  films would then be mainly hydrophobic interaction between macromolecule Mb and  $2C_{12}N^+PA^-$  films, in which tail-to-tail bilayer of surfactant constitutes the hydrophobic region of the films. This hydrophobic interaction would also be mainly responsible for the retention of Mb and excellent stability for Mb- $2C_{12}N^+PA^-$  films in blank buffers.

Mb- $2C_{12}N^+PA^-$  films seem to be more stable than films of Mb- $2C_{12}N^+Br^-$  or Mb- $2C_{12}N^+Br^-$ -Nafion composite films [16]. The Mb- $2C_{12}N^+PA^-$  films essentially retained their CV signals upon storage in buffers for about 2 months. The results suggest that  $2C_{12}N^+PA^-$  films have better adhesion to PG electrodes and strong interactions with Mb.

The gel-to-liquid crystal transition temperature ( $T_c$ ) at 18°C measured by DSC for  $2C_{12}N^+PA^-$  films (Table 2) suggests that surfactants  $2C_{12}N^+$  in  $2C_{12}N^+PA^-$  films are arranged in multiple bilayer structure similar to that proposed for  $2C_{12}N^+Br^-$  films [13]. This lamellar state contains considerable water between the bilayers [53,54]. Larger  $T_c$  value of 18°C for  $2C_{12}N^+PA^-$  films compared with 11°C for  $2C_{12}N^+Br^-$  films (Table 2) might be caused by some specific influences of  $PA^-$  backbone. Incorporation of Mb into  $2C_{12}N^+PA^-$  films caused a slight increase in  $T_c$ , which is also observed for Mb- $2C_{12}N^+Br^-$  films (Table 2). This suggests that Mb binding to the lipid films do not significantly disturb the alkyl chain order of the lipid bilayers.

Our voltammetric experimental temperature of  $25 \pm 2^\circ C$  is larger than  $T_c$  of 20°C for Mb- $2C_{12}N^+PA^-$  films, showing that the films were in the more fluid liquid crystal phase when CV scanned. This may also contribute to the enhanced electron transfer between Mb and PG electrodes in  $2C_{12}N^+PA^-$  films.

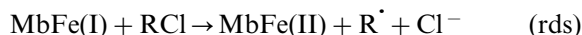
The sharp and well-defined X-ray diffraction peak (Fig. 6a), as well as DSC results (Table 2), supports the proposal that surfactants  $2C_{12}N^+$  are arranged in ordered bilayer structure intercalated between  $PA^-$  layers in the multibilayer composite films. Since the twice length of hydrocarbon chain for  $2C_{12}N^+$  is about 34 Å [55], the smaller layer spacing of 30.3 Å for  $2C_{12}N^+PA^-$  films suggests the possibility of tilting or intercalation of hydrocarbon chains of  $2C_{12}N^+$  to some extent in surfactant bilayer region between polyions layers. These findings indicate that  $2C_{12}N^+$  amphiphiles exist as well-oriented multibilayers complexing with polyanions of  $PA^-$ , which pile up parallel to the film plane. These structure data are also consistent with those of other polyions complex cast films from dialkylammonium amphiphiles and polyanions reported by Kunitake et al. [28]. Mb- $2C_{12}N^+PA^-$  films showed layer spacing of 29.9 Å (Fig. 6b), indicating that Mb did not expand the interlayer spacing of the films. This suggests that Mb binding to the lipid films does not disturb the multibilayer structure in a large fraction of the ordered polyions complex  $2C_{12}N^+PA^-$  films.

#### 4.3. Catalytic reactivity

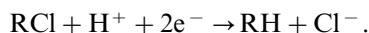
Cyclic voltammograms for Mb- $2C_{12}N^+PA^-$  films reacting with oxygen in the external solution demonstrate electrochemical catalysis at the potential of MbFe(III)/Fe(II) redox couple (Fig. 7). Similar voltammetric behaviors were observed previously in Mb- $2C_{12}N^+Br^-$  [56] and Mb-AQ [19] films, as well as on bare PG electrodes in aqueous buffers and in microemulsions containing Mb [57]. In the latter work [57], electrochemical reduction of MbFe(III) to MbFe(II) occurred at the electrode, followed by a fast reaction of MbFe(II) with oxygen. Mb is an oxygen carrier in biological systems and has a strong affinity for oxygen. This was proved by the large rate constant of  $2 \times 10^7 \text{ M}^{-1} \text{ s}^{-1}$  for the last reaction yielding MbFe(II)- $O_2$  at neutral pH [58]. The product of MbFe(II)- $O_2$  can then undergo electrochemical reduction at the potential of MbFe(III) reduction, producing hydrogen peroxide and MbFe(II) again [57]. While the mechanism of

catalytic reduction of oxygen at Mb-2C<sub>12</sub>N<sup>+</sup>PA<sup>-</sup> films has not yet been very clear, similar CV results to the solution work might be elucidated by the pathway suggested above for the solution work.

A highly reduced form of Mb, possibly MbFe(I) [35], is responsible for the second reduction peak for Mb-2C<sub>12</sub>N<sup>+</sup>PA<sup>-</sup> films. MbFe(I) most probably convert PCE or TCE to the less chlorinated species with positive shifts in electrode potential of about 1.0 V, compared to the potential for PCE or TCE in their direct reductions at blank 2C<sub>12</sub>N<sup>+</sup>PA<sup>-</sup> film electrodes. The mechanism of catalytic reduction of these organochlorides with Mb in 2C<sub>12</sub>N<sup>+</sup>PA<sup>-</sup> films might be expressed as follows [35]:



Thus, the overall reaction would be [59]:



The 1.0 V decrease of overpotential required for this reduction, combined with good stability of the films might be useful for practical applications in destroying or sensing pollutants.

## 5. Conclusions

Myoglobin in stable multibilayer films of 2C<sub>12</sub>N<sup>+</sup>PA<sup>-</sup> gave direct, reversible electron transfer with PG electrodes in buffer solutions. Effective electron transfer rates involving MbFe(III)/Fe(II) redox couple were greatly facilitated in microenvironment of 2C<sub>12</sub>N<sup>+</sup>PA<sup>-</sup> films compared with those on bare PG electrodes in Mb solutions. These ordered biomembrane-like films have excellent stability, and Mb is presumably stabilized mainly by hydrophobic interactions with the film components. Mb retained its native conformation in 2C<sub>12</sub>N<sup>+</sup>PA<sup>-</sup> films at medium pH. Mb-2C<sub>12</sub>N<sup>+</sup>PA<sup>-</sup> films on electrodes catalyzed reduction of some organohalide pollutants such as perchloroethylene and trichloroethylene, which provides a possibility of using the films for sensing pollutants.

## Acknowledgements

The support from the National Natural Science Foundation of China is acknowledged.

## References

- [1] K. Janacek, A. Kotyk, J. Koryta, *Biophysical Chemistry of Membrane Function*, Wiley, Chichester, UK, 1988.
- [2] G. Cevc, D. Marsh, *Phospholipid Bilayers*. Wiley, New York, 1987.
- [3] N. Nakashima, R. Ando, T. Kunitake, A. Harada, K. Okuyama, M. Takayanagi, *Chem. Lett.* (1983) 1577.
- [4] T. Kunitake, M. Shimomura, T. Kajiyama, A. Harada, K. Okuyama, M. Takayanagi, *Thin Solid Films* 121 (1984) L89.
- [5] T. Kunitake, A. Tsuge, N. Nakashima, *Chem. Lett.* (1984) 1783.
- [6] M. Shimomura, T. Kunitake, *J. Polym.* 16 (1984) 187.
- [7] J.H. Fendler, *Membrane Mimetic Chemistry*. Wiley, New York, 1982.
- [8] Z. Salamon, G. Tollin, *Bioelectrochem. Bioenerg.* 25 (1991) 447.
- [9] Z. Salamon, G. Tollin, *Bioelectrochem. Bioenerg.* 27 (1992) 381.
- [10] P. Bianco, A. Taya, J. Haladjian, *J. Electroanal. Chem.* 377 (1994) 299.
- [11] P. Bianco, J. Haladjian, *J. Electroanal. Chem.* 367 (1994) 79.
- [12] P. Bianco, J. Haladjian, *Electrochim. Acta* 39 (1994) 911.
- [13] J.F. Rusling, A.-E.F. Nassar, *J. Am. Chem. Soc.* 115 (1993) 11891.
- [14] A.-E.F. Nassar, Y. Narikiyo, T. Sagara, N. Nakashima, J.F. Rusling, *J. Chem. Soc., Faraday Trans.* 91 (1995) 1775.
- [15] A.-E.F. Nassar, W.S. Willis, J.F. Rusling, *Anal. Chem.* 67 (1995) 2386.
- [16] Q. Huang, Z. Lu, J.F. Rusling, *Langmuir* 12 (1996) 5472.
- [17] Z. Lu, Q. Huang, J.F. Rusling, *J. Electroanal. Chem.* 423 (1997) 59.
- [18] A.-E.F. Nassar, Z. Zhang, N. Hu, J.F. Rusling, T.F. Kumosinski, *J. Phys. Chem.* 101 (1997) 2224.
- [19] N. Hu, J.F. Rusling, *Langmuir* 13 (1997) 4119.
- [20] L. Stryer, *Biochemistry*, third ed., Freeman, New York, 1988.
- [21] E.F. Bowden, F.M. Hawkrige, H.N. Blount, in: S. Srinivasan, Y.A. Chizmadzhev, J.O.'M. Bockris, B.E. Conway, E. Yeager (Eds.), *Comprehensive Treatise of Electrochemistry*, vol. 10, Plenum, New York, 1985, pp. 297–346.
- [22] I. Taniguchi, K. Watanabe, M. Tominaga, F.M. Hawkrige, *J. Electroanal. Chem.* 333 (1992) 331.
- [23] S. Dong, Q. Chi, *Chin. J. Chem.* 11 (1993) 12.
- [24] B.C. King, F.M. Hawkrige, *J. Electroanal. Chem.* 237 (1987) 81.

- [25] J.F. Rusling, *Acc. Chem. Res.* 31 (1998) 363.
- [26] Y. Okahata, A. Shimizu, *Langmuir* 5 (1989) 954.
- [27] N. Hu, J.F. Rusling, *Anal. Chem.* 63 (1991) 2163.
- [28] N. Higashi, T. Kajiyama, T. Kunitake, *Macromolecules* 20 (1987) 29.
- [29] T. Kunitake, A. Tsuge, N. Nakashima, *Chem. Lett.* (1984) 1783.
- [30] K. Toko, N. Nakashima, S. Iiyama, K. Yamajuji, T. Kunitake, *Chem. Lett.* (1986) 1375.
- [31] Y. Okahata, G. Enna, K. Taguchi, T. Seki, *J. Am. Chem. Soc.* 107 (1985) 5300.
- [32] Y. Okahata, G. Enna, *J. Phys. Chem.* 92 (1988) 4546.
- [33] NSCA, *Pollution Handbook*, National Society for Clean Air and Environmental Protection, Brighton, UK, 1994.
- [34] C.C. Travis, S.T. Hester, *Environ. Sci. Technol.* 25 (1991) 815.
- [35] A.-E.F. Nassar, J.M. Bobbitt, J.D. Stuart, J.F. Rusling, *J. Am. Chem. Soc.* 117 (1995) 10986.
- [36] D. Lexa, J. Mispelner, J.-M. Saveant, *J. Am. Chem. Soc.* 103 (1981) 6806.
- [37] K.M. Kadish, in: A.B.P. Lever, H.B. Grey (Eds.), *Iron Porphyrins, Part II*, Addison-Wesley, Reading, 1983.
- [38] R.W. Murray, in: A.J. Bard (Ed.), *Electroanalytical Chemistry*, vol. 13, Marcel Dekker, New York, 1986, pp. 191–368.
- [39] A.J. Bard, L.R. Faulkner, *Electrochemical Methods*, Wiley, New York, 1980.
- [40] J.G. Osteryoung, J.J. O'Dea, in: A.J. Bard (Ed.), *Electroanalytical Chemistry*, vol. 14, Marcel Dekker, New York, 1986, pp. 209–308.
- [41] Z. Zhang, J.F. Rusling, *Biophys. Chem.* 63 (1997) 133.
- [42] J.J. O'Dea, J.G. Osteryoung, *Anal. Chem.* 65 (1993) 3090.
- [43] L. Meites, *Polarographic Techniques*, second ed., Wiley, New York, 1965.
- [44] A.M. Bond, *Modern Polarographic Methods in Analytical Chemistry*. Marcel Dekker, New York, 1980 pp. 27–45.
- [45] P. George, G. Hanania, *J. Biochem.* 52 (1952) 517.
- [46] M.J. Kamlet, J.L.-M. Abboud, M.H. Abraham, R.W. Taft, *J. Org. Chem.* 49 (1983) 2877.
- [47] C. Shi, J.F. Rusling, Z. Wang, W.S. Willis, A.M. Winiecki, S.L. Suib, *Langmuir* 5 (1989) 650.
- [48] E. Takahashi-Ushijima, H. Kihara, *Biochem. Biophys. Res. Commun.* 105 (1982) 965.
- [49] A.-S. Yang, B. Honig, *J. Mol. Biol.* 237 (1994) 602.
- [50] M. Brunori, G.M. Giacometti, E. Antonini, J. Wyman, *J. Mol. Biol.* 63 (1972) 139.
- [51] A. Bellelli, G. Antonini, M. Brunori, B.A. Springer, S.G. Sligar, *J. Biol. Chem.* 265 (1990) 18898.
- [52] A. Rossi-Fanelli, E. Antonini, D. Povoledo, in: A. Neuberger (Ed.), *Symposium on Protein Structure*, Methuen, London, 1958, pp. 144.
- [53] N. Hu, D.J. Howe, M.F. Ahmadi, J.F. Rusling, *Anal. Chem.* 64 (1992) 3180.
- [54] M.J. Kamlet, J.L.M. Abboud, M.H. Abraham, R.W. Taft, *J. Org. Chem.* 48 (1983) 2877.
- [55] J.F. Rusling, *Micropor. Mater.* 3 (1994) 1.
- [56] A.C. Onuoha, J.F. Rusling, *Langmuir* 11 (1995) 3296.
- [57] A.C. Onuoha, X. Zu, J.F. Rusling, *J. Am. Chem. Soc.* 119 (1997) 3979.
- [58] T. Wazawa, A. Matsuoka, G. Tajima, Y. Sugawara, K. Nakamura, K. Shikama, *Biophys. J.* 63 (1992) 544.
- [59] D.J. Dobson, S. Saini, *Anal. Chem.* 69 (1997) 3532.

# Simultaneous determination of catecholamines by ion chromatography with direct conductivity detection

C.L. Guan<sup>a</sup>, J. Ouyang<sup>a,\*</sup>, Q.L. Li<sup>a</sup>, B.H. Liu<sup>b</sup>, W.R.G. Baeyens<sup>c</sup>

<sup>a</sup> Department of Chemistry No. 15, Beijing Normal University, Beijing 100875, People's Republic of China

<sup>b</sup> Schmidt & Co. (H.K.) Ltd., Beijing 100037, People's Republic of China

<sup>c</sup> University of Ghent, Faculty of Pharmaceutical Sciences, Department of Pharmaceutical Analysis, Laboratory of Drug Quality Control, Harelbekestraat 72, B-9000 Ghent, Belgium

Received 7 April 1999; received in revised form 7 July 1999; accepted 16 July 1999

## Abstract

A simple method for simultaneous determination of three catecholamines using ion chromatography (IC) with direct conductivity detection (CD) based on the ionization of catecholamines in acidic medium without chemical suppression is developed in the present paper. The method could be used for the determination of these catecholamines in pharmaceutical preparations for the purpose of drug quality control. The recovery of catecholamines was more than 97% ( $n = 3$ ) and the relative standard deviation (R.S.D.) ( $n = 11$ ) was less than 2.1%. In a single chromatographic run, norepinephrine (NE), epinephrine (E) and dopamine (DA) can be determined in less than 10 min. The detection limits were found to be 0.001  $\mu\text{g/ml}$  for NE, 0.01  $\mu\text{g/ml}$  for E and DA respectively. Linear ranges were 0.01–50  $\mu\text{g/ml}$  for NE ( $r^2 = 0.9998$ ), 0.1–50  $\mu\text{g/ml}$  for E ( $r^2 = 0.9995$ ) and DA ( $r^2 = 0.9999$ ), respectively. © 2000 Elsevier Science B.V. All rights reserved.

**Keywords:** Catecholamine; Conductivity detection; Dopamine; Epinephrine; Ion chromatography; Norepinephrine

## 1. Introduction

Catecholamine drugs, such as epinephrine (E), norepinephrine (NE) and dopamine (DA), are important markers for the diagnosis of several diseases and are widely used in the treatment of bronchial asthma, hypertension, heart failure associated with organic heart disease and cardiac

surgery [1]. A number of methods have been reported for the determination of catecholamines by spectrophotometry [1–3], capillary electrophoresis [4] and chromatography with electrochemical detection [5–13], chemiluminescence detection [14] and fluorescence detection [15], etc. Amongst them high-performance liquid chromatography (HPLC) coupled to electrochemical detection offers advantages of high resolution with low detection limits. It has therefore been used as a very sensitive method for the determination of catecholamines in recent years. Although

\* Corresponding author. Tel.: +86-10-62348263; fax: +86-10-62200567.

E-mail address: jinoyang@ihw.com.cn (J. Ouyang)

octadecylsilyl (ODS) columns have been frequently used for the separation of the different catecholamines, an important limitation with such columns is that an organic solvent is required in order to achieve a good resolution which leads to complicated electrochemical behaviors when using electrochemical detection. Besides this limitation, electrochemical detection is not so popular in average analytical laboratories where ion chromatographic instruments have been installed because commercial ion chromatography instruments are normally equipped with only a conductivity detector. An electrochemical detector can of course be purchased but it is expensive and responds only to a limited number of compounds.

Therefore, a method was developed for the determination of catecholamines by using ion chromatography with conductivity detection. This method offers three advantages: Firstly, a commercial ion chromatography instrument can be applied directly to the determination of the three biologically important compounds without any modification. Secondly, a C18 column is replaced by an ion exchange column for the separation of the catecholamines, which allows an aqueous solution to be used as mobile phase. Thirdly, an expensive electrochemical detector becomes unnecessary. With this method, three important catecholamines, E, NE and DA, can be well separated using a cationic exchange column with dilute aqueous  $\text{HNO}_3$  solution as mobile phase.

## 2. Experiment

### 2.1. Apparatus

The ion chromatography (IC) apparatus was provided by Schmidt & Co. (H.K.) Ltd.; it consists of the 733 IC separation center, the 709 IC pump, and the 732 IC detector used to measure conductivity signal. An IBM personal computer employing IC metrodata software was used to record the chromatograms and to handle all data.

### 2.2. Reagents

Norepinephrine (NE), epinephrine (E) and dopamine hydrochloride (DA) were obtained from Sigma Chemical Co. (St. Louis, MO). The stock standard solutions of 210  $\mu\text{g/ml}$  NE and 406  $\mu\text{g/ml}$  E was prepared by dissolving NE and E in 0.12 mol/l hydrochloric acid, respectively. The stock standard solution of 210  $\mu\text{g/ml}$  DA was prepared with water. The stock standard mixed solution (50  $\mu\text{g/ml}$ ) was prepared by appropriately mixing three stock standard solutions with the mobile phase, which is described in the following section. These stock standard solutions were stored at 4°C for 1 month. The mobile phase was 1.0 mmol/l nitric acid. All other solutions were prepared by dissolving the analytical-reagent grade chemicals in water, except the stock solution of 25 mmol/l isonicotinic acid which was prepared with a mixture of water and anhydrous methanol (9:1).

### 2.3. Chromatographic conditions

The separation column was an IC column (Metrosep cation 1-2, 4.0  $\times$  125 mm) with a cationic pre-column. The mobile phase (1.0 mmol/l  $\text{HNO}_3$  solution) yielded an absolute conductivity of 325.0  $\mu\text{S/cm}$ . The optimum flow rate of the mobile phase was set to 1.0 ml/min, which resulted in a pressure of 5.4–6.0 MPa. The sample injection volume was 40  $\mu\text{l}$ . Catecholamine peaks were identified by comparing the retention time in the sample solution with that of standard solution. The content of NE, E and DA in the sample solution was quantified by comparing peak heights in elution profiles of sample with that of known standards.

## 3. Results and discussion

### 3.1. Optimization of chromatographic conditions

The key work of this study is to achieve separation of the three catecholamines by using ion exchange chromatography with an aqueous solution as mobile phase. To achieve baseline separa-



tion, a series of experiments were performed to examine the effects of various factors on the separation.

### 3.1.1. Optimization of mobile phase

Since the catecholamines are organo-amine species, a mobile phase that consisted of 2.5 mmol/l nitric acid and 5.0 mmol/l isonicotinic acid was used for the separation of NE, E and DA in the preliminary work. This condition is recommended by the Application Bulletin of Metrohm for the

separation of ammonium, methylamine, dimethylamine and trimethylamine. Under this condition, however, the E and DA were not completely separated. A series of new mobile phases had to be selected in order to obtain better separation. By keeping the concentration of isonicotinic acid at 5 mmol/l, the retention time of three components decreased with the change of nitric acid concentration in the 0.00–3.00 mmol/l range. Fig. 1 shows the effect of nitric acid on the separation at the concentrations of 0.75, 1.00, 1.25 and 1.50

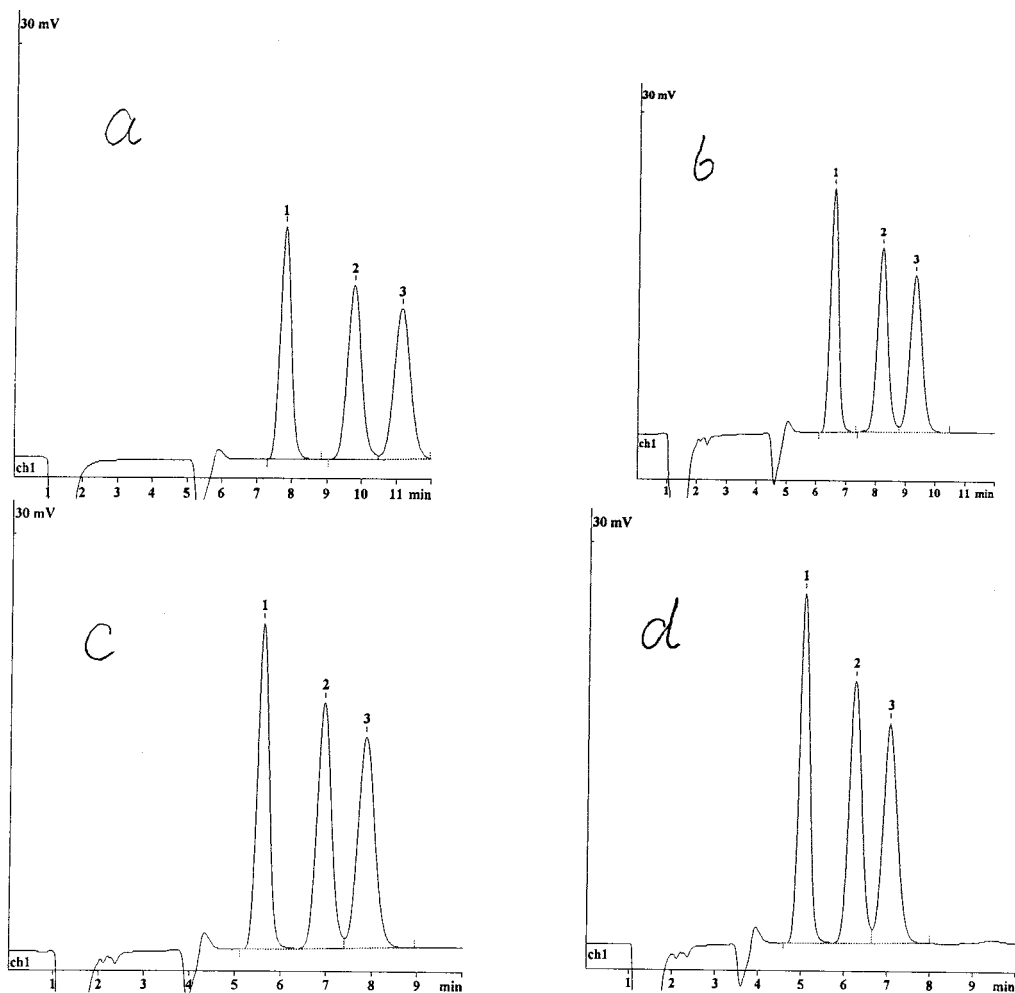


Fig. 1. Effect of nitric acid concentration on retention time of norepinephrine (NE), epinephrine (E) and dopamine (DA). 1, NE; 2, E; 3, DA. Chromatographic conditions: IC column, Metrosep cation 1-2 6.1010.000 ( $4.0 \times 125$  mm); flow rate, 1.0 ml/min; sample injection volume, 40  $\mu$ l. The mobile phase is described in the text. (a) 0.75 mmol/l of nitric acid; (b) 1.0 mmol/l of nitric acid; (c) 1.25 mmol/l of nitric acid; (d) 1.5 mmol/l of nitric acid.

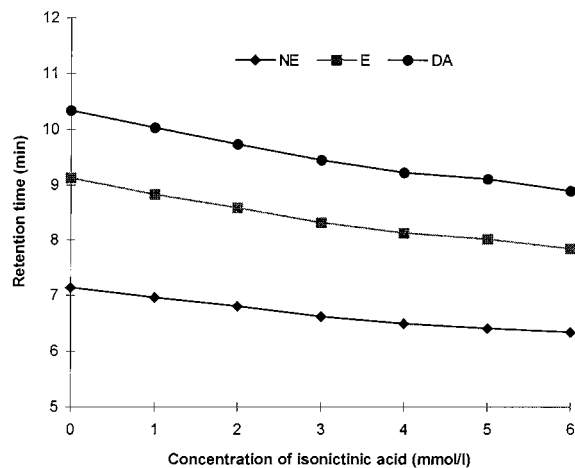


Fig. 2. Effect of isonicotinic acid concentration on retention time of norepinephrine (NE), epinephrine (E) and dopamine (DA). Chromatographic conditions are the same as listed in Fig. 1, except for the mobile phase, which is described in the text.

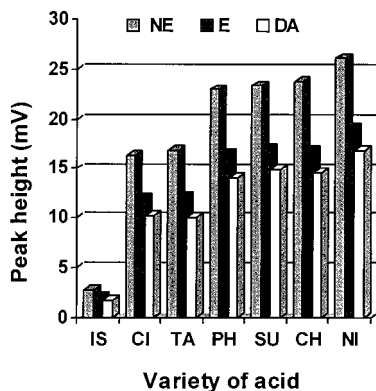


Fig. 3. Effects of varieties of acid. IS, isonicotinic acid (5 mmol/l); CI, citric acid (3 mmol/l); TA, tartaric acid (3 mmol/l); PH, phosphoric acid (1 mmol/l); SU, sulfuric acid (0.5 mmol/l); NI, nitric acid (1 mmol/l); CH, hydrochloric acid (1 mmol/l). IC chromatographic conditions: IC column, Metrosep cation 1-2 6.1010.000 (4.0 × 125 mm); flow rate, 1.0 ml/min; sample injection volume, 40  $\mu$ l; conductivity detection. NE, norepinephrine; E, epinephrine; DA, dopamine.

mmol/l. A good separation was observed at concentrations below 1.0 mmol/l nitric acid but lower concentrations led to a long retention time for the last peak. A concentration higher than 1.0 mmol/l, however, caused the last two peaks to overlap. Therefore, 1.0 mmol/l of nitric acid was applied to the subsequent study.

The effect of isonicotinic acid concentration on the catecholamine separation was also examined. The results showed that the effect on retention time was less significant with change in isonicotinic acid concentration in the range of 0.00–6.00 mmol/l (Fig. 2). In addition, a good separation could be obtained without the presence of isonicotinic acid. Therefore, isonicotinic acid was not used in the mobile phase for the subsequent study.

Besides nitric acid, the effects of a variety of acids on the separation of these three compounds were also examined. No significant improvement could be observed by using hydrochloric acid (1 mmol/l), sulfuric acid (0.5 mmol/l) or phosphoric acid (1 mmol/l). In fact, the peak height of each component reached the maximum value when 1.0 mmol/l nitric acid was used for determination of catecholamines (Fig. 3). Therefore, nitric acid was used throughout the subsequent study.

### 3.1.2. Effect of mobile phase flow rate

Flow rate affects not only separation efficiency but also the peak height of each component. The retention time and peak height of three compounds were examined at the flow rate of 0.6, 0.8, 1.0, 1.2 and 1.4 ml/min, respectively. The greatest peak height was achieved at 0.6 ml/min flow rate for E, NE and DA. Increasing the flow rate from 0.6 to 1.4 ml/min only led to a slight loss of peak height but a much longer retention time. To obtain efficient separation and adequate sensitivity, 1.0 ml/min flow rate was used throughout.

### 3.1.3. Effect of sample injection volume

Sample injection volume affects the peak height of the three compounds significantly. An increase in sample volume leads to an increase in peak height. Doubling the loop size brought an increase by a factor of 2 in peak height from 20 to 40  $\mu$ l but further increases in sample volume decreased resolution significantly. A 40- $\mu$ l sample volume was therefore used throughout the subsequent work.

Under the optimum conditions, the three catecholamines were well separated within 10 min, as indicated in Fig. 4.

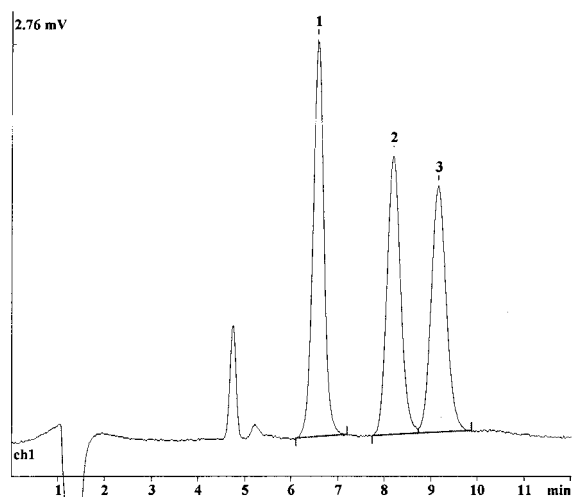


Fig. 4. Chromatogram of a standard containing 10  $\mu\text{g/ml}$  of norepinephrine (NE), epinephrine (E) and dopamine (DA). 1, NE; 2, E; 3, DA. Chromatographic conditions: IC column, Metrosep cation 1-2 6.1010.000 ( $4.0 \times 125$  mm); mobile phase, nitric acid (1 mmol); flow rate, 1.0 ml/min; sample injection volume, 40  $\mu\text{l}$ ; conductivity detection.

### 3.2. Linearity and detection limits

A series of working standard solutions containing NE, E and DA were prepared. The concentration range varied from 0.001 to 50  $\mu\text{g/ml}$ . Using the optimized conditions described above, the detection limit (signal-to-noise equal to 3) was 0.001  $\mu\text{g/ml}$  for NE, and 0.01  $\mu\text{g/ml}$  for E and DA. The linear range was 0.01–50  $\mu\text{g/ml}$  for NE and 0.1–50  $\mu\text{g/ml}$  for E and DA. The regression coefficient ( $r^2$ ) was 0.9998, 0.9995 and 0.9999 for NE, E and DA, respectively. The slope for NE, E and DA are 0.2377, 0.1811 and 0.1616, respectively, and

indicated that the sensitivity of the method is higher for NE than for E and DA. The relative standard deviation (R.S.D.) ( $n = 11$ ) for NE, E and DA was examined. No significant difference between the variation of inter- and intra-day data was observed. The values of R.S.D. are 1.23%, 1.10% and 2.10% for NE, E and DA, respectively. The results are summarized in Table 1.

### 3.3. Interference studies

The influences of common cations were investigated in the determination of 0.1  $\mu\text{g/ml}$  NE (6.58 min), E (8.20 min) and DA (9.18 min) using the proposed method. No significant interference was observed in the presence of 500-fold calcium (no signal detected), magnesium (no signal detected) and zinc (no signal detected), respectively. A 5-fold higher concentration of sodium (4.76 min) and 2-fold higher concentration of ammonium (5.09 min) did not cause significant influence. But the presence of potassium interfered with the determination of catecholamines because the retention time of potassium is 6.29, which is similar to the retention time of 6.58 for NE.

### 3.4. Sample analysis

The drug contents of injections of norepinephrine bitartrate, epinephrine hydrochloride and dopamine hydrochloride (a mixed sample containing: 2 mg/ml norepinephrine bitartrate, equivalent to 1 mg/ml norepinephrine; 1 mg/ml epinephrine; 10 mg/ml dopamine hydrochloride) were analyzed using the proposed method under the optimum conditions as described earlier.

Table 1  
Linearity, detection limit and relative standard deviation (R.S.D.)

Catecholamine	Linearity range ( $\mu\text{g/ml}$ )	Regression equation	Regression coefficient ( $r^2$ )	Detection limit ( $\mu\text{g/ml}$ )	R.S.D. (%) ( $n = 11$ )
NE	0.01–50	$y = 0.2377x + 0.0868$	0.9998	0.001	1.23
E	0.1–50	$y = 0.1811x - 0.0338$	0.9995	0.01	1.10
DA	0.1–50	$y = 0.1616x - 0.0174$	0.9999	0.01	2.10

Table 2  
Determination of catecholamines in pharmaceutical formulations

Preparation (injection)	Label (mg/ml)	Proposed method found (mg/ml)	R.S.D. (%) ( <i>n</i> = 3)
Norepinephrine bitartrate (Approval No. 921021)	2.0	1.98	1.43
Epinephrine hydrochloride (Approval No. 980929)	1.0	1.02	2.19
Dopamine hydrochloride (Approval No. 960803.1)	10.0	10.16	2.17

These injections were diluted directly using the mobile phase to the appropriate concentrations and injected into the sample loop for measurement. No clean-up procedure is involved. Catecholamine peaks were identified by comparing their retention times in the sample solution with those of standard solution and the content of NE, E and DA in the sample solution was quantified by comparing peak heights in elution profiles of sample with that of known standards. The presence of high concentration of sodium in the mixed injection had a slight influence on the assay for NE, but no other interference was found from the additives in the injections. The results are listed in Table 2. No significant differences could be observed between the present results and the label values.

In order to evaluate the validity of this method for the determination of the three compounds in pharmaceuticals, recovery studies were carried out on samples to which known amounts of NE, E and DA were added. The recoveries for the different concentration levels varied from roughly 97% to 103%, as shown in Table 3. The method shows

promise for the determination of pharmaceutical preparations.

#### 4. Conclusion

The present work demonstrated that ion chromatography can be successfully applied to the determination of biologically important compounds with aqueous solution as mobile phase. Although a conductivity detector suffers poor detection limits for the determination of the three pharmaceutical compounds in biological samples, it offers advantages of simple instrumentation and procedures and is therefore suitable for the routine control analysis of pharmaceutical preparations containing catecholamines.

#### Acknowledgements

The authors gratefully acknowledge Schmidt & Co. (H.K.) Ltd. for providing the ion chromatography apparatus.

Table 3  
Recovery of catecholamines added to pharmaceutical formulations

Preparation (injection)	Added (mg/ml)	Recovered (mg/ml)	Recovery (%) ( <i>n</i> = 3)
Norepinephrine bitartrate (Approval No. 921021)	0.8	0.81	101.3
	2.0	2.01	100.5
	4.0	4.06	101.6
Epinephrine hydrochloride (Approval No. 980929)	0.4	0.39	97.5
	1.0	1.01	101.0
	2.0	1.98	99.0
Dopamine hydrochloride (Approval No. 960803.1)	4.0	3.92	98.0
	10.0	10.20	102.0
	20.0	20.72	103.6

## References

- [1] J.J.B. Nevado, J.M.L. Gallego, P.B. Laguna, *Anal. Chim. Acta* 300 (1995) 293.
- [2] J.G. Li, J.R. Lu, *Fenxi Huaxue* 25 (1997) 314.
- [3] H.Y. Wu, J. Chen, W.G. Wang, L.L. Shen, *Fenxi Huaxue* 25 (1997) 496.
- [4] H.T. Chang, E.S. Yeung, *Anal. Chem.* 67 (1995) 1079–1083.
- [5] Y.H. Yang, Q. Li, *Hangtian Yixue Yu Yixue Gongcheng* 9 (1996) 217.
- [6] P. Kubalec, E. Brandsteterova, J. Lehotay, J. Cizmarik, *Pharmazie* 49 (1994) 12.
- [7] F. Mashige, Y. Matsushima, C. Miyata, R. Yamada, H. Anazawa, I. Sakuma, N. Takai, N. Shinozuka, A. Ohkubo, K. Nakahara, *Biomed. Chromatogr.* 9 (1995) 221.
- [8] M. Candito, F. Bree, A.M. Krstulovik, *Biomed. Chromatogr.* 10 (1996) 40.
- [9] H.B. He, C.M. Stein, B. Christman, A.J.J. Wood, *J. Chromatogr. B* 701 (1997) 115.
- [10] A.Z. Zhu, J. Liu, C.G. Fu, *Fenxi Ceshi Xuebao* 16 (6) (1997) 47.
- [11] M. Hay, P. Mormede, *J. Chromatogr. B* 703 (1997) 15.
- [12] M. Radjaipour, H. Raster, H.M. Liebich, *Eur. J. Clin. Chem. Clin. Biochem.* 32 (1994) 609.
- [13] J.M. Sanchis Mallols, J.R. Torres Lapasio, R.M. Villanueva Camanas, G. Ramis-Ramos, *Chromatographia* 39 (9/10) (1994) 591.
- [14] G.H. Ragab, H. Nohta, M. Kai, Y. Ohkura, K. Zaitso, *J. Pharm. Biomed. Anal.* 13 (1995) 645.
- [15] M.K. Lakshmana, T.R. Raju, *Anal. Biochem.* 246 (1997) 166.

# Hot-wire amperometric monitoring of flowing streams

Joseph Wang<sup>a,\*</sup>, Markus Jasinski<sup>b</sup>, Gerd-Uwe Flechsig<sup>b</sup>, Peter Grundler<sup>b,1</sup>,  
Baomin Tian<sup>a</sup>

<sup>a</sup> Department of Chemistry and Biochemistry, New Mexico State University, Las Cruces, NM 88003, USA

<sup>b</sup> Fachbereich Chemie, Universität Rostock, D-18051 Rostock, Germany

Received 31 March 1999; accepted 22 July 1999

## Abstract

This paper describes the design of a hot-wire electrochemical flow detector, and the advantages accrued from the effects of locally increased temperature, mainly thermally induced convection, upon the amperometric monitoring of flowing streams. A new hydrodynamic modulation voltammetric approach is presented, in which the solution flow rate remains constant while the temperature of the working electrode is modulated. Factors influencing the response, including the flow rate, temperature pulse, or applied potential, have been investigated. The hot-wire operation results also in a significant enhancement of the flow injection amperometric response. The minimal flow rate dependence observed with the heated electrode should benefit the on-line monitoring of streams with fluctuated natural convection, as well as various in-situ remote sensing applications. © 2000 Elsevier Science B.V. All rights reserved.

**Keywords:** Electrochemical detection; Flow analysis; Heat pulse; Hot wire electrochemistry; Hydrodynamic modulation

## 1. Introduction

Electroanalytical flow systems are being widely used in automated flow systems (such as flow-injection analysis), for on-line monitoring of environmental or industrial streams, or for the monitoring of chromatographic effluents [1–3]. Current–potential amperometry is usually employed in connection to several configurations of electrochemical flow detectors. Application of

hydrodynamic theory is commonly used for optimizing the performance of flow-through amperometric electrodes [4,5]. The limiting current response of flow-through electrodes is thus given by:

$$i_1 = nFAKDCU^\alpha \quad (1)$$

where  $n$  is the number of electrons transferred,  $F$  is the value of the Faraday,  $A$  is the surface area of the electrode,  $C$  is the bulk concentration,  $U$  is the flow rate,  $D$  is the diffusion coefficient, and  $K$  and  $\alpha$  are constants. Well-defined hydrodynamic conditions, with high rate of mass transport, are essential for the successful use of electrochemical detectors.

\* Corresponding author. Tel.: +1-505-646-2505; fax: +1-505-646-2649.

E-mail address: joewang@nmsu.edu (J. Wang)

<sup>1</sup> Also corresponding author.

The present paper describes a new approach for enhancing the performance of electrochemical detectors based on the use of hot-wire electrochemistry. Hot-wire electrochemistry has been shown recently to offer several advantages for electroanalytical work [6–8]. Such use of heated electrodes induces thermally efficient convection within a thin solution layer near the surface (with the bulk solution not being exposed to elevated temperatures). This is realized by integration of the working electrode both in the heating and potentiostatic circuitry, and applying an alternate heating current. The use of hot-wire electrochemistry has already been shown to be advantageous for electroanalytical applications ranging from stripping voltammetry [9] to voltammetry above the boiling point [7]. Similarly, in the following sections we will describe the design of a hot-wire flow detector and demonstrate the advantages accrued from the resulting hot-wire amperometric flow detection in connection to flow-injection analysis and a new form of hydrodynamic (thermal) modulation voltammetry.

## 2. Experimental

### 2.1. Apparatus

The flow system, shown in Fig. 1(B), consisted of a FIALab (Alitea, Sweden) peristaltic pump (b)

and an electrochemical detector (d) connected to a 264A Polarographic Analyzer/Stripping Voltmeter (f) (EG&G Princeton Applied Research). An OmniScribe recorder (Houston Instrument) was used to register the amperometric response signals. The detector (Fig. 1, A) was located downstream of the injection unit (c) (six-way valve, 200  $\mu$ l injection loop). A Ag/AgCl (3 M NaCl) reference electrode (Model RE-1, BAS Inc.) and a platinum wire counter electrode were located in the downstream waste beaker (e). Teflon tubing was used for interconnecting the various components. The two side-terminals of the detector were connected to the heating device and the middle one to the electrochemical analyzer. The heating device consisted of a laboratory-made sine-wave power generator that was connected to the assembly via a high frequency transformer. The frequency of the alternating current was 100 kHz in all experiments. Detailed information about the heating devices and techniques, as well as on the temperature calibration, has been described earlier [6–9].

### 2.2. Reagents

Ferrocyanide and potassium phosphate were received from Sigma. Sodium hydroxide was obtained from Aldrich. The ferrocyanide stock solution (0.1 M) was prepared by dissolving the appropriate amount of  $K_4[Fe(CN)_6]$  in deionized

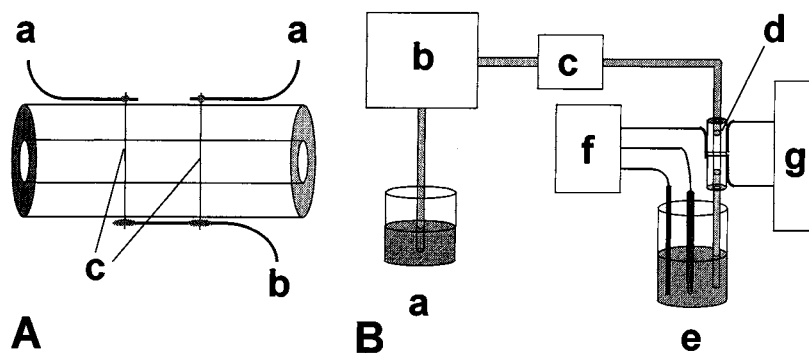


Fig. 1. Schematic of the hot-wire flow detector (A) and corresponding experimental setup (B). (A) Detector: (a) connections to the heating device; (b) connection to the potentiostat; (c) gold wires. (B) Experimental setup: (a) carrier reservoir; (b) pump; (c) injection valve; (d) detector; (e) waste collector with the reference and counter electrode; (f) potentiostat and recorder; (g) heating device.

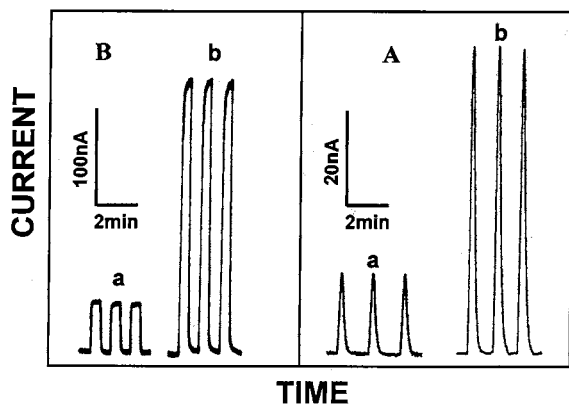


Fig. 2. Amperometric response to 0.2 mM  $K_4[Fe(CN)_6]$  in phosphate buffer (0.2 M, pH 7.3). Applied potential, +0.20 V. (A) Flow injection amperometry at 20°C (a) and 80°C (b), using a flow rate of 0.37 ml/min. (B) Continuous flow with (a) flow pulses (between 0.37 and 1.23 ml/min) at 20°C and (b) heat pulses (between 20 and 80°C) at 0.37 ml/min.

water. The phosphate buffer solution (0.2 M, pH 7.3) was prepared by dissolving the appropriate amount of potassium phosphate in deionized water. The pH was adjusted with sodium hydroxide solution.

### 2.3. Preparation of the gold fiber flow electrode

Following the principle design described in [10], a Tygon tube (1.5 mm inner diameter, 3 mm outer diameter, 30 mm long) was fixed together with three contact wires onto a ceramic plate ( $0.5 \times 10 \times 33.5$  mm) using 5-min epoxy resin. In the next step, two pieces of gold wire (25  $\mu$ m in diameter, delivered by Goodfellow, arranged in series, distance 4 mm) were implemented into the center of the tube at an angle of 90° to the length of the tube. To do this an injection needle was inserted through the tube. After that, a gold wire piece was inserted into the needle. Then the needle was removed, leaving the wire in the tube. The gold wire pieces were then connected to the contact wires by soldering in such a way that a symmetrical electrode design was obtained. In the last step, the whole arrangement was covered with epoxy resin to protect the damageable contacts.

### 2.4. Procedure

All results were obtained using a constant-potential amperometric detection mode. The phosphate buffer solution, which served as the carrier, was delivered by the FIA lab pump through the entire flow system. The analyte was either added to the phosphate buffer reservoir (before the pump) for continuous flow or injected with the six-way valve for flow injection experiments. On-line thermal modulation experiments were carried out by switching the heat 'on' and 'off' every 30 s, while maintaining a constant low flow rate. The flow rates were determined by weighing the volume of water pumped through the system over a 1 min period. All experiments were carried out in the presence of oxygen.

### 3. Results and discussion

Combining the concept of hot-wire electrochemistry and on-line amperometric monitoring can be readily accomplished by constructing a gold-fiber flow cell (Fig. 1A), analogous to the carbon-fiber flow electrode of Jagner and coworkers [10]. For this purpose, the gold fiber was inserted through the center of a Tygon tube flow channel, with the reference and counter electrode located in the downstream reservoir. The working electrode was then connected to both the heating device and the potentiostatic circuitry.

Fig. 2A displays flow-injection amperometric signals for  $2 \times 10^{-4}$  M ferrocyanide obtained in the conventional fashion (heat 'off'; a) and by heating the working electrode (b). The latter results in a substantial (four-fold) enhancement of the current response, without compromising the noise level or dynamic properties. Such signal amplification, associated primarily with the additional heat-induced convection (inherent to hot-wire electrochemistry), is achieved while maintaining low carrier flow rate (of 0.37 ml/min). Significantly higher flow rates would be required to achieve a similar sensitivity without heating the electrode.

The ability to thermally induce forced-convective transport in connection to low solution flow



rates can greatly benefit the monitoring of flowing streams. In particular, it paves the way for a new hydrodynamic modulation technique based on the use of periodic heating pulses. Hydrodynamic modulation voltammetry has been designed for discriminating against the major components of the background current at solid electrodes [11,12]. The application of hydrodynamic modulation voltammetry to flowing streams commonly re-

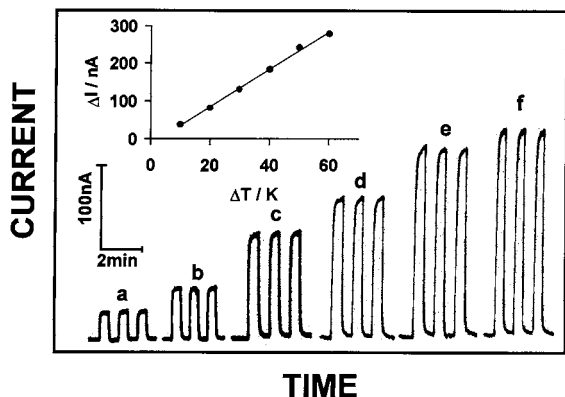


Fig. 3. Effect of the temperature pulses on the amperometric response to 0.2 mM  $K_4[Fe(CN)_6]$  with  $\Delta T$  of 10 (a), 20 (b), 30 (c), 40 (d), 50 (e) and 60 (f) K. Flow rate, 0.37 ml/min. Other conditions, as in Fig. 2B(b).

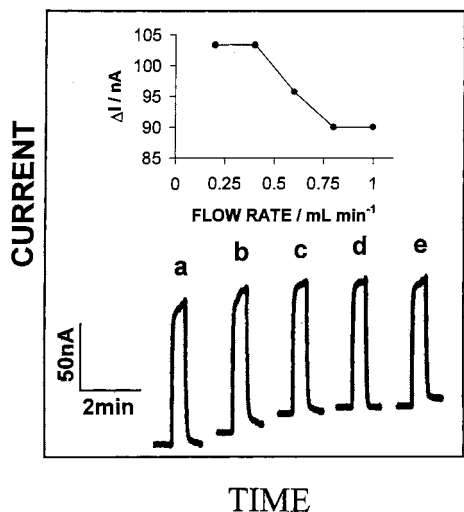


Fig. 4. Effect of flow rate upon the thermal modulation response to 0.2 mM  $K_4[Fe(CN)_6]$ . Flow rate: 0.2 (a), 0.4 (b), 0.6 (c), 0.8 (d) and 1.0 (e) ml/min.  $\Delta T = 30$  K. Other conditions, as in Fig. 2B(b).

quires a pulsation of the solution flow rate, which is not convenient in many practical situations [12]. The new thermal modulation approach is based on maintaining a constant low solution flow rate while switching the electrode heating 'on' and 'off'. Such thermal pulsing produces a temperature-dependent current amplitude. Fig. 2B compares the pulsed-flow (a) and pulsed-heat (b) amperometric response to ferrocyanide. The use of the thermal modulation results in a five-fold enhancement of the current amplitude (vs. the conventional pulsed flow operation). Such enhancement indicates that the flux of ferrocyanide to the surface at the 'on' temperature (80°C) is substantially higher than that at the 'high' flow rate (1.23 ml/min).

The resulting current difference (amplitude) is attributed to the effect of the thermal modulation upon different factors. In some cases, depending on the actual value of redox entropy, the temperature jump can add a thermo-e.m.f. contribution to the applied potential that may bring about a current increase if working in a specific potential region. In every case, independent of thermodynamic redox properties, there is a well-defined effect on the transport properties that can be described by changes in the thickness of the diffusion layer ( $\delta$ ) and upon the diffusion coefficient ( $D$ ). The difference in the limiting currents may thus be described by the following equation:

$$\Delta i_1 = i_{1,H} - i_{1,L} = nFAC \left[ \frac{D_H}{\delta_H} - \frac{D_L}{\delta_L} \right] \quad (2)$$

with the subscripts H and L designating the high and low temperatures of the electrode, respectively.

Fig. 3 shows the stopped-heating amperometric response for a flowing  $2 \times 10^{-4}$  M ferrocyanide solution obtained with different 'on/off' temperature differences ranging from 10 (a) to 60 (f) K. As expected (from the decreased  $\delta_H$ ; Eq. (2)), the current difference increases linearly with the temperature difference, i.e. increases over six-fold between  $\Delta T$  of 10–60 K (see also the resulting plot). Note also that the response times (both 'on' and 'off') increase upon raising the 'on' temperature. 'On'/'Off' response times of 8 and 22 s are observed for  $\Delta T$  of 10 and 50 K.

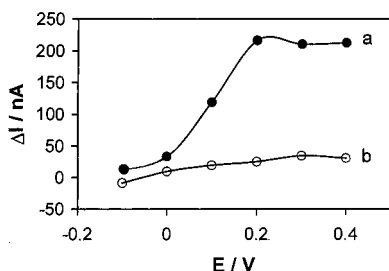


Fig. 5. Thermal-modulation hydrodynamic voltammogram for 0.2 mM  $K_4[Fe(CN)_6]$  (a), as well as for the blank phosphate buffer (0.2 M, pH 7.3) solution (b). Flow rate, 0.37 ml/min. Other conditions, as in Fig. 2B(b).

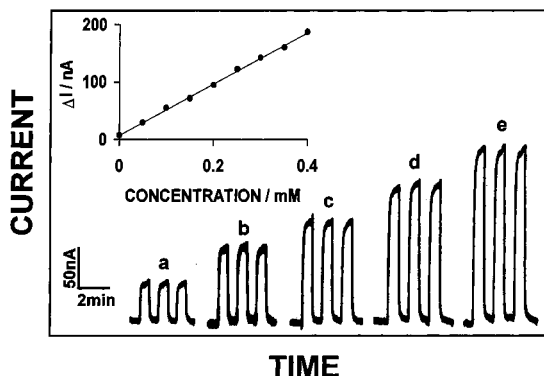


Fig. 6. Thermal modulation amperometric calibration data for  $K_4[Fe(CN)_6]$ . Amperometric current amplitudes for: (a) 0.05, (b) 0.1, (c) 0.15, (d) 0.2 and (e) 0.25 mM. The temperature difference was 30 K with a flow rate of 370  $\mu$ l/min. Also shown is the resulting plot over the 0–0.4 mM range. Other conditions, as in Fig. 2B(b).

Fig. 4 displays the influence of the solution flow rate upon the response. As expected (from the change in  $\delta_L$  in Eq. (2)), raising the flow rate between 0.2 and 1.0 ml/min increases primarily the baseline (heat ‘off’) current. In contrast, the heat ‘on’ current is nearly independent of the flow rate between 0.4 and 1.0 ml/min. The net result is that the current amplitude signal is decreasing at higher flow rates (see inset for resulting plot). These data indicate great promise for microanalytical systems employing very low solution flow rates. The on-line monitoring of environmental or industrial streams that is often influenced by fluctuations in the natural convection should also benefit from the minimal flow rate dependence

observed with the heated electrode. Similar advantages are expected for submersible remote electrochemical sensors.

Fig. 5 shows the thermal modulation current–potential curve for the oxidation of  $2 \times 10^{-4}$  M ferrocyanide (a), together with corresponding background current (b). These hydrodynamic voltammograms were developed and plotted pointwise by making 100-mV changes in the applied potential and measuring the current difference. The background current is very low, indicating good correction for non-conductive currents. Defined wave and plateau regions are observed. The thermal modulation half-wave potential is +0.10 V. This value is lower than the value (+0.20 V) observed in analogous pulsed-flow measurements (not shown). Such lowering of the half-wave potential is expected from the temperature dependence of the standard potential for the ferrocyanide couple.

Fig. 6 displays stopped-heating flow measurements of potassium ferrocyanide concentrations ranging from  $5 \times 10^{-5}$  M (a) to  $2.5 \times 10^{-4}$  M (b). The current difference increases linearly with the analyte concentration. These data, that are a part of a calibration experiment up to  $4 \times 10^{-4}$  M, resulted in a highly linear calibration plot (also shown), with a slope of 447 nA/mM and correlation coefficient of 0.999. A series of 38 successive stopped-heating flow measurements of a  $2 \times 10^{-4}$  M ferrocyanide solution was used for estimating the precision. A highly stable response was observed during this prolonged operation, to yield a relative standard deviation of 1.5% and a mean current difference of 96.8 nA. Such precision reflects the high reproducibility of the thermal modulation.

In conclusion, this exploratory investigation indicates that hot-wire electrochemistry can be exploited for developing a new thermal modulation amperometric approach for monitoring flowing schemes, and for enhancing the performance of on-line electrochemical detectors, in general.

## Acknowledgements

This work was supported by the US DOE

WERC Program and the Deutsche Forschungsgemeinschaft (DFG).

## References

- [1] H.B. Hanekamp, P. Bos, R.W. Frei, *Trends Anal. Chem.* 1 (1982) 135.
- [2] K. Stulik, V. Pacakova, *J. Electroanal. Chem.* 129 (1981) 1.
- [3] P.C. White, *Analyst* 109 (1984) 677.
- [4] V.G. Levich, *Physiological Hydrodynamics*, 2nd ed., Englewood Cliffs, Prentice Hall, 1962.
- [5] J. Wang, *Analytical Electrochemistry*, VCH, New York, 1994.
- [6] P. Grundler, *Fresenius J. Anal. Chem.* 362 (1998) 180.
- [7] P. Grundler, A. Kirbs, T. Zerihun, *Analyst* 121 (1996) 1805.
- [8] P. Grundler, T. Zerihun, A. Kirbs, H. Grabow, *Anal. Chim. Acta* 305 (1995) 232.
- [9] P. Grundler, G.U. Flechsig, *Electrochim. Acta* 43 (1998) 3451.
- [10] H. Huiliang, D. Jagner, L. Renman, *Anal. Chim. Acta* 193 (1987) 61.
- [11] J. Wang, *Talanta* 28 (1981) 369.
- [12] W.J. Blaedel, D. Iverson, *Anal. Chem.* 49 (1979) 1563.

# Speciation of iron in breast milk and infant formulas whey by size exclusion chromatography-high performance liquid chromatography and electrothermal atomic absorption spectrometry

P. Bermejo <sup>a,\*</sup>, E. Peña <sup>a</sup>, R. Domínguez <sup>a</sup>, A. Bermejo <sup>a</sup>, J.M. Fraga <sup>b</sup>,  
J.A. Cocho <sup>c</sup>

<sup>a</sup> *Department of Analytical Chemistry, Nutrition and Bromatology, Faculty of Chemistry, University of Santiago de Compostela, Avda de las Ciencias, 15705 Galeras SN, Spain*

<sup>b</sup> *Department of Pediatrics, Faculty of Medicine, University of Santiago de Compostela, Galeras SN, 15705 Santiago de Compostella, Spain*

<sup>c</sup> *Laboratory of Metabolic Disorders, Complejo Universitario, University of Santiago de Compostela, Galeras SN, 15705 Santiago de Compostela, Spain*

Received 5 January 1999; received in revised form 1 June 1999; accepted 23 July 1999

## Abstract

Speciation of iron in milk was carried out by high performance liquid chromatography (HPLC) and electrothermal atomic absorption spectrometry (ETAAS). Milk whey was obtained and low molecular weight protein separation was performed by size exclusion chromatography (SEC) with a TSK Gel SW glass guard (Waters) pre-column and a TSK-Gel G2000 glass (Toso Haas) column. After studying water as a possible mobile phase, this mobile phase was carefully selected in order to avoid alterations of the sample and to make subsequent iron determination in the protein fractions easier by ETAAS. The proposed method is sensitive (limit of detection [LOD] and LOQ 1.4 and 4.7  $\mu\text{g l}^{-1}$ , respectively) and precise (relative standard deviation [RSD] < 10%). Iron is principally found in the proteins of 3 and 76 kDa in breast milk, and it is irregularly distributed in infant formulas. © 2000 Elsevier Science B.V. All rights reserved.

*Keywords:* Iron speciation; Milk; SEC-HPLC; ETAAS

## 1. Introduction

Iron deficiency anemia (IDA) is a priority nutritional problem in industrialized as well as developing countries. Besides anemia per se, tissue iron deficiency may lead to a defect in learning capac-

\* Corresponding author. Tel.: + 34-981-591-079; fax: + 34-981-595-012.

E-mail address: qn1956@usc.es (P. Bermejo)

ity, cognitive performance and abnormalities in psychomotor development in infants and preschoolers. This deficiency also effects work performance in adults and an increase in the frequency of low birth weight, prematurity, and prenatal mortality in pregnancy can be found [1]. Because of the risk of cancer and heart disease in individuals with high iron stores [2,3] it is not recommended to supply iron to individuals who do not require it. A high priority must be assigned to the prevention of iron depletion among infants [4], and so, iron fortification has been widely used in the industrialized world.

Breast milk and/or milk formulas are the main nutrient fluids of newborn infants. Trace elements are usually added to infant formulas as inorganic salts, whereas in milk, these elements are bound to different compounds, which affect bioavailability. In order to carry out a rational supplementation, breast milk is used as a reference to evaluate the nutritional content of alternative formulas, assuming that the composition of breast milk may satisfy the growing demands of healthy infants during the early months of life [5]. It is interesting to know how the highest breast milk bioavailability might depend on the distribution among the different milk proteins and how inorganic salts are found in infant formulas after being added.

Few reports can be found in the literature. Previous results have been obtained by means of size exclusion chromatography-high performance liquid chromatography (SEC-HPLC) and inductive coupled plasma-atomic emission spectrometry (ICP-AES) [5–7]. Negretti de Brätter et al. [8] used instrumental neutron activation analysis (INAA) as the reference method for the quality control of the shape of the element profiles (Se, Fe, Zn) obtained with ICP-AES after chromatographic separation. When the sensitivity of ICP-AES is not sufficient ICP-MS may be used. However, instruments for these techniques are expensive and not available in many laboratories. Based on a cost-benefit analysis, atomic absorption spectrometry (AAS) seems to be the preferred method. The detection limits obtained by AAS methods, requiring a small sample volume, are low enough to allow the determination of most of the trace elements in speciation. Consequently,

the use of AAS, in particular electrothermal atomic absorption spectrometry (ETAAS) needs to be considered [9,10]. Thus, in an earlier study Fransson and Lönnnerdal [11] determined the distribution of iron among various fractions of breast milk by HPLC, ultrafiltration and AAS. The samples were freeze dried, ashed at 600°C for 5 h, and dissolved in 1:1:1 HCl/HNO<sub>3</sub>/H<sub>2</sub>O before analysis.

In this work, iron speciation in milk was carried out by SEC-HPLC and ETAAS. Milk fat and casein micelles were removed and the milk whey obtained was chromatographed. Special attention was paid to the column and mobile phase selection, when looking for the best separation in the lowest range of molecular weights, where iron presence had been reported [5–8,11].

Water was studied as mobile phase [12,13]. Then, the mobile phase was carefully selected, salinity was decreased, in order to avoid contaminations, stability problems of the organometal complex, undesired interactions with the sample to a great extent and interferences of our mobile phase in the direct determination of iron in protein fractions by ETAAS.

## 2. Experimental

### 2.1. Apparatus

Milk whey was obtained using an *ultracentrifuge* L8-Beckmann with a SW-40 rotor.

A Crison pH-meter equipped with a combined electrode gas-calomel INGOLD U455-Ag 7.0 DIN pH 0–14 was utilized to determine pH of mobile phases.

For the chromatographic separation of whey proteins, a High Performance Liquid Chromatograph 625-LC System (Waters, USA) equipped with a TSK gel SW glass guard pre-column, 4 cm × 8 mm, and a TSK gel G 2000 glass, 30 cm × 8 mm (Toso Haas, Japan) column was employed. The column has a selected silica-based packing, derivatized using the glycol ether function containing spherical 10 μm particles with pore sizes of 13 nm. The Waters 625 LC system is a non-metallic HPLC solvent delivery system for

liquid chromatography applications where wetted surface material is made of inert, polymeric materials and flexible PEEK tubing. Peaks were detected by an UV detector model 486 (Waters, USA) at 254 nm, and acquisition and processing of data were performed by the Millennium Chromatography Manager System, version 2.15 (Waters, USA) programme.

Iron measurement in milk and milk whey was carried out using an Atomic Absorption Spectrophotometer Perkin Elmer model 5000 (Perkin Elmer, Germany) at 248.3 nm, a hollow cathode lamp operating at 30 mA, a slit of 0.2 nm, and an acetylene air-flame.

Iron measurement in protein fractions was carried out using an Atomic Absorption Spectrophotometer 1100 B (Perkin Elmer, Germany) with a hollow cathode lamp and a HGA-700 graphite furnace (Perkin Elmer, Germany). The instrument was fitted with an AS-70 autosampler. Pyrolytic graphite tubes with L'vov platforms were used throughout the course of this study. Instrument settings for Fe determination are summarized in Table 1.

## 2.2. Reagents

All solutions were performed with ultrapure water, specific resistivity 18 M $\Omega$  cm, from a Milli-Q purification system (Millipore).

In order to prepare mobile phases, different reagents (ammonium nitrate, NH<sub>4</sub>NO<sub>3</sub>, Suprapur (Merck, Germany), ammonia solution, NH<sub>3</sub>, Suprapur (Merck, Germany), sodium azide, NaN<sub>3</sub> (Sigma, St. Louis, MO) were used. The calibration column was performed using protein standards ribonuclease A, ovalbumine, albumine, aldolase, coming from HMW Gel Filtration calibration Kit and LMW Gel Filtration Calibration Kit (Pharmacia Biotech, USA), and cyanocobalamin (Sigma).

A previously diluted stock solution of iron 1 g l<sup>-1</sup> (Merck, Germany), was employed to optimize ETAAS temperature programme and to obtain the calibration graphs. Finally, magnesium nitrate, MgNO<sub>3</sub>, Suprapur (Merck, Germany), was assayed as a possible modifier.

A Reference Material A-11 non-fat milk of the International Atomic Energy Agency (IAEA) with a certified iron content was used.

## 2.3. Procedure

### 2.3.1. Sampling

Breast milk samples were collected following strict precautions in order to minimize contamination and avoid alterations. The samples were collected by hoc trained personnel in polyethylene flasks using a motorized pump. Care was paid to avoid touching the inner wall of the device or flask.

Table 1  
Instrumental conditions and furnace programme for iron determination in protein fractions

Step	T (°C)	t (s)		Gas flow (ml min <sup>-1</sup> )	Signal read out
		Ramp	Hold		
Dry	100	15	30	300	—
Pyrolysis <sub>1</sub>	700	10	25	300	—
Pyrolysis <sub>2</sub>	1350	5	20	300	—
Atomization	2400	0	3	0	+
Clean	2600	1	3	300	—
Wavelength (nm)	248.3	Purge gas	Argon		
Background corrector	Deuterium	Graphite tubes	Pyrolytic		
Lamp (mA)	30	Injection volume (μl)	20		
Signal processing	Peak area	Slit width	0.2 nm		
Sample volume	20 μl				

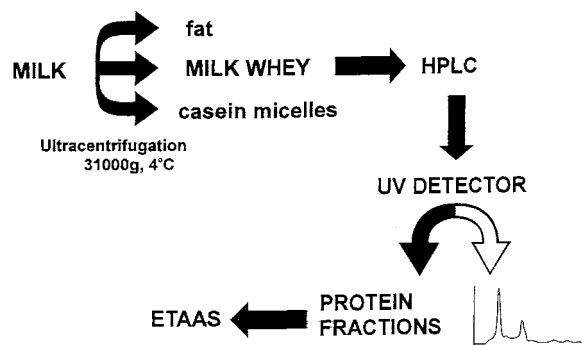


Fig. 1. Total procedure.

With regard to infant formulas, commercially available, solutions were prepared by dissolving milk powder using ultrapure water, following the manufacturer's instructions.

Containers and covers (polyethylene) were kept in nitric acid for at least 48 h, rinsed three times with ultrapure water and maintained dried until used. Samples were stored at  $-20^{\circ}\text{C}$  until treatments were performed.

### 2.3.2. Iron determination in milk and milk whey

Total values of iron concentration in milk and milk whey were directly determined by an AAS flame [14] using a high performance nebulizer. The addition procedures were always used.

### 2.3.3. Sample preparation: ultracentrifugation

Milk samples were ultracentrifuged [14–16] at 31 000 rpm ( $160\,000 \times g$ ) for 60 min, with 1 min acceleration and 1 min deceleration times. Milk whey was taken out with a micropipette after fat separation. The lower phase (casein micelles) remained in the bottom of the tube.

### 2.3.4. Iron speciation

**2.3.4.1. Chromatographic separation.** Milk wheys were filtered using Millex GV<sub>13</sub> 0.22  $\mu\text{m}$  sterile units (Millipore, France), and 100  $\mu\text{l}$  were injected in the chromatographic system, with a flow rate of 1  $\text{ml min}^{-1}$ . Measurement wavelength was 254 nm (Fig. 1). As each milk can present a different protein profile it was always necessary to perform a first injection to know the protein profile and

the retention time of the different peaks. A second injection of 100  $\mu\text{l}$  was performed afterwards and the eluent emerging from the UVA-VIS detector was collected in different fractions according to the number of different chromatographic peaks obtained for each sample.

**2.3.4.2. Iron determination.** Iron was directly determined in the collected fractions by ETAAS, without addition of a chemical modifier. Calibration was performed using standards of iron diluted with the mobile phase at concentrations of 0, 10, 20, 30  $\mu\text{g l}^{-1}$ . The volume of sample injected was 20  $\mu\text{l}$ . As the volumes of fractions are known (0.5–1.5 ml), the iron concentration was given as  $\text{ng fraction}^{-1}$ .

## 3. Results and discussion

### 3.1. Water as a mobile phase

Water was assayed to find a simple mobile phase which avoids interferences in iron measurement and undesirable interactions with the sample. Chromatograms of an infant formula were compared, using only water as the mobile phase and using a solution of the bactericide sodium azide 0.05%  $\text{m V}^{-1}$  [6], these results are shown in Fig. 2. Negative peaks and signal distortions appeared indicating that the aforementioned compound must be taken out of the mobile phase. Nevertheless to avoid the rapid deterioration of the column the use of the sodium azide was proposed only in the washing programme of the column.

### 3.2. Chromatographic conditions

The term 'non size effects' in SEC includes attractive interactions, such as ion exchange and hydrophobic binding, which tend to increase the elution volumes of solutes, and increase forces of electrostatic repulsion with the opposite effect. A balance must be made between the need to increase ionic strength to reduce ionic electrostatic interactions and to decrease ionic strength to limit hydrophobic interaction [17].

Early in the development of electrothermal atomization L'vov [18] found that molecular absorption by alkali halides was one of the major causes of interferences, when these halides are present in a concentration four or five orders of magnitude higher than the analyte element. Due to the very high sensitivity of the graphite furnace technique, this relationship is very quickly reached. For this reason the utilization of sodium chloride at concentrations of 0.05–0.3 M as one of the components of the mobile phase, as other authors using ICP-AES [5–8] had reported, was not possible here.

Ammonium nitrate concentration was optimized in the range of 0.1–0.4 M using a protein mixture (0.02 mg of cyanocobalamin, 0.19 mg ribonuclease A, 0.21 mg of ovalbumin, 0.19 mg of albumin, 0.77 mg of aldolase). Using ammonium nitrate 0.2 M the best separation at higher retention times (lower molecular weights) was obtained. This fact was observed because of the peak appearance corresponding to the aggregate which elutes slightly before the true peak of ribonuclease A (retention time = 15 min, Fig. 3). Different pHs around neutrality were assayed (pH 6.1, 6.7, 7.3) without observing significant changes in the elution. Ammonia solution was added to obtain pH 6.7, reported as milk pH [19]. The final composition of mobile phase was 0.2 M  $\text{NH}_4\text{NO}_3$  and  $3.24 \times 10^{-4}$  M  $\text{NH}_3$ .

Using this mobile phase the best peak definition was obtained, as can be seen in the chro-

matograms shown in Fig. 4, for a breast milk sample and the same infant formula used in the chromatograms of Fig. 2.

### 3.3. Column calibration

In order to know the molecular weight of the proteins found in the milk whey, the column was calibrated using a series of standard proteins with certified molecular weight. These proteins were chromatographed and the retention times obtained as well as the molecular weight are shown in Table 2.

The equation obtained to column calibration was:

$$\text{Log MW (kDa)} = -0.276 + 7.591t_R \text{ (min)}$$

with a correlation coefficient  $r = 0.974$ .

### 3.4. Precision in the protein separation

The final aim of this work is to determine iron in the different proteins of the milk whey, and for this reason it is necessary to know the repeatability of the protein retention times in order to be able to separate the protein fractions. To perform this study ten replicates of a breast milk sample and 12 replicates of an infant formula sample were chromatographed; the results obtained for the different proteins found in both types of milk are shown in Table 3. The retention times for all proteins were constant, and the relative standard

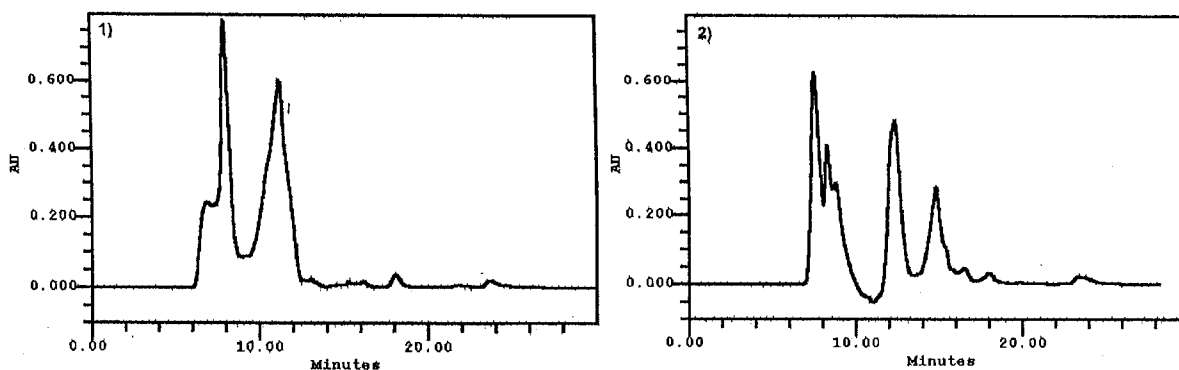


Fig. 2. Chromatograms demonstrating the negative effect of sodium azide addition (used as bactericide) in the elution. Mobile phase: (1) water; (2) sodium azide 0.05% (w/v).



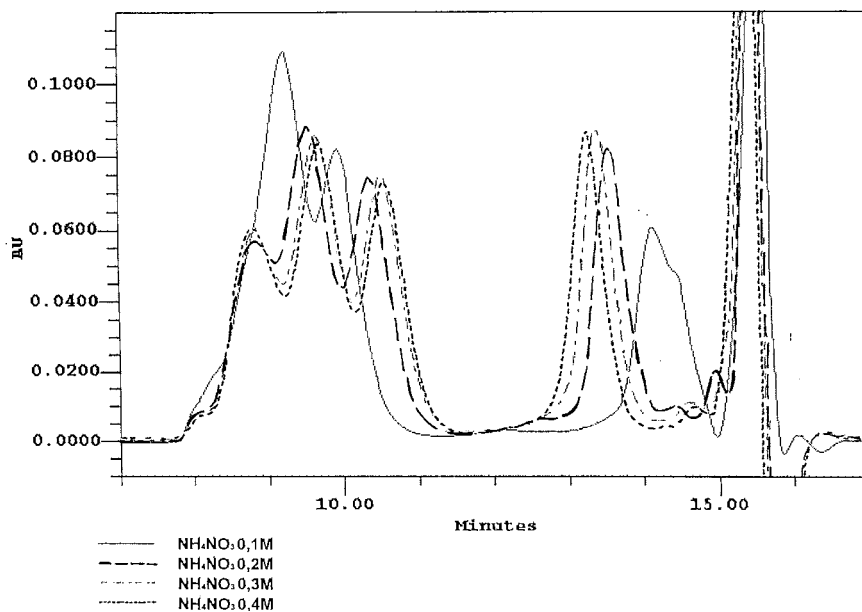


Fig. 3. Effect of different concentrations of ammonium nitrate in the elution of a standard protein mixture.

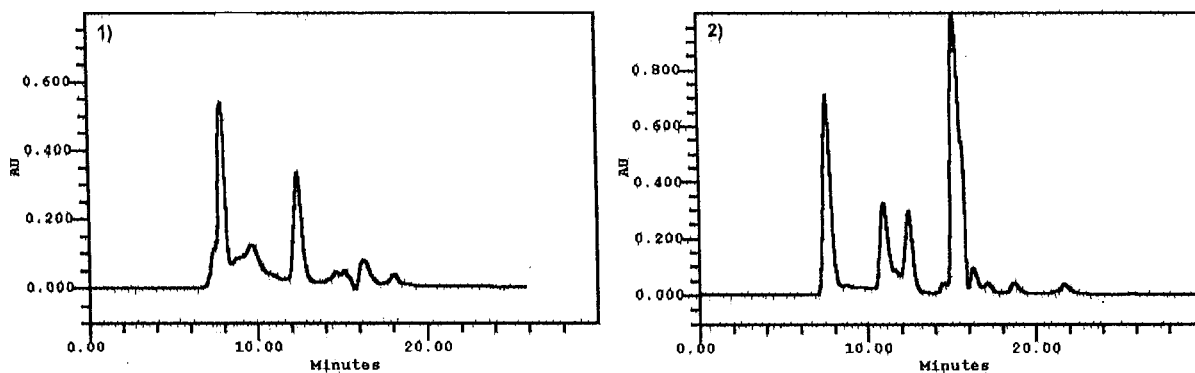


Fig. 4. Chromatograms: (1) breast milk sample; (2) infant formula sample.

deviation (RSD) for the absorbance expressed in height or area peak mode can be considered good in all cases. An R.S.D. of 12.3% was obtained for the peak corresponding to 2 kDa, this value could be produced because of being the nearest peak to the separation limit of the column.

### 3.5. Graphite furnace programme

The chemical modifier proposed for the iron determination in ETAAS is magnesium nitrate.

Table 2  
Column calibration

Standard protein	MW (kDa)	Retention time (min)
Cianocobalamine	1.355	15.5
Ribonuclease A	13.700	13.6
Ovalbumine	43.000	10.5
Albumine	67.000	9.6
Aldolase	158.000	8.9

Table 3  
Precision in protein separation

Breast milk ( <i>n</i> = 10)				Infant Formula ( <i>n</i> = 12)			
MW (kDa)	RSD (%)			MW (kDa)	RSD (%)		
	Retention time	Peak height	Peak area		Retention time	Peak height	Peak area
101	0.0	2.3	2.9	25	0.0	2.2	1.6
78	0.0	0.8	2.4	15	0.0	1.4	0.9
53	0.0	2.0	5.0	4	0.0	3.7	3.7
14	0.0	1.0	0.6	3.5	0.0	2.7	4.0
3	0.0	9.1	5.6	2	0.0	3.8	12.3
2	0.0	9.0	8.3				

To optimize the pyrolysis and atomization temperatures an aqueous iron standard solution of  $10 \mu\text{g l}^{-1}$  with  $\text{Mg}(\text{NO}_3)_2$  and without  $\text{Mg}(\text{NO}_3)_2$  were used. No important improvement in the iron stabilization was observed. For this reason and to avoid risk of contamination and to shorten the analytical procedure we propose the elimination of the use of the  $\text{Mg}(\text{NO}_3)_2$  and thus the direct introduction of the protein fractions become possible. The optimum pyrolysis and atomization temperatures were 1350 and 2400°C, respectively. An intermediate pyrolysis step at 700°C was necessary to follow a complete mineralization of the sample. Finally a cleaning step at 2600°C was introduced to avoid possible memory effects. The instrumental conditions and the furnace programme are summarized in Table 1.

### 3.6. Calibration

Solutions prepared in mobile phase with iron standard concentrations between 0 and  $30 \mu\text{g l}^{-1}$  were used to determine a calibration curve. The equation obtained was:

$$A = 4.48 \times 10^{-3} [\text{Fe}] - 5.0 \times 10^{-3} \quad r = 0.999$$

where *A* is the absorbance (peak area) and [Fe] is the iron concentration expressed in  $\mu\text{g l}^{-1}$ .

### 3.7. Sensitivity

The limit of detection (LOD) is defined as 3 S.D./*m* and the limit of quantification is given by

$10 \text{ S.D.}/m$  (*m* = slope of the calibration graph and S.D. = the within-run standard deviation of the blank signals). The values based on ten replicates of the blank were 1.4 and  $4.7 \mu\text{g l}^{-1}$ , respectively.

The characteristic mass (*m*<sub>0</sub>) defined as the mass of analyte that provides an integral absorbance of 0.0044 for an aliquot sample of 20  $\mu\text{l}$  was 20.4 pg.

### 3.8. Iron–protein complex stability

To know the stability of the Fe–protein complexes a study about the time effects on the chromatographic protein separation was performed. A milk whey sample (infant formula) was chromatographed at different times after preparation 1.0–2.0–3.0–4.0 and 24 h later. The results are shown in Fig. 5(1). It can be seen that only the absorbance of the protein corresponding to 2 kDa changes with the time and this absorbance was constant after 24 h. For this reason, the performance of chromatographic separation 24 h after the milk preparation was proposed.

On the other hand to know the effect of the sample freezing, the same sample was chromatographed before and after freezing, both chromatograms are shown in Fig. 5(2). It can be seen that the freezing did not affect to the protein separation.

In the same way the iron determination in the different protein fractions was performed before and after freezing. The levels of iron obtained are in Table 4 and it can be seen that there are no significant differences due to the sample freezing.

### 3.9. Precision in the iron determination

The within-run precision (RSD) of the method (instrumental and matrix factors) was studied us-

ing both types of milk. The iron content of the fractions obtained for a breast milk sample (six replicates) and for infant formula milk (nine replicates) was determined using the proposed proce-

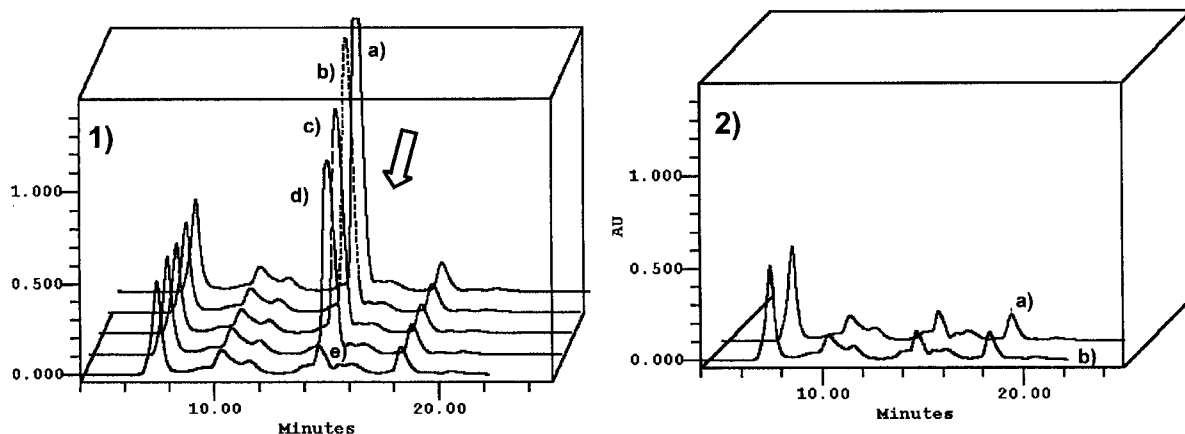


Fig. 5. (1) Chromatograms of a sample after ultracentrifugation: (a) 1 h later; (b) 2 h; (c) 3 h; (d) 4 h; (e) 24 h. 2) Chromatograms of a sample stabilized: (a) after ultracentrifugation; (b) after defreezing.

Table 4

Iron distribution in fractions of an infant formula sample before and after freezing

MW (kDa)	Before freezing		After freezing	
	[Fe] (ng fraction <sup>-1</sup> )	%	[Fe] (ng fraction <sup>-1</sup> )	%
321	74.7 ± 0.6	12.0	86.5 ± 1.8	14.0
59	110.3 ± 1.6	17.8	106.7 ± 5.4	17.3
38	207.0 ± 0.0	33.4	211.2 ± 1.6	34.2
15	162.4 ± 3.5	26.2	150.4 ± 0.0	24.3
3	46.1 ± 0.8	7.4	39.6 ± 0.8	6.4
2	19.6 ± 0.1	3.2	23.4 ± 0.1	3.8

Table 5

Precision in iron determination by electrothermal atomic absorption spectrometry (ETAAS)

Breast milk (n = 6)				Infant formula (n = 9)			
MW (kDa)	Fe (ng fraction <sup>-1</sup> )	S.D.	RSD (%)	MW (kDa)	Fe (ng fraction <sup>-1</sup> )	S.D.	RSD (%)
101	1.6	0.1	6.3	25	26.5	1.5	5.7
78	11.2	1.0	9.0	15	19.8	1.4	7.1
53	14.4	1.0	7.0	4	109.2	8.8	8.1
14	ND <sup>a</sup>	–	–	3.5	144.3	9.2	6.4
3	3.4	0.4	11.8	2	22.8	1.6	6.9
2	ND <sup>a</sup>	–	–				

<sup>a</sup> ND, not detected.

Table 6  
Mass balance study

	Before freezing [Fe] (ng fraction <sup>-1</sup> )	After freezing [Fe] (ng fraction <sup>-1</sup> )
$\Sigma[\text{Fe}]_{\text{fractions}}$ (ng 100 $\mu\text{l}^{-1}$ )	619.9	617.6
$[\text{Fe}]_{\text{milk}}$ (ng 1000 $\mu\text{l}^{-1}$ )	1150.0 $\pm$ 0.0	
$[\text{Fe}]_{\text{whey}}$ ( $\mu\text{g ml}^{-1}$ )	720.0 $\pm$ 20.0	
$\frac{[\text{Fe}]_{\text{fractions}}}{[\text{Fe}]_{\text{whey}}} \times 100$ (%)	86.1	86.1

ture. The results obtained are shown in Table 5. The values of RSD (%) obtained are acceptable in all cases because this precision includes all the analytical procedure: the chromatographic separation, the fraction collection and the iron determination.

### 3.10. Accuracy for the Fe determination in total milk and milk whey

The accuracy of the total iron concentration in milk was performed using a Certified Reference Material, non-fat milk A-11 of the IAEA with a certified content of  $3.65 \pm 0.76 \mu\text{g Fe g}^{-1}$ . This reference material was prepared at 15% (W/V) and the Fe content was determined using the addition procedure. The results obtained for five replicates were  $3.04 \pm 0.17 \mu\text{g Fe g}^{-1}$ . On the other hand the recovery of the method was studied measuring iron added to whole milk, due to the fact that this sample has a more complex matrix than milk whey. Different amounts of Fe added to the milk sample were studied, the results obtained were 100.0, 96.0 and 102.0% for 0.50, 1.00 and  $1.5 \mu\text{g ml}^{-1}$  of Fe added.

### 3.11. Mass balance study

To check the accuracy in the iron determination in the protein fraction a study about the mass balance in a milk sample was performed. The sample was studied after its collection and after freezing and each sample was chromatographed by duplicate. The iron levels for the total milk, the milk whey and for different fractions are shown in

Table 6. It can be seen that the iron mass balances always approached to 100% (86.1%), and it can be concluded that there is no contamination or loss problems.

### 3.12. Applications

The proposed method has been applied to the study of the iron distribution in the milk whey proteins of ten infant formulas and ten breast milk samples. The infant formula samples of different brands were prepared at the concentrations suggested by the manufacturer, whereas breast milk was individual samples from women living in Galicia, North West of Spain with most of them corresponding to the first stage of lactation.

The protein identification of the milk whey is usually performed by comparison of the retention times of standards and samples, but in case of an incomplete separation metals can not be clearly attributed to proteins [13], or may be attributed to the wrong one. To avoid this problem the iron found in a protein fraction was only associated with the molecular weight of the protein obtained in the calibration column.

The iron in the protein fractions was determined by ETAAS using the established conditions at least twice. The iron concentrations in milk and milk whey are reported in Table 7.

Previous researchers concluded that a more careful speciation should be performed in the range of low molecular weight compounds. First, Fransson and Lönnnerdal [11] demonstrated using ultrafiltration (membrane molecular weight cut-off of 15 kDa) and SEC that a considerable fraction of the iron was bound to LMW compounds in breast milk. Brätter and al. [5] found iron in a fraction of HMW (> 600 kDa) and in the fraction of LMW (9–10 kDa) eluting together with citrate. Suzuki et al. [6] studied daily changes in components of breast milk with number of lactation days. They found iron in one or two peaks, whose elutions times coincided with the transferrin peak and citrate peak time. However, their chromatographic separation seems to be worse. Negretti de Brätter [8] studied a wide range of MWs protein obtaining a complicate chro-

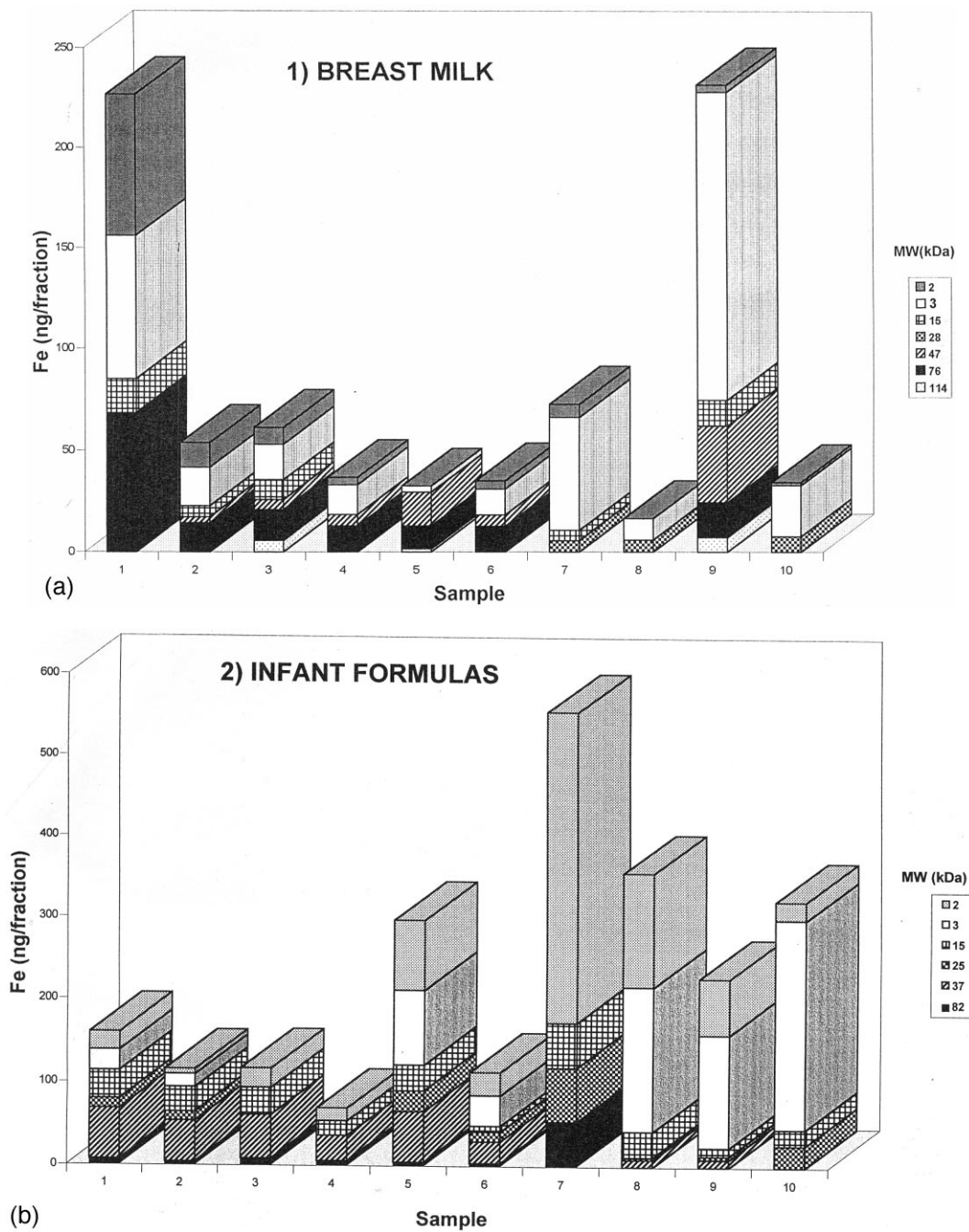


Fig. 6. Iron distribution among protein fractions: (1) breast milk; (2) infant formula. Concentration is expressed as  $\text{ng Fe fraction}^{-1}$ .

Table 7  
Iron concentration in milk and milk whey

Breast milk			Infant formula		
Sample	Milk	Milk whey	Sample	Milk	Milk whey
	[Fe] ( $\mu\text{g ml}^{-1}$ )			[Fe] ( $\mu\text{g ml}^{-1}$ )	
1	0.28 ± 0.01	0.22 ± 0.00	1	3.6 ± 0.30	1.8 ± 0.00
2	0.23 ± 0.00	0.12 ± 0.00	2	5.8 ± 0.10	1.6 ± 0.00
3	0.60 ± 0.01	0.41 ± 0.00	3	5.7 ± 0.10	1.6 ± 0.10
4	0.33 ± 0.00	0.24 ± 0.00	4	4.2 ± 0.10	1.1 ± 0.10
5	0.19 ± 0.00	0.17 ± 0.00	5	3.3 ± 0.10	2.0 ± 0.20
6	0.23 ± 0.00	0.17 ± 0.00	6	3.1 ± 0.30	1.8 ± 0.00
7	0.22 ± 0.00	0.13 ± 0.00	7	5.7 ± 0.10	1.8 ± 0.10
8	— <sup>a</sup>	— <sup>a</sup>	8	6.3 ± 0.30	1.4 ± 0.10
9	0.28 ± 0.01	0.17 ± 0.00	9	4.4 ± 0.60	1.5 ± 0.00
10	0.24 ± 0.00	0.22 ± 0.00	10	2.9 ± 0.10	1.5 ± 0.00

<sup>a</sup> Results not available.

matographic pattern and concluded that columns with a separation range < 250 kDa should be used for a detailed human milk speciation. The chromatographic patterns are similar to that obtained by Coni et al.[7]. They found a homogeneity of iron distribution in protein fractions of infant formulas, whereas there is an increase in the amounts of elements in those intermediate fractions of mature breast milk that are related to substances with molecular weights ranging between 10 and 100 kDa. Underlying this distribution, an important role is played by the differences in percentage of these proteins in the composition of cow, cow-based formulas and human milk. Colostrum shows a different element composition from that of mature milk.

It was found that the behaviour of the infant formulas is very different and the iron distribution in the proteins is not regular. This can be explained by the different chemical composition of the formulas, which are prepared in different proportions of whey, proteins and minerals according to the needs of the infants. For the studied breast milks, the iron was bound principally to the proteins corresponding to molecular weights of 3 and 76 kDa (Fig. 6), these results agree with the results obtained by other authors.

#### 4. Conclusions

A speciation method for iron in milk by HPLC and ETAAS has been developed in order to compare the iron distribution among low molecular weight proteins in breast milk and infant formulas. With the use of a simple mobile phase a good protein separation was obtained, and moreover its use does not present problems in the iron determination by ETAAS.

The results obtained showed a different iron distribution in the proteins of the milk whey of infant formulas and human milk, and this can be important in the iron bioavailability of both types of milk. For this reason it is necessary to continue these studies in order to prepare new infant formulas where the iron distribution is more similar to human milk.

#### Acknowledgements

This work was partially supported by the research project 1997, CEO12 Laboratorios Ordesa, Barcelona, Spain.

## References

- [1] J.D. Cook, B.S. Skikne, R.V. Baynes, *Progress in Iron Research, Advances in Experimental Medicine and Biology*, Plenum Press, New York, 1994.
- [2] R.G. Stevens, D.Y. Jones, M.S. Micorzi, P.R. Taylor, *N. Engl. J. Med.* 319 (1988) 1047.
- [3] T.J. Salonen, K. Nyssonen, H. Korpela, J. Tnomilehto, R. Seppanen, R. Salonen, *Circulation* 86 (1992) 803.
- [4] E.E. Ziegler, S.J. Fomon, *Nutr. Rev.* 54 (1996) 348.
- [5] P. Brätter, B. Gercken, U. Rösick, A. Tomiak, *Analytical Chemistry in Medicine and Biology*, vol. 5, Walter de Gruyter, Berlin, 1988, p. 145.
- [6] K.T. Suzuki, H. Tamagawa, S. Hirano, E. Kobayashi, K. Takahashi, N. Shimojo, *Biol. Trace Elem. Res.* 28 (1991) 109.
- [7] E. Coni, A. Alimonti, A. Bocca, F. La Torre, D. Pizzuti, S. Caroli, *Element Speciation in Bioinorganic Chemistry*, Wiley, Chichester, 1966.
- [8] V.E. Negretti de Brätter, S. Recknagel, D. Gawlik, *Fresenius J. Anal. Chem.* 353 (1995) 137.
- [9] Y. Havezov, *Fresenius J. Anal. Chem.* 355 (1996) 452.
- [10] A.K. Das, R. Chakraborty, *Fresenius J. Anal. Chem.* 357 (1997) 1.
- [11] G.B. Fransson, B. Lönnerdal, *J. Pediatr.* 96 (1980) 380.
- [12] B. Michalke, D.C. Münch, P.S. Schramel, *J. Trace Elem. Electrolytes Health Dis.* 5 (1991) 251.
- [13] B. Michalke, *Fresenius J. Anal. Chem.* 350 (1994) 2.
- [14] P. Bermejo, R. Domínguez, A. Bermejo, *Talanta* 45 (1997) 325.
- [15] M. Martin, F. Jacobs, J. Brushmiller, *J. Nutr.* 14 (1984) 869.
- [16] A. Conti, L. Napolitano, J. Libratori, *Milchwissenschaft* 38 (1983) 392.
- [17] M.E. Himmel, J.O. Baker, *Size Exclusion Chromatography of Proteins, Handbook of Size Exclusion Chromatography*, Marcel Dekker, New York, 1995.
- [18] B.V. L'vov, *Spectrochim. Acta* 24B (1969) 53.
- [19] F.M. Luquet, *Leche y productos lácteos. Vaca. Oveja. Cabra, Societé Scientifique d'Hygiene Alimentarie*, Ed. Acribia S.A., 1991.

# Poly(ester sulphonic acid) coated mercury thin film electrodes: characterization and application in batch injection analysis stripping voltammetry of heavy metal ions

Christopher M.A. Brett <sup>a,\*</sup>, Denise A. Fungaro <sup>a,b</sup>

<sup>a</sup> *Departamento de Química, Universidade de Coimbra, 3049 Coimbra, Portugal*

<sup>b</sup> *Instituto de Pesquisas Energéticas e Nucleares (IPEN), Divisão de Química, Ambiental-MQA, Travessa 'R' no. 400, Cidade Universitária, CEP 05508-900 São Paulo-SP, Brazil*

Received 18 March 1999; received in revised form 9 July 1999; accepted 23 July 1999

## Abstract

Mercury-thin film electrodes coated with a thin film of poly(ester sulphonic acid) (PESA) have been investigated for application in the analysis of trace heavy metals by square wave anodic stripping voltammetry using the batch injection analysis (BIA) technique. Different polymer dispersion concentrations in water/acetone mixed solvent are investigated and are characterised by electrochemical impedance measurements on glassy carbon and on mercury film electrodes. The influence of electrolyte anion, acetate or nitrate, on polymer film properties is demonstrated, acetate buffer being shown to be preferable for stripping voltammetry applications. Although stripping currents are between 30 and 70% less at the coated than at bare mercury thin film electrodes, the influence of model surfactants on stripping response is shown to be very small. The effect of the composition of the modifier film dispersion on calibration plots is shown; however, detection limits of around 5 nM are found for all modified electrodes tested. This coated electrode is an alternative to Nafion-coated mercury thin film electrodes for the analysis of trace metals in complex matrices, particularly useful when there is a high concentration of non-ionic detergents. © 2000 Elsevier Science B.V. All rights reserved.

*Keywords:* Poly(ester sulphonic acid) modified electrodes; Mercury thin-film electrode; Batch injection analysis; Anodic stripping voltammetry

## 1. Introduction

The protection of electrode surfaces against interferences which block the electrode by irreversible adsorption is extremely important in the

analysis of untreated environmental samples, such as effluents. The electrochemical batch injection analysis (BIA) technique [1,2] using polymer modified electrodes is useful in this regard, since blocking problems are reduced by the small contact time between sample and electrode, samples, usually of volume 50  $\mu$ l, being injected directly over the electrode. This approach has been ex-

\* Corresponding author. Tel./fax: +351-239-835295.

E-mail address: brett@ci.uc.pt (C.M.A. Brett)



plored for the analysis of heavy metal ions by anodic stripping voltammetry [3] at cation-exchange polymer coated mercury thin film electrodes (MTFEs) [4,5] and with size exclusion polymer coatings [5]. Detection limits are slightly higher than in continuous flow systems at around 5 nM for zinc, cadmium, lead and copper ions. Cation exchange polymers investigated were Nafion [4] and mixtures of Nafion with other sulphonated polymers [5]. It was found that there was a slightly superior performance from Nafion/poly(vinyl sulphonic acid) (Nafion/PVSA) films with respect to discrimination against concentrations up to 20 mg dm<sup>-3</sup> of model surfactants: Triton-X-100 detergent; sodium dodecylsulphate polyelectrolyte and protein standard [5]. Size exclusion polymers investigated were based on cellulose acetate [5]; the major problem with these was the fragility of the films, so they were not pursued further.

A different type of sulphonate polymer with some similar cation-exchange characteristics as Nafion is poly(ester sulphonic acid) (PESA) also known as Eastman-AQ. This polymer exists as AQ55, AQ38 and AQ29 with equivalent weights of 1500, 2500 and 2500, respectively [6]. The complete structure is not known but in all cases the cation-exchange character is due to a sulphonate group in the 5-position on an aromatic ring, the polymer chain being through the 1 and 3 positions by links to ester (-CO<sub>2</sub>-) groups [6]. Coatings of this polymer show good substrate adhesion. It has been shown that PESA-modified electrodes permit the exchange of cations for trace analysis [7], and that they discriminate well against electrode fouling [8]. Differential pulse anodic stripping voltammetry at PESA-coated mercury thin film electrodes (PCMTFE) in the presence of surfactants has also been demonstrated [9]. Further successful applications have been as ion-exchanger in acetonitrile solutions [6], and mixing with an enzyme as modifier layer [10–12] or to protect an enzyme-polymer modifier layer against external interferents [13].

The objective of this paper is to investigate the properties of PCMTFEs for application in batch injection analysis with square wave anodic stripping voltammetry (BIA-SWASV). The character-

istics of the formed films are probed by electrochemical impedance techniques. Discrimination against model surfactants is investigated.

## 2. Experimental

The BIA cell was as described previously [2]. A glassy carbon disc electrode, diameter 5 mm, is fixed directly under the tip of a programmable, motorised, electronic micropipette (Rainin EDP-Plus 100) at a distance of 2–3 mm. The internal diameter of the micropipette tip was 0.47 mm and a calibrated dispensation rate of 24.5 μl s<sup>-1</sup> was used in experiments to be described. The cell also contains a platinum foil auxiliary electrode and a saturated calomel electrode (SCE) as reference, and is filled with ~40 cm<sup>3</sup> of inert electrolyte.

Voltammetric experiments were controlled by a BAS CV-50W voltammetric analyser. Impedance spectra were recorded using a Solartron 1250 Frequency Response Analyser coupled to a Solartron 1286 Electrochemical Interface, controlled by a personal computer with Zplot software. A sinusoidal voltage perturbation of rms amplitude 10 mV was applied, scanning from 65 kHz to 0.1 Hz with 5 measurements per decade of frequency, and signal auto-integration (*t*-test at 99% confidence level) up to 50 s.

All reagents were of analytical grade and solutions were prepared using Millipore Milli-Q ultra-pure water (resistivity > 18 MΩ cm). Electrolytes employed included 0.1 M KNO<sub>3</sub>/5 mM HNO<sub>3</sub> and 0.1 M acetate buffer (pH 4.6). Experiments were done at temperatures of (25 ± 1°C) without deaeration.

A small quantity of solid PESA (Eastman AQ55) was a kind gift from Professor J. Pingaron, Universidad Complutense de Madrid, Spain.

### 2.1. Preparation of the GC electrode coated with PESA

Water/acetone solvent in the ratio 1:2 or 5:1 (v/v) was added to a known mass of solid PESA to obtain a dispersion with final concentration of 0.93 or 0.25%. It has been noted previously that it

is only possible to make dispersions of this polymer e.g. [8]. It was attempted to make true solutions with a number of solvents, but without success. The glassy carbon electrode was covered with polymer by applying 10  $\mu\text{l}$  of the dispersion to the surface with a micropipette. After evaporating the solvents with a jet of air at room temperature, whilst the electrode was rotating at 50 rpm, the polymer film was cured with a jet of warm air at 70°C for about 1 min.

## 2.2. Preparation of the PESA-coated mercury thin film electrode

In order to prepare the PCMTFE, the PESA-modified electrode was placed in a BIA cell [2] and mercury deposition was done *in situ* by injection of 10  $\mu\text{l}$  of 0.1 M Hg (II) in 0.1 M  $\text{KNO}_3$ /5 mM  $\text{HNO}_3$  directly over the centre of the electrode, applying a potential of  $-1.0$  V during 64 s [5].

## 3. Results and discussion

The results to be described used three different polymer solutions for electrode coatings. This is because PESA does not form a true solution, as mentioned in the experimental section; it is only possible to make a dispersion. Water and acetone solvent mixtures were employed: in the first two of these the water/acetone ratio was 1:2, the concentrations of PESA being 0.93 and 0.25 wt% in order to investigate the effect of concentration on polymer solubility. In the third, the water/acetone ratio was 5:1, with a 0.25 wt% concentration of PESA. The identity and ratio of the solvents can influence the morphology of the film obtained and the re-formation of the crystalline phases of the polymer. Most studies in the literature describe dispersions in the range 1–1.5 wt% concentration [6–9], higher than those used here. Nevertheless, the aim in this work was to produce a reproducible film as thin as possible.

### 3.1. Characterisation of the modified electrodes

The films formed were homogeneous and opaque with no visible differences between the

three types of prepared film. Film thickness was estimated by optical microscopy as 1  $\mu\text{m}$  for application of 10  $\mu\text{l}$  of polymer dispersion. The PCMTFEs also showed a visually uniform formation of mercury over the entire electrode surface. Preliminary experiments showed that they could be used for BIA-SWASV — see Fig. 1 for examples, which also demonstrates that some difference in stripping response at the various types of PESA-modified electrode is observed.

Further characterisation of the films of PESA on the glassy carbon substrate and of the polymer-coated MTFEs was done using electrochemical impedance in acetate buffer and nitrate electrolyte solutions. The reason for the choice of two electrolytes was that previous work on Nafion-coated electrodes has shown that there is a possible influence from the identity of the electrolyte anion, but not the cation [5]. Fig. 2 shows some typical impedance spectra in the complex plane for a PESA film formed from a 0.93% concentration dispersion in 1:2 water/acetone solvent, without deaeration of the solution. Several points can be readily deduced. At 0.0 V there is little evidence of charge transfer processes, the capacitive response being reduced by film roughness and porosity effects [14] (this is also observed at bare glassy carbon electrodes [15]). At applied potentials of  $-0.5$  and  $-1.0$  V the curvature in the plots can be attributed to oxygen permeating through the polymer film and possibly reduction of the carbon surface itself, as confirmed by experiments in the absence of dissolved oxygen. The influence of the anion identity is significant at  $-0.5$  V. At more negative potentials, as is observed at  $-1.0$  V, this difference would be expected to be less owing to the negative anionic charge. Similar observations of the permeation of nitrate anion have been made at Nafion membranes, where the cation exchange behaviour is also due to sulphonate groups [16].

Impedance plots at the PCMTFE at  $-0.5$  and  $-1.0$  V are shown in Fig. 3. At  $-1.0$  V the spectra exhibit a similar behaviour to Fig. 2 without mercury. However, at  $-0.5$  V there is evidence of a charge transfer process, ascribed to oxygen reduction, verified by removing oxygen, and the impedance values for oxygen reduction are much

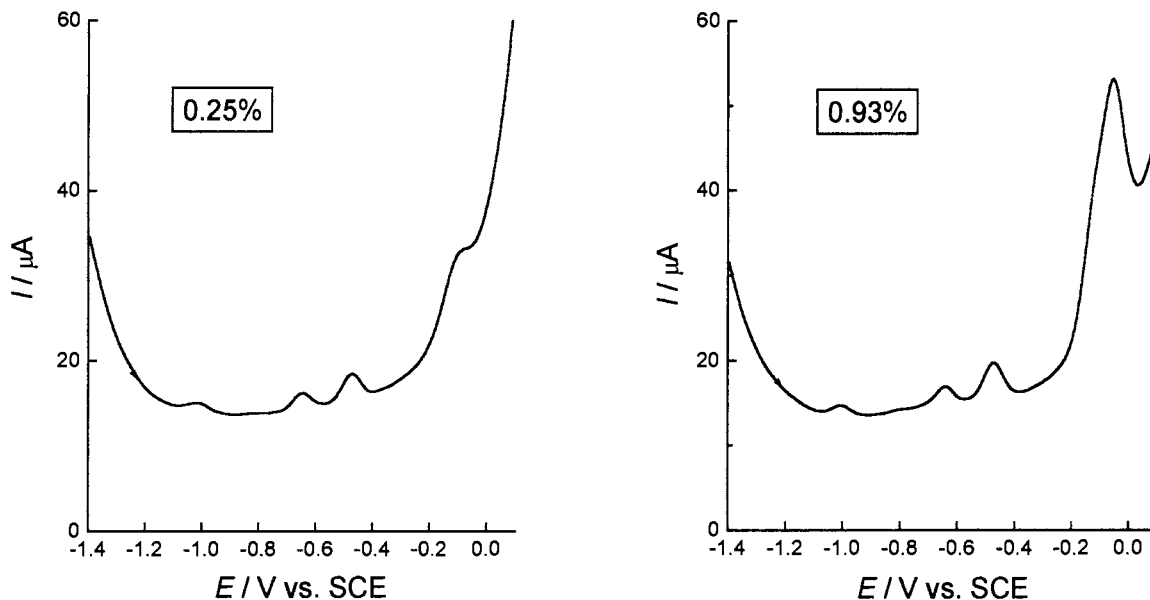


Fig. 1. BIA-SWASV traces for injection of 50  $\mu\text{l}$  of a sample containing  $10^{-7}$  M  $\text{Zn}^{2+}$ ,  $\text{Cd}^{2+}$ ,  $\text{Pb}^{2+}$  and  $\text{Cu}^{2+}$  onto PCMTFE in pH 4.6 0.1 M acetate buffer (modifier dispersion 0.25 and 0.93% concentration, 1:2 water/acetone solvent). Deposition time 30 s at  $-1.3$  V vs. SCE, SW parameters: amplitude 25 mV; frequency 100 Hz; potential increment 2 mV.

less in nitrate electrolyte than in acetate buffer, which means that oxygen can diffuse much more easily through the polymer film. The straight line portion at low frequency in nitrate electrolyte can be ascribed to charge separation within the polymer film again in agreement with [16]. This can be modelled by a capacitance, tak-

ing into account roughness effects, in series with the  $RC$  parallel combination describing the semi-circle. Fitting of the experimental results for nitrate electrolyte gives  $R = 120 \Omega$  and  $C = 12 \mu\text{F}$ , and 0.25 mF for the low frequency capacitance. For acetate buffer electrolyte  $R = 10 \text{ k}\Omega$  and  $C = 15 \mu\text{F}$ .

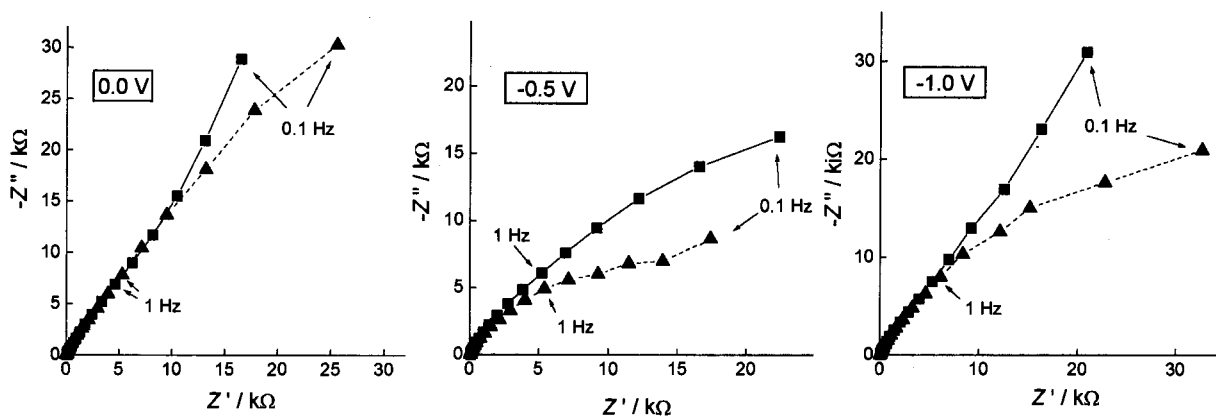


Fig. 2. Complex plane impedance plots for PESA-modified glassy carbon electrodes (0.93% dispersion in 1:2 water/acetone solvent) in  $\blacksquare$  0.1 M pH 4.6 acetate buffer, and  $\blacktriangle$  0.1 M  $\text{KNO}_3/5$  mM  $\text{HNO}_3$  electrolyte.

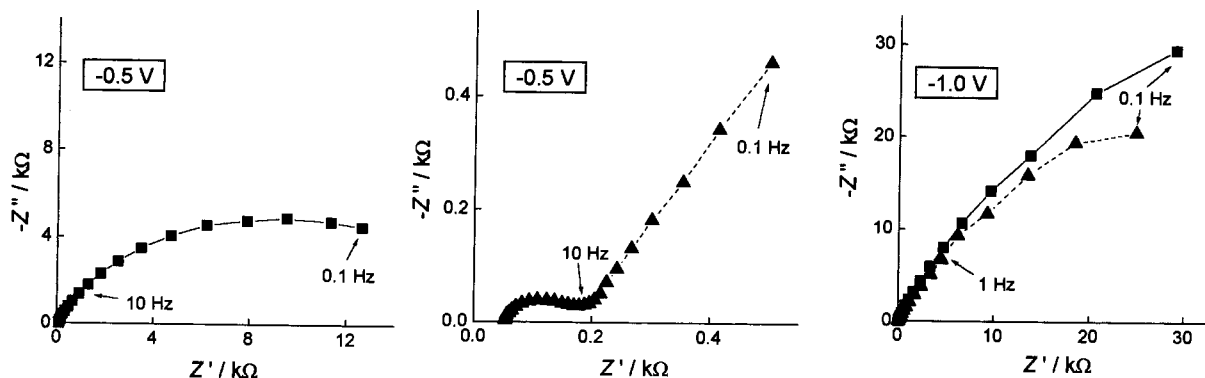


Fig. 3. Complex plane impedance plots for a PCMTFE (0.93% dispersion in 1:2 water/acetone solvent) in ■ 0.1 M pH 4.6 acetate buffer, and ▲ 0.1 M  $KNO_3/5$  mM  $HNO_3$  electrolyte.

In Fig. 4 the responses in nitrate electrolyte at the PCMTFE formed from the three types of dispersion are compared. Some differences between the types of film are evident at  $-0.5$  V, but there are essentially no differences at  $-1.0$  V. At  $-0.5$  V the impedance is small and the semicircle which appears is attributed to oxygen reduction; additionally, the adsorption capacitances due to nitrate ion adsorption and permeation are of almost equal value. The high frequency semicircle  $R$  and  $C$  values are very similar for the two dispersions in 1:2 water/acetone solvent; however, for the 5:1 water/acetone solvent the values become

$R = 300 \Omega$  and  $C = 50 \mu F$ . Thus, the general conclusion is that there is an influence from the concentration of the dispersion and the solvent. This influence must be on the morphology and structure of the film in such a way that the anions enter the film together with water solvent and cations, presumably swelling it to different extents, opening pores through which species can travel to the electrode substrate, and permitting the passage of oxygen. Such an effect will be less at more negative potentials when it will be more difficult for anions to enter the film, as observed at  $-1.0$  V.

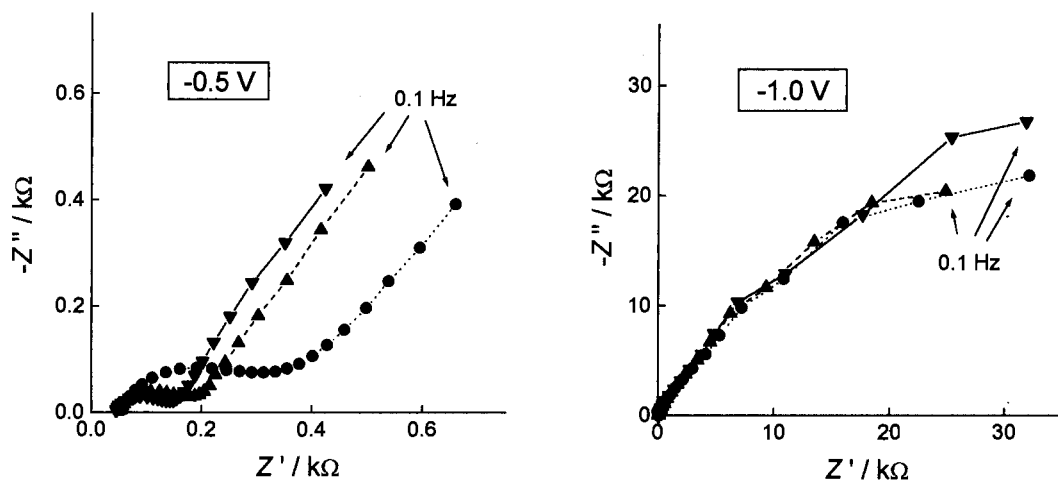


Fig. 4. Complex plane impedance plots for a PCMTFE in 0.1 M  $KNO_3/5$  mM  $HNO_3$  electrolyte: ▲ 0.93% in 1:2 water/acetone, ▼ 0.25% in 1:2 water/acetone and ● 0.25% in 5:1 water/acetone solvent.

The results presented in Figs. 2 and 3 can be re-examined in the light of these observations. Nitrate anion probably penetrates the film more easily during membrane swelling and opens up the structure in such a way as to permit the easier passage of oxygen. Although some influence from the different pH values could be expected, various studies have shown it not to be a significant parameter.

Thus, it is the identity of the electrolyte anion, rather than the composition of the modifier solution which has greatest effect on the film characteristics in the absence of electroactive species, except dissolved oxygen. The conclusion for ASV experiments—where the influence of oxygen should be excluded as much as possible—is that acetate buffer is to be preferred.

### 3.2. BIA-SWASV experiments at PCMTFEs

As mentioned above, Fig. 1 illustrates the stripping responses for a mixture of four heavy metal ions and shows the viability of the BIA-SWASV approach.

The influence of model surfactants was investigated for comparison with other polymer-modified electrodes. These were Triton X-100 detergent, sodium dodecyl sulphate (SDS) polyelectrolyte and protein standard ( $5.0 \text{ g dl}^{-1}$

albumin and  $3.0 \text{ g dl}^{-1}$  globulin, Sigma). Fig. 5 demonstrates the influence of Triton X-100 detergent on the height of the cadmium signal using a 0.93% film. Results from such experiments with all three types of surfactant are shown in the plots of Fig. 6. From these several deductions can be made:

- the stripping currents at PCMTFEs are lower than those at MTFEs by  $\approx 30\%$  (cadmium) and 70% (lead) in the absence of surfactants.
- There is generally a lesser alteration in the stripping current response at the PCMTFE with increasing surfactant concentration, in contrast to that at the MTFE. This partially reduces any negative effects due to the presence of the film.
- The behaviour of the PCMTFE on removing the surfactant (ensured by injecting blank electrolyte between successive injections of sample) shows no memory effect.

With respect to the last point, the data were registered using a procedure to ensure a clean surface without adsorbed species. This was done by injecting electrolyte between each injection of surfactant-containing sample, with application of a potential of  $-0.3 \text{ V}$  versus SCE for 10 min. In normal analyses, it was found that a period of 1 min is enough to remove any memory effect; however, for evaluation a longer period was em-

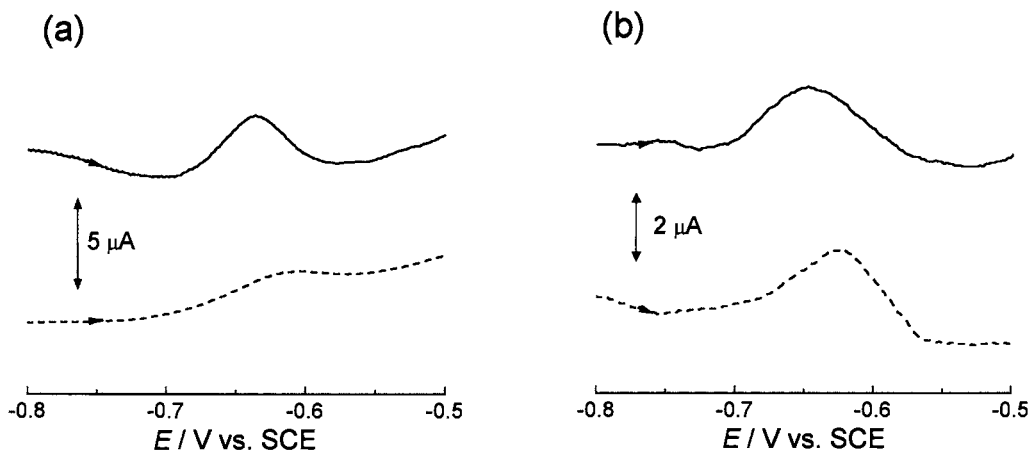


Fig. 5. BIA-SWASV traces showing influence of Triton X-100 on the height of the cadmium stripping signal at (a) MTFE (b) PCMTFE (0.93% concentration, 1:2 water/acetone solvent) in the presence (---) and absence (—) of  $1 \text{ mg dm}^{-3}$  Triton X-100. Experimental conditions as Fig. 1.

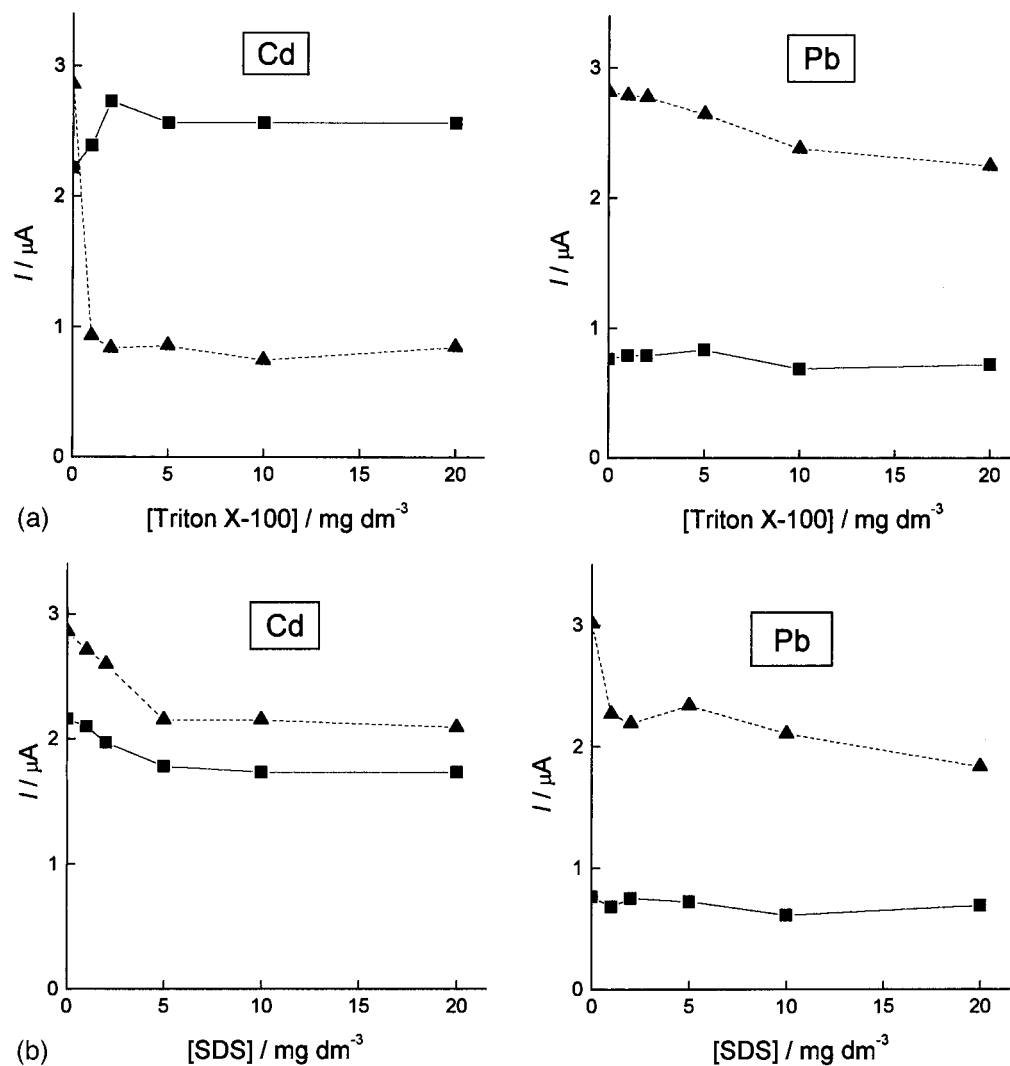


Fig. 6. Plots showing influence of increasing surfactant concentration on stripping response at ▲ MTFE and ■ PCMTFE (0.93% in 1:2 water/acetone) for the BIA-SWASV of  $10^{-7}$  M  $\text{Cd}^{2+}$  or  $\text{Pb}^{2+}$ : (a) Triton X-100; (b) sodium dodecylsulphate; (c) protein standard. Experimental conditions as Fig. 1.

ployed to be absolutely certain. If there were large amounts of copper ion in the solutions analysed then this procedure would not be sufficient, it being necessary to apply +0.1 V for a short period. This was avoided when possible to ensure that there is no oxidation of the mercury film.

There is some variation in the stripping current obtained in the absence of surfactant at the PCMTFE. This has been noted previously for various different polymer coatings [17] and may

be due partly to varying thickness of the films but to a greater extent to the internal structure of the film which is very difficult to control. In general the variation between different films is <10%. It suggests that the standard addition method is to be preferred for accurate measurements of concentration.

Calibration data for the three types of film from BIA-SWASV experiments for cadmium and lead are collected in Table 1. The data in Table 1

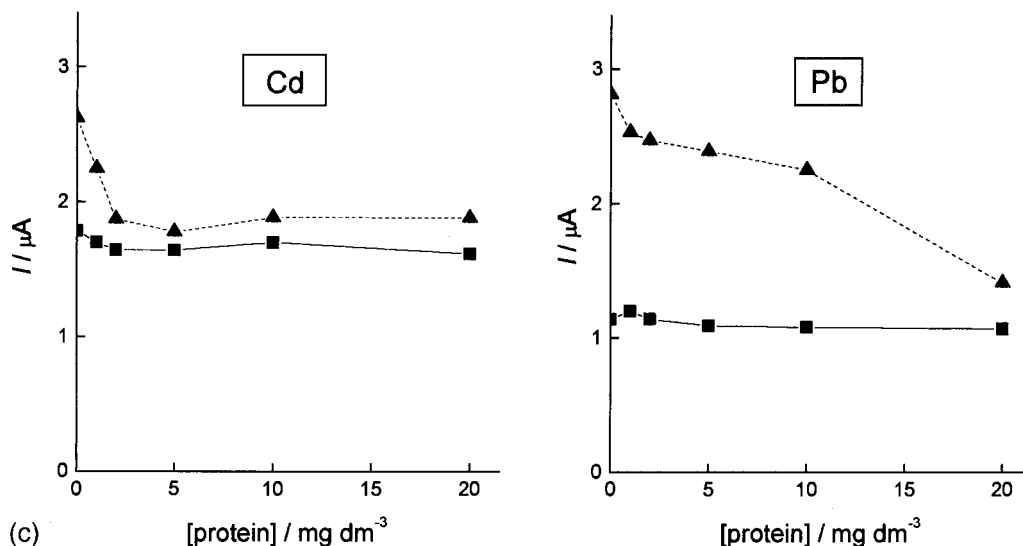


Fig. 6. (Continued)

were obtained over the range 10–100 nM; above 100 nM the linearity begins to fall off. It can be seen that the film morphology and thickness have significant influence on the calibration plots, complementing the deductions from impedance experiments. In particular, the first two films show the influence of the film concentration. However, the thicker film (higher concentration in the dispersion) leads to higher BIA-SWASV signals. The reason for this can be traced to the more particulate nature of the film in the latter case, i.e. a more particulate film-forming dispersion, such that the cations can traverse the film more easily.

On increasing the ratio of water to acetone, however, there is a significant increase in signal and the lead signal becomes larger than the cadmium signal. This is slightly surprising since the lead is much larger than the cadmium cation. However, the more hydrophilic environment during film formation with 5:1 ratio water/acetone solvent almost certainly leads to different orientations between the neighbouring polymer chains than for the case of the 1:2 water/acetone ratio and may result in there being fewer sulphonate groups available to interact with the cations in an exchange mechanism. The data suggest that the best

Table 1

Results from calibration plots in the determination of lead and cadmium by BIA-SWASV at PCMTFES in pH 4.6 acetate buffer

Dispersion of PESA		Slope ( $\mu\text{A nM}^{-1}$ )	Intercept ( $\mu\text{A}$ )	Correlation coefficient ( $n = 6$ ) (%)	Detection limit ( $3\sigma$ ) (nM)
0.93% in 1:2 water/ acetone	Cadmium	$0.0214 \pm 0.0011$	$0.0674 \pm 0.0455$	99.4	4.8
	Lead	$0.0106 \pm 0.0006$	$0.0640 \pm 0.0248$	99.4	5.5
0.25% in 1:2 water/ acetone	Cadmium	$0.00341 \pm 0.00092$	$0.0124 \pm 0.0378$	99.5	3.4
	Lead	$0.00140 \pm 0.00021$	$0.00243 \pm 0.00891$	99.6	5.9
0.25% in 5:1 water/ acetone	Cadmium	$0.0125 \pm 0.0005$	$0.00652 \pm 0.02015$	99.7	3.7
	Lead	$0.0246 \pm 0.0010$	$0.0893 \pm 0.0361$	99.7	3.8

film is the last one, 0.25% in 5:1 water/acetone solvent. Detection limits are very similar in all cases at around 5 nmol dm<sup>-3</sup>.

It is interesting to compare these data with those obtained at Nafion-coated electrodes [4,5]. In that case, the currents at coated electrodes are higher but there is some influence of surfactants (a drop in signal of  $\approx 20\%$  up to 20 mg dm<sup>-3</sup>). Detection limits for the two types of coating are very similar. However, as noted previously [5], there appears to be a specific interaction between Pb<sup>2+</sup> and non-ionic detergents (e.g. Triton), which leads to higher accumulations and larger stripping responses by up to 20%, possibly via weak complex formation on the Nafion surface. Indeed, it may be that such electrochemical experiments offer a useful probe for these interactions. In analyses of effluents containing large but variable quantities of non-ionic detergents this influence in the response at Nafion-coated electrodes could be problematic in which case the use of PESA films would be a useful and viable alternative.

#### 4. Conclusions

It has been demonstrated that PCMTFE coated mercury thin film electrodes can be used successfully in BIA with anodic stripping voltammetry. Characterization of films made from dispersions of different concentrations and in different solvent mixtures showed their importance in film optimisation. It was shown to be preferable to fill the cell with acetate buffer rather than nitrate electrolyte. Of the films tested, best results were obtained with a 0.93% dispersion concentration in 1:2 water/acetone solvent. Discrimination against model surfactants is excellent and the method provides a viable alternative to the use of Nafion coatings, particularly for application to samples

containing large quantities of non-ionic detergents.

#### Acknowledgements

The support of Fundação para a Ciência e Tecnologia (FCT), Portugal, project PEAM/SEL/526/95, is gratefully acknowledged. D.A.F. thanks FAPESP, Brazil for a post-doctoral fellowship. The authors thank Professor J. Pingarron, Universidad Complutense de Madrid, for the gift of a sample of poly(ester sulphonic acid).

#### References

- [1] J. Wang, Z. Taha, *Anal. Chem.* 63 (1991) 1053.
- [2] C.M.A. Brett, A.M. Oliveira Brett, L.C. Mitoseriu, *Electroanalysis* 7 (1995) 225.
- [3] C.M.A. Brett, A.M. Oliveira Brett, L. Tugulea, *Anal. Chim. Acta* 322 (1996) 151.
- [4] C.M.A. Brett, A.M. Oliveira Brett, F.-M. Matysik, S. Matysik, S. Kumbhat, *Talanta* 43 (1996) 2015.
- [5] C.M.A. Brett, D.A. Fungaro, J.M. Morgado, M.H. Gil, *J. Electroanal. Chem.* 468 (1999) 26.
- [6] T. Gennett, W.C. Purdy, *Anal. Chem.* 62 (1990) 2155.
- [7] J. Wang, Z. Lu, *J. Electroanal. Chem.* 266 (1989) 287.
- [8] J. Wang, T. Golden, *Anal. Chem.* 61 (1989) 1397.
- [9] J. Wang, Z. Taha, *Electroanalysis* 2 (1990) 383.
- [10] J. Wang, D. Leech, M. Ozsoz, S. Martinez, M.R. Smyth, *Anal. Chim. Acta* 245 (1991) 139.
- [11] L. Gorton, H.I. Karan, P.D. Hale, T. Inagaki, Y. Okamoto, T.A. Skotheim, *Anal. Chim. Acta* 228 (1990) 23.
- [12] J. Wang, A.J. Reviejo, *Anal. Chem.* 65 (1993) 845.
- [13] J. Wang, E. Dempsey, A. Eremenko, M.R. Smyth, *Anal. Chim. Acta* 279 (1993) 203.
- [14] C.M.A. Brett, A.M. Oliveira Brett, *Electrochemistry. Principles, Methods, and Applications*, Oxford University Press, Oxford, 1993, pp. 244–248.
- [15] P. Heiduschka, A.W. Munz, W. Göpel, *Electrochim. Acta* 39 (1994) 2207.
- [16] E.K. Umnikrishnan, S.D. Kumar, B. Maiti, *J. Membr. Sci.* 137 (1997) 133.
- [17] M.E.R. Dam, K.N. Thomsen, P.G. Pickup, K.H. Schröder, *Electroanalysis* 7 (1995) 70.



# Liquid chromatographic assessment of total and protein-bound homocysteine in human plasma

E. Bald \*, E. Kaniowska, G. Chwatko, R. Glowacki

*Department of Environmental Chemistry, University of Łódź, 163 Pomorska Street, 90-236 Łódź, Poland*

Received 9 April 1999; received in revised form 16 July 1999; accepted 23 July 1999

## Abstract

Homocysteine present in human blood plasma is derivatized with thiol selective ultraviolet labelling reagent, 2-chloro-1-methylpyridinium iodide, and separated from other plasma thiol derivatives by high-performance liquid chromatography (HPLC) with detection at 312 nm. The separation is carried out isocratically on LiChrospher RP-18 column using mobile phase consisting of pH 2.5 0.04 M trichloroacetic acid buffer and methanol in the ratio 9:1 (v/v) pumped at 0.5 ml min<sup>-1</sup> at 40°C. The homocysteine S-pyridinium derivative elutes at 6.5 min. To determine total and protein-bound homocysteine it is necessary to cleave disulphide bounds by the use of tri-n-butylphosphine in order to form free sulphhydryl group. The method provides quantitative information on total and protein-bound homocysteine based on assays with derivatization after reduction of whole plasma, and derivatization after reduction of acid precipitated proteins. The calibration graph is linear over the concentration range covering most experimental and clinical cases. The assay has a low pmol sensitivity and is reproducible; intra- and inter-day, relative standard deviation range from 1.79 to 5.09% and from 2.80 to 5.60%, respectively. The method is applied to the determination of total and protein-bound homocysteine in the plasma of healthy individuals. © 2000 Elsevier Science Ireland Ltd. All rights reserved.

*Keywords:* Homocysteine; Plasma; HPLC; UV detection

## 1. Introduction

Homocysteine is an intermediate amino acid formed during the metabolism of methionine, a sulphur-containing essential amino acid. The values of total homocysteine, understood as the sum of free and protein bound homocysteine, between

5 and 15  $\mu\text{mol l}^{-1}$  plasma in fasting subjects are considered normal. Above normal concentrations are referred to as hyperhomocysteinemia [1]. The two major acquired causes of increased homocysteine levels are chronic renal failure and absolute or relative deficiencies of folate, vitamin B12 or vitamin B6, three vitamins involved in the normal metabolism of methionine [2]. An increased interest in the metabolism of homocysteine emerged during last decade because moderate hyperhomocysteinemia is common in the general population

\* Corresponding autor. Tel.: +48-42-6355835; fax: +48-42-6783924.

*E-mail address:* ebald@kryisia.lodz.pl (E. Bald)

and has been linked with premature cardiovascular disease [3–5].

It was shown [6] that erythrocytes are responsible for most of the increase in plasma homocysteine and suggested that homocysteine is derived from adenosylmethionine dependent protein carboxymethylation in cells. Intracellular homocysteine is assumed to exist in sulfhydryl form because of a high concentration of reduced glutathione and is exported to plasma when the rate of its production exceeds the metabolic capacity [7].

In plasma, most of homocysteine is in the disulfide form bound either to protein or to low-molecular-mass thiols [8]. Accurate and precise determination of plasma levels of homocysteine is essential for understanding its role in the pathogenesis of vascular disease. Because plasma homocysteine concentrations can be lowered by administration of folic acid or cobalamin [9] assessment of homocysteine in subjects involved in dietary modification or vitamin supplementation programs, as well as in cardiovascular disease patients at large, requires rapid and reproducible assays.

Several methodologies for the determination of total homocysteine in plasma have been described in the literature. To determine total plasma homocysteine, the sum of all protein-bound, oxidized low-molecular-mass, and free reduced homocysteine, it is necessary to reduce disulfide bonds followed by derivatization and gas chromatography-mass spectrum (GC-MS) [10], HPLC [11–17], ion-exchange chromatography [18,19], or high-performance capillary electrophoresis (HPCE) [20–22], separation with ultraviolet absorbance or fluorescent detection. Electrochemical detection does not require derivatization [23–26]. Most of HPLC methods for homocysteine determination are reviewed in details in excellent papers [27,28]. A fluorescence polarization immunoassay procedure for homocysteine with no pretreatment and chromatographic step has also been proposed [29].

In this report we describe a HPLC method for determination of homocysteine in human plasma. Free oxidized and protein-bound homocysteine is converted to its reduced counterpart by the use of

tri-*n*-butylphosphine (TNBT), and, following derivatization with 2-chloro-1-methylpyridinium iodide (CMPI), the homocysteine S-pyridinium derivative is quantified by reversed-phase HPLC with UV absorbance detection. This CMPI-HPLC method provides quantitative information on total and protein-bound homocysteine based on assays with derivatization after reduction of whole plasma, and derivatization after reduction of acid precipitated proteins.

## 2. Experimental

### 2.1. Apparatus

The liquid chromatography equipment used for the analysis was made by Hewlett–Packard (1100 Series system, Waldbronn, Germany) and consisted of a quaternary pump, autosampler, thermostated column compartment, vacuum degasser, and diode-array detector. For instrument control, data acquisition and data analysis an Hewlett–Packard ChemStation for LC 3D system including single instrument Hewlett–Packard ChemStation software and Vectra color computer was used. UV spectra were recorded on a Hewlett–Packard HP 8453 diode array UV–vis spectrophotometer. For pH measurement, a Hach One pH meter was used. Water was purified using a Millipore Milli-QRG (Vien, Austria) system.

### 2.2. Chemicals and reagents

CMPI [30], 2-chloro-1-propylpyridinium iodide (CPPI) and internal standard, cysteine-CPPI derivative, were prepared in this laboratory. CMPI is also commercially available from Fluka (Buchs, Switzerland) and Sigma (St. Louis, MO). For homocysteine derivatization (Fig. 1) prior to HPLC analysis, a 0.1 M water solution of CMPI was used. Stock internal standard solution was prepared as a 1 mM water solution of cysteine-CPPI derivative and used after appropriate dilution. Ethylenediaminetetraacetic acid disodium salt (EDTA), tris(hydroxymethyl)aminomethane (Tris), perchloric acid (PCA), and HPLC-grade methanol and acetonitrile were from J.T. Baker

(Deventer, Netherlands). Trichloroacetic acid (TCA) and tri-*n*-butylphosphine (TNBP) were from Fluka. L-Cysteine hydrochloride (CSH), DL-cystine (CSSC) and glutathione (GSH) were from Reanal (Budapest, Hungary). DL-Homocysteine (HCSH) and cysteinylglycine (CGSH) were from Sigma and DL-homocysteine (HCSSCH) was purchased from Serva (Heidelberg, Germany). All other reagents were HPLC or analytical reagent grade. Purified water from Millipore Milli-QRG was used throughout the experiments. All liquids used for HPLC system were filtered through 0.2  $\mu\text{m}$  membranes.

The pH of the buffers was adjusted by potentiometric titrations. The titration system was calibrated with standard pH solutions.

### 2.3. Methods

#### 2.3.1. Blood collection and subject

Blood was collected by venipuncture from apparently healthy subjects in a fasting state to the tube containing EDTA, cooled on ice and centrifuged at  $800 \times g$  for 15 min at room temperature within 30 min of collection. The plasma supernatant was stored at  $-20^\circ\text{C}$  until analysis.

#### 2.3.2. Determination of total plasma homocysteine, procedure 1

To 500  $\mu\text{l}$  of plasma 500  $\mu\text{l}$  of pH 8.2 1 M Tris buffer, 250  $\mu\text{l}$  of 0.1 M EDTA solution and, 25  $\mu\text{l}$  of 10% TNBP in methanol was added. The reac-

tion mixture was incubated at  $60^\circ\text{C}$  for 30 min, and after cooling, 50  $\mu\text{l}$  of 0.1 M CMPI was added, vortex-mixed and kept at room temperature for 30 min, followed by addition of 300  $\mu\text{l}$  of 3 M PCA solution and 40  $\mu\text{l}$  of 0.025 mM internal standard solution. Precipitated protein was removed by centrifugation ( $11\,500 \times g$ , 10 min, room temperature) and supernatant was transferred to a vial, followed by injection (20  $\mu\text{l}$ ) into the chromatographic system.

#### 2.3.3. Determination of protein-conjugated homocysteine, procedure 2

To 500  $\mu\text{l}$  of plasma 300  $\mu\text{l}$  of 3 M PCA solution was added and the mixture was vortex-mixed followed by 15 min centrifugation. After removing of supernatant and washing with 200  $\mu\text{l}$  of water the protein was resuspended with 500  $\mu\text{l}$  of water and 500  $\mu\text{l}$  of pH 2.0 M 8.2 Tris buffer and reduced with TNBP, derivatized with CMPI, deproteinized with PCA and chromatographed as described in Section 2.3.2.

#### 2.3.4. Chromatographic conditions

HPLC analysis was performed with Hewlett-Packard 1100 Series system. Separation was carried out with an analytical reversed-phase column C18 LiChroCART,  $125 \times 4$  mm I.D. packed with 5  $\mu\text{m}$  particles of LiChrospher RP-18 (Hewlett-Packard, Waldbronn, Germany). The autosampler injected 20  $\mu\text{l}$  aliquots of final analytical solutions. Separations were isocratic using mobile

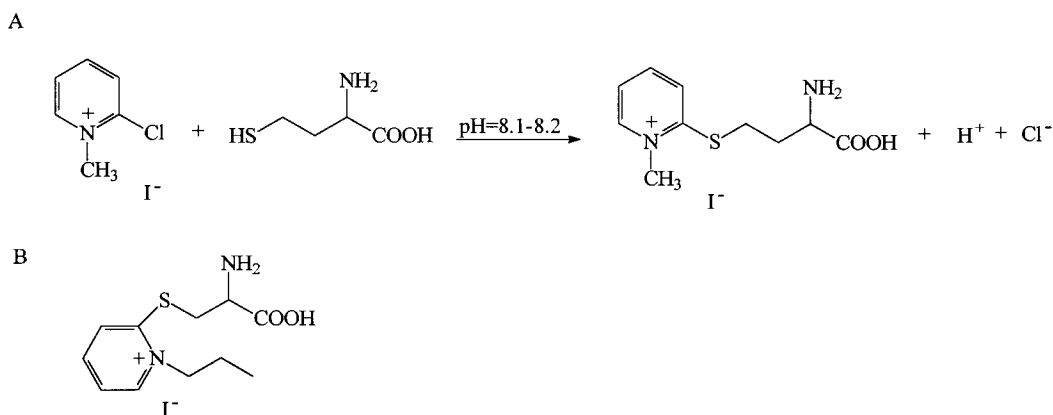


Fig. 1. Chemical derivatization reaction of homocysteine (A); chemical structure of the internal standard (B).

phase consisting of 0.04 M trichloroacetic acid buffer adjusted to pH 2.5 with lithium hydroxide and methanol in the ratio of 9:1 (v/v) pumped at 0.5 ml min<sup>-1</sup> at 40°C. The absorbances were measured at 312 nm. Identification of peaks was based on comparison of retention times and diode-array spectra with the corresponding set of data obtained by analyzing authentic compounds.

### 2.3.5. Internal standard approach

In order to minimize the contributions of sample preparation, injection variations and column deterioration to the final results, the internal standard were used. The cysteine-CPPI derivative applied here as an internal standard possesses similar chemical structure and chromatographic properties to that of homocysteine-CMPI derivative (Fig. 1).

### 2.3.6. Preparation of calibration standards

Stock solutions of 10 µmol ml<sup>-1</sup> homocysteine, homocystine, cysteine, cysteinylglycine, and reduced glutathione were prepared as described in our previous work [31] on urine analysis. These solutions could be kept at 4°C for several days without noticeable change of the thiols content. The working solutions were prepared by appropriate dilutions with water as needed and processed without delay. For preparation of calibration standards of human plasma, a 500 µl portions of plasma from a apparently healthy donor were placed each in a polypropylene tube and spiked with the appropriate amount of working standard solution of homocysteine. Calibration standards for construction of standard curve for plasma homocysteine were spiked with homocysteine to provide concentration of exogenous homocysteine of 2.5, 5, 7.5, 10, 20, 30, and 50 nmol ml<sup>-1</sup> plasma (assuming 100% of the future reduction of the disulphide bond of homocysteine).

### 2.3.7. Stability of the homocysteine S-pyridinium derivative in plasma matrix

To test the stability of the S-pyridinium derivative of homocysteine in plasma matrix, a 10 nmol ml<sup>-1</sup> of homocysteine calibration standard was prepared, derivatized with CMPI and deproteinized as described under Section 2.3.2 and

kept at ambient temperature. Aliquots of 20 µl were chromatographed at time zero and in successive h.

### 2.3.8. Calibration curve

Calibration curve for plasma total and protein-bound homocysteine was constructed by processing a 500 µl calibration standard samples of plasma spiked with homocystine according to procedure 1. The ranges of homocystine added were from 1.25 to 25 nmol ml<sup>-1</sup>. The peak height ratios of homocysteine derivative to that of internal standard were plotted versus analyte concentration and the curve was fitted by least-square linear regression analysis.

### 2.3.9. Recovery

Recovery was determined by adding different amounts of homocystine solution in water to human plasma samples with known endogenous homocysteine level and processed in the manner described in Section 2, and calculated with the use of formula:

$$\text{Recovery(\%)} = \frac{(\text{measured level} - \text{endogenous level}) \times 100\%}{\text{added amount}}$$

### 2.3.10. Application of the method

To show the performance of the method, blood samples were taken from 12 fasting volunteers, 23–57 years old (six men and six women) in the morning. The blood was processed as described under Section 2.3.1, and total and protein-bound homocysteine in plasma were determined following the procedures 1 and 2, respectively.

## 3. Results and discussion

Homocysteine in plasma exists in different forms (Fig. 2), including the major protein-bound fraction, free oxidized fraction where cysteine-homocysteine mixed disulphide predominates along with mixed disulphides with other endogenous thiols present in plasma, and homocysteine dimer. Free reduced homocysteine represents the third and minor fraction [32]. To determine total and

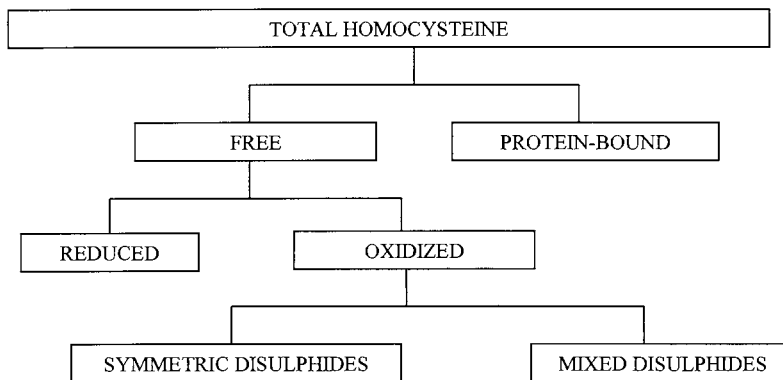


Fig. 2. Forms of homocysteine in human blood plasma.

protein-bound homocysteine, it is necessary to cleave disulphide bounds in order to form the free sulphhydryl group. For this purpose we have used TNBP. For derivatization of reduced homocysteine we have used the selective thiol UV-labeling reagent CMPI. Optimal conditions for cleavage of disulphide bond of homocysteine with TNBP and subsequent derivatization via the  $-SH$  group with CMPI are described in our earlier reports [31,33].

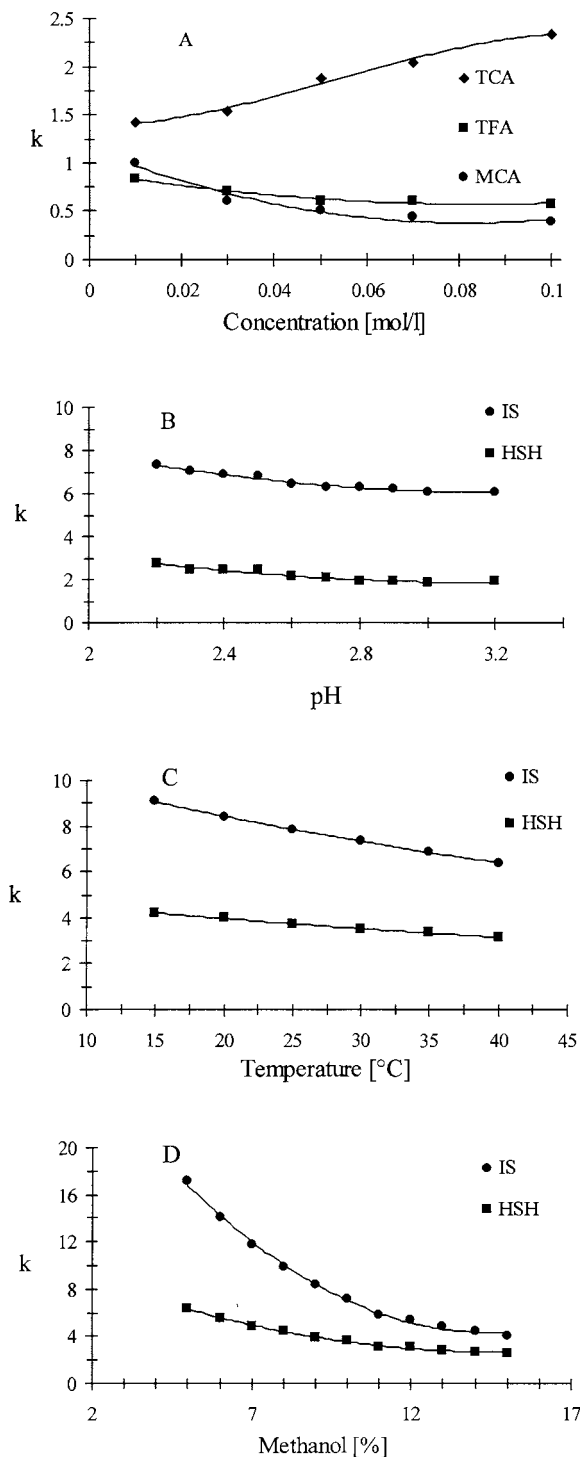
### 3.1. Optimization of chromatographic conditions

Standard reversed-phase chromatography yields little retention for S-pyridinium derivatives of biological thiols because of their hydrophilic and ionic character. They elute close to the solvent front and separation is impossible. Depending on mobile phase pH, within the pH range acceptable for reversed-phase silica-based columns, homocysteine moiety of the S-pyridinium derivative may be anionic, zwitterionic, or cationic, whereas derivative as a whole possesses net positive charge as a result of the permanent positive charge on quaternary nitrogen atom in pyridine ring. This net positive charge increases when pH decreases as a result of the homocysteine primary amino group protonation, as well as ionization suppression of carboxylic acid residue. Retention of cationic analytes can be enhanced by the addition of alkyl sulphonates pairing agents, as described in our earlier work [33]. These types of pairing reagents are expensive, can strongly adsorb to the stationary phase, require long column-equilibration time,

and low pH ionic strength buffer. Recently, we have learned [31] that the retention of the cationic S-pyridinium derivatives of homocysteine and metabolically related thiols can be modified dramatically by chromatographing them with the mobile phases containing trichloroacetic acid. In this work, the increased retention of cationic homocysteine S-pyridinium derivative by the use of trihaloacetate buffers as pairing agents was investigated. In addition to pH, the chromatographic variables that were investigated include ionic strength, concentration and size of the trihaloacetate anion, counter cation size, organic modifiers, and temperature and flow-rate of the mobile phase.

#### 3.1.1. Effect of buffer type, its concentration and counter cation size

The buffers examined include monochloroacetic acid (MCA), tribromoacetic acid (TBA), trichloroacetic acid (TCA) and trifluoroacetic acid (TFA). Initial experiments with TBA showed lack of sufficient UV-transparency at analytical detection wavelength, so this buffer was not considered further. The influence of the remaining three buffers and their concentration on retention of homocysteine derivative is shown in Fig. 3(A). These results show that retention was influenced both by the nature of the buffer and concentration. Retention of homocysteine was increased significantly with TCA and was positively correlated to the concentration of the buffer. In the case of MCA and TFA, poor retention was ob-



served with slightly negative correlation to concentration. This retention behaviour can be accounted for in terms of solvophobic ionic interaction of the analyte with the pairing agent which enhances reversed-phase partitioning, as well as the inductive effect that the halogens have on the electron density of the carboxylate anion. The trifluoride is more electronegative, withdrawing electrons from the anion, and it interacts less with the net-cationic S-pyridinium derivatives than trichloroacetate. Similar retention behaviour was observed by others [34] in the case of underivatized biogenic aminothiols.

The effect of the charge density of the counter cation used for the adjustment of the pH of the TCA buffer on the retention and resolution of the cationic S-pyridinium derivatives was also studied. Using the chromatographic conditions described in Section 2, retentions of cysteine and homocysteine S-pyridinium derivatives were highest for the counter cation with the lowest charge density ( $K^+$ ), whereas resolution was highest for the counter cation with the highest charge density ( $Li^+$ ). Relevant data for cysteine and homocysteine-CMPI derivatives are shown in Table 1.

### 3.1.2. Effect of pH, organic modifier, temperature, and mobile phase flow-rate

The influence of pH, organic modifier, temperature, and mobile phase flow-rate on retention was also studied. Resolution was examined for homocysteine and two neighbouring peaks—cysteine and glutathione. These results are shown in Figs. 3 and 4. The retention factor for homocysteine does not change with variation of the mobile phase flow-rate (data not shown).

After thorough study of the above mentioned chromatographic variables, the separation conditions chosen constitute a necessary compromise between maximum detectability and chromatographic resolution. The chromatogram shown in

Fig. 3. Retention factor of the homocysteine-CMPI derivative and the internal standard (IS) as a function of: (A), the buffer type and concentration; (B), the eluent pH; (C), the column temperature; and (D), the organic modifier content. Other chromatographic condition as described in Section 2.

Table 1

Influence of counter cation charge density on retention and resolution.

Base	Retention factor <sup>a</sup>		Resolution
	CSH-CMPI	HCSH-CMPI	
KOH	1.55	2.06	2.48
NaOH	1.46	1.99	2.95
NH <sub>4</sub> OH	1.42	1.94	2.75
LiOH	1.12	1.88	5.38

<sup>a</sup> Chromatographic conditions as described in Section 2

Fig. 5 is the final result of the procedure, and it does indeed yield a satisfactory distribution of the peaks over the chromatogram. The plasma matrix does not interfere with the resolution and quantitation of the resulting homocysteine-CMPI and internal standard peaks. Commonly used drugs, e.g. drugs routinely administered to diabetics, captopril, or aspirin, do not disturb the assay. All these drugs show no absorption in this relatively clean ultraviolet region (312 nm) or like captopril, elute after much longer time. Fig. 5 displays typical chromatogram resulting from CMPI-HPLC analysis of acid precipitated protein from 0.5 ml of plasma. As shown, homocysteine-CMPI derivative eluting after 6.5 min and the internal standard, eluting after 12 min, were resolved and separated from endogenous plasma thiol components and derivatization reagent excess under the optimum analytical conditions used. The overall chromatographic run time was established at 16 min. Under the optimum conditions for homocysteine determination, cysteine and cysteinylglycine appear as a double peaks.

### 3.2. Validation

#### 3.2.1. Linearity

Four replicates of different concentrations of exogenous homocysteine added to the normal

Fig. 4. Variation of the resolution of homocysteine derivative and adjacent peaks as a function of: (A), the eluent pH; (B), the TCA buffer concentration; (C), the column temperature; (D), the methanol content in the mobile phase. Other chromatographic parameters as described in Section 2. Symbols: ◆ resolution between CSH and HCSH; and ● resolution between HCSH and GSH.

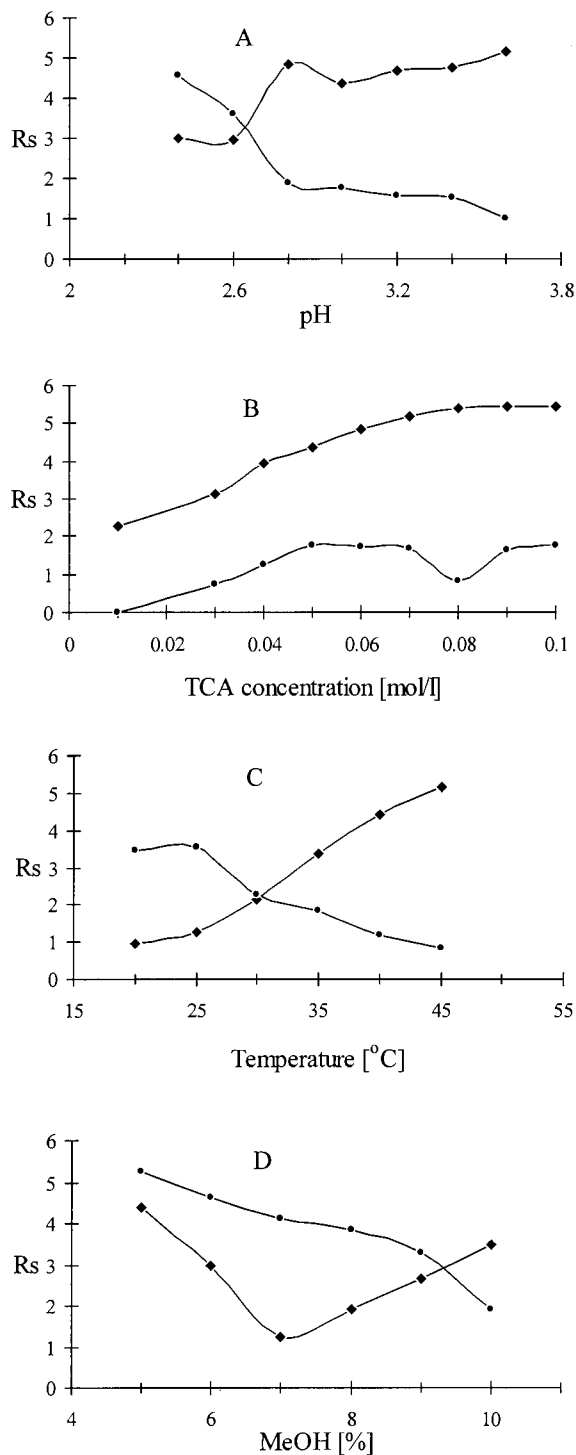


Fig. 4.

plasma sample as specified in Section 2.3.6 were processed according to the procedure described in Section 2. The correlation between analyte concentration and the detector response was linear. The equation for the linear regression line and the coefficient of correlation for these data are  $y = 0.069x + 0.552$  and  $R^2 = 0.9965$ , respectively. Corresponding data for standard water solution of homocysteine are  $y = 0.1338x - 0.0343$  and  $R^2 = 0.9996$ , respectively. The values obtained during calibration with the use of another ten plasma samples, obtained from ten different

donors, within the validation procedure were similar. In each case the correlation coefficient was above 0.996.

### 3.2.2. Reproducibility

A series of sequential determinations ( $n = 5$ ) were performed with normal plasma samples spiked with different amounts of homocysteine and the mean values, standard deviations and relative standard deviation were calculated. The typical results for the within-day reproducibility are shown in Table 2. The between-day reproducibil-

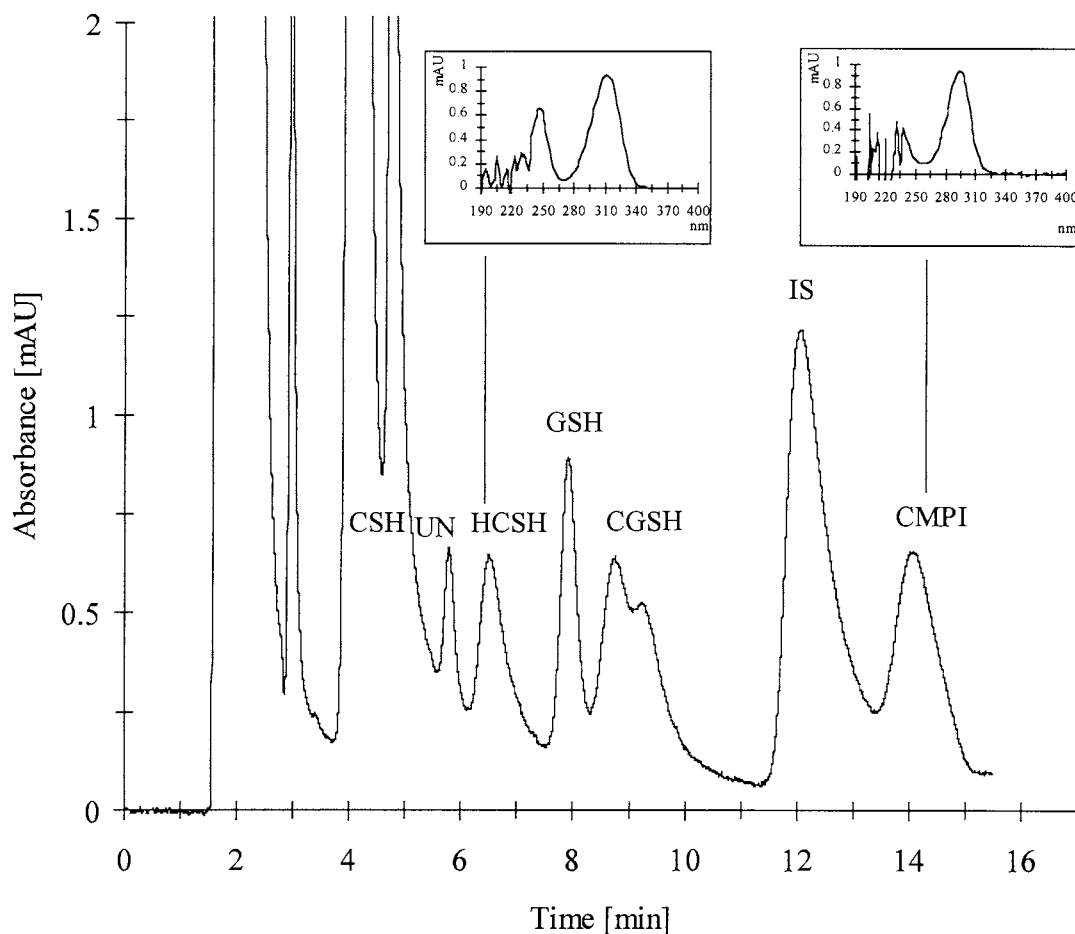


Fig. 5. Chromatogram of the derivatized plasma sample for determination of protein-bound homocysteine from a healthy donor. Insets are characteristic absorption spectra of the HCSH-CMPI derivative and derivatization reagent (CMPI) as recorded by diode-array detection. Protein-bound homocysteine content is  $4.08 \text{ nmol ml}^{-1}$  plasma. Analysis was performed according to procedure 2. Separation and quantitation are as described under Section 2. Peaks: CSH, cysteine; UN, unknown; HCSH, homocysteine; GSH, glutathione; CGSH, cysteinylglycine; IS, internal standard; CMPI, excess of the derivatization reagent.



Table 2

Absolute recoveries and within-analysis imprecisions of total homocysteine in human plasma, spiked at three levels ( $n = 5$ )

Concentration [nmol/ml]	Recovery [%]	R.S.D. [%]
3	95.80	2.45
25	96.10	1.85
55	104.15	1.50

ity was estimated by performing the same determinations on the same batch of sample every day for period of 8 days ( $n = 6$ ). The reproducibility for total homocysteine was 5.6 and 2.8% for level of 6.4 nmol ml<sup>-1</sup> (endogenous homocysteine) and 46.4 nmol ml<sup>-1</sup> (endogenous spiked with 40 nmol ml<sup>-1</sup>), respectively.

### 3.2.3. Recovery

The absolute recovery was determined by analysis of replicate sets of plasma samples of known concentration of endogenous homocysteine from an equivalent plasma matrix. Three concentrations of exogenous homocysteine were studied: one near the lower limit of quantitation, one near the center, and one near the upper boundary of the standard curve. The results calculated from formula described in Section 2.3.9 are displayed in Table 2.

### 3.2.4. Detection and quantitation limits

Lower limit of detection of homocysteine in standard water solution was 0.1 nmol ml<sup>-1</sup> (2 pmol in peak). At this concentration the signal-to-noise ratio was three. At 0.3 nmol ml<sup>-1</sup> the percent deviation from the nominal concentration and the relative standard deviation were both less than 20. Thus, according to specific recommendations for method validation [35], 0.3 nmol ml<sup>-1</sup> was defined to be the lower limit of quantitation. At all other concentrations up to the upper limit of quantitation (50 nmol ml<sup>-1</sup>) the imprecision and deviation from the nominal concentration were less than 4%.

In the case of plasma matrix, 2.5 nmol ml<sup>-1</sup> serving as the lowest concentration on the standard curve was recognized as the lower limit of quantitation. At this point recovery and imprecision were 96.0% and 2.7%, respectively. The concentration of added homocysteine equal to 1 nmol ml<sup>-1</sup> was also measured with acceptable [35], accuracy, and im-

precision (83.5% and 17.5%, respectively). According to the best of our knowledge, total and protein-conjugated homocysteine at concentrations lower than 3 nmol ml<sup>-1</sup> is exceedingly rare in either patients or healthy donors.

### 3.2.5. Stability

As we have previously indicated [31] homocysteine-CMPI derivative is stable at room temperature in water and urine matrix for more than 24 h. In plasma, no significant change in peak height was noted during the first 10 h, however, after 25 h the peak lost 6% of its initial size (data not shown). It remains unclear whether this loss is as a result of decomposition of the derivative or to the occlusion to the sample test tube walls.

### 3.3. Application of the method

The validated method was used to analyze total and protein-bound homocysteine in 12 samples taken from apparently healthy individuals (detailed data not shown). Total and protein-bound homocysteine were higher in men than in women (mean  $\pm$  S.D.: 7.42  $\pm$  0.37 for total; 6.44  $\pm$  0.25 for protein-bound; and 5.39  $\pm$  0.24 for total; 4.42  $\pm$  0.22 nmol ml<sup>-1</sup> for protein-bound homocysteine, respectively). The share of protein-bound fraction (mean  $\pm$  S.D.) in total homocysteine was: 72.9  $\pm$  3.5% for men; and 69.0  $\pm$  5.5% for women. Our results are similar to the findings of previous works which have demonstrated that normal human plasma contains 5–12 nmol ml<sup>-1</sup> total homocysteine [12,19,35–37,39]. They are also consistent with reports indicating that the total values for homocysteine is higher in males than in females [37,38,40].

## 4. Conclusion

In conclusion, the recommended CMPI-HPLC method consists of two procedures developed for determination of the total, and protein bound homocysteine in human plasma. The oxidized and protein-bound fractions are converted into reduced form employing tri-*n*-butylphosphine, and following derivatization with 2-chloro-1-

methylpyridinium iodide, the homocysteine S-pyridinium derivative is separated and quantified by ion-pair reversed-phase liquid chromatography and ultraviolet absorbance detection. The assay has proven its usefulness for the determination of total and protein-bound homocysteine in normal human plasma. Separation of homocysteine from the other plasma components was achieved by isocratic HPLC elution in 16 min. Several experimental conditions were optimised to ensure a relatively long column life. First, the column was operated at pH 2.5 which is within the range recommended by most manufacturers of the silica-based columns. Second, the salt concentration of the mobile phase is low. Finally, the low flow rate creates low back pressure.

Sensitivity, precision, and accuracy of the method are sufficient for determination of total and protein-bound homocysteine in clinical and experimental investigations. The sensitivity of the method is not sufficient enough for measurement of the free fraction of homocysteine, but can be calculated from the difference between total and protein-bound fractions. Total homocysteine is more reliable in the diagnosis of inborn errors of homocysteine metabolism and in cardiovascular risk assessment than free fraction, which vary according to specimen history. The work on the automation of the assay with the use of an on line biological sample processor is now in progress.

## Acknowledgements

The authors thank Małgorzata Kędzior, M.Sc. from Voivodeship Blood Station in Łódź for providing access to the plasma samples. This work was supported in part by Grant No 505/469 and 505/600 from the University of Łódź.

## References

- [1] M.R. Malinow, M.J. Stampfer, *Clin. Chem.* 40 (1994) 857.
- [2] V.W. Dennis, K. Robinson, *Kidney Int. Suppl.* 57 (1996) S11.
- [3] P.M. Ueland, H. Refsum, L. Brattström Jr, in: R.B. Francis Jr (Ed.), *Atherosclerotic cardiovascular disease*, homeostatis, and endothelial function, Marcel Dekker, New York, 1992.
- [4] I.J. Perry, H. Refsum, R.W. Morris, S.B. Ebrahim, P.M. Ueland, A.G. Shaper, *Lancet* 346 (1995) 1395.
- [5] G. Montalescot, A. Ankri, B. Chadeaux-Vekemans, J. Blacher, F. Philippe, G. Drobinski, R. Benzidia, P. Kamoun, D. Thomas, *Int. J. Cardiol.* 60 (1997) 295.
- [6] A. Andersson, A. Isaksson, B. Hultberg, *Clin. Chem.* 38 (1992) 1311.
- [7] B. Christensen, H. Refsum, O. Vintermyr, P.M. Ueland, *J. Cell Physiol.* 146 (1991) 52.
- [8] P.M. Ueland, M.A. Mansoor, A.B. Guttormsen, F. Müller, P. Aukrust, H. Refsum, A.M. Svardal, *J. Nutr.* 126 (1996) 1281S.
- [9] L. Brattström, B. Israelsson, B. Norrving, D. Bergqvist, J. Thörne, B. Hultberg, A. Hamfelt, *Atherosclerosis* 81 (1990) 51.
- [10] S.P. Stabler, J. Lindenbaum, D.G. Savage, R.H. Allen, *Blood* 81 (1993) 3403.
- [11] R.C. Fahey, G.L. Newton, R. Dorian, E.M. Kosower, *Anal. Biochem.* 111 (1981) 357.
- [12] A. Araki, Y. Sako, *J. Chromatogr.* 422 (1987) 43.
- [13] H. Refsum, P.M. Ueland, A.M. Svardal, *Clin. Chem.* 35 (1989) 1921.
- [14] D.W. Jacobsen, V.J. Gatautis, R. Green, *Anal. Biochem.* 178 (1989) 208.
- [15] J.B. Ubbink, W.J.H. Vermaak, S. Bissbort, *J. Chromatogr.* 565 (1991) 441.
- [16] B. Vester, K. Rasmussen, *Eur. J. Clin. Chem. Clin. Biochem.* 29 (1991) 549.
- [17] T. Fiskerstrand, H. Refsum, G. Kvalheim, P.M. Ueland, *Clin. Chem.* 39 (1993) 263.
- [18] A. Andersson, L. Brattström, A. Isaksson, B. Israelsson, B. Hultberg, *Scand J. Clin. Lab. Invest.* 49 (1989) 445.
- [19] A. Briddon, *Amino Acids* 15 (1998) 235.
- [20] E. Jellum, A.K. Thorsrud, E. Time, *J. Chromatogr.* 559 (1991) 455.
- [21] E. Jellum, *J. Cap. Elec.* 2 (1994) 97.
- [22] S.H. Kang, J.W. Kim, D.S. Chung, *J. Pharm. Biomed. Anal.* 15 (1997) 1435.
- [23] E.G. Demaster, F.N. Shirota, B. Redfern, D.J.W. Goon, H.T. Nagasawa, *J. Chromatogr.* 308 (1984) 83.
- [24] L.A. Smolin, J.A. Schneider, *Anal. Biochem.* 168 (1988) 374.
- [25] D.L. Rabenstein, G.T. Yamashita, *Anal. Biochem.* 180 (1989) 259.
- [26] M.R. Malinow, S.S. Kang, L.M. Taylor, P.W.K. Wong, B. Coull, T. Inahara, D. Mukerjee, G. Sexton, B. Upson, *Circ. Res.* 79 (1989) 1180.
- [27] P.M. Ueland, H. Refsum, S.P. Stabler, M.R. Malinow, A. Andersson, R.H. Allen, *Clin. Chem.* 39 (1993) 1764.
- [28] D.W. Jacobsen, *Anal. Chem.* 65 (1993) 367.
- [29] M.T. Shipchandler, E.G. Moore, *Clin. Chem.* 41 (1995) 991.
- [30] E. Bald, *Talanta* 27 (1980) 281.
- [31] E. Kaniowska, G. Chwatko, R. Głowacki, P. Kubalczyk, E. Bald, *J. Chromatogr. A* 798 (1998) 27.

- [32] P.M. Ueland, *Clin. Chem.* 41 (1995) 340.
- [33] S. Sypniewski, E. Bald, *J. Chromatogr. A* 676 (1994) 321.
- [34] W.A. MacCrehan, D. Shea, *J. Chromatogr.* 457 (1988) 111.
- [35] V.P. Shah, K.K. Midha, S. Dighe, I.J. McGilveray, J.P. Skelly, A. Yacobi, T. Layloff, C.T. Viswanathan, C.E. Cook, R.D. McDowall, K.A. Pittman, S. Spector, *J. Pharm. Sci.* 81 (1992) 309.
- [36] P.M. Ueland, H. Refsum, *J. Lab. Clin. Med.* 114 (1989) 473.
- [37] A.M. Svardal, M.A. Mansoor, P.M. Ueland, *Anal. Biochem.* 184 (1990) 338.
- [38] M.A. Mansoor, A.M. Svardal, P.M. Ueland, *Anal. Biochem.* 200 (1992) 218.
- [39] D.W. Jacobsen, V.J. Gatautis, R. Green, K. Robinson, S.R. Savon, M. Secic, J. Ji, J.M. Otto, L.M. Taylor Jr, *Clin. Chem.* 40 (1994) 873.
- [40] L. Brattström, A. Lindgren, B. Israelsson, A. Andersson, B. Hultberg, *J. Intern. Med.* 236 (1994) 633.

# Gradient flow titration for the determination of fluoride ion in natural waters

A.C. Lopes da Conceição <sup>a,\*</sup>, M.M. Correia dos Santos <sup>a</sup>,  
M.L.S. Simões Gonçalves <sup>a</sup>, Fernando J.V. Santos <sup>b</sup>

<sup>a</sup> Instituto Superior Técnico, Centro de Química Estrutural, Av. Rovisco Pais, 1049-001 Lisbon, Portugal

<sup>b</sup> Departamento de Química e Bioquímica da F.C.U.L., Campo Grande, 1700 Lisbon, Portugal

Received 16 April 1999; received in revised form 9 July 1999; accepted 23 July 1999

## Abstract

The determination of fluoride ions in water samples was accomplished by using a gradient flow titration. A standard commercial combined electrode is used in a cell configuration that combines the gradient chamber and the electrode in a single unit. The methodology developed gives results with a relative standard deviation of about 3%. The average recoveries after spiking natural samples with fluoride are in the range 100–102%. The method was used successfully in determining the fluoride concentration in water samples. © 2000 Elsevier Science B.V. All rights reserved.

*Keywords:* Gradient flow titration; Fluoride; Water analysis.

## 1. Introduction

Flow-injection analysis (FIA) is a mature technique with a wide variety of applications [1]. On the other hand, determination of fluoride in water samples with a fluoride selective electrode has become an officially accepted method because of the fact that this sensor is one of the best behaving ion selective electrodes [2]. The incorporation of a fluoride selective electrode in flow systems has been described earlier and its performance

and benefits are quite well documented [3–8]. Recently a flow injection (FI) system with potentiometric detection has been developed for the speciation of fluoride using a fluoride ion selective electrode with a single flow-through detector [9].

Most of the methods reported use remarkably little of the data recorded, usually one point (the peak height) or two points (the peak width). However, each point in a response curve in FI represents a different mixture of reactant and sample. This concentration gradient is generated by the reproducible timing and controllable sample dispersion, a unique feature of FI [10].

This paper proposes the use of the entire time-dependent response, instead of the final potential

\* Corresponding author. Tel.: +351-1-8419269; fax: +351-1-8464455.

E-mail address: pcqac@alfa.ist.utl.pt (A.C. Lopes da Conceição)

reading alone, as an improved ion activity assessment with ion-selective electrodes and a flow-through system.

In this work the concentration gradient in a flow injection system for the potentiometric determination of fluoride ion in water samples based on a gradient flow injection titration is explored. Determination of fluoride ion is accomplished by switching the injection valve between a standard and a sample solution. A titration curve is produced that contains information regarding the performance of the detection unit (gradient chamber and electrode) as well as the fluoride ion concentration in the sample.

Throughout the experiments a commercial combined fluoride electrode, ORION model 96-09, is used in a cell configuration that combines the gradient chamber and the electrode into a single unit [11,12].

Optimisation of the FIA variables and the features of the method have been studied before application of the developed methodology for the determination of the fluoride ion in water samples.

## 2. Theory

The theory of gradient chamber operation has been described by several authors [13–16]. In order to make use of the full information in a titration curve, it is necessary to relate the measured potential with the time dependent concentration in the mixing chamber. If we assume that: (I) the dispersion as a result of the valve is small compared to what happens in the cell; (II) the solution within the gradient chamber is at equilibrium at all times; (III) the time constant for the electrode response is shorter than that for the mixing in the gradient chamber; (IV) pH and ionic strength are kept constant throughout the titration, the fluoride content in the solution in the chamber as a function of time is given by (see Appendix A):

$$[F]_t^{\text{tot}} = [F]_{\text{st}}^{\text{tot}} - ([F]_{\text{st}}^{\text{tot}} - [F]_{\text{sa}}^{\text{tot}}) \times \exp\left[\frac{Q}{V}(t_0 - t)\right] \quad (1)$$

In this expression  $[F]_t^{\text{tot}}$  is the total concentration of fluoride at time  $t$  following a step change in

inflowing concentration from a standard solution  $[F]_{\text{st}}^{\text{tot}}$  to a sample solution  $[F]_{\text{sa}}^{\text{tot}}$  at time  $t_0$ ,  $V$  is the gradient chamber volume and  $Q$  the flow rate.

The measured quantity, the combined fluoride electrode potential  $E$ , is given by the Nernst-type equation:

$$E_t = K - S \times \ln[F]_t^{\text{tot}} \quad (2)$$

where  $K$  and  $S$  are empirical values.

Introducing Eq. (1) into Eq. (2) the titration curve  $E_t$  versus  $t$  can be calculated according to:

$$E_t = K - S \times \ln\left\{[F]_{\text{st}}^{\text{tot}} - ([F]_{\text{st}}^{\text{tot}} - [F]_{\text{sa}}^{\text{tot}}) \times \exp\left[\frac{Q}{V}(t_0 - t)\right]\right\} \quad (3)$$

The above equation contains information regarding the performance of the detection unit ( $K$ ,  $S$ ,  $Q/V$  and  $t_0$ ) as well as the concentration of the sample ( $[F]_{\text{sa}}^{\text{tot}}$ ).

The experimental data were fitted according to Eq. (3) using the program Solver from Excel being the sample solution concentration of one of the fitted parameters. Initial values of the parameters to be fitted were given and the quality of the fit was judged in terms of the sum of the residuals  $\Sigma(E_t - E_t^{\text{exp}})^2$ . It is worthwhile to point out that of the five parameters involved, good guesses for those regarding the characteristics of the sensor as well of the mixing chamber, i.e.  $K$ ,  $S$ ,  $Q/V$  and  $t_0$  were taken, which turns out to be an advantage when to many parameters have to be fitted.

## 3. Experimental

### 3.1. Chemicals

The water used in the experiments, to rinse and to prepare the solutions, was distilled and deionized from a Milli-Q-water purification system. All solutions were prepared with pro-analysis grade reagents. A stock solution of fluoride ion (201 mg  $l^{-1}$ ) was prepared from the sodium salt. In all experiments a 1.0 M sodium chloride, 0.25 M acetic acid, 0.75 M sodium acetate and 0.02 M sodium citrate (TISAB) solution was used.

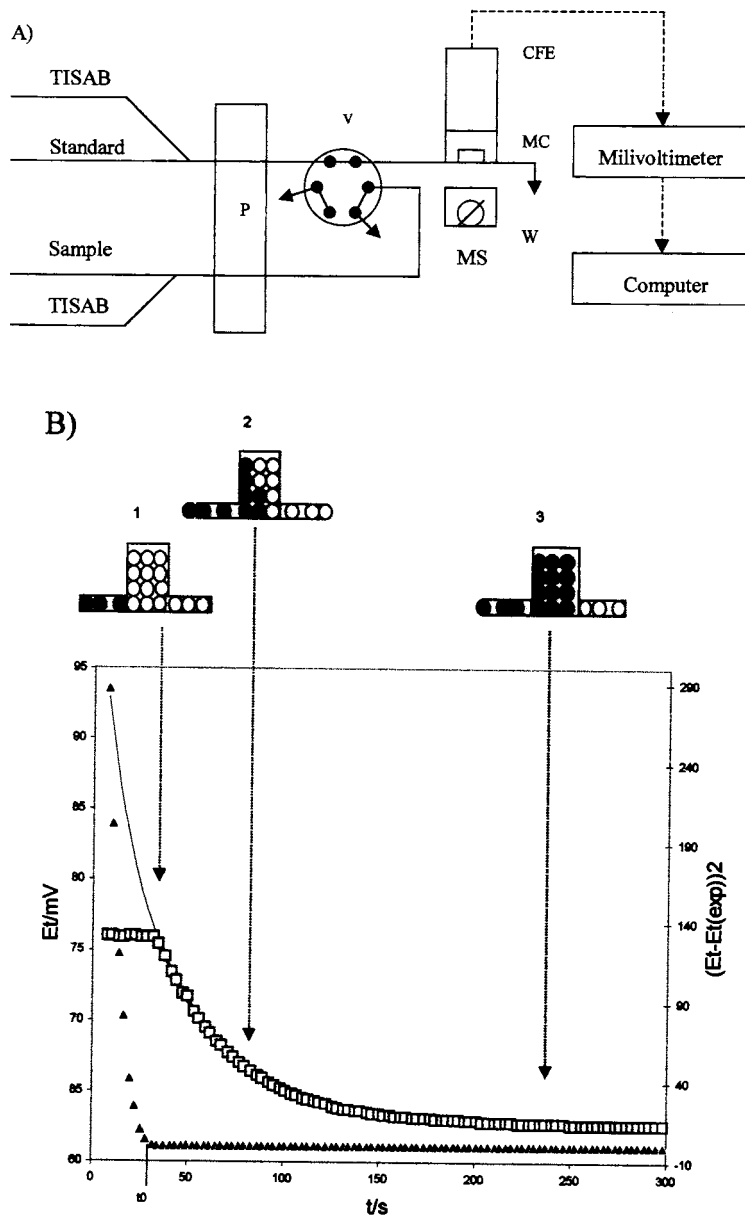


Fig. 1. (A) Block diagram of the flow-injection titration manifold: W, waste; MS, magnetic stirrer; MC, mixing chamber; P, pump; CFE, combined fluoride electrode; V, valve. (B) Typical gradient FI titration curve of fluoride system between concentrations 1.28 and 2.22  $\text{mg.l}^{-1}$  with  $Q = 1.7 \times 10^{-2} \text{ ml s}^{-1}$ ; experimental ( $\square$ ), fit ( $-$ ), and residuals ( $\triangle$ ). The three arrows indicate, respectively, the situations where: (1) the second solution is going to enter the chamber; (2) the chamber is half filled with the first and the second solution and; (3) the chamber is fully filled with the second solution.

Table 1

Effect of the flow rate on the fitting: titration of a standard solution, 2.01 mg l<sup>-1</sup>, with a sample solution, 1.21 mg l<sup>-1</sup>

$Q_{\text{pump}}$ (ml s <sup>-1</sup> ) × 10 <sup>2</sup>	$(Q/V)_{\text{fitted}}$ (s <sup>-1</sup> ) × 10 <sup>2</sup>	$\Sigma(E_t - E_t^{\text{exp}})^2$ (mV) <sup>2</sup>	$K_{\text{fitted}}$ (mV)	$S_{\text{fitted}}$ (mV)	$(C_{\text{sample}})_{\text{fitted}}$ (mg l <sup>-1</sup> )
0.25	0.35				
0.33	0.44				
0.50	0.63	0.52	177.94	26.67	1.25
0.83	1.1	0.30	178.24	26.72	1.26
1.0	1.3	1.31	177.77	25.18	1.23
1.3	1.8	0.80	177.15	26.40	1.22
1.7	2.2	1.07	177.16	26.38	1.23
2.5		0.84	177.34	26.56	1.23
3.3		0.68	177.30	26.61	1.25
3.7	4.9	0.90	176.65	26.33	1.23
4.3	5.5	1.25	176.49	26.25	1.20
4.8	6.4	0.51	176.47	26.44	1.30
5.8	7.0				
6.7	10				
Average			177 ± 1	26 ± 1	1.24 ± 0.03

### 3.2. Equipment

The gradient chamber and FI manifold have previously been described [11,12], and is shown in Fig. 1(A). A combined fluoride electrode from ORION, model 96-90 was used as the sensor in all measurements. The electrode forms one wall of the gradient chamber, allowing efficient monitoring of the chamber contents. The manifold also consists of an injection valve Rheodyne 4 way (RH5020) and of a peristaltic pump Gibson Minipuls 2 (Villius le Bel, France). A pH/ISE Meter Orion Model 720A with an interface RS232C coupled to a personal computer was used to take the potentiometric measurements.

### 3.3. Procedure

A number of different pairs of solutions were used covering different concentrations of fluoride ion.

The experiments were performed by introducing in to the flow system a standard followed by the sample solutions (or vice versa), which were mixed in the gradient chamber, at a constant pH and ionic strength. So each titration experiment covered a continuous transition between the fluoride concentration in the standard and that of the sample solution, resulting in a plateau attained at the end.

Potentials versus time were recorded on the automated data acquisition system formed by the ISE meter interfaced to the personal computer. Readings were taken at a frequency of 0.5 Hz.

The FI manifold was not thermostatted so all results reported are obtained at room temperature (20–25°C).

## 4. Results and discussion

### 4.1. Optimisation of the FI procedure

In Fig. 1(B) a typical titration curve (experimental and fitted curve) are shown together with the residuals about the fitted curve, and as can be seen the fit is quite good.

In order to check some of the variables that may affect the quality of the results different flow rates,  $Q$ , have been used, the direction of titration (i.e. lower to higher concentrations and vice-versa) were analysed, as well as the concentration range during the titration.

Tables 1 and 2, show that the flow rates between 0.005 and 0.05 ml s<sup>-1</sup> do not significantly affect the results, which means that there are no kinetic limitations. So higher flow rates can be used to improve the time of analysis.

The direction of the titration does not have a significant effect on the results as can also be seen from Tables 1 and 2 where both titrations are shown. Although there is an indication that the best fits are obtained when the direction of the titration goes from the higher to a lower concentration, as follows from Fig. 2, the differences founded are within the precision of the method. In any circumstances the fluoride electrode behaves according to theory with a slope close to  $60 \pm 1$  mV; (Nernstian type equation with slope  $RT/F2.3$ ) as can be observed in Tables 1 and 2 where values of  $S = (RT)/F2.3$  mV are shown.

Additional evidence for the quality of the fit can be seen in Fig. 3 where the fitted flow rate,  $Q_{\text{fit}}$ , is plotted as a function of the experimental flow rate,  $Q_{\text{pump}}$ , and a correlation coefficient,  $r = 0.9993$ , is obtained.

As to the concentration of the standard relatively to the sample, best results are produced when  $C_{\text{sample}}$  is of the order of  $0.5 \times C_{\text{standard}}$ , as can be concluded from the residuals about the fitted curve as shown in Table 3. For stationary measurements the best results are obtained when  $C_{\text{sample}}$  approaches  $C_{\text{standard}}$  but this would not work here because the fitting procedure requires time-dependent changes.

Table 2

Effect of the flow rate on the fitting: Titration of a sample solution,  $1.21 \text{ mg l}^{-1}$ , with a standard solution,  $2.01 \text{ mg l}^{-1}$

$Q_{\text{pump}}$ ( $\text{ml s}^{-1}$ ) $\times 10^2$	$(Q/V)_{\text{fitted}}$ ( $\text{s}^{-1}$ ) $\times 10^2$	$\Sigma(E_t - E_t^{\text{exp}})^2$ ( $\text{mV})^2$	$K_{\text{fitted}}$ (mV)	$S_{\text{fitted}}$ (mV)	$(C_{\text{sample}})_{\text{fitted}}$ ( $\text{mg l}^{-1}$ )
0.25	0.34				
0.33	0.40				
0.50	0.59	0.85	-177.96	26.58	1.94
0.83	1.0	1.42	-178.25	26.63	1.96
1.0	1.3	0.53	-177.85	26.48	1.94
1.3	1.7	0.94	-177.15	26.40	1.96
1.7	2.0	1.57	-177.16	26.38	1.98
2.5		1.95	-177.45	26.42	1.85
3.3		1.42	-177.35	26.54	1.92
3.7	4.6	0.98	-176.72	26.20	1.87
4.3	5.5	0.47	-176.60	26.09	1.78
4.8	5.8	1.07	-176.49	26.25	1.92
5.8	6.8	1.47	-176.63	26.40	1.92
6.7	8.8				
		Average	$-177 \pm 1$	$26.4 \pm 0.4$	$1.91 \pm 0.06$

## 4.2. Features of the method

The conditions just discussed for the variables influencing the FI system were used in the assessment of the proposed FI methodology for the analysis of fluoride ion in water samples. A summary of the usual features are shown in Table 4. The precision of the analytical signal and the determination limit were evaluated by repeated titrations (at least  $n = 10$  experiments). An important aspect is whether the electrode still shows a Nernstian type behaviour in the flow system. Throughout all experiments the combined fluoride electrode incorporated in the mixing chamber showed an excellent response with an average slope of  $60 \pm 1$  mV.

The analysis time is taken as the time elapsed from the moment the sample is mixed with the carrier until the fit produces the sample concentration for a flow rate of  $0.05 \text{ ml s}^{-1}$ .

## 4.3. Application to real samples

The above results show that the developed FI methodology can be used for the fluoride determination in water samples. So the method was applied to the analysis of water samples such as tap water and commercially available mineral waters. In the analysis of tap water samples, fluoride



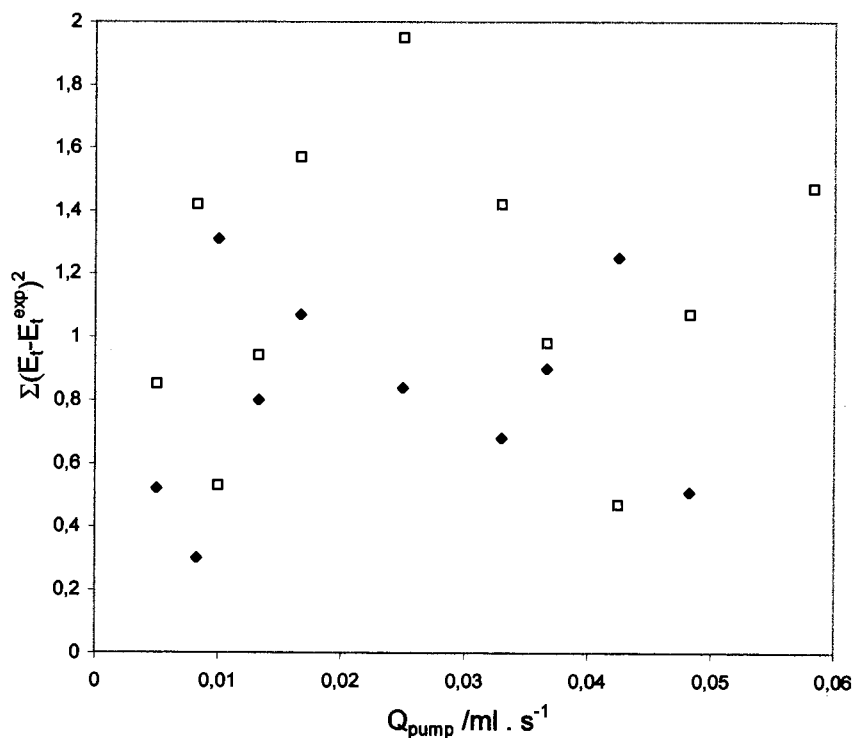


Fig. 2. Residuals about the fitted curve as a function of the pump flow rate,  $Q_{\text{pump}}$  ( $\text{ml s}^{-1}$ ), of the FI titrations; higher ( $2.01 \text{ mg l}^{-1}$ ) to lower concentration ( $1.21 \text{ mg l}^{-1}$ ) (◆); and lower ( $1.21 \text{ mg l}^{-1}$ ) to higher concentration ( $2.01 \text{ mg l}^{-1}$ ) (□).

additions were made since no fluoride was detected.

The quality of the results obtained by the FI methodology was evaluated by comparing them with those of reference methods. So determinations of fluoride were carried out using a reference batch procedure, i.e. a direct potentiometric determination with the same combined fluoride electrode.

A summary of the results obtained is shown in Tables 5 and 6.

Recoveries of fluoride added to tap water samples with a fluoride content below the detection limit of the method are presented in Table 5, and as can be seen average recoveries of 101% were obtained.

Application of the method to fluoride analysis in mineral waters is shown in Table 6. As can be concluded from this set of values the results provided by the FI method compared quite well with those obtained by the reference procedure. A cor-

relation coefficient  $r = 0.997$  was found thus showing a good agreement between the two methods.

From the above results one may conclude that proposed FI method yields good accuracy.

As previously mentioned the direction of the titration does not have a significant effect on the concentration results and this can also be easily checked in Table 6 where both results are shown.

## 5. Conclusions

The developed FI methodology based on a gradient titration is a good alternative to other procedures for fluoride determination in water samples. In fact:

(1) This proposed FI method uses a very simple system requiring only equipment generally available in analytical routine laboratories, i.e.; conventional fluoride electrode, pH meter, peristaltic pump and computer with Excel program.

Emphasis should be placed on the fact that a commercial available combined fluoride electrode was used throughout the experiments. Nernstian behaviour was found in the FIA system with an average slope of  $-60 \pm 1$  mV per concentration decade.

Table 3

Optimisation of the ratio  $C_{\text{sample}}/C_{\text{standard}}^a$ 

$C_{\text{sample}}$ (mg l <sup>-1</sup> )	$C_{\text{sample}}/C_{\text{standard}}$	$\Sigma(E_t - E_t^{\text{exp}})^2$ (mV <sup>2</sup> )
1.21	0.6	1.1
$8.05 \times 10^{-1}$	0.4	4.5
$4.03 \times 10^{-1}$	0.2	12.3
$2.01 \times 10^{-1}$	0.1	30.5

<sup>a</sup>  $C_{\text{standard}} = 2.01$  mg.l<sup>-1</sup>;  $Q = 0.017$  ml s<sup>-1</sup>.

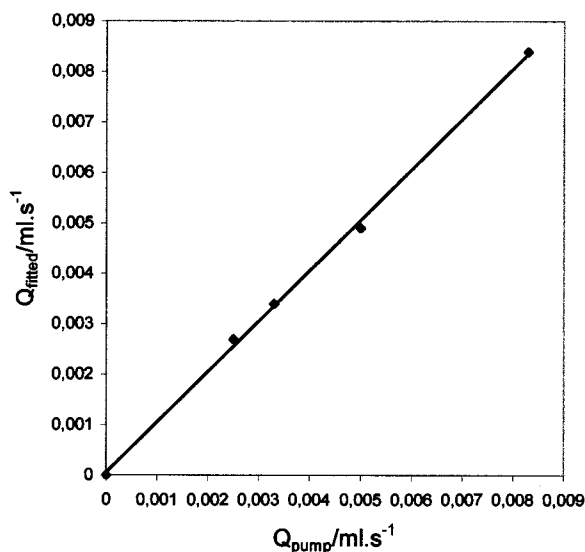


Fig. 3. Fitted flow rate,  $Q_{\text{fit}}$  (ml s<sup>-1</sup>), as a function of experimental flow rate,  $Q_{\text{pump}}$  (ml s<sup>-1</sup>). Other conditions as in Table 1.  $Q_{\text{fit}} = (6 \pm 10) \times 10^{-5} + (1.00 \pm 0.02) \times Q_{\text{pump}}$ , ( $n = 5$ ,  $\sigma_r = 1.3 \times 10^{-4}$ )

Table 4

Features of the method

Precision of the analytical signal	3%
Determination limit	$1.90 \times 10^{-1}$ mg l <sup>-1</sup>
Time of analysis	1.5 min
Slope	$60 \pm 1$ mV

The data-acquisition system as well as the non-linear regression fit used, only require computer capabilities present in the everyday desk top computer.

(2) The configuration adopted overcomes problems arising for the possible formation of dead volumes in the modular devices when conventional electrodes are interposed in the flow systems.

(3) The proposed methodology where the entire time-dependent response is used is much faster than batch titrations (1.5 vs 10–15 min typically) and more precise than direct determination in FIA with only a few standard solutions.

Indeed while in FI potential readings do not require the attainment of equilibrium, because of the reproducible timing and controlled simple dispersion, in batch titration equilibrium must be reached in each point.

As happens with any titration procedure the precision is improved towards a simple calibration curve where relative standard errors of 4% are common unless several standards are used.

## Appendix A

The variation of fluoride concentration with time in the mixing chamber is given by:

$$\frac{d[F]_t^{\text{tot}}}{dt} = \frac{Q}{V}[F]_{\text{sa}}^{\text{tot}} - \frac{Q}{V}[F]_t^{\text{tot}} \quad (\text{A1})$$

where  $[F]_t^{\text{tot}}$  is the total fluoride concentration inside the chamber,  $[F]_{\text{sa}}^{\text{tot}}$  is the total fluoride concentration in the sample,  $V$  is the volume of the chamber and  $Q$  is the flux. After separation of variables and integrating we have:

$$\ln([F]_{\text{sa}}^{\text{tot}} - [F]_t^{\text{tot}}) = \frac{Q}{V}t + K \quad (\text{A2})$$

where  $K$  is the integration constant, this value can be determined for the initial condition, since for  $t = t_0$  we have  $[F]_t^{\text{tot}} = [F]_{\text{st}}^{\text{tot}}$ , where  $[F]_{\text{st}}^{\text{tot}}$  is the total concentration of fluoride in the standard solution. Considering the value of  $K$  we have:

$$[F]_t^{\text{tot}} = [F]_{\text{st}}^{\text{tot}} - ([F]_{\text{st}}^{\text{tot}} - [F]_{\text{sa}}^{\text{tot}}) \exp\left[\frac{Q}{V}(t_0 - t)\right] \quad (\text{A3})$$

Table 5  
Recovery of fluoride added to tap water using FI method

Sample	Fluoride determined (mg l <sup>-1</sup> )	Fluoride added (mg l <sup>-1</sup> )	Fluoride recovery (%)
Tap water	2.01	2.01	100
Tap water	4.10 × 10 <sup>-1</sup>	4.03 × 10 <sup>-1</sup>	102
Tap water	1.22	1.21	101
Tap water	1.64	1.61	102

Table 6  
Comparison of the results provided by the FI method with those from the reference procedure<sup>a</sup>

Sample	FI C <sub>sample</sub> (mg l <sup>-1</sup> )		Batch C <sub>sample</sub> (mg l <sup>-1</sup> )
	Low to high	High to low	
Tap water	1.94 ± 0.06	2.08 ± 0.06	2.0 ± 0.1
Mineral water (Carvalhelhos)	3.2 ± 0.1	3.3 ± 0.1	3.3 ± 0.2
Mineral water (Vidago Salus)	5.4 ± 0.2	5.3 ± 0.2	5.6 ± 0.2
Mineral water (Pedras Salgadas)	3.2 ± 0.1	3.08 ± 0.09	3.0 ± 0.1

<sup>a</sup> Low to high, titration of a low concentration solution with a high concentration solution; high to low, titration of a high concentration solution with a low concentration solution.

## References

- [1] M. Valcarcel, M.D. Luque de Castro, *Flow Injection Analysis Principles and Applications*, Ellis Horwood, Chichester, England, 1987.
- [2] A.D. Eaton, in: L.S. Clesceri, A.E. Greenberg (Eds.), *Standard Methods for the Examination of Water and Wastewater*, nineteenth ed, APHA-AWWA-WEF, Washington, 1995.
- [3] J. Slanina, W.A. Lingerak, F. Bakker, *Anal. Chim. Acta* 117 (1980) 91.
- [4] P. Van den Winkel, G. De Backer, M. Vandeputte, N. Mertens, L. Dryon, D.L. Massart, *Anal. Chim. Acta* 145 (1983) 207.
- [5] W. Frenzel, P. Brätter, *Anal. Chim. Acta* 185 (1986) 127.
- [6] W. Frenzel, P. Brätter, *Anal. Chim. Acta* 187 (1986) 1.
- [7] W. Frenzel, P. Brätter, *Anal. Chim. Acta* 188 (1986) 151.
- [8] J. Fucskó, K. Tóth, E. Pungor, *Anal. Chim. Acta* 194 (1987) 163.
- [9] M. Trojanowicz, P.W. Alexander, D.B. Hibbert, *Anal. Chim. Acta* 366 (1998) 23.
- [10] B. Karlberg, G.E. Pacey, *Techniques and Instrumentation in Analytical Chemistry*. In: *Flow Injection Analysis a Practical Guide*, vol. 10, Elsevier, Amsterdam, 1989.
- [11] D.R. Turner, S. Knox, M. Whitfield, M. Santos, C. Pescada, M.L. Gonçalves, *Anal. Chim. Acta* 226 (1989) 229.
- [12] D.R. Turner, S. Knox, M. Whitfield, M. Santos, C. Pescada, M.L. Gonçalves, *Anal. Chim. Acta* 226 (1989) 239.
- [13] J.F. Tyson, *Anal. Chim. Acta* 179 (1986) 131.
- [14] H.L. Pardue, B. Fields, *Anal. Chim. Acta* 124 (1981) 39.
- [15] H.L. Pardue, B. Fields, *Anal. Chim. Acta* 124 (1981) 65.
- [16] H.L. Pardue, P. Jager, *Anal. Chim. Acta* 179 (1986) 169.

# Copper determination in natural water samples by using FAAS after preconcentration onto amberlite XAD-2 loaded with calmagite

Sérgio L.C. Ferreira \*, Janeide R. Ferreira, Alailson F. Dantas,  
Valfredo A. Lemos, Neyla M.L. Araújo, A.C. Spinola Costa

*Universidade Federal da Bahia, Instituto de Química, Campus Universitário da Federação, Salvador, Bahia, 40170-290, Brazil*

Received 19 January 1999; received in revised form 26 July 1999; accepted 29 July 1999

## Abstract

A procedure for separation and preconcentration of trace amounts of copper in natural water samples, has been proposed. It is based on the adsorption of copper(II) ions onto a column of Amberlite XAD-2 resin loaded with calmagite reagent. This way amounts of copper within the range from 0.0125 to 25.0  $\mu\text{g}$ , in a sample volume of 25 to 250 ml, and pH from 3.7 to 10.0 was concentrated as calmagite complex in a column of 0.50 g of Amberlite XAD-2 resin. Copper (II) ion was desorbed by using 5.0 ml of 2 mol  $\text{l}^{-1}$  hydrochloric acid. Detection and determination limits of the proposed procedure for 250 ml sample volume were 0.15 and 0.50  $\mu\text{g l}^{-1}$ , respectively. Selectivity test showed that (in the indicated concentration), calcium(II) (500 mg  $\text{l}^{-1}$ ), magnesium(II) (500 mg  $\text{l}^{-1}$ ), strontium(II) (50 mg  $\text{l}^{-1}$ ), iron(III) (10 mg  $\text{l}^{-1}$ ), nickel(II) (10 mg  $\text{l}^{-1}$ ), cobalt(II) (10 mg  $\text{l}^{-1}$ ), cadmium(II) (10 mg  $\text{l}^{-1}$ ) and lead(II) (10 mg  $\text{l}^{-1}$ ) did not interfere in copper determination by this procedure. Precision of the method, evaluated as the relative standard deviation by analyzing a series of seven replicates, was 2.42% for a copper mass of 1.0  $\mu\text{g}$  in a sample volume of 100 ml. The accuracy of the proposed procedure was evaluated by means of copper determination in reference biological samples. The achieved results were in good agreement with certified values. The extractor system had a sorption capacity of 1.59  $\mu\text{mol}$  of copper per gram of resin loaded with calmagite. The proposed procedure was applied for copper determination by FAAS in natural water samples. Samples were collected from different places of Salvador city, Bahia, Brazil. The achieved recovery, measured by the standard addition technique, showed that the proposed procedure had good accuracy. A good enrichment factor (50  $\times$ ) and simplicity are the main advantages in this analytical procedure. © 2000 Elsevier Science B.V. All rights reserved.

*Keywords:* Copper determination; Natural water samples; FAAS; Calmagite

## 1. Introduction

Copper is an essential element not only for life in mammals but also for plants and lower forms

\* Corresponding author. Fax: + 55-71-2374117.

of organisms. It has varied and many biologic effects as an essential element as a toxic one. It is usually used as algicide and herbicide [1,2]. In natural water and biological samples its level is low, and previous steps of separation and enrichment are usually required. This way many preconcentration procedures for copper determination [3–13] have been developed and they involve different analytical techniques and several materials. Liquid–liquid extraction by using dithiocarbamate [3] and trioctylmethylammonium chloride [4] as complexing reagents, coprecipitation with magnesium hydroxide as collector [5], precipitation as rubeanic acid complex and filtration by using membrane filter [6], and also several systems of adsorption that uses sorbents such as polyurethane foam loaded with diethyldithiocarbamate [7], activated carbon [8,9], Amberlite XAD resins [10,11] naphthalene [12] and silica gel loaded with diethyldithiocarbamate [13]. Solid phase extraction process [6–13] has received more acceptance due to a number of possible advantages including availability and easy recovery of the solid phase, reach of high preconcentration factors and easiness of separation and enrichment using continuous flow systems. Besides they usually do not need organic solvents, which may be toxic.

This paper proposes an analytical procedure for determination of trace copper in natural water sample by FAAS, using a column packed with Amberlite XAD-2 resin loaded with calmagite for preconcentration and separation.

Calmagite or 1-(1-hydroxy-4-methyl-2-phenylazo)-2-naphthol-4-sulfonic acid has been used as spectrophotometric reagent in several procedure

[14], its reaction with copper(II) ions was studied by Mutsuo and Miyamoto [15]. In aqueous solution the complex copper(II)-calmagite has a maximum absorption at 550 nm.

Amberlite XAD-2 (polystyrene-divinylbenzene polymer) is a very used resin in preconcentration procedures, thanks to its good physical and chemical properties such as porosity, high surface area, durability and purity [10]. In our laboratory, it has been used in column loaded with PAN and TAC for preconcentration and determination of nickel [16] and cobalt [17], respectively.

## 2. Experimental

### 2.1. Apparatus

A Varian Model SpectraAA 220 flame atomic absorption spectrophotometer was used for copper determination. The absorption measurements were made under conditions described in Table 1.

A 300 ANALYSER pH meter was used to measure pH values.

### 2.2. Reagents

All reagents were of analytical reagent grade unless otherwise stated. Double distilled water was used for the preparation of solutions. Nitric and hydrochloric acids were of suprapur quality (Merck). Laboratory glassware was kept overnight in a 5% nitric acid solution. Before use the glassware was rinsed with deionized water and dried in a dust-free environment.

Copper(II) solution ( $1.00 \text{ mg l}^{-1}$ ). Prepared by diluting a  $1000 \text{ mg l}^{-1}$  copper solution (atomic absorption Aldrich) in a 5% hydrochloric acid solution.

Calmagite solution (0.10%). Prepared by dissolving 0.25 g calmagite (Sigma Aldrich) in 250 ml of ethanol.

Acetate buffer solution (pH 4.75). Prepared by mixing 68.0 g of trihydrate sodium acetate and 29.4 ml of glacial acetic acid in 1 l of deionized water.

Table 1  
Operating parameters for flame atomic absorption spectrophotometer

Wavelength	324.8 nm
Lamp current	4.0 mA
Slit width	0.50 nm
Burner height	13.5 mm
Acetylene flow	$2.00 \text{ l min}^{-1}$
Air flow	$13.50 \text{ l min}^{-1}$
Aspiration rate	$3.2 \text{ ml min}^{-1}$

### 2.3. Conservation and preparation of the water samples

Samples were collected from the surface of the aqueous systems by using Teflon flasks in different places of Salvador city, Bahia, Brazil on August 1998. They were acidified with 1.0 ml of concentrated nitric acid per liter of sample. The samples were filtered through a cellulose membrane (Millipore) of 0.45  $\mu\text{m}$  pore size.

### 2.4. Preparation of Amberlite XAD-2 column loaded with calmagite

Amberlite XAD-2 (Aldrich) was treated with an ethanol: hydrochloric acid: water (2:1:1) solution overnight. Then resin was rinsed with deionized water until supernatant water pH got neutral. Afterwards it was dried in an oven at temperature of 110°C for 3 h.

The packing of the column must be done using ethanol as eluent since water makes resin beads float.

The resin was saturated with the reagent by passing 10.0 ml of a 0.10% calmagite solution in ethanol at a flow of 0.50  $\text{ml min}^{-1}$ . Afterwards it was washed with water until reagent excess was eliminated from the resin. All experiments were done in glass columns with a 0.40 cm internal diameter and length of 15 cm that held 0.50 g of XAD-2. Before sample loading the column must be preconditioned by passing a buffer solution. Then the column could be used repeatedly for ten times at least.

### 2.5. Procedure for the sorption of copper on the column

It was transferred 25 to 250 ml of sample solution of copper ions in the range of 0.0125 to 25.00  $\mu\text{g}$  into a becker and it was added 10 ml of buffer solution pH 4.75. This solution must be passed through the column at a flow rate of 1.80  $\text{ml min}^{-1}$ . After this solution had been passed the column was washed with 10 ml of deionized water. The adsorbed copper chelate on the column was then eluted with 5.0 ml of 2 mol  $\text{l}^{-1}$  hydrochloric acid solution at a flow rate of 1.0 ml

$\text{min}^{-1}$ . The eluent was collected in a 5 ml volumetric flask and copper was determined by FAAS technique under conditions described in Table 1.

## 3. Results and discussion

In order to determine the optimum conditions for quantitative extraction of copper by using Amberlite-XAD2 resin loaded with calmagite several parameters were assessed.

### 3.1. pH effect on copper sorption

The effect of pH on sorption of copper(II) ions showed that the recovery of copper is maximum and quantitative (> 95%) within a pH range from 3.7 to 10.0. This can be seen in the Fig. 1. pH control was kept by using pH 4.75 acetate buffer, pH 6.66 hexamine buffer, pH 7.56 triethanolamine buffer, pH 8.0 and 8.5 borate buffer and pH 9.0 and 10.0 ammonium buffer. The acetate buffer at pH 4.75 was suggested since solutions of acetate buffer are very stable. At pH 4.75 the acetate buffer has its highest buffer index.

### 3.2. Effect of flow rate and aqueous volume

The effect of flow rate on the copper sorption was studied by varying the flow rate from 0.30 to 2.8  $\text{ml min}^{-1}$  under optimum conditions. Results demonstrated that copper(II) retention on the resin was complete at a flow rate equal or lower than 2.0  $\text{ml min}^{-1}$ , as can be seen in Fig. 2. The effect of sample volume on copper extraction was investigated by passing 25, 50, 100, 200 250, and 400 ml volume solution through the column at a constant flow rate of 1.8  $\text{ml min}^{-1}$ . In all cases the achieved recovery was higher than 95%, what is advantageous for copper determination in water samples. The restriction on use of 400 ml was the spent time on sample elution.

### 3.3. Sorption capacity

The sorption capacity of the Amberlite XAD-2 resin loaded with calmagite for copper was also evaluated. The resin had a sorption capacity of

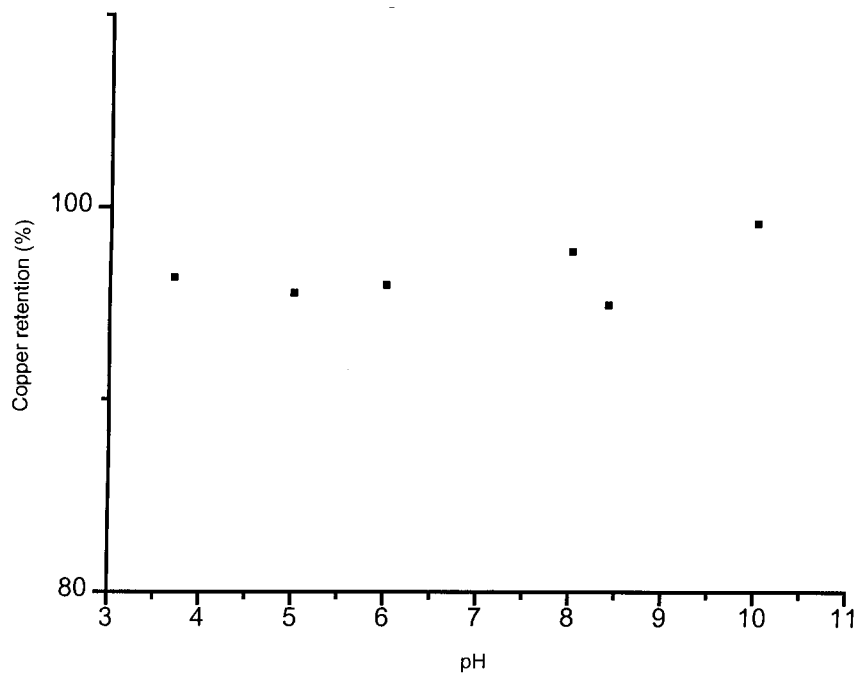


Fig. 1. Effect of pH on the copper retention on calmagite loaded Amberlite XAD-2 resin. Copper: 1.00  $\mu\text{g}$  /100 ml.

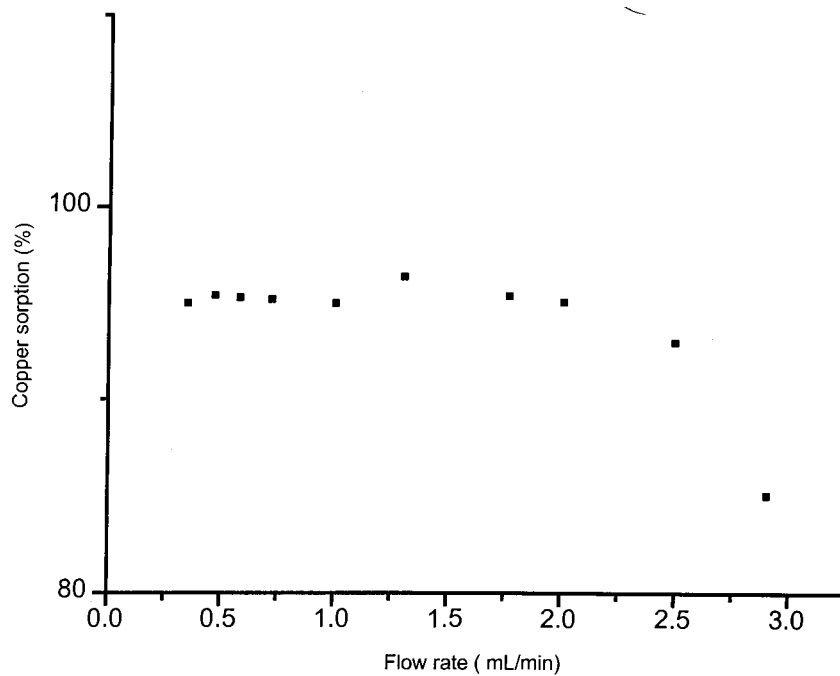


Fig. 2. Effect of flow rate on copper retention on calmagite loaded Amberlite XAD-2 resin. Copper: 1.00  $\mu\text{g}$ /100 ml. pH: 4.75.

1.59  $\mu\text{mol}$  of copper per gram of XAD-2 resin. Under conditions of maximum adsorption distribution coefficient was higher than  $1.0 \cdot 10^4 \text{ l kg}^{-1}$ . The extractor system has  $2.36 \cdot 10^{-4} \text{ mol}$  of calmagite by gram of Amberlite XAD-2 resin.

### 3.4. Copper elution from XAD-2 resin

In order to determine the copper elution from resin 5.0 ml of hydrochloric acid in concentrations of 0.25, 0.50, 1.0, 2.0, 3.0, and 4.0  $\text{mol l}^{-1}$  was used. The elution was quantitative ( $> 95\%$ ) for solutions at concentrations equal or higher than 0.50  $\text{mol l}^{-1}$ . Hydrochloric acid solution with concentration 2.0  $\text{mol l}^{-1}$  has been suggested to guarantee the complete extraction of the copper from resin and also the efficiency of column wash.

### 3.5. Selectivity of the proposed procedure

In order to determine the selectivity of method several solutions that contained copper ( $1.0 \mu\text{g l}^{-1}$ ) and other ions were prepared. The proposed procedure was applied using a solution volume of 200 ml. Results showed that in the indicated concentration calcium(II) ( $500 \text{ mg l}^{-1}$ ), magnesium(II) ( $500 \text{ mg l}^{-1}$ ), strontium(II) ( $50 \text{ mg l}^{-1}$ ), iron(III) ( $10 \text{ mg l}^{-1}$ ), nickel(II) ( $10 \text{ mg l}^{-1}$ ), cobalt(II) ( $10 \text{ mg l}^{-1}$ ), cadmium(II) ( $10 \text{ mg l}^{-1}$ ) and lead(II) ( $10 \text{ mg l}^{-1}$ ) did not interfere in copper determination by this procedure.

The influence of electrolytes on the copper sorption was also studied. Results demonstrated

that the recovery of the copper in 100 ml solution was quantitative even in the presence of 20% sodium chloride or 20% potassium nitrate.

### 3.6. Characteristics of the proposed procedure

The proposed procedure can be applied to preconcentration and separation of copper within the range from 0.0125 to 25.0  $\mu\text{g}$ , in a solution volume of 25 to 250 ml, by using 0.50 g of Amberlite XAD-2 resin loaded with calmagite reagent.

The determination by FAAS was made by an analytical curve built with copper solutions (5 ml volume) at concentrations from 0.0 to 0.4  $\mu\text{g ml}^{-1}$ , which were prepared by dilution of copper solution  $1.0 \mu\text{g ml}^{-1}$  in 2  $\text{mol l}^{-1}$  hydrochloric acid solution. Detection and determination limits of the proposed procedure for 250 ml of sample volume were 0.15 and 0.50  $\mu\text{g l}^{-1}$ , respectively.

The precision of the method, evaluated as the relative standard deviation by analyzing a series of seven replicates, was 2.42% for a copper mass of 1.0  $\mu\text{g}$  in a sample volume of 100 ml.

The accuracy of the enrichment system proposed was evaluated by means of copper determination in reference biological samples. Found results described in Table 2 were in good agreement with the certified values.

A test could evaluate the accuracy of both preconcentration procedure and analytical technique used (FAAS) in copper determination in seawater sample. Copper masses were added before and after the preconcentration steps and the recoveries were determined. Table 3 shows results from this test, as well as the efficiency of the proposed method.

### 3.7. Copper determination in natural water samples

The proposed preconcentration procedure was applied to determine this element in natural water samples from Salvador city, Bahia-Brazil. Two hundred millilitres of volume sample was used. Results are described in Table 4. In order to evaluate the accuracy of the preconcentration procedure, known masses (1.0 to 5.0  $\mu\text{g}$ ) of copper were added in sample volumes of 200 ml. The

Table 2  
Achieved results for the analyzed certified reference materials

Sample	Copper found by proposed methodology ( $\mu\text{g g}^{-1}$ )	Certified values ( $\mu\text{g g}^{-1}$ )
Rice flour NIST-1568 <sup>a</sup>	$2.41 \pm 0.10$	2.4
Citrus leaves NIST-1572	$16.02 \pm 1.76$	16.5
Pine needles NIST-1575	$2.94 \pm 0.30$	3.0

<sup>a</sup> NIST, National Institute of standards and Technology.



Table 3  
Copper recovery before and after the preconcentration step<sup>a</sup>

	Recovery (%)
Copper mass found in the sample	0.34 <sup>b</sup> –
Copper mass found in the sample +	1.26 <sup>b</sup> 92
Copper mass added (1.0 and 2.0 µg) in the sample before the preconcentration step	2.22 <sup>b</sup> 94
Copper mass found in the sample + copper mass added (1.0 µg) in the sample solution after the preconcentration step	1.30 <sup>b</sup> 96

<sup>a</sup> Rio Vermelho sea water sample, sample volume: 200 ml.

<sup>b</sup> Average of three determinations.

Table 4  
Copper determination in natural water samples from Salvador City

Sample	Mass of added copper <sup>b</sup> (µg)	Found copper <sup>a</sup> (µg l <sup>-1</sup> )	Recovery (%)
Canto do sol lake water	0	0.80 ± 0.15	
	1	5.40 ± 0.57	92
Tororo lake water	0	1.15 ± 0.13	
	1	5.80 ± 0.56	93
Abaeté lake water	0	25.3 ± 3.1	
	5	51.3 ± 4.98	104
Pituaçu lake water	0	7.10 ± 0.39	
	5	33.85 ± 4.34	107
Joanes river water	0	3.58 ± 0.04	
	1	8.90 ± 1.02	106
Rio Vermelho sea water	0	1.72 ± 0.25	
	1	6.37 ± 0.75	93
Canto do Sol sea water	0	0.95 ± 0.13	
	1	5.55 ± 0.69	92

<sup>a</sup> At 95% confidence level.

<sup>b</sup> Mass of added copper in 200 ml of sample volume.

proposed procedure was applied and achieved recoveries varied from 92 to 107%, what demonstrated that the used method had a good accuracy. This evaluation was made for all the analyzed samples, what proved that this procedure can be used for copper determination in natural water samples.

#### 4. Conclusions

The main advantages of this procedure are: (i) the preparation of the extractor system is simple and fast; (ii) the elution step does not involve use of organic solvents as other procedures does; (iii) during copper desorp-

tion the calmagite reagent remains in the resin, what allows using the column several times; (iv) a good enrichment factor (50 ×) can be achieved.

The achieved recovery measured by standard addition technique, showed that the proposed procedure had good accuracy.

The proposed procedure has been applied for copper determination in natural water samples by using FAAS, yet it can be used for other samples and other analytical methods like ICP-AES.

The copper concentration found in sea water samples demonstrated that the collected samples are polluted, considering the reported values for copper in sea water [18].

## Acknowledgements

The authors acknowledge the grants from CNPq, FINEP and CAPES.

## References

- [1] F.W. Oehme, Toxicity of Heavy Metals in the Environment, Marcel Dekker, New York, 1978.
- [2] J.M. Moore, Inorganic Contaminants of Surface Water, Springer Verlag, New York, 1991.
- [3] S. Sachsenberg, T. Klenke, W.E. Krumbein, E. Zeeck, Fresenius J. Anal. Chem. 342 (1992) 163.
- [4] X.Y. Zhang, S. Keiichi, A. Satoh, K. Sawada, T. Suzuki, Anal. Sci. 13 (1997) 891.
- [5] J. Wu, E.A. Boyle, Anal. Chem. 69 (1997) 2464.
- [6] J.L. Itoh, T. Miyake, M. Komata, Nippon Kagaku Kaishi 7 (1996) 645.
- [7] D. Atanasova, V. Stefanova, E. Russeva, Talanta 45 (1998) 857.
- [8] R.E. Santelli, M. Gallego, M. Valcárcel, Talanta 41 (1994) 817.
- [9] A. Uzawa, T. Narukawa, T. Okutani, Anal. Sci. 14 (1998) 395.
- [10] L. Elci, M. Soylak, M. Dogan, Fresenius J. Anal. Chem. 342 (1992) 175.
- [11] V.K. Jain, S.S. Sait, P. Shrivastav, Y.K. Agrawal, Talanta 45 (1997) 397.
- [12] T. Nagahiro, G.F. Wang, M. Satake, Microchem. J. 52 (1995) 247.
- [13] B. Perez-Cid, S. Rio-Segade, C. Bendicho, Microchem. J. 55 (1997) 319.
- [14] K.L. Cheng, K. Ueno, I. Imamura, Handbook of Organic Reagent, CRC Press, Boca Raton, USA, 1992.
- [15] M. Mutsuo, K. Miyamoto, Bull. Chem. Soc. Jap. 42 835. Chem. Abs. 71 (1969) (1969) 18461b.
- [16] S.L.C. Ferreira, C.F. Brito, A.F. Dantas, N.M.L. Araújo, A.C.S. Costa, Talanta 48 (1999) 1173.
- [17] S.L.C. Ferreira, C.F. Brito, Anal. Sci. 15 (1999) 189.
- [18] S.N. Willie, Y. Iida, J.W. McLaren, Atomic Spec. 19 (1998) 67.

# Voltammetric determination of 5-hydroxydole-3-acetic acid in human gastric juice

Ying Liu <sup>a</sup>, Yanxia Jiang <sup>a</sup>, Wenbo Song <sup>a</sup>, Nan Lu <sup>a</sup>, Mingzhu Zou <sup>a</sup>,  
Hongding Xu <sup>a,\*</sup>, Zhenxiang Yu <sup>b</sup>

<sup>a</sup> Department of Chemistry, Jilin University, Changchun 130023, People's Republic of China

<sup>b</sup> The First Clinic Hospital Attached to Bethun Medical College, Changchun 130023, People's Republic of China

Received 22 January 1999; received in revised form 26 July 1999; accepted 29 July 1999

## Abstract

A method for the determination of the major serotonin metabolite — 5-hydroxyindole-3-acetic acid (5-HIAA) in human gastric juice by cyclic voltammetry was described. The measurement conditions were investigated. The potential window was chosen from +0.1 to +0.9 V, the supporting electrolyte was 0.025 M PBS solution (pH 2.0). The method allowed determination in the concentration range from  $2.0 \times 10^{-7}$  to  $2.0 \times 10^{-5}$  M and a detection limit of 80 nM. When samples of gastric juice were analyzed with the method, we obtained the mean content of 5-HIAA in the gastric juice. Meanwhile, interference from other ions and substances were examined. The experimental results indicate that the method for the determination of gastric juice samples is successful. © 2000 Elsevier Science B.V. All rights reserved.

**Keywords:** 5-HIAA; Cyclic voltammetry; Human gastric juice

## 1. Introduction

5-HIAA, the major metabolite of 5-HT, is found in significant concentrations in the central nervous system, plasma and gastrointestinal tract. The catabolic pathway of 5-HT is by the action of the enzyme monoamine oxidase to form 5-HIAA. 5-HIAA is much more stable than serotonin and is often used to assess serotonin level [1]. Recently, Several groups have reported various ways

for determination of 5-HIAA in urine [2–5], blood, plasma [6–10], brain tissue [11–13], platelets [14,15], incised skin wounds of guinea-pig [16], bovine eye [17], and cerebrospinal fluid [18,19]. But very few papers concern for the measurement of 5-HIAA in gastric juice [20]. The content of 5-HIAA in the gastric juice with gastric diseases such as atrophic gastritis is higher than that in healthy peoples, whereas the content of 5-HIAA in people who have gastric carcinoma is much higher [20]. These results are of considerable significance in early diagnosis of gastric carcinoma and chronic atrophic gastritis. Therefore

\* Corresponding author. Fax: +86-431-394334.

E-mail address: jian-zh@263.net (H. Xu)

we aim to develop a simple, sensitive, rapid procedure based on electrochemical technique for the routine quantitative determination of 5-HIAA in gastric juice.

Electrochemistry has a distinct advantage compared to most analytical techniques. This is because it involves a direct conversion of chemical information to an electrical signal without need for intermediate optical or magnetic carriers. Many studies have demonstrated that the electroanalytical techniques — voltammetry, chronoamperometry and various pulse methods — are useful for making concentration measurements as well as for studying homogeneous reaction mechanisms of electroanalytically detectable chemical species in neurobiology [21–23]. In this paper, to our knowledge, the cyclic voltammetry is the first used to determine 5-HIAA in human gastric juice, the results are rather satisfied. In addition, because of high sensitivity of determination, operational simplicity, and cheap instruments, this makes it possible to measure 5-HIAA of gastric juice with the electrochemistry method in clinical laboratory analysis. Thus, the method is an effective way found to be suitable for routine determination of 5-HIAA without the restriction of time and place.

## 2. Experimental

### 2.1. Apparatus and chemicals

Electrochemical measurements were performed with a JSH-1 Voltammeter analyzer, DCG-multi-function programmer (Jilin Longjing Analytical Instrument Plant, China), and a Ground X–Y recorder (England). A conventional single-compartment cell equipped with a platinum wire counter-electrode and Ag–AgCl reference-electrode was employed. The working electrode was a homemade Teflon-shrouded glassy carbon electrode (geometric area 0.147 cm<sup>2</sup>). All potential values were measured and reported vs. Ag–AgCl reference electrode and experimental were made at room temperature (about 22°C).

5-HIAA was purchased from Sigma. A stock solution of 5-HIAA was prepared freshly every

day and used directly for detection in open air at room temperature. All other compounds used in this work were of analytical grade. Because Na<sub>2</sub>HPO<sub>4</sub>-NaH<sub>2</sub>PO<sub>4</sub> buffer solution was similar to the composition of body fluid, 0.025 M pH 2 phosphate buffered saline (PBS) solution was chosen as the supporting electrolyte. The 5-HIAA quantitation was achieved by measuring the oxidation peak current between +0.1 and +0.9 V in pH 2 PBS solution.

### 2.2. Treatment and cleaning of the electrode

The glassy carbon electrode used for experiment was treated by the following method: at first, the GCE was polished to a mirror with 0.05 μm alumina powder, and then was polished successively on a piece of deer-skin. Immediately after polishing, it was rinsed with double-distilled water, and was further cleaned ultrasonically in 1:1 nitric acid and finally in water successively, followed to air-drying. After cyclic voltammetry had been carried out, the electrode surface absorbed the electrooxidation product of 5-HIAA. Besides the treatment method as before, the electrode was set to a clean cell only containing 10 ml of 0.025 M PBS solution and successive cyclic scans were applied between +0.1 and +0.9 V for 5 min. The cleaned electrode surface was monitored by a cyclic voltammogram recorded at the above potential until there was only the background current in a cyclic voltammogram.

## 3. Results and discussion

### 3.1. Voltammetric behavior of 5-HIAA

After manually polishing the surface of the electrode, the cyclic voltammogram of 10 μM 5-HIAA in 0.025 M PBS solution (adjusted to pH 2.0 with 1% HCl) was shown in Fig. 1. On the potential window, the use of a very high potential may enhance the fouling of the GCE by polymers formed as end-products of the oxidation of 5-HIAA. The very low potential may increase the coverage of the electrode by hydrogen gas. Both effects may increase the ‘irreversibility’ of the

electrode process. Therefore, the potential window was chosen from +0.1 to +0.9 V. As can be seen, the 5-HIAA exhibited an oxidative peak (0.65 V), however, no corresponding reductive peak appeared when the signal was reversed. This suggests that the electrode reaction may be regarded irreversible [24].

Further investigation was made to the transport characteristics of 5-HIAA in the GCE. The cyclic

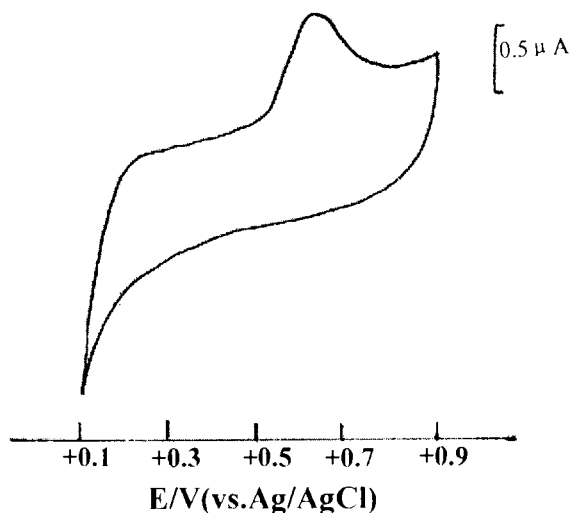


Fig. 1. Cyclic voltammogram for 10  $\mu\text{M}$  5-HIAA in 0.025 M, pH 2.0 phosphate buffer at a GCE. Scan rate was 100  $\text{mVs}^{-1}$ .

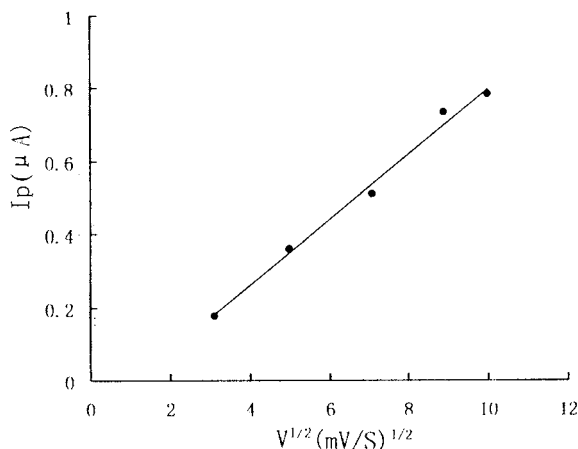


Fig. 2. Dependence of the peak currents  $I$  of the cyclic voltammogram on  $v^{1/2}$ . Experimental peak currents were measured for  $10^{-5}$   $\text{mol L}^{-1}$  5-HIAA.

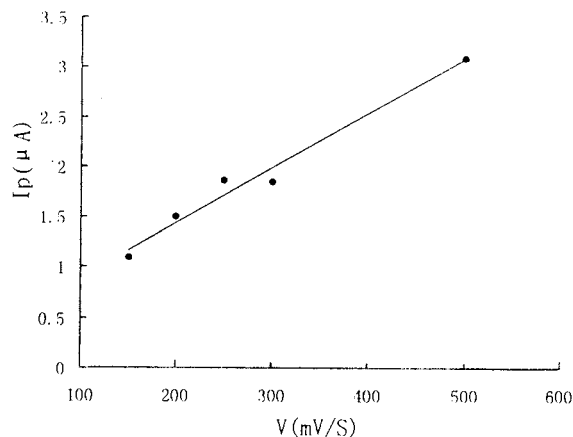


Fig. 3. Dependence of the peak currents  $I$  of the cyclic voltammogram on  $v$ . Experimental peak currents were measured for  $6.0 \times 10^{-5}$   $\text{mol L}^{-1}$  5-HIAA.

voltammetry current response obtained was found to be linearly proportional to square root of the scan rate when  $v$  (scan rate)  $\leq 100$   $\text{mVs}^{-1}$ . It illustrates that the process was diffusion-controlled [25]. While  $v > 100$   $\text{mVs}^{-1}$ , the cyclic voltammetry current response is linearly proportional to the scan rate, which demonstrates that process is adsorption-controlled [26]. The two plots were shown separately in Figs. 2 and 3. More evidence for the adsorptive behavior of 5-HIAA was demonstrated by the following experiment. When the GCE was switched to a medium containing only pH 2 PBS solution after being used in measuring a 5-HIAA solution, peak signal was still observed.

### 3.2. Optimization of pH

pH values, as an important factor, directly influenced determination of 5-HIAA. Thus the effect of pH on the voltammetric response of the GCE was studied. The peak current values in the differ-

Table 1  
Effect of pH values in 25  $\mu\text{M}$  5-HIAA

pH	2.0	3.0	4.0	5.0	6.0	7.0	8.0
$I_p$ ( $\mu\text{A}$ )	0.88	0.76	0.43	0.38	0.30	0.26	0.23

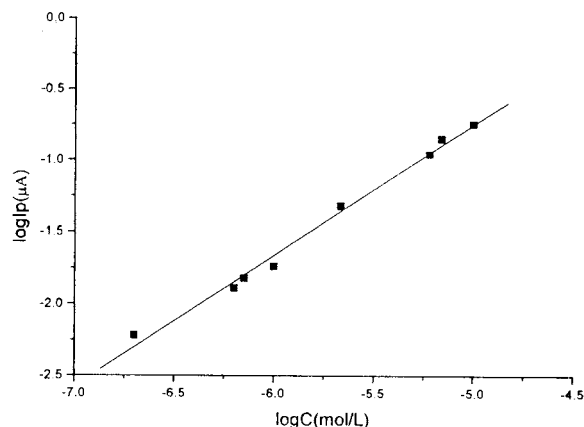


Fig. 4. Calibration plot for 5-HIAA obtained at the GCE.

ent pH values of the analyte solutions for 25  $\mu\text{M}$  5-HIAA were listed in Table 1. As can be seen, when pH values increased from 5 to 9, the peak current changed unobviously. But when pH values  $< 4$ , the peak current increased obviously. In acidic media, the protonization of indolic nitrogen in 5-HIAA is beneficial to its electrooxidation, or electroactivity of protonated 5-HIAA was more stronger. Thus, the stronger the acidity was, the

Table 2  
Effect of foreign species; concentration of 5-HIAA: 20  $\mu\text{M}$

Foreign species	Tolerance limit	Content in gastric juice
$\text{K}^+$	200 mM	10 mM <sup>a</sup>
$\text{Ca}^{2+}$	200 mM	4 mM <sup>a</sup>
$\text{Cl}^-$	2 M	125–127 mM <sup>a</sup>
Phosphate	200 mM	6 mM <sup>a</sup>
$\text{Fe}^{3+}$	0.2 mM	0.14–0.20 $\mu\text{M}$ <sup>b</sup>
$\text{Cu}^{2+}$	0.2 mM	0.11–0.17 $\mu\text{M}$ <sup>b</sup>
$\text{Zn}^{2+}$	0.2 mM	0.25–0.35 $\mu\text{M}$ <sup>b</sup>
$\text{Ni}^{2+}$	0.2 mM	0.01–0.02 $\mu\text{M}$ <sup>b</sup>
$\text{Mo}^{2+}$	0.2 mM	0.003–0.007 $\mu\text{M}$ <sup>b</sup>
Ascorbic acid	80 $\mu\text{M}$	55–59 $\mu\text{M}$ <sup>c</sup>
$\text{Al}^{3+}$	20 mM	–
$\text{Mg}^{2+}$	0.2 mM	–
$\text{Pb}^{2+}$	0.8 mM	–
Glucose	30 mM	–
Urea	40 mM	–
Uric acid	0.2 mM	–

<sup>a</sup> Ref. [27].

<sup>b</sup> Ref. [28].

<sup>c</sup> Ref. [29].

higher the peak current was. The data show an optimum performance above pH value of 2 and therefore pH 2 PBS solution was chosen for all the subsequent electrochemical measurement.

### 3.3. Calibration curves and precision

Linear calibration curves ( $\lg I$  vs.  $\lg C$ ) were obtained in pH 2 PBS solution with scan rate 100 mV/S between the concentration ranges from 0.2 to 10  $\mu\text{M}$  with correlation coefficients of 0.9956, slope 0.9124, respectively as shown in Fig. 4. The detection limit for 5-HIAA was 80 nM (signal-to-noise ratio = 3). In order to prove the precision of the method, repetitive measurements were carried out in 25  $\mu\text{M}$  5-HIAA after the electrode was polished and cleaned every time as before. The results of eight time measurements showed a SD of 0.046, RSD of 2.4%. Thus the method can give a good reproducibility.

### 3.4. Determination of 5-HIAA in human gastric juice

#### 3.4.1. Gastric juice samples

Human gastric juice samples were obtained from volunteers with moderate and severe gastric diseases. Gastric juice of empty stomach 3–4 ml was collected into a plastic test tube by gastroscopy. The gastric juice was centrifuged at  $4000 \times g$  for 10 min, 1.0 ml of the supernatant was isolated to another test tube, 1.0 ml of the perchloric acid used for deproteinization was then added. The mixture shaken vigorously for 12 min, was centrifuged again  $4000 \times g$  for 10 min. Fifty microlitres of the supernatant collected was added into 10 ml of PBS analyte solution to be determined under the optimum conditions.

#### 3.4.2. Sample determination

Interference is an important factor in analyzing correctly 5-HIAA in a sample, because the 5-HIAA content in samples is usually very low. The various foreign species were examined to detect their effect on the determination of 5-HIAA. The results and the content of the potential interference species in gastric juice were listed in Table 2. Though the concentration of the ascorbic acid in

Table 3  
Results of the determination of 5-HIAA in human gastric juice

Sample	Determination concentration ( $\mu\text{g ml}^{-1}$ )	Recovery (%)
1	4.096	96.2
2	3.643	96.0
3	4.162	95.1
4	4.343	95.9
5	3.091	95.7

body fluids was high and oxidative potential is close to the 5-HIAA's, in the patients with moderate or severe gastric diseases, the content of in the gastric juice was less than that of the tolerance limit [29]. Thus the measurement of 5-HIAA wasn't interfered by ascorbic acid.

The determination of 5-HIAA in human gastric juice had the following advantages: fast response time, high sensitivity, low detection limit and simple operation. In order to avoid any effect of the sample matrix on the response characteristics, the standard additional method was used to analyze the samples. When spiked with exogenous standard 5-HIAA solution (0.2, 0.5, 1.0, 2.0, 3.0  $\mu\text{M}$ ), a good linearity in human gastric juice level (such as the sample 1) was observed with a correlation coefficient 0.9988. The 5-HIAA level in gastric disease was found to be 4.029  $\mu\text{g ml}^{-1}$  gastric juice (mean values), which was in good agreement with the certified value [20]. The results were list in Table 3.

#### 4. Conclusion

The present method allows simple, sensitive and accurate quantitative determination of 5-HIAA in the sample of gastric juice. The procedure offers an attractive possibility for clinical laboratory analysis. This method will stimulate further research on its application in the study of the chemical and biochemical processes relevant to neuropharmacology and neurobiology.

#### Acknowledgements

This work was supported by the Jilin Provincial Natural Science Foundation of China.

#### References

- [1] L. Bertilsson, *Life Sci.* 41 (1987) 821.
- [2] A.R. Bonfigli, G. Coppa, R. Testa, I. Testa, G. Desio, *Eur. J. Clin. Chem. Clin. Biochem.* 35 (1997) 57.
- [3] A. Helander, O. Beck, M. Wennberg, T. Wikstrom, G. Jacobsson, *Anal. Biochem.* 196 (1991) 170.
- [4] G. Alemany, A. Gamundi, C. Rossello, R. Rial, *Biomed. Chromatogr.* 10 (1996) 144.
- [5] A.M. Kumar, J.B. Fernandez, K. Goodkin, N. Schneiderman, C. Eisdorfer, *J. Liq. Chromatogr. Relat. Technol.* 20 (1997) 1931.
- [6] A.J. Dunn, *Life Sci.* 42 (1988) 1847.
- [7] S. Wright-Honari, E.F. Marshall, C.H. Ashton, F. Hasanyeh, *Biomed. Chromatogr.* 4 (1990) 201.
- [8] F.C. Cheng, J.S. Kuo, L.G. Chia, T.H. Tsai, C.F. Chen, *J. Chromatogr. B* 654 (1994) 177.
- [9] J. Ishida, R. Iizuka, M. Yamaguchi, *Clin. Chem.* 39 (1993) 2355.
- [10] K. Thorre, M. Pravda, S. Sarre, G. Ebinger, Y. Michotte, *J. Chromatogr. B* 694 (1997) 297.
- [11] J.S. Soblosky, L.L. Colgin, C.M. Parrish, J.F. Davidson, M.E. Carey, *J. Chromatogr. B* 712 (1988) 31.
- [12] P.T. Kissinger, C.S. Bruntlett, R.E. Shoup, *Life Sci.* 28 (1981) 455.
- [13] P. Tuzhi, W. Guoshun, L. Huiping, S. Baoen, *Anal. Letts.* 28 (1995) 395.
- [14] Y. Xia, G. Dai, Y. Zhou, B. Zhou, H. Guo, *Zhong Hua Yixue Jian Yan Zazhi* 12 (1989) 176.
- [15] T.H. Tsai, W.J. Tsai, C.F. Chen, *J. Chromatogr.* 669 (1995) 404.
- [16] Y. Maeno, F. Takabe, Y. Mori, M. Iwasa, H. Inove, *Forensic Sci. Int.* 51 (1991) 51.
- [17] S.A. Best, T.M. Midgley, W. Huang, D.G. Watson, *J. Pharm. Biomed. Anal.* 11 (1993) 323.
- [18] C.S. Hong, B. Bush, R.F. Seegal, K.O. Brosch, *Anal. Letts.* 20 (1987) 435.
- [19] A.M. Kumar, M. Kumar, K. Deepika, J.B. Fernandez, C. Eisdorfer, *Life Sci.* 47 (1990) 1751.
- [20] Y.J. Xun, Z.Y. Zhen, Y.S. Jie, *J. Norman Bethune Univ. Med. Sci.* 16 (1990) 376.
- [21] J.A. Stamford, J.B. Justice Jr., *Anal. Chem.* 68 (1996) 359A.
- [22] R.N. Adams, *Anal. Chem.* 48 (1976) 1128A.
- [23] M.P. Brazell, R.J. Kasser, K.J. Renner, J. Feng, B. Moghaddam, R.N. Adams, *J. Neurosci. Methods* 22 (1987) 167.
- [24] F. Anson. Translated by W.Z. Huang. *Electrochemistry and Electroanalytical Chemistry*, first ed., Beijing University Press, Beijing, 1983, p. 16.

- [25] A.J. Bard, L.R. Faulkner, *Electrochemical Methods*, John Wiley & Sons, New York, 1980, p. 218.
- [26] A.J. Bard, L.R. Faulkner, *Electrochemical Methods*, John Wiley & Sons, New York, 1980, p. 488.
- [27] C.B. Shi, *Modern Clinical Analytical Handbook*, first ed., Chinese Medical Press, 1998. p. 415.
- [28] D.L. Li, Z.L. Lu, W.L. Liu, *Chin. J. Dig.* 9 (1989) 301.
- [29] B.J. Rathbone, A.W. Johnson, J.I. Wyatt, J. Kelleher, R.V. Heatley, M.S. Losowsky, *Clin. Sci.* 76 (1989) 237.



# A new study of the enzymatic hydrolysis of carboxymethyl cellulose with a bulk acoustic wave sensor

Deliang He, Lili Bao, Yumei Long, Wanzhi Wei, Shouzhuo Yao \*

College of Chemistry and Chemical Engineering, Hunan University, Changsha 410082, People's Republic of China

Received 12 April 1999; received in revised form 16 July 1999; accepted 29 July 1999

## Abstract

A new bulk acoustic wave (BAW) cellulase sensing technique, which is based on the enzymatic hydrolysis process of sodium carboxymethylcellulose (CMC) by cellulase, was established. The frequency shift curves of BAW sensor indicated that the viscosity of the tested solutions decreased during the hydrolysis process. The hydrolysis rate of CMC by cellulase was calculated from the frequency shift curves. The hydrolysis rate of CMC under different pH conditions at 30°C showed that cellulase had high hydrolysis ability approximately at pH 5.0. Kinetic parameters (the Michaelis constant  $K_m$  and the maximum rate  $V_{max}$ ) of the process were estimated by using a linear method of Lineweaver–Burk plot.  $K_m$  is  $1.95 \pm 0.25 \text{ mg ml}^{-1}$  and  $V_{max}$  is  $-(4.25 \pm 0.58) \times 10^{-3} \text{ g}^{1/2} \text{ cm}^{-3/2} \text{ cP}^{1/2} \text{ min}^{-1}$ . Also the activation energy ( $E_a$ ) of the enzymatic hydrolysis, with a value of  $51.99 \pm 1.26 \text{ kJ mol}^{-1}$ , was estimated in this work. © 2000 Elsevier Science B.V. All rights reserved.

**Keywords:** Bulk acoustic wave sensor; Cellulase; Carboxymethyl cellulose; Kinetics parameters; Enzymatic hydrolysis

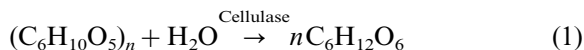
## 1. Introduction

Cellulose is the major component of all vegetation, ranging from one-third to one half of dry plant materials. Natural cellulose is a high polymer of a chair conformational structure which is combined by  $\beta$ -1,4-glucoside linkage [1–4]. No vertebrates can utilize cellulose directly as an energy source. To use it as food it must first to be hydrolyzed to glucose. Under mild conditions cellulose can be hydrolyzed by acid. But this process

requires strong mineral acid acting at elevated temperatures over an extended period of time. In addition, the digests must be neutralized and the sugar must be recovered and separated from excess salt and toxic by-products such as furfural. The process has not proved economical under normal conditions. Biological degradation of cellulose by many remen and soil microorganisms and cellulases is the greatest natural mass hydrolytic reaction. Enzymatic hydrolysis of cellulose, if it can be achieved efficiently, could give glucose at moderate temperatures and pH conditions. The enzymatic hydrolysis of cellulose can be expressed by:

\* Corresponding author. Tel.: +86-731-882-2286; fax: +86-731-882-4525.

E-mail address: szyao@mail.hunu.edu.cn (S. Yao)



A great deal of cellulose occurs in manufactured products such as paper, textile and building materials. The enzymatic hydrolysis of cellulose is high efficient and valuable. So it is extremely important to investigate the catalytic reaction mechanism and the catalytic activity and kinetic parameters of the enzymatic hydrolysis of cellulose. Many investigations were developed to obtain cellulases possessing high activity [5–9]. Reese proposed  $C_1$ – $C_x$  concept for cellulases capable of degrading native cellulose and a brief description of each component of cellulase complex [10]. Mandels and Weber introduced the production of cellulases [11]. Cellulase is a complex of enzymes (including  $C_1$  and  $C_x$ ) showing various types of activities [2,12,13]. There are many assaying methods to detect or measure the catalytic activity of cellulase [2,5,13,14]. Principal methods have included: (1) reduction of viscosity of a solution of a cellulose derivative; (2) production of reducing sugar from a soluble cellulose derivative; (3) production of reducing sugar or loss of residue weight from solid cellulose; (4) reduction in optical density of a cellulose sol or suspension; and (5) measurements of reduction in breaking strength of thread, yarn, or fabric, swelling of cotton or paper, maceration of filter paper, and microfragmentation of cellulose micelles. These methods differ markedly in sensitivity, and in cellulase components detected, depending on the substrate used, the effect measured, and the duration and conditions of the assay. Also the kinetic parameters of the enzymatic hydrolysis process were measured by many investigators. Zhang and co-workers determined the Michaelis constant  $K_m$  of free cellulase and cellulase immobilized by the complexes of chitosansodium carboxymethyl cellulose and chitosanpolyacrylic acid [15]. Cavaco-Paulo and Almeida measured the kinetic parameters during cellulase treatment of cotton [16]. Busto and et al. measured  $K_m$  and  $V_{max}$  values when carboxymethyl cellulose was used as substrate [17]. Cavaco-Paulo and his co-workers measured the kinetic and adsorption parameters for *Trichoderma reesei* cellulases during simulated cotton processing [18]. The assay of

activity and kinetic parameters of cellulase achieved mainly by the determination of production of reducing sugar, reduction of viscosity and reduction of optical density of the tested solutions. However, it is difficult for them to monitor the enzymatic hydrolysis process of cellulose on-line and conveniently, and other reagents such as dinitrosalicylic acid (DNS) is necessary during the determination process sometimes, moreover the expensive equipments are needed for the determination of activity and kinetic parameters. Therefore, in producing cellulase for a specific application, the ideal assay should be simple and closely approximate the using conditions.

The bulk acoustic wave (BAW) sensor has been extensively used as a kind of highly sensitive chemical and biological sensor in various fields, since it oscillated successfully in liquid phase in the 1980s [19–23]. The resonant frequency of the piezoelectric quartz crystal (PQC) changes with the viscosity and density of the liquid, the following equation is effective under certain experimental conditions:

$$\Delta F = -F_s^{3/2}(\eta_L \rho_L / \pi \mu \rho_Q)^{1/2} \quad (2)$$

where  $\Delta F$  is the resonant frequency change of the crystal,  $F_s$  is the resonant frequency,  $\eta_L$  is the viscosity of the liquid,  $\rho_L$  is the density of the liquid,  $\mu$  is the shear modulus of the quartz crystal,  $\rho_Q$  is the density of the quartz crystal. Based on relationship 2, the BAW sensor can be used as a viscosity and density detector just like the technique presented in this paper. The viscosity of the tested solutions has an obvious decline while cellulase was used to hydrolyze cellulose under experimental conditions [1,13]. According to the response of BAW sensor, the enzymatic hydrolysis process can be monitored as well as the kinetic parameters can be estimated. The application of BAW sensor in studying of the enzymatic hydrolysis of cellulose by cellulase has not been reported in previous literatures.

Cellulase from *Trichoderma viride* and sodium carboxymethylcellulose (CMC) were used as enzyme source and substrate source in this paper. The frequency shift curves were recorded during the enzymatic hydrolysis process under certain conditions. The hydrolysis rate of CMC could

clinch from the rate of  $\Delta F$  of the BAW sensor. The optimum pH of the enzymatic hydrolysis of CMC was obtained by determining the initial rate under different pH conditions at 30°C. And the Michaelis constant  $K_m$  and the maximum rate  $V_{max}$  of cellulase were gained by fitting the Lineweaver–Burk equation [24]. Also the activation energy of the enzymatic reaction was obtained by measuring the reaction rate at different temperature. The results gained in this work are coincident with the values reported in previous literatures [12,17]. It can be anticipated that BAW sensor will be used in studying the enzymatic hydrolysis of cellulose by cellulase as a new method.

## 2. Experimental

### 2.1. Apparatus

The measuring system was constructed from an Au-plated (diameter 5.5 mm), AT-cut 9 MHz quartz crystal (diameter 12.5 mm) with a well-type cell to position one side of the crystal at the bottom. The laboratory-made IC-TTL oscillating circuit was supplied with 5 V by a d.c. voltage regulator (Model JWY-30B, Shijiazhuang Electronic Factory No. 4). Frequency changes were measured with a digital counter (Model SS3341A, Shijiazhuang Electronic Factory No. 4). The tested solutions were stirred with a magnetic stirrer (Shanghai Electro-communication Instrumentation Factory). A thermostat was used to control the reaction temperature through a thermostatic water jacket.

### 2.2. Reagents and chemicals

Cellulase (from *Trichoderma viride*, E. C. 3. 2. 1. 4, enzyme activity:  $\geq 15\,000\ \mu\text{g}^{-1}$ ) was provided by Shanghai Lizhu Dongfeng Biological Technology Limited Corporation. One unit will liberate 1.0  $\mu\text{mol}$  of glucose from cellulose in 1 h at pH 5.0 at 37°C. Sodium CMC was presented by Shanghai Chemical Reagents Station, it is a cellulose derivative with a degree of substitution between 6.5 and 8.5 and was used as substrate.

Other chemicals were of analytical grade. The double distilled deionized water was used throughout.

Ten  $\text{mg ml}^{-1}$  stock solution of cellulase was prepared. The concentrations of CMC stock solutions employed were from 2.5 to 20  $\text{mg ml}^{-1}$ . The acetic acid and sodium acetate solution (0.2 M, pH from 3.0 to 6.0) was used as buffer solution.

### 2.3. Frequency shifts of enzymatic hydrolysis process of CMC by cellulase

Five ml CMC solution and 2.5 ml of 0.2 M buffer solution were put into the detection cell and mixed uniformly. A total of 2.5 ml of 10  $\text{mg ml}^{-1}$  cellulase solution was taken out from the stock and let in a thermostatic bath for 10 min. After this process, it was also put into the detection cell, and the resonant frequencies of BAW sensor were recorded during the enzymatic hydrolysis process. The experimental temperature was controlled at 30 and 35°C, respectively. The experimental pH was from 3.0 to 6.0. The range of initial concentration of CMC solutions was from 2.5 to 20  $\text{mg ml}^{-1}$ .

### 2.4. Measurements of enzymatic hydrolysis process of CMC by spectrophotometry

The enzymatic hydrolysis rates of CMC under different CMC concentrations and different temperatures were measured by spectrophotometry according to the method adopted by Zhang et al. [15]. The range of initial concentration of CMC solutions was from 2.5 to 20  $\text{mg ml}^{-1}$ . The experimental temperatures were selected at 30 and 35°C.

## 3. Results and discussion

### 3.1. Typical response curves

The response curves of enzymatic hydrolysis of CMC solutions with different concentrations at 30°C are shown in Fig. 1 (pH 5.0). The responses of BAW sensor change with the viscosity of the tested solutions while CMC was hydrolyzed by

cellulase. Moreover, the response shifted more when the concentration of CMC is higher. That is to say, the reaction rate of enzymatic hydrolysis increases with the concentration of CMC while the same cellulase solution was used.

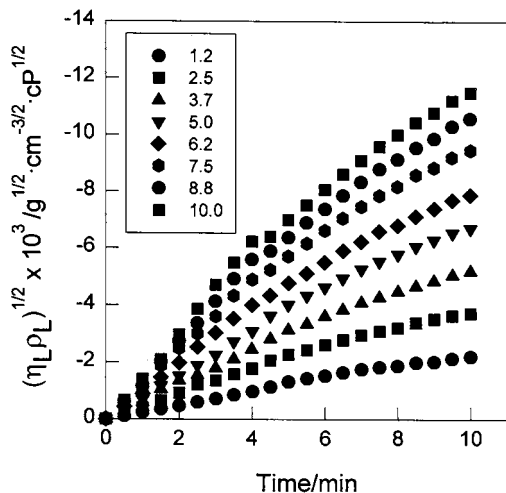


Fig. 1. The response curves of carboxymethylcellulose (CMC) solutions of different concentrations (30°C, pH 5.0, 2.5 mg ml<sup>-1</sup> cellulase).

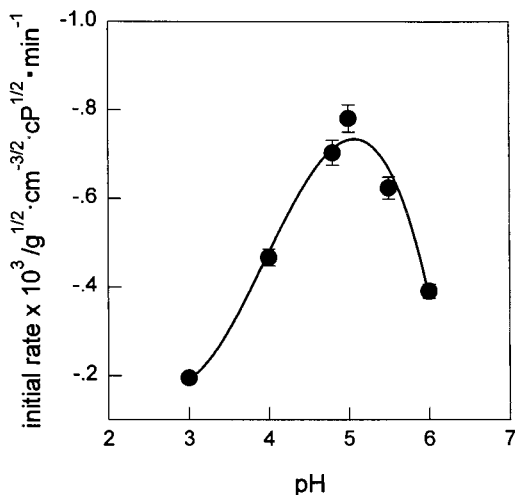


Fig. 2. The dependence of initial hydrolysis rates on pH values (30°C, 2.5 mg ml<sup>-1</sup> cellulase, 5.0 mg ml<sup>-1</sup> carboxymethylcellulose [CMC]).

### 3.2. Effect of pH value

The frequency shifts of enzymatic hydrolysis of CMC solutions by cellulase under different pH conditions at 30°C were recorded. The frequency shift curves are not identical at different pH value, this means that the rate of enzymatic hydrolysis of CMC by cellulase is diverse. In other words, cellulase has dissimilar enzymatic ability to hydrolyze CMC under different pH conditions.

The initial rate of enzymatic hydrolysis reaction of CMC solutions was obtained from the shifting rate of the resonant frequency of BAW sensor within 3 min. The curve of the initial hydrolysis rate with pH values was shown in Fig. 2. It can be found that the initial rates are diverse at different pH, and the maximum initial rate of enzymatic hydrolysis appears approximately at a pH value of 5.0 at 30°C. So the pH value of buffer solution for aftermentioned experiments was selected at 5.0.

### 3.3. Estimation of kinetic parameters

Kinetic parameters of the enzymatic reaction can be estimated by using BAW sensor system from the data of initial hydrolysis rates by the direct linear method of Lineweaver–Burk plot [24,25]:

$$\frac{1}{V} = \frac{K_m}{V_{\max}} \frac{1}{[S]} + \frac{1}{V_{\max}} \quad (3)$$

where  $V$  and  $V_{\max}$  are the initial hydrolysis rate and maximum hydrolysis rate in g<sup>1/2</sup> cm<sup>-3/2</sup> cP<sup>1/2</sup> min<sup>-1</sup>,  $K_m$  is the Michaelis constant in mg ml<sup>-1</sup>,  $[S]$  is the CMC concentration in mg ml<sup>-1</sup>. Thus a plot of the reciprocal of initial rate versus the reciprocal of CMC concentration for experiments at a fixed enzyme concentration should give a straight line. Furthermore, the intercept with the ordinate gives  $1/V_{\max}$  and the slope is  $K_m/V_{\max}$ , from which  $V_{\max}$  and  $K_m$  can be calculated. In this work, the concentration range of CMC was from 1.2 to 10 mg ml<sup>-1</sup>, the experimental temperature was controlled at 30°C. The dependence of  $1/V$  and  $1/[S]$  is shown in Fig. 3, it can be seen that  $1/V$  is linear to  $1/[S]$ . By fitting Eq. (3) ( $n = 8$ ,  $r = 0.995$ ), the kinetic parameters are obtained,

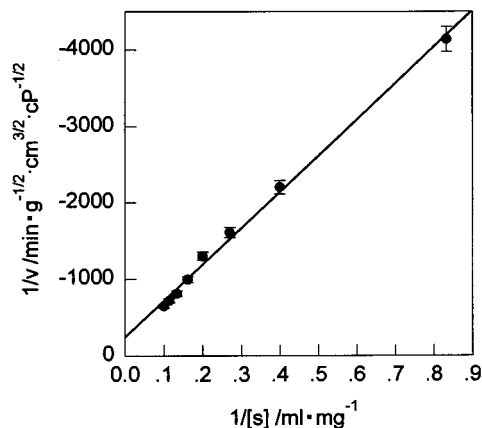


Fig. 3. The relationship between  $1/[S]$  and  $1/V$  (30°C, pH 5.0, 2.5 mg ml<sup>-1</sup> cellulase).

$K_m$  is  $1.95 \pm 0.25$  mg ml<sup>-1</sup> and  $V_{max}$  is  $-(4.25 \pm 0.58) \times 10^{-3}$  g<sup>1/2</sup> cm<sup>-3/2</sup> cP<sup>1/2</sup> min<sup>-1</sup>.

#### 3.4. Activation energy of the enzymatic hydrolysis of cellulase

The activation energy can be calculated from two reaction rate constants at two experimental temperatures according to the Arrhenius equation [26]:

$$\log k = -\frac{E_a}{2.303R} \frac{1}{T} + \log A \quad (4)$$

where  $k$  is the reaction rate constant,  $E_a$  is the activation energy,  $R$  is the gas constant,  $T$  is the absolute temperature,  $A$  is a constant. Eq. (4) can be rewritten to next equation if the two reaction rate constants ( $k_1$  and  $k_2$ ) at two temperatures ( $T_1$  and  $T_2$ ) have been determined.

$$E_a = \frac{2.303RT_1T_2}{T_2 - T_1} \log \frac{k_2}{k_1} \quad (5)$$

Table 1

Comparisons of  $K_m$  and  $E_a$  value estimated by bulk acoustic wave (BAW) sensor with that obtained by spectrophotometry

Different methods	$K_m$ (mg ml <sup>-1</sup> )	$E_a$ (kJ mol <sup>-1</sup> )	Reference
Value in reference	1.72		[15]
Value estimated by BAW sensor	$1.95 \pm 0.25$	$51.99 \pm 1.26$	This paper
Value obtained by spectrophotometry	$1.86 \pm 0.14$	$51.65 \pm 1.13$	This paper

While the concentrations of CMC and cellulase are identical,  $k_2/k_1$  can be substituted by  $V_2/V_1$  because the reaction rate is of direct proportion to the reaction rate constant [26]. In this work, 30 and 35°C were selected, the initial rates ( $V_1$  and  $V_2$ ) of the enzymatic hydrolysis reaction were  $-(7.65 \pm 0.15) \times 10^{-4}$  and  $-(10.70 \pm 0.20) \times 10^{-4}$  g<sup>1/2</sup> cm<sup>-3/2</sup> cP<sup>1/2</sup> min<sup>-1</sup>, respectively ( $n = 3$ ). So  $E_a$  can be calculated as follows:

$$E_a = \frac{2.303RT_1T_2}{T_2 - T_1} \log \frac{V_2}{V_1} \\ = 51.99 \pm 1.26 \quad (\text{kJ mol}^{-1}) \quad (n = 3) \quad (6)$$

#### 3.5. Comparisons of $K_m$ and $E_a$ with that obtained by spectrophotometry

The comparisons of experimental results estimated by BAW sensor with that in reference and that obtained by spectrophotometry are shown in Table 1. It can be found that  $K_m$  and  $E_a$  agree well with that obtained by other methods.

## 4. Conclusion

A new BAW cellulase sensing technique, which is based on the enzymatic hydrolysis process of sodium CMC by cellulase, was established. The advantages of this method compared with measurement of reduction of viscosity and production of reducing sugar are shown in Table 2. The response curves of BAW sensor indicate that the viscosity of the tested solutions decreased during the hydrolysis process. The hydrolysis rate of CMC by cellulase could clinch from the response curves within a short reaction period. The different initial hydrolysis rates of CMC under dissimilar pH conditions showed that cellulase has high hydrolysis ability approximately at pH 5.0 at

Table 2  
Comparisons of bulk acoustic wave (BAW) sensor method with measurement of reduction of viscosity and production of reducing sugar

Method	Apparatus	Other reagents	Measuring procedure	Measuring object	Sample needed (ml)	Reference
Reduction of viscosity	Cheap	Not necessary	Troublesome and intermittent	Viscosity of solution	10 <sup>b</sup>	[2,11]
Production of reducing sugar	Expensive	Requisite <sup>a</sup>	Rather troublesome and intermittent	Production of cellulose	502.5	[2,11,15]
BAW sensor	Cheap	Not necessary	Easy and continuous	Viscosity of solution	≤10 <sup>c</sup>	This paper

<sup>a</sup> Glucose oxidase (GOD), ammonium molybdate, potassium iodide, *o*-toluidine or dinitrosalicylic acid (DNS).

<sup>b</sup> It is related to viscometer used, and more measuring times is needed to accomplish the determination.

<sup>c</sup> It could be reduced when little cell is used.

30°C. The kinetic parameters of the enzymatic hydrolysis by cellulase are estimated using a linear method of Lineweaver–Burk plot. While CMC is employed as substrate, the Michaelis constant  $K_m$  and the maximum rate  $V_{max}$  of  $1.95 \pm 0.25 \text{ mg ml}^{-1}$  and  $-(4.25 \pm 0.58) \times 10^{-3} \text{ g}^{1/2} \text{ cm}^{-3/2} \text{ cP}^{1/2} \text{ min}^{-1}$  are obtained. Also the activation energy ( $E_a$ ) of the enzymatic hydrolysis, with a value of  $51.99 \pm 1.26 \text{ kJ mol}^{-1}$ , is estimated in this work. The experimental results agree well with that in reference and that obtained by spectrophotometry.

### Acknowledgements

This work was financially supported by the National Science Foundation of China and the Project of Hunan Science and Technology Commission.

### References

- [1] C. Liu, Chemical basis of cellulose (Chinese), Sci. Press 2 (1985).
- [2] S. Zhang, Fundamentals of enzyme preparation industry (Chinese), Sci. Press 595 (1984).
- [3] E.B. Cowling, T.K. Kirk, Biotechnol. Bioeng. Symp. 6 (1976) 95.
- [4] E.T. Reese, M. Mandels, A.H. Weiss, Adv. Biochem. Eng. 2 (1972) 181.
- [5] Cellulase Research Laboratory, Shanghai Institute of Plant Physiology, Academia Sinica and Shanghai Distillery No. 2, Acta Microbiol. Sinica (Chinese), 18(1) (1978) 27.
- [6] K. Osmundsvag, J. Goksoyr, Eur. J. Biochem. 57 (1975) 405.
- [7] M. Mandels, J. Weiber, R. Parizek, Appl. Microbiol. 21 (1971) 152.
- [8] E.S. Morozova, Symp. on Enzymatic Hydrolysis of Cellulose, Aulauko, Finland, 1975, p. 193.
- [9] M.G. Myers, B. Eberhart, Biochem. Biophys. Res. Commun. 24 (1966) 782.
- [10] E.T. Reese, M. Mandels, Dev. Ind. Microbiol. 5 (1964) 115.
- [11] M. Mandels, J. Weber, Adv. Chem. Ser. 95 (1969) 391.
- [12] A.N. Pathak, T.K. Ghose, Process Biochem. 8 (4) (1973) 35.
- [13] G.G. Guilbault, Handbook of Enzymatic Methods of Analysis, Pergamon Press, New York, 1976, p. 213.
- [14] G. Halliwell, in: E.T. Reese (Ed.), Advances in Enzymatic Hydrolysis of Cellulose and Related Materials, Pergamon Press, London, 1963, p. 71.
- [15] C. Zhang, L. Wang, Y. Jiang, Gongneng Cailiao/J. Funct. Mater. (Chinese) 26 (4) (1995) 364.
- [16] A. Cavaco-Paulo, L. Almeida, Journal of the Textile Institute, Part 1: Fibre Science and Textile Technology, 87(1) (1996) 227.
- [17] M.D. Busto, N. Ortega, M. Perez-Mateos, Bioresour. Technol. 57 (2) (1996) 187.
- [18] A. Cavaco-Paulo, L. Almeida, D. Bishop, Niches in the World of Textiles World Conference of the Textile Institute, Proceedings v 2. Textile Inst., Manchester, UK, 1997, p. 268.
- [19] T. Normura, M. Maruyama, Anal. Chim. Acta 147 (1983) 365.
- [20] K.K. Kanaeawa, J.G. Gordon, Anal. Chim. Acta 175 (1985) 99.
- [21] S.Z. Yao, T.A. Zhou, Anal. Chim. Acta 212 (1988) 61.
- [22] S.Z. Yao, T.A. Zhou, Kexue Tongbao (Chinese) 15 (1985) 1153.
- [23] S.Z. Yao, L.H. Nie, Anal. Proc. (London) 24 (1987) 336.
- [24] H. Lineweaver, D.J. Burk, J. Am. Chem. Soc. 56 (1934) 658.
- [25] R.H. Wang, Q.Y. Cai, L.Y. Wu, L.L. Nie, S.Z. Yao, Anal. Lett. 29 (1) (1996) 59.
- [26] I.H. Segel, Biochemical Calculations, Wiley, New York, 1976, ch. 3.

# The electrogenerated chemiluminescent behavior of hemin and its catalytic activity for the electrogenerated chemiluminescence of lucigenin

Guo Nan Chen <sup>a,\*</sup>, Lin Zhang <sup>a</sup>, Rong Er Lin <sup>b</sup>, Zhen Cong Yang <sup>a</sup>, Jian Ping Duan <sup>a</sup>, Hong Qing Chen <sup>a</sup>, D. Brynn Hibbert <sup>c</sup>

<sup>a</sup> Department of Chemistry, Fuzhou University, Fuzhou, Fujian, 350002, China

<sup>b</sup> Bureau of Commodity Inspection, Samming, Fujian, 365000, China

<sup>c</sup> School of Chemistry, The University of New South Wales, Sydney, 2052, Australia

Received 24 March 1999; received in revised form 28 July 1999; accepted 3 August 1999

## Abstract

The electrogenerated chemiluminescent (ECL) behavior of hemin at a platinum electrode in the alkaline solution has been investigated in detail. Under the optimum conditions the linear response range of hemin is  $1.0 \times 10^{-5}$ – $1.0 \times 10^{-8}$  g ml<sup>-1</sup>, the detection limit was  $1.0 \times 10^{-8}$  g ml<sup>-1</sup>, and the relative standard derivation for  $1 \times 10^{-7}$  g ml<sup>-1</sup> hemin was 2.8%. It has been also found that hemin would catalyze the ECL of lucigenin at a platinum electrode in a neutral solution in the presence of hydrogen peroxide, the catalytic ECL intensity was linear with the concentration of hemin in the range of  $1.0 \times 10^{-14}$ – $1.0 \times 10^{-10}$  g ml<sup>-1</sup>. IgG labeled with hemin was used to examine the ECL catalytic activity of hemin after conjugating to protein, and the results showed that hemin retained ECL catalytic activity when conjugated to protein. © 2000 Elsevier Science B.V. All rights reserved.

**Keywords:** Hemin; Electrogenerated chemiluminescence; Lucigenin; IgG

## 1. Introduction

Recently nonradioactive labels such as enzymes, stable free radicals and chemiluminescent (CL) reagents have been used in attempts to overcome the intrinsic shortcoming of radioimmunoassay. Of these labels an enzyme is a promising alternative label, as an enzyme is a

catalyst and it can be determined with high sensitivity by various methods. For example, horseradish peroxidase (HRP) is an effective catalyst for the luminol-H<sub>2</sub>O<sub>2</sub> CL system that has been widely used [1–3]. However, in enzyme immunoassay, the steric hindrance of macromolecular compound and the instability of high molecular labeling enzymes would affect the antigen–antibody reaction. Therefore, some mimetic enzymes have been developed to be used as a substitute for natural enzyme in analytical appli-

\* Corresponding author. Fax: +86-591-3713866.

E-mail address: gnchen@fzu.edu.cn (G. Nan Chen)



cations. Various metalloporphyrins have been used as mimetic peroxidase in fluorescence and CL analysis [4–6].

Hemin is a well-known natural metalloporphyrin compound. The difference between hemin and synthetic metalloporphyrin is that hemin has no substituted group at positions 9, 10, 11, 12, and it has two carboxyl groups, which can condense with a hydroxyl or amino group in protein. Ikarlyama [7] developed a method termed chemiluminescent catalytic immunoassay in which he used hemin as the labeling agent to label human serum albumin (HAS), which would catalyze the CL reaction between luminol and  $\text{H}_2\text{O}_2$ . However, no attention has been paid to the ECL behavior of hemin. We have recently found that hemin gave a reproducible ECL signal at a platinum electrode in NaOH-KCl solution when a triangular pulse voltage was applied. We also found that hemin could catalyze the ECL reaction of lucigenin at a platinum electrode by using KCl as the supporting electrolyte.

In this paper, the ECL behavior and mechanism of hemin itself at a platinum electrode in alkaline solution have been investigated in detail, and the catalytic characteristics of hemin for the ECL reaction of lucigenin at a platinum electrode in a neutral solution have also been discussed. IgG labeled with hemin was used to examine the catalytic activity of hemin after conjugating to protein.

## 2. Experimental

### 2.1. Apparatus

A Shimadzu RF-540 spectrofluorimeter, a Perkin-Elmer Lambda 9 Spectrophotometer and a BAS-100 Electrochemical Analyzer (Bioanalytical System, Purdue, In, USA) were used. ECL experiments were performed with a system made in our laboratory, which consisted of an HFC-Chemiluminescent Detector, a potentiostat, an electrochemical cell and a recorder. A block diagram of this system has been shown in the literature [8,9]. The details of the HFC-I CL Detector have been given previously [10]. The potentiostat used was

XHD-I (Precision Instrumental Company of Xiamen University, Xiamen, China) it mainly included a waveform generator, which could perform linear, triangular voltage, square wave and double-step pulse voltage sweep. ECL experiments utilized a platinum plate working electrode ( $4 \times 6.5$  mm, sealed in glass) in a conventional three electrode cell configuration. The auxiliary electrode was a platinum ball electrode ( $d = 2.2$  mm, sealed in glass), and the reference electrode was an Ag-AgCl electrode. The photomultiplier tube, GDB-413 (Nanjing Electron Tube Works) with a detection range of 300–700 nm was housed directly in front of the electrochemical cell.

### 2.2. Reagents

Solution of hemin: 10.0 mg of hemin (Sigma) was dissolved in 5 ml of  $0.2 \text{ mol l}^{-1}$  NaOH, and was then diluted to 100 ml to give a stock standard solution containing  $1 \times 10^{-4} \text{ g ml}^{-1}$  of hemin. This solution was diluted to the required concentration with water.

Solution of lucigenin: 52.2 mg of lucigenin (Aldrich) was dissolved in 100 ml of water to obtain a stock standard solution containing  $1.0 \times 10^{-3} \text{ mol l}^{-1}$  lucigenin. This solution was diluted to the required concentration with water.

IgG was obtained from Shanghai Biological Product Institute, 1-ethyl-3-(3-dimethylamino-propyl) carbodiimide hydrochloride (EDC) was obtained from Sigma. All the other reagents used were analytical reagents or better and all water used were doubly distilled in a fused-silica apparatus.

### 2.3. Procedure

#### 2.3.1. Measurement of ECL of hemin

The cell filled with 10 ml solution containing hemin,  $0.4 \text{ mol l}^{-1}$  KCl and  $0.03 \text{ mol l}^{-1}$  NaOH was placed in the detector chamber. A potential was then applied to the working electrode and the ECL signal was recorded. After each measurement, the working electrode and the auxiliary electrode were exchanged and electrolyzed at 1.0 V for 1 min in  $0.5 \text{ mol l}^{-1}$   $\text{HNO}_3$  before the next measurement.

### 2.3.2. Measurement of ECL of lucigenin catalyzed by hemin

The cell filled with 10 ml solution containing hemin,  $0.1 \text{ mol l}^{-1}$  KCl,  $1 \times 10^{-6} \text{ mol l}^{-1}$  lucigenin and  $1 \times 10^{-6} \text{ mol l}^{-1}$   $\text{H}_2\text{O}_2$  was placed in the detector chamber. The subsequent procedure was the same as measurement of ECL of hemin.

### 2.3.3. Preparation of hemin-labeled IgG

Thirteen milligrams of hemin was dissolved in 3 ml of water, 27.2 mg EDC was then added. The mixture was incubated for 10 min at room temperature with stirring. A mass of 10.2 mg IgG in 4 ml of water was added to the above mixture and the mixture was allowed to stand at room temperature for 10 h with stirring. Ten milligrams of glycine was added to stop the reaction. The reaction mixture was dialyzed 24 h at  $4^\circ\text{C}$  against the pH 7 phosphate buffer solution (the buffer solution was changed five times during dialysis). The resulting labeled protein was chromatographed on a Sephadex G-25 column (diameter, 17 mm; l, 400 mm), and eluted with  $0.1 \text{ mol l}^{-1}$  phosphate buffer solution (pH 7). All fractions eluted from the column (3 ml) was used for spectrophotometric and ECL studies.

## 3. Results and discussion

### 3.1. The ECL behavior of hemin

#### 3.1.1. Selection of the conditions for ECL reaction of hemin

The preliminary investigation showed that hemin gave ECL in alkaline KCl solution at the platinum electrode when triangular voltage was

applied. Considering that some oxidants and reductants would enhance the ECL of some metallic complex system [11,12], the ECL behavior of hemin in different media: KCl-NaOH, KCl-NaOH- $\text{H}_2\text{O}_2$ , KCl-NaOH- $\text{NH}_4\text{S}_2\text{O}_8$ , KCl-NaOH- $\text{Na}_2\text{C}_2\text{O}_4$  solutions were investigated in detail. The results are shown in Table 1. It can be seen from Table 1 that the presence of the oxidants and reductants would inhibit the ECL of hemin, and the inhibition was increased with the concentration of oxidants and reductants. We attempt to use a buffer solution containing carbonate, phosphate and acetate to control pH, however, we found that all these anions would decrease the ECL of hemin. Therefore, KCl-NaOH system was used for the subsequent investigation.

The effect of NaOH concentration on the ECL intensity of hemin was investigated, and the result showed that the ECL intensity was increased with NaOH when its concentration was lower than  $0.02 \text{ mol l}^{-1}$ . When concentration of NaOH was higher than  $0.02 \text{ mol l}^{-1}$ , the ECL intensity reached maximum and became constant. Thus,  $0.03 \text{ mol l}^{-1}$  NaOH was selected for subsequent studies.

KCl was used as the supporting electrolyte. The ECL intensity of hemin did not change much when the KCl concentration was varied between  $0.3\text{--}0.5 \text{ mol l}^{-1}$ , when KCl was lower than  $0.3 \text{ mol l}^{-1}$ , the ECL intensity was decreased greatly, and after  $5 \times 10^{-2} \text{ mol l}^{-1}$ , hemin almost did not give ECL. Meanwhile, we also found that KCl itself gave an ECL background;  $0.4 \text{ mol l}^{-1}$  KCl was used for subsequent investigation.

Square, triangular and symmetric double step pulse voltages were selected to examine the ECL behavior of hemin at the platinum electrode.

Table 1

The ECL intensity of hemin in various media (hemin =  $1.0 \times 10^{-6} \text{ g ml}^{-1}$ )<sup>a</sup>

ECL system	KCl-NaOH	KCl-NaOH- $\text{H}_2\text{O}_2$		KCl-NaOH- $(\text{NH}_4)_2\text{S}_2\text{O}_8$		KCl-NaOH- $\text{Na}_2\text{C}_2\text{O}_4$	
		A <sub>1</sub>	A <sub>2</sub>	B <sub>1</sub>	B <sub>2</sub>	C <sub>1</sub>	C <sub>2</sub>
I <sub>ECL</sub>	21	14.5	9.2	12.0	8.0	7.0	9.0

<sup>a</sup> NaOH,  $0.03 \text{ mol l}^{-1}$ ; KCl,  $0.4 \text{ mol l}^{-1}$ ; A<sub>1</sub>:  $\text{H}_2\text{O}_2$ ,  $3.0 \times 10^{-3} \text{ mol l}^{-1}$ ; A<sub>2</sub>:  $\text{H}_2\text{O}_2$ ,  $3.0 \times 10^{-2} \text{ mol l}^{-1}$ ; B<sub>2</sub>:  $(\text{NH}_4)_2\text{S}_2\text{O}_8 = 1.0 \times 10^{-3} \text{ mol l}^{-1}$ ; B<sub>1</sub>:  $(\text{NH}_4)_2\text{S}_2\text{O}_8 = 1.0 \times 10^{-3} \text{ mol l}^{-1}$ ; C<sub>1</sub>:  $\text{Na}_2\text{C}_2\text{O}_4$ ,  $1.0 \times 10^{-4} \text{ mol l}^{-1}$ ; C<sub>2</sub>:  $\text{Na}_2\text{C}_2\text{O}_4$ ,  $1.0 \times 10^{-3} \text{ mol l}^{-1}$ .

Table 2  
Optimum conditions for the ECL of hemin

Electrochemical parameters	Solution conditions (mol l <sup>-1</sup> )		
Pulse waveform	Triangular	NaOH	0.03
Pulse amplitude	1.5 V	KCl	0.4
Static stand time	15 s		
Pulse period	8 ms		

Hemin gave only a very weak ECL under symmetric double-step and square pulse voltages, but the ECL of hemin was strong when triangular pulse voltage was applied. Therefore, the triangular pulse voltage was selected for subsequent studies.

A triangular pulse voltage was selected to examine the relationship between the potential and ECL intensity. It was found that when the potential was lower than 1.0 V, the ECL signal was very weak, above which the intensity increased with increasing potential. The intensity reached a maximum and constant value above 1.5 V. Thus a 1.5 V triangular pulse voltage was selected for subsequent studies.

The effect of pulse duration of the range 0.22–22 ms was tested, and the results showed that the ECL intensity of hemin increased with increasing pulse duration; when the pulse period was 8.0 ms, the intensity was strongest and the peak shape was better. For a fast ECL reaction system, after each measurement, the solution should be stood for some time to let the diffusion layer around the electrode return to its original state, thus better reproducibility could be obtained. It was found that a 15 s static time was enough to give repeatable measurement. The optimum conditions for the ECL of hemin used in subsequent studies is shown in Table 2.

### 3.1.2. Linear response range, detection limit and precision

Under the above optimum conditions, the linear response range was  $1 \times 10^{-5}$ – $2 \times 10^{-8}$  mol l<sup>-1</sup> hemin. The minimum detectable concentration of hemin (defined as the concentration which could be detected for a signal-to-noise ratio of 3) was  $1 \times 10^{-8}$  mol l<sup>-1</sup>, and the relative standard

deviation for measurement of  $1 \times 10^{-1}$  mol l<sup>-1</sup> hemin was 2.8% ( $n = 10$ )

### 3.2. The ECL of lucigenin catalyzed by hemin

Hemin has been used as mimetic enzyme to catalyze the CL reaction between luminol and H<sub>2</sub>O<sub>2</sub> [7]. We also found that hemin would catalyze the ECL of luminol at a platinum electrode in a strong alkaline solution, however, the catalyzed ECL emittance of luminol was much weaker than CL emittance of luminol. Therefore, it was not possible to be used for immunoassay. The ECL of lucigenin in aqueous alkaline solution saturated with oxygen at a platinum electrode has been investigated [13], and the result indicated that the ECL of lucigenin is emitted at the peak potential of -0.30 V, but it was similar to luminol, the sensitivity of the lucigenin ECL system was much lower than its CL system. Our experiments showed that the sensitivity of the ECL of Lucigenin would be increased greatly in the presence of trace H<sub>2</sub>O<sub>2</sub>, and some metal ions would catalyze this system. Thus, there is no doubt that this system can be applied to determination of trace metals in a similar way to luminol, but it can be used only for determination of metals, as lucigenin does not have any group which can be conjugated to other compound. Therefore it cannot be used as the label and further used for immunoassay. Fortunately, we found that hemin would catalyze the ECL of lucigenin in a neutral KCl solution at a platinum electrode in the presence of trace H<sub>2</sub>O<sub>2</sub>. It has been confirmed that hemin can be used as the label to conjugate to protein, such as human serum albumin (HAS), and this catalyst label can be sensitively quantitated by catalytic activity in a manner similar to enzyme immunoassay [7].

### 3.2.1. The ECL of lucigenin in the presence of hemin

Haapakka's experiments showed that lucigenin would give ECL at  $-0.3$  V in alkaline solution at the platinum electrode [13]. We found that addition of trace  $\text{H}_2\text{O}_2$  would greatly increase the ECL of lucigenin at platinum electrode. Unfortunately, as stated above the highly sensitive detection of lucigenin has no significance in analytical practice as it lacks of conjugation group.

It is well known that lucigenin will react with  $\text{H}_2\text{O}_2$  to give CL in alkaline solution, but not in neutral solution. Conversely, lucigenin would give ECL at a platinum electrode in neutral solution, especially in the presence of  $\text{H}_2\text{O}_2$  and hemin. Therefore the neutral solution was used for subsequent experiment to avoid producing CL. As the determination was based on the catalytic activity of hemin, so the conditions should be optimized to minimize the non-catalytic ECL and maximize the catalytic ECL.

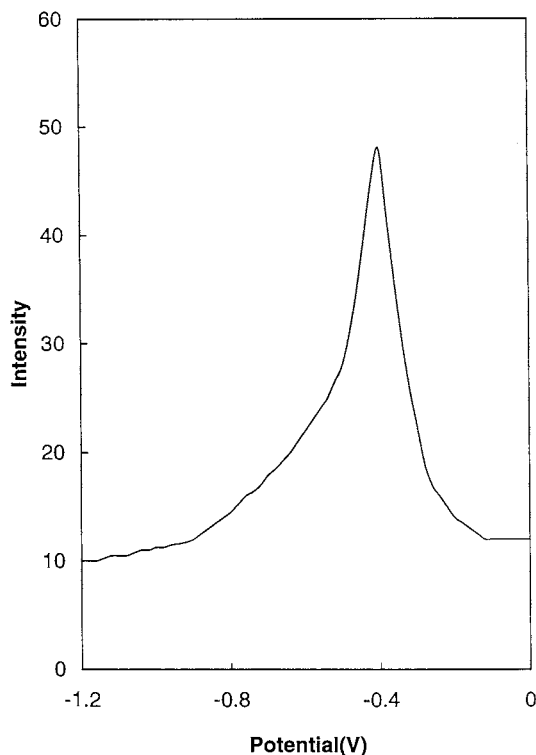


Fig. 1. ECL intensity of lucigenin as a function of potential (Lucigenin) =  $1.0 \times 10^{-6}$  mol  $\text{l}^{-1}$ ; (KCl) = 0.1 mol  $\text{l}^{-1}$ .

KCl was used as the electrolyte in our experiment. The effect of KCl on the catalytic ECL has been examined and the result showed that KCl would not effect the catalytic ECL in the range of 0.02–0.2 mol  $\text{l}^{-1}$ , 0.1 mol  $\text{l}^{-1}$  was used for the subsequent experiment.

The  $\text{H}_2\text{O}_2$  concentration had a marked influence on the catalytic ECL intensity. The experiment showed that  $\text{H}_2\text{O}_2$  can enhance catalytic ECL intensity greatly and the enhancement of intensity increases linearly with concentration of  $\text{H}_2\text{O}_2$  in the range of  $1 \times 10^{-5}$ – $5 \times 10^{-5}$  mol  $\text{l}^{-1}$ . Above this concentration the catalytic ECL intensity decreases with increasing  $\text{H}_2\text{O}_2$  concentration. This is due to the increasing of non-catalytic ECL (background) in higher concentration of  $\text{H}_2\text{O}_2$ . Therefore,  $3 \times 10^{-5}$  mol  $\text{l}^{-1}$   $\text{H}_2\text{O}_2$  was selected for subsequent experiment.

The effect of lucigenin concentration has been examined and the results showed that the catalytic ECL intensity would be increased with the concentration of lucigenin, but the non-catalytic ECL (background) was increased as well. It was found that when the concentration of lucigenin was  $1 \times 10^{-9}$  mol  $\text{l}^{-1}$  the difference between catalytic and non-catalytic ECL could be maximized, therefore,  $1 \times 10^{-9}$  mol  $\text{l}^{-1}$  lucigenin was used in the subsequent experiment.

Linear sweep, square, triangular and symmetric double step pulse voltages were selected to examine the catalytic ECL behavior of lucigenin at the platinum electrode in the presence of hemin. It was found that the catalytic ECL was stronger when linear sweep was performed. Fig. 1 shows the ECL intensity observed during the electrolysis of lucigenin in the presence of hemin at the platinum electrode as a function of potential under the stated conditions. The curve shows the intensity maximum with peak potential at  $-0.40$  V versus Ag–AgCl. Unlike non-catalytic ECL of lucigenin, the light life of catalytic ECL of lucigenin is shorter, therefore, the intensity was related to the scan rate. The experiment showed that the lower scan rate lower scan rate was better than higher, the best scan rate was in the range of 10–30  $\text{mV s}^{-1}$ ; 20  $\text{mV s}^{-1}$  was used in the subsequent experiments.

Table 3  
Optimum conditions for the ECL of lucigenin catalyzed by hemin

Electrochemical parameters		Solution conditions (mol l <sup>-1</sup> )	
Waveform	Linear sweep	KCl	0.1
Scan rate	20 mV s <sup>-1</sup>	H <sub>2</sub> O <sub>2</sub>	3 × 10 <sup>-5</sup>
		Lucigenm	1 × 10 <sup>-9</sup>

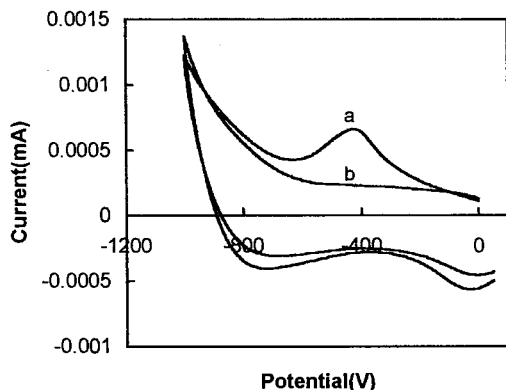
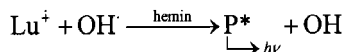
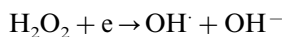
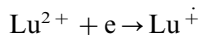


Fig. 2. Cyclic voltammogram of lucigenin (Lucigenin) = 1.0 × 10<sup>-4</sup> mol l<sup>-1</sup>; (KCl) = 0.1 mol l<sup>-1</sup>. a: Lucigenin + KCl; b: KCl.

The optimum conditions for the ECL of lucigenin catalyzed by hemin are shown in Table 3.

Fig. 2 presents the cyclic voltammogram of lucigenin under the stated conditions. An irreversible reduction process of lucigenin can be observed from Fig. 2. The peak potential of lucigenin reduction wave is -0.40 V versus Ag-AgCl, which can match the peak potential versus ECL intensity.

It has been confirmed that hydrogen peroxide should be involved in the ECL reaction of lucigenin at a platinum electrode. The formation of a reduction product of lucigenin, which is most probably a radical, is necessary for the lucigenin to produce ECL [13]. Based on the results obtained by cyclic voltammetry and the intensity versus potential curves, the following general reaction scheme is proposed for the ECL reaction of lucigenin at the platinum electrode in the presence of H<sub>2</sub>O<sub>2</sub> and hemin,



Here, P\* is the light-emitting species, which, most probably peroxides, decompose via an intermediate of the emitter, *N*-methylacrdone [14].

Under the above optimum condition, the linear logarithmic calibration range cover several order of magnitude of concentration of hemin (1.0 × 10<sup>-10</sup>–1.0 × 10<sup>-15</sup> g ml<sup>-1</sup>). The calibration curve of catalytic activity hemin for ECL is shown in Fig. 3. The minimum detectable concentration of hemin (defined as the concentration which could be detected for a signal-to-noise ratio of 3) was 1.0 × 10<sup>-15</sup> g ml<sup>-1</sup>, and the relation standard deviation for measurement of 1.0 × 10<sup>-12</sup> g ml<sup>-1</sup> hemin is 7.5% (*n* = 10).

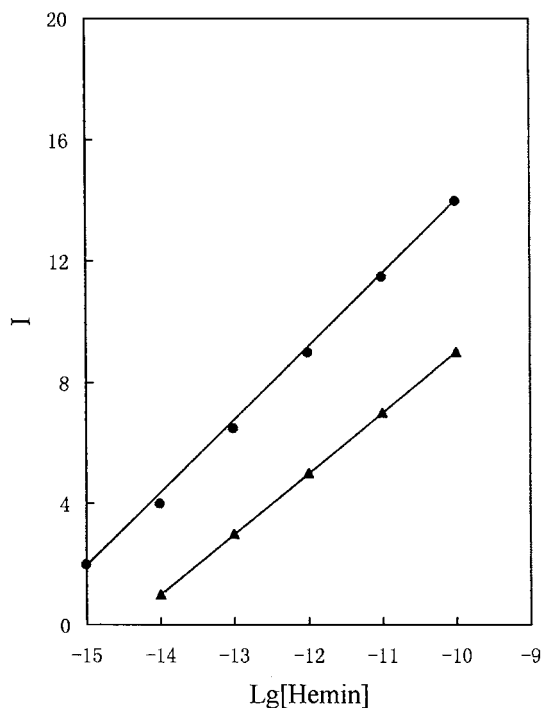


Fig. 3. Calibration curves. ●, Catalytic activity hemin for ECL; ▲, conjugated hemin for ECL.

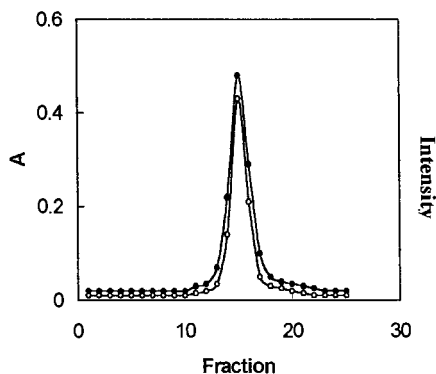


Fig. 4. Sephadex G-25 chromatogram of hemin-IgG. ●, Absorbance; ○, ECL intensity.

### 3.3. ECL catalytic activity of the conjugated hemin-IgG

IgG labeled with hemin was used to examine the ECL catalytic activity of hemin after conjugating to protein. The Sephadex G-25 chromatogram of the hemin-IgG is shown in Fig. 4. Each fraction (3 ml) was monitored at 280 nm for its absorbance and ECL intensity. It can be seen from Fig. 4 that fraction 15 shows the maximum absorbance and ECL intensity. The sharp peak in the elution pattern is ascribed to the hemin-IgG conjugated. No noticeable fraction of free hemin was obtained, as the free hemin was eliminated by dialysis prior to chromatography. Fraction 15 was used for further investigation because of its higher hemin–protein molar.

Conjugated hemin has been tested for ECL catalytic activity. Under the above mentioned optimum conditions, ECL intensity was measured at different concentration of conjugated hemin against fixing lucigenin and hydrogen peroxide concentration. The linear response range was  $1.0 \times 10^{-14}$ – $1.0 \times 10^{-10}$  g ml<sup>-1</sup>. The calibration curve of conjugated hemin for ECL is also shown in Fig. 3. Conjugated hemin can be quantitated in this concentration range by measuring ECL intensity under the above conditions. It is obvious that hemin retains ECL catalytic activity when conjugated to protein.

## 4. Conclusion

Three conclusions can be drawn: (1) hemin displays ECL behavior at a platinum electrode in alkaline solution when a triangular pulse voltage is applied; (2) hemin would catalyze the ECL reaction of lucigenin at a platinum electrode in neutral solution in the presence of H<sub>2</sub>O<sub>2</sub>; (3) hemin retains ECL catalytic activity when conjugated to protein, which indicates that hemin is possible to be used as the mimetic enzyme for labeling of antigen and antibody and further used for immunoassay.

## Acknowledgements

This project was financially supported by the Natural Sciences Foundation of China (296750003) and the Natural Sciences Foundation of Fujian Province, China.

## References

- [1] G.H.G. Thorpe, L.J. Kricka, in: M.A. Deluca, W.D. Mcelroy (Eds.), *Methods in Enzymology*, Academic Press, Florida, Vol. 133, (1992) p. 331.
- [2] Y.X. Ci, W.B. Chang, J.K. Tie, *Fenxi Huaxue* 20 (1990) 1100.
- [3] G.H. Aherne, *Anal. Proc.* 27 (1990) 100.
- [4] T. Hara, M. Toriyama, H. Miyoshi, S. Syogase, *Bull. Chem. Soc. Jpn.* 57 (1984) 3009.
- [5] T. Hara, M. Toriyama, K. Kitamura, M. Imaki, *Bull. Chem. Soc. Jpn.* 58 (1985) 2135.
- [6] T. Hara, K. Tsukagoshi, *Anal. Sci.* 6 (6) (1990) 797.
- [7] Y. Ikarlyama, S. Suzuki, *Anal. Chem.* 54 (1982) 1126.
- [8] G.N. Chen, R.E. Lin, Z.F. Zhao, J.P. Duan, L. Zhang, *Anal. Chim. Acta* 341 (1997) 251.
- [9] G.N. Chen, R.E. Lin, H.S. Zhuang, Z.F. Zhao, X.Q. Xu, F. Zhang, *Anal. Chim. Acta* 375 (1998) 269.
- [10] G.N. Chen, J.P. Duan, Q.F. Hu, *Mikrochim. Acta* 116 (1994) 227.
- [11] I. Rubinstein, A.J. Bard, *J. Am. Chem. Soc.* 103 (1981) 512.
- [12] H.S. White, A.J. Bard, *J. Am. Chem. Soc.* 104 (1982) 6891.
- [13] K.E. Haapakka, J.J. Kankare, *Anal. Chim. Acta* 130 (1981) 415.
- [14] R. Maskiewicz, D. Sogah, T.C. Bruice, *J. Am. Chem. Soc.* 101 (1979) 5347.

# Determination of surfactant concentration using micellar enhanced fluorescence and flow injection titration

Charles A. Lucy \*, Josephine S.W. Tsang

Department of Chemistry, The University of Calgary, 2500 University Drive NW, Calgary, Alberta, Canada T2N 1N4

Received 4 May 1999; received in revised form 29 July 1999; accepted 3 August 1999

## Abstract

Flow injection titration was used for the determination of anionic, cationic, nonionic and zwitterionic surfactants. The procedure was based on the micellar-enhanced fluorescence of 1,8-anilino-naphthalene sulfonate (ANS). Samples were injected into a carrier stream of phosphate buffer and  $1.0 \text{ mol l}^{-1}$  NaCl. The sample then passed through a mixing chamber which generated the exponential peak shape needed for the titration as well as diluted the sample in the carrier stream to control the pH and ionic strength of the sample. The peak width was linearly related to the logarithm of the surfactant concentration. The minimum detectable concentration was governed by the critical micelle concentration for anionic, zwitterionic and nonionic surfactants, but below the critical micelle concentration for cationic surfactants. The linear range extended for  $\sim 1.5$  orders of magnitude. Reproducibility ranged from 12% at the lower end of the calibration range to 1.1% at higher concentrations. For SDS recoveries of 82–108% were achieved in matrices as concentrated as  $1 \text{ mol l}^{-1}$  in NaCl or  $\text{Na}_2\text{SO}_4$ . © 2000 Elsevier Science B.V. All rights reserved.

*Keywords:* Titration; Phosphate buffer; Micelle; Surfactant

## 1. Introduction

Since its introduction over two decades ago [1], flow-injection titrations have shown steady development. In its original and simplest form, a flow-injection titration manifold disperses or dilutes a plug of sample to generate a concentration gradient. This sample gradient is then monitored di-

rectly or through the sample's interaction with an indicator dye. The width of the resultant peak is related logarithmically to the original concentration of sample.

Numerous means of generating concentration gradients of sample and reagents have been developed. Many of these methods are based on hydrodynamic mixing. These include: exponential mixing chambers [1–3]; wide bore tubing [4,5]; as well as simple single tube manifolds in both flow injection analysis [4,6,7] and sequential injection analysis [8,9]. Using a single tube has the advantages of simplicity and high throughput. Whereas

\* Corresponding author. Present address: Department of Chemistry, University of Alberta, Edmonton, Alberta, Canada. Tel.: +1-780-4920315; fax: +1-780-4928231.

E-mail address: charles.lucy@ualberta.ca (C.A. Lucy)

use of an exponential dilution chamber allows for the analysis of samples with concentrations varying over several orders of magnitude. There also exist a wide array of flow titrations based on electrochemically generated reagent gradients [10–15].

Thus, the manifolds used for flow-injection titrations have proliferated. In contrast the range of samples analyzed using this technique has remained relatively narrow. The original application for flow-injection titrations was acid-base titrations [1], and that remains the most common application [2,4,7–9]. Flow-injection titrations have also been performed for: zinc using a complexometric titration [4] and potassium triiodide using an iodimetric titration [4]; chloride [6], sulfate [3] and acid dissociation [16–18] and stability constants [19] using potentiometric titrations; and sulfide, cysteine and thiol-containing drugs by chemiluminescence [5].

In this paper, the application of flow-injection titrations is extended to the analysis of surfactants, including zwitterionic surfactants. Our interest in surfactant analysis arose from our previous studies in which zwitterionic sulfobetaine surfactants were found to be extremely useful additives in capillary electrophoresis [20–22]. However, we could not find a methodology to assay the concentration of such surfactants. In this paper, we develop a methodology for flow-injection titration analysis of all types of surfactants.

Titrimetric methods are commonly used for surfactant assay due to their speed and low cost [23]. Anionic surfactants may be titrated with a cationic surfactant [24,25], cationic surfactants may be titrated with a hydrophobic anion [23], and nonionic polyether surfactants can be titrated based on ion pair formation with large cations such as  $\text{Ba}^{2+}$  [23]. However, for zwitterionic surfactants, which contain both cationic and anionic functionalities, the titration procedure is not so well defined. In some cases, the zwitterionic surfactant can be made cationic under acidic conditions, at which point titrations developed for cationic surfactants can be used for the analysis of the zwitterionic surfactant [26]. However, such a procedure is not suitable for sulfobetaine zwitterionic surfactants.

Similarly, flow injection analysis has been used for determination of a variety of types of surfactants. Anionic surfactants have been analyzed using ion pair extraction with methylene blue [27,28] and malachite green [29]. Cationic surfactants have been analyzed using ion pair extraction with Orange II [30,31]. Nonionic polyethylates have been analyzed by ion pair extraction of their  $\text{K}^+$  adducts with the anionic dye tetrabromophenolphthalein ethyl ester [32]. However, there have been no reports of analyses of zwitterionic surfactants using flow injection analysis.

Our approach is to monitor the micelles formed when the sample surfactant is above its critical micelle concentration. The presence of micelles will be detected using 1,8-anilino-naphthalene sulfonate (ANS). Typically, ANS is used as a fluorescent probe for studies of biological membranes [33] and protein structure [34]. However, it has also been used to determine critical micelle concentrations (cmc) of surfactants [35–37]. ANS does not fluoresce in water, but fluoresces strongly in hydrophobic environments, such as the core of a micelle. Thus, the response in our system corresponds to the surfactant concentration above the critical micelle concentration. However, the critical micelle concentration varies with the ionic strength and nature of the counter ion in the matrix. Thus, use of ANS in a classical FI system would result in errors if the matrix composition changed. To circumvent this problem, flow injection titration is used to dilute the sample into a high ionic strength solution, thereby making the matrix composition constant.

## 2. Experimental

### 2.1. Apparatus

The apparatus is as shown in Fig. 1. A Waters 625 LC Solvent Delivery System (Milford, MA) was used to pump the carrier stream. Sample was injected using a Rheodyne (Berkeley, CA) model 9125 injector. The injection volume was 50  $\mu\text{l}$  in preliminary flow injection experiments and 300  $\mu\text{l}$  in flow-titration experiments. In preliminary flow injection experiments, the sample then merged



with a ANS reagent stream from an Alitea peristaltic pump (Medina, Washington), and then flowed through a Waters 470 Fluorescence detector ( $\lambda_{\text{ex}} = 370 \text{ nm}$ ;  $\lambda_{\text{em}} = 490 \text{ nm}$ ).

In flow-titration experiments, the mixing chamber was added to the manifold, as depicted in Fig. 1. The mixing chamber has been described previously [38], and consisted of a circular chamber of 3.40 ml stirred by a magnetic stirrer. Baffles within the mixing chamber ensure complete mixing, and a near ideal exponential response function [38]. Signal was recorded using a OmniScribe series D5000 chart recorder.

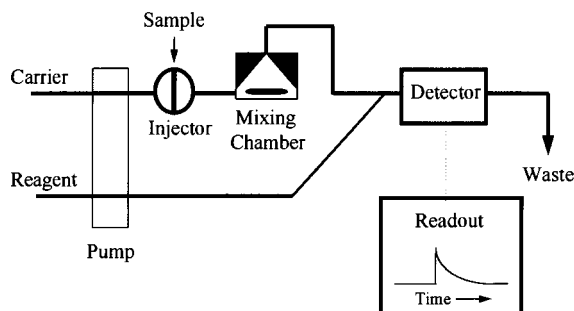


Fig. 1. Manifold for flow-titration determination of surfactants based on micellar enhanced fluorescence of 1,8-anilino-naphthalene sulfonate (ANS). See Section 2.1 for details.

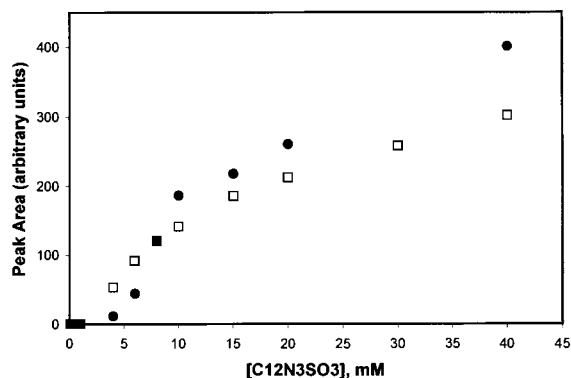


Fig. 2. Flow injection response of the zwitterionic surfactant dodecyltrimethyl(3-sulfopropyl)ammonium ( $C_{12}N_3SO_3$ ) to 1,8-anilino-naphthalene sulfonate (ANS) reagent at low (●) and high (□) ionic strength. Experimental conditions: carrier stream,  $1.0 \text{ ml min}^{-1}$  d.  $H_2O$ ; reagent stream,  $2 \text{ ml min}^{-1}$   $0.011 \text{ mol l}^{-1}$  phosphate buffer (pH 7.2) with  $2 \times 10^{-5} \text{ mol l}^{-1}$  ANS (●) and with  $2 \text{ mol l}^{-1}$  NaCl (□); excitation wavelength, 370 nm; emission wavelength, 490 nm.

## 2.2. Reagents

All reagents were of analytical grade and solutions were prepared in Nanopure ultrapure water (Barnstead). Buffers were prepared from orthophosphoric acid (BDH) and sodium hydroxide (BDH). 8-Anilino-1-naphthalene-sulfonic acid (ANS; Aldrich), dodecyl sulfate sodium salt 98% and 70% (SDS), hexadecyltrimethylammonium bromide 99% (CTAB; Sigma), dodecyltrimethyl(3-sulfopropyl)ammonium hydroxide 98% ( $C_{12}N_3SO_3$ ; Aldrich), Triton X-100 (Aldrich) and coco (amidopropyl)hydroxyl-dimethylsulfobetaine (Rewoteric AM CAS U; Witco) were used as received without further purification.

ANS (Aldrich) was weighed accurately and dissolved in water to obtain a stock solution of  $5 \times 10^{-4} \text{ mol l}^{-1}$ . New stock solution was made each week to ensure its fluorescence sensitivity.

Orthophosphoric acid was stored as a  $1 \text{ mol l}^{-1}$  stock solution. New stock solution was made when necessary. NaOH was used to adjust the buffer pH to 7.2.

## 2.3. Procedures

Experimental conditions for the flow injection titration were: carrier stream,  $1.0 \text{ ml min}^{-1}$  of  $0.010 \text{ mol l}^{-1}$  phosphate buffer (pH 7.2) with  $1.0 \text{ mol l}^{-1}$  NaCl; reagent stream,  $1.5 \text{ ml min}^{-1}$   $2 \times 10^{-5} \text{ mol l}^{-1}$  ANS in distilled water; injection volume, 300  $\mu\text{l}$ .

## 3. Results and discussion

### 3.1. Flow injection

Fig. 2 shows the flow injection response of the zwitterionic surfactant dodecyltrimethyl(3-sulfopropyl)ammonium ( $C_{12}N_3SO_3$ ) to ANS. Below 2 mM surfactant there is no fluorescence signal. As the surfactant concentration is increased, there is a sudden onset of fluorescence signal. This onset is said to coincide with the cmc of the surfactant [35]. Extrapolation of the initial fluorescence signals back to zero fluorescence yields estimates of the cmc of dodecyltrimethyl(3-sulfo-

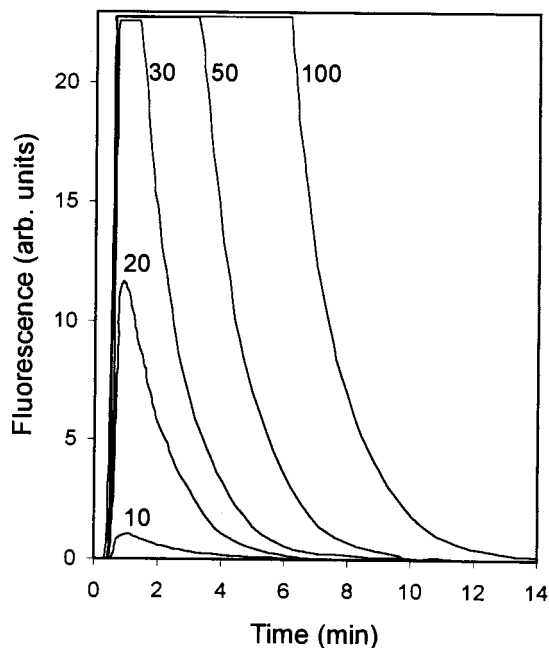


Fig. 3. Flow-titration response for the zwitterionic surfactant dodecyldimethyl(3-sulfopropyl)ammonium ( $C_{12}N_3SO_3$ ) to 1,8-anilino-naphthalene sulfonate (ANS). Experimental conditions: carrier stream,  $1.0 \text{ ml min}^{-1}$   $0.010 \text{ mol l}^{-1}$  phosphate buffer (pH 7.2) with  $1.0 \text{ mol l}^{-1}$  NaCl; reagent stream,  $1.5 \text{ ml min}^{-1}$   $2 \times 10^{-5} \text{ mol l}^{-1}$  ANS; excitation wavelength, 370 nm; emission wavelength, 490 nm.

propyl)ammonium as 4 mM at low ionic strength ( $\bullet$ ) and 1.3 mM at  $1.3 \text{ mol l}^{-1}$  NaCl ( $\square$ ). These values are in reasonable agreement with the literature values (3.6 mM at zero ionic strength and 1.7 mM at  $1.0 \text{ mol l}^{-1}$  NaCl at  $30^\circ\text{C}$  [39]). At surfactant concentrations significantly above the cmc, the fluorescence signal showed a negative deviation from linearity.

The general behavior observed for  $C_{12}N_3SO_3$  in Fig. 2 was also observed for other zwitterionic (CAS U), nonionic (Triton X-100), cationic (CTAB) and anionic (SDS) surfactants studied. However for SDS the fluorescence signal was rectilinear above the cmc over the entire SDS concentration range studied (0–40 mM). Also, for CTAB the onset of fluorescence (0.03 mM at  $0.015 \text{ mol l}^{-1}$  ionic strength) occurred well below the literature cmc value (0.8 mM at zero ionic strength and  $25^\circ\text{C}$ ). This is consistent with the

observation of de Vendittis et al. [35] that ANS was not appropriate for determining cmc values of cationic surfactants.

Regardless, direct flow injection analysis based on micellar enhanced fluorescence is not appropriate for the determination of surfactant concentrations. As is apparent in Fig. 2, the fluorescence response is altered in two ways by the matrix. Firstly, the cmc changes with ionic strength and matrix counter-ion. In Fig. 2, the cmc of dodecyldimethyl(3-sulfopropyl)ammonium ( $C_{12}N_3SO_3$ ), as indicated by the onset of fluorescence, decreases 3-fold upon increasing the ionic strength. More dramatic changes in the cmc (10–100-fold) would occur for anionic and cationic surfactants which experience much greater electrostatic head group repulsion [39–41].

A second effect apparent in Fig. 2 is that the fluorescence response is altered by the matrix. In Fig. 2, the sensitivity of the fluorescence response is decreased by the addition of NaCl. However, the effect of the matrix on fluorescence did not seem to be a quenching phenomenon. Indeed, the fluorescence signal for other surfactants such as CTAB and Triton X-100 was somewhat enhanced by the addition of salt to the matrix.

In many industrial applications of surfactants, such as in enhanced oil recovery, the sample matrix can vary significantly in composition. Thus the use of micellar enhanced fluorescence in direct flow injection analysis is inappropriate. Rather, a technique that is insensitive to the sample matrix is required.

### 3.2. Flow titration

The most commonly quoted characteristic of flow-titrations is that the peak width is logarithmically related to the sample concentration. However another often overlooked characteristic is that the response from the tail of the peak results from exponentially diluted sample. Thus in our system (Fig. 1), the sample passes through a mixing chamber to generate an exponential peak shape. This dilutes the sample in a high ionic strength buffer. The diluted sample then mixes with the ANS reagent stream. As shown in Fig. 3, the resultant signal has a sharp front followed by

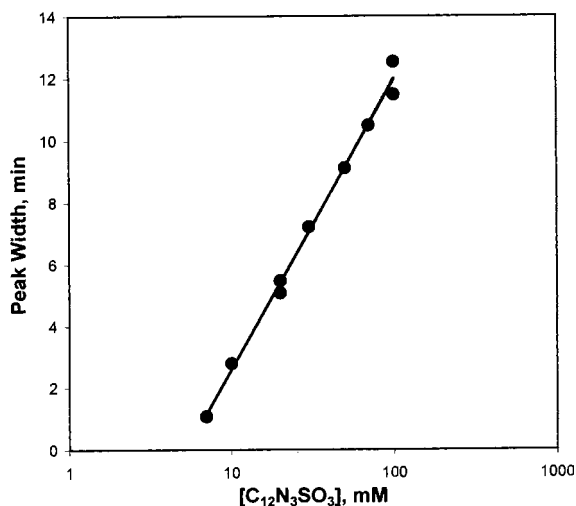


Fig. 4. Flow-titration response for the zwitterionic surfactant dodecyltrimethyl(3-sulfopropyl)ammonium ( $C_{12}N_3SO_3$ ) to 1,8-anilino-naphthalene sulfonate (ANS). Experimental conditions as in Fig. 3. Peak width measured 0.2 units above the baseline.

a gradual exponential tail. In the tail region, the matrix is dominated by the high ionic strength buffer, thus minimizing sample matrix effects. Typically, the width was measured near the baseline (0.6 arbitrary units) to maximize the dynamic range.

The width of the peaks shown in Fig. 3 are linearly related to the logarithm of the dodecyltrimethyl(3-sulfopropyl)ammonium ( $C_{12}N_3SO_3$ ) concentration, as shown in Fig. 4. Statistics for

this calibration curve, as well as that for other surfactants, are given in Table 1. The linearity of response was excellent for the anionic SDS, cationic CTAB and zwitterionic  $C_{12}N_3SO_3$ . The dynamic linear range was  $\approx 1.5$  orders of magnitude. The linear range started about one order of magnitude above the cmc for anionic, nonionic, and zwitterionic surfactants. For CTAB, a linear response was observed as low as the cmc, presumably due to interaction between the anionic ANS and the cationic surfactant [35]. The maximum surfactant concentration which could be analyzed was limited by the maximum peak width that can be tolerated ( $\sim 15$  min).

For SDS, CTAB and  $C_{12}N_3SO_3$ , the linearity of the calibration was independent of the height above the baseline used for calibration. Thus to maximize the dynamic range, peak width measurements were generally made at the lowest signal that was practical. However under such measurement conditions the linearity of calibration curves for CAS U and Triton X-100 were poor. For CAS U, it was found that if the width was measured at a height of 0.6 arbitrary units, the calibration curve appeared sigmoidal in shape. However, if the width were measured at a greater height (7 arbitrary units) above the baseline, the linearity improved greatly. For Triton X-100, the calibration curve was simply scattered. Altering the height at which the peak width was measured did not affect the degree of scatter. It is unknown why the calibrations for CAS U and Triton X-100

Table 1

Calibration statistics for flow-titration analysis of surfactants based on 1,8-anilino-naphthalene sulfonate (ANS) fluorescence<sup>a</sup>

Surfactant	Conc range (mM)	$R^2$	cmc (mM) [39]
Sodium dodecyl sulfate (SDS)	8–100	0.9943	0.9 <sup>c</sup>
Hexadecyltrimethyl ammonium bromide (CTAB)	0.01–0.5	0.9945	0.01 <sup>d</sup>
Dodecyl dimethyl (3-sulfopropyl) ammonium hydroxide ( $C_{12}N_3SO_3$ )	7–100	0.9991	1.7 <sup>c</sup>
Triton X-100 <sup>b</sup>	0.06–3 w/v%	0.974	0.002 w/v% <sup>d</sup>
Coco (amidopropyl)hydroxyl-dimethylsulfobetaine (CAS U)	0.7–10	0.985	0.05 [20]

<sup>a</sup> Experimental conditions: carrier stream,  $1.0 \text{ ml min}^{-1}$  0.01 mol  $l^{-1}$  phosphate buffer (pH 7.2) with  $1.0 \text{ mol l}^{-1}$  NaCl; reagent stream,  $1.5 \text{ ml min}^{-1}$   $2 \times 10^{-5}$  mol  $l^{-1}$  ANS; injection volume, 300  $\mu$ l; excitation wavelength, 370 nm; emission wavelength, 490 nm.

<sup>b</sup> Experimental conditions as in <sup>a</sup>, except: carrier stream,  $1.5 \text{ ml min}^{-1}$  0.01 mol  $l^{-1}$  phosphate buffer (pH 7.2) with  $1.0 \text{ mol l}^{-1}$  NaCl.

<sup>c</sup> In  $0.2 \text{ mol l}^{-1}$  NaCl.

<sup>d</sup> In  $1.0 \text{ mol l}^{-1}$  KCl.

<sup>e</sup> In  $1.0 \text{ mol l}^{-1}$  NaCl at 30°C.

were problematic. It is suspected that the problems arise from CAS U and Triton X-100 both having variable chain lengths. CAS U is prepared from coconut oil, and as a result the aliphatic chain length varies from C<sub>8</sub> to C<sub>18</sub>. Triton X-100's hydrophilic tail consists of 5–15 ethylene oxide units.

To determine the reproducibility of the technique six replicate injections of 20 mM and 100 mM SDS were made. The relative SDs for these measurements were 12 and 1.1%, respectively. The higher uncertainty associated with 20 mM SDS is a reflection that this measurement was made near the lowest concentration detectable.

To test the effect of sample matrix on the measurements, recovery studies were performed for 20 mM SDS in distilled water, 0.5 mol l<sup>-1</sup> NaCl, 1.0 mol l<sup>-1</sup> NaCl, 0.5 mol l<sup>-1</sup> Na<sub>2</sub>SO<sub>4</sub> and 1 mol l<sup>-1</sup> Na<sub>2</sub>SO<sub>4</sub>. Recoveries ranged from 82 to 108%, which represent quantitative recoveries.

#### 4. Conclusions

This paper presents a simple and easily automated procedure for determining surfactant concentration. It is applicable to all types of surfactants, including zwitterionic surfactants which cannot be determined by any other procedure. The peak width is linearly related to the logarithm of the surfactant concentration for about one and a half orders of magnitude. The bottom of the linear range is about one order of magnitude above the critical micelle concentration. Precision is strongly dependent on the sample concentration, but can be as good as 1.1% at higher concentrations. The technique is unaffected by matrices as concentrated as 1 M NaCl or Na<sub>2</sub>SO<sub>4</sub>. Future studies will focus on improving the sample throughput by decreasing the volume of the mixing chamber.

#### Acknowledgements

This work was supported by the Natural Science and Engineering Research Council of Canada and by The University of Calgary.

Funding provided for J.S.W.T. by the Summer Career Placements Program sponsored by the Government of Canada is gratefully acknowledged.

#### References

- [1] J. Ruzicka, E.H. Hansen, H. Mosbæk, *Anal. Chim. Acta* 92 (1977) 235–249.
- [2] D.R. Turner, S. Knox, M. Whitfield, M. Correia dos Santos, *Anal. Proc.* 24 (1987) 360–362.
- [3] O. Lutze, B. Roß, K. Cammann, *Fresenius J. Anal. Chem.* 350 (1994) 630–632.
- [4] A.U. Ramsing, J. Ruzicka, E.H. Hansen, *Anal. Chim. Acta* 129 (1981) 1–17.
- [5] I. López Garcia, P. Viñas, J.A. Martínez Gil, *Fresenius Z. Anal. Chem.* 345 (1993) 723–726.
- [6] M.B. Etxebarria, J.L.F.C. Lima, M.C.B.S.M. Montenegro, R. Pérez-Olmos, *Anal. Sci.* 13 (1997) 89–92.
- [7] K. Grudpan, P. Sritharathikhun, J. Jakmunee, *Anal. Chim. Acta* 363 (1998) 199–202.
- [8] G.D. Clark, J. Zable, J. Ruzicka, G.D. Christian, *Talanta* 38 (1991) 119–124.
- [9] J.F. van Staden, H. du Plessis, *Anal. Commun.* 34 (1997) 147–151.
- [10] G. Nagy, Z. Fehér, K. Tóth, E. Pungor, A. Ivaska, *Talanta* 26 (1979) 1143–1153.
- [11] Z. Fehér, G. Nagy, I. Slezsák, K. Tóth, E. Pungor, *Anal. Chim. Acta* 273 (1993) 521–530.
- [12] R.C. Schothorst, G. den Boef, *Anal. Chim. Acta* 181 (1986) 235–239.
- [13] R.H. Taylor, J. Ruzicka, G.D. Christian, *Talanta* 39 (1992) 285–292.
- [14] R.H. Taylor, C. Winbo, G.D. Christian, J. Ruzicka, *Talanta* 39 (1992) 789–794.
- [15] R.H. Taylor, J. Rotermund, G.D. Christian, J. Ruzicka, *Talanta* 41 (1994) 31–38.
- [16] D.R. Turner, S. Knox, M. Whitfield, M. dos Santos, C. Pescada, M.L. Gonçalves, *Anal. Chim. Acta* 226 (1989) 229–238.
- [17] D.R. Turner, S. Knox, M. Whitfield, M. dos Santos, C. Pescada, M.L. Gonçalves, *Anal. Chim. Acta* 226 (1989) 239–246.
- [18] D.R. Turner, M. Correia dos Santos, P. Coutinho, M.L. Gonçalves, S. Knox, *Anal. Chim. Acta* 258 (1992) 259–267.
- [19] A.C. Lopes da Conceição, M.L.S. Simões Gonçalves, M.M. Correia dos Santos, *Anal. Chim. Acta* 302 (1995) 97–102.
- [20] K.K.-C. Yeung, C.A. Lucy, *Anal. Chem.* 69 (1997) 3435–3441.
- [21] K.K.-C. Yeung, C.A. Lucy, *J. Chromatogr. A* 804 (1998) 319–325.
- [22] K.K.-C. Yeung, C.A. Lucy, *Anal. Chem.* 70 (1998) 3286–3290.

- [23] T.M. Schmitt, *Analysis of Surfactants*, Marcel Dekker, New York, 1992. Chapter 11.
- [24] American Society for Testing and Materials, *Standard Test Method for Synthetic Anionic Ingredient by Cationic Titration*, Philadelphia, PA. Method D3049–89.
- [25] American Society for Testing and Materials, *Standard Test Method for Active Material in Anionic Surfactants*, Philadelphia, PA. Method D4251–89.
- [26] M.J. Rosen, F. Zhao, D.S. Murphy, *J. Am. Oil Chem. Soc.* 64 (1987) 439–441.
- [27] J. Kawase, A. Nakae, M. Yamanaka, *Anal. Chem.* 51 (1979) 1640–1643.
- [28] Y. Sahleström, B. Karlberg, *Anal. Chim. Acta* 185 (1986) 259–269.
- [29] T. Sakai, H. Harada, X. Liu, N. Ura, K. Takeyoshi, K. Sugimoto, *Talanta* 45 (1998) 543–548.
- [30] J. Kawase, M. Yamanaka, *Analyst* 104 (1979) 750–755.
- [31] J. Kawase, *Anal. Chem.* 52 (1980) 2124–2127.
- [32] M.J. Whitaker, *Anal. Chim. Acta* 179 (1986) 459–462.
- [33] L.S. Bakas, E.A. Disalvo, *Biochim. Biophys. Acta* 1065 (1991) 114–120.
- [34] D.L. Gibbons, P.M. Horowitz, *J. Biol. Chem.* 270 (1995) 7335–7430.
- [35] E. de Vendittis, G. Palumbo, G. Parlato, V. Bocchini, *Anal. Biochem.* 115 (1981) 278–286.
- [36] V. Koppaka, J. Wang, M. Banerjee, B.R. Lentz, *Biochemistry* 35 (1996) 7482–7491.
- [37] O.W. Odom, W. Kudlicki, G. Kramer, B. Hardesty, *Anal. Biochem.* 245 (1997) 249–252.
- [38] C.A. Lucy, L.L.M. Glavina, F.F. Cantwell, *J. Chem. Ed.* 72 (1995) 367–374.
- [39] P. Mukerjee, K.J. Mysel, *Critical Micelle Concentrations of Aqueous Surfactant Systems*, National Bureau of Standards, U.S. Government Printing Office, Washington, DC, 1971.
- [40] D. Myers, *Surfactant Science and Technology*, second ed., VCH, New York, 1992, pp. 81–131.
- [41] K.W. Herrmann, *J. Colloid Interf. Sci.* 22 (1966) 352–359.

# Analysis of explosives using electrospray ionization/ion mobility spectrometry (ESI/IMS)

G. Reid Asbury, Jörg Klasmeier, Herbert H. Hill Jr. \*

*Department of Chemistry, Washington State University, Pullman, WA 99164-4630, USA*

Received 6 May 1999; received in revised form 2 August 1999; accepted 3 August 1999

## Abstract

The analysis of explosives with ion mobility spectrometry (IMS) directly from aqueous solutions was shown for the first time using an electrospray ionization technique. The IMS was operated in the negative mode at 250°C and coupled with a quadrupole mass spectrometer to identify the observed IMS peaks. The IMS response characteristics of trinitrotoluene (TNT), 2,4-dinitrotoluene (2,4-DNT), 2-amino-4,6-dinitrotoluene (2-ADNT), 4-nitrotoluene (4-NT), trinitrobenzene (TNB), cyclo-1,3,5-trimethylene-2,4,6-trinitramine (RDX), cyclo-tetramethylene-tetranitramine (HMX), dinitro-ethyleneglycol (EGDN) and nitroglycerine (NG) were investigated. Several breakdown products, predominantly  $\text{NO}_2^-$  and  $\text{NO}_3^-$ , were observed in the low-mass region. Nevertheless, all compounds with the exception of NG produced at least one ion related to the intact molecule and could therefore be selectively detected. For RDX and HMX the  $[\text{M} + \text{Cl}]^-$  cluster ion was the main peak and the signal intensities could be greatly enhanced by the addition of small amounts of sodium chloride to the sprayed solutions. The reduced mobility constants ( $K_0$ ) were in good agreement with literature data obtained from experiments where the explosives were introduced into the IMS from the vapor phase. The detection limits were in the range of 15–190  $\mu\text{g l}^{-1}$  and all calibration curves showed good linearity. A mixture of TNT, RDX and HMX was used to demonstrate the high separation potential of the IMS system. Baseline separation of the three compounds was attained within a total analysis time of 6.4 s. © 2000 Elsevier Science B.V. All rights reserved.

*Keywords:* Electrospray ionization; Ion mobility spectrometry; Reduced mobility constants; Baseline separation

## 1. Introduction

Trace analysis of explosives is of major importance in two different fields. One is the threat of an illegal use of these compounds, which has led

to major efforts in developing explosives' detection systems [1–3]. The other is growing concern about the health risks associated with the release of explosives from military sites and former ammunition plants into the environment [4–6]. Ion mobility spectrometry (IMS) is one of the most promising analytical techniques currently investigated for the detection of explosives. The major advantages of IMS are its fast response times and

\* Corresponding author. Tel.: +1-509-3355648; fax: +1-509-3358867.

*E-mail address:* hhhill@wsu.edu (H.H. Hill Jr.)

its sensitivity to many of the commonly used explosives due to their strong electron affinity [7].

Although a number of commercial IMS systems are already available, there are still some problems to overcome. The routine use of IMS as a detection method for explosives requires a reproducible response produced by clearly identified ions. The ion chemistry of the compounds, however, is different depending on the operation conditions (e.g. ionization method, drift tube temperature, drift gas) of the IMS system. Published IMS spectra often differ significantly due to temperature effects and the addition of reactants to the drift gas [8,9]. Hitherto, several different ions have been reported including molecular ions of the form  $M^-$  or  $[M-H]^-$ , multi-component cluster-ions (e.g.  $[M + Cl]^-$  or  $[M + NO_3]^-$ ) and fragment ions (e.g.  $NO_3^-$ ). The exact nature of the species formed in the IMS can only be decisively determined using an IMS/MS combination.

Thermally labile compounds like NG and EGDN tend to decompose at elevated temperatures and often only non-specific fragment ions (e.g.  $NO_2^-$  and  $NO_3^-$ ) are observed [1]. As high-temperature operation of the IMS provides several advantages such as, eliminating interference problems and enhancing the sensitivity, it would be desirable to establish such a system for the determination of explosives.

The use of electrospray ionization (ESI) instead of the standard  $^{63}Ni$  ionization source could also be advantageous. The combination of ESI with mass spectrometry (MS) has already been successfully applied to the analysis of explosives [10,11]. In our lab, recently a novel, cooled electrospray ionization system has been developed for the use with IMS. This enables the direct analysis of aqueous samples [12,13]. This methodology could provide a helpful tool for the screening of water samples suspected to be contaminated with explosives.

Using our ESI-IMS-MS, we investigated the response characteristics and the detection limits for a number of different explosives. The mass spectral data were used to identify the IMS peaks to enable a comparison of the calculated  $K_0$ -values with literature data. Also the ion patterns

observed for RDX and HMX were compared to results of previously published ESI-MS studies. 2-ADNT, one of the initial metabolic intermediates of TNT formed after release of TNT into the environment [5], was included in the study to address the possible tracing of environmental contamination with an IMS method.

## 2. Experimental

### 2.1. Chemicals and solvents

The explosives used in this study included 2,4,6-trinitrotoluene (TNT), 2,4-dinitrotoluene (2,4-DNT), 1,3,5-trinitrobenzene (TNB), 2-amino-4,6-dinitro-toluene (2-ADNT), 4-nitrotoluene (4-NT), cyclo-1,3,5-trimethylene-2,4,6-trinitramine (RDX), cyclo-tetramethylene-tetranitramine (HMX), ethyleneglycol-dinitrate (EGDN), and nitroglycerin (NG). All compounds were purchased as standards in sealed ampoules from either Supelco (Bellefonte, PA) or Radian International (Austin, TX). They came dissolved in acetonitrile at a concentration of  $1000 \text{ mg l}^{-1}$  and were diluted with methanol–water (9:1, v/v) to  $10 \text{ mg l}^{-1}$  or less. Solutions containing sodium chloride or ammonium acetate were prepared by diluting the stock standard solutions with an appropriate solution of the respective salt in methanol–water (9:1, v/v). All solvents used were reagent grade (J.T. Baker, Phillipsburg, PA).

### 2.2. Instrumentation

The ESI/IMS/MS-system was constructed at Washington State University and has been described in detail elsewhere [12,13]. A total spray voltage of  $-2500 \text{ V}$  was applied to the electrospray unit. The electrospray needle was kept cool by water cooled nitrogen flowing along the axis of the needle at a flow rate of about  $60 \text{ ml min}^{-1}$ . This cooling process was necessary to eliminate solvent evaporation inside the needle prior to electrospray. A continuous flow of solvent (methanol–water, 9:1, v/v) through the ESI source was provided by a dual piston syringe

pump (Brownlee Labs, Santa Clara, CA) with a flow rate of  $5 \mu\text{l min}^{-1}$ . Samples were injected via a six-port injector (C6W, Valco Industries, Houston, TX) with an external injection loop.

A detailed description of the IMS unit can be found in Wu et al. [13]. The instrument was operated in the negative mode, as explosives tend to produce negative ions. The electric field strength in the desolvation region and the drift region was  $280 \text{ V cm}^{-1}$  with a total drift voltage of  $-3650 \text{ V}$ . The drift tube was operated at  $250^\circ\text{C}$  at atmospheric pressure. A counterflow of preheated dry nitrogen ( $800 \text{ ml min}^{-1}$ ) was introduced as drift gas at the end of the drift region. This drift gas was further used to desolvate the electrosprayed ions in the desolvation region.

The ion mobility spectrometer was interfaced to a C50-Q quadrupole mass spectrometer (ABB Extrel, Pittsburgh, PA 15238). The ions entered

the MS via a 40-micron pin hole leak which served as the barrier between the atmospheric pressure of the IMS tube and the vacuum of the mass spectrometer.

All mobility data was collected by replacing the stock preamplifier with a Keithley 427 amplifier (Keithley Instruments, Cleveland, OH) and sending the amplified signal to the data acquisition system, which was constructed at WSU. A detailed description of the IMS control and data acquisition system can be found in [12]. All of the IMS spectra shown in this paper were the average of 256 individual spectra. Mobility spectra were collected in a non-selective and a mass selective mode. In the non-selective mode all ions were allowed to pass the mass filter, whereas in the mass selective mode the mass spectrometer was set to allow only a single  $m/z$  to pass. All identifications of distinct ions were based on the mass spectral data.

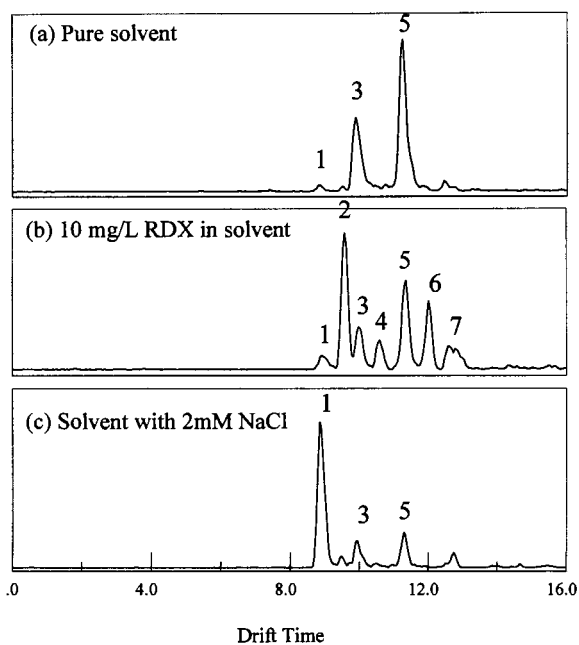


Fig. 1. Background ions in the low-mass region of the IMS monitored for pure solvent (a), a solution of  $10 \text{ mg l}^{-1}$  RDX (b) and a solution of  $2 \text{ mM NaCl}$  in the solvent (c). Notation: 1, chloride ( $\text{Cl}^-$ ); 2, nitrate ( $\text{NO}_3^-$ ); 3, formate ( $\text{HCOO}^-$ ); 4, nitrite ( $\text{NO}_2^-$ ); 5, acetate ( $\text{CH}_3\text{COO}^-$ ); 6, probably nitrite adduct ( $\text{CH}_3\text{OH} + \text{NO}_2^-$ ); 7, cluster of at least two unidentified ions ( $m/z$  89 and 97).

### 3. Results and discussion

#### 3.1. Low-mass background and breakdown ions

The low-mass region of the IMS spectra was studied in some detail in order to better characterize the high temperature atmospheric pressure ESI/IMS and its ion chemistry. The top spectrum of Fig. 1 shows the background signal of the IMS when spraying pure solvent. There are three distinct peaks (# 1, # 3, # 5), which were identified by mass analysis to be  $\text{Cl}^-$ ,  $\text{HCOO}^-$ , and  $\text{CH}_3\text{COO}^-$ , respectively. These ions are most likely formed by ESI from trace impurities of the solvents (e.g. acetic acid, chloride salts).

The middle spectrum of Fig. 1 shows the peaks observed in the low-mass region with a solution of RDX ( $10 \text{ mg l}^{-1}$ ). Besides the three background peaks a number of other peaks appeared. Peaks labeled # 2 and # 4 were identified as nitrite and nitrate. They were probably formed by thermal breakdown of RDX in the hot desolvation region. All of the investigated explosives produced significant amounts of these two ions, which is not surprising since most of the compounds are thermally labile [1].



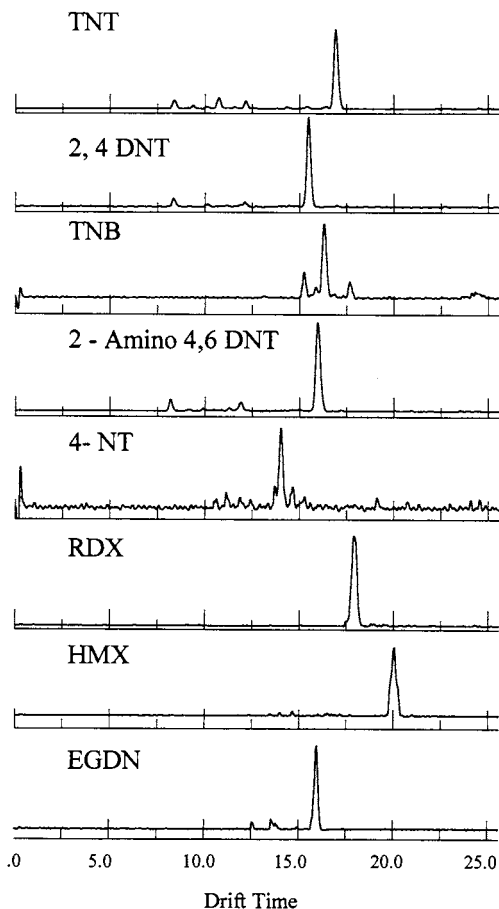


Fig. 2. Ion mobility spectra of eight explosives with low mass filter set to 140. Concentration of standard solutions was  $10 \text{ mg l}^{-1}$  in methanol–water (9/1, v/v), 2 mM NaCl was added for RDX and HMX.  $m/z$  values can be seen in Table 1.

The peak labeled # 6 has a mass of 78 amu and is suggested to be a  $(\text{CH}_3\text{OH} + \text{NO}_2^-)$  adduct ion. The final peak (# 7) appears to be a cluster of different ions. The mass spectral analysis revealed that it contains at least two ions with  $m/z$  89 and 97. The identity of these peaks is speculated to be adducts of nitrite and nitrate with other breakdown products. The same mass peaks have been previously observed in an ESI/MS study, but were also unidentified [11].

The bottom spectrum of Fig. 1 shows the low-mass region for pure solvent containing 2 mM sodium chloride. As expected the chloride peak (# 1) dominates this spectrum. The simultaneous

reduction of the other background ions is probably a result of charge competition.

### 3.2. IMS spectra of standard solutions of explosives

The different explosives were sprayed out of standard solutions at concentrations of  $10 \text{ mg l}^{-1}$  each. The respective spectra are shown in Fig. 2. They were taken with the low-mass filter set to 140, effectively eliminating any ions in the low-mass region from reaching the detector. Furthermore it should be noted that the spectra shown for RDX and HMX were taken with the addition of 2 mM NaCl to the standard solution, predominantly forming  $(\text{M} + \text{Cl}^-)$  adduct ions (see discussion below).

In the case of nitroglycerine only breakdown product ions (mainly nitrate) were produced and no ions could be detected in the high mass region. The thermal instability of NG in traditional IMS systems at temperatures above  $150^\circ\text{C}$  is known and has been reported before [1,9]. Obviously this is also valid for the ESI/IMS system at  $250^\circ\text{C}$ .

TNB showed at least three different peaks with the  $\text{M}^-$  ( $m/z$  213) being the dominant one. Mass spectral analysis revealed  $m/z$  values of 178 and 244 for the two other peaks seen in the IMS spectrum. The latter is speculated to be a  $(\text{M} + \text{CH}_3\text{CO}^-)$  adduct formed by the molecule clustering with the methanol solvent. All the other compounds showed only one main peak being either  $(\text{M}-\text{H})^-$  or  $\text{M}^-$ . The reduced mobility constants ( $K_0$ ) of the dominant peaks for each compound were calculated and are listed in Table 1. It can be seen that they are in good agreement with previously reported literature values obtained from experiments where the compounds have been introduced into the IMS as vapors.

### 3.3. Sensitivity enhancement by addition of Cl

It is known that the sensitivity of IMS systems using a  $^{63}\text{Ni}$  foil as ionization source to certain explosives can be enhanced by adding chlorinated reactants (e.g. dichloromethane) to the carrier gas [1,3,9]. This phenomenon has not yet been investigated with electrospray ionization. In our experi-

Table 1

 $K_0$ -values of different product ions of the investigated compounds compared to literature data

Compound	m/z	Species	LoD ( $\mu\text{g l}^{-1}$ )	$K_0$ ( $\text{cm}^2 \text{V}^{-1} \text{s}^{-1}$ ) <sup>a</sup>	Reference	
TNT	226	(M-H) <sup>-</sup>	15	1.48	1.54 (N <sub>2</sub> ) 1.45 (air)	[8] [1–3]
2 ADNT	196	(M-H) <sup>-</sup>	16	1.57	–	–
2,4 DNT	181	(M-H) <sup>-</sup>	26	1.62	1.67 (N <sub>2</sub> ) 1.57 (air)	[8] [1]
4-NT	136	(M-H) <sup>-</sup>	>1000	1.79	1.81 (air)	[8]
TNB	244	(M+CH <sub>3</sub> O <sup>-</sup> ) <sup>-</sup>	n.c.	1.42	–	–
	213	M <sup>-</sup>	1.54	–	–	–
	178	?	1.65	–	–	–
RDX	257	(M+Cl <sup>-</sup> ) <sup>-</sup>	40	1.40	1.39 (air)	[2,3]
HMX	331	(M+Cl <sup>-</sup> ) <sup>-</sup>	86	1.25	1.25 (air)	[2]
EGDN	152	M <sup>-</sup>	190	1.57	–	–
NG	226	(M-H) <sup>-</sup>	n.d.	–	1.45 (air)	[2]
	262	(M+Cl <sup>-</sup> ) <sup>-</sup>	n.d.	n.d.	1.47 (N <sub>2</sub> )	[9]

<sup>a</sup> First column: measured in this study with N<sub>2</sub> as drift gas. Second column: reference data, drift gas given in parentheses. n.d., not detected; n.c., not calculated; LoD, limit of detection.

ments the addition of small amounts of dichloromethane to samples of RDX and HMX showed no significant effects in the IMS, even with respect to the Cl<sup>-</sup> peak. However, a huge increase in the peak intensities for the Cl<sup>-</sup> peak and the (M + Cl<sup>-</sup>)<sup>-</sup> adduct peak could be achieved by adding sodium chloride to the samples. This seems reasonable taking into account that when using a <sup>63</sup>Ni foil the ions are created in the gas phase from volatile species, whereas electrospray creates the ions in solution from dissolved species. Significant increases in signal intensity for the (M + Cl<sup>-</sup>)<sup>-</sup> adduct were observed at concentrations as low as 0.02 mM NaCl. The optimal concentration was found to be about 2 mM with an overall increase in signal intensity compared to a pure standard solution of more than one order of magnitude (about 12 times).

Figs. 3 and 4 show the different spectra for RDX and HMX with and without the addition of 2 mM NaCl. The increase in the intensity of the chloride peak after adding NaCl can be seen from Fig. 3. No M<sup>-</sup> or (M-H)<sup>-</sup> ions were detected in either case. However, the spectra clearly indicate a significant increase in the peak intensity with the addition of the chloride salt. Apparently, both compounds are able to form stable (M + Cl<sup>-</sup>)<sup>-</sup> adduct ions with our operating conditions. None

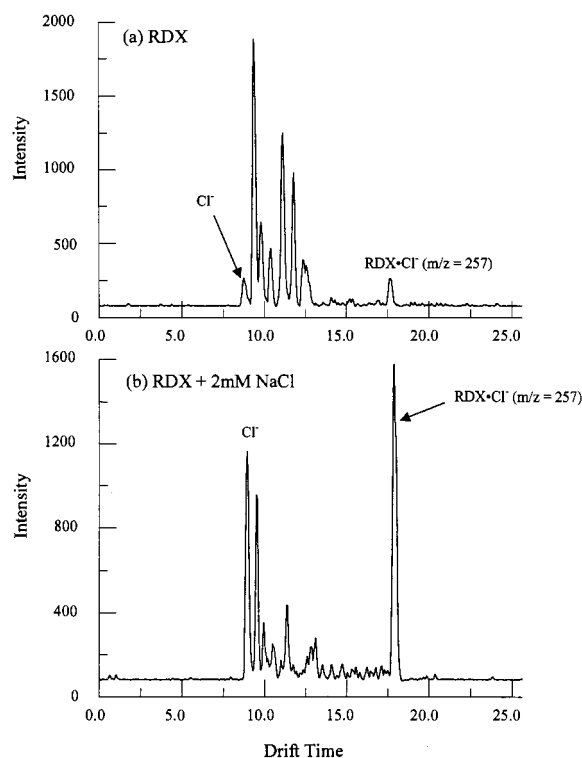


Fig. 3. Ion mobility spectra of RDX with (a) and without (b) addition of NaCl (2 mM). Concentration of standard solution was  $10 \text{ mg l}^{-1}$  in methanol–water (9/1, v/v) each.

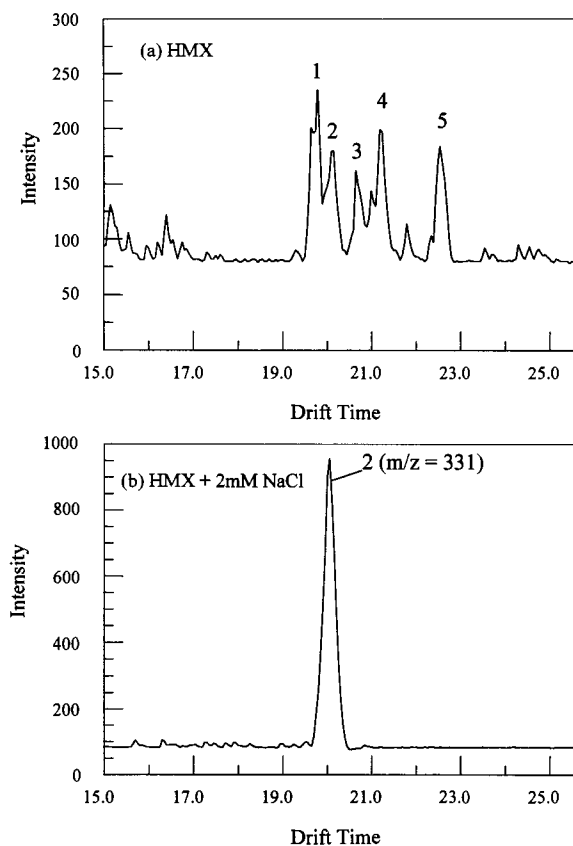


Fig. 4. Ion mobility spectra of HMX with (a) and without (b) addition of NaCl (2 mM). Concentration of standard solution was  $10 \text{ mg l}^{-1}$  in methanol–water (9/1, v/v) each. Notation: 1,  $m/z$  334, 2,  $m/z$  331; 3,  $m/z$  341; 4,  $m/z$  355; and 5,  $m/z$  357.

of the other explosives produced measurable amounts of  $(M + \text{Cl}^-)^-$  adduct ions. This is surprising for EGDN, as this compound has been shown to do so in vapor phase IMS systems [1,9].

The top spectra of Figs. 3 and 4 obtained with the pure standards also show the peak for the  $(M + \text{Cl}^-)^-$  adduct, but the signals are much weaker. Whereas for pure RDX no other ions appeared in the IMS spectrum, HMX showed a couple of additional peaks.  $M/z$  of these peaks were identified to be 334, 341, 355 ( $M + 59$ ) and 357. Similar observations were made in previously published ESI/MS studies, but the identity of the respective ions remains in question. Yinon et al [11] labeled the  $(M + 59)$  as a  $(M + \text{NNO}_2\text{-H})^-$  cluster ion, whereas Casetta and Garofolo [10]

refer to the same peak as an acetate adduct  $(M + \text{CH}_3\text{COO}^-)^-$  due to the fact that they sprayed standard solutions containing 2 mM of ammonium acetate. With our experimental design we could not achieve any increase in the  $(M + 59)$ -peak by adding 2 mM of ammonium acetate, but this might well be a temperature effect since the IMS was operated at  $250^\circ\text{C}$ .

#### 3.4. Detection limits and linearity of response

With the exception of NG, TNB and 4-NT all explosives produced signals significantly above the noise level (about 300 fA) at a concentration of  $10 \text{ mg l}^{-1}$ . Detection limits for these compounds were determined as the concentrations giving peak heights three times the noise level. The calculated values for the different compounds are given in Table 1. They were found to vary between  $15\text{--}190 \text{ } \mu\text{g l}^{-1}$  which is similar to detection limits reported for HPLC systems [6,14]. With the parameters used for data acquisition this calculates to absolute IMS detection limits of  $8\text{--}100 \text{ pg}$ , which compares to the lowest reported values for commercial vapor phase IMS systems [1,3].

The calibration curves of the compounds showed excellent linearity over a concentration range of at least two orders of magnitude having  $r^2$ -values greater than 0.99. These results are especially promising with respect to the need of establishing a quantitative IMS determination method for explosives.

#### 3.5. Separation of three common explosives by IMS

A number of different methods for analyzing explosives from complex environmental matrices using liquid chromatographic and gas chromatographic separations have been reported so far [4–6,14,15]. The separation capabilities of ESI-IMS-MS demonstrating a resolving power similar to liquid chromatography has already been demonstrated [13]. As the IMS also shows high sensitivity for many of the explosives, the use of ESI/IMS for analyzing environmental samples was taken into consideration.

The experimental data showed measurable differences in the  $K_0$ -values for most of the compounds (see Table 1). Thus, a mixture of three common explosives at concentrations of  $1 \text{ mg l}^{-1}$  (TNT) and  $2 \text{ mg l}^{-1}$  (RDX and HMX), respectively was analyzed to evaluate the separation capabilities of the instrument. In order to enhance the sensitivity of the system to RDX and HMX,  $2 \text{ mM NaCl}$  was added to the mixture. The resulting spectrum is shown in Fig. 5. Although the instrument was not optimized to give the highest possible resolution, the resolving power was sufficient to achieve baseline separation of the three compounds. The actual resolving power calcu-

lated from the data was  $57 \pm 5$  for the three peaks. In chromatographic terms, this corresponds to about 18 000 theoretical plates. Additionally, it must be pointed out that the whole separation was achieved in less than 25 ms per single spectrum resulting in a total analysis time of only 6.4 s for averaging 256 spectra.

This indicates that ESI-IMS could be a method to rapidly analyze environmental samples for mixtures of explosives at trace concentrations. Further investigations including improvement of resolution and analyzing real samples are currently in preparation.

### Acknowledgements

This project was in part supported by research grants from the Federal Aviation Administration (Grant # 97G009) and the U.S. Army Research Office (Grant DAAG559810107). Additionally, an ACS research fellowship was awarded to Reid Asbury sponsored by the Society of Analytical Chemistry of Pittsburgh.

### References

- [1] L.L. Danylewych-May, C. Cummings, Explosive and taggant detection with Ionscan, in: J. Yinon (Ed.), *Advances in Analysis and Detection of Explosives*, Kluwer Academic Publishers, Dordrecht, 1993, pp. 385–401.
- [2] R.K. Ritchie, F.J. Kuja, R.A. Jackson, A.J. Loveless, L.L. Danylewych-May, Recent developments in IMS detection technology, in: G. Harding, R.C. Lanza, L.J. Myers, P.A. Young (Eds.), *Substance Detection Systems*, International Society for Optical Engineering, Bellingham, WA, 1994, pp. 76–86.
- [3] D.D. Fetterolf, Detection of trace explosive evidence by ion mobility spectrometry, in: J. Yinon (Ed.), *Advances in Analysis and Detection of Explosives*, Kluwer Academic Publishers, Dordrecht, 1993, pp. 117–131.
- [4] S. Barshick, W.H. Griest, *Anal. Chem.* 70 (1998) 3015.
- [5] S.D. Harvey, H. Galloway, A. Krupsha, *J. Chromatogr. A* 775 (1997) 117.
- [6] C.A. Weisberg, M.L. Ellickson, *Am. Lab.* 30 (1998) 32N.
- [7] R. Wilson, A. Brittain, Explosives detection by ion mobility spectrometry, in: J.E. Dolan, S.S. Langer (Eds.), *Explosives in the Service of Man*, Royal Society of Chemistry, Cambridge, 1997, pp. 92–101.
- [8] G.E. Spangler, P.A. Lawless, *Anal. Chem.* 50 (1978) 884.
- [9] A.H. Lawrence, P. Neudorfl, *Anal. Chem.* 60 (1998) 104.

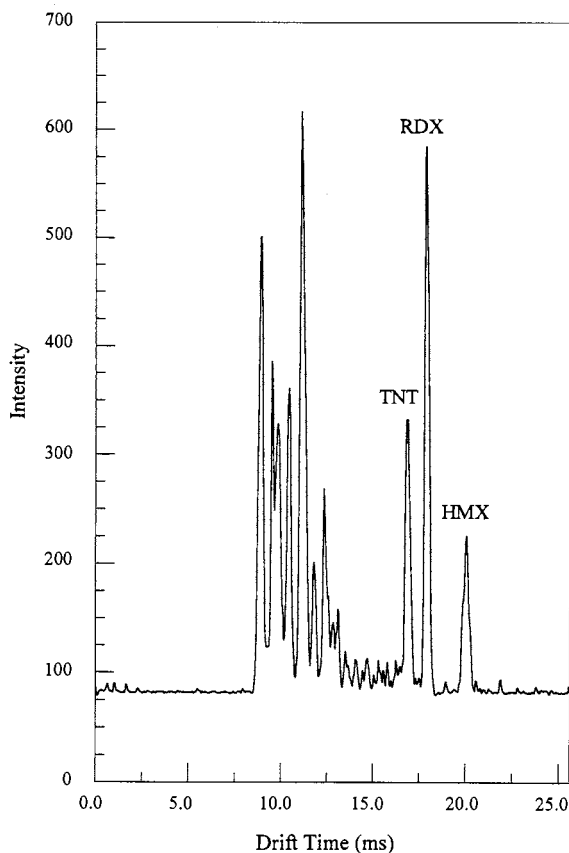


Fig. 5. Ion mobility spectrum of a mixture of TNT ( $m/z$  226), RDX ( $m/z$  257) and HMX ( $m/z$  331) showing baseline separation of these explosives. Concentrations were  $1 \text{ mg l}^{-1}$  for TNT and  $2 \text{ mg l}^{-1}$  for RDX and HMX in methanol–water (9/1, v/v) additionally containing  $2 \text{ mM NaCl}$ .

- [10] B. Casetta, F. Garofolo, *Org. Mass Spectr.* 29 (1994) 517.
- [11] J. Yinon, J.E. McClellan, R.A. Yost, *Rapid Commun. Mass Spectr.* 11 (1997) 1961.
- [12] D. Wittmer, Y.H. Chen, B.K. Luckenbill, H.H. Hill, *Anal. Chem.* 66 (1994) 2348.
- [13] C. Wu, W.F. Siems, G.R. Asbury, H.H. Hill, *Anal. Chem.* 70 (1998) 4929.
- [14] U. Lewin, J. Efer, W. Engewald, *J. Chromatogr. A* 730 (1996) 161.
- [15] F. Garofolo, V. Migliozi, B. Roio, *Rapid Commun. Mass Spectrometr* 8 (1994) 527.

# $(C_{70})_2$ -P-tert-butylcalix[6]arene complex films on electrodes catalyze the reduction of nitrite ions

Ting Liu, Mei-Xian Li, Nan-Qiang Li \*, Zu-Jin Shi, Zhen-Nan Gu, Xi-Huang Zhou

*Department of Chemistry, Peking University, Beijing 100871, PR China*

Received 1 June 1999; received in revised form 2 August 1999; accepted 3 August 1999

## Abstract

$(C_{70})_2$ -P-tert-butylcalix[6]arene complex films on GC electrode surface showed two couples of redox reactions in mixed solvent of (1:1, v:v) acetonitrile and water containing tetra-butylammonium perchlorate. The electrocatalytic reduction for nitrite by these films was observed, indicating that  $(C_{70})_2$ -P-tert-butylcalix[6]arene is capable of mediating the electron transfer to nitrite. © 2000 Elsevier Science B.V. All rights reserved.

*Keywords:*  $(C_{70})_2$ -P-tert-butylcalix[6]arene film; Catalysis; Nitrite; Cyclic voltammetry

## 1. Introduction

Recently, there is extensive interest in the host-guest complexes involving fullerenes. Both  $C_{60}$  and  $C_{70}$  form complexes with a variety of macromolecules, notably calixarenes [1–5], cyclotrimer-trylene (CTV) [6,7],  $\gamma$ -cyclodextrin [8], azacrown ethers [9] and a porphyrine [10]. Since Atwood discovered in 1994 that P-tert-butylcalix[8]arene selectively includes  $C_{60}$  in carbon soot and forms the precipitate with 1:1 stoichiometry [1], quite a few studies regarding the supramolecular chemistry of fullerene with calixarenes were carried out. Although the electrochemical properties of  $C_{60}$  and  $C_{70}$  have been widely studied in solution

as well as thin solid films on electrode surfaces [11–16], and their electrocatalytic abilities were gradually revealed [17–20], the electrochemical study of the supramolecular complex of fullerene and calixarene is still very limited. More recently, the electrochemistry of complex of  $C_{60}$ -P-tert-butylcalix[8]arene as well as  $(C_{70})_2$ -P-tert-butylcalix[8]arene were studied in our laboratory [21–23]. Bard also reported his recent study of  $C_{60}$ -P-tert-butylcalix[8]arene films using a scanning electrochemical microscope–quartz crystal microbalance [24]. The above work revealed that the electrochemistry of these complexes of fullerenes is different from that of fullerene themselves.

The present work is focused on the electrochemistry of  $(C_{70})_2$ -P-tert-butylcalix[6]arene [ $(C_{70})_2$ -L] complex films.  $C_{70}$  forms 2:1 complex with P-tert-butylcalix[6]arene from toluene solu-

\* Corresponding author. Fax: +86-10-62751708.

*E-mail address:* 1mwx@chemms.chem.pku.edu.cn (N.-Q. Li)

tion [1]. Voltammetry study showed that these films have two reversible electroreduction waves in mixed solvents of acetonitrile (MeCN) and water (1:1 v:v) between the potential range from 0.2 to  $-1.15$  V. In order to explore the possible biological and analytical application, the electrochemical catalytic reduction of nitrite ion by  $(C_{70})_2$ -L films was examined in this study. Since the electroreduction of nitrite ion usually requires a large overpotential at most electrode surfaces, study of electrocatalytic behavior of  $(C_{70})_2$ -L film for nitrite is important for better understanding its reactivity and application.

## 2. Experimental

### 2.1. Chemicals

The synthesis of  $C_{70}$  was described elsewhere [25]. Its purity (99%) was confirmed by mass spectrometry and HPLC. The *p*-tert-butylcalix[6]arene (L) (99%) was prepared in our laboratory according to a literature procedure [26,27]. Also, the  $(C_{70})_2$ -*p*-tert-butylcalix[6]arene [ $(C_{70})_2$ -L] was synthesized according to reference [1]. Elemental analysis found: C (92.7%), H (3.56%) calculated: C (93.2%), H (3.19%). Tetra-butylammonium perchlorate ( $Bu_4NClO_4$ ) was purchased from Sigma. Toluene and acetonitrile (MeCN) were distilled from  $P_2O_5$  prior to use. Sodium nitrite was of analytical reagent grade and used as received from Beijing Chemical. All other reagents were of analytical grade. Water was triply distilled from an all-quartz still. Fresh  $NaNO_2$  solutions were prepared daily. High purity nitrogen was used for deaeration.

### 2.2. Apparatus and procedures

A PAR (Princeton Applied Research) 273 potentiostat/galvanostat and a PAR Model 270 electrochemical system were used for cyclic voltammetry and Osteryoung square wave voltammetry. A combination of PARC Model 174A polarographic analyzer and a type 3086x-y recorder was also used for CV at lower scan rates. All electrochemical measurements were performed

by using a conventional electrochemical cell, with a glassy carbon (GC) as the working electrode, platinum plate as the counter electrode and a saturated calomel electrode (SCE) as the reference electrode. All electrochemical experiments were conducted under nitrogen atmosphere and at ambient laboratory temperature ( $25 \pm 2^\circ C$ ). Elemental analysis experiment was carried out by using a Vario EL Elementar (Germany). Model pHs-3 Meter (Shanghai, China).

### 2.3. Preparation of $(C_{70})_2$ -L films and $C_{70}$ films

The working electrode was a glassy carbon disk ( $d = 4$  mm), the effective electrode area was  $0.1228$  cm<sup>2</sup>, as determined by cyclic voltammogram of  $K_3Fe(CN)_6$  ( $1.0 \times 10^{-4}$  M) in  $0.10$  M KCl. The GC electrodes was polished with  $0.3$   $\mu$ m alumina slurry and washed ultrasonically for 3 min in distilled water, then in ethanol respectively. Two  $(C_{70})_2$ -L films with different thicknesses were used. GC electrodes were coated by dropping 5 or 3  $\mu$ l  $1.0 \times 10^{-4}$  M  $(C_{70})_2$ -L in toluene and dried under an infra-red lamp. The  $C_{70}$  films ( $5$   $\mu$ l  $2.0 \times 10^{-4}$  M  $C_{70}$  in toluene) were prepared in the same way.

## 3. Results and discussion

### 3.1. Voltammetric behavior of $(C_{70})_2$ -L film

Cyclic voltammetry shows that  $(C_{70})_2$ -L complex film have one pair of redox reactions in a mixed solvent of MeCN and water (1:1, v:v) containing  $0.04$  M  $Bu_4NClO_4$  as the supporting electrolyte from potential range of 0 to  $-0.75$  V (Fig. 1). Some difference between the first scan and subsequent scan was observed, indicating that there might be a structural rearrangement accompanying the release of the solvent which was entrapped during evaporation process and injection of  $Bu_4N^+$  and a small amount of anions into films [11,15,16,21–24]. Therefore, the third scan was used in further evaluations.

Osteryoung square-wave voltammetry was also used to study these films because of its better sensitivity (Fig. 2). The  $(C_{70})_2$ -L film electrodes

presents one couple of nearly reversible SWV forward and reverse waves, which can be attributed to redox of  $(C_{70})_2-L$ .

For comparison, the voltammetric behavior of  $C_{70}$  film in 1:1 mixture of MeCN and water containing 0.04 M  $Bu_4NClO_4$  was also carried out. A broad reduction wave and a reoxidation wave were observed (Fig. 3). The first reduction process of  $C_{70}$  was a slow, one electron-transfer reaction according to literature [23]. There is two  $C_{70}$  molecules in one  $(C_{70})_2-L$ . Accordingly, it was

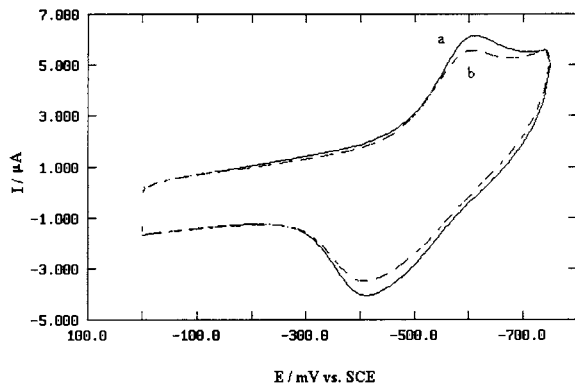


Fig. 1. Cyclic Voltammograms for  $(C_{70})_2-L$  ( $5 \mu l 1.0 \times 10^{-4} M$ ) film on a GC electrode in a mixed solvent of acetonitrile and water (1:1/v:v) containing 0.04 M  $Bu_4NClO_4$ . Scan rate is  $100 mV s^{-1}$ . (a) first scan; (b) third scan.

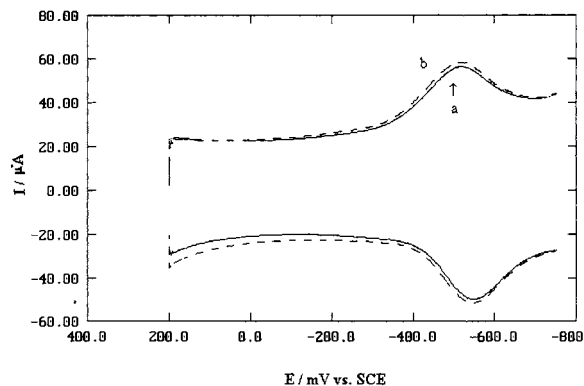


Fig. 2. Osteryoung square wave voltammograms at 25 mV pulse height (30 Hz) for  $(C_{70})_2-L$  ( $5 \mu l 1.0 \times 10^{-4} M$ ) film on a GC electrode in a mixed solvent of acetonitrile and water (1:1/v:v) containing 0.04 M  $Bu_4NClO_4$  (a) first scan; (b) third scan.

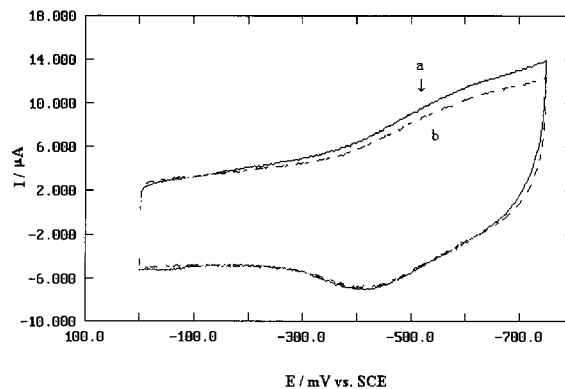
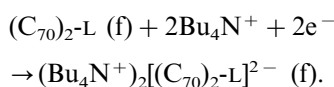


Fig. 3. Cyclic voltammograms for  $C_{70}$  ( $5 \mu l 2.0 \times 10^{-4} M$ ) film on a GC electrode in a mixed solvent of acetonitrile and water (1:1/v:v) containing 0.04 M  $Bu_4NClO_4$ . Scan rate is  $100 mV s^{-1}$ . (a) first scan; (b) third scan.

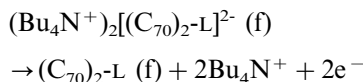
clear that the reduction reaction of  $(C_{70})_2-L$ , which was corresponded to the first reduction of  $C_{70}$  was a two-electron transfer reaction. Upon reduction,  $(C_{70})_2-L$  was reduced to  $[(C_{70})_2-L]^{2-}$ ,  $Bu_4N^+$  ions incorporated into the film to balance the negative charges. After reoxidation,  $Bu_4N^+$  left the film. The whole process caused the film reorganization. This might also be one of the reasons that the first CV scan is different from those of the following scans.

A possible mechanism for the reduction and reoxidation of  $(C_{70})_2-L$  film is suggested as follows:

The reduction process



The reoxidation process:



where 'f' represents the film on the GC electrode.

As the reduced form of  $(C_{70})_2-L$  is less soluble in the mixed MeCN and water (1:1, v:v);  $(C_{70})_2-L$  film had better stability. Its redox wave of CV and Osteryoung SWV did not change much after a dozen scans. Furthermore, at scan rates from  $50 mV s^{-1}$  up to  $300 mV s^{-1}$ , the cathodic and anodic peak currents are proportional to the scan



rate, indicating that the voltammograms are surface-confined waves and electro-transfer in the films displays thin-layer behavior [28]. For a surface-controlled process, the surface concentration ( $\Gamma^*$ ) could be calculated according to the following relation:

$$Q = nFA\Gamma^*$$

where  $n = 2$ , and  $A$  represents the effective elec-

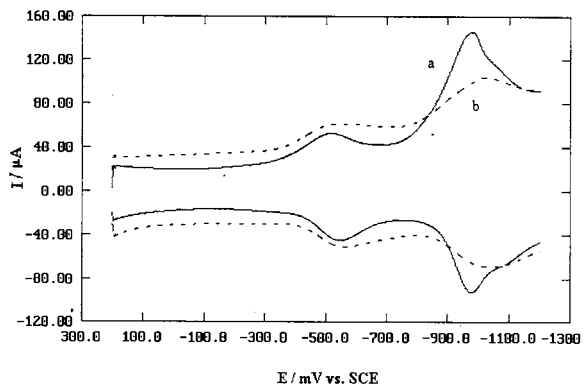


Fig. 4. Osteryoung square wave voltammograms at 25 mV pulse height (30 Hz) for  $(C_{70})_2$ -L ( $5 \mu\text{l } 1.0 \times 10^{-4} \text{ M}$ ) film on a GC electrode in a mixed solvent of acetonitrile and water (1:1 v:v) containing 0.04 M  $\text{Bu}_4\text{NClO}_4$  (a) first scan; (b) third scan.

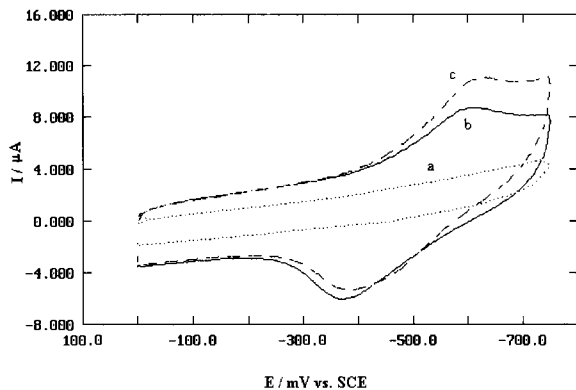


Fig. 5. Cyclic voltammograms for bare GC electrode (curve a) and  $(C_{70})_2$ -L ( $3 \mu\text{l } 1.0 \times 10^{-4} \text{ M}$ ) films on a GC electrode (curve b and curve c) in a mixed solvent of acetonitrile and water (1:1 v:v) containing 0.04 M  $\text{Bu}_4\text{NClO}_4$  (pH = 7.7). Scan rate is  $100 \text{ mV s}^{-1}$ . (a) presence of  $5.0 \times 10^{-3} \text{ M NO}_2^-$  (b) without  $\text{NO}_2^-$  (c) after added  $5.0 \times 10^{-3} \text{ M NO}_2^-$ .

trode area. The average reduction charge  $Q$  was then calculated to be  $3.26 \mu\text{C}$  by integration of the reduction peak, and  $\Gamma^*$  was calculated to be  $1.38 \times 10^{-10} \text{ mol cm}^{-2}$ , which was far smaller than the real surface coverage ( $4.07 \times 10^{-9} \text{ mol cm}^{-2}$ ). This confirms that only 3.39%  $(C_{70})_2$ -L molecules in  $(C_{70})_2$ -L films are electroactive.

If the final potential changed to  $-1.15 \text{ V}$ , two sets of nearly reversible Osteryoung SWV were observed (Fig. 4). The forward and reverse peak currents have remarkable decrease after continuous potential scan, but well-defined SWV still could be obtained. Based on above results, the electrocatalysis investigation was restricted to the first redox process of  $(C_{70})_2$ -L.

### 3.2. Electrocatalytic reduction of nitrite by $(C_{70})_2$ -L film

As is well known, the direct reduction of nitrite ion requires a large overpotential at most electrode surfaces, but reduction can be catalyzed in aqueous solution by various iso- and hetero-polyoxometalates [29–32]. As shown in Fig. 5, curve a, no electrochemical response was observed at the bare GC electrode in 0.04 M  $\text{Bu}_4\text{NClO}_4$ , a mixed solvent of MeCN and water (1:1 v:v). After the electrode was coated with  $(C_{70})_2$ -L, there was a pair of reversible  $(C_{70})_2$ -L electroreduction/electro-oxidation wave in the range 0 and  $-0.75 \text{ V}$  (Fig. 5, curve b). Noticeably, the cathodic peak current was remarkably increased and the corresponding anodic peak current decreased after addition of  $\text{NO}_2^-$  to the solution (Fig. 5, curve c).

Since cations play an important role in determining the electrochemical behavior of fullerene films, and anions could inject into  $(C_{70})_2$ -L films [11,15,16,21–24], the CV behavior of  $(C_{70})_2$ -L films as well as the catalytic activity of the  $(C_{70})_2$ -L films electrode toward nitrite ions was also examined at different pH value after addition various buffer solution. In a buffered mixed solution, such as in 0.05 M phosphate buffer solution (pH = 6.64–9.18), a mixed solvent of MeCN and water (1:1 v:v) containing 0.04 M  $\text{Bu}_4\text{NClO}_4$ ,  $(C_{70})_2$ -L films had better and stable electrochemical activity (Fig. 5). Moreover, in 0.1 M  $\text{NH}_3\text{-NH}_4\text{Cl}$

Table 1  
Effect of coating amount on the cathodic peak current<sup>a</sup>

Coating amount of (C <sub>70</sub> ) <sub>2</sub> -L (1 × 10 <sup>-4</sup> M)	1 μl	2 μl	3 μl	4 μl	5 μl	6 μl	7 μl
Cathodic peak current I (without NO <sub>2</sub> <sup>-</sup> ) (μA)	2.55	3.21	3.60	3.39	3.40	3.58	3.46
Cathodic peak current I <sub>c</sub> (added 5 × 10 <sup>-3</sup> NO <sub>2</sub> <sup>-</sup> ) (μA)	2.80	3.77	5.40	4.32	4.51	4.48	4.80

<sup>a</sup> Scan rate 0.1 V s<sup>-1</sup>.

buffered mixed solution (pH = 8–10), the CV response of (C<sub>70</sub>)<sub>2</sub>-L films was also well-defined, but the catalytic activity toward nitrite ions was not as good as that in phosphate buffered solution. These results indicated that (C<sub>70</sub>)<sub>2</sub>-L films displayed stable electrochemical activity and K<sup>+</sup>, Na<sup>+</sup>, NH<sub>4</sub><sup>+</sup>, Cl<sup>-</sup> and PO<sub>4</sub><sup>3-</sup>, had little effect on the voltammetric behavior of (C<sub>70</sub>)<sub>2</sub>-L films in the presence of Bu<sub>4</sub>NClO<sub>4</sub>. That is in the presence of 0.05 M K<sup>+</sup>, 0.1 M Na<sup>+</sup>, 0.1 M NH<sub>4</sub><sup>+</sup>, 0.1 M Cl<sup>-</sup> and 0.05 M PO<sub>4</sub><sup>3-</sup>, the change of cathodic peak currents did not exceed RSD 5%. It is known that NO<sub>2</sub><sup>-</sup> disproportionates to form NO and NO<sub>3</sub><sup>-</sup> in acidic solutions [29–32]. Therefore, the electrocatalytic study was carried out in phosphate buffer solution (pH = 7–8). (C<sub>70</sub>)<sub>2</sub>-L film showed better electrocatalytic behavior for nitrite ion in mixed solvent of MeCN and water containing phosphate buffer solution between pH = 7–8.

The influence of coating amount on the electrochemical behavior of (C<sub>70</sub>)<sub>2</sub>-L film and the electrocatalytic reduction of nitrite ion was also tested. As Table 1 showed, the catalytic peak current was significantly increased and the peak shape was well-defined when the surface coverage was between 2.44 × 10<sup>-9</sup> mol cm<sup>-2</sup> – 4.89 × 10<sup>-9</sup> mol cm<sup>-2</sup> [dropping 3, 4, 5 or 6 μl a sample of 1 × 10<sup>-4</sup> M solution of (C<sub>70</sub>)<sub>2</sub>-L in toluene on the electrode surface]. So dropping 3 μl 1 × 10<sup>-4</sup> M solution of (C<sub>70</sub>)<sub>2</sub>-L in toluene on the GC electrode surface was used in this study.

Fig. 6 illustrated the cyclic voltammogram of (C<sub>70</sub>)<sub>2</sub>-L film in the mixed solvent of MeCN and water containing nitrite ion at scan rate of 10 and 20 mV s<sup>-1</sup>. With the addition of NO<sub>2</sub><sup>-</sup>, a dramatic current increase is observed for the cathodic peak, while the corresponding anodic peak current decreased. Obviously, lower scan rate was beneficial for catalysis reaction. It was also found

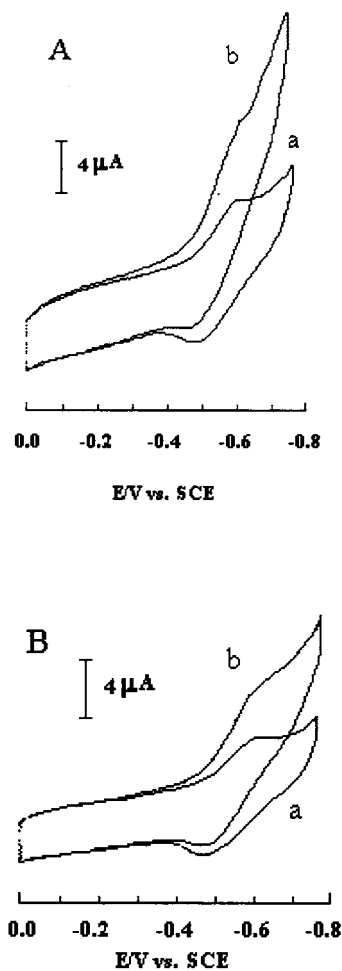


Fig. 6. Cyclic voltammograms for (C<sub>70</sub>)<sub>2</sub>-L (3 μl 1.0 × 10<sup>-4</sup> M) film on a GC electrode in a mixed solvent of acetonitrile and water (1:1/v:v) containing 0.04 M Bu<sub>4</sub>NClO<sub>4</sub>. (a) without NO<sub>2</sub><sup>-</sup> (b) after added 1.0 × 10<sup>-2</sup> M NO<sub>2</sub><sup>-</sup>. A. Scan rate is 10 mV s<sup>-1</sup>. B. Scan rate is 20 mV s<sup>-1</sup>.

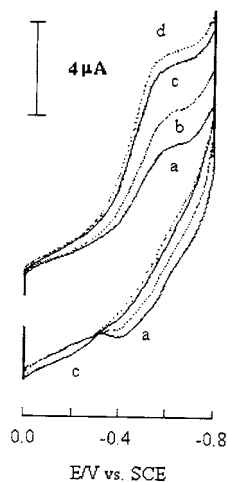


Fig. 7. Cyclic voltammograms for  $(C_{70})_2$ -L ( $3 \mu\text{l } 1.0 \times 10^{-4} \text{ M}$ ) film on a GC electrode in a mixed solvent of acetonitrile and water (1:1/v:v) containing  $0.04 \text{ M Bu}_4\text{NClO}_4$  ( $\text{pH} = 7.7$ ). Scan rate is  $10 \text{ mV s}^{-1}$ . (a) without  $\text{NO}_2^-$  (b) a +  $5.0 \times 10^{-3} \text{ M NO}_2^-$ . (c) a +  $1.0 \times 10^{-2} \text{ M NO}_2^-$  (d) a +  $1.2 \times 10^{-2} \text{ M NO}_2^-$

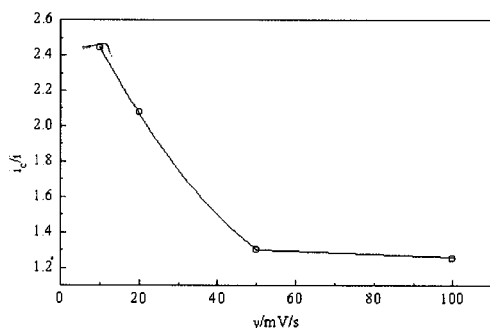
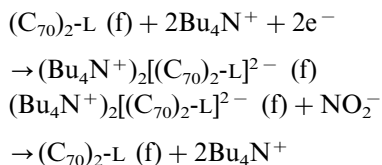


Fig. 8. Relationship of the cathodic current catalytic efficiency and scan rate.

that catalytic current increased with the concentration of nitrite ion at a fixed scan rate (Fig. 7). The insignificant decrease of anodic peak current is probably due to the lower  $\text{NO}_2^-$  concentration, and the lower kinetic constant of catalytic reaction. Catalytic efficiency expressed as the ratio of catalytic current ( $i_c$ ) to the cathodic current ( $i$ ) for  $(C_{70})_2$ -L film in solution not containing nitrite decreased with the increasing of scan rate (Fig. 8). This is another evidence of electrocatalytic reaction. A possible mechanism for the catalytic reaction might be described as follows:



+ products (containing N)

where 'f' represents the film on the GC electrode.

It has been well known that the electrochemical reduction of nitrite ion requires large overpotential at most electrode surfaces, but electrochemical catalysis using  $(C_{70})_2$ -L film electrode moves the applied potential needed to reduce the nitrite ion more positive. The rate of such reactions was enhanced by shuttling electrons between  $(C_{70})_2$ -L films and nitrite ion. The above experimental results demonstrate that the  $(C_{70})_2$ -L film electrode provides a possibility for the application in electroanalytical chemistry.

In summary, the  $(C_{70})_2$ -L films electrode have two couples of redox reaction in mixed solvents of MeCN and water(1:1, v/v). Its first reduction/reoxidation peaks are fairly stable, and can catalyze the reduction of nitrite ion.

## Acknowledgements

This project was supported by the National Natural Science Foundation of China (No. 29835110).

## References

- [1] J.L. Atwood, G.A. Koutsantonis, C.L. Raston, *Nature* 368 (1994) 229.
- [2] T. Suzuki, K. Nakashima, S. Shinkai, *Chem. Lett.* (1994) 699.
- [3] R.M. Williams, J.M. Zwier, G.H. Nachtgal, A.P. Kentgens, *J. Am. Chem. Soc.* 116 (1994) 6965.
- [4] T. Suzuki, K. Nakashima, S. Shinkai, *Tetrahedron Lett.* 36 (1995) 249.
- [5] W.M. Williams, J.W. Verhoeven, *Recl. Trav. Chim. Pays-Bas* 111 (1992) 531.
- [6] J.L. Atwood, M.J. Barnes, R.S. Burkhalter, P.C. Junk, J.W. Steed, C.L. Raston, *J. Am. Chem. Soc.* 116 (1994) 10346.
- [7] J.L. Atwood, M.J. Barnes, M.G. Gardiner, C.L. Raston, *Chem. Commun.* (1996) 1449.
- [8] T. Anderson, G. Westman, G. Stenhagen, M. Sundahi, O. Wennerstrom, *Tetrahedron Lett.* 36 (1995) 597.

- [9] F. Diederich, J. Effing, U. Jonas, L. Jullien, T. Plesnivy, H. Ringsdorf, C. Thilgen, D. Weinstein, *Angew. Chem. Int. Ed. Engl.* 31 (1992) 1599.
- [10] D.M. Eichhom, S. Yang, W. Jarrell, T.F. Baumann, L. S. Beall, A. White, D.J. Williams, A.J. Barrett, B.M. Hoffman, *J. Chem. Soc. Chem. Commun.* (1995) 1703.
- [11] F. Zhou, C. Jehoulet, A.J. Bard, *J. Am. Chem. Soc.* 114 (1992) 11004.
- [12] K. Meerholz, P. Tschunky, J. Heinze, *J. Electroanal. Chem.* 347 (1993) 425.
- [13] Y. Ohsava, T. Saji, *J. Chem. Soc. Chem. Commun.* (1992) 781.
- [14] Q. Xie, E. Perez-Coredero, L. Echegoyen, *J. Am. Chem. Soc.* 114 (1992) 3978.
- [15] C. Jehoulet, Y.S. Obeng, Y.T. Kim, F. Zhou, A.J. Bard, *J. Am. Chem. Soc.* 114 (1992) 4237.
- [16] C. Liu, S. Dong, G. Cheng, D.Y. Sun, *J. Electrochem. Soc.* 143 (1996) 3874.
- [17] Y. Huang, D.M. Wayner Danial, *J. Am. Chem. Soc.* 115 (1993) 367.
- [18] T. Fuchigami, M. Kasuga, A. Konno, *J. Electroanal. Chem.* 411 (1996) 115.
- [19] F. D'Souza, J.P. Choi, Y.Y. Hsieh, K. Shriever, W. Kutner, *J. Phys. Chem. B* 102 (1998) 212.
- [20] F. D'Souza, J.P. Choi, W. Kutner, *J. Phys. Chem. B* 102 (1998) 4247.
- [21] N. Li, B. Zhou, H. Lou, W. He, Z. Shi, Z. Gu, X. Zhou, *J. Solid State Electrochem.* 2 (1998) 253.
- [22] H. Luo, N. Li, W. He, Z. Shi, Z. Gu, X. Zhou, *Electroanalysis* 10 (1998) 576.
- [23] H. Luo, N. Li, W. He, Z. Shi, Z. Gu, X. Zhou, *J. Solid State Electrochem.* 2 (1998) 432.
- [24] D.E. Cliffel, A.J. Bard, S. Shinkai, *Anal. Chem.* 70 (1998) 4146.
- [25] Y. Zhou, Z. Gu, Y. Wu, Y. Sun, Z. Jin, Y. Xiong, Y. Sun, H. Fu, J. Wang, *Carbon* 32 (1994) 935.
- [26] C.D. Gutsche, *J. Am. Chem. Soc.* 103 (1981) 3782.
- [27] C.D. Gutsche, in: J.F. Stoddant (Ed.), *Calixarenes; Monographs in Supramolecular Chemistry*, Royal Society of chemistry, London, 1989.
- [28] A.J. Bard, L.R. Faulkner, *Electrochemical Methods*, Wiley, New York, 1980.
- [29] J.E. Toth, F.C. Anson, *J. Am. Chem. Soc.* 111 (1989) 2444.
- [30] B. Keita, A. Belhouari, L. Nadjo, R. Contant, *J. Electroanal. Chem.* 381 (1995) 243.
- [31] X. Xi, G. Wang, B. Liu, S. Dong, *Electrochim. Acta* 40 (1995) 1025.
- [32] S. Dong, X. Xi, M. Tian, *J. Electroanal. Chem.* 385 (1995) 227.

# Construction of a compact spectrofluorometer/spectrophotometer system using a flexible liquid core waveguide

Robert H. Byrne<sup>a,\*</sup>, Wensheng Yao<sup>a</sup>, Eric Kaltenbacher<sup>a</sup>,  
Robert D. Waterbury<sup>a,b</sup>

<sup>a</sup> University of South Florida, Department of Marine Science, 140 7th Ave., South, St. Petersburg, FL 33701, USA

<sup>b</sup> Ocean Optics, Inc., 380 Main Street, Dunedin, FL 34698, USA

Received 11 June 1999; received in revised form 30 July 1999; accepted 3 August 1999

## Abstract

A liquid-core waveguide made of Teflon AF-2400 has been used to construct a simple, sensitive and robust instrument capable of performing fluorimetric and spectrophotometric analyses on aqueous solutions. The instrument, which uses a CCD array detection system, is unique in that high performance is achieved for both measurement techniques with minimal changes in instrument configuration. The fluorimetric detection limits for quinine sulfate and chlorophyll-a are 0.06 nanomolar and 0.03 nanomolar, respectively. Absorbance measurements using the same instrument demonstrate nanomolar detection capacities for hydrogen sulfide and subnanomolar detection limits for methylene blue. © 2000 Elsevier Science B.V. All rights reserved.

**Keywords:** Spectrofluorometer; Spectrophotometer; Flexible liquid core waveguide; CCD array detection system

## 1. Introduction

Until recently, fluorimetric measurements have been more sensitive than measurements obtained via absorbance spectroscopy. However, with the development of long pathlength cells, the sensitivity of conventional absorbance measurements has been increased by as much as two orders of magnitude [1–3]. As an example of the expanded

sensitivity of spectrophotometric analysis, we have recently used a ten meter pathlength liquid core waveguide system to measure total iron concentrations between 0.1 and 3.5 nanomolar off the west coast of Florida. The decision to use fluorimetric or spectrophotometric procedures for a given type of environmental analysis involves consideration of analyte absorbance and fluorescence characteristics and the specificity of each type of analysis in the presence of a complex array of natural substances. Additional important considerations for measurements in the field include instrument availability, portability, durability and

\* Corresponding author. Tel.: +1-727-5531508; fax: +1-727-5531189.

E-mail address: byrne@seas.marine.usf.edu (R.H. Byrne)

power consumption. Fluorescence and absorbance measurements generally require the use of separate analytical devices, distinct in terms of optical configuration and components. In this work we demonstrate the performance of a small, sensitive and robust device that is capable of both fluorimetric and spectrophotometric analysis. The optical configuration employed for both types of analyses involves the use of a liquid core waveguide and requires very minor adjustments depending on which technique is chosen.

Liquid core waveguides (LCW) constrain light propagation within a liquid medium when the liquid has a higher index of refraction (RI) than the surrounding solid tubing. LCW's involving the use of Teflon AF-2400 (RI = 1.29) provide advantageous applications in Raman spectroscopy [4] and UV-VIS absorbance spectroscopy [1–3] relative to conventional optoelectronic designs. Fujiwara et al. [5] described the first application of liquid core capillary cells in fluorescence spectrometry. The LCW used by Fujiwara et al. was constructed of quartz (RI = 1.46) and was applicable only to liquids with indices of refraction much greater than those of aqueous solutions. Dasgupta et al. [6] were the first to report the performance of linear Teflon AF waveguides with transverse illumination (excitation) for measurement of fluorescence in aqueous systems. The use of a Teflon AF LCW with transverse excitation was reported to be highly effective for exclusion of excitation light from the detection system unless the LCW was used in coiled configuration [6]. Since Dasgupta et al. were interested in systems which were simple, yet very inexpensive and effective, the authors' system did not involve use of monochromators or spectrometers. In the present work we have investigated the use of LCWs, in coiled configuration, linked via fiber optics to a CCD array spectrometer. In coiled configuration with transverse illumination, our system is very compact and provides not only fluorescence but also highly sensitive absorbance measurements with no system re-configuration other than optional insertion or removal of blocking filters. This dual character greatly extends the analytical capabilities and sen-

sitivity of our system for use with virtually any solvent. The sample size requirement for measurements is very low. The internal volume of the 1.6 m LCW (560  $\mu\text{m}$  i.d.) used in this work is  $\approx 0.4 \text{ cm}^3$ .

## 2. Experimental

### 2.1. Apparatus

A schematic of our fluorometer/spectrometer optoelectronic layout is shown in Fig. 1. The centerpiece of the device is a liquid core waveguide (LCW) made of Teflon AF-2400 (Biogeneral), with an inner diameter equal to 560  $\mu\text{m}$  and an 800  $\mu\text{m}$  outer diameter. This 1.6 m length LCW is wound around a quartz tube (2.5 cm outer diameter). Two narrow spectrum UV lamps (JKL # BF350, peak emission near 370 nm) are mounted inside the quartz tube. The tube and helically wound LCW are enclosed in aluminum foil to maximize excitation from reflected light during fluorimetric analysis. At each end of the 1.6 m LCW, two custom 'T' couplers are used to interface the LCW to an optical fiber (Polymicro Technologies, 400  $\mu\text{m}$  core diameter) and the silicon tubing (5 mm ID) used for fluid introduction. These specially designed couplers allow light to be transmitted/collected from the ends of the LCW while simultaneously allowing fluid to be pumped through the cell. The numerical aperture of the source and detection fibers is 0.22 which closely matches the 0.27 numerical aperture of the LCW. Light output from one end of the LCW is measured with a palm-sized CCD array spectrometer (Ocean Optics S2000).

In absorbance mode light is introduced to the LCW from a fiber-coupled tungsten-halogen lamp (Ocean Optics LS-1), and the UV excitation lamps are off. In fluorescence mode the tungsten-halogen lamp is off and the UV lamps are used to excite fluorophores within the LCW's liquid core. Collected light in fluorescence mode is filtered using a high-pass filter (Melles Giot, O3FCG-459) to remove ultraviolet radiation before transmission to the spectrometer.

## 2.2. Reagents

Quinine sulfate was purchased from Fisher Scientific. Working solutions were freshly prepared by diluting the stock solution (0.1277 mM quinine sulfate in 0.05 M H<sub>2</sub>SO<sub>4</sub>) with 0.05 M H<sub>2</sub>SO<sub>4</sub>. Chlorophyll-a was purchased from Sigma. Methanol (Ultra Resi-Analyzed) was obtained from J.T. Baker. Chlorophyll working solutions were prepared by diluting a 2.150 μM stock solution with pure methanol. The chlorophyll concentration in the stock solution was determined spectrophotometrically based on absorbance measurements at 666 nm.

A hydrogen sulfide stock solution was prepared by dissolving Na<sub>2</sub>S·9H<sub>2</sub>O (washed free of oxidation product) in oxygen-free Milli-Q water. Mixed diamine reagent was prepared by dissolving 0.090 grams *N,N*-dimethyl-*p*-phenylenediamine chloride and 0.15 grams FeCl<sub>3</sub>·6H<sub>2</sub>O in 100 cm<sup>3</sup> of cool 50% (v/v) reagent grade hydrochloric acid.

Methylene blue was purchased from Sigma. Methylene blue working solutions were prepared by diluting a 20 μM stock solution in 0.005 mM HCl.

## 2.3. Procedures

Fluorescence measurement capabilities were demonstrated with quinine sulfate and chlorophyll-a. Fluorescence measurements of quinine sulfate were referenced to 0.05 M H<sub>2</sub>SO<sub>4</sub>. Chlorophyll-a fluorescence was referenced to methanol. For comparison with the work of Dasgupta et al. [6] fluorescence measurements were also obtained using methylene blue in 5 × 10<sup>-3</sup> molar HCl.

Absorbance measurement capabilities were demonstrated with sulfide, based on the methylene blue method [7]. Sulfide measurements were obtained by addition of 1 cm<sup>3</sup> of mixed diamine reagent to 100 cm<sup>3</sup> sample solutions. Absorbances were measured at 660 nm after 20 min for color development, and were referenced to absorbances at 710 nm to compensate for baseline drift. Additionally, direct absorbance measurements of methylene blue were obtained for comparison with fluorimetric measurements.

Sample solutions were introduced into the LCW capillary cell with a peristaltic pump (Rainin, model RP-1) at a flow rate of ≈ 2 cm<sup>3</sup> min<sup>-1</sup>. Samples can also be introduced to the LCW using plastic syringes. All measurements were made within a 22°C air conditioned room.

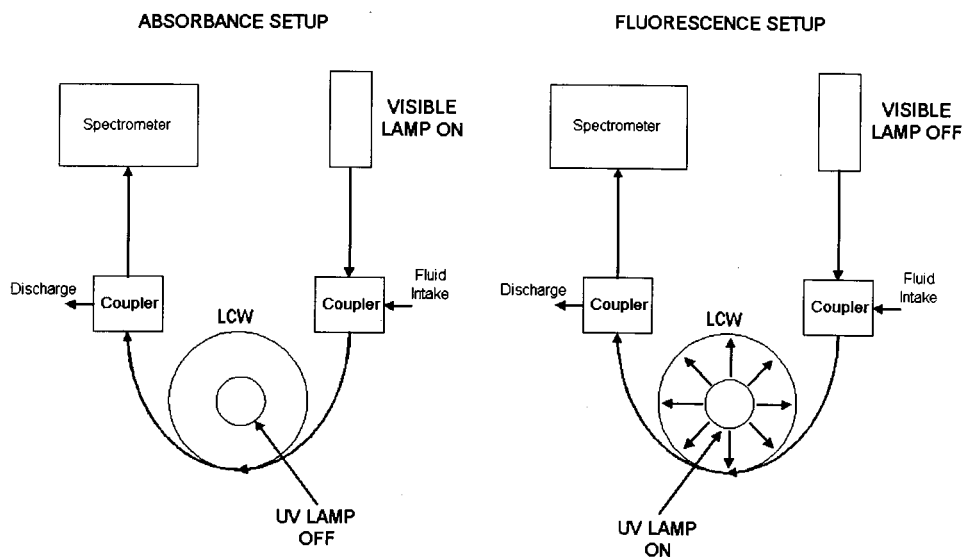


Fig. 1. Overview of the fluorometer/spectrometer optoelectronic layout.

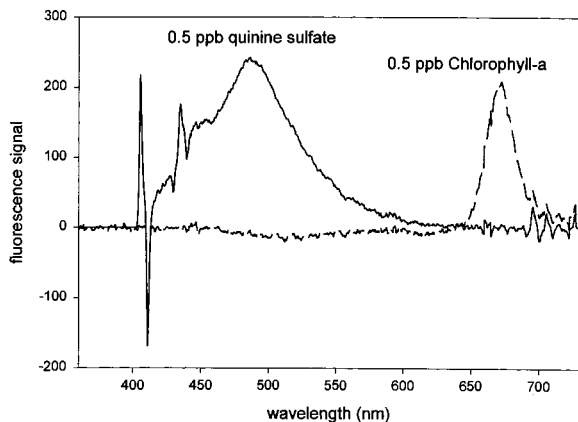


Fig. 2. Fluorescence spectra of 0.5 ppb quinine sulfate and 0.5 ppb chlorophyll-a.

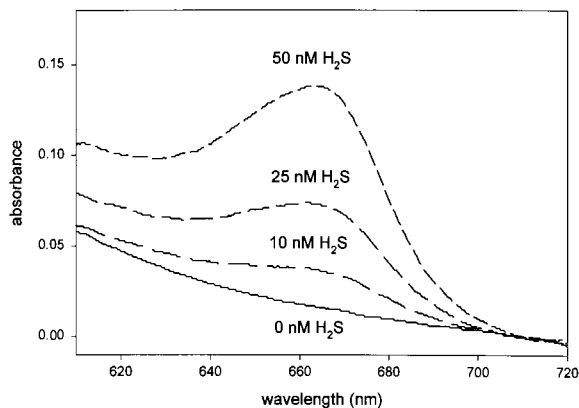


Fig. 3. Absorbance spectra of hydrogen sulfide obtained using the LPAS setup shown in Fig. 1.

### 3. Results and discussion

The fluorescence emission spectra of 0.5 ppb quinine sulfate (0.64 nanomolar) and 0.5 ppb chlorophyll-a (0.56 nanomolar) are shown in Fig. 2. Emitted light was collected for a period between 1.5 and 2 s. The quinine sulfate fluorescence response at 489 nm was linear for concentrations between 0.31 and 6.14 nanomolar:

$$\text{fluorescence signal} = (323.8 \pm 3.5)$$

$$\times [\text{quinine sulfate}] \text{ (nM)}$$

with  $r^2 = 0.999$  ( $n = 5$ ). The fluorescence response of chlorophyll-a at 671 nm was also linear over

the range of our observations (0.056 to 0.56 nanomolar), with a slope very similar to the fluorescence response (slope) obtained for quinine sulfate:

$$\text{fluorescence signal} = (365.0 \pm 4.0)$$

$$\times [\text{chlorophyll-a}] \text{ (nM)}$$

with  $r^2 = 0.998$  ( $n = 6$ ). The relative standard deviation for six measurements of 0.5 ppb quinine sulfate was 2.0%. The relative standard deviation for six measurements of 0.5 ppb chlorophyll-a was 3.3%. For measurements at higher concentrations the light collection time can be reduced to periods as short as 10 ms.

The absorbance spectra developed in our sulfide absorbance measurements are shown in Fig. 3.

$$\text{Absorbance} = (0.016 \pm 0.002)$$

$$+ (0.00240 \pm 0.00008)$$

$$\times [\text{H}_2\text{S}] \text{ (nM)}$$

with  $r^2 = 0.998$  ( $n = 4$ ). The sensitivity observed in this analysis is consistent with the subnanomolar detection limits we have observed [1–3] for iron, chromate, nitrate and other substances using long pathlength liquid core waveguides. The relative standard deviation for six measurements of 25 nanomolar sulfide was 5%.

In absorbance mode, the 1.6 meter pathlength LCW used in this work provided a detection limit for hydrogen sulfide on the order of 5 nanomolar. This detection limit can be improved with a longer LCW. This can be accomplished by extending the helical winding of the LCW at the end nearest the tungsten-halogen lamp. The fluorescence sensitivity will not be decreased as long as the excitation source is sufficiently close to the detector to minimize self absorption of fluorescence within the LCW.

In fluorescence mode the simple instrumentation used in this study provides detection limits of 0.06 nanomolar (0.05 ppb) and 0.03 nanomolar (0.03 ppb) for quinine sulfate and chlorophyll-a, where detection limits are defined here as three times the standard deviation of the solvent fluorescence. These detection limits correspond to analyte concentrations  $\approx 10\%$  as large as those



shown in Fig. 2. The fluorescence sensitivity (detection limit) of our device can be improved with a brighter excitation source, a larger radius of curvature in the helically-wrapped LCW and a more sensitive detector. A factor of two sensitivity improvement would provide a detection limit equal to that stated for a commercial fluorometer (Turner Designs, Model 10-AU-005-CE).

The LCW system used in the previous analyses was also used to perform fluorescence measurements on seawater collected off the West Coast of Florida. Fluorescence signatures can be used to characterize the dissolved organic matter (DOM) content of natural waters and provide a means of distinguishing between water mass sources in the ocean [8,9]. Fig. 4 shows the fluorescence spectra of seawater samples collected 8 miles and 140 miles off shore. The much higher fluorescence signal for the nearshore sample is consistent with a substantial increase in the biological productivity of nearshore waters.

Both fluorescence and absorbance measurements were performed on methylene blue (MB) solutions. The observed detection limit for MB fluorescence measurements was on the order of 50 nM (identical to the results obtained by Dasgupta et al. [6] with a linear LCW configuration). The detection limit obtained for methylene blue absorbance measurements was 0.2 nM. This represents a more than two orders of magnitude improvement in detection capabilities for this in-

tensely colored dye, which is widely used for measuring anionic surfactants in water and wastewater. This observation shows that combined spectrofluorometer/spectrophotometer systems offer greatly expanded detection capabilities compared to systems providing only a single mode of analysis.

The analytical apparatus described in this work is versatile, simple, sensitive and robust. Without using peristaltic pumps (which can be replaced with hand-held syringes) the power consumption of the device in either mode of operation is  $\approx 10$  watts (tungsten-halogen lamp 9.6 watts, excitation UV lamps 2 watts). The characteristics of the device make it quite amenable to autonomous in-situ analysis.

#### 4. Conclusions

In this work we have demonstrated a single photometric system capable of both fluorescence and absorbance measurements. Depending on the physical-chemical characteristics of the analyte being considered, analysts are then free to choose the type of procedure that provides optimum quantitation characteristics. For efficient fluorophores and/or substances with large molar absorptivities, detection limits much lower than 1 nanomolar are easily achieved using one or both procedures. Interconversion between the fluorescence and the absorbance configuration involves only the insertion or removal of a blocking filter and utilization of either the axial source lamp for absorbance measurements or the UV excitation lamp for fluorescence measurements.

In fluorescence configuration our measurements differ from those of Dasgupta et al. [6] in our use of a CCD array spectrometer for wavelength discrimination. Wavelength discrimination is important in natural solutions as a means of resolving the independent fluorescence contributions of multiple fluorophores. Fig. 2 clearly demonstrates that deterioration in quantitation accuracy will occur for measurements of solutions containing multiple fluorophores unless dispersive optics are an integral part of the detection system.

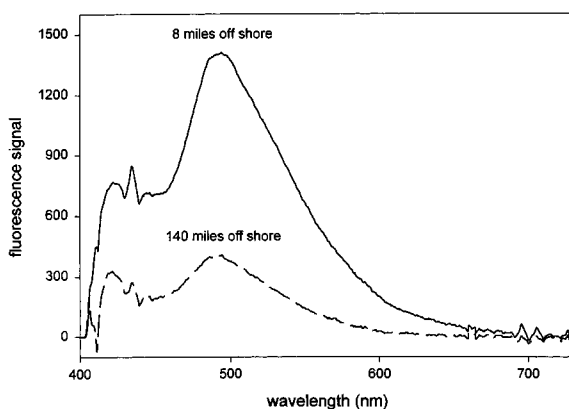


Fig. 4. Fluorescence spectra of seawater collected in the Gulf of Mexico.

The analyses of Dasgupta et al. [6] indicated that light losses occur for coil diameters smaller than 5 cm. The closely comparable fluorometric sensitivities obtained for methylene blue in their work (linear LCW configuration) and our work (2.5 cm diameter coil) is probably due to lost fluorescence output being offset by the improved signal to noise ratio inherent in systems with wavelength discrimination. In any event, we strongly emphasize that the geometrical configuration of the LCW system we have used is highly flexible. As an example, larger coil diameters and larger numbers of excitation sources can be added inside and/or outside of the coil. Alternatively, the sensitivities of both absorbance measurements and fluorescence measurements can be improved through the use long lengths of LCW (five or more meters [3]) followed by a short linear section of LCW for fluorescence measurements as in the design of Desgupta et al. [6]. With such improvements, it should be anticipated that system performance can be significantly improved relative to the design tested in the present work.

In addition, with suitable excitation optics, it should be anticipated that LCW fluorescence systems could include excitation–emission matrix spectroscopy wherein repeated emission scans are

collected at numerous excitation wavelengths. Such analyses are capable of resolving the diverse component fluorescence contributions of dissolved organic matter in natural aqueous systems (e.g. [9] and references therein).

### Acknowledgements

This work was supported by the Office of Naval Research under contract # N00014-96-1-5011.

### References

- [1] R.D. Waterbury, W. Yao, R.H. Byrne, *Anal. Chim. Acta* 357 (1997) 99.
- [2] W. Yao, R.H. Byrne, R.D. Waterbury, *Environ. Sci. Tech.* 32 (1998) 2646.
- [3] W. Yao, R.H. Byrne, *Talanta* 48 (1999) 277.
- [4] R. Altkorn, I. Koev, R.P. Van Duyne, M. Litorja, *Appl. Opt.* 36 (1997) 8992.
- [5] K. Fujiwara, J.B. Simeonsson, B.W. Smith, J.D. Winefordner, *Anal. Chem.* 60 (1988) 1065.
- [6] P.K. Dasgupta, G. Zhang, J. Li, C.B. Boring, S. Jambunathan, R. Al-Horr, *Anal. Chem.* 71 (1999) 1400.
- [7] J.D. Cline, *Limnol. Oceanogr.* 14 (1969) 454.
- [8] M.M. De Souza Sierra, O.F.X. Donard, M. Lamotte, C. Belin, M. Ewald, *Mar. Chem.* 47 (1994) 127.
- [9] P.G. Coble, *Mar. Chem.* 51 (1996) 325.

Short communication

# Study of the parameters affecting the binding of metals in solution by *Chlorella vulgaris*

C.E. López-Suárez, J.M. Castro-Romero \*, M.V. González-Rodríguez, E. González-Soto, J. Pérez-Iglesias, H.M. Seco-Lago, J.M. Fernández-Solís

Universidad de A Coruña, Departamento de Química Analítica, Escuela Universitaria Politécnica, Serantes, s/n, 15405-Ferrol, A Coruña, Spain

Received 12 March 1999; received in revised form 20 May 1999; accepted 8 July 1999

## Abstract

The ability of *Chlorella vulgaris* to accumulate heavy metals in solution (Mn, Cr, Ni, Zn and Cu) was investigated. Various parameters (algal biomass, pH and contact time of the algae with the sample) have been studied. Nine mg of algal biomass, pH 8 and 15 min of contact time, with 1 ppm of each metal, were the optimized conditions. At pH 8, the optimum value to rise the maximum binding, a fraction of metals in solution precipitates forming hydroxides. Combining both processes, a chemical–biological system for the removing of metals at ppb levels from the environment is obtained. The simultaneous determination of these five metals was performed by capillary electrophoresis (CE) with a UV/Vis detector. © 2000 Elsevier Science B.V. All rights reserved.

**Keywords:** Binding; Capillary electrophoresis; *Chlorella vulgaris*; Heavy metals

## 1. Introduction

Numerous applications of microorganisms in different technologic fields such as water treatment, wastewater treatment, biologic detoxification and heavy metals control in natural waters or industrial waste streams have been proposed and developed [1].

Microalgae have been used to remove heavy metals from waste streams due to the well-known ability of microorganisms to accumulate metal cations [2].

So, at Napa (California), where several tanneries emit chromium compounds, algae in a series of facultative ponds have been shown to adsorb chromium and settle to the pond bottom where they remain [3]. Traces of uranium, gold and silver can also be removed from solutions by mixing with freshly cultured algae and then harvesting the algae plus the adsorbed metal ions [3].

\* Corresponding author. Tel.: + 34-981-337-400; fax: + 34-981-337-401.

E-mail address: jmcr@udc.es (J.M. Castro-Romero)

At Concord (California), more than half of the calcium and magnesium in wastewaters could be removed by algal-induced precipitation in a shallow pond [3]. The operative problems that present these systems are due to the difficulty to establish standard patterns. So, these systems are only used at experimental levels and none of them have been applied at industrial level [1].

Unicellular green algae (*Chlorophyceae*) have been used because of their resistance and small mortality in the laboratory, which makes the counting of the cells easy. So, they have been chosen for different experiments in natural waters by the US Environmental Agency [3].

Darnall et al. [4] and Kubiak et al. [5] have established the binding of single metals to *Chlorella vulgaris*, studying the dependence of this process upon pH, mass and time.

Differences in adsorption profiles have also been demonstrated by using various strands of algae freeze-drying or heat-killing the algal biomass to reduce the matrix effects from living algae [6].

Harris and Ramelow [7] studied the metal-binding properties of particulate materials derived from *C. vulgaris* and *Scenedesmus quadricauda*. Both algae were able to bind strongly the four studied metals (Ag, Cu, Cd and Zn) by immobilization of the algal biomass in a cross-linked polymer, having a particularly strong affinity for Ag and Cu.

Pascucci [8] studied the effects of a multielement solution of four metals on the binding process of *C. vulgaris*. Samples were analyzed by a multielement flame atomic absorption spectrometer.

The ability of microalgae to adsorb metals from the environment reducing the toxicity levels of the industrial wastewaters is a subject of great interest for this paper. The main purpose of this work is the study of the ability of *C. vulgaris* to accumulate heavy metals as Mn, Cr, Ni, Zn and Cu.

A chemical–biological system for elimination of metals from the environment is obtained by adjusting the optimum pH for the chemical precipitation of the metals and their adsorption by the algae. The simultaneous determination of the metals was performed by capillary electrophoresis

(CE), an analytical technique that allows a rapid and efficient simultaneous analysis of ionic species at low sample concentrations.

CE has some advantages such as the high resolution of the results in a very short analysis time and significantly lower operative costs than other analytical techniques [9]. These advantages have allowed the use of CE in the determination of different ions in biological and environmental samples, foods, industrial and pharmaceutical products [10–13].

## 2. Experimental

### 2.1. Reagents and standards

Water used was obtained from a Milli-Q water purification system (Millipore, Bedford, MA) and contained no detectable analyte cations. Mn, Cr, Ni, Zn and Cu standards were prepared by mixing and diluting different 1000 mg l<sup>-1</sup> Titrisol concentrates of these elements (Merck). BGE containing 6 mM  $\alpha$ -hydroxyisobutyric acid (Waters CIA-Pak HIBA) was prepared by dissolving 0.068 g of HIBA in a volumetric flask and adding 64  $\mu$ l of UV Cat-1 reagent (Waters CIA-Pak UVCat-1 Reagent). The final pH of the BGE was 4.4 for all the analysis.

### 2.2. Instrumentation

A Waters Quanta 4000 (Waters, Milford, MA) Capillary Electrophoresis System with a 20-sample carousel, a positive power supply and a mercury lamp detector (185 nm) was used. A personal computer (466 NEC installed with a Millennium Data Station, version 2.15 Millennium Chromatography Manager) was used to control the instrument setting, data acquisition and analysis. Fused-silica capillaries 75  $\mu$ m I.D. (363  $\mu$ m O.D.) and 60 cm total length, were used in all analysis. A positive voltage of 15 kV was applied. The sample injections were carried out in electromigration mode at +15 kV for 7 s. The capillary was cleaned and prepared every morning according to the following procedure: washing for 1 min with ultrapure water, for 5 min with 0.1 M KOH, and

with ultrapure water for 2 min. Finally, the capillary was conditioned with the BGE for 10 min.

### 2.3. Validation of the method

The reproducibility of the analytical method was studied by making ten consecutive runs of a sample. Precision, in terms of relative standard deviation (R.S.D.), was 6.7, 5.2, 4.8, 4.9 and 7.6% for Mn, Cr, Ni, Zn and Cu, respectively.

The linearity of the calibration graphs, expressed as peak area versus metal ion concentration was evaluated. For most ions, a good linearity ( $R^2 = 0.9934$ – $0.9984$ ) was obtained. Table 1 summarized calibration curves and regression coefficients for each metal.

The following detection limits were obtained: 13, 30, 24, 43 and  $64 \mu\text{g l}^{-1}$  for Mn, Cr, Ni, Zn and Cu, respectively.

### 2.4. Procedure

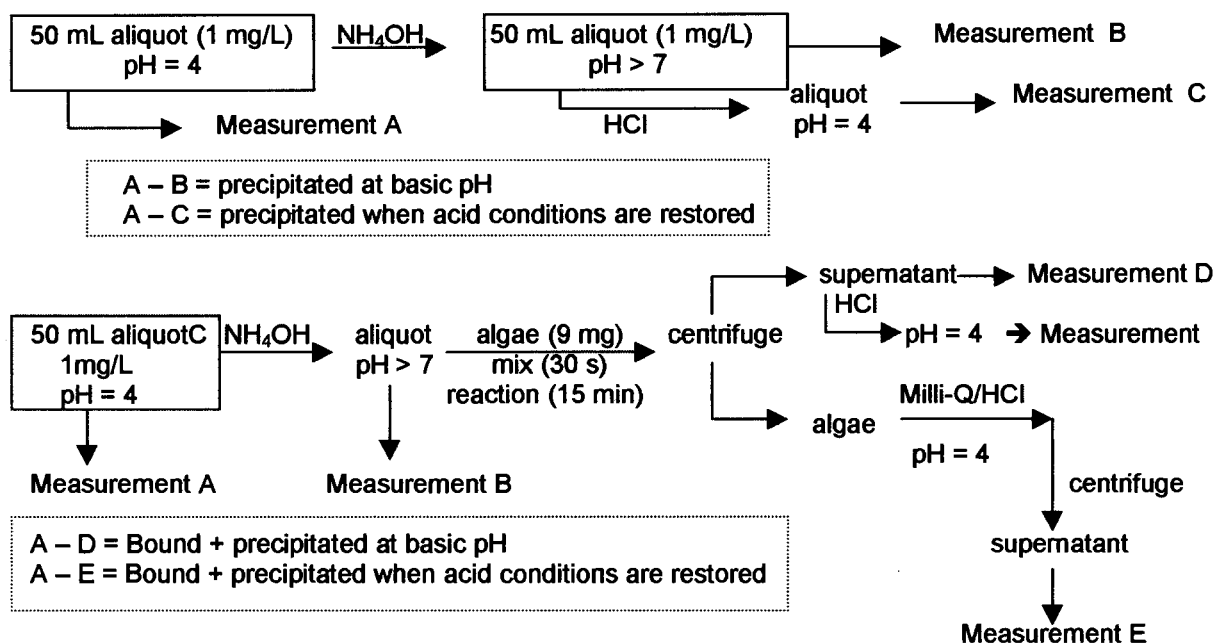
The effects of pH, mass of algae and contact time in the binding process of the algae have been studied. Ten ml aliquots of prepared solution of  $1 \text{ mg l}^{-1}$  each of Mn, Cr, Ni, Zn and Cu, were

Table 1  
Calibration curves

Metal	Calibration curve	$R^2$
Mn	$y = 6706.6x + 396.58$	0.9951
Cr	$y = 12466x + 91.758$	0.9980
Ni	$y = 11358x + 237.07$	0.9934
Zn	$y = 11457x + 282.75$	0.9984
Cu	$y = 11216x + 424.23$	0.9966

added to algae samples, and mixed for 30 s. The pH of the samples was modified with  $0.10 \text{ M NH}_4\text{OH}$  for the different experiments. The samples were subsequently centrifuged at 4000 rpm for 15 min. The supernatant was decanted for the algal pellet and simultaneously analyzed by CE for the five metals. The fraction of metal bound to the algae can be indirectly determined comparing the electropherograms performed with and without algae. The algae decanted were taken to perform biomass monitoring. Then, sedimented cells were washed three times in distilled water containing  $15 \text{ mg l}^{-1}$  of  $\text{NaHCO}_3$ , transferred to porcelain cups, dried overnight in a hot-air oven at  $105^\circ\text{C}$  and weighed [14].

After establishing the standard conditions for the binding process of algae, the percentage of



metal released from a sample at a basic pH was studied. To avoid the risk of considering the precipitated metal as metal bound, the indirect determination has been performed using the following steps:

### 3. Results and discussion

The traditional methods for heavy metals removal from industrial wastewaters consist of its basic precipitation. This process is carried out by formation of the respective metal hydroxides, whose solubility constants are usually low enough to allow the water flow after removing the suspended solids generated by the precipitation. A pH readjustment of the water before its final discharge or subsequent biological process can be necessary depending on the pH at which metal precipitation takes place. The disadvantages of this traditional method are apparent when several metals are to be removed. The high costs to achieve the precipitation of all metals and neutralize the residual water for its final discharge would be reduced if the different heavy metals could be released at a suitable discharge pH.

#### 3.1. Optimization of the binding process

The influence of different parameters (pH, algal biomass, time of contact of the algae with the sample) in the binding process of the Mn, Cr, Ni, Zn and Cu by *C. vulgaris* have been established.

#### 3.2. pH effect

The results obtained show that the pH is the main parameter in the binding process. Different experiments were made at three pH values: 4.0, 6.0 and 8.0. The higher percentage of binding was found at pH 8. When the pH of the sample was higher, a metal precipitation was observed. Fig. 1 shows that algae are able to bind a higher amount of metal at pH 8, its affinity being particularly high for Cr and Cu. It appears as though a competition for binding sites on the algal surface is occurring amongst the five metals studied.

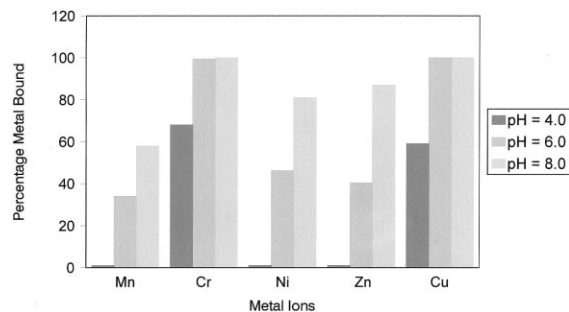


Fig. 1. Effect of the pH on the simultaneous binding of five metals by *Chlorella vulgaris* (3 mg algal biomass was mixed with  $1 \text{ mg l}^{-1}$  solution of each metal. After a 15-min reaction time the solution was centrifuged and the supernatant analyzed for metals).

Mn is scarcely bound at pH 4. At pH 6 Mn reaches a 34% binding percentage. At pH 8 the binding percentage increases in a factor near 2 over the previous value.

The obtained data show the easiness of Cr to be bound independently of the pH value. At pH 4 a 68% value is obtained. A 100% binding is obtained both at pH 6 and 8.

Ni and Zn show a very similar binding profile as a pH function. At pH 4 they are scarcely bound. At pH 6 the binding percentages obtained are 46.3 and 40.4% for Ni and Zn, respectively. At pH 8 the highest binding percentage is obtained (81% for Ni and 87% for Zn).

Cu, like Cr, has a high binding capacity independently of the pH value showing at pH 4 a 59% binding percentage and a 100% binding both at pH 6 and 8.

#### 3.3. Time effect

The effect of the contact time of the algae with the sample at pH 8, being the mass of algae and the temperature constants (5 mg and  $20^\circ\text{C}$ , respectively) was studied. Analysis were performed every 15 min during 2.5 h of contact with the sample. The higher binding occurs in the first 15 min. Cu, Cr and Zn remain unchanged starting from 15 min. Mn and Ni suffer fluctuations reaching the greatest stability starting from 90 min and recovering the binding percentage reached at 15 min.

### 3.4. Effect of the mass of the algae sample

It has been observed that the variation in the mass of *C. vulgaris* has a much greater effect on the fraction of metals bound than the other parameters studied. The residence time of the algae in the samples was 15 min at a pH 8.0 and 20°C. The alga shows again a high affinity for Cr and Cu. Only 3 mg of alga biomass is able to bind the 100% of these metals in solution. For Zn, Ni and Mn 9 mg of algae are needed to achieve the highest binding percentage.

After optimizing these parameters, the subsequent studies were made at pH 8, with 9 mg of alga biomass and 15 min contact time.

### 3.5. Study of the precipitation/redissolution of the metal ions

Increasing the pH of the sample to a value around 8 implies a loss of dissolved metals due to the formation of metal hydroxides. The recovery of the initial pH allows the quantification of the redissolved precipitated metal, obtaining a 0, 35, 45, 57 and 41% redissolution for Mn, Cr, Ni, Zn and Cu, respectively. The results obtained show that it is not possible to achieve a 100% redissolution because of the formation of stable soluble complexes that prevent the detection of the cations by CE. The comparison of these results with those obtained when algae are introduced in the sample allows the quantification of the precipitated metal that is removed with the algal biomass.

### 3.6. Study of the binding of metals by the algae at pH 8

Table 2 shows the fraction of precipitated and remainder metal in solution after modification of the initial pH value of the sample to pH 8.0. It also shows the binding percentages after introducing the algal biomass in the sample at pH 8. It is observed that the alga is able to bind almost the totality of metals that remain in solution. The totality of metals in solution competes for a number of binding sites or functional groups within the algae cells by any of the two mechanisms associated with living cells (entrapment by cellular components or active transport across the cell membrane). The binding efficiency of metals increases rapidly with the pH of the sample.

### 3.7. Study of the total amount of removed metal by the algal sample

The metallic hydroxides can be removed by the alga (bound to the algae or incorporated to the algal biomass) or remain in the final solution as solid in suspension. It is observed that the redissolved amounts in the supernatant are not significant. This may be due to the fact that the greater part of precipitate is carried down with biomass algal in the centrifugation process. The final solution would have ppb levels of metal in solution. The real results of the final solution show that Mn, Cr and Cu are below the detection limit whereas Ni and Zn appear at 20 and 40 ppb, respectively.

Table 2  
Metal binding capacity of *Chlorella vulgaris* at pH 8.0 (9 mg algal biomass, 15 min residence time)

Metal	pH 4		pH 8			
	Metal in solution (mg l <sup>-1</sup> ) <sup>a</sup>		Precipitated metal (%)	Metal in solution (%)	Metal in solution (mg l <sup>-1</sup> ) <sup>b</sup>	Metal bound (%)
Mn	1.005		7.5	92.5	0.925	95.2
Cr	1.090		49	51.0	0.556	100
Ni	1.003		24	76.0	0.762	100
Zn	1.111		33	67.0	0.744	100
Cu	1.048		39	61.0	0.639	100

<sup>a</sup> Initial metal concentrations at pH 4.0.

<sup>b</sup> Metal concentrations at pH 8.0 (after increasing the initial pH value).

#### 4. Conclusions

*C. vulgaris* is able to strongly bind the five studied metals in solution. It is observed that the optimum value to rise the maximum binding efficiency for the five studied metals is a pH near 8. The binding efficiency was more remarkable for Cr and Cu. A fraction of metals in solution precipitates forming hydroxides at this pH value. So, alga is able to bind the remainder fraction in solution.

A waste treatment method integrating microalgal adsorption (biological process)-induced precipitation (chemical process) allows removing or reducing the amount of toxic metals in wastewaters to ppb levels.

The removal of toxic metals from wastewaters appears to be very promising by using microorganisms in suspension. The treatment by precipitation as hydroxides is the most generally used technique for removing metals from waste streams. An alternative treatment system that uses inexpensive materials to remove and reclaim metals could be of technical and commercial interest [3].

#### Acknowledgements

This work has been supported by Xunta de Galicia, XUGA 17202A95.

#### References

- [1] J. Abalde, A. Cid, J.P. Fidalgo, C. Herrero, *Microalgas: Cultivo y Aplicaciones*, Servicio de Publicaciones da Universidade da Coruña, A Coruña, 1995.
- [2] L.E. Shubert, *Algae as Ecological Indicators*, Academic Press, London, 1984.
- [3] M.A. Borowitzka, L.J. Borowitzka (Eds.), *Micro-Algal Biotechnology*, Cambridge University Press, Cambridge, 1988.
- [4] D.W. Darnall, B. Greene, M.T. Henzl, J.M. Hosea, R.A. McPherson, J. Sneddon, M.D. Alexander, *Environ. Sci. Technol.* 20 (1986) 206.
- [5] W.W. Kubiak, J. Wang, D. Darnall, *Anal. Chem.* 61 (1989) 468.
- [6] C.A. Mahan, V. Majidi, J.A. Holcombe, *Anal. Chem.* 61 (1989) 624.
- [7] P.O. Harris, G.J. Ramelow, *Environ. Sci. Technol.* 24 (1990) 220.
- [8] P.R. Pascucci, *Anal. Lett.* 26 (1993) 445.
- [9] S.F.Y. Li, *Capillary Electrophoresis-Principles, Practice and Applications* (Journal of Chromatography Library, Vol. 52), Elsevier, Amsterdam, 1992.
- [10] Q. Yang, M. Jimidar, T.P. Hamoir, J. Smeyers-Verbeke, D.L. Massart, *J. Chromatogr. A* 673 (1994) 275.
- [11] J.P. Romano, J. Krol, *J. Chromatogr.* 640 (1993) 403.
- [12] P.E. Jackson, P.R. Haddad, *J. Chromatogr.* 640 (1993) 481.
- [13] S.A. Oehrle, R.D. Blanchard, C.L. Stumpf, D.L. Wulfeck, *J. Chromatogr. A* 680 (1994) 645.
- [14] A.E. Greenberg, L.S. Clesceri, A.D. Eaton (Eds.), *Standard Methods for the Examination of Water and Wastewater*, 18th edition, American Public Health Association, Washington, DC, 1992.



## Author Index

### Volume 50 (1999)

---

- Abdel-Aziz, M.S., 913  
Abu-Eid, M.A., 819  
Ahmad, H.M., 913  
Ahmed, M., 625  
Akyilmaz, E., 87  
Alia, J.M., 291, 391  
Al-Jallad, T., 1089  
Al-Kurdi, Z., 1089  
Aller, A.J., 307  
Allonier, A.-S., 227  
Al-Majed, A.A., 765  
Almeida, A.A., 253  
Al-Obaid, A.M., 765  
Alonso-Chamarro, J., 337  
Altimira, P., 695  
Amagai, T., 851  
Amézquita López, F.J., 269  
Araújo, A.N., 337  
Araújo, N.M.L., 1253  
Arikawa, Y., 799  
Arnold, M.A., 491  
Arslan, Z., 929  
Asano, Y., 595  
Astruc, A., 1  
Astruc, M., 1  
Auger, J., 423  
Azambre, B., 359
- Badwan, A., 1089  
Baeyens, W.R.G., 1197  
Balasubramanian, S., 457  
Bald, E., 1233  
Baniwal, S., 499  
Bao, L., 1267  
Baret, M., 541  
Basavaiah, K., 887  
Becerra, E., 695  
Becker, W., 283  
Belal, F., 765  
Beltran Lucena, R., 413  
Bendicho, C., 905  
Bermejo, A., 1211
- Bermejo, P., 1211  
Bermond, A., 227  
Bernal, J.L., 527  
Berzas, J.J., 261  
Birri, J., 25  
Bi, S., 1011  
Bitar, H., 743  
Blanco, M., 527  
Bosch Reig, F., 269  
Bosco Bharathi, J.R., 79  
Bottari, E., 993  
Brett, C.M.A., 1223  
Bruhn, C.G., 967  
Brynn Hibbert, D., 1275  
Bubnis, B., 1073  
Buisson, J.-F., 737  
Byrialsen, K., 367  
Byrne, R.H., 1307
- Cadoux, F., 423  
Camacho-Frias, E., 509  
Cámara, C., 165  
Camel, V., 227  
Cañabate Díaz, B., 401  
Cao, M., 1011  
Capelo, J.L., 905  
Caramão, E.B., 1035  
Cardosi, M.F., 103  
Cardoso, A.A., 959  
Caroli, S., 327  
Carreira, L.A., 827  
Carsol, M.-A., 141  
Castañeda, G., 261  
Castro-Romero, J.M., 1313  
Cayré, I., 445  
Cellulosi, D., 993  
Ceppi, S.B., 1057  
Cerdà, V., 695  
Chandra, S., 499  
Chen, H., 95  
Chen, W.-Y., 977  
Chen, Y., 1011
- Chiswell, B., 1109  
Choppin, G.R., 641  
Chow, A., 193  
Christensen, J.M., 367  
Chunshan, C., 947  
Chwatko, G., 1233  
Cladera, A., 695  
Cocho, J.A., 1211  
Conesa, F., 541  
Cong Yang, Z., 1275  
Correia dos Santos, M.M., 1245  
Cosnier, S., 219  
Costa, R.C.C., 337  
Cruces-Blanco, C., 401, 1099  
Czae, M.-z., 921
- Dai, L., 1011  
Danielsson, B., 787  
Dantas, A.F., 1253  
Dasgupta, P.K., 481, 617  
Davis, J., 103  
de Celis, B., 307  
Del Castillo, B., 261  
Deliang, L., 947  
del Olmo, M., 1141  
De Pauli, C.P., 1057  
Deyhimi, F., 1129  
Dinçkaya, E., 87  
Dominguez, R., 1211
- Ecker, S.T., 569  
Edwards, H.G.M., 291, 391  
Eid, A.F., 819  
Eisenreich, N., 283  
El Khorassani, H., 743  
Emmert, G.L., 1073  
Er Lin, R., 1275  
Estela, J.M., 695  
Etxebarria, N., 345  
Eyerer, P., 283
- Fabry, P., 541

- Fang, Y., 953  
 Fan, J., 893  
 Färber, J.-M., 239  
 Fatibello-Filho, O., 899  
 Feher, Z., 939  
 Feng, S., 893  
 Feo, J.C., 307  
 Fernandes, J.C.B., 661  
 Fernández Band, B.S., 881  
 Fernández-de Córdova, M.L., 277  
 Fernández Gutiérrez, A., 401, 1099  
 Fernández, L.A., 345  
 Fernández Recamales, M., 413  
 Fernández Romero, J.M., 57  
 Fernández Sánchez, M.L., 207  
 Fernández-Solís, J.M., 1313  
 Ferreira, J.R., 1253  
 Ferreira, S.L.C., 1253  
 Festa, M.R., 993  
 Filgueiras, A.V., 905  
 Flechsig, G.-U., 1205  
 Fomin, V.V., 113  
 Forte, G., 327  
 Forteza, R., 695  
 Fraga, J.M., 1211  
 Fu, C., 953  
 Fungaro, D.A., 1223  
  
 Galer, K., 985  
 Gallegos-Perez, J.L., 509  
 Galoppi, B., 327  
 Gámiz-Gracia, L., 875  
 Ganguly, M.K., 669  
 Gan, N., 1011  
 Gao, L., 1163  
 Garcia-Olalla, C., 307  
 Garcia-Navarro, F.J., 291, 391  
 Gaur, R.D., 1073  
 Genfa, Z., 617  
 Gesser, H.D., 193  
 Gimeno Adelantado, J.V., 269  
 Giné, M.F., 247  
 Glowacki, R., 1233  
 Gómez-Álvarez, E., 121  
 Gonzalez, C., 751  
 González LaFuente, J.M., 207  
 González-Rodríguez, M.V., 1313  
 González-Soto, E., 1313  
 Gordon, G., 1073  
 Górecki, T., 985  
 Goreti, M., 1035  
 Gorton, L., 787  
 Grundler, P., 1205  
 Guan, C.L., 1197  
 Guerin, T., 1  
 Guillaume, Y.C., 533  
  
 Gu, J., 35  
 Guo, Z., 1157  
 Gutiérrez, A.M., 165  
 Gu, Z.-N., 1299  
  
 Hanna, W.G., 809  
 Hansen, Á.M., 367  
 Hasebe, T., 677  
 Hasegawa, M., 799  
 Hassan, S.S.M., 491  
 Hassan, Y.A.M., 841  
 He, D., 1267  
 Heintz, O., 359  
 Heredia Mira, F.J., 413  
 Hernández, J., 183  
 Hernanz Vila, D., 413  
 Hilal, S.H., 827  
 Hill Jr., H.H., 1291  
 Hu, N., 1183  
 Hu, Y., 1183  
  
 Iamiceli, A.L., 327  
 Ibrahim, K.E.E., 841  
 Idriss, K.A., 913  
 Ikebukuro, K., 799  
 Ínam, R., 609  
 Isengard, H.-D., 239  
  
 Jaber, A.M.Y., 1089  
 Jacintho, A.O., 247  
 Jacobsen, B.N., 717  
 Jaffrezic-Renault, N., 219  
 Jaillais, B., 423  
 Jambunathan, S., 481  
 Jasinski, M., 1205  
 Jiang, Y., 1261  
 Jiao, K., 95  
 Jia, Y.-H., 1027  
 Jingwei, Z., 947  
 Jones, B.T., 649  
 Jun, X., 253  
 Jurado, A.B., 1141  
  
 Kaltenbacher, E., 1307  
 Kane, J.S., 25  
 Kaniowska, E., 1233  
 Karickhoff, S.W., 827  
 Karube, I., 799  
 Karuna, R., 381  
 Katakya, R., 939  
 Katsumata, H., 41  
 Kawashima, T., 41, 677  
 Khalanski, M., 227  
 Khayyami, M., 787  
 Klasmeier, J., 1291  
 Kölle, S., 283  
 Kristiansen, J., 367  
  
 Krzton, A., 359  
 Kubo, K., 73  
 Kubota, L.T., 661  
 Kurihara, M., 41, 677  
 Kuselman, I., 1135  
  
 Lajunen, L.H.J., 67  
 Larsson, P.-O., 787  
 Lavilla, I., 905  
 Lemos, V.A., 1253  
 Liang, H., 1011  
 Li, J., 617  
 Li, K.A., 585  
 Lima, J.L.F.C., 253  
 Li, M.-X., 1299  
 Li, N.-Q., 1299  
 Lin, X., 1175  
 Li, Q.L., 1197  
 Lista, A.G., 881  
 Liu, B.H., 1197  
 Liu, T., 1299  
 Liu, Y., 1261  
 Liu, Z.-L., 1027  
 Li, W., 469  
 Locatelli, C., 1079  
 Long, Y., 1267  
 Lopes da Conceição, A.C., 1245  
 López-Suárez, C.E., 1313  
 Lucy, C.A., 1283  
 Lukaszewski, Z., 299  
 Lumbreras, J.M., 307  
 Lu, N., 1261  
 Luque de Castro, M.D., 57, 875  
 Luque-Pérez, E., 121  
 Lynggaard-Jensen, A., 707  
  
 MacDonald, B., 25  
 Machado, L.F.R., 247  
 Madariaga, J.M., 345  
 Malhotra, R.K., 601, 669  
 Marcelloni, A.M., 409  
 Marchante-Gayón, J.M., 207  
 Marshall, G.D., 481  
 Martelet, C., 219  
 Martínez-Lozano, C., 49  
 Martínez, M.T., 149  
 Martín, J., 49  
 Masadome, T., 595  
 Mascini, M., 141  
 Massart, D.L., 541  
 Masuda, Y., 799  
 Matsushita, H., 851  
 McComb, M.E., 193  
 McKeegan, K.J., 103  
 Meadows, F., 1149  
 Menardo, C., 541  
 Mendoza Olivares, D., 269

- Menegário, A.A., 247  
 Mengual, O., 445  
 Merino Boyle, E., 1099  
 Meunier, G., 445  
 Miller, K.E., 1045  
 Miller, M.J., 491  
 Molina-Díaz, A., 277  
 Monsallier, J.M., 641  
 Montes, R., 959  
 Moosa Hasany, S., 625  
 Mori, A., 73  
 Moskvín, A.L., 113  
 Moskvín, L.N., 113  
 Moszhuchin, A.V., 113  
 Moya Moreno, M.C.M., 269  
 Mufazzal Saeed, M., 625
- Nagourney, S.J., 25  
 Nakamura, H., 799  
 Nakamura, T., 595  
 Namieśnik, J., 985  
 Nan Chen, G., 1275  
 Narayanan, N., 1149  
 Neira, J.Y., 967  
 Neto, G.O., 661  
 Neto, J.A.G., 959  
 Nicolai, Y., 433  
 Nicolaï, M., 433  
 Nielsen, J.L., 367  
 Nóbrega, J.A., 967  
 Nomura, Y., 799
- Okamoto, Y., 787  
 Olansandan, 851  
 Oleschuk, R.D., 193  
 Oliveira, A.F., 899  
 Olson, D.C., 481  
 Olszowy, H., 1109  
 Ortiz Boyer, F., 57  
 Ouyang, J., 1197
- Pacey, G.E., 175  
 Padmasubashini, V., 669  
 Palmer, S., 939  
 Palomeque, M.E., 881  
 Panebianco, A., 409  
 Pang, C., 1175  
 Pan, J., 35  
 Panwar, A., 499  
 Parras-Armenteros, J., 291  
 Parvinen, P., 67  
 Patonay, G., 1149  
 Peist, K., 25  
 Peña, E., 1211  
 Pérez-Conde, M.C., 165  
 Pérez-Iglesias, J., 1313  
 Pérez, M., 149
- Pérez-Ruiz, T., 49  
 Peter, S., 79  
 Petruniöck, N., 865  
 Peyrin, E., 533  
 Ping Duan, J., 1275  
 Pinilla, M.J., 261  
 Plaza, M., 149  
 Plebani, C., 409  
 Pouet, M.-F., 429  
 Pouly, F., 737  
 Prasada Rao, T., 1065  
 Puech, K., 445  
 Pugalenthi, V., 457
- Qing Chen, H., 1275  
 Quesada, J.M., 57  
 Quigley, W.W.C., 569  
 Quijano, M.A., 165
- Ramamohan, T.R., 79, 1065  
 Ramanathan, K., 787  
 Ramírez García, M.I., 401  
 Razek, T.M.A., 491  
 Reddy, M.L.P., 79, 1065  
 Reid Asbury, G., 1291  
 Ren, S., 1163  
 Ribas, K.C.L., 1003  
 Richter, P., 183  
 Robles, L.C., 307  
 Rohe, T., 283  
 Roig, B., 751  
 Ríos, A., 121  
 Rosin, C., 433  
 Rover, L., Jr., 661  
 Rufini, I.A., 247  
 Ruiz-Medina, A., 277
- Sabry, S.M., 133  
 Saji, J., 1065  
 Sakai, T., 41  
 Sakurai, T., 73  
 Salerno, A., 409  
 Salido, A., 649  
 Sanchez-Jimenez, C.J., 291  
 San Francisco, N.A., 967  
 Santos, F.J.V., 1245  
 Sanz, J., 149  
 Sanz-Medel, A., 207  
 Sasaki, K., 175  
 Sashidhar, R.B., 381  
 Satyanarayana, K., 601, 669  
 Schneider, M., 359  
 Seco-Lago, H.M., 1313  
 Sedaira, H., 913  
 Segura Carretero, A., 401, 1099  
 Senillou, A., 219  
 Serrano, D., 527
- Shao, X., 1175  
 Shih, Y., 635  
 Shin, H.-S., 641  
 Shi, Z.-J., 1299  
 Shojania, S., 193  
 Shraim, A., 1109  
 Silva, M.M., 1035  
 Simões Gonçalves, M.L.S., 1245  
 Singh, A.K., 499  
 Sitjar, P., 695  
 Skogerboe, K.J., 1045  
 Snabre, P., 445  
 Somer, G., 609  
 Song, W., 1261  
 Spinola Costa, A.C., 1253  
 SriLatha, 887  
 Strochkova, E., 1135  
 Sukhan, V., 865  
 Sultan, S.M., 841  
 Sun, I.-W., 977  
 Su, X., 469  
 Svanberg, K., 787  
 Swamy, J.M., 887  
 Synovec, R.E., 569, 1045  
 Szymanski, A., 299
- Taher, M.A., 559  
 Tanaka, H., 799  
 Tapia, A.E., 183  
 Teshima, N., 41, 677  
 Thomas, O., 729, 737, 743, 751  
 Tian, B., 1205  
 Tomás, V., 49  
 Tomaszewski, K., 299  
 Tong, S.Y., 585  
 Torabi, F., 787  
 Toral, M.I., 183  
 Torsi, G., 1079  
 Toth, K., 939  
 Touraud, E., 737, 743  
 Tousset, N., 433  
 Tranfo, G., 409  
 Tsang, J.S.W., 1283  
 Tummillo, N.J., Jr., 25  
 Tur'yan, Y.I., 1135  
 Tyson, J.F., 929
- Vahey, P.G., 569  
 Vaillant, S., 729  
 Valcárcel, M., 121  
 Vale, R., 1035  
 Vaughan, D.H., 103  
 Velasco, M.I., 1057  
 Vera-Avila, L.E., 509  
 Vilchez, J.L., 1141
- Wang, J., 893, 921, 1205

Wang, L., 953  
Wang, M., 95  
Wang, X., 1011  
Waterbury, R.D., 1307  
Weber, J.V., 359  
Wei, W., 469, 1267  
Wei, W.-z., 1019  
Wen, X.-L., 1027  
Wolcott, D.K., 481  
Wolska, L., 985  
Wu, S., 1175  
  
Xie, Y.-t., 1019  
Xuezi, D., 947  
Xu, H., 1261

Yang, H.-Y., 977  
Yao, G., 585  
Yao, S., 469, 1267  
Yao, S.-z., 1019  
Yao, W., 1307  
Ye, C., 893  
Ye, L., 1011  
Yu, T.-y., 635  
Yu, Z., 1261  
  
Zafra, A., 1141  
Zaia, C.T.B.V., 1003  
Zaia, D.A.M., 1003  
Zaporozhets, O., 865  
Zatar, N.A., 819

Zeng, H.-s., 1019  
Zeng, Y., 1183  
Zen, J.-M., 635  
Zhang, G., 893  
Zhang, L., 677, 1275  
Zhang, S., 95  
Zheng, X., 1157  
Zhou, X.-H., 1299  
Zou, G., 1011  
Zou, M., 1261  
Zuloaga, O., 345  
Zuo, X., 469



ELSEVIER

Talanta 50 (2000) 1333–1337

Talanta

www.elsevier.com/locate/talanta

## Subject Index

### Volume 50 (2000)

- Acetylsalicylic acid determination 661  
Acid-extractable 25  
Acid number 1135  
Activated carbon treatment 799  
Adsorption 625  
Adsorption chronopotentiometry 1011  
Adsorptive-catalytic stripping voltammetry 921  
Adsorptive stripping voltammetry 133  
Alcoholic group dissociation 993  
Aliphatic 641  
Alloys and biological samples 559  
Aluminium 1011  
Amberlite XAD-4 509  
Ammonium diethyl dithiophosphate 959  
Ammonium ion-selective electrode 1129  
Amperometric detection 953  
Anodic stripping voltammetry 1223  
Aromatic 641  
Arsenate 1109  
Arsenic 1, 959, 1109  
Arsenite 1109  
*Arthromyces ramosus* peroxidase 799  
Ascorbate oxidase 87  
Ascorbic acid 87, 893, 1027  
Atomic fluorescence 875
- Baseline separation 1291  
Batch injection analysis 1223  
Beclomethasone dipropionate 527  
Binding 1313  
Biogenic amines 141  
Biological fluids 765  
Biosensor 87, 219  
Bismuth 977  
Bisphenol A (BPA) 1141  
Bovine serum albumin 1149  
Bromazepam 841  
Bromide ion 595  
Bromide-selective electrode detector 595  
BTEX 193  
Bulk acoustic wave sensor 1267  
Butylated hydroxyanisole (BHA) 1099
- Butyltin chloride 149
- Cadmium 967, 1035  
Calcein 881  
Calcium 929  
Calmagite 1253  
Capillary electrophoresis 533, 1313  
Carbocysteine 1003  
Carboxyarsenazo 585  
Carboxyl groups 641  
Carboxymethyl cellulose 1267  
Catalysis 1299  
Catalytic hydrogen wave 609  
Catalytic potential titration 947  
Catalytic reaction 41  
Catecholamine 1197  
CCD array detection system 1307  
Cd(II) 1175  
Cellulase 1267  
Ceterizine hydrochloride 887  
Chemically based model 1065  
Chemically-modified electrode 635  
Chemical modifiers 967  
Chemical separation 601  
Chemiluminescence 677, 799  
Chemometric methodology 533  
Chemometrics 841  
*Chlorella vulgaris* 1313  
Chloride determination 67  
Chlorination 227  
Chlorine dioxide 1073  
Chromatomebrane extraction 113  
Circular dichroism (CD) 1149  
Coal analysis 1035  
Co-electroosmotic capillary electrophoresis 953  
Coiled reactor 899  
Cold vapor mercury method 175  
Colloids 729  
Complexation equilibria 913  
Conductivity detection 1197  
Continuous cleanup/preconcentration 57  
Copper 1035

PII: S0039-9140(99)00299-4

- Copper determination 41, 905, 1253  
(C<sub>70</sub>)<sub>2</sub>-P-tert-butylcalix[6]arene film 1299  
Crystal violet 947  
Cyanex 923 79  
Cyanex 301 79  
Cyano propyl stationary phase 569  
Cyclic voltammetry 1027, 1261, 1299  
Cyclodextrin 35  
β-Cyclodextrin 533  
Cyclodextrins 939  
Cysteine 41, 1003
- Dansyl chloride labelling 1099  
Degradation 1089  
Derivative fluorescence 1141  
Derivative spectrophotometry 559, 669  
Detection limits 921  
Developer 595  
Diamine oxidase 141  
Didodecyltrimethylammonium polyacrylate 1183  
Differential pulse mode 133  
Differential pulse polarography 609  
Differential scanning potentiometry 1057  
Dihaloacetonitriles 227  
Dimethylarsenic acid 1109  
Dithizone 865  
D-Mannite 993  
Domestic microwave oven 899  
Dopamine 677, 1027, 1197  
Dosage forms 765  
Double chamber bulk acoustic wave detector 1019  
Double-focusing sector field inductively coupled plasma mass spectrometry 207  
Drinking water 649  
Drug formulation 635  
Dynamic surface tension detector (DSTD) 1045
- Electroanalysis 977  
Electrocatalysis 921, 1183  
Electrochemical 103  
Electrochemical detection 1205  
Electrochemical immunoassay 95  
Electrogenerated chemiluminescence 1275  
Electrospray ionization 1291  
Electrothermal-AAS 905  
Electrothermal atomisation 67  
Electrothermal evaporation 67  
Enzymatic hydrolysis 1267  
Enzyme electrode 87  
Enzyme field effect transistor 219  
Enzyme immobilization 87  
Epinephrine 1197  
ETAAS 1211  
Experimental design 527  
Extraction 1065  
Extraction-chromatographic preconcentration 113  
Extractive second derivative spectrophotometry 183  
FAAS 1253  
Factorial design 149  
Fermentation 1019  
Ferritin 95  
FIA 881  
Filtration 985  
Fish spoilage 141  
Flame atomic absorption spectrometry 25, 457, 929  
Flexible liquid core waveguide 1307  
Flow analysis 1205  
Flow injection 121  
Flow-Injection 49, 677  
Flow injection 875, 893, 929  
Flow injection analysis 113, 595  
Flow-injection analysis 799  
Flow injection analysis 1045  
Flow-injection analysis 959  
Flow injection analysis (FIA) 787  
Flow injection spectrophotometric 899  
Flow-injection spectrophotometric method 41  
Fluorescence behavior 73  
Fluorescence detector 617  
Fluorescence quenching 491  
Fluoride 1245  
Fluorimetric determination 881  
Fluorimetry 1099  
Fluoroquinolones 765  
Fluorionophore 73  
Food analysis 1099  
Fractionation 729  
Frontal analysis 509  
Fruit juices 87
- Gas phase molecular absorption spectrometry 149  
Geological materials 669  
Glassy carbon electrode 1027  
Global nitrogen 751  
Glycerine 993  
Gradient flow titration 1245  
Grain 947  
Graphite furnace atomic absorption spectrometry 25, 1035  
Ground water 67
- Halophenols 227  
Heat pulse 1205  
Heavy metals 1313  
Hemin 1275  
Hg 881  
Hg(II)-SCN 625  
5-HIAA 1261  
High-performance liquid chromatography 207  
High performance liquid chromatography 165  
High resolution spectrophotometry 1073  
Homocysteine 1233  
Horseradish peroxidase (HRP) 95  
Hot wire electrochemistry 1205  
HPLC 1, 1089, 1233

- HPLC/post-column fluorimetric derivatisation 57  
Human gastric juice 1261  
Human urine 165  
Humic acid 641  
Humic acids 1057  
Hydraulic oils 1135  
Hydride generation 149, 959, 1109  
Hydrochloric acid 841  
Hydrodynamic modulation 1205  
Hydrogen peroxide 1157
- IgG 1275  
Imidazole 533  
Impurities 601  
INCAT 193  
Inclusion constant 35  
Indoor pollution 851  
Inductively coupled plasma atomic emission spectrometry 25  
Inductively coupled plasma-atomic emission spectrometry 457  
Inductively coupled plasma atomic emission spectrometry 601, 669  
Inductively coupled plasma mass spectrometry 165  
Industrial wastewater 737  
In(III) 1175  
Interferences 541, 1079  
Interfering ions 1129  
Inverse least-squares regression 527  
Ion-chromatography 1019  
Ion chromatography 1197  
Ionization equilibrium constant 827  
Ion mobility spectrometry 1291  
Ion-pair complex 887  
Ion selective electrode 947  
Ion-selective electrode (ISE) 1129  
Ion-selective electrodes 541, 939  
Ion sensor 499  
Iron determination 183  
Iron(II) 841  
Iron(III) 41, 1065  
Iron speciation 1211  
Isoniazid 469  
Isosbestic point 729  
ISP sensor 469
- Kinetically-hindered surface active analytes 1045  
Kinetics parameters 1267  
Kinetic spectrophotometric method 893
- Lactic acid 121  
L-cysteine 1109  
Lead 967, 1035  
Lidocaine 939  
Liquid chromatography 569  
Liquid core waveguide 617  
L-Serine 993  
Lucigenin 677, 1275  
Macrocycle 499
- Magnesium 929  
*m*-Aminophenol 95  
Manganese 947  
Manganese dioxide 1157  
Manganese(II) determination 913  
Mebendazole 1089  
Membrane sensor 499  
Mercury thin-film electrode 1223  
Metal ions determination 865  
Metals determination 25  
Metrological parameters 1135  
Mg-selective electrodes 499  
Micellar effect 1027  
Micelle 1283  
Microextraction 193  
Micro liquid-liquid extraction 1141  
Microscopic ionization constants 827  
Microwave digestion 25, 875  
Milk 1211  
Milk samples 121  
Modified carbon paste electrode 1157  
Modified silica gel 865  
Molecular absorption 67  
Molybdenum(VI) 609  
Monitor 1019  
Monitoring 743  
Monomethylarsonic acid 1109  
Multi-element Hollow Cathode Lamp 649  
Multivariate calibration 541  
Mussels 967  
Myoglobin 1183
- NAD<sup>+</sup> and NADH 787  
Natural water 113, 1011  
Natural water samples 1253  
*N*-Hydroxysuccinimidimido gel 799  
Nickel 559  
Niobate-tantalates 669  
Nitrate 819  
Nitrite 103, 819, 1299  
Nitroso-R salt 559  
Norepinephrine 1197  
Normal and cancer tissues 787
- Oil products and phenols 113  
On-line alkaline hydrolysis 661  
On-line analysis 1175  
Optical absorbance detectors 481  
Optical fiber coupled light emitting diode 481  
Optical sensor 491  
Overlapping spectrophotometric signals 1163  
Oxalic acid 953  
Oxidant 751  
Ozone 175
- Palladium 809  
*para*-Cl-phenylazo-R-acid 809

- Partial least squares 1163  
Particulate pollution 729  
Passive sampler 851  
*p*-Benzoquinone 1003  
Pb(II) 1175  
pH 827  
Pharmaceutical detection 469  
Pharmaceutical dosage forms 1089  
Pharmaceutical products 1003  
1,10-Phenanthroline 41  
Phenazopyridine hydrochloride 133  
Phenol 103, 509, 569  
3-Phenyl-4-benzoyl-5-isoxazolone 1065  
Phenylethyl alcohol 527  
Phloroglucinol 103  
pH-Metry 1135  
Phosphate buffer 1283  
Phosphate ion 799  
Phosphomolybdenum blue 819  
Phosphorus 751  
Photochemical reaction 49, 121  
Photoinduced electron transfer 73  
 $pK_a$  827  
Plasma 1233  
Plasma and urine samples 133  
Plasma samples 57  
Polychlorinated biphenyls 985  
Polycyclic aromatic hydrocarbons 985  
Poly(ester sulphonic acid) modified electrodes 1223  
Polyurethane foam 625  
Portland cement analysis 913  
Potentiometric selectivity coefficient 1129  
Potentiometric sensor 1157  
Procaine 35  
Protein determination 585  
Proteins 939  
Putrescine oxidase 141  
Pyruvate oxidase G 799
- Quadrupole inductively coupled plasma mass spectrometry 207  
Quality assurance 25  
Quality control 695  
4-Quinolones 765
- Rare earths 79  
Rayleigh light scattering 585  
Reactor-grade uranium 601  
Reduced mobility constants 1291  
Reducing sugars 899  
Reference materials 25  
Reflective flow-through cell 481  
Rhodamine 6G 893  
River water 799  
Rubenic acid 1011  
Ruthenium determination 183
- Salicylate tubular electrode 661
- SAR 827  
Sea water 227  
SEC-HPLC 1211  
Sediments 1079  
Selective reduction 1109  
Selenium 1, 875  
Selenium(IV) 609  
Selenium speciation 165  
Semi-micro mechanics 707  
Separation 1065  
Separation factors 79  
Sequential injection analysis 841  
Sewer systems 707  
Silicon removal 929  
Simultaneous quantitative analysis 1163  
Sludge 25  
Slurry sampling 1035  
Soil dissolution 929  
Solid-liquid extraction 905  
Solid phase extraction 509  
SPARC 827  
Speciation 1, 827, 1109  
Spectrofluorometer 1307  
Spectrophotometer 1307  
Spectrophotometric method 887  
Spectrophotometry 809, 819, 913, 959, 1003  
Spectroscopy 103  
Squarylium dye 1149  
Standard Reference Materials® 25  
Statistical analysis 457  
Stripping voltammetry 977  
Strontium determination 929  
Sulfur dioxide 491  
Surface water 985  
Surfactant 1283  
Surfactant-polymer multibilayer composite films 1183  
Suspended particulate matter 985  
Synergistic extraction 79  
Syringe 695
- Tea 635  
The constant current coulometric titration method 35  
Theophylline 635  
Thermodynamic characteristics 625  
Titanium(IV) 1065  
Titration 1283  
Tl(I) 1175  
TOC 743  
Tosflex 977  
Total chromium 457  
Total sulphide 737  
Toxic 1011  
Trace determination 1079  
Trace metals 921  
Treatment 717  
Tuberculosis 469  
Tungsten 669  
Tungsten coil electrothermal atomizer 967



- Ultrasound 905
- Univariate calibration 541
- Urban 717
- Urea 219
- Urease 219
- Urinary selenium speciation 207
- Urine 953
- UV detection 1233
- UV spectrophotometry 729, 737, 743
- UV-visible spectrometry 457
  
- Vitamin C tablets 87
- Vitamin D<sub>3</sub> hydroxymetabolites 57
- Vitamin K<sub>1</sub> 49
- VOC 193
- Volatile organohalogen compounds 851
  
- Voltammetric analyzer 1175
- Voltammetry 95, 1079
  
- Wastewater 717, 729, 743
- Waste water systems 707
- Water analysis 509, 1141
- Water analysis. 1245
- Water mobile phase 569
- Waters 695
- Wavelet multiresolution analysis 1163
- Wavelet transform 1175
- W-Coil atomic absorption spectrometer 649
  
- Zinc dithizonate 865
- Zwitterionic equilibria 827